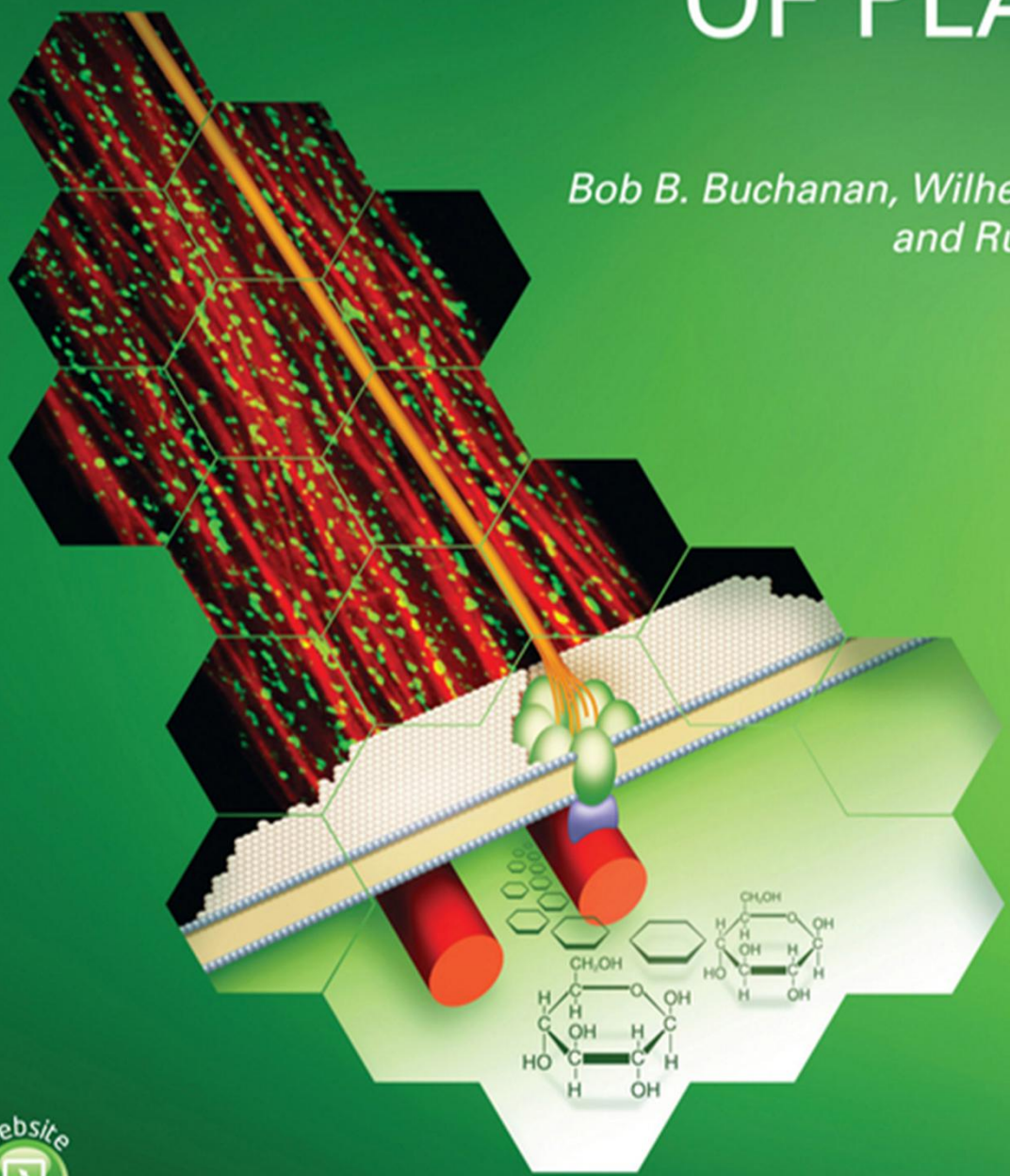
American Society of Plant Biologists

SECOND EDITION

BIOCHEMISTRY & MOLECULAR BIOLOGY OF PLANTS

EDITED BY
Bob B. Buchanan, Wilhelm Gruissem, and Russell L. Jones



with website

WILEY Blackwell

BIOCHEMISTRY & MOLECULAR BIOLOGY OF PLANTS

BIOCHEMISTRY & MOLECULAR BIOLOGY OF PLANTS



EDITED BY

Bob B. Buchanan, Wilhelm Gruissem, and Russell L. Jones

American Society of Plant Biologists

WILEY Blackwell

This edition first published 2015 © 2015 by John Wiley & Sons, Ltd

Registered Office
John Wiley & Sons, Ltd, The Atrium, Southern Gate, Chichester, West Sussex, PO19 8SQ, UK

Editorial Offices
9600 Garsington Road, Oxford, OX4 2DQ, UK
The Atrium, Southern Gate, Chichester, West Sussex, PO19 8SQ, UK
111 River Street, Hoboken, NJ 07030-5774, USA

For details of our global editorial offices, for customer services and for information about how to apply for permission to reuse the copyright material in this book please see our website at www.wiley.com/wiley-blackwell.

The right of the author to be identified as the author of this work has been asserted in accordance with the UK Copyright, Designs and Patents Act 1988.

All rights reserved. No part of this publication may be reproduced, stored in a retrieval system, or transmitted, in any form or by any means, electronic, mechanical, photocopying, recording or otherwise, except as permitted by the UK Copyright, Designs and Patents Act 1988, without the prior permission of the publisher.

Designations used by companies to distinguish their products are often claimed as trademarks. All brand names and product names used in this book are trade names, service marks, trademarks or registered trademarks of their respective owners. The publisher is not associated with any product or vendor mentioned in this book.

Limit of Liability/Disclaimer of Warranty: While the publisher and author(s) have used their best efforts in preparing this book, they make no representations or warranties with respect to the accuracy or completeness of the contents of this book and specifically disclaim any implied warranties of merchantability or fitness for a particular purpose. It is sold on the understanding that the publisher is not engaged in rendering professional services and neither the publisher nor the author shall be liable for damages arising herefrom. If professional advice or other expert assistance is required, the services of a competent professional should be sought.

Library of Congress Cataloging-in-Publication Data are available.

Paperback ISBN: 9780470714218
Hardback ISBN: 9780470714225

A catalogue record for this book is available from the British Library.

Wiley also publishes its books in a variety of electronic formats. Some content that appears in print may not be available in electronic books.

Cover image: The illustration on the cover shows a fluorescence image of an *Arabidopsis* epidermal cell depicting the localization of cellulose synthase (CESA, green) and microtubules (red). The overlying graphic shows how the synthesis of a cellulose microfibril (yellow) is related to the CESA complex, portrayed as a rosette of six light green particles embedded in the plasma membrane that are attached to a microtubule by a purple linker protein (CSI1). Fluorescent image courtesy of Chris Somerville and Trevor Yeats, Energy Biosciences Institute, University of California, Berkeley.
Cover design by Dan Jubb.
Complex illustrations by Debbie Maizels, Zoobotanica Scientific Illustration.

Set in 10/12pt Minion by SPi Global, Pondicherry, India

1 2015

BRIEF CONTENTS

I COMPARTMENTS

1 Membrane Structure and Membranous Organelles 2
2 The Cell Wall 45
3 Membrane Transport 111
4 Protein Sorting and Vesicle Traffic 151
5 The Cytoskeleton 191

II CELL REPRODUCTION

6 Nucleic Acids 240
7 Amino Acids 289
8 Lipids 337
9 Genome Structure and Organization 401
10 Protein Synthesis, Folding, and Degradation 438
11 Cell Division 476

III ENERGY FLOW

12 Photosynthesis 508
13 Carbohydrate Metabolism 567
14 Respiration and Photorespiration 610

IV METABOLIC AND DEVELOPMENTAL INTEGRATION

15 Long-Distance Transport 658
16 Nitrogen and Sulfur 711
17 Biosynthesis of Hormones 769
18 Signal Transduction 834
19 Molecular Regulation of Reproductive Development 872
20 Senescence and Cell Death 925

V PLANT ENVIRONMENT AND AGRICULTURE

21 Responses to Plant Pathogens 984
22 Responses to Abiotic Stress 1051
23 Mineral Nutrient Acquisition, Transport, and Utilization 1101
24 Natural Products 1132

CONTENTS

The Editors xi
List of Contributors xii
Preface xv
About the Companion Website xvi

I COMPARTMENTS

1 Membrane Structure and Membranous Organelles 2

Introduction 2
1.1 Common properties and inheritance of cell membranes 2
1.2 The fluid-mosaic membrane model 4
1.3 Plasma membrane 10
1.4 Endoplasmic reticulum 13
1.5 Golgi apparatus 18
1.6 Exocytosis and endocytosis 23
1.7 Vacuoles 27
1.8 The nucleus 28
1.9 Peroxisomes 31
1.10 Plastids 32
1.11 Mitochondria 39
Summary 44

2 The Cell Wall 45

Introduction 45
2.1 Sugars are building blocks of the cell wall 45
2.2 Macromolecules of the cell wall 51
2.3 Cell wall architecture 73
2.4 Cell wall biosynthesis and assembly 80
2.5 Growth and cell walls 90
2.6 Cell differentiation 99
2.7 Cell walls as sources of food, feed, fiber, and fuel, and their genetic improvement 108
Summary 110

3 Membrane Transport 111

Introduction 111
3.1 Overview of plant membrane transport systems 111
3.2 Pumps 120
3.3 Ion channels 128
3.4 Cotransporters 142
3.5 Water transport through aquaporins 146
Summary 148

4 Protein Sorting and Vesicle Traffic 151

Introduction 151
4.1 The cellular machinery of protein sorting 151
4.2 Targeting proteins to the plastids 153
4.3 Targeting proteins to mitochondria 157
4.4 Targeting proteins to peroxisomes 159
4.5 Transport in and out of the nucleus 160
4.6 ER is the secretory pathway port of entry and a protein nursery 161
4.7 Protein traffic and sorting in the secretory pathway: the ER 175
4.8 Protein traffic and sorting in the secretory pathway: the Golgi apparatus and beyond 182
4.9 Endocytosis and endosomal compartments 188
Summary 189

5 The Cytoskeleton 191

Introduction 191
5.1 Introduction to the cytoskeleton 191
5.2 Actin and tubulin gene families 194
5.3 Characteristics of actin filaments and microtubules 196
5.4 Cytoskeletal accessory proteins 202
5.5 Observing the cytoskeleton: Statics and dynamics 207
5.6 Role of actin filaments in directed intracellular movement 210
5.7 Cortical microtubules and expansion 216
5.8 The cytoskeleton and signal transduction 219
5.9 Mitosis and cytokinesis 222
Summary 238

II CELL REPRODUCTION

6 Nucleic Acids 240

Introduction 240
6.1 Composition of nucleic acids and synthesis of nucleotides 240
6.2 Replication of nuclear DNA 245
6.3 DNA repair 250
6.4 DNA recombination 255
6.5 Organellar DNA 260
6.6 DNA transcription 268
6.7 Characteristics and functions of RNA 270
6.8 RNA processing 278
Summary 288

7 Amino Acids 289

Introduction 289
7.1 Amino acid biosynthesis in plants: research and prospects 289
7.2 Assimilation of inorganic nitrogen into N-transport amino acids 292
7.3 Aromatic amino acids 302
7.4 Aspartate-derived amino acids 318
7.5 Branched-chain amino acids 326
7.6 Glutamate-derived amino acids 330
7.7 Histidine 333
Summary 336

8 Lipids 337

Introduction 337
8.1 Structure and function of lipids 337
8.2 Fatty acid biosynthesis 344
8.3 Acetyl-CoA carboxylase 348
8.4 Fatty acid synthase 350
8.5 Desaturation and elongation of C_{16} and C_{18} fatty acids 352
8.6 Synthesis of unusual fatty acids 360
8.7 Synthesis of membrane lipids 365
8.8 Function of membrane lipids 373
8.9 Synthesis and function of extracellular lipids 382
8.10 Synthesis and catabolism of storage lipids 389
8.11 Genetic engineering of lipids 395
Summary 400

9 Genome Structure and Organization 401

Introduction 401
9.1 Genome structure: a 21st-century perspective 401
9.2 Genome organization 404
9.3 Transposable elements 416
9.4 Gene expression 422
9.5 Chromatin and the epigenetic regulation of gene expression 430
Summary 436

10 Protein Synthesis, Folding, and Degradation 438

Introduction 438
10.1 Organellar compartmentalization of protein synthesis 438
10.2 From RNA to protein 439
10.3 Mechanisms of plant viral translation 447
10.4 Protein synthesis in plastids 450
10.5 Post-translational modification of proteins 457
10.6 Protein degradation 463
Summary 475

11 Cell Division 476

Introduction 476
11.1 Animal and plant cell cycles 476
11.2 Historical perspective on cell cycle research 477
11.3 Mechanisms of cell cycle control 482
11.4 The cell cycle in action 488
11.5 Cell cycle control during development 497
Summary 506

III ENERGY FLOW

12 Photosynthesis 508

Introduction 508
12.1 Overview of photosynthesis 508
12.2 Light absorption and energy conversion 511
12.3 Photosystem structure and function 519
12.4 Electron transport pathways in chloroplast membranes 529
12.5 ATP synthesis in chloroplasts 537
12.6 Organization and regulation of photosynthetic complexes 540
12.7 Carbon reactions: the Calvin–Benson cycle 542

12.8 Rubisco 548
12.9 Regulation of the Calvin–Benson cycle by light 551
12.10 Variations in mechanisms of CO_2 fixation 557
Summary 565

13 Carbohydrate Metabolism 567

Introduction 567
13.1 The concept of metabolite pools 570
13.2 The hexose phosphate pool: a major crossroads in plant metabolism 571
13.3 Sucrose biosynthesis 573
13.4 Sucrose metabolism 577
13.5 Starch biosynthesis 580
13.6 Partitioning of photoassimilates between sucrose and starch 587
13.7 Starch degradation 593
13.8 The pentose phosphate/triose phosphate pool 597
13.9 Energy and reducing power for biosynthesis 601
13.10 Sugar-regulated gene expression 606
Summary 608

14 Respiration and Photorespiration 610

Introduction 610
14.1 Overview of respiration 610
14.2 Citric acid cycle 613
14.3 Plant mitochondrial electron transport 620
14.4 Plant mitochondrial ATP synthesis 632
14.5 Regulation of the citric acid cycle and the cytochrome pathway 634
14.6 Integration of the cytochrome pathway and nonphosphorylating pathways 635
14.7 Interactions between mitochondria and other cellular compartments 639
14.8 Biochemical basis of photorespiration 646
14.9 The photorespiratory pathway 648
14.10 Role of photorespiration in plants 652
Summary 655

IV METABOLIC AND DEVELOPMENTAL INTEGRATION

15 Long-Distance Transport 658

Introduction 658
15.1 Selection pressures and long-distance transport systems 658
15.2 Cell biology of transport modules 664
15.3 Short-distance transport events between xylem and nonvascular cells 668
15.4 Short-distance transport events between phloem and nonvascular cells 673
15.5 Whole-plant organization of xylem transport 691
15.6 Whole-plant organization of phloem transport 696
15.7 Communication and regulation controlling phloem transport events 705
Summary 710

16 Nitrogen and Sulfur 711

Introduction 711
16.1 Overview of nitrogen in the biosphere and in plants 711
16.2 Overview of biological nitrogen fixation 715
16.3 Enzymology of nitrogen fixation 715
16.4 Symbiotic nitrogen fixation 718
16.5 Ammonia uptake and transport 735
16.6 Nitrate uptake and transport 735
16.7 Nitrate reduction 739
16.8 Nitrite reduction 744
16.9 Nitrate signaling 745
16.10 Interaction between nitrate assimilation and carbon metabolism 745
16.11 Overview of sulfur in the biosphere and plants 746
16.12 Sulfur chemistry and function 747
16.13 Sulfate uptake and transport 750
16.14 The reductive sulfate assimilation pathway 752
16.15 Cysteine synthesis 755
16.16 Synthesis and function of glutathione and its derivatives 758
16.17 Sulfated compounds 763
16.18 Regulation of sulfate assimilation and interaction with nitrogen and carbon metabolism 764
Summary 767

17 Biosynthesis of Hormones 769

Introduction 769
17.1 Gibberellins 769
17.2 Abscisic acid 777
17.3 Cytokinins 785
17.4 Auxins 795
17.5 Ethylene 806
17.6 Brassinosteroids 810
17.7 Polyamines 818
17.8 Jasmonic acid 821
17.9 Salicylic acid 826

17.10 Strigolactones 830
Summary 833

18 Signal Transduction 834

Introduction 834
18.1 Characteristics of signal perception, transduction, and integration in plants 834
18.2 Overview of signal perception at the plasma membrane 838
18.3 Intracellular signal transduction, amplification, and integration via second messengers and MAPK cascades 843
18.4 Ethylene signal transduction 847
18.5 Cytokinin signal transduction 850
18.6 Integration of auxin signaling and transport 852
18.7 Signal transduction from phytochromes 857
18.8 Gibberellin signal transduction and its integration with phytochrome signaling during seedling development 861
18.9 Integration of light, ABA, and CO_2 signals in the regulation of stomatal aperture 866
18.10 Prospects 870
Summary 870

19 Molecular Regulation of Reproductive Development 872

Introduction 872
19.1 The transition from vegetative to reproductive development 872
19.2 The molecular basis of flower development 881
19.3 The formation of male gametes 889
19.4 The formation of female gametes 897
19.5 Pollination and fertilization 902
19.6 The molecular basis of self-incompatibility 908
19.7 Seed development 913
Summary 923

20 Senescence and Cell Death 925

Introduction 925
20.1 Types of cell death 925
20.2 PCD during seed development and germination 930
20.3 Cell death during the development of secretory bodies, defensive structures and organ shapes 932
20.4 PCD during reproductive development 937
20.5 Senescence and PCD in the terminal development of leaves and other lateral organs 940
20.6 Pigment metabolism in senescence 948
20.7 Macromolecule breakdown and salvage of nutrients in senescence 951
20.8 Energy and oxidative metabolism during senescence 957
20.9 Environmental influences on senescence and cell death I: Abiotic interactions 961
20.10 Environmental influences on senescence and cell death II: PCD responses to pathogen attack 964
20.11 Plant hormones in senescence and defense-related PCD 974
Summary 982

V PLANT ENVIRONMENT AND AGRICULTURE

21 Responses to Plant Pathogens 984

Introduction 984
21.1 Pathogens, pests, and disease 984
21.2 An overview of immunity and defense 985
21.3 How pathogens and pests cause disease 989
21.4 Preformed defenses 1009
21.5 Induced defense 1012
21.6 Effector-triggered immunity, a second level of induced defense 1022
21.7 Other sources of genetic variation for resistance 1032
21.8 Local and systemic defense signaling 1033
21.9 Plant gene silencing confers virus resistance, tolerance, and attenuation 1042
21.10 Control of plant pathogens by genetic engineering 1044
Summary 1050

22 Responses to Abiotic Stress 1051

Introduction 1051
22.1 Plant responses to abiotic stress 1051
22.2 Physiological and cellular responses to water deficit 1054
22.3 Gene expression and signal transduction in response to dehydration 1061
22.4 Freezing and chilling stress 1068
22.5 Flooding and oxygen deficit 1076
22.6 Oxidative stress 1085
22.7 Heat stress 1094
22.8 Crosstalk in stress responses 1097
Summary 1099

23 Mineral Nutrient Acquisition, Transport, and Utilization 1101

Introduction 1101

23.1 Overview of essential mineral elements 1102

23.2 Mechanisms and regulation of plant K^+ transport 1103

23.3 Phosphorus nutrition and transport 1113

23.4 The molecular physiology of micronutrient acquisition 1118

23.5 Plant responses to mineral toxicity 1127

Summary 1131

24 Natural Products 1132

Introduction 1132

24.1 Terpenoids 1133

24.2 Biosynthesis of the basic five-carbon unit 1135

24.3 Repetitive additions of C_5 units 1138

24.4 Formation of parent carbon skeletons 1141

24.5 Modification of terpenoid skeletons 1143

24.6 Metabolic engineering of terpenoid production 1145

24.7 Cyanogenic glycosides 1146

24.8 Cyanogenic glycoside biosynthesis 1152

24.9 Functions of cyanogenic glycosides 1157

24.10 Glucosinolates 1158

24.11 Alkaloids 1159

24.12 Alkaloid biosynthesis 1164

24.13 Biotechnological application of alkaloid biosynthesis research 1171

24.14 Phenolic compounds 1178

24.15 Phenolic biosynthesis 1185

24.16 The phenylpropanoid-acetate pathway 1188

24.17 The phenylpropanoid pathway 1195

24.18 Universal features of phenolic biosynthesis 1202

24.19 Evolution of secondary pathways 1205

Summary 1206

Further reading 1207

Index 1222

THE EDITORS

Bob B. Buchanan
A native Virginian, Bob B. Buchanan obtained his PhD in microbiology at Duke University and did postdoctoral research at the University of California at Berkeley. In 1963, he joined the Berkeley faculty and is currently a professor emeritus in the Department of Plant and Microbial Biology. He has taught general biology and biochemistry to undergraduate students and graduate-level courses in plant biochemistry and photosynthesis. Initially focused on pathways and regulatory mechanisms in photosynthesis, his research has more recently dealt with the regulatory role of thioredoxin in seeds, plant mitochondria and methane-producing archaea. The work on seeds is finding application in several areas. Bob has served as department chair at UC Berkeley and was president of the American Society of Plant Physiologists from 1995 to 1996. A former Guggenheim Fellow, he is a member of the National Academy of Sciences and the Japanese Society of Plant Physiologists (honorary). He is a fellow of the American Academy of Arts and Sciences, the American Society of Microbiology, the American Society of Plant Biologists, and the American Association for the Advancement of Science. His other honors include the Bessenyei Medal from the Hungarian Ministry of Education, the Kettering Award for Excellence in Photosynthesis, and the Stephen Hales Prize from the American Society of Plant Physiologists, a Research Award from the Alexander von Humboldt Foundation, the Distinguished Achievement Award from his undergraduate alma mater, Emory and Henry College, and the Berkeley Citation.

Wilhelm Gruissem
Wilhelm Gruissem was born in Germany where he studied biology and chemistry. After obtaining his PhD in 1979 at the University of Bonn in Germany and postdoctoral research at the University of Marburg in Germany and the University of Colorado in Boulder, he was appointed as Professor of Plant Biology at the University of California at Berkeley in 1983. He was Chair of the Department of Plant and Microbial Biology at UC Berkeley from 1993 to 1998, and from 1998 to 2000 he was Director of a collaborative research program between the Department and the Novartis Agricultural Discovery Institute in San Diego. In 2000 he joined the ETH Zurich (Swiss Federal Institute of Technology) as Professor of Plant Biotechnology in the Department of Biology and the Institute of Agricultural Sciences. Since 2001 he has been Co-Director of the Functional Genomics Center Zurich. From 2006 to 2010 he served as President of the European Plant Science Organization (EPSO) and since 2011 as Chair of the Global Plant Council. From 2009 to 2011 he also served as Chair of the Department of Biology at ETH Zurich. In addition to his research on systems approaches to understand pathways and molecules involved in plant growth control, he directs a biotechnology program on trait improvement in cassava, rice, and wheat. In 2008 he founded Nebion, a bioinformatics company building the internationally successful Genevestigator database. He is an elected fellow of the American Association for the Advancement of Sciences (AAAS) and the American Society of Plant Biologists, he is Editor of *Plant Molecular Biology*, and he serves on the editorial boards of several journals and on advisory boards for various research institutions. He has received several prestigious awards, including a prize from the Fiat Panis Foundation in Germany and the Shang-Fa Yang award of Academia Sinica in Taiwan for his trait improvement work in cassava and rice. In 2007 he was elected lifetime foreign member of the American Society of Plant Biologists.

Russell L. Jones
Russell L. Jones was born in Wales and completed his BSc and PhD degrees at the University of Wales, Aberystwyth. He spent 1 year as a postdoctoral fellow at the Michigan State University Department of Energy Plant Research Laboratory with Anton Lang before being appointed to the faculty of the Department of Botany at the University of California at Berkeley in 1966. As Professor of Plant Biology at UC Berkeley he taught undergraduate classes in general biology and graduate courses in plant physiology and cell biology for over 45 years. He is now Professor Emeritus, Department of Plant and Microbial Biology at UC Berkeley. His research focuses on hormonal regulation in plants using the cereal aleurone as a model system, with approaches that exploit the techniques of biochemistry, biophysics, and cell and molecular biology. Russell was president of the American Society of Plant Physiologists from 1993 to 1994. He was a Guggenheim Fellow at the University of Nottingham in 1972, a Miller Professor at UC Berkeley in 1976, a Humboldt Prize Winner at the University of Göttingen in 1986, and a RIKEN Eminent Scientist, RIKEN, Japan, in 1996.

LIST OF CONTRIBUTORS

Nikolaus Amrhein Institute of Plant Science, ETH Zurich, Switzerland

Julia Bailey-Serres Department of Botany and Plant Sciences, University of California, Riverside, CA, USA

Tobias I. Baskin Department of Biological Science, University of Missouri, Columbia, MO, USA

Paul C. Bethke Department of Plant and Microbial Biology, University of California, Berkeley, CA, USA

Gerard Bishop Department of Life Sciences, Imperial College London, London, United Kingdom

Elizabeth A. Bray Erman Biology Center, University of Chicago, Chicago, IL, USA

Karen S. Browning Department of Chemistry and Biochemistry, University of Texas, Austin, TX, USA

John Browse Institute of Biological Chemistry, Washington State University, Pullman, WA, USA

Judy Callis University of California, Davis, CA, USA

Nicholas C. Carpita Department of Botany and Plant Pathology, Purdue University, Lafayette, IN, USA

Maarten J. Chrispeels Department of Biology, University of California, San Diego, CA, USA

Gloria Coruzzi Department of Biology, New York University, New York City, NY, USA

Shaun Curtin Department of Plant Pathology, University of Minnesota, St Paul, MN, USA

David Day Division of Biochemistry and Molecular Biology, Australian National University, Canberra, Australia

Stephen Day Deceased

Emmanuel Delhaize CSIRO, Clayton, Australia

Lieven De Veylder Universiteit Gent, Gent, Belgium

Natalia Dudareva Horticulture and Landscape Architecture, Purdue University, West Lafayette, IN, USA

David R. Gang Institute of Biological Chemistry, Washington State University, Pullman, WA, USA

Walter Gassmann Division of Plant Sciences, University of Missouri, Columbia, MO, USA

Jonathan Gershenzon Department of Biochemistry, MPI for Chemical Ecology, Jena, Germany

Ueli Grossniklaus Institute of Plant Biology, University of Zurich, Zurich, Switzerland

Kim E. Hammond-Kosack Rothamsted Research, Harpenden, United Kingdom

Dirk Inzé Universiteit Gent, Gent, Belgium

Stefan Jansson Umeå Plant Science Centre, Umeå University, Umeå, Sweden

Jan Jaworski Department of Chemistry, Miami University, Miami, FL, USA

Jonathan D. G. Jones The Sainsbury Laboratory, John Innes Centre, Norwich, United Kingdom

Michael Kahn Institute of Biological Chemistry, Washington State University, Pullman, WA, USA

Leon Kochian U.S. Plant, Soil and Nutrition Laboratory, Cornell University, Ithaca, NY, USA

Stanislav Kopriva Department of Metabolic Biology, John Innes Centre, Norwich, United Kingdom

Toni M. Kutchan Donald Danforth Plant Science Center, St. Louis, MO, USA

Robert Last Cereon Genomics LLP, Cambridge, MA, USA

Ottoline Leyser The Sainsbury Laboratory, University of Cambridge, Cambridge, United Kingdom

Birger Lindberg Møller Center for Synthetic Biology, Plant Biochemistry Laboratory, Department of Plant and Environmental Sciences, University of Copenhagen, Copenhagen, Denmark and Carlsberg Laboratory, Copenhagen, Denmark

Sharon R. Long Department of Biological Sciences, Stanford University, Stanford, CA, USA

Richard Malkin Department of Plant and Microbial Biology, University of California, Berkeley, CA, USA

Maureen C. McCann Department of Biological Sciences, Purdue University, West Lafayette, USA

A. Harvey Millar Australian Academy of Science, Acton, Australia

Tony Millar Research School of Biological Sciences, Australian National University, Canberra, Australia

Luis Mur Institute of Biological, Environmental and Rural Sciences, Aberystwyth University, Aberystwyth, Wales, UK

Krishna K. Niyogi Department of Plant and Microbial Biology, University of California, Berkeley, CA, USA

John Ohlrogge Department of Botany, Michigan State University, East Lansing, USA

Helen Ougham Institute of Biological, Environmental and Rural Sciences, University of Aberystwyth, Aberystwyth, Wales, UK

John W. Patrick School of Environmental and Life Sciences, University of Newcastle, Newcastle, Australia

Natasha V. Raikhel MSU–DOE Plant Research Laboratory, Michigan State University, East Lansing , MI, USA

John Ralph Department of Biochemistry and Great Lakes Bioenergy Research Center, University of Wisconsin, Madison, WI, USA

Peter R. Ryan Division of Plant Industry, CSIRO, Canberra, Australia

Hitoshi Sakakibara RIKEN Plant Science Center, Yokohama, Japan

Daniel Schachtman Department of Agronomy and Horticulture, University of Nebraska, Lincoln, NE, USA

Danny Schnell Department of Biochemistry and Molecular Biology, University of Massachusetts, Amherst, MA, USA

Julian L. Schroeder Biological Sciences, University of California, San Diego, CA, USA

Lance Seefeldt Department of Chemistry and Biochemistry, Utah State University, Logan, UT, USA

Mitsunori Seo RIKEN Plant Science Center, Yokohama, Japan

Kazuo Shinozaki RIKEN Center for Sustainable Resource Science, Yokohama, Japan

James N. Siedow Department of Botany, Duke University, Durham, NC, USA

Ian Small Plant Energy Biology, ARC Center of Excellence, The University of Western Australia, Crawley, Australia

Chris Somerville Department of Plant and Microbial Biology, University of California, Berkeley, CA, USA

Linda Spremulli Department of Chemistry, University of North Carolina, Chapel Hill, NC, USA

L. Andrew Staehelin Department of Molecular and Cell Development Biology, University of Colorado, Boulder, CO, USA

Masahiro Sugiura Centre for Gene Research, Nagoya University, Japan

Yutaka Takeda Okayama University, Okayama, Japan

Howard Thomas Institute of Biological, Environmental and Rural Sciences, University of Aberystwyth, Wales, UK

Christopher D. Town J. Craig Venter Institute, San Diego, CA, USA

Yi-Fang Tsay Institute of Molecular Biology, Academia Sinica, Taiwan

Stephen D. Tyerman School of Agriculture, Food and Wine, Adelaide University, Adelaide, Australia

Matsuo Uemura Iwate University, Morioka, Iwate, Japan

Aart J. E. van Bel Institute for General Botany, Justus-Liebig-University, Giessen, Germany

Alessandro Vitale Institute of Agricultural Biotechnology, Milan, Italy

John M. Ward College of Biological Sciences, University of Minnesota, MN, USA

Peter Waterhouse School of Molecular Bioscience, The University of Sydney, Sydney, Australia

Frank Wellmer Smurfit Institute of Genetics, Trinity College, Dublin, Ireland

Elizabeth Weretilnyk Department of Biology, McMaster University, Hamilton, Ontario, Canada

Ricardo A. Wolosiuk Instituto de Investigaciones Bioquímicas, Buenos Aires, Argentina

Shinjiro Yamaguchi RIKEN Plant Science Center,, Yokohama, Japan

Samuel C. Zeeman Institute of Plant Science, ETH Zurich, Switzerland

PREFACE

The second edition of the *Biochemistry & Molecular Biology of Plants* retains the overall format of the first edition in response to the enthusiastic feedback we received from users of the book. The first edition was organized into five sections dealing with organization and functioning of the cell (Compartments), the cell's ability to replicate (Cell Reproduction), generation of energy (Energy Flow), regulation of development (Metabolism and Developmental Regulation), and the impact of fundamental discoveries in plant biology (Plant, Environment, and Agriculture). Although the section organization of the second edition remains unchanged, many of the chapters have been written by new teams of authors, reflecting the retirement of some of our colleagues, but also the dynamic development of plant biology during the last 20 years that was driven by a cohort of younger investigators, many of whom have contributed to this second edition.

Changes in chapter authorship also reflect the impact that molecular genetics had on our field, and three chapters stand out in this regard: Chapter 9 on Genome Structure and Organization, Chapter 18 on Signal Transduction, and Chapter 19 on Molecular Regulation of Reproductive Development. Advances resulting from molecular genetics have been particularly dramatic in the field of plant hormones and other signaling molecules where the receptors for all of the major hormones and their complex signaling pathways have now been described in detail.

Soon after publication of the first edition, *Biochemistry & Molecular Biology of Plants* was translated into Chinese, Italian, and Japanese, and a special low-priced English-language version of the book was published in India. In this version the entire book was published in black and white, illustrating the costs involved in producing four-color versions of textbooks.

Another change that accompanied the writing and production of this second edition was the involvement of the publisher John Wiley and our interaction with the Editorial Office in the United Kingdom. Wiley had entered into an agreement with the American Society of Plant Biologists to lead the publication of books written by ASPB members. The second edition of *Biochemistry & Molecular Biology of Plants* is one of the first of hopefully many books that will be published jointly by ASPB and Wiley.

Production of this book required input from many talented people. First and foremost the authors, who patiently, in some cases very patiently, worked with the editors and developmental editors to produce chapters of remarkably high quality. The two excellent developmental editors, Justine Walsh and Yolanda Kowalewski, worked to produce a collection of chapters that read seamlessly; the artist Debbie Maizels produced figures of exceptional technical and artistic quality; the staff at John Wiley, who worked tirelessly on this project; and Dr Nik Prowse, freelance project manager, who efficiently handled the chapter editing and management during the production phase of the book.. Special thanks go to Celia Carden whose support, enthusiasm, and management across two continents have gone a long way to making this book successful. The support of ASPB's leadership and staff, notably Executive Director Crispin Taylor and Publications Manager Nancy Winchester, are gratefully acknowledged. We also appreciate the continuing/ongoing support that we received from ASPB as this book was being developed. The contributing authors thank reviewers for commenting on their chapters.

Most important, we want to express appreciation to our wives, Melinda, Barbara, and Frances, who during the past few years again tolerated and accepted the textbook as a demanding family member.

Bob B. Buchanan
Wilhelm Gruissem
Russell L. Jones
November, 2014
Berkeley, CA, and Zurich, Switzerland

Note: Following the common publishing convention, species names that appear in the italicized figure legends have been set in standard roman typeface so that they are easily identifiable.

ABOUT THE COMPANION WEBSITE

This book is accompanied by a companion website:

www.wiley.com/go/buchanan/biochem

This website includes:

- PowerPoint slides of all the figures from the book, to download;
- PDF files of all the tables from the book, to download.



I

COMPARTMENTS



1

Membrane Structure and Membranous Organelles

L. Andrew Staehelin

Introduction

Cells, the basic units of life, require **membranes** for their existence. Foremost among these is the plasma membrane, which defines each cell's boundary and helps create and maintain electrochemically distinct environments within and outside the cell. Other membranes enclose eukaryotic organelles such as the nucleus, chloroplasts, and mitochondria. Membranes also form internal compartments, such as the endoplasmic reticulum (ER) in the cytoplasm and thylakoids in the chloroplast (Fig. 1.1).

The principal function of membranes is to serve as a barrier to diffusion of most water-soluble molecules. Cellular compartments delimited by membranes can differ in chemical composition from their surroundings and be optimized for a particular activity. Membranes also serve as scaffolding for certain proteins. As membrane components, proteins perform a wide array of functions: transporting molecules and transmitting signals across the membrane, processing lipids enzymatically, assembling glycoproteins and polysaccharides, and providing mechanical links between cytosolic and cell wall molecules.

This chapter is divided into two parts. The first is devoted to the general features and molecular organization of membranes. The second provides an introduction to the architecture and functions of the different membranous organelles of plant cells. Many later chapters of this book focus on metabolic events that involve these organelles.

1.1 Common properties and inheritance of cell membranes

1.1.1 Cell membranes possess common structural and functional properties

All cell membranes consist of a bilayer of polar lipid molecules and associated proteins. In an aqueous environment, membrane lipids self-assemble with their hydrocarbon tails clustered together, protected from contact with water (Fig. 1.2). Besides mediating the formation of bilayers, this property causes membranes to form closed compartments. As a result, every membrane is an asymmetrical structure, with one side exposed to the contents inside the compartment and the other side in contact with the external solution.

The lipid bilayer serves as a general permeability barrier because most water-soluble (polar) molecules cannot readily traverse its nonpolar interior. Proteins perform most of the other membrane functions and thereby define the specificity of each membrane system. Virtually all membrane molecules are able to diffuse freely within the plane of the membrane, permitting membranes to change shape and membrane molecules to rearrange rapidly.

Biochemistry & Molecular Biology of Plants, Second Edition. Edited by Bob B. Buchanan, Wilhelm Gruissem, and Russell L. Jones.
© 2015 John Wiley & Sons, Ltd. Published 2015 by John Wiley & Sons, Ltd.
Companion website: www.wiley.com/go/buchanan/biochem

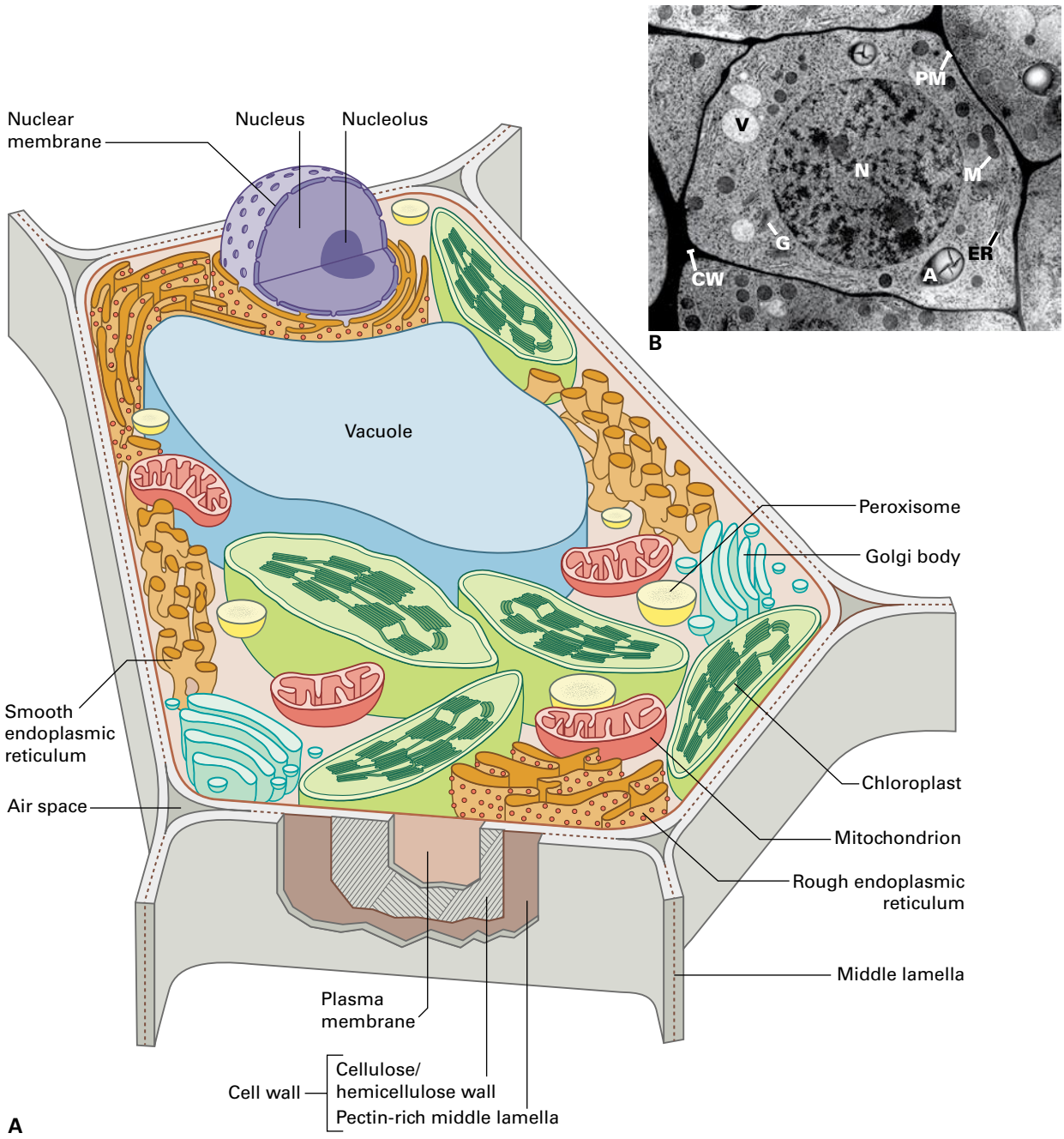


FIGURE 1.1 *(A) Diagrammatic representation of a mesophyll leaf cell, depicting principal membrane systems and cell wall domains of a differentiated plant cell. Note the large volume occupied by the vacuole. (B) Thin-section transmission electron micrograph (TEM) through a* Nicotiana *meristematic root tip cell preserved by rapid freezing. The principal membrane systems shown include amyloplast (A), endoplasmic reticulum (ER), Golgi stack (G), mitochondrion (M), nucleus (N), vacuole (V), and plasma membrane (PM). Cell wall (CW).*
Source: (B) Micrograph by Thomas Giddings Jr., from Staehelin et al. (1990). Protoplasma 157: 75–91.

1.1.2 All basic types of cell membranes are inherited

Plant cells contain approximately 20 different membrane systems. The exact number depends on how sets of related membranes are counted (Table 1.1). From the moment they are formed, cells must maintain the integrity of all their membrane-bounded compartments to survive, so all membrane systems must be passed from one generation of cells to the next in a functionally active form. Membrane inheritance follows certain rules:

- Daughter cells inherit a complete set of membrane types from their mother.
- Each potential mother cell maintains a complete set of membranes.
- New membranes arise by growth and fission of existing membranes.

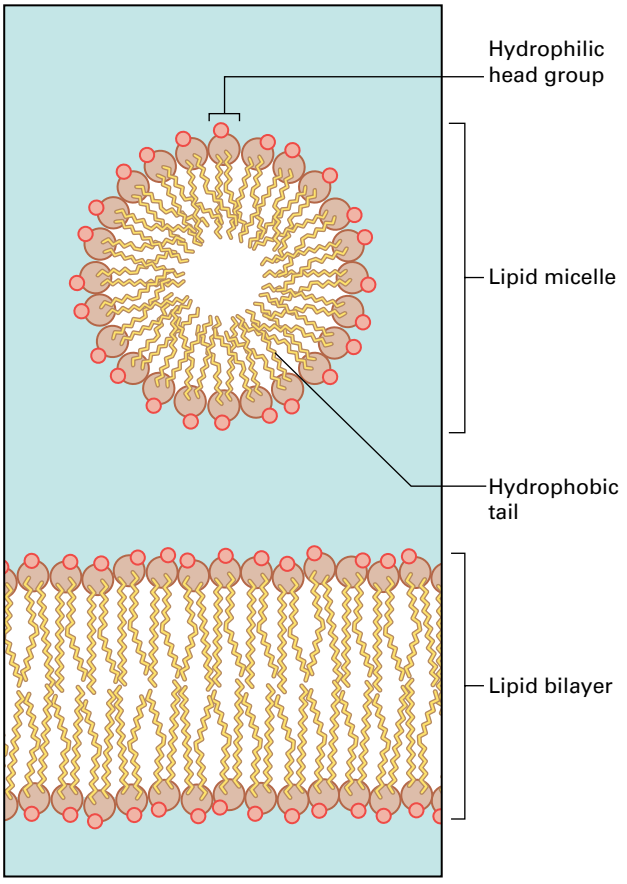


FIGURE 1.2 *Cross-sectional views of a lipid micelle and a lipid bilayer in aqueous solution.*

TABLE 1.1 *Membrane types found in plant cells.*

Plasma membrane
Nuclear envelope membranes (inner/outer)
Endoplasmic reticulum
Golgi cisternae (*cis*, medial, *trans* types)
Trans-Golgi network/early endosome membranes
Clathrin-coated,COPIa/Ib*, COPII*, secretory and retromer vesicle membranes
Autophagic vacuole membrane
Multivesicular body/late endosome membranes
Tonoplast membranes (lytic/storage vacuoles)
Peroxisomal membrane
Glyoxysomal membrane
Chloroplast envelope membranes (inner/ outer)
Thylakoid membrane
Mitochondrial membranes (inner/outer)

*COP, coat protein.

1.2 The fluid-mosaic membrane model

The **fluid-mosaic membrane model** describes the molecular organization of lipids and proteins in cellular membranes and illustrates how a membrane's mechanical and physiological traits are defined by the physicochemical characteristics of its various molecular components. This model integrates much of what we know about the molecular properties of membrane lipids, their assembly into bilayers, the regulation of membrane fluidity, and the different mechanisms by which membrane proteins associate with lipid bilayers.

1.2.1 The amphipathic nature of membrane lipids allows for the spontaneous assembly of bilayers

In most cell membranes, lipids and glycoproteins make roughly equal contributions to the membrane's mass. Lipids belong to several classes, including phospholipids, glucocerebrosides, galactosylglycerides, and sterols (Figs. 1.3 and 1.4). These molecules share an important physicochemical property: they are **amphipathic**, containing both **hydrophilic** ("water-loving") and **hydrophobic** ("water-fearing") domains. When brought into contact with water, these molecules spontaneously self-assemble into higher-order structures. The hydrophilic head groups maximize their interactions with water molecules, whereas hydrophobic tails interact with each other, minimizing their exposure to the aqueous phase (see Fig. 1.2). The geometry of the resulting lipid assemblies is governed by the shape of the amphipathic molecules and the balance between hydrophilic and hydrophobic domains. For most membrane lipids, the bilayer configuration is the minimum-energy self-assembly structure, that is, the structure that takes the least amount of energy to form in the presence of water (Fig. 1.5). In this configuration, the polar groups form the interface to the bulk water, and the hydrophobic groups become sequestered in the interior.

Phospholipids, the most common type of membrane lipid, have a charged, phosphate-containing polar head group and two hydrophobic hydrocarbon tails. Fatty acid tails contain between 14 and 24 carbon atoms, and at least one tail has one or more *cis* double bonds (Fig. 1.6). The kinks introduced by these double bonds influence the packing of the molecules in the lipid bilayer, and the packing, in turn, affects the overall fluidity of the membrane.

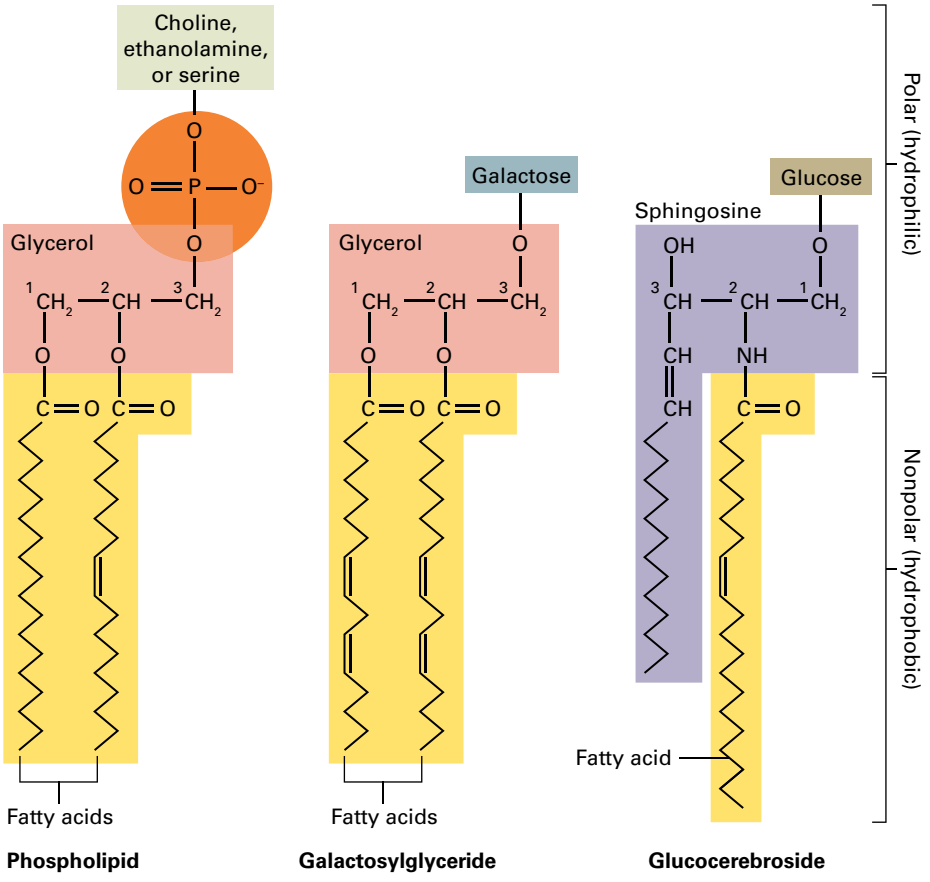


FIGURE 1.3 *Plant membrane lipids.*

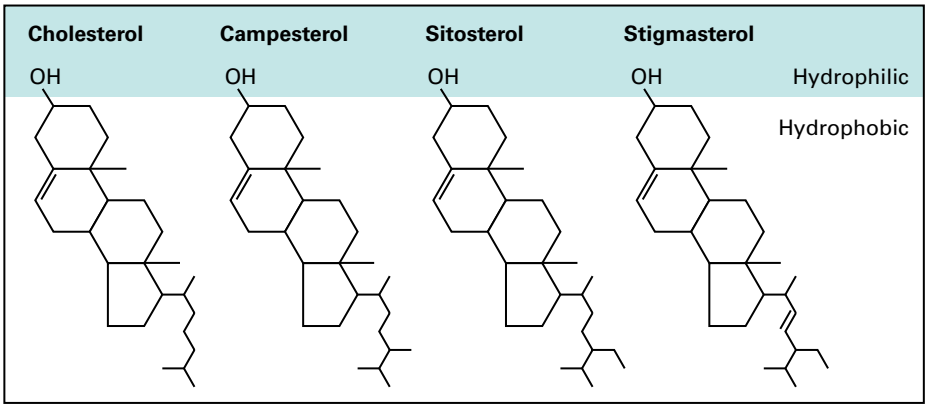


FIGURE 1.4 *Sterols found in plant plasma membranes.*

1.2.2 Phospholipids move rapidly in the plane of the membrane but very slowly from one side of the bilayer to the other

Because individual lipid molecules in a bilayer are not bonded to each other covalently, they are free to move. Within the plane of the bilayer, molecules can slide past each other freely. A membrane can assume any shape without disrupting the hydrophobic interactions that stabilize its structure. Aiding this general flexibility is the ability of lipid bilayers to close on themselves to form discrete compartments, a property that also enables them to seal damaged membranes.

Studies of the movement of phospholipids in bilayers have revealed that these molecules can diffuse laterally, rotate, flex their tails, bob up and down, and flip-flop (Fig. 1.7). The exact mechanism of lateral diffusion is unknown. One theory suggests that individual molecules hop into vacancies ("holes") that form transiently as the lipid molecules within each monolayer exhibit thermal motions. Such vacancies arise in a fluid bilayer at high frequencies, and the average molecule hops ~10^7 times per second, which translates to a diffusional distance of ~1 μm traversed in a second. Both rotation of individual molecules around their long axes and up-and-down bobbing are also very rapid events. Superimposed on these motions is a constant flexing of the hydrocarbon tails. Because this flexing

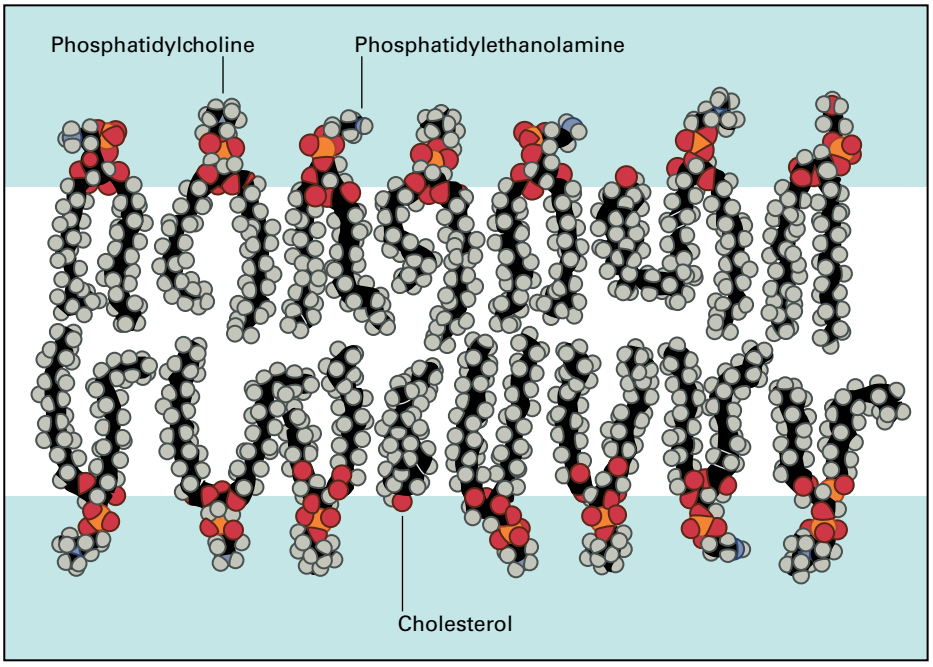


FIGURE 1.5 *Organization of amphipathic lipid molecules in a bilayer.*

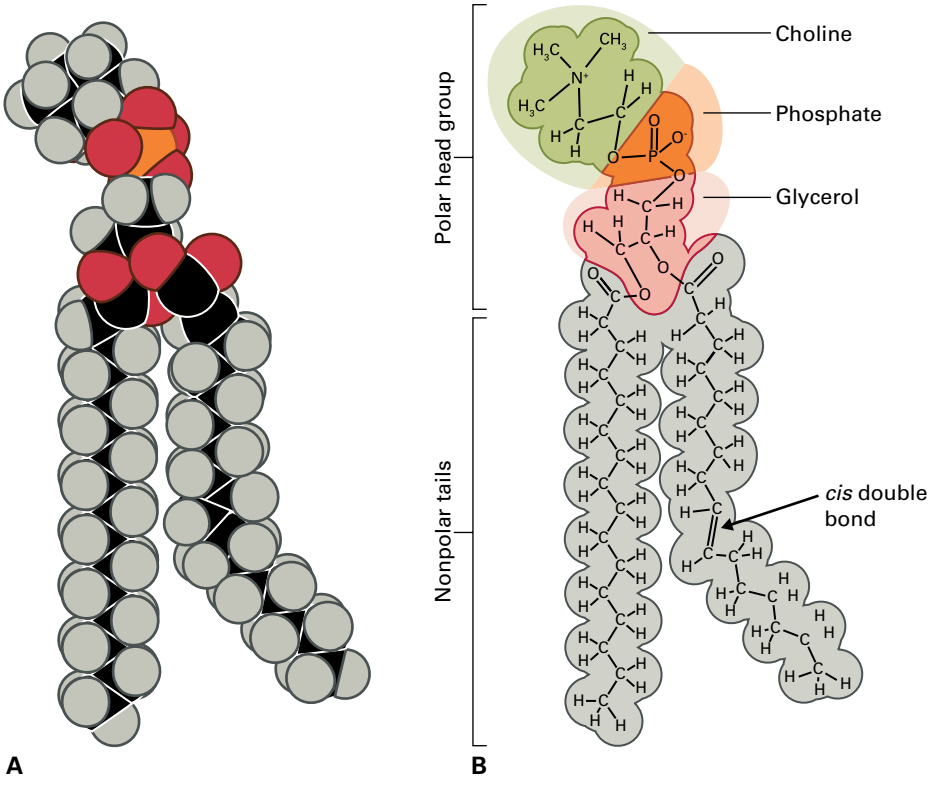


FIGURE 1.6 *(A) Space-filling model of a phosphatidylcholine molecule. (B) Diagram defining the functional groups of a phosphatidylcholine molecule.*

increases towards the ends of the tails, the center of the bilayer has the greatest degree of fluidity.

In contrast, spontaneous transfer of phospholipids across the bilayer, called flipping, rarely occurs. A flip would require the polar head to migrate through the nonpolar interior of the bilayer, an energetically unfavorable event. Some membranes contain "flippase" enzymes, which mediate movement of newly synthesized lipids across the bilayer (Fig. 1.8). Different flippases specifically catalyze translocation of particular lipid types and thus can flip their lipid substrates in only one direction. The energy barrier to spontaneous flipping and flippase specificity, together with the specific orientation of the lipid-synthesizing enzymes in the membranes, result in an asymmetrical distribution of lipid types across membrane bilayers.

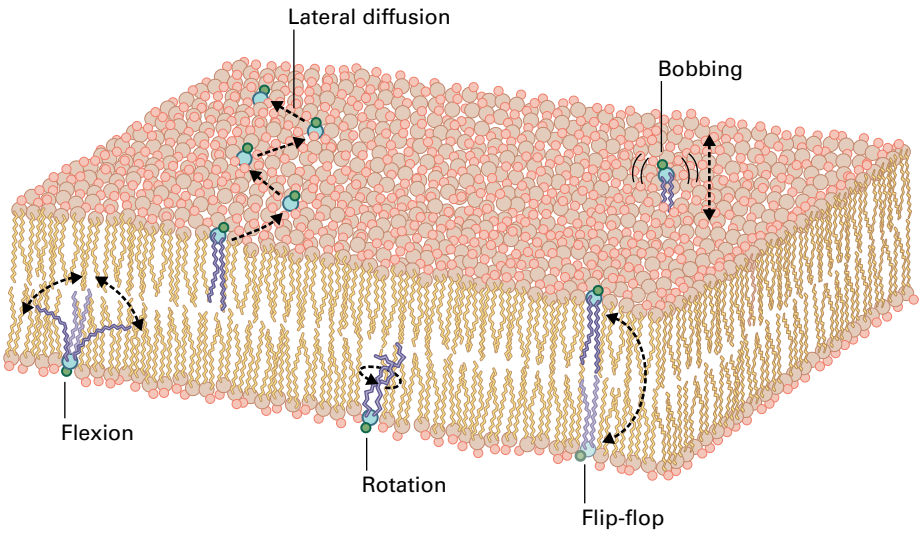


FIGURE 1.7 *Mobility of phospholipid molecules in a lipid bilayer.*

Membrane sterols in lipid bilayers behave somewhat differently from phospholipids, primarily because the hydrophobic domain of a sterol molecule is much larger than the uncharged polar head group (see Fig. 1.4). Thus, membrane sterols are not only able to diffuse rapidly in the plane of the bilayer, they can also flip-flop without enzymatic assistance at a higher rate than phospholipids.

1.2.3 Cells optimize the fluidity of their membranes by controlling lipid composition

Like all fatty substances, membrane lipids exist in two different physical states, as a semicrystalline gel and as a fluid. Any given lipid, or mixture of lipids, can be melted—converted from gel to fluid—by a temperature increase. This change in state is known as **phase transition**, and for every lipid this transition occurs at a precise temperature, called the temperature of melting (T_m, see Table 1.2). Gelling brings most membrane activities to a standstill and increases permeability. At high temperatures, on the other hand, lipids can become too fluid to maintain the permeability barrier. Nonetheless, some organisms live happily in frigid conditions, whereas others thrive in boiling hot springs and thermal vents. Many plants survive daily temperature fluctuations of 30°C. How do organisms adapt the fluidity of their membranes to suit their mutable growth environments?

To cope successfully with the problem of temperature-dependent changes in membrane fluidity, virtually all poikilothermic organisms—those whose temperatures fluctuate with the environment—can alter the composition of their membranes to optimize fluidity for a given temperature. Mechanisms exploited to compensate for low temperatures include shortening of fatty acid tails, increasing the number of double bonds, and increasing the size or charge of head groups. Changes in sterol composition can also alter membrane responses to temperature. Membrane sterols serve as membrane fluidity "buffers," increasing the fluidity at lower temperatures by disrupting the gelling of phospholipids, and decreasing fluidity at high temperatures by interfering with the flexing motions of the fatty acid tails. Because each lipid has a different T_m, lowering the temperature can induce one type of lipid to undergo a fluid-to-gel transition and form semicrystalline patches, whereas other lipids remain in the fluid state. Like all cellular molecules, membrane lipids have a finite life span and are turned over on a regular basis. This turnover enables plant cells to adjust the lipid composition of their membranes in response to seasonal changes in ambient temperature.

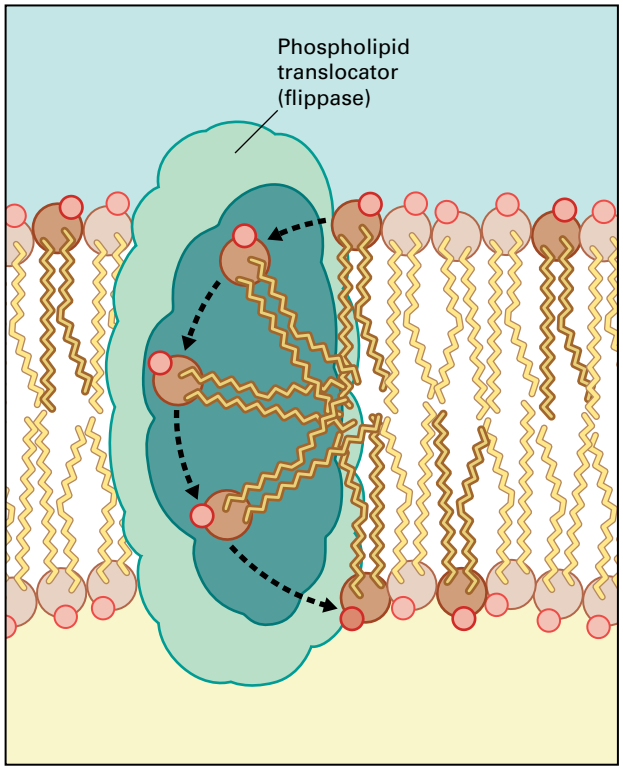


FIGURE 1.8 *Mechanism of action of a "flippase," a phospholipid translocator.*

1.2.4 Membrane proteins associate with lipid bilayers in many different ways

The different ways in which membrane-bound proteins associate with lipid bilayers reflect the diversity of enzymatic and structural functions they perform. The original fluid-mosaic membrane model included two basic types of membrane proteins: peripheral and integral (Fig. 1.9). More recent research has led to the discovery of three additional classes of membrane proteins—**fatty acid-linked**, **prenyl group-linked, and phosphatidylinositol-anchored**—all of which are attached to the bilayer by lipid tails (Fig. 1.10).

By definition, **peripheral proteins** are water-soluble and can be removed by washing membranes in water or in salt or acid solutions that do not disrupt the lipid bilayer. Peripheral proteins bind either to integral proteins or to lipids through

TABLE 1.2 *The effects of fatty acid chain length and double bonds on the temperature of melting (T_m) of some defined phospholipids.*

	T_m (°C)		
Types of chains*	**Phosphatidylcholine**	**Phosphatidyl-ethanolamine**	**Phosphatidic acid**
Two $C_{14:0}$	24	51	
Two $C_{16:0}$	42	63	67
Two $C_{18:0}$	55	82	
Two $C_{18:1}$ (*cis*)	–22	15	8

*The shorthand nomenclature for the fatty acyl chains denotes how many carbon atoms (first number) and double bonds (second number) they contain.

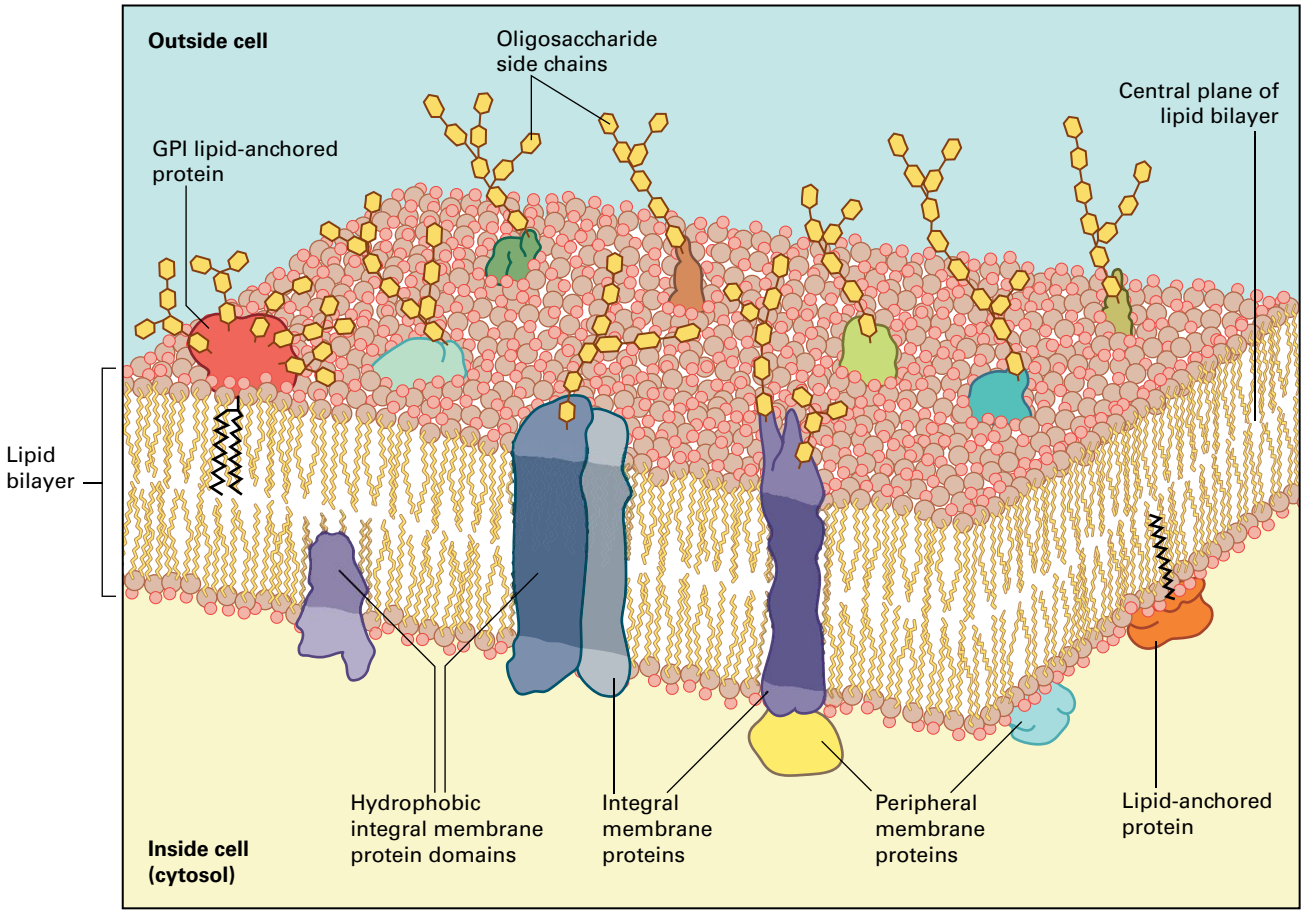


FIGURE 1.9 *A modern version of the fluid-mosaic membrane model, depicting integral, peripheral, and lipid-anchored membrane proteins. Not drawn to scale.*

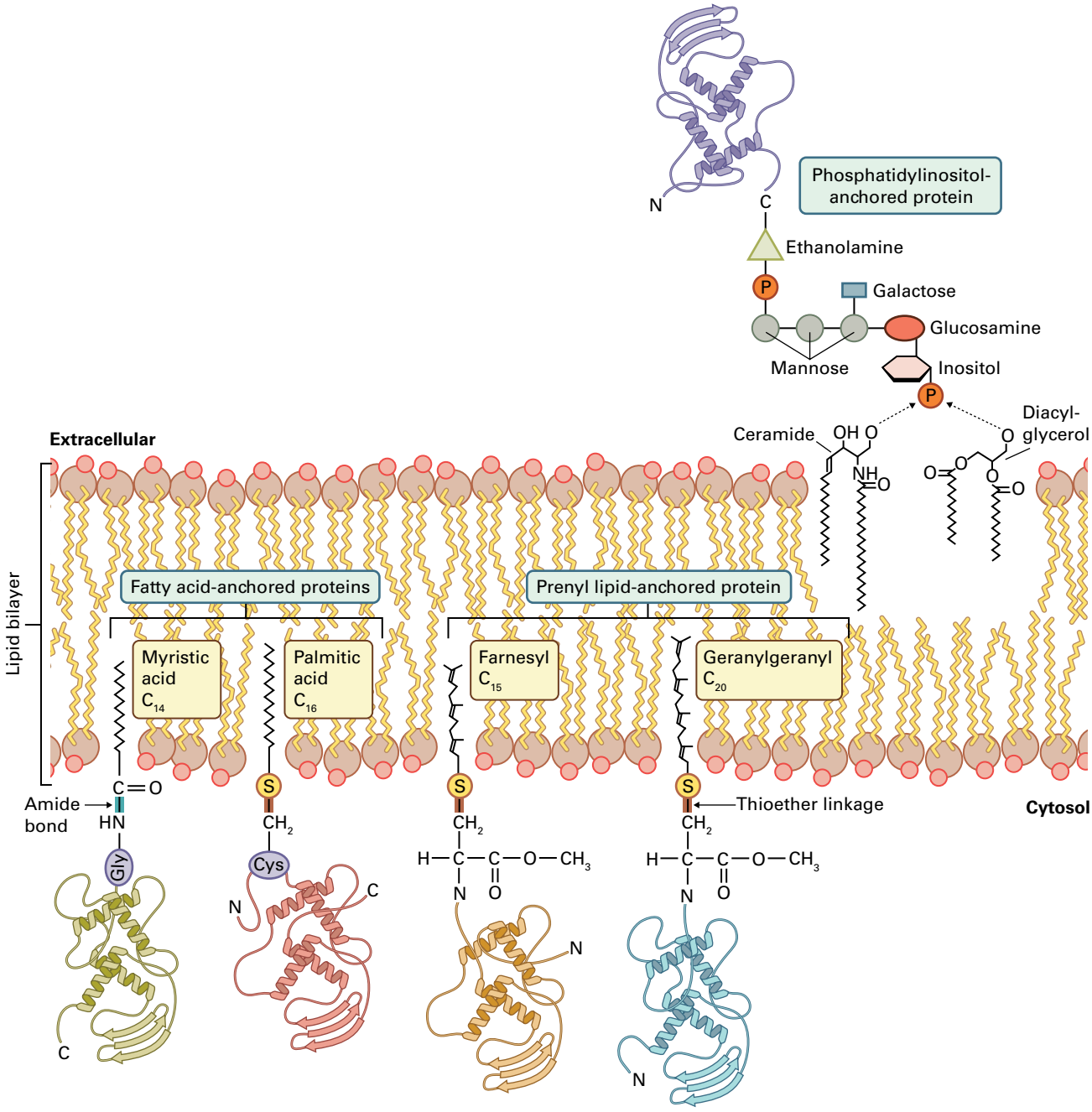


FIGURE 1.10 *Fatty acid-anchored, prenyl lipid-anchored, and glycosylphosphatidylinositol (GPI)-anchored proteins.*

salt bridges, electrostatic interactions, hydrogen bonds, or some combination of these, but they do not penetrate the lipid bilayer. Some peripheral proteins also provide links between membranes and cytoskeletal systems. In contrast, the amphipathic, transmembrane or partly embedded **integral proteins** are insoluble in water. Because the hydrophobic domains are sequestered in the hydrophobic interior of the bilayer, an integral protein can be removed and solubilized only with the help of detergents or organic solvents, which degrade the bilayer.

Both the fatty acid-linked and the prenyl group-linked proteins bind reversibly to the cytoplasmic surfaces of membranes to help regulate membrane activities. Cycling between the membrane-bound and free states is mediated in most cases by phosphorylation/dephosphorylation or by GTP/GDP binding cycles. The fatty acid-linked proteins are attached either to a myristic acid (C_{14}), by way of an amide linkage to an amino terminal glycine, or to one or more palmitic acid (C_{16}) residues, by way of thioester linkages to cysteines near the carboxyl terminus. Prenyl lipid-anchored proteins are attached to one or more molecules of farnesyl (C_{15}; 3 isoprene units) or geranylgeranyl (C_{20}; 4 isoprene units), which are also coupled to cysteine residues in carboxyl-terminal CXXX, CXC, and XCC motifs (Fig. 1.10).

In contrast to the fatty acid- and the prenyl group-linked proteins, the phosphatidylinositol-anchored proteins are

bound to the lumenal/extracellular surfaces of membranes (Fig. 1.10). Interestingly, these proteins are first produced as larger, integral proteins with one transmembrane domain. Enzymatic cleavage between the transmembrane domain and the globular surface domain produces a new C terminus on the globular domain, to which the lipid is coupled by ER-based enzymes (see Chapter 4, Section 4.6.4). The remaining transmembrane domain is then degraded by proteases. Many arabinogalactan proteins (AGPs) appear to be linked to the plasma membrane via a glycosylphosphatidylinositol (GPI) anchor. These molecules can be enzymatically released from the cell surface by phospholipase C.

1.2.5 The fluid-mosaic membrane model predicts structural and dynamic properties of cell membranes

Although the original fluid-mosaic membrane model was developed at a time when membrane researchers knew only of peripheral and integral proteins, slight modifications to its basic premises have accommodated more recent discoveries, including lipid-anchored proteins and membrane protein–cytoskeletal interactions.

Membrane fluidity involves the movement not only of lipid molecules, but also of integral proteins that span the bilayer and of the different types of surface-associated membrane proteins. This ability of membrane proteins to diffuse laterally in the plane of the membrane is crucial to the functioning of most membranes: Collisional interactions are essential for the transfer of substrate molecules between many membrane-bound enzymes and of electrons between the electron transfer chain components of chloroplasts and mitochondria (see Chapters 12 and 14). Such movements are also critical for the assembly of multiprotein membrane complexes. In addition, many signaling pathways depend on transient interactions among defined sets of integral membrane proteins and peripheral or lipid-anchored proteins.

Tethering structures regulate and restrict the movement of membrane proteins, often limiting their distribution to defined membrane domains. This tethering can involve connections to the cytoskeleton and the cell wall, bridges between related integral proteins, or junction-type interactions between proteins in adjacent membranes. A particularly striking example of the latter type of interaction occurs in the grana stacks of chloroplast membranes (see Section 1.10.4). Grana stack formation has been shown to affect the lateral distribution of all major protein complexes in thylakoid membranes and to regulate the functional activity of the photosynthetic reaction centers and other components of the photosynthetic electron transport chain.

Another mechanism for generating transient membrane microdomains of different composition involves membrane lipids organized in the form of **lipid rafts**. GPI-anchored proteins are typically associated with such membrane domains, which have been defined by cell biologists as membrane domains that are resistant to certain types of detergents. Biochemical analyses of these detergent-resistant membrane fractions have shown that they contain over 100 proteins and are enriched for phytosterols, and that the degree of fatty acid unsaturation affects their stability. However, due to their transient nature, there is no consensus on their *in vivo* size and composition. Indirect evidence suggests that lipid rafts participate in membrane sorting and signaling functions.

1.3 Plasma membrane

The plasma membrane forms the outermost boundary of the living cell and functions as an active interface between the cell and its environment (Fig. 1.11). In this capacity it controls the transport of molecules into and out of the cell, transmits signals from the environment to the cell interior, participates in the synthesis and assembly of cell wall molecules, and provides physical links between elements of the cytoskeleton and the extracellular matrix. In conjunction with specialized domains of the ER, the plasma membrane produces **plasmodesmata**, membrane tubes that cross cell walls and provide direct channels of communication between adjacent cells (Fig. 1.12). As a result of these plasmodesmal connections, almost all the living cells of an individual plant share a physically continuous plasma membrane. This contrasts sharply with the situation in animals, where virtually every

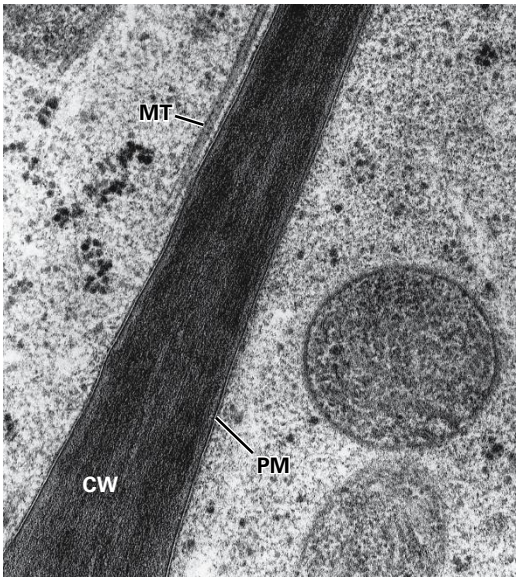


FIGURE 1.11 *The plasma membrane (PM) of a turgid plant cell is pressed tightly against a cell wall (CW). These adjacent cryofixed plant cells have been processed by techniques that preserve the close physical relationship between plasma membrane and cell wall. Cells preserved with chemical fixatives for observation under an electron microscope often demonstrate artifacts of specimen preparation, such as a wavy conformation of the plasma membrane and a gap between the membrane and the cell wall. Microtubule (MT).*
Source: TEM by A. Lacey Samuels, University of British Columbia, Vancouver, Canada.

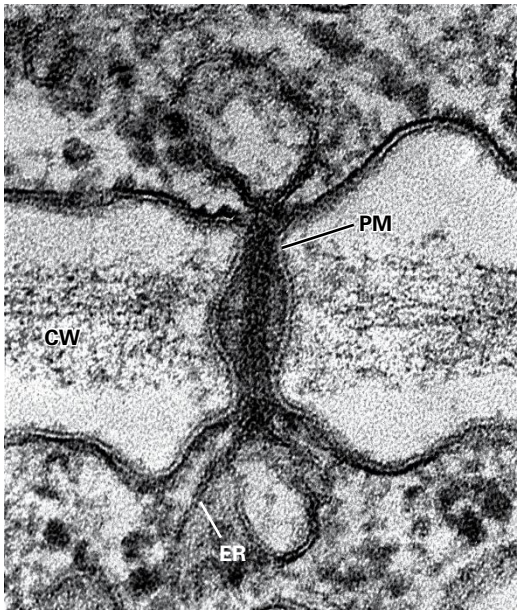


FIGURE 1.12 *Longitudinal section through a plasmodesma. Plasma membrane (PM), endoplasmic reticulum (ER), cell wall (CW). Source*: TEM by Lewis Tilney, from Tilney et al. (1991). J Cell Biol 112: 739–747.

cell has a separate plasma membrane, and cell-to-cell communication occurs instead through protein channels known as gap junctions.

Yet another important difference between plants and animals is that plant cells are normally under turgor pressure, whereas animal cells are isoosmotic with their environments. Turgor pressure forces the plasma membrane tightly against the cell wall (see Fig. 1.11).

1.3.1 The lipid composition of plasma membranes is highly variable

Plasma membranes of plant cells consist of lipids, proteins, and carbohydrates in a molecular ratio of ~40:40:20. The lipid mixture contains phospholipids, glycolipids, and sterols, the same classes found in animal plasma membranes. In plant plasma membranes, the ratio of lipid classes varies remarkably among the different organs in a given plant and among identical organs in different plants—in contrast to the far more constant ratios in animal cells. Barley (*Hordeum vulgare*) root cell plasma membranes, for example, contain more than twice as many free sterol molecules as phospholipids (Table 1.3). In leaf tissues this ratio is generally reversed, but varies: In barley leaf plasma membranes, the phospholipid to free sterol ratio is 1.3:1, whereas in spinach (*Spinacia oleracea*) it is 9:1.

This striking variability, which continues to puzzle researchers, indicates that ubiquitous plasma membrane enzymes can function in widely different lipid environments. These results have led to the suggestion that the lipid composition of plant plasma membranes may have little bearing on their functional properties and that the only important lipid parameter is membrane fluidity. If this were true, it would mean that virtually all lipid classes are interchangeable so long as a given combination of lipids yields a bilayer of desired fluidity at a particular temperature. This provocative idea may well be an overstatement, reflecting our ignorance about the functional roles of specific lipid types; moreover, it seems to be contradicted by the finding that the activity of proton-translocating ATPase (H^+-ATPase) molecules from corn (*Zea mays*) root reconstituted into artificial membranes can be modulated by changes in sterol composition. More research is needed to clarify how different lipid classes contribute to plasma membrane function.

The most common free **sterols** of plant plasma membranes are campesterol, sitosterol, and stigmasterol (see Fig. 1.4). Cholesterol, the principal free sterol of mammalian plasma membranes, is a minor component in the vast majority of plant species analyzed to date, oat (*Avena sativa*) being a notable exception to this trend. Sterol esters, sterol glycosides, and acylated sterol glycosides are more abundant in plants than in animals. Sterol glycosylation, a reaction catalyzed by UDP-glucose:sterol glycosyltransferase, has been exploited as a marker for isolated plant plasma membranes. Sphingomyelin, another major type of lipid formed in mammalian plasma membranes, has yet to be found in plants. Interesting differences in the fatty acid tails of plant and mammalian plasma membrane **glycerolipids** have also been reported. Whereas plants principally utilize palmitic ($C_{16:0}$), linoleic ($C_{18:2}$), and linolenic ($C_{18:3}$) acids, mammals use palmitic ($C_{16:0}$), stearic ($C_{18:0}$), and arachidonic ($C_{20:4}$) acids.

TABLE 1.3 *Lipid composition of plasma membranes from various non-cold-acclimated species and tissues (mole %).*

Lipid type	Barley root	Barley leaf	*Arabidopsis* leaf	Spinach leaf
Phospholipids	26	44	47	64
Free sterols	57	35	38	7
Steryl glucosides	7	–	5	–
Acylated steryl glycosides	–	–	3	13
Glucocerebrosides	9	16	7	14

1.3.2 Cold acclimation leads to characteristic changes in plasma membrane lipid composition

Low temperature is one of the most important factors limiting the productivity and distribution of plants. All plants able to withstand freezing temperatures possess the ability to freeze-proof their cells by a process known as **cold acclimation** (see Chapter 22). This metabolic process involves altering the composition and physical properties of membranes, cytoplasm, and cell walls so that they can withstand not only freezing temperatures but also freeze-induced dehydration. One of the most cold-hardy woody species is the mulberry tree (*Morus bombycis* Koidz). After cold acclimation in midwinter, these trees can withstand freezing below –40°C, but in midsummer, when they are not cold-acclimated, they can be injured by a freeze below –3°C.

Among the most pronounced and critical alterations that occur during cold acclimation are changes in lipid composition of plasma membranes. One might expect cold acclimation-induced lipid changes to vary among species, given the differences in plasma membrane lipid composition already noted (Table 1.3). However, in all cold-hardy herbaceous and woody species studied to date, cold acclimation has been reported to cause an increase in the proportion of phospholipids and a decrease in the proportion of glucocerebrosides. In addition, the mole percent of phospholipids carrying two unsaturated tails increases. Species in which the cold-acclimated plasma membranes contain the highest proportion of diunsaturated phospholipids and the lowest proportion of glucocerebrosides tend to be the most cold hardy.

1.3.3 Plasma membrane proteins serve a variety of functions

Among the prominent classes of proteins present in the plasma membrane are transporters, signal receptors, and proteins that function in cell wall interactions and synthesis. Most plasma membrane proteins involved in these transmembrane activities are of the integral type. However, these proteins often form larger complexes with peripheral proteins. The extracellular domains of many integral proteins are glycosylated, bearing N- and O-linked oligosaccharides.

The plasma membrane H^+-ATPase (P-type H^+-ATPase) couples ATP hydrolysis to the transmembrane transport of protons from the cytosol to the extracellular space. This proton pumping has two effects. First, it acidifies cell walls and alkalinizes the cytosol, thereby affecting cell growth and expansion (see Chapter 2) as well as many other cellular activities. Second, it produces an electrochemical potential gradient across the plasma membrane that can drive the transport of ions and solutes against their respective concentration gradients (see Chapters 3 and 23). The plasma membrane also contains specialized water-conducting channels known as aquaporins (see Chapter 3).

In plants, transmembrane signaling receptors (see Chapter 18) are essential for cell communication and for mediating interactions with the environment. They also play important roles in development and in orchestrating diverse defense responses. Receptors capable of responding to many types of signaling molecules, including hormones, oligosaccharins, proteins, peptides, and toxins have been identified, but only a small number of these have been characterized to date.

Plasma membrane proteins participate in a variety of interactions with the cell wall, including formation of physical links to cell wall molecules, synthesis and assembly of cell wall polymers, and creation of a highly hydrated, tissue-specific interfacial domain. The presence of physical connections between the plasma membrane and the cell wall was first deduced from the presence of thread-like strands connecting the protoplasts of plasmolyzed cells to the cell wall (Fig. 1.13). These strands are known as **Hechtian strands** in honor of Kurt Hecht, who is credited with their discovery in 1912. During cold acclimation, the number of Hechtian strands increases, suggesting that increasing the strength of the protoplast–cell wall interactions helps protect protoplasts from the stress of freeze-induced dehydration. Electron microscopic analysis has shown that these strands are thin

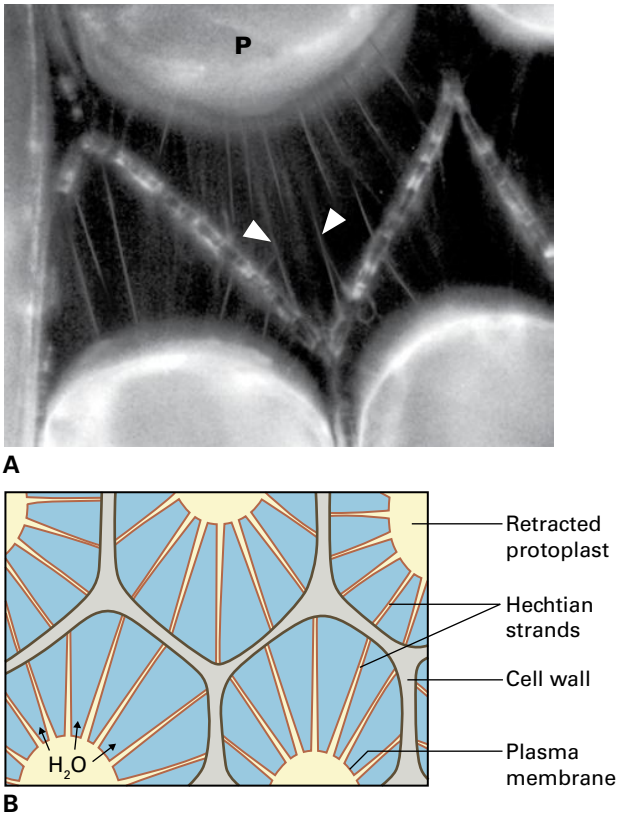


FIGURE 1.13 *(A) Light micrograph of plasmolyzed onion epidermal cells. Hechtian strands ("arrowheads") connect the protoplasts (P) to the cell walls (CW). (B) Diagram illustrating features of plasmolyzed plant cells.*
Source: TEM by Karl Oparka, from Oparka et al. (1994). Plant Cell Environ 17: 163–171.

tubes of cytoplasm delineated by a plasma membrane that retains tight contacts with the cell wall. These strands remain continuous with the plasma membrane. Although the molecules that link the plasma membrane to the cell wall have not yet been identified, indirect studies suggest they may be integrin-type receptors that recognize the amino acid sequence Arg-Gly-Asp (RGD) in cell wall constituents. A protein known as WAK1, a plasma membrane receptor with kinase activity, is another candidate protein.

AGPs, another class of cell surface proteins, are highly glycosylated proteoglycans that derive >90% of their mass from sugar. Classical-type AGPs appear to be anchored to the external surface of the plasma membrane by means of GPI lipid anchors (see Section 1.2.4), providing a carbohydrate-rich interface between the cell wall and the plasma membrane. The fact that AGPs are expressed in a tissue- and developmental stage-specific manner suggests they may play a role in differentiation. Additional plasma membrane proteins, the cellulose synthase and callose synthase complexes, extrude cellulose (ß-1,4-linked glucose) and callose (ß-1,3-linked glucose), respectively, directly into the cell walls (see Chapter 2).

1.4 Endoplasmic reticulum

The ER is the most extensive, versatile, and adaptable organelle in eukaryotic cells. It consists of a three-dimensional (3D) network of continuous tubules and flattened sacs that underlie the plasma membrane, course through the cytoplasm, and connect to the nuclear envelope but remain distinct from the plasma membrane. In plants, the principal functions of ER include synthesizing, processing, and sorting proteins targeted to membranes, vacuoles, or the secretory pathway as well as adding N-linked glycans to many of these proteins and synthesizing a diverse array of lipid molecules. The ER also provides anchoring sites for the actin filament bundles that drive cytoplasmic streaming, and plays a critical role in regulating the cytosolic concentrations of calcium (Ca^{2+}), which influence many other cellular activities.

The classical literature distinguishes three types of ER membranes: **rough ER**, **smooth ER,** and **nuclear envelope**. However, researchers now recognize many more morphologically distinct subdomains that perform a variety of different functions (Fig. 1.14). Despite this functional diversity, virtually all ER membranes are physically linked and enclose a single, continuous lumen that extends beyond the boundaries of individual cells via the plasmodesmata.

1.4.1 The ER gives rise to the endomembrane system

The **endomembrane system** includes membranous organelles that exchange membrane molecules, either by lateral diffusion through continuous membrane or by transport vesicles that bud from one type of membrane and fuse with another (Fig. 1.15). The principal membrane systems connected in this manner include the nuclear envelope, membranes of the secretory pathway (ER, Golgi, *trans*-Golgi network, multivesicular body, plasma membrane, vacuole, and different types of transport/secretory vesicles), and membranes associated with the endocytic pathway (plasma membrane, clathrin-coated endocytic vesicles, *trans*-Golgi network/early endosome/recycling endosome, multivesicular body/late endosome, vacuole, and transport vesicles). Extensive traffic between these compartments not only transports secreted molecules to the cell surface and vacuolar proteins to the vacuoles, but also distributes membrane proteins and membrane lipids from their sites of synthesis, the ER and Golgi cisternae, to their sites of action, all of the endomembrane organelles. A plethora of sorting, targeting, and retrieval systems regulate traffic between the different compartments, ensuring delivery of molecules to the correct membranes and the maintenance of organelle identity (see Chapter 4).

All membranes of the endomembrane system are connected by both **anterograde** (forward) and **retrograde** (backward) **traffic** (Fig. 1.15). The anterograde pathway usually delivers newly synthesized molecules to their destination. In the retrograde pathway, membrane molecules dispersed by transport processes are recycled to their sites of origin, and "escaped" molecules are returned to their normal site of action. Because the volume of membrane traffic is large and the accuracy of sorting is <100%, a certain percentage of mislocalized proteins remain in all endomembrane systems. This normal "contamination" of endomembranes provides a never-ending challenge for biochemists interested in obtaining "pure" membrane fractions.

1.4.2 The ER forms a dynamic network, the organization of which changes during the cell cycle and development

In living plant cells, the spatial organization and kinetic behavior of ER membranes can be visualized by means of the lipophilic fluorescent stain $DiOC_6$ (3,3′-dihexyloxacarbocyanine iodide). Light microscopic images of such cells show a lace-like network of lamellar and tubular cisternae that continuously undergo architectural rearrangements (Fig. 1.16). Electron microscopic studies have shown that the lamellar regions correspond to sheets of polysome-bearing rough ER membranes (Fig. 1.17; see also domain 5 in Fig. 1.14), and the tubular regions to smooth ER membranes (Fig. 1.18; see also domain 6 in Fig. 1.14) that possess fewer or, in specialized tissues, no bound ribosomes. New tubules can grow from existing membranes and then fuse with other ER cisternae to create new network polygons while other tubules rupture and are reabsorbed into the network.

In interphase cells, the ER underlying the plasma membrane, called the cortical ER, is highly developed, and because of its links to the plasma membrane and to plasmodesmata, is less dynamic than the ER cisternae that pass through the cell

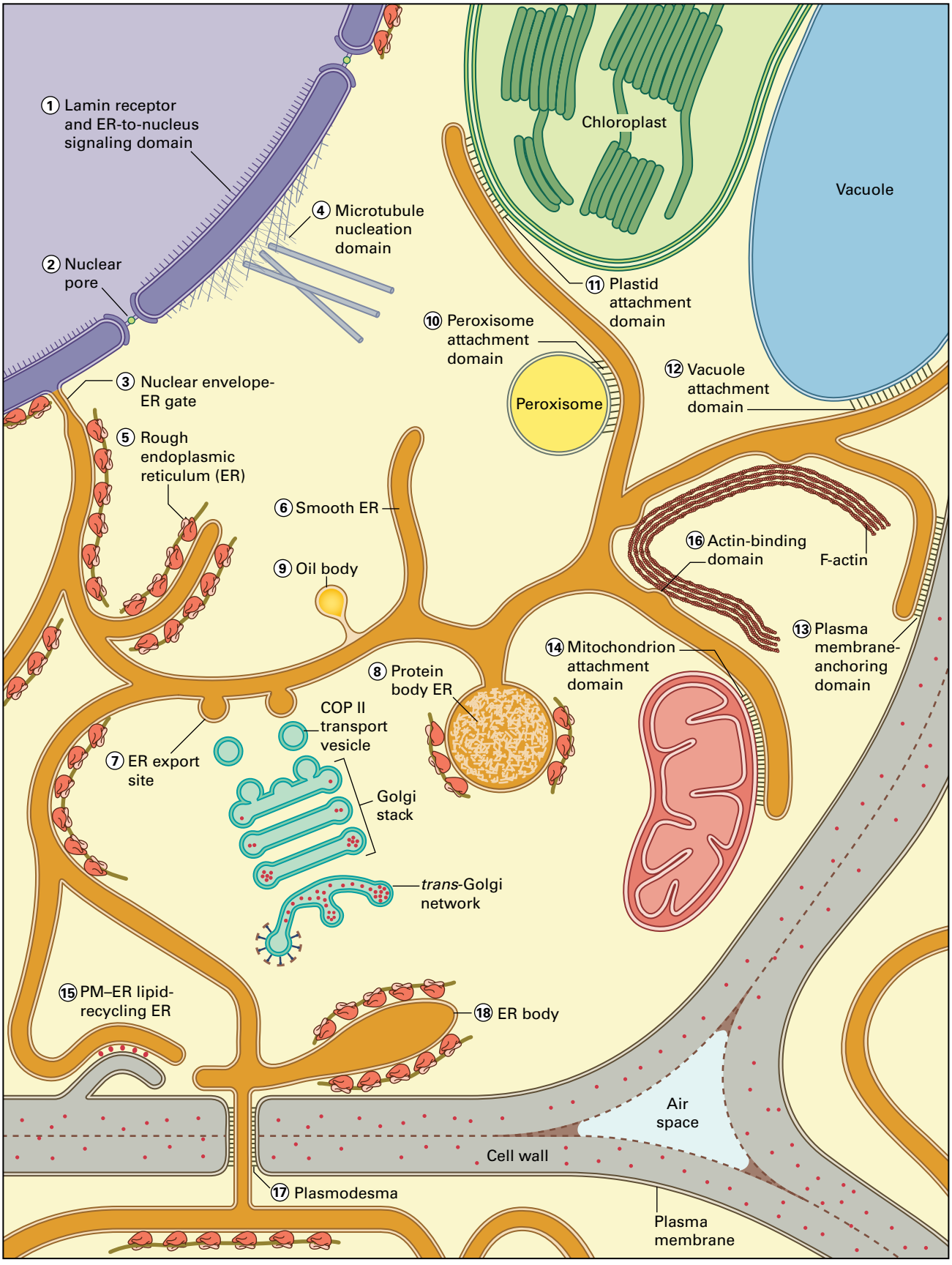


FIGURE 1.14 *Diagram illustrating 18 functional domains of the plant ER system.*

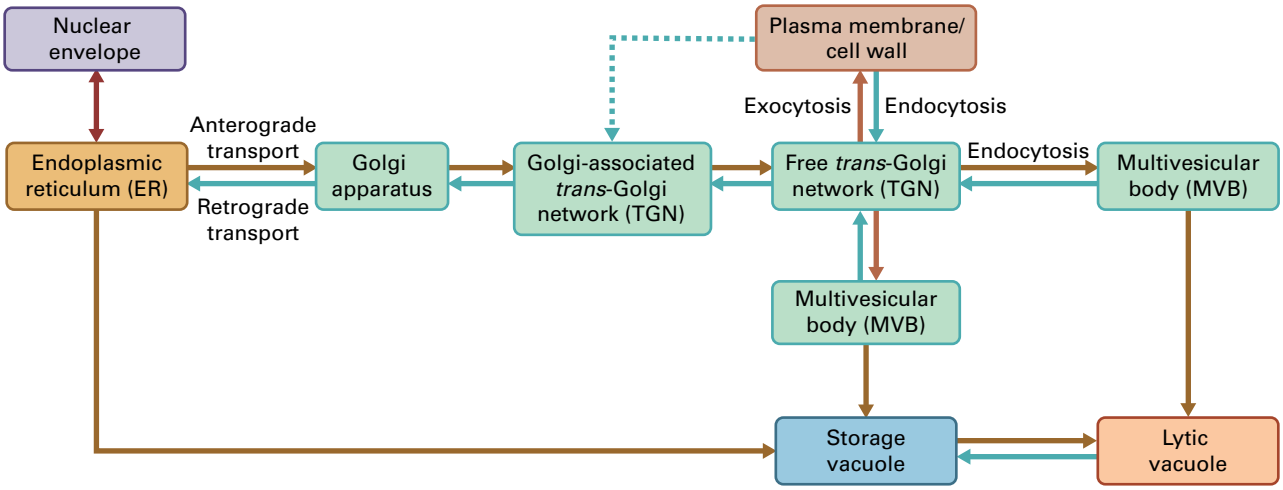


FIGURE 1.15 *Diagrammatic overview of the major membrane compartments of the endomembrane system and the directions of membrane trafficking between these compartments. Single-headed arrows represent anterograde and retrograde vesicle traffic. Double-headed arrows connected by a single line indicate that membrane components and lumen contents can diffuse laterally between these compartments (nuclear envelope and ER). Double headed arrow connected by two lines signals interconversion between vacuole types.*

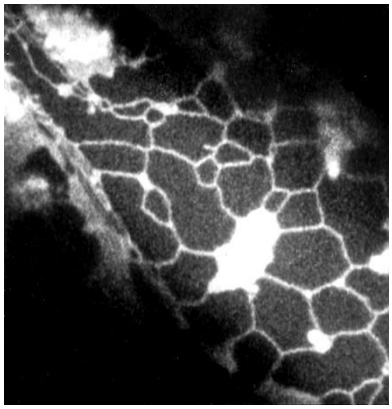


FIGURE 1.16 *Light micrograph of the cortical ER network in a living onion epidermal cell stained with the fluorescent dye $DiOC_6$. Lamellar and tubular membranes are organized in the form of a polygonal lattice that changes over time.*
Source: Micrograph by Helmut Quader, from Knebel et al. (1990). Eur J Cell Biol 52: 328–340.

interior. Indeed, the cortical ER often serves as a semi-immobile platform to which the actin filament bundles involved in cytoplasmic streaming are bound (Fig. 1.19; see also domain 16 in Fig. 1.14). During mitosis, the ER undergoes a series of characteristic rearrangements consistent with the idea that it might regulate spindle activities and cell plate assembly by controlling local Ca^{2+} concentrations. In gravity-sensing columella cells of root tips, ER membranes are confined to the cell cortex in a dense network, leaving the central cytoplasm free of ER cisternae to allow specialized amyloplasts (statoliths) to sediment freely (see Section 1.10.7). Gravitropic signaling appears to involve deformation of cortical ER membranes by the heavy statoliths and production of a Ca^{2+} flux. In seeds, extensive arrays of rough ER develop in storage cells during the accumulation of storage proteins. In contrast, intricate networks of smooth ER tubes are a characteristic feature of oil gland cells (see Fig. 1.18) that synthesize and secrete significant amounts of lipophilic substances such as volatile alcohols, terpenes, and flavonoids (see Chapter 24).

1.4.3 Oil bodies and some types of protein bodies are formed by specialized ER domains

Two important agricultural products, vegetable oils and dietary seed proteins, are produced by enzymes associated with the ER. The storage oils of seeds—triacylglycerols—provide energy and membrane lipid building blocks during early stages of seedling growth. During their synthesis by ER enzymes, triacylglycerols partition into the interior of the ER bilayer and then accumulate at sites defined by molecules known as oleosins. Oleosins have a thumbtack-like architecture, with the "shaft" portion consisting of hydrophobic amino acids and the head exhibiting an amphipathic structure. As the newly synthesized triacylglyceride molecules accumulate between the bilayer leaflets at the oleosin sites, they give rise to spherical **oil bodies** (Fig. 1.20; see also domain 9 in Fig. 1.14). The surface layer of each oil body consists of a phospholipid monolayer, embedded oleosins, and other proteins (see Chapter 8).

Seed storage proteins are synthesized during seed development and serve as the principal source of amino acids for germination and seedling growth. Cereal plants produce two classes of storage proteins, the water-soluble **globulin** proteins and the more hydrophobic, alcohol-soluble **prolamins**. Globulin proteins are synthesized by rough ER polysomes and subsequently accumulate in storage vacuoles (see Chapters 4 and 19). In contrast, prolamins assemble into disulfide-linked polymers, while still residing in the ER, giving rise to spherical structures known as **protein bodies** (Fig. 1.21; see also domain 8 in Fig. 1.14). **ER bodies** (Fig. 1.22;

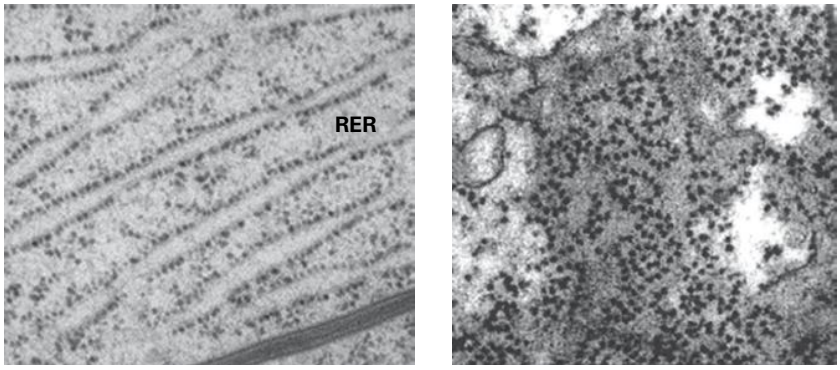


FIGURE 1.17 *(A) TEM of rough ER (RER) membranes in a eucalyptus root meristem cell. See domain 5 in Figure 1.14. (B) TEM showing polyribosome coils on the surface of a rough ER membrane domain in a young root epidermal cell of radish. See domain 5 in Fig. 1.14.*
Source: (A) Micrograph by Brian Gunning, Australian National University, Canberra. (B) Micrograph by Eldon Newcomb, from Bonnett, Newcomb. (1965). J Cell Biol 27: 423–432.

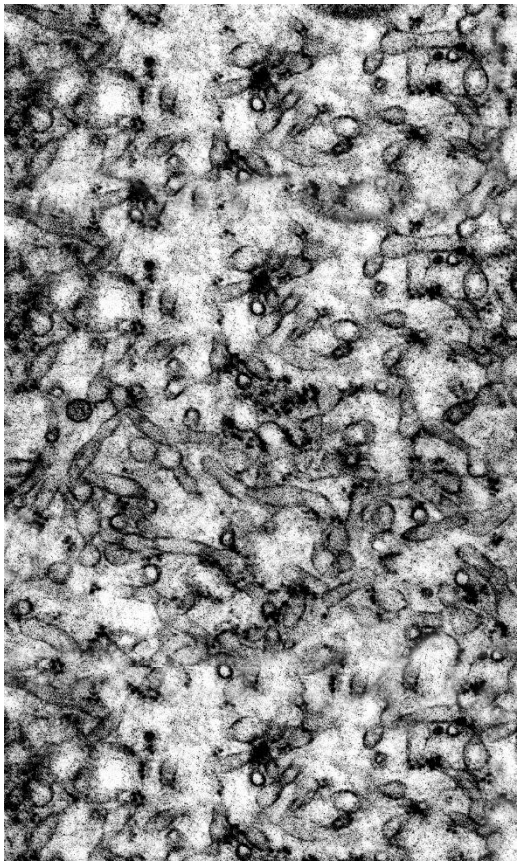


FIGURE 1.18 *TEM of smooth ER tubules in a glandular trichome cell of a mint leaf. See domain 6 in Figure 1.14.*
Source: Micrograph by Glenn W. Turner, Washington State University, Pullman, WA.

see also domain 18 in Fig. 1.14) resemble protein bodies but possess a more lens-shaped architecture and do not accumulate storage proteins. Some native ER bodies contain aggregated β-glucosidases, enzymes involved in pathogen defenses. However, ER bodies can also be induced to form in transgenic plants by the expression of green fluorescent protein (GFP) containing a signal peptide and an ER retention signal.

1.4.4 Transport vesicles mediate the transfer of newly synthesized secretory/storage/membrane proteins from the ER to the Golgi apparatus

COPII vesicles bud from specialized ER membrane domains and mediate ER-to-Golgi transport of soluble proteins destined for the cell surface and vacuoles, and membrane proteins for the different compartments of the endomembrane system (Fig. 1.23). ER domains that produce **COPII vesicles** are known as **ER export sites** (see domain 7 in Fig. 1.14). At these sites secretory proteins are separated from resident ER proteins and selectively packaged into the forming COPII vesicles for trafficking to *cis*-Golgi cisternae. In higher plants, budding COPII vesicles are unstable structures with a half-life of ~10 s, and they can only be observed in electron micrographs of cells preserved by high-pressure freezing. Furthermore, the identification of an ER export site, as defined by a localized ER region producing several budding COPII vesicles together with an associated Golgi stack with its *cis*-side facing this site, is often complicated by the 3D architecture of the ER membranes. Thus, the site often consists of budding COPII vesicles that are being formed on several adjacent tubular ER domains.

1.4.5 ER attachment domains appear to mediate non-vesicular lipid transport between the ER and other membrane systems

ER membranes possess several types of membrane attachment domains where the ER forms appositional contacts with other membrane systems. Such contact sites have been observed between ER and plasma membrane, cell plate membrane, mitochondria, plastids, peroxisomes, and vacuoles (see domains 10–15 in Fig. 1.14). In such regions, ER membranes approach these other membranes to within ~10 nm,

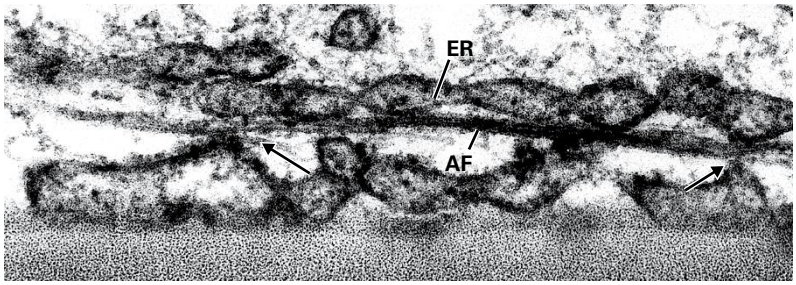


FIGURE 1.19 *TEM showing sites where an actin filament (AF) attaches to cortical ER (arrows). See domain 16 in Figure 1.14.*
Source: Micrograph by Irene Lichtscheidl, from Lichtscheidl et al. (1990). Protoplasma 155: 116–126.

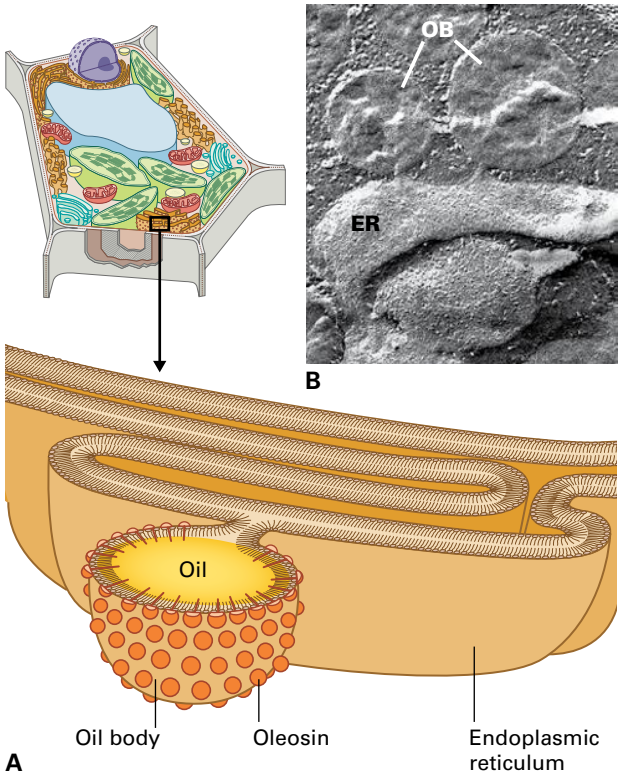


FIGURE 1.20 *(A) Triacylglycerides accumulate between the two lipid monolayers of a smooth ER membrane and bud off as oil bodies at sites defined by oleosin molecules. (B) TEM of oil bodies (OB) budding from an ER membrane into the cytoplasm. See domain 9 in Figure 1.14.*
Source: (B) Micrograph by Donna Fernandez, from Fernandez, D. and Staehelin, L.A. (1987). Plant Physiol 85: 487–496.

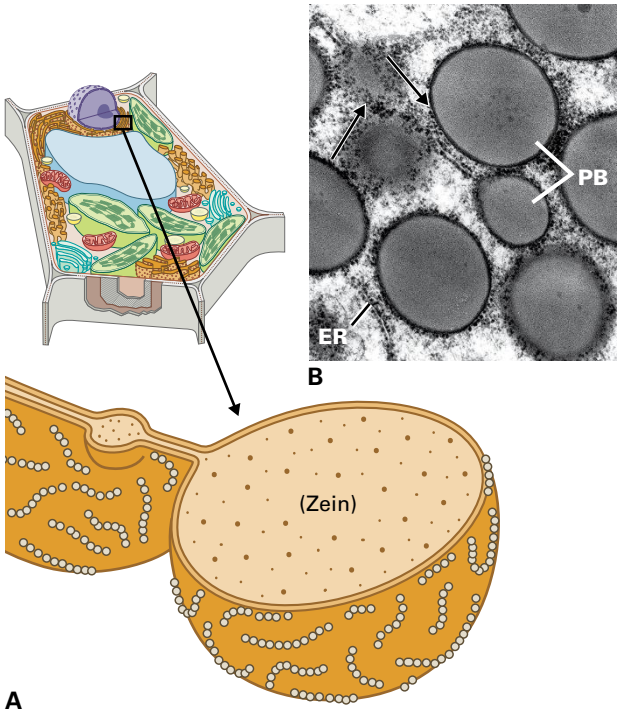


FIGURE 1.21 *(A) Prolamin storage proteins (e.g., zein) aggregate in protein bodies that bud from specialized rough ER. (B) TEM of protein bodies (PB) forming in maize endosperm. Polysomes (arrows) are attached to the delimiting ER membrane. See domain 8 in Fig. 1.14.*
Source: (B) Micrograph by Brian A. Larkins, University of Arizona, Tucson, AZ.

and in electron tomographic images the adjacent membranes can be seen to be connected through discrete bridging structures (Fig. 1.24A).

Preliminary evidence suggests that such attachment sites may serve as sites of calcium transport via calcium channels (for example, between plasma membrane and ER) and/or mediate non-vesicular, intermembrane lipid transport. Higher plants contain two distinct pathways for membrane lipid synthesis (see Chapter 8), and the enzymes of these pathways are located both in plastids (the **prokaryotic pathway**) and ER (the **eukaryotic pathway**). The prokaryotic pathway produces C_{16} and C_{18} fatty acids, and a significant fraction of these fatty acids are exported to the ER for synthesis of phospholipids, some of which are exported back to plastids. ER-plastid lipid trafficking occurs via lipid-transfer proteins, which are most likely concentrated in the ER-plastid attachment sites (Fig. 1.24B; see also domain 11 in Fig. 1.14). The ER–mitochondria contact sites most likely mediate transfer of phosphatidylserine from ER to mitochondria for the production of phosphatidylethanolamine, a major component of mitochondrial membranes. Molecular lipid recycling has also been shown to occur between the plasma membrane and ER (see Section 1.6.1 and domains 13 and 15 in Fig. 1.14). No information is available on the functional roles of ER–vacuole and ER–peroxisome attachment sites.

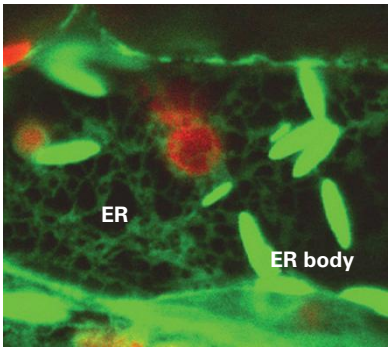


FIGURE 1.22 *Confocal microscope image of ER bodies in an* Arabidopsis *hypocotyl cell expressing a green fluorescent protein (GFP) with a signal sequence and an HDEL ER retention sequence. See domain 18 in Figure 1.14.*
Source: Micrograph by Brian Gunning, Australian National University, Canberra.

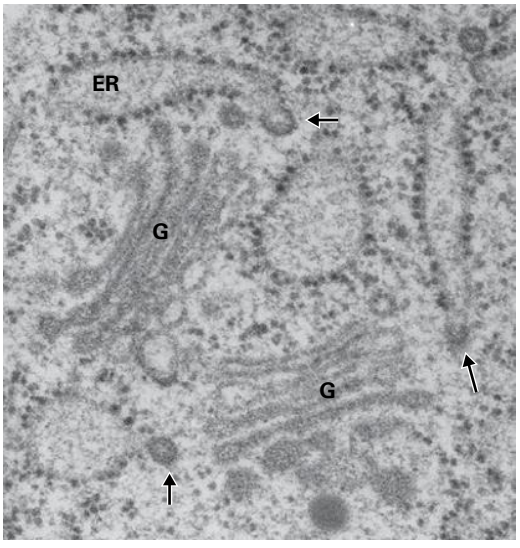
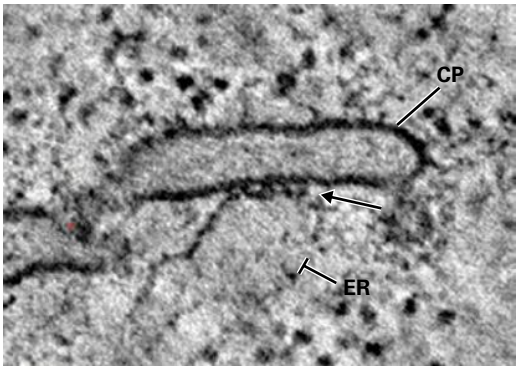
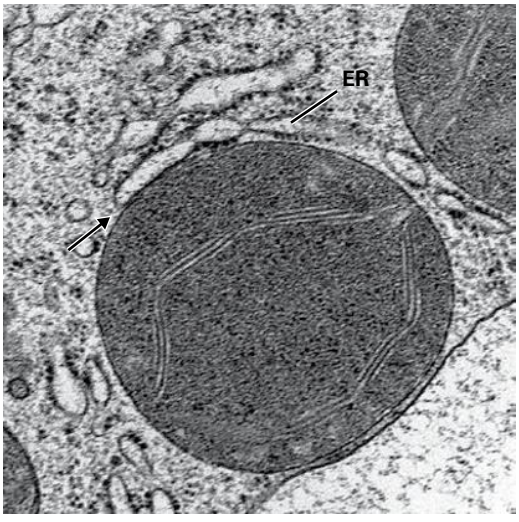


FIGURE 1.23 *TEM of COPII vesicles (arrows) budding from ER export sites adjacent to Golgi stacks (G) in an endosperm cell of an* Arabidopsis *seed. See domain 7 in Figure 1.14.*
Source: Micrograph by York-Dieter Stierhof, University of Tübingen, Germany.



A



B

FIGURE 1.24 *(A) Electron tomographic slice image of a contact region between an ER membrane and a late stage cell plate membrane (CP) on the verge of becoming a plasma membrane. Note the bridging structures (arrow) between the two membranes in the contact zone. See domain 13 in Figure 1.14. (B) TEM of a contact region (arrow) between an ER membrane and outer envelope membrane of a plastid in a pine epidermal cell. See domain 11 in Figure 1.14.*
Source: (A) Micrograph by Jose-Maria Segui-Simarro from Seguí-Simarro, J.M. et al. (2004). Plant Cell 16: 836–856. (B) Micrograph by A. Lacey Samuels, University of British Columbia, Vancouver, Canada.

1.5 Golgi apparatus

The term Golgi apparatus refers to the complement of **Golgi stacks** and associated ***trans*-Golgi networks** (TGNs) within a given cell. The Golgi apparatus occupies a central position in the secretory pathway, receiving newly synthesized proteins and lipids from the ER and directing them to either the cell surface or vacuoles (see Fig. 1.15). In plants, the Golgi apparatus is involved in assembling complex polysaccharides of the cell wall matrix, synthesizing and processing O- and N-linked oligosaccharide side chains of membrane, cell wall, and vacuolar glycoproteins, and producing glycolipids for the plasma and tonoplast membranes.

The glycosyltransferases and glycosidases that carry out these reactions are integral proteins. Most of these enzymes possess an active site that faces the interior space of the flattened Golgi cisternae. However, some of the enzymes that produce polysaccharide backbones have a transmembrane disposition with an active site on the cytosolic side of the membrane and a channel for transferring the growing polysaccharide chain across the membrane and into the cisternal lumen (see Chapter 2). Sugar nucleotides are used as substrates by the glycosyltransferases that synthesize the different carbohydrate products.

1.5.1 The plant Golgi apparatus consists of dispersed Golgi stack-Golgi associated TGN units that exhibit a polar cisternal organization

The functional unit of the plant Golgi apparatus is the Golgi stack, its associated Golgi-associated (early) TGN, and the **Golgi scaffold** (**Golgi matrix**), which encompasses both structures (Figs. 1.25, 1.26, and 1.28–1.30). Unlike in animal cells, where the Golgi apparatus occupies a position close to the cell center, the Golgi stack–Golgi-associated TGN units of plants are always dispersed throughout the cytoplasm, either as individual units or in small clusters (Fig. 1.27). This dispersed organization, together with the fact that the stacks can travel along actin filaments by means of myosin motors, ensures that secretory products reach their destinations even in large, vacuolated cells. The number of Golgi stack–TGN units per cell varies widely, depending on species, size, and developmental stage of the cell and the volume and type of secretory/storage materials produced. For example, small shoot apical meristem cells of *Arabidopsis thaliana* contain

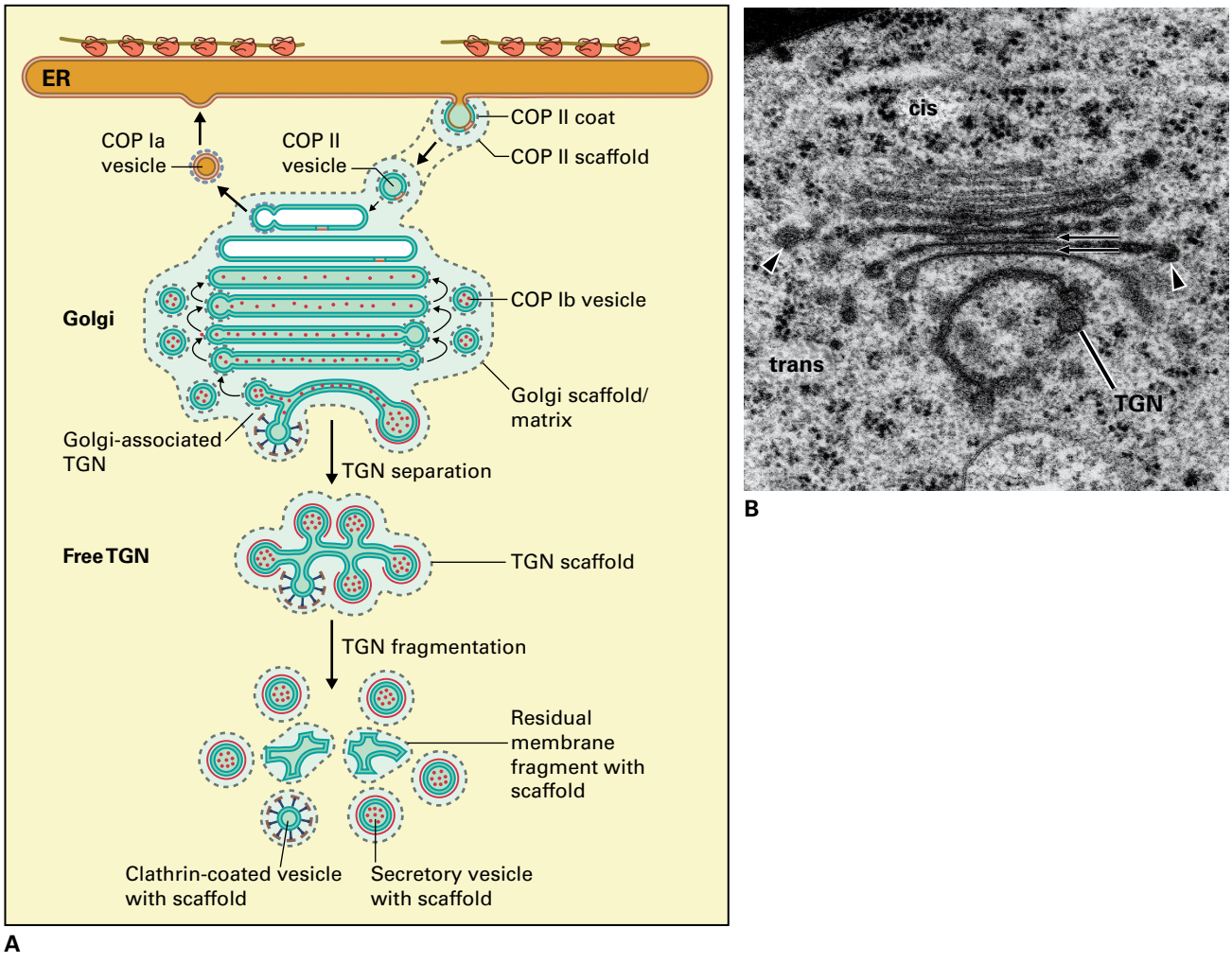


FIGURE 1.25 *(A) Schematic diagram illustrating the sites of origin and the trafficking routes of five types of ER/Golgi/TGN-associated vesicles. COPII-type vesicles bud from the ER and transport cargo molecules and membrane to the* cis*-Golgi cisternae. COPIa-type vesicles bud from* cis*-Golgi cisternae and recycle ER proteins back to ER. COPIb-type vesicles are produced by cisternae of the medial and* trans *Golgi and Golgi-associated TGN and recycle molecules between those compartments. Secretory and clathrin-coated vesicles are formed on TGN cisternae to transport the final products to their ultimate destinations: plasma membrane/cell wall and vacuoles. Cisternal fragmentation releases the latter vesicles and gives rise to residual cisternal membrane fragments. Note that the Golgi stack, the TGN cisternae and associated vesicles are all encased by protein scaffolds (matrices). (B) TEM of a cross-sectioned Golgi stack from a root cap columella cell. The cisternae exhibit a distinct* cis*-to-*trans *polarity with the lumenal contents of the* trans *side cisternae staining more densely. Arrowheads: COP-coated budding vesicles; arrows: intercisternal elements;* trans*-Golgi network (TGN).*
Source: (A) Adapted from Staehelin, L.A. and Kang, B.-H. (2008). Plant Physiol. 147: 1454–1468. (B) Micrograph by Thomas Giddings Jr., from Staehelin et al. (1990). Protoplasma 157: 75–91.

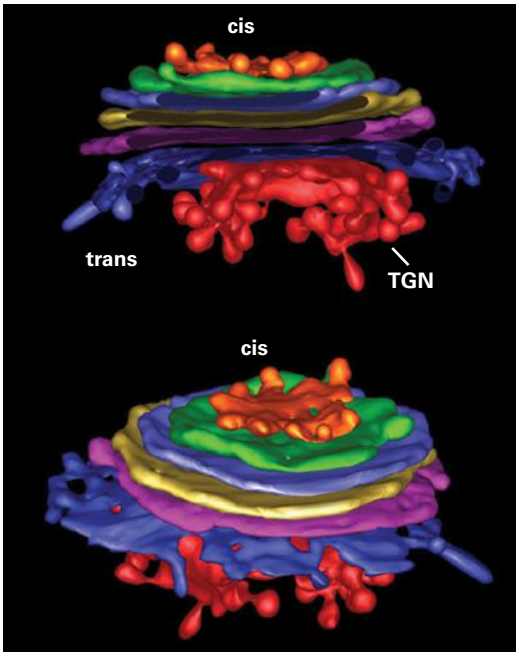


FIGURE 1.26 *Two views of a 3D tomographic model of a Golgi stack and an associated TGN cisterna of an* Arabidopsis *root meristem cell. Note the small size of the* cis*-side cisternae, the disc shape of the central Golgi cisternae, and the large number of budding vesicles being formed on the TGN cisterna.*
Source: Model by Byung-Ho Kang, University of Florida, Gainesville, FL.

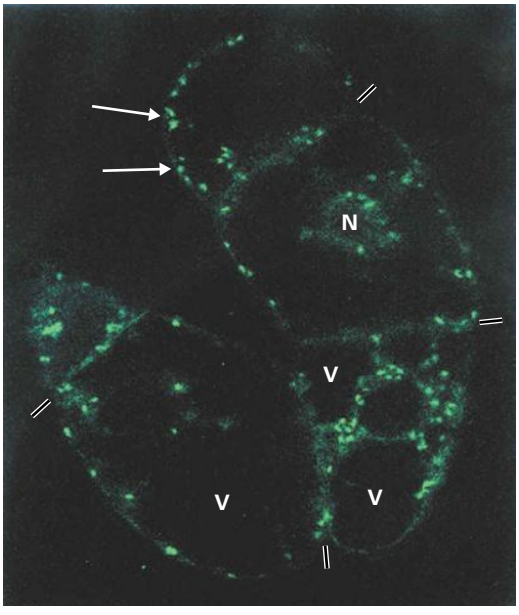
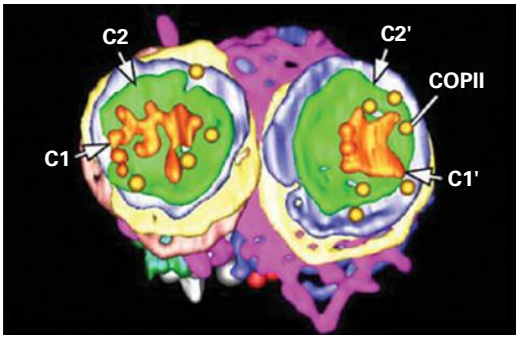
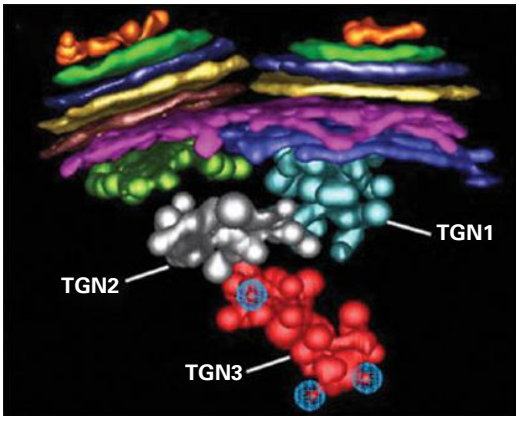


FIGURE 1.27 *Light micrograph of a group of transformed tobacco BY-2 cells expressing a mannosidase I–green fluorescent protein fusion protein. The chimeric protein is localized to Golgi stacks (arrows). Labeled Golgi are seen in the cortical cytoplasm as well as in transvacuolar cytoplasmic strands that connect the nucleus (N) with cortical cytoplasm. Cross-walls between cells are marked with double lines. Vacuoles (V).*
Source: Micrograph by Andreas Nebenfuehr, University of Tennessee, Knoxville, TN.



A



B

FIGURE 1.28 *Two views of a 3D tomographic model of a dividing Golgi stack of an* Arabidopsis *root meristem cell. (A)* Cis*-side, face-on view of the two forming daughter stacks. The C1 (orange) and the C2 (green)* cis*-cisternae display varying shapes reflecting the process of cisternal assembly. (B) Side view of the dividing Golgi stack showing that the two sets of* cis *and medial cisternae are held together by a larger* trans *Golgi cisterna (pink). On the* trans *side of the stack, three TGN cisternae at different stages of maturation are seen.*
Source: Model by Byung-Ho Kang, from Staehelin, L.A. and Kang, B.-H. (2008). Plant Physiol. 147: 1454–1468.

~35 Golgi stacks, suspension-cultured tobacco (*Nicotiana tabacum*) BY-2 cells up to 800, and giant fiber cells of cotton >10,000.

Each Golgi stack-TGN unit consists of a set of five to eight flattened **Golgi cisternae** that exhibit a distinct morphological polarity and possess fenestrated and bulbous margins, and a Golgi-associated TGN cisterna on the *trans*-side of the stack (see Figs. 1.25, 1.26, and 1.28). Three types of Golgi cisternae, *cis*, medial, and *trans*, can be distinguished based on their position in a stack, their staining properties, the types of vesicles that bud from their rims, and their biosynthetic functions. According to the **cisternal progression** model of Golgi trafficking, COPII vesicles from the ER are assembled into new cisternae on the *cis*-side of the stack (Figs. 1.25 and 1.28), and the *trans*-most cisternae are converted to Golgi-associated TGN cisternae before they are shed to become free TGN cisternae. This process leads to a net displacement of cargo-laden cisternae across the stack as new cisternae are added

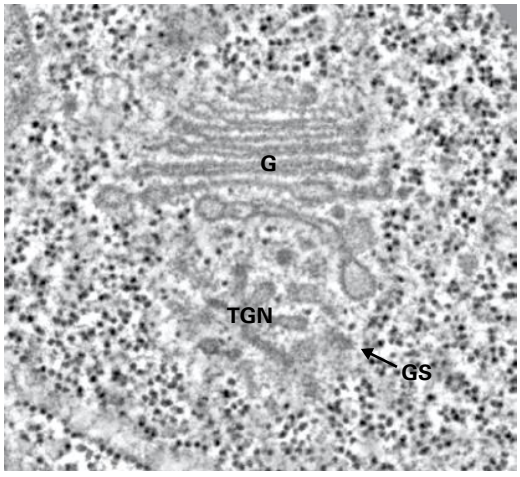


FIGURE 1.29 *Tomographic slice image of an* Arabidopsis *meristem Golgi stack (G) and TGN cisternae and their encompassing, ribosome-excluding scaffold/matrix (GS) systems.*
Source: Micrograph by Byung-Ho Kang from Staehelin, L.A. and Kang, B.-H. (2008). Plant Physiol 147: 1454–1468.

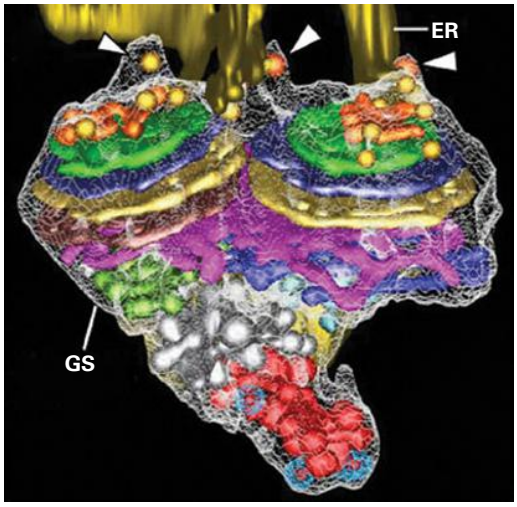


FIGURE 1.30 *3D tomographic model of a dividing Golgi stack docked to an ER export site in an* Arabidopsis *meristem cell. The docking is mediated by structural links (arrowheads) between the* cis*-side of the Golgi scaffold/matrix (GS) and the scaffolds on the budding COPII vesicles. See diagrams Figures 1.25A and 1.31.*
Source: Model by Byung-Ho Kang, from Staehelin, L.A. and Kang, B.-H. (2008). Plant Physiol 147: 1454–1468.

and old cisternae are shed. During their assembly the *cis*-Golgi cisternae remain biochemically inactive. Most of the biosynthetic activities are confined to the medial and *trans*-Golgi cisternae and to a lesser extent to the Golgi-associated TGN compartments.

To maintain the characteristic enzymatic properties of the different cisternal types during translocation of cisternae across the stack, the cisternae bud recycling vesicles that transport membrane proteins in a retrograde direction. These vesicles are known as **COPI vesicles** (see Fig. 1.25A). In plants, two types of COPI vesicles have been characterized: **COPIa vesicles** that recycle escaped ER proteins from *cis*-Golgi cisternae back to the ER, and **COPIb vesicles** that bud from medial- and *trans*-Golgi and Golgi-associated TGN cisternae and transport cisternal membrane proteins in a retrograde direction. This latter transport is responsible for maintaining the steady-state distribution of enzymes within Golgi stacks.

Intercisternal elements are another type of *trans*-Golgi cisterna–associated structure (see Fig. 1.25B). These parallel protein fibers lie sandwiched between cisternae and may serve as anchors for the glycosyltransferases involved in synthesis of large polysaccharide slime molecules, such as those secreted by the outermost cells of root caps.

1.5.2 The *trans*-most Golgi cisternae give rise to TGN cisternae that sort and package Golgi products

The function of the TGN is to sort and to package the products of the Golgi stacks into **secretory vesicles** and **clathrin-coated vesicles**. Secretory vesicles transport membrane and cargo molecules to the plasma membrane and cell wall, whereas clathrin-coated vesicles produced by the TGN deliver membrane and soluble molecules to multivesicular bodies and vacuoles. The TGN cisternae arise from the *trans*-most Golgi cisternae by a cisternal peeling process that yields free, independent TGN compartments (see Fig. 1.25). TGN cisternae in the process of peeling are called Golgi-associated or **early TGN cisternae**, and those that have become physically separated from the originating Golgi stack, **free** or **late TGN cisternae**. During cisternal peeling, the cisternae undergo multiple changes in architecture, including a 30–35% decrease in cisternal membrane surface area, most likely due to the removal of membrane by COPIb-type recycling vesicles. Concomitantly, the flattened cisternae are converted into grape-like membrane compartments as the number of budding secretory and clathrin-coated vesicles increases. This maturation process continues until all products have been sorted and packaged. Once this has happened, the fully matured free TGN cisterna breaks up, yielding free secretory and clathrin-coated vesicles together with small residual fragments of the cisternal membranes (see Fig. 1.25A). The fate of the residual membrane fragments is unknown.

The ratio of secretory to clathrin-coated vesicles budding from free TGN cisternae is highly variable, but typically secretory vesicles are more numerous. Even in a single root apical meristem cell, the ratio can vary from 5:1 to 1:3 on free TGN cisternae derived from adjacent Golgi stacks. This variability most likely reflects the composition of mRNAs (coding for secretory versus vacuolar proteins) that were translated by ER-bound polysomes close to a given ER export site. Upon transfer of each batch of locally produced

proteins to a forming *cis*-Golgi cisterna of an individual Golgi stack, and after passing through the stack, the biased set of vacuolar or secretory proteins reaches the TGN. There, the ratio of secretory to clathrin-coated vesicles formed is adjusted to the ratio of products in the cisternal lumen. This variability reflects the inherent flexibility of the sorting and packaging systems of the TGN cisternae. Free TGN compartments with a high ratio of clathrin-coated vesicles were given the name "partially coated reticulum" by early electron microscopists, but in light of the new findings, this name has outlived its usefulness and should be abandoned. *Trans*-Golgi and TGN cisternae are the most acidic compartments of the Golgi apparatus. They are acidified by vacuolar (V-type) H^+-ATPases (see Chapter 3). The low pH environment of the cisternal lumen appears to regulate enzyme activities and cause an osmotic collapse of the lumen, which is of critical importance for the sorting and packaging of the Golgi products.

1.5.3 The Golgi scaffold/matrix originates on COPII buds and mediates ER-to-Golgi COPII vesicle transport

The Golgi matrix is a fine, filamentous, cage-like structure that completely surrounds all Golgi and TGN cisternae and is comprised of long coiled-coil scaffolding proteins, hence the more recent name Golgi scaffold. This scaffold/matrix excludes ribosomes from the immediate vicinity of Golgi and TGN cisternae, thereby facilitating its visualization in electron micrographs of ribosome-rich cell types (Fig. 1.29). It also appears to prevent COPI-type intercisternal recycling vesicles from escaping from the immediate surroundings of the Golgi stack and helps maintain structural integrity of Golgi stacks and associated TGN cisternae as they move along actin filaments through the cytoplasm.

Analysis of Golgi stack dynamics has shown that stacks move in a stop-and-go manner. This has led to the hypothesis that stacks may pause at ER export sites to pick up cargo for processing by Golgi enzymes. The mechanism responsible for inducing Golgi stacks to pause at ER export sites has puzzled cell biologists for many years. It now appears that the Golgi scaffold/matrix is intimately engaged in this process (see Figs. 1.25 and 1.30). In particular, recent studies have shown that COPII vesicles originate with a ~40-nm-wide external layer of long, scaffold-type proteins, termed **COPII scaffold**. As illustrated in the "dock, pluck and go model" of ER-to-Golgi trafficking (Fig. 1.31), the scaffold layer of budding COPII vesicles appears to capture passing Golgi stacks by binding to the *cis*-side of the Golgi scaffold/matrix. Once bound to a COPII vesicle, the wiggling motion of the Golgi stack appears to provide the force needed to pluck the budding vesicle from the ER export site. The plucked COPII vesicle together with its scaffold layer is then transferred to the *cis*-side of the Golgi scaffold/matrix where it contributes to the assembly of a new *cis*-Golgi cisterna.

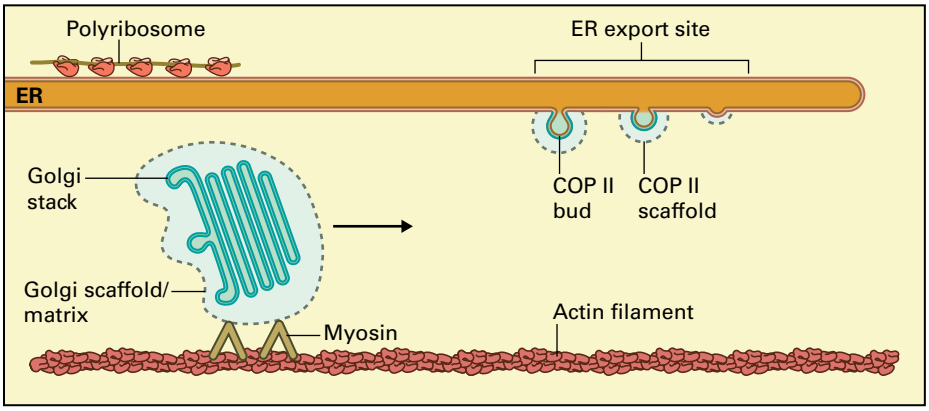
1.5.4 The sugar-containing molecules produced in Golgi cisternae serve diverse functions

The Golgi apparatus is involved in assembling the **N-linked** and **O-linked glycans** of glycoproteins and proteoglycans and in synthesizing complex polysaccharides (see Chapters 2 and 4). One of the principal functions of glycosylation is to protect proteins against proteolysis, thereby increasing their life span. Sugar groups increase protein solubility and may specify plasma membrane–cell wall interactions, prevent premature activation of lectins (highly specific sugar-binding proteins), and contribute to protein folding or assembly of multiprotein complexes. Most proteins subject to N-linked glycosylation perform enzymatic functions, whereas O-glycosylated proteins often serve structural roles. For example, the O-glycosylation of extensin molecules (see Chapter 2) is responsible for their rod-shaped architecture. Both N- and O-linked glycan side chains are present in many highly glycosylated AGPs that, at >90% sugars, are classified as proteoglycans. The complex cell wall polysaccharides produced by the Golgi apparatus perform structural functions and can bind water and heavy metals. In addition, these polysaccharides contain cryptic regulatory oligosaccharide domains that can be released by specific enzymes to yield regulatory molecules known as oligosaccharins.

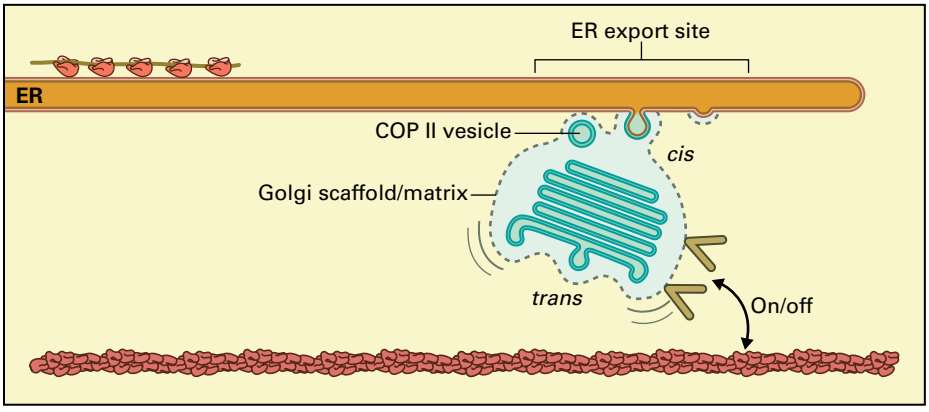
1.5.5 The Golgi apparatus is a carbohydrate factory

The synthesis of N-linked glycans starts in the ER with assembly of a 14-sugar oligosaccharide on a molecule of **dolichol**, a large lipid composed of 14–24 isoprene units. Once complete, this oligosaccharide is transferred by oligosaccharyl transferase to selected asparagine residues in nascent polypeptide chains. Most of the subsequent processing of the oligosaccharide occurs in the Golgi, including systematic removal of mannose residues and the addition of other types of sugars (see Chapter 4). The enzymes involved in these reactions are not randomly distributed among Golgi cisternae but become localized to medial, or *trans* cisternae, depending on which sequential step they catalyze as a given N-linked glycan moves through the stack from *cis* to *trans*. For example, the native enzyme mannosidase I, which mediates the first step of N-glycan processing in the Golgi is localized in medial Golgi cisternae. However, when this enzyme is expressed in transgenic plant cells as a mannosidase I-GFP fusion protein, the fusion protein is also seen in *cis*-Golgi cisternae and even in the ER. Apparently, when too many Golgi membrane enzymes of a given type are produced, they pile up in upstream compartments of the secretory pathway. For this reason, localizing Golgi membrane proteins by means of GFP fusion proteins yields unreliable results.

O-linked glycans are important components of hydroxyproline-rich glycoproteins and AGPs, many of which serve structural



A Go-phase (saltatory/directional movements)



B DOCK-and-PLUCK-phase (wiggling and slow directional movements)

FIGURE 1.31 *Dock, pluck, and go model of ER-to-Golgi vesicle trafficking. (A) Go-phase: Golgi stacks travel along actin filaments propelled by myosin motors. (B) Dock-and-pluck phase: The scaffold of a budding COPII vesicle attaches to the* cis*-side of the Golgi scaffold/matrix of a passing Golgi stack and pulls the Golgi off the actin track. Once the COPII scaffold binds to the Golgi matrix, the wiggling motion of the Golgi stack facilitates the release of the COPII vesicle from the ER by a "plucking" mechanism. Once it has harvested the COPII vesicle from the ER export site, the Golgi is free to resume its movement along the actin track.*
Source: Adapted from Staehelin, L.A. and Kang, B.-H. (2008). Plant Physiol. 147: 1454–1468.

roles. The sugars, mostly arabinose and galactose, are attached to amino acids that contain hydroxyl groups, such as hydroxyproline, serine, and threonine. Very little is known about the synthesis of O-linked glycans. On newly synthesized proteins destined for O-glycosylation, selected proline residues are converted to hydroxyproline in the ER, but where the enzymes are located that add the first arabinose sugars to those hydroxyprolines remains to be determined.

The matrix polysaccharides of plant cell walls are structurally complex molecules that play a central role in determining cell size and shape (see Chapter 2). Defined fragments of such molecules also function as signaling molecules in pathways that control plant growth, organogenesis, and the elicitation of defense responses. Unlike the linear polymers cellulose and callose, all branched cell-wall polysaccharides are synthesized by enzymes in Golgi and Golgi-associated TGN cisternae. The molecular details of the assembly pathways have yet to be elucidated. However, an outline of the spatial organization of the xyloglucan and pectic polysaccharide pathways in the Golgi stacks has been developed by using immunolocalization to track in which cisternae specific carbohydrate groups are added. Probably the most striking result of these studies is that assembly of pectic polysaccharides appears to involve enzymes localized in medial and *trans*-Golgi and possibly Golgi-associated TGN cisternae, whereas enzymes that produce xyloglucan appear to be confined to *trans*-Golgi and Golgi-associated TGN cisternae. To date, very few native enzymes and nucleotide sugar transporters involved in complex polysaccharide biosynthesis have been immunolocalized to specific types of Golgi cisternae.

1.6 Exocytosis and endocytosis

Exocytosis is the process by which secretory vesicles derived from the TGN fuse with the plasma membrane, releasing their contents into the extracellular space (Fig. 1.32A). In growing cells, this process delivers proteins and lipids needed

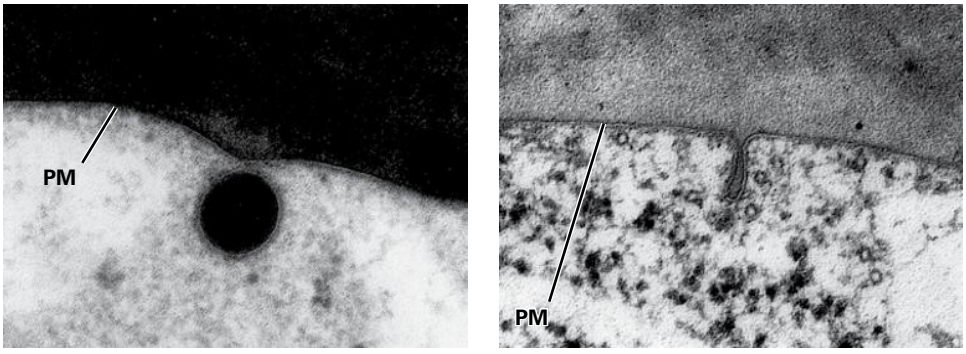


FIGURE 1.32 *Cross-sectional images of secretory vesicles. (A) TEM of a secretory vesicle in the process of initiating membrane fusion with the plasma membrane (PM). (B) TEM of a secretory vesicle that has fused with the plasma membrane and discharged its contents. The disc-shaped infolding of the membrane shown here is observed only in turgid cells.*
Source: (A) Micrograph by L. Andrew Staehelin, from Staehelin et al. (1990). Protoplasma 157: 75–91. (B) Micrograph by Yoshinobu Mineyuki, University of Hyogo, Himeji, Japan.

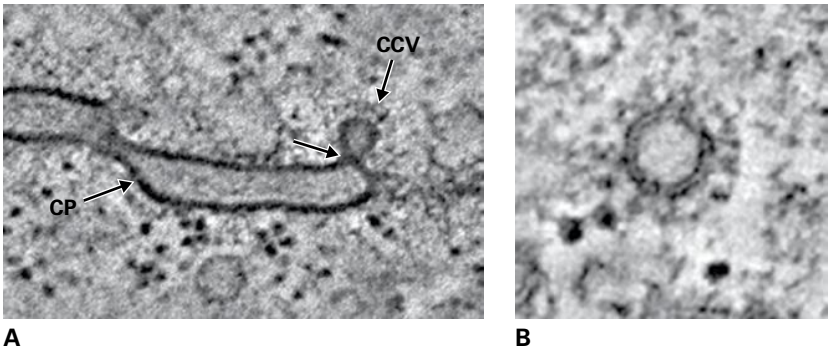


FIGURE 1.33 *Tomographic slice images of clathrin-coated vesicles. (A) A clathrin-coated vesicle (CCV) in the process of budding from a late-stage cell plate (CP) membrane. The arrow points to a dynamin motor protein ring that mechanically separates the vesicle from the membrane. (B) Higher magnification view of a cross-sectioned clathrin-coated vesicle.*
Source: (A) Micrograph by Jose-Maria Segui-Simarro, Universidad Politécnica de Valencia, Spain. (B) Micrograph by Mathias Gerl, University of Colorado, Boulder.

for expansion of the plasma membrane as well as complex polysaccharides, glycoproteins, and proteoglycans required for cell wall growth. Because of the large surface-to-volume ratio of secretory vesicles, exocytosis delivers more membrane to the cell surface than is needed for expansion of the plasma membrane. Excess plasma membrane molecules are returned to the cytoplasm by two mechanisms: (1) **endocytosis** mediated by clathrin-coated vesicles (Fig. 1.33) that contain membrane proteins and lipids, and (2) non-vesicular, intermembrane lipid transport at plasma membrane–ER interaction sites associated with fused vesicle membrane domains (see domain 15 in Fig. 1.14). Endocytosis is also used to turn over plasma membrane molecules and remove activated receptors from the cell surface. A **recycling pathway** allows endocytosed, but still functional plasma membrane proteins to be recycled back to the plasma membrane. In animal cells, endocytosis plays a major role in the uptake of nutrient molecules, but little evidence suggests such a role in plants.

1.6.1 In plants, turgor pressure affects membrane events associated with exocytosis, endocytosis and membrane recycling

When a secretory vesicle in an animal cell fuses with the plasma membrane, its contents are expelled to the extracellular space and the vesicle membrane becomes part of the plasma membrane. As this occurs, the plasma membrane is expanded slightly, an expansion that can be readily accommodated by changes in surface architecture of the animal cell. Turgor pressure prevents this from happening in plant cells. In turgid plant cells, the plasma membrane is pressed tightly against the cell wall (see Fig. 1.11) and cannot expand unless the cell wall expands as well. When a spherical secretory vesicle fuses with the plasma membrane of a turgid cell, turgor pressure not only forces the vesicle contents into the cell wall, but also flattens the vesicle into a disc-shaped infolding of the

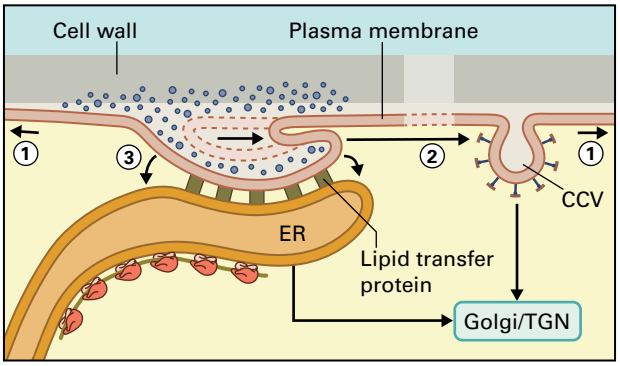


FIGURE 1.34 *Three mechanisms for removing excess membrane from a plasma membrane infolding generated by the fusion of a secretory vesicle with the plasma membrane (see Fig. 1.32B) of a turgid plant cell: 1. cell expansion; 2. formation of clathrin-coated endocytic vesicles (CCV); 3. direct transfer of lipid molecules from the plasma membrane to adjacent ER membrane via lipid transfer proteins.*
Source: Adapted from Staehelin, L.A. and Chapman, R.L. (1987). Planta 171: 43–57.

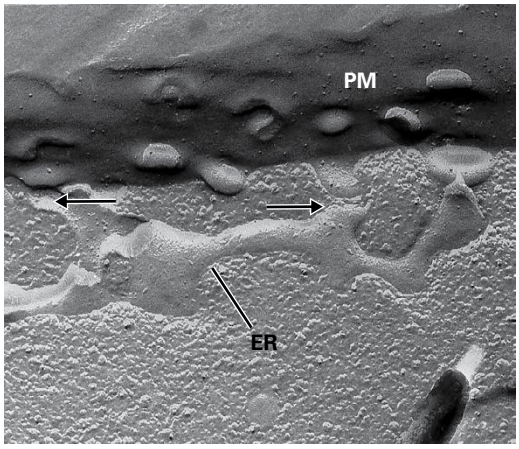


FIGURE 1.35 *TEM showing lipid-recycling ER domains. The ER cisterna has characteristic extensions that form specialized contact sites (arrows) with freshly fused and collapsed secretory vesicles in the plasma membrane (PM) of a cryofixed pea root tip cell. These structures correspond to domain 15 in Figure 1.14.*
Source: Micrograph by Stuart Craig, from Craig, S. and Staehelin, L.A. (1988). Eur J Cell Biol 46: 81–93.

plasma membrane (Fig. 1.32B). Because the plasma membrane cannot expand, the infolding remains in place until excess membrane is removed.

How then is excess membrane removed from plant plasma membranes? Plants, like animal cells, can recycle excess membrane from the plasma membrane via endocytosis of clathrin-coated vesicles (Fig. 1.34 and Section 1.6.2). However, endocytosis demands much more energy in plants than in animal cells because sizable hydrostatic pressure forces must be overcome to form plasma membrane invaginations. In contrast, retrieval of lipid molecules from the plasma membrane via non-vesicular, intermembrane lipid transport—lipid "hopping"—mediated by lipid transfer proteins (Fig. 1.34) circumvents this energy problem, and reduces the number of endocytotic vesicles needed for the removal of excess plasma membrane material.

Evidence for lipid hopping has come from both lipid uptake research and electron microscopic studies of ultra-rapidly frozen cells. To investigate lipid uptake, a fluorescent analog of the membrane lipid phosphatidylcholine was added to the outer surface of the plasma membrane. This molecular marker was quickly translocated to peripheral ER cisternae with no evidence of vesicular intermediates. However, this uptake required that an extracellular enzyme convert phosphatidylcholine to diacylglycerol, a membrane lipid that lacks a large, polar headgroup and can readily flip-flop across the plasma membrane before being transferred to the ER. Electron micrographs of cryofixed cells suggest that this rapid lipid transfer is mediated by unique ER membrane extensions that form tight caps over the plasma membrane appendages left behind by the fused secretory vesicles (Figs. 1.34 and 1.35; see also domain 15 in Fig. 1.14). During this process the disc-shaped appendages tip over to form characteristic horseshoe-shaped plasma membrane invaginations. Once capped by an ER extension, the invagination shrinks until excess membrane is gone. The ER then retracts from the plasma membrane.

1.6.2 The membrane compartments associated with endocytosis can be identified by following the uptake of tracer molecules

The process of endocytosis can be visualized by exposing cells to tracer molecules that are internalized by clathrin-coated endocytic vesicles. Two classes of molecular markers have been used in such investigations. Compounds in one group serve as membrane markers and bind to the plasma membrane (e.g., cationized ferritin); members of the other class, known as fluid-phase markers, are internalized with the aqueous phase (e.g., lanthanum nitrate). The widely used fluorescent endocytosis marker FM4-64 is generally portrayed as a membrane marker, but based on published micrographs it also appears to bind to cell-wall components. Compared to the vast literature on endocytosis in animal systems, the number of comparable plant studies remains remarkably small. Two factors have contributed to the slow development of the field: (1) the low level of endocytic activity of plant cells, and (2) the presence of cell walls that greatly impede access of tracer molecules to the plasma membranes, making experimentation more difficult. Protoplasts can be used for tracer uptake studies, but the concentrated sucrose medium that protects protoplasts from bursting also affects cell function, yielding results that may not be representative of what occurs in healthy turgid cells.

A schematic model of our current understanding of the endocytic pathway in plants is depicted in Figure 1.36. Much

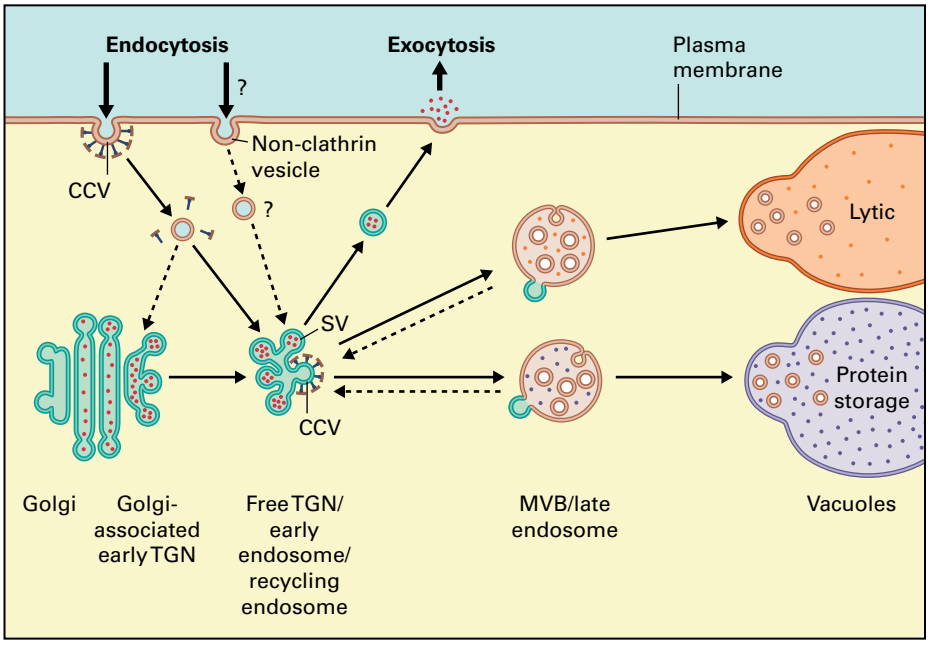


FIGURE 1.36 *Schematic diagram of the endocytic pathway of plant cells. Plasma membrane material internalized via clathrin-coated vesicles is delivered to compartments called early endosomes, most of which appear to correspond to free TGN cisternae (see Fig. 1.25A) where the different types of proteins are sorted and packaged into either secretory vesicles (SV) that recycle materials back to the plasma membrane or clathrin-coated vesicles (CCV) that deliver molecules to multivesicular bodies (MVBs), which serve as late endosomes. Some MVBs deliver molecules to lytic vacuoles, whereas others send materials to protein storage vacuoles.*

of the recent progress in plant endocytosis research has resulted from following the uptake of fluorescent tracer molecules into cells. The first compartments to receive endocytosed molecules are known as **early endosomes** and/or **recycling endosomes**, and those that receive the molecules later as **late endosomes**. In plants, the early endosomes correspond to TGN cisternae, and the late endosomes to **multivesicular bodies (MVBs)**. As discussed above, TGN cisternae serve as sorting and packaging compartments in the secretory pathway. The endocytosis pathway makes use of these capabilities to sort recyclable molecules from the plasma membrane into secretory vesicles so that they can be returned to the plasma membrane, and molecules destined for destruction into clathrin-coated vesicles for transport to MVBs and ultimately to lytic vacuoles. MVBs are spherical membrane compartments that contain distinct internal vesicles (Fig. 1.37A). Two types of vesicles bud from the boundary membrane of MVBs. Those that bud towards the cytoplasm and recycle membrane proteins back to the TGN are known as **retromer vesicles**. In contrast, budding of the boundary membrane into the MVB lumen gives rise to the **internal vesicles**. This latter process is employed to sequester membrane proteins—most notably activated, internalized plasma membrane receptors—into the interior of MVBs so that they can be functionally silenced and subsequently degraded by lytic vacuolar enzymes. Delivery of the vesicular contents of MVBs to storage or lytic vacuoles occurs by fusion of the MVBs with the vacuolar membranes (Fig. 1.37B).

Two types of structurally similar MVBs can be distinguished based on their cellular location and functional attributes. One type is seen in close proximity to the TGN, with both types of membrane compartments encompassed by a continuous TGN/MVB scaffold system. In developing *Arabidopis* embryo cells the proteolytic processing of seed storage proteins starts in these TGN-associated MVBs, which

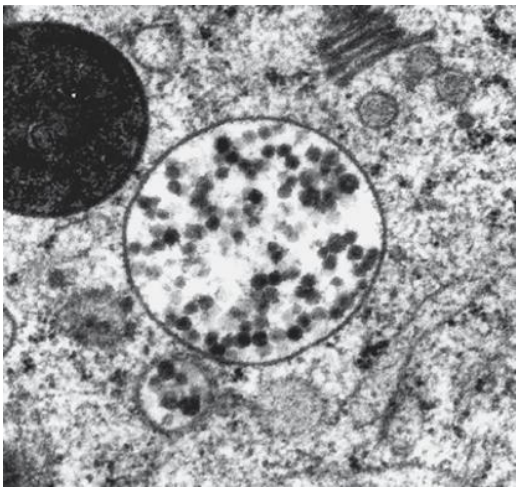


FIGURE 1.37 *(A) TEM of one large and one small multivesicular body in the cytoplasm of a tobacco cell cultured in suspension. (B) Multivesicular body (MVB) that has just fused with a vacuole (V) and is in the process of delivering its internal vesicles to the vacuolar lumen. Source*: (A) Micrograph by L. Andrew Staehelin. (B) Micrograph by Byung-Ho Kang, University of Florida, Gainesville, FL.

deliver the processed storage proteins to the protein storage vacuoles. MVBs that contain cargo molecules destined for vacuoles have also been called prevacuolar compartments, but because the definition of MVBs is more precise, the prevacuolar compartment nomenclature is now being phased out. MVBs not contained within the TGN/MVB scaffold system are capable of moving around cells in an independent manner and do not appear to process storage proteins. These independent MVBs, which receive endocytosed molecules, are also surrounded by a scaffold system, and deliver their contents to lytic vacuoles.

1.7 Vacuoles

Vacuoles, fluid-filled compartments encompassed by a **tonoplast membrane**, are conspicuous organelles of most plant cells: They typically occupy ~30% of the cell volume (Fig. 1.38), but in some cells, the space occupied by the vacuolar compartment(s) can approach 90%, with most of the cytoplasm confined to a thin peripheral layer connected to the nuclear region by transvacuolar strands of cytoplasm. During the cell cycle (see Chapter 11), vacuoles of apical meristem cells undergo major changes in shape and size. During interphase (G1 phase of the cell cycle), numerous small vacuoles are dispersed throughout the cytoplasm (see Fig. 1.1B). These vacuoles fuse into larger units during S and G2 phases and prometaphase. Coinciding with formation of the phragmoplast during cell plate formation, vacuolar volume shrinks by up to 80% and vacuoles assume a tubular configuration. This shrunken state persists until cytokinesis is complete and the two daughter cells enter the G1 phase. It has been postulated that the transient reduction in vacuole volume during early telophase provides a means for increasing the volume of the cytosol to accommodate the forming phragmoplast microtubule arrays and associated cell plate-forming structures.

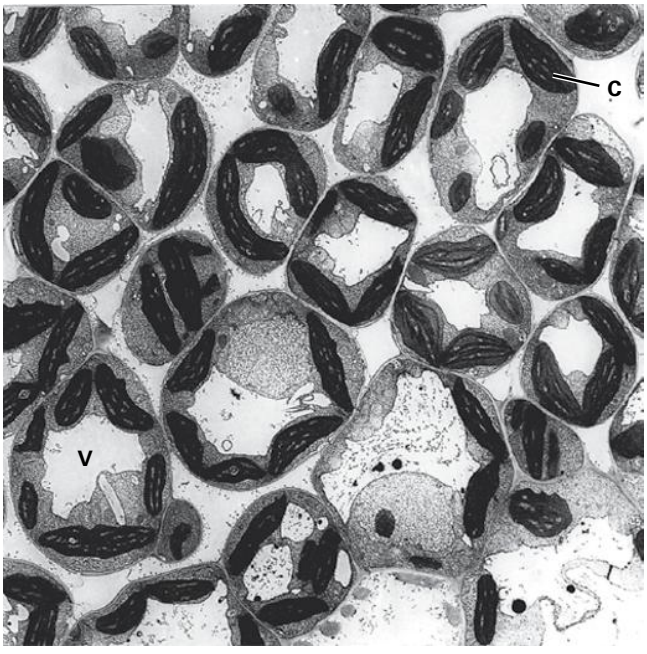


FIGURE 1.38 *TEM showing a cross-sectional view of spongy mesophyll cells in a bean leaf illustrating the large amount of cell volume occupied by the central vacuoles (V). Chloroplasts (C).* *Source*: Micrograph by L. Andrew Staehelin.

1.7.1 Plants use vacuoles to produce large cells cheaply

One of the major challenges faced by plants during evolution was to produce large solar collectors at a metabolic cost that could be recovered by the energy trapped and utilized by chloroplasts in a growing season. This problem was solved by increasing the volume of the vacuolar compartment to drive cell enlargement while keeping the amount of nitrogen-rich cytoplasm constant. This latter point is particularly important for plants, whose growth is often limited by N availability. By filling a large volume of the cell with "inexpensive" vacuolar contents, mostly water and minerals, plants are able to drastically reduce the cost of making expanded structures such as leaves, which are essentially throwaway solar collectors.

Plant cell expansion is driven by a combination of osmotic uptake of water into the vacuoles and altered cell wall extensibility. The water taken into vacuoles generates turgor pressure which expands the primary cell wall and creates stiff, load-bearing structures in conjunction with the walls. This exploitation of internal hydrostatic pressure to stiffen thin primary cell walls resembles the use of air pressure in an inner tube to convert a pliable, flat bicycle tire into a stiff circle capable of supporting heavy loads. Wilting and the associated softening of plant organs are caused by the loss of water from the vacuoles.

To maintain turgor pressure of continuously expanding cells, solutes must be actively transported into the growing vacuole to maintain its osmolarity. An electrochemical potential gradient across the tonoplast membrane provides the driving force for uptake of solutes. The gradient, in turn, is produced and maintained by two electrogenic proton pumps: V-type H^+-ATPase and vacuolar H^+-pyrophosphatase (H^+-PPase). The principal solutes in vacuoles include the ions K^+, Na^+, Ca^{2+}, Mg^{2+}, Cl^-, SO_4^{2-}, PO_4^{3-}, and NO^{3-}, and primary metabolites such as amino acids, organic acids, and sugars. Movement of water across the tonoplast membrane is mediated by aquaporin channels (see Chapter 3).

1.7.2 Plant vacuoles are multifunctional compartments

Vacuoles play several metabolic roles in addition to promoting cell expansion.

Storage: In addition to the solutes and primary metabolites mentioned above, plants also store large amounts of proteins in their vacuoles, especially in seeds. Stored reserves

can be retrieved from vacuoles and used in metabolic pathways to sustain growth. Interestingly, most of the flavors of fruits and vegetables can be traced to compounds that are stored in vacuoles.

Digestion: Vacuoles have been shown to contain the same types of acid hydrolases found in animal cell lysosomes. These enzymes, which include proteases, nucleases, glycosidases, and lipases, together allow for the breakdown and recycling of nearly all cellular components. Such recycling is needed not only for the normal turnover of cellular structures, but also for the retrieval of valuable nutrients during programmed cell death associated with development and senescence (see Chapter 20).

pH and ionic homeostasis: Large vacuoles serve as reservoirs of protons and metabolically important ions, such as Ca^{2+}. Typically, plant vacuoles have a pH between 5.0 and 5.5, but the range extends from ~2.5 in vacuoles of lemon (*Citrus limon*) fruit to >7.0 in unactivated protein storage vacuoles. By controlling the release of protons and other ions into the cytosol, cells can regulate not only cytosolic pH but also the activity of enzymes, the assembly of cytoskeletal structures, and membrane fusion events.

Defense against microbial pathogens and herbivores: Plant cells accumulate an amazing variety of toxic compounds in their vacuoles, both to reduce feeding by herbivores and to destroy microbial pathogens. These compounds include:

- phenolic compounds, alkaloids, cyanogenic glycosides, and protease inhibitors to discourage insect and animal herbivores
- cell wall-degrading enzymes such as chitinase and glucanase, and defense molecules such as saponins to destroy pathogenic fungi and bacteria
- latexes, wound-clogging emulsions of hydrophobic polymers that possess insecticidal and fungicidal properties and also serve as antiherbivory agents

Sequestration of toxic compounds: Plants cannot escape from toxic sites. Nor can they efficiently excrete toxic elements (e.g., heavy metals) and metabolites (e.g., oxalate). Instead, plants sequester these compounds into vacuoles. For example, to remove oxalate, specific cells develop vacuoles containing an organic matrix within which oxalate is allowed to react with Ca^{2+} to form calcium oxalate crystals. In other plant cell types, members of the **ABC family of transporters** (see Chapter 3) are used to transport **xenobiotics** (foreign compounds) from the cytoplasm into vacuoles. Accumulation of toxic compounds in leaf vacuoles is one reason leaves are shed on a regular basis.

Pigmentation: Vacuoles that contain anthocyanin pigments are found in many types of plant cells. Pigmented flower petals and fruits are used to attract pollinators and seed dispersers, respectively. In leaves, some vacuolar pigments screen out UV and visible light, helping prevent photo-oxidative damage to the photosynthetic apparatus.

1.7.3 Plants generate different types of vacuoles by means of vacuole transformation pathways

A fundamental question in plant vacuole research is whether plant cells produce multiple populations of functionally different types of vacuoles (multiple vacuole hypothesis), or if they produce one basic type of vacuole system that becomes specialized in response to developmental and/or physiological signals. Until recently, most researchers subscribed to the multiple vacuole hypothesis, which postulates that the large central vacuoles in root tip cells arise from the fusion of protein storage vacuoles and pre-existing lytic vacuoles. However, several recent investigations have yielded data that contradict this hypothesis. In particular, these new studies have demonstrated that the root tip cells of freshly germinated seedlings contain only protein storage vacuoles, which provide nutrients to the growing cells. As these nutrients are released from the vacuoles, the protein storage-type vacuoles are gradually converted into lytic vacuoles by means of cell type-specific transformation pathways. The transformation process includes changes in vacuole architecture as well as changes in composition of the vacuole membrane. Most notably, the protein storage vacuole marker protein α-TIP, an aquaporin-type protein, is replaced by the lytic vacuole aquaporin homolog, γ-TIP. Formation and maintenance of the different vacuole types also involves different types of vacuole targeting signals (see Chapter 4).

Senescing leaves of *Arabidopsis* and soybean (*Glycine max*) have been shown to produce two types of acidic vacuole systems in mesophyll and guard cells, a large central vacuole system with lytic properties, and smaller senescence-associated vacuoles. These latter vacuoles are more acidic than the central vacuole, accumulate a senescence-specific cysteine protease, and lack the γ-TIP of the central vacuole. Yet to be determined is whether these vacuoles arise *de novo*, or if they originate by budding from the central vacuole.

Autophagic vacuoles, also known as **autophagosomes**, are transient, large, double membrane vesicles responsible for delivering cytoplasmic materials to lytic vacuoles/lysosomes for degradation. The process begins with the entrapment of a targeted region of cytoplasm, including whole organelles, by cisterna-like membranes derived from collapsed vacuolar membranes and possibly ER membranes, followed by fusion with a lytic vacuole or lysosome. Autophagic vacuole formation is used to recycle old or damaged organelles, to provide nutrients during starvation, to generate large central vacuoles in root tip cells during germination, and to mobilize the cytoplasm during programmed cell death (Fig. 1.39).

1.8 The nucleus

The nucleus contains most of the cell's genetic information and serves as the center of regulatory activity (Fig. 1.40). Although the DNA–protein complexes that make up chromosomes are

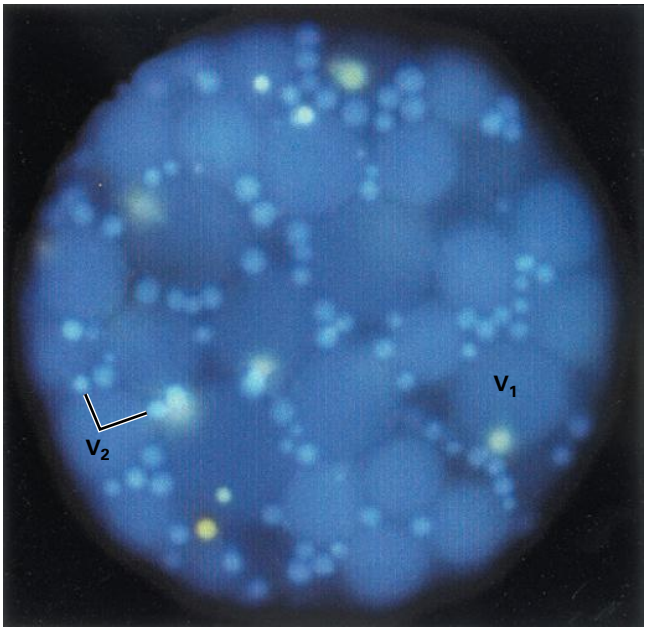


FIGURE 1.39 *Light micrograph of an aleurone protoplast stained with a fluorescent dye. Two types of vacuoles are depicted: large protein storage vacuoles (V_1) and smaller lytic/autophagic-type vacuoles (V_2) that may be involved in autophagy-associated programmed cell death.*
Source: Micrograph by Paul C. Bethke, University of Wisconsin, Madison, WI.

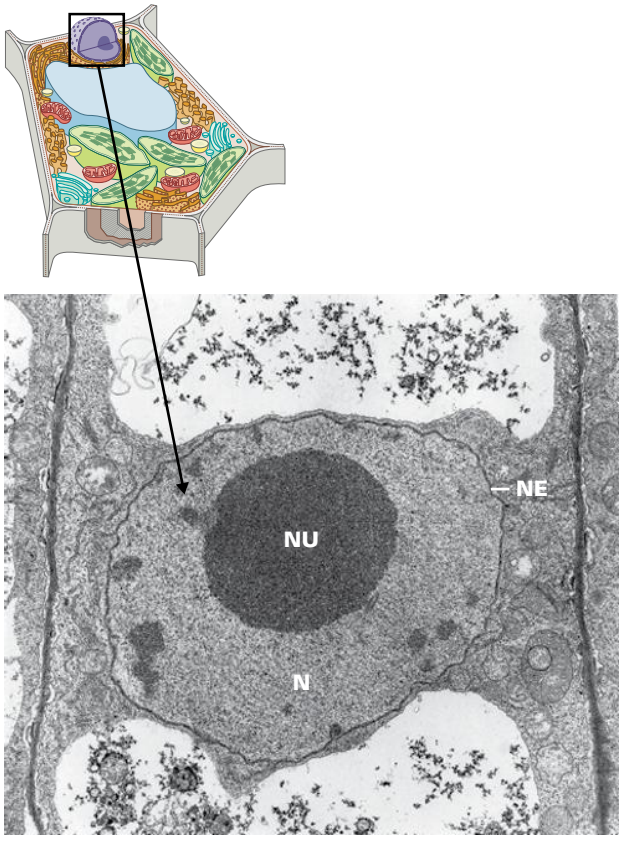


FIGURE 1.40 *TEM showing the nucleus (N) of a bean root tip cell. Note the two membranes of the nuclear envelope (NE) and the large central nucleolus (NU).*
Source: Micrograph by Eldon Newcomb.

evident only as an irregular network of chromatin during interphase, individual chromosomes nevertheless occupy discrete domains within the nucleus throughout this part of the cell cycle. Interphase is the most important stage of the cell cycle for gene expression because during this period chromosomes are actively transcribed.

A typical interphase plant cell nucleus also contains one to several **nucleoli** (singular: nucleolus) lying free in the nuclear matrix, or **nucleoplasm**. These prominent, densely staining, often spherical bodies house the cytoplasmic ribosome manufacturing machinery. A brief introduction is given below to the ultrastructure and activities of the nucleolus as well as to the structure of nuclear pores, through which nucleolar products must move to reach the cytoplasm.

1.8.1 The nuclear envelope is a dynamic structure with many functions

The **nuclear envelope** forms the outer boundary of the nucleus. It consists of two concentric membranes, the **inner nuclear membrane** and the **outer nuclear membrane**, separated by the **perinuclear space** (Fig. 1.41). The two principal functions of the nuclear envelope are to separate the genetic material in the nuclear compartment from the enzyme systems in the cytoplasm, and to regulate the exchange of molecules that traffic between the two compartments via the **nuclear pores** (Figs. 1.41 and 1.42). The inner and outer envelope membranes

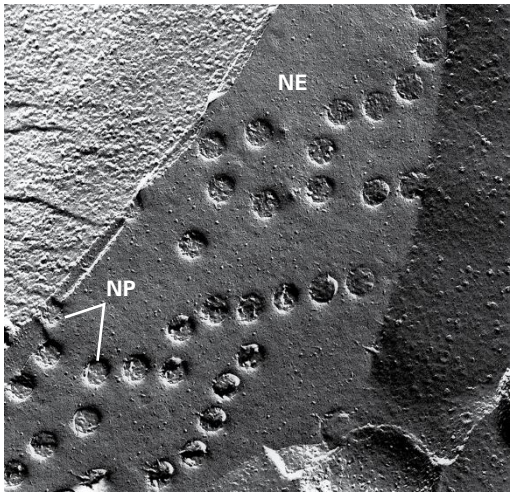


FIGURE 1.41 *TEM of a freeze-fractured nuclear envelope (NE) with nuclear pores (NP). The continuity of the inner and outer membranes becomes apparent where the membranes are seen in cross section.*
Source: Micrograph by L. Andrew Staehelin.

are connected to each other via the bridging bilayer regions of the pores. The outer membrane of the nuclear envelope is continuous with membranes of the ER through narrow (~20 nm in diameter) connections (see domain 3 in Fig. 1.14) and

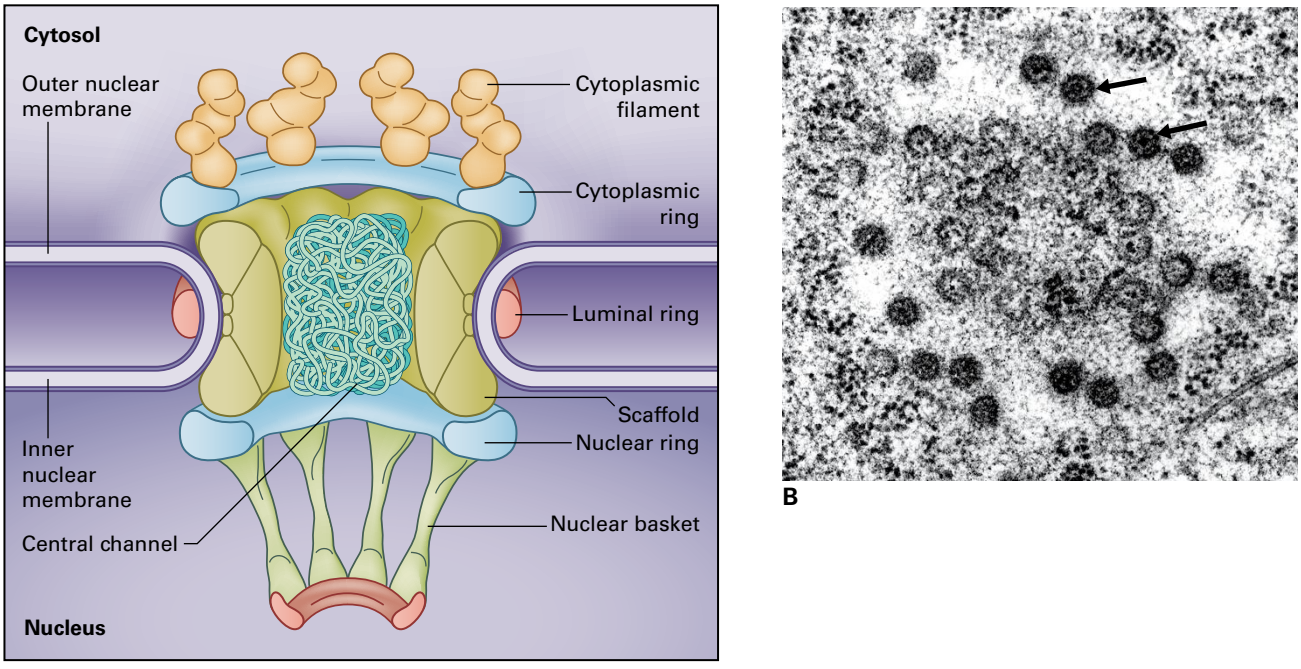


FIGURE 1.42 *(A) Diagram of a nuclear pore complex in a nuclear membrane. (B) TEM showing a tangential thin section through nuclear pore complexes of a tobacco root tip cell. Arrows indicate pores in which the central transporter plug depicted in (A) is clearly seen.*
Source: (B) Micrograph by Takashi Murata, National Institute of Basic Biology, Okazaki, Japan.

resembles the ER in having functional ribosomes on its cytoplasmic face. The perinuclear space is therefore continuous with the ER lumen. A meshwork of 10-nm-diameter filaments, called the **nuclear lamina**, underlies the inner envelope membrane (see domain 1 in Fig. 1.14). The lamina links the nuclear pore complexes and anchors and organizes the interphase chromatin at the nuclear periphery.

1.8.2 Nuclear pore complexes function as both molecular sieves and as active transporters

The density of nuclear pores embedded in the envelope varies considerably, depending on the type of cell. In plant cells, pores occupy from 8% to 20% of the envelope surface, at a pore density of 6–25 μm^{-2}. The pattern of pore distribution over the envelope varies in different organisms and cell types.

Each pore consists of an elaborate macromolecular assemblage known as the **nuclear pore complex** (Fig. 1.42). Nuclear pore complexes have an octagonal symmetry and appear similar in size and architecture throughout the plant and animal kingdoms. A nuclear pore complex is ~50 nm in diameter, has an estimated molecular mass of 125 MDa, and is composed of multiple copies of at least 30 different proteins, **nucleoporins**.

Nuclear pore complexes regulate trafficking between cytoplasm and nucleus. They permit rapid diffusion of small (<1 kDa), water-soluble molecules. Larger molecules (<40 kDa) can also diffuse across the pores, but more slowly. Proteins and protein–RNA complexes >40 kDa require an active transport system as do some smaller proteins such as histones. In electron micrographs the central pore region stains more darkly (Fig. 1.42), most likely due to the presence of translocating proteins.

Proteins translated in the cytoplasm can be targeted to the nucleus by a **nuclear localization signal** sequence of amino acids (see Chapter 4). Recognition of this signal by the nuclear import receptors causes the opening of the central channel region of the pore. An additional signal facilitates exit from the nucleus. Most imported proteins remain in the nucleus, even if they are in soluble form and can move freely in the nucleoplasm. However, some proteins are known to move back and forth between nucleus and cytoplasm. Energy in the form of ATP is required to transport larger proteins or particles through the pore in either direction. Hydrolysis of ATP probably leads to a conformational change in transporters that causes pores to open.

1.8.3 The nucleolus is the ribosome factory of the cell

Although the **nucleolus** is not membrane-bounded, it is a distinct organelle within the nucleus (Fig. 1.43). It consists of a large aggregate of macromolecules, including rRNA genes, precursor and mature rRNAs, RNA processing enzymes, snoRNPs (small nucleolar ribonuclear proteins), ribosomal proteins and partially assembled ribosomes. Its main function is to transcribe ribosomal DNA, which loops through the nucleolus, and to assemble the ribosomal RNAs and imported ribosomal proteins into ribonucleoprotein subunits

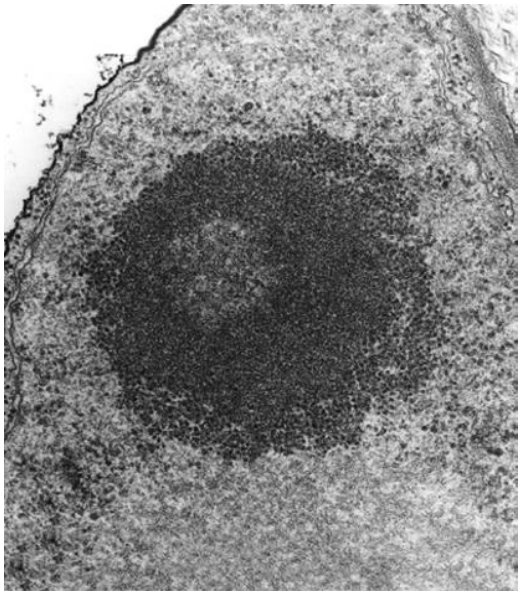


FIGURE 1.43 *TEM of a nucleolus within the nucleus of a carnation (*Dianthus caryophyllus*) cell. Note the three characteristic subdomains: fibrillar center, where ribosomal transcription takes place; surrounding dense fibrillar domain, where the rRNA transcripts are processed; and outermost granular layer that surrounds the whole structure.*
Source: Micrograph by Eldon Newcomb.

for transport to the cytoplasm. The size of the nucleolus is highly variable and reflects the number of ribosomes the cell is producing. Three types of subdomains can be identified by electron microscopy:

- one or more fibrillar centers, in which ribosomal transcription takes place,
- dense fibrillar components surrounding the centers, where ribosomal RNA transcripts are processed, and
- granular component that encompasses the fibrillar region.

The granular component consists of preribosomal particles and ribosomal subunits 15–20 nm in diameter. These are in various stages of assembly and are smaller than fully developed ribosomes in the cytoplasm. On maturation they are exported from the nucleus through the central channel of the nuclear pore. The nucleolus breaks down at the beginning of prophase and reforms when ribosomal genes of the chromosomal nucleolar organizing region become active in the young daughter nuclei during telophase.

1.8.4 During mitosis, the nuclear envelope disassembles into cisternal fragments that initiate the formation of new envelopes around the daughter nuclei

At the onset of mitosis (see Chapter 11), nuclear pore complexes disassemble, leaving holes in the envelope membranes before the envelope itself breaks down at the start of prometaphase. A cyclin-dependent protein kinase plays a central role in regulating disassembly and reassembly of the envelope during mitosis. Phosphorylation of the nuclear lamins on the inner surface of the envelope correlates with breakdown of the nuclear lamina and envelope and is also believed to play a part in assembly and disassembly of the pore complex. When the nuclear envelope breaks down, the membranes are converted into cisterna-like membrane compartments of the ER. After prometaphase, these nuclear envelope remnants are partitioned into the two halves of the dividing cell. During early telophase, dephosphorylation of nuclear lamins and other proteins triggers reassembly of the nuclear envelope on the surface of chromosomes in a process that excludes cytoplasmic proteins. This is followed by reassembly of the nuclear pore complexes between the borders of neighboring membrane compartments and completion of the nuclear envelope by membrane growth and coalescence.

1.9 Peroxisomes

Peroxisomes are structurally simple organelles composed of a single membrane that surrounds the finely granular peroxisome matrix (Fig. 1.44). Most peroxisomes are roughly spherical, with diameters ranging from 0.2 to 1.7 μm. The number of peroxisomes per cell is highly variable, as is their enzyme composition, which can change within a given cell during development and in response to environmental challenges. Peroxisomes contain over 300 nucleus-encoded proteins that function in fatty acid oxidation, metabolism of reactive oxygen species, photorespiration, and triglyceride metabolism. Catalase is present in all peroxisomes and used as a marker enzyme for the organelle (Fig. 1.44B). The concentration of enzymes in the peroxisome matrix is very high as evidenced by their high density (1.23 g cm^{-3}, compared to 1.18 g cm^{-3} for mitochondria), and the formation of strikingly beautiful catalase crystals in leaf peroxisomes (Fig. 1.45). In living cells of transgenic *Arabidopsis* plants in which GFP is fused to a peroxisome targeting signal, peroxisomes are seen to give rise to new peroxisomes via budding, and to translocate along actin filaments at peak velocities of 10 μm per second.

1.9.1 The role of peroxisomes depends on the organ or tissue in which they occur

In leaves of C_3 plants (plants that produce the three-carbon compound 3-phosphoglycerate as the first stable photosynthetic intermediate), peroxisomes play a key role in **photorespiration** (see Chapter 14), a light-dependent uptake of O_2 and release of CO_2 that arises from the dual function of the Calvin–Benson–Bassham cycle enzyme Rubisco (ribulose-1,5-bisphosphate carboxylase/oxygenase; see Chapter 12). Although Rubisco has much higher substrate affinity for CO_2, which it joins to ribulose 1,5-bisphosphate to form two molecules of 3-phosphoglycerate, the enzyme also combines abundant

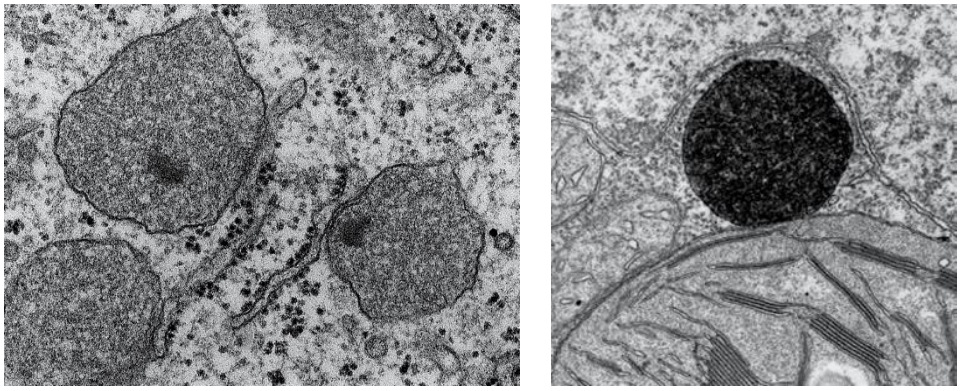


FIGURE 1.44 *(A) TEM showing three roundish, unspecialized peroxisomes closely associated with ER cisternae in a bean root cell. (B) TEM of a tobacco leaf peroxisome stained with diaminobenzidine and osmium to demonstrate the presence of catalase in the organelle.*
Source: (A) Micrograph by Sue E. Frederick, Mount Holyoke College, South Hadley, MA. (B) Micrograph by Sue E. Frederick, Mount Holyoke College, South Hadley, MA.

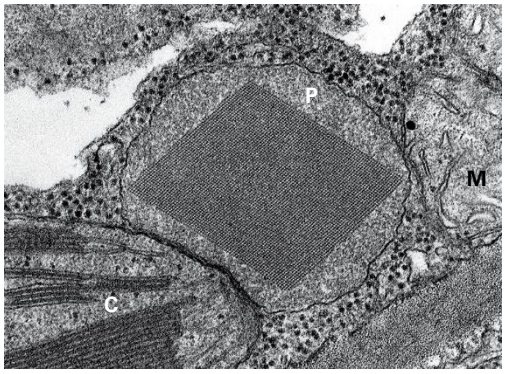


FIGURE 1.45 *TEM of a tobacco leaf peroxisome (P) in close physical contact with both a chloroplast (C) and a mitochondrion (M). Note large catalase crystal in the peroxisome.*
Source: Micrograph by Sue E. Frederick, from Frederick, S.E. and Newcomb, E. (1975). Protoplasma 84: 1–29.

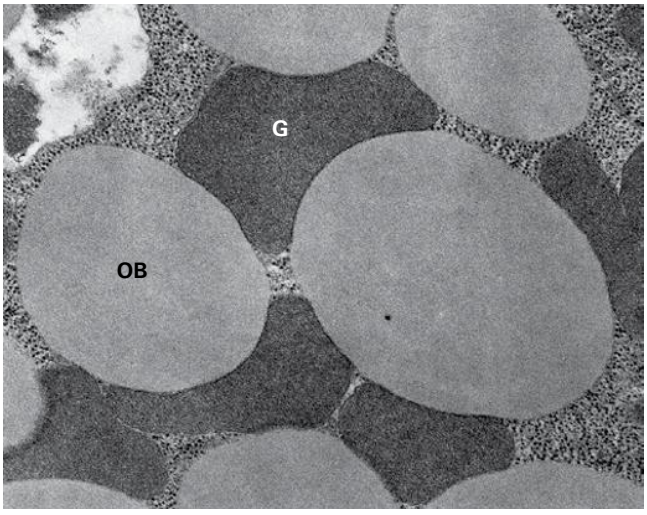


FIGURE 1.46 *TEM of glyoxysomes (G) surrounding oil bodies (OB) in a cotyledon of a germinating tomato seed.*
Source: Micrograph by Sue E. Frederick, Mount Holyoke College, South Hadley, MA.

atmospheric O_2 with ribulose 1,5-bisphosphate to form one molecule of 3-phosphoglycerate and one molecule of 2-phosphoglycolate. The photorespiratory carbon oxidation cycle salvages this 2-phosphoglycolate by converting it to 3-phosphoglycerate, returning to the Calvin–Benson–Bassham cycle up to 75% of the reduced carbon in 2-phosphoglycolate and releasing the remainder as CO_2.

The photorespiratory cycle involves interactions between a chloroplast, a leaf peroxisome, and a mitochondrion. Electron micrographs of leaf tissues in C_3 plants show that these three organelles are always closely associated physically and are often appressed to one another (Fig. 1.45). Recently, a protein called PEX10 has been shown to mediate attachment of peroxisomes to chloroplasts.

Because photorespiration is an inevitable accompaniment of C_3 photosynthesis, peroxisomes are large and abundant in the mesophyll tissues of C_3 plants. In C_4 plants, for which the first stable photosynthetic intermediate is a four-carbon organic acid, the Calvin–Benson–Bassham cycle occurs not in the mesophyll but in vascular bundle sheath cells (see Chapter 12), where the oxygenase activity of Rubisco is decreased because CO_2 concentration is much higher than in the ambient atmosphere. Leaf peroxisomes of C_4 plants are concentrated in bundle sheath cells, being smaller and relatively scarce in mesophyll cells. Specialized peroxisomes termed **glyoxysomes** participate in the mobilization of lipids in germinating oil seeds (Fig. 1.46; see also Chapter 8) and the breakdown and recycling of membranes during senescence (see Chapter 20). In some legume root nodules, peroxisomes are involved in the conversion of fixed N_2 into nitrogen-rich organic compounds (see Chapter 16).

1.10 Plastids

Plastids are major organelles found only in plant cells. They carry out photosynthesis, synthesize and store starch and oils, and contribute products to other biosynthetic pathways.

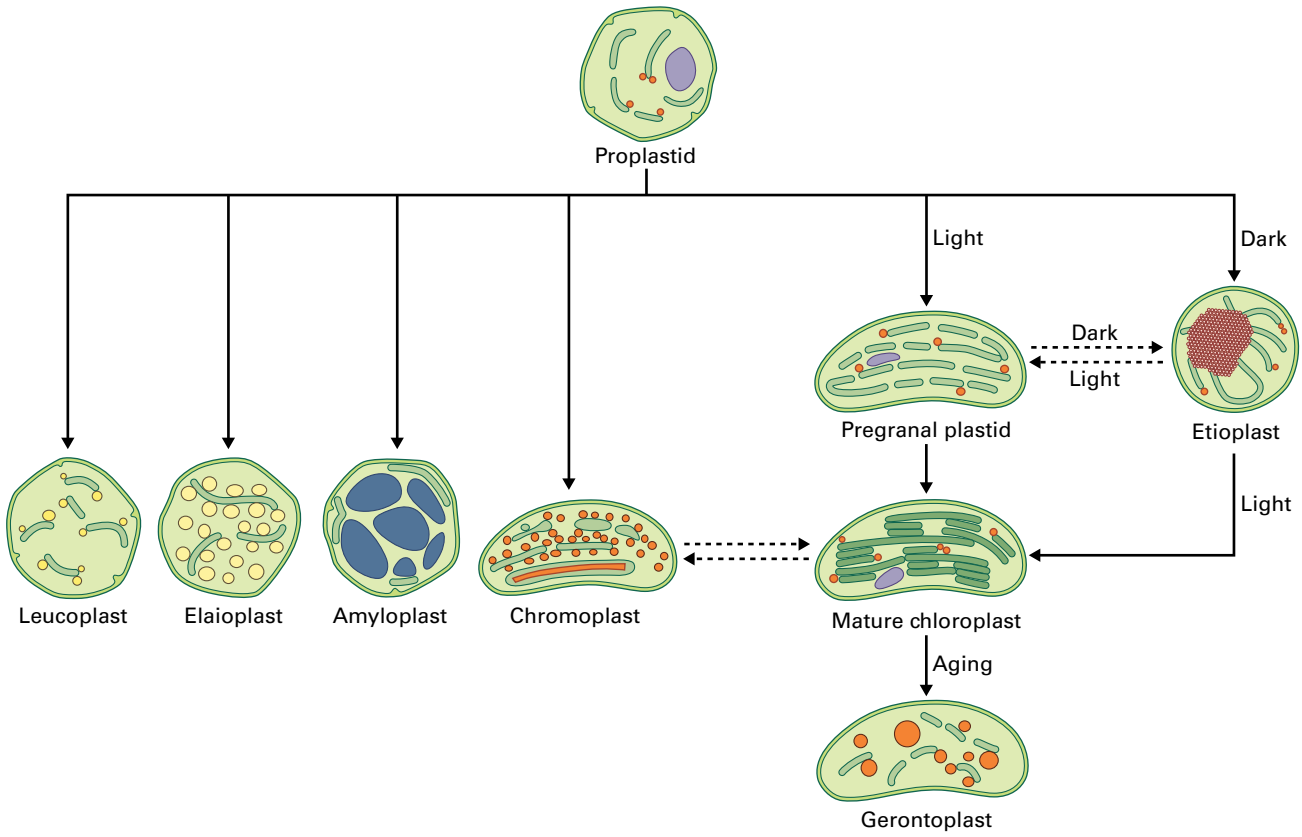


FIGURE 1.47 *Diagram illustrating the developmental relationships between the major types of plastids. All plastids in plants are derived from proplastids, which are passed on to the next generation in eggs and sperm, and are maintained in the meristems. Single arrows with solid lines depict normal steps of plastid development; dashed arrows show conversions that occur under special circumstances.*

Their outer boundary is formed by an envelope consisting of a pair of concentric membranes (Fig. 1.47). Plastids are semiautonomous and contain the genetic machinery required to synthesize some of their own proteins. The numbers of plastids per cell is highly variable and can change during development. They reproduce by division.

As is implied in the name (from the Greek *plastikos*: molded), plastids vary in size, shape, content, and function. Interest in this morphological plasticity was rekindled by studies of transgenic plant cells expressing GFP fused to a chloroplast stroma localization signal. Such GFP probes can be used to follow rapid changes in plastid shape, particularly the formation and retraction of 0.35 to 0.85-μm-wide tubular extensions known as **stromules** (stroma-filled tubules, Fig. 1.48). Stromules not only have the ability to grow and contract, they can also attach to each other and to other plastids, but they do not form tubular bridges that allow for the exchange of molecules.

Plastids also possess a remarkable capacity to differentiate, dedifferentiate, and redifferentiate (Fig. 1.47), and this plasticity has led to some confusion in plastid nomenclature. Most notably, the term leucoplast has been used in three different ways, as a generic term for some/all types of non-pigmented plastids, as a name for a postulated precursor type of plastid that gives rise to certain types of non-pigmented plastids, and as a name for non-pigmented plastids that produce essential oils (see below). In this chapter, we use the term leucoplast to describe essential oil-producing plastids. Using the term leucoplast as a generic name for some/all types of uncolored plastids no longer serves a useful purpose and should therefore be discontinued.

1.10.1 The outer and inner membranes of the plastid envelope differ in composition, structure, and transport functions

Plastid envelope membranes mediate bidirectional metabolic traffic flows between the interior of plastids and the surrounding cytosol. Unlike other membranes of most eukaryotic cells, the envelope and thylakoid membranes of the chloroplast are poor in phospholipids and rich in galactolipids, a difference that some investigators believe might reflect the evolution of plants in a marine environment, where phosphorus is a limiting element (see Chapter 8).

The **outer envelope membrane** contains a non-specific pore protein that freely permits water and a variety of ions and metabolites (<10 kDa) to pass into the **intermembrane space**, the aqueous compartment between the membranes. The outer membrane is smooth and never becomes confluent

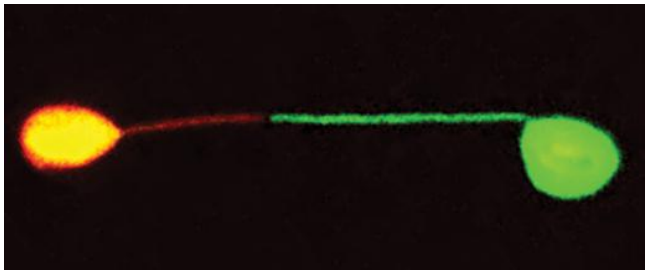


FIGURE 1.48 *Light micrograph of two fluorescently labeled plastids with thin, tubular stromule extensions that contact each other at their ends. Both plastids contain the same photoconvertable type of GFP, but the plastid on the left was irradiated to convert its fluorescent molecules from green to red. The lack of conversion of the green fluorescence on the right demonstrates that the stromules are not fused and do not exchange proteins. Micrograph courtesy of Jaideep Mathur, University of Guelph, Canada.*

with the inner membrane at any point. Electron microscopic studies, however, have revealed contact sites where proteins connecting the membranes mediate the transfer of nuclear-encoded chloroplast proteins from the cytosol to the chloroplast stroma (see Chapter 4). Among the polypeptides localized to the outer membrane are enzymes involved in galactolipid metabolism, some of which participate in cold acclimation.

The **inner envelope membrane** is freely permeable to small, uncharged molecules, including O_2 and NH_3, and to low-molecular-mass, undissociated monocarboxylic acids. Most metabolites, however, cross the inner membrane with the aid of specific transporters. The inner envelope membrane also contains enzymes involved in the assembly of thylakoid membrane lipids.

1.10.2 All types of plastids are developmentally related to proplastids

Proplastids are the precursors of all types of plastids (Fig. 1.47). They are the plastids that are passed on to the next plant generation in eggs and sperm, and are a characteristic feature of meristematic cells. Angiosperm meristem cells contain 10–20 spherical or ovoid proplastids with diameters from ~0.2 to 1.0 μm (Fig. 1.49). The internal milieu of the proplastid, called the **stroma**, appears uniformly dense and finely granular and contains fewer ribosomes than do the more highly differentiated etioplasts and chloroplasts. In chemically fixed cells one or more nucleoids are sometimes identifiable in the stroma as electron-lucent regions containing fine (3-nm-diameter) DNA fibrils. The internal membrane system remains poorly developed, consisting of a few invaginations of the inner membrane and a small number of flattened sacs called **lamellae** with associated plastoglobules (see Section 1.10.5). The proplastid

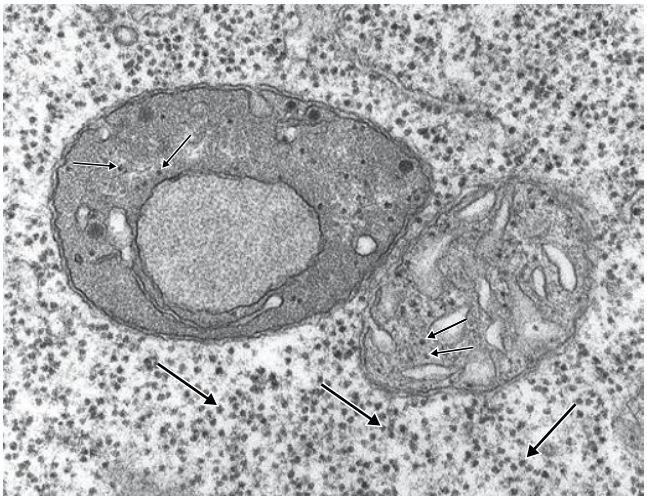


FIGURE 1.49 *TEM showing a proplastid (left) adjacent to a mitochondrion in a bean root cell. Note that ribosomes in the two organelles (small arrows) are smaller than cytoplasmic ribosomes (large arrows). The large electron-dense particles in the proplastid are plastoglobules, and the large round structure in the middle is a protein deposit.*
Source: Micrograph by Eldon Newcomb.

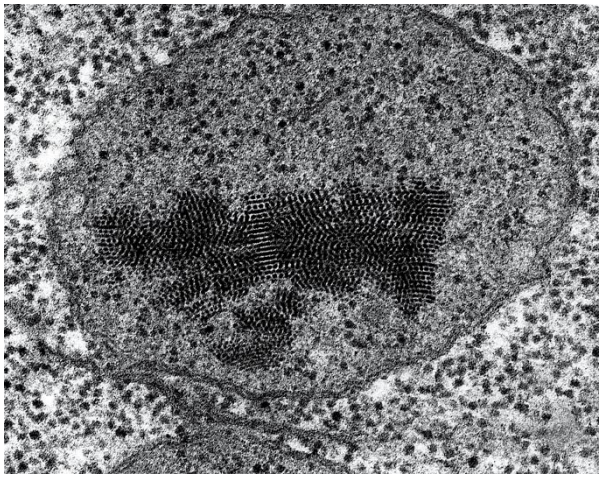


FIGURE 1.50 *TEM illustrating phytoferritin deposits inside a proplastid in a root apical meristem cell of soybean.*
Source: Micrograph by William P. Wergin.

stroma frequently contains starch granules, and occasionally deposits of phytoferritin (Fig. 1.50), a storage form of iron similar to the ferritin of animal cells. Such deposits are most frequently observed in the plastids of storage organs.

1.10.3 Chloroplasts house the photosynthetic machinery

Chloroplasts (Fig. 1.51), the green photosynthetic plastids responsible for energy capture, are commonly hemispherical or lens-shaped in vascular plants but vary considerably in

shape in mosses and algae. Plant chloroplasts commonly measure ~5–8 μm long and 3–4 μm thick. The photosynthetic apparatus of chloroplasts is contained within the expansive **thylakoid** membrane system (see Section 1.10.4).

The number of chloroplasts present in photosynthetic cells varies by cell type and species. In a leaf of the castor bean plant (*Ricinus communis*), a palisade mesophyll cell contains ~36 chloroplasts, but a spongy mesophyll cell only ~20. Of the ~500,000 chloroplasts per square millimeter of castor leaf, 82% occur in palisade mesophyll cells. Chloroplasts frequently store starch in quantities that vary according to the balance between sugar synthesis and sugar export. Developing chloroplasts in young leaves also possess many plastoglobules, thylakoid-associated lipid bodies (Figs. 1.51 and 1.57; see Section 1.10.5).

Etioplasts (Fig. 1.52A) are plastids for which the development from proplastids to chloroplasts has been arrested by the absence of light or by very low light conditions. They do not represent an intermediate stage in the normal, light-induced proplastid to chloroplast development. Instead, they constitute a special kind of plastid found only in white or pale-yellow etiolated tissues kept in the dark. Etioplasts lack the green, light-harvesting pigment **chlorophyll**, but accumulate large amounts of the colorless chlorophyll precursor called protochlorophyllide.

Etioplasts store membrane lipids in the form of a prominent, quasicrystalline membranous structure called the **prolamellar body** (Fig. 1.52A). This structure forms when membrane lipid synthesis continues in the absence of corresponding amounts of thylakoid protein synthesis, which requires light. The high concentration of lipids in prolamellar bodies (~75%) results in the formation of lipid tubes that branch in three dimensions to form a semi-crystalline lattice (Fig. 1.52B–D). When etioplasts are illuminated, they begin to develop into chloroplasts. Light triggers synthesis of chlorophyll from protochlorophyllide as well as the assembly of stable chlorophyll–protein complexes, resulting in the outgrowth of thylakoid membranes from the prolamellar body.

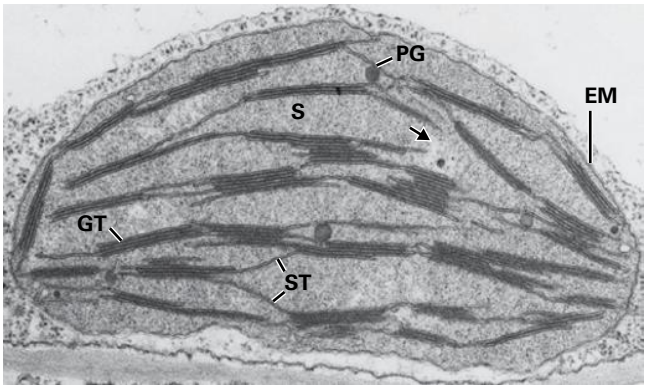


FIGURE 1.51 *TEM of a developing tobacco chloroplast. Two envelope membranes (EM) delineate the chloroplast stroma (S) within which stacked grana thylakoids (GT) and non-stacked stroma thylakoids (ST) are seen. The dark granules are plastoglobuli (PG). The arrows point to lightly stained DNA-containing regions of the stroma.*
Source: Micrograph by L. Andrew Staehelin, University of Colorado, Boulder, CO.

1.10.4 The photosynthetic grana and stroma thylakoid membranes form a physically continuous three-dimensional network

As illuminated proplastids differentiate into chloroplasts, a highly complex thylakoid membrane system develops in the stroma (Figs. 1.51 and 1.53). The electron transfer chain of the thylakoid membranes harnesses light energy to generate NADPH and a transmembrane proton gradient that drives ATP synthesis (see Chapters 3 and 12). The NADPH and ATP, in turn, power photosynthetic carbon fixation in the stroma (see Chapter 12).

Within each chloroplast, two distinct types of internal membrane domains—stacks of thylakoids, called **grana** (singular: granum), and non-stacked **stroma thylakoids**—form a continuous network that encloses a single anastomosing (branching and reconnecting) chamber, the thylakoid lumen (Figs. 1.53, 1.54, and 1.55). In young developing chloroplasts,

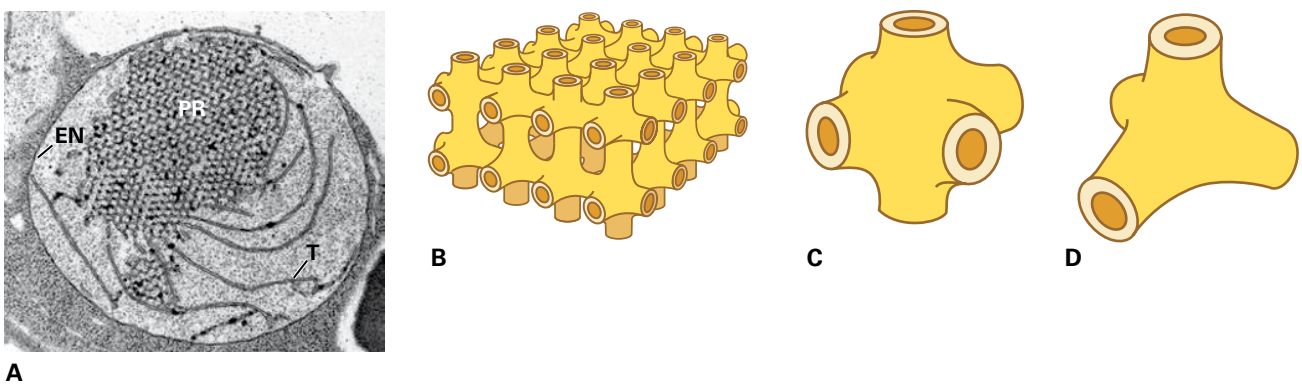


FIGURE 1.52 *(A) TEM of an etioplast with a large prolamellar body (PR) and associated non-stacked thylakoids (T) in a maize leaf. Envelope membranes (EN). (B–D) Three-dimensional models of membrane lattice structures that make up prolamellar bodies.*
Source: Micrograph by Eldon Newcomb.

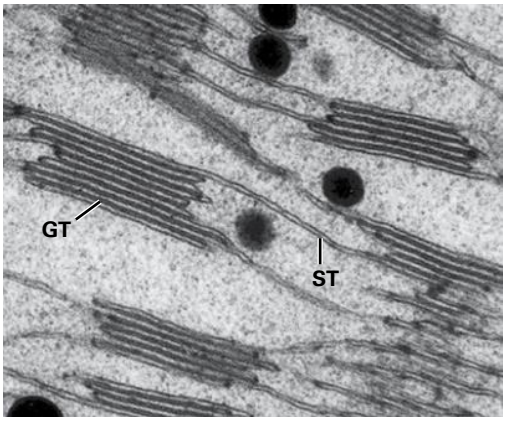


FIGURE 1.53 *High magnification TEM of stacked grana (GT) and non-stacked stroma (ST) thylakoids in a chloroplast of spinach. Note that a given membrane can be stacked in one area and not stacked in another.*
Source: Micrograph by L.Andrew Staehelin, University of Colorado, Boulder.

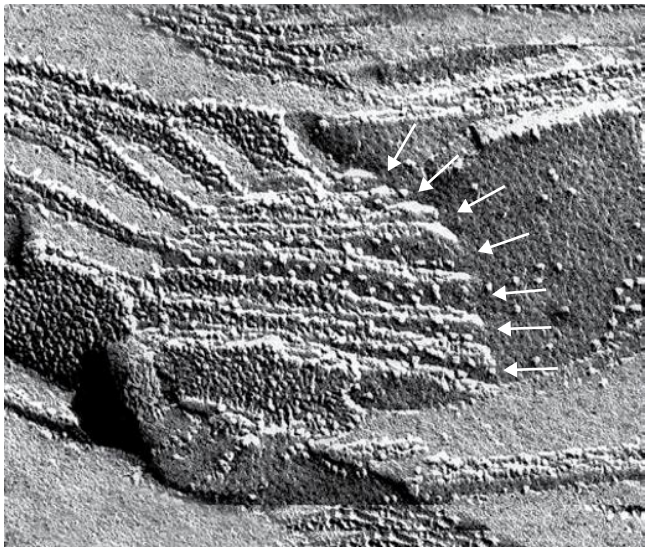


FIGURE 1.54 *TEM depicting a single granum and associated stroma thylakoids of a freeze-fractured pea chloroplast. Arrows point to sites where the two types of thylakoid domains are continuous. Compare with 3D model Figure 1.55.*
Source: Micrograph by L. Andrew Staehelin, University of Colorado, Boulder.

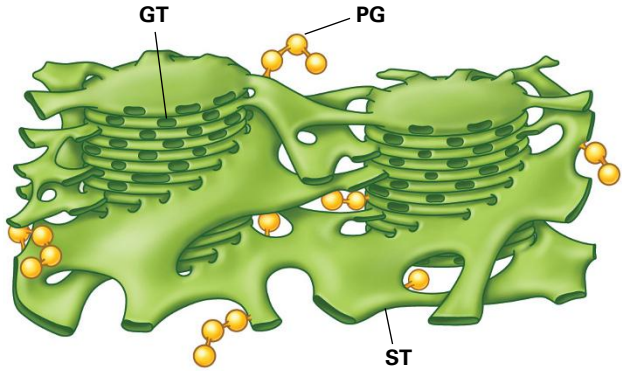


FIGURE 1.55 *Diagram illustrating the spatial relationship between stacked grana (GT) and interconnecting stroma (ST) thylakoids, and attached plastoglobules (PG). Notice the precision of the architectural organization.*

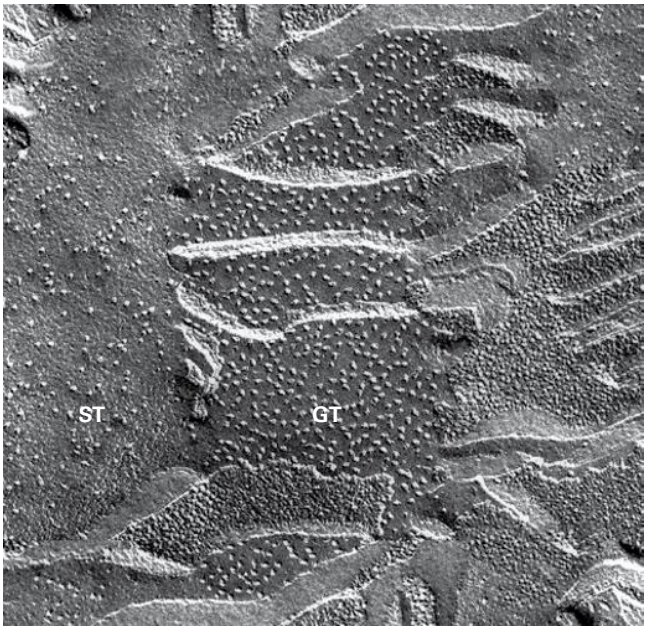


FIGURE 1.56 *Freeze-fracture TEM revealing differences in grana (GT) and stroma (ST) thylakoid composition. Large granules seen on the grana membrane fracture faces in the center correspond to photosystem II complexes.*
Source: Micrograph by L. Andrew Staehelin, University of Colorado, Boulder.

the initial thylakoids are unstacked and highly perforated. During chloroplast development, stacked grana arise from tongue-like outgrowths in the margins of the perforations of the originating thylakoids. As each outgrowth expands into a flattened sac, it contributes to the stacked grana membrane domain. As this process repeats, the grana stacks increase in height and differentiate further into intricate 3D thylakoid networks. The number of thylakoids in the grana of a mature chloroplast may vary from several to 40 or more, depending on the species and environmental conditions. In general, plants grown in the shade have more numerous and thicker grana than individuals of the same species growing in bright light.

Membranes of non-stacked, stroma and stacked, grana thylakoids differ in important ways from one another. For example, photosystem I and ATP synthase complexes reside exclusively in stroma thylakoids and unappressed regions of the grana stacks. Photosystem II and light harvesting complex II, on the other hand, are located in the appressed regions of grana stacks. This segregation of protein complexes between appressed grana thylakoids and unappressed stroma thylakoids is known as **lateral heterogeneity** of the photosynthetic membrane system (see Chapter 12). In the freeze-fracture

electron micrograph shown in Figure 1.56, this lateral heterogeneity is evidenced by nonrandom distribution of membrane particles (protein complexes) between grana and stroma membranes. Thylakoid stacking is ubiquitous in green plants and is believed to be involved in regulating the distribution of absorbed energy between photosystem I and photosystem II during photosynthesis.

1.10.5 Plastoglobules are thylakoid-associated lipoprotein bodies that contain structural proteins and enzymes involved in the synthesis and storage of lipid molecules

Plastoglobules (Figs. 1.51 and 1.57A) are lipoprotein bodies encompassed by a monolayer of polar lipids that is contiguous with the stroma-side leaflet of the thylakoid membrane (Fig. 1.57B). The lipid core contains several types of prenylquinones, (α-tocopherol [vitamin E], phylloquinone [vitamin K1], plastoquinone, and menaquinones), as well as carotenoids, neutral lipids, and breakdown products of chlorophylls. The boundary layer consists of a monolayer of galactosylglycerides, structural proteins called plastoglobulins and enzymes involved in the synthesis and metabolism of the core lipids. Plastoglobules vary in size and number during plastid development and differentiation, becoming more abundant in response to environmental stresses (e.g., high light levels, drought, high salinity, and exposure to ozone) and during senescence. During chromoplast development, accumulation of carotenoids in plastoglobules confers color to fruits and petals.

1.10.6 Chromoplasts and gerontoplasts derive their color from carotene and xanthophyll pigments

Chromoplasts (Fig. 1.58) are yellow, orange, or red, depending on the particular combination of carotenes and xanthophylls present. These pigments are produced during chromoplast differentiation, and are deposited in plastoglobules as well as in lycopene crystals within residual thylakoid membranes. Chromoplasts are responsible for the colors of many fruits (e.g., tomato [*Lycopersicon esculentum*], orange [*Citrus sinensis*]), flowers (e.g., buttercup [*Ranunculus* spp.], marigold [*Tagetes* spp.]), and roots (e.g., carrot [*Daucus carota*], sweet potato [*Ipomoea batatas*]). Chromoplasts can develop directly from proplastids or by the dedifferentiation of chloroplasts (Fig. 1.47), as happens in ripening tomato fruits. Occasionally chromoplasts will redifferentiate into chloroplasts, as they do in some yellow and orange citrus fruits that regreen under the appropriate conditions or in light-exposed surfaces of carrot roots.

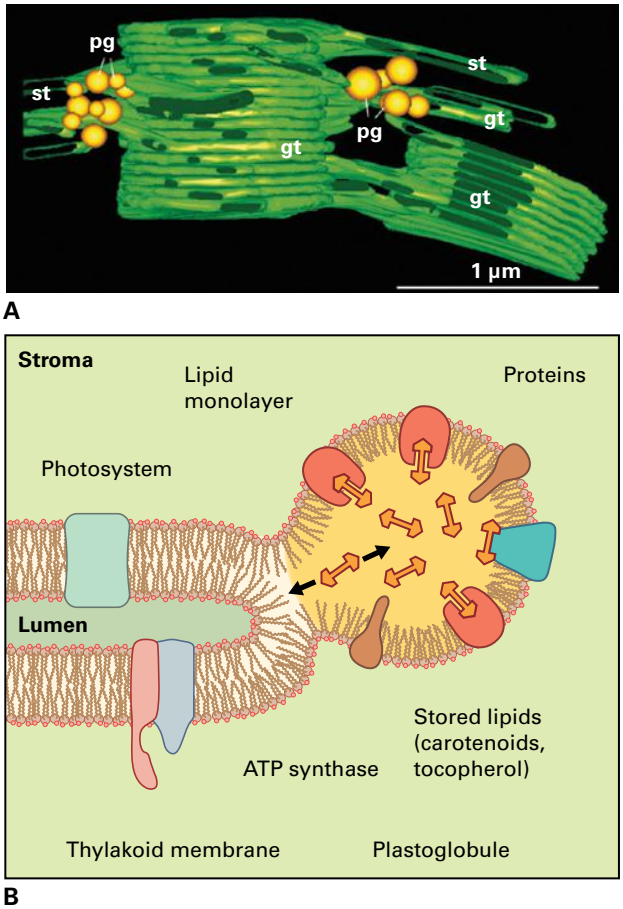


FIGURE 1.57 *(A) 3D tomographic model of thylakoid membranes and associated plastoglobules. Stacked grana thylakoids (gt), non-stacked stroma thylakoids (st), and plastoglobules (pg) are shown. (B) Diagram of a plastoglobule attached to a thylakoid membrane. The lipid monolayer that surrounds the plastoglobule is continuous with the outer leaflet of the thylakoid membrane and is studded with structural and enzymatic proteins. The functional domains of these latter proteins are located mostly in the plastoglobule interior.*
Source: (A) Tomographic model by Jotham R. Austin II, from Austin, J.R., II, et al. (2006). Plant Cell 18:1693–1703. (B) Adapted from Austin, J.R., II, et al. (2006). Plant Cell 18: 1693–1703.

Chromoplast development is accompanied by a massive induction of enzymes that catalyze carotenoid biosynthesis. Although inactive forms of these enzymes occur in the stroma, active forms occur only in plastid membranes, where the highly lipophilic precursors of carotenes, as well as carotenes themselves, are localized. The great variation in composition of large carotenoid deposits results in major differences in the size and shape of the internal structures of chromoplasts.

Gerontoplasts are formed from chloroplasts during senescence of foliar tissues. Chloroplast senescence involves a controlled dismantling of the photosynthetic apparatus including the thylakoid membranes, and the accumulation of massive amounts of plastoglobules that can become very large. The

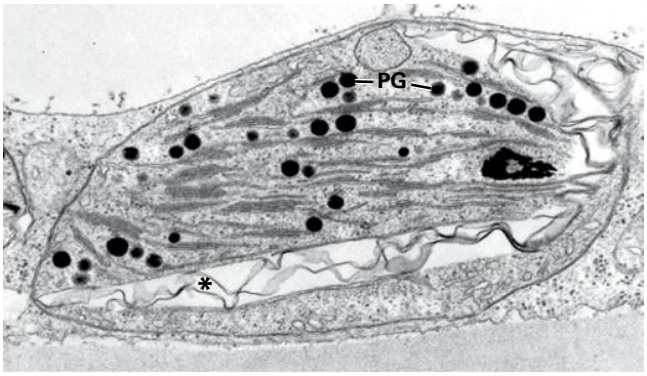


FIGURE 1.58 *TEM of a developing chromoplast in a ripening tomato. The relatively early stage of this chloroplast to chromoplast transformation (see Fig. 1.47) is evidenced by the presence of small grana thylakoid stacks, which later disappear. Mature chromoplasts only contain plastoglobules (PG) and crystals (*) of lycopene within residual membrane sacs.*
Source: Micrograph by Martin Steer, University College Dublin, North Ireland.

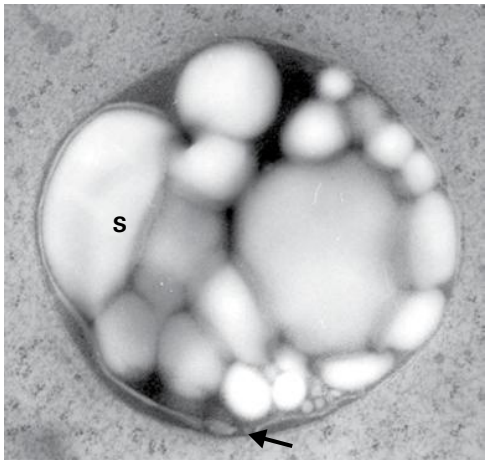


FIGURE 1.59 *TEM of an amyloplast with many starch granules (S) and flattened membrane sacs (arrow) that underlie the inner envelope membrane in an* Arabidopsis *columella cell. Columella cell amyloplasts serve as statoliths of the gravity-sensing apparatus of root tips. Amyloplasts also store starch in potato tubers.*
Source: Micrograph by Monica Schoenwaelder, University of Colorado, Boulder.

degraded thylakoid and stroma proteins provide a significant source of amino acids and nitrogen for the plant. In contrast, neither lipids nor pigments are recycled.

1.10.7 Different classes of colorless plastids synthesize and store starch and oils

Amyloplasts (Fig. 1.59) are unpigmented plastids that resemble proplastids but contain starch granules. Amyloplasts are especially common organelles in storage organs such as potato (*Solanum tuberosum*) tubers. Starch grains, which can be quite massive, occur free in the stroma together with a few flattened membrane sacs that line the inner envelope membrane. In gravity-sensing columella cells of root caps, amyloplasts serve as statoliths, sedimenting in response to gravity and thereby triggering the gravitropic response.

Elaioplasts are small, round plastids that store oil in the form of membrane-associated oil droplets. The oils contain triglycerides and sterol esters, and the droplets are delineated by a monolayer of polar lipids and proteins as in plastoglobules. Elaioplasts are produced in tapetal cells that surround developing pollen. When the tapetal cells lyse during the final stage of pollen maturation, the released sterol esters and oils become incorporated into the outer exine layer of the pollen wall.

Leucoplasts (Fig. 1.60), as defined in this chapter (see Section 1.10 introduction), are colorless plastids involved in synthesis of monoterpenes, and other volatile compounds contained in essential oils. Many of these compounds such as menthol, a derivative of mint oil, are exploited by humans as flavors or pharmacological agents. Their synthesis is carried out by specialized secretory gland cells associated with leaf and stem trichomes or within the secretory cavities of citrus peel. They possess a dense stroma, few internal membranes and ribosomes,

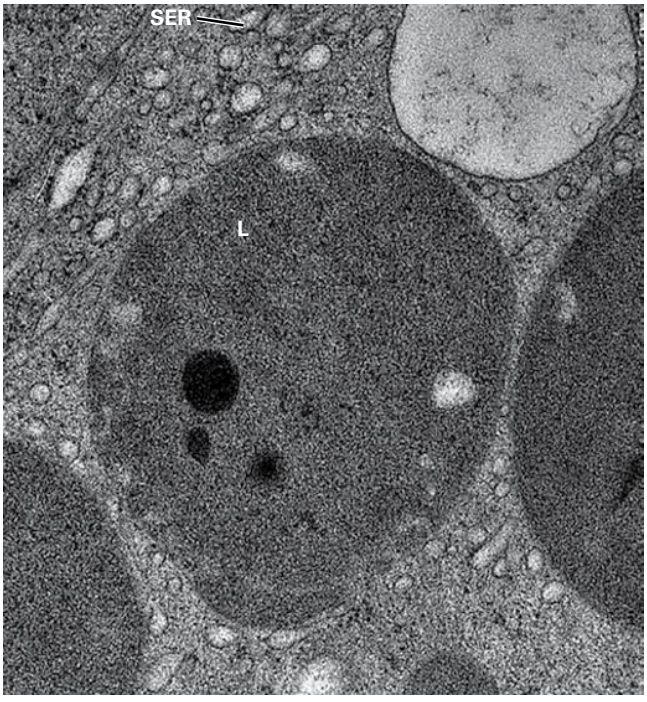


FIGURE 1.60 *TEM of a leucoplast (L) in an actively secreting glandular trichome of peppermint (*Mentha piperita*). Electron-dense globules correspond to lipid droplets. Note the near absence of internal plastid membranes and the presence of extensive tubular smooth ER cisternae (SER) in the surrounding cytoplasm.*
Source: Micrograph by Glenn W. Turner, Washington State University, Pullman, WA.

and the essential oil-containing plastoglobules that stain darkly with osmium. Leucoplasts are typically surrounded by an extensive network of tubular smooth ER membranes, which also participate in the synthesis of lipid molecules.

1.10.8 Plastids are partially autonomous, encoding and synthesizing some of their own proteins

Chloroplasts contain double-stranded, circular chromosomes and protein-synthesis machinery that accounts for as much as 50% of the total ribosomal complement of photosynthetic cells. Given that most chloroplast polypeptides are synthesized on cytoplasmic ribosomes, clearly the development of chloroplasts requires the integrated activities of both chloroplast and nuclear genomes.

Rubisco, the key enzyme in photosynthesis and photorespiration, serves as a good example. Although the small subunit of this enzyme is encoded in nuclear DNA and translated on cytoplasmic ribosomes, the large subunit is encoded in chloroplast DNA and translated on chloroplast ribosomes. Because the enzyme makes up ~50% of the total soluble protein in leaves and may be the most abundant protein in nature, the pattern of its continual breakdown and replacement helps explain the large number of ribosomes present in chloroplasts.

1.10.9 Plastids reproduce by division of existing plastids

Plastids arise from the binary fission of existing plastids. Division of proplastids, etioplasts, and young chloroplasts is most common, but even fully developed chloroplasts can divide. In meristematic cells, plastid division occurs during the G2 phase of the cell cycle (see Chapter 11), thereby enabling daughter cells to inherit the same number of plastids as parent cells. The number of plastids in interphase shoot apical meristem cells of *Arabidopsis* is ~11. During cell expansion, the number of plastids per cell can increase several-fold.

Plastid division is first made evident by a constriction in the center of the plastid (Fig. 1.61). The constriction deepens and tightens, creating an extremely narrow isthmus before the two daughter plastids separate completely. The division machinery includes two contractile ring systems, an internal ring located on the stromal side of the inner envelope membrane, and an external ring that forms on the cytosolic side of the outer envelope membrane. The inner ring subunits have been shown to be homologs of the *FtsZ* proteins that function in the cell division of cyanobacteria, the endosymbiotic precursors of chloroplasts (see Box 1.1). The outer ring contains a polysaccharide ring composed of polyglucan chains and associated dynamin proteins. Dynamin proteins are mechanoproteins that also form the contractile rings involved in budding of clathrin-coated vesicles (see Fig. 1.33A), and the dumbbell-shaped vesicles involved in cell plate assembly. Chloroplast division starts with the formation of the FtsZ ring, which recruits cytosolic glucosyltransferases to the site of constriction to produce the polyglucan molecules that form the polysaccharide ring. The polysaccharide ring, in turn, appears to serve as a template for the contractile force-generating dynamin molecules.

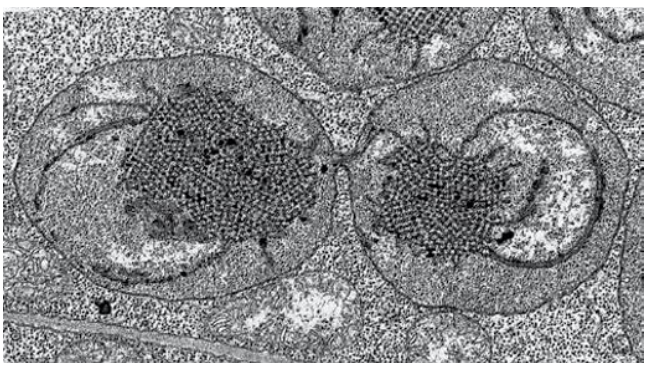


FIGURE 1.61 *TEM of a dividing etioplast in an etiolated leaf of a bean seedling. Note the central constriction.*
Source: Micrograph by Peter J. Gruber, Mount Holyoke College, South Hadley, MA.

1.10.10 Plastids are inherited maternally in most flowering plants but paternally in gymnosperms

Cytoplasmic organelles can be passed from one generation to the next by way of the egg (maternal inheritance), sperm (paternal inheritance), or both (biparental inheritance). Genetic evidence indicates that in most angiosperms, plastids (and mitochondria) are inherited maternally. These organelles from the male are either excluded from sperm cells or degraded during male gametophyte development or double fertilization. Whether from egg or sperm, plastids are in the proplastid stage of development at the time they are inherited.

Biparental inheritance of plastids and mitochondria has been documented both cytologically and genetically in a few flowering plant genera, including *Pelargonium* (geranium), *Plumbago* (leadwort), and *Oenothera* (evening primrose). In *Pelargonium*, male plastids and mitochondria differ ultrastructurally from those of the female, making it possible to establish that organelles from both are present in the developing embryo. *Plumbago*, a model of particular interest, has dimorphic sperm—one of the male gametes is rich in mitochondria, the other in plastids—and exhibits preferential fertilization, the plastid-rich sperm fusing with the egg most commonly and the mitochondrion-rich sperm doing so only rarely. Gymnosperms differ strikingly from angiosperms in their mode of plastid inheritance, with plastids typically passed to the next generation through sperm.

1.11 Mitochondria

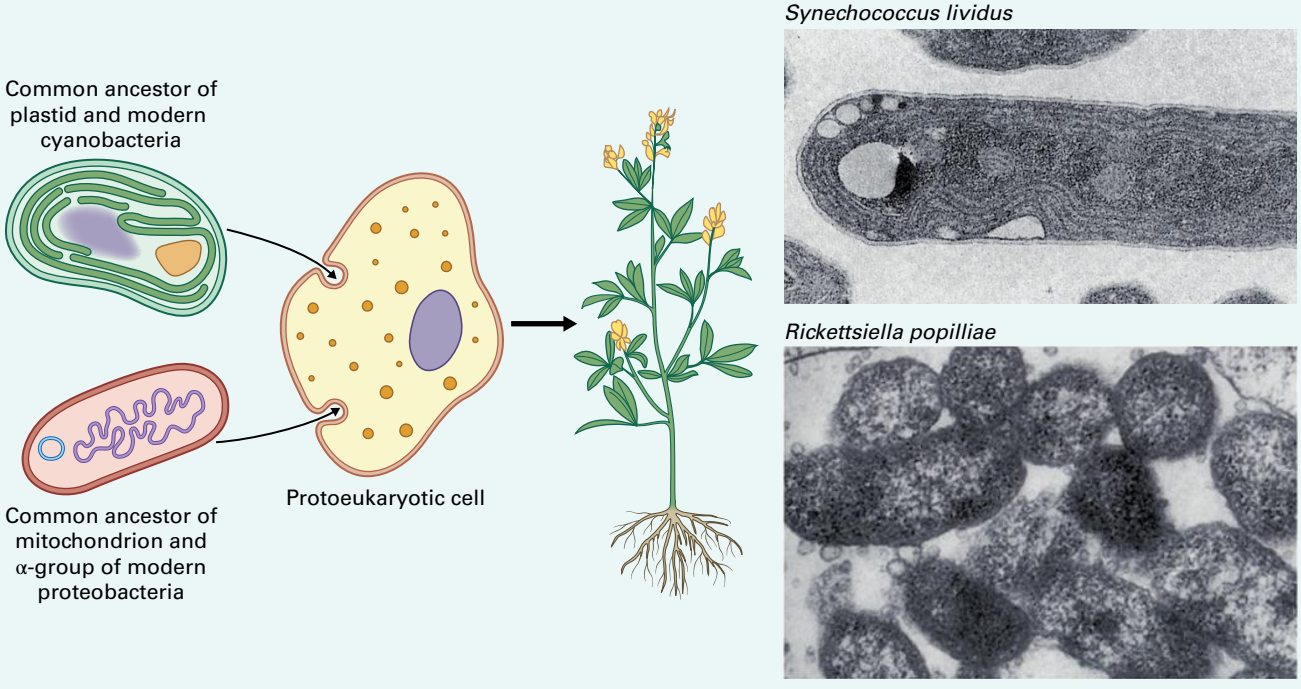
Mitochondria (singular: mitochondrion) are organelles that house enzymes and electron transfer chain components that produce ATP by ways of the citric acid cycle, respiration, and ATP synthase (see Chapter 14). In addition, mitochondria

BOX 1.1

Plastids and mitochondria evolved from endosymbiotic bacteria

Plastids and mitochondria are widely thought to have arisen from eubacteria that invaded or were engulfed by protoeukaryotic cells during the origin of the eukaryotic lineage. These organelles retain the genetic capacity to make some of their own proteins, but most of their genes have been transferred to the nucleus over time in what appears to be an ongoing process. Genes are first translocated from organelle to nucleus, so that they coexist for a time in both, before being gradually lost from the organelle. As a result of this gene loss, mitochondria and plastids now require nuclear gene products for function and replication.

Evidence for the endosymbiosis theory includes cellular and molecular traits that plastids and mitochondria share with free-living eubacteria. Similar to the genomes of eubacteria and unlike the nuclear genomes of eukaryotes, the DNA that remains within the organelles is predominantly circular and does not form extensive supramolecular complexes with proteins. In eubacteria, the DNA is organized in the form of a nucleoid that is attached to a specific region of the plasma membrane, but it is not segregated from the other cellular constituents by a membrane. Similarly, the DNA of chloroplasts and mitochondria is organized in the form of nucleoids that are attached to thylakoids and the inner membrane, respectively. Mitochondrial and plastid ribosomes are smaller than cytoplasmic ribosomes (see Figs. 1.49 and 1.62) and resemble those of eubacteria in shape and size, appearing in electron micrographs as electron-opaque particles ~15 nm in diameter. The organellar ribosomes, like those of eubacteria, are sensitive to certain antibiotics that are ineffective against cytoplasmic ribosomes (e.g., chloramphenicol). Comparison of ribosomal RNA (rRNA) sequences from organelles and certain free-living eubacteria suggests that plastids share a common ancestor with modern cyanobacteria and mitochondria with modern proteobacteria.



Evidence indicates that plants and other eukaryotic organisms evolved from endosymbiotic associations between different eubacteria. A comparison of ribosomal RNA sequences suggests that plant plastids share a common ancestor with modern cyanobacteria, such as the free-living organism Synechococcus lividus. *Mitochondrial rRNA sequences of extant eukaryotes share greatest homology with members of the α-group of the proteobacteria, which includes several genera of intracellular parasites (e.g.,* Agrobacterium, Rhizobium, *and* Rickettsia*). The electron micrograph at lower right shows cells of* Rickettsiella popilliae *within a blood cell of its insect host.*
Source: Photomicrographs: Madigan, M.T., Martinko, J.M. and Parker, J. (1997) Brock Biology of Microorganisms, 8th edition. Prentice Hall, Upper Saddle River, NJ.

produce organic acids and amino acids that are used in biosynthetic and multiorganelle metabolic pathways such as photorespiration (see Chapter 14), C_4 photosynthesis and Crassulacean acid metabolism (see Chapter 12), and gluconeogenesis (see Chapters 8 and 20). The two principal waste products of mitochondria are CO_2 and H_2O.



FIGURE 1.62 *Thin-section TEM of a mitochondrion in a eucalyptus root tip cell. A crista-forming infolding of the inner membrane is marked by the open arrow. Small eubacteria type ribosomes, ~15 nm in diameter (arrows), and hints of fibrous DNA strands are seen within the mitochondrial matrix.*
Source: Micrograph by Brian Gunning, "Plant Cell Biology on DVD, Information for Students and a Resource for Teachers," Springer Verlag, www.plantcellbiologyonDVD.com

1.11.1 Mitochondria comprise two membranes and two membrane-bounded compartments

Mitochondria are composed of two membranes and two membrane-bounded compartments: the **outer membrane**, the **inner membrane**, the **intermembrane space**, and the large internal space called **matrix** (Figs. 1.62 and 1.63). Most of the functional activities of mitochondria are located in the inner membrane and the matrix (see Chapter 14). The inner membrane can be divided into two subdomains, the **inner boundary membrane**, which is closely apposed to the outer membrane, and the **cristae membranes**, which give rise to the membrane infoldings, **cristae** that protrude into the matrix. Connecting these two inner membrane domains are the narrow **cristae junctions** located at the base of the cristae.

A defining feature of the outer membrane are proteins called **porins**, large, integral membrane proteins that form channels and enable molecules up to 10 kDa to diffuse freely into and out of the intermembrane space. Molecules capable of diffusing across these pores include ions, sugars, amino acids as well as ADP and ATP, but not proteins. The outer membrane also contains enzymes involved in the conversion of phosphatidylserine into phosphatidylethanolamine, but most of the lipids needed for mitochondrial membrane synthesis are produced by the ER and imported without modification.

The inner membrane has a high protein/lipid ratio (~75:25) and houses the protein complexes of the electron transport chain, which together with the ATP synthases, comprise ~80% of the membrane proteins. Mitochondrial ATP synthases, like

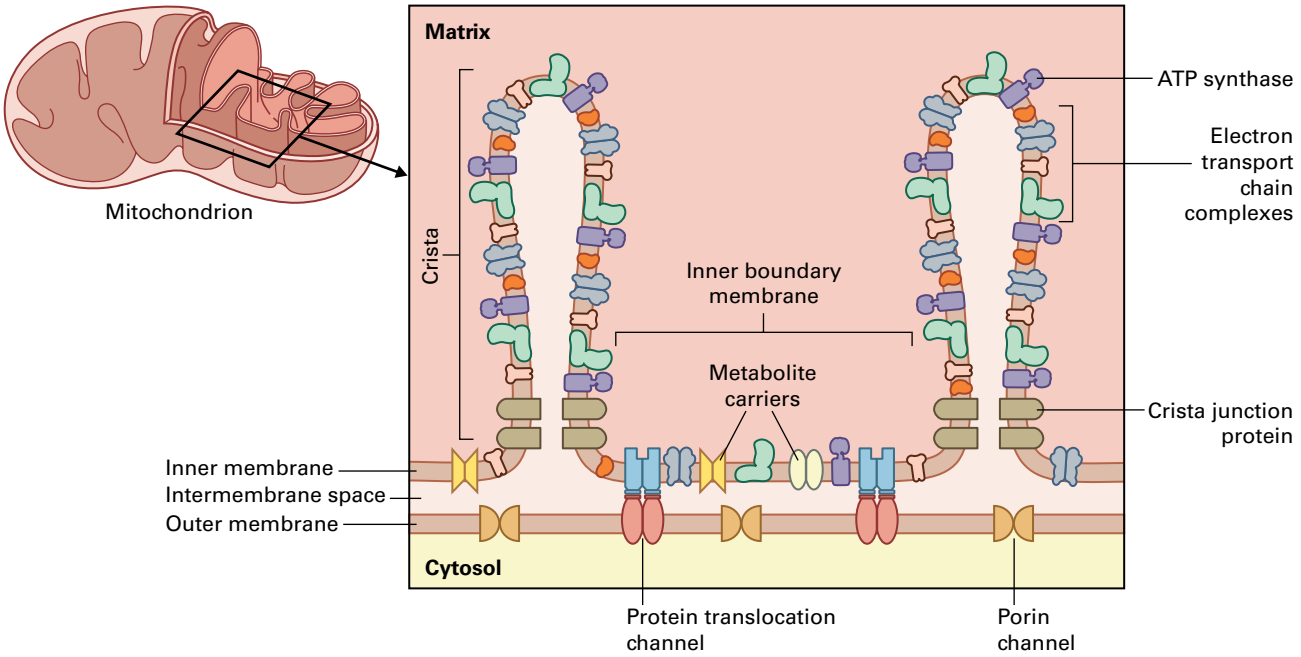


FIGURE 1.63 *Diagram depicting the 3D organization of mitochondrial cristae and the distribution, within its membranes, of associated protein complexes.*

those in chloroplasts, are driven by a transmembrane proton gradient produced by the action of the electron transfer chain (see Chapters 3 and 14). Recent studies have shown that these latter proteins are located preferentially in the cristae membrane domains of the inner membrane. In contrast, the inner boundary membrane domains are significantly enriched in protein translocation proteins and carriers that facilitate the movement of metabolites between the cytosol and intermembrane space and the mitochondrial matrix. The cristae junctions are, in part, responsible for the non-random distribution of these different types of proteins between the two inner membrane domains.

In dormant seeds, the **promitochondria of the embryo** are largely devoid of cristae and possess a matrix with a low protein content. During imbibition, new cristae are formed following the activation of the protein synthesis machinery and the assembly of new respiratory chain and ATP synthase complexes in the inner membrane. Simultaneously, the accumulation of citric acid cycle and biosynthetic enzymes increases the protein content of the matrix. When the demand for ATP increases, the number and size of the mitochondrial cristae can grow further to accommodate the additional electron transfer chain and ATP synthase proteins.

The inner membrane also contains a unique type of "double" phospholipid, **cardiolipin**, which has four fatty acid tails (Fig. 1.64). Cardiolipin binds to the transmembrane domains of the ATP synthase rotor proteins. In damaged mitochondria, it translocates to the outer membrane where it triggers autophagy.

The matrix is comprised of hundreds of soluble enzymes that metabolize pyruvate and fatty acids to acetyl-CoA and oxidize the acetyl-CoA via the citric acid cycle to produce NADH for the electron transfer chain. Other matrix components include multiple copies of the mitochondrial genome, mitochondrial ribosomes, tRNAs and various proteins required for the expression of mitochondrial genes.

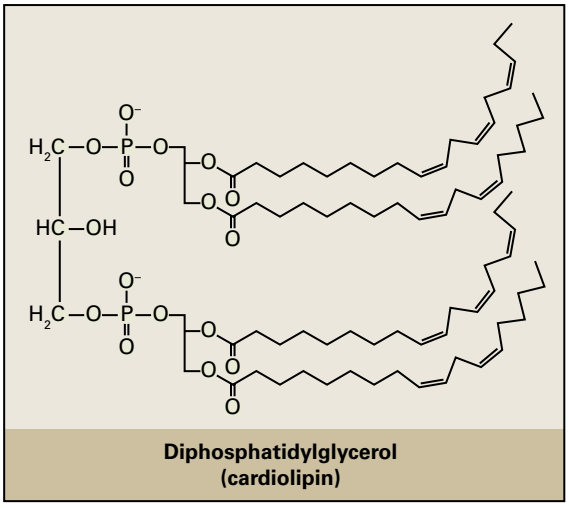


FIGURE 1.64 *Structure of cardiolipin, an unusual phospholipid component of the inner mitochondrial membrane.*

1.11.2 Shoot apical meristem cells are unique in that they contain two structurally distinct types of mitochondria

Until recently, plant mitochondria have been portrayed as being small, round to sausage-like organelles measuring 0.5–1 μm in diameter and 1–3 μm in length (Fig. 1.65A). This description appears to be correct for all cells of intact higher plants except for shoot apical meristem (SAM) cells, which

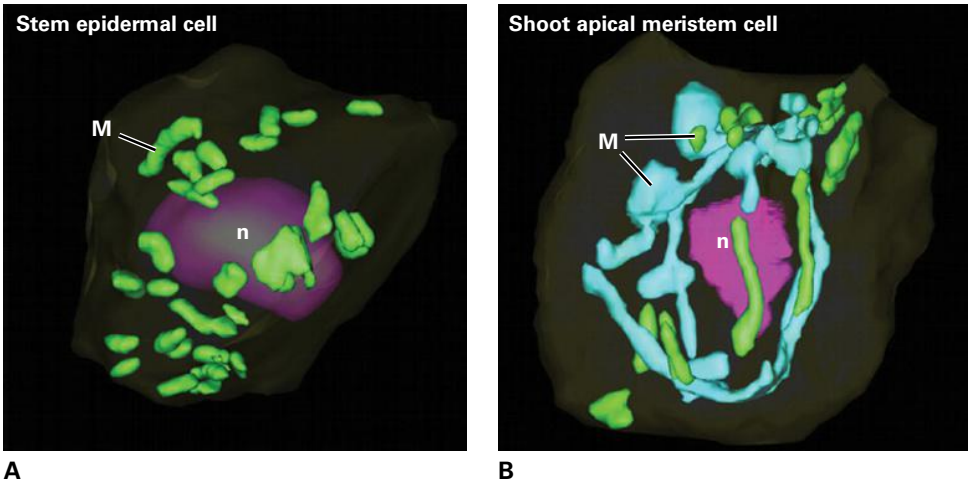


FIGURE 1.65 *(A) 3D reconstruction of the mitochondria and nucleus of an epidermal cell in* Arabidopsis *based on serial confocal microscopy sections. Typical of cells in most plant organs, the mitochondria (M, green) are small and dispersed throughout the cytoplasm. n, nucleus. (B) 3D reconstruction of an* Arabidopsis *shoot apical meristem cell based on serial thin-section TEMs. In this mitotic cell most of the mitochondria (M, green and light blue) are organized into a large, cage-like structure with only a few small, individual mitochondria seen in the cell cortex. n, nucleus.*
Source: Models by Jose-Maria Segui-Simarro, Universidad Politécnica de Valencia, Spain.

possess both the characteristic small mitochondria in the cell cortex as well as a large, central, reticulate mitochondrion (Fig. 1.65B) that undergoes characteristic cell cycle-dependent changes.

In living plant cells, the small mitochondria are seen to be highly dynamic organelles that can slide to different cellular locations and frequently undergo fission and fusion and occasional branching changes. The number of mitochondria per cell varies from fewer than 50 to several thousand depending on cell type and cell size. However, for a given type of cell the cytoplasmic volume occupied by mitochondria is fairly stable. For example, in SAM cells mitochondria make up ~10% of cell volume whereas in cell types with high energy requirements such as transfer cells (see Chapter 15) they make up to 20%. Mitochondria congregate around cellular areas with high energy needs; in plant cells their movements are mediated by the actin–myosin cytoskeletal system.

The large, central mitochondrion of *Arabidopsis* SAM cells varies in shape from tentaculate to cage-like during the cell cycle (Fig. 1.66). The tentaculate mitochondrial form, which wraps around one nuclear pole, is seen during the G1 and S phases of the cell cycle, where it contributes 40% of the mitochondrial volume. The remaining small mitochondria are scattered throughout the cortical cytoplasm. In G2, the tentaculate mitochondrion extends around the nucleus to produce a second cap-like domain on the opposite side of the nucleus. During this expansion, ~60% of the smaller mitochondria fuse with the large mitochondrion, whose volume increases to 80% of the total mitochondrial volume. The cage-like mitochondrion is formed during mitosis. It completely encompasses the mitotic spindle and the early phragmoplast. During late cytokinesis the cage-like mitochondrion divides into two tentaculate mitochondria that wrap around the opposite poles of the daughter nuclei, while simultaneously budding off new small mitochondria by fission. It has been postulated that the tentaculate/cage-like mitochondrion of SAM cells provides an efficient means for recombining the mitochondrial DNA during vegetative life prior to gamete production, thereby preventing speciation.

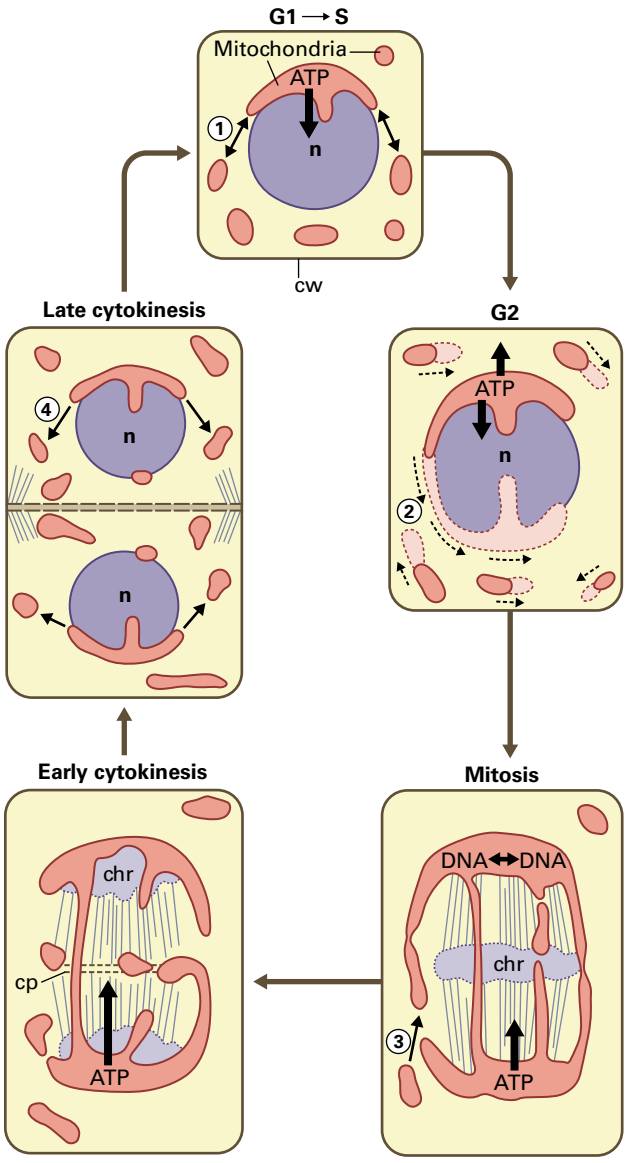


FIGURE 1.66 *Model of cell cycle-dependent changes in mitochondrial architecture in* Arabidopsis *shoot apical meristem cells and their potential functional roles. The model postulates that the large, tentacular/cage-like mitochondria provide a structural framework that enables mtDNA intermixing for mtDNA recombination prior to cytokinesis. (1) fusion/fission equilibrium; (2) net mitochondrial growth; (3) fusion during mitosis. n, nucleus; chr, chromosomes; cp, cell plate; cw, cell wall; G1, G2, and S, cell cycle stages.*
Source: Adapted from Segui-Simarro, J.M., Coronado, M.J. and Staehelin, L.A. (2008). Plant Physiol 148: 1380–1393.

1.11.3 Like plastids, mitochondria are semiautonomous and possess the genetic machinery to make some of their own proteins

Plant mitochondria, like the mitochondria of all eukaryotes, contain genomes that encode ribosomal RNAs (rRNAs), transfer RNAs (tRNAs), and a few proteins. However, enzymes concerned with DNA replication, transcription and processing, and translation are apparently all encoded in the nucleus. Among the distinctive features of plant mitochondrial genomes are their large size and complexity in comparison with mitochondria of other organisms (see Chapter 6). For example, whereas mammalian mtDNAs are 15,000–18,000 nucleotides long, plant mtDNAs range in size from ~200,000 nucleotides in some crucifers to a remarkable 2,500,000 nucleotides in watermelon (*Citrullus lanatus*). Related to this wide range in nucleotide number is variability in the sizes of mtDNA molecules. Mitochondrial genomes take the form of either a single large, circular chromosome or one large, circular molecule and several smaller circular molecules (representing recombination between repeated sequences), depending on species.

Another notable feature of plant mitochondrial genomes is that they do not contain a complete set of tRNA genes but encode only ~16 tRNAs, specific for 12–14 amino acids. Twenty tRNAs, at least one for each of 20 common amino acids, are generally necessary for protein synthesis. How, then, can plant mitochondria synthesize any proteins at all? The best evidence to date is that the "missing" tRNAs are encoded by nuclear genes and imported into mitochondria from the cytosol.

Still another special feature of plant mitochondria is the presence of some plastid DNA sequences in their genomes. These sequences, some of which are tRNA genes, represent DNA transferred from plastids and incorporated into the mtDNA during the course of evolution. Most of them are not functional in the mitochondria.

Plant mitochondria probably contain several hundred different proteins. Only a very few of these, some 15 or 20, are encoded and synthesized in mitochondria. Of these few, most are components of the electron transfer chain or part of the ATP synthase complex in the mitochondrial inner membrane. All remaining mitochondrial proteins must be encoded by nuclear genes, synthesized on ribosomes in the cytosol, and imported into the mitochondria.

Summary

This chapter provides an introduction to cell membranes and the endomembrane system with an emphasis on structural aspects.

Cell membranes are inherited structures that serve as barriers to the diffusion of most water-soluble molecules and enable cells to create compartments in which chemical composition can differ from the surroundings. Membranes are composed of polar lipids that form a bilayer continuum and proteins that are responsible for most membrane functions. The plasma membrane serves as the diffusional boundary of individual cells and controls the transport of molecules into and out of cells. The endomembrane system forms a dynamic network that permeates all regions of the cytosol and gives rise to specialized membranous organelles. Together, the components of the endomembrane system are involved in many important cellular processes, including transport and secretion, protein modification, and metabolic reactions. Vacuoles are organelles that enable plant cells to grow rapidly with the expenditure of minimal amounts of energy and proteins. They perform a multitude of functions, including storage, digestion, ionic homeostasis, defense against pathogens and herbivores, and sequestration of toxic compounds.

Plastids are members of a family of organelles specific to plants and algae. The principal types of plastids are the photosynthetic chloroplasts, starch-storing amyloplasts, carotenoid-forming and colorful chromoplasts, and essential oil-producing leucoplasts. All plastids are semiautonomous organelles, that is, they are capable of producing some but not all of their proteins, with the rest being imported from the cytoplasm.

Mitochondria are organelles in which the process of aerobic respiration produces ATP mostly from sugars and fatty acids. They also provide metabolic intermediates that serve as substrates for the synthesis of other molecules. Like plastids, they are semiautonomous organelles.



2

The Cell Wall

Nicholas C. Carpita, John Ralph, and Maureen C. McCann

Introduction

The shape of a plant cell is constrained by its cell wall. When a living plant cell is treated with cell wall-degrading enzymes, the resulting membrane-bound **protoplast** is spherical (Fig. 2.1). The cell wall limits the rate and direction of cell growth, exerting a profound influence on plant development and morphology. In certain cell types, walls are elaborated to carry out specialized functions, and in some, including tracheary elements and some trichomes, the protoplast disintegrates during development and the mature cell consists entirely of cell wall (Fig. 2.2).

The plant cell wall is a dynamic compartment, changing throughout the life of the cell. When cells of the meristem enlarge and elongate, new material is continuously integrated into the **primary cell wall**, which expands and increases in surface area, in some cases over a 1,000-fold. New walls are born in the **cell plate** during cell division and fuse with the existing side walls (Fig. 2.3). **A middle lamella** forms the interface between the primary walls of neighboring cells, and material is also added to this interface as their primary walls increase in area (Fig. 2.4). In older cells, the pectin-rich material in the cell corners is sometimes digested by hydrolytic enzymes, and an air space forms (Fig. 2.4). Finally, at differentiation, many cells, such as tracheids and fibers, elaborate within the primary wall a distinct **secondary cell wall**, building complex structures uniquely suited to the cell's function (Fig. 2.5).

The plant cell wall is a highly organized composite of many different polysaccharides, proteins, and aromatic substances. Some structural molecules act as fibers, others as a crosslinked matrix analogous to the glass fibers and plastic matrix in fiberglass. The molecular composition and arrangements of wall polymers differ among species, tissues of a single species, individual cells, and even regions of the wall around a single protoplast (Fig. 2.6).

Not all specialized functions of cell walls are structural. Some cell walls contain molecules that affect patterns of development and mark a cell's position within the plant. Walls contain signaling molecules that participate in cell–cell and wall–nucleus communication. Fragments of wall polysaccharides may elicit secretion of defense molecules, and the wall may become impregnated with protein and lignin to armor it against invading fungal and bacterial pathogens (Fig. 2.7). Cell wall surface molecules also allow plant cells to recognize their own kind in pollen-style interactions (Fig. 2.8).

2.1 Sugars are building blocks of the cell wall

Polysaccharides, polymers of sugars, are the principal components of the cell wall and form its main structural framework. Polysaccharides are long chains of sugar molecules covalently linked at various positions, and some are decorated with side-chains of various lengths. Familiarity with the chemistry and nomenclature of sugars greatly facilitates understanding of the many biological functions of polysaccharides.

Sugars are polyhydroxy aldehydes (**aldoses**) and ketones (**ketoses**) that can be grouped according to their chemical formula, configuration, and stereochemical conformation. Almost

Biochemistry & Molecular Biology of Plants, Second Edition. Edited by Bob B. Buchanan, Wilhelm Gruissem, and Russell L. Jones.
© 2015 John Wiley & Sons, Ltd. Published 2015 by John Wiley & Sons, Ltd.
Companion website: www.wiley.com/go/buchanan/biochem

all cell wall sugars are aldoses. Many sugars have the empirical formula $(CH_2O)_n$, from which the term **carbohydrate** is derived.

Numerical prefixes define how many carbons a sugar contains. For example, a triose has three carbon atoms, a pentose five, and a hexose six. All sugars can exist in a straight-chain conformation, and sugar molecules with four carbons or more can also rearrange to form heterocyclic rings (Fig. 2.9). Sugars that adopt a five-membered ring configuration (four carbons and an oxygen) are called **furanoses**, and those forming six-membered rings (five carbons and an oxygen) are **pyranoses**. The ring conformation a sugar adopts is not defined by the number of carbons: both pentoses and hexoses can occur in either ring form.

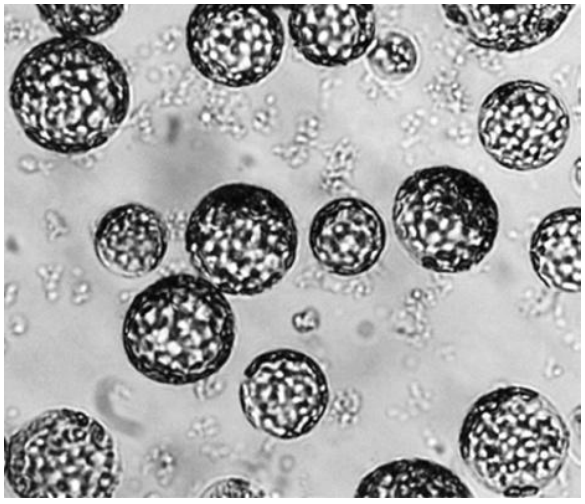


FIGURE 2.1 *Without their cell walls, protoplasts adopt a spherical form. Source*: N. J. Stacey, John Innes Centre, Norwich, UK.

Pyranose and furanose rings can be diagrammed using either flat **Haworth projections** or conformational models (Fig. 2.9). The pyranose sugars assume the so-called "chair" conformation, whereas the furanose sugars are a "puckered" five-membered ring. The five tetrahedral carbon atoms forming a pyranose ring project the hydrogen and hydroxyl groups either in **equatorial** positions away from the ring or in **axial** positions above and below the ring. Pyranoses adopt one of two possible "chair" forms to accommodate as many hydroxyl or other bulky groups as possible in the equatorial position. For common cell wall D-sugars, such as D-glucose, the $^4C_1$-chair conformation is the most energetically favorable, but for the deoxy-sugars L-fucose and L-rhamnose, the $^1C_4$-chair is the more favorable conformation (Fig. 2.10).

In aldoses, including the hexose glucose and the pentose arabinose, the C-1 is the **anomeric carbon**, the only carbon bound to two oxygen atoms. The other carbons are numbered sequentially around the ring. The hydroxyl group of the anomeric carbon can be in α or β position. In solution,

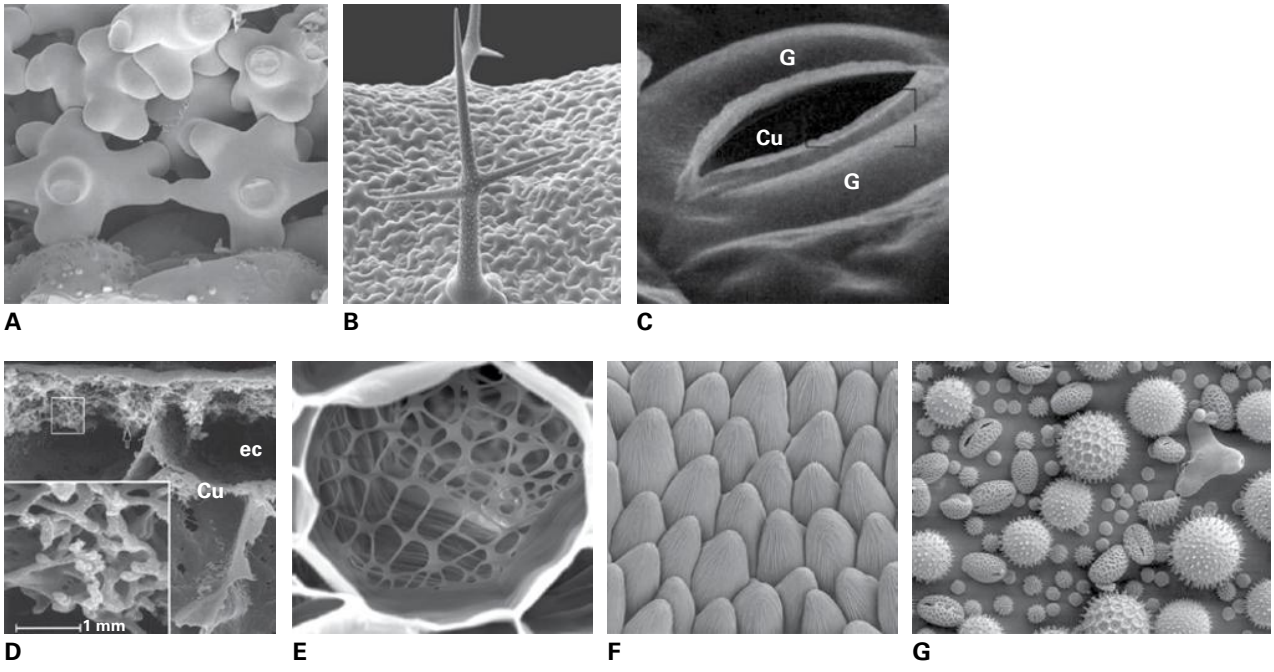


FIGURE 2.2 *A developing cell constructs its wall architecture to provide characteristic shapes. (A) The spongy parenchyma of a* Zinnia elegans *leaf minimizes cell contact and maximizes cell surface for gas exchange. Note how water droplets bead on the waxy lower epidermis but not on the spongy mesophyll cells. (B) An* Arabidopsis *trichome is an exquisitely branched, modified epidermal cell. (C) The thickened and elaborated inner wall of a guard-cell pair (G) provides the physical form needed to control aperture size of a stoma. The cuticle (Cu), a special wall outgrowth of waxy and phenolic substances, minimizes evaporative loss of water from the exterior surface. (D) Transfer cells elaborate a highly fenestrated wall to enhance surface area of the plasma membrane for sugar transport. (E) The end wall (sieve plate) of the sieve element is perforated with many canals as a result of selective wall hydrolysis. (F) The specialized shapes of these epidermal cells reflect light to enrich the colors of a snapdragon* (Antirrhinum *sp.) petal. (G) Pollen grains elaborate outer walls of many forms.*
Source: (A, F) K. Findlay, John Innes Centre, Norwich, UK. (B) P. Linstead, John Innes Centre, Norwich, UK. (C) Staples et al. (1988). Science 235: 1659–1662. (D) Talbot et al. (2001). Protoplasma 215: 191–203). (E) Michael Knoblauch, Washington State University. (G) http://www.newscientist.com/article/dn14136-microscope-on-a-chip-to-give-four-times-the-detail.html.

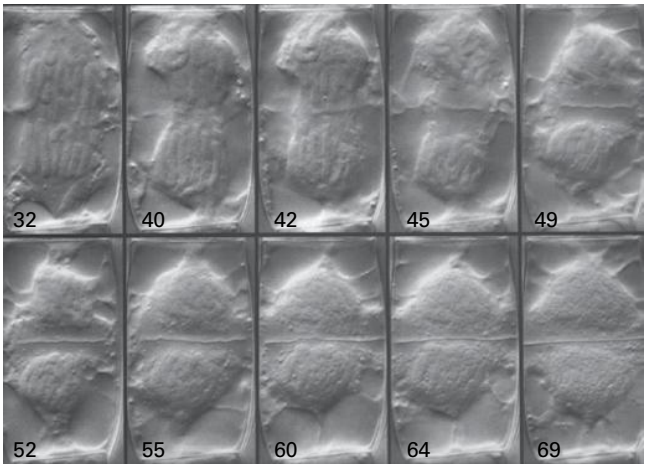


FIGURE 2.3 *Formation of the cell plate during cell division of a* Tradescantia *stamenal hair cell. The cell plate forms during cytokinesis and undulates until it contacts the mother wall. Coincident with partitioning of the mother cell into two daughter cells, the cell plate changes from a wavy appearance to a firm, flattened wall. Values in the corners of each plate are minutes from the onset of prophase.*
Source: P. Hepler in Gunning & Steer. (1996). Plant Cell Biology. Jones and Bartlett, London.

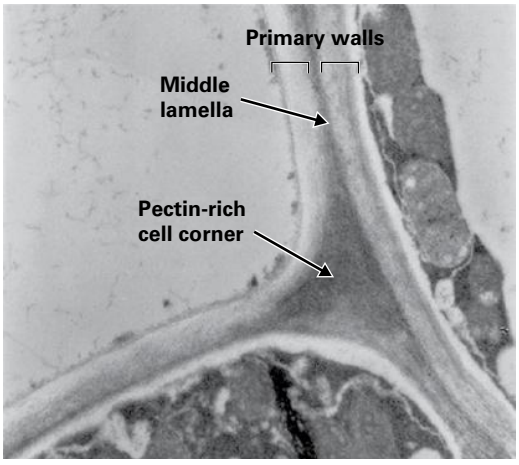


FIGURE 2.4 *Primary walls of cells are capable of expansion. Adhesion between certain cells is maintained by the middle lamella, and the cell corners are often filled with pectin-rich polysaccharides. The middle lamella forms during cell division and grows coordinately with the primary walls.*
Source: M. Bush, John Innes Centre, UK.

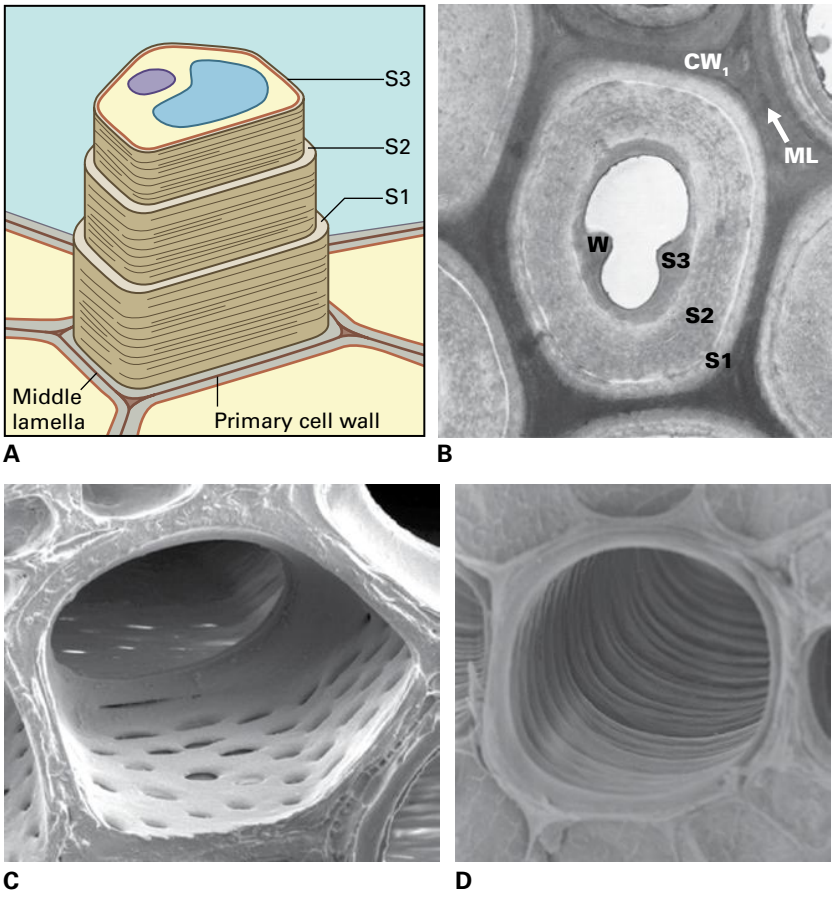


FIGURE 2.5 *When they have achieved their final size and shape, some cells elaborate a multilayered secondary wall within the primary wall. In this example of a fiber cell from a young stem of a locust (*Robinia *spp.) tree (A), three distinct layers of secondary wall (S1–S3) within the primary wall (CW1) and middle lamella (ML) are visualized in the electron microscope (B). Many fibers contain "warts" (W), which are a last stage of wall thickening before the protoplast disintegrates. Subfunctionalization is inherent in the pattern of the thickenings, from the netted appearance of stem tracheids that resist torsional strain (C) compared to the radially oriented thickenings of petiole tracheids that provide more flexibility (D).*
Source: (B, C) Maureen McCann, Purdue University.

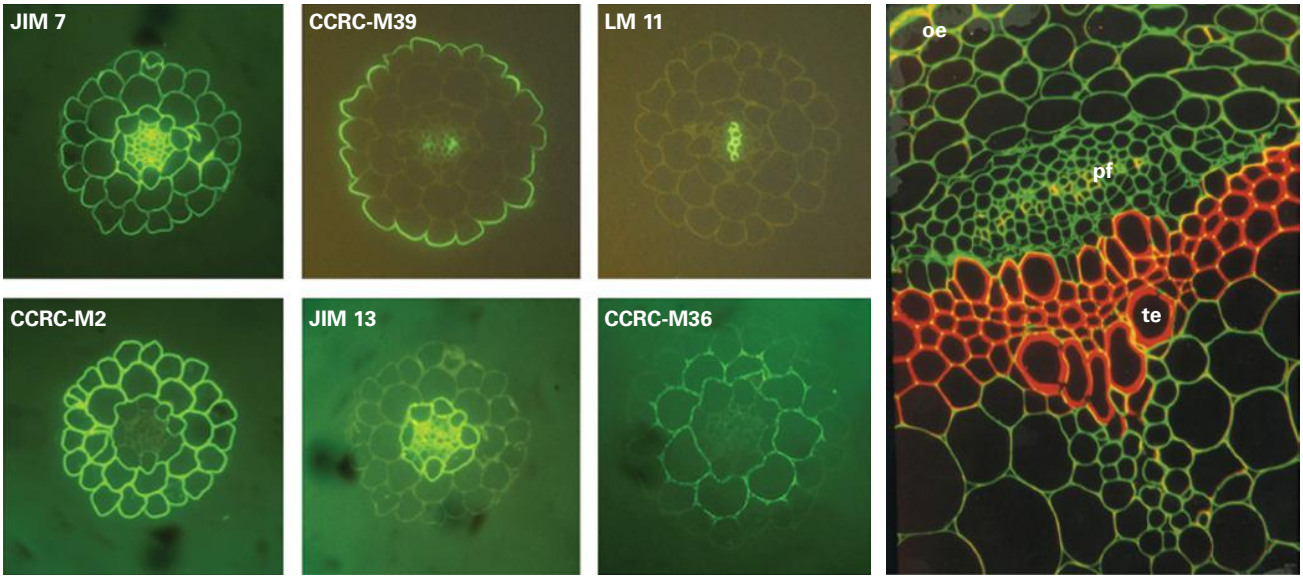


FIGURE 2.6 *Production of complex, chemically diverse molecules of cell walls is developmentally regulated. (A) Staining walls of* Arabidopsis *root with six monoclonal antibodies against cell-wall polysaccharides demonstrates they occur in specific cell and tissue types. JIM7 recognizes methyl-esterified homogalacturonan and stains all cells; CCRC-M2, which recognizes an epitope of sycamore maple rhamnogalacturonan I (RG I), stains epidermal and cortical cells, whereas CCRC-M39 recognizes fucosylated xyloglucans (and RG I), and stains only the outward facing wall of the epidermis; JIM13 recognizes an arabinogalactan-protein epitope in the stele; LM11 recognizes arabino-4-O-methyl glucurono-xylans and stains fiber cells of the stele, whereas CCRC-M36, which recognizes unbranched backbones of RG I, stains primarily cortical cells. (B) Cross-section of an* Arabidopsis *stem showing domains enriched in methyl-esterified pectin are labeled in green. De-esterified pectins, shown in yellow, are found in specialized cells, such as the outer epidermal wall (oe), fiber cells of phloem (pf), some cell corners and cross-walls, and tracheary elements of the xylem (te). Lignin autofluorescence is shown in red. Source*: (A) Glenn Freshour & Michael Hahn, CCRC, University of Georgia. (B) Paul Linstead, John Innes Centre, UK.

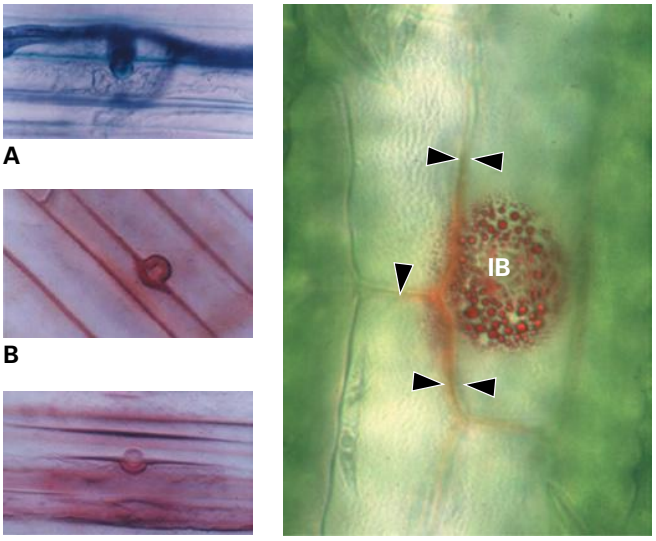


FIGURE 2.7 *Cells often alter their cell wall in response to environmental stimuli and potential pathogens and symbionts. (A) In response to attempted invasion by fungal hyphae of* Colletotrichum *(stained with lactophenol-cotton blue), a maize (*Zea mays*) cell produces a wall apposition called a papilla. Largely composed of callose, the papilla also accumulates lignin, as shown by staining with phloroglucinol (B) and by staining with syringaldehyde stain for laccase activity (C). (D) In its response to* Colletotrichum *invasion, an infected cell of sorghum (*Sorghum bicolor*) accumulates phytoalexins in inclusion bodies (IB), and neighboring cells armor their walls with reddish phenylpropanoids (arrowheads). Source*: R. L. Nicholson, Purdue University.

the hydroxyl group of the anomeric carbon **mutarotates**, flip-flopping between α and β configurations as the ring spontaneously opens and closes. However, the hydroxyl is locked into a specific configuration when the anomeric carbon becomes linked to another molecule.

The designation **D** or **L** should accompany any reference to an α or β configuration. The D or L designation refers to the position of the hydroxyl group on the asymmetric (**chiral**) carbon farthest from the C-1 (i.e., C-5 of hexoses and C-4 of pentoses). An asymmetric carbon is one in which all four substituent groups are different, so that **enantiomers** (mirror images) of the structures cannot be superimposed. In the D-configuration, when viewed in a **ball-and-stick model**, the three larger groups of the last asymmetric carbon increase in size clockwise; in the L-configuration, they increase in size counterclockwise (see Fig. 2.9). D and L are not related to the (+) or (–) designations for **dextrorotatory** or **laevorotatory** optical rotation, which define as clockwise or counterclockwise, respectively, the direction in which a chemical species rotates plane-polarized light.

2.1.1 Monosaccharides linked into cell wall polymers are derived from glucose

D-**Mannose** (Man) and D-**galactose** (Gal) are **epimers** of D-glucose (Glc) made by converting the C-2 and C-4 hydroxyl groups, respectively, from the equatorial to the axial positions

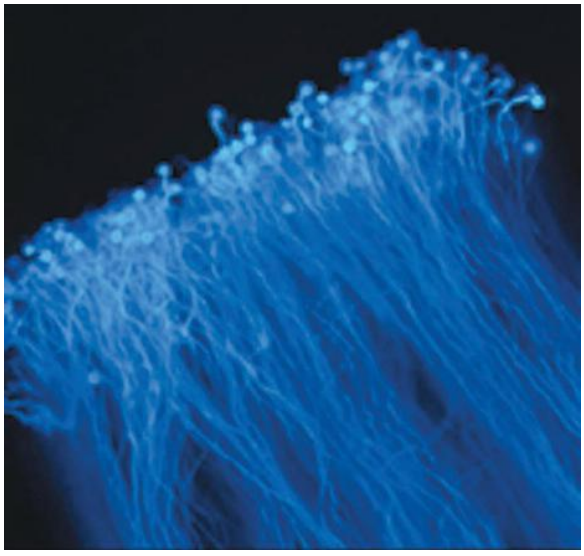


FIGURE 2.8 *In a self-incompatability response, growth of pollen tubes is terminated coincident with swelling of pollen tube tips and formation of callose plugs, as observed here by staining with aniline blue.* *Source*: Image by R. Cotter provided by Sheila McCormick, USDA-Albany, CA.

(Fig. 2.10). Replacement of the C-6 primary alcohols by carboxylic acid groups gives D-**mannuronic acid** (ManA), D-**galacturonic acid** (GalA), or D-**glucuronic acid** (GlcA). Removal of the carboxyl group from D-glucuronic acid forms the pentapyranose, D-**xylose** (Xyl), a sugar in which all of the carbons are in the heterocyclic ring. A rare branched sugar, **D-apiose** (Api), is also formed from D-GlcA. The C-4 epimer of D-xylose is L-**arabinose** (Ara). The D to L conversion occurs because, in this instance, epimerization occurs at C-4, the last asymmetric carbon. By convention, this places the C-1 hydroxyls of α-D-pyranoses in the axial position, and those of α-L-pyranoses in the equatorial position.

The C-6 of some hexapyranoses can also be dehydrated to methyl groups to create deoxysugars. In plants, the two major cell wall deoxysugars are 6-deoxy-L-mannose, called L-**rhamnose** (Rha), and 6-deoxy-L-galactose, called L-**fucose** (Fuc). This spontaneously changes the conformation of L-Rha and L-Fuc from the $^{4}C_{1}$-chair conformation to the more favorable $^{1}C_{4}$-chair conformation, which allows more hydroxyl groups to be in the equatorial rather than axial position (Fig. 2.10). Cell wall sugars are interconverted via nucleotide-sugar intermediates by reactions that take place largely at the endoplasmic reticulum (ER) and Golgi apparatus (see Section 2.4.3).

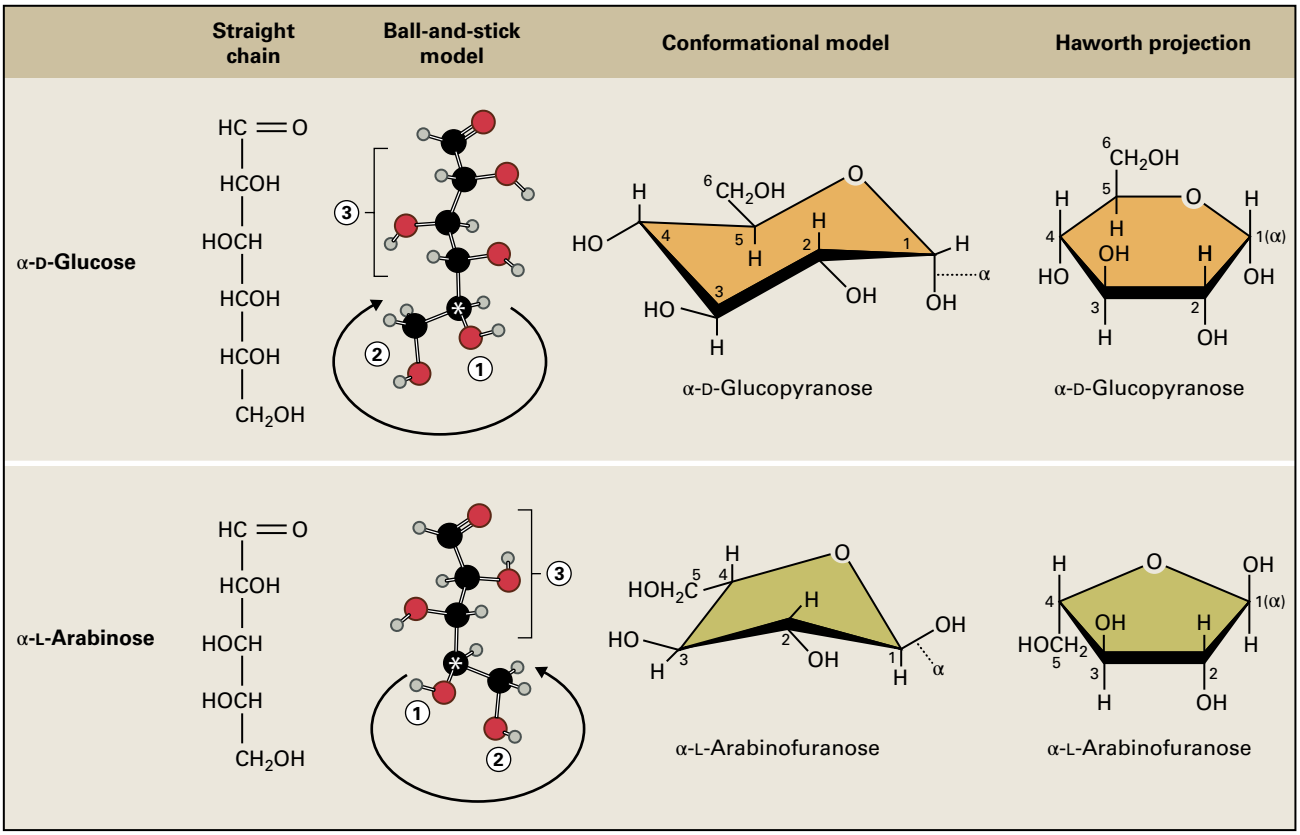


FIGURE 2.9 *Sugar nomenclature. Both D-glucose and L-arabinose are shown (from left to right) in straight-chain, ball-and-stick, and conformational models and as Haworth projections. The ball-and-stick model demonstrates the convention whereby the last asymmetric carbon (marked by asterisk) is oriented with the single hydrogen group in the rear. The three asymmetric groups are labeled numerically, with 1 being the smallest and 3 the largest. The size of the three asymmetric groups increases clockwise for D-sugars and counterclockwise for L-sugars. The conformational model distinguishes the relative axial and equatorial positions of the hydroxyl groups around the ring structure of pyranoses. α-D-Glucose is the most stable of the hexoses because every hydroxyl group of the ring and the C-6 primary alcohol group are in the equatorial position, which is energetically more favorable than any other orientation. By convention, the α-configuration of L-arabinofuranose is in the "up" equatorial position.*

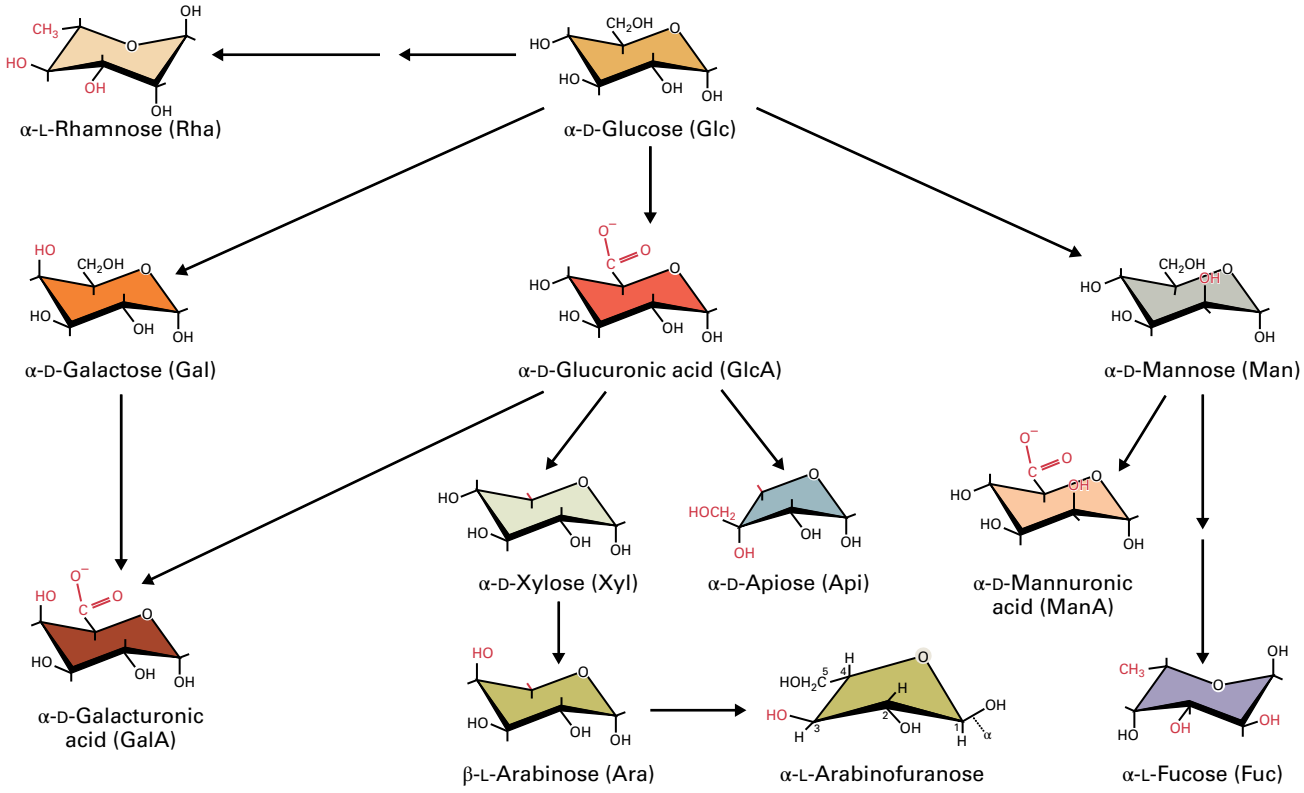


FIGURE 2.10 *Common sugars of plant cell walls and their interconversion. Modifications needed to convert D-glucose into other sugars are shown in red. For pyranoses, ring conformations can also spontaneously invert into two chair conformations—the $^4C_1$-chair or $^1C_4$-chair conformations—which switches equatorial groups to axial groups and vice versa at each position. The lowest energy conformation is one that places as many bulky hydroxyls in the equatorial position as possible. For most pyranoses, the $^4C_1$-chair is thus the preferred conformation, but by activity of a 3,5-epimerase, the $^1C_4$-chair becomes the preferred conformation for L-Rha and L-Fuc. The abbreviations of each of these sugars are specified by IUPAC-IUBMB convention and should be used exclusively. Note that L-Ara can assume both the α-furanose conformation shown in Figure 2.8 and the β-pyranose conformation shown here.*

2.1.2 Polymers of specific sugars are further characterized by their linkage types and configuration of their anomeric carbons

Sugars in polymers are always locked in pyranose or furanose rings. During sugar polymerization, the anomeric carbon of one sugar molecule is joined to the hydroxyl group of another sugar, sugar alcohol, hydroxylamino acid, or phenylpropanoid compound in a **glycosidic linkage**. A sugar can be attached to D-glucose at O-2, O-3, O-4, or O-6, that is, to the hydroxyl oxygens on C-2, C-3, C-4 or C-6. Only the O-5 position is unavailable, as it constitutes part of the ring structure.

A disaccharide can be described with respect to both linkage and anomeric configuration. For example, cellobiose is β-D-glucose-(1→4)-D-glucose: The anomeric linkage forms when the C-1 of one D-glucose residue is replaced by the equatorial hydroxyl at the C-4 position of another D-glucose (Fig. 2.11). Only one D-glucose is locked in the β-configuration; the other D-glucose is undesignated because its anomeric hydroxyl group is free to mutarotate in solution. Because the aldehyde of this sugar is able to reduce copper under alkaline conditions, it is classically described as a **reducing sugar**, and this end of even a very long polymer is called the **reducing end**. In branched polysaccharides there will be a nonreducing sugar at the end of each side-chain and at the terminus of the backbone, but there will only be a single reducing end.

In cellobiose, the anomeric carbon of one glucose is linked to the hydroxyl group farthest away from the anomeric carbon of the other glucose (Fig. 2.11). For the β-linkage to occur with the C-4 equatorial hydroxyl group, sugars to be linked must be inverted almost 180° relative to each other, and iteration of this linkage produces a nearly linear molecule. In contrast, the units of laminaribiose, or β-D-glucose-(1→3)-D-glucose, are linked somewhat askew (Fig. 2.11), and iteration of this linkage produces a helical polymer.

Polysaccharides are named after the principal sugars that constitute them. Most polysaccharides have a backbone structure, and the composition of this structure is indicated by the last sugar in the polymer's name. For example, xyloglucan is a backbone of (1→4)-β-D-glucosyl residues with xylosyl units attached, glucuronoarabinoxylan is a backbone of (1→4)-β-D-xylosyl residues with glucosyluronic acid and arabinosyl units attached to it, and so forth.

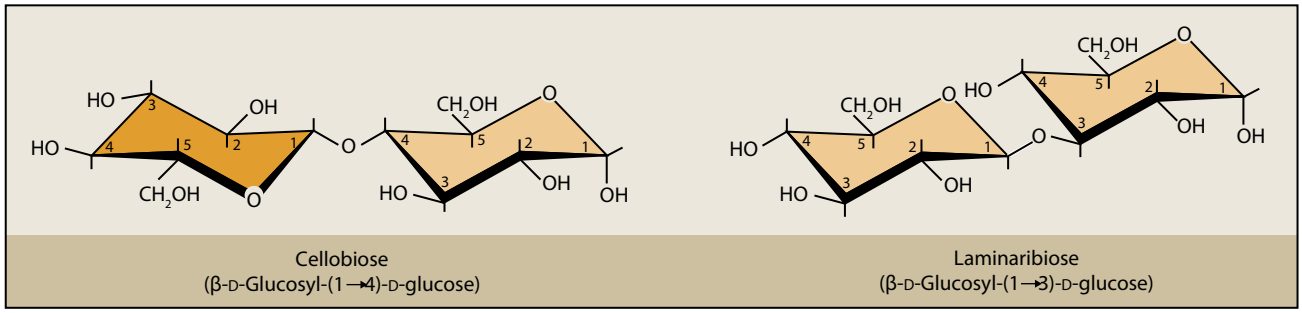


FIGURE 2.11 *Linkage structures of cellobiose and laminaribiose. The (1→4)-β-D-linkage of cellobiose inverts the glucosyl unit about 180° with respect to each other, whereas the (1→3)-β-D-linkage is only slightly askew. (Shading of the glucose units illustrates the 180° inversion.)*

2.1.3 Polymer branching produces great structural diversity

What makes sugar subunits such versatile building materials is their ability to form linkages at multiple positions. With 11 different sugars commonly found in plant cell walls (see Fig. 2.10), four different linkage positions, and two configurations with respect to the oxygen atom, the permutations of pentasaccharide structure zoom to over 5 billion! Glucose alone can form almost 15,000 different pentameric structures. Multiple bonding positions also make possible the formation of branched polysaccharides, enormously increasing the number of possible structures. Fortunately for cell wall researchers, the structures of some of the major wall components are relatively conserved among species.

The two major tools that carbohydrate chemists use to elucidate the structure of highly complex polysaccharides are methylation analysis (Box 2.1) and nuclear magnetic resonance (NMR) spectroscopy (Box 2.2). NMR spectroscopy is particularly useful for examining polysaccharides and aromatic molecules in the underivatized state.

2.2 Macromolecules of the cell wall

2.2.1 Cellulose is the principal scaffolding component of all plant cell walls

Cellulose is the most abundant plant polysaccharide, accounting for 15–30% of the dry mass of all primary cell walls and a much larger percentage of secondary walls. Cellulose exists in the form of **microfibrils**, which are *para*-crystalline assemblies of several dozen (1→4)-β-D-glucan chains hydrogen bonded to one another along their length (Fig. 2.12). In vascular plants, each microfibril consists of a crystalline core of about 24 chains coated with 12 more that can interact with other glycans and water. Microfibrils of 36 glucan chains have a theoretical diameter of 3.8 nm, but X-ray diffraction shows some microfibrils could be as small as 3.3 nm, or about 24 chains. Microfibrils of angiosperms have been measured to be between 5 and 12 nm wide in the electron microscope, but this estimate includes noncellulosic polymers tightly bound onto the surface. Microfibrils of algae can form either large, round cables or flattened ribbons of several hundreds of chains. Each (1→4)-β-D-glucan chain may be just several thousand units (≈2–3 μm long), but individual chains begin and end at different places within the microfibril to allow a microfibril to reach lengths of hundreds of micrometers and contain thousands of individual glucan chains. This structure is analogous to a spool of thread that comprises thousands of individual cotton fibers, each about 2–3 cm long.

From electron diffraction it can be seen that the (1→4)-β-D-glucan chains of cellulose are arranged parallel to one another, that is, all of the reducing ends of the chains point in the same direction. Bacterial cellulose is synthesized at the nonreducing ends of the glucan chains.

Callose differs from cellulose in consisting of (1→3)-β-D-glucan chains, which can form helical duplexes and triplexes. Callose is made by a few cell types at specific stages of wall development, such as growing pollen tubes and in the cell plates of dividing cells. Callose is also made in response to wounding or attempted penetration by invading fungal hyphae (see Fig. 2.7).

2.2.2 Crosslinking glycans interlock the cellulosic scaffold

Crosslinking glycans are a class of polysaccharides that can hydrogen bond to cellulose microfibrils: they may coat microfibrils, but are also long enough to span the distance between microfibrils and link them together to form a network. Crosslinking glycans are often called "hemicelluloses," a widely used term for all materials extracted from the cell wall with molar concentrations of alkali, regardless of structure.

The two major crosslinking glycans of all primary cell walls of flowering plants are **xyloglucans** (XyGs) and **glucuronoarabinoxylans** (GAXs) (Fig. 2.13). The XyGs crosslink the walls of all eudicots and about one-half of the monocots, but in the cell walls of the "commelinid" line of monocots, which includes bromeliads, palms, gingers, sedges, and grasses, the major crosslinking glycan is GAX (Fig. 2.13).

Most XyGs consist of linear chains of (1→4)-β-D-glucan with two or three contiguous α-D-Xyl units linked to the O-6 position of the Glc units between unbranched Glc residues.

Certain xylosyl units are substituted further with other monosaccharides, typically α-L-Ara, or β-D-Gal, to improve water solubility and possible recognition by wall-modifying enzymes, and sometimes the Gal is substituted further with α-L-Fuc (Fig. 2.13). Sequence-dependent hydrolases are used to elucidate the fine structure of XyGs by cleaving them at specific sites along the glucan backbone into fragments that are small enough to characterize fully (Boxes 2.3 and 2.4). A convention has been adopted to describe certain ubiquitous side-chains of XyG in which the entire subtending side-chain

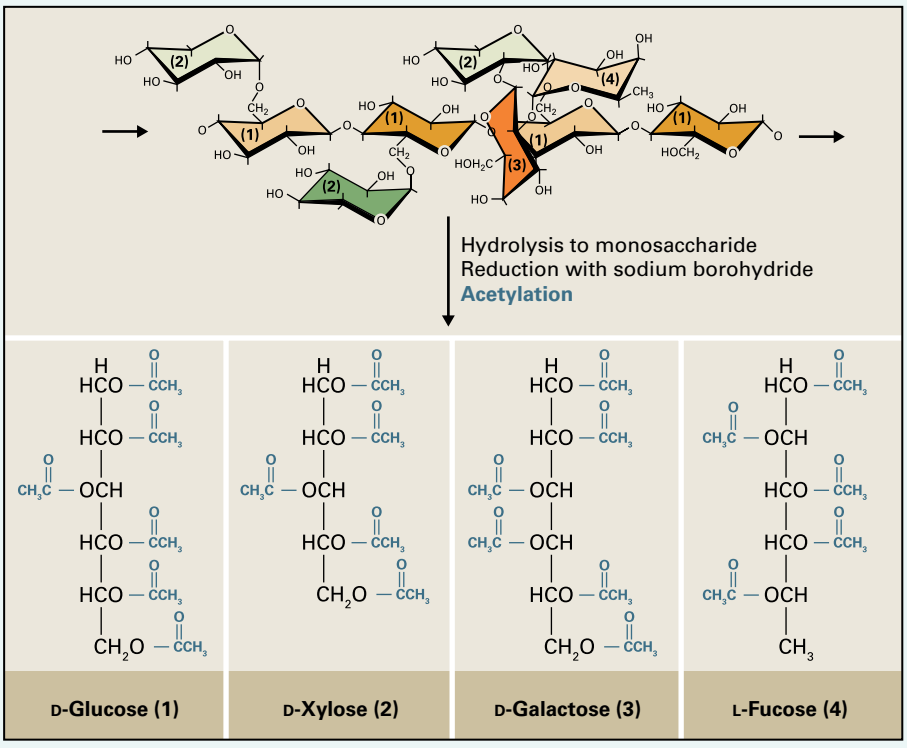
BOX 2.1 Methylation analysis determines carbohydrate linkage structure

Strong acids can break the glycosidic linkages of polysaccharides to release individual monosaccharides. The monosaccharides can then be chemically reduced with borohydride and acetylated with acetic anhydride to make **alditol acetates.** For example, the complex xyloglucan shown in (A) is hydrolyzed to its four major sugar components. The alditol acetates derived from different sugars are volatile at different temperatures and can be separated on that basis using **gas–liquid chromatography**. The derivatives are injected onto a thin capillary column coated with a highly polar waxy liquid phase to which they adhere. The temperature is then raised to the point at which the interaction with the wax is broken, and the derivatives are swept out of the column by an inert carrier gas to a detector. If a temperature gradient is applied, different sugars will elute at different times and be resolved in a chromatogram (B). By comparing these results with the behavior of similarly treated standards, one can determine the molar ratio of each sugar in the original sample. Frequently, the types of sugars present in the sample and their molar ratios will be indicative of a specific polysaccharide.

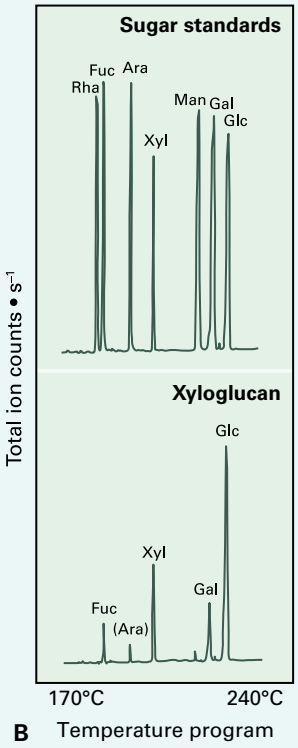
However, complex polysaccharides cannot be identified from their sugar composition alone. Polymer backbones are built from unit structures of one to a few repeated sugars and linkages, but are frequently substituted with appendant sugar units and side-chains that can themselves be further branched. Linkage structure of polysaccharides can be deduced indirectly by methylation analysis (C), a method in which polysaccharides are chemically methylated with methyl iodide at every free hydroxyl group. Carbon atoms that participate in glycosidic linkages and in the ring do not have a free hydroxyl group and so are not methylated. The methylated polysaccharide is hydrolyzed to its components of partly methylated monosaccharides, and these components are reduced and acetylated as before. However, because linkage analyses of certain derivatives depend upon the ability to differentiate the top (C-1 containing) of the molecule or molecular fragment from its bottom (C-5 or C-6 containing), the reducing agent borodeuteride is used to label the C-1 alcohol, thereby marking its position for further analyses. These partly methylated alditol acetates are resolved by gas–liquid chromatography. The xyloglucan methylated before hydrolysis yields an array of derivatives (C), the nature of which depends on the number and positions of the acetyl groups, which in turn indicate the positions of which another sugar was attached (see arrows). The *t-* designation refers to a nonreducing terminal sugar in a side-chain.

Unequivocal determination of the structure is made by **electron-impact mass spectrometry (EIMS)**. As the partly methylated alditol acetate derivatives exit the gas chromatography column, an electron beam breaks each derivative into fragments. The bonds in each derivative have different susceptibilities to breakage, so the molecule breaks into a characteristic set of fragments, which are like the pieces of a jigsaw puzzle. The larger fragments are more diagnostic, but each of these may be broken into smaller fragments that can be used to confirm the deduced structures. The relative abundance of the mass of each fragment in combination with the spectrum of masses for a particular derivative is diagnostic of its structure. Identification of the one or two extra acetyl groups instead of methyl groups indicates which carbons were participating in glycosidic bonds. For example (D), a 4-linked glucose unit in xyloglucan gives characteristic mass/charge ratios (*m/z* values) of 118 and 233, and the latter fragment indicates the acetyl group at the O-4 position, which was protected from methylation by the linkage of a sugar. Likewise, the 4,6-linked glucose branch point contains yet another acetyl group, increasing the mass of this fragment to *m/z* 261. Note the presence of the deuterium atom at C-1 is essential for discriminating between 2-Xyl and 4-Xyl, which are symmetrical derivatives. The major fragments from the 2-Xyl derivative are *m/z* 190 and *m/z* 117, whereas those from 4-Xyl are *m/z* 118 and *m/z* 189; without the deuterium at the C-1, both 2- and 4-Xyl would give *m/z* 117 and *m/z* 189, making them indistinguishable.

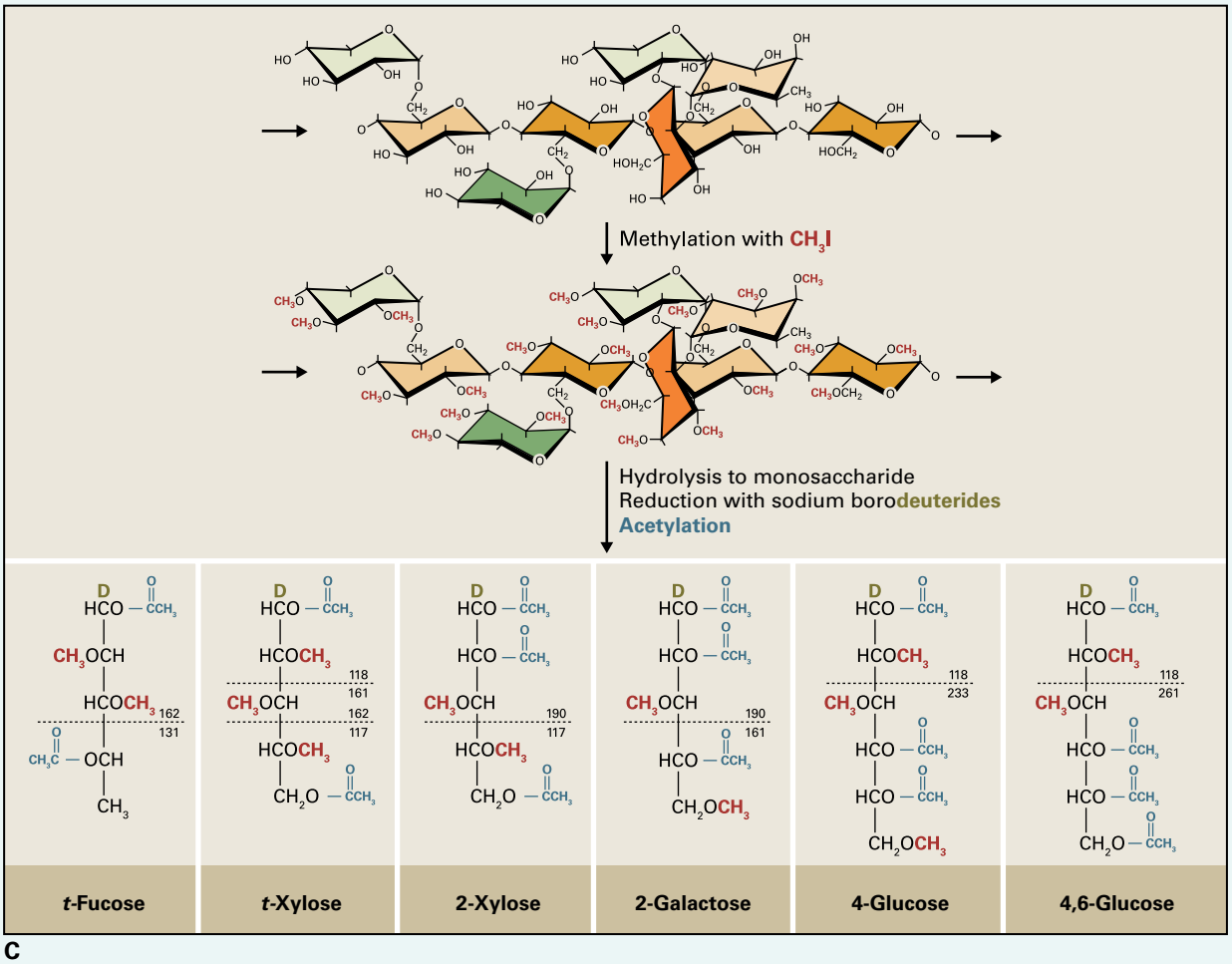
Uronic acids, such as the galactosyluronic acid of pectins, can be converted to their respective neutral sugars after coupling the carboxyl group with a water-soluble diimide and reducing it with sodium borodeuteride ($NaBD_4$). This reaction introduces two deuterium atoms onto the C-6 of the sugar, and the proportion of uronic acid originally present is inferred as a relative proportion of the corresponding neutral sugar. In (E), 4-Gal and 4-GalA are differentiated by the 2 amu shift in *m/z* 233 to give *m/z* 235.


Hydrolysis to monosaccharide
Reduction with sodium borohydride
Acetylation
D-Glucose (1)
D-Xylose (2)
D-Galactose (3)
L-Fucose (4)

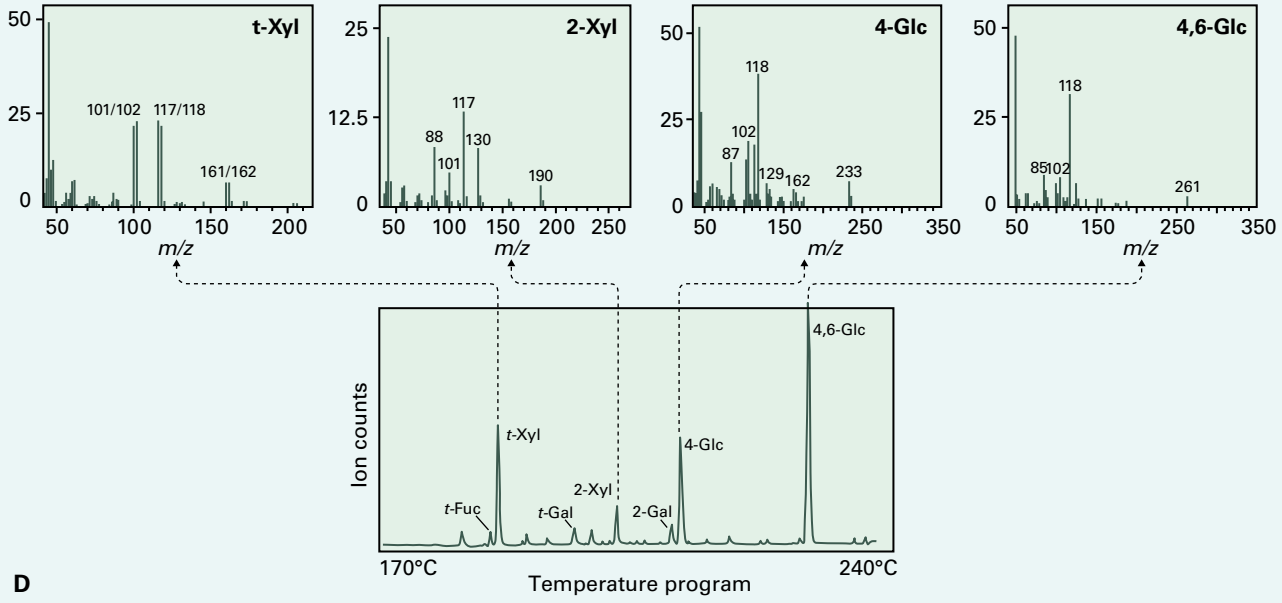
A


Sugar standards
Fuc
Rha
Ara
Xyl
Man
Gal
Glc
Xyloglucan
Glc
Xyl
Gal
Fuc
(Ara)
Total ion counts • s⁻¹
170°C
240°C
Temperature program

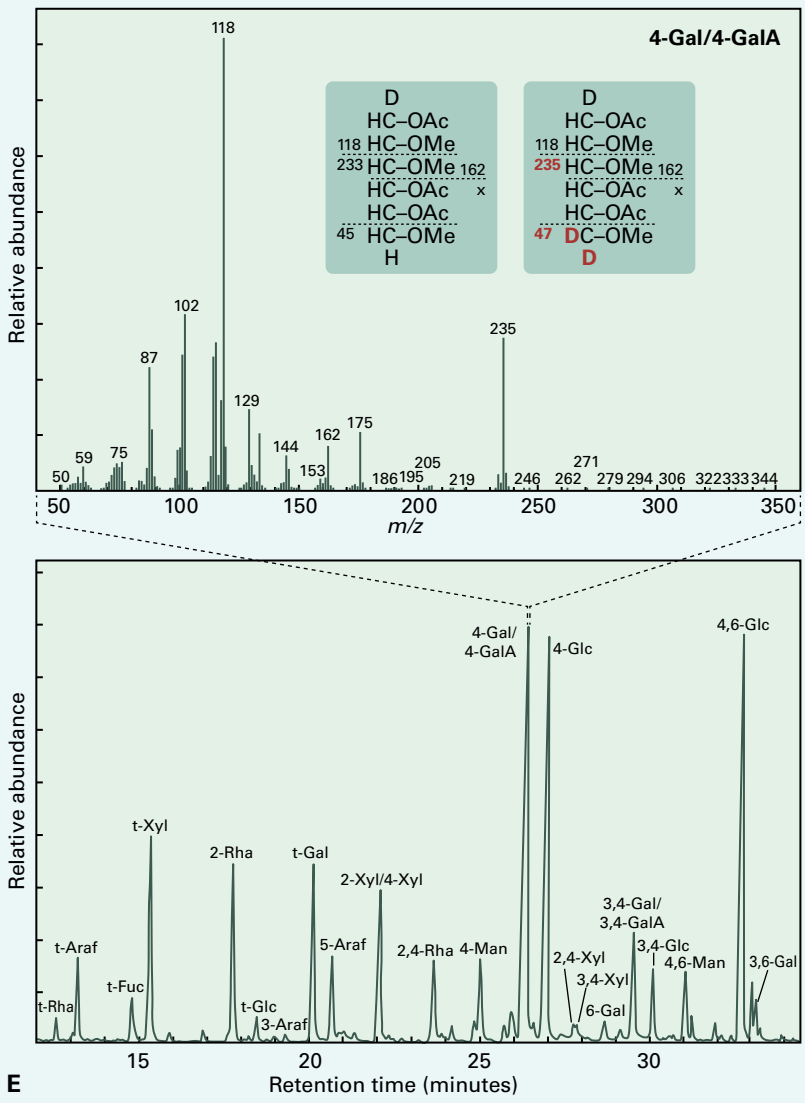
B


Methylation with CH3I
Hydrolysis to monosaccharide
Reduction with sodium borodeuterides
Acetylation
t-Fucose
t-Xylose
2-Xylose
2-Galactose
4-Glucose
4,6-Glucose

C


t-Xyl
101/102
117/118
161/162
2-Xyl
117
88
130
101
190
4-Glc
118
102
87
129
162
233
4,6-Glc
118
85
102
261
m/z
Ion counts
t-Fuc
t-Xyl
t-Gal
2-Xyl
2-Gal
4-Glc
4,6-Glc
170°C
240°C
Temperature program

D


4-Gal/4-GalA
D
HC–OAc
118 HC–OMe
233 HC–OMe 162
HC–OAc x
HC–OAc
45 HC–OMe
H
D
HC–OAc
118 HC–OMe
235 HC–OMe 162
HC–OAc x
HC–OAc
47 DC–OMe
D
Relative abundance
m/z
t-Xyl
2-Rha
t-Gal
2-Xyl/4-Xyl
t-Araf
t-Fuc
t-Rha
t-Glc
3-Araf
5-Araf
2,4-Rha
4-Man
4-Gal/
4-GalA
4-Glc
2,4-Xyl
3,4-Xyl
6-Gal
3,4-Gal/
3,4-GalA
3,4-Glc
4,6-Man
4,6-Glc
3,6-Gal
Retention time (minutes)

E

BOX 2.2

Polymer composition and structure can be determined by nuclear magnetic resonance (NMR) spectroscopy

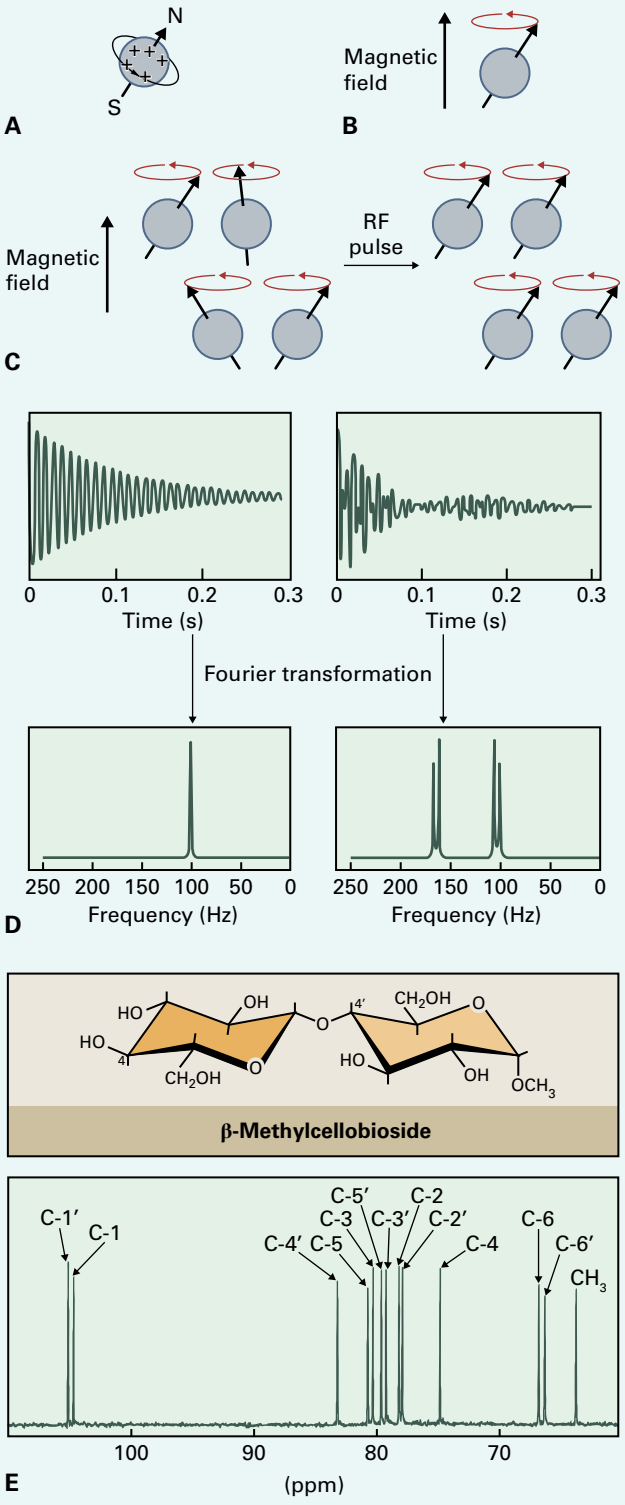
NMR spectroscopy is a nondestructive method that can provide information about the chemical structure and composition of polysaccharides and lignins, their relative orientations, their mobilities, and the nature of their interactions. An NMR spectrometer consists of a powerful magnet and electronic circuitry designed to measure the magnetic properties of the atomic nuclei contained in a sample. Asymmetric atomic nuclei – those with an odd number of protons and neutrons, such as ^{1}H and ^{13}C – have an intrinsic angular momentum, sometimes called the **nuclear spin**, which generates a magnetic field (A). When a magnetic nucleus is placed in the spectrometer magnetic field, a force is exerted that tends to line up its nuclear spin with the applied magnetic field. However, the rules of quantum mechanics do not allow a nucleus to arbitrarily adopt any orientation. That is, its angular momentum (or spin) is **quantized** (i.e., limited to a few well-defined values). For ^{1}H and ^{13}C nuclei, there are two spin states, often conceptualized as 'spin-up' and 'spin-down', or aligned with vs. against the magnetic field direction. The interplay of the quantized angular momentum and the magnetic force causes the nucleus to precess the way a spinning top does under the influence of gravity, wobbling as it spins (B). This precessive motion has a characteristic **resonance frequency** (frequency of the spin) that depends on the strength of the magnetic field, the magnetic properties of the nucleus, and its closest atomic neighbors. It is those interactions with its closest neighbors that give the most information about the nucleus of interest.

In an NMR experiment, populations of nuclei, rather than individual nuclei, are observed. Under most conditions, the precession of a population of nuclei is not coherent; that is, the individual nuclear spins in the sample tilt in different directions so the precession cannot be detected (C left). To be observed by NMR, a sample is subjected to a brief magnetic pulse, called a radio frequency (RF)-pulse, that oscillates at the nuclear resonance frequency delivered by small coils close to the sample. This redistributes the nuclear spin orientations so they become partially aligned and the precessing components of nuclear spin can be observed from the population of nuclei (C right).

The signal observed as a result of the RF-pulse is usually composed of a range of slightly different resonance frequencies. The RF-pulse itself comprises a range of frequencies, and is thus analogous to striking a bell simultaneously to produce a mixture of different audio frequencies. Just as we hear all of the frequencies of the ringing bell simultaneously, all the frequencies returning from the sample are picked up in the same RF coils and are recorded simultaneously. A mathematical operation called **Fourier transformation** is used to convert the time-domain (amplitude vs time) NMR response into a frequency-domain (amplitude vs frequency) spectrum that makes it easier to distinguish and tabulate signals with different frequencies (D).

Nuclei connected by three or fewer molecular bonds often exhibit an interaction called **scalar coupling**. The molecular geometry of this coupling leads to the splitting of signals that is a characteristic feature of ^{1}H-NMR spectra. The anomeric (H-1) resonance of a typical sugar is split into a doublet by scalar coupling with H-2—the larger the dihedral angle, the larger the frequency difference. For a β-linked glucosyl residue (as in cellobiose), the dihedral angle H1–C1–C2–H2 is approximately 180°, which results in a relatively large H1–H2 scalar coupling of 8 Hz, whereas the dihedral angle for an α-linked glucosyl residue (as in maltose) is only 60°, which results in a relatively small H-1–H-2 scalar coupling of 3.6 Hz. Thus, the anomeric configuration of a glucosyl residue can be unambiguously determined simply by measuring the distance (in Hz) between the two components of the anomeric proton doublet.

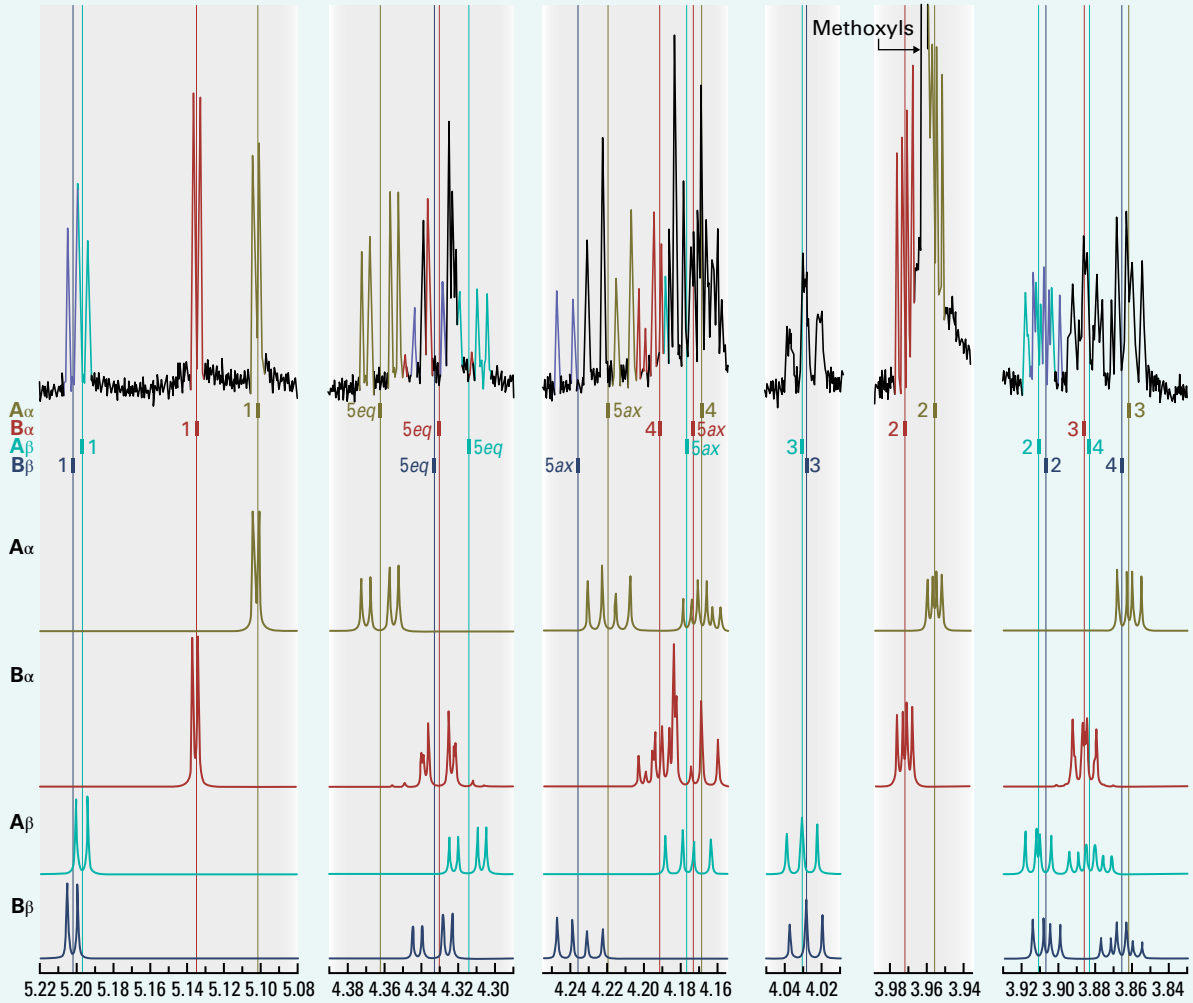
The different frequencies in the NMR spectrum arise because the electron cloud surrounding each nucleus shields it from the applied magnetic field. Neighboring atoms with differing degrees of electronegativity surrounding the nucleus being observed produce a change in its resonance frequency called the **chemical shift**. This chemical shift, which is measured in parts per million (ppm) relative to the resonance frequency of a nucleus in a standard compound such as tetramethylsilane (TMS), provides information about the chemical environment of the nucleus within the molecule. For example, the electron-withdrawing oxygen attached to C-6 of glucose decreases the electronic shielding for this nucleus, resulting in a chemical shift of approximately 60 ppm. On the other hand, two electron-withdrawing oxygen atoms are attached to the anomeric carbon (C-1) of glucose, which is thus much less shielded than C-6, and has a chemical shift of approximately 100 ppm. Chemical shifts can provide structural information, as illustrated in the ^{13}C-NMR spectrum of β-methyl cellobioside (E). Here, the glycosidic bond between two glucosyl residues causes the chemical shift (80.2 ppm) of C-4' (at the point of attachment) to be substantially greater than the chemical shift (71.0 ppm) of C-4. This difference is called a glycosylation effect, and is often used to establish the specific point at which two sugars are joined by a glycosidic bond.



The ^{1}H- and ^{13}C-NMR spectra of complex molecules are much more complicated, and multi-dimensional NMR, where more than a single NMR parameter is presented in a spectrum, has greatly improved structural analyses, such as **two-dimensional (2D) NMR**, **heteronuclear multiple-quantum coherence (HMQC)**, **heteronuclear single-quantum correlation (HSQC)**, and **three-dimensional (3D) NMR**. **Correlation spectroscopy (COSY)** is a type of 2D NMR where a proton's chemical shift in one dimension is correlated with the proton to which it is scalar-coupled in the second dimension (^{1}H–^{1}H COSY). **Total correlation spectroscopy (TOCSY)** experiments are particularly useful for identifying the side-chains in various lignin structures, or for identifying resonances in an individual saccharide unit of a polysaccharide — an example is given below. **Solid-state NMR** techniques can distinguish regions of a polysaccharide that differ in their mobility or conformation, facilitating the development of models for assembly of polysaccharides to form complex, dynamic structures within the cell wall.

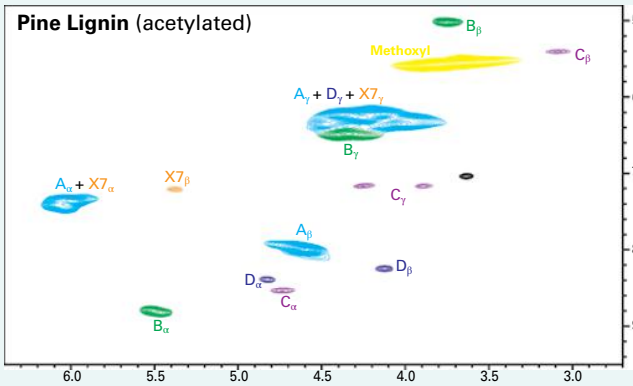
An example of the characterization of a complex structure containing both carbohydrate and phenolic structures is the diarabinosyl β-*O*-4-dehydrodiferulate from grass walls, formed by radical-coupling of two ferulates 5-linked to two arabinosyl units of two GAX polymers (Fig. 2.13) after hydrolysis from the xylan backbone. Simple inspection of the structure suggests that there should be two different arabinosyl moieties, and the NMR spectra resolve both the α- or β-orientation anomeric configurations of each arabinosyl moiety (F). The arabinosyl region of the proton-NMR spectrum, colored for clarity, show splitting patterns arising from scalar coupling between protons on neighboring carbons. Anomeric H-1 protons are each simple doublets, from coupling with their respective H-2 protons, but H-2 protons are more complex (basically doublets of doublets) because of coupling with both H-1 and H-3 protons (with different scalar coupling constants). Subspectra for each of the four arabinosyl moieties can be accurately calculated and plotted by computer simulation using the actual spectrum as input, and the correct chemical shifts and coupling constants are then revealed. The nonanomeric protons are found by tracing the coupling network in a 2D ^{1}H–^{1}H COSY experiment, starting from the easily identified anomeric H-1 with H-2, then H-2 with H-3 (and H-1), H-3 with H-4 (and H-2), and H-4 with the two H-5 protons (and vice versa) (F).

In an HMQC or HSQC 2D ^{13}C–^{1}H correlation experiment, protons at the chemical shifts centered on the contours in the horizontal (^{1}H) direction are directly attached to their respective carbons with the chemical shift given on the vertical (^{13}C) axis. Much of the power of these data comes from the dispersion created, that is, by the way signals from protons are resolved because of the differing chemical shifts of their attached carbons and, conversely, by the way the carbons are resolved by the chemical shifts of their attached protons. In this example, four complex 5-proton pairs are all clearly separated.

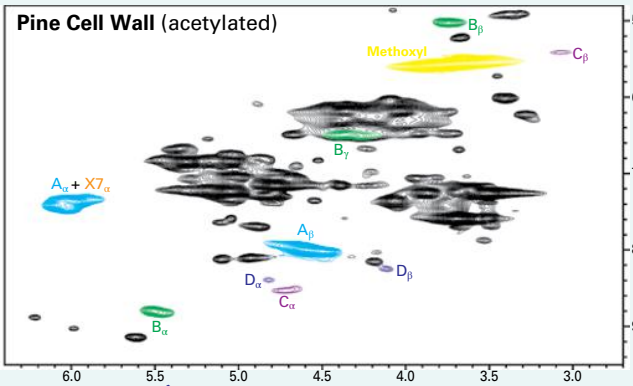


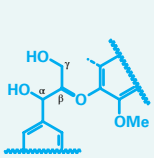
F ^{1}H NMR, Arabinosyl region

G

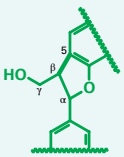


H

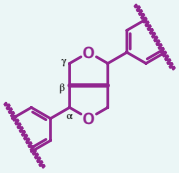




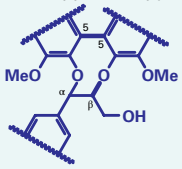
A
β-aryl ether
(β-*O*-4)



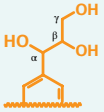
B
phenylcoumaran
β-5



C
resinol
β-β



D
dibenzodioxocin
5-5/β-*O*-4 (α-*O*-4)



X7
arylglycerol

Methoxyl

Unresolved,
Unassigned,
saccharides etc.

As a second example, we show a partial 2D NMR spectrum of a lignin isolated from pine (G). Lignins are more complex in that they are created from combinatorial free-radical coupling reactions in which the coupling can take several pathways (see Fig. 2.22) and produce chains with random sequence. It is possible to readily discern the types and distribution of interunit linkages from 2D ^{13}C–^{1}H correlation experiments, as shown in G. Because of the excellent dispersion in this experiment, many of the correlations in the same type of spectrum run on whole (unfractionated) cell wall (H), despite the dominance of the polysaccharide components.

Source: Original introductory text was provided by William York, CCRC, Georgia.

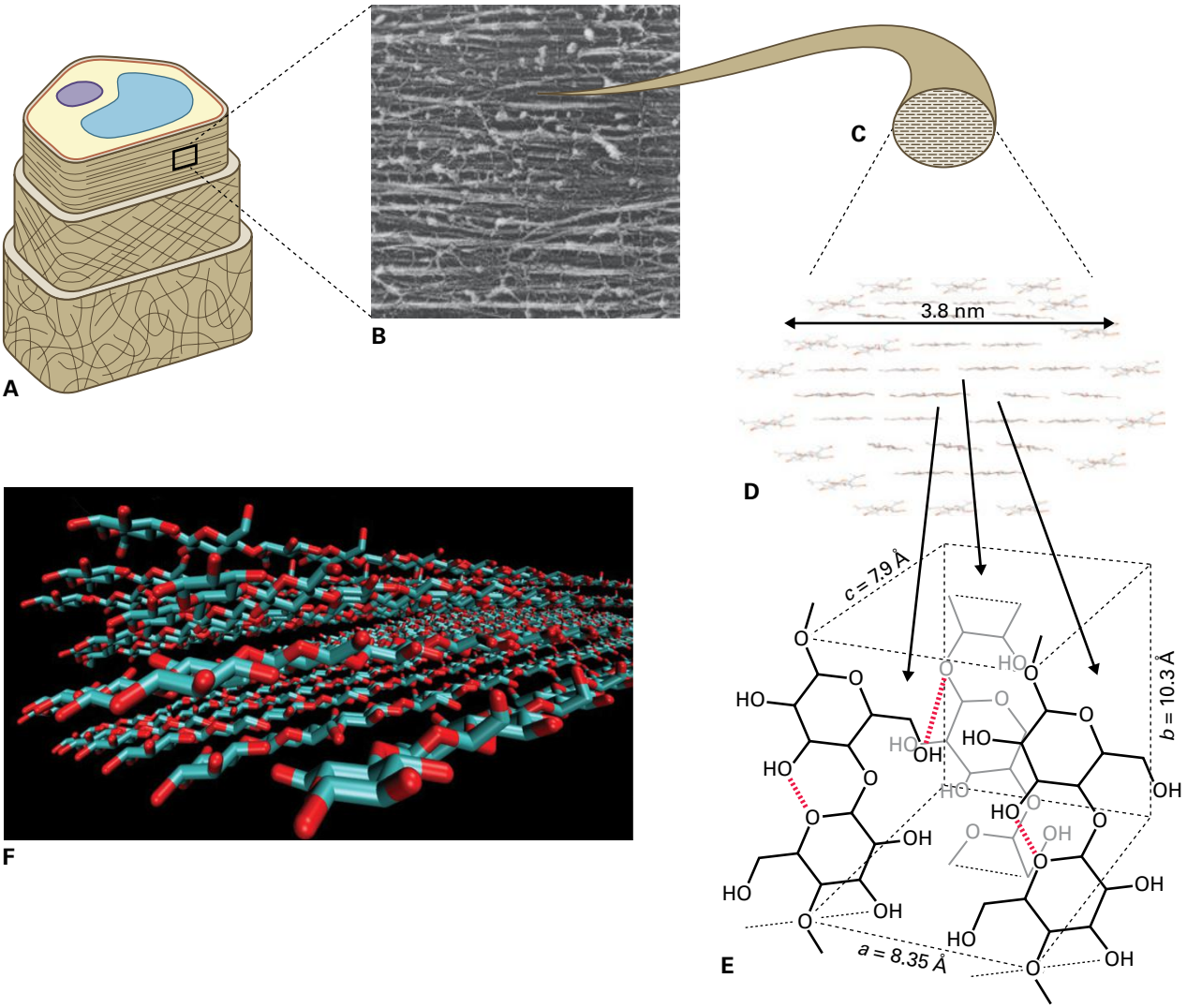
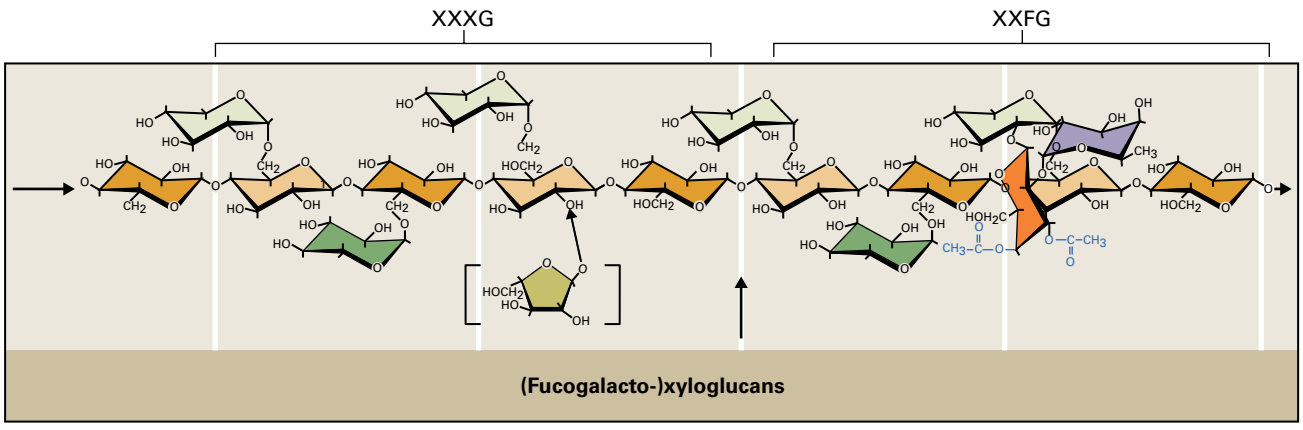
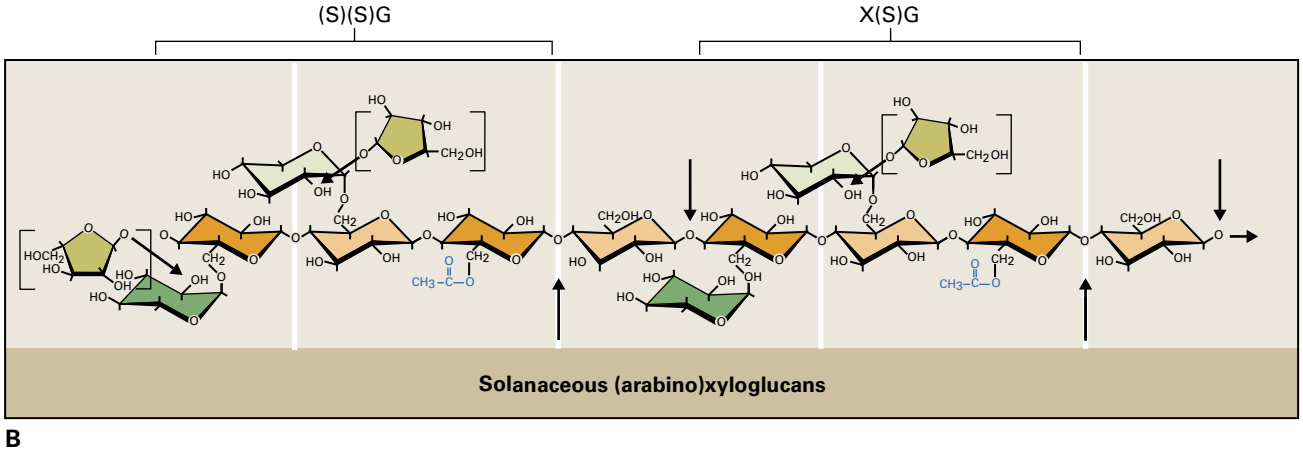


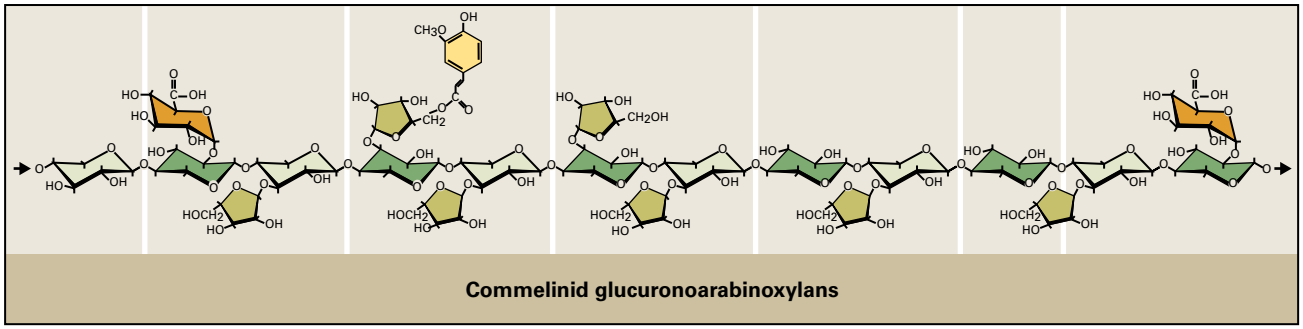
FIGURE 2.12 *Cellulose microfibrils are* para*-crystalline arrays of several dozen (1→4)-β-D-glucan chains that tightly hydrogen bond to each other, both side-to-side and top-to-bottom. The microfibrils can spool randomly around a spherical meristematic or a cell expanding isodiametrically (i.e., in all directions equally). However, in elongating cells (A), microfibrils wind around the cell in slightly helical arrays nearly transverse to the long axis of the cell, and can be seen in freeze-fracture replica of an elongating maize root cell wall (B). A single microfibril (C) is shown in cross-section (D). From solid-state NMR spectroscopy studies, glucan chains at the surface of the microfibril are thought to adopt a slightly different alignment. A microfibril of 36 chains in this arrangement is predicted to be 3.8 nm in diameter. The 18–24 glucan chains in the core of the microfibril have a precise spacing, representing a diameter of 2.6–3.0 nm. The arrangement of atoms in the unit structure of the microfibril core has been determined by X-ray diffraction (E). Molecular modeling of a cellulose microfibril predicts a slight right-handed twist from 180° (F).*
Source: (F) Mike Crowley, National Renewable Energy Lab, Golden, CO.



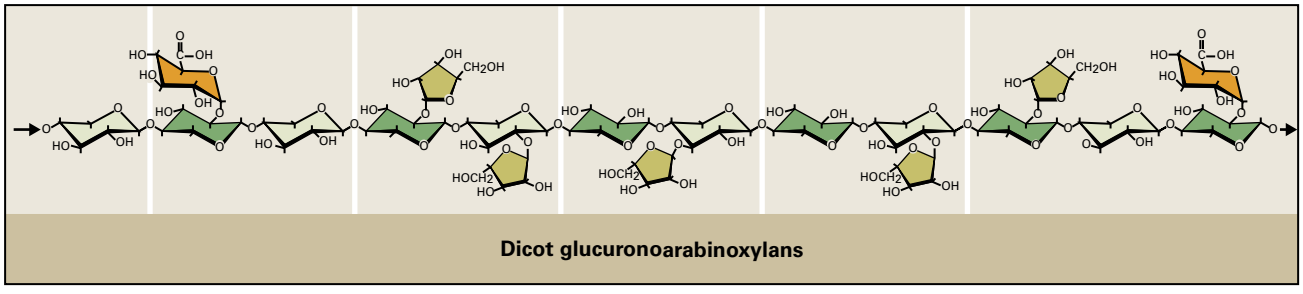
A



B



C



D

FIGURE 2.13 *Chemical structures of the major crosslinking glycans of the primary walls of flowering plants. Dotted lines delineate (1→4)-β-disaccharide units of glucose and xylose inherent in all crosslinking glycans. Such linkage requires backbone sugars to be oriented about 180° from each other. (A) Fucogalactoxyloglucans. In most xyloglucans, the α-D-xylosyl units are added to three contiguous glucosyl units of the backbone to produce a heptasaccharide unit structure. On about half of these unit structures, a t-α-L-Fuc-(1→2)-β-D-Gal- is added to the O-2 of the Xyl side-group nearest the reducing end, forming a nonasaccharide unit. Attachment of an α-L-Ara unit to the O-2 position of the backbone glucose unit at a few positions along the backbone blocks hydrogen bonding of the XyG to cellulose at these sites. The arrows denote the only linkages that can be cleaved by the* Trichoderma *endo-β-D-glucanase. According to the single letter designator convention (Table 2.1),*

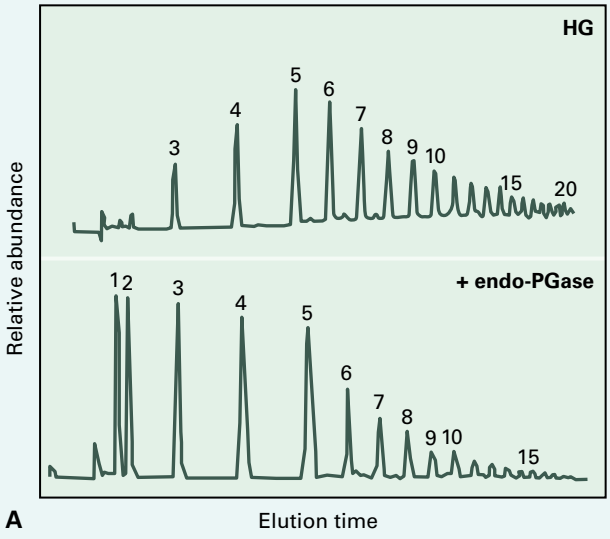
BOX 2.3 Oligosaccharide unit structure can be determined by sequence-specific glycanases and high-performance anion exchange chromatography (HPAEC)

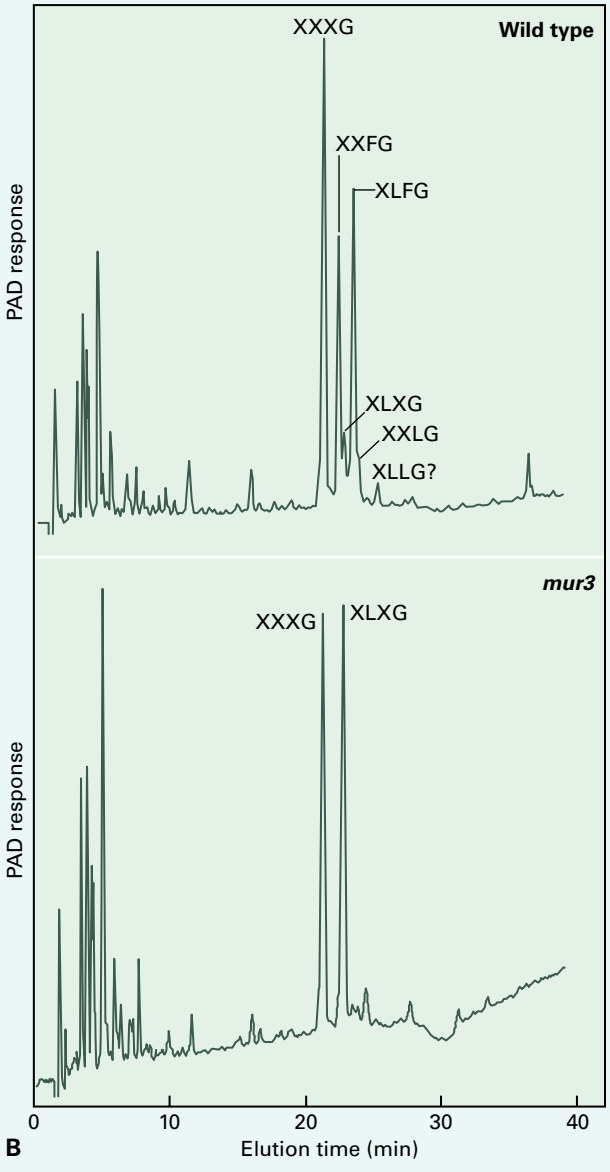
A direct method to determine the sequence of sugars in a complex carbohydrate is not presently available. However, much like the restriction endonucleases that recognize and cleave specific sequences of DNA, **sequence-dependent glycanases** that cleave polysaccharides at specific glycosidic linkages can be used to generate small oligosaccharides, the structure of which can be determined.

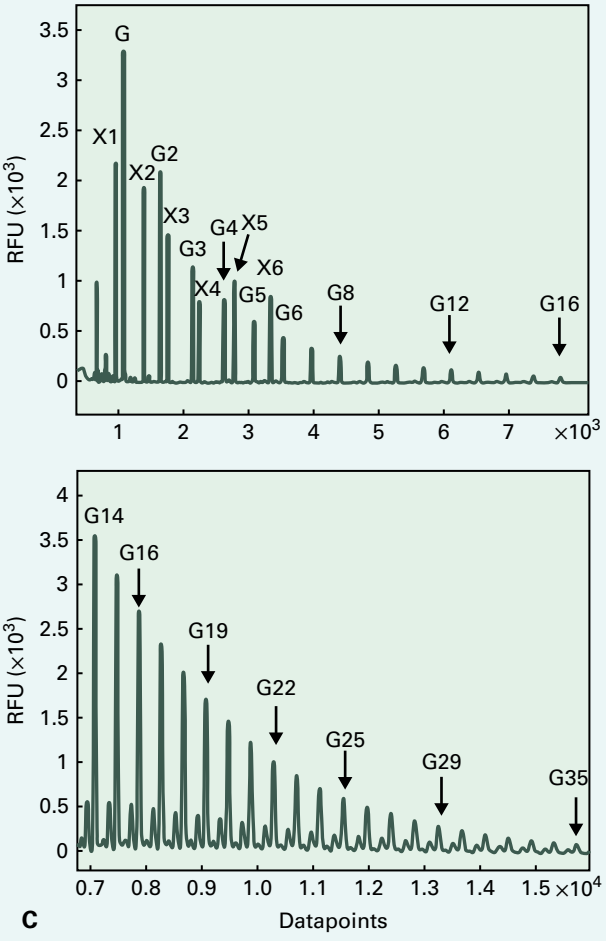
Sequence-dependent glycanases obtained from microbes either require or are restricted by structural features of the polysaccharide in addition to a specific sugar linkage. Several of these enzymes have been used to yield oligomers characteristic of repeating unit structures, indicating the characteristic unit composition of very large polymers. For example, a *Bacillus subtilis* endoglucanase cleaves a (1→4)-β-D-glucosyl linkage only if preceded by a (1→3)-β-D-linkage, and a *B. subtilis* glucuronoxylanase C cleaves (1→4)-β-D-xylosyl linkages only at sites with appendant glucuronic acid units. The activity of an endo-β-D-glucanase from the fungus *Trichoderma viride* is blocked by appendant groups of the glucan chain; the enzyme can only hydrolyze unsubstituted (1→4)-β-D-glucosyl linkages. This feature makes the enzyme useful in determining the frequency of contiguous attachment of xylosyl units onto the (1→4)-β-D-glucan chain of xyloglucan. For most flowering plants, the basic unit of structure of xyloglucan comprises glucose residues, three of which are substituted with three xylosyl groups. The first two xyloses can be decorated by galactose, and a fucose can be added to the first galactose to generate six characteristic oligomers (Table 2.1).

Conventional anion-exchange chromatography is a convenient method to separate uronic acid-containing polymers (A), but in general, neutral sugars and oligosaccharides are not well resolved by conventional **high-performance liquid chromatography (HPLC)**. However, special alkali-resistant HPLC apparatus can support **HPAEC**, a useful tool for analyzing oligosaccharide products of sequence-dependent glycanases. The hydroxyl groups of sugars are weak acids and become negatively charged at high pH. This property may be exploited since the relative retention on an anion-exchange column depends on the number, position, and degrees of freedom of the hydroxyl groups of the oligomer. The oligosaccharides become charged when introduced into a stream of up to 0.5 M NaOH. The anionic oligosaccharides bind to the column and are then eluted in a gradient of increasing sodium acetate in NaOH. As the sugars elute, they are detected by an electrochemical cell called a **pulsed amperometric detector** (PAD). A small proportion of the sugars are oxidized as they pass over the gold-plated detector, and when these oxidized sugars bind to the detector plate the concentration is measured as the relative decrease in the standing potential of the detector. A brief pulse of reversed polarity repels the oxidized sugar from the plate. This pulse-cycle is repeated every 300 ms or so. The measuring pulses are summed over time to produce a chromatogram. The PAD is reasonably specific for sugars as many other compounds are not oxidized by comparable electrical pulses. (B) The xyloglucan unit profiles of wild-type *Arabidopsis* and a *murus3* mutant lacking the entire α-L-fucose-(1→2)-β-D-galactose- side-chain from the first xylose. For wild-type XyG, all six possible oligomers are observed; because the galactosyl transferase that normally decorates the Xyl residues

FIGURE 2.13 (*Continued*) *these two oligomers are XXXG and XXFG. The decasaccharide XLFG can be a major unit structure in many species. (B) Arabinoxyloglucans. In the Solanales and Lamiales, the major repeating unit is a hexamer, rather than heptamer, with one or two α-L-Ara units added directly to the O-2 position of the Xyl units. The Solanaceae XyG units are separated by two unbranched Glc units rather than one, and the penultimate Glc contains an acetyl group at the O-6 position. The arrows denote the linkages able to be cleaved by the* Trichoderma *endo-β-D-glucanase. Using the single letter designator convention (Table 2.1), these two oligomers are XSGG or SSGG, if one or two Ara units are attached, or XXGG if they are not attached. Some Asterales and related orders have both arabinosyl and galactosyl units attached to XyG oligomers (not shown). Also, some storage XyGs in leguminous species can have XXXXG, and even XXXXXG, units that are decorated with up to four Gal units (not shown) (C) Commelinid glucuronoarabinoxylans. In the GAX from commelinid monocot walls, the α-L-Ara units are added strictly to the O-3 position of the xylosyl units of the backbone polymer. Feruloyl groups (and sometimes other hydroxycinnamic acids) are esterified to the O-5 position of the α-L-Ara units and are spaced about every 50 Xyl units of the backbone. The α-D-GlcAs are added to the O-2 position of the xylosyl units. The feruloyl units of adjacent GAX polymers can couple to crosslink GAXs in the wall. (D) Other glucuronoarabinoxylans. The noncommelinid monocots and all eudicots also contain GAX in addition to the more abundant XyG. However, the α-L-Ara units of these GAXs are attached mostly to the O-2 position instead of the O-3 position. As with the commelinid GAX, the α-D-GlcA units are attached only at the O-2 position.*







closest to the reducing end is defective in the *mur3* mutant, only XXXG and XLXG are found in great abundance.

Capillary electrophoresis, where small amounts of charged polymers are separated in liquid phase in columns of very small diameter in an electric field, is also effective in separating an oligomeric series of uronic acid-rich polymers. For neutral oligosaccharides, charged fluorescent dyes have been developed that couple to the reducing end of the oligomer to provide both the electrophoretic mobility and a sensitive means of detection (C). The upper trace shows separation of a mixture of hydrolyzed dextran and β-1,4-xylo oligosaccharides of DP1 to DP6; Larger dextran oligosaccharides are resolved by extending the electrophoresis time to 90 minutes. RFU, relative fluorescence units; G, Glucose; X, Xylose.

Source: Li et al. (2013). *Biotech. Biofuels* 6: Art. No. 94. (B) Carpita NC, McCann MC (2015). *J. Exp. Bot.*, in press.

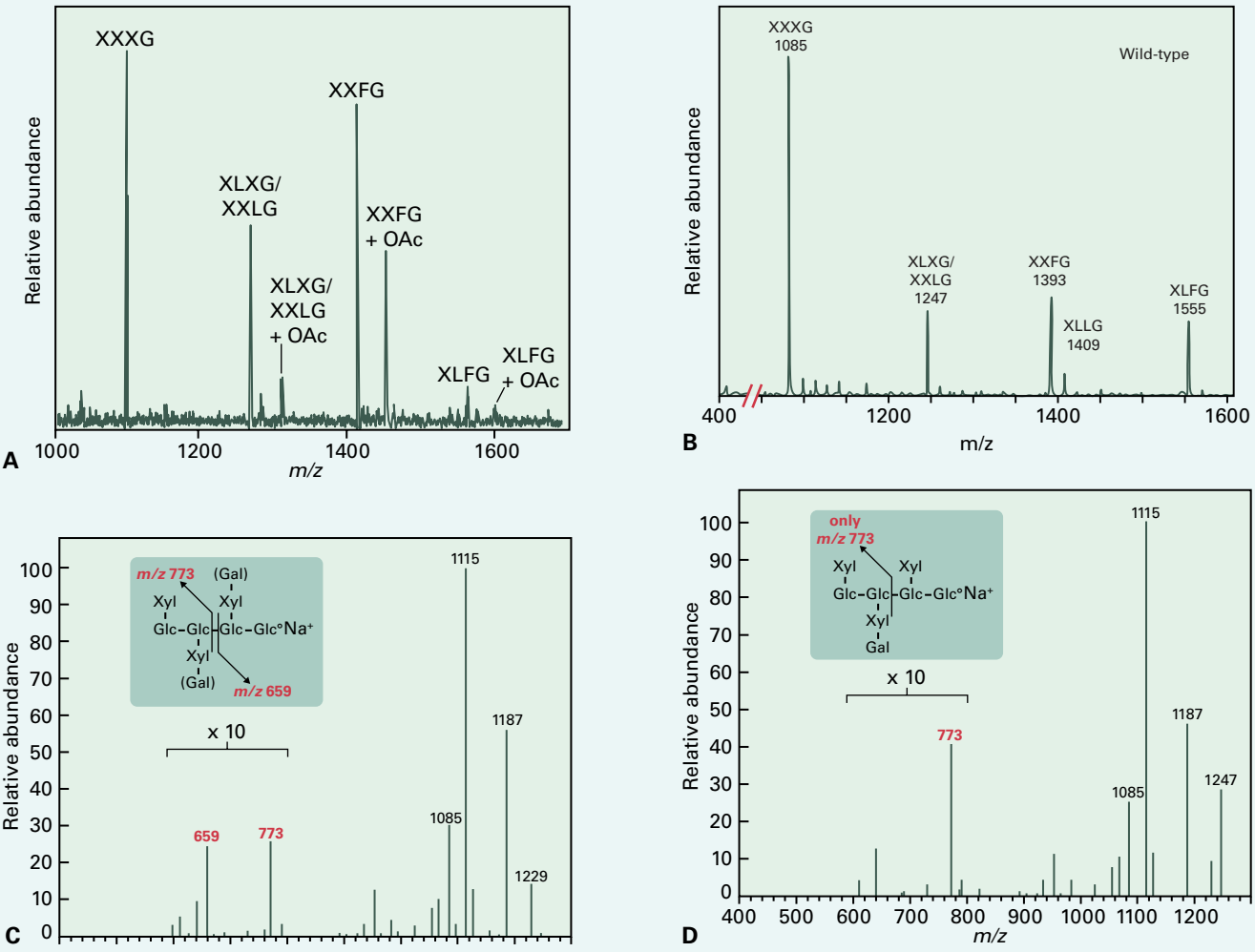
BOX 2.4

Polysaccharide sequence can be inferred by matrix-assisted laser desorption ionization (MALDI)-time of flight (TOF) and electrospray-ionization (ESI) tandem mass spectrometry (MS/MS)

Although EIMS of the partly methylated alditol acetates is the main procedure used by carbohydrate biochemists to establish the linkage structure of unknown polymers (see Box 2.1), new MS techniques greatly extend the mass range that can be analyzed and can provide linkage and sequence information for underivatized oligosaccharides.

One such technique is **matrix-assisted laser desorption ionization-time of flight (MALDI-TOF) MS**. Underivatized polymers are mixed with a material that ionizes them on exposure to brief pulses of a laser. The polymeric ions are differentially accelerated in the mass spectrometer, depending on their size, and molecular masses as great as 200 kDa are detected by a finely tuned calculation of the time interval between laser bombardment and contact with the mass spectrometer anode (A). For the xyloglucan oligomers in (A), the degree of acetylation is determined by ions of diagnostic mass (the molecular ion M^+ plus *m/z* 43 per acetyl group).

In **electrospray-ionization (ESI) MS**, water-soluble carbohydrate oligomers are 'nebulized' into a fine mist toward the entrance to the MS against a counter-current of warmed dry air. Oligomers trapped in microdroplets adsorb Na^+ atoms and are collected after evaporation in an **ion trap**. Samples of different mass/charge ratios can then be analyzed by MS for relative abundance of diagnostic ions of interest. In (B), masses diagnostic of additions of one and two galactose units and one fucose unit are detected in the oligomers from xyloglucan from wild-type *Arabidopsis*, whereas *mur2* is missing the fragments diagnostic of fucosylation, and *mur3* has only a single galactose addition. An advantage of ESI MS over MALDI-TOF is that the collection of trapped ions can be fragmented further to gain information on the positions of individual sugars in the



oligomer. In the example in (C), the addition of galactose on either the first or second xylose of a xyloglucan fragment yields *m/z* 1247. However, in MS/MS of *m/z* 1247, Gal at the first xylose yields a fragment *m/z* 659, whereas Gal at the second xylose yields *m/z* 773. In the wild-type, galactose is found at both positions (1), whereas in the *murus3* mutant, the galactose is only at the second xylose (2), revealing the effect of the mutation as a defective galactosyl transferase that is unable to decorate the xylose residue closest to the reducing end of the oligomer.

along the glucan is designated by a single letter on the basis of its terminal sugar (Table 2.1).

The XyGs are constructed in block-like unit structures containing 6–11 sugars, the proportions of which vary among tissues and species (Fig. 2.13). While cellotetraose with two or three contiguous xylosyl units is the base unit backbone structure for most XyGs, some variants have been found with cellopentaose and even cellohexaose units with four and five subtending xylosyl units, respectively. The XyGs comprise at least four major variants of structure. The XyGs of noncommelinid monocots and most of the eudicots are fucogalacto-XyGs. The fundamental structure is composed of nearly equal amounts of XXXG and XXFG, but variations can occur and α-L-Ara is added at some places along the glucan chain. Solanaceous species and peppermint (*Mentha x piperita*) have arabino-XyGs in which only two of every four glucosyl units contains a xylose unit, and the xylosyl units are substituted with either one or two α-L-Ara units to produce a mixture of SXGG, XSGG, and SSGG subunits, where S signifies the terminal arabinosylation in Solanaceous species. Curiously, an acetyl group replaces the third xylosyl unit in the arabino-XyGs.

Commelinid monocots also contain small amounts of XyG, but these contain random additions of one or two xylosyl units isolated along the glucan chain and the rare addition of a Gal as the only subtending sugar. Other members of the class Asteridae have units that have α-L-Ara and β-D-Gal in the same oligomer, and still others have additions of α-D-Xyl or β-L-Gal (Fig. 2.14). Still other types of side-chains, including branched chains, are seen in nonvascular and nonseed vascular plants (Table 2.1). In the laboratory, mutant plants affected in their ability to decorate the xylosyl units of their

TABLE 2.1 *Single-letter designators of simple and complex xyloglucan side groups.*

Single-letter designator	Terminal sugar	Side group on the glucan chain
G	D-Glucose	None
X	D-Xylose	α-D-Xyl-(1→6)-
L	D-Galactose	β-D-Gal-(1→2)-α-D-Xyl-(1→6)-
F	L-Fucose	α-L-Fuc-(1→2)-β-D-Gal-(1→2)-α-D-Xyl-(1→6)-
S	L-Arabinofuranose	α-L-Ara*f*-(1→2)-α-D-Xyl-(1→6)-
T	L-Arabinofuranose	β-L-Ara*p*-(1→3)-α-L-Ara*p*-(1→2)-α-D-Xyl-(1→6)-
U	D-Xylose	β-D-Xyl-(1→2)-α-D-Xyl-(1→6)-
J	L-Galactose	α-L-Gal-(1→2)-β-D-Gal-(1→2)-α-D-Xyl-(1→6)-
D	L-Arabinopyranose	α-L-Ara*p*-(1→2)-α-D-Xyl-(1→6)-
E	L-Fucose	α-L-Fuc-(1→2)-α-L-Ara*p*-(1→2)-α-D-Xyl-(1→6)-
P	D-Galacturonic Acid, D-Galactose	β-D-GalA-(1→2)-[β-D-Gal-(1→4)-]α-D-Xyl-(1→6)-
Q	D-Galactose (2)	β-D-Gal-(1→4)-β-D-GalA-(1→2)-[β-D-Gal-(1→4)] α-D-Xyl-(1→6)-
M	L-Arabinopyranose, D-Galactose	α-L-Ara*p*-(1→2)-[β-D-Gal-(1→4)] α-D-Xyl-(1→6)-
N	L-Arabinopyranose, D-Galactose	α-L-Ara*p*-(1→2)-[β-D-Gal-(1→6)-β-D-Gal-(1→4-] α-D-Xyl-(1→6)-

Most angiosperm eudicots possess the side groups of D-Gal (L) and L-Fuc (F) attached to the xylose units along the glucan backbone. Both furanose and pyranose forms of L-Arabinose are found, whereas all other sugars are understood to be in the pyranose form. Side groups S, T and U are found in the Asteridae and Solanaceae. The complex branched side groups, including those containing galacturonic acid residues are found in mosses and nonseed vascular plants.

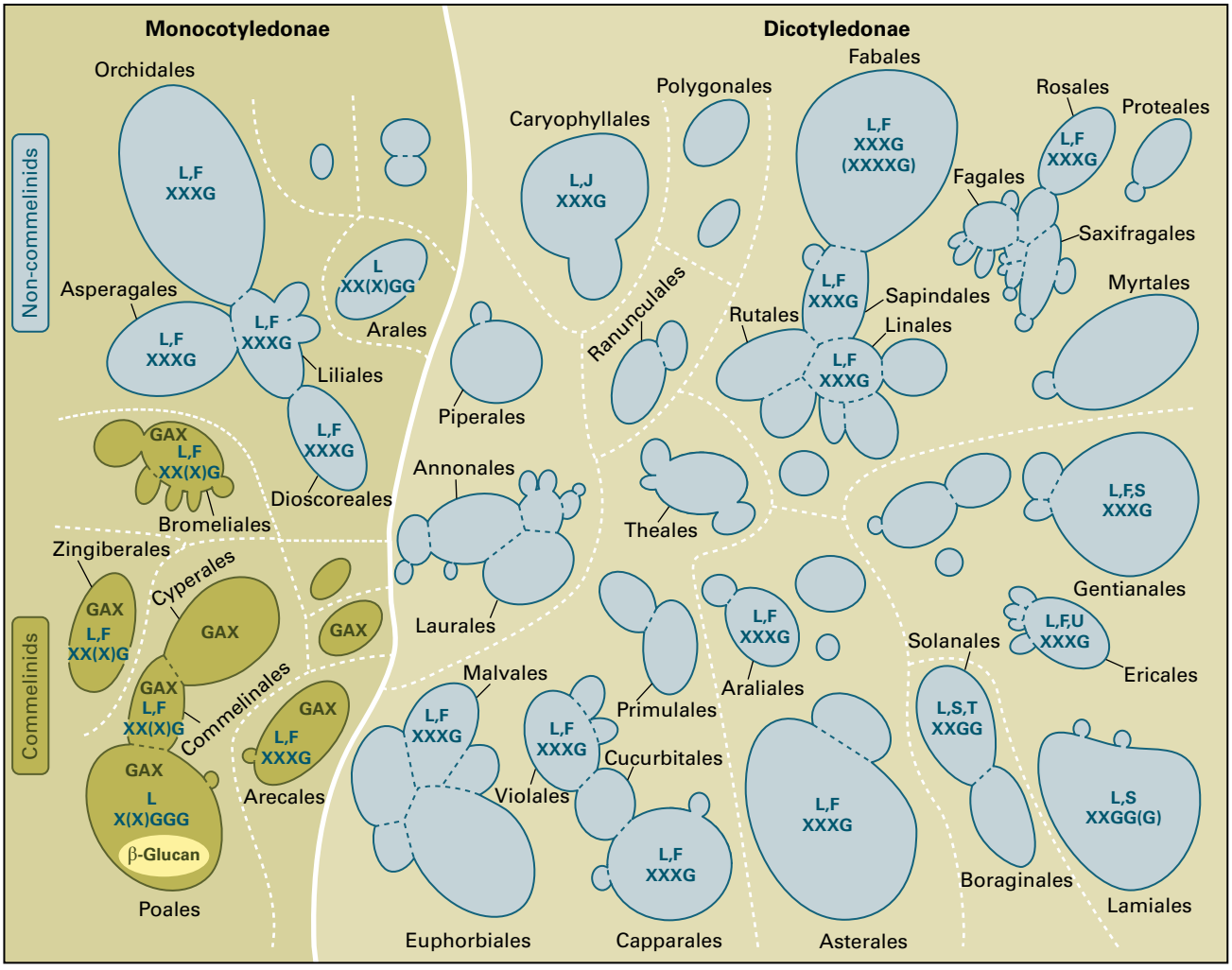


FIGURE 2.14 *Orders of the flowering plants, with symbolic descriptions of the major crosslinking glycans and major distinctions illustrated between grasses and other commelinid monocots, noncommelinid monocots, and eudicots. The fundamental XXXG backbone unit structure is found in most species (see Fig. 2.12), backbone variants in both monocots and eudicots are shown. The single letter code (Table 2.1) gives the extended side-groups that have been documented; L [β-D-Gal-(1→2)-α-D-Xyl-(1→6)-] and F [α-L-Fuc-(1→2)-β-D-Gal-(1→2)-α-D-Xyl-(1→6)-] are the most common sidegroups, with S [α-L-Araf-(1→2)-α-D-Xyl-(1→6)-], T [β-L-Arap-(1→3)-α-L-Arap-(1→2)-α-D-Xyl-(1→6)-], and U [β-D-Xyl-(1→2)-α-D-Xyl-(1→6)-] side groups found in the Solanales, Lamiales, and Ericales of the Asteridae line. GAX = glucuronoarabino-xylan (see Fig. 2.13); β-Glucan = mixed-linkage (1→3),(1→4)-β-D-glucan (Fig. 2.15).*

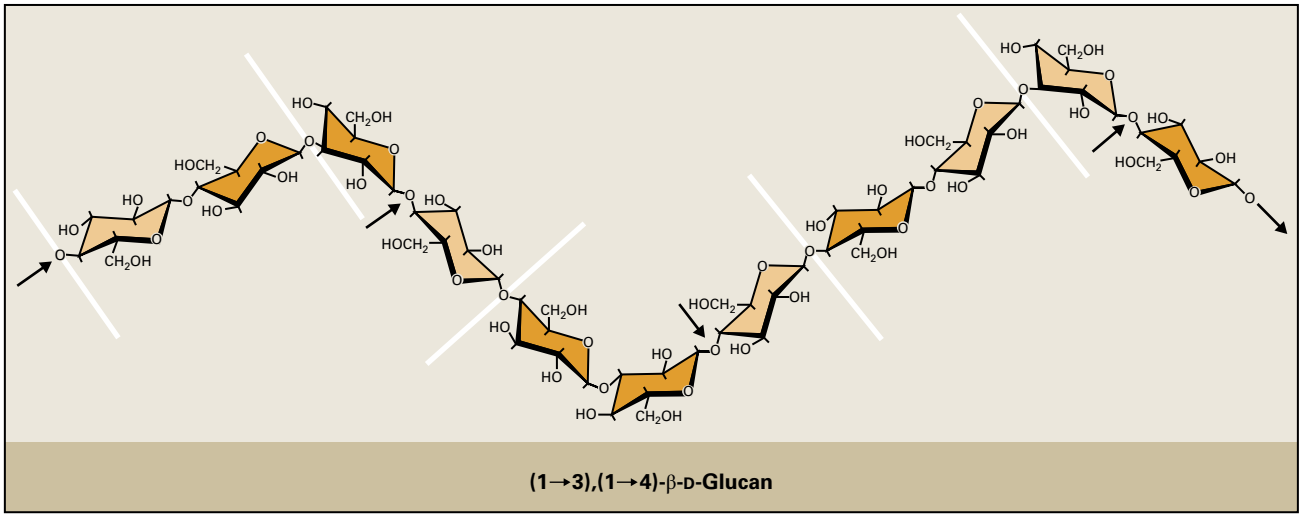


FIGURE 2.15 *Among the angiosperms, the mixed-linkage (1→3),(1→4)-β-D-glucan is unique to the Poales. Red arrows indicate cleavage sites by the* Bacillus subtilis *endoglucanase. The unbranched polymers are composed of mostly cellotriose and cellotetraose units connected by single (1→3)-β-linkages. Smaller amounts of larger cellodextrins up to about nine (1→4)-β-D-glucose residues are found (not shown).*

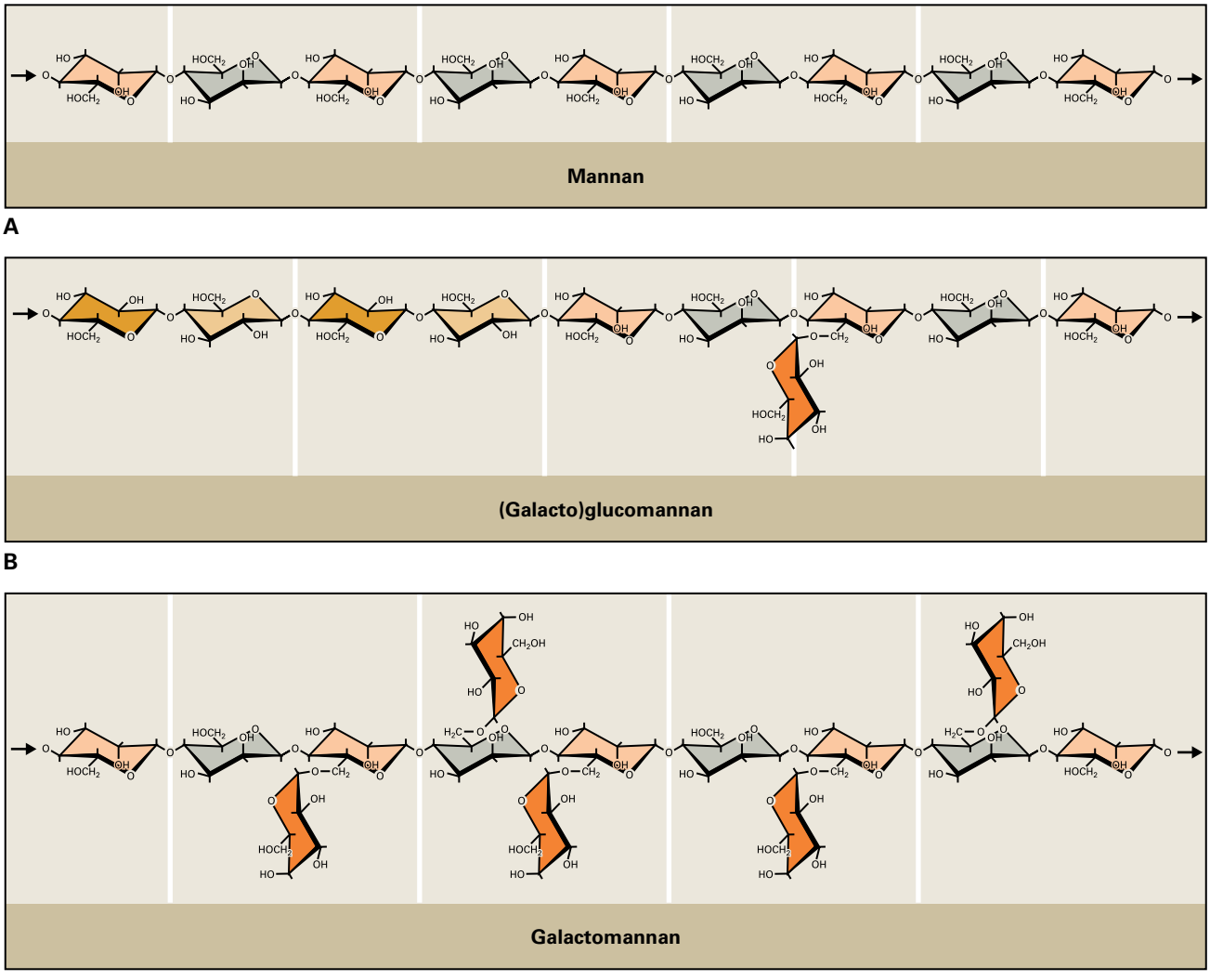


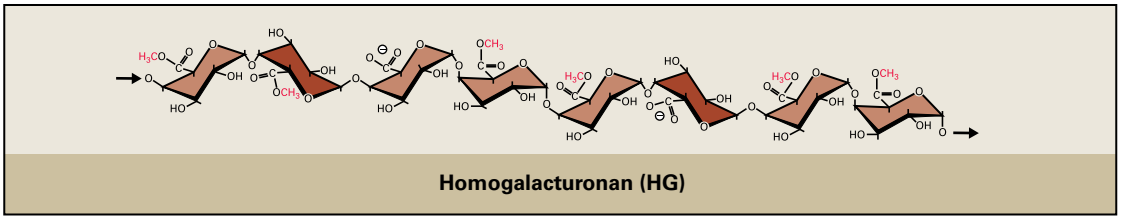
FIGURE 2.16 *Crosslinking glycans that contain mannose. The dotted lines mark the (1→4)-β-disaccharide unit structures (see Fig. 2.12). (A) Pure mannans can hydrogen bond into para-crystalline arrays, which are similar in structure to cellulose. (B) (Galacto)glucomannans are roughly equimolar mixtures of (1→4)-β-D-Man and (1→4)-β-D-Glc units, with occasional addition of terminal α-D-Gal units added to the O-6 position of the Man units. Glucomannans are tightly bound to the surface of cellulose microfibrils. (C) Galactomannans have backbones composed exclusively of (1→4)-β-D-mannan with the α-D-Gal units added at the O-6 positions. Gal units interrupt hydrogen bonding and greatly enhance water solubility.*

XyGs appear to grow as well as wild-type plants, although tensile strength of the primary walls is compromised if the galactosylated side-chains are missing.

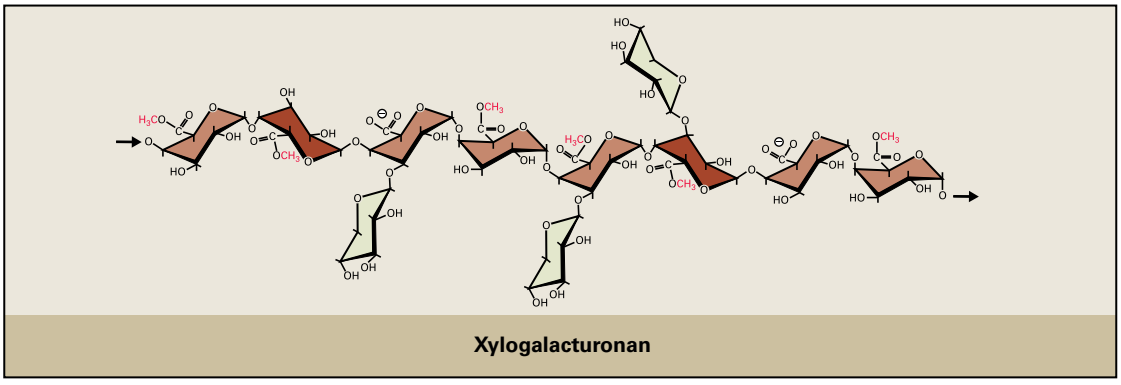
All angiosperms contain at least small amounts of GAX, but their structure may vary considerably with respect to the degree of substitution and position of attachment of α-L-Ara residues (Fig. 2.13). In commelinid monocots, in which they are the major crosslinking polymers, the Ara units are always on the *O*-3 position. However, in species in which XyG is the major crosslinking glycan, the α-L-Ara units are more commonly found at the *O*-2 position. In all GAXs, the α-D-GlcA units are attached to the *O*-2 position.

In the order Poales, which contains cereals and grasses, a third major crosslinking glycan, "**mixed-linkage" (1→3),(1→4)-β-D-glucans** (β-glucans), distinguishes these species from other commelinid species (Fig. 2.15). These unbranched polymers consist of mostly random mixtures of cellotriose and cellotetraose units in a ratio of about 2.5:1 and connected by single (1→3)-β-D-linkages. Additional cellodextrins of five to nine consecutive (1→4)-β-D-Glc units are all spaced by single (1→3)-β-D-linkages. In aqueous solutions, cellotriose and cellotetraose units result in corkscrew-shaped polymers of about 50 residues that are spaced by the longer cellodextrins. Although absent from all other angiosperms, mixed-linkage (1→3),(1→4)-β-D-glucans of altered cellodextrin unit structure are found in the lichen *Cetraria islandica* and the nonseed vascular plant *Equisetum*.

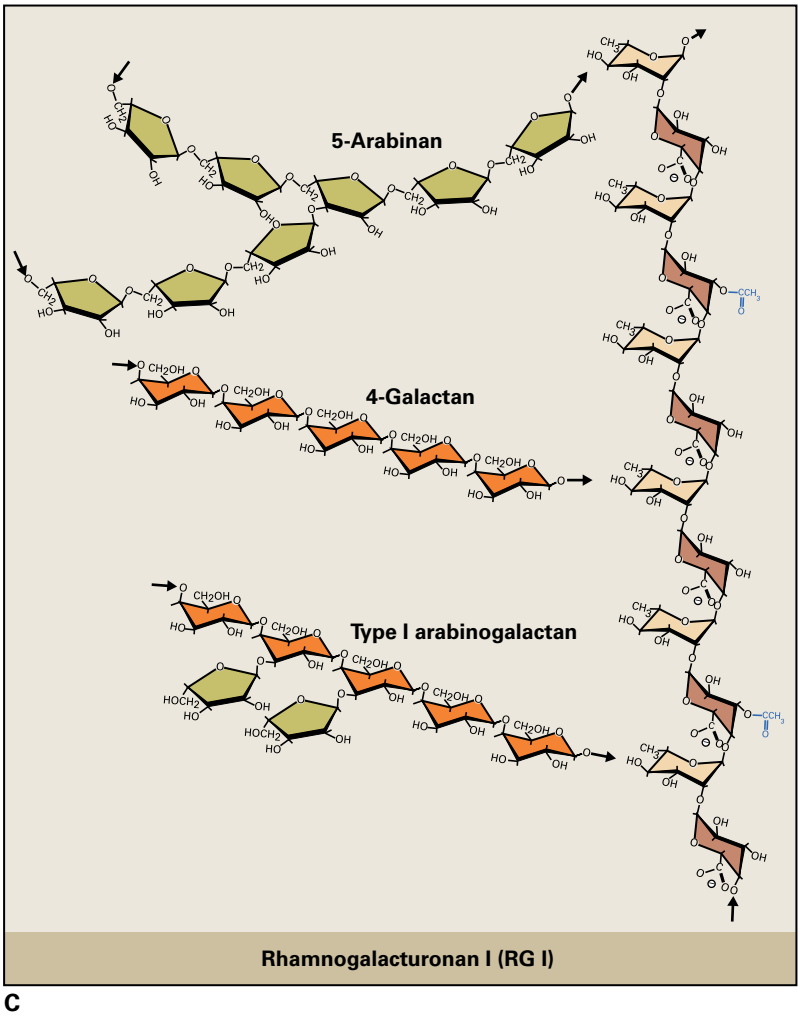
Other, much less abundant noncellulosic polysaccharides, **mannans**, are found in virtually all angiosperms. In certain algae mannan microfibrils substitute for cellulose as the fundamental scaffold (Fig. 2.16). **Glucomannans** and **galactoglucomannans** potentially interlock the microfibrils in some primary walls. In certain fern species, (gluco)mannans are the major crosslinking glycan, constituting a **type III** cell wall. Extensively substituted **galactomannans** are unable to bind to cellulose and form thick gels upon hydration.



A



B



C

FIGURE 2.17 *Pectic polysaccharides of plants. (A) Highly methyl esterified chains of (1→4)-α-D-GalA (HG) are secreted by the Golgi apparatus and are de-esterified to varying degrees in certain wall domains by pectin methyl esterases in the wall (see Section 2.3.2). (B) Xylogalacturonans are a separate class of substituted HG, with appendant α-D-Xyl units at the O-3 position of about half of the GalA units. (C) Contorted, rod-like RG I is composed of a repeating disaccharide, →2)-α-L-Rha-(1→4)-α-D-GalA-(1→. About one-third of the GalA units are acetylated at secondary alcohol groups. To the O-4 position of the rhamnosyl units are attached neutral sugar side-chains of branched and linear (1→5)-α-L-arabinans, (1→4)-α-D-galactans, and type I arabinogalactans. Some seed mucilages have nonreducing terminal residues of L-Fuc and L-Gal attached to the O-3 instead of the O-4 positions of Rha.*

2.2.3 Pectin matrix polymers are a diverse class of uronic acid-rich polysaccharides

Pectins comprise a mixture of heterogeneous, branched, and highly hydrated polysaccharides rich in D-galacturonic acid. Pectins are easily extracted from the cell wall by Ca^{2+}-chelators such as ammonium oxalate, EDTA, EGTA, or cyclohexane diamine tetraacetate (CDTA), or by de-esterifying agents such as Na_2CO_3 or alkali less than 0.1 M.

Pectins perform many functions: determining wall porosity and providing charged surfaces that modulate wall pH and ion balance, regulating cell–cell adhesion at the middle lamella, and serving as recognition molecules that alert plant cells to the presence of symbiotic organisms, pathogens, and insects. Particular cell wall enzymes may bind to the charged pectin network, constraining their activities to local regions of the wall. By limiting wall porosity, pectins may affect cell growth, thereby regulating access of wall-loosening enzymes to their glycan substrates (see Section 2.5.8).

Two fundamental constituents of pectins are **homogalacturonan** (HG) (Fig. 2.17A) and **rhamnogalacturonan I** (RG I) (Fig. 2.17C). HGs are homopolymers of (1→4)-α-D-GalA that contain up to ≈200 GalA units and are about 100 nm long. There are two kinds of structurally modified HGs, **xylogalacturonan** (Fig. 2.17B) and **rhamnogalacturonan II** (RG II) (Fig. 2.18). RG II is misnamed as it is not structurally related to RG I, but was first identified as a rhamnose-containing pectin. RG II has the richest diversity of sugars and linkage structures known, including apiose, aceric acid (3-C′-carboxy-5-deoxy-L-xylose), 2-*O*-methyl fucose, 2-*O*-methyl xylose, Kdo (3-deoxy-D-*manno*-2-octulosonic acid), and Dha (3-deoxy-D-*lyxo*-2-heptulosaric acid). The highly conserved structure of RG II among flowering plants suggests an important function despite its low abundance in cell walls. Dimers of RG II are crosslinked by borate, two diester bonds per boron atom, between apiose units in the complex sidegroups (Fig. 2.18B). In the *Arabidopsis murus1* mutant, dimers do not form because of a defect in the de novo synthesis of fucose, which alters side-chain structure and reduces its ability to bind to boron. Both the stature of *murus1* plants and the tensile strength of their cell walls are reduced, but normal stature and strength can be rescued by spraying plants with excess boron.

RG I is a rod-like heteropolymer of repeating (1→2)-α-L-Rha-(1→4)-α-D-GalA disaccharide units. RG Is can be isolated from the cell walls by enzymatic digestion with **polygalacturonase** (PGase), but the length of RG I is unknown because there may be runs of HG on the ends of the molecule. While HG and RG II appear to be covalently linked in a single polymer, it is not yet known whether RG I and HG form a continuous backbone, or if one of these molecules attaches as a side-chain to the backbone of the other.

Other polysaccharides composed mostly of neutral sugars, such as **arabinans, galactans**, and highly branched **type I arabinogalactans** (AGs) of various configurations and sizes, are attached to the *O*-4 of many of the Rha residues of RG I (see Fig. 2.17C). In general, about half of the Rha units of RG I have side-chains, but this ratio can vary with cell type and physiological state. Type I AGs are found only associated with pectins and are composed of (1→4)-β-D-galactan chains with mostly *t*-Ara units at the *O*-3 of the Gal units.

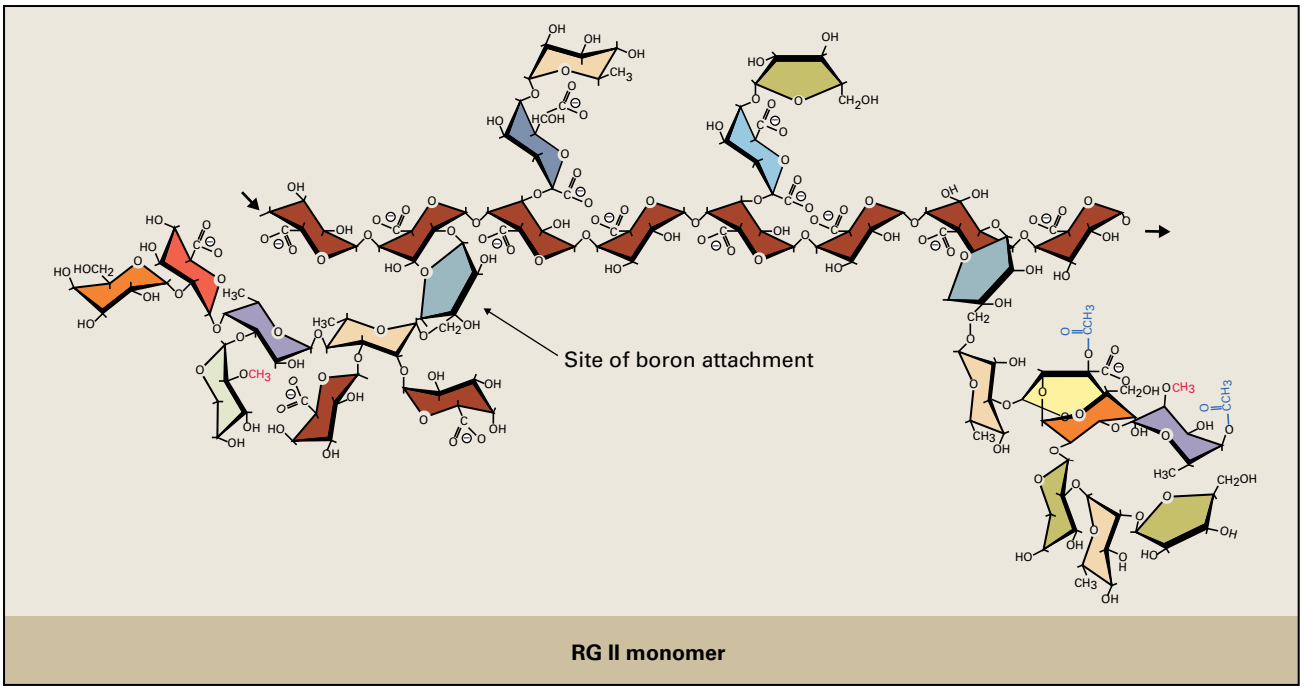
2.2.4 Structural proteins are encoded by large multigene families

Although the structural framework of the cell wall is largely carbohydrate, structural proteins may also form networks in the wall. There are three major classes of structural proteins named for their respectively enriched amino acid: **hydroxyproline-rich glycoproteins** (HRGPs), **proline-rich proteins** (PRPs), and **glycine-rich proteins** (GRPs) (see Fig. 2.19). All of them are developmentally regulated, with relative amounts varying among tissues and species (Fig. 2.20). All mRNAs for these structural proteins encode signal peptides that target the proteins to the secretory pathway, and like other secretory proteins destined for the cell wall, structural proteins are cotranslationally inserted into the ER.

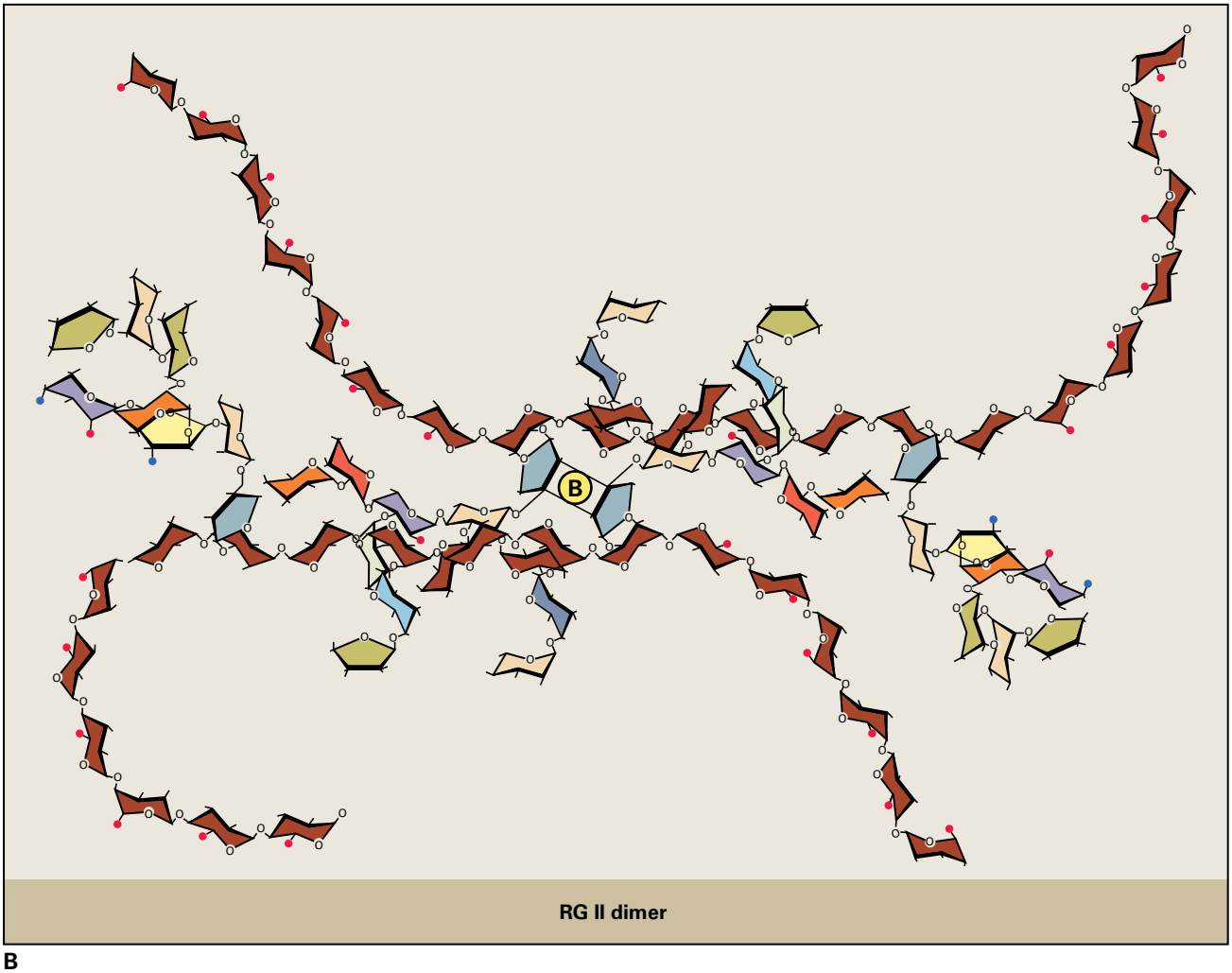
Extensin is one of the best studied plant HRGPs and consists of repeating Ser-$(Hyp)_4$ and Tyr-Lys-Tyr sequences that are important for secondary and tertiary structure (Fig. 2.19). The repeating Hyp units predict a "**polyproline II**" rod-like molecule. A single *t*-α-D-Gal residue is added to the Ser residues, whereas one to four arabinosyl units are added to one or all of the four Hyp residues. The conformational structure of PRPs is unknown, but their similarity to extensin suggests they may also be rod-shaped proteins. GRPs, some of which contain more than 70% glycine, are predicted to be β-pleated sheets rather than rod-shaped molecules. Like HRGPs, cell wall GRPs are difficult to extract and may become crosslinked into the wall.

2.2.5 Arabinogalactan proteins are developmentally regulated proteoglycans

Type II AGs are a diverse group of short (1→3)- and (1→6)-β-D-galactan chains connected to each other by (1→3,1→6)-linked branch-point residues, and they are associated with specific proteins and peptides to form **arabinogalactan proteins (AGPs)**. AGPs are more aptly described as proteoglycans, as they can consist of more than 95% carbohydrate. AGPs constitute a broad class of molecules located in Golgi-derived vesicles, the plasma membrane, and the cell wall. The site of AGP glycosylation remains undetermined, but it is likely the Golgi apparatus because it involves attachment of large, highly branched galactan chains and subsequent decoration with Ara units (Fig. 2.21). AGPs are often decorated with additional sugars, including *t*-β-D-GlcA-(1→3)- and *t*-α-L-Rha-(1→4)-β-D-GlcA-(1→3)- side groups on the (1→6)-β-D-galactan chains, where *t* is defined as the nonreducing terminal sugar. Characterization of the polysaccharide contents of the Golgi apparatus and secretory vesicles, including glycosylated proteins – shows that a majority of the material present is AGP. Another characteristic of



A



B

FIGURE 2.18 *Rhamnogalacturonans. (A) RG II is a complex HG with four distinct side groups containing several different kinds of sugar linkages. (B) RG II monomers of about 4,200 kDa can dimerize as boron di-diesters of the apiose residues. Red dots indicate methyl groups, blue dots acetyl groups.*

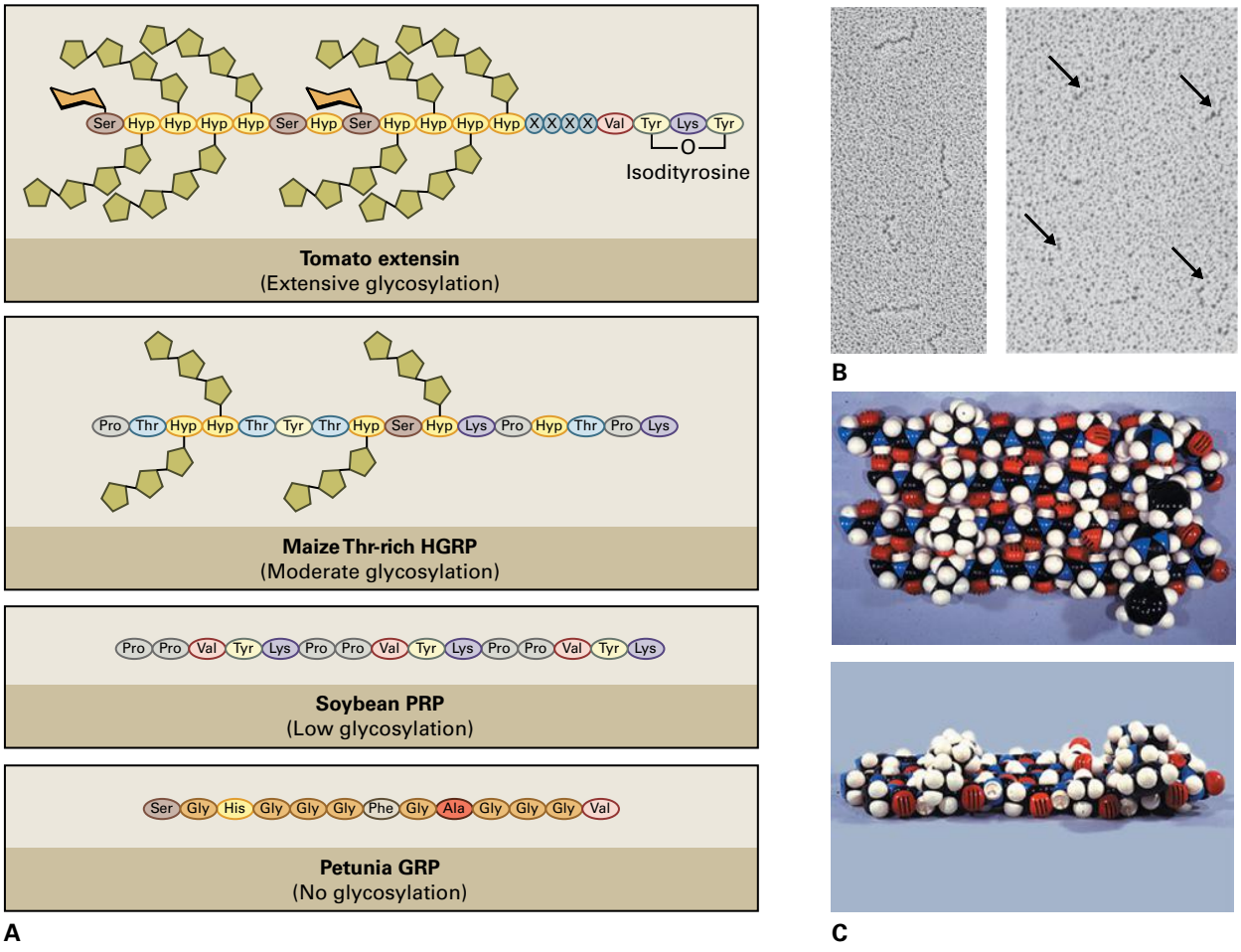


FIGURE 2.19 *Comparisons of repeated motifs of extensins, maize Thr-rich proteins, PRPs, and GRPs. (A) A Ser-(Hyp)$_4$ or related motif found in many flowering plants is heavily glycosylated with mono-, di-, tri-, and tetra-arabinosides that associate with the polyproline helix to reinforce a rod-shaped structure of tomato (*Solanum lycopersicum*) extensin molecules. A Gal unit is attached to the Ser residue. The Tyr-Lys-Tyr motif is the likely position of the intramolecular isodityrosine linkage. An extensin-like Thr-rich protein from maize is moderately glycosylated. The repeated motifs of PRP lack many contiguously hydroxylated Ser, Thr, and Hyp residues—a signal for glycosylation with arabinosides, so PRPs are not as heavily glycosylated. (B) Rotary-shadowed replicas of isolated extensin precursors reveal their rod-shaped structure (left). Removal of the arabinosides results in loss of the rod-shaped structure (right). (C) In contrast to the rod-shaped extensins, the GRPs may form β-sheet structures and are not glycosylated. A* Petunia hybrida *GRP has 14 repeats of the motif shown in (A), and the aromatic residues align on one face of the proposed β-sheet. Source*: (B) Stafstrom & Staehelin. (1986). Plant Physiol 81:242. (C) Condit & Meagher. (1986). Nature 323:178–181.

AGPs is their ability to bind Yariv reagent, a β-D-Glc derivative of phloroglucinol (Fig. 2.21).

Like structural proteins, AGPs are encoded by a large multigene family. Of the few proteins that have been isolated, they can be characterized as enriched in Pro(Hyp), Ala, and Ser/Thr. They possess distinguishing common motifs, but contain domains with similarity to some PRPs, extensins, and the Solanaceous lectins (Fig. 2.21). An interesting clade in the AGP gene family has similarity to fasciclin domain-containing proteins in animal cells, known to function in cell adhesion. While no clear-cut function has been described for AGPs, they are made only in specific cell types, at particular developmental stages, and in response to specific environmental stimuli. Many AGPs are glycosylphosphatidylinositol (GPI)-anchored; a GPI anchor is a glycolipid, with a carbohydrate link to a proteolytically trimmed C-terminus of a protein, attached post-translationally to diacylglyercol, anchoring the protein to the plasma membrane (Fig. 2.21). Phospholipase C is known to cleave glycosylated proteins from their membrane anchors, where they subsequently can migrate into the cell wall or be recovered into the cytoplasm by endocytosis. In addition to AGPs, many different classes of wall-associated proteins are GPI-anchored, including some proteases, glycosyl hydrolases, and several surface proteins involved in anisotropic cell growth.

2.2.6 Aromatic substances are present in the nonlignified walls of commelinid species

The primary walls of commelinid orders of monocots and Chenopodiaceae (such as sugar beet and spinach) contain significant amounts of aromatic substances incorporated into

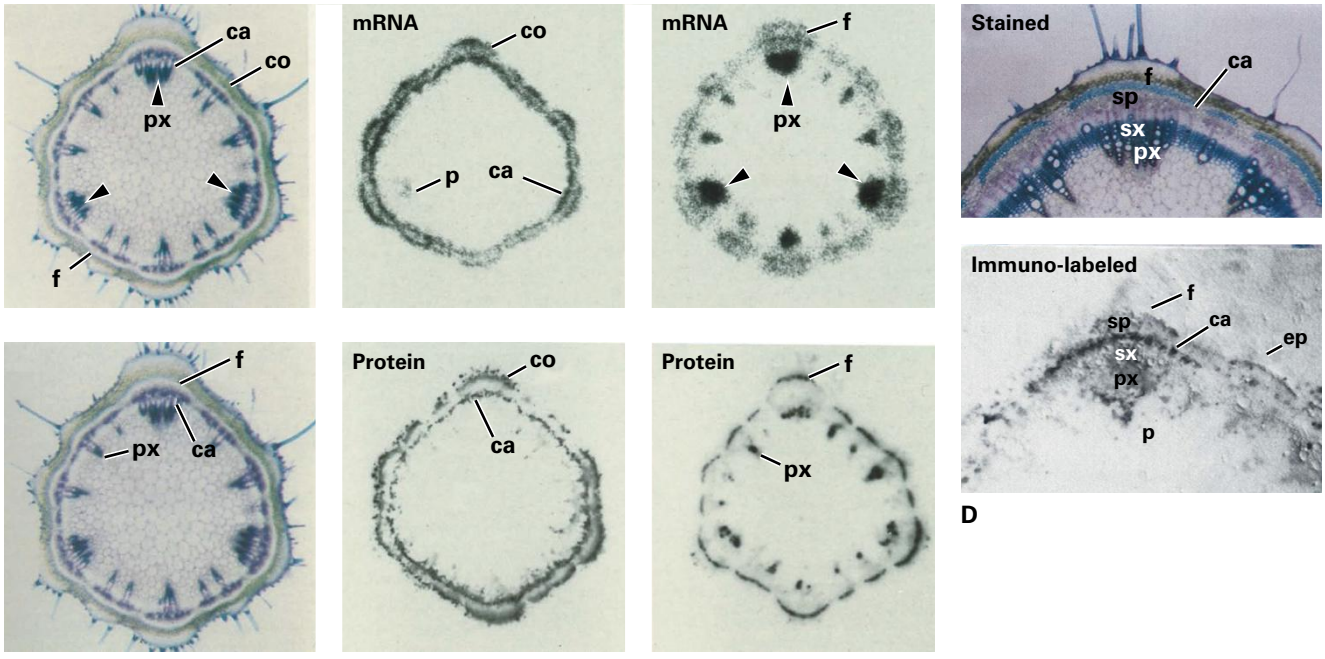


FIGURE 2.20 *When cleanly sliced sections of a plant are pressed firmly for a few seconds to a nitrocellulose sheet, soluble carbohydrate, protein, and nucleic acids are left behind, imprinted in a nearly cell-specific pattern. Coined tissue printing, this technique has been instrumental in providing biologists with an extremely simple experimental tool with many uses. (A) Stained sections of the elongating second internode of a soybean (*Glycine max*) stem are provided for comparison with other pairs of sections. (B) In situ hybridization with an HRGP cDNA probe and immunolocalization with an HRGP-specific antibody reveal that HRGPs and the mRNA transcripts that encode them are colocalized in cortical (co) and cambial (ca) cells. (C) The same techniques show that GRP mRNA transcripts and their protein products are enriched in phloem (f) and protoxylem (px). Thus, the GRP proteins and transcripts are found primarily in vascular or lignified cells, whereas the HRGPs are located in meristematic cells and cells around the cambium. (D) Magnification of the stained section and tissue print shows that HRGP can be immunolocalized to the cellular level. ep, epidermis; p, pith; sp, secondary phloem; sx, secondary xylem.*
Source: Ye & Varner. (1991). Plant Cell 3:23–38.

their unlignified cell wall polymers, a feature that makes them fluoresce under UV light. A large proportion of plant aromatics are the **hydroxycinnamates**, esters of primarily ferulic and *p*-coumaric acids (Fig. 2.22). In grasses, about one of every 20 Ara units of GAX are acylated at their O-5 positions by hydroxycinnamates. Up to half the ferulate units of neighboring GAXs may crosslink via radical dehydrodimerization to form a large variety of dehydrodiferulates, interconnecting GAX into a network (Fig. 2.23). In Chenopodiaceae, Gal or Ara side-chain units on some RG I molecules are acylated with feruloyl groups. The hydroxycinnamate *p*-coumarate, and possibly also ferulate, is also reduced to various hydroxycinnamyl alcohols, which form common precursors for lignin and lignan structures; in fact, much of the ferulate may derive from coniferaldehyde (Fig. 2.23).

2.2.7 Evolution of cell wall polymers can be correlated to gain of function

The structural complexity of plant cell walls can involve up to five classes of polymers: cellulose microfibrils, crosslinking glycans, pectins, structural proteins, and lignins and other phenylpropanoid substances. When did these classes of cell wall molecules appear in the tree of life (Fig. 2.24), and how is each primitive component later modified in structure during evolution to optimize its role in the functional composite? The nine most common monosaccharides found in angiosperm cell walls can all be traced to prokaryotic ancestors as well as the earliest plant species. When did specific glycosyl transferase activities appear, and in which ancestors?

Cellulose is an ancient polymer. It first appears in bacteria, not as a cell wall constituent but as an extruded ribbon of extracellular material that functions as attachment appendages for bacterial adhesion to host cells or a flotation device, called a "pellicle," on the surface of water to improve aeration. Cellulose microfibrils characteristic of plants are thought to have originated in charophytic algae and extend in distinct stages to nonvascular land plants (mosses, liverworts, and hornworts), primitive vascular plants (club mosses, ferns, and fern allies), and seed plants (gymnosperms, angiosperms) (Fig. 2.24). Cellulose is also found in most algae outside the plant lineage as well as in slime molds and tunicates.

The basic diagnostic structure of xyloglucan, the α-D-Xyl-(1→6)-D-Glu linkage (isoprimerverose), is not found in algae, but appears in mosses and all more recently evolved plants. Naked xyloglucans are poorly soluble in

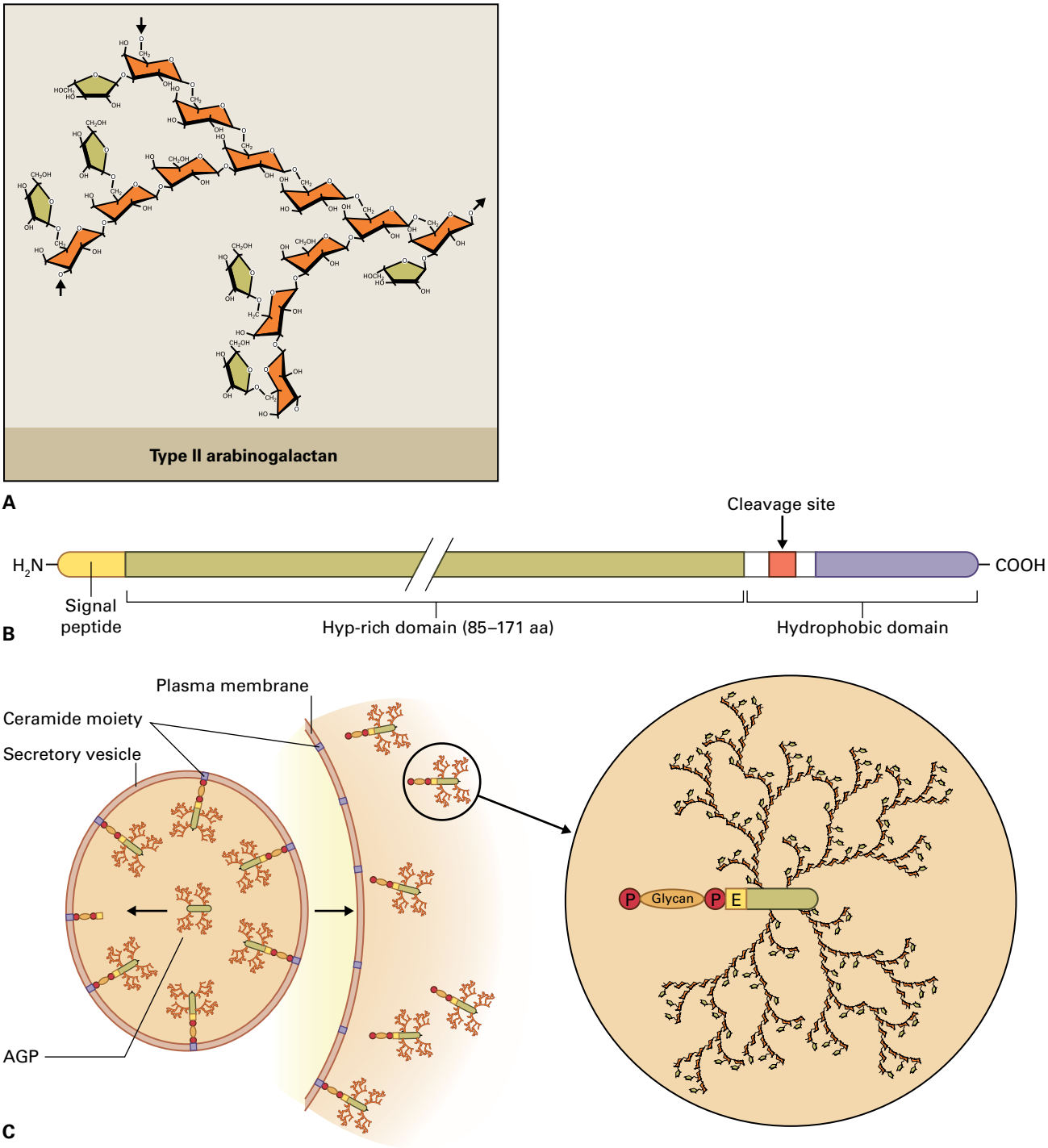


FIGURE 2.21 *(A) Arabinogalactan proteins (AGPs) are proteoglycans, many of which are glycosylated with type II AG structures. (B) The AGP genes are characterized by their enrichment in Hyp, Ala, and Ser/Thr residues in domains that are thought to contain the AG chains, but, as with the GRPs, there are no clear-cut unifying motifs. Some of the AGPs contain domains that are homologous to extensins or PRPs, and also contain Cys-rich domains. Each of these domains is glycosylated in different ways. (C) Some AGPs, after cleavage of the C terminus, covalently attach to glycosylphosphatidyl inositides (called GPI anchors) during synthesis and secretion in the ER and Golgi apparatus. Once at the exterior of the cell, the AGP portions can be cleaved from the GPI anchor and serve as signal molecules. E, ethanolamine.*

water, so appendant sugars are added to xylose residues to increase solubility. These appendant sugars are quite diverse among angiosperms (see Fig. 2.14 and Table 2.1), and this diversity extends to its earliest appearance in mosses, suggesting a function specific to the plant beyond water solubility.

Glucuronoxylans are major noncellulosic glycans of tracheary elements in all vascular plants, with arabinoxylans becoming the principal crosslinking glycan of commelinid monocots. The association with vascular tissues is consistent with its absence from the Charophyta as well as liverworts

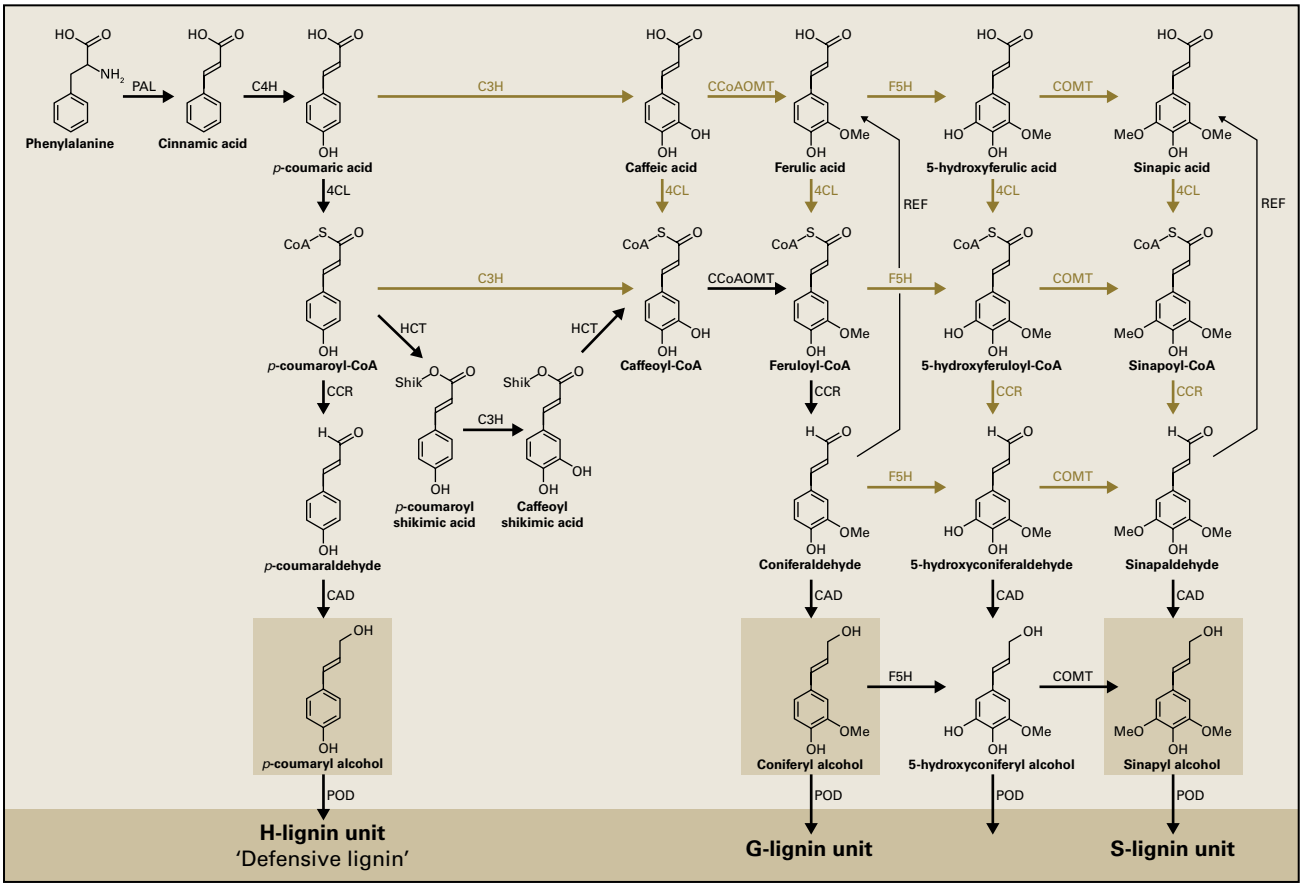


FIGURE 2.22 *Current view of the metabolic pathways from phenylalanine or tyrosine to hydroxycinnamic acids and monolignols. Modifications to the ring are shown left to right across the page, and modifications to the side-chain are shown down the page. Phenylalanine ammonia lyase (PAL) and cinnamate 4-hydroxylase (C4H) or tyrosine ammonia lyase (TAL) initiate the pathway by producing* p*-coumaric acid. Ring modifications are catalyzed by* p*-coumaroyl-shikimate/quinate 3-hydroxylase (C3H) and ferulate (coniferyl aldehyde/alcohol) 5-hydroxylase (F5H), caffeoyl-CoA 3-*O*-methyl transferase (CCoAOMT), and caffeic acid* O*-methyltransferase (COMT). Reduction of the side-chain is initiated by generation of* p*-coumaroyl-CoA from* p*-coumaric acid is catalyzed by HCT, and subsequent products of hydroxylation and methylation are catalyzed by 4-coumarate acid CoA ligase (4CL), cinnamoyl-CoA reductase (CCR), and cinnamyl alcohol dehydrogenase (CAD). Peroxidases couple the monolignols,* p*-coumaryl alcohol, coniferyl alcohol and sinapyl alcohol, into H-* (p*-hydroxylphenyl), G- (guaiacyl), and S- (syringyl) lignin units.*

and basal mosses and its appearance in the pre-vascular advanced mosses and hornworts. In contrast, mannans (glucomannans and gluco(galacto)mannans), like cellulose, are abundant in many algae including the characean algae and nonvascular land plants. Mannans replace cellulose in *Acetabularia*, a "mannan weed" in the Chrysophyta, as the major structural scaffold. Mannans are the major crosslinking glycan of certain ferns, but their abundance is greatly reduced in vascular plants. Curiously, a form of mixed-linkage (1→3),(1→4)-β-D-glucan found only in Poales and no other angiosperm is also detected in the primitive vascular plant, *Equisetum*. The widely variant distribution of cellotriose and cellotetraose unit composition between the β-glucans of *Equisetum* and Poales indicates a convergent evolution of synthases.

Though they contain no xyloglucans, charophytes, nonvascular liverworts, basal and advanced mosses, and hornworts all contain uronic acid-rich HGs as major matrix polymers. The appearance of the characteristic RG I disaccharide (1→2)-α-L-Rha-(1→4)-α-D-GalA remains to be established. However, monoclonal antibodies against the HG backbone detect the polymer in certain liverworts and mosses, and the typical neutral side-chains of (1→5)-α-L-arabinans and (1→4)-β-D-galactans are detected in a wide range of species. The complex pectic polysaccharide RG II, with side-group composition similar to angiosperms, is observed first in the Charophyta. Antibodies against the arabinogalactan portion of AGPs and 3-*O*-methyl Rha and 3-*O*-methyl Gal, monosaccharides that commonly decorate them, detect these proteoglycans widely among nonvascular plants.

The appearance of lignins coincides with the evolution of vascular plants. In general, primitive nonseed vascular plants contain only guaiacyl units, whereas the additional methoxy group in the syringyl groups appear in the angiosperms. Syringyl groups appear to be made by a different pathway in the earlier diverging nonseed vascular plant, *Selaginella*.

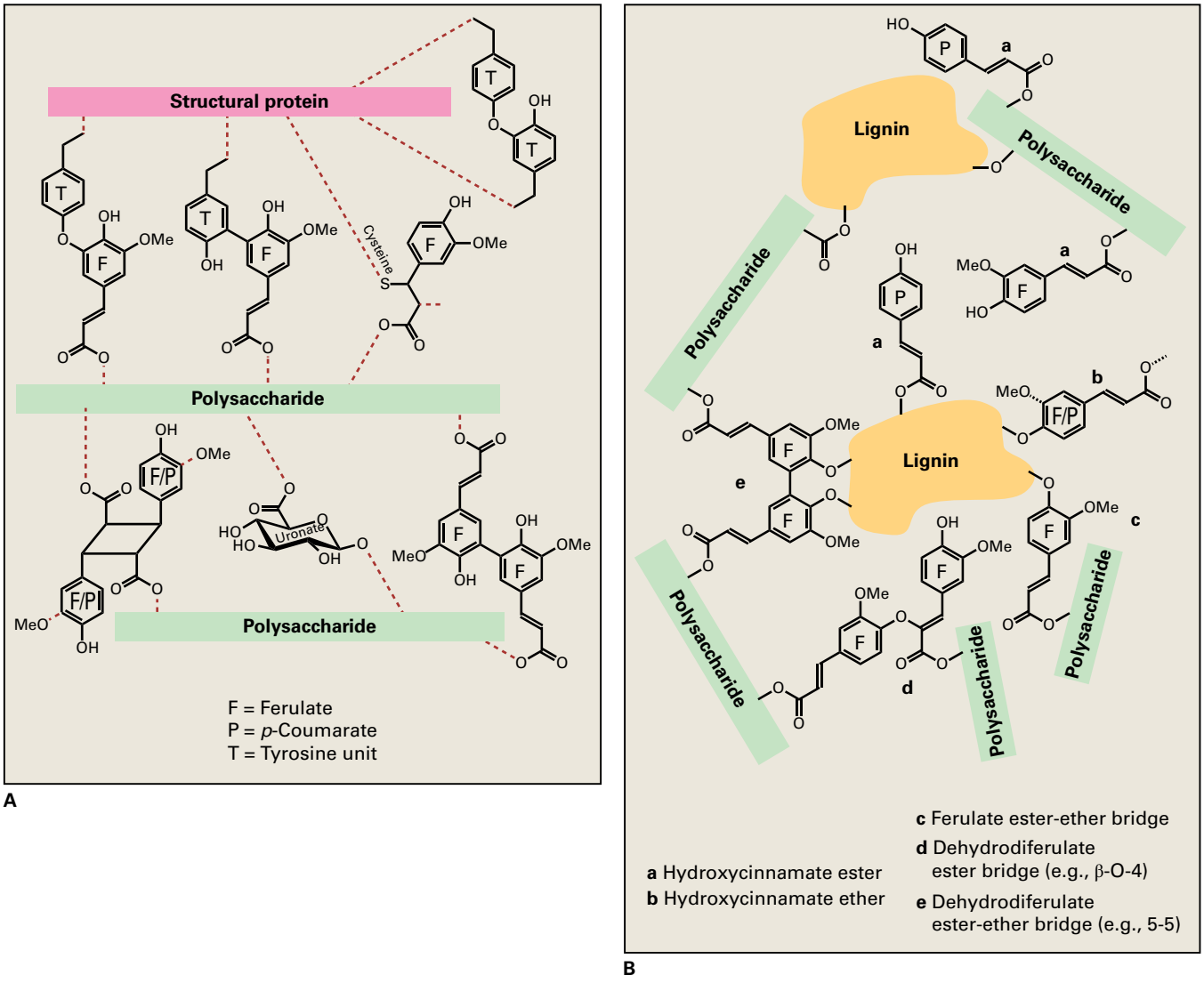


FIGURE 2.23 *Types of lignin interactions in plants. (A) Several kinds of polysaccharide–polysaccharide and polysaccharide–protein crossbridges are possible, and many of these involve aromatic substances. Isodityrosine forms an intrapeptide linkage may be needed to stabilize the extensin rods (a). Tyrosine, lysine (not shown), and sulfur-containing amino acids can form ether and aryl linkages with hydroxycinnamates acylating polysaccharides (b). Neighboring polysaccharides may contain crossbridges esterified directly to other polysaccharide chains (c). (B) The types of carbohydrate–lignin crossbridges are indicated by seven linkages. (C) Lignification differs substantially from dimerization of monolignols. Dehydrodimerization of all monolignols (i–iv) are able to produce dehydrodimers with a β-O-4 linkage (a) in comparable amounts. Sinapyl alcohol and syringyl units (ii and iv) are incapable of making β-5 units (b). Only monolignols are able to dehydrodimerize to produce β-β units (c). Crosscoupling of a hydroxycinnamyl alcohol with a G unit (iii) gives only β-O-4 and β-5 units; crosscoupling of a hydroxycinnamyl alcohol with an S-unit (iv) leads almost exclusively to β-O-4 units. Coupling of preformed G-oligomers (v) is the source of the 5-5- and 4-O-5 units. Red arrows indicate sites at which further radical coupling can occur during lignification; the arrows to the 5-positions in (d) and (e) structures shows where coupling can occur in G-units but not in S-units (where the 5-position is occupied by a methoxyl group).*

2.3 Cell wall architecture

2.3.1 The primary wall consists of structural networks

Just as buildings come in many styles, so too does the architecture of cell walls. Any wall model is generic, and in the following subsections, we establish architectural principles rather than describe specific cell wall architecture. Several technologies are now available to image cell wall architectures and even individual molecules used in their construction (Box 2.5).

The primary cell wall is made up of two, sometimes three, structurally independent but interacting networks. The fundamental framework of cellulose and crosslinking glycans lies embedded in a second network of matrix pectic polysaccharides. The third independent network consists of the structural proteins or a phenylpropanoid network. Subsequent sections of the chapter addresses two distinct cell wall types,

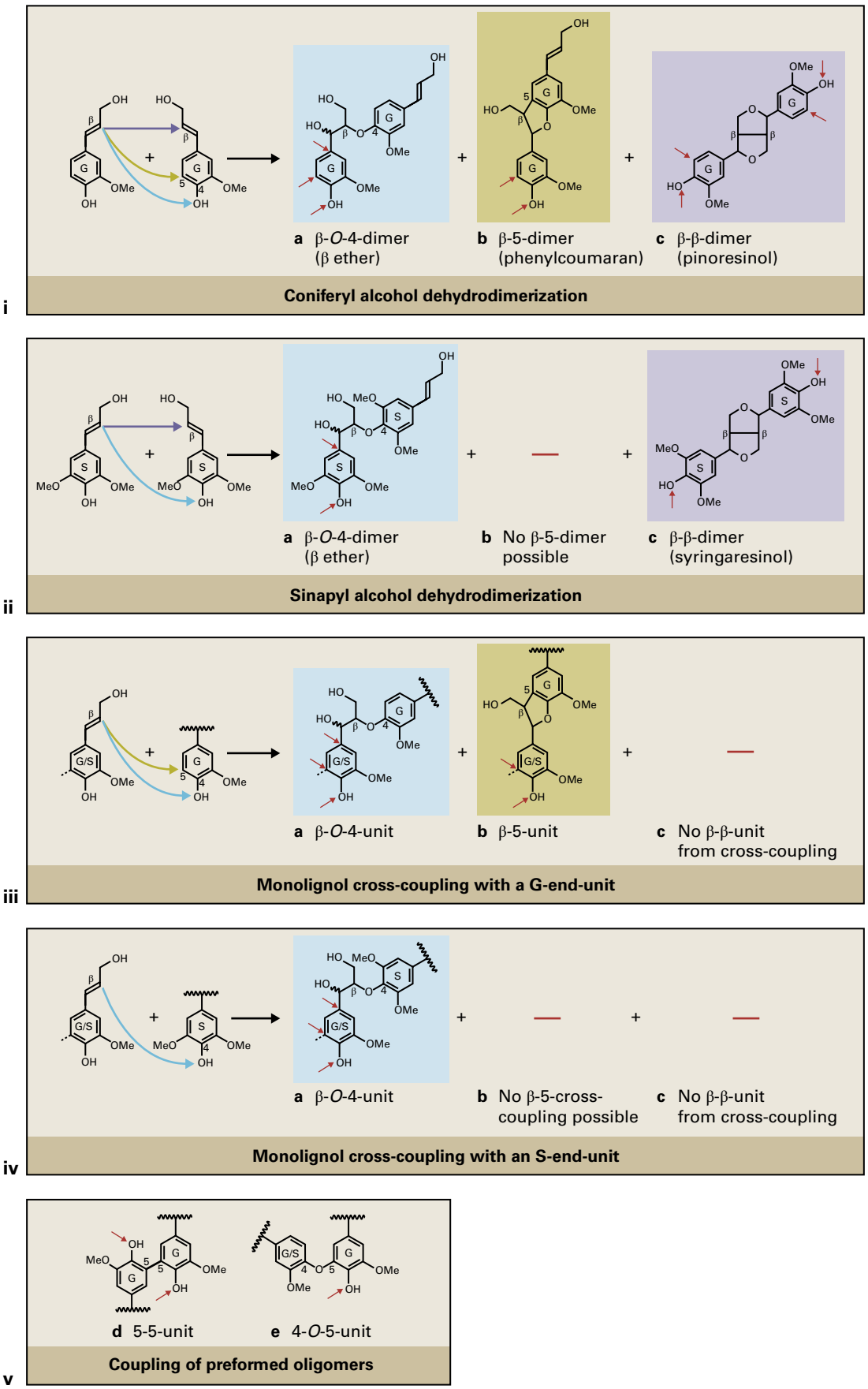


FIGURE 2.23 (*Continued*)

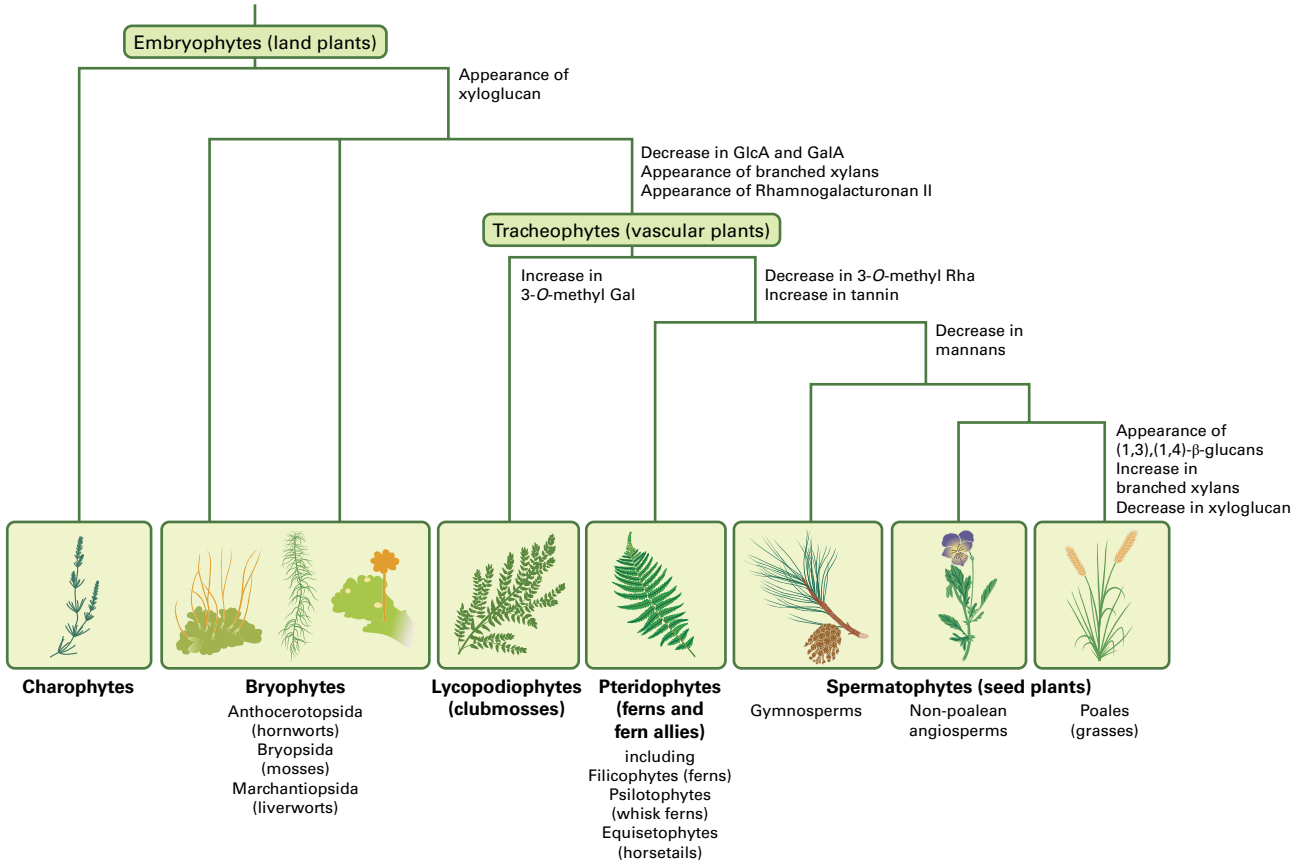


FIGURE 2.24 *Evolution of plant cell wall polysaccharides. Key transitions in polysaccharide composition are shown from the charophytes to nonvascular and vascular land plants.*

BOX 2.5

Cell walls and their component polymers can be imaged directly by novel microscopy techniques

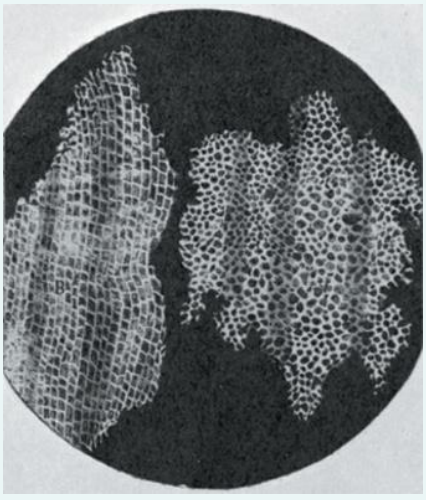
Cell walls were first imaged by Robert Hooke in the 17th century using light microscopy (A). When conventional techniques are used to stain plant tissues for electron microscopy, the cell wall appears as a fuzzy zone with little structural information (B). However, taking a series of electron micrographs of a sample tilted through a range of angles in the electron beam has been used to reconstruct the interior structure of a sample from its projections. **Dual-axis electron tomography** has been used to measure individual microfibrils of wood at about 3.2 nm with an unstained core of about 2.2 nm.

A technique called **fast-freeze, deep-etch, rotary-shadowed replica** allows one to visualize cell walls at high resolution and with good preservation of the three-dimensional spatial relationships of the polymers (C). This technique requires three steps:

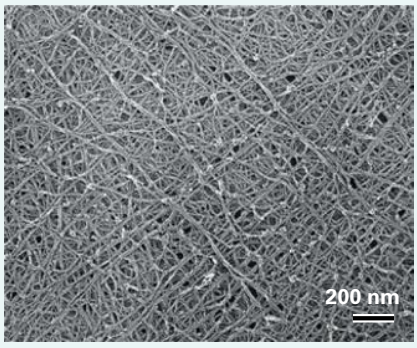
wall material is frozen rapidly with liquid nitrogen or helium
surface ice is removed under vacuum
the exposed surface is coated with a thin film of platinum and carbon to produce a replica, essentially a three-dimensional contour map of the cell wall polymers in their proper orientation
the underlying tissue is dissolved away, and the replica is viewed in the electron microscope.

Because the walls are frozen quickly, little ice damage occurs, and because no chemical fixatives or dehydrants are used, the normal spacing of components remains. Gentle extraction of pectic polysaccharides from cell walls before freezing can reveal fine thread-like crosslinking glycans spanning between the larger microfibrils (C). A glancing fracture through an onion epidermal wall prepared by this technique reveals the lamellar structure of the wall (D).

Isolated cell-wall molecules can also be imaged with the replica technique. The molecules are mixed in glycerol and sprayed on to a freshly cleaved sheet of mica. After



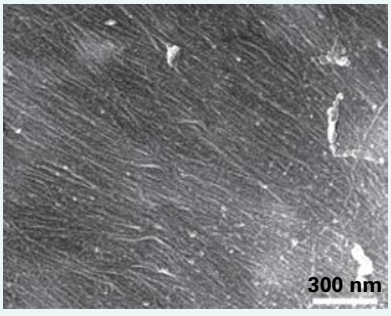
A



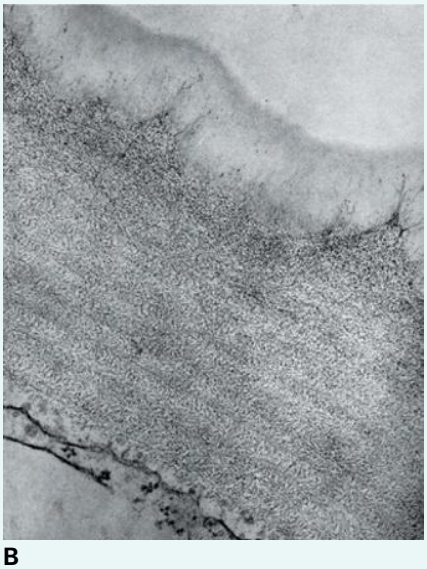
C



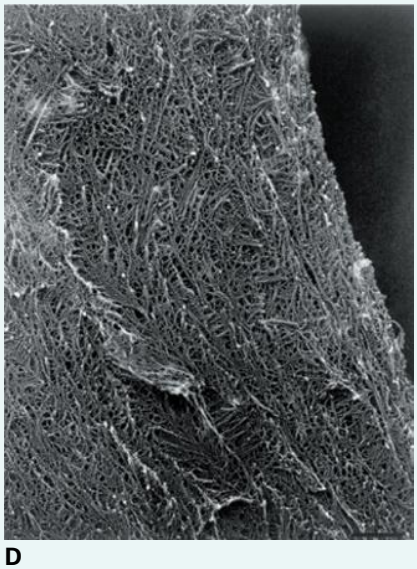
E



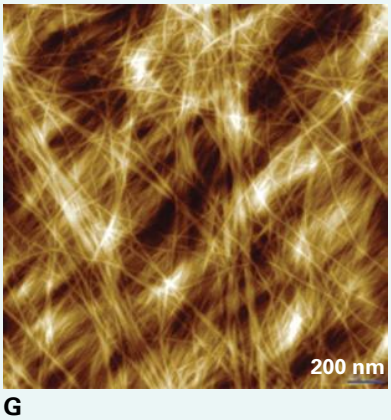
F



B



D



G

the glycerol has been dried under vacuum, a rotary-shadowed replica is made, and the mica is dissolved by strong acid. Length measurements made directly from electron micrographs allow a minimum molecular mass to be estimated, assuming each sugar residue corresponds to 0.5 nm (E).

However, making replicas is technically difficult and other imaging technologies provide an easier route to imaging at least microfibrils within walls. Field-emission scanning electron microscopy (FESEM) now provides the necessary resolution in scanning rather than transmission EM (F). High-resolution atomic force microscopy (AFM) has the versatility to make measurements in air or under fluid. Sample topography (height data) and elasticity (phase image) can be acquired simultaneously. In dried maize stalks, internal faces revealed microfibrils of minimum cross-section 5 by 10 nm^2 (G). In atomic force spectroscopy, the binding forces between a cellulose substrate and an AFM tip coated in xyloglucan or other polysaccharide can be measured. The xylogucan is covalently linked to the AFM tip and forces to remove the hydrogen-bonded xyloglucan from the cellulose are measured as tens of picoNewtons, approximating to one hydrogen bond per backbone glucose residue.

Source: (A) Hooke. (1664). Micrographia. The Council of the Royal Society of London for Improving Natural Knowledge, London. (B) McCann et al. (1990). J Cell Sci 96:323–334. (C) McCann et al. (1995). Can J Bot 73: S103–S113. (D) Ledbetter & Porter. (1970). Introduction to the Fine Structure of Plant Cells. Springer-Verlag, New York. (E) B. Wells, John Innes Center, Norwich, UK. (F) Sugimoto et al. (2000). Plant Physiol 124:1493–1506. (G) Ding & Himmel. (2006). J Agric Food Chem 54:597–606.

Types I and II, which differ in chemical composition and are associated with distinct plant taxa (see Fig. 2.14).

2.3.2 Walls of angiosperms are assembled in two distinct types of architecture

The walls of most eudicots and noncommelinid monocots contain equivalent amounts of XyGs and cellulose. These kinds of wall are denoted as Type I walls. XyGs occur in two distinct locations; they bind tightly to the exposed faces of glucan chains in cellulose microfibrils, and they span the distance between adjacent microfibrils, perhaps linking to other XyGs. With an average length of ≈200 nm, XyGs are long enough to span the distance between two microfibrils and bind to both of them. Such spanning XyGs have been observed by electron microscopy. Studies using NMR spectroscopy support this interpretation by finding different mobilities for XyG in the wall, an enzyme-accessible fraction with greater mobility and an enzyme-inaccessible fraction of lesser mobility. Studies of the rheological properties of cellulose–XyG composites made in vitro show that crosslinking of cellulose microfibrils by XyG greatly enhances the elastic properties of the composite.

In Type I walls (Fig. 2.25A), the cellulose–XyG framework is embedded in a pectin matrix that controls wall porosity, among other physiological properties. HG is thought to be secreted as highly methyl esterified polymers, and the enzyme **pectin methylesterase (PME)** located in the cell wall cleaves some of the methyl groups to initiate binding of carboxylate ions to Ca^{2+}. Helical chains of HGs can condense by crosslinking with Ca^{2+} to form "junction zones," thereby linking two antiparallel chains (Fig. 2.26A). The strongest junctions occur between two chains of at least seven unesterified GalA units each. If sufficient Ca^{2+} is present, some

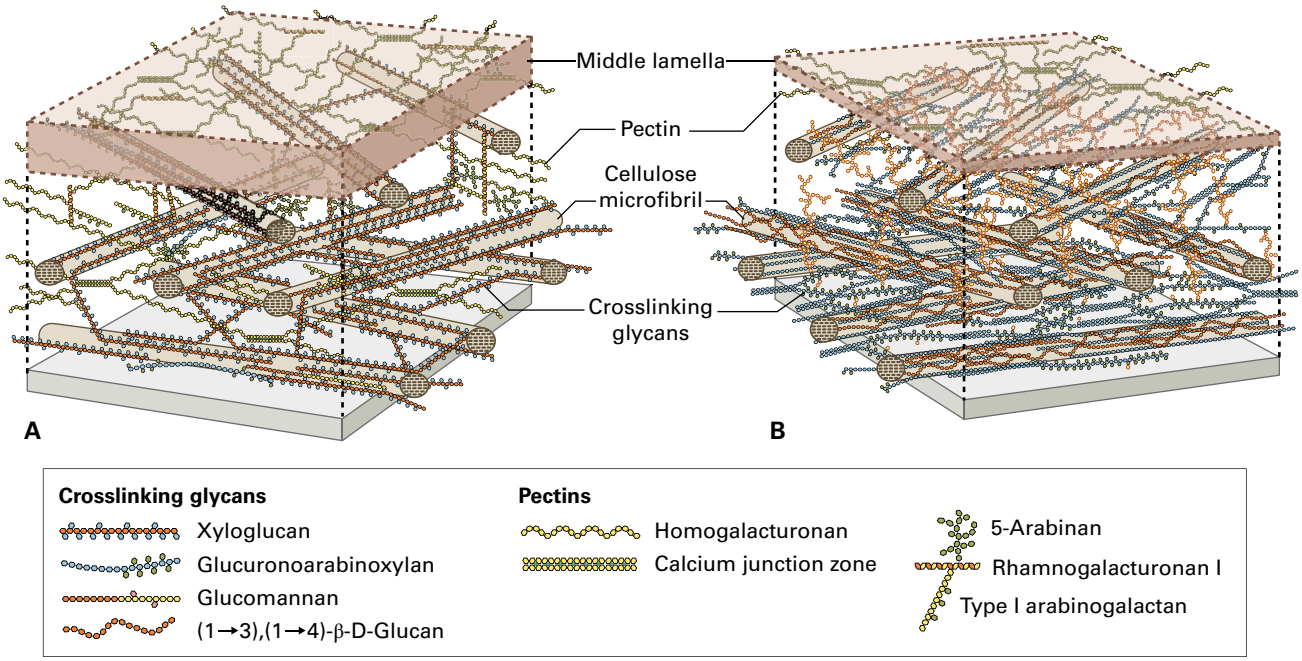


FIGURE 2.25 *(A) Three-dimensional molecular model of the Type I wall showing the molecular interactions between cellulose, XyG, pectins, and wall proteins. The framework of cellulose microfibrils and XyG polymers is embedded in a matrix of pectic polysaccharides, HG and RG I, the latter being substituted with arabinan, galactan, and arabinogalactan. Because XyGs have only a single face that can hydrogen bond to another glucan chain and can self-associate, we depict several XyGs as woven to interlace the microfibrils. Many other associations are possible, including bridging of two microfibrils by a single XyG. With hemicellulose-coated microfibril diameters of about 5 nm and a spacing of about 20–30 nm, a primary wall 80 nm thick can have only about five to 10 strata (only three lamellae of microfibrils are shown for clarity). During growth, cleavage or dissociation of XyGs by enzymes loosens the cellulose-XyG network allowing microfibrils to separate. After growth, extensin molecules may interlock the separated microfibrils to reinforce the architecture. Additional proteins may also be inserted to crosslink extensin, forming a heteropeptide network. (B) A three-dimensional molecular model of the Type II wall shows the molecular interactions between cellulose, GAX, pectins, and aromatic substances. The microfibrils are interlocked by GAXs instead of XyGs. Unlike XyGs, the xylans are substituted with Ara units, which block hydrogen bonding. The xylans are probably synthesized in a highly substituted form, and de-arabinosylated in the extracellular space to yield stretches of the xylan that can bind on either face to cellulose or to each other. Porosity of the GAX domain could be determined by the extent of removal of the appendant units. Some highly substituted GAX remains intercalated in the small amount of pectins that are also found in the primary wall. We depicted here the special Type II wall of the grasses (Poales), which synthesize β-glucans during cell enlargement and then hydrolyze most of the polymer after maximal growth rates have been achieved. These cork-screw-shaped molecules contain linear runs of cellodextrins about every 50 glucosyl units or so, and these runs are targets for endo-β-D-glucanases that cleave them. A combination of selective chemical extractions, immunolocalization, and scanning electron microscopy has shown that β-glucans are tightly bound to cellulose microfibrils and rarely extend between them. Unlike the Type I wall, a substantial portion of the noncellulosic polymers are "wired on" to the microfibrils by alkali-resistant phenolic linkages.*

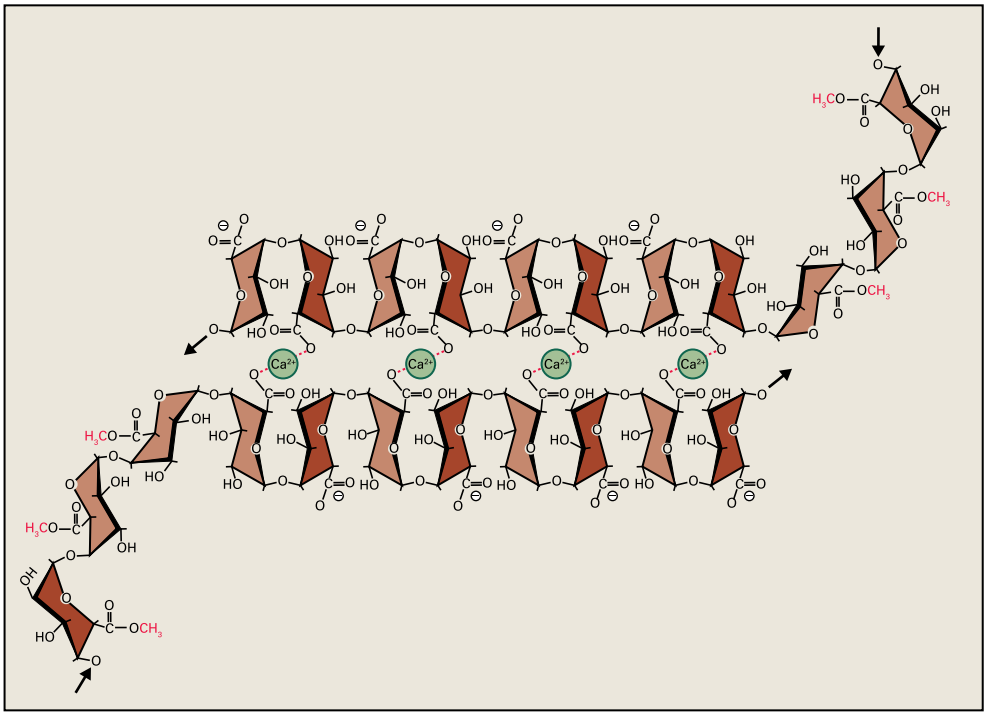


FIGURE 2.26 *Possible calcium–pectate interactions in the cell wall. (A) HG may complex with Ca^{2+} to form "junction zones." Loss of pectin esters generates contiguous runs of HG free acids that can then form "egg box" junctions with Ca^{2+} bridging two antiparallel chains. (B) Antiparallel or parallel chains of partly methylated HG can also be linked in less firmly bound calcium complexes.*

methyl esters can be tolerated in the junction, and the HGs can bind in both parallel and antiparallel orientation (Fig. 2.26B). The spacing of the junctions is postulated to create a cell-specific pore size. Rha units of RG I and their side-chains interrupt the Ca^{2+} junctions and contribute to pore definition (Fig. 2.27).

Other properties of the pectin network also regulate porosity. The extent of methyl esterification may remain high in walls of some cells, and a type of gel may form that contains highly esterified parallel chains of HGs. Some HGs and RGs are crosslinked by ester linkages to other pectins or other polymers held more tightly in the wall matrix and can only be released from the wall by de-esterifying agents. Other pectic polymers may separate sites of borate di-diester crosslinking by RG II dimers along the pectic backbone (see Fig. 2.18). In boron-deficient cell cultures walls swell and porosity

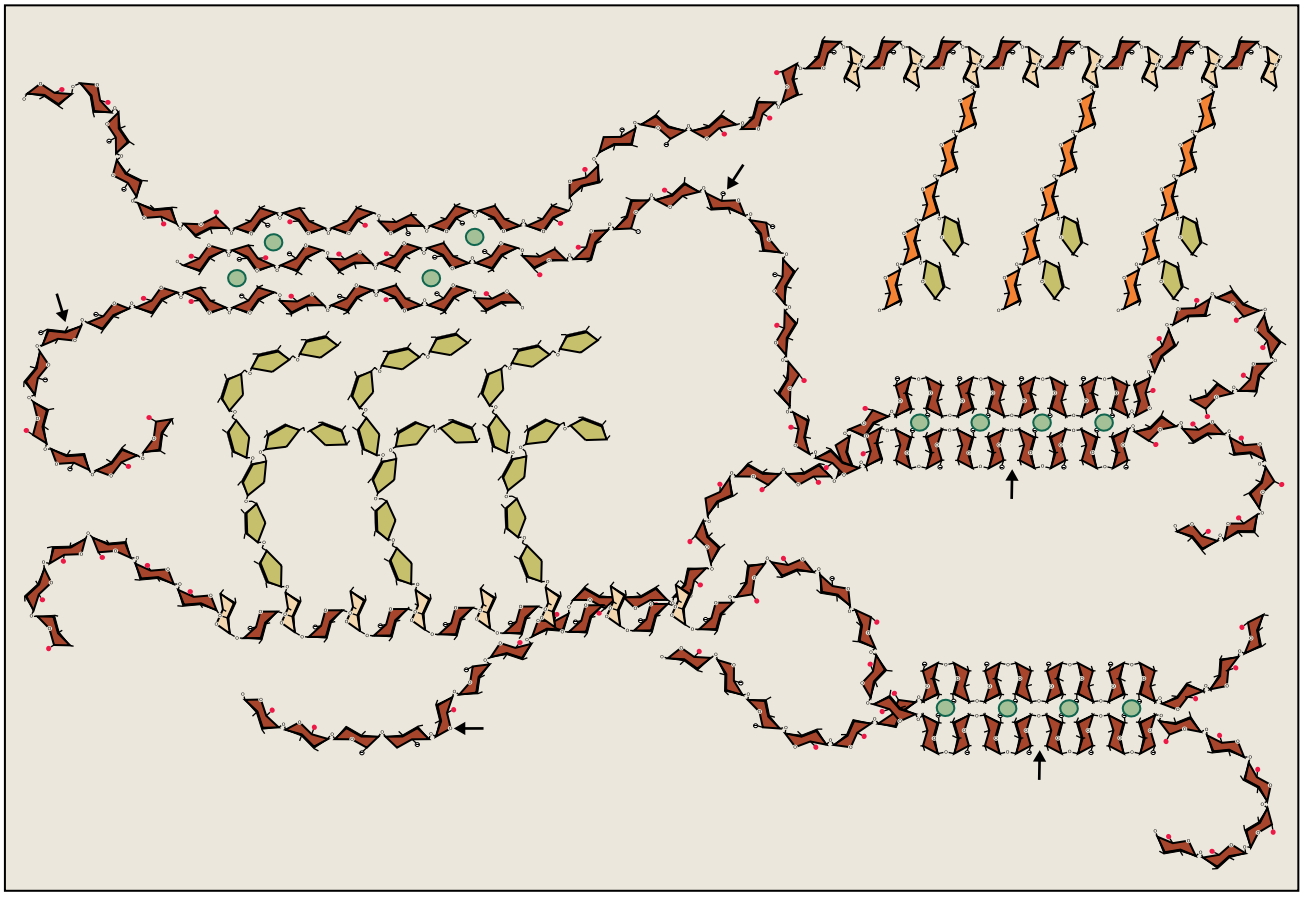


FIGURE 2.27 *Pectin matrix establishes the "pore size," that is, the relative size of the channels formed by the wall matrix that permit molecules to freely diffuse through the wall matrix. This pore size can be established by a combination of the frequency and length of the junction zones, the degree of methylesterification, and the length of the arabinans, galactans, and arabinogalactans attached to RG I that extend into the pores. Additional factors that influence pore size are the frequency of RG II and its dimerization by boron (not shown). The charge density depends on the extent of de-esterification of the HG to yield carboxyl acids unbound to Ca^{2+}. Arrows denote domains of negative charge density in HGs.*

increases. Neutral polymers (arabinans or galactans) are pinned at one end to the pectic backbone, but extend into and are highly mobile in wall pores (Fig. 2.27). These neutral polymers also regulate the amount of water that is tightly bound into the wall structure. At some stages of cell development, hydrolases are released that trim these neutral polymers, potentially increasing pore size. In meristems and elongating cells, where Ca^{2+} concentrations are kept quite low, significant de-esterification of HG can occur without Ca^{2+} binding, altering charge density and local pH.

Some Type I walls contain large amounts of protein, including basic proteins that can interact with the pectin network. In these instances, various structural proteins can form intermolecular bridges with other proteins without necessarily binding to polysaccharide components.

Type II walls of commelinid monocots contain cellulose microfibrils similar to those of the Type I wall, but instead of XyG, the principal polymers that interlock microfibrils are GAXs. Unbranched GAXs can hydrogen bond to cellulose or to each other. Attachment of α-L-Ara and α-D-GlcA side groups to the xylan backbone of GAXs prevents formation of hydrogen bonds, thereby blocking the crosslinking between two branched GAX chains or from GAX to cellulose. In contrast, α-D-Xyl units attached at *O*-6 of XyG, away from the binding plane, stabilize the linear structure and permit binding to one side of the glucan backbone. Despite the predominance of GAX, Type II walls contain small amounts of XyG that also bind tightly to cellulose.

In general, Type II walls are pectin-poor, but an additional contribution to charge density of the wall is provided by α-D-GlcA units on GAX. These walls have very little structural protein compared with eudicots and other monocots, but can accumulate extensive interconnecting networks of phenylpropanoids, particularly as cells stop expanding (see Fig. 2.25B).

2.3.3 Polymers remain soluble until they can be crosslinked at the cell surface

Many polymers are modified by esterification, acetylation, or glycosylation for solubility during transport. Later, extracellular enzymes de-esterify, deacetylate, or deglycosylate to

generate sites along the polymers available for crosslinking into the cell wall. These sites are determined by long-range binding order of polysaccharides, permitting their assembly into precise cell wall architectures. A range of crosslinking possibilities exists, including hydrogen bonding, ionic bonding with Ca^{2+} ions, covalent ester linkages, ether linkages, and van der Waals' interactions. Because AGPs constitute a majority of the material of secretory vesicles but never accumulate in the wall, they might function as a chaperone-like matrix that prevents premature associations and keeps enzymatic functions in a quiescent state until secretory materials are assembled in the wall.

Assembly processes occur in an aqueous environment, and one of the major components of cell walls is water. This is of structural importance from the viewpoint of maintaining polymers in their proper conformations. Water is the medium that permits passage of ions and signaling molecules through the apoplast; it also provides an environment for enzyme function. The apoplastic space is thought to be at a pH of ≈5.5, although this value averages much heterogeneity in wall structure, and pH can vary widely from the plasma membrane to the middle lamella, and as the wall becomes modified during growth. The pore diameter that limits diffusion of molecules through the primary wall is ≈4 nm, but some molecules larger than this limiting diameter can pass through the wall to the plasma membrane, perhaps by way of a small number of larger pores or because they are rod-like rather than globular.

2.4 Cell wall biosynthesis and assembly

2.4.1 New walls are initiated in the cell plate after mitotic division

While a vast majority of the cell wall mass is formed by integration of new polymers into an expanding pre-existing matrix, new cell walls originate de novo to form the developing cell plate. As plant chromosomes complete division during telophase of the mitotic cell cycle, the **phragmosome,** a flattened membranous vesicle containing cell wall components, forms across the cell within a cytoskeletal array called the **phragmoplast** (see Chapter 5). The noncellulosic cell wall polysaccharides synthesized in the Golgi and packaged in vesicles fuse with the growing cell plate. The plate grows outward until the edges of membranous vesicle fuse with the plasma membrane, creating two cells. Finally, the new cell wall fuses with the existing primary wall (see Fig. 2.3).

The plant Golgi apparatus is a factory for the synthesis, processing, and targeting of glycoproteins (Fig. 2.28). It has also been shown by autoradiography to be the site of synthesis of noncellulosic polysaccharides. Thus, with the exception of cellulose, the polysaccharides, structural proteins, and a broad spectrum of enzymes are coordinately secreted in Golgi-derived vesicles and targeted to the cell wall.

2.4.2 Cellulose microfibrils are formed at the plasma membrane surface

The only polymers made at the outer plasma membrane surface of plants are cellulose and callose. Cellulose synthesis is catalyzed by multimeric enzyme complexes located at the termini of growing cellulose microfibrils (Fig. 2.29). These **terminal complexes** are visible in freeze-fracture replicas of plasma membrane. In some algae, terminal complexes are organized in linear arrays, whereas in others—and in all angiosperms—they form six-membered **particle rosettes** (Fig. 2.29). Thus, each of the six components of the particle rosette is expected to synthesize two to six of the glucan chains, and an estimated total of 16, 24, or 36 chains are then assembled into a functional microfibril. In freeze-fracture, the particle rosettes are about 25 nm in diameter, but this size represents only portions of the membrane-spanning and short exterior domains (Fig. 2.29H, I). Hidden in surface views of rosette structures in the plasma membrane, the much larger catalytic domains of cellulose synthases are estimated to be 50 nm wide (Fig. 2.29J).

Terminal complexes appear in the plasma membrane coincident with the activity of cellulose synthesis. Kinetic studies monitoring the pathway of glucose to cellulose have established that UDP-Glc is the primary substrate for cellulose synthase. Isoforms of sucrose synthase, an enzyme that produces UDP-Glc directly from sucrose, are also associated with the plasma membrane and may contribute a localized source of UDP-Glc substrate.

Cellulose synthase produces one of the most abundant biopolymers on earth, yet the plant enzyme has proven curiously difficult to purify in active form. Cellulose synthase activity from plants generally disappears rapidly upon cell breakage, and even under conditions of gentle plasma membrane isolation. Use of certain stabilizing detergents has preserved associated cellulose synthase complexes to produce disorganized microfibrils with UDP-Glc of sufficient crystallinity to diffract X-rays, the first unequivocal demonstration of cellulose synthesis in vitro in microsomal membrane preparations from a cell culture. There is still much work to do to define all the accessory proteins of a cellulose synthase complex and to understand the regulation of its activity and turnover and associations with cytoskeletal and cell wall components that stabilize it in the membrane.

The unbranched (1→3)-β-D-glucan **callose** is a natural component of the initial cell plate, the pollen tube wall, and in transitional stages of wall development of certain cell types. Unlike the wound polymer, pollen tube callose is synthesized by enzymes that do not require Ca^{2+} as cofactors; moreover, these synthases are enzymes distinct from cellulose synthases, encoded by a distinct family of glycosyl transferases.

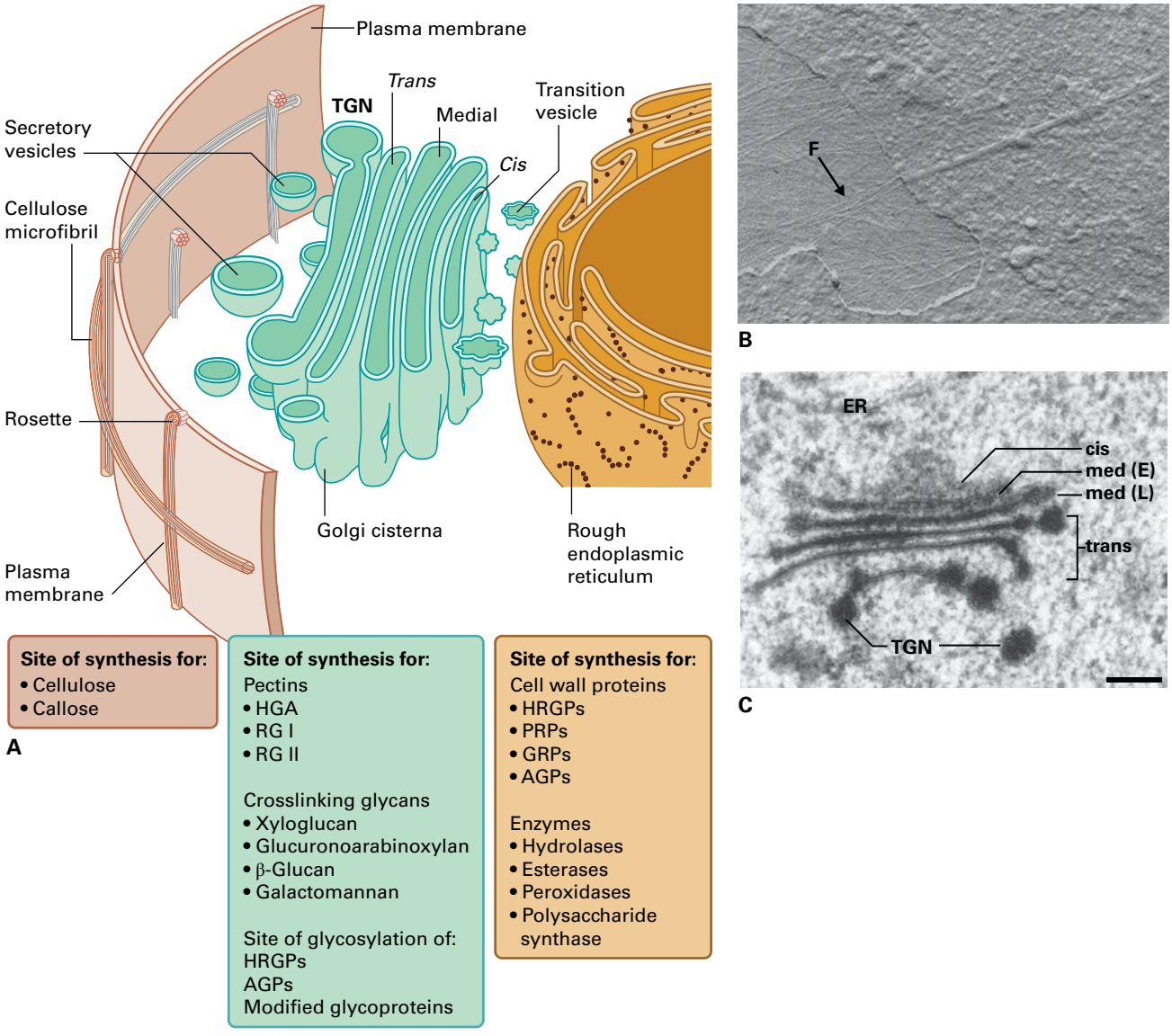


FIGURE 2.28 *(A) Cell wall biosynthesis requires coordination of the synthesis of cellulose microfibrils at the plasma membrane surface, the synthesis and glycosylation of proteins and wall-modifying enzymes at the rough ER, and the synthesis of all noncellulosic polysaccharides at the Golgi apparatus. Material destined for the cell wall is packaged into secretory vesicles, transported to the cell surface, and integrated with newly synthesized microfibrils. Assembly of the new wall stratum is estimated to begin when no more than 10 glucose residues of a cellulose chain are made. (B) A replica plate of the E-face (exterior leaf of a fractured membrane bilayer). Numerous vesicles aggregate at the surface. A portion of the membrane has torn away to reveal the underlying microfibrils (F). (C) Cross-section of a single dictyosome body of the Golgi apparatus showing the characteristic development of several membrane sheets, from the* cis*-face nearest the ER to the* trans*-face; these develop into the distinctive* trans*-Golgi-network (TGN), which is the principal vesicle-secreting body. E and L, early and late* medial*-Golgi stacks, respectively.*
Source: (B) Gunning & Steer. (1996). Plant Cell Biology, Jones and Bartlett, London. (C) Zhang & Staehelin. (1992). Plant Physiol 99:1070.

2.4.3 Golgi-associated enzymes interconvert the nucleotide sugar substrates for polysaccharide synthesis

The reactions that synthesize noncellulosic cell wall polysaccharides in the Golgi apparatus use several nucleotide sugars as substrates. Beginning with formation of UDP-Glc and GDP-Glc, pathways for **nucleotide sugar interconversion** produce various nucleotide sugars de novo in enzyme-catalyzed reactions (Figs. 2.30 and 2.31). Many of these interconversion enzymes (e.g., epimerases and dehydratases) appear to be membrane-bound and localized to the ER-Golgi apparatus. Guanosine-based nucleotide sugars, such as GDP-Glc and GDP-Man, are used in synthesis of glucomannan, and GDP-Fuc is a substrate in fucosylation of complex glycoproteins, pectins, and some crosslinking glycans (Fig. 2.32).

L-Arabinose is in the furanose ring conformation in most plant polymers containing this sugar, including GAX, 5-linked arabinans, AGP, and extensin, whereas UDP-Ara is exclusively in the pyranose form. Isomerization is catalyzed by UDP-Ara mutase, which interconverts the nucleotide-sugars,

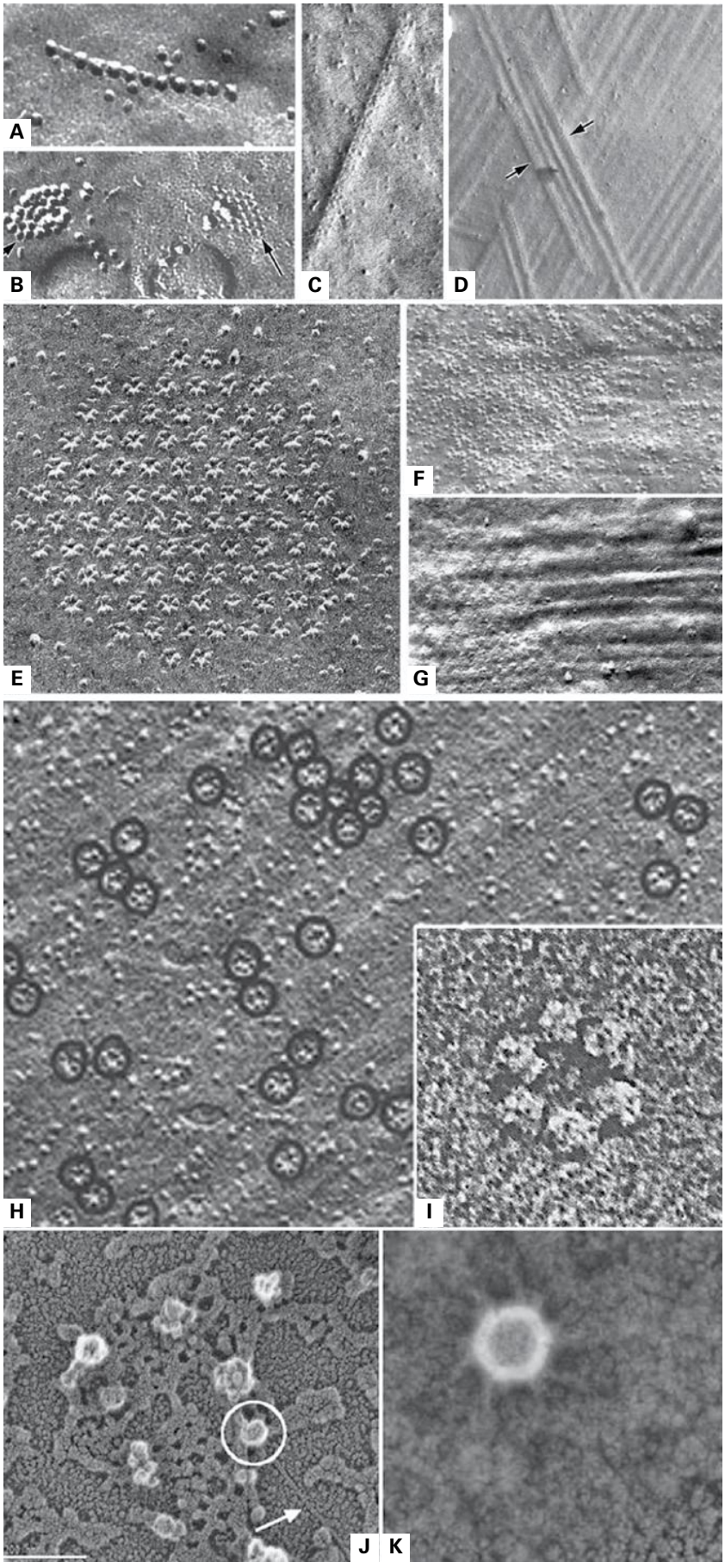


FIGURE 2.29 *Terminal complexes associated with cellulose microfibril biosynthesis as imaged by freeze-fracture and rotary shadowing of membranes. The cellular slime mold,* Dictyostelium discoideum*, forms two kinds of terminal complexes. A linear array is associated with the extracellular ribbon of cellulose formed by streaming cells (A), whereas the cell wall of the stalk cells is made by aggregate arrays that appear to be rudimentary rosettes (B). Some algae, such as* Oocystis*, have linear arrays of particles (C). These terminal complexes often pair up at the plasma*

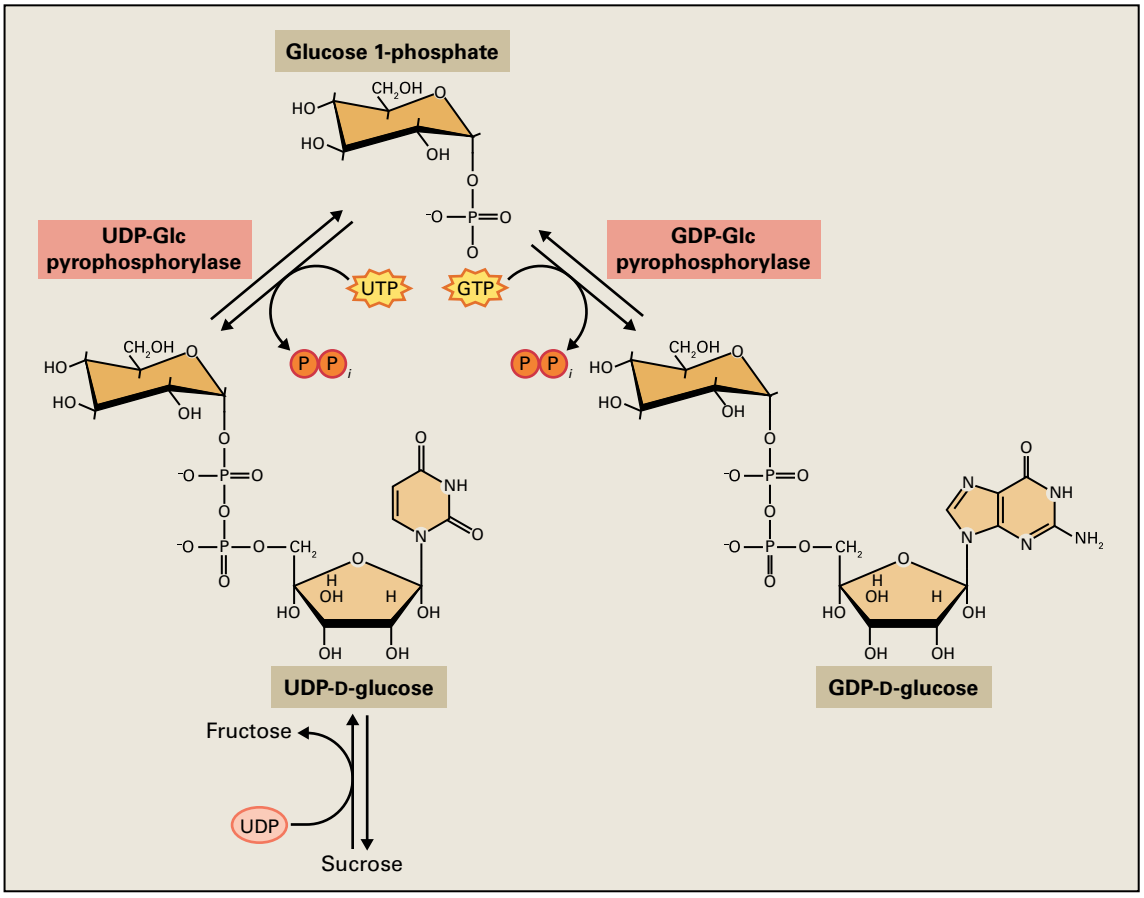


FIGURE 2.30 *Central molecule in cell wall biosynthesis, the nucleotide-sugar UDP-Glc. UDP-Glc and GDP-Glc are made from glucose-1-phosphate by action of a pyrophosphorylase, or from sucrose by action of a sucrose synthase.*

UDP-Ara*p* and UDP-Ara*f* (Fig. 2.31). UDP-Ara mutase is the enzymatic activity of "reversibly glycosylated protein," once thought to be an intermediate in xyloglucan synthesis.

Formation of nucleotide sugars occurs via two distinct pathways. De novo synthesis pathways initially produce the full array of nucleotide sugars, which are then used as substrates for synthesis of polysaccharides, glycoproteins, and several other glycosylation reactions. However, several monosaccharides other than Glc may be incorporated into nucleotide sugars via salvage pathways involving C-1 kinases and nucleotide diphosphate-sugar pyrophosphorylases (Fig. 2.31 and 2.32). Salvage pathways are essential to reuse these monosaccharides after they have been hydrolyzed from polymers during assembly and turnover in the cell wall. Some sugars, such as Rha and Xyl, do not have C-1 kinases, and their carbons must be reused via other pathways. Xyl is returned via the pentose phosphate pathway after isomerization to xylulose.

2.4.4 Crosslinking glycans and pectins are made at the Golgi apparatus

Many reports of the synthesis of noncellulosic wall polysaccharides in vitro include use of membrane preparations enriched in Golgi membranes. In mixed membrane preparations containing plasma membrane and Golgi and UDP-Glc as a substrate, the predominant products are callose, made by

FIGURE 2.29 (*Continued*) *membrane and initiate synthesis of microfibrils in opposite directions (see arrows) (D). The six-membered particle rosettes were first seen in the desmid* Micrasterias. *In this alga, the individual rosettes aggregate in the membrane to form even larger hexagonal arrays that are associated with formation of flat ribbons of cellulose (E). The rosettes are seen on the "P-face," the inner leaf of the plasma membrane bilayer (F), whereas the impression of the microfibrils and larger particles that apparently fit into the center of each rosette are located in the outer leaf, or "E-face" (G). The rosettes (circled) are found in great abundance only in the membrane underlying the developing thickenings of xylem root vessel elements in cress (H). The inset shows the sixfold symmetry of a single particle rosette from a* Zinnia elegans *tracheary element developing in vitro (I). A substructure can be observed in each of the particles. In these freeze-etch images, only portions of the membrane-spanning domains and extracellular loops of the CesA proteins can be observed. Cytoplasmic structures (circled) underlying the rosettes in plasma membrane footprints are always at the terminus of a microfibril (arrow) (J). A Markham rotational analysis of one of these shows the reinforcement of hexagonal shape with 60° rotational steps. All other angles of rotation cancel to a circular shape. Bar = 200 nm (K).*
Source: (A, B) Grimson et al. (1996). J Cell Sci 109:3079. (C, D), from D. Montezinos and R.M. Brown, Jr. (1976). J. Supramol. Struct. 5:277; (E–G), from Giddings et al. (1980). J. Cell Biol. 84:327; (H), from W. Herth (1985). Planta 164:12; (I), from C. Haigler, in D.P. Delmer (1999). Annu. Rev. Plant. Physiol. Plant Mol. Biol. 50:245; (J–K), from A.J. Bowling and R.M. Brown, Jr. (2008). Protoplasma 233:115.

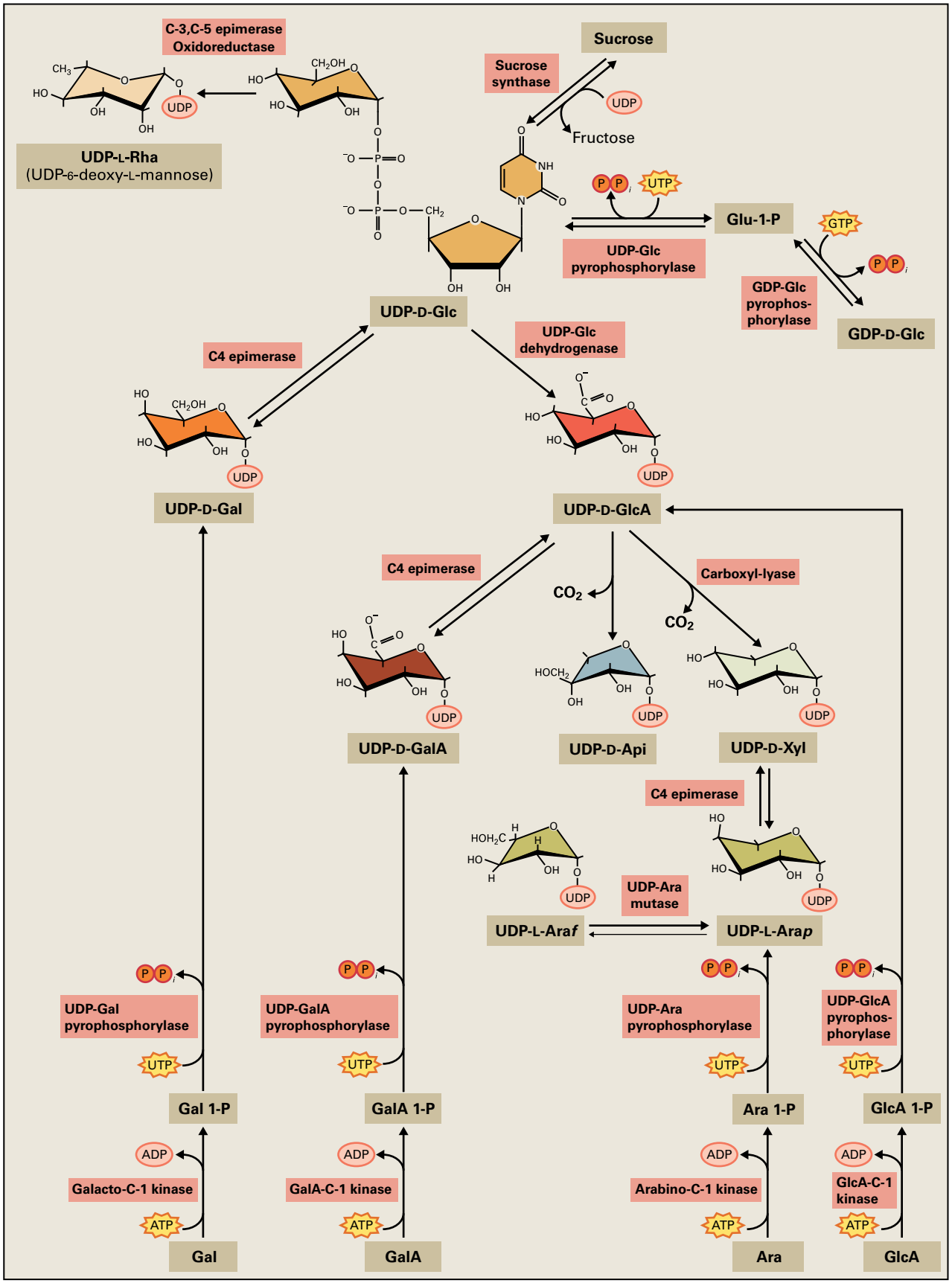


FIGURE 2.31 *Major uridine nucleotide-sugar interconversion pathways in plants. UDP-Gal*p *is made from UDP-Glc*p *in an equilibrium reaction catalyzed by a C-4 epimerase. A dehydrogenase oxidizes the O-6 primary alcohol of UDP-Glc*p *to UDP-GlcA*p*, which is interconverted to UDP-GalA*p *by a different C-4 epimerase. A carboxyl lyase cleaves the carboxyl group from UDP-GlcA*p *to produce UDP-Xyl*p*, which is subsequently interconverted by yet another C-4 epimerase to produce UDP-Ara*p*. All of the UDP-sugars made de novo are in the pyranose form; interconversion of the UDP-Ara*p *and UDP-Ara*f *is catalyzed by a mutase originally described as the 'reversibly glycosylated protein'. The deoxysugar, L-Rha, is made by action of an oxidoreductase and a C-3,5 epimerase using UDP-Glc as substrate. Several sugars, including Ara, Gal, GalA, and Fuc, are "salvaged" back into the nucleotide-sugar pool by C-1 kinases that generate sugar-1-phosphates as direct substrates for pyrophosphorylases.*

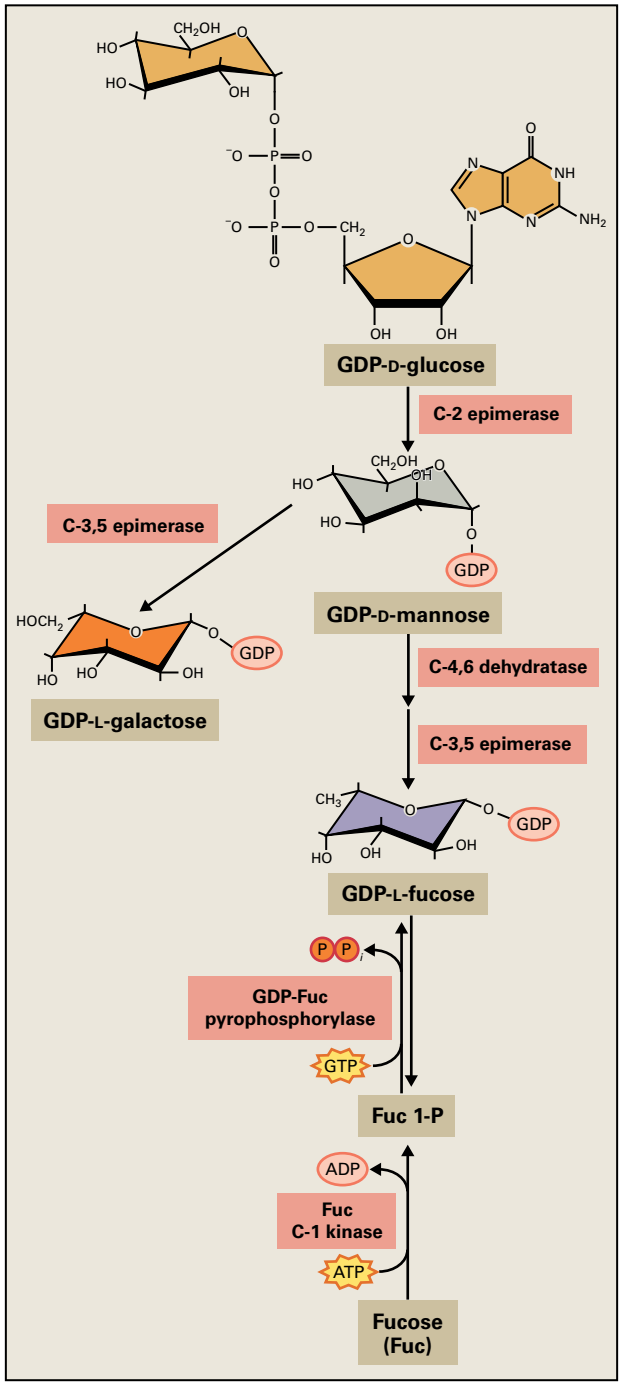


FIGURE 2.32 *The major guanosine nucleotide-sugar is GDP-Man, interconverted by C-2 epimerase action with GDP-Glc. Two key nucleotide-sugars are made from GDP-Man, GDP-Fuc by consecutive action of a C-4,6 dehydratase and C-3,5-epimerase, and GDP-L-Gal from action of a C-3,5 epimerase alone. A salvage pathway incorporates L-Fuc via a C-1 kinase into GDP-Fuc.*

wound-inducible contaminating plasma membrane callose synthases or damaged cellulose synthases. This reaction is activated by Ca^{2+}, the concentrations of which increase markedly in cells that have been damaged. Thus, the other noncellulosic polysaccharides of interest must be detected and quantified in the presence of a huge background of callose.

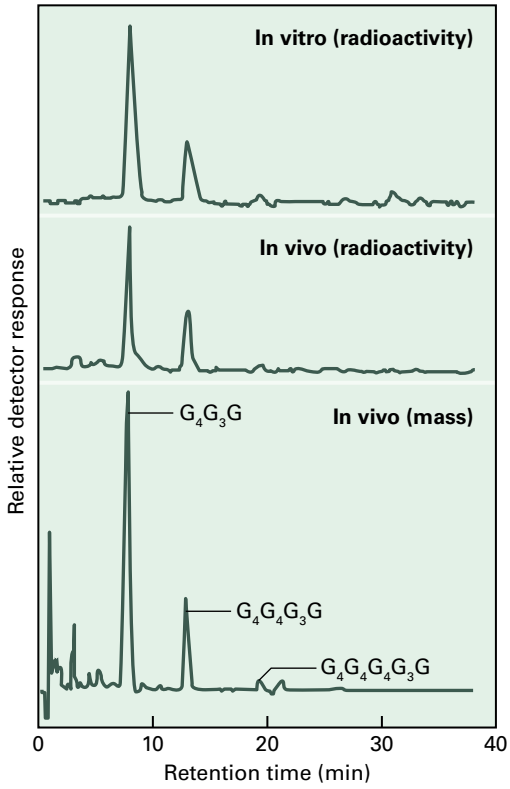


FIGURE 2.33 *The* B. subtilis *endoglucanase has the unusual ability to hydrolyze a (1→4)-β-D-glucosyl linkage* only *if the penultimate linkage is a (1→3)-β-D-glucosyl linkage. Because 90% of cereal β-glucans are composed of cellotriosyl and cellotetraosyl units in a ratio of about 2.5:1, the enzyme generates cellobiosyl-(1→3)-glucose (G_4G_3G) and cellotriosyl-(1→3)-glucose ($G_4G_4G_3G$) oligosaccharides in such a ratio. When the radioactive products of such a digest are separated by HPAEC, the ratio of these oligomeric units is the same from β-glucan synthesized in vivo by living plants fed ^{14}C-glucose or synthesized in vitro from isolated Golgi membranes and UDP-^{14}C-Glc. Characterization of polysaccharide synthase reaction products in such a way confirms that synthesis in vitro mimics that in vivo. $G_4G_4G_4G_3G$, cellotetraosyl-(1→3)-glucose.*

By treating polysaccharides with sequence-dependent glycanases, researchers can detect characteristic unit structures despite the presence of wound-induced callose. This technique, which verifies that isolated membranes are capable of synthesizing unit structures identical to those made in vivo, has been particularly useful for studying in vitro synthesis of XyG (Boxes 2.3 and 2.4).

The precise topographic location of polysaccharide synthase enzymes on or within Golgi membranes has been established only for unbranched mixed-linkage β-glucan. The catalytic domain of this synthase is located on the cytosolic side of the Golgi membrane, and the product is extruded into the lumen. UDP-Glc is substrate for the mixed-linkage β-glucan synthase of grass species, and either Mg^{2+} or Mn^{2+} is required as a cofactor. The preservation of β-glucan synthase activity is demonstrated by digestion of the β-glucan product with *Bacillus subtilis* endoglucanase into characteristic tri- and tetrasaccharides in the correct ratio (Fig. 2.33).

For branched polysaccharides, the nucleotide-sugar substrate used for backbone synthesis may be donated from either the cytosolic or luminal side of the Golgi, but branch units are probably added only from the luminal side. Hence, synthesis of complex polysaccharides must be coordinated with transport of some of the nucleotide sugars into the Golgi apparatus. The isolated Golgi apparatus of plants with Type I walls can synthesize very short (1→4)-β-D-glucan chains from either UDP-Glc or GDP-Glc, but the synthesis of XyG is greatly enhanced by addition of near millimolar levels of both UDP-Glc and UDP-Xyl, and also with Mn^{2+} or Mg^{2+} as co-factor. Cleavage of the XyG reaction products yields substantial amounts of the diagnostic XXXG heptasaccharide unit, verifying that the cellular machinery needed to make a complete unit structure can be preserved in a cell-free system. Because only very short chains of (1→4)-β-D-glucan backbone can be made from UDP-Glc in the absence of UDP-Xyl, the glucosyl- and xylosyltransferases appear to be tightly coupled, catalyzing formation of repeating heptasaccharide units cooperatively. Attachment of additional sugars to Xyl units may occur coordinately as well, but additional elaboration involving galactosyl and fucosyl transferases continues during later stages of transit through the Golgi apparatus (see Fig. 2.28). These types of coordinated glycosyl transfers are observed in synthesis of glucomannans with GDP-Glc and GDP-Man, galactomannans with GDP-Man and UDP-Gal, and arabinoxylans with UDP-Xyl and UDP-Ara. In addition, synthesis in vitro of HG appears to be coordinated with its methyl esterification.

2.4.5 Synthases of cellulose and other β-linked polysaccharides are encoded by the *Cellulose* and *Cellulose synthase-like* gene superfamily

Genes encoding vascular plant cellulose synthases have been identified, but the molecular groundwork for identifying *cellulose synthase* (*CesA*) genes was laid first in bacteria the *Acetobacter xylinum* and *Agrobacterium tumefaciens*, which extrude extracellular ribbons of cellulose. These synthase genes and those of other enzymes that bind nucleotide sugars encode four highly conserved domains thought to be critical for UDP-Glc (and certain other UDP-sugars) binding and catalysis (Fig. 2.34A). So far, all other kinds of synthases able to make contiguous (1→4)-β-glycosyl linkages, such as chitin synthases and hyaluronate synthases, contain these four sequences of high amino acid identity. All of these polysaccharide synthases are considered **processive** synthases, which means that the enzyme complex continually adds sugars to the terminus without releasing the polysaccharide.

Analysis of sequences in a cDNA library made from cotton fibers at the onset of secondary wall cellulose formation allowed identification of two highly expressed plant sequences homologous to the *Acetobacter* cellulose synthase gene and containing all four UDP-Glc binding sequences. The polypeptides that they encode (≈110 kDa) are predicted to have eight transmembrane domains, bind the substrate UDP-Glc, and contain two large domains unique to plants: the plant-conserved region (P-CR) and class-specific region (CSR). In addition, the N-terminal region of the protein contains a Zn-finger motif capable of protein–protein binding and thought to function in coupling individual CesAs into the particles of the rosette complex.

The biochemical mechanisms of synthesis for all (1→4)-β-linked polymers of xylose, mannose, and glucose solve a unique steric problem in that each sugar unit must be inverted nearly 180° with respect to its neighbors. To make such a linkage by addition of one glucose residue at a time, either the synthase or the growing chain must rotate 180°, or the sugar must be added in a constrained position and snap alternately into the proper orientation by some other factor associated with the synthase. Because a cellulose microfibril is composed of several dozen chains, each arising from a different synthase complex, a drastic reorientation of enzyme or substrate would not be expected. A variation of this scheme would be a biochemical "toggle" switch, whereby after each glycosyl transfer the catalytic function alternates between two amino acids within a single active site. The crystal structure of a bacterial cellulose synthase from *Rhodobacter sphaeroides* provides a single site of UDP-Glc substrate binding and catalysis, suggesting a toggling mechanism for this primitive synthase (Fig. 2.34B). The additional P-CR and CSR domains in plant CesAs and in vitro dimerization and interactions among CesA isoforms indicate a more complex structure and mechanism. Analysis, however, of the size of the catalytic domains by small-angle X-ray scattering studies indicates the size of the rosette complex demands that each monomer contribute a single (1→4)-β-D-glucan chain (Fig. 2.34C).

All angiosperm species examined have at least 10 distinct *CesA* genes. While some are expressed in a cell- or tissue-specific manner, at least three isoforms can be expressed in a single cell. Also, the three different *CesA*s expressed in cells making primary walls are distinct from the three expressed in cells making secondary walls (Fig. 2.34D). The CSR domain located within the catalytic sequence defines the subclass structure of the gene family by its cysteine-, basic-, and acidic-rich motifs, which are conserved across many species. Further, mutations that cause a deficiency in any of the three isoforms result in drastic loss of cellulose synthesis. When cellulose synthase complexes are extracted from plasma membrane with detergents, the three CesAs polypeptides remain associated, indicating that each may fill a specific position in the rosette complex. In a classic biochemical "pulldown" strategy, the use of an antibody specific against one CesA polypeptide immunoprecipitates a complex containing the two other CesA polypeptides.

How many microfibrils are made by a single rosette? Mounting evidence suggests that it may be only one. Rosettes are assembled in the Golgi membrane and delivered to the plasma membrane intact. From rates of cellulose synthesis, the length of the microfibrils, and the number of rosettes per

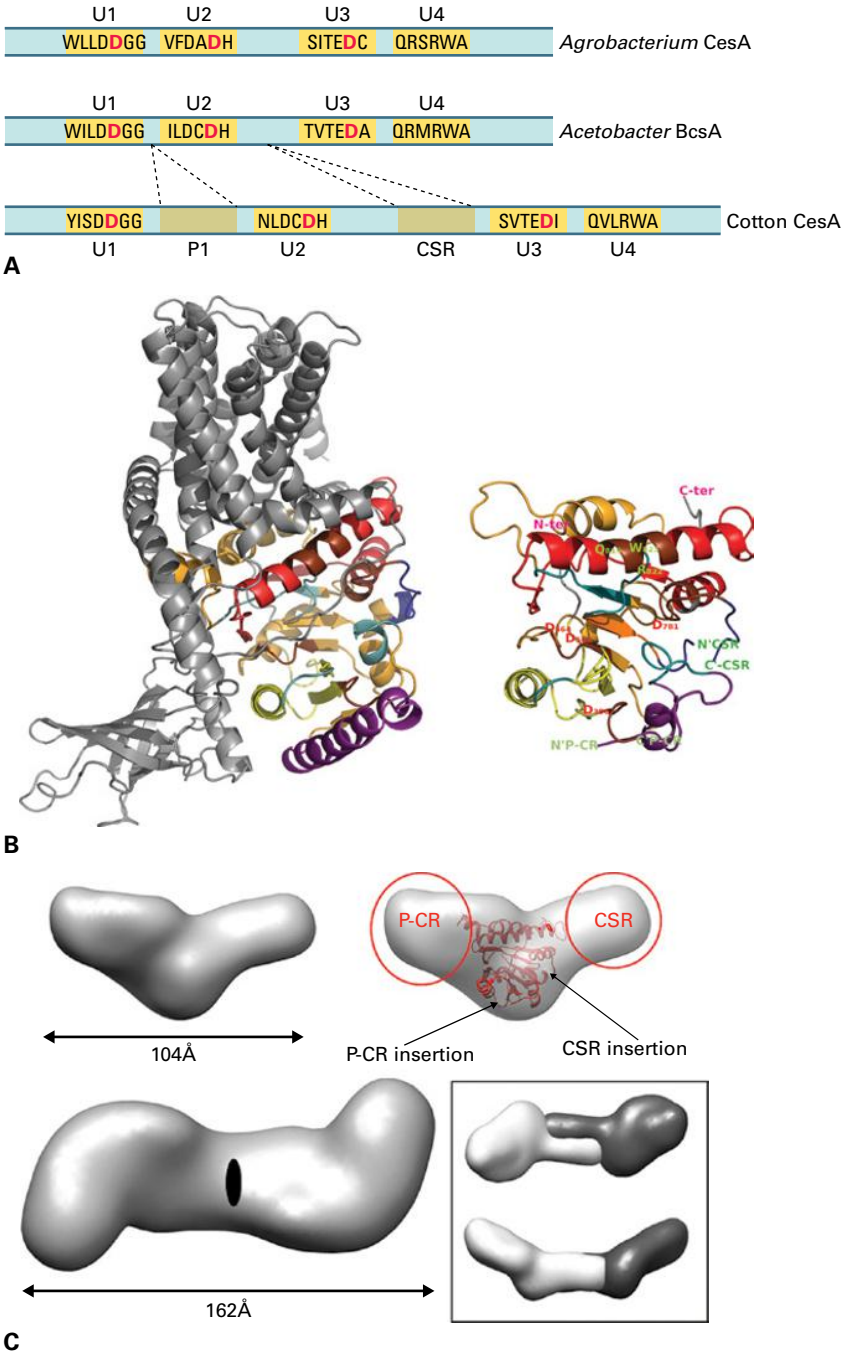


FIGURE 2.34 *(A) Cellulose synthase genes from* Acetobacter xylinum, Agrobacterium tumefaciens, *and* Gossypium hirsutum *(cotton) are characterized by four catalytic motifs; three of the four domains demonstrate absolute conservation of four aspartyl residues (D, DxD, D, in red) predicted to be necessary for substrate binding and catalysis of the glycosidic bond formation. In addition to the four aspartyl residues, the Q/RxxRW motif in the fourth catalytic motif is also conserved in every synthase of a polysaccharide with contiguous (1→4)-β-linked units in which one sugar is inverted with respect to its neighbors. Two sequences, P-CR and CSR, are plant-specific. (B) Crystal structure of a bacterial cellulose synthase, with the catalytic domain compared with a model of a homologous plant CesA catalytic domain minus the P-CR and CSR. N-ter and C-ter connect to the second and third membrane-spanning domains, respectively. The plant sequences containing the catalytic motifs homologous to the bacterial synthase are in yellow, orange, and red; nonhomologous gaps in sequence are in purple and teal. The four conserved aspartyl residues are in red, and the QxxRW in green; N' and C' P-CR and CSR indicate points of insertion of these plant-specific domains. (C) The surface envelope of a plant CesA catalytic domain (CatD) was determined by small-angle X-ray scattering of the recombinant protein in solution. The CatD is predicted to be a two-domain structure, with the smaller domain participating in the formation of a dimer. In the upper right is seen a molecular docking experiment that places the best fit of the domains homologous to the bacterial in the central portion of the CatD. This orientation places the plant-specific CSR sequences in the smaller domain that functions in dimerization. (D) Genes of the* CesA/Csl *superfamily of* Arabidopsis *(in red), rice (*Oryza sativa*; in yellow), and maize (*Zea mays*; in green). In all angiosperms studied thus far, at least three* CesA *genes are co-expressed during both primary wall formation –* Arabidopsis AtCesA1, AtCesA3, *and* AtCesA6 *– and secondary wall formation –* Arabidopsis AtCesA8,

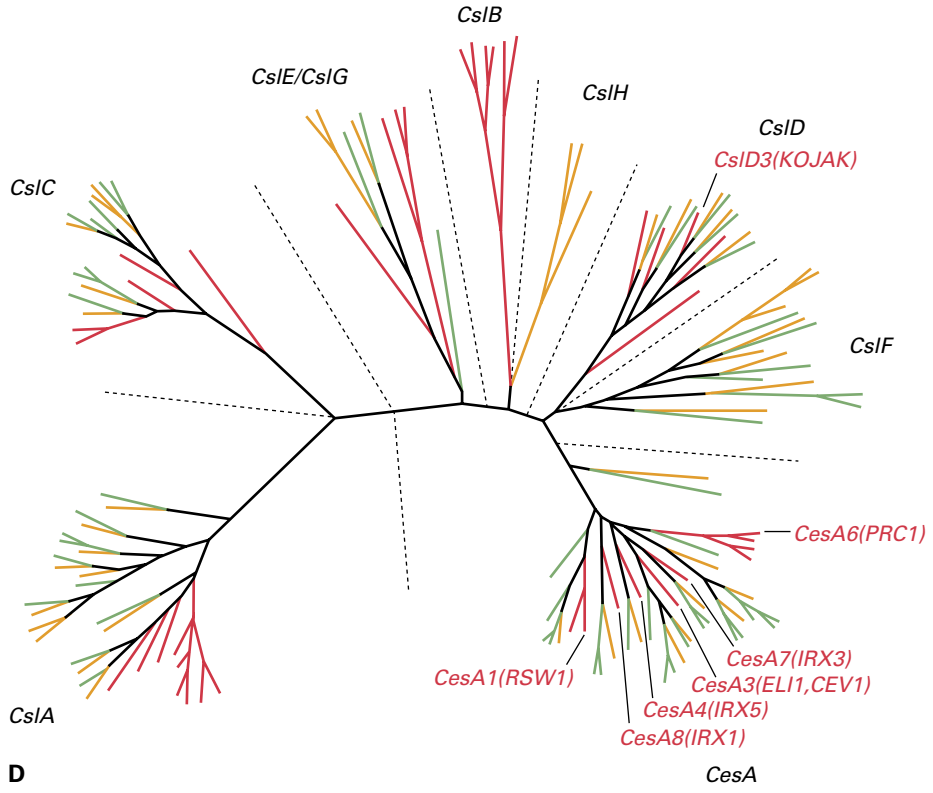


FIGURE 2.34 (*Continued*) AtCesA7, *and* AtCesA4. *Orthologous genes of* Oryza sativa *and maize are also expressed similarly. For* Arabidopsis, *mutations in any one gene (mutant name in parentheses) results in cellulose deficiencies in their respective primary or secondary wall, indicating that all three are essential for cellulose synthesis. The root-hairless mutant* kojak *was traced to a mutation in the* CslD3 *gene possibly encoding a cellulose synthase in these tip-growing cells, but the expression patterns and inferred sub-cellular locations suggest that isoforms function in all cells and produce a yet unknown product. Heterologous expression studies have established that at least some members of the* Arabidopsis CslA *group function in mannan synthesis and* CslC *group function in xyloglucan synthesis. The grass-specific* CslF *and* CslH *group members are likely to function in synthesis of the mixed-linkage (1→3),(1→4)-β-D-glucan.*

mm^2, it was estimated that synthesis of one microfibril takes 10 min. A continual supply of rosettes is delivered throughout cell growth; treatment of cells with cycloheximide, a potent protein synthesis inhibitor, results in loss of cellulose synthases from the membrane with a half-life of less than 30 minutes.

Plant cells possess arrays of cortical microtubules that underlie and connect to the plasma membrane. Orientation of the cortical microtubule array often pre-stages the orientation of cellulose microfibril deposition. The cortical array can align cellulose synthase complexes either by direct protein-mediated connection or by defining channels in the membrane in which the synthase can move. Cortical microtubules may guide cellulose synthase complexes in the plasma membrane as the complexes are propelled forward by crystallization of chains within a microfibril. CesA proteins fused to fluorescent marker proteins made it possible to image how rosettes move in the plasma membrane, and this has allowed researchers to establish that they follow the orientation of cortical microtubules. However, once microfibril orientation has been established, microtubules can be disrupted using chemical treatments and the orientation will persist, presumably using the previously deposited microfibrils for guidance. Thus, cellulose microfibrils appear to have the ability to self-align in the absence of cortical microtubules and/or pre-existing cellulose microfibrils, and cortical microtubules may, therefore, only be required for directing cellulose into a new orientation during cell differentiation.

This discovery opened the door for identification of the *CesA* superfamily of genes that includes the ***Cellulose synthase-like*** (*Csl*) genes (Fig. 2.34D). Several related *Csl* genes may function in the synthesis of many other crosslinking glycans that comprise the plant wall. All of these genes contain the four domains for nucleotide-sugar binding and catalysis, membrane-spanning domains, and plant-conserved regions, but with the exception that some *CslD* genes lack Zn-finger domains, and the CSRs are truncated to a variable extent. Eight subclasses of *Csl* genes are recognized. While most subclasses are represented in all angiosperms, *CslF*, and possibly *CslH*, contain only grass genes, and *CslB* and *CslG* are represented only in eudicots. Some of the *CslD* genes are suspected to be cellulose synthases of tip-growing cells. Heterologous expression of some of these *Csl*s has shown them to encode the probable components of the backbone synthases of mannans and glucomannans (*CslAs*), xyloglucan (*CslCs*), and (1→3),(1→4)-β-D-glucans (*CslFs*).

2.4.6 Diversity of polysaccharide structures is accomplished by numerous classes of glycosyl transferases

According to the Carbohydrate-Active enzymes (CAZy) database, which describes families of structurally-related catalytic and carbohydrate-binding modules (or functional domains) of enzymes that degrade, modify, or create glycosidic bonds, there are over 90 distinct families of **glycosyl transferases (GTs)**, with 44 families represented in plants (Box 2.6 for more information on CAZy and other useful on-line databases devoted to cell wall biology). GTs catalyze transfer of activated monosaccharides to another biological compound, usually another sugar, oligomer, or polysaccharide. Family membership is based on structurally related protein catalytic or functional motifs and domains, but implicit in this are the evolutionary relationships of the genes that encode them. Some families are found across many Kingdoms, but several are found only in plants. Family GT2 contains the processive transferases of cellulose and related glycan synthases that form the *CesA/Csl* gene superfamily described above. Families *GT8* and *GT47* are exceptionally well populated with members that function in nonprocessive substitution of cell wall pectic and crosslinking glycan backbones with several kinds of sugars (Fig. 2.35). Just as group structure of the *CesA/Csl* superfamily reflects divergence in cell wall composition, so do the families of GTs. For example, family *GT8,* which contains members mainly involved in pectin synthesis, comprises four major groups and one minor group, with *Arabidopsis* sequences more abundant in Groups A and B, and grass sequences more abundant in Groups C and D (Fig. 2.35A). The HG backbones are synthesized by at least two GT8 galacturonosyl transferases (GAUT), GAUT1 and GAUT7, that for a Golgi-resident dimer. While a single GT family can use different sugars in catalysis, the linkage configuration and the basic mechanism of glycosyl transfer is generally consistent. Two types of glycosyl transfer are the **retaining** and **inverting** mechanisms, which refer to whether the anomeric configuration is preserved or switched from that of the nucleotide sugar. Most nucleotide-sugars are in the α-D- conformation, and a retaining mechanism would preserve the α-D- (or β-L-) linkage typical for the HG backbone, whereas the inverting mechanism produces a β-D- (or α-L-) linkage.

BOX 2.6

Genomic resources for cell walls

A useful resource for cell wall-associated genes is contained in the Carbohydrate-Active enZYme (CAZy) database (http://www.cazy.org), which compiles evolutionarily related genes based on structural motifs and functionalities. Four groups of enzymes, glycosyl transferases, glycosyl hydrolases, lyases, esterases, and a broad collection of cellulose-binding modules function in substrate binding associated with catalysis. A large proportion of the genes in CAZy function in the synthesis and remodeling of the cell wall.

Several web sites are devoted specifically to plant cell-wall gene families. Cell Wall Genomics (http://cellwall.genomics.purdue.edu) has assembled over 1,200 genes per species, particularly those of *Arabidopsis*, rice, and maize, involved in sugar and monolignol substrate generation, polysaccharide synthesis and glycosyl transferase activities, ER-Golgi-plasma membrane targeting, wall assembly and remodeling, secondary wall formation, and signaling and response elements in the extracellular matrix. The site also reports on over 900 *Arabidopsis* and 200 maize insertional mutants and their biochemical and spectroscopic phenotypes. Growing collections of these and other mutants are available from the Arabidopsis Resource Center (http://abrc.org) and the Maize Stock Center (http://maize.org).

A similar site called Cell Wall Navigator (http://bioweb.ucr.edu/Cellwall/) is an integrated database and mining tool for protein families that are involved in plant cell wall biogenesis by comparison within angiosperm species and across Kingdoms. Other sites provide information about glycosyl transferases of rice (http://ricephylogenomics.ucdavis.edu/cellwalls/gt/), and a range of genomic resources for *Brachypodium* (http://brachypodium.pw.usda.gov/). The functions of specific gene and protein families, such as expansins (http://homes.bio.psu.edu/expansins/) and XTHs (http://labs.plantbio.cornell.edu/XTH/) contributed by individual labs.

Useful information about cell wall chemistry, as well as biochemical resources used in defining cell wall structure and architecture, are available at WallBioNet: Plant Cell Wall Biosynthesis Research Network (http://xyloglucan.prl.msu.edu/) and CarboSource Services, Complex Carbohydrate Research Center, University of Georgia, USA (http://www.ccrc.uga.edu/~carbosource/CSS_home.html).

Two sites are devoted to development and cataloguing of cell wall monoclonal antibodies and other reagents to probe polysaccharide fine structure at the single cell wall level or for development of tailored carbohydrate microarrays at the Complex Carbohydrate Research Center (http://www.ccrc.uga.edu/~carbosource/CSS_home.html) and PlantProbes, University of Leeds, UK (http://www.plantprobes.net).

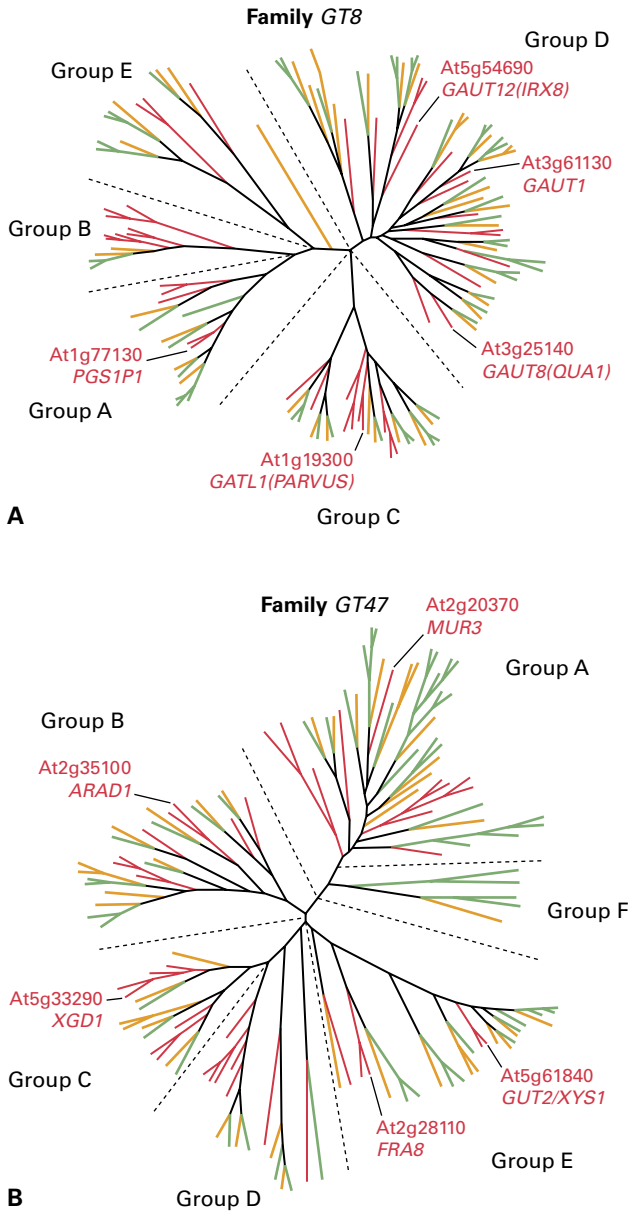


FIGURE 2.35 *Genes of major nonprocessive glycosyl transferase families of* Arabidopsis *(in red), rice (*Oryza sativa*; in yellow), and maize (*Zea mays*; in yellow). (A) In* Glycosyl Transferase Family8 *(*GT8*), the largest clade, Group D, encodes galacturonosyl transferases GAUT1 and GAUT7, which interact to iteratively extend GalA units typical of homogalacturonan. This large family of retaining-type transferase genes probably encodes several putative GAUTs, and three distinct subgroups of GAUT-like (GATL) proteins.* GAUT8, *or* QUASIMODO1 *(*QUA1*), is involved in the synthesis of rhamnogalacturonan II. The* PARVUS *gene is involved in the synthesis of the tetrasaccharide primer for xylan synthesis. (B)* GT47 *encodes inverting-type transferases that add several distinct types of side-group sugars to pectins and crosslinking glycans. Group A contains* MUR3, *which encodes a galactosyl transferase that adds the (1→2)-β-*D*-Gal residue of the first xylosyl residue from the reducing end of the repeating heptasaccharide unit of xyloglucan. In Group B,* ARABINOSE DEFICIENT1 *(*ARAD1*) functions in (1→5)-α-*L*-arabinan synthesis, and in Group C,* XYLOGALACTURONAN DEFICIENT1 *(*XGD1*)*

Family *GT47* consists of five groups of genes that encode at least four different types of activities, including galactosyl-, arabinosyl-, xylosyl-, and glucuronosyl-transferases, all using an inverting mechanism of glycosyl transfer (Fig. 2.35B). Group A, the largest group, contains *MUR3*, encoding a galactosyl transferase that adds the (1→2)-β-D-Gal residue of the first xylosyl residue from the reducing end of the repeating heptasaccharide unit of xyloglucan.

Members of several other gene families have also been functionally characterized (Table 2.2), but there is a long way to go to establish the function of every member. Although members of the *CesA/Csl* gene superfamily share the ability to synthesize (1→4)-β-D-glycans, the (1→4)-β-D-xylans are synthesized coordinately by members of the GT47 Group B xylan xylosyl transferases (IRX10B) and GT43 gene family (Table 2.2). Like cellulose and the (1→3),(1→4)-β-D-glucan synthases, at least two distinct isoforms of these xylosyl transferases combine to form a synthase complex.

2.5 Growth and cell walls

2.5.1 The cell wall is a dynamic structure

Cell expansion involves extensive changes in the mass and composition of the cell wall. Cell growth, an irreversible increase in cell volume, can occur by expansion (increase in cell size in two or three dimensions) or by elongation (expansion constrained to one dimension). Variety in cell shape may result if either of these two processes occurs at specific regions of the cell surface.

During elongation or expansion, existing cell wall architecture must change to incorporate new material, which increase the surface area of the cell and induces water uptake by the protoplast. The turgor pressure exerted by the protoplast is necessary to drive cell expansion, and this pressure usually remains a constant driving force for expansion. Regulation of wall loosening is considered the primary determinant of rates of cell expansion. Cell wall architecture must be extensible; that is, mechanisms must exist that allow discrete biochemical loosening of the cell wall matrix, permitting microfibril separation and insertion of newly synthesized polymers. Cells may extend tens, hundreds, or even thousands of times their original length while maintaining constant wall thickness. Thus, loosening and continued deposition of new material into the wall must be tightly integrated events (Fig. 2.36).

FIGURE 2.35 *(Continued) encodes a xylosyl transferase that adds the (1→3)-β-xylose units to homogalacturonan. Group E contains* FRAGILE FIBER8 *(*FRA8*), which functions in the synthesis of the tetrasaccharide primer for xylan synthase, and* GUT2/XYS1, *which encodes a xylosyltransferase involved in xylan elongation.*

TABLE 2.2 *Cell-wall-related glycosyl transferases.*

Gene family	Known substrates	Predicted activity
GT8	UDP-D-GalA; UDP-D-GlcA; UDP-D-Gal	Retaining transferases involved in pectin and xylan synthesis; galactinol synthesis
GT31	UDP-D-Gal, UDP-D-Glc-NAc, UDP-D-Gal-NAc	Inverting transferases involved in glycosylation of proteins and arabinogalactan synthesis
GT34	UDP-D-Xyl, UDP-D-Gal	Retaining transferases involved in side-group additions to xyloglucan and galactomannan synthesis
GT37	GDP-L-Fuc	Inverting type transferases involved in fucosylation of xyloglucans and glycoproteins.
GT43	UDP-D-Xyl	Inverting transferases involved in xylan polymerization
GT47	UDP-D-Gal, UDP-L-Ara, UDP-D-Xyl, UDP-D-GlcA	Inverting transferases involved in side-group additions to xyloglucan, xylans, and homogalacturonans; synthesis of α-arabinans; synthesis of xylans
GT48	UDP-D-Glc	Callose synthase
GT61	UDP-D-Xyl, UDP-L-Ara	Inverting transferases involved in side-group additions to xylan
GT64	UDP-D-*N*-acetyl-Glc	Glycoprotein synthesis
GT77	UDP-D-Xyl, UDP-L-Ara	Synthesis of complex pectins and O-linked glycoproteins

The Carbohydrate-Active enZyme (CAZy) database classifies glycosyl transferases based on sequences and common biochemical and protein motifs. Several of these function in the synthesis of cell wall polysaccharides or glycoproteins.

2.5.2 Most plant cells grow by uniform deposition of polymers on all of their cell wall surfaces, but some cells target polymers to a growing tip

In the vast majority of plant cells, growth and deposition of new wall material occur uniformly along the entire expanding wall. However, **tip growth**, growth and deposition of new wall material mostly at the tip of a cell, occurs in some plant cells, notably root hairs and pollen tubes (Fig. 2.37). Root hairs and pollen tubes have different wall compositions, even though they share a common mechanism of growth: pollen tubes contain callose and have distinct homogalacturonan epitopes, whereas root hairs do not. Tip-growing cells expand at prodigious rates for plant cells (>200 nm s^{-1} for pollen tubes). The site of expansion in tip-growing cells is focused to the dome-shaped apex, which is filled with secretory vesicles by myosin-mediated delivery on the tracks of actin microfilaments (see Chapter 5).

Cellulose microfibril orientation determines the axis of elongation. In cells that grow by uniform expansion, layers of microfibrils lie unaligned in the wall matrix, but in cells that elongate, microfibrils align in transverse or helical orientations to the axis of elongation.

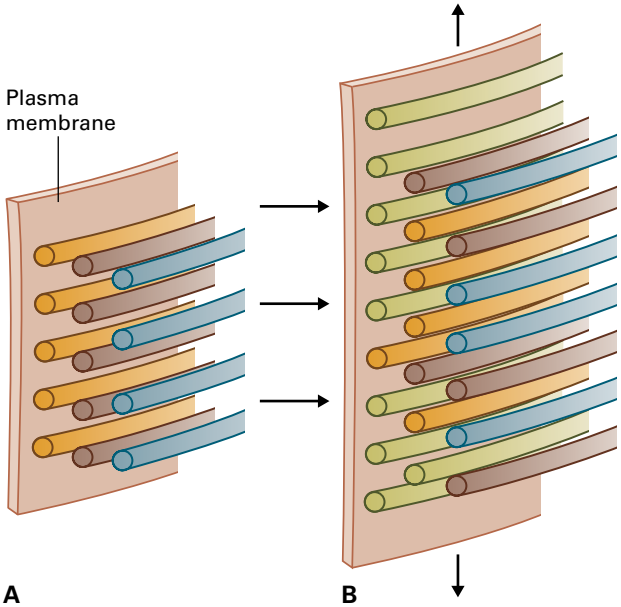


FIGURE 2.36 *Wall loosening and incorporation of new wall polymers are integrated events so that wall thickness is maintained during cell expansion. Because walls are only a few strata thick, loosening with no insertion of new wall material would very quickly thin the wall during growth and cause rupture. In contrast, deposition without loosening would increase wall thickness, because walls would not expand. Vertical arrows denote direction of expansion and separation of exterior microfibrils, and horizontal arrows show location of the addition of new microfibrils on the inner surface of the wall and integration into overlaying strata.*

2.5.3 The multinet growth hypothesis explains axial displacement of cellulose microfibrils during expansion of the cell wall

From studies of developing cotton fibers, the **multinet growth hypothesis** was developed to explain how cellulose microfibrils that have been deposited in a transverse or slightly helical orientation are displaced axially as elongation proceeds (Fig. 2.38A). New microfibrils deposited in strata on the inner surface of the wall in a generally transverse orientation functionally replace older microfibrils. Older microfibrils are displaced into the outer layers of the wall as new microfibrils are added and become reoriented in a longitudinal direction as the cell elongates. Consistent with this hypothesis, changes in diffraction patterns of polarized light by algal cells, induced by reorientation of the parallel microfibrils, occur primarily in the inner layers of the wall close to the plasma membrane. The driving force for wall extension is turgor pressure generated by the protoplast, but it is the tension created on the microfibrils perpendicular to the outward push of the protoplast that leads to separation of the microfibrils (Fig. 2.38B). A turgor pressure of 1 MPa can generate several hundreds of MPa of tension because the volume of a relatively large protoplast is resisted by a very thin cell wall.

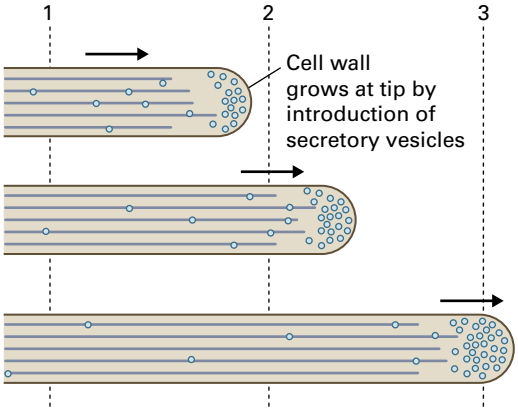


FIGURE 2.37 *Rates of vesicle delivery and deposition determine rate of tip growth. To withstand increase in tension in the axial wall of the cylinder of a tip-growing cell, microfibrils must be spooled transversely.*

The essence of the multinet growth hypothesis is descriptive for many kinds of cells, but microfibrils do not necessarily reorient axially, and significant extension is possible with little reorientation if many wall strata contribute to the expansion. Cellulose microfibrils woven in a shallow helix around the cell prevent the growing cell from becoming spherical. By analogy, the springlike toy, such as Slinky or Flexi, stretches easily along its longest axis, but resists attempts to increase its diameter (Fig. 2.38C); when stretched, the spring extends substantially with only a small change in helical angle, but with a wide separation of the coils. Extension of a cell wall might be viewed as a series of tightly interacting concentric Slinkys in both right-handed and left-handed orientations that reorient at crossed angles during separation (Fig. 2.38A). Given the estimated thickness of the primary wall (80–100 nm in meristematic and parenchymatous cells) and the dimensions of matrix

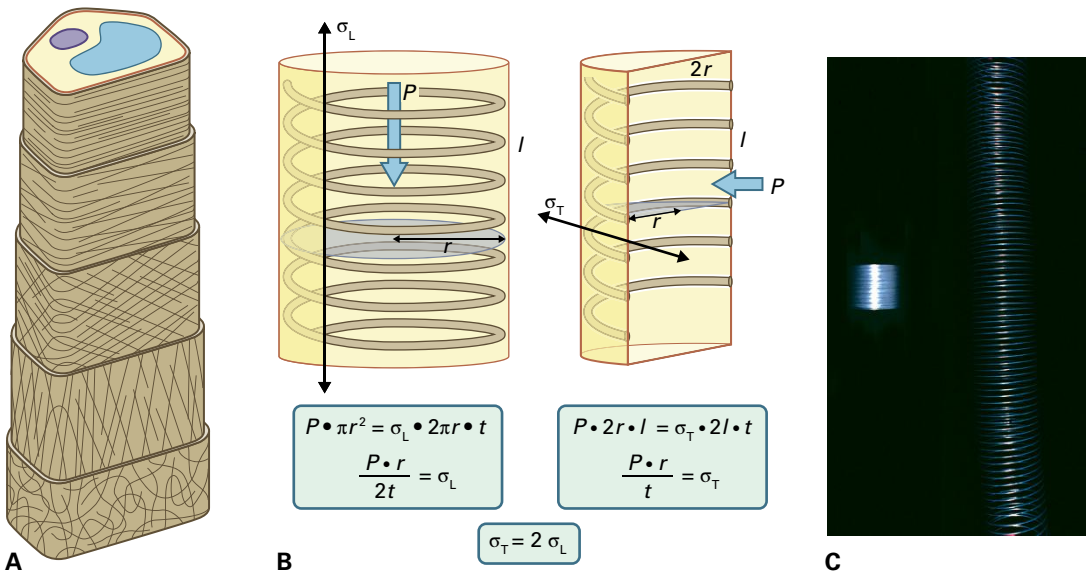


FIGURE 2.38 *(A) The original multinet growth hypothesis explains that as walls stretch during growth, microfibrils reorient passively from a transverse direction on the inner wall to a longitudinal direction at the outer wall. (B) Hydrostatic pressure developed by the protoplasm is resisted by a relatively thin cell wall, and tensile force pulling microfibrils apart is several orders of magnitude higher than cell turgor pressure. For example, a spherical cell with a radius (r) of 50 μm and 1 MPa of turgor (P), enveloped by a cell wall only 0.1 μm thick (t), develops 250 MPa of tension in the wall. This enormous tension changes as the cell geometry changes. When this cell begins to elongate and become cylindrical, the tension increases to 500 MPa tangentially because of change in cell dimension. l, length; σ_L, longitudinal stress; σ_T, tangential stress. (C) Although a Slinky is difficult to extend radially because of the orientation of the coils, it is easily extended lengthwise. Similarly, altering the interaction between tethering crosslinking glycans and transversely oriented cellulose may be the principal determinant of the rate of cell elongation.*

components, only five to ten strata make up the wall. Microfibrils from several strata may even merge somewhat to fill in gaps as new strata are deposited onto the inner surface (see Fig. 2.36).

2.5.4 The biophysics of growth underpins cell wall dynamics

Several different classes of cell wall polymers constitute nearly independent determinants of strength in elongating cells. These include (a) the microfibrils arranged in the transverse axis, which are interconnected with crosslinking glycans; (b) putative networks involving structural proteins or phenylpropanoid compounds; and (c) elements of the pectin network. When plant growth regulators, such as auxin and gibberellin, change *direction* of growth, they do so through changes in orientation of cortical microtubules and cellulose microfibrils. When they change *rate* of growth, their mechanisms include dissociation or breakage of tethering molecules from microfibrils. A mathematical formulation that describes the growth rate of plant cells allows us to define the cell wall properties that must be modified to permit growth.

The driving force for water uptake in elongating cells can be quantified by

$$\delta l/\delta t = Lp(\Delta\Psi_w), \qquad \text{(Eq. 2.1)}$$

where $\delta l/\delta t$ is the change in length per unit time, L*p* is hydraulic conductivity, i.e., the rate at which water can flow across the membrane, and $\Delta\Psi_w$ is the water potential difference between the cell and the external medium. The difference in water potential is the driving force for water movement and comprises two components, $\Psi_\pi + \Psi_p$, the osmotic potential and pressure potential (turgor), respectively. Revising Equation 2.1 to include changes in cellular volume (*V*) yields Equation 2.2, where growth is defined as a change in volume (*V*) per unit time, and depends on the surface area (*A*) of the plasma membrane available for water uptake.

$$\delta V/\delta t = A \bullet Lp(\Delta\Psi_w). \qquad \text{(Eq. 2.2)}$$

Thus, rate of growth is proportional to membrane surface area, the conductivity of the membrane, and the water potential difference driving water uptake. In nongrowing cells, $\Delta\Psi_w$, and thus $\delta V/\delta t$, equals zero, because the rigid cell wall prevents water uptake and the turgor pressure rises to a value equal to that of the osmotic potential of the cell. By contrast, in growing cells, the $\Delta\Psi_w$ does not reach zero because the wall tethers have been loosened. As a result, cell volume increases irreversibly. This wall-localized event, called **stress relaxation**, serves as the fundamental difference between growing and nongrowing cells (Fig. 2.39).

When turgor is reduced in growing cells by an increase in the external osmotic potential, growth ceases at some pressure before turgor reaches zero. This value, called the **yield threshold**, defines the pressure potential that must be exceeded before expansion can occur. The increment of growth rate change above the yield threshold is dependent not only on turgor but also on a factor called wall **extensibility**, which is the slope (m) of a general equation, shown as Equation 2.3, where *Y* is the yield threshold.

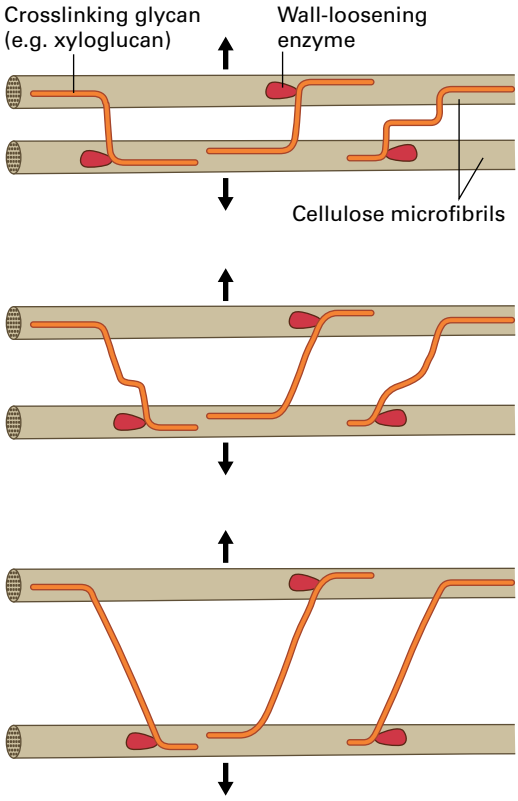


FIGURE 2.39 *Stress-relaxation is considered the underlying basis of cell expansion. When an elongating cell is stretched by turgor, longitudinal stress (indicated by arrows) is borne more or less equally by glycans tethering the cellulose microfibrils. If some tethers are dislodged from microfibrils, or hydrolyzed, they temporarily "relax" and the yield threshold is breached because other tethers are strained. Water uptake results in expansion of microfibrils to take up slack of the relaxed glycans, which once again experience tensile stress.*

$$\text{Rate} = m(\Psi p - Y) \qquad \text{(Eq. 2.3)}$$

The biochemical determinants of yield threshold and extensibility have yet to be identified.

2.5.5 The acid-growth hypothesis states that auxin-dependent acidification of the cell wall promotes wall extensibility and cell growth

Despite marked differences in the composition of Type I and Type II walls, the biophysics of growth of grasses and other flowering plants are similar. Although the chemical complexity of the wall is daunting, the similarity of the physiological responses of all flowering plants to acid, auxin, and light of

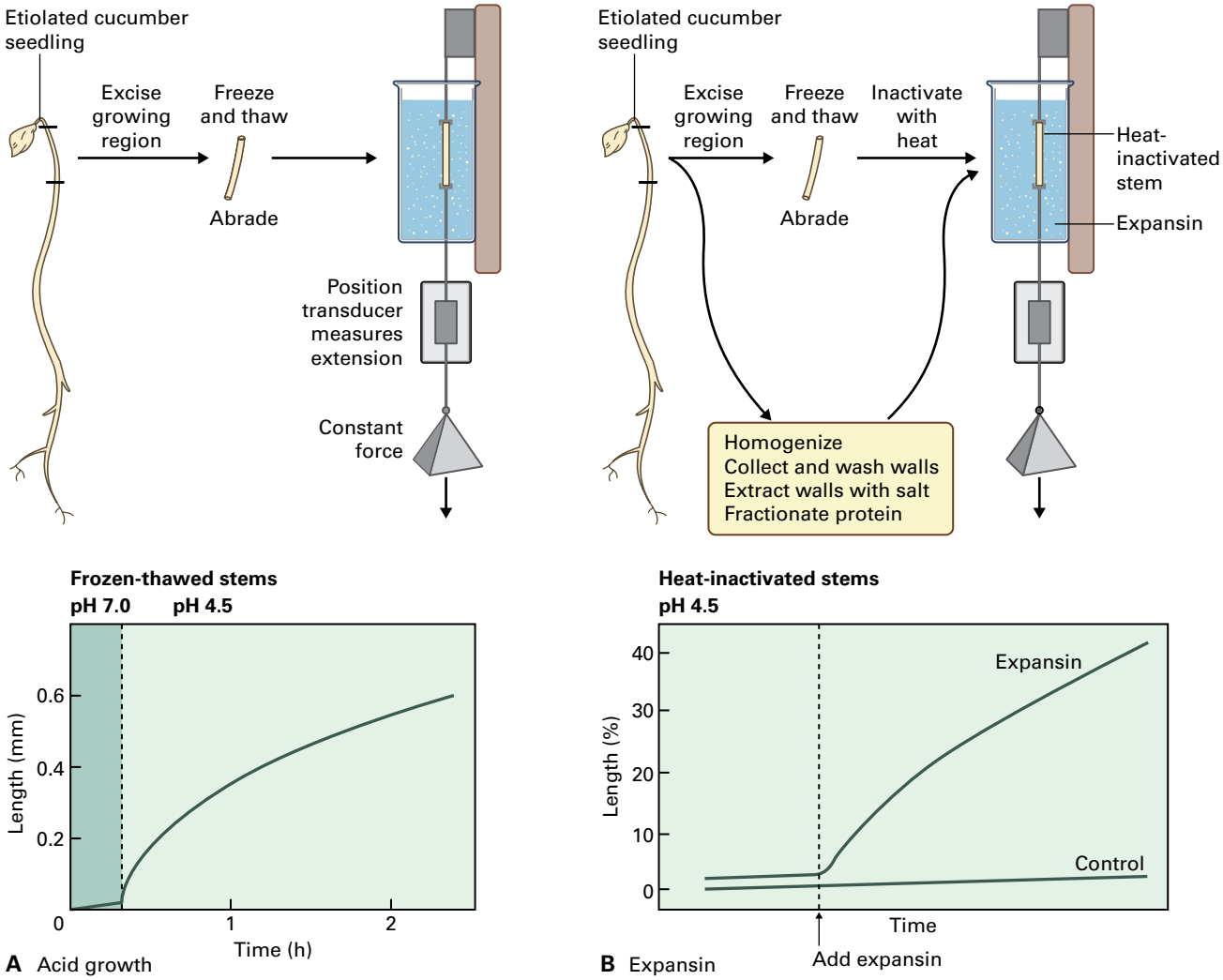


FIGURE 2.40 *Sections of growing epicotyl, hypocotyl or coleoptile are frozen, thawed and placed under a constant stress. A position transducer measures elongation continuously. (A) When the bathing solution of the frozen-thawed sections is changed from pH 7 to 4.5, extension occurs almost immediately. (B) If the sections are heat-inactivated, no extension occurs at any pH. However, when expansins are added, extension is restored at acidic pH. Neither plant hydrolases nor xyloglucan endo-β-transglucosylase is able to cause this effect in vitro.*

different qualities indicates that a few common mechanisms of wall expansion exist, regardless of the kinds of molecules that tether microfibrils.

Extraction of several kinds of polysaccharide hydrolases from cell walls of tissues rich in growing cells raised the possibility that regulation of these enzymes was a mechanism by which auxin could cause wall expansion. A major breakthrough came with the discoveries that auxin caused acidification of the medium in which elongating tissue sections were bathed, and that H^+ could substitute effectively for auxin (Fig. 2.40). This **acid-growth hypothesis** posits that auxin activates a plasma membrane proton pump that acidifies the cell wall. The low pH, in turn, activates apoplast-localized growth-specific hydrolases that cleave the load-bearing bonds that tether cellulose microfibrils to other polysaccharides. Cleavage of these bonds loosens the cell wall, which decreases turgor, and the resulting water potential difference causes uptake of water. Relaxation of the wall (i.e., separation of microfibrils) passively leads to an increase in cell size.

The basic tenets of the acid-growth hypothesis have stood the test of time, but three problems persist. First, no enzymes have been found that hydrolyze wall crosslinking glycans exclusively at pH lower than 5.0. Second, no reasonable explanation exists for how growth is kept in check once the hydrolases are activated. Third, no hydrolases extracted from the wall and added back to the isolated tissue sections, regardless of external pH, cause extension in vitro.

2.5.6 Regulation of the cellulose/crosslinking glycan network by expansins and xyloglucan-endotransglucosylases/hydrolases

Two large multigene families encode proteins implicated in restructuring the cellulose/crosslinking glycan network: **expansins**, which can catalyze wall extension in vitro without

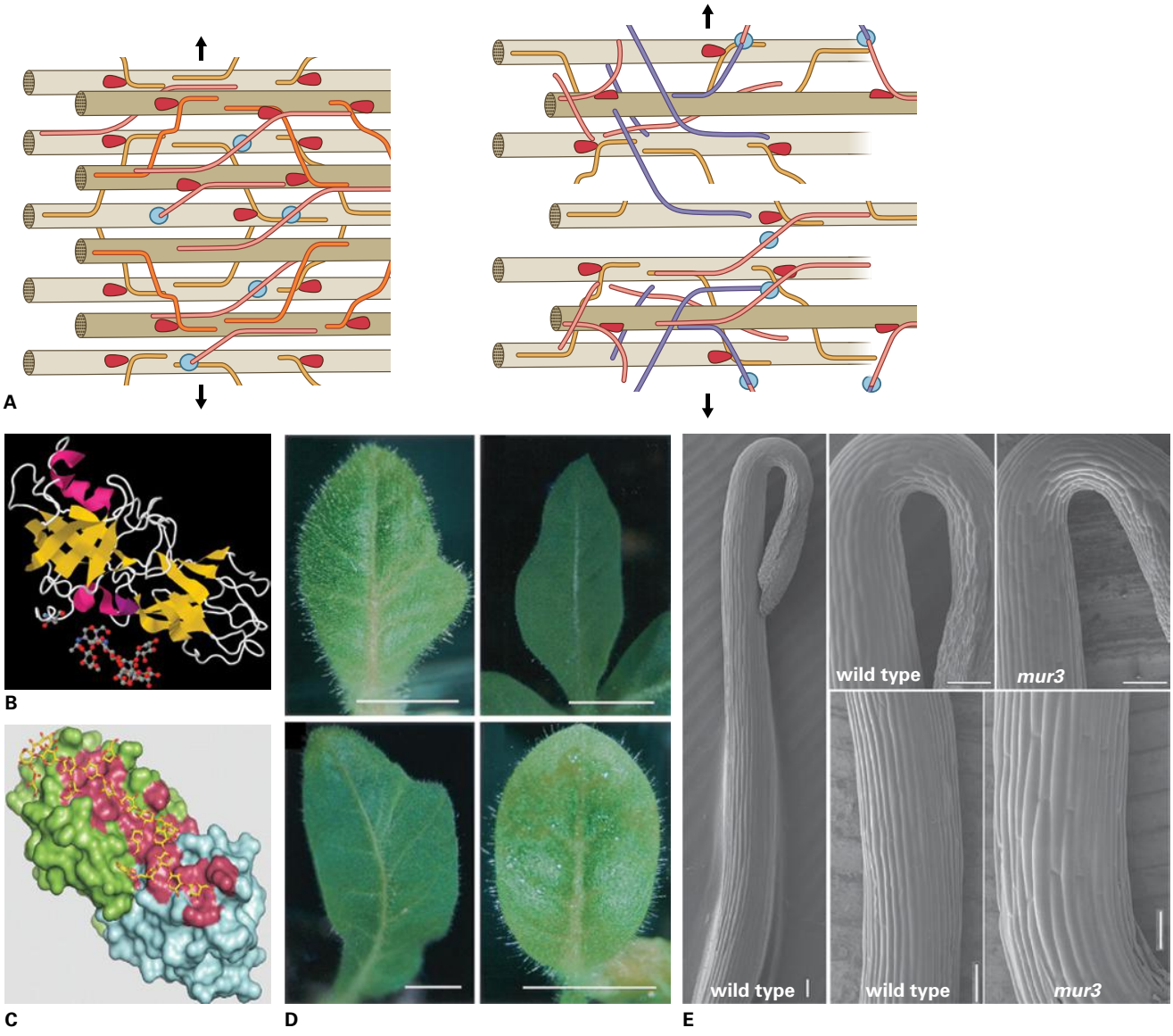


FIGURE 2.41 *(A) Microfibril separation driven by cellular osmotic pressure is facilitated by loosening of tethering crosslinking glycans. This is accomplished by expansins, which break steric interactions between crosslinking glycans and cellulose. Members of the endo-β-D-transglucosylase/hydrolase family (XTH) with only endo-β-D-transglucosylase (XET) activity hydrolyze a glycan and reattach one part of the chain to the nonreducing terminus of another. This action by XET functions in forming new tethers as microfibrils from inner lamellae merge with microfibrils of the outermost lamellae as they are pulled apart during wall extension. (B) The crystal structure of the* Zea mays *β-expansin shows the groove or cleft structure characteristic of endohydrolases (Fig. 2.42) but is missing a domain that would contain a catalytic amino acid for hydrolysis. This β-expansin is* N*-glycosylated, but α-expansins are typically unglycosylated. (C) Alignment of a glucuronoarabinoxylan is modeled in the groove of the* Z. mays *β-expansin. (D) Leaf shape can be manipulated by local induction of expansin expression (arrows), indicating that physical changes in cell wall structure can feed back to control developmental patterns. (E) The* mur3 *mutant produces a galactose-deficient xyloglucan in elongating hypocotyls that is poorly recognized by XETs. Cell elongation in* mur3 *just below the hook is indistinguishable from that of wild type (upper panels), but epidermal cell swelling at the base of the hypocotyl is observed in* mur3 *after elongation has ceased.*
Source: (E) Peña et al. (2004). Plant Physiol. 134:443–451.

any detectable hydrolytic or transglycolytic events, and **xyloglucan endo-β-transglucosylases** (XET), which cannot induce wall expansion in vitro.

Expansins are ubiquitous in growing tissues of all flowering plants, and they likely catalyze breakage of hydrogen bonds between cellulose and load-bearing crosslinking glycans. Such an activity could disrupt tethering of cellulose by XyGs in Type I walls and by GAXs in Type II walls and by GAXs and β-glucans in grass walls. Expansins are the only proteins shown to produce wall expansion in vitro (Fig. 2.41A).

Two major evolutionary groups of expansins, termed α and β, are found in all angiosperms, although the α-expansins are more numerous in plants with Type I walls and β-expansins are more numerous in grasses. Because grass α-expansins induce extension of tissues with Type I

walls, it is attractive to think expansins are ubiquitous enzymes involved in the rapid growth responses of both Type I and Type II walls. However, further studies show certain β-expansins have no appreciable activity on Type I cell walls. A notable difference between the two groups is extensive glycosylation of β-expansins, which appears to be absent in α-expansins. A maize (*Zea mays*) pollen allergen belonging to the expansin B family (EXP B1) binds strongly to xylans in Type II cell wall. The crystal structure of EXP B1 shows an unstructured glycosylated N-terminal extension and a two-domain folded structure with a highly conserved open surface spanning the two domains (Fig. 2.41B,C). The surface has many aromatic and polar residues suitable for binding a branched polysaccharide of about 10 residues in length. It has been proposed that expansin uses the strain energy stored in a taut cellulose-binding glycan to dissociate the glycan from the cellulose surface, using a 10-degree shift in angle between domains to cause a one-residue dislocation of the polysaccharide along the binding surface.

Exogenous expansins applied to a meristem induce bulging of the meristem at sites of application, an effect that later is followed by development of leaf primordia. Local transient induction of expansin expression on the flank of developing leaves leads to induction of ectopic lamina tissue and modulation of leaf shape (Fig. 2.41D). Thus, morphogenesis may be manipulated by alteration of the biophysical properties of the cell wall that then impacts gene expression and developmental pathways by yet-to-be-discovered signal pathways.

Several members of the **xyloglucan endotransglucosylase/hydrolase** (XTH) gene family carry out transglycosylation of XyGs, where one chain of XyG is cleaved and reattached to the nonreducing terminus of another XyG chain, an enzyme activity described as xyloglucan endo-β-transglucosylase (XET). Unlike expansins, XETs cannot induce wall expansion in vitro. However, transglucosylase activity could function in realignment of XyG chains in different strata during growth, where XET cleaves and ligates xyloglucans with new xyloglucan partners such that wall architecture may be modified without detectable changes in composition (Fig. 2.41A). Support for this proposed function comes from experiments with mutant plants with altered XyG structures for which XETs have reduced substrate affinities. These mutants are unaltered in growth rate and architecture but exhibit cell bulging when growth stops and suffer severe loss in tensile strength (Fig. 2.41E). A mannan transglycosylase/hydrolase has been described that can carry out a transglycosylation reaction in the presence of mannan-derived oligosaccharides. A mixed-linkage endo-β-transglucanase has also been found in *Equisetum*, but no such activity was detected in the grasses.

Since the wall composition of grass Type II wall differs from all other flowering plant species, researchers are also investigating the exo- and endo-β-D-glucanases that hydrolyze grass β-D-glucans to glucose. Addition of purified exo- and endo-glucanases to heat-killed coleoptiles cannot induce extension growth. However, when antibodies directed against these enzymes are added to enzyme-active walls, they inhibit growth, suggesting that hydrolases also play a role in extension growth.

2.5.7 In Type I walls, cell growth is associated with biochemical changes in the pectin network

The cellulose/crosslinking glycan network lies embedded in a pectin network that may control access of wall-modifying enzymes to their substrates. The self-hydrolysis of isolated walls by nascent enzymes, termed **autolysis**, yields substantial amounts of Ara and Gal from Type I walls, suggesting that changes in the arabinan and galactan side-branches of RG I (see Fig. 2.17C) or AGPs (see Fig. 2.21) occur during growth.

The most marked change revealed by biochemical analysis is the increase in the degree of methyl esterification of wall HGs when newly synthesized pectins are deposited during elongation. The deposition of highly esterified HGs is followed by a de-esterification event that can remove a large proportion of methyl ester groups from the wall when growth stops. Ionized carboxyl groups can form Ca^{2+}-HG junction zones, causing the matrix to become more rigid (see Fig. 2.26). The cell walls of meristematic and elongation zones are characteristically low in Ca^{2+}, and Ca^{2+}-HG junction zones are observed more frequently after cell elongation has stopped. Changes in the esterification of HG have been correlated with growth in many different systems. For example, the degree of methyl esterification is highest in etiolated *Zea mays* coleoptiles and tissue-cultured *Nicotiana tabacum* cells that are actively elongating. Pectic HG is implicated in cell adhesion maintenance simply because middle lamellae of many fruits and vegetables are rich in HG. A pectin glucuronyltransferase that transfers glucuronic acid to RG II is also required for intercellular attachment.

2.5.8 Glycosyl hydrolases and glycosyl lyases modify cell wall polysaccharide structures in situ

Over 130 different glycosyl hydrolase families are represented in the CAZy database (Box 2.6), with plant sequences represented in 35 of them. Glycosyl hydrolases cleave single sugars from polysaccharides in the cell wall. Arabinosidase, galactosidase, xylosidase, and fucosidase activities modify side-chains of pectins and crosslinking glycans during different stages of development. The same glycosyl hydrolase gene family can have multiple activities represented within it,

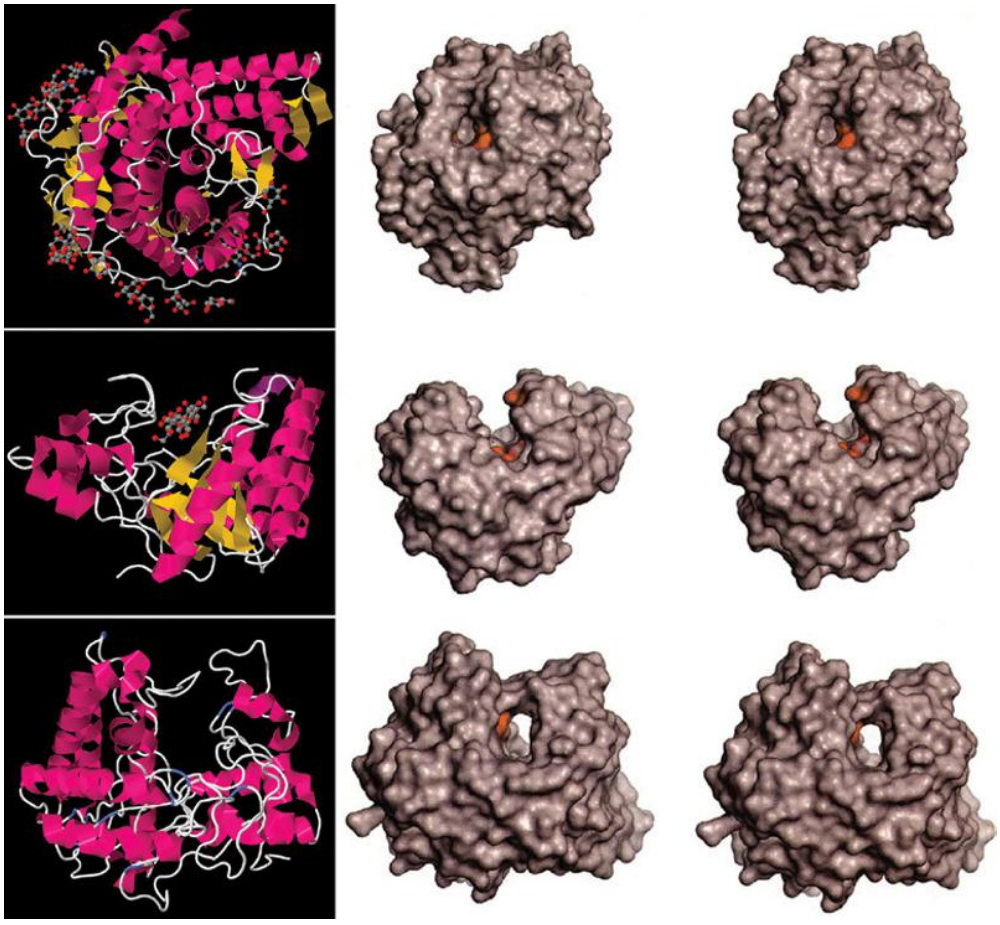


FIGURE 2.42 *Fundamental structures of hydrolases. Crystal structures and stereo pairs of three types of exo- and endohydrolytic enzymes. The top pair ("pocket") and bottom pair ("tunnel") are typical of exohydrolases, whereas the middle pair ("groove" or "cleft") is characteristic of endohydrolases. One can 'freeview' the image pair without a viewing device by relaxing one's eyes and looking* through *each image in parallel at a comfortable distance, where the apparent distance between the images matches that of your eyes. The 3D image should appear in good focus between the two.*

demonstrating that sequence similarity is not a sufficient basis for inferring biochemical function of homologs.

Polysaccharide degrading enzymes are classified as either **exo**- or **endohydrolases**. Typically exo-hydrolases cleave mono- or disaccharides from the nonreducing terminus of the polysaccharide chain, whereas endo-hydrolases break glycosidic bonds randomly along a chain that is uninterrupted by side groups. Crystal structures show that exo-hydrolases form cavities or tunnels for insertion of the end of a polysaccharide, but endo-enzymes form grooves that can attach to the polysaccharide anywhere along the chain (Fig. 2.42). Like glycosyl transferases, hydrolases have **retaining** and **inverting** mechanisms of catalysis, depending on whether an acyl intermediate is formed before water cleaves the glycosidic bond (Fig. 2.43A and B). Certain classes of carbohydrate-active enzymes possess tethered **carbohydrate-binding modules** (CBM) that provide substrate specificity. Over 60 families of CBMs have been discovered, including those of plant hydrolases. **Pectin, pectate,** and **RG lyases** are endo-enzymes that cleave uronic acid-rich polysaccharides without water, creating an anhydro-uronic acid (Fig. 2.43C).

2.5.9 Type I and Type II cell walls exhibit different biochemical changes during growth

Dramatic chemical changes occur in crosslinking glycans of Type II walls of commelinid monocots. A highly substituted GAX (HS-GAX), in which six out of every seven Xyl units bears an appendant group, is associated with the maximum growth rate of coleoptiles. The number of Ara and GlcA side groups along the GAX chains varies markedly, from GAXs for which Xyl units are nearly all branched to those with only 10% or less of Xyl units bearing side groups. Side groups not only prevent hydrogen bonding but also render GAX water

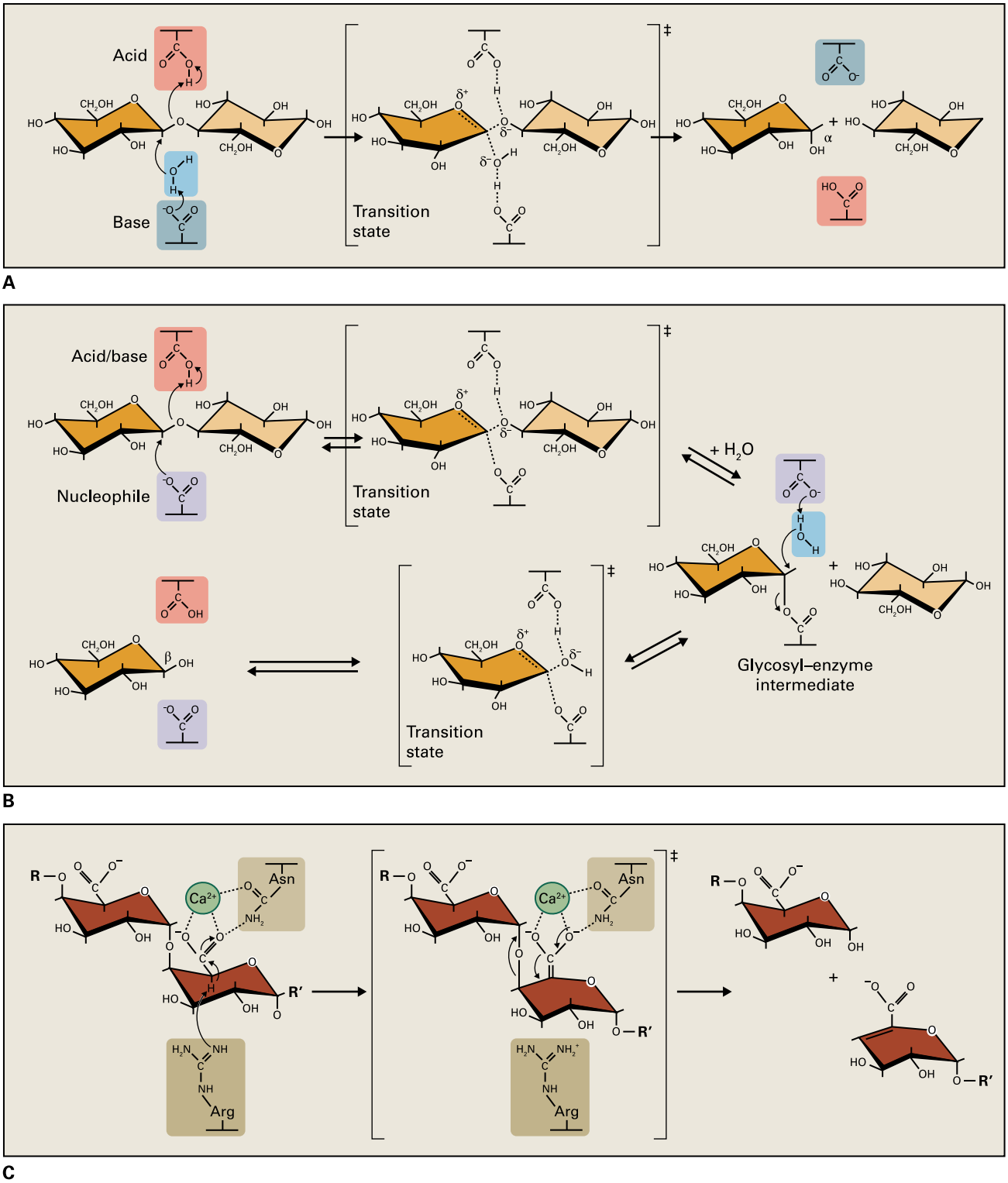


FIGURE 2.43 *Mechanisms of catalysis of hydrolases and lyases. (A) "Inverting" glycoside hydrolases break glycosidic bonds in a single step reaction that inverts the anomeric configuration in a reaction mechanism involving oxocarbenium ion-like transition states. In the example here, the β-linkage of the glycoside cellobiose is converted to the α-configuration upon hydrolysis. The reaction occurs with acid/base catalysis typically by two glutamic or aspartic acids. These reactions are carried out when the carboxylic acid/carboxylate groups of the two amino acids are about 6-10 Å apart, allowing enough room for both water and the glycoside in the active site. (B) In "retaining" glycoside hydrolases, the configuration is retained in a two-step reaction involving two oxocarbenium ion-like transition states and a glycosyl–enzyme intermediate. Like the inverting hydrolases, the acid/base and nucleophilic amino acids are typically aspartic and glutamic acids, but spacing of the reactive groups in the active site is about 5.5 Å. In this example, the β-linkage of cellobiose is retained in the β-configuration. In these types of reactions, water can be replaced by other glycosides, and the enzyme can perform transglycosylation reactions to make longer oligomers. (C) In contrast to hydrolases catalyzed by acidic amino acids, lyases use basic amino acids to catalyze the breakage of glycosidic linkages in the absence of water. In this example of a pectate lyase, deprotonation of the C5 carbon is made possible by the electrophilic nature of the carboxyl group of the uronic acid, catalytic divalent Ca^{2+} ions, and the two basic amino acid residues in the active site. Lyase activity results in desaturation of the uronosyl residue between the C4 and C5 carbons, resulting in a puckering of the normally relaxed chair of the pyranose.*

soluble. In dividing and elongating cells, highly branched GAXs are abundant, whereas after elongation and differentiation, more and more unbranched GAX polymers accumulate. Cleavage of the Ara and other side groups from contiguously branched Xyl units can yield runs of unbranched xylan capable of binding to other unbranched xylans or to cellulose microfibrils.

Type II walls are also low in pectin content. Chemically, pectins of the Type II wall include both HG and RG I, and HS-GAX is closely associated with these pectins. Interactions between HS-GAX, HG, and RG I could control wall-loosening activities, as suggested for Type I walls. Spacing of the appendant Ara and GlcA units of GAXs could determine porosity and surface charge, functionally replacing the predominant pectic substances in Type I cell wall, as illustrated in Fig. 2.25B. HGs of *Z. mays* pectins, which are methyl esterified, also contain nonmethyl esters, the formation and disappearance of which coincide with the most rapid rate of cell elongation. The chemical nature of the nonmethyl esters is not known. Some arabinans, particularly 5-linked arabinans, are found in walls of dividing cells but are not made during cell expansion.

When grass cells begin to elongate, they accumulate mixed-linkage **β-glucans** in addition to GAX (see Fig. 2.15). Among the angiosperms, β-glucans are unique to the Poales (see Fig. 2.14) and are one of the few known developmental stage-specific polysaccharides among the angiosperms. Absent from meristems and dividing cells, β-glucans accumulate to almost 30% of the noncellulosic cell wall material during the peak of cell elongation, and then are largely hydrolyzed by cells during differentiation. Because synthesis and hydrolysis of β-glucans occurs simultaneously throughout elongation, the amount that accumulates is a small fraction of the total synthesized. Appearance of β-glucans during cell expansion and acceleration of their hydrolysis by auxin treatment implicate direct involvement of the polymer in growth.

2.5.10 Once growth has ceased, cell wall shape must be locked in place by wall components

Once elongation is complete, the primary wall locks the cell into shape by becoming much less extensible. One component of the locking mechanism for Type I walls may be HRGPs, such as extensin. The flexible regions of these proteins could wrap around cellulose microfibrils, and the rod-like regions serve as spacers. However, we do not know how extensins are crosslinked in the wall. Loss of solubility of extensins in Type I walls is associated with an increase in tensile strength. Other proteins may be necessary to actually lock extensins together. Greater quantities of PRP are synthesized later in cell development and particularly in the same vascular cells as extensin. One hypothesis holds that extensin precursors accumulate in the cell wall during cell division and elongation, but cannot crosslink wall components in the absence of PRPs.

Instead of Hyp-rich extensin, Type II walls contain a threonine-rich protein, with sequences reminiscent of extensin; crosslinking phenolic compounds are also present. As with extensin, soluble precursors of Thr-rich protein accumulate early in the cell cycle and become insoluble during cell elongation and differentiation. This polymer is prevalent in vascular tissue and in special, reinforced wall structures, such as pericarp. However, much of the crosslinking function in Type II walls probably rests with esterified and etherified phenolic acids, and formation of these crosslinkages accelerates at the end of the growth phase. Once phenolic cross-bridges are in place, they may account for a substantial part of the load-bearing role in fully expanded cells (see Fig. 2.25B).

2.6 Cell differentiation

2.6.1 The plant extracellular matrix is a mosaic of cell wall architectures

At the light microscope level, histochemical stains reveal a diverse distribution of polysaccharides in different cells, and the complexity of polysaccharide structure is resolved even more effectively with highly specific probes. This has been achieved using the natural specificity of enzymes for their substrates and antibodies for particular antigens (Box 2.7). More recently, the advent of microspectroscopy, in which a microscope with modified optics is attached to a spectrometer, has made **chemical imaging** possible. The distribution of a functional group of a molecule can be mapped at the single-cell level (Box 2.7).

Even in a single cell, modifications occur that distinguish between transverse and longitudinal walls. For example, preferential digestion of end walls occurs in sieve tube elements. Some substances, such as waxes, are secreted only to a cell's outer epidermal face. Within a single wall there are zones of different architectures, the middle lamella, plasmodesmata, thickenings, channels, pit-fields and cell corners, and there are domains within the thickness of a wall in which degree of pectin esterification and abundance of RG I side-chains differ (Fig. 2.44).

Comparisons of the sizes of microdomains in the wall with those of the polymers that must fit within them implies that mechanisms exist for packaging and positioning of large molecules. For example, unesterified pectins can be as long as 700 nm, and yet in some cell types, are accommodated in a middle lamella that is only 10–20 nm wide, indicating they must be constrained to lie parallel to the plasma membrane. This microdiversity within walls reveals that the wall is not a homogeneous and uniform building material, but a mosaic of different wall architectures in which various components contribute to the multifunctional properties of the apoplast.

2.6.2 Fruit ripening involves developmentally regulated changes in wall architecture

Most fruits in which the pericarp or endocarp softens during ripening develop thickened primary walls that are markedly enriched in pectic substances, primarily HG and RG I (Fig. 2.45). Texture of ripe fruit pulp is governed by the extent of wall degradation and loss of cell–cell adhesion. For example, the walls of the apple (*Malus domestica*) cortex undergo little change in rigidity and exhibit little separation, whereas walls of the peach (*Prunus persica*) mesocarp and tomato (*Solanum lycopersicum*) pericarp soften considerably through wall swelling and loss of cell adhesion. In tomato, locules containing the seeds dissolve completely in a process called **liquefaction**.

Pectins can constitute more than 50% of the fruit wall. Softening in tomato parenchyma tissue is associated with loss of methyl esters of HG, the consequence of activity of PME, which removes methylester groups from the GalA residues of pectic polysaccharide backbones. The deesterified HG backbone is then susceptible to activity of PGase. PGase I, with a molecular mass of approximately 100 kDa, comprises a 46-kDa PGase II tightly complexed with a β-subunit. The β-subunit is a unique **aromatic amino acid-rich protein** that is synthesized early in fruit development and thought to function as an anchoring component for the PGase II subunit. The β-subunit may solubilize pectins from the cell wall, facilitating progressive hydrolysis by PGase II of the glycosidic bonds within the unbranched HG backbone. Pectin modification within the wall during ripening is tightly regulated, the result of such mechanisms as substrate modification, which restricts

BOX 2.7

Techniques to probe heterogeneity of wall composition at the single cell level

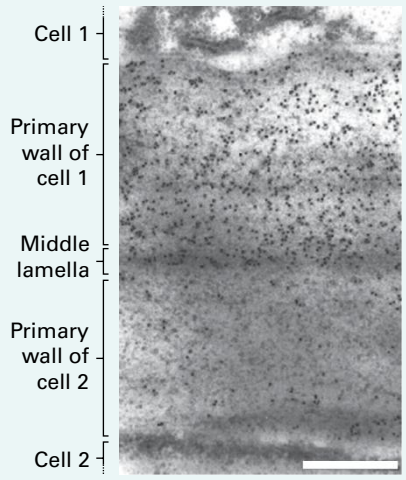
A wide range of antibodies has been raised against cell wall epitopes, most commonly using monoclonal antibody technology or from recombinant phage libraries. Two sites are devoted to development and cataloguing of cell wall monoclonal antibodies and other reagents to probe polysaccharide fine structure at the single cell wall level or for development of tailored carbohydrate microarrays at the Complex Carbohydrate Research Center (http://www.ccrc.uga.edu/~carbosource/CSS_home.html) and PlantProbes, University of Leeds, UK (http://www.plantprobes.net).

The complexity of polysaccharide structure has made precise characterization of epitopes difficult. These antibodies are used as "designer stains" to label cell walls (A), isolated polymers (B), or their sites of synthesis (C).

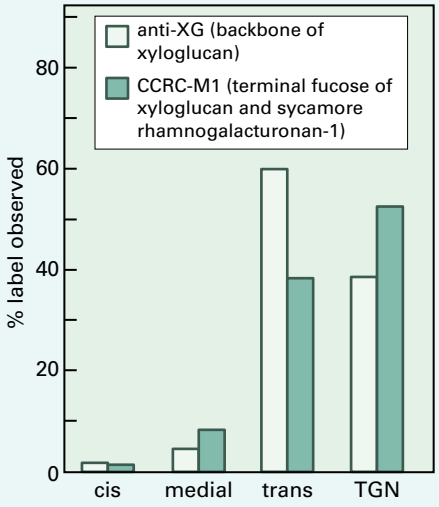
Some hydrolytic cell wall enzymes contain a polysaccharide-binding domain, such as the carbohydrate-binding module (CBM) of bacterial and fungal cellulases, and these enzymes can be conjugated directly with colloidal gold to produce probes for use in the electron microscope. Enzymes are denatured before coupling so that catalytic activity is eliminated, yet binding specificity remains. High-resolution images of their binding have been achieved by using semiconductor quantum dots incorporated into a recombinant CBM fused to a molecular tag of repeated histidine (or His) units for direct imaging. Water-soluble and highly luminescent quantum dots of (CdSe)ZnSe bind five histidines at the zinc surface while retaining desirable electronic properties for imaging by transmission electron microscopy (top) or scanning transmission electron microscopy (bottom) to decorate an individual cellulose microfibril (D).

Another means of probing the chemical composition of single cell walls is Fourier transform infrared (FTIR) microspectroscopy. FTIR spectroscopy is an extremely rapid, noninvasive vibrational spectroscopic method that can quantitatively detect a range of functional groups including carboxylic esters, phenolic esters, protein amides and carboxylic acids, and can provide a complex "fingerprint" of carbohydrate constituents and their organization (E). Several functional groups absorb infrared radiation at characteristic frequencies, making assignments of some specific wall components possible, for example, the methyl esters and carboxylate ions of pectins. The IR beam can be diverted via mirror optics to pass through a sample mounted on a microscope stage. Individual spectra from areas of these dimensions can be collected over a large tissue area by a computer-driven stage to produce chemical images of the sample, as in this map of methyl ester distribution in an *Arabidopsis* hypocotyl (F). Each frequency in the IR spectrum can be represented as a separate map. Another vibrational spectroscopy, FT-Raman spectroscopy, provides a complementary technique for chemical imaging. Raman scattering depends on changes in polarizability of functional groups due to molecular vibration, while infrared absorption depends on changes in intrinsic dipole moments. Spatial resolution of infrared chemical imaging is limited to 10 μm by diffraction effects. Improved resolution, to 1 μm, is obtained with Raman imaging. Sample fluorescence and the inherent weakness of Raman scattering can be problems. For the latter, recent developments in stimulated Raman spectroscopy provides the opportunity for local signal amplification and much improved Raman signal detection. (G) A Raman spectrum of maize cell walls with a red arrow indicating the absorbance at 1600 cm^{-1} corresponding to lignin, and a chemical image of a stem section showing where this signal is most abundant (red).

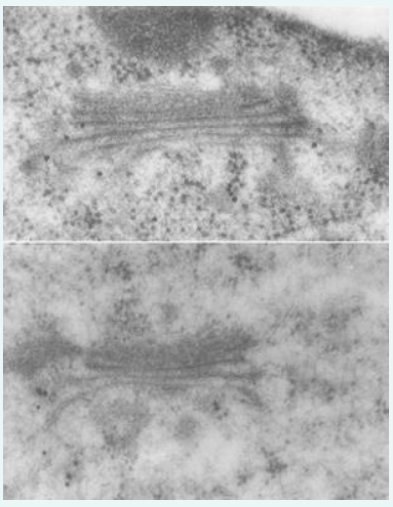
Source: (A) Steele et al. (1997). Plant Physiol 114:373–381. (B) McCann et al. (1995). Can J Bot 73: S103–S113. (D) Ding et al. (2006). Biotechniques 41:435–443. (E) M.C. McCann, John Innes Center, Norwich, UK. (G) Saar et al. (2010). Agnew Chem Int Ed 49:5476–5479.

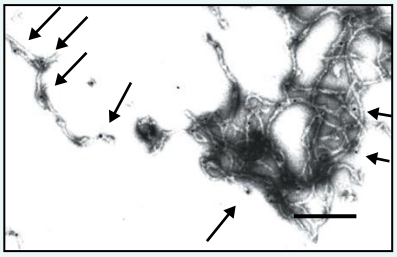

Cell 1
Primary wall of cell 1
Middle lamella
Primary wall of cell 2
Cell 2

A

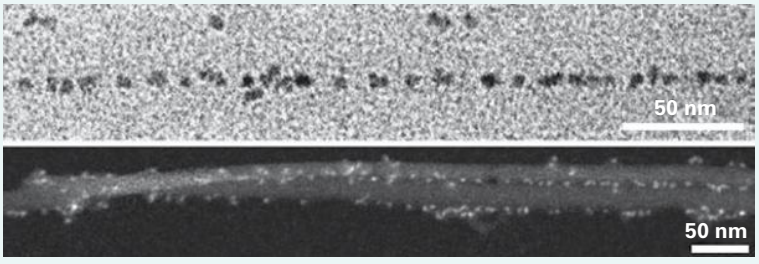

anti-XG (backbone of xyloglucan)
CCRC-M1 (terminal fucose of xyloglucan and sycamore rhamnogalacturonan-1)
% label observed
0
20
40
60
80
cis
medial
trans
TGN
Cisternal positioning in Golgi stack

C

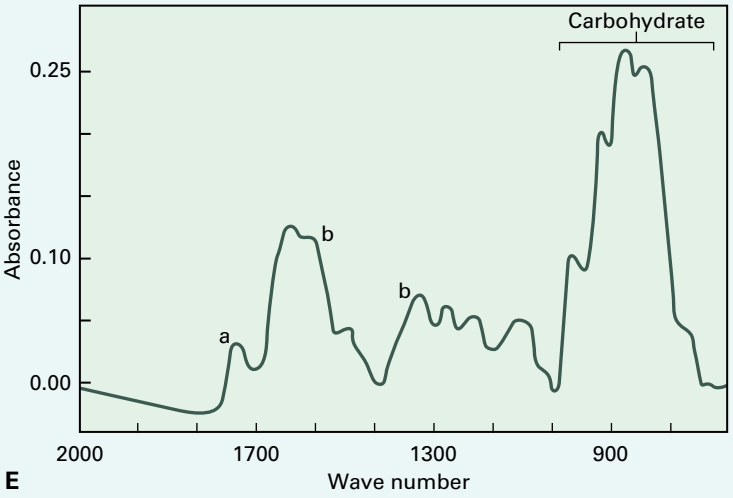




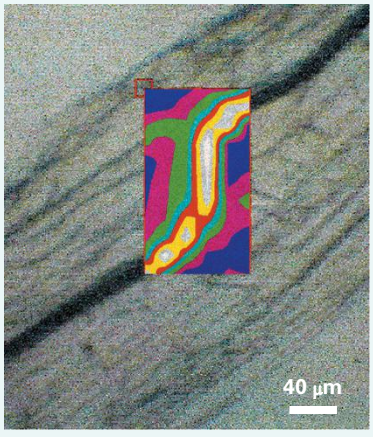
B


50 nm
50 nm

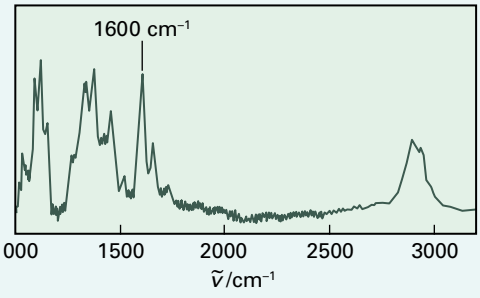
D


Carbohydrate
0.25
0.10
0.00
Absorbance
a
b
b
2000
1700
1300
900
Wave number

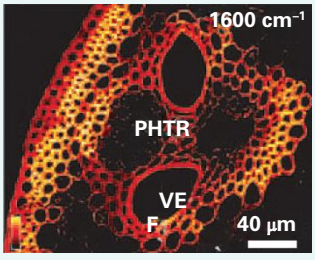
E


40 µm

F


1600 cm⁻¹
1000
1500
2000
2500
3000
ν̃/cm⁻¹

G


1600 cm⁻¹
PHTR
VE
F
40 µm

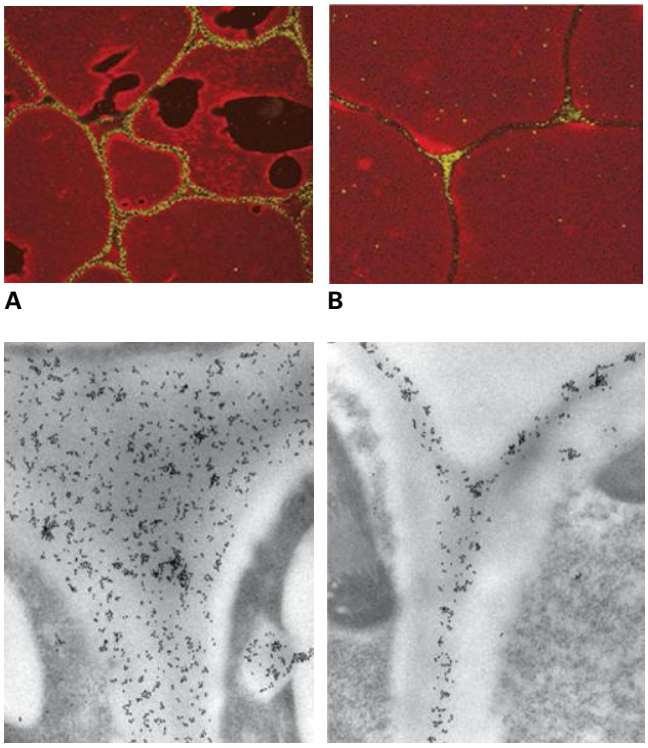


FIGURE 2.44 *Potato cell walls immunogold-labeled and silver-enhanced to reveal the localization of pectin galactan side-chains and calcium pectate junctions, with use of the monoclonal antibodies LM5 and 2F4, respectively, in the light microscope. The green color shows where light is reflected from silver-enhanced gold particles in the confocal microscope. The galactan side-chains are localized to the primary wall (A), whereas calcium pectate is predominantly in cell corners (B). A methyl-esterified pectic epitope is present throughout the cell walls of vascular cells (C) but restricted to an outer layer of the walls of palisade cells (D) in electron micrographs of a* Zinnia elegans *leaf immunogold-labeled with the JIM7 monoclonal antibody.*
Source: (A, B) Max Bush, John Innes Centre, UK. (C, D) Stacy et al. (1995). Plant J 8:891–906.

enzyme access to the substrate, or the presence of enzyme inhibitors, as in the inhibition of PGase II activity by the diffusible products of pectin depolymerization. Inhibitor proteins that inactivate PMEs and PGases have also been identified that endogenously regulate pectin depolymerization or protect against pathogenic organisms.

Despite extensive deesterification and depolymerization of pectin polymers during ripening, fruit softening does not appear to result directly from these modifications to HG. Using antisense inhibition of PGase, researchers were able to almost completely inhibit such activity, essentially preventing pectic depolymerization in transgenic fruit; however, little or no reduction in softening occurred. Although crosslinking glycans do not appear to undergo extensive ripening-related depolymerization, several glycan-degrading enzymes increase in activity including XET, expansin, and glycan hydrolases. These enzymes may be involved in restructuring the tethering by crosslinking glycans, thereby changing the properties of the network throughout the primary cell wall and contributing to softening of the pericarp tissue and whole tomato fruit.

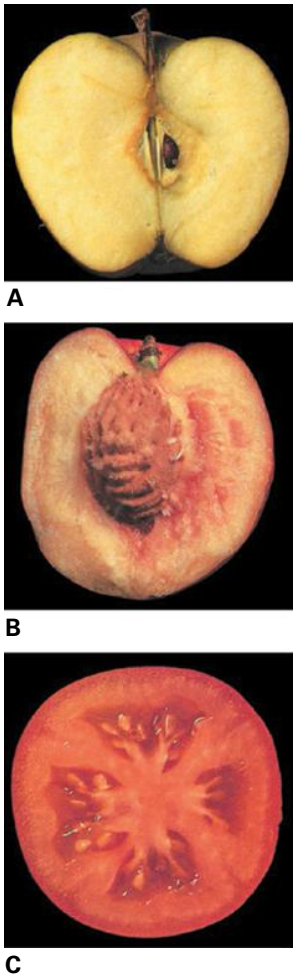


FIGURE 2.45 *Cell walls are the principal textural elements of fresh fruits and vegetables. The walls of fruit change their architecture in different ways during ripening. (A) Apple cortex walls may stiffen and maintain cell adhesions. The 'mealy' texture of an overripe apple is a result of loss of cell–cell adhesion by dissolution of the middle lamella. The middle lamella is enriched in many pectic substances. (B) The walls of the mesocarp cells of peach swell and soften during ripening, whereas those of the endocarp become an exceptionally tough protective shield for the seed. (C) Like the peach, the tomato pericarp walls swell and soften during ripening, but some of the walls completely disintegrate, by a process called liquefaction, to create locules for the developing seeds.*
Source: (A–C) Bowes. (1996). A Colour Atlas of Plant Structure. Manson Publishers, London.

2.6.3 Secondary walls are elaborated after growth of the primary wall has stopped

For many cell types, the differentiation process is associated with the formation of a distinct **secondary wall** on the plasma-membrane side of the primary wall. Regardless of chemical composition, the primary wall is always defined as the structure that participates in irreversible cell expansion. When cells stop growing, the wall is crosslinked into its ultimate shape. At that point, deposition of the secondary wall begins.

Secondary walls often exhibit elaborate specializations. The cotton (*Gossypium hirsutum*) fiber, for example, consists of nearly 98% cellulose at maturity. In some cells, such as

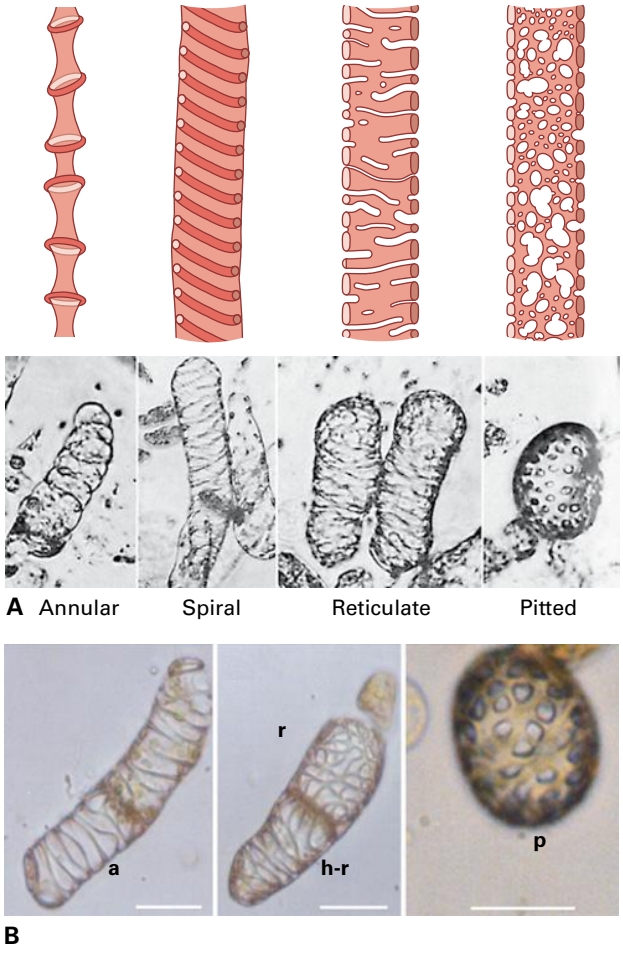


FIGURE 2.46 *Secondary wall thickening patterns of vessel elements in a single plant may be annular, spiral, reticulate, and pitted. Many of these patterns are emulated during formation of the tracheary elements in vitro by* Zinnia elegans *mesophyll cells in liquid culture (a = annular; r = reticulate; h-r = helical-reticulate; p = pitted). Source*: Falconer & Seagull. (1985). Protoplasma 125:190–198.

sclereids, vascular fibers, and the stone cells of pear, the secondary wall becomes uniformly thick, composed largely of cellulose microfibrils that can sometimes fill the entire cell lumen. The secondary wall can contain, however, additional noncellulosic polysaccharides, proteins, and aromatic substances such as lignin. In tracheids, secondary walls can form special patterns, such as annular or helical coils or reticulate and pitted patterns (Fig. 2.46). These walls typically contain glucuronoxylans or 4-*O*-methylglucuronoxylans in addition to cellulose. Unlike GAXs of grass walls, these xylans are devoid of Ara but contain a (1→2)-α-D-GlcA residue about every 6–12 xylosyl residues. Collenchyma cells elaborate a primary wall at thickened corners of these cells (Fig. 2.47).

The walls of many cells function long after the cells that produced them are dead and desiccated. For example, orientation of the polymers assembled in walls of living cells results in mechanical strains upon desiccation, strains that result in abscission of plant parts and the dehiscence of fruit coats along defined planes. The paper-thin wings of a maple (*Acer* spp.) samara and feathery tufts of hair cells of dandelion (*Taraxacum officinale*) and willow (*Salix* spp.) fruits form only upon drying: each structure aids in scattering of seeds (Fig. 2.48).

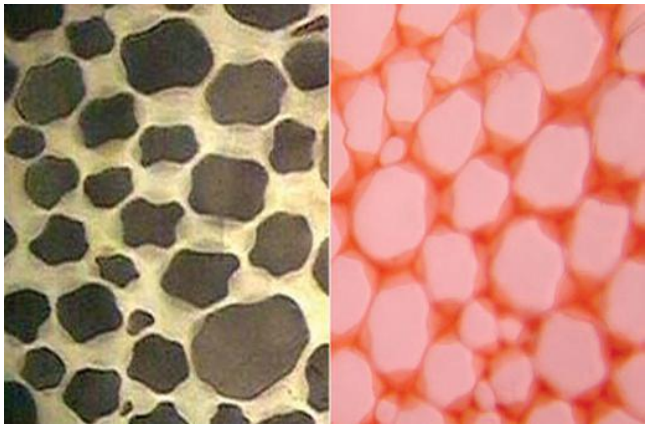


FIGURE 2.47 *(A) Collenchyma cell has reinforced thickenings only in the cell corners. (B) Cellulosic thickenings of the primary wall can be seen when pectins of the middle lamella are stained with Neutral Red. Source*: John Tiftickjian, Delta State University.

Many structural proteins are cell-specific, occurring only in the secondary wall. For example, some PRPs concentrate in secondary walls of protoxylem elements of bean (*Phaseolus vulgaris*), whereas some GRP family members are synthesized in xylem parenchyma cells and exported to primary walls of neighboring protoxylem elements. Other GRPs are found in sclereids, associated with both the primary and secondary walls. HRGPs generally are found in primary walls of all tissues, although in widely varying proportion, but a Thr-rich, extensin-like protein of *Z. mays* is more abundant in secondary walls of the firm pericarp of popcorn.

Not all cell wall secondary thickenings represent distinct secondary walls. Some thickened walls have a composition typical of a primary wall but simply contain more strata. Guard cells and epidermal cells thicken the wall facing the environment to a much greater degree than side walls or the inward-facing wall. Pairs of guard cells contain thickenings of radially arranged cellulose microfibrils, especially in walls adjacent to the stoma, which are needed to withstand the enormous turgor pressure generated by the cell during stomatal opening (see Fig. 2.2C). Pectic arabinans in guard cell walls are required for their ability to open and close reversibly. Epidermal cells form specialized exterior layers of cutin and suberin to prevent loss of water vapor, and endodermal cells suberize their contiguous side walls to form the Casparian band that forces water and dissolved solutes to move symplasmically into the stele.

2.6.4 Secondary deposition of suberin and cutin renders cell walls impermeable to water

Suberin is found in specific tissues and cell types, notably the root and stem epidermis, cork cells of the periderm, surfaces of wounded cells, and parts of the endodermis and bundle

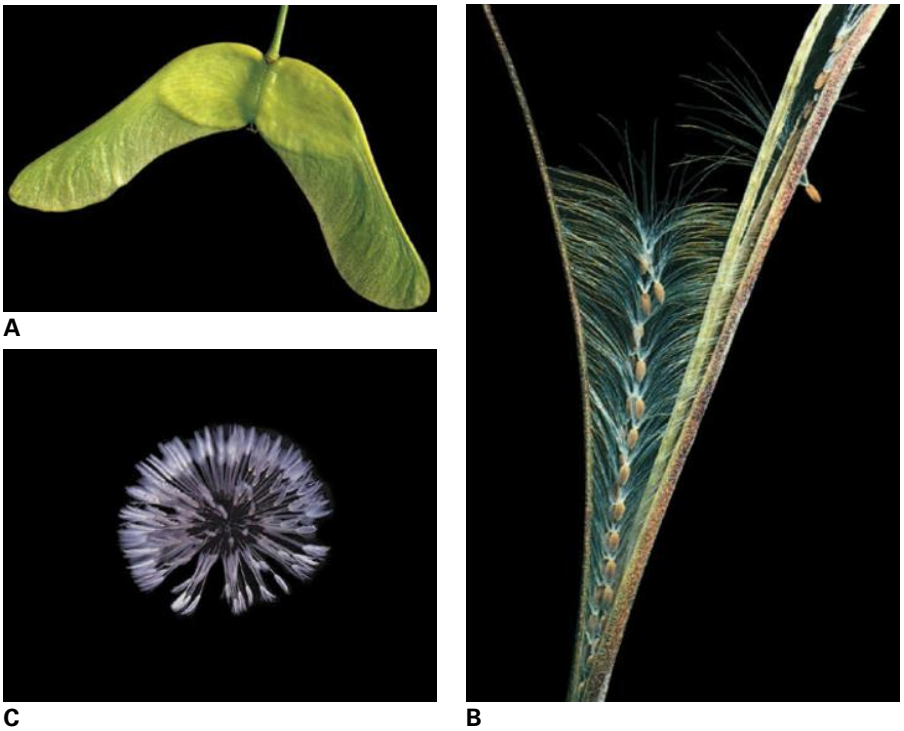


FIGURE 2.48 *Cells that produce special walls can function long after death. The sycamore-maple uses paper-thin walls of a samara as wings for seed dispersal (A). The hard fruit coat of a willow cracks open along a dehiscence zone upon desiccation (B). The pattern of microfibril deposition creates a physical tension that causes fruit to snap open. Like the dandelion (C), the feather tuffs of willow trichomes are used for long-distance seed dispersal.*
Source: Bowes. (1996). A Colour Atlas of Plant Structure. Manson Publishers, London.

sheath cells (Fig. 2.49). It is recognized by lipid-specific stains such as Sudan IV, which detects long-chain fatty acids and alcohols, dicarboxylic acids, and hydroxylated fatty acids. The core of suberin is lignin-like and incorporates ferulate esters of fatty alcohols via radical coupling reactions. The attachment of the long-chain hydrocarbons imparts a strongly hydrophobic character to material that prevents water movement.

The polyester cutin and its associated waxes also are found on leaf and stem surfaces, providing a strong barrier to diffusion of water. Waxes generally are esters of long-chain fatty acids and alcohols, but are better described as complex mixtures of these hydrocarbon esters with ketones, phenolic esters, terpenes, and sterols.

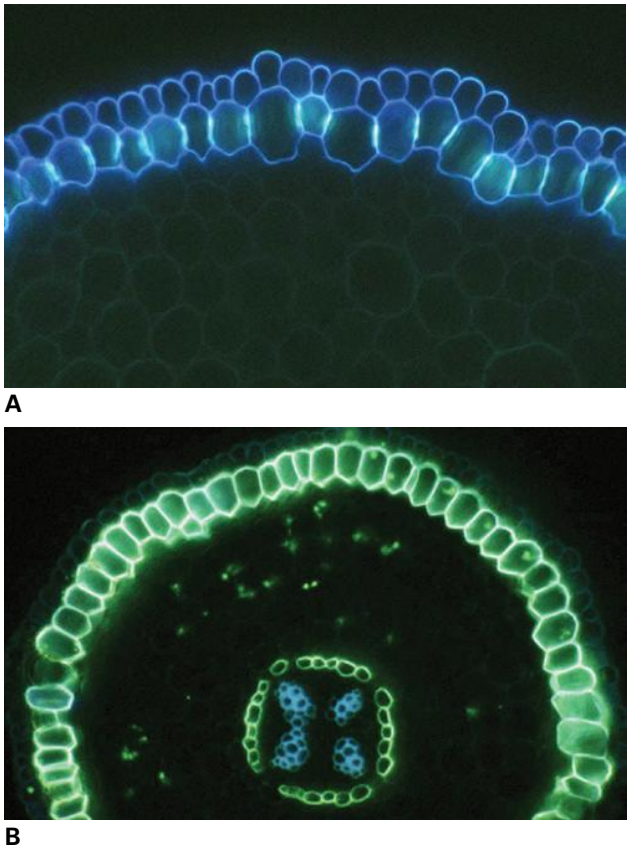


FIGURE 2.49 *Certain cell walls are waterproofed with suberin. (A) Cell walls of epidermis and exodermis of an onion (*Allium cepa*) root are detected with the blue fluorescent stain for suberin, berberine. (B) Exodermis and endodermis of an ash* (Fraxinus *spp.) are detected with the green fluorescent stain for lipids, fluorol. Lignin autofluorescence of xylem tracheary elements is shown in blue.*
Source: Brundrett. (2008). Mycorrhizal Associations: The Web Resource. Accessed May 7, 2015.

2.6.5 Lignin is a major component of some secondary walls

The most obvious distinguishing feature of secondary walls is the incorporation of lignins, complex networks of aromatic compounds called **phenylpropanoids**. With a few exceptions, no lignin exists in Type I primary walls, whereas networks of lignin and other phenylpropanoid compounds are present in Type II primary walls. For Type I walls, lignin synthesis is initiated when secondary wall deposition commences. Three primary phenylpropanoids, the hydroxycinnamyl alcohols or "monolignols"—*p*-coumaryl, coniferyl, and sinapyl alcohols—account for most of the lignin networks. The monolignols are linked by way of ether, or carbon–carbon bonds via radical coupling reactions (see Fig. 2.23), the predominant coupling reaction of a monolignol (invariably at its side-chain β-position) with the phenolic end of the growing polymer (at

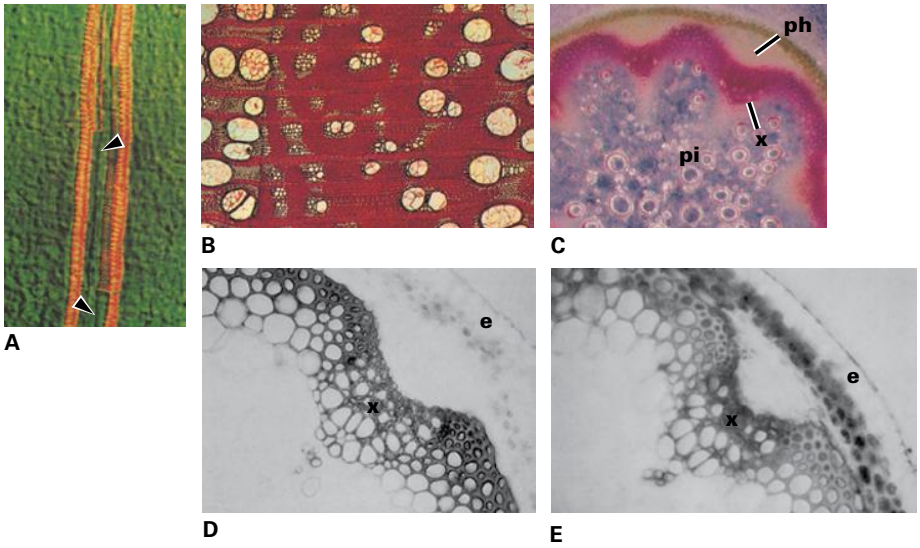


FIGURE 2.50 *Several different procedures can be used to visualize lignin, including (A) acid fuchsin, which produces an orange fluorescence. In this* Arabidopsis *leaf, lignin can be seen located in spiral thickenings of vessels. Phloroglucinol is a general stain for lignin as seen in cross-section of a* Robinia pseudoacacia *stem (B), or xylem (x) and extraxylary fibers of an* Arabidopsis *floral stem (C). Mäule reagent produces a red color with syringyl lignin, which is derived from sinapyl alcohols, but forms a brown-orange color on reacting with guaiacyl lignin, which is derived from coniferyl alcohol (D). This reagent differentiates a mutant of* Arabidopsis *unable to make syringyl lignin from wild-type plants (E). ph, phloem; pi, pith; e, epidermis. Source*: (A) Dharmawardhana et al. (1992). Can J Bot 70:2238–2244. (B) Bowes. (1996). A Colour Atlas of Plant Structure. Manson Publishers, London. (C) Zhong et al. (1997). Plant Cell 9:2159–2170. (E) Chapple et al. (1992). Plant Cell 4:1413–1424.

its 4-*O*- or 5-positions). The diversity of monolignols, their radical coupling at several possible sites on each phenolic moiety, and the racemic nature of polymerization all impart remarkable complexity to lignin structure.

Lignins can be detected in tissue sections by specific stains, such as acid fuchsin, the Wiesner reagent (phloroglucinol-HCl), and the Mäule reagent (Fig. 2.50). The Mäule reaction, in which a $KMnO_4$ oxidation is followed with ammonia, is particularly useful because it distinguishes syringyl lignin and guaiacyl lignin, indicating the former by a bright red color and the latter by yellow (Fig. 2.50). Total lignin is quantified by various methods, either chemically or by NMR and other spectroscopic methods. Degradative acidolysis and thioacidolysis, reductive cleavage, permanganate, nitrobenzene, and alkali/copper oxide oxidation are all used to detect lignin. The former procedures are considered the most diagnostic, specifically cleaving the characteristic β-aryl ether bonds to release monomers and higher oligomers. The **degradation followed by reductive cleavage (DFRC)** method partially cleaves lignins to peracetates of their constituent monomers (as peracetates after the full procedure). The products of oxidations include *p*-hydroxybenzaldehyde, vanillin, and syringaldehyde (and their corresponding acids) from *p*-hydroxyphenyl, guaiacyl, and syringyl lignin units, respectively. Because most plants contain only very low levels (<2%) of *p*-hydroxyphenyl units, lignins are classified by their guaiacyl and syringyl content. Gymnosperms contain predominantly guaiacyl units, whereas woody angiosperms, herbaceous eudicots and grasses exhibit a broad range of ratios of guaiacyl and syringyl residues.

Synthesis of monolignols in plants is well documented and appears to occur in the cytosol. Monolignols can be glycosylated in reactions associated with the ER and Golgi apparatus, but this glycosylation may simply be for protection and storage; it does not seem to be necessary for membrane transport and targeting. Once in the wall, monolignols polymerize via radical coupling reactions. The radicals are generated by **peroxidases**, which use H_2O_2 as a substrate, or by **laccases**, members of the "blue copper oxidase" family of enzymes that use O_2. Although monolignol–monolignol dehydrodimerization reactions are implicated in chain initiation, the main lignification event is the addition of a monolignol (radical) to the phenolic end of the growing polymer (see Fig. 2.23) in a so-called endwise process.

During lignification, there are opportunities for cell wall crosslinking by at least two mechanisms. First, each radical coupling reaction of a monolignol at its β-position produces an intermediate quinone methide structure that must be rearomatized by nucleophilic addition at its benzylic or α-position. This is chiefly accomplished by internal trapping to make phenylcoumaran and resinol structures, or simply by proton-catalyzed water addition to produce the α-hydroxy-β-ether compounds (see Fig. 2.23). Carbohydrate hydroxyls may also be coupled, however, to produce lignin-carbohydrate benzylic ethers and yield lignin–polysaccharide crosslinking, although evidence for such lignin-carbohydrate linkages has been difficult to find. In Type II cell walls ferulate esters on GAX undergo radical coupling reactions analogous to those of monolignols. Thus, combinatorial ferulate dehydrodimerization results in a range of dehydrodiferulates and effects powerful polysaccharide–polysaccharide crosslinking (see Fig. 2.23). Moreover, ferulate radicals and radicals from diferulates are compatible with radical coupling reactions going on within lignification. As a result, ferulates cross-couple with

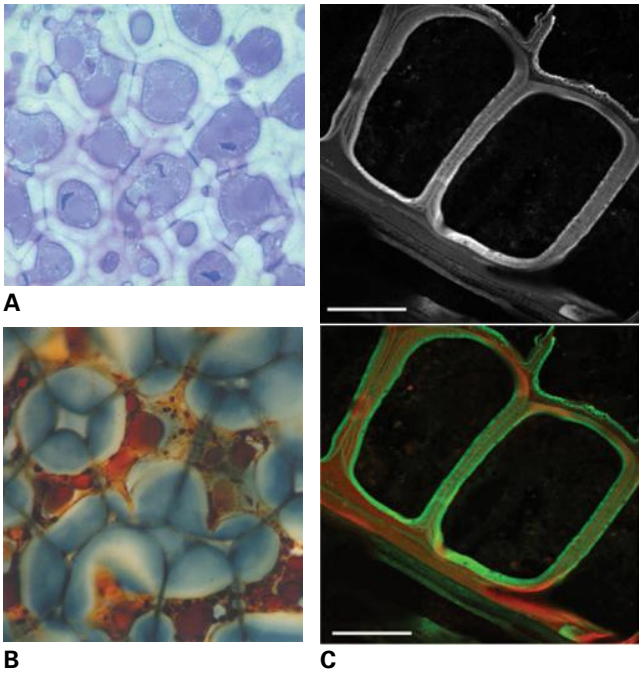


FIGURE 2.51 *Endosperm walls of date (*Phoenix dactylifera*) have extremely hard and thick walls of mannan. (A) A low-magnification light micrograph of date endosperm shows that these mannans exclude Toluidine Blue dye. (B) Cotyledon walls of Brazilian legume jatobá (*Hymanaea courbaril*) accumulate "amyloid" xyloglucans that stain lightly with iodine. (C) The aleurone layer, the outermost layer of endosperm cells of grass caryopsis, has cell walls enriched in mixed-linkage β-glucan. The β-glucan is detected with a monoclonal antibody against the (1→3),(1→4)-β-D-linkage. Immunofluorescence labeling is viewed by confocal microscopy. Bars = 25 μm.*
Source: (A) D. DeMason, University of California, Riverdale. (B) M. Buckeridge, Instituto de Botanica, Secao de Fisiologia e Bioquimica Plantas, Sao Paulo, SP, Brasil. (C) Fabienne Guillon, INRA, Nantes, France.

monolignols and higher oligomers to integrate into the lignin matrix. Although it is rarely noted as such, these ferulates, in addition to the monolignols themselves, are authentic therefore "monomers" in lignification.

2.6.6 Some secondary walls can serve as storage materials

Another site of diversity among plant species is the secondary walls of the cotyledon and endosperm of developing seeds. These walls contain little or no cellulose but rather consist of a single noncellulosic polysaccharide typically found in the primary wall. These secondary walls serve two functions. First, they provide a strong wall to protect the embryo or impose mechanical dormancy. Second, they contain specialized storage carbohydrates that are digested during germination and converted to sucrose for transport to the growing seedling.

Gal-rich XyG abounds on the cotyledon walls of *Tamarindus, Hymenaea courbaril* (jatobá), and similar legumes, as well as species of Primulaceae (primrose family), Linaceae (flax family) and Ranunculaceae (buttercup family) (Fig. 2.51). Glucomannans predominate in cotyledon walls of some lilies and irises. Seeds of date (*Phoenix dactylifera*), coconut (*Cocos nucifera*) and other palms, coffee bean (*Coffea arabica*), ivory nut (*Phytelephas aequatorialis*), and some Apiaceae all contain a thick cotyledon or endosperm wall of almost pure mannan (Fig 2.51). The endosperm of lettuce (*Lactuca sativa*) seeds, which constitutes the mechanical determinant of dormancy, is more than 70% mannan. All endospermic legumes store galactomannans, but the Man:Gal ratio can vary markedly, yielding a variety of galactomannans with very different physical properties. For example, fenugreek (*Trigonella*) makes an almost fully branched galactomannan, whereas guar (*Cyamopsis*) galactomannans and those of carob (*Ceratonia siliqua*) or locust bean (*Ectomyelois ceratoniae*) are much less branched, which changes their viscosities. Seeds of yet other species accumulate neutral polysaccharides typically found associated with pectins. For example, lupines contain large amounts of (1→4)-β-D-galactan, and some arabinan.

All grasses accumulate (1→3),(1→4)-β-D-glucan in walls of endosperm at some stage in embryo development. Oat (*Avena sativa*) and barley (*Hordeum vulgare*) brans are notably enriched in β-glucans, which make up as much as 70% of the aleurone layer cell walls at maturity (Fig. 2.51).

2.6.7 Global regulation of cell wall synthesis

It is clear that different gene family members must be coordinately regulated to build walls of specific composition. The expression patterns of individual gene family members are being measured using whole or custom microarrays or newer deep-sequencing technologies to define sets of genes that are coregulated. Secondary walls are typically deposited during specific phases of cell differentiation and provide an excellent system for global transcriptional analyses aimed at identifying secondary wall-related gene networks. The secondary wall-specific *CesA* genes and genes involved in lignin biosynthesis are used as markers for finding genes of unknown function that are coregulated with them.

Secondary walls also provide the opportunity to identify key regulatory proteins of gene involved in cell wall synthesis in specific cell types. Gain-of-function experiments with a family of transcriptional activators with conserved N-terminal amino acid domains (NAC domains) and oncogenes of an avian myoblastosis (MYB) viral transcriptional activator show increased and ectopic secondary wall formation (Fig. 2.52). The NAC domain proteins trigger expression of several *MYB* genes that directly activate genes encoding several enzymes of the monolignol synthesis pathway. These expression networks activated in xylem and fibers cells are balanced by certain WRKY genes that encode a class of repressors that silence vascularization of pith cells.

MicroRNA sequences have also been implicated in regulatory control of transcription factors in *Populus*, and they are upregulated during formation of tension wood. Some cellulose synthases occur as *cis*-oriented pairs, providing antisense transcripts to downregulate synchronously both these and

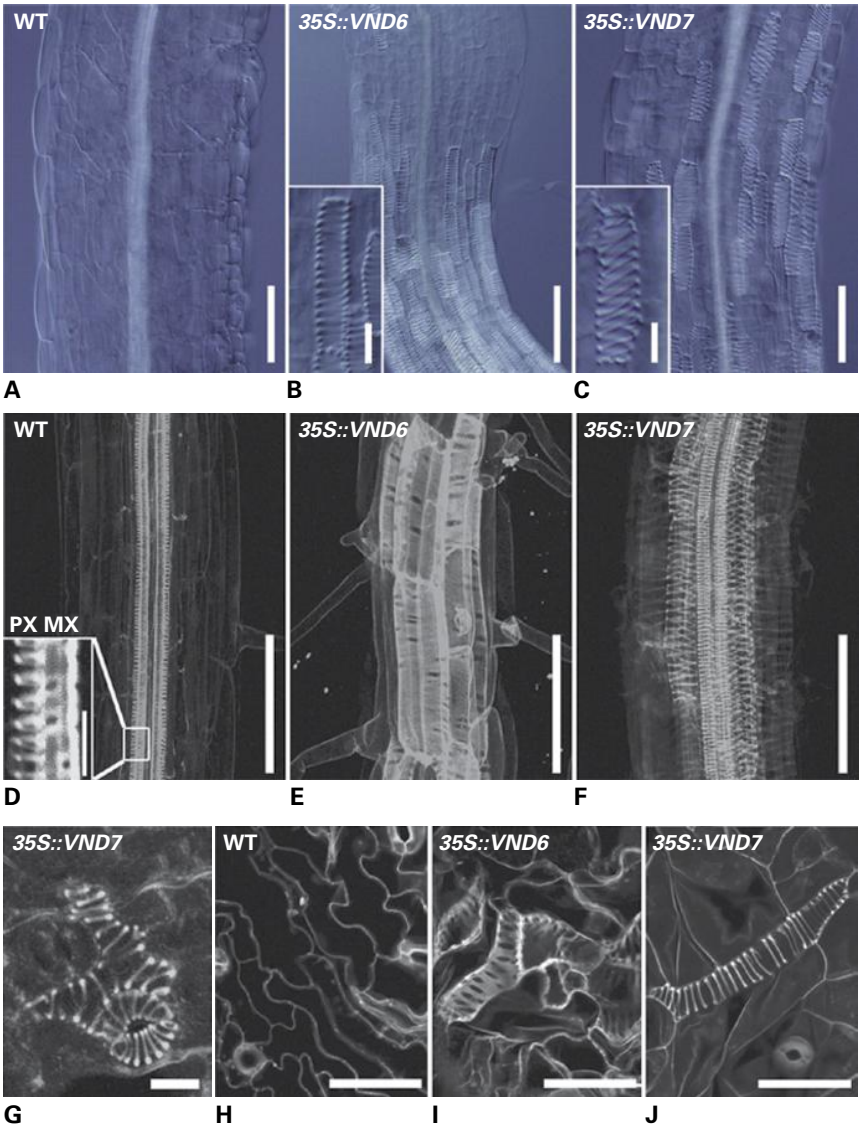


FIGURE 2.52 *Overexpression of two vascular-related "NAC" domain-containing (VND) proteins, VND6 and VND7, induce* trans*-differentiation of various cell types in* Arabidopsis *into metaxylem- and protoxylem-like vessel elements respectively. Wild-type hypocotyls contain a central vascular bundle (A, D), but cortical and epidermal cells are induced to form metaxylem by ectopic expression of* VND6 *(B, E) and protoxylem by ectopic expression of* VND7 *(C, F).* Arabidopsis *stomata (G) and poplar trichomes (J) form vascular-like thickenings by ectopic expression of the* Arabidopsis *VND7. Ectopic expression of VND6 also induces vascular thickenings in poplar trichomes (I), whereas no such thickenings are observed in wild-type poplar epidermis (H). Images were taken using differential interference contrast (A–C) and confocal laser scanning microscopy (D–J). Bars are 100 μm (A–F), 50 μm (H–J), and 10 μm (G); insets in b and c, 20 μm; inset in d is 10 μm.*
Source: Kubo et al. (2005). Genes Devel 19:1855–1860.

other wall-related genes in changing a cell's developmental program to secondary wall deposition.

2.6.8 Cell walls as sensory panels for signal transduction

Not all specialized functions of cell walls are structural. Cell walls contain molecular elements called receptor-like kinases (RLKs), which facilitate response mechanisms to biotic and abiotic stimuli as well as developmental and positional signals (Fig. 2.53). They can be viewed as sets of intricate sensory panels for signal transduction, although all molecular elements are not yet fully understood or placed clearly in physiological networks. Feedback mechanisms sensing and restructuring the biomechanical properties of walls and organs in response to stimuli are a major gap in this area. Two sets of molecules that are implicated in some aspects of the mediation of response are leucine-rich repeat (LRR) kinases and wall-associated kinases (WAKs).

LRR kinases populate the plasma membrane and allow signal transduction across this topological barrier. These LRR domains are specialized for interactions with ligands of the plasma membrane–cell wall interface. Examples include R gene disease resistance factors, chimeric LRR-extensin (LRX) proteins that function in root hair development, and proteins that function in meristem identity and transition to organ.

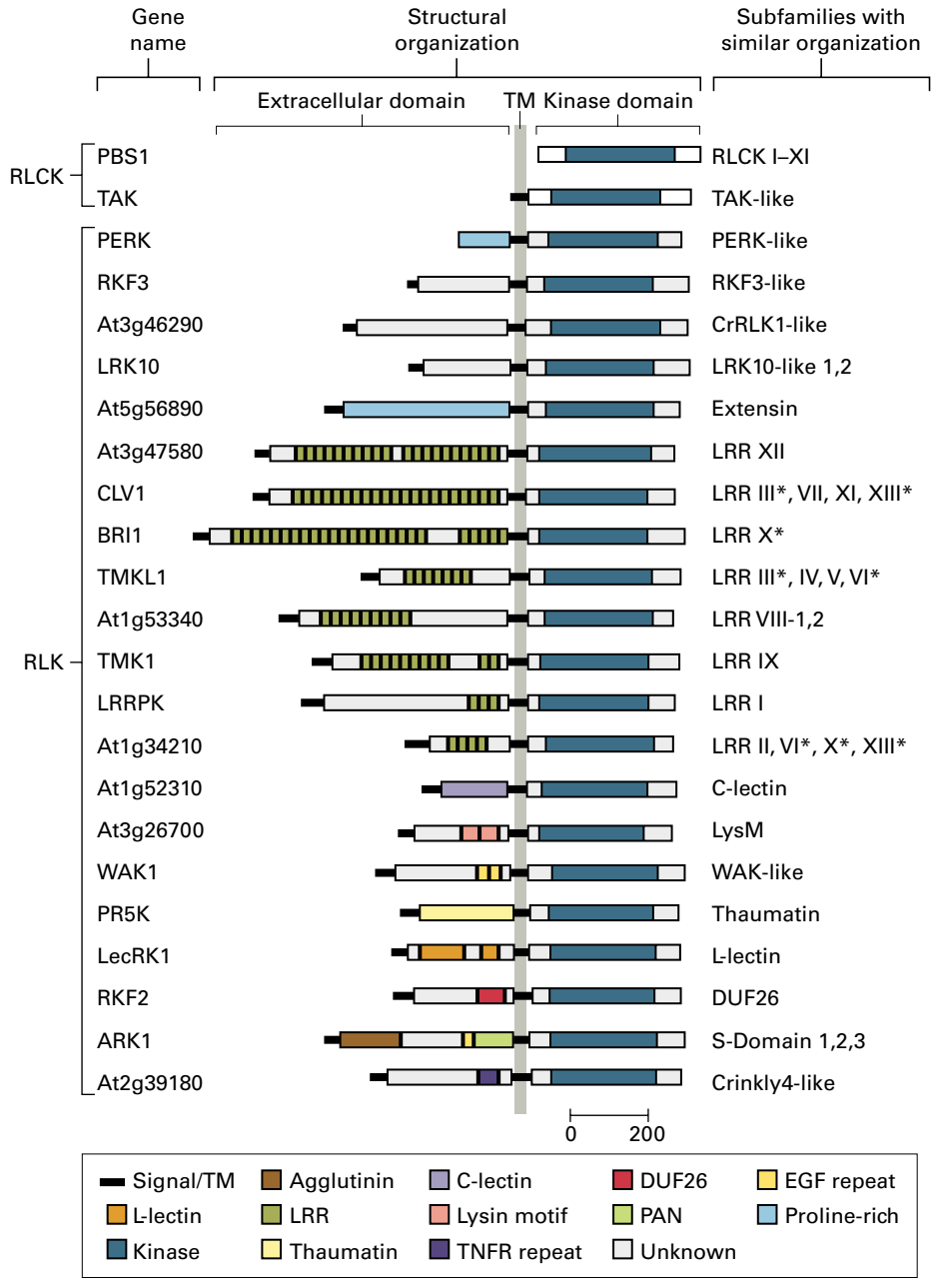


FIGURE 2.53 *Domain organization of representative receptor-like kinases (RLKs) and RLK-subfamily affiliations. Many plasma membrane-localized RLKs with different extracellular protein domains have been identified. Each of the structures shown here is representative of a subfamily of closely related sequences. Some of these RLKs, such as CLAVATA (CVL1), interact with small peptide ligands that are secreted to the apoplast, but others, such as WAK1, bind pectins or other cell wall components to form a cell wall–plasma membrane–cytoplasm signal pathway. Leucine-rich repeat (LRR) sequences include the extensin-containing domain protein, LRX1, which functions in cell development. The gray line indicates the position of the membrane-spanning domain.*

WAKs have a highly conserved serine/threonine kinase cytoplasmic domain, a plasma membrane-spanning region, and a more variable extracellular domain containing EGF (epidermal growth factor) repeats, which are likely to function in ligand recognition. Upon phosphorylation, WAKs bind to pectins and a glycine-rich protein to form a complex in conjunction with kinase-associated protein phosphatase, KAPP. Loss of WAK function results in disruption of normal cell expansion.

2.7 Cell walls as sources of food, feed, fiber, and fuel, and their genetic improvement

Cell walls directly impact the raw material quality of human and animal food, textiles, wood and paper, and they can play a role in human medicine. Modification of various cell wall



A B

FIGURE 2.54 Brown-midrib (bm) *mutants of* Sorghum *spp. or* Z. mays *have defects in lignin synthesis that results in a reddish-brown color of leaf vascular tissue (A). Depicted here is a* bm2-bm4 *double mutant. Certain* bm *mutants and their combinations in sorghum result in improved nutrition in ruminant animals because of enhanced digestibility; sheep will preferentially graze such mutants (B). Source*: (A) Vermerris et al. (2010). J Exp Bot 61(9):2479–2490. (B) Wilfred Vermerris, Univ. Florida; in reference to data in Li et al. (2008). Plant J 54:569–581.

constituents is a goal in the food processing, paper, agriculture and biotechnology industries. Achievement of this goal depends on understanding the molecular basis for the mechanical and textural properties of plant-derived materials.

The food industry uses isolated AGPs and pectins as gums and gelling agents. Fungal and bacterial wall hydrolases are used to adjust food textures. The cell walls of fruits and vegetables are now recognized as important dietary components, and they may protect against cancer of the colon, coronary heart disease, diabetes, and other ailments. β-Glucans are causal agents in the ability of oat and barley brans to lower serum cholesterol and reduce insulin demand of people with diabetes. Some pectins may have antitumor activities, possibly by stimulating the immune system after uptake through particular cells of the gastrointestinal tract.

Particular foods are being genetically engineered to improve their storage characteristics and maximize consumer appeal. Target enzymes include PGase, PME, and several polysaccharide hydrolases. The results of attempts to change only one parameter of wall metabolism are rarely those predicted, because of the inherent complexity of the wall and ability of plant cells to adapt to change. Such biotechnological applications will become more common as we understand more of the regulation of cell wall metabolism, particularly regulatory mechanisms for polymer synthesis and wall loosening.

With the advent of biotechnology, agricultural researchers are investigating particular enzymes involved in cell wall metabolism in hopes of producing crops with desired characteristics by enhancing commercially valuable traits (e.g., fiber production in flax, cotton, ramie, and sisal) or abolishing costly ones (e.g., modification of lignification of some plant tissues). For example, the pulp and paper industry, which processes trees to cellulose, and the livestock industry, which depends on the transformation of cell walls into muscle tissue, are striving to reduce the lignin content, or to alter the composition/structure to be less recalcitrant, in their respective sources of fiber and fodder. Reducing lignin content would reduce organochlorine wastes and cut costs tremendously for the paper industry, which currently uses chemical extractions to purify cellulose from wood. Alternatively, altering structure such that lignins can be more readily depolymerized and removed from polysaccharide fiber using simpler chemical treatments would be enormously beneficial. Lignin–carbohydrate interactions exert a great influence on digestibility of forage crops by ruminant animals, and the kind of lignin present rather than the total amount is often the crucial factor. Hence, mutants with altered lignin type may yield new forage crops that exhibit greater digestibility without sacrificing the strengthening function of lignin to the water-conducting cells of the plant; for example, certain natural **brown-midrib** mutants of sorghum (*Sorghum bicolor*) are already known to be more digestible (Fig. 2.54).

Bioenergy derived directly from plants, or the use of plants as feedstocks for fermentation by microbes, has an ever-increasing contribution to the diversifying energy portfolio, with positive impacts for energy security, mitigation of environmental consequences of elevated greenhouse gases, and in stimulation of rural economies. Sucrose and glucose from sugarcane (*Saccharum officinarum*) fermented to ethanol already provide Brazil with energy independence from petroleum fuels. In the USA, production of ethanol from corn (*Z. mays*) grain is a mature industry, but animal feed supplies and food products compete for this substrate. Lignocellulosic biomass consists principally of cell walls, harvested from dedicated bioenergy crops or from dried crop residues, such as sugarcane bagasse or maize and sorghum stover. Lignocellulosic biomass provides a rich source of solar energy trapped as lignin and carbohydrates in a broad range of plants unrestricted by climate or geographic location. Perennial grasses such as switchgrass (*Panicum virgatum*) and *Miscanthus* are considered superior potential feedstocks because they have C4 photosynthesis and a long growing season, can sequester nutrients in rhizomes at the end of the growing season, and exhibit high water use efficiency. However, integration of bioenergy crops

into the agricultural landscape must be sustainable, cost-effective, and present a small agronomic footprint in balance with food and feed production. For this reason, highly productive annual grasses such as sorghum and tropical maize are gaining notice as a bioenergy crop that integrates sustainably in a crop rotation system.

Cell wall polysaccharides are hydrolyzed to glucose and other sugars, which are then metabolized by microbes to produce biofuels. A general consensus is emerging that recalcitrance of lignified cell walls to hydrolysis by enzymes is a key obstacle that could be mitigated by identifying more efficient cell wall-degrading enzymes, expressing them recombinantly in transgenic plants, or modifying biomass composition or biomass quality to facilitate degradation. However, an equally important goal is to maximize the amount of carbohydrate biomass per hectare to reduce the energy and economic costs of production and transport to refineries.

In a broader view, fermentation is an inherently wasteful process—about one-half of the sugar used is lost as CO_2 during formation of ethanol by yeast. In this instance, enhancing fuel value of biomass as a combustible material, e.g., by elevating lignin content, becomes a worthwhile goal – lignin's fuel value is about 50% higher than that of polysaccharide. Researchers are already exploring ways to chemically convert lignocellulosic biomass to liquid biofuels and to a host of useful substrates that could replace petroleum. A better understanding of the control of cell-wall carbohydrate and aromatic domains and their architecture is likely to lead to major improvements in the energy potential of designed bioenergy crop plants.

Summary

Cell walls are composed of polysaccharides, proteins, and aromatic substances. The primary wall of the cell is extensible but constrains the final size and shape of every cell. Facing walls of adjacent cells adhere to each other at the middle lamella. In some cells, secondary walls are deposited on the inner surface of the primary wall after growth has stopped.

Cellulose microfibrils form the scaffold of all cell walls and are tethered together by crosslinking glycans; this framework is embedded in a gel of pectic substances. There are at least two types of primary walls. The Type I walls of eudicots and noncommelinid monocots have xyloglucan–cellulose networks embedded in a pectin-rich matrix and can be further crosslinked with a network of structural proteins. Type II walls of commelinid monocots have glucuronoarabinoxylan–cellulose networks in a relatively pectin-poor matrix. Ferulate esters and other hydroxycinnamic acids and aromatic substances crosslink the Type II walls.

Plants devote about 10% of their genome to cell wall biogenesis, which encompasses the synthesis of substrates, polymer assembly, and rearrangement during growth. A new cell wall is initiated at the cell plate. Cellulose microfibrils of all vascular plants and some algae are synthesized at the surface of the plasma membrane at terminal complexes called particle rosettes, whereas all noncellulosic crosslinking glycans and pectic substances are made at the Golgi apparatus and secreted. All cell wall sugars are synthesized de novo from interconversion of nucleotide sugars, which are the substrates for polysaccharide synthases and glycosyl transferases.

Cell shape is largely governed by the pattern of cellulose deposition, but cell enlargement is dependent on polymer remodeling enzymes, such as expansin and endo-β-transglucosylase. Cell enlargement is also accompanied by numerous changes in the structure of the wall's crosslinking glycans and pectin matrix. Termination of cell growth is accompanied by crosslinking reactions involving proteins and aromatic substances. Cell walls become specialized for the function of the approximately 40 cell types that plants comprise. The plasma membrane–cell wall interface is the cell's sensory panel for interaction with the environment, and many proteins and protein kinases have been implicated in signaling related to cell specification and growth as well as response to injury from abiotic and biotic factors.

In addition to their use in wood, paper, and textile products, cell walls are the major textural component in fresh fruits and vegetables, and constitute important dietary fibers in human nutrition. They provide a major source of calories for ruminant animals. Cell walls are the lignocellulosic biomass that will likely become a major substrate for biofuel production.



3

Membrane Transport

Julian I. Schroeder, Paul C. Bethke, Walter Gassmann, and John M. Ward

Introduction

Redistribution of ions and small organic molecules is essential for plant growth, cell signaling, nutrition, movements and cellular homeostasis. To fulfill these essential functions, plants have evolved numerous proteins that mediate the transport of ions, metabolites, and other compounds across the plasma membrane (PM) and organelle membranes of cells. Many of these transporters are selective for the substrate being transported and their activities are regulated. Most plant transporter genes are members of multigene families that show developmental and tissue-specific expression. Research is elucidating central functions of membrane transporters in response to physiological stimuli including abiotic and biotic stresses and how the activities of individual transporters are coordinated within a network at the cell and tissue levels.

3.1 Overview of plant membrane transport systems

3.1.1 Membranes facilitate compartmentalization

One of the earliest events in the evolution of life was the development of a barrier between the sensitive biochemical machinery of replication and the dispersive forces of the outside world. This barrier is the cell membrane. Delimited by its membrane, the cell can support metabolic, reproductive, and developmental activities that require a stable physicochemical environment. The hydrophobic nature of the membrane lipid bilayer ensures that hydrophilic compounds, including most nutrients and metabolites, can be sequestered on one side of the membrane or the other. During the 1930s, groundbreaking work established that the ability of most molecules to permeate plant cell membranes correlates with their oil : water partition coefficient (Fig. 3.1). The same principle applies to all biological membranes. The finding that the permeability of membranes for water is two orders of magnitude higher than predicted by the lipophilicity of water ultimately led to the identification of transporter-mediated water transport (see Section 3.5).

Plant cells contain many specialized organelles responsible for diverse biosynthetic, catabolic, and storage functions (see Chapter 1). The evolution of eukaryotes and the development of an endomembrane system allowed the homeostatic function of membranes to be carried one step further. Compartmentalization of solutes within membrane-bound organelles not only concentrates reactants and catalysts, but also segregates incompatible processes. This division of labor facilitates metabolic flexibility and efficiency.

3.1.2 Membrane transport underlies many essential cell biological processes

The complete sequence of the *Saccharomyces cerevisiae* nuclear genome reveals that about 2,000 of the 6,000 genes encode membrane-associated proteins, of which a large

Biochemistry & Molecular Biology of Plants, Second Edition. Edited by Bob B. Buchanan, Wilhelm Gruissem, and Russell L. Jones.
© 2015 John Wiley & Sons, Ltd. Published 2015 by John Wiley & Sons, Ltd.
Companion website: www.wiley.com/go/buchanan/biochem

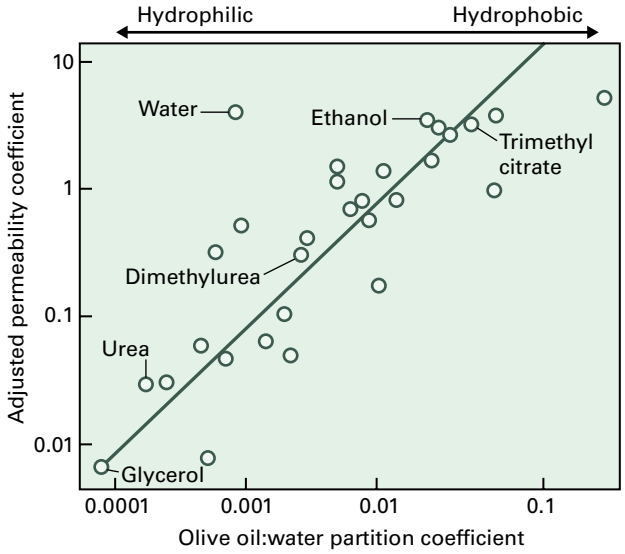


FIGURE 3.1 *Water displays anomalously high permeability in biological membranes. For most small, uncharged solutes, the ability to permeate biological membranes is correlated with their ability to dissolve in a hydrophobic phase, in this case olive oil. Water is an exception and is 2 orders of magnitude more permeant than predicted. The adjusted permeability coefficient,* $P_s \bullet \sqrt{M_r}$ *in units of* $cm \bullet h^{-1}$*, is the experimentally determined permeability coefficient for each solute (Ps) multiplied by the square root of the molecular mass of that solute, which adjusts for differences in rates of diffusion.*

proportion are transport system components. A similar percentage of the proteins encoded in the 26,000-gene *Arabidopsis* nuclear genome are associated with membranes. Of these, approximately 1,300 protein sequences have been assigned a transport function. In plant cells, membrane transport is central to a wide range of essential processes:

- *Nutrient acquisition.* Plants synthesize vital organic biomolecules from inorganic nutrients, many of which must be absorbed from the soil by roots for assimilation into amino acids and other metabolites. Thus, nitrogen can be absorbed as NH_4^+ or NO_3^-, sulfur as SO_4^{2-}, and phosphorus as PO_4^{3-} (see Chapters 16 and 23). Macronutrients such as potassium (K^+) and calcium (Ca^+) and trace elements such as boron, zinc, copper, and iron are absorbed in inorganic form. Uptake of these essential nutrients is mediated and regulated by specialized nutrient transport proteins (see Chapter 23).
- *Metabolite distribution.* In terrestrial plants, autotrophic tissues such as the photosynthetically active mesophyll cells in leaves supply reduced carbon and other metabolites to heterotrophic tissues. Long-distance transport from source tissues to sinks is accomplished by the phloem. Sucrose and amino acids cross the membranes of phloem companion cells and are loaded into the phloem by way of specific membrane-spanning transport proteins (see Chapter 15).
- *Compartmentalization of metabolites.* Given the many metabolic pathways present within a plant cell, compartmentalization of enzymes and metabolites prevents futile cycling. One classic example relates to starch, which can be synthesized and stored in amyloplasts even while glycolysis proceeds in the cytosol. Starch synthesis depends on importing glucose 6-phosphate across the double membrane of the amyloplast (see Chapter 13). Compartmentalization also enhances metabolic efficiency. In the mitochondrial matrix, for example, the ADP/ATP and NADH/NAD^+ ratios are greater than in the cytosol, which provides a substrate/product ratio that favors respiratory activity. The corresponding transport mechanisms are required for mitochondrial export of ATP and import of reducing equivalents (see Chapter 14).
- *Energy transduction.* Membrane transport lies at the heart of biological energy conversion. Light energy drives electron transfer in chloroplasts and accumulation of protons (H^+) in the thylakoid lumen. Similarly, oxidation of NADH provides energy for pumping H^+ from the mitochondrial matrix into the intermembrane space. In each case, spontaneous, exergonic flow of H^+ back across the membrane is used to generate ATP. Understanding the mechanisms by which light and high-energy electrons are harnessed to phosphorylate ADP therefore demands knowledge of membrane transport.
- *Turgor generation.* The presence of a rigid cell wall enables plant cells to generate turgor (positive hydrostatic pressure). Turgor generation is accomplished by accumulating salts via specific membrane transporters; this drives water uptake into the cell. In mature cells of most plants, K^+ accumulates in the cytosol and in the large central vacuole, whereas in halophytes the principal cations are K^+ and Na^+, with Na^+ accumulation in vacuoles. Cations must be balanced by a corresponding concentration of anions to achieve electroneutrality; in vacuoles, the principal anion is usually Cl^- (depending on its extracellular availability), malate, or a mixture of organic and inorganic anions.
- *Waste product excretion.* Metabolism inevitably generates waste products that must be removed from the cytosol.
- *Signal transduction.* Many environmental and hormonal signals that influence plant growth and development are transduced via transiently increasing the concentration of cytosolic free Ca^{2+}. First, Ca^{2+}-permeable channels open in response to particular stimuli and allow passive entry of Ca^{2+} into the cytosol, thus causing an increase in the cytosolic free Ca^{2+} concentration. Second, Ca^{2+}-translocating ATPases or H^+/Ca^{2+} exchange transporters subsequently remove Ca^{2+} from the cytosol by pumping it across the plasma membrane and intracellular membranes. Changes in intracellular Ca^{2+} concentrations are sensed by Ca^{2+}-binding proteins that can propagate numerous physiological stimuli (see Chapter 18).

3.1.3 Selective permeability of biological membranes depends on transport systems with integral membrane proteins

Controlled transport of ions, nutrients, and metabolites across the plasma membrane and intracellular membranes is required to integrate whole-plant and cellular metabolism. Transport is made possible by membrane-spanning proteins within the lipid bilayer. These so-called transport proteins can be regarded as conventional enzymes in many respects, with the important exception that transport events are vectorial (i.e., defined by a magnitude and a direction), whereas enzyme-catalyzed reactions are scalar (i.e., defined entirely by magnitude). Like enzymes, all transport systems exhibit some degree of substrate specificity and work by lowering activation energy required for transport.

All membrane transport systems have membrane-spanning, integral membrane proteins. These contain stretches of amino acids that are predominantly lipophilic (hydrophobic) and interact favorably with the fatty acyl chains of membrane phospholipids. Hydropathy analysis (Box 3.1) identifies putative integral membrane proteins using a previously determined amino acid sequence. An α-helix must contain about 20 amino acid residues to span the hydrophobic lipid bilayer. Hydropathy analysis identifies hydrophobic stretches of amino acids that may form a transmembrane helix. Although all transmembrane transport proteins have membrane-spanning components, some transport systems also require soluble regulatory protein subunits for full catalytic activity.

3.1.4 Pumps, channels, and cotransporters are components of membrane transport systems

Membrane transport systems have been categorized as pumps, channels, or cotransporters. Although contemporary biochemical analyses of membrane transporters have blurred the boundaries between these classes (see below), they remain useful. Pumps catalyze active transport, coupling the energy liberated from hydrolysis of ATP (or in a few cases pyrophosphate, PP_i) to transport of a specific molecule against an electrochemical gradient. The H^+-translocating ATPases in the plasma membrane and the H^+-translocating PPase in the tonoplast are classic examples of pumps.

In contrast to pumps, channels and cotransporters facilitate passive transport, utilizing energy stored in electrochemical gradients to power transport. Channels help a compound diffuse down its electrochemical gradient by forming aqueous pores in the membrane. The K^+ and anion channels in the guard cell plasma membrane are well-studied examples of plant ion channels (see Section 3.3). Unlike channels, cotransporters (often called carriers) transport specific molecules against an electrochemical gradient by linking transport of one molecular species in the energetically unfavorable "uphill" direction to transport of another molecular species, typically H^+, in an energetically favorable "downhill" direction. The net change in free energy for all molecules transported is negative, allowing the transport reaction to occur without need for direct chemical energy inputs from ATP or PP_i hydrolysis. Cotransporters that catalyze solute flux in the same direction as H^+ (or Na^+) flux are known as symporters. Because protons flow passively across most membranes in the direction of the cytosol, symporters typically energize uptake of solute into the cytosol, either from the external medium or from intracellular compartments. Conversely, excretion from the cytosol can be accomplished by antiporters, which exchange solutes for protons. Antiporters are present at the plasma membrane and at endomembranes. Sucrose transporters that link sugar accumulation to H^+ movement are examples of cotransporters. An overview of the above processes is shown in Figure 3.2.

These distinctions between transporter types do not serve to describe mechanisms of all transporters. As noted below, some ion channels also have cotransporter-like activity, and some cotransporters form an aqueous pore and act similarly to channels. Furthermore, even ATP-hydrolyzing pumps use channel-like domains to transport substrates across the membrane.

3.1.5 Transport rates vary across different transporter types

Transport activity is a function of the transporter rate (number of molecules transported per unit time per transporter) and the number of transporters in the membrane. Pumps are relatively slow with rates of 10^2 molecules s^{-1} transported. This is because pumps go through large conformational transitions to couple metabolic reactions to transport. Cotransporters may also undergo conformational changes during transport, but transport rates are greater than those of pumps, in the range 10^3–10^6 s^{-1}. Channels do not undergo conformational changes during transport and can catalyze ion fluxes of 10^6–10^7 s^{-1}.

These differences in transport rates explain why the abundance of different transport proteins varies markedly. Pumps have slow rates of transport, and, as described below, generate the proton gradients that drive an array of symporters and antiporters. A square micrometer of membrane may include several hundred to several thousand pump proteins, but typically contains only 1–10 channel proteins. The rapid transport rates of channels facilitate electrophysiological analysis of individual channel molecules (see Section 3.3.2).

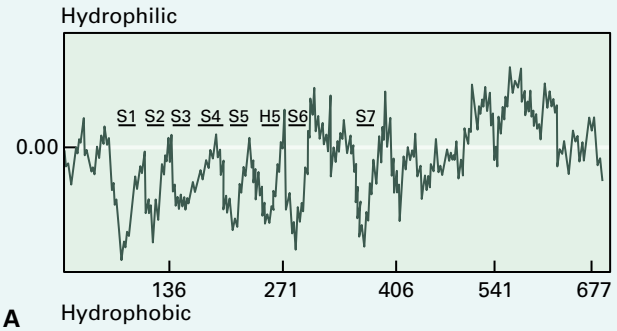
BOX 3.1

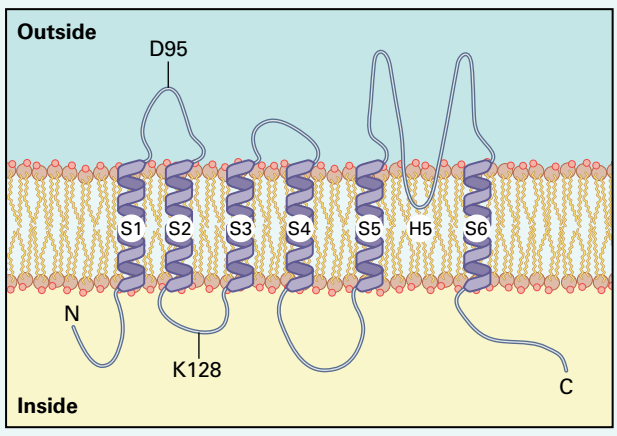
Hydropathy analysis uses amino acid sequence data to identify membrane-spanning polypeptides

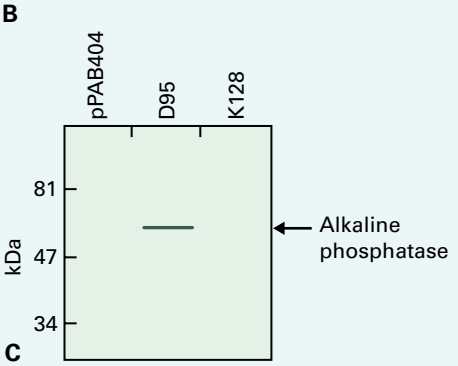
Because all transport systems contain intrinsic membrane proteins, an obvious pair of questions is, "Which domains of the protein traverse the membrane, and which are exposed to the aqueous phases?" For known protein sequences, a simple test has been devised. This test incorporates the recognition that a polypeptide in a predominantly hydrophobic environment (e.g., a membrane) will adopt an α-helical conformation. Given the well-established dimensions of an α-helix (one amino acid residue for every 0.15-nm rise along the helix), and the hydrophobic portion of the membrane lipid (about 3 nm total for the fatty acyl side chains from both leaflets of the phospholipid bilayer), about 20 amino acid residues are required to span the hydrocarbon core of a membrane, assuming that the α-helix is perpendicular to the membrane plane.

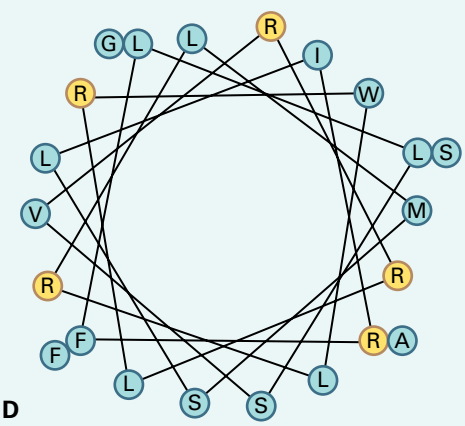
The propensity of a stretch of polypeptide to reside in a bilayer can be predicted on the basis of the mean hydrophilicity of component amino acid residues. Common amino acids are assigned a hydropathy index reflecting the aqueous solubility of the amino acid; values range from +4.5 for the most hydrophobic amino acid (isoleucine) to –4.5 for the most hydrophilic amino acid (arginine). The mean hydropathy index of stretches of a protein sequence can be determined by computer; 19 residues with a mean hydropathy index of greater than 1.6 distinguish transmembrane helices from hydrophobic domains buried in the center of globular proteins. Thus, a mean hydropathy index is calculated for residues 1 through 19 of a protein, then residues 2 through 20, and so on. The analysis predicts that highly hydrophilic, even charged, residues can reside in the membrane lipid, provided the number of hydrophobic residues in the vicinity is sufficient to favor stable partitioning in a hydrophobic phase. This prediction is supported by experimental evidence: mutations that introduce charged residues into transmembrane domains do not necessarily alter transport function.

A sample hydropathy plot for the plant K^+ channel protein KAT1 is shown in panel A of the accompanying figure, and the interpretation of the results in terms of transmembrane topology is shown in panel B. Experimental confirmation of predictions arising from hydropathy analysis is highly desirable. Ideally, transmembrane domains can be identified from crystal structures. An alternative experimental approach is to construct chimeric proteins, inserting a reporter enzyme, such as alkaline phosphatase, at various positions within the transmembrane protein. For example, a gene construct that encodes an alkaline phosphatase inserted at one of two locations within KAT1-glutamate-95 (D95) or lysine-128 (K128) (panel B)—is expressed in *Escherichia*









coli. If the alkaline phosphatase domain of the chimeric protein is located in the cytosol of *E. coli*, enzyme activity is unstable; if located in an extracellular domain, however, the activity of the enzyme is stable. Alkaline phosphatase activity is detected for chimera D95 but not for chimera K128 (panel C). This finding is consistent with the hydropathy analysis because D95 and K128 are on opposite sides of the membrane and therefore must be separated by a transmembrane domain. In practice, many such constructs must be used to determine the topology of the complete protein. This method confirmed the transmembrane topology of KAT1 shown in panel B.

More refined theoretical approaches have been devised since the advent of hydropathy analysis, including techniques to maximize charge–charge pairings within the membrane. Viewed from above the plane of the membrane, the α-helices of a membrane protein can be visualized as helical wheels (panel D). In this representation of the first 22 amino acids of the S4 transmembrane domain of KAT1, each letter represents an amino acid residue (standard amino acid code). Positively charged arginine residues are shown in yellow. Charged residues of opposite polarity on different helices tend to associate with each other, contributing to the tertiary structure of the protein.

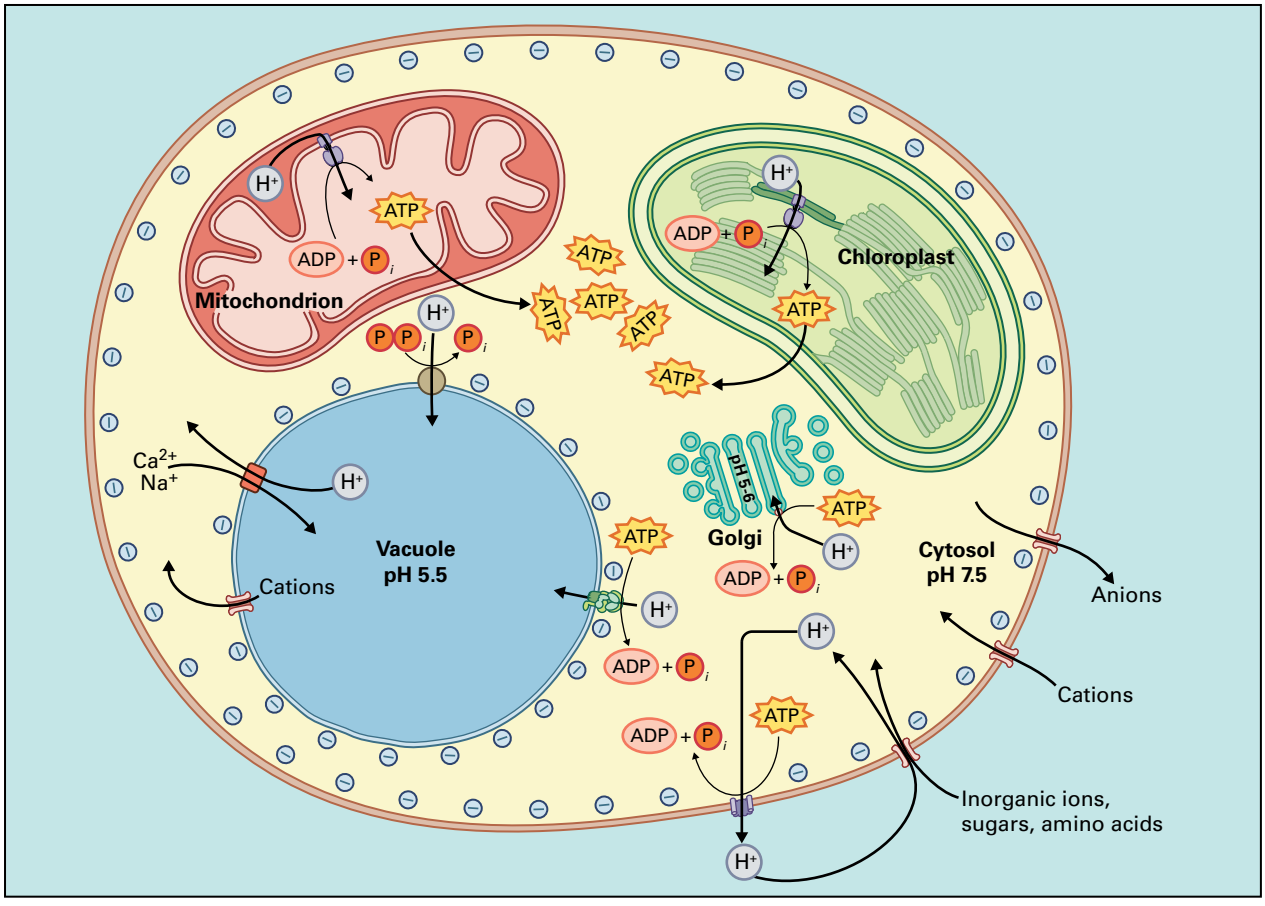


FIGURE 3.2 *Overview of chemiosmotic processes in an idealized plant cell. In mitochondria and chloroplasts, energy in H^+ gradients is harvested to synthesize ATP. Proton gradients are also established across the plasma membrane and tonoplast by pumps that hydrolyze ATP and PP_i. The electrochemical potential established by these pumps is used to move many ions and small metabolites through integral membrane channels and cotransporters.*

3.1.6 Chemical and electrical potential gradients drive transport across membranes

The net direction of transport across a membrane is dictated by the driving force on the transport system. Driving forces can be quantified in terms of the free energy relationships inherent in transmembrane solute potentials (Box 3.2), whether these involve H^+, other inorganic ions, or organic solutes such as sugars and amino acids. The magnitude of a transmembrane potential for an uncharged solute ($\Delta\mu$) or for an ion ($\Delta\bar{\mu}$) can be described in units of free energy (kJ mol^{-1}) normally associated with scalar reactions. The polarity (sign) of transmembrane electrochemical potential for a solute determines the direction of flow. At the plasma membrane, a

BOX 3.2 The electrochemical potential of a solute is defined by differences in concentration and charge

The **chemical potential** of an uncharged solute, S, in a given medium is defined by Equation 3.B1, where μ^{o}_{S} is the **standard chemical potential o**f S at 1 molar concentration (1 M), R is the gas constant (8.314 J mol^{-1}·K^{-1}), T is absolute temperature (in Kelvin), and ln(a) is the natural logarithm of the activity, a, of the solute. For uncharged solutes, a can be expressed as molar concentration, but for charged solutes, a is used to account for incomplete dissociation (solubilization) of the solute. The units of chemical potential are Joules per mole (J·mol^{-1}).

$$\mu_s = \mu^{o}_{s} + RT \cdot \ln(a) \qquad \text{(Eq. 3.B1)}$$

Suppose we have a membrane separating two aqueous media, one inside the cell (denoted by the subscript c for cytosol) and the other outside the cell (denoted by the subscript o), as shown in the figure. We can calculate the chemical potential of an uncharged solute S in each of the two media by using Equation 3.B1. For S in medium c and medium o, we can make the calculations shown in Equations 3.B2a and 3.B2b, respectively.

$$(\mu_s)_c = \mu^{o}_{s} + RT \cdot \ln[S]_c \qquad \text{(Eq. 3.B2a)}$$

and

$$(\mu_s)_o = \mu^{o}_{s} + RT \cdot \ln[S]_o \qquad \text{(Eq. 3.B2b)}$$

Now we can calculate the **chemical potential difference** for S, $\Delta\mu_S$, across the membrane simply by subtracting Equation 3.B2b from Equation 3.B2a. The standard chemical potential terms cancel each other out, and we are left with Equation 3.B3, the relationship that defines the energy stored in a transmembrane solute concentration difference.

$$\Delta\mu_s = RT \cdot \ln[S]_c - RT \cdot \ln[S]_o = RT \cdot \ln\{[S]_c/[S]_o\} \qquad \text{(Eq. 3.B3)}$$

The term RT·ln{[S]$_c$/[S]$_o$} is similar to the Mass Action Ratio term in the equation defining Gibbs free energy, RT·ln{[products]/[reactants]}, except that here the reactants and products are defined by their position in space (inside or outside of the cell), not by their chemical modification. The vectorial reaction for S is shown in the figure. Convention dictates that we relate the cytoplasmic compartment to the extracytoplasmic compartment when defining chemical potential differences (thus, Eq. 3.B2b was subtracted from Eq. 3.B2a, and not vice versa).

The polarity of $\Delta\mu_s$ is critical in expressing the energetic relationship of the solute across the membrane. A positive value indicates that free energy must be applied to translocate solute into the cytosol, whereas a negative value indicates that solute will move passively, given an appropriate transport system. A value of zero indicates equilibrium; i.e., solute concentration is the same on each side of the membrane. Just as the Gibbs free energy change describes the equilibrium position of a reaction but not the rate at which equilibrium is reached, so too the magnitude of the chemical potential difference describes the energetics of transport but cannot be used to predict rates of transport.

Let us now consider an ion, I, carrying a net charge of z, which is positive for cations and negative for anions. Because the ion bears a charge, the overall energetic potential of the ion will be influenced by the electrical potential (V_m) across the membrane. This involves adding an extra term to Equation 3.B1, so that we can now express the **electrochemical potential** of the ion as in Equation 3.B4, where $\bar{\mu}^{o}_{I}$ is the **standard electrochemical potential** of I at 1 molar concentration (1 M), F is the Faraday constant (96,500 C·mol^{-1} [coulombs per mole of electrons]), and v is the electrical potential of the medium in volts. Inclusion of F in the final term has the effect of converting electrical units into J·mol^{-1}, and since z is dimensionless, all terms in the equation have the same units.

$$\bar{\mu}_I = \bar{\mu}^{o}_{I} + RT \cdot \ln[I] + zFv \qquad \text{(Eq. 3.B4)}$$

If we now return to the model cell shown in the figure, we can calculate an **electrochemical potential difference** for the ion I across the membrane in a way analogous to that used to calculate the chemical potential difference for S. Thus, for ion I in media c and o, respectively, we can derive Equations 3.B5a and 3.B5b from Equation 3.B4.

$$(\bar{\mu}_I)_c = \bar{\mu}^{o}_{I} + RT \cdot \ln[I]_c + zF \cdot v_c \qquad \text{(Eq. 3.B5a)}$$

and

$$(\bar{\mu}_I)_o = \bar{\mu}^{o}_{I} + RT \cdot \ln[I]_o + zF \cdot v_o \qquad \text{(Eq. 3.B5b)}$$

Subtracting Equation 3.B5b from 3.B5a, we obtain Equation 3.B6, where $\Delta\bar{\mu}_I$ is the electrochemical potential difference for I, and V_m (= v_c – v_o) is the electrical potential difference or, more commonly, the membrane potential.

$$\Delta\bar{\mu}_I = RT \cdot \ln\{[I]_c/[I]_o\} + zF \cdot V_m \qquad \text{(Eq. 3.B6)}$$

The electrochemical potential difference for an ion is simply the sum of the chemical and electrical potentials. When chemical potential is equal and opposite to

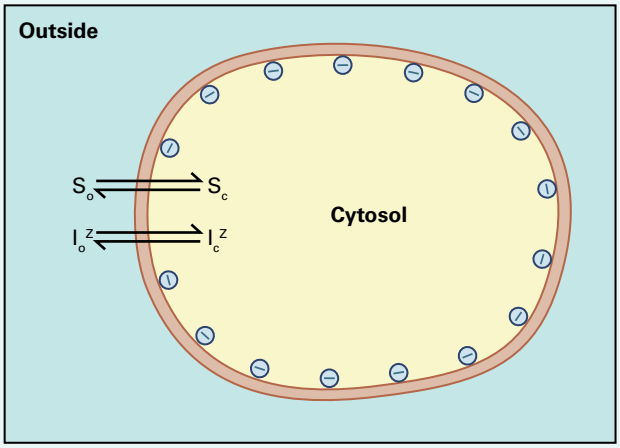
electrical potential, the sum is zero and there is no overall driving force on the ion (i.e., the ion is at equilibrium). For a single ion in media c and o, setting $\Delta\bar{\mu}_i$ in Equation 3.B6 equal to zero and solving for V_m gives the membrane potential at which the flow for a given ion reverses between inward and outward (Equation 3.B7).

$$V_m = E_{ion} = RT/zF \cdot \ln\{[ion]_o/[ion]_c\} \quad \text{(Eq. 3.B7)}$$

This equation can be brought into a more familiar form by replacing the constants R and F, assuming a temperature around 25°C (T = 298 K), and converting the natural logarithm into a base$_{10}$ logarithm by multiplying by 2.303:

$$V_m = E_{ion} = 59\,mV/z \cdot \log\{[ion]_o/[ion]_c\} \quad \text{(Eq. 3.B8)}$$

This potential is referred to as the **equilibrium potential**, E_{ion}, or the **Nernst potential** for that ion.



negative value of $\Delta\mu$ or $\Delta\bar{\mu}$ indicates passive flow from the external medium into the cytosol. Conversely, a positive value indicates that energy input is required for uptake of solute or ion because passive direction of flow is out of the cell.

For an uncharged solute, the free energy expended or released by its transport across a membrane is a function of its transmembrane concentration gradient. For a charged solute, three factors determine driving force: the charge of the solute, the transmembrane concentration gradient, and the difference in electrical potential across the membrane (Box 3.2). This last term is referred to as the membrane potential or membrane voltage and is given the symbol V_m or $\Delta\psi$. Each ionic species has its own concentration-dependent chemical potential, whereas the electrical potential has the same value for every ionic species across a given membrane at a given time. Normally, the membrane voltage across the plasma membrane of plant cells is about –150 mV on the cytoplasmic side relative to the extracellular side. Most organelle membranes are less polarized. A value of –20 mV is commonly cited for the tonoplast, that is, –20 mV in the cytosol relative to the vacuole lumen.

3.1.7 Transmembrane proton gradients are the foundation of the energy economy in plants

Proton electrochemical gradients, often expressed as proton motive force (pmf) in volts (Box 3.3), constitute one of the major energy currencies of the cell, on a par with ATP and NAD(P)H. Transmembrane H^+ potentials established by the electron transfer chains of the inner mitochondrial and chloroplast thylakoid membranes drive the synthesis of ATP (see Chapters 12 and 14). At other membranes in the cell, pumps hydrolyze ATP to power the transport of H^+ out of the cytosol and into the endomembrane system or extracellular matrix. The resulting transmembrane H^+ potentials are then used to power transport of other ions and solutes across membranes through channels and cotransporters (see Fig. 3.2). First elucidated in the context of ATP synthesis, this chemiosmotic coupling hypothesis is now widely accepted as a universal mechanism of biological energy conservation.

The H^+ pumps at the plasma membrane and organellar membranes are **electrogenic**: they create electrical current because the ions they remove from the cytosol carry charge. Therefore, these pumps not only contribute directly to ΔpH, the chemical component of the proton motive force, but also make V_m, the electrical component, more negative. The quantitative definition of pmf (Box 3.3, Eq. 3.B12) can be used to estimate the free energy contained in the electrochemical potential that is generated by pumping H^+ across the plasma membrane. Typically, cytosolic pH is 7.5 and extracellular cell wall space pH is near 5.5. This 100-fold proton gradient equates to a voltage of approximately –120 mV at 25°C. Assuming a V_m of –150 mV across the cell membrane, pmf is calculated as –150 mV + –120 mV = –270 mV. pmf values ranging from –200 to –300 mV are common in plant cells.

3.1.8 H^+ pumps and K^+ channels are key players in determining the membrane potential of a cell

A membrane potential or voltage results from gradients of cations and anions across the membrane. However, only those ions to which the membrane is permeable at a given time contribute to the membrane potential. For example, when anion channels are activated by signal transduction

BOX 3.3 Proton motive force relates transmembrane pH difference to membrane potential

As shown in Equation 3.B9, the pmf is a measure of the free energy stored in a transmembrane electrochemical potential difference for H^+, expressed in volts.

$$\text{pmf} = \Delta\bar{\mu}_{H^+}/F \qquad \text{(Eq. 3.B9)}$$

To calculate $\Delta\bar{\mu}_{H^+}$ (Eq. 3.B10), we write Equation 3.B6 from Box 3.2 explicitly for H^+.

$$\Delta\bar{\mu}_{H^+} = RT\cdot\ln\{[H^+]_c/[H^+]_o\} + zF\cdot V_m \qquad \text{(Eq. 3.B10)}$$

For H^+, the charge $z = +1$. Dividing both sides of Equation 3.B10 by F, and converting the natural logarithm into a base$_{10}$ logarithm by multiplying by 2.303, we obtain Equation 3.B11.

$$\text{pmf} = (RT/F)\cdot(2.303)\log\{[H^+]_c/[H^+]_o\} + V_m \qquad \text{(Eq. 3.B11)}$$

Equation 3.B11 can be simplified considerably, because R and F are constants, and the value for the absolute temperature in Kelvin T usually falls within a fairly narrow range. Furthermore, because $\log[H^+]_c = -\text{pH}_c$ and $\log\{1/[H^+]_o\} = \text{pH}_o$, we can write, for conditions at 25°C, Equation 3.B12, in which the first term on the right-hand side simplifies to 0.0591 V. However, it is more convenient in biological systems to express the pmf (and V_m) in mV, so after multiplying through by 10^3, Equation 3.B12 becomes $\text{pmf} = 59.1\text{ mV}\ [\text{pH}_o - \text{pH}_c] + V_m$, which states that each pH unit change is energetically equivalent to 59 mV of membrane potential.

$$\begin{aligned}\text{pmf} &= [(8.314)(298)(2.303)/(96{,}500)][\text{pH}_o - \text{pH}_c] + V_m \\ &= 0.0591\text{V}[\text{pH}_o - \text{pH}_c] + V_m \\ &= 59.1\text{mV}[\text{pH}_o - \text{pH}_c] + V_m \qquad \text{(Eq. 3.B12)}\end{aligned}$$

cascades, only then does the typical anion gradient across the plasma membrane actually affect the membrane potential. The amount of ions that need to flow across a biological membrane to change the membrane voltage is actually very small because the cell's capacitance—the amount of charge it can hold for a given V_m—is related to its surface area, and very few electrical charges are needed to charge the small capacitance of most cells (Box 3.4). Membrane potential is a macroscopic parameter. That is, if V_m is measured by comparing the potentials reported by two electrodes placed on each side of the membrane, then no matter how far from the membrane the electrodes are placed, the potential should be the same. Membrane potentials arise across biological membranes in several ways. As noted in Section 3.1.7, metabolically coupled pumps (usually ATPases) that transport H^+ out of the cytosol exert a major influence on the resting value of V_m in cells and tend to drive V_m to negative values (Fig. 3.3). At steady state, continuing operation of electrogenic pumps is compensated by movement of countercharges through other transport systems. Charge movement may consist of a flow of positive charges into the cytosol such as mediated by proton-coupled symporters (see Section 3.4) or a flow of negative charges out of the cell.

The second major factor exerting an effect on the resting value of V_m is the large gradient for K^+ across the plasma membrane and the ensuing transport of K^+ from the cytosol through K^+ channels (see Fig. 3.3). Plants maintain cytosolic K^+ concentrations at around 150 mM. The K^+ concentration in the extracellular wall space is low (e.g. 0.1–5 mM) and at least some K^+ channels are usually open. The tendency of K^+ to exit from the cell through K^+ channels generates an excess of negative charge inside the cell, yielding a negative value of V_m. However, when membrane voltage becomes too negative, leaking of K^+ from the cell stops. Assuming a 100-fold K^+ gradient across the cell membrane, the negative voltage at which channel-mediated K^+ efflux stops (i.e., the equilibrium potential for K^+, see Box 3.2) is approximately –120 mV.

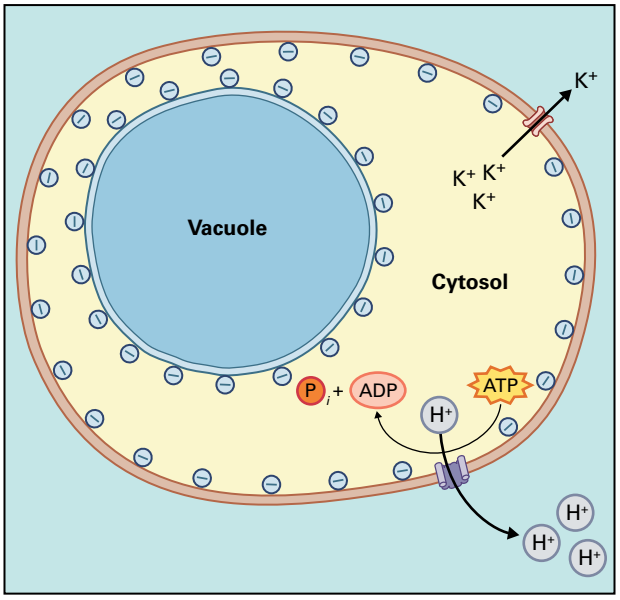


FIGURE 3.3 *Mechanisms that control the membrane potential of the plasma membrane. Transfer of positive charge across the membrane from inside to outside makes the membrane potential more negative. Proton pumps and outward K^+ channels are illustrated.*

BOX 3.4

Biological membrane potentials can change quickly when small amounts of cations or anions flow across the membrane

A membrane potential is the result of a charge difference across the membrane. The charge (Q, in coulombs [C]) stored on a membrane at a particular voltage is a function of the membrane capacitance (C, in coulombs per volt per square meter [$C \cdot V^{-1} \cdot m^{-2}$], i.e., farad per square meter [$F \cdot m^{-2}$]) according to the relationship $Q = CV$, where V is voltage. For most biological membranes, C is of the order 0.01 $F \cdot m^{-2}$, and for the plasma membrane of a plant cell, V_m averages –150 mV. This yields a net charge of 0.0015 $C \cdot m^{-2}$, with anions accumulating in excess of cations on the intracellular side of the membrane compared to the extracellular side.

For a 40-μm-long plant cell, the area of the plasma membrane is 10^{-8} m^2, assuming the shape of the cell approximates a cube. Hence, converting coulombs to molar equivalents by using the Faraday constant, the excess negative charge in the cytosol is $(1.5 \times 10^{-3}\ C \cdot m^{-2})$ $(10^{-8}\ m^2$ membrane)/(96,500 $C \cdot mol^{-1})$, or roughly 1.5×10^{-16} eq. (Because F refers to the number of ionized species, the results are expressed here in terms of molar equivalents rather than moles.) If the cytosol of this cell occupies 10% of the intracellular volume (with the vacuole occupying most of the rest), the volume of cytosol is 10^{-11} L, so the excess negative charge is $(2 \times 10^{-16}$ eq)/$(10^{-11}$ L) = 20 μeq·L^{-1}. Given that the total ionic strength of the cytosol is more than 200 meq·L^{-1}, the ionic imbalance does not exceed 1 part in 10,000. In simple terms this means that very few ions are needed to change the charge of the membrane, because the capacitance of the membrane is very small.

Although the balance between inherently high K^+ permeability and electrogenic H^+ pump activity in plant membranes is usually the main feature that determines their resting V_m, any transport system capable of conducting ions (and therefore current) across the membrane will affect V_m. Under some conditions, membranes exhibit transiently high permeabilities to anions or to Ca^{2+}. This will ordinarily lead to a transient, positive swing in V_m, or membrane depolarization, as anions flow out of the cell or Ca^{2+} ions flow into the cell (see Section 3.3).

3.1.9 Pump, channel, and cotransporter activities interact through their respective impacts on chemical gradients and membrane potential

While it is useful to study individual transporters in isolation, it is important to consider that the action of any transporter in a cell has effects on other transporters by altering the membrane potential or chemical gradients, or both. Thus, the integrated action of pumps, channels and cotransporters determines the ability of a cell to take up nutrients and carry out other physiological functions (Fig. 3.4). Whereas proton pumps actively expend energy to establish a pmf, passive transporters (cotransporters and channels) utilize the energy stored in the pmf. Depending on the transport mechanism of these passive transporters, the electrical potential, the chemical potential, or both are utilized to transport a given solute.

The pmf is especially useful to drive the uptake of negatively charged and neutral solutes. For example, uptake of NO_3^- is energetically unfavorable because V_m is negative, which would inhibit uptake of a negatively charged nutrient such as NO_3^-. By coupling the uptake of one NO_3^- to the uptake of two H^+, a H^+-NO_3^- symporter overcomes this obstacle by mediating the uptake of a net positive charge (see Fig. 3.4). In this way both the H^+ chemical potential and the favorable electrical potential are utilized to enable the uptake of NO_3^-.

The uptake of an uncharged solute like glycine (Gly), on which the negative V_m has no effect, can be mediated by a H^+-Gly symporter against a glycine gradient (see Fig. 3.4). The function of a 1 H^+ : 1 Gly transporter impacts both the chemical and electrical H^+ potential equally and is balanced out by the extrusion of one proton.

The negative V_m favors the accumulation of positively charged solutes such as K^+. K^+ is the most abundant cation in the cytosol, and its uptake usually occurs against a fairly steep chemical gradient. Depending on the electrochemical potential for K^+, uptake of K^+ can occur via channels at intermediate to high external K^+ concentrations (see Fig. 3.4) by utilizing the electrical potential. At lower external K^+ concentrations, K^+ uptake is coupled to the pmf or other favorable potential proposed to occur through a combination of K^+ channels and parallel high-affinity K^+ transporters for which the transport mechanism remains unknown. In the case of a K^+ channel, only the electrical component of the pmf is impacted. By extruding one H^+ per K^+ taken up, the H^+-pumping ATPase increases the H^+ chemical potential of the extracellular space while maintaining V_m. Therefore channel-mediated K^+ uptake is energetically efficient because it does not dissipate the chemical H^+ gradient.

The energetics of solute uptake has additional implications for regulation of transport function. The steep pmf directed into a plant cell under physiological conditions typically prevents situations where transport is reversed (e.g., release of

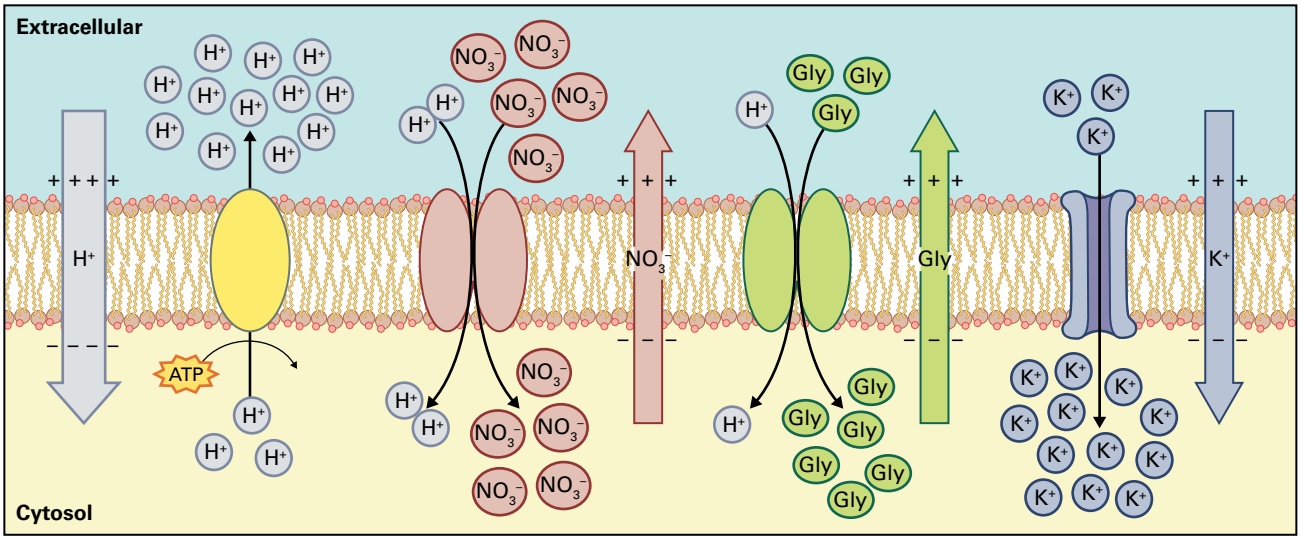


FIGURE 3.4 *Illustration depicting a plasma membrane H^+ pump (yellow), a channel that functions in K^+ uptake (blue), a H^+-coupled nitrate transporter (red), and a H^+-coupled amino acid transporter (green) that mediates the uptake of uncharged amino acids such as glycine (gly). Each solute has its own electrochemical potential (large colored arrows), which is determined by the solute's chemical concentration gradient across the membrane, its electrical charge (if any), and the charge difference across the membrane. If a solute has a higher concentration in the cytosol than in the apoplast, the chemical potential favors solute release. Because living cells generally have a negative membrane potential, the electrical potential favors release of negatively charged solutes and the uptake of positively charged solutes. The electrical potential does not act on uncharged solutes.*

NO_3^- and H^+ via a symporter), but when artificial proton and solute gradients are applied, many cotransporters are fully reversible. In either case, there is tight coupling between H^+ and solute transport. Recently obtained crystal structures of cotransporters are revealing how this coupling is achieved. In contrast, ion channels such as a K^+ channel might frequently encounter physiological states where the K^+ electrochemical potential favors K^+ release, for example, when external K^+ concentrations drop after a rain storm. With this class of transporters, gating is important. Gating—the regulation of channel opening and closing—determines under which conditions a channel will allow the movement of substrate (see Section 3.3.5).

3.2 Pumps

3.2.1 F-type ATPases at the inner mitochondrial and thylakoid membranes are H^+-pumps that synthesize ATP

F-type ATPases (also called ATP synthases) are found in plants at the inner mitochondrial and thylakoid membranes and function in ATP synthesis. These two kinds of membranes contain electron transfer chains driven by redox potential and light energy, respectively, and power the accumulation of protons in the inner membrane space of mitochondria and the lumen of thylakoids (see Chapters 12 and 14). The proton gradient established by these electron transport chains drives "reverse" H^+ flow through the F-type ATPases, thereby resulting in ATP synthesis. One sector of an F-type ATPase, called F_o in plant mitochondria and CF_o in chloroplasts, traverses the membrane and forms an H^+-permeable conduit. The other sector of the enzyme, called F_1 in mitochondria and CF_1 in chloroplasts, readily dissociates from the transmembrane sector, contains adenine nucleotide-binding sites and can hydrolyze ATP in vitro. The flow of H^+ through F_o causes long-range conformational transitions in F_1 that result in the synthesis of ATP.

The subunit composition of F-type ATPases varies according to the ATP-synthesizing membrane in which they are found. Nevertheless, members of this class of H^+-ATPase contain a "core" of common subunits that are essential for catalysis (Fig. 3.5). Additional subunits probably perform regulatory functions. Regulation is particularly important in chloroplasts at night, when ATP hydrolysis by CF_1 must be prevented in the absence of a light-imposed proton gradient (see Chapter 12).

Crystallographic studies of the F_1 sector $\alpha_3\beta_3\gamma$ complex from bovine mitochondria demonstrated that the three adenine nucleotide-binding sites of the complex (located primarily on the three β subunits), show three distinct conformations. At any given time, one binding site is in an open conformation, another is binding a nucleotide loosely, and the third is binding a nucleotide tightly. These studies lend structural support to the conformational model for proton-driven ATP synthesis, which postulates that ATP is synthesized by F-type ATPases through a process of rotational catalysis.

BOX 3.5

The energetics of solute uptake: some illustrative examples

To illustrate the energetics of solute uptake, let's consider a cell at room temperature that has a 10-fold K^+ gradient across its membrane (higher $[K^+]$ in the cytosol than outside). Using Equation 3.B8 in Box 3.2, we can calculate an E_{K+} of –59 mV. If the membrane potential is more negative than –59 mV, the cell can accumulate K^+ using a passive transporter like a channel. If the membrane potential is more positive than –59 mV, channel-mediated K^+ fluxes would be directed out of the cell. Hence, in this case, E_{K+} defines the cell membrane potential range that allows for passive influx of K^+ given the known K^+ concentration gradient. One could also ask the question: assuming a cytosolic $[K^+]$ of 100 mM, and an extremely negative membrane potential of –300 mV, what is the lowest external $[K^+]$ at which channel-mediated (passive) uptake is theoretically possible? Solving Equation 3.B8 for $[ion]_o$ one arrives at a concentration of approximately 0.7 μM K^+!

Although membrane potentials of –300 mV have been measured in plant cells and fungi, it may be very hard for plants to maintain such a negative membrane potential and only use channels when solute gradients are steep. For many nutrients, energetically unfavorable solute gradients are overcome by cotransporters, which in plants usually couple solute transport to the pmf. This mechanism has been confirmed for many nutrients, with the exception of K^+. The proton concentration is higher in the extracellular space (e.g. pH 5.5) than in the cytosol (e.g. pH 7.5). This difference of 2 pH units corresponds to a 100-fold higher proton concentration outside the cell than inside. In a coupled system, the equilibrium potential of each ion is combined to derive an overall equilibrium potential. Equation 3.B13 represents the equilibrium potential equation for uptake of an ion with a single positive charge coupled to the uptake of protons, where m and n designate the transport stoichiometry $m \bullet ion^+ : n \bullet H^+$:

$$V_m = 59/(m+n) \bullet (m \bullet \log\{[ion^+]_o/[ion^+]_c\} + n \bullet \log\{[H^+]_o/[H^+]_c\}) \quad \text{(Eq. 3.B13)}$$

Because pH is a logarithmic value, Equation 3.B13 can be simplified to:

$$V_m = 59/(m+n) \bullet (m \bullet \log\{[ion^+]_o/[ion^+]_c\} + n \bullet \Delta pH) \quad \text{(Eq. 3.B14)}$$

with $\Delta pH = pH_c - pH_o$.

Assuming $pH_c = 7.5$ and $pH_o = 5.5$, and $[K^+]_c = 100$ mM and $[K^+]_o = 1$ μM, Equation 3.B13 or 3.B14 tells us that a cell needs to hyperpolarize the cell membrane to more negative than –88.5 mV for a $1K^+ : 1H^+$ transport stoichiometry, or only –19.7 mV for a $1K^+ : 2H^+$ transport stoichiometry. Channel-mediated uptake would require a membrane potential more negative than –290 mV. Even though the logic of this equation is compelling, plant scientists have not yet unequivocally confirmed a $K^+ : H^+$ cotransporter for K^+ uptake. Thus, biology does not always conform to elegant theories. In addition, since K^+ channels can adjust the membrane potential to very negative voltages, they were proposed in early research to provide a mechanism for proton pump-driven K^+ uptake at low external K^+ concentrations. But other charged substrates, such as NO_3^-, have clearly been shown to be transported via proton cotransport.

As mentioned in Section 3.1.9, proton coupling is especially useful for the uptake of negatively charged (anionic) substrates. Equation 3.B8 illustrates why: for channel-mediated uptake of an anion with a single negative charge (e.g. NO_3^-) against a 10-fold concentration gradient, the membrane potential would need to be more positive than +59 mV inside the cell, a positive value that occurs only transiently, if at all, in most plant cells. Equation 3.B15 describes the equilibrium potential for a cotransporter that couples the uptake of one anion with one negative charge to the uptake of two protons, and thereby converts the uptake of one negative charge to the uptake of one net positive charge:

$$V_m = 59 \bullet (\log\{[ion^-]_o/[ion^-]_c\} + 2 \bullet \Delta pH) \quad \text{(Eq. 3.B15)}$$

Using the same proton gradient as above and uptake against a 10-fold anion gradient, Equation 3.B15 tells us that the membrane potential needs to be more negative than +177 mV, a condition that is likely always met.

According to the conformational model, ADP and inorganic phosphate (P_i) first bind to the open nucleotide binding site. Proton flow through the F_o sector of the enzyme causes a rotor composed of the $\gamma\varepsilon_{10}$ subunits to rotate relative to a stator formed from the $\alpha_3\beta_3\delta ab_2$ subunits. Thus proton flow through F_o is coupled to catalysis in F_1 by rotation of the γ subunit. Rotation of γ alters the conformation of all three nucleotide-binding sites. The tight-binding site opens and releases newly formed ATP into the aqueous medium, the open site is converted to a loose-binding site, and the

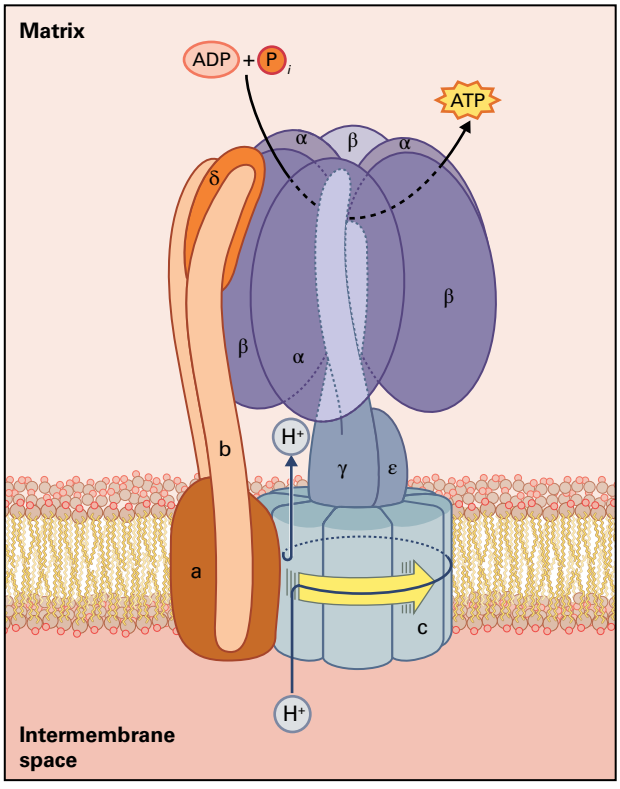


FIGURE 3.5 *Structure of the core subunits of the mitochondrial ATP synthase, an F-type H$^+$-ATPase. The common subunits of the F$_o$ sector are known as a, b, and c. In the complex from* E. coli, *these subunits are present in a stoichiometry of ab$_2$c$_{9-12}$. Subunit c is a small (8 kDa) and extremely hydrophobic subunit with two transmembrane spans. Subunit b possesses one transmembrane span and is thought to project from the membrane surface to interact with the F$_1$ sector. A core of five distinct subunit types are present in the F$_1$ sector in the stoichiometry α3β3γδε. Three nucleotide-binding sites are located primarily on the three β subunits. The yellow arrow indicates the direction in which the c subunits are proposed to rotate during proton translocation. Rotation of the c subunits is thought to drive rotation of the γ subunit and thereby alter the conformation of the nucleotide-binding sites (see Fig. 3.6).*

loose-binding site forms a tight pocket in which ATP is produced spontaneously (Fig. 3.6). In net terms, a total of three or perhaps four protons are admitted through the F$_o$ sector for each ATP synthesized. Video microscopy has been used to visualize rotational catalysis in experiments where either F$_1$ or F$_o$ was immobilized, and the other subunit complex was labeled with actin filaments or gold beads that could be observed directly. Rotation rates as high as 500 revolutions per second were observed for the enzyme from *E. coli* labeled with 40-nm gold beads.

3.2.2 P-type ATPases covalently bind the γ-phosphate of ATP during catalysis

The class of ion-motive ATPases known as P-type ATPases is named for the presence of a covalent enzyme–phosphate (E–P) transition state during the reaction cycle. During hydrolysis of MgATP, the γ-phosphate of ATP becomes transiently but covalently bound to an aspartyl residue on the enzyme, forming an acyl–phosphate bond. Structural studies of P-type ATPases suggest that both formation and hydrolysis of this acyl–phosphate bond, in addition to binding of ATP and release of ADP, orchestrate conformational changes within the pump to drive ion transport.

P-type ATPases include the plasma membrane (PM) H$^+$-ATPases of plants and fungi, the Na$^+$/K$^+$-exchanging ATPase ubiquitous in the plasma membrane of animal cells, Ca^{2+}-ATPases of the plasma membrane and endomembranes of animals and plants (see Section 3.2.6), and the H$^+$/K$^+$-exchanging ATPase of mammalian gastric mucosa. All P-type ATPases are inhibited by orthovanadate ($H_2VO_4^-$), which forms an analog of the E–P transition state and blocks the reaction cycle. Furthermore, all P-type ATPases share a common domain structure that reflects their functional attributes (Fig. 3.7).

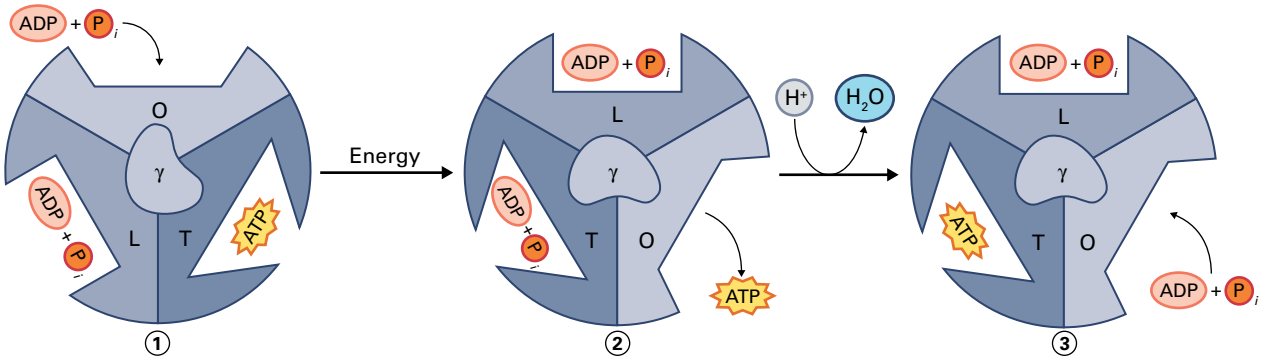


FIGURE 3.6 *Model for the synthesis of ATP by an F-type H$^+$-pumping ATPase. At any one time, each of the three nucleotide-binding sites has a distinct conformation: One site is open (O), another binds loosely (L), and the third site binds tightly (T). Proton flow through the ATP synthase causes the γ subunit to rotate. This rotation changes the conformation of the three nucleotide-binding sites in panel 1 to those in panel 2 such that the O site becomes an L site, the L site becomes a T site, and the T site becomes an O site. ADP + P$_i$ initially bind to a site in the O conformation and are condensed to form ATP on conversion of the binding site to the T conformation. Release of ATP is from the O site (panel 2) and binding of ADP + P$_i$ to the O site (panel 3) occurs prior to the next rotational event.*

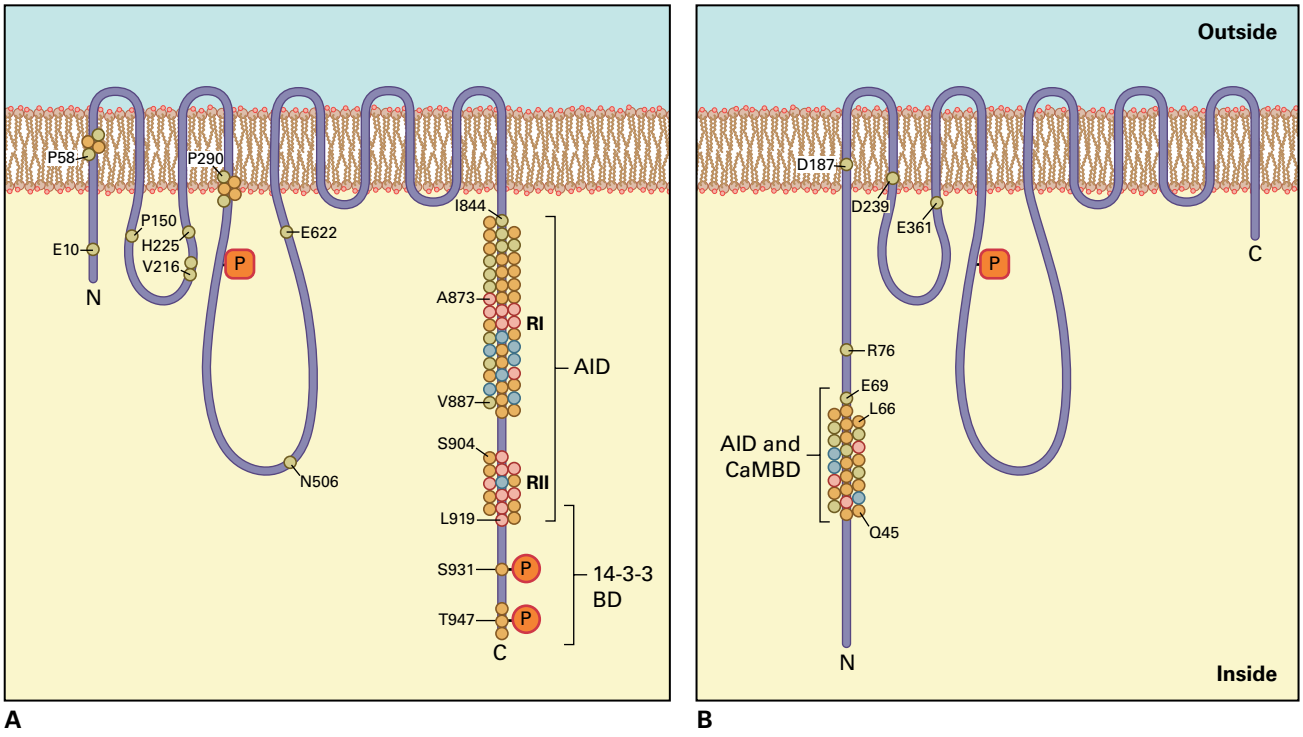


FIGURE 3.7 *Diagrams illustrating the membrane topology and location of the C-terminal auto-inhibitory domain (AID) in P-type H^+-ATPases (A) and the N-terminal AID in plant PM-type Ca^{2+}-ATPases (B). The two regions of the H^+-ATPase AID are designated RI and RII. The calmodulin-binding domain (CaMBD) of the Ca^{2+}-ATPase and essential phosphorylation sites in the 14-3-3 binding domain (BD) of the H^+-ATPase are also indicated.*
Source: Lone Bækgaard et al. (2005). J Bioenerg Biomembr 37:369–374.

3.2.3 Unlike the F-type ATPase, which harnesses pmf to drive ATP synthesis, the P-type PM H^+-ATPase generates pmf by hydrolyzing ATP

The PM H^+-ATPase is a single polypeptide of about 100 kDa that pumps one H^+ out of the cell for each MgATP hydrolyzed. Different conformations of the enzyme, known as the E1 and E2 states, expose the H^+-binding site to alternate sides of the membrane (Fig. 3.8). The conformational change that exposes the bound H^+ to the apoplast is linked to additional conformational transitions that lower binding-site affinity, permitting H^+ dissociation.

The proton gradient generated by PM H^+-pumping ATPase is utilized by a variety of cotransporters to energize transport and influences ion channel activity through its impact on V_m. PM H^+-ATPase is also critical in removing excess H^+ from the cytosol. Many metabolic pathways result in net production of protons, some of which must be removed to prevent acidification of the cytosol. In fact, cytosolic pH is remarkably stable, remaining at 7.1–7.5.

Unlike F-type H^+-ATPases, which synthesize ATP at the expense of the proton gradient, PM H^+-ATPases catalyze the same reaction in reverse. How is the direction of the reaction determined? The relative sizes of the driving forces do not answer this question; the ΔG for ATP hydrolysis in the mitochondrial matrix is probably similar to that in the cytosol, being about –50 kJ·mol^{-1}. Likewise, the electrochemical potential for protons (pmf·F) is similar across both the inner mitochondrial and plasma membranes, with a value near +25 kJ·mol^{-1}. To resolve this apparent paradox, we must also take into account the reaction stoichiometry, the number (n) of H^+ moved per ATP hydrolyzed or synthesized. In Reaction 3.1, H^+_i and H^+_o refer, respectively, to H^+ on the inside or outside

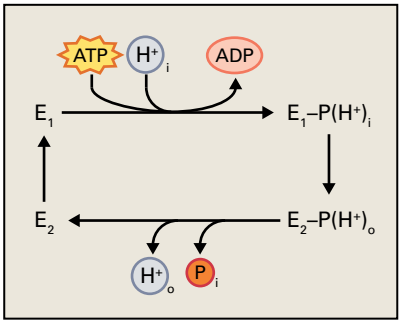


FIGURE 3.8 *Reaction cycle for P-type ATPases. Protons bind to the ATPase in the E_1 conformation. Hydrolysis of ATP and phosphorylation of the enzyme cause a change to the E_2 conformation. The lower affinity of E_2 for H^+ results in the release of protons on the other side of the membrane from where they were acquired. Hydrolysis of the enzyme–phosphate bond releases P_i and returns the ATPase to the E_1 state.*

of the membrane. The free energy relationship is defined in Equation 3.1. If ΔG_{pump} is negative, the pump reaction proceeds from left to right, as written, whereas a positive value indicates the reverse reaction. Thus, for PM H⁺-ATPase, which hydrolyzes one ATP for each proton pumped, $n = 1$ and $\Delta G_{pump} = -25$ kJ mol^{-1}. In contrast, for mitochondrial F-type ATPase, which translocates several protons per molecule of ADP phosphorylated, $n = 3$ and $\Delta G_{pump} = +25$ kJ mol^{-1}. This difference in net direction can be likened to pushing cars uphill. A person might make headway with one car, but additional cars will overcome the force applied by the person and will roll back down the hill.

Reaction 3.1

$$nH^+_i + ATP \leftrightarrow nH^+_o + ADP + P_i$$

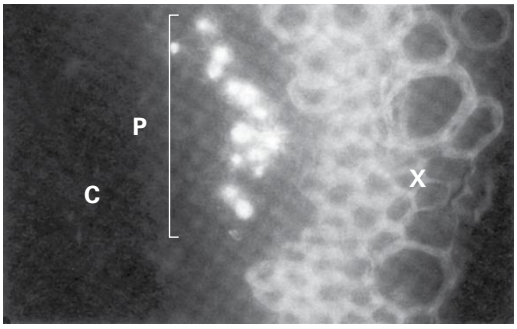
$$\Delta G_{pump} = n(pmf \cdot F) + \Delta G_{ATP} \qquad \text{(Eq. 3.1)}$$

3.2.4 PM H⁺-ATPases are encoded by a multigene family that exhibits tissue-specific expression

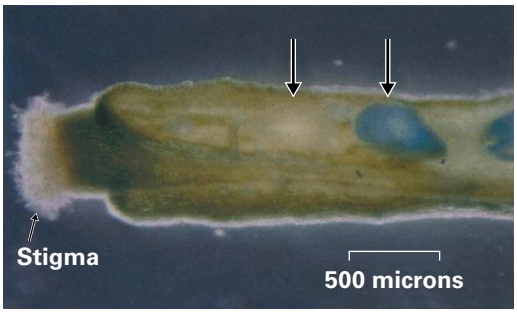
PM H⁺-ATPases in *Arabidopsis* are encoded by genes of the *AHA* family. At least 10 *AHA* genes have been identified, each encoding a distinct PM H⁺-ATPase isoform. The PM H⁺-ATPases of *Solanum lycopersicum*, *Nicotiana tabacum* and other plant species are also members of multigene families. Studies using the *GUS* reporter gene fused to the promoter regions of specific *AHA* genes have revealed that isoform expression is to a degree tissue specific. For example, *AHA3* is expressed selectively in phloem companion cells, the micropyle, and the developing seed funiculus (Fig. 3.9A). Analysis of plants with mutations in the *AHA3* gene demonstrated that AHA3 is essential for normal pollen formation. In contrast, *AHA10* is expressed principally in developing seeds, especially in the integument surrounding the embryo (Fig. 3.9B). Isoforms also have different biochemical activities. AHA1 and AHA2 have K_m values for ATP of 0.15 mM, while the K_m of AHA3 is 10-fold higher.

3.2.5 PM H⁺-ATPase is regulated by an array of mechanisms.

Most enzymes that play pivotal roles in metabolism are subject to intense regulation, and PM H⁺-ATPase is no exception. The pump is activated in response to lowered cytosolic pH. The C-terminal cytosolic region of the enzyme (see Fig. 3.7A) forms an auto-inhibitory domain consisting of two conserved regions, RI and RII. Removal of the auto-inhibitory domain by proteolytic cleavage or genetic modification activates the H⁺-ATPase considerably.



A



B

FIGURE 3.9 *Tissue-specific expression of genes for PM H⁺-ATPase isoforms in* Arabidopsis. *(A) Stem cross-section from* Arabidopsis *expressing an AHA3-c-Myc fusion protein and labeled for immunofluorescence detection of the H⁺-ATPase. Cell-specific labeling is seen in a subset of phloem (p) cells but not in cortical (c) or autofluorescent xylem (x) cells. (B) The* AHA10 *gene promoter is expressed in developing seeds, as shown by b-glucuronidase (GUS) staining. Two developing seeds (arrows) are shown in an* Arabidopsis *silique. The blue color in the seed to the right indicates expression of an AHA10-GUS fusion protein.*
Source: (A) DeWitt & Sussman. (1995). Plant Cell 7:2053–2067. (B) Harper et al. (1994). Mol Gen Genet 244:572–587.

Point mutations in either of the two conserved regions have a similar effect.

A striking twist to C-terminal H⁺-ATPase inhibition has been observed during studies with fusicoccin (FC) (Fig. 3.10), a toxin produced by the fungus *Fusicoccum amygdali,* a pathogen affecting peach and almond trees. FC elicits an increase in guard cell turgor, thereby opening stomata and causing leaves to wilt. The toxin's primary mode of action is stimulation of PM H⁺-ATPase, not only in stomatal guard cells but also in a range of plant cell types. FC activates the enzyme by relieving C-terminal auto-inhibition. The FC receptor is a 14-3-3 protein. These soluble proteins function as dimers and bind to target proteins at a defined consensus sequence that includes a phosphorylated Serine (Ser) or Threonine (Thr) residue. Regulation of the H⁺-ATPase by 14-3-3 proteins occurs in the absence of FC in uninfected plants through an interaction of 14-3-3 dimers at its C terminus. Phosphorylation of the penultimate Thr residue stabilizes 14-3-3 binding and increases pump activity. This phosphorylation is sensitive to environmental factors. For example, phosphorylation occurs in guard cells in response to blue light and in root cells in response to aluminum stress.

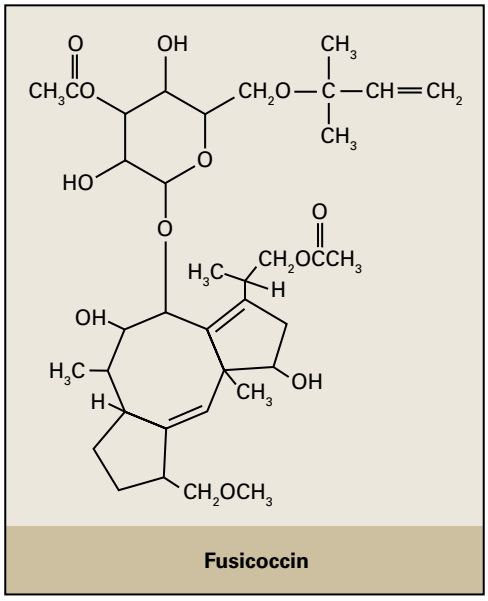


FIGURE 3.10 *Structure of fusicoccin, a toxin produced by a fungal pathogen of plants,* Fusicoccum amygdali, *that stimulates the P-type H⁺-ATPase.*

Mutational analysis and X-ray crystallography have been used to establish a model for H⁺-ATPase activation through 14-3-3 binding (Fig. 3.11). In this scheme, H⁺-ATPase exists in an inactive state as a dimer and interactions between the auto-inhibitory domains maintain the pump in an inactive state. Phosphorylation of the penultimate Thr residue promotes binding of a 14-3-3 dimer that prevents inhibition of pump activity by the auto-inhibitory domain. Further association with two additional 14-3-3 dimers and two pairs of H⁺-ATPase monomers results in the formation of an active, hexameric complex. *F. amygdali* has apparently co-opted this native scheme for the regulation of H⁺-ATPase activity, as FC binds to a preformed H⁺-ATPase-14-3-3 complex and stabilizes the enzyme in the active state.

An additional and separate mechanism of activation of H⁺-ATPase contributes to auxin-induced stimulation of proton pumping (see Chapter 2). In this case, auxin upregulates expression of the pump. For example, in *Zea mays* (maize) coleoptiles, auxin stimulates pump expression and cell wall acidification in nonvascular tissue but not in vascular tissue.

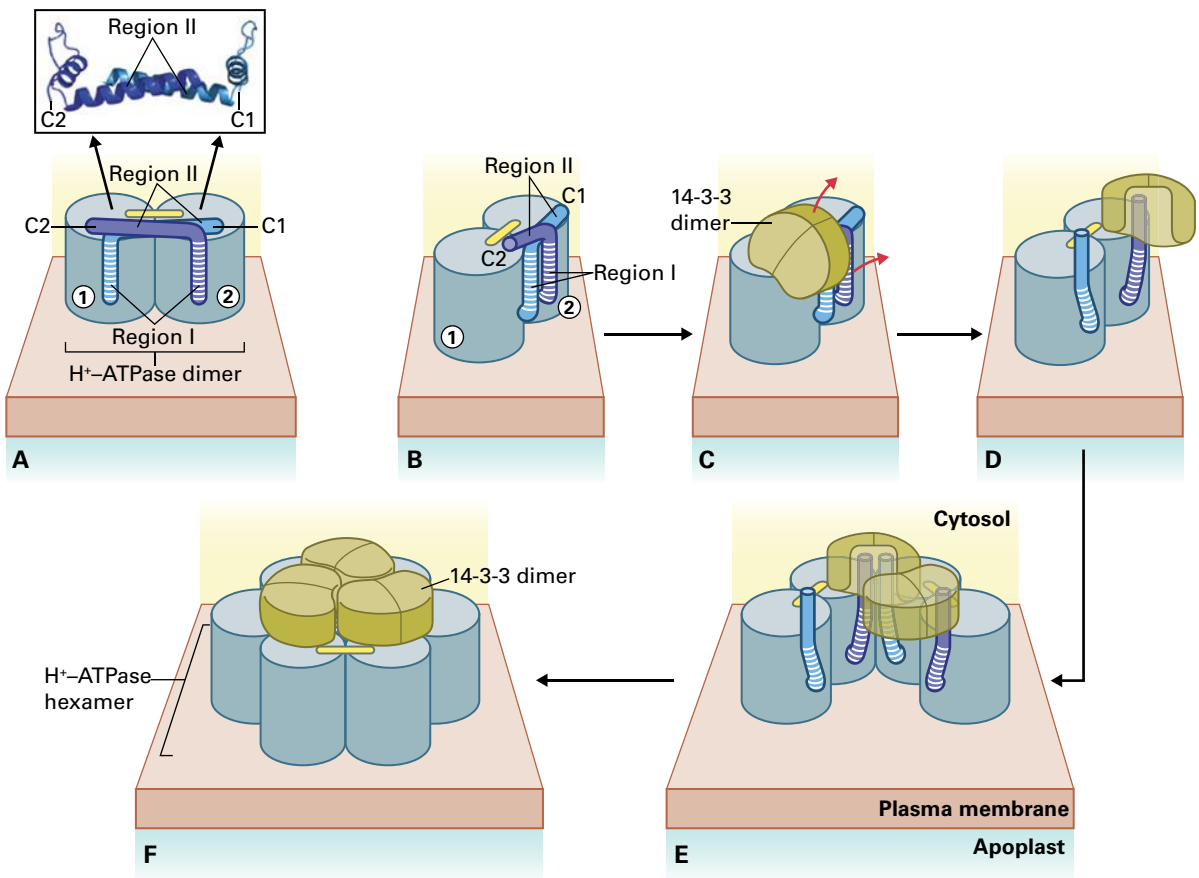


FIGURE 3.11 *A model for activation of the PM H⁺-ATPase by phosphorylation and binding of 14-3-3 proteins. In (A) and (B) a H⁺-ATPase dimer (monomers are blue and links between monomers are indicated as yellow links) is shown in an inactive state with interacting C-terminal auto-inhibitory domains (illustrated as blue tubes). In (C) through (E), phosphorylation of the penultimate Thr within the H⁺-ATPase allows 14-3-3 binding. Binding of the H⁺-ATPase with the 14-3-3 induces a conformational change (red arrows), which (D) abolishes the intermolecular contacts of the auto-inhibitory regions II, finally resulting in (E), a complex of two H⁺-ATPase dimers. (F) Association of a third 14-3-3/ATPase dimer generates the active hexameric complex.*
Source: Ottmann et al. (2007). Mol Cell 25:427–440.

3.2.6 Ca^{2+}-ATPases, another group of P-type ATPases, are distributed among various plant membranes

Calcium-pumping ATPases are distributed in the plasma membrane, ER, chloroplast envelope, and tonoplast. These enzymes pump Ca^{2+} out of the cytosol, thereby maintaining the cytosolic concentration of free Ca^{2+} at about 0.2 μM. This low concentration of free Ca^{2+} is essential in all cells to prevent precipitation of phosphates, but in eukaryotes it has become the basis for stimulus–response coupling pathways. Cytosolic Ca^{2+} can be increased many-fold in response to physiological stimuli without exceeding the low micromolar range.

Names for the two distinct classes of Ca^{2+}-ATPases found in plants reflect the cellular location of homologous pumps in animals. Unlike their animal counterparts which are only found in the plasma membrane, plant Ca^{2+}-ATPases of the plasma membrane type are found in plasma membrane, endomembranes (including ER), and the chloroplast inner envelope. These Ca^{2+}-ATPases are calmodulin (CaM) activated and possess an N-terminal CaM-binding domain (see Fig. 3.7B), in contrast to the C-terminal CaM-binding domain of animal PM-type Ca^{2+}-ATPases. In fact, plant PM-type Ca^{2+}-ATPases are the only examples yet reported of P-type ATPases regulated by their N termini. The second class of Ca^{2+}-ATPases is formed by ER type Ca^{2+}-ATPases, which in animals and plants have no CaM-binding domain. An *Arabidopsis* ER-type Ca^{2+}-ATPase identified by molecular cloning has been localized immunochemically to the ER.

The electrochemical potential against which Ca^{2+} must be pumped by these enzymes is vast, not only because the concentration of cytosolic free Ca^{2+} is several orders of magnitude less than that on the other side of the membrane, but also because the negative membrane potential opposes the export of divalent cations with double the effective force imposed on monovalent cations.

3.2.7 The tonoplast and other endomembranes are energized by vacuolar (V-type) H^+-ATPases

The lumen of plant vacuoles is acidic, with a pH near 5.5, about 2 pH units lower than that of the cytosol. In most unripe fruits and some citrus fruits, the vacuolar pH can drop below 3, imparting a sour taste to the tissue as a whole. Proton pumping into the vacuolar lumen is catalyzed by V-type H^+-ATPases that energize the membrane for cotransporter-mediated transport and generate the low pH of the vacuole, where hydrolases with acidic pH optima are located. Evidence is strong that V-type ATPases are also present in membranes of the ER, Golgi, and clathrin-coated vesicles of plant cells (as is the case in yeast and animal cells). The acidic pH of these compartments may contribute to vesicle sorting, membrane trafficking, and protein targeting (see Chapter 4).

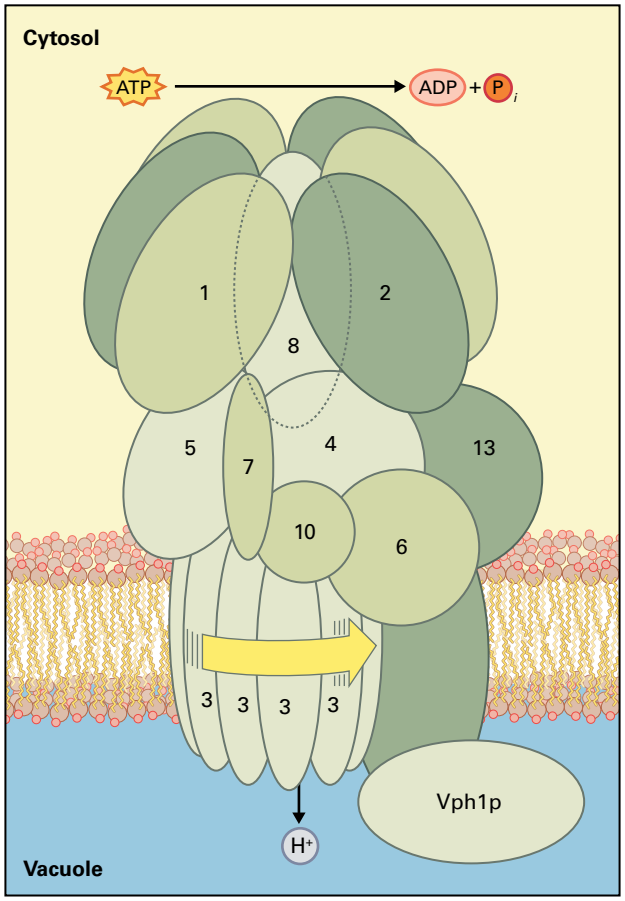


FIGURE 3.12 *Structural model of a V-type H^+-ATPase from* Saccharomyces cerevisiae. *The numbered subunits correspond to the protein products of* VMA1-VMA8, VMA10, *and* VMA13; *an additional subunit, Vph1p, is also shown. A hexameric subunit array in V_1 is generated by three copies each of subunit 1 and subunit 2 (homologous to the β and α subunits of the F-type ATPase, respectively). Another eight or so subunits also contribute to V_1. The V_o sector contains multiple copies of subunit 3 (a dominant, highly hydrophobic subunit of 16 kDa that arose from a duplication and fusion of the gene for the 8-kDa subunit c of F_o) and four additional subunits.*

Sequence analysis has demonstrated that V-type ATPases are distant relatives of F-type H^+-ATPases that operate solely in the direction of ATP hydrolysis. The ratio of H^+ translocated per ATP hydrolyzed has been measured as 2, although some evidence suggests that pump stoichiometry depends on luminal pH, with a low pH resulting in average ratios less than 2.

At the protein level, the structure–function partitioning in sectors of F-type and V-type H^+-ATPases has been retained (Fig. 3.12). Thus the V-type enzyme can be separated into a soluble V_1 sector, analogous to F_1 and including the adenine nucleotide binding sites, and a membrane-bound V_o sector, analogous to F_o and composing the H^+ pathway through the membrane. As might be anticipated, there is some sequence homology between subunits in the V_1 and F_1 sectors and also between subunits in the V_o and F_o sectors. However, V-type H^+-ATPases have a more complex subunit composition than F-type H^+-ATPases, and some evidence indicates that subunit composition for the V-type enzyme is variable. V-type

H^+-ATPases are potently and specifically inhibited by the macrolide antibiotic bafilomycin A_1, an extremely hydrophobic compound produced by *Streptomyces* that interacts with the V_o sector of the enzyme.

3.2.8 The tonoplast has a unique H^+-pumping inorganic pyrophosphatase (H^+-PPase)

A supplementary H^+ pump in the tonoplast of plants uses the free energy of hydrolysis of PP_i, rather than ATP, to pump H^+. Whether H^+-PPases may actually also transport K^+ remains controversial. In contrast to V-type ATPases, the PPase is a relatively simple enzyme composed of a single class of 80-kDa polypeptide that possesses as many as 17 membrane-spanning domains. The functional unit of the pump is probably a homodimer. The H^+-PPase is ubiquitous in plants, and is found in a few species of Protozoa, Eubacteria, and Archaea. In plants, H^+-PPases have been mainly localized to the tonoplast and Golgi.

3.2.9 ABC-type pumps are major players in sequestration of amphipathic metabolites and xenobiotics into the vacuole

A wide range of secondary metabolites, including flavonoids, anthocyanins, and breakdown products of chlorophyll, are sequestered in vacuoles where they are isolated from metabolic pathways or play a defense role. In addition, several xenobiotics—synthetic compounds such as herbicides—can be effectively detoxified by vacuolar sequestration. Transport of these compounds into vacuolar vesicles is dependent on ATP but is not sensitive to protonophores that dissipate the proton gradient. This indicates that transport is directly ATP dependent rather than indirectly dependent through secondary coupling to the pmf. Furthermore, transport is not sensitive to the V-type ATPase inhibitor bafilomycin but is sensitive to vanadate.

Amphipathic compounds are moved across the vacuolar membrane by pumps known as ATP-binding cassette (ABC) transporters. The ATP-binding cassette is widely distributed among enzymes that bind ATP (including F-type ATPases) and includes the so-called Walker A and B motifs (Fig. 3.13). The family of ABC transporters is ancient and is found in all domains of life. Mammalian ABC transporters, which have been extensively characterized, transport a wide range of compounds, including chemotherapeutic drugs and proteins. In bacteria, some ABC transporters are involved in uptake of simple nutrients such as phosphate and amino acids, and in *S. cerevisiae* an ABC transporter exports mating factor. The defining feature of ABC transporters is their domain structure: a stretch of transmembrane spans, followed by a nucleotide-binding fold that incorporates the Walker motifs. This domain structure is duplicated in both the N- and C-terminal halves of the transporter (Fig. 3.13). Crystal structures of ABC transporters show that a single transporter is composed of two transmembrane domains and two nucleotide-binding domains. However, not all ABC transporters are encoded by a single gene: some ABC transporter genes encode half a transporter, which presumably can form homo- or heterodimers,

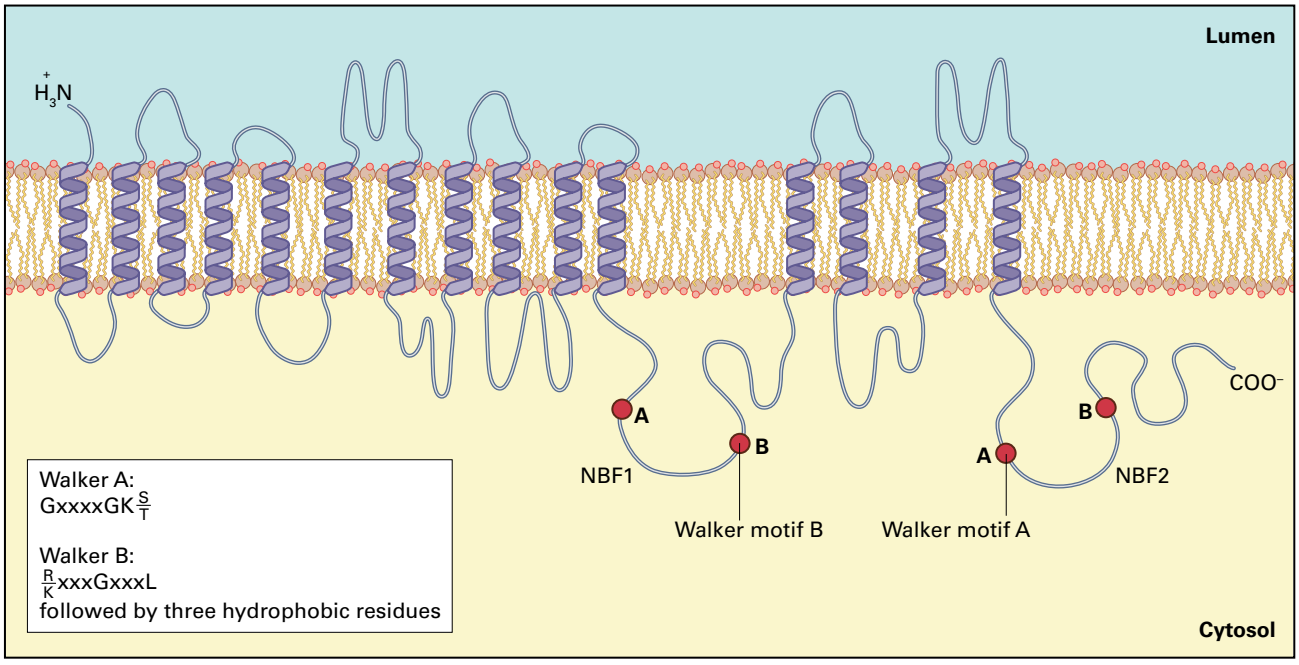


FIGURE 3.13 *Model of MRP2, a vacuolar ATP-binding cassette (ABC) transporter from* Arabidopsis. *Two nucleotide-binding folds, NBF1 and NBF2, each contain Walker motifs A and B. The NBFs are separated by transmembrane domains containing multiple integral membrane helices.*

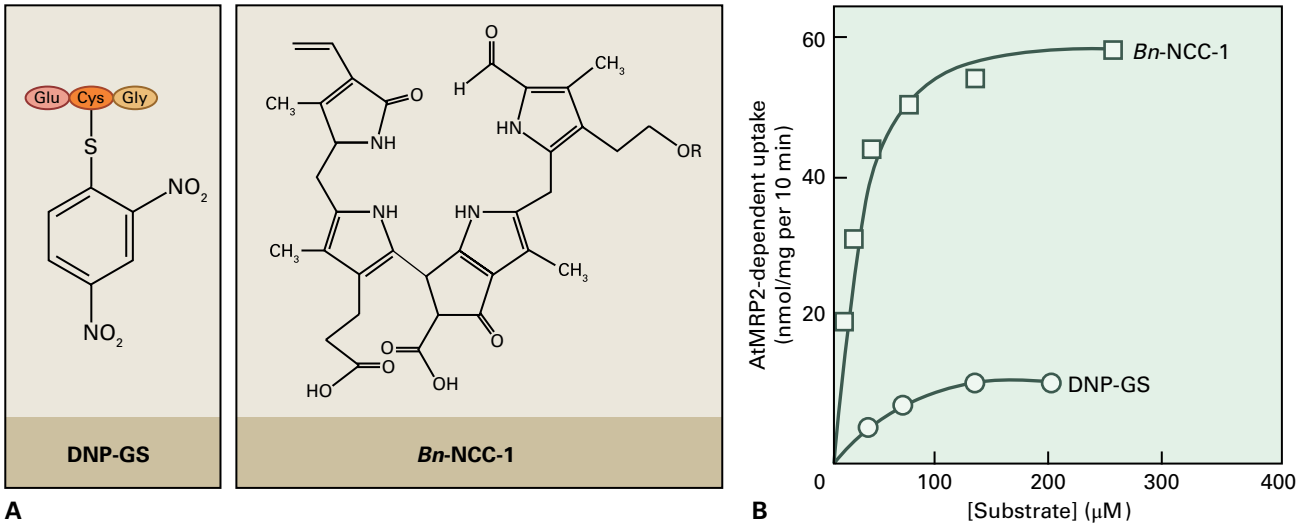


FIGURE 3.14 *Transport of a glutathione-conjugated xenobiotic and a chlorophyll catabolite by AtMRP2, an ABC transporter from* Arabidopsis. *(A) Structures of the glutathione-conjugated xenobiotic dinitrophenol (DNP-GS) and a linear tetrapyrrole from* Brassica napus *(*Bn*-NCC-1). In the* Bn*-NCC-1 structure, R represents a malonyl group. (B) Concentration-dependent uptake of DNP-GS and* Bn*-NCC-1 by AtMRP2.*

and some transporters are encoded by four genes (two transmembrane domain and two nucleotide binding domain genes), or a combination of these.

Whole genome sequences indicate that plants possess well over a hundred ABC transporter genes, constituting the largest transporter gene family, suggesting roles as diverse as those described for other organisms. For example, many xenobiotics are sequestered in plant vacuoles after glucosylation, and ABC transporters are possibly involved in sequestration. Other compounds, including flavonoids and some xenobiotics, are known to be transported by ABC transporters as glutathione conjugates (GS-conjugates). In these cases, the compound must first be linked to glutathione by a glutathione *S*-transferase reaction. Yet other compounds (e.g. the linear tetrapyrrole catabolites of chlorophyll) are transported without prior conjugation. One *Arabidopsis* ABC transporter, MRP1, appears to translocate GS-conjugates exclusively. Another, MRP2 (Fig. 3.13), translocates not only GS-conjugates but also unmodified chlorophyll catabolites (Fig. 3.14). Several mammalian ABC transporters also demonstrate broad substrate specificities that are atypical of transport systems in general; most non-ABC transporters exhibit strong selectivity for the preferred substrate.

A great deal remains to be discovered concerning plant ABC transporters. The complete crystal structures of two *E. coli* ABC transporters, the vitamin B12 importer BtuCD and the lipid exporter MsbA, suggest that transport mechanism might depend on each specific transporter. A comparison between the structures of BtuCD and MsbA showed that number and position of transmembrane helices varies. For example, the complete BtuCD transporter has 10 + 10 transmembrane alpha helices rather than the canonical 6 + 6, and they are arranged in such a way to accommodate entry of the large vitamin B12 substrate from the aqueous periplasm. The lipid substrate for MsbA is thought to enter from the inner leaflet of the plasma membrane between the transmembrane domains of the transporter. The MsbA structure was obtained in the absence of lipids, so it is not clear whether the transporter has a lipid-filled pore that can accommodate a hydrophobic substrate, or whether the substrate is "flipped" to the other side of the membrane in a reaction occurring at the interface of the ABC transporter and the membrane lipid.

3.3 Ion channels

3.3.1 Ion channels are ubiquitous in plant membranes

In the early 1950s, voltage-activated selective fluxes of ions that cause action potentials were described during classic studies on squid axons. Action potentials are generated when the membrane is depolarized to a voltage more positive than a threshold. A substantial further depolarization then follows, but this is transient and the membrane potential (V_m) returns rapidly to its negative resting potential, typically after 0.001 to 0.002 s in axons. Such cells are said to be "excitable." In the nervous systems of animals, action potentials have well-known signal propagation roles. Some types of plant cells are excitable, such as algal cells, although the action potentials are about three orders of magnitude slower than those of their animal counterparts. The best-studied action potentials in plants occur in the giant internodal cells of charophyte algae, where their function remains unknown (Fig. 3.15). A few terrestrial plant cells are also excitable, especially those exhibiting rapid changes in size. In *Mimosa pudica*, leaf stroking evokes an action potential that causes the pulvinus, a hinge region at the base of the leaf, to lose turgor and collapse the leaf. Some insectivorous plants (e.g., *Dionaea muscipula* and *Drosera* spp.) also use action potentials to couple the sensing of prey to subsequent leaf movements.

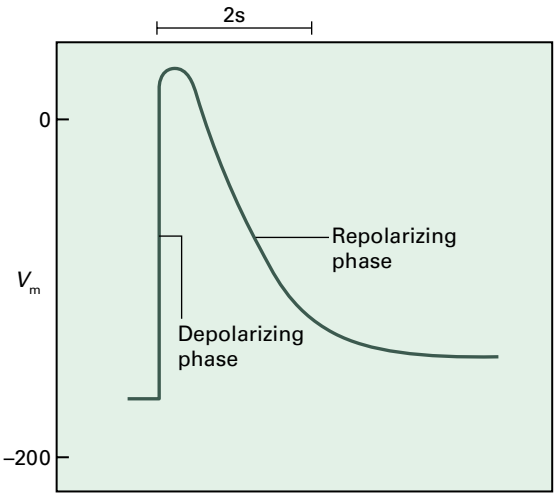


FIGURE 3.15 *An action potential as seen in the large internode cells of some algae. In response to a depolarizing, stimulating pulse, the membrane potential rapidly depolarizes further. This depolarization phase is followed by a much slower repolarizing phase, during which ion fluxes return the* V_m *to nearly its initial value.*

These rather specialized examples appear to be exceptions, and the major roles of plant ion channels are substantially different from animal paradigms. Little was known about plant ion channels before the mid 1980s, when technologies developed for neurophysiological investigations were applied to plant cells and demonstrated the presence of ion channels in a "non-excitable" plant cell, the guard cell. Ion channels are now known to be present in all plant cell types and at all membranes that have been analyzed. Research on guard cell ion channels has led to present models of the functions of a network of plant ion channels acting in concert to mediate physiological processes. Studies in specific cell types (e.g., guard cells, root epidermal cells, and xylem parenchyma) have employed the tools of electrophysiology, genetics, molecular biology, and genomics to assign and model specific properties and biological functions of various classes of plant ion channels.

3.3.2 Ion channels are studied with electrophysiological techniques

The **patch clamp** technique (Box 3.6) made possible dramatic advances in our understanding of plant ion channels. Developed by the early 80s for detecting and characterizing ion channels in excitable animal cells, the technique is also applicable to plant plasma membranes and intact plant vacuoles. In essence, the patch clamp technique allows detection of small electrical currents that ions carry as they flow through channels. The experimenter can control all the components of the electrochemical driving force, meaning the media on both sides of the membrane and, by using a feedback amplifier, the transmembrane voltage.

The patch clamp technique can be used to resolve the activity of single protein molecules (channels) as they conduct ions. Channel activity in single cells can also be measured. Using the whole-cell patch clamp technique, the activity of hundreds or thousands of ion channels in a single cell can be quantified, and changes in activity in response to diverse cellular messengers and stimuli can be studied. By comparing changes in ion fluxes to physiological responses, such as the swelling or shrinking of guard cells, the function of specific channel types has been determined. A major advantage of the patch clamp technique is that transport activity can be analyzed in relatively small cells, meaning that most if not all types of plant cells are amenable to this approach.

Alternatives to the patch clamp technique include the construction of planar lipid bilayers (Fig. 3.16) for the measurement of single channels, and classical microelectrode impalement techniques (Fig. 3.17) for the study of large, whole cells that are not cytoplasmically connected to one another by plasmodesmata. Lipid bilayers can be used to study the activities of channels at intracellular membranes that, by virtue of their dimensions, are not amenable to conventional patch clamp analysis (e.g., ER). Microelectrode impalement recordings can be made using cells with relatively intact cell walls, whereas the patch clamp technique requires the isolation of plant protoplasts.

3.3.3 Ionic fluxes through channels are driven solely by electrochemical potential differences

Ion flow through channels is passive. In contrast to pumps or ion-coupled cotransporters, the direction of ion flow through a channel is dictated simply by the electrochemical potential gradient for that ion, $\Delta\bar{\mu}_{ion}$ (see Box 3.2). The current passing through a single channel (Fig. 3.18) can be plotted as a function of the membrane potential to yield a current–voltage (I–V) relationship for the channel (Fig. 3.19). If the single channel I–V relationship is linear, it is said to be Ohmic and according to Ohm's law $I = V/R$, where R is the resistance. The slope of this relationship, $1/R$, is the single-channel conductance (g), measured in picosiemens (pS). The value of g is a measure of the transport rate of the channel and is characteristic for a given channel type under particular conditions. Typically, g increases with the concentration of the permeant ion, so it is important to specify the recording conditions under which g is measured.

Channel-mediated currents that flow into the cytosol are defined as negative, are shown as downward deflections on current traces, and may be carried either by an influx of cations into the cell or an efflux of anions leaving the cell. Conversely, outward currents carried by cation efflux or anion influx are defined as positive and are shown as upward (positive) deflections on current traces. When $\Delta\bar{\mu}_{ion} = 0$, there is no overall driving force acting on the ion, so the net flux of that ion through the channel is zero, and the current it carries

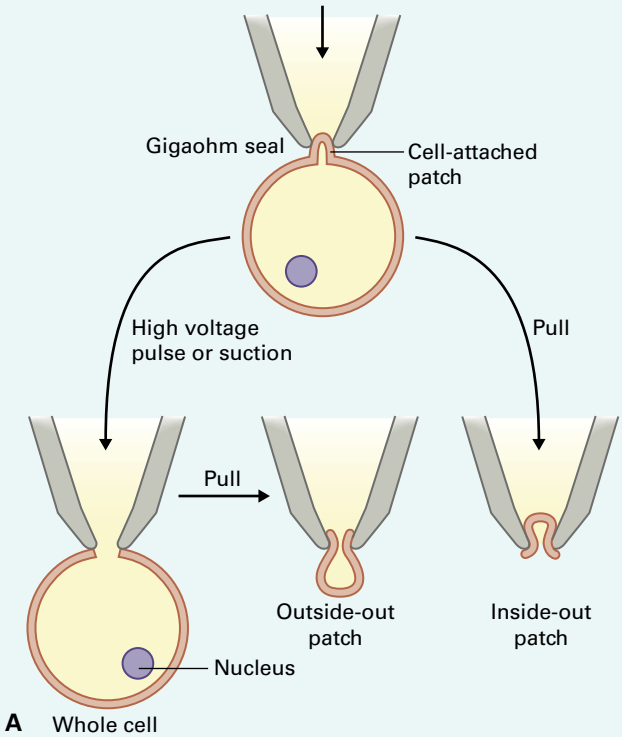
BOX 3.6 The patch clamp technique is used to measure ionic currents

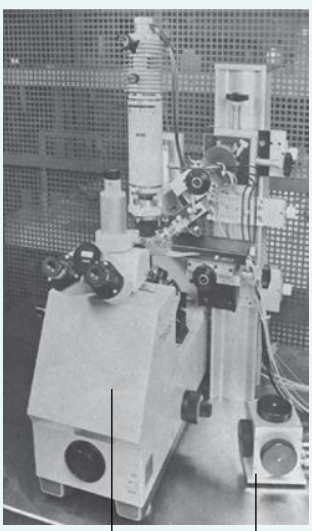
The patch clamp technique arose from elegant technical advances, theoretical considerations and early "noise" analyses of neurotransmitter activated ion currents. Pushing a blunt-tipped, heat-polished glass micropipette against a biological membrane, and simultaneously applying suction to the inside of the micropipette can form an electrically tight seal. The high resistance of this seal (>1 GΩ, or 10^9 ohms) limits current leak between the membrane and pipette (panel A), and the small size of the membrane patch that covers the pipette tip (a few square micrometers) greatly reduces the background noise, allowing the resolution of single proteins, channels.

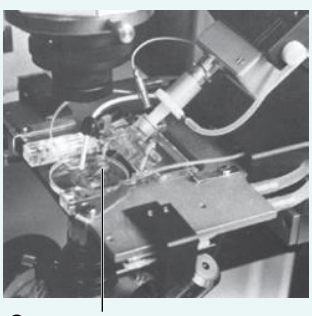
A typical patch clamp recording apparatus is shown in panels B and C. The patch clamp technique utilizes several recording modes (panel A). Initial seal formation attains cell-attached mode, which can record the activities of individual ion channels but does not allow control of medium composition on the cytosolic side of the membrane. Despite its limited use in plant cells, this recording mode can be applied to channels that lose activity when the cytoplasm is perturbed. Pulling the pipette away from the rest of the membrane generates an inside-out patch, in which the cytosolic face is exposed to the bathing medium. The solution composition on both sides of the membrane is now defined. Alternatively, the membrane patch that covers the pipette tip can be disrupted with a high-voltage pulse or suction, thereby giving electrical access to the inside of the cell. The activities of the ensemble of ion channels in the entire cell membrane can then be monitored in this frequently used whole-cell mode. The relatively large volume of medium in the pipette exchanges rapidly with the cell contents, and becomes the defined intracellular solution. Finally, if the pipette is pulled away from the cell after attainment of the whole-cell mode, a membrane bleb is also pulled away and reseals itself across the pipette tip as an outside-out patch.

To convert the electrical current through an open channel to a rate of transport (ions s^{-1}), the single channel current is divided by the absolute unitary electrical charge of an electron (1.6×10^{-19} A·s) and by the charge (valence) of the ion being investigated. For example, Ca^{2+} ions have a charge of +2. A channel-mediated current of 1 pA (10^{-12} A) for the divalent cation Ca^{2+} represents a turnover rate of more than 3 million Ca^{2+} ions per second:

$$[(10^{-12}\,A)/[(1.6\times10^{-19}\,A\cdot s)(+2)]=3.125\times10^{6}\,ions\,s^{-1}$$







Source: Adams & List Associates Ltd., Great Neck, NY.

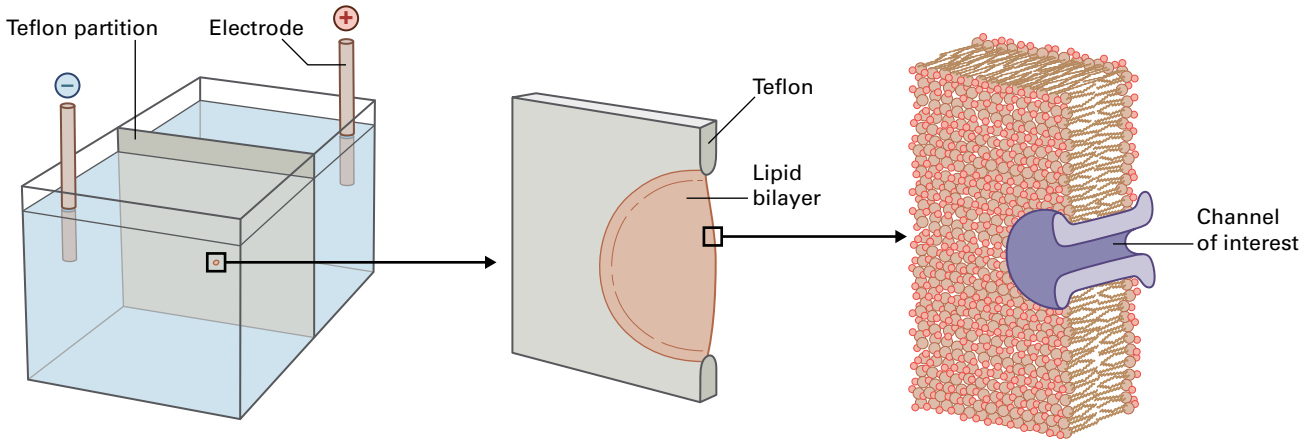


FIGURE 3.16 *Measurement of channel activity in planar lipid bilayers. A bilayer of purified lipids can be formed across a small (0.1-mm-diameter) hole in a Teflon partition that separates two chambers. Electrodes are dipped into solutions on either side of the partition and connected to an amplifier. Fractionated plant membrane vesicles introduced into one of the chambers fuse spontaneously with the artificial membrane, thereby incorporating channels into the bilayer and allowing the currents they carry to be measured.*

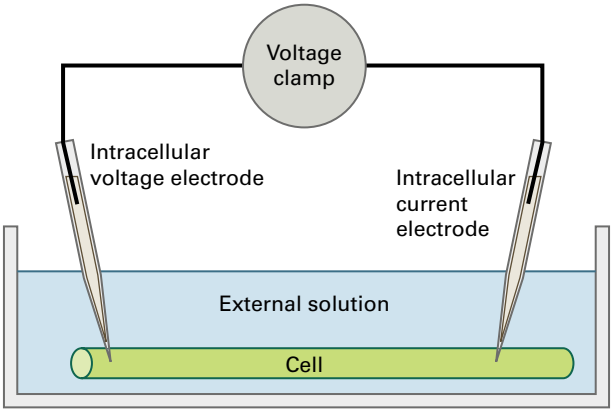


FIGURE 3.17 *Recording whole-cell membrane currents with a two-electrode voltage clamp. The cell is impaled with a voltage microelectrode, which is used to establish the electrical potential across the membrane, and a current electrode, which measures the current flowing in or out of the cell.*

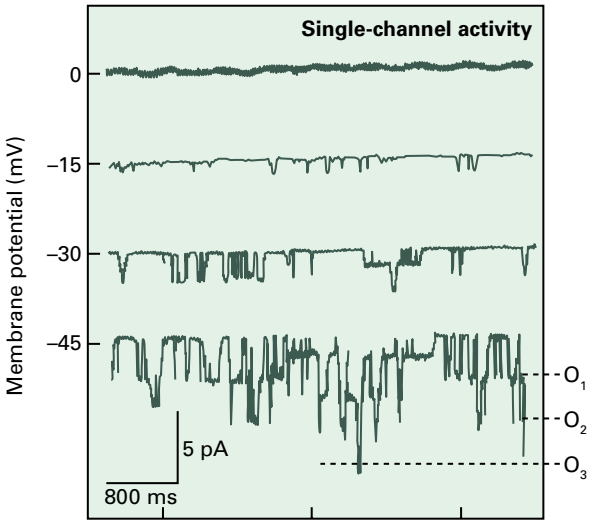


FIGURE 3.18 *The recorded activity of a single channel taken from a tonoplast membrane patch. The prevalence of the conductive (O state) increases with imposed membrane voltage in the negative range. O_1, one channel open; O_2, two channels open; O_3, three channels open.*

is also zero. The membrane potential at which the driving force on a specific ion is zero is called the equilibrium or Nernst potential, E_{ion}, for that ion. The equations to calculate E_{ion} were introduced in Box 3.2 (Equations 3.B7 and 3.B8).

3.3.4 Ion channels exhibit ionic selectivity

Channels are not thought to require large conformational changes to catalyze transport. Nevertheless, it would be wrong to think of channels merely as sieve-like pores in a membrane, because they exhibit two additional properties that are essential for their function: **ionic selectivity** and **gating**.

Ion channels display selectivity for their ionic substrates. Most classes of ion channels in plant cells usually discriminate in favor of either cations or anions. Cation channels can

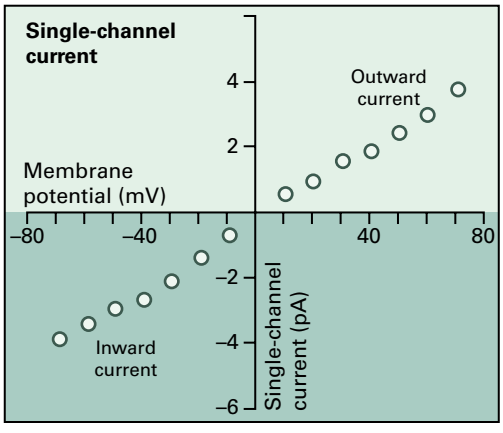


FIGURE 3.19 *Current–voltage (I–V) curve for a single channel.*

be further subdivided into those that select K^+ or Na^+ over other monovalent cations, those that are relatively nonselective among monovalent cations, and those that are permeable to divalent cations, particularly Ca^{2+}. Most plant plasma membrane anion channels appear to allow permeation of a wide range of anions, including Cl^-, NO_3^-, or organic acids. Distinct types of anion channels in the tonoplast have been described that select either for Cl^- or for organic acids such as malate.

Up to this point, we have emphasized that ion fluxes through channels are monitored as electrical currents. However, currents themselves provide no information on which ions are flowing. In general, this information on ionic selectivity of a channel can be gained through a measurement of the reversal potential (E_{rev}; see Box 3.7) of the channel under various ionic conditions. E_{rev} is defined as the voltage at which the current through the channel reverses from inward to outward. In other words, E_{rev} is the zero-current voltage, an experimentally derived parameter for a given transporter. If E_{rev} for the channel is in accord with E_{ion}, the equilibrium potential of a given ion based on biophysical theory (see Box 3.2), this is good evidence that the ion in question is carrying the current. However, channels are often not perfectly selective for a given ion; in these cases, E_{rev} can be evaluated to determine ionic selectivity of one type of ion relative to another type of ion (see Box 3.7). For example, the permeability of a channel for K^+ ions can be determined relative to that of Na^+ ions. The fact that channels are selective implies that sites capable of interacting with and distinguishing between specific ions must be located within channel pores. In some cases, these sites have been identified at a molecular level.

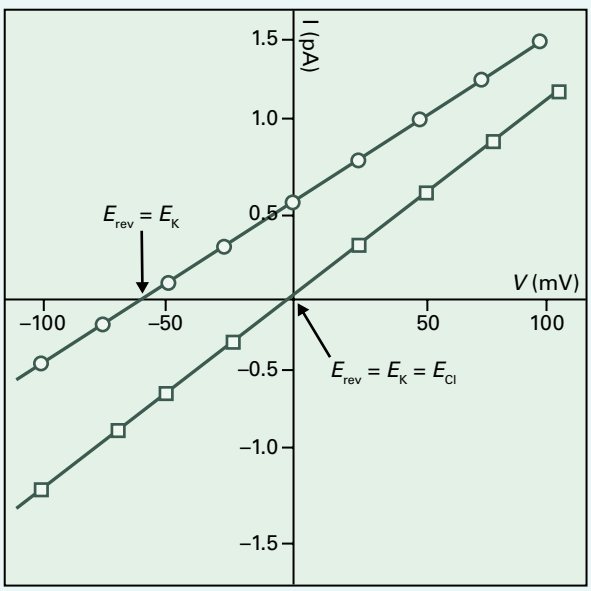
BOX 3.7 Ionic selectivity of ion channels can be determined by measurements of the reversal potential of the channel under various ionic conditions

From a biological point of view, one of the principal interesting features of ion channels in plant cells concerns the identities of the ions that flow through them. Frequently, this issue of ionic selectivity is addressed through measurement of E_{rev} for the channel-mediated currents in various ionic conditions.

Take the example of a channel for which patch clamp recordings of single-channel currents are obtained in symmetrical conditions (100 mM KCl on both sides of an outside-out membrane patch). These records of current can be plotted as a function of voltage in the form of a current–voltage (I–V) relationship (see figure). As seen for the curve with square data points, the zero-current potential (E_{rev}) is 0 mV under these symmetrical conditions. However, for either K^+ or Cl^-, the logarithm term in Equations 3.B7 or 3.B8 that define the E_{ion} reduces to 0 because the concentration ratio of either ion is 1 (and ln 1 or log 1 = 0). Now, let us suppose that the external KCl concentration is decreased to 10 mM in the continued presence of 100 mM KCl in the pipette. Now there is a 10-fold concentration difference across the pipette, which is reflected in the *I–V* curve with circular data points (see figure). The value for E_{rev} is now –59 mV. Comparing this value with E_K (–59 mV) and E_{Cl} (+59 mV) shows, by the coinciding values of E_{rev} and E_K, that the channel has perfect selectivity for K^+ over Cl^-. If the channel is permeable to more than one ionic species, its reversal potential is the mean of the individual ionic equilibrium potentials, weighted according to their respective permeabilities.

Selectivity ratios for different permeant ions are often determined in so-called bi-ionic conditions, in which each permeant ion is selectively present on just one side of the membrane. In graphs A and B, for example, the same outside-out patch was bathed with either 100 mM K^+ (A) or 100 mM Na^+ (B). In both cases, the pipette contained 100 mM K^+. As expected, E_{rev} was close to 0 mV with equal concentrations of K^+ across the membrane. With K^+ inside and Na^+ outside, however, E_{rev} shifted to -58 mV. This value can be used to compute a permeability ratio for Na^+ and K^+. For the example of a cation channel with permeability both to K^+ and Na^+, then $E_{rev} = (RT/zF) \ln\{P_{Na}[Na^+]_o/P_K[K^+]_i\}$, where P_{Na}/P_K is the permeability ratio for Na^+ with respect to K^+.

In this example, the channel has a 10-fold higher selectivity for K^+ over Na^+. A word of caution: calculated permeability ratios do not reflect precise transport selectivity, but do help distinguish more and less permeant ions.



3.3.5 Ion channels are gated by voltage or ligands, through changes in open state probability

Ion channels are tightly controlled by conformational shifts between open (O) or closed (C) states. To catalyze ion movement, the channel must first switch into its open state. This switching between O and C states is what gives rise to the discrete transitions in current shown in single-channel recordings (see Fig. 3.18). Alternation between the O and C states is represented by Reaction 3.2. In nearly all channels, activation is controlled by membrane voltage, a ligand/second messenger, covalent modification, or a combination of these. When a factor activates a channel, the equilibrium of Reaction 3.2 shifts from left to right.

Reaction 3.2

$$\text{Channel}_c \leftrightarrow \text{Channel}_o$$

The contribution of an individual type of channel to whole-cell or whole-vacuole currents can be defined as in Equation 3.2, where I is the ionic current across the whole cell or vacuole, N is the number of channels, i is the current that flows through the channel when open, and P_o is the probability that the channel is in its open state. Activation of a channel-mediated current usually involves an increase in P_o (Fig. 3.20). For example, voltage-dependent gating can transform a linear current to voltage relationship measured at the single-channel level (see Fig. 3.19) to a distinctly nonlinear current-voltage relationship across the whole plasma membrane (Fig. 3.21). Changes in N can also be achieved through covalent modification (e.g., phosphorylation) or ligand binding.

$$I = N \cdot i \cdot \boldsymbol{P}_o \qquad \text{(Eq. 3.2)}$$

3.3.6 Voltage-dependent K^+ channels at the plasma membrane

Whole-cell recordings made over a range of holding voltages indicate that currents flow across the plasma membrane in both directions, into and out of the cytosol. These inward and outward currents have two components: an instantaneous current, and a time-dependent current that increases over a period of several hundred milliseconds. Plotting the time-dependent currents as a function of membrane potential makes it apparent that the currents are voltage activated. Activation occurs only beyond a **threshold voltage**, which is more negative than E_K for the inward current and more positive than E_K for the outward current. These time-dependent currents were identified and characterized as inward-rectifying and outward-rectifying K^+-channel currents in guard cells and are now known to be widely distributed in different types of plant cells (see Fig. 3.21). Molecular (see Section 3.3.8) and biophysical evidence demonstrates definitively that time-dependent inward and outward currents are carried by separate

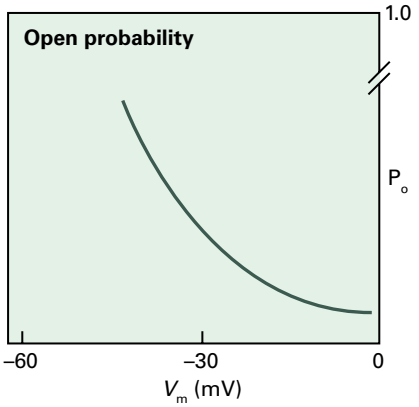


FIGURE 3.20 *The open state probability (P_o), defined as the proportion of total recording time that the channel resides in its open state, is plotted as a function of the holding voltage. Here, P_o shows a progressive increase as V_m becomes more negative.*

classes of ion channels. The channels carrying these currents are said to rectify. Like valves, rectifying channels carry current mainly in one direction. For this reason, the channels are referred to as inward-rectifying K^+ channels and outward-rectifying K^+ channels.

Outward K^+ channels contribute to net release of K^+ from guard cells during stomatal closure and from pulvinar cells during leaf movements. Research on guard cells led to the model that inward K^+ channels take up K^+ from the cell wall; the resulting K^+ accumulation contributes to cell turgor or K^+ nutrition as in root epidermal cells. Inward K^+ channels can take up K^+ only at potentials more negative than E_K. In cases where the membrane is depolarized or the extracellular K^+ is in the low micromolar range, K^+ is accumulated by both "low- or medium-affinity" K^+ channels and "high-affinity" K^+ transporters.

3.3.7 Plant cell inward-rectifying K^+ channels function in net K^+ uptake into plant cells and are encoded by a family of voltage-gated channels

Inward-rectifying K^+ channels, also called K^+ influx channels or K^+_{in}, preferentially conduct K^+ ions into the cytosol and are activated by more negative membrane potentials (hyperpolarization). They were first characterized in stomatal guard cells and proposed to mediate K^+ uptake into guard cells, which is required for stomatal opening. Inward-rectifying K^+ channels mainly activated by membrane voltages more negative than the cell resting membrane potential also exist in animal cells. These K^+ channels function to inhibit the electrical excitability of cells such as neurons and cardiac muscle cells. Although plant K^+ channels play a role in regulating the membrane potential of cells, the function of plant inward-rectifying K^+ channels in mediating long-term K^+ uptake differs from the typical function of inward-rectifying K^+ channels in animal cells. As we

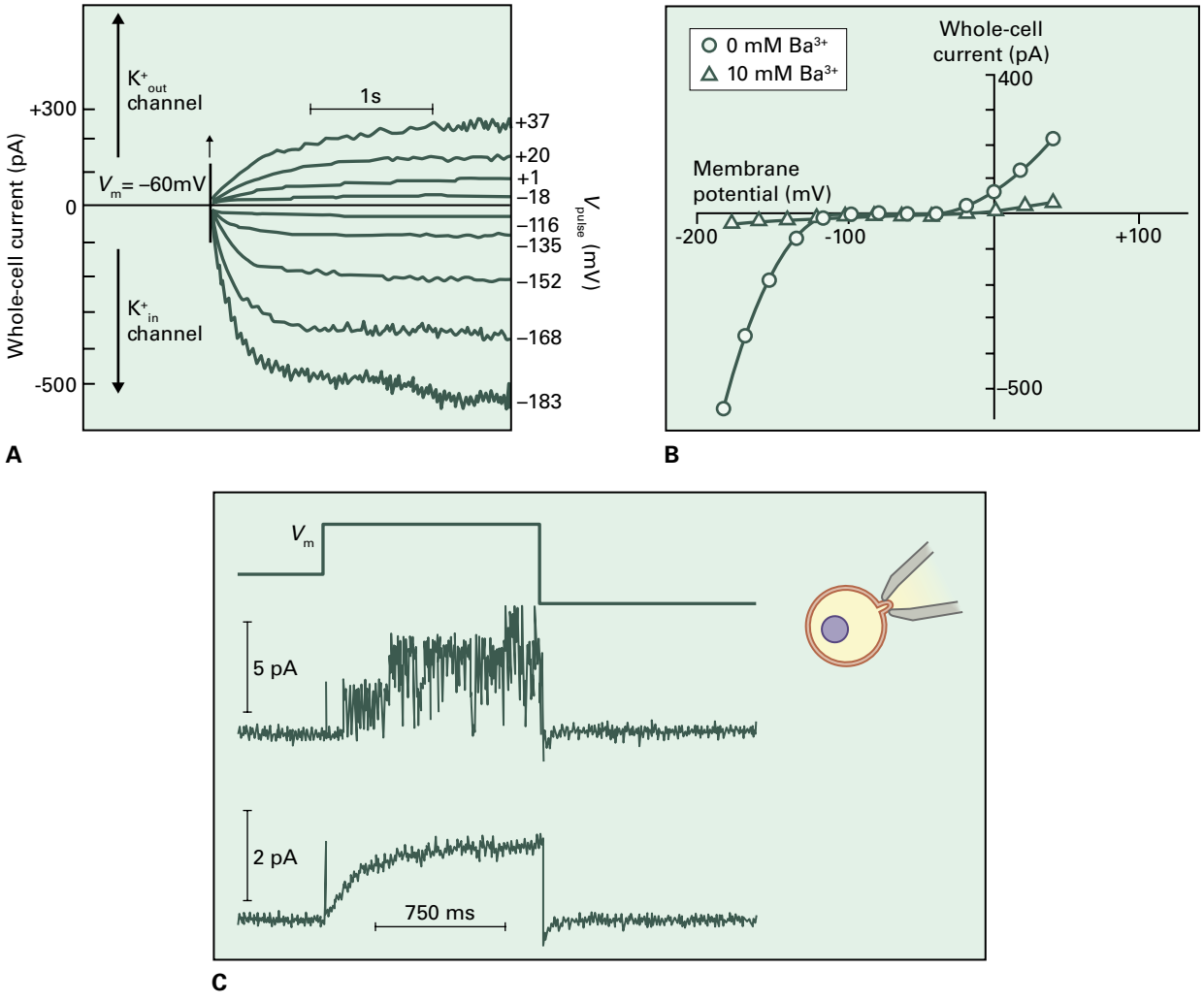
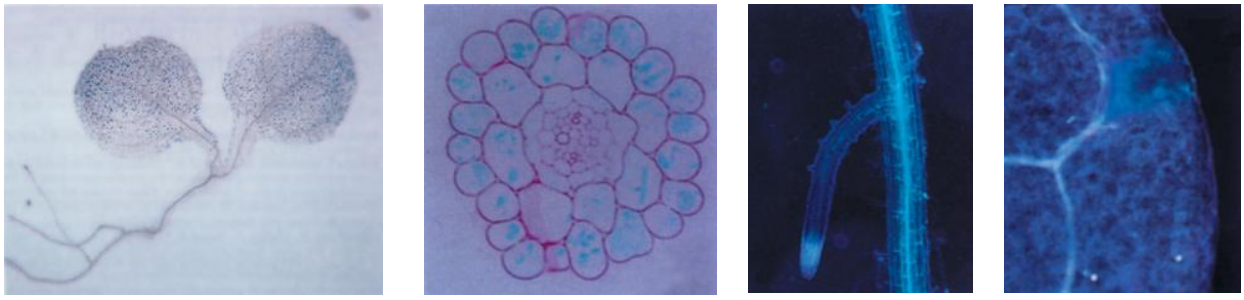


FIGURE 3.21 *Whole-cell K^+ channel currents in a guard cell as measured by the patch clamp technique (see Box 3.6A). (A) Electrophysiology data traces: In response to a series of successive voltage pulses, K^+ ions flow through channels in the plasma membrane. The sequentially recorded current traces, corresponding to the applied voltages between –183 and +37 mV, are superimposed in this plot. The applied voltages during each voltage step are indicated to the right of the steps. (B) Current–voltage relationship for the time-dependent currents measured toward the end of voltage pulses where currents reached a plateau (steady state) in (A). Downward-deflecting currents in (A) and the corresponding negative currents in (B) correspond to the plant inward-rectifying K^+ (K^+_{in}) channels identified in guard cells. Upward-deflecting currents in (A) and the corresponding positive currents in (B) correspond to the plant outward-rectifying K^+ (K^+_{out}) channels. (C) Measurement of single K^+_{out} channels in a small guard cell membrane patch. Top inset: applied positive voltage pulse to the plasma membrane. Middle: Example trace of single K^+_{out} channels recorded in response to the above voltage pulse. Lower: Averaging of many such successive single channel recordings shows the average time- and voltage-dependent activation of single K^+_{out} channels.*
Source: Schroeder et al. (1987). Proc Natl Acad Sci USA 84:4108–4112.

will see in Section 3.3.8, the molecular structure of plant K^+ influx channels differs substantially from that of animal inward-rectifying K^+ channels, and this further differentiates these two classes of channel.

The first eukaryotic K^+ influx channels were cloned from plants and functionally characterized by expression in *Xenopus* oocytes. *Xenopus* oocytes were found to provide a powerful system for characterizing the functions of plant transporters ranging from K^+ channels, to cotransporters and aquaporins, as described later. This class of K^+ channels has now been characterized in numerous cell types. Electrophysiological analyses of plant K^+ influx channels expressed in *Xenopus* oocytes have confirmed their unique properties.

Plant K^+ influx channel subunits are products of a multigene family, members of which exhibit tissue-specific expression. One member, KAT1 (see Box 3.1), is expressed selectively in guard cells (Fig. 3.22A); another, AKT1 (Fig. 3.23), is found in roots and hydathodes (see Fig. 3.22B). The *AKT1* gene of *Arabidopsis* has been disrupted using T-DNA insertional mutagenesis (see Chapter 6). The resulting mutant, referred to as *akt1-1*, exhibits reduced K^+ uptake (Table 3.1) and substantially less growth in media with low K^+ concentrations and added ammonium ions, which block high-affinity K^+ uptake transporters belonging to the KUP/HAK/KT family (Fig. 3.24). The analysis of K^+ uptake in *atk1-1* mutants indicates that *AKT1* encodes a medium-affinity K^+ uptake channel under physiological conditions.



A B

FIGURE 3.22 *Tissue-specific expression of plant inward-rectifying K^+ channels. (A) KAT1-mediated GUS expression in the guard cells of an* Arabidopsis *seedling. (B) AKT1-mediated GUS expression in (from left to right) mature roots, lateral roots, and hydathodes of* Arabidopsis.

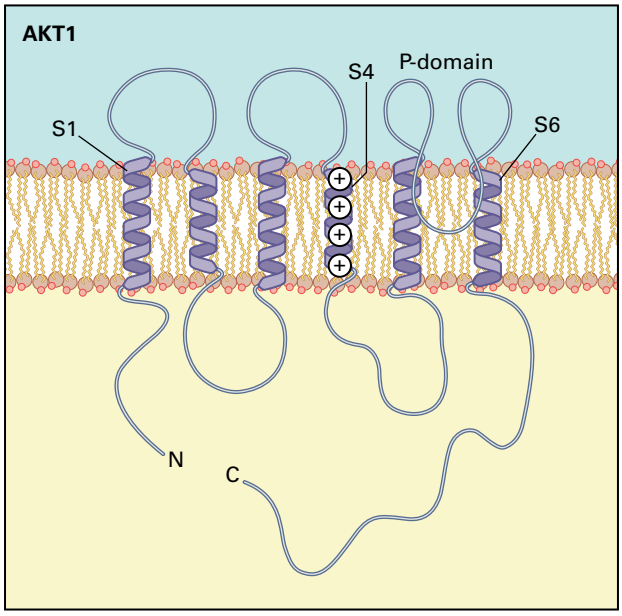


FIGURE 3.23 *Structure of the inward rectifying K^+ channel AKT1. There are six transmembrane spans, S1 through S6, with a membrane-intrusive loop between S5 and S6. This loop makes up the pore domain (P-domain) of the channel. Two helix-breaking proline residues at each end of a 20-residue span force the loop back into the membrane. The functional channel works as a tetramer, with the P-domains of each subunit interacting to form a narrow constriction that contains the K^+ selectivity site.*
Source: (A) Nakamura et al. (1995). Plant Physiol 109:371–374. (B) Lagarde et al. (1996). Plant J 9:195–203.

3.3.8 Plant cell K^+ influx channels are members of the Shaker family of voltage activated ion channels

Several structural features define plant K^+ influx channels as members of the *Shaker* family, a superfamily of voltage-gated K^+, Ca^{2+}, and Na^+ channels found in animal cells and named for the *Drosophila* mutant from which the first outward-rectifying K^+ channel was cloned. A characteristic feature of *Shaker* channels is evident in plant inward rectifying K^+ channels. The fourth transmembrane α helix, known as the S4 domain, exhibits a regular pattern of positively charged residues, lysine (Lys) or Arg, every third residue, so that the charged residues tend to project from one side of the helix. This region of the protein forms the **voltage sensor**, which is involved in opening the channel in response to a permissive voltage (Fig. 3.25). As a change in voltage is imposed across the membrane, the S4 helix is thought to screw into the membrane (for K^+_{in} channels), with the conformational transition opening the "gate" that controls ion flow through a separate part of the protein. Interestingly, all *Shaker*-type animal voltage-gated K^+, Na^+, and Ca^{2+} channels are activated by depolarization of the plasma membrane, whereas the *Arabidopsis* KAT1 channel was the first voltage-gated channel identified that is activated by hyperpolarization of the membrane, despite sharing a very similar predicted overall structure. This adaptability of the *Shaker* "bodyplan" to opposite gating requirements was discovered by analyzing KAT1 and is underscored by the fact that the major depolarization-activated K^+ channels in guard cells (GORK) and root stelar cells (SKOR) also belong to the *Shaker* family of ion channels.

Inward-rectifying K^+ channels are tetramers, in which each of the *Shaker* subunits contributes to the pore through which ions flow (Fig. 3.26). The pore domain (P-domain) of each subunit is located between the fifth and sixth transmembrane spans, looping into the membrane and out of it again. It is the P-domain that endows the channel with its ionic selectivity, with the conserved sequence TxGYGD providing a hallmark characteristic of many plant (and animal) K^+ channels. In addition to the four *Shaker* subunits, the functionally intact inward rectifying K^+ channels may include additional subunits, which might play a role in regulating channel properties.

3.3.9 The activity of voltage-dependent K^+ channels at the plasma membrane is regulated by voltage and phosphorylation

As befits their central role in cell biology, outward and inward transporting K^+ channels are also subject to regulation by factors other than membrane voltage. In guard cells (Fig. 3.27), where they have been studied most intensively, outward rectifying K^+ channels are activated by the small increase in cytosolic pH that can be elicited by abscisic acid (ABA). Inward K^+

TABLE 3.1 *Uptake of $^{86}Rb^+$ by roots of wild-type and mutant akt1-1* Arabidopsis *plants.*

	^{86}RbCl (μM)		
	10	100	1000
Wild type	44.8 ± 7.6*	112.1 ± 24.8	282.2 ± 44.1
akt1-1	3.1 ± 0.3	23.3 ± 1.3	145.9 ± 10.1

* Each value is the mean rate of uptake (nanomoles per gram fresh weight per hour) ± SEM (n = 4).

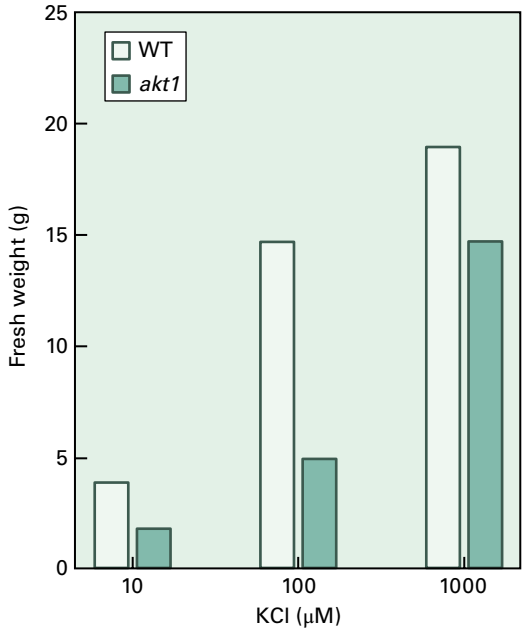


FIGURE 3.24 Arabidopsis akt1 *mutants deficient in the AKT1 inward rectifying channel demonstrate diminished growth in comparison with wild type (WT). The difference in growth rates is particularly pronounced at limiting concentrations of K^+.*

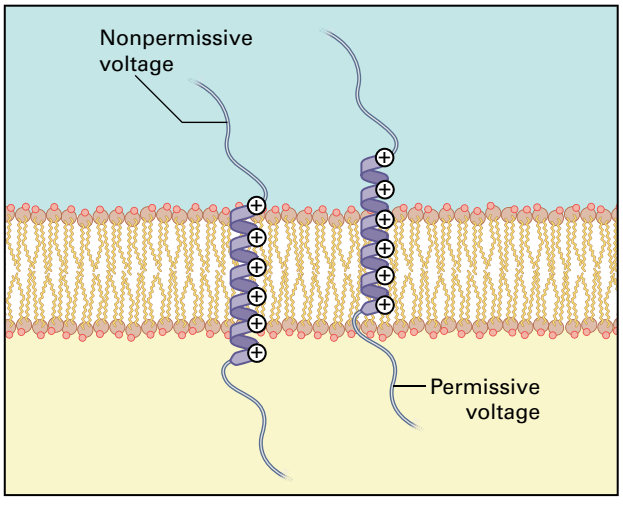


FIGURE 3.25 *The voltage-sensing S4 domain screws out of the membrane in response to application of a depolarizing voltage. By analogy with animal* Shaker *channels, this region is thought to twist slightly in the membrane when voltage is applied, so that it projects slightly from the membrane surface, just as a corkscrew does if twisted through a cork.*

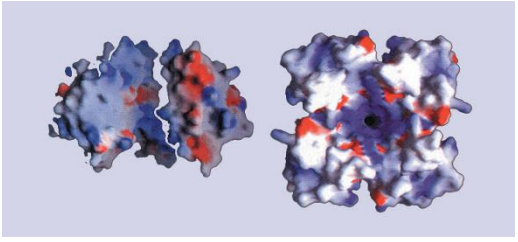


FIGURE 3.26 *Structure of the* Shaker *K^+ channel, viewed from the side (left) and top (right). In the side view, the foremost of the four subunits that contribute to the pore is omitted to show the center of the channel. Positively charged regions are shown in blue, negatively charged regions in red.*
Source: Kreusch et al. (1998). Nature 392:945–948.

channels are downregulated by increased cytosolic [Ca^{2+}]. Evidence for control by phosphorylation has come from a study of ABA-insensitive *abi1* mutants of *Arabidopsis*. The *ABI1* locus encodes a protein phosphatase 2C. Mutants display much less outward rectifying K^+ channel activity. In wild-type plants, ABA upregulates outward K^+ channel activity and downregulates inward K^+ channel activity (Fig. 3.27).

3.3.10 Monovalent cation channels at the vacuolar membrane are [Ca^{2+}]-sensitive and mediate vacuolar K^+ mobilization

Vacuoles are usually thought of as organelles for accumulation and storage of solutes, but in some circumstances massive solute loss from vacuoles is required. One important example is during osmotic adjustment, which can involve massive net salt loss from the cell and hence from the vacuole. Thus, hypoosmotic stress involves mobilization of ions from vacuoles to restore normal cell turgor, and during stomatal closure ions must be lost from guard cell vacuoles. Ion channels facilitate this mobilization of ions. In the case of guard cells, two different classes of K^+-permeable channel are competent in releasing K^+ from the vacuole. The interesting features of these channels relate to their complementary modes of regulation.

Both types of channels activate instantaneously in response to an imposed voltage. The fast vacuolar (FV) channel, which exhibits little selectivity among monovalent cations, is inhibited when cytosolic [Ca^{2+}] exceed 1 μM and is activated when cytosolic pH increases (Fig. 3.28). Conversely, the vacuolar K^+ (VK) channel, which is highly selective for K^+ over other

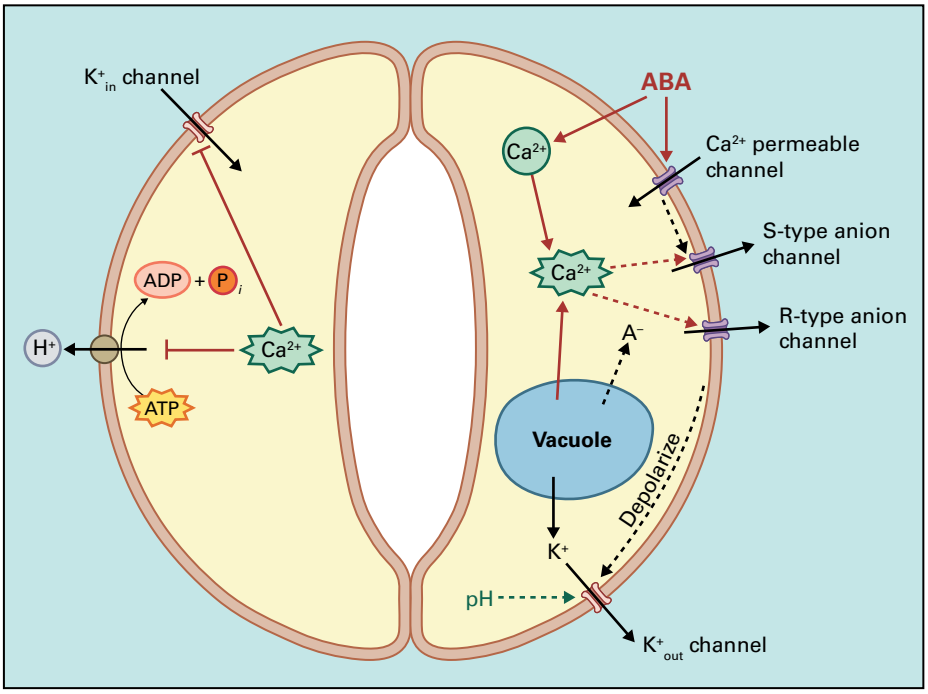


FIGURE 3.27 *Model describing how a network of ion channels functions in mediating stomatal closure by ABA or other stimuli. The right stomatal guard cell shows mechanisms that lead to solute efflux that mediates stomatal closing: Ca^{2+}-permeable channels, the S-type and R-type anion channels that are activated by Ca^{2+}-dependent and Ca^{2+}-independent pathways and the K^+_{out} channels. The left guard cell depicts parallel mechanisms that function in stomatal opening. Elevated Ca^{2+} down-regulates plasma membrane proton pumps and K^+_{in} channels thus inhibiting stomatal opening and contributing to the plant ion channel network.*
Source: Schroeder et al. (2001). Annu Rev P Physiol Plant Mol Biol 52:627–658.

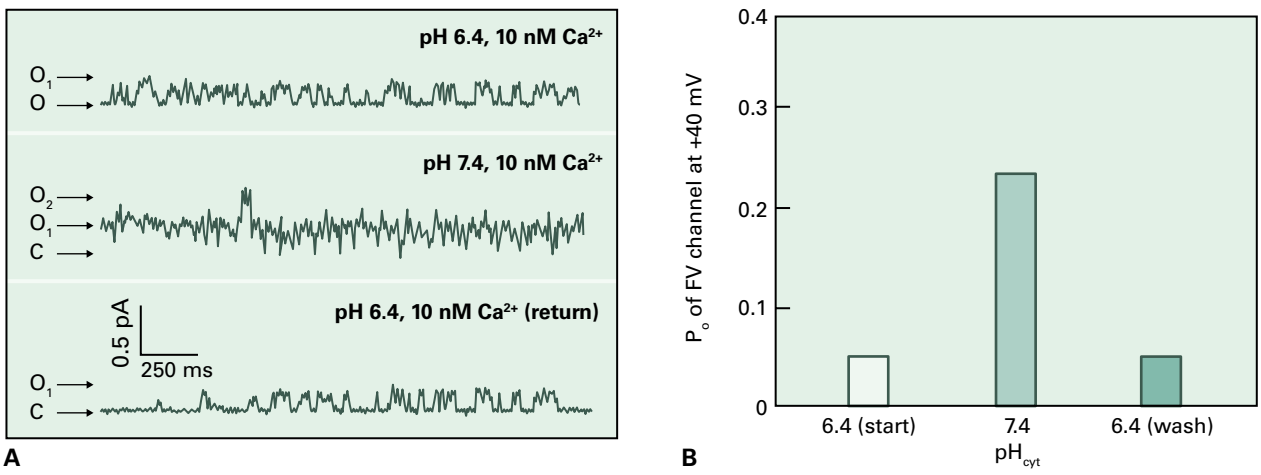


FIGURE 3.28 *Activities of vacuolar FV K^+ channels depend on cytosolic pH and Ca^{2+}. (A) The activity of a single FV channel from a* Vicia faba *guard cell tonoplast is strongly influenced by pH. O_1, one channel open; O_2, two channels open; C, closed. (B) Increasing cytosolic pH from pH 6.4 to 7.4 increases the open state probability (P_o) of the channel.*

monovalent cations, is activated by cytosolic [Ca^{2+}] in the nanomolar to low micromolar concentration range (Fig. 3.29) and is inhibited by increasing cytosolic pH.

Stomatal closure is often, but not always, preceded by an increase of [Ca^{2+}] in the guard cell cytosol, so VK channels are well poised to respond by opening and releasing K^+ from vacuoles (Fig. 3.27). However, stomata can also close in the absence of a change in [Ca^{2+}], in which case an increase in the sensitivity of signaling proteins to cytosolic [Ca^{2+}] and an increase in guard cell cytosolic pH are likely to play a role in responding to the primary closing stimulus. In these cases, FV channels will open. The presence of complementary channel types, each fulfilling the same function of vacuolar K^+ release, may provide an example of how parallel mechanisms often mediate biological processes.

While the molecular identity of FV channels is still unknown, a VK channel, TPK1, has been identified in *Arabidopsis*. TPK1 (Fig. 3.30) was originally isolated based on

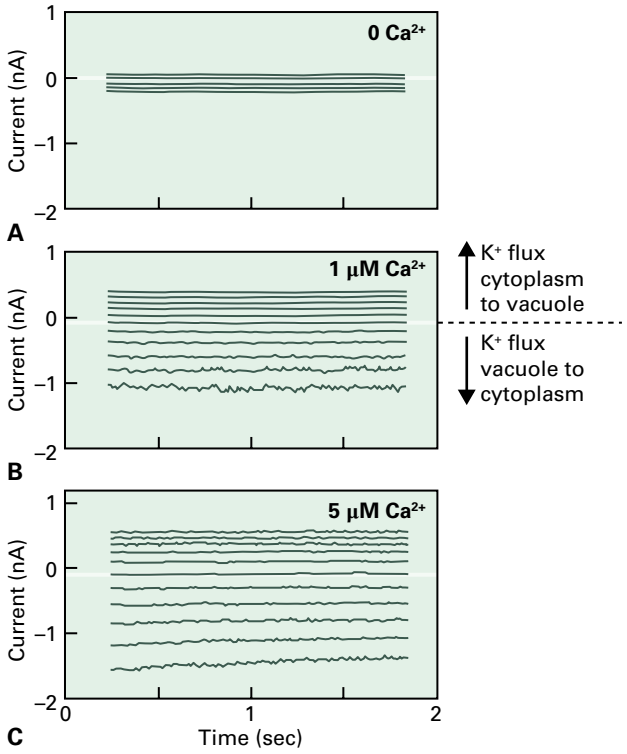


FIGURE 3.29 *(A) Vacuolar K^+-selective and Ca^{2+}-activated (VK) channel currents across the vacuolar membrane of guard cell protoplasts from* Vicia faba. *At a low cytosolic Ca^{2+} concentration (<0.1 μM) VK channels are not activated in guard cell vacuoles. (B and C) Elevation of the cytosolic Ca^{2+} concentration to 1 μM (B) or to 5 μM (C) causes a strong activation of the K^+-selective VK channels as identified and characterized in guard cells. In contrast to the strongly voltage dependent K^+_{in} and K^+_{out} channels in the plasma membrane (see Fig. 3.28), VK channels are active at both positive and negative voltages and are almost instantaneous, showing no lag after application of the voltage pulse. Source*: Ward & Schroeder. (1994). Plant Cell 6:669–683.

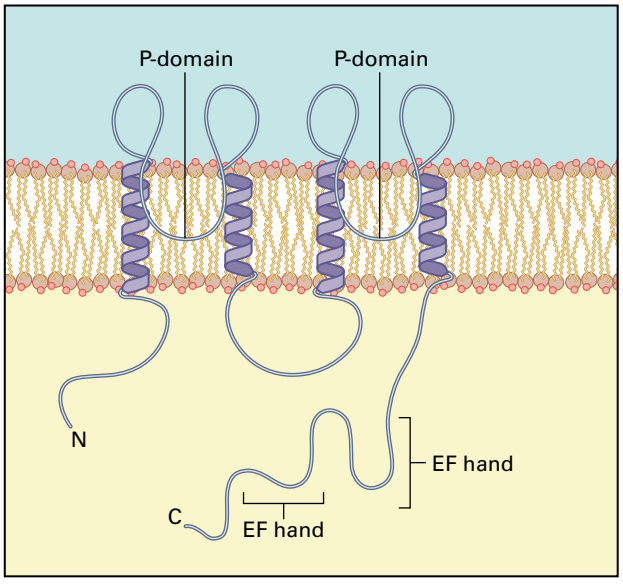


FIGURE 3.30 *An outward rectifying K^+ channel. TPK1 has just four predicted transmembrane spans but two P-domains. Toward the C terminus are two high-affinity Ca^{2+} binding motifs known as EF hands.*

an EST encoding a protein with the highly conserved pore-forming "P-domain" motif TxGYGD. This channel is a member of the "two-pore" K^+ channel family, so-called because there are two P-domains in each subunit. In contrast to *Shaker*-type channels, TPK1 has only four transmembrane spans in each subunit. Two potential Ca^{2+}-binding motifs, called EF hands, reside towards the C terminus of the protein. Although two-pore K^+ channels have been characterized in *S. cerevisiae* and *H. sapiens*, those channels do not possess EF hand sites. The functional attributes of TPK1 as a K^+ channel were confirmed by heterologous expression, and the channel was subsequently localized to the tonoplast.

3.3.11 High-affinity K^+ transporters are present at the plasma membrane

Besides the biophysically and physiologically well-studied functions of K^+ channels, plants possess a large number of K^+ transporters that do not belong to typical ion channel families. The KUP/HAK/KT family includes high-affinity K^+ uptake transporters and is conserved between plants and fungi. However, the transport mechanism of this important class of K^+ uptake transporters remains unknown and does not follow the dogma of proton coupled cotransport. In one study of *Arabidopsis* roots an apparent proton-coupled K^+ uptake mechanism was reported, but this has not been confirmed and may represent an exception or minor activity.

3.3.12 Calcium channels make use of steep gradients in $[Ca^{2+}]$ to mediate Ca^{2+} flow into the cytosol

Ca^{2+} ions are taken up into the cytosol predominantly by ion channels, rather than proton-coupled transporters. Why is this the case? Most likely because the cytoplasmic $[Ca^{2+}]$ is maintained at very low levels in all eukaryotic cells. Activity of the Ca^{2+}-ATPases discussed in Section 3.2.6 maintain cytoplasmic $[Ca^{2+}]$ at approximately 0.0001 millimolar (or 10^{-7} M), whereas the $[Ca^{2+}]$ in soils, the apoplast and vacuoles can be 0.1 to >1 mM. Thus negative membrane potentials at the plasma membrane and vacuolar membrane can easily pull Ca^{2+} ions into the cytosol through Ca^{2+} channels.

3.3.13 The activity of plasma membrane Ca^{2+} channels is regulated by low molecular weight signaling molecules and voltage

Patch clamp studies, mainly of guard cells, have provided ample evidence for the presence of Ca^{2+} channels in the plasma membrane. Plant Ca^{2+} channels are usually not perfectly selective for Ca^{2+}, but are permeable to other cations.

Still, because of the steep Ca^{2+} concentration gradient into the cell and the very low $[Ca^{2+}]$ in the cytosol, even a non-selective Ca^{2+}-permeable channel will cause a rapid rise in cytosolic $[Ca^{2+}]$ when activated. One of the major Ca^{2+} channels in the guard cell plasma membrane is most active at hyperpolarizing potentials, but the threshold of activation is also determined by signals such as ABA and reactive oxygen species. Although several gene families are likely candidates for Ca^{2+} channels, the molecular identity of the guard cell plasma membrane hyperpolarization-activated Ca^{2+} channels remains unknown.

Among likely candidates for plant Ca^{2+} channels are members of the cyclic nucleotide-gated channel (CNGC) and plant glutamate receptor-like homolog families. An *Arabidopsis* Ca^{2+}-permeable CNGC, called DND2, functions in transducing a Ca^{2+} signal in response to pathogen-specific molecules such as lipopolysaccharides. Another member of this family, CNGC18, is required for polarized tip growth of pollen tubes, a process that involves fluxes of ions such as Ca^{2+} into the growing tip. Glutamate (Glu) receptors in animals play important roles in regulating the excitability of neuronal cells. Surprisingly, plants possess homologs of these proteins: the *Arabidopsis* genome includes 20 members of the *GLR* gene family. In *Arabidopsis* roots, the *GLR3.3* gene is required for induction of transient depolarizations and Ca^{2+} influx upon exposure of roots to wounding, Glu and a few other amino acids. Pharmacological studies have implicated Glu-like receptors in microtubule depolymerization and growth cessation of *Arabidopsis* roots in response to aluminum; however, the biological function of Glu receptors in plants is still largely unknown.

3.3.14 Ca^{2+}-permeable channels in endomembranes are activated by both voltage and ligands

It appears that several different classes of Ca^{2+}-permeable channels may be present in intracellular membranes of plants. Although some studies had suggested that typical animal organellar Ca^{2+} channels, the IP_3 receptors and ryanodine receptors, exist in plants, plant genome sequences revealed that no close homologs exist to either of these animal counterparts. Thus it remains controversial whether the animal IP_3 and cADPR signaling paradigms are relevant in land plants. The recent sequencing of the *Chlamydomonas rheinhartii* genome has revealed that this unicellular alga expresses a canonical IP_3 receptor and other animal-like ion channels that have not been found in land plants.

In plant vacuoles, slow vacuolar (SV) channels are Ca^{2+}-permeable cation channels. These SV channels exhibit rather slow, time-dependent activation over several hundred milliseconds in response to membrane depolarization and are strongly activated by Ca^{2+}-calmodulin (Fig. 3.31). The plant vacuolar SV channel may be the best characterized plant ion channel located in a membrane other than the plasma membrane. This channel is ubiquitous and abundant in the vacuolar membrane of terrestrial plants. Channel density based on patch clamp data has been calculated to be 1 SV channel or more per μm^2. The SV channel is permeable to several cations including Ca^{2+}, K^+, Na^+, and Mg^{2+}. A physiological function of SV channels in Ca^{2+} wave propagation in roots has been found that supports the previous model that

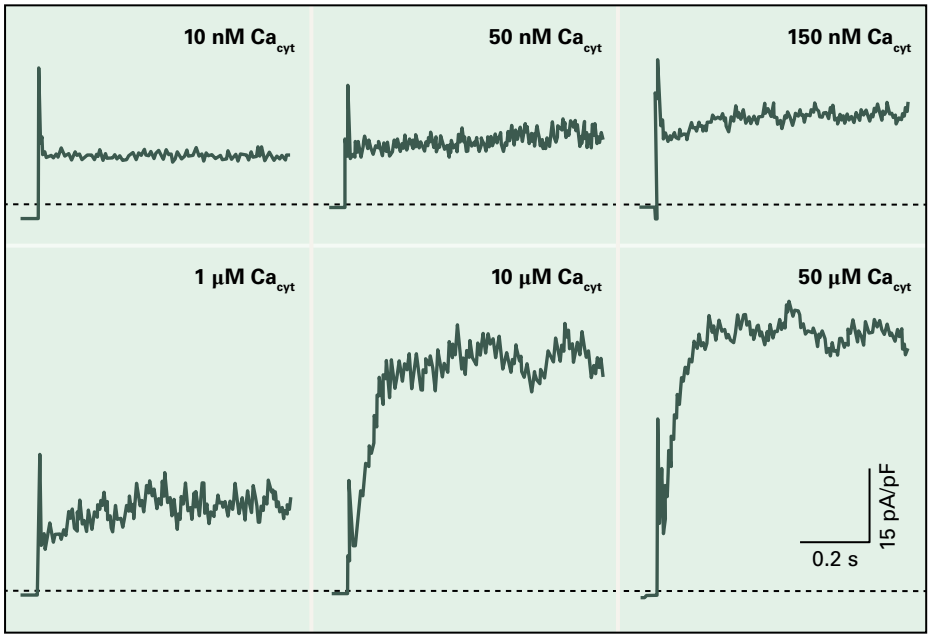


FIGURE 3.31 *Activity of the SV channel currents increases with increasing cytosolic concentration of Ca^{2+}. The free Ca^{2+} concentration on the cytoplasmic membrane side of guard cell vacuoles was increased from 10 nM (upper left) to 50 µM (lower right). The upward defecting time-dependent currents at elevated Ca^{2+} correspond to the ubiquitous SV channel currents in plant vacuoles. Current traces in each panel are in response to voltage pulses to +100 mV. pA, picoampere; pF, picofarads. Dashed lines show zero current level.*
Source: Pei et al. (1999). Pl Physiol 121:977–986.

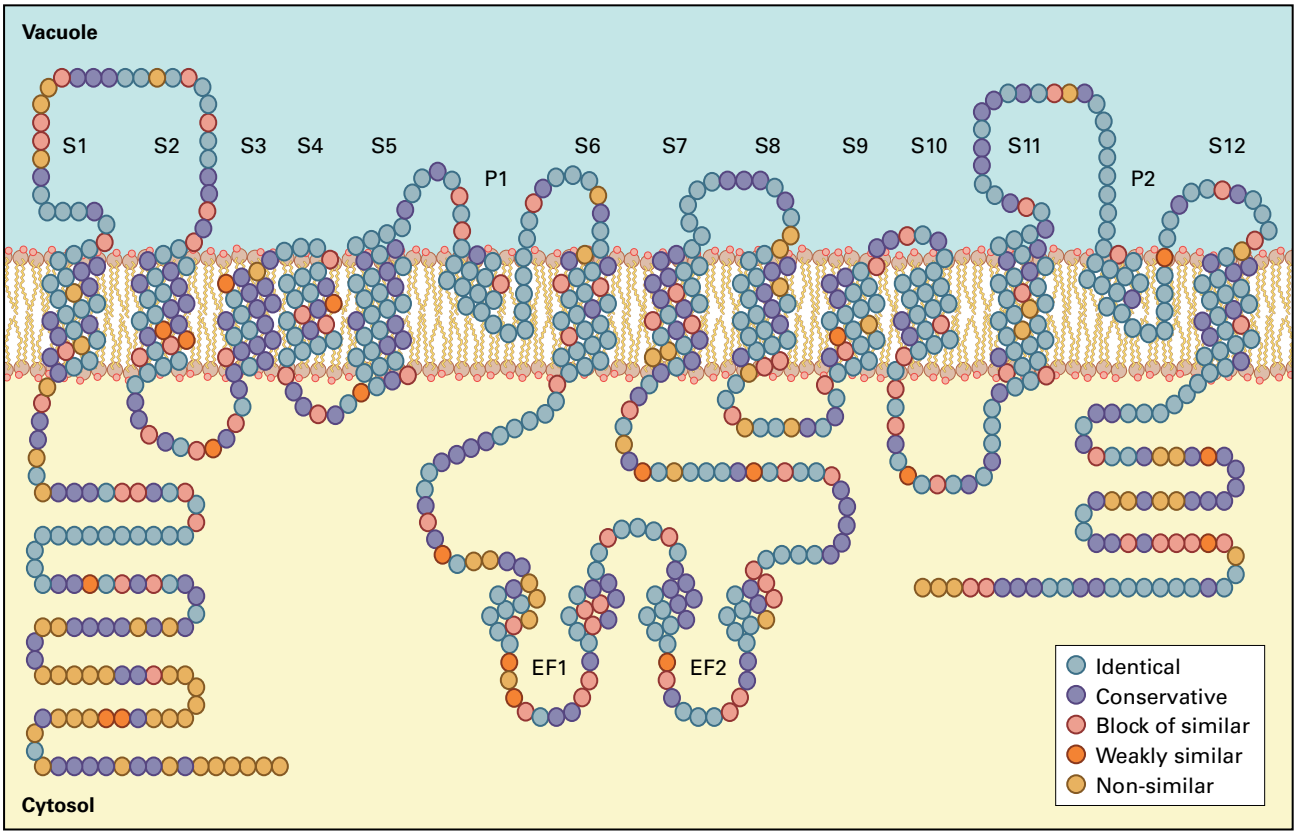


FIGURE 3.32 *Predicted structure of the rice SV channel, OsTPC1, showing 12 membrane spanning domains, labeled S1 to S12 and topology within the membrane bilayer. P1 and P2 are the two pore loops that consist of a pore helix and selectivity filter. Two calcium binding EF-hands (EF1 and EF2) are located between S6 and S7. Conservation of amino acids between OcTCP1 and the* Hordeum vulgare, Arabidopsis thaliana, Triticum aestivum, *and two* Nicotiana tabacum *TCP1 sequences is indicated by the color code on the right, below.*
Source: Pottosin & Schönknecht (2007). J Exp Bot 58:1559–1569.

these Ca^{2+}-permeable channels can allow conditional release of Ca^{2+} from vacuoles.

SV channel activity is tightly regulated by multiple factors including voltage, with positive membrane potentials promoting opening. Increases in cytosolic [Ca^{2+}] increase the channel open probability and shift the voltage dependence to less positive values. The sensitivity of the channel to [Ca^{2+}] is increased by the presence of calmodulin and magnesium. Vacuolar [Ca^{2+}] has an opposite effect and promotes channel closure. Protein phosphorylation and dephosphorylation regulate channel activity through action on more than one site. Channel activity is also inhibited by acidification on either side of the membrane.

The SV channel from *Arabidopsis*, TPC1, has been cloned, and is a member of the two-pore channel family. The TPC family contains voltage-gated cation channels consisting of two homologous domains, each having six transmembrane helixes and one pore domain (Fig. 3.32). Each of the homologous domains is likely to have an evolutionary relationship to the six transmembrane domains and single pore in *Shaker*-type K^+ channels. Two Ca^{2+}-binding EF-hands are located in a cytosolic loop that links the two halves of the SV channel and these are sites for potential regulation by calcium.

Why are there so many candidate types of Ca^{2+}-permeable channels in plant cells? There is as yet no definitive answer to this question, but we can speculate. The activation of different channel types might result in different dynamic patterns of the Ca^{2+} signal, for example, by mediating localized rises in [Ca^{2+}] and different rates of change in concentration. The additional information encoded by location and changes in concentration might render downstream responses stimulus specific. This notion is supported by stimulus-specific Ca^{2+} elevation patterns observed in plants, and by Ca^{2+}-based signaling pathways that rely on different Ca^{2+} pools.

3.3.15 Plasma membrane anion channels facilitate solute release during turgor adjustment and elicit membrane depolarization after stimulus perception

Anion channels are ubiquitous in the plant plasma membrane, where they are thought to play several essential roles. This class of ion channels was first characterized in guard cells, where they function in controlling solute release during turgor adjustment in response to physiological signals that cause stomatal closing. Cellular loss of anions is affected by Ca^{2+}-activated anion channels, of which at least two kinetically distinct classes, the rapidly activating R-type and the slowly activating S-type, have been identified in guard cells

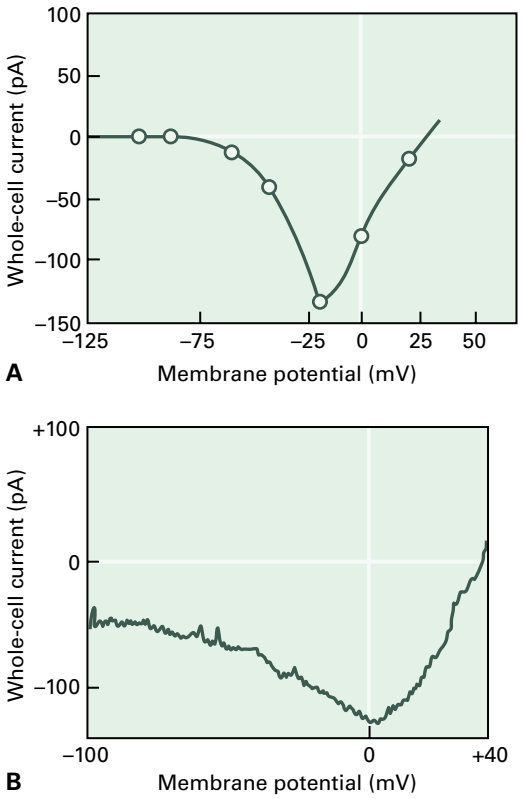


FIGURE 3.33 *Anion channels in guard cells. (A) Current–voltage relationship for rapidly activating (R-type) anion channels. (B) Steady-state current–voltage relationship for slowly activating (S-type) channels.*

(Fig. 3.27). These well-characterized Ca^{2+}-activated anion channels are also gated by voltage (Fig. 3.33). The equilibrium potential for Cl^- ions (E_{Cl}) is usually a positive value because cytosolic [Cl^-] exceeds the extracellular [Cl^-] (see Box 3.2). The opening of these channels results in massive efflux of Cl^- from cells and membrane depolarization. This depolarization can activate outward rectifying K^+ channels during salt loss. Anion channel activity is therefore the pacemaker of plant cell turgor reduction. Physiological stimuli that trigger stomatal closing via activation of S-type anion channels include ABA, elevated CO_2, pathogenic elicitors and ozone.

The *Arabidopsis SLAC1* gene was shown to encode the major subunit of S-type anion channels in the plasma membrane of guard cells. Studies had suggested that S-type anion channels are a central regulator of stomatal closing by allowing controlled release of anions from guard cells, which also depolarizes guard cells and drives K^+ release. Indeed, mutants in the *SLAC1* gene are impaired in stomatal closing in response to numerous physiological stimuli and second messengers, including ABA, CO_2, darkness, low humidity, [Ca^{2+}], and reactive oxygen species, including ozone.

Ca^{2+}-activated anion channels are also subject to additional types of regulation. In a range of cell types, including guard cells, ATP has an activating effect. Anion channel activity is not supported by nonhydrolyzable ATP analogs, and the inhibitory effects of ATP removal are prevented by protein phosphatase inhibitors. Ca^{2+}-dependent and Ca^{2+}-independent protein kinases function in anion channel activation in guard

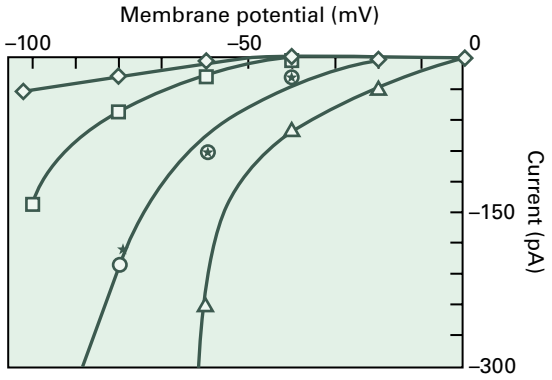


FIGURE 3.34 *Current–voltage relationship for vacuolar uptake of malate through time-dependent anion channels in the tonoplast. Malate uptake by anion channels is strongly promoted by negative membrane potentials and increases with cytosolic malate concentration. In this figure, cytosolic malate concentrations were 10 mM (open diamonds), 20 mM (open squares), 50 mM (open circles), and 100 mM (open triangles)—all with a vacuolar malate concentration of 10 mM. Malate uptake with equal concentrations of malate (50 mM) present on both sides of the membrane is indicated by stars.*

cells. All this evidence points to control of anion channel activity through phosphorylation by protein kinases, which has been further characterized in the oocyte system.

3.3.16 Vacuolar malate transporters that participate in malate sequestration have been identified

In most glycophytic plants, a major anionic constituent of the vacuole is malate. Plants exhibiting crassulacean acid metabolism (CAM) take up and release malate from vacuoles on a diurnal basis. Malate uptake into the vacuolar lumen is driven by the cytosol-negative V_m (Fig. 3.34). Ca^{2+}-dependent protein kinases can activate vacuolar malate uptake channels. Selectivity studies, in which the ionic forms of malate are titrated between the un-protonated (malate^{2-}) and the singly protonated (H•malate$^-$) forms, strongly suggest that the permeant form is malate^{2-} (Fig. 3.35), which would effectively maximize the use of V_m as a driving force. Because the vacuolar pH is notably lower than that of the cytosol (by about 2 pH units in most plants, but by as much as 4 pH units at the end of the night in CAM plants), the malate^{2-} that enters the vacuole will be rapidly protonated and its concentration effectively lowered in favor of the H•malate$^-$ and H_2•malate forms. The pH difference across the tonoplast helps sustain the concentration difference that drives malate^{2-} into the vacuole. Conversely, reverse flow into the cytosol is very unfavorable. Malate is therefore likely to exit vacuoles of CAM plants through a completely independent pathway, perhaps by way of a cotransporter.

Two kinds of vacuolar malate channels have been identified at the molecular level. One channel whose activity corresponds with previously characterized inward rectifying malate channels (because malate is negatively charged this corresponds to malate fluxes into the vacuole) is a member

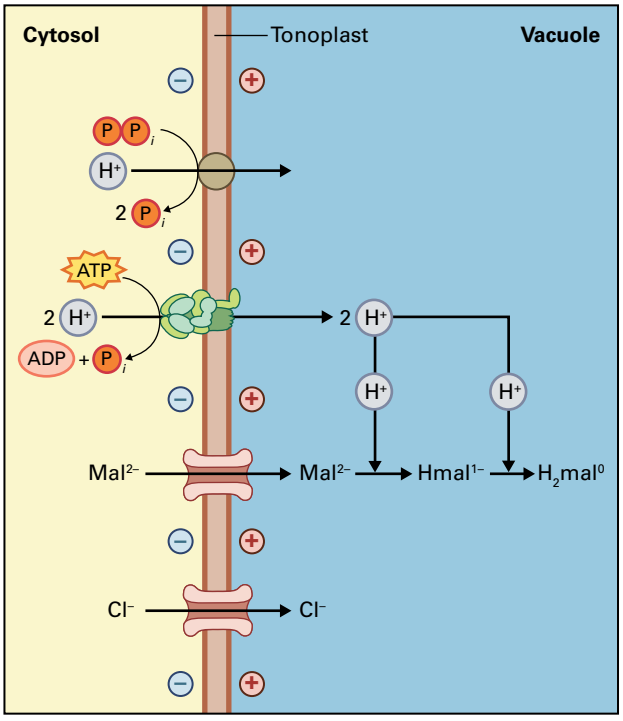


FIGURE 3.35 *Accumulation of malate in the roots of CAM plants. Malate^{2-} is thought to enter the vacuole through malate-selective channels. These channels are strongly inward rectifying and do not allow substantial malate^{2-} efflux. Once inside the vacuole, malate^{2-} is protonated to H•malate^{1-} and H_2•malate^{0}. This maintains the effective concentration difference for malate^{2-} across the membrane.*

of the *ALMT* (aluminum-activated malate transporter) gene family. Promoter fusions of the *AtALMT9* gene in *Arabidopsis* showed that it was preferentially expressed in mesophyll cells. T-DNA insertion mutants of *AtALMT9* had strongly reduced vacuolar malate channel activity.

The second kind of malate channel, the *Arabidopsis* tonoplast dicarboxylic acid transporter (AttDT9) was identified by homology with a sodium/dicarboxylic acid cotransporter in *H. sapiens* kidney. AttDT protein localizes to the vacuole in mesophyll cells. Mutant *Arabidopsis* plants lacking a functional *AttDT* gene had 25% less malate in leaves than wild type. Redundancy in function between AtALMT9 and AttDT is likely since knockout mutants in *AtALMT9* that strongly reduce channel activity as measured by patch clamp analysis have only slightly reduced amounts of vacuolar malate.

3.4 Cotransporters

3.4.1 Cotransporters facilitate transport against an electrochemical potential difference

Cotransporters utilize the downhill gradient of H^+ or Na^+ for the uptake or export of solutes against an uphill gradient. They couple a thermodynamically favorable influx of H^+ or Na^+ to drive an unfavorable transport reaction such as the uptake of Cl^-. Cotransporters that transport the substrate and coupling ion (usually H^+ in plants) in the same direction are called symporters. Symporters are uptake transporters, and most sugar, amino acid, peptide, Cl^-, NO_3^-, SO_4^{2-}, and phosphate uptake occurs via symporters. Antiporters transport the coupling ion and substrate in opposite directions and act as exporters. Antiporters for sucrose, Na^+, K^+, NO_3^-, and BO_3^{3-} are known. Symporters and antiporters are present in the plasma membrane and in endomembranes (see Fig. 3.2). Both symporters and antiporters use (and dissipate) the proton motive force, which needs to be continuously maintained by the action of H^+ pumps in the plasma membrane and organellar membranes.

Like the vast majority of enzymes, cotransporters are relatively specific for their substrates. In the case of organic substrates, for example, cotransporters readily distinguish between isomers, transporting L-amino acids and D-sugars in marked preference to the respective D- and L-isomers. Among amino acids, acidic, basic, and neutral amino acids are all transported by distinct plasma membrane cotransporters. A wide range of cotransporter types are found in all membranes. The prominence of H^+-coupled transport systems in the plant cell plasma membrane illustrates that organisms living in relatively dilute media depend on energized solute transport.

3.4.2 Cotransporters are often characterized in heterologous systems

Cotransporters are very difficult to identify by biochemical approaches because they are not abundant (see Section 3.1.5) and do not execute reactions (such as ATP hydrolysis) that can be assayed without reconstitution in membranes. The most widely applicable and successful approach applied to plant cotransporters has been *S. cerevisiae* complementation. For this approach, yeast mutants that are defective in growth on the solute of interest are transformed with cDNA from a plant library. Transformed yeast colonies able to grow on the particular solute express a functional plant transporter. The encoding DNA sequence can then be obtained. The large number of yeast transport mutants, and the ease and rapidity with which genetic studies can be conducted in yeast, make this an attractive experimental system. As a result, the first plant plasma membrane cotransporters for sugars, amino acids, peptides, inorganic cations (e.g., K^+), and inorganic anions (e.g., SO_4^{2-}) were identified using this approach.

Cotransporter proteins are highly hydrophobic. A structure predicted by hydropathy analysis often exhibits 12 transmembrane spans, with the most extensive hydrophilic loop appearing between transmembrane spans 6 and 7 (Fig. 3.36).

Single-celled oocytes from the South African clawed frog *Xenopus laevis* are a popular alternative heterologous

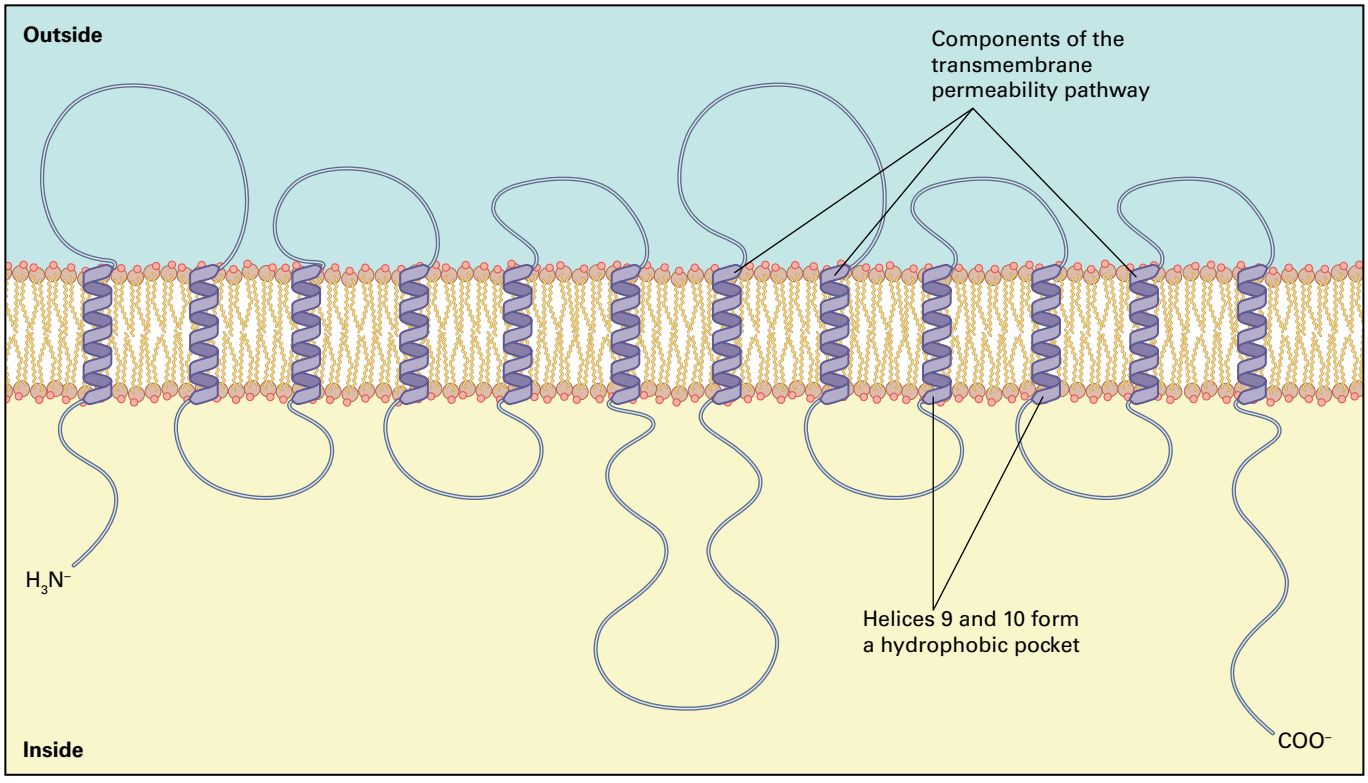


FIGURE 3.36 *Structural model illustrating the orientation of a generalized cotransporter in a membrane.*

expression system for plant channels and transporters. The large size of oocytes, around 1 mm in diameter, allows impalement by micropipettes and microelectrodes (Fig. 3.37), to monitor transporter-mediated membrane currents. Furthermore, the plasma membrane of oocytes is relatively quiescent with respect to transport activity, so the background activity of endogenous transporters rarely contributes substantially to the fluxes or currents measured in experiments with heterologously expressed transporters. Expression of heterologous transporters in oocytes is achieved by microinjection of in vitro synthesized cRNA into single cells, where the cRNA provides the template for translation. Typically, transport activity is monitored between 2 and 4 days after cRNA microinjection, when expression is at a maximum.

Experimental evidence for H^+-coupled transport has been derived from two classes of experiments. The first method, which uses microelectrodes to monitor the V_m across the cell membrane, is restricted to assessment of plasma membrane symporter activity (Fig. 3.38A). When a cell is bathed in substrate—even an uncharged one like a sugar—the plasma membrane often depolarizes very rapidly, indicating that positive electrical charge (usually H^+) is flowing into the cell. These depolarizations show that the H^+-coupled transport systems are electrogenic (carry electrical charge). An alternative experimental approach that is applicable to a variety of membranes involves the use of fractionated membrane vesicles (Fig. 3.38B). Vesicular uptake of a radioisotope-labeled substrate is compared in the presence and absence of a proton gradient. In the presence of a proton gradient of the appropriate polarity, substrate accumulation inside the vesicles indicates H^+-coupled transport (Fig. 3.38B).

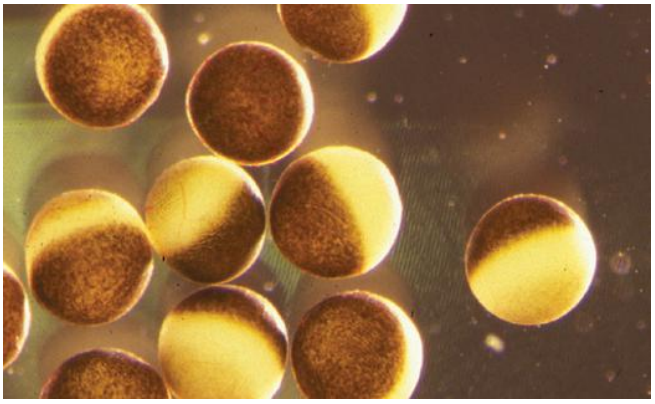


FIGURE 3.37 Xenopus *oocytes can be readily injected with cRNA encoding putative transporters using an injection pipette. After a few days incubation to allow time for translation of new protein, transport assays, such as electrophysiology or uptake of radiolabeled substrate, can be used to study transport activity.*
Source: GeneClamp 500. Axon Instruments Inc., Foster City, CA.

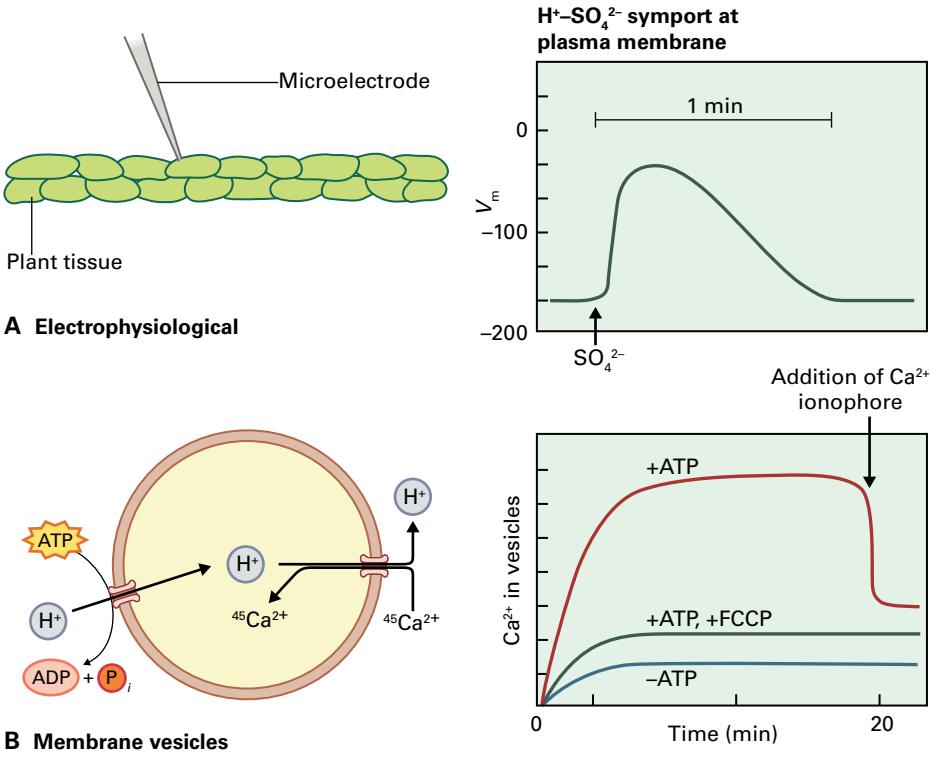


FIGURE 3.38 *Methodologies for demonstrating H^+-coupled solute transport by cotransporters. (A) The cell is impaled with a glass micropipette containing an electrolyte and an electrode. This microelectrode, in conjunction with another electrode in the bathing solution, is used to measure the voltage across the membrane. An uncharged or anionic substrate is introduced into the bathing solution. If a cation is cotransported with the substrate, positive charge flows into the cell, the membrane depolarizes, and V_m increases. Ion substitution experiments and alkalization of the medium often identify the cation as H^+. If the transported substrate is anionic, membrane depolarization implies that at least two H^+ are transported per monovalent anion, or three H^+ per divalent anion. (B) Vesicles are incubated with a radiolabeled substrate (e.g., $^{45}Ca^{2+}$), and filtered though narrow-pore nitrocellulose. The filter is then washed and the vesicle-associated radioactivity is quantified. This method allows comparison of vesicular uptake in the presence and the absence of a pmf. If the cytosolic face of a vesicle is exposed to the medium, endogenous H^+-ATPase activity can establish an inside-acid pmf. This gradient is used to drive uptake of the radiolabeled substrate, as shown in the accompanying graph of Ca^{2+} uptake (red line; +ATP). Addition of a Ca^{2+}-selective ionophore (indicated by vertical arrow above graph) results in Ca^{2+} leakage from the vesicle and demonstrates that Ca^{2+} has been accumulated within the vesicle rather than bound to it. In the absence of ATP (–ATP, blue line), or in the presence of compounds that eliminate the proton gradient (FCCP: carbonyl cyanide p-[trifluoromethoxy] phenylhydrazone; green line), Ca^{2+} accumulation is much reduced.*

3.4.3 In some cases, ion-coupled solute transport involves Na^+ rather than H^+

Although H^+-coupling prevails as a mechanism for energizing cotransporter-mediated transport in plants, examples of Na^+ symport have been found. In some marine algae, uptake of NO_3^- and some amino acids is Na^+ dependent. The plentiful concentration of Na^+ in sea water (approximately 480 mM) results in a large inwardly directed electrochemical gradient for Na^+ across the plasma membrane (Fig. 3.39). However, uptake of K^+ at micromolar concentrations is also Na^+ dependent in some freshwater aquatic plants and charophyte algae. Although the Na^+ concentration of freshwater is considerably less than that of sea water, it is nevertheless possible for Na^+ coupling to energize transport because the V_m component of the electrochemical driving force for Na^+ is sufficiently large to overcome the smaller concentration difference for this ion across the plasma membrane. The genes encoding this Na^+/K^+ transport activity have not yet been isolated from freshwater plants and charophyte algae. However, this Na^+/K^+ transport activity has been found for a subfamily of the HKT transporter gene family in grasses (see Chapter 23). At high Na^+ concentrations these HKT transporters can become Na^+ channel-like transporters, mediating Na^+ influx into cells. A different subfamily of plasma membrane HKT transporters (class 1 HKT transporters) are Na^+ transporters and provide a major mechanism for protecting land plants from over-accumulation of Na^+ in leaves by removing Na^+ ions from the xylem sap before it is unloaded into leaves. HKT marker-assisted breeding of highly active HKT transporters from wild plant varieties is producing domesticated crops that show improved salinity tolerance, an important agricultural trait.

3.4.4 Transcriptional and post-translational controls regulate cotransporter activity

H^+-coupled transport systems are capable of generating impressive amounts of solute accumulation. As a corollary, H^+-coupled cotransporters must be subject to tight regulation

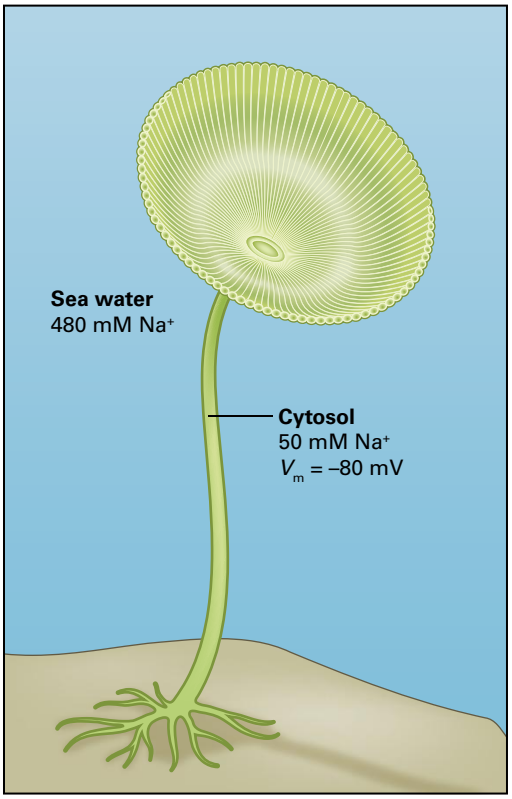


FIGURE 3.39 *A large electrochemical potential for Na^+ exists across the plasma membrane of marine algae, such as* Acetabularia, *shown here.*

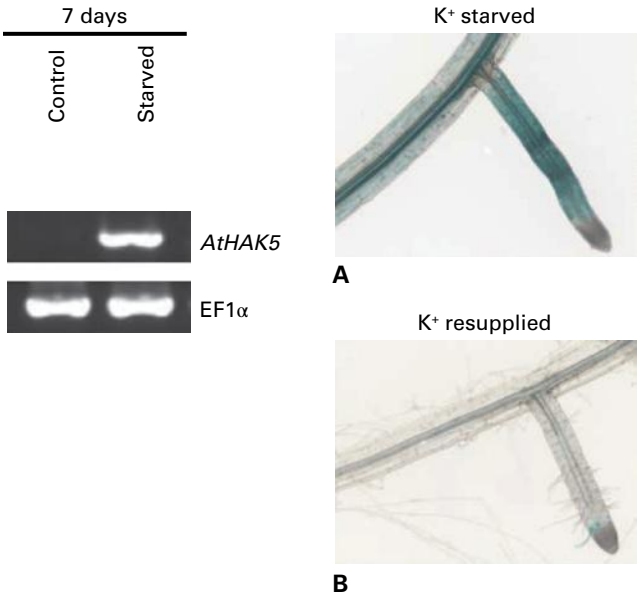


FIGURE 3.40 *Expression of K^+ transporter gene* AtHAK5 *is induced by K^+ starvation.* Arabidopsis *plants grown with sufficient K^+ have undetectable* AtHAK5 *mRNA expression in roots. Plants grown for 7 days in the absence of K^+ show expression of* AtHAK5 *in roots as detected by RT-PCR (left panel). K^+ starvation-induced* AtHAK5 *promoter-GUS activity is shown in the right panel. When K^+ is re-supplied,* AtHAK5 *expression returns to the low basal level. The AtHAK5 transporter was shown to mediate the major component of the "classical" K^+ starvation-induced high-affinity $K^+(Rb^+)$ uptake in* Arabidopsis *roots.*
Source: Gierth et al. (2005). Plant Physiol 137(3): 1105–1114.

if physiological concentrations of solutes are to be maintained in the cytosol. Two forms of control predominate. Transcriptional control is evident for many cotransporter genes, with expression being de-repressed during periods of substrate starvation. In the presence of substrate, expression of the cotransporter is repressed and transport is evident only at a low rate. An example of probable transcriptional control is shown in Figure 3.40 for uptake of K^+ into roots of *Arabidopsis:* K^+ starvation, which enhances K^+ uptake capacity in roots, correlates with expression of the K^+ uptake transporter AtHAK5, although no evidence has been obtained that AtHAK5 is a H^+-coupled cotransporter. Knockout of the *AtHAK5* gene in *Arabidopsis* results in a greatly reduced high-affinity $K^+(Rb^+)$ influx, showing that AtHAK5 is a major component of the classical inducible high-affinity K^+ influx activity identified in roots. Furthermore, double knockout of the *AtHAK5* gene and the inward K^+ channel gene, *AKT1*, leads to almost complete removal of $K^+(Rb^+)$ influx at low concentrations and severe growth defects. An exception to induction of transporters by nutrient starvation is cotransporter-mediated NO_3^- transport, which is induced rather than repressed by its substrate.

Post-translational control of cotransporters can also regulate transport activity. This has been documented in the giant internodal cells of the charophyte alga *Chara,* which can be internally perfused with defined media. There, a high rate of H^+-coupled Cl^- transport into the cell is observed in the absence of cytosolic Cl^-, but the rate declines almost to zero as cytosolic Cl^- increases to a modest concentration of 10 mM. This phenomenon, known as trans-inhibition, results from relatively tight binding of cytosolic Cl^- to the cotransporter at the active site. Thus, the greater the cytosolic Cl^- concentration, the more the cotransporter becomes locked up in its substrate-bound form, and the less the cotransporter is able to take up Cl^- from outside the cell.

3.4.5 Many metabolites are transported by specific cotransporters within the major facilitator superfamily

Plant cells contain a rich diversity of proton-coupled transporters for uncharged nutrients and metabolites. Many are encoded by genes in the major facilitator superfamily (MFS). Most is known about plant H^+-coupled uptake transporters (symporters) and relatively little about H^+-coupled efflux transporters (antiporters). This is primarily due to the efficiency of using *S. cerevisiae* mutants to identify uptake transporters by heterologous expression (see Section 3.4.2). *S. cerevisiae* is also used to study uptake transport activity in detail when radiolabeled substrates are available. The *Xenopus* oocyte expression system and electrophysiology have been very useful in identifying substrates for coupled transporters. One benefit to this system is that radiolabeled substrates are not necessary, however, transport needs to be

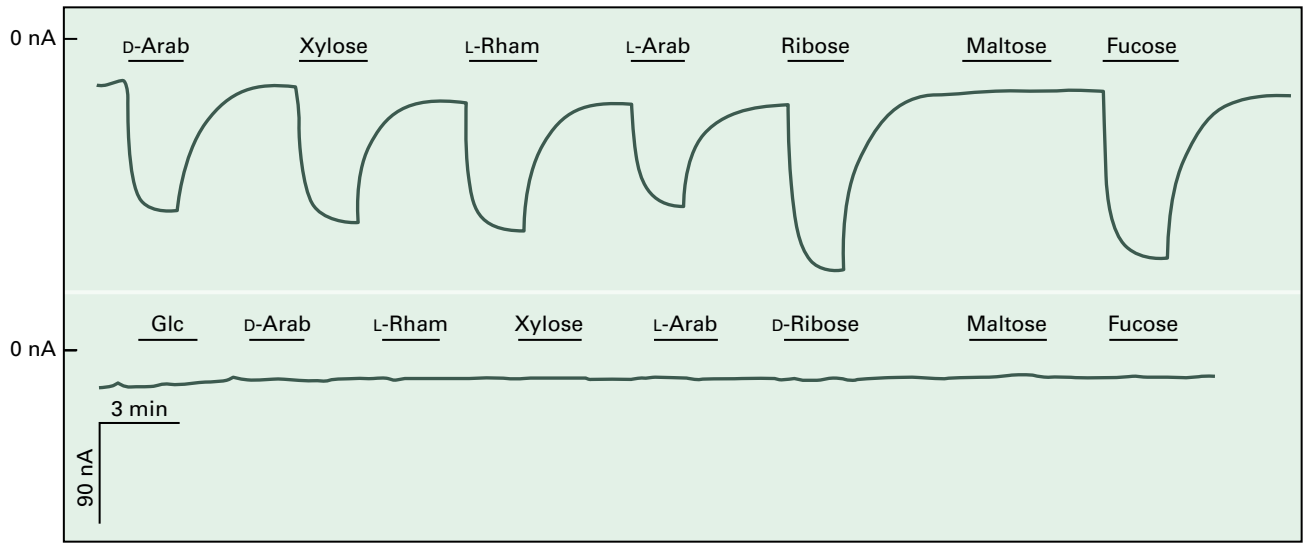


FIGURE 3.41 *Electrophysiological analysis of AtPLT5 (At3g18830) transport activity in* Xenopus *oocytes. Oocytes were clamped at –40 mV, and substrates were applied extracellularly as indicated. Downward deflections represent inward H^+ current coupled to substrate transport into the oocyte. Top trace: oocyte injected with* AtPLT5 *RNA; while bottom trace, uninjected oocyte. The results show that arabinose, xylose, rhamnose, ribose, and fucose are all transported by AtPLT5, but maltose is not.*
Source: Reinders et al. (2005). J Biol Chem 280(2): 1594–1602.

electrogenic—a charge must be transported across the membrane for transport activity to be detected. For example, AtPLT5, an *Arabidopsis* homolog of sugar alcohol permeases (within the MFS), was analyzed by expression in oocytes (Fig. 3.41). AtPLT5 transports a wide range of sugars including hexoses, pentoses and tetroses, as well as sugar alcohols such as sorbitol.

Many transporter genes are present in multiple copies and are members of gene families. The reason for this apparent redundancy is not completely understood. The transcribed proteins could be functionally redundant, but there are other likely possibilities. Multiple genes could provide fine-tuned expression patterns or differences in activity, regulation, localization, or protein turnover. The gene family that encodes sucrose transporters (SUTs) in *Arabidopsis* has provided some insight into the question of why plant transporters often exist as members of multigene families. *Arabidopsis* has nine *SUT* genes whose expression patterns differ. *AtSUC2*, for example, is expressed in companion cells and is essential for phloem loading, whereas *AtSUC1* has similar transport activity but is expressed in pollen, trichomes, and roots and is essential for pollen function. *AtSUC5* is expressed in seeds and is important for seed development. There are differences in transport activity as well. SUTs most closely related to AtSUC1 have a high affinity for sucrose with K_m values for sucrose of less than 2 mM. AtSUC9, one member of this group, has a very high affinity for sucrose ($K_m = 66$ μM) compared to other SUTs. At the other end of the spectrum, the less homologous gene *AtSUT4* encodes a transporter with a K_m for sucrose of 12 mM. There are differences in membrane localization: AtSUT4 is localized to the tonoplast while other SUTs reside in the plasma membrane. Two *SUT* genes, *AtSUC7* and *AtSUC8*, are pseudogenes. Therefore, even though nine *SUT* genes are present in *Arabidopsis*, there is little functional redundancy, and aside from the pseudogenes each SUT can be assigned a unique function.

Most plant sugar transporters, including H^+-coupled monosaccharide transporters for glucose, are members of the MFS. However, plant genes outside of the MFS also encode important proton-coupled transporters for uncharged solutes. Examples of symporters are purine permeases (PUPs), ureide permease (UPS), and the urea permease AtDUR3. Members of the multidrug and toxic efflux transport (MATE) family function as antiporters, and some transport uncharged solutes. For example, TT12 transports anthocyanins into the vacuole.

3.5 Water transport through aquaporins

3.5.1 The direction of water transport across membranes is determined by hydrostatic and osmotic pressures

Most biologists have, at some time or another, observed the simple effects of hyperosmotic treatment of plant tissue: The tissue becomes flaccid, and at the cellular level, plasmolysis occurs. The rapidity of plasmolysis bears testimony to the high degree of permeability that biological membranes exhibit towards water.

Two components of water potential, determine the directionality of water flow through membranes: the hydrostatic pressure difference ($\Delta\Psi_p$) across the membrane, and the osmotic pressure difference ($\Delta\Psi_s$) across the membrane (see Chapter 15, Box 15.1). Formally, the flux of water across the

membrane (J_v) is proportional to the driving force (Eq. 3.3), where L_p, the constant of proportionality, is the permeability of the membrane to water, expressed in terms of surface area, $m \cdot s^{-1}$ MPa^{-1} (i.e., $m \cdot s^{-1}$ m^2 N^{-1}, where N is the force in Newtons, $kg \cdot m \cdot s^{-2}$); σ; known as the reflection coefficient, expresses the ability of the osmotically relevant solutes to permeate the membrane relative to water. For completely impermeant solutes, $\sigma = 1$, whereas for solutes with equal permeability to water, $\sigma = 0$. In practice, most osmotically active solutes encountered in physiological conditions (ions, sugars, and so forth) are much less permeable than water, and σ can be considered to equal 1. In conditions of osmotic equilibrium, $J_v = 0$ by definition, so $\Delta\Psi_p$ and $\sigma\Delta\Psi_s$ are equal and opposite.

$$J_v = L_p(\Delta\Psi_p - \sigma\Delta\Psi_s) \qquad \text{(Eq. 3.3)}$$

3.5.2 Water movement occurs through the membrane lipid bilayer and through channels called aquaporins

Water passes through the lipid component of biological membranes, despite the fundamentally hydrophobic characteristics of the fatty acyl chains in the phospholipid bilayer. The permeability of bilayer membranes to water can be demonstrated in artificial systems—either liposomes or planar lipid bilayers. A parallel major pathway for water movement across membranes that allows for much more rapid water movement has been identified. This pathway uses water channel proteins called aquaporins.

3.5.3 Aquaporins are members of the major intrinsic protein family

Aquaporins are integral membrane proteins in the major intrinsic protein (MIP) family and are present in bacterial, plant and animal cells. They are small (25–30 kDa), very hydrophobic proteins with six transmembrane spans containing internal sequence homology indicative of origins from a gene duplication and fusion (Fig. 3.42). Aquaporins are also characterized by the highly conserved NPA (Asn-Pro-Ala) residues present in both the N- and C-terminal halves of the protein. Aquaporins are present in all plant membranes associated with the secretory system including the plasma membrane, tonoplast, ER and Golgi. Plants have many aquaporin genes (more than 30 in *Arabidopsis*) that are classified within four subgroups: plasma membrane intrinsic proteins (PIPs), tonoplast intrinsic proteins (TIPs), nodulin 26-like intrinsic membrane proteins (NIPs), and small basic intrinsic proteins (SIPs).

The discovery of aquaporin function was achieved in 1992 by expressing the complementary RNA from an animal MIP homolog in *Xenopus* oocytes. When the oocytes were then

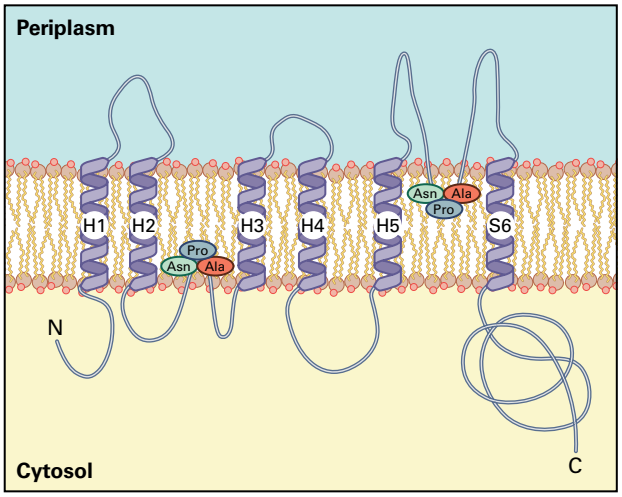


FIGURE 3.42 *Structure of an aquaporin showing the six transmembrane helices and two conserved NPA (Asn-Pro-Ala) residues.*

subjected to hypo-osmotic shock, the rate of swelling was considerably faster in the aquaporin-expressing oocytes than in controls. This work was followed by research showing similar functional aquaporin properties for a plant homolog expressed in *Xenopus* oocytes.

Intriguingly, some plant aquaporins can transport other small, uncharged solutes that are important for plant nutrition, stress responses, or signal transduction. The list of compounds that permeate some plant aquaporins includes CO_2, urea, glycerol, NH_4^+, methyl ammonium, boric acid, H_2O_2, silicic acid, lactic acid, formamide, arsenic, and acetamide.

Aquaporins exist as tetramers in membranes, but the functional pores are formed by monomers (Fig. 3.43). The X-ray crystallographic structure of plant aquaporins has been solved in both the closed and open gated states. The pore is formed by two loops containing NPA domains (see Fig. 3.42) that dip into the membrane from either side. Selectivity is conferred at the tightest constriction of the pore by the aromatic/arginine region. Gating of the pore depends on the position of loop D, the cytoplasmic domain between the fourth and fifth transmembrane spans. Loop D blocks the pore in the closed state (see Fig. 3.43).

3.5.4 Aquaporin expression and activity are regulated

Aquaporin gene expression is regulated by many environmental factors, including light quality and intensity, water and nutrient availability, salt stress, drought and anoxia. In addition, aquaporin activity is regulated by cytoplasmic pH and protein phosphorylation. Under some conditions, such as anoxia, cytoplasmic acidification causes aquaporin inhibition through protonation of a conserved histidine (His). Protein phosphorylation of conserved Ser residues also leads to channel closing. Phosphorylation is catalyzed by a

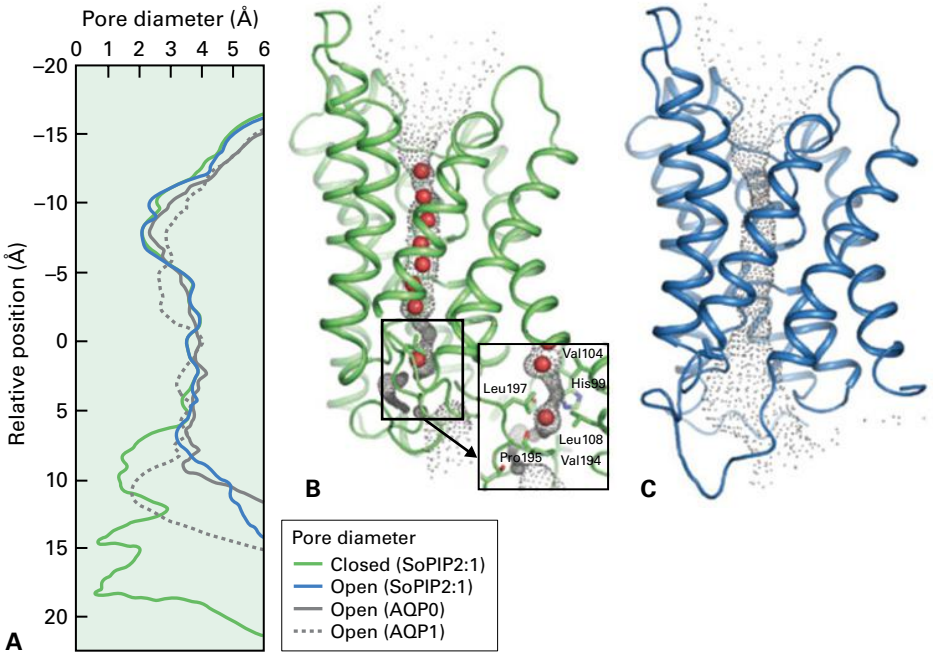


FIGURE 3.43 *(A) Pore diameter in closed conformation for SoPIP2:1 (green) and in open conformation for SoPIP2:1 (blue), AQP1 (solid gray) and AQP1 (dotted gray) is shown as a function of the distance from the NPA signature sequence. (B) The closed pore of SoPIP2;1 is represented as a funnel illustrating the pore boundaries. The inset shows the pore near the gating region of loop D characterized by Val 194, Pro 195, and Leu 197. (C) The open pore of SoPIP2;1.*
Source: Törnroth-Horsefield et al. (2006). Nature. 439 (7077): 688–694.

Ca^{2+}-dependent protein kinase that may form a component of a signaling pathway linking water stress to channel activity. Cytoplasmic Ca^{2+} may also have direct effects on aquaporin activity: a binding site for divalent cations was discovered during analysis of the X-ray structure.

Results from several studies using vesicles derived from the plasma membrane and tonoplast show a much higher (100-fold) water permeability of the tonoplast. It is likely that, in those studies, the activity of plasma membrane aquaporins was not maintained during vesicle isolation. However, the results may point out differences in regulation between plasma membrane and vacuolar aquaporins. More recent studies have shown that both plasma membrane and tonoplast have high water permeability (up to 500 μm s^{-1}). Water permeability across both plasma membrane and tonoplast is controlled predominantly by aquaporins.

Summary

Membrane transport plays a fundamental role in many biological processes in plant cells, including generation of cell turgor, energy, movements, signal transduction, nutrient acquisition, waste product excretion, and metabolite distribution and compartmentalization. Four fundamental classes of transport systems are present at all membranes. *Pumps* catalyze transport of ions or complex organic molecules against their thermodynamic gradients. At membranes other than the ATP-synthesizing membranes of mitochondria and chloroplasts, pumps are generally driven by ATP hydrolysis. At all membranes, H^+ pumps remove H^+ from the cytosol and generate a proton gradient and an electrical gradient (pmf) across each membrane. *Ion channels* mediate transport at very high rates and play diverse roles in plant biology. Channels can be regulated between open and closed states, and activation is frequently controlled either by membrane voltage or by protein modification through second messengers (e.g. Ca^{2+}) or through phosphorylation/dephosphorylation. Channels that are very highly selective for K^+ reside in the plasma membrane and tonoplast. Anion channels and less selective cation channels are also present in both membranes. These channels have essential roles in signal transduction, cell expansion, nutrient acquisition and

redistribution. *Cotransporters* translocate a wide range of simple solutes, including ions, sugars, and amino acids. Cotransporters are distinguished from pumps by not requiring ATP hydrolysis to drive transport, and from channels by coupling the uphill accumulation of a solute to the energetically favorable movement of a second solute. In plants, cotransporters are generally energized through coupling to proton motive force (pmf)-driven H^+ transport. Some examples of channels and cotransporters, many of which were discussed in more detail in this chapter, are summarized in Table 3.2 for cationic substrates, and in Table 3.3 for anionic substrates. *Aquaporins* facilitate rapid transport of water across the plasma membrane and tonoplast.

All classes of transport systems have been identified at the molecular level; in many cases, structural aspects of the transport system can be related to solute permeation and to control of transport system activity. These transport systems play important roles in numerous processes, including central roles in the responses of plants to abiotic and biotic stresses. Identifying specific transporters that fulfill particular roles requires consideration of four aspects of transport: the charge of the nutrient or metabolite, the concentration of the molecule on each side of the membrane under physiological conditions, the precise location of the transport step within the organism and the regulation of the proteins by physiological stimuli. These four aspects determine the type of transporters capable of carrying out specific transport functions. In virtually all cell types, transporters capable of facilitating translocation in either direction under a variety of conditions need to be present in order to maintain cellular homeostasis and promote growth and development. Consequently, plants have a large number of genes encoding transporters for the many solutes and transport steps encountered in the whole plant.

TABLE 3.2 *Transporters of cationic substrates and nutrients.*

Substrate	Transporter	Transporter Family	Membrane*	Function
K^+	K^+_{in} channel AtKAT1	Shaker-type voltage-gated K^+ channel	PM	K^+ influx channel; stomatal opening
K^+	AtAKT1	Shaker	PM	K^+ influx channel; K^+ uptake in roots
K^+	K^+_{out} channels GORK, SKOR	Shaker	PM	K^+ release in guard cells (GORK) and stelar cells
K^+	TPK1 (AtKCO1)	Two-pore K^+ channel (4 TM)	T	Vacuolar K^+ (VK) channel; K^+ release from vacuole activated by increase in cytosolic Ca^{2+} concentration, stomatal closing
K^+	AtHAK	KUP/HAK/KT	PM	High-affinity K^+ uptake into roots and likely other cells
Fe^{2+}	AtIRT1	ZIP	PM	iron uptake in roots
Fe^{2+}	AtNRAMP3/4	NRAMP	T	iron release from vacuole
Ca^{2+}	DND1/2	CNGC	PM	Ca^{2+} influx; signaling; e.g. in guard cells
Ca^{2+}	GLR3.3	glutamate receptor	PM	transient depolarization, Ca^{2+} signaling in roots
Ca^{2+}	TPC1	Two-pore channel (2 x 6 TM)	T	Slow vacuolar (SV) channel; Ca^{2+}, K^+, Na^+ and Mg^{2+} permeable

* PM, plasma membrane; T, tonoplast.

TABLE 3.3 *Transporters of anionic substrates and nutrients.*

Substrate	Transporter	Transporter family	Membrane*	Function
Anions	S-type anion channel, AtSLAC1		PM	anion release during stomatal closing
Malate	AtALMT		PM	Al^{3+}-activated malate release in roots, Al^{3+} detoxification
Malate	AtALMT9	ALMT family	T	Cl^- and malate transport into vacuoles in mesophyll cells
Malate	AttDT9	dicarboxylic acid transporter	T	malate transport into vacuoles
Anions	R-type anion channel, ALMT12	ALMT family	PM	Anion efflux from guard cells during stomatal closing
NO_3^-	AtNPF6.3/ AtNRT1.1	NPF	PM	low-affinity H^+-coupled nitrate transporter
NO_3^-	AtNRT2		PM	high-affinity H^+-coupled nitrate transporter; requires second integral membrane protein for function; no sequence homology between NRT1 and NRT2 family
NO_3^-	AtCLCa	CLC chloride channel	T	1 H^+/2 NO_3^- antiporter for nitrate transport into vacuole; nitrate storage
Phosphate		PHT family	PM	H^+-coupled phosphate uptake in roots
Sulfate		SULTR family	PM	members are low- or high-affinity H^+-coupled sulfate uptake transporters; some also permeable to molybdate and selenate

* PM, plasma membrane; T, tonoplast.



4 Protein Sorting and Vesicle Traffic

Alessandro Vitale, Danny Schnell, Natasha V. Raikhel, and Maarten J. Chrispeels

Introduction

To function properly, a plant cell must direct many thousands of different polypeptides to specific metabolic compartments, cytoplasmic structures, and membrane systems. Membrane-bound proteins occur in more than a dozen organelles and compartments, including the vacuolar membrane or tonoplast, the plasma membrane, membranes of the endoplasmic reticulum (ER), Golgi apparatus and peroxisomes, outer and inner envelopes of the chloroplast and mitochondria, and in thylakoid membranes. Soluble proteins are present in all subcellular compartments, including the cell wall and, with the only possible exception, the lumen of Golgi cisternae. Some proteins are unique to a particular structure, compartment, or membrane; other, very similar, proteins with comparable amino acid sequences, structures, and functions occur in more than one compartment. For example, invertases occur in the vacuole and cell wall, whereas water-channel proteins (aquaporins) are found in the tonoplast, plasma membrane and ER. Cells therefore require the necessary machinery to sort each protein and direct it to its proper destination.

4.1 The cellular machinery of protein sorting

4.1.1 Protein sorting requires peptide address labels and sorting machinery, and usually requires crossing at least one membrane

How do these thousands of proteins find their way to the correct subcellular location? All proteins, except those that remain in the compartment where they are made, have one or more **targeting domains** that act as an address label (see Box 4.1 on how they are identified). Targeting domains are short amino acid sequences or peptide motifs but can also be post-translational modifications, such as glycans (oligosaccharides). Targeting domains are often located at the N-terminus of a protein, but may be present in the C-terminus or elsewhere in the polypeptide.

Each compartment or membrane system requires a different targeting domain. Likewise, the compartment contains

Biochemistry & Molecular Biology of Plants, Second Edition. Edited by Bob B. Buchanan, Wilhelm Gruissem, and Russell L. Jones.
© 2015 John Wiley & Sons, Ltd. Published 2015 by John Wiley & Sons, Ltd.
Companion website: www.wiley.com/go/buchanan/biochem

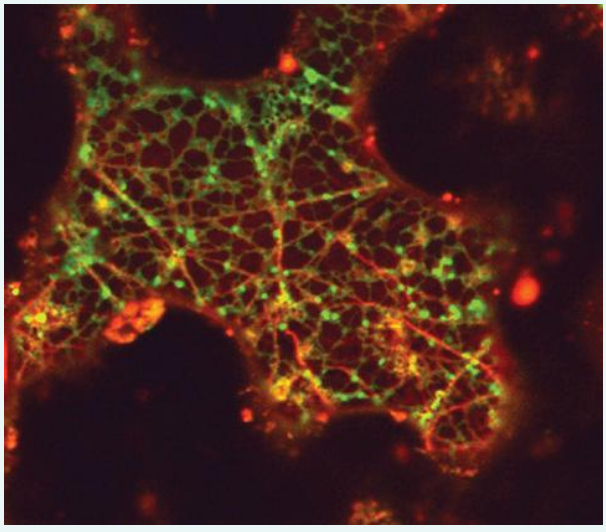
BOX 4.1 Targeting signals and machineries have been identified using isolated organelles, permeabilized cells, transient transformation and transgenic plants

Different approaches have been used to study targeting signals. Signals that target proteins to chloroplasts, mitochondria, and peroxisomes, can be studied in vitro by incubating purified organelles with precursor proteins and determining the conditions necessary for protein uptake into the organelle. This makes it possible to determine which cytosolic proteins and small molecules (e.g., ATP or GTP) are necessary for import. Instead of using isolated organelles, one can also incubate precursor proteins with permeabilized protoplasts.

The secretory system is too complex and cannot be reconstituted in vitro with isolated subcellular fractions. Researchers have relied on transient expression systems or stable transformed plants to study protein sorting in the secretory system. Immunocytochemistry or organelle fractionation is used to determine the subcellular compartment(s) in which the protein accumulates (see Box 4.2). Pulse-chase experiments (Box 4.3) provide information on protein processing, traffic routes, and turnover. Because targeting signals are conserved between plant species, one can delete or mutate a putative targeting signal or add it to another protein, and then examine the effect of these mutations on the subcellular location of the protein. When a signal peptide is fused at the N-terminus of a prokaryotic enzyme its presence is sufficient for the protein to enter the ER, traffic along the secretory pathway, and be secreted (see Section 4.7.2). Similar experiments led to the identification of signals for sorting to vacuoles (see Section 4.8.1).

The discovery of green fluorescent protein (GFP), and the subsequent development of other fluorescent proteins that emit different colors, has revolutionized studies of protein traffic, organelle biogenesis, and dynamics. Fluorescence microscopy allows one to identify precisely the subcellular localization of a given protein and visualize in vivo the dynamics of protein traffic and of organelle movement. By fusing GFP with sorting signals or with resident proteins of different compartments virtually any organelle, membrane, or cellular compartment can be "lit up" in a colored form within a living tissue. This approach has established that the Golgi stacks of plant cells, here seen as green dots in a leaf epidermal cell expressing a fusion between GFP and the transmembrane domain of a Golgi protein, move throughout the cytoplasm along tracks formed by actin microfilaments (red in the figure) and the ER network, unlike those of mammalian cells that are positioned in a perinuclear location in association with microtubules.

Source: Boevink et al. (1998). Plant J 15:441–447.



highly selective sorting machinery that recognizes a specific targeting domain. The interaction between targeting domain and sorting machinery directs the protein to the proper compartment by mediating translocation across one or more compartment membranes. Targeting domains have different names, depending on the location to which a protein is being targeted (Table 4.1). Although the targeting domain is essential for protein transport, it may not be part of the active protein, and proteases often remove the targeting domain to create a functional, mature polypeptide.

Because most proteins are made in the cytosol, the majority of proteins within organelles and compartments must be translocated across one or more membrane. Plastid and mitochondrial DNA encode a small number of proteins (<100) that are synthesized by ribosomes within these organelles, but the vast majority of chloroplast and mitochondrial proteins are nucleus encoded.

Most proteins have hydrophilic surfaces and therefore do not readily pass through the hydrophobic lipid bilayer. Proteinaceous channels or pores in membranes allow protein entry (Fig. 4.1). Usually, polypeptides are translocated in an extended or unfolded conformation, but a fully folded protein can sometimes pass through a membrane as in peroxisomes and chloroplast thylakoids. As a polypeptide passes through a channel, it is assisted by molecular **chaperones** (for a detailed discussion of chaperones, see Chapter 10). By inhibiting molecular interactions that may cause polypeptides to fold incorrectly and aggregate, chaperones increase the yield of

TABLE 4.1 *Peptide address labels for targeting to different organelles and compartments.*

Destination	Address label (targeting domain)
ER	Signal peptide (SP)
Chloroplast	Transit peptide
Mitochondrion	Presequence
Nucleus	Nuclear localization signal (NLS)
Peroxisome	Peroxisome targeting signal (PTS)
Vacuole	Vacuolar sorting signal (VSS)

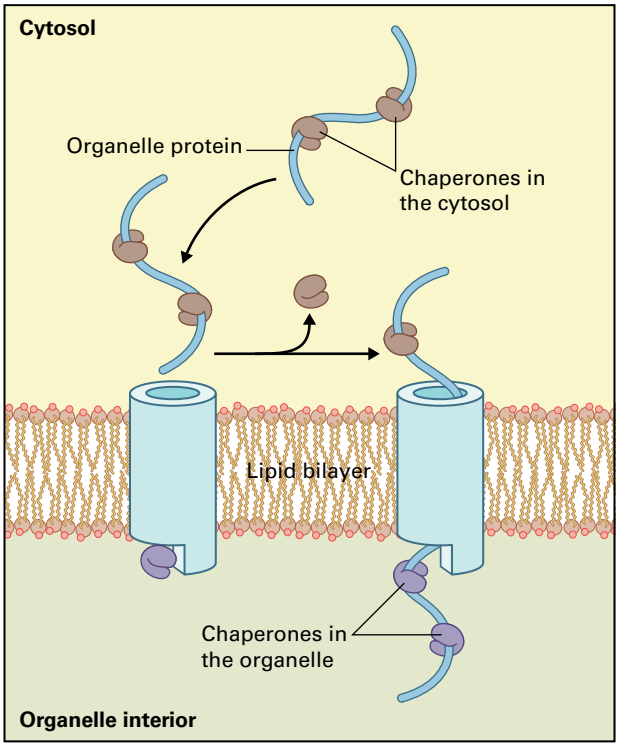


FIGURE 4.1 *A proteinaceous channel and chaperones facilitate the passage of a protein through the lipid bilayer. Chaperones bind a polypeptide on both sides of the membrane (in the cytosol and the organelle interior). They keep the polypeptide in an unfolded state in the cytosol and help it to fold correctly in the organelle interior.*

correct tertiary structures but not the rate of protein folding. Some cytosolic chaperones interact with nascent proteins, keeping them unfolded so they can pass through a protein channel. Other chaperones bind to the amino acid chain as it emerges from the membrane and facilitate folding. Still others function as repair stations to correct minor misfolding. The many members of one family of chaperones—the 70-kDa heat shock proteins (Hsp70)—fill all these roles, interacting with a wide spectrum of proteins.

4.1.2 Protein sorting can be a multistep process requiring more than one targeting domain

The general features of protein sorting appear to apply to all compartments. Proteins destined to locations other than the cytosol carry a targeting domain that is recognized by cytosolic factors needed to deliver the polypeptide to the sorting machinery at the compartment surface. These factors act together to deliver the unfolded protein to a specific receptor on the target membrane, thereby opening a channel consisting of several polypeptides. A translocation motor that hydrolyzes nucleoside triphosphates drives protein transport through the membrane, after which the transported protein folds with the help of additional chaperones and ATP.

Targeting of proteins from the cytosol to the compartment surface can occur after protein synthesis is complete (posttranslational) or during translation on cytoplasmic ribosomes (cotranslational). Proteins in the first group are released in the cytosol and targeted to a variety of destinations, including plastids, mitochondria, peroxisomes, and nuclei (pathways 1 and 2 in Fig. 4.2). Most proteins destined for the **secretory pathway** are synthesized on ribosomes bound to the ER. The synthesis and translocation of these proteins are coupled, such that the polypeptide chain is transported across the ER membrane as it emerges from the ribosome (pathway 3 in Fig. 4.2).

After passing through a membrane, proteins may be transported to special compartments within semi-autonomous organelles (e.g., the thylakoid membrane in plastids) or transported to other compartments after membrane translocation (e.g., vacuolar and plasma membrane proteins). Transport to a final destination or retention in a compartment usually requires a second targeting domain such as a vacuolar sorting signal. The domains of proteins with multiple targeting and retention signals interact sequentially with various sorting machineries until the final destination is reached. Integral membrane proteins typically insert into the membrane during the translocation process by laterally diffusing within the lipid bilayers once they enter the translocation channel. In many cases the transmembrane segments of these proteins serve the dual purpose of a targeting signal and a membrane anchor.

4.2 Targeting proteins to the plastids

4.2.1 Transport of proteins into chloroplasts involves a removable transit peptide

Although plastids (see Chapter 1) contain their own DNA and ribosomes, most of their proteins are encoded in nuclear DNA and synthesized in and imported from the cytosol. The biosynthesis of proteins encoded by chloroplast DNA is discussed

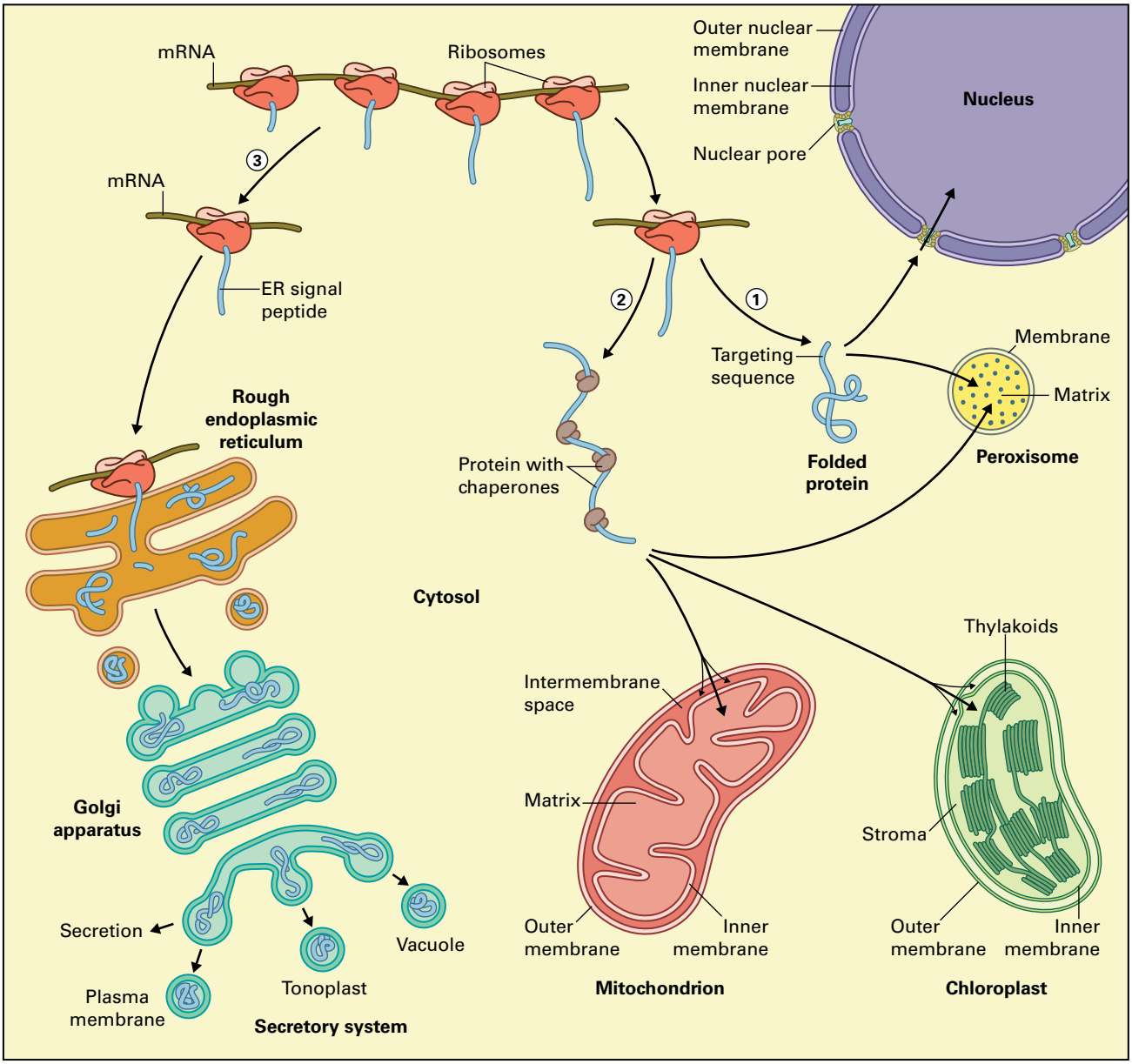


FIGURE 4.2 *All nuclear encoded mRNAs are translated in the cytosol. Pathways 1 and 2: proteins destined for mitochondria, chloroplasts, peroxisomes, or the nucleus and those that are to remain in the cytosol are released from the polyribosomes and may remain bound to chaperones (Pathway 2) or folded (Pathway 1). An exposed targeting sequence will cause the proteins to bind to a receptor (in the cytosol or on an organelle) and then be targeted to that compartment. Pathway 3: if the nascent polypeptide has a signal peptide then the polyribosome will attach to an ER membrane and the protein will be released in the lumen of the ER or become part of the ER membrane. Subsequently proteins will be sorted in the secretory system and either secreted or end up in the plasma membrane, or be transported to the vacuole or the tonoplast.*
Source: Lodish et al. (2013). Molecular Cell Biology, 7th edition. W.H. Freeman.

in Chapter 10. Chloroplasts have an envelope consisting of an outer and an inner membrane and an internal membrane system of thylakoids. These membranes define three aqueous compartments: the intermembrane space in the envelope, the stroma within the inner membrane, and the thylakoid lumen (Fig. 4.3). Thus, proteins must be directed not only into the plastid, but also to the proper location within the organelle.

Chloroplast proteins encoded by nuclear DNA are translated in the cytosol as precursors with an amino-terminal **transit peptide** of ≈30–100 amino acids that targets polypeptides to the chloroplast and enables their translocation into the stroma. After translocation, a peptidase removes the transit peptides of stromal precursor proteins. Proteins that lack a transit peptide cannot be imported, and if the transit peptide is added to the amino terminus of a protein that is foreign to the chloroplast this chimeric precursor protein is imported. The import of chloroplast precursors occurs at contact sites (proteinaceous channels) between the outer and inner envelope membranes and precursor proteins that are in transit span both envelope membranes.

Although the vast majority of the roughly 2,500 nucleus-encoded proteins that enter chloroplasts have a transit peptide,

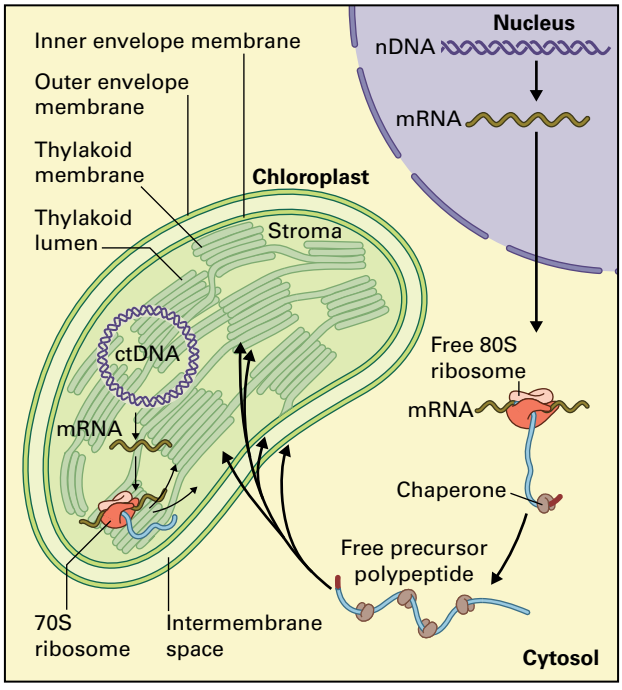


FIGURE 4.3 *Biosynthesis of chloroplast proteins and their targeting to five different compartments in the chloroplast. Chloroplast proteins may be encoded by nuclear DNA (nDNA) or chloroplast DNA (ctDNA); the respective mRNAs are translated by ribosomes in the cytosol (80S ribosomes) or in the chloroplast stroma (70S ribosomes). Proteins made as precursor polypeptides in the cytosol may be targeted to the outer or inner envelope membranes or may enter the chloroplast stroma. Once across the envelope membranes, proteins may remain in the stroma compartment or may be targeted to the thylakoid membrane, thylakoid lumen, or inner envelope membrane.*

a comparison of chloroplast proteomics data with genome sequence data suggest that several hundred proteins are targeted by mechanisms that do not involve a transit peptide. Among this group, a small number of chloroplast proteins (e.g., nucleotide pyrophosphatase/phosphodiesterase, α-amylase, and α-type family of carbonic anhydrases) appear to be targeted to the ER via a signal peptide and then directed to the chloroplast in a mechanism involving vesicle trafficking from the secretory pathway. These proteins are unique among chloroplast proteins in that they contain N-linked glycans that are added in the ER (see Section 4.6.7).

4.2.2 To enter chloroplasts, proteins pass through a proteinaceous channel with the aid of molecular chaperones

Import into chloroplasts can be studied by incubating purified chloroplasts with radioactively labeled precursor proteins (obtained by in vitro translation of mRNA in the presence of radioactive amino acids). The accepted model for chloroplast protein import entails two steps and requires chaperones on both sides of the chloroplast envelope and a group of proteins, collectively called the protein import translocons. The translocons are integral membrane complexes named Toc (translocon at the outer envelope membrane of the chloroplast) and Tic (translocon of the inner envelope membrane). Toc and Tic complexes come into contact at the point of protein import to allow transport directly from the cytosol into the chloroplast. To translocate proteins, both translocons use energy in the form of nucleoside triphosphates.

Cytosolic chaperones (Hsp70 homologs) hold proteins in an unfolded or partially folded state while their transit peptides interact with receptors within the Toc complex. The receptors are associated with a membrane channel through which the imported polypeptides pass (Fig. 4.4). The Toc receptors, Toc34 and Toc159, are specific GTP-binding proteins tightly anchored in the outer membrane with their GTP-binding domains exposed to the cytosol. A third protein, Toc75, forms the membrane channel through multiple β-barrel transmembrane segments. The GTP-binding and hydrolytic activities of the Toc receptors regulate the protein import process by controlling translocation of the polypeptide through the channel. Toc34 and Toc159 are encoded by gene families in most plants and genetic studies suggest that members of these families form distinct translocons that are important in regulating the import of different classes of proteins. A fourth protein, Hsp70 IAP (import intermediate-associated protein), a homolog of Hsp70, is found within the intermembrane space of the envelope. It is proposed to facilitate passage of the protein from the Toc to the Tic complex. Two Tic components, Tic110 and Tic40, associate with a molecular chaperone in the stroma, Hsp93 (93-kDa heat shock protein family member) and these three form a molecular motor that pulls proteins across the envelope via cycles of ATP hydrolysis.

After entering the chloroplast stroma a protease removes the transit peptide. If the protein is to remain in the stroma, it will be folded with the help of a class III chaperone called chaperonin (see Chapter 10). By contrast, soluble proteins that function in the thylakoid lumen, and membrane proteins that become part of the thylakoid, are held by chaperones in an unfolded state for passage to their next destination. Inner-membrane proteins are inserted into the membrane during translocation across the Tic complex or from the stroma after completion of translocation. Proteins targeted to the outer membrane do not enter the transport channel but instead enter the membrane directly from the cytosol.

4.2.3 Targeting into the thylakoid lumen requires a bipartite transit peptide and targeting to the thylakoid may follow four different paths from the stroma

After import, many chloroplast polypeptides are further sorted to the inner envelope membrane, to the thylakoid membrane, or to the thylakoid lumen. Proteins destined for

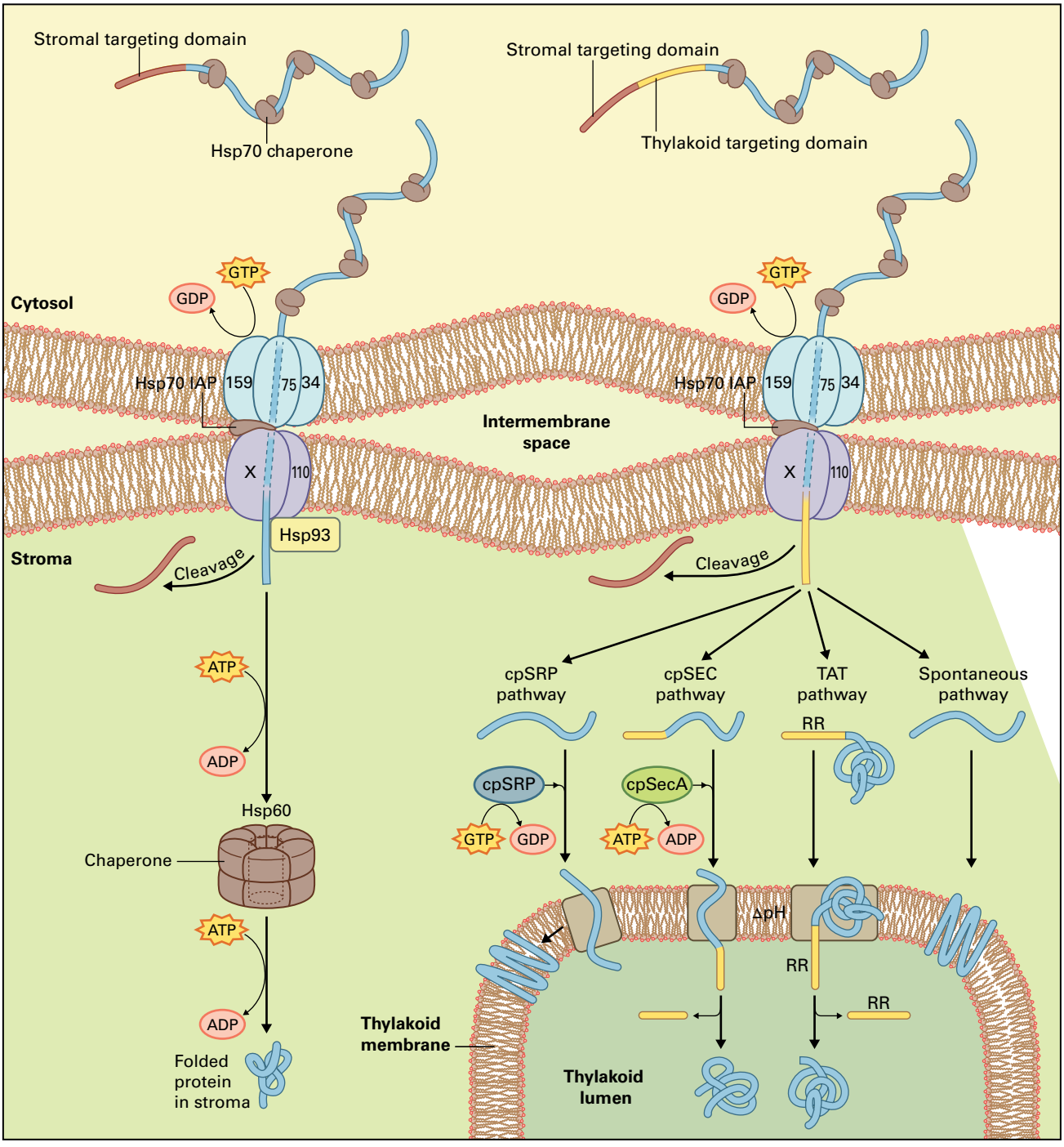


FIGURE 4.4 *Mechanism of protein import into chloroplasts. At the top of the figure, chaperones in the cytosol hold a protein with its transit peptide exposed in an unfolded conformation. The protein on the left has a stromal targeting domain only (red), whereas the protein on the right has a bipartite transit peptide with both stromal and thylakoid (yellow) domains. The transit peptide is bound by receptors in the outer membrane (Toc159 and Toc34). They deliver the protein to the Toc channel (Toc75) via a GTP hydrolysis cycle. The Toc complex associates with the Tic complex (X and Tic110), and the polypeptide is pulled into the stroma via ATP-dependent binding to the stromal Hsp93 chaperone. Proteins that remain in the stroma (e.g., Rubisco) lose their transit peptides and are folded and assembled with the assistance of the Hsp60 chaperone and ATP hydrolysis. Proteins that function in the thylakoid membrane enter the stroma via the same pathway, but are targeted to the thylakoid via one of four pathways. Thylakoid membrane proteins (e.g., LHCPs) are engaged by the chloroplast signal recognition particle (cpSRP) and are inserted into the membrane via GTP hydrolysis. Other membrane proteins (CFoII, PsbX,Y,K) insert spontaneously without the assistance of other proteins or nucleoside triphosphate hydrolysis. Some thylakoid lumenal proteins (e.g., OE33 and plastocyanin) are targeted by the chloroplast SEC (cpSEC) pathway by binding to chloroplast Sec A in an ATP-dependent reaction. Other lumenal proteins (e.g., OE23 and OE16) fold rapidly in the stroma and are targeted by the twin arginine translocation (TAT) pathway using the pH gradient (ΔpH) across the membrane.*

the thylakoid lumen, such as plastocyanin, contain a bipartite transit peptide. The stromal targeting domain of the transit peptide guides the protein to the stroma, where a protease removes it. This exposes a second targeting domain just behind the first one in the amino acid sequence (Fig. 4.4). This lumenal targeting domain then directs the protein across the thylakoid membrane to the lumen, where a second protease removes it. The transit peptides of proteins integral to the thylakoid membrane direct proteins into the stroma and hydrophobic transmembrane regions of the mature protein itself, rather than a removable targeting domain, direct the protein to and into the thylakoid membrane.

There are at least four pathways for targeting to the thylakoid: two for soluble lumenal proteins and two for membrane proteins (Fig. 4.4). In contrast to the Toc and Tic machinery, the components of the thylakoid targeting pathways are closely related to the protein targeting pathways that operate in bacteria, suggesting that protein targeting to the thylakoid has been conserved during evolution from the original bacterial endosymbiont.

(1) The translocation of lumenal proteins, such as OE33 and plastocyanin, by the **cpSEC pathway** requires ATP and a soluble protein and is stimulated by a pH difference (ΔpH) between the chloroplast stroma and the thylakoid lumen. Isolation and characterization of the targeting components show them to be homologous to the bacterial secretory translocation system and is therefore referred to as the cpSEC pathway (chloroplast SEC pathway). (2) Other thylakoid lumenal proteins, such as OE23 and OE17, are transported by an ATP-independent process that requires only the pH gradient. A twin-arginine motif (RR) located preceding the hydrophobic region in the second region of the transit peptide, is essential for protein transport on the ΔpH pathway. Consequently, this pathway is referred to as the twin arginine translocation or **TAT pathway**. It represents one of the rare cases in which fully folded proteins are transported across a membrane and appears to have evolved to accommodate proteins that rapidly fold into their three-dimensional structures in the stroma prior to transport into the lumen. Although the receptors and potential channel proteins have been identified for the TAT pathway, the mechanism by which transport occurs without disrupting membrane integrity is to date unknown.

(3) The third pathway, for integral thylakoid membrane proteins such as light-harvesting chlorophyll-binding protein (LHCP), requires GTP rather than ATP and is stimulated by the presence of a ΔpH. This pathway also requires a stromal factor, which has been identified as a chloroplast homolog of the signal recognition particle (SRP), a ribonucleoprotein complex involved in targeting proteins to the ER (see Section 4.6.2) and is therefore called the **cpSRP pathway**. (4) The fourth pathway is termed the **spontaneous pathway** because no energy requirements or protein components have been identified. Proteins such as the CFoII subunit of the thylakoid ATP synthase and the PsbX, K, and Y subunits of the photosystems utilize this pathway.

4.3 Targeting proteins to mitochondria

4.3.1 Transport into mitochondria relies on targeting domains, called presequences, and an import apparatus

Mitochondria, like chloroplasts, have both an outer membrane (OM) and an inner membrane (IM) that define two separate aqueous compartments: the intermembrane space and the mitochondrial matrix, each containing unique proteins (Fig. 4.5A). The enzymes of the electron transport chain lie in the inner membrane, whereas glycine decarboxylase and most of the enzymes of the tricarboxylic acid cycle are found in the matrix.

The majority of mitochondrial proteins (hundreds) are encoded by nuclear DNA, translated in the cytosol and synthesized as precursors with an amino-terminal targeting

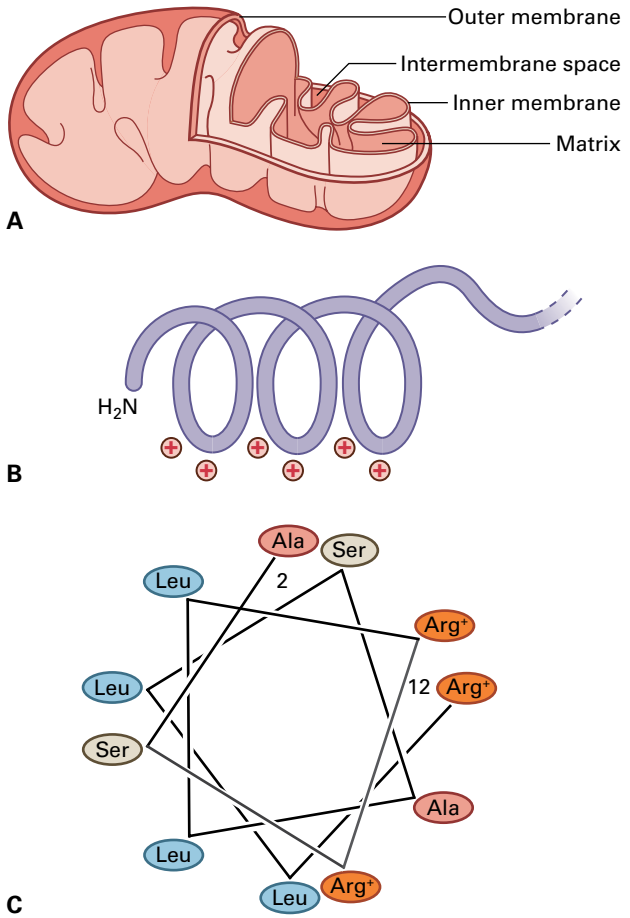


FIGURE 4.5 *(A) The four compartments of the mitochondrion. (B) Schematic representation of an amphipathic polypeptide helix with charged amino acids on one side and hydrophobic amino acids on the other side. (C) Two-dimensional projection of a typical presequence of an ATPase subunit imported into mitochondria, with hydrophobic amino acids to one side and charged amino acids on the other.*

domain, called a **presequence**, that facilitates entry into mitochondria. Despite the superficial resemblance between chloroplast transit peptides and mitochondrial presequences, the latter do not target proteins to chloroplasts, and transit peptides do not target proteins to mitochondria. Analysis of mitochondrial presequences indicates that many can form positively charged amphipathic α-helices; these have hydrophobic amino acid residues on one face of the helix and charged residues on the other (Fig. 4.5B,C). After a protein enters a mitochondrion, the presequence is cleaved by an endopeptidase, just as in the chloroplast.

Proteins are transported to mitochondria in an unfolded state with the help of the chaperone, cytosolic Hsp70, and imported by an import apparatus that spans both inner and outer membranes at a point of contact. Once the protein is in the matrix, folding is catalyzed by another chaperone, Hsp60, and by proteins called TOMs and TIMs (translocases of outer and inner membranes, respectively) (Fig. 4.6).

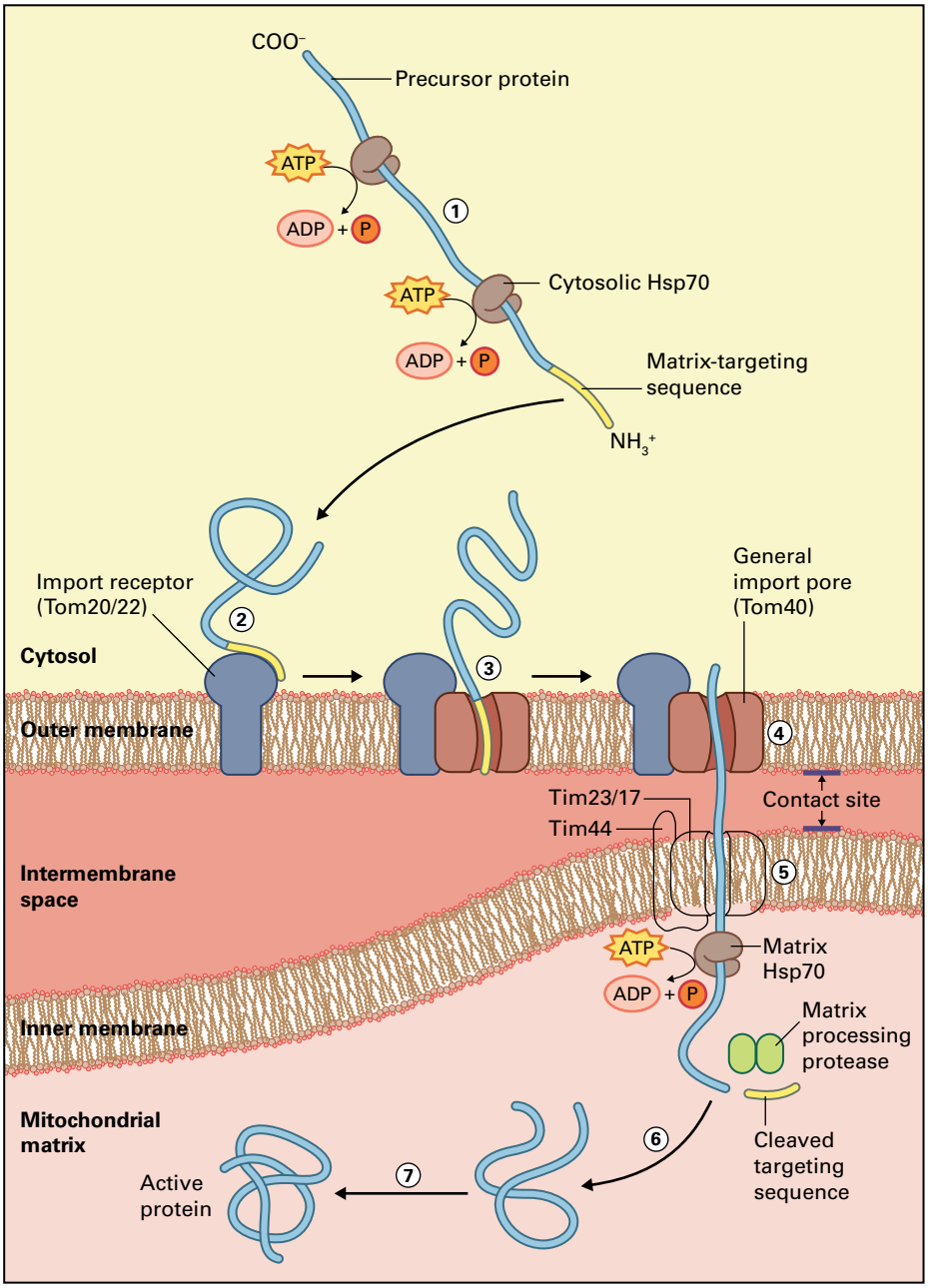


FIGURE 4.6 *Protein import into the mitochondrial matrix. Polypeptides are held in an unfolded configuration in the cytosol by chaperones such as Hsp70. After binding to an import receptor in the outer membrane the polypeptide is transferred to a proteinaceous pore and is threaded through it and through a pore in the inner membrane at a site where the two membranes are in contact. A matrix processing protease cleaves the presequence and chaperones help to fold the protein in the mitochondrial matrix. Numbers indicate sequence of events.*
Source: Lodish et al. (2013). Molecular Cell Biology, 7th edition. W.H. Freeman.

Several features distinguish mitochondrial from chloroplast protein transport. Mitochondrial import machinery proteins do not share sequence identity with those of the chloroplast. Furthermore, transport into the mitochondrial matrix requires an electrochemical potential across the inner membrane, in addition to ATP. Which mechanisms at the surface of these organelles contribute to the fidelity of protein sorting between mitochondria and chloroplasts? As in chloroplasts, transport of some proteins into the mitochondrial inner membrane and the intermembrane space requires two signals. Integral inner membrane proteins initially engage the Tom complex, but can utilize one of two Tim complexes to facilitate membrane insertion. Membrane proteins with a single transmembrane segment utilize the same Tim23 complex utilized by matrix proteins. Complex, multispanning membrane proteins, including the nucleotide and metabolite transporters, utilize the Tim22 complex. In both cases the hydrophobic amino acid sequences including one or more transmembrane segments serve to trigger insertion of the protein into the membrane during translocation. Mitochondria also contain numerous proteins in the intermembrane space that are involved in electron transport. These proteins are initially transported through the Tom complex, but do not engage the Tim complexes. Rather, a specific mitochondrial import and assembly (MIA) machinery in the intermembrane space exists to assist in their folding and assembly.

Some proteins can be dual-targeted to both chloroplasts and mitochondria. These proteins typically perform basic maintenance functions within the organelles, including DNA and RNA maintenance, protein translation, and protein processing. Dual targeting of proteins occurs by two mechanisms. In one case, the gene for a protein might encode two alternative targeting domains that are generated by selection of alternative transcription or translation start sites or alternative mRNA splicing. In the second case, proteins can carry a single targeting domain with characteristics of both chloroplast and mitochondrial targeting signals. These ambiguous targeting domains are recognized by the targeting components of both organelles.

4.4 Targeting proteins to peroxisomes

4.4.1 Uptake of proteins by peroxisomes involves removable or intrinsic peroxisome targeting signals

Peroxisomes are specialized organelles that participate in many essential metabolic pathways (see Chapter 1). Plants contain at least three types of peroxisomes: (1) germinating seeds, young seedlings, and senescent leaves contain glyoxysomes that metabolize fatty acyl chains (see Chapters 1, 14, and 20); (2) peroxisomes in leaves play a major role in photorespiration (see Chapters 1 and 14); (3) some root nodules of tropical legumes that export ureides contain peroxisomes with unique enzymes of nitrogen metabolism (see Chapters 1 and 16). Peroxisomal enzymes also mediate steps in the biosynthesis of important plant hormones and signals, including jasmonic acid, salicylic acid, indole acetic acid, reactive oxygen species (ROS), and nitric oxide (NO). The importance of peroxisomes for the plant life cycle is shown by the observation that mutants that disturb peroxisome biogenesis are often embryo lethal.

Peroxisomes are surrounded by a single membrane and do not contain DNA or ribosomes. It appears that the membrane component of peroxisomes is initially derived from the ER via a budding process. However, all soluble peroxisomal proteins and many membrane proteins must be synthesized by cytosolic ribosomes and imported from the cytoplasm into pre-existing peroxisomes. At least two distinct peroxisome targeting signals, PTS1 and PTS2, are involved in the import of proteins into the peroxisomal matrix.

The tripeptide PTS1 (Ser-Lys-Leu, SKL) or a closely related variant targets most proteins destined for the peroxisomal matrix. This short sequence is located at the carboxyl terminus of many peroxisomal proteins and is not removed after translocation into the peroxisome. Deletion of this carboxyl-terminal signal abolishes import of nearly all peroxisomal proteins that carry it. In a few proteins, import is not abolished, suggesting that additional peroxisome targeting signals may be present within the protein. PTS2 consists of a cleavable amino-terminal targeting domain and is used by a subset of peroxisomal matrix proteins. Passenger proteins fused to PTS-like sequences are directed correctly into peroxisomes.

Protein import to peroxisomes requires not only a peroxisomal targeting signal but also ATP. Although the transport of some PTS1-containing proteins requires cytosolic factors, such as members of the Hsp70 family, it is not known whether chaperones are needed for import of all proteins, and the relationship between chaperones and protein import is an active area of research. Peroxisomal protein import also is distinguished by the observation that fully folded and oligomeric proteins can be imported into the organelle.

Mutants deficient in peroxisome biogenesis, including mutants in the import machinery for peroxisomal matrix proteins, called *pex* mutants, have mutations in *Peroxin* or *PEX* genes. More than 30 *pex* mutants have been identified in yeast (*Saccharomyces cerevisiae*) and mammals and half a dozen in *Arabidopsis*. In addition, many of the remaining *PEX* genes for which there are no clear phenotypes have been identified in the *Arabidopsis* genome. In yeast and other fungi the PEX5 receptor protein in the cytosol binds cytosolic PTS1-containing proteins (Fig. 4.7) and the PEX7 receptor also in the cytosol binds PTS2-containing proteins. These complexes then dock at the peroxisomal membrane to other PEX proteins that constitute the proteinaceous pore for protein import.

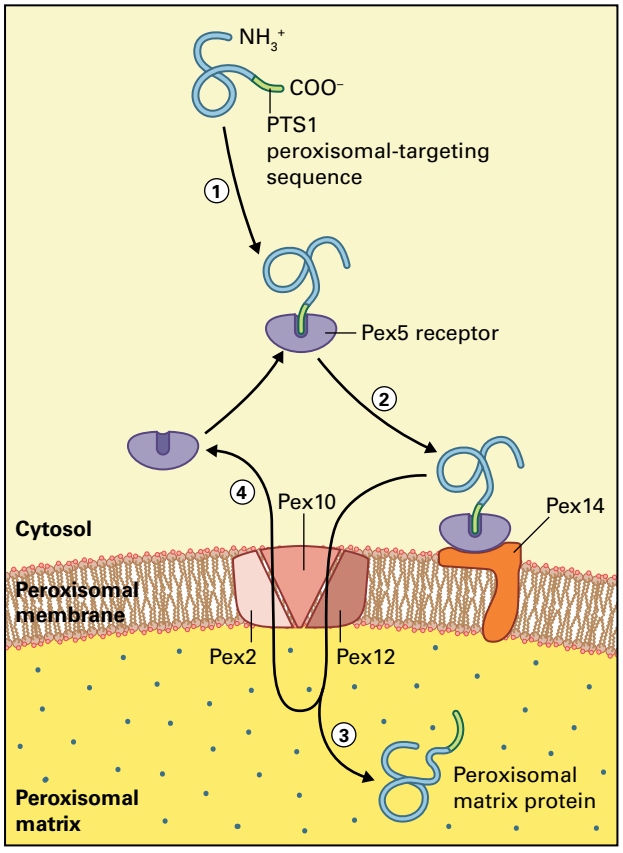


FIGURE 4.7 *Import of peroxisomal protein carrying the PTS1 targeting signal. A correctly folded protein in the cytosol such as catalase may carry an exposed PTS1 that will bind to a cytosolic receptor (PEX 5) and the complex docks at a receptor in the peroxisomal membrane (PEX 14). The polypeptide is transferred to a proteinaceous pore consisting of several PEX subunits and transported into the peroxisomal matrix. The cytosolic receptor is released and recycled. Numbers indicate sequence of events.* *Source*: Lodish et al. (2013). Molecular Cell Biology, 7th edition. W.H. Freeman.

4.5 Transport in and out of the nucleus

4.5.1 Proteins enter and leave the nucleus via nuclear pore complexes

Many macromolecules that function in the nucleus, including regulatory proteins, histones, RNA polymerases, and heterogeneous nuclear RNA-binding proteins, are synthesized in the cytoplasm (Fig. 4.2). In some cases, DNA from plant pathogenic bacteria and viruses is also selectively imported from the cytoplasm into the nucleus. Concurrently, tRNAs and mRNAs are synthesized, modified, and processed in the nucleus and exported to the cytoplasm. The nuclear envelope, which regulates these transport activities, comprises three structural elements: the outer and inner membranes with their intermembrane space (perinuclear space); nuclear pore complexes (NPCs); and the nuclear lamina. The outer nuclear membrane is continuous with the ER and, like rough ER, is studded with ribosomes (see Chapter 1 for a detailed description).

The nuclear envelope has hundreds of NPCs, located where the two nuclear membranes meet (Fig. 4.8). Proteins, ribonucleoprotein complexes, and RNA move in and out of the nucleus through these pores. Each NPC has multiple copies of at least 30 different proteins called nucleoporins (Nups). Each NPC constitutes a passive diffusion channel ≈9 nm in diameter. Small proteins of <40 kDa can diffuse passively through this pore, whereas larger proteins enter the nucleus through active transport. However, even small nuclear proteins such as the 20-kDa histones usually enter the nucleus by active transport rather than by diffusion.

4.5.2 Importins and exportins help transport proteins that contain specific localization signals into and out of the nucleus

Most polypeptides destined for the nucleus have address labels, called **nuclear localization signals** (NLSs), consisting of one or more short internal sequences with basic amino acids. NLSs share certain characteristics, but there is no strict consensus sequence. They generally contain several residues of arginine and lysine and may also have proline residues that disrupt helical domains. The position of the NLS within the amino acid sequence of a protein varies, and they are not cleaved from nuclear proteins after translocation. Therefore the proteins can re-enter the nucleus if they are exported to the cytosol or released when the nuclear envelope is disassembled during mitosis. Many nuclear proteins require more than one NLS for efficient nuclear targeting in vivo, which suggests that protein structure may play an important role in NLS presentation and in the ability of independent NLSs in the same polypeptide to function in a cooperative manner.

Many viral proteins have NLSs, and PKKKRKV is the NLS of the large T-antigen of the simian virus SV40, which has been studied in great detail. A mutation that causes a single amino acid change at the third position abolishes NLS function and prevents nuclear import causing the large T-antigen to remain in the cytosol. Another class of NLS, designated bipartite, is typified by nucleoplasmin and the *Zea mays* (maize) transcription factor opaque-2 (Table 4.2). Mutations in either basic motif alone do not affect function, whereas mutations in both basic motifs significantly impair nuclear targeting.

Three cytosolic proteins play a role in the import of a protein carrying an NLS: importin α, importin β, and Ran, a monomeric G-protein that can exist in either the GTP-bound or GDP-bound conformation. Importins can act singly or as a bimolecular αβ complex. The first step of nuclear import is the binding of an NLS-containing cargo protein to importin to form a bi- or trimolecular complex. This complex diffuses into the pore and binds successively to different Nups. After entering the nucleoplasm, interaction of the complex with

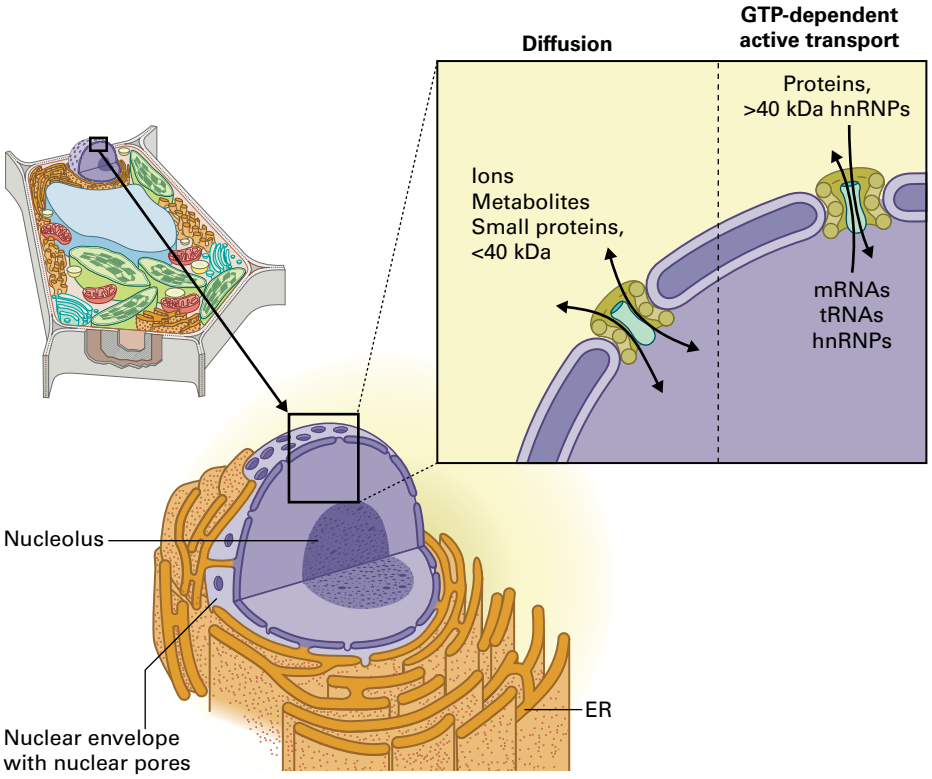


FIGURE 4.8 *Schematic representation of the basic processes of protein transport into the nucleus by diffusion or by active GTP-dependent transport. hnRNP, heterogeneous nuclear RNA-binding proteins.*

TABLE 4.2 *Nuclear localization signals in two maize transcription factors.*

Protein	NLS*	Class
opaque-2 (O2)	RKRKESNRESARRSRYRK	Bipartite
R	MSERKRREKL	SV40-like

*Basic residues are underlined.

Ran-GTP results in a conformational change that causes the cargo protein to be released with the formation of an importin–Ran-GTP complex. This complex will be exported back to the cytosol. Keeping this cycle going requires a GDP-GTP exchange factor (Ran-GEF) in the nucleoplasm and a GTPase accelerating protein (Ran-GAP) in the cytosol. The cycle is illustrated in Fig. 4.9. The rapid dissociation of the cargo complex in the nucleoplasm creates a concentration gradient of the complex that promotes its diffusion through the NPC, and the asymmetric distribution of Ran-GAP and Ran-GEF makes the cycle possible.

A similar mechanism is responsible for protein export. Three types of nuclear export signals (NESs) have been identified and the best understood are the leucine-rich motifs. Proteins with this motif bind to an exportin–Ran-GTP complex. This complex diffuses through the pore, interacting transiently with Nups and finally an interaction with NPC elements on the cytosolic side stimulates GTP hydrolysis and a change in the conformation of Ran, so that the complex falls apart and the exported protein is released into the cytosol.

Traffic into the nucleus can be regulated by complexing with a cytoplasmic protein that masks the NLSs, by phosphorylation and dephosphorylation, by association with membranes, or by environmental stimuli such as light. Some nuclear proteins show tissue-specific nuclear localization: they are present in the nucleus in some tissues but excluded in others. In the last few years evidence from several genetic screens indicates that Nups affect various processes like auxin response, cold-stress tolerance, flowering time, and plant microbe interactions.

mRNAs that have been processed in the nucleus remain associated with specific hnRNP (heterogeneous ribonucleoprotein) proteins in a messenger ribonucleoprotein (mRNP) complex. These complexes leave the nucleus after binding to the mRNP exporter, a heterodimeric protein.

4.6 ER is the secretory pathway port of entry and a protein nursery

Eukaryotic cells contain an extensive membrane network consisting of flattened sacs (cisternae), small vesicles, and other compartments—all of which are collectively referred to as the endomembrane system (see Chapter 1). Major components of the system are the ER, the Golgi apparatus, vacuoles, the plasma membrane, and different types of endosomes. This membrane network hosts the secretory pathway, a biochemical pathway that allows the secretion of proteins from the cell. Proteins synthesized by this pathway are termed secretory proteins, but not

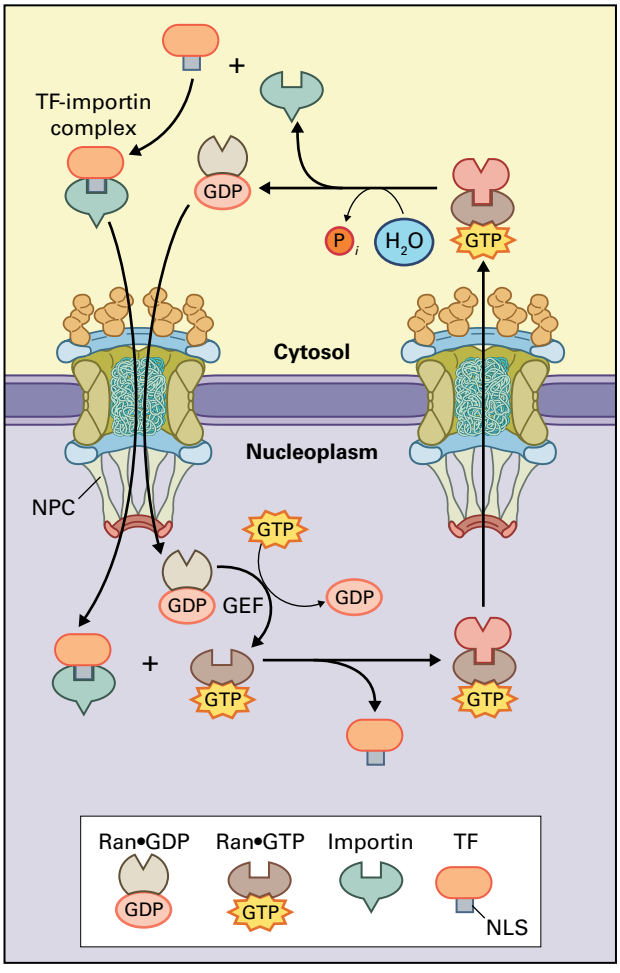


FIGURE 4.9 *Mechanism of import of a transcription factor (TF) into the nucleus. The cycle starts with the NLS of a TF binding to an importin molecule (see + sign); the complex enters the nucleus through the NPC and in the nucleoplasm it reacts with Ran-GTP so that the TF is released; Ran-GTP bound to importin will leave the nucleus; hydrolysis of GTP will cause a conformational change producing a Ran-GDP that can enter the nucleus and react with a GDP-GTP exchange factor to produce Ran-GTP.*
Source: Lodish et al. (2013). Molecular Cell Biology, 7th edition. W.H. Freeman.

all of them are secreted because many are sorted to and reside and function in the different compartments of the endomembrane system. Thus the secretory pathway also functions in the biogenesis of its own compartments and membranes, including the tonoplast and the plasma membrane. The major routes of traffic along the secretory pathway have been determined by fractionation of subcellular compartments (Box 4.2) coupled with radioactive pulse-chase experimentis (Box 4.3). These techniques are still used now, in addition to the more recent use of fusions with fluorescent proteins (Box 4.1).

Thousands of different proteins involved in every major process of plant development, reproduction, and response to the environment, as well as many storage proteins are synthesized by the secretory pathway. Essential functions of the plant endomembrane system, not shared with many other eukaryotes, include the biogenesis of multifunctional vacuoles, the use of the ER as a storage compartment, the formation of the cell plate during cytokinesis, the biosynthesis of cell wall polysaccharides and proteins, and polarized growth of certain cell types. The endomembrane system also stores calcium, synthesizes lipids for delivery elsewhere, and regulates steps in hormone synthesis, transport, and signaling. Many human and viral proteins of medical interest are also secretory proteins, and scientists are exploiting the plant endomembrane system for a safer and more cost-effective production of recombinant pharmaceuticals (Box 4.4).

4.6.1 Proteins travel in vesicles through the endomembrane system like cargo in containers

The major biosynthetic traffic route of the secretory pathway is from the ER to the Golgi and ultimately to the plasma membrane for secretion or to the tonoplast for delivery to vacuoles (Fig. 4.10). Passage from the Golgi to vacuoles is mediated by the *trans*-Golgi network (TGN) and multivesicular bodies (MVBs). As detailed in Section 1.5.2, two regions of the TGN can be morphologically identified: the early TGN (or Golgi-associated TGN) has a cisternal appearance and is strictly associated to the *trans*-cisternae of the Golgi apparatus, whereas the late TGN (or free TGN) has a grape-like appearance and is detached from the Golgi. The terms "early" and "late" refer to the direction of the biosynthetic secretory pathway. It should be noticed that the late TGN and MVBs are also involved in endocytosis from the cell surface (Fig. 4.10). Because endocytic traffic has an opposite direction compared to biosynthetic traffic, the late TGN is also termed "early endosomes", whereas MVBs are termed "late endosomes". A trademark of the secretory pathway is the formation of vesicles that bud off from one cisterna or compartment and then dock and fuse with the next one. The biosynthetic, forward or anterograde traffic must be matched by reverse or retrograde traffic of equal magnitude if the different compartments are to maintain their characteristic proteins. Furthermore, soluble and integral membrane proteins unique to each compartment must either remain behind when vesicles are formed to carry their cargo forward or be rapidly retrieved back to the compartment of residence by retrograde traffic (Fig. 4.11). The formation by budding of a vesicle requires that a coat of proteins be recruited from the cytosol. Before the vesicle can dock and fuse with its target compartment this coat must be stripped off again. Vesicles traveling between different compartments and in different directions have unique protein coats that contribute to the specificity of sorting.

4.6.2 The first sorting decision takes place during translation and requires the presence of signal peptides for entry into the ER

For nearly all secretory proteins, the first sorting decision is made when ribosomes involved in their synthesis become attached to the ER, creating rough ER (see Chapter 1). Rough

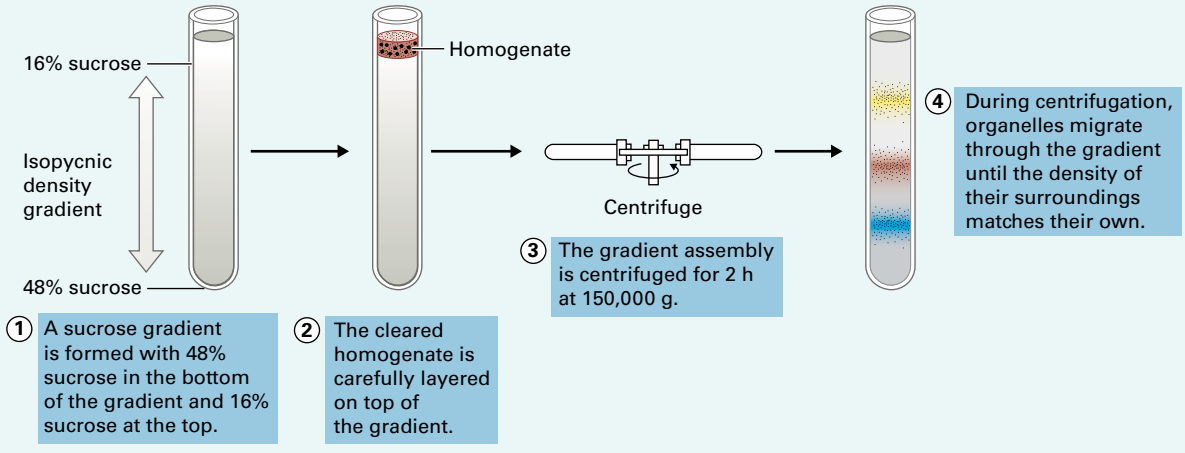
BOX 4.2

Sucrose density gradients are used to separate subcellular organelles for analysis of their contents

How do we find out in which subcellular compartment a protein is located? One way to answer this is to separate the organelles present in a homogenate on a sucrose gradient, on the basis of their density (isopycnic density centrifugation). The tissue must be homogenized gently in a buffered medium that is more or less isoosmotic with the cytosol to keep the organelles intact. Vacuoles, Golgi apparatus, plasma membrane, and ER usually fragment and form microsomes, most of which are from the ER, the most extensive endomembrane system. Newly synthesized proteins released in the lumen of the ER end up in the lumen of ER-derived microsomes. Removal of cell wall fragments, starch grains, and nuclei by a brief centrifugation at 2,000*g* results in a cleared homogenate that can be loaded on top of a sucrose gradient and centrifuged to separate the components.

In an isopycnic gradient with a sucrose concentration of 16% at the top and 48% or 60% at the bottom each organelle will travel to the region where the density of the gradient matches its own (figure). Such gradients can be used to separate organelles that have the same size, such as mitochondria and peroxisomes, or the microsomal vesicles that are derived from different membrane systems. The density of these vesicles reflects the protein-to-lipid ratio of the different compartments from which they are derived.

After centrifugation, the gradients are fractionated and assayed to determine which fractions have a particular protein of interest. Identification of each organelle (whether intact or fragmented into vesicles) is by means of a well-characterized marker enzyme or protein, preferably one unique to that organelle. Clathrin-coated vesicles and other organelles that lack characteristic enzyme activities can be identified with



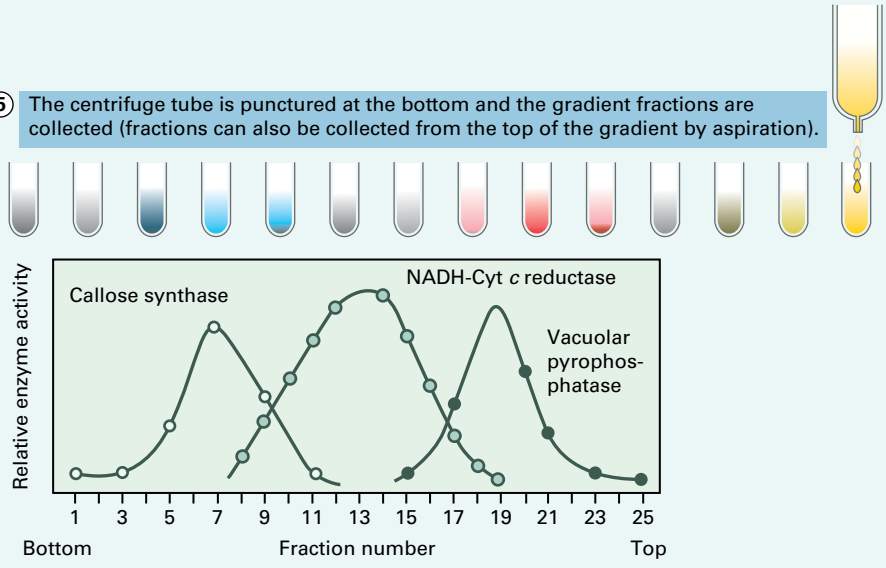
(1) A sucrose gradient is formed with 48% sucrose in the bottom of the gradient and 16% sucrose at the top.

(2) The cleared homogenate is carefully layered on top of the gradient.

(3) The gradient assembly is centrifuged for 2 h at 150,000 g.

(4) During centrifugation, organelles migrate through the gradient until the density of their surroundings matches their own.

(5) The centrifuge tube is punctured at the bottom and the gradient fractions are collected (fractions can also be collected from the top of the gradient by aspiration).



(6) The fractions are assayed for marker enzyme activity (or used for immunoblots). Here, callose synthase, NADH-cytochrome *c* reductase, and vacuolar pyrophosphatase serve as markers for the plasma membrane, ER, and tonoplast, respectively.

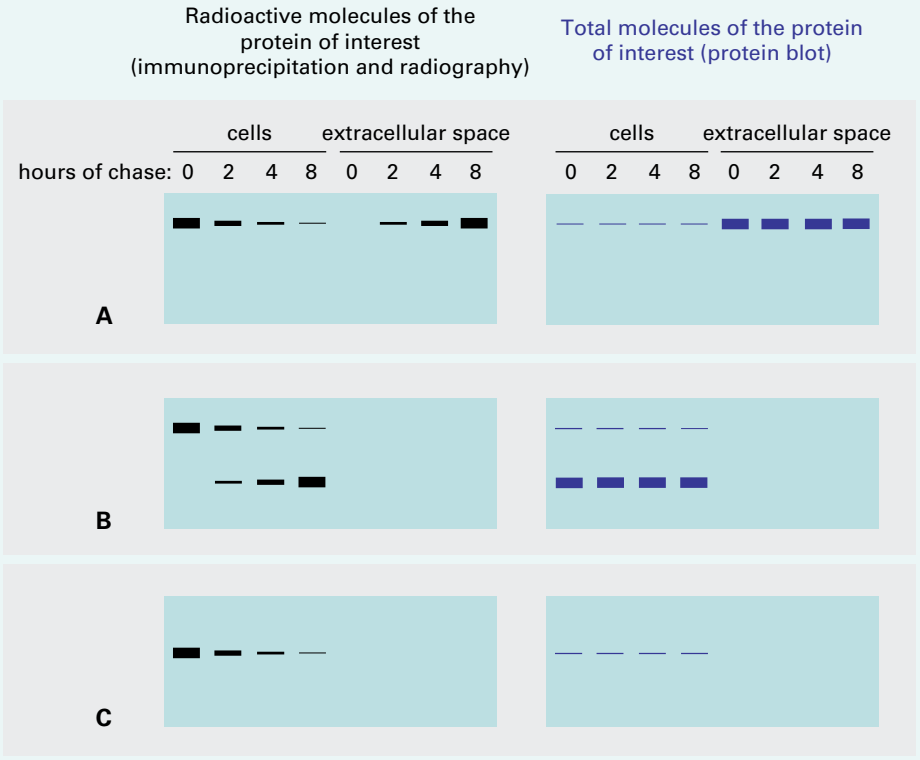
antibodies raised against a characteristic protein (e.g., clathrin). As proteomes of the different compartments are being characterized with growing speed, and genomics is providing thousands of gene sequences, the repertoire of antibodies available against proteins specific for each compartment is rapidly growing as well. An enzyme assay or immunoblot can be used to determine which gradient fractions contain the protein of interest and, by comparing its distribution with that of marker proteins, investigators can identify the subcellular location of the protein of interest.

Source: Ma & Hein. (1995). Trends Biotech 13:522–527.

BOX 4.3

Pulse-chase allows monitoring of traffic and protein stability

The fate of proteins can be followed by pulse-chase experiments in which cells or organs are exposed during a short time (pulse) to a radioactive precursor (amino acid or sugar). To stop incorporation of radioactivity, an excess of nonradioactive forms of the same amino acids is then added (chase) and a first sample is immediately collected (pulse, or zero time chase). Other samples are collected after different time intervals and represent the different chase time-points. The protein of interest is then selected from each sample with appropriate antibodies and analyzed by electrophoresis. Finally, proteins in the gel are revealed by autoradiography. The *total amount* of the protein of interest will obviously be the same in each sample (it can be visualized by protein blot, gels on the right in each panel), but the *radioactive* amount will vary with time (gels on the left in each panel). If a protein is destined to be secreted (A), its radioactive form will appear in the cell incubation medium during the chase and in parallel will disappear from the cells. To determine traffic routes, individual samples can be subjected to subcellular fractionation before immunoprecipitation: the radioactive protein will be detected in the compartment of synthesis at the end of the pulse (if the pulse time is not longer than the time taken to move to the next compartment) and then, at different chase times, in the compartments of transit and their final residence. Pulse-chase protein labeling was developed in the laboratory of Nobel Laureate George Palade in the 1960s and allowed him to determine that secreted proteins start their life in the ER and then travel through the Golgi. Pulse-chase also allows one to follow with time the processing of proteins from larger precursor to smaller mature forms (B, notice that a small amount of newly synthesized precursor is always present in the cell and can be revealed by protein blot) and to measure protein half life (C, protein with short half life). The administration, during the experiment, of specific inhibitors of protein processing or of trafficking steps also allows one to determine the role of processing on traffic and the influence of traffic on protein stability.

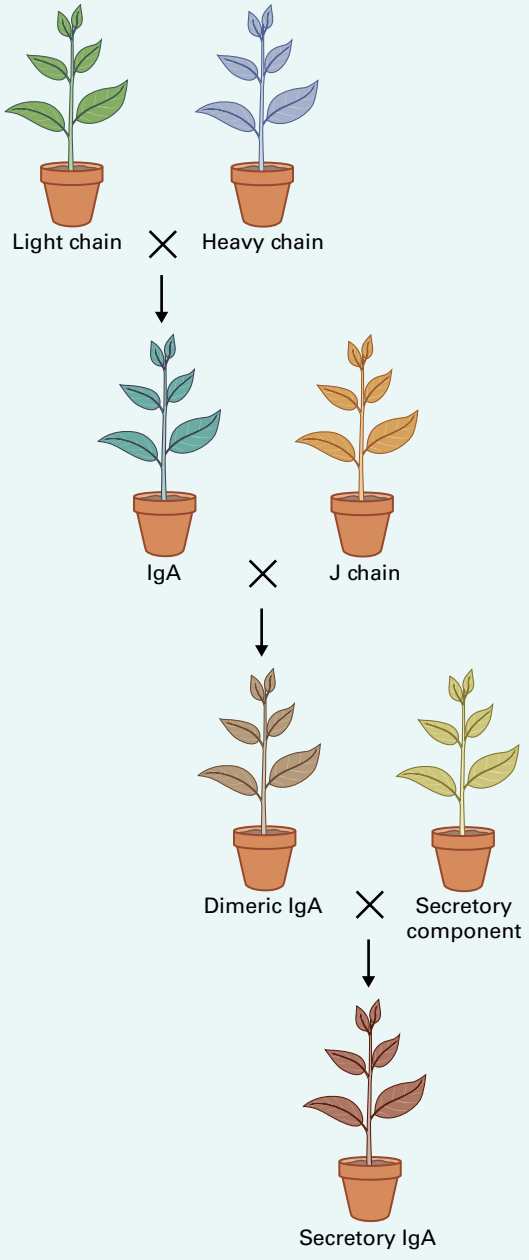


BOX 4.4

Many proteins that have important applications in the pharmaceutical industry are secretory proteins and can be produced in transgenic plants

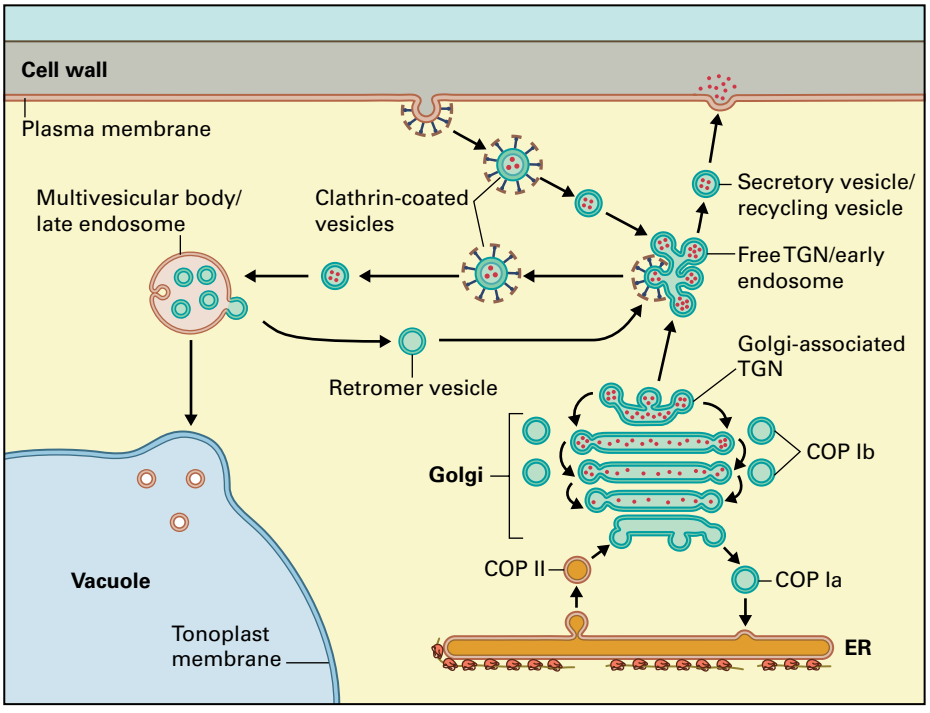
Many human and viral proteins that are used for medical applications are secretory proteins. Antibodies provide an excellent example, as today they are the single most important group of pharmaceuticals. The secretory protein family also includes all proteins of blood serum and of milk, peptide hormones, digestive enzymes, proteins of the extracellular matrix, such as collagen, and many viral antigens. Plants have been investigated as bioreactors for the production of many of these proteins, and antibodies produced in transgenic plants are already undergoing clinical trials. Growing plants is much less expensive than cell growth in fermentors, and plant-produced compounds are free from potential contamination by pathogenic viruses or prions. Plants could therefore be safer and more cost-effective bioreactors for the pharmaceutical industry, although this needs to be verified in large-scale production, and regulatory and public acceptance issues will need to be taken into consideration. The manufacture of drugs will only be permitted, if ever, in crop plants if the strictest containment conditions are observed by the manufacturers.

Antibodies are particularly stable in the apoplast and they can accumulate in transgenic plants up to 1% or even 10% of total protein, depending on the plant tissue and the specific antibody molecule. The production of secretory immunoglobulin A (SIgA), a very complex molecule, has been a remarkable success of plant biotechnology. SIgAs are the main antibodies found in mucosal secretions, such as saliva, tears, and gut secretions, and have the unusual characteristics of being produced by the cooperation of two cell types. Like most antibodies, the basic unit is a tetramer composed of two light and two heavy chains. This unit is assembled and dimerized by a joining (J) chain in the ER of plasma cells to form dimeric IgA (dIgA, actually a nonamer). dIgA is secreted and then recognized by a receptor present on the basolateral surface of epithelial cells. Transcytosis causes transport of the receptor/ligand complex to the apical surface, where a protease releases the dIgA associated with a portion of the receptor (called secretory component, SC), resulting in the formation of the full, 10-subunit SIgA molecule. SigA can be faithfully assembled in the ER when the four sequences (heavy and light chains, joining chain, and SC) are individually expressed in transgenic plants that are then crossed until the final form is synthesized in a single plant, opening the way for cost-effective, large-scale production of this pharmaceutical.



ER is particularly abundant in cells that specialize in protein secretion (e.g., cereal aleurone cells triggered to secrete hydrolases by gibberellic acid) or protein storage (e.g., storage parenchyma cells of developing seeds). The luminal (internal) space of the ER is topologically distinct from the cytosol and equivalent to the vacuolar and extracellular spaces, because of the mechanism of vesicle budding described above and illustrated in Figure 4.11. In other words, once a protein is in the lumen of the ER, the protein need not pass through another membrane to move from one compartment to another of the endomembrane system and become an extracellular or a vacuolar protein. Similarly, during intracellular traffic, integral

FIGURE 4.10 *Overview of the secretory pathway and endocytosis. Proteins synthesized on the rough ER travel to the Golgi and TGN. They can then be transported to the vacuole via MVBs or secreted. Proteins retrieved from the cell surface in endocytic vesicles arrive at the free TGN (early endosomes) and can then be recycled back to the plasma membrane or delivered to the vacuole via MVBs (late endosomes). The different types of vesicles involved are indicated.*



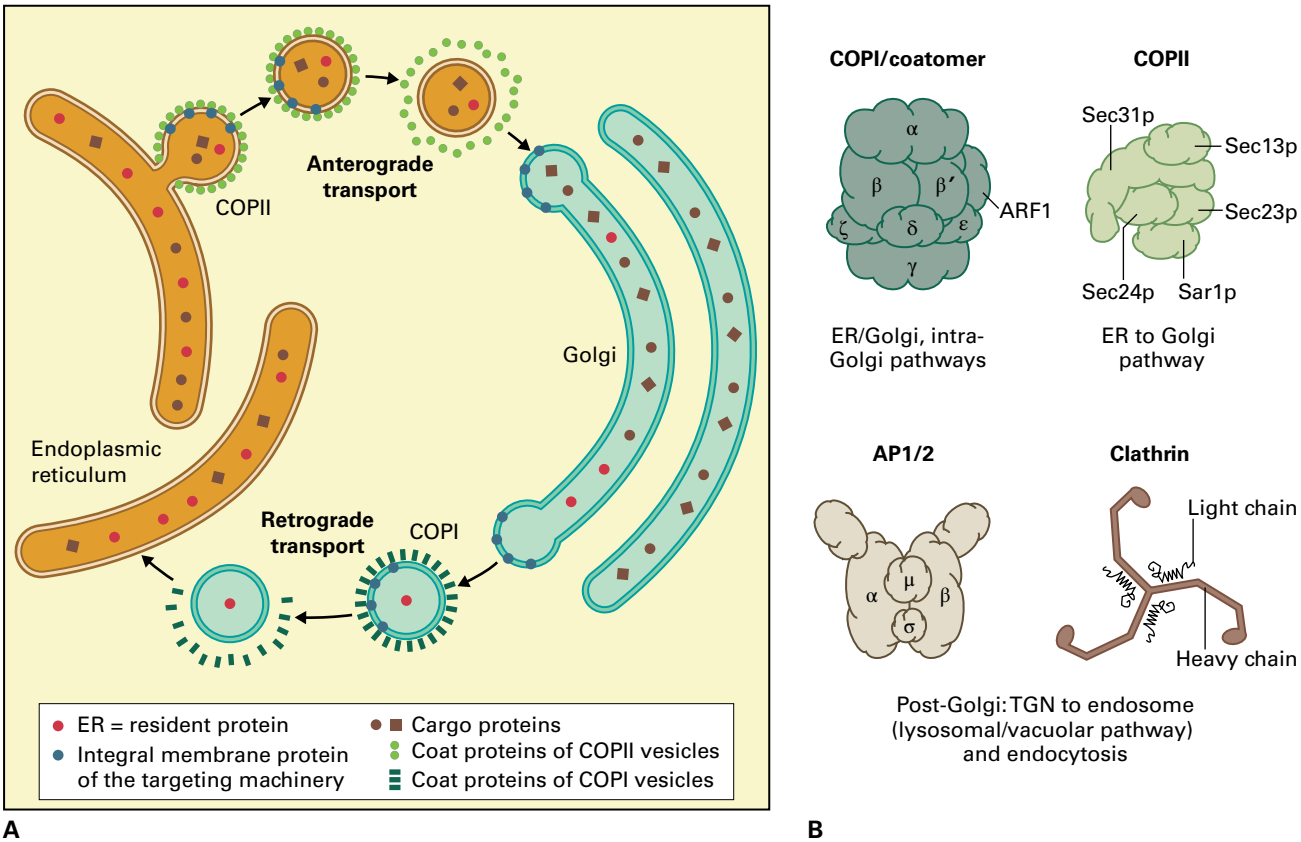


FIGURE 4.11 *Proteins travel as cargo in vesicles between compartments of the secretory system; shown here is traffic between the ER and the Golgi with vesicle traffic in two directions: forward or anterograde and return or retrograde. Top left: a bud forms when coat proteins are recruited from the cytosol to make a fully coated COP II vesicle that pinches off, is uncoated and then docks with a* cis*-Golgi cisterna. In retrograde transport a bud recruits COP Ia proteins, separates from the* cis*-Golgi, is then uncoated and fuses with the ER, bringing back soluble and membrane proteins that are ER residents.*

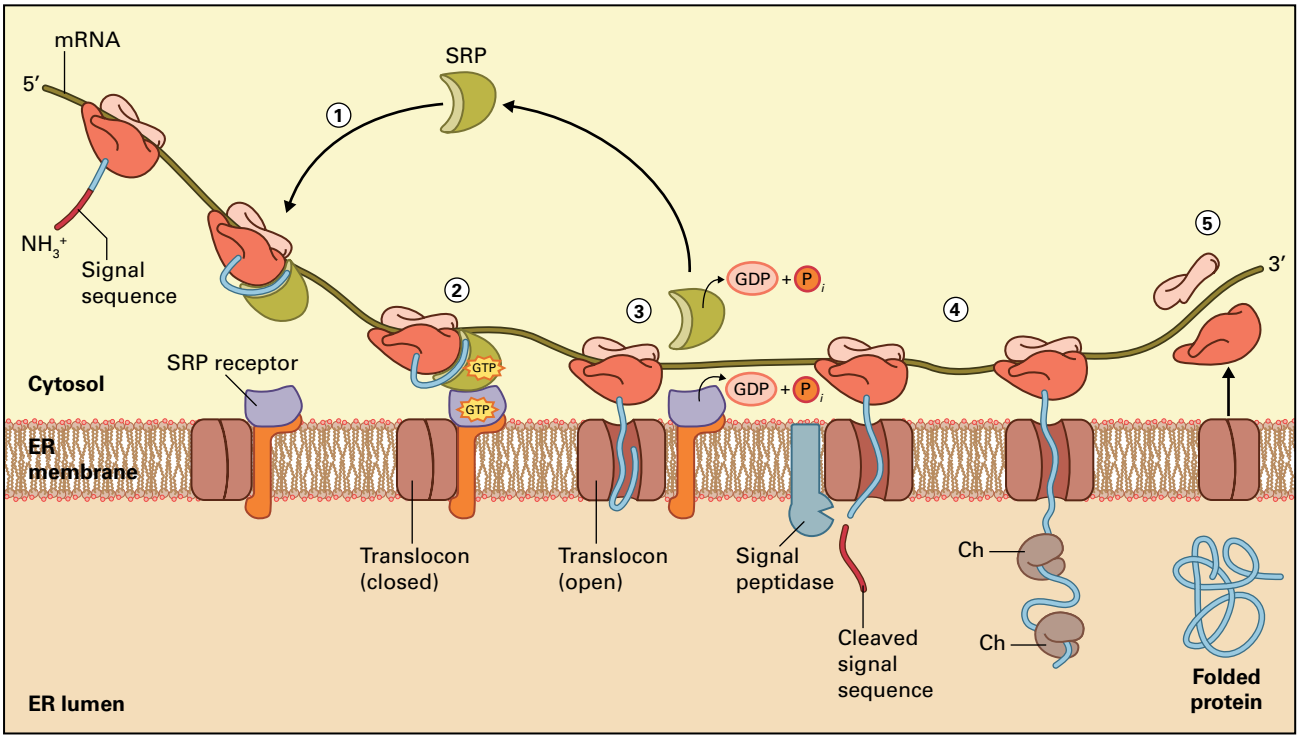


FIGURE 4.12 *Entry of a newly synthesized polypeptide into the lumen of the ER. Step 1: When a nascent polypeptide has about 70 amino acids the signal peptide protrudes far enough from the ribosome to be recognized by an SRP. Step 2: the SRP docks the entire complex onto the SRP receptor. Step 3: GTP hydrolysis opens the translocon, permits insertion of the nascent polypeptide and causes dissociation of the complex. Step 4: Signal peptidase cleaves the signal peptide and continued translation causes the nascent polypeptide to protrude further into the lumen so that it can be bound by chaperones (Ch). Step 5: When translation is finished the folded protein is released and the ribosomal subunits fall off the mRNA. Source*: Lodish et al. (2013). Molecular Cell Biology, 7th edition. W.H. Freeman.

TABLE 4.3 *Examples of signal peptide sequences.*

Protein	Final localization	Signal peptide sequence
Barley lectin *(Hordeum vulgare)*	vacuolar	MKMMSTRALALGAAAVLAFAAATAHA ↓ Q
Zein *(Zea mays)*	endoplasmic reticulum	MATKILALLALLALFVSATNA ↓ F
Insulin *(Homo sapiens)*	secreted	MALWMRLLPLLALLALWGPDPAAA ↓ F

The arrow indicates the cleavage site, and the first amino acid of the mature polypeptide is also shown. The stretch of hydrophobic amino acids is in green. Positively charged amino acids preceding it are in red.

membrane proteins maintain their orientation with respect to the membrane, and if they reach the plasma membrane their lumenal domains will become extracellular.

As they are being synthesized, soluble secretory proteins cross the membrane completely, whereas integral membrane secretory proteins become part of the ER membrane. Why do the ribosomes synthesizing these classes of proteins bind to the ER, and how do proteins cross the lipid bilayer? The nascent polypeptide chains of these proteins have at their amino terminus a sequence termed signal peptide (see Table 4.1), usually of about 16–30 amino acids, that directs the polypeptide chain to the ER membrane, begins the process of translocating the entire protein into the lumen of the ER, and is finally removed by a specific protease of the ER (Fig. 4.12). Such **signal peptides** are found on nearly all soluble secretory proteins and on many integral membrane proteins of the secretory system. Signal peptides differ from one another in amino acid sequence but share important structural features: located at the N-terminus of a polypeptide they typically consist of a short sequence containing one or more positively charged amino acids followed by at least six hydrophobic amino acids and then additional amino acids before the cleavage site (Table 4.3). Using recombinant DNA techniques to produce chimeric proteins, it has been found that a signal peptide attached to a cytosolic protein leads to translocation into the ER lumen, indicating that it is a

sufficient signal for this process to occur, and that the signal peptides of different secretory proteins are interchangeable among plant, animal, and yeast proteins.

A signal peptide is first recognized by the **signal recognition particle** (SRP), a ribonucleoprotein complex that contains a small RNA molecule of ≈300 nucleotides and six different proteins. SRPs ordinarily reside in the cytosol, where they await the protrusion of a signal peptide on a nascent protein being made on a polysome. Recognition between the signal peptide and the SRP must occur when the nascent polypeptide is ≈70 amino acids long, with ≈40 amino acids protruding beyond the surface of the ribosome. SRP binds to the hydrophobic core of the signal peptide causing arrest of translation until the entire assembly makes contact with the SRP receptor and docks on the ER membrane. The receptor is an integral membrane protein composed of two different GTP-binding polypeptides. Once docking has occurred, the SRP and one of the two polypeptides of the receptor dissociate from the signal peptide, utilizing the energy obtained by GTP hydrolysis. After the SRP is released into the cytosol, the ribosome and its nascent polypeptide dock onto the translocation complex, a transmembrane protein channel in the ER membrane consisting of three integral membrane proteins (Fig. 4.12). Release of SRP relieves the block in translation and the growing polypeptide extends across the channel into the ER lumen. As the polypeptide enters the lumen of the ER, the signal peptide is cotranslationally cleaved by signal peptidase, an enzyme complex at the luminal side of each ER translocation channel. The block and then release of translation makes it unnecessary that cytosolic chaperones maintain the growing polypeptide in an unfolded state (unlike what happens for translocation into mitochondria or chloroplasts). Furthermore, the block ensures that folding only occurs within the ER lumen, where a number of ER-specific modifications, necessary for the productive folding of many secretory proteins, occur (see Section 4.6.5).

4.6.3 Topogenic sequences are needed for the correct orientation of integral membrane proteins

Membranes of the endomembrane system contain integral proteins. Some have only one transmembrane segment whereas others have many transmembrane segments, connected by peptide loops on both sides of the membrane (Fig. 4.13) and with amino- and carboxy termini that can be located on either side of the membrane.

How are these proteins inserted into the ER in their correct orientation? Let us first consider the simplest case: a protein with a single transmembrane domain in which the amino terminus protrudes into the lumen of the ER. Such proteins have signal peptides that function exactly as described in the

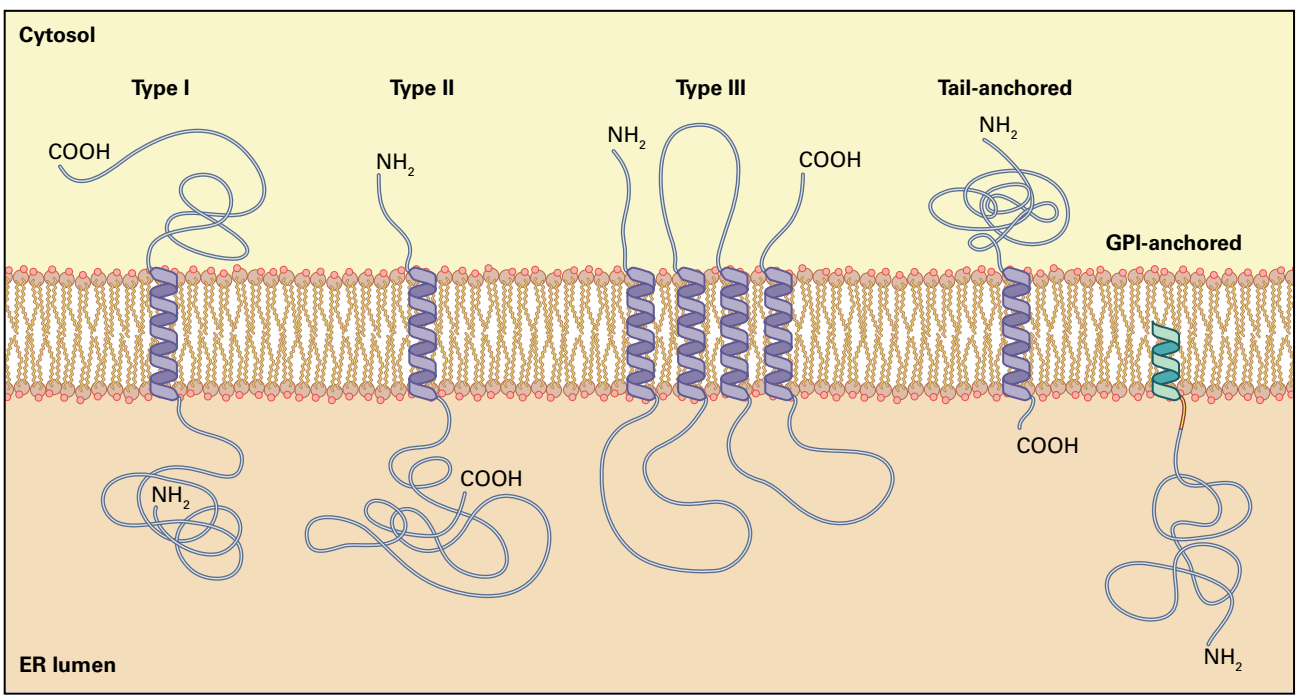


FIGURE 4.13 *Orientation of membrane proteins. Membrane proteins are classified according to their topological organization in the membrane. Type I and type II proteins have one transmembrane protein domain (an α-helix of 17–24 amino acids) located at the carboxyl (COOH) or amino (NH_3) termini, respectively Also, type I has a cleaved signal peptide, but type II does not. Multispanning proteins can have their two termini on the same side or on different sides of the membrane depending on number of spans. Tail-anchored proteins are similar to type II proteins but they have very few amino acids following the transmembrane domain. Unlike other transmembrane proteins, they are inserted post-translationally. Glycosylphosphotidyl inositol (GPI) anchored proteins are initially synthesized as type I proteins and the luminal portion is later transferred by a transamidase to a phospholipid in the membrane.*

previous section. The signal peptide is cleaved as the protein begins to traverse the membrane. Then, part way through the membrane, protein translocation stops. A hydrophobic transmembrane amino acid sequence acts as a "stop transfer," or **membrane anchor sequence**. The ribosome then detaches from the translocon and polypeptide synthesis is completed in the cytosol. This type of integral membrane protein, with a cytoplasmic carboxyl terminus, is called a type I membrane protein. Proteins that exhibit the reverse orientation, called type II, do not contain a removable signal peptide. Rather, the internal hydrophobic transmembrane domain acts as a nonremovable signal peptide: it directs translocation into the ER lumen of the sequence that follows it, leaving in the cytosol the domains that precede it. The glycosyl transferases in the Golgi have this orientation.

Tail-anchored (TA) proteins have the topology as that of type II but with a luminal C-terminal domain composed of only a few amino acids (often less than ten) or none; for this reason their active site is always exposed to the cytosol. During synthesis, the hydrophobic domain of TA proteins is still sequestered within the ribosome when the stop codon is reached and the ribosome starts to disassemble, so that it never becomes available to SRP interactions. TA proteins are therefore inserted post-translationally into the target membrane. A number of TA proteins are active in different compartments of the secretory pathway but are always first inserted into the ER membrane. Others are inserted and active on the outer envelope of mitochondria and plastids.

In proteins with multiple hydrophobic membrane-spanning domains (termed type III), the loops between the transmembrane domains are usually hydrophilic. The first transmembrane domain acts as a signal peptide (the amino terminus remaining in the cytosol), and the second domain functions as a membrane anchor sequence; the third domain acts again as a nonremovable signal peptide, the fourth as a membrane anchor sequence, and so on. Although both SRP and SRP receptors are necessary for the integration of the first transmembrane domain, they are not needed for the third, fifth, and subsequent domains.

4.6.4 Some proteins are anchored in the membrane by lipid molecules

Some membrane proteins are anchored to the membrane by a glycosylphosphatidyl-inositol (GPI) moiety. These proteins have a cleavable N-terminal signal peptide and a single C-terminal hydrophobic domain that terminates at the stop codon. Close to this domain there is a consensus recognized by an ER transamidase complex that removes the hydrophobic domain and replaces it with a preassembled GPI anchor. These GPI-anchored proteins are therefore membrane anchored but fully exposed to the ER lumen (Fig. 4.13). They then usually traffic along the secretory pathway to the plasma membrane, thus exposing the functional polypeptide on the cell surface. The consensus recognized by the transaminidase is rather complex, but algorithms have been developed to identify it. Using these algorithms combined with proteomic analysis of purified proteins, more than 200 *Arabidopsis* GPI-anchored proteins have been putatively identified. Arabinogalactan proteins, phytocyanins, lipid transfer proteins, and β-1,3 glucanases are highly represented members. The GPI anchor can be removed in vivo by the action of a phospholipase, thus releasing the protein in the cell wall as a soluble polypeptide (Fig. 4.14). Such processing may have a signaling function.

Protein modifications by the covalent linkage of lipids to the polypeptide chain occur in the cytosol (see Section 1.2.4 and Fig. 1.10 for a detailed description of these modifications). These modifications allow attachment to membranes leaving the whole polypeptide exposed to the cytosol and therefore

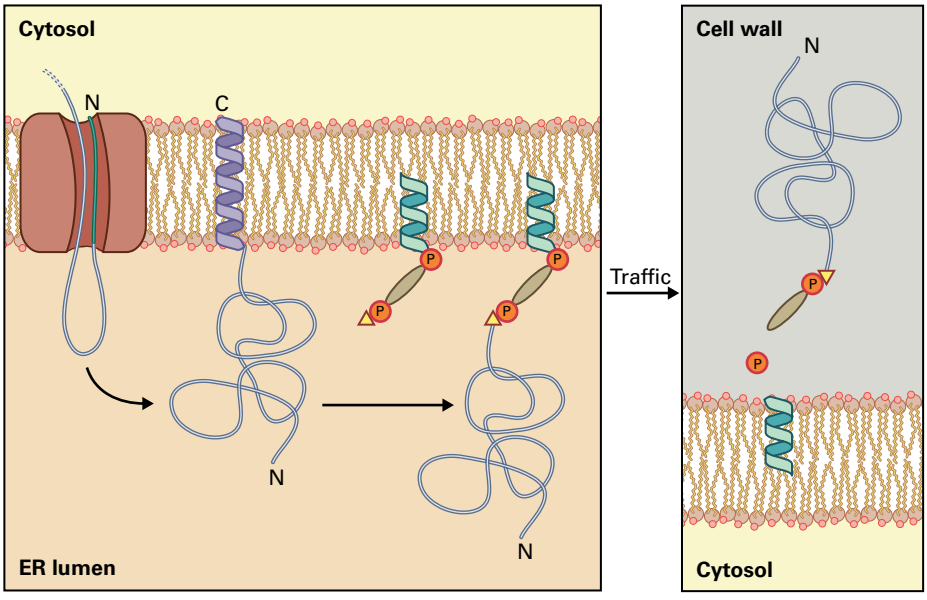


FIGURE 4.14 *Synthesis of GPI-anchored proteins. GPI-anchored proteins are initially synthesized as type I proteins. The luminal portion is later transferred by a transamidase to the preformed GPI anchor. After reaching the cell surface, the protein can remain membrane-anchored or be released by phospholipases into the cell wall environment. The signal peptide is in red; the original hydrophobic domain is in dark blue.*

have a function topologically similar to the transmembrane domain of TA proteins. Palmitoylation is the only reversible lipid modification and often occurs on myristoylated polypeptides: because myristic acid does not promote strong attachment, reversible palmitoylation can regulate cycles of membrane attachment and release that are used by signaling proteins. Prenyl transferases involved in this process are heterodimers. A unique geranylgeranyl transferase, with specific α and β subunits, is involved in the modification of Rab GTPases, which are a large family of regulators of vesicular traffic. Geranylgeranyl transferase and farnesyl transferase involved in the modification of many other proteins have instead a common α subunit and a specific β subunit. Loss-of-function mutants of the α subunit or the farnesyl transferase β subunit are lethal in yeast and in animals that have been investigated but not in *Arabidopsis*, where they give rise to enhanced ABA response and homeotic mutations. This is consistent with the finding that the *Arabidopsis* transcription factor APETALA1 (see Chapter 19) and a number of other plant proteins involved in tissue differentiation have prenylation signals, and that APETALA1 mutated in its farnesylation consensus loses its function.

4.6.5 Folding of secretory proteins occurs in the ER lumen in an environment that differs from the cytosol, and is assisted by helper proteins that constitute a large proportion of the ER proteome

The chemical environments of the ER lumen and the cytosol are different. Free calcium in the plant cytosol is normally at submicromolar concentrations whereas in the ER it is about 100 times greater. The most abundant proteins of the ER are Ca^{2+}-binding proteins and are regulated by Ca^{2+}. Examples include calnexin and calreticulin, proteins that act as molecular chaperones as well as Ca^{2+}-binding proteins.

The reducing environment of the cytosol makes disulfide bond formation a very rare event. By contrast, the ER lumen, like the extracellular space, is oxidizing and thus favors the formation of disulfide bonds that play fundamental roles in the folding and assembly of many secretory proteins.

Correct folding of newly synthesized proteins can fail. Adverse environmental conditions (such as oxidative stress and alterations in temperature), changes in protein synthesis rates due to stress, and gene mutations increase the chances of irreversible aggregation, but the results of in vitro denaturation/renaturation experiments show that, without the assistance of helpers, most proteins are anyway on the verge of failing to fold correctly. All subcellular compartments where protein synthesis occurs are equipped with chaperones and enzymes that have the role of avoiding unspecific aggregation of newly synthesized polypeptides, thus favoring folding efficiency.

Many proteins that reside in the ER are directly or indirectly involved as folding helpers (Fig. 4.15):

- Signal peptidase is a multisubunit membrane complex that removes the signal peptide of newly synthesized proteins. Removal is cotranslational and is usually required for correct folding.
- The binding protein (BiP) and endoplasmin, are the ER members of the heat shock chaperone 70 and 90 families. Both are very abundant soluble proteins in the ER lumen. BiP transiently associates in an ATP driven process with many, perhaps most, newly synthesized secretory proteins, inhibiting unspecific aggregation during polypeptide folding and the assembly of multimeric proteins. Endoplasmin plays a similar role but it is much less promiscuous than BiP and seems specific for multicellular eukaryotes, since it has not been found in yeast.
- Protein folding starts cotranslationally, thus often leading to erroneous disulfide (S–S) bond formation in the ER lumen. The S–S bonds that were formed need to be rearranged to allow correct folding. Protein disulfide isomerase (PDI), a soluble oxidoreductase, acts as a disulfide donor to folding intermediates. PDI is then reoxidized by flavoproteins of the ER so it can start a new round of isomerization (see Chapter 10).
- Peptidyl prolyl *cis-trans*-isomerases catalyze the *cis-trans* isomerization of prolyl-peptide bonds, which can be a rate-limiting folding step.
- Many secretory proteins are cotranslationally glycosylated on specific asparagine (Asn) residues by oligosaccharyltransferase, an enzyme complex active at the luminal side of any translocation channel of the ER membrane. This modification, termed N-glycosylation, increases the solubility of many folding intermediates.
- The enzymes glucosidase I and II and UDP-Glc:glycoprotein glucosyltransferase (UGGT) modify Asn-linked glycans in a reaction cycle that, together with transient association to the ER lectins calreticulin and calnexin, helps correct folding of glycoproteins.

Because of their fundamental role in the synthesis of the thousands of secretory proteins, the ER folding helpers are necessary for virtually any process of plant life. Mutations in their genes, overexpression or underexpression can affect plant development, reproduction, or stress resistance (Table 4.4).

4.6.6 The ER quality control system monitors proper folding and assembly of secretory proteins, and disposes of misfolded polypeptides

Incorrectly folded polypeptides are sequestered and degraded as soon as possible, to minimize harm to the cell. The ER lumen, being the folding compartment not only of its own

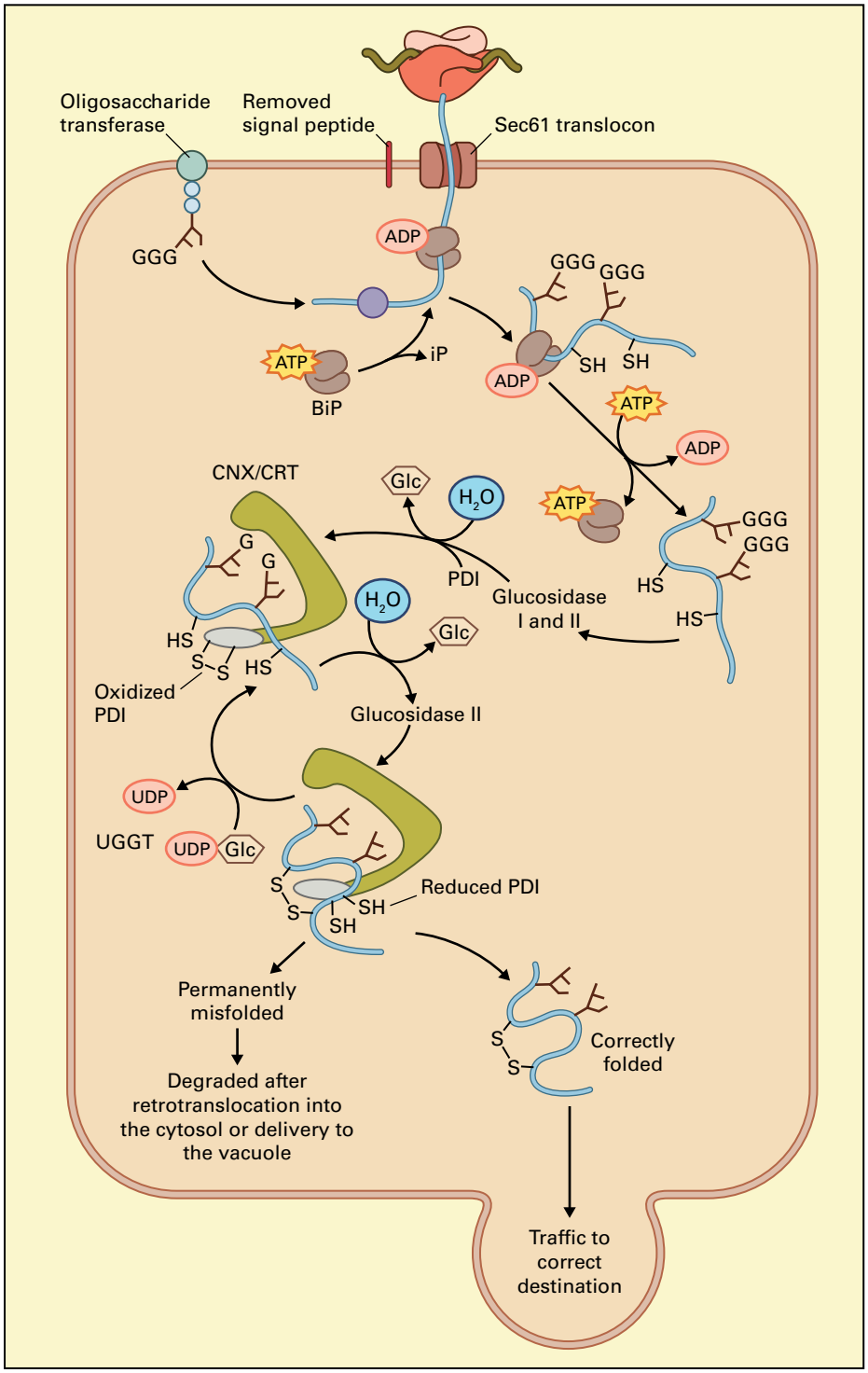


FIGURE 4.15 *Chaperones and folding helpers aid in the folding of proteins in the ER. BiP binds to hydrophobic motifs to prevent aggregation. If present, N-glycosylation sites are recognized by oligosaccharide transferase and glycans are transferred to the nascent polypeptide chain. Glucosidase I and II remove glucose residues (G) from the glycans and UDP-Glc-glycoprotein glucosyltransferase (UGGT) adds back one glucose. This cycle causes binding and release of the glycopolypeptide by the two lectins calnexin and calreticulin (CNX/CRT). Protein disulfide isomerase (PDI) catalyzes the formation of correct disulfide bonds. Eventually, the newly synthesized protein either completes correct folding and proceeds to traffic to its correct destination or remains permanently misfolded and is targeted for degradation in the cytosol or the vacuole.*
Source: Modified from Liu & Howell S.H. (2010). Plant Cell 22:2930–2942.

residents but also of proteins destined for many other locations, retains newly synthesized polypeptides until they have acquired their correct conformation. This function probably evolved to reduce the probability that malfunctioning proteins would reach their destinations. The three functions of promoting correct folding, retaining proteins until they are correctly structured and degrading defective proteins are collectively termed **ER quality control**.

TABLE 4.4 *Some effects of mutations in* Arabidopsis *genes encoding ER folding helpers.*

Protein	Mutation	Phenotype
Oligosaccharyltransferase subunits SST3a and SST3b	T-DNA insertions (double mutation)	Gametophytic lethal
Glucosidase I	point mutations at *knopf* locus (EMS treatment)	Seedling lethal Reduced content of cellulose
UDP-glucose:glycoprotein glucosyltransferase	Point mutation that causes an mRNA splicing defect	ER quality control is less stringent Restores brassinosteroid sensitivity in a *bri1* mutant, in which the brassinosteroid receptor is structurally defective but functionally active
BiP2	T-DNA insertion	Reduced secretion of pathogenesis-related proteins Reduced resistance to *Pseudomonas syringae* Hypersensitivity to salicylic acid analogs and to tunicamycin Hyperactivation of endoplasmin, calnexin and protein disulfide isomerase genes upon treatment with salicylic acid analogs
Endoplasmin	T-DNA insertion immediately upstream of the gene (expression is severely affected but not abolished)	*clavata*-like phenotypes inhibition of pollen tube elongation and pollen fertility

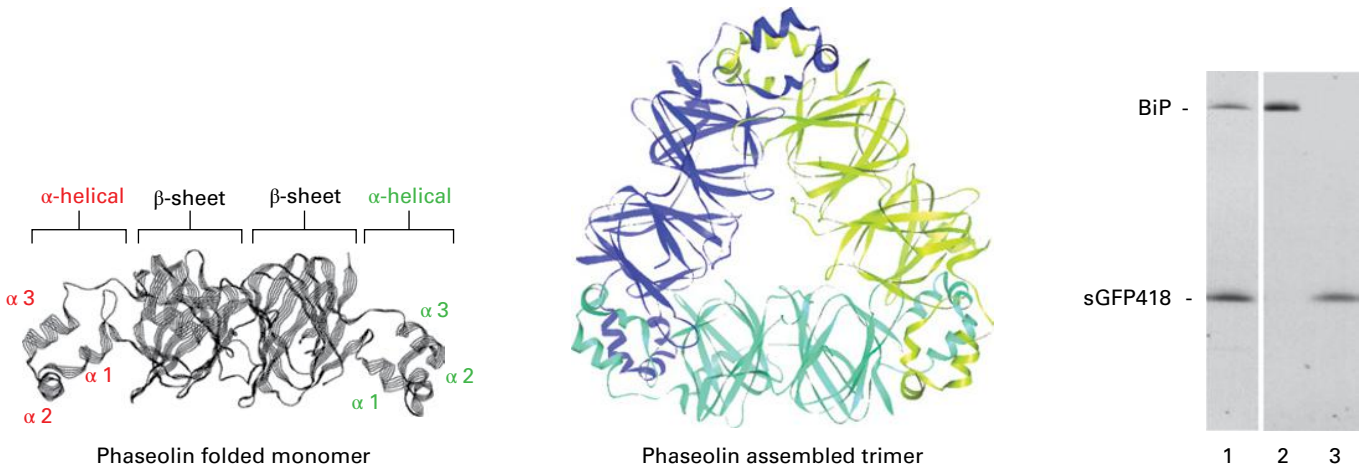


FIGURE 4.16 *BiP facilitates the assembly of trimers of the* Phaseolus vulgaris *protein phaseolin. Phaseolin homotrimers are mainly held together by hydrophobic interactions between α-helical domains: the three C-terminal domains indicated in green in the folded monomer interact with those indicated in red of an adjacent monomer, to form a trimer with a triangular shape. The C-terminal α-helical domains were fused to a secretory form of GFP (sGFP, consisting of GFP preceded by a signal peptide) and the chimeric polypeptide (termed sGFP418) was expressed in a transgenic plant. Protoplasts were prepared and pulse-labeled with radioactive amino acids. When proteins were immunoprecipitated with anti-BiP antibodies and analyzed by SDS-PAGE and fluorography, sGFP418 was shown to be the major polypeptide associated to BiP (lane 1). Treatment of the immunoprecipitate with ATP abolished this association (lane 2) and sGFP418 could be immunoprecipitated with anti GFP antiserum from the released material (lane 3). When a similar experiment was performed on sGFP, as a control, no association with BiP was detected (not shown). This indicates that the same domains involved in phaseolin assembly promote interactions with BiP. When phaseolin assembles into trimers these interactions are abolished.*
Source: Modified from Foresti et al. (2003). Plant Cell 15:2464–2475.

Many clues on ER quality control have been obtained studying the activity of the chaperone BiP. BiP binds preferentially to stretches of seven amino acids rich in hydrophobic amino acids. These sequences are not exposed at the protein surface in the folded and assembled proteins, thus providing an explanation for why, for example, BiP only binds to unassembled monomers of the bean (*Phaseolus vulgaris*) vacuolar storage protein phaseolin but not to assembled trimers. The domains of phaseolin monomers that directly interact to form trimers contain BiP binding sites that are masked upon assembly (Fig. 4.16). By binding, BiP prevents the nonspecific interaction of such domains during folding, thereby preventing proteins from denaturing or aggregating. BiP is an ATPase, and the hydrolysis of ATP causes it to release the

partially folded protein, affording additional chances to fold correctly. Correct folding of a protein may involve several cycles of BiP binding, ATP hydrolysis, and dissociation. The interactions with ER residents such as BiP provide a mechanism for the second feature of ER quality control that is the retention of not yet folded or assembled proteins in the ER.

When polypeptides are permanently misfolded or the subunits of multimeric proteins cannot assemble, the misfolded chains or the unassembled subunits are degraded. This is the third feature of ER quality control. Mechanisms have evolved that measure the time unproductively spent in the ER in the effort of folding or proper assembly, so that only defective proteins are degraded whereas normal intermediates of folding are not. Degradation in many cases occurs by first retrotranslocating the defective polypeptide back into the cytosol and then targeting it by ubiquitination for proteasome degradation. However, certain defective proteins are sorted to the vacuole for degradation, either through Golgi-mediated vesicular traffic or by autophagy of ER portions, both in yeast and plant cells.

4.6.7 Many secretory proteins are N-glycosylated during translocation in the ER

As mentioned before, N-glycosylation occurs in the ER. Attachment of N-linked glycans (oligosaccharides) occurs as the nascent polypeptide chain emerges into the ER lumen. Such glycans, which exhibit a $(glucose)_3(mannose)_9(N\text{-acetylglucosamine})_2$ ($(Glc)_3(Man)_9(GlcNAc)_2$) structure, are then modified, first in the ER and later in the Golgi apparatus (see Section 4.8.5). These glycans are built up, one sugar residue at a time, on dolichol pyrophosphate, a polyisoprenoid lipid of the ER, and are then transferred as a unit by the ER enzyme oligosaccharide protein transferase to certain Asn residues (Fig. 4.17). The residues that receive these glycans are almost invariably in an Asn-X-Ser or Asn-X-Thr configuration, where X can be any amino acid except proline. However, not all Asn-X-Ser/Thr configurations in a given secretory protein are necessarily N-glycosylated, because cotranslational folding of polypeptides can inhibit access of the oligosaccharyltransferase. Large-scale analysis indicates that two-thirds of potential N-glycosylation sites are actually glycosylated. After a glycan is transferred to a nascent polypeptide chain, the three glucose residues are quickly removed by two α-glucosidases that reside in the ER (glucosidase I and II). The resulting glycan, with the structure $(Man)_9(GlcNAc)_2$, is referred to as a high-mannose glycan.

N-linked glycans are highly hydrophilic and increase the water solubility of many polypeptides, thus allowing the production of a wider variety of protein conformations. They also protect proteins from proteolytic attack and have a major role in protein folding and quality control in the ER. Calnexin and calreticulin, two ER-resident lectins, help glycoproteins fold by binding to high-mannose chains from which two of the three glucose residues have already been removed. Such binding may result in the release of a correctly folded glycoprotein upon removal of the last glucose. In cases where these lectins release an incorrectly folded glycoprotein, an ER-located UDP-glucose:glycoprotein glucosyltransferase can add one glucose to the high-mannose chain. Cycles of addition and removal of glucose and interactions with the ER lectins take place until the glycoprotein is correctly folded. A folded glycoprotein is not a substrate for re-addition of glucose residues and thus cannot interact with calnexin or calreticulin. This system monitors the process of glycoprotein folding and may participate with other chaperones in retaining unfolded glycopolypeptides in the ER lumen.

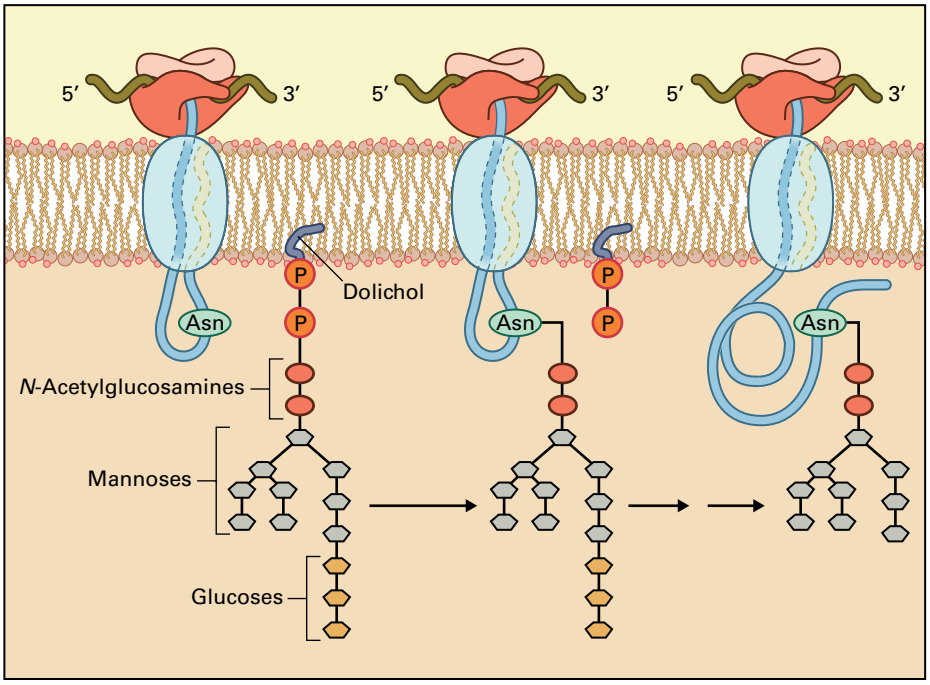


FIGURE 4.17 *Cotranslational transfer of a glycan (oligosaccharide) from a lipid carrier in the ER to an Asn residue of a nascent polypeptide chain. Glycans consisting of $(Glc)_3(Man)_9(GlcNAc)_2$ are assembled on dolichol carriers and transferred to an Asn residue as soon as a susceptible residue appears in the lumen of the ER. Removal of glucose residues and readdition of one residue is part of the folding process, which is aided by chaperones like BiP and protein disulfide isomerase (PDI).*

4.6.8 The unfolded protein response optimizes the quality control functions of the ER

The workload of the ER as a protein factory is not the same in all tissues and may depend on the stage of development or on environmental or biotic stresses. Plant cells, as well as other eukaryotic cells, have a sensing and signal transduction mechanism that regulates transcription and translation of specific genes to adapt the secretory pathway machinery to the level of ER loading needed. The genes encoding ER folding helpers are major targets of this signaling, and the most dramatic changes occur if the ER is loaded with an unusually high amount of newly synthesized misfolded proteins. For this reason, the mechanism has been termed unfolded protein response (UPR). Chemicals that inhibit correct protein folding in the ER, such as inhibitors of N-glycosylation, reducing agents or amino acid analogs, are potent UPR inducers and are used to study this mechanism, but the UPR is also involved when development or stress responses lead to rapid increases in secretory protein synthesis. The synthesis of individual secretory proteins with genetic defects that negatively affect their folding—by preventing signal peptide cleavage for example—also induces the UPR.

The UPR sensors/transducers are transmembrane proteins of the ER that monitor the accumulation of misfolded proteins and trigger the appropriate cellular responses. Four such sensors have been identified in plant cells: the membrane-associated transcription factors bZIP17, bZIP28, and bZIP60, and the kinase IRE1 (Fig. 4.18).

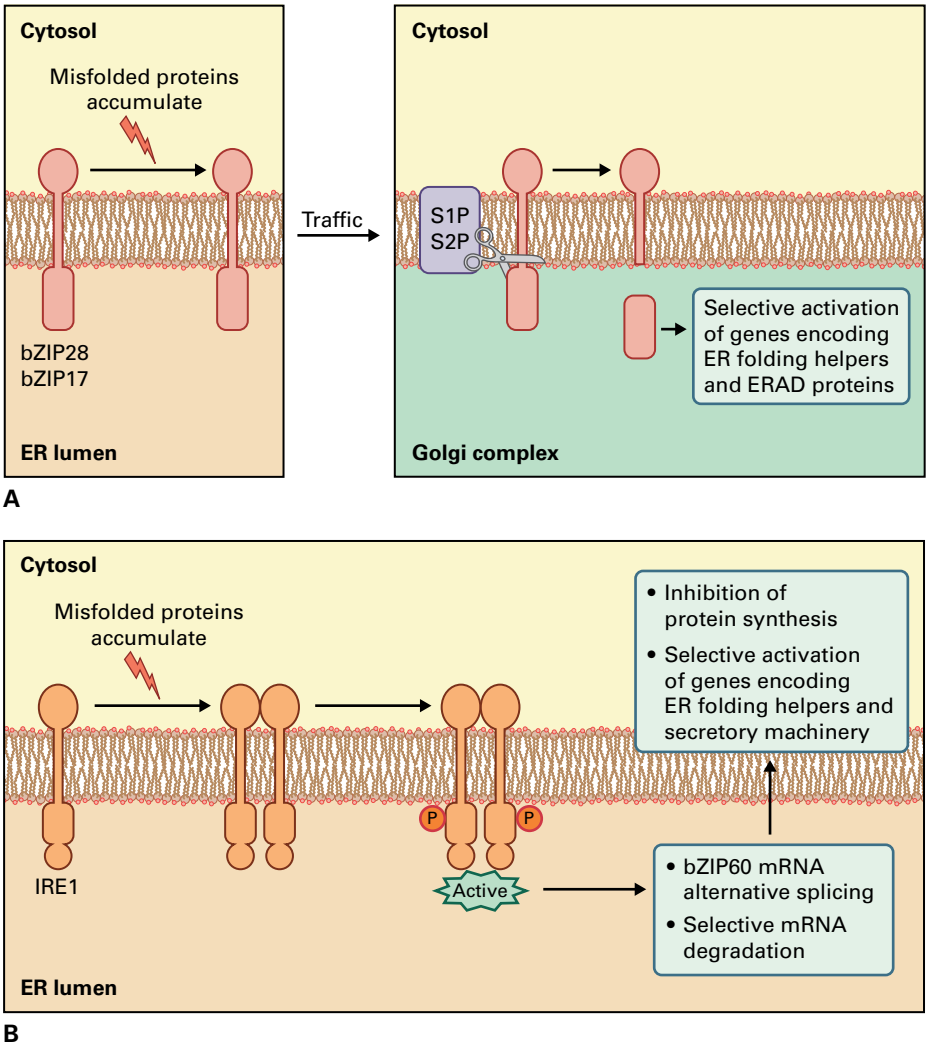


FIGURE 4.18 *Misfolded protein accumulation in the ER affects the behavior of at least four plant ER membrane proteins that signal the UPR. Upon misfolded protein accumulation the transcription factors bZIP28 and bZIP17 traffic to the Golgi complex, where their cytosolic domains are cleaved off by the Golgi-resident proteases S1P and S2P. They then enter the nucleus and activate transcription of target genes. The transmembrane protein ATF6 of mammalian cells has little sequence similarity with these plant proteins but has a very similar mechanism of action. IRE1 is present in plants, animals, and yeast. Upon ER stress IRE1 dimerizes and autophosphorylates its cytosolic portion, leading to the activation of an endonuclease domain. Plant IRE1 produces alternative splicing of the mRNA encoding the transmembrane transcription factor bZIP60, leading to the synthesis of a form without the transmembrane domain. This form reaches the nucleus where it upregulates the transcription of target genes. In mammalian and yeast cells, IRE1 instead splices the otherwise inactive mRNAs encoding the transcription factors XBP1 and HAC1, respectively. Besides this, active IRE1 also promotes degradation of specific mRNAs.*

Transcriptome analysis of *Arabidopsis* plants treated with folding inhibitors (e.g., tunicamycin) shows that virtually all ER folding helpers described in Section 4.6.5, many proteins of the secretory traffic machinery, subunits of the ER translocation channel and of protein degradation machineries, as well as certain transcription factors are all upregulated. Downregulated genes encode almost exclusively secretory proteins, mostly of the cell wall. This is consistent with the model in which UPR increases the synthesis of folding helpers and the machinery for the degradation of misfolded polypeptides, and lowers the workload of the ER by attenuating the synthesis of cargo secretory proteins and at the same time stimulating protein traffic.

A further level of ER sensing mechanism has been discovered by studying changes occurring during plant pathogen attack (the major pathogen-induced proteins are secreted or vacuolar hydrolases). It was found that transcriptional induction of BiP precedes that of the hydrolases, instead of following it, as would be expected by the general UPR model. Thus the ER appears to "prepare" itself for the increased load instead of responding to it. It was then determined that the promoters of many plant genes induced as part of the UPR have an additional *cis*-acting regulatory sequence that allows upregulation by NPR1, a master regulator of systemic acquired resistance, through the action of a novel transcription factor.

It should also be noted that, compared to mammals, plants have a higher copy number of certain ER folding helpers, which may reflect specialized functions. BiP is encoded by a single gene in the vertebrates that have been analyzed, but it is the product of multigene families in many plants. Out of the three BiP genes of *Arabidopsis*, BiP1 and 2 are constitutively expressed at high levels and induced to a limited extent upon UPR, whereas BiP3 is present at extremely low levels in normal conditions and is induced 40–50 times upon UPR. Besides canonical calreticulin (two proteins in *Arabidopsis*, CRT1 and CRT2), an additional isoform (CRT3) has been identified in plants. *Arabidopsis* CRT3 has a specific role in the synthesis of plasma membrane kinase-like receptors such as the brassinosteroid receptor BRI1 and the elf18-responsive EF-Tu receptor (EFR), which is involved in plant innate immunity. CRT3 has an unusual C-terminal domain and cannot be substituted by CRT1 or CRT2 in these functions.

4.7 Protein traffic and sorting in the secretory pathway: the ER

4.7.1 Vesicle budding and fusion is mediated by SNAREs and GTPases

Vesicle traffic occurs between many different compartments and it is therefore necessary for the vesicle and the target membrane to be appropriately identified. Vesicle budding is driven by the recruitment of cytosolic proteins that will form multimeric protein complexes, thus "coating" the vesicle. The different coats recognize the cytosolic tails of transmembrane proteins that will be incorporated into that specific vesicle. Four types of coats have been identified to date (see Fig. 4.10). (1) COP I (coat protein I) vesicles form at the Golgi apparatus and mediate retrograde traffic from the *cis*-Golgi to the ER (COP Ia-type vesicles) and between Golgi cisternae (COP Ib-type vesicles; see also Fig. 1.25A). (2) COP II (coat protein II) vesicles play the opposite role: they form at the ER and promote anterograde traffic to the Golgi apparatus. (3) Clathrin-coated vesicles (CCVs) mediate traffic from the late TGN (or free TGN) to MVBs and from the plasma membrane to the TGN and to MVBs (see also Fig. 1.36). Because MVBs serve as intermediate compartments between the TGN and vacuoles, some researchers also refer to them as prevacuolar compartments. Here, as in Chapter 1, we will use the term MVB. CCVs therefore mediate anterograde biosynthetic traffic to vacuoles as well as endocytotic traffic from the cell surface to the cell interior. Both types of vesicles share a common clathrin cage, but their coat contains different adaptor proteins that specifically link to clathrin the cytosolic tails of receptors that function in the different pathways (see Section 4.8.2). Although the term "adaptor protein" is used mainly in the case of CCVs, polypeptides with similar functions are part of the other type of coated vesicles. (4) Retromer-coated vesicles mediate the recycling of receptors from MVBs to the TGN. Other types of vesicles certainly exist, but their coats are yet to be identified. Recruitment of COP I, COP II, and clathrin, but not of the retromer, requires specific GTPases, which are part of the complexes. Before fusion to the target compartment, vesicles are uncoated by GTPase or ATPase activities. Assembly of the vesicle coat, budding of the vesicle, uncoating and subsequent fusion are shown in Fig. 4.19A–D. The discovery that the fungal metabolite brefeldin A inhibits specific coat recruitments has provided an important tool to study protein traffic along the secretory pathway (Box 4.5).

Proper identification and fusion to the target compartments is achieved through the interaction of vesicle proteins that include SNARE proteins (soluble *N*-ethylmaleimide-sensitive factor attachment protein receptor). SNAREs that occur on transport vesicles are called v-SNAREs, whereas t-SNARES are present on the targets with which the vesicles will fuse. In plants, t-SNAREs are also called syntaxins or SYPs; SYP stands for "syntaxin of plants". Plants have a complex secretory system and a large number of SNARE genes: 21–26 SNARE genes have been identified in yeast (the range is because some assignments are uncertain), 20 in *Drosophila*, 35–36 in humans, 60–69 in *Arabidopsis*, and 57–80 in rice (*Oryza sativa*). Some *Arabidopsis* T-DNA insertion mutations in SNARE genes have no obvious phenotype, suggesting genetic redundancy, whereas other insertions are embryo or gametophyte lethal even though they belong to small families with extensive sequence identity. Therefore, new and creative approaches are required to address the specific function of these SNAREs (Box 4.6).

SNAREs, which can vary considerably in size and structure, are sufficient for artificial vesicle fusion in vitro and

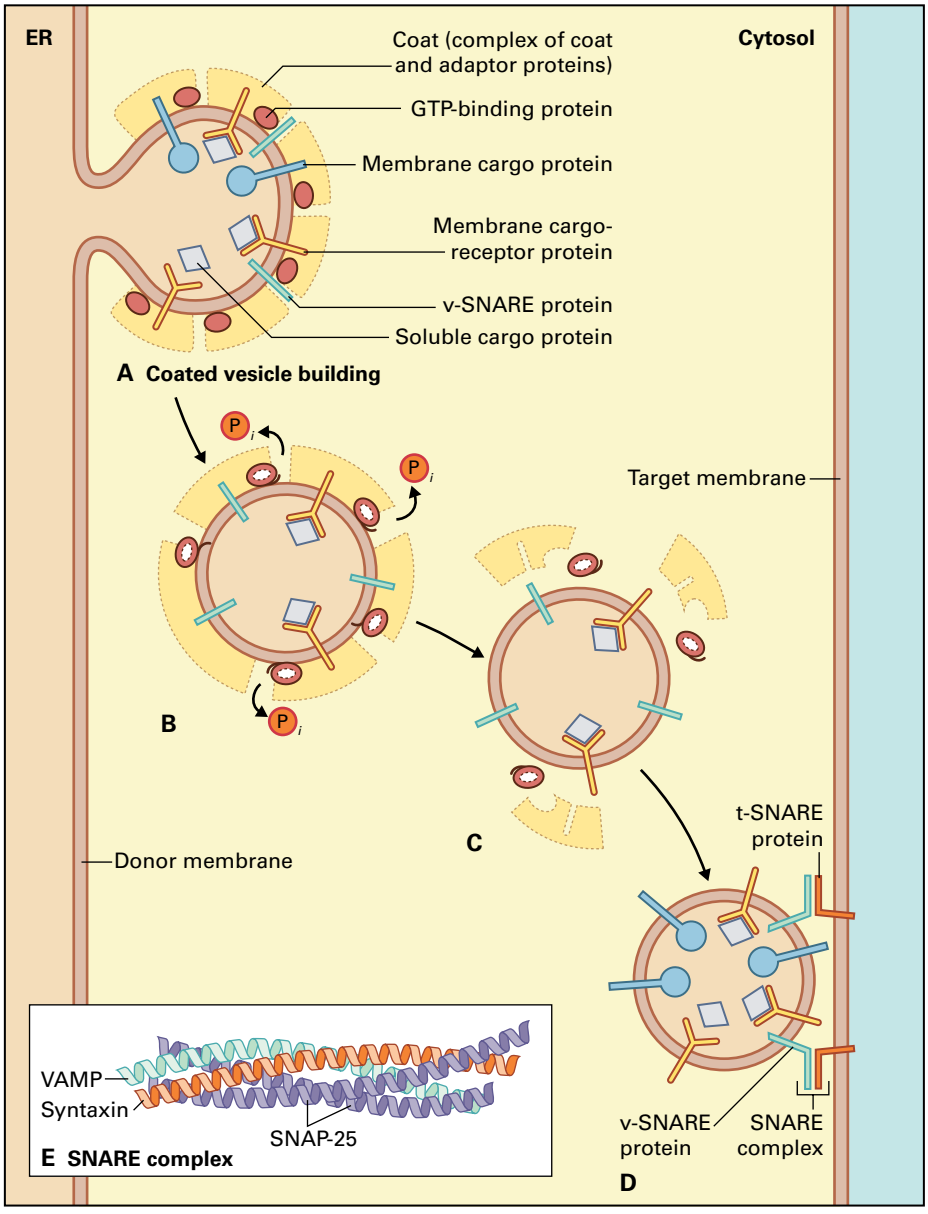


FIGURE 4.19 *Vesicle budding and fusion with a target membrane. (A) Vesicle budding starts with the recruitment of a small GTP-binding protein to a patch of the donor membrane. Complexes of coat proteins that are in the cytosol then bind to the cytosolic domains of receptors that are complexed with cargo proteins on the inside of the vesicle or to transmembrane proteins that may also be cargo. (B) Once the vesicle has pinched off, the GTPase activity of the GTP binding protein causes GTP hydrolysis and Pi release. (C) This results in uncoating of the vesicle. (D) Vesicle fusion occurs when the v-SNAREs encounter the right t-SNAREs on the target membrane so that they can form the four-helix bundles that involve the two SNAREs and another protein called α-SNAP. (E) Four-helix bundle of α-SNAP and SNAREs.*
Source: Lodish et al. (2013). Molecular Cell Biology, 7th edition. W.H. Freeman.

necessary for this process in vivo, but in cells they act in combination with other proteins to allow accurate and efficient recognition and fusion between vesicles and their target membranes. Among these proteins are Rab proteins, which constitute a large family of Ras-related GTPases. The GTP-bound form of a given Rab is recruited from the cytosol to its specific vesicle and interacts with effectors on the target membrane, probably acting as a tethering factor before SNAREs interact and promote actual fusion.

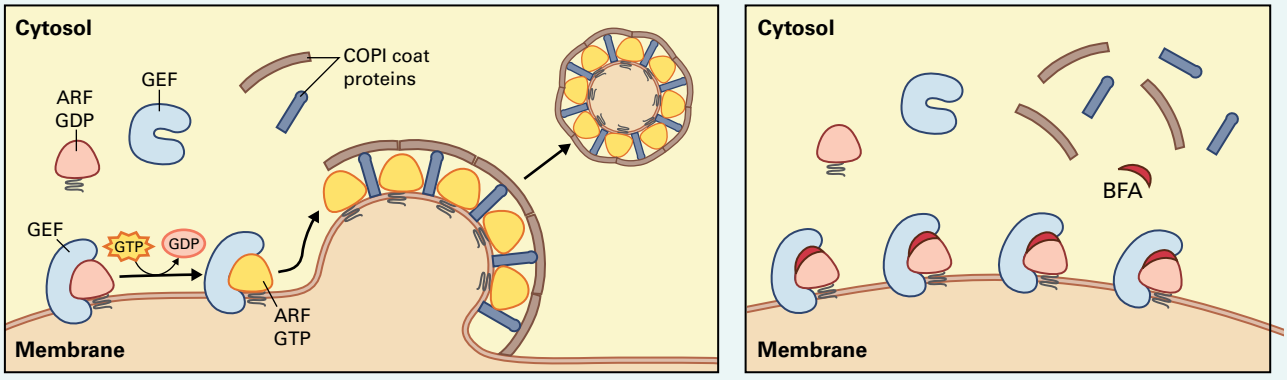
Most SNAREs are tail-anchored proteins, and they all share a coiled coil domain of 60–70 amino acids in their cytoplasmic portion that allows SNAREs to assemble in four-helix bundles called *trans*-SNARE complexes (Fig. 4.19E). One helix comes from a v-SNARE, one from its cognate t-SNARE, and two from a protein called α-SNAP that is tethered to the target membrane by a lipid anchor. These complexes are instrumental in facilitating the fusion of the vesicle membrane with its target membrane. The membrane fusion event allows the deposition of the vesicle contents into the target compartment. Once delivery is complete, the complex is dissociated. Dissociation of the four-helical bundle requires soluble NSF (*N*-ethylmaleimide sensitive factor). After the

BOX 4.5

Vesicle cycling and brefeldin A action

Brefeldin A (BFA) is a small fungal metabolite that has been a valuable tool to study vesicle trafficking because it blocks vesicle traffic from the ER to the Golgi. The molecular target of BFA is a Sec7-type GTP exchange factor (GDP/GTP exchange factor (GEF) for small G proteins of the ARF class; ARF-GEF) that catalyzes the activation of the GTPase ARF. Activated ARFs recruit COP I coat proteins and form transport vesicles. BFA traps the ARF*GDP/GEF complex on membranes, preventing GDP/GTP exchange, vesicle coat recruitment and vesicle formation. A major effect of BFA is the re-distribution of Golgi membranes and enzymes to the ER causing the formation of a BFA compartment that contains both ER and Golgi proteins. Thus, if the traffic of a given protein is inhibited by BFA or an unstable protein is stabilized by this drug, this is taken as an indication that the protein of interest normally travels through the Golgi apparatus. However, there are differences in the BFA response between mammalian and plant cells. In mammalian cells, the loss of COP I coats causes the formation of membrane tubules that eventually fuse with ER. By contrast, in plant cells, BFA treatment does not cause tubulation of the Golgi. The Golgi stacks initially retain their morphology except for the *cis*-cisternae. The remaining cisternae fuse with the ER to form hybrid stacks, or fuse with other Golgi to form oversized Golgi complexes that are continuous with the ER. Incorrect sorting in the TGN caused by BFA also gives rise to altered secretory vesicles that become trapped in aggregates known as Golgi bodies. Within a given cell there are multiple ARF-GEFs implicated in different trafficking steps. Eight genes have been identified in *Arabidopsis*. Not all of them are BFA-sensitive and the function of all of them is not known, but BFA also affects the ARF-GEF protein GNOM, which is localized in early endosomes (late or free TGN), thus preventing auxin efflux carrier proteins, the PIN proteins, from cycling between the plasma membrane and early endosomes.

Source: Anders & Jürgens. (2008). Cell Mol Life Sci 65:3433–3445.



A Coat recruitment

B BFA effect

BOX 4.6

Functional analysis of two homologous SNAREs

A clever genetic approach was used to study the cellular machinery that recognizes C-terminal vacuolar sorting signal (ctVSS). Seeds of transgenic plants that expressed a chimeric construct with an added ctVSS were mutagenized and the plants were examined for evidence that the protein had been secreted. The construct, called *VAC2*, encoded the clavata3 (CLV3) protein fused with a functional ctVSS at its carboxyl terminus. Wild-type CLV3 is a secreted protein that negatively regulates the proliferation of the shoot apical meristem by binding and activating the plasma membrane CLV1/2 LRR kinase receptor. Because VAC2 is sorted to the vacuole it cannot act on the CLV3 receptor on the plasma membrane and transgenic plants that express VAC2 have a normal phenotype. Mutations in the machinery that recognizes ctVSS may cause VAC2 to be secreted and the excess of CLV3 activity at the cell surface will reduce the size of the meristem. Such a phenotype can be readily identified by visual inspection of the plants.

Using this genetic assay the function of two conditionally redundant v-SNAREs, VTI11, and VTI12 that are 60% identical were identified. They localized at the TGN with a specific group of t-SNAREs, SYPs. However, analysis of both mutants showed that VTI11 and VTI12 can substitute for each other in their respective SNARE complexes. Interestingly, a double mutant cross between *vit11* and *vit12* is embryo lethal. By crossing plants expressing VAC2 with *vti11* and *viti12*, it was shown that trafficking of VAC2 (ctVSS) required the SNARE VTI12 but not VTI11.

Source: Adachi et al. (2003). Proc Natl Acad Sci USA 100:7395–7400.

SNARE complex is dissociated by a GTP-requiring process, the v-SNARE is recycled back to its original compartment.

4.7.2 Soluble proteins do not need sorting signals to travel from the ER lumen and be secreted, but most ER residents have signals that promote their recycling from the Golgi complex back into the ER

Soluble proteins that have been released into the lumen of the ER but have no other targeting or retention signals, are packaged at ER export sites, traffic through the Golgi apparatus and are eventually secreted. When plants or plant cells are transformed with transgenes that encode chimeric proteins consisting of a signal peptide from any secretory protein and a cytosolic or bacterial polypeptide that is not ordinarily secreted, the resulting protein enters the ER, and if it is not misfolded, it is secreted (see Box 4.1). For this reason, the pathway leading to secretion from the cell is often called the **default pathway**, and this holds true for any eukaryotic cell.

Some membrane proteins, on the other hand, appear to have motifs that promote their traffic to the Golgi. Investigation on a number of integral membrane proteins has identified di-acidic (such as DXE), dibasic ([RK]X[RK]), or dihydrophobic (YF) motifs that are present on their cytosolic tails, and when these motifs are mutated, the proteins remain in the ER. These sequences interact with components of the COP II complex, and it has been directly shown that increased synthesis of integral membrane cargo results in increased number of ER export sites, an effect that has not been obtained by overexpression of soluble secretory proteins. This suggests that default traffic of soluble proteins may take advantage of the traffic of certain membrane proteins.

If secretion is a default pathway for soluble proteins that enter the ER, it follows that retention in the ER needs signals. Most ER-resident proteins actually enter COP II-mediated anterograde traffic along the secretory pathway, but when they reach the Golgi apparatus they are retrieved to the ER by COP Ia-mediated retrograde traffic. For many soluble ER residents, retrieval occurs because they have a carboxyl-terminal tetrapeptide, in most cases HDEL or KDEL, recognized by the integral membrane receptor ERD2p, which shuttles between the Golgi apparatus and the ER. Affinity of ERD2p for the tetrapeptide is low at pH close to neutrality and higher at the slightly acidic pH of the Golgi apparatus, thus providing a mechanism for efficient retrieval of ER residents (Fig. 4.20). It should be kept in mind that in hetero-oligomeric proteins of the ER it is sufficient that the signal be present on just one subunit. Thus, polypeptides that do not have the tetrapeptide can also use this retrieval mechanism. Experimentally adding a KDEL or HDEL tail to proteins that ordinarily are secreted usually causes their efficient retention in the ER. This technique has been exploited to increase protein accumulation in transgenic plants avoiding possible degradation of the recombinant protein by acidic proteases present in the apoplast and vacuole, or by the proteasome if synthesis occurs in the cytosol. Conversely, removing HDEL from an ER resident such as calreticulin allows its secretion at a rate similar to that of naturally secreted proteins.

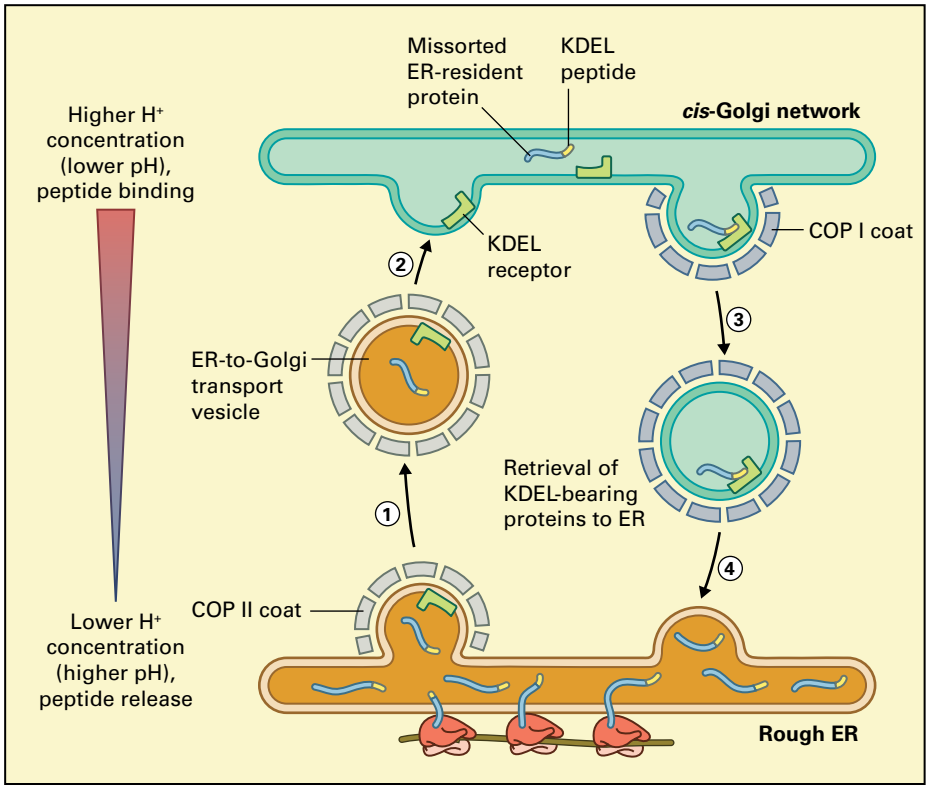


FIGURE 4.20 *The KDEL retention signal is recognized by the KDEL receptor ERD2p.Many ER residents are present at high concentrations and may passively diffuse into COP II vesicles that travel to the Golgi. They will be retrieved from the Golgi by COP Ia vesicles because at the lower pH of the Golgi, there is greater binding between the KDEL sequence and the ERD2p receptor. ERD2p cycles back to the ER because it has an ER retrieval motif recognized by COP Ia. At the pH of the ER the receptor releases its ligand.*
Source: Lodish et al. (2013). Molecular Cell Biology, 7th edition. W.H. Freeman.

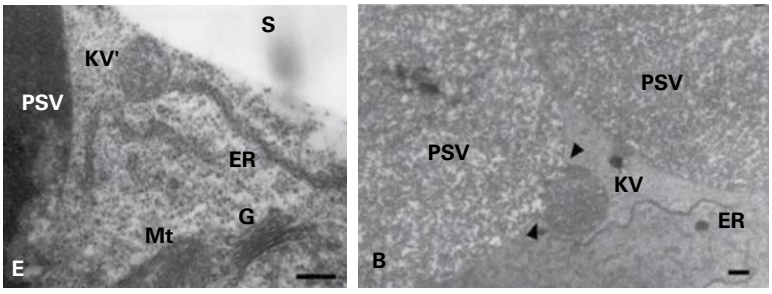


FIGURE 4.21 *Electron micrographs of cotyledon cells of germinating* Vigna mungo. *(A) An ER-derived vesicle (KV) loaded with the SH-EP protease. (B) A vesicle fusing with the protein storage vacuoles (PSV) where the protease is activated and then participates in storage protein hydrolysis. G, Golgi apparatus; Mt, mitochondrion; S, starch granule. Notice that these vesicles are much larger than the common traffic vesicles, such as COP I, II or clathrin coated vesicles. Bars: 200 nm.*
Source: Toyooka et al. (2000). J. Cell Biology 148:453–464.

How are integral membrane proteins of the ER retrieved? Many of them have two positively charged amino acids at positions −3 and −4 from the end of their cytosolic tail. The motif is KK if the tail is constituted by the C-terminus of the polypeptide and RR if it is the N-terminus. These motifs allow direct interactions with the COP Ia complex.

Not all ER residents use retrieval mechanisms. Some of them are retained without ever entering traffic to the Golgi. The mechanisms are not clear but the length of transmembrane domains may play a role. The membrane bilayer changes in lipid composition as it moves from one compartment to the next of the secretory pathway. Bilayers more distant from the ER are thicker. Proteins with short transmembrane domains (17 amino acids or fewer) have difficulty proceeding in forward traffic, simply because of mechanical constraints: the next membrane is too thick for them. By changing the length of the single transmembrane domain of a model chimeric type I protein it was found that a hydrophobic sequence of 20 amino acids allows anterograde traffic but the protein remains in the Golgi, and 23 amino acids allow progression to the plasma membrane.

4.7.3 Plant proteins with the KDEL signal can also be delivered to the cell surface or to vacuoles

Some plant proteins have a KDEL motif but function in a compartment different from the ER, thus having apparently the "wrong" localization signal. The first such protein to be discovered was the 22-kDa auxin-binding protein 1 (ABP1), located mainly in the ER. However, a minor proportion of ABP1 molecules are always present at the cell surface, where they positively regulate clathrin-mediated endocytosis of the PIN auxin efflux facilitators. Binding of auxin to ABP1 blocks this activity and inhibits PIN endocytosis. This led to the idea that, when necessary, the cell may be able to allow or regulate the secretion of ER residents. A conformational change in the protein could alter the way the KDEL tail is displayed and inhibit its interaction with the KDEL receptor, ERD2p.

The vacuolar cysteine proteases (they have a key cysteine residue in their active site) of the sulfhydryl-endopeptidase class, called SH-EP, have a transient KDEL signal. During seed germination, these proteases have a role in the hydrolysis of storage proteins and in cell death. Like many other proteolytic enzymes, SH-EPs are activated by post-translational removal of propeptides. In this case activation includes removal of the C-terminal propeptide that carries KDEL. SH-EP first accumulates in the ER as large accretions easily detectable with the electron microscope in enlarged ER cisternae and is subsequently delivered to the vacuole (Fig. 4.21). Deletion of the KDEL sequence by genetic engineering causes the enzyme to be secreted, indicating that, perhaps surprisingly, the ER retention motif is necessary for its correct sorting to the vacuole. Thus, in this case the KDEL signal functions as a mechanism to allow first high accumulation in the ER and then rapid, massive vacuolar delivery and activation.

4.7.4 In cereal endosperm cells, certain plant storage proteins assemble into large insoluble polymers that form protein bodies

The widespread globulin seed storage proteins of the 7S and 11S classes, as well as the less common 2S albumins (Box 4.7) traffic from the ER along the secretory pathway to vacuoles specialized for the high accumulation of proteins termed protein storage vacuoles, PSV (see also Section 1.7.3). In contrast, storage proteins of the prolamin class typical of cereals, form very large electron-dense, round-shaped, insoluble accretions with diameters of 0.5–2.0 mm within the ER lumen. These structures, which are in essence huge polymers, can be delivered to storage vacuoles by autophagy-like processes that bypass the Golgi apparatus or they are permanently stored in the ER-derived protein bodies (PB), formed when the ER membrane surrounding the aggregate pinches off from a cisterna (Fig. 4.22). Accumulation in PBs is particularly evident in maize, sorghum (*Sorghum bicolor*), millet

BOX 4.7 Seed storage proteins have unusual structures and accumulate in storage vacuoles or ER-derived protein bodies

Most plant seeds contain abundant storage proteins that constitute the major source of protein for human food and animal feed. Seed storage proteins are unique to plants and can be divided into four classes: 7S, 11S, 2S (named after their sedimentation coefficient expressed in Svedberg units), and prolamins. Each class usually includes polypeptides produced by a family of very similar genes. Their synthesis, transport and accumulation involve the different compartments of the secretory system. 7S, 11S, and 2S storage proteins accumulate in protein storage vacuoles (PSVs), whereas prolamins form protein bodies (PB) directly from the ER. Seed storage proteins evolved for the purpose of storing reduced nitrogen to be used in the first stages of seed germination. Seed PSVs also contain other abundant secretory proteins for plant defense such as lectins, enzyme inhibitors and ribosome inactivating proteins. For example, seeds of the common bean (*P. vulgaris*) contain ≈5% phytohemagglutinin, a lectin that is toxic to mammals and birds, and 1% α-amylase inhibitor, a protein that inhibits the α-amylases of mammals and insects.

The most common storage proteins are the salt-soluble 7S and 11S globulins, present in seeds of probably all plants although in different relative proportions. Both the **7S and 11S globulins** are synthesized as soluble polypeptides that form trimers in the ER and then proceed to PSVs via the Golgi and MVBs. In MVBs and PSVs, the polypeptides of the 11S class undergo a single event of proteolytic processing that forms subunits of 40 and 20 kDa. The two new subunits remain linked by a disulfide bond, and the proteolytic event exposes new hydrophobic residues that interact leading to the dimerization of the original trimers. Despite the low primary sequence similarity, 7S and 11S proteins have very similar secondary and tertiary structures, and the trimers that they form are nearly identical: compare the structure of the soybean (*Glycine max*) 11S trimer shown here with that of the phaseolin (the 7S storage protein of *P. vulgaris*) trimer shown in Fig. 4.16. The basic unit is repeated twice in a symmetrical fashion in each folded polypeptide and is comprised of a β-barrel and three α-helical segments. The latter are fundamental for trimer assembly. The β-barrel is unusual: it is termed "double-stranded β-helix" or "jelly-roll" barrel-like structure and is a hallmark of the large cupin superfamily of proteins. The cupin domain is considered by evolutionists to be an ancient protein-folding unit, having originated in prokaryotic ancestors and now present in all organisms with many diverse functions. The cupin domain is possibly the most compact existing form of polypeptide folding and is very resistant to heat and proteolysis, features that are probably important in storage proteins. It is also a major plant allergen.

2S storage proteins, particularly abundant in certain oilseeds such as oilseed rape (*Brassica napus*), are structurally unrelated to the 7S and 11S proteins. They traffic as monomers along the secretory pathway to PSVs. Post-translational proteolysis that starts in MVBs can remove an N-terminal propeptide or an internal propeptide, or both, depending on the species. The major feature of 2S albumins is the presence of four conserved disulfide bonds, two of which link the two subunits originating from internal proteolytic processing. Unlike the 7S and 11S globulins, this protein class has a remarkably high methionine content, a feature that has attracted the interest of biotechnologists for the improvement of the essential amino acid balance in seeds, until it was discovered that 2S albumins elicit allergic responses in mammals.

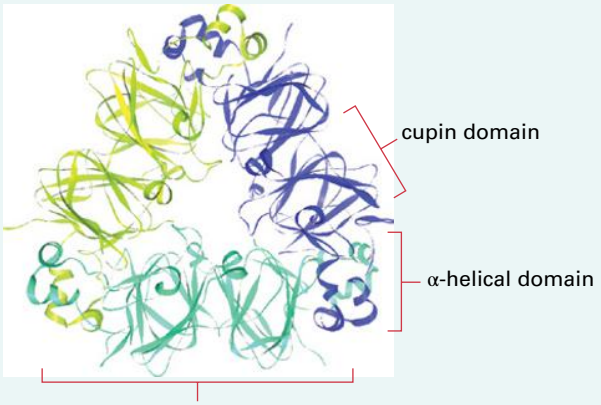
Prolamins are the least common but most diverse group of storage proteins. They are restricted to grasses and have been intensely investigated because they are the major seed proteins in wheat, maize, barley, sorghum and rye. They have the common feature of being soluble only in solutions containing more than 50% alcohol or upon reduction of their inter-chain disulfide bonds. The major prolamins in cereals of the Triticeae tribe (wheat, barley, and rye) can be divided into sulfur-rich, sulfur-poor, and high molecular weight proteins. The last have inter- and intra-chain disulfide bonds that lead to the formation of large polymers, whereas sulfur-rich prolamins have only intra-chain bonds. The sulfur-rich and high molecular weight prolamins have evolved by the attachment of a repeated sequence to a 2S albumin. The repeats are usually motifs of about six to eight amino acids, with a high content of proline or glutamine (hence the name prolamins), that occur several times in succession or are more dispersed within less conserved sequences. The sulfur-poor prolamins lack the 2S albumin domain. Glutenins, the high molecular weight prolamins of wheat, are responsible for the elastic properties of dough, and therefore for the bread-making performance of wheat flour. Inflammatory responses to gliadins, the sulfur-rich prolamins of wheat, and glutenin are the molecular basis of coeliac disease.

In wheat and sorgum, the prolamin types described above are less abundant and the major prolamins have evolved more recently, although they also contain repeats and polymerize thanks to disulfide bonds.

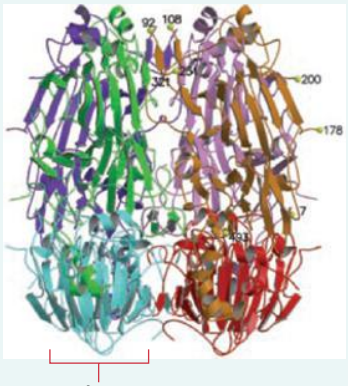
High molecular weight prolamins form large polymers that most probably constitute the fundamental core of a PB, to which other prolamins then associate. The protein

body is then essentially an extremely large heteropolymer that forms within the ER and is unable to enter vesicle-mediate traffic along the secretory pathway. In certain plant species, such as maize, PBs remain as isolated structures, whereas in others, such as wheat, they can end up in PSVs, probably through autophagy.

Trimer of glycinin, the 11S globulin from soybean (*Glycine max*)



Glycinin hexamer, rotated 90° about the vertical axis with respect to the trimer image



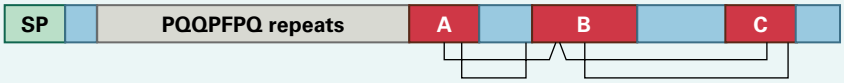
2S albumin from sunflower (*Helianthus annuus*)



SFA8: 2S albumin from sunflower (*Helianthus annuus*)



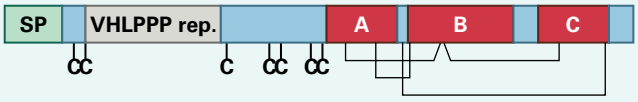
γ-gliadin: S-rich prolamin from wheat (*Triticum aestivum*)



C hordein: S-poor prolamin from barley (*Hordeum vulgare*)



27 kDa γ-zein: high molecular weight prolamin from maize (*Zea mays*)



SP signal peptide — propeptide — 2S albumin domain — repeated domain

conserved intrachain disulfide bonds — additional cysteine residues

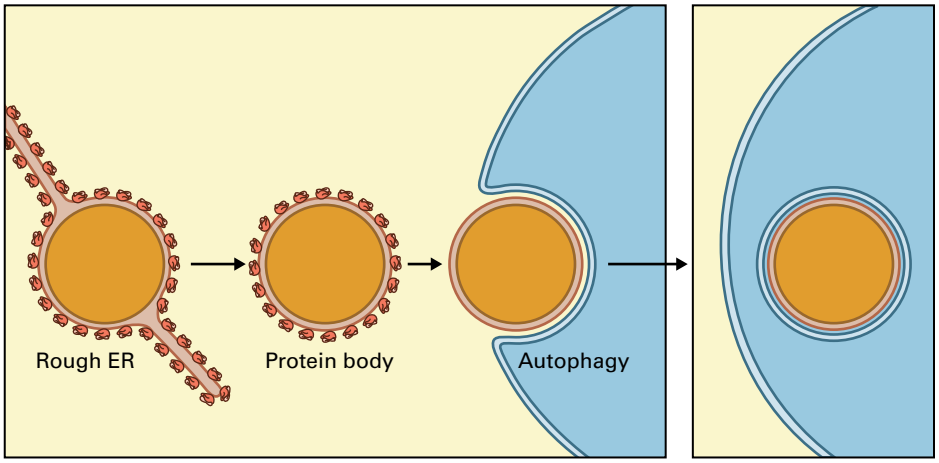


FIGURE 4.22 *Illustration of the formation of protein bodies and the transfer of protein bodies into vacuoles by autophagy. In some cereals, such as maize, protein bodies remain in the cytosol, surrounded by ribosomes. In other cereals, such as wheat, they undergo autophagy and end up in PSVs.*

and rice. Prolamins do not have transmembrane domains or KDEL-like signals. These proteins are unique to plants, and their polymerization and accumulation pose a number of interesting questions. Prolamins are the product of a number of gene families (see Box 4.6). They are in most cases insoluble in aqueous buffers and need either more than 50% alcohol or reducing agents to be solubilized. Apart from these characteristics, prolamins are far from being a homogeneous class of proteins in terms of sequence. How are PBs formed? The following features have been established:

- An individual PB is formed by the ordered assembly and accumulation of many different prolamin subunits. Some subunits are monomeric when expressed alone whereas others form homopolymers, often because of the formation of interchain disulfide bonds. An example of the former is wheat (*Triticum aestivum*) γ-gliadin, whereas maize γ-zein and wheat high molecular weight glutenin are polymeric (see Box 4.6).
- Unusually extensive interactions with chaperones like BiP occur during prolamin synthesis, suggesting prolonged exposure of hydrophobic sequences. Additional helpers are being discovered by analyzing cereal mutations: the distribution of the abundant 22-kDa α-zeins within maize PBs is altered when the *floury 1* gene, encoding a transmembrane protein of the ER, is mutated.
- Some prolamin subunits are able to form PBs with high efficiency when ectopically expressed in vegetative tissues of transgenic plants. This implies that PB formation does not require any tissue- or cereal seed-specific machinery apart from the prolamins themselves. Assembly into an insoluble polymer is sufficient to avoid entering protein trafficking from the ER to the Golgi apparatus.

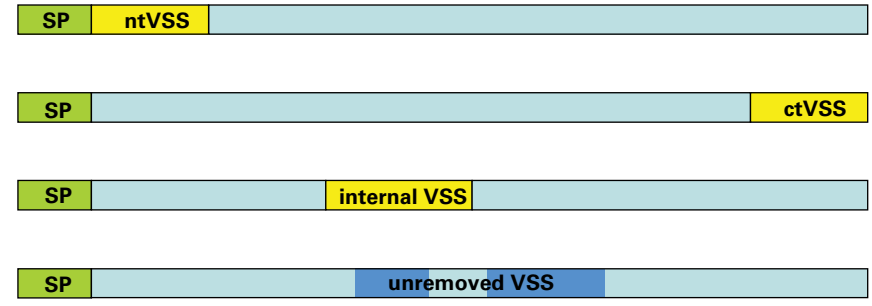
Electron-dense, insoluble accretions within the ER are also formed in mammalian cells in pathological conditions, when the ER quality control system is unable to rapidly dispose of defective proteins, but the developmentally regulated use of the ER to accumulate protein permanently as storage material, or temporarily for rapid mass delivery to vacuoles, is unique to plants.

4.8 Protein traffic and sorting in the secretory pathway: the Golgi apparatus and beyond

4.8.1 Targeting proteins to the vacuole depends on short vacuolar sorting signals

Plant cells have different types of vacuoles: lytic vacuoles that function in breakdown processes have an acidic pH and contain numerous hydrolases, whereas PSVs have a neutral pH and are especially prominent in cell types specialized for protein storage (see Chapter 1). The importance of the vacuole is shown by the observation that mutants in vacuolar biogenesis are embryo lethal. As discussed above, in certain cases, vacuolar delivery does not involve the Golgi apparatus, but most vacuolar proteins traffic though this compartment and are sorted at the TGN to MVBs and then finally they reach the vacuole.

Delivery of soluble proteins to the vacuole requires specific **vacuolar sorting signals** (VSSs) as well as targeting machinery. There are many similarities between plants and yeast with respect to vacuolar targeting, but plant VSSs do not function properly in yeast. In most cases VSSs are short stretches of amino acids that constitute, or are part of propeptides (Fig. 4.23). Propeptides are defined as peptides that are removed by proteolytic enzymes in MVBs or vacuoles as part of the protein maturation process. Propeptides can be either at the carboxyl terminus, at the amino terminus immediately following the signal peptide, or internal. These terminal propeptides carrying vacuolar sorting information are known as N-terminal (ntVSSs) and C-terminal VSSs (ctVSSs). In the



A

ntVSS	
Sweet potato sporamin	HSRFNPIRLPTTHEPA
Barley aleurain	SSSSFADSNPIRPVTDRAASTLE

ctVSS	
Barley lectin	VFAEAIAANSTLVAE
Tobacco chitinase	GLLVDTM
Brazil nut 2S albumin	IAFG
Common bean phaseolin	AFVY

Internal VSS	
Castor bean 2S albumin	STGEEVLRMPGDEN
Castor bean ricin	SLLIRPVVPNFN

B

FIGURE 4.23 *Vacuolar sorting signals. (A) Location of signals along the polypeptide. Green and yellow portions are absent from the mature protein. A signal peptide (SP, green) is present on any soluble secretory protein irrespective of the final location and is removed co-translationally; therefore it does not have a role in vacuolar sorting. Yellow boxes indicate propeptides, which are removed post-translationally upon vacuolar delivery and can contain a N-terminal VSS (ntVSS), C-terminal VSS (ctVSS), or internal VSS. The blue box indicates an unremoved VSS, which will be exposed on the surface of the folded protein and can be constituted by different portions of the polypeptide. (B) Examples of propeptides that contain or constitute VSSs. The loosely conserved motif of sequence specific VSS is shown in blue. The isoleucine (I) or leucine (L) residue that has been shown to be fundamental is in red.*

case of internal propeptides, after their removal the two remaining portions of the mature vacuolar protein remain often linked by a disulfide bond that had formed in the ER, as for example in the 2S storage albumins, or in ricin, the two-chain ribosomal inactivating protein of castor bean (*Ricinus communis*). Finally, VSSs exist that are located in surface loops of undetermined size and remain as part of the mature protein. Propeptides that contain VSSs are both necessary and sufficient for vacuolar targeting. If a gene construct is introduced into a plant cell and the VSS is absent from the coding sequence, the resulting protein is secreted. Conversely, a ctVSS, ntVSS, or internal VSS added to a nonvacuolar soluble secretory protein is sufficient to direct that protein to the vacuole, and this often occurs irrespective of the position in which the VSS is placed in the chimeric protein. These properties have not been demonstrated for the surface loops that appear to function as VSSs in proteins that lack propeptide-located VSSs.

Irrespective of their position in the polypeptide, a number of VSSs present in propeptides share a loose motif in which one isoleucine (Ile) or leucine (Leu) is fundamental: point mutations in Ile or Leu lead to loss of function of the signal and secretion of the protein. These signals are collectively termed sequence-specific VSS (ssVSS). Several VSSs however do not have this motif. Extensive site-directed mutagenesis of these other sequences, which are usually ctVSS, has shown that enrichment in hydrophobic amino acids is important, but no apparent consensus can be identified. Because these studies indicate that ctVSSs interact with components of the vacuolar sorting machinery, the sorting machinery presumably recognizes some structural feature or features of the ctVSS.

4.8.2 Vacuolar sorting receptors deliver cargo to the vacuole

Proteins that are transported to plant and yeast vacuoles or animal lysosomes are sorted from secreted proteins by transmembrane receptors that direct them to the appropriate forming vesicles (Fig. 4.24). These receptors bind specifically to the peptide domains (or glycans, in mammalian lysosomal

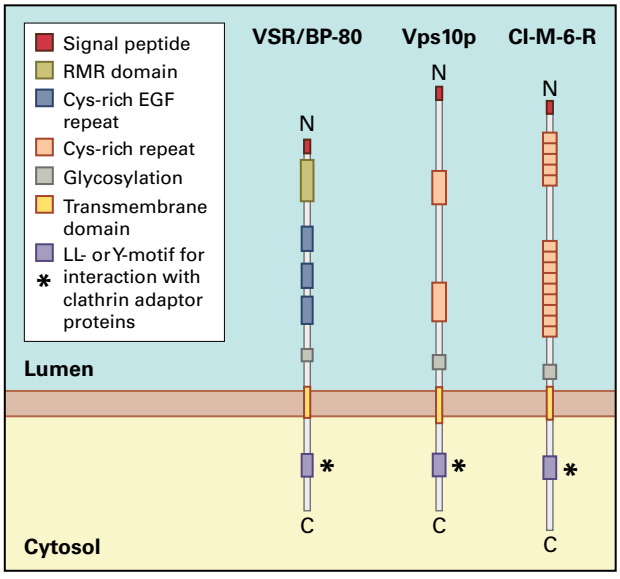


FIGURE 4.24 *Vacuolar and lysosomal sorting receptors. The structures of the plant vacuolar signal receptor VSR/BP80, the yeast vacuolar signal receptor Vps10 and the mammalian lysosomal cation-independent mannose-6-phosphate receptor (CI-M-6-R) are shown.*

hydrolases) that function as sorting signals. These receptors cycle continuously and move with their cargo in clathrin-coated vesicles from the TGN to MVBs and are returned empty in retromer vesicles. The different VSSs on plant vacuolar proteins are recognized by plant vacuolar sorting receptors (VSRs).

Like many integral membrane proteins of vacuoles or lysosomes, the sorting receptors for plant and yeast vacuoles or animal lysosomes contain in their cytosolic domains di-leucine (LL) or tyrosine-based (in most cases NPXY or YXXØ, where Ø represents a hydrophobic amino acid) motifs recognized by adaptor proteins of clathrin-coated vesicles. When these motifs are mutated the receptors are mis-sorted to the plasma membrane. Traffic of these proteins is blocked by brefeldin A, consistent with the fact that they pass through the Golgi apparatus.

The first plant VSR to be identified was purified from developing pea (*Pisum sativum*) cotyledons and shown to bind on an affinity column to immobilized ntVSS but not to ctVSS peptides. Most likely this VSR mediates the sorting of a subset of vacuolar proteins. This VSR is a type I transmembrane protein with a long luminal domain followed by a short transmembrane domain and a short cytoplasmic domain (Fig. 4.24). The cytoplasmic domain contains a diacidic motif for export from the ER and has a tyrosine motif that interacts with the clathrin coat adaptor proteins at the TGN. VSRs are encoded by a multi-gene family in pea and *Arabidopsis* (seven genes, not uniformly expressed in all tissues) and have been identified in *P. vulgaris*, *Cucurbita* sp., wheat and rice. Despite sharing high amino acid identity, VSRs have been implicated in different types of vacuolar transport pathways. In vitro binding studies indicate that receptors of the VSR class directly bind ssVSS, but their ability to recognize other VSSs is unclear. VSR homologs recycle between the Golgi apparatus and MVBs, where they are enriched at steady state, and are also found in highly purified preparations of clathrin-coated vesicles: these locations are expected based on the above described general mechanism of action of vacuolar receptors. Different VSR proteins may be needed for different sets of proteins (e.g., vacuolar hydrolases, lectins or storage proteins) and of course for different VSSs.

4.8.3 Traffic to protein storage vacuoles involves several different mechanisms

In storage parenchyma cells and other cell types in storage roots and in bark parenchyma that store proteins, a particularly large proportion of newly synthesized proteins enters the secretory pathway, to be delivered to PSVs (see Box 4.7). In the cotyledons of developing seeds PSVs appear to arise de novo as the storage parenchyma cells greatly enlarge and accumulate more protein. During this process, the central lytic vacuole eventually disappears.

The post-Golgi transport of storage proteins to PSVs involves electron-dense protein-filled vesicles, which can be readily observed by electron microscopy and have a high density in sucrose gradients (Fig. 4.25). These vesicles, termed dense vesicles (DVs), are then incorporated into MVBs and the storage proteins are finally delivered to the PSVs (Fig. 4.26). DVs do not have a clathrin coat and, surprisingly, they seem to lack any type of coat. This suggests that DVs may not originate by a budding process but rather they may be remnants of Golgi cisternae or TGN after clathrin-coated vesicles and vesicles destined for the cell surface have been released. The VSR cargo receptor is present at low levels in DVs, nevertheless, the abundant storage proteins of the 11S and 2S classes are in part secreted into the cell wall in the *vsr1* mutant of *Arabidopsis*. Furthermore, 2S albumins and ricin, which accumulate in the PSV of castor bean endosperm, have a ssVSS (see Box 4.6). The VSSs of many PSV proteins have been identified suggesting a role for one or more as yet unidentified VSRs.

It appears that the protein in DVs is highly condensed. This aggregation (or polymerization) can be seen by electron microscopy in the *cis-medial* Golgi of developing pea cotyledons (see Fig. 4.25) and *Arabidopsis* embryos and could have an important role in storage protein sorting to vacuoles. It is likely that sorting of a large aggregate or polymer does not require a 1:1 ratio between receptor and cargo molecules. The type I receptor-like protein RMR (abbreviation for receptor homology region transmembrane domain-Ring H2 motif protein) is found within DVs, MVBs and in PSVs, and binds several ctVSS. RMR proteins, encoded by a gene family, may have a role in the condensation of storage proteins and in their sorting, and may act in concert with receptors of the VSR class, which have a region of homology with RMR proteins in their luminal portion (see Fig. 4.24).

mRNA sorting also plays a role in the correct accumulation of storage proteins. Cereal endosperm contains rough ER as well as ER-derived PBs with attached polyribosomes. In rice, these PB contain prolamins, but the same cells also

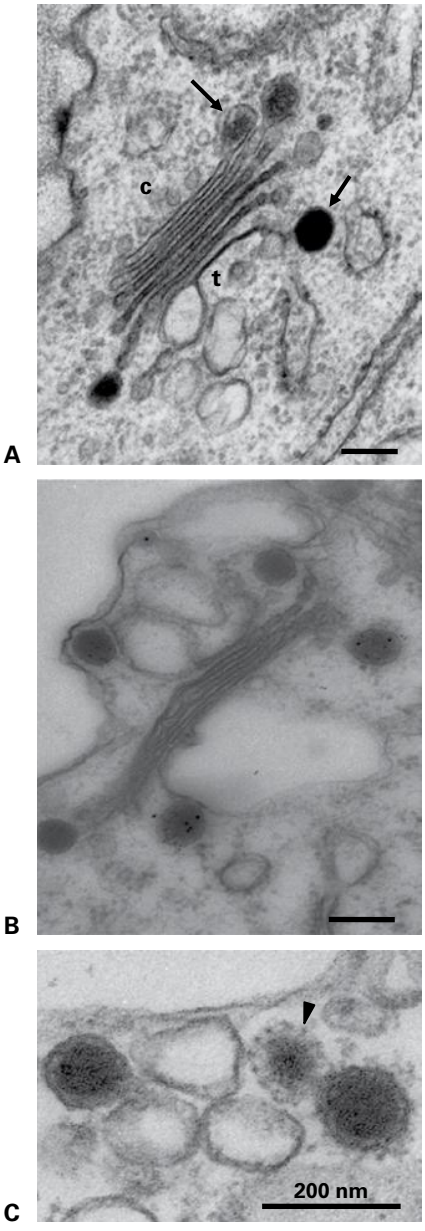


FIGURE 4.25 *Dense vesicles (DVs) in storage parenchyma cells of developing pea (*Pisum sativum *L.) cotyledons. (A) A clear* cis *(c) to* trans *(t) polarity in the cisternal structure of the Golgi apparatus is visible. Newly formed DVs (arrows) are seen attached to the first two* cis*-cisternae. Condensation of storage proteins proceeds as cisternal progression occurs, as indicated by the denser content of DVs. (B) Upon immunogold staining, the DV content is labeled with antibodies against the 7S and 11S seed storage proteins (large and small gold particles). (C) At right, a clathrin-coated vesicle is budding from a DV. The clathrin cage can be easily recognized (arrowhead). Bars: 200 nm. Courtesy of David G. Robinson.*

make glutelins, soluble storage proteins that accumulate in PSVs. Glutelin and prolamin mRNAs are not randomly distributed: prolamin mRNAs are preferentially associated with protein body ER and glutelin mRNAs with cisternal ER. This differential targeting is dictated by the 3′ untranslated regions of the respective mRNAs and is mediated by actin filaments.

4.8.4 Bypassing the Golgi apparatus: alternative pathways to vacuoles and secretion

The vast amount of information we have presented in the previous sections points to the Golgi apparatus as the major crossroad for biosynthetic secretory protein trafficking. However, protein delivery to vacuoles and the cell surface can in certain instances bypass this crossroad and even occur without translocation into the ER. So far the number of proteins known to follow these "alternative" routes is quite limited and therefore the extent of their contribution to total secretion or vacuolar delivery remains to be established. The mechanisms involved in these "alternative" routes are poorly characterized but the common landmark is that, unlike Golgi-mediated trafficking to the vacuole and cell surface, they are not sensitive to brefeldin A. This drug blocks the correct sorting of several tonoplast proteins, except for α-TIP, the tonoplast aquaporin of storage vacuoles. This observation has been the first indication that a plant secretory protein can bypass the Golgi apparatus, and indeed, known motifs for interaction with clathrin adaptor proteins or ER-exit motifs for interaction with COP II are not present in α-TIP.

The transport of soluble storage proteins to the vacuole may also bypass the Golgi (Fig. 4.26). For example, in developing *Cucurbita* sp. cotyledons, large vesicles filled with highly condensed storage protein, termed Precursor ACcumulating (PAC) vesicles appear to be transporting the abundant 2S storage proteins directly from the ER to the PSVs. This mechanism that transports highly condensed protein and bypasses the Golgi has also been demonstrated for the KDEL-containing SH-EP and for prolamins in the endosperm of certain cereals (see Sections 4.7.3 and 4.7.4). Thus, protein interactions can lead to protein accretion and traffic from the ER to the vacuoles without the involvement of the Golgi. In wheat endosperm cells, prolamin and the chaperone BiP, which ordinarily is an ER resident, are present both in the PB and in the vacuole. Perhaps ER-derived PBs are taken up directly into vacuoles, either by membrane fusion or, more likely, by engulfment akin to autophagy. As we illustrated in Section 4.7.4, in other cereals (e.g., maize and sorghum), the ER-derived PBs persist in the cytoplasm and do not enter the vacuoles. PBs, PACs, and DVs seem to reflect a common tendency of seed storage proteins to form polymers/large condensed structures that are either permanent or transient. Depending on the storage protein type this can occur already within the ER itself (PBs, PACs) or later along the secretory pathway (DVs). The final result can be either total inhibition of traffic (PBs) or vacuolar delivery, mediated (DVs) or not (PACs) by the Golgi apparatus. In any case, these mechanisms have probably evolved to allow high accumulation of very large amounts of protein at the lowest possible energy cost for the cell.

Cutin, a major component of the plant cuticle, is a polymer of fatty acids synthesized by the ER and polymerized in the extracellular space. *Arabidopsis* mutants that are affected in the final step of secretion of cuticular lipids accumulate lipid

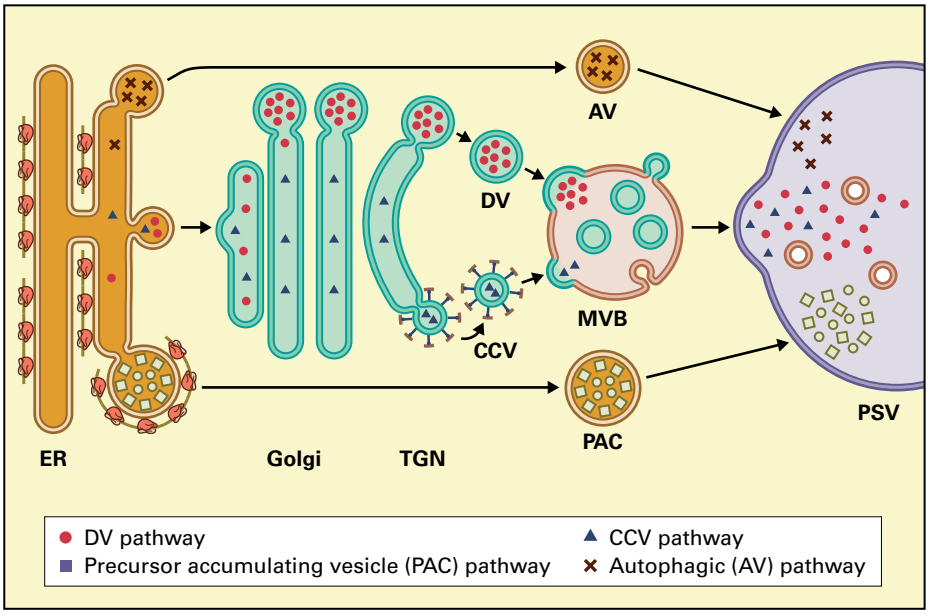
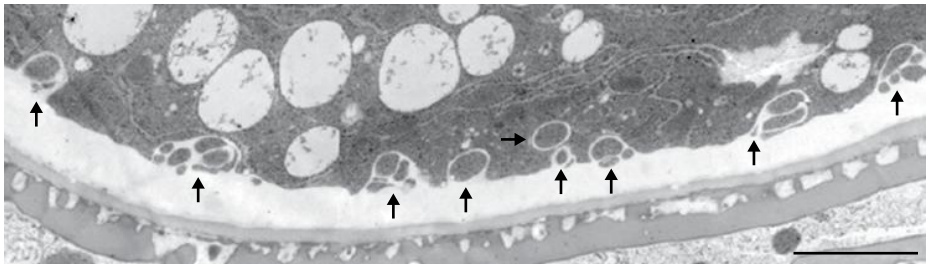
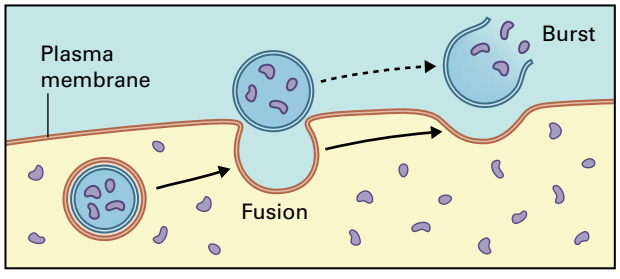


FIGURE 4.26 *The different pathways for the delivery of storage proteins to PSVs in seeds. Groups of closely spaced dots represent aggregation events. Dots, DV pathway; triangles, CCV pathway; squares, precursor accumulating vesicle (PAC) pathway; crosses, autophagic (AV) pathway.*



A



B

FIGURE 4.27 *Alternative secretion. (A) Electron micrograph of a tobacco pollen grain, showing vesicles that are being released into the cell wall (arrows). (B) Cartoon illustrating a mechanism for alternative secretion. Selected cytosolic proteins (blue) are incorporated into the vesicle, which is enclosed by an inner and an outer membrane, suggesting an autophagosomal origin. Upon fusion of the outer membrane with the plasma membrane the vesicle is released from the cell surface. Bursting may discharge the vesicle content into the apoplast.*
Source: Wang et al. (2010). Plant Cell 22:4009–4030.

inclusions in the ER but not in the Golgi, suggesting that the latter is not involved in the normal process of monomer secretion and that direct ER to plasma membrane trafficking exists. This is also supported by the fact that brefeldin A-insensitive trafficking from the ER to the cell surface of several proteins and lipids has also been observed in mammalian cells.

Finally, small vesicles containing soluble proteins that do not derive from precursors with a signal peptide are detectable in the cell wall of several plant tissues and plant cell cultures (Fig. 4.27A). They therefore constitute a direct cytosol-to-cell surface membrane trafficking pathway that does not involve the ER and Golgi apparatus. These secreted vesicles have a double membrane when they are still in the cytoplasm: their secretion occurs upon fusion between their outer membrane and the plasma membrane, a process morphologically similar to the release of internal MVB vesicles into the vacuolar lumen (Fig. 4.27B). However, the plant structures involved in this alternative secretion are immunologically distinct from plant MVB and are not affected by brefeldin A. The function of secreted vesicles in plants is not yet known. In animal cells, secreted vesicles originate from the fusion of MVB with the plasma membrane (generating exososmes) or by direct budding from the latter into the extracellular space (shedding microvesicles). They participate in cell-to-cell signaling either by discharging luminal content into the target cell cytosol by membrane fusion or through interactions between the extracellular domains of their membrane proteins and plasma membrane receptors.

4.8.5 Complex N-linked glycans are derived from high-mannose N-linked glycans during processing in the Golgi complex

When Asn-linked glycans become attached to nascent polypeptides they have three terminal Glc residues that play a role in protein folding and are removed by ER glucosidases (see Section 4.6.7). Furthermore, ER resident mannosidases can remove up to three Man residues. Therefore, at the moment of exit from the ER, N-glycosylated proteins have glycans, called **high-mannose glycans**, with the structure $(Man)_{9\text{-}6}(GlcNAc)_2$. These can be further modified by glycosidases and glycosyltransferases as the newly synthesized proteins travel through the Golgi complex. When the end product contains additional residues besides the original GlcNAc and Man, the glycan is termed a **complex glycan**. Golgi-mediated modifications follow defined pathways where in most cases the product of one reaction is the necessary substrate for the next. Distribution of processing enzymes in the *cis*-, medial, and *trans*-Golgi cisternae is polar, with mannosidase I enriched in the *cis*-Golgi and so on (see Chapter 1). The pathway of glycan modification until the formation of $(GlcNAc)_2(Man)_3(GlacNAc)_2$ is identical in animals and plants, whereas further modifications diverge (Fig. 4.28). The most extensively modified structure found in plants and also called the Lewis antigen, is $(Fuc)_2(Gal)_2(GlcNAc)_2$ $Xyl\mathbf{(Man)_3}Fuc\mathbf{(GlcNAc)_2}$, where the residues in bold are what remains of the original high mannose chain. This is often present in secreted plant glycoproteins. A common structure found in vacuolar glycoproteins is $Xyl\mathbf{(Man)_3}Fuc\mathbf{(GlcNAc)_2}$, which is derived from $(GlcNAc)_2$ $Xyl(Man)_3Fuc(GlcNAc)_2$ by the action of vacuolar *N*-acetylglucosaminidase. It should be noted that a wide variety of intermediate complex structures exist and that a number of glycoproteins have glycans that are not modified during transit through the Golgi, mainly because in a folded polypeptide glycans are not always fully exposed on the protein surface to the action of Golgi enzymes. Thus, the presence of complex glycans is used as evidence that a glycoprotein has passed through the Golgi, but the absence of modifications cannot be used as evidence that this has not occurred. There are marked differences between plants and mammals in residues added to N-linked glycans by Golgi glycosyltransferases and in the type of chemical linkages used. Unlike plants, mammalian complex glycans never have α1,3-Fuc or β1,2-Xyl residues attached to the proximal GlcNAc and to the core Man, respectively, and rarely have terminal β1,3-Gal residues. They instead often have α 1,6-Fuc linked to the proximal GlcNAc and terminal sialic acid linked to β1,4-Gal. These differences, in particular the α1,3-Fuc and β1,2-Xyl, make plant glycoproteins unusually immunogenic in mammals and contribute to plant food and pollen allergy in humans. This characteristic has implications in the use of plants as bioreactors for the production of pharmaceuticals. Scientists have developed different strategies to solve the problem. One is the addition of KDEL or HDEL at the C-terminus of a given pharmaceutical: rapid recycling from the Golgi apparatus does not allow glycan processing by Golgi enzymes and thus the oligosaccharides remain of the high mannose type. On some pharmaceuticals human complex glycans are important for function, and a more sophisticated approach is the "humanization" of the plant Golgi complex: knockout mutations are stacked together with expression of human Golgi enzymes, to eliminate unwanted plant modifications and substitute them with human ones. The strategy is feasible because, surprisingly, mutant *Arabidopsis* plants that lacks GlcNAc transferase I, a necessary enzyme to convert high-mannose glycans to complex glycans does not show defects when raised under normal growth conditions although it is more sensitive to environmental stress.

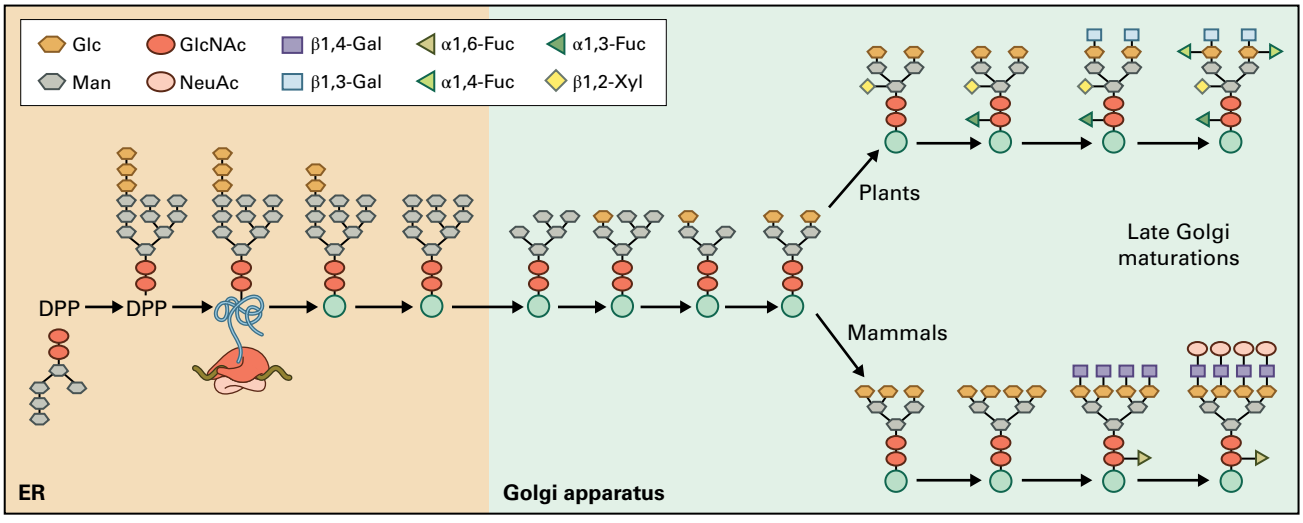


FIGURE 4.28 *Processing of plant and mammalian N-linked glycans in the ER and Golgi. The differences are in late Golgi maturation events, which occur in the* medial *and* trans*-Golgi cisternae. In the complex glycans of plants fucose (Fuc) is attached by an α1,3 linkage, vs α1,6 in mammals, and galactose (Gal) with a β1,3 linkage, vs β1,4 in mammals. The xylose (Xyl) residue attached by a β1,2 linkage is also found in invertebrates and is unusually antigenic in mammals. NeuAc, sialic acid.*
Source: Faye et al. (2005). Vaccine 23:1770–1778.

This indicates that processing of N-linked glycans into complex structures is not essential for plant growth, development or reproduction. Conversely, mice lacking GlcNAc transferase I die around the 10th day of gestation resulting from defects in cell–cell recognition and signaling.

4.8.6 Serine, threonine, and hydroxyproline residues can be O-glycosylated

Carbohydrates can be attached to the hydroxyl group of threonine, serine, or hydroxyproline. These structures are termed O-linked glycans and can be constituted by a single monosaccharide or may contain several residues. Proline hydroxylation also occurs in some animal proteins such as collagen, but hydroxyproline O-glycosylation has been found only in plants. Unlike N-linked glycans, polymeric O-linked glycans are formed by the post-translational, sequential addition of sugars. Conclusive evidence that all plant O-glycosylation reactions occur in the Golgi apparatus is still lacking, but immunomicroscopy studies, and analogy to O-glycosylation of serine and threonine residues in mammalian cells, suggest that this is the case. Bioinformatic analysis has identified 20 putative β1,3 galactosyl transferases in *Arabidopsis* which may be involved in O-glycosylation or in the modification of N-linked glycans: 17 are predicted to be type II membrane proteins with Golgi location.

The superfamily of hydroxyproline-rich glycoproteins (HRGPs) is unique to plants and includes arabinogalactan proteins (which are GPI-anchored proteins (see Section 4.6.4), proline-rich glycoproteins, extensins, and solanaceous lectins. In arabinogalactan proteins, short side chains containing arabinose, rhamnose, and glucuronic acid are attached to a branched Gal backbone core linked to hydroxyproline (see Chapter 2). In extensin, hydroxyproline residues are O-glycosylated with short side chains containing one to four arabinose residues, and many serine residues in the $Ser(Hyp)_4$ repeats are O-glycosylated with galactose. At least three types of arabinosyl linkages are involved; thus, the synthesis of these side chains requires three different arabinosyltransferases, enzymes that transfer an arabinose residue from UDP-arabinose to the polypeptide.

4.9 Endocytosis and endosomal compartments

4.9.1 Endosomal compartments

Cells have a vesicle-mediated pathway for uptake of extracellular macromolecules and internalization of plasma membrane proteins. This process is called endocytosis (see Chapter 1) and involves the TGN and MVB as sorting stations. Because of this role, the late (free) TGN and MVB are therefore also termed early and late endosomes, respectively (see Section 4.6.1).

In plant cells, endocytosis was first investigated using electron-dense cationized ferritin particles, because these are readily taken up in an endocytic process and easily visualized with the electron microscope. The pathway starts with an invagination of the plasma membrane and the formation of small, vesicles that bud towards the cytoplasm and traffic to the late (free) TGN (Fig. 4.29, see also Fig. 4.10). The process is analogous to the formation of coated vesicles described earlier (see Section 4.7.1). Two internalization pathways operate in parallel: one relies on CCVs, with coats similar to those of vesicles moving from the late (free) TGN to MVBs, but the protein coats of the vesicles in the other pathway have not been identified. In electron micrographs, CCVs appear to have spikes (see Fig. 1.33) and recruitment of clathrin from the cytosol requires specific adaptor protein complexes that bind clathrin on one side and the cytoplasmic domains of transmembrane receptors on the other. The extracellular domains of these transmembrane receptors interact with the proteins being internalized and determine the specificity of the endocytic process. After a cargo-laden clathrin-coated vesicle has formed, the neck region of the vesicle is severed by the motor protein dynamin, a small GTP-binding protein

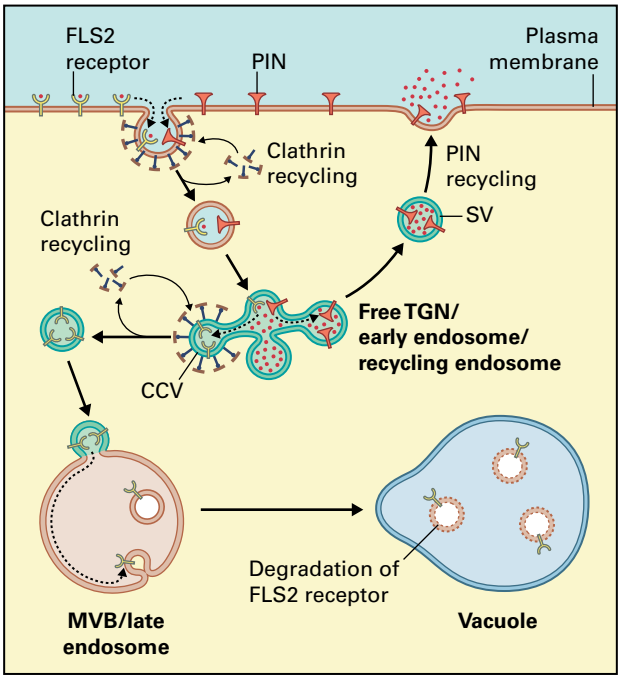


FIGURE 4.29 *Endocytic pathways. Endocytic vesicles form by invagination of the plasma membrane and can either have clathrin coats or coats of unknown composition. They will deliver their content to early endosomes (free TGN). From there, content can be delivered to late endosomes (MVBs) and finally to the vacuole or be recycled back to the plasma membrane. In the latter case the early endosomes function as recycling endosomes. Some receptors follow the traffic from the plasma membrane to the vacuole and are broken down there, others simply cycle between the plasma membrane and the early/recycling endosomes.*

(see Fig. 1.33A). A 70-kDa chaperone-like protein causes the released clathrin-coated vesicle to uncoat in a process that requires ATP. The uncoated vesicle can then fuse with the TGN. In the TGN, the internalized plasma membrane proteins can be either recycled back to the plasma membrane via secretory vesicles, or sorted into clathrin-coated vesicles and sent to MVBs (late endosomes) and vacuoles for degradation (Fig. 4.29). The borate transporter BOR1 provides an interesting example of the breakdown of a plasma membrane protein by endocytosis. When plants are borate starved the transporter is abundantly present on the plasma membrane of root cells. When borate is added to the growth medium, BOR1 is quickly endocytosed and transferred to vacuoles for breakdown.

The initial formation of the endocytic vesicles at the plasma membrane may be driven by the presence of the ligand (ligand induced endocytosis) or it may be constitutive. Both types of endocytosis have been observed in plants, as illustrated by studies on endocytosis and signaling treated in the next paragraph.

4.9.2 Endocytosis and signaling

Endocytosis plays an important role in plant signaling events that involve receptor-like kinases (RLKs), a large class of plasma membrane receptors with 600 members in *Arabidopsis* and more than 1000 in rice. A subclass of these receptors has extracellular leucine-rich repeats (LRRs) and is referred to as LRR-RLK. The first convincing example of ligand-induced endocytosis in plants was the isolation of the *Arabidopsis* LRR-RLK Flagellin Sensing 2 (FLS2) receptor that recognizes the bacterial elicitor flagellin (flg22). In transgenic lines that express a fusion of FLS2 and GFP, the plasma membrane is fluorescent indicating the location of the receptor. Only after activation of the receptor with flg22, was FLS2-GFP endocytosed and sent to vacuoles for degradation via MVBs (Fig. 4.29). Activation of a receptor may not always be required for its translocation to the late TGN/early endosomes and can also occur within this compartment. For example, the brassinolide receptor BRI1, also an LRR-RLK, is present at the cell surface and at the TGN, even in the absence of brassinolide, indicating constitutive endocytosis. BRI1 binds brassinolide at the cell surface, but the receptor does not initiate its signal transduction cascade there. It is first internalized via a constitutive recycling mechanism, transferred to the TGN and only then becomes active. It is possible that activation requires additional proteins found only at the TGN.

Another important regulatory process that involves endocytosis is the creation of auxin gradients, which requires two plasma membrane proteins: AUX1 involved in auxin uptake and the PIN family of auxin efflux carriers. The different PIN proteins in the plasma membrane have polarized distribution, either in the apical or basal part of cells. In roots the PIN2 carrier is constitutively recycled between the plasma membrane and the late TGN in a process that requires the ARF-GEF GNOM (see Box 4.5). This recycling along with PIN2 breakdown in the vacuole is responsible for creating auxin gradients.

Summary

Cells contain numerous metabolic compartments and membranes that have unique sets of proteins. Nearly all of these proteins are synthesized in the cytosol. How do they reach their correct destinations? Polypeptides have sorting domains that act as address labels for each destination. In some cases specific amino acids are part of the unique label, in other cases certain types of amino acids are required or the secondary structure is important. These sorting domains are usually short segments of polypeptide that may or may not be removed after the proteins reach their destination.

Many sorting domains interact with cytosolic receptors that in turn bind to one of the proteins that make up proteinaceous channels consisting of several polypeptides that are specific for each membrane (e.g., ER, chloroplast envelope, peroxisome, etc.). Passage of a polypeptide through a channel requires the participation of chaperones and energy in the form of ATP, GTP, or both. Chaperones help keep proteins unfolded in the cytosol before passage through the channel and are required to fold the protein correctly once it has crossed the membrane. In some cases proteins fold in their three-dimensional shape in the cytosol and then still can pass through a proteinaceous channel.

All living cells maintain an active secretory pathway having many functions besides protein secretion. The secretory pathway also transports proteins to vacuoles, maintains the protein complement of its various membrane systems and is involved in endocytosis. Proteins move between the various compartments of this pathway as cargo in vesicles. All proteins that have a signal peptide are translated on rough ER and enter the secretory pathway via translocation into the ER lumen. Correct folding is necessary not only for proper protein function, but also for transport. Proteins that are not correctly folded or cannot be assembled into oligomers are degraded by proteasomes after retrotranslocation back to the cytosol or in vacuoles. This degradation is part of the quality control system that the cell exerts over its complement of proteins. The folding process itself requires the participation of a number of chaperones and folding helpers that reside in the ER. When protein folding is impaired by

stress conditions the cell mounts an unfolded protein response (UPR) that causes enhanced expression of genes encoding ER chaperones and attenuation of the translation of proteins destined to enter the ER.

The secretory pathway targets proteins to the ER, Golgi, TGN (early endosomes), multivesicular bodies (late endosomes), vacuoles, and the plasma membrane. Transport between these various compartments generally requires vesicle budding and fusion. Vesicle formation and sorting are complex processes that involve integral membrane proteins (e.g., receptors and syntaxins) and cytosolic proteins (e.g., vesicle coat proteins). Coat formation is necessary for vesicle budding. Vesicles always uncoat before fusing with their target compartments. Cells make extensive use of highly regulated GTP-binding proteins/GTPases to regulate and provide energy for secretory pathway activity. Molecular genetics (finding mutants) and chemical genetics (applying chemicals to inhibit specific steps) are proving to be valuable tools in identifying components of this vesicle sorting machinery.

Cells also have a vesicle-mediated mechanism, called endocytosis, for taking up proteins and delivering them to endosomes for subsequent transfer to vacuoles. Endocytosis is also responsible for the back-and-forth transport of plasma membrane receptors that may become activated when they reach the TGN/early endosomes or routed to the vacuole for breakdown.



5

The Cytoskeleton

Tobias I. Baskin

Introduction

Despite the importance of membrane-bound organelles illustrated in the preceding chapters, the eukaryotic cell requires more than a set of defined compartments to function. Eukaryotic cells organize their components spatially, fixing some at defined locations in the cell, moving others to attain optimal positions. The contents of eukaryotic cells (and in some cases, the cells themselves) are mobile. Poking a cell with a fine needle stimulates its contents to move vigorously. A century ago, these directed movements were considered an unmistakable indicator of life; amusingly, this essential cellular property was described as *irritability*.

Directed movements of the cell and of its contents are mediated by the **cytoskeleton**, a network of filamentous protein polymers that permeates the cytosol. Plants contain two kinds of filaments, one built from the protein, actin, usually called *actin filaments* and the other built from the protein, tubulin, called *microtubules*. In this chapter, first each family is introduced and its properties described; second, principal cytoskeletal functions are illustrated; and, finally, the role of the cytoskeleton is described in mitosis and cytokinesis. The cytoskeleton evolved before plants diverged from animals and main features of the cytoskeleton have been conserved in both. Thus, much of the information presented applies to both animals and plants. However, the plant cytoskeleton has evolved unique functions, many of which will be highlighted.

5.1 Introduction to the cytoskeleton

5.1.1 Cells contain a dynamic, filamentous network called the cytoskeleton

When Robert Hooke viewed thin slices of cork through his microscope, he called the large empty spaces he saw "cells," because they reminded him of the spartan chambers inhabited by monks. Actually, Hooke was seeing only the walls of dead cells. Living cells, by contrast, are far from bare, empty spaces. Even the image of a cell with nucleus and organelles all floating in a more or less clear cytoplasm ignores the true complexity of the cell. Modern microscopes and staining techniques reveal that cells are packed with a dynamic filamentous network, a network that anchors, guides, and transports macromolecules, supramolecular complexes, and organelles (Fig. 5.1).

5.1.2 The cytoskeleton provides structure and motility and facilitates information flow

At any one time, a typical cell contains millions of protein molecules engaged in thousands of activities, ranging from biosynthesis to degradation. Few of these proteins function as single

Biochemistry & Molecular Biology of Plants, Second Edition. Edited by Bob B. Buchanan, Wilhelm Gruissem, and Russell L. Jones.
© 2015 John Wiley & Sons, Ltd. Published 2015 by John Wiley & Sons, Ltd.
Companion website: www.wiley.com/go/buchanan/biochem



FIGURE 5.1 *Different views of the same cells in the root of* Arabidopsis thaliana. *(A) Section stained with a reagent specific for cell walls. This image resembles what Hooke saw when he coined the term* cell. *(B) Adjacent section imaged with Nomarksi optics, a technique that makes visible many organelles, such as nuclei, mitochondria, or plastids. These and other organelles were discovered in the 19th and 20th centuries as microscopes improved. (C) The same section seen in B, imaged with fluorescence microscopy. The bright fibrous elements are microtubules, a major component of the cytoskeleton. The section was treated with an antibody that recognizes microtubules and then was stained with a fluorescence-tagged second antibody that binds the first. The cell cytoskeleton was discovered after further refinements in microscopy and the development of specific molecular reagents. Source*: T. Baskin, University of Missouri, Columbia.

polypeptide chains. Instead, they form complexes comprising anywhere from several to many hundred subunits. Moreover, the complexes themselves do not function in isolation. The products of a reaction sequence must find their way from one complex to another, for example, in biochemical pathways or as information flows from the exterior of the cell to the nucleus. All of this miniaturized machinery must withstand molecular bombardment from **Brownian motion** (see Box 5.1)—thermal noise—that occurs at physiological temperatures. The bombardment is intense: at 25°C, the standard temperature for biochemical measurements, a globular protein 5 nm in diameter will be hit by solutes about 1 billion times per second.

It should thus come as no surprise that cells have evolved means to organize their teeming internal contents, not only to dampen the effects of thermal noise but also to facilitate reactions of increasing duration and complexity. One such adaptation uses compartments to sequester and concentrate components (Chapter 1). A second such invention is the cytoskeleton.

5.1.3 The cytoskeleton consists of a network of fibrous polymers

The cytoskeleton is a network of interconnected fibrous polymers that run throughout the cell within the cytosol (Fig. 5.2). This network provides structural stability to cytoplasm, anchoring proteins and other macromolecules, and supporting organelles during and after their synthesis. Besides structural stability, the cytoskeleton also gives cells the property of motility, both internal and external. Cellular components can move actively within the cell, such as during cytoplasmic streaming, and many cell types change shape and move within their environment. The cytoskeleton also participates in processing cellular information. For example, elements of the cytoskeleton are known to converge on the plasma membrane at sites associated with transmembrane receptors. Finally, many elements of the cytoskeleton consist of asymmetric subunits so that the polymers themselves are like an arrow, providing directional cues within the cell (Fig. 5.3).

The cytoskeleton comprises three classes of polymer: intermediate filaments, actin filaments, and microtubules. These polymers are similar in being extremely long and formed from protein monomers polymerizing via noncovalent bonds; they differ in their specific behaviors and functions. Actin filaments and microtubules share many properties of assembly and regulation whereas intermediate filaments are somewhat distinct.

5.1.4 Intermediate filaments are probably absent from plants

In animal cell cytoskeletons, **intermediate filaments** are constructed from a group of well-described proteins, such as keratin or vimentin. The filaments are named for their thickness: at 10–15 nm in diameter, they are thinner than microtubules and thicker than actin filaments. Apparently, plant cells do not contain a filamentous system that is independent of microtubules and actin nor do plant genomes contain sequences unmistakably homologous to animal intermediate-filament proteins. In animal cells, intermediate filaments function primarily to add strength and resiliency (e.g., keratin filaments toughen skin cells). In plants, analogous functions can be handled by the cell wall.

One place where intermediate filaments might be needed in plants is inside the nucleus. Among animals and fungi, the intermediate filaments with the most conserved function are the lamins. These form the **nuclear lamina**, a sheet-like structure lying just inside the nuclear envelope, thought to maintain nuclear shape, to reinforce the large nuclear pore complexes, and to ensure that chromatin can be successfully anchored (see Chapters 1 and 4). In plants, a structure partially resembling the nuclear lamina is evident in electron

BOX 5.1

Not all movement in cells requires molecular motors and scaffolding

Robert Brown (1773–1858), pictured here in an 1835 portrait by Pickersgill (A), discovered the motion that bears his name while pursuing his passion, botany. Even though Brown studied medicine at university and was serving in the army, he had amassed so great a knowledge of botany that Sir Joseph Banks hired him to sail as a ship's naturalist aboard *The Investigator* on a voyage of discovery to Australia. The voyage lasted for years, circumnavigating Australia twice. During that time, Brown collected more than 4,000 species, most of them new to science and many in previously unknown genera. The difficulties he faced were physical and intellectual: *The Investigator* was cramped, damp, and unseaworthy, and the botany of his day had only just begun to classify plants "naturally" (that is, evolutionarily). Nonetheless, Brown's treatment of the Australian flora remains essentially intact today.

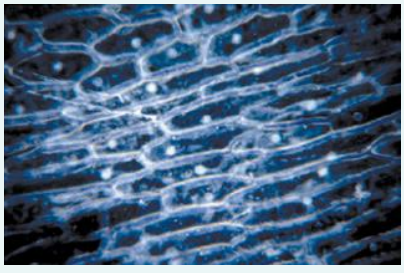
Brown's zeal for botany spurred him to become an excellent light microscopist. He realized that traits needed to support a natural classification of plants could be found in the early stages of development, which are microscopic. In Brown's day, the best microscopes had only a single lens, because the theory for properly correcting compound lenses had yet to be developed. Despite their simplicity, single-lens microscopes can reveal subcellular detail. The micrograph (B) shows a peel of onion epidermis viewed through a microscope used by Brown. Using dark-field illumination with the substage mirror shows the nuclei clearly against a dark background. From observations such as this, Brown coined the term "nucleus," and before the advent of cell theory he correctly surmised that it was a feature of every plant cell. He discovered cytoplasmic streaming in the stamen hairs of *Tradescantia* and delighted in showing this vivid cellular action to his friends, including such luminaries as Charles Darwin and William Hyde Wollaston (British chemist and inventor of the prism used in Nomarski optics, which today provides the best images of streaming in the stamen hairs—see Box Fig. 5.2A). Brown's major microscopical interest was the fertilization of plants. He was the first to correctly outline the anatomy of seeds and their embryos, and he discovered the naked ovule of gymnosperms, which allowed him to rationalize the classification of this group.

Important though these discoveries were, Brown's enduring fame rests on an 1827 discovery, made while examining pollen. He saw particles inside the grain moving randomly—rapidly and without cessation. (It was not the pollen itself he saw move, as often erroneously stated. Skepticism about his observations has been refuted by recent recreations of Brown's 1827 observations of Brownian motion with the very microscope Brown himself used, pictured here ready for use, C.) Brown was not the first person to observe this incessant movement; others had seen it before and surmised they were seeing the essence of life. But Brown observed the motion in pollen grains preserved for months in alcohol as well as in suspensions made by grinding a variety of rocks and minerals. He correctly concluded that the motion has a physical, not an organic, explanation. Later scientists quantified the motion to derive fundamental insight into the stochastic character of the molecular world. For example, French physicist and Nobel Prize winner Jean-Baptiste Perrin used Albert Einstein's formula for Brownian motion to calculate the size of the water molecule. It is apt that the incessant movement of particles bears the name of the indefatigable botanist, Robert Brown.

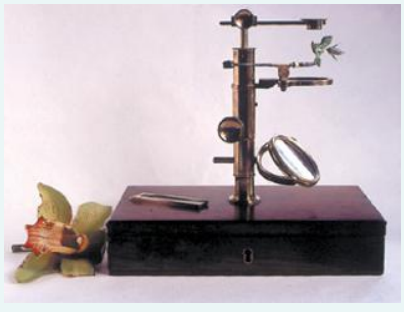
Source: (A) Portrait used by permission of the Linnean Society of London. (B, C) B.J. Ford, Rothay House, Cambridgeshire, UK.



A



B



C

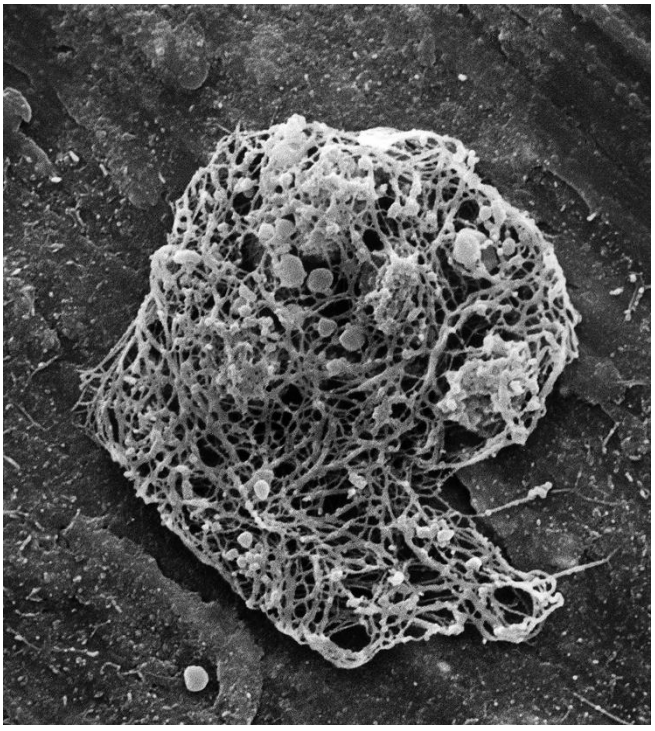


FIGURE 5.2 *Electron micrograph of cytoskeletal meshwork, showing detergent-resistant fibrous elements from a suspension-cultured carrot (*Daucas carota*) cell.*
Source: Xu et al. (1992). Plant Cell 4:941–951.

micrographs, and chromatin in plants no less than in animals requires anchoring for regulated gene expression. Nevertheless, while proteins arguably analogous to lamins are present in plant nuclei, their sequences are so distinct from those of animal lamins that it cannot be said whether they are deeply diverged homologs or independently evolved proteins. Therefore, while plants might possess filament-forming proteins in addition to actin and tubulin, these have yet to be characterized in detail and are almost certainly distinct evolutionarily from intermediate filaments.

5.2 Actin and tubulin gene families

5.2.1 Actin and tubulin are encoded by multigene families

Actin filaments are polymers of the protein actin; **microtubules** are polymers of the globular proteins, α- and β-tubulin. Actin binds ATP and is evolutionarily related to certain other ATP-binding proteins including heat-shock proteins and hexokinase; tubulin binds GTP and is distantly related to several types of G protein. Actin and tubulin occur in all eukaryotes, and homologs are present in prokaryotic genomes: for example, the tubulin-relative FtsZ forms a filamentous ring needed to effect cell division, and the actin-relative MreB

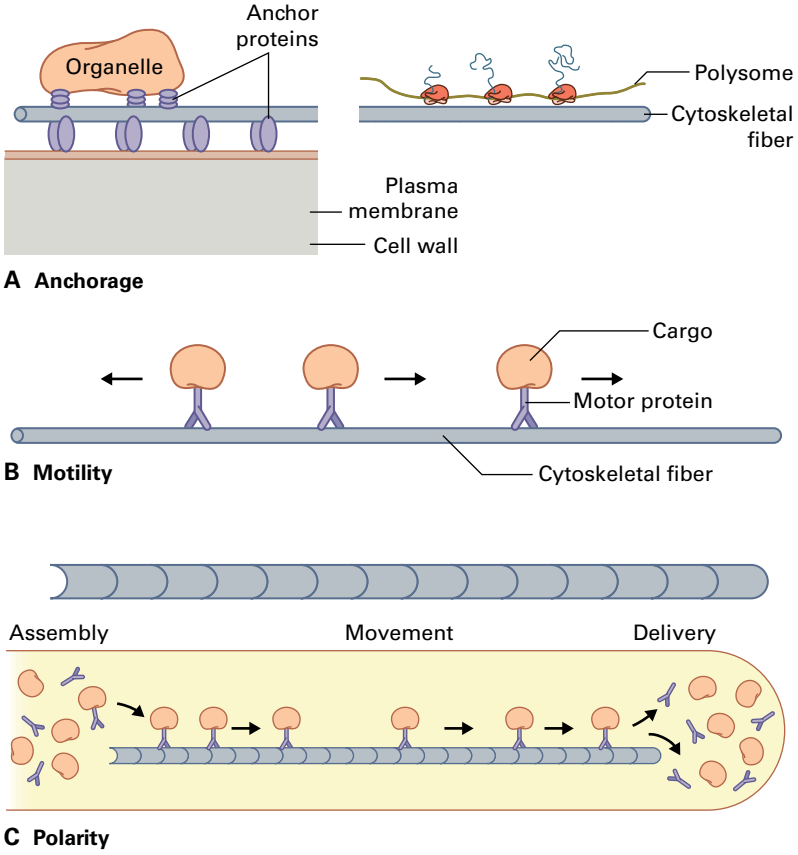


FIGURE 5.3 *Diagrams showing functions of the cytoskeleton. (A) Anchorage. The cytoskeleton anchors organelles and other macromolecular assemblies (e.g., polysomes). (B) Motility. The cytoskeleton supports active and directed intracellular movement of cellular components. (C) Polarity. The informational content of cytoskeletal fibers depends on the polarity of the fibers, which are formed from asymmetric subunits that define a direction along the polymer. In this example, cargo is assembled at one site, moved through the cell via the cytoskeleton, and delivered to a second location.*

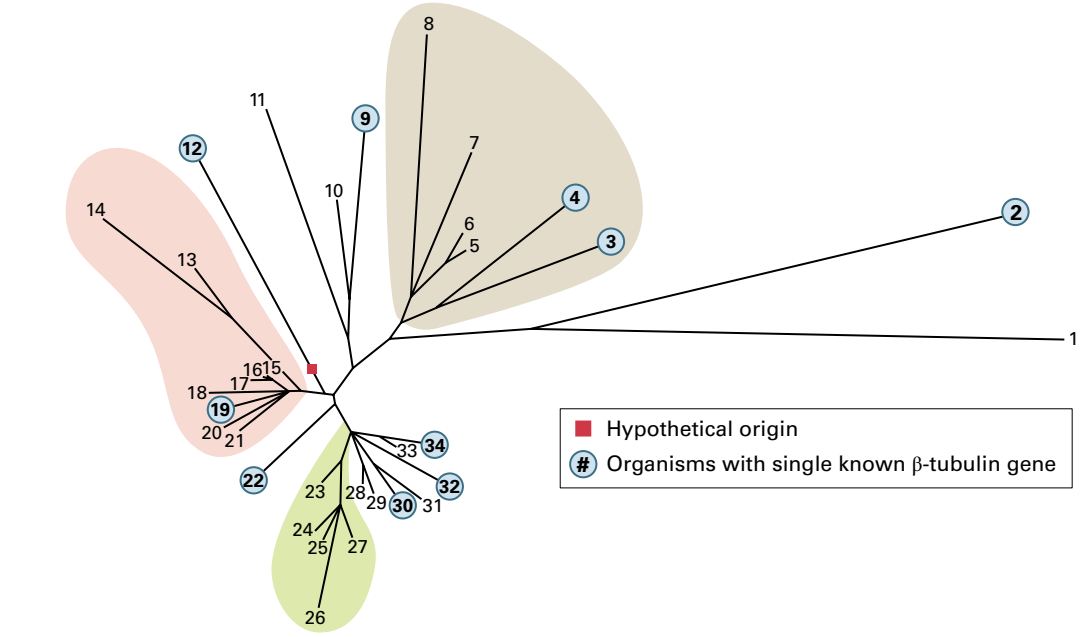
forms filaments required for the asymmetric cell shape of certain prokaryotic species. Evidently, the cytoskeleton was invented before the origin of eukaryotes.

In unicellular species, actin and tubulin are usually encoded by single-copy genes. In multicellular species, however, actin and tubulin are usually encoded by **gene families**. In vertebrates, actin and tubulin gene families typically contain between four and nine members, whereas in certain lineages of vascular plants, families are larger; for example, β-tubulin is represented by 20 genes in poplar (*Populus trichocarpa*), and actin by 100 genes in *Petunia hybrida*. Comparing the sequences within each family across kingdoms demonstrates they encode proteins that are usually at least 90% identical. Thus, actin and tubulin are in general highly conserved proteins that appear to have arisen from single-copy genes present before multicellular eukaryotes diverged (Fig. 5.4).

5.2.2 Several models explain gene family evolution

Why are these cytoskeletal proteins encoded by gene families? The different family members (called **isoforms**) could be distinct functionally, could allow for flexible regulation of transcription, or could reflect historical accident. These explanations are not mutually exclusive, and each probably describes part of the evolutionary process.

These explanations are well illustrated by experiments on the actin gene family in *Arabidopsis thaliana* (thale cress). Among plant genomes, this species has a relatively small collection of actin genes, expressing five isoforms in reproductive tissues and three others in vegetative tissue. Considering the vegetative isoforms, two of them (ACT2 and ACT8)



Fungi	Metazoa	Plants and green algae	Protozoa	Primitive eukaryotes
3: *S. pombe*	13: Chicken β6	23: *Chlamydomonas* β1	1: *Reticulomyxa* β2	2: *Entamoeba*
4: *S. cerevisiae*	14: Mouse β1	24: *Arabidopsis* β1	9: *Dictyostelium*	12: *Trichomonas*
5: *Colletotrichum* β2	15: *Xenopus* β2	25: Maize β2	10: *Physarum* β2	22: *Giardia*
6: *Aspergillus* BenA	16: Human β5	26: Soybean β1	11: *Reticulomyxa* β1	
7: *Aspergillus* TubC	17: Hamster β1	27: Pea β2	28: *Tetrahymena* β1	
8: *Colletotrichum* β1	18: *Haemonchus* β8		29: *Plasmodium* βA	
	19: *Caenorhabditis*		30: *Achlya*	
	20: *Drosophila* β3		31: *Ectocarpus* βb	
	21: Chicken β5		32: *Trypanosoma*	
			33: *Physarum* β1	
			34: *Euglena*	

A

FIGURE 5.4 *Evolutionary divergence of β-tubulin sequences. (A) Overview. The length of each branch is proportional to the rate of evolution of the sequence. The tree has been constructed to emphasize rates of divergence, not phylogenetic relationships. Note the clustering of tubulins within the major groups of eukaryotes and the predicted origin of β-tubulin before the radiation of the eukaryotes. As shown by the long branches, only a few β-tubulin sequences are thought to have undergone comparatively rapid evolutionary change. (B) Phylogenetic tree showing putative evolutionary relationships for the coding sequences of β-tubulins in plants. The tree was rooted with a green algal sequence. Clades include sequences from grasses (blue) and dicotyledons (brown), indicating that a gene family was present in the common ancestor and suggesting specialization. Similar conclusions have been reached for α-tubulin, as well as for actin. Arath, arabidopsis; Goshi, cotton; Medtr, medicago; Soltu, potato; Zinel, zinnia; Elein, goosegrass; Orysa, rice; Setvi, setaria; Triae, wheat; Zeama, maize.*

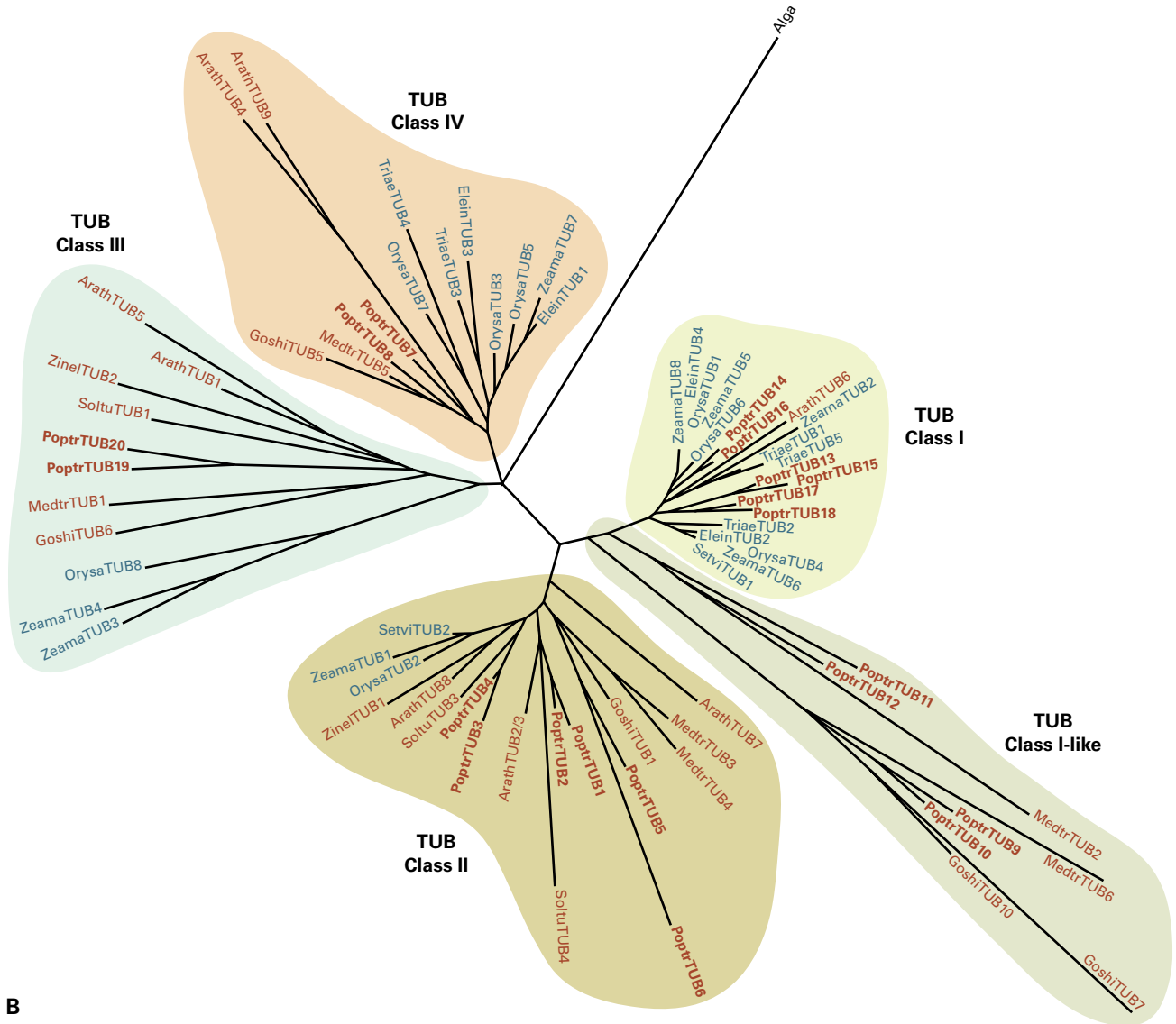


FIGURE 5.4 (*Continued*)

differ from each other by only two amino acids but by dozens of silent nucleotide changes, supporting the hypothesis that these have long diverged and are under strong selection. When these two genes are both knocked out, the double-mutant resembles wild-type plants closely, except for failing to make root hairs, a cell appendage that places large demands on the actin cytoskeleton (see Section 5.6). Furthermore, root hairs remain defective in this background even when the remaining vegetative isoform (ACT7) is expressed from one or both of the ACT2 and ACT8 promoters. Taken together these results show that ACT2 and ACT8 are distinct functionally from ACT7. However, reciprocal experiments show that ACT2 or ACT8 give rise to plants indistinguishable from wild type when either is the sole vegetative actin isoform expressed, provided that the amount of protein expressed is sufficiently great. Thus, ACT7 is functionally redundant with the other vegetative isoforms and its evolutionary trajectory is driven by regulatory demands or historical accident.

For tubulin, delineating the functions of specific isoforms is made even more complex because this protein is modified post-translationally (not only by phosphorylation, but also by acetylation, glutamylation, and detyrosination). Thus, each genetic isoform gives rise to several biochemical isoforms. Although certain tubulin genes have distinct expression patterns, others do not, and functional replacement experiments in plants have yet to be reported.

5.3 Characteristics of actin filaments and microtubules

Although made from distinct proteins, actin filaments and microtubules assemble by a similar process and share several characteristics. Like the synthetic polymer nylon, many biological polymers consist of molecular subunits linked by covalent bonds (e.g., as in RNA or polypeptides). In contrast, cytoskeletal

polymers have macromolecular subunits linked by non-covalent bonds, typical of quaternary protein structure. This allows microtubules and actin filaments to be dynamic, assembling or disassembling in response to factors that govern protein–protein interactions, such as ionic strength or temperature.

5.3.1 Spontaneous assembly of cytoskeletal polymers allows analysis of polymerization

The ability of actin filaments and microtubules to assemble spontaneously has the practical consequence that researchers can isolate and handle the protein in the form of subunits and can initiate polymerization in vitro by one of several simple manipulations. The time course of the polymerization reaction can be conveniently assayed by measuring the amount of light scattered by the solution, because light scattering increases as the polymer lengthens.

Polymerization occurs in three stages (Fig. 5.5). First, between the onset of conditions favoring polymerization and the first detected increase in polymer, a lag occurs. The lag reflects the need for an initial group of several subunits to associate correctly, forming a template for further assembly. This first stage of polymer assembly, the formation of a template, is called **nucleation.** The requirement for nucleation can be bypassed by adding small pieces of preformed polymer, often referred to as "seeds."

During the second stage, **elongation**, templates formed during nucleation grow by endwise addition of subunits. The rate of elongation represents the difference between the rate of subunit addition and the rate of subunit loss. The rate of subunit addition is the product of the association constant (k_{on}) and the concentration of free subunits in solution; the rate of subunit loss equals the dissociation constant (k_{off}). Consequently, the rate of elongation is proportional to the prevailing subunit concentration. Elongation continues until a plateau concentration of polymer is reached.

The third stage is a **steady state** in which a constant amount of polymer is maintained over time. The steady state is dynamic, the polymer gaining and losing subunits constantly. However, at steady state, the rate of subunit addition is balanced exactly by the rate of subunit loss (i.e., k_{on} [subunit] = k_{off}). Thus, steady state occurs when the concentration of subunits equals the ratio of the dissociation and association rate constants (i.e., [subunit] = k_{off}/k_{on}), the concentration known as the **critical concentration**. At concentrations less than this, polymer will not form spontaneously; at greater concentrations, the polymer will grow until the subunit concentration is depleted to the critical concentration.

5.3.2 Cytoskeletal polymers have an intrinsic polarity and hydrolyze nucleotides

Actin filaments and microtubules are polar structures because their protein subunits are asymmetrical. In polymer assembly, the asymmetric subunits line up end-to-end with a uniform orientation (Fig. 5.6A). The polarity thus conferred to the polymer means that each end has a different biochemical character. Therefore, each end of the polymer may have different rate constants for the assembly and disassembly reactions. In addition, each end of the polymer can be recognized specifically, so that cells may build polymer arrays with uniform polarity. The more dynamic end of the polymer is designated "plus" and the less active end "minus." Note that in this context these terms do not indicate electrical charge; the adjectives *positive* and *negative* are seldom if ever used to refer to this polarity.

Actin binds and hydrolyzes ATP, whereas tubulin binds and hydrolyzes GTP. These nucleotides play an important role in

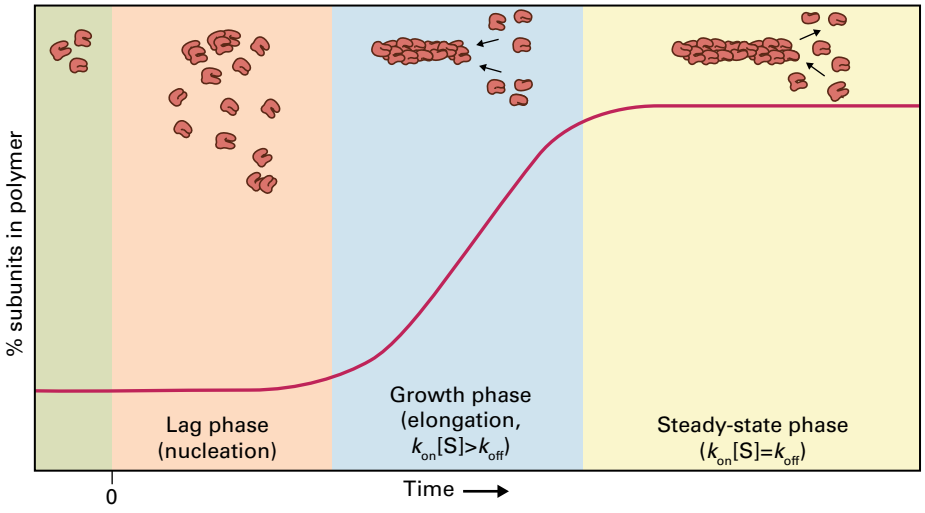


FIGURE 5.5 *Diagram illustrating process and kinetics of polymerization. A solution of individual subunits is induced to polymerize at time zero. During nucleation (pink panel), subunits must associate to create a stable template that serves as a platform for further elongation. In this example, using actin filaments, a template is formed when three subunits associate, generating a trimer. Because several subunits must interact simultaneously to form a template, this process is kinetically slower than that of adding subunits to the ends of an extant polymer and results in a lag phase. During elongation (growth phase, blue panel), subunits are rapidly added to the ends of growing polymers. A steady-state phase (yellow panel) is reached when the rate of subunit addition (k_{on}[S]) is balanced exactly by the rate of subunit loss (k_{off}).*

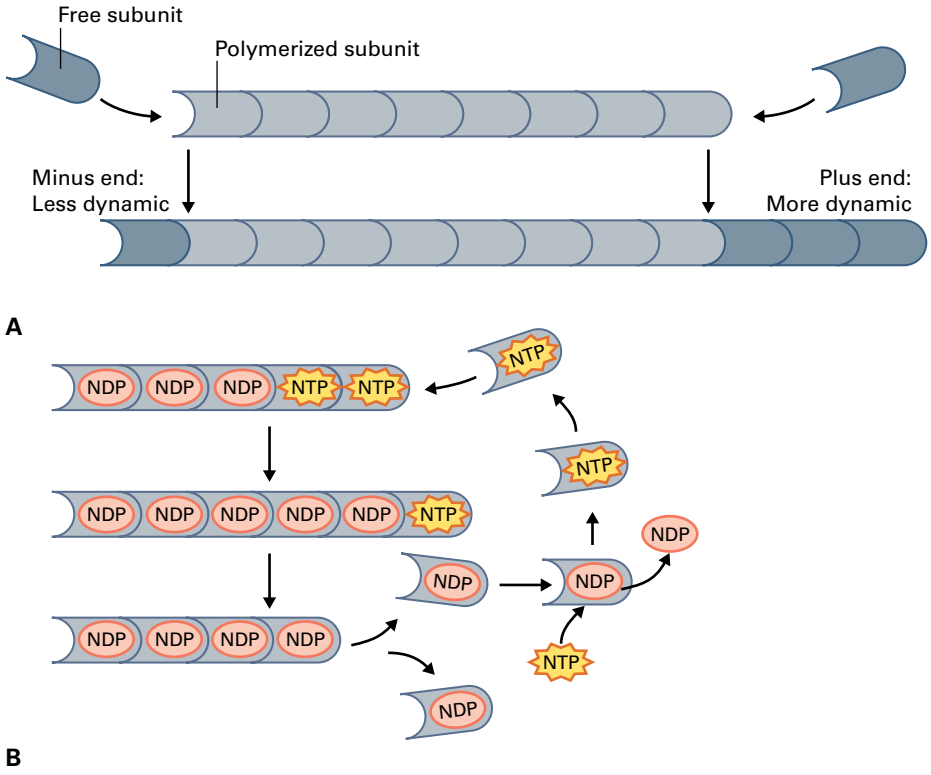


FIGURE 5.6 *(A) Actin filaments and microtubules form by head-to-head addition of intrinsically polar subunits, giving the polymers a defined polarity and each end distinct biochemical properties. One end of the filament is more dynamic than the other end, having increased rates of both subunit addition and loss. The more dynamic end is called the "plus" end and the less dynamic end is called the "minus" end (these terms do not refer to electric charge). (B) Actin and tubulin each bind nucleotides. The soluble proteins have a high affinity for the triphosphate form (NTP), and NTP-bound subunits have a high affinity for the assembled polymer (i.e., k_{on} S-NTP >> k_{on} S-NDP). After the subunit is incorporated into the polymer, the subunit's nucleotide is hydrolyzed. This lowers the affinity of the subunit for the polymer and might promote depolymerization. Subunits usually disassemble in the NDP-bound form and must exchange this nucleotide for NTP before again binding to the polymer.*

determining the properties of the polymers. The soluble subunit binds a nucleotide triphosphate (NTP), which greatly increases its assembly rate. This enhanced rate of assembly does not depend on energy from the γ-phosphate bond, because assembly is promoted equally by nonhydrolyzable nucleotide analogs. The γ-phosphate bond is hydrolyzed only after a subunit has bound to the polymer. The energy released by binding is stored in the polymer and used subsequently to enhance polymer dynamics, as described below. After a subunit dissociates, the bound nucleotide diphosphate (NDP) is rapidly exchanged for NTP, and the subunit is ready for another round (Fig. 5.6B). The involvement of nucleotides means that, in addition to the intrinsic difference between plus and minus polymer ends, each end may exist in at least two states, with subunits containing NDP or NTP. These different states extend the range of behavior possible for cytoskeletal polymers.

5.3.3 Differences in the biochemical properties of actin and tubulin give the polymers distinct dynamic behaviors

Soluble actin is a globular protein (sometimes termed *G-actin* in contrast to the polymeric or filamentous form called *F-actin*) of around 375 amino acids. Subunits polymerize into a tightly helical filament, ≈8 nm wide (Fig. 5.7). For historical reasons having to do with the appearance of actin filaments when decorated with the protein myosin, the minus end is sometimes called the *pointed* end, and the plus end called the *barbed* end.

The subunits that assemble into microtubules are heterodimers of the globular proteins α- and β-tubulin (Fig. 5.8). The dimers associate to form a hollow structure 25 nm in diameter. Each member of the dimer contains a bound guanine nucleotide, but only the β subunit engages in GTP hydrolysis and GDP–GTP exchange. In the microtubule, tubulin dimers bind together at their sides and at their ends. The dimers lie in straight columns called protofilaments. Most microtubules have 13 protofilaments, but the number can vary from 11 to 16. The lateral bonds between tubulin dimers displace dimers in adjacent protofilaments by several nanometers toward one end. Thus, the lattice of subunits that makes up the microtubule wall has a helical character. The plus end of the microtubule corresponds to the β-tubulin end of the dimer.

Several features besides nucleotide specificity distinguish actin filament and microtubule polymerization. For actin, the lag time for nucleation is proportional to the third power of concentration, which suggests that nucleation requires the assembly of a trimer. For microtubules, the nucleation lag is proportional to a much higher power of concentration, as

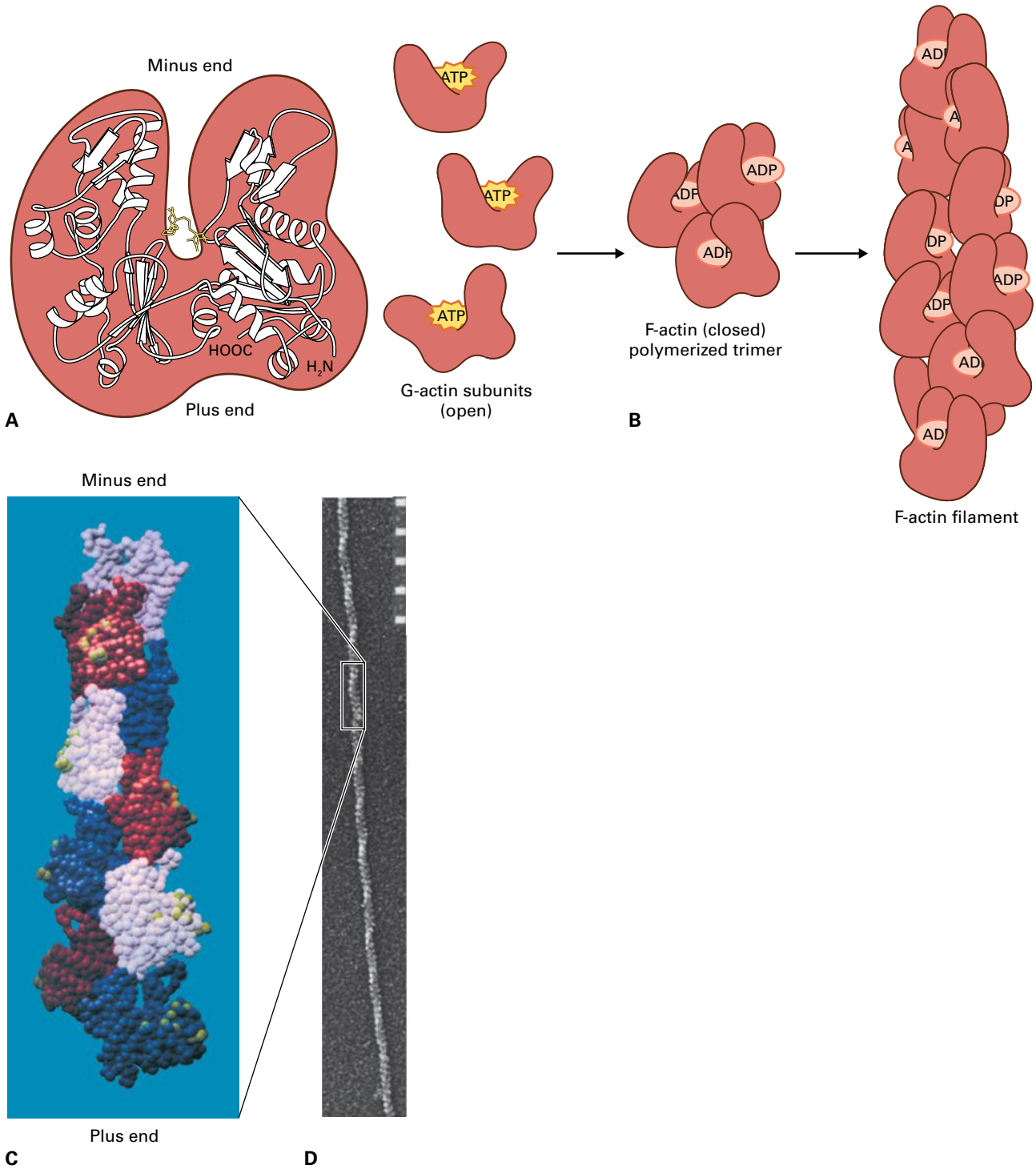


FIGURE 5.7 *The structure of actin and actin filaments. (A) Ribbon model of a single actin molecule. The yellow structure in the middle is the bound ATP. (B) Diagrams of G-actin monomers, a nucleated F-actin trimer, and a short actin filament, emphasizing the "open" and "closed" conformations. In the polymerized form, the conformation changes to enclose the active site, preventing the loss or exchange of nucleotide. Staggered subunit associations give the polymer its helical character. (C) Three-dimensional model of an actin filament, in which each ball represents an amino acid. Note the different shapes of the plus and minus ends. (D) Actin filament assembled from purified actin and imaged by high-resolution scanning electron microscopy. The helical nature of the filament is visible. Scale divisions equal 25 nm.*
Source: (C) Holmes et al. (1999). Nature 347:44–49. (D) Y. Chen, University of Wisconsin.

would be expected if as many as 13 subunits must assemble to form a template. The critical concentration for assembly of actin is ≈0.2 μM, very much lower than the concentration of actin typically found in cells (0.1–1 mM). Therefore, prevailing concentrations seldom present a barrier to nucleation of actin filaments; instead, cells must prevent unwanted polymerization. Cells have evolved accessory proteins to sequester soluble actin and to control its polymerization into filaments (see

Section 5.4; Box 5.2). By contrast, the critical concentration for microtubule assembly is ≈10 μM, only modestly below the usual cellular tubulin concentration (≈20 μM) and tubulin sequestration is usually not required.

Additionally, in the two types of polymer, nucleotide hydrolysis has different consequences. For actin, the presence of ATP at the plus (or barbed) end results in an assembly rate far exceeding that at the minus (or pointed) end, where the actin subunits contain ADP. This difference underlies a type of dynamic behavior called **treadmilling**, which occurs when the prevalent concentration of free subunits supports growth at the plus end but results in shrinkage at the minus end. The net rate of change in polymer length can be exactly zero, during which subunits incorporated at the plus end will

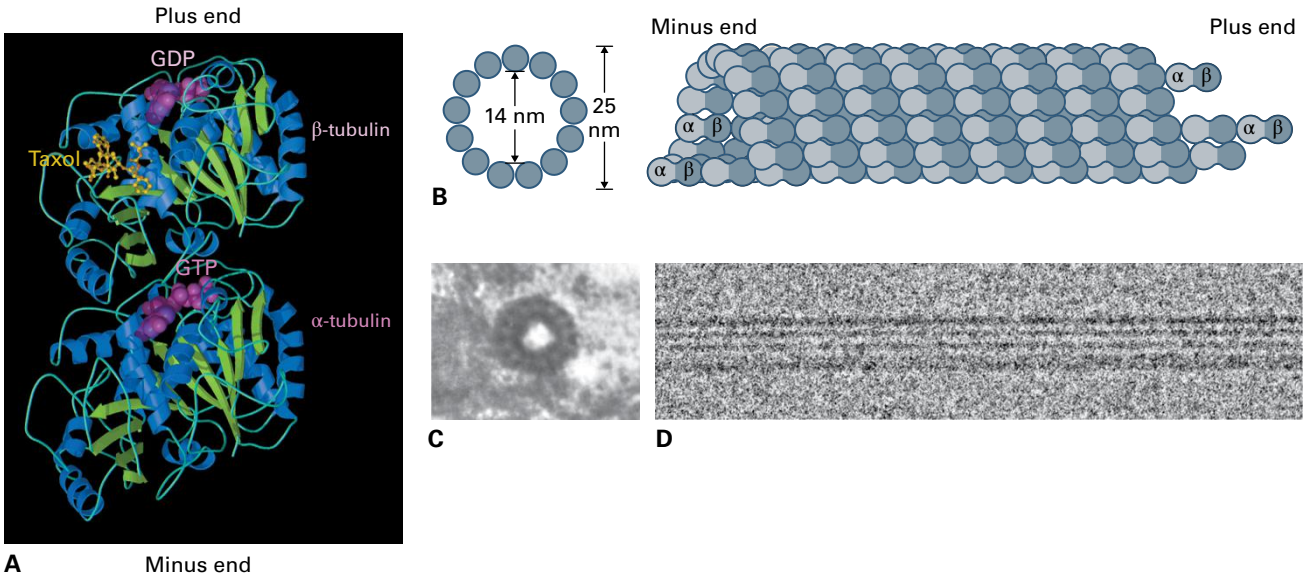


FIGURE 5.8 *The structure of tubulin and microtubules. (A) Ribbon diagram of the tubulin dimer, resolved at 0.37 nm. Regions of the β-sheet structure are shown in green and the α-helix in blue. Also shown are the positions of bound nucleotide (purple) and of taxol (yellow; a compound that stabilizes microtubules and used in the structural determination). Note the overall similarity of structure between α- and β-tubulin. (B) Diagrams of a microtubule in cross-section and side view. The subunits of the microtubule, dimers of α- and β-tubulin, align head to tail in long parallel columns called protofilaments. The protofilaments are displaced longitudinally from one another, giving a helical character to the lattice of subunits, but the microtubule itself is linear. The α-tubulin is exposed at the minus end of the polymer, β-tubulin at the plus end. (C) Electron micrograph of a microtubule in cross-section from a plant cell, showing thirteen protofilaments. (D) Electron micrograph of a microtubule assembled from purified tubulin and viewed from the side. Unlike (C), this side view was prepared by using cryotechniques, without chemical fixation or staining with heavy metals.*
Source: (A) Nogales et al. (1998). Nature 391:199–203. (C) Juniper & Lawton. (1979). Planta 145:411–416. (D) D. Chrétian, EMBO Laboratory, Heidelberg, Germany.

BOX 5.2 On the trail of plant profilin—from sneezes to signals

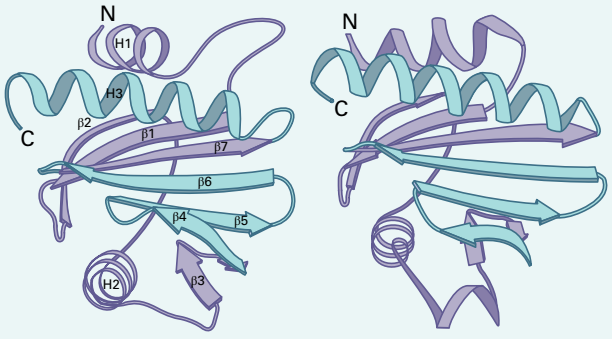
If flowering plants make you sneeze, your allergy might be triggered by a fascinating, ubiquitous actin-binding protein called profilin. Medical research and plant cell biology, usually worlds apart, were united in 1991 by the discovery that patients with pollen allergies often synthesize antibodies against profilin, which is packed into pollen. The antibodies recognize profilin from a variety of plants, a finding that offered the first explanation for the nonselectivity of many pollen allergies. Even more intriguing, certain patients had antibodies against human profilin, implying the allergy is aggravated through autosensitization. This finding has simplified diagnoses and is helping allergists evaluate preventative measures.

Beyond the etiology of allergy, the discovery of pollen as an abundant source of profilin was a boon for students of the plant cytoskeleton, enabling biochemical experiments. A small protein (10–17 kDa), profilin occurs in all cells, but its abundance increases 10- to 100-fold as pollen matures. Predicted amino acid sequences are typically 70–80% similar among plants, but when profilin sequences are compared across divergent taxa, the similarity drops to 20–40%. Despite sequence

divergence, profilin activity appears widely conserved. In fibroblasts, when profilin is overexpressed, the effects are identical, whether the encoding gene comes from a vertebrate or a plant. Furthermore, a profilin gene from maize (*Zea mays*) completely rescues a slime mold (*Dictyostelium discoideum*) mutant that lacks profilin. The similar activity of profilins from different sources might result from shared residues at both N- and C-termini and a similar three-dimensional structure. The ribbon diagrams (A) compare profilin from birch and acanthamoeba, a foraminifer. The conserved tertiary structure includes a core, six-stranded, antiparallel β-sheet, and the actin-binding domain, composed predominantly of the C-terminal α-helix (H3, blue) and the bottom three strands of the central sheet (β4, β5, and β6, blue).

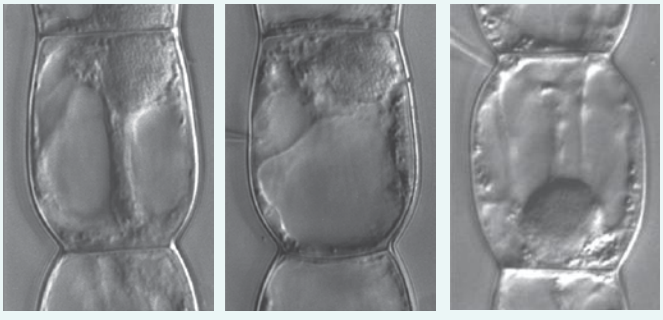
The first property of profilin to be characterized was its high affinity for soluble but not filamentous actin, which suggests that profilin sequesters actin monomers, releasing them locally, when and where the cell needs to polymerize actin. Indeed, the name profilin was derived from "profilamentous" actin, a term for sequestered actin that is otherwise competent to polymerize. The discovery of profilin in mature pollen fits this conception: mature pollen has few actin filaments but forms many within minutes of hydration. The ability of profilin to sequester actin is dramatically confirmed by microinjecting profilin into living *Tradescantia virginiana* stamen hair cells: the actin network is destroyed rapidly, thereby inhibiting cytoplasmic streaming (B) and cytokinesis. Presumably, profilin soaks up all of the actin monomers thus preventing new polymerization from balancing the ongoing depolymerization.

Since its discovery, activities reported for profilin have multiplied; these include stimulating nucleotide exchange, enhancing filament nucleation, interacting with regulatory subunits, and binding to membrane lipids. Thought to be important for profilin's multi-tasking is a binding site recognizing uninterrupted stretches of



Birch *Acanthamoeba*

A

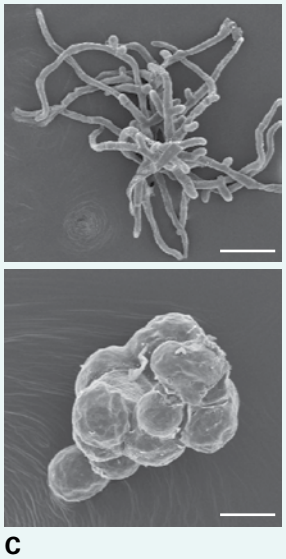


Cytoplasmic streaming along transvacuolar strands is evident in an uninjected cell

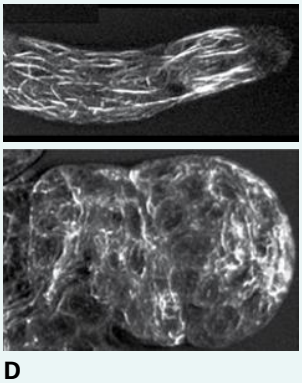
Ten minutes after profilin is microinjected, streaming has stopped and most of the transvacuolar strands have broken down

Streaming continues unabated 10 minutes after bovine serum albumin (BSA) is microinjected into a control cell

B



C



D

(C) Moss (Physcomitrella patens) gametophytes imaged with SEM. The control (top) has many thin branched protonemal filaments whereas when profilin expression is eliminated (bottom) cells are round, having lost the ability to polarize. Bars = 100 μm (top) and 10 μm (bottom). (D) Actin filaments imaged in control (top) and profilin RNAi (bottom) demonstrate that actin still polymerizes with reduced profilin but fails to be organized coherently.

the amino acid, proline, because polyproline stretches occur frequently in proteins that interact with profilin.

Which activity demonstrated in a test tube matters to a plant? Experiments with micro-injection (B) introduce the protein in super-abundance and thus the consequences might not be physiological. Progress toward elucidating key endogenous activities of profilin was made by taking advantage of the power of RNA interference in the moss, *Physcomitrella patens*. The moss gametophyte makes cellular filaments called protonemata, which grow by tip growth. Tip growing cells confine expansion to one region (the tip), giving rise to a slender, tube-like cell. Growth is confined to the tip by means of an extensive cellular polarization, long known to depend on actin. When protonemal cells express an RNAi construct that reduces if not eliminates profilin, they become spherical (C) and their actin organization becomes random (D). These phenotypes are rescued by wild-type profilin but not by a profilin engineered to be unable to bind actin and only partially rescued by a profilin unable to bind polyproline. These results imply that profilin is activated locally to specify actin organization, rather than globally to regulate the total amount of filamentous actin; the results also point to the essentiality of proflin's actin binding compared to polyproline binding. Sneezes in autumn remind us how much we have yet to learn about this tiny but fascinating polypeptide.

Source: (A) Ribbon diagrams adapted from Federov et al. (1997). Structure 5:33–45. (B) Valster et al. (1997). Plant Cell 9:1815–1824. (C, D) Vidali et al. (2007). Plant Cell 19:3705–3722.

"treadmill" through the polymer and eventually be released from the minus end (Fig. 5.9). Because the difference in assembly rate at the plus and minus ends is much larger for actin than for microtubules, treadmilling is presumed to be more common among actin assemblies. However, both polymers demonstrate this behavior.

Nucleotide hydrolysis gives rise to a different kind of behavior in microtubules, called **dynamic instability** (Fig. 5.10). Here, energy released by GTP hydrolysis accelerates depolymerization. Because GTP hydrolysis lags behind assembly, the growing ends of a microtubule will be rich in GTP-tubulin, a condition that stabilizes the microtubule lattice and favors growth. However, when the supply of tubulin dimers runs low, or when the rate of GTP hydrolysis accelerates, the end of the microtubule will contain few, or even no, GTP subunits. With only GDP subunits, the lateral bonds between protofilaments are strained. In this state, the protofilaments peel apart and initiate rapid disassembly, hundreds of times faster than the rate of growth. For a microtubule end, this transition from growing to shrinking is called *catastrophe*. Sometimes, the rapid disassembly stops, and growth resumes, a process called *rescue*. The mechanism for rescue is poorly understood, but might involve islands of GTP-tubulin remaining in the microtubule lattice.

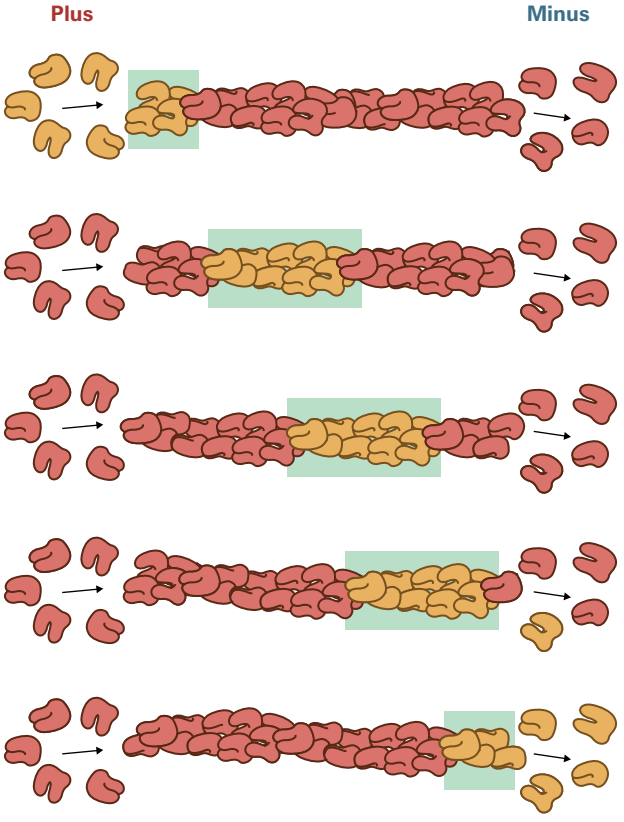


FIGURE 5.9 *Treadmilling, a dynamic behavior observed in cytoskeletal polymers, is supported by nucleotide hydrolysis. Because the bound nucleotide is hydrolyzed after subunit polymerization, the substrates of the assembly reaction differ from the products of the disassembly reaction. Therefore, each end of the polymer may have different values of* k_{on} *and* k_{off} *and hence exhibit different critical concentrations. As a result, subunits may add preferentially at the plus end and be lost preferentially at the minus end without changing the length of the polymer. As shown in the diagram, subunits (orange) added at one end "treadmill" through the polymer and are released from the other end. Although the diagram illustrates actin, treadmilling occurs also in microtubules.*

5.4 Cytoskeletal accessory proteins

If actin filaments and microtubules are the cell's bones, then accessory proteins are the muscles, tendons, and nerves animating that skeleton. The different functions performed by polymers of the highly conserved proteins actin and tubulin are mainly determined by a suite of accessory proteins, less highly conserved or entirely novel. Key accessory proteins allow the cytoskeleton to work whereas many others bind

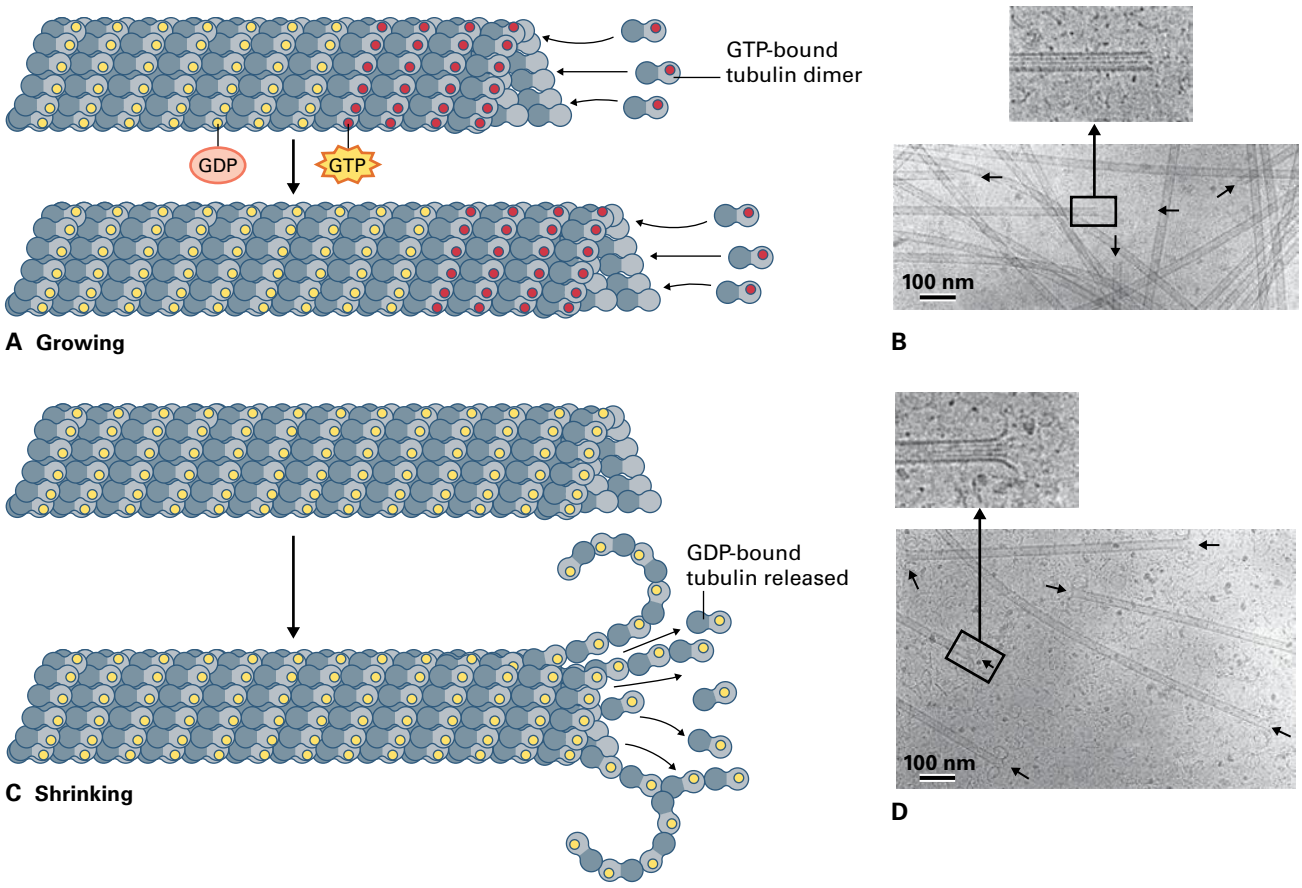


FIGURE 5.10 *Model for microtubule dynamic instability. (A) Diagram of growing microtubules. Since hydrolysis of GTP usually lags behind polymerization of new subunits, the growing ends of microtubules are rich in subunits in which β-tubulin monomers bind GTP. Such microtubules are said to have a "GTP-cap." In cells, the minus end of the microtubule is usually embedded in nucleating material, so GTP-caps are commonly considered only for the plus end. Note that the inert GTP bound to each α-tubulin is not shown. (B) Electron micrograph of growing microtubules. GTP-tubulin subunits pack into the microtubule lattice with minimal distortion, yielding straight ends for the growing microtubules (arrows; inset). (C) GTP hydrolysis causes a conformational change that tends to bend the protofilaments outward, weakening lateral contacts between dimers in adjacent protofilaments. In an intact microtubule, the GDP subunits in a protofilament are held in straight alignment by numerous lateral bonds to adjacent subunits and by the stability of the GTP cap. However, if the rate of polymerization decreases relative to the rate of hydrolysis, GTP subunits at the end become rare and the GDP subunits more readily assume their bent conformation. In this situation, the microtubule can undergo catastrophic depolymerization, during which subunits are released at a rate that far exceeds both the growth rate and the normal rate of subunit loss. (D) Electron micrograph of depolymerizing microtubules showing the protofilaments splaying outward (arrows; inset).*
Source: (B, D) Mandelkow et al. (1991). J. Cell Biol. 114:977–992.

and modify the characteristics of the polymer. Some of these proteins from plants have been implicated in human health (see Box 5.2).

5.4.1 Mechanochemical enzymes convert chemical energy into work

A pivotal type of accessory protein, mechanochemical enzymes, convert chemical energy to work, and are colloquially referred to as "motor proteins." There are three superfamilies of motor proteins—**myosin**, **dynein**, and **kinesin** (Fig. 5.11)—all represented by large and diverse gene families. Fundamentally, these proteins allow force to be generated between a cytoskeletal polymer and another cellular element, such as an organelle. Visualizing an organelle carried along a cytoskeletal polymer by a molecular motor invites comparison to a train carried along a track by a locomotive; however, a better comparison is to a person climbing a ladder using hands only. The climber has to grab the ladder, exert force to move at least as far as the next rung, and then let go of the ladder long enough to grab the next rung. To move along a cytoskeletal polymer, molecular motors work against thermal noise rather than gravity; they have high-affinity binding sites to grab the polymer, are built with long molecular lever arms to amplify a small conformational change driven by nucleotide hydrolysis into a large motion, and they alter the affinity for the cytoskeletal track in sync with the lever arm movement, thus allowing them to let go and rebind effectively.

Facing similar challenges, myosin, dynein, and kinesin share many features; having arisen eons ago, they differ in

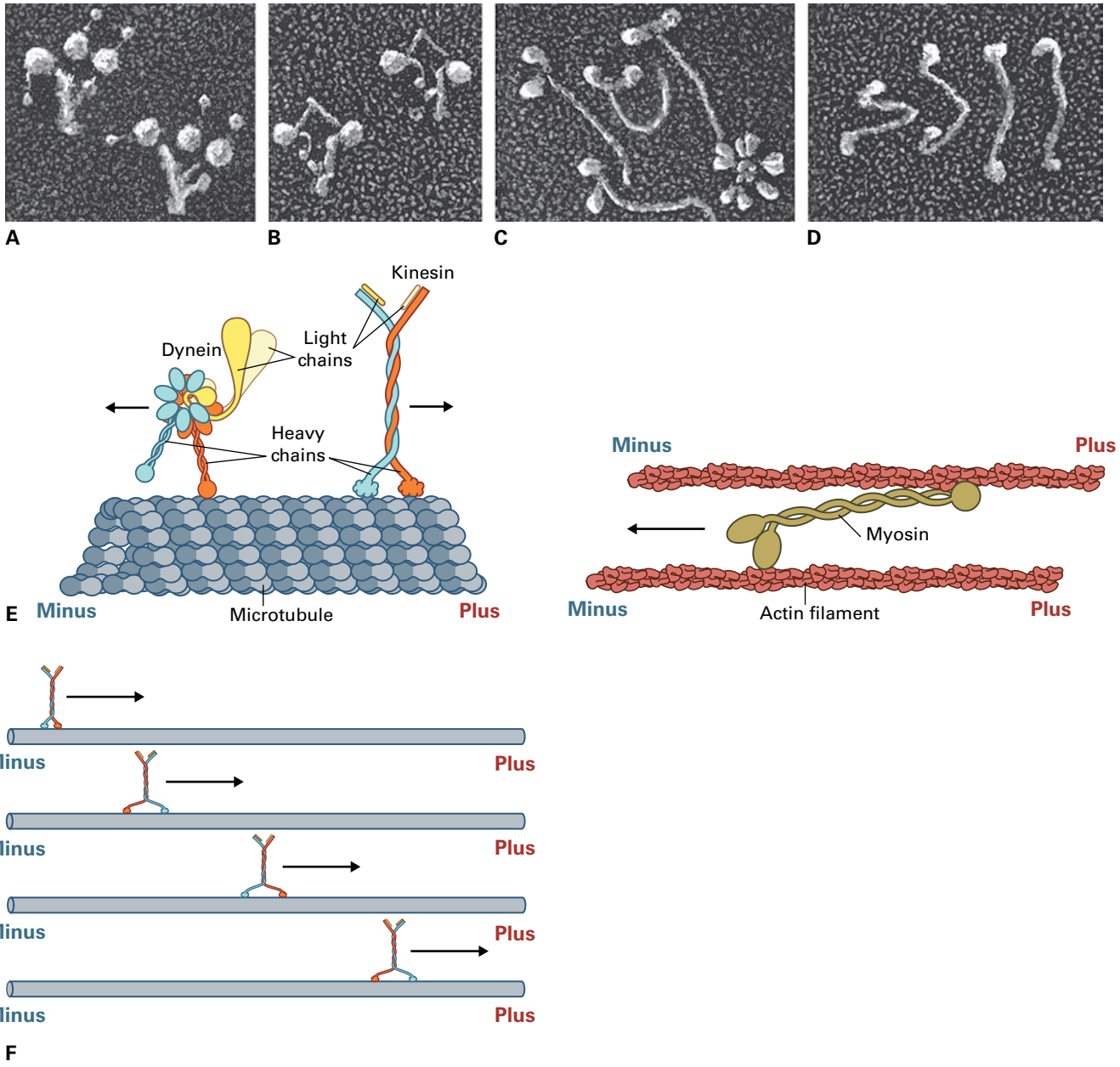


FIGURE 5.11 *Motor proteins. (A–D) Electron micrographs of motor proteins. (A) The ciliary form of dynein has three spherical head domains. (B) The cytoplasmic form of dynein has two head domains. (C) Myosin II. The asterisk-shaped structure in the lower right of the image is an IgM antibody used to purify the myosin. (D) Kinesin. In this image, the motor domains at one end of the rod-shaped protein and the light chains at the other end are not distinguishable. (E) Diagrams of motor proteins. Though not homologous, myosin and kinesin share a similar structural organization, each containing a pair of heavy chains and several accessory light chains. The heavy chains form globular head domains and elongated tail domains. The head binds to the cytoskeleton, contains the ATP binding site, and produces most if not all of the force. The tail domain is responsible for binding the specific cargo. The light chains regulate the activity of the motor or modify its binding properties. Dynein has its "head" domain in the middle, with cargo-binding and microtubule-binding domains emerging as projections. Force is generated in the central domain and acts to rotate one projection relative to the other. (F) Schematic view of kinesin in action. Alternate binding by the two heads ensures that a head is almost always bound; hence, the motor with cargo can move along the microtubule for long distances before dissociating. Although this action is often likened to a biped walking, the two heavy chains are the same, not mirror images (as are left and right legs), and so the head rotates by 180° with each step to be in proper orientation for binding the microtubule. Source*: (A–D) J. E. Heuser, Washington University of St Louis.

many others. They differ in which type of polymer they bind, what cellular cargo they transport, and the biochemical pathway they use to couple the changes in cytoskeletal affinity to steps of nucleotide binding, hydrolysis, and release. However all of them use ATP as their energy source. They all contain a globular, force-producing domain that binds ATP and a rod-shaped "tail" domain that binds cargo as well as regulatory peptides. Furthermore, these motor proteins usually function as dimers, which allows one subunit to bind the cytoskeletal substrate while the other remains free to move to and bind the

next site on the polymer (Fig. 5.11F). In other words, this gives the motor two hands with which to climb the ladder. With two heads, a motor can travel along a cytoskeletal track for tens of microns without letting go, an attribute called **processivity**.

5.4.2 Myosin moves along actin; dynein and kinesin move along microtubules

Myosin, the first motor protein discovered, was identified as the force-producing enzyme of muscle; we now know that members of the myosin family are present in most, but not all, eukaryotic cell types, powering motility involving actin filaments (Fig. 5.12). In myosin, the globular force-producing domain, the "head," also binds the actin substrate and force is developed by means of a long lever arm that connects head to tail (see Fig. 5.11E). With rare exception, myosins move to the plus end of the actin filament. Of the more than 20 different classes of myosin accepted to date, only two are present in plants, class VIII and XI, and these are unique to plants. Class XI myosin is similar to class V, which in animals and fungi plays a leading role in organelle motility. A class XI myosin isolated from the green alga, *Chara corallina,* holds the world's record for motor protein speed (60 μm s^{-1}).

Historically the next motor protein discovered was dynein, identified as the protein responsible for movement of eukaryotic cilia (note, "cilia" as used here includes flagella, which have a similar structure; prokaryotic flagella are totally different). The motile component of the cilium, the **axoneme**, comprises nine doublet microtubules encircling a central pair of microtubules (Fig. 5.13). Dynein motors are deployed along one side of the doublet microtubules and reach out to and exert force on the next doublet. This is an example, by no means unique, where the motor protein is fixed in place and moves its cytoskeletal track. If our climber is standing on a rooftop holding a ladder, then their climbing action will lower it. In studies of axonemal dynein, the green alga, *Chlamydomonas reinhardtii,* has been instrumental. Dynein of several isoforms is precisely arrayed into axonemes, subject to exquisitely complex regulation, and generates the waveforms required for ciliary propulsion.

Most eukaryotic cells also contain a cytoplasmic dynein isoform, which is distinct from axonemal isoforms although closely related. As its name suggests, this isoform functions in the cytoplasm with prominent roles in organelle movement and in the mitotic spindle (see Section 5.9). Although cytoplasmic dynein is present in animals and fungi, it was apparently lost in an early ancestor of green plants and algae. Additionally, seed plants no longer make cilia and have lost

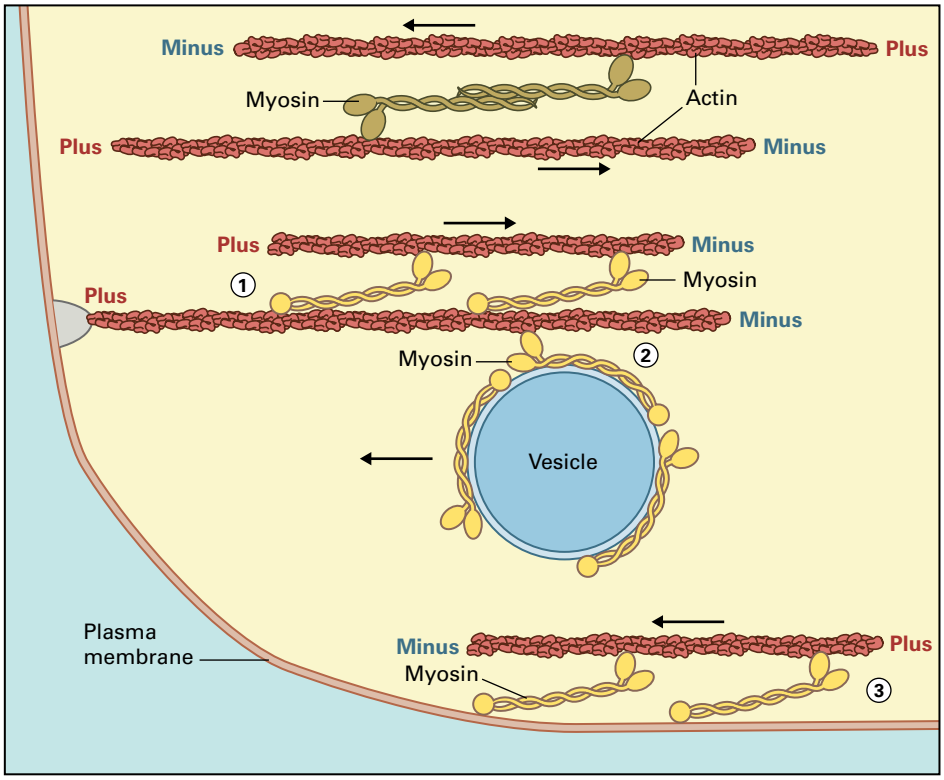


FIGURE 5.12 *Myosin proteins interact with actin filaments, moving from the minus (pointed) end to the plus (barbed) end of the polymer. Myosin II proteins, such as those in muscle, have long rod-like domains that promote assembly into bipolar (head-to-tail) filaments. Myosin II filaments pull actin filaments with opposite polarity towards one another, mediating local contractions. Other myosin motors usually form dimers that can bind an actin filament or a membrane. Plants contain class VIII and XI myosin, which form two-headed (i.e., dimeric) motors. Force transduction by the myosin head might then (1) move an actin filament relative to another, (2) move a vesicle along an actin filament, or (3) move an actin filament along a membrane. These three arrangements apply as well to the microtubule motors, dynein and kinesin.*

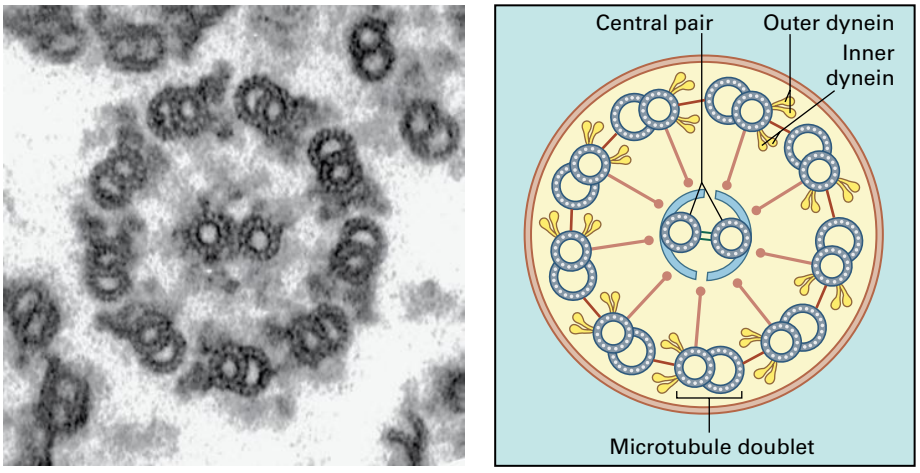


FIGURE 5.13 *Electron micrograph showing a cross-section of a cilium from* Chlamydomonas reinhardtii. *The axoneme has a ring of nine microtubule-like structures called doublets surrounding a central pair of microtubules. Dynein is bound statically to one doublet and reaches out to the neighboring doublet and tries to move it. Because the doublets are anchored at their bases and also to the central pair, the action of the force exerted by dynein causes the cilium to bend.*
Source: (micrograph) M. Hirono, University of Tokyo, Japan.

axonemal dynein. It is likely that some of the burdens lifted in animal cells by cytoplasmic dynein are shouldered in plants by kinesins (see below).

Dynein, whether axonemal or cytoplasmic, moves cargo to the minus end of the microtubule. It is a large polypeptide (>500 kDa), with its globular force-producing domain organized as a ring, and positioned in the middle of the molecule (see Fig. 5.11E). Two spokes emerge, one of which binds the microtubule and the other, longer and thicker, emerges on the other side of the ring and binds cargo and regulatory subunits. Force is generated by a contraction within the ring reducing the angle between the spokes. Dynein usually functions as a dimer, or even as a trimer, to increase processivity and perhaps to enhance scope for regulation.

Finally, the motor kinesin, although discovered third, is perhaps the best understood biochemically. Structurally, kinesin resembles myosin, with the globular head binding both ATP and microtubules and generating force by means of a lever arm connecting head to tail. In fact, kinesin and myosin might have evolved from the same ancestral peptide. Kinesins are diverse in most eukaryotes, with at least 14 classes defined, but have undergone particularly extensive radiation in plants, with *A. thaliana* containing 61 distinct kinesin genes, still a record among eukaryotic genomes, although poplar and rice (*Oryza sativa*) are close. Some classes of kinesin walk to the plus end (see Fig. 5.50 in Section 5.9.8) whereas others walk to the minus end. Plant kinesins, like those of animal cells, function in cell division and organelle motility; but we are just beginning to be able to assign functions to the multitude of plant kinesin motors.

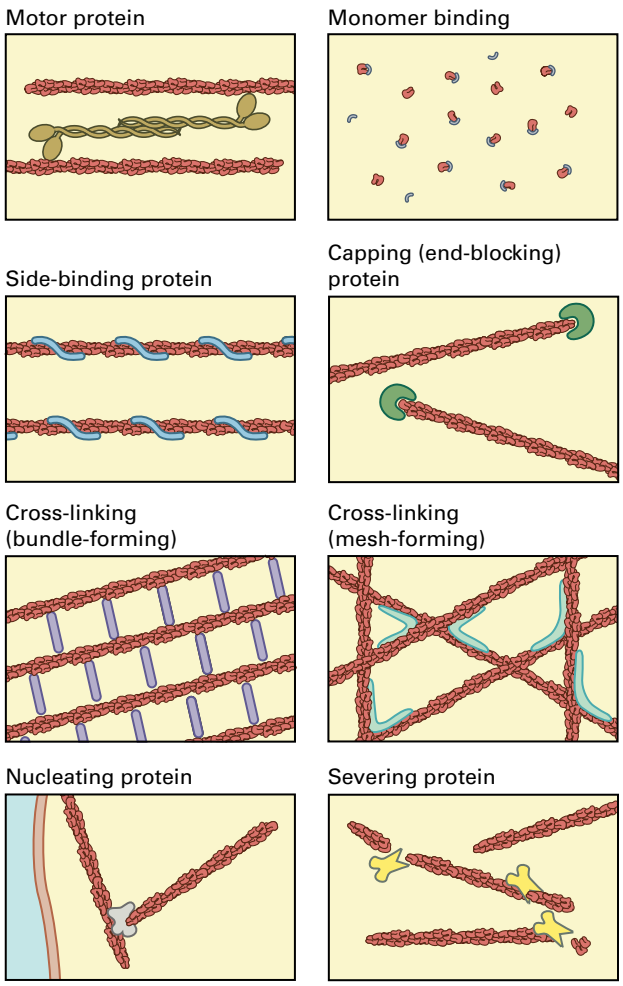


FIGURE 5.14 *Proteins that associate with the cytoskeleton have various functions, as illustrated here with actin filaments.*

5.4.3 Other accessory proteins bind, nucleate, or sever cytoskeletal polymers

Besides exerting force, accessory proteins help assemble, reinforce, and break down the cytoskeleton (Fig. 5.14). Knowledge about these accessory proteins comes mainly from studies on animals and fungi; in plants, some but not all of these proteins are present and new ones appear to have evolved. Dozens of such proteins exist, each with their own specialty. While unique in detail, the specialties can be categorized. Keep in mind that the following categorization refers to activity; some proteins have multiple activities.

A major distinction is between accessory proteins that interact with the monomer and the polymer. Proteins that

interact with monomers have two main activities, either to stimulate nucleotide exchange or to sequester the subunit. For example, **profilin** binds actin monomers and thereby lowers the concentration of subunits available for polymerization (see Box 5.2).

Accessory proteins that interact with polymer have three main activities: binding, nucleating, and severing (Fig. 5.14). All accessory proteins "bind" but the *binding protein* category refers to those that neither nucleate nor sever. Often the binding protein binds along the polymer (*side-binding*) and typically stabilizes it, exemplified by **tropomyosin** for actin and **MAP65** for microtubules, but some instead weaken the polymer lattice. An important subclass of binding proteins are those specific to one end of the polymer, often capping the polymer (*end-binding*). For example, the plus end of the microtubule is recognized specifically by the microtubule-associated protein, **EB1**, which remains at the plus end even as the microtubule grows and shrinks. Such proteins amplify the information contained in cytoskeletal polarity to generate or modify the polarity of the cell.

A large class of binding proteins is specifically crosslinking. This class includes proteins that link cytoskeletal elements to each other or to components of the cell, such as membranes, metabolic enzymes, or signal-transduction proteins. Proteins that crosslink one cytoskeletal polymer to another are of particular interest because the cytoskeleton nearly always is deployed as networks or bundles and these configurations require crosslinking for their formation and maintenance. The well characterized proteins of this class crosslink actin filament to actin filament or microtubule to microtubule, but newly discovered proteins, such as **anillin**, that link microtubules to actin filaments are attracting attention.

The structure of the cross-linking protein profoundly influences the type of network that forms. For example, **fimbrin** is a small, compact protein and has a pair of actin binding sites approximately 180° apart and therefore promotes the formation of tightly bundled actin filaments. Moreover, the binding sites on fimbrin are such that the two actin filaments have plus ends pointing in the same direction (so-called *parallel* polarity), ensuring that bundles form with uniform polarity. The uniformity supports movement in a single direction, as in cytoplasmic streaming (see Section 5.6.1). In contrast, **filamin** has a long and flexible region between actin-binding sites, which tends to promote a random, gel-like network. In addition to mechanical integrity, a gel-like network provides a path for transmitting a signal through the cell rapidly, because a mechanical disturbance initiated at one location in the gel can propagate through the network much faster than a chemical messenger can diffuse.

Nucleating proteins form a template from which the polymer can grow readily, overcoming the kinetic barrier to polymerization (see Section 5.3.1). For microtubules, **γ-tubulin**, a divergent member of the tubulin family, along with several other proteins forms a ring complex that serves as a base from which the αβ-tubulin heterodimers assemble. For actin, nucleation is accomplished by a protein complex containing **ARP2/3,** and several other proteins; alternatively, actin may be nucleated by **formins**. ARP2/3 nucleates filaments on existing actin filaments thereby forming a branched, mesh-like structure, whereas formin nucleates filaments on a membrane and tends to establish parallel filaments. By regulating the sites where nucleating proteins are deployed, the cell can control the sites from which cytoskeletal polymers emerge.

Severing proteins break down filaments. Although, as described (see Section 5.3), pure cytoskeletal polymers break down, the cell does not rely on spontaneous breakdown. Typical severing proteins bind anywhere on the filament and break it. An example of a protein that severs microtubules is **katanin** and one that severs actin filaments is **actin depolymerizing factor**. By creating free ends, severing proteins allow cytoskeletal arrays to be remodeled rapidly, for example promoting depolymerization or making easily translocated fragments. Some proteins break down cytoskeletal polymers from their ends, essentially by enhancing the rate for loss of subunits. Interestingly, several members of the kinesin class of motors have evolved to break down microtubules rather than to move cargo.

5.5 Observing the cytoskeleton: Statics and dynamics

To understand how the cytoskeleton works in a cell, we must go beyond reaction rate constants, genealogies, and catalogs of accessory proteins, and image the cytoskeleton within the cell. With few exceptions, the cytoskeleton in living cells is invisible through the light microscope. To increase its contrast, researchers can attach a fluorescent molecule (a **fluorophore**) to a cytoskeletal protein. Fluorescence offers high contrast because the light from the fluorophore is observed against a dark background. For this approach to succeed, the fluorophore must not alter the behavior of the protein and, likewise, subjecting the cell or organism to fluorescence microscopy must not alter its physiology.

5.5.1 Microinjection of labeled proteins was the first method used to image specific cytoskeletal polymers in living cells

The name "cytoskeleton" evokes a static, bony, armature, and this metaphor dominated early discussions of cytoskeletal function. Although clues were available to cytoskeletal dynamics—for example, from polarized-light microscopy—not until scientists imaged actin filaments and microtubules directly in living cells did the extraordinary dynamics of these polymers become widely appreciated.

Researchers found that a chemical fluorophore (e.g., fluorescein) could be conjugated covalently to tubulin without appreciably altering the biochemical properties of the protein. The labeled subunits, introduced into living cells

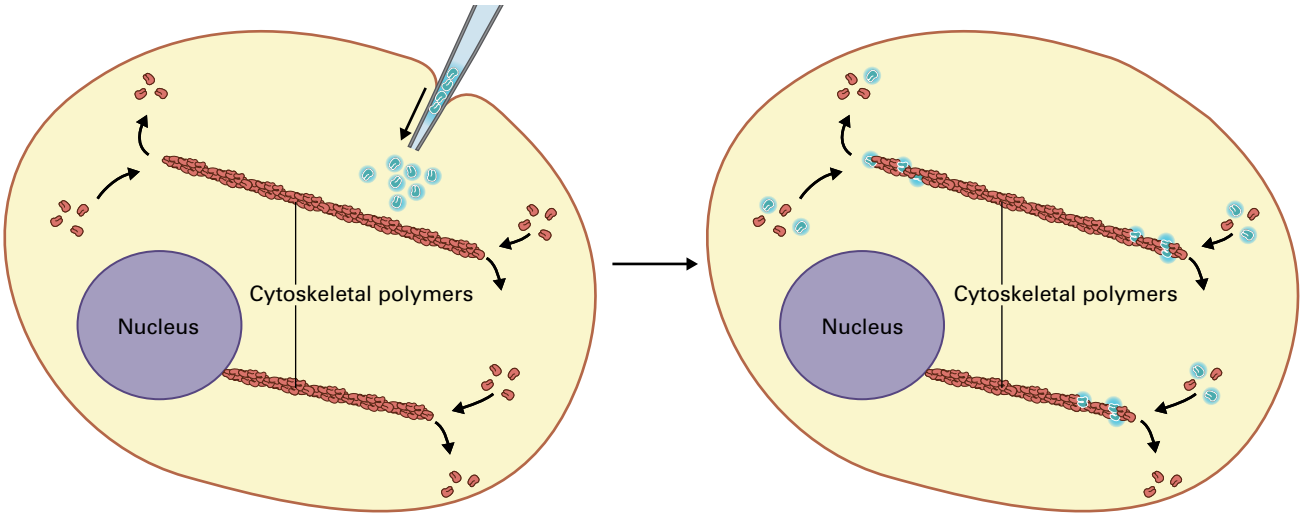


FIGURE 5.15 *Schematic representation of fluorescent analog cytochemistry as applied to cytoskeletal polymers. A cell is microinjected with a small volume of a solution containing the protein of interest conjugated to a bright fluorescent molecule (a fluorophore). A short time later, fluorescent subunits (as well as native subunits) are incorporated into cytoskeletal structures, rendering them visible in fluorescence microscopy.*

by microinjection, would incorporate into the native microtubules, rendering them visible with fluorescence microscopy (Fig. 5.15). Although this technique allowed microtubules to be observed in living animal cells in the 1980s, plant cells were more difficult to microinject because of their thick cell walls and large turgor pressures. In the 1990s, these obstacles were first overcome with stamen hair cells (Fig. 5.16), and soon thereafter in other cell types. In all cases, microtubule arrays were found to be extraordinarily dynamic, with the average individual microtubule half-life being about one minute.

For live imaging studies, actin filaments have also been tagged; however, in plant cells, all attempts have failed to introduce derivitized actin. An alternative has been to use a fluorescent conjugate of the small bicyclic peptide, phalloidin, which binds filamentous actin with high specificity and has been injected successfully into plant cells (Fig. 5.17; see Fig. 5.39). Nevertheless, not only can phalloidin affect actin filament behavior, it can become sequestered in vacuoles and be lost from the cell through plasmodesmata, hindering observations.

5.5.2 Fluorescent proteins have become reporters of choice for live cell imaging

Despite successes, the technical difficulty of microinjection slowed widespread adoption of this method. Instead, fluorescent proteins have become the reporters of choice for localizing proteins in living cells (see Fig. 1.27). Plants expressing labeled tubulin have been widely used and allow dynamics of microtubules to be followed in real time (Fig. 5.18). In contrast to labeled tubulin, where anomalous behavior is minimal, labeled actin has proved problematic. As with chemical fluorophores (see Section 5.5.1), actin tagged with GFP functions poorly in plants, and instead actin-binding proteins are tagged. One promising approach has been to make a chimera between GFP and an actin-binding domain from fimbrin (Fig. 5.19). But even though some of these tagged proteins give rise to plants without apparent defects, the reporter's fluorescence shows the actin-binding protein, which is not necessarily contiguous with the entire actin cytoskeleton. Illustrating this, pollen tubes expressing one of three different tagged actin-binding proteins give three different staining patterns (Fig. 5.20).

5.5.3 Cryofixation offers the highest resolution images of the cytoskeleton

Beyond revealing dynamics, imaging a living cell appeals to our sense of wonder at cellular animation. Nonetheless, there are good reasons for imaging dead cells. Dynamics become a liability when the cell responds to being squeezed beneath a coverslip or irradiated with a laser. Light microscopy works best on objects within a few dozen micrometers of the coverslip; as distance increases, aberrations accumulate and obtaining informative images becomes increasingly difficult. Light microscopy also has limited resolving power, whereas electron microscopy, although having higher resolving power, is incompatible with liquid water and living cells. Therefore, to avoid unwanted cellular reactions, to image deep within a sample, or to take advantage of the resolution of electron microscopy, scientists have long relied on imaging dead cells, and they are likely to continue to do so for the foreseeable future.

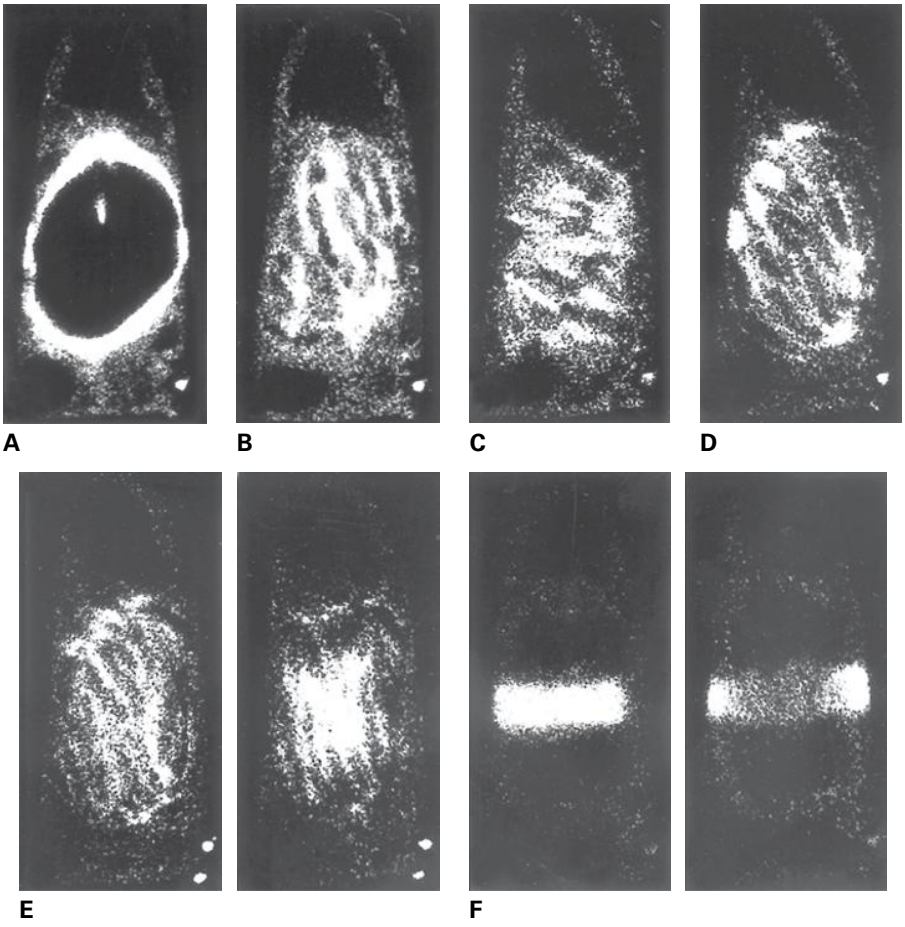


FIGURE 5.16 *Confocal fluorescence micrographs of a living stamen hair cell that was microinjected with tubulin purified from cow brain and derivatized with a fluorophore. These images represent the first use of fluorescent-analog cytochemistry to label the cytoskeleton in living plant cells. The disposition of microtubules is shown as the cell moves from (A) prophase through (B) prometaphase, (C) metaphase, (D) anaphase, (E) telophase, and (F) cytokinesis.*
Source: Zhang et al. (1990). Proc Natl Acad Sci USA 87:8820–8824.

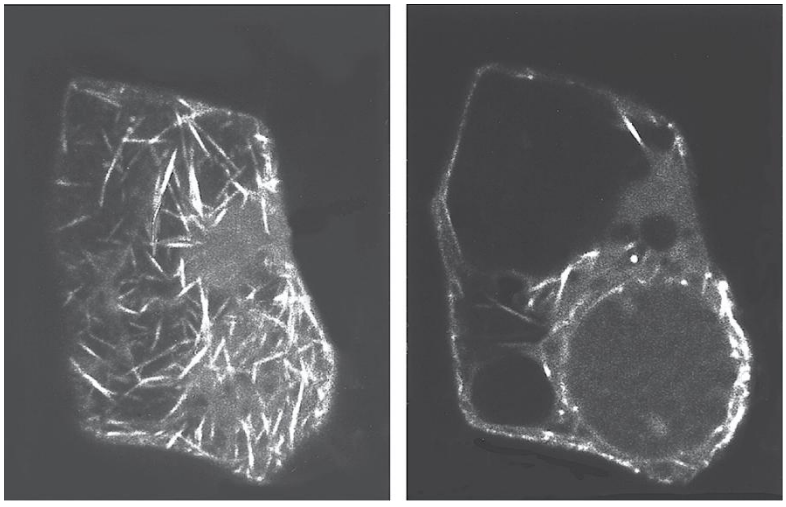


FIGURE 5.17 *Confocal fluorescence micrographs of a living leaf epidermal cell of* Tradescantia virginiana *microinjected with an actin-binding fluorophore (rhodamine-phalloidin). Left-hand panel shows the cell cortex, rich in filamentous actin; right-hand panel shows a focal plane at the nuclear level, showing the basket of actin that typically surrounds this organelle.*
Source: Cleary. (1995). Protoplasma 185:152–165.

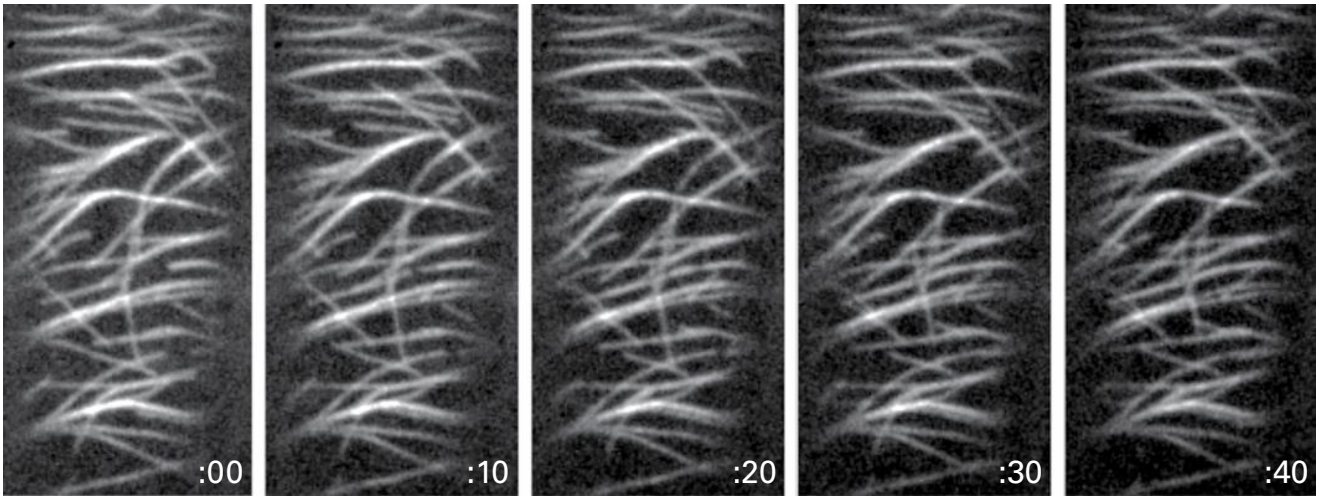


FIGURE 5.18 *Green fluorescent protein (GFP) provides a powerful alternative to microinjection for labeling cytoskeletal structures. This example shows cortical microtubules imaged with confocal fluorescence microscopy in the hypocotyl of* A. thaliana*. The images were taken at 10-second intervals. At first glance the array looks static, but following individual microtubules shows that many of them are growing and shrinking dynamically. Source*: S. Shaw, Indiana University.

For years, the way to kill a cell for microscopy, called fixation, was with alcohol. In the 1960s, after the introduction of an improved chemical fixation, based on glutaraldehyde, microtubules were imaged for the first time, a breakthrough that occurred with plant material. However, even the best chemical fixatives require minutes to halt the dynamic activities of cells. This is time enough for unnatural changes to occur while some cell components are fixed while others continue to move and react.

To overcome this problem, microscopists have turned to **cryofixation**. Samples are cryofixed by plunging them into a cryogenic liquid with a high heat capacity (e.g., propane) at a low temperature (−180°C). This removes heat from the sample so rapidly that insufficient energy remains to form ice (because ice expands, its formation damages the sample). The sample freezes in milliseconds, leaving little time for changes to occur. At ambient pressure, heat can be removed efficiently only from the outer 5–10 μm of the sample, restricting plunge freezing to single cells. However, using specialized apparatus, **high-pressure freezing** allows cryofixation under pressure, which prevents water crystallization for a considerable thickness (as much as 1–2 mm in favorable samples). Following cryofixation, the supercool water in the sample is exchanged with a solvent, such as acetone, at a temperature that is warmer (−80°C) but still too cold for formation of ice crystals. This exchange is called **freeze substitution**. Once the water is replaced with solvent, the sample can be processed for electron microscopy as usual.

Cryofixation halts all dynamic processes within milliseconds, the structures revealed often appear more life-like than those obtained with chemical fixation (Fig. 5.21). Recently, cryofixation has been used to address the problem of actin localization in the pollen tube. Contradictory images of actin in pollen tubes had been reported by different laboratories and sometimes even by the same laboratory in different papers. Discordant images were likewise produced by living-cell reporters (see Fig. 5.20). Cryofixing pollen tubes followed by freeze-substitution and staining with anti-actin revealed two features of actin (Fig. 5.22). First, fine actin filaments fill the shank of the tube: the thick bundles previously reported probably represent a bundling induced by fixation. Second, a dense fringe of cortical actin subtends the apex. This unusual structure is believed to play a pivotal role in the process of tip growth.

5.6 Role of actin filaments in directed intracellular movement

In all cells, the cytoskeleton interacts with organelles to move them specifically or to prevent their moving by providing anchorage. In plant cells, organelles move mainly on actin, whereas in animal cells organelles mainly ride microtubules. There are exceptions, and in both kingdoms microtubules and actin are increasingly realized to cooperate to direct organelle traffic optimally. Curiously, a similar reversal occurs in cell shaping, which in animals is directed by actin but in plants by microtubules (see Section 5.7). These evolutionary role reversals underscore the idea that eukaryotes invented cytoskeletal polymers early and, as they subsequently evolved, used them with considerable modularity. Animals and plants represent just two branches of the eukaryotic tree—once this diversity is sampled more richly for cytoskeletal function, we should have a better context for understanding these global shifts in function.

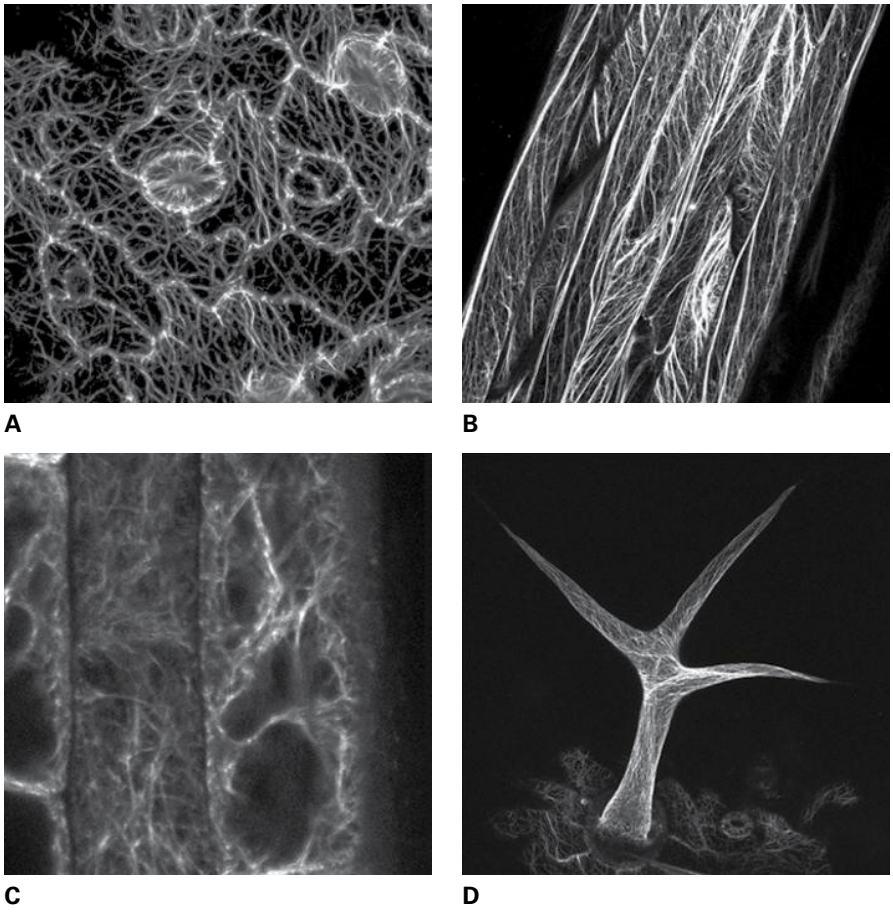


FIGURE 5.19 *The actin cytoskeleton can also be labeled with GFP reporters, albeit indirectly. These images are confocal fluorescence micrographs of various cell types in* A. thaliana *expressing a reporter containing GFP and sequences from the actin-binding protein, fimbrin. Dense networks of actin are seen in many cell types, including (A) the epidermis of a cauline leaf (the oval shapes are stomata), (B) a leaf vein, (C) cortical parenchyma of the root's elongation zone, and (D) a trichome.*
Source: E. Blancaflor, Noble Foundation, Ardmore, Oklahoma.

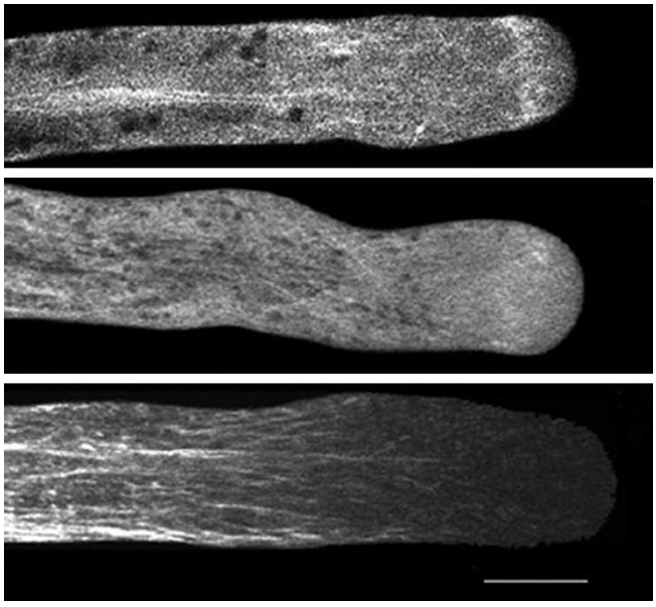


FIGURE 5.20 *Actin reporters based on fluorescent actin-binding proteins label only a subset of actin structures. These are confocal fluorescence micrographs of lily pollen tubes expressing reporters using different actin-binding proteins. Each reporter gives rise a distinct pattern of "actin". Bar = 10 μm.*
Source: Modified from Wilsen et al. (2006). Sex Plant Reprod 19:51–62.

5.6.1 Cytoplasmic streaming requires actin

Cytoplasmic streaming is the bulk movement of cytoplasm, literally streaming through the cell. Streaming is prominent in large, highly vacuolated cells (see Box Fig. 5.2A), such as the giant, algal internodal cells of the Characeae. The enormous size of these cells facilitated development of a pioneering model, allowing reactivation of motility with purified components (Fig. 5.23). In these cells, the cytoplasm is partitioned into a stationary layer in the cell cortex and an internal streaming layer, called the endoplasm. Near the boundary between layers lie long parallel bundles of actin filaments with uniform polarity. These bundles are firmly anchored to rows of chloroplasts, immobilized in the cortex by ramifying connections ultimately reaching the cell wall. The endoplasmic reticulum (ER) and other large organelles have myosin on their membranes, which drives organelle movement in a uniform direction, as specified by the polarity of the fixed actin filaments. The motion of the large organelles causes the entire endoplasm to flow.

Streaming in cells of land plants likewise involves myosin-bound organelles moving along actin filaments. Unlike the algal internodes, plant cells have dynamic actin so that

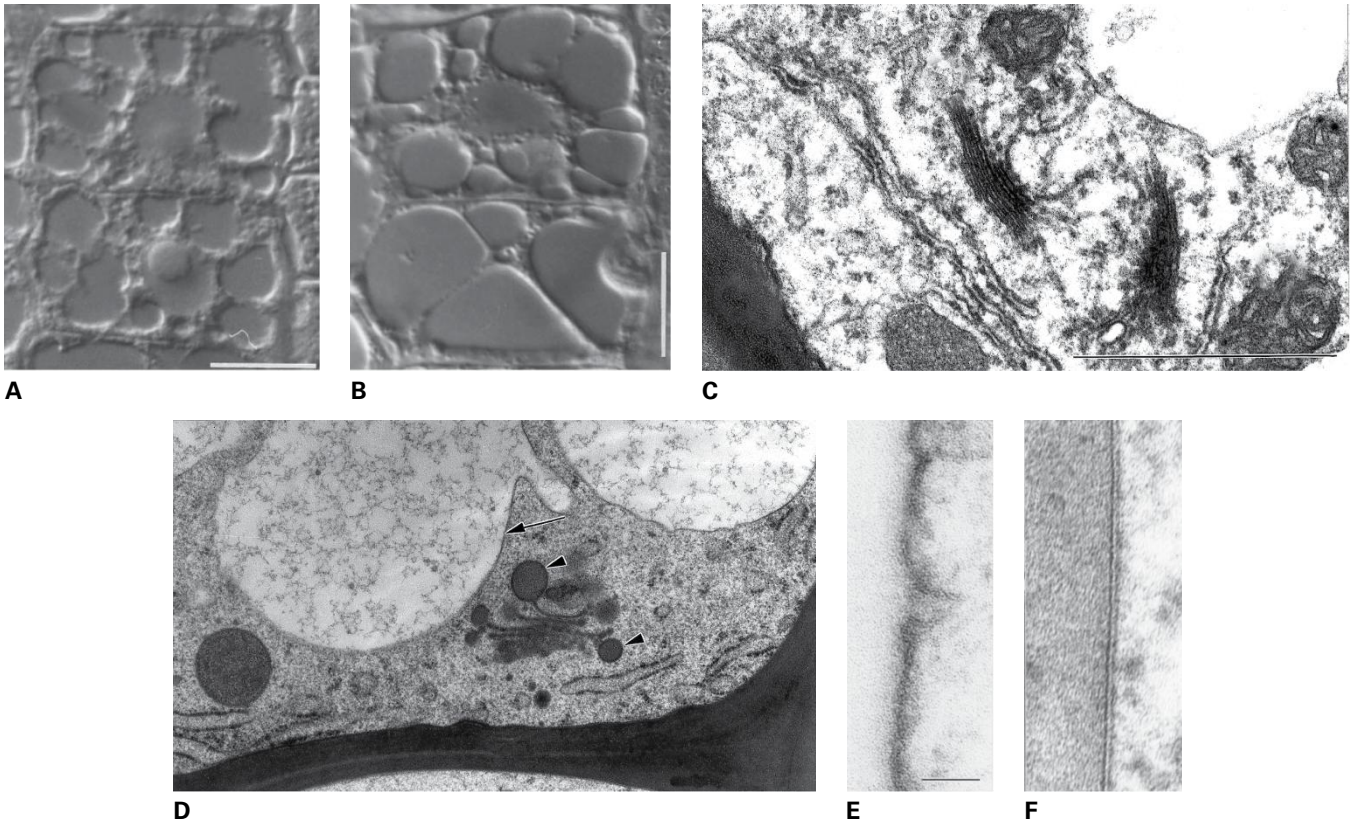


FIGURE 5.21 *Comparisons of chemical and cryofixation. (A,B) Nomarski optics of sectioned* A. thaliana *roots prepared by (A) chemical fixation and (B) cryofixation. Note the coagulated cytoplasm in A compared to B, where the transvacuolar strands almost seem to remain under tension. Bars = 10 μm. (C–F) Transmission electron micrographs of tobacco (*Nicotiana tabacum*) roots comparing chemical fixation (C and E) with high-pressure cryofixation (D and F). Note the smooth membranes (arrow), spherical organelles (arrowheads) and dense cytoplasm present in the cryofixed sample (D). At higher magnification, the plasma membrane of the chemically fixed cell is distorted (E), whereas that of the cryofixed cell appears as a smooth bilayer (F). Bars = (C, D) 2 μm, (E, F) 25 nm.*
Source: (A, B) Baskin et al. (1996). J Microsc 182:149–161. (C–F) Kiss et al. (1990). Protoplasma 157:64–74.

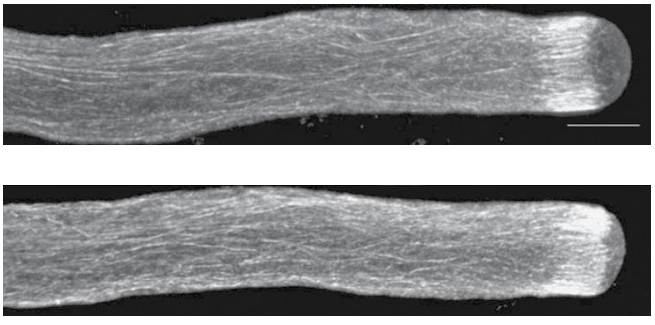


FIGURE 5.22 *Cryofixation defines the instantaneous state of actin filaments in the pollen tube and provides a reference to optimize a protocol for chemical fixation. Confocal micrographs of lily (*Lilium longiflorum*) pollen prepared by cryofixation (top) and an optimal chemical fixation (bottom). The dense ring of subapical actin and the finely divided filaments filling the shank are a consistent feature of actin images from cryofixed pollen tubes of many species. The cryofixed image provided a reference that allowed the development of a chemical fixation protocol that yielded similar images (bottom). Bar = 10 μm.*
Source: Lovy-Wheeler et al. (2005). Planta 221:95–104.

streamlines meander as actin filaments rearrange. Nevertheless, the result is similar, a thorough mixing of organelles within the cytoplasm despite the massive vacuole. In cells without large vacuoles, organelles also undergo sustained movements along actin filaments but without causing bulk flow (i.e., streaming) within the cytoplasm (see Fig. 5.26B,C).

5.6.2 Sustained movement and anchoring of organelles depend on actin filaments.

By far the most well-studied organelle movements in plants are those of chloroplasts. In photosynthetic cells, as the light environment changes, chloroplasts move to absorb light optimally, maximizing absorption in dim light but minimizing absorption in bright light (Fig. 5.24). Light-induced movement of chloroplasts, and their subsequent anchorage, depends on actin filaments (Fig. 5.25). In some plants, a meshwork of actin filaments encases chloroplasts when they are anchored and this arrangement changes to a more linear pattern ("tracks") when the chloroplasts are moving; however,

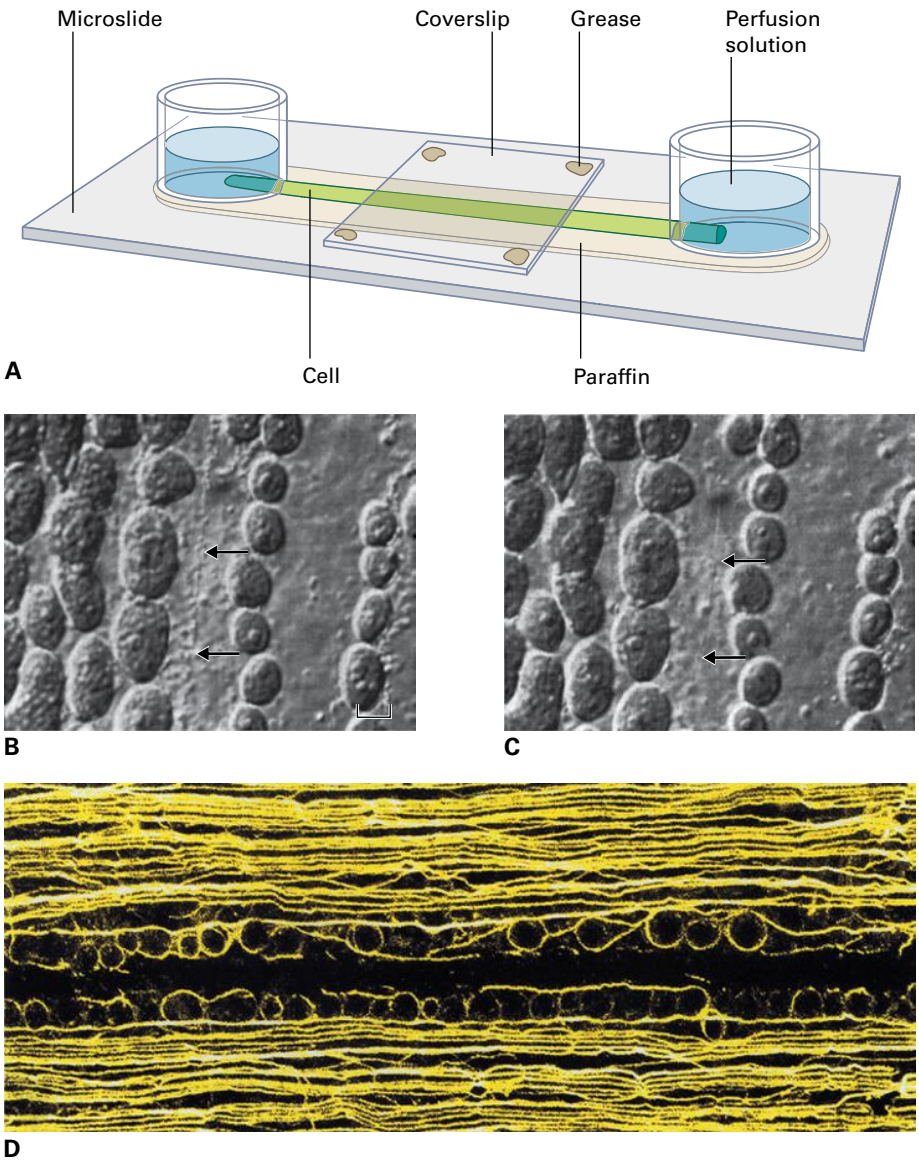


FIGURE 5.23 *The giant internodes of characean algae were used in early functional studies of cytoplasmic streaming. (A) Perfusion chamber. An internode is placed on a microscope slide and each end of the cell is placed under a glass ring with a notch cut to accommodate the cell. The perfusion solution is placed in the rings, and the portion of the cell between the rings is covered with liquid paraffin. Under these conditions, intact cells continue to stream for more than a week. To begin an experiment, one severs the ends of the cell and perfuses through solution. This removes the central vacuole and much of the endoplasm; however, the cortical cytoplasm containing the chloroplasts and associated cytoskeletal elements remain. (B, C) Light micrographs of a perfused cell in the chamber. Arrows point to a bundle of actin filaments that has been dislodged from a nearby row of chloroplasts. In (B), the bundle is covered with small particles. In (C), a solution containing ATP was perfused through, which reactivates streaming, moving the particles along the bundle and out of the field of view. This movement is now known to be powered by myosin and to underlie cytoplasmic streaming in many plant cells. (D) Fluorescence micrograph showing a region of the cortical cytoplasm from a giant algal internode stained with fluorescent phalloidin to localize actin filaments (yellow). Files of chloroplasts are also visible beneath the bundles. Source*: (B, C) Williamson. (1975). J Cell Sci 17:655–668. (D) G. Wasteneys, Australian National University, Canberra.

in other plants structural changes in the actin network are not observed. Given the importance of optimal light capture and the range of conditions where leaves photosynthesize, it should not be surprising that chloroplasts are moved by the actin system in more than one way. Plastid movements are also important in tissues that sense gravity; in these tissues, plastids (called amyloplasts because of their prominent starch grains) sediment in response to gravity. It is not known precisely how the cell senses the direction in which the amyloplasts fall, but several lines of evidence point to the importance of an actin meshwork that surrounds these organelles.

The Golgi apparatus, ER, mitochondria, and peroxisomes, all move along actin filaments in plants, contrasting their microtubule-based movement in animal and fungal cells. Because actin filaments pervade the plant cytosol in a dense meshwork, even forming thin, membrane-covered protrusions

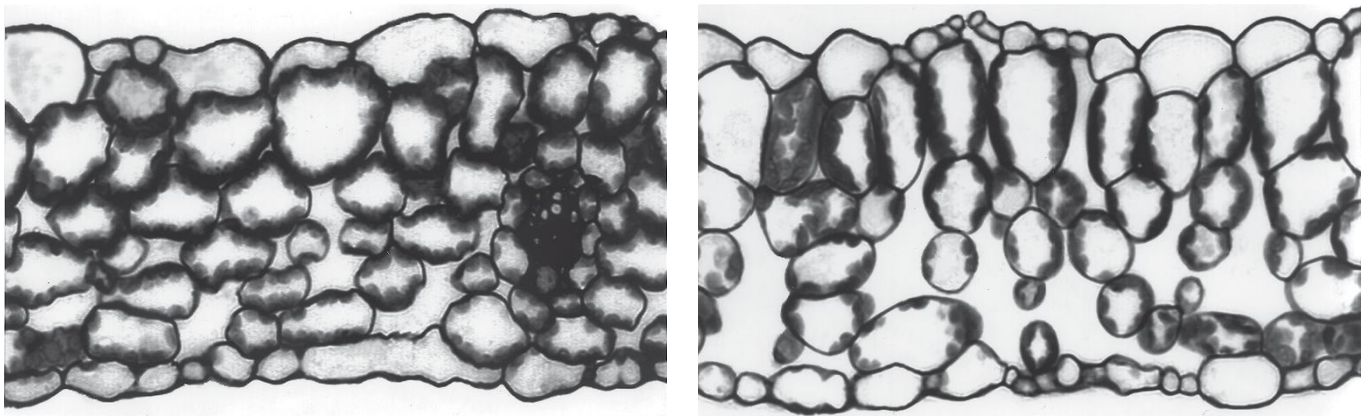
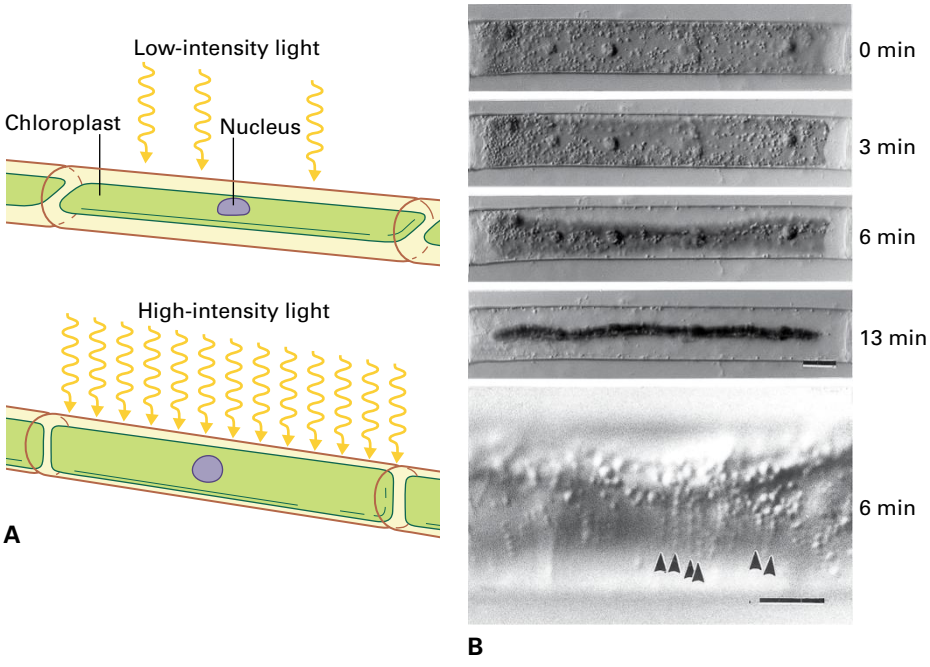


FIGURE 5.24 *As shown in cross-sections through the leaf of* A. thaliana, *chloroplasts move to maximize or minimize their absorption of light. (A) Exposed to dim light, chloroplasts move to walls parallel to the leaf surface, and stay there, thus maximizing light absorption for photosynthesis. (B) Exposed to bright light, chloroplasts migrate to cell walls perpendicular to the leaf surface, thus minimizing light absorption and photodamage.*
Source: Trojan & Gabrys. (1996). Plant Physiol 111:419–425.

FIGURE 5.25 *Studies of chloroplast movement have taken advantage of the green algal genus,* Mougeotia, *the cells of which contain a single, plate-shaped chloroplast that spans the entire cell. (A) In dim light, the flat side of the chloroplast faces the light, whereas in bright light, the edge faces the light. (B) Time course of chloroplast rotation in response to bright light, incident perpendicular to the page. The final image is at higher magnification and shows the edge of the chloroplast associated with cytoplasmic filaments, demonstrated to contain actin (arrowheads). Scale bar = 10 μm.*
Source: (B) Mineyuki et al. (1995). Protoplasma 185:222–229.



through the large central vacuole, organelles tracking actin thus are dispersed throughout the cell. The Golgi apparatus in animal cells is clustered beside the nucleus by means of minus-end-directed microtubule motor proteins that move the Golgi stacks toward the centrosome; whereas in plant cells, Golgi stacks move along actin filaments, albeit in a stop-and-go fashion, and are everywhere (see Fig. 1.27). In the cell cortex, the ER spreads out into a network of fine tubules connected by polygonal cisternae (see Fig. 1.16), an arrangement that depends on actin filaments anchored to the plasma membrane. Ribosomes and other structures for RNA processing also interact with actin filaments, an association attracting recent interest.

Plant mitochondria and peroxisomes also depend on actin to move, but interestingly these organelles also interact with microtubules, an interaction whose physiological relevance remains conjectural. Peroxisomes illustrate some of the puzzling features of organelle motility. These organelles have a myosin isoform on their membrane and their location and movement closely follow actin filaments. However, peroxisomes tend to be static in leaf mesophyll cells, unlike Golgi or plastids, and the extent of their motility in other cells varies with cell type and development. Surprisingly, peroxisomes aggregate at cytokinesis around the forming cell plate in members of the genus *Allium* but Golgi remain dispersed, as do peroxisomes in numerous other genera, both monocot and eudicot (Fig. 5.26). No one knows why alliacious peroxisomes aggregate so strikingly, nor why other organelles with actin-dependent motility are left behind. Evidently, cells have evolved layers of regulation to control which organelle moves where, and under what circumstances, regulatory mechanisms that are completely undiscovered.

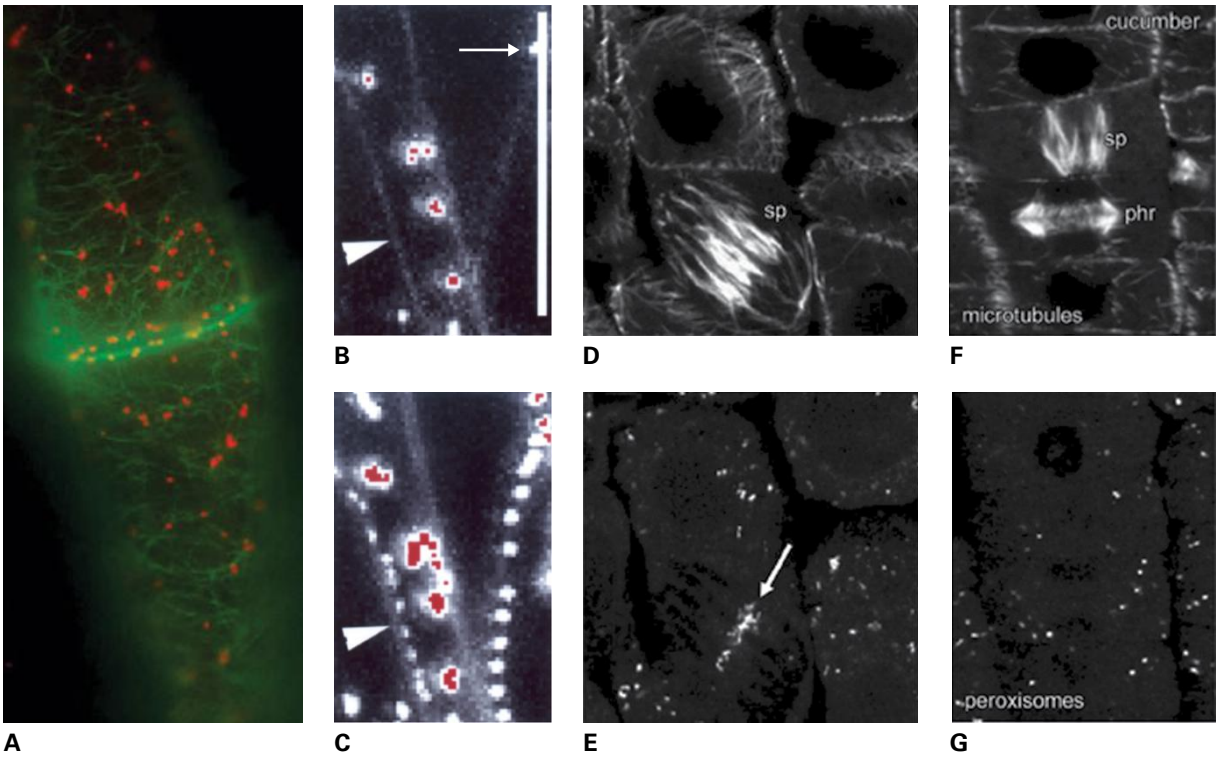


FIGURE 5.26 *Organelle motility. (A) Confocal fluorescence micrograph of a pair of tobacco cultured cells expressing a fluorescent reporter for actin (green) and Golgi (red) and showing their association, typical of plant organelles. (B, C) Confocal fluorescence micrographs of peroxisomes (arrow) moving on actin (arrowhead) in onion epidermis. B is a single frame and C is a superposition of several frames, where moving peroxisomes appear as a train of dots. Bar in B = 25 μm. (D–G) Curious peroxisome behavior in* Allium. *Fluorescence micrographs of sections double labeled for (D, F) microtubules and (E, G) peroxisomes. At mitosis and cytokinesis, cells in* Allium cepa *(D, E) accumulate peroxisomes strikingly at the equator (arrow), whereas this aggregation does not occur in other genera, such as in* Cucumis *(F, G). Furthermore in* Allium, *the Golgi apparatus remains dispersed (not shown) despite both organelles using actin for motility.*
Source: (A) A. Nebenführ, University of Tennessee. (B, C) Jedd & Chua. (2002). Plant Cell Physiol 43:384–392. (D–G) Collings & Harper. (2008). Int J Plant Sci 169:241–252.

5.6.3 Actin filaments participate in traffic to and from the plasma membrane

As described in Chapter 1, cells are congested with vesicular traffic, carrying membrane and soluble cargo from one organelle to another. The best-understood road runs from Golgi apparatus to plasma membrane, an outflow of material termed **secretion**. It is often assumed that secretory vesicles always move on actin filaments but this probably depends on cell type. Actin inhibitors do not always diminish rates of secretion measured biochemically, and given the proximity of Golgi bodies to the plasma membrane, a dedicated secretory "highway" is likely to be needed only in cell types that place particular demands on the secretory system, for example, root cap cells that secrete large volumes of slime to condition the rhizosphere.

Secretion is balanced by returning vesicles, going from plasma membrane to either Golgi or vacuole, an inflow of material called **endocytosis**. This pathway absolutely requires actin in animal and fungal cells; whereas, in plants, endocytosis can occur without actin, although rates and targeting are affected. In general, the role of actin in plant vesicle transport, both inward and outward, requires further study.

Two examples where actin filaments play an undisputed role in vesicle transport are in cells responding to pathogen attack and in tip-growing cells. Many pathogens initiate their attack by pushing against a cell, forming a structure called an **apressorium**. The plant cell responds to the pressure with a massive reorganization of both microtubules and actin filaments, with that of actin having been most clearly linked to a successful resistance. The actin filaments become focused on the apressorium and drive the accumulation of organelles and a localized cell wall thickening that hinders pathogen ingress (Fig. 5.27).

In pollen tubes, which grow by tip growth, actin filaments are polarized along the cell cortex to move secretory vesicles (and organelles) toward the tip and are polarized in the center of the tube to move endocytic vesicles (and organelles) away from the tip (Fig. 5.28). The vesicles associate with actin filaments and have myosin in their membranes. The high rates of relative expansion sustained by tip-growing cells require delivery of a large quantity of wall precursors without interruption. Moreover, streaming is *less* sensitive to the disruption of the actin cytoskeleton than is growth itself, an observation that has been interpreted as indicating a requirement for actin beyond vesicle transport to the tip. The exact roles of the actin cytoskeleton in inward and outward vesicle trafficking await their Mendel.

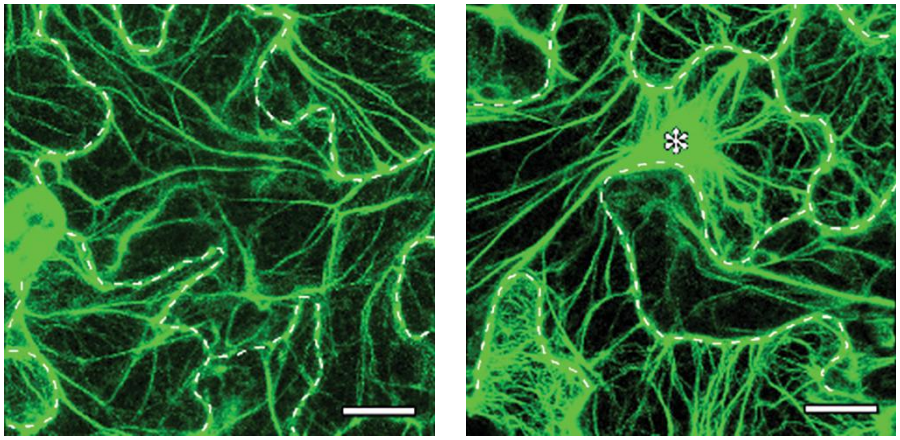


FIGURE 5.27 *Actin filaments help plants resist infection by pathogens. In this example showing cotyledon epidermal cells before (left) and 1 day after infection with powdery mildew (right), actin filaments, labeled with a GFP actin-binding protein, in the infected cell form a radial array focused on the infection site (asterisk). This configuration is thought to support the formation of wall thickening making it more difficult for the pathogen to enter the cell. Bar = 20 μm.*
Source: D. Takemoto, Univesity of Nagoya, Japan.

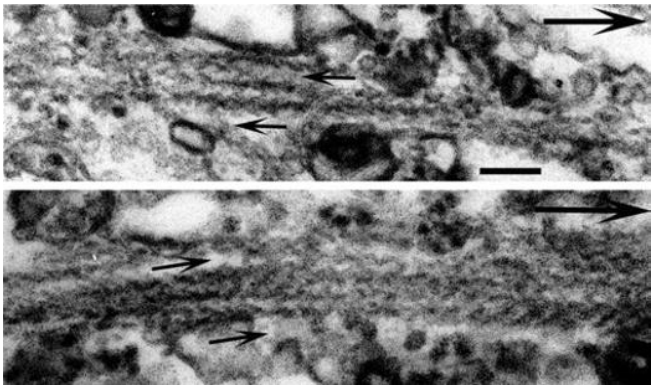


FIGURE 5.28 *Actin filaments are polarized in the growing pollen tube to support movement of vesicles to the tip along the tube cortex (top) and away from the tip in the center of the tube (bottom). Transmission electron micrographs of pollen tubes where, prior to embedding, the cells were incubated in a fragment of myosin which binds asymmetrically, forming arrowheads. Small black arrows show direction of myosin pointed ends and large black arrows point to the pollen tube tip. Bar = 100 nm.*
Source: Lenartowska & Michalska. (2008) Planta 228:891–896.

5.7 Cortical microtubules and expansion

Whereas actin stars in intracellular motility with microtubules supporting, the casting is reversed in the process of diffuse growth (so-called when growth occurs throughout the cell). Diffuse-growing plant cells usually expand faster in one direction than in another, that is, anisotropically. Anisotropic expansion underlies the plant's ability to make cylindrical stems, flat leaves, not to mention a petal shaped like a bee (made by certain orchids to lure pollinators). Anisotropic expansion depends on microtubules; when they are inhibited, the rate of increase in volume remains constant but the anisotropy of expansion decreases, often becoming isotropic.

5.7.1 An array of cortical microtubules controls the anisotropy of expansion

A dense array of microtubules lies just inside the plasma membrane of interphase plant cells, in the cortical cytosol (see Fig. 5.18). These so-called **cortical microtubules** are found in nearly all plant cell types although they are broken down during mitosis. In immunofluorescence light micrographs, the array looks like a single structure, encircling the cell; however, in electron micrographs, the array is resolved into a series of short (<10 μm), partially overlapping microtubules (Fig. 5.29). The microtubules within the array run mostly parallel one another and are close to and often touching the plasma membrane. The orientation of cortical microtubules was originally thought to be uniform per cell, but we now know that orientation can differ on different walls of a single cell. In elongating cells, their net orientation is perpendicular to the direction of most rapid expansion, an orientation that is referred to as "transverse." As elongation stops, transverse microtubules reorient to form helices around the cell, which is the typical orientation for non-growing cells.

A major function of the cortical array is to influence the direction of cellulose microfibril deposition, which in growing cells specifies the direction of maximal cell expansion (see Chapter 2). Except in tip-growing cells (such as pollen tubes and root hairs), the alignment of the cellulose microfibrils parallels that of the microtubules (Fig. 5.30). Cellulose microfibrils parallel the underlying cortical microtubules when protoplasts regenerate a cell wall. Both cellulose and microtubules become oriented in helices as cells mature, with a helical arrangement of cellulose microfibrils providing plywood-like reinforcement for the wall. Cellulose microfibrils also parallel the microtubules in developing secondary walls. When cell wall thickenings form in tracheids, the banded deposition of cellulose is preceded by a bundling of cortical microtubules. Finally,

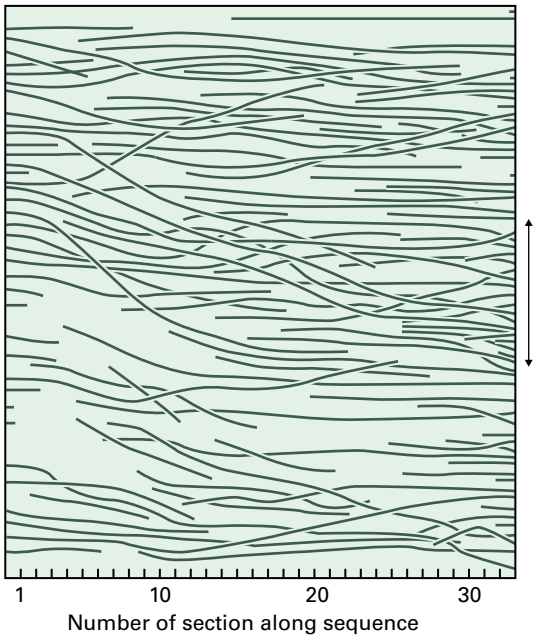


FIGURE 5.29 *A map of the cortical array of microtubules from a cell in the root of* Azolla pinnata*, based on reconstructions from serial sections examined with electron microscopy. The double-headed arrow represents the direction of maximum expansion rate.*

when microtubules are lost, either by experimental treatment with inhibitors or naturally, as in the leaf sheath cells of certain bulb-forming monocots, cellulose microfibrils are usually deposited with less organization and expansion is no longer as anisotropic.

Although such evidence makes it clear that cortical microtubules influence the orientation of cellulose, the mechanism behind this influence has not been discovered. Furthermore, microtubules might also influence other attributes of cellulose microfibrils, for example, their strength or their integration within the cell wall, both properties being important for expansion anisotropy. The strength of the microfibril could be influenced by proteins binding the microtubule that keep the cellulose synthase running optimally, like the coal-car behind a locomotive. Microfibril integration could be influenced by transmembrane proteins that bind microtubules with their cytosolic domains and, with their extracellular domains, promote reactions that integrate cellulose microfibrils into the cell wall fabric. Combining live-imaging and structural analysis of the cell wall is beginning to let us evaluate these possibilities and discover new ones.

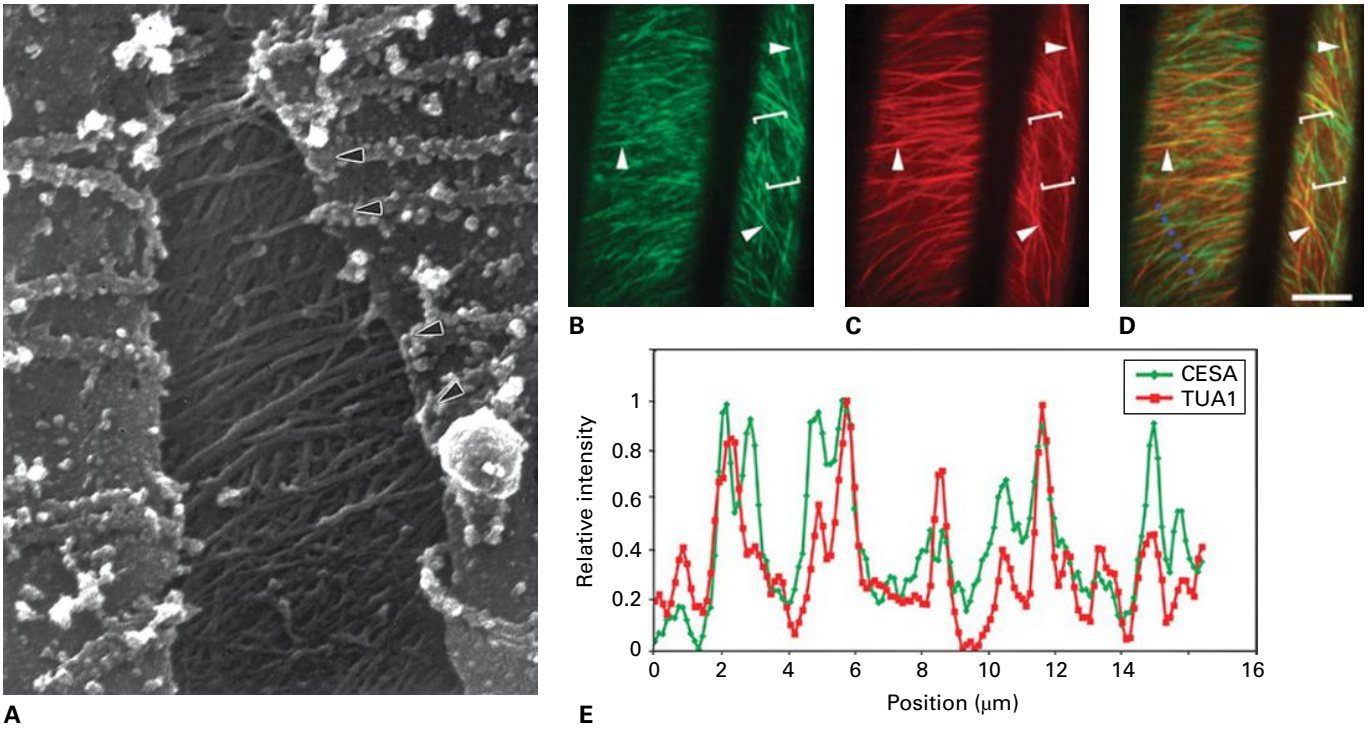


FIGURE 5.30 *Cellulose microfibrils parallel cortical microtubules. (A) Field-emission scanning electron micrograph of the interior of an onion root cell, looking toward the cell wall. Shown is the cortical cytoplasm on either side of a tear in the plasma membrane through which the cell wall is visible. The orientation of cortical microtubules (arrowheads) can be seen to parallel the direction of many of the microfibrils in the cell wall. (B–E) Live cell imaging of* A. thaliana *hypocotyls expressing fluorescently tagged tubulin (C, red) as well as cellulose synthase tagged with a yellow fluorescent protein (B, green). At a single time, the cellulose synthase labeling is point-like; the image (B) was made by summing consecutive frames so that the movement of the point becomes a line, defining the trajectory of motion (arrowheads in B). D merges both green and red signals into a single image, in which overlap of green and red appears yellow. Bar = 10 μm. The graph (E) plots the intensity of the green and yellow signal along the purple dotted line (in D). The cellulose synthase trajectories closely parallel the underlying microtubules, as seen by the many yellow lines in D and the correlated intensity profiles (E).*
Source: (A) Vesk et al. (1996). Protoplasma 195:168–182. (B–E) Paredez et al. (2006). Science 312:1491–1495.

5.7.2 Cortical microtubules collaborate with actin filaments in cell shaping

In contrast to the roughly cylindrical or polyhedral shapes of most plant cells, certain cell types are marvels of miniature sculpture. These shapes are carved by actin filaments and microtubules working together. Well-studied examples are leaf epidermis and mesophyll, which are highly sinuous at maturity (Fig. 5.31). In both cell types, microtubules and actin are deployed complementarily. In mesophyll, microtubules form thick bands here and there and actin filaments are enriched between the bands. Importantly, the microtubule bands form back-to-back in neighboring cells. In an epidermal cell, actin filaments are enriched within outward bulges whereas microtubules form preferentially within inward bulging regions; because an outward bulge of one cell is an inward bulge of its neighbor, microtubules and actin filaments have alternating deployments in neighboring cells. Within a cell, the mechanisms driving this complementary deployment are being actively investigated and apparently involve feedback in which actin filaments bind proteins that destabilize microtubules, and vice versa.

The complementary deployment of these systems contributes to cell shaping although this is clearer for mesophyll than for epidermis. In mesophyll, cells separate between expanding lobes, a separation that creates the airspaces essential to photosynthesis. The microtubule bands cause the underlying cell wall to thicken, thereby restricting expansion, while the actin filaments, perhaps by promoting secretion, locally enhance expansion; in concert, this pushes cells apart by growth at the lobes with air spaces forming where the cells are restricted (Fig. 5.31). In contrast, epidermal cells remain fully contiguous. Therefore, a lobe reflects an overlying area of rapid expansion rate (over an actin-rich region) adjacent to a region of slow expansion rate (over a microtubule-rich region). In these cells with elaborate shapes, as well as others such as trichomes and guard cells, antagonistic roles of microtubule and actin systems are being discovered and elucidated.

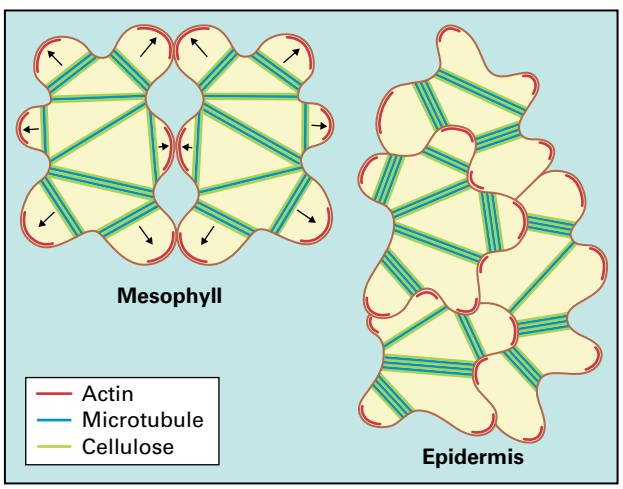


FIGURE 5.31 *The cytoskeleton is involved in producing complex cell shapes, as exemplified by spongy mesophyll and epidermal pavement cells. In mesophyll (left), microtubule bands (blue) girdle the cell while actin patches (red) form between microtubule bands; importantly, microtubule bands form opposite each other in neighboring cells, as do the actin patches. The microtubule bands cause congruent wall reinforcement (green) whereas the actin patches promote expansion, giving rise to lobes and cavities, and hence to the characteristic sponginess of mesophyll. However, in epidermis (right), actin patches and microtubule bands alternate between neighbors. This organization partitions the periclinal cell wall into regions of high and low expansion rate, and the lobes reflect this underlying variation.*

5.7.3 The cortical array is organized by a mechanism that separates nucleation and orientation

The mechanism that organizes the cortical array is an outstanding problem in plant cell biology. Virtually all known microtubule arrays, whether plant, animal, or fungal, are organized with respect to a prominent structure, such as the centrosome or the basal body, that houses the γ-tubulin complexes responsible for nucleating microtubules (see Section 5.3). By controlling where microtubules can form, these organizing structures determine the position of microtubules as well as their polarity (the minus end is at the nucleating site). The plant cortical array forms diffusely, with neither prominent organizing structures nor defined patterns of microtubule polarity. The cortical array contains γ-tubulin complexes, scattered throughout the array and supporting microtubule nucleation (Fig. 5.32). The nucleated microtubules often form at an acute angle to the original microtubule, giving rise to diverging microtubules, which are organized subsequently into the parallel alignment desired by the cell. Evidently, for the cortical array, the processes of nucleation and organization are distinct.

The problem of organizing the microtubules can be usefully broken down into three steps: (a) a signal must specify a direction, (b) that signal must be perceived by some cellular components and transmitted to the microtubules, and (c) the microtubules themselves must line up accordingly. The signal providing a polarity cue (step a) could be mechanical, electrical, or chemical. The transduction mechanism (i.e., perception, step b) is widely thought to involve a transmembrane protein or protein complex, in which the extracellular domain "senses" the signal, and the cytosolic domain constrains microtubule behavior. Behavior (i.e., the response, step c) can include specific interactions between microtubules, moving microtubules into correct alignment with a motor protein or treadmilling, and selectively stabilizing those microtubules that happen by chance to form at the correct angle. Cortical microtubule behavior is known to be affected

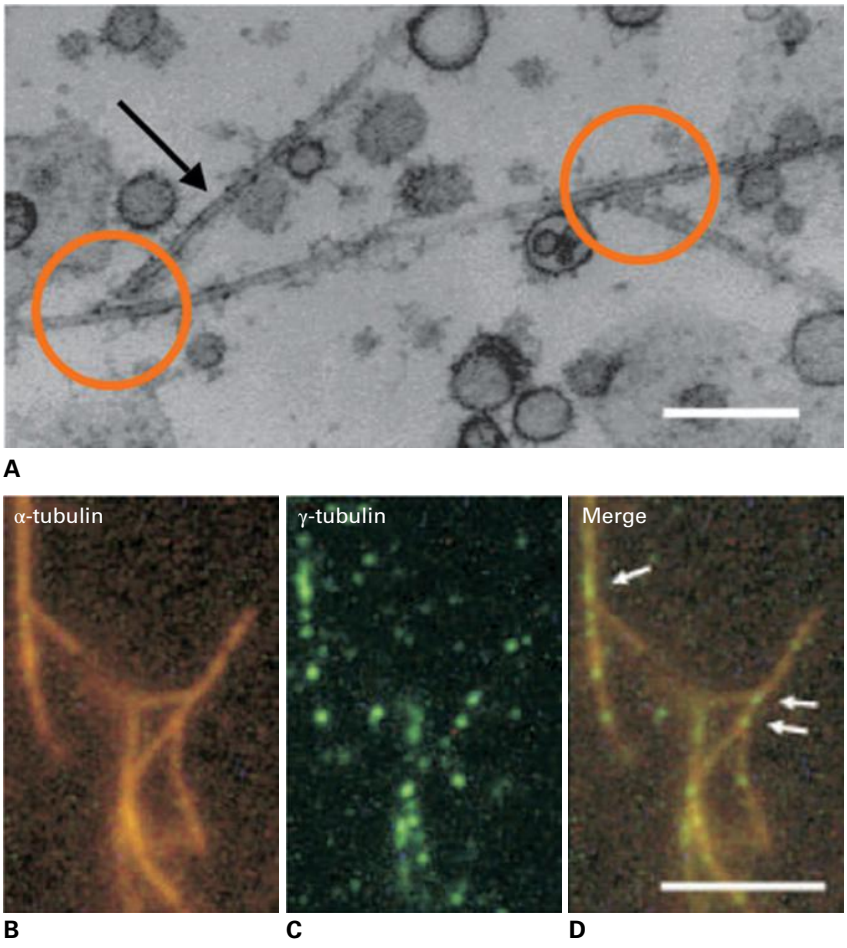


FIGURE 5.32 *The formation of the cortical array can be studied in vitro. Microtubules form de novo when fragments of the plasma membrane are incubated in a cell extract. The extract contains αβ-tubulin as well as γ-tubulin nucleating complexes, but new microtubules form only when the membrane fragment retains cortical microtubules. (A) Transmission electron micrograph showing microtubules nucleated along the side of an existing microtubule (circles). Bar = 200 nm. (B–D) Fluorescent micrographs showing microtubules (B) and γ-tubulin (C), and overlay (D). The γ-tubulin binds all along microtubules and is present at branch points (arrows in the merged image). Bar = 5 μm. It is believed that, in cells, continuous turnover of cortical microtubules is supported by γ-tubulin complexes binding to an existing microtubule, nucleating a microtubule, detaching after a while from that microtubule, and then binding another microtubule to repeat the process. Source*: Murata et al. (2005). Nature Cell Biol 7:961–968.

by interactions between microtubules, as well as by signal transduction elements, such as protein phosphorylation (Fig. 5.33; see Chapter 18). However, we are far from understanding the means whereby the plant lines up its cortical microtubules in a particular direction.

5.8 The cytoskeleton and signal transduction

Only connect. This motto was coined as advice for humanity; it also applies to cellularity. The cytoskeleton—large, pervasive, and filamentous—connects the cell. This connectivity means that the cytoskeleton is more than a substrate for motility; additionally, the cytoskeleton forms a compartment, providing a restricted space, and the cytoskeleton responds to mechanical forces. These related features of cytoskeletal function are subsumed here under the heading of *signal transduction* and described below. Ultimately, the machinery of signal transduction, such as G-proteins and kinases (see Chapter 18), is modulated, but specific pathways will not be elaborated here.

5.8.1 The cytoskeleton acts as a metastable compartment

Among the types of proteins discovered to bind the cytoskeleton, a large class are enzymes. Some of these are involved in metabolism, some are involved in protein translation, and many are regulatory. We do not fully understand the reasons for such associations, or even if they are functional rather than accidental, but there is a case for functionality. Several glycolytic enzymes localize to microtubules, apparently taking advantage of **metabolic channeling**, a term that describes the product of one enzyme being channeled to the next enzyme, for which it is a reactant (Fig. 5.34). Channeling occurs because propinquity limits diffusion to an effective surface as opposed to a volume, and diffusion in two dimensions is faster than in three.

In view of channeling, the cytoskeleton and its bound proteins can be thought of as a cellular compartment, albeit less restricted than the inside of a vesicle. However, as the cell responds to a change in its environment, the cytoskeleton often disassembles within minutes, freeing the contents of the cytoskeletal compartment to acquire new associations. Reassembly happens soon thereafter, often bringing about new

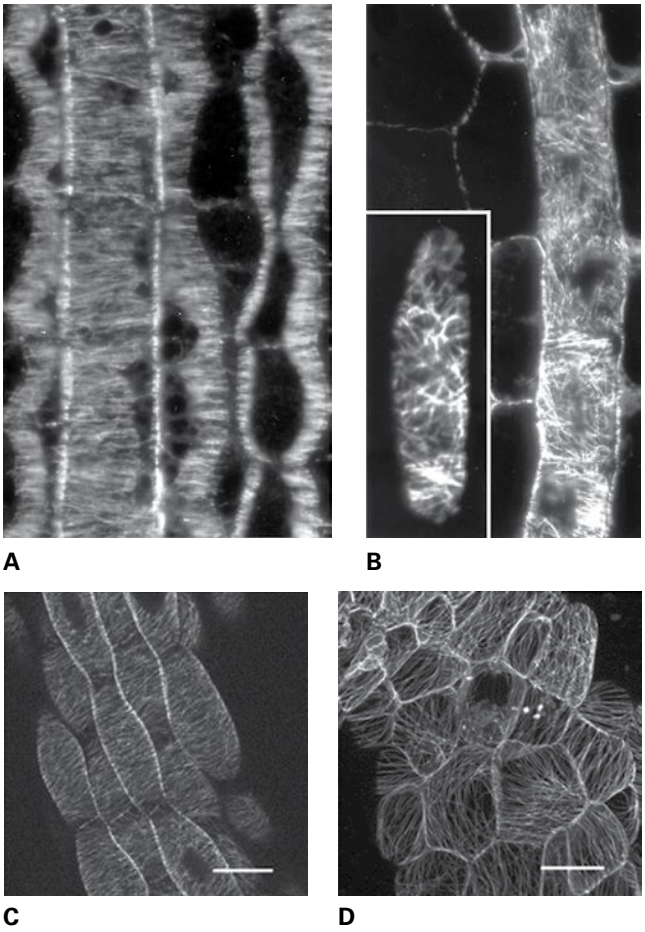


FIGURE 5.33 *Protein phosphorylation plays a role in microtubule organization. (A) Cortical microtubule arrays in a growing region of the* A. thaliana *root have transverse orientation. (B) Cortical arrays in a similar region of a root treated with staurosporine, an inhibitor of protein kinases, are organized aberrantly within each cell. Inset is at higher magnification. (C) Cortical microtubules in the growing hypocotyl with transverse orientation. In the* A. thaliana tonneau2 (ton2*) mutant (D), the arrays become disorganized on a tissue level, with different orientations in different cells. The* TON2 *gene encodes a protein phosphatase. Bars in C and D = 50 μm.*
Source: (A, B) Baskin & Wilson (1997). Plant Physiol. 113: 493–502. (C, D) Camilleri et al. (2002). Plant Cell 14:833–845.

orientations or structures. Insofar as much of the cytoskeleton is within the cortical cytoplasm, these widespread changes affect plasma-membrane components disproportionately. Responses to aluminum, salt, cold, and water deficit, among others, have been shown to include transient depolymerization of cytoskeletal elements and concomitant changes in signaling, such as elevated levels of cytosolic calcium or increased activities of regulatory enzymes. As an example, the opening and closing of stomata requires complex changes to both actin and microtubules, and actin filaments have been implicated in the gating of the potassium channels that potentiate guard cell movements. Just as the opening of an ion channel can change a cell's membrane potential by tens of millivolts, thereby changing the status of the plasma membrane throughout the cell in

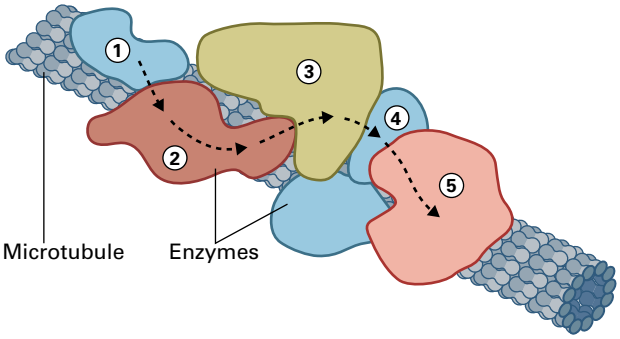


FIGURE 5.34 *Metabolic channeling might occur when the enzymes for a sequence of reactions bind to a microtubule. This makes it easier for the product of the first reaction to diffuse to the active site for the second reaction. The same principle occurs in multi-subunit complexes, such as pyruvate decarboxylase (see Chapter 22), in which several individual enzymes aggregate into a superstructure, again enhancing diffusional coupling between successive active sites.*

seconds, so too depolymerizing actin filaments or microtubules affects the cytoplasm throughout the cell. We are only beginning to understand the role of the cytoskeleton as a labile repository of information.

5.8.2 The cytoskeleton is connected to the cell wall

Unable to see, hear, or smell, plants rely widely on sensing mechanical forces. When the wind blows or the caterpillar chews, the plant vibrates; as rain and drought change water status, turgor pressure and cell wall stress respond in step; when the plant grows, the cell wall deforms. To sense these changes, the plant cell might relay the mechanical status of the wall to the cytoskeleton, a relay requiring connection points. In principle, attachment to the cell wall would amplify the range of mechanical perturbations that the cell could sense (Fig. 5.35).

Certainly, the cytoskeleton is anchored to the cell wall. This has been inferred from static images where cross-bridges extend from the cytoskeleton into the membrane (Fig. 5.36) and also from experiments. When intact cells are lysed, turgor pressure completely expels the contents of the cell, except for a skein of cortical microtubules and subtending patches of plasma membrane affixed to the wall. Similarly, when protoplasts settle on a slide and are lysed, the slide retains fragments of plasma membrane ("ghosts") with cortical microtubules; however, when protoplasts are treated briefly with a protease prior to lysis, microtubules are lost, presumably because the protease degrades a transmembrane attachment protein that binds both slide and microtubules.

The plasma membrane is also attached to the cell wall. This has been demonstrated by placing cells in a solution that is sufficiently hypertonic to cause the cell to shrink to a volume smaller than the space enclosed by the cell wall, a process called **plasmolysis**. In plasmolyzed cells, the protoplast seldom becomes spherical but remains stuck to the wall in

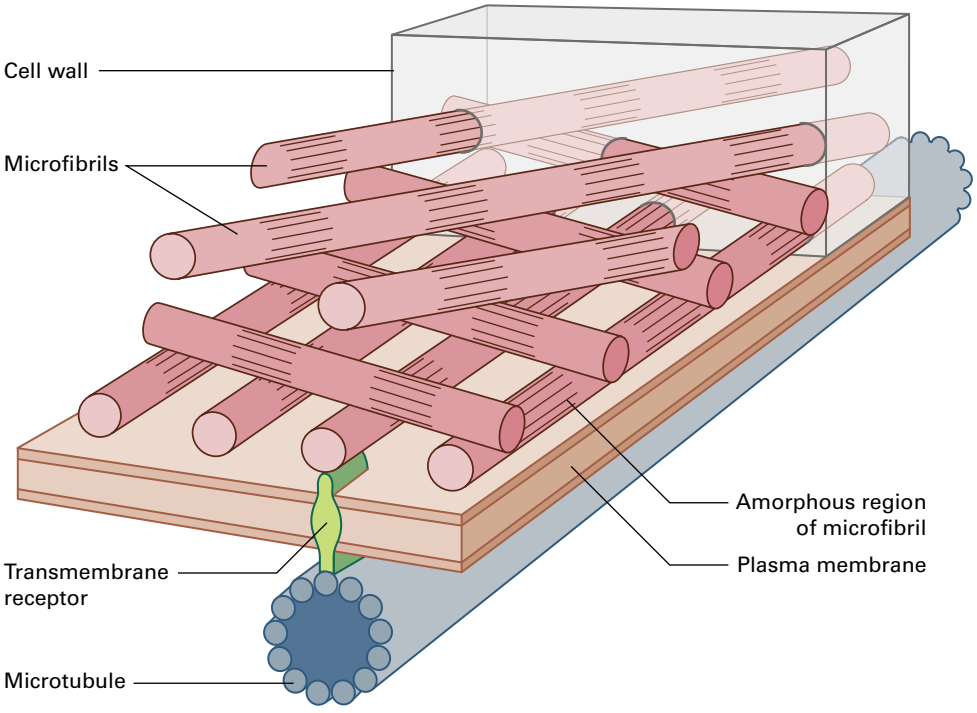


FIGURE 5.35 *Schematic view of how mechanical information may be sensed at the plasma membrane. This cutaway view of the cell wall illustrates a putative relationship between cellulose microfibrils, receptors in the membrane, and cortical microtubules. Amorphous regions on the microfibrils (or on other wall polymers) are deformed by the substantial tensions generated by turgor pressure. Receptors that span the plasma membrane have two binding sites: At their extracellular domain they bind the deformed regions of the microfibrils, and at their cytosolic domain they bind microtubules (or other cytoskeletal polymers). Changes in the mechanical loading will change the extent of deformation of the microfibril, which in turn could increase or decrease its binding affinity to the receptor. As with conventional receptors (e.g., for hormones), occupancy of the receptor's extracellular binding site determines the activity of its cytosolic site. The cytosolic site could have kinase activity and participate in signal transduction directly, or it could affect the behavior of cytoskeletal polymers. We can even imagine this relationship working in reverse, where the extracellular binding site influences reactions in the cell wall based on the status of the microtubules.*

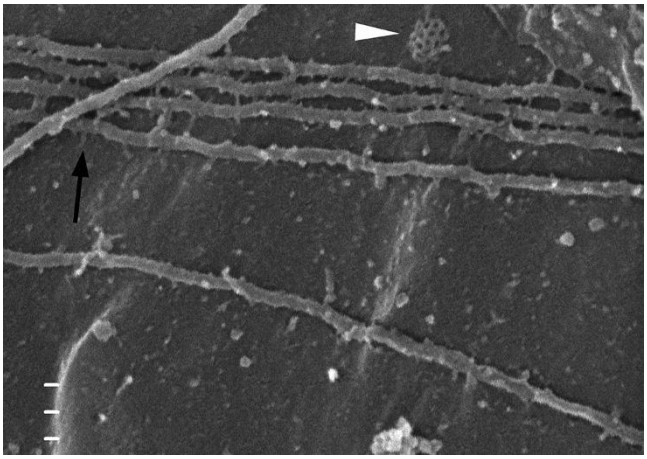


FIGURE 5.36 *Field-emission scanning electron micrograph of the cortex of a tobacco hypocotyl cell. The cell has been lysed, ejecting the cytoplasm but leaving behind the plasma membrane (note the geometrical lattice of a forming clathrin-coated vesicle (white arrowhead; see Chapters 1 and 4) and microtubules, apparently cross-bridged to the membrane (e.g., black arrow). Scale divisions = 50 nm. Source*: T. Baskin, University of Massachusetts, Amherst.

many regions. Often, the wall and protoplast are linked by a large number of thin, membranous strands, called Hechtian strands, after the botanist who described them in the 1910s (see Fig. 1.13). We don't know whether the attachment sites revealed through concave plasmolysis and Hechtian strand formation are the same as those that anchor the cytoskeleton to the cell wall, but they are likely to represent at least an overlapping set.

5.8.3 Probing the functionality of attachment sites leaves open the involvement of the cytoskeleton

What is the function, if any, of the attachment between cytoskeleton and cell wall? The relevance of such specialized attachment sites is suggested by analogy to animal cells, in which transmembrane receptor proteins, called **integrins**, physically link the actin cytoskeleton to the extracellular matrix and mediate signal transduction based on the status of that linkage. Integrins

are a large and complex family of plasma-membrane receptors that form connections needed for cell adhesion and locomotion, as well as for the bidirectional flow of information between cytoplasm and extracellular matrix. Integrins bind a variety of proteins in the extracellular matrix that contain a tripeptide, RGD (in the one-letter amino acid code). Consequently, exposing cells to small peptides containing RGD breaks connections between integrin and extracellular matrix and allows their relevance to be assayed, often with striking results.

That plants contain integrins was initially suggested by antibodies against integrins recognizing plasma-membrane proteins, as well as by RGD peptides disrupting various processes, including embryogenesis, gravity sensing, acclimation to salt stress, pollen tube growth through the pistil, and pathogen resistance. However, plant genomes contain sequences recognizable by similarity as homologues neither to integrins nor to their extracellular matrix ligands, although an RGD-containing protein, secreted by a pathogen and used to promote infectivity through disrupting plant cell adhesion, has been argued to be a homolog of an integrin ligand based on structural similarity rather than sequence. Furthermore, a plant plasma-membrane protein that binds RGD has been identified as being a serine/threonine receptor kinase of the lectin class and hence not homologous to integrins.

While attachment sites between cell wall and membrane are clear in plants, and both actin and microtubules undoubtedly participate in the cell's response to mechanical perturbation, in the absence of recognizable integrins any linkage between those sites and the cytoskeleton is undefined. There have been only a few studies of the plant cytoskeleton as affected by RGD peptides, and these have produced contradictory results. In addition to providing physical connections, it is logical that these attachment sites constitute conduits through which information about the cell's surroundings flows between cell wall and cytoskeleton (see Fig. 5.35). A grand challenge for the future will be to detect this information flow and to decipher its meaning.

5.9 Mitosis and cytokinesis

Every cell on earth was formed by division. **Mitosis** describes the physical separation of replicated chromosomes into two new nuclei. **Cytokinesis** describes the physical division of one cell into two. Mitosis and cytokinesis are accomplished by elaborate molecular machines constructed from the cytoskeleton: the **mitotic spindle**, which separates chromosomes, and (in plants) the **phragmoplast**, which builds the new wall between daughter cells. Comparing plants and animals, cytoskeletal machines for mitosis are largely the same whereas those for cytokinesis are distinct (Fig. 5.37). In both kingdoms, mitosis and cytokinesis represent the capstone function of the cytoskeleton. To grasp how these machines work, we need to know how the cytoskeletal structures are assembled and how forces are exerted to move chromosomes or to separate newly formed cells.

Mitosis and cytokinesis occur during a short phase of the cell cycle, called the M phase (see Chapter 11) and generally the processes are linked, with the spindle giving rise to the phragmoplast. However, the linkage is facultative; mitosis can occur without cytokinesis, forming multi-nucleated cells, and cytokinesis can happen long after the mitotic spindle has disassembled. In animal cells, the cytoskeletal involvement in cytokinesis begins in metaphase, whereas in plants, cytokinesis begins in prophase (part of M phase) or even earlier. Perhaps because cell walls are immobile and all but permanent, the plant cell takes pains to build them in the right place.

5.9.1 The preprophase band defines a cortical division site, which defines the placement of the new cell wall

The major cytoskeletal structure involved in orienting the cell wall built between dividing cells is the **preprophase band,** a ring of actin filaments and microtubules that encircles the cell just inside the plasma membrane (Fig. 5.38; see Fig. 5.45). Despite its name, the band is mature and functional in prophase, although it sometimes initiates earlier. The preprophase band forms at the site where the cell plate will eventually join the parent wall. Initially, the band is wide and rather loosely organized; as prophase continues, the band narrows and nearly all of the actin filaments and microtubules become closely parallel. Around the time of nuclear envelope breakdown, the polymers of the preprophase band depolymerize. This removes all microtubules from the cortical cytoplasm, whereas actin filaments remain in the rest of the cortex and are depleted, but not eliminated from the location previously occupied by the preprophase band (Fig. 5.39). The complete depolymerization of preprophase band actin and microtubules is surprising because it is only as telophase ends, long after the preprophase band polymers have vanished, that its former location is zeroed-in on by the edges of the enlarging phragmoplast, thus ensuring that the forming cell plate fuses with the parental wall at the right place.

We now believe that the preprophase band somehow modifies the underlying membrane or cell wall (or both) to establish the **cortical division site**, which is recognized subsequently by the edges of the phragmoplast. The preprophase band (or cortical division site) also plays a role in orienting the mitotic spindle; however, the phragmoplast edges can find the cortical division site even when the spindle has been considerably displaced, for example, by centrifugation, implying that orienting the spindle is a function for the band distinct from defining the placement of the new cell wall. In addition to guidance, the cortical division site might also promote a seamless integration of daughter and parental walls (Fig. 5.40).

How the preprophase band establishes the division site is obscure, as is how that site carries out its functions; however, there are some clues. A microtubule-associated protein, TANGLED, colocalizes with preprophase band microtubules but then remains at the division site thereafter (Fig. 5.41).

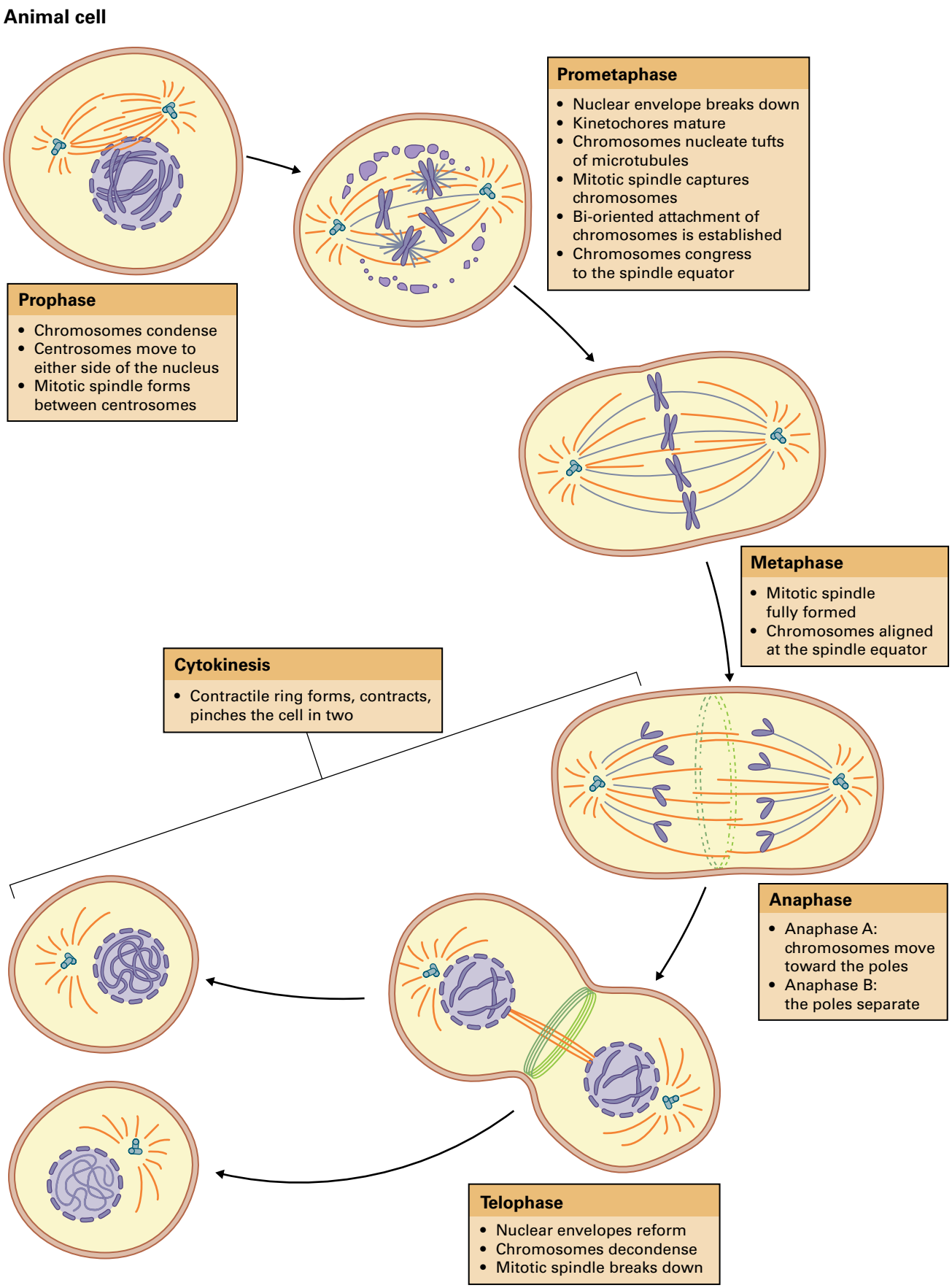


FIGURE 5.37 *Mitosis in animal and plant cells.*

Plant cell

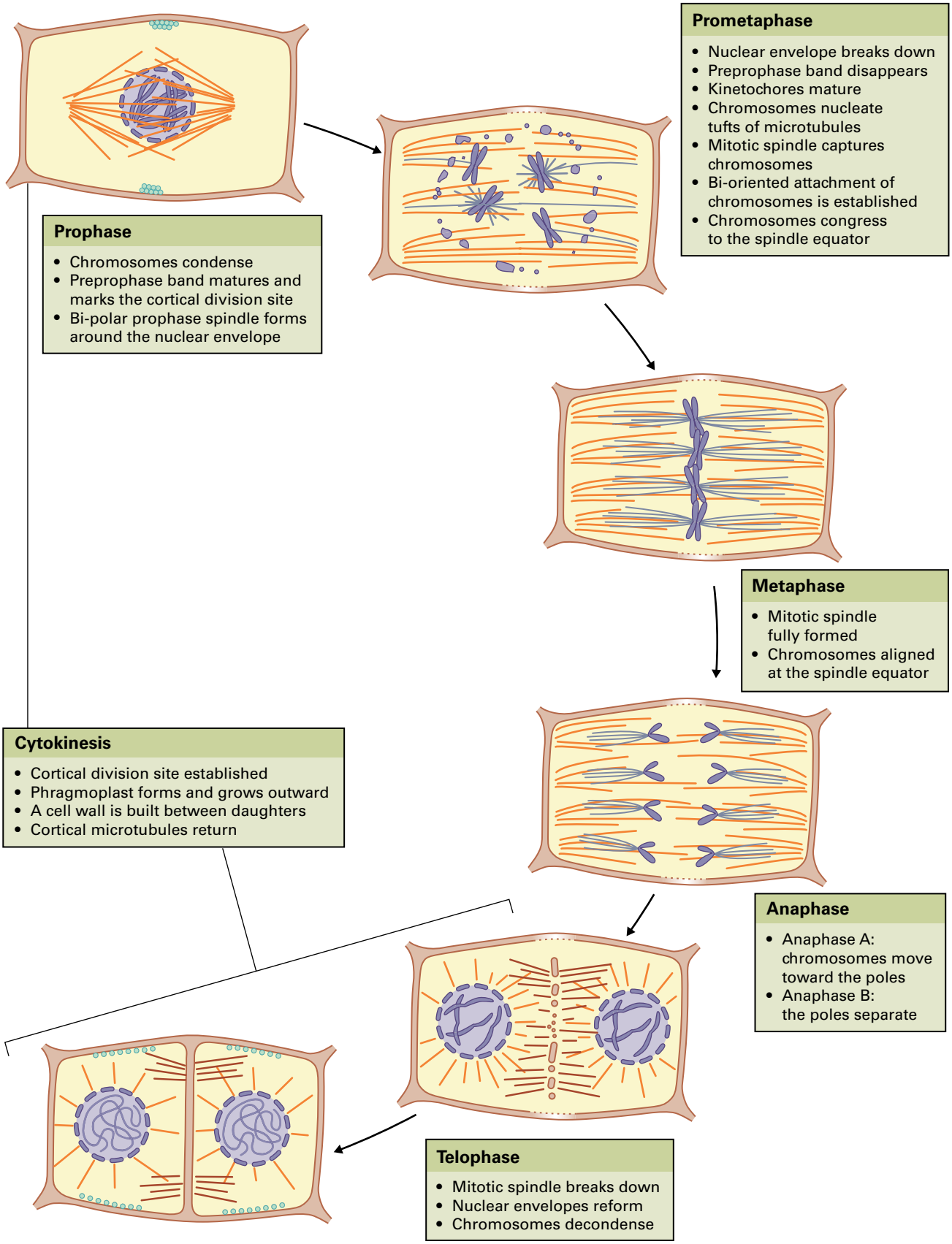


FIGURE 5.37 (*Continued*)

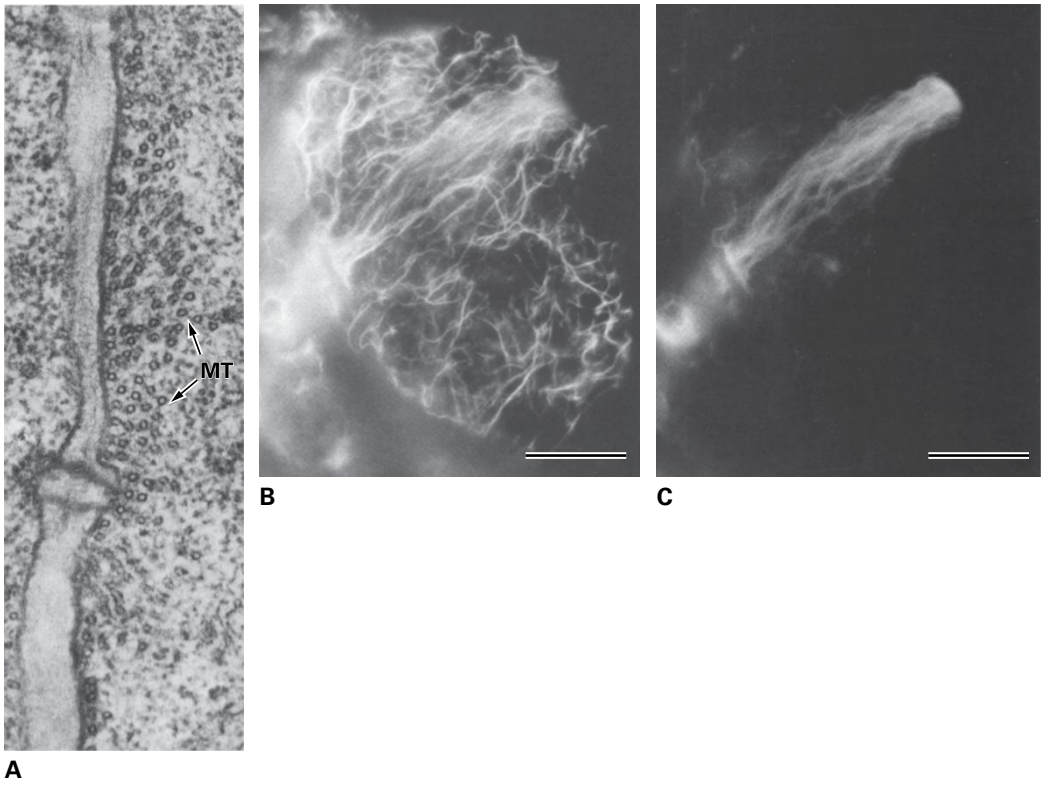


FIGURE 5.38 *Structure of the preprophase band. (A) Electron micrograph of a leaf epidermal cell, showing a cross-section through a preprophase band with abundant microtubules (MT). (B, C) Fluorescence micrographs of a suspension-cultured tobacco cell double-labeled to show actin (B) and microtubules (C). The microtubule band is narrow and the rest of the cortex lacks cortical microtubules, whereas the actin band is wider and actin filaments are present throughout the cortex. Bars = 10 μm.*
Source: (A) Galatis et al. (1984). Protoplasma 122:11–26. (B, C) Kakimoto & Shibaoka. 1987. Protoplasma 140:151–156.

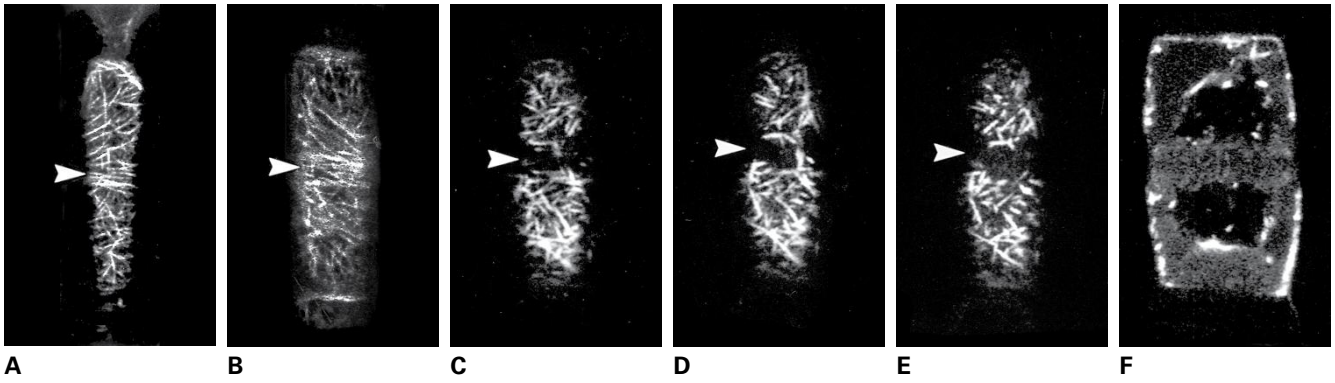


FIGURE 5.39 *Before prophase, actin filaments form a band, which is selectively removed as the cell goes through prometaphase. Confocal fluorescence micrographs of a living stamen hair cell during mitosis, microinjected with fluorescent phalloidin to label actin filaments. (A, B) In prophase, a loosely organized transverse band of actin filaments forms at the division site (arrowhead). Images shown are from the upper and lower cortex of the same cell. (C) Prophase, (D) metaphase, and (E) anaphase of the same cell. (F) Telophase of another cell. Actin filaments are depleted from the cortical division site (arrowheads) but remain elsewhere in the cortex. (A–E) A focal plane at the cell cortex; (F) a mid-plane.*
Source: (A–F) Cleary et al. (1992). J Cell Sci 103:977–988.

We do not know its biochemical function but loss of tangled activity gives rise to plants in which cell divisions are somewhat misoriented, suggesting that TANGLED participates in cortical site function.

A cortical division site forms in cells that divide with specific orientation but is generally absent from cell types where the division plane is inconsequential, cell types such as free endosperm, callus, and male and female gametophytes. Despite being nonessential for division per se, the preprophase band continues to tantalize researchers with its accurate forecast of cell plate placement and subsequent disappearing act.

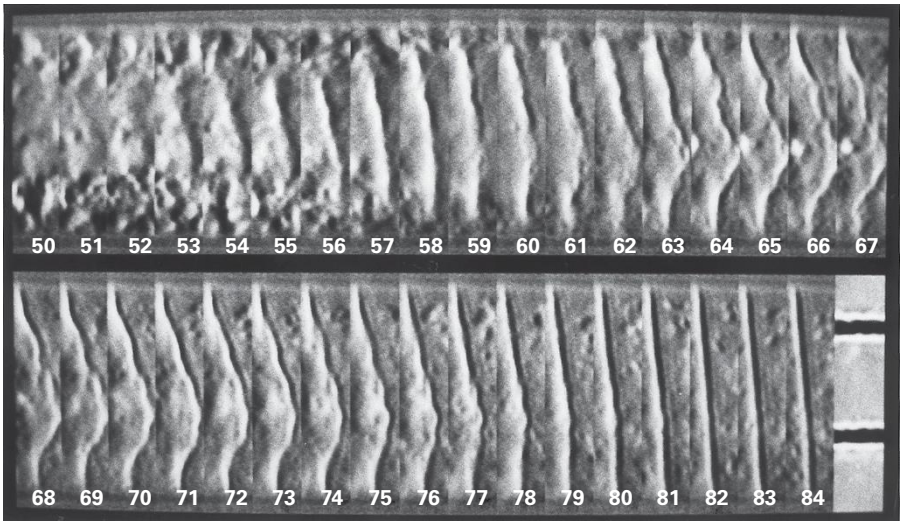


FIGURE 5.40 *Time-lapse light micrographs at 1-minute intervals during cell plate formation in a living stamen hair cell. The cell plate undulates as it forms; a short time after the plate reaches the parent wall (77 to 81 minutes), the undulations vanish abruptly. The cortical division site may condition the wall for subsequent events involving cell plate fusion. Scale division = 10 μm.*
Source: Mineyuki & Gunning. (1990). J Cell Sci 97:527–538.

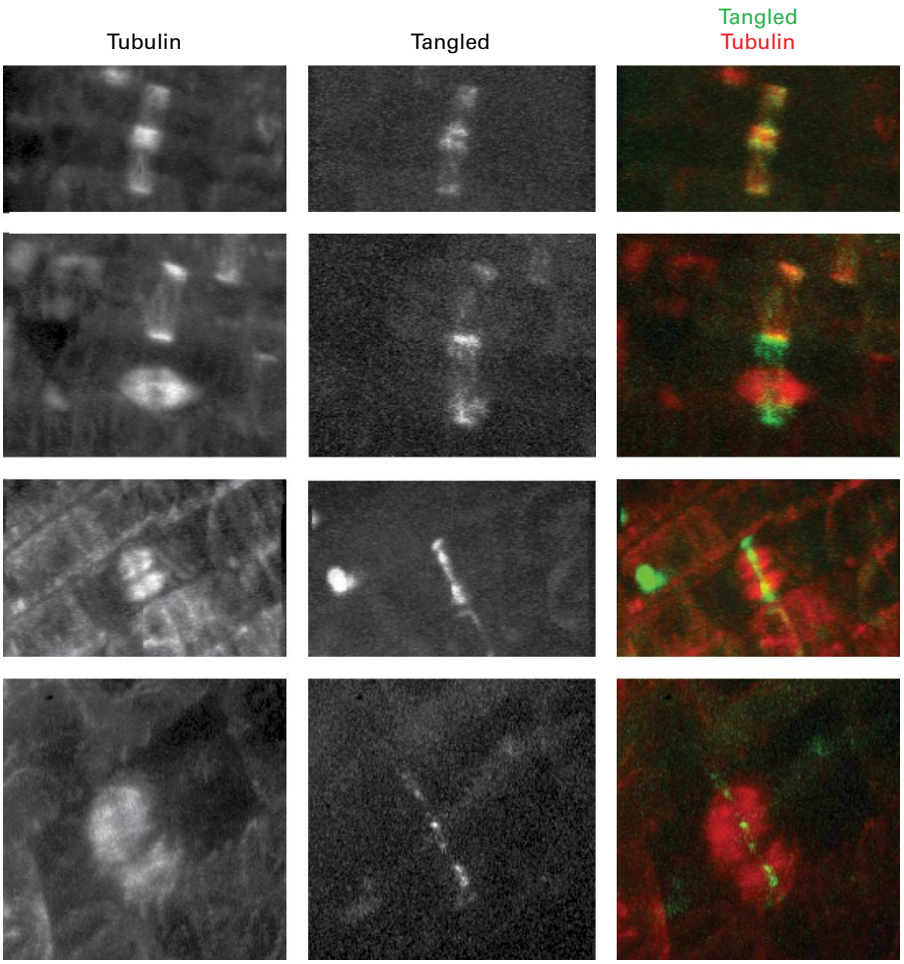


FIGURE 5.41 *The TANGLED protein remains at the cortical division site throughout mitosis. Confocal fluorescence micrographs of* A. thaliana *roots expressing fluorescent tubulin (left) and TANGLED, fused to a distinct fluorophore (center). The right-hand column shows the overlay with tubulin in red and tangled in green. In prophase (top row), TANGLED is localized to the preprophase band. However, at later stages of mitosis, when the microtubule preprophase band is gone, the TANGLED band remains (middle rows). As cytokinesis advances, the tangled band narrows until it is essentially the same thickness as the daughter cell wall (bottom row).*
Source: Walker et al. (2007). Curr Biol 17:1827–1836.

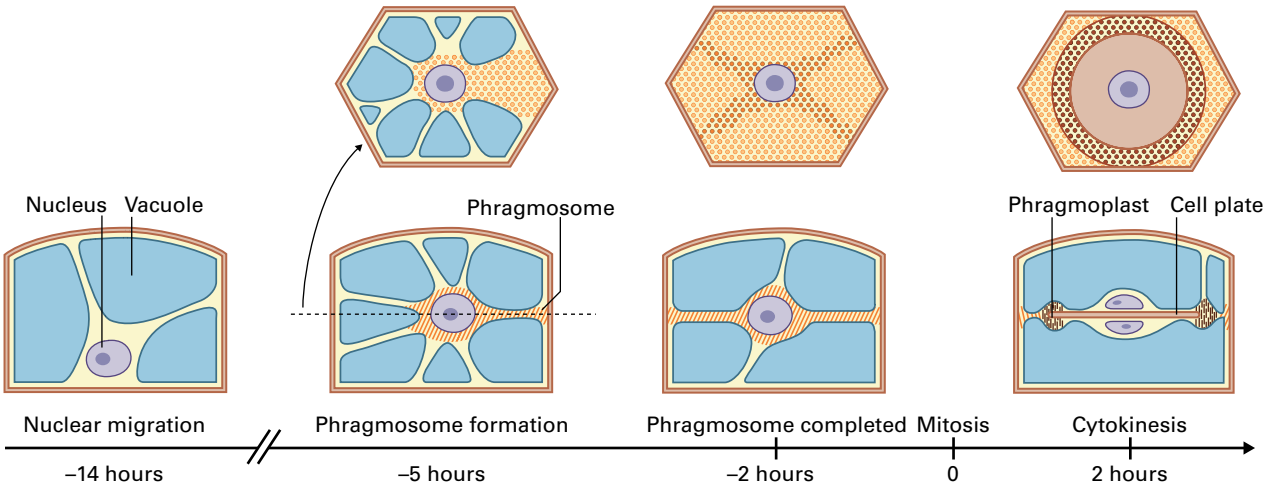


FIGURE 5.42 *Formation of the phragmosome. When highly vacuolated cells divide, such as the parenchyma cell sketched here, first the nucleus migrates to the center of the cell and the cytoplasm coalesces in the plane of the future cell wall. This sheet-like accretion of cytoplasm is called the phragmosome (orange), which might provide a conduit for the growing cell plate. Construction of the cell plate (dark red) begins at the cell center and must move outward through the vacuole to reach the parent cell wall. Top row shows the cell from the top and bottom row from the side.*

5.9.2 Division in large, vacuolated plant cells places unusual demands on the cytoskeleton

Usually, division is the business of shoot and root meristems (see Chapter 11), which contain densely cytoplasmic cells, little wider than the spindle itself; however cells of the secondary meristem, the cambium, are far larger. Furthermore, fully differentiated cells in plants are readily induced to divide, for example, by wounding or hormonal treatment, and such cells often reach dimensions of hundreds or even thousands of micrometers. Building a cell plate across a full grown cell is a Herculean task for the phragmoplast, taking for example an entire day to partition a 2-mm vascular cambium cell, longer than the entire cell cycle of a typical meristem cell.

Cytoskeletal involvement in the division of large, vacuolated cells begins well before prophase. Probably during S phase, the nucleus migrates to a central position in the cell, a migration that depends on both actin and microtubules. In certain cells, the cortical division site is marked by a thick ring of cytoplasm rich in actin filaments and depending on them for formation. However, the most conspicuous structure that forms in dividing vacuolated cells is the **phragmosome**.

The phragmosome (not to be confused with the phragmoplast) is a thin, reticulated layer of cytoplasm that forms in the plane of the future cell wall. The phragmosome contains both actin and microtubules and can be nearly a continuous sheet or a just a few strands. The phragmosome forms as the nucleus attains its central position, perhaps by means of the coalescence of the cytoplasmic, cytoskeleton-rich strands that support its migration (Fig. 5.42). Subsequently, at the periphery of the phragmosome, the preprophase band forms. Experiments show that once a phragmosome is present, reprogramming the plane of division becomes difficult. Specific functions for the phragmosome are not clear. It appears to anchor the nucleus at its central position and to help program the division site. In addition, a popular idea is that cytoskeletal elements within the phragmosome help the phragmoplast forge a coherent path through large vacuolar spaces.

5.9.3 The mitotic spindle comprises balanced forces and rapid microtubule turnover

The structure and general properties of the mitotic spindle are well conserved among eukaryotes. The spindle consists of hundreds to thousands of microtubules as well as their associated proteins. Other components are actin filaments and membrane-bound organelles derived from the ER. The mitotic spindle has two poles, which define not only the sites where the separated chromosomes will finally arrive but also the spindle's bipolar organization. Microtubules radiate away from each pole with their minus ends toward the nearest pole and their plus ends away (Fig. 5.43). Some microtubules run from the pole to specialized sites of attachment on the chromosomes, called kinetochores (see Section 5.9.6), whereas others extend from the pole for various lengths. Some of the latter meet and interact at the spindle equator with microtubules emanating from the opposite pole, forming a zone of overlap that stabilizes the spindle structure (see Box Fig. 5.3A).

The structure of the spindle is maintained by opposing forces. In general terms, forces at the midzone pushing outward are balanced by forces at the poles pushing in. Despite these forces, microtubules in the spindle are highly dynamic, with half-lives on the order of 1 minute. Kinetochore microtubules are longer lived but still turn over many times during mitosis. Many microtubules also undergo treadmilling (see Section 5.3.3), in which microtubule subunits are added at the kinetochore and

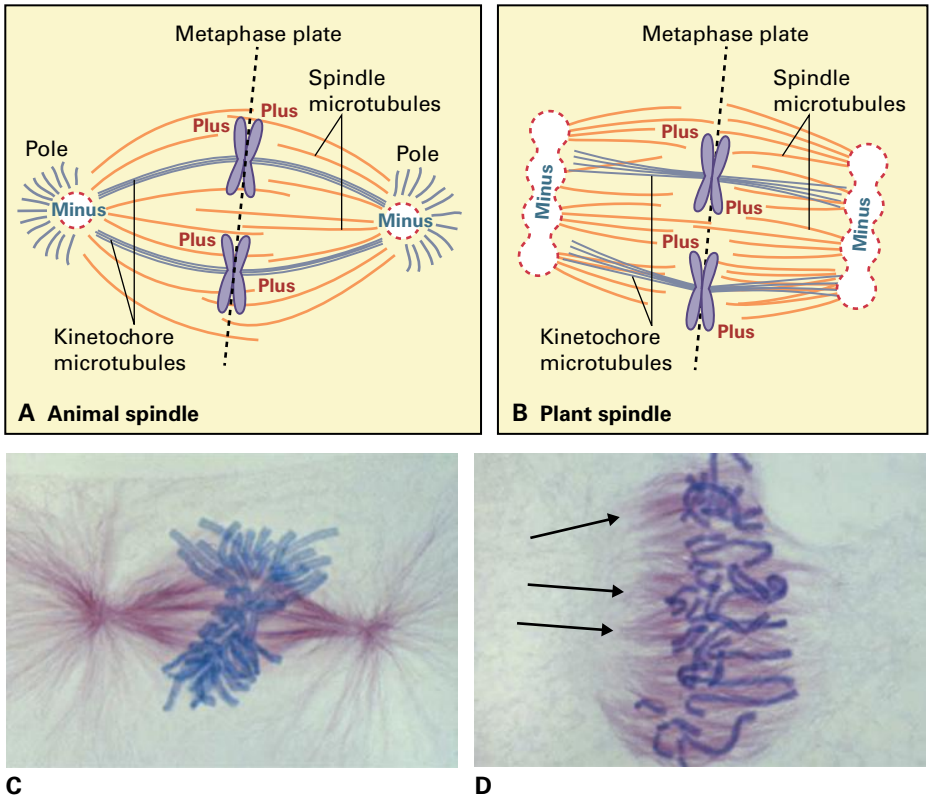


FIGURE 5.43 *Comparison of the mitotic spindle in cells of animals and plants. (A, B) Schematic. Both spindles are at metaphase. The plane occupied by the chromosomes (the equator, or metaphase plate) is a plane of symmetry for the spindle. Each half-spindle contains a pole, kinetochore microtubules (prominent bundles of microtubules that run from the kinetochore up to or near the pole), and many spindle microtubules, some of which enter the area occupied by the other half-spindle but never penetrate as far as the opposite pole. The minus ends of most microtubules are near the poles, whereas the plus ends grow away from the poles. In animal cells, the poles are tightly focused at the centrosome, whereas in plant cells, the poles are a group of subsidiary foci. (C–D) Bright-field micrographs of metaphase spindles from (C) a newt (*Taricha granulosa*) lung epithelial cell and (D) endosperm of the plant,* Haemanthus katherinii. *DNA is blue and microtubules are reddish brown. The newt spindle has focused poles and prominent kinetochore bundles typical of animal spindles whereas the endosperm spindle is barrel-shaped. However, although lacking an overall polar organizing center, numerous subsidiary foci of microtubules are present (arrows).*
Source: (C, D) Wadsworth & Khodjakov. (2004). Trends Cell Biol 14:413–419.

are lost at the pole. Treadmilling creates a coherent **flux** of tubulin dimers moving through the spindle, from kinetochore to pole. Underscoring the complexity of the spindle, microtubule turnover and flux are themselves able to generate forces and the motor proteins must be able to exert forces against microtubules even while the polymers assemble and disassemble.

5.9.4 A major difference between the spindles of animals and plants is assembly

Eukaryotes invented the spindle early in their evolution and for the most part mitosis in plant, fungal, and animal kingdoms is similar, but differences do occur. A fundamental difference between animal and plant mitotic spindles is in the manner of assembly. Animal cells have two known pathways for spindle assembly. The first discovered (and best understood) pathway involves **centrosomes** (Fig. 5.44). At interphase, the centrosome is adjacent to the nucleus and nucleates a radial array of microtubules; during S phase it replicates, and during prophase the replicated centrosomes separate to form two radial arrays of microtubules (each often called an aster) that become the spindle poles (Fig. 5.44E). The second pathway involves chromatin. Here, spindles form in a process in which the condensed chromosomes nucleate randomly oriented microtubule bundles and the bipolar organization of the mature spindle subsequently emerges as the divergent microtubules coalesce, apparently bundled and focused by dynein along with other proteins. Although discovered in oocytes where centrosomes are absent, we now know that a chromatin-mediated spindle assembly pathway operates alongside of the centrosome pathway, presumably to ensure a well-built spindle.

In interphase plant cells, most microtubules are part of the cortical array but some radiate from the nuclear envelope, nucleated there by proteins that are related to constituents of the animal centrosome, including γ-tubulin. In prophase, cortical microtubules disappear, except for those in the preprophase band (see Section 5.9.1) and spindle assembly starts with myriad microtubules polymerizing on the nuclear envelope. Soon, these microtubules radiate from foci on opposite sides of the nucleus that define the future poles of the mitotic spindle. This structure is called the **prophase spindle** (see Fig. 5.26A, Fig. 5.45H).

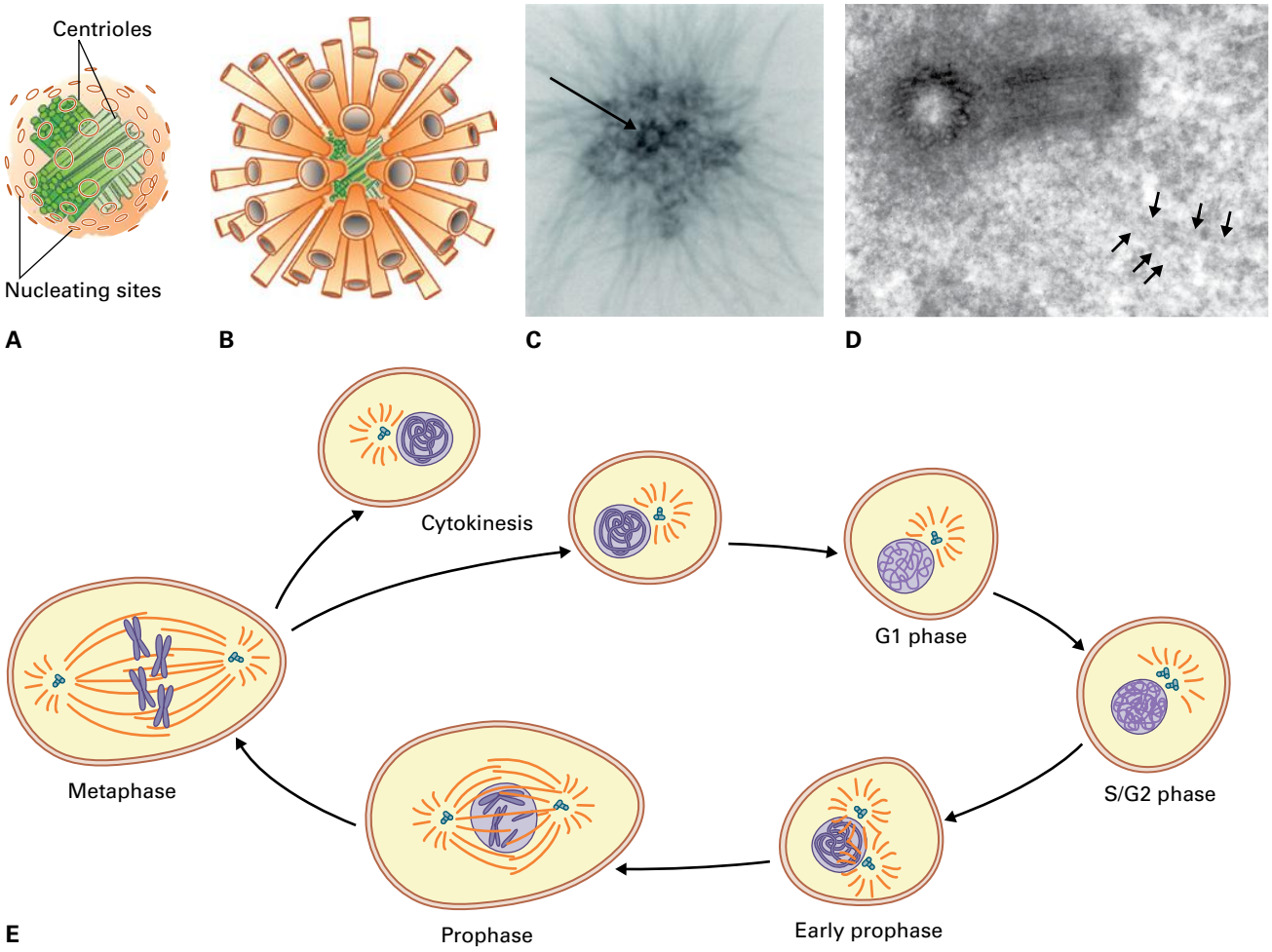


FIGURE 5.44 *The animal centrosome. (A–B) Schematics. The centrosome comprises a pair of centrioles, oriented at right angles, surrounded by a protein-rich matrix of indeterminate structure, termed pericentriolar material. One component of this material is γ-tubulin, which along with other proteins forms ring-shaped templates that play a role in nucleating microtubules. (C) Electron micrograph of an isolated centrosome from* Drosophila melanogaster. *One of the centrioles is just visible as a dark ring near the center of the pericentriolar material (arrow). (D) Electron micrograph through a centrosome from a mouse embryo. A pair of dark centrioles is seen with (faint) radiating microtubules (arrows). (E) The centrosomal cycle of an animal cell. The pair of centrioles duplicates during S phase, but the two pairs remain closely associated in a single complex. In early prophase, the complex splits, forming two separate centrosomes, each nucleating a radial array of microtubules, called an aster. As prophase continues, the centrosomes separate further and define the two poles of the mitotic spindle, which forms between them. By the end of mitosis, when the chromosomes have reached the poles, each daughter nucleus reforms near the centrosome. After cytokinesis, each new cell inherits a single centrosome.*
Source: (C) Moritz et al. (1995). J Cell Biol 130:1149–1159. (D) H. Schatten, University of Missouri, Columbia.

Lacking centrosomes, plant cells cannot use the centrosome-mediated pathway. Moreover, the bipolar organization of the plant spindle is typically established before nuclear envelope breakdown, ruling out the involvement of chromatin. Evidently plants assemble their spindle by a pathway that is at least partially distinct from those of other eukaryotes.

Some evidence on how the plant spindle forms implicates the preprophase band. In plant suspension cultured cells, which divide haphazardly, some of them divide without making a preprophase band. When the band is present, spindle bipolarity emerges during prophase as usual, but interestingly when the band is absent, a bipolar spindle forms after nuclear envelope breakdown, perhaps by the chromatin-mediated pathway described above. That the preprophase band appears to participate in the pathway of spindle organization underscores the importance of the cortical division site. Because the band bisects the position of the nucleus, usually by early in prophase, the band is sited ideally to enforce bipolarity on the myriad microtubules polymerizing along the surface of the nuclear envelope, perhaps by stimulating turnover of those microtubules in the middle of the nucleus (i.e., nearest to the band).

5.9.5 The structure of the plant and animal spindle pole is superficially different but fundamentally the same

For many years, a notable difference between plant and animal spindles was said to be the structure of the mitotic spindle pole. Animal spindle poles contain centrosomes and

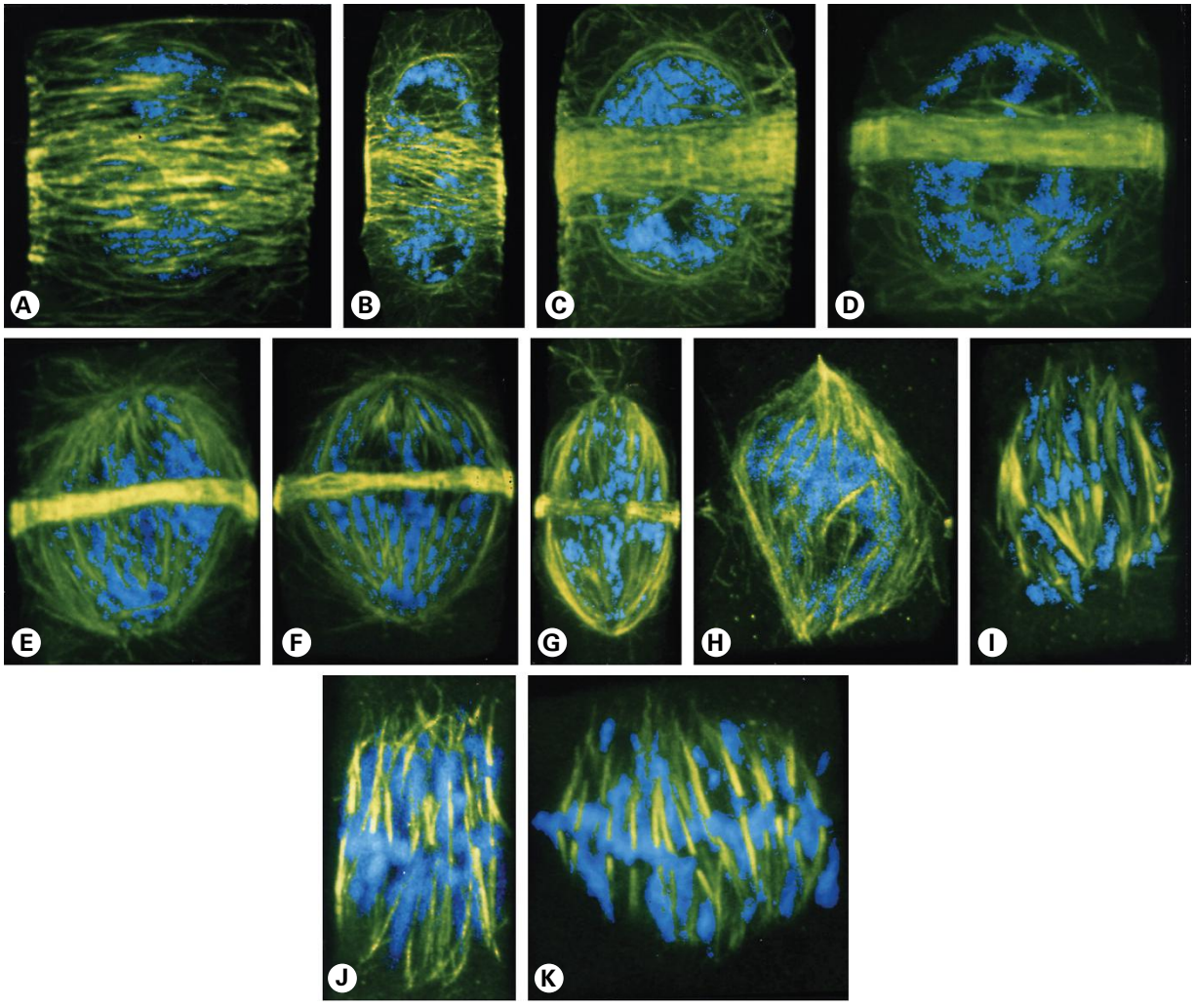


FIGURE 5.45 *Confocal fluorescence micrographs of fixed wheat (*Triticum aestivum*) root cells, showing the assembly of the mitotic spindle. Microtubules are green and yellow, DNA is blue. (A–D) The preprophase band develops from the coalescence of cortical microtubules before or during prophase. (E–H) The prophase spindle forms around the nuclear envelope. In late prophase (G, H), the preprophase band disassembles. (I–K) The mitotic spindle forms after breakdown of the nuclear envelope as the poles spread laterally and kinetochores capture bundles of spindle microtubules. Source*: (A–K) Gunning & Steer. (1996). Plant Cell Biology: Structure and Function. Jones and Bartlett, Sudbury, MA.

are tightly focused, whereas in plant cells, the mitotic spindle pole lacks centrosomes and is usually broad (see Fig. 5.43). The tight focus of the animal mitotic spindle pole was formerly ascribed to centrosomes, but poles are focused in oocytes and in somatic cells when centrosomes are removed surgically; what is more, poles become unfocused, despite centrosomes, when specific motor proteins are inhibited. Furthermore, the plant spindle pole is well focused during prophase, and the broad poles found at other phases, in fact, contain subsidiary microtubule foci ("little poles") linked by interdigitating microtubules. Because this resembles the canopy of a conifer forest, this organization is described as *fir-tree*-like. Although unfocused as a whole, each fir-tree top represents a focused structure. We now know that polar focusing, whether in broad or narrow spindles, is determined mainly by activity of minus-end directed motor proteins and cross-bridging proteins. In animals, a notable role is played in polar focusing by cytoplasmic dynein (see Section 5.4.2), a role that in plant cells has presumably been usurped by a minus-end directed kinesin.

5.9.6 Chromosomal movements at mitosis are similar in plant and animal cells

At the end of prophase, the nuclear envelope breaks down, and spindle microtubules begin to interact with chromosomes. The main sites of interaction are **kinetochores**, which form on each sister chromatid at opposite sides of the paired centromeric region (Fig. 5.46). For correct attachment of chromosomes to the spindle, each kinetochore must bind microtubules from only one spindle pole, and sister kinetochores must bind microtubules from opposite poles; mechanisms to resolve inappropriate associations rely on balancing

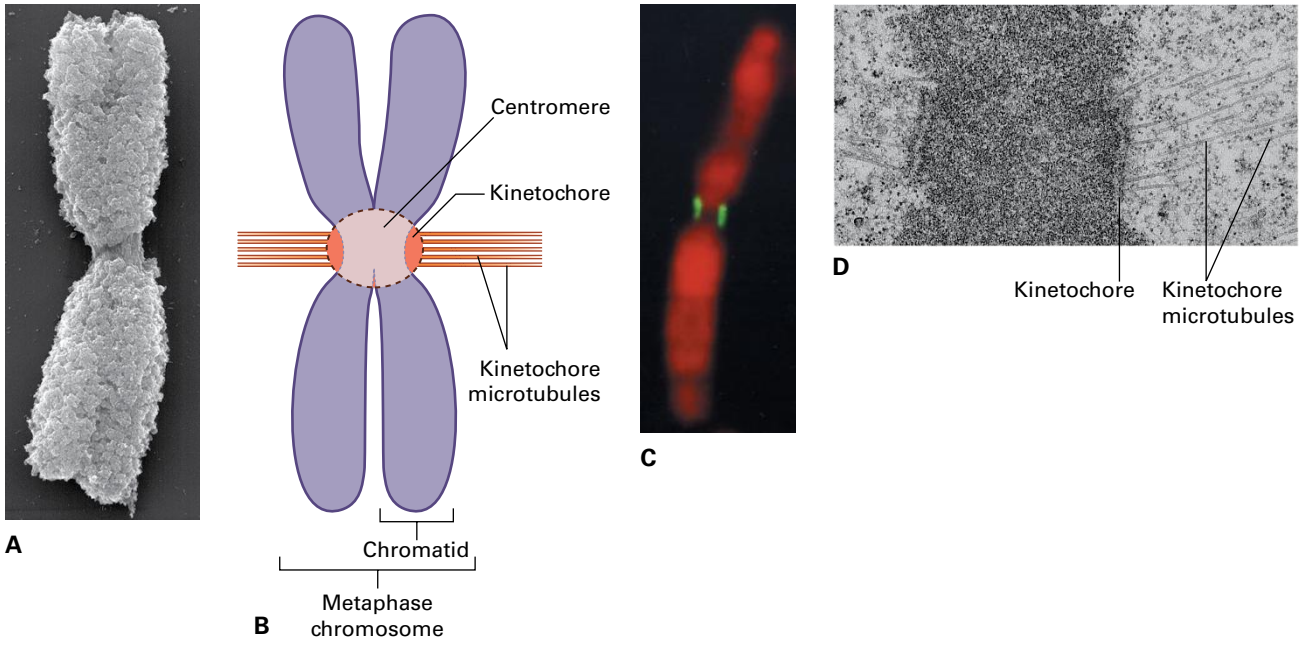


FIGURE 5.46 *The kinetochore. (A) Classical studies of genetics and cytology identified a chromosomal region that lacked genes and recombined infrequently as the location where sister chromatids attach to each other. This region, termed the centromere, can often be discerned in light micrographs as a constriction of the chromosome and is clear in this scanning electron micrograph of a plant metaphase chromosome. (B) The centromeric region of the chromosome is now known to mediate attachment of the mitotic spindle to the microtubules by virtue of a protein-rich plaque that forms at each sister centromere, called the kinetochore. The kinetochore binds to the plus ends of microtubules. (C) The kinetochore is a flat, plate-like structure. A Barking deer (*Muntiacus muntjak*) chromosome in metaphase is shown double-labeled for DNA (red) and for several kinetochore proteins (green). Two distinct kinetochores are visible, one for each chromatid. (D) Electron micrograph through the centromeric region of a chromosome at metaphase, showing both kinetochores. Note the layered structure of the kinetochore and the microtubules terminating there. A kinetochore typically binds 30–50 microtubules but, depending on its size, might bind just one or more than 100.*
Source: (A) R. Martin, Gerhard Wanner, University of Munich, Germany. (C) Van Hooser & Brinkley. 1999. Methods Cell Biol 61:57–80. (D) K. McDonald, University of California, Berkeley.

the tension forces across the two sister kinetochores. These usually are resolved during the 10–30 minutes of prometaphase but even one persisting bad attachment will arrest the cell in metaphase.

Chromosomes move mainly in two phases of mitosis, prometaphase and anaphase (see Fig. 5.37). At prometaphase, the chromosomes congress, moving from the random positions they held when first captured by the mitotic spindle to gather at the spindle midzone, termed when the chromosomes arrive, the **metaphase plate**. At anaphase, the replicated sister chromatids, previously held together by the cohesin complex, uncouple synchronously and move apart. Chromosomes move toward the poles (**anaphase A**) and the poles themselves move apart (**anaphase B**). Anaphase A is powered by forces exerted cooperatively on the kinetochore fiber; forces are exerted at the kinetochore, at the poles, and even from within the spindle. Anaphase B is powered by pulling forces exerted on each spindle pole from outside the spindle or pushing forces exerted by microtubule motor proteins on microtubules of opposite polarity (i.e., emanating from opposite spindle poles) located in the zone of overlap in the middle of the spindle (Box 5.3). The force generating mechanisms overlap and current research efforts are directed toward understanding where the forces originate and how they are regulated.

5.9.7 Plants have evolved a unique structure, the phragmoplast, for cytokinesis

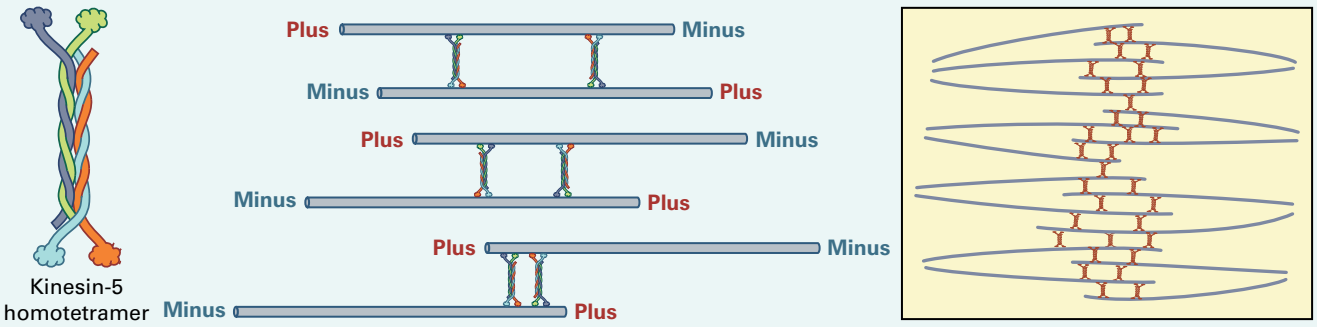
An animal cell physically pinches itself in two, whereas a plant cell erects a partition, in the form of a new cell wall. To divide, animal cells have evolved a cytokinetic organelle called the **contractile ring**, a band of actin filaments encircling the cell in the future plane of division, anchored to the plasma membrane (see Fig. 5.37). The contractile ring contains myosin, which pulls together adjacent, antiparallel actin filaments, shortening the circumference of the ring and squeezing the cell in two. We also know that some motile animal cells can divide by each half of the cell crawling in opposite directions, somewhat like the medieval punishment of being pulled apart by horses, but here too the cell periphery controls the process. In fungi and algae, construction of the new wall also typically begins at the edges and moves to the center, analogous to the animal contractile ring. In contrast, plants begin construction on the new wall within the cell (between the two daughter nuclei) and the process expands to reach the edges (see Fig. 5.37). The phragmoplast contains actin and myosin as well as microtubules, and both cytoskeletal systems contribute to function

BOX 5.3

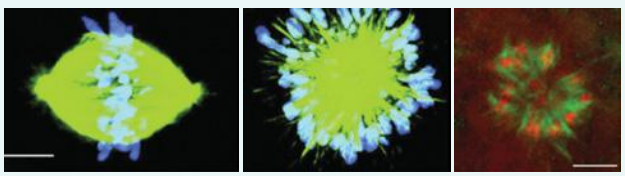
Holding the middle ground: the power at the spindle midzone

Watching a cell divide, one is struck by symmetry. At prophase, the preprophase band encircles the nucleus neatly around its equator. At metaphase, chromosomes come to rest in the middle of the spindle, precisely. After that, the cytokinetic apparatus bisects the spindle, exactly along the mid-plane. How is this symmetry established? The preprophase band helps orient the prophase spindle, the mitotic spindle in animal cells helps orient the contractile ring, and yet these structures are separated spatially by many micrometers. How does information from one structure propagate through the cell to another?

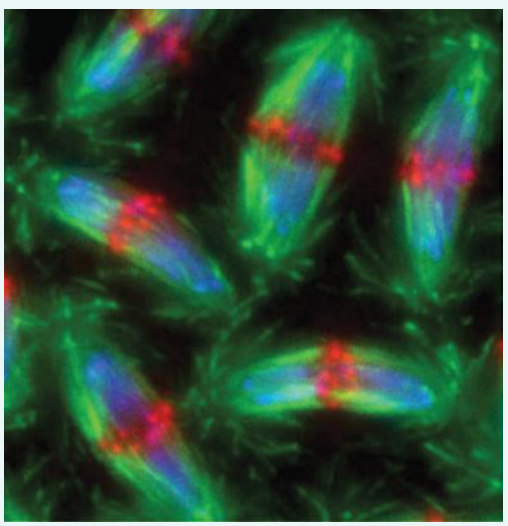
We are far from answering such questions but an important clue has been provided by special behavior of the zone of microtubule overlap in the spindle mid-plane. In both plants and animals, the zone of overlap is stabilized in part by kinesin-5 motor proteins. This type of kinesin forms a tetramer, organized so that each pair of heads binds a microtubule of opposite polarity, as



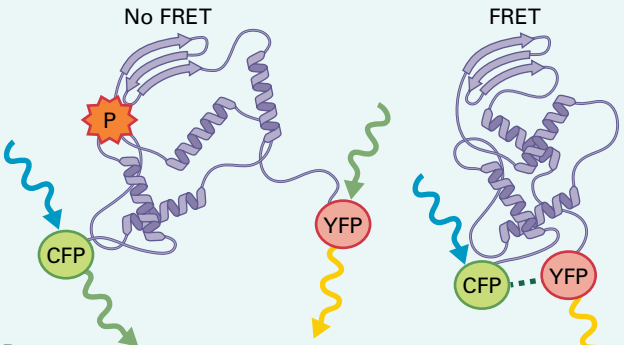
A



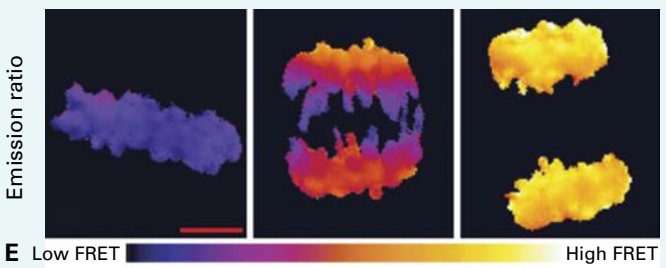
B



C



D



E

(A) Schematics of kinesin-5 arrangements. (B) Inhibiting kinesin-5 causes mono-polar spindles, exemplified by a vertebrate cell exposed to a chemical inhibitor of kinesin-5 (left, center: tubulin = green; DNA = blue) and by a plant cell mutant for KIN5c (right: tubulin = green; DNA red). (C) Passenger proteins (red) are dropped off at the spindle midzone during metaphase where they remain through cytokinesis. This image shows spindles in a Drosophila *embryo (tubulin = green; chromosomes = blue). (D) The FRET sensor consists of an Aurora-B phosphorylation site placed between two domains incorporating fluorescent protein tags. When phosphorylated, the fluorescent proteins are held apart; when dephosphorylated, the fluorescent proteins come within FRET range, detectable as YFP emission given CFP excitation. (E) The FRET sensor targeted to chromosomes reveals phosphorylation is high (low FRET) when the chromosomes are at the midzone (left) and low when they are at the poles (right), with a gradient of phosphorylation in between (middle). Depositing an active kinase at the spindle midzone communicates this position to the surrounding cytoplasm. Bars = 5 μm.*

present in the spindle midzone (A). When kinesin-5 function is inhibited, either chemically or genetically, the midzone fails and a mono-polar spindle results (B). In humans, a chemical inhibitor, monastrol, specific to this motor, is in clinical trials as a cancer therapeutic agent because of its specificity for dividing cells.

The spindle midzone is important not only for holding the halves of the spindle together but also because it defines the mid-plane of the mitotic apparatus. Kinesin-5 is a plus-end-directed motor. When the tetramer binds a pair of microtubules of opposite polarity, by walking to the plus ends of each, but not falling off, it produces a pair of microtubules of opposite polarity linked by a small region of overlap at their plus ends. The overlapping microtubules or the motor protein itself can serve as a binding site for other proteins, which thereby accumulate at the middle of the spindle. Certain proteins that accumulate there are called passenger proteins: during interphase and prophase, they bind chromatin, but when chromosomes reach the metaphase plate, these passengers disembark at the spindle midzone, where they remain for the remainder of mitosis and cytokinesis (C). One of these passengers is a kinase, aurora B. Is it just taking a ride?

Aurora B is active. This kinase actually signals the position of the spindle mid-plane, according to an ingenious piece of biosensor engineering. The engineered sensor combines two fluorescent proteins (YFP and CFP) separated by a flexible linker and a short sequence that is phosphorylated by aurora B specifically (D). The sensor operates based on the principle of fluorescence resonance energy transfer (FRET): when two fluorophores are side by side, energy can resonate from one to the other so that energy exciting one can be emitted by the other. In this case, exciting CFP when YFP is close enough for resonance yields emission characteristic of YFP. The ratio of emission from CFP and YFP quantifies the efficiency of energy transfer. This efficiency decreases with the sixth power of distance: even relatively small increases in distance lead to an essentially complete loss of energy transfer. With the phosphorylation site interposed between the fluorophores, the energy transfer efficiency becomes a function of phosphorylation by aurora B. The final step was to add a sequence to target the sensor to a specific cellular component; for instance, a histone sequence incorporates the sensor into chromatin. Following transformation of a vertebrate cell line with a construct encoding the sensor, phosphorylation due to aurora-B kinase can be observed in living cells on a specific cellular component.

The sensor reveals a striking phosphorylation gradient, centered at the midzone (E). The gradient is driven by aurora-B and in this instance functions to site the contractile ring in relation to the spindle. It is irresistible to extrapolate this mechanism to other processes related to the midzone. The ability of the preprophase band to modify behavior of microtubules at the nuclear equator, the force exerted on metaphase chromosomes being strongest in the spindle midzone, the ability of the phragmoplast to recruit new sets of overlapping microtubules at its periphery in precise alignment, all follow plausibly from the output of a localized kinase. The challenge now is to find those signals, elucidate their formation, and put together a complete picture of the forces and fluxes that divide the chromosomes and cleave the cell.

Source: (B) Left and middle panels, Meyer et al. (1999). Science 286:971; right panel, Bannigan et al. (2007). J Cell Sci 120:2819–2827. (C) http://homepages.ed.ac.uk/rradams/passengers.html (E) Fuller et al. (2008). Nature 453:1132.

although microtubules play the lead. The phragmoplast and the contractile ring are structurally so dissimilar it is difficult to visualize a common ancestor.

5.9.8 The phragmoplast initially forms between the separating chromosomes at late anaphase and then expands centrifugally to reach the parental cell wall

As the phragmoplast begins to form, residual microtubules in the spindle midzone are joined by abundant, newly polymerized microtubules emanating from the poles and reforming nuclei (Fig. 5.47). Initially, the phragmoplast mid-plane is defined by a narrow band, where microtubules emanating from each nucleus overlap. Soon thereafter, the band narrows until microtubules no longer overlap. Ultimately, a gap forms between microtubules as the new cell plate coalesces. Actin filaments also assemble into the phragmoplast, following the microtubules and generally parallel to them (Fig. 5.48). Both actin and microtubules have their plus ends at the phragmoplast mid-plane, meaning that nucleation occurs at or near the nuclei and new polymers grow toward the mid-plane.

The phragmoplast forms in the center of the cell between reforming nuclei. It then grows centrifugally toward the cell edges. As it grows, new microtubules are recruited to the periphery and lost from the interior, so that soon the phragmoplast attains a ring-like structure (Fig. 5.49). Initially, microtubules are long, reaching most of the way from nucleus to midzone but as the phragmoplast matures, microtubules become progressively shorter, losing any connection to the nuclear envelope. A progressive shorting also happens to

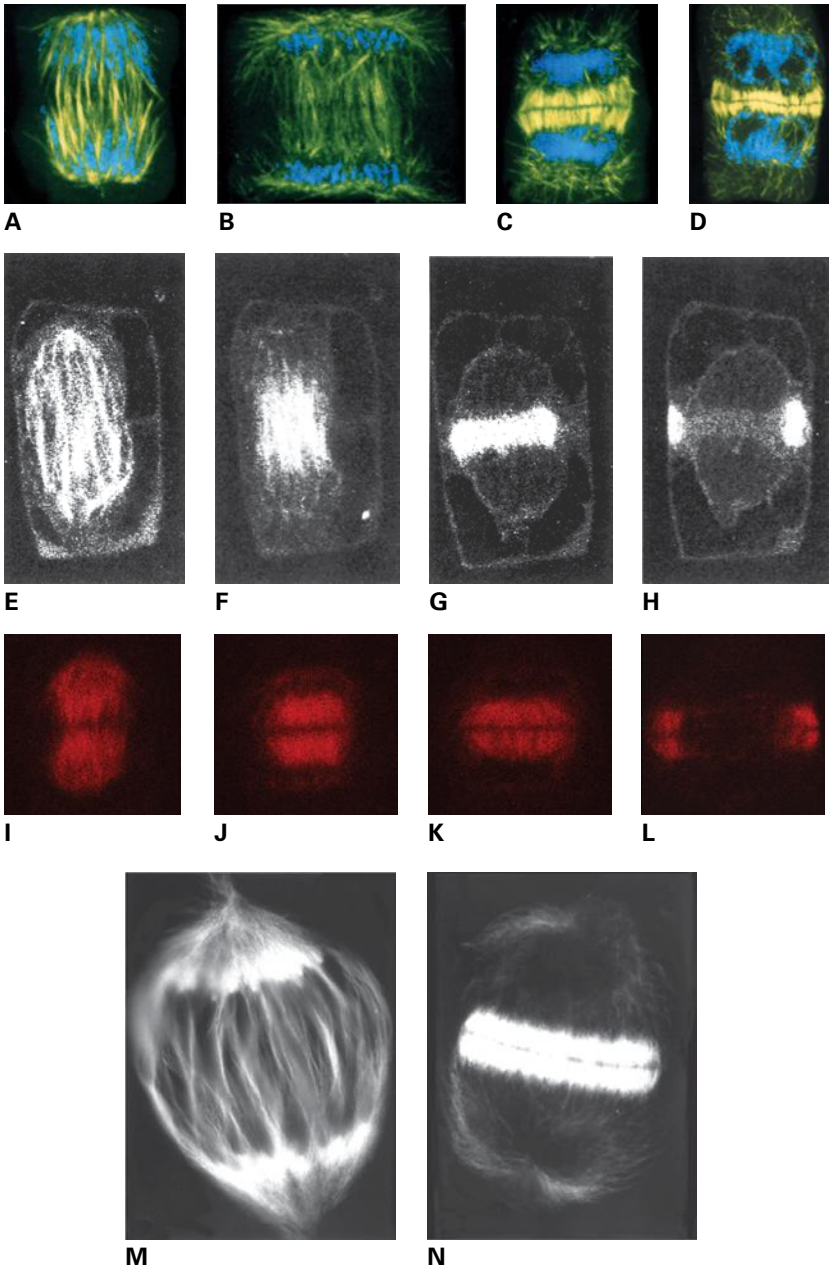


FIGURE 5.47 *Microtubule organization in the phragmoplast, as shown by fluorescence micrographs of phragmoplast microtubules from different plant cell types. (A–D) Fixed wheat root cells, with microtubules in green or yellow and DNA in blue. (E–H) Living* T. virginiana *stamen hair cells microinjected with labeled neural tubulin. (I–L) Living tobacco BY-2 cells with the GFP-tubulin signal shown in red. (M, N) Fixed endosperm cells of* H. katherinii. *The phragmoplast begins to form at late anaphase (A, E, I, M), as interzonal microtubules of the spindle are joined by newly polymerized microtubules at the equator. By telophase (B, F, J), the organization of the phragmoplast is well established: The plane of the forming cell wall is defined by a line where microtubules meet. Soon a gap between microtubules appears as the cell plate is deposited. As telophase progresses, phragmoplast microtubules tend to shorten, and disappear from the central region, forming an annulus of overlapping microtubules that expands centrifugally, eventually reaching the parental wall (C, D; G, H; K, L; N).*
Source: (A–D) Gunning & Steer. (1996). Plant Cell Biology: Structure and Function. Jones and Bartlett, Sudbury, MA. (E–H) Zhang et al. (1993). Cell Motil Cytoskel 24:151–155. (I–L) T. Murata, National Institute for Basic Biology, Okazaki, Japan. (M–N) Smirnova et al. (1995). Cell Motil Cytoskel 31:34–44.

actin filaments, but they are generally retained in the center (see Fig. 5.48). Microtubules and actin in the phragmoplast are highly dynamic, with half-lives for microtubules recorded to be on the order of 1 minute. The dynamic state of these polymers presumably facilitates phragmoplast growth, although the mechanism behind the ordered expansion is not known.

One of the first plant microtubule motor proteins to be characterized biochemically, a member of the kinesin-5 family and a relative of the motor protein that holds the spindle midzone together (see Box 5.3), was purified from isolated phragmoplasts (Fig. 5.50). This protein might be responsible for microtubule translocation observed in vitro in the phragmoplast or for stabilizing the bipolar arrangement of microtubules in the phragmoplast, plausible functions for a kinesin-5 motor. Many other kinesins have been implicated in phragmoplast structure and function, largely on the basis of mutant phenotypes. However, we do not understand what orchestrates the activities of all of these motors into a harmonious performance.

5.9.9 The phragmoplast coordinates the deposition of polysaccharide for the new wall

Both microtubules and actin filaments within the phragmoplast coordinate the intense secretory activity needed to build the cell plate. The phragmoplast harbors swarms of

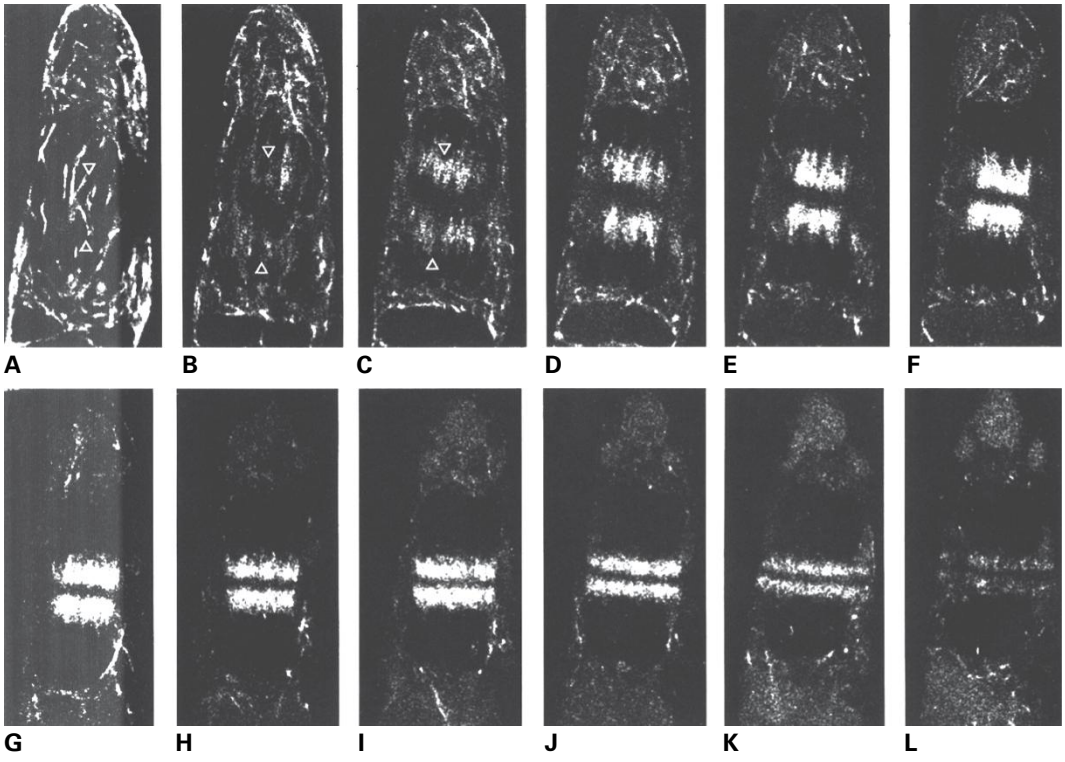


FIGURE 5.48 *Confocal fluorescence micrographs of actin filaments, labeled with fluorescent phalloidin, in the phragmoplast of living stamen hair cells. Actin filaments do not form as obvious an annular structure but instead tend to remain present throughout the forming cell plate. The persistent dark band at the equator indicates that actin filaments never overlap significantly across the equator.*
Source: Zhang et al. (1993). Cell Motil Cytoskel 24:151–155.

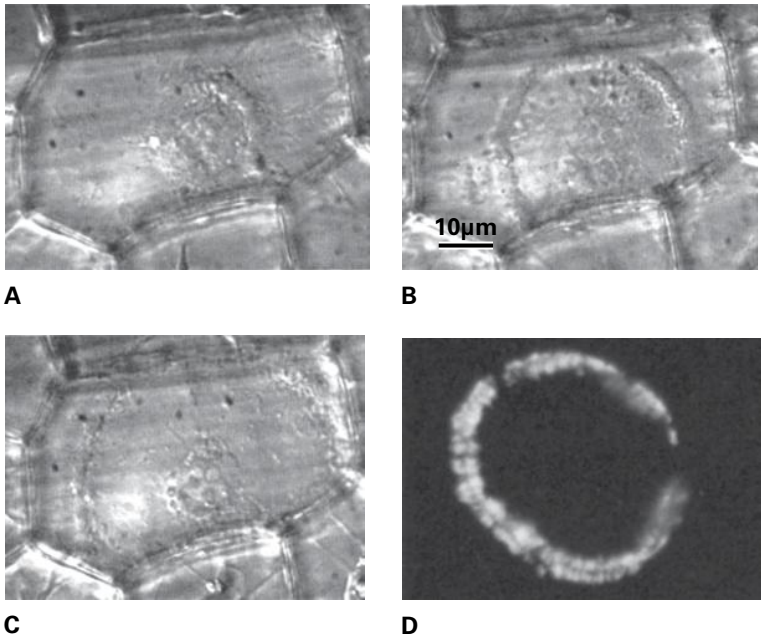


FIGURE 5.49 *The annular structure of the phragmoplast. (A–C) Light micrographs of division in a large, highly vacuolated leaf epidermal cell, taken at 30-minute intervals. The plane of the forming cell wall is parallel to the page, and the phragmoplast is viewed from above. An annulus, formed by the phragmoplast microtubules viewed end on, grows outward and eventually reaches the cell periphery. If fixed and stained to show microtubules, the annular structure in (C) would resemble the phragmoplast shown in (D).*
Source: (A–C) Venverloo & Libbenga. (1981). Z Pflanzenphysiol. 102:389–395. (D) Asada & Shibaoka. (1994). J Cell Sci 107:2249–2257.

vesicles and membranous organelles (Fig. 5.51). Vesicles deliver proteins and polysaccharides to the nascent cell wall and deliver plasma membrane to the growing cell plate. Additionally, vesicles return from the cell plate to the Golgi apparatus, removing excess membrane and recycling cell wall components. While some vesicles might move diffusively, most of this motility is powered by motor proteins bound to the vesicle membrane. Actin might also be directly involved in membrane fusion machinery, as is known for yeast, but this remains to be defined for plants.

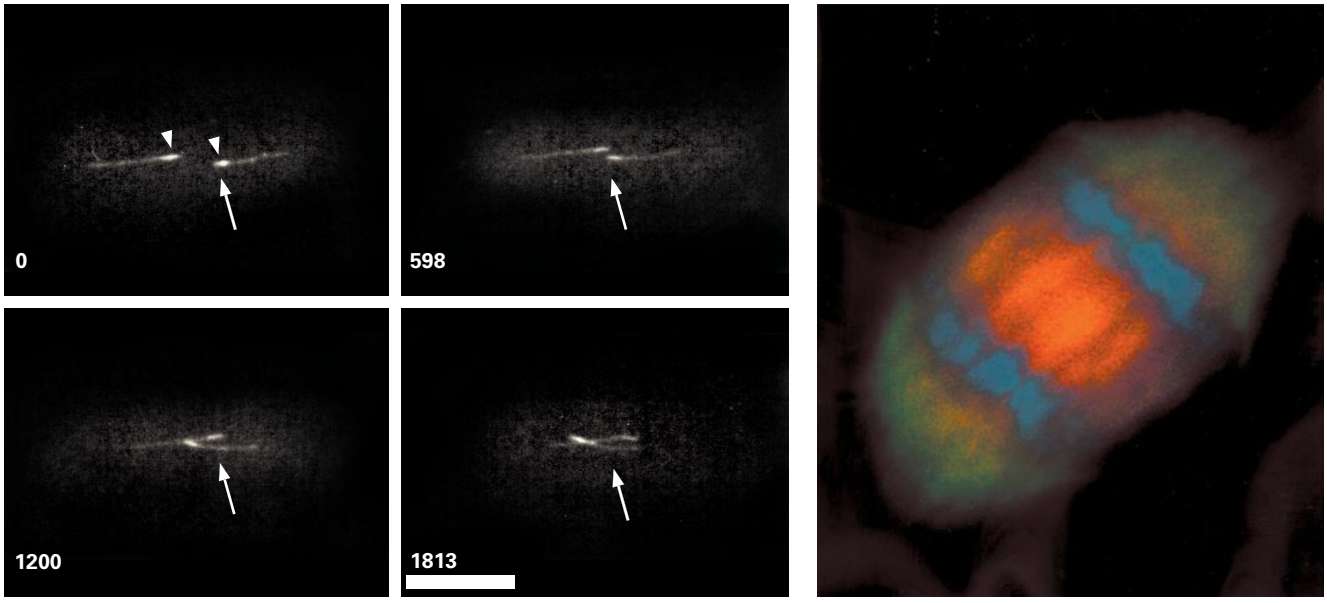


FIGURE 5.50 *The phragmoplast contains the first microtubule motor protein to be purified and characterized from plants, tobacco kinesin-related protein of 125 kDa (TKRP125), a member of the kinesin-5 family. (A) TKRP125 purified from the tobacco phragmoplast moves microtubules toward their minus ends. The purified protein was used to coat one surface of a microscopic observation chamber and was allowed to bind fluorescently labeled microtubules, prepared with a small region of heightened fluorescence marking their minus ends (arrowheads). ATP was added to the chamber and images captured at successive intervals (time is given in seconds; the arrow marks a fixed reference location). The microtubules move minus-end first, which is equivalent to a protein moving cargo toward the plus end of an anchored microtubule. (B) The motor protein is abundant in the spindle midzone. Here, an anaphase mitotic spindle from a tobacco cell has been triple-labeled to show DNA (blue), microtubules (green), and TKRP125 (red). The orange color in the spindle midzone, where the phragmoplast is forming, results from co-localization of microtubules and TKRP125. In this location, the motor is poised to help cement the microtubule overlap in the phragmoplast mid-plane.*
Source: (A) Asada & Shibaoka. (1994). J Cell Sci 107:2249–2257. (B) T. Asada, Osaka University, Japan.

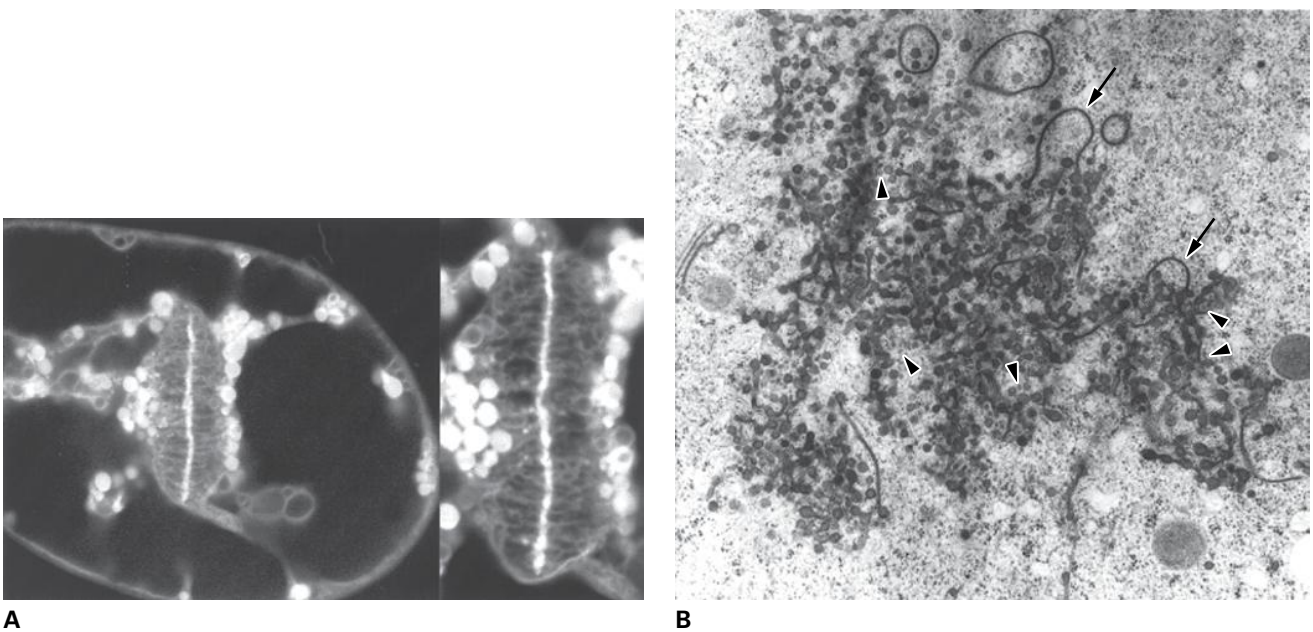


FIGURE 5.51 *The phragmoplast teems with vesicles for cell plate construction. (A) Fluorescence micrograph of a vacuolated suspension-cultured tobacco cell at telophase, stained with a membrane marker, indicating the abundant membranous material throughout the phragmoplast and the forming cell plate. The right-hand panel is an enlargement of the forming cell plate. (B) Electron micrograph prepared by high-pressure cryofixation of an early stage phragmoplast (section is parallel to and at the mid-plane) showing the abundance of vesicles and membranes. Microtubules can be seen in cross-section (arrowheads), as can the unusual, tubular, membrane extensions (arrows), believed to be associated with endocytosis.*
Source: (A) Gunning & Steer. (1996). Plant Cell Biology: Structure and Function. Jones and Bartlett, Sudbury, MA. (B) Samuels et al. (1995). J Cell Biol 130:1345–1357.

Membrane structures within the phragmoplast have been comprehensively imaged through electron tomography on material prepared by high-pressure cryofixation and the following model has been proposed (Fig. 5.52). In the initial stage of cell plate formation, an aggregation of vesicles with tubular extensions coalesce to form the **tubulovesicular network.** These tubules are long, thin, and curved and are surrounded by a protein-rich "fuzzy" matrix. This membranous network occurs at the phragmoplast midzone, where microtubules are abundant: first in the center of the cell where the phragmoplast forms, and then moving out to the periphery. After this stage, the continued delivery of vesicles and synthesis of polysaccharides widens the tubules to form an interwoven membranous layer, the **tubular network**. At this point, microtubules and the fuzzy matrix are lost. The network gradually loses reticulation, passing through a stage called the fenestrated sheet, and eventually becomes continuous. Each of these stages is associated with deposition of specific polysaccharide components of the cell plate. Interestingly, in a growing phragmoplast, all of these stages are present—the earliest being found at the periphery, and later ones succeeding progressively toward the center.

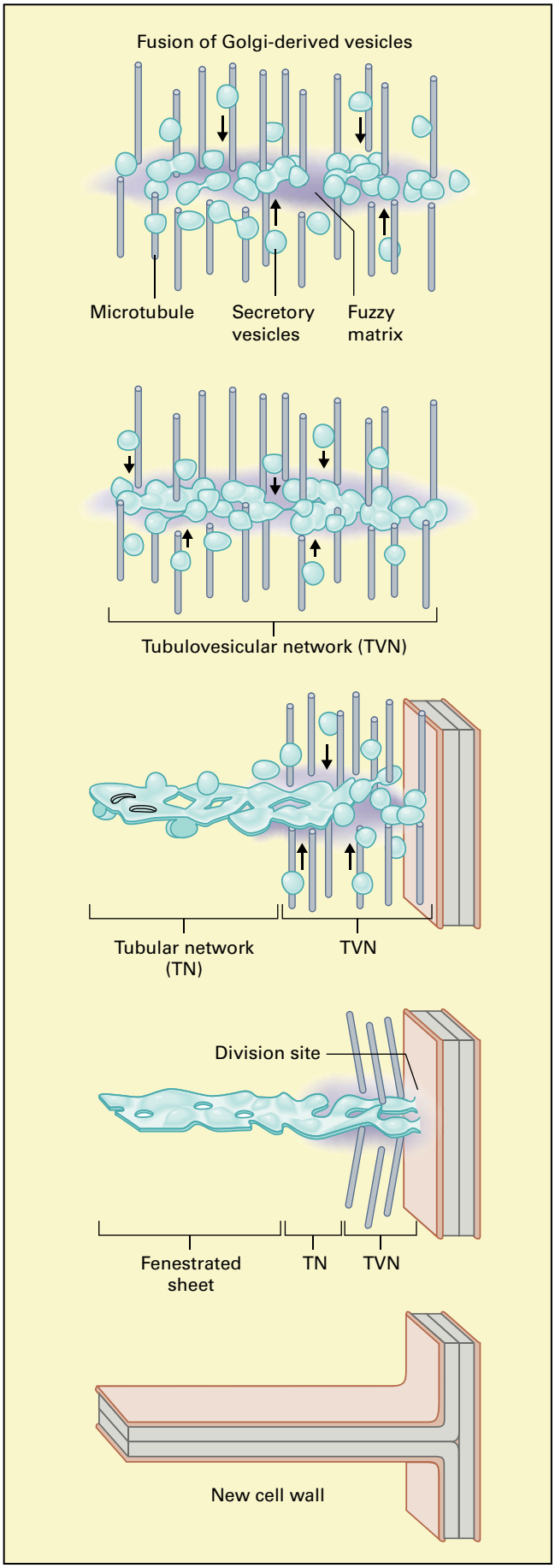


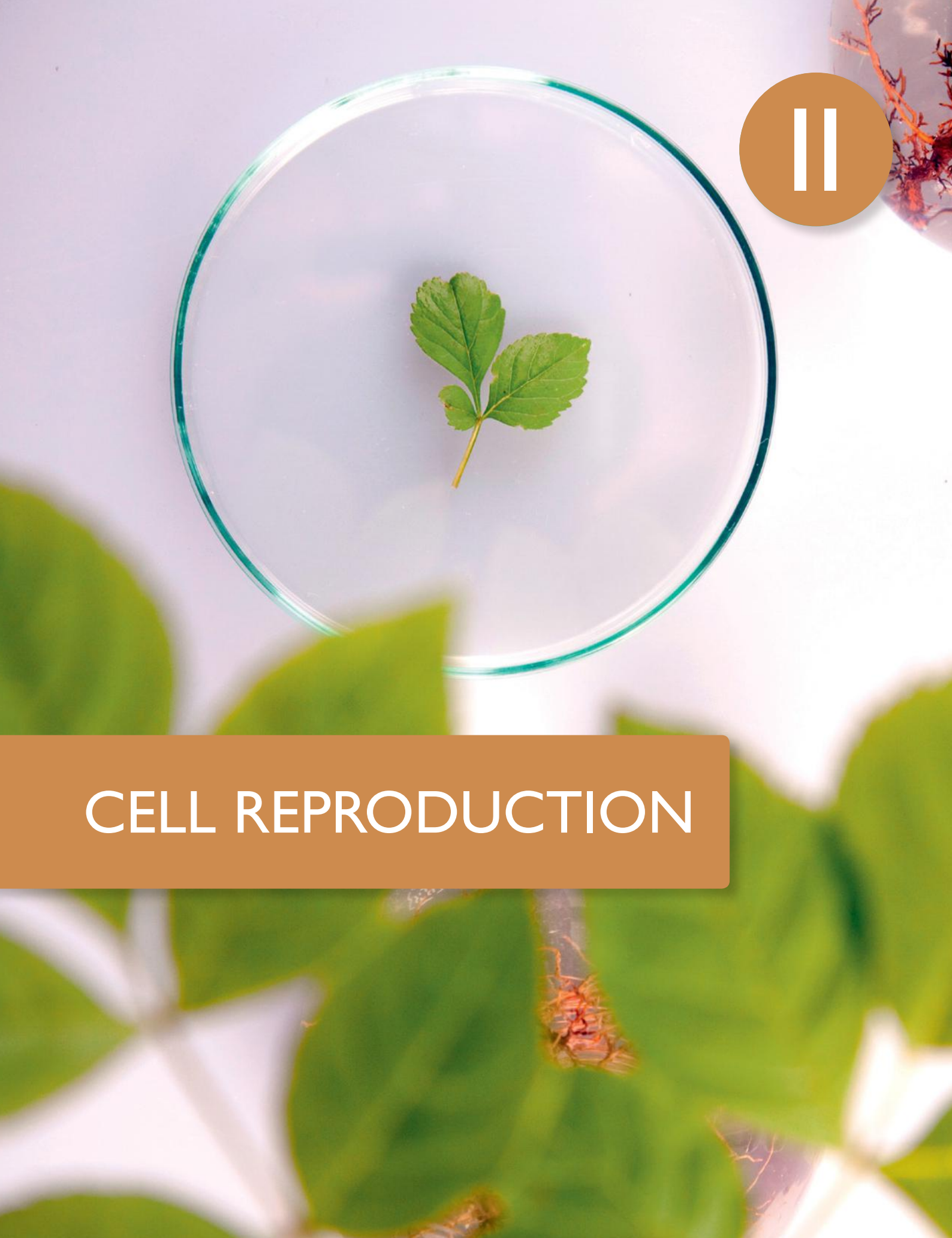
FIGURE 5.52 *Model showing the succession of membrane states in the developing phragmoplast. Initially, the region surrounding the zone where former spindle microtubules meet and overlap is called the fuzzy matrix and is rich in small vesicles which begin to fuse in the mid-plane. This forms the tubulovesicular network, where the volume of the membrane compartments at the mid-plane increases (forming tubules and cisternae) still surrounded by the fuzzy matrix. Continued secretion results in larger sheet-like cisternae forming, still with many tubular projections, called the tubular network, and the loss of the fuzzy matrix. Cisternae coalesce further to form the fenestrated sheet and eventually the mature cell plate. Note that as the phragmoplast grows, all of these stages can be found starting at the edge and moving to the center.*

Summary

In plants, the cytoskeleton comprises filamentous protein polymers of two types: actin filaments, and microtubules. Actin filaments and microtubules are not only skeletal but also "muscular"; they are responsible for the movements of cytoplasm and organelles. Actin filaments and microtubules are dynamic, turning over continually. These polymers are also polar in the sense of having different biochemical properties at each end. Their dynamic behavior and polarity are enhanced by free energy from the hydrolysis of nucleoside triphosphates. The biochemical properties of cytoskeletal polymers themselves appear to be widely conserved among eukaryotes. The different functions of the cytoskeleton, whether among cell types or taxa, are mediated by accessory proteins, which assemble, disassemble, bundle, sever, cap, crosslink, or move the polymers. In plants, actin filaments play starring roles in organelle movement. Microtubules are important for cell polarity and for controlling the anisotropy of expansion.

The cytoskeleton provides the machinery that separates the replicated chromosomes at mitosis and that partitions the daughter cells at cytokinesis. Mitosis depends on the mitotic spindle, a structure built largely from microtubules. Spindle microtubules interact with chromosomes at the kinetochore, a specialized protein-rich region that forms at the centromere. The dynamic properties of the microtubules, the architecture of the spindle, and force-generating proteins participate jointly in chromosome movement. The importance of each may vary at different phases of mitosis and in different cell types. Cytokinesis depends on cytoskeletal structures to ensure the appropriate orientation of the cell's new wall and to build it. During interphase, the phragmosome, a raft of cytoskeletal-rich cytoplasmic strands, often forms in the plane in which cell division will take place. In prophase, the preprophase band, a ring of microtubules and actin filaments, usually marks the location where the new cell plate will later fuse with the parental cell wall. During cytokinesis itself, the phragmoplast, a structure built from microtubules and actin filaments, orchestrates the intense secretory activity needed to build the forming cell plate and guides the growing cell plate to the parent cell wall.

II



CELL REPRODUCTION



6

Nucleic Acids

Masahiro Sugiura, Yutaka Takeda, Peter Waterhouse, Ian Small, Shaun Curtin, and Tony Millar

Introduction

The nucleic acids—deoxyribonucleic acid (DNA) and ribonucleic acid (RNA)—are polymers that can store and transmit genetic information. The blueprints for the biochemical machines that manufacture living organisms are encoded in the DNA molecules that make up the **genome** of the cell. During **transcription**, sequences of DNA serve as templates for the synthesis of RNA. Certain RNAs provide structural scaffolds in riboprotein complexes, others are important regulatory molecules that govern gene expression, and yet others, called messenger RNAs (mRNAs), are decoded by ribosomes during **translation** (see Chapter 10). The information in the translated sequences of mRNA specifies the amino acid sequence of proteins that ultimately contribute to the phenotypic characteristics of the organism. When cells divide, DNA **replication** generates a duplicate set of genetic instructions for the new cell (Fig. 6.1). DNA replication and repair are important processes because the survival of the individual organism depends on the stability of its genome. However, long-term survival of a population can be promoted by the genetic variation that results from changes in the DNA blueprints of its individual members.

Living cells store genetic information in the form of double-stranded DNA. In contrast, viral genomes consist of either double- or single-stranded nucleic acids and contain either DNA or RNA. The genomes of viruses are generally small and encode only a few of the proteins required for viral propagation. To replicate their nucleic acids and multiply, viruses must, therefore, exploit the biochemical machinery of a host cell. For example, when an RNA virus infects a cell, the cellular machinery can translate the viral RNA directly into protein, or it can use the viral genome as a template and synthesize complementary RNAs for subsequent translation. Some RNA viruses encode reverse transcriptase, an enzyme that uses RNA as a template for DNA synthesis. Once this enzyme has catalyzed the **reverse transcription** of a DNA copy of the viral RNA genome, the transcriptional and translational machinery of the host cell produce the other components necessary for virus multiplication (Fig. 6.1).

6.1 Composition of nucleic acids and synthesis of nucleotides

6.1.1 DNA and RNA are polymers of purine and pyrimidine nucleotides

DNA and RNA are long, unbranched polymers composed of four types of building blocks, called **nucleotides.** Each nucleotide comprises a purine or pyrimidine base, a pentose sugar, and a phosphate group (Fig. 6.2). The ribonucleotides in RNA contain ribose, a sugar with the chemical formula $(CH_2O)_5$. The deoxyribonucleotides that make up DNA contain 2-deoxyribose, from which the hydroxyl group linked to C-2 has been removed. Reactive 2′-hydroxyl groups make RNA much less stable than DNA, particularly in alkaline solutions.

Biochemistry & Molecular Biology of Plants, Second Edition. Edited by Bob B. Buchanan, Wilhelm Gruissem, and Russell L. Jones.
© 2015 John Wiley & Sons, Ltd. Published 2015 by John Wiley & Sons, Ltd.
Companion website: www.wiley.com/go/buchanan/biochem

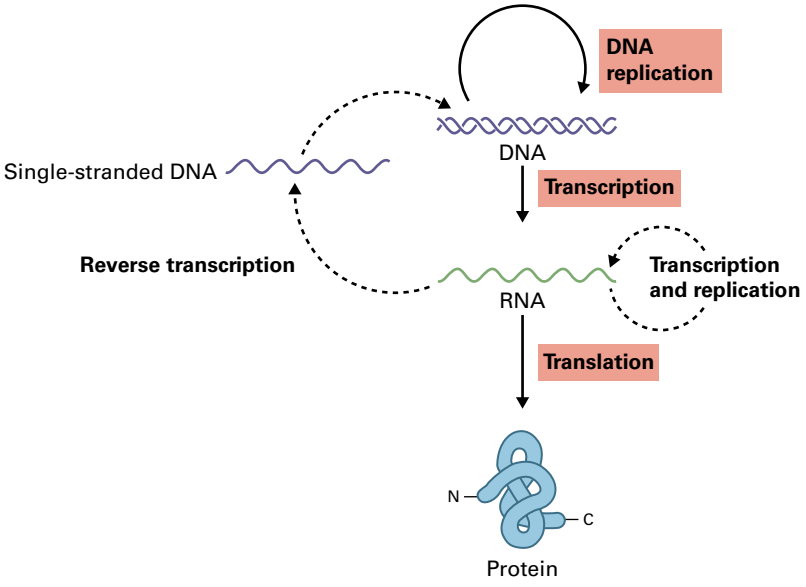
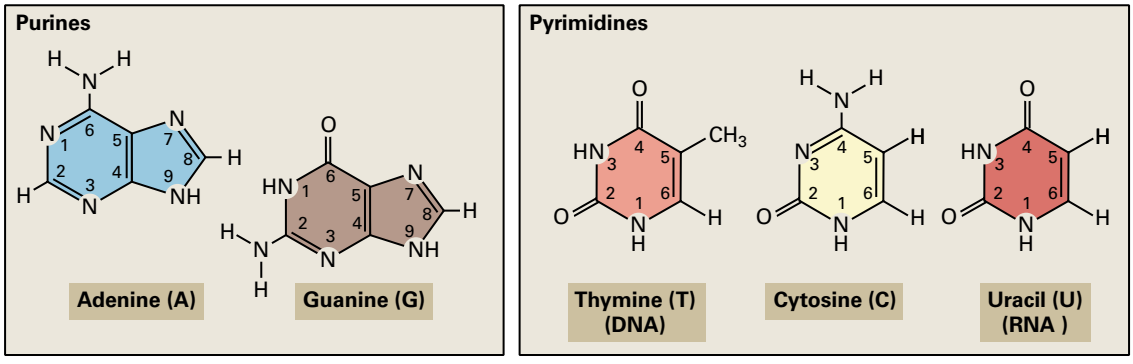
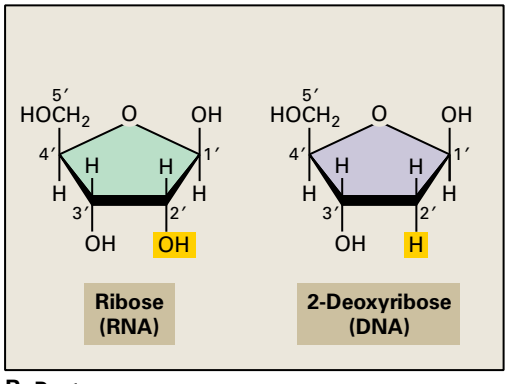


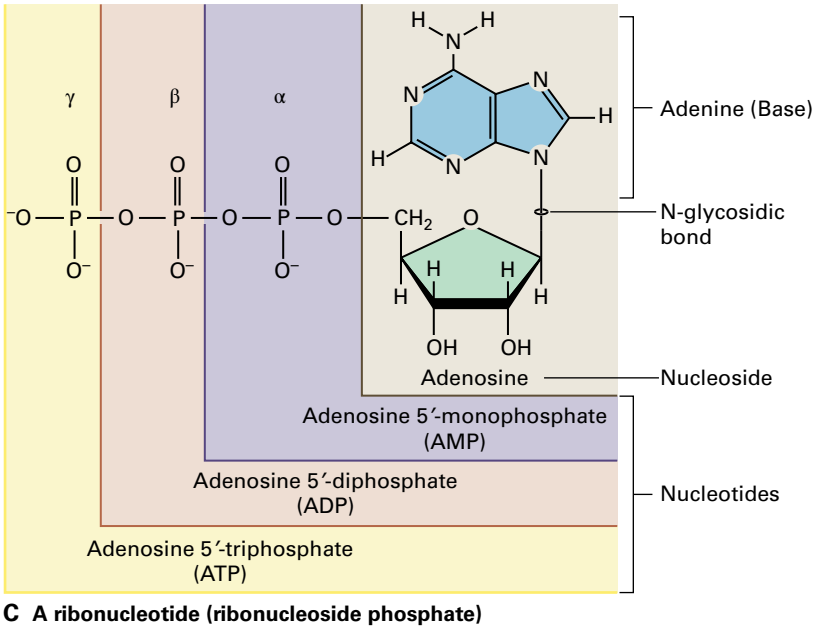
FIGURE 6.1 *In living organisms, genetic information is stored in genomes of double-stranded DNA. Single-stranded RNA is transcribed from this DNA template. Some RNA molecules encode instructions for the synthesis of specific proteins. Others participate in RNA processing or translation of RNA sequences into proteins. In contrast, viral genomes are varied; different viruses encode the genetic information required for their amplification in either single-stranded or double-stranded genomes that contain either DNA or RNA. The dotted lines indicate pathways involved in the reproduction of single-stranded RNA and single-stranded DNA viruses.*



A Bases



B Pentose sugars



C A ribonucleotide (ribonucleoside phosphate)

FIGURE 6.2 *The chemical components of nucleic acids. (A) The purine bases adenine and guanine are present in both DNA and RNA, as is the pyrimidine base cytosine. The pyrimidine base thymine is present in DNA. Uracil replaces thymine in RNA. (B) RNA nucleotides contain the pentose sugar ribose. DNA contains a less reactive pentose, 2-deoxyribose. In nucleosides and nucleotides, the carbons of the pentose sugar are numbered 1′ to 5′, as shown here. (C) A nucleoside comprises a purine or pyrimidine base and a pentose sugar. A nucleotide is a nucleoside in which C-5′ is linked to one, two, or three phosphate groups by a phosphoester bond.*

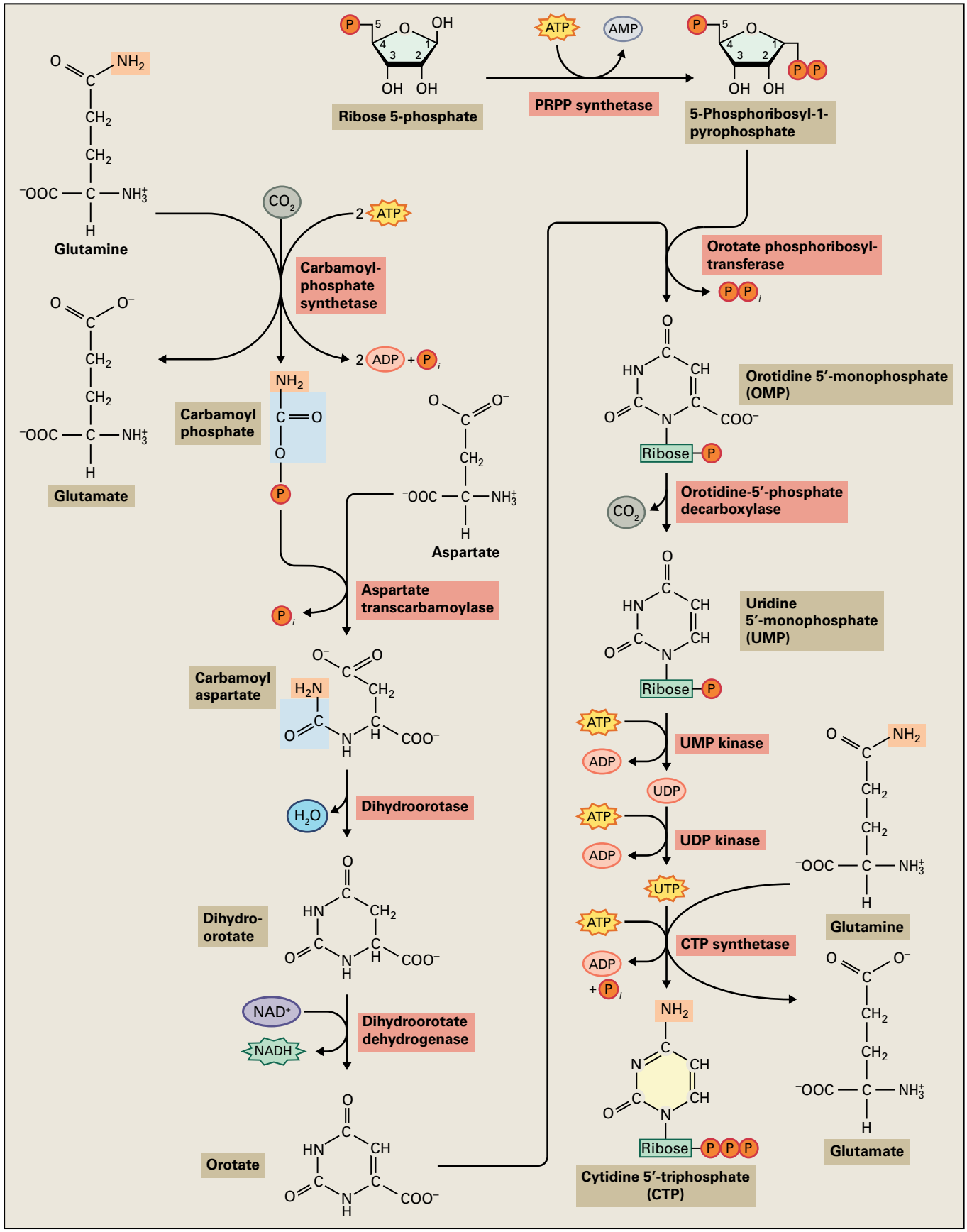


FIGURE 6.3 *The pathway of de novo pyrimidine nucleotide synthesis. Orotate, the first product with a complete pyrimidine ring, reacts with 5-phosphoribosyl-1-pyrophosphate (PRPP) to form the nucleotide orotidine 5′-monophosphate (OMP). Decarboxylation of OMP produces UMP. CTP is synthesized from uridine 5′-triphosphate (UTP) by amination; the probable amino donor is glutamine. Alternatively, cytidine 5′-monophosphate is synthesized from UMP (not shown). UDP, uridine 5′-diphosphate.*

Each nucleic acid includes four nitrogenous bases: two purines and two pyrimidines. DNA contains the purines adenine and guanine, and the pyrimidines cytosine and thymine. RNA also contains adenine, guanine, and cytosine, but thymine is replaced with another pyrimidine, uracil. Unusual or modified bases are also found in some ribonucleic acids, particularly transfer RNAs (tRNAs, see Section 6.7.3).

6.1.2 Plant cells synthesize pyrimidine and purine nucleotides de novo as well as by way of salvage pathways

The de novo synthesis of pyrimidine nucleotides begins with a series of six reactions that make up the orotic acid pathway. The pyrimidine orotate is produced from simple molecules: CO_2, aspartate, and the amide group of glutamine (Fig. 6.3). Once synthesized, orotate is joined to 5-phosphoribosyl-1-pyrophosphate (PRPP), and is subsequently modified to form the ribonucleotides uridine triphosphate (UTP) and cytidine triphosphate (CTP). In plants, all enzymes required for pyrimidine nucleotide biosynthesis are found in plastids, which are thought to be the primary site of cellular pyrimidine biosynthesis.

Purine nucleotide synthesis in plants is not well understood but is thought to proceed by a pathway defined in other organisms. Whereas the pyrimidine orotate is first synthesized as a free base and then linked to PRPP by an N-glycosidic bond, purine nucleotides are synthesized directly from PRPP by sequential addition of purine moiety precursors: glycine, CO_2, amide groups from aspartate and glutamine, and methenyl and formyl tetrahydrofolates (Fig. 6.4). Unlike pyrimidine biosynthesis, purine nucleotide synthesis is thought to occur in the cytosol.

Deoxyribonucleotides are derived from the corresponding ribonucleotides. The ribose moiety of the ribonucleotide is reduced by ribonucleotide reductase. The enzyme thymidylate synthase catalyzes the formation of deoxythymidine 5′-monophosphate (dTMP) by transferring a methyl group from methenyl tetrahydrofolate to the C-5 of deoxyuridine 5′-monophosphate (dUMP). Because the thymidylate synthase reaction is the only intracellular source of de novo dTMP, this enzyme is essential for maintaining a balanced supply of the four deoxynucleotide triphosphates required for DNA replication. The enzyme also has an important role in regulating the concentration of deoxyuridine nucleotides, which must be kept low to prevent incorporation of these nucleotides into DNA. Indirect evidence suggests certain plants (e.g., *Lemna major*) may contain an alternative pathway that methylates deoxycytidine 5′-diphosphate and deaminates the resulting product to yield deoxythymidine 5′-diphosphate.

The catabolism of nucleotides in plants is not well understood. DNA or RNA is first hydrolyzed to oligonucleotides by deoxyribonucleases or ribonucleases, respectively. The oligonucleotides are further hydrolyzed by phosphodiesterases to yield mononucleotides, which are then hydrolyzed by nucleotidases and phosphatases to yield nucleosides. The free nucleosides and bases that are formed during the breakdown of nucleotides can be converted back to nucleotides by way of salvage pathways. Unlike the de novo pathways of purine and pyrimidine synthesis, which are well established and thought to be similar in animals and plants, the salvage pathways of nucleotide biosynthesis are less understood and more diverse. These pathways have received considerable attention following the discovery that some diseases in animals and humans result from deficiencies in salvage pathway enzymes (Box 6.1).

Most salvage pathways of nucleotide biosynthesis fall into one of two principal categories. The first is a one-step pathway catalyzed by phosphoribosyltransferase (Reaction 6.1). This reaction is reversible in the presence of pyrophosphatase, which is found in the plastids but not the cytosol of plant cells (see Chapter 13).

Reaction 6.1 Phosphoribosyltransferase

$$\text{Base} + \text{PRPP} \leftrightarrow \text{Ribonucleotide} + \text{PP}_i$$

The second type of salvage pathway requires two steps that are catalyzed by nucleoside phosphorylase (Reaction 6.2) and nucleoside kinase (Reaction 6.3), respectively. The latter reaction is irreversible.

Reaction 6.2 Nucleoside phosphorylase

$$\text{Base} + (\text{deoxy})\text{Ribose1-P} \leftrightarrow (\text{deoxy})\text{Nucleoside} + \text{P}_i$$

Reaction 6.3 Nucleoside kinase

$$(\text{deoxy})\text{Nucleoside} + \text{ATP} \rightarrow (\text{deoxy})\text{Nucleotide} + \text{ADP}$$

Not all of the possible reactions suggested by the two pathways above occur in vivo. For example, while the nucleoside cytidine is present in plants, the free base cytosine has not been observed. Although certain deoxynucleosides can be salvaged by comparable reactions, experimental analysis has focused primarily on thymidine metabolism.

6.1.3 Nucleic acids are composed of nucleotides linked by phosphodiester bonds

In a nucleic acid, nucleotides are linked together in a polynucleotide chain. Covalent phosphodiester bonds join the 5′ carbon of one nucleotide to the 3′ carbon of the next, forming a sugar–phosphate backbone to which the four bases are attached (Fig. 6.5A). The directional nature of these bonds means that a linear nucleotide chain has two distinct ends with different biochemical characteristics. The 5′ end of a nucleic acid usually has a free phosphate group, and the 3′ end is typically hydroxylated. By convention, polynucleotide sequences are written 5′ to 3′, from left to right (Fig. 6.5B).

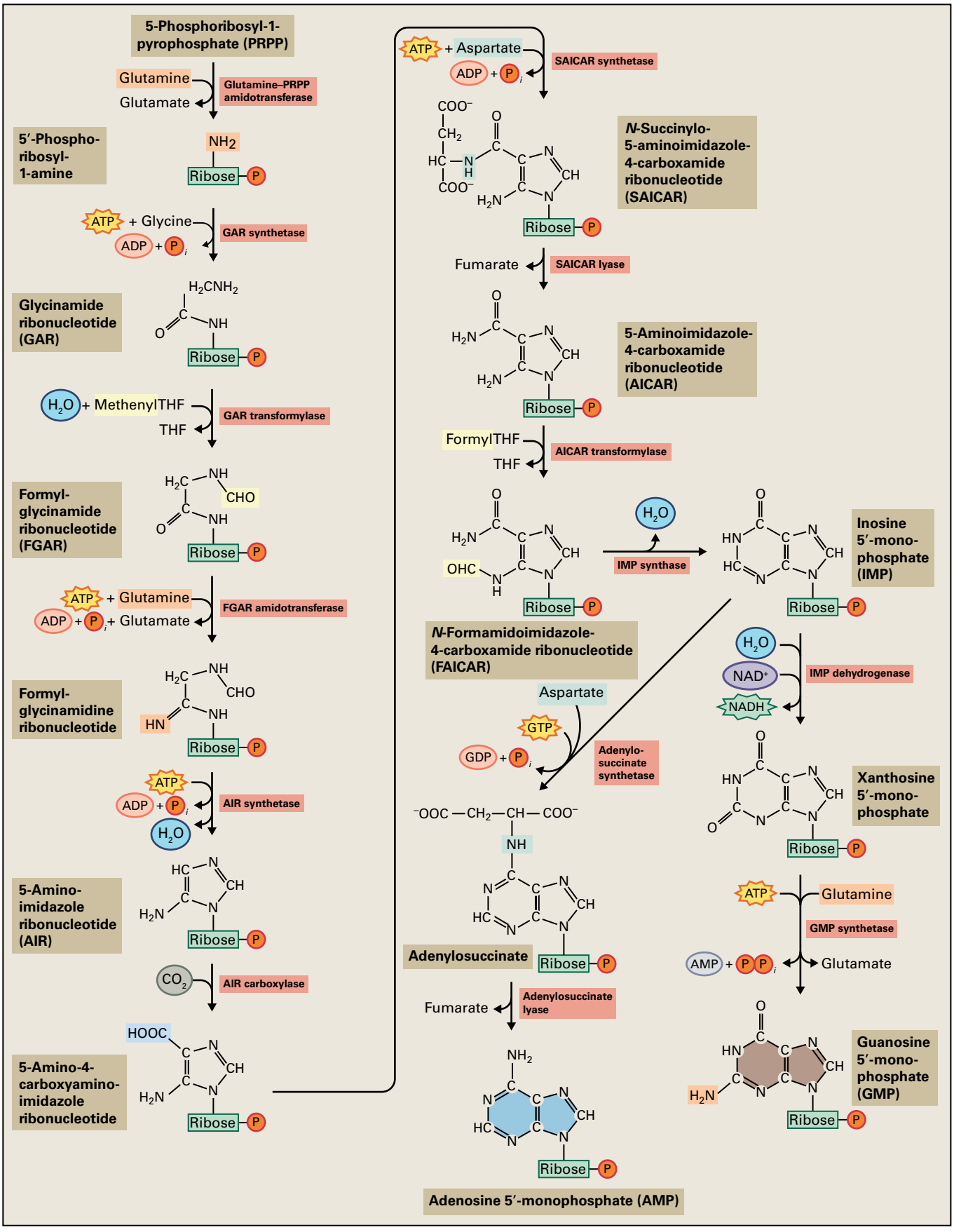


FIGURE 6.4 *The pathway of de novo purine nucleotide synthesis. In contrast to de novo synthesis of pyrimidine nucleotides, in which the nitrogenous base is formed prior to ribosylation, purine nucleotide synthesis modifies PRPP to create inosine 5′-monophosphate (IMP), the first product with a complete purine ring. Both AMP and GMP are derived from IMP. To generate AMP, first an aspartate is added to IMP, and then the carbon skeleton of the amino acid (fumarate) is removed, resulting in a net amination. IMP is oxidized and then aminated by glutamine to create GMP. THF, tetrahydrofolate.*

BOX 6.1

Defects in the salvage pathways of nucleotide biosynthesis are associated with diseases in humans

The importance of the salvage pathways of nucleotide biosynthesis is illustrated by the severity of the diseases that result from deficiencies in salvage pathway enzymes. For example, **Lesch–Nyhan syndrome,** a severe genetic disorder that occurs mostly in boys, is caused by lack of functional hypoxanthine-guanine phosphoribosyltransferase (HGPRTase), which catalyzes the condensation of hypoxanthine and PRPP. The inability to use PRPP results in its accumulation, which in turn stimulates glutamine-PRPP amidotransferase, thereby causing the overproduction of purine nucleotides. Oxidation of the excess purines results in the production of high concentrations of uric acid and affects especially the central nervous system, which may reflect the brain's particular dependence on the salvage pathways. Symptoms of the disease include mental retardation, poor coordination, and self-mutilating behavior.

Reduced activities of purine-nucleoside phosphorylase and adenosine deaminase affect the development and function of both T cells and B cells, causing a severe human immunodeficiency disease. Purine nucleoside phosphorylase deficiency results in a large accumulation of dGTP in T cells, which most likely is toxic during T-cell development. Adenosine deaminase deficiency leads to accumulation of deoxyadenosine in T cells, which has a negative effect on the activity of ribonucleotide reductase and thereby lowers the concentration of other deoxynucleotide triphosphates. The basis for B-cell toxicity is less understood.

The predominant form of DNA is a double-stranded, double helical structure formed from two separate polynucleotide chains by specific pairing of bases. Hydrogen bonds form between a larger, purine base on one chain (A or G, respectively) and a smaller, pyrimidine base on the other chain (T or C, respectively). A–T pairing involves two hydrogen bonds, whereas G–C pairing involves three hydrogen bonds (Fig. 6.6). The free energy that drives the hybridization of two single strands to form a duplex DNA results from the overall increase in entropy that occurs when the hydrophobic bases are moved from an aqueous environment into the center of the duplex. (Although duplex formation decreases the entropy of the nucleotide chains, it increases the entropy of the surrounding water molecules.) The two chains are antiparallel, such that the sugar–phosphate backbones of the two strands are oriented in opposite directions. The 5′ and 3′ ends of the genomes of single-stranded DNA viruses are typically linked by a phosphodiester bond, resulting in a circular molecule.

Most cellular RNA is single stranded, although the nucleotide chain often folds locally. The resulting domains generally contain stems, double-stranded regions that contain both "Watson–Crick" base pairs (i.e., G–C and A–U), many types of atypical base pairs (e.g., G–U, U–U, G–A, etc.), and terminal, single-stranded loops. These domains then associate with each other through various types of specific tertiary interactions. As a result, RNAs can assume very compact structures.

6.2 Replication of nuclear DNA

Before a cell can divide, it must produce a new copy of each of its chromosomes. In eukaryotic cells, chromosomes are made up of **chromatin**, a filamentous complex of DNA and proteins (see Chapter 9). Considering the long DNA molecules are tightly packaged into DNA–protein complexes, it is not surprising that the replication of DNA involves a large number of enzymes and regulatory proteins. Replication of nuclear DNA has been studied extensively in bacteria, yeast, and mammalian cells. Regulation of this process during the eukaryotic cell cycle is discussed in more detail in Chapter 11.

In all organisms, DNA replication involves three stages: initiation, elongation, and termination. In eukaryotes, the ends of the linear chromosomes are also modified to prevent DNA loss during subsequent rounds of replication. This section focuses on the general enzymology of nuclear DNA replication in eukaryotes. The prevailing view is that this process is very similar in all eukaryotes, although some of the regulatory mechanisms of DNA replication in plants may be tailored to their unique developmental and physiological functions.

6.2.1 Nuclear DNA synthesis begins at discrete origins of replication and requires complex cellular machinery composed of many proteins

Nuclear DNA replication occurs during the S phase of the cell cycle (see Chapter 11) and is a highly regulated process. Replication initiates simultaneously at a number of specific sites, termed **origins of replication** (Fig. 6.7). The identification of eukaryotic chromosomal replication origins has been most successful in the budding yeast *Saccharomyces cerevisiae*, where a specific sequence of 200 base pairs (bp)—called the autonomously replicating sequence (ARS)—is the minimal sequence requirement for the initiation of chromosomal DNA replication. In mammalian cells, initiation of DNA

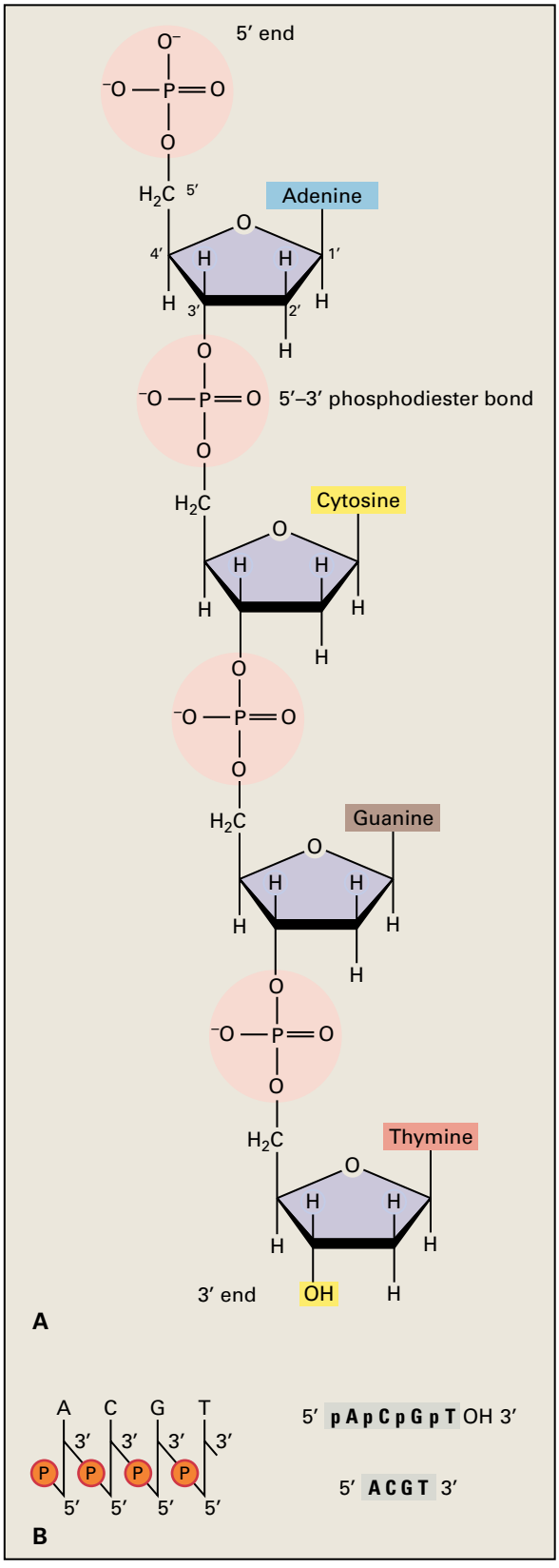


FIGURE 6.5 *(A) A polynucleotide chain of DNA. The alternating sugar–phosphate polymer forms the backbone of the polynucleotide chain. In RNA, a 2′-hydroxyl group replaces the 2′-hydrogen. (B) Representations of nucleic acids are drawn 5′ to 3′, from left to right. In most cases, nucleic acid sequences are presented in a format that does not include symbols for the sugar–phosphate backbone (lower right).*

replication occurs in specific regions that are more than 10,000 bp (i.e., 10 kilobases, or kb) apart. The minimal sequence that constitutes the DNA replication origin in these regions is still unknown. Specific replication origins have not been identified in plants.

Many possible origins of replication exist in the chromosome, but not all function in every cell. The segment of DNA that is replicated from a single origin is termed a replicon. In plant cells, for example, a typical replicon is 50–70 kb in length. *Triticale*, a hybrid allohexaploid grain, has replicons of about 22 kb. In contrast, the parent plants (rye and wheat) have replicons of 50 to 60 kb. Apparently, replication origins that remain silent in the cells of the parental species can become active in *Triticale*. Experiments with synchronized cell populations have also shown that not all replication origins on a given chromosome are activated at the same time when DNA replication is initiated during S phase. Origins of replication are activated ("fire") in a reproducible order. The timing of firing at a given origin is tightly regulated by the cell and may depend on the state of condensation of the chromatin in which the replication origin resides (see Section 6.2.4).

The activation of replication origins during S phase is now understood best in yeast and mammalian cells (see Chapter 11). DNA replication initiates as the chromatin structure unfolds. The two DNA strands separate at an AT-rich region and replication-specific proteins bind to the DNA (Fig. 6.8). Because the DNA double helix is very stable under normal conditions, specific ATP-dependent enzymes, called DNA helicases, must catalyze strand separation at the origin and ahead of the replication fork. Following DNA helicase activity, replication protein A (RP-A) binds to single-stranded DNA and stabilizes its structure. As DNA replication proceeds, DNA topoisomerases remove supercoils that form in front of the replication fork (Box 6.2).

6.2.2 Nuclear DNA replicates semi-conservatively and semi-discontinuously

As DNA replication proceeds from the replication origin, a multienzyme complex that contains **DNA polymerase** catalyzes the addition of deoxyribonucleotides to the 3′ end of a template-bound nucleic acid. Thus, DNA synthesis proceeds in the 5′ to 3′ direction, while the template strand is read 3′ to 5′, creating an asymmetric structure at the replication fork (Fig. 6.8). DNA polymerases can only add nucleotides to a pre-existing chain **(primer)** and are not active unless a primer with a free 3′ hydroxyl is hydrogen bonded to the DNA template being replicated. Primers are synthesized by specific ribonucleotide polymerases, called DNA primases, which initiate primer synthesis with a purine ribonucleotide.

As a result of the asymmetric structure of the replication fork, DNA synthesis is **semi-discontinuous**. Addition of nucleotides to one strand of newly synthesized DNA is continuous. This **leading strand** begins at a single primer,

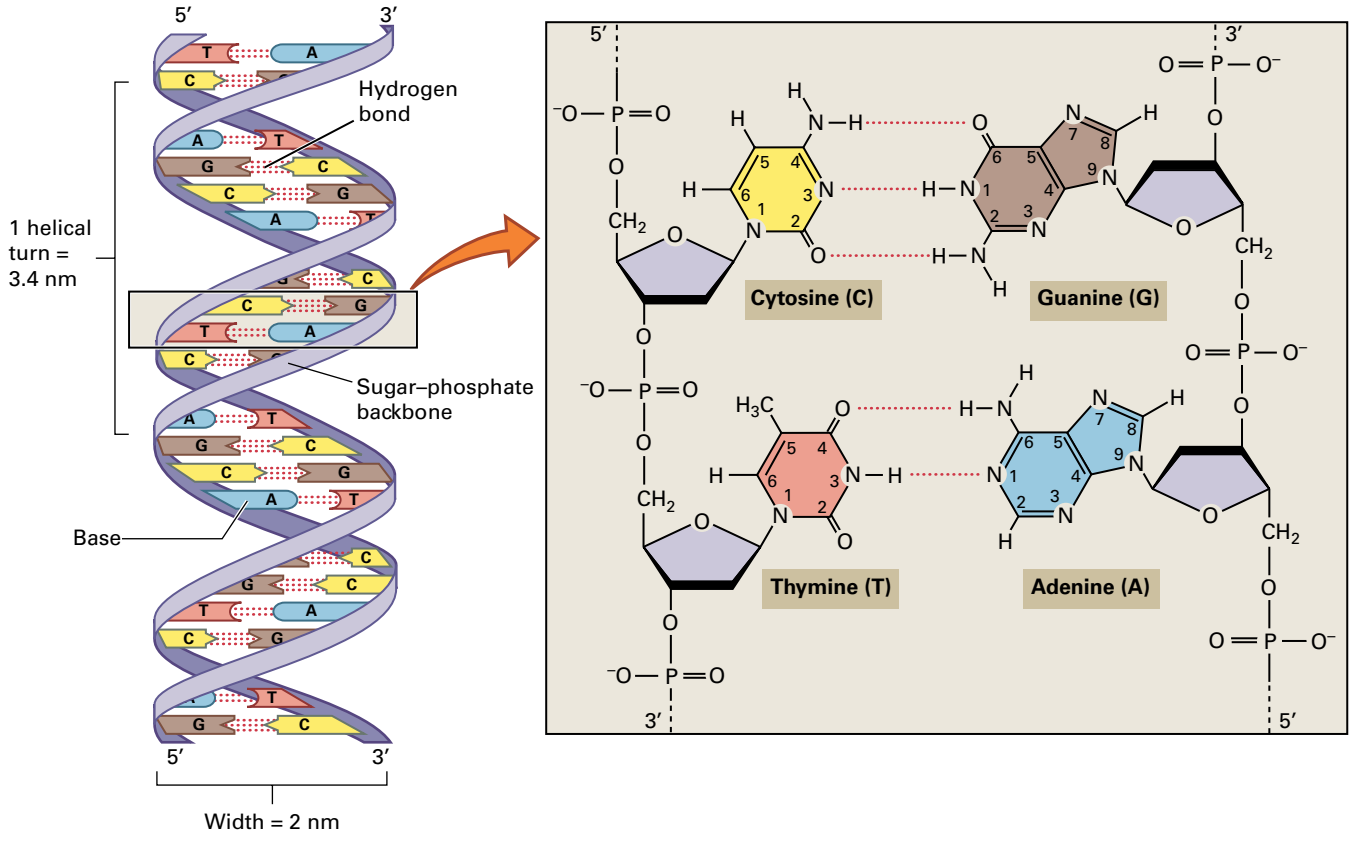


FIGURE 6.6 *The DNA double helix. Two DNA strands associate when their complementary bases pair. Three hydrogen bonds link cytosine and guanine, whereas only two hydrogen bonds form between thymine and adenine. The two DNA strands are antiparallel, running from 5′ to 3′ in opposite directions.*

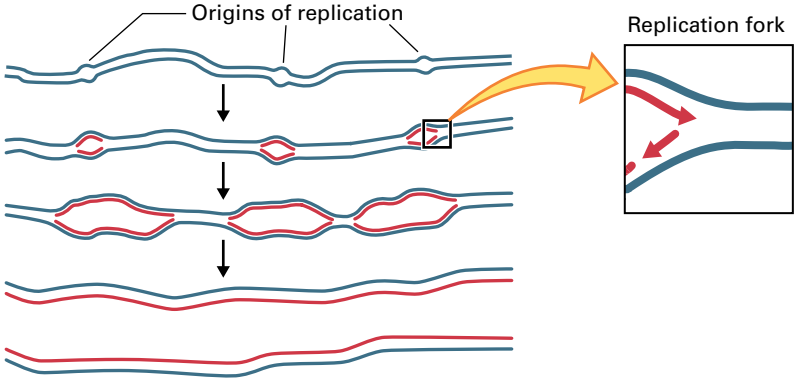


FIGURE 6.7 *DNA replication initiates at specific DNA sequences, called origins of replication, which are spaced apart in the DNA. Each origin produces two replication forks that move in opposite directions until they meet replication forks initiated at neighboring origins. The parental DNA strands are shown in blue, the newly synthesized strands in red.*

and the other **lagging strand** is synthesized in short, discontinuous segments of DNA called Okazaki fragments, each of which requires its own primer (Fig. 6.8). To produce a continuous DNA strand from the many fragments of the lagging strand, a special DNA repair system that includes a specific ribonuclease, RNase H, removes the RNA primer and replaces it with DNA. Another enzyme, DNA ligase, joins the 3′ end of the new DNA fragment to the 5′ end of the downstream DNA fragment. Since both strands of nuclear DNA serve as templates for DNA synthesis, the replication products each contain one original and one newly synthesized complementary strand. This type of DNA replication is termed **semi-conservative** (see Fig. 6.7).

Three principal DNA polymerase holoenzymes that replicate nuclear DNA have been identified in the nuclei of eukaryotes, including plants: α, δ, and ε. DNA polymerase α often dissociates from the template and, therefore, does not synthesize long chains of nucleotides, but two of its four subunits have DNA primase activity. DNA polymerase α, therefore, is thought to function primarily as a primase in lagging strand DNA synthesis (Fig. 6.8). After DNA polymerase α dissociates from the template, a primer terminus is exposed.

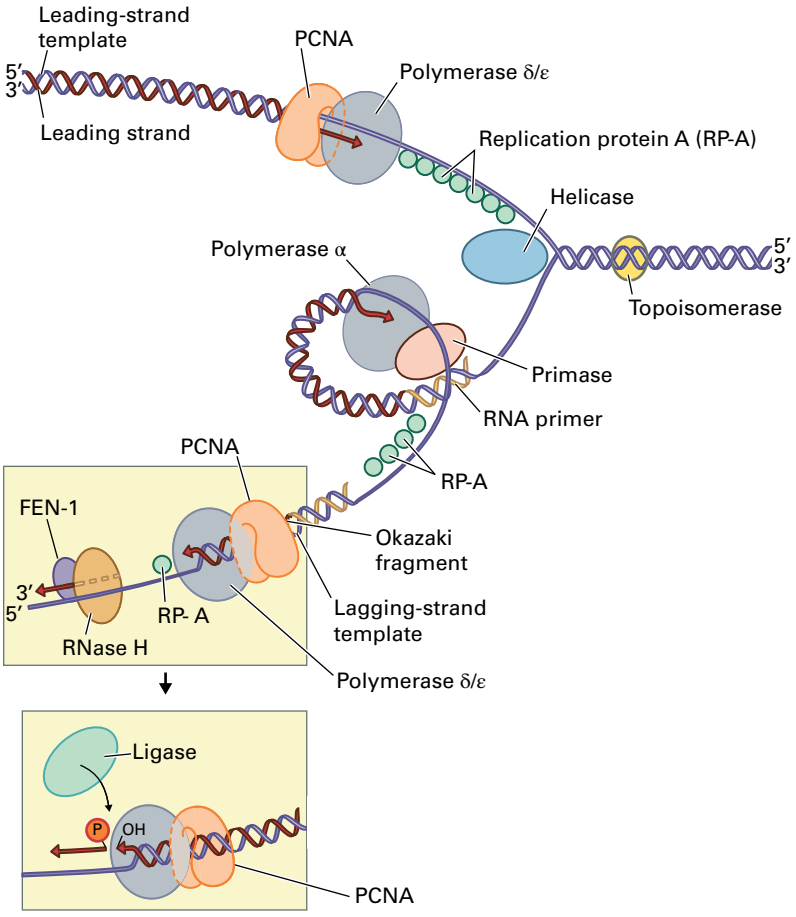


FIGURE 6.8 *Schematic representation of the organization of the eukaryotic DNA replication fork, showing discontinuous replication of the lagging strand. The model shown in this figure is based primarily on research in yeast. A complex containing helicase and two molecules of DNA polymerase carries out the coordinated synthesis of both the leading strand and the lagging strand. Topoisomerase acts ahead of the replication fork to remove the supercoils generated by unwinding the DNA (see Box 6.2). The leading DNA strand is lengthened continuously towards the fork as nucleotides are added. In contrast, the lagging DNA strand is synthesized in discrete segments, called Okazaki fragments. As leading strand synthesis progresses and the fork opens, priming sites on the lagging strand template are exposed. Following synthesis of a short RNA primer by primase, DNA polymerase α adds nucleotides to the new fragment until its 3′ end reaches the primer of the adjacent fragment. Gaps are produced by the concerted action of FEN-1 nuclease, which cleaves between the RNA primer and the new DNA strand, and RNase H, which degrades the RNA primers. The gaps are filled by DNA polymerases δ/ε, and the lagging DNA strand fragments are joined by DNA ligase. PCNA (proliferating cell nuclear antigen) is a protein cofactor of the DNA polymerase complex. RP-A (replication protein A) binds to and stabilizes single-stranded DNA.*

A multisubunit replication factor complex binds the terminus, facilitating the assembly of a functional DNA polymerase δ or ε complex to complete the synthesis of the Okazaki fragment. In contrast to DNA polymerase α, DNA polymerases δ and ε remain tethered to the DNA template by PCNA (proliferating cell nuclear antigen), an essential protein cofactor of the DNA polymerase complex that forms a ring-like structure around the DNA. For pedagogical reasons, most of the components involved in DNA replication are shown as individual complexes in Fig. 6.8. These proteins, however, cooperate to form a large, multisubunit complex of replication machinery at the replication fork. In addition, DNA replication occurs at discrete foci in the nuclei of mammalian cells. Called replication centers, these foci may contain as many as 100 replication forks.

DNA replication proceeds with remarkably high fidelity, producing on average only one error for every 10^9 base pairs replicated. Mismatch repair and the 3′ → 5′ exonuclease function of DNA polymerases δ and ε maintain this high fidelity. DNA polymerases are self-correcting enzymes that remove their own polymerization errors during replication. Separate, intrinsic 3′ → 5′ exonuclease activities enhance fidelity by a process called **proofreading.** These enzymatic activities can clip mismatched nucleotides from the 3′ end of the newly synthesized strand. DNA polymerase α lacks this 3′ → 5′ exonuclease activity, but demonstrates high fidelity nonetheless. The lack of proofreading by DNA polymerase α may be compensated for by the removal of the RNA primers and the few deoxyribonucleotides polymerized by the enzyme, followed by DNA mismatch repair (see Section 6.3.4).

BOX 6.2

DNA topoisomerases perform a number of functions during DNA replication

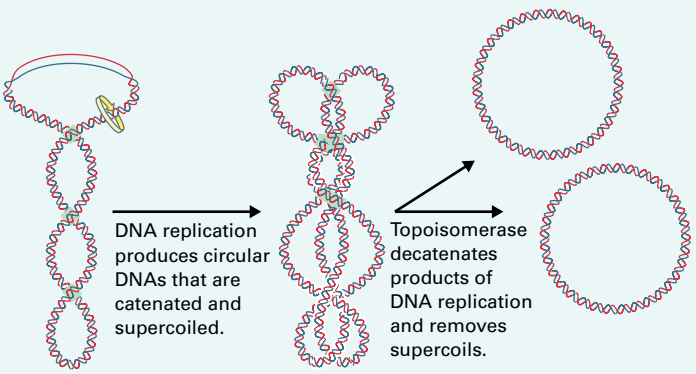
In double-stranded DNA, approximately 10 base pairs correspond to one complete turn about the axis of the double helix structure. As DNA replication begins, the DNA double helix must unwind to expose the leading and lagging strand templates. When one section of the molecule is underwound, the regions proximal and distal to it become overwound, thereby creating supercoils (Fig. 6.B2, left panel). The DNA ahead of the replication fork would have to rotate rapidly to remove these supercoiled regions and allow DNA replication to proceed. DNA in circular molecules or chromosomes, however, is not free to rotate. Instead, DNA topoisomerases remove (or in some cases add) supercoils to maintain favorable DNA topologies and allow DNA replication to continue. The electron micrograph shows a supercoiled circular DNA molecule (A) and a relaxed circular DNA molecule (B) for comparison.

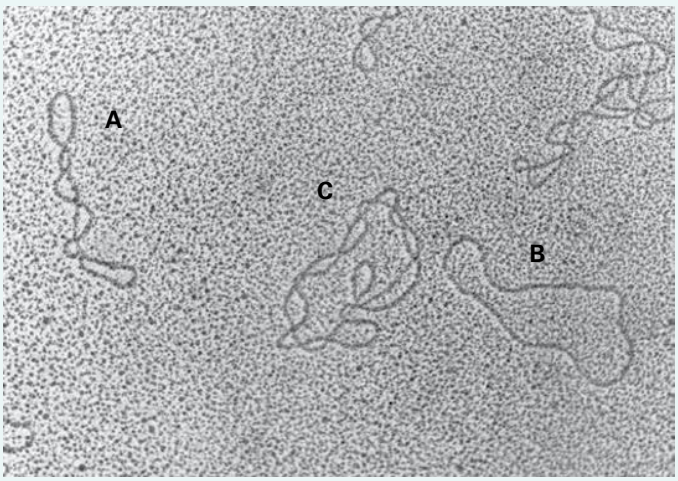
During replication of circular DNA molecules such as the chloroplast genome (see Section 6.5.4), the oppositely oriented replication forks eventually collide to yield two catenated (linked) circles of double-stranded DNA (see middle panel of diagram and structure C in the electron micrograph). In addition to removing supercoils, DNA topoisomerases are also required for separation of the interlocked circular replication products (see right panel of diagram).

Two classes of DNA topoisomerase that can attach covalently to a DNA phosphate, type I and type II, are found in both prokaryotes and eukaryotes. Topoisomerase I causes a single-strand break (or nick) in a DNA duplex by breaking a phosphodiester bond. Topoisomerase II creates transient double-strand breaks. Cleavage of the phosphodiester bonds is reversible and rapid, and it does not require additional energy. Topoisomerase I can only remove supercoils from DNA, whereas topoisomerase II (also called DNA gyrase) can either add or remove supercoils and can either catenate or decatenate circular duplex DNA molecules. Genetic analysis of topoisomerase function in yeast has shown topoisomerase II is essential for cell growth and division. In addition to decatenating the products of replication, this class of enzymes participates in chromosome condensation during mitosis and meiosis, constitutes a major component of the chromosome scaffold and nuclear matrix, and may also play a role in the structure of the DNA matrix complex.

The topoisomerases found in plant nuclei resemble their yeast and animal counterparts. A type I enzyme isolated from chloroplasts, however, is more similar to prokaryotic topoisomerase I, which is consistent with the prokaryotic origin of this organelle (see Section 6.5.1). Topoisomerases of types I and II have also been found in the mitochondria of mammals and trypanosome, but not in plant mitochondria.

Source: Sugiura, Nagoya University, Japan; previously unpublished.





6.2.3 Unlike prokaryotic DNA, eukaryotic chromosomes have ends that are protected by telomeres

Termination occurs in regions where newly synthesized DNA strands from two replication origins meet. In the *Escherichia coli* chromosome, specific sequences near the termination region, called *Ter* sites, arrest new strand synthesis in one direction. The newly synthesized strand from the other direction passes through the *Ter* site, and homologous recombination (see Section 6.4.2) occurs between the two newly synthesized strands. A similar mechanism may operate in eukaryotes, as DNA sequences resembling *Ter* sites have been found in yeast.

As described above, DNA polymerases require nucleotide primers to initiate DNA replication. If a priming site is located at the end of a linear chromosome, this short DNA segment would remain unreplicated after the primer is degraded and would not be available during the next round of DNA replication. As a result, a short segment of the chromosome would be deleted during each round of DNA replication. Normally, however, such deletions do not occur and chromosome length remains stable because chromosomes terminate in special sequences of DNA called **telomeres**. These sequences, which are similar in all eukaryotic cells, consist of multiple tandem repeats of a short DNA sequence—TTAGGG in humans and TTTAGGG in *Arabidopsis* (Fig. 6.9).

An enzyme called telomerase recognizes the G-rich strand of the telomere and extends the 3′ end of chromosomal DNA by adding new repetitions of the telomeric sequence. All known telomerases contain specific RNA molecules that are part of the enzyme complex and serve as the complementary template for the telomeric repeat unit (Fig. 6.10). After telomerase has copied several telomere repeats from its integral RNA template, the complementary C-rich DNA strand is synthesized. The telomeric repeats may serve as a primer site for chain elongation, allowing DNA polymerase to complete the unfinished strand.

Telomerase was discovered in the protist *Tetrahymena* and has also been isolated from yeast and animals. Plant chromosomes have highly conserved telomeric sequences, and telomerase activity has been found in plants, suggesting plant telomeres are maintained by mechanisms similar to those identified in other eukaryotes.

Human	TTAGGGTTAGGGTTAGGGTTAGGG
Paramecium	TTGGGGTTGGGGTTGGGGTTGGGG
Trypanosoma	TTAGGGTTAGGGTTAGGGTTAGGG
Arabidopsis	TTTAGGGTTTAGGGTTTAGGG

FIGURE 6.9 *Telomeres are simple, repeated DNA sequences found at the ends of eukaryotic chromosomes. Despite the evolutionary divergence of eukaryotic organisms, the repeated sequences of telomeric DNA are remarkably conserved.*

6.2.4 The timing of nuclear DNA replication is tightly regulated, although the mechanisms involved are not well understood

All chromosomal DNA replicates during the S phase of the cell cycle, but the timing of replication of a DNA segment depends in part on the structure of the chromatin region in which the DNA segment resides. The chromatin that remains in a highly condensed conformation during the interphase of the cell cycle is called **heterochromatin**; replication of DNA in segments of heterochromatin occurs very late in S phase. Studies in the budding yeast *S. cerevisiae* have also revealed the DNA located near telomeres is replicated late in S phase, whereas the DNA associated with centromeres (see Chapter 9) is replicated earlier. A telomere-associated ARS replicates sooner if relocated to another site on the chromosome. Similarly, if small segments of telomeric DNA sequence are inserted into a chromosome near an origin of replication that initiates DNA replication early, activation of the origin is delayed. In contrast, DNA segments that are actively transcribed are located in **euchromatin**, regions of the chromosome in which the chromatin is less condensed. These DNA segments are replicated early during S phase, suggesting gene expression can affect the timing of DNA replication. For example, genes that are transcribed constitutively in all cells replicate early, whereas genes that encode proteins with tissue-specific functions are replicated early in cells that express the genes but late in cells where they are inactive. Together, these observations suggest the DNA sequence of the replication origin does not necessarily dictate replication timing—other regulatory elements probably control initiation of DNA replication.

6.3 DNA repair

6.3.1 Damage to DNA can result in mutations

DNA molecules are constantly subjected to physical and chemical stresses in vivo. Oxygen, ultraviolet (UV) light, alkylating agents, and radicals all can cause random changes in the DNA sequence. These changes can result from strand breaks, chemical modification of bases, and incorporation of mismatched bases during replication. Common types of DNA changes include the formation of pyrimidine dimers, alkylation of bases, and deamination of bases (Fig. 6.11). If left uncorrected, spontaneous and induced DNA changes would rapidly alter the DNA sequence. For example, spontaneous deamination of cytosine to uracil is estimated to occur at a rate of 100 bases per genome per day. During replication, uracil would permanently change the DNA sequence at this

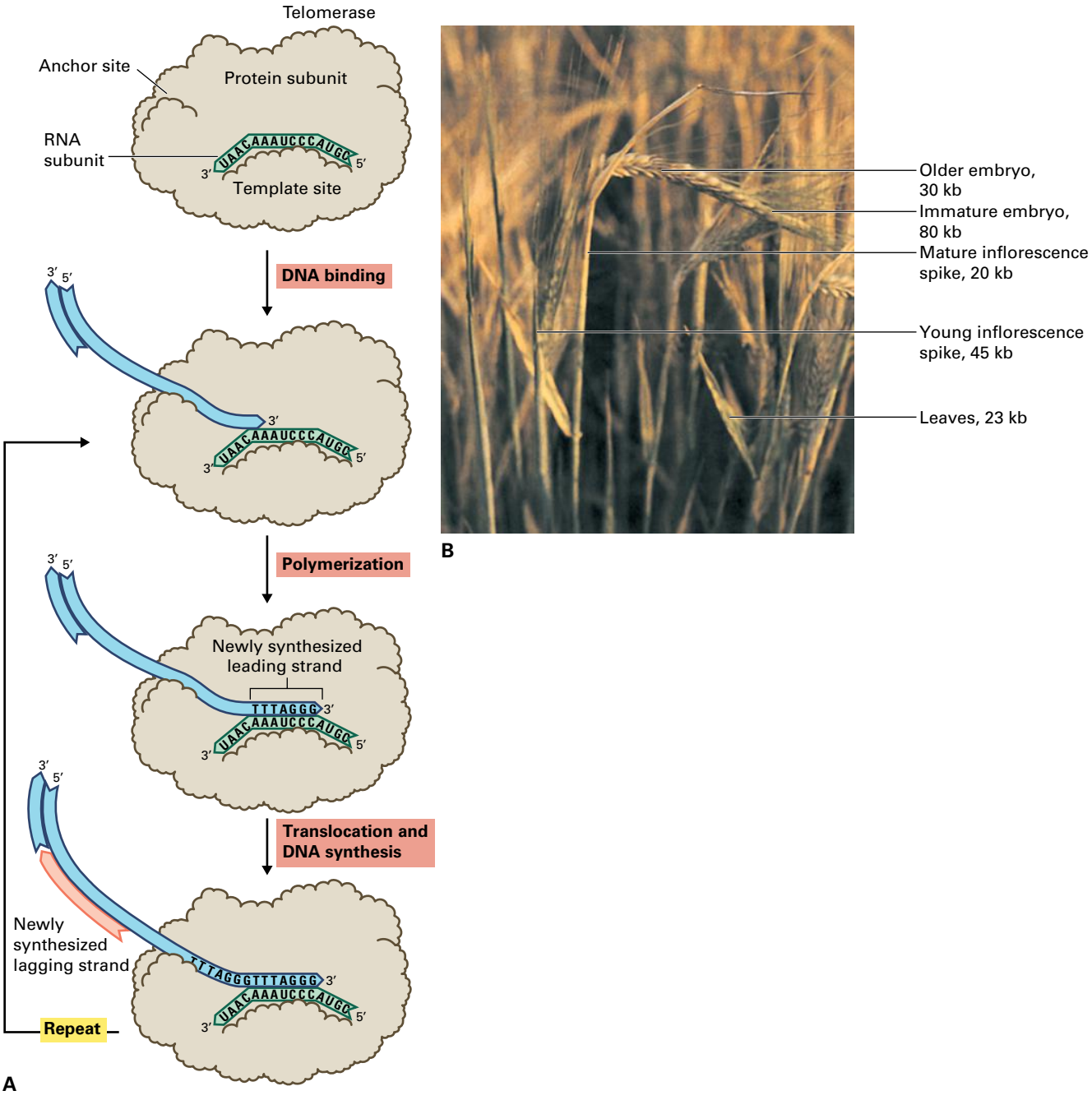


FIGURE 6.10 *(A) Elongation of telomeres. Telomerase recognizes the overhanging 3′ telomere sequences of the chromosome. An RNA molecule that is complementary to the telomeric DNA is part of the telomerase enzyme complex. The overhanging DNA of the leading strand hybridizes with the telomerase RNA and is elongated by telomerase, which uses the RNA as a template. Telomerase then translocates to the end of the leading strand. Primase and DNA polymerase subsequently elongate the lagging strand of telomere DNA. (B) Telomere length does not remain constant during development. The length of the telomeres of barley chromosomes varies among different organs and developmental stages.*
Source: (B) Shippen & McKnight (1998). Trends Plant Sci. 3:126–129.

site by pairing with adenine instead of guanine. Most DNA changes occur in sequences that do not encode genes; such events are therefore inconsequential. However, the possibility that DNA damage may result in mutations that disrupt the function of essential enzymes or structural proteins poses a significant risk to the cell. Several efficient DNA repair mechanisms have evolved to protect organisms against the potential deleterious effects of mutations.

6.3.2 Pyrimidine dimers, which are caused by UV-B, are repaired using visible light or UV-A

UV light can fuse pyrimidines to create cyclobutane dimers (Fig. 6.11) and pyrimidine(6 → 4)pyrimidinone dimers. Plants and humans incur approximately equal amounts of

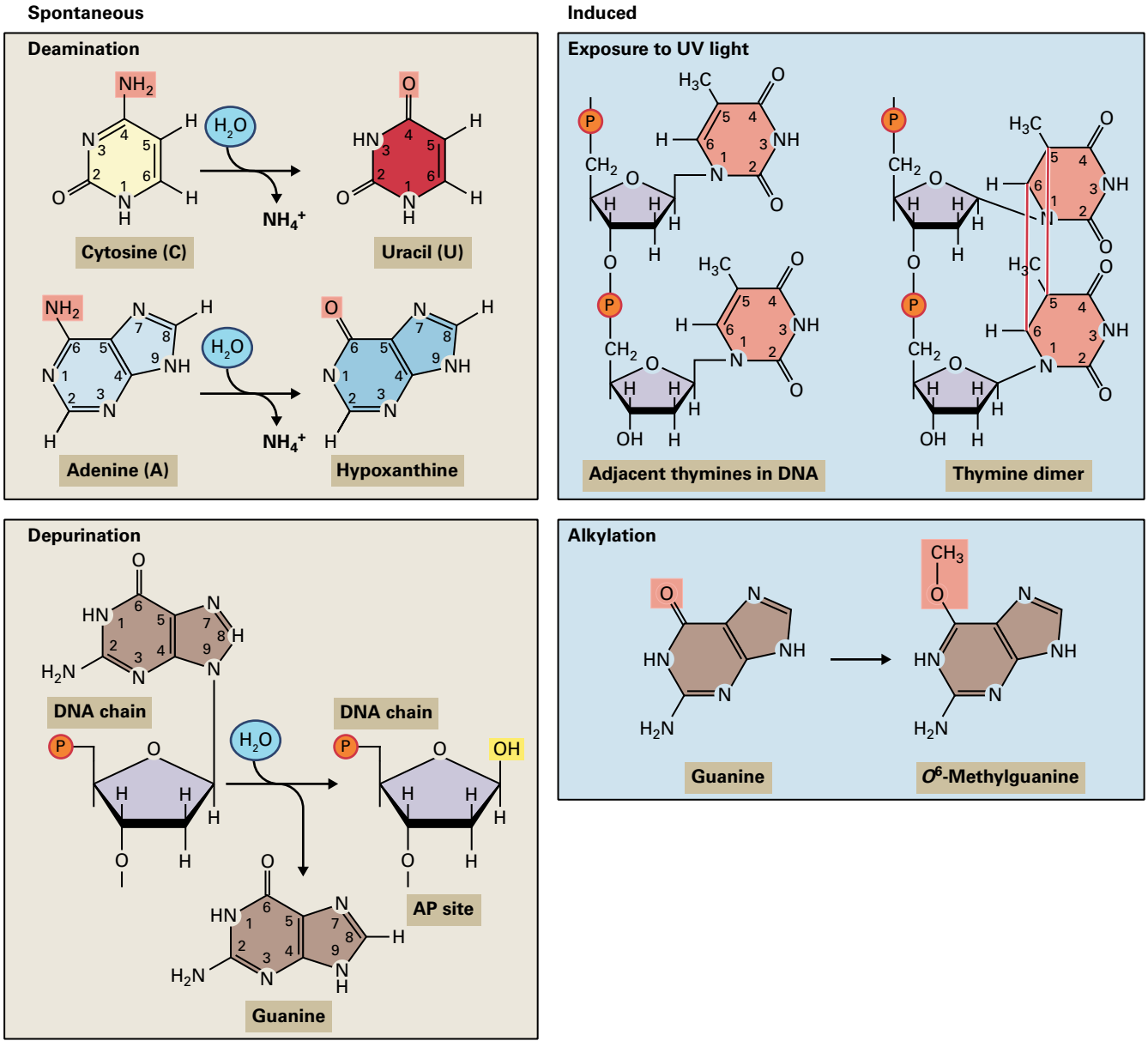


FIGURE 6.11 *Chemical reactions that cause DNA mutations can either occur spontaneously or be induced by radiation or chemicals. One major type of spontaneous DNA damage results from deamination of the bases cytosine or adenine. Depurination, another type of spontaneous event, forms an apurinic (AP) site in the DNA. UV light induces the formation of pyrimidine dimers between adjacent pyrimidine bases. Alkylation of DNA bases results in the addition of methyl groups (or sometimes ethyl groups, not shown) at various positions in the ring structure.*

DNA damage from the UV-A (320–400 nm) and UV-B (280–320 nm) wavelengths of sunlight. In bacteria and plants, some UV-induced mutations can be reversed by high-energy wavelengths of visible light or by UV-A. This conversion is called **photoreactivation** and is catalyzed by photolyases, enzymes that absorb radiant energy of wavelengths 300–600 nm and convert cyclobutane dimers to pyrimidine monomers (Fig. 6.12). In plants, the activation of certain photolyases is regulated by light and mediated by the photoreceptor phytochrome (see Chapter 18). A photolyase required for repair of pyrimidine(6 → 4)pyrimidinone dimers has been identified in *Arabidopsis* and wheat (*Triticum* spp.). This photolyase appears to be expressed constitutively.

6.3.3 Excision repair mechanisms can remove either individual bases or longer nucleotide chains

Two major pathways have been identified for DNA excision repair: **base excision repair** and **nucleotide excision repair**. In base excision repair, the chemically modified base (e.g., uracil, 5-methylcytosine, or 3-methyladenine) is first removed by a DNA glycosylase that is specific for that type of DNA lesion. The action of DNA glycosylase results in an apurinic or apyrimidinic (AP) site with an intact sugar–phosphate backbone. Next, an AP endonuclease cleaves a phosphodiester bond at

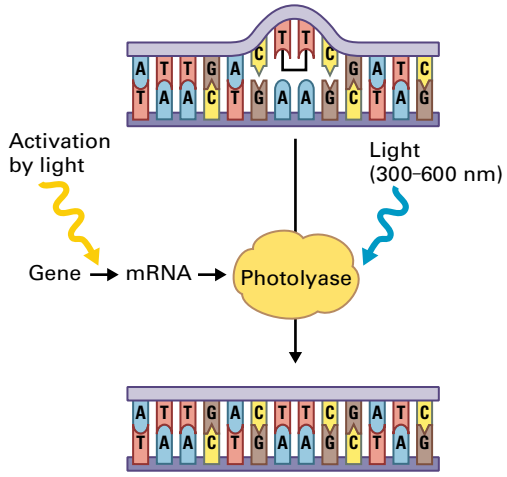


FIGURE 6.12 *Photolyases catalyze the repair of pyrimidine dimers. The enzyme uses energy from visible light to break the carbon–carbon bonds that join adjacent pyrimidine residues, such as UV-induced thymine dimers.*

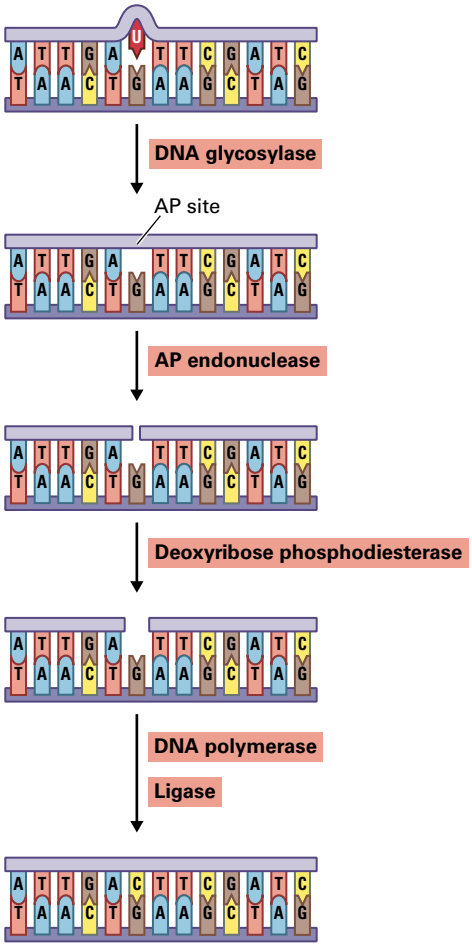


FIGURE 6.13 *The base excision repair pathway. In the pathway shown in this figure, a uracil formed by deamination of cytosine is removed from the sugar–phosphate backbone of the DNA strand by DNA glycosylase. AP endonuclease recognizes the resulting AP site and cleaves the DNA strand at that site. Deoxyribose phosphodiesterase then removes the remaining deoxyribose molecule. DNA polymerase and ligase repair the gap, restoring the cytosine/guanine base pair.*

the AP site, and a pathway that includes several enzymes then repairs the resulting nick. First, DNA deoxyribose phosphodiesterase removes the deoxyribose-phosphate molecule. Next, repair polymerase (DNA polymerase β in animal and yeast cells) adds a single nucleotide to the 3′ end of the DNA strand at the gap. Finally, DNA ligase seals the nick (Fig. 6.13). Plant homologs of the yeast genes that encode proteins involved in base excision repair have been isolated, and their gene products can excise specific DNA damage products in vitro.

The second pathway, nucleotide excision repair, involves the DNA replication machinery. This repair pathway can remove DNA damage that distorts the DNA double helix, including various pyrimidine dimers created by UV light. In eukaryotic cells, nucleotide excision repair removes and replaces a DNA fragment approximately 30 bases long. A multienzyme complex that recognizes the distortion in the DNA cleaves the damaged strand on both sides of the lesion. The oligonucleotide is then removed by DNA helicase. The resulting gap is repaired by DNA polymerase δ or ε and closed by DNA ligase (Fig. 6.14). With few exceptions, these activities have been identified in plants, and mutant plants defective in light-independent DNA repair have been identified. The mutations are located in genes that are homologous to human genes required for nucleotide excision repair, indicating plants utilize the same repair pathways identified in other eukaryotes.

6.3.4 Mismatch repair corrects errors made during DNA replication

In *E. coli,* adenine residues in the palindromic sequence GATC are methylated shortly after DNA replication. If DNA polymerase introduces an error during DNA replication that results in a mismatched base pair, repair occurs before methylation, when the newly synthesized DNA strand is unmethylated and the two strands can be distinguished (Fig. 6.15). This repair requires the function of three proteins that form a complex: MutS recognizes and binds to the base mismatch, MutH binds to DNA at the hemimethylated GATC sites and cleaves the unmethylated (newly synthesized) strand, and MutL binds to MutS and MutH and is required for the final repair steps. The combined action of additional proteins, namely the UvrD helicase and exonucleases, results in the removal of the damaged DNA strand beginning at the MutH cleavage site. The resulting gap is filled by DNA polymerases and sealed by DNA ligase.

Mismatch repair is a highly conserved mechanism that appears to function similarly in eukaryotes and bacteria. Several homologs of the bacterial *mutS* and *mutL* genes have been found in the genomes of yeast and mammals, and a *mutS* homolog is also present in human mitochondrial DNA. The mechanism that allows the bacterial MutS–MutL–MutH complex to discriminate between the parental and newly synthesized strands of DNA is not known in eukaryotes, in which GATC methylation has not been detected and *mutH*

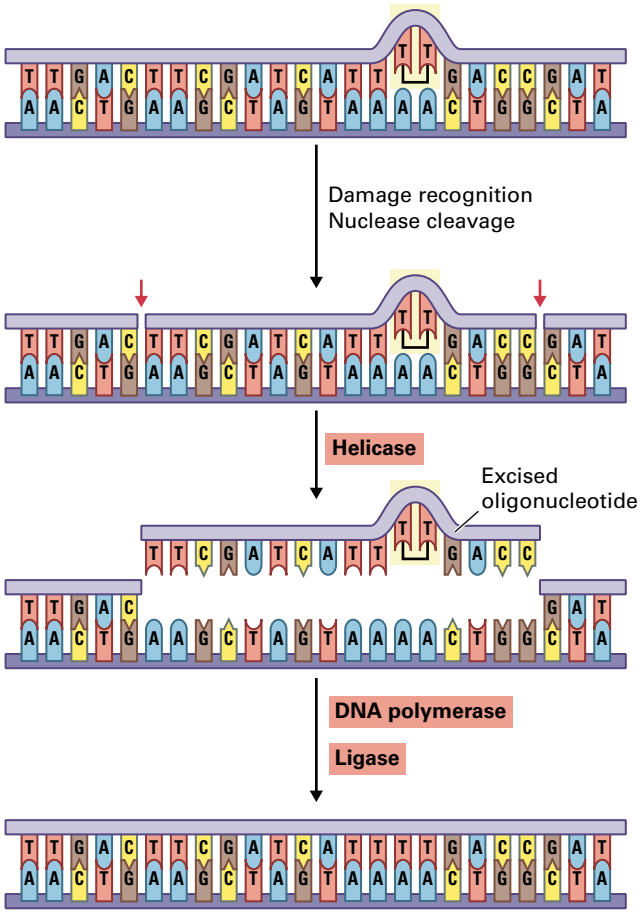


FIGURE 6.14 *Nucleotide excision repair of a pyrimidine dimer. The nucleotide excision repair pathway utilizes the DNA replication machinery to remove large distortions in the DNA double helix, such as pyrimidine dimers induced by UV light. Damaged DNA is first recognized by endonucleases and cleaved (red arrows). The oligonucleotide that contains the damaged bases is then excised after helicase unwinds the DNA at this site. DNA polymerase and ligase repair the resulting gap.*

homologs have not been identified. Families of eukaryotic genes that are homologous to *mutS* and *mutL* arose before the evolutionary divergence of animals, plants, and fungi. Homologs of these two genes have been cloned from several plants, suggesting this type of mismatch repair system is similar in all eukaryotic cells.

6.3.5 Error-prone repair allows DNA polymerase to read through damaged sites on the template

If during DNA replication the DNA polymerase complex encounters damage in the template strand, the enzyme complex bypasses the damaged site and continues DNA synthesis. This process is potentially mutagenic because the DNA polymerase does not repair the damage but instead inserts adenine nucleotides at the gap regardless of the original DNA sequence that would otherwise result at the damaged site.

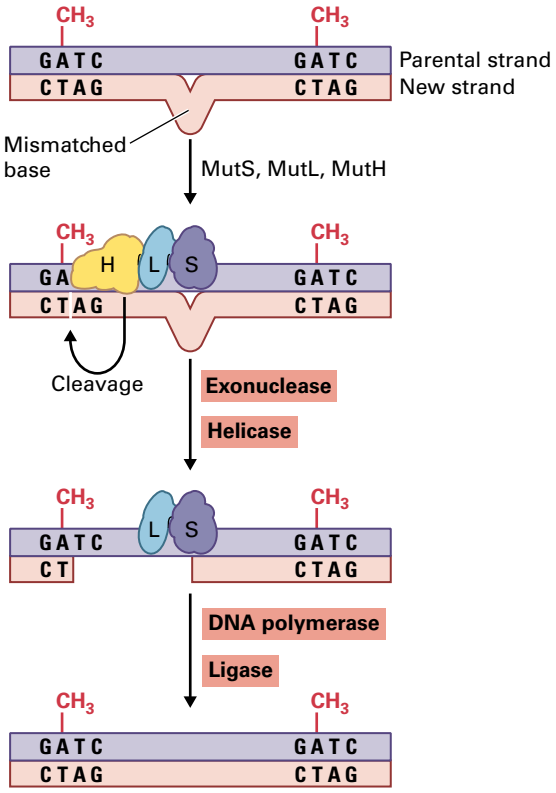


FIGURE 6.15 *Mismatch repair in* Escherichia coli. *A complex of three proteins—MutH, MutL, and MutS—recognizes mismatched bases introduced by DNA polymerase into the newly synthesized, unmethylated DNA strand. MutH cleaves the new DNA strand opposite the methylated site. The damaged DNA is then removed by the combined action of helicase and exonuclease. DNA polymerase and ligase subsequently repair the gap.*

In bacteria subjected to potentially lethal conditions, such as extensive UV irradiation, this **error-prone repair** mechanism, also called **translesion replication**, is activated. In *E. coli*, the proteins UmuC and UmuD bind to DNA polymerase and alter the stringency of nucleotide incorporation. Adenines are inserted into the newly synthesized strand at the lesion site irrespective of the sequence of the parental DNA strand. If the damaged sites are thymidine dimers, the newly synthesized DNA is not mutated. However, cytosine dimers result in mutations at the lesion sites. Although this type of repair can generate a large number of mutations, it may allow the cells to survive extensive DNA damage. A similar bypass mechanism has been identified in yeast. The products of the *umuC* gene family are required for dimer bypass and include proteins active in both error-prone and high fidelity repair mechanisms. A gene homologous to one member of the *umuC* gene family, the human XP-V gene, has been identified in plants.

6.3.6 Extensive DNA damage can also be repaired by homologous recombination

When DNA damage is extensive or affects a longer stretch of nucleotides, an alternate repair pathway can be induced as well. In recombination repair (Fig. 6.16), DNA polymerase stops

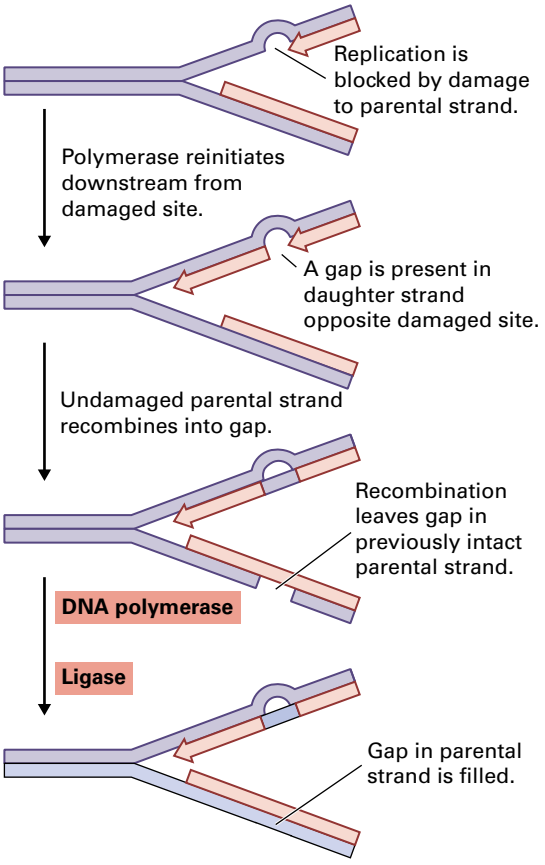


FIGURE 6.16 *Post-replication repair. When the DNA replication machinery encounters an unrepaired lesion (e.g., a pyrimidine dimer), DNA polymerase can bypass the block and reinitiate at a downstream site. The resulting gap in the newly synthesized DNA strand is then repaired by recombination with the undamaged parental strand. DNA polymerase and ligase fill the resulting gap in the previously intact parental DNA. The pyrimidine dimer can later be removed by excision repair (not shown) to produce two intact, double-stranded DNA molecules.*

replication when a lesion is encountered in the parental (template) strand. DNA replication resumes at the next priming site on the template, which may be several hundred nucleotides downstream from the damaged site. The discontinuity, or daughter strand gap, in the newly synthesized strand is then repaired by homologous DNA recombination with the complementary parental strand using specific recombination enzymes (see Section 6.4.2). DNA polymerases and DNA ligase repair the resulting gap in the complementary parental strand.

6.4 DNA recombination

6.4.1 DNA recombination plays an important role in both meiotic cell division and evolution

Although accurate DNA replication and repair are crucial for genetic stability in individuals, the long-term survival of a species as a whole is also influenced by genetic variation that

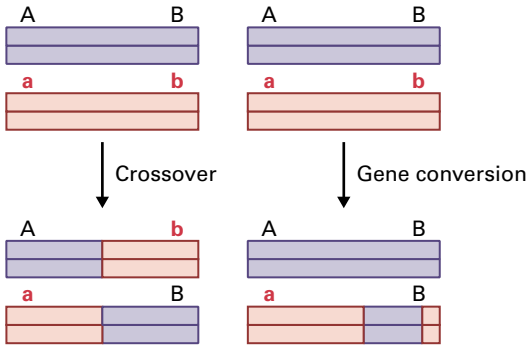


FIGURE 6.17 *Two types of homologous DNA recombination produce different results. Crossover between two molecules of double-stranded DNA results in the reciprocal exchange of DNA sequences (left panel). Gene conversion involves a nonreciprocal transfer of a nucleotide sequence from one double-stranded DNA molecule to another. The donor sequence (purple) remains unchanged while the recipient sequence (pink) loses genetic information (right panel).*

allows its members to adapt to changing environments. **Genetic recombination** of DNA has an important role in evolution because it rearranges DNA sequences to generate new combinations of DNA molecules. The novel genes that result can yield new types of RNAs and proteins and, therefore, new phenotypes. Furthermore, during meiotic cell division, DNA recombination can produce genetically distinct gametes and thereby promote the production of varied genotypes, which are acted on by environmental factors in the process of natural selection. The mechanisms involved in genetic recombination are related to DNA replication and repair. DNA recombination events are not rare; they have been observed in all classes of living organisms and in viruses.

6.4.2 Homologous recombination occurs between long nucleotide sequences that are similar

Three types of DNA recombination mechanisms have been identified: homologous recombination, site-specific recombination, and illegitimate recombination. Homologous recombination requires the DNA sequences involved to have regions that are substantially similar (i.e., homologous). The frequency of recombination generally increases with the length of the homologous DNA segments. The mechanisms used in homologous recombination can be inferred from the structure of the products (Fig. 6.17). When no information encoded in the two DNA duplexes is lost during the exchange of sequences by **crossover**, the recombination event is termed reciprocal. Nonreciprocal recombination, or **gene conversion**, results when one DNA duplex donates sequence information rather than exchanging it. Three molecular models—single-strand annealing, double-strand break repair, and one-sided invasion—have been proposed to explain the particular products of specific DNA recombination events as well as the general finding that double-strand DNA breaks enhance homologous recombination rates (Fig. 6.18).

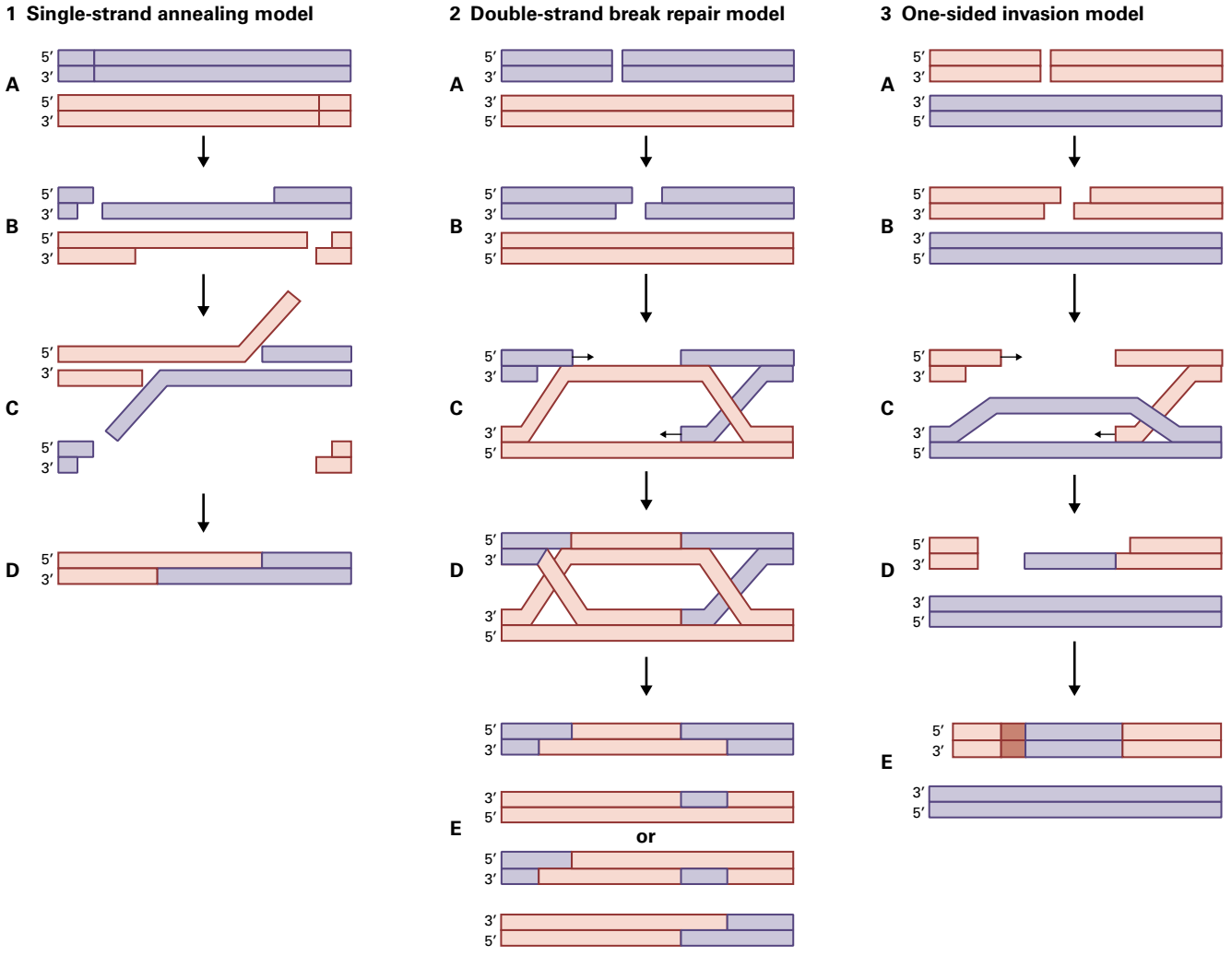


FIGURE 6.18 *Three models of homologous recombination. The donor DNA is purple, the recipient DNA pink. In the single-strand annealing model (1), a double-strand break must occur in both DNA duplexes (A). Exonucleases remove nucleotides beginning at the double-strand breaks and expose single-stranded homologous regions (B). The complementary single strands of DNAs anneal to each other (C), followed by the removal of the nonhomologous DNA overhangs and gap repair (D). This recombination mechanism is nonconservative, because only one chimeric DNA duplex can survive. In the double-strand break repair (DSBR) model (2), the recombination event initiates with a double-strand break in one of two DNA duplexes (A). After the double-strand break is enlarged by exonucleases (B), the overhanging 3′ ends of the DNA bind to complementary sequences on the other duplex and act as primers for DNA repair synthesis (C). The remaining gaps are repaired using the intact donor DNA as a template (D). The branched DNA molecules resulting from this process resolve into one of two possible combinations (E). DSBR is a conservative recombination mechanism because both DNA duplexes participating in the recombination event are restored. In the one-sided invasion model (3), a double-strand break in the acceptor DNA (A) is enlarged by exonucleases (B). One of the two resulting 3′ ends invades a complementary DNA sequence on an intact DNA duplex (C). DNA synthesis lengthens the invading strand. (D) Illegitimate recombination occurs upstream from the double-strand break, resulting in gene conversion (E).*

Plant breeding practices applied by humans over the course of thousands of years to select for desired traits in crop species have, in fact, been utilizing homologous recombination. Recent advances in molecular breeding techniques and transgenic plant technologies (see Box 6.3 and Box 6.4) are providing insights into the processes that underlie meiotic and somatic DNA recombination events in plants. The double-strand break repair model (Fig. 6.18) may explain the recombination events that occur during meiosis in plants. The single-strand annealing model (Fig. 6.18) best describes the extrachromosomal recombination events that can occur at a low frequency in somatic plant cells when plasmid DNA molecules that contain overlapping parts of a specific reporter gene are transferred into plant cells and recombine to restore an intact reporter gene. Naturally occurring extrachromosomal DNA molecules, such as the transferred DNA (T-DNA) of *Agrobacterium tumefaciens* (see Chapter 21) or viral DNAs show a similar recombination behavior.

6.4.3 Some proteins involved in homologous recombination have been identified in plants

Homologous recombination in both meiotic and mitotic cells requires the function of many gene products. Of these, the yeast proteins RAD51 and DMC1 are well characterized.

BOX 6.3 Gene targeting is a powerful technology for investigating gene function

Homologous recombination, the integration of transfected DNA molecules into homologous sequences of genomic DNA, has many possible applications for manipulating the plant genome. It has been used extensively to analyze the function of genes in yeast and mouse cells. The moss *Physcomitrella patens* has been developed into a plant model system over the last two decades (see figure). Its haploid gametophyte produces filamentous protonema and the leafy gametophore. In the haploid genome of the moss, homologous recombination is the normal pathway of DNA integration, and gene targeting experiments in this organism are generating insights into gene function. In the cells of angiosperms, homologous recombination between transfected DNA and homologous sequences within the genome occurs at a lower frequency than illegitimate recombination (see Section 6.4.5). Site-specific mutagenesis using novel restriction enzymes (see Section 6.4.6) has become a promising way of targeting and enhancing this process.



Source: R. Reski, University of Freiburg.

BOX 6.4 Site-directed mutagenesis using novel restriction enzymes

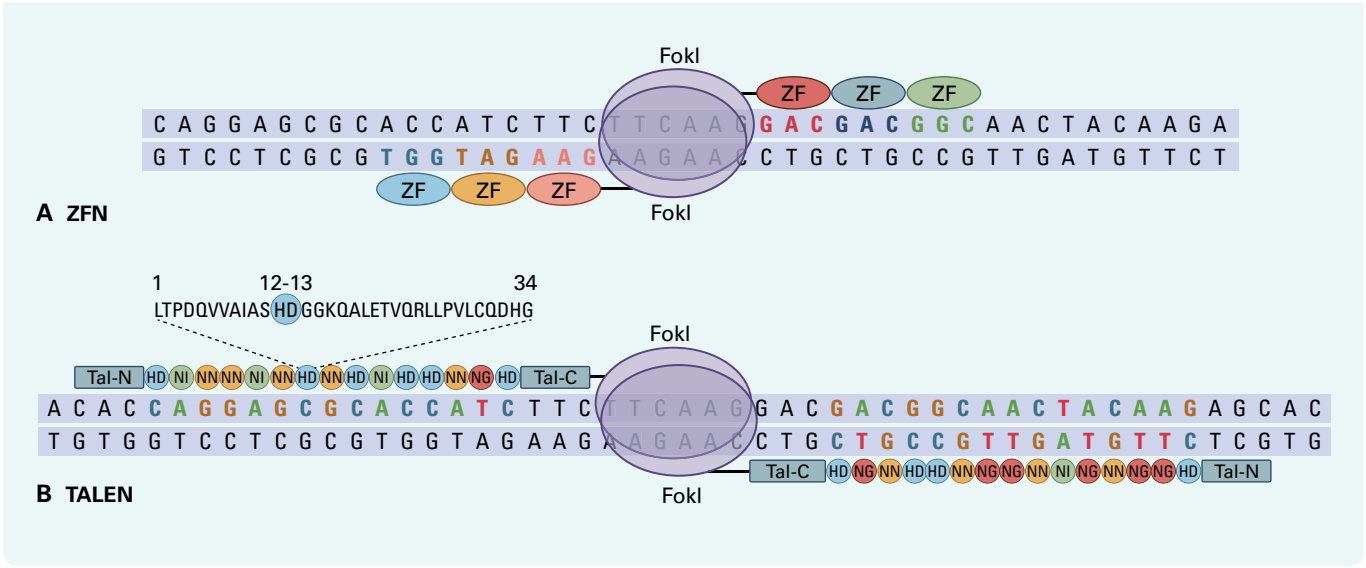
Hybrid nucleases can be expressed in plant cells to generate site-specific double-stranded breaks in genomic DNA. These nucleases can be used to either replace a target DNA sequence (knock-in) or disrupt the open reading frame (ORF) of the target (knockout). For knock-in experiments, the nuclease is used with a DNA donor template that contains an engineered sequence for the nuclease's target gene; this facilitates repair by homologous recombination and results in replacement of the target DNA sequence with the engineered sequence. For knockout experiments, the nuclease is expressed without a donor DNA template, which causes imperfect repair by nonhomologous end-joining mechanisms and perturbs the targeted DNA sequence, often disrupting the ORF.

The hybrid nucleases typically comprise two protein subunits that dimerize at their nuclease domains to generate a functional enzyme. Each subunit has a DNA-binding domain fused to the nonspecific cleavage domain of the FokI endonuclease. Several methods have been developed for the construction and selection of the DNA-binding domains that target the hybrid nucleases to specific DNA sequences. The most commonly used hybrid nucleases (see Fig. 6.B4) are zinc-finger nucleases (ZFNs) and transcriptional activator-like effector nucleases (TALENs).

ZFNs contain eukaryotic transcription factor zinc-finger DNA-binding motifs that bind to specific DNA sequences (see Chapter 9). To create a ZFN, three or more 25-amino acid zinc-finger peptides are fused to the FokI endonuclease cleavage domain. Each peptide can bind to specific nucleotide triplets via the zinc-finger's interchangeable seven-amino acid recognition helix. Three fused zinc-finger regions provide specificity to bind to a unique 9-bp sequence. ZFN dimers are context-dependent, so specific binding to a DNA sequence requires cooperative binding of the fingers and subunits. This means that not all sequences can be efficiently targeted and that, prior to their use, thorough screening and testing of the combined binding affinities is required.

Like the ZFNs, the DNA-binding domains of TALENs are also fused with cleavage domains from the FokI endonuclease (see Fig. 6.B4). The difference is in the DNA-binding domains. For TALENs the binding domain, called a TALE, is a central domain that typically holds 15 to 30 single-repeat monomers, each of 34 amino acid residues. The monomers are highly conserved with the exception of a hypervariable region at amino acid positions 12 and 13. The hypervariable regions bind to specific nucleotides, the repeat-variable diresidues (RVDs). There are four classes of RVDs determined by their hypervariable region. For example, an RVD with the following diamino acid residues will bind to these specific nucleotides NI = adenosine (A), HD = cytosine (C), NG = thymine (T), NN = guanine (G) or adenosine (A). TALENs appear to be more reliable and more specific than ZFNs, most likely due to the fact that because each RVD binds to a single nucleotide whereas ZFNs bind to DNA codons.

ZFNs and TALENs hold great promise as tools for targeted gene replacement and disruption. Substituting the nuclease domains with other enzymatic activities may also become powerful tools for regulating gene expression through epigenetic modifications, such as DNA methylation.



RAD51 is required for both mitotic and meiotic recombination, while DMC1 is expressed and active only during meiosis. Both are homologous to the *E. coli* protein RecA, which plays a central role during homologous recombination in bacteria. RecA catalyzes the strand transfer reaction, allowing single-stranded DNA to invade a DNA duplex at a homologous region (Fig. 6.19). In the presence of RP-A, which binds to single-stranded DNA, RAD51 and DMC1 also catalyze strand transfer. Strand transfer activity is required by all three mechanisms of homologous recombination (see Fig. 6.18).

A number of plant genes that share homology with *recA* have been identified, some of which may encode proteins that function in the chloroplast. Homologs of *RAD51* have been cloned from several plants, including *Lilium, Arabidopsis,* rice (*Oryza sativa*), wheat (*Triticum* spp.), and maize (*Zea mays*). Interestingly, expression of this gene is activated after treatment of plants with X-rays, suggesting somatic DNA recombination is induced by DNA damage. Plant proteins homologous to RecA or RAD51 most likely function in homologous recombination. A cDNA homologous to *DMC1* has been isolated from *Arabidopsis.* DCM1 and RAD51 colocalize during some stages of meiosis in *Lilium*; these proteins may act cooperatively in the alignment and pairing of complementary DNA strands during homologous recombination. Both proteins are attached to chromatin loops during the leptotene and zygotene stages of meiosis, and are associated with the synaptonemal complex during pachytene (Fig. 6.20).

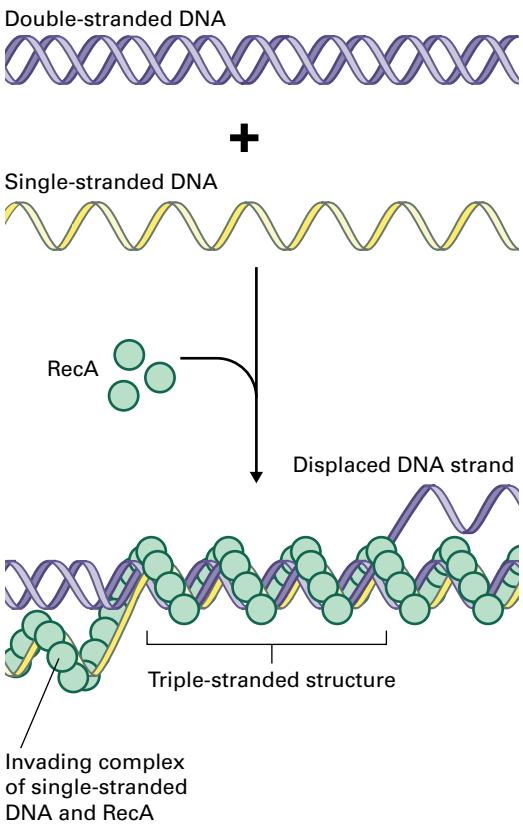


FIGURE 6.19 *The role of RecA in strand transfer. The* Escherichia coli *protein RecA is a 38-kDa monomer that binds to single-stranded DNA by a cooperative and stoichiometric mechanism. The resulting nucleoprotein complex aggregates with double-stranded DNA in triple-stranded DNA complex in which the nucleotide bases do not pair. This complex facilitates invasion of the single-stranded DNA and complementary pairing of base. Strands are subsequently exchanged. A stable heteroduplex region forms and functions as a template for branch migration (not shown).*

6.4.4 Site-specific recombination involves enzymatic activities and defined DNA loci

Another mechanism of DNA exchange that occurs in *E. coli,* called **site-specific recombination**, occurs at specific loci, does not require long regions of homologous DNA, and is independent of RecA. The experimental system in which

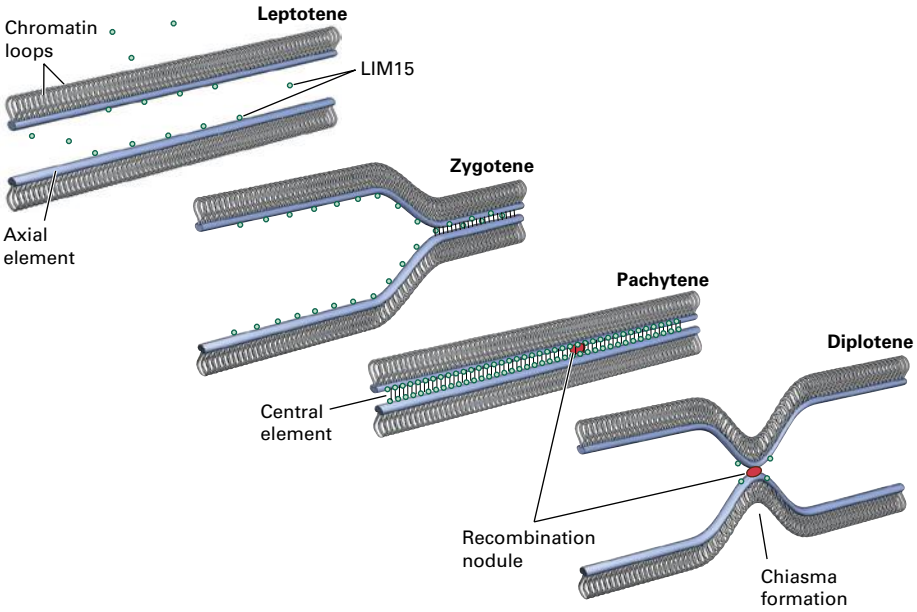


FIGURE 6.20 *The LIM15 protein of* Lilium *participates in the formation of the synaptonemal complex during meiosis. The synaptonemal complex may provide the structural framework for recombination events mediated by protein complexes at the recombination nodule.*

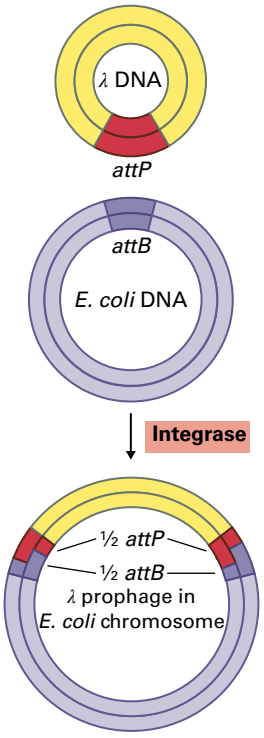


FIGURE 6.21 *Integration of λ phage into the* Escherichia coli *chromosome involves site-specific recombination between the* attP *sequence of the phage genome and the* attB *sequence of the bacterial genome. The recombination is catalyzed by an integrase.*

site-specific recombination is best characterized is the integration of bacteriophage λ into the *E. coli* chromosome. Two proteins and a shared DNA sequence are necessary and sufficient for λ integration. The proteins are a phage-encoded recombinase activity (integrase) and a host-encoded DNA-binding protein (IHF). The sequence requirement is a 31-bp palindrome that is present in both phage DNA and the host chromosome (Fig. 6.21).

Site-specific recombination also occurs in eukaryotes. For example, the 2μ plasmid of budding yeast encodes a recombinase (FLP) that is required for site-specific recombination at inverted repeats during DNA replication (see Section 6.5.4). In mammalian B and T cells, the rearrangement of immunoglobulin genes results from site-specific recombination. Although site-specific recombination events in the plant nucleus have not been identified, this process appears to be important during replication of plastid DNA and the rearrangement of many plant mitochondrial genomes (see Sections 6.5.4 and 6.5.5).

6.4.5 Illegitimate recombination does not require long segments of homologous DNA

Recombination events that do fall under any of the categories described above are generally referred to as **illegitimate recombination.** Several models for this type of DNA recombination have been proposed; some of these proposed mechanisms involve short sequences of homologous DNA, but others do not require any DNA homology. In *E. coli,* two mechanisms of illegitimate recombination are particularly well characterized: one is a homology-dependent process catalyzed by RNA polymerase, the other a homology-independent reaction catalyzed by DNA gyrase (topoisomerase II). Although illegitimate recombination does not appear to be a general mechanism in yeast, some gene products that participate in this type of DNA recombination have been identified.

Recombination products that cannot be explained by typical meiotic or somatic homologous DNA recombination mechanisms are often observed in plants. Illegitimate recombination models are often used to explain these novel recombinants. If this assumption is correct, plant genomes appear to experience illegitimate recombination more frequently than

they do homologous recombination. Since integration and excision of transposable DNA elements (see Chapter 9) and insertion of *Agrobacterium tumefaciens* T-DNA into plant chromosomes (see Chapter 21) do not require significant DNA homology, these events are often considered illegitimate recombination as well.

6.5 Organellar DNA

One of the major features by which eukaryotic cells differ from prokaryotes is the presence of various subcellular organelles (see Chapter 1), including the mitochondria (present in almost all eukaryotes) and plastids (present only in plants and algae). Plastids perform a wide variety of anabolic reactions that include photosynthetic carbon reduction (see Chapter 12), synthesis of amino acids (see Chapter 7), and fatty acid production (see Chapter 8). Plant mitochondria engage in respiration (see Chapter 14) and act in concert with other organelles to perform photorespiration (see Chapter 14) and gluconeogenesis (see Chapters 10 and 14).

Among the organelles of eukaryotic cells, plastids and mitochondria are unique because they possess their own genetic systems and protein synthesis machinery. In different taxa of algae and plants, transmission of these organelles (and thus of their genomes) varies, but is typically uniparental. Since the discovery almost 40 years ago that plastids and mitochondria contain DNA, much of the molecular research has focused on the structure and function of the organellar genomes. We now know that the genomes in plastids and mitochondria encode a small number of genes for proteins that function in the organelles, as well as components for the maintenance of their own genetic system. Expression of organellar genomes is under the tight control of the nuclear genome, but regulatory mechanisms have also evolved in plants that coordinate the expression of nuclear, plastid, and mitochondrial genes for proteins that function in the cytoplasmic organelles.

6.5.1 During evolution, chloroplasts and mitochondria originated from endosymbiotic bacteria

Plastids and mitochondria share many traits with free-living prokaryotic organisms. For example, the organization of organellar and bacterial genomes is similar. Likewise, chloroplasts carry out photosynthesis in much the same way as cyanobacteria. Comparison of ribosomal RNA (rRNA) sequences from organelles and certain free-living prokaryotes suggests plastids share a common ancestor with modern cyanobacteria, and mitochondria with modern proteobacteria. This RNA evidence supports the **endosymbiont hypothesis,** that chloroplasts and mitochondria probably evolved from prokaryotes that were engulfed by protoeukaryotic cells during the origin of the eukaryotic lineage (Fig. 6.22). Extant

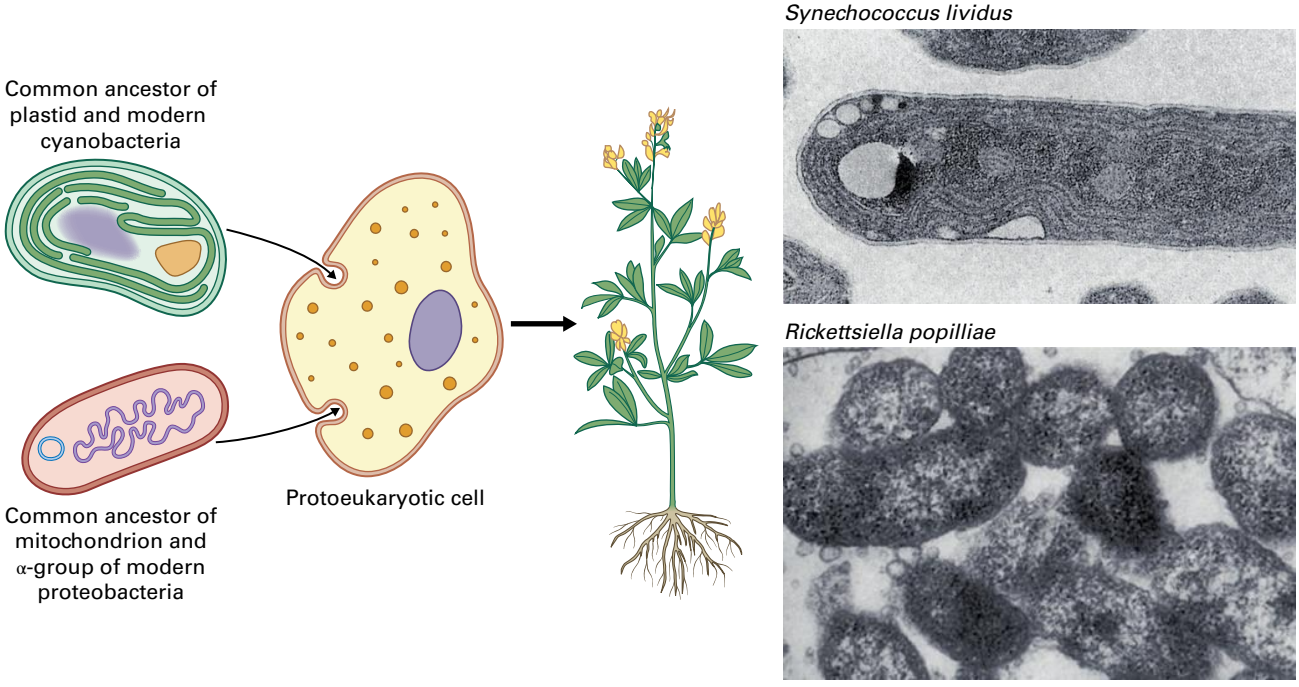


FIGURE 6.22 *Eukaryotes probably evolved from endosymbiotic associations between different prokaryotic organisms. A comparison of ribosomal RNA (rRNA) sequences suggests plant plastids share a common ancestor with modern cyanobacteria, such as the free-living* Synechococcus lividus*. Mitochondrial rRNA sequences of extant eukaryotes share greatest homology with members of the α-group of the proteobacteria, which includes several genera of intracellular parasites (e.g.,* Agrobacterium, Rhizobium, *and* Rickettsia*). The electron micrograph shows* Rickettsiella popilliae *cells within a blood cell of its insect host.*
Source: Madigan et al. (1997). Brock Biology of Microorganisms, 8th ed. Prentice Hall, Upper Saddle River, NJ.

symbioses between photosynthetic organisms and nonphotosynthetic hosts lend additional support to the endosymbiont hypothesis. For example, the biflagellate protist *Cyanophora paradoxa* acquires an endosymbiotic cyanobacterium, called a cyanelle, which functions as a chloroplast and provides the host cell with photosynthetically reduced carbon. Other examples are marine nudibranchs (sea slugs) that feed on algae. These animals can incorporate the algal chloroplasts into their own tissue and maintain the foreign organelles for nearly two months, receiving nourishment from plastid photosynthesis. Considering these contemporary examples, it is not difficult to envision that endosymbiotic events gave rise to oxygen-tolerant, photosynthetic eukaryotes.

Neither the chloroplasts nor the mitochondria of contemporary organisms can exist autonomously outside of the eukaryotic cell. During evolution, most of the DNA once present in the organelles was transferred to the nuclear genome. This process of gene transfer is ongoing. Some organellar DNA sequences resemble the **operons** of prokaryotes, in which genes encoding proteins that function in a common pathway or assemble into a complex are clustered together. Some sequences in the plastid genome are similar to the corresponding operons in cyanobacteria, including some regulatory elements, gene clusters (e.g., the *rpl23* operon), and ATPase subunit genes (*atp*). In general, however, some transcriptional and a majority of post-transcriptional regulatory factors in plant organelles are novel, and show no relationship to those in bacteria.

6.5.2 The structure of the plastid genome is conserved among plants

The plastid genome is composed of a single, circular chromosome of double-stranded DNA that typically comprises four segments (Fig. 6.23A): a large region of single-copy genes (LSC), a small region of single-copy genes (SSC), and two copies of an inverted repeat that separate the single-copy regions (IR_A and IR_B, respectively). However, other modes of plastid DNA organization have also been found. Plastid DNA is generally homogeneous within a given plant species, although in genomes that contain IR regions, plastid DNA often consists of two groups of molecules differing in the relative orientation of the single-copy regions. In the same way that all somatic cells in an organism possess the same set of nuclear genes but may express those genes in different combinations, all plastids in a single plant contain identical genetic material but may differ in developmental fate and metabolic activity.

The plastid DNAs of different plant and algal species vary greatly in length. The chlorarachniophyte alga *Bigelowiella natans* has one of the smallest known plastid genomes of any photosynthetic eukaryote, 69 kb. In contrast, the chloroplast genome of the chlorophycean alga *Floydiella terrestris* is 521 kb. Most plastid genomes, including those of tobacco, maize, rice, and *Marchantia,* range in size from 120 to 160 kb and share similar gene distribution and organization (Fig. 6.23B). Some of the size variation observed among land plant plastid genomes can be accounted for by changes in the length of the IR region, which ranges from 0.5 to 76 kb. The presence or absence of IR regions in plastid DNA has been used to categorize plastid genomes. Most plants contain IR regions but the plastid genomes of certain legumes, conifers, and algae lack them. It is likely that IR regions existed in the plastids of the common ancestor of plastids, and that one IR region was lost in some legumes and conifers during evolution.

6.5.3 Plastids contain both plastid-encoded and nuclear-encoded gene products

Complete sequences are available for the chloroplast genomes of more than 200 plants, including tobacco, maize, rice, and pine, and the mitochondrial genomes of more than one dozen plant species. Most plastid DNAs contain all the genes for plastid rRNAs and a full complement of genes for plastid tRNAs. They include, however, only about 100 single-copy genes, and most encode proteins required for photosynthetic functions (Table 6.1). Although the functions of most plastid-encoded proteins have been identified, a few open reading frames (ORFs) in the plastid genome have unknown functions. Chloroplast transformation technologies developed in tobacco (*Nicotiana tabacum*) and the unicellular alga *Chlamydomonas* are, however, providing powerful approaches for investigating these genes. Interestingly, the plastid genomes of nonphotosynthetic plants (e.g., *Rhizanthella gardneri*) are small (50–73 kb) and have lost many of the genes required for photosynthesis. In contrast, algal plastid genomes are generally larger than the plastid DNAs of plants and contain many additional genes not found in plant plastids. For example, the red alga *Porphyra purpurea* contains 70 novel protein-encoding plastid genes; in plants, these genes are found in the nuclear genome.

Many genes in the plastid genome are organized into **polycistronic** transcription units, that is, clusters of two or more genes that are transcribed by RNA polymerase from a single promoter. Some of these resemble prokaryotic operons (Fig. 6.24), although unlike prokaryotic operons, plastid genomes also contain polycistronic transcription units composed of functionally distinct genes. Often, mRNA from genes encoding proteins that are required during photosynthesis can be detected in nonphotosynthetic plastids, such as amyloplasts in root or chromoplasts in red tomato fruit (see Chapter 1). Apparently, these mRNAs are not translated into functional proteins. These findings and others have established that post-transcriptional regulation plays a significant role in the regulation of plastid gene expression.

While the plastid genome encodes several of the RNAs and proteins involved in translation of organellar mRNA, most of the genes that encode proteins required for photosynthesis are found in the nuclear genome. As discussed above,

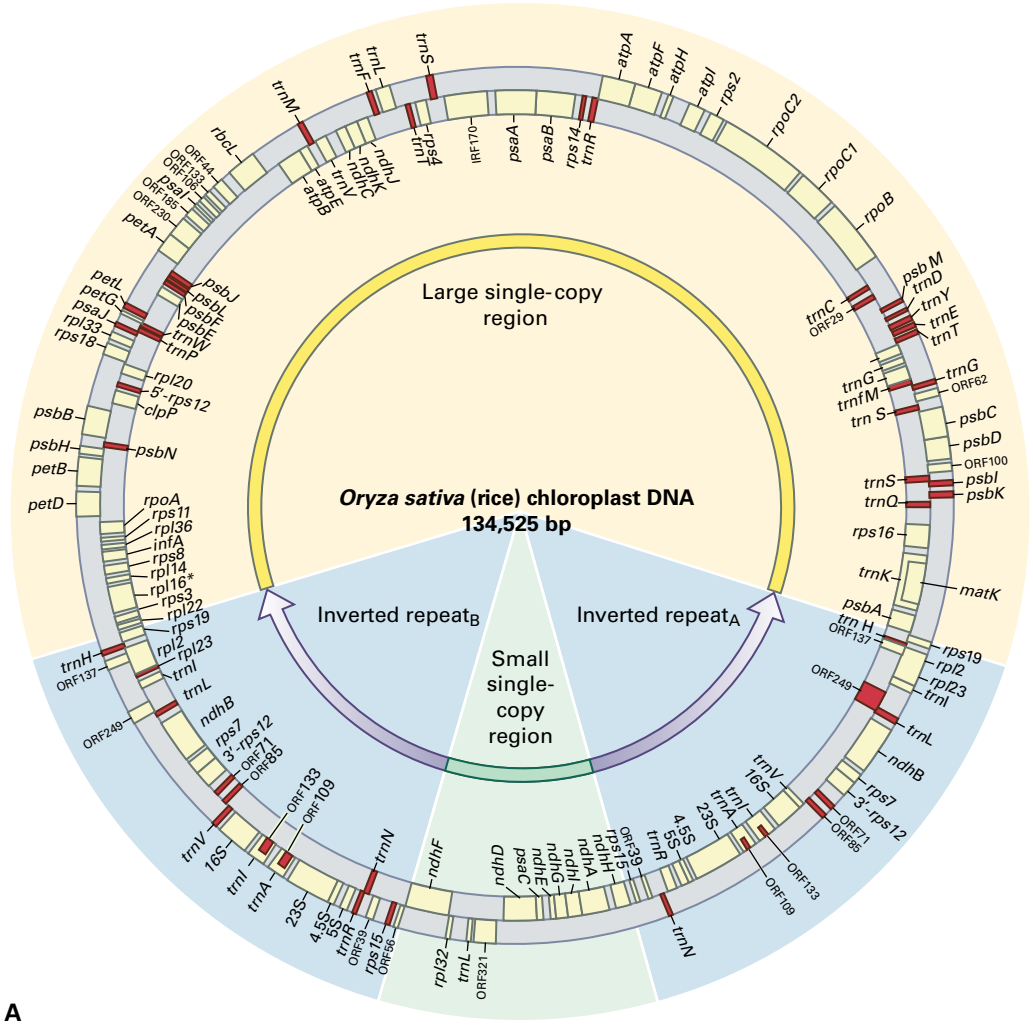


FIGURE 6.23 *(A) The chloroplast genome map of rice (*Oryza sativa*) is representative of the organization of plastid genes in most flowering plants. ORF, open reading frame. (B) Schematic representations of several plant plastid genomes, showing the conserved features: two regions of single-copy genes and two inverted repeats (IRs). The length of the IRs can vary widely among plastid genomes of different species. The single-copy regions in the plastid genome of the nonphotosynthetic parasitic plant* Epifagus *are quite small because most of the genes encoding photosynthetic proteins have been eliminated. The number beneath each DNA segment refers to its length in base pairs.*

TABLE 6.1 *Genes identified in complete plastid genome sequences.*

		Plants		Algae	
Gene products	**Gene acronym**	**Photosynthetic plants**	***Epifagus****	***Euglena***	***Porphyra**†*
Number of genes		101–150	40	82	182
Genetic system					
rRNA	rrn	4	4	3	3
tRNA	trn	30–32	17	27	35
Ribosomal protein	rps, rpl	20–21	15	21	46
Other		5–6	2	4	18
Photosynthesis					
Rubisco and complexes of the thylakoid membrane system	e.g., rbcL, psa, psb, pet, atp	29–30	0	26	40
NADH dehydrogenase‡	ndh	11	0	0	0
Biosynthesis and miscellaneous functions		1–5	2	1	40
Number of introns		18–21	6	155	0

* *Epifagus* (beechdrops) is a nonphotosynthetic, parasitic flowering plant.
† *Porphyra* is a red alga.
‡ The plastid genome of black pine does not encode genes for NADH dehydrogenase.

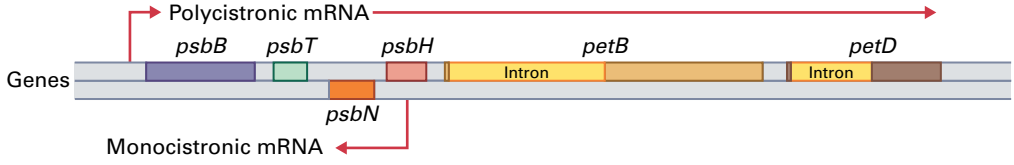


FIGURE 6.24 *The* psbB *operon of plant plastids exemplifies the typical organization of plastid genes into operons similar to those of prokaryotic genomes. Operons are transcribed into polycistronic mRNAs that often encode several related gene products. In the case of the* psbB *operon, the* psbN *gene encoded by the opposite strand appears to be transcribed as a monocistronic mRNA that encodes only one gene product.*

many genes present in the progenitor organelle were probably transferred to the nucleus during evolution. For example, the enzyme required for CO_2 fixation, ribulose-1,5-bisphosphate carboxylase/oxygenase (Rubisco), is a multiprotein complex with two types of subunits. The gene for the smaller subunit (*RBCS*) is found in the nucleus, whereas the gene for the larger subunit (*rbcL*) is present in the plastid genome (see Chapter 12). This distribution of genes between the nuclear and plastid genomes is typical of proteins that participate in the assembly of photosynthetic protein complexes. For example, photosystems I and II contain proteins encoded in both the nuclear and plastid genomes, as does the cytochrome b_6f complex and the plastid ATP synthase (see Chapter 12). Chloroplasts and other types of plastids contain many important biochemical pathways for which all of the enzymes are encoded in the nuclear genome, translated in the cytoplasm, and transported into the plastids (see Chapter 4).

6.5.4 The mechanism of plastid DNA replication is not well understood

Usually each chloroplast contains many copies of its circular genome, often as many as 150. However, the copy number of plastid genomes can vary widely with the developmental stage and the type of plastid. A large number of DNA molecules in chloroplasts probably reflects a high demand for expression of proteins active in photosynthesis, because substantially fewer DNA molecules are found in root amyloplasts and other nonphotosynthetic plastids. Our understanding of

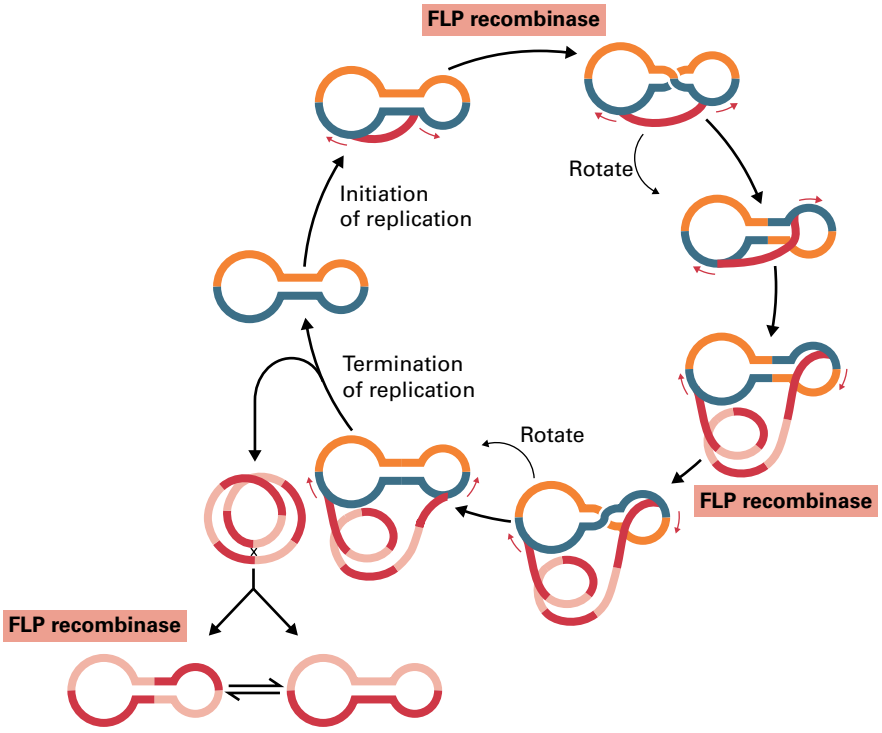


FIGURE 6.25 *The double rolling-circle model was first developed to describe the amplification of the yeast 2μ plasmid, but also serves as a model for the replication of chloroplast DNA. The small red arrows indicate the direction of DNA synthesis. During double rolling-circle replication, a single initiation event produces two replication forks with opposite orientations. A site-specific recombination catalyzed by FLP recombinase reorients the forks so they move in the same orientation. A second recombination event returns the replication forks to their initial, opposing orientations, allowing the forks to meet and replication to terminate. The resulting replication product is a long concatameric DNA from which monomers can be generated by FLP-mediated recombination or other recombination mechanisms. These concatameric DNA molecules have been observed in plastids.*

the regulation of plastid DNA replication is limited, but it is established that DNA replication in organelles is mostly independent of DNA replication in the nucleus. Plastid DNA amplification appears to be regulated by the frequency of DNA replication initiation, either in synchrony with the cell cycle in rapidly dividing cells, or by a cell cycle-independent mechanism during cellular differentiation. The process of plastid DNA replication is probably similar to the double rolling-circle model that describes the replication of the 2μ plasmids of budding yeast (Fig. 6.25). In these plasmids, as in the plastid genome, replication origins and site-specific recombination sites are located within long inverted repeats.

Electron microscopic analysis of DNA replication intermediates has been used to map the replication origins of plastid DNAs in some plants. In *Oenothera* and tobacco (*N. tabacum*), DNA replication begins at specific origins in the IR regions, near the gene for the 16S rRNA. Although pea (*Pisum sativum*) and *Euglena* do not have IR regions, the replication origin still appears to be close to the rRNA genes, suggesting the rRNA operon has retained DNA sequences that interact with the DNA replication machinery to initiate replication. However, in the chloroplast DNAs of *Oenothera,* pea, maize, and tobacco, displacement or D-loops have been observed at multiple sites. The presence of more than two D-loops, replicative intermediates, in which the unidirectional synthesis of a single new strand displaces one parental strand, suggests plastid genomes may contain DNA replication origins in addition to those associated with the rRNA operon.

DNA sequences available from several different plants indicate all the enzymes and regulatory proteins essential for plastid DNA replication are encoded in the nuclear genome. Specific enzymatic activities, including DNA polymerases, primase, topoisomerases, and helicases, have been detected in plant plastids; their function in replication is under investigation. DNA sequences in the chloroplast genomes of *Chlamydomonas* and *Porphyra* share homology with the *E. coli* genes *dnaA* and *dnaB,* which encode proteins that function in DNA replication and repair. The presence of these sequences in chloroplast DNA suggests the mechanisms of plastid DNA replication are similar to those of *E. coli.*

6.5.5 The size and arrangement of plant mitochondrial genomes are highly variable

Plant mitochondrial genomes, which range from about 200 kb in *Oenothera* and *Brassica* to over 10 Mb in *Silene conica*, are the most variably sized genomes in any group of organisms. Part of this variability results from an unusual accumulation of noncoding DNA sequences in the regions between genes (Fig. 6.26). Surprisingly, in *Arabidopsis* the nuclear genome is more information dense than the mitochondrial genome:

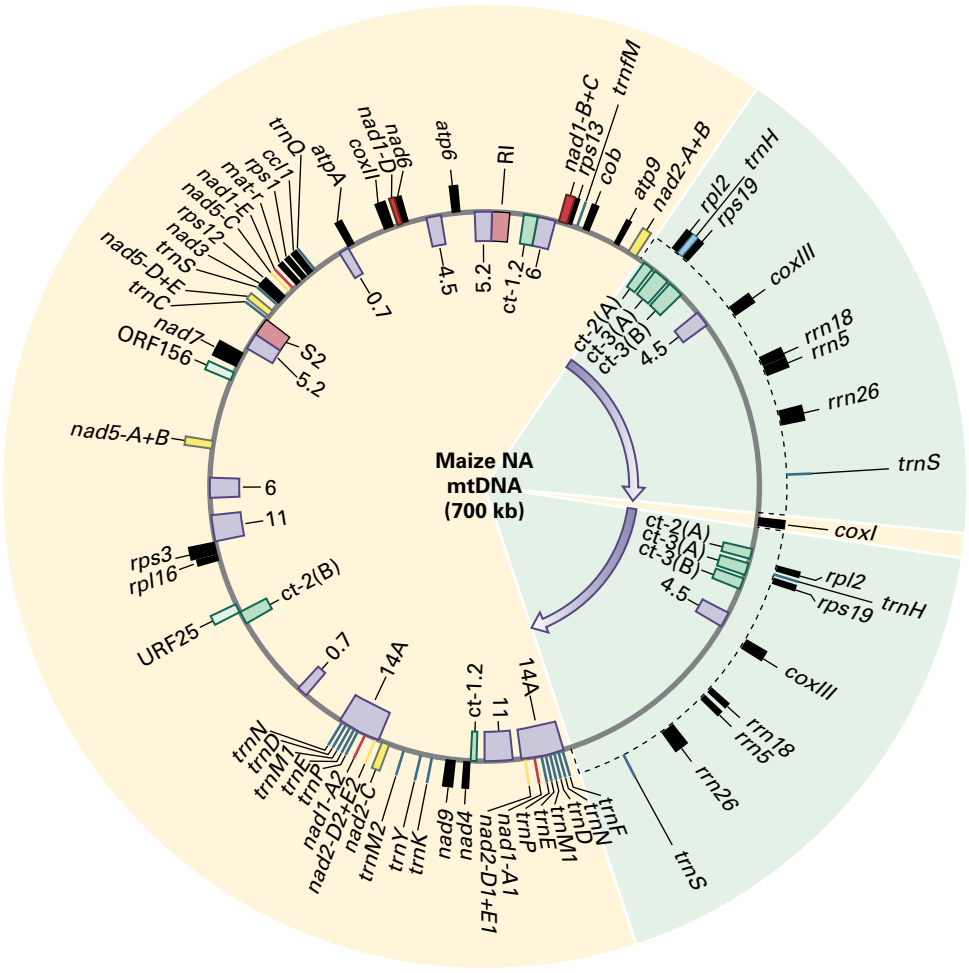


FIGURE 6.26 *The map of the mitochondrial genome of maize (*Zea mays*) is based on a hypothetical master circle DNA molecule that contains all of the mitochondrial genes. Although the mitochondrial DNA in maize is considerably larger than the chloroplast DNA, it contains fewer genes. Several inverted and direct repeat DNA sequences (shown in blue, green, and magenta boxes on the inner circle) have been identified that participate in recombination events to produce the small subgenomic circular DNA molecules shown in Figure 6.27.*

coding regions make up less than 10% of the 367-kb mitochondrial DNA, and 60% of the genome contains no characterized information. Unlike much of the noncoding intergenic DNA in the nuclear genome, plant mitochondrial intergenic regions are not made up of repetitive DNA sequences. In stark contrast, animal mitochondrial genomes are compact (about 16 kb) and essentially lack noncoding intergenic sequences.

Plant mitochondrial genomes sometimes exist as circular DNA molecules of variable size. Sequence analysis suggests the smaller DNA circles, called **subgenomic circles**, are derived from a larger circle, and the combined DNA sequence content of subgenomic circles can account for the entire mitochondrial genome. The subgenomic circles of maize (*Zea mays*) mitochondrial DNA are typical of this type of mitochondrial genome organization (Fig. 6.27). The largest possible maize mitochondrial circular DNA molecule, the **master circle**, would encode the complete set of mitochondrial genes. However, the master circle DNA has never been isolated; in fact, it is conceivable this large circular DNA molecule does not exist. Several short regions of different repeated DNA sequences that are distributed throughout the maize mitochondrial genome participate in the recombination events that form subgenomic DNA circles. These direct and inverted DNA repeat sequences probably shield the functional genes from deleterious rearrangements. Formation of subgenomic DNA circles has been observed in vivo. It remains to be established whether some or all subgenomic DNA circles replicate independently or whether they can be generated only from the hypothetical master circle. Recombination and fragmentation of plant mitochondrial DNA is not universal: The linear genome of *Chlamydomonas* and the circular genomes of *Marchantia* and white mustard (*Brassica hirta*) are homogeneous and do not appear to form subgenomic DNA circles.

6.5.6 The genetic content of the mitochondrial genome is conserved among plant species

The unicellular green alga *Chlamydomonas* was the first photosynthetic organism whose mitochondrial DNA was fully sequenced and the genome organization elucidated (Fig. 6.28). Complete nucleotide sequences of mitochondrial

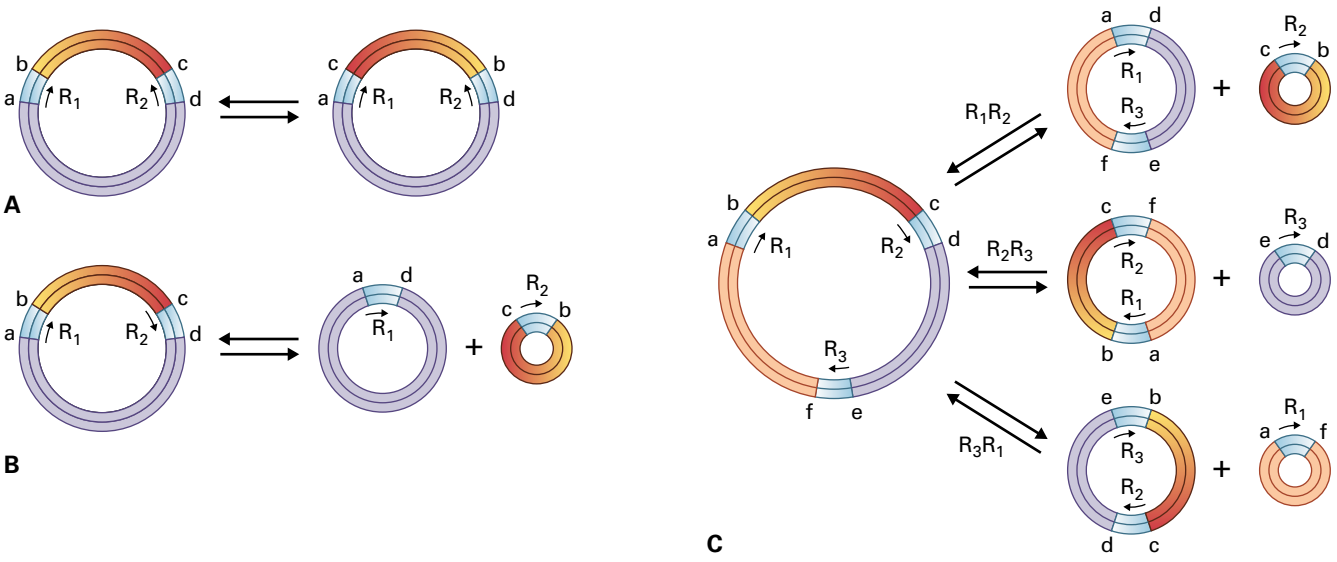
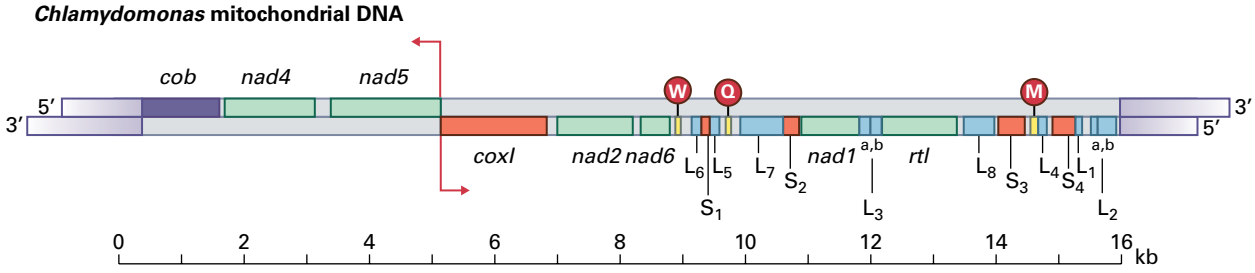


FIGURE 6.27 *Homologous recombination occurs at repeated DNA sequences within the plant mitochondrial genome. The DNA repeats can be either direct or inverted; their orientation influences how a recombination event reorganizes the genome. Three hypothetical master circle DNAs are shown, as are some of the subgenomic circles they can generate (A) Recombination between one pair of inverted repeats yields two isomeric forms of the master circle DNA. (B) Recombination between one pair of direct repeats yields two subgenomic circles. (C) Three distinct recombination events can occur in a master circle containing a three-copy direct repeat. Each possible recombination event produces a different pair of subgenomic circles.*



Gene content of *Chlamydomonas* mitochondrial DNA

	Gene	Gene product
Protein-coding genes	*cob*	Apocytochrome
	coxI	Cytochrome oxidase subunit I
	nad1, nad2, nad4, nad5, nad6	Subunits of NADH dehydrogenase
	rtl	Reverse transcriptase-like reading frame
rRNA genes	$L_1 - L_8$	Segments encoding large subunit of rRNA
	$S_1 - S_4$	Segments encoding small subunit of rRNA
tRNA genes	W	Tryptophan tRNA
	Q	Glutamine tRNA
	M	Methionine tRNA (elongator, not initiator)

FIGURE 6.28 *The mitochondrion of* Chlamydomonas *contains a linear DNA duplex of 15.8 kb. The genome contains eight genes that code for proteins. One striking and unique feature is the scrambled arrangement of rRNA gene segments. Both LSU and SSU rRNA genes are discontinuous. Throughout a 6-kb region, segments encoding specific rRNA domains are interspersed with one another and with intact genes that encode protein and tRNA. The rRNA-coding segments are numbered S1 through S4 and L1 through L8, according to the 5′ to 3′ order in which the homologous segments occur in the 16S and 23S rRNAs of* Escherichia coli, *respectively. The mtDNA encodes only three tRNAs, necessitating import of numerous tRNAs from the cytoplasm. The ends of the genome are characterized by terminal inverted repeats with single-stranded 3′ extensions. These extensions, which are identical in sequence (not complementary), exclude the possibility of genome cyclization or the formation of concatamers.*

BOX 6.5

Mitochondria in all eukaryotes are likely derived from the same endosymbiotic event

At one time, it was thought that only plant mitochondrial DNA contained a 5S rRNA gene, which is absent from the mitochondrial genomes of animals, fungi, and algae. This observation, combined with the striking differences in the size of mitochondrial DNA in plants, led to the hypothesis that plant mitochondria may have a separate evolutionary origin from the mitochondria of other eukaryotes.

When the mitochondrial genome of the green alga *Prototheca* was sequenced, however, it was found to contain a gene for 5S ribosomal RNA. Also encoded by the mitochondrial DNA of *Prototheca* is a set of genes for ribosomal proteins similar to those encoded by the mitochondrial genome of liverwort (Marchantiophyta), but absent from that of *Chlamydomonas*. These findings challenge the proposal that mitochondria originated separately in different eukaryotic taxa. Instead, they suggest a complex pattern of gene loss from a commonly inherited mitochondrial genome. Further DNA sequence analysis of mitochondrial genomes from divergent algae and plants has confirmed the evolutionary links shared by the mitochondrial DNAs of all eukaryotic organisms.

TABLE 6.2 *Types of genes identified in the maize mitochondrial genome.*

Gene products	Gene abbreviations	Function
rRNAs	rrn18, rrn26, rrn5	Protein synthesis
tRNAs	trn	Protein synthesis
Ribosomal proteins	rps, rpl	Protein synthesis
NADH dehydrogenase	nad	Respiratory electron transport
Cytochrome *c* oxidase	cox	Respiratory electron transport
Apocytochrome	cob	Respiratory electron transport
F_0F_1-ATPase proteins	atp	ATP synthesis

genomes are now available for over 65 species of plant and algae, including *Arabidopsis, Marchantia,* the green alga *Prototheca* (Box 6.5), and the red alga *Chondrus.* Although plant mitochondrial DNAs are complex and variable in size, they all contain essentially the same genetic information. Mitochondrial genomes do not code for many genes, as most of the enzymes required for DNA replication, transcription, and translation are encoded by the nucleus. The products of genes encoded in the mitochondrial genome participate predominantly in oxidative respiration, ATP synthesis, or mitochondrial translation (Table 6.2).

6.5.7 Homologous DNA sequences found in more than one plant genome suggest extensive movement of DNA between genomes

DNA sequencing projects revealed that mitochondrial genomes of plants contain nucleotide sequences homologous to sequences in chloroplast DNA (Fig. 6.29). In addition, sequences of mitochondrial and chloroplast DNA were found in nuclear genomes. These discoveries indicated the possibility of DNA transfer between organelles and nuclei, and the name "promiscuous DNA" was coined to describe a DNA sequence that occurs in more than one of the three genetic systems of eukaryotic cells—the nuclear, mitochondrial, and plastid genomes. To date, many types of promiscuous DNA segments have been reported in yeast, fungi, animals, and plants.

Promiscuous DNA sequences may be relics of extensive DNA transfer between progenitor organelles and nuclei. These transfers occurred over a long time span and provide insights into the evolution of plants. For example, the *tufA* gene, which encodes the plastid protein synthesis factor EF-Tu, is a plastid gene in algae but a nuclear gene in plants. The transfer of *tuf* A from the plastid to the nuclear genome was probably an early event during the evolution of the Charophyceae more than 500 million years ago. Another example is *rpl21,* a gene that encodes the plastid ribosomal protein L21. This gene is present in the plastid genome of liverwort and the nuclear genomes of angiosperms. Thus, *rpl21* was probably transferred to the nuclear genome some time after the divergence of nonvascular plants and flowering plants. The *rpl22* gene for the plastid ribosomal protein L22 may represent an even later transfer event because it is present in the plastid DNA of all plants except legumes, in which it is a nuclear gene.

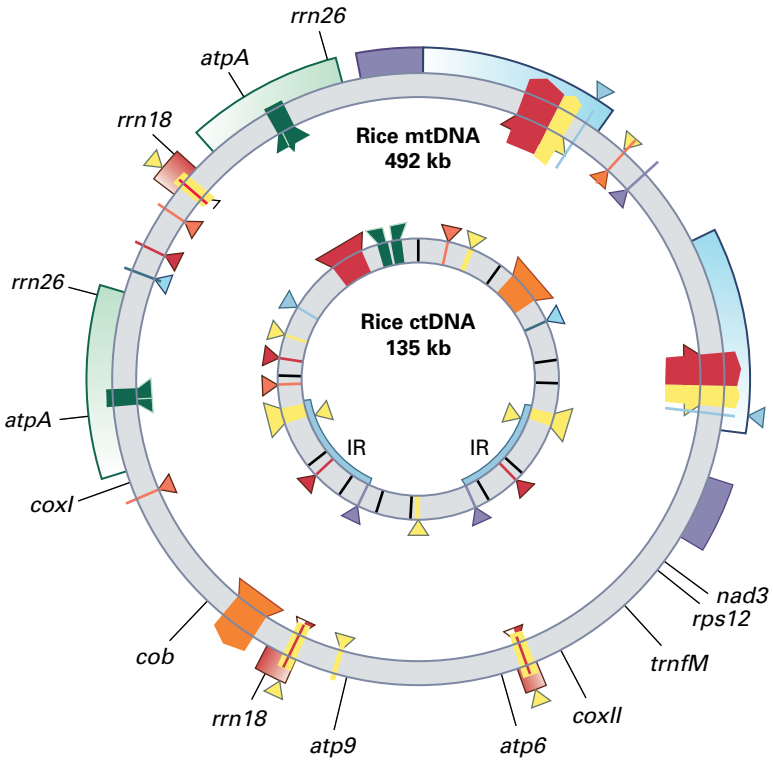


FIGURE 6.29 *Comparison of mitochondrial and chloroplast DNA sequences from rice (*Oryza sativa*) reveals the extent of promiscuous DNA. The colored triangles and boxes shown on the chloroplast genome (inner circle) represent DNA sequences that have been transferred to the mitochondria and inserted at different sites in the mitochondrial DNA (outer circle). It is interesting to note that mitochondrial DNA sequences have not been found inserted into the chloroplast genome, suggesting DNA transfer may be unidirectional, or the chloroplast may have an effective mechanism to protect itself against invading DNA molecules.*

6.6 DNA transcription

The nuclear and organellar genes discussed in previous sections contribute to the function of individual cells and the development of the multicellular organism. Expression of these genes must be regulated for cells to respond to changes in their environment and coordinate their activities within the tissues that make up complex organisms. Particularly in the nucleus, the organization of genes into chromatin and chromosomes is an important aspect of their regulation. However, **DNA transcription**, the synthesis of RNA on the DNA template, constitutes the primary control step.

The transcription from DNA to RNA is performed by DNA-dependent RNA polymerases. Subsequent modification of the resulting RNAs is discussed later in this chapter. This section briefly reviews the types of DNA-dependent RNA polymerases found in the nuclei and organelles of plants. The control of transcription by these RNA polymerases and associated regulatory proteins is described in Chapter 9.

6.6.1 Five nuclear RNA polymerases each transcribe different types of RNAs

Eukaryotic nuclei contain three classes of DNA-dependent RNA polymerases, called RNA polymerases I, II, and III (Table 6.3). RNA polymerases bind to and initiate transcription at specific sites on the chromosome, termed **promoters** (see Chapter 9). Although bacterial RNA polymerases can begin transcribing at promoters in the absence of additional proteins, eukaryotic RNA polymerases must interact with specific proteins called transcription factors to initiate transcription (Fig. 6.30).

Nuclear RNA polymerases are complex enzymes that contain two large subunits (125–220 kDa) and several smaller subunits. Five of the smaller subunits are common to all

TABLE 6.3 *The nuclear DNA-dependent RNA polymerases of plant cells.*

Polymerase	Location	Products
I	Nucleolus	25S, 17S, and 5.8S rRNAs
II	Nucleoplasm	mRNAs, pri-miRNAs, U1, U2, U4, U5,
III class 1	Nucleoplasm	5S rRNA
III class 2	Nucleoplasm	tRNAs
III class 3	Nucleoplasm	U3; U6; other small, stable RNAs
IV	Nucleoplasm	Transcripts from transposon and repeat elements that are processed into siRNAs
V	Nucleoplasm	Short transcripts from intergenic noncoding (IGN) regions

three RNA polymerases. As a result of these structural similarities, the three nuclear RNA polymerase share several functional properties, including the requirement for accessory proteins to initiate transcription correctly at cognate promoter regions.

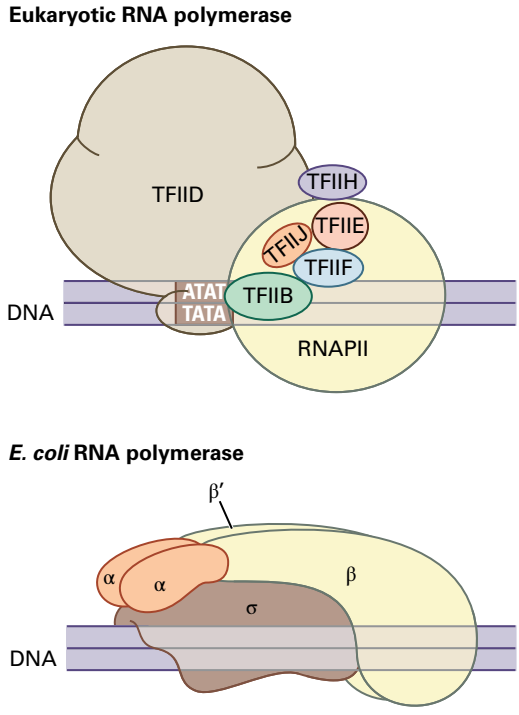


FIGURE 6.30 *Comparison of eukaryotic and prokaryotic RNA polymerases reveals these enzymes differ in complexity. Eukaryotic RNA polymerase II (RNAPII) is a multisubunit complex that requires several accessory proteins and regulatory protein complexes for promoter recognition at the TATA box region. In contrast, prokaryotic RNA polymerases, typified by* Escherichia coli *RNA polymerase, consist of four core subunits (α, α, β, and β′) and regulatory σ subunits. The increased complexity of the eukaryotic RNA polymerase II reflects the regulation of nuclear transcription by numerous signals (see Chapters 7 and 18). TFII, transcription factors for RNA polymerase II.*

The largest subunit of RNA polymerase II has a C-terminal domain that contains multiple repeats of the consensus sequence Tyr-Ser-Pro-Thr-Ser-Pro-Ser. A regulatory protein complex called transcription factor II H (TFIIH), which interacts with RNA polymerase II following recruitment of the enzyme to the promoter, contains a protein kinase that can phosphorylate Ser and Thr residues in the C-terminal domain. This phosphorylation is thought to release RNA polymerase II from its association with the promoter-initiation complex and allow the enzyme to begin synthesis of the mRNA from the template strand of the DNA.

Though many details of the mechanisms by which the three nuclear RNA polymerases initiate transcription in yeast and mammalian cells are known, additional regulatory proteins remain to be discovered. Plant RNA polymerases I, II, and III are similar to those of other eukaryotes. Moreover, genetic and biochemical data suggest the initiation of transcription in plants is controlled by regulatory mechanisms that resemble those in yeast and mammals. In plants, two other RNA polymerases (IV and V) produce RNAs for the epigenetic regulation of gene expression (Table 6.3).

6.6.2 Plastids contain multiple DNA-dependent RNA polymerases

The principal RNA polymerase of plastids resembles that of *E. coli*, which has five core subunits—α (×2), ω, β, and β′—and one of several regulatory σ subunits. Chloroplast DNA contains genes that encode proteins similar to the *E. coli* subunits α, β, and β′ that can form an enzyme complex in the plastid (Fig. 6.31). Several genes for σ-like subunits have also been identified in the nuclear genomes of plants. In a current model, plastid and nuclear gene products combine to form an *E. coli*-like plastid RNA polymerase required for the transcription of plastid genes.

As would be expected for genes transcribed by the plastid-encoded, prokaryote-type RNA polymerase, most chloroplast genes have regions proximal to their transcription initiation

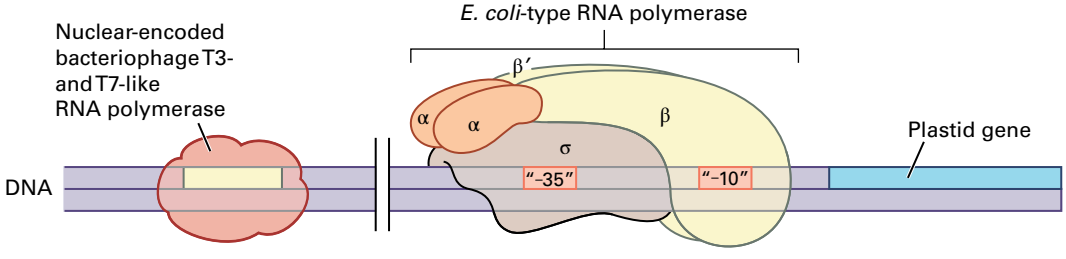


FIGURE 6.31 *Plant chloroplasts have two types of RNA polymerases. The existence of plastid genes encoding proteins similar to subunits α, β, and β′ of the* Escherichia coli *RNA polymerase, combined with biochemical analyses, suggest the presence of a prokaryotic-type chloroplast RNA polymerase (right). Genes for σ-like subunits have been identified in the nuclear genomes of many plants, indicating that both plastid and nuclear genomes cooperate in the regulation of chloroplast transcription. The plastid-encoded RNA polymerase recognizes chloroplast promoters that contain typical "–10" and "–35" prokaryotic consensus sequences. Recent results suggest chloroplast genes can also be transcribed by a nuclear-encoded, single-subunit RNA polymerase that resembles the RNA polymerases of bacteriophage T3 and T7 (left). When specific inhibitors of translation protein synthesis are used to block protein synthesis in the chloroplast, the nuclear-encoded RNA polymerase activity continues to transcribe chloroplast genes. The promoter sequences recognized by this novel type of RNA polymerase are not well understood.*

sites that often contain DNA sequences similar to the *E. coli* "–10" and "–35" consensus promoter motifs. Analysis of these DNA sequences by mutagenesis has shown the RNA polymerase recognizes this *E. coli*-type chloroplast promoter during initiation of transcription. However, subsequent investigations of chloroplast transcription in the presence of inhibitors of plastid protein synthesis, combined with analysis of mutants defective in chloroplast-localized protein synthesis, revealed transcriptional activity was reduced but not abolished when the *E. coli*-type RNA polymerase was impaired. Plastids must, therefore, import a nuclear-encoded RNA polymerase that functions alongside the *E. coli*-type RNA polymerase. This novel RNA polymerase, which resembles the single-peptide RNA polymerases of bacteriophage T3 and T7, recognizes promoter regions that differ in DNA sequence from the conserved "–10" and "–35" consensus promoter motifs. The nuclear-encoded enzyme is active in all plastid types (e.g., etioplasts, chromoplasts, and amyloplasts). Results suggest constitutive gene transcription of the plastid genome maintains chloroplasts and nonphotosynthetic plastids.

6.6.3 The genes of plastids and mitochondria can have multiple promoters

Unlike nuclear genes, which typically have one promoter that is recognized by RNA polymerase, transcription of many plastid genes and operons is initiated either at multiple promoters or at multiple sites. One example of this is the dicistronic *atpB–atpE* transcription unit (Fig. 6.32). Transcription of many plastid genes, especially of those encoding proteins involved in photosynthesis, is regulated by the developmental program and environmental factors, such as changing light conditions. Overall transcriptional efficiency can be controlled by adjusting the number of active promoters or by altering promoter strength, and plastids appear to utilize both these mechanisms. Certain mitochondrial genes also have multiple promoters that may control their differential expression. It is not known whether the different types of plastid RNA polymerases or the cofactors for these enzymes are involved in either promoter selection or control of transcription initiation at multiple sites.

6.7 Characteristics and functions of RNA

RNA is the primary product of gene expression and has essential roles in protein synthesis and other cellular functions. Coding mRNAs are central to protein synthesis, and other, noncoding RNAs are involved in guiding mRNA processing and degradation. Ribosomal RNA (rRNA) molecules form complex three-dimensional structures that combine with polypeptides to create ribosomes, the organelles responsible for protein synthesis (see Chapter 9). Ribosomes serve as a platform for reading mRNAs, which carry the instructions that dictate the amino acid sequences of proteins. Transfer RNAs (tRNAs) act as adapters to translate the codons of mRNA (specific three-nucleotide sequences) into particular amino acids (see Chapter 10).

In addition to its roles in protein synthesis, the versatile RNA molecule has biochemical properties that allow it to function as a genome or as a catalyst. One such characteristic is the ability of RNA to self-replicate, which is key to the evolutionary success of many RNA viruses that infect eukaryotic cells (see Chapters 10 and 21). Another trait is the ability of RNA to catalyze the breakage and formation of covalent bonds between nucleotides (e.g., during RNA splicing, see Section 6.8). Some RNA molecules can assume specific structures that cause particular chemical groups in one or more of its constituent nucleotides to become highly reactive. These RNAs, often referred to as **ribozymes,** can catalyze the cleavage and rejoining of polynucleotide chains. Some RNAs, such as the small nuclear RNAs (snRNAs) and the RNA component of telomerase (see Section 6.2.3), are found in eukaryotic nuclei and participate in RNA processing and DNA replication. The following sections discuss the different types of RNAs found in eukaryotic cells and their functions in plants.

6.7.1 RNAs are classified according to their function and size

When bulk RNA is extracted from cells, it consists of a complex mixture of polynucleotide chains that vary in lengths. RNA molecules are commonly designated according to the



FIGURE 6.32 *Multiple promoters direct transcription of the* atpB–atpE *gene cluster in tobacco (*Nicotiana tabacum*) chloroplasts. The* atpB *and* atpE *genes encode the β and ε subunits of ATP synthase, and their coding regions overlap each other by a few nucleotides. There are five transcription initiation sites (P1 through P5), indicated by red arrows. Four of the transcription initiation sites contain "–10" and "–35" consensus sequence motifs, but the sequence around the –290 site (P3) has no such motifs.*

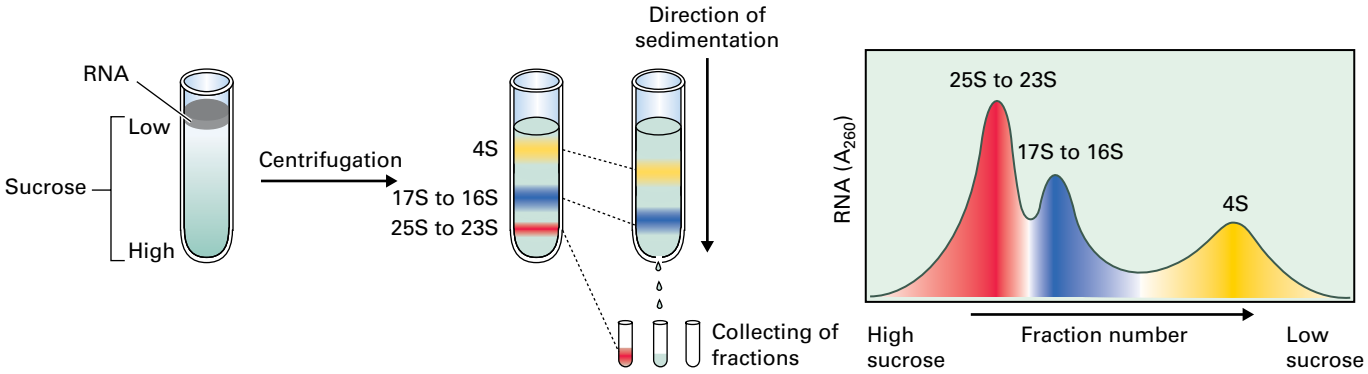


FIGURE 6.33 *The separation of RNA species by zone centrifugation. A solution containing a mixture of RNA molecules is loaded onto the top of a sucrose gradient (typically ranging from 2.5% to 15% sucrose) and centrifuged at high speed. When subjected to strong gravitational field, large RNA molecules sediment more rapidly than small RNA molecules. After centrifugation, sequential fractions are collected from the bottom of the centrifugation tube and the amount of RNA in each fraction is determined by measuring UV absorption at 260 nm (A_{260}).*

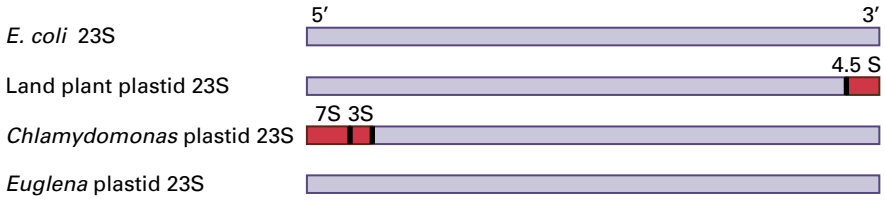


FIGURE 6.34 *Comparison of plastid 23S rRNAs from various organisms with the 23S rRNA of* Escherichia coli *reveals differences in organization. The 23S rRNA of* E. coli *is 1904 nucleotides long. The 4.5S rRNA encoded by the plastids of plants (shown in red) is homologous to the 100 nucleotides at the 3′ end of the* E. coli *23S rRNA. The* Chlamydomonas reinhardtii *chloroplast genome contains 7S and 3S rRNAs (shown in red) that are homologous to the 5′ end of* E. coli *23S rRNA. In contrast, the plastid-encoded 23S rRNA of* Euglena *is continuous, as are those of cyanobacteria and several algae (not shown).*

sedimentation coefficient, measured in Svedberg units (S, or 10^{-13} seconds). Three main RNA fractions (23S to 25S, 16S to 17S, and 4S RNA) can be separated by zone sedimentation (Fig. 6.33). The 23S to 25S and 16S to 17S fractions contain rRNAs, while the 4S fraction includes tRNAs and small noncoding RNAs. Most of the RNAs in these three classes are relatively stable molecules that can be detected easily using agar gel electrophoresis and ethidium bromide staining. In contrast, mRNAs are far less abundant in the cell and typically make up only 1–2% of the total cellular RNA. Molecules in this class of RNA, which vary considerably in size and stability, do not separate as a discrete fraction when subjected to zone sedimentation or gel electrophoresis.

6.7.2 The bulk of cellular RNA is ribosomal

All ribosomes consist of a large subunit and a small subunit. The small ribosomal subunit contains only one type of rRNA molecule (small-subunit rRNA), whereas the large subunit contains one long rRNA molecule (large-subunit rRNA) and one or more short rRNA molecules. Plants, algae, and photosynthetic protists each contain three classes of ribosomes: cytoplasmic, plastid, and mitochondrial. The short 5.8S rRNA is unique to cytoplasmic ribosomes and associates with 25S rRNA. Interestingly, the 5.8S rRNA is homologous to sequences in the 5′ end of *E. coli* 23S rRNA. Plastid 23S rRNAs resemble those of *E. coli* and cyanobacteria, both in sequence and length (Fig. 6.34), although it is broken into shorter RNA chains in some plants or algae. Plant mitochondrial ribosomes also contain a short 5S rRNA molecule, which is absent in animal mitochondria. Prokaryotic rRNAs typically contain methylated nucleotides, up to 10 in 16S rRNA and up to 20 in 23S rRNA, but little is known about the methylation states of plant and animal rRNAs because their sequences have been deduced from their genes.

Both small and large rRNAs fold into complex secondary structures (Fig. 6.35). Comparisons of rRNA sequences from many different organisms and organelles suggest the secondary structures of rRNAs are highly conserved despite considerable sequence divergence among organisms. The proposed structures receive additional support from experimental analysis, because many regions that are predicted by comparative analysis to form intramolecular base pairs also resist digestion by RNases and chemical reagents that degrade single-stranded RNA.

6.7.3 Plant cells contain three distinct sets of transfer RNAs

The second type of abundant RNA, tRNA, makes up most of the 4S RNA fraction in a whole-cell rRNA extract (see Fig. 6.34). Acting as adapters, tRNAs bind specific amino

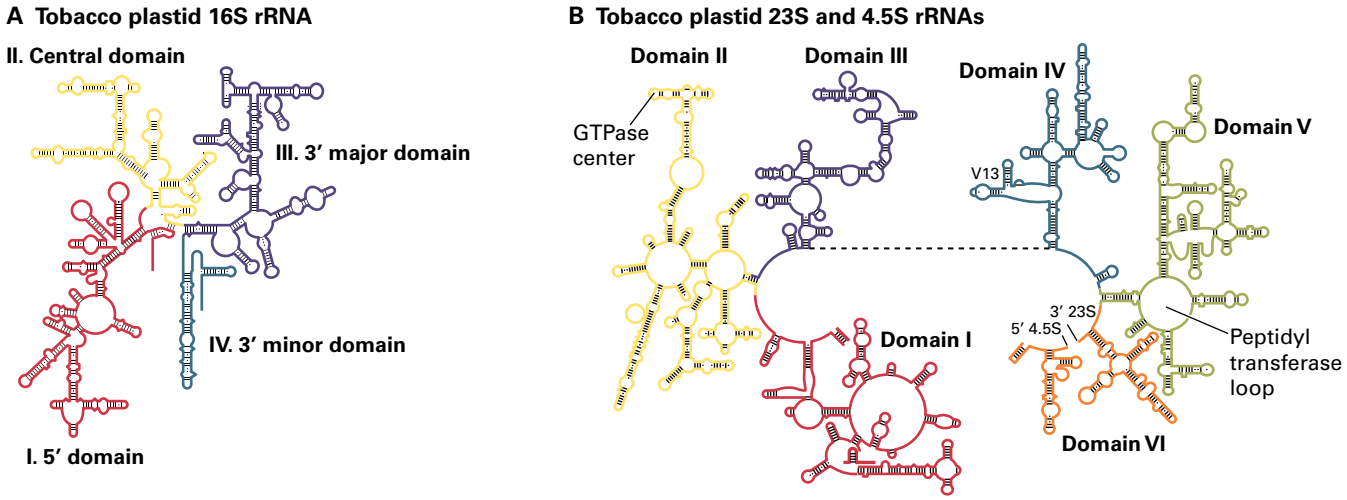


FIGURE 6.35 *Ribosomal RNAs can fold into complex secondary structures by pairing of complementary sequences. (A) The predicted secondary structure of tobacco plastid 16S rRNA reveals four major domains (I to IV). The structure of the tobacco 16S rRNA is based on the model for the structure of* Escherichia coli *16S rRNA. (B) Secondary structure predictions for tobacco plastid 23S and 4.5S rRNAs also reveal a conserved organization with six major domains (I–VI). Domain V is the principal site of tRNA binding to the 50S subunit.*

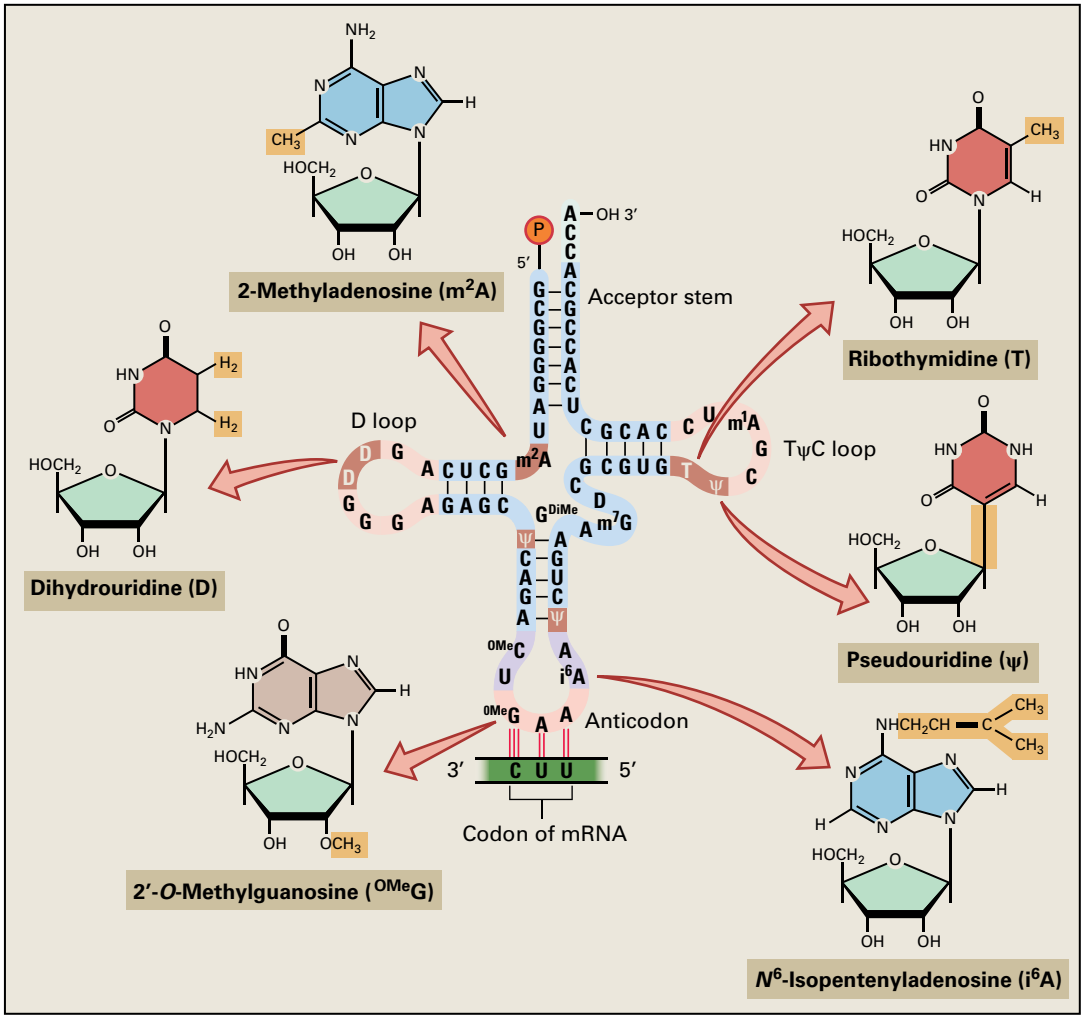


FIGURE 6.36 *The cloverleaf representation of wheat germ* $tRNA^{Phe}$*, the first plant tRNA to be sequenced. The structures of the modified nucleotides that occur at specific positions in plant tRNAs are shown. The four arms are named for their structure and function. The acceptor stem consists of a stem of nucleotide base pairs that extends to an unpaired CCA sequence at the 3′ end. The TψC loop is named for its pseudouridine residue (ψ). The anticodon, which varies among different tRNAs, constitutes the three nucleotides that interact with mRNA during translation (see Chapter 9). The D-loop is named for its dihydrouridine residue (D). A notable feature of all tRNA molecules is the presence of modified (or unusual) bases.*

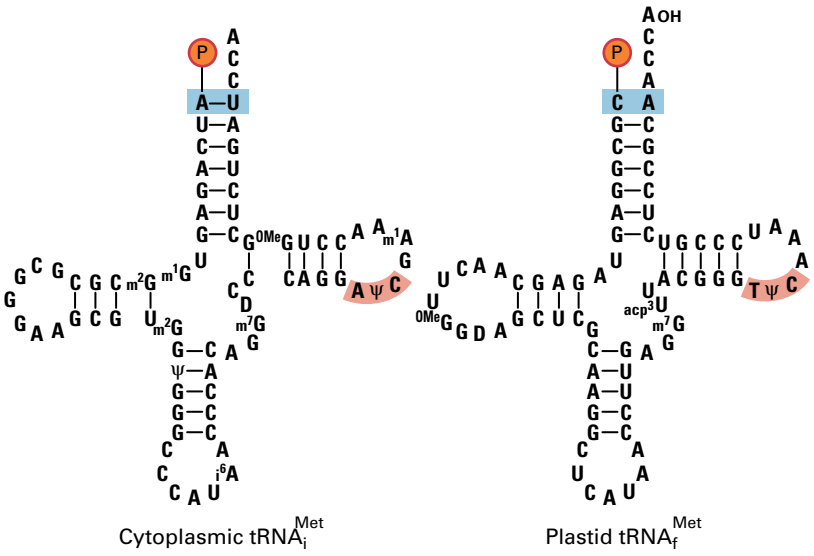


FIGURE 6.37 *The cytoplasmic initiator tRNA^{Met} of bean (left) is typical of eukaryotic cytoplasmic tRNAs. In contrast, the plastid initiator tRNA^{Met} (right) resembles those of prokaryotes. Initiator tRNAs, which are distinct from elongator tRNA^{Met}, have certain unique features. All cytoplasmic initiator tRNAs contain the sequence AψC instead of TψC in the TψC loop, Although the plastid tRNA^{Met} has the typical TψC sequence, its 5′ nucleotide is unusual in that it cannot base pair to the acceptor stem.*

acids and base pair with defined mRNA codons, facilitating the translation of nucleic acid sequences into polypeptides (see Chapter 10). A particular tRNA can accept only one of the 20 standard amino acids, but in most cases several different tRNA species, called isoaccepting tRNAs, bind the same amino acid. All tRNAs sequenced fit the cloverleaf model (Fig. 6.36). The conserved primary and secondary structures that characterize this class of molecules make purification of individual tRNA species difficult. In plants, the cytoplasm, plastids, and mitochondria each contain a unique population of tRNAs.

While mammalian mitochondrial DNA encodes all the tRNA genes necessary for translation, mitochondria from plants and many other organisms lack a full set of tRNA genes. Mitochondrial import of tRNAs from the plant cytoplasm was first suggested by the findings of hybridization experiments in which genes encoding some mitochondrial tRNAs were detected in nuclear DNA. Direct evidence was subsequently obtained from transgenic potato (*Solanum* spp.) plants that expressed a nuclear tRNA gene from bean. The bean tRNA could be detected in both the cytoplasm and the mitochondria of the transgenic potato plants. The mechanism of mitochondrial tRNA import remains unknown. In *Arabidopsis,* a single base mutation of tRNA^{Ala} blocks both its aminoacylation and import, suggesting that aminoacyl-tRNA synthases (see Chapter 10) participate in tRNA import into plant mitochondria. In contrast to mitochondrial DNA, the plastid genome of most plants encodes approximately 30 species of tRNAs (see Table 6.1), which are generally assumed to be sufficient for translation of proteins within the organelle. However, the chloroplast DNA of the nonphotosynthetic parasitic plant *Epifagus* contains only 17 tRNA genes (see Table 6.1). Translation in *Epifagus* plastids must therefore involve tRNAs of nuclear origin, suggesting that plastids may also be able to import tRNAs.

Plant cytoplasmic tRNAs are similar in sequence to those found in the cytoplasm of yeast and other eukaryotes, but many plastid tRNAs have attributes that are typically prokaryotic (Fig. 6.37). Consistent with their mixed origin, some plant mitochondrial tRNAs resemble those of prokaryotes, while others resemble those found in plant cell cytoplasm.

6.7.4 Cytoplasmic mRNAs are modified extensively after transcription

Messenger RNAs encode the amino acid sequences of proteins. The number of distinct mRNA species in a given cell, which can exceed tens of thousands, is comparable to the number of different proteins present in the cell. As discussed above, mRNAs constitute no more than 1–2% of total cellular RNA. Consistent with the range of molecular masses observed for polypeptides, mRNAs vary in length from a few hundred to several thousand nucleotides. In addition, mRNAs are generally more labile than rRNAs and tRNAs, although the turnover rate for some mRNAs is quite slow. Since individual mRNA species are usually of low abundance and, therefore, cannot be visualized directly by staining a gel with ethidium bromide, their detection requires hybridization with labeled probes of complementary DNA.

A typical cytosolic mRNA consists of five distinct regions (Fig. 6.38):

- a “cap” structure at the 5′ end
- a 5′-untranslated region
- the protein coding region
- a 3′-untranslated region
- a polyadenylic acid tract added to the 3′ end

The 5′ of the mRNA is first modified, or “capped,” by addition of a 7-methylguanosine nucleotide (m^{7}G). In the nucleus, shortly after the mRNA emerges from the RNA polymerase complex, a guanosine residue is joined to the 5′ nucleotide by way of a triphosphate bridge. The N-7 of the guanine is subsequently methylated (Fig. 6.39). The 5′ cap

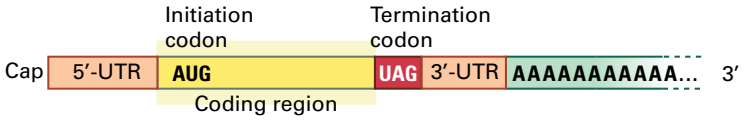


FIGURE 6.38 *Structure of a typical mature, nuclear-encoded, eukaryotic mRNA. Most mature mRNAs have 5′ and 3′ untranslated regions (UTRs) that often contain cis-regulatory sequences involved in the regulation of translation or mRNA stability. Specific regulatory sequences in the 3′-UTR are recognized by poly(A) polymerase, which synthesizes the addition of a polyadenylic acid tail at the 3′ end.*

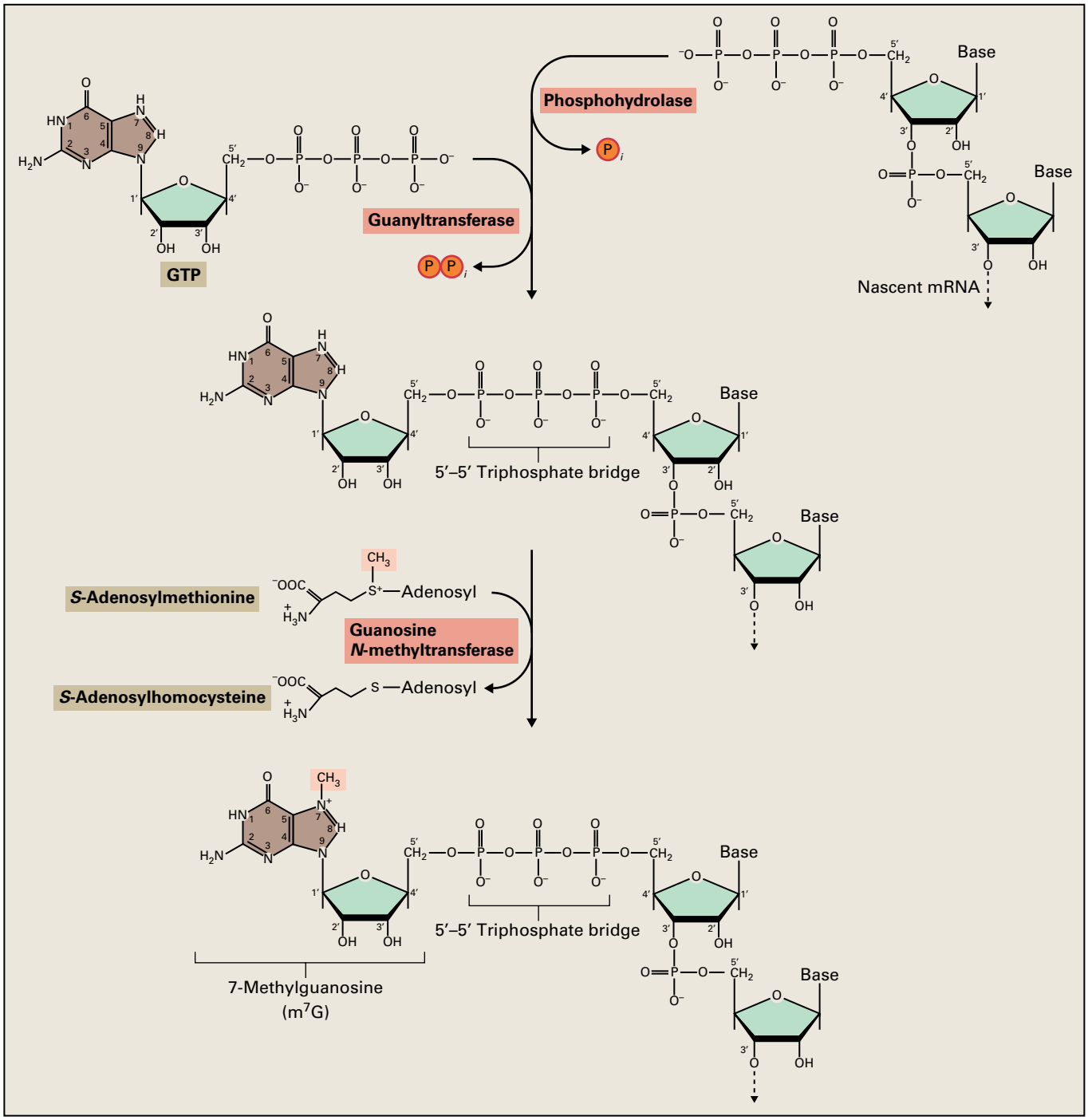


FIGURE 6.39 *5′ cap formation. The first nucleotide in an mRNA transcript, usually an A or a G, retains its 5′ triphosphate group. Phosphohydrolyase cleaves a phosphate from the 5′ terminal residue of the mRNA. The subsequent reaction of the 5′ triphosphate of a GTP and the 5′ diphosphate of the mRNA, catalyzed by guanylyltransferase, releases pyrophosphate and generates a 5′-triphosphate-5′ nucleotide linkage. Guanine methyltransferase then transfers a methyl group from* S*-adenosylmethionine to the 7 position of the guanine residue.*

plays an important role during the initiation of translation (see Chapter 10) and also seems to protect the mRNA from degradation during its synthesis.

The coding region, which is the nucleotide sequence translated into the amino acid sequence, begins with an initiation codon (usually AUG), and ends with a termination codon (UAG, UAA, or UGA). The sequence between start and stop codons constitutes an ORF (see Chapter 10). It is flanked by 5′ and 3′ untranslated regions (UTRs) that are highly variable in length. Consequently, the length of an mRNA does not always correlate with the length of the amino acid sequence it encodes. The precise function of the 5′ and 3′ UTRs is poorly understood for many mRNAs, but often these regions contain RNA sequences that can form secondary structure and interact with proteins that regulate transport, translation, and stability of the mRNA.

Most cytoplasmic mRNAs contain a 3′ sequence of polyadenylic acid. This poly(A) tail is not encoded in the DNA, but is added post-transcriptionally before the mRNA is exported from the nucleus to the cytoplasm. An enzyme complex that includes an endonuclease and poly(A) polymerase recognizes a signal sequence (5′-aauaaa-3′) near the 3′ end of the transcript, cleaves the pre-mRNA downstream from the signal, and adds 20–250 adenosine residues to the 3′ end. The poly(A) tail facilitates export of the mRNA from the nucleus, stabilizes the mRNA against exonucleolytic degradation, and appears to have a role in the initiation of translation.

The structure of plastid and mitochondrial mRNAs differs from that of cytoplasmic mRNA. The organellar mRNAs lack both the 5′ cap and 3′ poly(A) tail (Fig. 6.40). As a result of differences in post-transcriptional RNA processing, mitochondrial mRNAs commonly retain the 5′ triphosphate group, while the 5′ ends of most plastid mRNAs are monophosphorylated. Similar to prokaryotic mRNAs, the 5′- and 3′-UTRs of most organellar mRNAs can form stem–loop structures that have regulatory and stabilizing functions. These RNA structures often interact with proteins and serve as signals that affect the processing, translation, and degradation of the mRNA. A small fraction of plastid mRNA contains a short poly(A) segment or A-rich tract at the 3′ end. These poly(A) sequences are added to plastid mRNAs after endolytic cleavage at a 3′ sequence and at internal sites within the transcript. Unlike the poly(A) tail of cytoplasmic mRNAs, the 3′ polyadenylate sequences of plastid mRNAs appear to promote efficient degradation of the modified mRNA fragment.

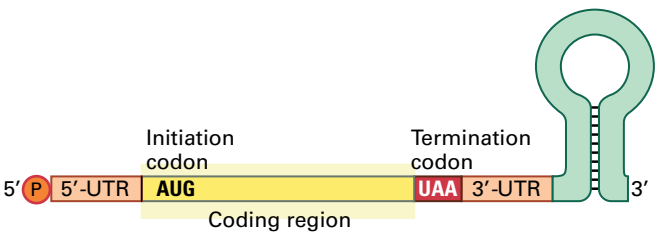


FIGURE 6.40 *Structure of a typical mature chloroplast mRNA. Chloroplast mRNAs resemble prokaryotic mRNAs and are not modified at the 5′ end. The mRNAs usually end in a 3′ stem-loop structure that appears to be important for the processing and stability of the transcript.*

6.7.5 Eukaryotic cells contain different classes of small RNAs

The majority of small RNAs in a plant cell have extremely important roles and can be divided into two main classes. One class comprises small nuclear RNAs (snRNAs) and small nucleolar RNAs (snoRNAs) of 60–300 nt in length. The other class is made up of very small (20–24 nt) RNAs that are generated from longer primary RNAs by Dicer-like endonucleases.

Small nuclear and small nucleolar RNAs (snRNAs and snoRNAs) are critical components of the small ribonucleoproteins snRNPs and snoRNPs that play essential roles in the maturation of mRNAs and rRNAs, respectively. They are numbered from U1 onward, reflecting the chronological order of their discovery. Most are found in the nucleolus and are, therefore, designated snoRNAs (small nucleolar RNAs). Several snRNAs contain unique 5′ cap structures as well as nucleotides that are methylated or modified. Most of the snRNAs in snRNPs are involved in splicing (removal) of intervening noncoding regions that from the precursor mRNA in the nucleus (see Section 6.8.2). Other snRNAs (e.g., U7) participate in processing of the 3′ terminus of histone pre-mRNA, which lacks a poly(A) tail. Most of the snoRNAs in the nucleolus, the site of transcription of ribosomal RNA genes (see Chapter 9), are involved in the processing of rRNA precursors. Although not all homologs of yeast and animal snRNA and snoRNA species have been identified in plants, the similarity of RNA processing mechanisms among all eukaryotes suggests the undetected ones likely exist.

6.7.6 Small regulatory RNAs derived from dsRNA mediate gene silencing

Small, 20–25-nt RNAs were first discovered in plants in which introduced transgenes were being silenced, and in plants infected with viruses. These **small RNAs** contained sequences from the "invading" transgene mRNA or viral genomic RNA. Because these RNAs are short and interfere with the expression of the gene or survival of the virus, they are called short interfering RNAs (siRNAs), and the process in which they act is called RNA interference (RNAi).

siRNAs are made by **Dicer-like (DCL) endonucleases**, which cleave long double-stranded (ds)RNAs that have themselves been generated either by host RNA-dependent RNA polymerases (RdRPs) or viral RdRPs (see Section 6.8.7). siRNAs are usually 21 nt long, and one strand of the DCL-generated duplex RNA is loaded on to another endonuclease called **Argonaute** (AGO), which in turn uses it as a guide to find target RNAs (Fig. 6.41). The siRNA-guided AGO is the main component of an **RNA-induced silencing complex**

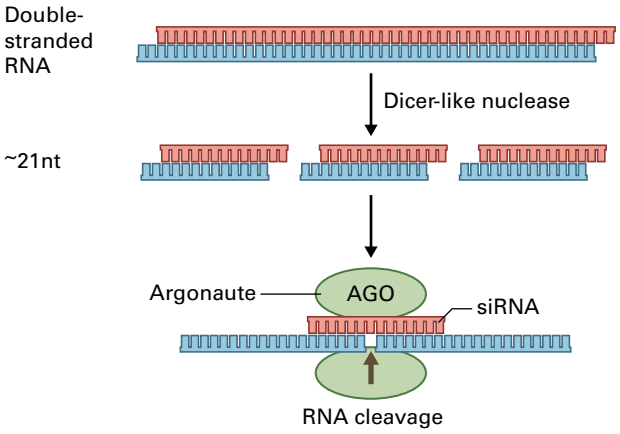


FIGURE 6.41 *In the basic mechanism of RNA interference, double-stranded RNA is recognized by a Dicer-like (DCL) endonuclease, which cleaves it into 21 nt RNA duplexes. One of the duplex strands, termed a short interfering (si) RNA, is loaded onto the Argonaute (AGO) endonuclease, which uses it to recognize single-stranded (ss) RNAs with a complementary sequence. AGO cleaves the cognate ssRNA in the middle of the target region.*

(RISC), which cleaves its target RNA and diminishes expression of the transgene or replication of the virus.

The mechanism that produces and utilizes siRNAs is related to pathways that produce and use four other classes of 20–25-nt RNAs (see Section 6.8.7 and Fig 6.42). These pathways produce microRNAs (miRNAs), trans-acting siRNAs (tasiRNAs), natural-antisense siRNAs (natsiRNAs), and heterochromatic siRNAs (hcsiRNAs). All four small RNA types are methylated at their 3′ nucleotide to protect them from polyuridylation and degradation. miRNAs range in size from 20 to 24 nt, tasiRNAs and natsiRNAs are predominantly 21 nt long, and hcsiRNAs are 24 nt in length. The differences in their sizes reflect the different DCL enzymes that produce them.

All eukaryotes encode miRNAs. Over 350 miRNAs have been identified in *Arabidopsis*, and almost 2000 in humans. Because of the wide distribution of miRNAs across species and the ongoing discovery of new members, their current nomenclature is inconsistent. A central miRNA registry (http://www.mirbase.org) provides a new number from its

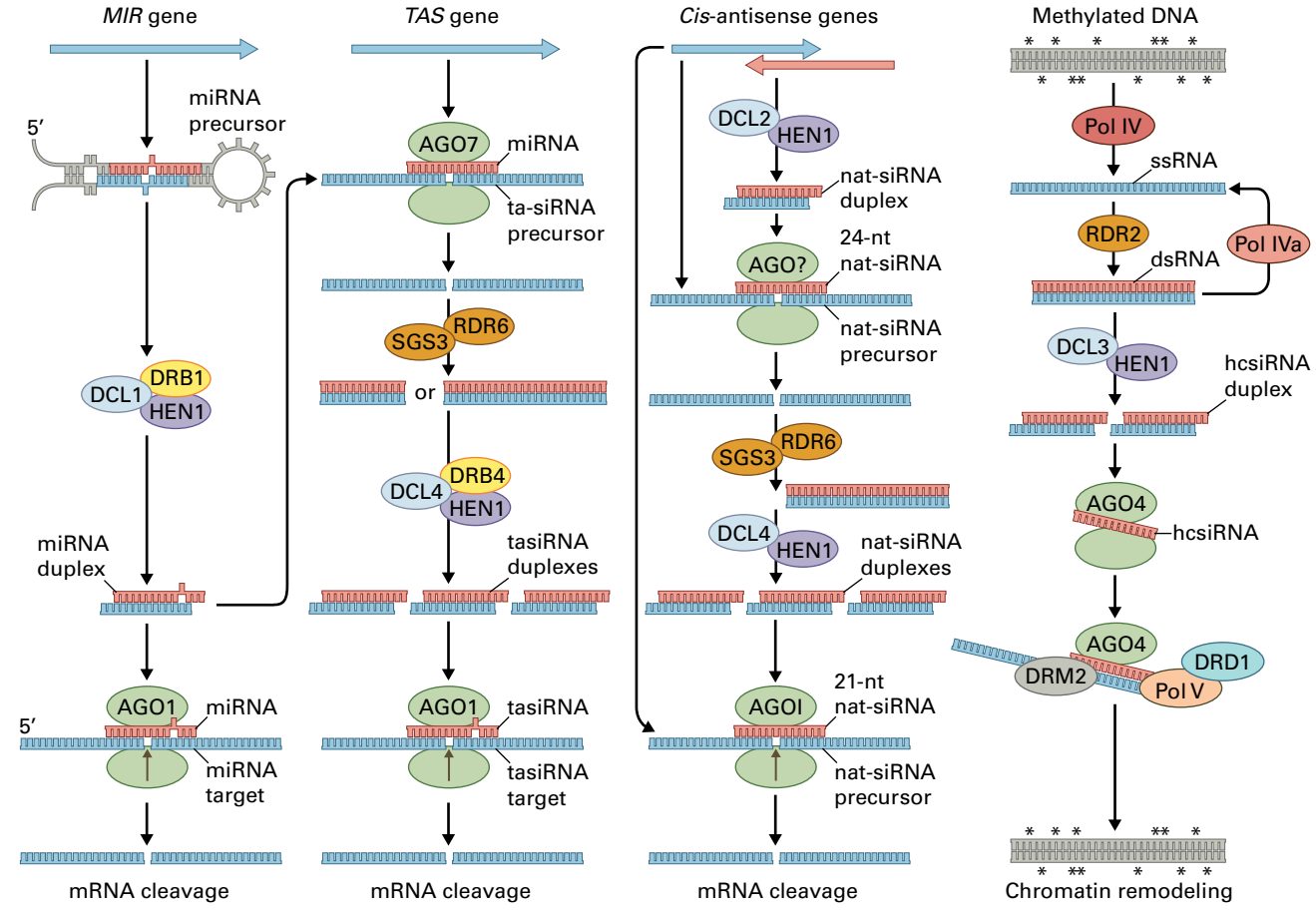


FIGURE 6.42 *In* Arabidopsis, *four different Dicer-like (DCL) endonucleases produce small RNAs to direct a number of different pathways. DCL1 generates microRNAs (from imperfect hairpin-like RNA precursors) that regulate development-associated genes. DCL2 and 4 produce siRNAs (from perfect dsRNA from replicating RNA viruses) for viral defense, and DCL3 produces hcsiRNAs (from dsRNA from transposons and other genomic sequences) to target chromatin repression. The pathways are intertwined, sharing some common or similar components, such as RNA-dependent polymerases, double-stranded RNA binding proteins, and Argonaute (AGO) endonucleases. Two other pathways produce tasi- or natsiRNAs, which are involved in regulating plant development and responses to environmental stress.*

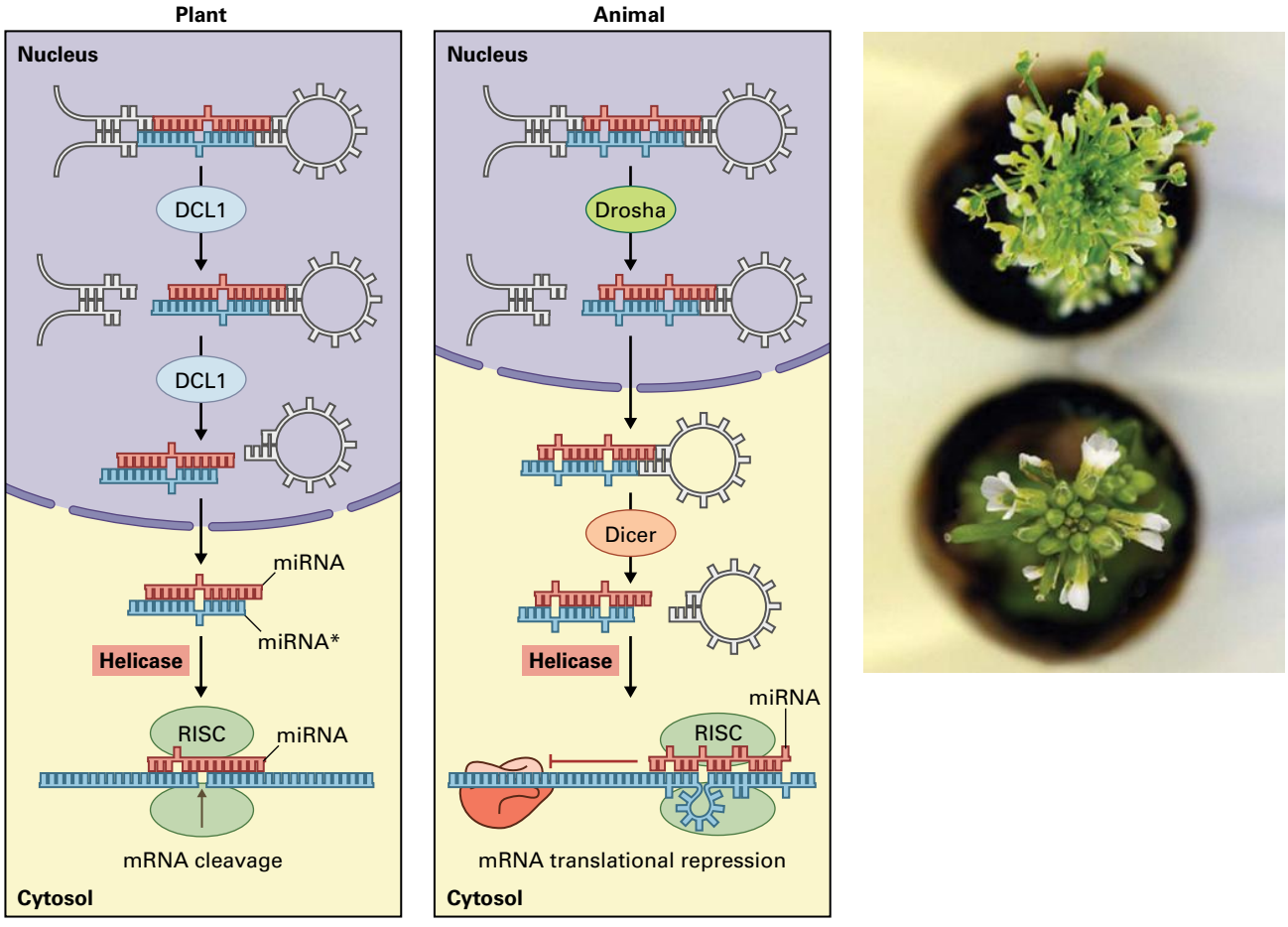


FIGURE 6.43 *Plants and animals produce microRNAs by DCL enzymes cleaving imperfect hairpin-like RNA precursors. The miRNA is shown in red. The compartments in which the processing steps occur are different between plants and animals, as is the method of directed gene repression. In plants, the mRNAs of the target genes are cleaved by miRNA-directed Argonaute (AGO), whereas in animals the AGO operates by translational repression. In the photographs, the top* Arabidopsis *mutant plant has a defective DCL1 protein and shows a severely distorted developmental phenotype. The bottom* Arabidopsis *plant has a wild-type DCL1 gene and shows normal inflorescence development.*

ascending register to each newly discovered miRNA, regardless of the species from which it was discovered. The first plant miRNA recorded in the registry was its 156th miRNA, and it came from *Arabidopsis*, so it is called *At*miR156. Ten different loci in the *Arabidopsis* genome encode this miRNA, so the miRNA from each locus is differentiated by an alphabetic suffix (i.e., *At*miR156a to *At*miR156j).

Overall, hundreds of genes are regulated by miRNAs, which downregulate their expression levels in different tissues or at different times. In some cases, miRNAs control developmental transitions and responses to environmental stresses, and in others they provide sharp, tissue-specific expression boundaries. In contrast to animal miRNAs, which act by translational repression, plant miRNAs operate mostly by cleaving the mRNA of the target gene (Fig. 6.43).

Like miRNAs, tasiRNAs and natsiRNAs downregulate gene expression by directing AGO-mediated cleavage of target gene mRNAs. In *Arabidopsis*, tasiRNAs are generated from only four template RNAs, and their main function is to regulate the expression of auxin response factors. In contrast, there are more than 2000 potential natsiRNA-targeted *Arabidopsis* genes. The principal role of natsiRNAs is thought to be the provision of an additional layer of gene regulation in response to environmental stresses.

The most abundant DCL-produced small RNAs in plants are hcsiRNAs. They are produced from and act upon transposons, repeated elements, and the heterochromatic regions of the plant genome. Unlike mi-, si-, tasi-, and natsi-RNAs, the 24-nt hcsiRNAs do not regulate gene expression by cleavage of mRNAs. Instead they operate by inhibiting transcription (see Section 6.8.7) by recruiting histone modifiers and DNA methyltransferases to their target regions in the chromosome. hcsiRNA-directed chromatin remodeling protects the genome from the deleterious effects of mobile transposons. It is increasingly implicated in short-term epigenetic alterations in response to environmental stresses and in determining the developmental fate of a cell.

In addition to snRNAs, snoRNAs, and the DCL-generated small RNAs, other types of small, stable RNA molecules have also been identified (Table 6.4). RNase P, an enzyme required for processing tRNAs, contains an integral RNA component. The 7SL RNA of the signal recognition

TABLE 6.4 *Small RNAs in plants.*

Type	Names	Location	Proposed function
Small nuclear RNAs (snRNAs)	Ul, U2, U4 through U9, U11, U12,	Nucleoplasm	Pre-mRNA splicing
	U7	Nucleoplasm	Histone pre-mRNA processing, poly(A) addition
Small nucleolar RNAs (snoRNAs)	U3, U8, U13 through U40	Nucleolus	Pre-rRNA processing
Short interfering RNAs (siRNAs)	siRNA	Cytoplasm	Virus defense
MicroRNAs (miRNAs)	miR156 to miR5666	Cytoplasm	Regulation of development and stress responses
Trans-acting siRNAs (tasiRNAs)	siR255 to siR1778	Cytoplasm	Regulation of auxin response factors
Natural-antisense siRNAs (natsiRNAs)	natsiRNA	Cytoplasm	Gene self-regulation
Heterochromatic siRNAs (hcsiRNAs)	hcsiRNA	Nucleus	Epigenetic regulation
Other small RNAs	RNase P	Nucleoplasm, plastids, mitochondria	Pre-tRNA processing
	7SL	Cytoplasm	Protein transport

particle functions in conjunction with proteins during the transport of proteins into the endoplasmic reticulum (see Chapter 4).

6.8 RNA processing

Although transcription is a complex and highly regulated step in the expression of a gene, it represents only the first in a series of events necessary to produce a functional RNA. RNA can be modified extensively, but most primary transcripts in eukaryotic cells must also be processed to yield mature RNA products. The coding regions of many eukaryotic genes are interrupted by sequences that do not appear in the mature RNA. The primary transcripts synthesized by RNA polymerases, therefore, include stretches of RNA that contribute to the final gene product **(exons)** and noncoding, intervening sequences that must be removed before the RNA can function **(introns)**. In the case of pre-mRNAs transcribed from genes containing introns, the intron sequences must be removed to produce an mRNA molecule that codes directly for the protein. The process by which the introns are excised from a pre-RNA and the exons are rejoined to yield the mature RNA sequence is called **RNA splicing**.

6.8.1 Introns are found in RNAs encoded in all three genomes of plant cell

Introns have been found in most classes of genes and occur in the nuclear, chloroplast, and mitochondrial genomes. However, the number of introns and frequency of intron-containing genes varies among plant species and organelles. For example, 155 introns account for 40% of the plastid genome of *Euglena,* whereas the chloroplast DNA of the red alga *Porphyra* lacks introns entirely. Most protein-coding genes in the plant cell nucleus contain one or more introns, but some, such as the maize (*Zea mays*) zein gene, do not. It is not unusual for some members of a gene family to have multiple introns and other members to contain none. No introns have been reported in 5.8S and 5S rRNA genes or in any of the plant snRNA genes.

Most introns can be classified into four general categories based on their structural features and the mechanisms by which they are spliced (Table 6.5). Nuclear pre-mRNA introns are the most prevalent type. In mammalian genes, these introns are highly variable in length, ranging from less than 100 nt to 100 kb, but they are typically shorter in plant genes. Nuclear pre-tRNA introns, which are found only in a subset of nuclear tRNA genes, are usually short and distinct from mRNA introns. Group I and II introns, which are classified

TABLE 6.5 *The four major types of introns.*

	Structural features		
Type	**Length (nucleotides)**	**Splice sites**	**Occurrence**
Nuclear pre-mRNA	>70	G↓GU…AG↓N*	Nuclear mRNAs
Nuclear pre-tRNA	11–13	not conserved	Nuclear tRNAs
Group I-type	>200	U↓N…G↓N	Plastid tRNA, rRNA, and mRNAs
Group II-type	<200 to >400	N↓GYGCG….AY↓N†	

*Minor classes of nuclear pre-mRNA introns contain the splice site sequence N↓GC….AG↓U and N↓AU….AC↓N, in which N represents any nucleotide.
†Y represents a pyrimidine nucleotide.

according to their primary and secondary structures, occur in the mitochondrial genomes of fungi, as well as in plant mitochondria and plastids. A fifth category of introns, Group III, was identified in the genus *Euglena,* in which more than 100 examples of this type of intron are now known.

6.8.2 The introns of plant nuclear pre-mRNA tend to be AU-rich and have conserved sequences at their splice junctions

Introns in plant pre-mRNAs vary considerably in length—from 70 nt to well over 7 kb—but most range from 80 to 140 nt. A minimum length is required for efficient splicing of these introns, because introns of less than 70 nt are rarely found in protein-coding genes. In contrast to the introns in the nuclear genes of animals, plant nuclear pre-mRNA introns tend to be enriched for adenosine and uridine ribonucleotides. In dicots, these introns contain 70% A-U base pairs on average. The composition of the pre-mRNA introns of monocots is 60% A-U on average, although some contain as few as 30% A-U base pairs.

The nucleotide sequences surrounding each exon–intron junction are highly conserved. In almost all plant nuclear mRNA introns, the boundary sequences at the 5′ splice site (donor site) and the 3′ splice site (acceptor site) consist of 5′ GU and AG 3′; this characteristic is known as the GU-AG rule. In rare instances, the intron splice site sequences are 5′ GC…AG 3′ or 5′ AU…AC 3′. An additional structural element, the branch site, is usually located 20–40 nt upstream from the 3′ splice site. During intron excision, the 5′ end of the intron binds to an adenine residue at the branch site, forming a lariat (Fig. 6.44). A conserved branch site sequence, UACUAAC is found in yeast introns, but this sequence is not strictly conserved in plant or mammalian introns. The branch site adenine in the conserved sequence has been underlined.

Unlike the case with animals, it has been difficult to obtain from plant tissues an in vitro splicing system that faithfully reproduces the in vivo pre-mRNA splicing reaction. However, the fundamental mechanism of pre-mRNA splicing in plants probably resembles that of mammals and yeast, because all of the conserved elements present in plant introns, that is, the 5′ and 3′ splice sites and the branch site, are similar to those found in the introns of mammals and yeast.

6.8.3 The position of nuclear tRNA introns is conserved, but their sequences are not

Introns in eukaryotic nuclear tRNA genes are short (11–60 nt). The 5′ splice site is located one nucleotide distal to the anticodon. There is no conserved sequence at the splicing junctions, but the introns contain a sequence that is complementary to the anticodon of the tRNA. Nuclear tRNA splicing is best understood in yeast. An in vitro pre-tRNA splicing system from wheat germ has provided a model for nuclear pre-tRNA splicing in plants, which is similar to that in yeast cells (Fig. 6.45).

6.8.4 Group I introns can self-splice and act as mobile genetic elements

Group I introns are distributed in the mitochondria of yeasts and other fungi, the nuclear rRNA genes of certain unicellular eukaryotes (e.g., *Tetrahymena*), and the organellar genes of plants. Group I introns are ribozymes (RNA molecules with catalytic activity) and reflect the presumed importance of RNA-catalyzed splicing reactions early in evolution. Group I intron sequences, which fold into complex secondary structures, begin the splicing reaction by binding and activating a G nucleotide. The 3′-hydroxyl of the activated G attacks the 5′ splice site group and catalyzes the cleavage of the phosphodiester bond at that site, releasing an exon (Fig. 6.46A). The 3′-hydroxyl of the free exon then attacks the 3′ splice site to release the intron and ligate the exons. Some self-splicing group I introns remain today, for example in the nuclear

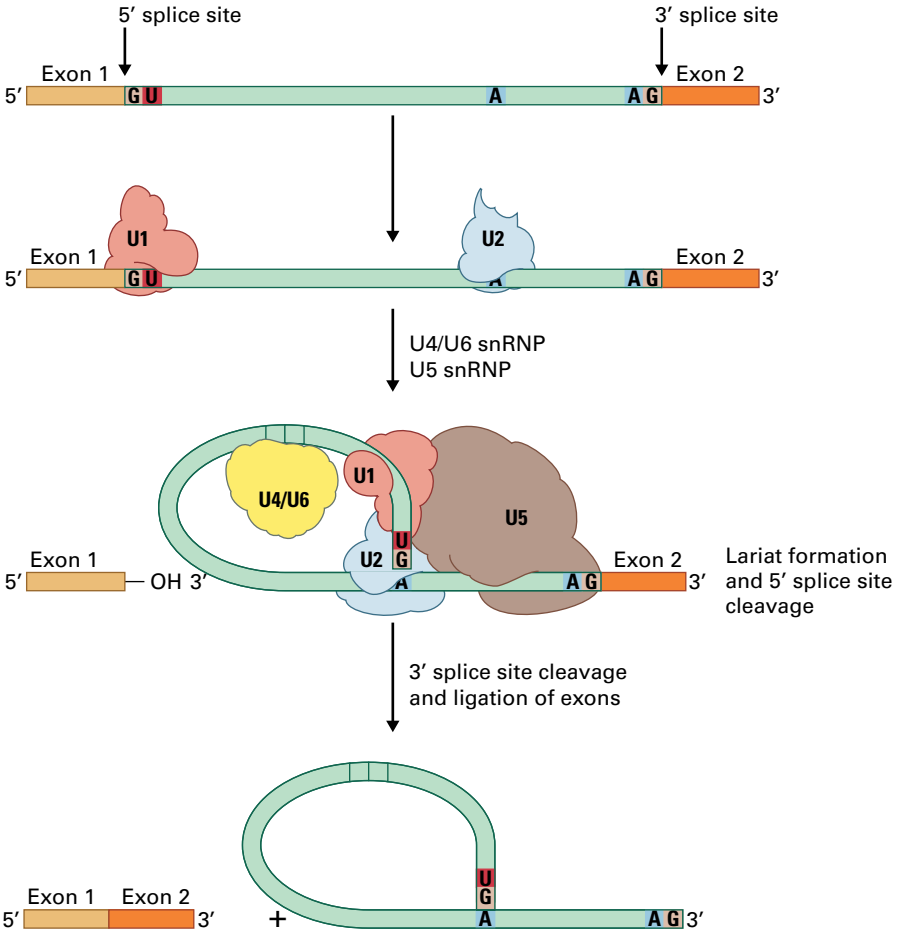


FIGURE 6.44 *Steps in the intron splicing of nuclear pre-mRNA. Pre-mRNA intron splicing occurs within a large ribonucleoprotein complex, called the spliceosome, which assembles on pre-mRNA. The spliceosome contains the snRNAs U1, U2, the U4/U6 complex, and U5, which are associated with small ribonuclear proteins (snRNPs), and non-snRNP protein factors. The splicing reaction is initiated by the nucleophilic attack of the 2′-hydroxyl group of the branch site adenosine on the 3′ → 5′-phosphodiester bond at the 5′ splice site. The 5′ guanosine of the exon–intron boundary and the branch site adenosine together form a 2′ → 5′ phosphodiester bond, generating the lariat intermediate and releasing the 5′ exon. Splicing is completed with a second nucleophilic attack by the 3′-hydroxyl group of the 5′ exon on the phosphodiester bond at the 3′ splice site, which ligates the exons and releasing the intron lariat.*

rRNA genes of *Tetrahymena* (where they were first discovered) and in certain chloroplast and mitochondrial genes.

Several group I introns, including the intron of the plastid 23S rRNA gene from *Chlamydomonas reinhardtii,* are mobile genetic elements. In a process known as "intron homing," these mobile introns are transmitted with high frequency to the progeny of genetic crosses between parents that have the intron and parents that do not. All mobile introns encode a DNA endonuclease that specifically recognize the intron-less allele and generates a double-strand break in the DNA near the insertion or "homing" site. This break is thought to initiate the replicative integration of the intron into the intron-less allele.

6.8.5 Group II introns and nuclear pre-mRNA introns share the same splicing mechanism

Group II introns are found in fungal mitochondrial genes, as well as in plant mitochondrial and plastid genes (see Box 6.6). Although group II introns differ significantly from nuclear pre-mRNA introns in their structure, they do share certain common features. Group II introns follow the GU-AG rule: the sequences at their 5′ and 3′ splice sites resemble those of nuclear pre-mRNA introns and contain a conserved branch site adenine. This finding indicates the group II introns and nuclear pre-mRNA introns have a common evolutionary origin and share the same splicing mechanism. Some of the group II introns in yeast mitochondria self-splice in vitro, using a particularly reactive A residue in the intron sequence as the attacking group for the formation of the lariat structure (Fig. 6.46B). Autocatalytic splicing has not been observed in Group II introns from plant plastids or mitochondria, suggesting these introns require additional factors for efficient splicing.

6.8.6 Precursor RNAs are processed extensively to create functional RNA molecules

Most eukaryotic genes are transcribed as precursor RNA (pre-RNA) molecules, which are then processed into shorter RNA species (mature RNAs). Extensive processing and modification are highly regulated, critical aspects in the production of functional RNA forms. Only certain species of small, stable RNAs that are transcribed by RNA polymerase III do not undergo extensive processing.

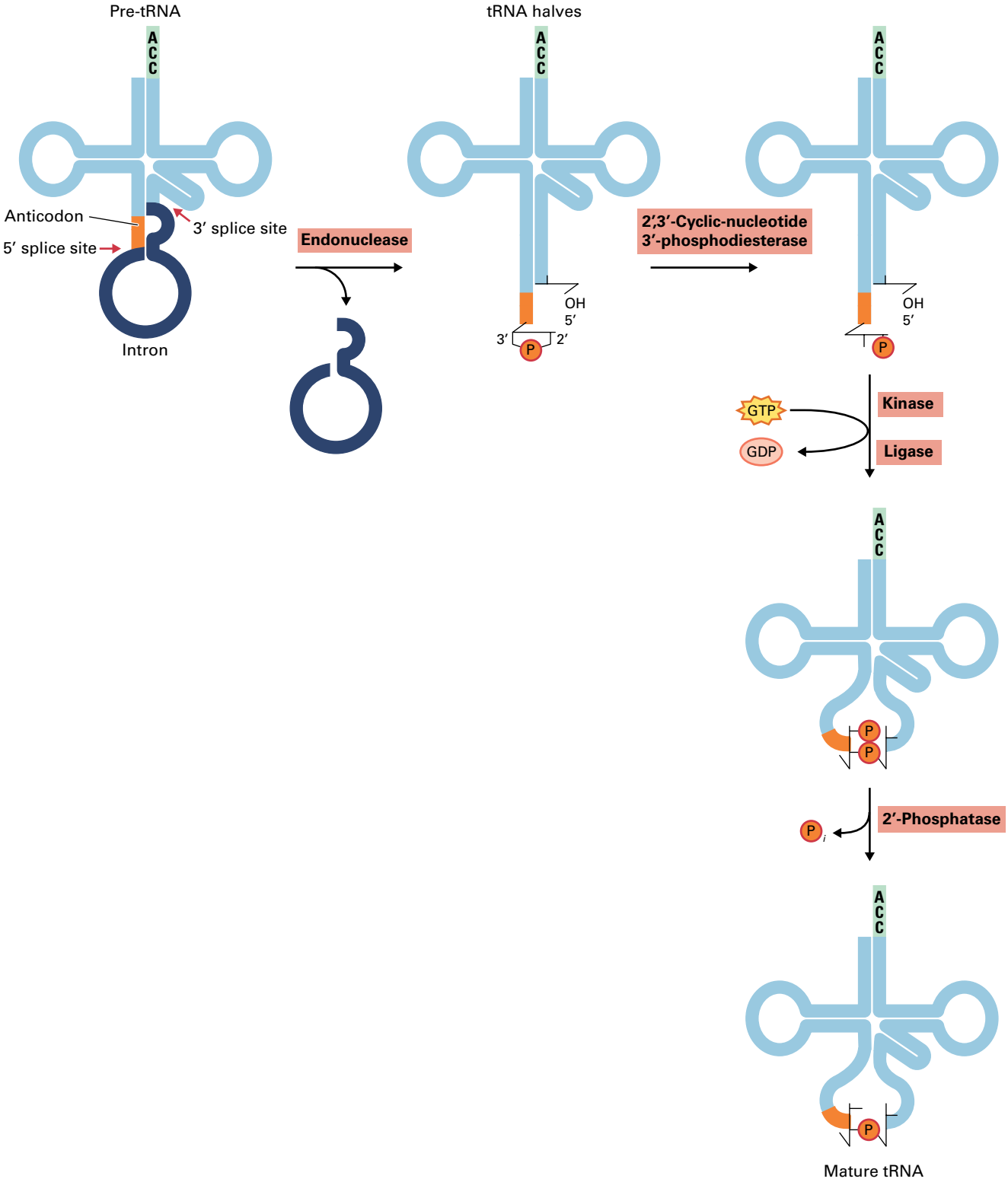


FIGURE 6.45 *The splicing pathway of pre-tRNA. An endonuclease cleaves the pre-tRNA at both ends of the intron (red arrows). This results in the formation of a cyclic 2′,3′-phosphate group at the 3′ end of the 5′ tRNA segment, as well as a free 5′-hydroxyl group at the 5′end of the 3′ tRNA segment. The cyclic phosphate group is cleaved to form a 2′-phosphate group. After the free 5′ hydroxyl of the 3′ tRNA segment is phosphorylated, both halves of the tRNA are joined by an RNA ligase. A 2′-phosphatase removes the 2′-phosphate group to yield the mature spliced tRNA.*

The transcription units in the nuclear rRNA gene cluster that encode the 17S, 5.8S, and 25S rRNA molecules are transcribed by RNA polymerase I into a single, long precursor molecule. The rRNA precursor molecule then undergoes a series of cleavage and methylation steps to yield mature the 17S, 5.8S, and 25S rRNA molecules (Fig. 6.47). The 5.8S rRNA is derived from the same RNA intermediate as the 25S rRNA; the bases of these two RNA products remain paired even after the intergenic RNA spacer sequences have been removed. Transcription of the 5S rRNA from the corresponding nuclear genes is independent and is catalyzed by RNA polymerase III. This cytoplasmic 5S rRNA is unusual in that it requires no processing.

All four plastid rRNA molecules are encoded as a polycistronic transcription unit that also includes the two tRNA genes encoding $tRNA^{Ile}$ and $tRNA^{Ala}$, each of which contains an unusually long intron. Following a complex processing pathway involving specific nucleases, the precursor RNA is then cleaved into 16S, 23S, 4.5S, and 5S rRNAs (Fig. 6.48). Once removed from the polycistronic RNA, the cleaved tRNA precursors are also processed and their introns are spliced to produce functional $tRNA^{Ile}$ and $tRNA^{Ala}$ molecules. Ribosomal

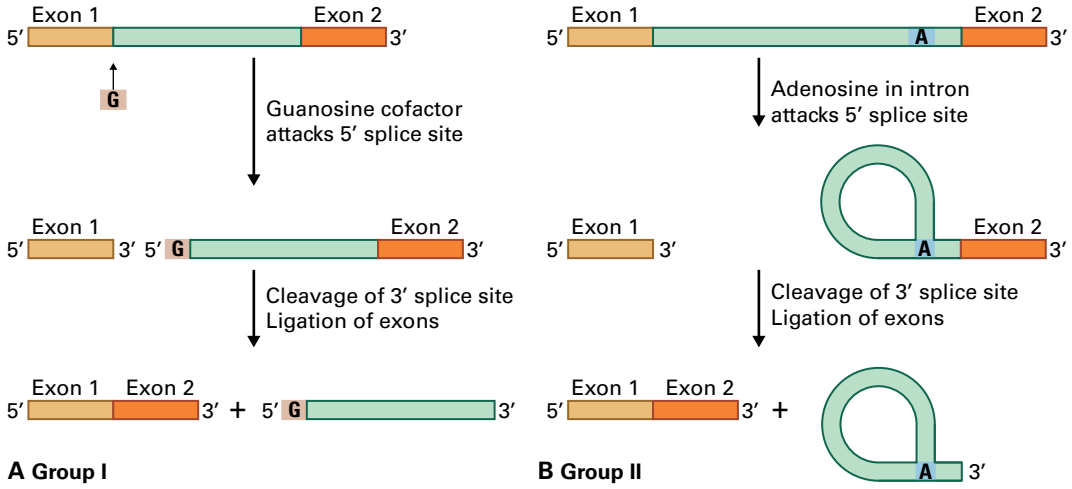
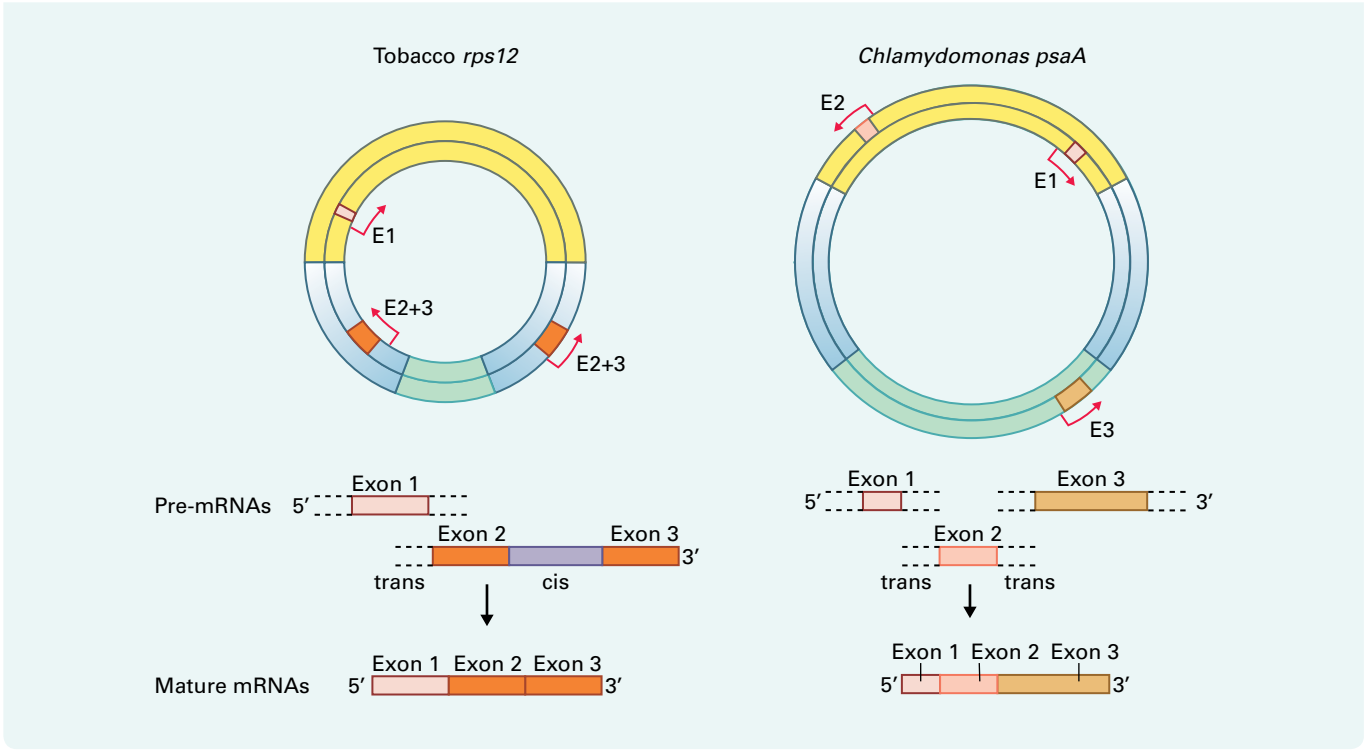


FIGURE 6.46 *Self-splicing mechanisms remove Group I- and Group II-type introns. Splicing of Group I introns is initiated when a guanosine molecule or its 5′ phosphorylated derivative binds to an intron sequence. The 3′ OH group of the bound guanosine attacks the phosphate group at the 5′ splice site, cleaving the phosphodiester bond at that site. The 3′ OH at the end of exon 1 reacts with the phosphate at the 3′ splice site, ligating the two exons and releasing a linear intron that is subsequently circularized (not shown). In contrast, the mechanism of group II introns self-splicing resembles splicing of nuclear pre-mRNAs, but does not involve the formation of a spliceosome (see Fig. 6.44).*

BOX 6.6 Certain Group II introns of plant organelles are removed by a *trans*-splicing mechanism

Splicing reactions are typically intramolecular and join exons from a single transcript (*cis*-splicing). However, splicing events discovered in plant chloroplasts and mitochondria involve two or more RNA molecules (*trans*-splicing). The tobacco (*Nicotiana tabacum*) chloroplast *rps12* gene (see Fig. 6.46B) is organized as two separate loci in the genome. Each locus produces an independent transcript: one encodes exon 1, and the other encodes the RNA product exon 2-intron-exon 3. Following transcription, trans-splicing joins exons 1 and 2; exons 2 and 3 are spliced in *cis* after removal of the intron. The *Chlamydomonas* chloroplast *psaA* gene (see Fig. 6.46B) is another example of a discontinuous gene in which three exons are encoded by three separate loci in the genome. In this case, two *trans*-splicing events generate the mature mRNA from three different transcripts.

In angiosperm mitochondria, the *nad1*, *nad2*, and *nad5* genes are also discontinuous, and their transcripts require *trans*-splicing to produce functional mRNAs. In contrast, the *nad2* and *nad5* genes in the mitochondrial genomes of ferns are continuous, and their introns are spliced in *cis*. These continuous genes are thought to be the ancestral genes that gave rise to the discontinuous genes of flowering plants. The unique *trans*-splicing mechanism may have co-evolved with the angiosperm genes as the latter were cleaved into separate transcription units.



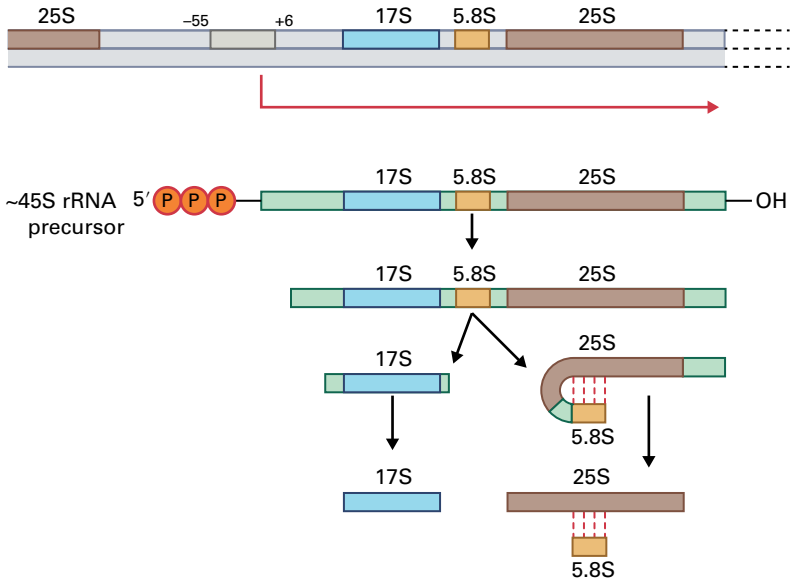


FIGURE 6.47 *Processing of the nuclear-encoded 45S rRNA precursor molecule produces three mature rRNAs. The 17S, 5.8S, and 25S rRNAs are derived from a common precursor rRNA molecule by processing reactions that require several RNases. During processing, the 25S and 5.8S rRNAs become hydrogen bonded and remain paired after the processing is complete.*

RNAs and tRNAs in plant mitochondria are also extensively processed from precursor molecules.

Unlike 5S rRNA, the tRNAs encoded by clusters of nuclear genes are transcribed by RNA polymerase III into precursor molecules that contain additional sequences at both the 5′ and 3′ ends. These extra sequences are then removed by specific nucleases, followed by the addition of three nucleotides, CCA, to the 3′ end. As discussed earlier, some tRNA precursors also contain introns that are spliced during processing to produce the functional tRNA molecule (see Fig. 6.45).

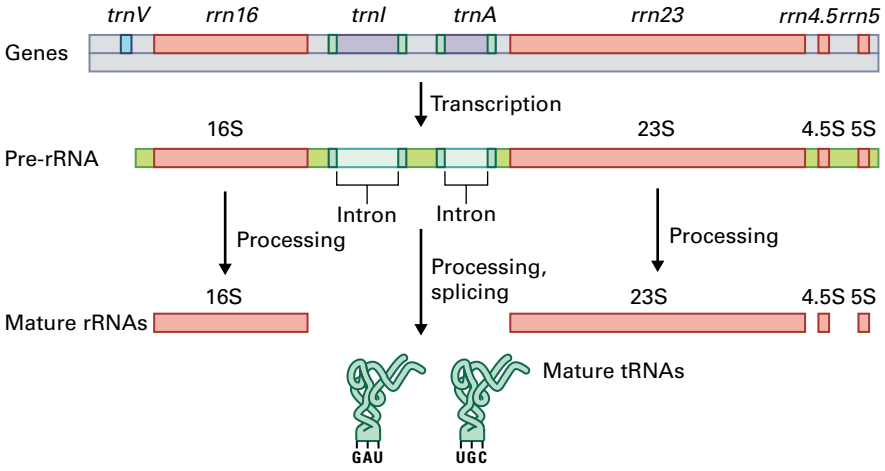


FIGURE 6.48 *Processing of chloroplast pre-rRNA from plants. Unlike nuclear-encoded rRNAs, the chloroplast rRNA operon also encodes two tRNAs in the spacer regions that separate the 16S and 23S rRNA. These tRNAs are interrupted by long introns (approximately 1 kb) and require both processing and splicing to produce the mature tRNAs.*

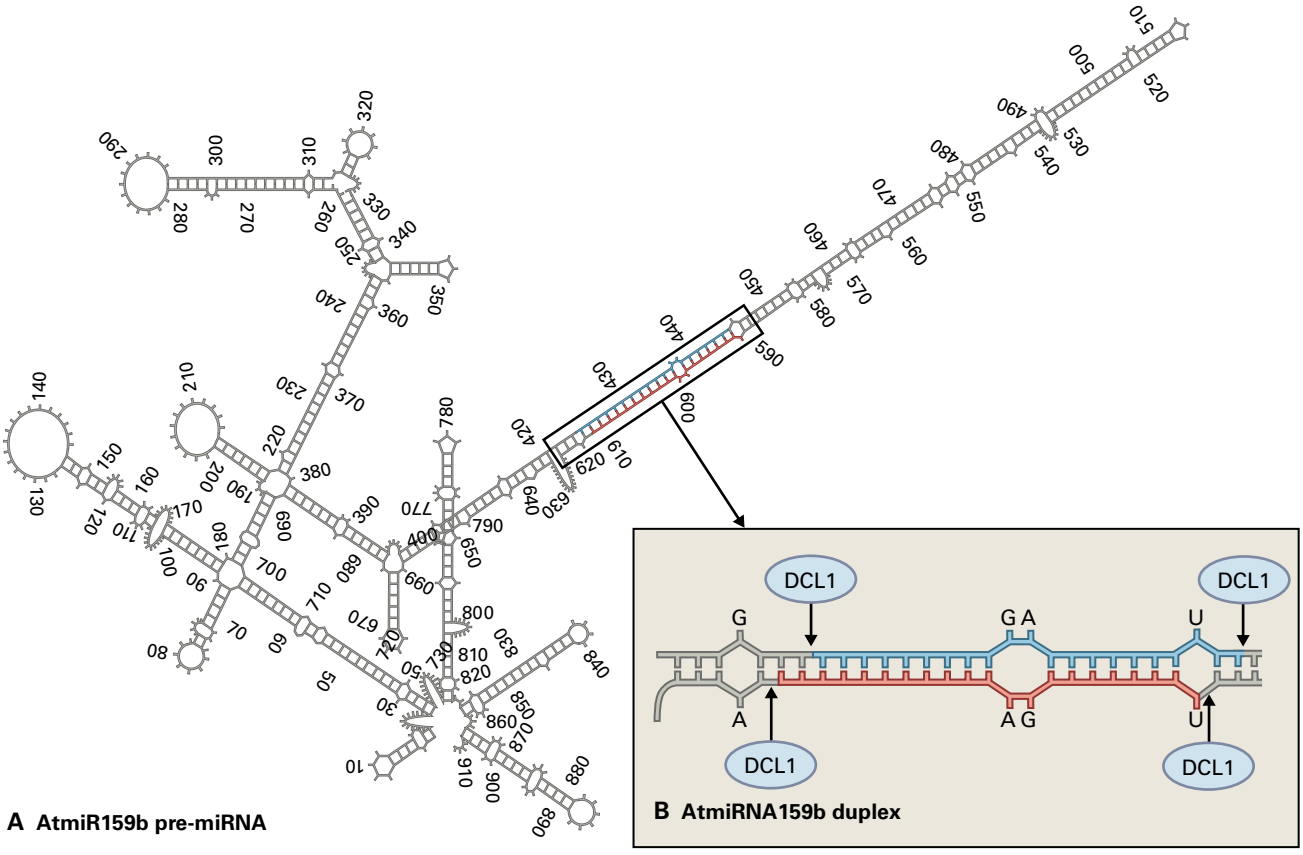


FIGURE 6.49 *(A) A mature microRNA (indicated by red lines) is precisely cleaved from its primary transcripts by Dicer-like1 (DCL1) endonuclease. (B) The microRNA is excised as a 21-nt duplex made up of the miRNA (red line) and its partner miR* strand (blue line). The DCL1 cleavage sites are indicated by the arrows. When excised, the duplex RNA molecule has a 19-nt overlap between the strands and two nucleotide 3′ overhangs.*

6.8.7 RNA transcripts are processed into small regulatory RNAs

The small RNAs that regulate endogenous gene expression by guiding specific mRNA degradation and chromatin modification are processed from long double-stranded or self-complementary single-stranded RNA molecules. Each of the four types of endogenous regulatory small RNAs are generated by a Dicer-like (DCL) endonuclease (Fig. 6.43). In plants there are four types of DCLs (DCL1-DCL4). DCL1 cleaves a miRNA duplex out of a hairpin-like single-stranded transcript (Fig. 6.49A). This transcript is made by DNA-dependent

RNA polymerase II from *MIRNA* genes that reside in the intergenic regions of the genome. DCL1 specifically cleaves a 21-nt duplex from the hairpin-RNA with a staggered cut at each end to produce two nucleotide 3′ overhangs. The tasi-, natsi-, and hcsiRNAs are cut by other DCLs from dsRNA molecules synthesized by **RNA-dependent RNA polymerases** (RdRPs) from single-stranded templates. The same cytoplasmic RdRP produces dsRNA for tasi- and natsiRNA production, but is recruited to the tasiRNA template by a specific miRNA, and by a DCL2-produced small RNA for the natsiRNA template. The dsRNA precursor for hcsiRNA production is generated in the nucleus by a different RdRP acting on a transcript made by DNA-dependent RNA polymerase IV. No matter which DCL or which dsRNA or hairpin-like RNA substrate is being acted upon, the DCL excises a duplex of dsRNA from the substrate and transfers only one strand of the duplex of the Argonaute (AGO) endonuclease. In the case of miRNA production the loaded strand is the miRNA and the discarded strand is called the miR* or passenger strand (Fig. 6.49B). The cleavage of target mRNAs guided by mi-, tasi-, and natsi-RNAs is predominantly mediated by AGO1. The recruitment of histone modifiers and DNA methyltransferases guided by hcsiRNAs is mediated by AGO4, which has a binding but not cleaving activity. The current model is that intergenic repeat regions of the genome have short transcripts produced by DNA-dependent DNA polymerase V which somehow remain associated with their template DNA and are accessible for recognition by hcsiRNA-loaded AGO4. This provides a way of recruiting the epigenetic modifiers to the appropriate genomic location (Fig. 6.43).

6.8.8 Some plastid mRNAs are polycistronic

Since the chloroplast genome of most plants contains about 150 genes, but only about 60 transcription units, it is likely most plastid mRNAs are first synthesized by chloroplast RNA polymerase into polycistronic mRNAs. While polycistronic bacterial mRNAs can be translated without further processing, polycistronic chloroplast mRNAs are first cleaved and processed to create monocistronic mRNAs (Fig. 6.50). The significance of this difference between bacterial and chloroplast

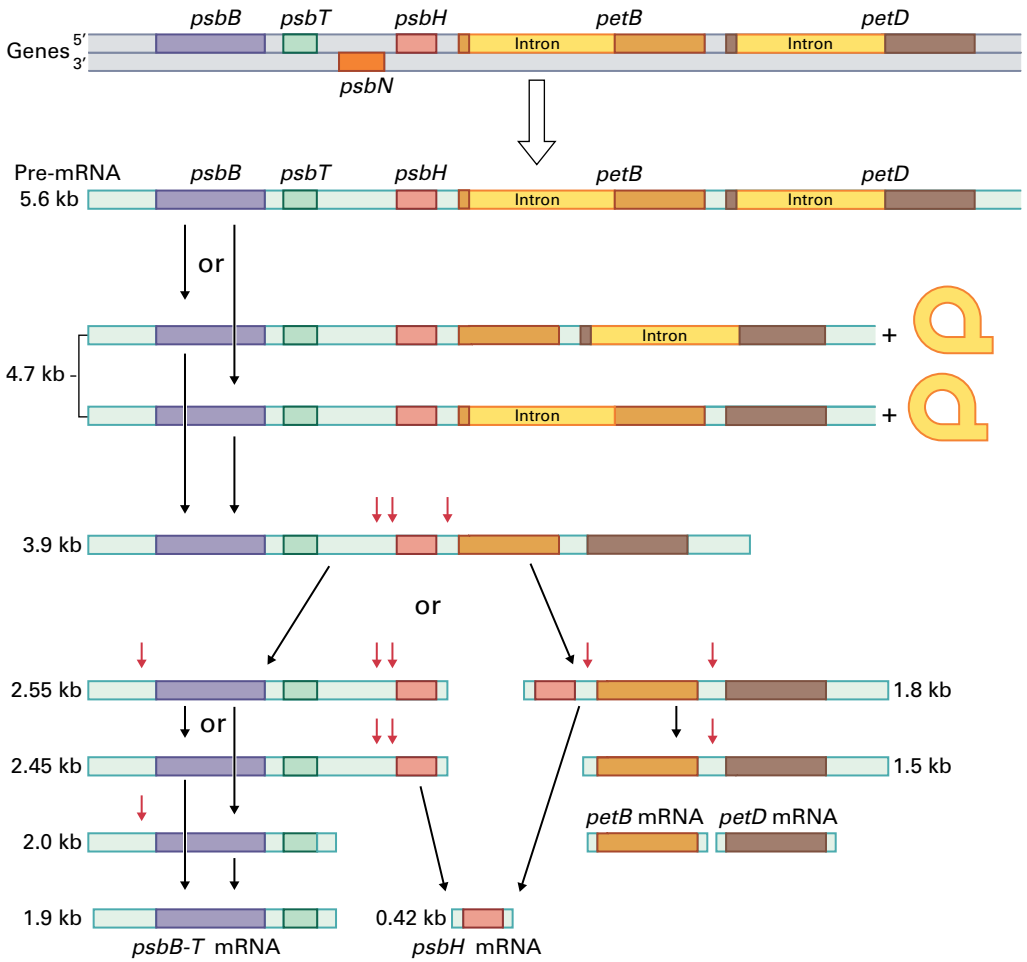


FIGURE 6.50 *The transcript from the* psbB *operon in plant plastids is a typical example of the complex processing and splicing reactions that are required to cleave the polycistronic mRNA precursor into mature monocistronic mRNAs that can be efficiently translated. Black arrows indicate possible alternative processing steps, and red arrows indicate cleavage sites that have been experimentally confirmed. The* psbN *gene is encoded by the opposite DNA strand and, therefore, is not part of the polycistronic transcript.*

polycistronic mRNAs is not well understood, although analysis of mutants that lack chloroplast functions has shown that, in some cases, processing is required for plastid mRNA translation. This suggests some details of the mRNA translation process in plastids differ from those in prokaryotes. With the exception of some closely linked genes, plant mitochondrial protein-coding genes are transcribed into monocistronic mRNAs.

6.8.9 RNA editing occurs in transcripts from plant organelles

RNA editing alters the protein-coding sequence of some mRNAs. This type of processing was first discovered in transcripts from mitochondrial genes of a trypanosome, in which the sequence of the RNA differs from the corresponding DNA sequence. Since then, RNA editing has been found in a number of different genetic systems, including plant mitochondria and chloroplasts.

Two types of RNA editing mechanisms alter primary transcripts: (a) insertion or deletion of nucleotides and (b) nucleotide conversion (i.e., modification or substitution), such as C to U (Table 6.6). Nucleotide insertion and deletion editing was first examined in the mitochondria of trypanosomes (Fig. 6.51A) and the slime mold *Physarum,* where transcripts are often extensively edited by insertion of long stretches of U. Short RNA molecules, called guide RNAs, contain the information required for editing. The guide RNAs are complementary to the edited portions of the mature mRNA. These guide RNAs contain short poly-U sequences at their 3′ end that donate the Us inserted during editing by a mechanism that resembles RNA splicing.

Nucleotide conversions, which occur in transcripts of plant mitochondria and chloroplasts, mammals, viruses, and lower eukaryotes, result in less dramatic changes to the mRNA sequence. Multiple site-specific conversions from C to U (or, rarely, U to C) occur in primary transcripts from both plastid and plant mitochondrial genomes (Fig. 6.51B). The frequency of RNA editing is organelle and gene specific, and the distribution of editing sites appears to be random. In mitochondria, C to U conversion occurs in nearly all protein-coding regions of transcripts. The total number of editing sites per genome has been estimated at 1,200 in wheat (*Triticum*) mitochondria, but only about 30 in the chloroplasts of flowering plants.

Editing of certain plant organellar mRNAs is essential for translation of a correct protein. Most nucleotide conversions change the first or second nucleotide in a codon, thereby altering the amino acid sequence of the protein (Fig. 6.52). Usually the amino acid change results in translation of a more highly conserved protein, as predicted by comparing the DNA sequence of a given gene and its edited mRNA transcript with DNA sequences for the same gene from organisms that do not edit mRNA. In rare cases, RNA editing occurs at the third codon position. Often, as a result of redundancy in the genetic code, such editing is silent and does not modify the predicted protein (see Chapter 9).

Editing can also shorten ORFs predicted from DNA sequences or produce new ORFs. The editing of glutamine codons (CAA and CAG) and the arginine codon (CGA) yields termination codons (UAA, UAG, and UGA), thereby introducing a premature termination of the ORF in both mitochondria and plastids. These edited stop codons generally convert the predicted C-terminal extension of a protein to the conserved protein size. Likewise, a threonine codon (ACG) can be converted to AUG. C to U editing can thus create both an initiation and a termination codon within the same transcript, producing a new ORF. These examples demonstrate that genomic DNA sequencing alone is not always sufficient to predict the products of organellar genes.

Editing processes in plant mitochondria and chloroplasts share certain features: C to U conversion and strong preferences for second codon positions and certain codon transitions. Furthermore, common sequence motifs around the editing sites are found in the transcripts of both organelles. These

TABLE 6.6 *Occurrence of RNA editing.*

Type	Organism	Organelle	Transcript	Modification
Insertion/deletion	Trypanosome	Mitochondria	mRNAs	U insertion/deletion
	Physarum	Mitochondria	mRNAs	C insertion
Conversion	Plants	Mitochondria	mRNAs	C → U, U → C
			tRNAs	C → U
			rRNAs	C → U
		Plastids	mRNAs	C → U, U → C
	Mammals	Nuclei	mRNAs	C → U
	Metazoans	Mitochondria	tRNAs	Various

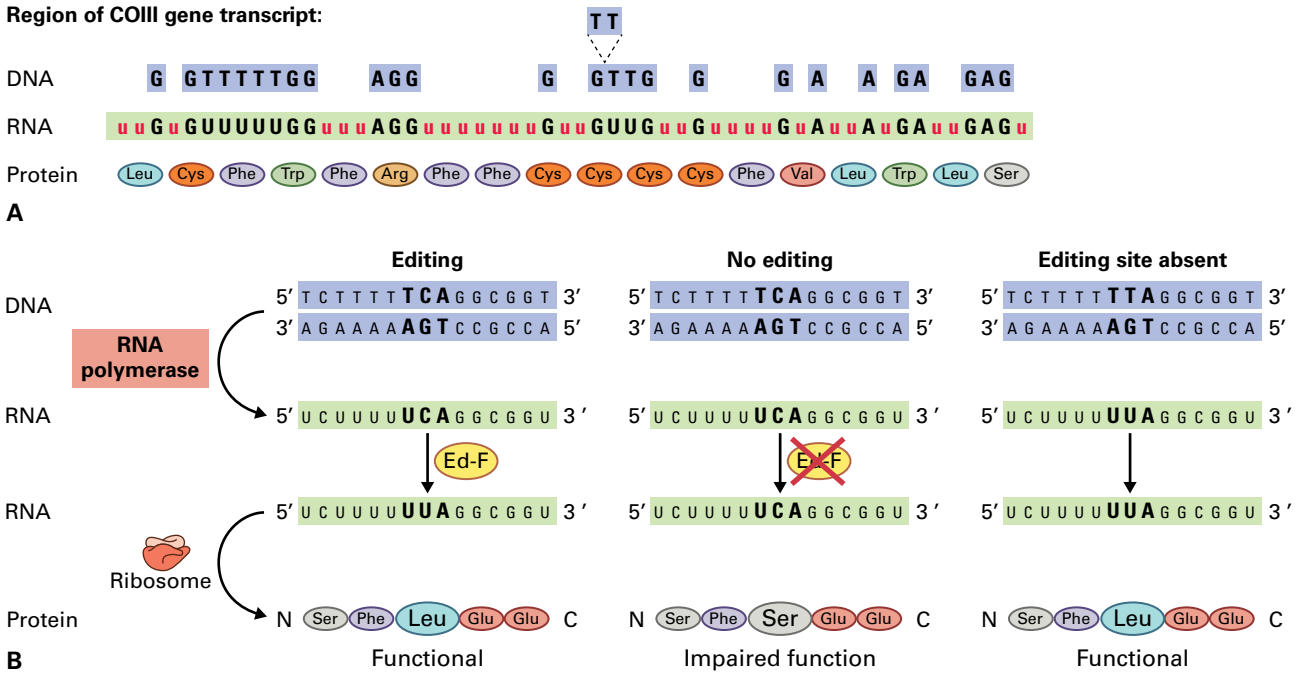


FIGURE 6.51 *RNA editing in protein-coding regions of mitochondrial transcripts from the protozoan* Trypanosome brucei. *(A) Comparison of the DNA sequence (purple) and RNA sequence (green) for the mitochondrial cytochrome oxidase III reveals striking differences. The RNA sequence is made considerably longer than the DNA sequence as the result of RNA editing, in this case the insertion of long stretches of Us. The protein encoded by the edited, mature mRNA has an amino acid sequence resembling the consensus sequence of cytochrome oxidase III proteins. The information required for RNA editing is provided by guide RNAs (not shown), which are complementary to portions of the edited mRNA. (B) RNA editing in chloroplasts of land plants changes specific cytidines into uridines on the RNA level. Often, editing affects TCA-serine codons and converts them into UUA-leucine codons (left panel). Nonediting of an editing site (middle panel) leads to defects usually resembling loss-of-function mutants of the gene whose transcripts remain unedited. Whether amino acids specified by nonedited codons are incorporated into the peptide chain, as depicted here, has not been thoroughly investigated yet. The absence of an editing site, for example a T being present already on the level of DNA (right panel), does not lead to a mutant phenotype.*

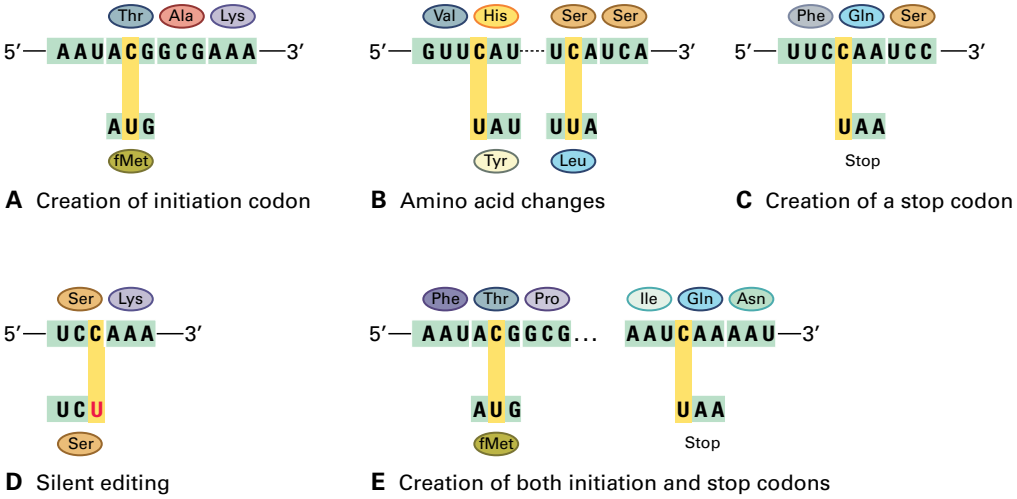


FIGURE 6.52 *Several types of mRNA editing involving base substitutions can significantly alter the polypeptide products encoded by the RNA sequences. Base substitutions can produce translation initiation codons (A), result in amino acid changes (B), or create a stop codon (C), possibly leading to premature termination of translation. Certain base substitutions within coding regions may not alter the amino acid sequence (D), whereas others may introduce initiation and stop codons that result in a new open reading frame (E).*

similarities suggest editing systems in chloroplast and mitochondria share components and perhaps mechanisms, although it is likely organelle-specific factors are also required. RNA editing in chloroplasts does not require translation, indicating that all protein components necessary for editing are encoded by the nuclear genome and imported into the chloroplast.

Summary

Genetic information is encoded in the nucleotide polymer of DNA. The DNA molecule is a double-stranded helix of two complementary strands of nucleotides that form hydrogen bonds between A-T and G-C base pairs. The genetic information is duplicated during DNA replication when DNA polymerases synthesize a new complementary nucleotide polymer, using each of the two parental strands in the double helix as templates. Although DNA is a stable molecule, it sometimes suffers damage from UV light or chemicals, or errors introduced by DNA polymerase during replication. If not repaired, this damage can cause mutations. Several repair mechanisms function to remove damaged nucleotides or incorrectly paired bases. Exchange of genetic information between DNA molecules in chromosomes is an important mechanism that drives evolution and establishes diversity among organisms. Exchange of genetic information occurs during recombination, when double-stranded DNA molecules are broken and rejoined with different DNA molecules. Before the genetic information stored in DNA can be expressed into a collinear sequence of amino acids in proteins, it must be transcribed into RNAs by multiprotein enzyme complexes called RNA polymerases. Plants contain the three well-known types of eukaryotic nuclear RNA polymerase and an additional two that are involved in RNA-directed epigenetic regulation. Chloroplast (and probably mitochondrial) genes are transcribed by prokaryote-type RNA polymerases, which reflects their evolutionary origin. Most RNAs transcribed by RNA polymerases must undergo extensive processing before they can function in the translation of proteins, the formation of ribonucleoprotein complexes such as ribosomes, or the guidance of mRNA degradation systems. The protein-coding regions of many genes are also interrupted by noncoding sequences, called introns, which must be spliced out to produce functional RNAs. In some cases, the genetic information contained in genes differs from the information found in their corresponding RNAs, which have nucleotides added, deleted, or substituted. This RNA editing usually restores cryptic DNA information to produce proteins with evolutionary conserved amino acid sequences.



7

Amino Acids

Gloria Coruzzi, Robert Last, Natalia Dudareva, and Nikolaus Amrhein

Introduction

Amino acids are compounds that contain both an amino group and a carboxyl group, and the term "amino acid" is usually associated with one of the 20 "proteinogenic" amino acids that are incorporated into proteins during translation (Fig. 7.1 and see Chapter 10). In addition to these, plants also make several hundred structurally diverse, nonproteinogenic amino acids with no obvious roles in protein synthesis. The proteinogenic amino acids are L-α-amino acids of the general structure R-CαH(NH_2)COOH, with the exception of proline, which is a cyclic secondary amino acid.

In addition to their role in protein synthesis, amino acids perform essential functions in both primary and secondary plant metabolism. Some amino acids serve to assimilate nitrogen (N) and transport it from sources to sinks, and others serve as precursors to phytohormones, such as indoleacetic acid and ethylene (see Chapter 17), or to an immense variety of secondary compounds involved in the interaction of plants with their abiotic and biotic environments (see Chapters 21 and 22). Traditionally, many amino acid biosynthetic pathways were investigated by researchers interested in plant secondary metabolism; most were originally uncovered in microorganisms and found to be phylogenetically conserved between bacteria, fungi, and plants. Thus, investigation of these pathways in plants appeared to provide few opportunities for original research on topics such as the reaction mechanisms of the respective enzymes.

The progress, however, in plant molecular biology and genome research has allowed questions specific to these pathways in plants to be addressed, such as the regulation of the expression of the isoenzymes involved in amino acid metabolism and their compartmentation, allosteric regulation, and specific functions. These investigations have revealed that amino acid biosynthesis and degradation are dynamic processes controlled by metabolic, environmental, and developmental factors. This chapter highlights examples in which combined molecular, biochemical, and genetic approaches have helped to define the pathways and uncover regulatory mechanisms of amino acid biosynthesis in plants. Knowledge of amino acid biosynthesis in plants has implications for applied research, because several enzymes of amino acid biosynthesis are targets for herbicide action, and a number of genes have been targets in the metabolic engineering of transgenic crop plants.

7.1 Amino acid biosynthesis in plants: research and prospects

7.1.1 Amino acid biosynthesis pathways in plants have been inferred largely from microbial pathways

The carbon skeletons used by plants for amino acid biosynthesis are derived from only a handful of intermediates of glycolysis, photosynthetic carbon reduction, the oxidative pentose phosphate pathway, and the citric acid cycle (Fig. 7.1).

Biochemistry & Molecular Biology of Plants, Second Edition. Edited by Bob B. Buchanan, Wilhelm Gruissem, and Russell L. Jones.
© 2015 John Wiley & Sons, Ltd. Published 2015 by John Wiley & Sons, Ltd.
Companion website: www.wiley.com/go/buchanan/biochem

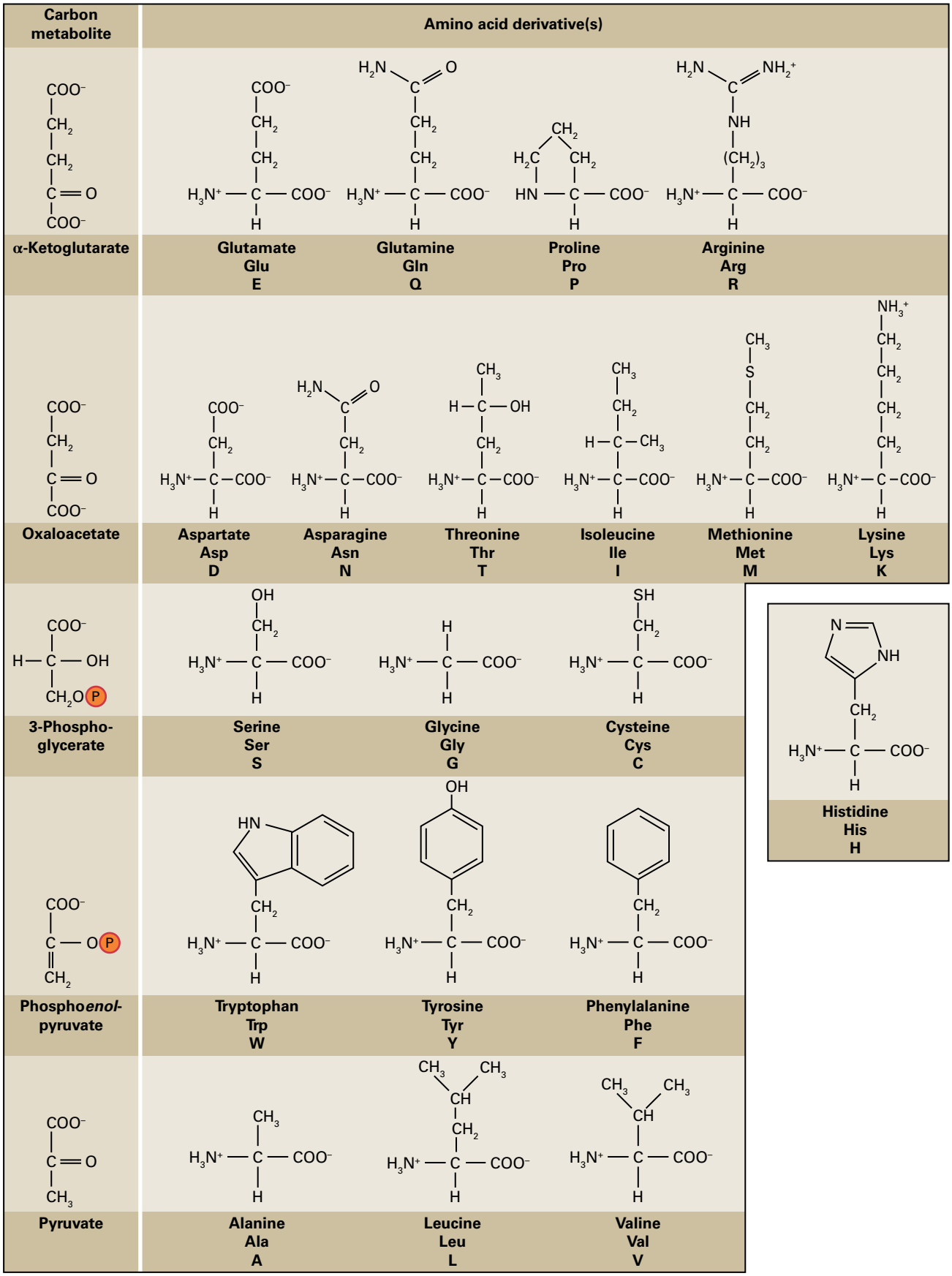


FIGURE 7.1 *Organic acid products of glycolysis, the citric acid cycle, and the Calvin-Benson cycle provide the carbon skeletons from which 19 of the 20 standard amino acids are synthesized. Not shown is erythrose 4-phosphate, a substrate in the synthesis of all three aromatic amino acids, and ribose 5-phosphate, a substrate in both histidine and tryptophan synthesis (see Fig. 7.2). Histidine is a special case, because formation of the carboxyl group is the last step in its biosynthesis. In this scheme, amino acids are arranged in relation to their respective common organic acid precursor. In textbooks of biochemistry, you usually find amino acids arranged with respect to side chain hydrophobicity. Both the one- and three-letter codes, respectively, are indicated.*

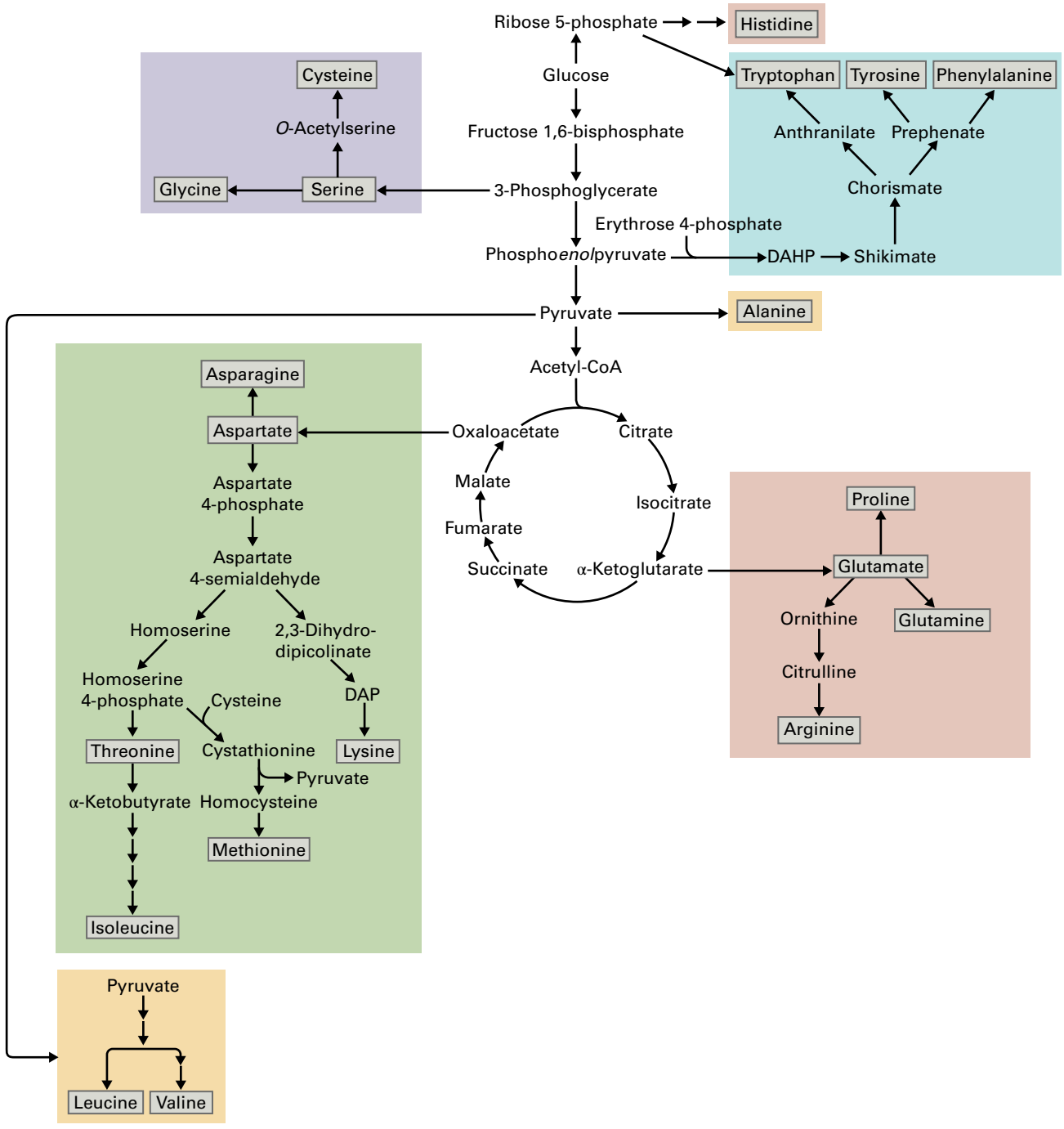


FIGURE 7.2 *Overview of the biosynthesis of the 20 proteinogenic amino acids in plants. Biosyntheses of serine, glycine, and cysteine are referred to in Chapters 14 and 16, respectively. Alanine is derived from the glycolysis intermediate pyruvate in a single transamination step. Ribose-5-phosphate is produced in the oxidative pentose phosphate cycle.*

The pathways generally accepted for amino acid biosynthesis in plants (Fig. 7.2) have been inferred in large part from those defined for bacteria and fungi, and these were identified through the combined use of auxotrophic mutants, isotopically labeled precursors, enzyme studies, and the analysis of the corresponding genes. Historically, the isolation of comparable amino acid biosynthesis mutants in plants was hampered by several factors, including gene redundancy and problems associated with supplementing auxotrophs.

It is not known whether plants use all the enzymatic pathways and control points observed in bacteria and yeast, as some variation also exists within these microorganisms. Indeed, plant amino acid biosynthetic pathways demonstrate levels of complexity not found in microbes. Whereas bacteria possess small genomes and lack organelles, plants may contain multiple genes for each step in a pathway, and sequential or even identical steps may occur in distinct subcellular compartments. In addition, although a number of plant **amino**

acid transporters have been identified, the mechanisms controlling the intra- and intercellular transport of amino acids and their intermediates are poorly understood. Furthermore, it is impossible to predict the in vivo function of an **isoenzyme** based solely on in vitro biochemistry. Plant extracts often contain mixtures of isoenzymes that do not coexist in the same organelle or even cell type within a plant tissue; therefore, the in vitro flux measurements used to define rate-limiting steps in the biosynthetic pathways of unicellular organisms have limited significance for study in multicellular plants.

In recent years, however, several different types of **genetic screens** have identified plant mutants in amino acid biosynthetic enzymes. Additionally, genes homologous to those known to be involved in amino acid biosynthesis, metabolism, and transport in other organisms can be identified in the increasingly available number of sequenced genomes, and their function in vivo can be examined using genetic approaches. Though investigations of amino acid biosynthesis mutants in plants have centered on *Arabidopsis,* progress in genomics, transcriptomics, proteomics, and metabolomics now allows extension of these investigations to crop plants, weeds, medicinal plants, or other species of interest in phylogenetic or ecological contexts.

7.1.2 Amino acid pathways in plants are targets for basic and applied research

Uncovering the features of amino acid biosynthesis unique to plants should stimulate both fundamental and applied research. One goal is to understand the genes that control growth-limiting processes (e.g., the assimilation of inorganic nitrogen into amino acids) and the factors that regulate the synthesis of plant secondary compounds from amino acid precursors. Such studies should also provide a framework for manipulating amino acid biosynthesis pathways in transgenic plants. For example, enzymes in several pathways have been identified as targets for herbicides, and in some cases, the genes encoding these enzymes have been used for engineering herbicide resistance (see Box 7.1). Eventually, insights from amino acid biosynthesis research may also provide enhanced crop resistance to osmotic stress (see Chapter 22), improved food protein composition, and production of pharmaceutically useful compounds. Therefore, the structural and regulatory genes controlling amino acid biosynthesis in plants are of interest not only to biochemists, but also to agricultural biotechnologists.

7.2 Assimilation of inorganic nitrogen into N-transport amino acids

The acquisition of N-containing ions, predominantly **nitrate**, and their conversion to the fully reduced form of inorganic nitrogen, that is, the **ammonium ion**, are described in Chapter 16. Here, we consider the entry of the reduced nitrogen into the amide and amine nitrogen of amino acids.

The initial assimilation products, mainly glutamate and glutamine, fulfill immediate functions as substrates in protein biosynthesis, but they also function in N-transport and readily donate nitrogen to the biosynthesis of amino acids, nucleobases, and a host of other N-containing compounds. Alternatively, nitrogen assimilated into glutamate and glutamine may be incorporated into aspartate and asparagine.

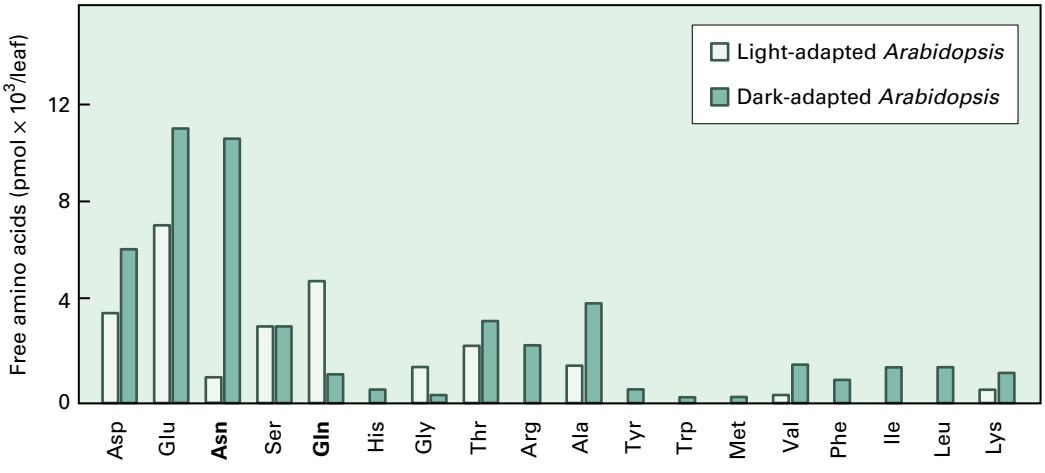


FIGURE 7.3 *Concentrations of free amino acids in light- and dark-adapted* Arabidopsis, *determined by high-performance liquid chromatography. Aspartate, glutamate, asparagine, and glutamine constitute 70% of total free amino acids. Asparagine concentrations are induced dramatically in dark-adapted plants, whereas glutamine concentrations increase in the light. These light-induced reciprocal changes in concentrations of asparagine and glutamine reflect the distinct natures of these amino acids. Glutamine, a metabolically very reactive amino acid, is preferentially synthesized in the light, whereas asparagine, which is relatively inert, is preferentially synthesized in the dark. Asparagine carries more nitrogen atoms per carbon atom than does glutamate and so is a more economical compound to transport nitrogen when carbon skeletons are limiting (in the dark). Increased concentrations of glycine in light-adapted plants result from photorespiration, which produces glycine as a byproduct.*

Aspartate is a metabolically reactive amino acid that serves as the nitrogen donor in numerous **aminotransferase** reactions and is the precursor of a large family of amino acids (see Fig. 7.2); asparagine, on the other hand, is relatively inert and serves primarily as a nitrogen transport and storage compound. Glutamate, glutamine, aspartate, and asparagine are the major amino acids translocated in the phloem, but also the xylem, of most species, including corn (*Zea mays*), pea (*Pisum sativum*), and *Arabidopsis.* Total amino acid concentrations in the phloem are in the range of 100–200 mM and are about tenfold lower in the xylem. Tissue and phloem concentrations of these transported amino acids are not static; they are modulated by factors such as light (Fig. 7.3) and nutritional or developmental stage.

The following sections focus on the enzymes that synthesize N-transport amino acids: **glutamine synthetase** (GS), **glutamate synthase** (GOGAT), **glutamate dehydrogenase** (GDH), **aspartate aminotransferase** (AspAT), and **asparagine synthetase** (AS) (Fig. 7.4). These enzymes are involved in the **primary assimilation** of inorganic nitrogen from the soil as well as in the reassimilation (**secondary assimilation**) of free ammonium within the plant. In plants, ammonium is released from organic compounds during several metabolic processes, including the **deamination of amino acids** during either seed germination or the formation of phenylpropanoid compounds (e.g., lignins), and, in particular, photorespiration in green tissues. Unlike animals, plants do not excrete nitrogenous wastes: the liberated ammonium must be reassimilated to support plant growth. **Photorespiratory ammonium release** (see Chapter 14) may exceed primary nitrogen assimilation by a factor of ten, so a plant unable to recycle ammonium would quickly suffer from severe ammonia toxicity.

7.2.1 The GS/GOGAT cycle is the principal nitrogen assimilation pathway in plants

GS catalyzes the ATP-dependent assimilation of ammonium into glutamine, using glutamate as a substrate, and it functions in a cycle with **GOGAT** (glutamine-2-oxoglutarate aminotransferase), which catalyzes the reductive transfer of the amide group from glutamine to **α-ketoglutarate** (2-oxoglutarate), forming two molecules of glutamate (Fig. 7.5). In the coupled reactions of GS and GOGAT, α-ketoglutarate is reductively aminated to form glutamate, and ATP is hydrolyzed. In fact, GS transfers the terminal phosphoryl group of ATP first to glutamate to form **γ-glutamyl phosphate**, and the activated carboxyl group of this compound then reacts with ammonia to form glutamine. The **GS/GOGAT cycle** is considered the principal route of **ammonium assimilation** in plants.

Distinct isoenzymes of both GS and GOGAT have been identified in all plant species examined. The two GS isoenzymes, GS1 and GS2, have been localized to the cytosol and chloroplast, respectively (Fig. 7.6), but GS2 has also been detected in mitochondria of *Arabidopsis*. The mechanism by which GS2 is directed to either organelle (e.g., through splice variants or alternative use of initiation codons) is unknown, but the mitochondrial GS2 would ensure that ammonia released from glycine during photorespiration is immediately recaptured. Either of two alternative shuttles, an **ornithine–citrulline shuttle** (see Section 7.6.4) or a **glutamine–glutamate shuttle**, may move toxic ammonia in bound form from the mitochondria to the chloroplasts. GS1 is encoded by a small multigene family, and the expression profiles and physicochemical properties of the isoforms differ (see below).

The two major classes of plant GOGAT enzymes are a **ferredoxin-dependent GOGAT** (Fd-GOGAT, found also in cyanobacteria) and an **NAD(P)H-dependent GOGAT** (NAD(P)H-GOGAT); the eubacterial enzyme is NADPH dependent. Subcellular fractionation and identification of plastid-targeting sequences have shown that both Fd-GOGAT and NADPH-GOGAT are plastid localized (Fig. 7.6). Some proteins in the latter class are more active in the presence of NADH than NADPH and are, therefore, termed NADH-GOGAT, which are expressed preferentially in nonphotosynthetic tissues, such as roots.

GS has a high affinity for ammonium and so can operate at the low ammonium concentrations present in living cells (K_m 3–5 μM). Labeling studies that trace the fate of $^{15}NH_4^+$ confirm that the label is incorporated primarily into the amide group of glutamine and then appears in the amino group of glutamate (see Fig. 7.5) and other amino compounds, including glutamine. The addition of GS inhibitors, for example, the glutamate analogs **methionine sulfoximine** or **L-phosphinothricin** (MSO or L-PPT, respectively; Fig. 7.7), inhibit, but do not completely block labeling of the amido group of glutamine and the amino group of glutamate. GS transfers the phosphate group from ATP to MSO, and the phosphorylated product forms an irreversible dead-end complex with the enzyme. This complex has been used to determine the intermediate state structure of GS1 from maize (*Zea mays*) after formation of **γ-glutamyl phosphate** (see above). Maize GS1 has a unique homodecameric structure of ≈400 kDa, whereas bacterial GS are homododecamers. **Phosphinothricin** (also known as **glufosinate**) forms a dead-end complex with GS as well and is used as an herbicide. Another GS inhibitor is **tabtoxinine-β-lactam** (Fig. 7.7) which is produced by plant pathogenic *Pseudomonas syringae* as a phytotoxin. The GOGAT inhibitor **azaserine** (a glutamine analog) blocks incorporation of the radiolabel into glutamate. These results, among others, support the hypothesis that the majority of inorganic nitrogen is assimilated through the GS/GOGAT pathway in plants.

At first glance, the GS/GOGAT pathway with its two coupled reactions and energy consumption looks unnecessarily complicated in comparison with the alternative direct reductive amination of α-ketoglutarate by **glutamate dehydrogenase**, but as discussed in Section 7.2.4, this is not the case.

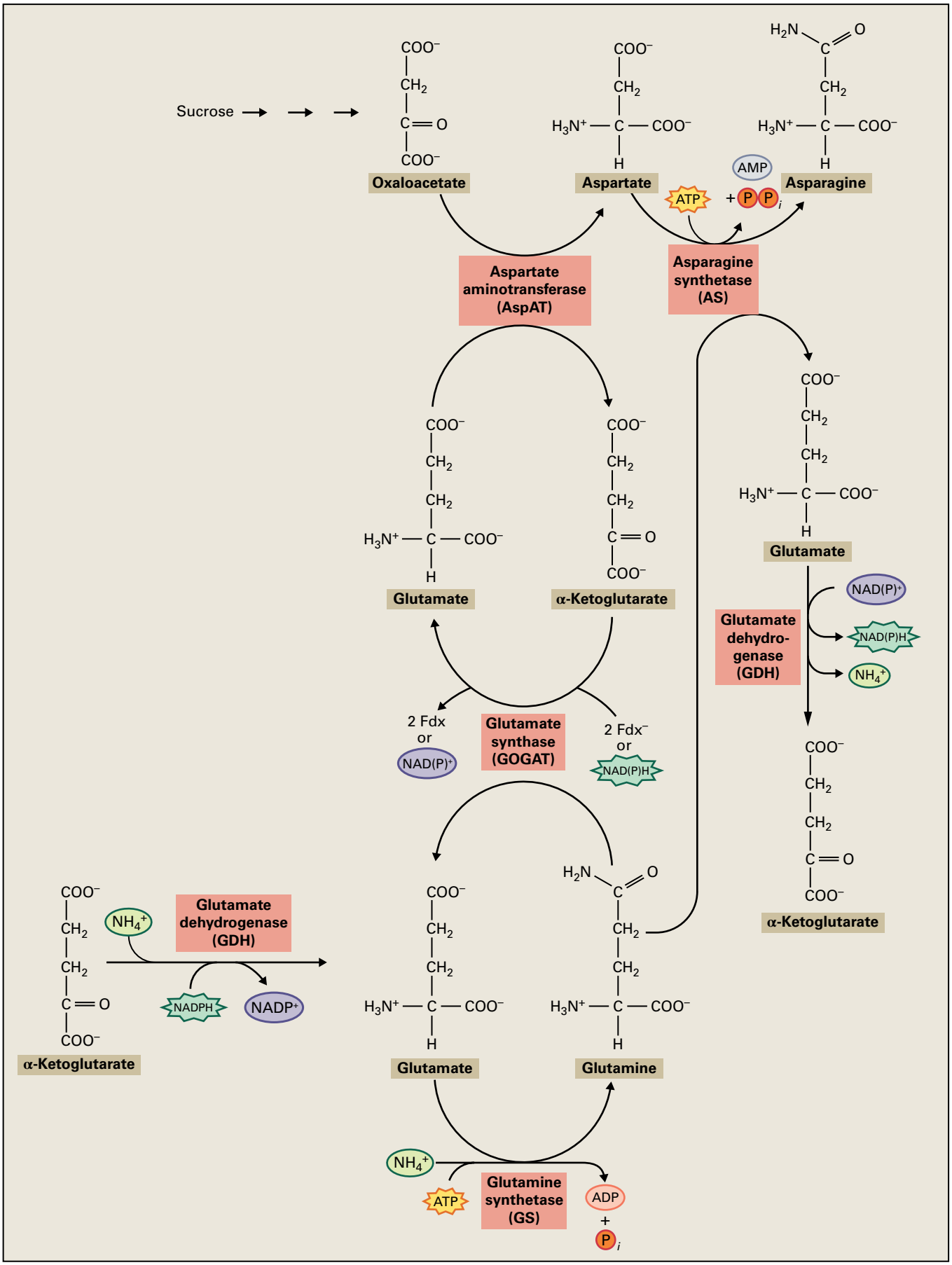


FIGURE 7.4 *An overview of the enzymes that participate in ammonium (NH_4^+) assimilation into the N-transport amino acids glutamate, glutamine, aspartate, and asparagine. Fdx, ferredoxin.*

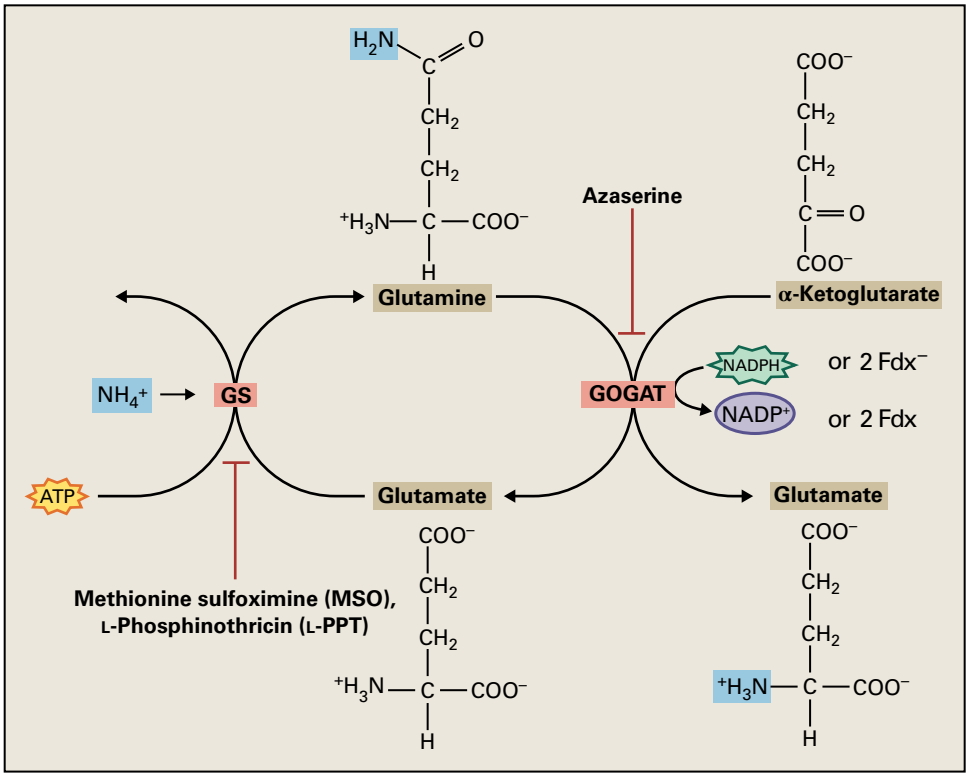


FIGURE 7.5 *The glutamine synthetase–glutamate synthase (GS/GOGAT) pathway is thought to be the principal mechanism of primary and secondary ammonium assimilation. Sites of action are shown for several enzyme inhibitors. Fdx, ferredoxin.*

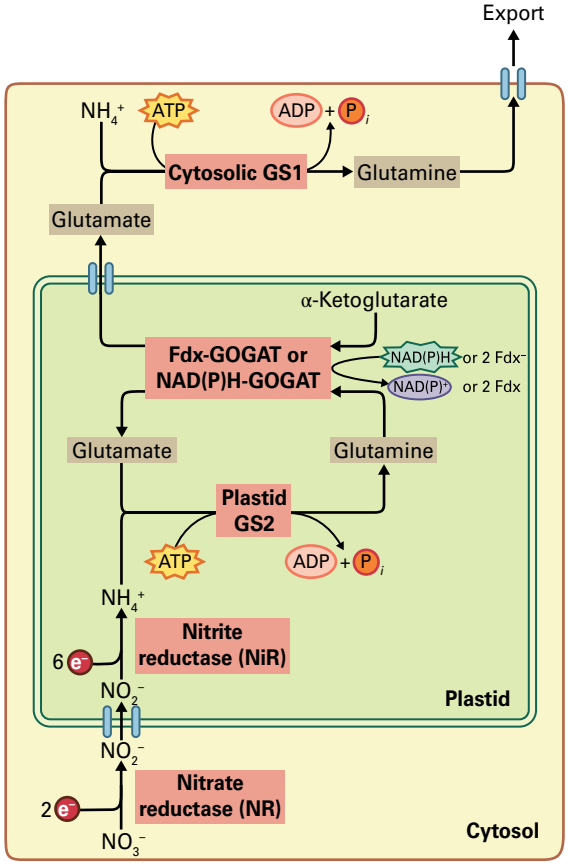


FIGURE 7.6 *Isoenzymes of glutamine synthetase (GS) are present in both the plastids (GS2) and the cytoplasm (GS1). Fdx, ferredoxin.*

7.2.2 Molecular and genetic studies demonstrate that cytosolic and chloroplast GS isoenzymes perform distinct roles in vivo

GS1 and GS2 can be separated by ion-exchange chromatography and so can be assayed and studied individually from plant extracts. Although the biochemical properties of these enzymes do not differ significantly when assayed in vitro, GS1 and GS2 have distinct physiological functions in vivo. GS2 is the predominant isoenzyme in leaves, where it may function both in primary ammonia assimilation and the reassimilation of photorespiratory ammonia. **Cytosolic GS1** isoenzymes are present at low concentrations in leaves and at higher concentrations in roots, suggesting this isoenzyme has a role in primary assimilation in roots. In some nitrogen-fixing legumes, nodule-specific cytosolic GS isoenzymes (termed GSn) assimilate nitrogen fixed by rhizobia (see Chapter 16).

Gene expression analyses carried out in various model and crop plants have revealed specific spatial, developmental, and seasonal patterns for GS1 and GS2. The gene encoding GS2 is expressed in mesophyll cells, whereas the genes for GS1 isoenzymes appear to be expressed specifically in phloem, suggesting that the chloroplast (and perhaps mitochondrial) and cytosolic GS isoenzymes perform distinct functions in vivo. The phloem-specific GS1 likely synthesizes glutamine for long-distance nitrogen transport, whereas GS2 in mesophyll cells is involved in primary nitrogen assimilation (in chloroplasts) or

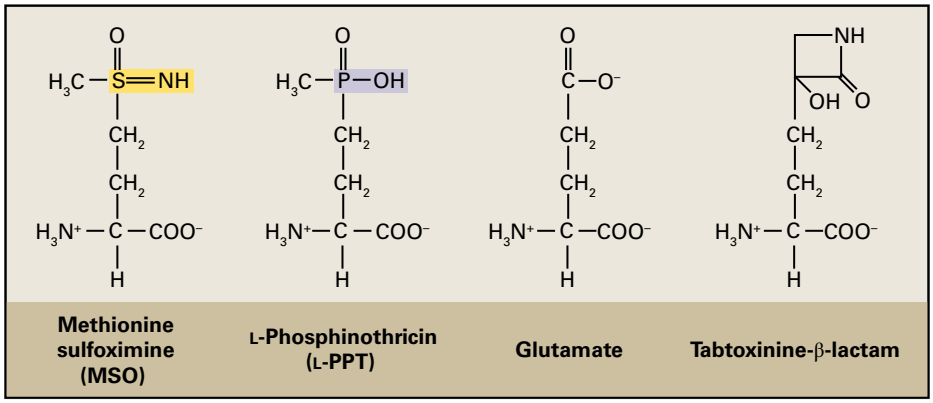


FIGURE 7.7 *Methionine sulfoximine, phosphinothricin, and tabtoxinine-β-lactam are inhibitors of glutamine synthetase. Phosphinothricine is part of the tripeptide bialophos, an antibiotic produced by certain streptomycetes, and tabtoxinine-β-lactam is part of the dipeptide tabtoxin produced by the plant pathogen* Pseudomonas syringae.

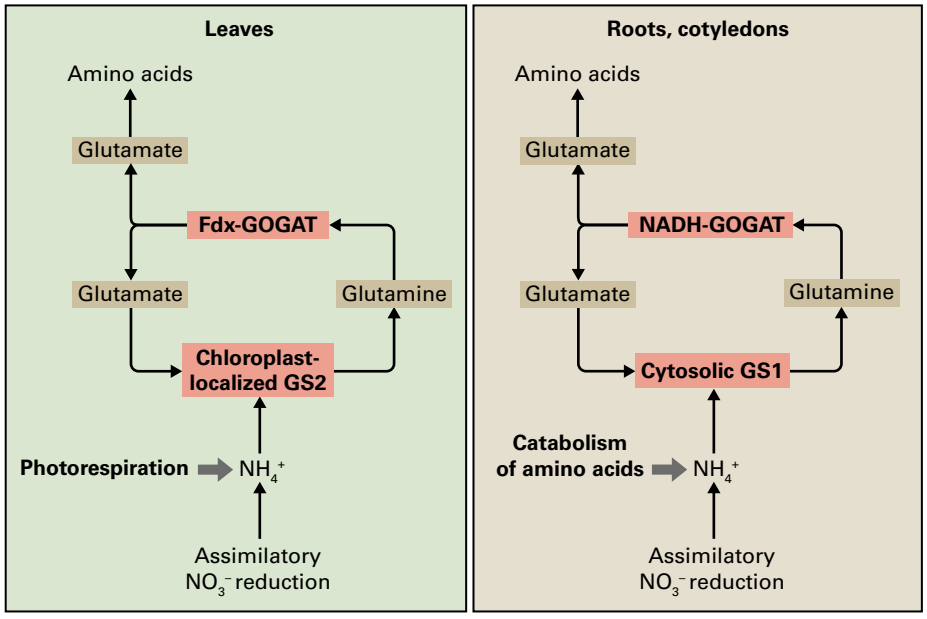


FIGURE 7.8 *NADH-dependent and ferredoxin-dependent isoenzymes (NADH-GOGAT and Fd-GOGAT, respectively) of GS play different physiological roles in plant metabolism.*

the reassimilation of **photorespiratory ammonium** (in chloroplasts and mitochondria). Mutants in chloroplast GS2 display a conditional lethality: they die in air (0.03–0.04% CO_2) but grow in a 1% CO_2 atmosphere that suppresses photorespiration. Thus, the chloroplast/mitochondrial GS2 enzyme is responsible for reassimilating ammonium released by mitochondrial photorespiration. GS1 is unable to compensate for the loss of GS2 function in leaf mesophyll cells of GS2 photorespiratory mutants, but it can take over its function in primary ammonia assimilation.

7.2.3 Mutants indicate a major role for Fd-GOGAT in photorespiration

GOGAT enzymes are flavoproteins containing iron–sulfur (Fe–S) clusters. Eubacterial NADPH-GOGAT has a basic (αβ) subunit structure, in which the **glutamine amidotransferase** activity releases the first glutamate and ammonia. The ammonia is then channeled through a **tunnel** within the α subunit to the oxoglutarate-binding site, where an iminoglutarate is formed. The iminoglutarate is then reduced to the second glutamate; electrons from NADPH arrive from the β subunit via Fe–S clusters and flavin mononucleotide (FMN). Eukaryotic GOGAT enzymes consist of a single polypeptide chain, which in case of NADH-GOGAT seems to have evolved through a fusion of the α and β subunits, while Fd-GOGAT shares similarity only with the α subunit.

In *Arabidopsis*, **Fd-GOGAT** is encoded by two genes (*GLU1* and *GLU2*), and NADH-GOGAT by a single gene (*GLT*). Unlike the situation with GS, all GOGAT isoforms are located exclusively in plastids. Fd-GOGAT is the predominant GOGAT isoenzyme in leaves and accounts for as much as 95–97% of total leaf GOGAT activity. In contrast, the NADH-GOGAT isoenzyme is present in low amounts in leaves, but it constitutes the predominant isoenzyme in non-photosynthetic tissues such as roots, where it has the same expression pattern as GS1. These organ-specific distribution patterns suggest a major role for Fd-GOGAT in primary nitrogen assimilation and photorespiration in leaves, whereas NADH-GOGAT may function predominantly in primary assimilation in the roots (Fig. 7.8). Light (mediated in part by phytochrome), carbon (in particular sucrose), and nitrogen signals, such as nitrate and ammonium, interact in the complex regulation of both Fd- and NADH-GOGAT (Fig. 7.8).

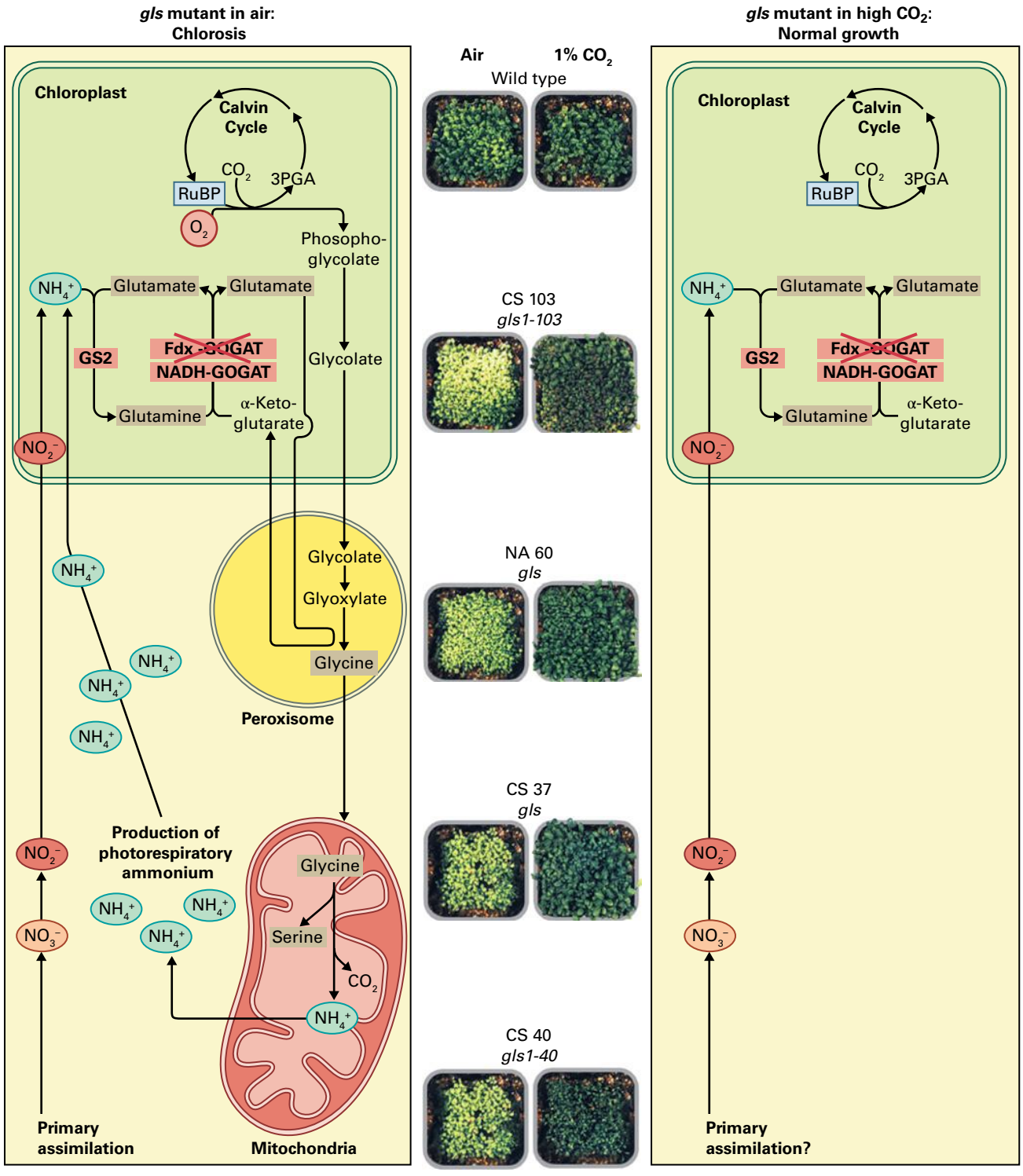


FIGURE 7.9 *Proposed role of Fd-GOGAT in primary nitrogen assimilation and in assimilation of ammonium produced as a byproduct of photorespiration.* gls *(Fd-GOGAT) mutants of* Arabidopsis *demonstrate a chlorotic phenotype when grown in air (0.03–0.04% CO_2), but can tolerate growth in a 1% CO_2 atmosphere that suppresses photorespiration.*
Source: Photographs: Coschigano et al. (1998). Plant Cell 10:741–752.

The importance of Fd-GOGAT in photorespiration can be seen in the *Arabidopsis gluS* mutants of GLU1, in which leaf Fd-GOGAT activity is reduced to less than 5% of wild-type levels (the low amounts of NADH-GOGAT activity detected in wild-type plants remain unaffected). All Fd-GOGAT-deficient mutants have a conditional lethal phenotype: they are chlorotic when grown in atmospheric conditions and are rescued when photorespiration is suppressed (1% CO_2) (Fig. 7.9). This indicates that primary ammonia assimilation is intact, due to the low level of GOGAT activity (<5% of the total activity)

provided by expression of *GLU2* and *GLT*. On the other hand, NADH-GOGAT deficiency in the *Arabidopsis* mutant (*glt1*-T) has only a weak phenotype (in particular, reduction in glutamate levels), and this is not related to impaired photorespiration because the phenotype persists in the presence of 1% CO_2.

7.2.4 Evidence suggests GDH plays primarily a catabolic role

GDH, an enzyme present in nearly all organisms, can catalyze both the synthesis and catabolism of glutamate. In the forward direction, GDH catalyzes the **reductive amination of α-ketoglutarate** using NAD(P)H; in the reverse reaction, it catalyzes the **oxidative deamination of glutamate**, with $NAD(P)^+$ as oxidant, to yield α-ketoglutarate and ammonium (Fig. 7.10). Plants contain two classes of GDH enzymes: an **NADH-dependent GDH** found in the mitochondria, and an NADPH-dependent GDH in the chloroplast.

GDH was long thought to represent a primary route of ammonium assimilation in plants because it is also present in microbes grown in ammonium-rich media. However, the discovery of the GS/GOGAT cycle in plants argued against a major role for GDH in ammonium assimilation. GDH has a high K_m for ammonium (10–80 mM), whereas tissue concentrations of ammonia typically range 0.2–1.0 mM. Furthermore, experiments in which $^{15}NH_4^+$ is fed to plants indicate a precursor–product relationship between glutamine and glutamate, consistent with primary nitrogen assimilation by GS/GOGAT (see Section 7.2.1). Additionally, treatment of plants with the GS inhibitor MSO (see Fig. 7.7) prevents incorporation of ammonium into glutamate and glutamine, even though both GDH activity and ammonium concentrations remain high in the treated plants. The high K_m of GDH for ammonium and its mitochondrial localization suggested this enzyme might instead be involved in reassimilating the large amount of photorespiratory ammonium released in mitochondria; however, screens for mutants in photorespiration did not identify GDH mutants, so any role that GDH plays in photorespiration is probably minor.

It is generally accepted that the primary role for GDH in vivo is in **glutamate catabolism**, for example, in darkness to provide carbon skeletons to fuel the citric acid cycle, or in germinating seeds and senescing leaves, when rates of amino acid catabolism are high (see Chapters 19 and 20). Under these conditions, GDH transcripts and enzyme activities are both upregulated. GDH may, however, play an anabolic role under certain conditions. GDH activity is induced in plants exposed to high concentrations of ammonium, likely as a detoxification mechanism, and possibly under salt stress, when there is a high demand for glutamate-derived proline (see Section 7.6.2), indicating a limited assimilatory role for GDH under conditions of ammonium toxicity (Fig. 7.10).

Energetic considerations may reveal why the GS/GOGAT pathway is preferentially, or almost exclusively, used for ammonia assimilation: in the net reactions catalyzed by GDH and GS/GOGAT, respectively, α-ketoglutarate is reductively aminated to glutamate. The GS/GOGAT reaction consumes ATP, while the GDH reaction does not. Hydrolysis of ATP ensures that glutamate formation in the GS/GOGAT reaction is irreversible, while the equilibrium is unfavorable for glutamate in the GDH reaction.

At least two genes encode GDH in plants, *GDH1* and *GDH2*. As GDH has a hexameric structure, a total of seven isoforms of the holoenzyme can be formed, and these can be separated electrophoretically: the two homohexamers of GDH1 and GDH2, and a total of five GDH1/2 heterohexamers,

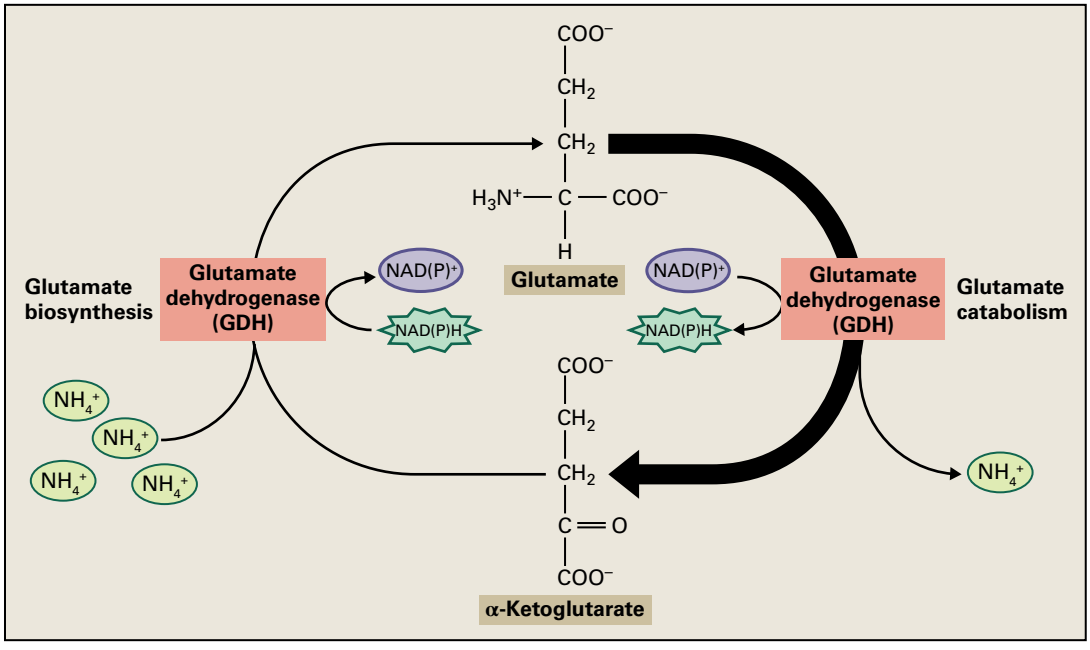


FIGURE 7.10 *GDH is thought to function primarily in glutamate catabolism (deamination), but may produce glutamate when ammonium concentrations are high, primarily as a detoxification mechanism.*

provided *GDH1* and *GDH2* are coexpressed in the same cells. The *gdh1* mutant of *Arabidopsis* displays an impaired growth phenotype under conditions of excess inorganic nitrogen (nitrate + ammonium; Fig. 7.11). The *gdh1/gdh2* double mutant is particularly sensitive to prolonged dark periods, during which plants suffer carbon starvation. Thus, the main function of GDH appears to be the provision of the C_5 carbon skeleton (α-ketoglutarate) of glutamate.

7.2.5 Studies of mutant plants have defined the isoenzymes that control nitrogen assimilation into the N-transport amino acid aspartate

After its initial assimilation into glutamine and **glutamate**, nitrogen can be distributed to many other compounds by **transaminases** or **aminotransferases** (AT). Because glutamate-utilizing transaminations regenerate **α-ketoglutarate**, these reactions permit primary assimilation to continue in the absence of de novo α-ketoglutarate synthesis. In particular, synthesis of **aspartate** regenerates the carbon skeletons required for further nitrogen assimilation by transferring an amino group from glutamate to **oxaloacetate**. Note that two electrons are transferred with the amino group, thus in the course of the transamination the donor of the amino group is oxidized and the recipient of the amino group is reduced. In this way, **aspartate amino transferase (AspAT)** plays a key role in nitrogen assimilation in plants (see Fig. 7.4).

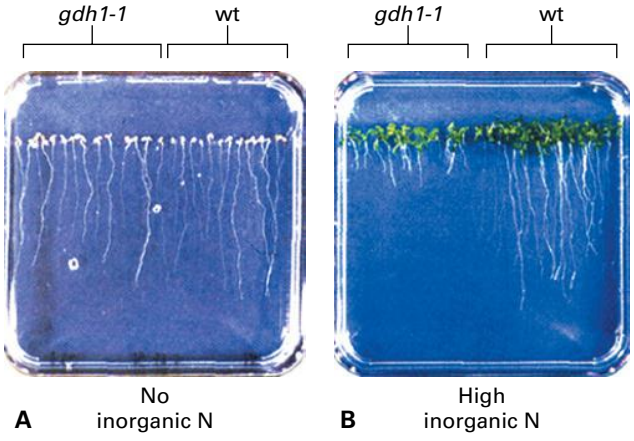


FIGURE 7.11 gdh1-1 *mutant seedlings can grow in the absence of inorganic nitrogen (B), but their growth is inhibited (A) by high nitrogen concentrations (20 mM ammonium plus 40 mM nitrate). Source*: Melo-Oliveira et al. (1996). Proc. Natl. Acad. Sci. USA 93:4718–4723.

In addition, aspartate is active in the transport of carbon and nitrogen within and between cells. In some C_4 plants, aspartate mobilizes carbon and reducing equivalents from the mesophyll to bundle sheath cells (see Chapters 12 and 14). In C_3 plants, the **malate–aspartate shuttle** allows transfer of reducing equivalents from mitochondria and chloroplasts into the cytoplasm (see Chapter 14 for detailed discussion of a similar malate–aspartate shuttle in mitochondria).

AspAT, the best characterized aminotransferase in plants, plays a central role in both aspartate synthesis and catabolism (Fig. 7.12). AspAT, also known as **glutamate:oxaloacetate aminotransferase (GOT)**, is a **pyridoxal phosphate**-dependent enzyme, like all transaminases (Fig. 7.13). The ability of AspAT to interconvert these important carbon and nitrogen compounds places it in a key position to regulate plant metabolism.

In line with the fact that aspartate is used to transfer carbon, nitrogen, and reducing equivalents between intracellular compartments, isoenzymes of AspAT have been localized to four cellular compartments: the cytosol, mitochondria, chloroplasts, and peroxisomes. In *Arabidopsis,* the entire gene family of AspAT isoenzymes has been characterized, and mutants of the two major AspAT isoenzymes (cytosolic AAT2 and plastid AAT3) have been identified. The *aat2* mutant plants are small, and they have greatly reduced content of free aspartate in the light and decreased asparagine content in the dark. It appears that aspartate produced during the day under control of AAT2 is converted to asparagine in the dark. The function of AAT3 has not been defined, because the *aat3* mutant has no visible phenotype. This is likely due to the activity of a recently identified nuclear-encoded novel prokaryotic-type AAT (PT-AAT) that is localized to chloroplasts in *Arabidopsis*, rice (*Oryza sativa*), and pine (*Pinus* sp.). It has been proposed, but needs to be substantiated, that AAT3 is primarily involved in shuttling reducing equivalents, while PT-AAT provides aspartate for the biosynthesis of the **aspartate-derived amino acids** threonine, lysine, and methionine, which occurs in the plastid (see Section 7.4.1). The lack of a visible phenotype of the *aa3* mutant plants is, therefore, likely due to the presence of PT-AAT.

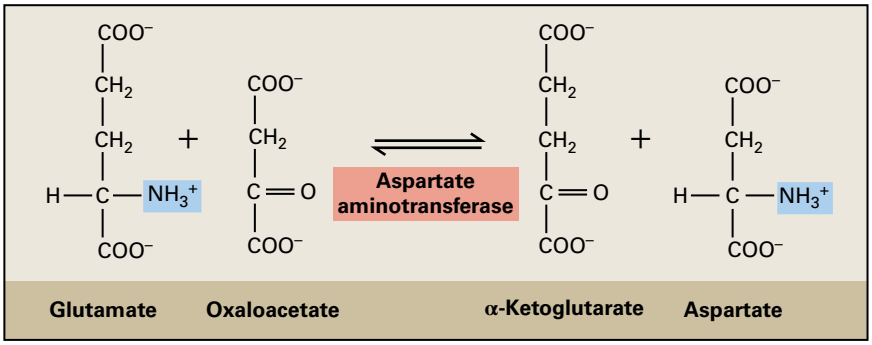


FIGURE 7.12 *Aspartate aminotransferase catalyzes the reversible transamination of oxaloacetate by glutamate to yield α-ketoglutarate and aspartate.*

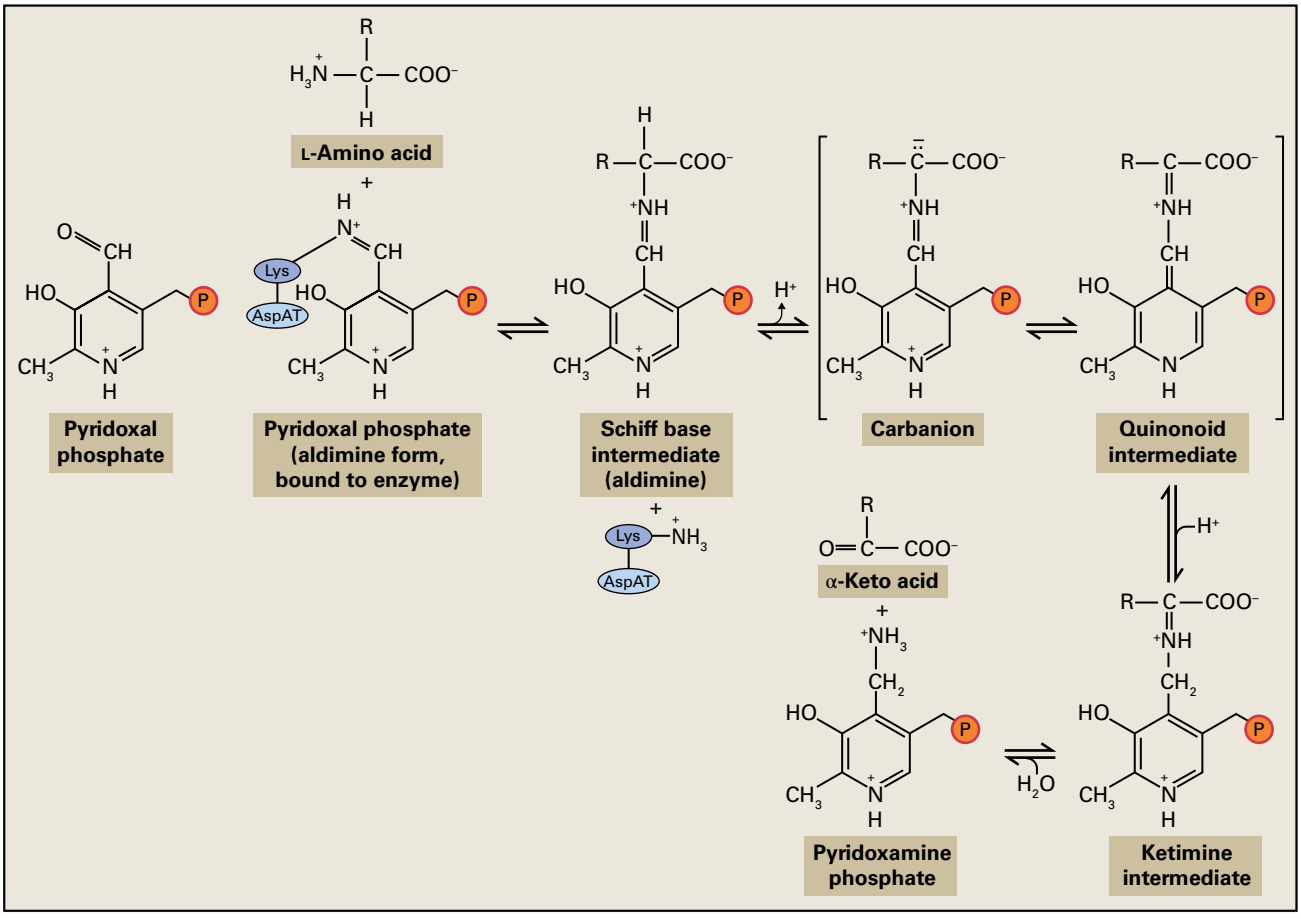


FIGURE 7.13 *Pyridoxal phosphate mechanism/Schiff base formation. The deamination half-reaction catalyzed by a transaminase is diagrammed from left to right. In the case of AspAT, the L-amino acid substrate at left is glutamate, and the α-keto acid product at right is α-ketoglutarate. Note the carbanion (in the brackets) is formed by deprotonation of the α-C of the bound amino acid, and the pyridinium N serves as an electron sink driving the formation of the quinonoid intermediate. Reprotonation gives rise to a ketimine, which is then hydrolyzed to form the α-keto acid and pyridoxamine phosphate. The subsequent amination half-reaction reverses the steps from right to left. For AspAT, the α-keto acid substrate at right is oxaloacetate, and the L-amino acid product to the left is aspartate. Pyridoxal phosphate also participates in racemization and decarboxylation of amino acids (not shown), forming similar carbanion and quinonoid intermediates.*

7.2.6 Light represses the biosynthesis of asparagine, an amino acid used for N-transport and storage

Amidation of aspartate by glutamine or ammonia yields asparagine, an inert amino acid used to store nitrogen and transport it from sources to sinks. Asparagine is the major nitrogenous compound detected in the phloem of several legumes, with concentrations as high as 30 mM. Crystallized out of **asparagus** extracts almost 200 years ago, asparagine was actually the first amino acid discovered. In the early 1800s, it was already known that this compound, which gives the distinct flavor to white asparagus, increases in the dark, while the formation of woody tissue is suppressed in this condition. Thus, etiolated asparagus is both tasty and soft. Asparagine is converted to **acrylamide** (a compound that is of concern as a carcinogen) during the heating of starchy food to high temperatures, as in the frying of French fries and potato chips.

The enzymology of asparagine biosynthesis in plants has been complicated by the instability of the enzyme.

In prokaryotes, separate genes, *asnA* and *asnB*, encode structurally distinct ammonium- and glutamine-dependent **asparagine synthetases** (ASs), respectively, whereas in plants, only genes encoding glutamine-dependent AS have been identified. The plant AS catalyzes the ATP-dependent transfer of the amido group from glutamine to aspartate, generating glutamate and asparagine (Fig. 7.14A). Note that AS releases pyrophosphate (PP_i) from ATP, so the activated intermediate in the amidation reaction is the adenylate, that is, **aspartyl AMP**, rather than the respective phosphate, as in the case of glutamine biosynthesis (see Section 7.2.1). Thus two energy-rich bonds are eventually cleaved in the amidation of aspartate. Although glutamine is the preferred substrate for nearly all of the AS enzymes studied in plants, some evidence indicates that ammonium-dependent asparagine synthesis may also occur (Fig. 7.14B). K_m values for ammonium, however, are more than 10-fold higher than in the case of glutamine

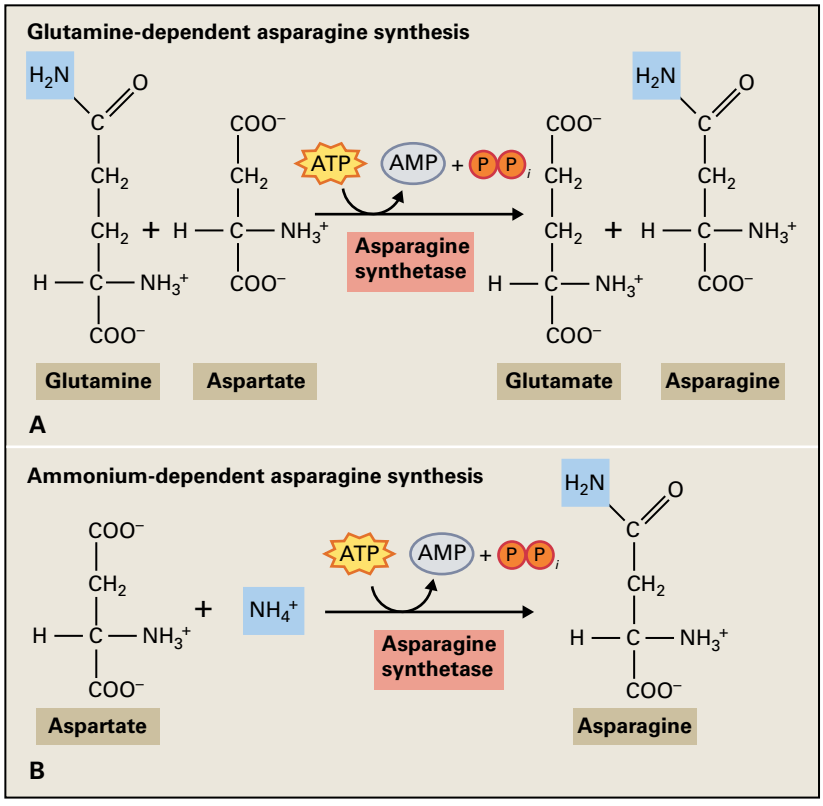


FIGURE 7.14 *Asparagine synthetases from plants preferentially use glutamine as a nitrogen donor (A), but can catalyze the assimilation of inorganic nitrogen when ammonium is plentiful (B).*

synthesis, and tracer studies with $^{15}NH_4^+$ have shown that glutamine is labeled efficiently, so the direct amidation of aspartate does not appear to occur at significant rates in vivo unless plants may encounter toxic concentrations of ammonium.

The genes encoding AS in *Arabidopsis* are differentially expressed: AS encoded by *ASN1* appears to be primarily involved in nitrogen mobilization during seed germination and in nitrogen remobilization in senescing leaves, while the enzyme encoded by *ASN2* is involved in nitrogen remobilization under stress conditions.

7.2.7 Light and carbon metabolism regulate the assimilation of nitrogen into amino acids

The incorporation of inorganic nitrogen into the assimilatory amino acids glutamate, glutamine, aspartate, and asparagine is a dynamic process that is regulated by external factors, such as light, and by internal stores of carbon and nitrogen metabolites. As early as the 1850s, studies showed that asparagine concentrations are dramatically influenced by light in several plant species (see Section 7.2.7). Later, it was found that the asparagine content of phloem exudates and the amount of AS enzyme activity are negatively regulated by light or by sucrose, and they increase during dark adaptation, while glutamine shows the opposite behavior (see Fig. 7.3).

Expression of the genes controlling assimilation of inorganic nitrogen into amino acids is subject to control by both light and metabolic factors. For example, genes for **nitrate reductase** and **nitrite reductase** are induced by light and by sucrose (Chapter 16). Similarly, light upregulates the expression of genes involved in ammonium assimilation into glutamine and glutamate, particularly that of chloroplast GS2 and Fd-GOGAT. By contrast, light represses the expression of genes for AS. In all three cases, this transcriptional regulation is mediated, at least in part, by the plant photoreceptor **phytochrome** (Chapter 18). Additionally, the light-driven synthesis of carbohydrates also affects the expression of genes involved in nitrogen assimilation. Sucrose or glucose can at least partially substitute for light in inducing the expression of genes for GS2 or Fd-GOGAT, as demonstrated in tobacco (*Nicotiana tabacum*) and in *Arabidopsis*. In contrast, sucrose represses the expression of AS genes when supplied to dark-adapted maize explants or to whole *Arabidopsis* plants. The effects of sucrose on GS/AS gene expression can be antagonized by amino acids. Sucrose induction of GS expression is repressed by amino acids, whereas amino acids relieve sucrose repression of AS gene expression.

Based on the reciprocal effects of carbon and organic nitrogen on the expression of GS2 and ASN1, a metabolic control model has been proposed (Fig. 7.15). In this model, GS2 expression is induced by light or when carbon skeletons required for ammonia assimilation are abundant. Thus, in the light, nitrogen is assimilated and transported as metabolically reactive **glutamine**, a substrate in numerous anabolic reactions. In contrast, ASN1 expression is induced when darkness prevents photosynthetic carbon reduction, or when concentrations of organic nitrogen are high relative

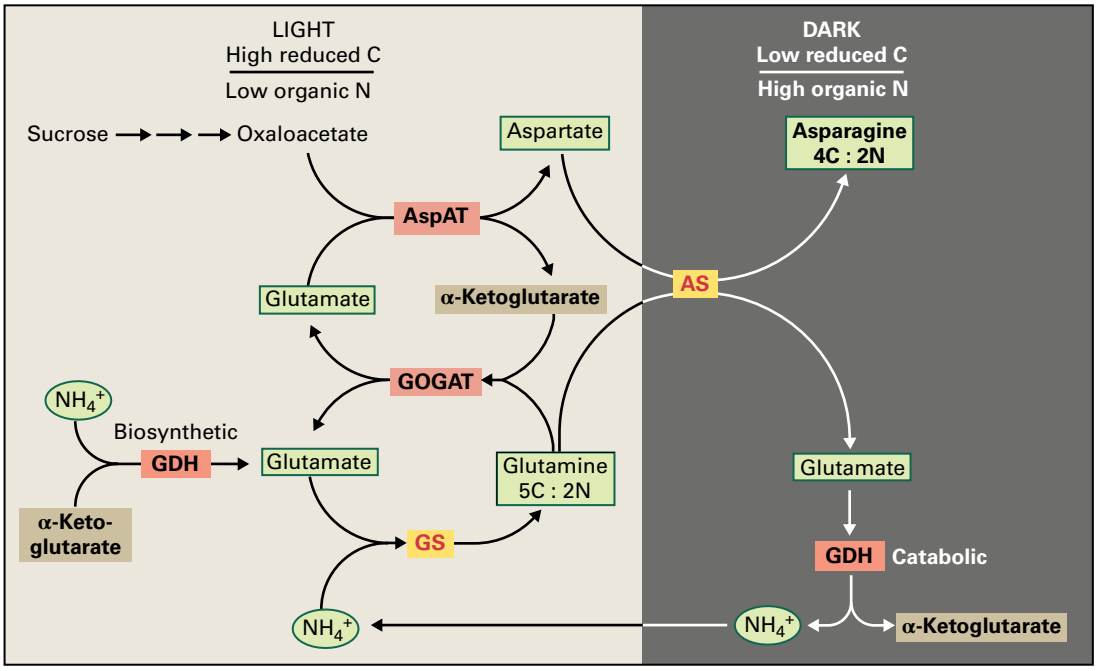


FIGURE 7.15 *Synthesis of glutamine and asparagine is sensitive to light and to the availability of reduced carbon. Expression of plastid-localized GS is upregulated by light or sucrose, promoting formation of the metabolically reactive nitrogen donor, glutamine. AS is inhibited by light or sucrose, and this inhibition can be released by increasing the concentration of amino acids in plant tissues. Darkness promotes AS expression and enhances synthesis of the inert nitrogen storage compound, asparagine. Note that asparagine represents a more efficient use of reduced carbon than glutamine does: Both amino acids bind two nitrogen atoms, but glutamine contains five carbon atoms, asparagine four.*

to those of carbon. Thus, under conditions of low carbon availability or high organic nitrogen, plants direct assimilated nitrogen into inert **asparagine**, which has a higher N:C ratio than glutamine and, therefore, can transport and store nitrogen more efficiently when carbon skeletons are limiting.

7.3 Aromatic amino acids

All living cells require the **aromatic amino acids** phenylalanine, tryptophan, and tyrosine for protein biosynthesis. In plants, the aromatic amino acid pathways also provide precursors for the production of numerous aromatic primary and secondary metabolites, such as plant hormones (the auxin, indole-3-acetic acid, and salicylic acid), pigments (anthocyanins), volatiles, defensive phytoalexins (see Chapter 21), feeding deterrents (tannins), UV protectants (flavonoids), signal molecules (isoflavonoids), bioactive alkaloids, and structural components (lignin, suberin, and cell wall-associated phenolics) (Fig. 7.16; see also Chapter 24). The importance of these pathways in plants is underscored by the fact that about 30% of the fixed carbon can flow through the common aromatic amino acid pathway, largely to make **lignin** (Chapters 2 and 24). Owing to their pharmacological and biological activities, aromatic amino acid-derived plant natural products are widely used in medicine (e.g., condensed tannins and morphine) and as food supplements (e.g., flavonoids and tocopherols) (see Chapter 24). The aromatic amino acid pathways are absent in animals; the enzymes of these pathways, therefore, became targets for the development of antibiotics against human and animal pathogens and plant herbicides.

7.3.1 Synthesis of chorismate constitutes the common aromatic amino acid pathway

Chorismic acid, the final product of the **shikimate pathway**, is the last common precursor in the synthesis of the three aromatic amino acids (**phenylalanine, tryptophan**, and **tyrosine**) as well as ***p*-aminobenzoic acid** (a precursor for the C_1 carrier tetrahydrofolate), the electron transport cofactor phylloquinone, other naphtho- and anthraquinones (see Chapters 12 and 14), and **salicylic acid** (see Chapter 17). Plastids have a prominent function in this biosynthesis, because a full set of the shikimate pathway enzymes has been localized to these organelles, while the occurrence of a full set of extraplastidial shikimate pathway enzymes has not been proven.

The seven-step synthesis of **chorismate** via the shikimate pathway (Fig. 7.17) begins with the condensation of two intermediates of carbohydrate metabolism, **phospho*enol*pyruvate** (PEP) from glycolysis and **erythrose 4-phosphate** from the pentose phosphate pathway (Chapter 13). This reaction is catalyzed by **3-deoxy-D-*arabino*-heptulosonate-7-phosphate (DAHP) synthase**. Based on the absence or presence of certain domains in the protein as well as amino acid sequence similarity, DAHP synthases have been classified into two types (type I and II) with less than 10% sequence identity. *E. coli* DAHP synthase belongs to the **type I DAHP synthase** family with molecular masses less than 40 kDa. Type II enzymes (≈50 kDa)

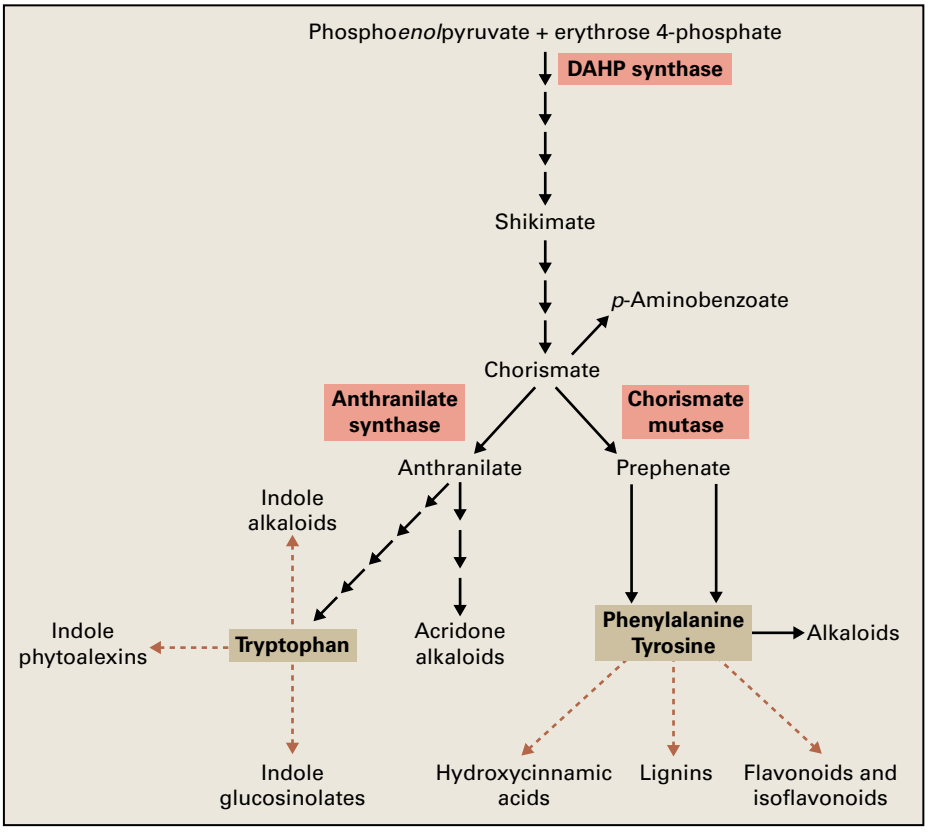


FIGURE 7.16 *Synthesis of the aromatic amino acids in plants. In addition to their functions in proteins, phenylalanine, tyrosine, and tryptophan serve as precursors for the synthesis of numerous primary and secondary metabolites.*

were first identified in plants, but were later also identified in some microorganisms. As more sequenced genomes became available, it appeared the **type II DAHP synthase** family contains a subset of plant enzymes that are clustered within a more divergent set of microbial enzymes.

High-resolution protein crystal structures have been determined for both types of enzymes and revealed similarities in tertiary structure and function between them. In fact, all DAHP synthases have a core $(\beta/\alpha)_8$ barrel monomer structure, and the key residues that interact with phospho*enol*pyruvate and the required divalent metal ion (Mn^{2+}) are conserved and positioned almost identically in both types, despite their minimal sequence identity. This common active site architecture and chemistry suggest that type I and type II enzymes evolved from a common ancestor. Type I and II DAHP synthases appear to differ in the possession of peripheral small domains (type II) that decorate the core $(\beta/\alpha)_8$ fold and are responsible for **aromatic amino acid-mediated allosteric regulation**.

In contrast to microbial enzymes, plant DAHP synthases are not feedback-inhibited by any of the aromatic amino acids, with the possible exception of those from maize and pea, which are feedback inhibited by tryptophan and tyrosine, respectively. Given that plant DAHP synthases contain domains that in microorganisms function as aromatic amino acid-binding elements, the correct conditions or combinations of aromatic amino acids that affect plant DAHP synthase activity may not have been found yet. Despite the divergence in their primary sequence and differences in regulatory properties, the plant enzyme can substitute for a defective *E. coli* or yeast enzyme and restore prototrophy.

Plants appear to contain two DAHP synthase genes (*DAHPS1* and *DAHPS2*) that are differentially expressed, suggesting they have distinct functions in vivo. *DAHPS1* is strongly induced in response to wounding and pathogen infection, whereas *DAHPS2* is constitutively expressed. In addition to plant DAHP synthases, which require Mn^{2+}as cofactor, a Co^{2+}-dependent DAHP synthase activity has been detected in the cytosol of several plant tissues. However, the corresponding protein has not been isolated; hence, its substrate specificity is unknown. Likewise, the corresponding gene(s) have not been identified, and the physiological function of this activity is currently unknown.

The second enzyme of the shikimate pathway, **3-dehydroquinate synthase**, catalyzes the cyclization step to a cyclohexane ring, which eventually becomes the benzene ring of the aromatic amino acids (see Fig. 7.17). The activity requires Co^{2+} and NAD^+ as cofactors (even though the overall reaction is redox neutral), and the plant enzyme has a K_m of 25 μM for DAHP. The conversion of DAHP to 3-dehydroquinate by the plant enzyme likely proceeds through the same five consecutive steps identified in the reaction sequence of the bacterial enzyme: alcohol oxidation, β-elimination of inorganic phosphate, carbonyl reduction, ring opening, and intramolecular aldol condensation. The crystal structure of a bacterial 3-dehydroquinate synthase revealed that the enzyme performs

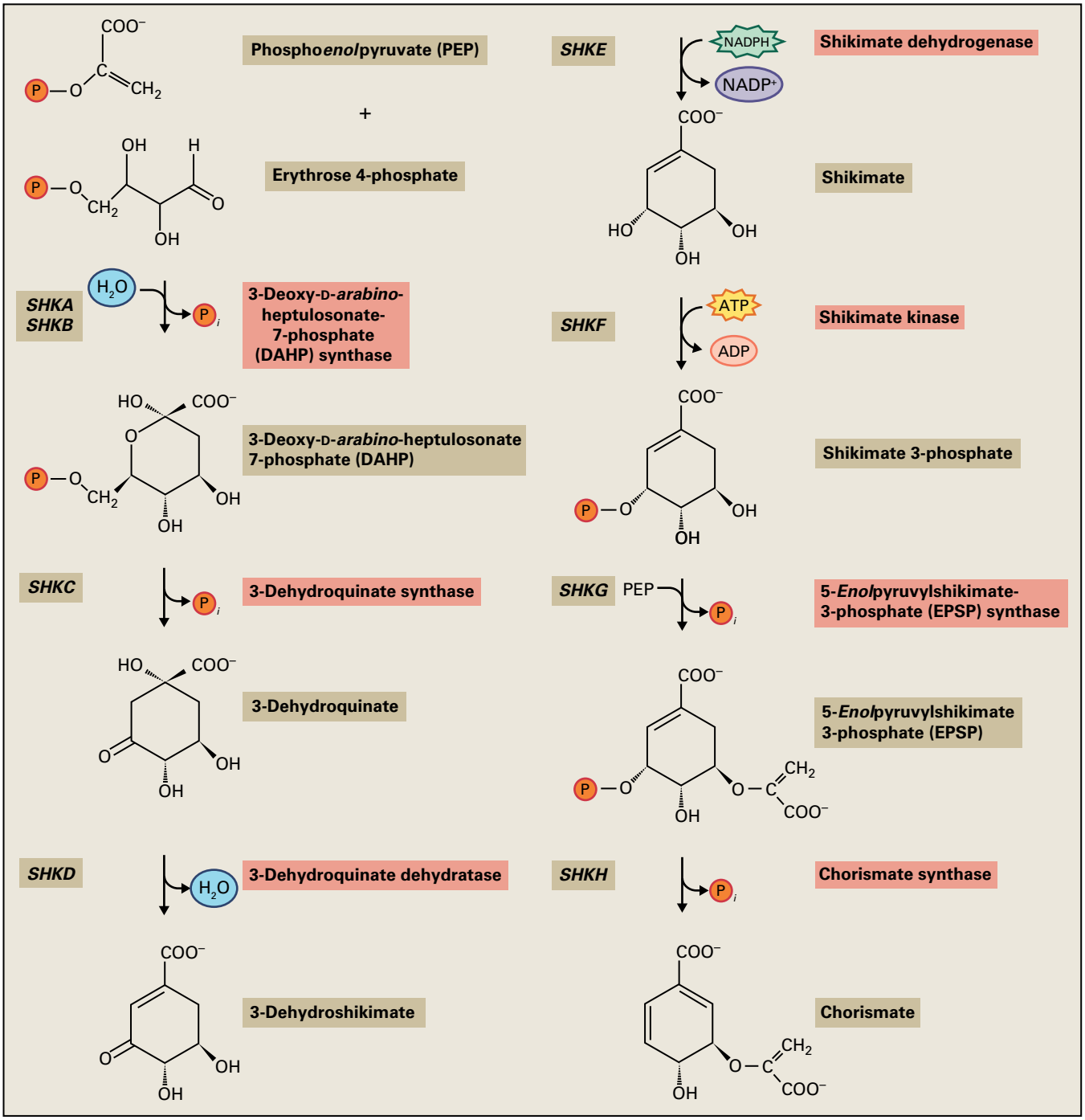


FIGURE 7.17 *Chorismate biosynthesis from phosphoenolpyruvate and erythrose 4-phosphate. The abbreviations* SHKA *through* SKKH *are notations proposed for the genes encoding shikimate pathway enzymes in plants.*

this multistep catalysis in a single active site without forming byproducts. A plant gene encoding 3-dehydroquinate synthase has been isolated from tomato (*Solanum lycopersicum*) by complementation of an *E. coli aroB* mutation that causes 3-dehydroquinate synthase deficiency. This single-copy gene is highly expressed in tomato roots, and its expression is induced by elicitor treatment in suspension culture cells. Plant and *E. coli* (AroB) 3-dehydroquinate synthases are monofunctional enzymes, while those from fungi are part of a pentafunctional **AROM complex** that catalyzes five consecutive reactions of the shikimate pathway, that is, the conversion of DAHP to 5-*enol*pyruvylshikimate 3-phosphate.

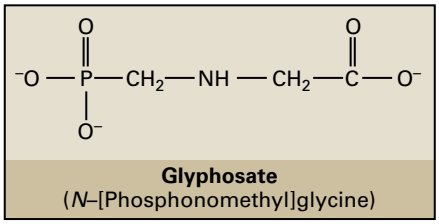
The third and fourth reactions in the shikimate pathway include the dehydration of 3-dehydroquinate to introduce the first double bond in the ring and form **3-dehydroshikimate**, which is subsequently reduced to **shikimate** at the expense of NADPH. 3-**Dehydroquinate dehydratase** (also known as **dehydroquinase**) and **shikimate dehydrogenase**

(also known as **shikimate:NADP$^+$ oxidoreductase**) catalyze these respective reactions, and their activities are found on a bifunctional enzyme in plants. This combined activity has been purified to homogeneity from spinach (*Spinacia oleracea*) chloroplasts. The specific activity of the first enzyme, 3-dehydroquinate dehydratase, is 10% of that of shikimate dehydrogenase, which presumably helps to efficiently convert 3-dehydroshikimate to shikimic acid. This assumption is supported by the observation that, in the crystal structure of the *Arabidopsis* enzyme, the active sites of 3-dehydroquinate dehydratase and shikimate dehydrogenase are proximal and face each other, obviously to facilitate optimal local 3-dehydroshikimate concentration for effective shikimate dehydrogenase catalysis. Many plant species, including *Arabidopsis*, contain a single gene encoding 3-dehydroquinate dehydratase-shikimate dehydrogenase. The only known exception is tobacco (*Nicotiana tabacum*), whose genome possesses two genes encoding functional plastid and cytosolic enzymes. The function of the cytosolic protein remains to be determined.

The fifth step in the pathway is catalyzed by **shikimate kinase**, which phosphorylates shikimate at the 3-hydroxyl, using ATP as a co-substrate, to produce **shikimate 3-phosphate** (Fig. 7.17). Shikimate kinases belong to the family of nucleoside monophosphate (NMP) kinases and are composed of four domains: the core, lid, shikimate- and NMP-binding domains. Although plant shikimate kinases share at most 30% identity with their bacterial counterparts and are approximately 10 kDa larger, comparison of their crystal structures reveals high conservation in the architecture of the enzyme active site between plants and microbes. Similar to bacterial enzymes, plant shikimate kinases are controlled primarily by the cellular energy status (**energy charge**: the relative concentrations of ATP, ADP, and AMP in the cell).

Plant genomes contain variable numbers of genes encoding shikimate kinases: one in tomato (*Solanum lycopersicum*), two in *Arabidopsis,* and three in rice (*Oryza sativa*), among others. In *Arabidopsis*, the two shikimate kinase isoforms AtSK1 and AtSK2 exhibit differential expression profiles. AtSK1 is coexpressed with stress response-related genes, and its expression is induced more than tenfold in response to heat stress. In contrast, AtSK2 is coexpressed with genes involved in processes directly associated with the shikimate pathway, including amino acid and secondary metabolism. The AtSK1 and AtSK2 proteins have almost identical structures; however, their biophysical properties are distinct. AtSK1 forms a homodimer and remains stable at elevated temperatures (37°C), whereas AtSK2 exists as a monomer and is rapidly inactivated at high temperatures. Screening of plants with deficiencies in AtSK1 and AtSK2, respectively, for metabolic or growth phenotypes in response to heat stress should facilitate detailed investigation of the functions of these enzymes in vivo.

The penultimate enzyme of chorismate biosynthesis, **5-*enol*pyruvylshikimate-3-phosphate (EPSP) synthase**, catalyzes the reversible production of EPSP and phosphate from shikimate 3-phosphate and PEP. EPSP synthase is the best studied enzyme of the shikimate pathway, as it is the prime target of the commercially important herbicide **glyphosate** (Fig. 7.18). Cocrystallization of EPSP synthase with shikimate 3-phosphate alone and in combination with glyphosate revealed that binding of the first substrate, shikimate 3-phosphate, to the enzyme triggers a global conformational change from an "open" to a "closed" conformation, thereby forming the active site in the interdomain cleft of EPSP synthase. Glyphosate occupies the PEP-binding site of the enzyme–shikimate 3-phosphate complex, thereby competitively inhibiting the EPSP synthase with respect to the second substrate, PEP. Based on glyphosate sensitivity, EPSP synthases from different organisms have been divided into two classes. All plants and most bacteria, including *E. coli*, have glyphosate-sensitive **class I EPSP synthases**, whereas some bacteria, such as *Agrobacterium* sp. strain CP4, have **class II EPSP synthases** that are relatively resistant to glyphosate and, therefore, have been used to generate **glyphosate-resistant transgenic crops**.



Glyphosate
(*N*–[Phosphonomethyl]glycine)

FIGURE 7.18 *Glyphosate, herbicidal constituent of the commercial herbicide Roundup® is a competitive inhibitor of EPSP synthase.*

EPSP synthase genes have been cloned from a number of plant species, and mutations and the structural basis of the glyphosate tolerance have been identified (see Box 7.1). The *Arabidopsis* genome contains two genes encoding one putative and one functional EPSP synthase, which is constitutively expressed at low levels.

The final enzyme of the pathway, **chorismate synthase**, catalyzes the elimination of phosphate and a hydrogen atom from EPSP to produce chorismate (see Fig. 7.17). The reaction (a 1,4-*trans*-elimination) is unusual and unique in nature. It requires a reduced flavin nucleotide cofactor ($FMNH_2$; see Fig. 14.4) typically associated with redox reactions, even though the reaction does not involve an overall change in redox state. Despite the fact that chorismate synthases from different kingdoms are highly homologous and have similar structural folds, cofactor specificity, and kinetic properties, two classes have been distinguished based on their ability to reduce the oxidized FMN. Chorismate synthases from fungi are associated with a NADPH-dependent flavin reductase as part of a bifunctional enzyme, whereas plants and most bacteria have monofunctional enzymes that depend on an external source of $FMNH_2$. Genes encoding chorismate synthases have been isolated from a number of plant species. The tomato (*Solanum lycopersicum*) genome contains two chorismate synthase genes that are differentially expressed.

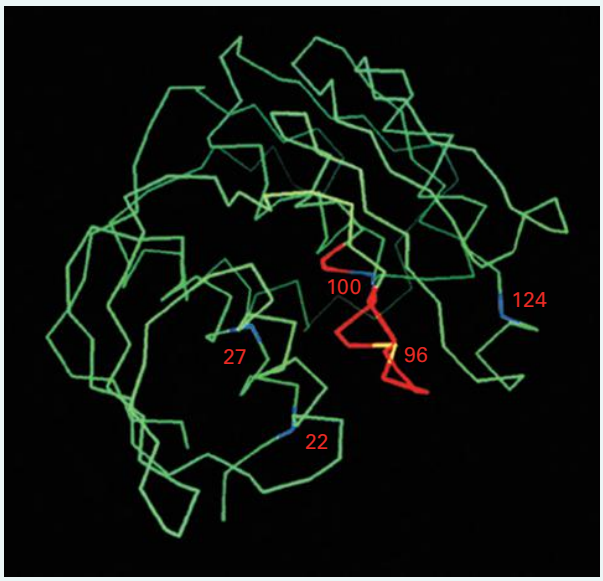
BOX 7.1

Detoxification genes and resistant target enzymes can provide crop plants with herbicide tolerance

Several enzymes of amino acid biosynthesis are targets for commercially significant herbicides: GS is inhibited by L-PPT (**Basta®**) (see Section 7.2.1), **acetohydroxy acid synthase** (**AHAS**) is inhibited by five classes of herbicides (the major ones belonging to the **imidazolinones**, **sulfonylureas**, and **triazolopyrimidines** as will be discussed in Section 7.5.2), and EPSP synthase is inhibited by glyphosate (**Roundup®**), as discussed above.

Herbicide tolerance is considered a desirable agricultural trait because it allows farmers to control weeds without affecting crop plant growth. Both classical breeding and molecular genetic strategies have been used to introduce these traits into economically important plants. Among the successful approaches for genetically engineering herbicide tolerance is the expression of enzymes that detoxify or degrade the inhibitor, and the introduction of mutant target enzymes that are less sensitive to the inhibitor. For example, expression of the *Streptomyces hygroscopicus* ***bar* gene**, encoding **phosphinothricin acetyltransferase**, makes plants resistant to L-PPT, whereas a naturally occurring form of EPSP synthase from an *Agrobacterium* strain provides tolerance to high concentrations of glyphosate. Mutant EPSP synthase has also been characterized in *E. coli*. Here, a backbone plot of the *E. coli* enzyme highlights active site residues (blue, numbered in red) and a conserved region (red). Conversion of the yellow Gly^{96} residue to Ala makes the protein resistant to glyphosate.

Source: Padgette et al. (1996). S. O. Duke, ed. CRC Press, Boca Raton, FL, pp. 53–84.



7.3.2 Chorismate mutase is the committing enzyme in phenylalanine and tyrosine synthesis

The biosynthesis of **phenylalanine** and **tyrosine** may occur via two alternative pathways with either **arogenate** or **phenylpyruvate/*p*-hydroxyphenylpyruvate** as intermediates (Fig. 7.19). Recent genetic evidence suggests that the arogenate route is predominant in plants. This means that plants differ from enteric bacteria and fungi, which primarily use the phenylpyruvate route.

Chorismate mutase (CM) catalyzes the intramolecular rearrangement of the enolpyruvyl side chain of chorismate to produce prephenate, and it is the committing enzyme for phenylalanine and tyrosine biosynthesis. In many plants, this activity exists in two isoenzyme forms, **CM1** and **CM2**, which are regulated quite differently from one another. The plastid localization and regulatory behavior of CM1 are consistent with a role for this activity as a committing enzyme in an amino acid biosynthetic pathway.

CM1 is feedback-inhibited by each of the end products, phenylalanine and tyrosine, and is activated by tryptophan, the product of the other branch of the pathway. Tryptophan reverses the inhibition by phenylalanine or tyrosine (Fig. 7.20). This mechanism regulates flux into the two competing pathways by increasing synthesis of phenylalanine and tyrosine when tryptophan is plentiful, and suppressing synthesis of phenylalanine and tyrosine when the supply of these amino acids is adequate.

The contrasting features of the CM2 isoform make this enzyme enigmatic. The activity of CM2 is not regulated by any of the aromatic amino acids, and unlike the other aromatic amino acid biosynthetic enzyme, CM2 lacks any obvious N-terminal plastid targeting sequence (transit peptide) and is cytosolic (Fig. 7.21). CM2 has roughly a 10-fold higher affinity toward chorismate than CM1. This is consistent with a presumably lower chorismate concentration in the cytosol, as chorismate is likely transported from plastids, in the absence of evidence for the existence of a cytosolic (partial or complete) shikimate pathway.

The *Arabidopsis* genome contains an additional gene encoding **CM3**. Like CM1, CM3 contains a putative plastid transit peptide and is subject to allosteric regulation, but its affinity toward chorismate is closer to that of CM2. All three *Arabidopsis* genes display differential expression, with *CM1* and, to a lesser extent, *CM3* being induced in response to elicitors and pathogen treatments. The different properties of CMs suggest their distinct physiological roles in plants.

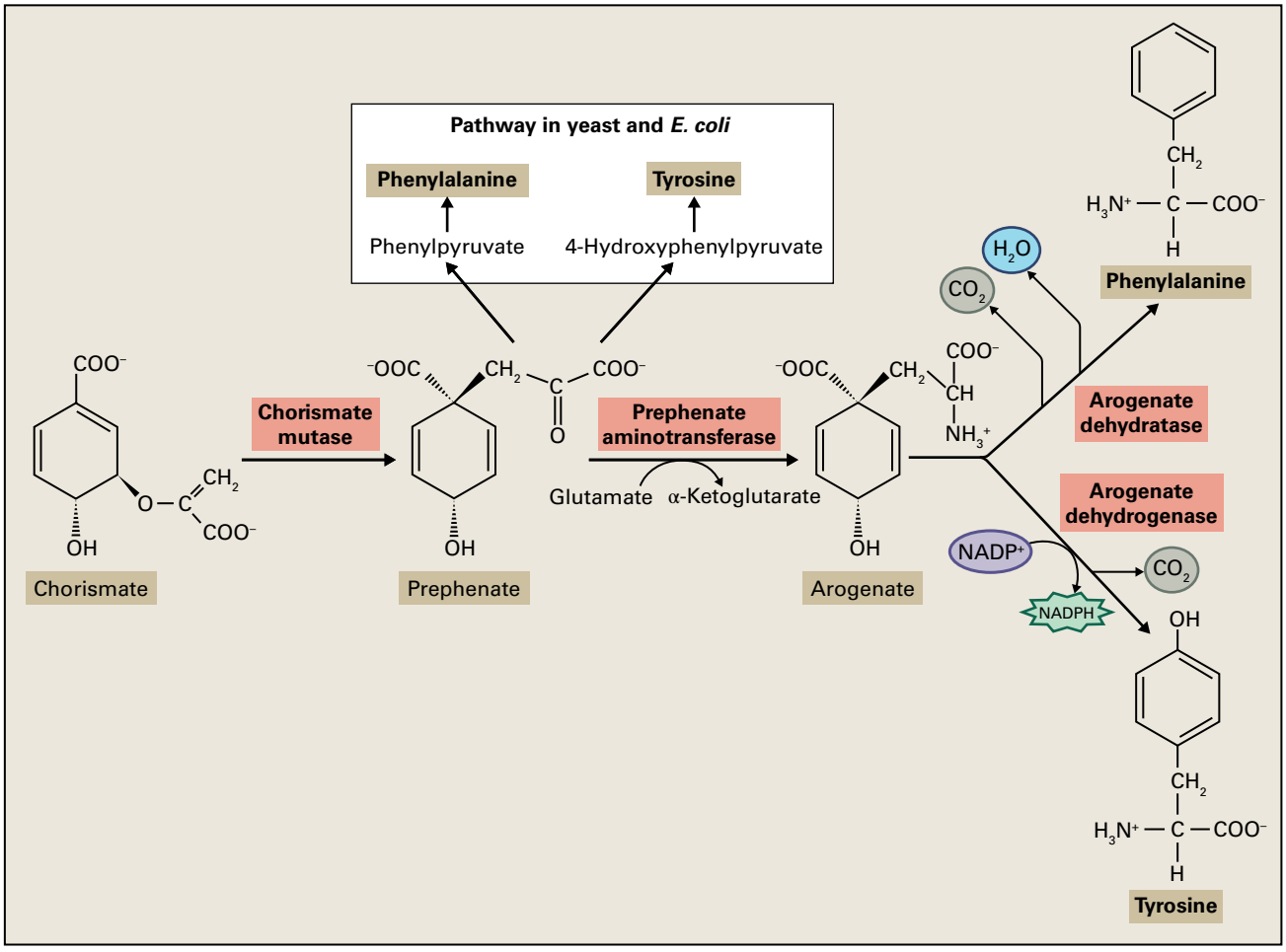


FIGURE 7.19 *Phenylalanine and tyrosine are predominantly synthesized from arogenate in plants. This is in contrast to the major pathway in* Saccharomyces cerevisiae *and* E. coli, *where phenylpyruvate and 4-hydroxyphenylpyruvate are intermediates.*

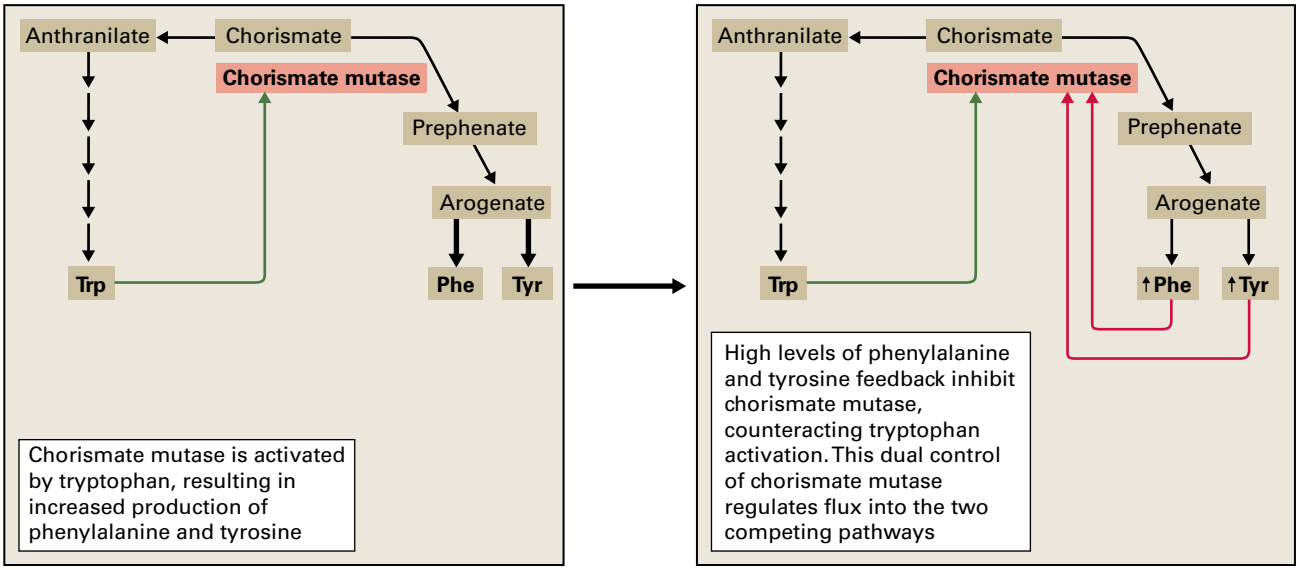


FIGURE 7.20 *Allosteric regulation of chorismate mutase controls flux from chorismate into phenylalanine and tyrosine.*

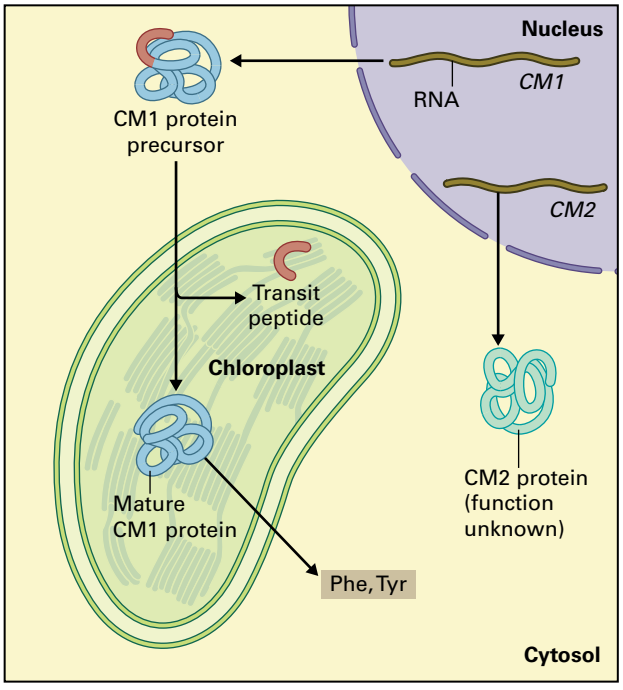


FIGURE 7.21 *CM1 and CM2 isoforms have distinct subcellular localization and appear to have different physiological roles. CM1 is plastid-localized, whereas CM2 is cytosolic. Because the substrate for CM is produced in the plastid, the function of the cytosolic isoenzyme remains unknown. Export of chorismate from the plastid has not been investigated.*

Interestingly, CM plays a critical role in interactions of phytoparasitic nematodes and phytopathogenic fungi (*Ustilago maydis*) with their host plants. Both nematodes and fungi inject their own CMs into the cytoplasm of plant cells. Probably in conjunction with plant CM2, these additional CM activities are assumed to increase the flow of chorismate from plastids to the cytosol and redirect the plant metabolome in favor of the parasite. This "**metabolic colonization**" is far from being understood.

The initial step of the **arogenate pathway**, the final step common to phenylalanine and tyrosine biosyntheses, is catalyzed by **prephenate aminotransferase**. This heat-stable PLP-dependent enzyme catalyzes a reversible transamination between prephenate and arogenate. A 10-fold higher affinity toward prephenate as compared to arogenate suggests that prephenate aminotransferase preferentially catalyzes the forward reaction under physiological conditions and directs the carbon flux from prephenate to arogenate. It utilizes either glutamate or aspartate as amino donor and is not inhibited by end products, consistent with it not acting at a branch point in the pathway. Prephenate aminotransferase genes have been cloned from a number of plant species, including *Arabidopsis*, petunia (*Petunia hybrida*), and tomato (*Solanum lycopersicum*), where they are coexpressed with other proteins involved in the shikimate pathway. *Arabidopsis* and tomato genomes appear to contain a single copy of prephenate aminotransferase, and a loss-of-function mutation in *Arabidopsis* is lethal at the one-cell stage of embryo development.

7.3.3 In plants, the pathway that synthesizes phenylalanine and tyrosine is regulated by its final reactions

The biosynthesis of **phenylalanine** and **tyrosine** in plants via the arogenate pathway represents an unusual case, wherein the committing reactions are also the last steps of the pathways.

The final enzyme of phenylalanine biosynthesis is **arogenate dehydratase**, which catalyzes the decarboxylation and dehydration of arogenate. Multiple genes encoding arogenate dehydratase have been isolated from a number of plant species. These plant genes encode monofunctional dehydratases that contain two domains: a catalytic domain and a C-terminal regulatory domain that is involved in the allosteric regulation by phenylalanine. Plant arogenate dehydratases display strict or preferred substrate specificities toward arogenate. However, some of them can also use prephenate as a substrate and convert it to phenylpyruvate, even though with V_{max} always being 10- to 100-fold lower with prephenate than with arogenate. Tyrosine can activate arogenate dehydratases to redirect flux from tyrosine to phenylalanine biosynthesis.

Arogenate dehydrogenase (ADH) catalyzes the oxidative decarboxylation of arogenate to tyrosine. This $NADP^+$-dependent enzyme lacks an additional tyrosine-binding domain, independent of the substrate binding site (unlike arogenate dehydratase), but it is feedback-inhibited by tyrosine competitively with respect to the arogenate substrate. ADH activities have been detected in a variety of plant species, however, genes encoding these enzymes have been isolated only from *Arabidopsis* and maize (two and four, respectively). *Arabidopsis* ADH1 exhibits strict substrate specificity toward arogenate, whereas ADH2 can also accept prephenate, but with a V_{max} by three orders of magnitude lower than that with arogenate. The individual functions of ADH1 and ADH2 in *Arabidopsis* remain to be determined.

Biosynthesis of phenylalanine and tyrosine can also occur via the alternative phenylpyruvate and *p*-hydroxyphenylpyruvate routes, respectively, in which aromatization precedes the transamination reaction (see Fig. 7.19), which then is the final step. Arogenate dehydratases with activities toward prephenate, as well as ADH2, can catalyze the conversion of prephenate to the corresponding pathway intermediates, **phenylpyruvate** and ***p*-hydroxyphenylpyruvate**. However, **prephenate dehydratase** and **dehydrogenase** activities, respectively, have rarely been detected in plant tissues. This raises the question about the contribution of these pathways to phenylalanine and tyrosine biosynthesis under physiological conditions. The final steps in these pathways are catalyzed by phenylpyruvate and *p*-hydroxyphenylpyruvate aminotransferase, respectively. Genes encoding **aromatic amino acid aminotransferases** have been isolated from melon (*Cucumis melo*) and opium poppy (*Papaver somniferum*) (see Chapter 24). In *Arabidopsis*, seven genes were annotated as **tyrosine aminotransferases**, and two of the corresponding enzymes possess tyrosine aminotransferase activity. Owing to the reversibility of the aminotransferase reaction, tyrosine

aminotransferases can also be involved in the biosynthesis of **tocopherol** and **plastoquinone** by conversion of tyrosine to **homogentisate** via *p*-hydroxyphenylpyruvate.

In animals and some microbes, phenylalanine can be converted to tyrosine by **phenylalanine hydroxylase** (therefore, tyrosine is not an **essential amino acid** in our diet). Phenylalanine-specific aromatic amino acid hydroxylases (monooxygenases) have been identified in non-flowering plants including algae, mosses, and gymnosperms, but not in angiosperms. These plastid plant phenylalanine hydroxylases use 10-formyltetrahydrofolate, rather than a tetrahydropterin like the animal enzymes, as a cofactor and molecular oxygen to provide the oxygen of the phenolic hydroxyl group. They provide an alternative biosynthetic path to tyrosine.

7.3.4 The tryptophan biosynthesis pathway in plants has been dissected with molecular genetic techniques

Conversion of chorismate to **tryptophan** has significance beyond amino acid biosynthesis. Plants use this pathway to produce precursors for numerous secondary metabolites, including the hormone auxin, indole alkaloids, phytoalexins, cyclic hydroxamic acids, indole glucosinolates, and acridone alkaloids (Fig. 7.22). These metabolites serve as growth regulators, defense agents, and signals for insect pollinators and herbivores. Some of these alkaloids, including the anticancer drugs vinblastine and vincristine, have great pharmacological value.

The biosynthetic pathway for tryptophan was the first proven to be amenable to detailed molecular genetic analysis (see Box 7.2); as a result of these studies, a generally accepted in vivo pathway has been constructed (Fig. 7.23). Genes for all of the enzymes have been characterized, and mutants have been identified for all but one of the seven proteins (indole-3-glycerol-phosphate synthase; IGPS; an antisense approach was chosen to downregulate this enzyme in *Arabidopsis*). The plant pathway comprises the same sequence of reactions seen in microorganisms.

7.3.5 Anthranilate synthase catalyzes the committing step in tryptophan biosynthesis

Anthranilate synthase (AnS) is an amino-accepting chorismate-pyruvate lyase that catalyzes the first step in tryptophan biosynthesis, the formation of anthranilate. It is a two-subunit enzyme in plants that functions as an $\alpha_2\beta_2$ complex. The α subunit catalyzes the amination of chorismate and removal of the *enol*pyruvyl side chain (yielding pyruvate), acting in concert with the **glutamine amidotransferase** activity of the

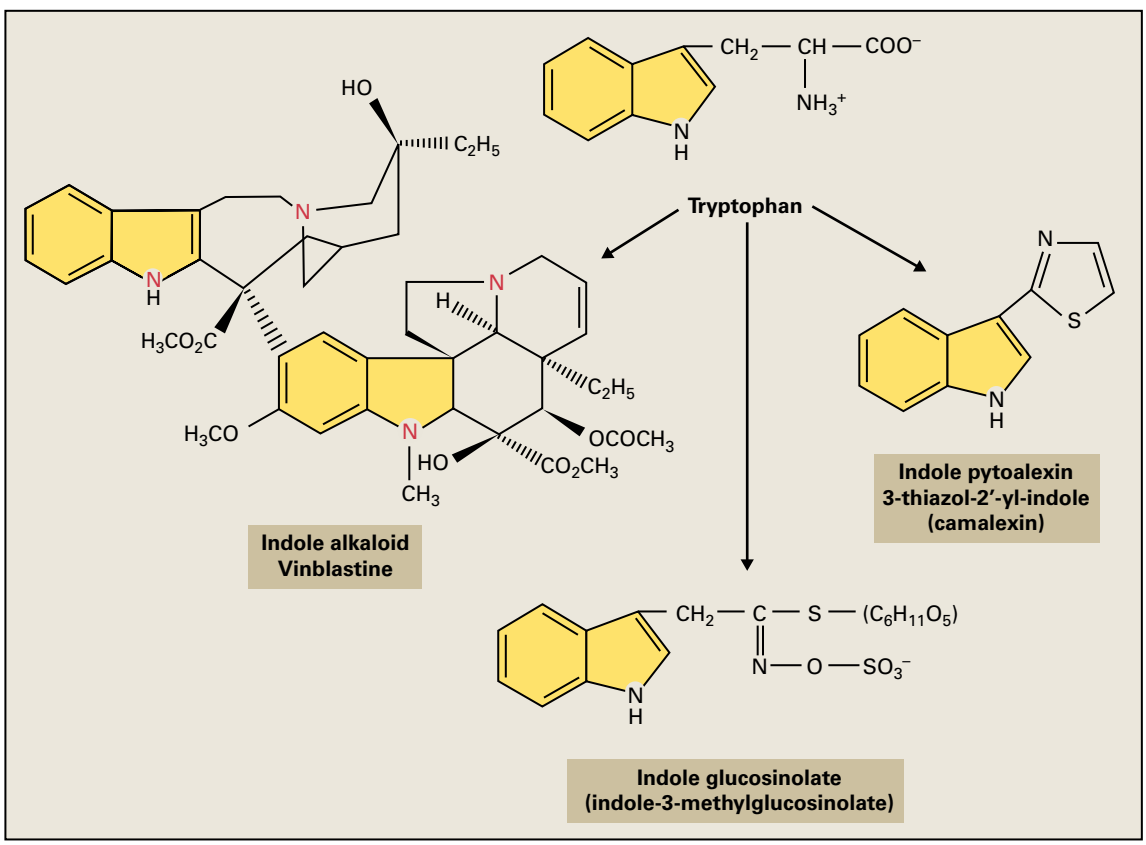


FIGURE 7.22 *The indole ring (highlighted in yellow) derives from the amino acid tryptophan and is a common feature of many secondary metabolites in plants.*

BOX 7.2

Various mutant screens have been used to elucidate the tryptophan biosynthesis pathway

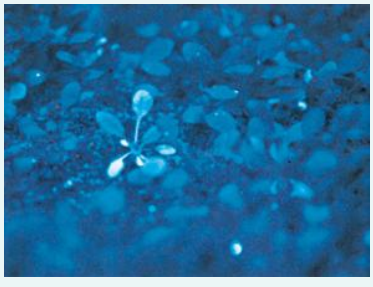
In microorganisms, it is easy to identify mutants auxotrophic for amino acids by replica-plating colonies and comparing their growth on minimal and supplemented media. Auxotrophic colonies are identified by their inability to grow without the addition of amino acids. Because replica plating is not an option for plant geneticists, the search for mutants that require medium supplementation is much more difficult, and plant biosynthetic pathways were less amenable to genetic analysis before the advent of comparative genomics. This problem was overcome by devising rapid screens for mutants that accumulate an intermediate in the biosynthetic pathway, or that continue to grow in the presence of compounds that would be converted into toxic products if all the enzymes in the pathway were present and active. There are several such examples in the tryptophan pathway.

The strong blue fluorescence of **anthranilic acid**, the first intermediate in the tryptophan pathway, provides a phenotype for identifying *Arabidopsis* mutants with reduced activities for the first three pathway enzymes. Loss-of-function mutants of **phosphoribosyl anthranilate** (PR-anthranilate) **transferase** *(trp1)* or PR-anthranilate isomerase (*pai;* see Box 7.3) have strikingly blue fluorescent leaves under UV light. These leaves are filled with anthranilate compounds because they are unable to effectively convert this intermediate to downstream products. This screen also provides a method for identifying *trp4* mutants with reduced **anthranilate synthase** (AnS) β subunit activity by screening *trp1* mutants for **second-site suppressor mutations** that decrease the ability to convert chorismate to anthranilate. Here, a diagram (A) of the phenotypic effects of mutations that abolish the activity in the first three enzymes of the pathway is accompanied by a photograph (B) taken under UV light, which reveals a single blue fluorescent *trp1* mutant plant growing among many wild-type *Arabidopsis* plants.

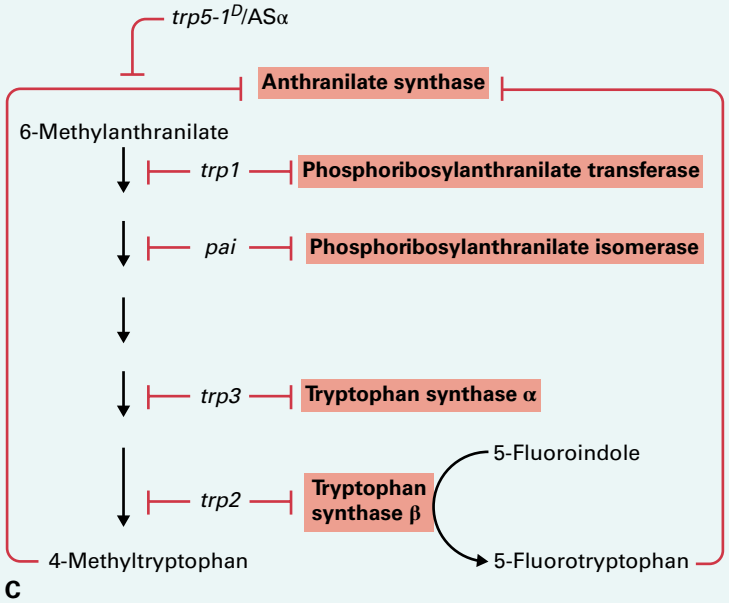
Toxic analogs of tryptophan and pathway intermediates have been used to identify both loss- and gain-of-function mutants. Analogs of pathway intermediates are toxic to plants because the enzymes of tryptophan biosynthesis convert them to tryptophan analogs (C). For example, 6-methylanthranilate is metabolized to 4-methyltryptophan, and 5-fluoroindole metabolizes to 5-fluorotryptophan-compounds that starve the plant for tryptophan because they inhibit AnS. Anthranilate analog-resistant plants fall into two categories: those with reduced activity of the enzymes that convert anthranilate to tryptophan (*trp1, pai, trp3,* and *trp2* mutants), and gain-of-function feedback-insensitive AnS *trp5D* mutants. These **relaxed allosteric regulation mutants** are also obtained by directly selecting

Genotype	Anthranilate synthase	PR-anthranilate transferase	PR-anthranilate isomerase	Phenotype in UV light
Wild type	Chorismate → Anthranilate	→ PR-anthranilate	→ CDRP	No fluorescence
trp1	Chorismate → Anthranilate	✗ PR-anthranilate	→ CDRP	Strong fluorescence
trp1; trp4	Chorismate ✗ Anthranilate	✗ PR-anthranilate	→ CDRP	No fluorescence
pai	Chorismate → Anthranilate	→ PR-anthranilate	✗ CDRP	Weak fluorescence

A



B



C

for resistance to tryptophan analogs (α-methyltryptophan, for example). Just as mutants of the first three steps of the pathway were targeted by use of anthranilate blue fluorescence screening, tryptophan synthase (TS)-deficient mutants have been identified by screening for resistance to exogenous 5-fluoroindole, which is converted by the TS β subunit to toxic 5-fluorotryptophan.

Source: (B) R. Last, Cereon Genomics LLC, Cambridge, MA, previously unpublished.

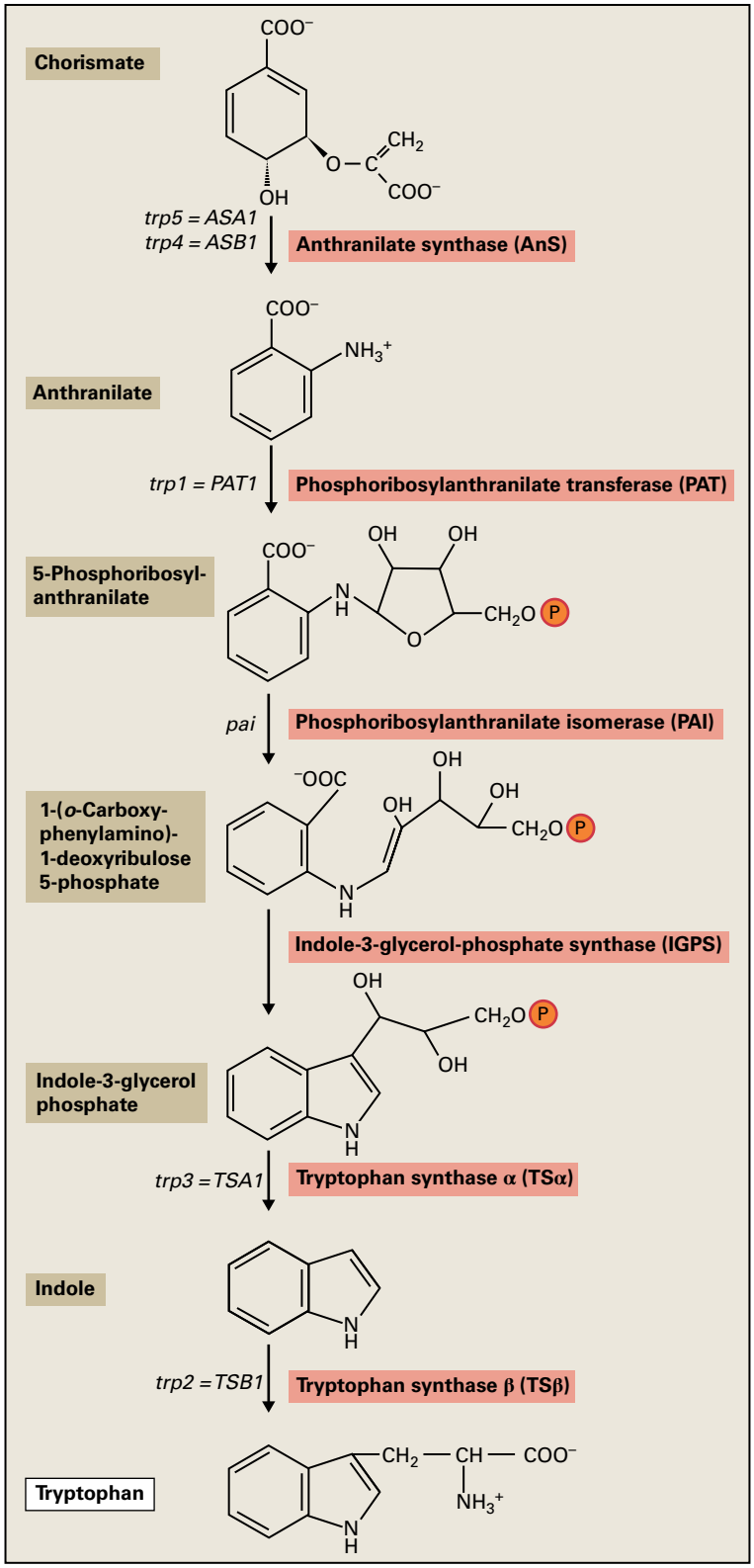


FIGURE 7.23 *Tryptophan biosynthetic pathway of* Arabidopsis. *The wild-type gene names (e.g.,* ASA1*) and mutant designations (e.g.,* trp5*) are indicated to the left of the arrows.*

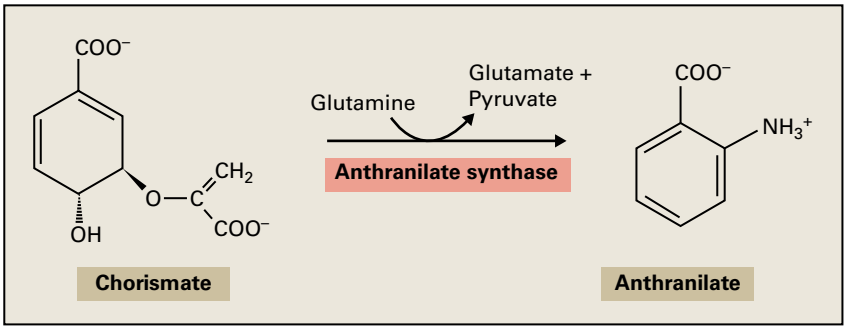


FIGURE 7.24 *Anthranilate synthase catalyzes the first step of tryptophan biosynthesis. Note that the γ-amide group of glutamine becomes the aromatic amino group of anthranilate. This activity, often called a glutamine aminotransferase, is therefore correctly called a glutamine amidotransferase. Glutamine amidotransferases, which are PLP-independent, generally catalyze a reaction in which ammonia generated by hydrolysis of glutamine is channeled to a second active site where it acts as a nucleophile. The hydrophobic tunnel prevents protonation of NH_3 and thus maintains its nucleophilicity.*

β subunit (Fig. 7.24). Analysis of the crystal structure of the bacterial enzyme suggests that the binding of chorismate to the α subunit triggers a conformational change to an active state and creates an intermolecular **tunnel for ammonia transfer** from the β to α subunit. As is the case in microorganisms, the α subunit can function in the absence of β subunit amidotransferase activity, provided ammonium is present at sufficient concentration (Reaction 7.1). However, the glutamine amidotransferase activity is likely of primary importance for AnS function in plants. The *trp4* mutation in the *Arabidopsis* AnS β subunit gene 1 suppresses accumulation of anthranilate, which possesses a strong blue fluorescence under UV light (see Box 7.2).

Reaction 7.1: Anthranilate synthase

$$\text{Chorismate} + NH_4^+ \rightarrow \text{anthranilate} + \text{pyruvate}$$

As expected for the committing enzyme in the tryptophan pathway, plant AnS activities are feedback-inhibited by micromolar concentrations of tryptophan in vitro. Tryptophan binds to the α subunit and restricts the AnS conformational change, suggesting the α subunit is responsible for the allosteric feedback inhibition by tryptophan. Most AnS α subunits in plants are feedback-sensitive to tryptophan, with the exceptions of feedback-insensitive tobacco and *Ruta graveolens* (common rue) α-subunit isoforms (see Box 7.3).

The use of toxic tryptophan analogs as false-feedback inhibitors allowed the identification of mutants with altered AnS regulation. Dominant *trp5-1D Arabidopsis* mutants that are resistant to **tryptophan analogs** have feedback-insensitive AnS activity. All four of these mutants resulted from the same aspartate to asparagine change in the AnS α-subunit gene *ASA1,* a mutation close to a region of microbial AnS enzymes important for feedback regulation. The *trp5-1* mutant has a threefold increase in free tryptophan, illustrating the importance of allosteric control in regulating tryptophan pools. Plants contain at least two genes encoding the α subunit and one gene encoding the β subunit. One of the α-subunit genes is constitutively expressed, whereas the other is regulated developmentally and is induced in response to wounding and pathogens, suggesting its involvement in the production of tryptophan pathway-derived natural products as a part of plant defense.

7.3.6 Biochemical characterizations of PAT, PAI, and IGPS lag behind molecular and genetic analyses

The second enzyme in the tryptophan biosynthesis is phosphoribosylanthranilate transferase (PAT), which catalyzes the formation of 5-phosphoribosyl anthranilate by transferring the phosphoribosyl moiety from phosphoribosylpyrophosphate to anthranilate (Fig. 7.25). A single-copy gene encodes PAT in the *Arabidopsis* genome. *PAT* is constitutively expressed, and its mRNA level is post-transcriptionally enhanced by the first two introns in *Arabidopsis*.

While relatively little is known about the enzymology of plant PATs, the *Arabidopsis* enzyme has been the subject of detailed genetic and molecular analysis. PAT mutants fall into two general classes: auxotrophic plants, which have such low PAT enzyme activity that seedlings cannot grow on sterile medium without the addition of tryptophan, and prototrophs, which have enough residual activity to survive without amino acid supplementation. Unlike the **prototrophic mutants**, which grow with a normal morphology, adult *trp1* **auxotrophic mutants** are small, bushy, and have greatly reduced fertility, even when tryptophan is added to their growth medium (Fig. 7.26). Perhaps these developmental defects are caused by an inability to produce auxin (indole-3-acetic acid, IAA) or other metabolites derived from this pathway. Biochemical analysis of the prototrophic *trp1* mutants indicates the PAT enzyme activity is present in vast excess of that required for maintaining pathway flux. Five of the prototrophic mutants have 1% of wild-type enzyme activity or less, yet grow normally without tryptophan supplementation.

BOX 7.3 An alkaloid-producing plant has a feedback-insensitive AnS

While feedback regulation of AnS is a logical mechanism for controlling the accumulation of tryptophan, it could reduce the plant's ability to rapidly synthesize secondary metabolites in response to environmental stimuli.

The existence of naturally occurring **tryptophan-insensitive AnS** isoforms is one mechanism by which plants appear to avoid this potential difficulty. After treatment with fungal cell wall elicitor, ***Ruta graveolens*** cell cultures rapidly accumulate anthranilate-derived antimicrobial **acridone alkaloids** (e.g., **rutagravin**; A); during this period, AnS activity and AnS α-subunit mRNAs increase dramatically. Both control and elicitor-induced cultures have similar amounts of tryptophan-sensitive AnS activity, but elicited cultures accumulate a large amount of feedback-resistant AnS.

These biochemical data correlate well with results of gene expression studies. *R. graveolens* has two characterized AnSα genes: ASα1 mRNA accumulation is stimulated after elicitation, whereas the amount of ASα2 mRNA does not change (B). Further characterization of the two AnS α-isoforms expressed in *E. coli* showed that the inducible AnSα1 activity is barely affected by the presence of unusually high concentrations of tryptophan (up to 100 μM). In contrast, the non-inducible AnSα2 product has an apparent K_i of less than 3 μM tryptophan, very similar to that observed for other characterized plant AnS activities. These results suggest that this alkaloid-producing plant makes an inducible AnS that is not subject to tryptophan inhibition and thus allows synthesis of anthranilate for secondary metabolism even under conditions where free tryptophan is plentiful.

Source: (B) Bohlmann et al. (1995). Plant J. 7:491–501.



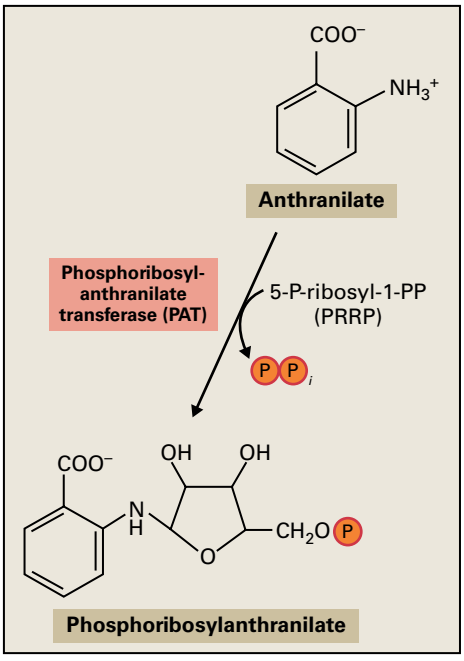


FIGURE 7.25 *Phosphoribosylanthranilate transferase (PAT) catalyzes the second step of tryptophan biosynthesis.*



FIGURE 7.26 *Morphology of the tryptophan-requiring* trp1 *mutants is dramatically altered from that of wild-type plants and includes small stature and reduced apical dominance.*
Source: Last, Cereon Genomics LLC, Cambridge, MA; previously unpublished.

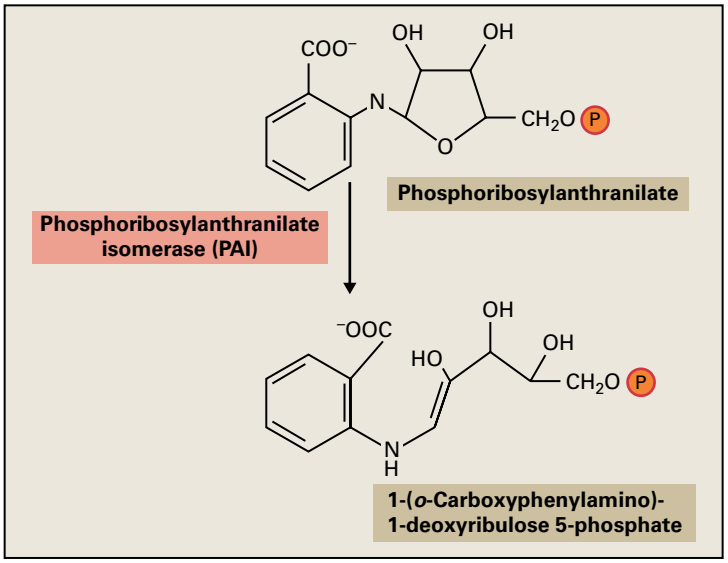


FIGURE 7.27 *Phosphoribosylanthranilate isomerase (PAI) catalyzes the third step of tryptophan biosynthesis.*

The third enzyme in the tryptophan biosynthetic pathway is **phosphoribosylanthranilate isomerase** (PAI; Fig. 7.27), which converts 5-phosphoribosylanthranilate to 1-(*o*-carboxyphenylamino)-1-deoxyribulose 5-phosphate (CDRP). Depending on ecotypes, *Arabidopsis* possesses three or four highly homologous *PAI* genes. In the Columbia ecotype, *PAI1* and *PAI2* are 99% identical, including their untranslated regions. This differs from the low degree of conservation observed for prokaryotic PAI proteins and suggests a recent **gene duplication** event or other mechanism that actively maintains the similarity of these genes. Each *PAI* gene exhibits a spatially and developmentally distinct expression pattern and a differential response to environmental stimuli. Owing to *PAI* gene redundancy, loss of any one gene does not reduce enzyme activity sufficiently to produce a distinct mutant phenotype. Even transgenic antisense-RNA plants with 10–15% of wild-type PAI enzyme activity do not show reduced growth rate, nor do they require tryptophan for growth. These observations suggest that PAI activity is present in excess of that required for normal growth. In the single PAI-deficient *Arabidopsis* mutant for which data have been published, deletion of one locus and DNA methylation-associated epigenetic silencing of the other gene were required to reduce the enzyme activity sufficiently to an undetectable level and to observe a visible phenotype (see Box 7.4; see also Chapter 9).

The penultimate enzyme of tryptophan biosynthesis, **indole-3-glycerol-phosphate synthase** (IGPS), catalyzes the decarboxylation and ring closure of CDRP (Fig. 7.28). It is the only enzyme known to catalyze the formation of the indole ring. One of two *Arabidopsis* genes encoding IGPS was isolated based on its ability to complement an *E. coli trpC*⁻ mutation despite low amino acid identity (22–28%) with microbial enzymes. Plant IGPSs exist as monofunctional enzymes, in contrast to fungal and bacterial IGPSs, which are synthesized as fusion proteins containing one or two other enzymes of the tryptophan biosynthetic pathway. Analysis of tryptophan and IAA levels in different *Arabidopsis* tryptophan biosynthesis mutants, as well as in transgenic plants with antisense suppression of *IGPS*, suggested that indole-3-glycerol-phosphate might be the branch-point intermediate in tryptophan-independent auxin biosynthesis. It appears, however, that IAA in these mutants is a decomposition product of the chemically unstable IGPS that accumulates in tryptophan synthase mutants (see below). A **tryptophan-independent auxin biosynthesis** is, therefore, unlikely (see Chapter 17).

7.3.7 Tryptophan synthase catalyzes the final step in tryptophan synthesis

Tryptophan synthase (TS) is a bifunctional enzyme that catalyzes the last two-step reaction of tryptophan biosynthesis, the conversion of indole-3-glycerol phosphate (IGP) and serine to tryptophan (Fig. 7.29). The best characterized of the microbial tryptophan biosynthetic enzymes, TS exists as an $\alpha_2\beta_2$ heterotetramer, and the separate subunits are capable of catalyzing independently two partial reactions of the reaction sequence:

Reaction 7.2: TS α-subunit

$$\text{IGP} \rightarrow \text{indole} + \text{glyceraldehyde 3-phosphate} \quad [\text{IGP lyase (IGL) activity}]$$

Reaction 7.3: TS β-subunit

$$\text{Indole} + \text{serine} \rightarrow \text{tryptophan} + H_2O$$

Biochemical and X-ray crystallographic studies of the *Salmonella typhimurium* TS enzyme have revealed that the indole intermediate generated at the active site of the α-subunit (TSA) is not ordinarily released from the enzyme, but rather travels through a 25-Å **intermolecular tunnel** to the β-subunit (TSB) active site (Fig. 7.30). This is comparable to the "**ammonia tunnel**" in glutamine amidotransferases (see Fig. 7.24). The two partial reactions are kept in phase by allosteric interactions between the two subunits, and each subunit can cause conformational changes that affect the catalytic

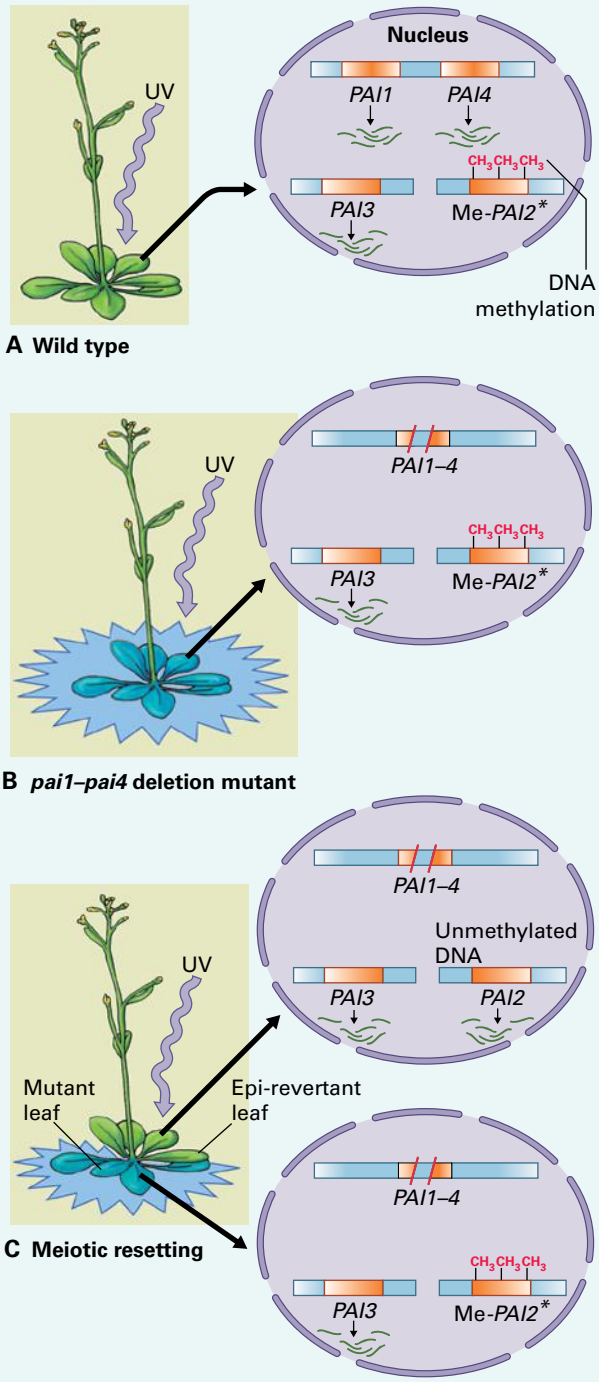
BOX 7.4

Epigenetic regulation of *PAI2* results in partial tryptophan auxotrophy

Although blue fluorescence screening failed to reveal *pai* mutants in the *Arabidopsis* Columbia ecotype, an unusual blue fluorescent mutant with diminished PAI activity was identified in the Wassilewskija ecotype. Unlike the large number of *trp1* mutants and antisense-*PAI* lines that are uniformly fluorescent, the phenotype of this mutant is unstable, showing a high frequency of somatic reversion to wild type (see figure).

Unlike Columbia, which has three genes, wild-type Wassilewskija (A) has four *PAI* genes, with *PAI4* found in an inverted repeat with *PAI1* at the same genetic site as the Columbia *PAI1* locus. The blue fluorescent *pai* mutant contains a deletion that simultaneously inactivates the linked *PAI1* and *PAI4* genes, leaving only *PAI2* and *PAI3* intact and making the plant dependent on *PAI2* expression. The Wassilewskija *PAI2* gene is subject to epigenetic regulation and is normally hypermethylated (shown as Me-*PAI2** in B), which leads to low mRNA expression. The instability of the mutant phenotype can be accounted for by random reduction in methylation of Me-*PAI2** (C), which reactivates the gene and creates epi-revertant regions of the plant that are phenotypically wild type (not blue fluorescent). These revertant tissues have enough PAI enzyme activity to prevent accumulation of anthranilate and thus allow normal growth of the plant. Because the blue fluorescence is cell-autonomous, the phenotype of each part of the plant accurately reflects its epi-genotype.

This is an example of how genetic tools that became available from studies of biochemical genetics can open up new approaches to studying seemingly unrelated areas of biology. In fact, because of the powerful blue fluorescence phenotype and well-characterized *PAI* gene family, the epigenetically silenced *PAI2** gene led to new approaches for studying the interesting areas of gene silencing and epigenetics, which have since developed into a fascinating field (see Chapter 7).



activity of the other. For example, α-subunit binding stimulates β activity (Reaction 7.3) 30-fold compared with uncomplexed β subunit. Conversely, the rate of cleavage of IGP at the α-subunit active site (Reaction 7.2) is increased 20-fold by binding of serine to the pyridoxal phosphate cofactor at the β-subunit active site (Fig. 7.30). In contrast to mutual activation of the subunits in bacteria, only an activation of the α-, but not the β-subunit, by the respective other subunit was observed upon formation of the $\alpha_2\beta_2$ TS complex of maize.

Fungi possess a single gene encoding a bifunctional TSA–TSB enzyme, whereas *E. coli* and plants have separate genes encoding TSA and TSB. In the *Arabidopsis* genome, there are at least two and four putative genes encoding TSA and TSB, respectively. The functional relevance of TSA1 and TSB1 in

FIGURE 7.28 *The indole-3-glycerol-phosphate synthase (IGPS) reaction produces the indole ring found in tryptophan and secondary metabolites.*

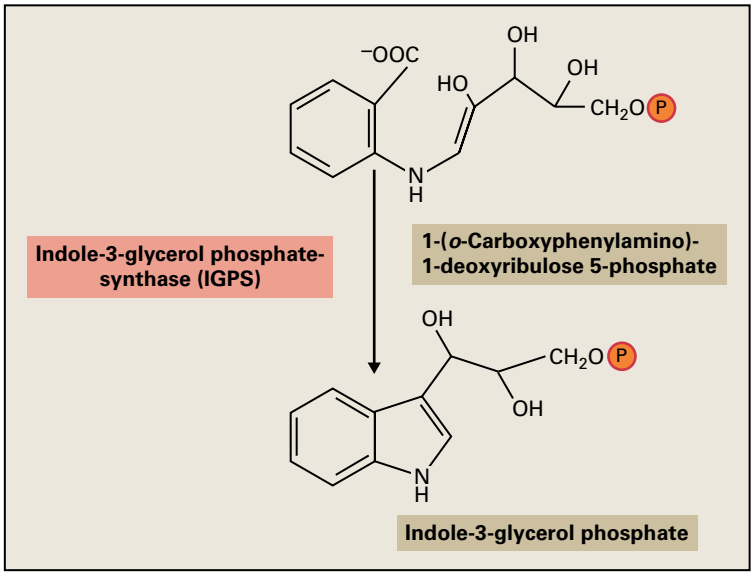
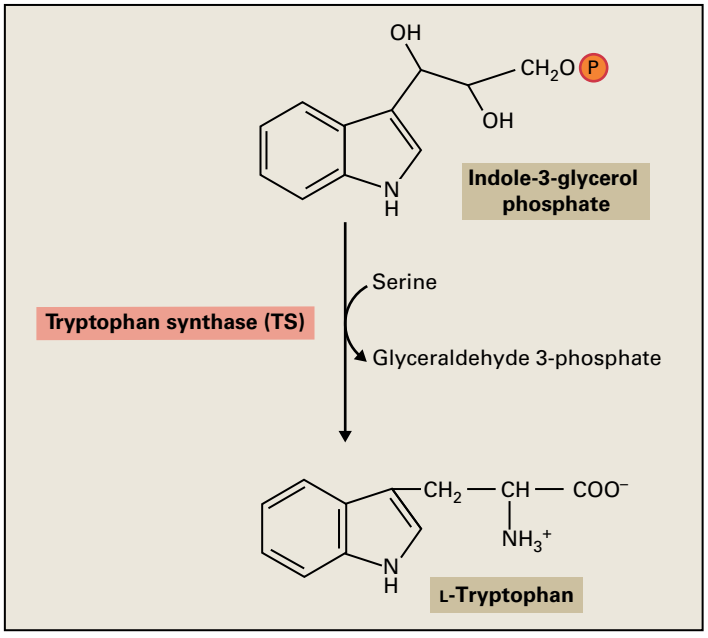


FIGURE 7.29 *Tryptophan synthase (TS) catalyzes the final step in tryptophan biosynthesis.*



tryptophan biosynthesis has been demonstrated by the tryptophan auxotrophic phenotype of the *trp3* and *trp2* mutants, respectively. However, the function of the other isoforms is not fully understood. In contrast to *Arabidopsis*, maize (*Zea mays*) contains one TSA and two highly identical and redundant TSB genes. Only simultaneous loss of both TSB functions leads to tryptophan auxotrophy.

Plants possess additional enzymes besides TSA that produce indole from IGP. Indole is a common precursor not only of tryptophan, but also of other plant natural products. Thus, in maize, a separate **indole-3-glycerolphosphate lyase** (IGL) is responsible for the formation of **volatile indole** under herbivore attack, while BX1 (see Box 7.5) catalyzes the first step in the biosynthesis of natural **benzoxazinoid pesticides**. The *Arabidopsis* genome also contains an indole-producing TSA-like enzyme (IGL). While all three genes are TSA paralogs, the corresponding proteins catalyze indole formation independent of a TSB-like subunit. As production of indole or benzoxazinoids sometimes exceeds that of tryptophan, the heterocomplex formation between TSA and TSB prevents the release of the indole intermediate and ensures a basal level of tryptophan for protein and auxin biosynthesis.

7.3.8 Aromatic amino acid biosynthesis occurs in the plastid

Aromatic amino acids are synthesized in the chloroplast, and several lines of evidence show that the total set of enzymes for the biosynthesis of phenylalanine, tryptophan, and tyrosine is found in plastids. Isolated chloroplasts incorporate $^{14}CO_2$ into

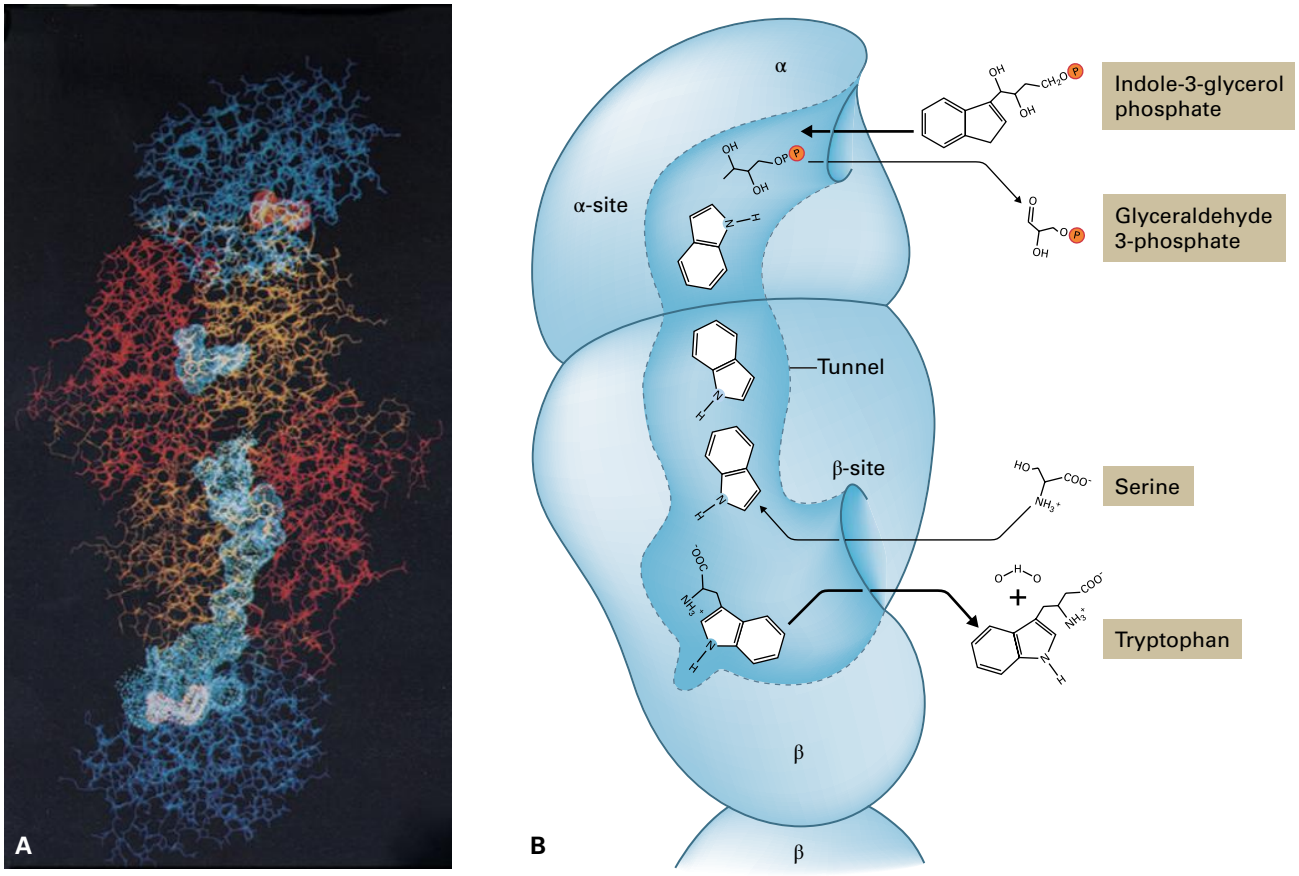


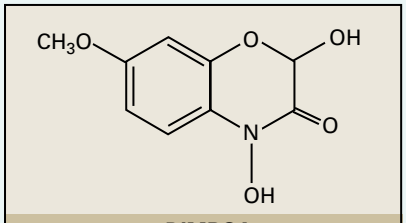
FIGURE 7.30 *Tryptophan synthase (TS) consists of α- and β subunits that join to form two active sites with a hydrophobic tunnel between them that channels indole from the site where it is released from indole-3-glycerol phosphate to the site where it is condensed with serine. (A) The structure of TS from* Salmonella typhimurium *with α subunits in blue, β subunit N-terminal residues in yellow, and C-terminal residues in red. A molecule of indole-3-glycerol phosphate (red) is bound to the active site of the α subunit. (B) Schematic drawing of the tunnel that guides indole from the active site of the α subunit to that of the β subunit.*
Source: (A) Hyde et al. (1998). J. Biol. Chem. 263:17857–17871.

BOX 7.5

Plants have an alternative single-subunit TSA enzyme efficient in indole synthesis

Indole has been implicated as an intermediate in the synthesis of some secondary metabolites, for example, cyclic hydroxamic acids such as 2,4-dihydroxy-7-methoxy-1,4-benzoxazin-3-one (DIMBOA), the structure of which is shown. This would appear to create a dilemma, because in the well-characterized bacterial TS enzyme, indole moves through a tunnel from the TSA active site to TSB, and does not escape from the TS heteroenzyme. A novel variation on the TS mechanism is found in maize (*Zea mays*), where a mutant (*bx1*, for benzoxazin-less) that fails to accumulate the normally abundant DIMBOA has a defect in a *TSA*-like gene *(BX1)*.

Unlike the *Arabidopsis* TSA1 protein, expression of the BX1 protein complements a *trpA*⁻ mutation even in the absence of a plant β subunit. This result argues that the BX1 protein can efficiently cleave IGP to form free indole without being activated by a TSB subunit. Kinetic analysis of the BX1 protein expressed in *E. coli* has confirmed that the homomeric BX1 enzyme is 30-fold more efficient in catalyzing IGP cleavage than the *E. coli* $\alpha_2\beta_2$ heteroenzyme. This suggests that plants have modified an enzyme of tryptophan biosynthesis to serve as the committing enzyme of indole-derived secondary metabolism while retaining the $\alpha_2\beta_2$ heteroenzyme for tryptophan biosynthesis.



DIMBOA
(2,4-Dihydroxy-7-methoxy-1, 4-benzoxazin-3-one)

aromatic amino acids, and activities of almost all enzymes involved in chorismate and aromatic amino acid biosynthesis have been detected in chloroplast extracts. Consistent with this view, genes containing plastid targeting sequences have been cloned for at least one isoenzyme responsible for a given biochemical step in the plant aromatic amino acid pathway. Plastid localization for most pathway enzymes was confirmed using GFP (green fluorescent protein) fusion proteins. Import of precursor proteins of DAHP synthase, shikimate kinase, EPSP synthase, PAI, and TSA into isolated chloroplasts has been also been demonstrated.

Subcellular fractionation and localization studies have uncovered a **cytosolic DAHP synthase** activity in some plants, and cytosolic isoforms both of CM (probably all plants) and **dehydroquinate dehydratase-shikimate dehydrogenase** (so far only found in tobacco; see Section 7.3.2) as well. The last two enzymes were confirmed at both biochemical and genetic levels. Genes encoding cytosolic tobacco (*Nicotiana tabacum*) dehydroquinate dehydratase/shikimate dehydrogenase 2 and *Arabidopsis* and petunia (*Petunia hybrida*) CM2 have been identified, and the cytosolic localization of the corresponding proteins was demonstrated. However, a gene encoding cytosolic DAHP synthase has not been identified, though several cytosolic enzymes catalyze the same reaction as DAHP synthase and are activated by Co^{2+} rather than Mn^{2+}. It seems unlikely that these are true enzymes of chorismate biosynthesis, because they can utilize a wide variety of aldehyde substrates in place of erythrose 4-phosphate, and their K_m values for erythrose 4-phosphate are tenfold higher than that of the Mn^{2+}-activated enzyme. Thus, these enzymes probably have metabolic roles in the cytosol unrelated to aromatic amino acid biosynthesis.

7.3.9 Aromatic amino acid biosynthesis is stress inducible

Unlike the aromatic amino acid biosynthetic enzymes in well-studied microbes such as *E. coli* and yeast, plant enzymes are regulated by environmental signals. This is logical, considering that, in contrast to the low abundance of the amino acids themselves, plants produce abundant, and in many cases highly inducible, secondary metabolites from intermediates or end products of these pathways. In fact, these enzymes of intermediary metabolism appear to be coordinately regulated with the pathways of aromatic secondary metabolism.

Evidence for this was first obtained in studies of the committing enzyme of aromatic amino acid biosynthesis. Mn^{2+}-dependent DAHP synthase activity and corresponding mRNA abundance increase in response to several treatments that induce secondary metabolite accumulation: wounding of plants, treatment of suspension cells with fungal elicitor, and bacterial pathogen treatment. The kinetics of wound-inducible DAHP synthase mRNA induction are similar to that of phenylalanine ammonia-lyase (PAL), the committing enzyme of aromatic secondary metabolism (Fig. 7.31A). This coinduction of gene expression in response to the environment is not limited to the first enzyme of the shikimate pathway, because shikimate kinase, EPSP synthase, chorismate synthase, and PAL are all maximally induced within several hours after fungal elicitor treatment of tomato (*Solanum lycopersicum*) suspension cells. Similarly, CM1 activity is induced by wounding in potato (*Solanum tuberosum*) tubers, and *CM1* and *PAL* mRNA are coordinately induced in elicited *Arabidopsis* suspension culture cells. In contrast, shikimate pathway genes exhibit different induction kinetics upon exposure of plants to ozone with DAHP synthase, 3-dehydroquinate dehydratase/shikimate dehydrogenase, and EPSP synthase showing the strongest induction. Only weak upregulation was observed for the other genes of the pathway.

There is also a strong correlation in *Arabidopsis* between upregulation of the genes of tryptophan biosynthesis and accumulation of the indolic secondary metabolite **camalexin** (see Fig.7.22) in response to a variety of stressful environmental conditions. Both mRNAs and proteins for all of the enzymes of the tryptophan pathway are induced after treatment with bacterial pathogens, and the rates of induction are similar to that for camalexin accumulation. Not only is the timing of the responses coordinated, but the amount of camalexin that accumulates is tightly correlated with the degree of tryptophan pathway enzyme induction in response to various bacterial pathogens (Fig. 7.31B).

Recent progress in transcriptome analysis allowed use of bioinformatics to dissect and obtain a global view of the regulation of plant metabolic responses to a variety of abiotic and biotic stresses. This analysis revealed that genes encoding enzymes involved in catabolism of amino acids are generally much more sensitive and respond more quickly at the transcriptional level to environmental and stress-associated signals than genes encoding anabolic (allosteric and nonallosteric) enzymes. Thus, **amino acid catabolism** is subjected primarily to transcriptional regulation, whereas in the regulation of amino acid biosynthesis, post-translational allosteric feedback inhibition plays an important role. However, a strong transcriptional response of both anabolic and catabolic genes in the tryptophan pathway was observed in response of *Arabidopsis* shoots to UV-B treatment.

7.4 Aspartate-derived amino acids

Three pathways lead directly from aspartate to the amino acids **lysine**, **threonine**, and **methionine** (see Figs. 7.2 and 7.32). Threonine is then a precursor to **isoleucine**, and methionine is activated to ***S*-adenosylmethionine** (SAM), which is the most important donor of the methyl group in many methylation reactions and also serves as a precursor in the formation of ethylene, polyamines, and in the chain elongation pathway of glucosinolate formation.

Aspartate-derived amino acids are required in the diets of nonruminant animals, including humans. Some diets that rely on plant foods are deficient in one or more of these protein building blocks and can lead to health problems if the

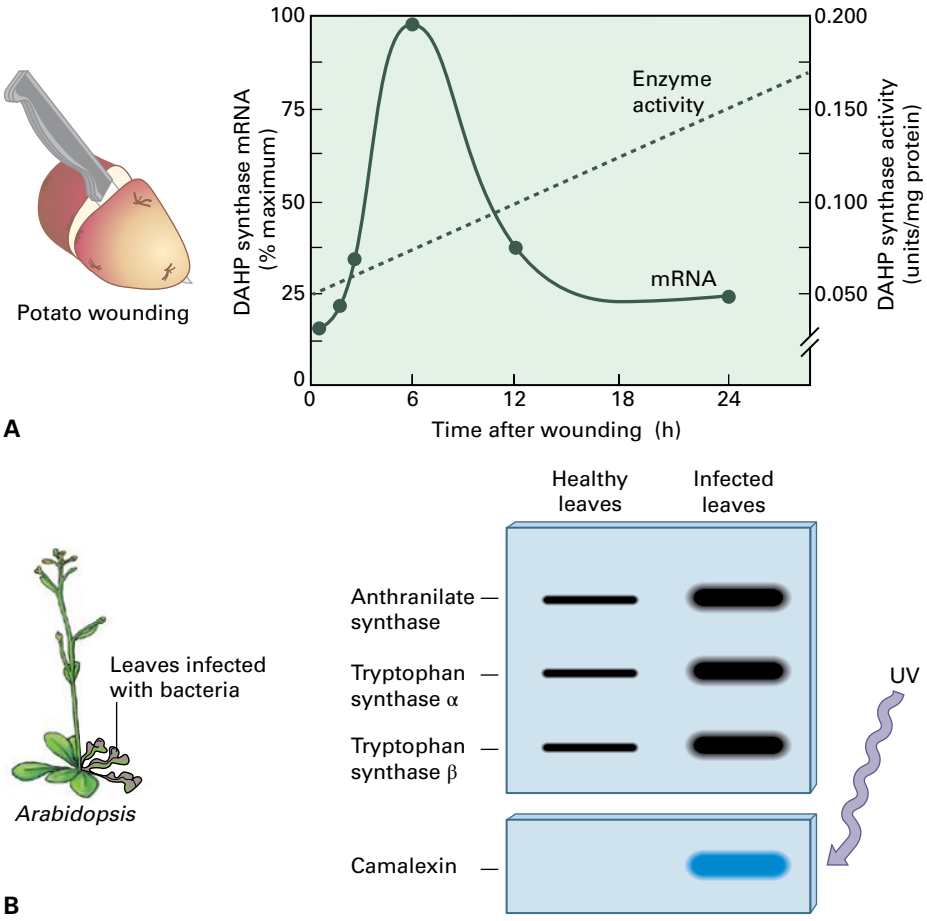


FIGURE 7.31 *Plants induce the enzymes of aromatic amino acid biosynthesis under conditions that cause increases in aromatic secondary metabolism. (A) Wounding of potato tubers causes increased DAHP synthase mRNA and enzyme activity. (B) Infection with a bacterial pathogen increases mRNAs for* Arabidopsis *tryptophan pathway enzymes and increases production of the antimicrobial indolic secondary metabolite camalexin, which fluoresces blue under UV light.*

amino acid deficiencies of grains and legume seeds are not complemented by eating both in combination. Human vegetarians who do not eat any animal products must balance their diets with care to provide all essential amino acids in the proportions that are needed for protein synthesis.

Like humans, farm animals cannot subsist on a diet composed entirely of grain. For example, corn is commonly used in animal feed because it provides calories at low cost, but it has a poor amino acid content and composition, being especially deficient in lysine, but also tryptophan and methionine. On the other hand, soybean is lysine-rich but methionine- and threonine-poor. Supplementing the diets of soybean- or grain-fed animals with lysine, threonine, or methionine increases the growth rate of these animals but is expensive. Not surprisingly, researchers are interested in using conventional breeding and transgenic metabolic engineering approaches to increase the amounts of nutritionally important amino acids, in particular those derived from aspartate, in crop plants.

7.4.1 Threonine, lysine, and methionine are products of a branched pathway with complex biochemical regulation

Aspartate provides the entire carbon skeleton for **threonine**, making it useful to consider threonine biosynthesis as the main pathway (Fig. 7.33), with branches to lysine and methionine (see Figs. 7.34 and 7.35). Aspartate is activated by phosphorylation by **aspartate kinase** (AK; also called aspartokinase), the committing enzyme for all aspartate-derived amino acid biosynthesis. **Aspartate 4-phosphate** (β-aspartyl phosphate) then goes through two NADPH-mediated reductions, which are catalyzed sequentially by **aspartate-semialdehyde dehydrogenase** and **homoserine dehydrogenase** (HSDH), to yield homoserine. Homoserine is then phosphorylated at the 4-position by **homoserine kinase**. **Homoserine 4-phosphate** is at the branching point of threonine and methionine biosynthesis. **Threonine synthase**, a pyridoxal phosphate-dependent enzyme that is allosterically activated by SAM (see Section 7.4.3), is a phospholyase that cleaves the carbon–oxygen bond of homoserine phosphate and then adds water to form the hydroxyl group of threonine.

Lysine biosynthesis presents a deviation from the general rule that the sequences of chemical reactions in complex amino acid biosynthetic pathways are uniform and evolutionarily conserved between all organisms possessing these pathways. It has been known for almost 50 years that the biosynthetic pathways leading to lysine are fundamentally different between bacteria and plants on the one hand, and fungi (asco- and basidiomycetes) on the other hand. In bacteria and plants, lysine is synthesized from aspartate via the **diaminopimelate** (DAP) **pathway** (Fig. 7.34). DAP is a component of the cell wall peptidoglycan in most bacteria, and the DAP pathway, therefore, fulfills two important functions in these organisms by supplying both DAP and lysine.

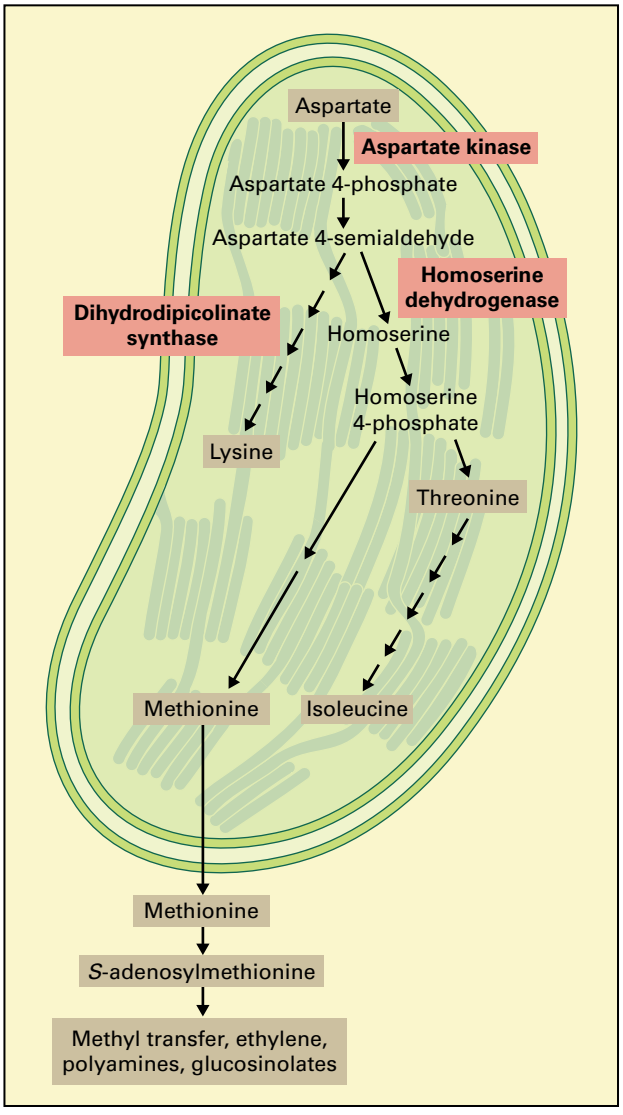


FIGURE 7.32 *The aspartate-derived amino acids are produced in the plastid. Methionine activation to* S*-adenosylmethionine and methionine regeneration occur in the cytosol.*

The fungal pathway proceeds through the intermediate α-**aminoadipate**, from which the name AAA pathway is derived. The starting point in AAA formation is the condensation of α-ketoglutarate and acetyl-CoA to give homocitrate (analogous to citrate formation in the TCA cycle), which is then converted in further TCA cycle-analogous reactions to α-ketoadipate (corresponding to an α-ketoglutarate extended by a methylene group) that is transaminated to yield α-aminoadipate. A variant of the AAA pathway has been found in thermophilic bacteria and in archaea, and the evolutionary background of these convergent pathways of lysine biosynthesis is a challenging topic.

The committing enzyme in the DAP pathway of lysine biosynthesis is **dihydrodipicolinate synthase** (DHPS), which condenses aspartate 4-semialdehyde with pyruvate and cyclizes the product to 2,3-dihydrodipicolinate. For a long time, it was not clear by which reactions ***meso*-2,6-diaminopimelate** is then formed in plants, because even within the bacteria several variants were found, none of which could be verified in plants. After an intensive search for orthologs of bacterial lysine biosynthesis genes in the *Arabidopsis* genome, followed by functional analysis of the gene products, it was uncovered that plants use yet another variant (Fig. 7.34): as in all bacterial variants, dihydrodipicolinate is reduced to **tetrahydrodipicolinate**. Then the pathways diverge; in plants, the acyclic form of tetrahydrodipicolinate is transaminated to give rise to L,L-DAP, which is then epimerized to *meso*-DAP.

(The term epimer is used when in a compound containing two or more chirality centers only one of these is converted to opposite chirality. The two compounds would then be diastereomers rather than enantiomers. A *meso*-form has a plane of symmetry, so the compound is overall achiral. The best known example is tartaric acid.)

At *meso*-DAP the variant pathways meet again, and lysine is formed by decarboxylation of *meso*-DAP. Within an amazingly short time, the crystal structure of the novel enzyme had been determined, giving testimony to the powerful support of biochemistry by genomics.

7.4.2 Methionine formation requires sulfur

In bacteria and plants, the continuous four carbon atoms in **methionine** are derived from the homoserine carbon skeleton. To replace the oxygen function by sulfur, the hydroxyl group must be activated. In bacteria and yeast, the activated form is *O*-succinylhomoserine and *O*-acetylhomoserine, respectively, while in plants it is *O*-phosphohomoserine (homoserine 4-phosphate).which is also the precursor of threonine (Fig. 7.35). In the **trans-sulfuration pathway**, the thiol group of cysteine is transferred to homoserine to produce homocysteine, through a cystathionine intermediate. **Cystathionine γ-synthase**, another pyridoxal phosphate-dependent enzyme, catalyzes the sulfur-linked joining of cysteine and homoserine 4-phosphate to form cystathionine (a thioether) and orthophosphate. Next, the C_3 skeleton of cysteine is cleaved by **cystathionine β-lyase** (again pyridoxal phosphate-dependent), now leaving the sulfur atom attached to the homoserine carbon skeleton; this produces **homocysteine**, pyruvate, and ammonium, making the reaction essentially irreversible. Direct sulfhydration of the activated homoserine with sulfide to give rise to homocysteine is the rule in bacteria and yeast, while in plants it seems to be of minor physiological significance. Homocysteine is then converted to methionine, with N^5-methyltetrahydrofolate serving as the methyl donor, in a reaction catalyzed by **methionine synthase** (homocysteine methylase). This activity not only is involved in de novo methionine synthesis, but also functions in recycling the ***S*-adenosyl-L-homocysteine** produced when **SAM** donates its methyl group in a methylation reaction (Fig. 7.36). While all steps of aspartate-derived amino acids were known to occur in plastids, it seemed puzzling that the final step in methionine synthesis should be localized to the

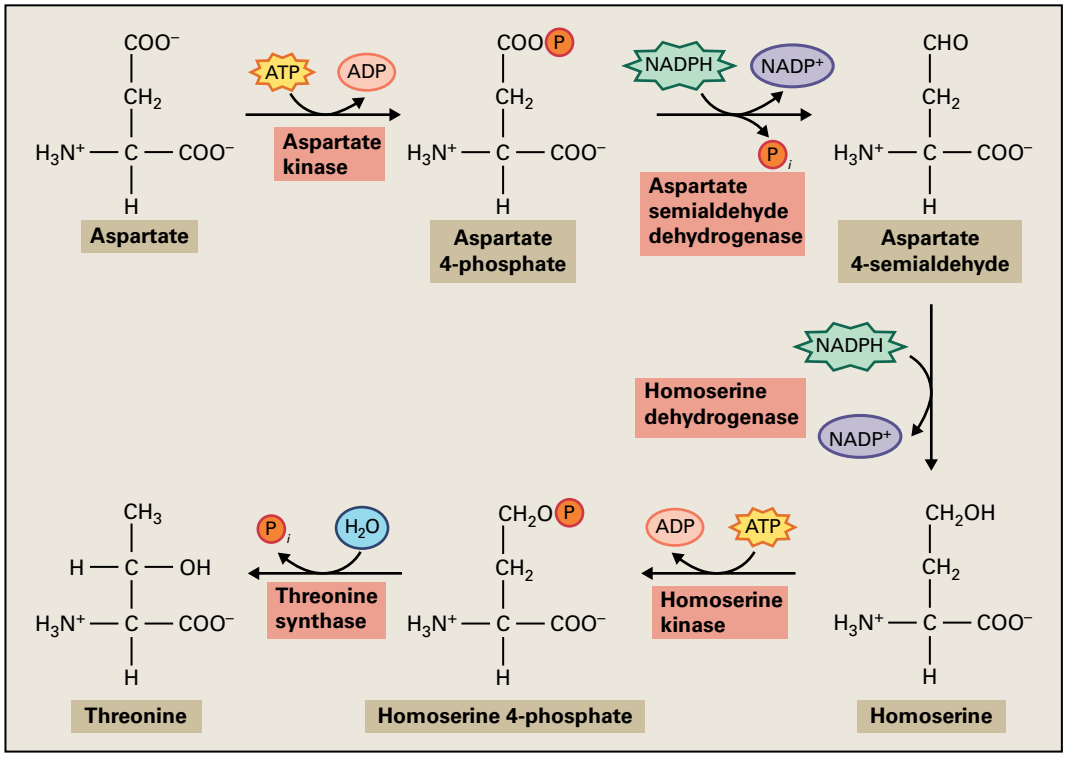


FIGURE 7.33 *The threonine biosynthetic pathway.*

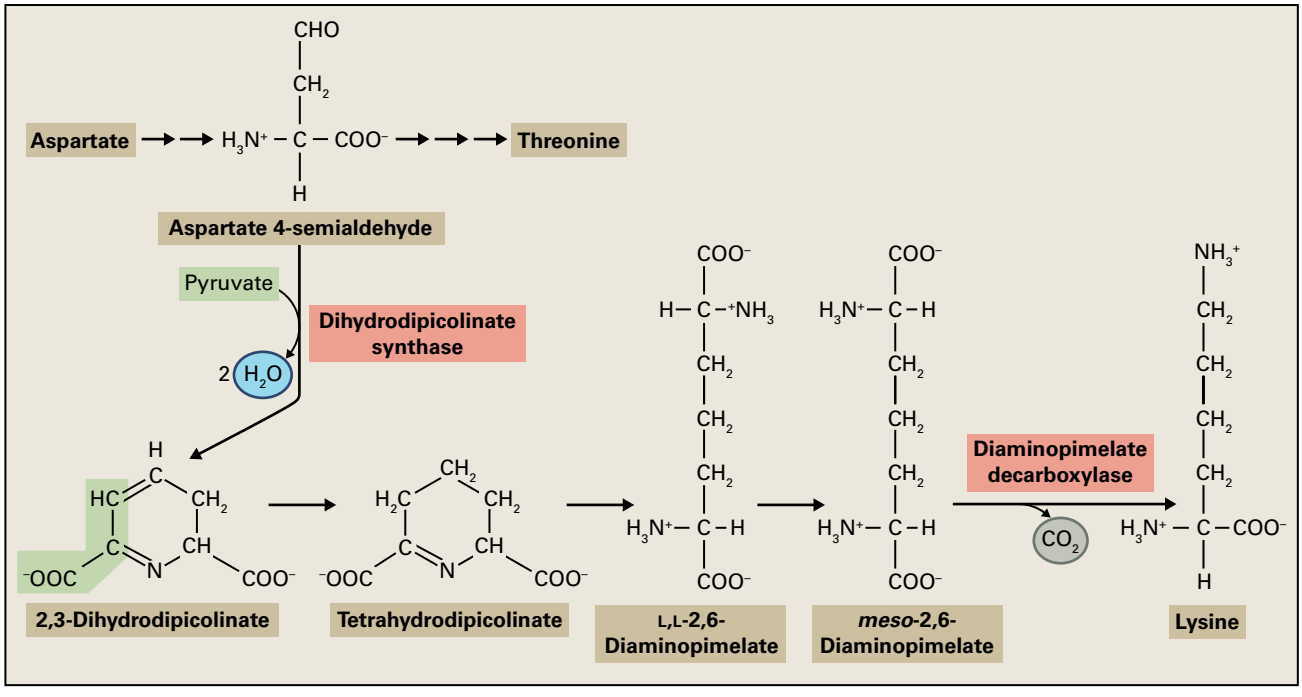


FIGURE 7.34 *Lysine biosynthesis branches from the threonine pathway.*

cytoplasm. This puzzle has been finally solved, however (see Section 7.4.4).

Methionine has two major fates: incorporation into proteins or conversion into SAM. SAM is a methyl donor used in DNA and RNA modification and in synthesis of abundant plant structural components, including lignin precursors, choline and its derivatives, and **pectin** (methyl esters of polygalacturonic acid). The carbon skeleton of the methionine moiety of SAM is also used as a precursor to the plant hormone ethylene and to polyamines (see Chapter 17), and in the chain elongation pathway of glucosinolate biosynthesis (see Chapter 24). Radiotracer experiments with the aquatic

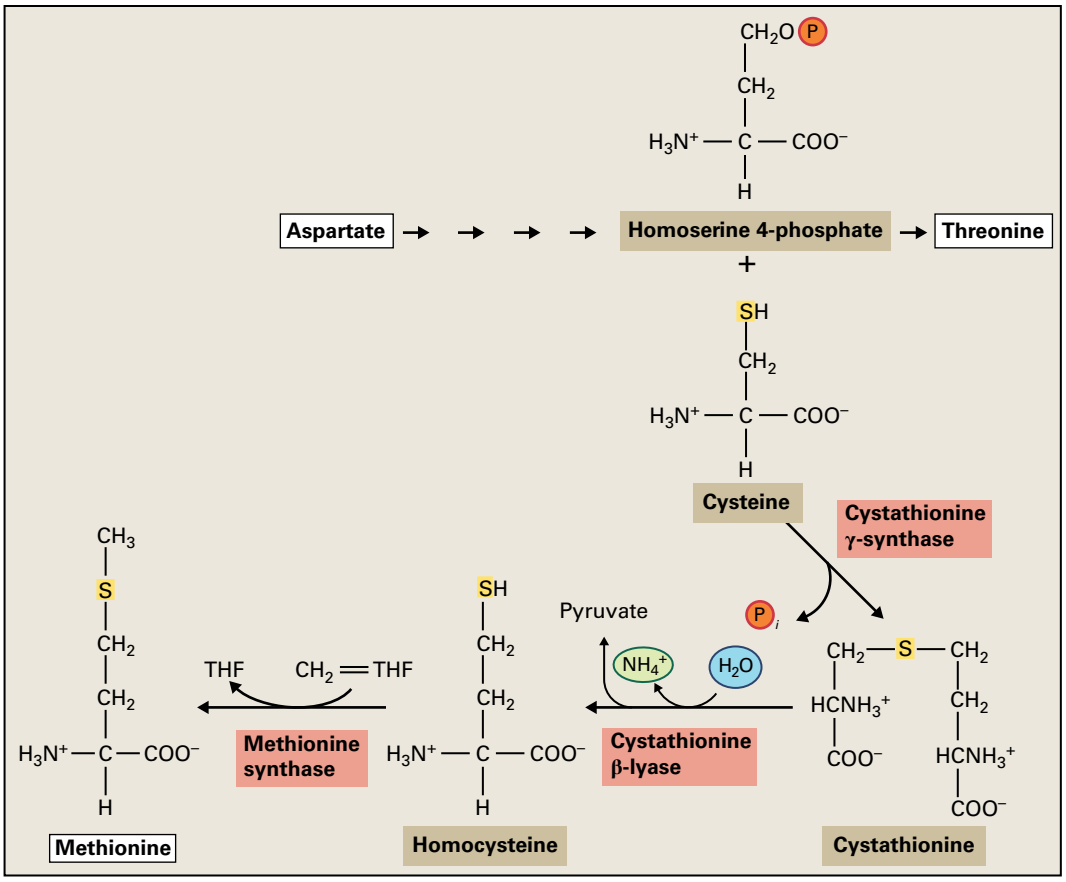
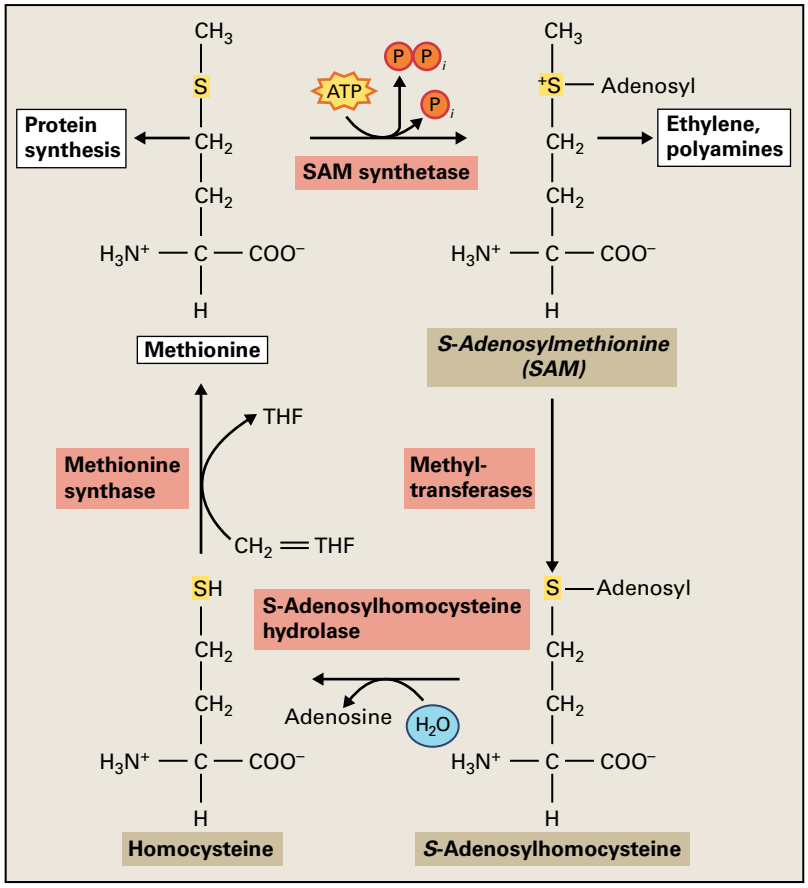


FIGURE 7.35 *The methionine biosynthetic pathway. THF, tetrahydrofolate.*

FIGURE 7.36 *S-Adenosylmethonine is produced from methionine and can be recycled to regenerate methionine. THF, tetrahydrofolate.*



plant *Lemna paucicostata* (duckweed) indicate that more than 80% of the label from ^{14}C-methyl-labeled methionine was incorporated into lipids, pectins, chlorophyll, and nucleic acids, whereas less than 20% appeared in protein. Thus, apparently the majority of methionine is converted into SAM for transmethylation reactions in plants. Production of SAM is an energy-demanding process in the unusual course of which the entire triphosphate chain is displaced from ATP by SAM synthetase and pyro- and orthophosphate, respectively, are released (Fig. 7.36).

As is the case for most amino acids, their catabolism has been investigated to a much lesser extent than their biosynthesis. For methionine, it became only recently clear in *Arabidopsis* that in addition to its transamination, cleavage of methionine by **methionine γ-lyase** is the initial reaction in its degradation. This pyridoxal phosphate-dependent enzyme occurs in microorganisms, and based on amino acid sequence similarity an ortholog was identified in the *Arabidopsis* genome and the corresponding protein characterized. This cytosolic enzyme converts methionine to **methanethiol** (CH_3-SH), **α-ketobutyrate,** and ammonia. α-Ketobutyrate is the precursor of **isoleucine** (see Section 7.5.1) and is thus not exclusively formed by threonine deaminase as had been generally believed.

7.4.3 Regulation of threonine, lysine, and methionine synthesis is complex

Not surprisingly, the biochemical mechanisms regulating flux through the branches of the aspartate-derived amino acid pathway are complex. First, aspartate-derived metabolism can follow three major routes, creating at least five branch point enzymes: **aspartate kinase** (AK), **dihydrodipicolinate synthase** (DHDPS), **homoserine dehydrogenase** (HSDS), **threonine synthase** (TS), and **cystathionine γ-synthase** (CγS). Of these, the first four are allosterically regulated in plants, and CγS is regulated at the transcriptional and, in some plants, at the posttranscriptional level. Second, the products of these pathways are expected to be needed by the plant in different amounts at each stage of development. An overview of the types of regulatory mechanisms inferred by in vitro studies is shown in Figure 7.37. As described below, experiments with feedback-insensitive mutants and transgenic plants are clarifying the in vivo importance of these regulatory phenomena.

AK, the committing enzyme for the overall pathway, is a critical regulatory enzyme occurring in multiple classes of AK isoenzymes, which have divergent primary sequences and contrasting allosteric properties. Biochemical studies indicated the existence of at least two forms of AK activity that are separable by column chromatography. For example, barley AK-I is inhibited by lysine, an inhibition potentiated by SAM. AK-II and AK-III, however, are both sensitive to threonine inhibition. Molecular analysis has identified genes that express two classes of AK: monofunctional proteins that resemble the *E. coli* lysine-sensitive isoform, and bifunctional enzymes homologous to the *E. coli* threonine-sensitive isoform that contain an HSDH coding region at the C-terminus (AK-HSDH).

If feedback regulation of AK is primarily responsible for regulating flux to all three end products (threonine, lysine, and methionine/SAM), deregulating this enzyme should increase accumulation of all three amino acids, and this is indeed the case. Mutants with deregulated **lysine-sensitive AK** were

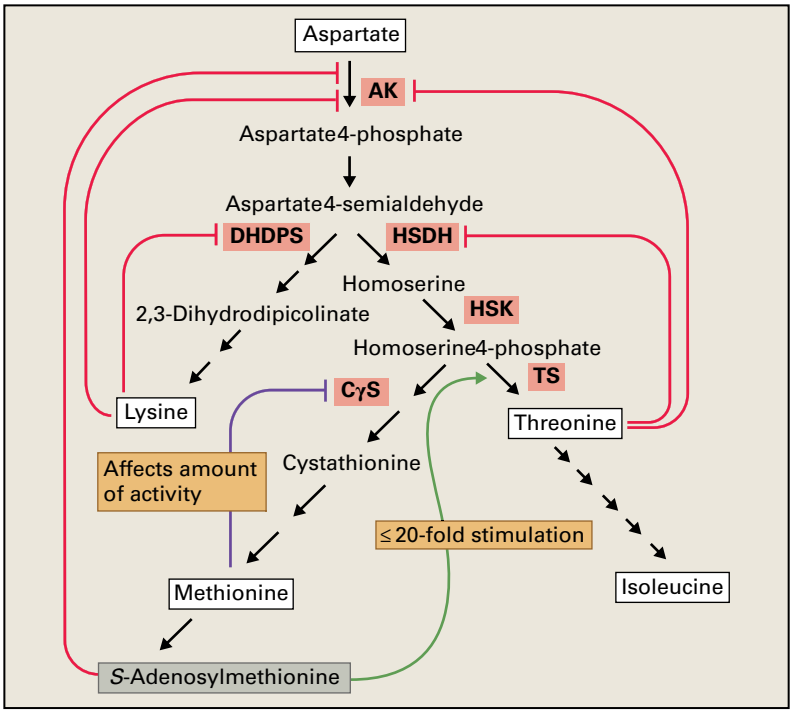


FIGURE 7.37 *Biochemical regulatory mechanisms proposed to regulate the synthesis of amino acids derived from aspartate. Red lines indicate end-product inhibition, the purple line refers to a reduction in detectable enzyme, and the green lines indicate stimulation of activity.*

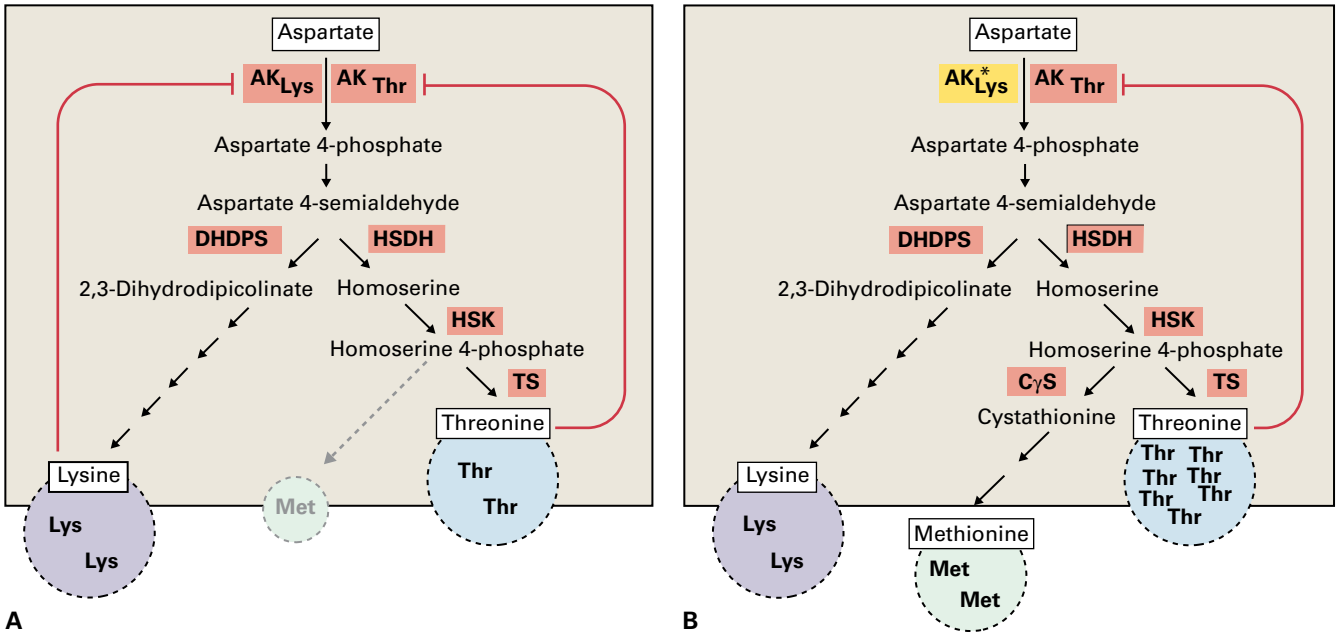


FIGURE 7.38 *Treatment of plants with lysine plus threonine allows selection for feedback-insensitive aspartate kinase mutants. AK_{Lys} and AK_{Thr} refer to AK isoforms that are inhibited by lysine or threonine, respectively. (A) Growth of wild-type plants or plant cell cultures on medium containing a mixture of lysine and threonine causes death by methionine starvation because of inhibition of AK activity. (B) Mutants arise that are insensitive to this normally toxic amino acid mixture. These plants (AK^*_{Lys}) contain amino acid changes in their lysine-sensitive aspartate kinase activities, which make them insensitive to feedback inhibition. This restores the plant's ability to synthesize methionine.*

selected by taking advantage of the fact that administration of threonine and lysine causes starvation for methionine by reducing total AK activity through feedback inhibition. Mutants were selected with AK activities that were less sensitive to lysine inhibition (Fig. 7.38). In an analogous approach, transgenic tobacco (*Nicotiana tabacum*) or potato (*Solanum tuberosum*) plants were constructed to express a *lysC* gene encoding a feedback-desensitized AK protein from *E. coli*. That these mutants and transgenic plants overaccumulated threonine shows both that AK plays an important role in modulating threonine accumulation in plants and that lysine and methionine accumulation are influenced at later steps in the pathway.

In plants, DHDPS activity is very sensitive to lysine inhibition (the concentration to achieve 50% inhibition, or I_{50}, is 10–50 μM), making it a likely candidate for a key regulator of lysine accumulation. Plant mutants with desensitized DHDPS were identified in several species by selection for resistance to the toxic lysine analog ***S*-aminoethyl-L-cysteine** (AEC). This molecule competes with lysine for incorporation into proteins and allows the identification of lysine-overproducer plants. AEC resistance in *Nicotiana sylvestris,* caused by production of a lysine-insensitive mutant DHDPS enzyme with a single amino acid change, led to these plants accumulating about 10-fold more lysine than did the wild type (Fig. 7.39). Similar results were obtained with transgenic plants that expressed bacterial DHDPS proteins, which are naturally about 20-fold less sensitive to lysine inhibition than plant enzymes are. In agreement with the mutant results, tobacco (*Nicotiana tabacum*) and oilseed rape (*Brassica napus*) transformants accumulated greater amounts of lysine than did controls. These results demonstrate the importance of allosteric regulation of DHDPS in regulating lysine accumulation in plants.

Transgenic plants and mutants that simultaneously express both feedback-insensitive AK and DHDPS accumulate free lysine concentrations that exceed those in plants expressing the mutant DHDPS alone, and have less threonine than plants with the desensitized AK alone. These results provide two important lessons about regulation of flux through this pathway. First, the relative accumulation of threonine and lysine seems to be affected by the ability of DHDPS and HSDH to compete for limiting amounts of aspartate 4-semialdehyde. Second, the very high sensitivity of DHDPS to feedback inhibition ordinarily restricts flux into lysine biosynthesis, explaining why AK single-mutant plants preferentially accumulate threonine rather than lysine.

Homoserine 4-phosphate is the final intermediate common to synthesis of threonine/isoleucine and methionine/SAM. Thus, the relative ability of threonine synthase and cystathionine γ-synthase to compete for this intermediate is likely to be important for regulating metabolic flux through these pathways. Two mechanisms have been proposed to influence this partitioning (see Fig. 7.37): (a) stimulation of threonine synthase activity by the product of the competing pathway, SAM; and (b) modulation of cystathionine γ-synthase activity by methionine availability. Thus, flux from homoserine 4-phosphate into threonine or methionine biosynthesis may be primarily regulated by the amounts of methionine and SAM present.

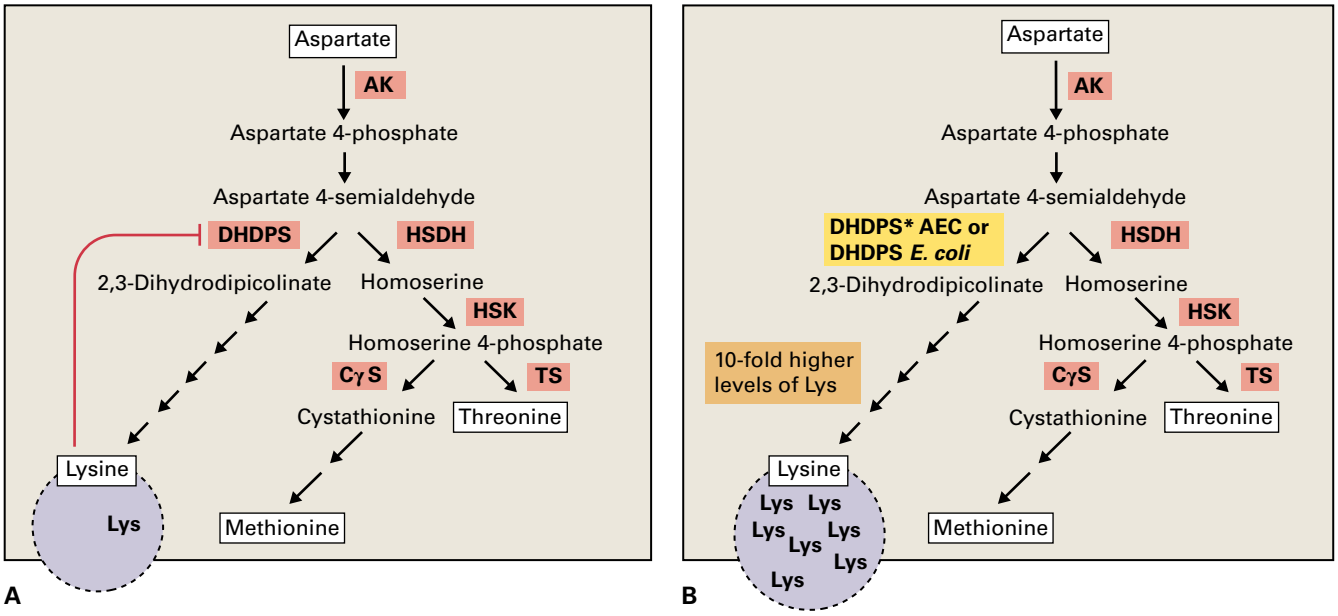


FIGURE 7.39 *Dihydrodipicolinate synthase (DHDPS) regulates the accumulation of lysine in plants. (A) Feedback inhibition of DHDPS acts to control the flux from aspartate 4-semialdehyde into lysine. (B) Dominant feedback-insensitive DHDPS mutants can be selected by use of classical genetics (DHDPS* AEC) or by expression of feedback-insensitive* E. coli *enzyme in transgenic plants (DHDPS* E. coli*). These plants overproduce lysine in comparison with the plant that expresses the wild-type DHDPS activity.*

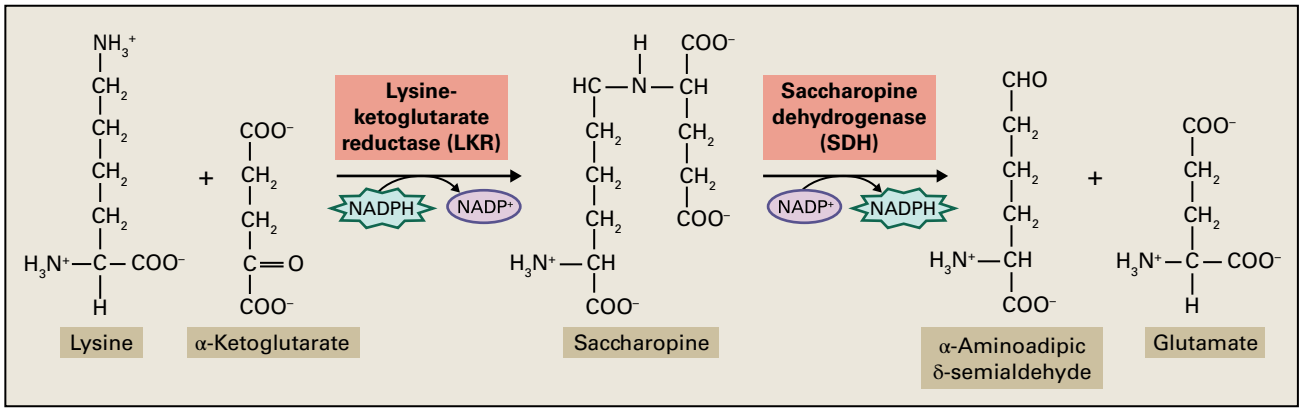


FIGURE 7.40 *Initial reactions in lysine catabolism.*

7.4.4 Biosynthesis and degradation regulate lysine levels in a concerted manner that must be understood to produce high-lysine plants

High quantities of lysine accumulate in plants expressing feedback-insensitive mutant DHDPS, but this perturbation of metabolism, which also affects other amino acids, causes severe developmental defects. Increasing the nutritional value of crops requires engineering increased lysine content in seeds, but simply increasing lysine biosynthesis by expressing mutant DHPS in a seed-specific manner may not be enough to achieve this goal. Targeting high-level expression of deregulated enzyme activities to seeds actually causes an enhancement of lysine breakdown. The first enzyme of **lysine catabolism** is **lysine-ketoglutarate reductase** (LKR), which reduces the labile Schiff base that is formed between the ε-amino group of lysine and α-ketoglutarate, to a stable opine, **saccharopine** (Fig. 7.40). In the subsequent reaction, catalyzed by saccharopine dehydrogenase (SDH), the amine function is transferred to the α-ketoglutarate skeleton, giving rise to glutamate while the ε-C of the lysine C-skeleton now carries the carbonyl function (α-aminoadipic δ-semialdehyde, which is further degraded to yield acetyl-CoA). The bifunctional polypeptide LKR/SDH is induced by lysine through complex transcriptional and posttranslational controls and is also subject to regulation by stress-associated signals. In addition to encoding the bifunctional polypeptide, the complex *LKR/SDH* locus may encode monofunctional

LKR and monofunctional SDH (depending on the plant species). The independent function of these two monofunctional enzymes is not fully understood.

7.4.5 All aspartate-derived amino acids are synthesized in the plastid

Many of the enzymes of lysine, threonine, and methionine biosynthesis have been localized to the chloroplast by measuring their activities in chloroplast lysates. In addition, comparison of the DNA sequences of cloned plant genes for pathway enzymes with those of microbes has revealed N-terminal extensions that resemble characterized plastid-targeting sequences. The final steps of methionine biosynthesis were long thought to be the exception to this rule; however, there are three functional isoforms of **methionine synthase** (MS) in *Arabidopsis*, one localized to chloroplasts and the other two to the cytosol. The current understanding is, therefore, that chloroplasts are fully autonomous in the biosynthesis of all aspartate-derived amino acids, including methionine (see Fig. 7.32). The cytosolic forms of MS are thought to be involved in the regeneration of methionine from homocysteine that remains after SAM-dependent methylation reactions. SAM synthase is exclusively cytosolic, and carriers have been identified that mediate the transport of SAM into chloroplasts and mitochondria.

7.5 Branched-chain amino acids

Isoleucine, **leucine**, and **valine** form the small group of **branched-chain amino acids** classified as such based on their small branched hydrocarbon residues. The biosynthesis of the branched-chain amino acids by plants attracts considerable attention for several reasons: First, they represent three of the 10 **essential amino acids** that animals must obtain from their diet and are, therefore, nutritionally important. Second, this pathway is a significant target for a variety of commercially successful herbicides. Finally, the amino acid products serve as precursors for secondary metabolites (Fig. 7.41).

7.5.1 Threonine deaminase participates in the synthesis of isoleucine but not of valine

A unique feature of branched-chain amino acid biosynthesis is that isoleucine and valine are synthesized in chloroplasts from two parallel pathways utilizing the same set of four enzymes. Each of the four enzymes has dual substrate specificity, starting with either **pyruvate** (leading to valine) or **α-ketobutyrate** (leading to isoleucine). While pyruvate (C_3) is an intermediate of glycolysis, its C_4 counterpart, α-ketobutyrate, is produced by **threonine deaminase** (TD, also known as **threonine dehydratase**). TD is thus the committing enzyme of the isoleucine pathway and has no role in valine metabolism (Fig. 7.42). As described in Section 7.4.2, α-ketobutyrate can also be produced from methionine by **methionine γ-lyase**, but the normal activity of this enzyme is insufficient for rescuing the isoleucine deficiency in TD knockdown mutants. Thus, while TD and methionine γ-lyase appear to have overlapping functions in isoleucine biosynthesis, TD plays the dominant role in controlling the threonine flux toward isoleucine under normal growth conditions.

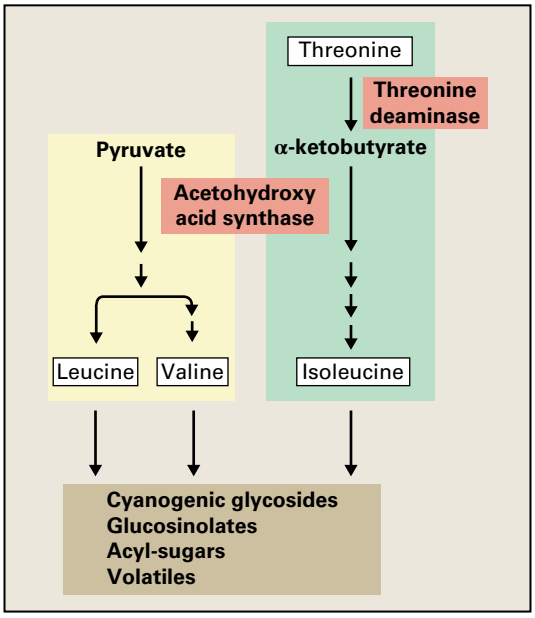


FIGURE 7.41 *The branched-chain amino acids serve as precursors to plant secondary metabolites.*

Similar to the bacterial enzyme, plant TD is a tetramer composed of identical subunits with a molecular mass of 59.6 kDa in *Arabidopsis*. In contrast to the *E. coli* enzyme, however, the plant TD dissociates into less active dimers at elevated isoleucine levels. Each subunit consists of an N-terminal PLP-binding catalytic domain and a C-terminal regulatory domain that is subject to feedback inhibition by isoleucine. Within the regulatory domain, there are two structurally different isoleucine allosteric binding sites. Binding of an isoleucine molecule to a high-affinity site promotes conformational changes that then allow the low-affinity site to bind a second isoleucine molecule, which leads to inhibition of the enzyme. The high-affinity binding site can also interact with valine. Such interactions induce conformational changes that trigger dissociation of isoleucine from the binding sites and thus the reversion of inhibition. An isoleucine-insensitive TD was identified in a screen for *Arabidopsis* mutants resistant to the isoleucine analog **L-*O*-methylthreonine**. Two amino acid substitutions, each in a different regulatory region, render the enzyme resistant to inhibition by isoleucine, and the mutant plants accumulate 20-fold more isoleucine than wild-type plants.

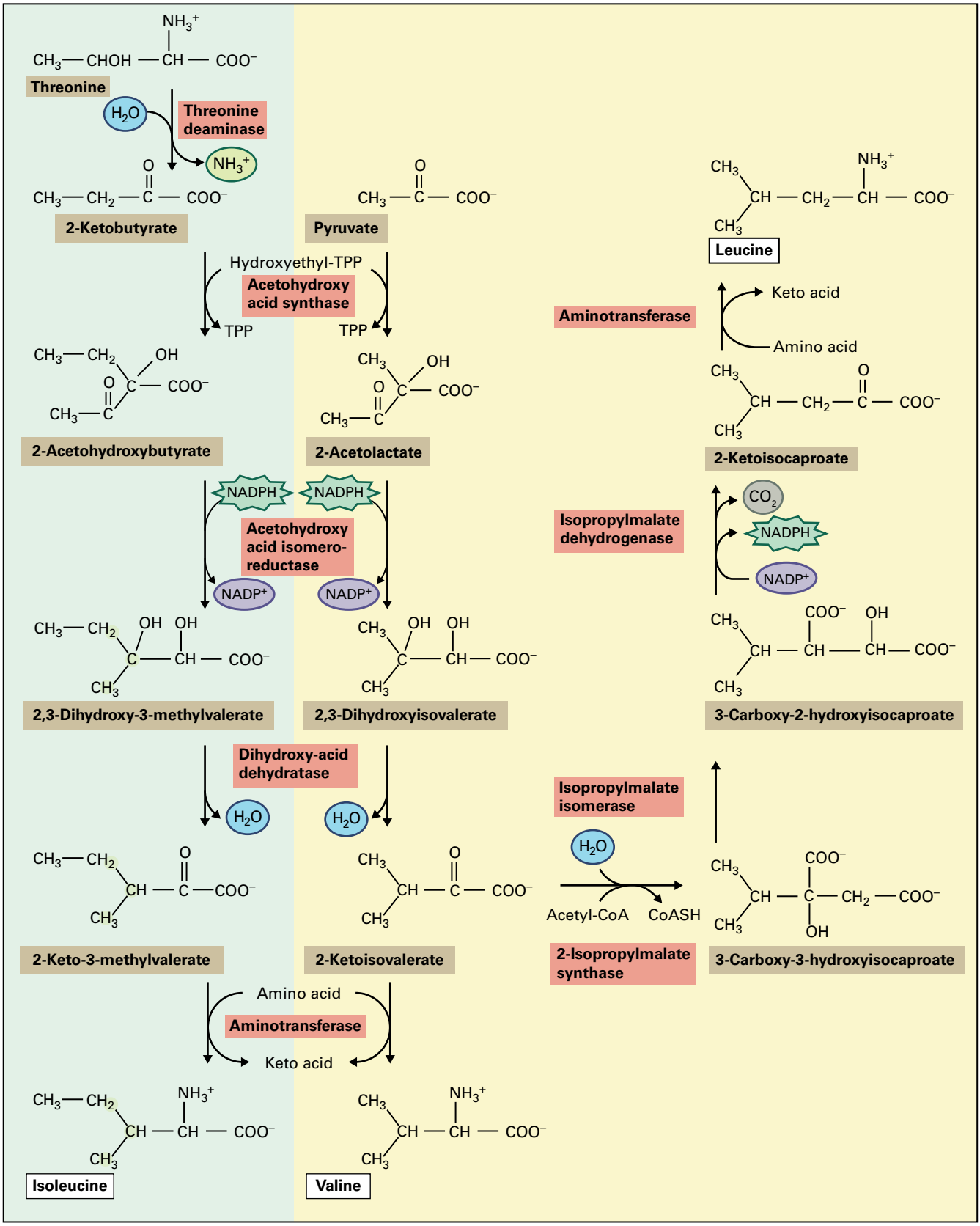


FIGURE 7.42 *Biosynthesis of isoleucine, leucine, and valine.*

BOX 7.6 Threonine deaminase 2 is involved in plant defense against herbivores in *Solanum* species

Many plant species have a single *TD* gene, and defects in this gene result in isoleucine deficiency and impaired growth and development. However, cultivated tomato (*Solanum lycopersicon*) and related *Solanum* species contain a duplicated *TD* gene (*TD2*) that encodes a protein with 51% identity to *TD1*. In contrast to the constitutive expression of *TD1*, *TD2* transcripts accumulate to high levels in immature buds and unopened flowers. Moreover, *TD2* expression in leaves is activated by the jasmonate signaling pathway in response to herbivore attack. Analysis of TD2-deficient tomato plants revealed that TD2 reduces herbivory by degrading threonine in the insect gut and thereby functions as an antinutritive defense by limiting threonine supply needed for the growth of the lepidopteran larvae. In the gut, TD2 undergoes proteolytic activation catalyzed by a chymotrypsin-like protease of the insect, which removes the C-terminal regulatory domain and generates an enzyme that degrades threonine without being inhibited by isoleucine. Truncated TD2 can also use serine as a substrate (producing pyruvate and ammonia) and thus affect the availability of this amino acid as well. Interestingly, in *Nicotiana attenuata,* a single *TD* gene serves a dual role in both isoleucine biosynthesis and protection against lepidopteran herbivores.

7.5.2 The isoleucine and valine biosynthetic pathways share four enzymes

The first common enzyme in the biosynthesis of the branched-chain amino acids is **acetohydroxyacid synthase** (AHAS; also known as **acetolactate synthase**), which catalyzes the decarboxylation of pyruvate followed by its condensation with either pyruvate or 2-ketobutyrate to form 2-acetolactate or 2-acetohydroxybutyrate, respectively (Fig. 7.42). AHAS requires thiamine diphosphate as cofactor, which is anchored to the active site of the enzyme by a divalent metal ion such as Mg^{2+}. AHAS also requires flavin adenine dinucleotide (FAD), even though this cofactor does not participate in the principal reactions and may have instead a structural function.

Like the bacterial and yeast enzymes, plant AHAS comprises both a large catalytic subunit and a smaller regulatory subunit. The large subunit alone is insensitive to allosteric inhibition, but reconstitution in vitro with the small subunit stimulates enzymatic activity and confers sensitivity to inhibition by valine, leucine, and isoleucine. The inhibition of AHAS by all three branched-chain amino acids is an unusual feature of the plant enzyme, since most bacterial and fungal enzymes are sensitive to inhibition by valine only.

Moreover, valine and leucine act synergistically on the plant enzyme. Such synergistic inhibition is the result of the presence of a sequence repeat in the AHAS regulatory subunit. As confirmed by site-directed mutagenesis, one repeat binds leucine, while the other binds valine or isoleucine. Presumably as a result of this allosteric regulation, plant growth is inhibited when valine is added to the medium. Valine tolerance has been found in mutants of tobacco and *Arabidopsis* with feedback-insensitive AHAS activity. The tobacco *Val^R-1* mutant has a single amino acid change in the AHAS protein responsible for the altered allosteric regulation and *in vivo* amino acid resistance.

AHAS has been intensely studied because it is the target of five commercially important and structurally highly divergent classes of herbicides: **imidazolinones**, **sulfonylureas**, **triazolopyrimidines**, pyrimidyl-oxy-benzoates and sulfonylaminocarbonyltriazolinones (Fig. 7.43). Mutant plants that are resistant to inhibitors of some, or in certain cases even all, of these different herbicide classes express AHAS proteins with mutations in the large catalytic subunit that cause increased inhibitor resistance. In many cases, single nucleotide mutations confer resistance without affecting the catalytic efficiency of AHAS, and hence do not reduce the fitness of plants possessing these mutant enzymes. Thus, resistance to these herbicides can evolve rather readily in the field. The crystal structure of *Arabidopsis* AHAS with bound sulfonylurea or imidazolinone herbicides has revealed that these compounds do not bind to the active site itself, but rather block a protein channel through which the substrates have access to the active site.

The 2-acetohydroxybutyrate and 2-acetolactate intermediates are subjected to alkyl rearrangement and NADPH-mediated reduction by **acetohydroxy acid isomeroreductase** (also called reductoisomerase) to form the corresponding 2,3-dihydroxyvaleric acids (see Fig. 7.42). The crystal structure of the homodimeric enzyme from spinach (*Spinacia oleracea*) has been determined, and inhibitors of this enzyme also have herbicidal activity.

The next step is catalyzed by **dihydroxy-acid dehydratase**, a 2Fe-2S cluster protein, to produce the 2-ketovalerate products. The importance of this enzyme in branched-chain amino acid biosynthesis was confirmed through identification of isoleucine- and valine-requiring *Nicotiana plumbaginifolia* mutants that lack dihydroxy-acid dehydratase activity. Then the final step in isoleucine and valine biosynthesis is transamination of the keto acids to the respective amino acids. A single aminotransferase activity appears to be involved in both isoleucine and leucine (see below) biosynthesis, while a distinct 2-ketoisovalerate aminotransferase

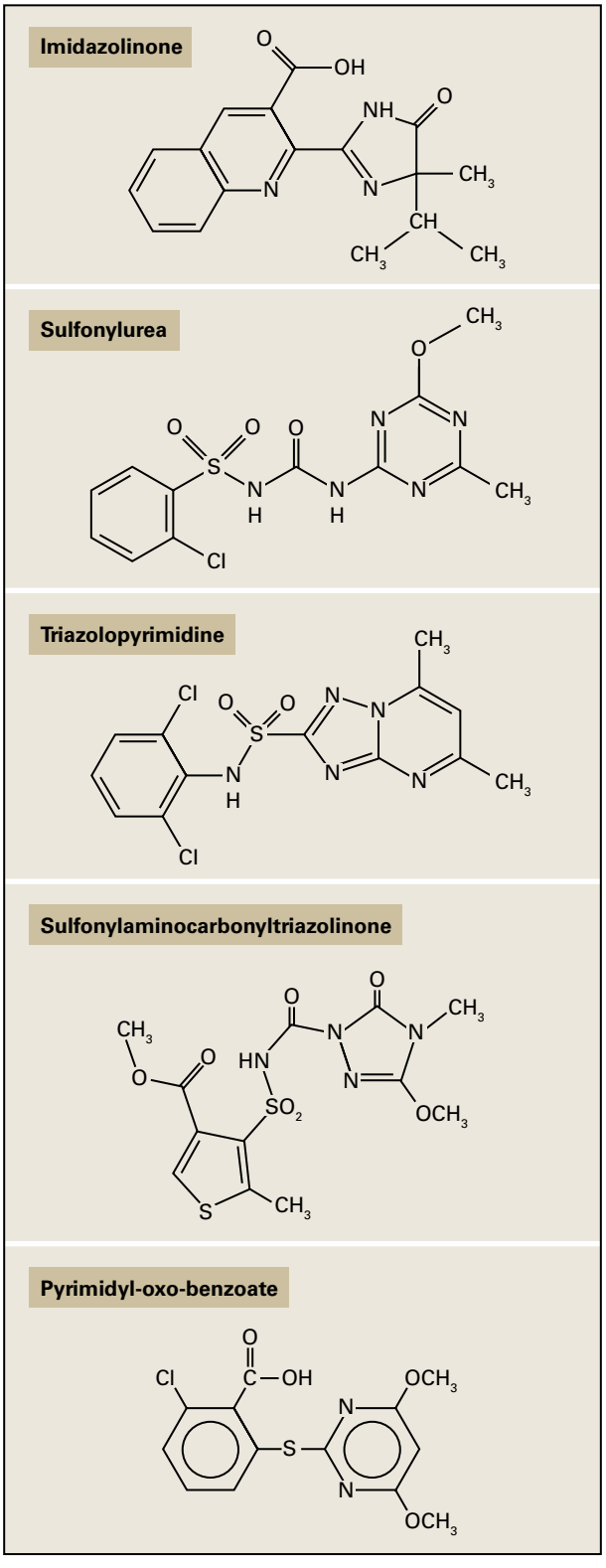


FIGURE 7.43 *Examples of the five classes of commercial herbicides that are AHAS inhibitors.*

produces valine. The *Arabidopsis* genome contains a small gene family of **branched-chain aminotransferases** (BCAT). Three of these (BCAT2, BCAT3, and BCAT5) appear to be targeted to the plastid, where they likely participate in the biosynthesis of the branched-chain amino acids, whereas BCAT1 is targeted to the mitochondrion and likely initiates the degradation of these amino acids. (BCAT4 actually transaminates methionine.)

7.5.3 Plant leucine biosynthesis follows the bacterial pathway

Leucine biosynthesis branches from 2-ketoisovalerate, the last intermediate of the valine biosynthetic pathway, and evidence indicates that plants use the pathway found in microbes (see Fig. 7.42). The committing enzyme for the pathway, **2-isopropylmalate synthase** (IPMS), catalyzes the transfer of an acetyl group from acetyl-CoA to 2-ketoisovalerate to produce 3-carboxy-3-hydroxyisocaproate (2-isopropylmalate or α-isopropylmalate). This enzyme is subject to feedback inhibition by micromolar concentrations of leucine. Biochemical characterization of recombinant proteins in conjunction with analysis of knockout mutants revealed that the *Arabidopsis* genome contains two IPMS genes encoding active IPMS proteins involved in leucine biosynthesis. The two genes are expressed in all organs at all developmental stages and can fully compensate for the absence of each other.

The second step in leucine biosynthesis is catalyzed by **isopropylmalate isomerase** (IPMI, also known as isopropylmalate dehydratase), which reversibly converts 3-carboxy-3-hydroxyisocaproate to 3-carboxy-2-hydroxyisocaproate (3-isopropylmalate or β-isopropylmalate). Similar to the bacterial enzyme, plant isopropylmalate isomerase has a heterodimeric structure with a large and a small subunit. In the *Arabidopsis* genome, a single gene encodes the large subunit, and three genes encode the small subunit. Detailed metabolic profiling of several mutants revealed the involvement of the large subunit in the biosynthesis of both leucine and chain-elongated methionine derivatives (see Section 7.4.2). In contrast, the small subunit determines the substrate specificity of the respective heterodimeric IPMI. One of the three *Arabidopsis* IPMI small subunits is responsible for leucine formation, while the other two mediate **methionine chain elongation**. As a result of differential tissue-specific expression of the small subunits, various IPMI heterodimers can be formed.

The penultimate reaction in leucine biosynthesis is the NAD^+-dependent oxidative decarboxylation of 3-isopropylmalate to 2-ketoisocaproate (4-methyl-2-oxovalerate) catalyzed by **isopropylmalate dehydrogenase** (IPMDH). The partially purified enzyme is a target of the herbicidal compound *O*-isobutenyl oxalylhydroxamate. IPMDH genes have been cloned from several plant species, and they can complement yeast with a mutation in the Leu2 gene, which encodes a functional IPMDH. The *Arabidopsis* genome contains three *IPMDH* genes, of which *IPMDH1* encodes a major enzyme with dual function in leucine biosynthesis and in methionine chain elongation in the course of aliphatic glucosinolate biosynthesis. Interestingly, IPMDH1 activity is regulated by thiol-based redox modification. Leucine biosynthesis is

completed by a transamination step catalyzed by the same BCATs that are involved in the formation of valine and isoleucine (see Section 7.5.2).

7.6 Glutamate-derived amino acids

Proline, **arginine**, and the (nonproteinogenic) amino acid **ornithine** are biosynthetically derived from **glutamate**. Proline has received major attention in plant biology because of its accumulation in responses to salt, drought, and metal stress. Although biochemical studies have rather neglected the synthesis of arginine in plants in the past, genomic annotations have provided missing information.

7.6.1 Proline metabolism is a target for metabolic engineering of stress tolerance

Understanding and manipulating proline biosynthesis in plants is largely motivated by observations that this cyclic secondary amino acid is one of several organic compounds that can function as **compatible solutes.** Compatible solutes are molecules that can accumulate to high concentrations in the cytoplasm without disrupting cellular activity and allow plants to lower their water potential and maintain turgor during dry or saline conditions (see Chapter 22). Proline also scavenges **reactive oxygen species** (ROS), which are formed under stressful conditions (see Chapters 21 and 22), and its function in stress situations is thus multifaceted. Water stresses cause considerable loss of agricultural productivity, making it desirable to develop **drought-tolerant plants** by conventional or transgenic strategies. Studies of genetically engineered plants that accumulate high levels of proline have provided clear evidence for the ability of proline to confer increased osmotic tolerance.

7.6.2 In plants, proline may be produced by two distinct pathways

Proline can be synthesized by two different pathways in plants. One originates from glutamate, the other from ornithine, although the details of the ornithine pathway are less clear (Fig. 7.44). The committing enzyme of the glutamate pathway, **pyrroline-5-carboxylate synthetase** (P5CS), is a bifunctional enzyme in plants. Its first activity, **γ-glutamyl kinase**, catalyzes the ATP-dependent phosphorylation of L-glutamate, and the γ-glutamyl phosphate produced is then reduced to **glutamic γ-semialdehyde** (GSA) by the NADPH-dependent GSA reductase. This intermediate spontaneously cyclizes to form Δ^1-pyrroline-5-carboxylate (P5C, a Schiff base). The *Arabidopsis* genome harbors two closely related P5CS genes with nonredundant functions (see Section 7.6.3). P5C is then converted to proline by the NADPH-dependent enzyme P5C reductase.

Two routes proposed for the synthesis of proline from ornithine (Fig. 7.44) differ as to whether Δ^1-pyrroline-5-carboxylate or Δ^1-pyrroline-2-carboxylate (an imino acid) is the final intermediate in the pathway. In the first instance, transamination of ornithine occurs at the δ-C, while in the second instance it occurs at the α-C. Ornithine δ-aminotransferase (δOAT) has been characterized at both the biochemical and molecular levels in plants.

7.6.3 Proline synthesis and breakdown are environmentally regulated in plants

Regulation of proline accumulation in plants occurs both at the enzyme level and through changes in gene expression. The committing enzyme P5CS appears to be rate limiting in plants, and its transcript as well as free proline increase rapidly in response to desiccation, salt stress, and treatment with abscisic acid, and they return to normal level when dehydrated plants are watered. In several plant species, PC5S overexpression (but not that of P5C reductase) leads to plants with increased soluble proline content and reduced sensitivity to osmotic stress. As the γ-glutamyl kinase activity of PC5S is feedback-inhibited by proline, this feedback loop paradoxically appears to counteract the effect of increased expression of the enzyme. Loss of feedback inhibition by a conformational change of the P5CS protein under stress conditions has been proposed. Expression of a wild-type feedback-sensitive, and a mutagenized feedback-insensitive, *Vigna aconitifolia* PC5S in tobacco (*Nicotiana tabacum*) revealed a higher accumulation of proline in control conditions. Proline accumulated to even higher levels under salt stress in those plants expressing the feedback-insensitive PC5S, indicating that feedback inhibition is not (fully) abolished under normal conditions.

Of the two *PC5S* genes of *Arabidopsis*, *PC5S1* responds to osmotic stress, and the loss-of-function mutant displays increased ROS levels and hypersensitivity to stress. Mutant *pc5s2* plants, on the other hand, have developmental defects, in particular embryo abortion during late seed development (desiccation stage). Tissue-specific expression patterns of the two genes differ considerably, and the two genes, therefore, do not complement each other.

The contribution of the ornithine pathway to proline synthesis was investigated both in **δOAT** loss-of-function mutants and in transgenic plants overproducing δOAT. In *Arabidopsis* loss-of-function mutants, proline accumulates normally under stress conditions, whereas arginine and ornithine can no longer be catabolized. This indicates a purely catabolic function of δOAT in arginine degradation, which occurs in mitochondria where δOAT is localized. On the other hand, transgenic *Nicotiana plumbaginifolia* and rice (*Oryza sativa*) expressing *Arabidopsis* δOAT accumulate more proline and are less sensitive to osmotic stress than wild-type plants. This discrepancy has not yet been resolved, but expression studies have shown that δOAT transcript levels actually decreased slightly under salt stress, whereas those of P5CS

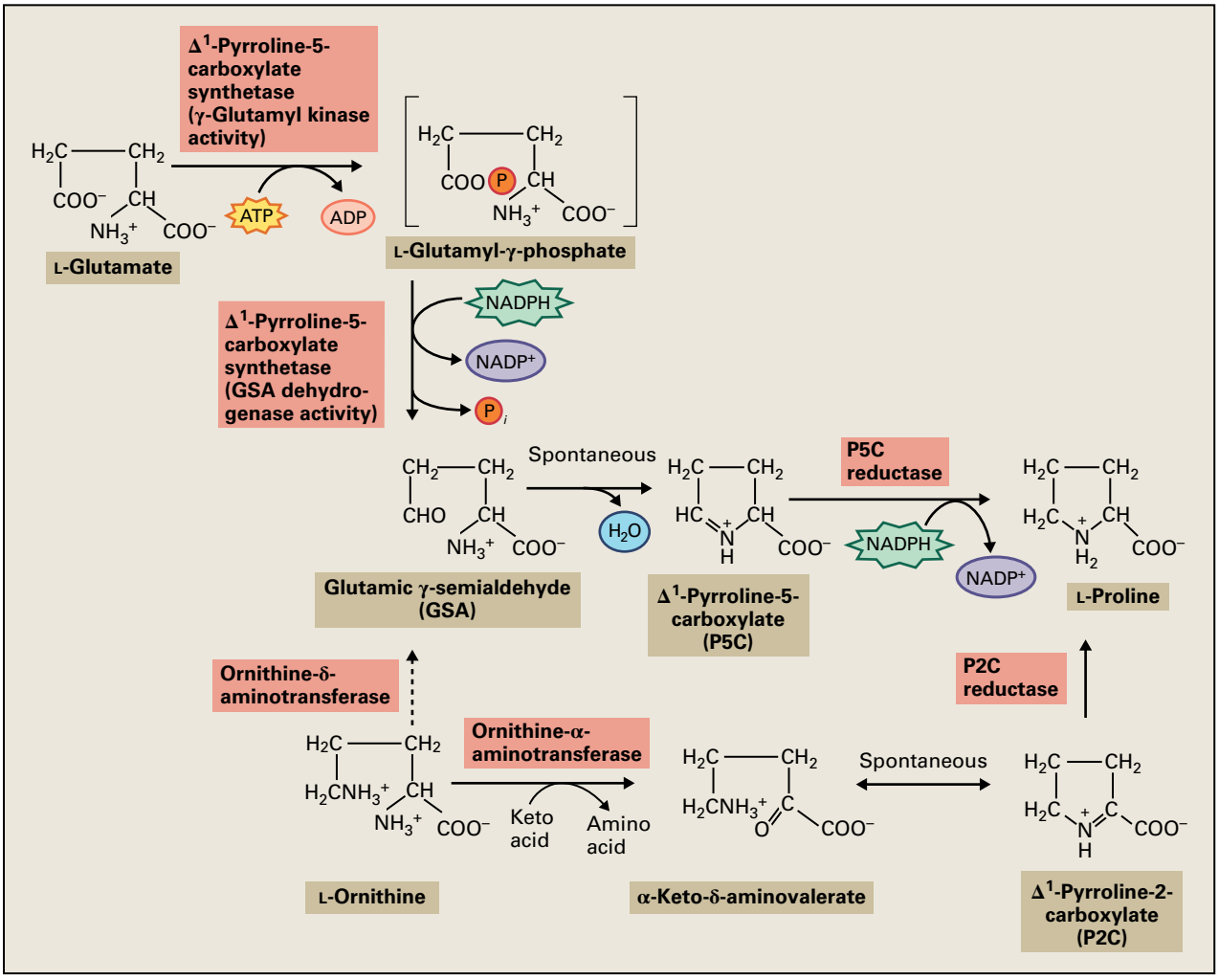


FIGURE 7.44 *Multiple pathways are proposed for proline biosynthesis in plants. A glutamate-derived pathway is well established (black arrows), and increasing evidence suggests the importance of ornithine as a precursor (red arrows). The relative importance of the pathways through ornithine-δ-aminotransferase (dotted red arrow) or ornithine-α-aminotransferase (pathway with all red arrows) remains to be determined. In plants, the γ-glutamyl kinase (proB in* E. coli*) and GSA dehydrogenase (proA in* E. coli*) are synthesized in a protein fusion. This activity is referred to as Δ¹-pyrroline-5-carboxylate synthetase.*

increased. This would again point to the predominance of the glutamate-dependent pathway of proline biosynthesis.

As discussed in Section 7.4.4, catabolism can play an important role in determining the concentration of a free amino acid. We can expect this particularly for proline, because its levels fluctuate considerably with environmental conditions. **Proline dehydrogenase** catalyzes conversion of proline back to Δ¹-pyrroline-5-carboxylate (P5C). The enzyme is a flavoprotein and is localized to the inner mitochondrial membrane. As P5C is in equilibrium with glutamic γ-semialdehyde (GSA), an NAD^+-dependent P5C dehydrogenase will form glutamate, which can move into the cytosol. The resulting **proline–glutamate exchange** between the cytosol and the mitochondria feeds electrons into the mitochondrial electron transport chain. Proline dehydrogenase mRNA is regulated in a manner reciprocal to that of the biosynthetic enzyme P5CS during both dehydration/rehydration of a plant and salt stress and recovery. This suggests that proline degradation is suppressed during periods of rapid de novo synthesis to prevent a futile cycle, and is then activated to bring proline concentrations back to prestress conditions.

When expression of an *E. coli* proline-insensitive γ-glutamyl kinase and a γ-glutamylphosphate reductase in tobacco or *Arabidopsis* is combined with simultaneous suppression of proline catabolism by expression of a *ProDH* antisense construct, the level of free proline increases up to 50-fold when the anabolic enzymes are targeted to plastids, and less when they are targeted to the cytosol. Apparently, proline can be synthesized both in the cytosol and in plastids.

7.6.4 Arginine is an amino acid rich in nitrogen

Arginine has a high N:C ratio (4:6) and serves as **nitrogen storage compound** in seeds, either in free form (e.g., in pea seeds) or in protein-bound form. In addition, it serves as a

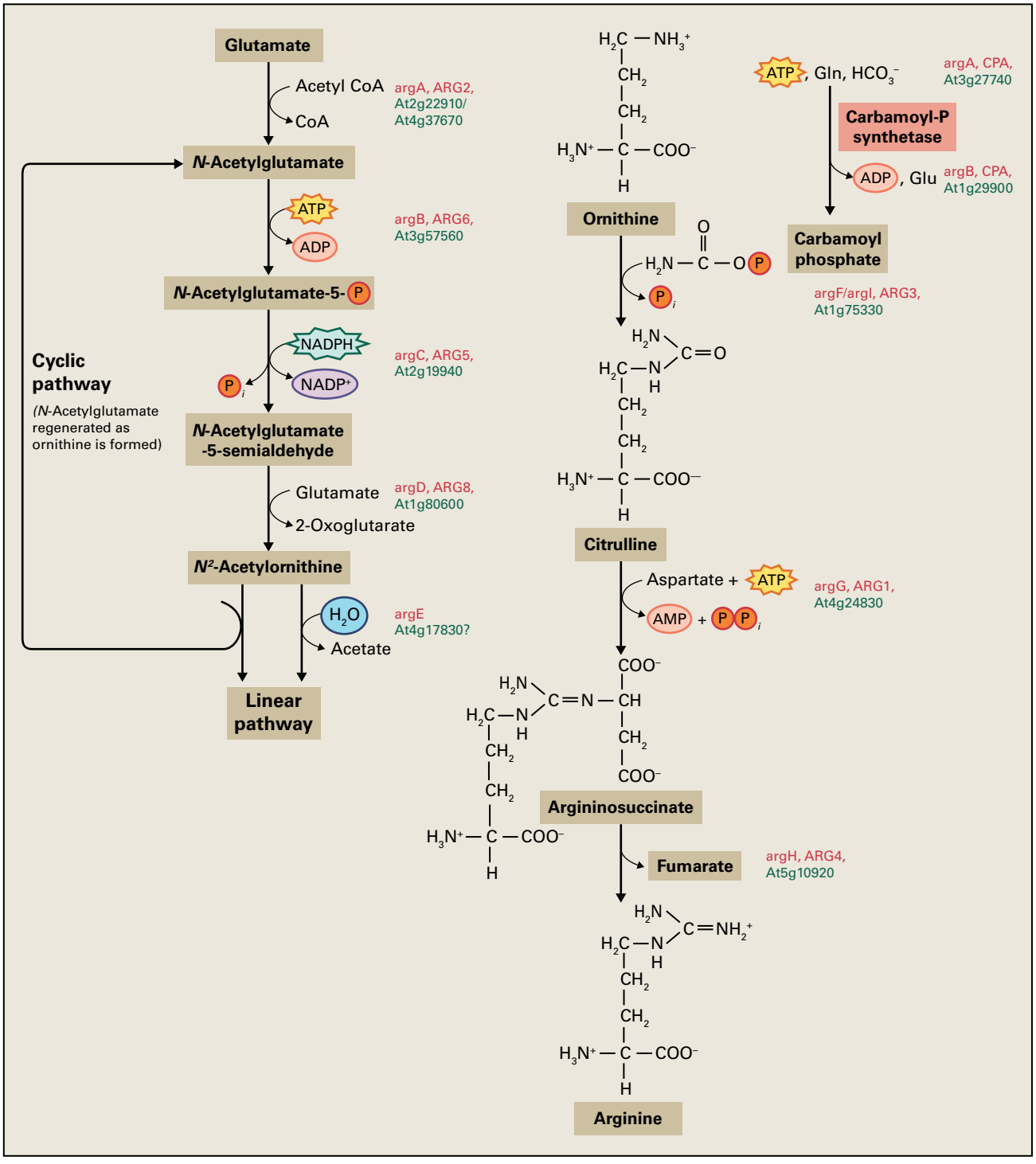


FIGURE 7.45 *Biosynthesis of arginine. Structures are only shown for the pathway from ornithine to arginine. Structures in the ornithine pathway correspond to those also seen in Figure 7.42, with the notable difference that they are N-acetylated.*

precursor in the biosynthesis of **polyamines**, certain alkaloids, and the signal molecule **nitric oxide** (**NO**). In terrestrial (*ureotelic*) vertebrates, it is the immediate precursor of **urea**, the nitrogen excretion product in urine. The urea cycle and arginine biosynthesis pathway, therefore, figure prominently in textbooks of general biochemistry. A limited number of biochemical and in silico genome mining studies have allowed elucidation of the pathway of arginine biosynthesis in plants, and these reactions are more or less identical to those in other organisms (Fig. 7.45). The pathway can be divided into two parts: from glutamate to ornithine, and from ornithine to arginine.

The ornithine pathway begins with the *N*-acetylation of glutamate by ***N*-acetylglutamate synthase** (NAGS). The

following γ-phosphorylation and subsequent reduction to the semialdehyde are analogous to the reactions of free glutamate in proline biosynthesis (see Fig. 7.44). Because acetylation of the amino group prevents spontaneous cyclization to the pyrroline carboxylate, *N*-acetylglutamic semialdehyde can be transaminated to give rise to ***N*-acetylornithine**, from which ornithine is released either by hydrolysis or by transfer of the acetyl moiety to glutamate (transacetylation) within the cyclic pathway shown in Fig. 7.45.

Arginine synthesis is initiated by the carbamoylation of the δ-amino group of ornithine with **carbamoyl phosphate** as the activated intermediate in a reaction catalyzed by **ornithine carbamoyl transferase** (OCT) that produces **citrulline** (Fig. 7.45). Carbamoyl phosphate is also required in pyrimidine synthesis, and the enzyme catalyzing its synthesis, carbamoyl phosphate synthetase (CPS), is feedback-inhibited by UMP and activated by IMP. Ornithine thus serves the needs of both pathways. The N atom required to convert citrulline to arginine is transferred from aspartate via **argininosuccinate**, which is cleaved to yield arginine and fumarate. Direct measurement of enzyme activities, chloroplast proteome data, and prediction of putative target sequences that direct the respective proteins to plastids, have demonstrated that the pathway is likely localized entirely in chloroplasts.

Only a limited number of reports detail either the overexpression or downregulation/knockout of any enzyme of the ornithine and arginine pathway, respectively. Overexpression of tomato (*Solanum lycopersicon*) NAGS in *Arabidopsis* increases ornithine content and enhances salt tolerance. A metabolomic analysis of the *ven3* and *ven6* mutants of *Arabidopsis* (which have a defect in mesophyll development and, therefore, exhibit a reticulate leaf phenotype) revealed that the mutants have an increased ornithine and a decreased citrulline content and can be rescued by citrulline complementation. The two *VEN* genes encode subunits of CPS, and the functionality of the respective polypeptides in CPS has been confirmed. How the arginine biosynthetic pathway functions in leaf development remains to be shown.

As pointed out above, arginine serves as a nitrogen storage pool. The branch point enzyme in the formation of ornithine and arginine, NAGS, is subject to control by a protein named **PII**, which was first discovered in *E. coli* as a coordinator of C:N interactions and then found to be highly conserved in bacteria, archaea, and plants. The plant homolog is targeted to the plastid and binds α-ketoglutarate and ATP. High N conditions reduce α-ketoglutarate concentrations because of its function in N assimilation (see Section 7.2), and this favors the interaction of PII and NAGS, which leads to activation of arginine synthesis and eventually to increased N storage.

7.7 Histidine

The elucidation of the **histidine** biosynthetic pathway in *Salmonella typhimurium* more than 50 years ago was a milestone in the biological sciences, not only because of the novel and complex reactions it involved, but because of the insight provided into the regulation of the pathway, which was instrumental in the development of the operon concept. Comparatively little work had been done on the plant pathway until the 1990s, when histidine biosynthesis was considered a potential target for the development of novel herbicides.

The plant research was instigated by the findings that a number of herbicidal compounds interfere with the biosynthesis of aromatic and branched-chain amino acids (see Sections 7.3.1 and 7.5.2). To date, plant genes encoding all of the eight enzymes required for histidine synthesis shown in Figure 7.46 have been identified. Although several textbooks list histidine as a member of the glutamate family, this is incorrect, because glutamate and glutamine contribute only N atoms to histidine synthesis rather than the C skeleton, as we saw for glutamate in the case of proline and arginine.

Histidine synthesis begins with the attachment of **5-phosphoribose** from 5-phosphoribosyl-1-pyrophosphate to ATP in an N-glycosidic linkage. Note the similarity of this reaction with the phosphoribosylation of anthranilate in tryptophan biosynthesis (see Fig. 7.25). Release of pyrophosphate by hydrolysis produces 5′-phosphoribosyl AMP. The six-membered ring of AMP opens by hydrolysis, and then isomerization to the ketone occurs, again as in the corresponding step in tryptophan biosynthesis (see Fig. 7.27). Ammonia provided by hydrolysis of glutamine in a **glutamine amidotransferase** reaction and being guided through a tunnel (see Fig. 7.24) affects the production of **imidazole glycerol phosphate** (IGP) and 5-aminoimidazole-4-carboxamide ribonucleotide (AICAR). AICAR is used in a salvage pathway to regenerate ATP, while IGP is converted by consecutive dehydration, transamination, hydrolysis of the phosphate group, and two dehydrogenation steps to histidine (Fig. 7.46). This is a significant difference to tryptophan biosynthesis, where tryptophan synthase replaces the glycerol phosphate side chain of **indole glycerol phosphate** with serine to produce tryptophan directly (see Fig. 7.29).

All proteins involved in the histidine pathway carry an N-terminal extension either proven or assumed to direct the proteins to the plastids. It is generally accepted that the complete pathway operates in the plastid.

Of all the genes of the histidine biosynthetic pathway, only overexpression of either of the two genes encoding **ATP-phosphoribsyltransferase** (ATP-PRT), the first committed enzyme of the pathway, significantly increased the levels of free histidine in transgenic *Arabidopsis* (up to 40-fold). This indicates that ATP-PRT controls substrate flux through the pathway, which conforms with its feedback inhibition by histidine. ATP-PRT overproducing plants had a specifically increased Ni tolerance (the imidazole ring of histidine is an efficient Ni chelator; this is why His-tagged proteins bind to Ni columns and can be specifically eluted with imidazole), and in wild-type plants, Ni tolerance correlates with ATP-PRT transcript levels. Plants overexpressing ATP-PRT are less

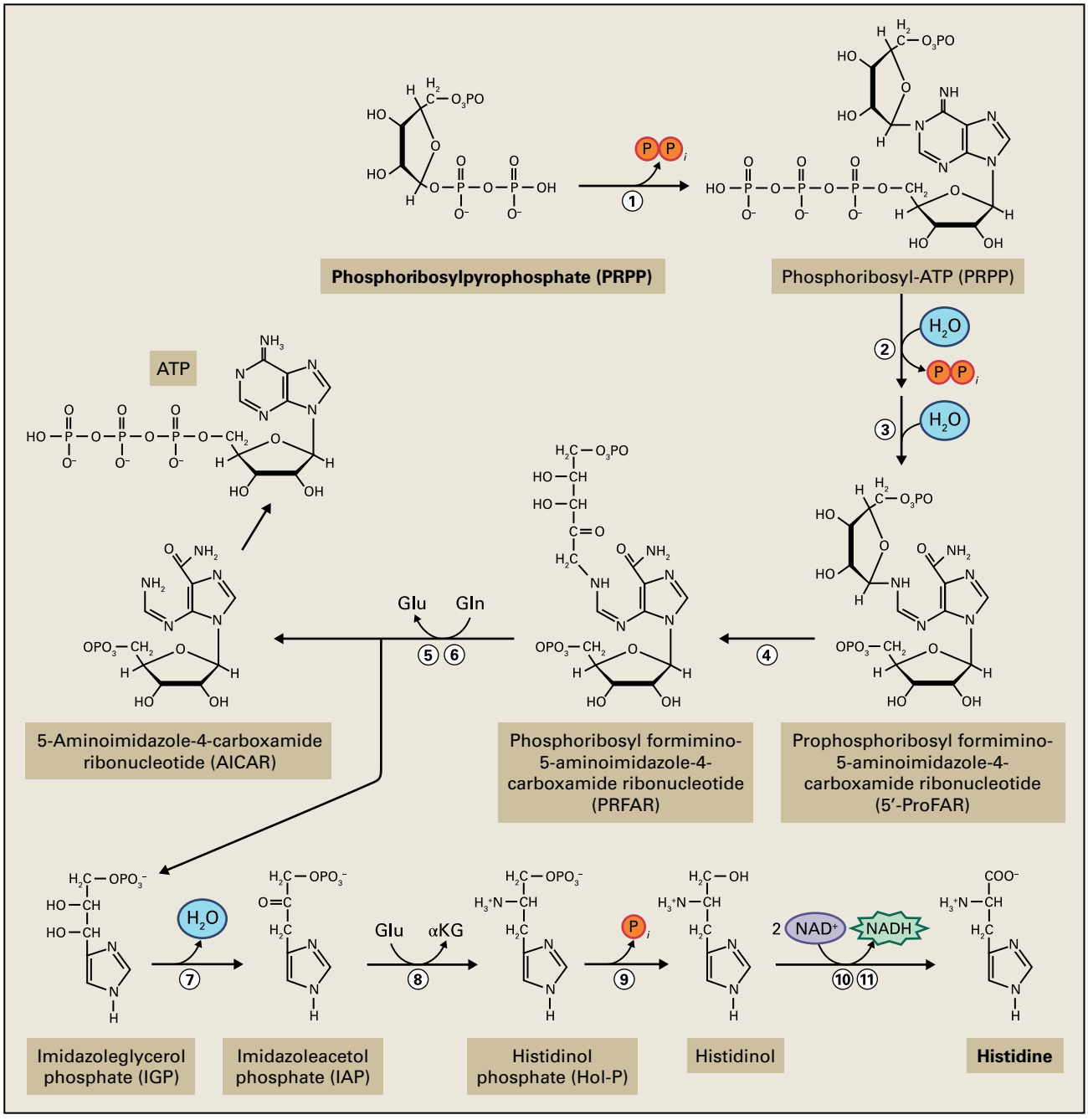


FIGURE 7.46 *Biosynthesis of histidine.*

tolerant to Co and Zn, and tolerance to Cd and Cu is unaffected. His overproduction has a negative effect on biomass production, which is apparently related to the high energy (ATP) costs of its production.

The *Arabidopsis hpa1* mutant, which is deficient in one of the two histidinol aminotransferases (Fig. 7.46), is defective in root meristem maintenance, and this results in a short root system related to the moderately reduced histidine content. The *apg10* mutant of *Arabidopsis*, which has pale green cotyledons and leaves in the juvenile stage, has a defect in the fourth enzyme of the histidine biosynthetic pathway that catalyzes the isomerization step after the ribose ring opening (Fig. 7.46). A similar phenotype had been seen in the *cue1* mutant, which has a defect in the plastid inner membrane phospho*enol*pyruvate (PEP)/phosphate translocator that provides PEP for aromatic amino acid biosynthesis. In both mutants, levels of the other amino acids are affected as well, which is taken as evidence for a crosspathway regulation of amino acid metabolism (see Box 7.7 and Box 7.8).

BOX 7.7 Does crosspathway regulation of gene expression exist in plants?

Prokaryotes and fungi use different mechanisms to coordinate the regulation of amino acid biosynthetic enzymes. In Gram-negative bacteria, the structural genes for a pathway are cotranscribed from operons. Starvation for a single amino acid causes derepression of the transcription of that biosynthetic operon by a mechanism involving a repressor protein and transcriptional attenuation. However, many fungal amino acid biosynthetic enzymes are under complex global control. In yeast, starvation for a single amino acid leads to transcriptional derepression of three dozen biosynthetic enzymes in at least 12 pathways. This general control response in yeast is mediated by the **transcription factor GCN4p**, a leucine-zipper protein whose synthesis is translationally regulated in response to amino acid starvation. Thus, the transcription of amino acid biosynthetic enzyme genes is sensitive to the translational state of the yeast cell, even though these two processes are separated by the nuclear envelope. This strategy is similar to, yet mechanistically different from, bacterial transcriptional attenuation: both allow the translational state of the cell to influence transcription of amino acid biosynthetic enzymes. Transcriptional profiling has more recently revealed that GCN4p is actually a master regulator of stress-induced gene expression, since out of several hundred yeast genes whose expression is affected by GCN4p, only about one quarter encode enzymes of amino acid metabolism.

Is there evidence for crosspathway regulation of amino acid biosynthesis in plants? Evidence is increasing for such a regulation, but no coherent picture has emerged yet. Starvation for aromatic amino acids, branched-chain amino acids, or methionine induces expression of the tryptophan pathway enzymes, but this response is not seen for a variety of other pathway enzymes. Starvation for histidine, however, by treatment of *Arabidopsis* seedlings with IRL 1803, an inhibitor of the histidine pathway enzyme imidazoleglycerol-phosphate dehydratase (see Fig. 7.46), increases accumulation of mRNAs for eight genes that encode enzymes involved in the biosynthesis of aromatic amino acids, lysine, histidine, and purines. It remains to be seen why starvation for histidine has unique consequences.

BOX 7.8 Plant amino acid biosynthetic pathways exhibit numerous gene duplications but few protein fusions

Notwithstanding the evolutionarily conserved reaction sequences of amino acid biosynthetic pathways between microorganisms and plants, the genetic organization of their enzymes in plants is in some ways quite different from what is found in microorganisms. In prokaryotes and fungi it is relatively unusual to discover **enzymes** with multiple **isoforms** encoded by separate genes. In contrast, many plant biosynthetic enzymes are encoded by multiple genes. In cases such as aspartate kinase, Δ^1-pyrroline-5-carboxylate synthetase, threonine deaminase, or the anthranilate α subunit from *Ruta graveolens*, these isoforms have different biochemical properties. In other instances, the genes are regulated differently or encode proteins with distinct subcellular locations (e.g., GS). However, for the majority of proteins encoded by multigene families, we still do not know what, if any, functional significance can be ascribed to the existence of multiple isoforms.

Another clear difference between plants and microbes is that **multifunctional proteins** are unusual in plants, and most enzymes of amino acid metabolism catalyze a single pathway step. Exceptions to this rule include the bifunctional Δ^1-pyrroline-5-carboxylate synthetase, 3-dehydroquinate dehydratase-shikimate dehydrogenase, and the lysine catabolic enzyme lysine-ketoglutarate reductase-saccharopine dehydrogenase. In prokaryotes and fungi, fusion proteins are common and can include three or more different activities. For example, the **ARO1 protein** of yeast is a pentafunctional protein that catalyzes all but the first and final steps of chorismate biosynthesis.

Summary

Amino acids, the building blocks of proteins in all organisms, play additional roles in plants. In plants, amino acids serve as precursors to a plethora of natural products that provide defense against pathogens and herbivores and tolerance to abiotic stress. They also store or transport nitrogen from sources to sinks. The control of amino acid synthesis in plants, therefore, affects many aspects of growth, development, and survival.

The synthesis of essential amino acids in plants and the amino acid composition of seeds relate indirectly to animal and human nutrition. Thus, understanding the pathways that allow and control amino acid synthesis in plants has significance with regard to basic research on the control of metabolic pathways as well as practical implications. Although amino acid biosynthetic pathways have been well defined in microbes, the situation in plants is still less defined, in part because of additional unique complexities. For example, in many instances, plants have multiple isoenzymes that catalyze the same biosynthetic reactions. These isoenzymes may be localized in distinct organelles or distinct cell types, or may be present at different developmental stages. Defining each step in an amino acid biosynthetic pathway and determining how each step is regulated, not only within the context of the respective pathway but rather in the context of the general metabolic network, are some of the key aspects of current research in amino acid biosynthesis in plants.

This chapter selectively highlights examples in which molecular, genetic, and biochemical approaches have been combined to elucidate the steps of these pathways in plants and to understand the regulation of these pathways at the level of gene regulation and beyond. Plant mutants in amino acid biosynthetic enzymes, which can now readily be identified in T-DNA insertion lines, have shown that the synthesis of amino acids in vivo affects numerous diverse processes, including photorespiration, hormone biosynthesis, and plant development. Use of transgenic approaches has revealed the feasibility of manipulating amino acid biosynthesis pathways in plants, with applications to engineering herbicide resistance and altering amino acid composition in seeds. Thus, while being products of primary metabolism, amino acids also control many diverse aspects of plant growth and development.



8

Lipids

John Ohlrogge, John Browse, Jan Jaworski, and Chris Somerville

Introduction

The term **lipid** refers to a structurally diverse group of molecules that are preferentially soluble in a nonaqueous solvent such as chloroform. Lipids include a wide variety of fatty acid-derived compounds, as well as many pigments and secondary compounds that are metabolically unrelated to fatty acid metabolism. Although we limit our discussion of lipids to those compounds with origins in fatty acid synthesis, this limitation still provides a broad group of compounds to explore, many of which are vital to the normal functioning of a cell. Each plant cell contains a diverse range of lipids, often located in specific structures. Furthermore, different plant tissues contain different lipids.

Although the metabolism of fatty acids and lipids in plants has many features in common with other organisms, the lipid pathways in plants are complex and some are not yet well understood. The complexity arises primarily from cellular compartmentalization of the pathways and the extensive intermixing of lipid pools between these compartments (Fig. 8.1). In addition, plants collectively accumulate more than 200 different fatty acids, so there are many open questions about the nature of the enzymes involved in the synthesis of these compounds. Among the many challenges facing plant biochemists today is the complete elucidation of these pathways and the mechanisms that regulate them.

8.1 Structure and function of lipids

8.1.1 Lipids have diverse roles in plants

Lipids serve many functions in plants (Table 8.1). As the major components of biological membranes, they form a hydrophobic barrier that is critical to life (see Chapter 1). Membranes not only separate cells from their surroundings; they also separate the contents of organelles, such as chloroplasts and mitochondria, from the cytoplasm. Cellular compartmentalization depends on polar lipids forming a bilayer that prevents free diffusion of hydrophilic molecules between the cellular organelles and prevents diffusion in and out of the cells. The membranes of chloroplasts, in which the light reactions of photosynthesis take place, primarily contain **galactolipids**. Membranes external to plastids are composed mainly of mixtures of **phospholipids.** Although a single gram of leaf tissue may contain as much as 1 m^2 of membrane, lipids make up a relatively small proportion of the total mass of plant tissue (Fig. 8.2).

Lipids also represent a substantial chemical reserve of free energy. Because fatty acids are substantially more reduced organic molecules than carbohydrates, fatty acid oxidation has a higher potential for producing energy. Furthermore,

Biochemistry & Molecular Biology of Plants, Second Edition. Edited by Bob B. Buchanan, Wilhelm Gruissem, and Russell L. Jones.
© 2015 John Wiley & Sons, Ltd. Published 2015 by John Wiley & Sons, Ltd.
Companion website: www.wiley.com/go/buchanan/biochem

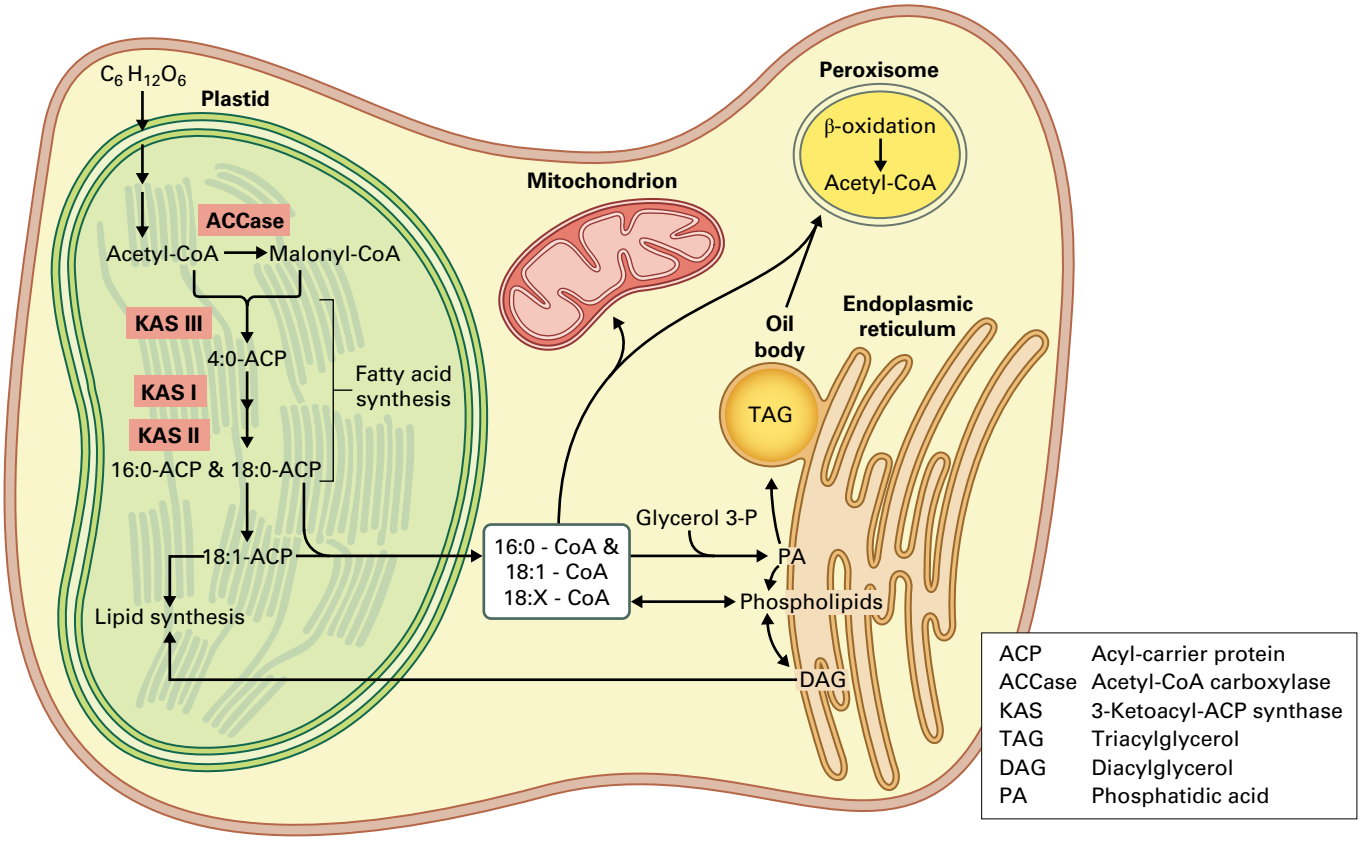


FIGURE 8.1 *Lipid synthesis and metabolism take place in various organelles, and in many cases involve movement of lipids from one cellular compartment to another.*

triacylglycerols are largely hydrophobic and exist in an essentially anhydrous environment. Carbohydrates, however, are hydrophilic, and the water of hydration adds substantially to their mass. Thus, on a mass basis, the ATP yield from catabolism to CO_2 and H_2O is approximately twice as high for triacylglycerols as for carbohydrates (Fig. 8.3). In cases where a compact seed mass is advantageous for facilitating dispersal or other processes, the carbon and energy required for seed germination are often stored in the form of triacylglycerols rather than as starch.

Fatty acids are also the precursors for other significant components of plant metabolism. The **waxes** that coat and protect plants from the environment are complex mixtures of long-chain hydrocarbons, aldehydes, alcohols, acids, and esters derived almost entirely from fatty acids. The **cutin** layer of epidermal cells also is composed of oxygenated fatty acids esterified with one another to produce a tough, polyester skin. Thus, in epidermal cells of aerial organs, the bulk of fatty acid synthesis is devoted to production of wax and cutin for protection (Fig. 8.4).

Some fatty acids play major roles in certain signal transduction pathways. The synthesis of the growth regulator **jasmonic acid** from linolenic acid and the activities of jasmonates as plant hormones and second messengers are widely studied (see Section 8.8.5 and Chapters 17 and 21). Similarly, phosphatidylinositol and its derivatives are messengers with regulatory roles, similar to messenger compounds found in other eukaryotes, which play important roles in signal transduction pathways (see Chapter 18). Fatty acids may also be involved in regulating various cellular processes via protein acylation.

8.1.2 Most, but not all, lipids contain fatty acids esterified to glycerol

Fatty acids are carboxylic acids of highly reduced hydrocarbon chains. The typical fatty acids found in the membranes of plants contain 16 or 18 carbons and are listed in Table 8.2, along with some unusual fatty acids that typically accumulate only in the storage triacylglycerols of seeds. Some of the nomenclature used in abbreviations for fatty acids and lipids is described in Box 8.1.

A major fraction of the fatty acids in plants are the polyunsaturated fatty acids linoleic acid ($18:2^{\Delta 9,12}$) and α-linolenic acid ($18:3^{\Delta 9,12,15}$). Only a few plants accumulate fatty acids with double bonds closer to the carboxyl group than the Δ9 position. In addition to the C_{16} and C_{18} common fatty acids, some plants also produce fatty acids of 8–32 carbons in length that usually accumulate in storage lipids or epicuticular wax. The fatty acid composition of lipids can be determined using gas chromatography to separate the methylated derivatives of the fatty acids.

TABLE 8.1 *Functions of lipid molecules in plants.*

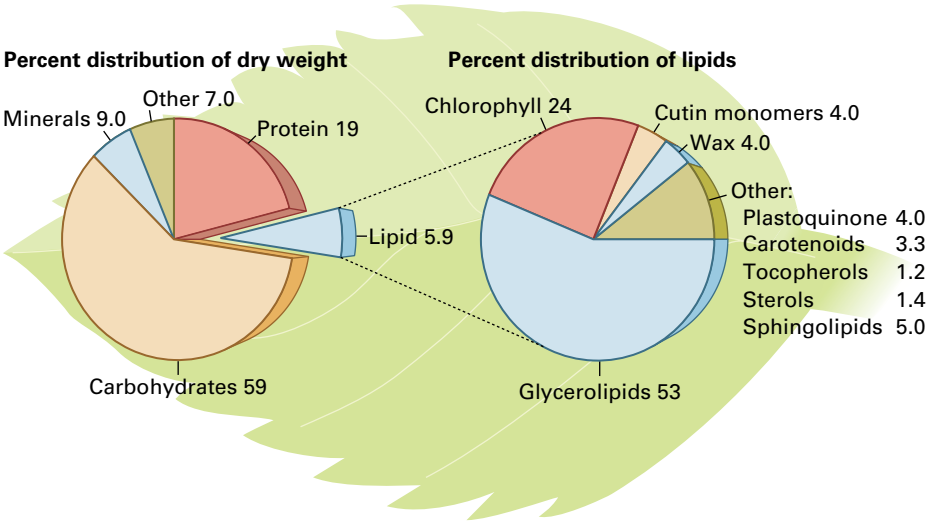
Function	Lipid types involved[a]
Membrane structural components	Glycerolipids Sphingolipids Sterols
Storage compounds	Triacylglycerols Waxes
Compounds active in electron transfer reactions	Chlorophyll and other pigments Ubiquinone, plastoquinone
Photoprotection	Carotenoids (xanthophyll cycle)
Protection of membranes against damage from free radicals	Tocopherols
Waterproofing and surface protection	Long-chain and very-long-chain fatty acids and their derivatives (cutin, suberin, surface waxes) Triterpenes
Protein modification	
Addition of membrane anchors	
Acylation	Mainly 14:0 and 16:0 fatty acids
Prenylation	Farnesyl and geranylgeranyl pyrophosphate
Other membrane anchor components	Phosphatidylinositol, ceramide
Glycosylation	Dolichol
Signaling	
Internal	Abscisic acid, gibberellins, brassinosteroids 18:3 Fatty acid precursors of jasmonate Inositol phosphates Diacylglycerols
External	Jasmonate Volatile insect attractants
Defense and antifeeding compounds	Essential oils Latex components (rubber, etc.) Resin components (terpenes)

[a]The isoprenoids and related lipids are described in Chapter 24.

Glycerolipids consist of fatty acids esterified to derivatives of glycerol. Four principal types are found in plants: triacylglycerols, phospholipids, galactolipids, and a sulfolipid. In addition, plants contain sphingolipids, which can be major components of the plasma membrane. In most cases, purification of a particular type of lipid from a plant extract yields a complex mixture. For example, seven different classes of phospholipids (Table 8.3) are defined by the structure of the head group, and each class is composed of distinct molecular species defined by the fatty acids attached to the *sn*-1 and *sn*-2 positions of the glycerol backbone. Thus, the phosphatidylcholine molecule depicted in Figure 8.5A has a saturated fatty acid esterified to the *sn*-1 position and a di-unsaturated fatty acid esterified to the *sn*-2 position. Some of the factors that control the fatty acid composition of lipids are discussed in Sections 8.5.3, 8.7.1, and 8.7.4.

Lipids are usually stored as triacylglycerols, three fatty acids esterified to glycerol (Fig. 8.5B). Triacylglycerols are frequently referred to as neutral lipids because of their nonpolar nature. Found primarily in seeds and pollen, triacylglycerols serve as energy and carbon stores. Because neutral lipids are not soluble in the aqueous phase of cells, they do not contribute to the osmotic potential of the cell. This is important to their role as storage materials because they accumulate in

FIGURE 8.2 *Approximate distributions of cellular constituents (as a percentage of total dry weight) and lipid types (as a percentage of total lipids by weight) in* Arabidopsis *leaf tissues. Some values were extrapolated from results obtained with other species.*



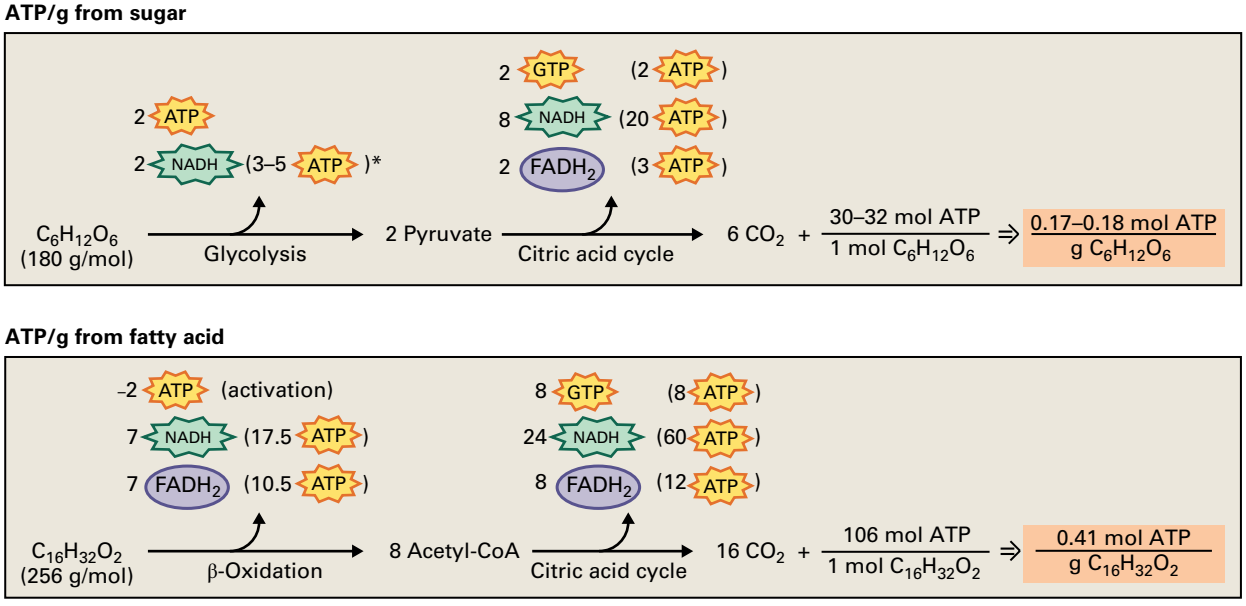


FIGURE 8.3 *Comparison of energy yield in animals from metabolism of fatty acids and carbohydrates to CO_2 and H_2O. Metabolism of fatty acids produces 0.41 mol of ATP per gram of fatty acid, whereas metabolism of carbohydrate yields 0.17 to 0.18 mol/g. Oxidation of one NADH by the mitochondrial electron transport chain is assumed to yield 2.5 ATP, whereas oxidation of one $FADH_2$ is assumed to yield 1.5 ATP. The number of ATPs derived from one NADH oxidized in the cytosol or peroxisome varies according to the mechanism by which the reducing equivalents (electrons) are transferred into the mitochondrion (see Chapter 14).*

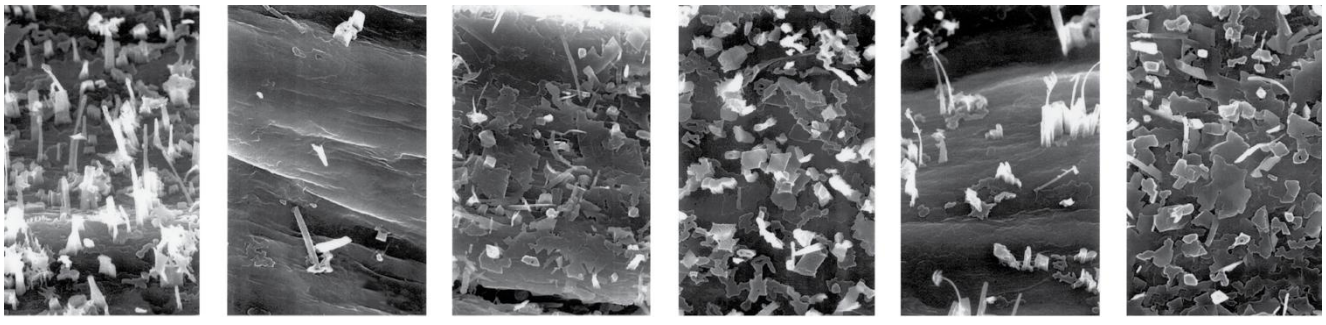


FIGURE 8.4 *Scanning electron micrographs of wild-type and mutant* Arabidopsis *stems (A–C) and siliques (D–F). Wild-type surfaces (A, D) are covered with various tubes and lobed plates of wax. Surfaces of the* cer7 *mutant (B, E) have both fewer wax crystals and altered crystalline structures. Surfaces of* cer17 *mutants (C, F) have fewer tubes than the wild-type plants.*
Source: Kunst & Samuels (2003), Progress in Lipid Research, Volume 42, Issue 1, Pages 51–80.

TABLE 8.2 *Selected fatty acids present in plants.*

Common name	Systematic name	Structure	Abbreviation[a]
Saturated fatty acids			
Lauric acid	*n*-Dodecanoic acid	$CH_3(CH_2)_{10}COOH$	12 : 0
Palmitic acid[b]	*n*-Hexadecanoic acid	$CH_3(CH_2)_{12}CH_2CH_2COOH$	16 : 0
Stearic acid[b]	*n*-Octadecanoic acid	$CH_3(CH_2)_{12}CH_2CH_2CH_2CH_2COOH$	18 : 0
Arachidic acid	*n*-Eicosanoic acid	$CH_3(CH_2)_{12}CH_2CH_2CH_2CH_2CH_2CH_2COOH$	20 : 0
Behenic acid	*n*-Docosanoic acid	$CH_3(CH_2)_{12}CH_2CH_2CH_2CH_2CH_2CH_2CH_2CH_2COOH$	22 : 0
Lignoceric acid	*n*-Tetracosanoic acid	$CH_3(CH_2)_{12}CH_2CH_2CH_2CH_2CH_2CH_2CH_2CH_2CH_2CH_2COOH$	24 : 0
Unsaturated fatty acids			
Oleic acid[b]	*cis*-9-Octadecenoic acid	$CH_3(CH_2)_7C(H)=C(H)(CH_2)_7COOH$	18 : $1^{\Delta 9}$
Petroselenic acid	*cis*-6-Octadecenoic acid	$CH_3(CH_2)_{10}C(H)=C(H)(CH_2)_4COOH$	18 : $1^{\Delta 6}$
Linoleic acid[b]	*cis,cis*-9,12-Octadecadienoic acid	$CH_3(CH_2)_4C(H)=C(H)-CH_2-C(H)=C(H)(CH_2)_7COOH$	18 : $2^{\Delta 9,12}$
α-Linolenic acid[b]	*all-cis*-9,12,15-Octadecatrienoic acid	$CH_3CH_2C(H)=C(H)-CH_2-C(H)=C(H)-CH_2-C(H)=C(H)(CH_2)_7COOH$	18 : $3^{\Delta 9,12,15}$
γ-Linolenic acid	*all-cis*-6,9,12-Octadecatrienoic acid	$CH_3(CH_2)_4C(H)=C(H)-CH_2-C(H)=C(H)-CH_2-C(H)=C(H)(CH_2)_4COOH$	18 : $3^{\Delta 6,9,12}$
Roughanic acid[b]	*all-cis*-7,10,13-Hexadecatrienoic acid	$CH_3CH_2C(H)=C(H)-CH_2-C(H)=C(H)-CH_2-C(H)=C(H)(CH_2)_5COOH$	16 : $3^{\Delta 7,10,13}$
Erucic acid	*cis*-13-Docosenoic acid	$CH_3(CH_2)_7C(H)=C(H)(CH_2)_{11}COOH$	22 : $1^{\Delta 13}$
Some unusual fatty acids			
Ricinoleic acid	12-Hydroxyoctadec-9-enoic acid	$CH_3(CH_2)_5C(OH)(H)-CH_2-C(H)=C(H)(CH_2)_7COOH$	12-OH-18 : $1^{\Delta 9}$
Vernolic acid	12,13-Epoxyoctadec-9-enoic acid	$CH_3(CH_2)_4-CH(O)-CH-CH_2-C(H)=C(H)(CH_2)_7COOH$	

[a] See Box 8.1 for an explanation of abbreviation nomenclature.
[b] These five fatty acids are commonly found as the principal constituents of membrane lipids. The others are found principally in storage lipids.

BOX 8.1 Abbreviations make lipid nomenclature more manageable

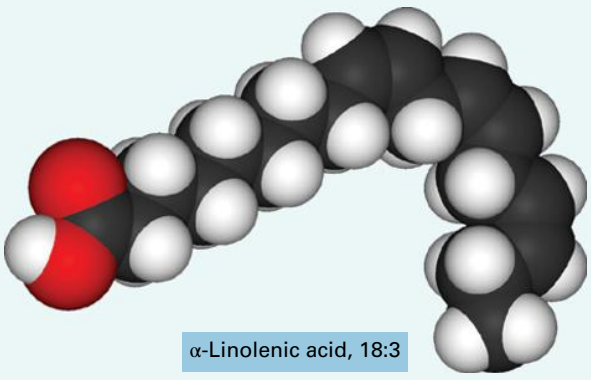
A simple shorthand notation based on molecule length and the number and position of double bonds has been developed to designate fatty acids. For example, the saturated C16 fatty acid, palmitic acid (hexadecanoic acid), is designated 16:0. The first value, 16, represents the number of carbon atoms. The second value, 0, indicates the number of double bonds. The monounsaturated 18-carbon fatty acid, oleic acid (*cis*-9-octadecenoic acid), is designated $18:1^{\Delta 9}$. The Δ9 superscript designates the position of the single double bond, counting the carboxyl group as carbon atom number 1. Because the double bonds in fatty acids are almost exclusively *cis* isomers, usually no designation for the configuration of double bond is used unless it is a *trans* isomer, as in $16:1^{trans\ \Delta 3}$. As shown in the illustration of palmitic and linolenic acids, major saturated and unsaturated fatty acids in photosynthetic tissues, introduction of *cis* unsaturations creates bends in the acyl chain.

Double bonds are usually separated by one carbon in the fatty acid chain (e.g., in the polyunsaturated α-linolenic acid, $18:3^{\Delta 9,12,15}$). It is sometimes useful to designate the position of the double bonds relative to the terminal methyl group (the omega carbon). Thus, an omega-3, or *n*-3, fatty acid contains a double bond three carbons from the methyl end of the fatty acid (e.g., $18:3^{\Delta 9,12,15}$ is an omega-3 fatty acid).

Abbreviations are also used to designate the position at which a fatty acid is esterified to the glycerol backbone of glycerolipids. *sn*-3 (stereospecific nomenclature-3) denotes the terminal hydroxyl that is phosphorylated in glycerol 3-phosphate, *sn*-2 refers to the central hydroxyl, and *sn*-1 is the terminal hydroxyl that is not phosphorylated.



Palmitic acid, 16:0



α-Linolenic acid, 18:3

amounts that would otherwise disrupt the maintenance of normal cellular osmolality.

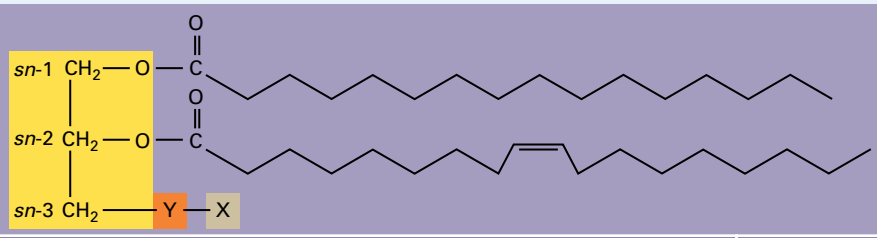
Phospholipids are synthesized by esterification of fatty acids to the two hydroxyl groups of *sn*-glycerol 3-phosphate to produce phosphatidic acid. All other phospholipids are derived from phosphatidic acid by esterification of a polar "head group" to the phosphoryl group (Table 8.3). Phospholipids are **amphipathic,** containing both hydrophobic (noncharged, nonpolar) fatty acids and a hydrophilic (charged, polar) head group. This property allows phospholipids—and other amphipathic glycerolipids—to form a bilayer in which the hydrophilic heads are in contact with an aqueous environment such as the cytosol, while the hydrophobic tails remain in contact with other hydrophobic tails (Fig. 8.6; see also Chapter 1).

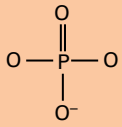
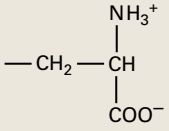
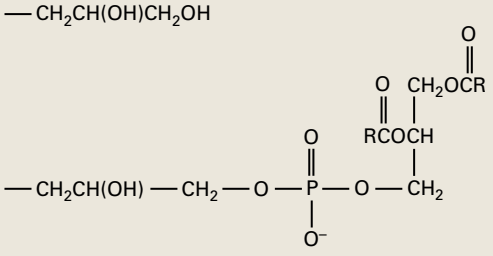
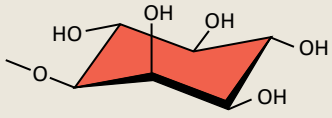
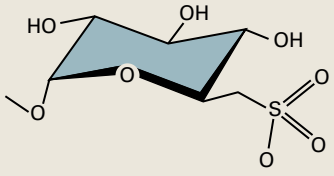
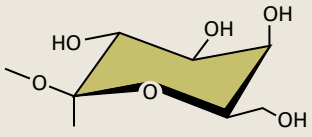
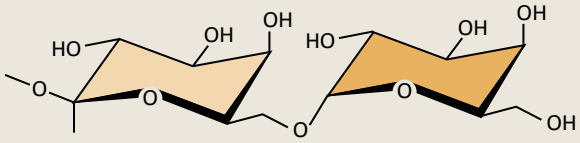
Galactolipids, another major class of glycerolipids, are localized in the plastid membranes. In these lipids, a galactosyl or sulfoquinovosyl group replaces the phosphoryl head group of the phospholipids (Table 8.3). The three major lipids belonging to this class of lipids are the two galactolipids monogalactosyldiacylglycerol and digalactosyldiacylglycerol and the plant sulfolipid sulfoquinovosyldiacylglycerol. These **glycolipids** contain high concentrations of polyunsaturated fatty acids. In the photosynthetic tissue of some plants, α-linolenic acid ($18:3^{\Delta 9,12,15}$) can constitute as much as 90% of the fatty acids in glycolipids. Plants such as peas (*Pisum sativum*), in which glycolipids contain exclusively C_{18} polyunsaturated fatty acids, are sometimes referred to as "18:3 plants." Others, such as spinach (*Spinacia oleracea*), contain glycolipids having appreciable amounts of a C_{16} polyunsaturated fatty acid, $16:3^{\Delta 7,10,13}$, localized exclusively in the *sn*-2 position, and are called "16:3 plants." The underlying difference between 18:3 plants and 16:3 plants is now understood: 18:3 plants synthesize most or all of their lipids in the endoplasmic reticulum (ER), whereas 16:3 plants utilize biosynthetic pathways in the plastid as well (see Sections 8.7.2 and 8.7.3).

Sphingolipids (Fig. 8.7), which represent approximately 5% of the total membrane lipids, are concentrated in the plasma membrane, where they make up as much as 26% of the mass of plasma membrane lipids. The sphingoid bases are generally toxic and are present in very low concentrations so that only the ceramides and glycosylceramides accumulate to any extent. Sphingolipids are unusual in that they are not esters of glycerol, but rather consist of a long-chain amino alcohol that forms an amide linkage to a fatty acid; the

TABLE 8.3 *Major classes of membrane lipids.*

Glycerophospholipid (general structure)



Substituent			Name of lipid
Formula of Y	**Name of X—OH**	**Formula of X**	
	Water	—H	Phosphatidic acid (PA)
	Choline	$-CH_2CH_2N^+(CH_3)_3$	Phosphatidylcholine (PC)
	Ethanolamine	$-CH_2CH_2NH_3^+$	Phosphatidylethanolamine (PE)
	Serine		Phosphatidylserine (PS)
	Glycerol	$-CH_2CH(OH)CH_2OH$	Phosphatidylglycerol (PG)
	Phosphatidylglycerol		Diphosphatidylglycerol (cardiolipin)
	myo-Inositol		Phosphatidylinositol (PI)
None	Sulfoquinovose		Sulfoquinovosyldiacylglycerol (SQD), also called sulfolipid (SL)
	Galactose		Monogalactosyldiacylglycerol (MGD)
	Digalactose		Digalactosyldiacylglycerol (DGD)

The basic structure of a glycerolipid is shown at the top. The C3 backbone (highlighted in dark yellow) is usually esterified to two fatty acids at the carbons labeled *sn*-1 and *sn*-2. The modifications of the *sn*-3 carbon can be described by the substituents *X* and *Y*, which correspond to the compounds shown in the lower part of the table. *sn* numbers refer to the stereochemical nomenclature system, which is, by convention, based on the structures of D- and L-glyceraldehyde. The convention with respect to glycerol is that, in a Fisher projection of L-glycerol (not shown), the central hydroxyl is shown to the left. By definition, the carbon above the *sn*-2 carbon is the *sn*-1 position and the position below is the *sn*-3 position.

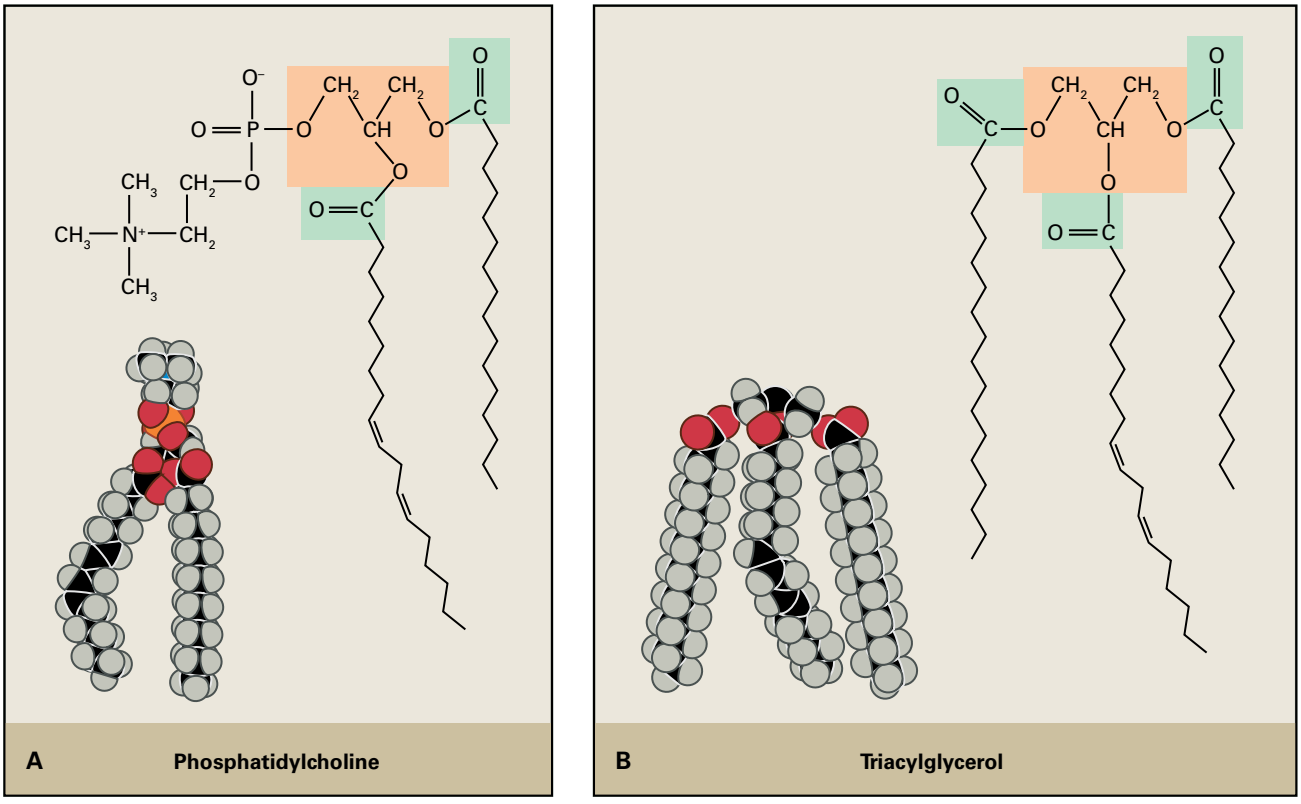


FIGURE 8.5 *Space-filling and conformational models of (A) the phospholipid phosphatidylcholine and (B) triacylglycerol. The ester linkages are highlighted in yellow, and the glycerol backbone is in orange.*

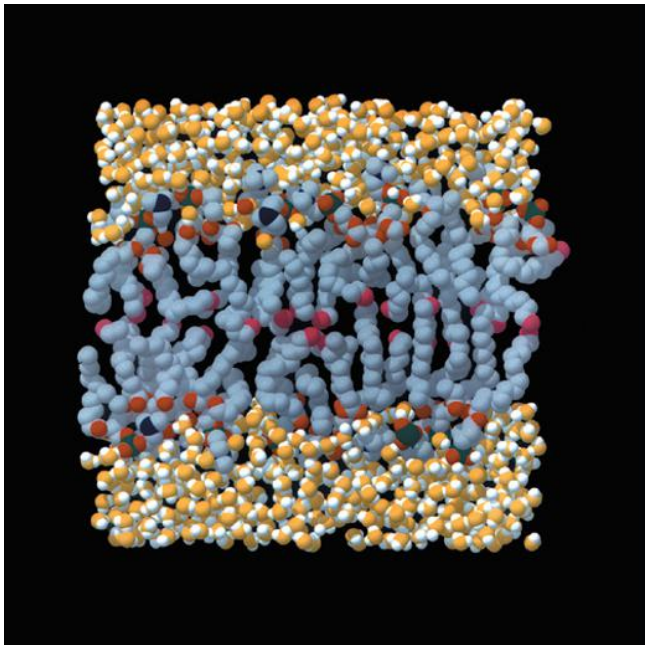


FIGURE 8.6 *Computer simulation of a cross-section of a membrane. The coloring is as follows: phosphorus, dark green; nitrogen, dark blue; lipid oxygens, red; terminal chain methyl groups, magenta; other carbons, gray; water oxygens, yellow; water hydrogens, white. For clarity, the radii of heavy atoms are reduced slightly from their van der Waals values, the radii of water hydrogens are increased, and carbon-bound hydrogens are omitted.*

acyl group is often longer than C_{18}. Complex sphingolipids, such as glucosylceramide, form from a simple sphingolipid (e.g., ceramide) by the addition of phosphocholine or one or more sugars. The synthesis of these lipids is discussed in Section 8.7.10.

8.2 Fatty acid biosynthesis

8.2.1 Fatty acid biosynthesis in plants is similar to that in bacteria

Fatty acid biosynthesis in plants takes place within plastids, organelles widely thought to have originated from a photosynthetic bacterial symbiont. Thus it is perhaps not surprising that fatty acid metabolism in plants closely resembles that of bacteria.

Acetyl-CoA is the initial substrate for synthesis of the carbon backbone of all fatty acids. A central intermediate in many aspects of cellular metabolism, it is produced and consumed by dozens of reactions in the cell (Fig. 8.8). Within plastids, pyruvate dehydrogenase directly produces acetyl-CoA from pyruvate generated during glycolysis (see Chapter 13).

During fatty acid biosynthesis, a repeated series of reactions incorporates acetyl moieties of acetyl-CoA into an acyl

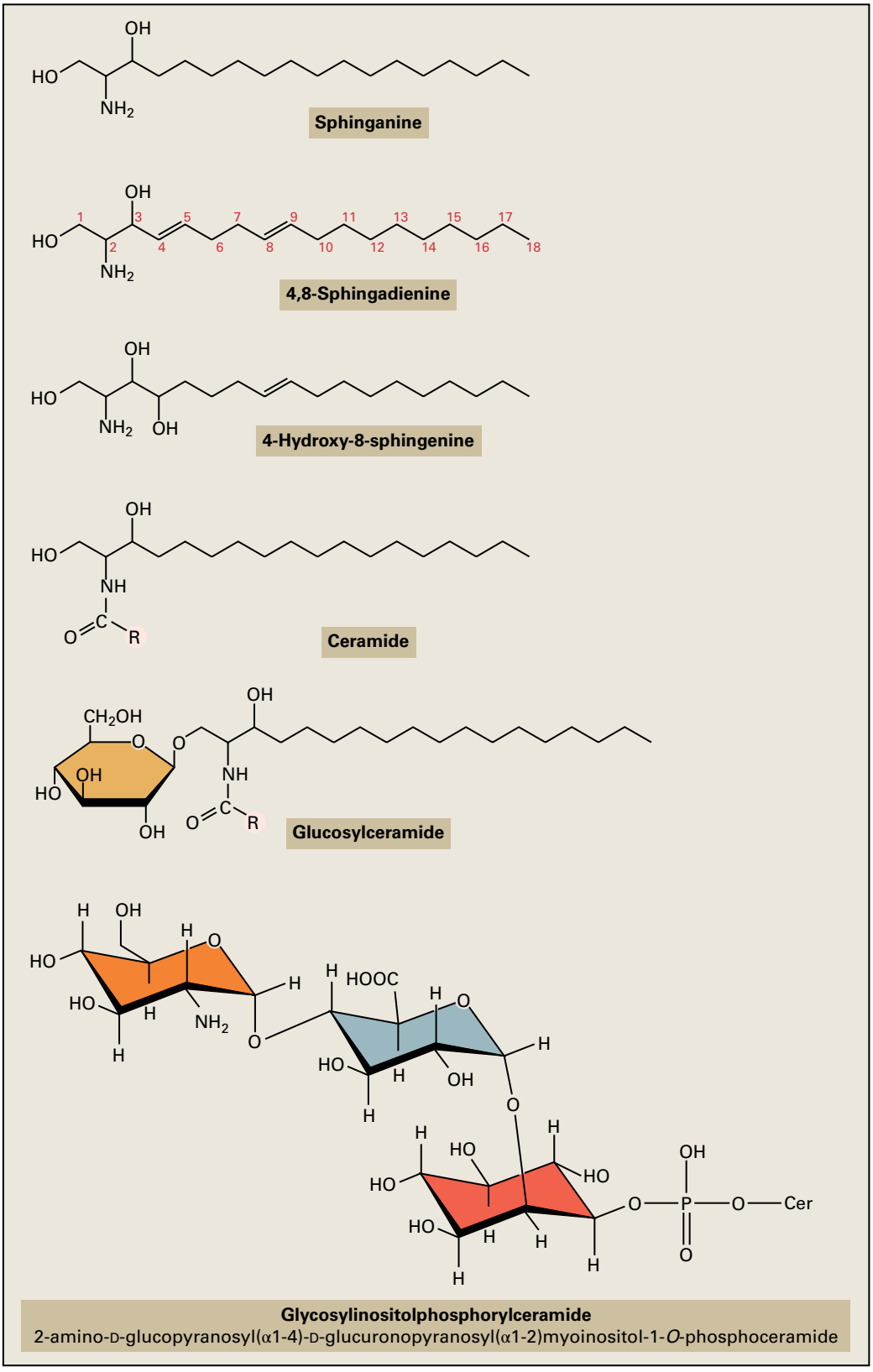


FIGURE 8.7 *Structures of selected plant sphingolipids. Sphinganine, 4,8-sphingadienine, and 4-hydroxy-8-sphingenine are called "sphingoid bases." The carbons are numbered from the primary hydroxyl. The numbers in the names refer to the position of double bonds or of other functional groups as indicated. The fatty acids (R) are usually saturated or monounsaturated C_{16}–C_{26} hydroxy fatty acids.*

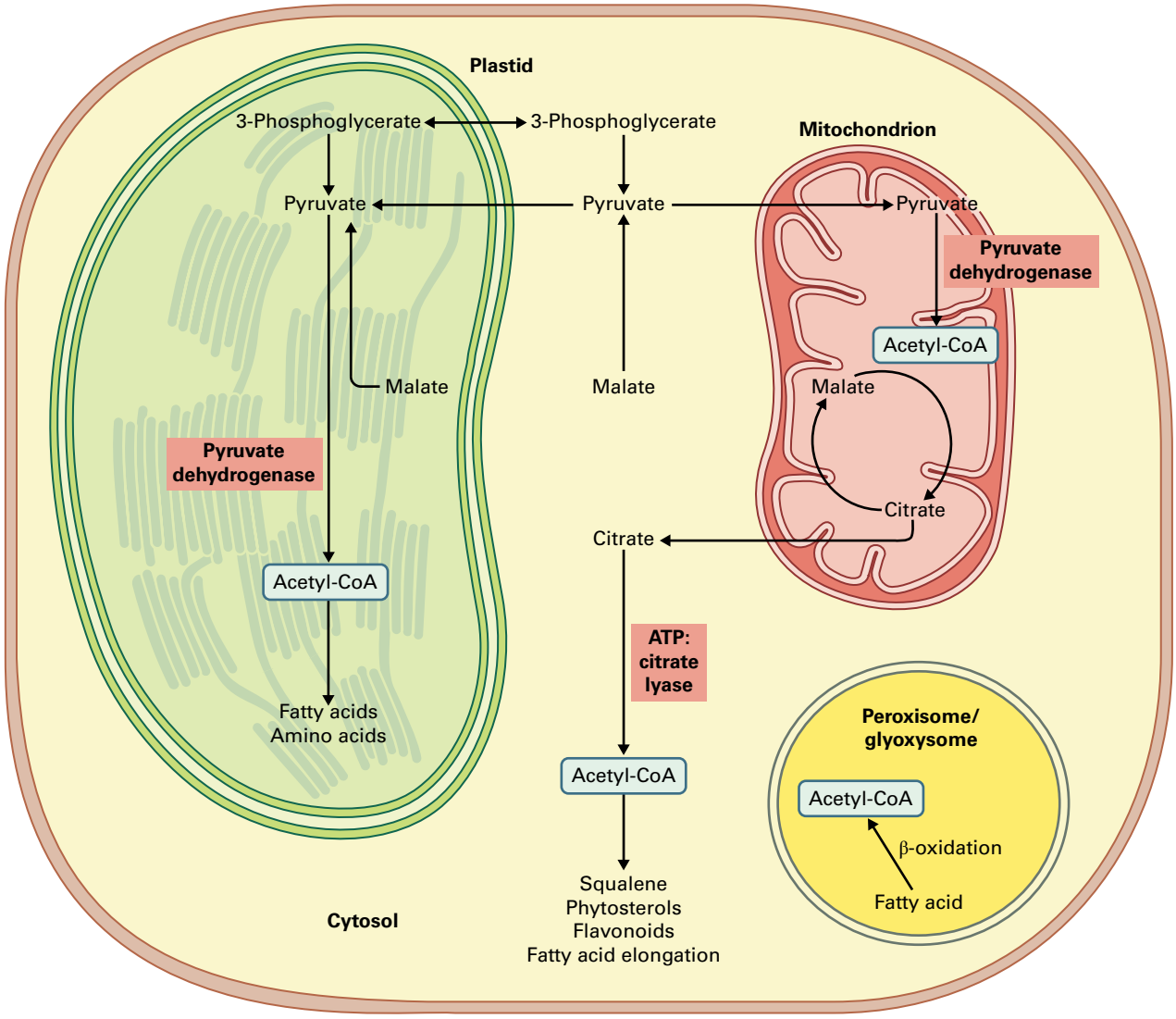


FIGURE 8.8 *Acetyl-CoA may be the most central intermediate in cellular metabolism, providing a link between many pathways. The major pathways involved in its production include glycolysis (via pyruvate dehydrogenase) and fatty acid oxidation. Acetyl-CoA is the starting material for biosynthesis of fatty acids, several amino acids, flavonoids (via chalcone synthase), sterols, and many isoprenoid derivatives synthesized in the cytosol. During respiration, acetyl-CoA is the source of carbon input into the citric acid cycle in the mitochondria. Despite this central role, acetyl-CoA is not believed to cross membranes and must be produced in the compartment in which it is utilized.*

group of 16 or 18 carbons. The enzymes involved in this synthesis are acetyl-CoA carboxylase (ACCase) and fatty acid synthase (FAS) (Fig. 8.9). The name fatty acid synthase refers to a complex of several individual enzymes that catalyze the conversion of acetyl-CoA and malonyl-CoA to 16:0 and 18:0 fatty acids (see Section 8.4). **Acyl-carrier protein** (ACP), an essential protein cofactor, is generally considered a component of FAS.

Fatty acid biosynthesis is initiated by the ATP-dependent carboxylation of acetyl-CoA to form malonyl-CoA. Next, the malonyl group is transferred to ACP. Assembly of the fatty acid begins when a carbon–carbon bond forms between C-1 of an acetate "primer" and C-2 of the malonyl group on ACP, which releases CO_2. This two-carbon chain length extension results initially in the formation of acetoacetyl-ACP. Subsequently, a sequence of three reactions—reduction, dehydration, and reduction again—leads to the formation of the fully reduced acyl-ACP. This sequence, progressing in three steps from a 3-ketoacyl group to a saturated acyl group, is a common reaction series found in biochemical pathways. For example, both β-oxidation and the citric acid cycle use the same series of reactions, but in reverse order.

Fatty acyl chains and their derivatives are among the most reduced molecules found in cells. Producing these molecules from their more-oxidized precursors requires a large investment of reducing power. As indicated above, each cycle of two-carbon addition involves two reduction steps. Thus, for a typical C_{18} fatty acid, 16 molecules of NAD(P)H are consumed. In illuminated chloroplasts, abundant reducing power is available from Photosystem I. In the dark and in tissues

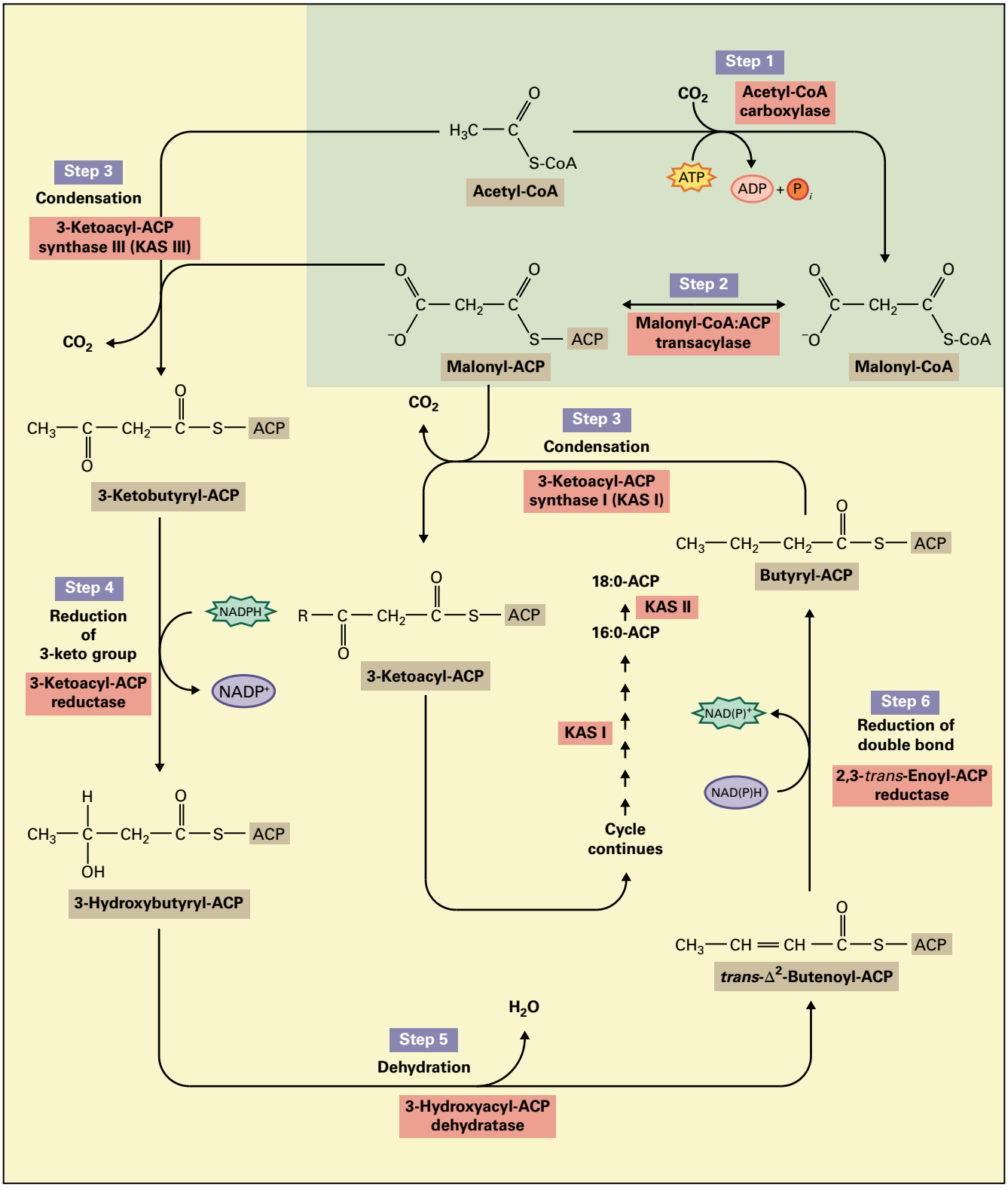


FIGURE 8.9 *Overview of fatty acid synthesis. Fatty acids grow by addition of two-carbon (C_2) units. The reactions highlighted in yellow show how malonyl-CoA enters the cycle; those highlighted in orange represent the cyclic reactions. Synthesis of a C_{16} fatty acid requires that the cycle be repeated seven times. During the first turn of the cycle, the condensation reaction (step 3) is catalyzed by ketoacyl-ACP synthase (KAS) III. For the next six turns of the cycle, the condensation reaction is catalyzed by isoform I of KAS. Finally, KAS II is used during the conversion of 16:0 to 18:0.*

lacking chloroplasts, the oxidative pentose phosphate pathway is the most likely origin of reduced NADPH (see Chapter 13).

8.3 Acetyl-CoA carboxylase

8.3.1 Malonyl-CoA formation is catalyzed in a two-step reaction by acetyl-CoA carboxylase

Long-chain fatty acids are assembled two carbons at a time from acetyl-CoA; however, formation of the carbon–carbon bond between successive acetate units is an energy-consuming process. To provide an energetically favorable leaving group for the subsequent condensation reaction, cells first carboxylate acetyl-CoA. This ACCase reaction occurs in two steps: first, a biotin prosthetic group is carboxylated in an ATP-dependent process, and then acetyl-CoA reacts with carboxybiotin to produce malonyl-CoA (Reaction 8.1; see also Fig. 8.10). ACCase activity is highly regulated and a major biochemical control point that determines the overall rate of fatty acid synthesis in plant cells.

8.3.2 Plants contain both homomeric and heteromeric forms of ACCase

ACCase catalyzes the initial step in fatty acid synthesis; indeed, in most plant cells, the major pathway consuming malonyl-CoA is plastid-localized fatty acid synthesis. However, plants also require malonyl-CoA outside the plastid, where it serves as a substrate for the flavonoid biosynthetic pathway, for fatty acid elongation reactions at the ER, for malonylation of some amino acids, and for the ethylene precursor, aminocyclopropanecarboxylic acid (Fig. 8.11).

In most plants, the plastid form of ACCase has four subunits: biotin carboxyl carrier protein (BCCP), biotin carboxylase (BC), and the α- and β subunits of carboxyltransferase (CT). These four subunits form a membrane-associated heteromeric complex of more than 650 kDa (Fig. 8.12). Three of the subunits are encoded by nuclear genes, whereas the fourth (β-CT) is encoded in the chloroplast genome.

The cytosolic form of ACCase is a single, large (greater than 500 kDa) homodimeric protein. The four subunits described above are integrated into domains of a single polypeptide, two of which associate to make up the homodimer (Fig. 8.12). This structure is similar to the ACCase found in animals and fungi. Indeed, there is as much as 50% amino

Reaction 8.1: Acetyl-CoA carboxylase

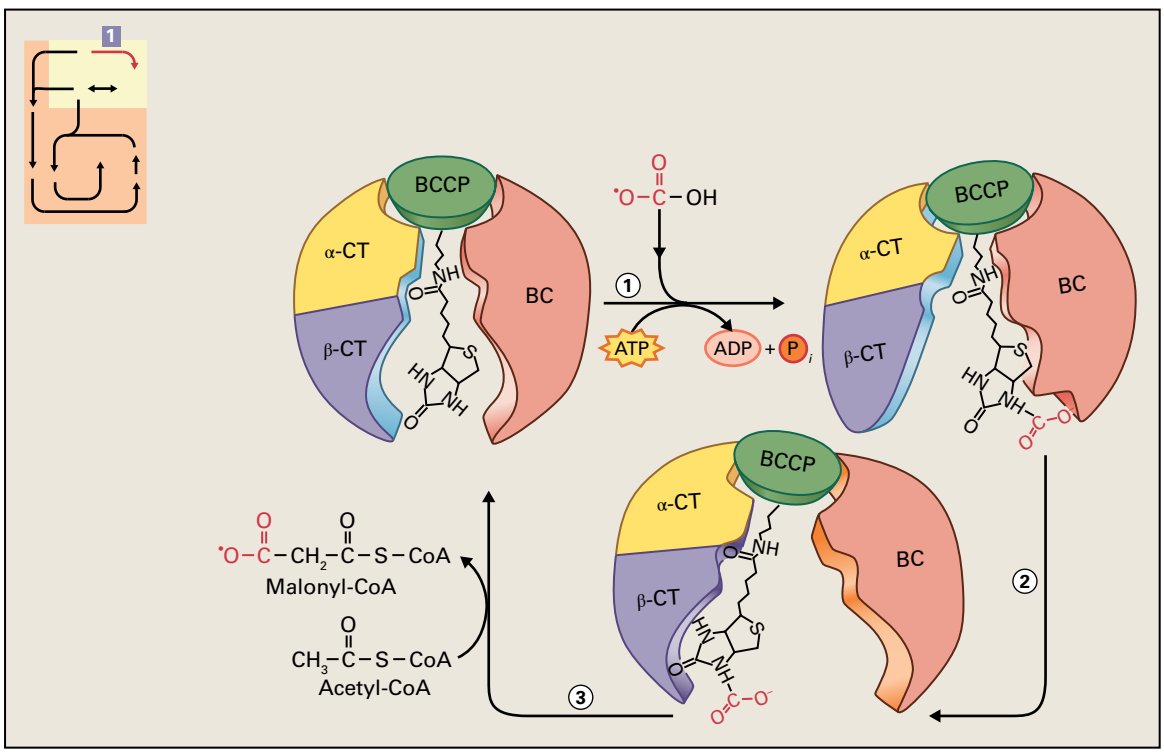


FIGURE 8.10 *The acetyl-CoA carboxylase (ACCase) reaction. ACCase catalyzes step 1 in the reaction sequence shown in Figure 8.9. ACCase has three functional components that form malonyl-CoA from acetyl-CoA. (1) In an ATP-dependent reaction, biotin carboxylase activates CO_2 (as HCO_3^-) by attaching it to a nitrogen in the biotin ring of biotin carboxyl carrier protein (BCCP). (2) The flexible biotin arm of BCCP carries the activated CO_2 from the biotin carboxylase active site to the carboxyltransferase site (α-CT and β-CT). (3) The transcarboxylase transfers activated CO_2 from biotin to acetyl-CoA, producing malonyl-CoA.*

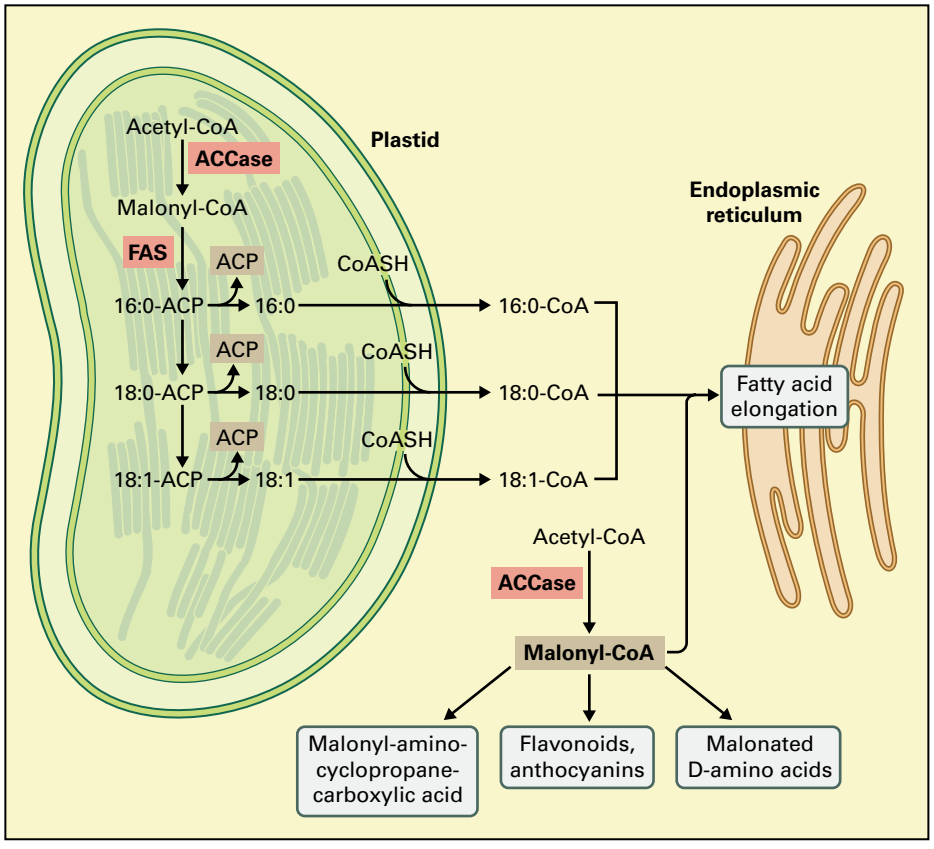
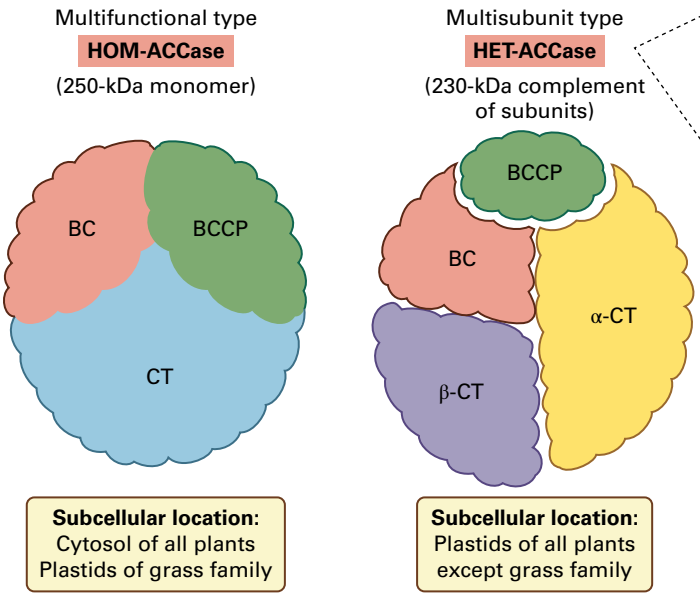


FIGURE 8.11 *Multiple fates of malonyl-CoA. Malonyl-CoA produced by the ACCase reaction enters several pathways in plants. Within the plastid, malonyl-CoA is used exclusively for the production of fatty acids. In the cytosol, malonyl-CoA is the carbon donor for fatty acid elongation, producing the precursors for surface waxes and certain seed lipids. Condensation of three molecules of malonyl-CoA produces a diverse range of flavonoids and their derivatives (see Chapter 24). In many plant tissues, the major form of the ethylene precursor 1-aminocyclopropane-1-carboxylic acid is the inactive malonylated derivative, produced by reaction with malonyl-CoA. Finally, many D-amino acids and other secondary metabolites react with malonyl-CoA to form malonylated derivatives. CoASH, coenzyme A.*



Subunit name	Abbreviation	Approx. size
Biotin carboxylase	BC	50 kDa
Biotin carboxyl carrier protein	BCCP	21 kDa
α-Carboxyl-transferase	α-CT	91 kDa
β-Carboxyl-transferase	β-CT	67 kDa

FIGURE 8.12 *Two different forms of ACCase occur in plants: a homodimeric form (HOM-ACCase) with three functional domains encoded in a single polypeptide of about 250 kDa, and a heteromeric form (HET-ACCase) consisting of four subunits that together form a plastid-localized complex of 650–700 kDa.*

acid identity between the sequences of the enzymes from organisms in these kingdoms.

Almost all monocot and eudicot plants so far examined have the two types of ACCase described above—with the heteromeric, multisubunit form in the plastid and the homodimeric form in the cytosol. The grass family (Poaceae) is an exception, with similar homodimeric forms being found in both plastids and cytosol. Furthermore, the β-CT

gene is partially or completely missing from the chloroplast genome, and none of the subunits of the heteromeric ACCase can be found in sequenced grass genomes. Although the reason for the different ACCase organization in grasses remains unknown, it has substantial practical significance in agriculture. Several widely used grass-specific herbicides kill grasses by specifically inhibiting the homodimeric form of ACCase in the plastid, thereby blocking plastid fatty acid biosynthesis.

8.3.3 Malonyl-CoA formation is the first committed step in fatty acid synthesis and is highly regulated

In many primary metabolic pathways, biochemical regulation occurs at the first committed step. Although malonyl-CoA is used in several pathways in the cell, fatty acid biosynthesis is the only known fate for malonyl-CoA within the plastid. Therefore, the ACCase reaction in plastids is the first committed step for fatty acid synthesis. Several lines of evidence indicate plastid ACCase activity is tightly regulated and this regulation determines, in large part, the overall rate of fatty acid synthesis. First, the concentration of malonyl-CoA in chloroplasts changes quickly during light–dark transitions and remains proportional to the rate of fatty acid synthesis. Second, for herbicides that specifically target the plastid ACCase, the same concentrations inhibit foliar fatty acid synthesis both in vivo and in vitro. Finally, addition of exogenous lipids to suspension cultures slows production of new fatty acids. Analysis of the substrates and products of plastid fatty acid metabolism indicates this regulation occurs at the ACCase reaction. Thus, plastid-localized ACCase appears to be a highly regulated enzyme subject to feedback and other biochemical controls. Post-translational activation of ACCase occurs by multiple mechanisms including feedback by acyl-ACP, phosphorylation, and redox regulation mediated by thioredoxin.

8.4 Fatty acid synthase

8.4.1 Different types of FAS exist in different kingdoms

FAS refers to all enzyme activities in fatty acid biosynthesis except ACCase. Although the reactions catalyzed by FAS are essentially the same for all organisms, two different types of FAS are found in nature. Animals and yeast use a Type I FAS, a single multifunctional enzyme complex characterized by large subunits (250 kDa). Each subunit can catalyze several different reactions. By contrast, plants and most bacteria have a Type II FAS, in which each enzyme activity resides on an individual protein that can be readily separated from the other activities participating in fatty acid synthesis. Type II FAS also includes ACP. The Type II FAS functions much like a metabolic pathway, whereas Type I FAS functions like a large protein complex (e.g., pyruvate dehydrogenase).

The assembly of a C_{18} fatty acid from acetyl-CoA in Type II fatty acid synthesis requires 48 reactions involving at least 12 different proteins. How is this complex pathway organized? Although no direct evidence has been established to date, supramolecular organization seems very likely. The estimated concentrations of many acyl-ACP intermediates of the pathway are in the nanomolar range, far below the K_m values predicted by kinetic analyses of the enzymes involved. Calculations suggest the enzyme activities available at these low substrate concentrations are not sufficient to support observed in vivo rates of fatty acid synthesis. Accordingly, some form of

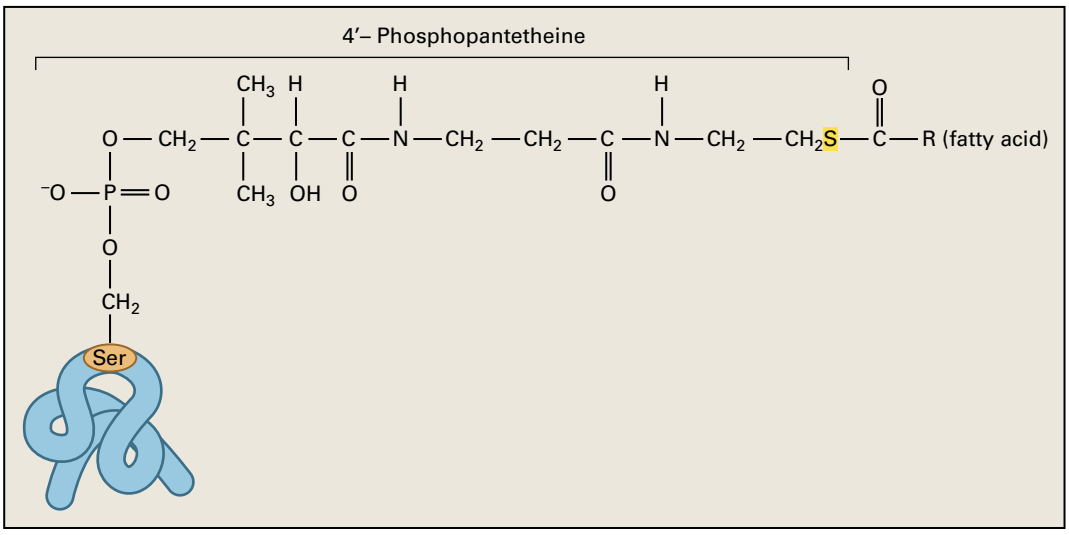


FIGURE 8.13 *Acyl-carrier protein (ACP), a small protein of 80–90 amino acids, participates as an acyl carrier in all reactions of fatty acid synthesis, as well as in desaturation and acyltransferase reactions. The prosthetic group is 4′-phosphopantetheine, which is covalently attached to the hydroxyl group of a serine residue in ACP. Shown is the structure of acyl-ACP.*

substrate channeling seems essential. Furthermore, in osmotically lysed chloroplasts, neither acetyl-CoA nor malonyl-CoA competes with radiolabeled free acetate for incorporation into fatty acids, suggesting acetate is channeled directly into fatty acid synthesis. Thus, Type II fatty acid synthesis is catalyzed by separate enzymes that appear to be complexed in a tightly coupled synthesis pathway.

8.4.2 ACP transports intermediates of fatty acid synthesis through the pathway

After formation of malonyl-CoA in the ACCase reaction (step 1, Fig. 8.9), the assembly of fatty acids involves a central cofactor, ACP (Fig. 8.13). This small protein is about 80 amino acids long and contains a phosphopantetheine prosthetic group covalently linked to a serine (Ser) residue near the middle of the polypeptide chain. The phosphopantetheine group, also found in coenzyme A (CoASH), contains a terminal sulfhydryl. The thioester linkage that forms between a fatty acid and this sulfur is a high-energy bond with a free energy of hydrolysis similar to that for ATP.

8.4.3 Malonyl-CoA:ACP transacylase transfers a malonyl moiety from CoASH to ACP

ACP first becomes involved in the fatty acid synthesis pathway when the malonyl group produced by ACCase is transferred from CoASH to the sulfhydryl of ACP by the reactions catalyzed by malonyl-CoA:ACP transacylase (Reaction. 8.2; see also step 2, Fig. 8.9).

The reaction mechanism involves a covalent malonyl–enzyme intermediate (Fig. 8.14). Analysis of the malonyl transacylase (note: the terms transacylase and acyltransferase are equivalent) from *E. coli* has demonstrated this intermediate is a serine ester. After the malonyl-transacylation, all subsequent reactions of fatty acid synthesis involve ACP.

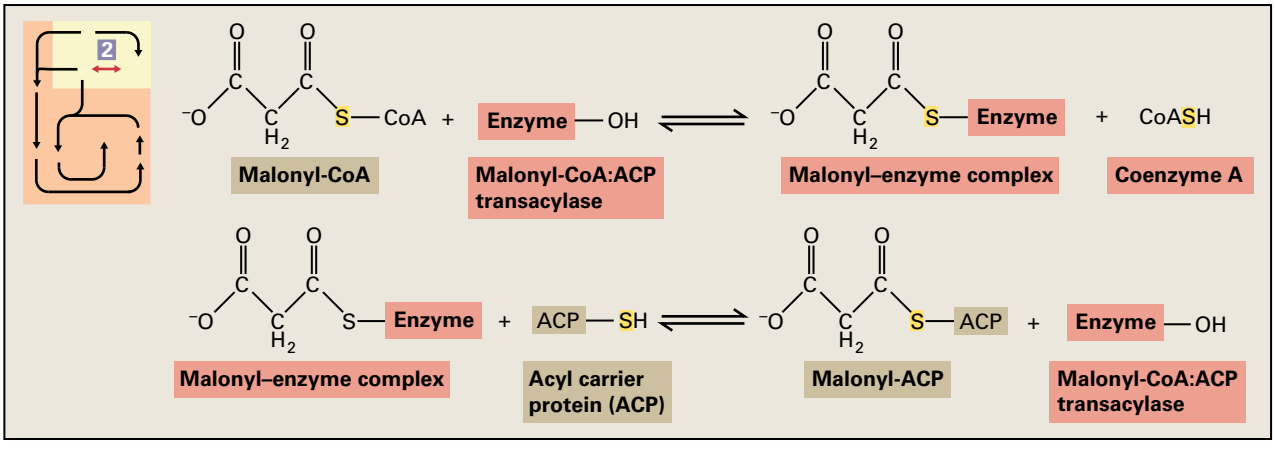
8.4.4 The three plant isoforms of 3-ketoacyl-ACP synthase demonstrate different substrate specificities

The defining reaction of fatty acid synthesis is the elongation of a "primer" acyl chain by two carbons donated from malonyl-ACP (step 3, Fig. 8.9). The condensation reaction to form a new carbon–carbon bond is catalyzed by 3-ketoacyl-ACP synthase (KAS), commonly called condensing enzyme (Fig. 8.15). All plants examined to date contain three KAS isoenzymes (I, II, and III), each distinguished by its substrate specificity. The general reaction for KAS occurs in two steps (Reaction 8.3; see also step 4, Fig. 8.9). The in vitro substrate specificity of each of the KAS isoenzymes suggests the role each plays in fatty acid biosynthesis. KAS I is most active with C_4–C_{14} acyl-ACPs. KAS II accepts only longer-chain (C_{10}–C_{16}) acyl-ACPs as substrates. KAS III has a strong preference for acetyl-CoA rather than acyl-ACP. These in vitro activities suggest KAS isoenzymes act in sequence. KAS III initiates fatty acid biosynthesis, using acetyl-CoA as a primer. KAS I then extends the acyl chain to C_{12}–C_{16}. Finally, KAS II completes the synthesis to C_{18}.

8.4.5 The last three steps of the fatty acid synthesis cycle reduce a 3-ketoacyl substrate to form a fully saturated acyl chain

The initial reductive step of fatty acid biosynthesis is the conversion of a 3-ketoacyl-ACP to a 3-hydroxyacyl-ACP (Reaction 8.4; step 4, Fig. 8.9). Native 3-ketoacyl-ACP reductase has a molecular mass of 130 kDa and a subunit mass of 28 kDa, suggesting it is a tetramer. The predominant form

Reaction 8.2: Malonyl-CoA:ACP transacylase



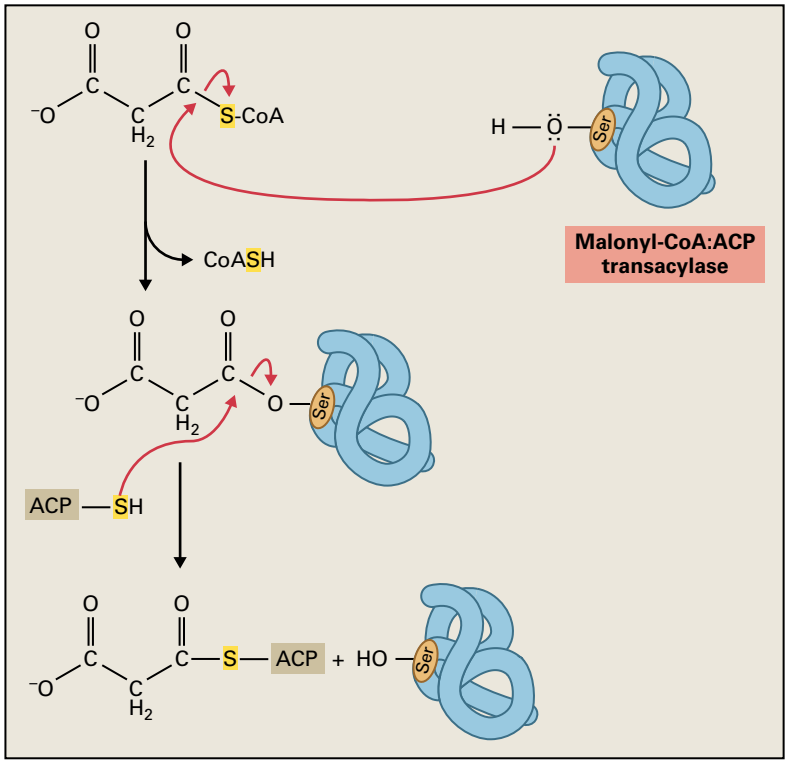


FIGURE 8.14 *Mechanism of the malonyl-CoA:ACP transacylase reaction. In the first step of the reaction, the malonyl group is transferred to a serine residue on the enzyme and CoASH is released. In the second step, the acyl group is transferred to the phosphopantetheine sulfhydryl group of ACP to form the malonyl-ACP thioester.*

is NADPH-dependent and can account for all the required 3-ketoacyl-ACP reductase activity for fatty acid synthesis.

The removal of water from 3-hydroxyacyl-ACP to form 2,3-*trans*-enoyl-ACP is catalyzed by 3-hydroxyacyl-ACP dehydrase (Reaction 8.5: step 5, Fig. 8.9). The purified dehydrase from spinach (*Spinacia oleracea*) has a molecular mass of 85 kDa and a subunit size of 19 kDa. Thus, it appears to be a homotetramer. Its substrate specificity is very broad, with high activity demonstrated for acyl groups ranging from C_4 to C_{16}.

In the final reduction step, enoyl-ACP reductase converts the 2,3-*trans*-enoyl-ACP to the corresponding saturated acyl-ACP (Reaction 8.6; step 6, Fig. 8.9). Enoyl-ACP reductase exists in two isoforms. The major form is specific for NADH and a homotetramer with a native molecular mass of 115–140 kDa and a subunit molecular mass of 32.5–34.8 kDa. A second isoform uses either NADPH or NADH and is specific for longer-chain (C_{10}) enoyl-ACPs.

8.4.6 Thioesterase reactions terminate the fatty acid biosynthesis cycle

Each cycle of fatty acid synthesis adds two carbons to the acyl chain. Typically, fatty acid synthesis ends at 16:0 or 18:0, when one of several reactions stops the process. The most common reactions are hydrolysis of the acyl moiety from ACP by a thioesterase, transfer of the acyl moiety from ACP directly onto a glycerolipid by an acyl transferase, or double-bond formation on the acyl moiety by an acyl-ACP desaturase. The thioesterase reaction yields a sulfhydryl ACP (Reaction 8.7).

Two principal types of acyl-ACP thioesterases occur in plants (Fig. 8.16). The major class, designated FatA, is most active with 18:$1^{\Delta 9}$-ACP. A second class (FatB), typified by 16:0-ACP thioesterase, is most active with shorter-chain, saturated acyl-ACPs. In both cases, however, the metabolic consequence of these reactions is the same. Cleavage of the acyl moiety from ACP prevents extension and targets the acyl group for export out of the plastid by an unknown mechanism. Thioesterases play an important role in plants that have unusually short fatty acids, such as coconut (*Cocos nucifera*), many species of *Cuphea,* and California bay (*Umbellularia californica*). These plants have thioesterases that are especially active with C_{10}–C_{12} acyl-ACPs; by prematurely terminating fatty acid biosynthesis, thioesterase activity results in the accumulation of 10:0 and 12:0 fatty acids in the seed triacylglycerols.

8.5 Desaturation and elongation of C_{16} and C_{18} fatty acids

If membranes contained only saturated or *trans*-unsaturated fatty acids, the hydrophobic lipid tails would form a semicrystalline gel, impairing the permeability barrier and interfering with the mobility of membrane components. By contrast, *cis*-double bonds, which introduce "kinks" into a fatty acid chain, can enhance membrane fluidity by dramatically lowering the temperature at which these ordered matrices melt.

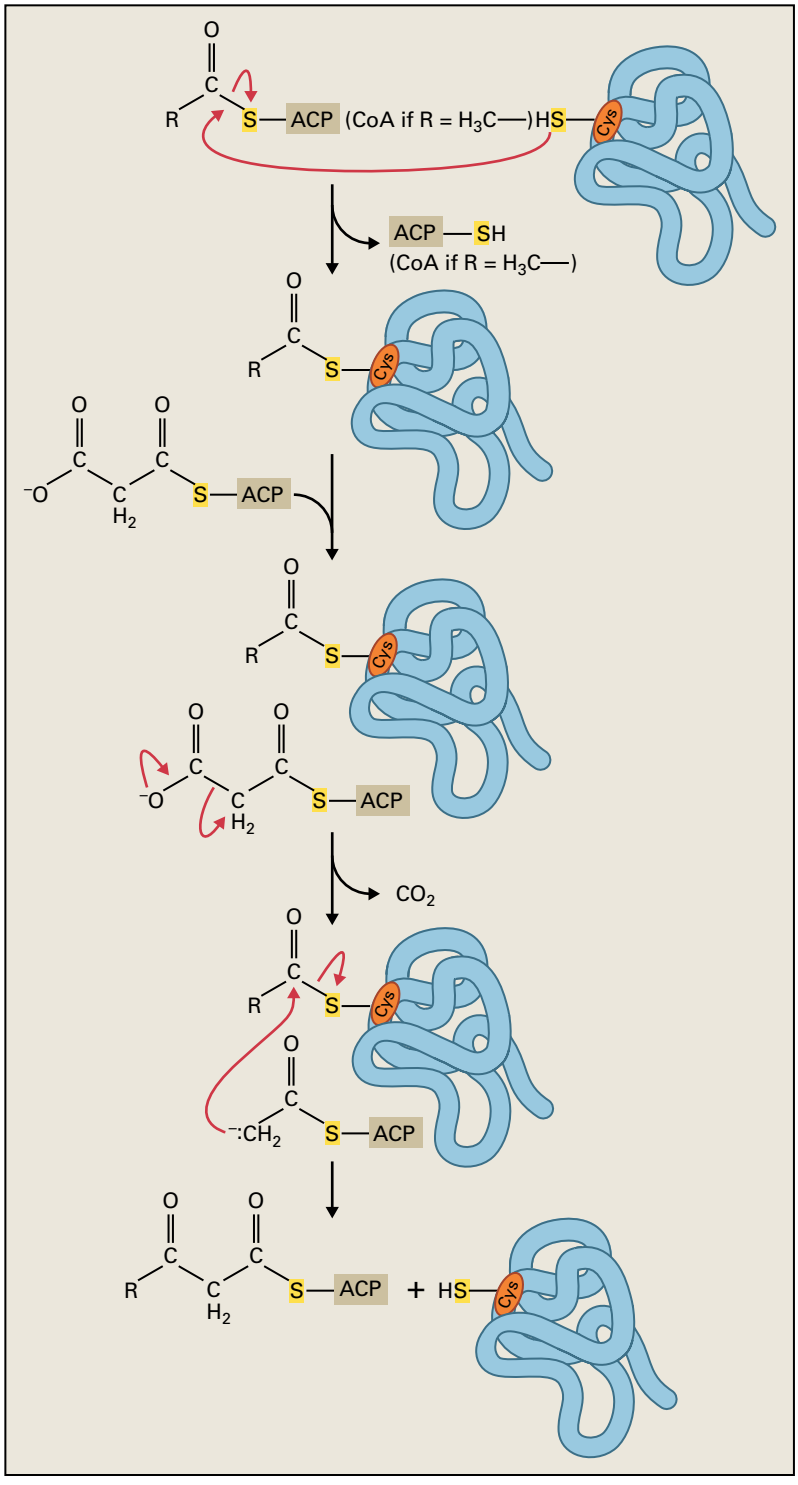


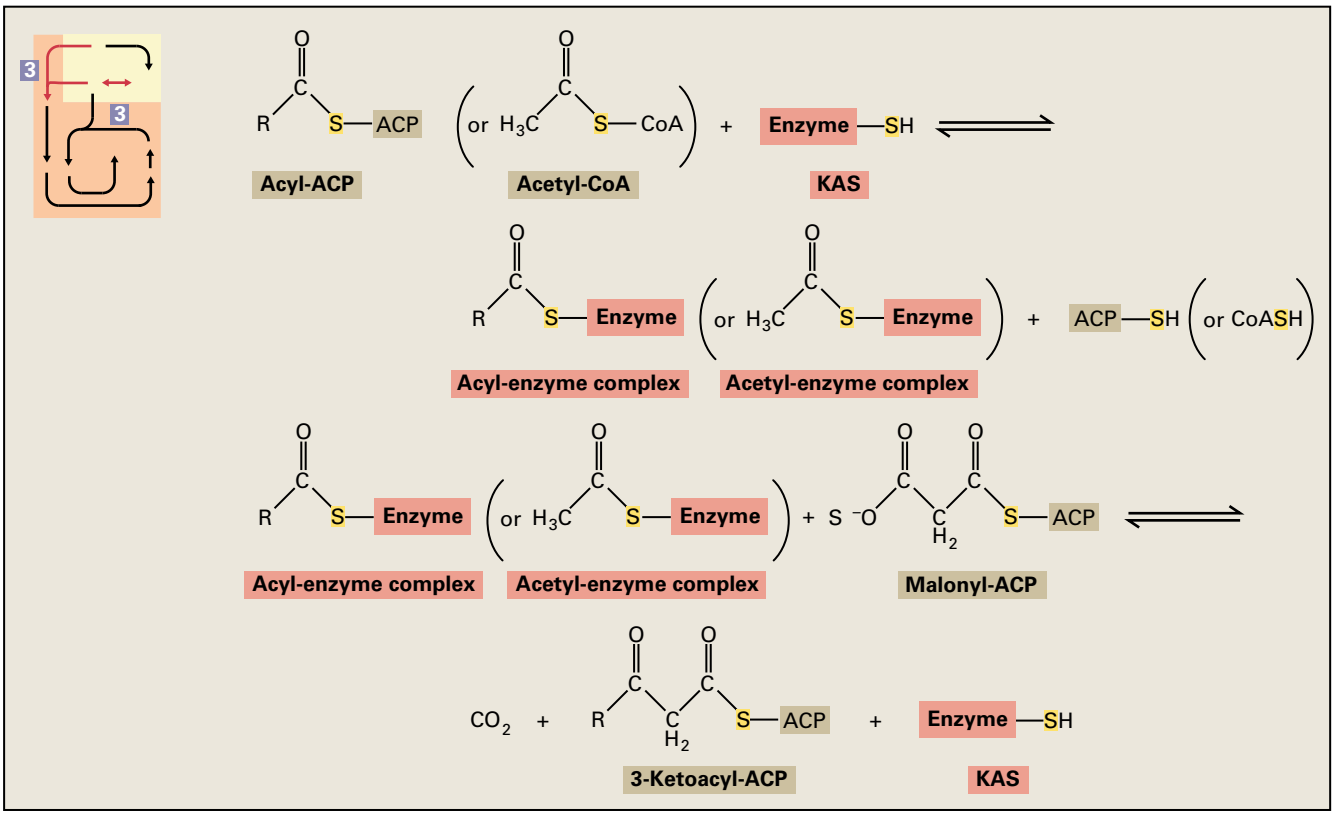
FIGURE 8.15 *3-Ketoacyl-ACP synthases catalyze Claisen condensations. This sequential reaction involves, first, the acyl transfer from an ACP or CoA thioester to an active site cysteine, followed by the entry of malonyl-ACP and decarboxylation of the malonate. The resulting carbanion then condenses with the acyl group to form a new C–C bond before release of the acyl group from the cysteine.*

For example, the desaturation step that converts stearic acid (18:0) to oleic acid ($18:1^{\Delta 9}$) lowers the melting point of the fatty acid from 69°C to 13.4°C. Double bonds at other positions in the chain also exert large effects on the melting temperature of fatty acids and of the lipids that contain them (Fig. 8.17; see also Chapter 1, Table 1.2). Formation of such double bonds is catalyzed by various desaturase enzymes, which generate a diverse array of unsaturated lipids found in membranes, storage reserves, and extracellular waxes.

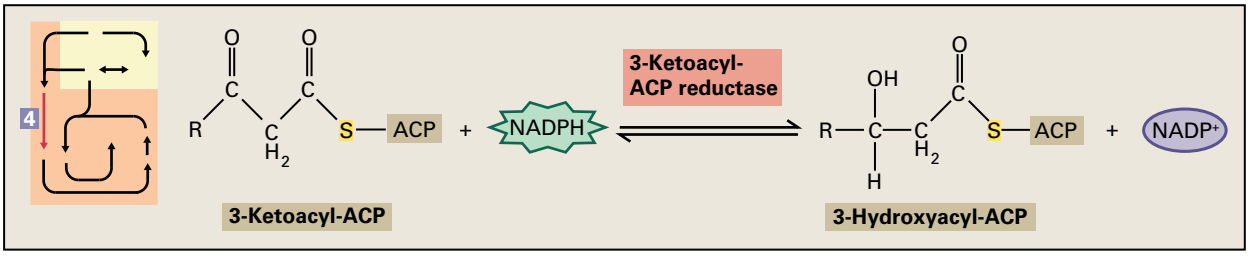
8.5.1 Plants contain a soluble, plastid-localized stearoyl-ACP desaturase

Unsaturated C_{18} acyl chains found in membrane lipids throughout the plant cell are products of a soluble chloroplast enzyme, stearoyl-ACP Δ9-desaturase (Fig. 8.18). All eukaryotes and some prokaryotes have desaturases that catalyze similar reactions, but in all cases these enzymes are integral

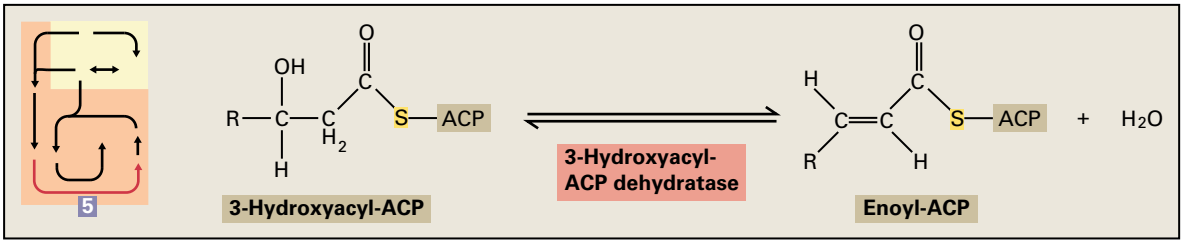
Reaction 8.3: 3-Ketoacyl-ACP synthase (KAS)



Reaction 8.4: 3-Ketoacyl-ACP reductase



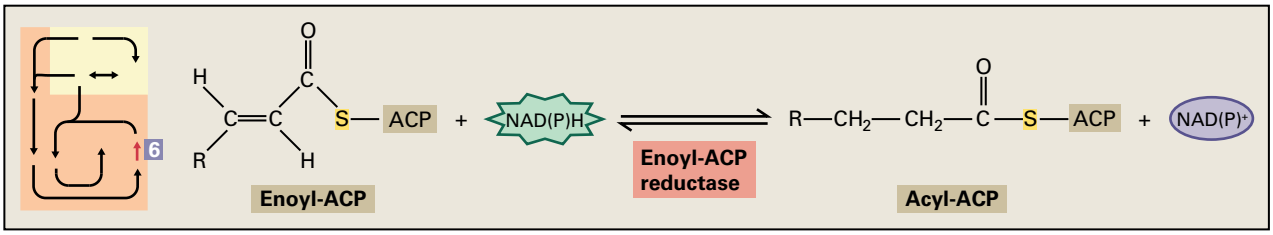
Reaction 8.5: 3-Ketoacyl-ACP dehydratase



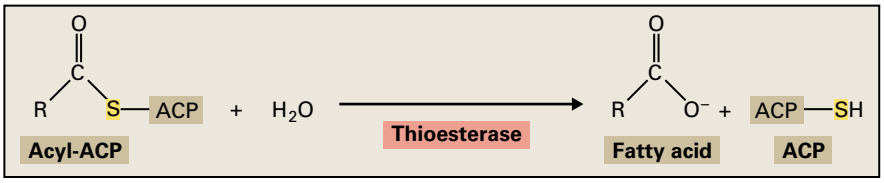
membrane proteins. Recently, stearoyl-ACP Δ9-desaturase has come to be recognized as the prototype of a distinct family of structurally similar enzymes that introduce double bonds at various locations along the acyl chain. Species-specific genes for two isoforms, which catalyze desaturations of palmitic acid at the Δ4 or Δ6 position, have recently been isolated from coriander (*Coriandrum sativum*) and black-eyed susan (*Thunbergia alata*), respectively.

Unlike the stearoyl-CoA desaturases of fungi and animals, which are located in the ER membranes, the members of the

Reaction 8.6: Enoyl-ACP reductase



Reaction 8.7: Thioesterase



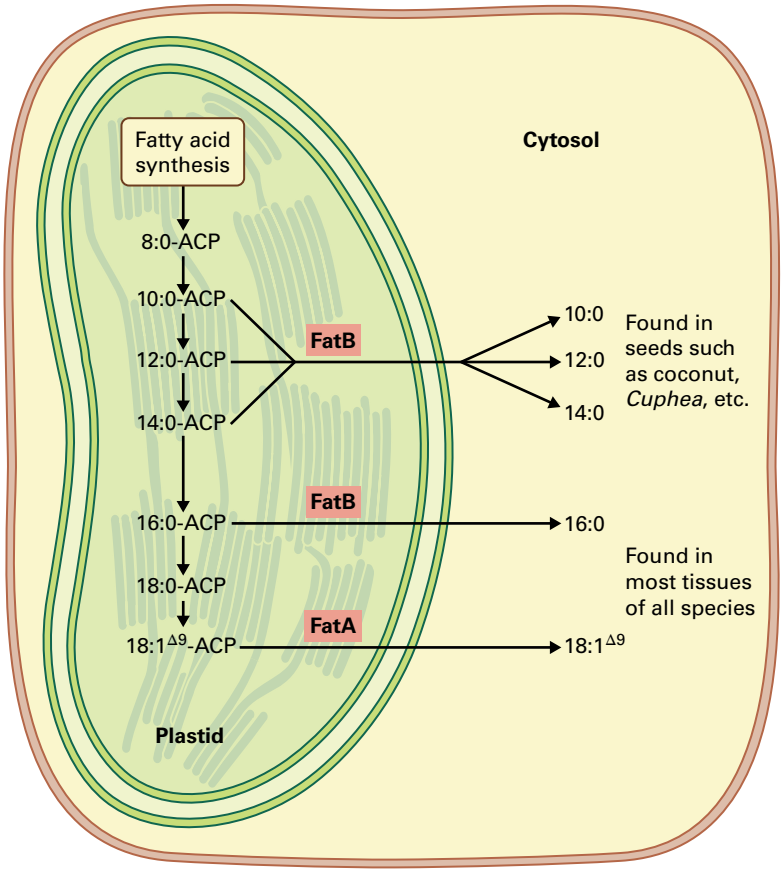


FIGURE 8.16 *Principal types of acyl-ACP thioesterases in plants. The FatA class is most active with 18:1$^{\Delta 9}$ and the FatB class is most active with saturated acyl-ACPs. The FatA 18:1$^{\Delta 9}$ thioesterase and the FatB 16:0-ACP thioesterase are found in all plant tissues. Some FatB thioesterases, especially those most active on acyl-ACP acyl groups shorter than C_{16}, are species specific.*

stearoyl-ACP desaturase enzyme family are soluble, a fact that has greatly facilitated structural and mechanistic studies. The tertiary structure of castor bean (*Ricinus communis*) stearoyl-ACP Δ9-desaturase has been solved by X-ray crystallography (Fig. 8.19A). As the crystal structure shows, the protein contains a cavity that can bind the 18:0 substrate in the correct orientation with respect to the active site (Fig. 8.19B). The amino acid sequences of known soluble desaturases from several plants are sufficiently homologous that we can deduce their active sites by mapping the sequences of the Δ4- and Δ6-desaturases onto the structure of the Δ9-desaturase. When the gene encoding the castor bean enzyme was expressed in *E. coli*, it produced a functional enzyme that could be purified in large amounts. Mössbauer spectrometry of the recombinant castor bean enzyme from cultures of *E. coli* grown in ^{57}Fe revealed the presence of a nonheme iron

center in the desaturases—a structure now known to be a Fe-O-Fe (diiron) center of the type found in bacterial methane monooxygenase (Fig. 8.19C). This provides an explanation for many properties of the desaturases, such as the observation that the overall desaturation reaction requires transfer of two electrons from a donor such as ferredoxin or cytochrome b_5 (Fig. 8.20).

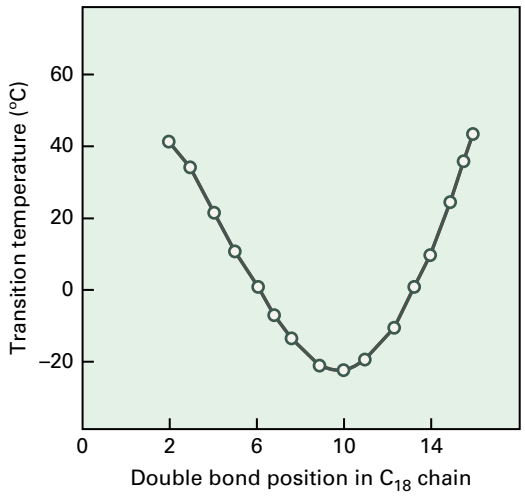


FIGURE 8.17 *The transition temperature, or melting temperature, of a lipid is strongly influenced by the presence and position of double bonds in the acyl groups. In this example, the transition temperature has been determined for several molecular species of phosphatidylcholine in which the two acyl groups are C_{18} fatty acids that contain double bonds at various positions along the chains. Thus, for instance, when the two acyl groups have double bonds between C-2 and C-3, the transition temperature is approximately 40°C, whereas for molecules with double bonds near the center of the acyl groups, the melting temperature is decreased by about 60°C. Thus, by controlling the position of the fatty acyl unsaturations, organisms can exert control over the physical properties of lipids.*

8.5.2 Most fatty acyl desaturases are membrane-localized proteins

Except for the soluble acyl-ACP desaturase family, all other fatty acid desaturases from animals, yeast, cyanobacteria, and plants are integral membrane proteins. The plant and cyanobacterial enzymes desaturate fatty acids of glycerolipids, whereas some yeast and animal desaturases act on acyl-CoAs.

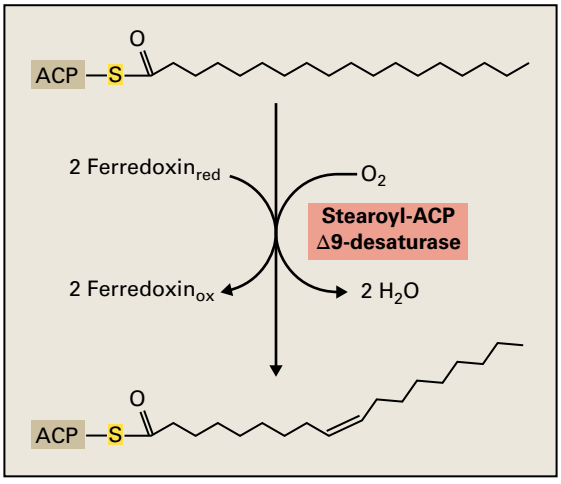


FIGURE 8.18 *Desaturation of stearic acid is catalyzed by stearoyl-ACP Δ9-desaturase.*

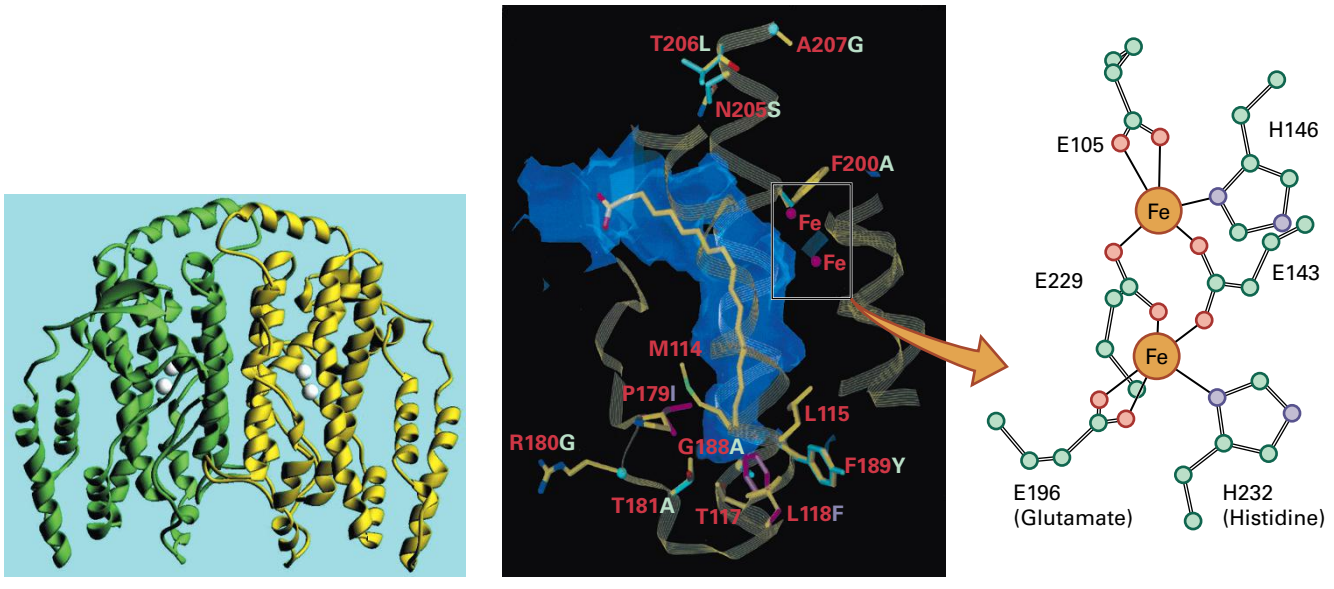


FIGURE 8.19 *(A) Tertiary structure of stearoyl-ACP Δ9-desaturase dimer from* Ricinus communis. *The four white spheres near the center of the enzyme are two pairs of iron ions that catalyze the desaturation reaction. (B) Schematic view of the substrate channel of a stearoyl-ACP Δ9-desaturase monomer. A model of the stearoyl substrate moiety is fitted in the binding pocket of the desaturase. (C) Details of the residues that coordinate the diiron-oxo group at the active site.*

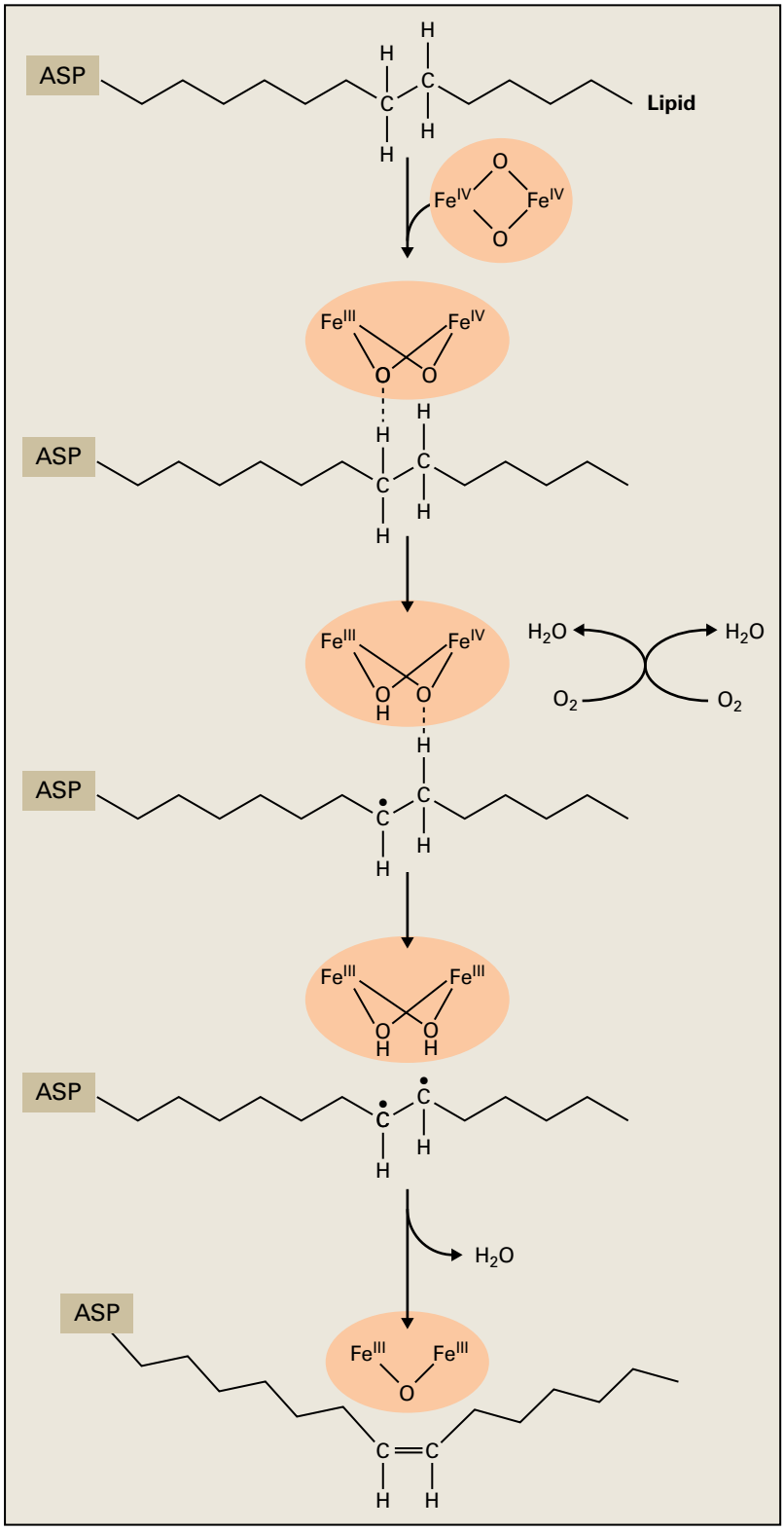


FIGURE 8.20 *Proposed catalytic mechanism for fatty acid desaturation. In the resting state, the diiron center is in the oxidized (diferric, or Fe^{III}–Fe^{III}) form with a μ-oxo bridge. Reduction of both iron ions by electron transfer from two ferredoxins (Fdx) results in the reduced (diferrous, or Fe^{II}–Fe^{II}) form. The reduced enzyme binds molecular oxygen, resulting in the formation of a peroxo intermediate, "P." Scission of the O–O bond results in the formation of an activated form of the diiron center, "Q" (diferryl, or Fe^{IV}–Fe^{IV}). By analogy with the methane monooxygenase reaction, Q has been proposed to perform an energy-demanding hydrogen abstraction from the methylene group of the unactivated fatty acid to yield a radical intermediate. Loss of the second hydrogen results in formation of the double bond along with the loss of H_2O and regeneration of the oxidized active site and the μ-oxo bridge.*

Solubilizing and purifying the plant enzymes have proven very difficult, limiting investigation by traditional biochemical techniques. Genetic analysis in *Arabidopsis* has provided an alternative approach to biochemical methods for assessing the function of the enzymes.

The number and properties of different desaturases in plants are known from the isolation of a comprehensive collection of *Arabidopsis* mutants with defects in each of eight desaturase genes. The enzymes encoded by these genes differ in substrate specificity, subcellular location, mode of regulation, or some combination of these (Table 8.4). The mutants were identified by analyzing lipid samples from leaves or seeds of individual plants from heavily mutagenized populations. The biochemical defect of each class of mutants is shown by breaks in the pathway in Figure 8.21. The mutations that disrupt the activity of specific fatty acid desaturases are designated *fab2* and *fad2* through *fad8.* Two of the desaturases are ER-localized enzymes, oleate desaturase (FAD2) and linoleate desaturase (FAD3). Three structurally related enzymes are located in the plastids: one oleate desaturase (FAD6) and two functionally similar linoleate desaturases (FAD7 and FAD8). The identities of these enzymes have been confirmed by cloning the corresponding genes and using the cloned genes to complement the mutations in transgenic *Arabidopsis* plants, thereby restoring enzyme activity.

The ER-localized enzymes act on fatty acids esterified to phosphatidylcholine and possibly other phospholipids, and they utilize cytochrome b_5 as an intermediate electron donor. Cytochrome b_5 is reduced by another membrane protein, cytochrome b_5 reductase. Thus, three proteins are required for the overall desaturation reaction catalyzed by the ER-localized desaturases. In contrast, the membrane-localized chloroplast enzymes use soluble ferredoxin as an electron donor and act on fatty acids esterified to galactolipids, sulfolipids, and phosphatidylglycerol (PG). Analysis of the mutants suggests the FAD4 enzyme is completely specific for PG, and the FAD5 enzyme appears to be specific for monogalactosyldiacylglycerol (Fig. 8.21). Despite differences in the glycerolipid substrates and electron donors used, and the position in which they insert the double bond, the majority of membrane-localized plant desaturases are structurally related to each other and to the membrane-localized desaturases from animals and yeast. They contain three histidine-rich sequences (typically HXXHH) that have been proposed to bind the two iron ions required for catalysis. Although the tertiary structure of the membrane-bound desaturases is not known, the iron-binding site may resemble that found in the diiron protein hemerythrin (Fig. 8.22).

From analysis of the effects of the mutations on glycerolipid fatty acid composition, a loss-of-function mutant appears to be available for every desaturase in *Arabidopsis* except stearoyl-ACP Δ9-desaturase, which is encoded by a family of genes. Thus, the *fab2* mutation, which is one of the genes encoding stearoyl-ACP desaturase, causes a significant increase in stearate concentrations but does not completely eliminate unsaturated fatty acids.

8.5.3 What factors determine glycerolipid desaturation?

Of central importance to the mechanisms that control desaturation are the factors that determine the extent of desaturation of a specific glycerolipid in a particular membrane. In cyanobacteria, the steady-state concentration of an oleate Δ12-desaturase mRNA is inversely correlated with temperature

TABLE 8.4 *Fatty acid desaturases of Arabidopsis.*

Name	Subcellular location	Fatty acid substrates	Site of double-bond insertion	Notes
FAD2	ER	$18{:}1\Delta^{9}$	Δ12	Preferred substrate is phosphatidylcholine
FAD3	ER	$18{:}2\Delta^{9,12}$	ω3	Preferred substrate is phosphatidylcholine
FAD4	Chloroplast	16:0	Δ3	Produces 16:1-*trans* at *sn*-2 of phosphatidylglycerol
FAD5	Chloroplast	16:0	Δ7	Desaturates 16:0 at *sn*-2 of monogalactosyldiacylglycerol
FAD6	Chloroplast	$16{:}1\Delta^{7}$ $18{:}1\Delta^{9}$	ω6	Acts on all chloroplast glycerolipids
FAD7	Chloroplast	$16{:}2\Delta^{7,11}$ $18{:}2\Delta^{9,12}$	ω3	Acts on all chloroplast glycerolipids
FAD8	Chloroplast	$16{:}2\Delta^{7,11}$ $18{:}2\Delta^{9,12}$	ω3	Isoenzyme of FAD7 induced by low temperature
FAB2	Chloroplast	18:0	Δ9	Stromal stearoyl-ACP desaturase

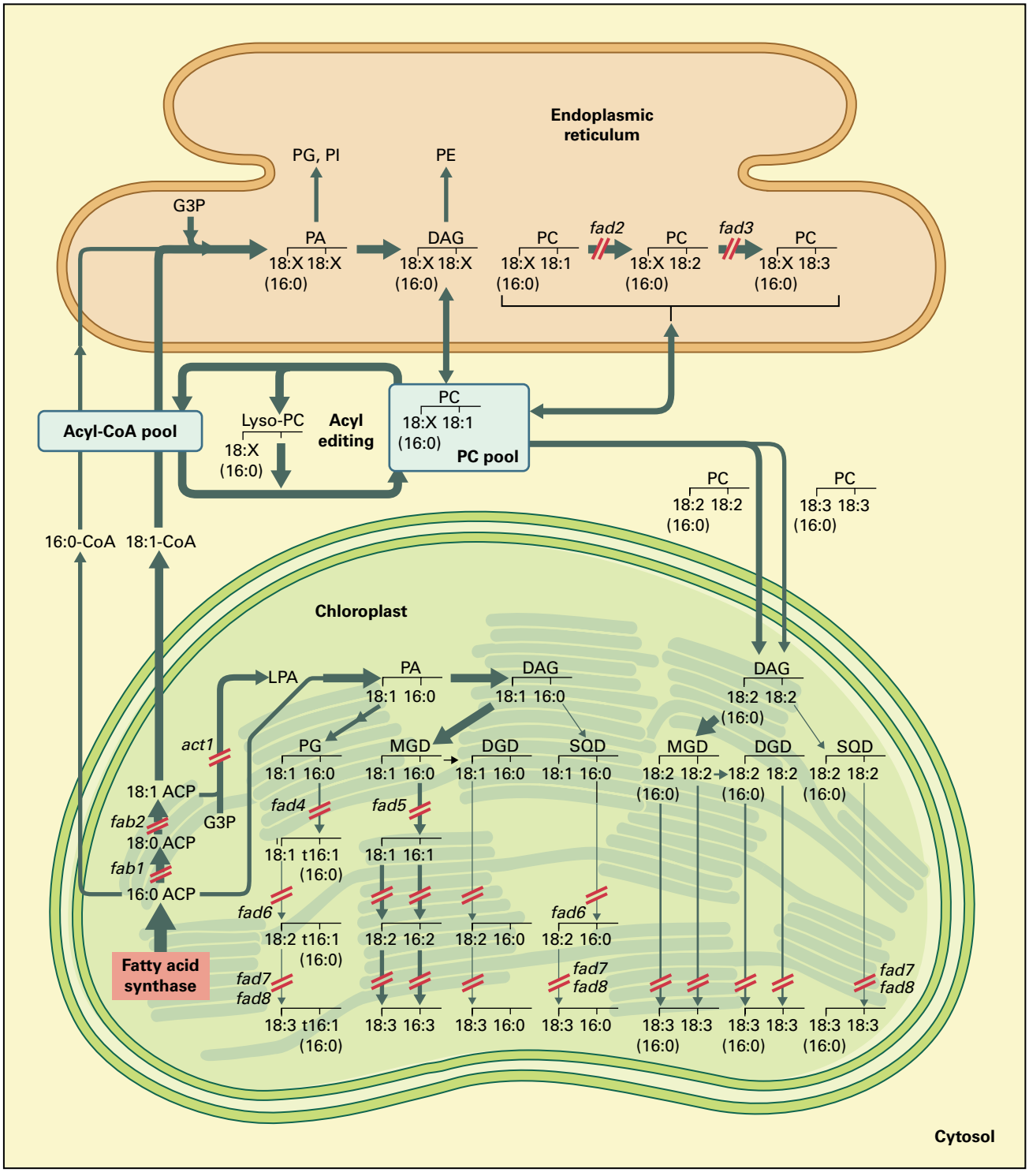


FIGURE 8.21 *Abbreviated scheme for lipid synthesis in leaves of* Arabidopsis. *The set of reactions occurring solely within the chloroplast are termed the prokaryotic pathway; those that involve glycerolipid synthesis in the ER and subsequent transfer to the chloroplast constitute the eukaryotic pathway. After fatty acids leave the chloroplast, the largest flux measured in pea leaf labeling experiments is the exchange of acyl groups between the acyl-CoA pool and PC. Therefore, most fatty acids that exit the plastid are first esterified to PC rather than glycerol-3-phosphate. It is possible this reaction occurs at the chloroplast envelope or the plastid associated membrane. The breaks in the pathway (red) represent some of the enzymes for which mutations have been obtained in their genes in* Arabidopsis *(see Table 8.4). DAG, diacylglycerol; DGD, digalactosyldiacylglycerol; G3P, glycerol 3-phosphate; LPA, lysophosphatidic acid; PA, phosphatidic acid; PC, phosphatidylcholine; PE, phosphatidylethanolamine; PG, phosphatidylglycerol; PI, phosphatidylinositol; MGD, monogalactosyldiacylglycerol; SQD, sulfoquinovosyldiacylglycerol.*

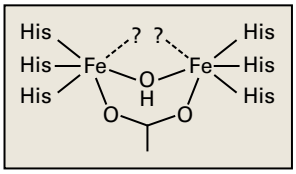


FIGURE 8.22 *Proposed ligation sphere of the integral membrane desaturases and related enzymes possessing two HXXHH motifs, in which all of the histidine residues have been shown to be essential for catalysis. The model is based on the structure of hemerythrin and shows a hydroxo bridge and a single carboxylate ligand that has yet to be defined. Question marks indicate the presence of two undefined ligands.*

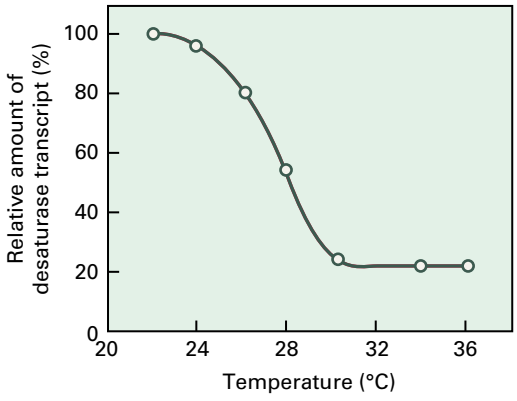


FIGURE 8.23 *In cyanobacteria, the amount of desaturase mRNA is regulated by growth temperature.*

(Fig. 8.23). Molecular and mutational analysis in *Synechocystis* PCC6803 demonstrated two-component regulators act as temperature sensors and induce the expression of desaturases and other genes in response to decreased temperature. These histidine kinase sensor components likely respond to changes in fluidity of the plasma membrane.

Most plants also increase the extent of membrane glycerolipid desaturation when grown at low temperature. The amount of mRNA for the desaturases genes in *Arabidopsis*, however, does not appear to change significantly in response to changes in growth temperature, with one exception: the *FAD8* gene, which exhibits a strong increase in mRNA abundance at low temperature. If a regulatory mechanism controlled desaturase gene expression in response to changes in the physical properties of membranes, we would expect this mechanism to detect large changes in membrane composition and to signal an increase in desaturase gene expression. However, expression of the cold-inducible *FAD8* gene is not altered in *fad7 fad8* double mutants, which are highly deficient in $16{:}3^{\Delta 7,10,13}$ and $18{:}3^{\Delta 9,12,15}$ fatty acids. Indeed, none of the loss-of-function *fad* mutations alters *FAD* gene expression. There is evidence the FAD8 desaturase is regulated by increased turnover of the protein at high temperatures. Presumably, the complexities associated with regulating the composition of many intracellular membranes in plants may require posttranscriptional mechanisms that can adjust the composition of each membrane independently.

8.5.4 Specialized elongase systems produce long-chain fatty acids

Fatty acid synthesis generally results in C_{16} and C_{18} fatty acids, yet plants have numerous requirements for longer fatty acids. All plants produce waxes, usually derived from C_{26} to C_{32} fatty acids. Often, sphingolipids contain C_{22} and C_{24} fatty acids. And, in some plants, triacylglycerols contain large amounts of C_{20} and C_{22} fatty acids. Where and how are these very-long-chain fatty acids synthesized?

Plants and most other eukaryotic organisms have a specialized elongase system for extension of fatty acids beyond C_{18}. These elongase reactions have several important features in common with FAS reactions (see Fig. 8.9). Each uses a reaction series that condenses two carbons at a time from malonyl-CoA to an acyl primer, followed by reduction, dehydration, and a final reduction. The result is the same acyl intermediates are used for the two processes. Although the enzymology of the elongase is not well understood, several important differences between the two systems are known (Fig. 8.24):

- Fatty acid elongases are localized in the cytosol and are membrane-bound.
- ACP is not involved in this process.
- The elongase 3-ketoacyl-CoA synthase (elongase KCS) catalyzes the condensation of malonyl-CoA with an acyl primer.

Recent cloning of elongase KCS genes from *Arabidopsis* and jojoba (*Simmondsia chinensis*) has revealed these 60-kDa enzymes bear little sequence similarity to any other condensing enzymes. Identification of additional clones suggests the elongase KCSs in *Arabidopsis* belong to a complex gene family with 21 members. The requirement for multiple genes may be related to the relatively narrow acyl substrate specificity of elongase KCSs, so several different elongase KCSs would be required to synthesize a C_{30} fatty acid. Elongase KCSs may also be specific for a particular physiological function, such as wax biosynthesis or sphingolipid biosynthesis.

The additional components of the elongase system have only recently been identified in yeast, and *Arabidopsis* homologs have also been identified. The reductases and dehydrase are also membrane-localized, and the reductases prefer NADPH.

8.6 Synthesis of unusual fatty acids

8.6.1 More than 200 fatty acids occur in plants

Extensive surveys of the fatty acid composition of seed oils from different plants species have identified more than 200 naturally occurring fatty acids that can be broadly classified into 18 structural classes. The classes are defined by the number and arrangement of double or triple bonds and various

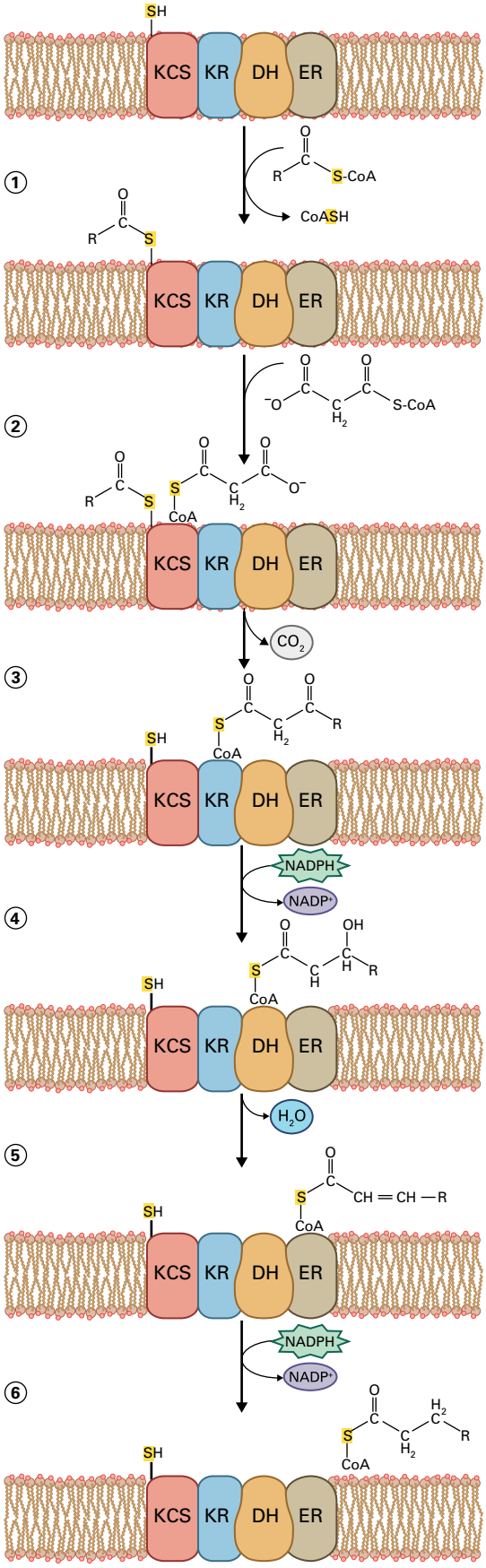


FIGURE 8.24 *Sequence of events during a single cycle of fatty acid elongation by the membrane-bound fatty acid elongase system, which*

functional groups, such as hydroxyls, epoxys, cyclopentenyl or cyclopropyl groups, or furans (Fig. 8.25).

The most common fatty acids, which often occur in both membrane and storage lipids, belong to a small family of C_{16} and C_{18} fatty acids that may contain as few as zero or as many

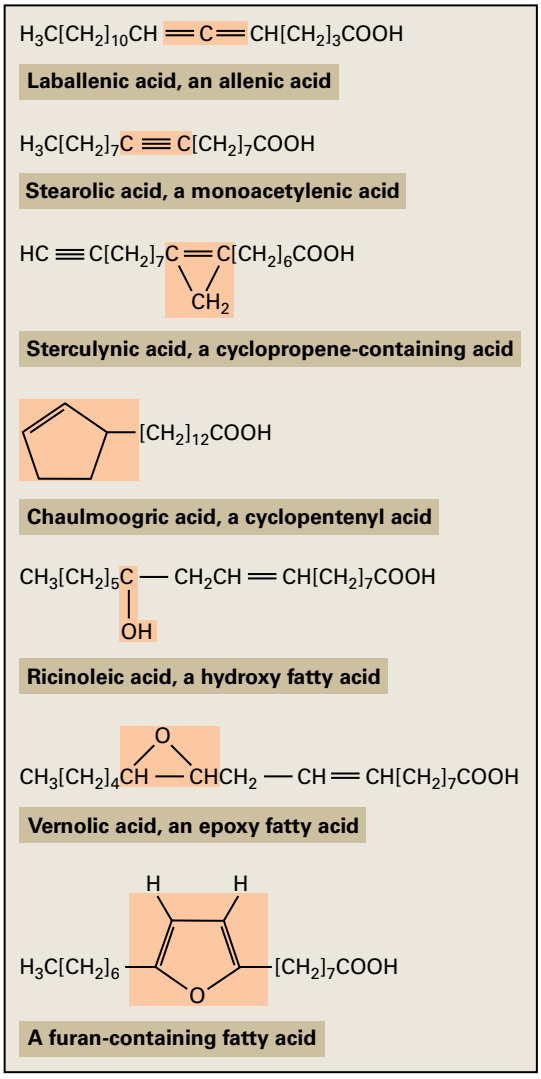


FIGURE 8.25 *Some of the functional groups found in unusual plant fatty acids.*

FIGURE 8.24 (*Continued*) *consists of at least four components: 3-ketoacyl-CoA synthase (KCS), 3-ketoacyl-CoA reductase (KR), 3-hydroxyacyl-CoA dehydrase (DH), and enoyl-CoA reductase (ER). The initial cycle of elongation starts with a C_{18} acyl-CoA, either stearoyl-CoA or oleoyl-CoA. Steps 1–3 are catalyzed by KCS. First, the acyl-CoA acylates an active-site cysteine. Next, the malonyl-CoA binds to the active site. Finally, a concerted reaction occurs in which the malonyl moiety is decarboxylated and a Claisen condensation with the acyl group results. Then steps 4–6, a reduction, a dehydration, and a second reduction, occur sequentially on the remaining components of the elongase system and result in the release of an acyl-CoA that is two carbons longer than the starting acyl-CoA. This acyl-CoA may then undergo additional cycles of elongation or be used in other pathways of lipid metabolism.*

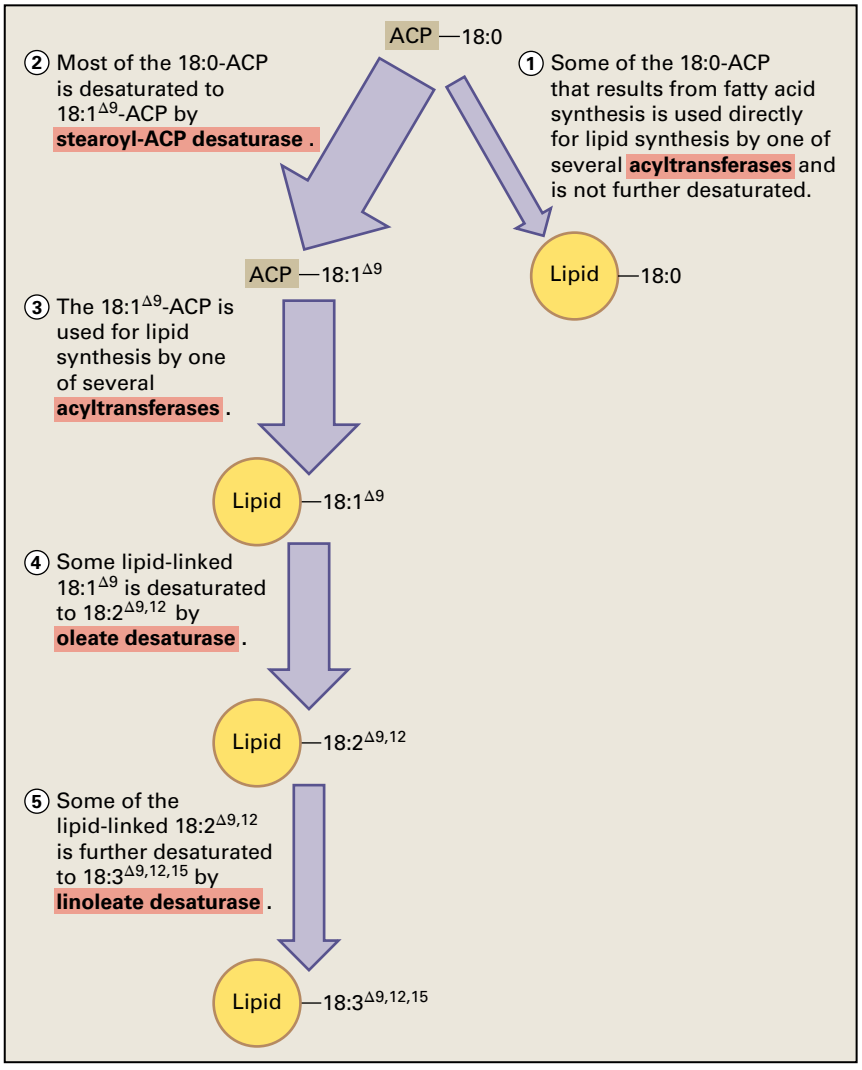


FIGURE 8.26 *Double bonds are introduced into fatty acids by a series of desaturases. The amount of a particular fatty acid that accumulates in a membrane varies from one membrane to another and is thought to be controlled partially by the activity of the various desaturases.*

as three *cis*-double bonds. All unsaturated members of the family descend from the fully saturated species as the result of a series of sequential desaturations that begin at C-9 and progress in the direction of the methyl carbon (Fig. 8.26). Fatty acids that cannot be described by this simple model are generally considered "unusual" because each is found in only a few plant species and almost exclusively in the seed oil. Several of these unusual fatty acids, such as lauric (12:0), erucic (20:1$^{\Delta 14}$), and ricinoleic (12-OH, 18:1$^{\Delta 9}$) acids, are of substantial commercial importance (see Section 8.11.4).

8.6.2 Some enzymes that synthesize unusual fatty acids resemble enzymes involved in the biosynthesis of common fatty acids

Much of the research concerning unusual plant fatty acids has focused on identifying new structures or cataloging the composition of fatty acids found in various plant species. Less is known about the mechanisms responsible for the synthesis and accumulation of unusual fatty acids, or of their significance to the fitness of the plants that accumulate them. However, the gene for the oleate Δ12-hydroxylase that catalyzes the synthesis of ricinoleic and other hydroxylated fatty acids of castor bean (*Ricinus communis*) and *Lesquerella fenderli* exhibits about 70% amino acid sequence similarity to the microsomal oleate Δ12-desaturase from the same species. To identify the amino acid differences responsible for causing the enzyme to be a hydroxylase instead of a desaturase, investigators have used site-directed mutagenesis to test the importance of the amino acids conserved in one class of enzymes but not in the other. On the basis of these studies, it appears the hydroxylase can be converted to a desaturase by as few as seven amino acid substitutions that alter the geometry of the active site.

The fact that such a small number of amino acid substitutions can alter the outcome of the enzymatic reaction indicates the diiron center used by these enzymes can catalyze different reactions, depending on the precise geometry of the active site. Indeed, evidence also indicates the enzymes that introduce epoxy groups and triple bonds are also structurally similar to the desaturases and hydroxylases. In contrast to the desaturases and hydroxylases, which act on saturated bonds, the epoxidases and acetylene forming enzymes are thought to act on double bonds, such that desaturation of a double bond

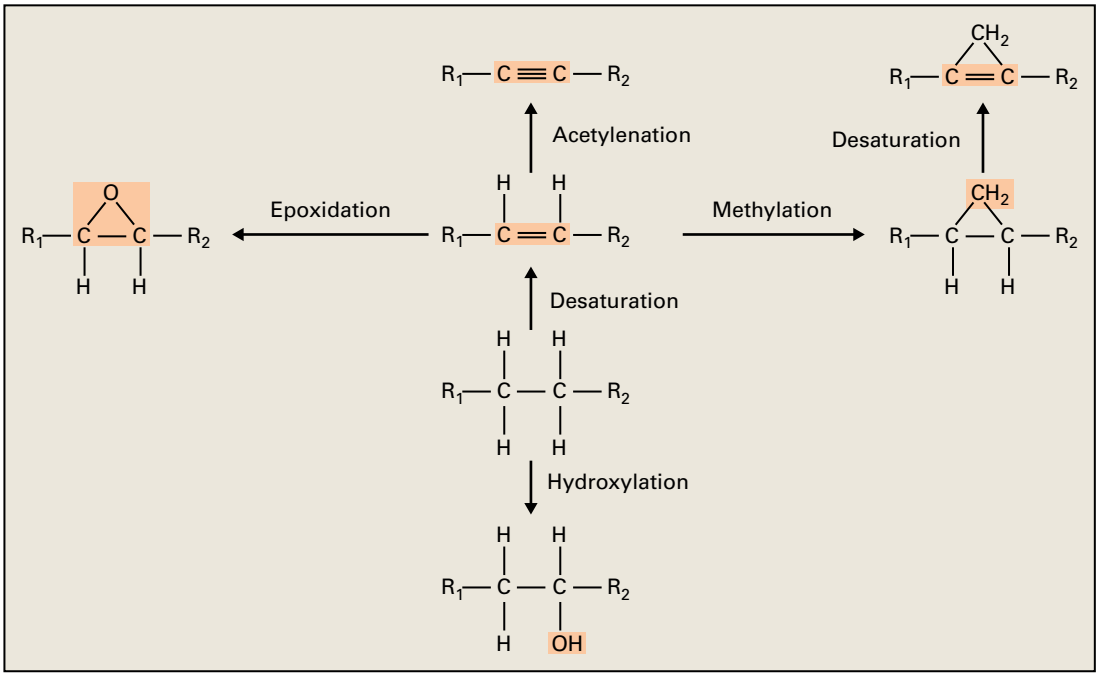


FIGURE 8.27 *A small number of reactions can account for much of the chemical diversity observed in plant fatty acids. Desaturation and hydroxylation reactions can be catalyzed by enzymes that differ by as few as four amino acids. Epoxidases and acetylenases are also closely related to desaturases. Additional chemical diversity may arise through the action of enzymes that methylate double bonds to produce cyclopropanes and cyclopropenes.*

gives rise to a triple bond, and oxidation of a double bond gives rise to an epoxy group. The formation of conjugated double bonds also requires a modified desaturase (a "conjugase"') acting on an unsaturated fatty-acyl substrate. Thus, many of the modifications found in fatty acids can be accounted for by a family of structurally related enzymes that can evolve from one specificity to another with only a few amino acid substitutions (Fig. 8.27).

These structural relationships have facilitated identification of many enzymes responsible for unusual fatty acid synthesis by their homology to sequences of enzymes involved in synthesis of usual fatty acids. For example, all membrane-bound desaturases described from animals, microbes, and plants contain three highly conserved histidine-rich sequences. Therefore, new enzymes related to the desaturase gene family can be identified relatively easily, even when overall homology is low. High-throughput sequencing of randomly selected cDNAs (expressed sequence tags) has facilitated the identification of dozens of enzymes responsible for unusual fatty acid synthesis. For instance, production of gamma-linolenate (18:3$^{\Delta 6,9,12}$) in seeds of borage (*Borago officinalis*), involves a Δ6-desaturase active on 18:2$^{\Delta 9,12}$ at the *sn*-2 position of phosphatidylcholine. To clone the glycerolipid Δ6-desaturase gene, cDNAs from developing borage seeds were sequenced. One class of cDNAs showed low overall homology to other desaturases (about 30% identity at the amino acid level), but contained characteristic histidine boxes with spacings similar to those in the Δ6-desaturase of *Synechocystis*. Expression of the borage cDNA in transgenic plants led to production of gamma-linolenate and 18:4$^{\Delta 6,9,12,15}$. Similarly, as was successful for identifying the castor hydroxylase, enzymes responsible for acetylenic, epoxy, and conjugated fatty acid production have been identified by their similarity to the Δ-12 desaturase sequence.

8.6.3 Unusual fatty acids occur almost exclusively in seed oils and may serve a defense function

Given that the ability to synthesize various unusual fatty acids must have evolved independently, their confinement to seed triacylglycerols indicates some selective constraint or functional significance. One possible function of unusual fatty acids is that, by being toxic or indigestible, they protect the seed against herbivory. Some unusual fatty acids may be inherently toxic, such as the acetylenic fatty acids or some of their metabolites. Other unusual fatty acids are toxic upon catabolism by the herbivore, such as the 4-fluoro fatty acids of *Dichapetalum toxicarium*. Cyclopentenyl fatty acids were long used in the treatment of leprosy, and the activity of hydnocarpic acid against many *Mycobacterium* species has been demonstrated. Cyclopropenoid fatty acids also appear to have biological activities, possibly because of accumulation in animal tissues of partial catabolites containing the cyclopropene ring, which inhibits β-oxidation of fatty acids. Malvalic and sterculic acids, produced by cotton (*Gossypium hirsutum*) plants, inhibit the growth of seed-eating lepidopteran larvae and may be part of a defense mechanism against these insects. These fatty acids may also be effective antifungal agents, inhibiting the growth of some plant pathogenic fungi at concentrations that appear biologically relevant.

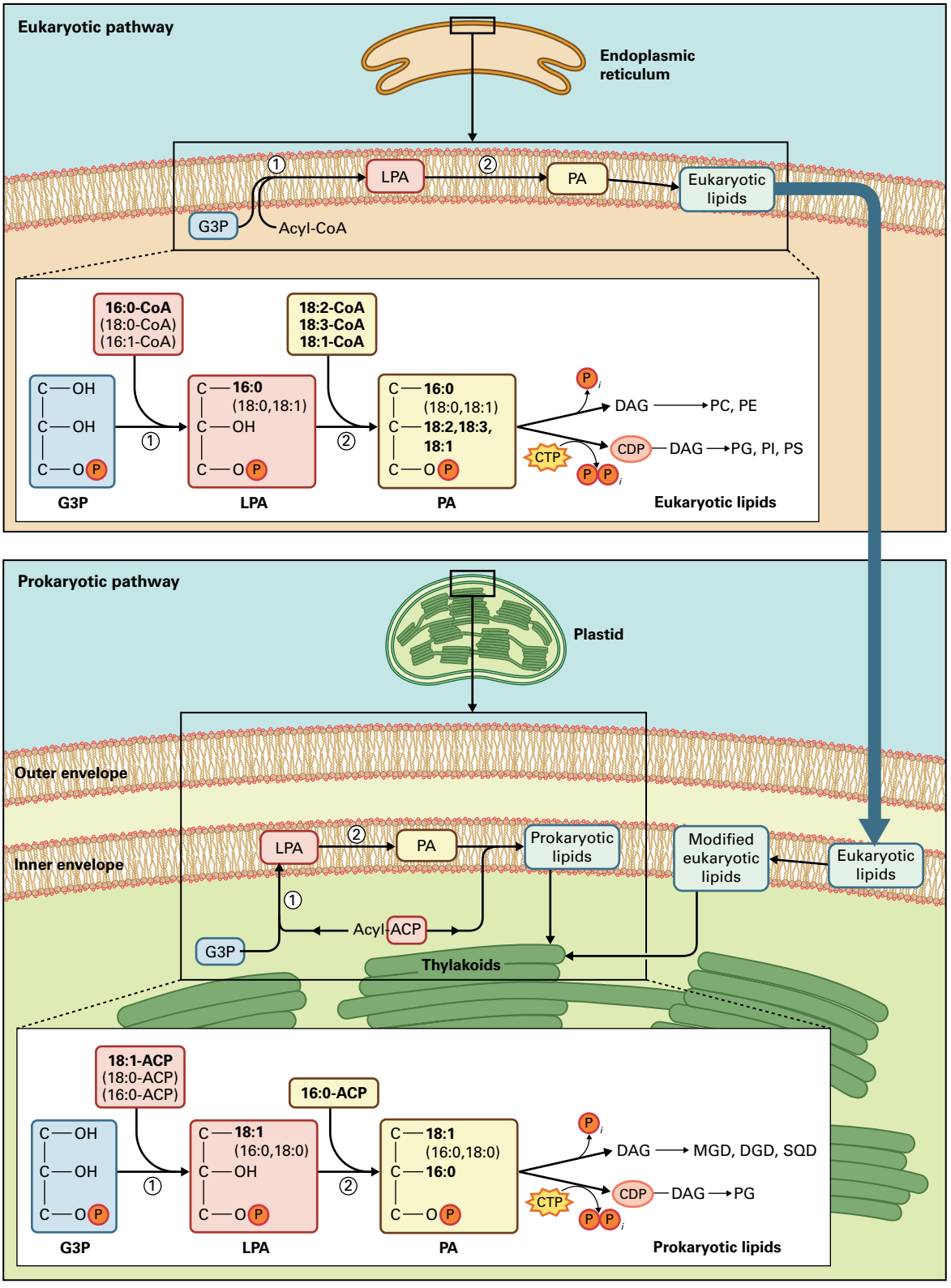


FIGURE 8.28 *The prokaryotic and eukaryotic pathways of plant glycerolipid synthesis. The prokaryotic pathway (lower panel) takes place in plastids and esterifies mainly palmitate to the* sn*-2 position of lysophosphatidate (LPA). The eukaryotic pathway (top panel) occurs outside the plastid, primarily in the ER and results in 18-carbon fatty acids esterified to the* sn*-2 position of glycerolipids. In the prokaryotic pathway, acyl-ACP is condensed with glycerol-3-phosphate (G3P) by a soluble enzyme, G3P acyltransferase (reaction 1). The product, LPA, partitions into the membranes where LPA is converted to phosphatidic acid (PA) by a membrane localized LPA-acyltransferase (reaction 2). PA is then converted to the other lipids found in chloroplasts. It is thought that most of the reactions of lipid synthesis by the prokaryotic pathway take place in the inner envelope of the plastids. The initial reactions of the eukaryotic pathway are similar except that acyl-CoA substrates are used and the G3P acyltransferase is associated with the ER. After desaturation of 18:1 to 18:2, lipids move from the ER to the other organelles, including the outer envelope of plastids. Eukaryotic lipids in the outer envelope are transferred into the inner membranes and modified by the replacement of headgroups and by the action of additional desaturases. CDP-DAG, cytidine diphosphate-diacylglycerol; DAG, diacylglycerol; PC, phosphatidylcholine; PE, phosphatidylethanolamine; PG, phosphatidylglycerol; PI, phosphatidylinositol; PS, phosphatidyserine; DGD, digalactosyl diacylglycerol; MGD, monogalactosyl diacylglycerol; SQD, sulfoquinovosyl diacylglycerol.*

8.7 Synthesis of membrane lipids

Two distinct pathways—the "prokaryotic" and the "eukaryotic" pathways—exist for membrane glycerolipid synthesis in plants (Fig. 8.28). The prokaryotic pathway refers to the synthesis of lipids within the plastid. The eukaryotic pathway refers to the sequence of reactions involved in synthesis of lipids in the ER, transfer of some lipids between the ER and the plastid, and further modification of the lipids within the plastid. Superimposed on the main pathways for glycerolipid synthesis are several additional pathways for the synthesis of other lipids, such as waxes, cutin, suberin, sphingolipids, and sterols. Less is known about the cellular localization of these pathways. Sphingolipid synthesis is likely to take place in the ER, as are elongation of fatty acids for wax synthesis and production of oxygenated fatty acids for cutin synthesis.

8.7.1 Phosphatidic acids formed in the plastids via the prokaryotic pathway and in the ER via the eukaryotic pathway differ in fatty acyl composition and position

Glycerolipid synthesis involves a complex and highly regulated interaction between the chloroplast, where fatty acids are synthesized, and other membrane systems of the cell. The 16:0-, 18:0-, and $18:1^{\Delta 9}$-ACP products of plastid fatty acid synthesis may be either incorporated directly into chloroplast lipids by the plastid-localized prokaryotic pathway or exported to the cytoplasm as CoA esters, which are then incorporated into ER lipids by an independent set of eukaryotic pathway acyltransferases (Fig. 8.28).

The first steps of glycerolipid synthesis are two acylation reactions that transfer fatty acids from acyl-ACP or acyl-CoA to glycerol 3-phosphate, forming phosphatidic acid (Fig. 8.29). Because of the substrate specificities of the plastid acyltransferases, the phosphatidic acid made by the prokaryotic pathway has 16:0 at the *sn*-2 position and, in most cases, $18:1^{\Delta 9}$ at the *sn*-1 position (see Fig. 8.28). In contrast to the plastid isoenzymes, the acyl-transferases of the ER produce phosphatidic acid that is highly enriched with C18 fatty acids at the *sn*-2 position; 16:0, when present, is confined to the *sn*-1 position (see Fig. 8.28).

8.7.2 Membrane lipid synthesis requires a complex collaboration between cell compartments

Both the prokaryotic and eukaryotic pathways were proposed initially on the basis of labeling studies and have subsequently been tested by genetic studies in *Arabidopsis*. Both are initiated by the synthesis of phosphatidic acid. In the chloroplast pathway, phosphatidic acid is used for the synthesis of PG or is converted to diacylglycerol (DAG) by a phosphatidic acid–phosphatase located in the inner plastid envelope. The DAG pool can act as a precursor for the synthesis of the other major chloroplast lipids: monogalactosyldiacylglycerol (MGD), digalactosyldiacylglycerol (DGD), and sulfoquinovosyldiacylglycerol (SQD), also called sulfolipid (see Fig. 8.28). In contrast to most other eukaryotic membranes, phospholipids (mostly PG) constitute 16% or less of the glycerolipids in chloroplast membranes (Fig. 8.30); the remainder is primarily galactolipid.

In the eukaryotic pathway, phosphatidic acid is synthesized in the ER from the acyl-CoA pool. This pool likely derives both from acyl-exchange reactions that reversibly equilibrate acyl groups in phosphatidylcholine (and other lipids) with acyl-CoA and from acyl-CoA that forms when fatty acids are exported from the plastid. ER-derived phosphatidic acid gives rise to the phospholipids, such as phosphatidylcholine, phosphatidylethanolamine, phosphatidylinositol, and phosphatidylserine, which are characteristic of the various membranes external to the chloroplast. However, the DAG moiety of phosphatidylcholine is returned to the chloroplast envelope, where it enters the DAG pool and contributes to the synthesis of plastid lipids (see Fig. 8.21). This lipid exchange between the ER and the chloroplast is reversible to some extent (see Section 8.7.4). The eukaryotic pathway is the principal route of glycerolipid synthesis in all nonphotosynthetic tissues as well as in the photosynthetic tissues of many plants. Among the angiosperms, only so-called 16:3 plants, such as spinach and *Arabidopsis,* produce more than 10% of their glycerolipids by the prokaryotic pathway (see Section 8.1.2 and below).

8.7.3 The fatty acid composition of lipids can reveal their pathway of origin

The relative amount of glycerolipid synthesized in plastids and the ER may vary in different tissues or in different plant species. In species such as pea (*Pisum sativum*) and barley (*Hordeum vulgare*), PG is the only product of the prokaryotic pathway, and the remaining chloroplast lipids are synthesized entirely by the eukaryotic pathway. By contrast, in leaves of 16:3 plants as much as 40% of cellular glycerolipid in leaf cells is synthesized within the chloroplasts. Because $16:3^{\Delta 7,10,13}$ is a major product of the pathway of glycerolipid synthesis in the chloroplast (see Fig. 8.21), the relative flux through the chloroplast prokaryotic pathway can be determined readily by the presence of this fatty acid (hence the name 16:3 plants). Plants with little or no $16:3^{\Delta 7,10,13}$ are called 18:3 plants. The contribution of the eukaryotic pathway to MGD, DGD, and sulfolipid synthesis is diminished in nonvascular plants, and in many green algae the chloroplast is almost entirely autonomous with respect to membrane lipid synthesis.

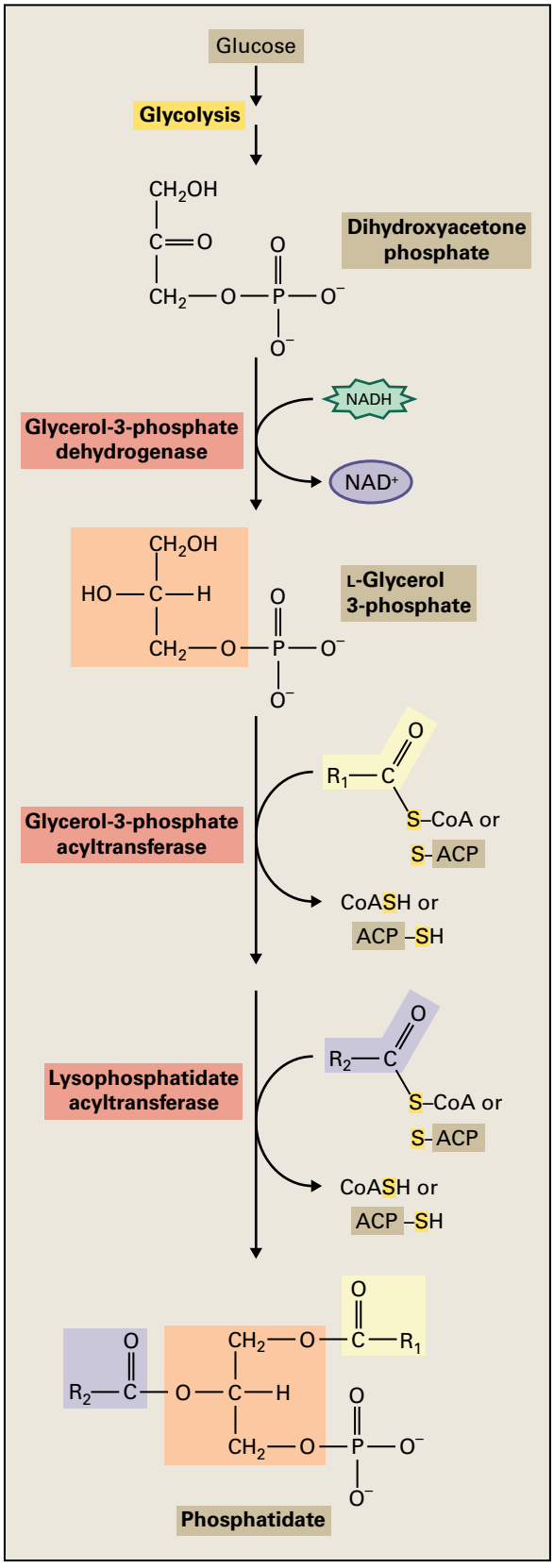


FIGURE 8.29 *The biosynthetic pathway to phosphatidate. Fatty acids activated by esterification to CoASH or ACP are transferred by acyltransferases to the hydroxyl groups of glycerol 3-phosphate. The plastid glycerol-3-phosphate acyltransferase is a soluble enzyme. Other known acyltransferases are membrane-associated.*

8.7.4 Large quantities of lipid move between the ER and chloroplasts

Each plant cell is autonomous with respect to glycerolipid synthesis, and there is no extensive transport of fatty acids or glycerolipids between cells. However, membrane biogenesis in plants involves a massive movement of fatty acids or lipids from one organelle to another (see Fig. 8.21). Quantitatively, the most significant movements of lipids are the export of fatty acids from plastids and the return of further desaturated acyl groups from the ER to the chloroplasts. In epidermal cells, there is also substantial movement of wax and cutin monomers from the ER to the extracellular space.

In the last few years, considerable progress has been made in understanding the mechanism of lipid transfer between the ER and the chloroplast. In particular, a series of mutants in *Arabidopsis* has allowed the identification of protein components of the transfer pathway. The current model proposes phosphatidic acid is generated from phosphatidylcholine in the ER and transported to the chloroplast inner envelope. An ATP-binding cassette (ABC) transporter transfers the phosphatidic acid through the inner envelope and makes it available to the enzymes of galactolipid and sulfolipid synthesis (Fig. 8.31). In terms of lipid trafficking, it is likely the plastid envelope is the most dynamic organellar membrane in nature.

Several lines of evidence indicate the existence of regulatory mechanisms that coordinate the activity of the two pathways for glycerolipid synthesis in plants. The *act1* (*acyl-CoA transferase1*) mutants of *Arabidopsis* are deficient in activity of chloroplast acyl-ACP:*sn*-glycerol-3-phosphate acyltransferase, the first enzyme of the prokaryotic pathway (see Fig. 8.21). This deficiency severely diminishes the flux through the prokaryotic pathway but is compensated for by increased synthesis of chloroplast glycerolipids via the eukaryotic pathway (Fig. 8.32). These and related results indicate that, even in case of a major disruption of one of the pathways of glycerolipid synthesis, mechanisms exist to ensure the synthesis and transfer of enough glycerolipids to support normal rates of membrane biogenesis. This striking example raises many unanswered questions. In particular, how is the demand for increased glycerolipid synthesis communicated to the lipid biosynthetic pathways during membrane expansion?

8.7.5 During de novo glycerolipid synthesis, the change in free energy that drives attachment of the polar head group is provided by nucleotide activation of either diacylglycerol or the head group itself

A general reaction common to all phospholipid biosynthesis pathways involves attachment of the phospholipid head group. In one case, a hydroxyl located on the head group carries out a nucleophilic attack on the β-phosphate group of

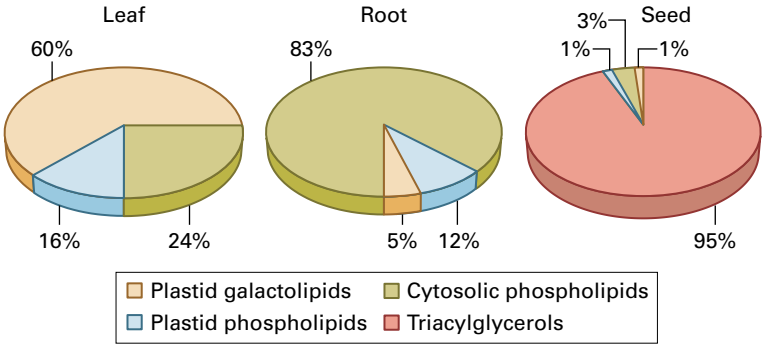


FIGURE 8.30 *Glycerolipid compositions differ in different cell types. In leaves, where the most abundant membranes are chloroplast lamellae, galactolipids are the most abundant class. In roots, by contrast, most of the membranes are present in extraplastidic systems such as the ER and Golgi apparatus. Seeds of oilseed species, such as* Arabidopsis, *contain mostly TAGs.*

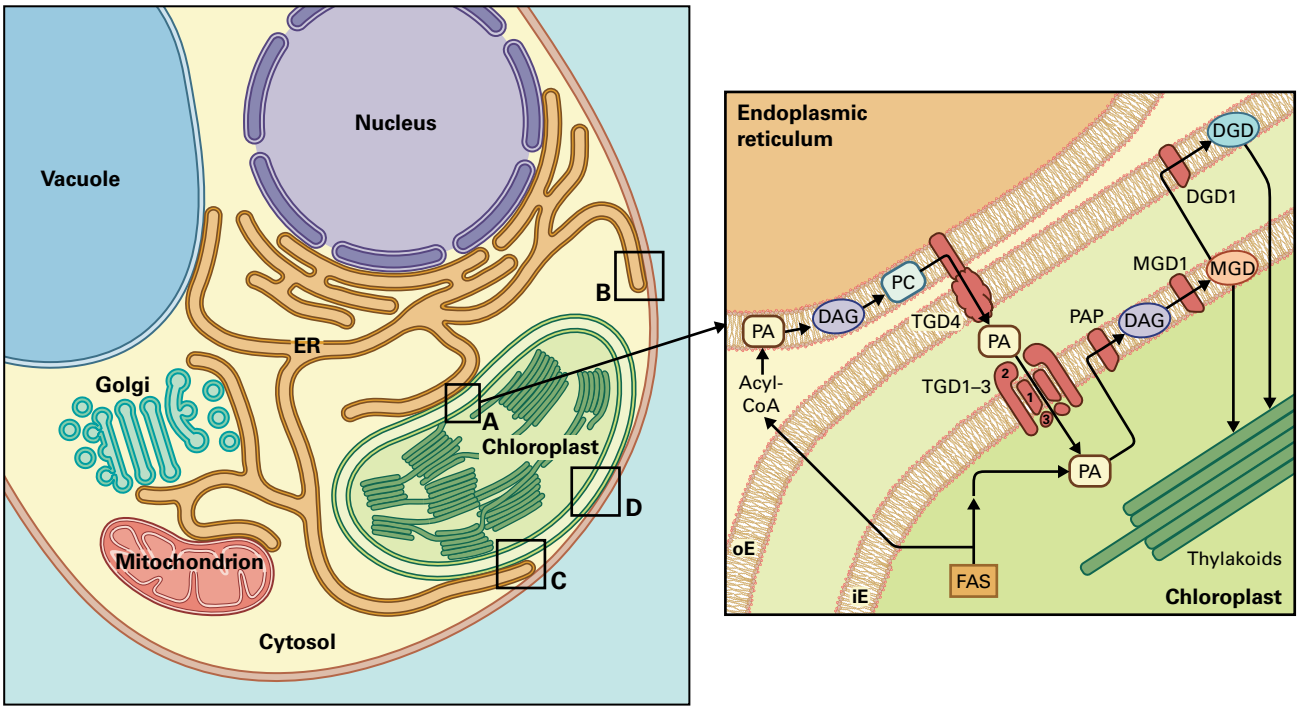


FIGURE 8.31 *Possible routes for lipid trafficking between ER, chloroplasts, and other membranes via membrane contact sites in a plant cell. (A–D) denote proposed contact zones for lipid trafficking between membranes: (A), chloroplast–ER contact; (B), plasma membrane-ER contact; (C), ER in contact with both chloroplast and plasma membrane; and (D), contact between chloroplast and plasma membrane. Other possible membrane contact sites pictured are between the ER and mitochondria,* trans*-Golgi and tonoplast, respectively. Inset: steps in the movement of glycerolipid from the ER to the chloroplast and synthesis of chloroplast MGD and DGD by the prokaryotic and eukaryotic pathways. TGD1–3 and TGD4 are component proteins of an ATP binding cassette (ABC) transporter. FAS, fatty acid synthesis; iE, inner envelope; oE, outer envelope.*

CDP-DAG. In the other, the *sn*-3 hydroxyl of DAG attacks the β-phosphate of a CDP-activated head group (Fig. 8.33). Thus, phospholipid biosynthesis can be divided into two general types of pathways: the CDP-DAG and DAG pathways.

Unlike prokaryotes, in which only the CDP-DAG pathway is present, plants, yeast, and animals synthesize phospholipids by using both the CDP-DAG and the DAG pathways, but the contributions of each pathway vary. For example, yeasts can synthesize all their phospholipids by using the CDP-DAG pathways, but under some conditions, they can repress a CDP-DAG pathway and use DAG instead. Animals make their major phospholipids—phosphatidylcholine and phosphatidylethanolamine—by using DAG pathways. The details of the synthesis of phospholipids in plants are not well characterized, and much of what is known has been learned by analogy to other organisms. Many of the pathways present in animals and yeast, for example, also are present in plants, although the extent to which each pathway

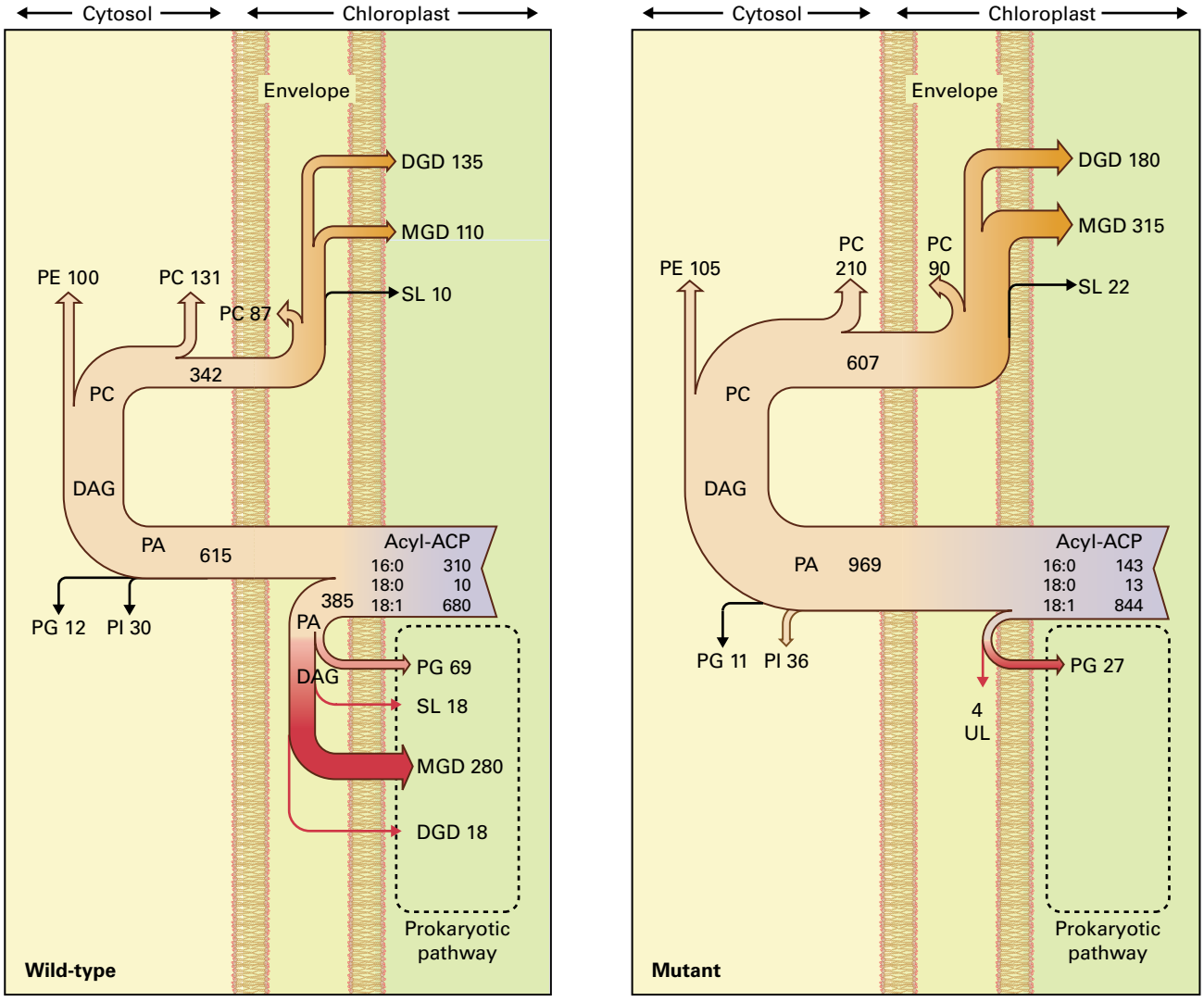


FIGURE 8.32 *Flux diagrams for wild-type* Arabidopsis *and* act1 *mutant, showing how fatty acids synthesized in chloroplasts are directed to different lipids in the chloroplasts and extraplastidic membranes. The diagram shows the average fate of 1,000 molecules of fatty acid. In wild-type* Arabidopsis *approximately 39% of the fatty acids are used for lipid synthesis within the chloroplast. Of the remaining fatty acids, about 27% are used for synthesis of lipids for extrachloroplast membranes such as the ER, Golgi, and plasma membrane, and roughly 34% are transferred to the chloroplast for lipid synthesis. In a mutant of* Arabidopsis *deficient in plastid glycerol-3-phosphate acyltransferase activity, most of the fatty acids are exported to the cytoplasm and then approximately 61% are reimported into the chloroplast. This suggests a mechanism that adjusts the flow of lipid between the membranes when necessary. SL, sulfolipid; UL, unknown lipid; other abbreviations as in Figure 8.28.*

contributes to the final phospholipid components of a cell may vary among organisms.

8.7.6 Phosphatidate is a substrate for both the CDP-DAG and DAG pathways

CDP-DAG is synthesized from phosphatidate and CTP by CDP:diacylglycerol cytidylyltransferase (Fig. 8.33). In plants, this membrane-bound enzyme is associated with several different organelles, localized in the inner chloroplast envelope and the inner mitochondrial envelope. Two CDP:diacylglycerol cytidylyltransferases occur in *Ricinus communis* endosperm: one localized in the mitochondria, the other in a microsomal fraction. DAG is produced by the dephosphorylation of phosphatidate by phosphatidate phosphohydrolase, an enzyme located in the inner chloroplast envelope membrane, microsomes, and soluble fractions. Analogy to yeast phospholipid synthesis makes it likely a mitochondrial form of this enzyme also exists, although it has not yet been detected in plants.

8.7.7 CDP-DAG and DAG pathways generate distinct types of lipids

Phospholipids derived from CDP-DAG include PG, the only phospholipid found in chloroplast thylakoids, and diphosphatidylglycerol (cardiolipin), which occurs exclusively in

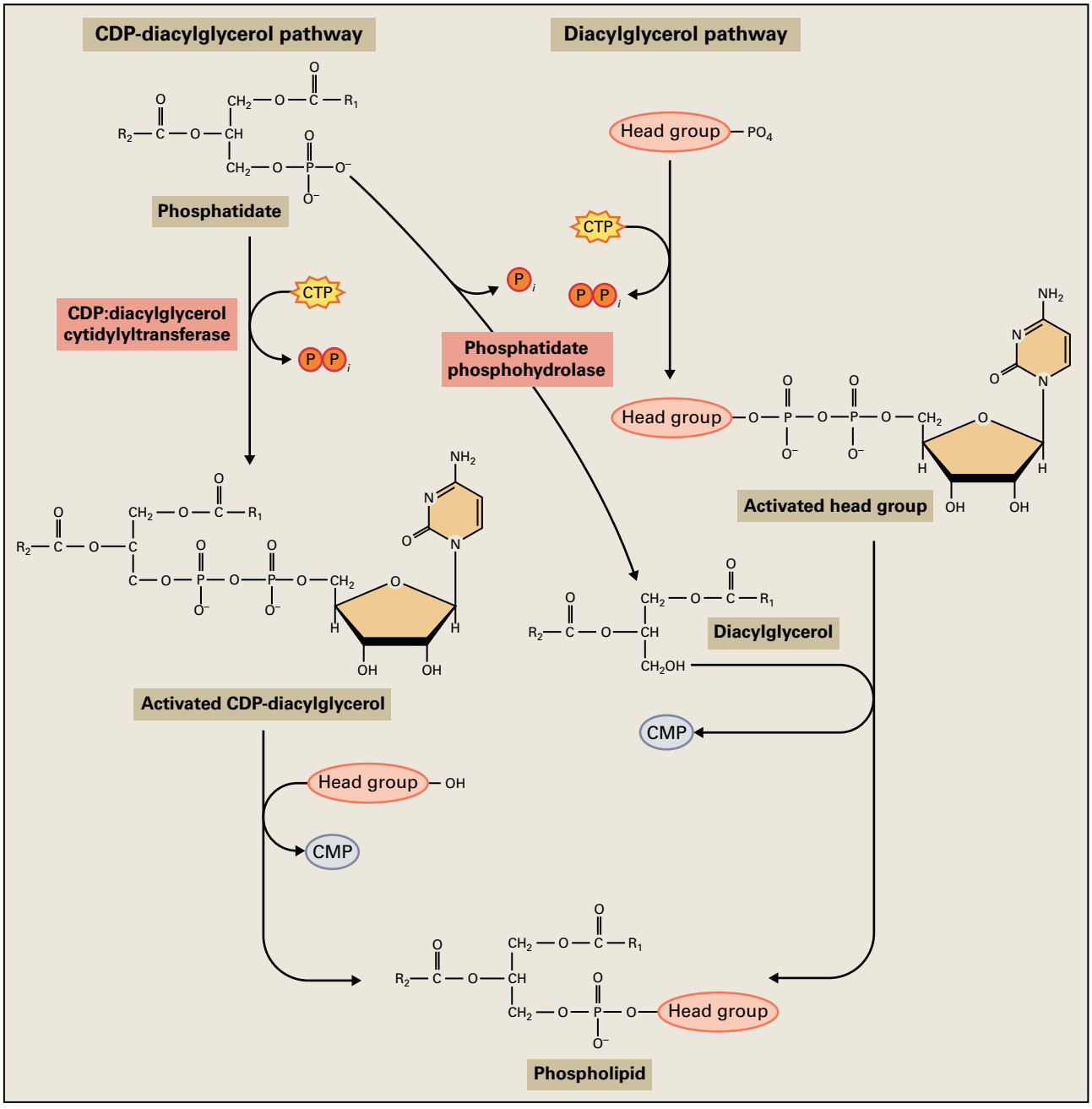


FIGURE 8.33 *Two general strategies for forming the phosphodiester bond of phospholipids. In the CDP-diacylglycerol pathway, an activated DAG is used. In the diacylglycerol pathway, the head group is activated by CTP.*

the inner mitochondrial membrane. As in *E. coli*, PG is synthesized in two steps in plants. Reaction of CDP-DAG with glycerol 3-phosphate produces phosphatidylglycerol phosphate, which is then dephosphorylated to yield PG (Fig. 8.34). This reaction also can take place in the ER. In mitochondria, diphosphatidylglycerol is synthesized by the reaction of PG with a second molecule of CDP-DAG.

Other phospholipids synthesized from CDP-DAG include phosphatidylinositol and phosphatidylserine (Fig. 8.34). Phosphatidylinositol is synthesized from free inositol in a reaction catalyzed by phosphatidylinositol synthase. Phosphatidylserine synthesis in most plant tissues uses Ser and is catalyzed by phosphatidylserine synthase in a reaction similar to that found in *E. coli* and yeast. This contrasts with phosphatidylserine synthesis in animals, in which phosphatidylserine is a product of the DAG pathway, arising from phosphatidylethanolamine by exchanging ethanolamine with a Ser (see next section).

The DAG pathway is used primarily for the synthesis of phosphatidylethanolamine and phosphatidylcholine in both plants and animals. In each case, DAG displaces a CMP from CDP-ethanolamine or CDP-choline to produce phosphatidylethanolamine or phosphatidylcholine, respectively (Fig. 8.35). The synthesis of the two CDP-alcohols parallels the synthesis of

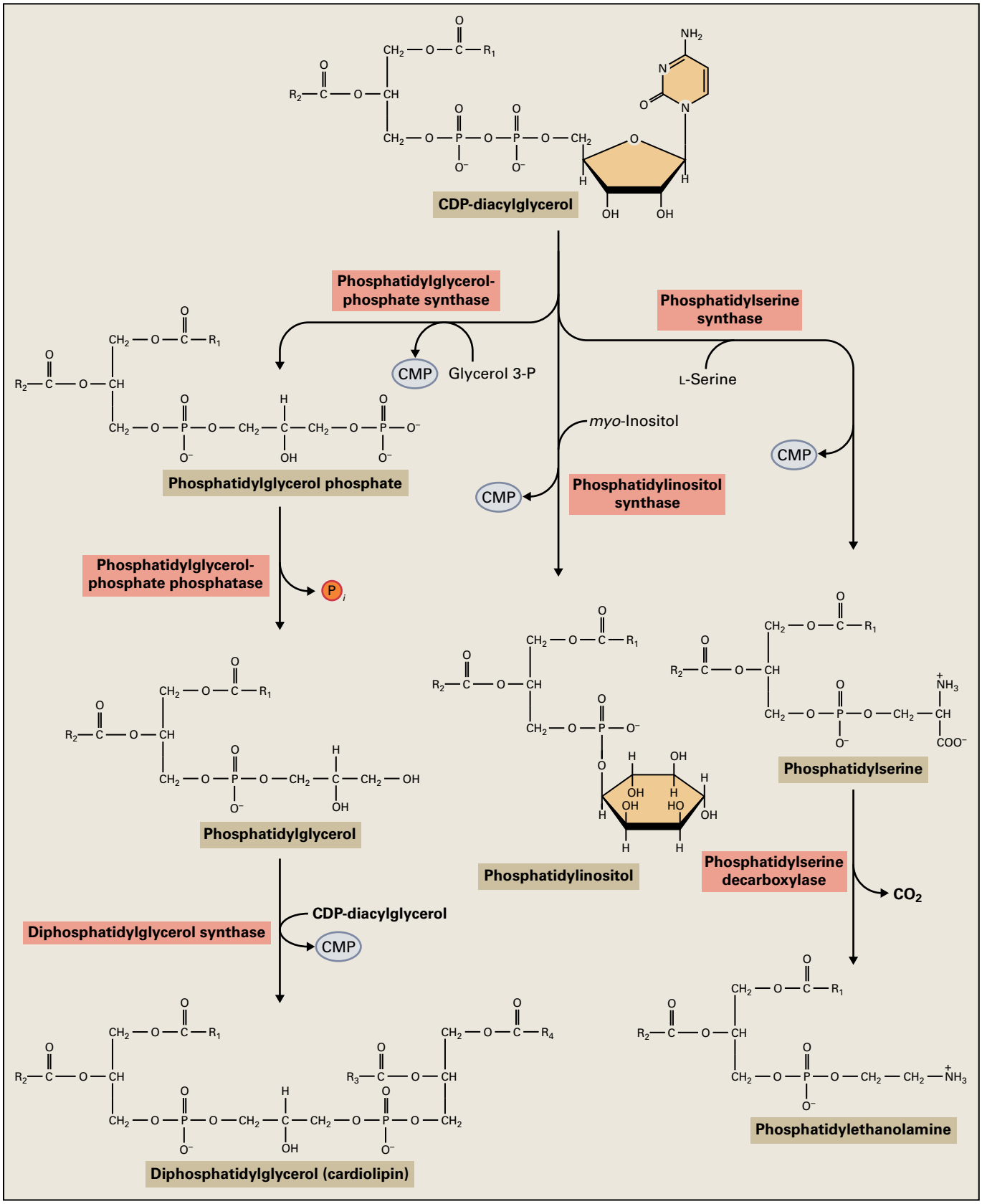


FIGURE 8.34 *Synthesis of phospholipids by the CDP-diacylglycerol pathway. Phosphatidylserine, phosphatidylinositol, and phosphatidylglycerol phosphate are synthesized when the head group displaces CMP from CDP-diacylglycerol. Phosphatidylglycerol phosphate is dephosphorylated to phosphatidylglycerol. Diphosphatidylglycerol (cardiolipin) is formed by reaction of phosphatidylglycerol with a second molecule of CDP-DAG.*

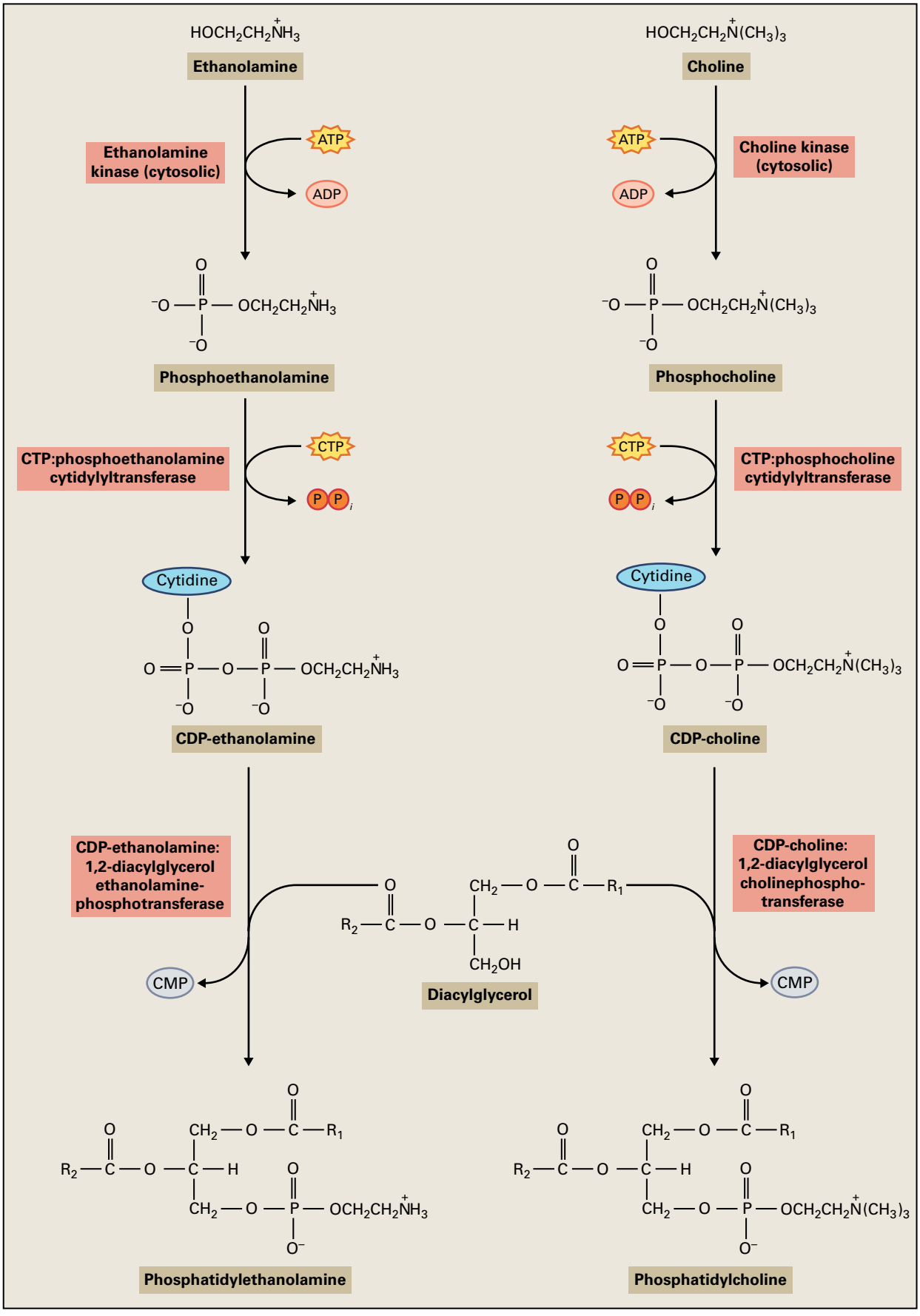


FIGURE 8.35 *The diacylglycerol pathway is the principal route for synthesis of phosphatidylcholine and phosphatidylethanolamine in plants.*

CDP-DAG. For example, choline is first phosphorylated to form phosphocholine before reacting with CTP to produce CDP-choline.

8.7.8 Pools of CDP-DAG-derived phospholipids and DAG-derived phospholipids interact in plants and in animals

Tracing the origin of specific lipids is often more difficult than the preceding section might suggest. For example, phosphatidylethanolamine, a phosphatidylserine precursor in animals, is a product of the DAG pathway in both animals and plants. In germinating *Ricinus communis* endosperm, phosphatidylserine appears to be made exclusively from DAG by the phosphatidylethanolamine exchange reaction (Fig. 8.36). Likewise, phosphatidylethanolamine can be generated from phosphatidylserine by decarboxylation. The net effect of this cycle is to produce ethanolamine from Ser. Indeed, this may be the primary metabolic source of ethanolamine. Direct conversion of phosphatidylethanolamine to phosphatidylcholine occurs in animals and yeast by sequential methylation of phosphatidylethanolamine by *S*-adenosylmethionine. In plants, however, this appears to be only a minor pathway, with phosphatidylcholine synthesized almost entirely from CDP-choline and DAG. Phosphocholine is synthesized by the methylation of phosphoethanolamine, with *S*-adenosylmethionine acting as the methyl donor. Thus in plants, choline originates mainly from ethanolamine, but phosphatidylcholine does not typically originate from phosphatidylethanolamine.

8.7.9 Galactolipids and sulfolipids are synthesized from DAG

DAG produced from phosphatidic acid by a specific phosphatase in the plastid is the substrate for galactolipid and sulfolipid synthesis. Cleavage of uridine diphosphate (UDP) esters provides energy for several of the reactions. UDP-galactose and UDP-sulfoquinovose are substrates for MGD and sulfolipid synthesis, respectively. The synthesis of DGD involves transfer of a second galactose from UDP-galactose to monoacylglyceroldiacylglycerol (Fig. 8.37). UDP-sulfoquinovose synthesis has been studied in *Arabidopsis* and the purple photosynthetic bacterium *Rhodobacter sphaeroides*. In *Arabidopsis*, the *SQD1* gene encodes the enzyme that catalyzes the synthesis of UDP-sulfoquinovose from UDP-glucose and sulfite (Fig. 8.38).

All organisms that carry out oxygenic photosynthesis contain sulfolipid as a major component of their photosynthetic

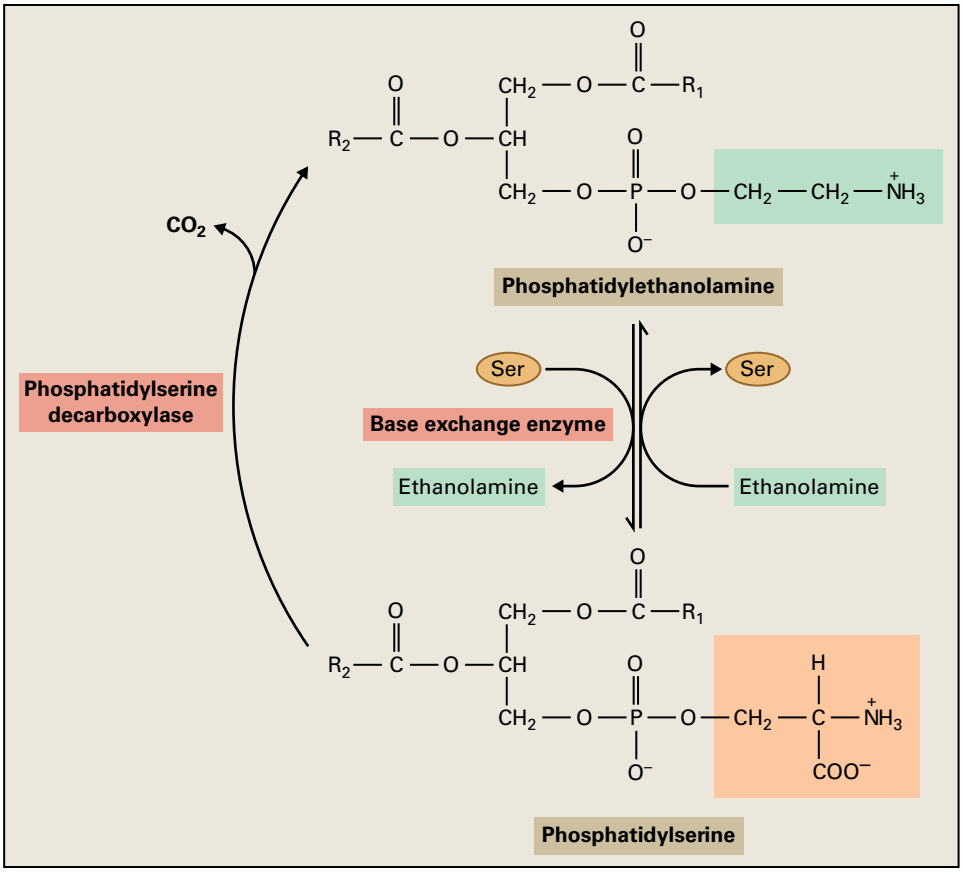


FIGURE 8.36 *Synthesis of phosphatidylserine from phosphatidylethanolamine has been observed in some plant tissues.*

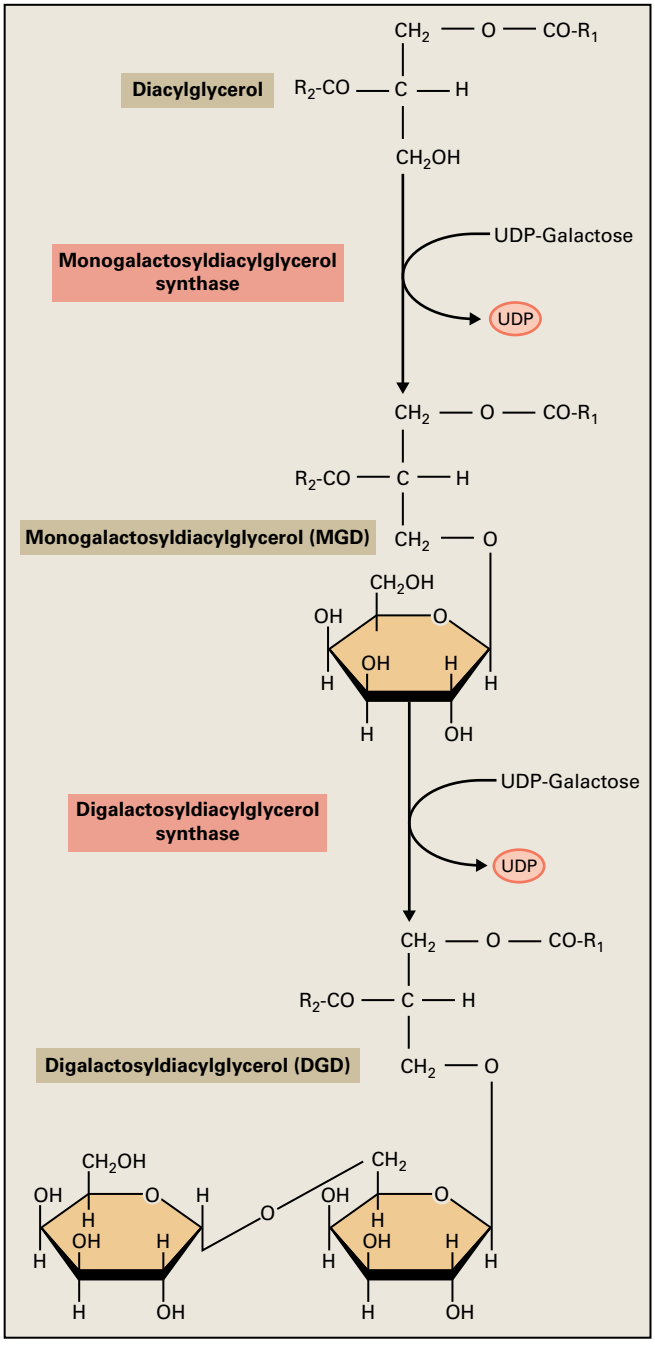


FIGURE 8.37 *Pathway of synthesis of galactolipids. The synthesis of MGD is catalyzed by a typical glycosyltransferase that transfers galactose from the nucleotide sugar-activated UDP-galactose to DAG. Similarly, the synthesis of DGD involves a second transfer from UDP-galactose to MGD.*

lamellae—a fact stimulating sustained interest in the possibility this lipid plays an essential role in supporting the light reactions of photosynthesis. Mutants of *R. sphaeroides* or cyanobacteria that are unable to synthesize sulfolipid, however, have normal rates of photosynthesis. Apparently, the main reason photosynthetic organisms have sulfolipid is to minimize the phosphate required for synthesizing the large amounts of membrane necessary to support high rates of light capture (Box 8.2).

8.7.10 Ceramide is the building block of plant sphingolipids

Just as DAG is the basic component of all glycerolipids, ceramide is the basic component of all sphingolipids. Complex sphingolipids, such as the glucosylsphingolipids and glucosylinositolphosphorylceramides (GIPC) that predominate in plants, are formed by modification of ceramide. The structures of the most commonly occurring long-chain bases, glucosylceramide and glycosylinositolphosphorylceramide are shown in Figure 8.7.

The initial phase of ceramide synthesis involves condensation of a palmitoyl-CoA with Ser, resulting in a 3-ketosphinganine (Fig. 8.39). This reaction is analogous to the condensation reactions catalyzed by FAS and elongases. Subsequently, the 3-keto group is reduced to the alcohol to produce sphinganine. Much of the sphinganine is then hydroxylated at the C-4, although in some plants there is a competing C-4 desaturase. The ceramide is then synthesized using sphinganine *N*-acyl transferase to transfer an acyl-CoA to the modified sphinganine. The acyl groups can range from C16 to C26, although C24 followed by C16 are the predominate fatty acids found in the ceramides. Also, the C16 fatty acids are predominately found in the glucosylceramides, whereas the very long chain fatty acids are found in glycosylinositolphosphorylceramides. Often, the fatty acid is hydroxylated at C-2 subsequent to formation of the ceramide.

In the second phase of synthesis, ceramide is converted to the complex sphingolipids. Glucosylceramide synthase is used to attach glucose to the ceramide from either UDP-glucose or steryl glucoside. Ceramides can also be converted to inositolphosphorylceramide using inositolphosphorylceramide synthase and the inositol phosphate donated from phosphatidyl inositol. Nothing is known about the subsequent reactions in plants that lead to glycosylinositolphosphorylceramide and its derivatives.

There is much interest in the function of sphingolipids in plants. They are enriched in detergent-resistant membranes, where they are presumed to play a structural role. In addition, mounting evidence suggests they function in signaling pathways involved with regulation of stomatal opening and programmed cell death. With mutants of sphingolipid metabolism becoming available, characterization of these roles should be forthcoming.

8.8 Function of membrane lipids

8.8.1 Membrane lipid composition affects plant form and function

Each membrane in a plant cell has a characteristic and distinct complement of lipid types (Fig. 8.40), and within a single membrane, each class of lipids has a distinct fatty acid

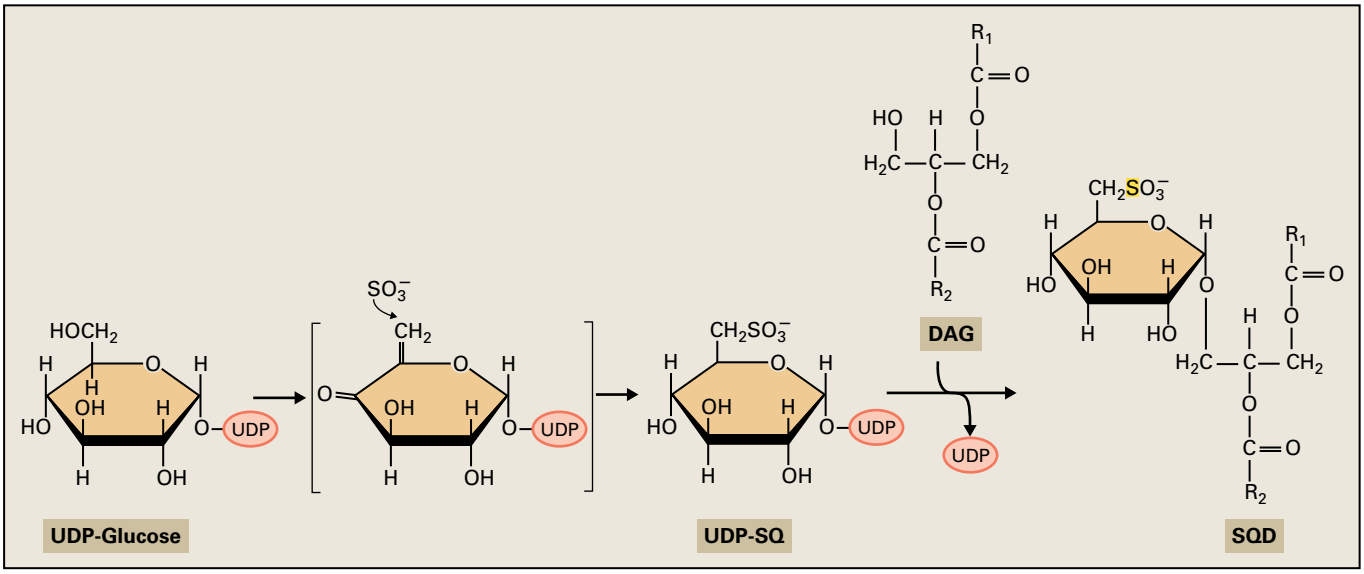


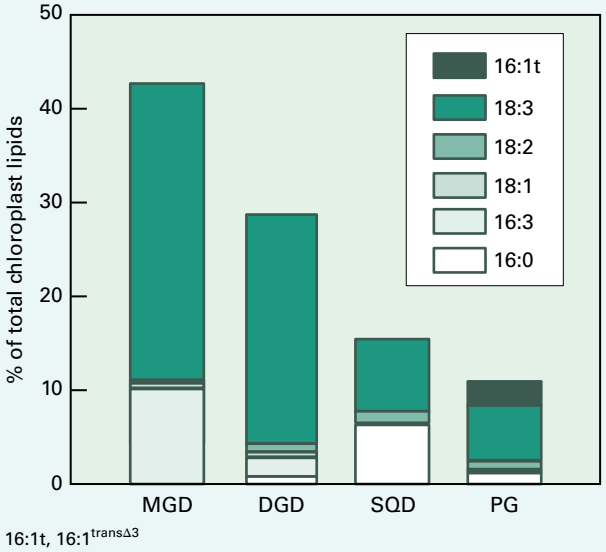
FIGURE 8.38 *Sulfolipid biosynthesis. SQD1 protein adds sulfite to UDP-glucose, and the resulting UDP-sulfoquinovose (UDP-SQ) is then used to transfer sulfoquinovose to DAG to form sulfoquinovosyldiacylglycerol (SQD).*

BOX 8.2

Plants conserve phosphate by using sulfolipids and galactolipids for chloroplast membrane synthesis

Each gram of leaf material contains approximately 1 m^2 of chloroplast membrane. If this membrane were composed primarily of phospholipids, as the membranes from animals and fungi are, plants would require much more phosphate for growth than they currently do. Given that phosphate is a limiting nutrient in many natural ecosystems, it is advantageous to plants to minimize the need for phosphate in membrane synthesis. In what appears to be an evolutionary adaptation to the problem of phosphate limitation, plants and other photosynthetic organisms use monogalactosyldiacylglycerol (MGD), digalactosyldiacylglycerol (DGD), and sulfoquinovosyldiacylglycerol (SQD, or sulfolipid) as substitutes for phospholipids such as phosphatidylglycerol (PG). For example, in the chloroplast membranes of spinach (a 16:3 plant), less than 15% of the bilayer lipids are phospholipids (see graph).

Evidence in support of this concept was obtained by the isolation of sulfolipid-lacking mutants of the photosynthetic purple bacterium *Rhodobacter sphaeroides* and the cyanobacterium *Synechococcus* PCC7942. When the mutants were grown in the presence of high concentrations of phosphate, their growth rate and photosynthetic characteristics were indistinguishable from those of the wild type. Under conditions of limiting phosphate, however, the growth of the mutants was inhibited. In addition, as the amount of phosphate available for membrane synthesis became limiting, several novel glycolipids accumulated to high concentrations.



composition. Until recently, we knew almost nothing about the reasons for this remarkable diversity. Our knowledge remains limited, but the examples discussed in this section demonstrate some of the important developmental processes and responses to environmental factors that are affected by membrane lipid composition.

One of the most visually dramatic phenotypes produced by a change in lipid composition is that of the *fab2* mutant of

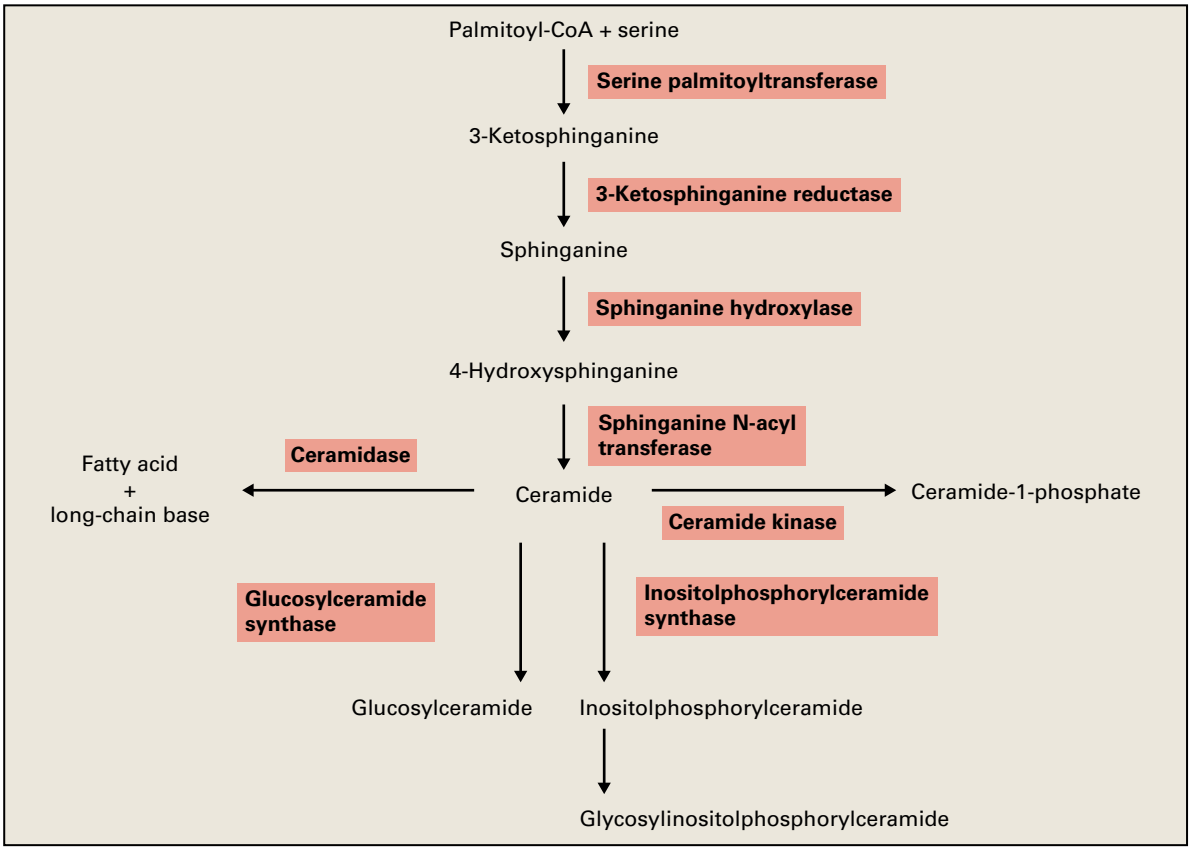


FIGURE 8.39 *Sphingolipid biosynthetic pathway in plants. All enzymatic reactions have been demonstrated* in vitro. *Reactions involved in long-chain base desaturation and acyl chain hydroxylation apparently occur following ceramide formation.*

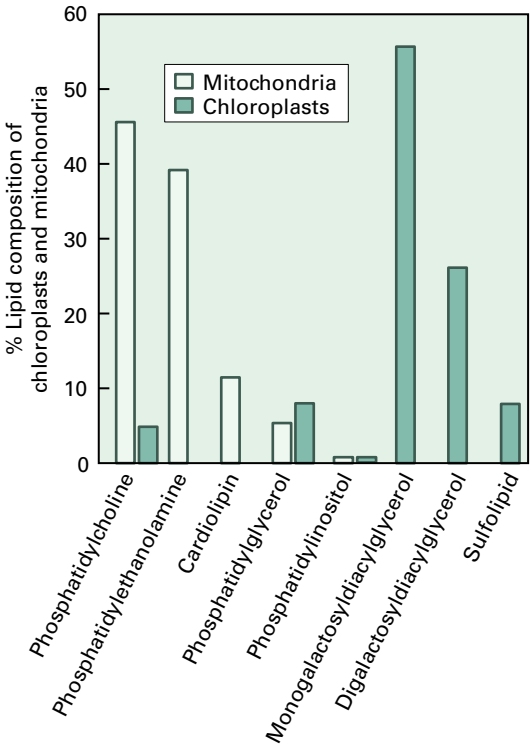


FIGURE 8.40 *Comparison of the lipid compositions of chloroplasts and mitochondria.*

Arabidopsis. The *fab2* plants are miniatures, a result of the accumulation of 18:0 in membrane lipids (Fig. 8.41A). The decrease in leaf size results from decreased size of several specific cell types. The failure of mesophyll and epidermal cells to enlarge produces a dramatic "brick-wall" appearance to the cross-section of a mutant leaf, contrasting with the characteristic, less compact leaf anatomy evident in the wild type (Fig. 8.41B,C). We do not know the mechanism by which increased 18:0 produces the miniature phenotype, but biophysical principles lead to the expectation that increased temperature would ameliorate the effects of increased saturation on the bilayer. Accordingly, the morphology of *fab2* more closely resembles that of the wild type when plants are grown at 35°C (Fig. 8.41D,E). Furthermore, at this temperature, *fab2* leaves develop typical palisade and spongy mesophyll layers.

8.8.2 Photosynthesis is impaired in plants that lack polyunsaturated membrane lipids

Highly unsaturated $18{:}3^{\Delta 9,12,15}$ and $16{:}3^{\Delta 7,10,13}$ fatty acids account for approximately 70% of all the thylakoid membrane fatty acids in plants and more than 90% of the fatty acids in MGD, the most abundant chloroplast lipid (see Fig. 8.40). These high amounts are noteworthy because free radical

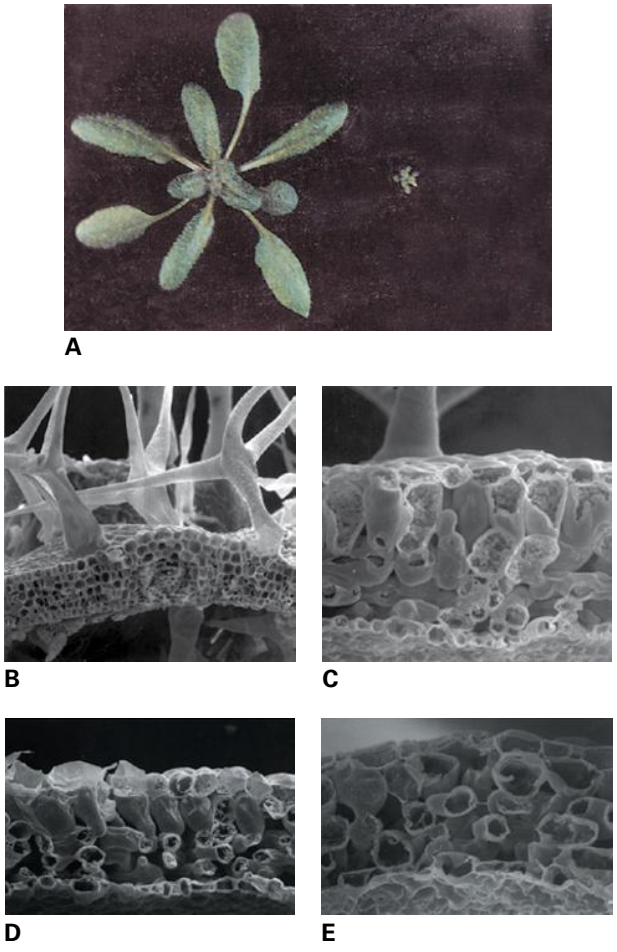


FIGURE 8.41 *Morphology of the* fab2 *mutant of* Arabidopsis. *(A) The growth of the mutant (at right) at 22°C is strongly reduced. The mutant plant is small because its cells (B) compared to wild type (C) do not enlarge to the same extent. Growth at higher temperature partially suppresses the deleterious effects of the* fab2 *mutation (D) on growth and development. The mutant grown at 36°C more closely resembles the wild-type control (E).*
Source: (A–E) Lightner et al. (1994). Plant J. 6:401–412.

byproducts of the photosynthetic light reactions stimulate oxidation of polyunsaturated fatty acids. If plants maintain high levels of unsaturation in thylakoids despite the risk of oxidation, one might reason photosynthesis is critically dependent on membrane unsaturation. Surprisingly, an *Arabidopsis* triple mutant (*fad3 fad7 fad8*) completely lacking $18{:}3^{\Delta 9,12,15}$ and $16{:}3^{\Delta 7,10,13}$ exhibits normal rates of growth and photosynthesis at 22°C (Fig. 8.42), demonstrating that $18{:}3^{\Delta 9,12,15}$ and $16{:}3^{\Delta 7,10,13}$ are not essential for photosynthesis in plants. These two fatty acids are not irrelevant, but their role is more subtle than expected. In fact, the loss of $18{:}3^{\Delta 9,12,15}$ and $16{:}3^{\Delta 7,10,13}$ has noticeable effects on photosynthesis only at low (below 10°C) and high (above 30°C) temperatures.

Although eliminating triunsaturated $18{:}3^{\Delta 9,12,15}$ and $16{:}3^{\Delta 7,10,13}$ has only minor consequences for photosynthesis, the process is greatly affected in an *Arabidopsis fad2 fad6* mutant lacking the diunsaturated fatty acids $18{:}2^{\Delta 9,12}$ and $16{:}2^{\Delta 7,10}$ and their downstream triunsaturated derivatives $18{:}3^{\Delta 9,12,15}$ and $16{:}3^{\Delta 7,10,13}$. These mutants lose nearly all photosynthetic capacity and cannot grow autotrophically. Nevertheless, *fad2 fad6* plants grow on sucrose media, where growth and organ development are remarkably normal (Fig. 8.42). These observations indicate the vast majority of receptor-mediated and transport-related membrane functions required to sustain the organism and induce proper development are well supported in this double mutant, which contains almost no polyunsaturated lipids. Apparently, therefore, photosynthesis is the only vegetative cell function that requires high levels of membrane polyunsaturation.

The work with *Arabidopsis* mutants indicates plants require polyunsaturated lipids to maintain the photosynthetic machinery, but this is not true of cyanobacteria. Mutants of *Synechocystis* PCC6803 that lack polyunsaturated fatty acids can photosynthesize normally, except at low temperature.

8.8.3 Does lipid composition affect chilling sensitivity?

One of the most extensively studied issues in membrane biology is the relationship between lipid composition and the ability of organisms to adjust to temperature changes. Chilling-sensitive plants undergo sharp reductions in growth rate and development at temperatures between 0°C and 12°C (Fig. 8.43). **Chilling injury** includes physical and physiological changes induced by low temperatures as well as subsequent symptoms of stress. Many economically important crops are sensitive to cold, including cotton, soybean (*Glycine max*), maize (*Zea mays*), rice (*Oryza sativa*), and many tropical and subtropical fruits. In contrast, most plants of temperate origin that continue to grow and develop at low temperatures are classified as chilling-resistant plants, including *Arabidopsis*.

In attempts to link the biochemical and physiological changes that characterize chilling injury with a single "trigger" or site of damage, investigators have suggested the primary event of chilling injury is a phase transition from the liquid crystalline state to the gel state in cellular membranes (Fig. 8.44). According to this proposal, the phase transition from liquid crystalline to gel alters the metabolism of chilled cells and leads to injury and death of the chilling-sensitive plants. Because desaturation of membrane lipids favors membrane fluidity (see Section 8.5), researchers have sought to define the relationship between membrane composition and chilling sensitivity. A related hypothesis specific to chloroplast membranes has been proposed, in which molecular species of chloroplast PG containing a combination of saturated fatty acid (16:0 and 18:0) at the *sn*-1 position of the glycerol backbone and either a saturated fatty acid or $16{:}1^{\Delta 3}$-*trans* fatty acid at the *sn*-2 position are suggested to confer chilling sensitivity on plants. Because the *trans*-double bond leaves the $16{:}1^{\Delta 3}$-*trans* fatty acid with a structure similar to 16:0 (see illustration in Box 8.1), these molecules are termed disaturated PG. The presence of significant quantities of disaturated PG in the chloroplast membranes would presumably promote the change from liquid crystalline to gel phase at chilling temperature, and the phase separation within the membranes would cause chilling sensitivity.

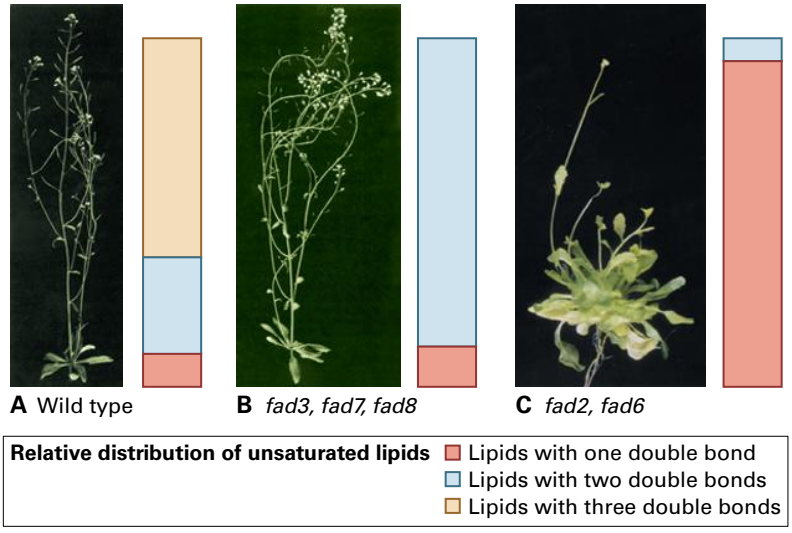


FIGURE 8.42 Arabidopsis *mutants reveal the roles of polyunsaturated fatty acids. Compared with a wild-type plant shown in (A), a mutant lacking* $18{:}3^{\Delta 9,12,15}$ *and* $16{:}3^{\Delta 7,10,13}$ *fatty acids (B) grows normally at 22°C. However, this mutant is male-sterile because jasmonate derived from* $18{:}3^{\Delta 9,12,15}$ *is required for pollen maturation and release. A mutant deficient in all polyunsaturated fatty acids cannot grow autotrophically. When grown in sucrose-enriched medium (C), this mutant is robust, indicating that photosynthesis is the only process that absolutely requires a polyunsaturated membrane.*
Source: (A, B) McConn & Browse (1996). Plant Cell 8:403–416. (C) McConn & Browse (1998). Plant J. 15:521–530.



FIGURE 8.43 *Exposure of chilling-sensitive plants such as cucumber* (Cucumis sativus) *to 2°C for 1 day causes severe injury. The plant on the right was kept at 25°C.*
Source: Somerville, Carnegie Institute of Washington, Stanford, CA; unpublished results.

As shown in studies with five different *Arabidopsis* mutants, diminished unsaturation resulted in plants that grew well at 22°C but were less robust than wild type when grown at 2–5°C. These results were observed even though the lipid changes in most of the mutants were insufficient to cause a lipid-phase transition. In addition, the low-temperature symptoms that developed in these lines appeared to be quite distinct from classic chilling sensitivity (Fig. 8.45A,B). Increased concentrations of disaturated PG (to as much as 60% of total PG) were obtained in transgenic *Arabidopsis,* and in these plants the damaging effects of low temperature became evident more quickly.

A complementary series of experiments was carried out in tobacco (*Nicotiana tabacum*), a chilling-sensitive plant. Transgenic expression of exogenous genes was used to specifically decrease the concentrations of disaturated PG or to bring about a general increase in membrane unsaturation, and the damage caused by chilling was alleviated to some extent. These findings indicate the extent of membrane unsaturation or the presence of particular lipids such as disaturated PG can affect the low-temperature responses of plants. However, some research indicates the relationship between membrane unsaturation and plant temperature responses is subtle and complex. In the *Arabidopsis fab1* mutant, disaturated molecular species of PG accounted for 43% of the total leaf PG—a higher percentage than is found in many chilling-sensitive plants. Nevertheless, the mutant was completely unaffected (when compared with wild-type controls) by a range of low-temperature treatments that quickly led to the death of cucumber (*Cucumis sativus*) and other chilling-sensitive plants. Growth of *fab1* plants slowed, relative to the wild type, only after more than two weeks' exposure to 2°C (Fig. 8.45C,D). These results indicate membrane unsaturation does contribute to chilling damage but that other processes are also important.

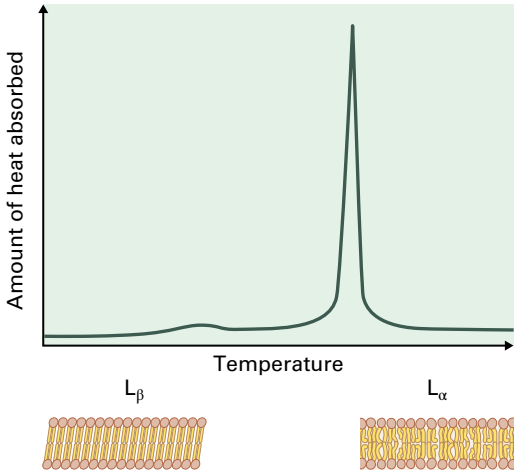


FIGURE 8.44 *Thermal transition from the gel phase (Lβ) to liquid crystalline phase (Lα) in a pure phosphatidylcholine bilayer (lower panel). At low temperatures, motion of the fatty acid chains is limited by Van der Waals forces. As the temperature is raised through the phase transition, heat is absorbed (upper panel) and Van der Waals forces are disrupted to form a bilayer with melted fatty acid chains (Lα).*

8.8.4 Membrane lipid composition can influence plant cell responses to freezing

Freezing stress in plants differs from chilling stress, and tolerance of freezing requires a specialized set of biological mechanisms. During initial freezing of plant tissue (down to –5°C), ice forms outside the plasma membrane. Because solutes are excluded from the ice, the solute concentration in the remaining extracellular aqueous phase increases, forcing water out through the plasma membrane by osmosis, and plasmolyzing the cell. When the temperature increases again and the ice melts, cellular damage may result.

If plants are allowed to acclimate to cold by growth at low, but not freezing, temperatures for a few days before exposure to freezing, many can withstand freezing to temperatures that would otherwise cause extensive damage or death (Fig. 8.46). Protoplasts from rye (*Secale cereale*) leaves have been used as a model system to investigate the molecular basis for this acclimation response (Fig. 8.47).

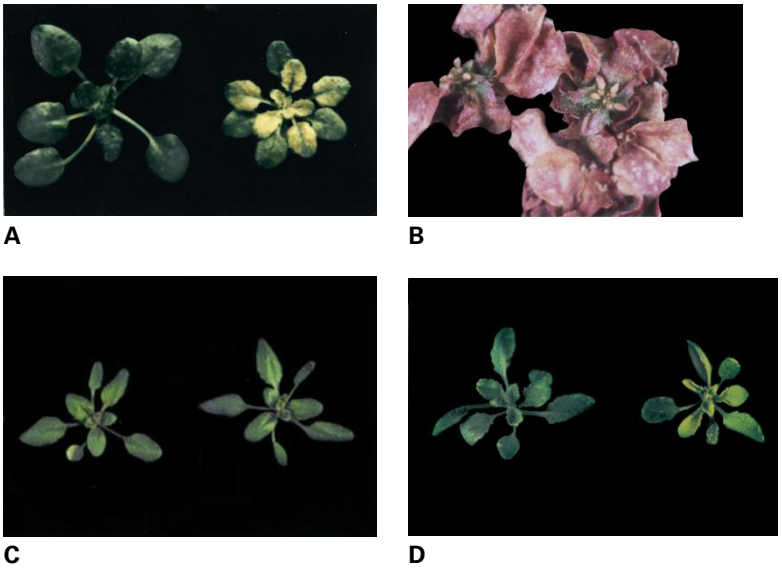


FIGURE 8.45 *Three different chilling responses in lipid mutants of* Arabidopsis. *(A) Compared with wild-type plants (left), the* Arabidopsis fad6 *mutant (right) becomes chlorotic after three weeks at 5°C. (B)* fad2 Arabidopsis *plants die after seven weeks at 6°C. (C) Compared with wild-type plants (left), the* fab1 *mutant (right) is unaffected by up to one week of exposure to chilling at 2°C. (D) After four weeks at 2°C, however,* fab1 *plants (right) show clear symptoms of chlorosis and reduced growth.*
Source: (A) Hugly & Somerville (1992). Plant Physiol. 99:197–202. (B) Miquel et al. (1993). Proc. Natl. Acad. Sci. USA 90:6208–6212. (C, D) Wu et al. (1997). Plant Physiol. 113:347–356.



FIGURE 8.46 *Cold acclimation allows plants to survive freezing. The* Arabidopsis *plants on the right were incubated at 4°C for 4 days to acclimate the plants, after which both pots were kept at –5°C for 4 days, and then transferred to growth conditions at 23°C for 10 days.*
Source: M. Thomashow, Michigan State University, East Lansing; previously unpublished.

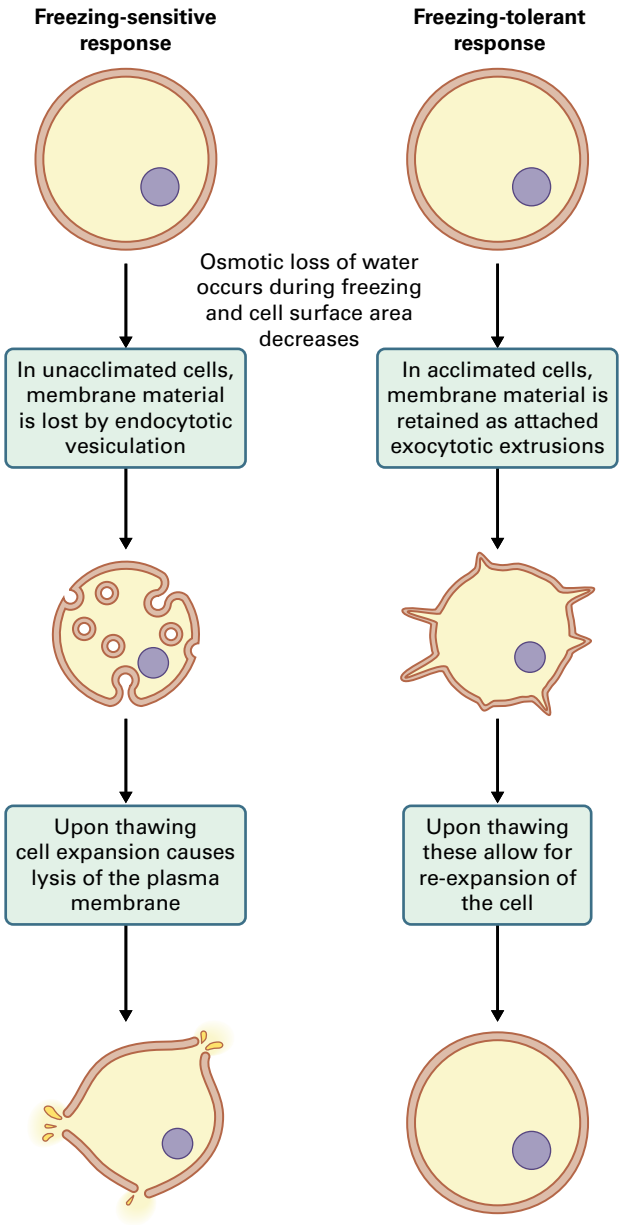


FIGURE 8.47 *During freezing stress, changes in plasma membrane morphology determine death or survival of the cell.*

When nonacclimated protoplasts are placed in a hyperosmotic medium, the plasma membrane buds off endocytotic vesicles, as shown in Figure 8.47. However, if the protoplasts are first preincubated with monounsaturated or diunsaturated species of phosphatidylcholine, so that the phospholipid is incorporated into the plasma membrane, hyperosomotic treatment results in the formation of exocytotic extrusions. Disaturated species of phosphatidylcholine do not induce this change. These differences in plasma membrane behavior correlate with protoplast survival during freezing: Preincubation of nonacclimated protoplasts with monounsaturated or diunsaturated phosphatidylcholine is as effective as cold acclimation in promoting protoplast survival, whereas preincubation with disaturated phosphatidylcholine has no beneficial effect. These observations suggest cold acclimation increases unsaturated phospholipids in the plasma membrane. Physicochemical considerations indicate such changes could mediate the shift from formation of endocytotic vesicles to formation of exocytotic extrusions.

8.8.5 Membrane lipids function in signaling and in defensive processes

Plants, animals, and microbes all use membrane lipids as precursors for the synthesis of compounds that have intracellular or long-range signaling activities. Intriguingly, many of the lipid derivatives characterized as signaling molecules in animals may also have roles in plant signaling. These include phosphatidic acid, DAG, ceramide, lyso-phosphatidylcholine, and *N*-acylethanolamine.

Phosphatidylinositols, frequently referred to as phosphoinositides, have important functions in signal transduction pathways. Their role in regulation of metabolic pathways has been most extensively studied in animal systems, but recent studies suggest they may serve a similar function in plants (see Chapter 18). In the principal active molecule, the phosphatidylinositol 4, 5-bisphosphate (PIP_2), the inositol moiety is phosphorylated at C-4 and C-5. In animals, phosphoinositides serve as second messengers to extracellular signals. The signal activates a phosphatidylinositol-specific phospholipase C, which cleaves PIP_2 to produce inositol 1,4,5-triphosphate (IP_3) and DAG, each of which acts as a second messenger (Fig. 8.48).

Jasmonate is another lipid-derived plant growth regulator (see Chapter 17). The structure and biosynthesis of jasmonate have intrigued plant biologists because of the parallels to some eicosanoids, which are central to inflammatory responses and other physiological processes in mammals. In plants, jasmonate derives from $18{:}3\Delta^{9,12,15}$ that is released from membrane lipids by specific lipases. The linolenic acid is oxidized by lipoxygenase, and the resulting product, 9-hydroperoxylinolenic acid or 13-hydroperoxylinolenic acid, may be further metabolized by one of three routes to produce a wide variety of derivatives, collectively referred to as oxylipins (Fig. 8.49).

The pathways by which 13-hydroperoxylinoleic acid may be metabolized are shown in Figure 8.50. The enzyme hydroperoxide lyase catalyzes α-scission of the *trans*-11,12-double bond to produce a C_6 aldehyde, *cis*-3-hexenal, and a C_{12} compound, 12-oxo-*cis*-9-dodecenoic acid. The acid is subsequently metabolized to 12-oxo-*trans*-8-dodecenoic acid, also known as the wound hormone traumatin. The enzyme allene-oxide synthase catalyzes the dehydration of 13-hydroperoxylinolenic acid to an unstable allene oxide, which readily decompose to form 9,12-ketols or 12,13-ketols. However, allene-oxide cyclase catalyzes the synthesis of the 9S,13S isomer of 12-oxo-phytodienoic acid, which can be further metabolized to (3R,7S) jasmonic acid.

The actions of jasmonate are dramatic and wide-ranging. Jasmonate is a key component of a wound-signaling pathway that allows plants to protect themselves against insect attack. When applied to plants at low concentrations, jasmonate induces expression of genes that lead to the production of proteinase inhibitors and other defense compounds. Furthermore, mutants of tomato (*Solanum lycopersicum*) and *Arabidopsis* that are deficient in jasmonate synthesis are much more susceptible to insect damage (Fig. 8.51).

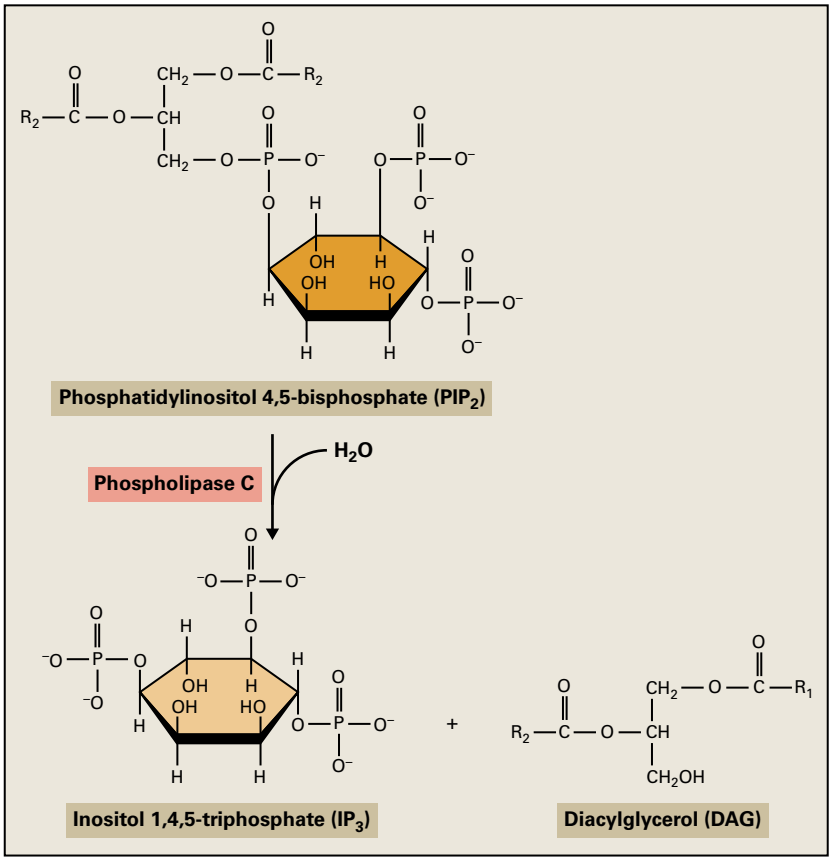


FIGURE 8.48 *Phospholipase C hydrolyzes phosphatidylinositol 4,5-bisphosphate to inositol 1,4,5-triphosphate and DAG.*

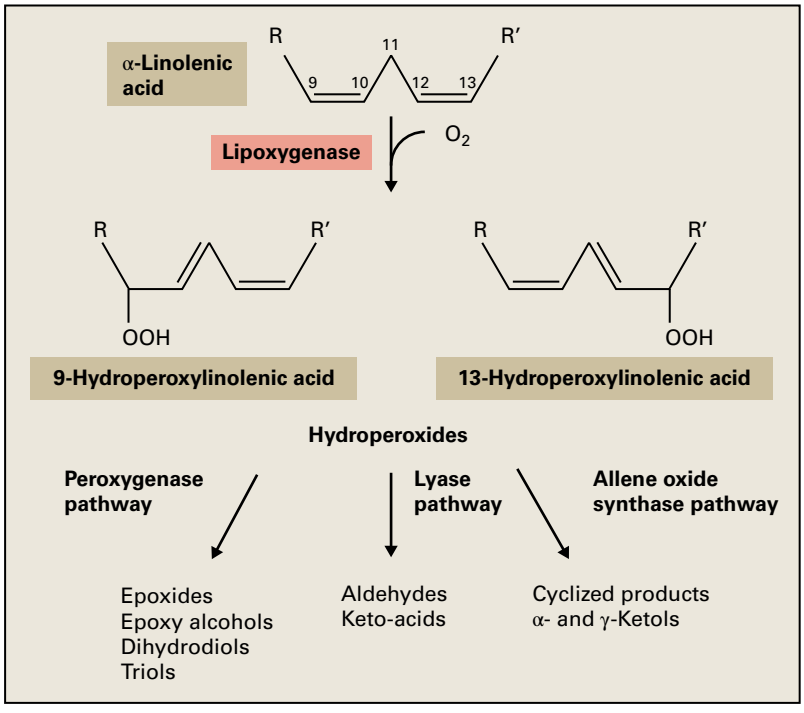


FIGURE 8.49 *The lipoxygenase pathway. In the dioxygenase reaction catalyzed by lipoxygenase, there is no net oxidation or reduction. A* cis–trans *conjugated diene, 13-hydroperoxylinolenic acid, forms in the reaction. The hydroperoxy acid can be metabolized by three separate pathways to a wide variety of products, including jasmonate. The pathway starts with the action of lipoxygenase on 18:3$^{\Delta 9,12,15}$ to produce 9-hydroperoxylinolenic acid or 13-hydroperoxylinolenic acid, depending on the source of the enzyme.*

Jasmonic acid itself is not an active hormone—it must be converted to an amino acid conjugate such as jasmonoyl-isoleucine, a ligand for the jasmonate receptor (see Chapter 17). A different role for jasmonate was revealed by the *fad3 fad7 fad8* triple mutant of *Arabidopsis*, which cannot synthesize jasmonate because it lacks the precursor 18:3$^{\Delta 9,12,15}$. The plants are male-sterile because pollen does not mature properly and is not released from the anthers. Application of jasmonate or linolenic acid to the anthers restores fertility, demonstrating jasmonate is a key signal in pollen development. The same mutant has been

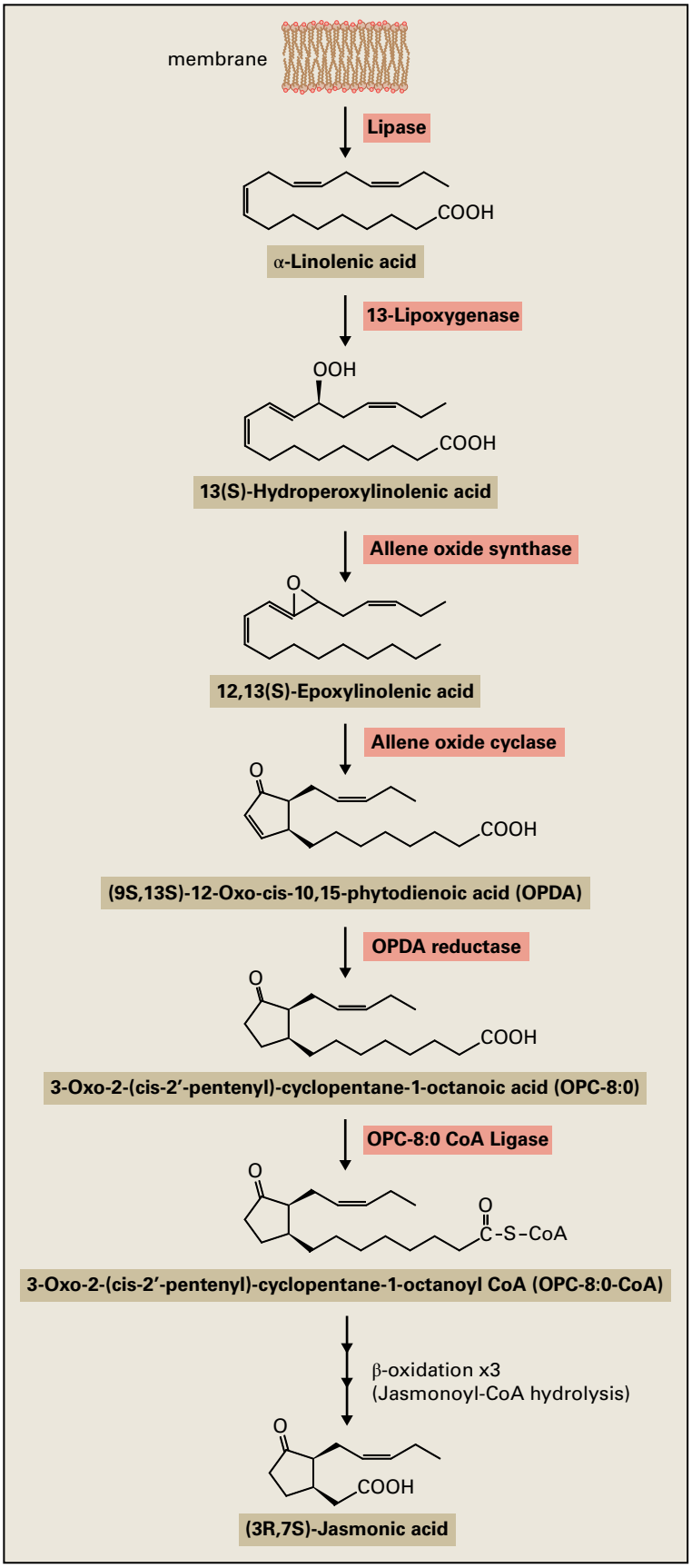


FIGURE 8.50 *Metabolism of 13-hydroperoxylinolenic acid. Additional reactions not shown include conversion of 11,12-epoxylinolenic acid to 13-hydroxylinolenic acid by peroxygenase and rearrangement of the 13-hydroxylinolenic acid to form 15,16-epoxy-13-hydroxyoctadecenoic acid. Also* cis*-3-hexenal and its corresponding alcohol are thought to give rise to several isomers.*

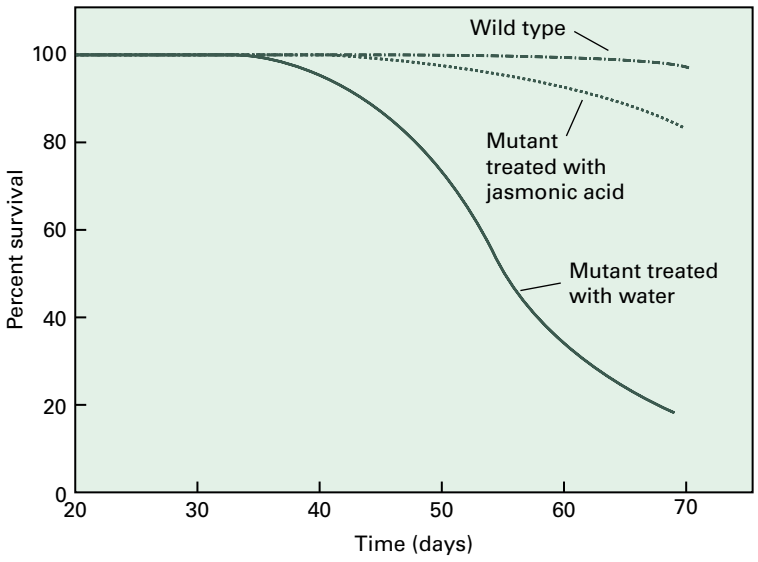


FIGURE 8.51 *Jasmonic acid signaling protects plants from insect predation. Wild-type* Arabidopsis *and a fad3 fad7 fad8 mutant were enclosed with adult flies of the fungal gnat* Bradysia impatiens*. The larvae of the flies feed on roots and stems, leading to plant death. The mutant plants, which were unable to synthesize jasmonic acid because of the fad mutations, were sprayed with either water or low concentrations of jasmonic acid.*

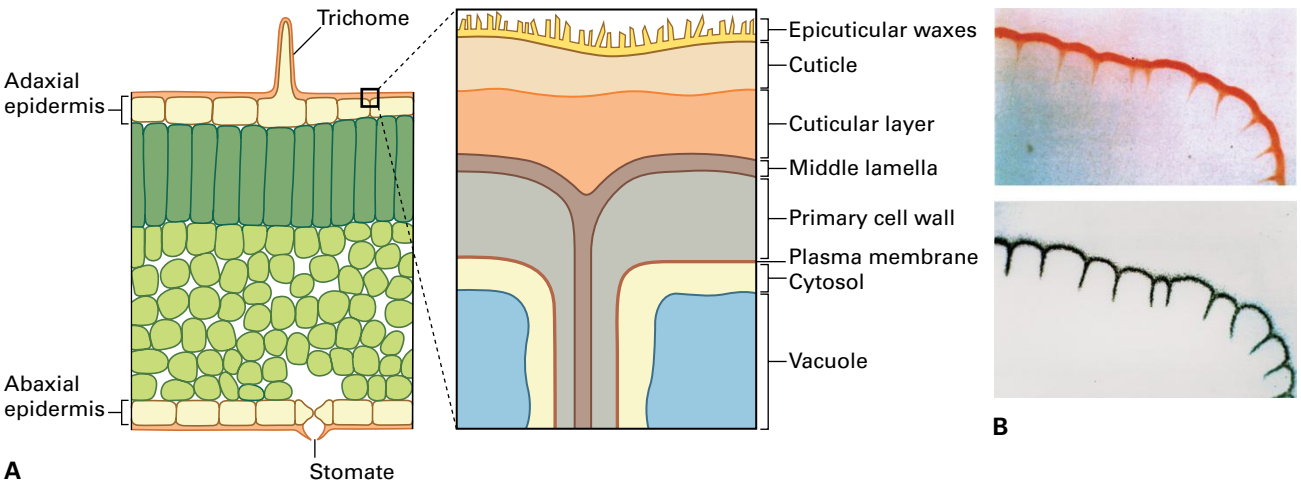


FIGURE 8.52 *(A) Schematic of cutin deposition in a leaf. Cutin covers the outer wall of epidermal cells. Thickness, structure and composition of the various layers of the cuticle can vary significantly depending on species, organs or developmental stage. Wax crystals are not always present on the surface. Epicuticular waxes cover the cuticle proper, which is cutin embedded with intracuticular waxes. The cuticular layer is thought to contain cutin and polysaccharides of the cell wall but might also contain intracuticular waxes. Included for illustration are a trichome on the adaxial surface and a stomate on the abaxial surface. (B) Cutin is deposited on the outer surface of epidermal cells. In the upper panel, a section of a leaf has been stained with Sudan III, which stains lipophilic materials. The lower panel is an autoradiograph of a leaf after incubation with radioactive fatty acids for 24 h. Subsequent extraction with methanol and methanol:chloroform (1:1 by vol.) removed the soluble fatty acids, leaving only cutin in place.*

used to demonstrate jasmonate (with ethylene) is an important chemical signal in nonhost resistance against fungal pathogens. Transcriptional profiling of the jasmonate response in *Arabidopsis* stamens led to the identification of jasmonate ZIM-domain (JAZ) proteins that are repressors of jasmonate signaling. The active form of jasmonate hormone, jasmonoyl-isoleucine, relieves repression by promoting binding of JAZ proteins to the F-box protein, coronatine-insensitive 1 (COI1), and their subsequent degradation by the ubiquitination/26S-proteasome pathway (see Chapters 10 and 17).

In addition to jasmonate, several other oxylipins have been reported to function as signal molecules. In particular, the oxylipin traumatin has been suggested to trigger cell division at the site of wounds, leading to the development of a protective callus. The lipoxygenase product 13-hydroxylinolenic acid triggers phytoalexin production. Similarly, C6–C8 alkenals act as volatile elicitors of a defense response in cotton.

8.9 Synthesis and function of extracellular lipids

8.9.1 Cutin, suberin, and their associated waxes provide lipophilic barriers to water loss and pathogen infection

Plants synthesize two types of lipid polymer that provide a crucial interface for interaction with and protection from the environment. The aerial parts of terrestrial plants are covered by a film of soluble and polymerized lipids, collectively called the cuticle (Fig. 8.52). This cuticle is synthesized by and deposited on the surface of epidermal cells that surround all aerial organs. The development of cuticles gave early land plants the ability to survive in dry environments. Indeed, one primary

role of this layer is to provide a permeability barrier against water loss; it also provides important resistance to pathogens, insects, and UV penetration.

The cuticle is composed of two types of lipids: an insoluble lipid polyester called cutin, which is a structure unique to plants, and the surface waxes, which cover the cutin matrix and are soluble in organic solvents (Fig. 8.52; see also Section 8.9.2). Cutin is a polymeric network of oxygenated C_{16} and C_{18} fatty acids and glycerol linked primarily by ester bonds. The monomers that give rise to cutin have largely been deduced by analyzing the composition of chemically depolymerized cutin. The principal constituents are monohydroxy-, polyhydroxy-, and epoxy fatty acids (Fig. 8.53, Table 8.5). In addition, at least *Arabidopsis* and *Brassica napus* contain dicarboxylic acids as major monomers.

The interesterified acyl chains of cutin form a relatively inelastic meshwork with a strongly hydrophobic character. However, because of the relatively large "pore size" of the cutin network, cutin does not provide the major barrier to plant water loss. Rather, it may act as a relatively inelastic outer skin that contributes to rigidity in turgid plant tissues. Because of its physical strength, cutin also provides defense against penetration of pathogens. To penetrate the cutin layer, some pathogens probably need to secrete cutinases, enzymes that hydrolyze the ester linkages. Furthermore, some mutants in cutin biosynthesis are more susceptible to bacterial and fungal pathogens. Plants with certain alterations in cutin biosynthesis also have fusions of organs such as petals and sepals, indicating cutin also plays a role in maintaining organ identity and plant morphology.

Many aspects of cutin structure and assembly are poorly understood. For example, although esters formed between the carboxyl group of one fatty acid to glycerol or to a primary or secondary hydroxyl group of another fatty acid are considered the major linkages, the three-dimensional architecture of the monomers is a major unknown (Fig. 8.53). Possible arrangements of the acyl chains and glycerol include dendrimeric (tree-like) or cross-linked structures. In addition, the number of monomers that determine the overall size of the polymer

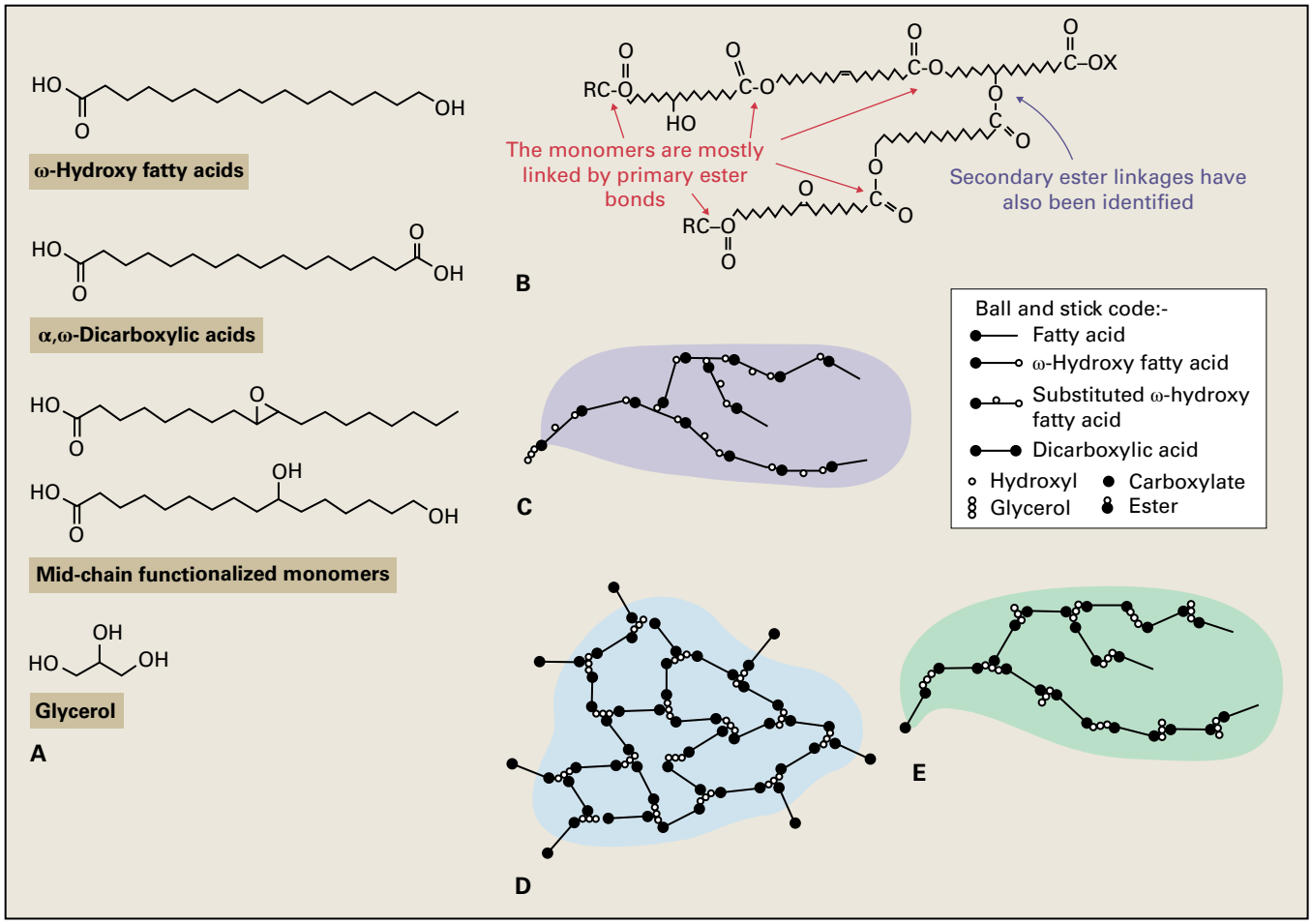


FIGURE 8.53 *Structures of common cutin monomers, and hypothetical monomer connectivity patterns. (A) Representative structures within each monomer group. Mid-chain oxygen-functionalized monomers, which include epoxy, hydroxy, vicinal dihydroxy and oxo groups, can be found in addition to normal fatty acids, ω-hydroxy fatty acids and α,ω-dicarboxylic acids (DCAs). (B) A small segment of ω-hydroxy fatty acid-rich polyester is illustrated to show the dominant primary ester linkages that form chains, along with a secondary ester linkage to enable a branch point. (C–E) Two-dimensional ball-and-stick representations of possible monomer connectivity patterns to give hypothetical local polyester domain structures. Only mid-chain OH groups are depicted; other mid-chain functional groups are not shown, as are possible nonester connectivities and esterification to a cell wall substrate. (C) Organization of fatty acid and ω-hydroxy fatty acid monomers to produce a dendrimer. (D) Organization of DCA and glycerol monomers to produce a cross-linked domain. (E) Organization of DCA and glycerol monomers to produce a dendrimer structure, achieved by allowing free OH groups on some of the glycerol monomers.*

TABLE 8.5 *Monomer composition of cutin and suberin.*

Monomer	Cutin	Suberin
Glycerol	10–50% of monomers	20–60% of monomers
Unmodified fatty acids	Minor (C_{16}–C_{18})	Minor (C_{16}–C_{26})
α,ω-Dicarboxylic fatty acids	Minor[a]	Common and substantial (C_{16}–vC_{26})
ω-Hydroxy fatty acids	Major (C_{16}–C_{18})	Common and substantial (C_{16}–C_{26})
Mid-chain modified ω-hydroxy fatty acids (C_{16}-C_{18})	Major	Minor[b]
Fatty alcohols	Rare and minor (C_{16}–C_{18})	Common and substantial (C_{18}–C_{22})
Ferulate	Low	High

[a] C_{16}–C_{18} dicarboxylates are major monomers in *Arabidopsis* and *Brassica napus* cutin (>50%).
[b] In some cases is substantial. Substituted dicarboxylic acids are also frequently found in suberins.

has not been defined. Cross-linking of cutin to the cell wall is believed to occur, but the extent and nature of such linkages has not been determined.

The cutin monomers that are produced in epidermal cells are synthesized from fatty acid precursors by CYP450 oxidases that introduce hydryoxyl groups. Apparently, cutin components are transported to the plasma membrane and secreted into the cell wall space (Fig. 8.54). How the cutin monomers are polymerized and transported to the site of cutin deposition is not well understood. At least some acyl monomers are attached to glycerol-3-phosphate inside the cell, by an acyltransferase reaction similar to the first reaction of membrane glycerolipid assembly. Unlike the reaction producing intracellular glycerolipids, however, the acyl precursors of cutin are esterified to the *sn*-2 position of glycerol, rather than the *sn*-1 position. Furthermore, some of these acyltransferases are plant-specific bifunctional enzymes that remove the phosphate to produce monoacylglycerol (MAG) products. Whether MAG is exported from cells, or if larger oligomers are assembled before export, is unknown. Additional assembly steps presumably occur outside the plasma membrane or, indeed, outside the cell wall. Movement of monomers or oligomers through the cell wall might be facilitated by lipid transfer proteins, after which "polyester synthase" may catalyze further growth of the cutin polymer. Specific GDSL-motif lipases can catalyze the transacylation of hydroxy fatty acid-monoacylglycerols to form oligomers at the cell wall–cuticle interface and are postulated to be "polyester synthases".

All plants also produce suberin, another extracellular lipid polymer associated with cell walls. The two polymers have similarities in their chemical composition and in the enzymes involved in their synthesis. However, there are a number of key differences. First, cutin accumulates outside the epidermal cell wall, whereas suberin is deposited on the inner side of the primary cell wall facing the plasma membrane. Second, cutin deposition is polar; it accumulates on only the outermost surface of epidermal cells and at the interface between the plant and its environment. In contrast, suberin can surround the entire plasma membrane of cells. Third, whereas cutin synthesis is restricted to epidermal cells, a much wider range of cell types and organs produces suberin. In roots, suberin is deposited as the Casparian bands/strip of endodermal cells, and suberin lamellae also surround these cells (Fig. 8.55; see also Chapter 24). The Casparian band/strips of very young portions of roots is thought to be comprised primarily of lignin or lignin-like substances whereas the canonical suberin lamellae are found in the zone of maturation. Suberin is also present in the periderm of mature roots and on the surface of tubers of roots and stems, and in seed coats. Suberin is a major component of the phellem of stems (e.g., cork) of woody plant species. Cork oak trees produce a commercially important phellem layer that is several centimeters thick and 50% suberin by weight. Suberin also surrounds the plasma membrane of bundle sheath cells of C4 species, where it may prevent CO_2 diffusion from bundle sheath cells. In many other tissues suberin is deposited in response to wounding and abiotic stresses, even in those tissues that normally synthesize cutin.

To accomplish the uptake of water and minerals from the soil, roots maintain hydrophilic contact with soil moisture through an extensive network of root hairs. The suberized Casparian bands/strip in the endodermal cells of plant roots is one system of control employed by plants to regulate what enters and exits the vasculature, and what is distributed to the aerial portions of the plant. The hydrophobic nature of the Casparian strip restricts movement of water and nutrients through the apoplast. This ensures solutions only enter endodermal cells by crossing the plasma membrane (embedded with selective transport proteins), where they then move symplastically to the vasculature. The suberized endodermal cells are also thought to prevent water and mineral movement out of the vasculature, thereby contributing to "root pressure," which aids in the initial movement of water and nutrients up the xylem to the aerial portions of the plant.

The main compositional differences between cutin and suberin are in their fatty acids. In suberin, they usually do not

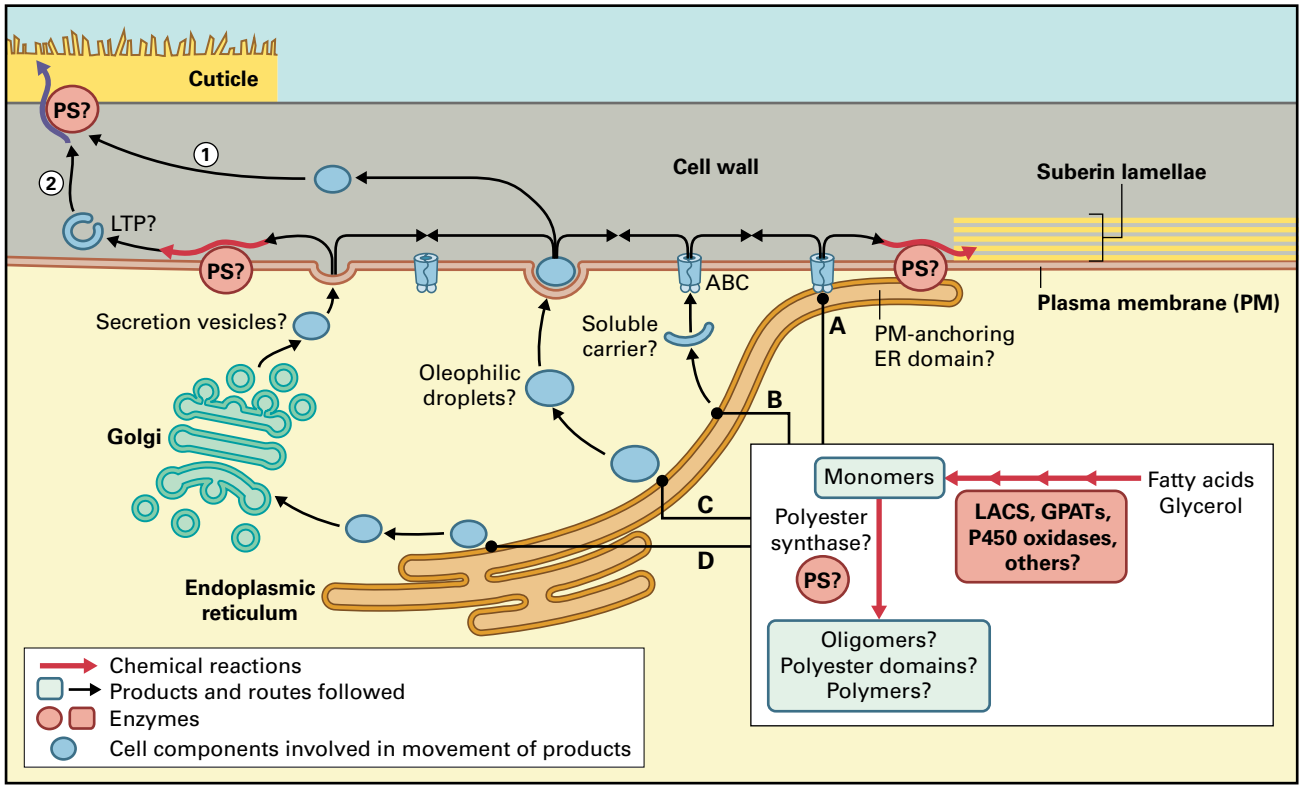


FIGURE 8.54 *Mechanisms and cellular locations of cutin and suberin assembly and deposition. The enzymes of monomer synthesis, including acylglycerol synthesis, are thought to be localized to the ER. Polyester synthases (PS) are broadly defined as enzymes catalyzing the formation of ester bonds between monomers, and also between putative polyester oligomers or domains. Additional enzymes may also anchor the polymers to the cell wall (CW). Four possible mechanisms and associated routes leading from the ER to the external face of the plasma membrane are shown (A–D). In addition, two possible mechanisms of passage of lipophilic precursors from the plasma membrane (PM) through the apoplast to the final site of assembly and deposition are depicted for the case of cutin synthesis (i and ii). Similar mechanisms may be operating for suberin assembly and deposition, but are not shown. The mechanisms are not necessarily mutually exclusive, and not every possibility is shown. (A) PM-anchoring ER domain. This could involve a spatial coupling of monomer synthesis and transport across PM. Transport may be accomplished via an ABC transporter (ABC). (B) Cytoplasmic carrier protein. (C) Oleophilic droplets. Osmophilic particles have been observed in the outer CW of rapidly expanding epidermis and could constitute oleophilic droplets on their way to the cuticle. These droplets could originate from ER, in a way similar to the budding process proposed for the ontogeny of seed oil-bodies. (D) Golgi-mediated secretion vesicle mechanism. This would be a likely possibility if polyester domains or polymers were formed in the ER or if polyesters were attached to polysaccharides inside the cell. It is also possible that a polyester attachment site is added intracellularly to CW polysaccharides. Mechanisms (A) and (B) would most likely accommodate transport of monomers or oligomers. By contrast, mechanisms (C) and (D) could also accommodate polymer domains. (1) Unchaperoned movement of lipidic precursors or oleophilic droplets across the apoplast. (2) Movement of monomers, oligomers of polymers bound to a protein carrier (e.g., lipid transfer proteins) or after attachment to a carrier such as a CW polysaccharide.*

have secondary alcohols or epoxy groups and are often longer than 18 carbons (Table 8.5). In addition, suberin has a relatively high content of dicarboxylic acids and a polyaromatic domain (Fig. 8.55). Despite differences in the deposition sites and composition of suberin and cutin monomers, their biosynthesis involves similar reactions catalyzed by isoforms of the same enzyme families (see Fig. 8.53 and Fig. 8.54).

Similar to cutin, solvent-soluble waxes are embedded in or associated with suberin. However, suberin has some associated waxes that are not typically found in the cuticle. Similar to the cuticle, suberin-associated waxes consist of alkanes, primary alcohols, and fatty acids. Unique to suberin waxes are alkyl hydroxycinnamates and monoacylglycerols, which are metabolically related to suberin.

8.9.2 Epicuticular wax reduces water loss

Cutin alone is not sufficient for determining the barrier/water-retarding properties of the cuticle. The aerial surfaces of plants are covered with a layer of chloroform-soluble, nonvolatile lipids, collectively called wax (see Fig. 8.52). Waxes are embedded into the polymeric cutin matrix, and in many plants waxes also extend beyond the cutin to the plant surface. The wax layer reduces water loss by orders of magnitude, making terrestrial plant life possible.

The amounts and composition of wax deposited are controlled by the plant in response to environmental factors such as relative humidity, soil moisture, and light intensity (Fig. 8.56). Wax composition varies from one plant species to

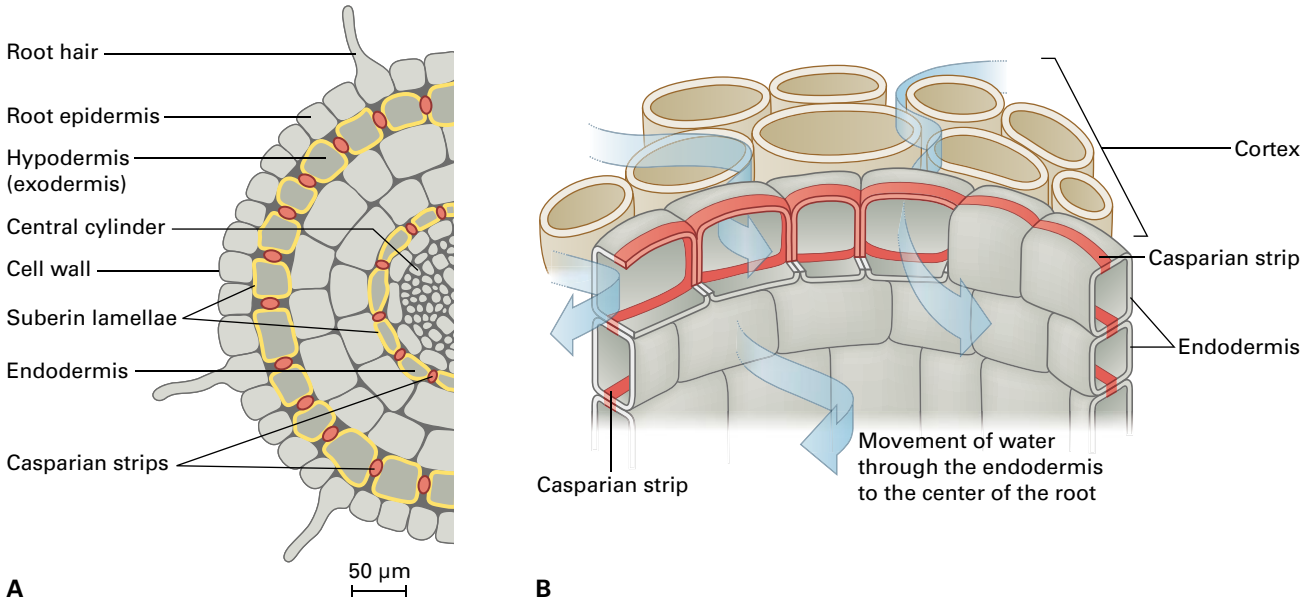
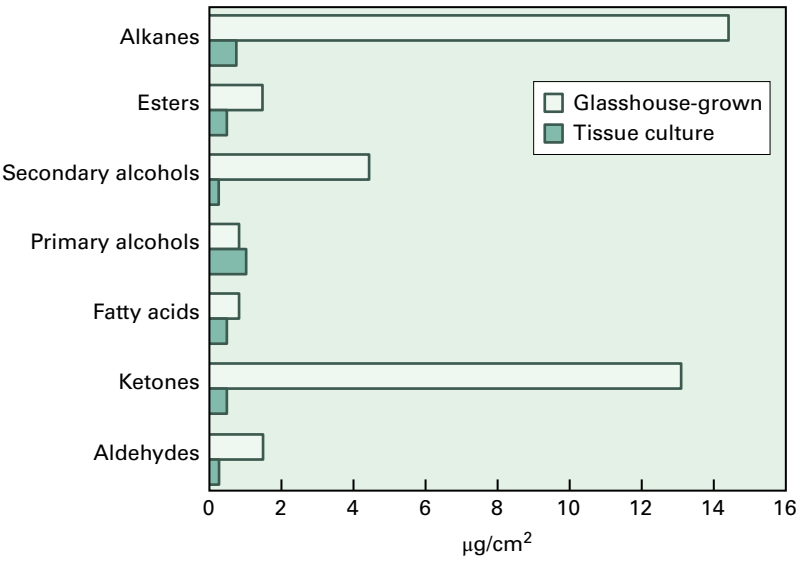


FIGURE 8.55 *Suberin deposition in the root endodermis. (A) Cross-section of a dicotyledonous root in its primary developmental state showing the suberized endodermis and hypodermis (exodermis), both with characteristic Casparian strips (red dots) in the radial cell walls and suberin lamellae (yellow) deposited onto the inner surfaces of the primary cell walls (gray). (B) Representation of the barrier function of the Casparian strip which restricts water flow through the apoplast into the root vasculature. Most water and solute uptake by roots occurs via the symplast.*

FIGURE 8.56 *Wax composition of* Brassica oleracea *plant grown in high-humidity conditions in tissue culture or in low-humidity conditions in a glasshouse.*



another, but wax generally contains a mixture of long-chain hydrocarbons, acids, alcohols, ketones, aldehydes, and esters. In addition, triterpenoids are frequently extracted in the wax fraction. The functional significance of interspecies differences in wax composition is not known. However, the study of mutants with altered wax composition indicates wax composition affects wax crystal structure. Some plants produce filaments, others produce plates or tubes or spiral-shaped forms (Fig. 8.57). The chemical composition of epicuticular waxes correlates with wax crystal structure: tubules are formed when secondary alcohols are abundant, whereas triterpenoids or primary alcohols form platelets in certain species. Different crystal structures may vary in their ability to reflect light—a property that may be useful for adaptation to growth in different light intensities. More importantly, perhaps, some pathogens and herbivorous insects are attracted to or repelled by specific wax compositions. Thus, wax composition may reflect the balance of selective biotic and abiotic pressures exerted on a particular plant species.

Wax monomers are synthesized from C_{16} and C_{18} fatty acids by an elongase complex located in the ER (Fig. 8.58). Although most enzymes involved in elongation, reduction, and oxidation

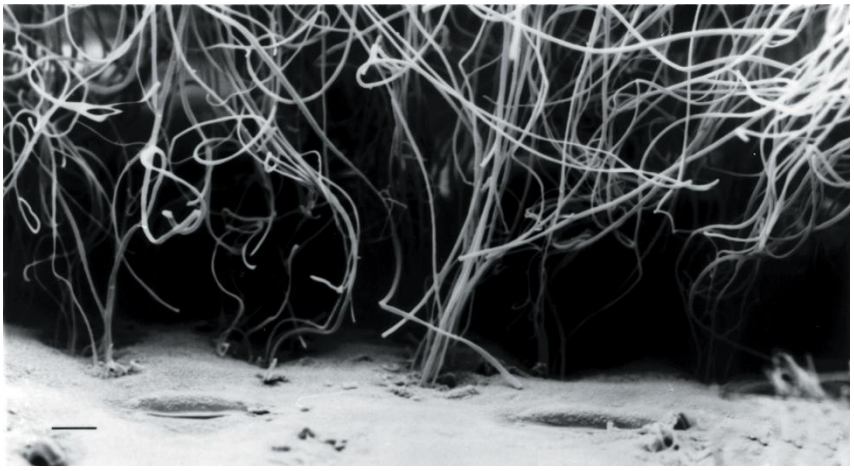


FIGURE 8.57 *Scanning electron micrograph of the surface of a* Sorghum bicolor *leaf sheath. In this species, the wax crystallizes as filaments that appear to emerge from defined regions of the cuticle. Scale bar (lower left) = 10 μm.*
Source: Jenks et al. (1994). Int. J. Plant Sci. 155:506–518.

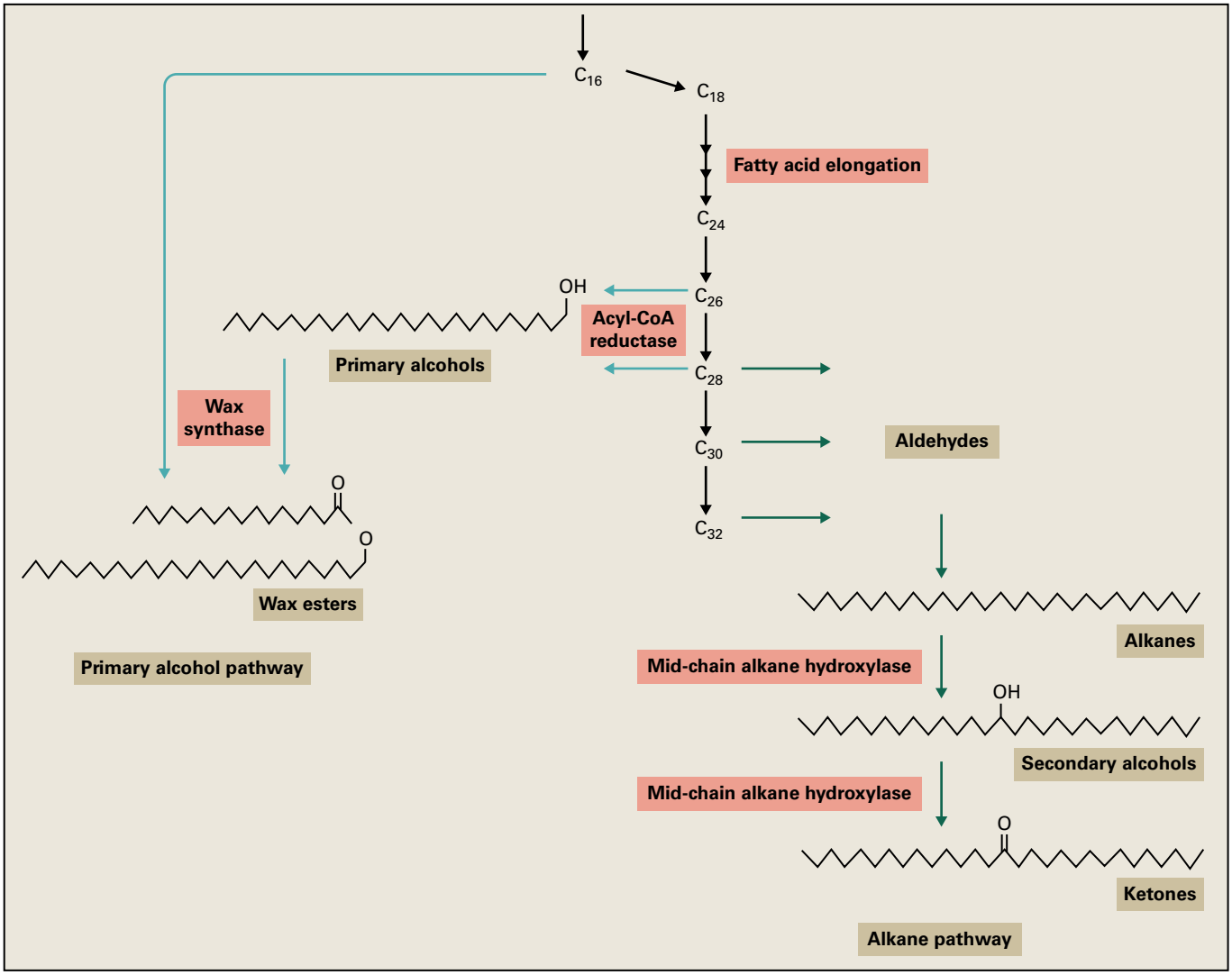


FIGURE 8.58 *Simplified pathways for surface wax biosynthesis.*

have been identified, the decarbonylation step, which produces the major alkane components of waxes, is still uncertain. Transport of wax across the plasma membrane involves ABC transporters, which results in wax accumulation inside the epidermal cells when mutated (Fig. 8.59). As with cutin biosynthesis, it is not well understood how wax monomers move from the plasma membrane through the cell wall to reach the outermost surface of epidermal cells. Because the principal

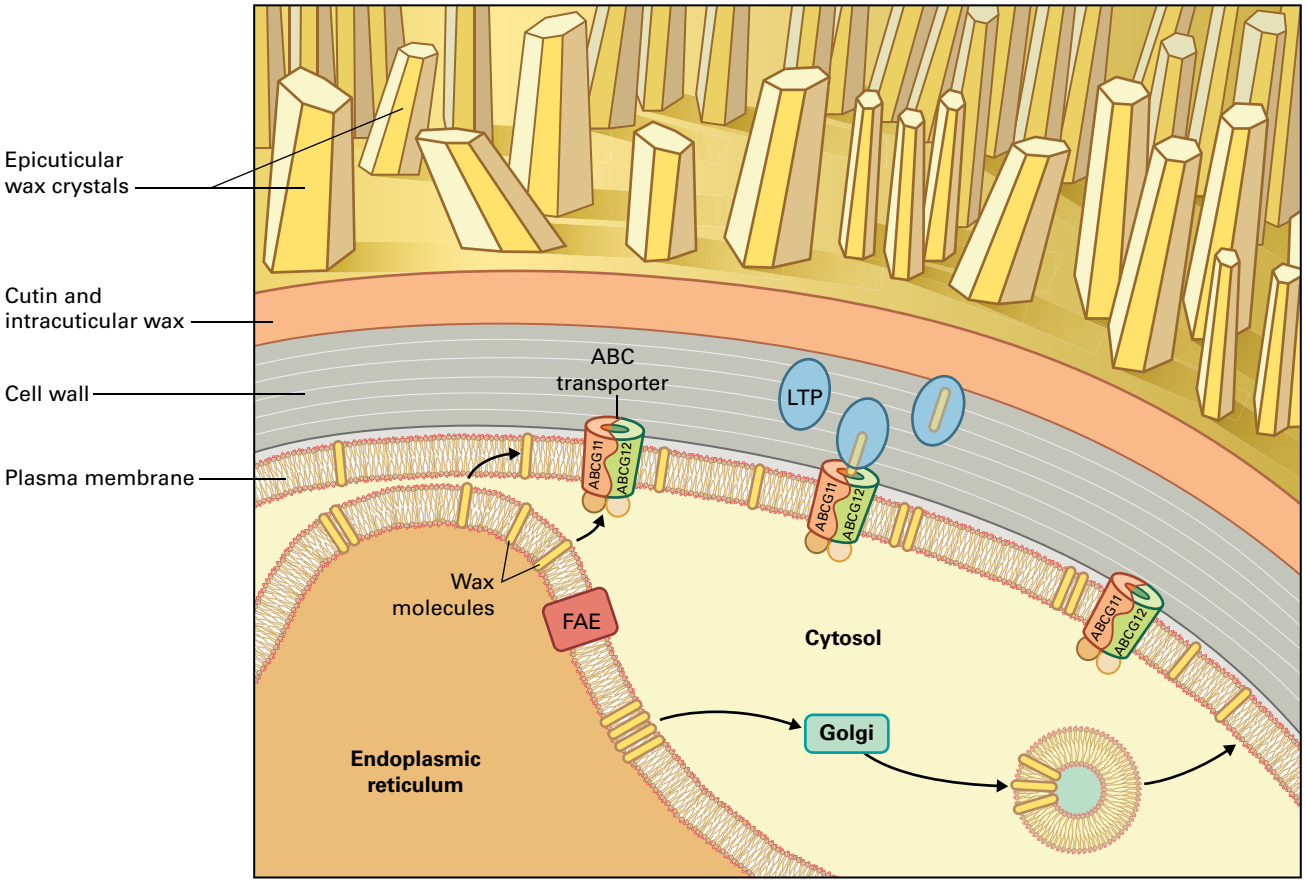


FIGURE 8.59 *Current models of wax export to the cuticle. The mechanisms for transport of wax molecules from epidermal cells to the surface of plants are currently unknown. Two hypothetical routes for movement of wax from the ER to the PM are shown: direct molecular transfer at ER-plasma membrane contact sites, or Golgi-mediated vesicular traffic through the secretory pathway. In either case, wax molecules cross the plasma membrane via ABC transporters (ATP-binding cassette transporter); movement through the cell wall to the cuticle may involve lipid transfer proteins, (LTP). Lipids may accumulate at the air interface based on their insolubility in the aqueous apoplast. FAE, fatty acid elongase.*

components are completely insoluble in aqueous solutions, the monomers are possibly transported by lipid-transfer proteins (Fig. 8.59). Lipid-transfer proteins are the most abundant proteins secreted at the surface of plant cells, and their small size may allow them to permeate the pores of the cell wall-carbohydrate matrix.

8.9.3 Surface lipids are required for male fertility and productive pollen–pistil interactions

Pollen grains are covered with a waxy layer called the exine, which is composed of a complex polymer called sporopollenin. This polymer is related to cutin, and mutations in its synthesis result in male sterility. Embedded in the exine is a layer of lipophilic material called tryphine or pollenkitt (Fig. 8.60; see also Chapter 19). In *Arabidopsis*, the tryphine layer includes small lipid bodies that appear to contain primarily C_{28} and C_{30} wax monomers. Probably an important function of the tryphine layer is to reduce water loss from the

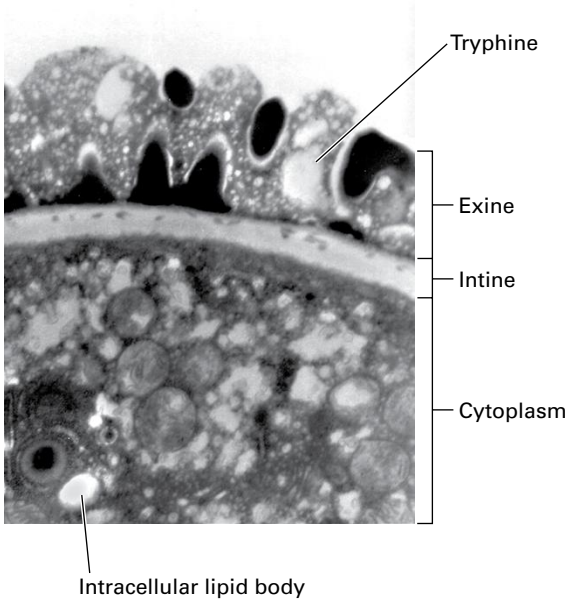


FIGURE 8.60 *Transmission electron micrograph through an* Arabidopsis *pollen grain.*
Source: D. Preuss, University of Chicago; previously unpublished.

pollen grain. However, experiments using *Arabidopsis*, rice, and other mutants with altered exine composition hint at a more complex role for these lipids. Some mutants are male-sterile; however, the fertility of their pollen can be rescued by mixing irradiation-killed wild-type pollen with mutant pollen. Accordingly, some factor in the wild-type pollen appears to complement the defective pollen. These experiments suggest the normal exine coat may play a signaling role in pollen–pistil interactions (see Chapter 19).

8.10 Synthesis and catabolism of storage lipids

Lipids in the form of triacylglycerols are widely found as a major carbon and chemical energy reserve in seeds, fruits, and pollen grains (Fig. 8.61). One of the few plants that stores lipids in a form other than triacylglycerols is jojoba (*Simmondsia chinensis*), a perennial shrub that stores fatty acids as wax esters in seeds. Plant storage lipids are also an important source of dietary fats for humans and other animals. Approximately 40% of the daily energy requirement of humans in industrialized countries is supplied by dietary triacylglycerols, of which more than half is from plant sources. Furthermore, triacylglycerols find use in manufacturing industries, particularly in the production of detergents, coatings, plastics, and specialty lubricants. For both food and industrial applications, the fatty acid composition of the oil determines its usefulness and, therefore, its commercial value.

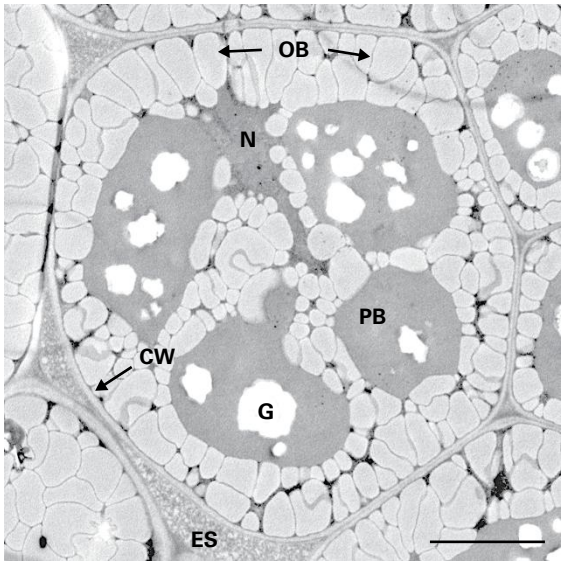


FIGURE 8.61 *Electron micrograph from a mature* Arabidopsis *seed showing a cotyledon cell containing abundant oil bodies (OB), protein bodies (PB), and globoid spaces (G). CW, cell wall; ES, extracellular space; N, nucleus. Bar = 2 μm.*
Source: J. Dyer, USDA, Maricopa, Arizona, USA.

8.10.1 Triacylglycerol synthesis involves acyltransferase and acyl-exchange reactions that move fatty acids between pools of membrane and storage lipids

Many of the biochemical reactions and some aspects of subcellular compartmentalization of triacylglycerol synthesis in developing oilseeds are the same as for membrane lipids. Because of interest in the factors that control the precise fatty acid composition of triacylglycerols, however, it is useful to consider seed lipid biosynthesis in terms of a pathway that emphasizes the acyltransferase and acyl-exchange reactions (Fig. 8.62). This pathway was proposed based on results from many oilseed species but is shown to describe the metabolism of developing *Arabidopsis* seeds. *Arabidopsis* seed lipids contain substantial proportions of both unsaturated C18 fatty acids (30% $18{:}2^{\Delta 9,12}$, 20% $18{:}3^{\Delta 9,12,15}$) and long-chain fatty acids (22% $20{:}1^{\Delta 11}$) derived from $18{:}1^{\Delta 9}$. As a result, *Arabidopsis* is a good model for the biochemistry of oilseeds rich in $18{:}2^{\Delta 9,12}$/$18{:}3^{\Delta 9,12,15}$ fatty acids and oilseeds from other species containing longer fatty acids.

As they are in other tissues, 16:0-ACP and $18{:}1^{\Delta 9}$-ACP are usually the major products of plastid fatty acid synthesis and 18:0-ACP desaturase activity in oilseeds. In seed tissues, these products are hydrolyzed to free fatty acids by thioesterases in the plastid stroma and transferred through the plastid envelope by an unknown mechanism. The free fatty acids are converted to acyl-CoAs in the outer plastid envelope, forming the substrates for subsequent acyltransferase reactions. Newly produced $18{:}1^{\Delta 9}$-CoA,18:0-CoA, and 16:0-CoA can be used for the synthesis of phosphatidylcholine and phosphatidic acid, as shown in Figure 8.62. Phosphatidylcholine is the main substrate for the sequential desaturation of $18{:}1^{\Delta 9}$ to $18{:}2^{\Delta 9,12}$ and $18{:}3^{\Delta 9,12,15}$. CDP-choline:diacylglycerol cholinephosphotransferase is responsible for net synthesis of phosphatidylcholine. In addition, phosphatidylcholine to DAG interconversions are catalyzed by phosphatidylcholine: diacylglycerol cholinephosphotransferase (PDCT) through the phosphocholine headgroup exchange between PC and DAG (Fig. 8.62), providing an alternate route for entry of $18{:}1^{\Delta 9}$ into phosphatidylcholine for desaturation and transfer of $18{:}2^{\Delta 9,12}$and $18{:}3^{\Delta 9,12,15}$ to the DAG pool for triacylglycerol synthesis.

The acyl-CoA pool does not contain only 16:0 and $18{:}1^{\Delta 9}$; exchange of $18{:}1^{\Delta 9}$from $18{:}1^{\Delta 9}$-CoA with the fatty acid at position *sn*-2 of phosphatidylcholine releases $18{:}2^{\Delta 9,12}$ and $18{:}3^{\Delta 9,12,15}$ back into the cellular acyl-CoA pool. In some oilseeds, including *Arabidopsis* and rapeseed (*Brassica napus*), $18{:}1^{\Delta 9}$-CoA can be modified by elongation to $20{:}1^{\Delta 11}$-CoA and $22{:}1^{\Delta 13}$-CoA. Synthesis of DAG may also involve these components of the acyl-CoA pool, as does the final acylation of DAG to form triacylglycerol by the enzyme acyl-CoA:1,2-diacylglycerol *O*-acyltransferase. At least two rather different forms of this enzyme occur in plants: one with at least six membrane-spanning domains and a smaller enzyme with three predicted membrane

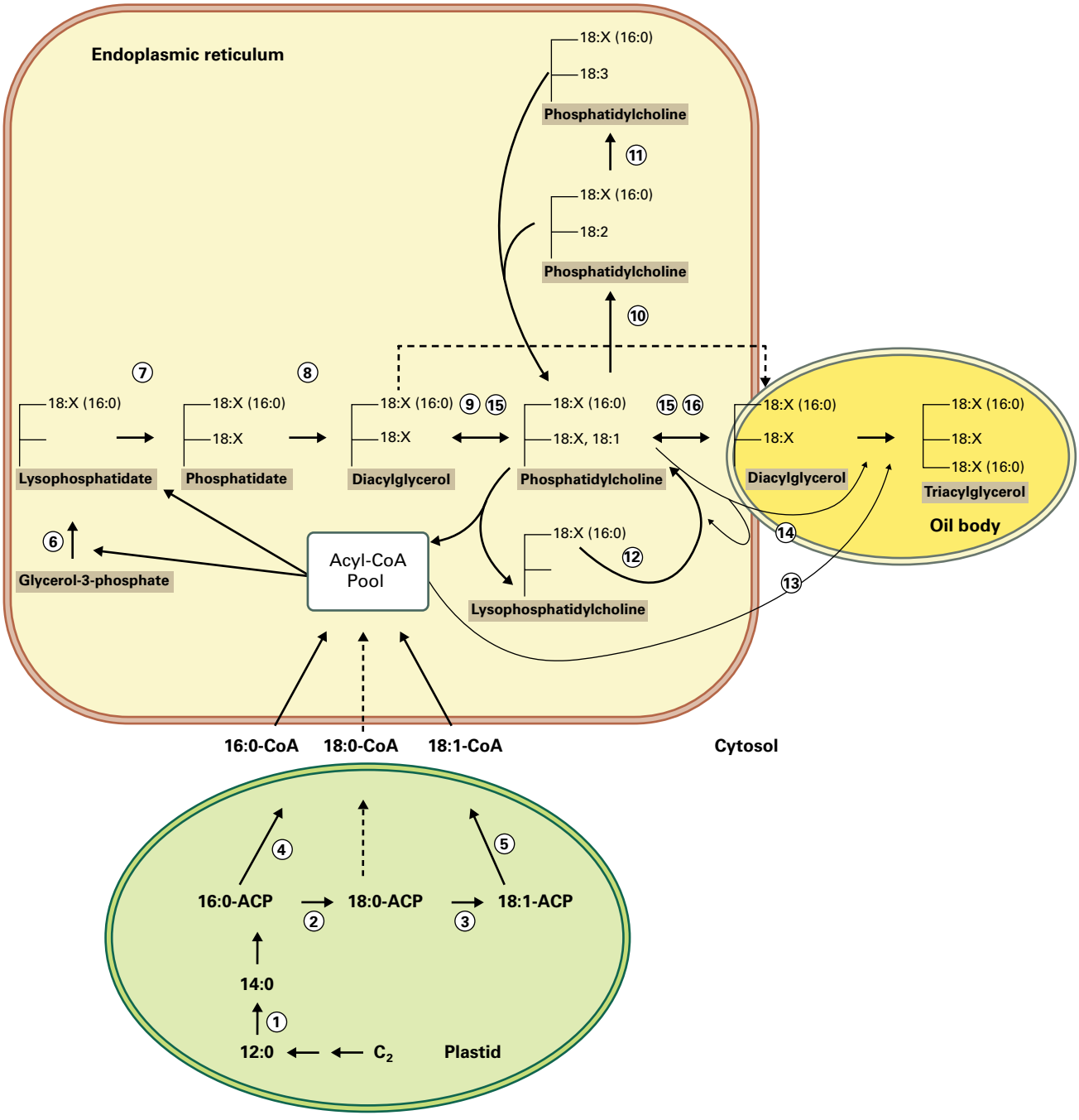


FIGURE 8.62 *Pathway of triacylgylcerol synthesis as deduced from in vivo labeling of developing soybean embryos and* Arabidopsis *seeds. The largest flux measured during labeling experiments is reaction 12, the exchange of acyl groups between the acyl-CoA pool and PC. Therefore, most fatty acids that exit the plastid are first esterified to PC rather than glycerol 3-phosphate. The dotted line represents that a small flux of de novo synthesized DAG can be used to make TAG however most DAG fluxes through PC prior to TAG synthesis. 1, KAS I- and KAS III-dependent FAS; 2, KAS II-dependent FAS; 3, stearoyl-ACP desaturase; 4, palmitoyl-ACP thioesterase; 5, oleoyl-ACP thioesterase; 6, acyl-CoA:glycerol-3-phosphate acyltransferase (GPAT); 7, acyl-CoA:lysophosphatidate acyltransferase (LPAT); 8, phosphatidate phosphatase (PAP); 9, CDP-choline:diacylglycerol cholinephosphotransferase (CPT); 10, oleate desaturase (FAD2); 11, linoleate desaturase (FAD3); 12, acyl-CoA:lysophosphatidylcholine acyltransferase (LPCAT); 13, acyl-CoA:diacylglycerol acyltransferase (DGAT); 14, phospholipid:diacylglycerol acyltransferase (PDAT); 15, phosphatidylcholine:diacylglycerol cholinephosphotransferase (PDCT); 16, other possible reactions for conversion of PC to DAG include phospholipase C, phospholipase D together with reaction 8, and the reverse of reaction 9.*

spanning domains. Evidence suggests, for both plants and animals, these two isozymes occur in different subcellular locations. Triacylglycerol can also be formed by transfer of an acyl group from phosphatidylcholine to DAG by the enzyme phosphatidylcholine:diacylglycerol acyltransferase. The relative contribution of these alternative enzymes to the in vivo flux of triacylglycerol synthesis in oilseeds varies in different species.

8.10.2 Triacylglycerols accumulate in discrete subcellular organelles called oil bodies

In oilseeds, oil bodies are droplets of triacylglycerols surrounded by a monolayer of phospholipids, with the hydrophobic acyl moieties of the phospholipids interacting with the triacylglycerols and the hydrophilic head groups facing the cytosol. Oil bodies also contain major protein components called oleosins, which are not found in significant amounts in any other cellular location (Fig. 8.63). Oleosins are low-molecular-mass proteins (15–25 kDa) that contain a sequence of 70–80 hydrophobic amino acids toward the middle of the protein. The sequence of this hydrophobic domain is conserved in oleosins from different plant species, but these proteins are not found in animals, bacteria, or fungi. Although some question of the protein secondary structure in the hydrophobic domain (β-strand or β-sheet) remains, there is general agreement that it protrudes into the triacylglycerol core of the oil body. Possibly, the more hydrophilic N- and C-terminal domains form amphipathic helices at the oil body surface.

Oleosins are found only in oil bodies of seeds and pollen, both of which undergo dehydration during maturation. In contrast, lipid droplets in fruit mesocarp (such as those of avocado and olive (*Olea europaea*) do not contain oleosin homologs. Thus, oleosins may stabilize oil bodies at low water potential in mature seeds and pollen when hydration of the surface phospholipids is not sufficient to prevent the oil bodies from coalescing and fusing. Oleosins also may regulate the size of oil bodies by imparting a defined curvature to the surface, which could be important for regulating the surface-to-volume ratio to facilitate rapid breakdown of oil bodies during germination. In this respect, the mesocarp lipids in avocado and olive are not thought to contribute to the germination or growth of the seedling, but are probably made by the plant to facilitate seed dispersal by animals.

The ontogeny of oil bodies is not absolutely clear, but one model suggests they arise by deposition of triacylglycerols between the two leaflets of the ER and then develop into discrete organelles that may or may not remain attached to the ER membranes (Fig. 8.64). This model accounts for the monolayer membrane of oil bodies and is consistent with biochemical results demonstrating triacylglycerol synthesis by microsomal membrane preparations. However, enzymes of oil synthesis are also reported to be associated with isolated oil bodies. The exact nature of the relationship between the oil bodies and ER takes on extra significance because DAGs are precursors for the synthesis of both triacylglycerols and the major membrane

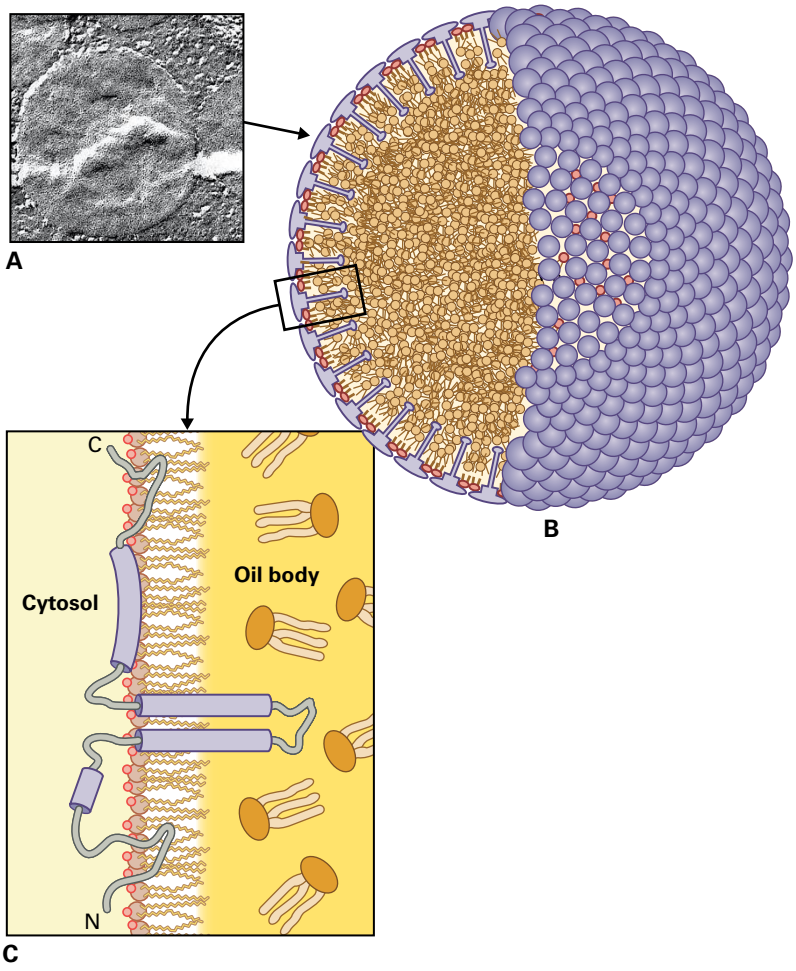


FIGURE 8.63 *(A) Transmission electron micrograph close-up of oil body. (B) Scale-model of an oil body. The oleosin molecule is depicted in the shape of an 11-nm-long hydrophobic stalk attached to an amphipathic and hydrophilic globular structure that forms the outer surface of the oil body. (C) Proposed model of the conformation of an 18-kDa oleosin. Cylinders depict helices.*
Source: (A) Fernandez & Staehelin (1987). Plant Physiol. 85:487–496.

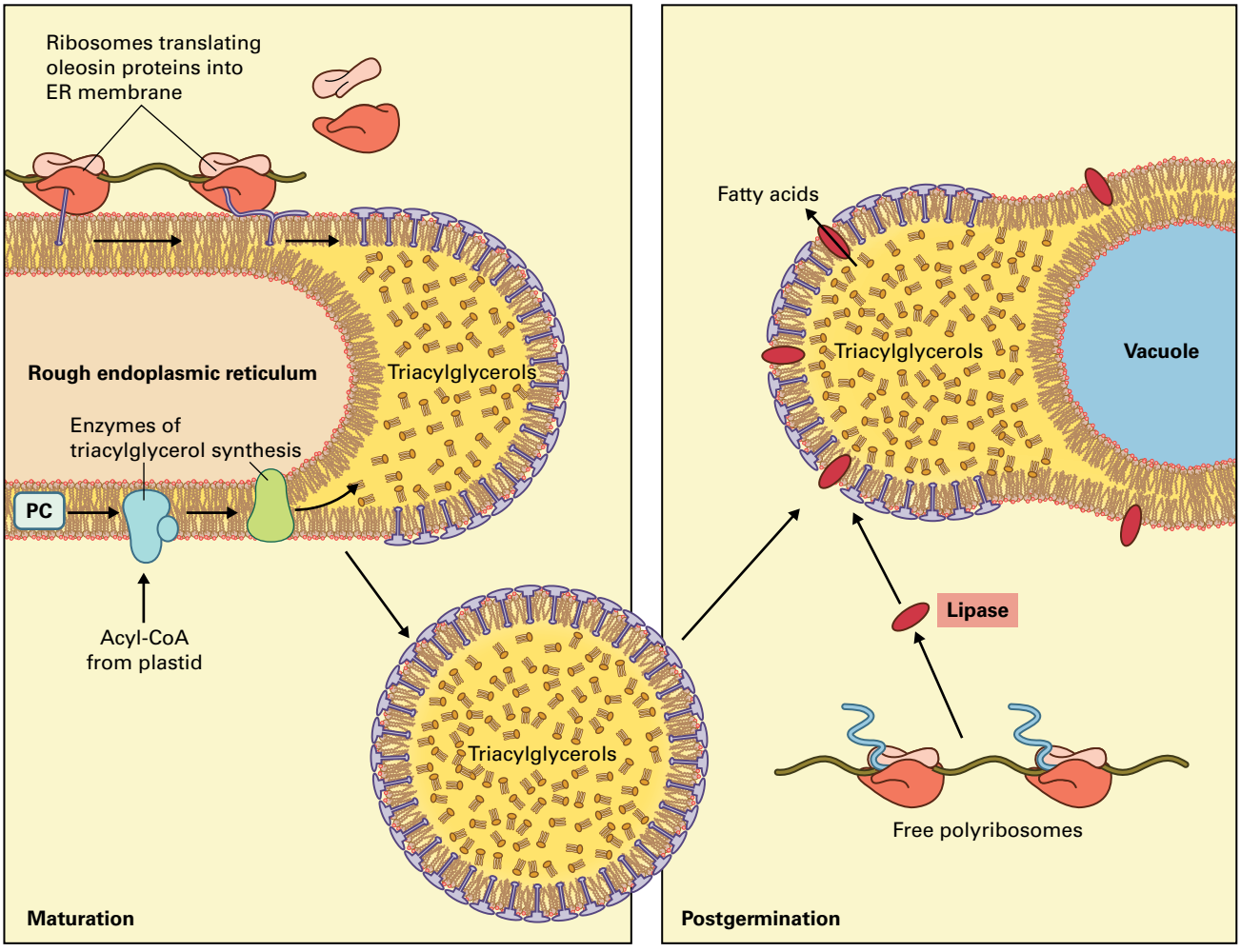


FIGURE 8.64 *Model of the synthesis and degradation of an oil body in an embryo during seed maturation and post germination. For clarity this model is not drawn to scale. The oil body diameter of 1–2 μM is actually 50–100 fold larger than an ER cross-section.*

phospholipids. Because many oilseeds contain high amounts of unusual fatty acids that are largely excluded from the membrane phospholipids, it follows DAGs must occupy a critical branch point in oilseed lipid metabolism.

8.10.3 Membrane and storage lipids often have distinct compositions

Unusual fatty acids (see Table 8.2 and Fig. 8.25) often constitute 90% or more of all fatty acids produced in the seed, but in almost all cases these fatty acids are present almost exclusively in triacylglycerols and are excluded from membrane lipids. This probably occurs because fatty acids with unusual structures could create undesirable physical or chemical properties in the membrane or perturb membrane fluidity. Therefore, plants that produce such unusual fatty acids must also have mechanisms to prevent accumulation of these compounds in membranes. Furthermore, hydroxy-fatty acids, epoxy-fatty acids, and some other unusual fatty acids are first synthesized on phosphatidylcholine, a major membrane lipid. What mechanisms ensure first the removal of these modified fatty acids from phospholipids and then their targeting to storage oils? At present, no clear or complete answer is available. However, developing seeds from species that produce unusual fatty acids might rely on phospholipases that can remove the fatty acids from polar lipids. Furthermore, these seeds usually have a suite of specialized acyltransferases and other enzymes specific for metabolizing unusual fatty acids.

Another possible method for keeping membrane and storage fatty acids distinct is subcellular compartmentation. Although membrane and storage lipid synthesis proceed by similar pathways and share common chemical intermediates (phosphatidate, DAG, and phosphatidylcholine; see Fig. 8.62), the specialized enzymes involved in storage oil biosynthesis may reside in domains of the ER distinct from enzymes that process the "common" fatty acids for incorporation into membranes.

8.10.4 Regulation of seed oil biosynthesis

Most plant vegetative tissues have a lipid content of 5% or less by dry weight, and, of this, less than 1% is in the form of triacylglycerol. In contrast, the total lipid content of many oilseeds

is over 50% of the dry weight, and more than 95% of this lipid is in the form of triacylglycerol. The conversion of sugars into triacylglycerol in developing oilseeds is thus a classic example for the developmental and tissue-specific regulation of metabolism.

Regulation of oil synthesis in seeds occurs by multiple mechanisms. One level of control involves allosteric enzyme regulation, for example at the enzyme acetyl-CoA carboxylase. In addition, analysis of mRNAs expressed in developing seeds indicates enzymes of fatty acid biosynthesis and oil body assembly are, for the most part, coordinately regulated at the level of mRNA expression. In addition, a number of enzymes of lipid metabolism belong to gene families and sometimes there is a specific member of the family that is only expressed in seeds. The transcription factor WRINKLED 1 (WRI1) plays a major role in controlling expression of genes involved in seed oil biosynthesis. Oil content in the *wri1* mutant of *Arabidopsis* is 80% reduced, whereas overexpression of the *WRI1* gene increases seed oil content. Some direct targets of this transcription factor are genes encoding enzymes of fatty acid biosynthesis and genes of glycolysis that provide precursors for fatty acid synthesis. Other transcription factors including LEAFY COTYLEDON1 (LEC1) act upstream of *WRI1* and are involved in the complex network of transcriptional regulation of embryo development in seeds. Metabolite (sugar)-sensing mechanisms also provide input for integration of primary metabolism in seeds, but are not yet understood at the mechanistic level. Identifying the factors and understanding the mechanisms that control oil biosynthesis in plants is providing one basis for successful engineering of oil content in seeds and perhaps in other plant tissues.

8.10.5 In some seeds, Rubisco acts without the Calvin–Benson cycle to provide a higher efficiency of carbohydrate to oil conversion

During seed development, photosynthate from the mother plant is imported in the form of sugars, and the seed converts these into precursors of fatty acid biosynthesis. In many seeds, the traditional glycolysis pathway plays a central role in this conversion (see Chapter 13). Pyruvate produced by glycolysis is then converted to acetyl-CoA by the plastid pyruvate dehydrogenase complex. In this reaction, the three carbons of pyruvate are converted to two carbons of acetyl-CoA with the loss of one carbon as CO_2. Thus, the conversion of carbohydrate to oil results in the loss of one third of the carbon.

Many seeds, however, are green and express substantial levels of Rubisco. It has been discovered that Rubisco and enzymes of the pentose phosphate pathway can act together to increase the efficiency of carbohydrate to oil biosynthesis. In this alternative pathway, the glyceraldehyde-3-phosphate dehydrogenase (GAP-DH) and phosphoglycerate kinase (PGK) reactions that normally produce phosphoglycerate (PGA) during glycolysis are bypassed, and PGA is instead produced by Rubisco. The net result is 20% more acetyl-CoA available for oil synthesis and 40% less loss of carbon as CO_2. However, the GAP-DH and PGK reactions normally provide reductant and ATP cofactors. To make up for the loss of these cofactors, in the Rubisco bypass pathway the seeds are green and produce cofactors through the light reactions of the photosystems.

8.10.6 Mobilization of storage lipids provides carbon and chemical energy for germination and pollination

Triacylglycerols function as an efficient source of carbon and energy for germination of seeds and pollen because lipids are a far more compact form of storage than is carbohydrate or protein (see Fig. 8.3). Relatively few species accumulate significant quantities of storage lipids in roots, tubers, or other storage organs where compact size is not important. Because of their hydrophobicity and insolubility in water, triacylglycerols are segregated into lipid droplets, which do not raise the osmolarity of the cytosol. Furthermore, unlike polysaccharides, triacylglycerols do not contain extra weight as water of solvation. The relative chemical inertness of triacylglycerols allows their intracellular storage in large quantity without risking undesired chemical reactions with other cellular constituents.

The same properties that make triacylglycerols good storage compounds present problems in their utilization. Because of their insolubility in water, triacylglycerols must be hydrolyzed to fatty acids before they are available for metabolism. The relative stability of the C–C bonds in the alkyl moiety of a fatty acid is overcome by activation of the fatty acid carboxyl group at C-1 by attachment to CoASH, followed by oxidative attack at the C-3 position. This latter carbon atom is also called the β-carbon in common nomenclature, from which the oxidation of fatty acids gets its common name: β-oxidation. The oxidation of long-chain fatty acids to acetyl-CoA by a four-step cycle is a central energy- and carbon precursor-yielding pathway during the germination of seeds and during the germination and growth of pollen tubes during fertilization. The acetyl-CoA formed during β-oxidation may be converted, via the glyoxylate cycle and gluconeogenesis, to carbohydrate (Fig. 8.65; see also Chapter 14). Mutants that are blocked in triacylglycerol hydrolysis, β-oxidation, or some steps of the glyoxylate cycle require an additional supply of carbohydrate to successfully establish seedlings after germination.

In addition to its special role in triacylglycerol mobilization after seed and pollen germination, the β-oxidation pathway also occurs in essentially all other plant cells. In most cells there is a continual slow turnover of membrane lipids and carbon from their fatty acids is recycled via β-oxidation. In addition, the synthesis of the hormone jasmonic acid requires three cycles of β-oxidation (see Fig. 8.50). Although the biological role of fatty acid oxidation differs in different

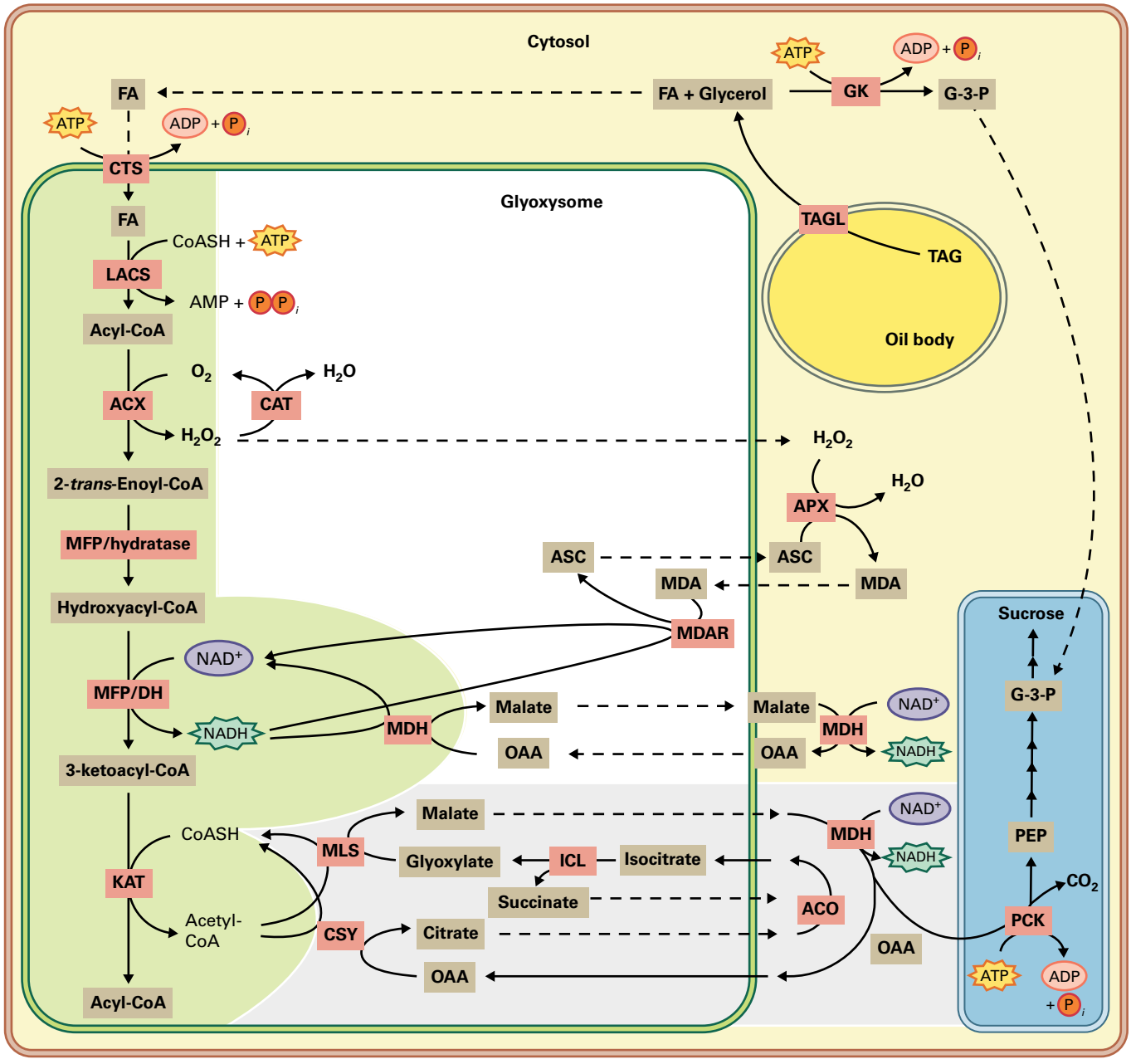


FIGURE 8.65 *Mobilization of storage lipids after seed germination and their conversion to carbohydrate involves multiple pathways and subcellular compartments (see also Fig. 14.41). The triacylglycerol (TAG) lipase TAGL hydrolyzes TAG stored in oil bodies to produce fatty acids (FAs) and glycerol. Glycerol kinase (GK) produces glycerol 3-phosphate (G-3-P), which can enter gluconeogenesis (blue shading). FAs are imported into the glyoxysome via the COMATOSE (CTS) ATP-binding cassette (ABC) transporter. FAs are activated by a long-chain acyl-CoA synthetase (LACS) and enter the core reactions of β-oxidation (light green background): acyl-CoA oxidase (ACX), multifunctional protein hydratase (MFP/Hydratase), multifunctional protein dehydrogenase (MFP/DH), and 3-ketoacyl-CoA thiolase (KAT). Hydrogen peroxide (H_2O_2) is broken down in the glyoxysome matrix by catalase (CAT) or is broken down as it passes through the membrane by an ascorbate peroxidase (APX)/monodehydroascorbate reductase (MDAR) electron transfer system. Glyoxysomal malate dehydrogenase (MDH) operates in the reverse direction to convert oxaloacetate (OAA) to malate and is dedicated to regenerating NAD+ from NADH for the continued operation of β-oxidation. Citrate synthase (CSY) is also essential for β-oxidation and plays a role in the glyoxylate cycle. Malate synthase (MLS) and isocitrate lyase (ICL) are unique to the glyoxylate cycle and localize to the glyoxysome. The aconitase (ACO) and MDH reactions of the glyoxylate cycle are cytosolic; MDH operates in the forward direction to produce OAA and NADH. Phosphoenolpyruvate (PEP) carboxykinase (PCK) is the major controlling step of gluconeogenesis (blue background), producing PEP from OAA. The contribution of the mitochondrial tricarboxylic acid (TCA) cycle to the production of OAA is not included. MDA, monodehydroascorbate; ASC, ascorbate.*

tissues and from organism to organism, the central enzyme reactions are essentially the same. Details of the enzymatic mechanisms can be found in biochemistry textbooks that focus primarily on animal metabolism. Therefore, the discussion below highlights those features of the pathway that differ between plants and animals.

8.10.7 β-Oxidation takes place in peroxisomes

The major site of fatty acid oxidation in animal cells is the mitochondrial matrix. In contrast, fatty acid oxidation in plants occurs primarily in the peroxisomes. In germinating seeds peroxisomes are often referred to as glyoxysomes, because they are also the site of several reactions of the glyoxylate cycle (Fig. 8.65).

In animals the glyoxylate cycle does not exist and most acetyl-CoA produced by the β-oxidation pathway enters the TCA cycle and is completely oxidized to CO_2 with production of additional metabolic energy. However, in plants the biological role of β-oxidation in peroxisomes is also to provide biosynthetic precursors from stored lipids. During germination, a large proportion of the triacylglycerols stored in seeds is converted into glucose, sucrose and a variety of essential metabolites. In many plants, sucrose produced from fatty acids is translocated from the seed tissues to the emerging shoots and roots of the seedlings. This process begins when fatty acids released from triacylglycerols are activated to form their CoA derivatives and are oxidized in peroxisomes. The acetyl-CoA produced is converted by way of the glyoxylate cycle to C_4 precursors for gluconeogenesis (Fig. 8.65; see also Chapter 14, Fig. 14.41). Peroxisomes contain high concentrations of catalase, which converts the H_2O_2 produced by β-oxidation to H_2O and O_2.

The β-oxidation enzymes of peroxisomes form a protein complex. As in the oxidation of fatty acids in mitochondria, the intermediates are CoA derivatives, and the process consists of four steps (Fig. 8.66):

- dehydrogenation to a $^{\Delta 2}$-*trans* unsaturated molecule
- addition of water to the resulting double bond
- oxidation of the β-hydroxyacyl-CoA to a ketone
- thiolytic cleavage by CoASH.

The difference between the peroxisomal and mitochondrial pathways lies in the first step. In peroxisomes, the flavoprotein dehydrogenase that introduces the double bond passes electrons directly to O_2, producing H_2O_2. This strong and potentially damaging oxidant is immediately cleaved by catalase to H_2O and ½O_2 (Fig. 8.66). In contrast, in mitochondria, the electrons removed in the first oxidation step pass through the respiratory chain to O_2, leaving H_2O as the product, a process accompanied by ATP synthesis. In peroxisomes, the energy released in the first oxidative step of fatty acid breakdown is dissipated as heat.

8.11 Genetic engineering of lipids

8.11.1 Improvement of oil quality is a major objective of plant breeders

Rapeseed and many other members of the Brassicaceae, as well as some other species, contain large proportions of very-long-chain (20- to 24-carbon) monounsaturated fatty acids. These are synthesized by chain elongation of 18:1$^{\Delta 9}$, as discussed earlier. Erucic acid (22:1$^{\Delta 13}$), which accounts for about 50% of the fatty acids in rapeseed oil, can cause heart disease when included in the diet of laboratory animals. Although high erucic acid content made rapeseed oil useful for certain industrial applications, it prevented the widespread use of rapeseed as an edible oil crop. In the 1950s, an extensive search was made for varieties of *B. napus* with low erucic acid and glucosinolate content, another antinutritional component of oil from *Brassica* species (Fig. 8.67; see also Chapter 16). During a period of about 20 years, several natural isolates containing reduced amounts of erucic acid were identified, and the two loci responsible for the phenotype were introgressed into cultivars of *B. napus* by many rounds of back-crossing. To distinguish the cultivars that produced oil with low erucic acid (LEAR) from those with high erucic acid (HEAR) content, the LEAR cultivars are now called canola (Fig. 8.67). Expression of a 3-ketoacyl-CoA synthase in transgenic canola plants restored the high erucic acid trait. Thus, the two genes introgressed into *B. napus* to produce canola are now known to encode naturally occurring mutations in two genes for 3-ketoacyl-CoA synthase.

8.11.2 Edible oils can be improved by metabolic engineering

Approximately 20% of the calories consumed by humans in developed countries are derived from plant oils. The fatty acid composition of dietary oils, particularly the saturated fatty acid content, is believed to influence the etiology of major diseases such as atherosclerosis and cancer. Many attempts have been made to alter the fatty acid compositions of food oils and reduce the proportions of 16:0, 18:0, 18:2$^{\Delta 9,12}$, and 18:3$^{\Delta 9,12,15}$ in favor of 18:1$^{\Delta 9}$. The move to develop monounsaturated oils is based on epidemiological data and laboratory experiments that suggest these oils reduce atherosclerosis (and associated heart attacks and strokes) by increasing the ratio of high-density lipoproteins to low-density lipoproteins in the blood. Furthermore, oils low in 18:2$^{\Delta 9,12}$ and 18:3$^{\Delta 9,12,15}$ are much more stable, particular in high-temperature food frying.

The targets for reducing polyunsaturates are the 18:1$^{\Delta 9}$- and 18:2$^{\Delta 9,12}$ desaturases of the ER, which, in *Arabidopsis,* are encoded by the *FAD2* and *FAD3* genes. Isolation of these genes by **gene-tagging** (*FAD2*) and **map-based**

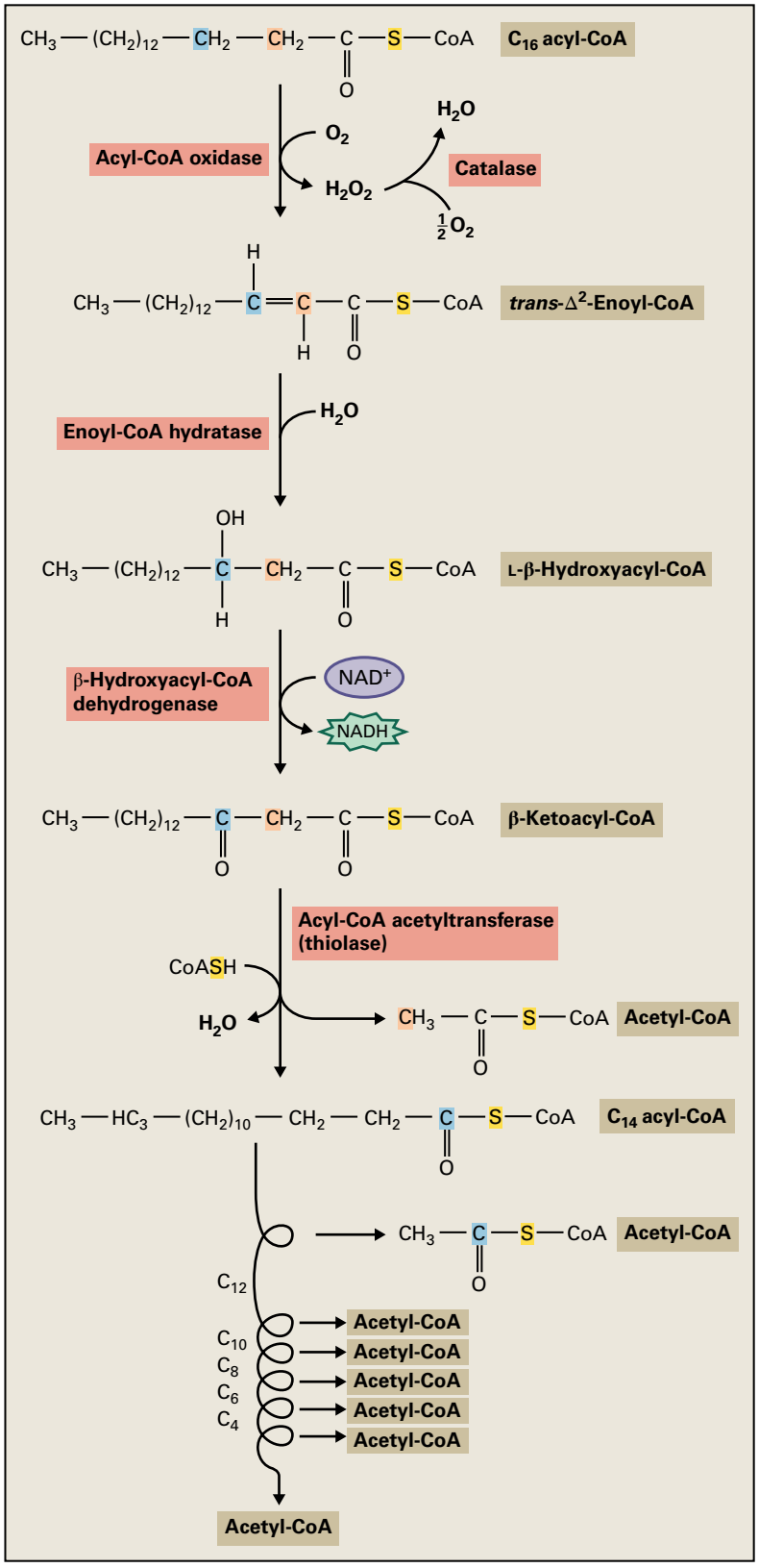


FIGURE 8.66 *β-Oxidation pathway in peroxisomes. In each pass through the sequence, one acetyl residue is removed in the form of acetyl-CoA from the carboxyl end of an acyl-CoA. Seven passes through the cycle are required to oxidize a C_{16} fatty acid to eight molecules of acetyl-CoA.*

cloning (*FAD3*) in *Arabidopsis* led quickly to identification of analogous genes in soybean, canola, and other crops, enabling genetic engineering of edible oils with improved nutritional properties. One success involves cosuppression of the oleoyl desaturase in soybean, which increased oleic acid levels from less than 10% to more than 85% of the total fatty acids; at the same time, saturated fatty acids were reduced from more than 15% to less than 5%. Oil from

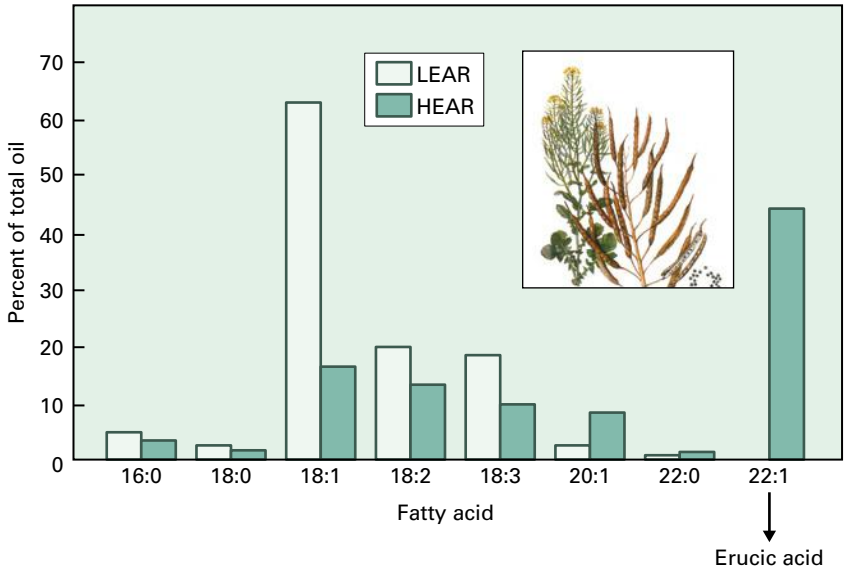


FIGURE 8.67 *Fatty acid composition of seed oil from high and low-erucic acid rapeseed (HEAR and LEAR, respectively) varieties. Additional improvements by plant breeding have reduced the 18:3 content of the most recent cultivars to a small percentage of the total fatty acids, with corresponding increases in the 18:1 content. Rapeseed is the major oilseed crop of Europe, Canada, and many countries with short growing seasons. After soybean and oil palm, it is the world's third largest source of vegetable oils. Varieties that have been bred to contain low amounts of erucic acid are referred to as canola. Because of its high oil content (45% of seed weight) and relative ease of transformation, canola has become the first crop genetically engineered to produce new oils.*

these soybean varieties is similar in composition to olive oil and has both improved health benefits due to the reduction in omega-6 fatty acids and improved oxidative stability. Mutation breeding programs have also led to the production of high-oleate lines of canola, sunflower (*Helianthus annuus*) and other oilseed crops.

The 20- and 22-carbon ω-3 fatty acids in fish oils, particularly eicosapentaenoic acid and docosahexaenoic acid, have health benefits that include likely reductions in heart disease, stroke, and other metabolic syndromes. Producing these fatty acids in seed oils is an attractive goal in oilseed engineering and has been achieved by the transgenic expression of a condensing enzyme (3-ketoacyl-CoA synthetase) to catalyze fatty acid elongation and up to three fatty acid desaturases (Δ6-, Δ4-, and ω-3 desaturase). This type of multienzyme pathway engineering is complex, but the availability of suitable genes from many animals and microbes allowed the testing of several different enzyme combinations. Some transgenic lines produce >20% of the target ω-3 polyunsaturated fatty acids and represent examples where plant genetic engineering may contribute substantially to improving health benefits of some foods.

8.11.3 Molecular genetic approaches have been used to increase oil yields

In addition to efforts to modify the types of fatty acids produced in plant seeds, there is considerable interest in increasing the yield of oil obtainable from oilseed crops. But a major unanswered question in plant lipid metabolism remains: What determines the quantity of oil stored in a seed? In addition to its interest to basic researchers, this question is of considerable practical importance if chemicals or fuels derived from oilseeds are to compete economically with petrochemical alternatives.

More than 30 reactions are required to convert acetyl-CoA to triacylglycerol, so many genes could control the yield of the end-product storage oil. Several approaches have resulted in increased oil content in seeds. For example, expression of diacylglycerol acyltransferase in soybean or rapeseed increased seed oil content and overexpression of the *WRINKLED1 (WRI1)* transcription factors also led to a higher level of oil in seeds.

In addition to their major use as food, plant oils are also considered as a source of fuel such as "biodiesel." Methyl esters of plant fatty acids have similar performance characteristics as petroleum-derived diesel fuel but produce less greenhouse gas and lack some pollutants produced by burning diesel fuel. In Europe approximately 12 billion liters of biodiesel were produced in 2014. Nevertheless, due to the large quantities of transportation fuel needed, this biodiesel accounted for less than 5% of the total fuel market. Greater production might be possible from perennial tropical species such as oil palm (*Elaeis* sp.) that produce as much as 4,000 liters of oil per hectare per year with low inputs of agrochemicals. If it becomes possible to genetically engineer oil palm, or expand its range, it may be viable to produce fuels and chemicals from a renewable source at a cost that is competitive with petroleum.

8.11.4 Fatty acids have numerous industrial applications

Soybean, palm, rapeseed, and sunflower oils account for approximately 80% of the world production of vegetable oil, with approximately 140 million metric tons of oil consumed in 2011. Most plant-derived oil is currently used for food, and over 90% of the fatty acids found in food oils are restricted to four structures: 16:0, 18:1, 18:2, and 18:3. However, nonfood industrial uses of plant lipids include the manufacture of soaps and detergents, paints, varnishes, lubricants, adhesives, and plastics (Table 8.6). These nonfood uses often depend on the special physical and chemical properties of "unusual" fatty acid structures that are not found in oils consumed for food. The largest nonfood use, by volume, is lauric acid (C_{12}) from coconut and palm kernel for the production of detergents and soaps. The castor plant produces ricinoleic acid (12-hydroxyoctadecenoic acid), which is used for the production of a wide variety of compounds. For example, ricinoleic acid can be pyrolyzed to sebacic acid, which is used to produce certain types of nylon. The lithium salts of sebacic acid are also used as high-temperature greases for jet engines. Erucic acid from rapeseed is used to make erucamide, a slip agent in the plastics industry that makes plastic films and other products easier to handle.

At present, genetic engineering of oilseeds is concerned with altering the quality of oil produced in temperate crops. An immediate goal is to expand the range of fatty acids available from crop species so that the uses of plant fatty acids can be expanded.

8.11.5 High-lauric-content rapeseed: a case study in successful oilseed engineering

Many of the unusual fatty acids found in nature have important industrial uses; however, the plants producing them are often poorly suited for high-production agriculture. As an alternative, the isolation of key genes directing the synthesis of a particular fatty acid can provide the means to genetically engineer agronomically suitable oilseed crops to produce the desired oil more easily and cheaply. The acyl-ACP thioesterases were the first enzymes of lipid biosynthesis for which genes were engineered and introduced into transgenic plants to produce a commercial product. A major ingredient of soaps, shampoos, detergents, and related products are the surfactants derived from lauric (12:0) and other medium-chain fatty acids that are obtained from coconut or palm kernel oils grown in the tropics. Worldwide, several billion dollars worth of such oils are used for production of surfactants. In part because of periodic price instability in these raw material supplies, a long-term goal of the surfactant industry has been to establish a temperate crop that could produce medium-chain fatty acids. Such a crop could provide alternative supplies and thereby lower or stabilize prices.

The advent of plant gene transfer techniques raised the question of whether temperate oilseed crops could be engineered to produce medium-chain fatty acids and other novel fatty acid compositions with the use of foreign genes. For example, it was unclear whether addition of new, unusual fatty acids might disrupt lipid metabolism, or some other process, in oilseed cells. More specifically, would a new fatty acid such as lauric acid be correctly targeted to triacylglycerol and excluded from membranes?

Research led first to biochemical demonstration of the existence of medium-chain acyl-ACP thioesterases and then to the cloning of a 12:0-ACP specific thioesterase from the California bay tree *(U. californica)*. Introduction of a single gene encoding the 12:0-ACP thioesterase into transgenic plants dramatically altered the chain length of fatty acids stored in the seed oils. In 1995, the first commercial production of a genetically engineered oil was obtained when about 1 million pounds of oil was extracted from rapeseed plants engineered to produce 40% to 50% lauric acid (Fig. 8.68).

TABLE 8.6 *Some nonfood uses of plant fatty acids. In all cases the genes responsible for synthesis of the specialty fatty acid composition in these oils have been identified.*

Lipid type	Example	Major sources	Major uses
Medium-chain	Lauric acid (12:0)	Coconut, palm kernel	Soaps, detergents, surfactants
Long-chain	Erucic acid (22:1)	Rapeseed	Lubricants, slip agents
Epoxy	Vernolic acid	Epoxidized soybean oil, *Vernonia*	Plasticizers, coatings, paints
Hydroxy	Ricinoleic acid	Castor bean	Coatings, lubricants, polymers
Trienoic	Linolenic acid (18:3)	Flax	Paints, varnishes, coatings
Wax esters	Jojoba oil	Jojoba	Lubricants, cosmetics

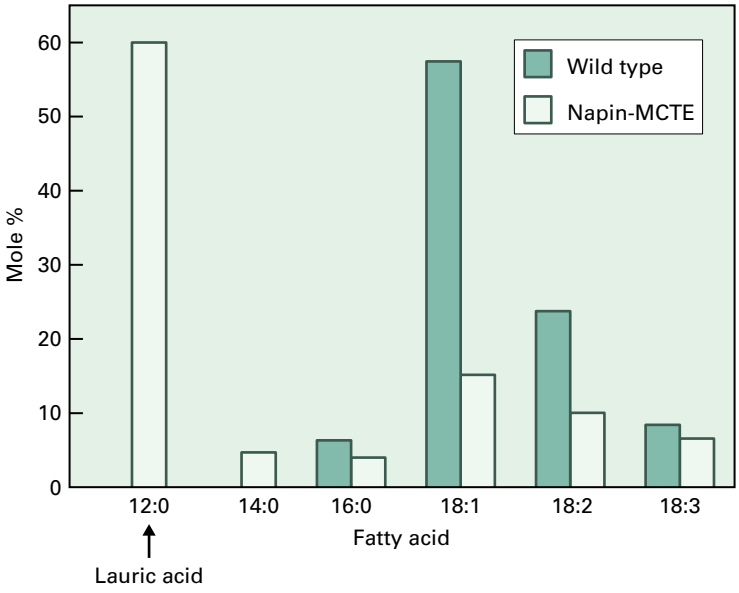


FIGURE 8.68 *Expression of a cDNA from California bay that encodes a medium-chain acyl-ACP thioesterase (MCTE) under control of the seed-specific napin promoter (Napin-MCTE) diverts carbon into medium-chain fatty acids to produce an oil with high laurate content.*

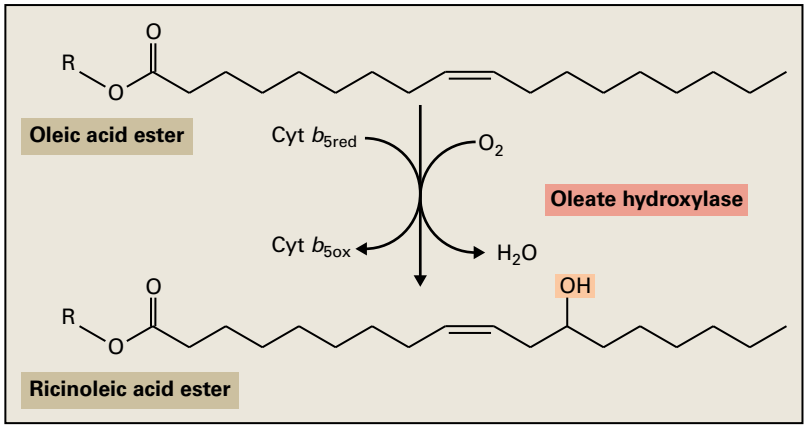


FIGURE 8.69 *Reaction catalyzed by oleate hydroxylase. Analogously to the FAD2 oleate desaturase that produces linolenate, the oleate substrate is esterified to phosphatidylcholine during the reaction.*

8.11.6 Expression of a glycerolipid hydroxylase from castor bean can drive synthesis of ricinoleic acid in transgenic plants

Ricinoleic acid (12-OH-18:1$^{\Delta 9}$) produced by castor bean is an extremely versatile natural product with industrial applications that include the synthesis of nylon-11, lubricants, hydraulic fluids, plastics, cosmetics, and other materials. However, castor bean contains ricin, an extremely toxic lectin (see Chapter 10, Box 10.1), as well as other poisons and allergens. In addition, agronomic problems result in poorer yields than other crops. As a result of these and other factors, castor bean is a minor crop grown mainly in nonindustrialized countries.

The successful cloning of a gene that encodes the hydroxylase responsible for 12- OH-18:1$^{\Delta 9}$ synthesis from 18:1$^{\Delta 9}$ relied on a detailed understanding of the biochemistry involved. For some time, the conversion of 18:1$^{\Delta 9}$ to 12-OH-18:1$^{\Delta 9}$ was thought to involve a single enzyme inserting a hydroxyl group at the same position as the double bond introduced by FAD2 desaturase (Fig. 8.69). Consideration of the probable reaction cycle of the desaturases suggested that 12-OH-18:1$^{\Delta 9}$ might be produced by a stalled desaturase. Partial sequencing of randomly chosen cDNAs from a library derived from developing castor bean endosperm identified a relatively abundant cDNA that encodes a protein with homology to the glycerolipid desaturases of other oilseeds. Expression of the castor bean cDNA in transgenic *Arabidopsis* and other plants led to the synthesis of 12-OH-18:1$^{\Delta 9}$ in seed tissues.

Unfortunately, when a transgene encoding a fatty acid modification enzyme is expressed in a heterologous host, accumulation of derivatized fatty acids is far less than in the species from which the gene was cloned. While castor oil contains >90% ricinoleate, transgenic *Arabidopsis* expressing the castor hydroxylase contain a maximum of only 17% hydroxy fatty acids in the seed oil. Understanding and overcoming the factors limiting accumulation of novel fatty acids is currently the major challenge in oilseed engineering. It is likely that accumulation of ricinoleic acid in castor bean seeds required

not only the evolution of the hydroxylase enzyme from an ancestral FAD2 desaturase (Section 8.6.2), but also the coevolution of one or more of the enzymes of lipid synthesis to efficiently incorporate ricinoleic acid into triacylglycerol. In support of this hypothesis, it was shown that coexpression of a castor isozyme of acyl-CoA:diacylglycerol acyltransferase with the hydroxylase increased the hydroxy fatty acid content of *Arabidopsis* seed oil from 17% to nearly 30%.

Summary

Lipids have diverse and essential roles in plants. As the hydrophobic barrier of membranes, they are essential for integrity of cells and organelles. Surface lipids protect plants from desiccation and from pathogen attack. In addition, they are a major form of chemical energy storage in seeds and are now recognized as a key component of some signal transduction pathways. Most lipids, but not all, contain fatty acids esterified to glycerol, and consideration of this area of metabolism involves, first, the synthesis of the fatty acid and, second, the assembly of a range of glycerolipid structures after esterification of two or three fatty acids to a glycerol backbone.

Fatty acid biosynthesis in plants is carried out in the plastid and begins with the carboxylation of acetyl-CoA by acetyl-CoA carboxylase to produce malonyl-CoA. This is the first committed step of the pathway and is a major site for biochemical regulation of fatty acid production. Acetyl-CoA and malonyl-CoA are subsequently converted into fatty acids by a series of reactions that add two carbons at a time to a growing chain. Acyl carrier protein is a 9-kDa cofactor protein that transports the intermediates of fatty acid synthesis through the pathway. Three condensing enzymes with different chain length specificity are required to assemble the 18 carbon fatty acids that are the major product of plastid fatty acid synthesis.

The first double bond is introduced by stearoyl-ACP desaturase, a soluble plastid enzyme unlike all subsequent fatty acyl desaturases that are membrane proteins localized in the ER or the plastid. Fatty acid biosynthesis can be terminated by hydrolysis of the thioester bond of acyl-ACP or by transfer of the acyl group to a glycerolipid. Free fatty acids released by the acyl-ACP thioesterases are exported from the plastid and converted to acyl-CoA at the plastid envelope.

There are two distinct pathways for the synthesis of membrane glycerolipids. The prokaryotic pathway, located primarily at the chloroplast inner envelope, uses 18:1-ACP and 16:0-ACP for the sequential acylation of glycerol 3-phosphate and synthesis of glycerolipid components of the chloroplast membranes. The eukaryotic pathway involves (a) export of 16:0 and 18:1 fatty acids from the chloroplast to the ER as acyl-CoAs and (b) their incorporation into phosphatidylcholine and other phospholipids that are the principal structural lipids of all the membranes of the cell except the chloroplast. In addition, the DAG moiety of phosphatidylcholine can be returned to the chloroplast envelope and used as a second source of precursors for the synthesis of chloroplast lipids.

Membrane lipids serve as a hydrophobic barrier, delimiting the cell and dividing it into functional compartments. The membrane lipid composition also affects plant form as well as many cellular functions. For example, photosynthesis is impaired in plants lacking polyunsaturated membrane lipids, and lipid composition can affect chilling sensitivity and influence plant cell responses to freezing. In addition, membrane lipids function in signal transduction pathways and defensive processes.

Storage lipids play a distinctly different role from membrane lipids. Storage lipids are almost exclusively triacylglycerols and accumulate in discrete subcellular organelles called oil bodies. The mobilization and catabolism of triacylglycerols provides energy and carbon for seedling growth after germination. The catabolism of the fatty acids released from triacylglycerol occurs via β-oxidation in peroxisomes. Acetyl-CoA produced by β-oxidation is converted to sugars for seedling growth by the glyoxylate cycle.

Plants are capable of synthesizing unusual fatty acids, with more than 200 different fatty acids having been found in different species. Some of the enzymes that synthesize unusual fatty acids show close resemblance to common fatty acid enzymes, such as membrane-bound desaturases. These unusual fatty acids are found almost exclusively in seed oils, and it is thought that they may serve a defense function.

Although several key steps remain uncertain, plant biochemists have defined almost all the enzymatic reactions involved in the biosynthesis and degradation of the major lipid components of plant cells. Many of the remaining questions center on the regulation of lipid biosynthesis, the details of signaling, and the cellular organization and transport of lipids. Furthermore, of over 700 genes in *Arabidopsis* annotated as potentially involved in lipid metabolism, there remain at least 500 whose function has not been demonstrated experimentally.



9

Genome Structure and Organization

Christopher D. Town and Frank Wellmer

Introduction

The essence of every characteristic of a species, from its morphology to timing of senescence, resides in information stored in its DNA, its genome. Large-scale, relatively inexpensive DNA sequencing has yielded complete genome sequences for a large number of microorganisms and complete, or nearly complete, sequences for numerous higher eukaryotes, including many plant species. In this chapter, we present a DNA sequence-centric view of the plant genome, its organization, and the mechanisms by which the encoded genes are expressed and their expression regulated.

Most of an organism's genes reside on nuclear DNA; however, plastids and mitochondria also contain DNA, which encodes some of the gene products required for organelle function and reproduction (see Chapter 6). Several traits encoded by organellar genes are in commercial use in plant crops, such as cytoplasmic male sterility in sorghum (*Sorghum* sp.) and maize (*Zea mays*). Traits arising from organellar genes can be clearly recognized by their uniparental inheritance patterns, because in most species mitochondria and chloroplasts are inherited only through the maternal contribution to the seed.

In the 1950s, plant geneticists found that pieces of genetic material could move from place to place in the genome. These mobile genetic elements were subsequently found to be ubiquitous components of genomes. This raised the possibility that such mobile elements could be responsible for larger-scale genomic changes than the accumulation of single-point mutations, and that they could, in fact, facilitate evolutionary change. While genome sequencing has, in general, simply added greater detail and specificity to what we have learned previously from genetics, cytogenetics, and molecular biology, there have also been major advances in the fields of epigenetics and the regulation of gene expression by families of small RNA molecules.

9.1 Genome structure: a 21st-century perspective

The first complete plant genome sequence, that of *Arabidopsis thaliana*, was published in 2000. Until then, our view of the structure and content of plant genomes was based on a number of techniques that had evolved over the entire 20th century. While informative, these techniques lacked the resolution provided by DNA sequencing. Some of these 20th-century methodologies and results are described here, followed by a description of the various approaches used for whole genome sequencing and the wealth of information and insights that these methods have generated.

9.1.1 Microscopy at progressively higher resolution reveals increasing detail of chromosome structure

Chromosomes were first visualized at the turn of the 20th century, and they were recognized as the bearers of a cell's hereditary material. As more became known about DNA,

Biochemistry & Molecular Biology of Plants, Second Edition. Edited by Bob B. Buchanan, Wilhelm Gruissem, and Russell L. Jones.
© 2015 John Wiley & Sons, Ltd. Published 2015 by John Wiley & Sons, Ltd.
Companion website: www.wiley.com/go/buchanan/biochem

chromosomes of higher eukaryotes were found to contain many centimeters, even meters, of double-stranded DNA molecules in compact chromosomal structures that, when visualized in cells at the metaphase of mitosis, are only microns in length. Increasing microscopic resolution allowed visualization of different features of chromosomes at a level that can now, to some extent, be described in terms of DNA sequence (Fig. 9.1).

Visualization of mitotic metaphase chromosomes using light microscopy reveals their basic features: the centromeres (responsible for orderly segregation of sister chromatids at mitosis), the chromosome arms, and the telomeres (tips of the chromosomes) (Fig. 9.1). Chromosomes can be visualized in a less condensed state during the pachytene stage of meiosis; in fact, chromosomes at this stage are frequently used as the substrates for fluorescence in situ hybridization (FISH, Box 9.1) to determine the chromosomal localization of particular types of DNA sequence. At this level of resolution, the distinction between hetero- and euchromatin is more evident, as are structures known as heterochromatic knobs. At the limits of resolution of light microscopy, DNA fibers can be visualized and either subjected to FISH (fiber-FISH) or even digested by restriction enzymes to produce an optical map.

For the highest levels of resolution, whole chromosomes can be visualized by scanning electron microscopy, and they can be partially disassembled to reveal the nucleoprotein scaffold to which the DNA strands attach. Ultimately, chromosomes can be resolved to a "beads on a string" level, which reveals how histones are involved in the packing of DNA into chromatin (see Fig. 9.1). The most basic level

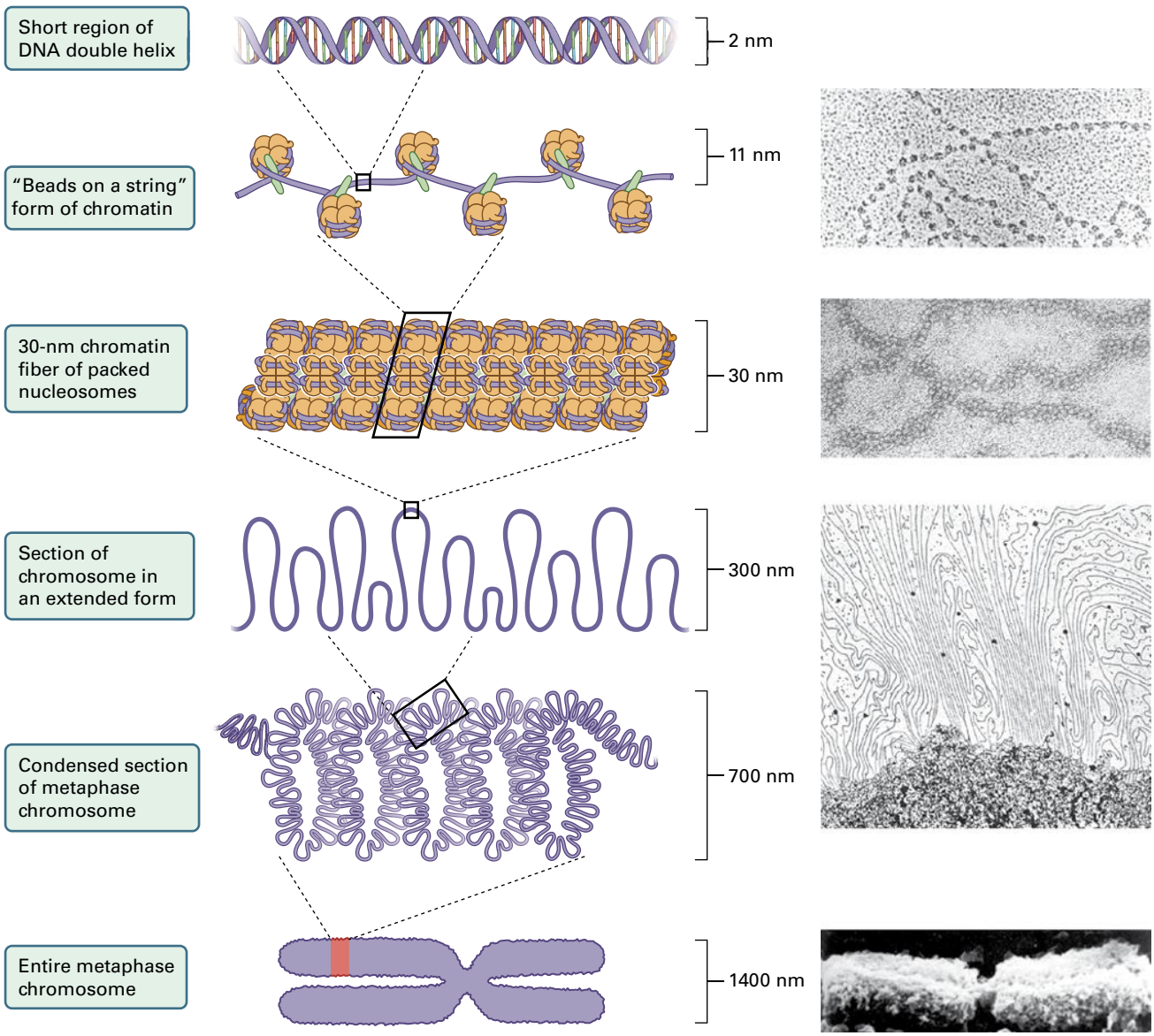
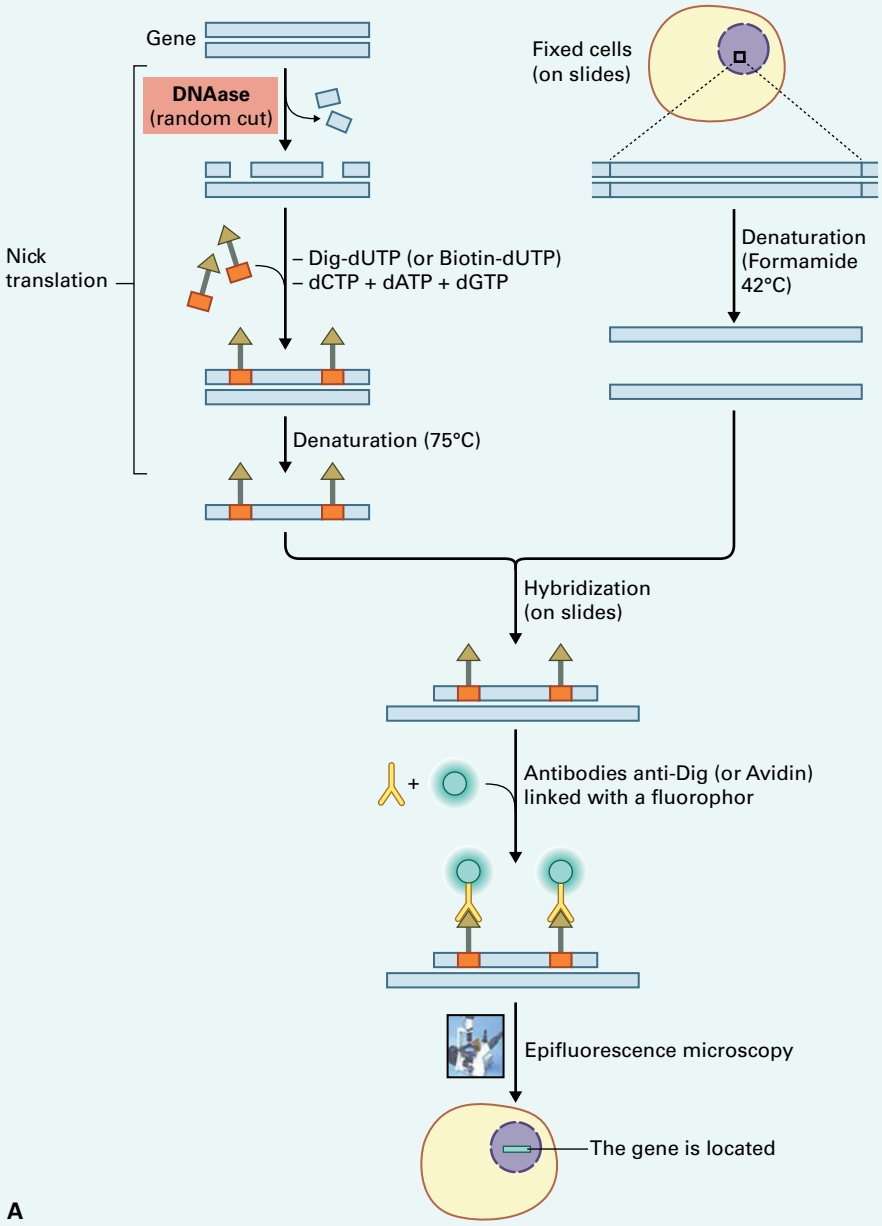


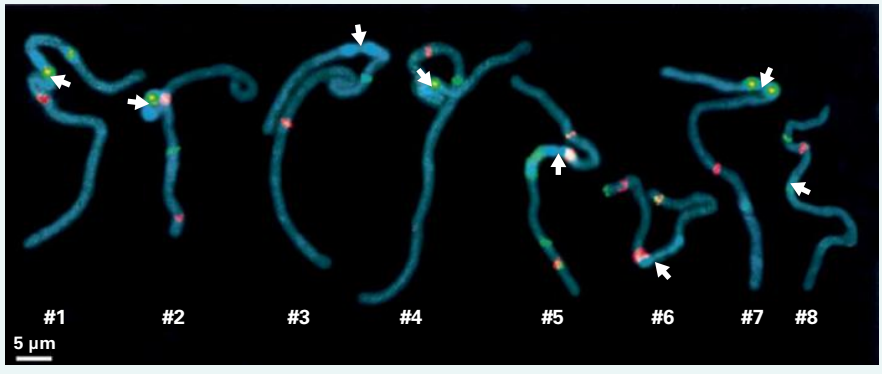
FIGURE 9.1 *Organization of DNA and proteins into chromatin at different levels of condensation. The cartoons on the left show DNA, DNA wrapped around nucleosomes, packed nucleosomes, extended loops of packed nucleosomes, DNA as it might be condensed into metaphase chromosomes, and a complete metaphase chromosome. Images at right are scanning electron micrographs at different levels of resolution that can be inferred from the scales on the cartoons.*

BOX 9.1

Fluorescence in situ hybridization is a technique used to localize DNA sequences on chromosomes



A



B

Fluorescence in situ hybridization (FISH) is a cytogenetic technique used to detect and localize specific DNA sequences on chromosomes. In FISH, DNA molecules representing a feature of a genome are labeled with a fluorescent dye, hybridized to chromosomes or DNA molecules immobilized on a glass slide, and then examined by fluorescence microscopy (A).

(A) Scheme of a FISH experiment designed to localize a gene to a particular chromosome. (B) Assignment of linkage group to chromosomes by FISH. For identification of chromosomes, pachytene preparations were probed with 5S rDNA (red) and *Mt*R1, a repetitive element found near centromeres (green). Centromeres are indicated by arrowheads.

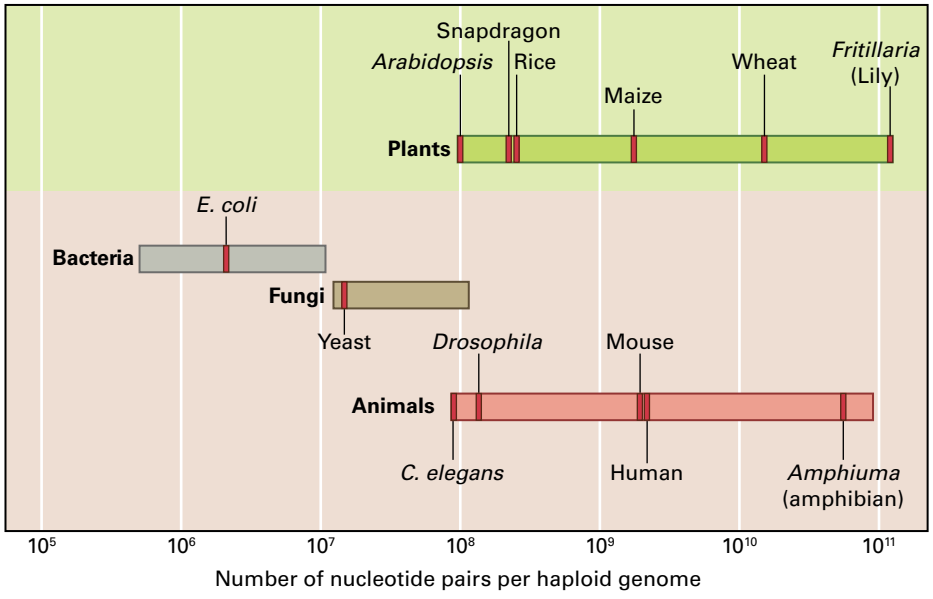


FIGURE 9.2 *C values (haploid genome size in base pairs) from various organisms. Most eukaryotes have haploid genome sizes between 10^7 and 10^{11} bp of DNA.*

of chromatin structure is the **nucleosome** array, called first-order condensation to distinguish it from subsequent higher-order condensation. A nucleosome consists of DNA wrapped two full turns (166 bp) around a globular octamer of histone proteins made up of two tetramers, each consisting of H2A, H2B, H3, and H4.

9.1.2 Genome size is highly variable among flowering plants

The size of the nuclear genome varies widely among organisms, with haploid DNA content (**C value**) ranging from 10^7 to 10^{11} base pairs (bp). The human genome is in the middle of this range, at 3×10^9 bp. Although it has been assumed that the apparent complexity of an organism correlates roughly with genome size—humans have larger genomes than most insects, and insects have larger genomes than fungi—this correlation is not universal. For example, some amphibians have genomes almost 50 times larger than that of humans, and cartilaginous fish generally have larger genomes than bony fish. Plant genomes are represented throughout the size range, with one of the smallest known plant genomes belonging to *Arabidopsis thaliana*, and one of the largest to a member of the lily family, *Fritillaria assyriaca* (Fig. 9.2).

In the mid-20th century, the term **C-value paradox** was coined to describe the lack of a direct relationship between genome size and organismal complexity. With the sequence of many genomes in hand, the sequence features of different classes of DNA that contribute to the paradox are known, although their significance and contribution to organismal complexity are still not well understood. In plants, at least, some of the size variation can be attributed to one or more rounds of genome duplication, and often much more to the expansion of families of (retro)transposons, as well as to present-day polyploidy (see Section 9.3).

DNA sequencing has provided more accurate estimates for the sizes of plant genomes; however, for the many plant and animal genomes for which DNA sequence data are not available, estimation of DNA content in isolated nuclei stained with a fluorescent dye has become accepted as a reliable and quite precise measure of genome size.

9.2 Genome organization

9.2.1 Nuclear genomes contain unique, single-copy sequences as well as repetitive DNA

Before the advent of DNA sequencing, one method for studying a genome's sequence composition was Cot analysis (see Box 9.2). By this method, a genome could be divided into

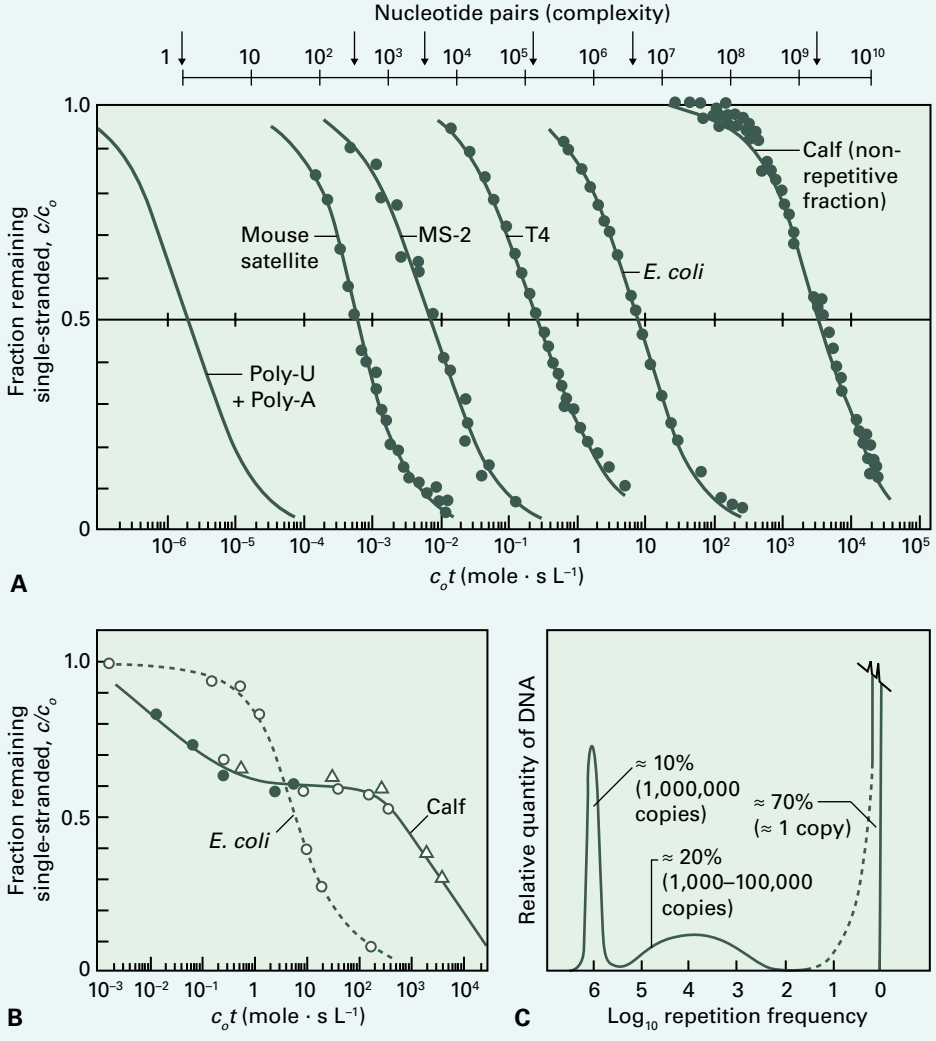
BOX 9.2

Cot analysis can be used to quantify repetitive DNA in a sample

Cot analysis is a technique used to measure the amount of repetitive DNA in a sample. It is based on the principles of DNA reassociation kinetics and involves denaturing a DNA sample and then allowing it to reanneal and following the fraction of DNA remaining single stranded over time (which can be days for a complex DNA sample).

In a typical plot, the fraction of single-stranded DNA is plotted against the product of the DNA concentration at zero time (c_o) and the measurement time (t), hence the term "Cot." This is a second-order reaction in which single-stranded molecules must find their complement to renature. As genome size increases, the number of copies of each sequence per gram of DNA decreases, and hence renaturation takes longer.

(A) Reassociation kinetics of a series of homogeneous DNA samples of increasing complexity (length of unique sequence). For any single DNA species, reassociation is a second-order reaction as the separated single-stranded molecules seek out and reassociate with their complements. As the length of the molecular species increases, its molar concentration (for a fixed mass of DNA) decreases and hence reassociation takes longer. (B) Comparison of reassociation kinetics of *E. coli* and calf thymus DNA. (C) The complex reassociation curve for calf thymus DNA can be reconstructed as the sum of three simple second-order components, with different $Cot_{1/2}$ values present in different amounts as shown here.



three components: highly repetitive, intermediately repetitive, and single-copy DNA. Even with the large amounts of DNA sequence now available, these broad categories still provide a useful framework for thinking about plant genome structure, although the boundaries between each of these categories are fluid.

By definition, single-copy DNA is present in only one copy per haploid genome; in practice, this is now considered low-copy DNA. This class of DNA sequences contains almost all of the gene-coding sequences in a genome. However, in most plant genomes more than half of the genes belong to gene families of various sizes. Thus, depending upon the criterion of sequence similarity being considered (e.g., >80% nucleotide identity), closely related genes would hybridize in a reassociation experiment and align with high fidelity in an in silico analysis, and so would no longer be classified as single copy.

Highly repetitive DNA is easier to define, and a good example is the tandem repeats found in plant centromeres. Some highly repetitive sequences that have a base composition significantly different from the average for that genome were originally called satellite DNA, because they were found at a different buoyant density in cesium chloride density gradient separations; this name persists today. In most animals and yeast, satellite DNA is AT rich, but examples from plants tend to be GC rich. Satellite DNA is primarily associated with either the centromere, or the telomeres in plants, and it is usually heterochromatic; that is, it remains condensed and inactive in interphase.

Intermediate repeated DNA sequences generally occur in a few tens to tens of thousands of copies in the genome. There are many thousands of families of intermediate repeat DNA, with the members of any one family being very similar, but not identical. Considered in terms of classical Cot analysis, members of one family would cross-hybridize during reassociation experiments. These sequences would be 80% or more identical at the nucleotide level. Within this broad category of repetitive DNA, one can find transposons, retrotransposons, structural RNAs including ribosomal, transfer and other RNA species, and some large protein-coding gene families. A significant number of these families of repeated sequences occur as tandem repeats, as exemplified by the ribosomal RNAs in the nucleolar organizer region (NOR) and the 5S RNA clusters. Some examples of large protein-coding gene families that occur as tandem repeats are the histone genes and the disease resistance genes.

9.2.2 Genetic and physical maps provide complementary views of genome organization.

Genetic maps are essentially ordered lists of the distinctive features (markers) along each chromosome and the relative distance between them (determined by the frequency of recombination between them during meiosis). These markers may be based upon either DNA sequence or phenotypic traits (e.g., plant height, leaf shape, disease resistance, stress tolerance).

Where genetic maps have been aligned with sequenced genomes, there is excellent correspondence between the order of sequence-based markers in the genetic map and the occurrence of these marker sequences in the genome itself. In some genome sequencing projects, genetic maps can facilitate the ordering and orientation of DNA sequence assemblies. The alignment of a genetic map with the corresponding annotated genome sequence also allows identification of candidate genes that lie close to the position on the genetic map of a phenotype of interest (e.g., seed yield, oil composition, etc.). A variety of methods can then be used to determine which of the candidate genes may actually control the phenotype of interest.

While a genetic map defines a chromosome in terms of recombination among loci to give a relative genetic distance between them (genetic space), a **physical map** is an ordered representation of many large DNA fragments (typically ≈100 kb) into which the genome has been decomposed. Given the number and sizes of plant genomes of interest to researchers, a prelude to large-scale sequencing is often the creation of a physical map. High-resolution physical mapping uses cloned sections of DNA to create maps of contiguous, overlapping fragments of DNA that can span very long distances. The region defined by such a map is called a **contig**, since it is constructed from contiguous clones.

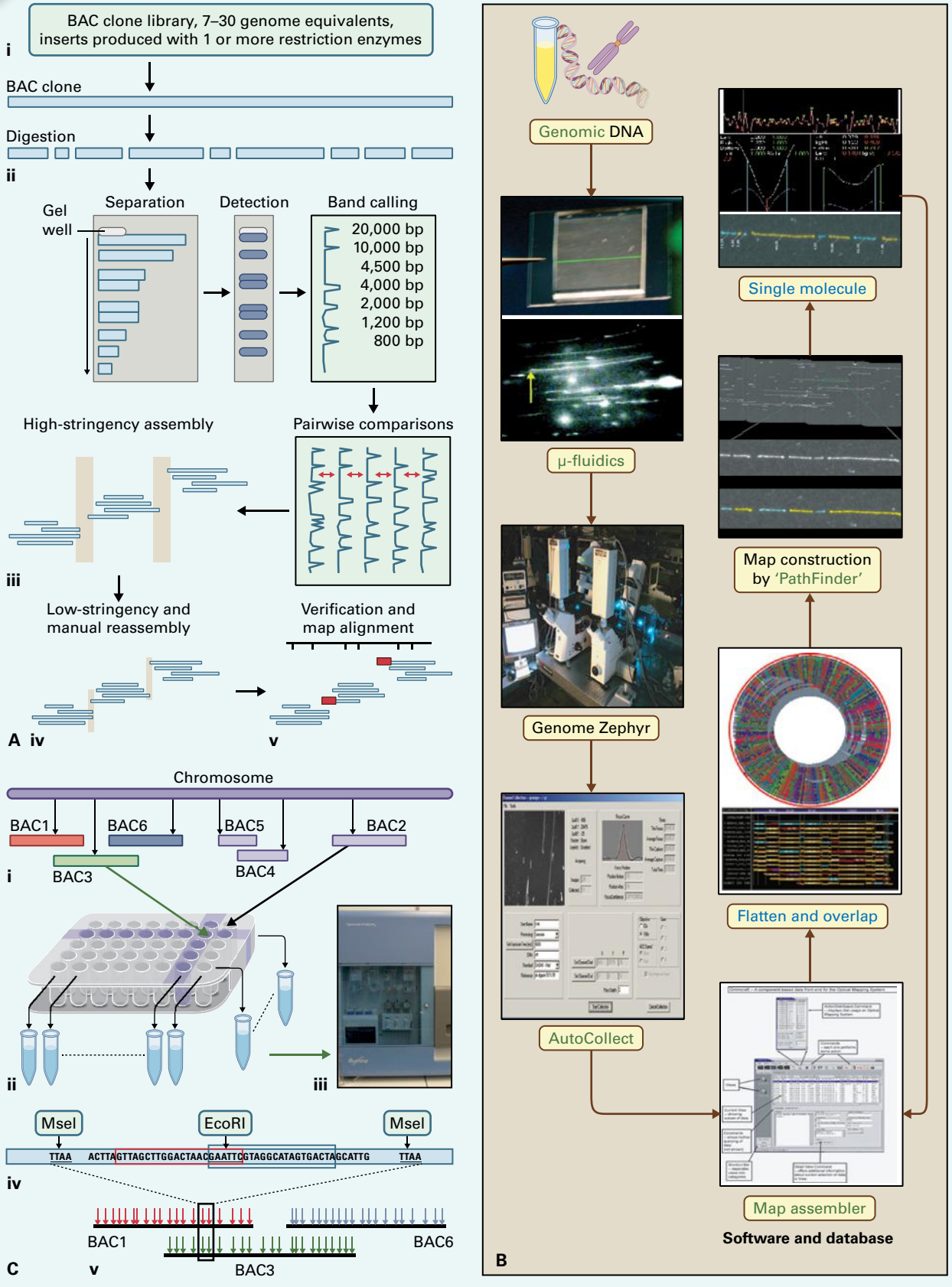
A common strategy for building a physical map involves the construction of a bacterial artificial chromosome (BAC) library. BACs are plasmid cloning vectors that use the replication origin of F-factors and so are propagated in *E. coli* as single (or very low copy) plasmids. The low copy number and use of recombination-deficient host cells contribute to the stability of the DNA molecules. Most BAC libraries have inserts of 100–150 kb genomic DNA, but larger insert sizes can also be generated. A technique called "fingerprinting" is then used to determine how these randomly cloned fragments overlap (see Box 9.3): The DNA of each BAC is digested with one or more restriction enzymes, and the sizes of the resultant fragments determined. Each BAC produces a characteristic set of fragments; two BACs overlap (their DNA inserts came from the same region of the genome) if they have a certain number of band sizes in common.

Originally, sizing was carried out on long agarose gels, but a newer technique, high information content fingerprinting, uses a combination of multiple restriction enzymes and four-color labeling, followed by resolution on a capillary DNA sequencing machine to produce a larger number of more accurately sized fragments and thus, a higher resolution map. This method of determining fragment overlap is being superseded by the generation of a set of sequence tags for each BAC using BAC pools and multiplexed sequencing (whole genome profiling, see Box 9.3).

Optical mapping (see Box 9.3) represents a further refinement of physical mapping. Here, isolated DNA molecules, typically a few hundred kilobase pairs in length, are immobilized on glass slides and digested with a restriction enzyme. Regardless of which method is used to tag each BAC or DNA fiber (band size or sequence), contigs of overlapping BACs or fibers are then assembled on the basis of shared tags.

BOX 9.3

The physical mapping of large genomes involves different methods



BAC fingerprinting. (A) (i) Bacterial artificial chromosome (BAC) library that represents 7–30 (or more) genome equivalents is constructed using a number of different restriction enzymes. (ii) Each clone is digested, and the resultant fragments are separated to produce a set of sized fragments, the DNA "fingerprint". (iii) A full pairwise comparison of all clones is performed to detect the proportion of shared bands among each pair of clones, and contigs of overlapping clones are constructed. At high-stringency, some overlaps are not detected (blue bands indicate gaps in the assembly). (iv) End clones from each contig can be compared at a relaxed cutoff score to detect smaller overlaps. (v) The contigs are aligned to the genetic map using shared markers to verify the map and to further merge contigs. The pink boxes indicate BAC-end sequences that have been used as genetic markers to align contigs to the genetic map.

Optical Mapping. (B) High molecular weight DNA from isolated nuclei is gently spread and fixed on a slide to produce long, isolated DNA fibers. The DNA is digested with an appropriate restriction enzyme, resulting in visible nicks in the DNA. The stained DNA is scanned with high-resolution automated microscopes, and the lengths of the succession of restriction fragments are profiled. Optical maps generally produce longer contigs (up to ≈50 Megabase pairs) than either the classical fingerprinting or whole genome profiling approach.

Whole genome profiling (C) (i) BAC clones are available in a 384-well plate format. (ii) BAC DNA is extracted after pooling each row (24 BACs) and each column (16 BACs). (iii) Pooled BAC DNA is digested (for example, with *Eco*RI/*Mse*I) and amplified after barcoded adapters are ligated for pool identification after sequencing. (iv) Deconvolution: sequence tags (30–50 per BAC) are assigned to individual BACs based on presence in one row and one column pool. (v) Overlapping (sets of) sequence tags from individual BAC clones generate contigs. Together, these contigs represent a sequence-based physical map of the genome.

9.2.3 Plant genome sequencing has provided a high-resolution view of genome structure

The sequencing of plant nuclear genomes began in 1997, following the adoption of *Arabidopsis thaliana* as a model for plant genomics and the recognition of two features critical for success: a small genome (initially estimated to be ≈120 Mb) and relatively little repetitive DNA. Over the next decade, sequencing technologies, sequence assembly techniques, and genome-oriented bioinformatics improved significantly. As a result, larger and more complex genomes, such as that of wheat (*Triticum* sp., see Fig. 9.2) are being sequenced. The following discussion provides a basis for understanding the various methods used for generating sequences of a whole genome, as well as the advantages and limitations of the different methods. Embedded in this discussion are concepts of strategy and technology, with strategy changing as technology develops.

The first genome-sequencing projects used a BAC-based strategy (see Box 9.4), in which a physical map was constructed from BACs, and BACs were sequenced individually. Individual BAC sequences were assembled separately and then joined together based upon sequence overlaps, aided by physical and genetic maps, to form complete chromosomes (also known as pseudomolecules). Because this approach is labor intensive and requires sequencing of thousands of BACs, methods for whole genome shotgun (WGS) sequencing were developed (Box 9.4).

WGS, in which the whole genome is fragmented and DNA sequenced as a single preparation, became more feasible as sequence assembly algorithms became increasingly sophisticated, and computers increasingly powerful. WGS has the disadvantage, however, that highly similar sequences arising from different parts of the genome co-assemble and, therefore, cannot be easily resolved. This problem remains with less expensive DNA sequencing technologies that have a higher output but also higher error rates and shorter read lengths.

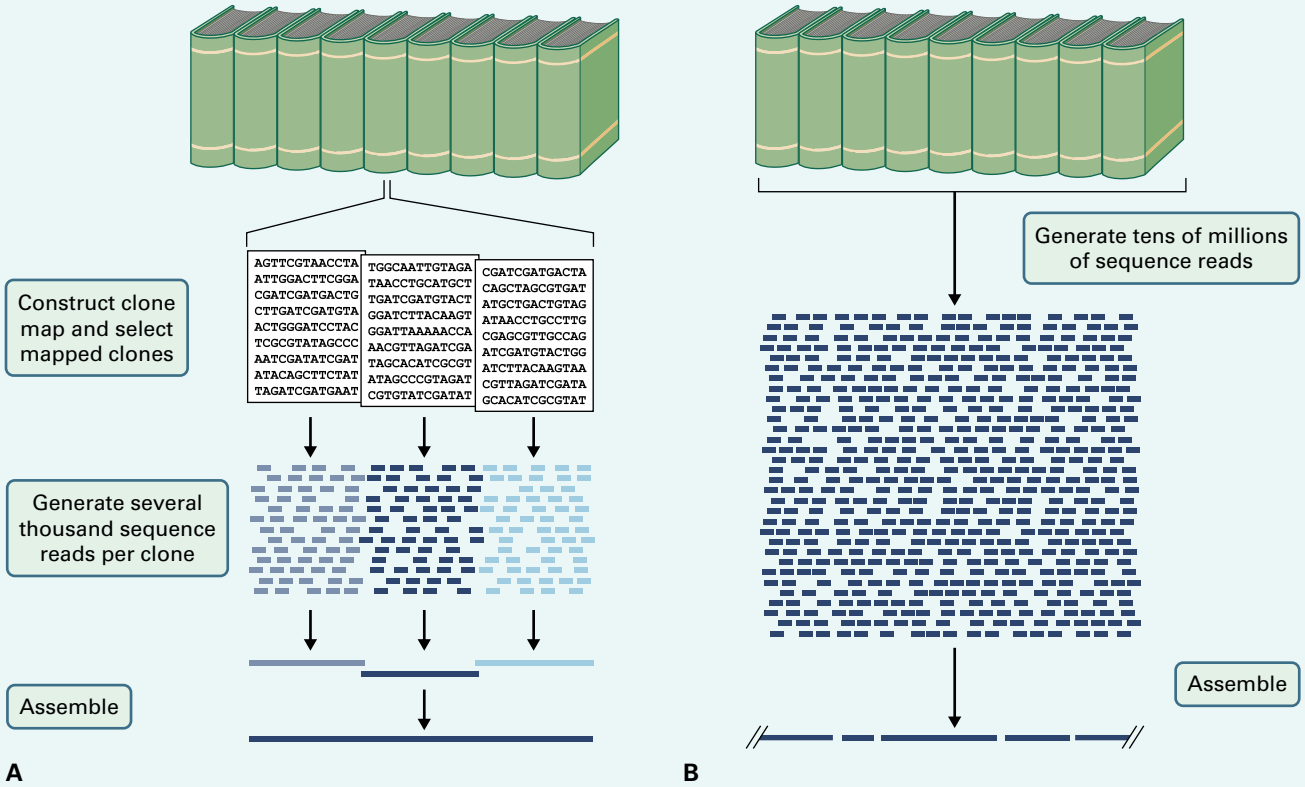
In most genome projects, some effort is made to sequence the ends of various defined-size fragments to produce "mate pair" sequences that are often useful in resolving DNA repeats. It is, nevertheless, not uncommon to find that genomes with even modest amounts of repetitive DNA cannot be fully assembled, so a significant fraction of the genome remains uncharacterized as a collection of collapsed reads. Genetic and physical maps originally used to validate BAC-based sequenced genomes now play important roles in the ordering and orienting of genome assemblies that may contain hundreds to thousands of sequence scaffolds.

9.2.4 Genome annotation reveals the biological functions encoded in the DNA sequence

The DNA sequence alone is not particularly informative. **Genome annotation** is the process by which regions of the genome (DNA sequence) are recognized as encoding genes and the structure of the gene is defined (exons, introns, and other features) and its function inferred. Two general methods are used to define gene structures.

BOX 9.4 Genome sequencing involves different strategies

In a BAC-based sequencing project (A), genomic DNA is partially digested with restriction enzymes such that BAC clones each contain ≈100–150 kb DNA. The clones are organized into a physical map (see Box 9.3), after which individual BAC clones representing a minimum tiling path through the genome are sequenced and used to reconstruct the genome. In a whole genome shotgun (WGS) approach (B), the entire genome is fragmented usually by sonication or hydrodynamic shearing followed by size selection into pieces that vary according to the sequencing technology to be used. This collection of unordered fragments (numbering many millions) is then sequenced, and sophisticated assembly algorithms are used to reconstruct the entire genome. Although the assemblies produced by WGS approaches are generally slightly less accurate or complete, this approach is far less laborious or costly than the BAC-based approach, which has become essentially obsolete.



One method is based on available sequences of mRNAs (sequenced as cDNA) and proteins (generally inferred from nucleotide sequences, but sometimes also from direct protein sequencing). Various algorithms can be used to align pre-existing sequences to a new genome, and many of these algorithms can also recognize conserved splice sites (GT….AG; so-called spliced alignment) to define exon-intron boundaries. The most accurate gene structures are defined by full-length cDNAs that have captured the entire protein coding sequence of a particular gene. Alignments of nucleotide and protein sequences from other species are also informative, but become progressively less so as the evolutionary distance between the new genome and available sequence increases. Overall alignments between two related genomes can also be highly informative, as sequences that are conserved between two genomes are thought to have functional significance and, thus, to encode either genes or regulatory sequences.

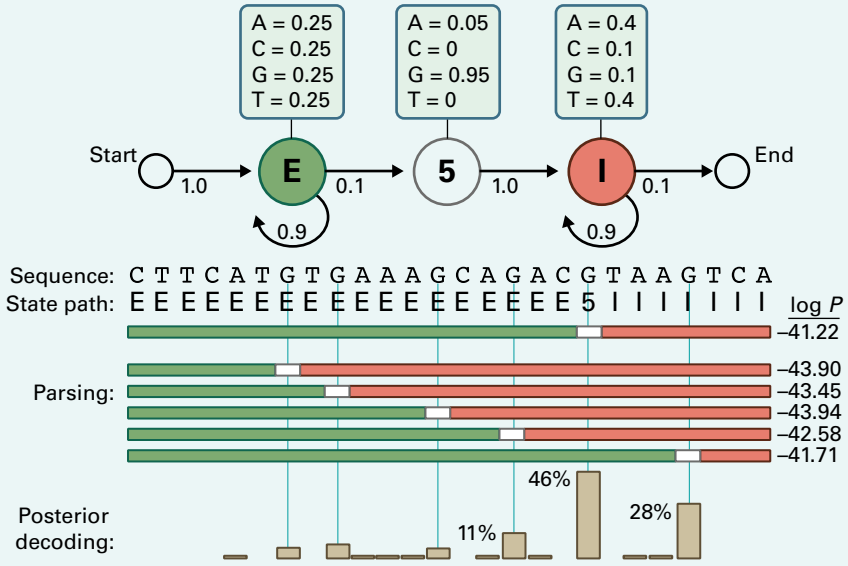
The second method for defining gene structures is strictly computational and relies on differences in base composition and adjacent nucleotide frequencies (di-, tri-, tetranucleotides, etc.) and their transition probabilities between exons, introns, and intergenic sequences. These sophisticated programs frequently involve hidden Markov models (HMMs; see Box 9.5) and are generally trained on a small, well-defined set of structures that have been identified in the new genome (or that of a close relative) using existing sequences.

Together, these two methods are used to identify gene structures throughout a new genome, both in regions where there is supporting evidence from nucleotide and protein sequences and in those where there is not. Gene structures

BOX 9.5 Hidden Markov models (HMMs) underlie many gene prediction programs

Hidden Markov models (HMMs) are statistical methods used to help define gene structures. In this example, the DNA sequence begins in an exon, contains one 5′ splice site, and ends in an intron, as shown in the "state path." To infer where the switch from exon to intron occurs (i.e., the location of the 5′ splice site), the sequences of exons, splice sites, and introns must have different statistical properties, including base composition and higher order oligonucleotide frequencies, etc.

Suppose exons have a uniform base composition (25% probability of each base), introns are A/T rich (for example, 40% each for A/T, 10% each for C/G), and the 5′ splice site consensus nucleotide is almost always a G (for example, 95% G and 5% A). We can construct an HMM that invokes three *states* we might assign to a nucleotide: E (exon), 5 (5′ splice site), and I (intron). Each state has its own *emission probabilities* (shown above the states), which model the base composition of exons, introns, and the consensus G at the 5′ splice site. Each state also has *transition probabilities* (arrows), the probabilities of moving from this state to a new state. The transition probabilities describe the linear order in which we expect the states to occur: one or more Es, one 5, one or more Is. In practice, HMMs are given training sets of genes with known structures (inferred from full-length cDNAs), from which transition probabilities can be calculated and gene structures predicted on new DNA sequence.



supported only by computational methods are considered unreliable predictions in some plant genomic communities.

Prediction of gene structures (Box 9.6) results in the definition of a protein coding sequence (CDS) for each gene. Assignment of function to these genes then relies upon their matches to other genes in databases such as GenBank or SwissProt. Here, the matching is done at the amino acid level, since protein sequences are generally more conserved across species than nucleotide sequence. The function of the database match is then transferred to the new protein. This method can result in potentially erroneous annotations because only a fraction of all the proteins in GenBank or similar databases have actually had their annotated function confirmed experimentally. This phenomenon of "transitive error propagation" is well recognized in the annotation community and will gradually decrease as the functions of more proteins are elucidated experimentally.

9.2.5 DNA sequencing has informed our understanding of genome organization at the DNA level

The organization of the *Arabidopsis* genome provides an excellent model and starting point from which to understand the overall structure of many plant genomes. The genome sequencing project produced approximately 105 Mb of DNA sequence, with the unsequenced portions around the centromeres estimated to be ≈15 Mb, for a total genome size of 120 Mb. Subsequent measures using flow cytometry have suggested that the amount of unsequenced DNA was larger, with a total genome size of ≈150 Mb, but this does not affect our description of the basic genome features, which are found in most of the other plant genomes. As with a number of plants and animals, the small genome size of *Arabidopsis*

BOX 9.6 Various kinds of evidence are used to support gene structure predictions

The support of gene structure predictions includes computational gene predictions, spliced alignments to the genome sequence of cDNAs, expressed sequence tags (ESTs) from the same species, and spliced alignments of proteins from the same or related species. The alignment algorithms are splice-site aware and, thus, identify and support the correct structure for the gene under study. The view shows an approximately 4.5-kb window along the minus strand of *Arabidopsis* chromosome 1 in the region encoding the 3-methylcrotonyl-CoA carboxylase 1 (At1g03090). The curated gene structures are shown in dark green on the white background towards the bottom of the window, with exons shown as solid bars and introns and UTRs as open bars. The box with the black background above this curation shows the collective evidence (from bottom to top): splice site predictions, computational gene predictions, protein alignments shown in orange, EST alignments from searching the various plant Gene Indices in varied colors, and *Arabidopsis* transcript assembly alignments at the top shown in bright pink. The vertical marker line indicates the position of a skipped exon (supported by both cDNA and protein alignments) that results in two protein isoforms.

Screenshot is from the Annotation Station gene editor, proprietary software that is similar to the open source Apollo editor.



correlates with its short life cycle: Plants with larger genomes tend to reproduce more slowly.

The main features of the chromosome shown in Figure 9.1 can now be described at the DNA sequence level.

Most genes are found in the euchromatic chromosome arms

The chromosome arms stretching from the telomeres to the pericentromeric regions close to the centromeres comprise ≈100 Mb of sequence and are more or less uniformly gene rich. The *Arabidopsis* genome encodes approximately 30,000 protein-coding genes, as well as many transfer RNA (tRNA) genes and various classes of noncoding RNA genes with a variety of regulatory functions. These numbers continue to increase as more small genes (both protein-coding and regulatory) are discovered. The average *Arabidopsis* protein-coding gene contains five exons and occupies approximately 2 kb of genomic sequence from start to stop codon. As described below, a gene's regulatory sequences may lie upstream, downstream, or within this region, although most promoter functions are typically found upstream of the transcription start site. Genes are separated by ≈2.5 kb of DNA (including regulatory regions), for a gene density of one gene every 4.5 kb. This is among the highest gene densities found in plants and is comparable to the genomes of *Brachypodium*, the moss *Physcomitrella*, and the unicellular *Chlamydomonas*. With few exceptions, only one strand of any particular region of the

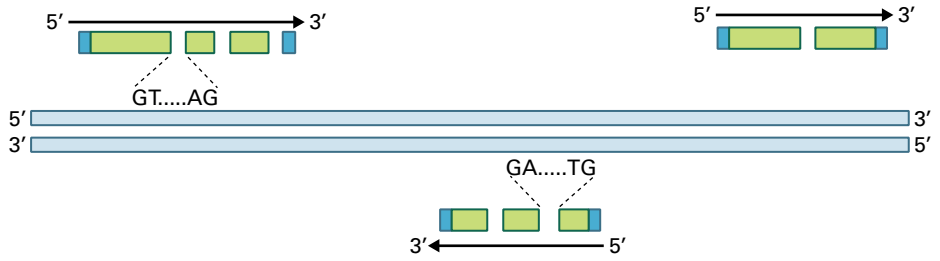


FIGURE 9.3 *Genes (protein-coding sequences) are found on either DNA strand, but rarely in the same region on both strands. Because transcription is always 5′ → 3′, genes on opposite strands are transcribed in opposite directions; transcription may be convergent or divergent. Note the orientation of the conserved splice site boundaries on the two strands. Green boxes represent the protein coding region of the transcripts (CDS), and blue depicts the 5′ and 3′ untranslated regions (UTRs). On rare occasions, two genes may occur in the same region of the DNA, but on opposite strands, with one gene lying within the intron of the other.*

double helix actually encodes a protein. Thus, protein-coding genes may lie on either strand and be transcribed in either direction (Fig. 9.3).

Telomeres guard the ends of chromosomes

Chromosome arms end in telomeres, which are specialized structures that protect chromosome ends, ensure their faithful replication, and prevent the shortening of chromosomes during successive rounds of DNA synthesis (see Chapter 6). The canonical plant telomeric repeat (TTTAGGG) is found in almost all plant species for which this element has been sequenced. In *Arabidopsis*, telomeres are ≈2–3 kb in length.

In eukaryotes, a specialized enzyme called **telomerase** maintains the single-stranded overhang remaining after chromosome DNA replication to keep it from being shortened during each cell division (see Fig. 6.10). Telomerase is a reverse transcriptase with a segment of RNA integrated into its three-dimensional structure. The RNA functions as the template for the new telomere sequence. Telomeres also seem to function in maintaining "nonsticky" ends on the chromosomes. By contrast, according to cytogenetic analyses, the ends of broken chromosomes are very sticky, readily joining with any other available DNA fragment. Telomeres also appear to play a role in the organization of chromosomes in the nucleus, attaching the chromosome to the fibrous nuclear lamina on the inner surface of the nuclear envelope (see Chapter 5).

Centromeres are responsible for the precise segregation of chromosomes into daughter cells during division

Cytologically, chromosome centromeres (Fig. 9.4) are heterochromatic (highly condensed) chromatin constrictions to which the spindle fibers attach to facilitate the separation of replicated chromatids in mitosis and meiosis. Among the simplest of characterized centromeres are those of the budding yeast *Saccharomyces cerevisiae* and the fission yeast *Schizosaccaromyces pombe*, which are only tens to hundreds of nucleotides in length. However, plant centromeres are almost invariably much larger and more complex. Analogous to the alpha satellite repeat that characterizes the centromeres of human genomes, plant centromeres typically contain tandem arrays of one or more species-specific sequences, generally between 150 and 200 bp in length (approximately the length of DNA wrapped around a nucleosome). In addition, centromeres are rich in retrotransposon sequences. Despite information about their sequence content, the essential sequence components of plant centromeres are not well defined. Centromeres are better recognized by the proteins that bind to the DNA in this region, especially histone CENH3. Approximately 50 proteins are constitutively or transiently associated with yeast centromeres, and homologs of many of these are found in plants, including CENP-C, CENP-H-1 and CCAN, ASK, CBF5, and Bub-like proteins.

The size of the centromeres varies between species and even across chromosomes within an individual species, ranging from 50 kb to many megabases. Despite a limited understanding of the functional elements of plant centromeres, both DNA sequence and the associated proteins, it is becoming possible to construct artificial chromosomes capable of sustained autonomous replication and of moving parts or all of important metabolic or developmental modules into other varieties or species for crop improvement (Fig. 9.5).

The **pericentromeric regions** flanking the centromeres extend many megabases and have a low gene density, high content of transposons, and, predominantly, retrotransposons (see Section 9.3). Genetic recombination is also suppressed in these regions.

Genes encoding the RNA components of ribosomes are localized to a small number of genome regions

Nucleolar organizer regions (NORs) are cytologically identifiable regions of the chromosome around which ribosomal RNA transcription, biogenesis, and assembly occur. Ribosomal RNA (rRNA) is needed in such large quantities for ribosome structure and protein synthesis in active cells that it would be impossible for one or a few copies of rRNA genes to keep up with translational needs. At the DNA sequence level, these regions consist of many tandem repeats of an approximately 10-kb sequence that encodes the 28S, 18S, and 5.8S RNA components of the ribosome (Fig. 9.6). The coding

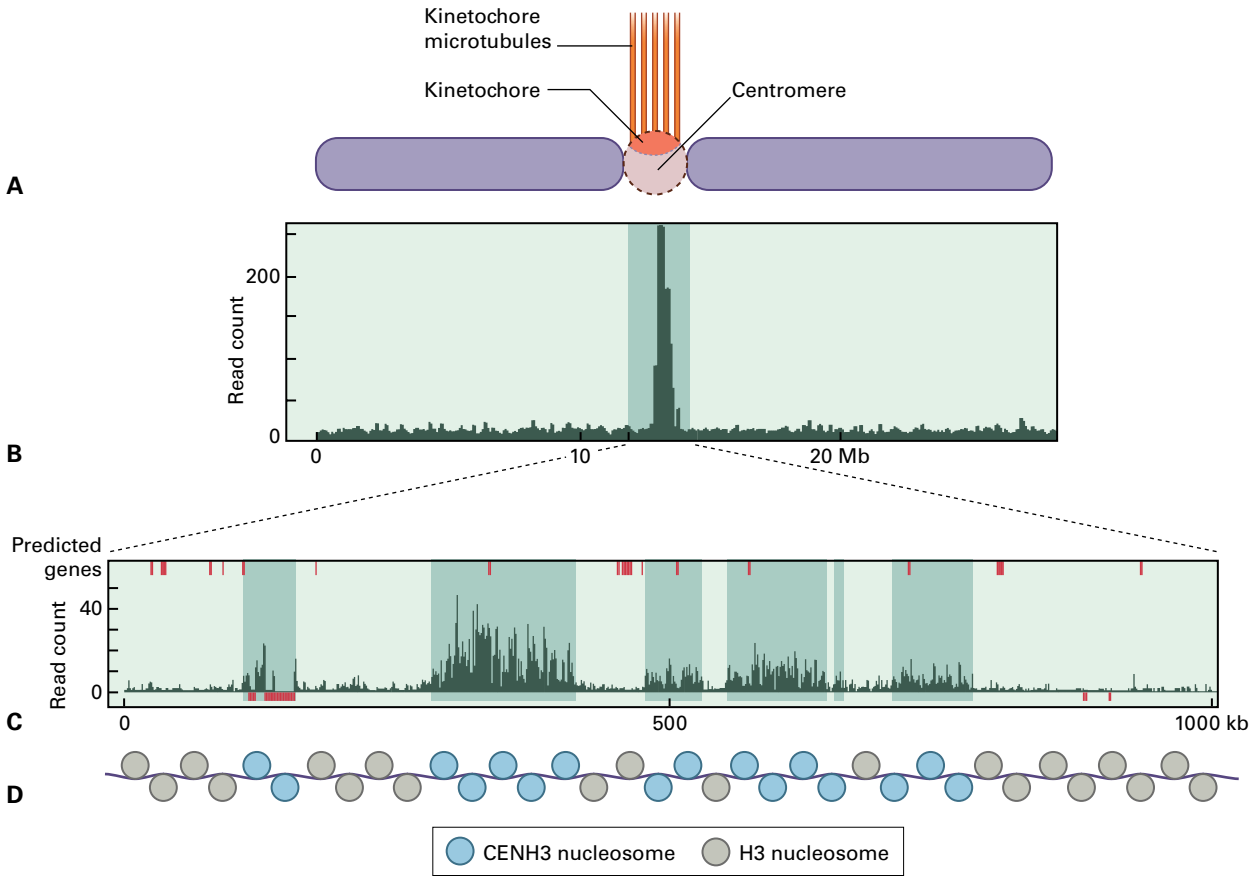


FIGURE 9.4 *Structure of the centromere of chromosome 8 of rice* (Oryza sativa). *(A) General structure of a chromosome displaying chromosome arms (blue), centromere (red), kinetochore (yellow), and microtubules (purple). Only one sister chromatid is shown for simplicity. (B) Localization of CENH3 (a centromere-specific histone 3 variant) to the centromeric region deduced from ChIP-Seq (see Box 9.10) against CENH3 across the entire chromosome. The gray box indicates the crossing over-suppressed region of the chromosome. (C) Expanded view of the CENH3-binding domain. Predicted genes (red boxes) are located predominantly outside CENH3 binding domains (gray boxes), and the 155-bp centromeric repeat (CentO) arrays are shown as red boxes beneath the mapped reads. (D) Representation of nucleosome pattern across Cen8 in rice. Gray circles represent nucleosomes with canonical histone H3, and cyan circles represent CENH3-containing nucleosomes. Not drawn to scale.*

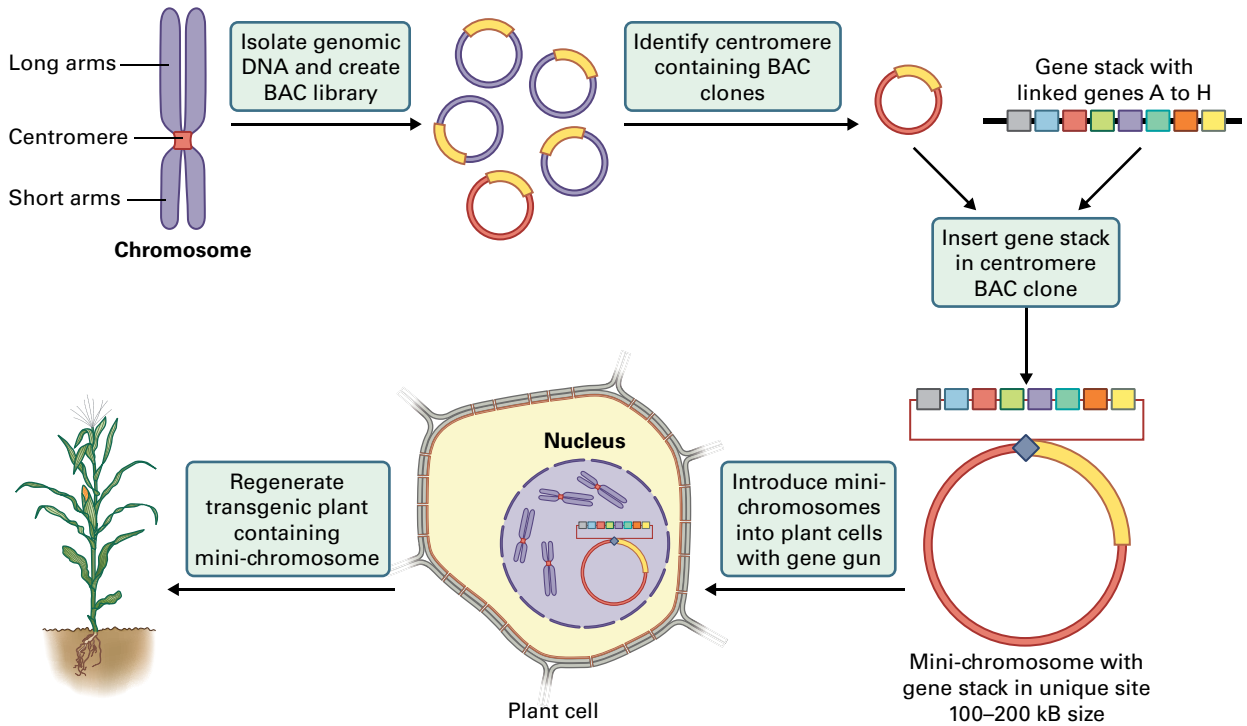


FIGURE 9.5 *Artificial mini-chromosomes carrying sets of genes can be constructed for plant genetic engineering.*

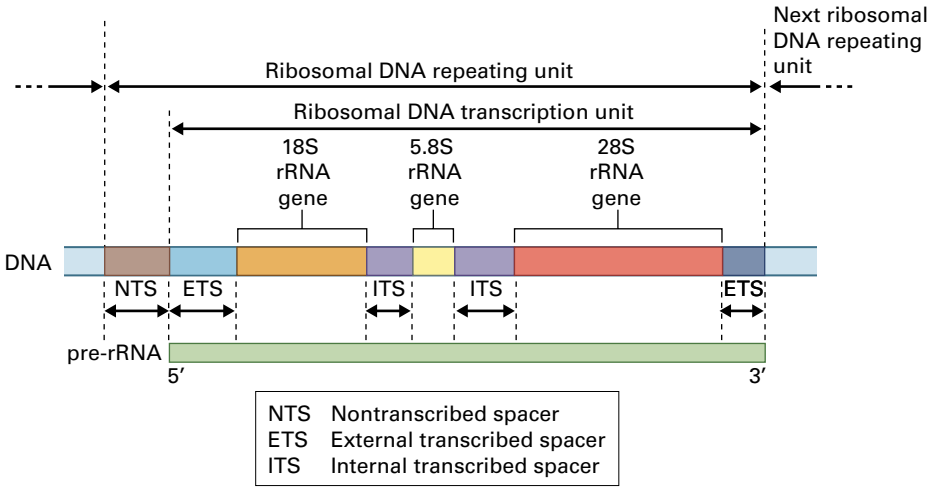


FIGURE 9.6 *The eukaryotic ribosomal DNA repeating unit. Most plant ribosomal genes lie within a repeating unit ranging from 7,800 to 185,000 bp long. The repeating unit is composed of highly conserved rRNA genes separated by short stretches of spacer sequences that are not transcribed (NTS, ETS, and ITS). Ribosomes contain four distinct RNA molecules of sizes 18S, 5.8S, 28S, and 5S that contribute to their structure. Genes for the first three are contained on a rDNA repeating unit, whereas the 5S gene is found elsewhere in the genome.*

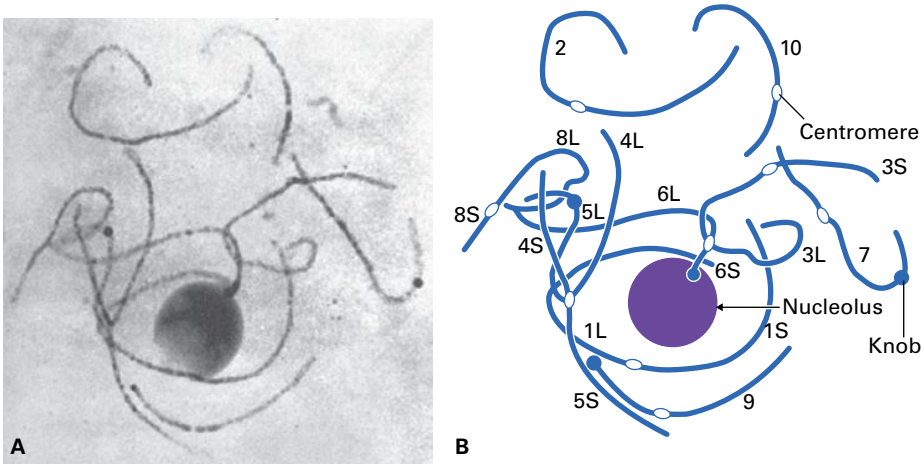


FIGURE 9.7 *Maize (*Zea mays*) chromosomes provide an example of heterochromatic knob(s). (A) A micrograph of a maize microsporocyte nucleus at the pachytene stage, showing the ten chromosomes and the nucleolus. (B) Schematic drawing identifying the chromosomes. In the pachytene stage, homologous chromosomes reside side-by-side and appear thick enough to enable the identification of individual chromosomes by their structural features (e.g., positions of centromere and knobs).*

sequences of these three genes are highly conserved across species, but the intergenic transcribed spacer (ITS) is much more variable and has been used for exploring relationships between species. Each species typically contains only one or two NORs; their number and chromosomal location(s) being determined by FISH. The other RNA component of the ribosome (5S RNA) is also encoded in tandem arrays, but these are found at other chromosomal locations. In *Arabidopsis*, the principal 5S RNA gene clusters are found in the centromeric regions of chromosomes 3, 4, and 5.

Condensed chromatic can often be visualized as heterochromatic knobs

Heterochromatic knobs are recognized cytologically as regions of highly condensed chromatin separated from the centromeres. They are more common in plants with larger genomes, such as maize (Fig. 9.7). The single heterochromatic knob in *Arabidopsis* lies on chromosome 4; it has been fully sequenced and found to consist in large part of retrotransposons.

9.2.6 Larger genomes are structurally more complex, with gene islands interspersed between large regions of repetitive sequence

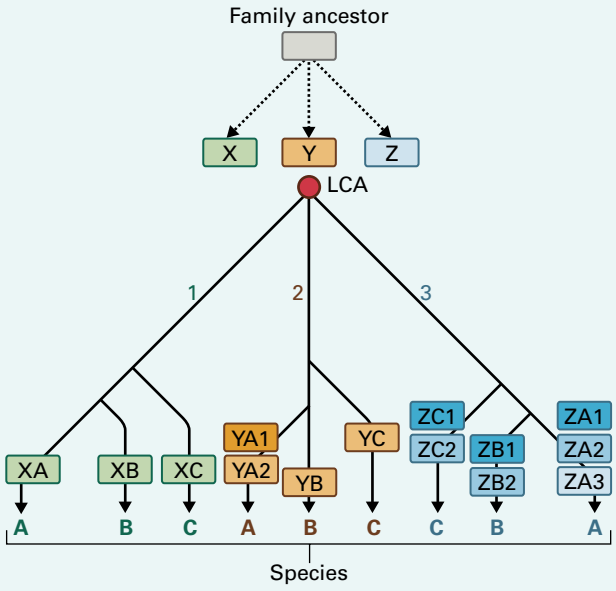
The structural features described above are common for many of the smaller plant genomes (<1 Gb); the maize genome, however, presents a somewhat different picture of genome organization that may also be characteristic of other large genomes of the Poaceae (grasses/cereals) and other families or genera. The maize (*Zea mays*) genome consists of approximately 80% repetitive DNA, much of which encodes

BOX 9.7

Homology, orthology, and paralogy are important concepts in plant evolution and speciation

Homologs are genes that share a common origin. From an evolutionary perspective, there are two types of homologous genes: orthologs are genes that originated from the same gene in the last common ancestor of the two species, and paralogs are genes that are related by duplication. Successive rounds of genome duplication can generate complex ortholog and paralog relationships.

In the figure, X, Y, and Z represent three paralogous genes that existed prior to the last common ancestor of the hypothetical tree. In branch 1, XA, XB, and XC in the three species A, B, C involves only vertical inheritance and the genes are orthologs. Branch 2 shows lineage-specific duplication in species A, such that YA1 and YA2 are paralogs (in-paralogs) within species A and co-orthologs to YB and YC. In branch 3, lineage-specific duplications or triplications in each species mean that ZA1–ZA3 are in-paralogs to each other and co-orthologs to ZB1-2 and ZC1-2. The situation can be further complicated by subsequent differential gene loss in individual lineages.



retrotransposons (see Section 9.3). In contrast to most plant genomes, which are organized into gene-rich euchromatic chromosome arms and gene-poor heterochromatic centromeres, the maize genome consists of gene islands within oceans of retrotransposons. The gene islands are small, containing from one to seven genes (an average of four) and covering ≈50 kb, with several times this distance between adjacent gene islands. While this model likely holds for other members of the Poaceae with large, highly repetitive genomes, such as wheat (*Triticum* sp.) and barley (*Hordeum vulgare*), it remains to be seen if it also applies to monocots outside the grasses or to large dicot genomes such as lettuce (*Lactuca sativa*), sunflower (*Helianthus annuus*), or onion (*Allium cepa*).

9.2.7 Ancestral genome duplications have played a major role in plant genome structure

Plant genome sequences provide striking and clear evidence of large-scale duplication events that may have occurred from a few to more than 100 million years ago (Box 9.7). Evidence for such events is frequently displayed in the form of a dot plot (Fig. 9.8), in which the coordinates of the two axes represent the position of a genome feature, and each dot represents a region of similarity between two parts of the genome. Dot plots are frequently performed in protein space, since these protein sequences are generally more conserved over greater evolutionary time than DNA sequences, thus permitting detection and visualization of older duplication events. In a dot plot of a genome against itself, the central diagonal (if shown) simply represents the position of the same conserved feature on the two coordinates, while series of dots forming diagonals off this central line show evidence for segmental duplications.

The timing of genome duplication events can be inferred from the divergence of the two sequences. This is calculated as the synonymous substitution rate in protein-coding sequences (inferred from either genomic or EST sequences), which in turn is calibrated by cross-reference to fossil records. Synonymous substitutions refer to changes in the third base positions of codons that do not affect a protein's amino acid sequence and are thus not under selective pressure.

Basing plant evolutionary history on DNA sequence is becoming increasingly complex and sometimes controversial as data accumulate and more sophisticated methods of analysis are applied. Duplication events become progressively more difficult to detect as one looks further back in time. As more sequence divergence occurs, there may be successive changes at the same nucleotide position, making it increasingly difficult to recognize paralogous pairs.

Following genome duplication events, gene loss and changes in gene function are both possible. The terms subfunctionalization and neofunctionalization were first proposed many years ago in the context of the duplication of individual genes, rather than large-scale genome duplication. Subfunctionalization describes how the two progeny from an originally single copy gene may take on different roles that collectively amount to the same activity of the original gene,

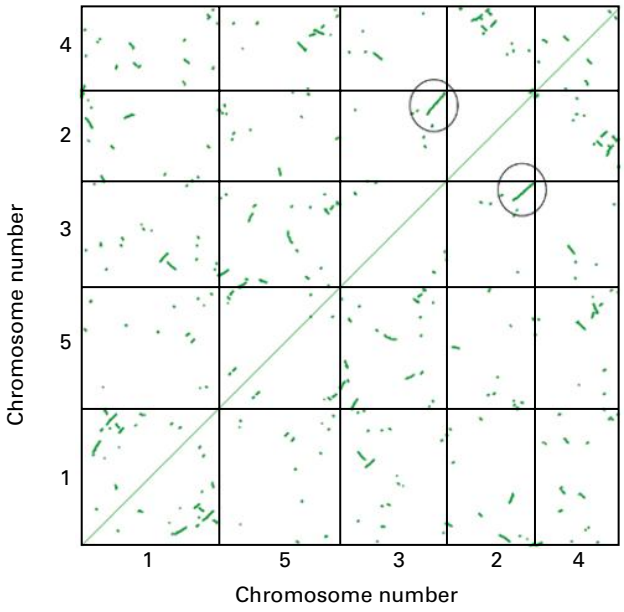


FIGURE 9.8 *Dot plot of the* Arabidopsis thaliana *genome against itself showing evidence of ancestral duplication events. Chromosomes are arranged in the order of descending size. Each dot represents a cluster of similar genes found at two different places in the genome. The lines circled represent a region at the bottom of chromosome 2 that is duplicated at the bottom of chromosome 3 (note the symmetry around the diagonal line that denotes self-identity). The figure was produced using the CoGe software suite.*

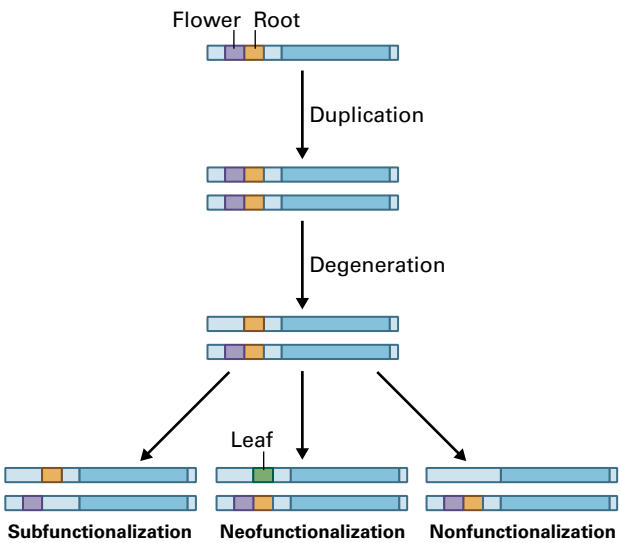


FIGURE 9.9 *Subfunctionalization and neofunctionalization. A single gene contains promoter elements that drive expression in both flowers and roots. After duplication and degeneration, there are three possible outcomes. Under the subfunctionalization scenario, each gene retains only one of the promoter elements and becomes specialized for expression in only one of the two organs. Under the neofunctionalization scenario, one of the promoter elements mutates (or the gene acquires a new element) that now drives expression in leaves. Under the third (nonfunctionalization) scenario, one copy of the gene is no longer expressed and is often referred to as a pseudogene.*

both in terms of pattern of expression and biochemical activity. Neofunctionalization describes the situation where one of the duplicated genes takes on a function not previously associated with its parent gene (Fig. 9.9). These changes can occur in either the regulatory or structural (protein-coding) region of the gene. Once duplicated, at least one of the duplicate genes is free to diverge or evolve without maintaining its original function, which might be essential for survival of the organism.

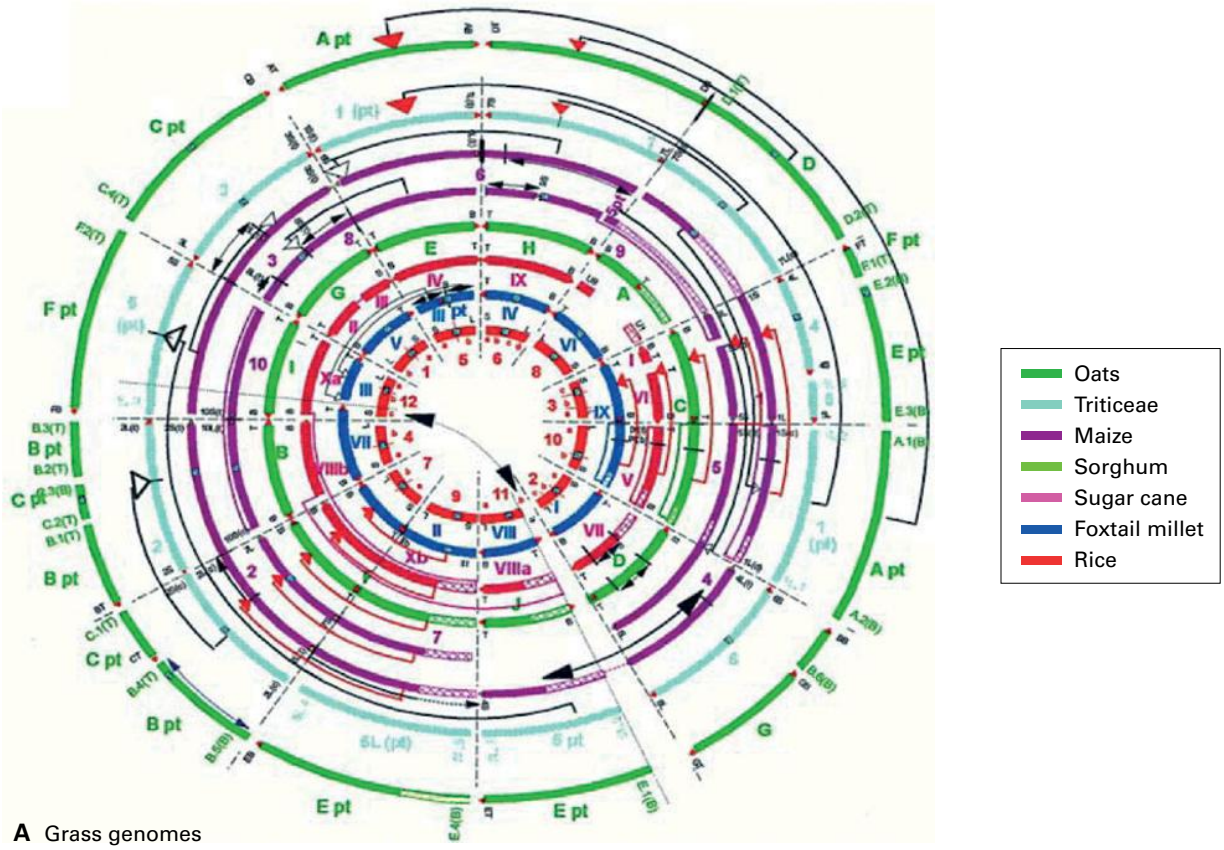
9.2.8 Related plant species display evolutionarily conserved organization and arrangement of single-copy genes

Genetic mapping and genome sequencing projects have revealed that gene content and order along large segments of chromosomes are often conserved among related species in both the plant and animal kingdoms. This colinearity of genetic loci or genes is called **synteny**. The first striking example of synteny across multiple plant species was demonstrated for the grasses (Fig. 9.10A), but as more sequence-based genetic maps and sequenced genomes have been generated, it is clear that the same kinds of relationships can be found within other families, for example the Solanaceae (tomato, potato, pepper, eggplant, etc.) and the legumes (*Medicago*, *Lotus*, common bean, soybean, pea, etc.).

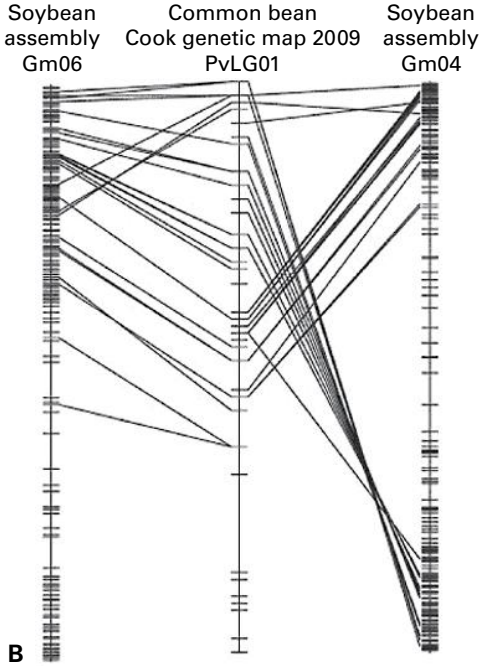
With more distant species, synteny is usually inferred from the order of presumed orthologous protein sequences, rather than directly from comparison of nucleotide sequences. An example of rice–maize synteny is shown in Figure 9.10B. The lengths of synteny blocks decrease as one compares progressively more distant species; however, even between species that lie in different families and diverged as much as 50 million years ago, or more, many short synteny blocks can still be found (known as microsynteny). Synteny is not only of academic interest, but can be used to exploit knowledge about a sequenced genome to infer positional and sequence information about a gene of interest in a related genome that may be considered too large for cost-effective sequencing (for example, leveraging information from the *Medicago truncatula* genome to identify a candidate symbiosis gene in *Pisum sativum*).

9.3 Transposable elements

Transposable elements are sections of DNA (sequence elements) that move, or **transpose**, from one site in the genome to another. These mobile DNA elements can make up a significant portion of the nuclear genome, and they carry genetic information with them as they transpose, making them important features of genome organization. Transposable elements from organisms as diverse as *Drosophila*, yeast (*Saccharomyces cerevisiae*), and maize (*Zea mays*) show a substantial conservation in organization, sequence, and mode of transposition and are classified according to their sequence organization and mode of transposition (Table 9.1).



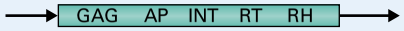
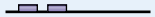
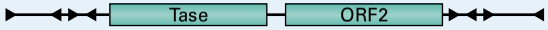
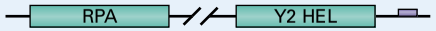
A Grass genomes



B

FIGURE 9.10 *Synteny between different grass genomes. (A) Consensus grass comparative map. The data have been drawn from many sources: Oats–wheat–maize–rice; wheat–rice; maize–rice; maize–wheat; maize–sorghum–sugarcane; and foxtail millet–rice. Arrows indicate inversions and transpositions necessary to describe present-day chromosomes. Locations of telomeres (Δ) and centromeres (□) are shown where known. Hatched areas indicate chromosome regions for which very little comparative data exist. Chromosome nomenclatures indicate arm (short/long or top/bottom). (B) A more detailed view of synteny between soybean and common bean is shown in the alignment of their genetic maps.*

TABLE 9.1 *Classification of plant transposons based upon structural features.*

Order	Superfamilies		TSD
Class I (retrotransposons)			
LTR	Copia, Gypsy		4–6
DIRS	DIRS,		0
PLE	Penelope		Variable
LINE	L1		Variable
	I		Variable
SINE	tRNA, 7SL		Variable
Class II (DNA transposons) – Subclass 1			
TIR	Tc1-Mariner, hAT, Mutator, P		2–11
	PIF-Harbinger		
	CACTA		0
Class II (DNA transposons) – Subclass 2			
Helitron	Helitron		0
Structural features			
Long terminal repeats	Terminal inverted repeats	Coding region 	Noncoding region
Diagnostic feature in noncoding region		Region that can contain additional ORF(s)	
Protein-coding domains			
AP: Aspartic proteinase	APE: Apurinic endonuclease	EN: Endonuclease	ENV: Envelope protein
GAG: Capsid protein	HEL: Helicase	INT: Integrase	ORF: Open reading frame of unknown function
RH: RNase H	RPA: Replication protein A	RT: Reverse transcriptase	Tase: Transposase (*with DDE motif)
YR: Tyrosine recombinase	Y2: YR with YY motif		

TSD, target site duplications.

9.3.1 Retrotransposons are mobile elements that move via an RNA intermediate.

The two basic types of transposable elements are classified according to their mode of transposition: Class I elements transpose via an RNA intermediate and are known as **retrotransposons**, and LTR retrotransposons possess long terminal repeats and encode a GAG protein (involved in the production of virus-like particles), a POL protein (reverse transcriptase) and sometimes also an ENV (envelope protein), frequently fused together as a polyprotein. Retrotransposons are likely viral in origin, as evidenced by their transposition mechanism, which proceeds through an intermediate in much the same way that a retrovirus replicates in a host genome (Fig. 9.11A), although there is scant evidence for actual viral particle intermediates in the case of

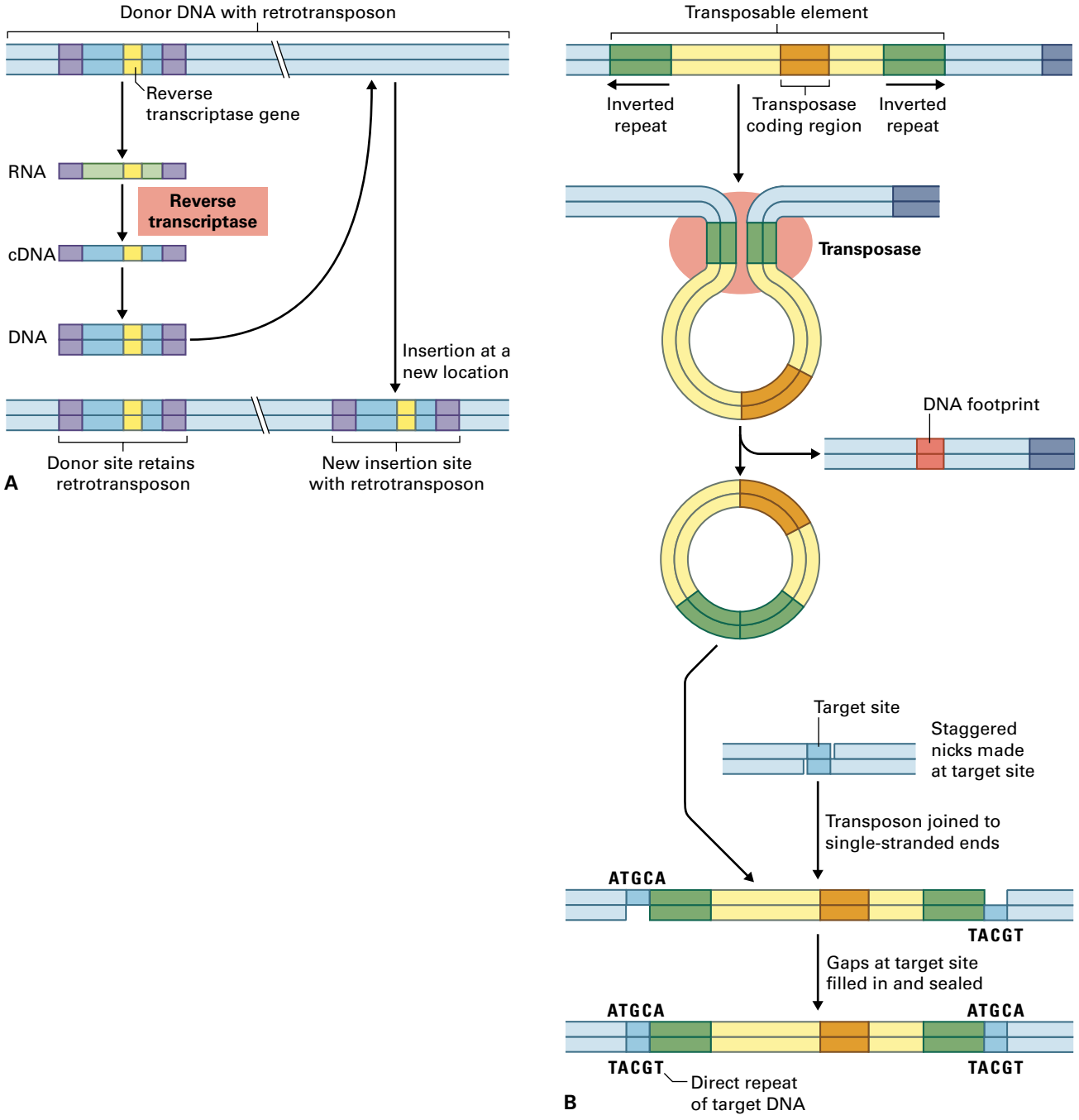


FIGURE 9.11 *(A) Mechanism of retrotransposon transposition. The element to be transposed is copied (transcribed) into an RNA intermediate. This is reverse-transcribed into cDNA which is then inserted into a new location. (B) Structure and transposition of a class II transposable element. A common feature of transposable elements is the flanking of the element by short inverted repeat sequences. A model for transposition suggests that the enzyme transposase recognizes these sequences, creates a stem/loop structure, and then excises the loop from that region of the genome. A staggered cut is made at the new insertion site. After the transposon is inserted the single-stranded regions resulting from the staggered cut are filled in resulting in target site duplication.*

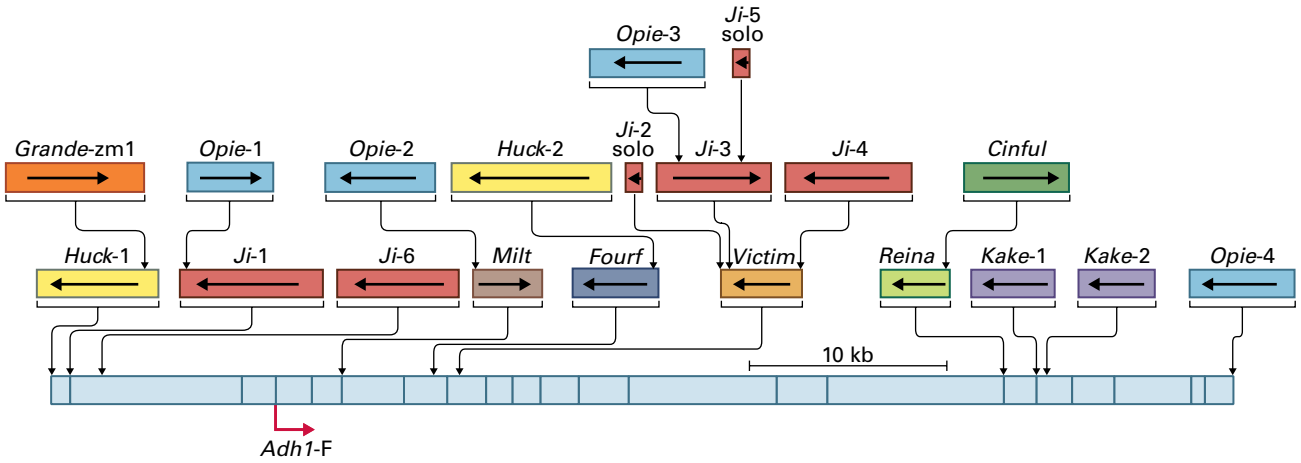


FIGURE 9.12 *Multiple transposition events in the maize genome. Repetitive DNA sequences of the maize genome in the region around the* Adh1 *gene. Retrotransposons make up much of the region of the maize genome around the* Adh1 *gene. Classes of sequence motifs are named (e.g.,* Opie *for blue) and have been placed on the map in the positions where the insertions occur.*

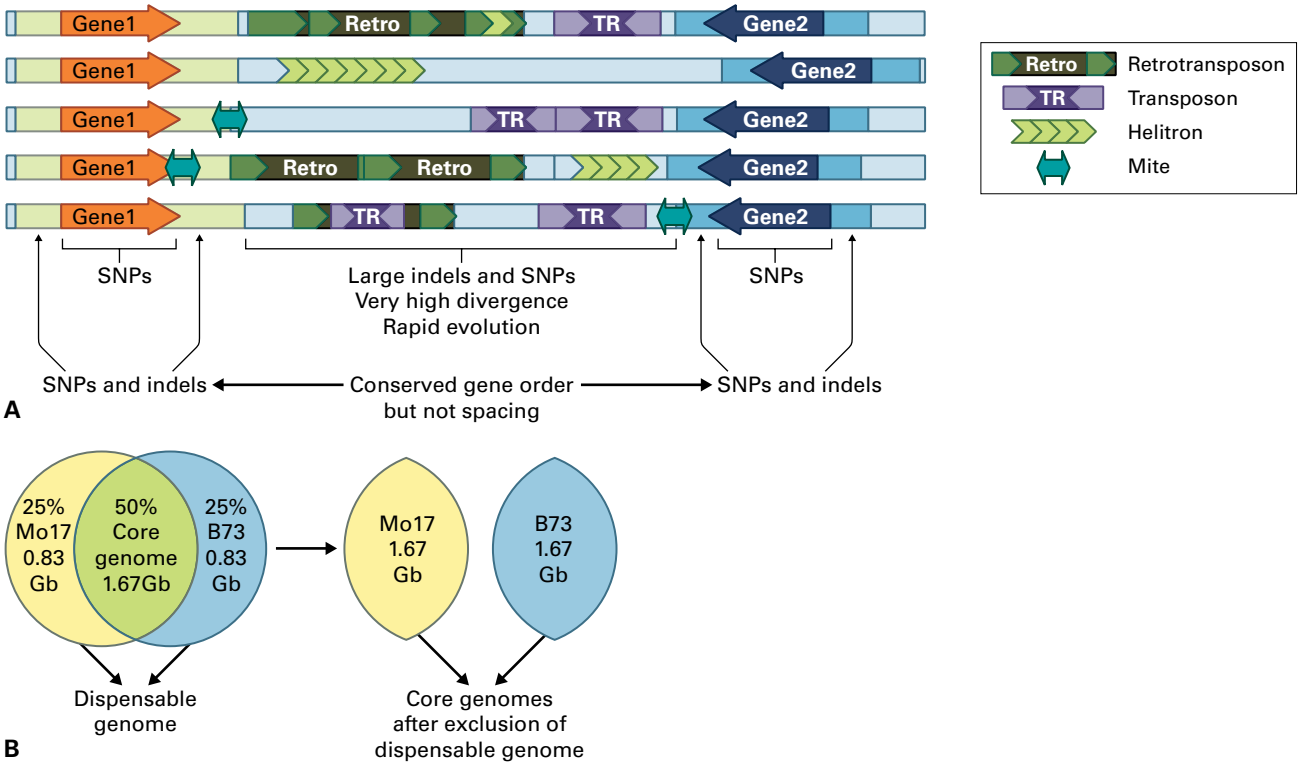


FIGURE 9.13 *Diversity within different maize cultivars and the pan-genome concept. (A) Sequence variation in a short segment of the maize genome. Five different alleles of a short segment encompassing two genes are represented. (B) The pan-genome concept. About two-thirds of the maize genome is shared by the Mo17 and B73 cultivars, while the other one-third is unique to each cultivar.*

plant retrotransposons. Class II elements are **DNA transposons** that transpose via a DNA intermediate and upon excision often leave an altered DNA sequence (footprint) behind at the original position (Fig. 9.11B).

In terms of quantity or copy number, retrotransposons (either active or degenerate versions thereof) greatly outnumber DNA transposons in plant genomes. In large genomes such as those of cereals and other species, such as iris or lily, they can make up 50–90% of the genome. A now classic example of how transposons and transposon expansion can contribute to genome size can be seen in an analysis of a group of nested transposons found in the maize genome

(Fig. 9.12). By comparison of the sequence similarities between the LTR ends of the different members of this complex array of insertions, it was possible to determine the relative age of these events as this build-up occurred (the repeats at the ends of the most recent insertion event being most similar to each other while those at the ends of the oldest insertion event being most diverged).

Sequence analysis of multiple maize accessions has revealed surprising genome diversity. Although many accessions/varieties have the same genetic map (gene order), with only minor variations within genes, there is great sequence diversity between genes (Fig. 9.13A) as well as some variation in gene content, including copy number of multigene families. This kind of variation is likely to be found in other species in which there has been recent transposon activity (i.e., within the last few million years). As a result of this activity, not all members of a single species have the same genetic content. This has led to the concepts of a species' core genome and pan genome, originally proposed for bacterial species. The core genome refers to the set of genes shared by all members of the species, whereas the pan genome describes the total collection of genes in that species as a whole (essentially the intersection and union of each individual's genetic repertoire respectively; Fig. 9.13B).

Many regions of the genome classified as retrotransposon-related based upon their sequence are no longer functional retrotransposons due to sequence changes that disrupt their protein-coding ability. Some of these DNA sequences may still transpose under the influence of intact retrotransposons, and their promoters may also influence the expression of normal genes near their site of insertion into the genome.

Other class I transposons are LINEs (long interspersed elements) and SINES (short interspersed elements). Full-length LINEs range from 4 to 9 kb in length; their transposition requires element-encoded endonuclease, reverse transcriptase, and nucleic acid binding activities. SINEs are small (80–500 bp) nonautonomous elements that use the LINE enzymatic machinery for transposition.

9.3.2 Maize DNA transposons were discovered as elements responsible for chromosome breakage and color variation

Class II elements (see Box 9.8) were the first to be discovered as the Ac/Ds transposable element system in maize (Fig. 9.14). The *Ac/Ds* system consists of two types of elements: the **autonomous element** (*Ac; activator*), and the **nonautonomous element** (*Ds; dissociator*). The Ac element is autonomous because it encodes all products required for its transposition in a 4.6-kb DNA sequence. The central region encodes a 3.5-kb transcript of the transposase that excises both *Ac* and all members of the *Ds* family. Inverted repeats of 11 bp on each end of the *Ac* DNA region function in transposase recognition. In addition, when the element inserts into a new position in the genome, a pair of 8-bp direct repeats generated from the host genome is added to flank the element. These direct repeats, which remain fixed in the genome even after the element transposes out again, are referred to as a **footprint** of the transposition event (see Fig. 9.11B). Inverted repeats at the ends and footprints of insertion/excision events are characteristic of DNA transposable element families like Ac/Ds, but the size and sequences of these signatures are specific characteristics of each family.

Ds elements are a family of related DNA sequences recognized by the transposase encoded by *Ac*. They are nonautonomous because they do not encode their own transposase; rather, *Ds* transposition depends on the presence of *Ac* and its gene products. To date, seven different superfamilies of Class II transposons have been discovered in plants, and examples of at least some of these families are found in all plant genomes. MITES (miniature inverted-repeat transposable elements) are short, nonautonomous DNA elements that are widespread and abundant in plant genomes and require transposases from other elements for their transposition. Most MITEs have been divided into two major groups on the basis of shared structural and sequence characteristics: *Tourist*-like and *Stowaway*-like.

9.3.3 Transposable elements can function in diverse species

Transposable elements from one species can also be active in other species, and this has given rise to the technology of **transposon tagging** to create gene disruptions and mutant phenotypes. For example, a tobacco transposon TnT has been introduced into *M. truncatula* by *Agrobacterium*-mediated transformation. Transposon-tagged lines can be screened for a phenotype of interest, after which the insertion site can be identified by target site rescue and sequencing. Alternatively, in the case of a sequenced genome, the location of random insertion sites can be identified by sequencing, leading to the identification of plant lines containing insertions in genes of interest.

9.3.4 Transposition events can cause mutations and changes in gene expression

Most plant genomes contain a small number of intact, potentially active transposons and a much larger number of defective elements. Transposition events can cause mutations. Unlike Class I elements, Class II elements generally produce unstable mutations. After excision, the impact of the residual target site duplication depends on its location in the regulatory or coding regions and on whether it allows restoration of a disrupted reading frame. Many of the variegated

BOX 9.8 Transposable elements are classified according to their mechanism of transposition and the sequence of the genes that they encode

Order	Example of structure at superfamily level		TSD	Code	Occurrence
Class I (retrotransposons)					
LTR	*Copia*	GAG AP INT RT RH	4–6	RLC	P,M,F,O
	Retrovirus	GAG AP RT RH INT ENV	4–6	RLR	M
DIRS	*DIRS*	GAG AP RT RH YR	0	RYD	P,M,F,O
	Ngaro	GAG AP RT RH YR	0	RYN	M,F
PLE	*Penelope*	RT EN	Variable	RPP	P,M,F,O
LINE	*R2*	RT EN	Variable	RIR	M
	L1	ORF1 APE RT	Variable	RIL	P,M,F,O
SINE	*tRNA*		Variable	RST	P,M,F
Class II (DNA transposons) - subclass 1					
TIR	*Tc1-Mariner*	Tase*	TA	DTT	P,M,F,O
	CACTA	Tase* ORF2	2–3	DTC	P,M,F
Crypton	*Crypton*	YR	0	DYC	F
Class II (DNA transposons) - subclass 2					
Helitron	*Helitron*	RPA Y2 HEL	0	DHH	P,M,F
Maverick	*Maverick*	C-INT ATP CYP POL B	6	DMM	M,F,O

Structural features

- Long terminal repeats
- Terminal inverted repeats
- Coding region
- Noncoding region
- Diagnostic feature in noncoding region
- Region that can contain one or more additional ORFs

Protein coding domains

AP	Aspartic proteinase
APE	Apurinic endonuclease
ATP	Packaging ATPase
C-INT	C-integrase
CYP	Cysteine protease
EN	Endonuclease
ENV	Envelope protein
GAG	Capsid protein
HEL	Helicase
INT	Integrase
ORF	Open reading frame of unknown function
POL B	DNA polymerase B
RH	RNase H
RPA	Replication protein A (found only in plants)
RT	Reverse transcriptase
Tase	Transposase (* with DDE motif)
YR	Tyrosine recombinase
Y2	YR with YY motif

patterns in flowers and in maize kernels are due to transposon excision events (Fig. 9.14). Transposons may affect the expression of neighboring genes, both by read-through transcription into the gene and by the spread of epigenetic silencing from the transposon into nearby regions of the genome (Fig. 9.15).

9.4 Gene expression

The development of plants and their ability to respond to changes in the environment depend largely on the readout of the information within their genome. This process of **gene expression** requires the transcription of genes into RNA and in many cases the translation of these RNAs into the ultimate gene products—proteins. This section examines the molecular machinery that mediates gene expression and describes some of the most common regulatory mechanisms that control gene activities in plants.

9.4.1 RNA polymerases have distinct functions in the transcription of nuclear genes

RNA polymerases (RNAPs) are the enzymes that synthesize the different types of RNA found in plant cells. In plants, up to five different RNAPs mediate the transcription

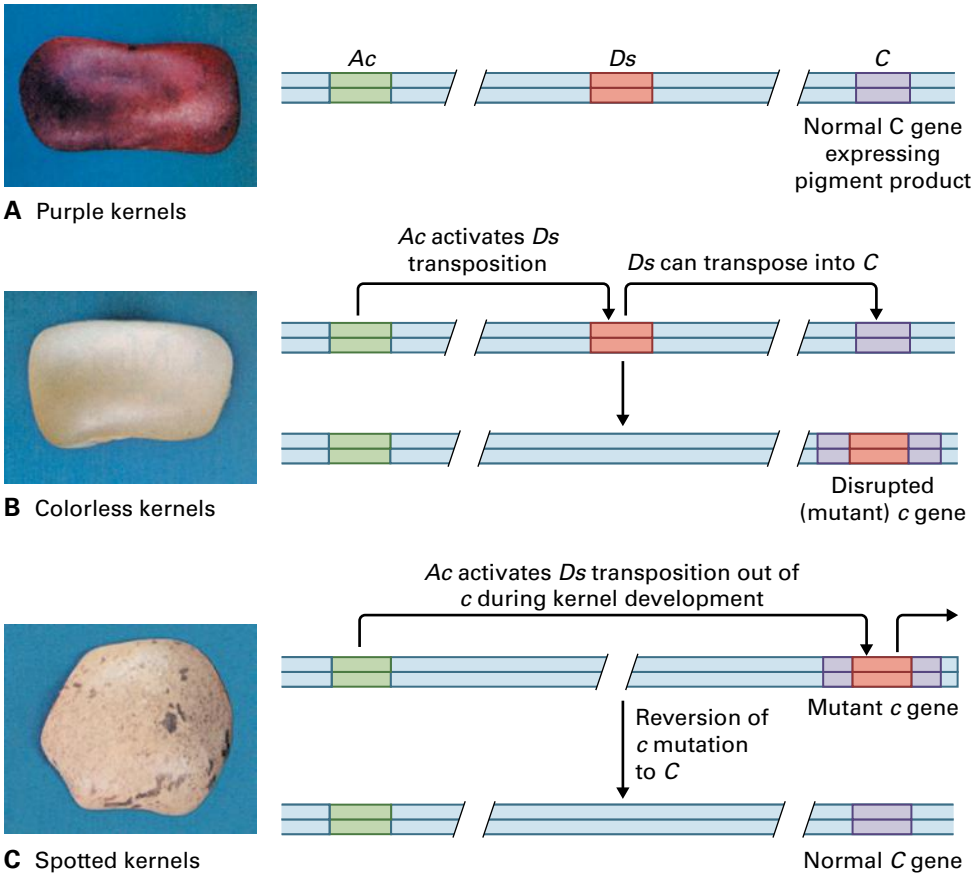


FIGURE 9.14 *Variegated corn and effects of transposition of the color patterns in corn kernels. Barbara McClintock was the first scientist to recognize the existence of transposable DNA elements in the genome. She proposed that genes, or sections of genes, could "jump" from one position in the genome to another, based on her observations of the genetics of certain maize kernel phenotypes. The following example illustrates the progression of events: (A) The* C *gene encodes maize pigments that make the kernels purple, so when* C *is active, kernels are purple. (B)* Ac *encodes a transposase that mediates transposition of the* Ds *element.* C *is inactivated when the transposable element Ds is inserted into it, resulting in a colorless mutant phenotype (*c*). (C) If* Ds *is transposed ("jumps") out of the mutant* c *gene during the course of development,* C *is restored to activity, and purple sectors are seen within a colorless background.*

of genes in the nuclear genome, and additional RNAPs are responsible for transcription of organellar genomes (see Chapter 6). The nuclear RNAPs (designated RNAP I–V) have distinct functions and synthesize different types of RNAs (Table 9.2).

The role of **RNAPI** in gene expression is highly specific in that it only transcribes the 45S ribosomal RNA (rRNA) precursor, which is processed into 5.8S, 18S, and 28S rRNAs. Despite this limitation, RNAPI-mediated transcription accounts for up to 50% of RNA synthesis in growing cells.

RNAPII is responsible for the transcription of protein-coding genes and thus synthesizes messenger RNAs (mRNAs). In addition, it transcribes microRNA (miRNA) genes and synthesizes small nuclear RNAs (snRNAs), as well as *trans*-acting small interfering RNAs (ta-siRNA) (see Chapter 6). Because of its central importance for the expression of proteins, RNAPII has been studied extensively and its structure has been resolved in atomic detail (Fig. 9.16).

RNAPIII transcribes genes coding for transfer RNAs (tRNA), 5S rRNA, and a variety of other small RNAs. **RNAPIV** and **RNAPV** have been discovered only relatively recently, and in contrast to RNAP I to III, which are present in all eukaryotes, appear to be plant-specific (RNAPV is only found in angiosperms, or flowering plants). Furthermore, these RNAPs are not essential for the viability of a plant, unlike RNAPs I, II, and III. The function of RNAPIV is to synthesize small interfering RNAs (siRNAs). RNAPV transcribes noncoding RNAs involved in siRNA-mediated gene silencing (see Chapter 6).

Because of structural differences, RNAPs differ in their sensitivity to inhibitors of transcription. For example, RNAPII is highly sensitive to α-amanitin, a cyclic octapeptide found in the *Amanita* genus of mushrooms and one of the main sources of mushroom poisoning. In contrast, RNAPI is insensitive to α-amanitin, and RNAPIII has intermediate sensitivity. RNAPIII can be further selectively inhibited by tagetitoxin, a bacterial phytotoxin. Because of these differences in sensitivity, RNAP-specific inhibitors such as α-amanitin and tagetitoxin are useful in distinguishing between transcripts generated by different RNAPs.

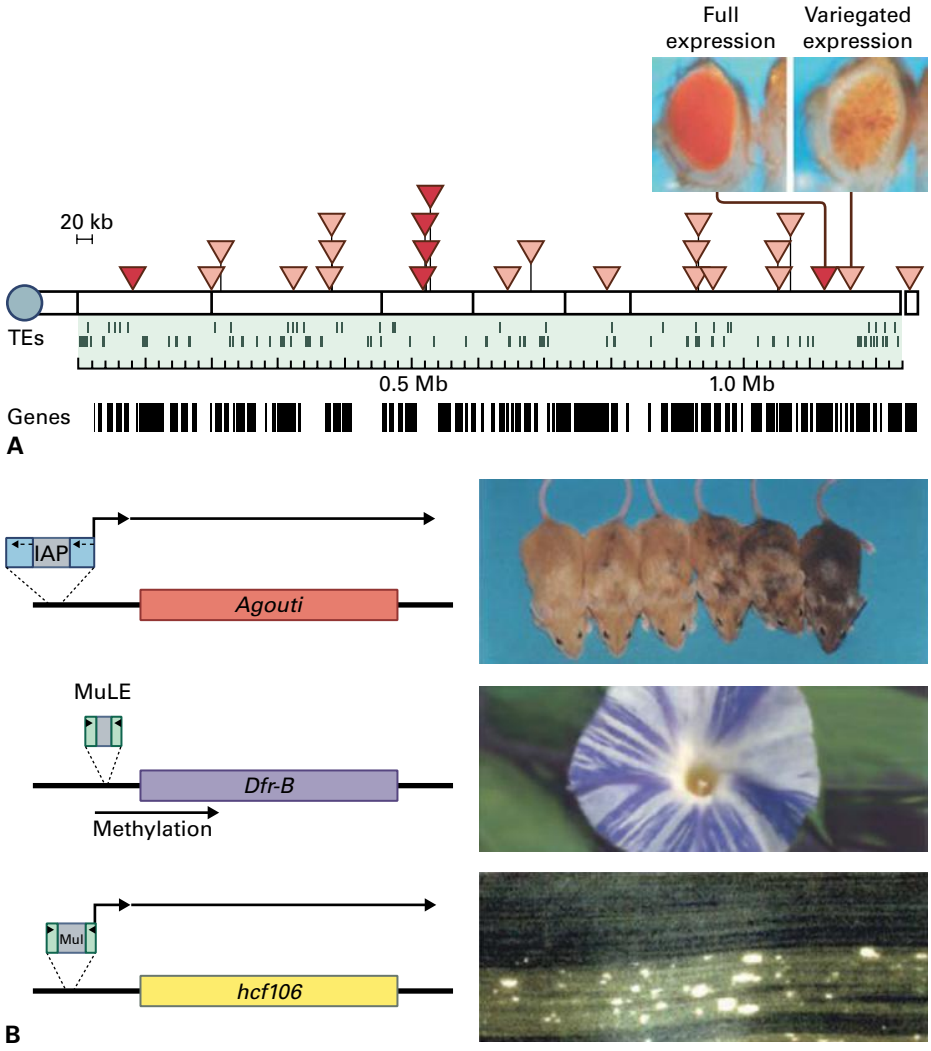


FIGURE 9.15 *Transposable elements can have a variety of effects on nearby genes. (A) Position effect variegation in* Drosophila melanogaster. *The expression of a transgene conferring red eye color depends on its proximity to transposable elements. Solid red triangles indicate insertion sites that confer full red color in a white-eyed mutant, while transgenes inserted at sites shown by hatched triangles produce variegated eye color due to modulation of expression by nearby transposable elements. (B) Three examples of variegation induced by transposon insertion close to a protein-coding gene. In mice, the IAP retrotransposon produces an outward-reading transcript that extends into the agouti coat-color gene. The level of agouti transcript, and the color of the coat, is subject to the epigenetic status of the retrotransposon and is heritable. In morning glory (*Ipomoea *sp.) flowers, DNA methylation of a nonautonomous MuLE transposon can spread to the promoter of the dihydroflavonol reductase gene, creating petal-color streaks. In maize (*Zea mays*), the activity of one TE family regulates two epialleles. In sectors where the Mutator transposon family is active, the mutant phenotypes of both epialleles occur, generating single sectors of pale green (high chlorophyll fluorescence, hcf106 mutant) and necrotic spotted (les28 mutant) tissue on leaves92. hcf106 transcripts are initiated by a nonautonomous (Mu1) transposon only when the autonomous transposon elsewhere in the genome is inactive.*

TABLE 9.2 *Plant nuclear RNA polymerases and their products.*

RNAP	RNA synthesized
I	5.8S, 18S and 28S rRNAs
II	mRNAs, miRNAs, snRNAs, ta-siRNAs
III	5S rRNA, tRNAs, snRNAs
IV	siRNAs
V	noncoding RNAs

9.4.2 General transcription factors and RNA polymerases form the basal transcriptional machinery

The process of transcription can be divided into three consecutive phases: (i) initiation of transcription, (ii) an elongation step that leads to the formation of an RNA product through RNAP activity, and (iii) termination.

The initiation of transcription is an important control step that depends on the formation of a **transcription preinitiation complex** (Fig. 9.17). This multisubunit protein complex is composed of an RNAP and associated proteins (Table 9.3)

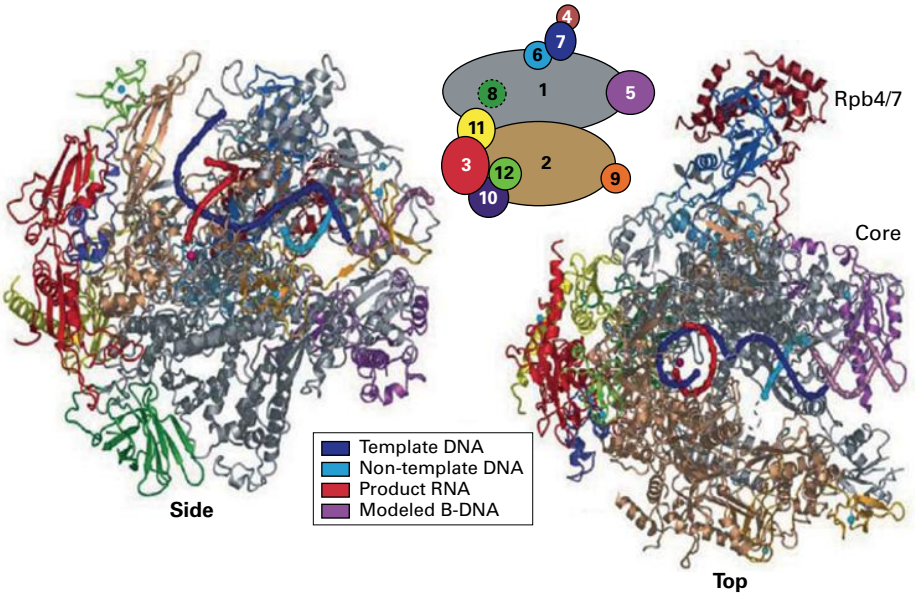


FIGURE 9.16 *Crystal structure of the RNAPII elongation complex from yeast (*Saccharomyces cerevisiae*). The polymerase subunits are color-coded according to the key between the top and side views. Template DNA, nontemplate DNA, and product RNA are shown in blue, cyan, and red, respectively.*

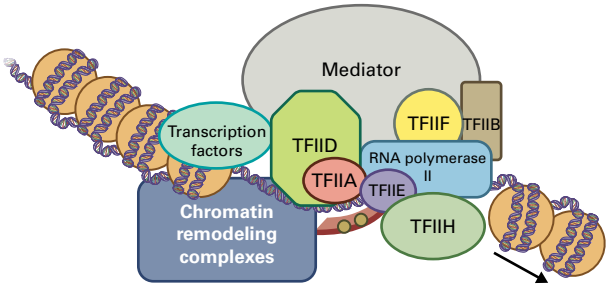


FIGURE 9.17 *Schematic representation of the RNAPII preinitiation complex and its interactions with transcription factors and chromatin remodeling complexes on DNA. Light-brown beads symbolize nucleosomes.*

that modulate RNAP activity and recruit the enzyme to the promoters of genes. For example, RNAPII cannot bind to DNA alone; rather, it requires the presence of several **general transcription factors** (TFIIA, B, D, E, F, and H). TFIID, itself a multiprotein complex, constitutes the key set of proteins in the transcription preinitiation complex.

One of the TFIID components, **TATA binding protein** (TBP) recognizes the **TATA box** (Fig. 9.17), a DNA sequence motif located in the promoters of many protein-coding genes around position –30 (i.e., 30 nucleotides upstream from the transcription initiation site, which corresponds to the first nucleotide of the RNA). TBP-mediated binding of the TFIID complex to a promoter leads to the sequential recruitment of additional general transcription factors and RNAPII into the preinitiation complex and subsequently to the initiation of transcription.

9.4.3 The expression of many plant genes changes during development or in response to environmental cues

Some plant genes are constitutively expressed, meaning that they are transcribed in all cells of a plant. These genes often function as **housekeeping genes**, because they encode proteins that are involved in basic cellular functions such as carbohydrate metabolism or protein biosynthesis. However, not all genes in a nuclear genome are expressed at all times; many are transcribed only at certain stages of plant development or in specific tissues or cell types. The expression of even other genes depends on environmental signals or stresses to which the plant has to adapt. The term **differential gene expression** refers to such changes in transcriptional activities during development or in response to environmental

TABLE 9.3 *Components of the RNAPII preinitiation complex in* Arabidopsis.

Factor	Number of subunits	Function
TFIIA	3	Stabilizes TBP-TATA interaction
TFIIB	1	Selection of the transcription initiation site
TFIID	TBP and 12-15 TAFs	Recognition of promoter elements
TFIIE	2	Formation of the initiation complex
TFIIF	2	Recruits TFIIE and TFIIH
TFIIH	10	Allows RNAPII promoter escape and elongation
RNAPII	12	Initiation, elongation and termination of transcription
Mediator	≈34	Relays information of DNA-bound transcription factors to RNAPII

TAF: TBP-Associated Factor.

BOX 9.9 Gene expression in plants can be analyzed by different methods

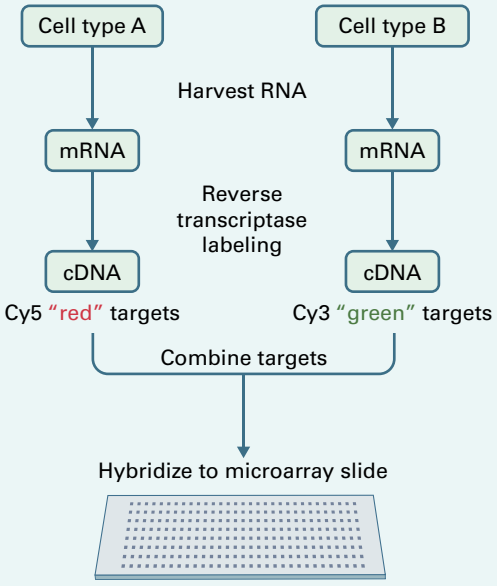
Methods for analyzing gene expression in plants can be divided into single-gene and genome-wide approaches. To determine the expression pattern of a single gene in a plant, a number of established experimental methods can be used, and the most common include **reverse transcriptase PCR** (RT-PCR), in situ hybridization, and reporter gene approaches.

RT-PCR is based on the synthesis of complementary DNA (cDNA) from mRNA isolated from specific tissues or cell types. This reaction is catalyzed by the enzyme reverse transcriptase, which was first isolated from RNA viruses. A PCR reaction with gene-specific primers then leads to the detection of cDNAs from specific genes. Through the use of DNA-binding dyes, the amplification of cDNA fragments by PCR can be followed in real time, allowing the quantitation of transcripts in a sample. This approach, known as **quantitative real time RT-PCR** (qRT-PCR), has become a standard in molecular biology.

In situ hybridization is based on direct detection of mRNA in a tissue sample. An RNA probe complementary to the mRNA of interest is synthesized and labeled with an epitope tag for detection. This probe is then incubated with entire plant organs (known as whole-mount *in situ* hybridization) or with tissue sections. After hybridization of the probe to the target mRNA, antibodies directed against the epitope tag are added. These antibodies are coupled to an enzyme that catalyzes a color reaction to allow detection.

Commonly used reporter proteins in plants are **β-glucuronidase** (GUS) as well as **Green Fluorescent Protein** (GFP) and its many derivates. These reporter proteins are either expressed under control of the promoter of a gene or they are translationally fused to the amino- or carboxyl-terminal end of the protein under study. Detection of the GUS reporter in plant tissue is based on a colorimetric reaction; in contrast, GFP signal is detected through the use of fluorescent or confocal microscopes.

Genome-wide approaches used for the detection of differentially expressed genes are microarray analysis and RNA sequencing. **Microarrays** (see figure) are based on single-stranded DNA probes that are complementary to gene transcripts. These probes are usually synthesized chemically and then spotted and immobilized onto glass slides. For the detection of transcripts in a sample, mRNA is isolated and reverse-transcribed into cDNA. The cDNAs are then labeled with a fluorescent dye, and the resulting material is incubated with a microarray so the different cDNAs can hybridize to their complementary probes. After washing the microarray thoroughly, it is scanned to reveal and quantitate the fluorescent signals. **RNA-sequencing** (RNA-Seq) is based on the direct sequencing of cDNA libraries using ultra high-throughput DNA sequencing technologies. This technique is likely to supersede microarray analysis for the genome-wide detection of gene expression because it is more sensitive and does not require the time-consuming and expensive preparation of DNA probes.



cues. Many different experimental approaches have been established to study gene expression in plants (see Box 9.9).

To understand the importance of differential gene expression for plant growth and development, it is important to take a look at how different cell types are formed through the process of **cellular differentiation**. It is now well-established throughout the biological kingdom that, with few exceptions, cellular differentiation does not involve loss of genetic information. This was demonstrated first in the plant kingdom by classic experiments on carrot and tobacco, where tissue explants or isolated cells from a mature plant could be induced to regenerate into a complete plant that was identical to the root cell donor. This notion of the **totipotency** of nuclei from adult cells was replicated in frogs by the demonstration that the cytoplasm of an enucleated frog egg is capable of development when guided by the genome of a nucleus transferred from a differentiated frog cell. These classic experiments have now been superseded by the isolation first of embryonic stem cells from mice, humans, and other animal species and the more recent demonstrations of reprogramming of differentiated adult mammalian cells by transfection with an appropriate suite of transcriptional regulators. Cell differentiation that accompanies an organism's development can therefore be seen as the orchestrated activation and repression of appropriate

sets of genes in different organs and tissues over developmental time. How is this process controlled to ensure that certain gene sets are active only at specific stages of development or in certain parts of the plant body? The answer to this question involves the regulatory regions of the genome, the promoters of genes.

9.4.4 Promoters are composed of regulatory DNA sequence elements

A promoter contains various sequence elements that collectively recruit the protein factors that regulate the transcription of a gene. Each class of RNA polymerase binds to its cognate promoters to initiate transcription. Promoters consist of two types of regulatory elements, **basal elements** and ***cis*-elements**. Basal elements are necessary for RNA polymerase binding and positioning and generally lie within 50 bp up- or downstream of the transcription initiation site. They are often relatively conserved between different genes and together form the **core promoter**. One example for a basal element is the TATA box (see Section 9.4.2), and other examples for elements in core promoters are the **TFIIB recognition elements** (BREs), which are found immediately upstream and downstream of TATA boxes (Fig. 9.18) and recognized by the general transcription factor TFIIB, and the **downstream promoter element** (DPE), which is located around 30 bp downstream of the transcriptional start site and bound by subunits of the TFIID complex. Not all types of basal elements are always present in a given promoter; instead, the composition of core promoters shows a large degree of variability. In contrast to other eukaryotes, basal elements are as yet not well defined in plants due, at least in part, to the limited sequence data of precisely defined transcription start sites.

Unlike basal elements, which show some degree of conservation between different genes, *cis*-elements vary greatly from gene to gene. "*Cis*" (from Latin, meaning "on the same side") refers to the fact that these regulatory elements are located on the same DNA molecule as the genes they control. *Cis*-elements are responsible for the activation, repression or modulation of gene expression. They are bound by ***trans*-acting factors**, proteins encoded elsewhere ("in *trans*") in the genome that can interact directly with the basal transcriptional machinery (for example, with components of the TFIID general transcription factor complex) or indirectly through **mediator**, a large protein complex that acts as a transcriptional coregulator (see Fig. 9.17). This, in turn, influences the rate at which transcription by the appropriate RNA polymerases occurs. The *trans*-acting factors that bind *cis*-elements are usually transcription factors. They are also called **specific transcription factors** to distinguish them from the general transcription factors discussed above.

Most *cis*-elements in plants lie within 1–2 kb of sequence upstream of the transcription start site (Fig. 9.18). However, they may also be found further upstream, in a gene's introns or exons, or downstream of the site where termination of transcription occurs. *Cis*-elements are usually short (<10 bp) in sequence and vary greatly in their base composition (Table 9.4).

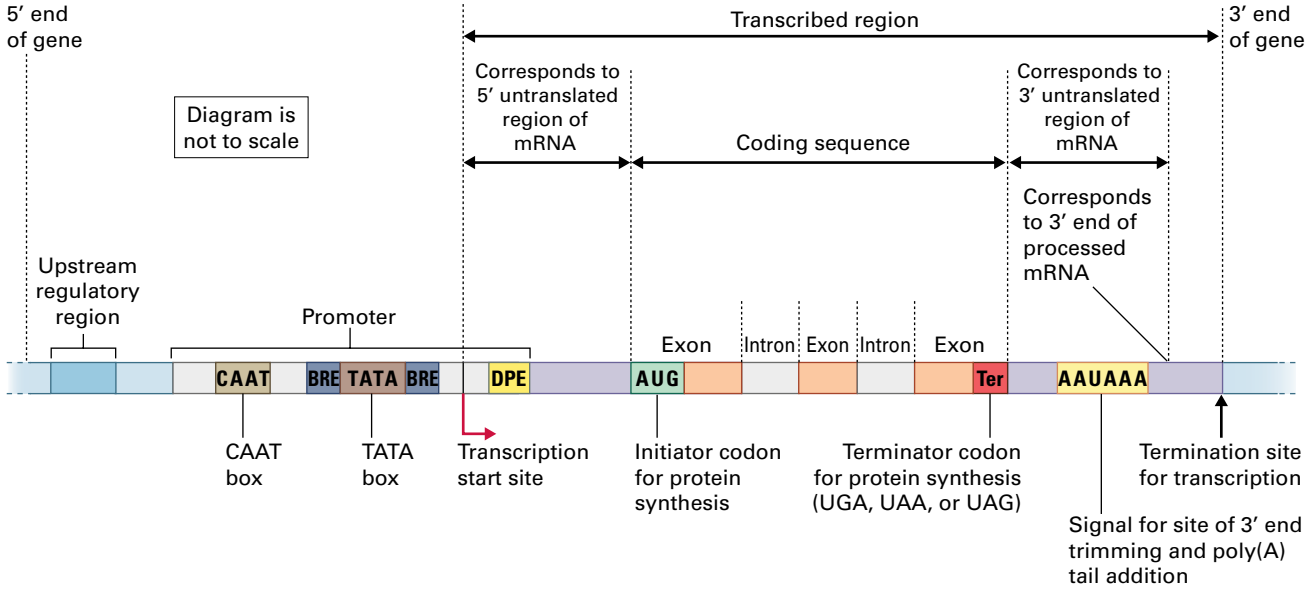


FIGURE 9.18 *Structure and organization of a eukaryotic gene. A gene is divided into several functional units. The transcribed region acts as a template for synthesis of mRNA, which is then edited and translated into the protein product of the gene. The transcribed region is interspersed with noncoding sequences that partition the region into coding sections (exons) and noncoding sections (introns). The transcribed region is flanked on either side by noncoding sequences that play a role in regulation of the gene. Most of the regulatory sequence elements are in the 5′ flanking region. The first 1,000 bp or so of the 5′ flanking region is referred to as the gene promoter, as it contains sequence motifs important for the "promotion" of transcription. One of the most highly conserved regulatory elements is the TATA box, which is usually found within the first 50 bp of the transcription start site. The TATA box coordinates the recruitment of RNAPII to the gene.*

TABLE 9.4 *Examples for DNA sequence motifs bound by* Arabidopsis *transcription factors, and their functions in plant growth and development.*

Motif name	Sequence	Bound by	Function
ABA-responsive element (ABRE)	CACGTGGC	ABRE-binding factors (bZIP proteins)	ABA response
Auxin response element (ARE)	TGTCTC	Auxin response factors	Auxin response
CArG box	$CC(A/T)_6GG$	MADS domain proteins	Flower development, etc.
Evening element	AAAATATCT	Certain MYB proteins	Gene regulation by the circadian clock
G box	CACGTG	bZIP and bHLH proteins	Light response, etc.
GATA promoter motif	(A/T)GATA(G/A)	GATA transcription factors	Various

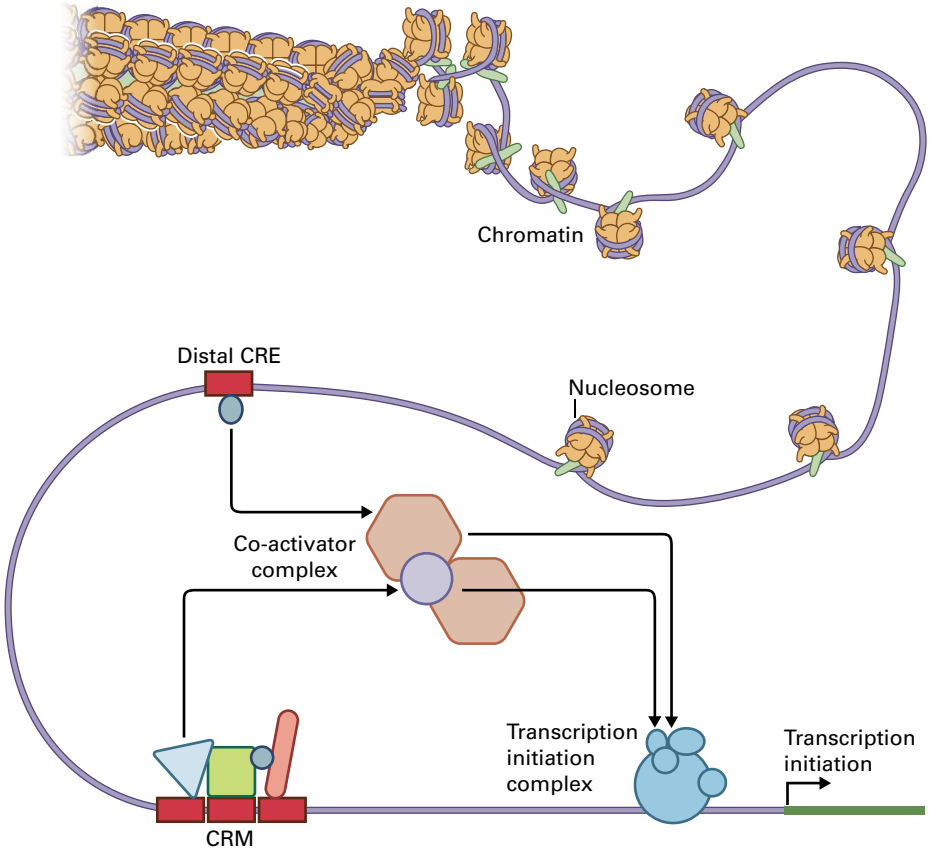


FIGURE 9.19 *Example for the function of* cis*-regulatory modules and enhancers. A* cis*-regulatory module in the promoter of a gene is bound by several transcription factors. This transcription factor complex, together with an input from a distal* cis*-regulatory element (CRE), which acts as an enhancer, leads to the recruitment of a co-activator complex and ultimately, to the promotion of transcription.*

A promoter can contain several different *cis*-elements, and more than one copy of the same element can be present. These elements often cluster together to form ***cis*-regulatory modules**. The function of these modules likely allows the cooperative action of several (different or identical) transcription factors in the regulation of gene expression by bringing them in close proximity to one another (Fig. 9.19). *Cis*-regulatory modules are often classified as **enhancers** or **silencers**, depending on whether they promote or inhibit the expression of a gene. Some biologists use the terms enhancer and silencer to refer to regulatory elements that are located a great distance away from the transcribed region of a gene to distinguish them from **proximal promoter elements** (regulatory elements found in the vicinity of the transcription start site). *Cis*-regulatory modules can also function as **insulators** to block signals from enhancers and silencers and prevent them from influencing gene expression activities of certain genes (Fig. 9.20).

Cis-elements can mediate expression of specific genes during development or in response to internal or external signals. One example is the auxin response element (AuxRE; sequence: 5′-TGTCTC-3′), which is found in the promoters of genes controlled by the phytohormone auxin (see Chapter 18). The occurrence of specific *cis*-elements in a

promoter, therefore, determines where and when a gene is expressed in a plant. Hence, the capacity of cells for differential gene expression is hardwired into the genome in the form of a ***cis*-regulatory code**.

9.4.5 Diverse transcription factor families control gene expression

As discussed above, *cis*-elements are bound by transcription factors that in turn promote or inhibit gene expression by interacting with components of the transcriptional machinery. These transcription factors usually bind DNA in a sequence-specific manner so that a given transcription factor targets a specific *cis*-element; for example, the ARE mentioned above is bound by members of a family of transcription factors called auxin response factors (ARFs).

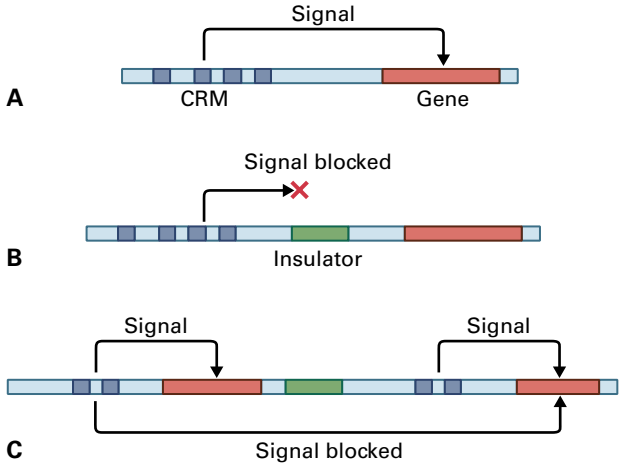


FIGURE 9.20 *Function of genetic insulators. The effect of a* cis*-regulatory module (CRM) on a gene (A) can be blocked by the presence of an insulator (B). Insulators can also limit the effects of a CRM on a specific gene, preventing neighboring genes from responding to CRM activity (C).*

Transcription factors are typically composed of at least two domains with different functions. The **DNA-binding domain** mediates the recognition of and binding to a *cis*-element, while the **transactivating domain** interacts with the transcriptional machinery and determines the activity of the protein. Transcription factors also typically contain a **nuclear localization sequence** (NLS), which allows the proteins to enter the nucleus after they have been synthesized in the cytoplasm.

Several different types of DNA-binding domains have been identified, and their structures have been resolved in atomic detail, yielding detailed insights into how they interact with DNA (Fig. 9.21). For example, **zinc finger** transcription factors are characterized by a domain that carries a duplicated set of projections that insert into the major groove of the DNA double-helix. The projections are created by coordinating a zinc ion with four amino acids (often a combination of two histidine and two cysteine residues). Another structural motif frequently found in transcription factors is the **basic leucine zipper** (bZIP) domain. Proteins with this domain form dimers that bind to the major groove of the DNA molecule. Each bZIP monomer contains an α-helix in which every seventh amino acid residue is a leucine. The leucine residues face each other in the dimer and their structural arrangement "zips" the helices together into a coiled coil arrangement. The coiled coil holds the dimer together and holds the basic region in place within the major groove. Compared to DNA-binding domains, transactivating domains are structurally not well defined (note that a transactivating domain, despite its name, can also act to repress the transcription of a gene).

Transcription factors can thus be divided into **repressors** and **activators**, depending on their effect on gene expression. However, some transcription factors carry both repressor and activator function. These proteins are said to be **bifunctional**. Which of the two functions dominates in the control of a given gene may depend on the presence of additional transcription factors at that gene's promoter or on posttranslational modifications of the bifunctional transcription factor that render one of the transactivating domains inactive.

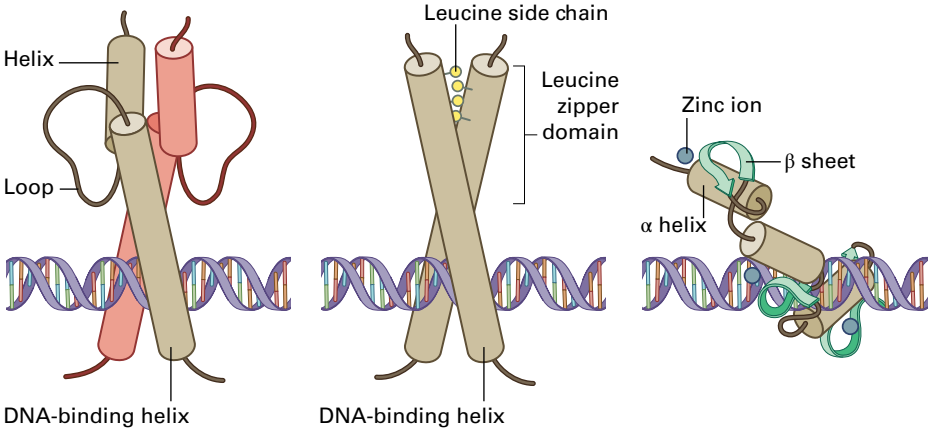


FIGURE 9.21 *Three major types of DNA binding domains. (A) Helix–loop–helix motif. (B) Basic leucine zipper. (C) Zinc finger domain. Each model illustrates the DNA/protein complex.*

TABLE 9.5 *Examples for transcription factor families in* Arabidopsis *and rice. The number of family members, and whether the families are plant specific, is indicated.*

Family	*Arabidopsis*	Rice (*Oryza sativa*)	Plant specific
AP2/ERF	147	161	No*
bZIP	74	94	No
GRAS	32	57	Yes
MADS	108	77	No
MYB	198	182	No
NAC	100	149	Yes
WRKY	71	109	No*

*But predominantly found in plants.

The pivotal role of transcription factors for the regulation of plant growth and development is demonstrated by the large number of transcription factor-coding genes in plant genomes. For example, the *Arabidopsis* genome contains approximately 2,000 genes that encode transcription factors. This number corresponds to roughly 6% of all *Arabidopsis* genes, considerably higher than that observed in many other model organisms. The different transcription factors found in higher plants can be grouped into 50 or so families, depending mainly on sequence similarities. The names of these families sometimes refer to common structural features (e.g., **basic helix–loop–helix proteins** (bHLH) contain a DNA-binding domain composed of two α-helical segments separated by an intervening loop) (Fig. 9.21), but they are also often named after their physiological function in the plant (e.g., the ARFs mentioned above) or after the founding member(s) of a family (e.g., the **AP2-like transcription factors**, which constitute one of the largest transcription factor families in plants, were named after the APETALA2 (AP2) protein, a key regulator of flower development).

Many plant transcription factor families are also found in other eukaryotes (e.g., bZIP and MYB proteins) (Table 9.5); however, the number of family members is often considerably enlarged or reduced in plants when compared to those of animals or fungi. One example is the family of **MADS domain transcription factors** (named after the four founding members of the family), which has over 100 members in *Arabidopsis*, but only two in *Drosophila*. At the same time, the *Drosophila* genome encodes many more zinc-finger transcription factors than *Arabidopsis* despite having fewer genes. In addition to evolutionary conserved transcription factor families, plants contain many transcription factors that are not found outside of the plant kingdom, including, for example, the ARFs mentioned above.

The large number of transcription factors in plants implies a high degree of complexity in the regulation of gene expression activities. This complexity is further increased by the fact that many transcription factors, such as the bZIP proteins, act as dimers. In addition to **homodimers** (pairs of identical proteins), many transcription factors also form **heterodimers** (pairs of different transcriptional regulators). Because a single transcription factor can form heterodimers with many different partner proteins, the number of possible transcription factor complexes is staggering. Moreover, the activities of transcription factors can be regulated through a plethora of posttranslational modifications that often occur in response to the activation of a specific signal transduction pathway (see Chapter 18). For example, phosphorylation of a transcription factor by a specific protein kinase may alter DNA-binding activities or serve as a signal for its degradation. The activities of other transcription factors are controlled by changes in their intracellular localization; while retention of a transcription factor in the cytoplasm renders it inactive, the induction of its nuclear import leads to its activation.

A key problem in regulatory biology is identifying the genes that a transcription factor controls and the *cis*-elements to which it binds. To address this problem, a number of experimental approaches have been developed to locate the binding site of a transcription factor in a genome. A particularly powerful technique for the identification of **target genes** of transcription factor is **chromatin immunoprecipitation** (ChIP; see Box 9.10). The results of genome-wide analyses of binding sites of several transcription factors in *Arabidopsis* suggest transcription factors can bind to hundreds, if not thousands, of regions across the genome. At the same time, not all binding events result in changes in gene expression, perhaps because these sites lie outside of functional *cis*-regulatory modules.

9.5 Chromatin and the epigenetic regulation of gene expression

9.5.1 Nuclear DNA is packaged into chromatin, a dynamic structure

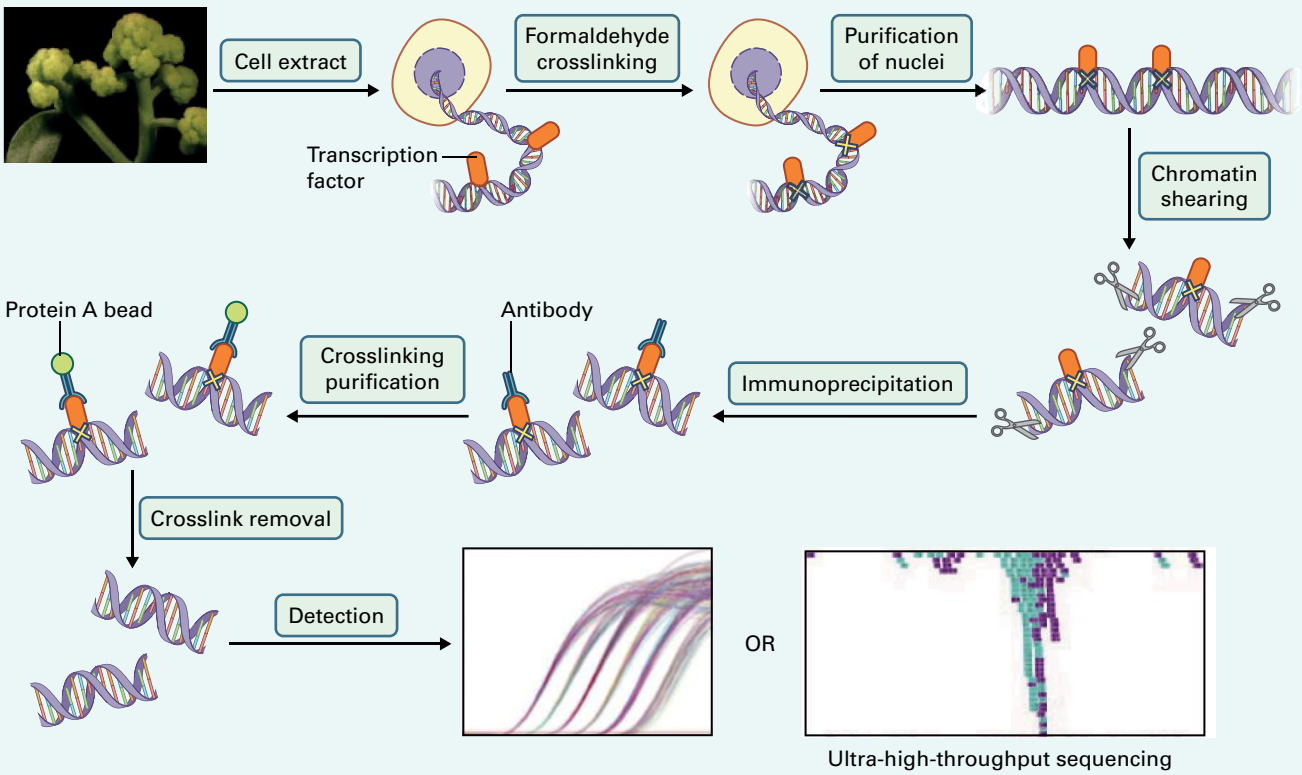
The nuclear genomes of many plants are exceptionally large, and to fit this amount of DNA into a nucleus that is only a few micrometers in diameter, the nuclear DNA is condensed to reduce its length. This efficient packaging strategy is made possible through the association of DNA with different types of proteins into **chromatin**. The most important and abundant of these proteins are the histones. Histones are relatively small proteins that contain many basic amino acid residues in their sequence, resulting in a high positive net charge that allows them to bind strongly to the negatively charged DNA. As described earlier (see Section 9.1.1), the main function of histones is the formation of nucleosomes (see Fig. 9.1).

BOX 9.10

The binding sites of transcription factors can be identified through chromatin immunoprecipitation (ChIP)

A chromatin immunoprecipitation (ChIP) assay begins with fixation of plant tissue with a crosslinking agent such as formaldehyde, which covalently attaches DNA-binding proteins to the nucleic acid. Subsequently, chromatin is isolated from the cells and broken into small fragments. These chromatin fragments are then incubated with antibodies against the protein of interest. After purifying the DNA–protein–antibody complexes, for example, through the use of immobilized protein A, which has a high affinity for certain antibody types, the crosslinks are reversed and the immunoprecipitated DNA is isolated. The genomic fragments can then be tested for an enrichment of specific genomic regions through real-time PCR ("ChIP-qPCR"), or on a genome-wide scale through the use of DNA microarrays ("ChIP-chip") or ultra-high-throughput DNA sequencing ("ChIP-Seq") methods. Genomic regions found to be overrepresented in the immunoprecipitated chromatin relative to negative control regions (i.e., regions that are not bound) likely contain binding sites of the protein of interest.

The ChIP procedure can also be employed for epigenetic marks (especially histone modifications) using antibodies directed against these chromatin modifications.



The high degree of condensation of nuclear DNA within chromatin poses a considerable challenge for the process of gene expression (as well as for other processes, such as DNA replication), because transcriptional units and promoter sequences are inaccessible for RNA polymerases and transcription factors. Early studies on the correlation between gene expression and chromatin structure established that active genes are generally more sensitive to digestion by the nuclease DNase I than are inactive genes (Fig. 9.22). These differences are due to the fact that chromatin surrounding a transcriptionally active gene is less condensed than genomic chromatin as a whole and is thereby more accessible to nuclease digestion. Regions of DNA that are hypersensitive to DNase I are thought to be nucleosome free, allowing transcription factors greater access to promoter *cis*-elements. These regions of low chromatin condensation are also termed **euchromatin**, whereas regions that are highly condensed are referred to as **heterochromatin**.

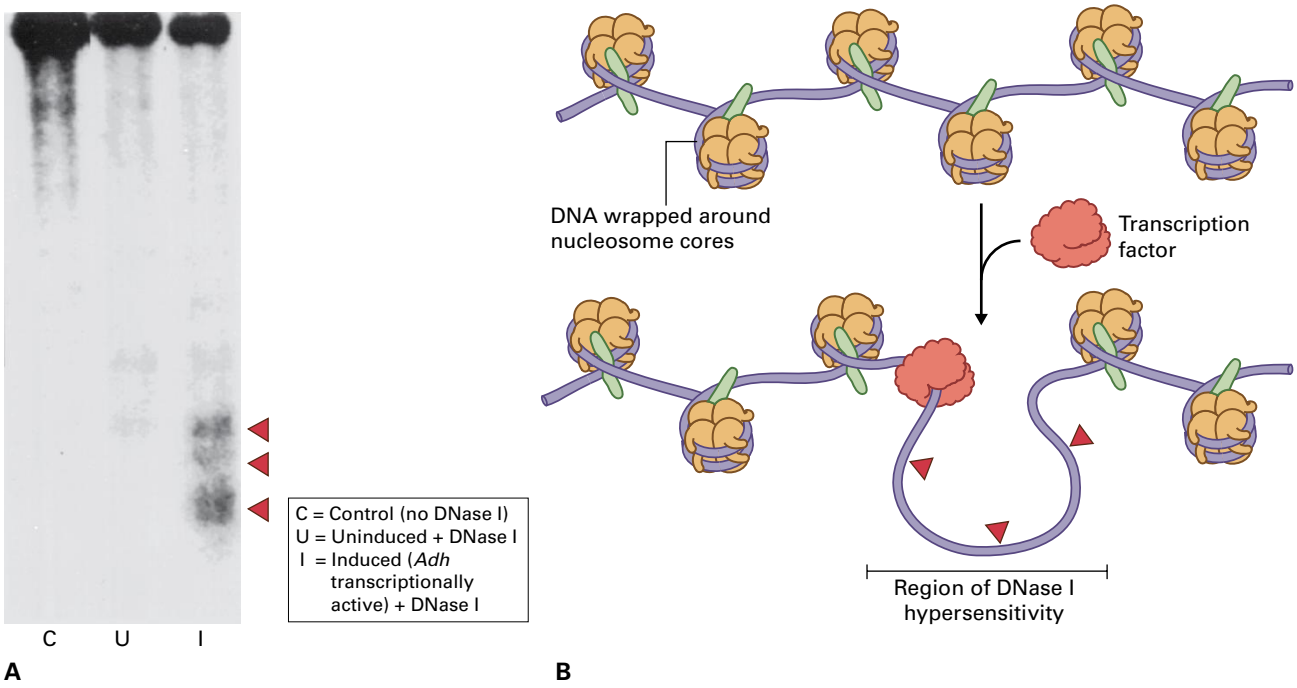


FIGURE 9.22 *DNase I hypersensitive sites in the maize Alcohol Dehydrogenase 1 (ADH1) promoter. As a gene becomes transcriptionally active, regions of the promoter become less condensed, to accommodate transcription factors. This opening of the promoter chromatin can be visualized as an increase in accessibility to DNase I digestion. DNase I is an endonuclease with very little sequence specificity. DNA held in a condensed chromatin configuration is difficult for DNase I to access, but when the chromatin of a gene promoter becomes less condensed—to afford access to the transcriptional machinery—it also becomes more accessible to DNase I. Thus, hypersensitivity to DNase I is a hallmark of the less-condensed chromatin configuration necessary for a gene to become transcriptionally active. (A) The ADH1 gene promoter is less accessible to DNase I in cells where the gene is "off" (uninduced, U) than in cells where it is transcriptionally active (induced, I). The transcriptionally active promoters from induced cells show more regions of DNase I hypersensitivity (indicated with the filled triangles) than do those where the gene is not being transcribed (C is the control). (B) The hypersensitive region may reflect a nucleosome-free region, a state potentiated by the binding of one or more transcription factors.*

The existence of euchromatic and heterochromatic regions implies that chromatin structure can be modified or remodeled. In fact, chromatin is a dynamic entity that can undergo considerable structural change. Chromatin structure is directly remodeled through the activity of at least two different protein classes, **histone chaperones** and **ATP-dependent chromatin remodeling enzymes**. Histone chaperones, such as chromatin assembly factor 1 (CAF-1), are involved in the deposition of histones during DNA replication and remodeling. They are also thought to prevent misfolding and aggregation of histones. Chromatin remodeling enzymes alter the position of nucleosomes in chromatin to reduce or increase the accessibility of other proteins to the DNA. They contain a DNA-dependent ATPase that is the powerhouse of the system. Classic examples of chromatin remodeling proteins are the products of the SWI and SNF genes in yeast, which affect mating type switch (SWI) and the ability to ferment sucrose (SNF), respectively, and actually function together in the same complex. Homologs of SWI/SNF have been identified in plants and are involved in the control of diverse developmental processes.

The ability of a cell to modify the structure of its chromatin raises the question as to how this process is controlled at the molecular level and what signals determine the locations within chromatin targeted by remodeling enzymes.

9.5.2 Gene expression may also be controlled by epigenetic mechanisms

The traditional view of the relationship between genotype and phenotype is that all the heritable traits that determine the patterns and timing of gene expression, and hence an individual's phenotype, are encoded in the primary sequence of its DNA. Over the decades, there have been sporadic examples of heritable changes that apparently do not involve alterations in an organism's primary DNA sequence. Such changes are said to be **epigenetic** (literally: "on top of genetics").

Early examples of epigenetic phenomena are **paramutation** (Fig. 9.23) and **cosuppression**, but epigenetic

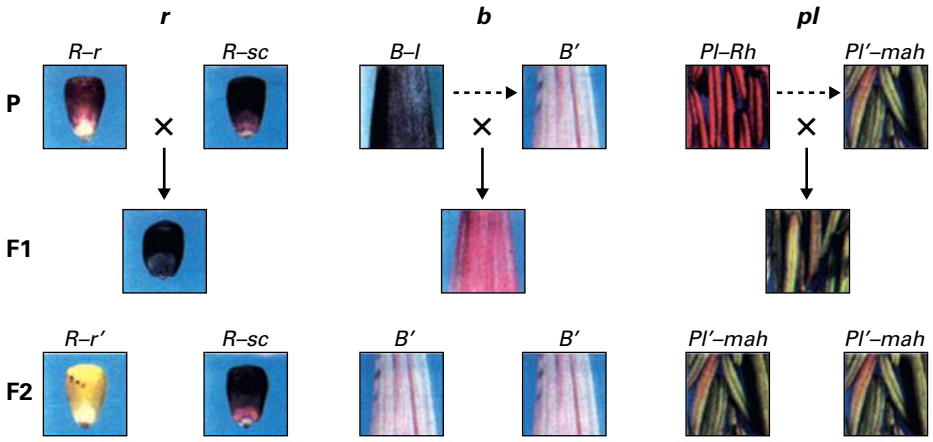


FIGURE 9.23 *Paramutation describes an allelic interaction whereby the expression of one allele in a heterozygote is altered by the presence of the other. Several cases of paramutation have been described for loci that control pigmentation in* Zea mays. *The examples shown are those affecting coloration of seed (*r *expression), husk (*b *expression), and anther (*pl *expression). Parental, F1, and the resulting segregant phenotypes are represented in successive rows of the figure. (A) Activity of the paramutable* R–r *allele is heritably reduced after exposure to the paramutagenic* R–sc *allele in the F1 heterozygote. The* R–r *and* R–sc *alleles are structurally distinct from one another and the* R–sc *allele is always strongly expressed. (B) Weakly expressed paramutagenic B′ states can arise spontaneously from strongly expressed paramutable* B–I *alleles (dashed arrow). B–I alleles change exclusively to* B′ *when exposed to* B′ *in the F1 heterozygote. (C) Weakly expressed paramutagenic* Pl′–mah *(Pl′) states can arise spontaneously from strongly expressed paramutable* Pl–Rh *(Pl) alleles (dashed arrow).* Pl–Rh *alleles change exclusively to* Pl′–mah *when exposed to* Pl′–mah *in the F1 heterozygote.*

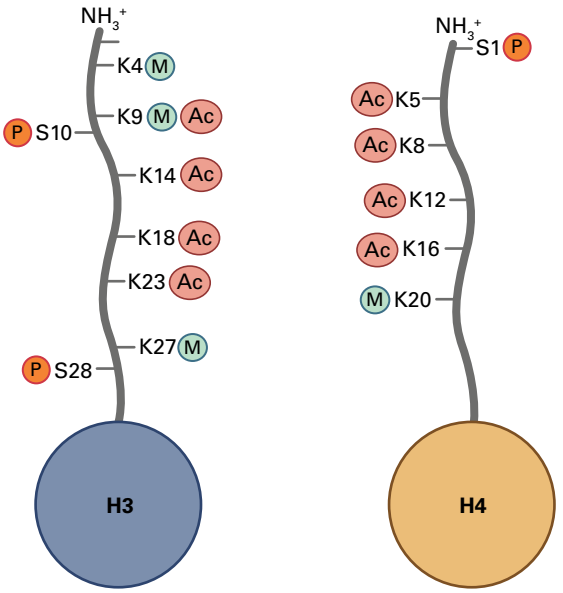


FIGURE 9.24 *Covalent modifications of histones H3 and H4. "M" symbolizes methylation, "Ac" acetylation, and "P" phosphorylation. Modified amino acid residues (single letter abbreviations are used) and their positions relative to the N-terminus of a protein are indicated.*

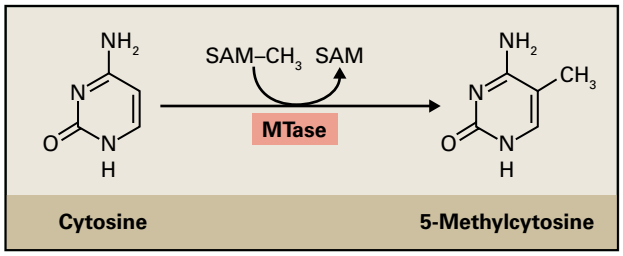


FIGURE 9.25 *Cytosine methylation. A methyltransferase (MTase) transfers a methyl group from S-adenosyl methionine (SAM) to cytosine, resulting in the formation of 5-methylcytosine.*

mechanisms play key roles in many cellular and developmental processes and in particular in the regulation of gene expression. Epigenetic mechanisms are largely based on a multitude of different types of covalent chromatin modifications, which are also called **epigenetic marks**. These include DNA methylation, as well as an array of posttranslational histone modifications that occur preferentially at the amino- (Fig. 9.24) and carboxyl-terminal tails of these proteins. While epigenetic mechanisms in plants and animals show many commonalities, there are also some differences, some of which will be briefly touched on below.

DNA methylation is based on the methylation of cytosine bases in the nuclear DNA by enzymes called **DNA methyltransferases** (Fig. 9.25). Unlike in animals, where the methylation of cytosines is found mainly in the context of CG dinucleotides, in plants, cytosines in the context of CHG and CHH (recall that in the IUB code, H = C, T, or A) sequences are also targets of DNA methyltransferases. DNA methylation is an attractive model for epigenetic changes because mechanisms exist to ensure both mitotic and meiotic inheritance of specific DNA methylation patterns. Newly replicated DNA that contains hemi-methylated sites is a strong substrate for methyltransferase activity that ensures the maintenance of preexisting methylation patterns in both daughter

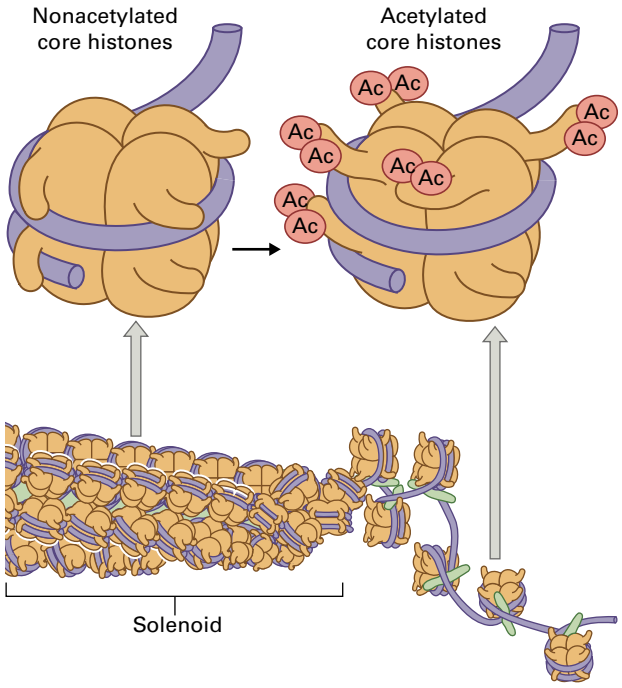


FIGURE 9.26 *Histones can be modified by acetyltransferases and deacetylases to influence the degree of chromatin condensation. Both histones within the nucleosome and the linker histone H1 can be modified at the N-terminal region by acetyltransferases. An acetyl group on a histone creates steric hindrance for surrounding structures, thereby generating a local region of decondensation. Decondensation of chromatin can facilitate recruitment of transcription factors to the surrounding sequence. Histone deacetylases (not shown) remove acetyl groups to allow the N-termini of histones to interact more tightly with DNA.*

chromosomes. Three distinct pathways of DNA methylation with overlapping functions have been characterized in *Arabidopsis* and likely exist in many, if not all, plant species. METHYLTRANSFERASE 1 (MET1), a homolog of mammalian DNMT1, primarily maintains methylation at CG sites while CHROMOMETHYLASE3 (CMT3), which is plant-specific, maintains methylation at CHG sites. The third pathway involves DOMAINS REARRANGED METHYLASES 1 and 2 (DRM1/2; homologs of mammalian DNMT3a/3b) and maintains cytosine methylation in all sequence contexts. This process requires the active targeting of sites by siRNAs (see Chapter 6).

The occurrence of DNA cytosine methylation can be studied through **bisulfite sequencing**. This technique is based on the treatment of genomic DNA with sodium bisulfite, which converts cytosines, but not of methylated cytosines, into uracil. The subsequent sequencing of the treated DNA can then distinguish between cytosines that were methylated or not. Using this approach, it has been shown that about 20% of the *Arabidopsis* genome is methylated and that the proportion of methylated DNA increases with genome size and repeat content. The largest fraction of methylated DNA occurs within transposons and other repeats. In fact, methylation plays an important role in silencing transposon activity, as evidenced by the observation of genome-wide transcriptional activation of transposons in mutants lacking maintenance methylation activity. The effect of DNA methylation on gene expression varies according to the location of the methylated cytosines. Promoter methylation is usually associated with decreased transcription, whereas methylation in the body of a gene often correlates with moderate to high expression levels.

Post-translational modifications of histones include, for example, methylation, acetylation, and phosphorylation (see Fig. 9.24), and of these, the best understood are histone acetylation and methylation.

Histone acetylation occurs via the transfer of the acetyl group from acetyl coenzyme A to the ε-amino group of different lysine residues of mainly histones H3 and H4 by enzymes known as **histone acetyl transferases** (HATs). Acetylated histones regulate transcription through interaction with proteins that contain a **bromodomain**, a 110 amino acid sequence motif present in a variety of transcription factors as well as in some chromatin remodeling complexes. In general, histone acetylation is thought to activate gene expression by reducing chromatin condensation (Fig. 9.26). Histone acetylation can be reversed by a class of enzymes called **histone deacetylases** (HDACs).

Histone methylation occurs predominantly, but not exclusively, on lysine residues of histones H3 and H4 and is carried out by **histone methyl transferases** (HMTases) that use *S*-adenosyl methionine as the methyl donor. Unlike histone acetylation, where only single acetyl groups are added, histone methylation can lead to the addition of either mono-, di- or tri-methyl groups. The effects of histone methylation on gene expression depend on the amino acid residues in the histone tails that are modified. While methylation of certain residues increases gene expression, methylation of other residues has the opposite effect. For example, tri-methylation of lysine 27 of histone H3 by **polycomb repressive complex 2** (PRC2) leads to the repression of genes. In contrast, tri-methylation of lysine 4 of histone H3 through **trithorax** group (trxG) proteins counteracts PRC2 activity and leads to gene activation. For other residues in histones, the exact methylation status determines the effect on gene expression. One example is the di-methylation of lysine 9 of histone H3, which serves as a repressive mark, whereas tri-methylation of the same residue is commonly associated with actively transcribed genes.

9.5.3 Epigenetic mechanisms are often based on an interplay with transcription factors

As described above, a bewildering array of different epigenetic marks exist that can have opposite effects on the transcription of a gene. How does a cell use this wealth of

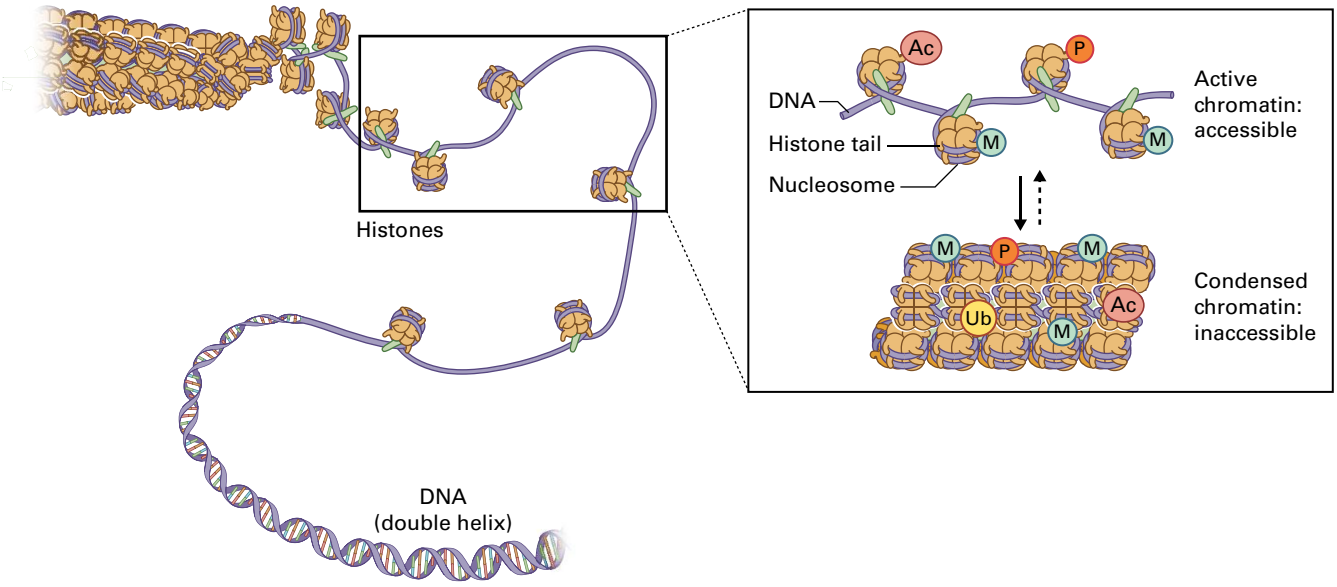


FIGURE 9.27 *Chromatin states. A combination of specific epigenetic marks in a genomic region leads either to chromatin condensation or to a more relaxed chromatin configuration. These changes in chromatin structure prevent or facilitate transcription.*

information to control gene expression activities during development or in response to environmental stimuli? The now generally accepted view is that different combinations of epigenetic marks can be read and interpreted by specialized proteins that then activate or repress the expression of a gene for example through the modification of chromatin structure. This idea was initially put forward as the **histone code hypothesis**, which has now been incorporated into the more generally applicable concept of the **epigenetic code**.

Because of the multitude of different epigenetic marks, the number of combinations that could theoretically occur in a genome is staggering. However, analyses of the epigenomes (i.e., the genome-wide distribution of epigenetic marks) of plants and animals have led to the realization that not all possible combinations actually occur in vivo. Instead, certain patterns of epigenetic marks, the so-called **epigenetic states**, are prevalent (Fig. 9.27). The number of different epigenetic states appears to be relatively small, but this view may change in the future when further in-depth studies are conducted and the epigenomes of specific cell types are analyzed.

One key question in regulatory biology is how epigenetic mechanisms are linked to the activity of transcription factors. The emerging picture suggests that transcription factors provide the general inputs for the control of gene expression, and enzymes that set or erase epigenetic marks use the information from these inputs to modify chromatin structure. At a molecular level, there is ample evidence that these enzymes are targeted to genes through the direct or indirect interaction with transcription factors. One example for an indirect mechanism involves **transcriptional co-repressors** (Fig. 9.28). These proteins bind to certain transcription factors and then recruit histone deacetylases to the promoters of genes, which leads to the removal of acetyl groups from histones and ultimately to changes in chromatin structure.

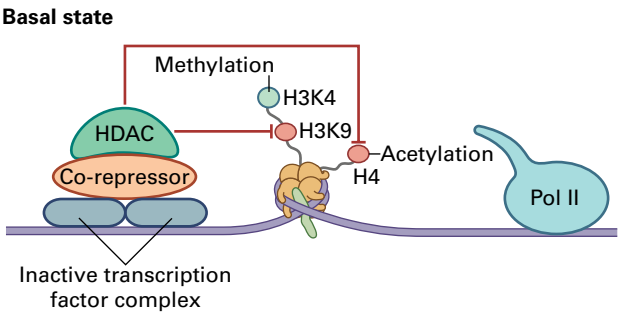


FIGURE 9.28 *Mechanism of transcriptional co-repressor function. Binding of a co-repressor to a transcription factor complex leads to the recruitment of a histone deactytelase (HDAC) to a target gene promoter. The HDAC then removes acetyl groups from histone H3 in specific positions. This change in chromatin state inactivates transcription.*

9.5.4 Epigenetic mechanisms control plant growth and development

As briefly mentioned above, epigenetic mechanisms control many cellular and developmental processes during plant development (see also Chapter 19). One well-studied

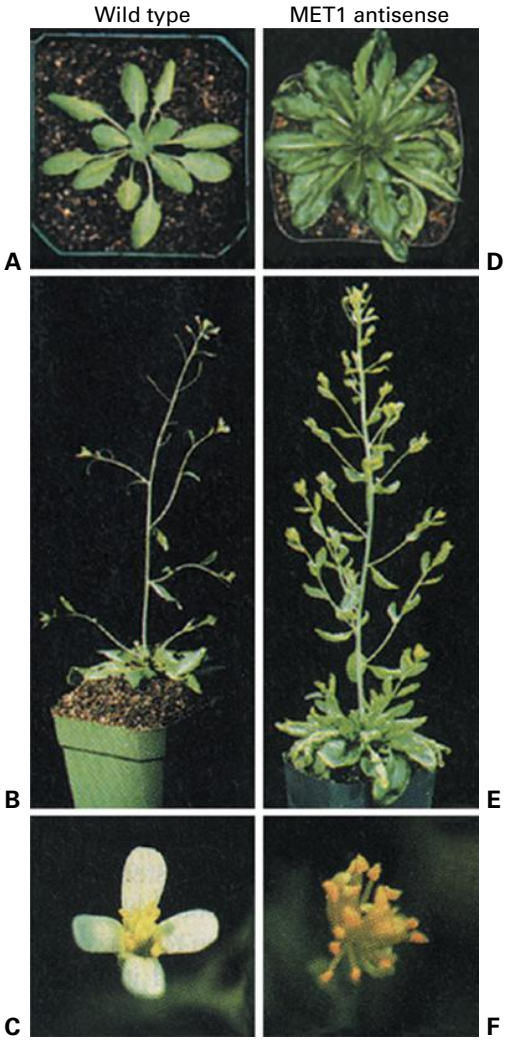


FIGURE 9.29 *Interference with DNA methyltransferase activity. Phenotypic comparisons of wild-type (A–C) and a MET1 antisense line (D–F) of* Arabidopsis thaliana. *Interference with cytosine methylation activity by an antisense knockout approach for the MET1 gene is associated with abnormal phenotypes during vegetative (A, D), inflorescence (B, E), and floral (C, F) development.*

example is the regulation of flowering time in *Arabidopsis*. In winter annuals (plants that typically germinate in fall, survive the winter period, and then flower in spring), the gene *FLOWERING LOCUS C* (*FLC*) represses the initiation of flowering. This repression is removed during winter, when the plant experiences a prolonged cold period, through a process termed **vernalization**. The underlying molecular mechanism appears to depend mainly on the activity of the polycomb repressive complex 2 (see Section 9.5.2), which represses the *FLC* gene by tri-methylation of lysine 27 of histone H3. Once *FLC* expression is turned off, flowering can commence in response to certain environmental signals, such as the photoperiod.

Polycomb group (PcG) proteins are also involved in the repression of entire developmental programs (for example, genes that are involved in seed and embryo development). A loss of PcG activity leads to a depression of such genes in vegetative tissue of the plant and can, in extreme cases, result in **somatic embryogenesis**, where embryo formation is initiated by somatic cells (i.e., cells of the plant body) without fertilization.

Another example for involvement of epigenetic mechanisms in the control of plant growth is the role of DNA methylation in a phenomenon called **genomic imprinting**. This term refers to an unusual mode of inheritance, in which alleles are active or inactive, depending on whether they were passed on from the mother or the father. Imprinting is to a large extent based on differences in cytosine methylation patterns between the paternal and maternal genomes. These differences are caused, for example, by the DNA-demethylating glycosylase DEMETER, which is expressed primarily in the female gametophyte and reduces the methylation state of the maternal genome.

DNA methylation also has a direct effect on the development of a plant. For example, a disruption of MET1 activity (see Section 9.5.2) leads to a reduction in genome methylation and to a late-flowering phenotype, as well as to abnormal shoot and flower development (Fig. 9.29).

Summary

The genome of a plant contains the blueprint for the structure and function of the organism. Starting with the concept of genes as units of inheritance and chromosomes as the visible carriers of these genes, our understanding of genome structure has progressed over the last century from cytogenetics, through increasingly sophisticated microscopy methods to DNA sequencing. Our view of the genome was dramatically refined by the first complete sequence of a plant genome (*Arabidopsis*) and subsequently by many others. Plant genomes vary considerably in size, with the larger genomes containing more repetitive DNA in the form of transposable elements and other sequences. Movement of transposable elements has played roles both in genome evolution and diversity within species. Most plant genomes appear to contain 25,000–50,000 genes, somewhat more than animal genomes (including humans) and larger gene families. This is due to one or more whole genome duplications that have occurred in different lineages from a few million to a hundred or more million years ago. DNA

sequencing has also allowed us to associate specific sequences with cytological features such as centromeres, telomeres, and nucleolar organizer regions.

The expression of genes in a genome gives a plant its life, its form, and its ability to respond to environmental cues and stimuli. A great deal is now known about the basic mechanisms of transcription and about how specific transcription factors regulate gene expression in temporally, spatially and environmentally specific fashions by interacting with regulatory elements in the promoters of genes. There is now ample evidence that a multitude of epigenetic mechanisms, which are based on covalent modifications of histones and of the DNA itself, contribute to the regulation of gene expression and are involved in controlling various physiological and developmental processes in plants.



10

Protein Synthesis, Folding, and Degradation

Judy Callis, Karen S. Browning, and Linda Spremulli

Introduction

Proteins constitute a large percentage of plant cellular dry weight and carry out many different and essential cellular functions. Proteins also serve as nitrogen and energy stores in the seed endosperm or embryo of seed plants. Protein metabolism is central to cell growth, differentiation, and reproduction, and cells respond to internal and external signals by regulating both protein synthesis and degradation to adjust the amounts of specific proteins to suit cellular requirements.

Although plants share many features of protein synthesis and degradation in common with other eukaryotic organisms, some aspects are unique to plant cells and photosynthetic single-celled organisms such as *Chlamydomonas* and *Euglena*. This chapter highlights the protein synthetic processes that are distinct from those in other organisms and describes how translation (the "reading" of the messenger RNA, or mRNA, template and "writing" of the corresponding peptide sequence) may be affected by intrinsic, biotic, and abiotic factors. The basic steps of protein biosynthesis outlined in general biochemistry textbooks are directly applicable to plant systems, and the reader is referred to such sources for a general introduction as needed. This chapter also illustrates how the polypeptide chain folds to form a precise three-dimensional structure that can carry out specific biological functions. Finally, this chapter elaborates how all cellular compartments have specific pathways for removing proteins by hydrolyzing peptide bonds.

10.1 Organellar compartmentalization of protein synthesis

In plants, protein synthesis occurs in three subcellular compartments (Fig. 10.1): the cytosol, plastids, and mitochondria each contain distinct protein synthetic machinery. About 75% of cell proteins are made in the cytosol, where mRNAs transcribed from the nuclear genome are translated. About 20% of the proteins in a photosynthetically active cell (e.g., a young leaf cell) are synthesized in the chloroplast using mRNA templates transcribed from the chloroplast genome, and a small amount of protein synthesis (2–5% of total protein) occurs in mitochondria. In the cytosol, more than 25,000 different proteins may be synthesized, whereas in chloroplasts, about 40 proteins are synthesized, though plastid genomes can encode over 200 proteins. The number of proteins synthesized in mitochondria varies widely among species; about 20–40 proteins appear to be synthesized in the mitochondria of the liverwort *Marchantia polymorpha*, for example, whereas the mitochondrial genomes of most plants typically encode far fewer proteins. The overall mechanisms responsible for protein synthesis in the cytosol, plastids, and mitochondria are similar, but are clearly distinct from each other; accordingly, plant cells contain three different types of ribosomes,

Biochemistry & Molecular Biology of Plants, Second Edition. Edited by Bob B. Buchanan, Wilhelm Gruissem, and Russell L. Jones.
© 2015 John Wiley & Sons, Ltd. Published 2015 by John Wiley & Sons, Ltd.
Companion website: www.wiley.com/go/buchanan/biochem

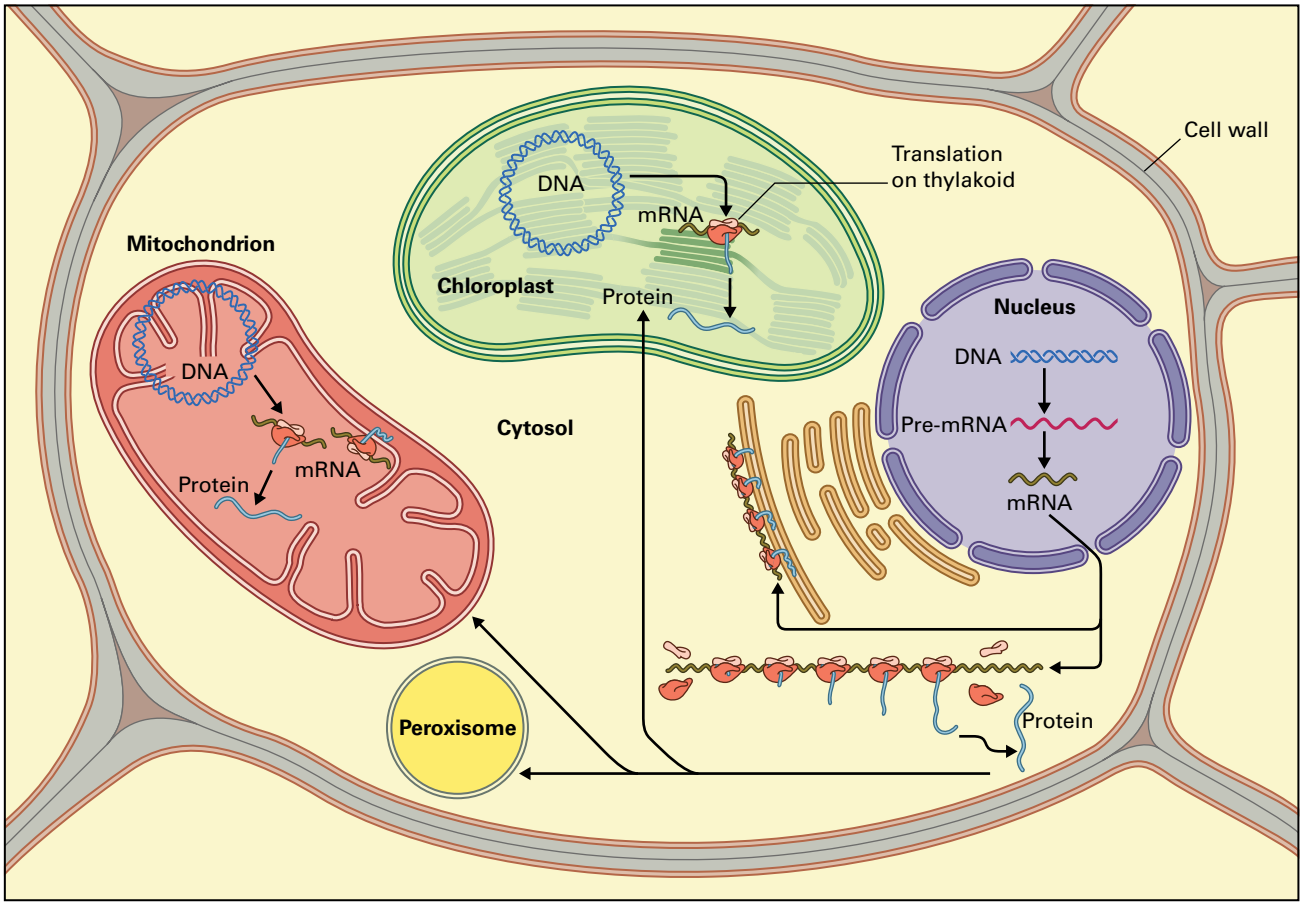


FIGURE 10.1 *Sites for protein synthesis in a plant cell. A typical plant cell synthesizes proteins in three distinct compartments—the cytosol, plastids, and mitochondria. Translation of mRNAs transcribed in the nucleus occurs in the cytosol, either on soluble or membrane-bound ribosomes. In contrast, both transcription and translation of plastid and mitochondrial mRNA take place within those organelles. Similarly, ribosomes can be membrane-localized in the organelles. Proteins synthesized in the cytosol can be imported into one or more organelles— the plastid, mitochondria, or microbody. Shown here is the leaf-type microbody, the peroxisome (see Chapter 4). Organellar genomes are shown in circular form, but can exist in other conformations.*

three groups of transfer RNA (tRNA), and three sets of translation factors for protein synthesis (see Section 10.2).

In many cases, plant plastid and mitochondrial genomes encode tRNAs that are used specifically for protein synthesis within the organelle; there are cases, however, in which tRNAs encoded within the nuclear genome are imported into mitochondria for use in mitochondrial protein biosynthesis. Plastids and mitochondria presumably arose through the endosymbiosis of ancient prokaryotic organisms (see Chapters 1 and 6). Consistent with this theory, the protein synthetic machineries in plastids and mitochondria are closely related to those of bacterial systems, as evidenced by the similarity of ribosome composition and structure (see Table 10.1). However, the capacity of the organellar genomes to synthesize proteins is limited, and, as a result, both organelles require proteins imported from the cytosol after synthesis (see Chapter 4). Most organelle-encoded proteins function in oligomeric protein complexes that contain subunits from both nuclear and organelle genomes. Assembly of such complexes requires close coordination of transcription and translation between the nucleus, cytosol, and organelle.

10.2 From RNA to protein

10.2.1 Protein biosynthesis occurs on ribosomes

Ribosomes are large complexes of proteins and ribosomal RNA (rRNA, see Chapter 6) that hold tRNA and mRNA in position and catalyze the formation of peptide bonds between amino acid residues. They can be isolated intact or as two subunits—one large and one small (Table 10.1, Fig. 10.2)—that reversibly associate and dissociate during protein synthesis. Surprisingly, it is not the protein component, but the largest RNA species of the large subunit that catalyzes peptide bond formation. The importance of this RNA species (a ribozyme) is highlighted by the toxicity of ribosome-inactivating proteins (RIPs), which remove an adenine base from the large subunit RNA to inactivate protein synthesis (see Box 10.1).

The protein composition of eukaryotic ribosomes is highly conserved. Plant cytosolic ribosomes contain

TABLE 10.1 *Summary of the composition and properties of various plant ribosome types.*

Ribosome (in S value*)	Subunits (in S value*)	rRNAs (in S value*)	Number of proteins
Plant cytosolic, 80S	40 60	18 28, 5.8, 5	32 48
Plant plastids, 70S	30 50	16 23, 5, 4.5	≈25 ≈33
Plant mitochondria, ≈70S	30 50	18 26, 5	>25 >30
Bacterial, 70S	30 50	16 23, 5	21 31

*Ribosomes, their subunits, and resident RNAs are designated by their tendency to sediment in a sucrose gradient. The higher the S (Svedberg) value, the faster the ribosome sediments, typically a reflection of a greater mass.

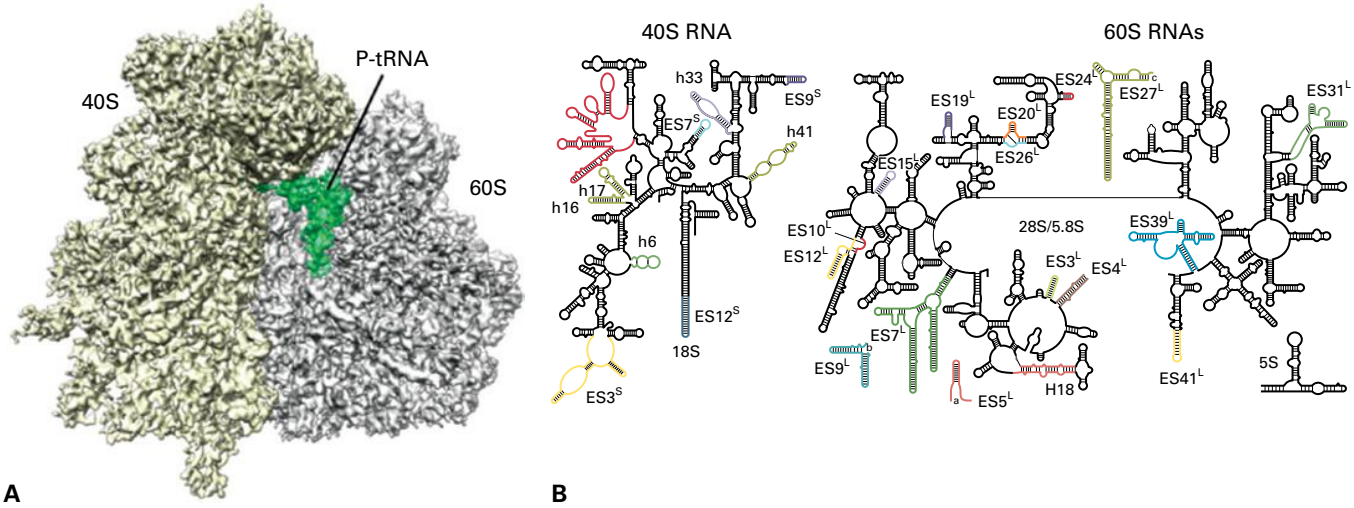


FIGURE 10.2 *(A) CryoEM structure of translating wheat (*Triticum aestivum*) ribosome at 5.5 Å resolution, with the small (40S) and large (60S) subunits colored yellow and gray, respectively, and the peptidyl-tRNA, in green, in the P site. (B) Secondary structures of the rRNAs in the 40S and 60S wheat subunits, left and right, respectively. Colored regions represent expansion segments (ES), which are additional rRNA sequences found in eukaryotic ribosomes but absent from prokaryotic ribosomes. Most ES sequences are located at the ribosome surface and are of variable lengths among eukaryotes.*
Source: Armache et al. (2010) PNAS 107: 19748–19753.

orthologs of mammalian ribosomal proteins (RPs) and have one additional plant-specific subunit (the RPP3, a member of the acidic ribosomal protein family, discussed below). Plant ribosomes contain an estimated 80 proteins, each typically encoded by a small gene family. For example, in *Arabidopsis* the number of family members ranges from two to eleven. The multiple isoforms of RPs suggest that there may be a wide diversity of ribosomes, some with specific functions or roles.

Most ribosomal proteins are basic in nature, which facilitates their interaction with the negatively charged rRNA; however, ribosomes also contain a small family of acidic proteins, called P-proteins. In addition to the conserved RPP0, RPP1, and RPP2 proteins found in all eukaryotes, plant ribosomes also contain a unique member, RPP3. RPP3 interacts with RPP1 and RPP2 to form a mobile acidic stalk complex on the large subunit, which interacts with an elongation factor (eEF2) to promote GTP hydrolysis tRNA translocation within the ribosome following peptide bond formation.

Many ribosomal proteins undergo post-translational modifications. For example, several ribosomal proteins are substrates for various kinases, and phosphorylation of the small subunit ribosomal protein, S6, is affected by various metabolic and environmental conditions including heat, cold, hypoxia, and sugar signaling. The physiological significance of these modifications is of great interest in understanding ribosome heterogeneity. In addition, nonribosomal proteins copurify with ribosomes. One such protein is a scaffold protein called receptor for activated C kinase 1 (RACK1), which binds to the 40S subunit and eIF6, likely facilitating 80S ribosome assembly. RACK1 also has non-ribosomal functions.

BOX 10.1

RIP: Ribosome-inactivating proteins (RIPs) have an appropriately grim acronym

Ricin, a toxic protein from the seeds of the castor bean plant (*Ricinus communis*), is the best-known member of a class of plant polypeptides known as ribosome-inactivating proteins (RIPs). Ricin was made famous as the poison used by the Bulgarian secret police to assassinate the defector Georgi Markov in London in 1978. In a plot that reads like a popular spy novel, a dart-tipped umbrella was used to deliver the toxin to its unfortunate victim.

Ricin cleaves the glycosidic bond between the sugar and an adenine residue at a specific position on the 28S ribosomal RNA. Loss of this adenine irreversibly inactivates the ribosome. RIPs are thought to provide protection of seeds and plants from predators and viral infections. RIPs are being investigated as potential therapeutic agents that could be targeted to kill malignant cells, and in particular, ricin, has been implicated as a possible bioterrorism agent.

Source: M. Williams, Veterinary Medicine Library, University of Illinois; previously unpublished.



10.2.2 Initiation of protein synthesis establishes the reading frame on the mRNA and positions the first amino acid for incorporation

Initiation of protein synthesis is a complex series of events that is largely conserved in eukaryotes. The initiation of translation is facilitated by a group of auxiliary protein factors referred to as **eukaryotic initiation factors** (eIFs), which are classified on the basis of the general reaction they promote. Each may consist of a single or multiple polypeptides (Table 10.2), and many mechanisms that regulate cytosolic protein synthesis in eukaryotes affect the activities of one or more of these factors.

Initiation (Fig. 10.3) begins when eIF2 interacts with an initiator Met-tRNA^{Met} in the presence of GTP to generate a tRNA–protein complex called the ternary complex. eIF2 is a heterotrimer of alpha, beta, and gamma subunits. Once formed, the ternary complex binds to a free 40S ribosomal subunit, a process facilitated by several other eIFs (Fig. 10.3). The small subunit of the ribosome, bound to the Met-tRNA and several eIFs, then interacts with the mRNA. This step requires the eIF4 family of initiation factors, which includes eIF4A (DEAD box helicase), eIF4B (RNA-binding protein), eIF4G (protein interactions), and eIF4E (cap-binding protein). The eIF4s facilitate recognition of the cap structure and interaction between the 40S subunit with other associated eIFs and the mRNA. In addition, there is circularization of the mRNA through interactions of eIF4G and the poly(A)-binding protein (PABP) bound to the 3′ poly(A) tail. Any secondary structures in the 5′ portion of the mRNA are presumably removed by the helicase and the ATP hydrolysis activities of eIF4A in complex with eIF4F (eIF4G/eIF4E) and eIF4B.

The 40S subunit must then identify the correct AUG codon to begin reading the mRNA. Typically, the 40S subunit carrying the bound Met-tRNA migrates away from the cap along the 5′ untranslated region (UTR) of the mRNA in a 5′ to 3′ direction, a process referred to as **scanning**. Based on model plants, the 5′ UTRs range from <10 to >200 nucleotides (nt), but on average are ≈125 nt. mRNAs with 50–75 nt 5′ UTRs are over-represented in polysomes, suggesting this is the optimum leader length in protein synthesis. For initiation, the ribosome generally selects the first AUG codon it encounters; however, there are significant exceptions (especially with viral templates; see Box 10.2). AUG selection is facilitated by codon:anticodon hydrogen bonding between the AUG codon and the Met-tRNA bound to the ternary complex on the 40S subunit with the associated factors eIF1, eIF1A, and eIF5B. This pairing fixes the start site on the mRNA and establishes the correct reading frame.

Ribosomal selection of the initiation AUG codon is not strongly dependent on the nucleotide sequence surrounding the codon. A consensus sequence surrounding the AUG translation initiation codon for *Arabidopsis* and rice (*Oryza sativa*) was identified through in silico analysis of predicted translation initiation sites. The consensus sequence is highly degenerate: aa(A/G)(A/C)aAUGGcg and c(g/c)(A/G)(A/C)(G/C)AUGGCg, where lower-case letters are variable and upper-case letters are conserved nucleotides. These sequences are similar to the human translation initiation consensus, with the G following the AUG codon being the most important

TABLE 10.2 *Eukaryotic initiation factors (eIFs) and their roles in initiating translation.*

Class	Members	General role
eIF1	eIF1, eIF1A	Multiple effects in enhancing initiation of complex formation and AUG selection
eIF2	eIF2, eIF2B*	GTP-dependent recognition of Met-tRNA and nucleotide exchange
eIF3	eIF3†	Ribosomal subunit dissociation; promotion of Met-tRNA and mRNA binding to 40S subunits
eIF4	eIF4A, eIF4B, eIF4F‡, eIF(iso)4F‡, eIF4H*	Recognition of 5′ cap on mRNA, binding 40S subunit to mRNA, and unwinding mRNA secondary structure
eIF5	eIF5, eIF5B*	Promotion of eIF2 GTPase activity, AUG selection, and release of factors from ribosome; joining of the 60S subunit
eIF6	eIF6	Binds to 60S subunits and may function in regulation and assembly of ribosomes
PABP	Poly(A)-binding protein	Binds to poly(A) at 3′ end of mRNA and interacts with eIF4F at the 5′ end, facilitating circularization

*The presence of eIF2B, eIF5B, and eIF4H in plants is based only on the presence of gene sequences similar to other eukaryotes. eIF2B and eIF4H have not been purified or characterized from plants.
†eIF3 is composed of 13 nonidentical subunits (designated a–m) ranging from 180 to 28 kDa.
‡These factors are composed of two subunits. eIF4F consists of eIF4G and eIF4E (cap-binding protein); and plant-specific eIFiso4F consists of eIFiso4G and eIFiso4E (cap-binding protein).

residue neighboring the AUG codon. *Arabidopsis* mRNAs that lack the optimal context at the initiator AUG are more likely to be poorly translated in leaves under dehydration stress. Thus, the initiation context may be particularly important when protein synthesis is constrained, such as under suboptimal growth conditions. Other properties of the 5′ UTR that can affect translation of its downstream open reading frame (ORF) are the presence of potential secondary structures, such as a loop of self-complementarity, or short ORFs called upstream ORFS (uORFS, see Box 10.3).

Next, the large ribosomal subunit binds to the small subunit, with the mRNA and Met-tRNA^{Met} remaining in the correct position (Fig. 10.3). During this stage, eIF5 acts as a GTPase-activating protein and stimulates the hydrolysis of GTP by eIF2 present in the ternary complex; eIF2-GDP is then released. The final step of joining of the 60S subunit requires eIF5B, another GTPase that interacts with both the large and small subunits.

This mechanism for the initiation of protein biosynthesis in the cytosol of plants appears to be very similar to that in other eukaryotes. One difference, however, is the presence of two forms of eIF4F, the protein complex involved in recognizing the 5′ mRNA cap before the interaction between the mRNA and 40S ribosomal subunit. Plants have two forms of this initiation factor, eIF4F and eIF(iso)4F, each comprised of two subunits, eIF4G/eIF4E or eIFiso4G/eIFiso4E. The purpose of these two forms in plants is not known, but likely reflects the need for specialized translation or regulation of translation for some plant mRNAs.

10.2.3 Initiation of protein synthesis in the cytosol is tightly regulated

In all eukaryotes, translation is primarily regulated at the initiation. In mammals and yeast, phosphorylation of eIF2 by several different kinases prevents the exchange of GDP bound by eIF2. Whether phosphorylation of eIF2 is also a major regulatory event in plant cells is still unknown and an area of active research. Several lines of evidence suggest this regulatory system may function in plants. Unphosphorylated eIF2α is barely detectable under normal growth conditions, but the phosphorylated form increases in seedlings depleted for amino acids. Concomitantly, overall protein synthesis declines (Fig. 10.4). An *Arabidopsis* kinase (GCN2) that phosphorylates plant eIF2α subunit has been identified. GCN2 is activated by amino acid deprivation, among other stresses, and eIF2 is phosphorylated in a GCN2-dependent manner under the same conditions (Fig. 10.4). These changes correlate with an overall reduction in protein synthesis; however, a direct effect on initiation of translation by phosphorylation of eIF2α by plant GCN2 kinase has not been demonstrated.

A second major regulatory pathway in yeast and mammals is through a small protein that competes with eIF4G for binding to eIF4E. These eIF4E-binding proteins, known as 4E-BPs in mammals, are regulated through phosphorylation by kinases in signal transduction cascades. This group of regulatory proteins has not been detected yet in plants, either biochemically or through bioinformatics.

The regulation of translation by small RNAs is a rapidly growing area of research. The exact mechanisms of how small RNAs regulate the translation of targeted mRNAs are still being explored. While microRNAs (miRNAs) were thought to act primarily by degrading mRNAs in plants, it appears that, as in animals, miRNAs can inhibit translation specifically without affecting mRNA levels. Small RNAs may not only downregulate translation of mRNAs; they can also enhance translation under certain conditions.

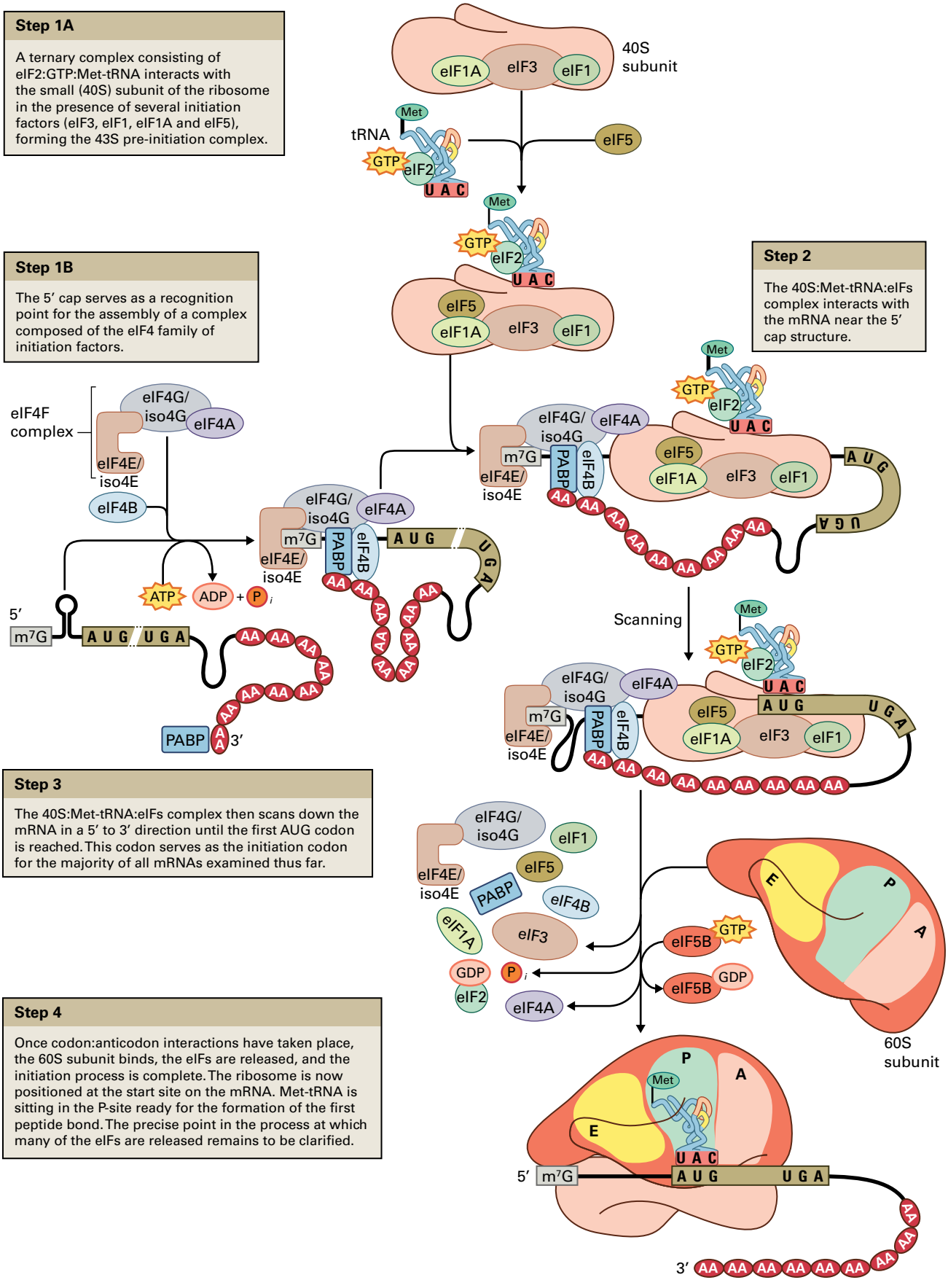
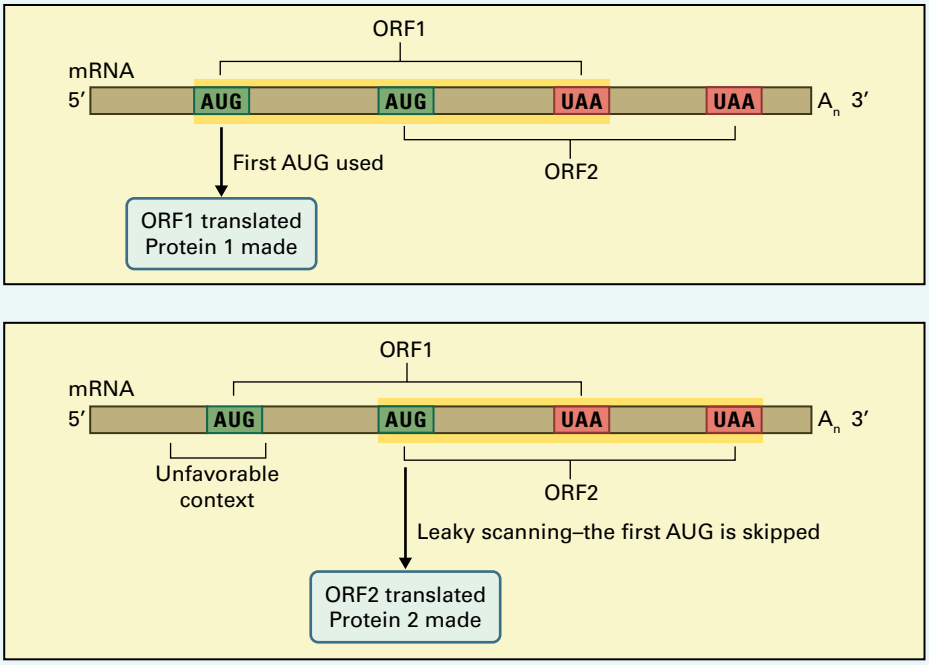


FIGURE 10.3 *Overview of the mechanism of polypeptide chain initiation in the plant cell cytosol.*

BOX 10.2

Leaky scanning allows plant viruses to translate multiple polypeptides from a single mRNA

Most eukaryotic mRNAs are monocistronic, initiating protein synthesis from the AUG codon closest to the 5′ end. Several features of a particular mRNA—including the nucleotide sequence surrounding the first AUG, the secondary structure of the mRNA, and the distance between the cap and the first AUG codon—can affect the efficiency of initiation at the first AUG. If the first AUG is in an unfavorable context, some ribosomes may bypass it and initiate translation at the second AUG codon, in a process referred to as **leaky scanning**. If the two AUG codons set different reading frames, the two proteins made will have very different sequences and likely carry out different biological functions. Many plant viruses, such as many of the luteoviruses (e.g., barley yellow dwarf virus), use this strategy because it allows the virus to minimize its genome size while maximizing the coding capacity of the genome.



10.2.4 Polypeptide chain elongation involves sequential addition of amino acid residues to the growing polypeptide chain

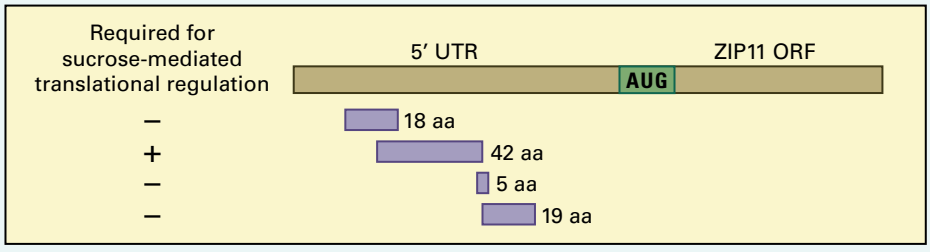
The sequential addition of amino acids to the growing polypeptide chain involves the use of three sites (the A-, P-, and E-sites, Fig. 10.5) on the fully assembled 80S ribosome. The P-site (peptidyl-tRNA binding site) participates in chain initiation and donates the growing polypeptide chain to the incoming aminoacyl-tRNA (aa-tRNA) in the A-site. The A-site (aa-tRNA binding site or decoding site) exposes the next codon to be read on the mRNA, where the incoming charged tRNA binds. The P-site tRNA occupies the E-site (exit site) after it has released its growing polypeptide chain, just before it leaves the ribosome. These three sites are used sequentially as the polypeptide chain is synthesized, and a complete cycle requires as little as 0.05 seconds.

The overall chain elongation process occurs in three steps (Fig. 10.5) and requires three elongation factors: eEF1A, eEF1B, and eEF2 function similarly to bacterial elongation factors. eEF1A in the GTP-bound form binds to the aa-tRNA and delivers it to the ribosome, accompanied by GTP hydrolysis. eEF1B exchanges the GDP for GTP on eEF1A to allow recycling of eEF1A. eEF2 catalyzes translocation of the mRNA through GTP hydrolysis after formation of the peptide bond. eEF2, unlike other G proteins involved in translation, such as eIF2 and eEF1A, does not require a recycling factor to replace the GDP for GTP. eEF2 is a target of regulation through phosphorylation and ADP ribosylation, processes that are conserved across eukaryotes. Both eEF1A and eEF2 are believed to interact with the

BOX 10.3 Translation of certain mRNAs is regulated by upstream open reading frames

A classical eukaryotic mRNA harbors only a single open reading frame (ORF), and ribosomes scan across the 5′ untranslated region (5′ UTR) to find the main AUG start codon (see text). Thus, it comes as a surprise that an estimated one third of mRNA species contain additional AUG codons within their 5′ UTR (5′ leader). These upstream AUGs and their associated **upstream open reading frames** (uORFs) complete with a stop codon terminate before the AUG of the major ORF.

uORFs often serve a regulatory purpose. For example, the mRNA for the *Arabidopsis* transcription factor, AtbZIP11, contains a 42-amino acid uORF (uORF2) with a phylogenetically conserved peptide sequence that represses translation of the main ORF when sucrose levels are high. Given that AtbZIP11 induces transcription of asparagine synthetase mRNA, its uORF may serve to coordinate sugar and amino acid metabolism. The sucrose-regulatory uORF is embedded into a cluster of additional uORFs that fine-tune its regulatory activity. Specific components of the general translation initiation machinery, including 60S ribosomal proteins and subunits of the largest initiation factor, eIF3, allow the ribosome to **reinitiate** translation after terminating at a uORF stop codon. Without such reinitiation, the main ORF could not be translated effectively.



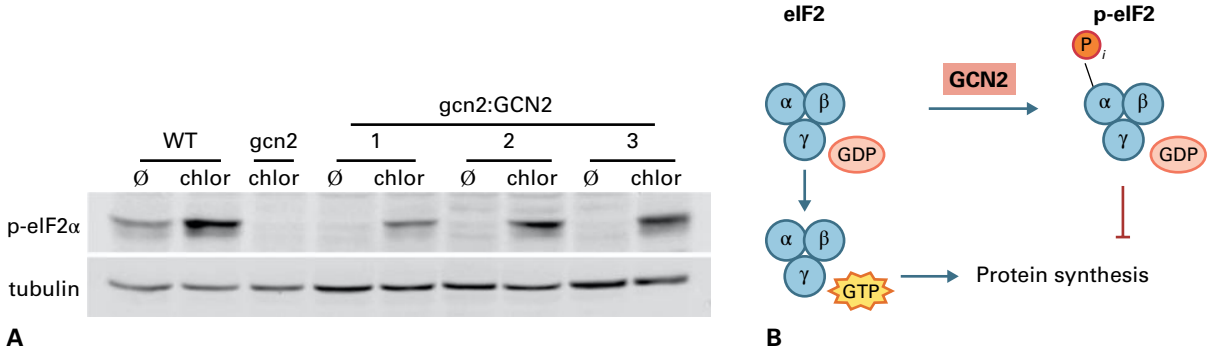


FIGURE 10.4 *(A) The alpha subunit of eIF2 is phosphorylated in response to amino acid deprivation (here by treatment of seedlings with the herbicide chlorosulfuron (chlor), an inhibitor of branched amino acid synthesis). Phosphorylation is detected with an antibody that specifically detects the phosphorylated form. eIF2α phosphorylation is not seen in a* gcn2 *mutant background, but is restored when a GCN2 expression construct is re-introduced into the mutant background. Three independent transgenic lines are shown. The tubulin immunoblot (below) indicates that equal protein was present in each sample. (B) Schematic of the proposed control of protein synthesis initiation by eIF2α phosphorylation. Phosphorylation correlates with reduced overall protein synthesis; however, the mechanism of the inhibition has not been shown to be similar to that in mammals and is currently unknown. Source*: (A) Lageix et al. (2008). BMC Plant Biology 8:134.

P-protein stalk on the large ribosomal subunit, which is essential for GTP hydrolysis.

As a ribosome starts to read an mRNA, it moves downstream, exposing the start codon and allowing a second ribosome to initiate translation of the mRNA. Thus, mRNAs generally associate with several ribosomes to form structures referred to as polysomes, or polyribosomes (Fig. 10.6). The ribosomes are often spaced as close as 80–100 nt apart on the mRNA. An 80S ribosome occupies about 30–35 nt on an mRNA. The presence of an mRNA in a polysome suggests translation of that mRNA, although exceptions exist. Recent studies have shown that mRNA associated with polysomes may be a distinct population of mRNA from the total mRNA isolated from cells, and may more accurately represent the protein synthetic activity of the cell. The method of ribosome footprinting can identify not only which mRNAs are actively being translated, but the position of the ribosome on the mRNA.

Step 1

A growing polypeptide chain is covalently attached to the tRNA in the P-site. The A-site is empty, exposing the next codon in the mRNA. The E-site is occupied by the uncharged tRNA from the previous cycle.

Step 2

A charged tRNA binds to the ribosomal A-site only if its anticodon matches the exposed codon on the mRNA. When this occurs, the tRNA in the E-site is ejected from the ribosome. A required elongation factor, eEF1, forms a ternary complex with GTP and the charged tRNA and promotes the binding of the charged tRNA to the A-site of the ribosome.

Step 3

The ribosome uses the peptidyl transferase center to catalyze the formation of a peptide bond between the growing polypeptide chain and the new amino acid. Recent experiments suggest that rRNA plays a particularly important role as a ribozyme in this catalytic step. The net result of this process is that the nascent polypeptide has been transferred from the tRNA in the P-site to the new amino acid attached to its tRNA in the A-site. The polypeptide is one residue longer, the peptidyl-tRNA now occupies the A-site, and the tRNA in the P-site is free of its amino acid. This tRNA is said to be deacylated.

Step 4

The complex must rearrange, exposing the next triplet. This process, called translocation, involves three rearrangements: the deacylated tRNA in the P-site moves into the vacant E-site; the peptidyl-tRNA in the A-site moves into the P-site; and the ribosome moves relative to the mRNA by exactly three nucleotides (one codon), exposing a new triplet in the A-site. Moving one or two nucleotides too little or too much would initiate a new reading frame, probably resulting in an inactive polypeptide.

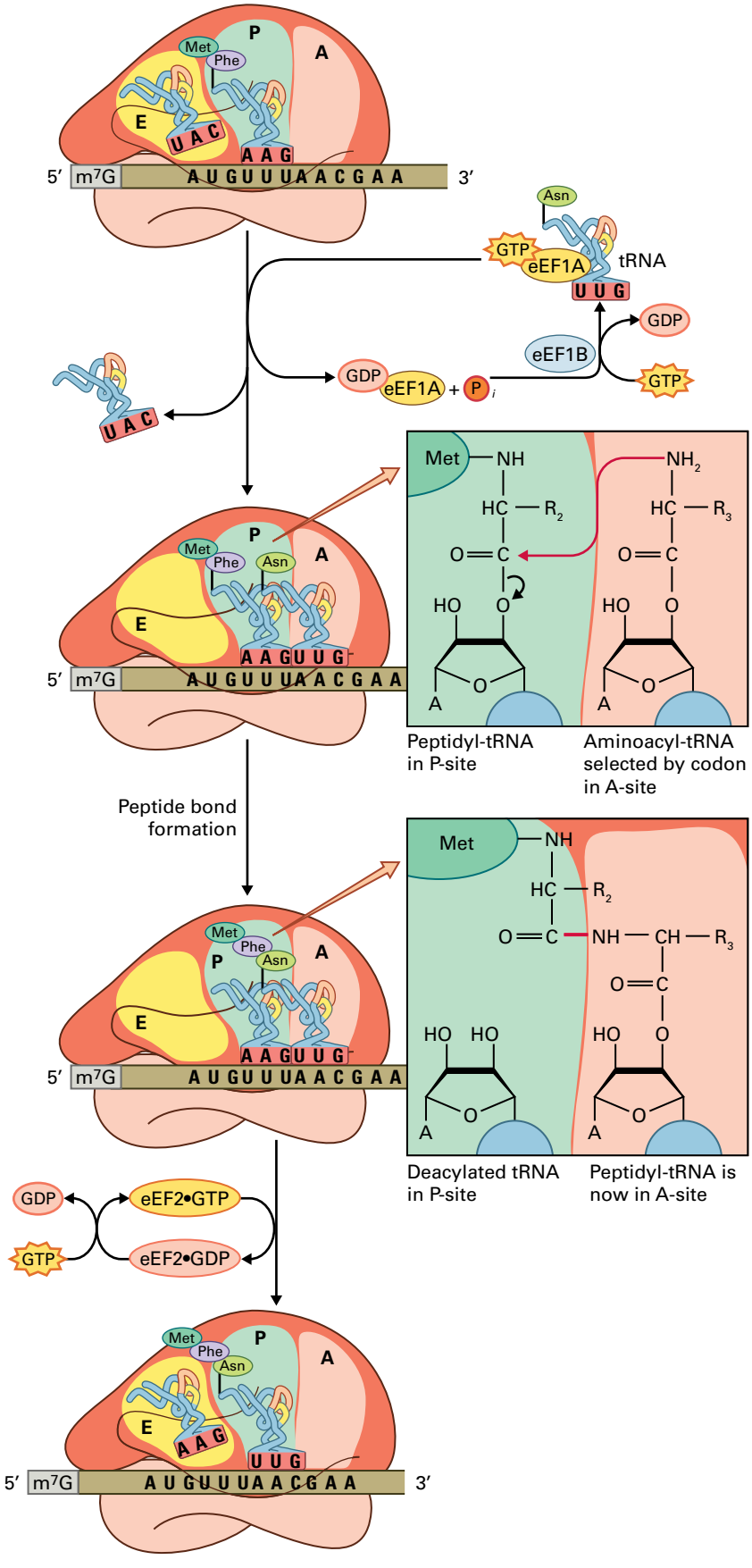


FIGURE 10.5 *The elongation phase of cytosolic protein synthesis in plants.*

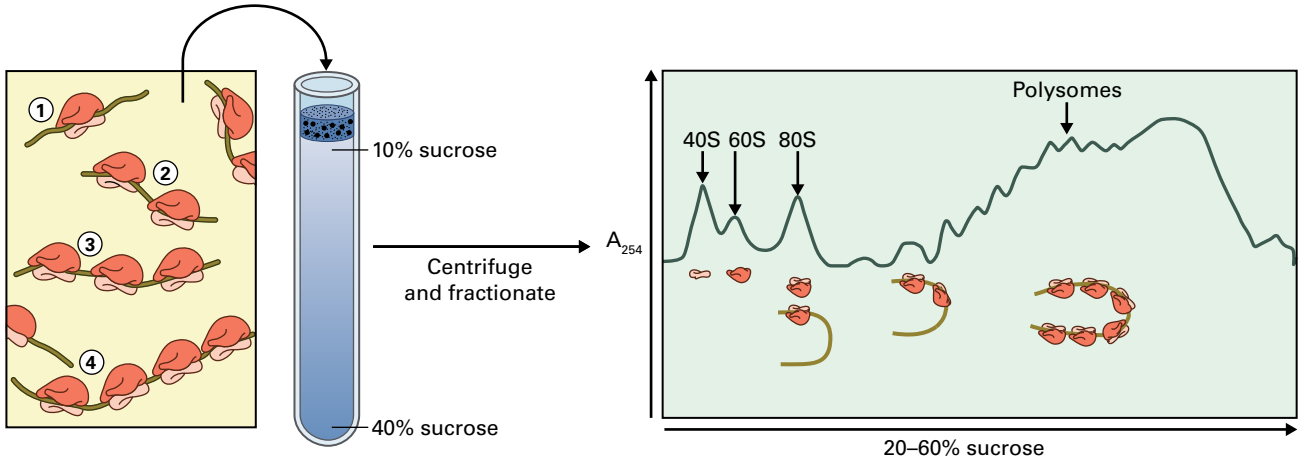


FIGURE 10.6 *Most mRNAs are translated by more than one ribosome at a time. The term polysome refers to an mRNA that binds multiple ribosomes. Sucrose density-gradient centrifugation can be used to separate the mRNAs that bind different numbers of ribosomes. The more ribosomes bound, the more massive the polysome, and the greater the distance traveled during sedimentation.*

Polysomes fall into two classes—free and membrane-bound. The proteins synthesized by free polysomes are released after translation and are directed to their final destination by protein sequences that act as targeting signals. By contrast, the protein products of membrane-bound polysomes are inserted directly into the membrane during translation, typically the endoplasmic reticulum (ER), but also the thylakoid and inner membrane of the plastid and mitochondria, respectively. This mechanism is referred to as **cotranslational translocation** (see Chapter 4 for more details).

10.2.5 Termination of protein synthesis occurs at specific signals in the mRNA

Polypeptide elongation ceases when a ribosome reaches one of three stop codons on the mRNA: UAA, UAG, or UGA (Fig. 10.7). Termination of protein synthesis requires two proteins, known as **release factors** (RFs), eRF1 and eRF3, to bind to the A-site. eRF1 is a structural mimic of tRNA, and it recognizes all three stop codons and binds eRF3 and GTP. eRF3 has GTPase activity. RF interaction with the ribosome triggers a series of events, including hydrolysis of the bond between the completed protein and the final tRNA at the P-site. GTP hydrolysis by RF3 stimulates release of the polypeptide and the RFs from the ribosome. The tRNA and the ribosome are also released from the mRNA and become available to participate in another cycle of translation.

Dissociation of the 80S ribosome into 40S and 60S subunits is promoted by eIF6 and ATP-binding cassette E (ABCE1) protein in an ATP-dependent process, and may not occur until 40S subunits are required for preinitiation complex formation. Consequently, 80S ribosomes lacking an mRNA accumulate when initiation of translation is limited, such as under conditions of stress (e.g., hypoxia, heat shock, or dehydration stress).

10.2.6 Translation of plant cytosolic mRNAs is affected by stress conditions

Protein synthesis in the cytosol of plants does not occur at a constant rate. Rather, it is regulated in response to numerous physiological and environmental changes. Stresses such as anaerobiosis, heat shock, or viral infection diminish cytosolic protein synthesis (see Chapters 21 and 22). For example, plants growing in flooded fields can suffer oxygen deficit (hypoxia) as soil gases are displaced by water and less air reaches the roots. During hypoxia, oxidative phosphorylation can no longer provide energy for the cell, and fermentative metabolism dominates. The cell responds by decreasing the synthesis of most of the normal cellular proteins while maintaining synthesis of select enzymes required for glycolysis and ethanolic fermentation. mRNAs for the enzymes involved in anaerobic metabolism remain bound to polysomes, whereas other mRNAs decrease dramatically from the polysome population. Upon reintroduction of oxygen, mRNAs for all cellular processes rapidly return to polysomes. Presumably, this mechanism of reduction of protein synthesis and sequestration of cellular mRNAs during this stress helps to conserve ATP and preserve energy when aerobic metabolism is limited. The regulatory mechanisms that control how the translational machinery responds to physiological and environmental changes are currently the focus of considerable research.

10.3 Mechanisms of plant viral translation

10.3.1 Viral mRNAs are translated despite the absence of a 5′ CAP

Many plant viral RNAs lack a 5′ cap structure, so the RNA is translated in a cap-independent manner. These viral RNAs harbor a cap-independent translation enhancer or element

Step 1

A complex of release factors (including eRF1 and GTP-bound eRF3) binds to the stop codon exposed in the A-site. Most likely, although it is not yet proven, the deacylated tRNA in the E-site is released at this point.

Step 2

The peptidyl transferase center on the ribosome catalyzes the hydrolysis of the ester bond that links the completed polypeptide to the final tRNA.

Step 3

eIF6 and ABCE1 promote release of the protein and the mRNA is dissociated from the ribosomal subunits, making the mRNA available for another round of protein synthesis. (Note: the precise timing and function of GTP hydrolysis remain to be investigated more fully.)

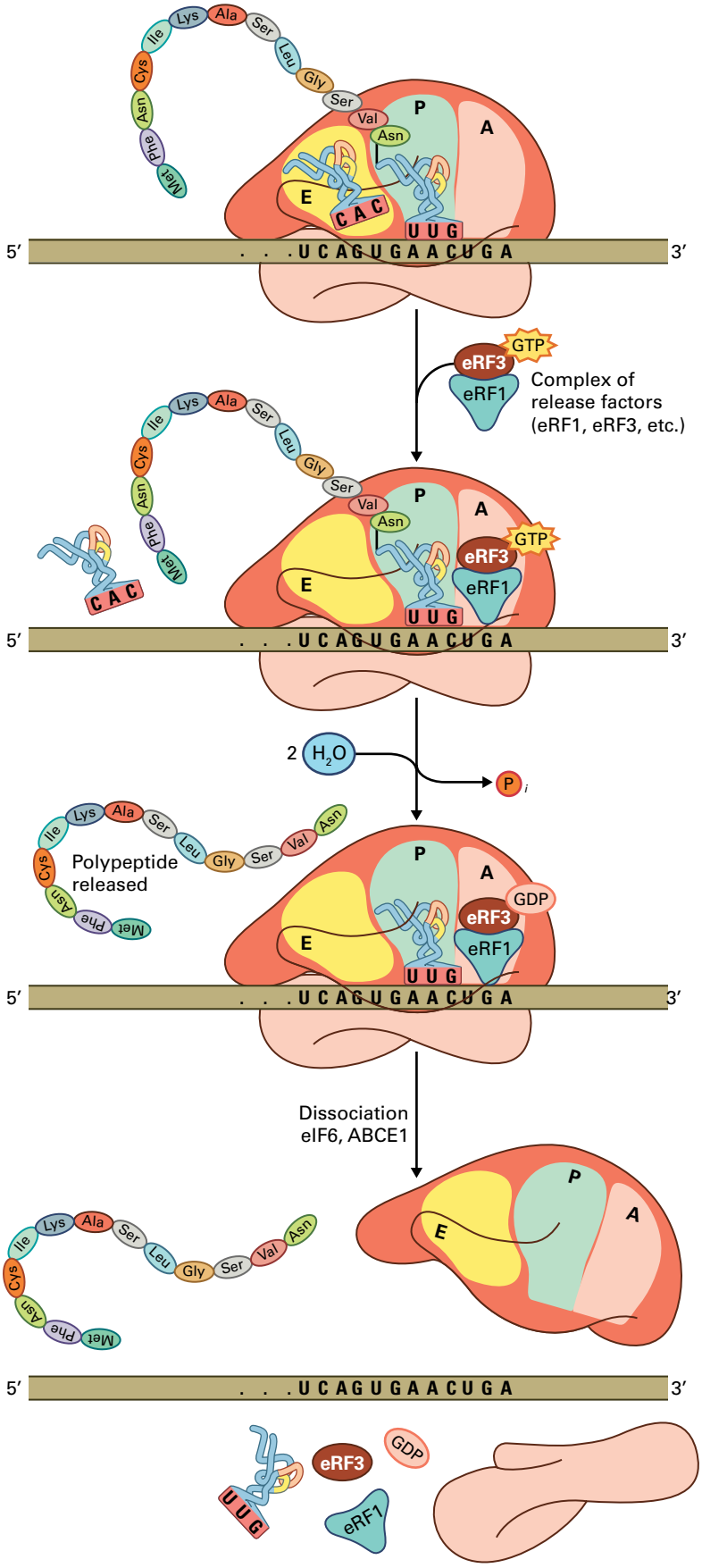


FIGURE 10.7 *Events during the termination of protein synthesis. Polypeptide chain termination occurs when one of three stop codons appears in the A-site of the ribosome.*

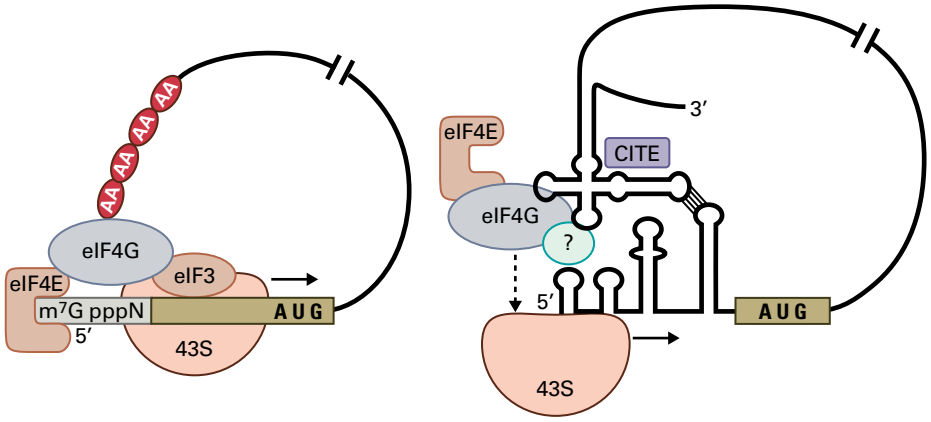


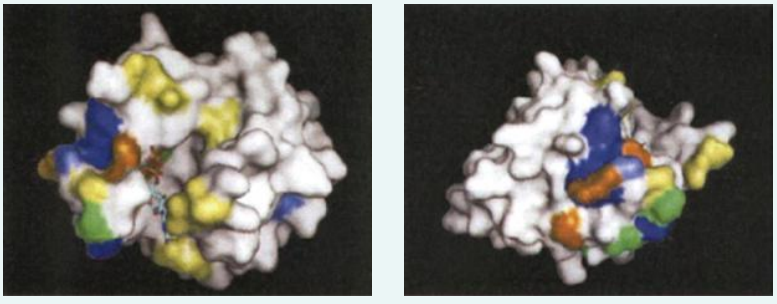
FIGURE 10.8 *Plant viral RNAs initiate translation differently than cytosolic mRNAs. The viral RNA (right) contains a 3′ CITE that binds the eIF4 complex, mimicking the cap structure of cytosolic mRNA (left). The viral cap-like structure interacts with the pre-initiation complex (43S) to position the RNA correctly at its 5′ UTR.*
Source: W. Allen Miller, Iowa State University.

BOX 10.4

Plants have naturally occurring virus resistance genes

A number of naturally occurring plant virus resistance genes in lettuce, tomato, pepper, pea, melon, rice, and barley correspond to genes encoding the cap-binding complex subunits, eIF4E, eIFiso4E, eIF4G, or eIF(iso)4G. The majority, but not all, of these resistance factors function against RNA viruses (potyvirus, cucumovirus, carmovirus, bymovirus, sobemovirus, polerovirus) carrying a virus-encoded protein (VPg) linked at the 5′ end of their genomes. Translation initiation factor-mediated resistance results from a small number of amino acid changes, most of which are not conservative and are on the surface of the protein (see colored areas in protein images). Interestingly, the mutations (often single amino acid changes) occur at sites generally distinct from the cap-binding region of the host protein, suggesting that cap-binding ability is not affected by the mutation (because eIF4E must still function for host mRNA translation). Although the exact mechanism for viral resistance has not been determined, it appears that these host initiation factor genes are required in some capacity for the translation and/or replication of the viral RNA genome that is mediated by direct interaction with the viral VPg protein.

Select known VPg resistance mutations



(CITE) in a UTR. This RNA tract has a high affinity for translation initiation factors that, in turn, recruit the ribosome to the mRNA.

Plant viral CITEs are usually about 100 nt long and come in a variety of sequences and structures. Those of potyviruses and crucifer-infecting tobamovirus are located in the 5′ UTR of the viral mRNA. In contrast, CITEs of viruses in the large, diverse Tombusviridae family (e.g., the Carmovirus, Tombusvirus, and Panicovirus genera) are located in the 3′ UTR. Some of these 3′ CITEs bind subunits of translation initiation factor eIF4F or eIF(iso)4F, which normally requires a cap structure on the RNA to bind with high affinity. Most 3′ CITEs are known or predicted to base pair to a sequence in the 5′ UTR mimicking the circularization of cellular mRNAs by the interaction of eIF4G and PABP (Fig. 10.8). The essential role of translation initiation factors, eIF4E, eIFiso4E, eIF4G, or eIF(iso)4G in the virus replication cycle is made evident by the fact that alleles of genes encoding these factors are often recessive resistance genes (see Box 10.4). This means the wild-type alleles are essential for virus infection. Coordination of translation with replication is a key to successful viral infection (see Box 10.5).

BOX 10.5

Viruses coordinate replication and translation

Why do some viruses have such a complicated system to control translation initiation at the 5′ end via a sequence in the 3′ UTR? One reason is that it may prevent collisions between ribosomes and the viral replicase during early infection events. All positive-sense RNA viruses must translate the viral replicase-coding region before the viral RNA can be replicated. A problem is that translation must be shut off to allow the replicase to copy the viral RNA without interference from the ribosomes translating the RNA. Replicase initiates complementary RNA synthesis at the 3′ end of the viral template RNA. As the replicase moves in the 5′ direction in the 3′ UTR of the template, it would encounter and disrupt the CITE structure in the 3′ UTR and interfere with CITE base pairing to the 5′ UTR, thereby turning off translation initiation at the 5′ end. This would depopulate the RNA of ribosomes translating upstream of the replicase. By the time the replicase moves upstream along its template to the translated region, the translated region would be ribosome-free and available to be copied by the viral replicase. Thus, blocking the base pairing between the 3′ CITE and the 5′ UTR would serve as a molecular switch to turn off translation and promote replication.

10.3.2 Viruses use recoding mechanisms, such as shifting the translation reading frame and reading through stop codons, to increase the diversity of proteins synthesized

Plant viruses often use recoding mechanisms (noncanonical reading of the genetic code) to increase the variety of products they can make. Ribosomal frameshifting allows translation of overlapping open reading frames (Fig. 10.9).

All ribosomes initiate at the same start codon in "zero frame," and most read only this ORF. In the region of reading frame overlap, however, a small fraction (1–10%) of translating ribosomes change reading frames. The vast majority of programmed frameshifts are into the –1 frame. Frameshifting at –1 occurs at a slippery heptanucleotide that usually fits the consensus XXXYYYZ, where X is any base, Y is A or U, and Z is any base except G. This is followed by a highly structured region, usually consisting of a pseudoknot, beginning six to eight bases downstream. It is thought that, as the leading edge of the ribosome encounters the structured region, the slippery site is positioned inside the ribosome bound to the tRNAs at the A- and P-sites. The tension created by the inability of the ribosome to "melt" the pseudoknot forces the tRNAs in the A- and P-sites to slip one base backward relative to the mRNA and into the –1 frame. tRNAs then repair to the mRNA, the pseudoknot secondary structure is melted, and translation resumes normally.

Many viruses also can incorporate an aa-tRNA instead of a release factor at a stop codon in a process called in-frame stop codon readthrough, or codon redefinition. Like frameshifting, this is an infrequent event performed by <1% to perhaps 10% of ribosomes, depending on the readthrough sequence. It provides a high ratio of the shorter protein encoded by the first ORF to the C-terminally extended version of the protein encoded by the first ORF plus the sequence downstream of the stop codon. Readthrough signals in the mRNA are quite diverse and less well characterized than those that confer –1 frameshifting. Perhaps the best characterized example is that of tobacco mosaic virus (TMV). Expression of the polymerase gene requires readthrough of a stop codon at the consensus motif UAGCARYYA, where UAG is the stop codon, R is any purine, and Y is any pyrimidine. The mechanism of readthrough remains unknown.

10.4 Protein synthesis in plastids

10.4.1 Plastid protein synthesis shows many similarities to bacterial protein synthesis

Plastid protein synthesis differs from cytosolic protein synthesis in several details. In general, the ribosomes, mRNAs, and auxiliary factors required at each step are not interchangeable between the cytosol and the plastid, and the numbers and functions of specific initiation factors differ considerably between the cytosol and the plastid. Bioinformatic analyses indicate plants have plastid translation factors that can be recognized based on their homology to bacterial translational factors. These include homologs of prokaryotic initiation factors (IF1, IF2, and IF3), elongation factors (EF-Tu, EF-Ts, and EF-G), termination factors (RF1, RF2, RF3), and the ribosome recycling factor RRF (Table 10.3). Very little enzymology has been carried out on the translation factors required in the plastid. The best studied are those of the unicellular photosynthetic organism *Euglena gracilis*, which have many functional similarities to the bacterial factors, but also have a number of unique structural features that may facilitate their function within the chloroplast.

Plastid ribosomes (see Table 10.1) have a single 16S rRNA in the small subunit, but three rRNAs in the large subunit (23S, 5S, and 4.5S); however, the total amount of RNA in plastid ribosomes is only a few nucleotides more than in bacterial ribosomes. Homologs of almost all of the bacterial ribosomal proteins occur in plastid ribosomes, and several

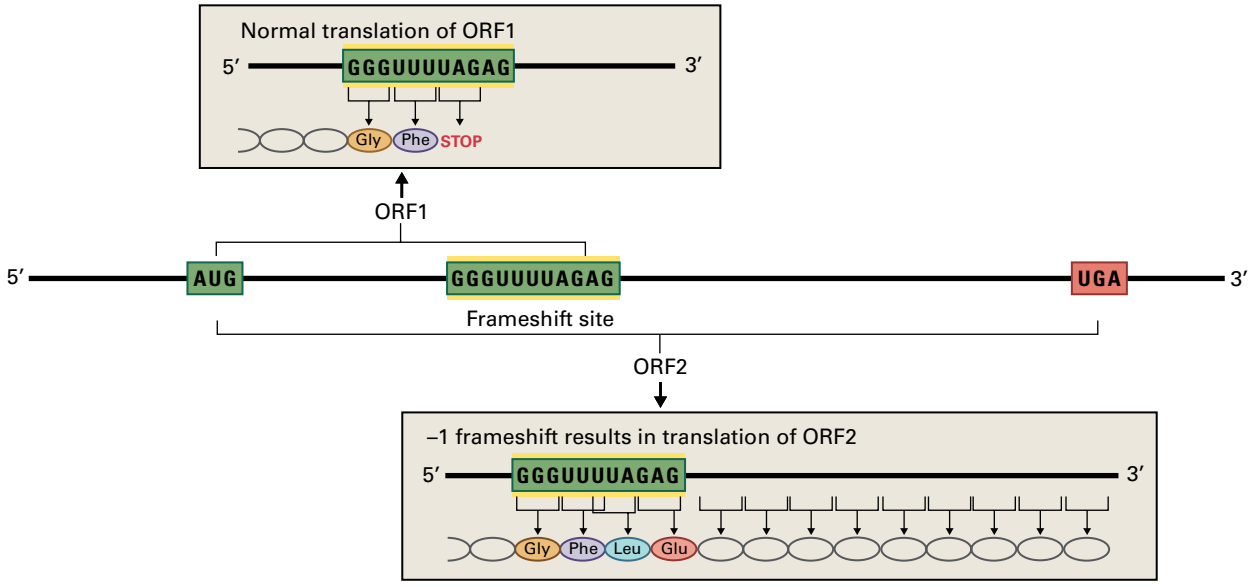


FIGURE 10.9 *Recoding mechanisms are used in viruses. Frameshifting occurs when two overlapping ORFs share a start codon but terminate at different sites. The reading frame of one ORF shifts, made possible by a recoding signal positioned at the site where the frameshift occurs. The ribosome slips back one nucleotide (into the –1 frame), then continues until reaching a different stop codon.*

TABLE 10.3 *Plastid translation factors and their relationship to bacterial translation factors.*

Factor	Role in prokaryotes	Approximate conservation between *Arabidopsis* and bacterial factor	Comments
IF1	Facilitates the functions of IF2 and IF3	≈58% identical to *E. coli* IF1 after removing the import signal	Very small protein, probably <80 amino acids after import signal removed
IF2	Binds the initiator tRNA (fMet-tRNA) to the ribosome	≈34% identical to *E. coli* IF2 after removing the import signal	Lengths variable, with the *E. gracilis* chloroplast IF2 over twice the size of the *E. coli* factor
IF3	Mediates dissociation of ribosomal subunits, proofreads the initiation complex	≈42% identical to *E. coli* IF2 after removing the import signal	Generally longer than the bacterial factors, with the *E. gracilis* chloroplast IF3 over twice the size of the *E. coli* factor
EF-Tu	Binds aa-tRNA to A-site of the ribosome	≈69% identical to *E. coli* IF2 after removing the import signal	Generally a highly conserved factor; encoded in chloroplast genome in some species
EF-Ts	Mediates guanine nucleotide exchange with EF-Tu	≈34% similar to *E. coli* EF-Ts, but percentage unclear due to overall poor alignment	Polyprotein with chloroplast ribosomal protein S7
EF-G	Translocase	≈57% identical to *E. coli* EFG after removing the import signal	GTPase
RF-1	Release factor 1, recognizes UAA/UAG	≈41% identical to *E. coli* RF after removing the import signal	Essential gene
RF-2	Release factor 2, recognizes UAA/UGA	≈41% identical to *E. coli* RF after removing the import signal	Also important for mRNA stability
RF3	Mediates release of RF1 and RF2 from the ribosome	33% identical to *Chlamydomonas* RF3	Homolog not yet clear in *Arabidopsis*
RRF	Ribosome recycling factor	≈44% identical to *E. coli* RF after removing the import signal	Has been isolated from spinach and preliminary enzymology studies done

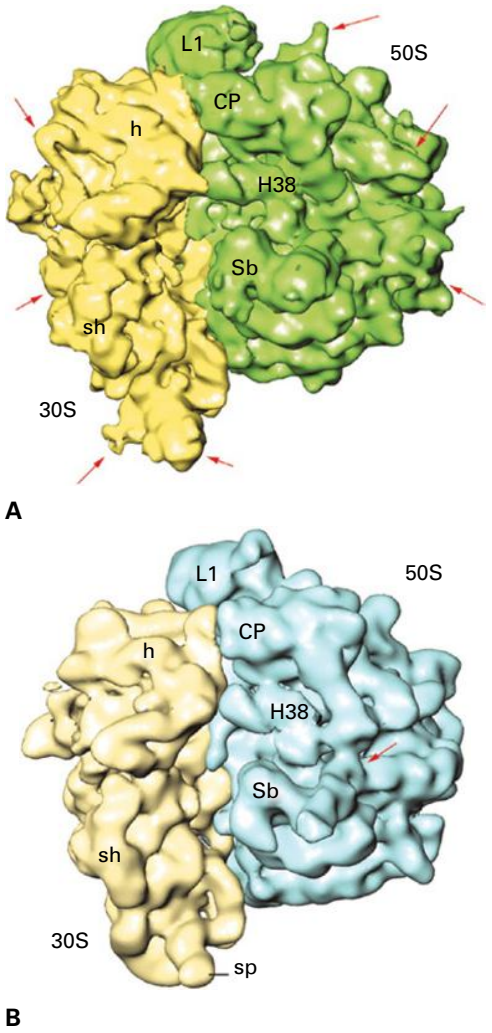


FIGURE 10.10 *Comparison of the cryoelectron microscopy maps of the spinach* (Spinacia oleracea) *chloroplast 70S ribosome at 9.4-Å resolution and the* E. coli *70S ribosome. (A) The chloroplast ribosome is shown with the 30S subunit in yellow and the 50S subunit in green. (B) The* E. coli *70S ribosome with the 30S subunit in pale yellow and the 50S subunit in blue. Structural differences between chloroplast an* E. coli *ribosomes are indicated by the red arrows in A. Landmarks of the 30S subunit: h, head; sh, shoulder; and sp, spur. Landmarks of the 50S subunit: CP, central protuberance; H38, 23S rRNA helix 38; L1, protein L1 protuberance; and Sb, stalk base.*
Source: Sharma et al. (2007). Proc. Natl. Acad. Sci. USA. 104: 19315–19320.

plastid-specific ribosomal proteins (PSRPs) have no counterparts in bacteria. The exact number of these varies between the plastids of different organisms. For example, spinach (*Spinacia oleracea*) chloroplast ribosomes have six plastid-specific ribosomal proteins (four in the small subunit and two in the large subunit). Cryoelectron microscopy of these ribosomes (Fig. 10.10) has allowed an estimation of the location of these plastid-specific proteins. One of them (PSRP1) is located on the decoding face of the small subunit and blocks both the ribosomal A- and P-sites to prevent translation. It has been postulated that this protein must be released or moved before initiation occurs, and that this process may be directly involved in the regulation of chloroplast protein synthesis by light (see below).

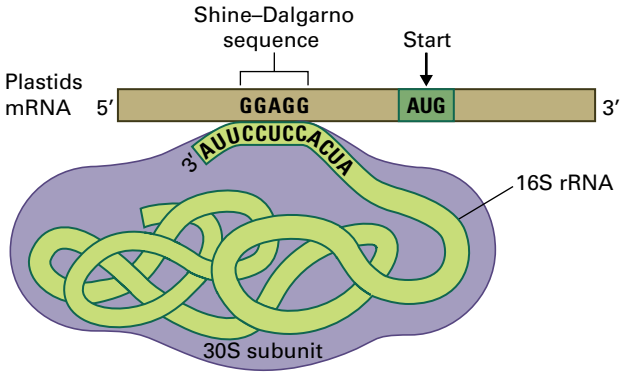


FIGURE 10.11 *The Shine–Dalgarno interaction for selection of the start codon. Initiation at the correct AUG codon is facilitated by hydrogen bonding between a polypurine sequence in the mRNA (the Shine–Dalgarno sequence) and a polypyrimidine sequence near the 3′ end of the small subunit 16S rRNA.*

Perhaps one of the most fundamental differences between the translation systems found in the plastid and cytosol of plants can be seen in the process by which the initiation signal on the mRNA is selected. As discussed earlier, cytosolic mRNAs have a 5′ cap that flags the 5′ end for initiation factors. By contrast, plastid mRNAs are not capped and are often transcribed as polycistronic messages that contain several reading frames, similar to bacterial mRNAs.

In bacterial systems, the small (30S) subunit of the ribosome selects the correct AUG codon for initiation. The 16S rRNA in this subunit base pairs with the Shine–Dalgarno sequence, a short sequence found just upstream of the initiation AUG and named after its discoverers (Fig. 10.11); binding this sequence facilitates selection of the start codon. The mechanism by which plastid ribosomes recognize the correct AUG for initiation has been studied most extensively in *E. gracilis,* spinach, and *Chlamydomonas*. Chloroplast mRNAs from these organisms tend to fall into two classes. One group does not contain a Shine–Dalgarno sequence within 20 nt of the start codon. Further, they have no conserved sequence signal in the 5′ UTR. The translational start site in these mRNAs is specified by the presence of an AUG codon in an unstructured or weakly structured region of the mRNA (Fig. 10.12) and in many cases probably requires one or more nuclear-encoded *trans*-acting proteins to facilitate initiation. The chloroplast mRNAs in the second group contain a Shine–Dalgarno sequence upstream from the start codon. In this class of mRNAs, the sequences surrounding the start codons demonstrate a greater degree of secondary structure, and the Shine–Dalgarno sequences typically play a role in initiation.

10.4.2 Thylakoid membrane proteins encoded in plastid DNA are translated on membrane-bound ribosomes

The light reactions of photosynthesis occur in the thylakoid membranes, and several of the proteins synthesized by the chloroplast are destined for incorporation into enzyme complexes

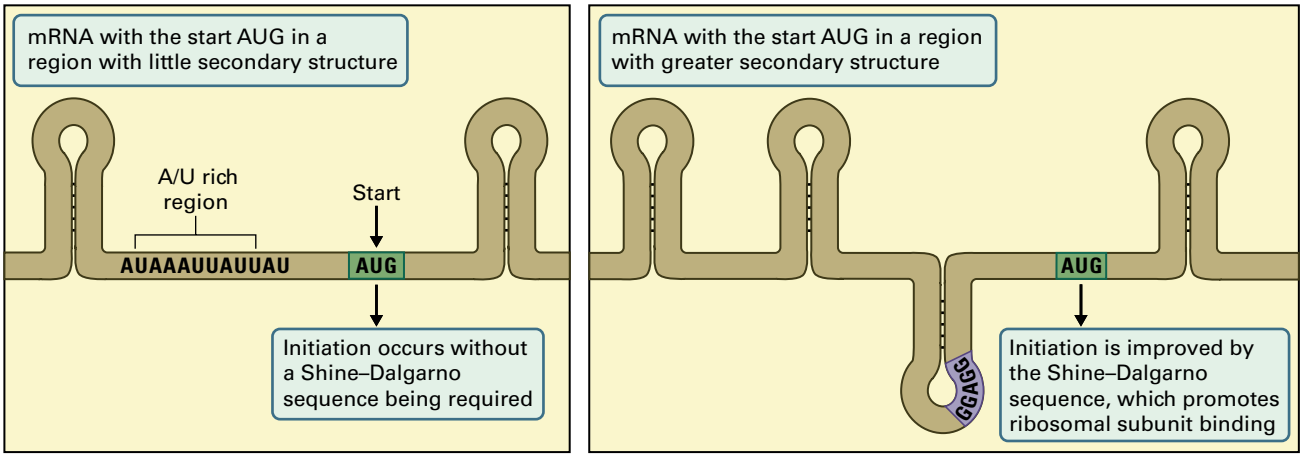


FIGURE 10.12 *Selection of the start site on chloroplast mRNAs proceeds by one of two routes, as dictated by the mRNA sequence. In the first route (left), the start codon is located in a weakly structured region and may be facilitated by a trans-acting factor. In the second route (right), a Shine–Dalgarno sequence is located near the start codon facilitating its selection for initiation.*

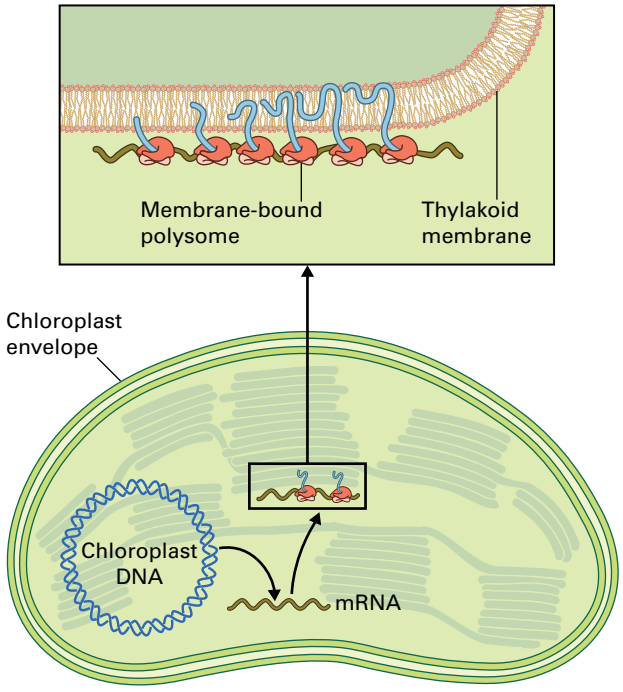


FIGURE 10.13 *Proteins targeted to multimeric complexes in the thylakoid membrane are synthesized on membrane-bound ribosomes. Translation of these mRNAs is initiated in the soluble portion of the chloroplast (stroma). Signals in the nascent peptides then direct the polysomes to the thylakoid membranes, where protein synthesis is completed.*

found in these membranes (Fig. 10.13). Synthesis of chloroplast membrane-bound proteins appears to occur in two steps. Protein synthesis in the chloroplast is believed to be initiated on free ribosomes. Once the nascent protein chain emerges from the ribosome, the amino acid sequence near its N-terminus acts as a signal sequence, directing the ribosome to the thylakoid membrane. This process is mediated by a protein complex, the chloroplast signal recognition particle. Once the ribosome and its nascent chain associate with the membrane, translation continues, and the polypeptide is inserted into the membrane as it is synthesized. In some cases, it is believed that certain mRNAs are directed to thylakoid membranes directly by binding to membrane associated RNA-binding proteins.

10.4.3 Chloroplast protein synthesis is regulated by light

Photosynthetically active chloroplasts arise from proplastids as a leaf develops, or from etioplasts in dark-grown tissues upon light exposure. Dramatic morphological and biochemical changes occur within these organelles during these transitions.

In the thylakoids, major protein complexes, most notably photosystems I and II (PSI, PSII), are assembled from nuclear- and plastid-encoded proteins. To achieve this, synthesis of many chloroplast proteins is greatly enhanced during the light-induced greening of the plastid. Translation of certain chloroplast mRNAs increases as much as 100-fold, sometimes without significant changes in the amount of mRNA present. For example, the mRNA for the large subunit of Rubisco (LSU) is present in dark-grown amaranth (*Amaranthus* sp.) and is bound to polysomes, but translation is minimal. When the cotyledons are illuminated, LSU mRNA remains constant, but LSU protein synthesis can be detected within 3–5 hours. Similarly, in barley (*Hordeum vulgare*), initiation complexes with the LSU mRNA are formed both in the light and dark, but the subsequent elongation step is enhanced in the light.

In addition to this translational control, changes in transcription, mRNA stability, cofactor availability, and protein degradation also participate in regulating the synthesis of chloroplast proteins (Fig. 10.14). Each protein shows a distinct pattern of regulation. The synthesis of some proteins appears to be controlled to a large extent by transcription, whereas the quantities of other proteins are regulated by changes in translation initiation rates or protein degradation.

It has become clear that nuclear gene products act as regulators of chloroplast protein synthesis, in some cases affecting the translation of a single species of chloroplast mRNA by interacting with its 5′ UTR, or more globally affecting

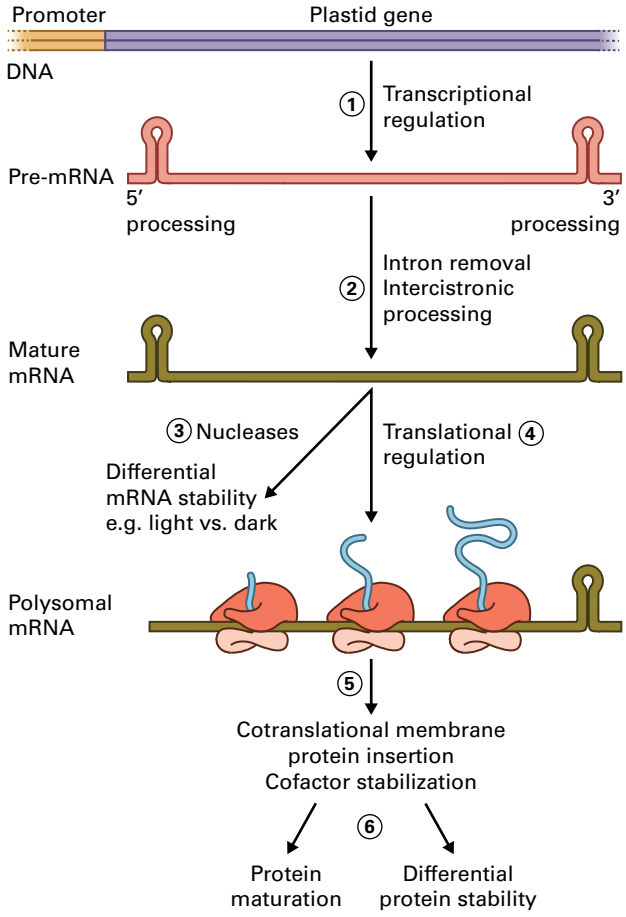


FIGURE 10.14 *Many regulatory processes act together to control the quantities of chloroplast proteins present during different phases of growth and development. (1) Gene expression can be regulated at the transcription of the DNA into RNA. (2) Regulation also occurs in the maturation of the pre-mRNA into the mature mRNA. These steps include processing the 3′ and 5′ ends, removing introns, and processing polycistronic mRNAs in intercistronic regions. (3) The stability of the mRNA is regulated through the action of the nucleases that determine how long the RNA will be available for translation. (4) The translation of the mRNA into protein is regulated in several ways, including through the action of specific mRNA-binding proteins. (5) The rate of protein synthesis and the stability of the nascent chain may be regulated during the cotranslational insertion of the polypeptide into the membrane and by the binding of a cofactor such as chlorophyll. (6) The amount of the final protein product from a gene is also regulated by its maturation (folding, modification, localization) and by sequence signals that regulate its lifespan.*

translation of many mRNAs. These protein–mRNA complexes increase in the light, correlating with enhanced translation of the mRNA component (Fig. 10.15, see Box 10.6).

10.4.4 mRNA-binding proteins can be regulated by redox potential

During light-activated protein synthesis, binding of the translational activator proteins must be coordinated with the photosynthetic activity of the chloroplast. At least two pathways seem to link these processes: The first involves the redox potential of the chloroplast, whereas the second couples translation to the availability of energy in the organelle.

Within the chloroplast, photosynthetic electron transfer generates reducing power and drives synthesis of the energy-rich nucleotide ATP (see Chapter 12). Both of these processes appear to regulate translation of *psbA* transcripts in the chloroplast of *Chlamydomonas*. The *psbA* gene product, the D1 protein, is a core component of PSII. The redox environment of the chloroplast and the availability of ATP are thought to influence the formation of a multiprotein complex that binds to the 5′ UTR of the *psbA* mRNA. Formation of this mRNA–protein complex is promoted by light and correlates with a 50- to 100-fold enhancement of *psbA* translation.

During the light reactions of photosynthesis, water is split and its electrons are transferred to $NADP^+$ by means of a series of electron carriers. One of these redox-active carriers, the small iron–sulfur protein ferredoxin, can donate electrons to several proteins, including the enzyme ferredoxin-thioredoxin reductase (FTR). While best known for mediating the transfer of electrons from reduced ferredoxin to the regulatory disulfide protein thioredoxin (see Chapters 12 and 13), FTR can also reduce a chloroplast enzyme called disulfide isomerase (RB60), which catalyzes the interconversion of cysteinyl sulfhydryls and disulfides. In the current model for regulation of psbA protein synthesis by light in *Chlamydomonas*, the light-dependent reduction of RB60 leads to reduction of disulfides within the mRNA-binding protein RB47 (Fig. 10.16). Reduced RB47 as part of an oligomeric complex can then bind to the 5′ UTR of the *psbA* mRNA and upregulate its translation.

In chloroplasts, light-dependent phosphorylation of ADP produces energy for the plant cell. In the dark, ATP concentrations fall while ADP concentrations rise. Exposing leaves to light results in a rapid increase in ATP and a concomitant decrease in ADP. These light-dependent shifts in the ADP/ATP ratio may play a role in linking the status of the light environment to translational activity in the chloroplast.

Synthesis of the *Chlamydomonas* D1 protein encoded by *psbA* provides the best-studied case for regulation of translation by ADP/ATP ratios. When activated by high ADP concentrations, a serine-threonine protein kinase is thought to phosphorylate RB60 in an unusual reaction that transfers the β-phosphate from ADP to the protein (Fig. 10.16). The phosphorylated form of RB60 not only fails to promote the reduction of RP47, but also may actively oxidize this protein, leading to accumulation of the oxidized form of RB47. Because the reduced form of RB47 must bind to the *psbA* mRNA to activate translation, the net result of this process is a decrease in the synthesis of D1. Thus, in the current model, a dual system acts to regulate the translation of the *psbA* mRNA. In the dark, when there is an abundance of ADP, RB60 is phosphorylated, reducing its ability to activate the binding of RB47 to the mRNA; in the light, the kinase is inhibited, and the redox environment of the plastid activates RB60. As a result, the reduced form of RB47 accumulates, increasing the ability of that protein to bind mRNA and activate translation.

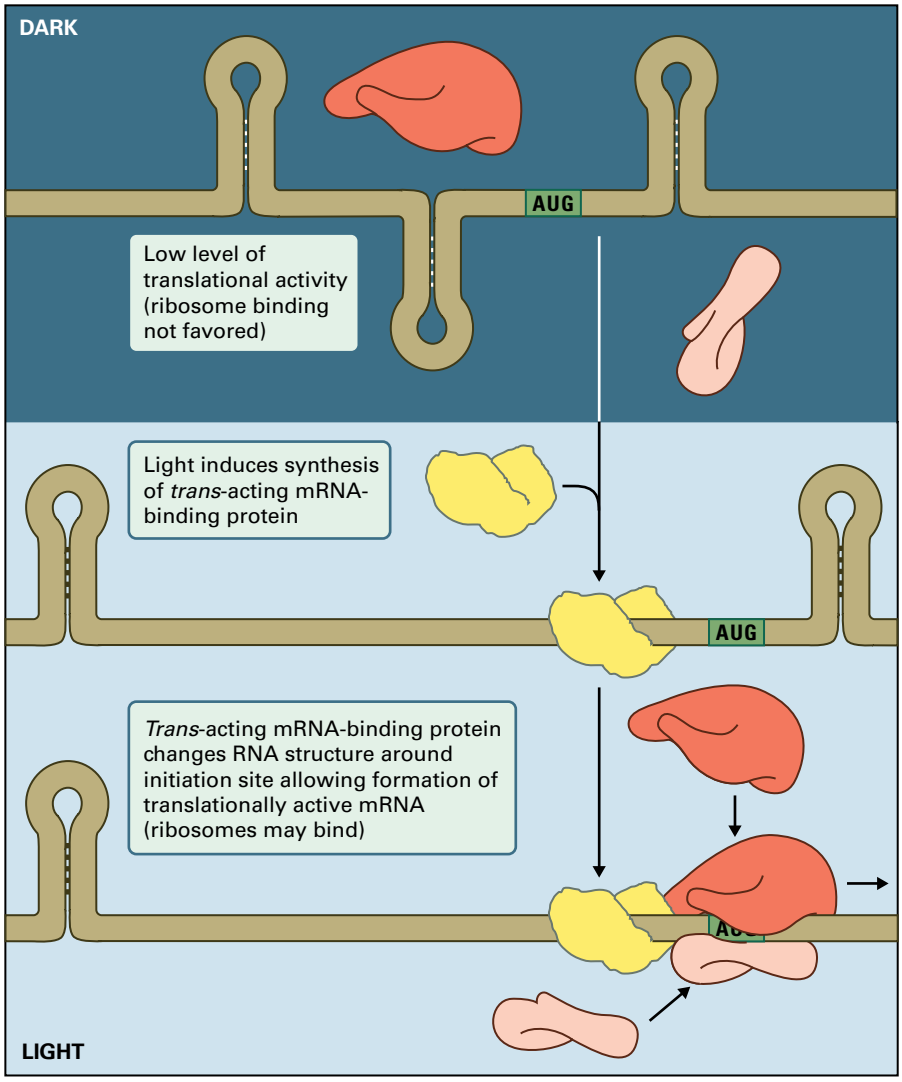


FIGURE 10.15 *Trans-acting factors that bind to the 5′ UTRs of chloroplast mRNAs are thought to play a role in light-dependent activation of translation.*

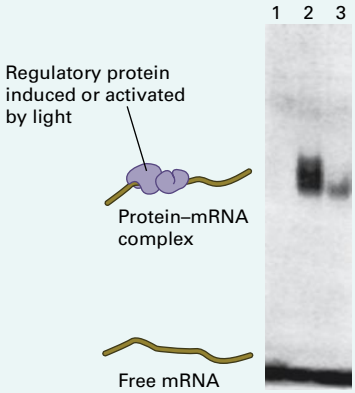
BOX 10.6

Binding of proteins to mRNAs can be detected by gel-mobility shift assays

Protein binding to RNA can often be detected by a gel-mobility shift assay, in which the RNA is labeled with radioactivity, and its migration during polyacrylamide gel electrophoresis is detected by autoradiography. If a protein binds to the RNA, the protein/RNA complex migrates more slowly in the gel than the unbound RNA molecules. The *trans*-acting factors that bind to chloroplast mRNAs can be detected by this method.

In a specific example, suppose a portion of *psbA* mRNA is subjected to electrophoresis alone (lane 1) or is incubated with an extract of light-grown cells that contain an mRNA-binding protein (lane 2). A protein–mRNA complex forms that migrates at a slower rate during gel electrophoresis. Much less of the mRNA–protein complex is observed when the mRNA is incubated with extracts of dark-grown cells (lane 3).

Source: Danon & Mayfield (1991). EMBO J. 10:3993–4001.



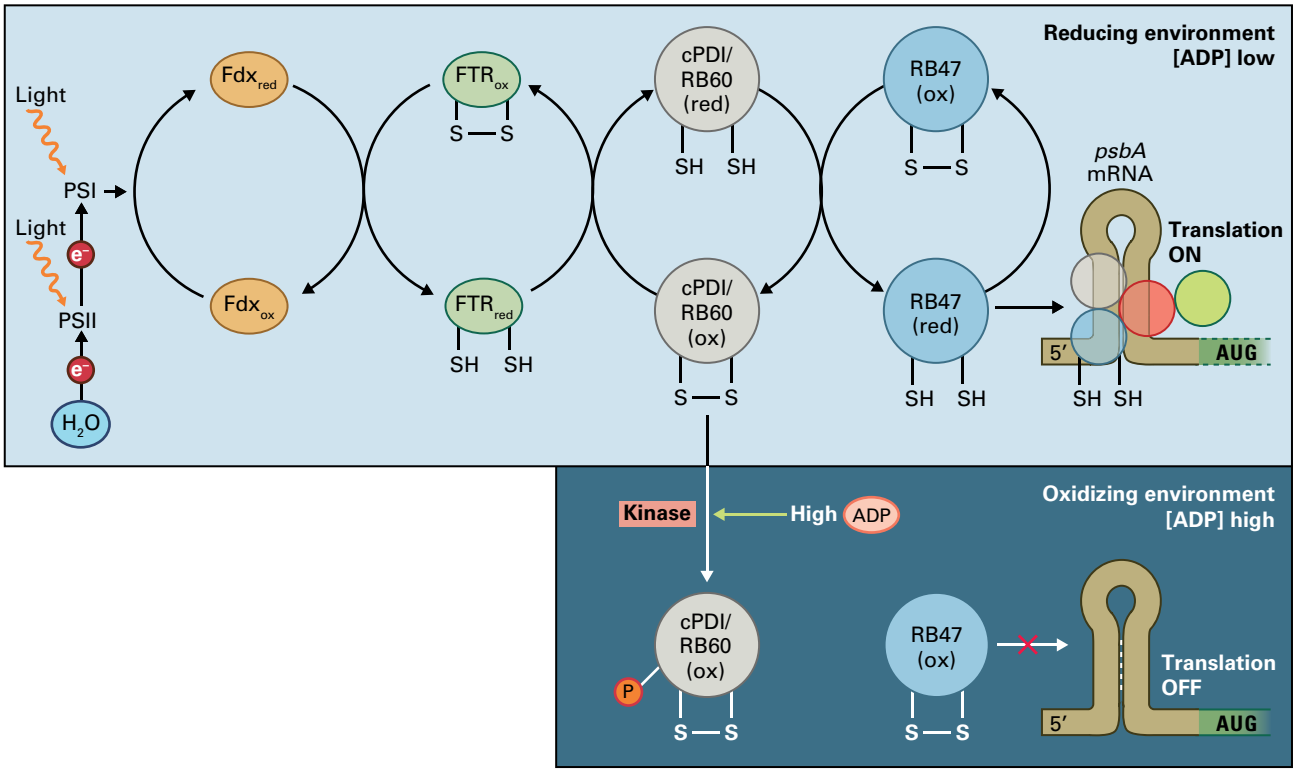


FIGURE 10.16 *Model for how light affects synthesis of the chloroplast protein D1, the product of the* psbA *mRNA. In* Chlamydomonas*, a unicellular alga, translation of* psbA *mRNA is enhanced dramatically when a protein complex consisting of at least four distinct polypeptides binds to the 5′ UTR. The current model postulates that in the dark, concentrations of reduced ferredoxin (Fdx_{red}) are low and cPDI/RB60 is oxidized. As a consequence, the RB47 mRNA-binding protein is also oxidized and binds poorly to the 5′ UTR of the* psbA *mRNA. In the absence of reduced RB47, there is little translation of the* psbA *mRNA. In the light, electrons flow from water to ferredoxin via photosystems (PS) II and I. Fdx_{red} donates electrons to ferredoxin-thioredoxin reductase (FTR), which in turn reduces disulfides in cPDI/RB60. The reduced cPDI/RB60 via PSII and PSI subsequently donates electrons to reduce disulfides in RB47, which can then bind* psbA *mRNA, greatly enhancing its translation. A second level of control is exerted by the concentration of ADP in the chloroplast. In the dark, high concentrations of ADP activate a protein kinase that phosphorylates cPDI/RB60. The phosphorylated form of cPDI/RB60 not only fails to promote the accumulation of reduced RB47 but also appears to actively promote its oxidation. Because the oxidized form of RB47 does not bind well to the* psbA *mRNA, translation is not activated in the dark.*

10.4.5 Cofactor insertion often occurs during translation of photosynthetic components

Numerous proteins involved in photosynthesis require prosthetic groups such as chlorophylls, carotenoids, quinones, or hemes to carry out their biological functions. Often, a protein must bind its cofactors before it can accumulate in a stable conformation. Perhaps the best-studied group of proteins in this category is the group that binds chlorophyll. Chloroplast thylakoid membranes include several proteins that bind chlorophyll, six of which are synthesized within the plastid itself. These proteins are essential components of PSI, PSII, and the light-harvesting complexes. In addition to chlorophyll, they also contain several other prosthetic groups, such as quinones (see Chapter 12).

These proteins cannot be detected in cells from emerging leaves and cotyledons before exposure of these organs to light. However, in most plants, mRNA transcripts for these chlorophyll-binding proteins are present whether the plants are kept in the light or the dark. Surprisingly, some of these mRNAs associate with thylakoid membrane-bound polysomes even in the dark. This indicates that synthesis of chlorophyll-binding proteins is initiated in the dark, but some mechanism prevents the accumulation of mature protein products under those conditions.

Plants must have light to synthesize chlorophyll, since light is required for the conversion of protochlorophyllide to chlorophyll (see Chapter 12). The accumulation of chlorophyll-binding proteins appears to depend on the ability of the chloroplast to complete the process of chlorophyll synthesis. If chlorophyll is not present, the apoprotein is degraded, presumably because it fails to fold properly (Fig. 10.17). In this way, the accumulation of chlorophyll-binding proteins is coupled to the light-dependent synthesis of their cofactors.

To allow time for the chloroplast to coordinate the synthesis of a protein, its insertion into a membrane, and the binding of its required cofactors, the ribosomes pause at discrete sites during the synthesis of the nascent polypeptide chain. The best-studied example of the cotranslational insertion of cofactors is the D1 protein. During its synthesis, the ribosome

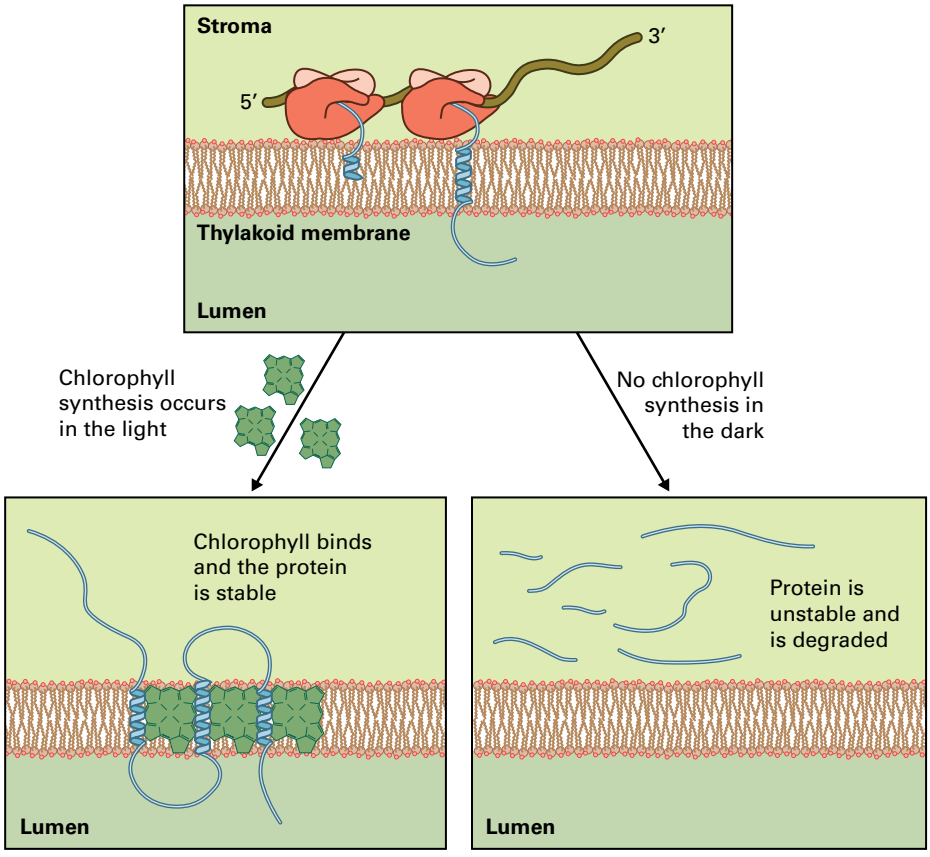


FIGURE 10.17 *Regulation of protein synthesis by cofactor availability: model for stabilization of a chloroplast protein by cofactor binding. Proteins in the thylakoid membranes bind cofactors such as chlorophyll, quinones, or iron–sulfur clusters. Many proteins that bind chlorophyll do not accumulate in dark-grown chloroplasts, although the mRNA for these proteins is present and is often found in polysomes. Plants require light to complete the synthesis of chlorophyll. Although chlorophyll-binding proteins are believed to be synthesized in the dark, the apoprotein (protein without the bound cofactors) formed is unstable and is rapidly degraded. In the light, the plants make chlorophyll, which binds to the growing polypeptide chain and stabilizes it.*

pauses at discrete positions (see Box 10.7), and these pauses facilitate interaction of the nascent chain with the thylakoid membrane, the insertion of segments of the growing polypeptide into the membrane, and assembly of the protein into PSII. The binding of cofactors to the protein occurs during its synthesis and assembly (Fig. 10.18).

10.5 Post-translational modification of proteins

10.5.1 Proteolytic processing can be used to modify the final protein product

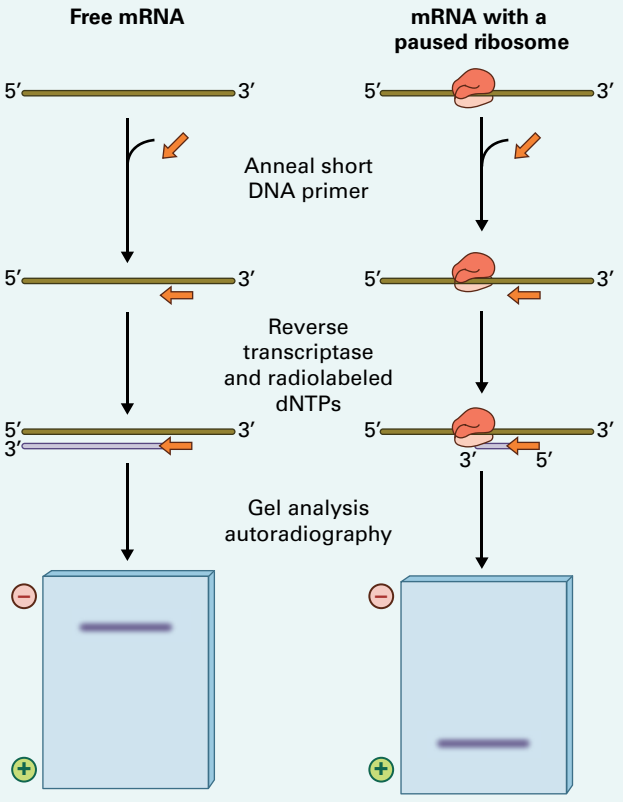
Initially, all polypeptides begin with either formylmethionine (in bacteria, plastids, and mitochondria) or methionine (in the eukaryotic cytosol). The formyl group is almost always removed by a ribosome-associated deformylase. In about half of all proteins, the initiating methionine is removed from the nascent chain by a ribosome-associated protease called Met-aminopeptidase. Removal of the N-terminal methionine is determined largely by which amino acid occupies the second position; small neighboring residues favor removal of the initial amino acid. Occasionally, the second amino acid is also removed, although the protease responsible for this step has not been identified.

As proteins reach their appropriate subcellular location, proteolytic processing may remove any N-terminal signal sequences (see Chapter 4) and other segments of the original polypeptide. One example of proteolytic processing in plant chloroplasts occurs during D1 maturation. Before complete assembly of photosystem II, a C-terminal peptide of D1 (consisting of nine or 16 amino acids, depending on the organism) is removed. The newly formed C-terminus binds to a manganese atom in the oxygen-evolving center, and this interaction is essential for subsequent photosystem function.

Proteolytic processing is also involved in generating active peptide hormones. The 18 amino acid peptide hormone, systemin, is produced in response to wounding in members of the Solanaceae, such as tomato (*Solanum lycopersicum*) and potato (*S. tuberosum*) (Fig. 10.19). Systemin is secreted by wounded plant cells and is transported to other regions of the affected plant to participate in inducing the synthesis of proteins involved in plant defense. Like many peptide hormones

BOX 10.7 Toeprinting can be used to determine where ribosomes pause during protein synthesis

The positions where ribosomes pause on an mRNA can be determined by mapping the edge of the ribosome on the 3′ side of the region of the mRNA covered by the ribosome. In this procedure, known as **toeprinting**, mRNAs with ribosomes bound at the stalled position are isolated, and a short DNA primer is hybridized to the mRNA downstream from the predicted pause site. Reverse transcriptase is used to synthesize a cDNA from the mRNA/primer complex. When no ribosomes are present on the mRNA, the reverse transcriptase can potentially copy the mRNA all the way to the 5′ end; however, if a ribosome is present between the site where the primer is annealed and the 5′ end of the mRNA, the progress of the reverse transcriptase is blocked. When it reaches the edge of the ribosome, the enzyme stops and dissociates from the mRNA, creating a shorter cDNA that locates the leading edge of the ribosome.



in animals, systemin is initially synthesized as a much larger precursor of 200 amino acids, and proteolytic processing produces the active peptide hormone. Phytosulfokines, sulfated penta-, and tetrasulfated peptides discovered for their role in cultured cell proliferation, are produced from an 89 amino acid precursor that includes an N-terminal signal sequence. RALF (rapid alkalinization factor) is also synthesized as a pre-proprotein and undergoes several proteolytic cleavages to produce the biologically active molecule, while others, such as ENOD40 and CLAVATA3, only have an N-terminal signal sequence removed to produce the mature form.

10.5.2 Proteins must fold into a precise three-dimensional structure to carry out their biological function

During or after the completion of translation, the polypeptide chain rearranges to give rise to the well-defined three-dimensional conformation of the protein. Much remains to be learned about this process, but according to the current model, a newly synthesized protein first folds into a structure in which most of the elements of secondary structure (e.g., α-helices and β-sheets) are present (Fig. 10.20). These structures align with each other so that the orientation approximates the final structure of the folded protein. This partially folded molecule, referred to as a **molten globule**, is the starting material from which the final three-dimensional structure of the protein will emerge after numerous interactions among the amino acid side chains.

In vitro, many proteins can unfold and then refold correctly within a few microseconds, re-establishing their native conformations in the absence of other cellular components. This protein behavior has led to the idea that the primary sequence of the polypeptide contains all the information necessary to confer the correct structure on the folded protein. Similar assumptions have been made regarding the formation of oligomeric complexes. However, high concentrations of cellular proteins and the presence of many surfaces with which a folding protein can interact may interfere with proper folding. In the eukaryotic cytosol, most protein folding occurs cotranslationally. In chloroplasts, at least a portion of protein folding occurs post-translationally. The folding of proteins *in vivo* is regulated by **molecular chaperones**, proteins that promote proper folding of polypeptides and suppress folding patterns that would result in protein aggregation or nonfunctional protein products (Fig. 10.21, see Section 10.5.3).

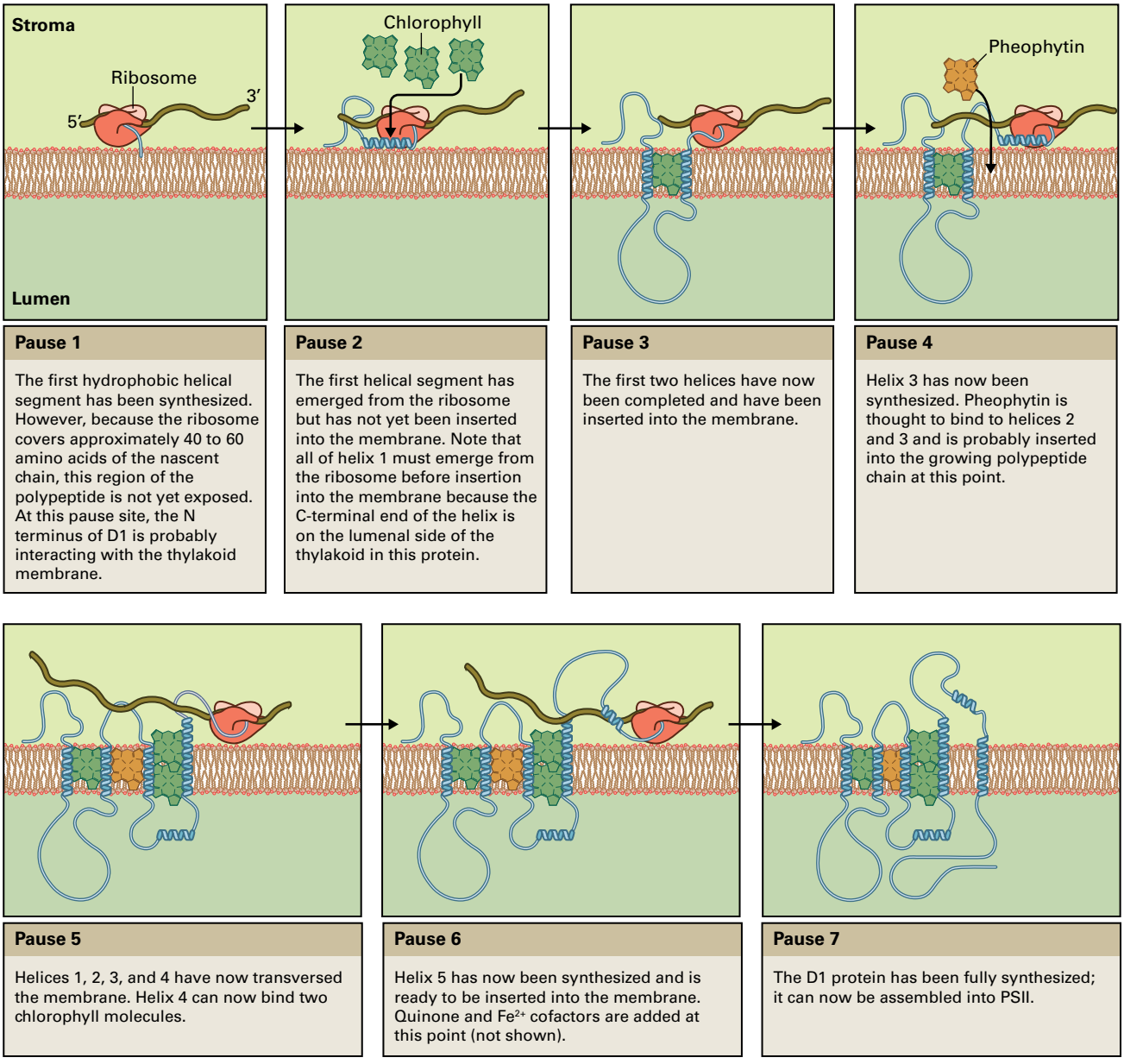


FIGURE 10.18 *Model for cotranslational insertion of cofactors into the D1 proteins. Ribosomes synthesizing D1 pause during translation to allow the protein to interact with the membrane with the correct topology and allow insertion of cofactors such as chlorophyll, pheophytin, and quinones.*

10.5.3 Protein-assisted folding occurs in the cell

Molecular chaperones are proteins that bind and stabilize otherwise unstable protein conformations. Through coordinated and repeated binding and release of partially folded polypeptides, chaperones facilitate several processes, including protein folding, oligomer assembly, subcellular localization, and protein degradation. Chaperones do not direct specific folding patterns; rather, they prevent the formation of incorrect interactions within a polypeptide, between polypeptides, or between polypeptides and other macromolecules. Thus, chaperones increase the yield of fully functional proteins.

Chaperones fall into several major classes, including the Hsp70 family (named for their approximate mass in kilodaltons), and the chaperonin family (Table 10.4 and Fig. 10.21). The Hsp70 family is found in bacteria and in most compartments of eukaryotic cells. Similarly, chaperonins are found in all cells, from bacteria and the eukaryotic cytosol to subcellular organelles, such as chloroplasts and mitochondria.

10.5.4 The Hsp70 family of molecular chaperones maintains polypeptides in an unfolded state

During protein synthesis, stable folding cannot occur until at least one complete domain (i.e., 100–200 amino acids) of a nascent protein chain emerges from the ribosome. These nascent

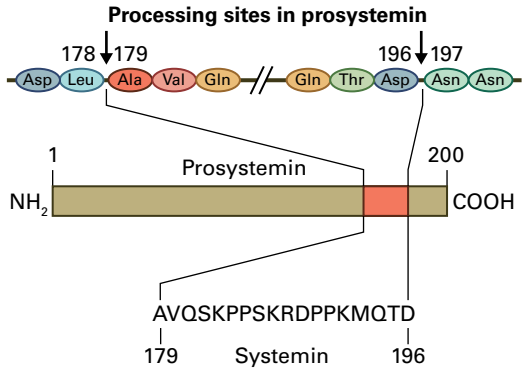


FIGURE 10.19 *The 18-amino-acid peptide hormone, systemin, is formed by plant cells in response to wounding. It is produced by proteolytic processing of prosystemin, a much larger precursor polypeptide (200 amino acids).*

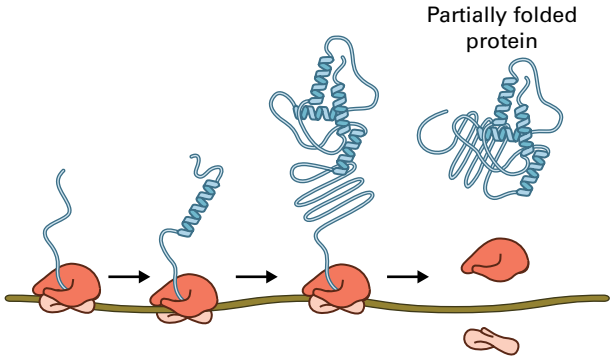


FIGURE 10.20 *Steps in protein folding. Protein folding in the cell cytosol is primarily cotranslational. Many proteins, especially multidomain proteins, fold as they are being synthesized. Each domain folds as it emerges fully from the ribosome. Proteins in bacteria, and at least some proteins in chloroplasts and mitochondria, often fold after the completion of their synthesis (i.e., post-translationally).*

chains contain hydrophobic amino acids that tend to aggregate so as to minimize their interaction with the aqueous environment. A cell must maintain these aggregation-prone nascent chains in a nonaggregated, folding-competent state.

Molecular chaperones in the Hsp70 family bind to amino acid chains emerging from the ribosome during protein synthesis (Fig. 10.22). These proteins bind and release hydrophobic segments of unfolded proteins in an ATP-dependent manner. Hsp70 binding stabilizes unfolded proteins and prevents their aggregation. The controlled release of the unfolded protein may permit it to proceed successfully along the folding pathway once a complete domain is synthesized (Fig. 10.23). This process is facilitated by cochaperones such as Hsp40 and GrpE. Hsp40 facilitates the interaction of Hsp70 with the nascent chain, while GrpE functions as a nucleotide exchange factor, increasing the rate of conversion of the Hsp70 family member between the ATP (loose protein affinity) and ADP (tight protein binding) bound conformations (Fig. 10.23).

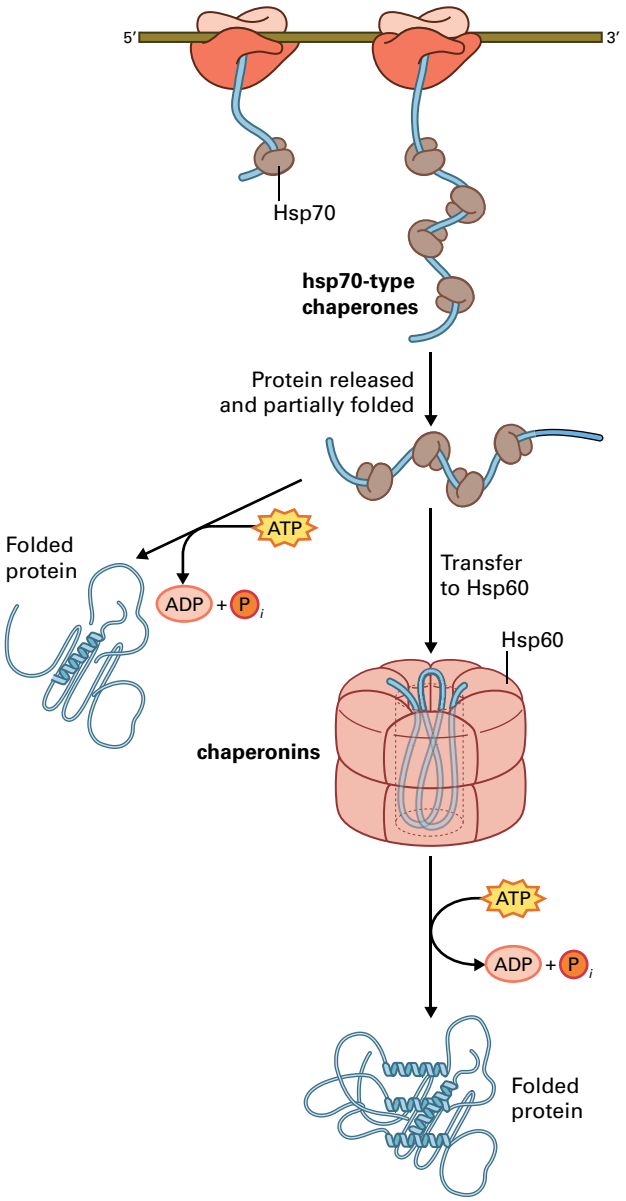


FIGURE 10.21 *Molecular chaperones are divided into two classes. The Hsp70 chaperones function in the early stages of the protein-folding process, often during translation, by recognizing small hydrophobic patches on the surface of the nascent polypeptide. Many polypeptides can fold with the aid of the Hsp70 pathway alone. The chaperonins act later in the process, after translation, and provide a central cavity in which protein folding is facilitated. Both Hsp70 and chaperonin pathways require energy in the form of ATP hydrolysis for proper functioning.*

10.5.5 Chaperonins play a crucial role in facilitating the folding of many proteins

In the current model for protein folding in bacteria, chloroplasts, mitochondria, and the eukaryotic cytosol, nascent polypeptide chains interact with the Hsp40/Hsp70 proteins while a portion remains positioned on the ribosome. For some cellular proteins, particularly in chloroplasts and mitochondria, subsequent successful folding requires transfer to a second folding complex, the chaperonin system.

TABLE 10.4 *Examples of chaperones found in plants, bacteria, and organelles.*

Hsp70 family		Chaperonins	
Bacteria	dnaK	Bacteria	GroEL (cpn60), GroES (cpn10)
Eukaryotic cytosol	Hsp70, Hsp40	Mitochondria	Mt-cpn60
Endoplasmic reticulum	BiP	Chloroplasts	Rubisco-binding protein (ch-cpn60), ch-cpn10
Mitochondria	Grp25	Cytosol	TRiC (or CCT)

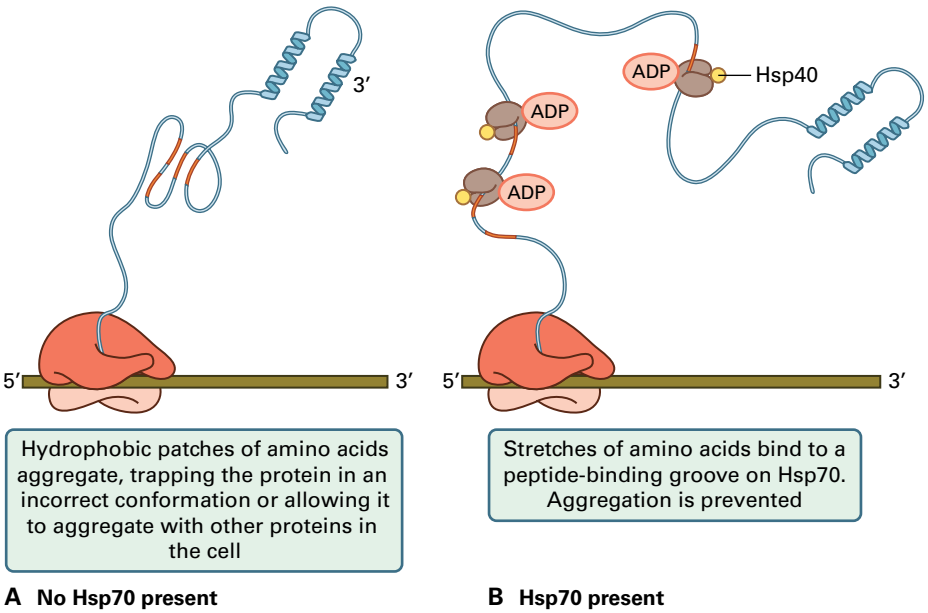


FIGURE 10.22 *Hsp70 is believed to play a role in preventing improper folding and aggregation of nascent polypeptide chains and newly released polypeptide chains. (A) The three-dimensional structure of a protein often involves interactions between distant segments of the polypeptide chain. As the nascent peptide emerges from the ribosome, the side chains of hydrophobic amino acids cluster together to avoid contact with water. As a result, the protein may fail to fold correctly, or the peptide chain may aggregate with other cellular proteins. (B) Hsp70 and its cochaperone Hsp40 bind to the nascent chain, impeding unfavorable interactions within the nascent chain and between the unfolded polypeptide and other proteins in the cell. Hsp70 thus prevents the protein from becoming trapped in an incorrectly folded conformation and prevents the aggregation of the nascent polypeptide with other proteins in the cell.*

Chaperonins are the most varied and structurally complex class of molecular chaperones, and they are divided into two families: the GroEL group (also called the Hsp60, chaperonin 60, or cpn60 group), and the TRiC (TCP-1 ring) family (see Table 10.4). The GroEL group is found in bacteria, mitochondria, and chloroplasts, whereas the TRiC family functions in the eukaryotic cytosol.

The best-studied member of the GroEL family is from *E. coli*, but the organellar chaperonins are believed to share similar structures and functions. All are oligomeric proteins, consisting of ≈60 kDa subunits. Bacteria and mitochondria appear to contain one chemical species of GroEL subunit, whereas chloroplasts have two. In plants, plastid and mitochondrial GroEL are encoded in the nuclear genome and imported into the organelle. In mitochondria and chloroplasts, as in bacteria, GroEL chaperonins consist of two stacked rings with seven subunits, arranged in the shape of a barrel ≈150 Å in height and 140 Å in diameter with a central cavity ≈50 Å wide (Fig 10.24). Unfolded polypeptides bind in this central cavity in a collapsed molten globule-like conformation.

GroEL works in cooperation with a smaller protein, GroES. In *E. coli*, GroES consists of 10 kDa subunits that form heptameric rings. The plastid protein is sometimes referred to as cpn10, based on the molecular mass of its subunit in *E. coli*. However, this nomenclature can be misleading because one chloroplast homolog has a molecular mass of ≈24 kDa, consisting of two GroES-like units (Fig. 10.25). GroES plays a crucial role in promoting the binding and release of the unfolded polypeptide and induces significant conformational changes in GroEL (Fig. 10.26).

A few polypeptides synthesized in the cytosol are thought to use a chaperonin referred to as the TRiC complex. This complex is not as well understood as the GroEL–GroES complex, but it may play a similar role in folding. In plants, the

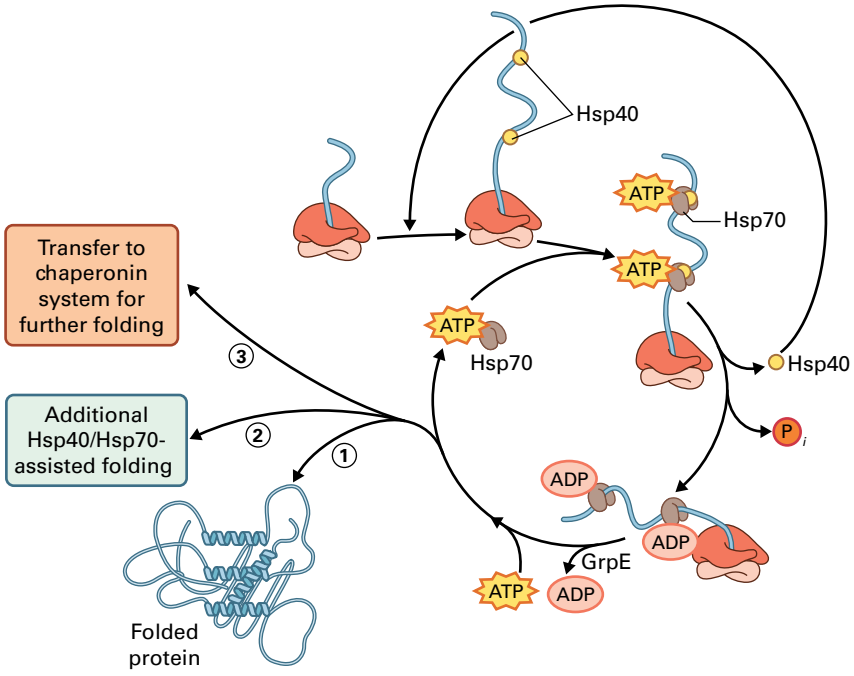


FIGURE 10.23 *Model for the role of Hsp70 in protein folding. The unfolded polypeptide is bound by Hsp40, a cochaperone that facilitates the interaction of an Hsp70:ATP complex with the unfolded polypeptide. The Hsp70 protein contains two domains: The N-terminal domain contains the ATP-binding site, whereas the C-terminal domain folds into a conformation that can bind short peptide sequences exposed on an unfolded protein. After ATP hydrolysis, a stable ternary complex of the unfolded polypeptide, Hsp70, and ADP forms. A nucleotide exchange factor, often designated GrpE, promotes the exchange of ADP for ATP. In the presence of ATP, the interaction of Hsp70 with the polypeptide is reduced, and Hsp70 dissociates from the folding protein. The protein can then (1) complete its folding and enter the native state, (2) interact with Hsp40 and Hsp70 again to undergo additional folding steps, or (3) be transferred to an additional folding system, the chaperonin system.*

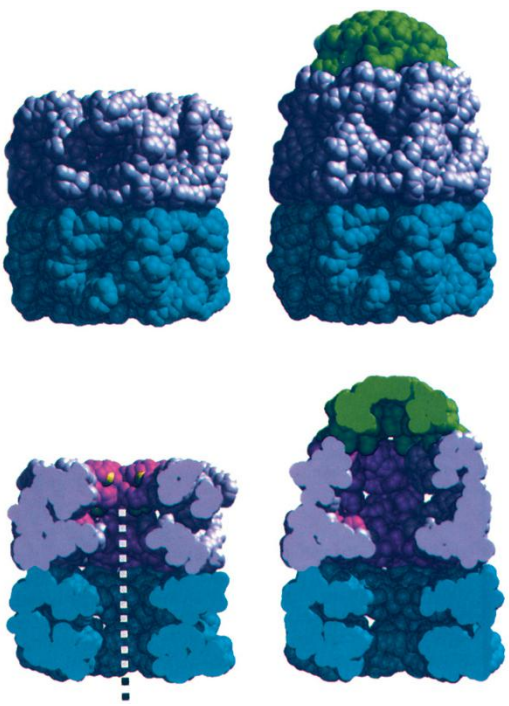


FIGURE 10.24 *Structures of GroEL and GroES. These space-filling representations illustrate the central cavity in which folding takes place.*

TRiC complex contains at least six distinct polypeptides, many of which appear to be related to each other in sequence. As with GroEL, TRiC subunits are arranged in two stacked rings with a hole in the center. Many of the general principles discussed above for protein folding in chloroplasts and mitochondria probably apply to plant cytosol as well. However, much work remains to be done to develop a detailed understanding of this process.

10.5.6 Protein folding is coordinated with transport

Many proteins are secreted from cells or localized in subcellular compartments other than their sites of synthesis. Protein synthesis, transport, and folding events vary according to where the protein is localized. Proteins destined for secretion from the cell or localized to membrane-bound organelles of the secretory pathway are simultaneously synthesized on ER-bound polysomes and translocated into the ER lumen, which contains molecular chaperones that facilitate folding in this compartment. Nuclear-encoded proteins targeted to the plastids, mitochondria, or peroxisomes are synthesized in the cytosol and then imported into their target organelles. In all these examples, protein transport and folding must be tightly

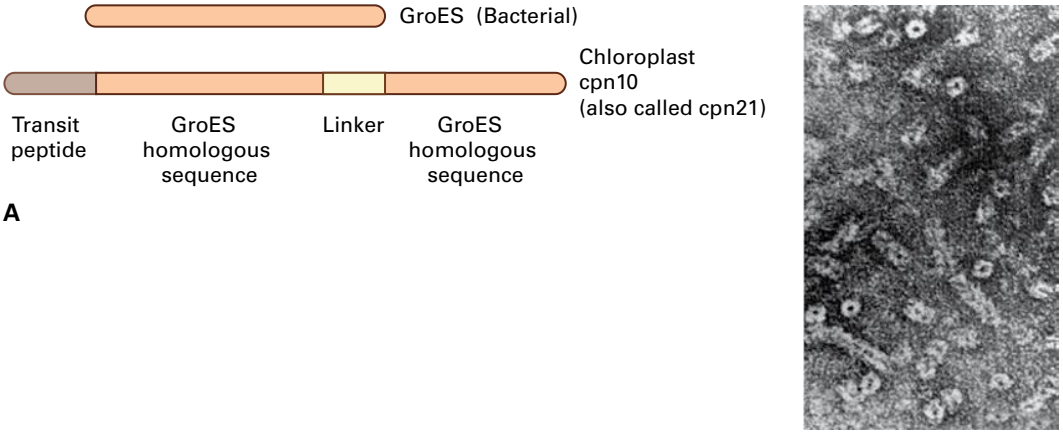


FIGURE 10.25 *(A) The chloroplast homolog of GroES (cpn10, also referred to as cpn21) has an unusual structure. The N-terminal region contains a transit peptide specifying chloroplast localization. The remainder of the protein consists of two sequences of ≈100 amino acids, each of which is analogous to the bacterial GroES. These two repeats are separated by a short linker region. (B) In this electron micrograph, cpn10 can be seen forming a ring-like structure analogous to that observed in bacterial GroES.*
Source: (B) Baneyx et al. (1995) J. Biol. Chem. 270:10695–10702.

coordinated. Chapter 4 examines in detail the synthesis at the ER and folding in the ER lumen, formation of correct disulfide bonds between cysteine residues, and import of newly synthesized proteins into organelles.

10.5.7 Assembly of soluble oligomeric complexes is essential for many biological processes

Many biological processes require oligomeric protein assemblies consisting of more than one copy of the same polypeptide or many different polypeptides. It is crucial that these oligomeric complexes be assembled correctly. Much remains to be learned about the molecular details of the assembly processes.

The chloroplast enzyme Rubisco has been studied as an example of the assembly of a soluble oligomeric protein complex. In plants, Rubisco consists of eight copies of a large subunit (LSU, 53 kDa) and eight copies of a small subunit (SSU, ≈14 kDa) (see Fig. 12.39). The large subunits form an octameric core, whereas the small subunits form two layers of four subunits each, on opposite sides of the core. As shown in Figure 10.27, the LSU is encoded by chloroplast DNA and synthesized in the chloroplast, whereas the SSU gene is transcribed in the nucleus, its mRNA translated in the cytosol, and protein imported into the chloroplast.

Rubisco assembly requires the active participation of the chloroplast chaperonin (cpn60), another plastid-localized product of a nuclear gene. Cpn60 forms a large complex with the LSU shortly after the subunit is released from the ribosome. In an ATP-dependent step, folding of the LSU is facilitated. Once folded, the LSU is released from the chaperonin. In cyanobacteria, the protein RbcX facilitates Rubisco assembly after chaperonin release by organizing an LSU octamer capable of associating with SSUs. The generality of this RUBISCO-specific chaperone to higher plants has yet to be established.

10.6 Protein degradation

10.6.1 Protein degradation plays many important physiological roles

Degradation of cellular proteins is a constant and ongoing process that serves a number of physiological roles, one of which might be called "cellular housekeeping." Abnormal proteins arise in cells as a result of mutations, errors in protein synthesis or folding, spontaneous denaturation, disease, stress, or oxidative damage. If not removed, these damaged proteins eventually poison the cell, often by forming large insoluble aggregates that affect basic cellular processes. Plant cells do not divide rapidly enough to keep concentrations of damaged proteins dilute, so eliminating these proteins is essential. Photoinhibited D1 protein in PSII is a good example of a damaged protein that is proteolyzed during the repair process (see Box 10.8).

A second role for protein degradation is to modulate accumulation of subunits of oligomeric protein complexes in the correct stoichiometry and to maintain the correct ratio of enzymes and their cofactors. One example can be seen in the coordinated accumulation of the large and small subunits of Rubisco. When the concentration of LSUs in the chloroplast decreases—for example, if synthesis is experimentally prevented—SSUs synthesized in the cytosol are rapidly degraded when imported into chloroplasts. Another example is seen with the synthesis of the chlorophyll a/b-binding protein: When chlorophyll synthesis is prevented, the apoprotein is rapidly degraded (see Fig. 10.17).

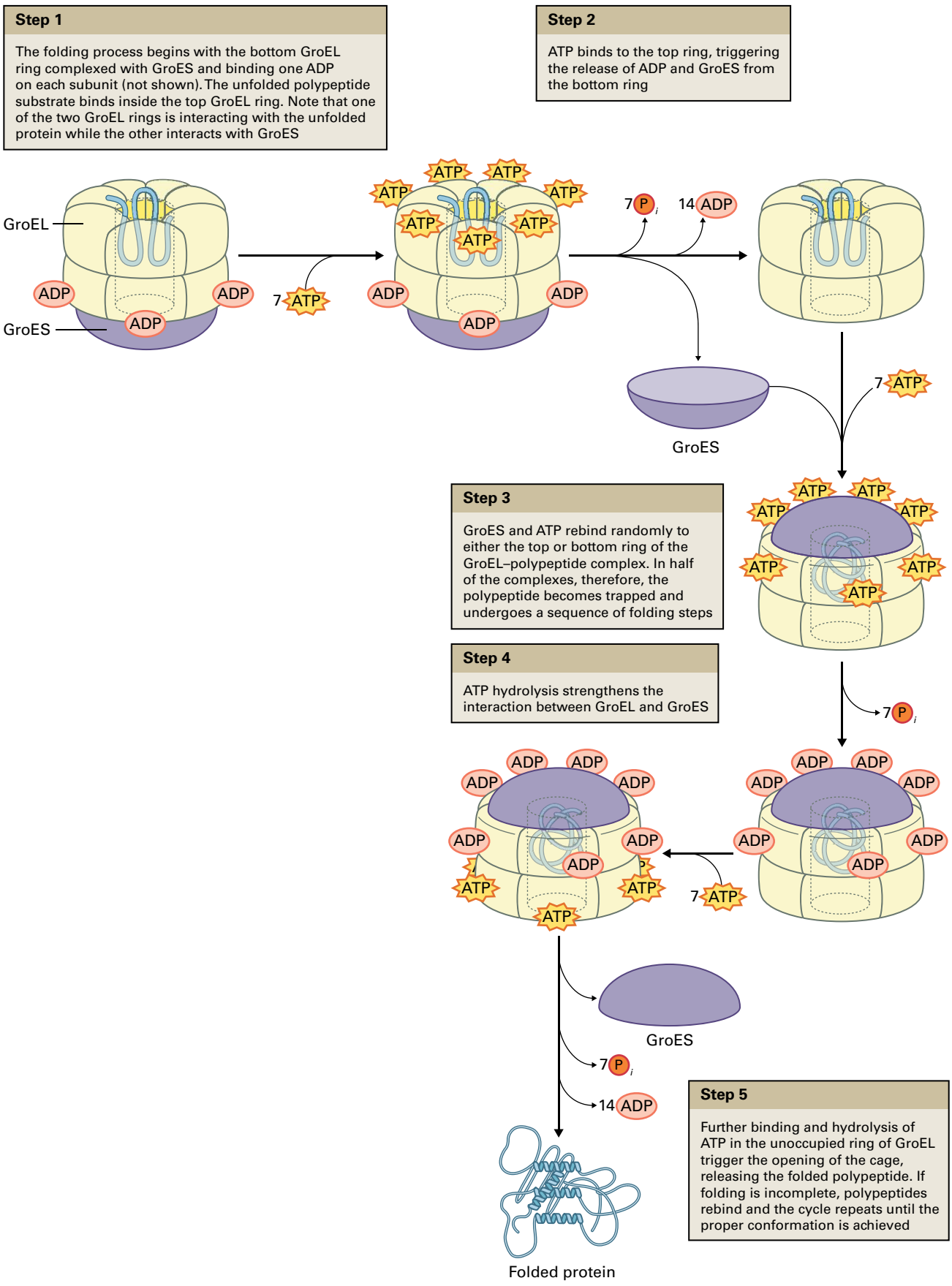


FIGURE 10.26 *Model for the roles of GroEL and GroES in protein folding. This type of system is thought to be present in chloroplasts and mitochondria.*

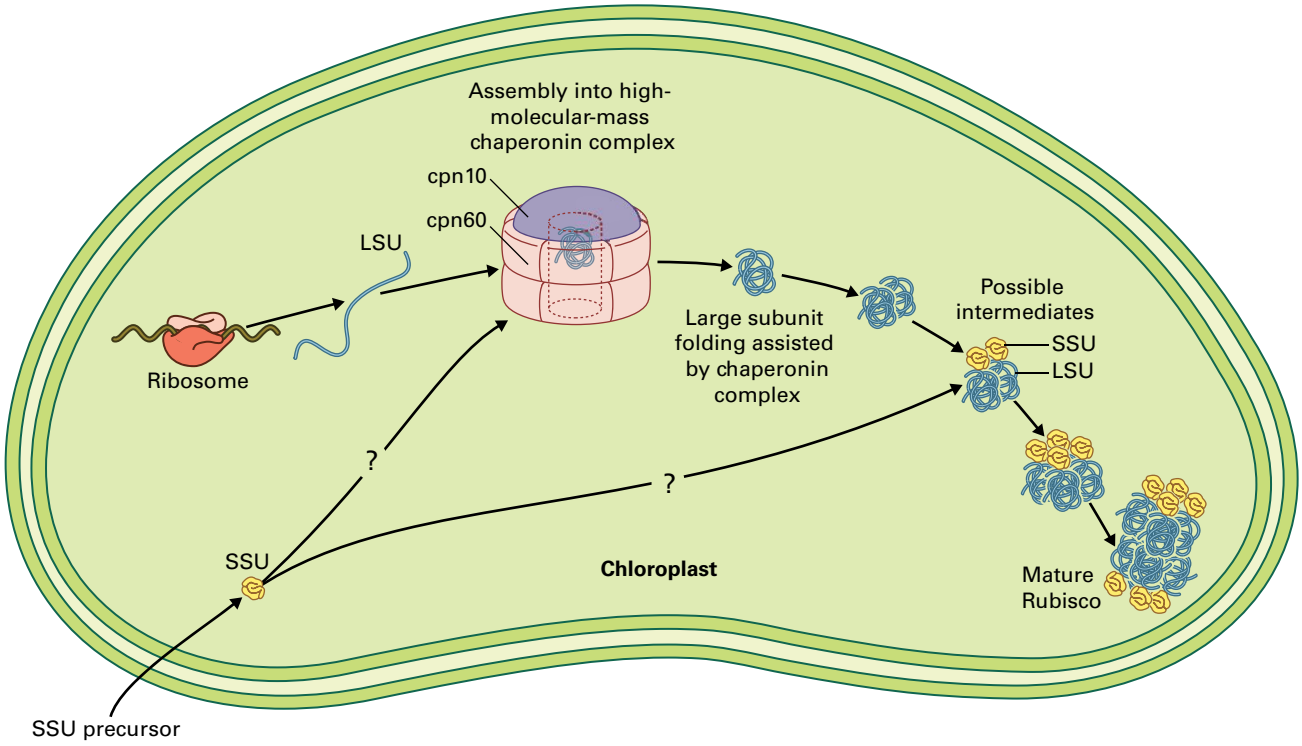


FIGURE 10.27 *Synthesis and assembly of Rubisco requires the participation of two genomes and two translational systems as well as chloroplast chaperones. The large subunit of Rubisco is encoded in the chloroplast genome, and for correct folding, it requires the chaperonin system consisting of cpn60 (the analog of GroEL) and its cochaperonin cpn10 (the analog of GroES). Both cpn60 and cpn10 are synthesized in the cell cytosol as precursors. After they are imported into the chloroplast, their transit peptides are removed, and the mature proteins assemble into the chaperonin complex. The folding of the large subunit of Rubisco is facilitated by interaction with the chaperonin complex. The small subunit of Rubisco is synthesized in the cytosol as a precursor protein. After transport across the chloroplast membranes, the precursor is processed into its mature form. Eight copies of the folded large subunit must then assemble with eight copies of the small subunit to form the active oligomeric enzyme complex.*

BOX 10.8

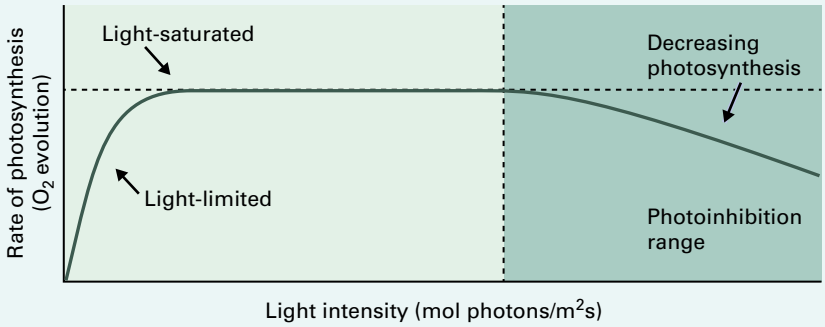
The D1 repair cycle operates to repair photodamage to PSII

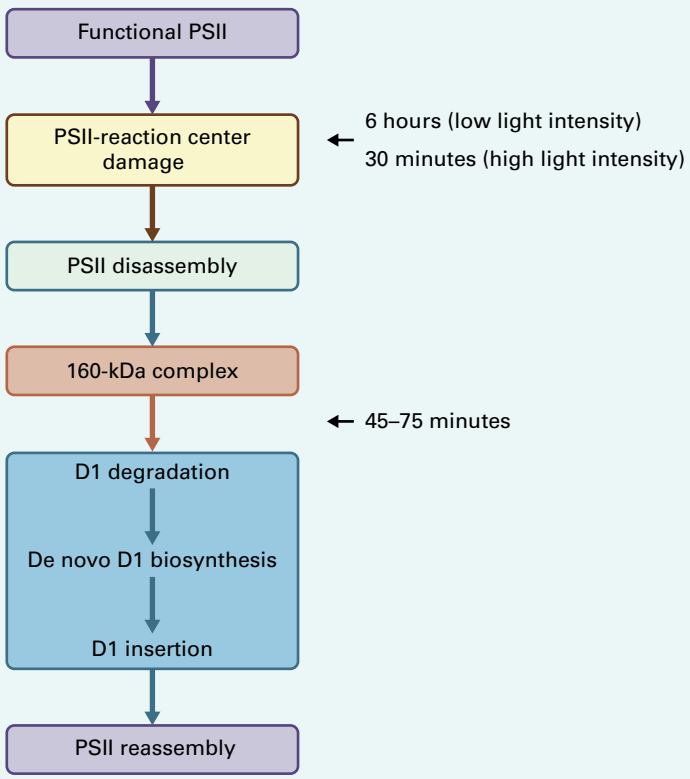
Although light is the source of energy for photosynthesis, it can also cause extensive damage to the photosynthetic apparatus, especially PSII. Light can lead to the inactivation of electron transport and can promote oxidative damage to the reaction centers, particularly to proteins D1 and D2. Plants have evolved a complex and energetically expensive mechanism to repair photoinduced damage, which occurs at a rate directly proportional to the intensity of the incident light. When damage to PSII outpaces the plant's ability to repair itself, photoinhibition results, and this can lead to reduced growth. The severity of photoinhibition varies with the plant species, physiological state, and its life history. The extent of photoinhibition is greatly affected by other environmental conditions, including temperature and water availability.

D1 and D2 constitute the core polypeptides of the photosynthetic reaction center of PSII (see Chapter 13). When D1 is damaged during the photochemical reactions of PSII, it is targeted for degradation by proteolysis. Presumably, oxidative damage to D1 by singlet oxygen or superoxide anion radicals alters its conformation, rendering it vulnerable to proteases. D1 is an integral thylakoid membrane protein with both luminal and stromal loops. The degradation pathway has several steps, and the initial step requires cleavage of a soluble loop in either stroma or lumen. Once D1 has been cleaved, PSII is thought to undergo a partial disassembly. The photodamaged D1 is degraded, new D1 protein is synthesized de novo on chloroplast ribosomes and inserted into the thylakoid membrane, and the PSII complex is reassembled. Direct D1 degradation and de novo D1 biosynthesis can become rate-limiting under high light intensities, resulting in the accumulation of 160-kDa complexes containing partially disassembled PSII and additional proteins of an unknown nature.

The D1 repair cycle poses significant logistical problems for the chloroplast. Thylakoid membranes

demonstrate lateral heterogeneity. PSII is located primarily in closely adjacent, or appressed, membranes. By contrast, D1 synthesis occurs in unappressed membranes exposed to the stroma, where ribosomes can bind and insert the growing polypeptide into the membrane during synthesis. How the lateral movement of damaged PSII complexes to unappressed regions to reassemble with newly synthesized D1 remains an interesting question.





Protein degradation probably plays its most important role, however, in regulating numerous biological processes through the degradation of biologically active molecules. In this sense, protein degradation can be viewed as the final mechanism for regulating gene expression, that is, the final regulatory mechanism controlling the levels of protein gene products. As an example, consider enzymes catalyzing the first step or the rate-limiting step of a metabolic cascade. When these enzymes are short-lived because of proteolytic degradation, the plant can alter the output of a particular metabolic pathway simply by decreasing or increasing the rate of proteolysis of the enzyme catalyzing the rate-limiting step. For example, synthesis of the hormone ethylene is controlled by the activity of ACC synthases (see Chapter 17 for details of ethylene synthesis pathway). These enzymes are short lived in cells and modulation of their degradation rates results in alteration of ethylene production.

Likewise, the concentration of key regulatory proteins such as transcription factors or signaling proteins regulates downstream processes and, as a consequence, these proteins are also almost always subject to proteolytic regulation. In plants, phytochrome A (PhyA) provides a good example (see Chapter 18). Phytochromes exist in two forms that can be interconverted by light. The P_R form of PhyA absorbs red light, has little biological activity, and is long lived in plant cells, whereas the P_{FR}

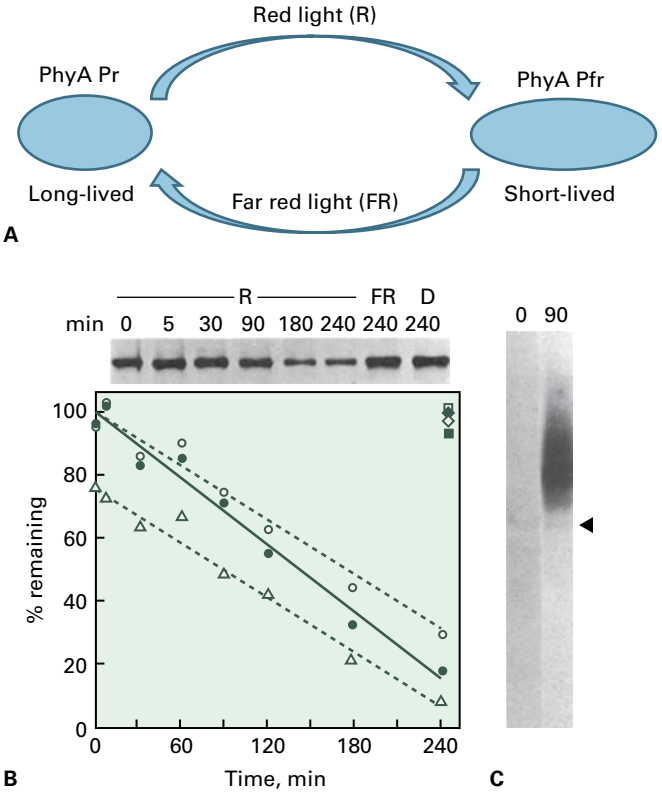


FIGURE 10.28 *(A) The conformation of phytochrome in dark-grown (D) seedlings (Pr) is long-lived, while the phytochrome form (Pfr) after red (R) light absorption is short-lived. Pfr reverts back to the Pr long-lived form after absorption of far red light (FR). (B) The rapid loss of Pfr can be detected by measuring amount of spectrally active PhyA (open triangles) or by ELISA and immunoblot assays visualizing PhyA with anti-PhyA antibodies (immunoblot analysis is shown above graph, and represented by open circles in the graph; ELISA assay results are represented by closed circles). The reduction in PhyA is quantified as the percentage remaining as a function of the time of exposure to light. The amount of Pr (spectrally, open symbols, or immunologically, closed symbols), whether from dark-grown seedlings (square symbols) or from far-red light-treated seedlings (diamond symbols) stays the same over time (top horizontal line). (C) Pr and Pfr were isolated from cells by immunoprecipitation and separated by size. The presence of ubiquitinated Pfr, but not ubiquitinated Pr was visualized, indicating that ubiquitination of Pfr correlated with its degradation, suggesting that PhyA in the Pfr form is a substrate of the ubiquitin system. Arrowhead indicates migration of unmodified Pfr. Ubiquitinated species migrate more slowly due to presence of one or more covalently attached ubiquitin proteins. Different species of PhyA have different numbers of ubiquitins attached, giving rise to the heterogeniety in size observed.*
Source: (B, C) Shanklin et al. (1987) PNAS 84:359–363.

form absorbs far-red light, acts as a photoreceptor to initiate many light-regulated developmental processes, and is rapidly degraded (Fig. 10.28). Another well-characterized example is the DELLA family of proteins. These proteins function as negative regulators of gibberellin signaling, and their degradation is required for proper response to this hormone (see Chapter 17).

Proteolysis in plants also supplies amino acids necessary for maintaining cellular homeostasis and for new growth. Approximately half of the complete set of proteins in a plant is replaced every 4–7 days, and in many cases, new proteins are synthesized from recycled amino acids. A good example of the role of proteolysis in supplying amino acids is seed germination (see Chapter 19). During germination, most of the amino acids required for growth of seedlings are supplied by degradation of seed storage proteins synthesized during embryo maturation. In senescing leaves, some proteases play an important role in activating the senescence process, whereas others likely produce amino acids for use by other parts of the plant (see Chapter 20).

10.6.2 Proteases are classified by catalytic mechanism

In contrast to other enzymes, proteases are classified by their catalytic mechanism, not by the nature of their substrate or biological function. The aspartate-, cysteine-, serine/threonine-, and metalloproteases have the side chain of the indicated amino acid or a metal ion (often zinc) in the active site to catalyze peptide bond hydrolysis. Chemicals can inhibit a specific protease class or subset of classes, and class-specific inhibitors are useful in protease identification. For example, metalloproteases are inactive without a bound metal cation, so incubation with a metal chelator inhibits metalloprotease activity, leaving aspartate, cysteine, and serine/threonine activities unaffected.

Another distinction among proteases is whether they catalyze peptide bond hydrolysis at the end of the protein (either N- or C-terminus) or at an internal site. This property separates the exoproteases, which release either a single amino acid residue or di- or tripeptides located at the ends of a polypeptide, from the endoproteases that cleave peptide bonds further within. The exoproteases process the termini of proteins or remove peptides remaining after endoprotease action.

10.6.3 Proteolysis can be selective or nonselective

At specific times, degradation of proteins occurs without reference to the nature of the protein. For example, during autophagy (self-digestion, see Chapter 20) new membrane structures are produced that encircle cytoplasmic contents inside a closed vesicle. Proteins and membranes trapped within the vesicle are degraded independent of identity. Both the encapsulation and subsequent digestion in the vacuole by resident proteases do not show preference for any specific protein.

In contrast, most proteins are selectively degraded, that is, the protein is specifically recognized and degraded while proteins in the same compartment and presumably accessible to the same proteases are not. One can easily imagine the advantages of this selectivity. A single plant cell may contain more than 5,000 different proteins at any given time. It is imperative that cells have precise mechanisms for targeting individual proteins for degradation. Without such regulation, proteolytic enzymes would degrade cellular proteins indiscriminately.

Multiple proteases require ATP hydrolysis for activity. Because the hydrolysis of peptide bonds is energetically favorable and thus does not require coupled ATP hydrolysis, ATP is thought to act to increase specificity. The addition of an ATP requirement necessitates accessory proteins to link ATP hydrolysis to proteolysis. Thus, protease systems are complex, including both catalytic and specificity activities.

10.6.4 Protease activity is highly regulated

It also is evident that unregulated protease activity could have dire consequences, for example, by removing a substrate protein at inappropriate times. So, in addition to a high degree of specificity, protease activities are controlled by similar mechanisms that control the activities of other cellular proteins; some of these include control of synthesis, compartmentalization of the protease away from substrate until proteolysis is desired, synthesis as an inactive precursor, or changes in the activity of the protease by modification, such as phosphorylation, or by interaction with ligands. This is only a partial list of the possible ways that protease activity is regulated in cells to prevent unwanted destruction of its substrates.

10.6.5 Plant cells contain a large number of proteases that are found at several sites in the cell

An indication of the significance of proteolysis is the large number of genes in a single organism dedicated to the processing and cleavage of proteins. For example, in rice (*Oryza sativa*) and *Arabidopsis*, whose genomes have been extensively annotated, bioinformatics studies identify approximately 700 and 800 predicted proteases, respectively. In addition, predicted components of the proteolytic pathway called the ubiquitin pathway (see below) that are not proteases per se, but are required for proteolysis, add approximately another 1,000 proteins. This large number of genes encoding proteases and/or components of proteolytic pathways within a single organism indicates the diversity and significance of protein processing and degradation throughout the life of an organism.

Proteases are localized to multiple cellular compartments (Fig. 10.29). Thus, distinct systems are present in vacuoles, in the cytosol, in the nucleus, in chloroplasts, and in mitochondria. The proteolytic machinery in each compartment reflects the evolutionary origin of that compartment. Thus, the proteolytic mechanisms observed in chloroplasts and

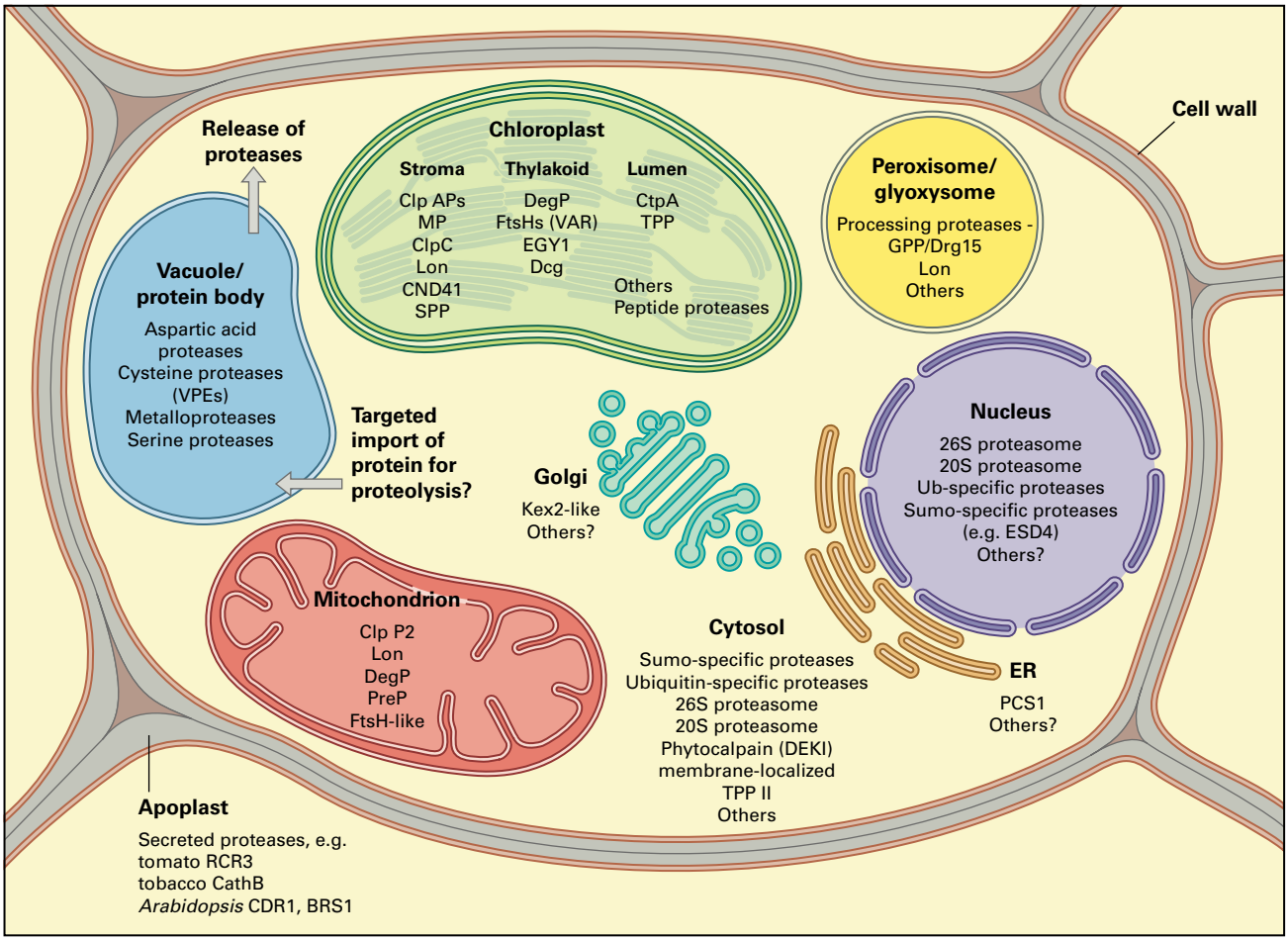


FIGURE 10.29 *Most subcellular compartments in a plant cell (the cytosol, nucleus, chloroplasts, mitochondria, ER, and vacuole) contain proteases. In addition, many plant cells secrete proteases.*

mitochondria are more closely related to bacterial systems than to those localized in the plant cell cytosol.

Vacuoles are very conspicuous organelles and may occupy as much as 95% of the plant cell volume. Rich in hydrolytic enzymes, vacuoles perform a variety of functions. The proteases they contain may play a role in protein degradation similar to that of lysosomes in animal cells. During nutrient starvation, the vacuole is the site of digestion of autophagic vesicles, where proteins are degraded to generate needed amino acids in an autophagic process (see Chapter 20). In seed-reserve tissues, specialized vacuoles called protein bodies have been observed. Proteins deposited in the protein body during seed maturation remain there in a stable state until the seed germinates. During germination, protein bodies fuse with a different vacuole containing proteases, and the storage proteins are degraded, supplying amino acids to the new seedling.

Plastids contain a complement of proteases distinct from the cytosol. In addition to processing proteases, there are proteases involved in protein removal. In *Arabidopsis*, bioinformatic analyses predicted 11 different protease types in chloroplasts encoded by ≈50 genes. Three different types of ATP-dependent proteases with prokaryotic relatives have been experimentally verified to reside in the chloroplast. They are named after the homologous proteins in *E. coli*: Clp, FtsH, and Lon, each encoded by multigene families in plants. In addition, chloroplasts contain ATP-independent proteases, including the Deg family, involved in removal of damaged PSII proteins (see Box 10.8).

The ATP-dependent proteases contain both proteolytic and ATPase activities, either on a single polypeptide or on different proteins. Clp is a stromal multimeric enzyme complex, consisting of multiple catalytic subunits; these ClpP or ClpP-like proteins in are a heterotetradecamer subcomplex that interacts with a regulatory subunit possessing the ATP hydrolysis activity (Fig. 10.30). FtsH is a homomultimeric complex bound to thylakoids and is also involved in damaged D1 proteolysis. In addition to degradation inside the chloroplast, recent evidence suggests that during autophagy, portions of the chloroplast segment into vesicles, which fuse with the tonoplast. Once inside the vacuole, chloroplast-derived components are degraded.

Other plant organelles, including mitochondria, microbodies, such as peroxisomes, and the ER also have the ability to degrade proteins, but the mechanisms are poorly understood in plants. In the case of ER-localized proteins, in yeast and mammals, translocation of proteins from the ER to the cytosol occurs before breakdown, but such a mechanism has not yet been described in plants.

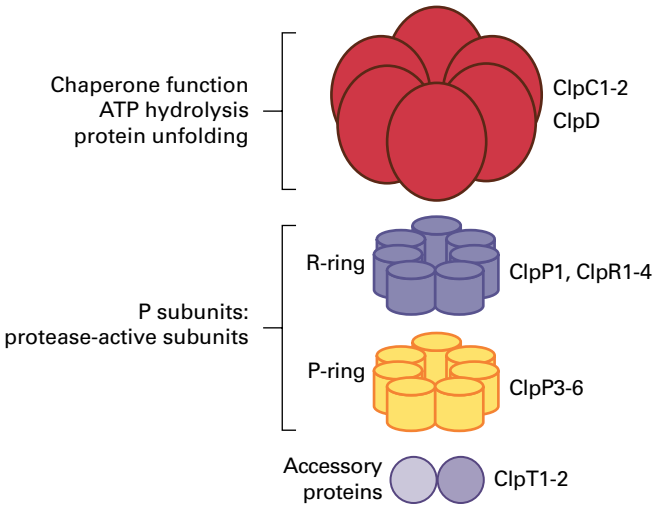


FIGURE 10.30 *Representation of chloroplast Clp protease complex. The P subunits are active serine proteases, R subunits are related inactive subunits, which form two heptameric rings. Names of the individual subunits in* Arabidopsis *are indicated to the right; the P ring subunits P3, P4, P5, and P6 are in a 1:2:3:1 stoichiometry. The R ring contains ClpP, the only chloroplast-encoded subunit and R proteins R1, R2, R3, and R4 subunits in 3:1:1:1 stoichiometry. ClpC1, ClpC2, and ClpD form a hexameric RING, hydrolyzing ATP to unfold proteins and feed them into the internal chamber and access to protease active sites. ClpT2 proteins are thought to play a role in assembly.*

10.6.6 The ubiquitin pathway is a major intracellular pathway for selective proteolysis in the cytosol and nucleus

The ubiquitin pathway is the major proteolytic pathway in the cytosol and nucleus. It is unusual because it requires prior modification of the substrate protein by another protein, ubiquitin (Fig. 10.31), which is not degraded, but is recycled for future attachment (Fig. 10.32). This conserved eukaryotic pathway is essential, likely because of its role in modulating the abundance of key regulators of the cell cycle and of developmental transitions. The ubiquitin pathway includes all enzymes required for ubiquitin attachment, the protease complex that hydrolyses the substrate and removes ubiquitin intact, accessory proteases that hydrolyze various ubiquitin linkages, and the myriad of proteins that modulate any one of these processes (Fig. 10.32). The number of genes in this pathway in a single organism is estimated at >1,200, and new components are still being identified.

Conjugation of ubiquitin to a substrate requires ATP and is carried out by a multienzyme pathway (Fig. 10.33). This pathway first catalyzes the formation of an isopeptide bond between the C-terminus of ubiquitin and typically the ε-amino group on the side chain of a lysine residue on a substrate protein. Proteins with a single attached ubiquitin are known, but many have multiple covalently bound ubiquitins. Additional ubiquitin molecules typically are added onto an ε-amino lysyl group of a previously attached ubiquitin, forming an ubiquitin chain. Ubiquitin has seven lysine residues (see Fig. 10.31), and all have been found in ubiquitin–ubiquitin linkages formed *in vivo*, although the major site of ubiquitin attachment to ubiquitin is lysine 48. In addition, multiple lysine residues on the substrate protein can be conjugated in this manner, giving rise to more than one ubiquitin chain on a single protein.

The enzymes responsible for ubiquitin conjugation, E1 (ubiquitin activating enzyme), E2 (ubiquitin conjugating



FIGURE 10.31 *Ribbon (left and center, opposite faces) and space-filling (right) models of ubiquitin. Ubiquitin consists of a compact globular domain with a flexible protruding C-terminal segment, where it attaches to proteins. The three hydrophobic residues on the surface are indicated in blue, and these residues function in noncovalent protein–protein interactions with other components of the ubiquitin pathway. The seven lysine residues that serve as attachment sites for a second ubiquitin are indicated in red, with the major attachment site, lysine-48 indicated in magenta. Source*: Vijay-Kumar et al. (1987). J. Mol. Biol. 194:531–544.

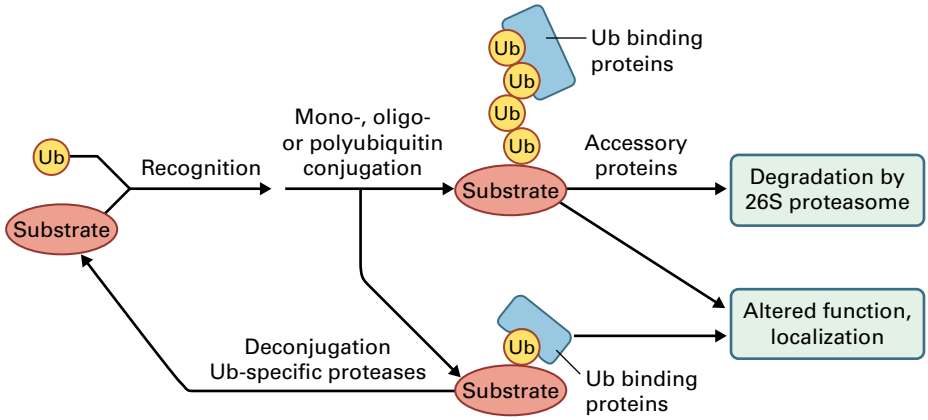


FIGURE 10.32 *Modification of proteins by covalent ubiquitin addition has diverse consequences. Typically, polyubiquitylation via ubiquitin lysine-48 targets a protein for proteasomal degradation. Monoubiquitylation can affect the protein's subcellular localization, intermolecular interactions, enzymatic activity, and possibly other properties.*

enzyme), and E3 (ubiquitin ligase) act sequentially (Fig. 10.33). E1 activates the C-terminus of ubiquitin through adenylate formation, transfers the ubiquityl moiety to a cysteinyl group on itself to form thioester-linked ubiquitin, and then transfers the ubiquitin to a cysteinyl group on an E2, the second protein in the cascade. The E2 with a thioester-linked ubiquitin then binds to E3, and ubiquitin is transferred to the substrate, either directly or indirectly. In one type of E3, the HECT type, ubiquitin is first thioester-linked to the HECT E3 and then transferred to a peptide linkage on the substrate. For all other E3s, ubiquitin transfer is directly from the E2 to the substrate (Fig. 10.33). Hence, interaction of the substrate with the E3 is a key step, and modulation of this interaction provides a means of controlling the rate and extent of ubiquitylation.

It is not surprising, then, that the largest group of proteins in the ubiquitin pathway is the E3 ligases (Table 10.5). These proteins can be divided into two mechanistic types: The HECT E3 type covalently attach ubiquitin prior to substrate ubiquitylation, whereas the RING/U box E3 type serves as a scaffold to position the substrate protein adjacent to the E2 carrying a thioester linked ubiquitin (Fig. 10.34). RING proteins and U box proteins are named after the domain that interacts with the E2. RING and U box domains form similar structures using different mechanisms, Zn chelation and hydrophobic interactions, respectively. Some E3s are multimeric, of which the cullin-RING ligases (CRLs) are the best characterized in plants. In one type of CRL (the SCF type), one subunit (F-box protein) interacts with the substrate protein, while the other SCF subunits position the E2 for optimum ubiquitin transfer (Fig. 10.34, Table 10.5). Other CRL E3 ligases are similar, with one subunit serving the substrate interaction function (Table 10.5).

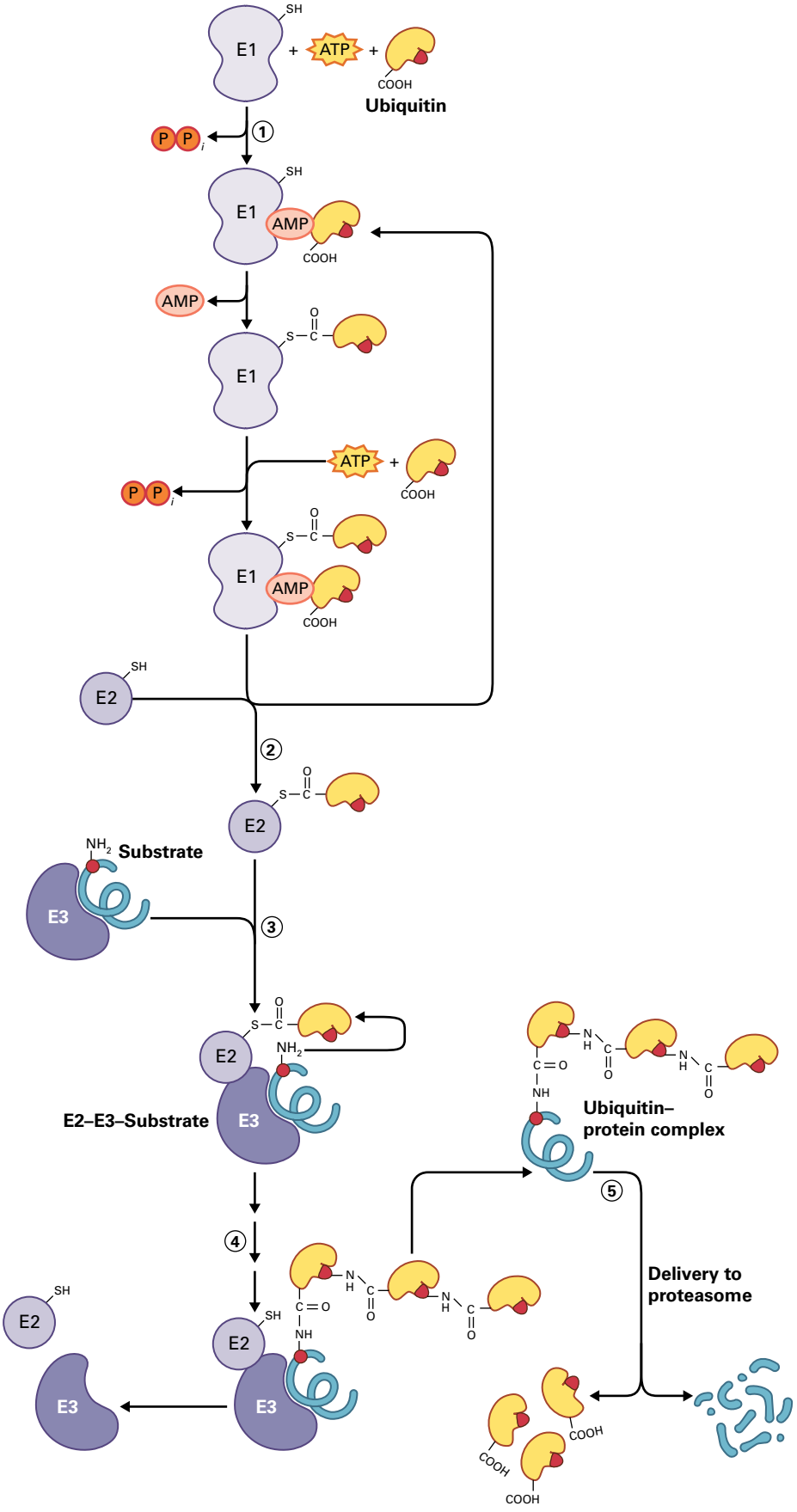


FIGURE 10.33 *Covalent attachment of ubiquitin to substrate proteins requires three enzymes, E1, E2, and E3. The first step is activation of the ubiquitin C-terminus, which is analogous to amino acid activation in amino acyl tRNA synthesis and fatty acid activation (see Fig. 10.8). Using ATP, E1 (ubiquitin activating enzyme) forms an ubiquitin adenylate, releasing pyrophosphate. The C-terminal carboxyl of ubiquitin is then covalently attached to the Cys residue sulfhydryl of E1 in a thioester linkage similar to that found in acyl CoA esters. In step 2, the ubiquitin*

TABLE 10.5 *Types of ubiquitin E3 ligases and selected examples of specific E3s and their substrates.*

E3 ligase type	Mechanism for ubiquitin conjugation	Subunit composition	Substrate recognition (approximate number of genes in *Arabidopsis*)	Select identified substrate proteins (interacting ligase subunit)
CUL1-based Cullin-RING-Ligase (CRL) type, this specific CRL called SCF	Scaffold	4 well-characterized subunits, CULLIN1, RBX, SKP1, F-box protein	F-box proteins (700)	Aux/IAAs (TIR1, AFBs, interaction regulated by IAA) DELLAs (GID2,SLY1, interaction regulated by gibberellins) EIN3 (EBF1, EBF2) JAZs (COI1, interaction regulated by jasmonate conjugates) D15 (MAX2/D3, regulated by strigolactones)
CUL3-based CRL	Scaffold	3 subunit proteins, CULLIN3, RBX, BTB protein	BTB proteins (80)	ABF2 (ARIA) ACS5 (ETO1) NPR1 (NPR4, interaction regulated by salicylic acid)
CUL4-based CRL	Scaffold	4 subunit proteins, CULLIN4, RBX, DDB1, DCAF/WD40 + others?	DCAF/WD40 proteins (90)	
Non-CRL RING	Scaffold	Unknown	Other domain on RING or unknown (480)	NAC1 (SINAT5) ABI3 (AIP2)
U box	Scaffold	Unknown	Other domain on U box, unknown (40)	
HECT	Forms ubiquitin thioester	Unknown	Other domain on HECT, unknown (7)	
RBR	Both: Scaffold, then forms ubiquitin thioester	Unknown	Other domain on RBR protein (42)	
APC	Scaffold	11 proteins and modulators (CDC20, CDH1)	CDC20, CDH1	Mitotic cyclins

FIGURE 10.33 (*Continued*) *is transferred to a Cys residue, a sulfhydryl of E2 (ubiquitin carrier enzyme). In step 3, the protein targeted for modification is bound by E3 (ubiquitin ligase). An E2 with a thioester-linked ubiquitin also interacts with the E3. Thus, the E3 brings ubiquitin and the substrate in close proximity, and evidence suggests that conformational changes occur upon E2 binding that facilitate ubiquitin transfer from E2 to the substrate. The ubiquitin is attached to the substrate protein through an isopeptide bond between the C-terminal carboxyl of ubiquitin and typically the side-chain amino group of a lysine (shown as a red dot). In step 4, multiple additional ubiquitin residues are added to the substrate protein. The C-terminal carboxyl of each additional ubiquitin is attached to an internal lysine residue (red dot) of the preceding ubiquitin chain. In general, a series of about four ubiquitins must be attached to the substrate protein before it can be delivered to the proteasome effectively. Some proteins are only modified with a single ubiquitin. In step 5, the ubiquitin-conjugated protein is delivered to the proteasome for degradation.*

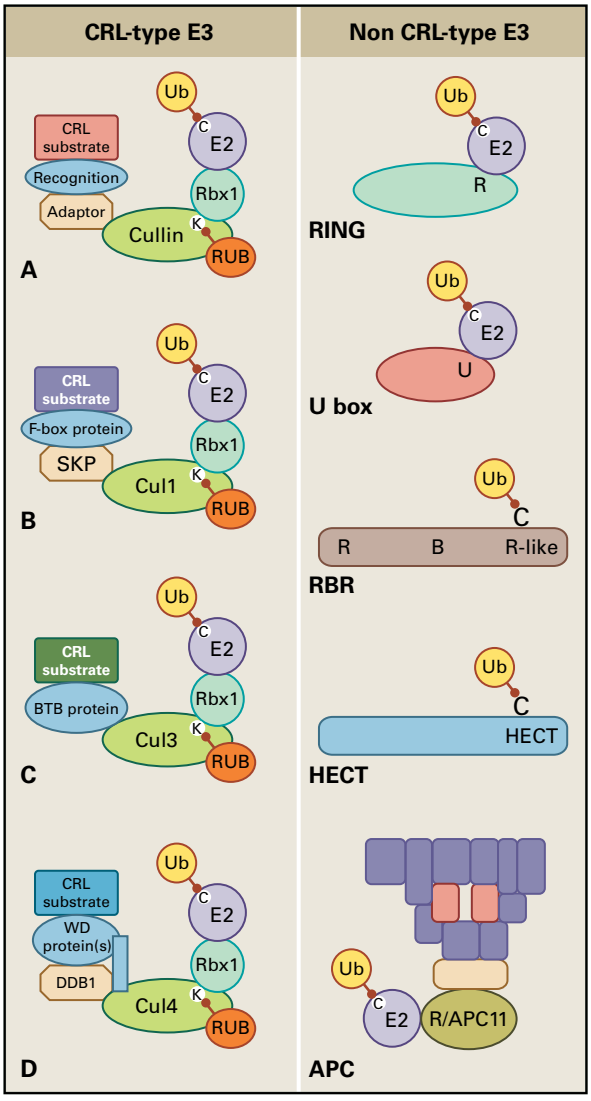


FIGURE 10.34 *Two major types of ubiquitin E3 ligases: CRL-type (left) and non-CRL-type (right). E3 ligases interact with both the substrate and E2. Many different proteins are ubiquitin-modified, and different E3s modify a specific protein or group of proteins. CULLIN-RING-ligase (CRL)-type E3s (left) are multimeric: One subunit interacts with the substrate, the other binds E2, and the CULLIN protein in between serves as a scaffold. (A) The generic architecture of CRLs is shown. All share the same RING protein (RBX) and for full activity in vivo, all CULLINs must be modified by a single ubiquitin-like protein (RUB). CUL1-based CRL is called an SCF (SKP-CULLIN1-F box); F-box proteins bind substrate (B). CUL3-based CRL with BTB proteins as the substrate binding subunit are shown (C), and the CUL4-based CRL (D). The exact composition of CUL4 CRLs is uncertain, but WD-repeat containing proteins in some cases are substrate-interacting subunits. Non-CRL types (right) include RING, U box, RBR and HECT types, named for the domains that interact with the E2 (in the case of RING and U box) or carry ubiquitin in a thioester linkage (HECT domain). RBR proteins are named after the 3 RING-like domains, the first binds E2 and the third contains a catalytic cysteine that carries activated ubiquitin, similar to the HECT domain E3s. Evidence suggests these non-CRL ligases could be oligomeric, but little is known. The anaphase promoting complex (APC) is multimeric E3 with several substrate-binding subunits, and the small RING protein APC11 binds the E2. It functions to modify cell cycle regulators, such as cyclins.*

10.6.7 The 26S proteasome is a unique protease complex that recognizes ubiquitylated proteins

Ubiquitylated proteins are processed to peptides by the 26S proteasome, an extremely large oligomeric protein complex with a molecular mass of >1.5 megadaltons (MDa). The proteasome is an assembly of complexes, most notably the 20S core proteasome and the 19S regulatory complex, or 19S cap. The 20S core consists of four stacked rings, each made of seven subunits (note the similarity to the GroEL chaperone). The active sites for proteolysis face inward, into a channel through the center of the stacked rings (Fig. 10.35). Placement of these catalytic centers inside the channel limits accessibility. The pores into the channel are normally in a closed configuration, and binding of the 19S cap and ATP hydrolysis are required to switch the pores to the open configuration. The 19S cap also binds ubiquitylated proteins, helps unfold substrate proteins using ATP hydrolysis, removes ubiquitin, and inserts the unfolded, de-ubiquitylated polypeptide into the channel within the stacked ring structure, where peptide bond hydrolysis occurs.

Thus, a major fate of ubiquitylated proteins is delivery to the proteasome for degradation. Several types of ubiquitin-binding proteins facilitate the interaction between ubiquitylated proteins and the proteasome. Some of these ubiquitin-binding proteins are part of the regulatory particle, while others only transiently interact.

10.6.8 Ubiquitin attachment is highly regulated

Ubiquitin attachment is highly regulated to prevent unwanted or excessive ubiquitin attachment. Substrate interaction with ligases is regulated by multiple mechanisms. In some cases, modification of the ligase occurs, either a covalent modification, such as phosphorylation, or by interaction with an activator or inhibitor subunit. Alternatively, the substrate protein can be covalently modified or interact with another protein or small molecule to promote interaction with the ligase. Additionally, the presence or absence of specific pathway components can regulate ubiquitylation. For example, upon phosphate starvation in *Arabidopsis*, the miR399 miRNA targets the RNA encoding the E2 enzyme UBC24/PHO2 for degradation, reducing UBC24 synthesis. Although the molecular mechanism is not known, reduction of UBC24 allows plant roots to respond to conditions of low phosphate by enhancing uptake of external phosphate and conserving internal sources.

10.6.9 The ubiquitin pathway is essential in plant hormonal responses

The CRLs are essential ubiquitin ligases in all organisms, including plants where they are implicated in numerous processes, including hormonal responses, progression through

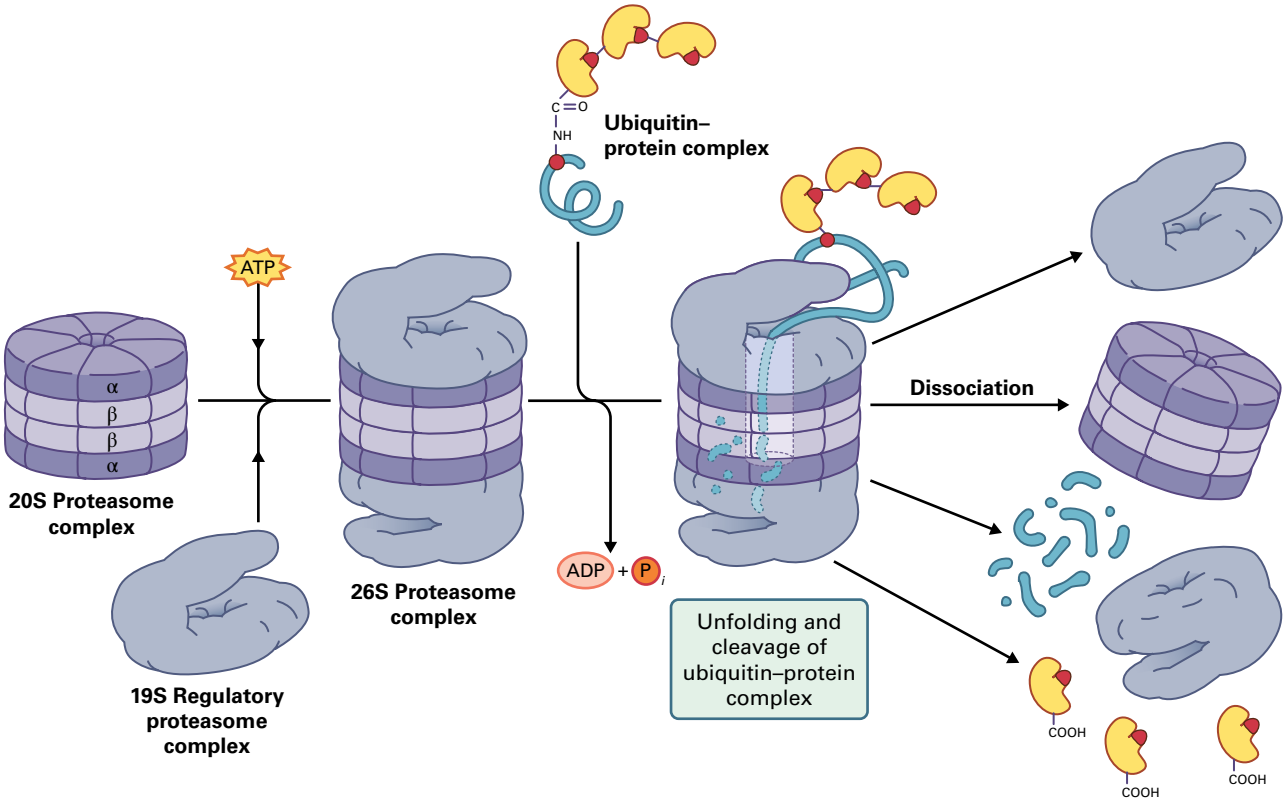


FIGURE 10.35 *Structure of the 26S proteasome. The core 20S proteasome has a distinctive hollow cylindrical shape created by the assembly of four stacked rings. Each ring contains seven polypeptides. A 19S regulatory subunit binds to the ends of the 20S proteasome, forming the 26S proteasome. Ubiquitylated proteins are delivered to the proteasome for degradation, likely by ubiquitin-binding proteins either free or bound to the proteasome. The regulatory subunit contains ATPases and ubiquitin-specific proteases for unfolding the substrate and removing the ubiquitin, respectively.*

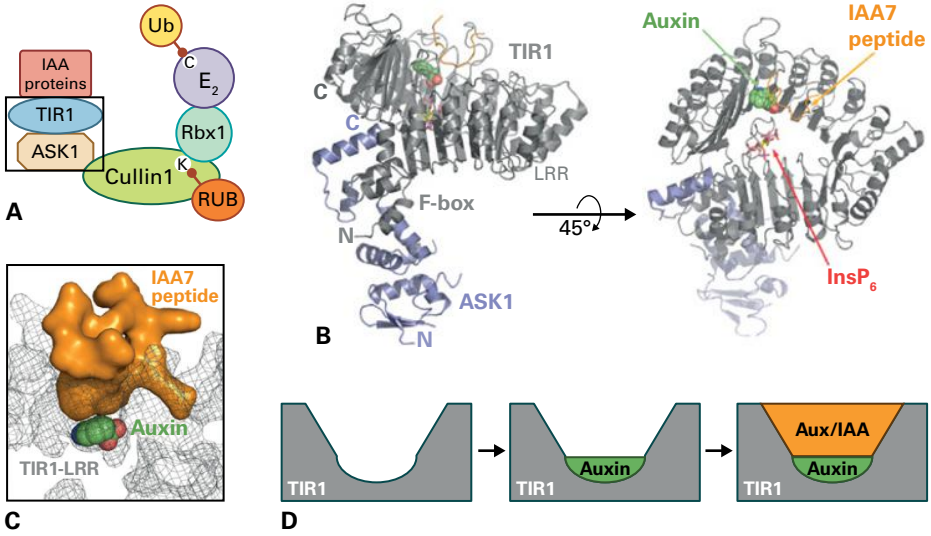


FIGURE 10.36 *SCF^{TIR1} is an auxin-regulated E3 ligase. (A) Schematic representation of a specific SCF E3 ligase containing the F-box protein TIR1. This ligase interacts with the Aux/IAA proteins (called IAA proteins in* Arabidopsis*) in an auxin-dependent manner, which explains the observation that auxin modulates Aux/IAA degradation rates. The rate of ubiquitylation would be modulated by auxin, and in turn the rate of recognition and degradation by the proteasome then depend on auxin. The X-ray structure of the boxed region is shown in B. (B) X-ray structure of TIR1 in complex with the substrate adaptor, ASK1, and a peptide of an* Arabidopsis *IAA protein, IAA7. The peptide-binding pocket requires auxin (in green) at the base. (C) Expanded view of the IAA-auxin-TIR1 binding site, with the IAA peptide in a space -filling model. (D) Schematic model of the requirement for auxin to facilitate IAA interaction with TIR1. Auxin has been coined the "molecular glue" that holds together the substrate, IAA proteins, and E3 ligase subunit. This is an example of ligand-regulated degradation, where auxin is important for the ubiquitylation reaction, which is required for substrate degradation by the proteasome.*
Source: Tan X et al. (2007). Nature 446:640–645.

the cell cycle, and biotic responses. The substrate-recognizing subunit of one type of CRL, the F-box protein of the SCF-type of CRL, is encoded by a large gene family, presumably because each F-box protein interacts with a different substrate protein or protein family. The best characterized F-box protein is TIR1, which was first identified genetically as an auxin response mutant. The X-ray crystal structure of TIR1 has been solved, and members of the Aux/IAA protein family have been identified as substrates. The Aux/IAA proteins are transcriptional regulators of the auxin response. Some of these proteins are short-lived in cells, and their degradation rates are modulated by the level of auxin. Remarkably, auxin itself binds to TIR1 and helps form the Aux/IAA-binding site. These results provide a molecular explanation for the ability of auxin to change proteolytic rate through changing the rate of ubiquitylation (Fig. 10.36).

The stimulation of ubiquitylation by the auxin-TIR1-Aux/IAA interaction is not an isolated example of how small molecules regulate proteolysis. Multiple hormone signaling pathways utilize regulated proteolysis. The jasmonate signaling pathway requires proteolysis of JAZ transcription factors, and binding of a jasmonate conjugate to the F-box protein called COI1 regulates degradation of JAZ proteins. Gibberellin (GA) signaling requires the inactivation of the DELLA family of proteins, and a major mechanism of down-regulation is through proteolysis. Active GAs and DELLAs bind to a receptor, and this GA-DELLA-receptor complex interacts with the SLY F-box protein to facilitate ubiquitylation of DELLA proteins and promote their degradation. Thus, direct modulation of the ubiquitin pathway enzymes by small molecules appears to be a reiterated theme, rather than an exception in plants.

10.6.10 Ubiquitylated proteins can have fates other than proteasome-mediated degradation

The consequence of marking proteins with ubiquitin is not limited to hydrolysis by the proteasome. There is evidence with yeast and mammalian proteins that, in addition to proteolysis, ubiquitylation can affect subcellular location and activity. In these aspects, ubiquitin functions as a posttranslational modification. Studies on the nonproteolytic role of ubiquitin are in their infancy in plants.

Summary

Plants have three compartments in which proteins are synthesized. Protein synthesis mechanisms differ among these compartments, probably reflecting their distinct evolutionary origins. Protein synthesis is carefully regulated in response to the physiological needs of the plant. This regulation is particularly apparent in chloroplasts, where protein synthesis is coordinated with the photosynthetic activity of the organelle. After synthesis, proteins must be localized to the appropriate cellular location and may also be modified. Chaperones are required for the proper folding of proteins in cells. Protein folding and localization are coupled. Proteins are degraded to modulate the quantities of key metabolites, to provide amino acids, to modulate signaling pathways and to remove improperly folded proteins.



11

Cell Division

Dirk Inzé and Lieven De Veylder

Introduction

Every cell originates from the division of an existing cell. This process is regulated precisely to ensure cells divide only at appropriate times and replicate critical cellular components with high fidelity.

The cell cycle consists of two events: **cell division**, during which a cell replicates its genome and partitions it to daughter cells, and **cell growth**, during which cells increase their mass by synthesizing proteins, membrane lipids, and other essential components. Whereas cell growth and most biochemical processes are continuous, the cell cycle proceeds in discrete, incremental steps. Eukaryotic cells have evolved specialized protein kinases, phosphatases, and proteases that function as switches to impose this stepwise mode of progression on the processes of DNA replication and partitioning of the duplicated genetic information in two daughter cells during **cytokinesis**. This network of regulatory proteins involved in monitoring cell cycle progression is also suited for coupling cell cycle stages with environmental conditions, such that cell divisions only occur when conditions are favorable.

In addition to regulating the timing of cell division, cell cycle control mechanisms perform a quality control function to prevent transmission of incompletely replicated or damaged genomes to daughter cells. Incomplete genome replication, rereplication of DNA without division, DNA damage, or division before DNA has been completely replicated can all wreak havoc on the cell's progeny. To prevent such errors, all organisms utilize molecular mechanisms to monitor cell division progress at specific steps in the cell cycle, called **checkpoints**.

The basic mechanisms governing cell division arose early in eukaryotic evolution and are highly conserved. Though the basic principles of cell cycle control are similar in all eukaryotes, plants possess a number of species-specific modifications in the mechanisms that regulate cell division. This chapter provides an overview of the basic principles that control cell division, with an emphasis on plant-specific modifications.

11.1 Animal and plant cell cycles

The last common ancestor of plants, animals, and fungi lived over 1.5 billion years ago, well after eukaryotes had evolved. Despite the great evolutionary distance and distinctly different appearances of modern multicellular organisms, the cellular machinery that performs fundamental functions, including the molecules that regulate the division cycle, is highly conserved in all extant eukaryotes. Among these conserved molecules are the protein kinases that control major cell cycle transitions and their regulatory subunits, the enzymes responsible for DNA replication, the cytoskeletal structures necessary for chromosome movements during mitosis, and the components of the ubiquitin-dependent

Biochemistry & Molecular Biology of Plants, Second Edition. Edited by Bob B. Buchanan, Wilhelm Gruissem, and Russell L. Jones.
© 2015 John Wiley & Sons, Ltd. Published 2015 by John Wiley & Sons, Ltd.
Companion website: www.wiley.com/go/buchanan/biochem

pathway for protein degradation, which plays essential roles during the cell cycle (see Chapter 10). Somatic cells also share the fundamental four-phase subdivision of the cell division cycle. Although all eukaryotic cells employ a similar molecular machinery to duplicate themselves, animal and plant cells have also evolved distinct mechanisms for controlling cell division, and these are related to the structural and developmental features that differ between plant, mammalian, and fungal cells.

One notable distinction is that during mitosis in mammals, chromosomes move toward a discrete pole, and when the two daughter nuclei move apart, this process involves progressive constriction of the plasma membrane at the central contractile ring. In plant cells, the two daughter nuclei become separated by a **cell plate** that grows at the equator of the mother cell. The cell plate ultimately fuses with the plasma membrane and cell wall that now surround both daughter cells. To generate these two daughter cells, plants have developed two unique cytoskeletal structures, the **preprophase band** and the **phragmoplast** (Fig. 11.1).

Plant cells also differ from mammalian cells in that they have a rigid cell wall and cannot move. Plant organogenesis, therefore, depends on cell division and cell expansion at the site of new organ formation. In addition, cell division in plants is mostly confined to specialized regions called **meristems**, which produce new cells that differentiate as they move away from the meristem (Fig. 11.2). Meristem cells are pluripotent, meaning they allow their progeny to become committed to a spectrum of developmental fates. During the plant life cycle, the identity of the shoot meristem itself can change from a vegetative to a reproductive program, resulting in the formation of flowers (see Chapter 19).

Also in contrast to mammals, plants and plant organs develop their characteristic shapes and functions after the embryo emerges from the seed. The root–shoot axis becomes established and the first leaves (the cotyledons) develop during embryogenesis, but most plant growth occurs after germination by iterative proliferation at the meristems. Because of the sessile life of plants, development and cell division are strongly influenced by environmental factors, such as light, gravity, nutrients, and biotic and abiotic stress conditions. All these specific features contribute to the plant-specific regulation of the factors controlling cell division.

11.2 Historical perspective on cell cycle research

DNA replication and chromosome segregation are the fundamental processes required for cell division. Proliferating cells alternate between these two mutually incompatible states, and the transitions between these states are regulated by cell cycle control mechanisms. Elucidation of these mechanisms has been an active area of research for many years.

11.2.1 The beginnings of cell cycle research can be traced to important discoveries in several areas of biology

In 1869, DNA was discovered to be the major component of the nucleus, and by the end of the 19th century, microscopic examination had revealed that proliferating cells alternate between two stages: **interphase** and **mitosis**. In interphase, no substantial nuclear structures are discernible, whereas in mitosis, chromosomes become visible, are distributed to opposite poles of the cell, and disappear again when the newly formed cells separate by division. By 1944, DNA was shown to be the genetic material, highlighting the importance of the nucleus in cell division. Later, DNA synthesis was found to occur during interphase in bean root tip cells. Together with the discovery of "gap phases" in which cells grow, and of the fact that progression to the next cell cycle phase can be controlled by a variety of intracellular and extracellular signals, the cell cycle was determined to consist of four phases, rather than two: interphase is subdivided into a synthesis phase (S) and two gap phases (G1 and G2) that separate DNA synthesis from mitosis (M). In the sequence G1, S, G2, M, the four phases constitute one complete round of the cell cycle (Fig. 11.3). The discovery in 1953 by James Watson and Francis Crick that the nucleotide bases of DNA are arranged as a complementary double helix immediately suggested a likely mechanism for how the encoded genetic information is replicated during S phase. The stage was set for the remarkable advances in cell cycle research that have characterized the past decades.

11.2.2 Genetics, biochemistry, and cell biology have been instrumental in elucidating molecular details of the cell cycle

Progress in several fields of biological research has rapidly advanced our understanding of how cells divide. Genetic analysis, biochemical complementation, and cell fusion experiments have provided important pieces of evidence that together reveal a great deal about the cell cycle.

In 1970, cell cycle regulation was dissected genetically in the single-celled budding yeast *Saccharomyces cerevisiae*. Genetic analysis was used extensively to identify the genes encoding the essential components of the cell division machinery and clarify the functional relationships of the gene products. Conditional cell cycle mutants were especially useful because they could grow at permissive temperatures (around 20–25°C), but not at a restrictive temperature (usually 36°C). Fortunately, the cell cycle of budding yeast has a readily visible marker, **bud formation**, which facilitates screening for mutants. The nascent bud, which appears approximately at the time of initiation of DNA synthesis, grows throughout the cell cycle, so a mutant phenotype can

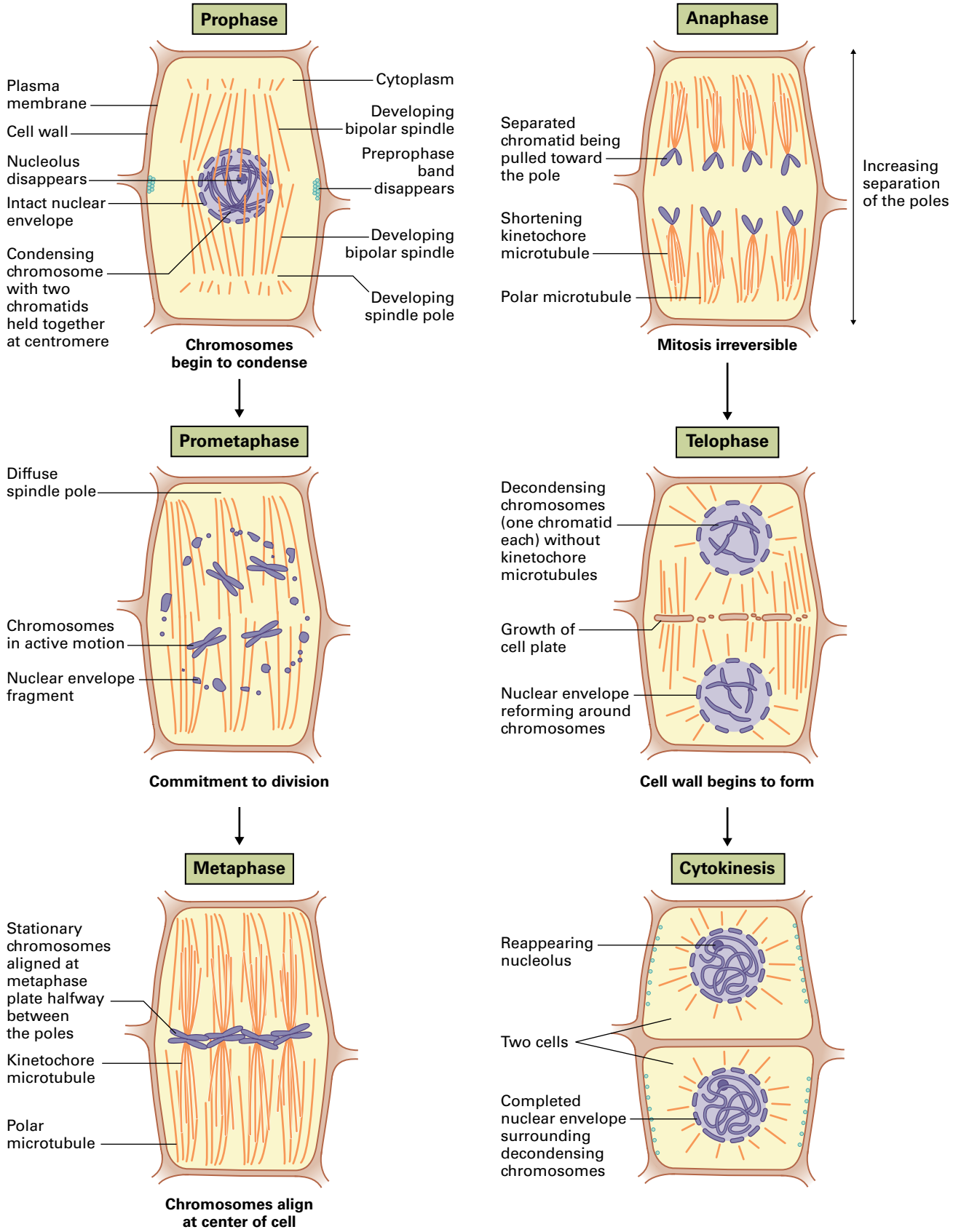


FIGURE 11.1 *Mitosis in plants. By the end of the 19th century, microscopy of plant cells had shown that steady increases of cell volume in proliferating cells were punctuated by the disappearance of the nucleus and appearance of condensed chromosomes (prophase), followed by their alignment along the equator of the cell (metaphase). Chromosomes appeared to separate and move toward the cell poles (anaphase), which was followed by reappearance of two nuclei (telophase), and the subsequent formation of separate daughter cells (cytokinesis). Most aspects of mitosis in plant cells are similar to those in animal cells, but the two types of cells differ in their spindle poles (which are more diffuse in plant cells) and in the mechanisms by which daughter nuclei are separated. Animal cells constrict their plasma membrane during telophase, while in plant cells, a cell plate is built that forms the new cell wall.*

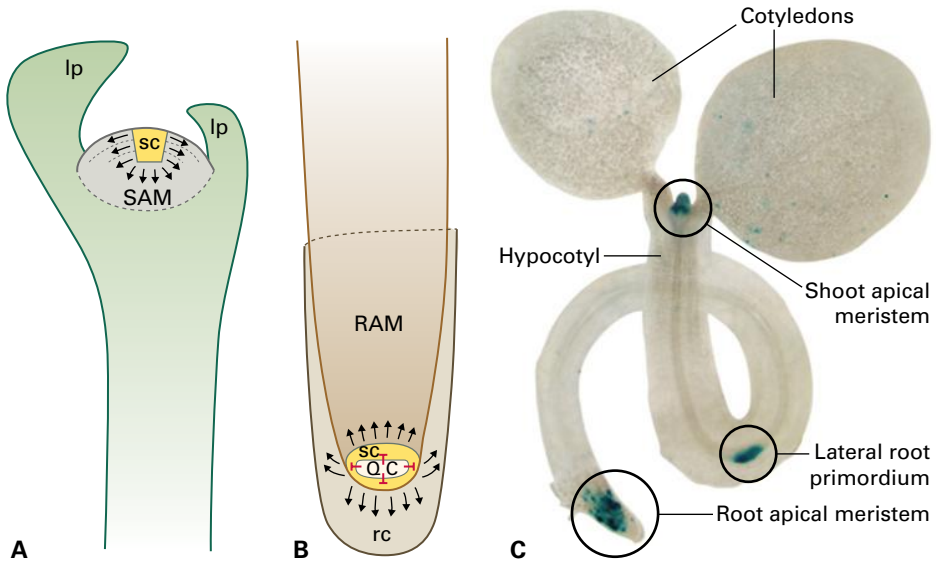


FIGURE 11.2 *Continuous development after embryogenesis in plants. Unlike animals, plants can form new organs and tissues continuously throughout their life span. The tissues responsible for maintenance of this open growth mode are shoot apical meristems (SAMs) (A) and root apical meristems (RAMs) (B). Both meristems consist of undifferentiated and dividing cells that deliver new cells to the growing structures. Small populations of stem cells (sc) within the meristems are essential for the self-perpetuating capacity of meristems. After asymmetric divisions, the stem cells form daughter cells with distinct cell fates. One daughter cell will maintain the stem cell fate, whereas the other will receive instructions to differentiate into a specific cell type. However, the final differentiation is postponed and will only occur after several rounds of symmetric divisions that give rise to growing cell files (arrows). In the shoot apex, leaf primordia (lp), also made of dividing cells, are formed in close proximity to the SAM. In the root, no new organs are formed near the RAM and the entire structure is covered by a protective root cap (rc). At the apex cap boundary of the root, a small group of nondividing cells occurs, the quiescent center (QC). Signals emitted by these cells maintain the immediate surrounding cells in a stem-cell fate and prevent them from differentiation. (C) The sites of cell division can be visualized in an* Arabidopsis *seedling by the activity of a CYCLIN–GUS fusion protein produced exclusively in mitotic cells (blue). Next to the SAM and RAM, cell division activity can be observed at the lateral root primordia, sites at which new lateral roots initiate.*

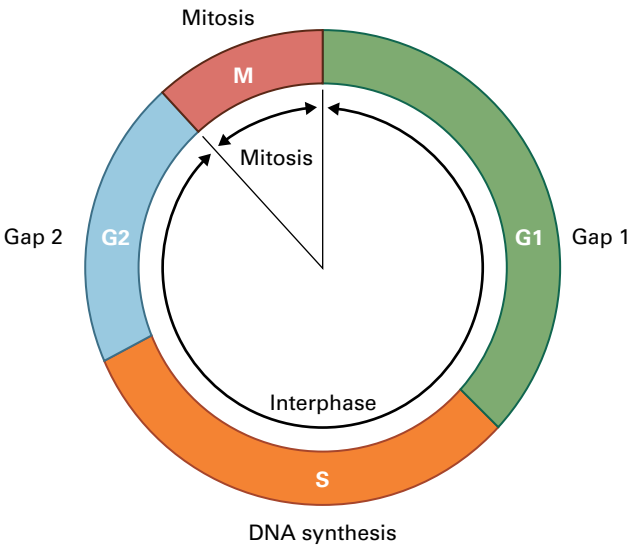


FIGURE 11.3 *Phases of the cell cycle. Microscopic investigation of the cell cycle reveals two distinct states: mitosis, characterized by chromosome condensation and nuclear division, and interphase, during which chromosomes appear diffuse and cells do not divide. The discovery that DNA synthesis occurs during interphase led to the identification of four cell cycle phases: mitosis (M), DNA synthesis (S), and two gap phases (G1 and G2) that separate these events.*

be related to a specific ratio of the volumes of the mother and daughter cells.

The goal of screening for **cell division control** (*cdc*) mutants was to isolate colonies in which growth was arrested at a particular stage when the culture was transferred to the restrictive temperature (Fig. 11.4). In contrast, mutations in genes not related to the cell cycle (e.g., genes encoding metabolic enzymes) were predicted to arrest proliferation at random time points of the cell cycle, that is times at which the cell was deprived of a particular metabolite (Fig. 11.4). The arrest phenotype of the *cdc* mutant identified by time-lapse photography revealed how far the cell cycle could progress without the presence of the wild-type gene product, called the **termination** or **arrest point**; however, it did not reveal when the wild-type gene product was normally required. Accomplishing this task required the use of another technique, **synchronization**.

In a proliferating population, individual cells are in different phases of the cell cycle, making it extremely difficult to study proteins or RNA molecules that are specific to individual phases of the cell cycle. Cell cultures can be synchronized, however, by blocking the progression of cells at a specific point in the cell cycle with drugs that inhibit crucial processes, such as DNA synthesis. Once all the cells in a culture

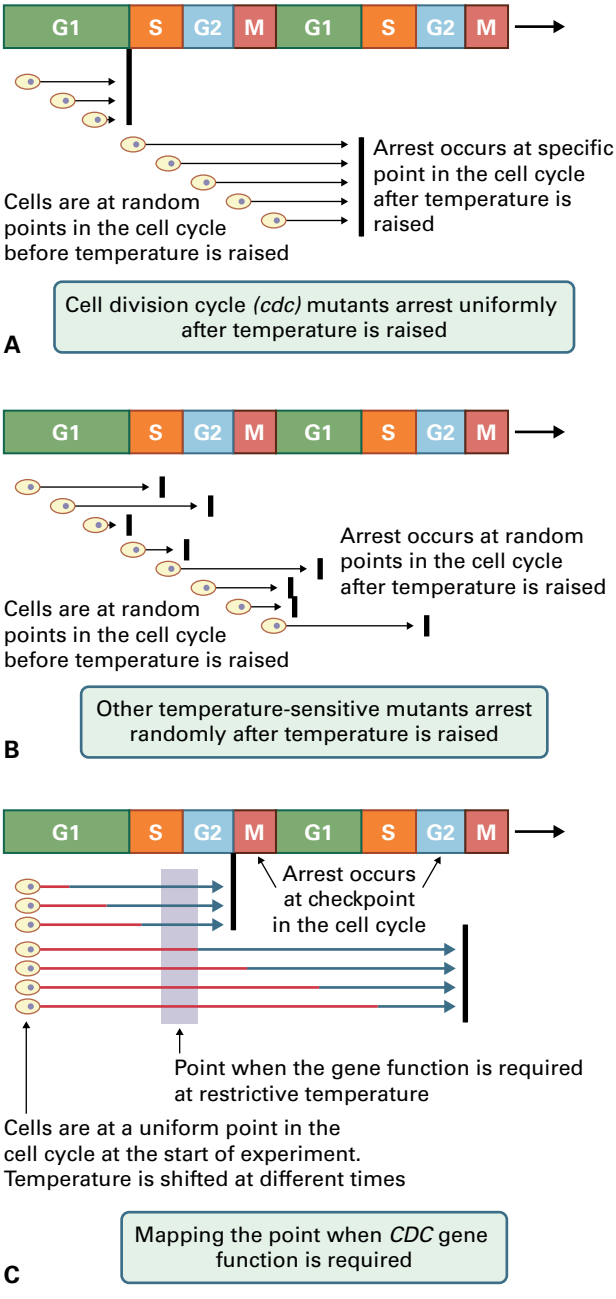


FIGURE 11.4 *Genetic screen for identifying conditional cell division cycle (*cdc*) mutants of yeast. Unlike conditional* cdc *mutants (A) that arrest at the same phase in the cell cycle after the temperature is increased to the restrictive temperature, other conditional mutants (B) arrest at random points in the cell cycle after exposure to the restrictive temperature. Such experiments allow identification of the termination, or arrest, point—the point in the cell cycle beyond which mutant cells cannot progress without the gene product. Once a* cdc *mutant is identified, synchronized cell cultures can be used to determine the execution point—the point in the cell cycle at which the gene product is required (C). The temperature is shifted at different times for different synchronized cell cultures, as denoted by the transition of the arrow color from red to blue. Cultures exposed to the restrictive temperature before they reach the execution point arrest at the next termination point, whereas those exposed to the restrictive temperature after they reach the execution point can proceed through another round of the cell cycle before arresting.*

have been arrested at the same stage of the cell cycle, the inhibitor can be removed to relieve the cell cycle block and allowing the cells to proceed synchronously through the cell cycle for one or two rounds. By transferring synchronized cells at successive stages of the cycle to a restrictive temperature and monitoring their fate by time-lapse photography, investigators can identify the point in the cycle at which the wild-type gene product is required—the **execution point** (Fig. 11.4).

Biochemical analysis, particularly when used in combination with cell biology, also provides powerful tools for examining the function of specific cell cycle proteins. Two techniques often used together are analysis of phase-specific protein extracts and biochemical complementation (Fig. 11.5). In one experiment, clam oocytes were stimulated to divide, protein extracts from the cells were prepared at different times after stimulation, and the protein patterns were analyzed. This

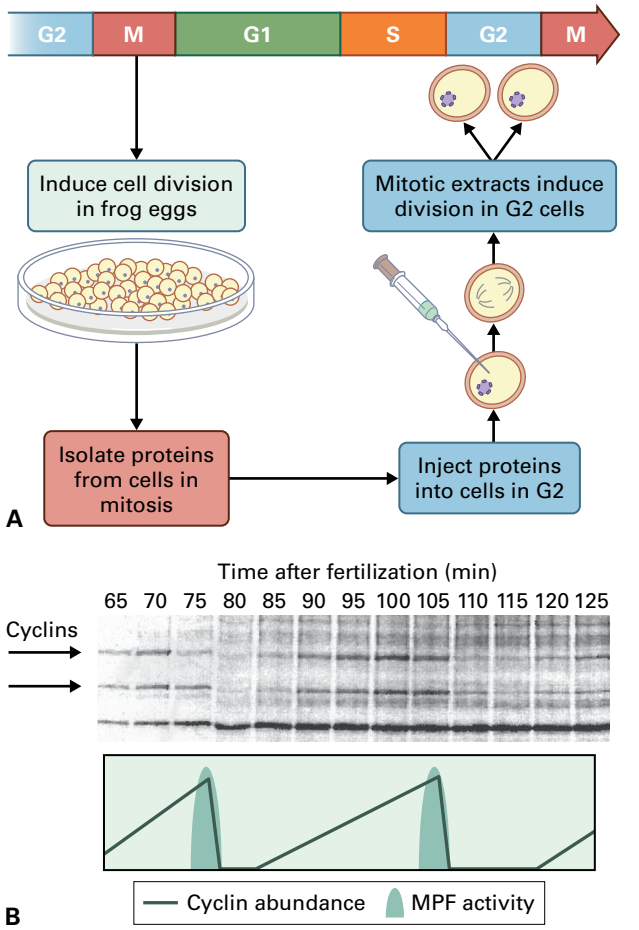
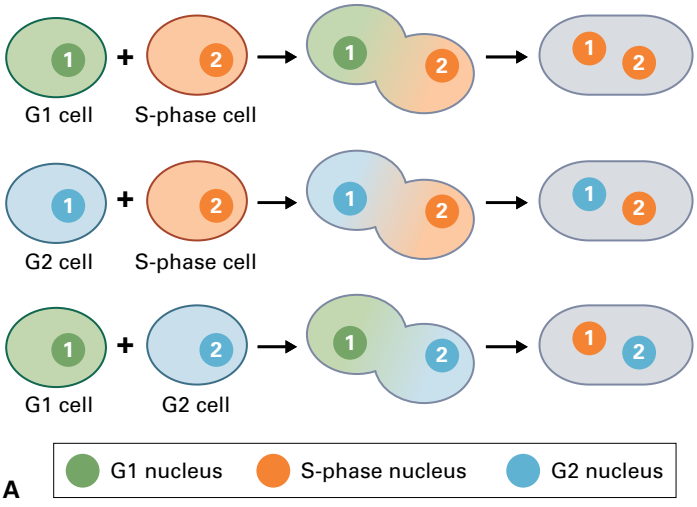


FIGURE 11.5 *Identification of a mitosis-promoting factor (MPF). (A) Extracts are taken from mitotic* Xenopus *oocytes. The extracts contain proteins that induce G2 cells to undergo mitosis. Similar experiments were used to isolate an MPF capable of triggering G2 cells to divide. (B) Biochemical analyses of fractions of cell extracts taken at various stages of the cell cycle reveal the presence of cyclins, soluble protein factors that demonstrate cyclic changes in abundance during the cell cycle. Cyclin abundance correlates with the activity of MPF. Source*: (B) Minshull (1989). J. Cell Sci. Suppl. 12:77–98.

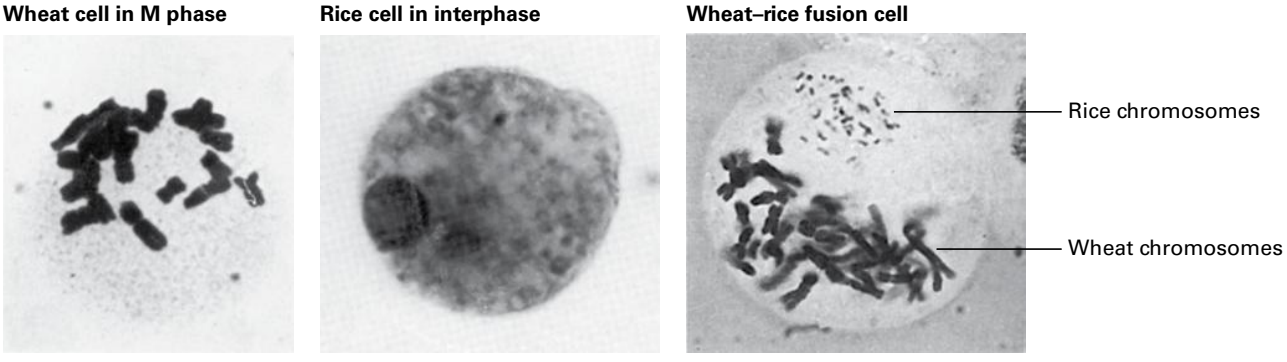
approach identified a set of unstable proteins called **cyclins,** which appear and disappear at specific phases of the cell cycle. In other experiments, protein extracts from cells undergoing mitosis were fractionated, and the fractions were either combined with extracts from arrested oocytes or were injected into arrested oocytes. Determination of which fractions released the arrested extracts or oocytes allowed identification of a **mitosis-promoting factor** (MPF).

Finally, cell fusion experiments were performed, first with human cell lines and later with plant cells (Fig. 11.6). In these experiments, cells in different stages of the cell cycle were fused to observe how the nuclei responded. When cells in G1 were fused with S-phase cells, the G1 nuclei rapidly advanced into DNA replication. This indicated that although G1 cells were competent to replicate their DNA, this process required activation by a factor already present in S-phase cells. When G2- and S-phase cells were fused, however, only the S-phase nucleus continued to replicate its DNA. Moreover, the G2 nucleus did not progress into the M phase after this fusion, as it ordinarily would have. This indicated the G2 nuclei were not competent to rereplicate and that a factor in S-phase cells prevented them from entering mitosis. When G2 cells and G1 cells were fused, the G1 nucleus replicated DNA, but on a schedule similar to that of unfused G1 cells, whereas the G2 nucleus did not replicate. Together, these observations demonstrated that S-phase cells contain a labile activator that can stimulate G1 nuclei (but not G2 nuclei) to enter S phase. Cells also contain a repressor of mitosis, which is active in S-phase cells and inhibits DNA rereplication before mitosis.



A

Observations	Conclusions
G1 nucleus replicates. Early S-phase nucleus continues replication.	G1 nucleus is competent to replicate. S-phase cells contain activator.
G2 nucleus does not replicate. S-phase nucleus continues replication. G2 nucleus does not progress into M phase.	G2 nuclei are not competent and do not rereplicate. G2 cells do not inhibit replication. S-phase nuclei retard mitosis in G2 nuclei.
G1 nucleus replicates at normal time; G2 nucleus does not replicate.	G2 cells do not suppress S-phase entry of G1-phase nuclei.



B

FIGURE 11.6 *Examples of cell fusion experiments. (A) Fusion experiments conducted with animal cells revealed diffusible factors regulate cell division progress, whereas nondiffusible factors associated with chromosomes determine whether the chromosomes are competent to respond to the diffusible factors. (B) Cell fusions of plant cells at different stages of the cell cycle. Plant cell protoplasts, from which cell walls were removed by enzymatic digestion, can be fused together. To readily distinguish the origin of chromosomes in the fused protoplasts, cells from different species with distinct chromosome morphologies are used. In this experiment, mitotic wheat protoplasts (condensed chromosomes, left panel) were fused with rice protoplasts in interphase (chromosomes not condensed and, therefore, not visible, middle panel). After fusion, the rice chromosomes rapidly condensed and became visible (right panel). This suggests the mitotic wheat cells contain diffusible factors sufficient to initiate chromosome condensation in interphase cells.*
Source: (B) Szabados & Dudits (1980). Exp. Cell Res. 127:441–446.

These different approaches led to the identification of a group of kinases, known as **cyclin-dependent kinases** (CDKs). CDK activity is controlled in a cell cycle phase-dependent manner by the regulatory **cyclin** subunits. The conserved nature of cell cycle control by CDKs is reflected in the fact that a human *CDK* gene can complement a yeast *CDK* mutant despite the 1–1.5 billion years of evolutionary divergence between these organisms. CDKs and cyclins also make up the MPF, an observation that again supports the idea that cell cycle control is conserved among all eukaryotes, including plants. Peak cyclin abundance was later found to correlate well with the maximum biochemical activity of MPF (see Fig. 11.5).

In the following sections, we discuss the molecular components that advance and regulate cell division in plants and illustrate their temporal action in DNA replication and mitosis. The nomenclature of cell cycle proteins, which can be confusing, has been simplified wherever possible. For historical reasons, a protein conserved in many organisms can have many different names in the literature, but only one name is used here for homologous genes or proteins.

11.3 Mechanisms of cell cycle control

11.3.1 Specific kinase complexes facilitate cell cycle progression

Cell cycle progression is controlled by changes in CDK activity. CDK protein complexes are composed of at least two different subunits, one functioning as a protein kinase (CDK) and the other as an activator (cyclin). The protein kinase alone lacks activity; association with a cyclin is the first step in activating the complex. Many single-celled eukaryotes such as yeast have a single CDK, whereas all multicellular eukaryotes appear to have multiple CDKs. All eukaryotic cells also have multiple classes of cyclins, each of which is required for specific regulatory steps during the cell cycle.

In yeast, these different cyclins interact sequentially with the single CDK subunit, thereby changing the substrate specificity of the enzyme complex during the cell cycle. In multicellular organisms, certain CDKs interact specifically with different classes of cyclins, and these interactions determine the activity and substrate specificity of the CDK complexes at particular points in the cell cycle. Thus, the association of CDKs with specific cyclins is generally thought to be a key regulatory mechanism for advancing the cell through the various stages of the cell cycle.

Cyclins are not, however, the only factors controlling CDK activity. The activity of CDKs also depends on their phosphorylation status and association with other regulatory proteins, such as substrate docking factors and CDK inhibitory molecules. Furthermore, proteases selectively destroy cyclins and CDK inhibitory proteins at defined time points during the cell cycle. The irreversible destruction of these proteins contributes to the unidirectional progression through the cell cycle.

11.3.2 Multicellular eukaryotes have a complex pathway of CDKs

CDKs are a highly conserved class of eukaryotic protein kinases with several characteristic features. When complexed with a cyclin subunit, they phosphorylate substrates on serine or threonine residues within an S/TPXR/K recognition motif found in most CDK substrates. Crystallographic studies have revealed their structure has two lobes, the N-terminal (upper) and C-terminal (lower) lobes, with the catalytic site residing in a deep cleft between the two lobes. Other amino acids required for CDK activity are located throughout the molecule, and they are organized into their appropriate spatial context only after the CDK protein has folded into its three-dimensional structure and interacted with a cyclin subunit.

Cyclin binding is required for entrance of substrates into the catalytic site, which is initially shielded by a flexible CDK domain, called the T-loop. When cyclin binds, the T-loop shifts into an open configuration that is stabilized by the phosphorylation of a conserved threonine residue in the T-loop (Fig. 11.7). This phosphorylation is catalyzed by CDK-activating kinases (CAKs), which are CDKs themselves.

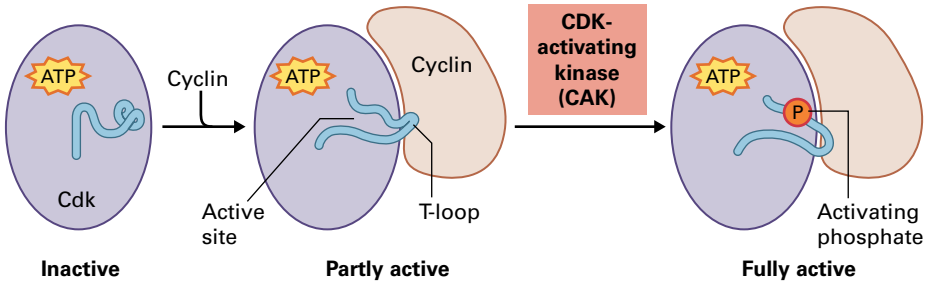


FIGURE 11.7 *The structural basis of CDK activation. The activity of CDKs is highly regulated, and association of the CDK catalytic subunit with an activating cyclin subunit is essential for protein kinase activity. Subsequent phosphorylation of the conserved Thr residue at position 161 by a CAK is required for full activity.*

Plants have two functional classes of CAKs: CDKDs and CDKFs. CDKD is functionally related to the CAKs of vertebrates, whereas CDKF is a plant-specific CAK with unique enzyme characteristics. The functional diversity between the two CAKs is exemplified by their substrate specificity and cyclin dependence, and the activation of CDKs by CAKs is complex (Fig. 11.8). In addition to activating CDKs for substrate binding, CDKDs phosphorylate the C-terminal domain (CTD) of the largest subunit of the RNA polymerase II, which allows cells to coordinate transcription with cell cycle progression. Unlike CDKD, CDKF activation does not require association with cyclins. CDKF phosphorylates CDKD and, therefore, functions as a CAK-activating kinase. CDKF itself has a conserved site at Thr290, which probably needs to be phosphorylated by an unknown upstream protein kinase before it can phosphorylate CDKD (Fig. 11.8). Such a phosphorylation cascade may link CDK activation to developmental pathways or hormonal regulation.

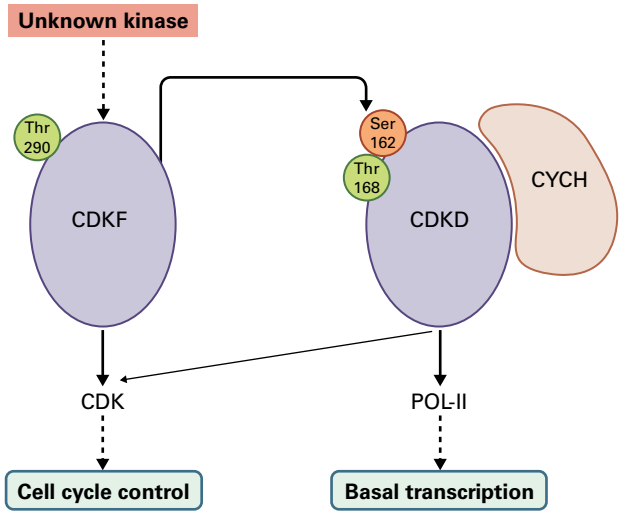


FIGURE 11.8 *Two classes of plant CAKs. CDKF is responsible for phosphorylation and activation of CDKD. Phosphorylated CDKD forms a stable complex with CYCH, and the CYCH–CDKD complex has kinase activity toward both the C-terminal domain of RNA polymerase II (POL-II) and CDKs. The CDK kinase activity of CYCH–CDKD is significantly lower than that of CDKF.*

Amino acid domains required for cyclin binding reside in the N-terminal (upper) lobe of the CDK and are named according to the single-letter codes of the amino acids they comprise. All eukaryotic organisms studied to date have at least one CDK with the PSTAIRE motif. In plants, PSTAIRE-containing CDKs are designated **A-type CDKs** (CDKAs), and they play a pivotal role at both the G1-to-S and G2-to-M transitions. The requirement of CDKA activity for cell division is demonstrated by a reduction in the cell division rate in plants with low CDKA activity, or the arrest of the second mitotic division during male gametogenesis in *CDKA* null mutants (Fig. 11.9).

Other CDKs have variations of the PSTAIRE motif. Plants possess a unique class of CDKs, the **B-type CDKs** (CDKBs), which have either PPTALRE or PPTTLRE motifs, reflecting the two subgroups, CDKB1 and CDKB2. In contrast to CDKAs, expression and activity of CDKBs are more confined to specific phases of the cell cycle, and the two subgroups differ slightly in timing of transcription: *CDKB1* transcripts accumulate during S, G2, and M phases, whereas *CDKB2* expression is specific to the G2 and M phases. Accumulation of CDKB proteins follows their transcription pattern, while their associated kinase activities reach a maximum during mitosis. CDKB1 activity is required for cell cycle progression through mitosis; plant cells with reduced CDKB1 activity arrest at the G2-to-M transition. Moreover, such plants display abnormal stomata and reduced numbers of stomatal complexes (Fig. 11.10). This mutant phenotype indicates CDKB1 has a role in the series of sequential cell divisions required to form a stomatal complex. A role for CDKB2 in cell cycle regulation is illustrated by the abnormal shoot apex and altered phylotaxis of plants with reduced *CDKB2* expression (Fig. 11.10).

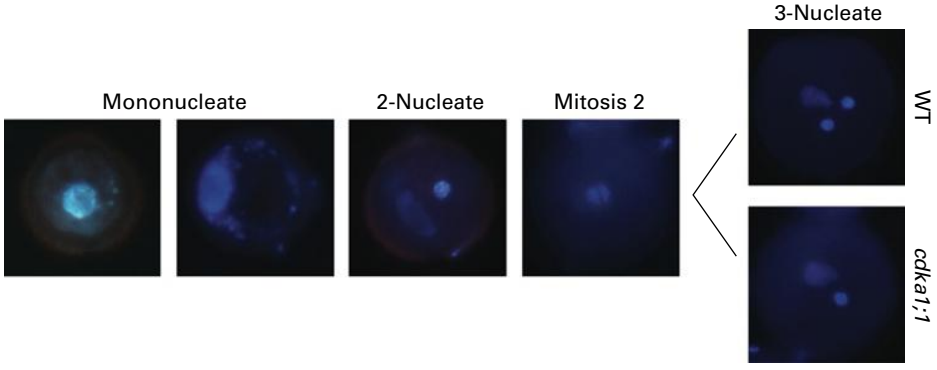


FIGURE 11.9 *Two rounds of mitotic divisions in wild-type haploid microspores derived from a microspore mother cell. After the first division, the developing gametophyte contains two cells: a vegetative cell with a large nucleus that encloses a generative cell with a small nucleus (2-nucleate stage). Next, the generative cell divides again (mitosis 2) so that the mature pollen contains one large vegetative and two small sperm cells (3-nucleate stage). In CDKA null mutants* (cdka1;1), *the generative nucleus fails to progress through the second mitosis, resulting in pollen with one vegetative and only one sperm cell.*

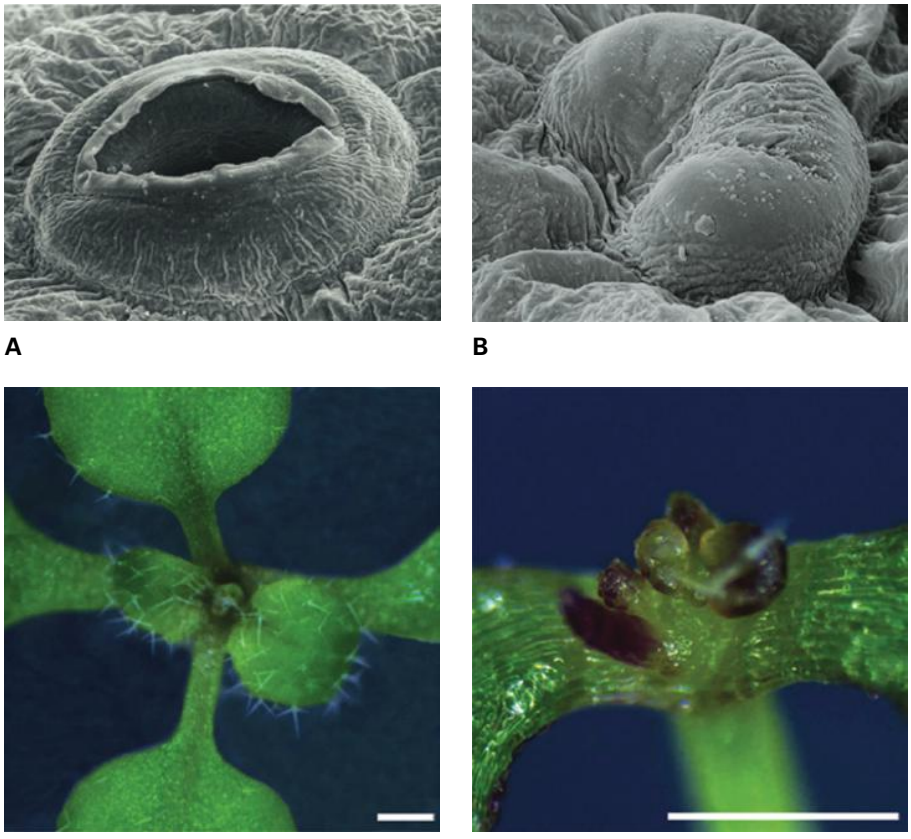


FIGURE 11.10 *B-type CDKs control plant-specific aspects of the cell cycle. (A–B) Plants with reduced CDKB1 activity have a high number of stomata with aberrant morphology. In contrast to wild-type plants (A), the stomata in these mutants show a unicellular round or kidney-shaped appearance and lack pores (B). Remarkably, the aberrant cells still acquire typical stomatal features, such as guard cell shape formation and cell wall thickening, indicating CDKB1 activity controls stomatal divisions, but not the differentiation of cells toward their stomatal identity. (C–D) In plants with reduced CDKB2 activity, the typical meristem organization observed in wild-type plants (C) is disrupted because of a strong inhibition of cell division, which results in an abnormal meristem structure and defects in phyllotaxy (D).*

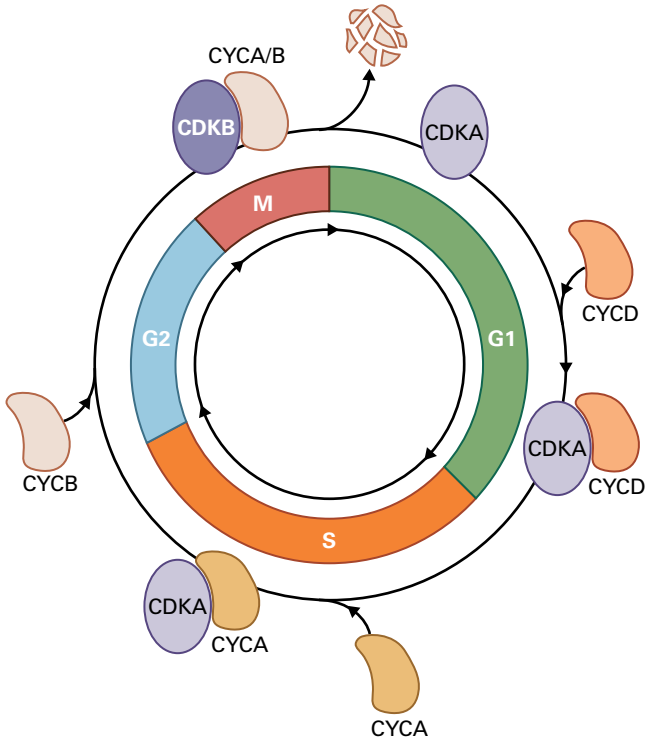
Plants also contain more distantly related CDKs, designated C-type (CDKC) and E-type (CDKE) CDKs, which do not have a clear role in cell cycle control. CDKC may have a role in transcription elongation by phosphorylating the CTD of the RNA polymerase II, as well as in linkage of transcription with RNA splicing. CDKE (also known as HUA ENHANCER3) controls cell fate specification in floral organs by a currently unknown mechanism.

11.3.3 Cyclins determine the specificity and subcellular localization of CDKs

Association with cyclins is required for CDK protein kinase activity. As mentioned previously, cyclin binding induces structural changes needed for substrate recognition, including the repositioning of the T-loop (see Fig. 11.7). Cyclins also confer substrate specificity to the cyclin–CDK complex and are involved in targeting CDKs to specific subcellular compartments during the cell cycle.

Plants contain more cyclins than other organisms. For example, despite its small genome size, the *Arabidopsis thaliana* genome encodes up to 50 different cyclins. Plant cyclin nomenclature is based on functional similarities with mammalian counterparts within a **cyclin box**, a largely conserved central domain that interacts with the kinase subunit. Plant cyclins are classified as types A, B, C, D, H, L, P, and T. Until now, a clear role in cell cycle progression has been demonstrated for A-, B-, D-, and H-type cyclins. In a broad sense, D-type cyclins are anticipated to control the G1-to-S transition; A-type cyclins, the S-to-M phase control; B-type cyclins both the G2-to-M and intra-M-phase control; and the H-type cyclins control the activity of CDKDs (Fig. 11.11).

D-type (CYCD) cyclins diverge largely in their sequence and were originally identified by functional complementation of a yeast strain deficient for G1-specific cyclins. In mammals, accumulation of CYCDs is stimulated by growth hormones. Similarly, expression of plant *CYCD*s is modulated by growth factors, such as cytokinins, auxins, brassinosteroids, sucrose, and gibberellins. This indicates these cyclins act as key switches linking the hormonal and nutritional status of plant cells with cell cycle progression. In agreement with this model, expression of *CYCD*s precedes cell division in germinating seeds, and correspondingly, mutant plants with *CYCD*



CDK	Cyclin
CDKA;1	CYCA1;1, 1;2 CYCA2;1, 2;2, 2;3, 2;4 CYCA3;1, 3;2, 3;3, 3;4
CDKB1;1, 1;2	CYCB1;1, 1;2, 1;3, 1;4 CYCB2;1, 2;2, 2;3, 2;4 CYCB3;1
CDKB2;1, 2;2	CYCD1;1 CYCD2;1 CYCD3;1, 3;2, 3;3 CYCD4;1, 4;2 CYCD5;1 CYCD6;1 CYCD7;1

FIGURE 11.11 *The central regulator of the cell cycle is a CDK–cyclin heterodimer.* Arabidopsis *has five genes encoding CDKs that directly control the cell cycle, and more than 50 cyclin genes encoding mitotic A- and B-type cyclins and D-type cyclins. These classes can be further subdivided in subclasses, for which several of the family members are indicated on the right. They form different combinations of pairs and control progression of distinct cell cycle phases.*

loss-of-function alleles show that CYCDs are rate limiting for cell cycle reactivation in the root apex during germination (Fig. 11.12A). Analogously, expression of the *CYCD3;1* gene depends on cytokinin and appears to affect cell division of cytokinin-deprived calli (Fig. 11.12B). Thus, *CYCD* expression seems important for coupling development to nutrient and growth factor availability.

Progression through S phase and entry into mitosis is probably controlled by the **A-type** (CYCA) **cyclins** and **B-type** (CYCB) **cyclins,** respectively. Besides a cyclin box, both types of cyclins also carry a protein domain called the **mitotic destruction box** (D-box) that mediates cyclin degradation late in mitosis. The potential of plant B-type cyclins to trigger the G2-to-M transition was originally shown by microinjection experiments into *Xenopus* oocytes, which illustrated that plant cyclins could overcome the natural G2/M arrest of oocytes. Later, ectopic expression of a *CYCB* was demonstrated to stimulate cell division in roots and trichomes. Promoters of plant *CYCB* genes contain a common *cis*-acting element, called the **M-specific activator** (MSA) element, which is necessary and sufficient to direct G2/M-specific gene expression.

11.3.4 CDK activity is regulated by kinases, phosphatases, and specific inhibitors

The activities of CDK–cyclin complexes are controlled by specialized kinases and phosphatases, which have important functions in regulating cell cycle progression. In yeast, these complexes are subject to inhibitory phosphorylation of the Tyr15 residue in the CDK, whereas in vertebrates CDKs are phosphorylated on both Thr14 and Tyr15. Tyr phosphorylation is catalyzed by the Wee1 kinase, and both Tyr and Thr phosphorylation is counteracted by the dual-specific phosphatase Cdc25 (Fig. 11.13). Thus, Cdc25 and Wee1 act as "on" and "off" switches of CDK activity, respectively, and together play an important role as a timer of M-phase onset.

Plant CDKs are likely also negatively controlled by phosphorylation. Tyr phosphorylation of CDKA has been detected upon cytokinin deprivation, osmotic stress, and DNA damage. This phosphorylation is probably catalyzed by the plant WEE1 kinase, because overexpression of this gene inhibits cell cycle progression. However, no *CDC25* homolog has been identified in a plant genome, indicating the mechanism that controls the timing of M-phase onset is fundamentally different in plants. Likely candidates that have taken over the role of Cdc25 as timer of mitosis are the B-type CDKs or CDK inhibitory proteins (CKIs).

CKIs can be found in all organisms, and they inhibit cell cycle progression through direct association with activated CDK–cyclin complexes, preventing them from phosphorylating substrates. In humans, two different classes of CKIs are known. Members of the INK4 protein family, which operate as important regulators of the G1-to-S transition, are frequently mutated in neoplastic cells that have lost the ability to control proliferation. Members of the CIP/KIP family inhibit a broad range of CDK–cyclin complexes involved in the control of both the G1-to-S and G2-to-M transitions and operate as important effectors of anti-mitogenic stimuli.

Plants also have two classes of CKIs. One class shares a conserved domain with the mammalian CIP/KIP family at

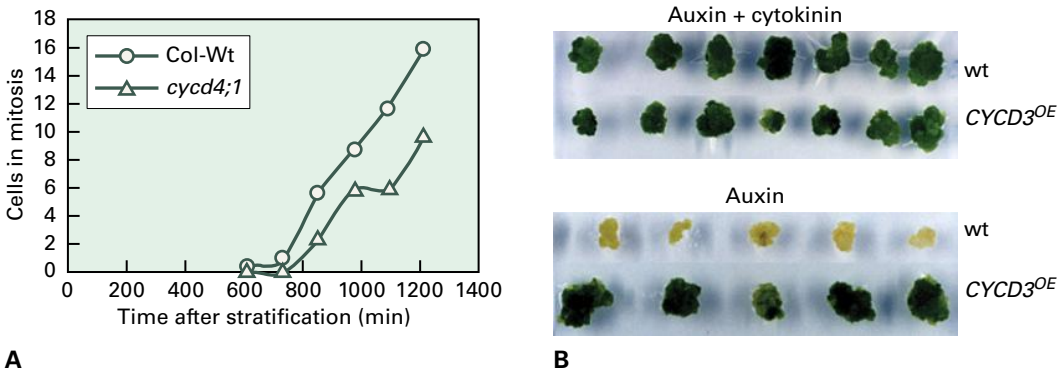


FIGURE 11.12 *D-type cyclins (CYCD) regulate cell cycle progression according to the nutritional and hormonal status of plant cells. (A) Effect of CYCD levels on the activation of cell division in the root meristem during germination.* CYCD4;1 *loss-of-function mutants* (cycd4;1) *have a delayed onset of cell division activity and fewer dividing RAM cells, resulting in a lower rate of cell division than that of wild-type plants (Col-Wt). (B) Effect of CYCD levels on hormone-regulated callus formation. Wild-type leaves produce calli efficiently when exogenous cytokinin and auxin are present (top), but in the absence of cytokinin (bottom), only a few, slow-growing calli are formed; these fail to become green, and they degenerate after a period in culture. In contrast,* CYCD3*-overexpressing transgenic plants* (CYCD3^{OE}) *produce healthy green calli in both the presence and absence of exogenous cytokinin.*

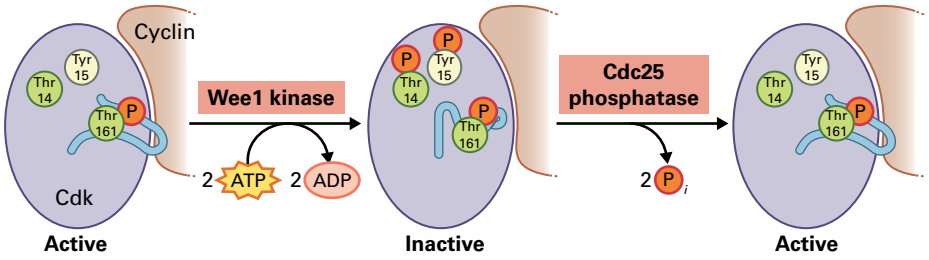


FIGURE 11.13 *The protein kinase activity of a yeast CDK is regulated by phosphorylation and shown here as an example. Phosphorylation by a Wee1 kinase of conserved threonine and tyrosine residues (Thr14 and Tyr15) near the N-terminus of the CDK catalytic subunit inhibits protein kinase activity. Dephosphorylation by a Cdc25 phosphatase removes these inhibitory phosphate residues and regulates the timing of entry into mitosis. Although the amino acids are conserved in plant CDKs, it is still unknown if they are regulated by enzymes with similar functions.*

the extreme C-terminus that is involved in binding CDKs and cyclins and is essential for CKI activity. Because this conserved domain shares similarity with the N-terminal CKI domain of mammalian CIP/KIP proteins, these plant CKIs are known as **Kip-related proteins** (KRPs). Elevated KRP levels in plants restrain CDK activity and inhibit cell division, resulting in dwarfism and other alterations in plant morphology (Fig. 11.14A,B). The main targets of KRPs are the CDKA–CYCD complexes. Expression of the *Arabidopsis KRP1* gene (also known as *ICK1*) is induced by abscisic acid (ABA), probably contributing to the ability of ABA to arrest cell cycle progression. KRPs are also transcriptionally and post-transcriptionally controlled by other hormones, including auxin, cytokinin, and gibberellin.

The other class of plant CKIs includes the *Arabidopsis* SIAMESE (SIM) and SIAMESE-RELATED (SMR) proteins. The *SIM* gene was originally identified as a suppressor of cell division in trichomes (Fig. 11.14C,D). The SIM and SMR proteins share with KRPs a six-amino acid domain that is essential for cyclin binding and inhibition of CDK activity, and, like KRPs, they inhibit D-type cyclin-containing CDK complexes. *SIM* and *SMR* genes respond strongly to diverse stress conditions, suggesting they play a major role in connecting cell cycle progression with biotic and abiotic stress perception.

11.3.5 Ubiquitin-dependent proteolysis occurs at key transitions in the cell cycle

Proteolysis ensures the unidirectional progression of the cell cycle by rapidly triggering the irreversible breakdown of target proteins. For example, proteolysis of CKIs is necessary to trigger the G1-to-S transition. Similarly, degradation of the cohesion proteins that connect sister chromatids is required for the irreversible transition from metaphase to anaphase. In all cases, the route to destruction runs via the ubiquitin-proteasome system, which uses the highly conserved polypeptide **ubiquitin** as a tag to mark target proteins for degradation by the 26S proteasome (see Chapter 10).

For ubiquitination, polyubiquitin chains must be generated on target proteins through the combined action of ubiquitin-carrying enzymes (E2s) and ubiquitin protein ligases (E3s),

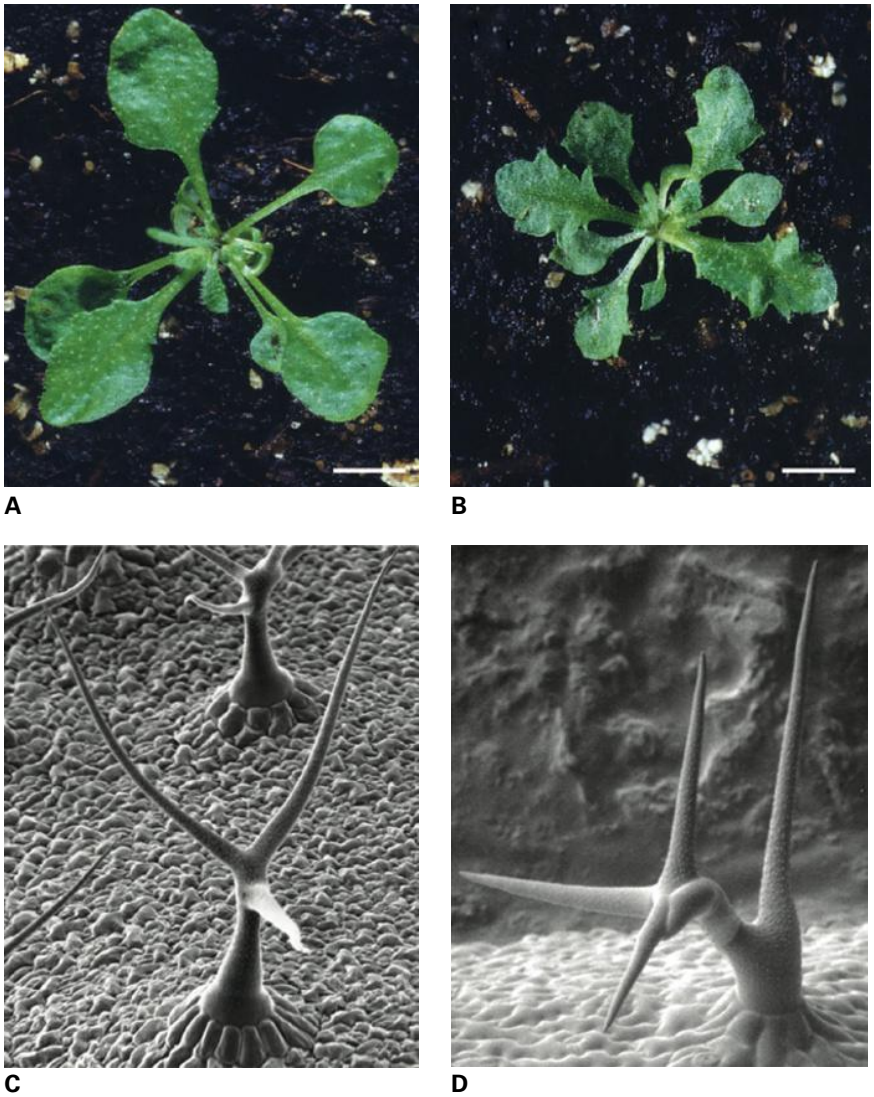


FIGURE 11.14 *CDK inhibitors and their effects on plant morphogenesis. (A, B) Wild-type (A) and* KRP2*-overexpressing (B) plants.* KRP2*-overproducing plants have narrow leaves that are serrated. These two phenotypes result from a strong reduction in leaf cell number. (C, D) Wild-type (C) and* sim *mutant (D) trichomes. Wild-type trichomes are unicellular, whereas* sim *mutants show a high frequency of multicellular trichomes.*
Source: (A, B) Based on figure published by De Veylder et al. (2001). Plant Cell 13:1653–1668. (C, D) Based on figure published by Churchman et al. (2006). Plant Cell 18:3145–3157.

which bring targets and E2s together. Two different E3 complexes are most intimately dedicated to the basic cell cycle control, namely **Skp1-Cullin-Fbox** (SCF)-**type of E3 ligases** and the **anaphase-promoting complex/cyclosome** (APC/C), which operate at the G1-to-S transition and in M phase, respectively.

Plant D-type cyclins are likely subjected to degradation in an SCF-dependent manner, as observed for their mammalian counterparts. Many D-type cyclins also contain PEST sequences, regions rich in Pro, Glu, Ser, and Thr that can confer protein instability. Other cell cycle regulators that are targets of the SCF include CDC6, CDT1a, E2Fc, and the KRPs. Among the SCF-type of E3 ligases, the F-box protein recognizes the substrates that need to be degraded. It is still unknown which of the 694 F-box proteins of *Arabidopsis* are involved in the specific recognition of the cell cycle regulatory proteins. An exception is the F-BOX-LIKE 17 (FBL17) protein, which targets the KRP CDK inhibitors for destruction.

The APC/C comprises at least 12 proteins, and recognizes and ubiquitinates several proteins, including proteins that contain the D-box (mitotic destruction box, see Section 11.3.3). Like SCF, APC/C can occur in several forms with different selector proteins (Fig. 11.15). The activation and substrate specificity of the APC/C complex are in part determined by two adaptor proteins, CDC20 and CDH1. The *Arabidopsis* genome encodes five *CDC20* genes as well as three genes that encode CDH1-related proteins, designated *CCS52A1*, *CCS52A2*, and *CCS52B*. The three *Arabidopsis CCS52* genes probably have nonredundant functions: *CCS52B* is expressed from G2 to M, whereas *CCS52A1* and *CCS52A2* are expressed from late M until early G1, suggesting consecutive actions of these APC/C activators in the plant cell cycle. The CCS52 proteins interact with different subsets of mitotic cyclins, either in free or CDK-bound forms.

Well-characterized target proteins that are ubiquitinated by APC/C are A- and B-type cyclins containing D-box sequences. The destruction of these cyclins is essential for exit from mitosis. Constitutive overexpression of a nondegradable CYCB, lacking the destruction box, causes severe growth retardation and abnormal development due to an abnormal mitosis and inhibition of cytokinesis.

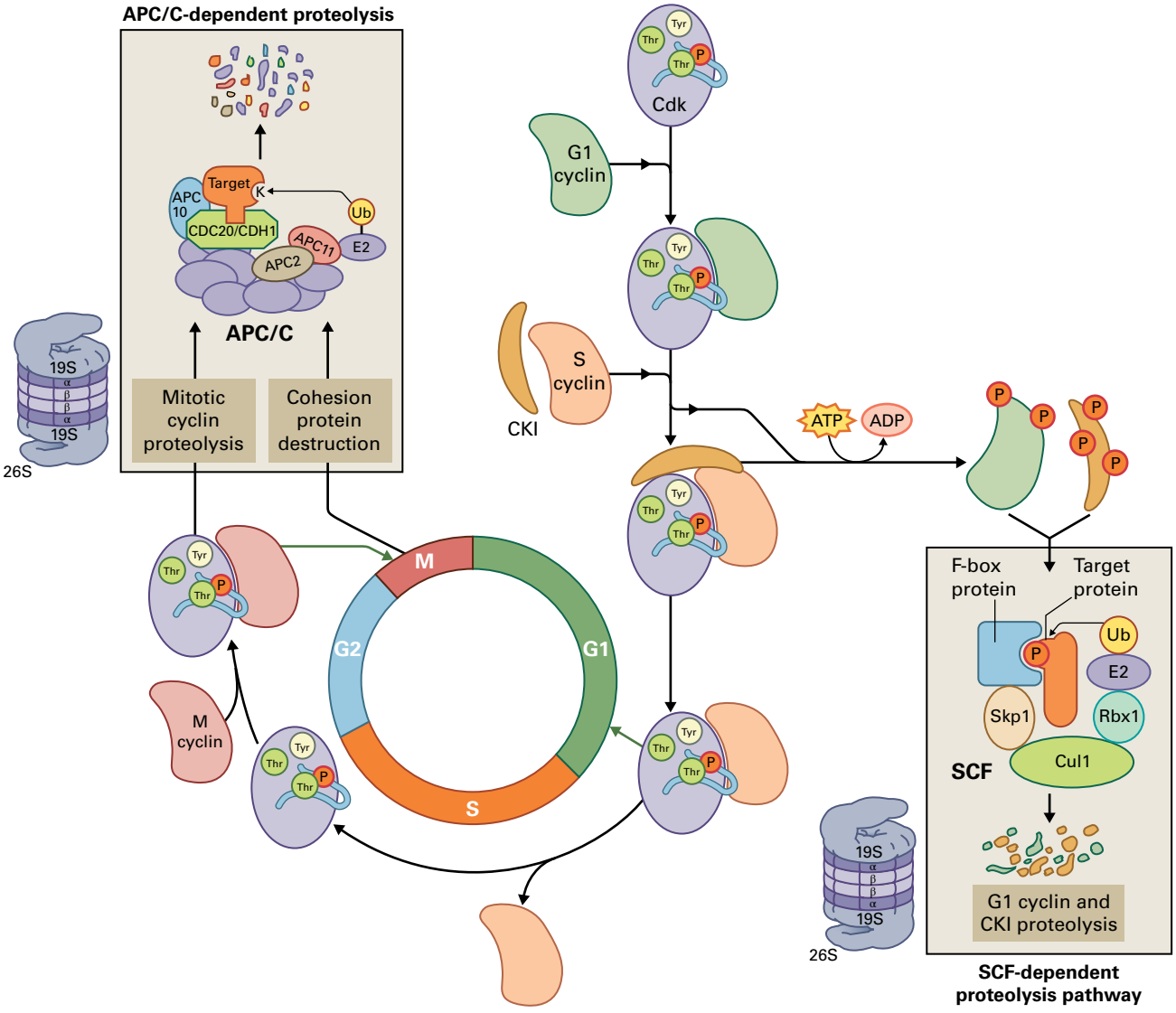


FIGURE 11.15 *Protein degradation is instrumental in controlling cell cycle progression at two major transitions. At the G1-to-S transition, two types of cell cycle proteins are substrates for regulatory proteolysis: CKIs, which bind to S-phase cyclin – CDK complexes and prevent CDK activity, and G1 cyclins, which must be degraded to commit the cell irreversibly to the start of a new cycle. CKIs and G1 cyclins are targeted by Skp1-Cullin-F-box (SCF)-type of E3 ligases for degradation in the proteasome. At the metaphase-to-anaphase transition, anaphase-promoting complex/cyclosome (APC/C) complex-controlled proteolysis degrades mitotic cyclins and severs the links between sister chromatids to permit chromosome segregation. SCF-type E3 ligases contain three core subunits, the RING protein Rbx1, a cullin (Cul) protein, and an F-box substrate receptor. The cullin protein functions as a scaffold by bringing together the catalytic module (RBX1 and the E2 enzyme) and the substrate receptors. Recognition by SCF often requires substrate phosphorylation, which creates a signal for interaction between substrate and the SCF complex. The APC/C is the largest and most complex E3 ligase known so far and contains at least 12 subunits. The APC/C requires WD40 activator proteins (CDC20/FZ and CCS52/FZR) and most likely also the APC10 subunit to recruit its substrates and target them for degradation by the proteasome. The RING-H2 finger subunit APC11 interacts with an E2 enzyme to stimulate the ubiquitination reaction. APC/C substrates carry different degradation motifs (degrons), including the well-known destruction box (D-box).*

11.4 The cell cycle in action

11.4.1 Control of the G1-to-S transition by the RBR/E2F pathway

In mammals, G1-to-S entry is initiated by the synthesis of D-type cyclins after mitogenic stimulation by serum growth factors. When complexed with specific CDKs, D-type cyclins initiate phosphorylation of the retinoblastoma (RB) tumor suppressor protein, which negatively regulates cell proliferation through association with members of the E2F transcription factor family (Fig. 11.16).

E2F transcription factors are required for transcriptional activation of genes encoding proteins that are essential during DNA replication. Thus, E2F transcription factors are critical effectors of the decision to pass the G1-to-S restriction point and allow cells to proceed into S phase. When RB binds an

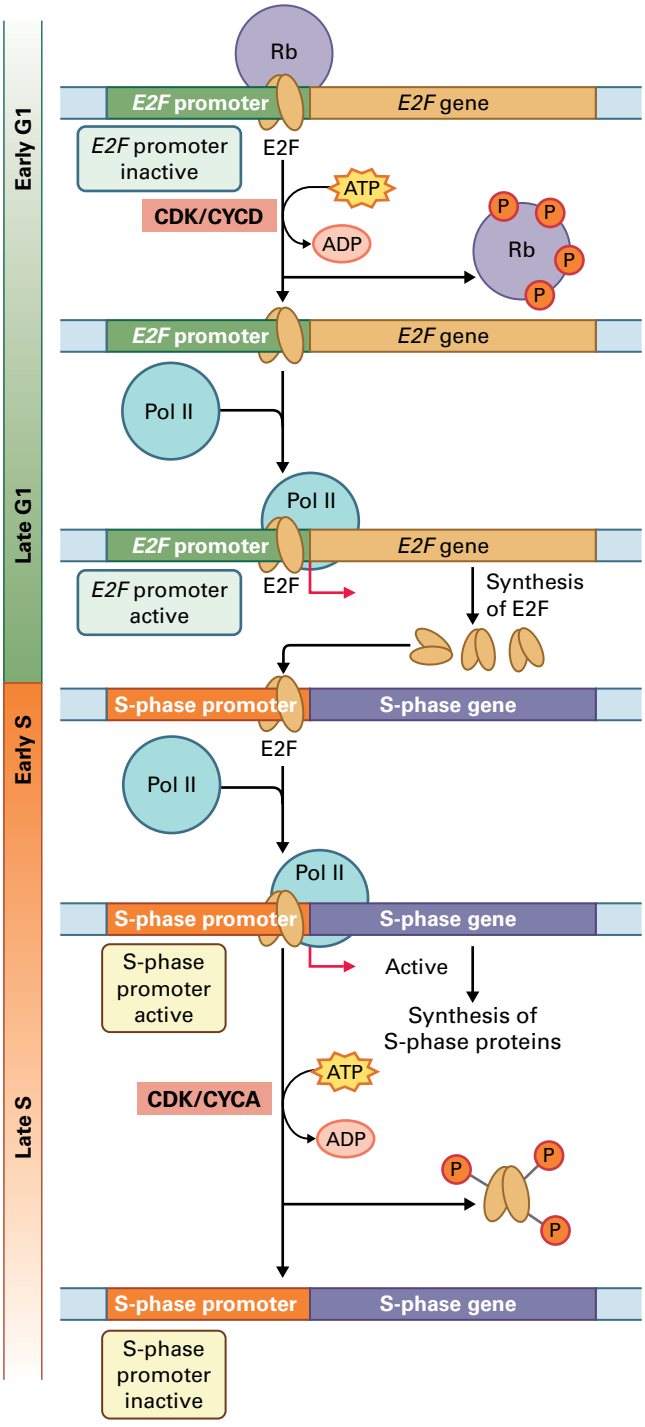


FIGURE 11.16 *E2F transcription factor activation at the G1-to-S transition enforces the commitment to S phase. The E2F transcription factor activates its own transcription by binding to a site in its own promoter. In G1, E2F activity is suppressed by binding the retinoblastoma protein (RB). As a consequence of passage through the restriction point, the CDK/CYCD complex phosphorylates RB, resulting in its dissociation from E2F and relieving the inhibition of E2F. This activates E2F transcription, resulting in a positive-feedback loop that leads to accumulation of large amounts of E2F protein as well as other S-phase-specific proteins and subsequent transcription of S-phase-specific genes by RNA polymerase II (Pol II). Phosphorylation of E2F by the CDK–CYCA complex then inactivates E2F-dependent S-phase transcription.*

E2F transcription factor, it inactivates it by masking its transcriptional activation domain. Moreover, under certain conditions, RB stimulates the recruitment of DNA-modifying proteins that can repress the promoter activity of E2F target genes by inducing chromatin condensation. RB phosphorylation by CDK–CYCD complexes counteracts the inhibitory function of RB, thereby releasing transcriptionally active E2Fs and, consequently, initiating DNA replication. By this mechanism, RB proteins enforce the decision to proliferate and activate the cell cycle-dependent transcription of genes that encode the DNA synthesis machinery at the G1-to-S transition.

Despite the 1.5 billion years of evolution that separates mammals from plants, both types of organisms use the same RB/E2F pathway to control the G1-to-S transition. Even the canonical DNA *cis*-acting element (TTTCCCGC) recognized by the E2F transcription factors within the promoter region of the E2F target genes is identical. *Arabidopsis* encodes one RB-related gene (*RBR*) and three E2F transcription factors (E2Fa, E2Fb, and E2Fc), which can be classified into two groups. The domain organization of all E2Fs is similar and is characterized by a single, conserved DNA-binding domain, followed by a DP dimerization domain (Fig. 11.17A). Dimerization of the E2Fs with the DP proteins, which contribute a second DNA-binding domain, is a prerequisite for tight sequence-specific binding to the promoter regions of E2F-responsive genes. Both E2Fa and E2Fb possess a transcriptional activation domain and, correspondingly, have been demonstrated to induce cell proliferation upon their overexpression. By contrast, E2Fc lacks a clear activation domain and operates as a negative regulator of E2F-responsive genes, thereby forming a second class within the family of E2F transcription factors. *E2Fc* overexpression inhibits cell division, whereas plants without functional E2Fc show increased proliferative activity.

As in animals, RBR is phosphorylated in a cell cycle phase-dependent manner by CDKs in complex with D-type cyclins; this phosphorylation probably inactivates RBR and subsequently releases activating E2F-DP transcription factors. Simultaneously, CDK-mediated phosphorylation of E2Fc targets E2Fc for destruction in an SCF-dependent manner. Combined, these two events induce expression of genes encoding proteins involved in DNA replication, such as nucleotide biosynthetic enzymes (e.g., ribonucleotide-diphosphate reductase and thymidine kinase) and replication factors (such as DNA polymerases and PCNA).

Upon completion of the *Arabidopsis* genome sequencing project, a new class of E2F-related proteins was discovered that binds E2F target genes in a DP-independent manner through a duplicated DNA-binding domain (Fig. 11.17A). These atypical E2F proteins were first described in *Arabidopsis* as DP-E2F-like (DEL) proteins, but they are also known as E2Fd-E2Ff. Because they lack a transcriptional activation domain, they are postulated to act as repressors and might play a role in a negative feedback loop to repress E2F-activated promoters. Until now, no role for DEL proteins in the timing of S-phase onset has been described. Rather, results obtained

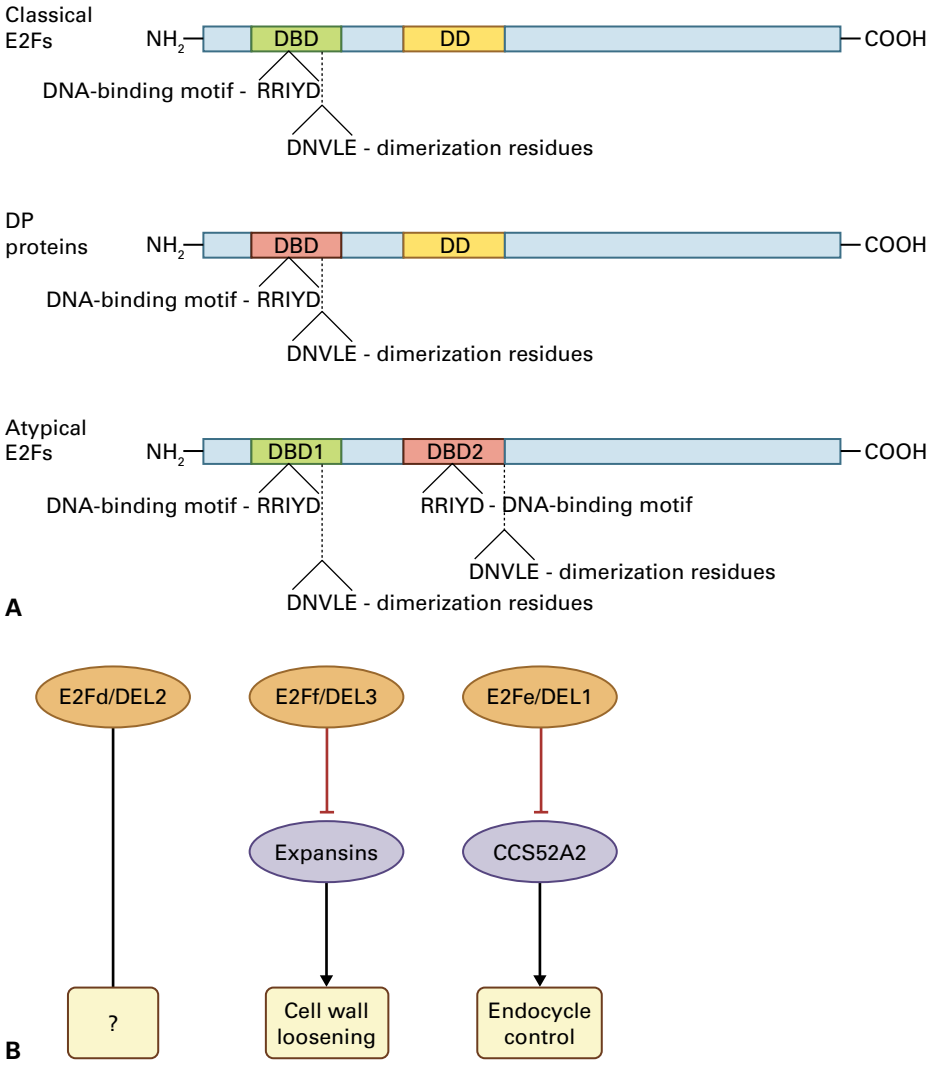


FIGURE 11.17 *Typical and atypical E2F transcription factors. (A) Structural differences between typical and atypical E2F proteins. E2F proteins and the related DP proteins have both a DNA-binding domain (DBD) and a dimerization domain (DD). Atypical E2F proteins have two DBDs and no DD. Atypical E2Fs must dimerize with a DP protein to bind DNA, but the two DBDs enable atypical E2Fs to bind DNA as monomers. (B) Overview of identified biological roles of atypical E2F proteins in* Arabidopsis. *The observed cell elongation and upregulated expression of expansin genes in* E2Ff/DEL3 *loss-of-function mutant plants suggest the atypical E2Ff transcription factor functions in the control of cell wall loosening.* E2Fe/DEL1 *expression controls the onset of DNA endoreplication through the transcriptional regulation of* CCS52A2, *which encodes an APC/C activator protein implicated in the regulation of DNA endoreplication. E2Fd/DEL2 could, therefore, control the balance between cell proliferation and differentiation, but the underlying molecular mechanism is still unknown.*

with knockout lines suggest a function in the coordination between cell division and post-mitotic cell differentiation. DEL3 operates as an inhibitor of cell elongation in dividing cells by transcriptional repression of cell wall-modifying enzymes (such as expansins), whereas DEL1 prevents dividing cells from entering the endocycle prematurely (see below) (Fig. 11.17B). After their initial discovery in plants, DEL-related proteins were found in animals, where they play an important role in the coordination between cell proliferation and apoptosis.

RBR also plays an important role outside the cell cycle. Equally important as the control of cell cycle entry for normal plant development are the restraint mechanisms that prevent precocious activation of cell division. RBR is required for cell differentiation of both male and female gametophytes. In case of embryo development, the central cell of the embryo sac must be kept in a quiescent state until fertilization has occurred, and chromatin remodeling seems to be an important control mechanism in this process. RBR and RBR-binding proteins of the polycomb group, such as FERTILIZATION INDEPENDENT SEED (FIS) and MULTICOPY SUPPRESSOR OF IRA1 (MSI1), form a multiprotein complex that is essential for inducing formation of the heterochromatin that probably silences expression of cell cycle genes. In *RBR1* knockout lines of *Arabidopsis*, this heterochromatin is not formed, resulting in mitotic divisions in the unfertilized egg cell and autonomous endosperm development, with sterility as a consequence. Likewise, RBR-mediated

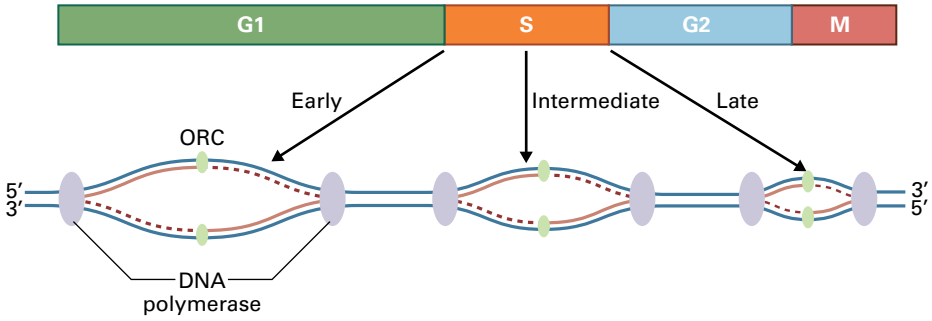


FIGURE 11.18 *The origin of recognition complex (ORC) is a landmark that instructs the cell where to initiate DNA replication. The ORC also serves as a docking point for replication proteins. Individual origins initiate replication at different times during S phase (early, middle, and late origins). This model for replication of discrete origins was developed from electron microscopy data. Dotted lines represent lagging DNA strands.*

chromatin modeling might dictate the differentiation status of cells, as indicated by the observed delay in cell differentiation in RBR-deficient cells.

11.4.2 Many proteins are involved in controlling S-phase progression

Most of the progress in the field of DNA replication has been made by combining the knowledge obtained by genetic experiments in yeast and biochemical data resulting from work in frog oocytes. Replication is initiated at multiple origins along DNA by a conserved mechanism that consists of four steps: origin recognition, assembly of a **prereplication complex** (preRC), activation of the helicase, and loading of the replication machinery, also referred to as the **replisome**.

Origins of DNA replication are sites in the genome where replication begins. Except for budding yeast, origins of replication are not defined by primary DNA sequences, but by a unique structure dictated by epigenetic determinants. Usually, replication starts at an origin and proceeds bidirectionally, making two Y-shaped DNA structures, called **replication forks**. Eventually, the replicons fuse, resulting in complete genomic duplication. Not all origins initiate DNA synthesis simultaneously at the beginning of S phase; DNA synthesis is initiated throughout S phase. Therefore, origins of DNA replication are classified into early, intermediate, and late types (Fig. 11.18).

Many proteins interact directly and indirectly with the origins of replication to control progression through S phase. DNA replication begins with the assembly of a preRC, which consists of many different proteins (Fig. 11.19). First, an **origin recognition complex** (ORC) binds to DNA in newly replicated chromatin during the S to early G1 phases of the cell cycle. The ORC is a six-protein complex containing ORC1 to ORC6 proteins in equal stoichiometry, and its binding provides a docking platform for additional replication proteins, including the CELL DIVISION CYCLE 6 (CDC6) and CHROMATIN LICENSING AND DNA REPLICATION FACTOR 1 (CDT1). During G1, the CDC6 and CDT1 proteins load the **MINICHROMOSOME MAINTENANCE helicase** (MCM) onto the ORC to complete the preRC. MCM

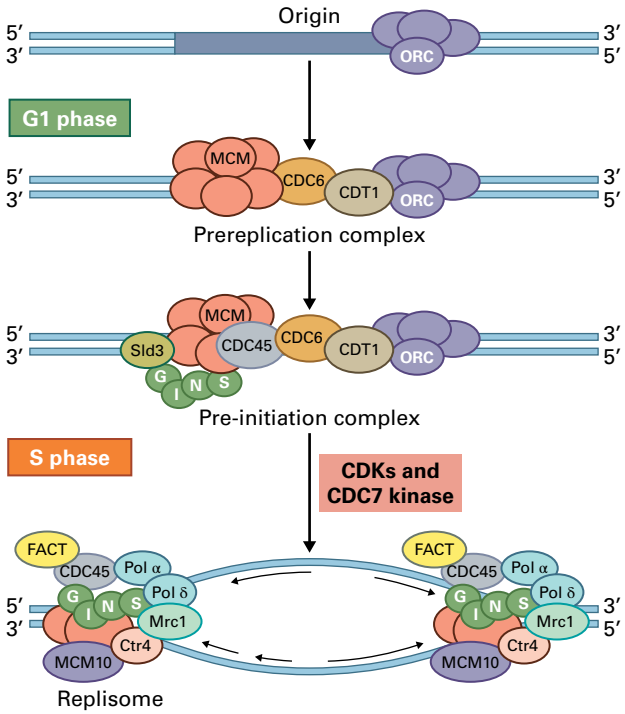


FIGURE 11.19 *Stepwise assembly of the prereplication complex. The ORC is a complex of six proteins, and its binding to DNA provides a docking platform for additional proteins. To prevent premature DNA replication, the proteins that associate with the ORC are assembled in steps. CDC6 and CDT1 proteins bind first, followed by MCM proteins and the CDC45 protein, forming the prereplication complex. The prereplication complex is activated by protein phosphorylation (by CDKs and CDC7 kinase), which commits the cell to a round of cell division, defining the start of S phase. Phosphorylation of MCMs and the GINS complex loads the replisome complex with several other replication proteins including the DNA polymerases, and establishes the replication fork. Subsequent phosphorylation of CDC6 and other origin-binding proteins results in their destruction and ensures that the origins of replication are only activated once in each cell cycle.*

proteins, a family of six related and essential proteins, assemble into a large doughnut-shaped complex around the DNA helix, which unravels the DNA at the replication origin and then travels along the DNA with the rest of the replication machinery, unwinding the DNA at the replication forks.

Loading of the MCM helicase onto the DNA is referred to as **DNA replication licensing** to indicate that chromatin-bound MCM proteins give the cell a license for one round of DNA replication.

The actual onset of DNA replication is regulated by the recruitment of the replisome to the origins of replication. The CDC45 protein and a large number of other proteins (e.g., the four-subunit GINS complex, Sld2, and Sld3) are needed for loading of the replisome. The large multiprotein complex that is created at this step is designated the **pre-initiation complex** (preIC), and it opens the DNA helix, stabilizes the formed single-stranded DNA, and allows enzymes (including DNA polymerases) to copy the DNA. Helicase activation and replisome loading are coupled events, ensuring coordinated replication. By a lack of coordination, the helicase might produce unreplicated single-stranded DNA at the fork, which occurs when DNA replication is blocked.

Many other proteins are needed to establish conditions favorable for DNA replication, but they do not regulate DNA replication itself. For example, the biochemical pathways required to synthesize the nucleotide triphosphates used during DNA synthesis are stimulated just before the onset of S phase. During replication, chromosomal DNA remains organized in chromatin, a complex composed largely of histone proteins. Therefore, a substantial amount of new histones must be synthesized in S phase. Histone gene expression and protein accumulation are strongly stimulated in early S phase (Fig. 11.20).

Little is known about how plant replicons are regulated. It is likely, however, that the process of DNA replication is conserved in plants, as evidenced by the presence of genes homologous to most of the key players involved in preRC and preIC formation (e.g., MCMs, ORCs, CDC6, CDC45, and CDT1). Moreover, the embryo- and gametophyte-lethal phenotypes of mutations in genes such as *MCM7* and *CDC45* illustrate their importance in the plant DNA replication cycle.

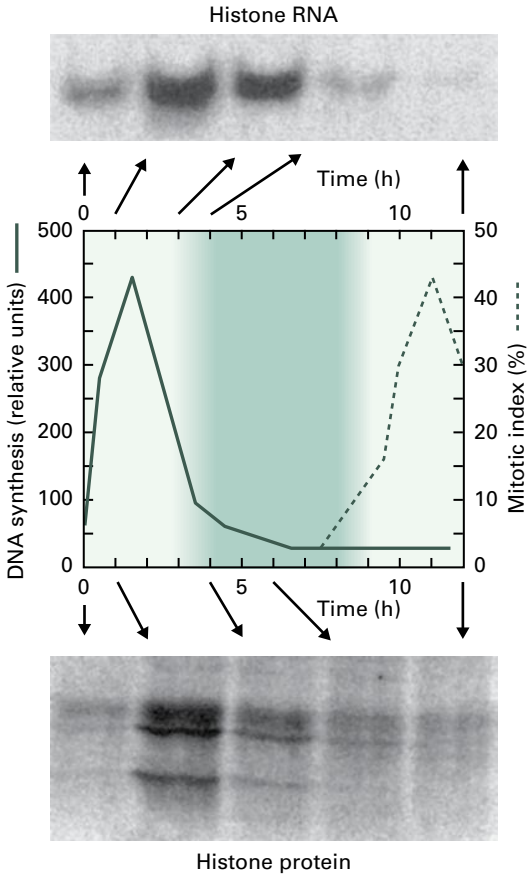


FIGURE 11.20 *Histone expression is regulated by the cell cycle. Histones are basic proteins involved in organizing chromatin structure. During S phase, the cellular content of histones must be doubled to assemble with the newly replicated DNA. Therefore, the synthesis of histone-specific RNA (top) and the accumulation of histones (bottom) is strongly stimulated in S phase (0–4 hours in this experiment) but not in M phase (8–12 hours). The activity of cell cycle phase-specific transcription factors is responsible for this peak of histone mRNA accumulation.*
Source: Adapted from Reichheld et at. (1998). Nucleic Acids Res. 26:3255–3262.

11.4.3 DNA replication is strictly controlled during the cell cycle

Initiation of DNA synthesis is inhibited during G2, M, and G1 phases, and this avoids two major types of cell cycle errors. DNA synthesis in G2 and early M would lead to a change in **ploidy** (DNA content and genome copy number) and interfere with chromosome segregation, and DNA synthesis in anaphase, telophase, or G1 would not be coupled to cell growth. The "once-and-only-once" nature of DNA replication is achieved through a temporal separation between the formation of the preRC and preIC.

Although DNA replication is restricted to S phase, assembly of the protein complexes that mediate initiation of DNA synthesis is promoted at late M and early G1 phases. The chromosomal cycle starts at the transition from metaphase to anaphase, which is accompanied by the activation of the APC/C. The APC/C facilitates the destruction of the mitotic cyclins, causing a dramatic decrease in CDK activity. This reduced activity allows CDC6, which is otherwise marked by CDK-mediated phosphorylation for protein destruction, to accumulate and interact with ORCs. Thus, CDC6–ORC complexes can form only after M phase is complete and before S phase begins (Fig. 11.19).

In late G1 phase, the cell decides whether to proceed with proliferation at the **restriction point** (or START in the budding yeast cell cycle). Once the cell has passed this point in the cell cycle, it is committed to S phase. Although replication origins are competent to initiate DNA synthesis at this time, cells are not able to enter S phase before expression of S-phase genes (such as histone genes) has been stimulated. S phase is then initiated when primed preRCs are activated by phosphorylation, which requires the collaborative action of CDKs and the Dbf4-dependent kinase (DDK4).

DDK4 is a heteromeric protein kinase complex that consists of a catalytic CDC7 subunit and regulatory DBF4 subunit.

It is tethered to origins of replication and is activated at the beginning of S phase. DDK4 phosphorylates the MCM2–MCM7 complex, which is thought to cause a conformational change in the MCM5 protein. This triggers the DNA unwinding activity of the MCM complex and signals to preIC proteins to bind, including the CDC45 protein and GINS complex. The GINS complex is phosphorylated by CDKs and together with CDC45 binds the DNA polymerase B subunit. The GINS–CDC45–DNA polymerase B subunit complex then binds chromatin and recruits the replisome, resulting in the start of DNA replication. MCM phosphorylation thus appears to be a key event in switching preRCs to the replicative state. Simultaneously, CDK-dependent phosphorylation of CDC6 and other replication proteins target these proteins for destruction. This ensures the initiated origins of replication cannot be reactivated a second time and the DNA is copied only once.

Thus, replication of nuclear DNA in S phase is the critical event of the chromosomal cycle, but it depends entirely on the cell acquiring competence during the M and G1 phases to initiate replication later in S phase. Although DNA synthesis remains inhibited during M and G1 phases, assembly of the protein complexes that mediate the initiation of DNA synthesis is promoted. In contrast, DNA synthesis is promoted during S phase, while assembly of the protein complexes that facilitate the initiation of DNA synthesis is inhibited.

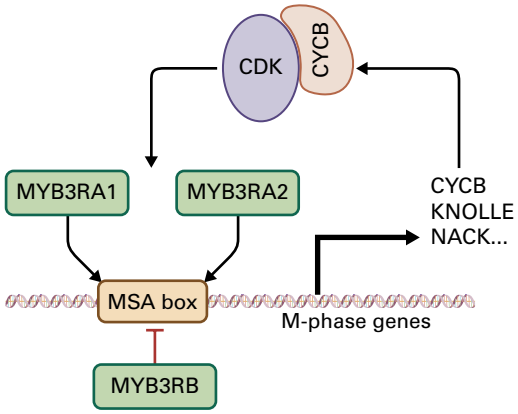


FIGURE 11.21 *Binding of MYB3R proteins to the M-specific activator (MSA) element. The MSA element is necessary and sufficient for the G2-to-M-specific transcriptional activation of M-phase genes. In tobacco, three MYB3R proteins are structurally related to animal c-Myb proteins. Whereas the MYB3RA1 and MYB3RA2 genes display a cell cycle phase-dependent transcription profile, levels of MYB3RB remain constant during the cell cycle, and MYB3RB cannot activate MSA-containing promoters. The extent of transcriptional activation of MSA-containing promoters by MYB3RA2 depends on the cell cycle phase and on its C-terminal domain, which is a target for CDK phosphorylation. This implies feedback mechanisms in which the cyclins induced by the MYB3R proteins form a complex with CDKs that activates MYB3R activity. Likewise, controlled proteolysis of cyclins might result in rapid inactivation of MYB3R proteins. Both mechanisms may account for the observed sharp peak of mitosis-specific cyclins during the cell cycle. This feedback mechanism is strengthened by MSA elements in the promoters of MYB3R transcription factors. The initial trigger for transcriptional activation of MYB3RA1 and MYB3RA2 remains unknown.*

11.4.4 Multiple regulatory factors are required for the G2-to-M transition

Once DNA replication is complete, synthesis of the M-phase cyclins in late G2 prepares the cell for mitosis. The rapid increase in mitotic CDK activity at the G2-to-M transition initiates mitosis and, subsequently, cytokinesis, beginning with chromosome condensation and alignment of the chromosomes at the metaphase plate. In mammals, the G2-to-M transition is specifically regulated by CDKs that associate with A- and B-type cyclins. In plants, the CDKs that regulate the G2-to-M transition are probably CDKA and CDKB, as both are active at this transition point. On the basis of their peak of transcription during the G2 and M phases, both A- and B-type cyclins are probably responsible for the mitotic events.

Plant B-type CDKs and other genes expressed during mitosis (such as KNOLLE and the kinesin NACK) contain a common *cis*-acting element, the **MSA element**, which is necessary and sufficient to direct G2-to-M-specific gene expression. The MSA element binds two types of MYB3R transcription factors, which are structurally related to animal c-Myb proteins: *MYB3RA*, which displays a cell cycle phase-dependent transcription profile, and *MYB3RB*, the levels of which remain constant during the cell cycle. The MYB3RB protein cannot activate MSA element-containing promoters. A model has been proposed in which MYB3RA and MYB3RB proteins antagonistically control the expression of the G2-to-M-specific genes (Fig. 11.21). Interestingly, the activity of the MYB3Rs is stimulated by their phosphorylation by CDKs. The cyclins induced by MYB3R proteins form a complex with CDKs that hyperactivates MYB3R activity, and this probably contributes to the sharp peak of mitosis-specific genes during the cell cycle. This positive feedback mechanism is strengthened by the presence of MSA elements in the promoter of the *MYB3R* genes. The trigger of initial transcriptional activation of *MYB3RA* remains unknown.

11.4.5 How does a cell become competent for mitosis?

Most of our understanding of the molecules involved in organizing mitosis is drawn from genetic experiments with animal cells and yeast. Although little is known about the nature and regulation of the molecules involved in mitosis in plants, current experimental evidence hints at similarities.

As discussed above, mitosis is suppressed during G1, S, and G2 phases, and the stepwise process that promotes mitosis is initiated in S phase. Mitosis commences with the initiation of chromosome condensation and disassembly of

the nuclear envelope that separates the nuclear matrix from the cytoplasm (Fig. 11.22). This is often referred to as the onset of the M phase, but the cells are not yet competent for chromosome segregation. Full competence for separation of the duplicated DNA is achieved only when condensed chromosomes are aligned along a plane in the center of the cell, with each chromosome comprising two **chromatids** that, although attached to each other, are connected by microtubules to opposite ends of the cell. Chromosome segregation is then initiated when the link between sister chromatids is severed.

Several different classes of molecules are involved in establishing the full competence for mitosis. Proliferating cells synthesize proteins collectively called condensins and cohesins, which are essential for assembling the long chromatin fibers into chromosomes and thereby permit the replicated DNA to be segregated without damage. The molecular details of how chromosome condensation and cohesion are achieved have been discovered mainly in yeast. Cohesion proteins such as SMC1, SMC3, and SCC1 are synthesized during S phase. These proteins interact with both sister chromatids (daughter strands) of a chromosome to establish and maintain their tight linkage until anaphase. Cohesion occurs at both centromeres, where it plays an essential role during chromosome segregation during mitosis and meiosis. Cohesion also locates along the chromosomes, enabling higher order chromosome dynamics and recombination between sister chromatids in response to DNA damage. Plants also have cohesins and condensins, and their inactivation causes a premature arrest in embryo development.

Condensation of chromosomes compacts the chromatids into short, rod-like structures to facilitate their separation during mitosis and meiosis. Condensing chromosomes are assembled around a central axis of scaffold proteins, presumably arrays of cohesin and condensin molecules that bind to long loops of DNA. During the early steps of chromosome

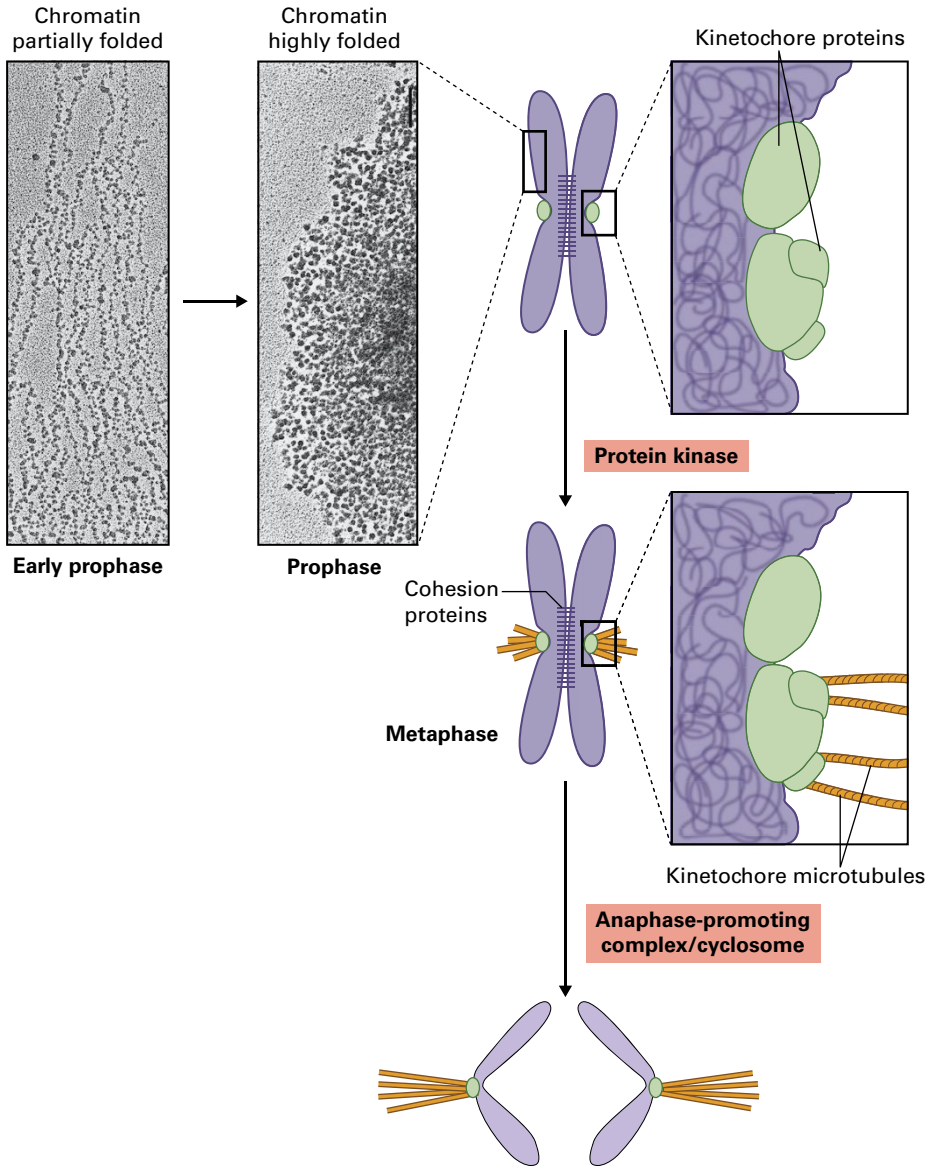


FIGURE 11.22 *Chromosome condensation and the kinetochore complex. In its unpackaged state, the long, fragile DNA molecule would be sheared into pieces during chromosome aggregation and segregation. DNA is packaged into higher order chromatin structures by winding around histones. The chromatin, however, which provides access to transcription factors and RNA polymerase to allow gene expression, is still too diffuse to permit segregation of sister chromosomes in mitosis. Further condensation and disentangling of chromosomes occur in prophase to prepare for chromosome segregation (see photos). The kinetochores are protein complexes that bind to centromeres and serve as attachment points for the spindle microtubules that pull apart the sister chromatids to opposite cell poles. The APC/C, which is activated by protein phosphorylation, tags the mitosis inhibitor securin for proteolysis. This ultimately leads to the destruction of the cohesion proteins that join sister chromatids and results in chromatid separation during anaphase. Source*: Photographs: Sitte et al. (1998). Strasburger Lehrbuch der Botanik, 34th ed. Gustav Fischer Verlag.

condensation, the two sister chromatids condense into one large cylinder. Upon further condensation in late prophase and early metaphase, topoisomerases introduce supercoils into the DNA helix. The supercoils increase the packing density of DNA even further and, at this point, the sister chromatids are distinguishable by light microscopy. The chromosome structure at this phase exposes the cohesins to regulatory factors that break the linkage between sister chromatids in anaphase. Throughout this process, inhibitory proteins such as securin begin to accumulate, and they safeguard against precocious entry into mitosis. Securin binds to and antagonizes the separase protein, which breaks the linkage between sister chromatids and triggers chromosome separation at the onset of anaphase. Genetic analysis in yeast indicates securin must bind to separase for correct targeting to the site where it acts in late metaphase. Thus, securin binding simultaneously suppresses premature activation of separase and ensures its correct localization. Based on sequence similarity, no clear ortholog for securin can be found in plants; however, the separase AESP is required for cohesin removal from meiotic chromosomes and is essential for embryo development.

A second large complex, the kinetochore, attaches to the centromeres of chromosomes. The microtubule network, which is ultimately responsible for congregation of the chromosomes along the metaphase plate and their subsequent movement toward the cell poles, binds to the kinetochores (Fig. 11.22). Kinetochore assembly is coupled with the completion of DNA replication. The molecular composition of the plant kinetochore complex is still poorly understood.

11.4.6 Proteases regulate the initiation of chromosome separation and M-phase exit

The capacity of the cell to undergo ordered mitosis is established during S phase and continues until mitosis is complete. Ordered mitosis begins with insertion of cohesins into the newly replicated helices and removal of catenations that would preclude chromosome separation. Once chromosomes are disentangled and condensed, they are fully competent for segregation. The cell, however, is not competent for mitosis until the sister chromatids are aligned along its equator. Cells at this time also monitor whether the kinetochores of paired chromatids are attached to the opposite cell poles. To prevent premature sister chromatid separation while these processes are in progress, segregation is suppressed during metaphase by inhibition of separase (see above). At the end of metaphase, the protein complexes required for chromosome separation are fully poised, in a state analogous to the primed prereplication complex at the G1-to-S transition.

The metaphase-to-anaphase transition is activated by CDK-mediated phosphorylation of the APC/C, which in turn results in the ubiquitination of securin. Ubiquitinated securin is recognized by the 26S proteasome as a substrate and is degraded. This activates separase, which breaks the cohesin-established linkages between sister chromatids. Once these bonds are broken, the mechanical forces generated by motor proteins along the kinetochore microtubules draw each "sister" of the formerly paired chromatids to opposite ends of the cell (Fig. 11.22). Activated APC/C also causes destruction of mitotic cyclins, marking the exit from mitosis. Simultaneously, the decline in mitotic CDK activity relieves the repression of the G1 cyclin synthesis, allowing accumulation of A-type cyclins, which had been suppressed from S phase through telophase. Thus, G1 CDK activity can gradually increase, allowing assembly of new replication complexes and maintaining APC/C activity to prevent any residual mitotic CDK activity.

11.4.7 Checkpoint controls are activated by DNA damage or incomplete cell cycle events

Cell proliferation often occurs under unfavorable conditions. Consequently, cells may incur DNA damage or may lag in completing DNA synthesis or in attaching chromosomes to the spindle apparatus. All cells are capable of restoring normal cell cycle activities using special repair mechanisms, but cell cycle progression must be arrested to prevent the damage from progressing to a **mitotic catastrophe**. When damage occurs, cell cycle progression is arrested at a checkpoint. Three major types of checkpoints have been discovered: arrest at a checkpoint can occur prior to the restriction point at the G1-to-S transition, prior to the S-to-M transition that couples mitosis to the completion of DNA synthesis, or prior to sister chromatid separation, at either the G2-to-M or the metaphase-to-anaphase transition. Each of these three checkpoints immediately precedes a committing event that is irreversible (Fig. 11.23).

Although it is still largely unknown how plants control the checkpoints during mitosis, there is clear evidence that the replication-associated checkpoints are partly conserved between animals and plants. When DNA is damaged, two important global cellular responses are needed for survival of the cells: activation of the DNA repair machinery and delay, or even arrest, of the cell cycle progression. This coordinated action ensures that cells repair their damaged DNA before they proceed into mitosis. At the crossroads of both pathways, two related kinases are found, the **ATAXIA TELANGIECTASIA MUTATED** (ATM) and **ATM AND RAD3-RELATED** (ATR) proteins. These proteins are highly conserved and are triggered in response to different types of DNA stress: double-strand breaks (DSBs) activate ATM, whereas ATR primarily responds to single-strand breaks or stalled replication forks. Mutations in *ATM* or *ATR* render organisms hypersensitive to DNA damage-inflicting agents. In plants, the *atm* mutants show growth defects when treated with γ-rays (Fig. 11.24A) or DSB-causing methyl methanesulfonate. By contrast, the *atr* mutants primarily exhibit hypersensitivity to drugs (such as hydroxyurea and aphidicolin) that inhibit the progression of the replication fork (Fig. 11.24B).

FIGURE 11.23 *Checkpoint controls monitor the state of the cell during the cell cycle. If serious DNA damage has been incurred or any biosynthetic process is incomplete, progression of the cell cycle is arrested before any irreversible, committing steps are taken. Checkpoint controls are active before the cell cycle reaches START (in budding yeast) or the restriction point (its equivalent in animals), as well as at the metaphase-to-anaphase transition (in yeast and animals) and at the G2-to-M transition (in animals).*

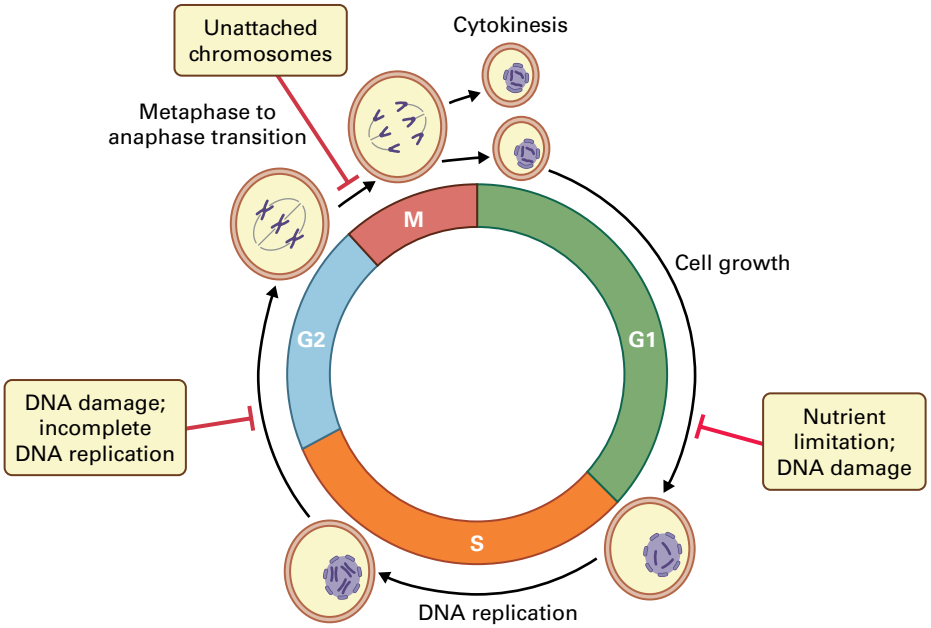
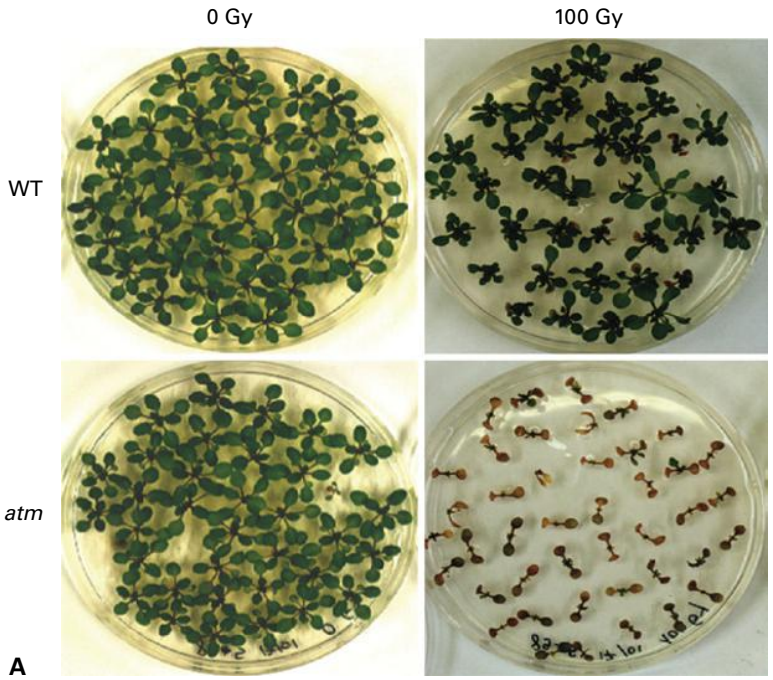
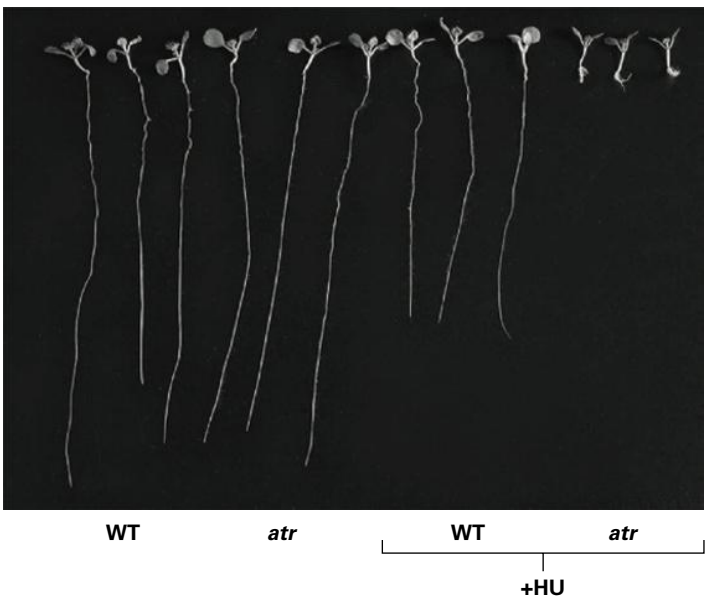


FIGURE 11.24 *Hypersensitivity of* ATM *mutant plants to treatments that induce double-strand breaks, such as irradiation with γ-rays. (A) Five-day-old wild-type (WT) and atm1 mutant seedlings were either left untreated (0 Gray units, Gy) or subjected to 100 Gy of irradiation. Photographs were taken 21 days after irradiation. The growth of wild-type plants resumes (top right), whereas that of the mutant seedlings is arrested (bottom right). (B) Sensitivity of wild-type (WT) and atr mutant plants to replication-arresting agents, such as the nucleotide biosynthesis inhibitor hydroxyurea (HU). Seeds were germinated on control medium or medium supplemented with HU and grown for 3 weeks. Both the wild-type and* atr *mutants grow at similar rates on control plates (left). By contrast, on plates containing HU (right, +HU), wild-type root growth is reduced, whereas that of the* atr *is almost completely inhibited.*





DNA damage-induced cell cycle arrest is mediated by CDK inactivation. In animals, ATM and ATR signal the tumor suppressor protein p53 and the checkpoint kinases CHK1 and CHK2. Activation of these proteins induces the transcription of CKIs and inactivation of the CDC25 phosphatase, an essential timer of mitosis in nonplant species (see above). In plants, the mechanism by which the cell cycle is arrested in response to DNA damage must be in part different, because a functionally homologous *CDC25* gene is absent. Correspondingly, the counteracting WEE1 kinase, not CDC25, has been shown to arrest the plant cell cycle in times of DNA stress. *WEE1* expression is rapidly induced by DNA stress in an ATM- and ATR-dependent manner, resulting in the Tyr phosphorylation of CDKs and subsequent cell cycle arrest. Likely targets of WEE1 are the A-type CDKs and CAKs. Plants without a functional *WEE1* gene fail to arrest their cell cycle in response to replication defects, with a growth arrest as a consequence.

Currently, the plant signaling cascades that operate between ATM/ATR and WEE1 are unknown (Fig. 11.25). The signaling pathways through which ATM and ATR signal DNA stress to the cell cycle machinery must be different from those in mammals, because genes for p53 and functionally homologous CHK1/CHK2 kinases have not been identified in plant genomes. Instead, plants possess a plant-specific transcription factor named SOG1 that operates immediately downstream of ATM/ATR, suggesting the signaling pathways that activate cell cycle arrest upon DNA damage evolved differently in plants.

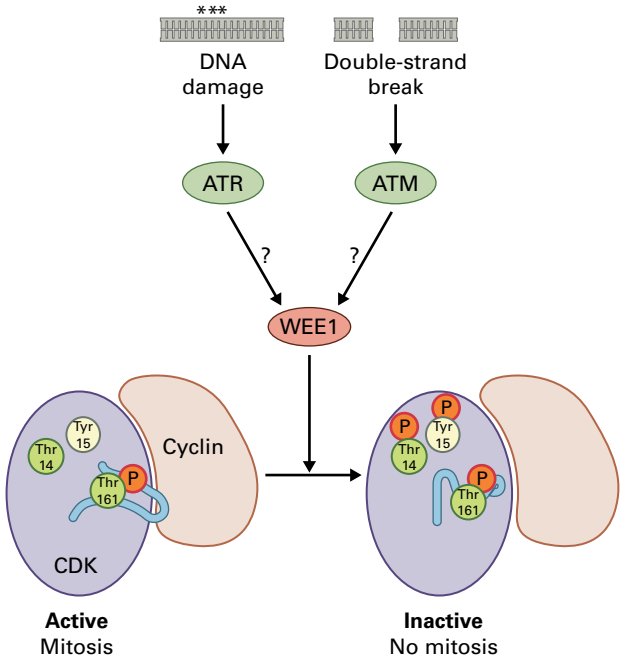


FIGURE 11.25 *ATR- and ATM-mediated signaling of single- and double-strand DNA breaks. Transcriptional induction of the* WEE1 *kinase gene occurs through an unknown pathway (indicated by question marks). WEE1 phosphorylates CDK–CYC complexes, resulting in their inhibition and preventing mitotic entry.*

WEE1 is likely not the only mediator of DNA damage checkpoint. In mammals, checkpoint activation involves transcriptional induction of the CKIs CIP/KIP, but for plants no obvious link between KRPs and DNA stress has been reported. In contrast, some *SMR* genes are strongly induced in an ATM-dependent manner by DNA stress, demonstrating their potential to operate as checkpoint regulators upon genotoxic stress.

11.5 Cell cycle control during development

11.5.1 Cell division is tightly controlled in shoot meristems and during organ formation

Plants, unlike animals, continue to develop after embryogenesis, and new organs and tissues can be formed throughout the entire life span. The tissues responsible for this growth strategy are the apical meristems situated at the tips of shoots (shoot apical meristem, SAM) and roots (root apical meristem, RAM) (see Fig. 11.2). In addition, the cambium is a specialized form of meristem that generates only vascular cells during secondary growth of tissues and is not involved in organogenesis. Lateral roots are generated de novo by the induction of cell division in selected root pericycle cells.

Organ formation in shoots occurs on the flanks of the SAM, where cell division activity is generally increased to produce the large number of required new cells (Fig. 11.26A). A slowly dividing population of self-renewing stem cells at the centers of the root- and shoot apical meristems is important not only for maintenance of the meristem, but for ensuring low cumulative mutation rates in long-lived plants such as bristlecone pines, in which meristems can function for millennia.

Several genes essential for SAM function have been identified by mutations that disrupt the structure of the SAM. They all display characteristic expression patterns in the SAM that develops gradually during embryogenesis. Genetic analysis of the SAM has allowed these genes to be grouped into three classes (Fig. 11.26B): one class of genes is required to establish and maintain the indeterminate central zone necessary for self-renewal of the meristem, and the second and third classes direct differentiation and regulated localized cell division in organ primordia, respectively. Mutations in genes of each of these classes affect all aspects of normal shoot meristem activity, indicating that the individual activities of domains in the meristem in which these genes are expressed are not autonomous.

The first class of genes is defined by several different homeodomain-type transcription factors required to establish and maintain meristems. The maize *KNOTTED* gene was the first gene of this type to be discovered. When *KNOTTED1*

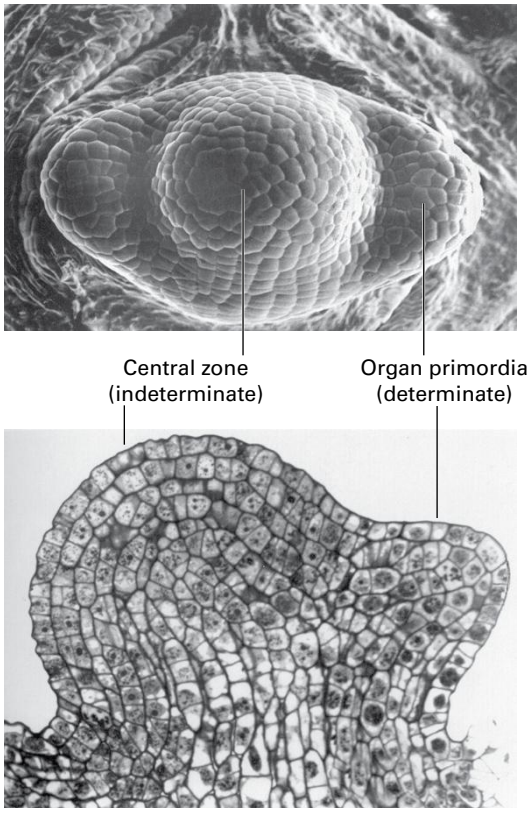


FIGURE 11.26 *Organization of the shoot apical meristem (SAM). (A) Two different views of a SAM. The top-down view reveals the incipient organ primordia on the periphery of the meristem. The longitudinal section shows the layered tissue organization of the SAM as well as a developing new organ. (B) Regulatory genes required for the establishment and maintenance of the SAM are expressed in specific domains. The* WUS *gene is expressed at the base of the meristem and is required for expression of the* STM *gene in a domain above it. The products of the* CLV1 *and* CLV3 *genes (receptor and ligand, respectively) presumably interact to determine the size of the indeterminate central zone of the meristem.*
Source: (A) Lyndon (1998). The Shoot Apical Meristem: Its Growth and Development. Cambridge University Press, Cambridge UK.

or the related *Arabidopsis* gene *KNAT1* is activated inappropriately, shoot meristems appear ectopically, for example, on leaves. Another *Arabidopsis* gene, *SHOOT MERISTEM-LESS* (*STM*), is necessary to maintain the capacity for self-renewal or indeterminate growth in the center of the meristem. In the absence of a functional *STM* gene, the SAM disappears and cells at its location differentiate. *STM* appears to keep the shoot meristem cells undifferentiated by promoting cytokinin biosynthesis (cytokinins promote cell division via *CYCD3* expression) and reducing levels of gibberellins. Another homeobox protein, WUSCHEL (WUS), is also required for meristem maintenance, and its production in a central cell population immediately below the apical layer is necessary for specifying stem cells. WUS represses several A-type *ARABIDOPSIS RESPONSE REGULATOR* (*ARR*) genes, which are negative regulators of cytokinin signaling (see Fig. 11.26 and Chapter 18).

Expression of *WUS* is also under the negative control of a second class of genes that promote differentiation in organ primordia. When these genes are disrupted by mutation, the meristem increases in size because cells fail to differentiate. In *Arabidopsis*, loss of *CLAVATA* (*CLV*) gene function results in extremely enlarged meristems and increased organ numbers. *CLV* encodes a receptor-like protein kinase and might function to process intercellular signals. *clv3* mutants have phenotypes very similar to those of *clv1* plants. *CLV3* codes for a short polypeptide that is the ligand for *CLV1*. Currently, little is known about how the various homeodomain proteins control cell cycle activity in the meristems.

Leaf organ primordia initially resemble needles, but they soon broaden in the plane of the future leaf blade. The third class of genes required for meristem function controls proliferation locally in the developing organ. The *PHANTASTICA* (*PHAN*) gene in *Antirrhinum majus* regulates cell proliferation along the upper (dorsal) lamina to generate the leaf blade. The phenotype associated with recessive mutations in this gene is a ventralized, radially symmetrical, needle-like leaf consisting of just the midrib. Furthermore, impaired leaf development in *phan* mutants suppresses proliferation and further organogenesis in the apex, indicating retrograde signaling from nascent organs is important for maintaining shoot meristem function. ASYMMETRIC LEAVES 1 is the *Arabidopsis* ortholog of PHAN.

11.5.2 Specific patterns of cell division might not be required for appropriate root cell speciation

In contrast to the apparently random arrangement of cells in shoot organ primordia, the root apex is highly structured, and tissues derived from the RAM are often organized into long, contiguous cell files. This organization results from an underlying pattern of cell division. The cell files appear to converge onto a central zone within the root apex, the **quiescent center** (QC), in which cells divide only infrequently (Fig. 11.27). The QC is a small group of cells that emit signals to surrounding cells that prevent them from differentiating.

The transcription factors SCARECROW (SCR) and SHORT ROOT (SHR) are crucial for specification of the QC.

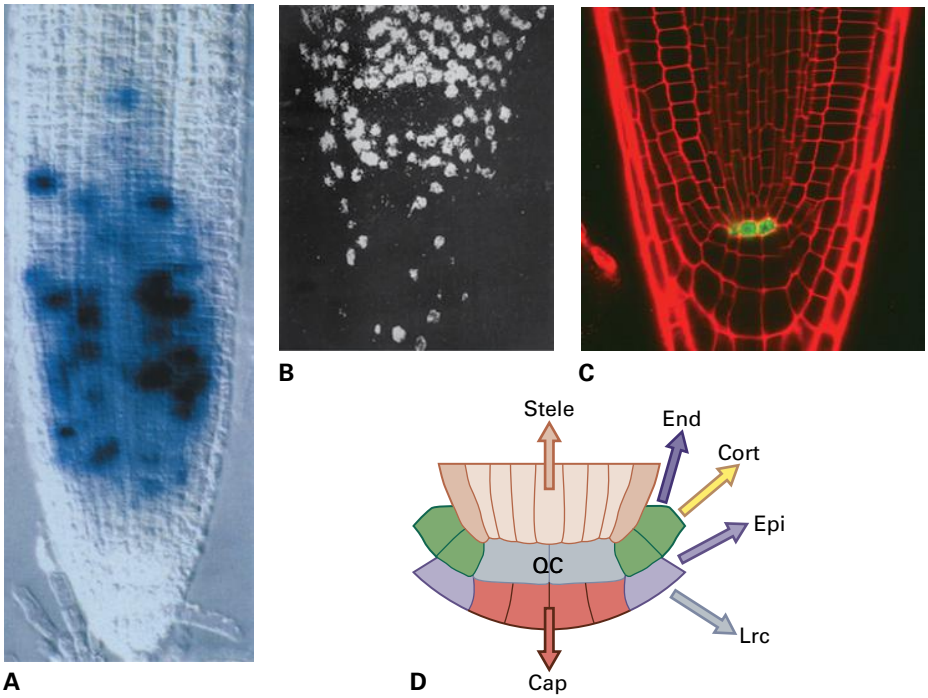


FIGURE 11.27 *Mitotic activities in the root apical meristem. (A) A longitudinal section through the root apex of* Arabidopsis*, as viewed by light microscopy. Patterns of mitotic activity are visualized by the activity of a CYCLIN–GUS fusion protein produced exclusively in mitotic cells. (B) Patterns of DNA synthesis in growing* Arabidopsis *roots. Roots were grown in a solution of radioactive thymidine, which was incorporated into the newly synthesized DNA. The longitudinal section was exposed to a photographic emulsion, and white spots represent cells with newly synthesized DNA. Reduced cell proliferation can be seen in the quiescent center (QC), the dark void in the center of the root. (C) A promoter:GFP reporter line highlighting cells of the root QC (green). (D) Organization of the root stem cell niche. Arrows indicate how stem cell division produces regular vertical files of cells. Above and around the QC are the stem cells for the root tissues: lateral root cap (Lrc, purple) and epidermis (Epi, purple), cortex (Cort, green) and endodermis (End, green), pericycle (dark brown) and vascular tissue (light brown). Below are the stem cells for the central portion of the root cap (pink).*
Source: (A) Colón-Carmona et al. (1999). Plant J. 20:503–508. (B) O'Brien & McCully (1969). Plant Structure and Development–A Pictoral and Physiological Approach. Macmillan, New York.

Mutations in *SCR* and *SHR* result in the inability to specify a QC in the root and, as a consequence, all stem cells are lost. Interestingly, QC function and its capacity to produce stem cells can be restored in an *SCR* mutant by reducing *RBR* expression levels. Also, in a wild-type background, local reduction of *RBR* increases the number of stem cells in the RAM, whereas its overproduction results in depletion of stem cells. Likewise, other elements of the RBR-E2F pathway have been found to control the size of the stem cell pool in the root meristem. These data suggest the RBR-E2F pathway operates downstream of SCR to determine the stem cell state of cells. SHR and SCR also regulate the spatiotemporal expression of a specific D-type cyclin involved in formative cell divisions.

The PLETHORA (PLT) group of transcription factors is important for delimiting the meristematic and elongation zones of roots. High and intermediate PLT activity levels promote stem cell maintenance and proliferation, respectively, whereas reduction in activity is required for cells to exit proliferation and enter differentiation. The plant hormone auxin plays an essential role in root patterning, and PLETHORA transcription factors are likely integrators of the auxin gradients in roots. Expression of *PLETHORA* genes overlap with the auxin maximum in the roots.

11.5.3 Cell division underlies several theories of plant development

The role of the cell cycle machinery in plant development has been the subject of much debate. Obviously, cell division is essential for generating the cells that constitute tissues and organs; however, whether cell division drives growth and development (**cellular theory**) or, alternatively, cell division merely follows a developmental plan (**organismal theory**) is more difficult to answer (Fig. 11.28). Experiments in the late 1950s and early 1960s suggested cell division had little function in growth and morphogenesis. Seedlings from γ-irradiated wheat grains grow to some extent without cell division and resemble untreated seedlings in many aspects of growth. These data provided the first experimental evidence that genetic information, and not the number and orientation of cell divisions, specify the shapes of leaves.

Thanks to the ability to alter cell cycle parameters in transgenic plants, the question of the importance of cell division in determining organ size has been revisited. Transgenic plants that constitutively overproduce any of the KRPs have more than 10-fold fewer cells, but they are, on average, sixfold larger than those of wild-type plants. The reduction in cell

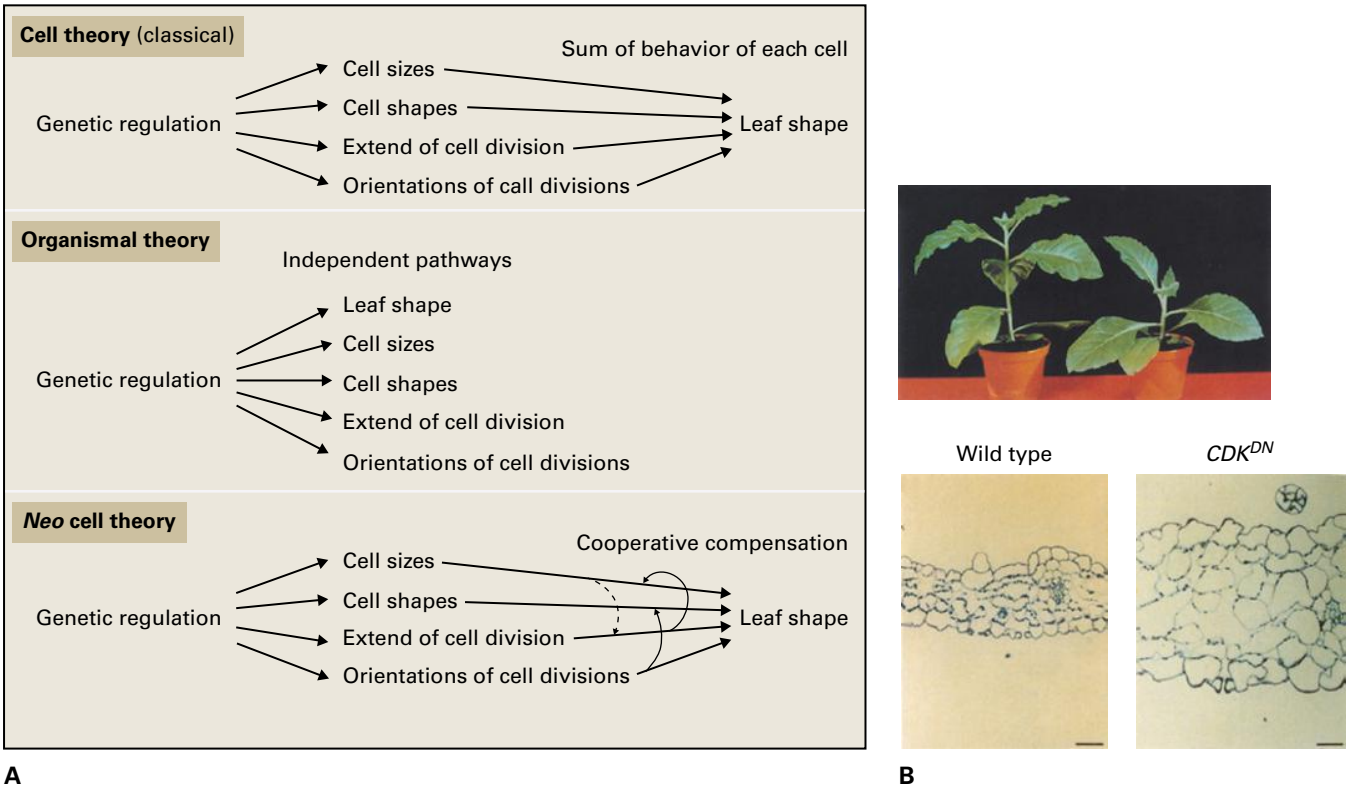


FIGURE 11.28 *Plant growth and cell division are not tightly coupled. (A) A comparison of the cell theory, the organismal theory, and the* neo *cell theory. The cell theory refers to the concept that cells are the basic units controlling the shape and size of organs, including leaves. The organismal theory holds that the organism, rather than the cell, is the basic unit of life. In this case, genetic information specifies form independently of genetic influences on cell size and shape, or on the number and orientation of cell divisions. The neo cell theory reconciles both theories, taking into account that cells are the unit of morphogenesis and that through regulatory feedback mechanisms each cell is controlled by factors that govern the morphogenesis of the organ in which the cell resides. (B) Altered CDK activity does not significantly affect plant morphology or stature. In transgenic tobacco (*Nicotiana tabacum*) plants, reduction of CDK activity by expression of a dominant-negative mutant (*CDK^{DN}*) gene that encodes an inactive A-type CDK protein inhibits proliferation. The resulting plant (top panel, right) has fewer, but larger, cells than the wild type, as shown in cross-sections of leaves (bottom panels). The overall stature of the mutant plant is remarkably similar to that of the wild type (top panel), indicating increased cell expansion compensates for decreased proliferation.*
Source: (B) Hemerly et al. (1995). EMBO J. 14:3925–3936.

number is compensated by an increase in cell size. Similarly, overexpression of a dominant-negative *CDKA* (Fig. 11.28B) or a nondegradable *CYCB1;1* in tobacco (*Nicotiana tabacum*) retards the cell cycle and causes formation of larger cells. On the other hand, constitutive overexpression of positive regulators of the cell cycle, such as *E2Fa* or *CYCD3;1*, results in more, but smaller cells; here, the increase in cell number is compensated by a decrease in cell size. All these observations support the organismal theory of plant development, in which the size and shape of an organ or organism is set to some extent by a certain endogenous mechanism independent of the cell division processes. In other words, plants can sense the size of developing organs and compensate for changes in cell division activity with modifications in cell expansion. This phenomenon is known as **compensation**. It is not known what determines the blueprint for leaf shape and size, but hormonal gradients probably play an important role.

However, not all experimental data fit the organismal theory. For example, overexpression of a dominant-negative *CDKA;1* under the control of a seed storage promoter deregulates embryo development. The strong inhibition of cell division upon *KRP* overexpression results in altered leaf shape. Furthermore, overexpression of *CYCB1;1* under the control of the *CDKA;1* promoter accelerates root growth, as would be expected under the cellular theory. These data suggest the organismal theory might only hold true to a certain degree, and that in extreme situations, growth is controlled both at the level of the organism and of the cell.

To reconcile these contrasting views, the ***neo* cell theory** was formulated (Fig. 11.28B). This theory states cell division and cell expansion are the building blocks of growing organs, but there is also a regulatory feedback from organ-wide control systems on cell division and cell expansion. Both the short- and long-range signaling components interacting with the cell cycle machinery need to be defined. Numerous genes have been identified that enhance plant organ size, mainly by extending the timing of cell proliferation during organ development. Examples are the transcriptional regulators AINTEGUMENTA and GROWTH REGULATING FACTORS, which stimulate by an unknown mechanism the expression of cell cycle genes.

11.5.4 Cell division may be independent of cell differentiation

Evidence suggests cell division acts independently of cell differentiation. Neither inhibition nor stimulation of cell division (through overexpression or knockout of cell cycle genes) severely affects cell differentiation. For example, trichome-specific expression of *CYCD3;1* in *Arabidopsis* converts unicellular trichomes in multicellular hairs without affecting differentiation. Another example is found in transgenic plants with reduced CDKB1 activity. In these plants, many stomata, normally built of two guard cells, consist of only one kidney-shaped cell due to inhibition of cell division. These aberrant cells still acquire stomatal identity (see Fig. 11.10), illustrating that cell division and differentiation are uncoupled events.

11.5.5 Totipotency is a rarely used alternative developmental path

In many plant cell cultures and under appropriate conditions, single cells can regenerate an entire plant through two alternative pathways: **organogenesis** and **embryogenesis**. In the former, morphogenesis proceeds by forming shoot organs, followed by root organs. Plants also proliferate asexually in this manner; in many species, roots can generate new shoots, or vice versa. During somatic embryogenesis, embryos are formed directly in the culture. This ability of single cells to recapitulate embryogenesis and pattern formation somatically, without an intervening reproductive phase (flowering), is called **totipotency**.

In some genera (such as *Kalanchoe*), somatic embryogenesis can occur in intact plants and does not depend on the loss of tissue integrity (Fig. 11.29). Thus, organogenesis and somatic embryogenesis are alternative reproductive strategies to flowering. These asexual mechanisms might be developmental relics that predate the evolution of flowering plants. They may have been preserved in some plant species to allow clonal propagation.

Totipotency has been used in tissue culture to regenerate various plant organs. Even highly specialized plant cells can retain full totipotency, as illustrated, for example, by the stomatal guard cells of sugar beet (*Beta vulgaris*), from which plants can be regenerated. Regardless of the tissue type used as source material, at least three main steps toward plant regeneration are required: cellular dedifferentiation, cell cycle reentry, and induction of redifferentiation.

Cellular dedifferentiation and cell cycle reentry are intimately linked, making it difficult to disentangle these processes at the molecular level. Significant progress has come from studies with protoplast cultures. Plant protoplasts can be obtained from intact tissues by enzymatic removal of the cell wall and, under appropriate conditions, they can be regenerated into intact plants. Before they can reenter the cell cycle, however, protoplasts that originate from differentiated tissues must undergo an abrupt switch from a fully differentiated to a dedifferentiated status. Evidence indicates that this transition is accompanied by a change in the chromatin structure, thereby altering the portion of the genome that is accessible for transcription (euchromatin) versus the one that is repressed (heterochromatin). At the onset of cell division, the proportion of euchromatin increases considerably. It is thought the RBR-E2F pathway is involved in this process, as there is a change in chromatin structure of E2F target genes upon the dedifferentiation of protoplasts. Dynamic changes in chromatin structure are primarily orchestrated by posttranscriptional modifications of the histones in nucleosomes, for example acetylation by histone acetyltransferases.



A



B

FIGURE 11.29 *Totipotency as an alternative developmental path. (A) Cells from many plant species can be cultured in vitro and induced to regenerate vegetative organs by application of suitable combinations of plant hormones. The photograph shows plantlets growing leaves from disorganized tissues called calli. (B) For some plant species (such as* Kalanchoe*), the formation of clonal offspring is a competitive advantage. Small plantlets formed in the axils of serrated leaves are viable and can root if the parent leaf is torn off or when it senesces. Source*: (A) Smith, University of Edinburgh, Scotland; previously unpublished. (B) Raven et al. (1992) Biology of Plants, 5th ed. Worth Publishers, New York.

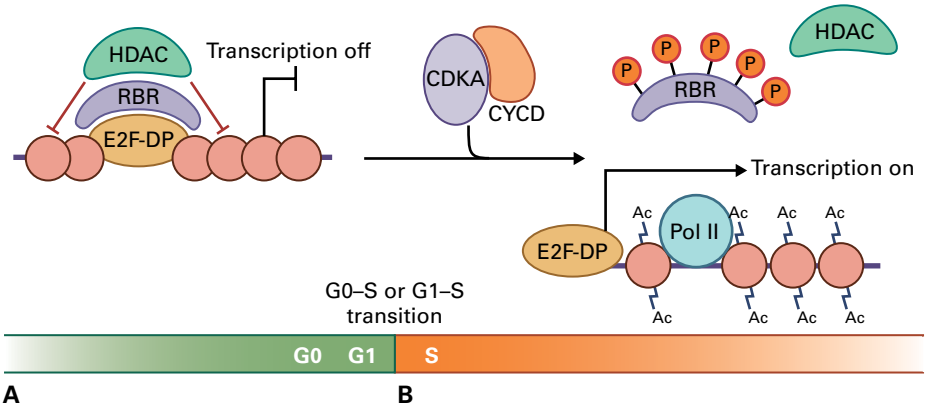


FIGURE 11.30 *Model for the role of chromatin remodeling in the switch from quiescent to dividing cells. (A) In quiescent (or G1-arrested) cells, the retinoblastoma-related protein (RBR) targets histone deacetylases (HDAC) to the promoters of important regulatory genes required for the G0/G1-to-S transition. RBR itself represses the activity of E2F/DP transcription factors. Through HADC activity, the chromatin is condensed, thereby obstructing the accessibility of DNA for transcriptional regulatory proteins and preventing transcription of the E2F/DP target genes. (B) Cell cycle entry is facilitated by the activation of CDKA–CYCD complexes that phosphorylate RBR, thereby releasing it and HDAC from the E2F/DP transcription factors. In the absence of HDAC, the activity of unidentified histone acetyltransferases becomes dominant. This results in the acetylation of histones and, consequently, in a less condensed nucleosomal conformation. The DNA in this relaxed chromatin structure is now accessible to transcriptional regulatory proteins. Ac, acetyl group; Pol II, RNA polymerase II.*

In maize, the histone deacetylase Rpd3I is associated with the RB-related protein (RBR), and together, these proteins probably repress genes required for cell cycle entry. After stimulation with growth factors, CDKs complexed with D-type cyclins might phosphorylate RBR, which may release both the RBR and histone deacetylase from the promoters of downstream genes that are required for cell cycle entry (Fig. 11.30). This model is supported by the observation that expression of D-type cyclins precedes the resumption of cell division in germinating seeds, and that the knockout of specific D-type cyclins delays cell cycle reactivation in the root meristem. A role for RBR in controlling the differentiation status of cells is corroborated by the delay in cell differentiation by RBR deficiency, whereas its induced expression pushes meristematic cells into the differentiation pathway.

11.5.6 Developmental ploidy increases are common in plants

During development, cells exit the cell cycle and start to differentiate. Exit from the cell cycle is sometimes accompanied by the onset of an alternative cycle, called the endocycle. The endocycle occurs in a wide variety of cell types in arthropods, mammals, and plants. During the endocycle, no cytokinesis occurs between successive rounds of DNA replication, and the DNA content of the cell doubles with every round of replication. These increases can be dramatic: the suspensor cells of *Phaseolus coccineus* go through 12 additional cycles of DNA replication without intervening mitosis, resulting in an approximately 8,000-fold increased DNA content per cell.

The ploidy level of individual cells can increase by various mechanisms. When DNA replication is accompanied by mitosis but without cytokinesis, polynucleated cells are formed in a process called **endomitosis**. Alternatively, when repeated replication of DNA takes place without formation of new nuclei during telophase, **endoreplication** can result in **polyploidy** or **polyteny**. In polyploid cells, the sister chromatids separate and return to the interphase state as in the mitotic cell cycle, resulting in more chromosomes that retain their individual identity within the original nuclear envelope. On the contrary, polyteny is characterized by the occurrence of chromosome duplication without DNA condensation/decondensation steps and without sister chromatid segregation, forming "giant" multistranded chromosomes with $2n$ chromatids. As a consequence, the number of chromosomes within the nuclear envelope remains the same. In addition, any variation between polyteny and polyploidy is possible.

Endoreplication is often tissue specific (such as in the maize kernel and the tomato fruit), but it can sometimes be found in most vegetative cells, as observed for *Arabidopsis* (Fig. 11.31). The physiological relevance of endoreplication is subject to debate. It probably plays an important role in the differentiation of post-mitotic cells, because endocycle onset usually characterizes the switch between cell proliferation and differentiation. Often, a correlation between DNA ploidy level and cell size is seen (Fig. 11.32). Endoreplication may also provide the increased gene dosage needed to accommodate cell enlargement. As plant species that endoreduplicate are often characterized by a rapid life cycle, endoreplication may also represent an evolutionary strategy to support fast development. Endoreplicating species may combine the advantages of both small- and large-genome species; a small genome allows cells to duplicate quickly at a low energy cost, whereas a large genome enables maintenance of large cells. These features can be valuable under conditions that limit cell division but not cell elongation, such as cold climates.

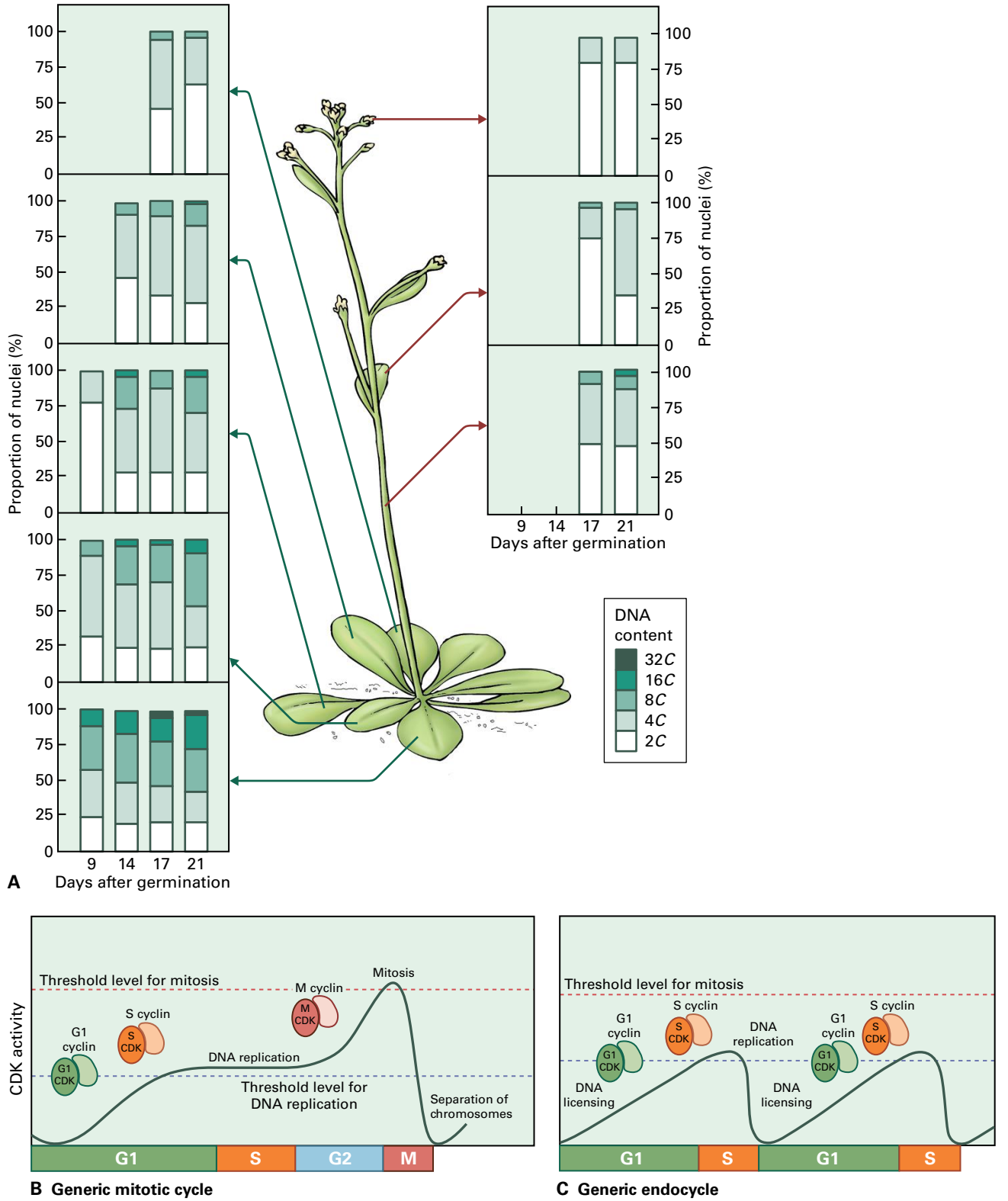


FIGURE 11.31 *Control of DNA endoreplication and polyploidy during development. (A) Developmental control of DNA content. Analysis by flow cytometry of interphase nuclei isolated from* Arabidopsis *tissues at different developmental stages shows a strong correlation between polyploid DNA content and increased tissue age. For a given species, C is the mass of DNA present in the haploid genome. (B, C) Roles of CDK–cyclin complexes in mitotic and DNA endoreplication cycles. (B) Typical mitotic cycle. During early G1, CDK activity must be low to allow licensing of replication origins. Late in G1, CDK levels rise due to increasing levels of G1 cyclins until the level of CDK activity is sufficient to inactivate RBR and trigger S phase, including firing of replication origins and S-phase transcription. Maintenance of S phase requires specific CDK–cyclin complexes. During G2, transcription of M-phase cyclins increases until a high level of active CDK–cyclin complexes is reached and M phase begins. In mid-M phase, mitotic cyclins are destroyed by APC/C and CDK levels once again drop to early G1 levels. (C) Typical DNA endoreplication cycle. CDK levels of G1 and S continue to cycle between low levels in a G1-like phase for licensing of the replication origins and the increased levels are needed to trigger S. Mitotic CDK complexes either never form or their activity is suppressed, with CDK activity never reaching the level necessary to trigger M phase as a consequence.*

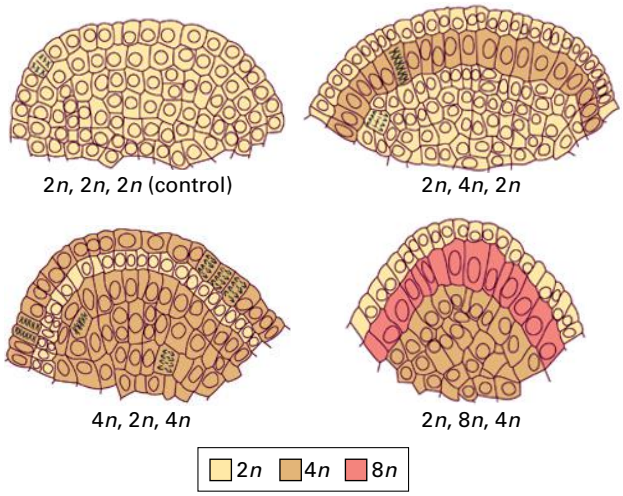


FIGURE 11.32 *Correlation of ploidy with cell size. Chimeras (individuals composed of cells with different genotypes) can be readily generated in plants by use of grafting techniques. Analysis of plants with chimeric meristems demonstrates that cell volume is determined not by position but by genome copy number (ploidy, n). A strong positive correlation was observed between increased ploidy and cell size.*

The endoreplication cycle can be viewed as a mitotic cell cycle in which the M phase is skipped. In contrast, because cells that divide and endoreplicate both need to duplicate their DNA, they probably share the components required for DNA replication. As each endoreplication cycle has to activate the replication origins, it is not surprising that many proteins controlling the assembly of the preRC (such as CDC6 and CDT1) have an impact on endocycle regulation and progression. Increased endoreplication levels are also observed upon overexpression of E2F transcription factors, suggesting that the E2F-RBR pathway contributes to the endocycle onset.

Elimination of mitotic CDK activity involves transcriptional repression and proteolytic destruction of the G2-to-M-specific CDK/cyclin complexes. CDKs to be inhibited are the B1-type CDKs, as illustrated by the observation that plants with reduced CDKB1 activity display a faster onset of the endocycle. An increase in the activity of CCS52A-activated APC/C probably accounts for the selective destruction of CDKB1-associated cyclins through ubiquitination. Also A-type CDK activity needs to be reduced, a process that likely involves CKIs from both the KRP and SIM families.

11.5.7 Plant cells must replicate and maintain three genomes

Unlike cells of animals or fungi, plant cells have three different genomes in three cellular compartments: the nucleus, the plastids, and the mitochondria. Plant mitochondrial genomes are generally much larger than their animal or yeast counterparts and often range from 200 to 2,400 kb. The plastid genome is approximately 130 to 150 kb. Genomes in mitochondria and plastids generally encode only a fraction of the proteins required for the functioning of these organelles, which, therefore, depend on the import of proteins encoded by nuclear genes.

Within a plant, the copy numbers of mitochondrial and plastid genomes are surprisingly flexible. The organellar genomes are primarily replicated within meristems and organ primordia. The copy number of the organellar genomes can be very high: 20–100 copies per mitochondrion and 50–150 copies per plastid. In rapidly dividing cells, however, the number of organelles remains relatively low. As post-mitotic cells mature, replication of organellar DNA gradually ceases and mitochondrion/plastid division proceeds, eventually reducing the genome copy number per organelle (Fig. 11.33).

The strict maintenance of plastid populations in dividing plant cells and regulation of plastid numbers in different cell types indicate a mechanism that coordinates plastid division with cellular division. This coordination is strict in species bearing a single plastid, such as some algae and diatoms. In the red alga *Cyanidioschyzon merolae*, inhibition of the degradation of a DNA replication-specific cyclin by a tetrapyrrole-mediated signaling pathway coordinates organellar and nuclear DNA replication. Also in higher plants, inhibition of plastid retrograde signaling affects cell cycle exit and onset of nuclear DNA endoreplication. Nevertheless, the coordination between organellar and nuclear DNA replication is probably less stringent in higher plants as compared to unicellular algae because multiple proplastids are present in every meristematic cell. The replication factor CDT1 also has been proposed to coordinate nuclear DNA replication with proplastid division. The *Arabidopsis* CDT1 protein is targeted to both the nucleus and chloroplasts, and plants with reduced CDT1 levels show defects in plastid size and number. However, the molecular mechanisms by which this replication factor controls plastid division are still unknown.

11.5.8 Plant growth regulators affect the activity of specific cell cycle regulators

Terrestrial plants are **sessile**, attached to an immobile substrate. As plants deplete nearby reserves, they must grow continuously toward new points of access to soil nutrients and light. To fully exploit their environment, plants require flexible growth rates and patterns. Although growth is not the only plant response to a changing environment, cell division and expansion are essential to bringing the plant body into contact with untapped resources.

Like other multicellular organisms, plants use long-range signaling mechanisms to communicate between distant organs (e.g., shoots and roots) and to coordinate their growth. Small molecules play a pivotal role in such mitogenic signaling. Plant growth regulators, including hormones (e.g., auxins, cytokinins, ethylene, ABA, jasmonic acid, strigolacton,

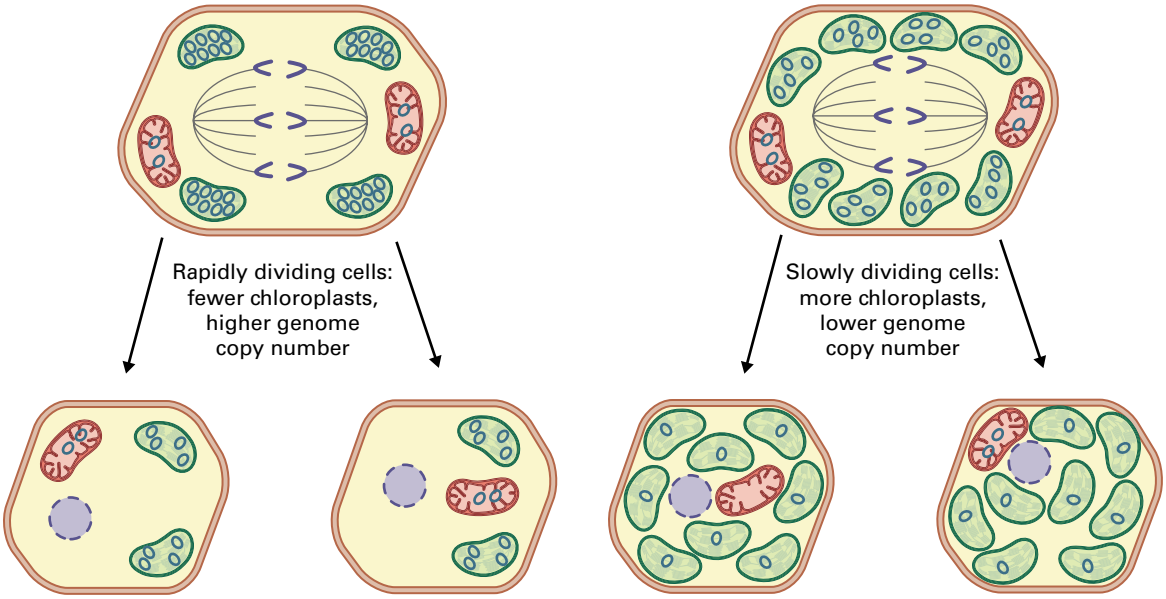


FIGURE 11.33 *Replication of chloroplast DNA is not coupled to nuclear DNA replication. Rapidly dividing cells in young leaves contain relatively few chloroplasts but each chloroplast has a high copy number of the circular plastid genome. DNA synthesis in these chloroplasts continues even when nuclear DNA is not being replicated. When cells gradually cease to proliferate and begin to expand during leaf growth, the genome copy number of individual chloroplasts decreases because the chloroplasts continue to divide one or two more times even in the absence of plastid DNA synthesis.*

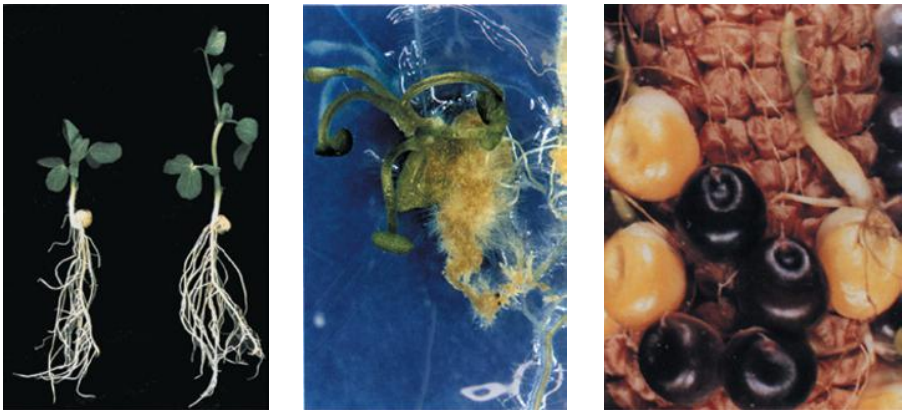


FIGURE 11.34 *Abnormalities in hormone synthesis, perception, or response strongly affect plant growth. (A) A block in brassinosteroid synthesis compromises the appropriate expansion of plant cells and affects their ability to respond to light (compare mutant pea plant on left with the wild-type plant on the right). (B) Enhanced synthesis of auxin stimulates excessive lateral root formation. In the* Arabidopsis *superroot mutant, this phenotype is ultimately lethal. (C) The inability of the maize* vp1 *mutant to maintain seed dormancy in response to ABA results in premature germination on the ear (vivipary) and jeopardizes the ability of the seed to survive desiccation.*
Source: (A) Yokota (1997). Science 2:137–143. (B) Boerjan et al. (1995). Plant Cell 7:1405–1419. (C) McCarty et al. (1991). Cell 66:895–905.

gibberelin, and brassinosteroids), lipo-oligosaccharides (such as nodulation factors), and peptides (such as PSK, GRF, PSY, and CLV), have been implicated in various aspects of growth regulation (see Chapter 18). Mutants defective in hormone synthesis, perception, or response often show drastic changes in their appearance and growth habits (Fig. 11.34).

Auxins and cytokinins are two plant growth regulators with likely roles in cell division regulation. Freshly established plant cell cultures require auxins and cytokinins for continued proliferation; for example, withdrawal of auxin or cytokinin from the medium of fresh tobacco (*Nicotiana tabacum*) cell cultures results in arrest in G1 or G2, respectively. The lack of cytokinin in tobacco cell cultures is correlated with increased tyrosine phosphorylation of a tobacco CDK that probably inhibits kinase activity. When such arrested cultures are supplied with cytokinins, tyrosine phosphorylation is reduced and cell division activity resumes. In *Arabidopsis*, cytokinin is also necessary to stimulate expression of a D-type (G1) cyclin (*CYCD3*), and constitutive expression of this cyclin relieves the need for cytokinin in

tissue explants (see Fig. 11.12). By contrast, constitutive expression of *E2Fb* can sustain cell division under auxin-limiting conditions.

Treatment of intact plants with plant hormones does not stimulate growth in all tissues. For instance, application of auxins to roots induces branch root formation but inhibits apical meristem activity. Reducing cytokinin concentrations in roots enhances growth, but represses shoot growth. Changes in the expression of cell division regulators such as cyclin and E2Fs and overall cell division activity are early responses to such hormone treatments (Fig. 11.35). Although modifications in the concentrations of auxin or cytokinin clearly affect cell division activity, the nature of the response is not uniform and depends on the tissue.

In contrast to auxin and cytokinin, jasmonic acid exerts an inhibitory affect on cell proliferation, arresting the cell cycle at both the G1-to-S and G-to-M transition points. The G2 arrest correlates with a strong decrease in M-phase genes (such as B-type CDKs, cyclins, and kinesins), but the molecular mechanism involved is unknown. The inhibitory effect of jasmonic acid corresponds with its observed negative impact on plant growth and might represent a mechanism for cross-talk between cell cycle progression and stress perception.

ABA, which is primarily involved in stomatal aperture closure and in signaling drought stress responses, also negatively influences plant growth. ABA concentrations in the root increase during water stress, and the RAM is arrested under such conditions. Expression of the CDK–cyclin complex inhibitor *ICK1/KRP1* is induced, suggesting the inhibitor regulates CDK activity in roots during stress conditions. Similarly, the hormone ethylene is involved in arresting the cell cycle by inhibiting CDK activity upon exposure of plants to mild stress.

Brassinosteroids and gibberellins mostly enhance cell growth and expansion; in the dark, however, brassinosteroids suppress activation of leaf organogenesis, presumably by controlling cell division. Gibberellins stimulate cell division in both *Arabidopsis* root meristems and shoot internodes of deep-water rice, where cells divide and expand rapidly in response to flooding. The role of gibberellins on cell proliferation depends on DELLA proteins (see Chapter 18), which are thought to restrain cell proliferation by enhancing expression of the cell cycle inhibitory genes *KRP2* and *SIAMESE*. In general, much has yet to be learned about how plant hormones and developmental signals control cell cycle activity and tissue and organ sizes.

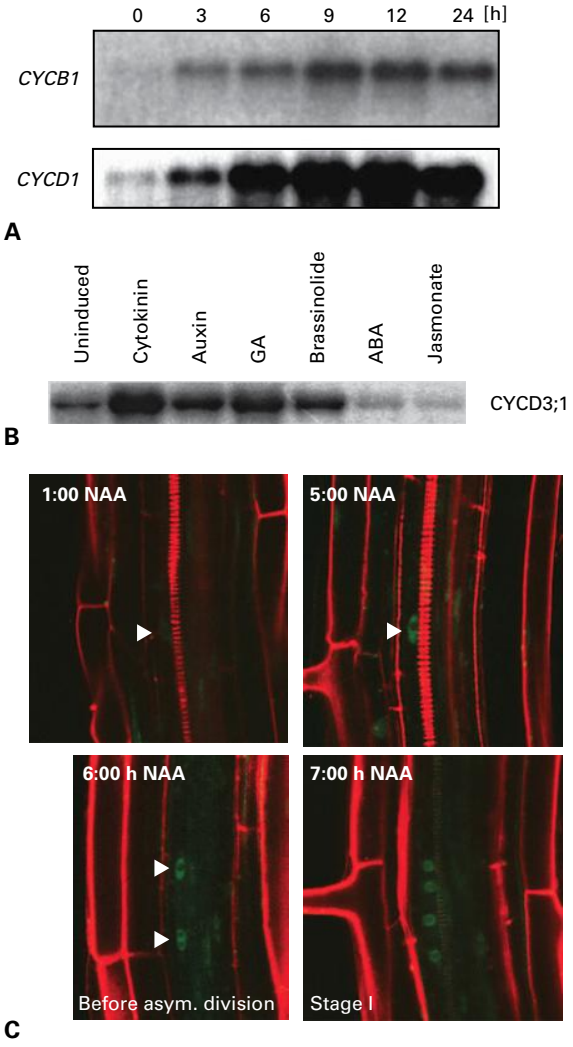
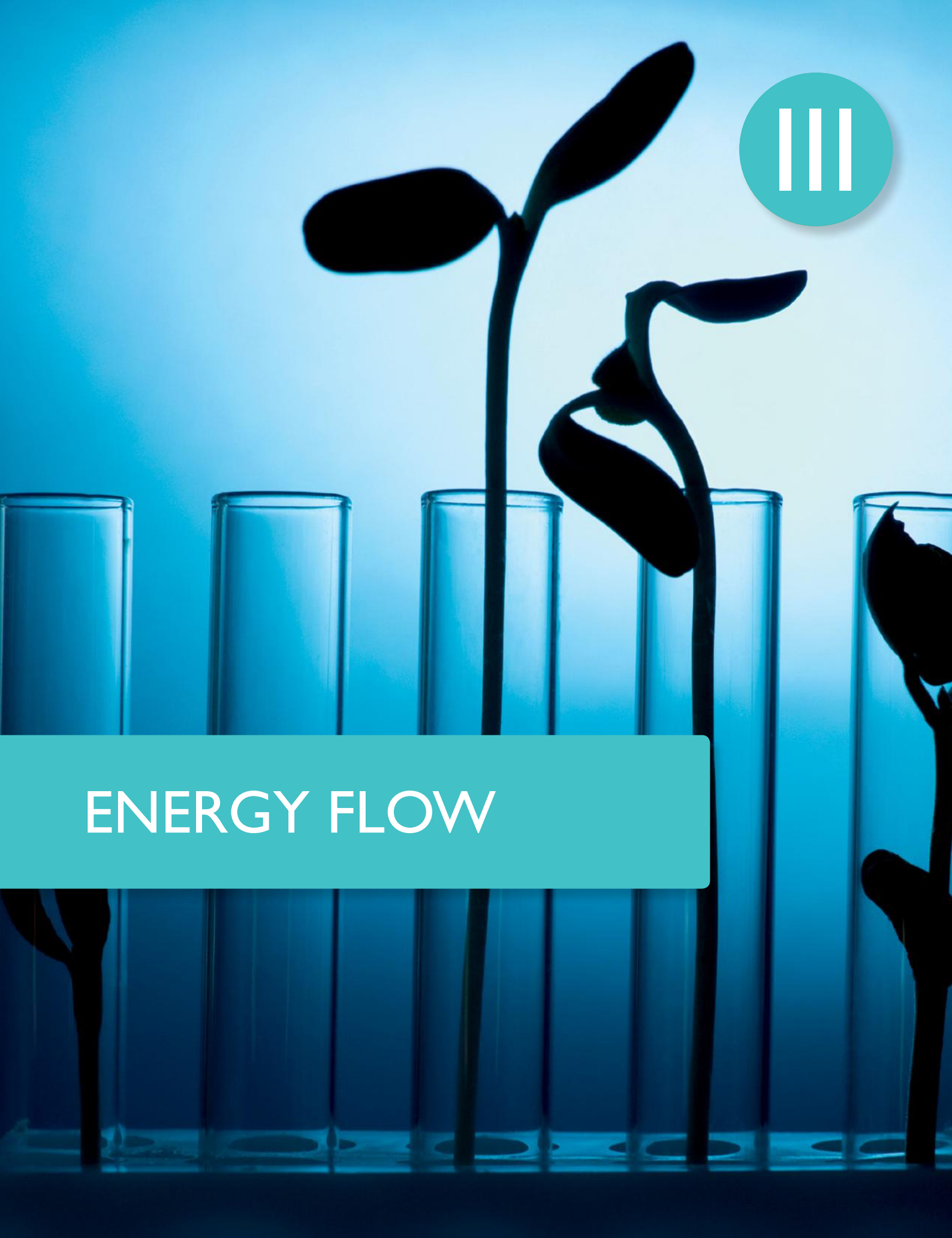


FIGURE 11.35 *Plant growth stimulators affect the expression of cell cycle regulators. (A) Accumulation of mRNAs for mitotic* (CYCB1) *and G1* (CYCD1) *cyclins increases after stimulation of* Arabidopsis *roots with auxin. The accumulation is the greatest 12 hours after stimulation and then decreases. (B) Transcriptional induction of* CYCD3 *in response to different hormone treatments in cell cultures. (C) Accumulation of the E2Fa–GFP fusion protein in lateral root initiation cells after auxin (NAA) treatment. The E2Fa–GFP signal increases rapidly between 1 and 5 hours after NAA treatment, marking the lateral root initiation sites before the occurrence of the first asymmetric cell division that marks the outgrowth of a new lateral root. Source*: (A) Top: Doerner et al. (1996). Nature 380:520–523. Bottom: P. Doerner, University of Edinburgh, Scotland; previously unpublished.

Summary

In proliferating cells, cell growth is coupled with cell division. The most fundamental roles of cell division are replication of chromosomes and subsequent distribution of the chromosomes to daughter cells. These events are controlled by protein kinases and proteases that have been identified in plants as well as in other model systems (animals and yeast). Although functional characterization of these regulatory proteins is not complete, initial observations indicate that they function in a similar manner, but might be regulated differently.



III

ENERGY FLOW



12

Photosynthesis

Krishna K. Niyogi, Ricardo A. Wolosiuk, and Richard Malkin

Introduction

The synthesis of organic compounds from inorganic precursors requires energy and reducing power (low-potential electrons). Autotrophic organisms use carbon dioxide (CO_2) as the sole carbon source for production of organic molecules. For **chemoautotrophic** bacteria and the living communities dependent on their activity (e.g., the fauna of deep-sea hydrothermal vents), the ultimate sources of this energy are the chemical bonds found in inorganic molecules. Such organisms are, however, a minority. In nearly all biological systems, the synthesis of organic molecules is driven directly or indirectly by energy from the sun. The overall process whereby plants, algae, and prokaryotes directly use light energy to synthesize organic compounds from CO_2 is called **photosynthesis.**

All photosynthetic organisms are **photoautotrophic**. Some prokaryotes can use light as an energy source for ATP synthesis, but they require organic molecules as sources of carbon for growth; such organisms are **photoheterotrophic**, but not photosynthetic. Photosynthesis sustains most autotrophic producers of organic material, as well as the heterotrophic consumers they support. In addition to providing food, biomass, and fossil fuels, photosynthesis in plants and algae produces the oxygen (O_2) required for respiratory activity by all multicellular and many unicellular organisms.

Photosynthesis encompasses both a complex series of reactions that involve light absorption, light conversion, and electron transfer and a multistep enzymatic pathway that converts CO_2 and water into carbohydrates. This chapter explores these life-sustaining processes in detail. Other topics frequently covered in discussions of photosynthesis are discussed elsewhere, such as sucrose and starch metabolism in Chapter 13 and photorespiration in Chapter 14.

12.1 Overview of photosynthesis

12.1.1 Photosynthesis is a biological oxidation–reduction process

Most photosynthetic organisms convert light energy into stable chemical products. As shown in Reaction 12.1, photosynthesis is a biological **oxidation–reduction** (or **redox**) process. CO_2 is the electron acceptor, and H_2A is any reduced compound that can serve as the electron donor. (CH_2O) represents the carbohydrate generated by the reduction of CO_2, and A represents the product formed by oxidation of H_2A.

Reaction 12.1: Photosynthesis

$$CO_2 + 2H_2A \xrightarrow{h\nu} (CH_2O) + 2A + H_2O$$

In the case of O_2-evolving (**oxygenic**) photosynthesis, the focus of this chapter, water serves as the reductant (Reaction 12.2). Water is oxidized, and the electrons released are energized and ultimately transferred to CO_2, yielding O_2 and carbohydrate. Plants, algae, and prokaryotic cyanobacteria are capable of this light-driven, **endergonic** (energy-requiring) reaction, which has a free energy change ($\Delta G^{\circ\prime}$) of +2840 kJ mol^{-1} for the synthesis of hexose. Oxygenic photosynthesis

Biochemistry & Molecular Biology of Plants, Second Edition. Edited by Bob B. Buchanan, Wilhelm Gruissem, and Russell L. Jones.
© 2015 John Wiley & Sons, Ltd. Published 2015 by John Wiley & Sons, Ltd.
Companion website: www.wiley.com/go/buchanan/biochem

was an evolutionary innovation of cyanobacteria that led to the accumulation of O_2 in the Earth's atmosphere more than 2 billion years ago.

Reaction 12.2: Oxygenic photosynthesis

$$CO_2 + 2H_2O \xrightarrow{h\nu} (CH_2O) + O_2 + H_2O$$

Many prokaryotes perform **anoxygenic** photosynthetic reactions that are consistent with Reaction 12.1 but utilize electron donors other than water. For example, purple sulfur bacteria use electron donors such as H_2S, producing elemental sulfur rather than O_2 as a photosynthetic product (Reaction 12.3). These bacteria retain the capacity to reduce CO_2 to carbohydrate, and in some cases, the carbon fixation reactions are almost identical to those found in oxygenic organisms. Anoxygenic photosynthetic bacteria are essential components of many terrestrial and aquatic ecosystems. In addition, these prokaryotes have served as important models for studying various aspects of photosynthesis (Box 12.1).

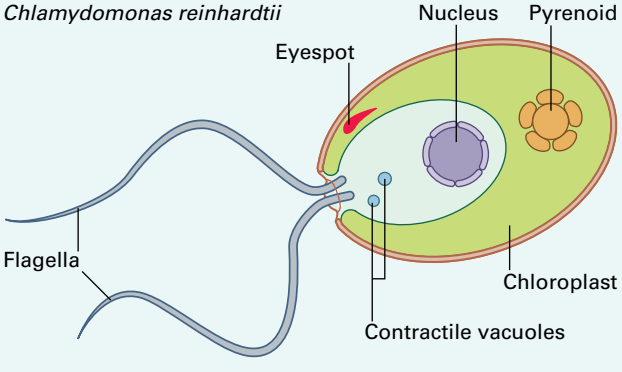
BOX 12.1 Model organisms are used to study photosynthesis

Like other areas of plant biology, contemporary research in photosynthesis has benefited from the development of techniques of molecular genetics and molecular biology. Several model organisms are used in studies of photosynthesis, each of which has characteristics that make it attractive to researchers.

Photosynthetic bacteria have played a major role in the discovery of important concepts in photosynthesis. The anoxygenic purple bacteria (e.g., *Rhodobacter sphaeroides*) and some cyanobacteria (e.g., *Synechocystis* sp. PCC 6803) are metabolically flexible and can grow either photoautotrophically or heterotrophically. In the case of *R. sphaeroides*, most of the genes involved in photosynthesis are located together in the genome in a photosynthesis gene cluster, which facilitates molecular analysis. The functions of specific genes can be tested by constructing deletion mutants. Because these prokaryotic organisms can grow under heterotrophic conditions, they can be used to study mutations of the photosynthetic apparatus that would be lethal in obligate photoautotrophs. Detailed structure–function analysis of the encoded proteins can be performed by transforming cells with strategically modified DNA. Such techniques have been used extensively in studies of photochemical reaction center complexes and electron transfer proteins, providing insight into the specific functions of many individual subunits of these photosynthetic complexes.

In studies of eukaryotic organisms, the requirement for cooperation of the nuclear and chloroplast genomes (see Chapters 6 and 9) in photosynthesis presents additional challenges. *Chlamydomonas reinhardtii,* a unicellular green alga, has emerged as one of the best eukaryotes for molecular studies of chloroplast biogenesis. Like the photosynthetic bacteria described above, *C. reinhardtii* can grow heterotrophically in the dark if supplied with a carbon substrate such as acetate, allowing researchers to study mutations that abolish photosynthesis. Another major advantage of *C. reinhardtii* is its amenability to transformation of both the nuclear and chloroplast genomes. Genome sequencing and phylogenomic approaches have identified hundreds of conserved genes that are hypothesized to have a role in photosynthesis or chloroplast biogenesis. The functions of these genes are being tested using reverse genetic approaches, such as random insertional mutagenesis of the nuclear genome or targeted mutagenesis of the chloroplast genome (in which targeted deletion mutants can be easily made, as in the photosynthetic bacteria mentioned above).

Although somewhat limited by the lethality of mutations that completely abolish photosynthesis, genetic approaches using plants such as *Arabidopsis thaliana*, maize (*Zea mays*), and tobacco (*Nicotiana tabacum*) have also been very fruitful in photosynthesis research. *A. thaliana* is especially amenable to high-throughput mutant screening approaches and reverse genetics, exploiting the large T-DNA insertion mutant collections that have been developed for this model organism. An advantage of maize is the fact that lethal photosynthetic mutants are easily maintained as heterozygotes, and the large seeds enable substantial growth of nonphotosynthetic seedlings to provide ample material for biochemical studies. In tobacco, chloroplast transformation is also possible, and the use of antisense and other gene silencing technologies to study nuclear genes has been very informative. Concentrations of specific enzymes active in the Calvin–Benson cycle have been diminished through this approach. In some cases, this technique has yielded plants having reduced rates of photosynthesis; in other cases, antisense plants have revealed unknown complexities in the regulation of photosynthesis.



Reaction 12.3: Photosynthetic oxidation of sulfur compounds, such as H_2S

$$CO_2 + 2H_2S \xrightarrow{h\nu} (CH_2O) + 2S + H_2O$$

12.1.2 In photosynthetic eukaryotes, photosynthesis takes place in the chloroplast, a specialized organelle

In eukaryotes, the biophysical and biochemical reactions of photosynthesis occur in a specialized plastid, the **chloroplast** (see Chapter 1). All the reactions required for photosynthesis take place in this organelle, which arose from the endosymbiotic association of a protoeukaryotic cell and a photosynthetic bacterium related to modern cyanobacteria (see Chapters 1 and 6). The complex structure of the chloroplast reflects its diverse biochemical functions. Chloroplasts from land plants (Fig. 12.1) are surrounded by a double-membrane system consisting of an **outer and inner envelope** and also contain a complex internal membrane system. The internal membrane system, known as the **thylakoid** membrane, contains distinct regions. Some thylakoids (**granal thylakoids**) are organized into **grana**, stacks of appressed membranes, whereas others (**stromal thylakoids**) are unstacked and are thus exposed to the surrounding fluid medium, the chloroplast **stroma**. The thylakoid membranes are interconnected and enclose an internal space known as the **lumen**.

12.1.3 Photosynthesis consists of light reactions and carbon reactions

During the 1950s and 1960s, experiments showed that isolated chloroplasts can convert CO_2 to carbohydrate in the light (see Reaction 12.2) and that the photosynthetic process involves two phases: the light reactions, which produce O_2, ATP, and NADPH; and carbon reactions (the carbon reduction cycle, also called the **Calvin–Benson cycle**, after its co-discoverers, Melvin Calvin and Andrew Benson), which reduce CO_2 to carbohydrate and consume the ATP and NADPH produced in the light reactions.

The two phases of photosynthesis occur simultaneously, but they reside in different regions of the chloroplast (Fig. 12.2). The thylakoid membranes contain the multiprotein photosynthetic complexes, photosystems I and II (PSI and PSII), which include the reaction centers responsible for converting light energy into chemical bond energy. These reaction centers are part of a photosynthetic electron transfer chain that also contains a transmembrane cytochrome complex (cytochrome b_6f), a water-soluble copper protein (plastocyanin), and a lipid-soluble quinone (plastoquinone). Located primarily in the thylakoids, the photosynthetic electron transport chain moves electrons from water in the thylakoid lumen to soluble redox-active compounds in the stroma (e.g., $NADP^+$). This electron transport is coupled to the generation of a **proton motive force** (pmf) across the thylakoid membrane. Using the potential energy of the pmf, ADP is phosphorylated by the chloroplast ATP synthase, a large stroma-exposed protein complex located in thylakoid

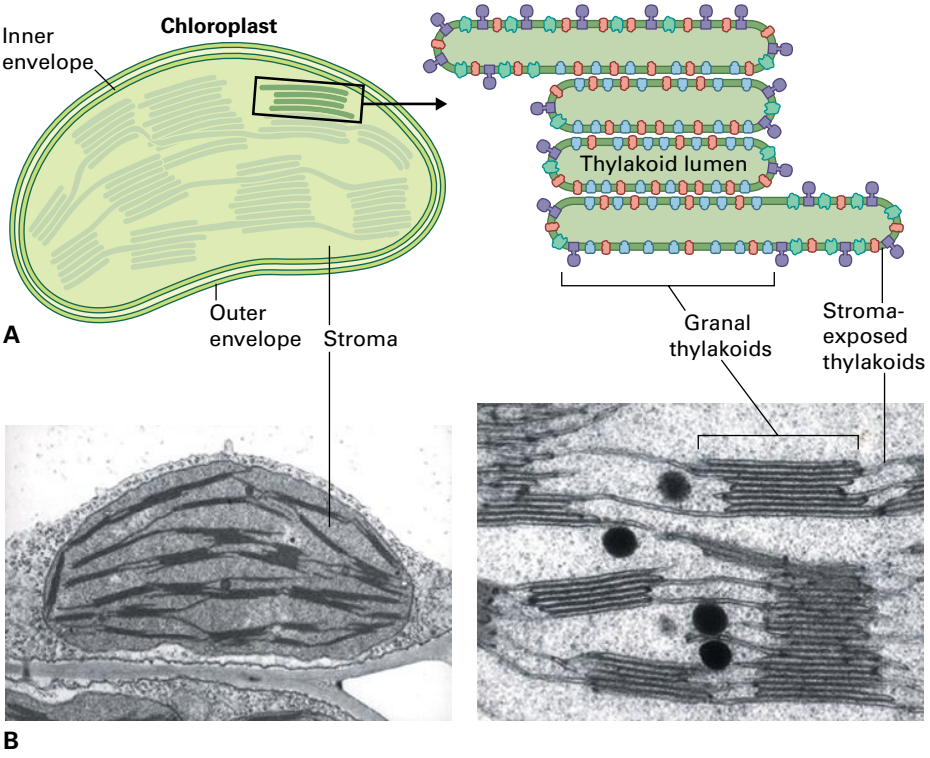


FIGURE 12.1 *Plant chloroplast. (A) Schematic diagram showing compartmentalization of the organelle. In a typical plant chloroplast, the internal membranes (thylakoids) include stacked membrane regions (granal thylakoids) and unstacked membrane regions (stromal thylakoids). (B) Transmission electron micrographs reveal plant chloroplast ultrastructure. The higher magnification emphasizes the membrane stacking and includes electron-dense lipid bodies known as plastoglobuli.*
Source: (B) Staehelin & van der Staay (1996). Structure, composition, functional organization and dynamic properties of thylakoid membranes. In Oxygenic Photosynthesis: The Light Reactions, D. R. Ort and C. F. Yocum, eds. Kluwer Academic Publishers, Dordrecht, The Netherlands, pp. 11–30.

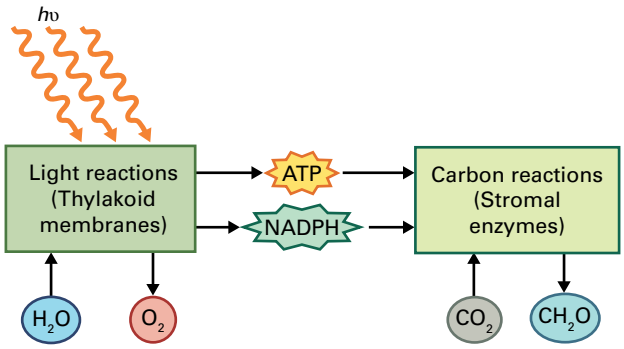


FIGURE 12.2 *The light and carbon (formerly "dark") reactions of photosynthesis occur in separate chloroplast compartments. Light is required for the synthesis of ATP and NADPH substrates in a series of reactions that occur in thylakoid membranes of the chloroplast. These products of the light reactions are then used by a series of stromal enzymes that fix CO_2 into carbohydrates during the carbon reactions.*

membranes. In contrast, the Calvin–Benson cycle reactions occur in the stroma.

In the past, the Calvin–Benson cycle was referred to as the "dark" reactions of photosynthesis. This terminology may be misleading, because these reactions occur during the day. Furthermore, some of the enzymes involved in CO_2 fixation require activation by light. It is, therefore, more accurate to say the carbon reactions depend on the light reactions, for both high-energy products and regulatory signals.

12.2 Light absorption and energy conversion

12.2.1 Light has properties of both particles and waves

One of the major advances of 20th-century physics was the finding that light, a form of electromagnetic radiation, has properties of both waves and particles. In the case of the quantum mechanical description, radiant energy is visualized as being a stream of energy-carrying particles called quanta (singular: quantum). Each quantum of light, or **photon**, contains a discrete quantity of energy. The energy of a single photon is equal to Planck's constant, h (6.626×10^{-34} Joule s), multiplied by the frequency of the radiation, ν, in cycles per second (s^{-1}) (see Equation 12.1).

Equation 12.1: Energy is directly proportional to frequency

$$E = h\nu$$

Thus, not all colors of light (wavelengths) have equal energy. The energy of a photon of a particular wavelength can be described by Equation 12.2, where c is the velocity of light (3.0×10^8 m s^{-1}) and λ is wavelength (m). As this relationship indicates, the energy content of light is inversely proportional to its wavelength. For example, 1 mol of photons of 490-nm blue light has an energy of 240 kJ, whereas 1 mol of photons of 700-nm red light has only 170 kJ. Relating these numbers to the +2840 kJ mol^{-1} required for CO_2 fixation gives some idea of the minimum number of quanta required to convert six CO_2 molecules to one molecule of hexose sugar. Oxygenic photosynthetic organisms use visible light, with wavelengths of 400–700 nm, whereas many anoxygenic photosynthetic organisms can harness the less energetic wavelengths in the near infrared at wavelengths greater than 700 nm.

Equation 12.2: Energy is inversely proportional to wavelength

$$E = hc/\lambda$$

12.2.2 Light is absorbed by pigment molecules

For light energy to be used by any system, the light must first be absorbed. This is a significant problem for photosynthetic organisms, because shading and reflection can result in large losses of available light. Molecules that absorb light are called **pigments**. The absorption of a photon by a pigment molecule converts the pigment from its lowest-energy (ground) state to an excited state (pigment*):

Reaction 12.4: Pigment excitation

$$\text{Pigment} \xrightarrow{h\nu} \text{Pigment}^*$$

A pigment molecule becomes excited when absorption of light energy causes one of its electrons to shift from a lower-energy molecular orbital, which is closer to the pigment's atomic nuclei, to either of two more-distant, higher-energy orbitals. The laws of quantum mechanics (Equation 12.3) dictate that transitions to an excited state occur only when the energy exactly matches the energy gap between the ground state energy (E_g) and the excited state energy (E_e)—in this case, the gap between the ground state and the excited state energies of the pigment molecule. That is, not all transitions are allowed.

Equation 12.3: Quantitative requirements for pigment excitation

$$E_e - E_g = hc/\lambda$$

In the case of molecules, in contrast to atoms, the ground state and the excited states have many closely spaced substates, the result of molecular vibration and rotations. These are shown in Figure 12.3, along with the first and second excited **singlet states** for a molecule that has two major absorption bands, such as chlorophyll (see Section 12.2.3), which has one absorption band in the blue spectral region

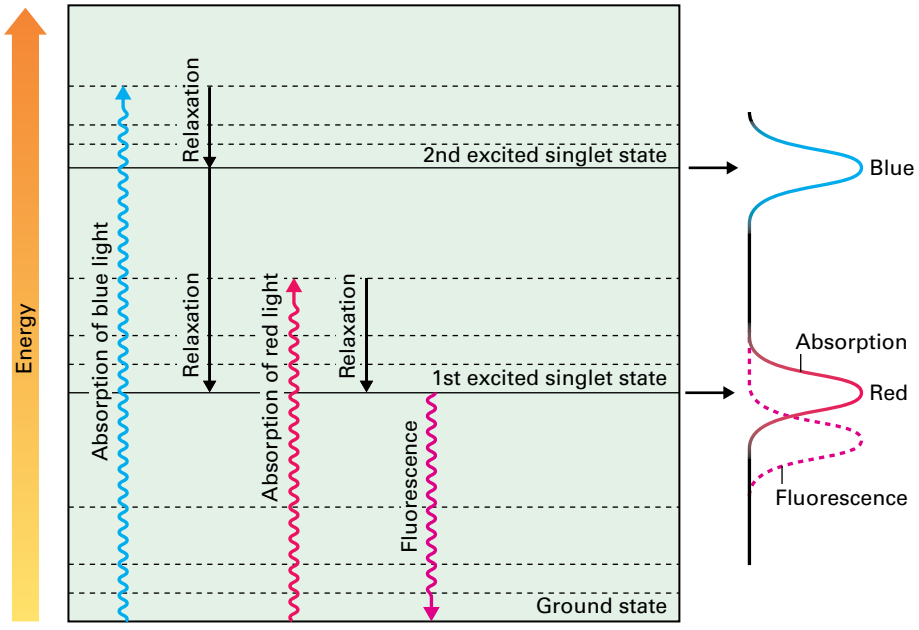


FIGURE 12.3 *Energy levels in the chlorophyll molecule. Absorption of blue or red light causes the chlorophyll molecule to convert into an excited state, with blue light absorption resulting in a higher excited state because of the greater energy of blue light relative to red light. Internal conversions or relaxations convert higher excited states to the lowest excited state, with a concomitant loss of energy as heat. Light may be reemitted from the lowest excited state through fluorescence. The spectra for fluorescence and absorption are shown at the right of the figure. The short-wavelength absorption band corresponds to a transition to the higher excited state, and the long-wavelength absorption band corresponds to a transition to the lower excited state.*

and one in the red. Excitation causes transitions from the lowest substate of the ground state to any one of these higher-energy substates, depending on the energy relationship shown in Equation 12.3. The existence of this series of substates in molecules yields broad absorption bands rather than the sharp absorption bands found with atoms.

In molecules, two types of excited states can exist. The singlet state is relatively short-lived and contains electrons with opposite (antiparallel) spins; the more long-lived **triplet state** has electron spins that are aligned (parallel). Triplet states generally have much longer lives (take longer to de-excite) than singlet states and are at a lower energy level. Transitions from the singlet state to the triplet state can occur, but these are low-probability events.

Once excited, an electron can return to the more stable ground state by one of several paths, and in each, the energy released may take several forms. In the simplest case, the energy is released as heat during a nonradiative decay (**relaxation**) (Fig. 12.3). A second mechanism involves the emission of a photon in a process known as **fluorescence** (Fig. 12.3). The emitted light has a longer wavelength than the absorbed light because fluorescence always arises from decay from the first excited state to the ground state and is preceded by de-excitation from higher substates to the first excited state via vibrational relaxations. Measurements of chlorophyll fluorescence are used to investigate the efficiency and regulation of photosynthesis (Box 12.2). A third mechanism, **energy transfer**, involves the transfer of energy to another molecule, usually one in close proximity to the excited molecule. This process is an important vehicle for the movement of absorbed light energy through an array of pigment molecules. Finally, the excited molecule may lose an electron to an electron-acceptor molecule through a **charge separation** event, in which the excited pigment reduces an acceptor molecule. This last mechanism, called **photochemistry**, converts light energy into chemical products (Reaction 12.5) and is central to the process of photosynthesis.

Reaction 12.5: Photochemistry

$$\text{Pigment} + \text{acceptor} \xrightarrow{h\nu} \text{pigment}^{*} + \text{acceptor} \rightarrow \text{pigment}^{+} + \text{acceptor}^{-}$$

With several avenues of relaxation available, what dictates the fate of the excited state? Simply this: the process with the fastest rate is favored over others and predominates. For many of the pigments found in the photosynthetic apparatus, fluorescence occurs in nanoseconds (ns, 10^{-9} s); however, photochemistry in photosynthetic organisms occurs more rapidly, in picoseconds (ps, 10^{-12} s) (Section 12.3.2). Thus, when the 1,000-fold more rapid pathway of photochemistry is available, little fluorescence is observed and photosynthesis proceeds with high efficiency. The singlet state of the photosynthetic pigment chlorophyll (see Section 12.2.3) participates in energy transfer and photochemistry. The relatively long half-life for triplet-state chlorophyll (as evidenced by how long it takes the molecules in the triplet state to diminish to one-half their original number) suggests that it is not an intermediate in the charge separation events in photosynthesis.

Using Equation 12.4, we can estimate the efficiency of photochemistry in any system by determining the **quantum yield,** phi (Φ), of the photochemical event. According to this equation, a quantum yield of 1.0 would indicate that every absorbed photon is converted into chemical product; lower values indicate other decay pathways diminish the efficiency of the photochemical reaction. In photosynthetic systems under optimum conditions, the measured quantum yield of photochemistry is approximately 1, indicating that other decay routes do not occur to any substantial extent and that almost all absorbed photons are utilized for photochemical charge separation. Losses in efficiency in other steps of the primary photochemical event are associated with the stabilization of some of the photochemical reaction products.

BOX 12.2

Biophysical techniques are used to investigate photosynthesis

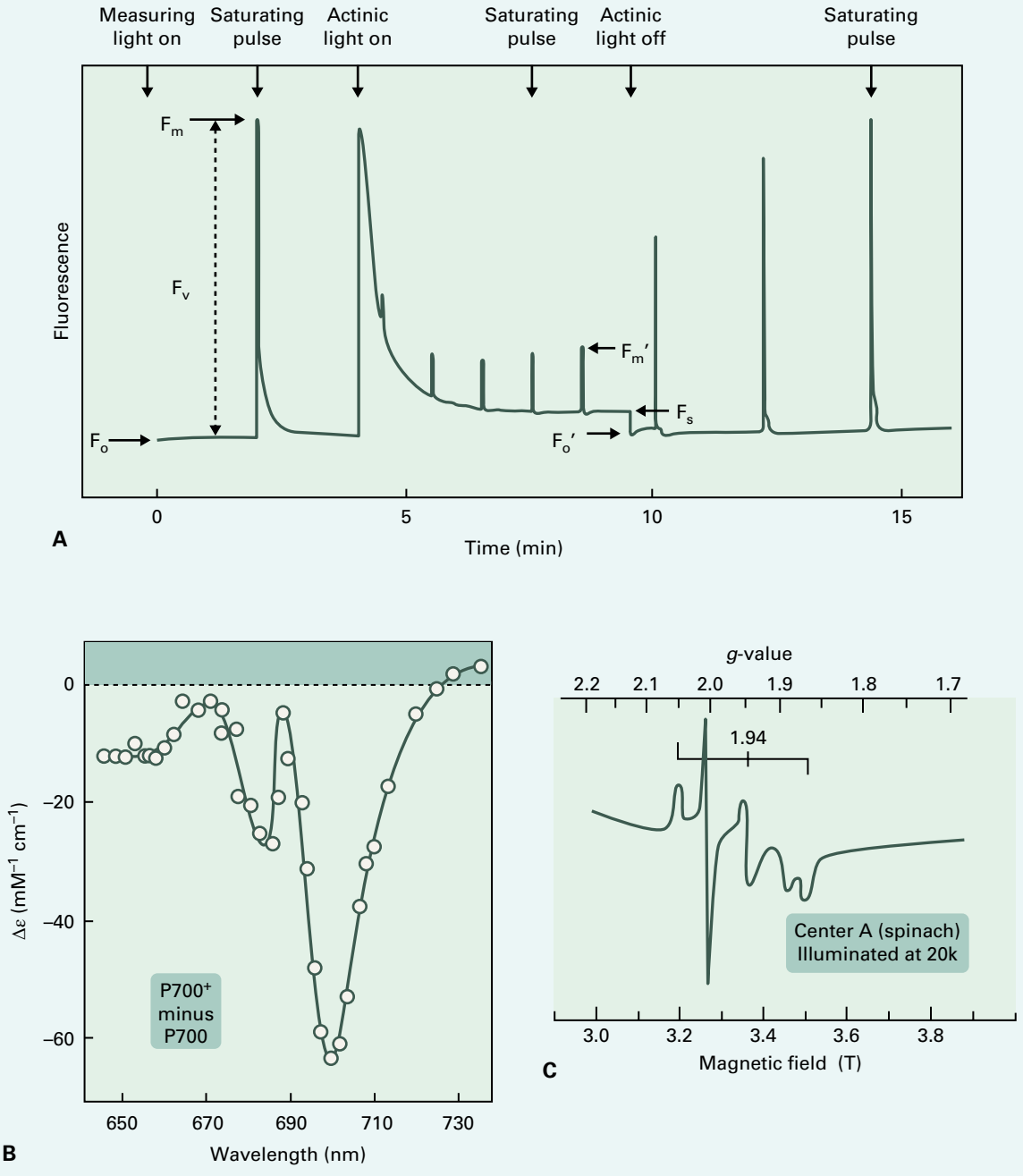
Studies of photosynthesis, particularly those related to the light reactions, have benefited from a vast array of techniques used to examine specific components of the photosynthetic apparatus and their function. For example, measurements of chlorophyll fluorescence are used to investigate the efficiency of photosynthesis and energy transfer during photosynthetic light harvesting. At ambient temperatures, most fluorescence comes from chlorophyll *a* molecules associated with PSII. Although the quantum yield of chlorophyll *a* fluorescence in plants is only 0.6–3% under these conditions, it provides useful information about energy transfer, photochemistry, and nonradiative dissipation of absorbed light energy. These mechanisms all involve the singlet excited state of chlorophyll, so changes in these pathways for de-excitation of singlet excited chlorophyll affect chlorophyll fluorescence yield. A pulse-amplitude-modulated (PAM) fluorometer can measure parameters that reflect several aspects of photosynthesis in varying light, such as the maximum efficiency of PSII (F_v/F_m, where the variable fluorescence F_v is the difference between the maximum fluorescence F_m and the minimum fluorescence F_o in the dark-acclimated state) and the nonradiative dissipation of energy (NPQ = $F_m/F_m' - 1$, where F_m' is the maximum fluorescence in the light) (A). Chlorophyll fluorescence can also be measured at low temperature (77K), which enables one to distinguish and measure the antenna associated with both PSII and PSI.

Various spectroscopic techniques are also used in studies of the light reactions, taking advantage of the many oxidation–reduction reactions that occur during photosynthesis as a result of light conversion and subsequent electron transfer events. These approaches rely on characteristic "signatures" that distinguish the oxidized and reduced species of a given molecule. When these molecules engage in electron transfer reactions, changes in their redox state can be monitored. Two techniques that have been widely applied to these systems are optical absorption spectroscopy, based on the interaction of light with the molecules, and electron paramagnetic resonance (EPR) spectroscopy, based on the magnetic properties of the molecules.

Absorption spectroscopy has been used extensively to detect the state of pigment molecules. Such measurements have provided important details on the kinds of pigments found in photosynthetic membranes and their organizational features. An extension of this technique is absorption difference spectroscopy, which has been applied to the study of pigments that show absorption changes under differing conditions, for example, when they undergo oxidation–reduction reactions in the light. Because the concentration of these molecules in the photosynthetic membrane is low and is masked by the large absorption of pigmented molecules that do not undergo redox changes, these small absorption changes are difficult to detect. By measuring the difference in the redox state of the molecule in the light versus that in the dark, one can detect these small absorption changes without needing to obtain the absolute spectrum of the component. For example, the reaction center chlorophyll P700 takes its name from such a change, a decrease centered at approximately 700 nm when this pigment undergoes oxidation in the light (B). Other electron carriers also have characteristic absorption changes associated with their oxidation or reduction. This trait allows the monitoring of any individual component in a complex mixture of components, such as are found in a photosynthetic membrane. To obtain these spectra, one can activate the samples by using either steady-state illumination lasting 1 or more seconds or ultrashort flashes, in the range of picoseconds, nanoseconds, or microseconds. The latter technique allows determination of the time-resolved kinetics of a particular redox process. In the case of submicrosecond measurements, the technology is rather sophisticated, using high-energy lasers as the light source. Such measurements have been used to identify early intermediates in the charge separation events in photosynthesis, as well as to monitor the overall kinetics of specific electron transfer events.

Another useful spectroscopic technique applied to photosynthetic systems is electron paramagnetic spin resonance (EPR) spectroscopy, also known as electron spin resonance (ESR). Instead of measuring changes related to the optical properties of molecules as occur during optical absorption spectroscopy, EPR is based on the magnetic properties of paramagnetic molecules, those that contain unpaired electrons. For example, in all photosynthetic reaction centers, both the oxidized and the reduced products of the primary charge separation event are paramagnetic (having been generated by the transfer of a single electron), and both can be detected by the EPR technique. In addition, the process of oxidation and reduction of electron carriers in the electron transfer chain alters the number of unpaired electrons in these molecules. EPR detects transitions that occur between electron spin states that have been established by placing the paramagnetic molecule in a magnetic field. Researchers can use this technique not only to follow the redox state of the electron carrier, but also to gather information on the chemical nature of the paramagnetic species. Different paramagnetic species are characterized by different values for *g* (a unitless number associated with paramagnets). For example, the free electron

(a theoretical construct) has a *g*-value of 2.0023, whereas the unpaired electron in a photooxidized molecule of the reaction center of chlorophyll has a *g*-value of 2.0026 and the plastosemiquinone free radical has a *g*-value of 2.0045. These slight differences are related to the environment of the unpaired electron in each molecule, relative to a free electron not subject to environmental influences. Metal ion-containing centers, such as iron–sulfur (Fe–S) centers found in ferredoxin and PSI, have more-complex EPR spectra because of the involvement of different orbitals for their unpaired electrons compared with those for free radicals. The first-derivative EPR spectrum of F_A (Fe–S center A) in PSI in liquid helium is shown in C. This Fe–S center is characterized by three *g*-values: 2.04, 1.94, and 1.86. F_B and F_X, the other Fe–S centers of PSI, have slightly different *g*-values, allowing for their spectral resolution. Copper-containing proteins in the Cu^{2+} state, such as the oxidized form of the copper-containing soluble protein plastocyanin, have *g*-values of 2.22 and 2.05, substantially different from the *g*-values for Fe–S centers. Cu^{+} is diamagnetic, so reduction of plastocyanin results in a loss of its EPR signal.



Equation 12.4: Quantum yield

$$\Phi = \frac{\text{number of products formed photochemically}}{\text{number of quanta absorbed}}$$

12.2.3 All photosynthetic organisms contain chlorophyll or a related pigment

All photoautotrophic organisms contain some form of the light-absorbing pigment **chlorophyll**. Plants, algae, and cyanobacteria synthesize chlorophyll, whereas anaerobic photosynthetic bacteria produce a molecular variant called **bacteriochlorophyll** (Fig. 12.4). (Some photoheterotrophic prokaryotes can synthesize ATP with light as the energy source by using retinal as a pigment bound to a rhodopsin-like protein; these species do not contain chlorophyll and, though fascinating, are tangential to the chlorophyll-based light reactions discussed here.)

Chlorophyll molecules contain a **tetrapyrrole** ring (porphyrin) structure like that found in the heme prosthetic group of hemoglobin and the cytochromes (see Chapter 14, Fig. 14.17). Several steps in the biosynthesis of chlorophyll and heme are shared; however, chlorophyll binds a magnesium (Mg) atom in the center of its tetrapyrrole ring, whereas heme binds an iron (Fe) atom. In addition, a long (C_{20}) hydrophobic side chain, known as a phytol tail, is attached to the tetrapyrrole ring structure of chlorophyll and renders the molecule extremely nonpolar. The biosynthetic pathway for

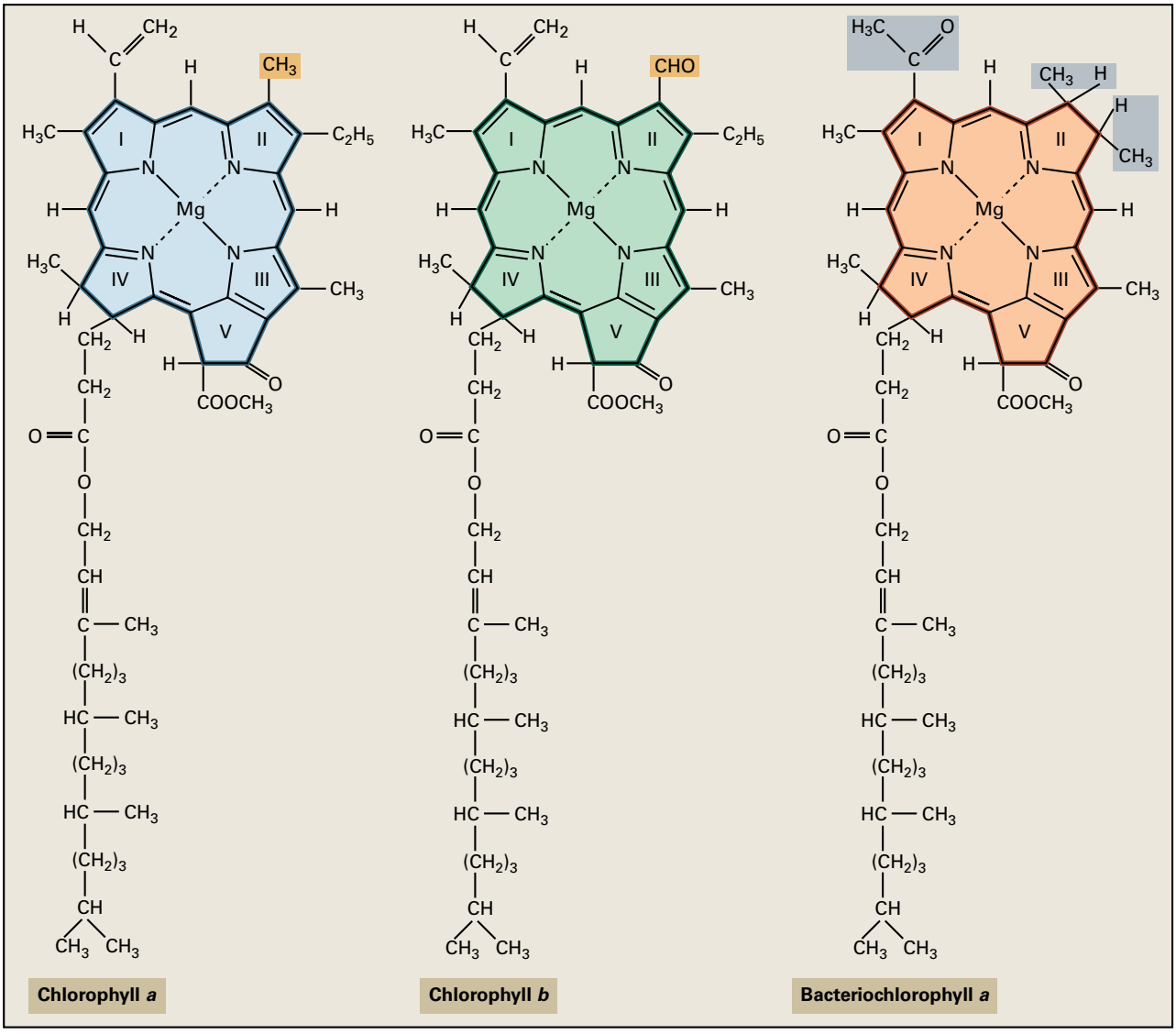


FIGURE 12.4 *Structures of chlorophylls. Chlorophyll molecules have a porphyrin-like ring structure that contains a central magnesium (Mg) atom coordinated to the four modified pyrrole rings. Chlorophylls also contain a long hydrocarbon tail that makes the molecules hydrophobic. Various chlorophylls differ in their substituents around the ring structure. In chlorophyll* a*, a methyl group is present, whereas in chlorophyll* b*, a formyl group is present at the same position. Bacteriochlorophyll, found in prokaryotic photosynthetic bacteria, also shows side-chain modifications when compared with the chlorophyll* a *molecule.*

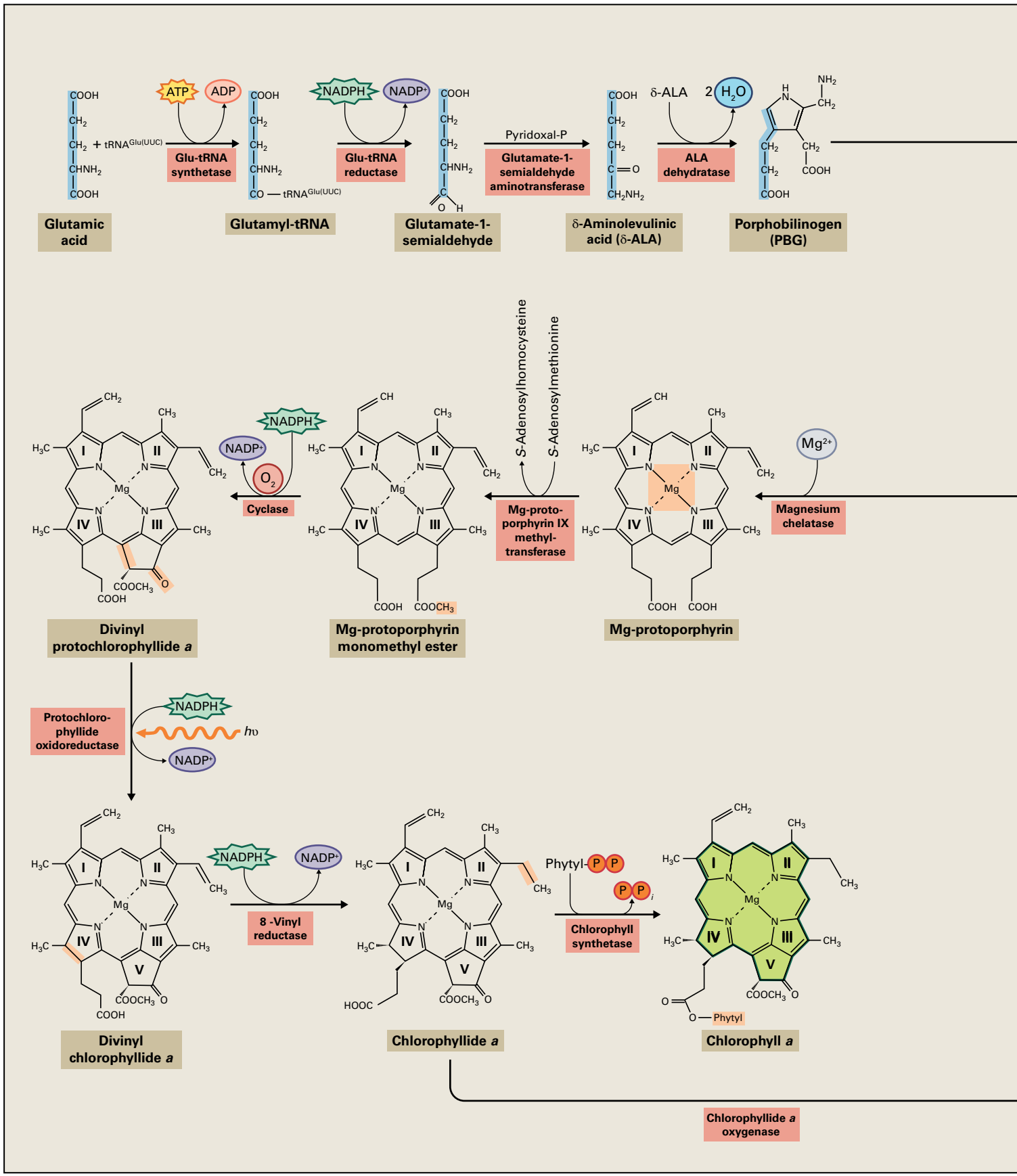
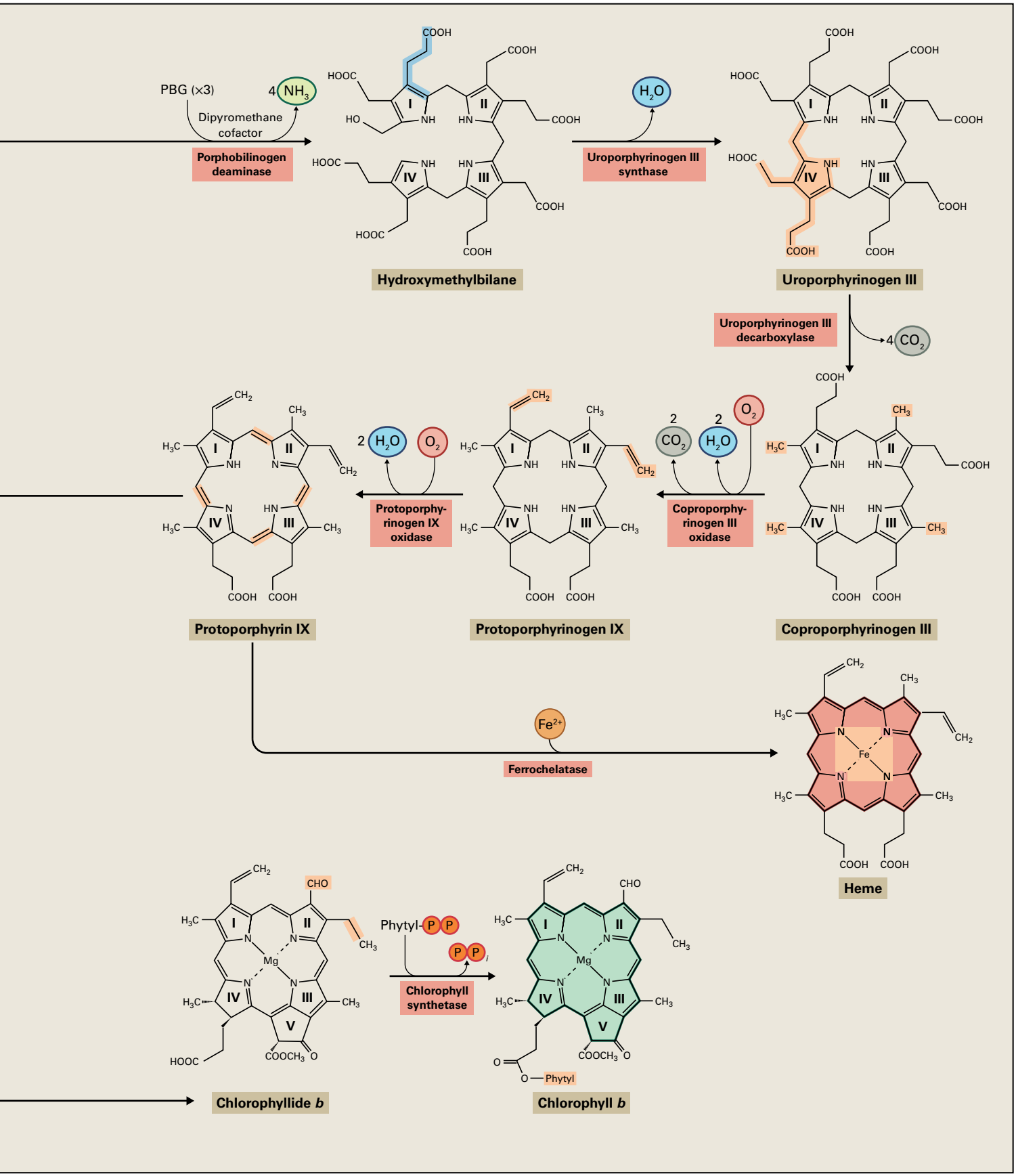


FIGURE 12.5 *Biosynthesis of chlorophylls and heme. The biosynthesis of chlorophylls and heme begins with the synthesis of δ-aminolevulinic acid (ALA) from glutamic acid. Two molecules of ALA react to yield porphobilinogen (PBG). Four molecules of PBG form the ring structure of protoporphyrin IX, the common branch point for the synthesis of heme and chlorophyll. To make chlorophyll, a magnesium chelatase inserts Mg into the protoporphyrin IX ring; during heme synthesis, an iron chelatase inserts Fe into the ring. Chlorophyll synthesis involves further modifications of the porphyrin structure, including formation of a fifth ring (V) and attachment of the phytyl chain. In angiosperms, synthesis of chlorophyll* a *requires a light-dependent protochlorophyllide reductase enzyme; synthesis of chlorophyll* b *is believed to occur with chlorophyllide* a *as the substrate.*

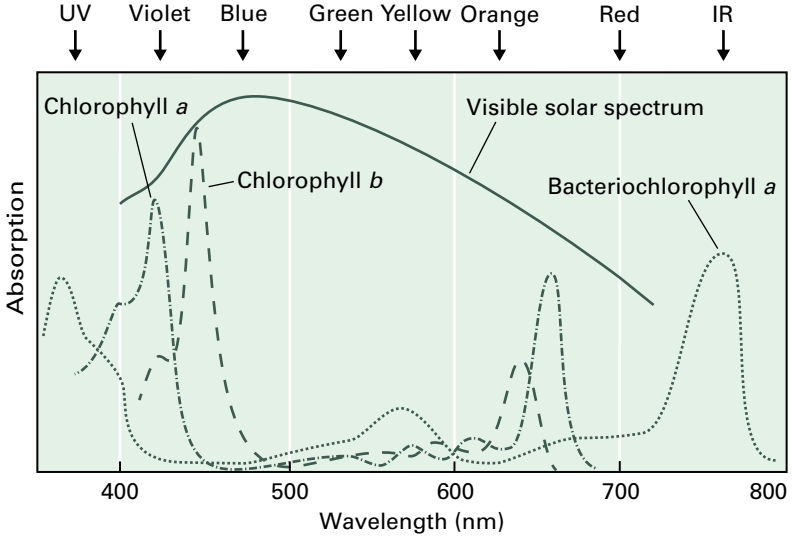

PBG (×3)
4 NH3
Dipyromethane cofactor
Porphobilinogen deaminase
Hydroxymethylbilane
H2O
Uroporphyrinogen III synthase
Uroporphyrinogen III
Uroporphyrinogen III decarboxylase
4 CO2
Coproporphyrinogen III
2 CO2
2 H2O
O2
Coproporphy-rinogen III oxidase
Protoporphyrinogen IX
2 H2O
O2
Protoporphy-rinogen IX oxidase
Protoporphyrin IX
Fe2+
Ferrochelatase
Heme
Phytyl-PP
PPi
Chlorophyll synthetase
Chlorophyllide b
Chlorophyll b
Phytyl

chlorophyll has been elucidated through a combination of labeling studies, enzyme biochemistry, and mutant analysis.

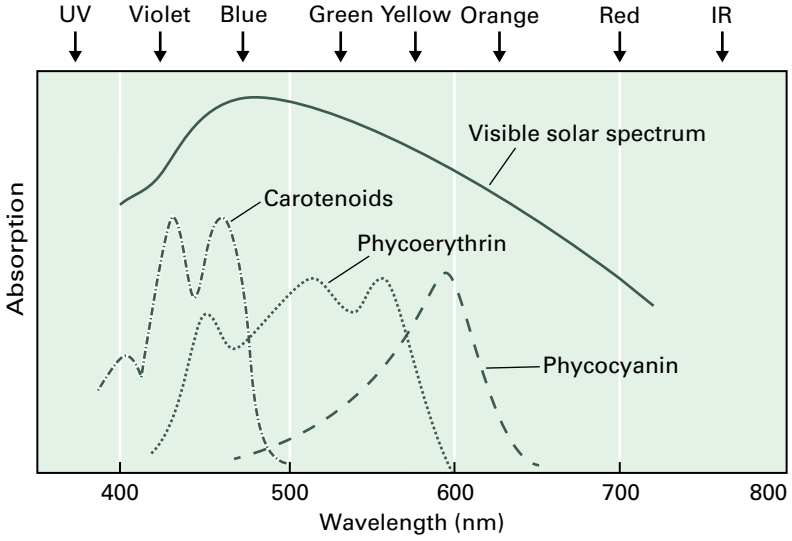
The first committed precursor in the biosynthesis of chlorophyll and heme is δ-aminolevulinic acid (ALA). In plants and cyanobacteria, ALA is produced from glutamate in a series of reactions involving $tRNA^{Glu}$ (Fig. 12.5). Although ALA synthesis differs in plants and animals, the reactions that convert ALA to the branch point intermediate, protoporphyrin IX, are common to both groups of organisms. Protoporphyrin IX can be converted to heme by ferrochelatase, which inserts the iron atom into the center of the ring.

In the first step of the chlorophyll branch of the pathway, magnesium (Mg)-chelatase inserts a magnesium atom instead of iron. Subsequent reactions, including a cyclization to form a fifth ring, convert Mg-protoporphyrin IX into protochlorophyllide, which is reduced to generate chlorophyllide. In angiosperms, protochlorophyllide reduction is strictly light dependent, whereas gymnosperms, many algae, and photosynthetic bacteria contain light-independent protochlorophyllide reductase, which allows these organisms to synthesize chlorophyll in the dark. The final step in synthesis of chlorophyll *a* involves esterification of the hydrophobic phytol side chain.

The distinct forms of chlorophyll have different side chains on the ring or different degrees of saturation of the ring system (see Fig. 12.4). For example, chlorophyll *b* is synthesized through the action of an oxygenase enzyme that converts a methyl to a formyl side group. These small changes in chemical structure substantially alter the absorption properties of the different chlorophyll species (Fig. 12.6A). Absorption is also affected by excitonic interactions with neighboring pigments and the noncovalent interaction of the molecule with chlorophyll-binding proteins found in the photosynthetic membrane. Chlorophyll is green because it absorbs light in



A Chlorophylls



B Other photosynthetic pigments

FIGURE 12.6 *(A) Absorption spectra of chlorophylls. The absorbance spectra of pigments dissolved in nonpolar solvents are shown for chlorophylls* a *and* b *and bacteriochlorophyll* a. *The visible region of the solar spectrum is also diagrammed. Note the spectra of these pigments show substantial shifts in absorption in vivo, where they are associated with specific proteins. (B) Absorption spectra of other photosynthetic pigments. The absorption spectrum of the carotenoids is for pigments dissolved in nonpolar solvents; the remaining spectra are for pigments in aqueous solution. UV, ultraviolet; IR, infrared.*

the 430-nm (blue) and 680-nm (red) wavelengths of the visible spectrum more effectively than it absorbs green light. The green light not absorbed is reflected, which makes it visible. It is worth noting that some oxygenic photoautotrophs, such as cyanobacteria and red algae, contain additional pigments, called phycobilins, that are linear tetrapyrroles. These pigments absorb green and blue-green light (Fig. 12.6B), enabling utilization of more of the visible light spectrum.

12.2.4 Carotenoids participate in light absorption and photoprotection

A second group of pigment molecules found in all photosynthetic organisms is the **carotenoids** (Fig. 12.7). This class of molecules includes the carotenes, which contain a conjugated double-bond system of carbon and hydrogen, and the xanthophylls, which in addition contain oxygen atoms in their terminal rings.

Carotenoids are tetraterpene (C_{40}) molecules derived from eight isoprene units, the products of the nonmevalonate pathway located in the chloroplast (see Chapter 24). Phytoene, the precursor to all carotenoids, is synthesized from two molecules of geranylgeranyl diphosphate. In plants, two desaturases, phytoene desaturase and zeta-carotene desaturase, and two isomerases, zeta-carotene isomerase and carotene isomerase, catalyze the reactions that convert phytoene to lycopene, which is cyclized on both ends to generate either β-carotene, with two β-ionone rings, or α-carotene, with one β-ionone ring and one ε-ionone ring (Fig. 12.7). Hydroxylation of α-carotene produces **lutein**, the most abundant xanthophyll in the plant chloroplast. Hydroxylation of β-carotene results in formation of zeaxanthin. Epoxidation of zeaxanthin yields violaxanthin, which can be converted to neoxanthin by formation of an allene bond and isomerization. Zeaxanthin can also be synthesized by de-epoxidation of violaxanthin in the so-called **xanthophyll cycle**, which is especially important at high light intensities (see Section 12.6.3). Many other carotenoids with diverse structures are synthesized by algae and photosynthetic bacteria.

Several steps of the carotenoid pathway are affected in mutants of plants such as maize (*Zea mays*) and *Arabidopsis*. The genes encoding many enzymes of the plant carotenoid biosynthesis pathway have been cloned by expression in *E. coli,* which does not ordinarily make carotenoids (Fig. 12.8). Carotenoids, which are responsible for the orange-yellow colors observed in the leaves of plants, absorb light between 400 and 500 nm, a range in which absorption by chlorophyll *a* is relatively weak (see Fig. 12.6B). As such, carotenoids play a minor role as accessory light-harvesting pigments, absorbing and transferring light energy to chlorophyll molecules. Carotenoids play an important structural role in the assembly of light-harvesting complexes (LHCs, see Section 12.3.8).

Carotenoids have an indispensable function in protecting the photosynthetic apparatus from photooxidative damage (see Chapter 22). They can accept excitation energy from both the triplet state of chlorophyll and the singlet state of oxygen. Singlet oxygen, generated by energy transfer from triplet chlorophyll, is toxic and the major type of reactive oxygen species that causes photooxidative damage in plants. If carotenoid biosynthesis is blocked by addition of inhibitors or by mutation, and the organism is then exposed to light in the presence of O_2, lethal concentrations of singlet oxygen are formed.

12.3 Photosystem structure and function

12.3.1 A photosystem consists of a photochemical reaction center and a light-harvesting antenna system

In photosynthesis, light energy is absorbed and converted into relatively stable chemical products by integral membrane pigment-protein complexes called **photosystems**. All photosystems contain a **reaction center**, where photosynthetic electron transfer begins with a charge separation, as well as an array of light-harvesting, or **antenna**, pigments that are bound by proteins. These antennae absorb light energy and transfer it to the reaction center, where excitation of specially bound chlorophyll (Chl) molecules results in transfer of an electron to an acceptor (A), as shown in Reaction 12.6. This is the primary photochemistry that initiates conversion of light energy into chemical energy.

Reaction 12.6: Photochemistry in a reaction center

$$\text{Chl A} \xrightarrow{h\nu} \text{Chl}^{*}\,\text{A} \rightarrow \text{Chl}^{+}\,\text{A}^{-}$$

The special chlorophyll in the reaction center can be excited directly by absorption of a photon, or it can be excited upon receipt of excitation energy from the antenna. Thus, the antenna, which consists of many pigment molecules, increases the absorption cross-section of the reaction center. Transfer of excitation energy in the antenna from one chlorophyll molecule to another occurs by a mechanism known as Förster energy transfer or resonance (Reaction 12.7). Proximity of the donor and acceptor molecules within the antenna is critical, because the efficiency of energy transfer is inversely proportional to the sixth power of the distance separating the two molecules. For two chlorophylls separated by approximately 10 Å, an energy transfer time of less than 1 ps has been observed. The relative orientation of the two pigments is also significant, and the fluorescence spectrum of the donor pigment and absorption spectrum of the acceptor pigment must overlap for efficient energy transfer. For antenna pigments in close proximity and proper spatial orientation, energy transfer can proceed with high speed and efficiencies approaching 99%.

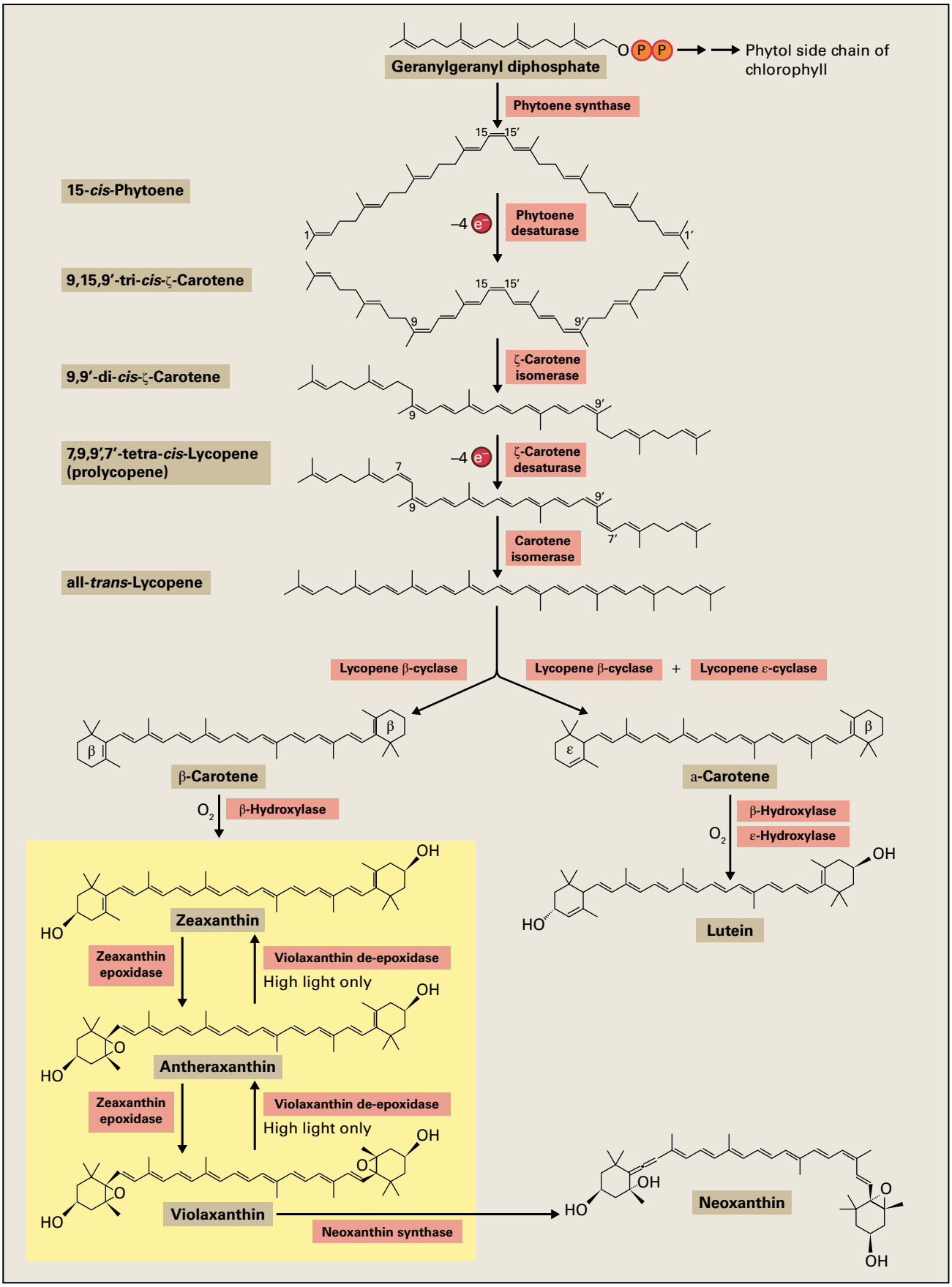


FIGURE 12.7 *Biosynthesis of carotenoids and xanthophylls in plants. The pathway for conversion of geranylgeranyl diphosphate to lycopene, shown in the upper half of the figure, involves desaturation and isomerization reactions. Two desaturases, phytoene desaturase (PDS) and zeta-carotene desaturase (ZDS), and two isomerases, zeta-carotene isomerase (Z-ISO) and carotene isomerase (CRTISO), participate in these reactions. The conversion of lycopene to carotenoids and xanthophylls is illustrated in the lower half. The Greek letters β and ε designate the ring structures of the two carotene species. The xanthophyll cycle (lower left) protects plants from high light intensities by converting violaxanthin into zeaxanthin, which participates in thermal dissipation of excess absorbed light energy.*

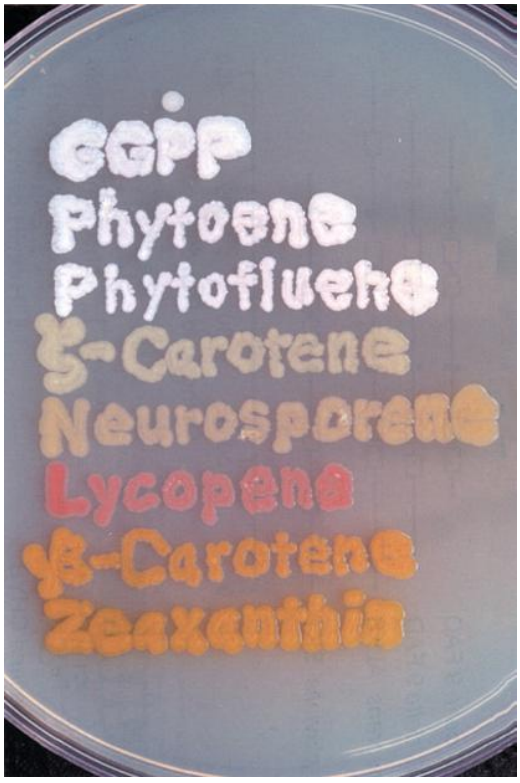


FIGURE 12.8 *E. coli colonies expressing genes in the carotenoid biosynthesis pathway. The name of each product is spelled out in colonies expressing that product.*
Source: Cunningham Jr. & Gantt (1998). Annu. Rev. Plant Physiol. Plant Mol. Biol. 49:557–583.

Reaction 12.7: Excitation energy transfer

$$Chl^*_{donor} + Chl_{acceptor} \rightarrow Chl_{donor} + Chl^*_{acceptor}$$

12.3.2 Reaction centers contain both special chlorophyll and electron acceptor molecules involved in energy conversion

Biochemical fractionation of detergent-solubilized photosynthetic membranes has led to the isolation of reaction centers from anoxygenic bacteria, cyanobacteria, algae, and plants that are capable of performing the initial photochemistry in vitro. Spectroscopic studies have indicated that the reaction center chlorophyll participating in the primary charge separation event shown in Reaction 12.7 is composed of more than one chlorophyll or bacteriochlorophyll molecule. In the case of the reaction center complex from the purple bacterium *Rhodobacter sphaeroides,* this pigment is a pair of bacteriochlorophylls that has been named P865 after the wavelength of light for which oxidation-linked changes in absorbance are greatest (Box 12.2). This absorbance change associated with the primary charge separation provides a means to detect and quantitate reaction centers.

In addition to chlorophyll, reaction center complexes contain a series of electron acceptors. The chemical nature of these acceptor molecules depends on the type of reaction center. A general feature of electron transfer events in all reaction centers is the transfer of an electron from the special chlorophylls, such as P865, to another pigment molecule, such as a bacteriopheophytin (pheophytin is a chlorophyll derivative lacking Mg), or even to another chlorophyll molecule. This reaction is followed by subsequent electron transfer to nonpigment molecules, either quinones or Fe–S centers, that further stabilize the charge-separated state. The generalized sequence of events is described in Reaction 12.8.

Reaction 12.8: Primary charge separation in the reaction center

$$P^* ChlA_0A_1A_2 \rightarrow P^+Chl^-A_0A_1A_2 \rightarrow$$
$$P^+ChlA_0{}^-A_1A_2 \rightarrow P^+ChlA_0A_1{}^-A_2 \rightarrow P^+ChlA_0A_1A_2{}^-$$

The kinetics of the primary photochemistry in reaction centers have been studied in great detail. Within several picoseconds of the initial charge separation event of photosynthesis, the light energy conversion reaction is complete and chemical products have been formed. The technique of ultrafast absorbance spectroscopy, in which extremely short laser flashes activate electron transfer components in the reaction center complex, has made it possible to follow the electron transfer steps, from the special chlorophylls to the sequential electron acceptors. In the purple bacterial reaction center, the initial charge separation event, resulting in the formation of oxidized bacteriochlorophyll ($P865^+$) and a reduced adjacent bacteriochlorophyll ($BCh a^-$), takes place in approximately 3 ps. The next step, reduction of the bacteriopheophytin electron acceptor ($BPh a^-$), occurs in only 1 ps. After an additional 100–200 ps, the electron has been transferred to a bound quinone (Q_A).The terminal quinone electron acceptor (Q_B) is reduced on a slower (microsecond) time scale (Fig. 12.9).

12.3.3 Oxygenic photosynthetic organisms contain two photochemical reaction centers, PSI and PSII

Reaction centers can be divided into two basic types, depending on the nature of the electron acceptor. A reaction center that ultimately reduces an Fe–S cluster is a Type I (or Fe–S type) reaction center, whereas one that reduces a quinone is a Type II (or Q type) reaction center. The photosynthetic membranes of anoxygenic photosynthetic bacteria contain only one type of reaction center, which varies among organisms. For example, green sulfur bacteria and heliobacteria contain a Type I reaction center; purple bacteria have a Type II reaction center.

By contrast, all O_2-evolving organisms, including cyanobacteria, algae, and plants, contain both Type I (PSI) and Type II (PSII) reaction center complexes. Thus, PSII contains electron carriers similar to those in the purple bacterial

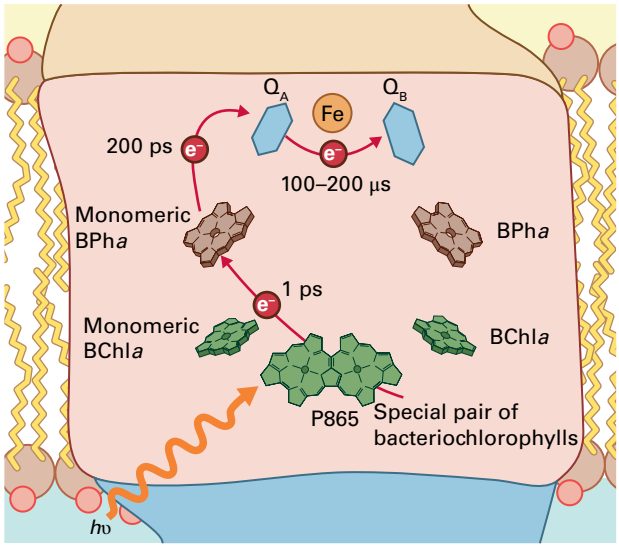


FIGURE 12.9 *Kinetics of electron transfer in the purple bacterial reaction center. The special pair of bacteriochlorophylls in the reaction center undergoes oxidation in the light. The electron lost from P865 is rapidly transferred to a monomeric bacteriochlorophyll (BChla) and then on to bacteriopheophytin (BPha). These initial reactions occur in only a few picoseconds. In approximately 200 ps, this electron is transferred to one of two ubiquinone molecules, Q_A, and then on to a second ubiquinone, Q_B, on a slower time scale. The electron transfer proceeds unidirectionally through one of the two symmetrical cofactor branches.*

TABLE 12.1 *Electron transfer carriers in the PSI and PSII reaction centers.*

Carrier	PSI	PSII
Reaction center chlorophylls	P700, Chl_A, and Chl_B	P680 and Chl_{D1}
A_0	Chlorophyll *a*	Pheophytin *a*
A_1	Phylloquinone	Plastoquinone (Q_A)
A_2	F_X (Fe–S center)	Plastoquinone (Q_B)

reaction center (pheophytin, quinones), whereas PSI contains bound Fe–S centers as stable electron acceptors (Table 12.1). The chlorophylls that undergo light-induced oxidation in PSI and PSII have been named P700 and P680, respectively, referring to absorbance bands in the difference spectra (Box 12.2) for these pigments.

12.3.4 All reaction centers have a homologous core structure

A major advance in understanding the structure and function of reaction centers came with the determination of the structure of the Type II reaction center complex from the photosynthetic purple bacterium *Rhodopseudomonas viridis* by X-ray crystallography. The core of the structure consists of a heterodimer of two homologous proteins, L and M, each of which has five transmembrane α-helices (Fig. 12.10A). The similarity of L and M suggests they arose by gene duplication of an ancestral reaction center, a homodimer. Together, these two proteins bind all the pigments and cofactors involved in the primary charge separation and electron transfer. The electron carriers are organized in a pseudosymmetrical arrangement of two branches (Fig. 12.10B); however, only one of the two symmetrical pathways available to the electron is used. The second arm remains inactive for reasons that seem to be related to the dynamics of the protein environment.

Subsequent determination of the crystal structures of PSII and PSI from cyanobacteria revealed that these reaction centers share a conserved core structure with the purple bacterial reaction center. The heterodimer in PSII is composed of the D1 and D2 proteins, which are homologous to L and M in the bacterial reaction center. In addition to the symmetrical pair of five transmembrane helices contributed by D1 and D2, two related proteins with six transmembrane helices each (CP47 and CP43) constitute the core antenna of PSII (Fig. 12.10A). In PSI, the cofactor-binding and core antenna domains are combined in the PsaA and PsaB proteins, which have 11 transmembrane helices each (Fig. 12.10A). Although the primary amino acid sequences of the PSII and PSI core proteins have diverged substantially, the arrangement of the transmembrane helices and the positions of the electron carriers are similar (Fig. 12.10). This structural homology suggests that all photosynthetic reaction centers (Type I and Type II) evolved from a common ancestor.

12.3.5 PSII is a light-driven water-plastoquinone oxidoreductase

PSII is an integral membrane complex containing the P680 reaction center, and X-ray crystallography of the cyanobacterial complex confirmed it is a dimer of two reaction centers, as indicated by earlier biochemical studies. PSII from plants is also found as a dimer, but its molecular structure has not been determined.

In addition to the electron transport components involved in the primary charge separation, each monomer in the PSII complex contains more than 20 proteins plus antenna pigments and several lipids. The core of the monomeric form of the PSII reaction center complex is shown schematically in Figure 12.11. As mentioned above, two proteins (D1 and D2) bind electron transfer prosthetic groups, such as P680, pheophytin, and plastoquinone. Other proteins, such as CP43 and CP47, bind core antenna pigments (chlorophyll *a* and β-carotene). Still other PSII proteins on the luminal side of the complex are involved specifically in water oxidation. The functions of many of the remaining low molecular-mass subunits, including cytochrome b_{559}, remain unknown.

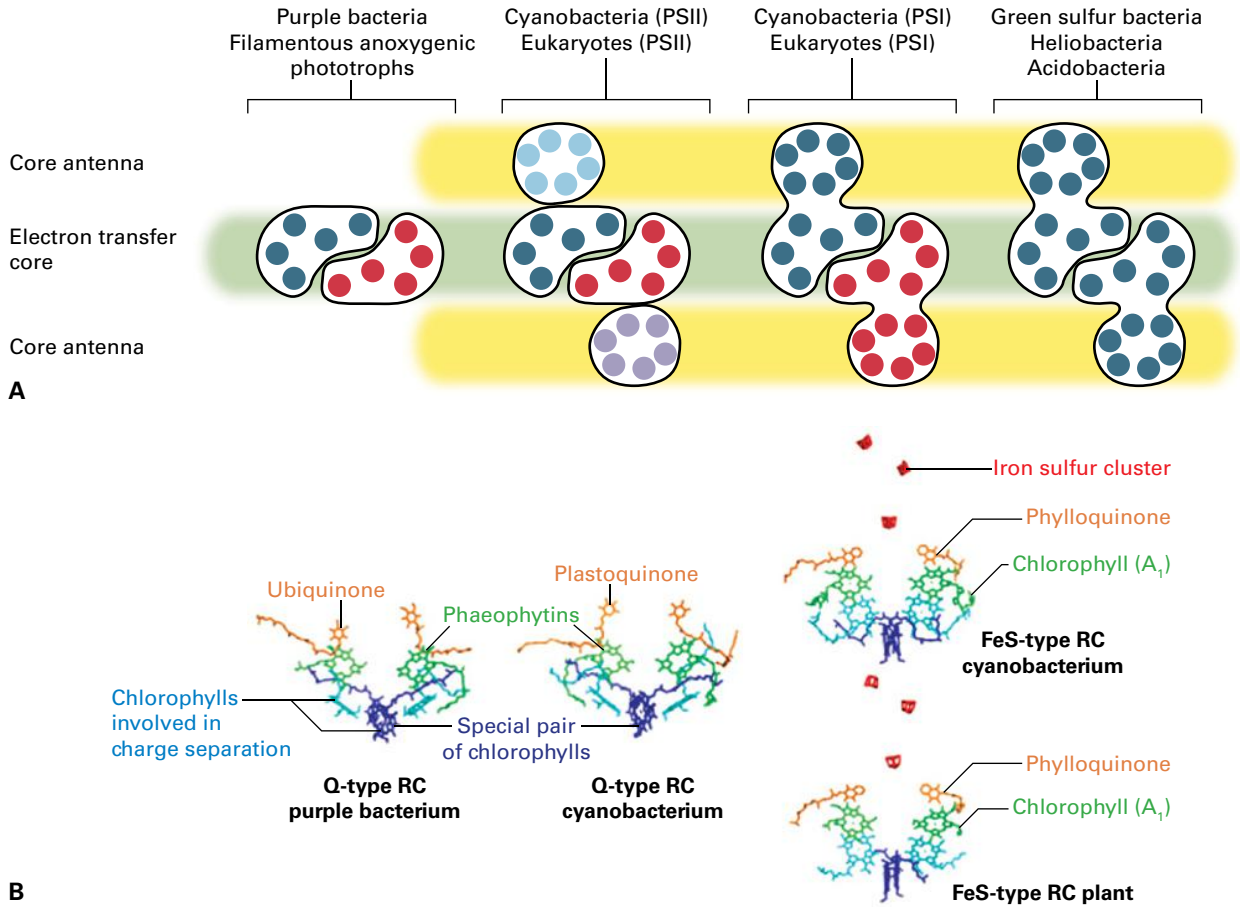


FIGURE 12.10 *(A) Schematic depiction of the organization of homologous transmembrane helices (shown as circles) in different photosynthetic reaction centers. Photosynthetic purple bacteria, such as* Rhodopseudomonas viridis *and* Rhodobacter sphaeroides*, have a Type II reaction center with a heterodimeric core of L and M subunits, represented by the proteins with five blue and five red circles, respectively. PSII of cyanobacteria and photosynthetic eukaryotes is a Type II reaction center with a heterodimeric core of D1 and D2 subunits (proteins with five blue and five red circles, respectively) and two core antenna subunits (CP47 and CP43, depicted as proteins with six purple and six light blue circles, respectively). In PSI, the core antenna moiety is fused with the core domain in a heteromer of PsaA and PsaB proteins (shown as proteins with 11 blue and 11 red circles, respectively) that constitute a Type I reaction center. Green sulfur bacteria, heliobacteria, and acidobacteria have a Type I reaction center that is homodimeric (depicted as two proteins with 11 circles each). (B) Organization of electron transfer carriers in different photosynthetic reaction centers, based on X-ray crystallography. Each series of electron carriers is organized around a pseudo-twofold axis of symmetry.*

Table 12.2 summarizes the properties of some of the polypeptide components of the PSII core complex (most of the smaller and more peripheral subunits are not included). Molecular genetic studies have revealed that several of the low molecular-mass proteins in PSII are required for assembly and stabilization of active PSII complexes.

In the light, PSII functions as a water-plastoquinone oxidoreductase, transferring electrons from water to plastoquinone via only one of the two cofactor branches. The kinetics of the electron transfer reactions in PSII, by which plastoquinone is reduced, are shown in Figure 12.12. Following excitation of the special chlorophylls in the reaction center, the $P680^{+}Pheo^{-}$ radical pair is established quickly, within a few tens of picoseconds. Like the purple bacterial reaction center, the PSII reaction center complex binds two quinones, denoted Q_A and Q_B. Q_A is bound tightly to the PSII reaction center and functions as the first relatively stable electron acceptor. Q_B, which is bound more loosely, functions as a secondary electron acceptor. Reduction of the two quinones proceeds through a five-step process:

1. The first electron is released from P680 and transferred to Q_A to produce a plastosemiquinone, Q_A^{-}.
2. This electron is then transferred to Q_B to yield the semiquinone Q_B^{-}. The loss of the electron returns Q_A^{-} to Q_A.
3. A second electron is then transferred from P680 to Q_A to produce a second Q_A^{-}.
4. The second electron is subsequently transferred from Q_A^{-} to Q_B^{-} to produce a fully reduced Q_B^{2-} molecule. Again, Q_A^{-} reverts to Q_A.
5. Finally, the fully reduced Q_B^{2-} takes up two protons from the stromal side of the membrane, yielding a plastoquinol, Q_BH_2.

According to this model, under physiological conditions Q_A is capable only of single electron reduction to the semiquinone

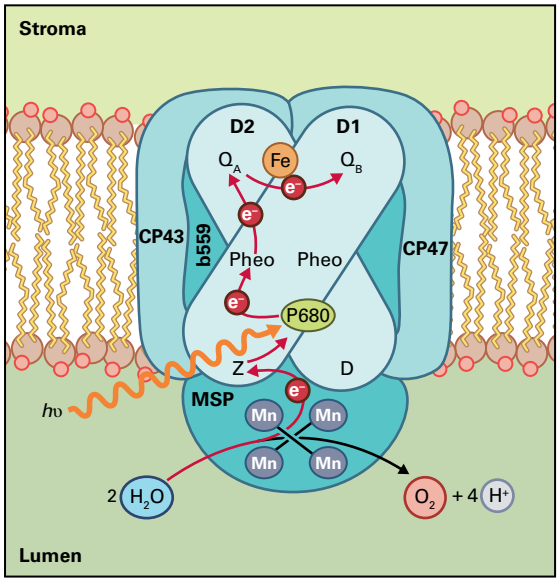


FIGURE 12.11 *Schematic diagram of the reaction center core of monomeric PSII. The D1 and D2 proteins bind most of the cofactors involved in charge separation and electron transport. Electrons are transferred from P680 to pheophytin (Pheo) and subsequently to two plastoquinone molecules, Q_A and Q_B. The nonheme iron (Fe) does not have a direct role in electron transfer. $P680^+$ is reduced by Z, a tyrosine residue in the D1 subunit. Also indicated is the oxidation of water by the Mn cluster, which is bound to the luminal side of the complex and stabilized by a peripheral protein, PsbO (labeled as MSP). CP43 and CP47 are chlorophyll* a*-binding core antenna proteins. D1 is susceptible to photooxidative damage and undergoes active turnover (see Chapter 10, Box 10.8).*

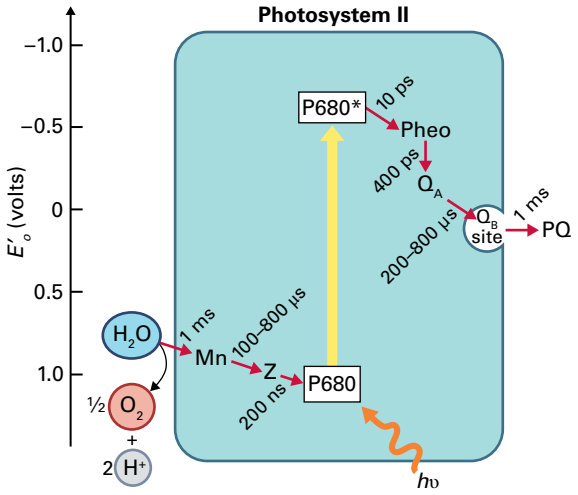


FIGURE 12.12 *PSII electron carriers and the kinetics of electron transfer. Pheophytin receives an electron from P680 and transfers it to the first of two plastoquinones (Q_A), which is bound tightly to the complex; the second plastoquinone, being mobile, is able to bind the Q_B site when oxidized (PQ), but not when fully reduced (PQH_2). Transfer of a single electron to Q_A occurs in approximately 400 ps. Reduction of PQ bound in the Q_B site to form the semiquinone PQ^- occurs in approximately 200–400 μs, whereas the second reduction to form PQH_2 takes place in 800 μs. Overall, within 1 ms, the oxygen-evolving complex is oxidized by one electron and the quinone is reduced by one electron for each charge separation in PSII.*

TABLE 12.2 *Protein subunits of the plant PSII core complex. Most of the smaller and more peripheral subunits are not included.*

Protein	Gene	Location of gene[b]	Mol. mass (kDa)	Function
Hydrophobic subunits				
D1	*psbA*	Chloroplast	32	Reaction center protein
D2	*psbD*	Chloroplast	34	Reaction center protein
CP47	*psbB*	Chloroplast	51	Core antenna
CP43	*psbC*	Chloroplast	43	Core antenna
Cyt. *b*-559 α Subunit	*psbE*	Chloroplast	9	Unknown
Cyt. *b*-559 β Subunit	*psbF*	Chloroplast	4	Unknown
PsbH	*psbH*	Chloroplast	10	Unknown
PsbI	*psbI*	Chloroplast	4.8	Assembly
Hydrophilic subunits				
33 kDa	*psbO*	Nucleus	33	O_2 evolution
23 kDa	*psbP*	Nucleus	23	O_2 evolution
17 kDa	*psbQ*	Nucleus	17	O_2 evolution

level, whereas Q_B can switch between three states: the fully oxidized quinone Q_B, the semiquinone Q_B^-, and fully reduced quinol Q_B^{2-}. After reduction and protonation, Q_BH_2 dissociates from the PSII reaction center complex and diffuses into the lipid bilayer of the membrane to function as a mobile electron carrier. The Q_B site on the reaction center complex is filled with another plastoquinone from the pool of quinone molecules diffusing in the membrane.

The reduction of Q_A occurs in about 200 ps because this reaction is linked to the primary charge separation. The reduction of Q_B is slower, requiring 100 µs. This indicates that Q_B^- must bind to the PSII reaction center complex while waiting to receive a second electron. In contrast, the binding of Q_BH_2 is relatively weak: This quinol is easily displaced from its binding site by fully oxidized quinones.

12.3.6 Oxidation of water produces O_2 and releases electrons required by PSII

P680, the reaction center chlorophyll of PSII, undergoes light-induced oxidation to produce the strong oxidant, $P680^+$, which can oxidize water to release O_2. This implies that the oxidation-reduction midpoint potential of the $P680/P680^+$ couple is greater than +820 mV at pH 7, because splitting water requires at least this much oxidizing potential. In fact, the midpoint potential of $P680^+$ is estimated to be between +1.2 and +1.4 V, making it the most oxidizing molecule in biology. The oxidation of water is not a direct process, but involves a complex series of reactions on the oxidizing (luminal) side of PSII. The oxidation of water involves the transfer of four electrons:

Reaction 12.9: Oxidation of water

$$2H_2O \rightarrow O_2 + 4H^+ + 4e^-$$

Analysis of the thermodynamics of water oxidation has been used to predict that this reaction occurs in either two steps involving two electrons each, or one step involving four electrons. Single-electron transfers would form highly energetic oxidant intermediates that would destroy components of the photosynthetic membrane system. This implies the existence of a charge-storage apparatus on the oxidizing side of PSII that can couple the single positive charges produced in the reaction center at P680 with the multiple positive charges required for water oxidation.

The mechanism of O_2 evolution has been investigated by measuring the amount of O_2 evolved after a series of short flashes of light. With dark-adapted chloroplasts, little O_2 appears after the first two flashes, but maximum amounts of O_2 appear after the third flash and after every subsequent fourth flash. The evolution finally reaches a steady-state level after a large number of flashes (Fig. 12.13).

The S-state model (Fig. 12.14) was proposed to explain these observations. This model postulates a light-driven charge-

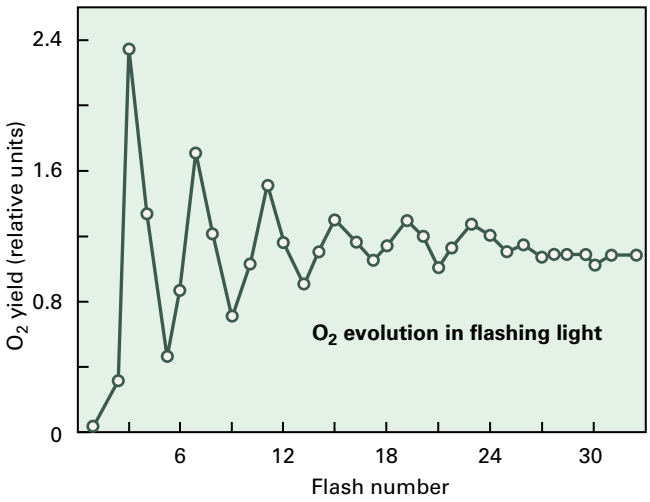


FIGURE 12.13 *O_2 evolution in flashes. The pattern of O_2 evolution is shown in response to a series of short flashes of light. The maximum amount of O_2 is produced on the third flash, after which a periodic spike is observed after every fourth flash. The flash yield damps out after approximately 20 flashes to a steady-state value.*

accumulation mechanism by which the oxygen-evolving machinery of PSII progresses through five successive states of increasing oxidation, S_0 through S_4, with S_4 being a strong oxidant capable of oxidizing water. Each charge separation event in the P680 reaction center yields $P680^+$, which ultimately oxidizes the charge accumulator, advancing it to the next S-state and increasing its charge by +1. The only state from which O_2 is evolved is S_4.

In dark-adapted chloroplasts, the charge accumulator is predominantly in the S_1 state, resulting in a maximum yield of O_2 on the third flash, as observed experimentally (see Fig. 12.13). The first flash advances the oxidation state from the dark-adapted S_1 to S_2. The second flash oxidizes S_2 to S_3, and the third flash yields the strong oxidant, S_4, triggering the evolution of oxygen and returning the charge accumulator to the S_0 state. Each succeeding cycle required four flashes because four photons are required per O_2 evolved. The reactions are complicated by "misses" (a flash that fails to oxidize P680), "double hits" (one flash oxidizes P680 twice), and "relaxations" (S_2 or S_3 decays to S_1 in the dark). Such events cause the oxygen yield to stabilize over a series of many flashes. In general terms, however, the S-state scheme has provided an excellent explanation for many of the basic observations on O_2 evolution.

12.3.7 The catalytic site for water oxidation is a Mn_4CaO_5 cluster

The S-state model does not provide a direct biochemical framework for understanding O_2 evolution, so what is the chemical nature of the S-state charge accumulator? Early findings that manganese (Mn) deficiency in algae or chloroplasts affects O_2 evolution, as well as findings in subsequent studies, have led to acceptance that Mn is the main charge

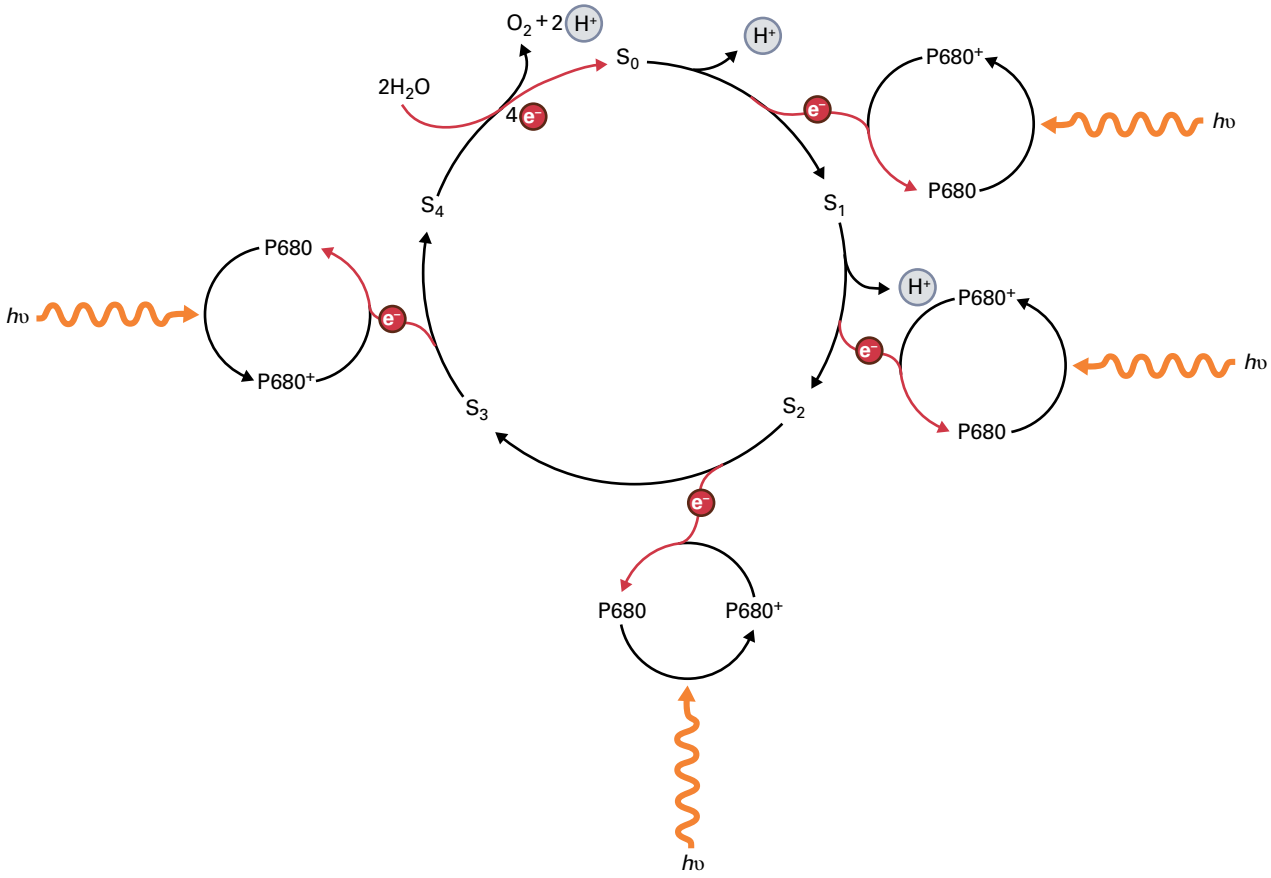


FIGURE 12.14 *The O_2 evolution apparatus exists in five different oxidation states (S_0 through S_4). The cycle is advanced sequentially by photons trapped by PSII until the highly oxidized (positively charged) state (S_4) is produced. S_4 is the only state capable of water oxidation. Shown is the light-driven oxidation of P680 and subsequent reduction by electrons that are derived ultimately from water.*

accumulator in the S-state model. Mn atoms appear to undergo successive oxidations to yield a strongly oxidizing complex in the S_4 state that is capable of water oxidation. A large number of biophysical measurements have helped define the oxidation state and structure of four Mn atoms associated with the O_2-evolving complex of PSII.

Determination of the structure of cyanobacterial PSII at 1.9-Å resolution has provided important insight into the detailed arrangement of the manganese cluster. As shown in Figure 12.15, the catalytic site for water oxidation is a Mn_4CaO_5 cluster. The structure resembles a distorted chair, with three Mn, one Ca, and four oxygen atoms forming a cubane-like structure (the base of the chair), and one Mn and one oxygen atom as the back of the chair. The oxygen atoms form oxo bridges between the Mn and Ca atoms. In addition, four water molecules are associated with the Mn_4CaO_5 complex (Fig. 12.15), at least one of which is likely a substrate for water oxidation. This structure presumably represents the cluster in the dark S_1 state. Advances in time-resolved X-ray diffraction techniques may enable determination of the structure of the Mn_4CaO_5 cluster in the other S states.

The link between $P680^+$ and the Mn_4CaO_5 cluster is indirect. An additional electron carrier intermediate, Z (see Reaction 12.10), is a tyrosine residue in the D1 subunit of the reaction center complex of PSII (Tyr-161). The identity of this residue has been confirmed by site-directed mutagenesis studies with PSII complexes from cyanobacteria, and the high-resolution crystal structure showed it is linked to the Mn_4CaO_5 cluster by a hydrogen bond network (Fig. 12.15B). To function as an intermediate between P680 and the S-state, the tyrosine radical formed in Reaction 12.10 must be a strong oxidant, capable of advancing the S-state. Measured kinetics of Z^+ formation and decay are consistent with this proposed role.

Reaction 12.10: Oxidation and reduction of P680 during oxygenic photosynthesis

$$S\ Z\ P680 \xrightarrow{h\nu} S\ Z\ P680^+ \rightarrow S\ Z^+\ P680 \rightarrow S^+\ Z\ P680$$

12.3.8 Plants use light-harvesting chlorophyll *a*/*b*-binding proteins as their major peripheral antennae

Thylakoid membranes from plants and green algae contain two different forms of chlorophyll (see Fig. 12.4): Chlorophyll *a* is found in all reaction center complexes as well as antennae, whereas chlorophyll *b* is found only in peripheral antenna

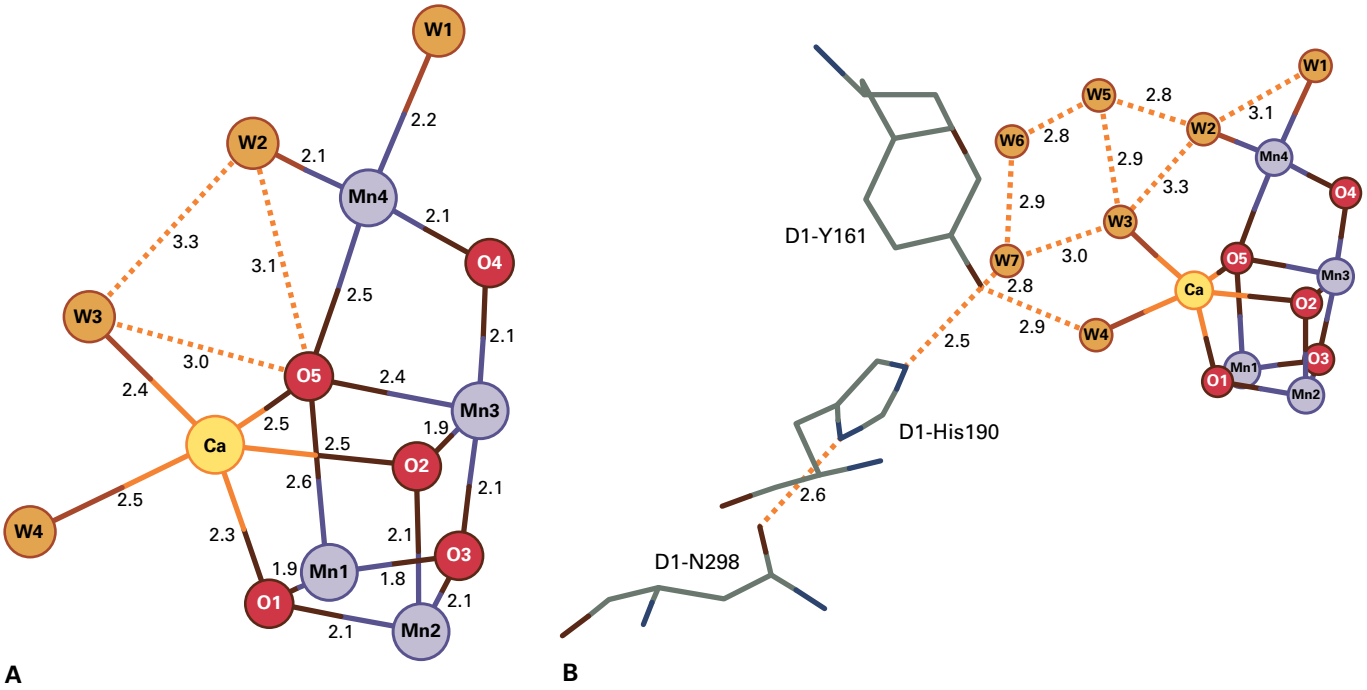


FIGURE 12.15 *Structure of the water-oxidizing Mn_4CaO_5 cluster in PSII determined at 1.9 Å resolution. (A) Structure of the metal cluster with oxo bridges and water ligands. The bond distances are shown in Å. Hydrogen bonds are depicted as dashed lines. (B) Hydrogen bond network linking the Mn_4CaO_5 cluster and tyrosine Z (D1-Y161).*

complexes. These peripheral antennae are in addition to the core antennae associated with the CP47 and CP43 proteins in PSII and the PsaA and PsaB proteins in PSI. Analyses of the total antenna sizes of PSII and PSI show that, in most plants, approximately 250 chlorophyll molecules are associated with each reaction center.

At least 10 different integral membrane **light-harvesting complex** (LHC) proteins that bind chlorophylls and xanthophylls have been identified by fractionation of chloroplast membranes with nondenaturing detergents followed by electrophoresis (Table 12.3). This analysis shows that all of the chlorophyll in thylakoids is associated with specific proteins, some with PSI and others with PSII. All are encoded in the nucleus and must, therefore, be imported into the chloroplast before binding with chlorophyll and associating with their proper photosystem. Similar LHC proteins are found in nearly all photosynthetic eukaryotes.

The major pigment-binding protein in plant thylakoid membranes is a trimeric complex called **LHCII**. Estimated to represent about half of the total protein in the thylakoid membrane, it is arguably the most abundant membrane protein on Earth. The structure of LHCII has been determined at a resolution of 2.5 Å (Fig. 12.16). Each 25-kDa protein monomer has three transmembrane helices that bind eight chlorophyll *a*, six chlorophyll *b*, and four xanthophyll molecules. Two lutein molecules serve as scaffolding for the first and third helices, and a neoxanthin and a violaxanthin are bound more peripherally.

Mild detergent fractionation of plant thylakoid membranes yields intact PSI and PSII complexes with full arrays of pigment molecules. As described in Section 12.3.9, the structure of the PSI reaction center–antenna supercomplex has been solved. A detailed structure of plant PSII has not yet been obtained, but researchers have constructed a model of the

TABLE 12.3 *Properties of light-harvesting chlorophyll protein complexes.*

Complex	Number of Chls	Gene*	Mol. mass (kDa)
Light-harvesting complexes (LHC) associated with PSI			
LHCI 680	14	*lhca3*	24.9
	14	*lhca2*	23.2
LHCI 730	14	*lhca1*	21.5
	14	*lhca4*	22.3
Light-harvesting complexes associated with PSII			
CP29	13	*lhcb4*	27.3–28.2
LHCII	14	*lhcb1*	24.7–24.9
	14	*lhcb2*	24.9
	14	*lhcb3*	24.3
CP26	9	*lhcb5*	26.1
CP24	10	*lhcb6*	23.2

* Genes are nuclear-encoded.

PSII supercomplex based on single particle cryoelectron microscopy (Fig. 12.17). The positions of the reaction center core (C), trimeric LHCII (S and M types), and monomeric antenna complexes were assigned by fitting the X-ray structures of individual components to the electron microscopy data. The resulting $C_2S_2M_2$ supercomplex shows the overall architecture of PSII, with LHCII connected to the dimeric reaction center core via the monomeric LHC proteins CP29, CP26, and CP24 (Fig. 12.17).

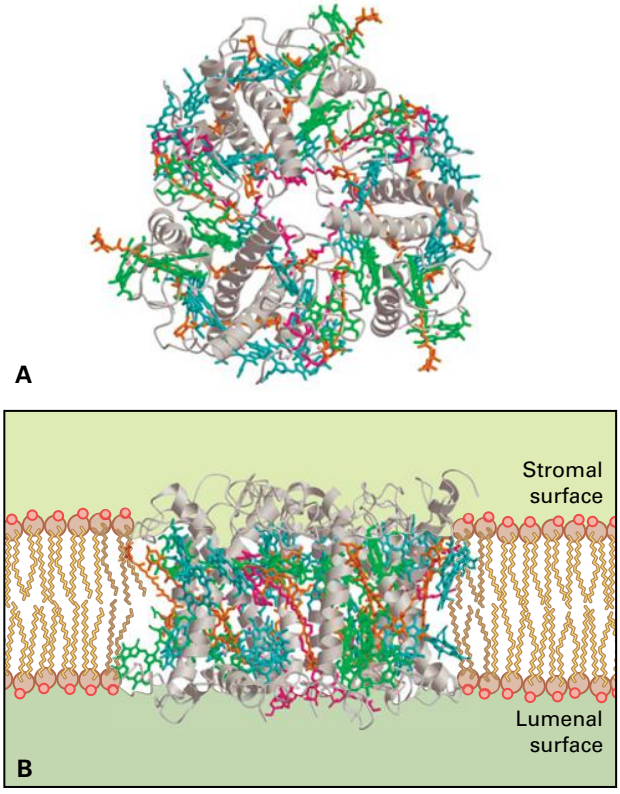


FIGURE 12.16 *Trimeric structure of LHCII. Each monomer in the complex contains three transmembrane-spanning helices and binds 14 molecules of chlorophyll* a *and* b*, as well as four xanthophyll molecules. (A) View from the stromal side of the membrane. (B) Side view within the plane of the membrane.*

12.3.9 PSI is a light-driven plastocyanin-ferredoxin oxidoreductase

PSI from plants contains approximately 15 protein subunits (Table 12.4). PsaA and PsaB (each ≈80 kDa) form the central heterodimer of the reaction center and are involved in binding the major electron transfer carriers, such as P700 and accessory chlorophylls, the chlorophyll *a* acceptor molecule (A_0), phylloquinone (vitamin K1, the A_1 acceptor), and the bound Fe–S center F_X. The low molecular-mass PsaC subunit (9 kDa) binds two additional Fe–S centers, F_A and F_B. Like PSII, PSI contains a large number of protein subunits that do not bind prosthetic groups, many of which have undefined function.

The midpoint potentials of the electron carriers and the kinetics of electron transfer through PSI are shown in Figure 12.18. Unlike PSII, both of the symmetrical cofactor branches in PSI appear to be active, so electron transfer from P700 is bidirectional (Fig. 12.19), with the A branch on PsaA being dominant. The two branches converge at F_X, so there is still only one pathway for electrons exiting PSI via F_A and F_B. The terminal electron acceptor is ferredoxin, a soluble Fe–S protein located in the stroma (a part of ferredoxin is bound to thylakoids in plants such as pea). On the luminal side, plastocyanin is a copper-containing protein that serves as the electron donor to PSI by reducing $P700^+$. Thus, the PSI complex functions as a light-dependent plastocyanin-ferredoxin oxidoreductase. Ferredoxin is a very strong reductant with a redox midpoint potential of –420 mV. The reduced ferredoxin generated by PSI is capable of reducing $NADP^+$ in a thermodynamically favorable reaction in the physiological pH range.

FIGURE 12.17 *Structural model of the plant PSII $C_2S_2M_2$ supercomplex. (A) Top view of the projection map determined by single particle cryoelectron microscopy. (B) Assignment of subunits by fitting of high-resolution structures. The dimer of PSII cores (C) is in the center of the supercomplex, with monomeric LHCs (CP29, CP26, and CP24) connecting the strongly bound (S) and moderately bound (M) peripheral LHCII trimers to the core.*
Source: Kouril et al. (2012). Biochim. Biophys. Acta 1817:2–12.

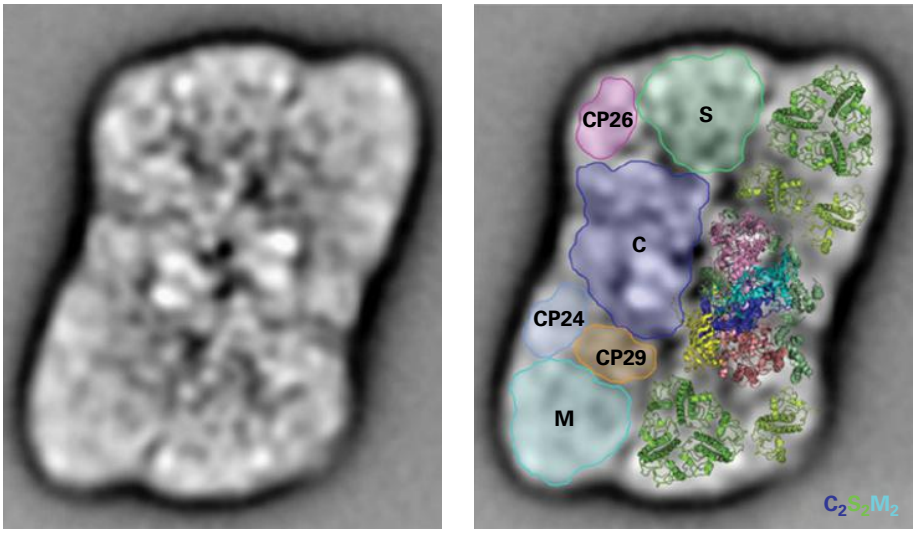


TABLE 12.4 *Protein subunits of the plant PSI core complex.*

Protein	Gene	Location of gene	Mol. mass (kDa)	Function
Hydrophobic subunits				
PsaA	*psaA*	Chloroplast	83	Reaction center protein
PsaB	*psaB*	Chloroplast	82	Reaction center protein
PsaF	*psaF*	Nucleus	17	PC docking
PsaG	*psaG*	Nucleus	11	LHCI binding
PsaH	*psaH*	Nucleus	10	LHCII-P docking
PsaI	*psaI*	Chloroplast	4	Unknown
PsaJ	*psaJ*	Chloroplast	5	Interaction with PsaF
PsaK	*psaK*	Nucleus	9	LHCI binding
PsaL	*psaL*	Nucleus	18	LHCII-P docking
PsaO	*psaO*	Nucleus	10	LHCII-P docking
PsaP	*psaP*	Nucleus	14	LHCII-P docking
Hydrophilic subunits				
Stromal orientation				
PsaC	*psaC*	Chloroplast	9	Fe–S apoprotein
PsaD	*psaD*	Nucleus	18	Ferredoxin docking
PsaE	*psaE*	Nucleus	10	Ferredoxin docking
Luminal orientation				
PsaN	*psaN*	Nucleus	10	PC docking

High-resolution crystal structures are available for PSI from both cyanobacteria and plants. Cyanobacterial PSI is a trimer of reaction centers, with 96 chlorophylls, 22 carotenoids, two phylloquinones, and three 4Fe–4S clusters per reaction center. This structure revealed the detailed structure of the core antenna, the symmetrical cofactor branches, and their interactions with the protein subunits. By contrast, the plant PSI structure shows a supercomplex with a monomeric reaction center core and a peripheral antenna composed of four LHCI proteins (Fig. 12.20). The peripheral LHCI antenna array is located on one side of the reaction center in a crescent shape. The locations of 12 core protein subunits have been determined, ten of which are also found in cyanobacterial PSI. The positions of the electron transfer components and core antenna chlorophylls are conserved between plant and cyanobacterial PSI.

12.4 Electron transport pathways in chloroplast membranes

12.4.1 The chloroplast noncyclic electron transport chain produces O_2, NADPH, and ATP and involves cooperation of PSI and PSII

Between the 1940s and the early 1960s, three seminal findings formed the basis for our current understanding of the coordinated operation of the two photosystems in the chloroplast electron transport chain. The first discovery was of the "red

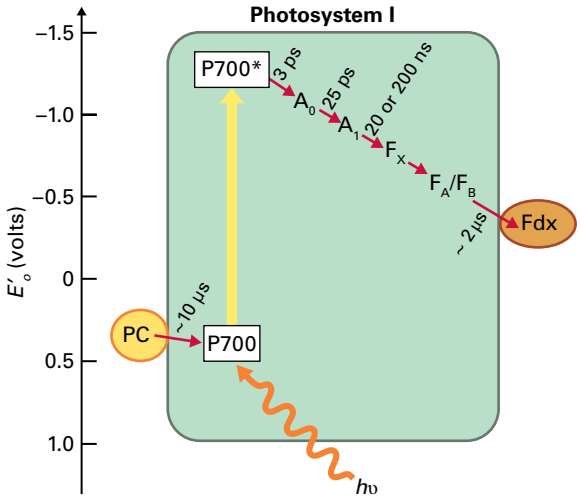


FIGURE 12.18 *PSI electron carriers and the kinetics of electron transfer. The pathway of electron transfer through the PSI complex is shown to involve P700, a monomeric chlorophyll* a *(A_0), a phylloquinone (A_1), and a series of additional electron carriers that include three different Fe–S centers (F_X, F_A, and F_B). Electron transfers through these carriers occur in the time range of picoseconds to nanoseconds, with the terminal electron acceptor, ferredoxin (Fdx), being reduced in approximately 2 μs. For simplicity, only one path of electron transfer is indicated, and the accessory chlorophyll near P700 is not shown.*

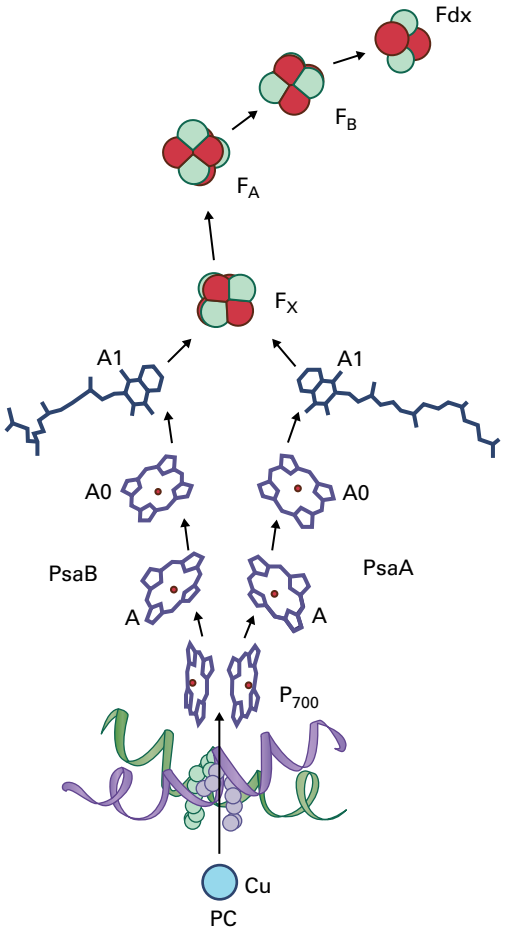


FIGURE 12.19 *Organization of electron carriers and electron transfer pathways in the PSI reaction center complex. The P700 dimer is located on the luminal side of the structure and two symmetrical cofactor branches radiate out from P700. Each includes an accessory chlorophyll* a *molecule (A), a monomeric chlorophyll* a *molecule identified as A_0, and a phylloquinone (A_1). The two branches converge at the Fe–S center F_X. On the stromal side of the complex, two additional Fe–S centers (F_A and F_B) have been identified on the path to the soluble acceptor ferredoxin (Fdx). The electron donor on the luminal side of PSI is the soluble copper protein plastocyanin (PC).*

drop," where the efficiency of photosynthesis was found to decrease dramatically at wavelengths greater than 680 nm, though there was still substantial absorption of light by chlorophyll. In effect, light of wavelengths longer than 680 nm appeared ineffective in photosynthesis, regardless of absorption by the photosynthetic pigments. Questions raised by the red drop were answered by the second observation, the "enhancement effect." When red and far-red light were used in combination, the rate of photosynthesis was greater than the sum of the rates achieved by using only red or only far-red light. The third finding revealed that red and far-red wavelengths had an antagonistic effect on the oxidation and reduction of cytochromes in the electron transport chain: red light causing reduction of cytochromes, and far-red causing their oxidation.

These three findings form the basis for the **Z-scheme** (Fig. 12.21), a model of the chloroplast electron transfer chain that takes into account the different pigment and reaction center compositions of the two photosystems. PSI, with its longer-wavelength reaction center P700, is more efficient in far-red light. PSII, however, operates more efficiently in red light because of its relatively shorter wavelength reaction center, P680. For photosynthesis to occur with optimal efficiency, the two photosystems must cooperate.

This cooperation of two photosystems that absorb optimally in different spectral regions explains the red drop phenomenon and the enhancement effect; the efficiency of photosynthesis would be expected to diminish if one of the two photosystems were preferentially activated, as would happen under either red or far-red light alone, but not under both combined. The Z-scheme also explains the antagonistic effects of red and far-red light. The far-red light that activates PSI photochemistry oxidizes the photosystem, which in turn oxidizes electron carriers located between the photosystems (e.g., cytochromes). By contrast, the red light that activates PSII photochemistry and oxidizes P680 generates reduced compounds, which would reduce subsequent electron carriers in the chain.

The Z-scheme remains the preeminent model of **noncyclic photosynthetic electron transfer** and has been elaborated in detail. In the light, the primary charge separation in PSII produces a strong oxidant ($P680^+$) and a weak, relatively stable reductant, a plastosemiquinone (Q_A^-); in PSI the charge separation produces a strong, stable reductant (a reduced Fe–S center, F_X^-) and a weak oxidant ($P700^+$). $P680^+$ produced by PSII provides the oxidizing power to remove electrons from water, whereas Q_A^- provides the reducing power that ultimately donates electrons to $P700^+$ via a series of energetically "downhill" electron transfers involving additional electron carriers,

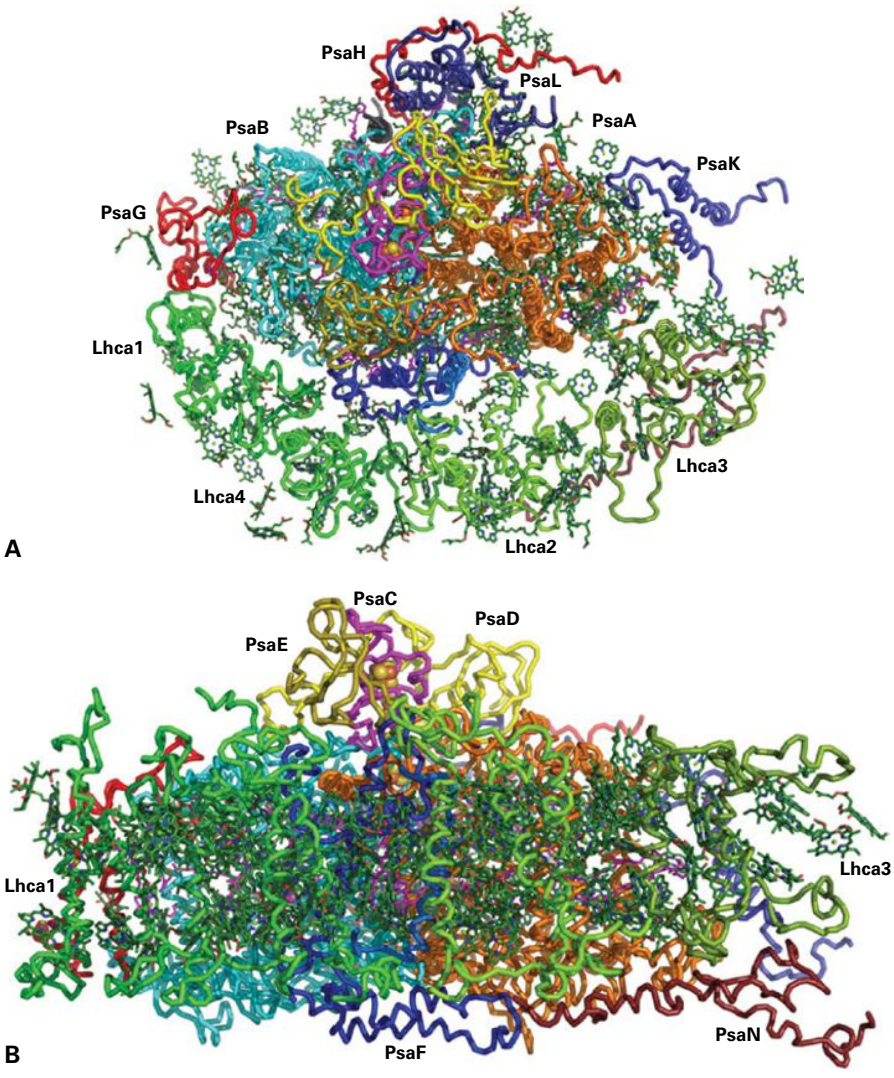


FIGURE 12.20 *Structure of plant PSI. (A) View from the stromal side of the membrane. The peripheral antenna composed of Lhca1-4 proteins is shown on the lower side of the monomeric reaction center core. "Gap chlorophylls" that connect peripheral antenna to the core antenna are evident in the space between the Lhca proteins and the reaction center. (B) Side view within the plane of the membrane. The PsaC, PsaD, and PsaE subunits protrude into the stroma and facilitate electron transfer to the soluble terminal acceptor, ferredoxin.*

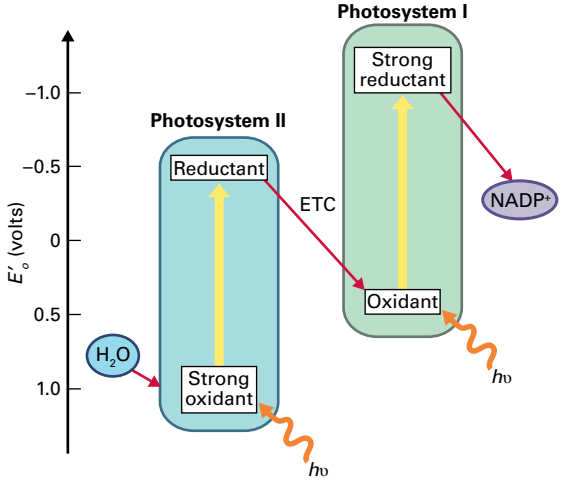


FIGURE 12.21 *Conceptual diagram of the Z-scheme, showing the cooperation of PSII and PSI in the transfer of electrons from water to NADP⁺. In the light, PSII generates a strong oxidant capable of oxidizing water, and a reductant. Illuminated PSI, in contrast, generates a strong reductant capable of reducing NADP⁺, and a weak oxidant. The two photosystems are linked by an electron transfer chain (ETC) that allows the PSI oxidant to receive electrons from the PSII reductant.*

including the transmembrane protein complex, cytochrome b_6f. The energy released by this **exergonic** electron transfer contributes to the formation of a proton gradient that can be used for the synthesis of ATP. An intermediate product of P700 oxidation, reduced ferredoxin, serves as an electron donor in many important reactions, including reduction of $NADP^+$, assimilation of nitrogen (see Chapter 8), and reduction of the regulatory disulfide protein thioredoxin (see Section 12.9.4).

A current depiction of the Z-scheme describing the electron carriers in reference to their midpoint oxidation-reduction potentials is shown in Figure 12.22A. A corresponding schematic, Figure 12.22B, illustrates the movement of electrons and protons during noncyclic electron transfer in oxygenic photosynthetic organisms. This electron transfer pathway generates three principal products: O_2, ATP, and NADPH. The two photosystems are connected by a series of electron carriers that include plastoquinone, the cytochrome b_6f complex, and plastocyanin. Oxidation of water and exergonic electron transport produce a proton electrochemical gradient that drives synthesis of ATP by the transmembrane ATP synthase. A structural view of the protein complexes involved in the Z-scheme is shown in Figure 12.23.

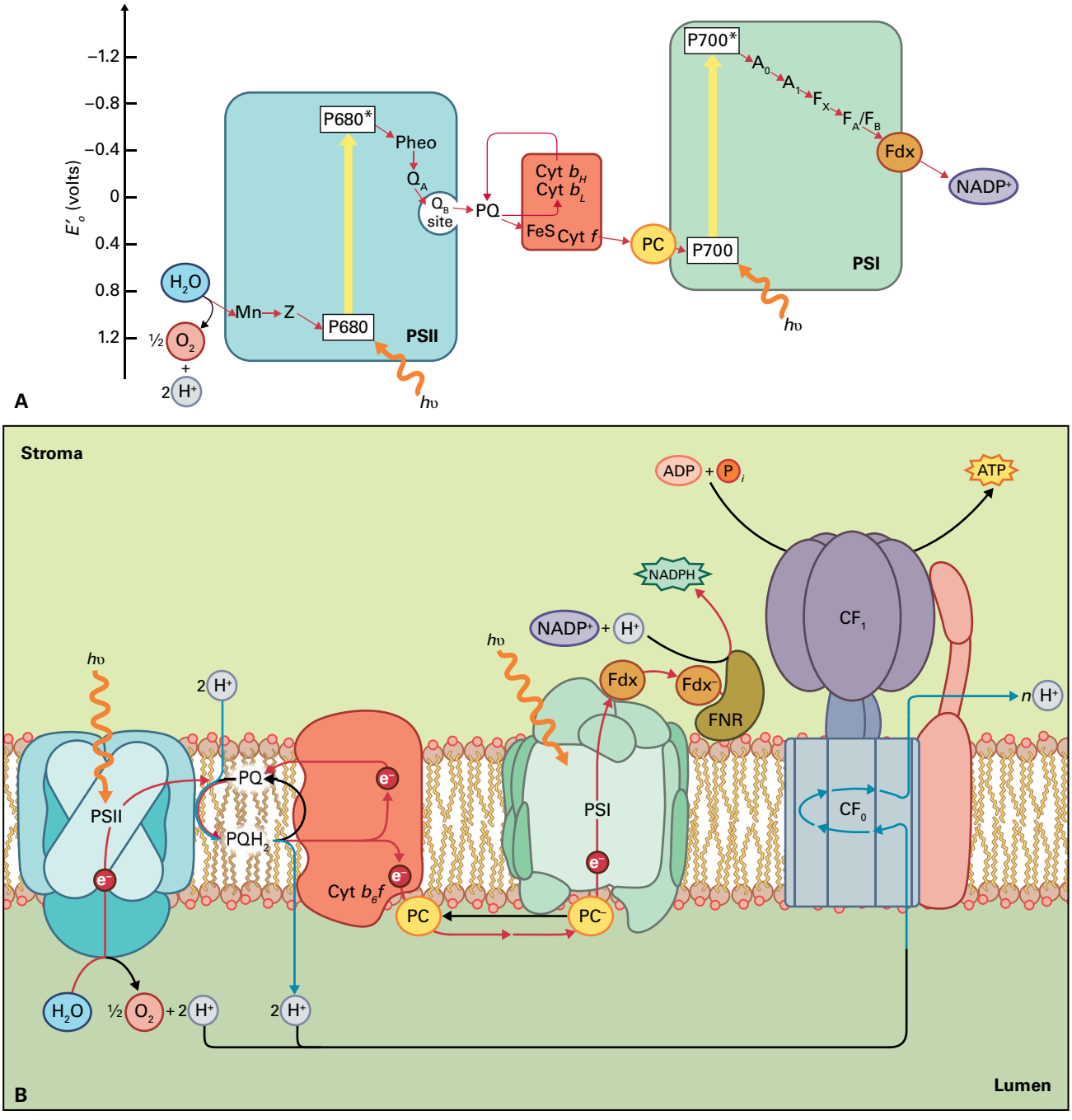


FIGURE 12.22 *(A) The current Z-scheme, showing E_m values of electron carriers. The vertical placement of each electron carrier of the noncyclic electron transfer chain corresponds to the midpoint of its redox potential. These voltage values have been verified experimentally. (B) Membrane organization of the Z-scheme. The components of the chloroplast electron transport chain and the ATP-synthesizing apparatus are illustrated in the thylakoid membrane. Four membrane complexes (PSII, PSI, the cytochrome b_6f complex, and the ATP synthase) are shown. Electrons are transferred from water to NADP⁺; accompanying this electron transfer, a proton gradient is established across the membrane. This electrochemical gradient is ultimately utilized for the synthesis of ATP by the ATP synthase. Fdx, ferredoxin; FNR, ferredoxin-NADP⁺ reductase.*

12.4.2 The cytochrome b_6f complex transfers electrons from reduced plastoquinone to oxidized plastocyanin

Oxidation of plastoquinol occurs by an integral membrane protein complex, the cytochrome b_6f complex, which is similar in structure and function to the cytochrome bc_1 complex (Complex III) of the mitochondrial respiratory chain (Chapter 14). Both complexes are dimers, with each monomer containing a conserved core of four electron carriers: a high-potential *c*-type cytochrome (cytochrome *f* or c_1), a high-potential 2Fe–2S Fe–S protein (the Rieske Fe–S protein), and a *b*-type cytochrome (cytochrome b_6 or *b*) with two *b*-type hemes (see Figs. 14.20 and 14.22); however, determination of the high-resolution structures of the cytochrome b_6f complex

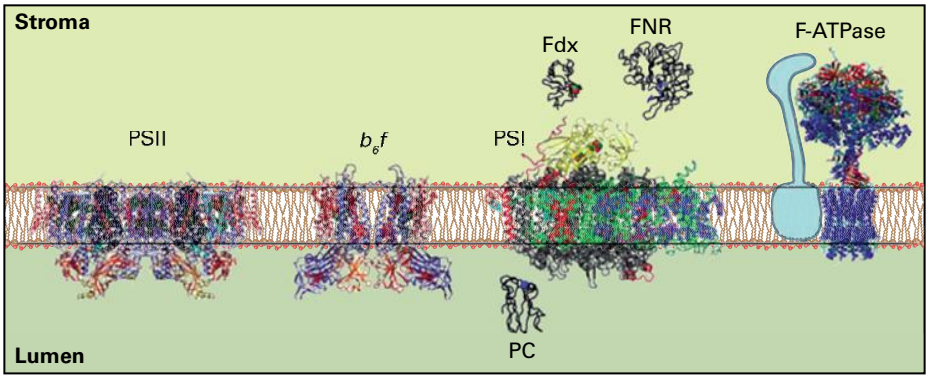


FIGURE 12.23 *A structural view of the Z-scheme showing structures of the major thylakoid membrane complexes (PSII, cytochrome b_6f complex, PSI, and ATP synthase) involved in the light reactions of oxygenic photosynthesis. Also shown are the structures of the soluble proteins Fdx and FNR on the stromal side of PSI, as well as PC in the lumen."*

TABLE 12.5 *Protein subunits of the cytochrome* b_6f *complex.*

Protein	Gene	Location of gene	Mol. Mass (kDa)	Function
Cyt *f*	*petA*	Chloroplast	32	Cyt *f* apoprotein
Cyt b_6	*petB*	Chloroplast	24	Cyt b_6 apoprotein
Rieske FeS	*petC*	Nucleus	19	Rieske Fe–S apoprotein
Subunit IV	*petD*	Chloroplast	17	Quinone binding at Q_p
PetG	*petG*	Chloroplast	4.0	Stability
PetL	*petL*	Chloroplast	3.4	Stability
PetM	*petM*	Nucleus	4.0	Stability
PetN	*petN*	Chloroplast	3.3	Stability

from a cyanobacterium and a green alga revealed several surprising features. In addition to four small protein subunits unique to the b_6f complex, there is an extra *c*-type heme bound to cytochrome b_6, a chlorophyll *a* molecule, and a β-carotene. Like PSII and PSI, the cytochrome b_6f complex contains both nuclear and chloroplast gene products (Table 12.5).

The cytochrome b_6f complex functions as a plastoquinol-plastocyanin oxidoreductase, transferring electrons from plastoquinol to plastocyanin, which resides in the lumen of the thylakoid membrane. This transfer is accompanied by the translocation of protons across the membrane, from stroma to lumen. An unusual feature of the cytochrome complex mechanism permits translocation of two protons for every electron transferred to plastocyanin, facilitating formation of the proton gradient that drives ATP synthesis.

12.4.3 Proton translocation via cytochrome b_6f is thought to involve a Q-cycle

The most widely accepted mechanism to describe the reactions of the cytochrome complex is the Q-cycle (Fig. 12.24). According to this model, the cytochrome complex contains one quinol-binding site (Q_p) and one quinone-binding site (Q_n) on opposite sides of the membrane. Quinol oxidation proceeds in two steps at the Q_p site, located at the luminal side of the membrane. At Q_p, quinol is oxidized to the semiquinone by the Rieske Fe–S center, and the released electron passes from the Fe–S center to cytochrome *f*, then on to plastocyanin. The plastosemiquinone is then oxidized by one of the two hemes, known as b_l, (*b*-low potential), located in cytochrome b_6 near the luminal side of the membrane. Accompanying this oxidation, protons are released from the quinol into the lumen. The electron in the b_l heme is transferred across the membrane to the second *b*-type heme, known as b_h (*b*-high potential). This electron is then transferred to a quinone molecule that has bound at the Q_n site on the stromal side of the membrane, producing a semiquinone. This cycle repeats itself once again to oxidize a second plastoquinol, with one electron being passed to plastocyanin and the second being transferred to the Q_n site to produce a fully reduced quinol molecule (PQH_2); the fully reduced quinol picks up two protons from the stroma and dissociates from the Q_n site. The net result of this cycle is that a plastoquinol molecule is oxidized to a quinone (PQ; at the Q_p site), two electrons are transferred to plastocyanin (PC), and four protons are transferred from the stroma to the chloroplast lumen (Reaction 12.11). The arrangement of the electron carriers involved in the cytochrome b_6f complex is shown in Figure 12.25.

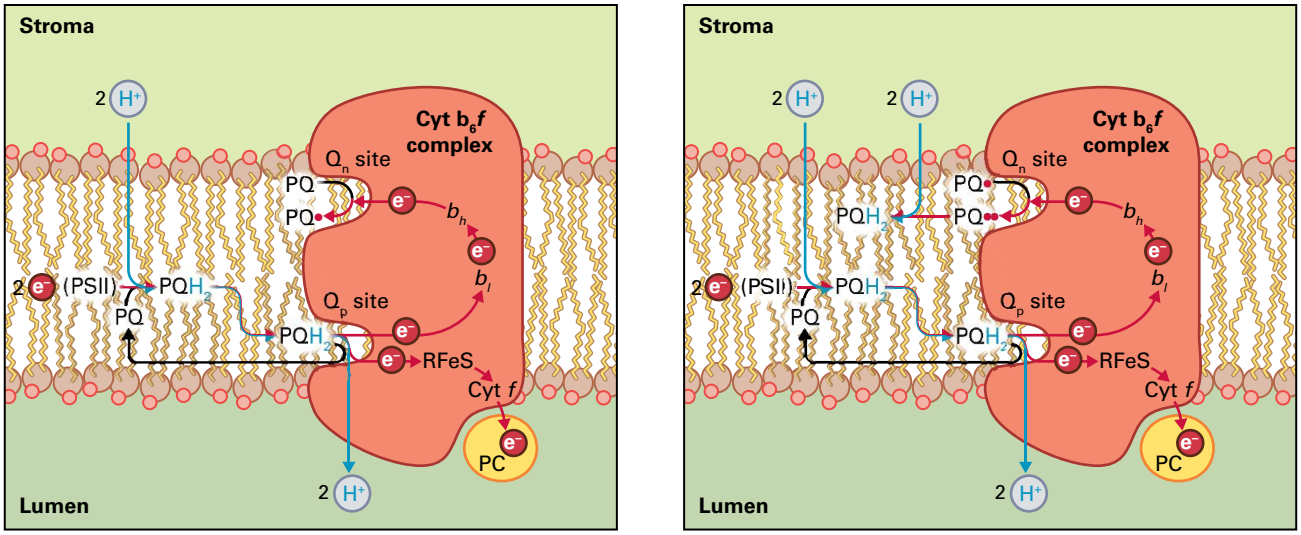


FIGURE 12.24 *The Q-cycle. The transmembrane organization of the cytochrome b_6f complex is shown schematically. At the quinol-binding site, Q_p, a plastoquinol molecule (PQH_2) is oxidized and two protons are released to the lumen. During the first turnover of the complex (A), one electron released from plastoquinol is passed through the high-potential electron carriers, the Rieske Fe–S protein (RFeS) and cytochrome f, to the electron acceptor, plastocyanin. The other electron passes through the cytochrome b_6 hemes (b_l and b_h/c_h) to a quinone binding site on the stromal side of the membrane, Q_n, where it reduces a quinone molecule to form a plastosemiquinone ($PQ^{\bullet}$). During the oxidation of a second plastoquinol molecule (B), the pathways of electron transfer are identical except that the second electron reduces the plastosemiquinone at the Q_n site to a fully reduced plastoquinol ($PQ^{\bullet\bullet}$), which takes up protons from the stroma, is released from the complex, and enters the plastoquinone pool.*

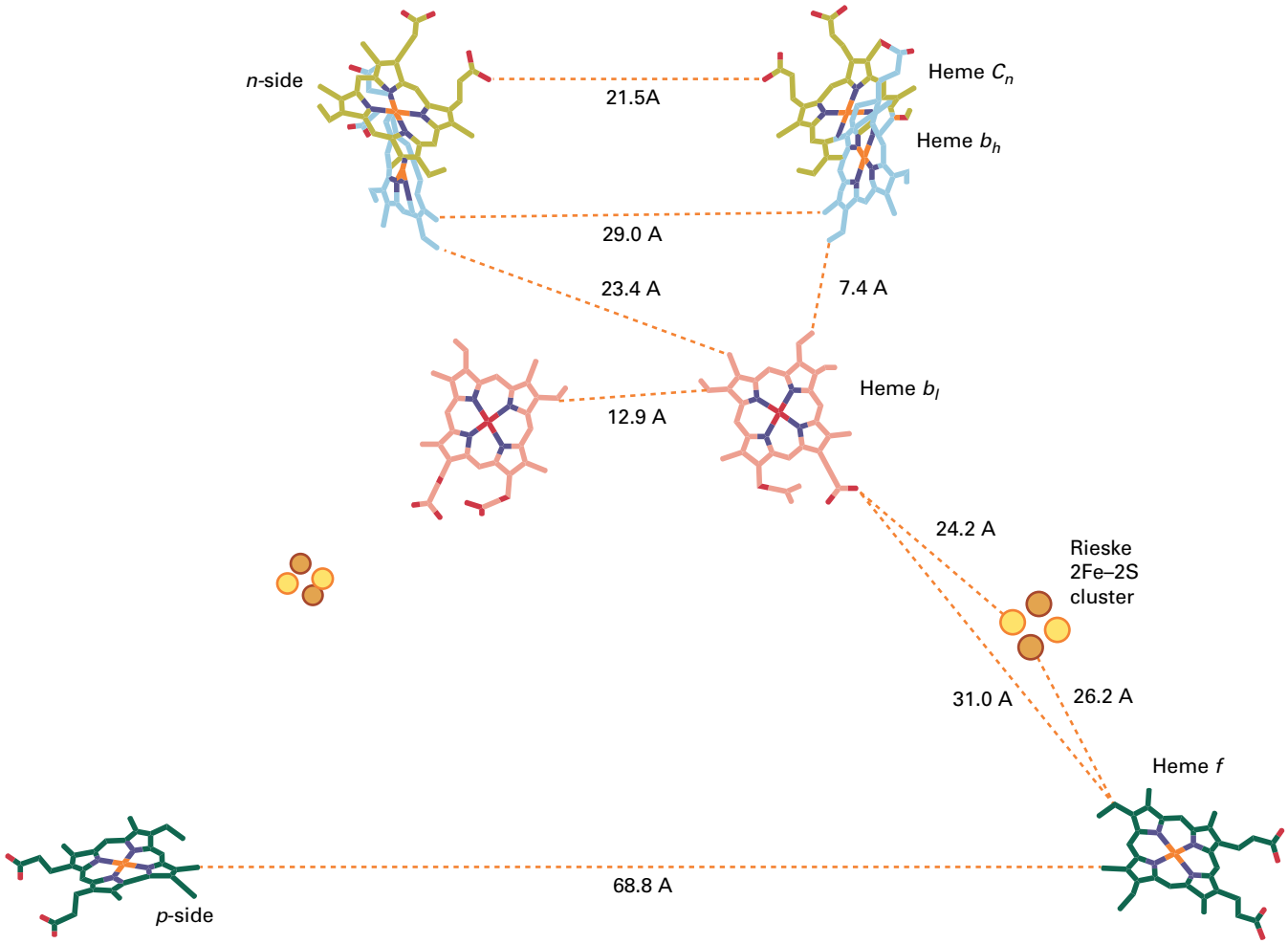


FIGURE 12.25 *Organization of electron carriers and electron transfer pathways in the dimeric cytochrome b_6f complex. The Q_p site is located near heme b_l and the Rieske Fe–S center on the luminal side of the complex. One electron from oxidation of plastoquinol passes through the Rieske Fe–S center on its way to cytochrome f and then plastocyanin. Movement of the Rieske protein is hypothesized to facilitate the electron transfer to cytochrome f. The second electron from plastoquinol is transferred to heme b_l and then to hemes b_h and/or c_n near the Q_n site on the stromal side of the complex. It is possible that a two-electron pathway for reduction of plastoquinone occurs at the Q_n site.*

Reaction 12.11: The Q-cycle in the chloroplast

$$PQH_2 + 2PC_{ox} + 2H^+_{stroma} \rightarrow PQ + 2PC_{red} + 4H^+_{lumen}$$

The reactions of the cytochrome b_6f complex are among the most important in limiting the rate of electron flux. Whereas Q_BH_2 is formed in approximately 100 µs, quinol oxidation occurs in 10–20 ms. Direct measurements of the rate of reactions through the high-potential carriers, including oxidation of cytochrome *f* by plastocyanin, have shown half-reaction times no longer than 1–2 ms. However, the reactions of cytochrome b_6, particularly the kinetics of the oxidation of the high-potential heme, b_h, are considerably slower and appear to be the rate-limiting steps in the complex.

12.4.4 Plastocyanin, a soluble protein, links cytochrome b_6f and PSI

The cytochrome b_6f complex reduces the mobile electron carrier plastocyanin, a low molecular-mass (11 kDa), copper-containing protein. Electron transfers involving plastocyanin are very rapid: Its reduction by the cytochrome b_6f complex takes about 100–200 µs, and its oxidation by PSI requires about 10 µs. Docking of plastocyanin to PSI involves electrostatic interactions with the PsaF subunit and hydrophobic interactions with PsaA and PsaB on the luminal side of the reaction center complex.

In some algae and cyanobacteria, the biosynthesis of plastocyanin is controlled by the extent of copper availability in the growth medium. In the absence of copper, these cells are unable to accumulate plastocyanin and instead synthesize a *c*-type cytochrome, cytochrome *c*-553, which is functionally interchangeable with plastocyanin.

12.4.5 Electrons from PSI are transferred to NADP⁺ in the stroma in a reaction requiring ferredoxin and ferredoxin-NADP⁺ reductase

Electrons from PSI are transferred to the 2Fe–2S Fe–S protein ferredoxin in the chloroplast stroma. This electron carrier does not transfer electrons directly to $NADP^+$, rather through activity of an intermediate enzyme called ferredoxin-$NADP^+$ reductase (FNR; see Fig. 12.22 and Fig. 12.23). Evidence indicates that ferredoxin and FNR form a complex through electrostatic interaction. FNR is an FAD-containing enzyme that can be reduced in two single-electron steps: The first electron reduces FNR to the flavin semiquinone state, and the second to the fully reduced state, $FADH_2$ (see Chapter 14, Fig. 14.6). FNR then transfers the two electrons to $NADP^+$. FNR is loosely associated with the thylakoid membrane and is easily dissociated. High-resolution structures of both ferredoxin and FNR are available from X-ray crystallography (see Fig. 12.23), and models for the interaction of the two proteins have been developed from the structural data.

12.4.6 Chloroplasts also contain cyclic electron transport chains that involve PSI

As described above, the noncyclic electron transport chain in chloroplasts links the oxidation of water (O_2 evolution) to the reduction of $NADP^+$ and production of ATP. Chloroplasts also carry out a cyclic electron transport process that involves PSI, plastoquinone, the cytochrome b_6f complex, and plastocyanin. In a model that describes this pathway (Fig. 12.26), PSI reduces

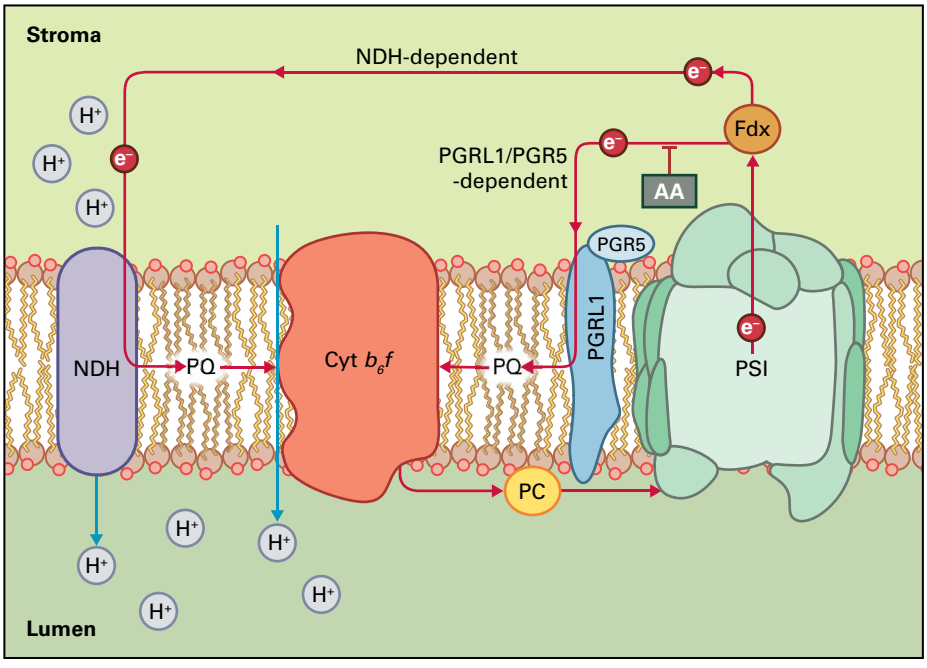


FIGURE 12.26 *Two pathways of cyclic electron transport around PSI in plants. One pathway uses the NADH dehydrogenase-like (NDH) complex, whereas a putative ferredoxin-plastoquinone oxidoreductase activity involving PGRL1 and PGR5 is necessary for the other pathway, which is sensitive to antimycin A (AA). Both pathways involve PSI, reduced ferredoxin, the cytochrome b_6f complex, and plastocyanin. The only net product of the pathway is ATP, which is synthesized by using the proton gradient generated through plastoquinol oxidation.*

ferredoxin in the light, but instead of transferring an electron to $NADP^+$, reduced ferredoxin donates electrons to the plastoquinone pool. Reduced plastoquinol can then be oxidized by the cytochrome b_6f complex, allowing proton translocation across the membrane. Electrons complete the cycle by returning to PSI via plastocyanin, and the pmf resulting from operation of a Q-cycle (Fig. 12.26) drives ATP synthesis. Thus, cyclic electron transport produces only ATP as a product without net production of NADPH. It seems to be involved in adjusting the ratio of ATP to NADPH production from the light reactions to meet the demands of downstream metabolism.

Biochemical and molecular genetic studies have suggested that two different enzymes catalyze the ferredoxin-dependent reduction of plastoquinone during cyclic electron transport around PSI (Fig. 12.26). One pathway is catalyzed by the **NADH dehydrogenase-like** (NDH) **complex** in the thylakoid membrane. This large complex is similar to mitochondrial Complex I, except the electron donor appears to be reduced ferredoxin instead of NADH. The formation of supercomplexes of PSI with the NDH complex depends on two minor LHCI antenna proteins, Lhca5 and Lhca6. The NDH pathway is especially prominent during oxidative stress. The second pathway involves a **ferredoxin-quinone oxidoreductase** that is sensitive to antimycin A. This activity depends on a complex of two thylakoid proteins, PGRL1 and PGR5. PGRL1 accepts electrons from ferredoxin and contains redox-active cysteine residues and an Fe-containing cofactor that are necessary for quinone reduction. Thioredoxin *m* (Trx *m*, see Box 12.4) has been implicated in the regulation of both types of cyclic electron transport. In the green alga *Chlamydomonas reinhardtii*, PGRL1 has also been found in a supercomplex with PSI, FNR, and the cytochrome b_6f complex.

12.4.7 Specific inhibitors and artificial electron acceptors have been used to study chloroplast electron transport

Several compounds specifically inhibit the chloroplast electron transport chain and act as herbicides (Fig. 12.27). One class of inhibitors binds at the Q_B site on the D1 protein in PSII and prevents the reduction of Q_B. The most widely studied of these is the inhibitor Diuron, 3-(3,4-dichlorophenyl)-1,1-dimethylurea (DCMU). Atrazine also acts at this site. A second class of inhibitors acts at the reducing side of PSI, inhibiting reduction of ferredoxin. The herbicide Paraquat (methyl viologen) is a member of this class, and its action as a herbicide results from its autoxidizability, which results in the formation of a superoxide radical that is highly reactive and damaging to the photosynthetic apparatus. Paraquat has been used experimentally as a nonphysiological electron acceptor, substituting for ferredoxin.

Another set of inhibitors includes plastoquinone analogs, such as 2,5-dibromo-3-methyl-6-isopropyl-*p*-benzoquinone (DBMIB; or dibromothymoquinone), which block electron transfer by competing with plastoquinol for binding at the quinol oxidizing (Q_p) site in the cytochrome b_6f complex. The site of action of these inhibitors in relation to the electron carriers of the chloroplast noncyclic electron transfer chain is shown in Figure 12.28. In addition to their commercial value as herbicides, these inhibitors are useful for defining the electron transfer events that take place in the photosynthetic membrane. For example, cyclic electron transport is blocked by inhibitors of the cytochrome b_6f complex, such as DBMIB, but not by PSII inhibitors, such as DCMU.

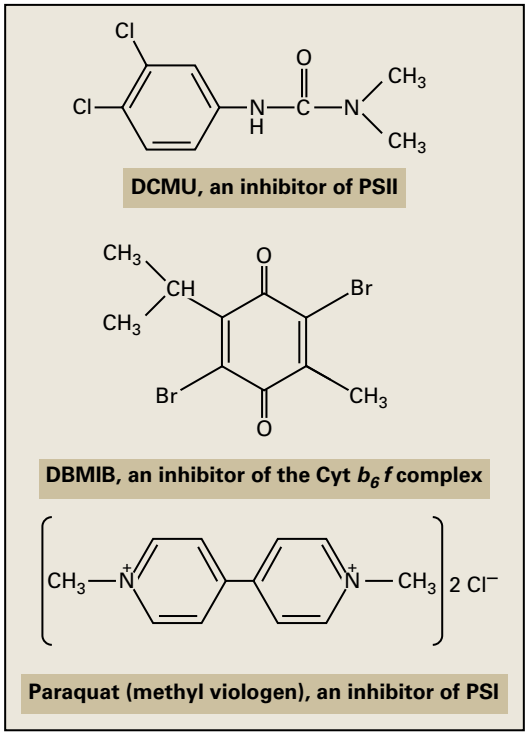


FIGURE 12.27 *Chemical structures of three inhibitors of the photosynthetic electron transport chain: DCMU, 3-(3,4-dichlorophenyl)-1,1-dimethylurea; DBMIB, 2,5-dibromo-3-methyl-6-isopropyl-p-benzoquinone; and Paraquat.*

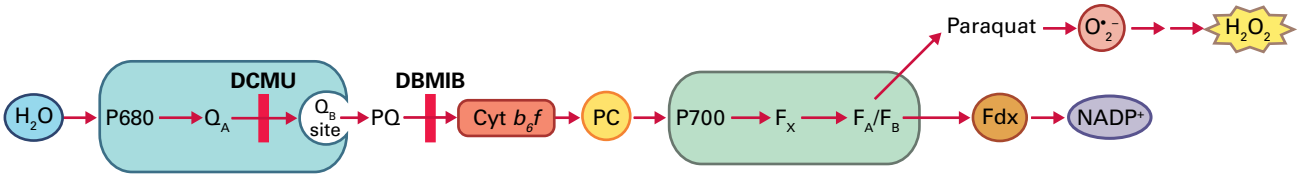


FIGURE 12.28 *Sites of action for the inhibitors of the chloroplast electron transport chain diagrammed in Figure 12.22. DCMU and DBMIB block electron transfer reactions, whereas reduced Paraquat autooxidizes to a radical, resulting in the formation of superoxide and other reactive oxygen species.*

12.5 ATP synthesis in chloroplasts

Photophosphorylation, the light-dependent synthesis of ATP, is mechanistically similar to the oxidative phosphorylation processes in mitochondria. Chloroplasts can synthesize ATP using either noncyclic electron transfer, with a concomitant synthesis of O_2 and NADPH, or cyclic electron transfer, in which there is no net utilization of substrate and no end product other than ATP.

12.5.1 Electron transport and ATP synthesis are coupled in vivo

A major feature of both oxidative phosphorylation and photophosphorylation in vivo is that ATP synthesis is energetically coupled to electron transport. This means that no phosphorylation of ADP occurs in the absence of electron transport, and that electron transfer is restricted in the absence of ATP synthesis. In vitro, however, it is possible to obtain high rates of electron transfer in the absence of ATP synthesis under certain nonphysiological conditions, most notably upon addition of compounds known as uncouplers. Uncouplers prevent ATP synthesis but allow electron transfer to proceed unimpeded. Their behavior is explained by the chemiosmotic model (see Section 12.5.2).

There are two coupling sites for energy conservation in the chloroplast noncyclic electron transport chain. These sites involve regions of the electron transport chain where proton accumulation in the thylakoid lumen is coupled to electron transport. One site involves protons liberated when water is oxidized by PSII, given that the protons released are localized in the luminal space of the chloroplast thylakoid membrane system. The second site involves protons released when plastoquinol is oxidized by the cytochrome b_6f complex; in this case, the quinol oxidation results in the release of protons into the luminal space.

The amount of ATP synthesized during noncyclic electron transport, expressed as the P/2e$^-$ or ATP/2e$^-$ ratio, has long been a subject of controversy. To some extent, this is because the isolation of well-coupled chloroplasts is challenging. An accurate measurement of the maximum amount of ATP synthesized during electron transfer is difficult to obtain. Values for noncyclic photophosphorylation in chloroplasts are generally in the range of 1.0–1.5 ATP molecules synthesized from ADP and Pi for every two electrons transferred from water to NADP$^+$.

12.5.2 Chloroplasts synthesize ATP by a chemiosmotic mechanism driven by a proton gradient

The chemiosmotic model was proposed in the 1960s to explain ATP synthesis in chloroplasts and mitochondria. According to this model, the main energetic driving force for ATP synthesis is an ion gradient across a selectively permeable biological membrane—in chloroplasts and mitochondria, this is a proton gradient generated as a consequence of electron transfer. This gradient establishes a concentration difference of protons and can also result in a difference in electric potential across the membrane. These sources of potential energy can be used for the phosphorylation of ADP by ATP synthase, an enzyme that can couple this energetically favorable proton flow to the synthesis of ATP (see Fig. 12.22B and Chapters 3 and 14).

Several important features of the chemiosmotic model have been verified experimentally. First, this mechanism requires an intact membrane system with low intrinsic permeability to protons. Second, the electron transport components in the membrane must be arranged vectorially to allow electrons to cross the membrane at defined sites. As electrons pass through this series of electron carriers, protons are also translocated across the membrane at these coupling sites. In chloroplasts, protons move from the stroma to the thylakoid lumen as electrons are transferred along the chain. In the noncyclic electron transport pathway, protons are "deposited" in the lumen at the oxygen-evolving complex of PSII and at the Q_p site near the luminal face of the cytochrome b_6f complex, which act to oxidize water and plastoquinol, respectively. This unidirectional proton accumulation results in a high concentration of protons on the luminal side of the membrane and a lower concentration on the stromal side. The resulting gradient supplies the **proton motive force** (pmf).

As summarized by Equations 12.5 and 12.6, there is a linkage between the pH component, arising from a concentration difference of protons across the membrane (ΔpH), and the electrical potential component, arising from a difference in charge across the membrane (Δψ). According to the chemiosmotic model, the $\Delta\bar{\mu}_{H+}$ (in kilojoules per mole) or pmf (in volts) is the driving force for ATP synthesis.

Equation 12.5: Contribution of pH and membrane potential to the proton motive force

$$\Delta\bar{\mu}_{H+} = \Delta pH + \Delta\psi$$

Equation 12.6: The proton motive force

$$pmf = \Delta\bar{\mu}_{H+}/96.5\,kJ\,V^{-1}mol^{-1}$$

The final element in the chemiosmotic model is the presence in the membrane of an ATP synthase capable of using the pmf to convert ADP into ATP. This enzyme complex is oriented in the thylakoid membrane with a hydrophilic head group on the stromal side of the membrane and a hydrophobic channel that allows H$^+$ ions to diffuse spontaneously from the lumen to the stroma (Fig. 12.29). The chemiosmotic model predicts a fixed stoichiometry between the number of protons transported across the membrane and the number of ATP molecules synthesized, the H$^+$/ATP ratio. Most estimates

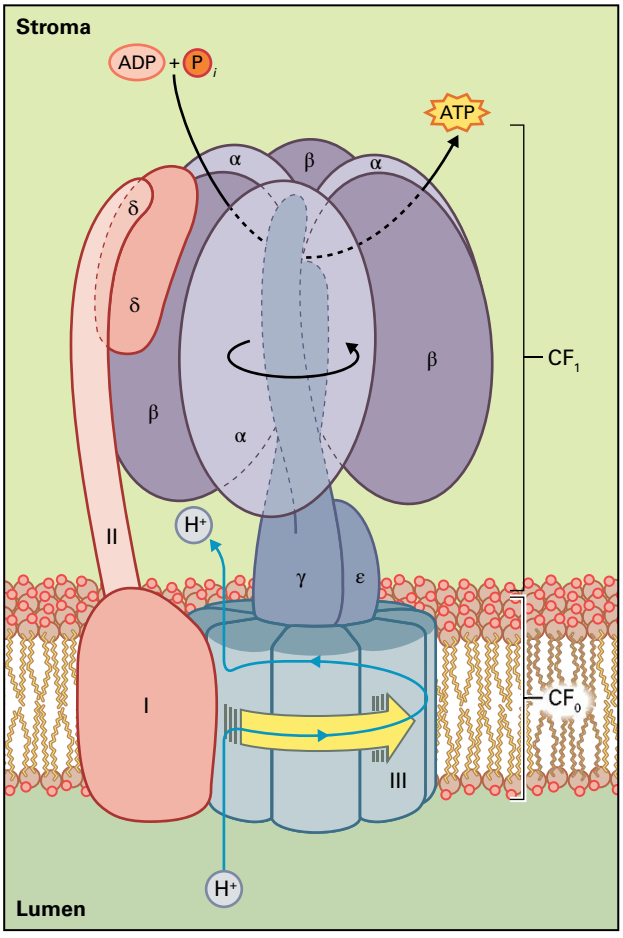


FIGURE 12.29 *Model for the chloroplast ATP synthase complex. The subunit structure of the ATP synthase indicates two major regions in the protein: an integral membrane protein portion (CF_0), which functions as a channel for protons passing through the membrane, and an extrinsic portion (CF_1), which contains the catalytic sites involved in ATP synthesis. CF_1 consists of five different subunits (α, β, γ, δ, and ε), whereas CF_0 contains four different subunits (I, II, III, and IV, of which three are shown), including 14 copies of subunit III in the membrane.*

indicate a value of 4.67 H$^+$/ATP. According to the present model of the noncyclic electron transport chain, the net transfer of two electrons through the chain results in the accumulation of six protons in the lumen. These numbers are critical in understanding proton translocation sites, as well as the energetics of ATP synthesis in chloroplasts.

The chemiosmotic model explains many observations of coupled ATP synthesis in both chloroplasts and mitochondria. For example, the coupling of phosphorylation and electron transfer can be understood as a feedback system. As the electron transport chain moves protons into the lumen, the luminal concentration of protons increases, generating a back pressure that slows further proton pumping. As the ATP synthase transports protons out of the lumen, the luminal concentration of protons decreases, relieving the back pressure and facilitating the accumulation of more protons in this space. The ability of nonphysiological uncoupling agents to overcome this effect is easily understood: Most uncouplers are weak acids that enter the lumen in their unprotonated form and diminish the luminal H$^+$ concentration by binding protons. Transmembrane diffusion of these bound protons provides an alternative pathway to the reactions catalyzed by the ATP synthase. Thus electron transport proceeds at high rates in the presence of the uncoupling agent, even though no ATP is being synthesized.

The most convincing experimental result in support of the chemiosmotic model was "acid–base phosphorylation." In this experiment, chloroplasts were first incubated at around pH 4, allowing them to establish this pH internally. The chloroplast suspension was then rapidly adjusted to pH 8 to establish an artificial pH gradient across the membrane. This gradient energized ATP synthesis until the pH difference was insufficient to drive ADP phosphorylation. Acid–base ATP synthesis required no light and was insensitive to electron transport inhibitors, such as DCMU, indicating that a pH gradient alone was sufficient to drive ATP synthesis. However, the acid–base ATP synthesis was sensitive to the addition of uncoupling agents, which affect the proton gradient directly. Subsequent research has confirmed and extended the original observations, and the chemiosmotic model is now widely accepted as the mechanism for ATP synthesis by both chloroplasts and mitochondria.

12.5.3 The thylakoid ATP synthase complex contains numerous subunits

The chemiosmotic model proposed a key role for a vectorial ATP synthase that would use the energy stored in a proton electrochemical potential for the synthesis of ATP. This enzyme was first identified on the basis of its ability to hydrolyze ATP (see F-type ATPase in Chapter 3). In native membranes, the ATPase activity of this enzyme is inactive, allowing for a unidirectional synthesis of ATP in the light. The pmf established across the thylakoid membrane in the light activates the ATP synthase and inhibits the wasteful ATPase activity of this enzyme.

The thylakoid ATP synthase consists of two segments: a transmembrane segment (CF_0) and a hydrophilic segment on the stromal surface (CF_1). CF_0 participates in translocating protons across the membrane to the catalytic portion of the enzyme, CF_1; CF_1 is involved in the actual conversion of ADP and P_i to yield ATP, using energy stored in the proton gradient. The enzyme is often referred to as the CF_0–CF_1 complex (Fig. 12.29).

Chloroplast ATP synthase is a 400-kDa enzyme that contains nine different subunits (Table 12.6) and includes both chloroplast and nuclear-encoded gene products. CF_1 consists of two large subunits (≈50 kDa), α and β, plus three smaller subunits called γ, δ, and ε (Fig. 12.29). CF_1 contains three copies of each of the large subunits and one copy each of the other subunits to give an overall stoichiometry of $\alpha_3\beta_3\gamma\delta\varepsilon$. The α and β subunits bind ADP and phosphate and catalyze

TABLE 12.6 *Protein subunits of the ATP synthase complex.*

Protein	Gene	Location of gene	Mol. mass (kDa)	Function
CF_1				
α Subunit	*atpA*	Chloroplast	55	Catalytic
β Subunit	*atpB*	Chloroplast	54	Catalytic
γ Subunit	*atpC*	Nucleus	36	Proton gating
δ Subunit	*atpD*	Nucleus	20	Binding CF_1 to CF_0
ε Subunit	*atpE*	Chloroplast	15	ATPase inhibition
CF_0				
I	*atpF*	Chloroplast	17	Binding CF_0 to CF_1
II	*atpG*	Nucleus	16	Binding CF_0 to CF_1
III	*atpH*	Chloroplast	8	Proton translocation
IV	*atpI*	Chloroplast	27	Binding CF_0 to CF_1

the phosphorylation of ADP into ATP. The δ subunit links CF_0 to CF_1, and the γ subunit appears to control proton gating through the enzyme. The ε subunit blocks catalysis in the dark, preventing the breakdown of ATP, and may also be involved in proton gating through interactions with the γ subunit. The γ subunit also participates in a regulatory mechanism mediated by the ferredoxin/thioredoxin system, which results in activation of ATP synthase in the light at a low pmf and deactivation of the enzyme complex in the dark, thereby blocking wasteful hydrolysis of ATP at night.

The hydrophobic CF_0 portion of ATP synthase is composed of four additional subunits, I, II, III, and IV. These subunits are present as single copies, except for subunit III, which appears to be present in 14 copies per complex in plant chloroplasts. Subunit III may form a pathway for proton translocation from the luminal space to the stroma.

12.5.4 Structural resolution of the F_1 complex from mitochondrial ATP synthase provides insight into the coupling of proton transport and ATP synthesis

Homologous enzymes involved in the synthesis of ATP have been identified in other energy-transducing membranes, such as the inner mitochondrial membrane (F_0–F_1 complex; Chapter 14) and bacterial membranes. A high-resolution structure of the F_1 portion of the mitochondrial enzyme has provided new and important structural information related to the mechanism of ATP synthesis. An important feature of the structure is the description of the alternating α and β subunits, with the γ subunit extending up through a hydrophobic cavity of the $\alpha_3\beta_3$ hexamer of F_1 down into the stalk region. Other low-molecular-mass subunits (δ and ε) were not resolved in the structure. The orientation of the γ subunit is consistent with its proposed role, wherein this subunit transmits the energy of the proton gradient to the catalytic sites for ATP synthesis that are localized on the α and β subunits.

The most widely accepted mechanism of ATP synthesis is the **binding change mechanism** (Fig. 12.30). In this mechanism, conformational changes in the protein are critical and the energy stored in the proton gradient is not directly used to drive the synthesis of ATP in a classical sense; rather, it is used to release a tightly bound form of ATP from its catalytic binding site on the enzyme. The CF_1 portion of the enzyme has three nucleotide binding sites, each of which can exist in one of three conformational states: a loose nucleotide binding (L), a tight nucleotide binding (T), and an open binding site (O), which is free of nucleotides. At any time, all three states are present in the CF_1 complex, each associated with one of the three catalytic centers present in the enzyme. According to the binding change mechanism, ADP and P_i initially bind to an unoccupied site in the open state. As protons move from the lumen to the stromal region through the CF_0 channel, energy is released that results in a rotation of the γ subunit of CF_1, and this rotation causes conformational changes in the three nucleotide binding sites. The T site, which contains bound ATP, is converted to an O site as the ATP is released, while the L site (containing the bound ADP and P_i) is converted into a T site, where the formation of ATP is favored.

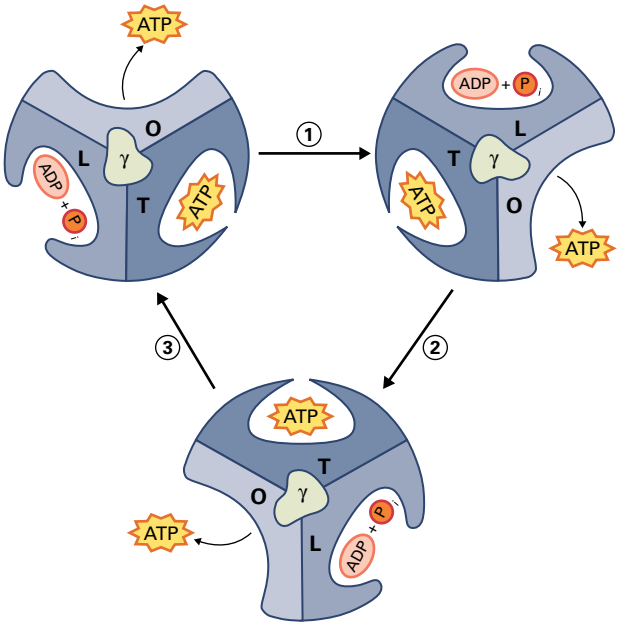


FIGURE 12.30 *Binding change mechanism of ATP synthesis by the CF_0–CF1 complex. Three nucleotide-binding sites are shown on the enzyme—the O-site (open), available to bind ADP and P_i; the L-site (loose), in which ADP and P_i are loosely bound; and the T-site, a tight nucleotide-binding site where ATP is formed. The movement of protons across the membrane drives rotation of the γ subunit in the enzyme, causing conformation changes that interconvert the three sites.*

Evidence from several laboratories supports the binding change mechanism, based on observations of the rotation of the γ subunit within the complex. Assuming one proton is transferred per copy of subunit III, the passage of 14 protons would allow a full rotation of the γ subunit and release 3 ATP molecules. Thus, the structure of the chloroplast ATP synthase suggests a H^+/ATP ratio of 4.67.

12.6 Organization and regulation of photosynthetic complexes

12.6.1 Protein complexes of the thylakoid membrane exhibit lateral heterogeneity and variable stoichiometry

Two types of internal membranes are present in the chloroplast: stacked or appressed thylakoid membranes (grana) and exposed or unstacked membranes (stromal thylakoids) (see Fig. 12.1). An important organizational feature of thylakoids in plants and green algae is that PSI and PSII are not distributed randomly throughout the membrane system: PSI lies primarily in the unstacked and stroma-exposed membranes, whereas PSII is found mostly in the appressed (stacked or granal) membranes (Fig. 12.31).

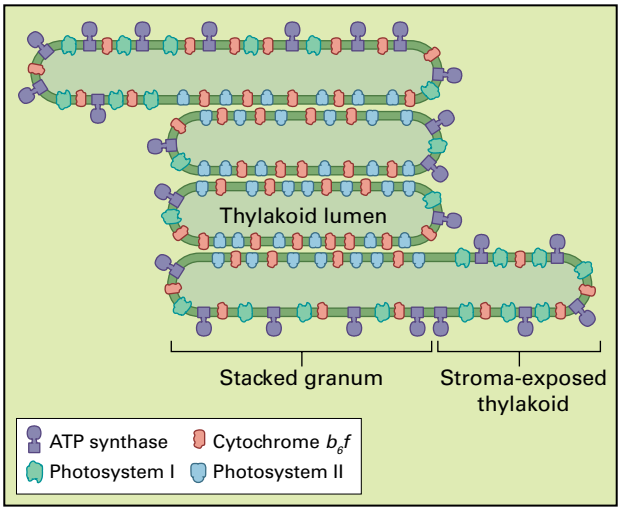


FIGURE 12.31 *Lateral heterogeneity of the chloroplast membrane complexes. PSII is localized primarily in the stacked membrane regions of the thylakoid membrane, whereas PSI and ATP synthase are almost exclusively localized in the stroma-exposed membrane regions. The cytochrome b_6f complex is distributed evenly throughout the membrane regions. The separation of the photosystems necessitates mobile electron carriers such as plastoquinone and plastocyanin, which shuttle electrons between the spatially separated membrane complexes.*

TABLE 12.7 *Distribution of photosynthetic components in chloroplast membrane regions.*

	Thylakoids (%)	
Component	**Appressed**	**Stroma exposed**
PSII	85	15
PSI	10	90
Cytochrome b_6f complex	50	50
LHCII	90	10
ATP synthase	0	100
Plastocyanin*	40	60

* Percentages indicate relative distribution of each component in either appressed or stroma-exposed thylakoid membranes, except in the case of plastocyanin, where localization refers to the lumen of the respective membrane region.

Other protein complexes integral to the thylakoid membrane are also distributed unequally among these two membrane domains (Table 12.7). For example, the ATP synthase is located almost entirely in the stroma-exposed membrane. Even soluble electron transfer proteins such as plastocyanin are distributed unequally within granal and stromal regions of the continuous thylakoid lumen. This **lateral heterogeneity** indicates that the two photosystems, which cooperate in

transferring electrons from H_2O to $NADP^+$ in the electron transport chain, are spatially separated from each other. According to this model, mechanisms for long-distance electron transfer must exist. Note that not all membrane-bound proteins are distributed unequally in the thylakoid. The cytochrome b_6f complex, which transfers electrons between the two photosystems, is distributed evenly (Fig. 12.31).

The concept that PSII and PSI cooperate in the noncyclic transport of electrons from water to $NADP^+$ led to the expectation that the two photosystems would be present in equal amounts in thylakoid membranes. Experimental evidence, however, has not supported this prediction. The ratio of PSII to PSI (photosystem stoichiometry) can vary between 0.4 and 1.7 among various wild-type photosynthetic organisms, such as green and red algae, cyanobacteria, and plants, and the ratio in mutants may vary even more. Photosystem stoichiometry can also be regulated by light quality, demonstrating the ability of the photosynthetic organisms to alter their membrane composition in response to gradients of light quality, such as those observed in a forest canopy or in aquatic environments.

12.6.2 Phosphorylation of LHCII influences the distribution of energy between PSI and PSII

LHCII, the light-harvesting protein complex that functions as a peripheral antenna for PSII, is found almost exclusively in grana (see Table 12.7). Extensive stacking of membranes correlates with the presence of LHCII. Chloroplasts from some mutant plants lacking LHCII have greatly reduced stacking but remain photosynthetically competent. The function of membrane stacking in chloroplasts may be related to the efficient distribution of light energy between PSI and PSII complexes. Because balanced excitation of both photosystems is required for maximum electron transport efficiency, it is critical that one photosystem does not receive preferential photon delivery. The spatial separation of the two photosystems may aid in this regulation. In addition, chloroplasts are able to adjust LHCII association with PSII to regulate distribution of quanta between the photosystems.

A small pool of the total LHCII undergoes reversible phosphorylation in the light. Phosphorylation of LHCII changes the surface charge on the protein. After phosphorylation, LHCII molecules become negatively charged and are displaced from the hydrophobic core of the granal stacks to the less hydrophobic, exposed stromal membrane region. This migration of a portion of the PSII antenna complex decreases light absorption by PSII in the granal membrane by decreasing the antenna associated with PSII (Fig. 12.32).

The most widely accepted model for how chloroplasts sense an imbalance in excitation and phosphorylate LHCII in response involves a redox-activated kinase, STN7. STN7 is activated only when the pool of plastoquinone, a mobile

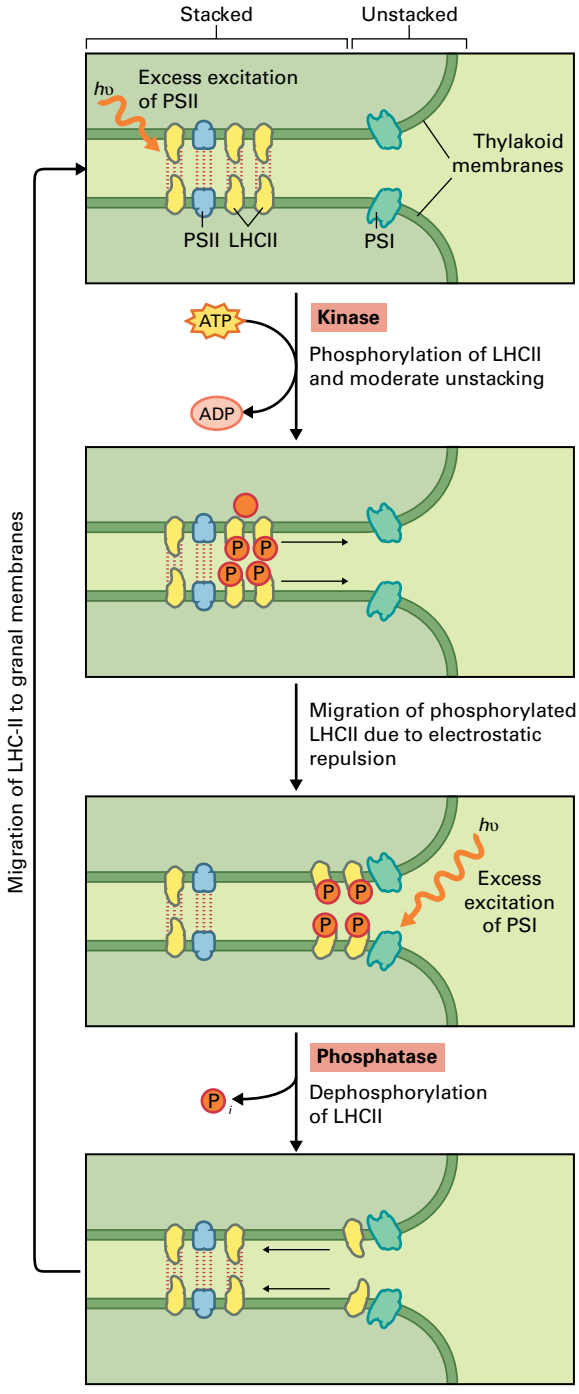


FIGURE 12.32 *Phosphorylation of LHCII controls energy distribution. Excess excitation of PSII relative to PSI increases the level of reduced plastoquinone, which activates a kinase that phosphorylates LHCII. This results in a partial unstacking of the membranes because of electrostatic repulsion of negatively charged LHCII molecules and a migration of some phosphorylated LHCII from the stacked membrane region to the unstacked membrane region, where it can associate with PSI. This effectively reduces the PSII antenna size and favors absorption of quanta by PSI. Excessive PSI activation results in plastoquinol oxidation and kinase de-activation. A phosphatase is able to hydrolyze the phosphate group of LHCII, allowing it to migrate back to the more hydrophobic environment of the stacked membrane region. This mechanism allows for adjustment of the relative excitation of PSI and PSII.*

electron carrier that shuttles electrons between PSII and the cytochrome b_6f complex, is in a highly reduced state (see Section 12.4). When PSII receives more light than PSI, plastoquinone becomes predominantly reduced, resulting in activation of the LHCII kinase. The kinase phosphorylates LHCII, resulting in migration of LHCII away from the granal region where it can associate with PSI, thereby adjusting the relative excitation of PSII and PSI. As plastoquinone becomes more oxidized by PSI activation, the kinase becomes less active and a phosphatase acts to dephosphorylate LHCII, allowing it to migrate back to the granal membrane, thereby increasing the amount of light absorbed by PSII. This feedback system allows for a subtle control of light distribution between the two photosystems, even though they lie in different parts of the thylakoid (Fig. 12.32).

12.6.3 Light harvesting is regulated by nonphotochemical quenching processes that dissipate excess light energy

Under the high light intensities found in nature, plants may absorb more light energy than they can use for photosynthesis. This excessive excitation of chlorophylls can increase formation of the triplet state of chlorophyll and the singlet state of oxygen (see Section 12.2). Damage caused by singlet oxygen and its reactive products can decrease the efficiency of photosynthesis in a process known as **photoinhibition** (see Box 10.8).

All oxygenic photoautotrophs regulate light harvesting to protect against photoinhibition when light is in excess. In plants, various **nonphotochemical quenching** (NPQ) processes act as safety valves for photosynthesis that dissipate excess absorbed light energy harmlessly as heat (Fig. 12.33). NPQ results in de-excitation of the singlet state of chlorophyll in the antenna of PSII, and it is routinely measured using chlorophyll fluorescence (Box 12.2). In addition to their photoprotective roles in quenching triplet chlorophyll and singlet oxygen, specific carotenoids (e.g., zeaxanthin and lutein) have been implicated in NPQ.

Several components of NPQ occur with different induction and relaxation kinetics. A flexible, rapidly reversible type of NPQ is induced by the buildup of a high thylakoid ΔpH in the presence of excess light. The resulting low pH in the thylakoid lumen activates an enzyme (violaxanthin de-epoxidase) that converts violaxanthin into zeaxanthin (see Fig. 12.7), and it also leads to protonation of a membrane protein (PSBS) that promotes a dissipative state of LHC proteins in the PSII antenna (Fig. 12.33). This is the major form of NPQ that regulates light harvesting in natural, fluctuating light, and mutants that lack flexible NPQ exhibit decreased fitness. Sustained types of NPQ are more prominent in some plants that experience chronic excess light on a seasonal basis (e.g., overwintering evergreens).

12.7 Carbon reactions: the Calvin–Benson cycle

12.7.1 The Calvin–Benson cycle in the chloroplast stroma utilizes the energy stored in the thylakoid membranes for the assimilation of atmospheric CO_2

Conversion of inorganic carbon into carbon skeletons of organic material (autotrophy) is required for building all the molecules necessary for life (Box 12.3). In plants, light energy drives the oxidation of water, which produces molecular oxygen (O_2) in thylakoid membranes and yields ATP, reduced ferredoxin, and reduced pyridine nucleotide (NADPH). The

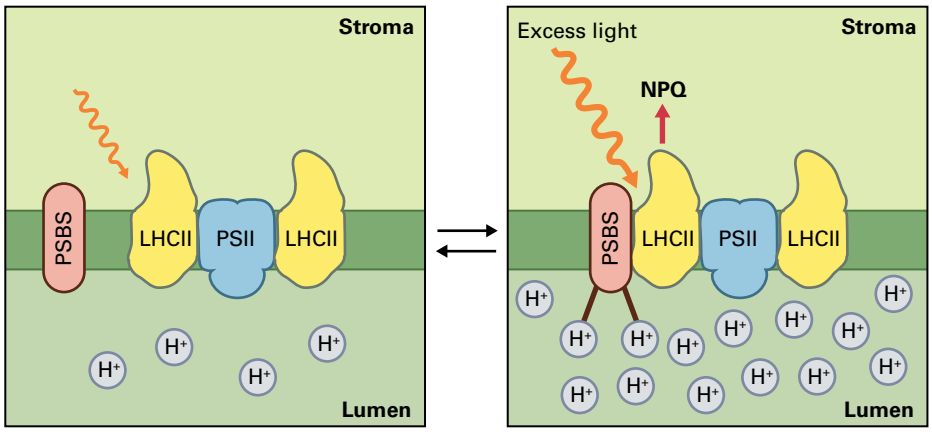


FIGURE 12.33 *Nonphotochemical quenching regulates light harvesting by PSII. In limiting light, LHC proteins efficiently transfer excitation energy to the reaction center of PSII. In excess light, when the rate of photosynthesis is saturated and protons accumulate to a high concentration in the thylakoid lumen, a flexible type of nonradiative dissipation is induced in the PSII antenna on a timescale of seconds to minutes. Proton binding to the PSBS protein and accumulation of zeaxanthin (not shown) causes a conformational change or reorganization of PSII that switches the antenna into a dissipative state that prevents overexcitation of chlorophyll and overreduction of the electron transport chain.*

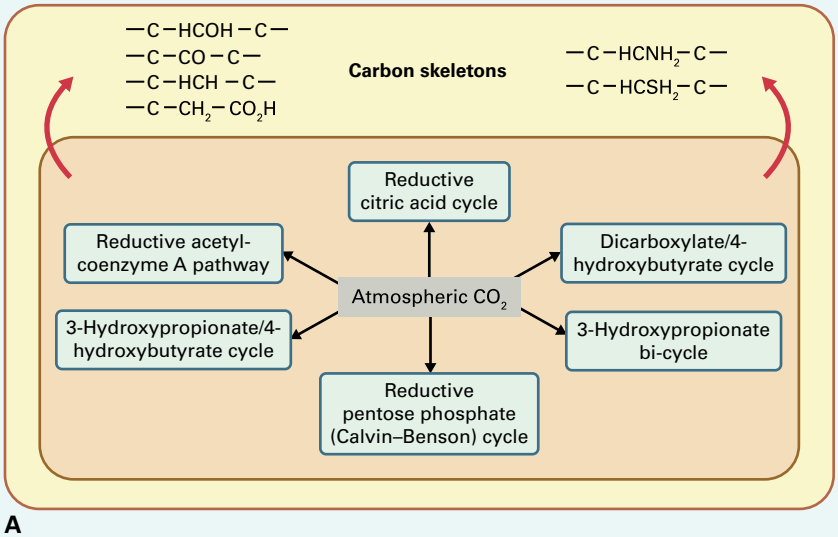
BOX 12.3

Autotrophy is the transition from the inorganic to the organic world

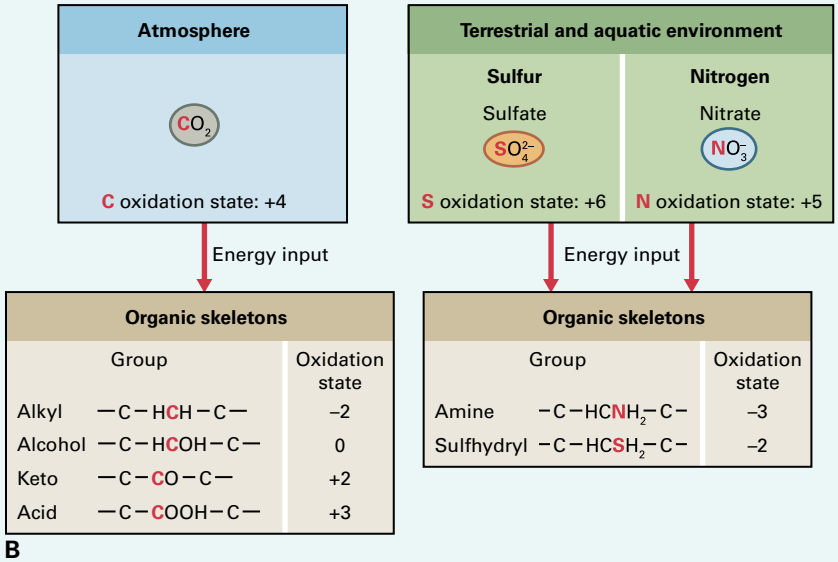
All the organic carbon found in living organisms ultimately comes from inorganic sources, such as gaseous CO_2 and soluble and insoluble HCO_3^- and CO_3^{2-}, the distribution of which in the biosphere depends on environmental parameters, such as temperature, pH, and pressure. Land and marine organisms and many specialized microbes developed the ability to use inorganic carbon as the sole source for building up the organic molecules required to sustain cell metabolism (A). This process, autotrophy, requires a constant flux of energy for converting carbon and other elements from the high oxidation state they hold in the environment (CO_2: +4) to the low oxidation states of organic molecules that participate in cell metabolism $-CO_2H$: +3; –CO–: +2; –CHO: +1; –CHOH–: 0; $-CH_2OH$: –1; $-CH_2-$: –2; $-CH_3$: –3; CH_4: –4) (B).

Two environmental sources provide the energy that sustains autotrophy: chemical compounds (used by chemoautotrophs) and light (used by photoautotrophs). Membrane protein complexes channel the external energy for driving the endergonic flow of electrons. Subsequently, the reducing power is used for the transformation of chemical bonds catalyzed by specific enzymes.

Assimilation of CO_2 proceeds through six different pathways (A): the reductive acetyl-CoA pathway, reductive citric acid cycle (reverse citric acid cycle), dicarboxylate/4-hydroxybutyrate cycle, 3-hydroxypropionate bi-cycle, 3-hydroxypropionate/4-hydroxybutyrate cycle, and reductive pentose phosphate cycle (Calvin–Benson cycle). The former five autotrophic pathways function in prokaryotes and yield acetyl-coenzyme A or pyruvate at



A



B

early stages of CO_2 fixation. Large organic molecules are subsequently built up through unique gluconeogenic pathways. There is renewed interest in these pathways for improving oxygenic photosynthesis through synthetic biology.

The remaining pathway for CO_2 fixation—the reductive pentose phosphate cycle (Calvin–Benson cycle or C_3 pathway)—constitutes the major aerobic mechanism for the formation of biomass (i.e., synthesis of structural and storage polysaccharides). The Calvin–Benson cycle is used for CO_2 assimilation by many chemo- and photoautotrophic prokaryotes and all photoautotrophic eukaryotes.

Autotrophy. (A) CO_2 assimilation in the biosphere through autotrophic pathways. Atmospheric CO_2 is the building block for carbon skeletons in autotrophic organisms. (B) Oxidation state of carbon, nitrogen and sulfur in the biosphere. The oxidation state of these elements decreases when they are transferred from the environment to the organic molecules of living organisms.

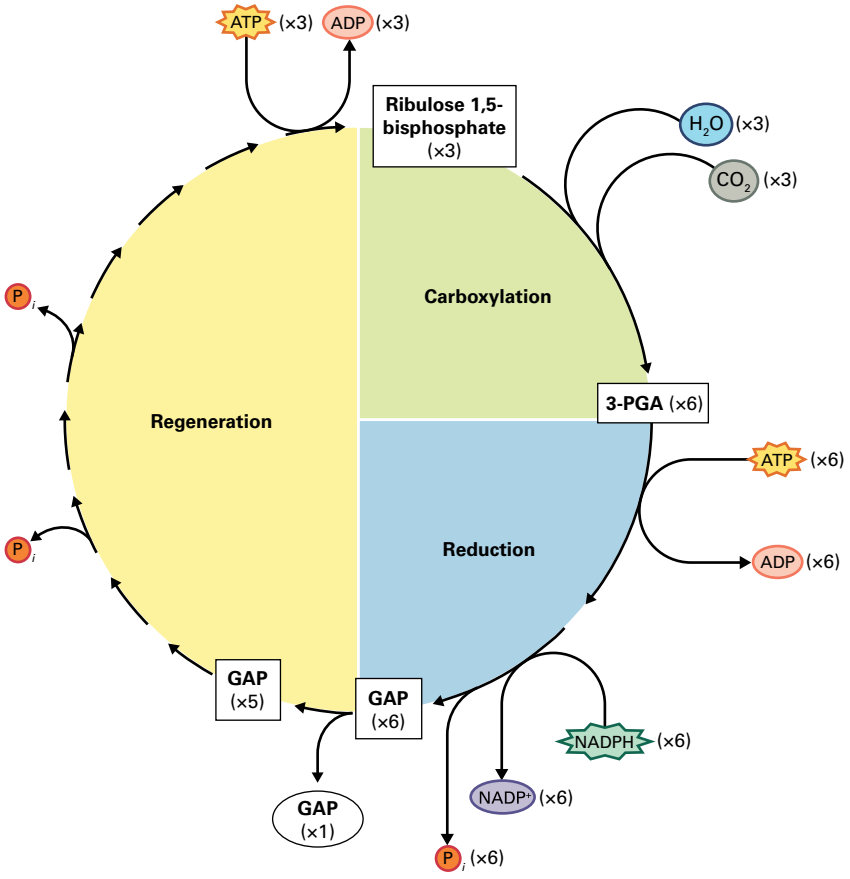


FIGURE 12.34 *Three phases of the Calvin–Benson cycle: carboxylation, reduction, and regeneration. Overall, the fixation of three molecules of CO_2 into one molecule of triose phosphate requires six molecules of NADPH and nine of ATP (3 CO_2: 6 NADPH : 9 ATP ≡ CO_2: 2 NADPH : 3 ATP). The net glyceraldehyde 3-phosphate (GAP) formed is utilized either for immediate metabolic needs or converted to a storage form of carbohydrate—starch in the chloroplast or sucrose in the cytosol. 3-PGA, 3-phosphoglycerate.*

ATP and NADPH released in the chloroplast stroma are used for the conversion of atmospheric CO_2 to carbohydrates.

The pathway by which this conversion occurs, the Calvin–Benson cycle, is crucial for sustaining most life forms. It was discovered in the 1950s, in experiments in which illuminated green algae (*Chlorella*, *Scenedesmus*) were pulsed with $^{14}CO_2$ and sampled at short intervals by injecting the cell suspensions into boiling alcohol. The ^{14}C-containing compounds were successively separated by two-dimensional paper chromatography, detected by autoradiography, and analyzed for the exact position of the ^{14}C label by co-chromatography and degrading the isolated intermediates. The presence of the enzyme activities needed for the photosynthetic CO_2 assimilation in green algae validated the predicted pathway. Some photosynthetic prokaryotes (photosynthetic bacteria, cyanobacteria) and all photosynthetic eukaryotes (algae and plants) fix CO_2 into biomass using the Calvin–Benson cycle (Box 12.3).

12.7.2 The Calvin–Benson cycle proceeds through 13 biochemical reactions

The Calvin–Benson cycle proceeds through 13 biochemical reactions that can be analyzed separately in three highly coordinated phases: carboxylation, reduction, and regeneration (Figs. 12.34 and 12.35).

- Carboxylation of the CO_2-acceptor molecule: ribulose 1,5-bisphosphate (RuBP; five-carbon acceptor molecule) reacts with one molecule each of CO_2 and water to yield two molecules of 3-phosphoglycerate (3-PGA) in the first enzymatic step of the cycle (see Section 12.7.3).
- Reduction of 3-PGA: Photochemically generated ATP and NADPH (see Section 12.4.1) are used in two enzymatic reactions for the reduction of 3-PGA to glyceraldehyde 3-phosphate (GAP) (see Section 12.7.4).
- Regeneration of RuBP: The regeneration of the CO_2 acceptor RuBP closes the cycle through ten enzyme-catalyzed reactions, one requiring ATP (see Section 12.7.5).

12.7.3 Carboxylation of RuBP is the first committed reaction of the Calvin–Benson cycle

In the carboxylation phase, three molecules of CO_2 and three molecules of H_2O react with three molecules of RuBP to produce six molecules of 3-PGA (Reaction 12.12, Fig. 12.35). The enzyme ribulose-1,5-bisphosphate carboxylase/oxygenase (Rubisco) catalyzes these reactions (see Section 12.8). Plants that form 3-PGA (a three-carbon molecule) as the first stable compound after feeding with $^{14}CO_2$ in the light are called **C_3 plants**.

Reaction 12.12: Ribulose-1,5-bisphosphate carboxylase/oxygenase (Rubisco)

$$3\ \text{Ribulose 1,5-bisphosphate (RuBP)} + 3CO_2 + 3H_2O \rightarrow 6\ \text{3-phosphoglycerate (3-PGA)} + 6H^+$$

12.7.4 Reduction of 3-PGA follows CO_2 fixation and employs products of the light reactions

The reductive phase of the Calvin–Benson cycle converts the six molecules of 3-PGA coming from the carboxylation stage into six molecules of GAP (Fig. 12.35). This two-step process employs ATP and NADPH, the products of the light reactions. First, the enzyme 3-phosphoglycerate kinase (Reaction 12.13) catalyzes the reaction of ATP with the carboxyl group of 3-PGA, yielding the mixed anhydride 1,3-bisphosphoglycerate (1,3-bis-PGA). Next, NADPH converts 1,3-bis-PGA to GAP and inorganic phosphate (P_i) in a reaction catalyzed by the chloroplast enzyme NADP–glyceraldehyde-3-phosphate dehydrogenase (NADP–GAPD; Reaction 12.14).

Reaction 12.13: 3-phosphoglycerate kinase

$$6\ \text{3-Phosphoglycerate (3-PGA)} + 6\ \text{ATP} \rightarrow 6\ \text{1,3-bisphosphoglycerate (1,3-bis-PGA)} + 6\ \text{ADP}$$

Reaction 12.14: NADP–glyceraldehyde-3-phosphate dehydrogenase (NADP–GAPD)

$$6\ \text{1,3-Bisphosphoglycerate (1,3 bis-PGA)} + 6\,\text{NADPH} + 6H^+ \rightarrow 6\ \text{glyceraldehyde 3-phosphate (GAP)} + 6\ NADP^+ + 6\ P_i$$

12.7.5 Regeneration of RuBP is necessary for continuous operation of the Calvin–Benson cycle

One of the six molecules of GAP (1 molecule × 3 carbons/molecule = 3 carbons) accounts for the net fixation of three molecules of CO_2 (3 molecules × 1 carbon/molecule = 3 carbons) and represents the newly formed photosynthetic product. The other five molecules of GAP (5 molecules × 3 carbons/molecule = 15 carbons) enter the last and largest set of reactions to regenerate three molecules of RuBP (3 molecules × 5 carbons/molecule = 15 carbons) and allow continuous uptake of atmospheric CO_2.

Ten of the 13 enzymes of the Calvin–Benson cycle catalyze the reshuffling of the carbons from five molecules of GAP to form three molecules of RuBP (Reactions 12.15–12.24, Fig. 12.35):

- Triose phosphate isomerase catalyzes the conversion of two molecules of GAP into two molecules of DHAP (Reaction 12.15). Together, GAP and DHAP are referred to as triose phosphate.

Reaction 12.15: Triose phosphate isomerase

$$2\ \text{Glyceraldehyde 3-phosphate (GAP)} \leftrightarrow 2\ \text{Dihydroxyacetone phosphate (DHAP)}$$

- Aldolase catalyzes the aldol condensation of a third molecule of GAP with one molecule of DHAP, yielding the six-carbon sugar fructose 1,6-bisphosphate (FBP) (Reaction 12.16).

Reaction 12.16: Aldolase

$$\text{Glyceraldehyde 3-phosphate (GAP)} + \text{Dihydroxyacetone phosphate (DHAP)} \rightarrow \text{Fructose 1,6-bisphosphate (FBP)}$$

- FBP is hydrolyzed to the sugar monophosphate fructose 6-phosphate (F 6-P) in a reaction catalyzed by a specific chloroplast fructose-1,6-bisphosphatase (Reaction 12.17).

Reaction 12.17: Fructose-1,6-bisphosphatase

$$\text{Fructose 1,6-bisphosphate (FBP)} + H_2O \rightarrow \text{Fructose 6-phosphate (F6-P)} + P_i$$

- The F6-P molecule donates a two-carbon unit (C_1 and C_2) to a fourth molecule of GAP via the enzyme transketolase,

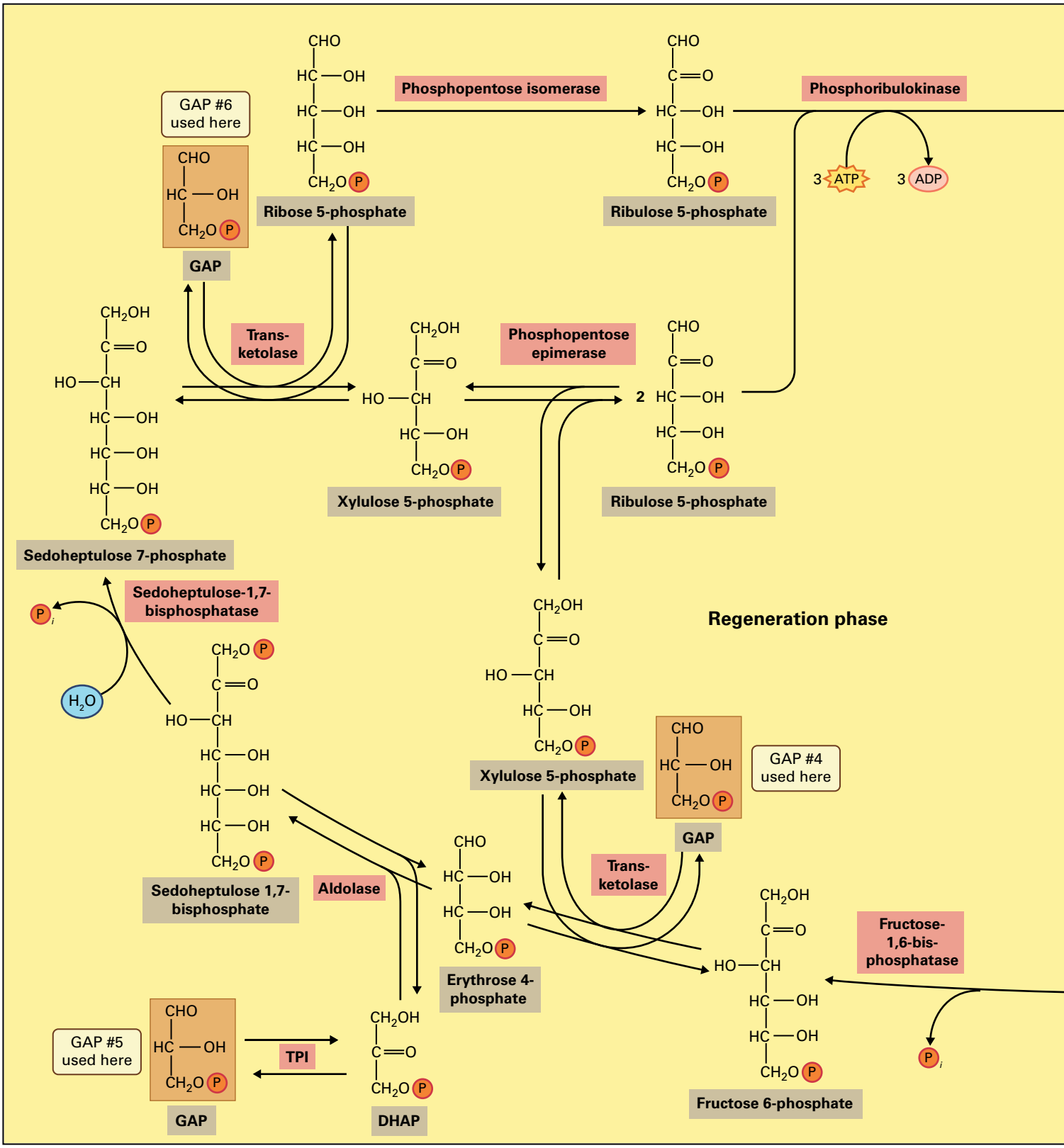
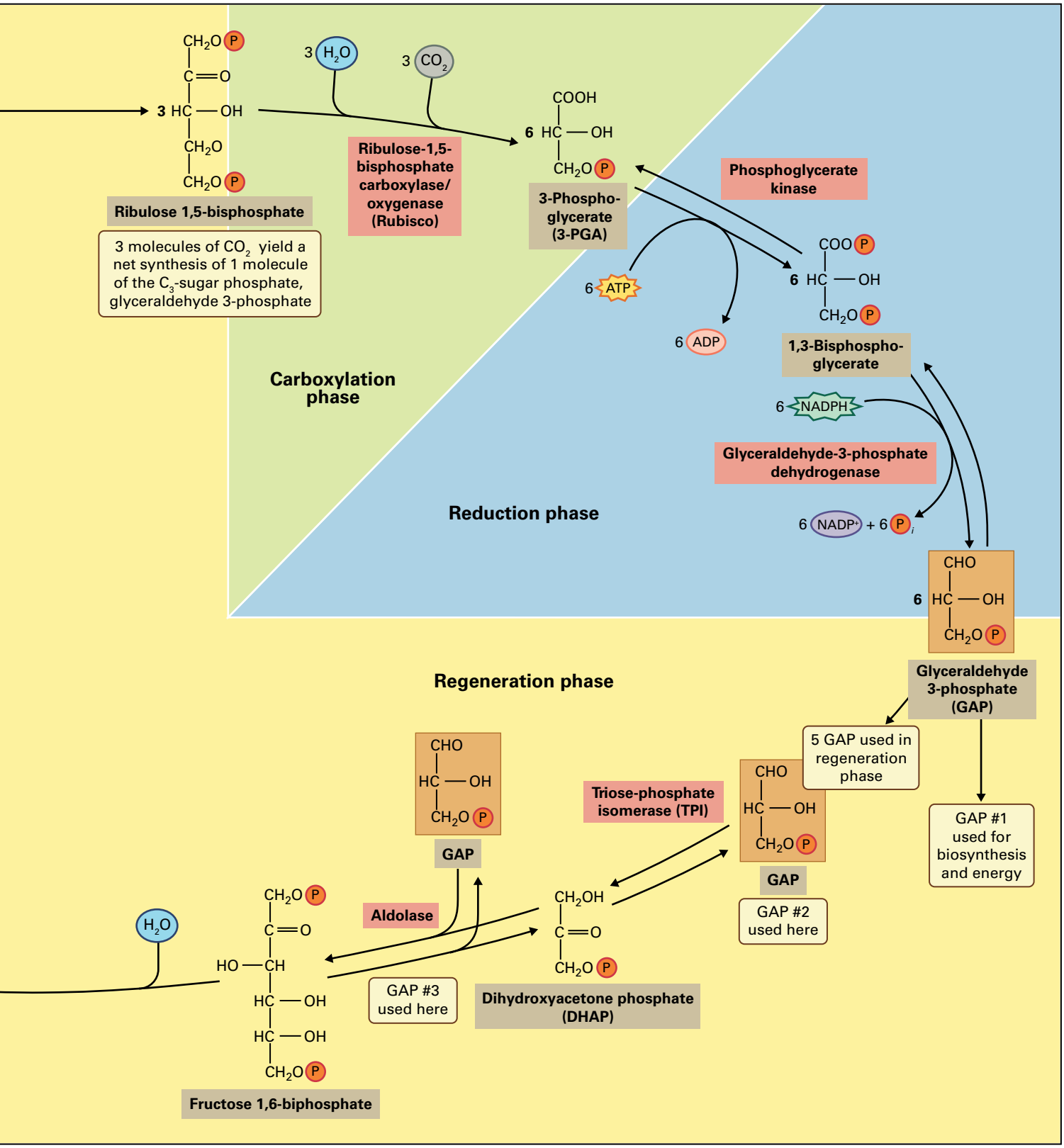


FIGURE 12.35 *Individual reactions of the Calvin–Benson cycle.*


Ribulose 1,5-bisphosphate
3 molecules of CO_2 yield a net synthesis of 1 molecule of the C_3-sugar phosphate, glyceraldehyde 3-phosphate
Ribulose-1,5-bisphosphate carboxylase/ oxygenase (Rubisco)
3-Phospho-glycerate (3-PGA)
Phosphoglycerate kinase
1,3-Bisphospho-glycerate
Glyceraldehyde-3-phosphate dehydrogenase
Glyceraldehyde 3-phosphate (GAP)
Carboxylation phase
Reduction phase
Regeneration phase
5 GAP used in regeneration phase
GAP #1 used for biosynthesis and energy
GAP
GAP #2 used here
Triose-phosphate isomerase (TPI)
Aldolase
GAP #3 used here
Dihydroxyacetone phosphate (DHAP)
Fructose 1,6-biphosphate

yielding xylulose 5-phosphate (Xu 5-P). The other four carbons of the F6-P molecule (C_3, C_4, C_5, and C_6) form erythrose 4-phosphate (E4-P) (Reaction 12.18).

Reaction 12.18: Transketolase

Fructose 6-phosphate (F 6-P) + Glyceraldehyde 3-phosphate (GAP) → Erythrose 4-phosphate (E4-P) + Xylulose 5-phosphate

- E4-P combines, via aldolase, with the remaining molecule of DHAP to yield the seven-carbon sugar bisphosphate sedoheptulose 1,7-bisphosphate (SBP) (Reaction 12.19).

Reaction 12.19: Aldolase

Erythrose 4-phosphate (E4-P) + Dihydroxyacetone phosphate (DHAP) → Sedoheptulose 1,7-bisphosphate (SBP)

- SBP is hydrolyzed to the respective sugar monophosphate sedoheptulose 7-phosphate (S7-P) by a specific chloroplast sedoheptulose-1,7-bisphosphatase (Reaction 12.20).

Reaction 12.20: Sedoheptulose-1,7-bisphosphatase

Sedoheptulose 1,7-bisphosphate (SBP) + H_2O → Sedoheptulose 7-phosphate (S7-P) + P_i

- A two-carbon unit of S 7-P (C_1 and C_2) is transferred to the fifth (and last) molecule of GAP, via transketolase, producing a second molecule of Xu 5-P. The remaining five carbons (C_3, C_4, C_5, C_6, and C_7) of the S 7-P molecule yield ribose 5-phosphate (R 5-P) (Reaction 12.21).

Reaction 12.21: Transketolase

Sedoheptulose 7-phosphate (S 7-P) + Glyceraldehyde 3-phosphate (GAP) → Ribose 5-phosphate (R 5-P) + Xylulose 5-phosphate (Xu 5-P)

- Ribulose 5-phosphate epimerase catalyzes the transformation of two molecules of Xu 5-P in two molecules of ribulose 5-phosphate (Ru 5-P) (Reaction 12.22).

Reaction 12.22: Ribulose-5-phosphate epimerase

2 Xylulose 5-phosphate (Xu 5-P) → 2 Ribulose 5-phosphate (Ru 5-P)

- Ribose-5-phosphate isomerase catalyzes the conversion of R 5-P into a third molecule of Ru 5-P (Reaction 12.23).

Reaction 12.23: Ribose-5-phosphate isomerase

Ribose 5-phosphate (R 5-P) → Ribulose 5-phosphate (Ru 5-P)

- Finally, three additional molecules of ATP phosphorylate the three molecules of Ru 5-P, forming three molecules of RuBP in the reaction catalyzed by phosphoribulokinase (PRK) (also called ribulose-5-phosphate kinase) (Reaction 12.24).

Reaction 12.24: Phosphoribulokinase (PRK)

3 Ribulose 5-phosphate (Ru 5-P) + 3 ATP → 3 Ribulose 1,5-bisphosphate (RuBP) + 3 ADP + $3H^+$

Net : 3 CO_2 + 5 H_2O + 6 NADPH + 9 ATP → Glyceraldehyde 3-phosphate (GAP) + 6 $NADP^+$ + $3H^+$ + 9 ADP + 8 P_i

In summary, the addition of three molecules of CO_2 to three molecules of the five-carbon sugar RuBP yields six molecules of 3-PGA, which in turn generate six molecules of GAP after successive phosphorylation and reduction with six molecules of ATP and six molecules of NADPH, respectively. Five molecules of GAP and three additional molecules of ATP regenerate the three molecules of RuBP that set the Calvin–Benson cycle for another turn of CO_2 fixation. The remaining molecule of GAP formed in the carboxylation and reduction phases of the Calvin–Benson cycle constitutes the net product of carbon fixation that plants use to build storage carbohydrates and other cellular constituents (Fig. 12.35).

12.8 Rubisco

Rubisco, the predominant protein in plant leaves, catalyzes the initial reaction of the Calvin–Benson cycle, the carboxylation of RuBP. In addition, Rubisco catalyzes a competing oxygenation reaction (**photorespiration**, see Sections 12.8.3 and 14.8.2), which reduces the efficiency of photosynthetic carbon fixation. This section describes the structure of Rubisco and mechanisms of its catalysis and regulation.

12.8.1 Four distinct forms of Rubisco are found in nature

Enzyme analyses and genome sequencing projects have revealed distinct forms of Rubisco that are present in organisms that fix CO_2, as well as in microorganisms that do not use CO_2 as a major carbon source. From a comparison of primary structures, four forms of Rubisco have been identified with different arrangements of large subunits (L, ≈50 kDa) and small subunits (S, ≈15 kDa) (Table 12.8). Homodimers of the catalytic large subunits are the common unit to all forms. Forms I, II, and III are catalytically competent, while members of form IV lack Rubisco activity and play other roles in metabolism.

Form I is found in most autotrophic organisms. Contributing up to 50% of soluble leaf protein, it is the predominant protein in plant leaves. Its high levels in the photosynthesizing cells of plants and its presence in phytoplankton,

which provide more than 45% of global net primary production annually, make Form I the most abundant protein on earth. Owing to its abundance and importance in plant photosynthesis, we restrict our analysis to aspects of molecular biology and biochemistry of Form I.

Form I is the only type of Rubisco that harbors small subunits, and it consists of eight large and eight small subunits $[L_8S_8]$: Four dimers of large subunits $[L_2]_4$ capped by four small subunits at the top and the bottom $[S_4]_2$ build the hexadecameric structure $\{[S_4]\bullet[L_2]_4\bullet[S_4] = L_8S_8\}$. Although the hexadecameric L_8S_8 is confined to chloroplasts in photosynthetic eukaryotes, the biosynthesis and assembly of the constituent subunits follow different pathways (Table 12.9). The *rbcL* gene encoding the large subunit is in the plastid genome of algae and land plants, whereas it is in the nucleus in dinoflagellates. The *rbcS gene* that encodes the small subunit is located in the plastid genome of red and brown algae. In the green lineage of photosynthetic eukaryotes (green algae and land plants), the *rbcS* gene is in the nucleus, and so the latter small subunit is expressed as a pre-protein that translocates to the chloroplast, where its transit peptide is cleaved at the chloroplast envelope prior to assembly with the large subunit into the hexadecameric L_8S_8. In plants, a suite of nuclear and chloroplast factors modulate the gene expression of chloroplast and nuclear DNA at the posttranscriptional, translational, and posttranslational levels.

TABLE 12.8 *Different forms of Rubisco.*

Form	Quaternary Structure	Organism(s)
I	L_8S_8	Plants, algae, proteobacteria, cyanobacteria
II	$(L_2)_n$	Proteobacteria, dinoflagellates
III	$(L_2)_n$; $(L_2)_5$	Archaea
IV	L_2	Proteobacteria, cyanobacteria, archaea, algae

TABLE 12.9 *Subcellular localization of DNA encoding eukaryotic Rubisco.*

Organism	Quaternary Structure	Subunits	
		Large	Small
Plants, green algae	L_8S_8	Chloroplast	Nucleus
Red and brown algae	L_8S_8	Chloroplast	Chloroplast
Dinoflagellates	L_2	Nucleus	–

12.8.2 The assembly of Rubisco requires molecular chaperones

A conserved nuclear encoded protein (MRL1), found in green algae and plants, regulates biogenesis of Form I (L_8S_8) Rubisco at a posttranscriptional stage through accumulation of the large subunit (L) mRNA. Moreover, prior to formation of L_8S_8 Rubisco, three main processes involving molecular chaperones prevent the misalignment and off-pathway aggregation of large subunits (Fig. 12.36).

12.8.3 Rubisco also functions as an oxygenase

In addition to its role as a carboxylase, Rubisco has an oxygenase activity that uses O_2 as a substrate instead of CO_2 to produce 3-PGA and the two-carbon molecule, 2-phosphoglycolate (Fig. 12.37). All Rubisco enzymes characterized thus far can act as oxygenases, even those isolated from obligately anaerobic prokaryotes that cannot grow in the presence of O_2. This indicates the oxygenase activity is intrinsic to Rubisco.

The two substrates, CO_2 and O_2, compete for the same active site on the enzyme, and the activity of the enzyme toward these substrates is dictated by the relative amounts of O_2 and CO_2 in the environment. In air, the carboxylation reaction proceeds approximately three times faster than the oxygenation reaction; the oxygenase activity, however, proceeds at a rate that can have profound effects on the overall

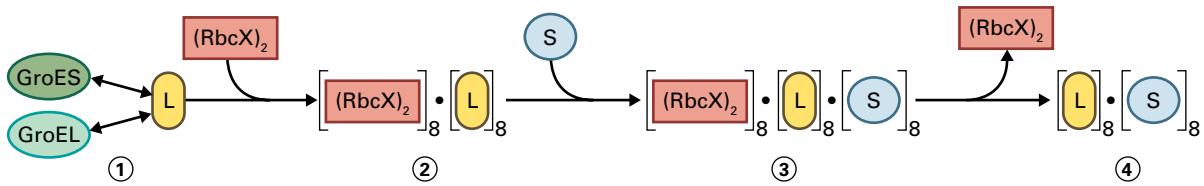


FIGURE 12.36 *Chaperones assist the assembly of Rubisco subunits. (1) Chaperonins GroEL and GroES sequester and ensure the correct folding of the newly synthesized large subunit (L). (2) The assembly chaperone $(RbcX)_2$ binds the large subunit and provides positional information for proper association of large subunit dimers to form the L_8–$((RbcX)_2)_8$ complex. (3) The small subunit (S) associates with L_8–$((RbcX)_2)_8$, triggering a conformational change in RbcL and eliciting (4) the release of $(RbcX)_2$ and formation of the catalytically mature Rubisco holoenzyme $[L]_8$–$[S]_8$.*

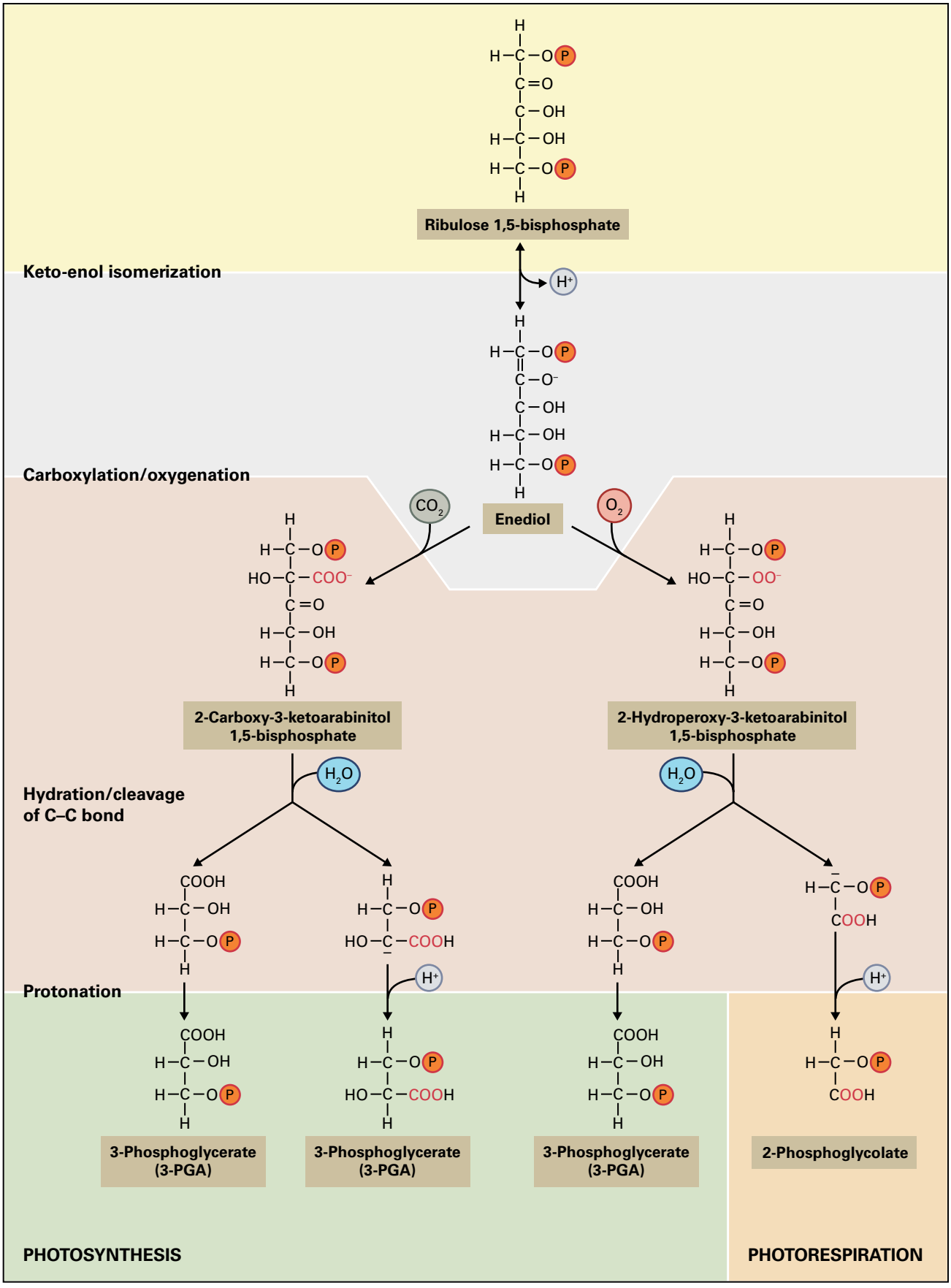


FIGURE 12.37 *Rubisco-mediated carboxylation or oxygenation of RuBP. The 3-PGA and 2-phosphoglycolate formed are metabolized through the Calvin–Benson cycle and the C_2 oxidative photosynthetic carbon cycle, respectively.*

efficiency of CO_2 fixation in C_3 plants: in some cases, an estimated 50% of CO_2 fixed via photosynthesis is lost through this process of photorespiration (see Section 14.8).

12.8.4 Rubisco catalyzes carboxylation or oxygenation in five steps

The active form of Rubisco catalyzes carboxylation or oxygenation reactions in five steps that involve intermediates of variable stability (Fig. 12.37):

1. Enolization of RuBP: Carbamylated Rubisco with bound Mg^{2+} binds to and attracts a proton from the C_3 of RuBP, yielding the 2,3-enediolate form of RuBP linked to Rubisco (the five-carbon-enediol–Rubisco complex) (see Section 12.9.3).
2. Carboxylation or oxygenation of the 2,3-enediolate: Addition of gaseous CO_2 (or O_2) to the unstable Rubisco-bound enediol intermediate discriminates the carboxylase and oxygenase activities. The competing reactions—carboxylase and oxygenase—are an inevitable consequence of the enzyme mechanism, because both CO_2 and O_2 react with the 2,3-enediolate form of RuBP bound to the active site of Rubisco. CO_2 and O_2 yield 2-carboxy-3-ketoarabinitol 1,5-bisphosphate (carboxylase activity) and 2-peroxy-3-ketoarabinitol 1,5-bisphosphate (oxygenase activity), respectively.
3. Hydration of the resulting ketone: the resulting ketone is hydrated to produce unstable intermediates.
4. Cleavage of a specific carbon–carbon bond: the carbon–carbon bond between C_2 and C_3 of the RuBP is cleaved.
5. Protonation of the resulting carboxylate: the carboxylate product is protonated, yielding two molecules of 3-PGA (carboxylase activity) or one molecule of 3-PGA and one molecule of 2-phosphoglycolate (oxygenase activity).

The reaction of the enediol-RuBP bound to Rubisco with CO_2 initiates the Calvin–Benson cycle for inorganic carbon assimilation; its reaction with O_2 initiates the process of photorespiration (see Chapter 14).

12.9 Regulation of the Calvin–Benson cycle by light

Light regulates flux through the Calvin–Benson cycle. This regulation is critical because the chloroplast stroma contains enzymes of the Calvin–Benson cycle that catalyze carbohydrate synthesis as well as oxidative enzymes of pathways that catalyze carbohydrate degradation. To prevent futile cycling and ensure optimal activity of these competing pathways, it is essential for the synthetic apparatus to be "on" and the degradative apparatus "off" in the light.

Chloroplasts ensure appropriate rates of biochemical transformations through modification of both the level and catalytic activity of enzymes. Specific regulatory mechanisms activate enzymes of the Calvin–Benson cycle when needed in the light and turn them off at night; degradative enzymes, such as glucose-6-phosphate dehydrogenase of the pentose phosphate pathway, behave in the opposite manner and are inactive in the light and active in the dark, adjusting production of triose phosphates and preventing futile cycles caused by competing processes (see Chapter 13).

12.9.1 Light modulates the levels of stromal enzymes encoded in nuclear and chloroplast genomes

The levels of stromal enzymes encoded in both the nucleus and chloroplast depend on the rates of their gene expression and protein synthesis. Like the Rubisco small subunit, nuclear-encoded polypeptides are translated on cytosolic 80S ribosomes and have an N-terminal transit signal that is removed at the chloroplast envelope as the mature form of the enzyme enters the plastid and is released into the stroma. Like the Rubisco large subunit, plastid-encoded proteins are translated in the stroma on prokaryotic-like 70S ribosomes. To build up the correct amount of each enzyme for the plastid, nuclear gene expression must be coordinated with the expression of other components of the photosynthetic apparatus encoded in the plastid DNA. Upon stimulation by light, the synthesis of both chloroplast and nuclear mRNAs is coordinated, ensuring that new polypeptides are present together and in sufficient amounts for the function of pathways.

Most of the regulation between nucleus and plastids is **anterograde**: products of nuclear genes control the transcription and translation of plastid genes. For example, the precursor of the small subunit of Rubisco is encoded in the nuclear genome, whereas the large subunit in encoded in the chloroplast. The abundance of the small subunit in the stroma controls the translation of the large subunit mRNA, thereby achieving efficient stoichiometry of Rubisco subunits in the hexadecameric complex (L_8S_8).

In other cases, signal transduction mechanisms can be **retrograde**: The signals flow from the chloroplast to the nucleus. For example, plastidial ferrochelatase I catalyzes the synthesis of heme, which in turn regulates the expression of nuclear-encoded, chloroplast-targeted proteins in greening leaves.

12.9.2 Light-linked posttranslational modifications of enzymes regulate the Calvin–Benson cycle

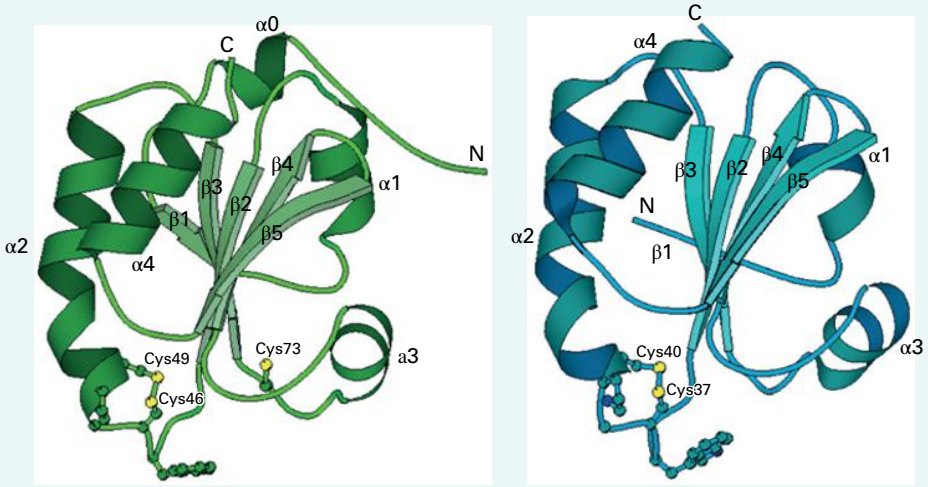
Whereas accumulation of chloroplast enzymes causes slow changes in overall catalytic rates, posttranslational modifications change catalytic rates rapidly in response to

BOX 12.4

Thioredoxins occur in multiple forms and have conserved structures to interact with target enzymes

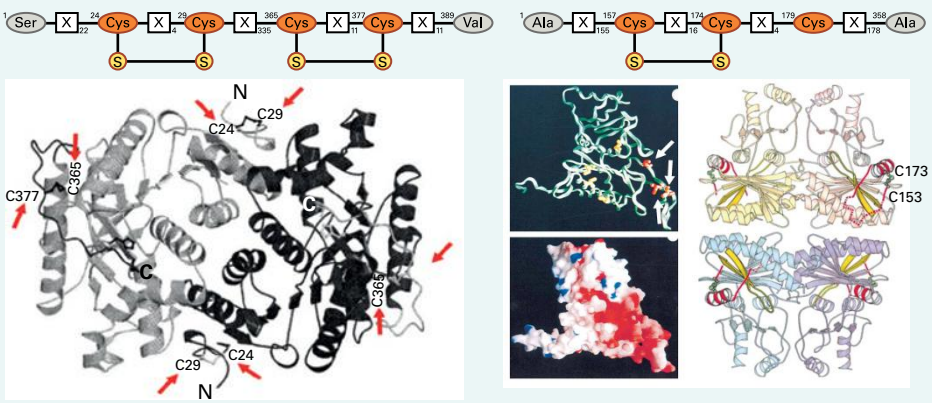
Biochemical and genomic studies have uncovered isoforms of Trx in different organisms. The nuclear DNA of land plants, for example, has genes coding for seven different types of thioredoxin (*f*, *m*, *x*, *y*, *z*, *h*, *o*). Trx *f*, *m*, *x*, *y*, and *z* are located in the chloroplasts, *o* in mitochondria, and *h* in the cytosol, endoplasmic reticulum, and plasma membrane. The proteins are characterized by a canonical disulfide active site consisting of Cys-Gly-Pro-Cys and a common tertiary structure called the thioredoxin fold, which consists of five antiparallel beta sheets sandwiched between three alpha helices (A). Surface charges contribute to specificity for interacting with partner enzymes, such as the interaction between Trx *f* and regulatory enzymes of the Calvin–Benson cycle.

Chloroplast enzymes interacting with Trx appear to have evolved from redox-insensitive counterparts inherited from heterotrophic ancestors by acquiring regulatory cysteines. The most extensively studied chloroplast enzymes regulated by Trx have specific sequences at the N- or C-terminus (NADP-malate dehydrogenase) (B) or in the core of the polypeptide (fructose-1,6-bisphosphatase) (C). This structural information has made possible the introduction of specific regulatory sequences through genetic engineering to convert nonregulatory enzymes to regulatory forms that show activity changes following Trx-linked redox transitions.



Thioredoxin *f* Thioredoxin *m*

A Crystal structures of spinach chloroplast thioredoxins



B NADP–MDH **C CFBPase**

modifications in the chloroplast stroma that are coupled to photosynthetic electron transport.

Enzymes of the cycle can acquire different catalytic rates via one of two mechanisms that alter protein structure: (1) Rubisco activase regulates the activity of Rubisco through removal of bound, inhibitory sugar derivatives (see Section 12.9.3), and (2) the ferredoxin–thioredoxin system (FTS) regulates the activity of four enzymes (fructose-1,6-bisphosphatase, sedoheptulose-1,7-bisphosphatase, PRK, and NADP–GAPD) by the reduction of specific disulfide bonds (Box 12.4 and Section 12.9.4).

12.9.3 Rubisco activase modulates Rubisco activity

The unique mechanisms that regulate Rubisco activity are related to the enzyme's slow capacity for CO_2 fixation (1–12 CO_2 fixations per second, per active site).

Prior to catalysis, Rubisco must be activated by a molecule of CO_2 (modulation, Fig. 12.38A), which reacts with the ε-NH_2 group of a specific lysine within the active site through carbamylation. The carbamate derivative then binds Mg^{2+} to yield the catalytically active enzyme. In catalysis, the ternary complex [E–CO_2^-•Mg^{2+}] binds another CO_2 molecule (the substrate) in the active site, which then reacts with RuBP to yield two molecules of 3-PGA.

Both decarbamylated and carbamylated Rubisco are inhibited by sugar phosphates, even by the substrate RuBP (Fig. 12.38B). The natural sugar phosphate, 2-carboxyarabinitol 1-phosphate (CA1P), which resembles the six-carbon intermediate of the carboxylation reaction, is a strong inhibitor that reversibly inhibits both uncarbamylated and carbamylated Rubisco. CA1P and the other bound sugar phosphates are specifically removed by the ATP-dependent enzyme, **Rubisco activase**, which prepares Rubisco for the catalytic cycle.

Many plant species contain two different Rubisco activases (42 and 47 kDa) that are the results of alternative splicing of a unique pre-mRNA. The two isoforms are identical, except for the extra peptide at the C-terminal region of the longer form, which contains two cysteines that alternate reversibly between the sulfhydryl and disulfide forms in a reaction catalyzed by

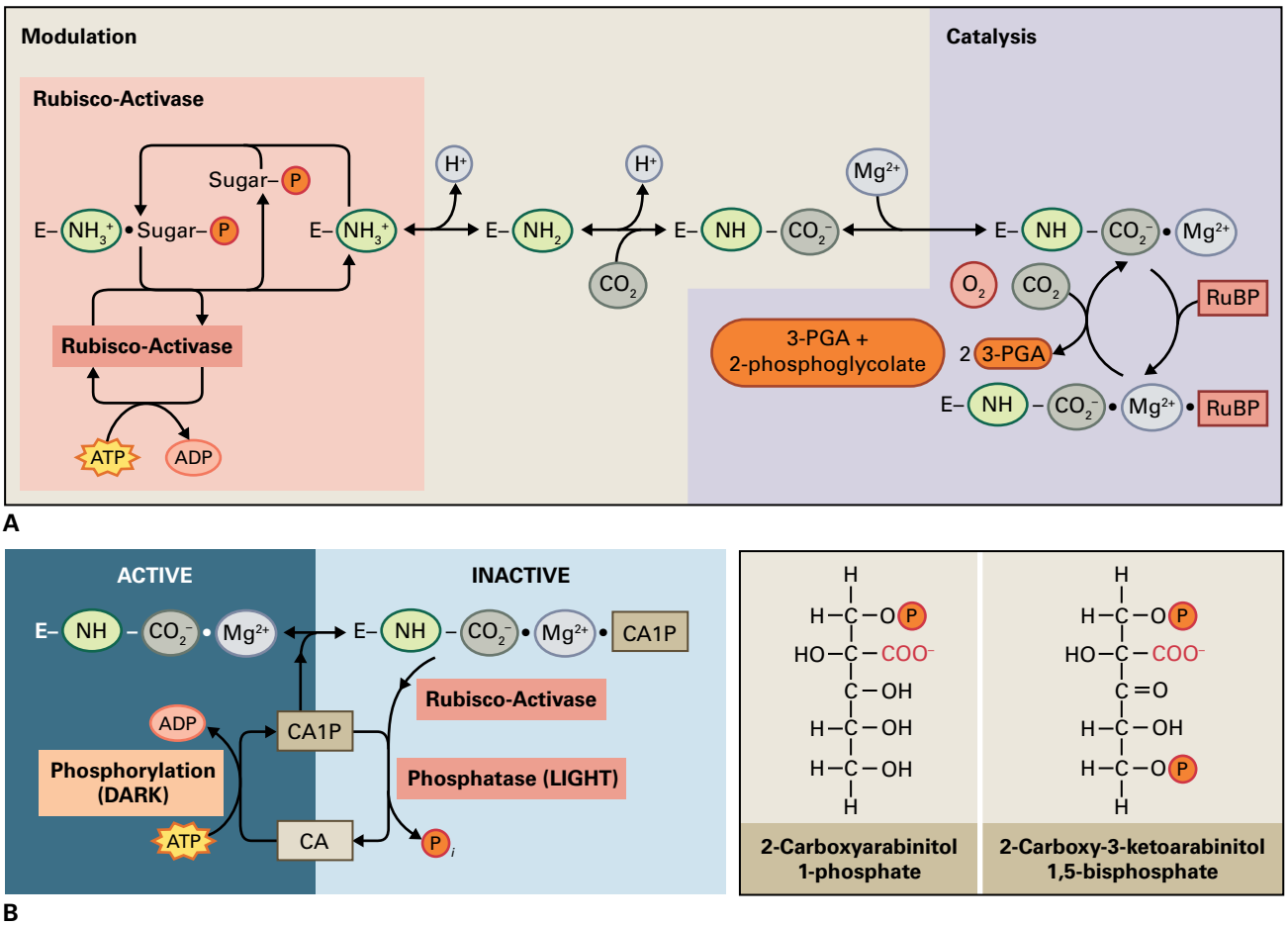


FIGURE 12.38 *Regulation of Rubisco activity. (A) The CO_2 molecule plays a dual role in the activity of Rubisco (E): it transforms the enzyme from an inactive to an active form (modulation) and is the substrate for the carboxylase reaction (catalysis). (B) Rubisco is inhibited by tightly bound sugar phosphates, including the natural inhibitor 2-carboxyarabinitol 1-phosphate (CA1P), that is a structural analog of the six-carbon intermediate of the carboxylation reaction (see Fig. 12.37). CA1P turns the enzyme off at night in some plants and Rubisco activase removes these inhibitory sugar derivatives.*

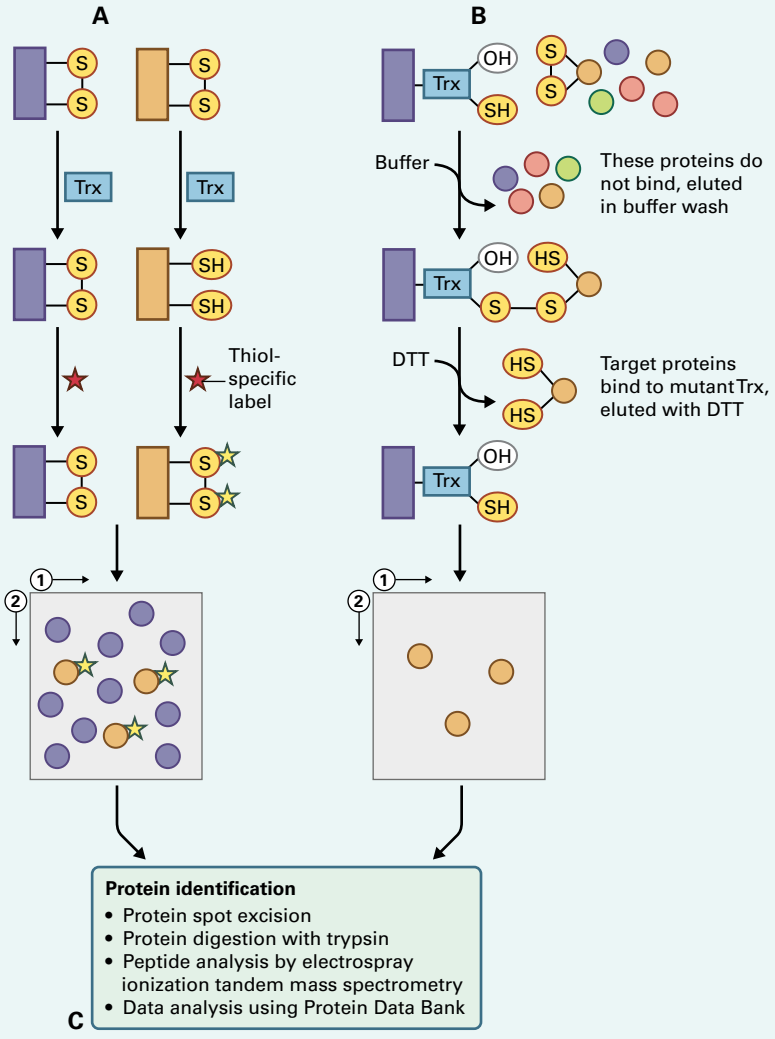
BOX 12.5

Proteomics has greatly increased our understanding of redox regulation in plants

Experimental advances in proteomics have uncovered the role of Trx far beyond the regulation of the Calvin–Benson cycle as was originally envisaged. With this approach, specific disulfide bonds of proteins linked to Trx can be identified by one of two procedures.

One procedure is to label target proteins chemically with a thiol-specific reagent, such as monobromobimane (mBBr) after reduction with Trx (A). An alternative strategy relies on the mechanism of the dithiol-disulfide exchange reaction taking place between reduced Trx and oxidized target proteins (B). Immobilized, mutated Trx in which the internal cysteine has been replaced by a serine (–Trp-Cys-Gly-Pro-Ser–) binds covalently to specific proteins through a disulfide bond; however, the column does not release the heterodisulfide intermediate because the substitution of the second (resolving) cysteine with serine interrupts the dithiol-disulfide exchange reaction. Elution with a disulfide-reducing agent, such as dithiothreitol, provides an enriched fraction of proteins sensitive to Trx reduction. In both approaches, Trx-sensitive proteins are isolated by two-dimensional gel electrophoresis and identified by mass spectrometry (C).

By applying these proteomics approaches, more than 300 potential Trx-linked targets proteins have been identified, many of which have been confirmed biochemically or genetically. These proteins occur throughout the plant and participate in processes as diverse as chloroplast development and hormone synthesis. Some are redox-regulated enzymes that are deactivated in the light by reactive oxygen species. Once these toxic oxidants are scavenged, the enzymes are reduced again to restore the original activity. Upon oxidation, enzymes regulated oxidatively typically bind glutathione (see Chapter 14) through a disulfide linkage by a mechanism known as glutathionylation, which stabilizes the deactivated form and gives it protection against oxidative damage. In some cases, the bound glutathione is removed by Trx, but more often, the related protein glutaredoxin acts in this capacity. Glutaredoxin is a widely distributed dithiol oxidoreductase that is reduced by the reduced form of glutathione.



thioredoxin (see Section 12.9.4). Both isoforms of the activase activate Rubisco. Studies with transgenic *Arabidopsis* plants indicate that photosynthesis in plants expressing only the longer isoform is more sensitive to inhibition by heat stress than photosynthesis in the wild type or in plants expressing only the shorter isoform; however, whether these isoforms are associated with thermal tolerance is unclear.

12.9.4 The ferredoxin–thioredoxin system regulates enzymes by redox transitions

During the day, light-mediated electron transport generates intermediates with highly reducing potential that transform oxidized inorganic precursors into reduced metabolites; simultaneously, a network of redox pathways transfers information from thylakoid membranes to the stroma for the regulation of enzymes. The ability of cysteine residues to reversibly form intra- and intermolecular disulfide bonds is of primary significance for the dynamic regulation of enzyme activity in response to redox conditions of chloroplasts. This post-translational modification, in which disulfide (-S–S-) bonds are reduced to the sulfhydryl (-SH) level in the light, has been the subject of intense research in plants since the discovery of the **ferredoxin–thioredoxin system** in the 1970s (Box 12.5).

During photosynthesis, electrons flow from the photosynthetic electron transport system to regulatory disulfide bridges of target proteins (Fig. 12.39). This change is achieved by the ferredoxin–thioredoxin system, which is made up of Fdx (Section 12.4.5), the Fe–S enzyme ferredoxin–thioredoxin reductase (FTR), and the small protein-disulfide oxidoreductase, thioredoxin (Trx) (Box 12.4). These three proteins form a complex (Fig. 12.40A) that converts reducing power originating from light-dependent electron transport in the thylakoid membranes to a regulatory thiol signal in the stroma to change the activity of target enzymes.

The redox transformations begin with the light-dependent reduction of Fdx, which then transfers electrons to FTR, cleaving its disulfide bond (see Fig. 12.40B, reactions 1 and 2). Next, FTR converts the disulfide bond of Trx to two sulfhydryl groups, forming the Trx-FTR complex (Fig. 12.40B, reactions 3 and 4). X-ray diffraction studies of crystals have demonstrated that the electron donor –Fdx– and the electron acceptor –Trx– dock on opposite sides of the FTR molecule (Fig. 12.40A). Fdx then delivers two successive transfers of one-electron through the [Fdx•FTR] complex to the two-electron acceptor, Trx (Fig. 12.40B, reaction 5). In the reduction of Trx, the [4Fe–4S] cluster of FTR stabilizes a one-electron-reduced intermediate that prevents the release of reactive intermediates. The light-induced redox transformations are complete once reduced Trx converts the disulfide bonds of target chloroplast enzymes to the sulfhydryl level, thereby leading to a change in activity (Reaction 12.25, see Fig. 12.39).

Reaction 12.25

$$\text{Trx}-(\text{SH})_2 + \text{Enzyme}-(\text{S})_2 \rightarrow \text{Trx}-(\text{S})_2 + \text{Enzyme}-(\text{SH})_2.$$

The mechanisms that restore Trx-reduced (active) enzymes to the oxidized (less active) forms in the dark are not clear. Trx becomes oxidized when electron flow from Fdx to the enzyme ceases in the dark.

12.9.5 Light-mediated changes in noncovalent interactions of enzymes also control the Calvin–Benson cycle

Noncovalent interactions of enzymes with other proteins and metabolites can also alter catalytic activity within minutes of a light–dark transition. Moreover, the assembly of noncovalently linked complexes causes rapid responses of the associated enzymes to subtle changes in the intensity and quality of sunlight (for example, those caused by cloud cover or canopy shading). Enzymes of the Calvin–Benson cycle undergo intramolecular and intermolecular noncovalent interactions when they associate with regulatory proteins and yield supramolecular complexes, bind chloroplast metabolites (e.g., ATP, NADPH), respond to ionic composition of the cellular milieu (e.g., pH and Mg^{2+}), and bind to the surface of thylakoid membranes. Overall, these noncovalent mechanisms act in concert with posttranslational modifications to rapidly control the structure and activity of individual enzymes.

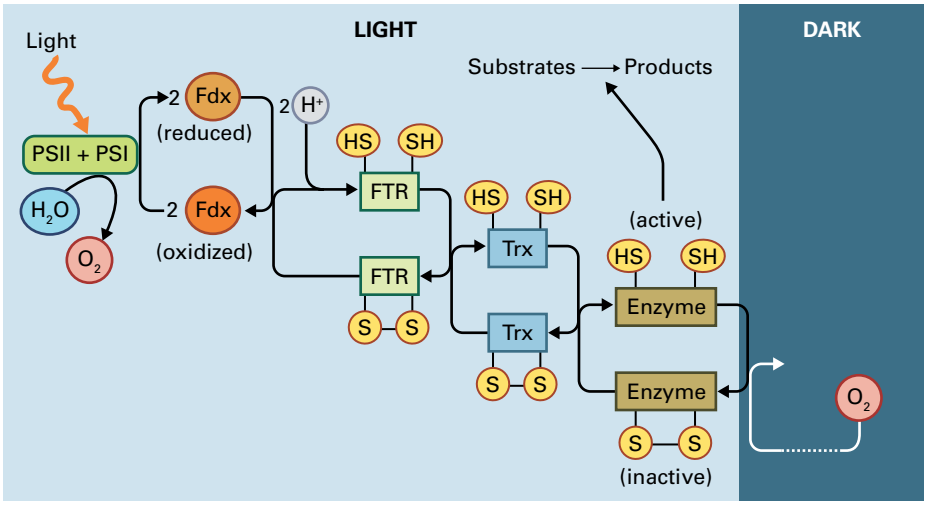


FIGURE 12.39 *The ferredoxin–thioredoxin system (FTS) provides a mechanism for light-dependent activation or deactivation of enzymes. Photosynthetic electron transfer by PSI leads to reduction of ferredoxin (Fdx). In turn, reduced Fdx reduces thioredoxin (Trx), a regulatory disulfide protein, via the Fe–S enzyme ferredoxin–thioredoxin reductase (FTR). Reduced Trx can then reduce the disulfide bonds of numerous target proteins, modulating their activity. In the dark, O_2 oxidizes both the target enzymes and Trx (not shown) by an unknown mechanism.*

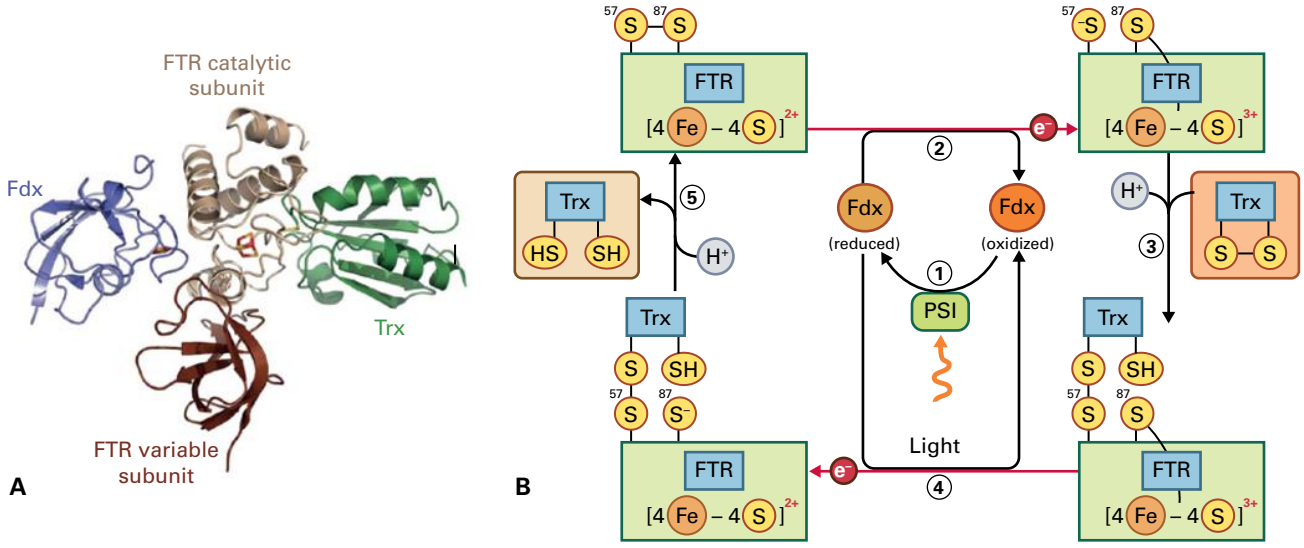


FIGURE 12.40 *Details of the ferredoxin–thioredoxin system. (A) Structure of the Fdx–FTR–C49S Trx-f complex. Fdx, the catalytic subunit of FTR, the variable subunit of FTR, and C49S Trx-f are colored blue, beige, brown, and green, respectively. (B) Mechanism proposed for the catalytic activity of FTR. Light reduces Fdx via the photosynthetic electron transport chain (reaction 1). Cleavage of the disulfide bond linking Cys57 and Cys87 of FTR takes one electron from one molecule of reduced Fdx, while the second electron comes from the reduced prosthetic group $[4Fe–4S]^{2+}$ of FTR (reaction 2). Cys 57 yields a thiolate anion and Cys 87 is stabilized by forming the fifth ligand to the newly oxidized cluster $[4Fe–4S]^{3+}$. The thiolate form of Cys57 and a proton cleave the unique disulfide bond of Trx yielding the heterodisulfide complex [FTR–(Cys57)–S–S–Trx] (reaction 3). A second molecule of reduced Fdx provides one electron for the reduction $[4Fe–4S]^{3+} \Rightarrow [4Fe–4S]^{2+}$ releasing the Cys87 of FTR from binding to the prosthetic group (reaction 4). The thiolate form of Cys87 and a proton cleave the heterodisulfide complex, releasing reduced Trx and restoring the disulfide bond of FTR for another catalytic cycle (reaction 5). In summary, FTR drives the reduction of Trx using two electrons from reduced Fdx and two protons from the surrounding stroma. Subsequently, the reduced Trx reduces a target enzyme, thereby leading to a change in activity.*

Phosphoribulokinase and NADP–glyceraldehyde-3-phosphate dehydrogenase bind to the small protein CP12

In addition to being regulated by Trx, plastid phosphoribulokinase (PRK) and NADP–glyceraldehyde-3-phosphate dehydrogenase (NADP–GAPD) are regulated by noncovalent associations with the nuclear-encoded chloroplast protein CP12 (an ≈8.5-kDa protein found in cyanobacteria, green algae, and plants) in supramolecular complexes. In the light (reducing conditions), chloroplasts of land plants and most algae contain active NADP–GAPD (which forms a homotetramer), active PRK (which forms a dimer harboring cysteines), and the reduced form of the CP12 protein, which harbors four sulfhydryl groups (Fig. 12.41).

In the dark (oxidizing conditions), sulfhydryl groups of both PRK and CP12 are oxidized to disulfides, and these oxidized forms recruit the NADP–GAPD homotetramer for the formation of a supramolecular complex. Both enzymes exhibit marginal enzyme activity when associated with CP12 in the supramolecular complex. Illumination of dark-adapted cyanobacteria and chloroplasts activates the ferredoxin–thioredoxin system, which cleaves the disulfide bonds of PRK and CP12. This reduction releases the constituent enzymes from the complex, imparting full catalytic capacity to both NADP–GAPD and PRK (Fig. 12.41).

While CP12 assembles with NADP–GAPD and PRK in dark-adapted pea (*Pisum sativum*) leaves, suppression of CP12 in tobacco (*Nicotiana tabacum*) by genetic manipulation causes minor changes in both photosynthetic carbon fixation and the activity of the two enzymes. However, it leads to significant changes in plant growth, carbohydrate partitioning, and morphology. This considerable heterogeneity between species indicates that the role of CP12 extends beyond regulation of the Calvin–Benson cycle.

The ferredoxin–thioredoxin system also regulates NADP–GAPD itself

Chloroplasts of land plants contain not only the NADP–GAPD homotetramer, (A_4)–NADP–GAPD, and its associated regulatory system, but also a second form of the enzyme, the heterotetramer (A_2B_2)–NADP–GAPD. Although the primary structure of the B subunit is homologous to the A counterpart, it holds a C-terminal extension with two cysteines that are controlled by the ferredoxin–thioredoxin system (Fig. 12.41). In the light, NADP–GAPD is catalytically active because the cysteine residues are reduced $\{[A_2]\bullet[B–(SH)_2]_2\}$; in the dark, formation of disulfide bonds promotes aggregation of heterotetramers into enzymatically inactive hexadecamers $\{[A_8]\bullet[B–(S)_2]_8\}$.

Light actuates changes in stromal pH and Mg^{2+} concentration

When dark-treated chloroplasts are exposed to light, the pH of the stroma increases as protons are translocated from that compartment to the thylakoid lumen. As light drives H^+ into the thylakoid lumen, Mg^{2+} is released from the lumen to compensate for the influx of positive charges. As a consequence, the stromal pH increases from 7 to 8, and the concentration of Mg^{2+} increases from 1–3 mM to approximately 3–6 mM. Changes in

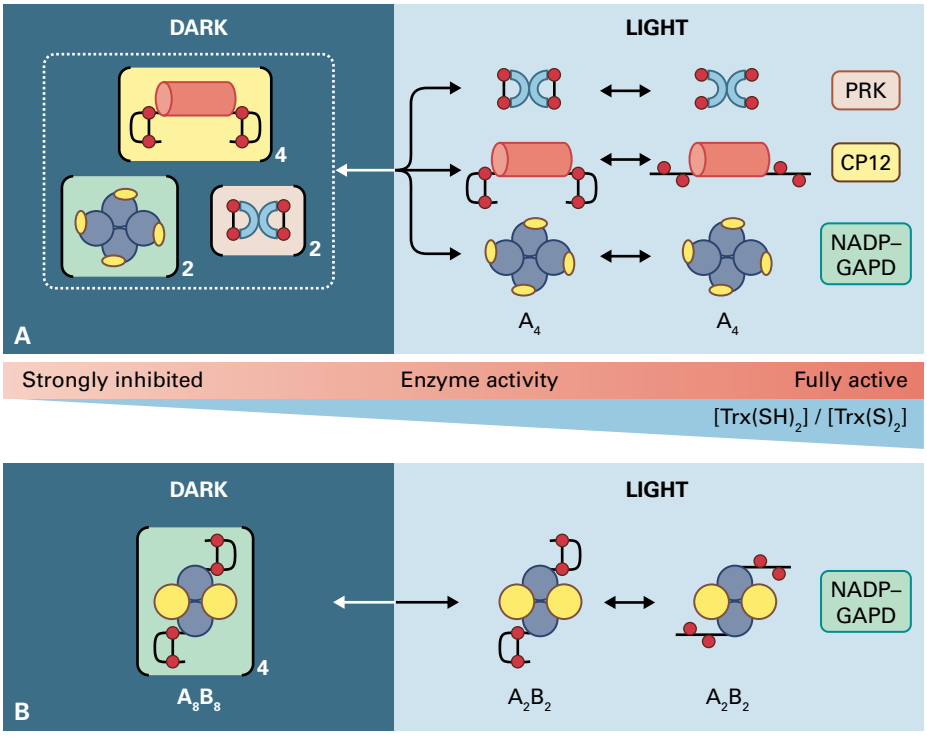


FIGURE 12.41 *Regulation of NADP–glyceraldehyde 3-phosphate dehydrogenase (NADP–GAPD) and phosphoribulokinase (PRK). Two forms of NADP–GAPD function in the Calvin–Benson cycle: the homotetramer (A_4)–NADP-GAPD and the heterotetramer (A_2B_2)–NADP–GAPD. (A) The activity of the homotetramer (A_4)–NADP-GAPD depends on the small protein CP12. Under light conditions, the high ratio [Trx–$(SH)_2$]/[Trx–$(S)_2$] reduces disulfide bonds of CP12 and PRK, making (A_4)-NADP-GAPD and PRK catalytically active. Under dark conditions, the low ratio [Trx–$(SH)_2$]/[Trx–$(S)_2$] allows the formation of intramolecular disulfide bonds in CP12 and PRK. The oxidized states of CP12 and PRK recruit the homotetramer (A_4)–NADP–GAPD for the formation of the heterocomplex [CP12•PRK•(A_4)–NADP-GAPD]. Both PRK and (A_4)–NADP–GAPD are catalytically inactive in this supramolecular complex. CP12 regulates the activity of GAPD and PRK in some photosynthetic organisms (for example, in cyanobacteria, diatoms, red and green algae, and certain plant species such as pea and spinach, but not in others like tobacco). (B) The activity of the heterotetramer (A_2B_2)–NADP–GAPD depends on the C-terminal extension of (A_2B_2)–NADP-GAPD. Under light conditions, the high ratio [Trx–$(SH)_2$]/[Trx–$(S)_2$] causes the reduction of the B subunit of (A_2B_2)–NADP-GAPD, thereby (A_2B_2)–NADP-GAPD exhibits maximum activity. Under dark conditions, the low ratio [Trx–$(SH)_2$]/[Trx–$(S)_2$] promotes formation of disulfide bonds in the C-terminal extension of the heterotetramer (A_2B_2)–NADP-GAPD. The oxidized state of (A_2B_2)–NADP–GAPD contributes to the self-association into the hexadecameric complex A_8B_8 that is catalytically inactive.*

stromal pH and Mg^{2+} concentration complement the ferredoxin–thioredoxin system and are important for the activation and maximum catalysis of enzymes such as Rubisco, fructose-1,6-bisphosphatase, sedoheptulose-1,7-bisphosphatase, and PRK.

12.10 Variations in mechanisms of CO_2 fixation

12.10.1 Some autotrophic bacteria and archaea do not fix carbon via the Calvin–Benson cycle

Although the Calvin–Benson cycle is the mechanism for conversion of CO_2 into carbohydrates that sustains most life in the biosphere, it is not universal. In some prokaryotes, CO_2 fixation proceeds by five other pathways. These variants of microbial autotrophy synthesize organic acids from atmospheric CO_2, employing acetyl-CoA as an intermediate, and have survived eons of evolution in specific ecological niches (see Box 12.3).

12.10.2 In plants, C_4 and CAM metabolism increase the efficiency of Rubisco carboxylation

As described in Section 12.8.3, Rubisco catalyzes both carboxylation and oxygenation of RuBP, and photosynthetic organisms have developed strategies to overcome the problems caused by photorespiration. Land plants have adapted two different mechanisms to suppress photorespiration and increase the use of atmospheric CO_2 (Fig. 12.42): **C_4 photosynthetic carbon fixation** (see Section 12.10.3) and **Crassulacean acid metabolism** (CAM) (see Section 12.10.7). These two mechanisms are additions to the Calvin–Benson cycle that separate the uptake of atmospheric CO_2 from the

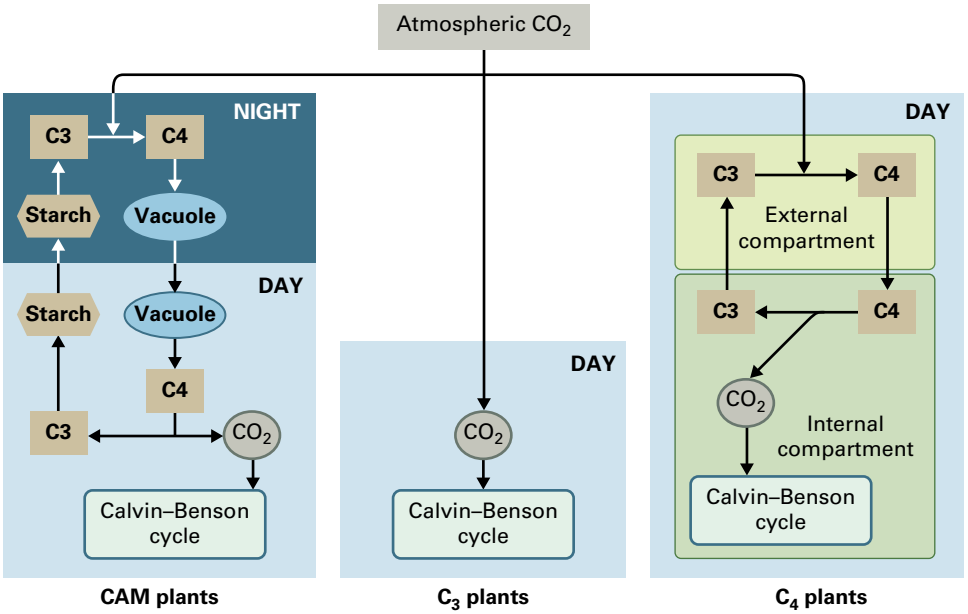


FIGURE 12.42 *Photosynthetic CO_2 assimilation in C_3, C_4, and CAM plants. The C_4 cycle and CAM are additions to the Calvin–Benson cycle for the efficient capture of CO_2. The C_4 cycle and CAM separate spatially and temporally, respectively, the capture of atmospheric CO_2 from the CO_2 fixation by the Calvin–Benson cycle.*

supply of substrate to Rubisco inside the leaf. They act as CO_2 pumps to increase the concentration of CO_2 around the carboxylation site of Rubisco, thereby reducing the competing effect of O_2.

12.10.3 C_4 plants utilize two distinct metabolic compartments for fixing CO_2

Not all organisms that contain the Calvin–Benson cycle produce 3-PGA as the first stable photosynthetic intermediate. Studies in the 1960s identified several plant species that form large amounts of four-carbon organic acids as the first products of CO_2 fixation when supplied with $^{14}CO_2$. On this basis, plants are classified as C_3 or **C_4 plants** based on the primary product of carbon fixation in photosynthesis: three-carbon (3-PGA) and four-carbon (oxaloacetic acid, OAA) compounds are the primary products of carbon fixation in C_3 and C_4 plants, respectively (Fig. 12.42).

C_4 photosynthesis involves the primary carboxylation of a three-carbon precursor (phospho*enol*pyruvate, PEP) to OAA, catalyzed by PEP carboxylase, followed by the decarboxylation of the four-carbon intermediate prior to secondary (final) carboxylation at the active site of Rubisco. These two biochemical functions are separated between two intracellular compartments, which allow the primary and the secondary carboxylations to occur simultaneously.

Sugar cane (*Saccharum* sp.), maize (*Zea mays*), and numerous tropical grasses are among the species that exhibit the C_4 labeling pattern. The leaves of these and almost all C_4 species exhibit an unusual anatomy involving two different types of chloroplast-containing cells: mesophyll cells surround enlarged bundle sheath cells, which in turn are arranged concentrically with respect to vascular tissues (Fig. 12.43). Reduced interveinal distance and limited leaf thickness maximize the contact between mesophyll and bundle sheath cells. The 19th-century German botanists who originally described this feature called it **Kranz anatomy** (German: wreath). The biochemical differentiation of mesophyll cells and bundle sheath cells is essential for the effective operation of C_4 photosynthesis: PEP carboxylase (PEPCase) accumulates in the cytosol of mesophyll cells (external compartment), and Rubisco in the chloroplasts of bundle sheath cells (internal compartment). The biphasic C_4 system reduces photorespiration dramatically by increasing levels of CO_2 near Rubisco to enable Rubisco carboxylation to outcompete the oxygenation reaction. The low photosystem II activity in the bundle sheath also minimizes the Rubisco oxygenation reaction.

C_4 photosynthesis also occurs, however, in numerous organisms devoid of Kranz anatomy, including a number of aquatic and land plants. In some of these cases, photosynthetic enzymes and dimorphic chloroplasts occur in separate cytoplasmic domains within a single photosynthetic cell (Fig. 12.44). The subcellular localization of photosynthetic functions in *Bienertia sinuspersici*, for example, revealed that chloroplasts of peripheral and central compartments differ and function in an analogous manner to the mesophyll and bundle sheath chloroplasts of Kranz anatomy. Thus, diffusion gradients between and within cells shuttle metabolic intermediates of the C4 cycle between the two compartments. In addition to the mechanisms employed by plants, cyanobacteria and green algae have also developed alternative CO_2 concentrating mechanisms for increasing the availability of CO_2 for Rubisco.

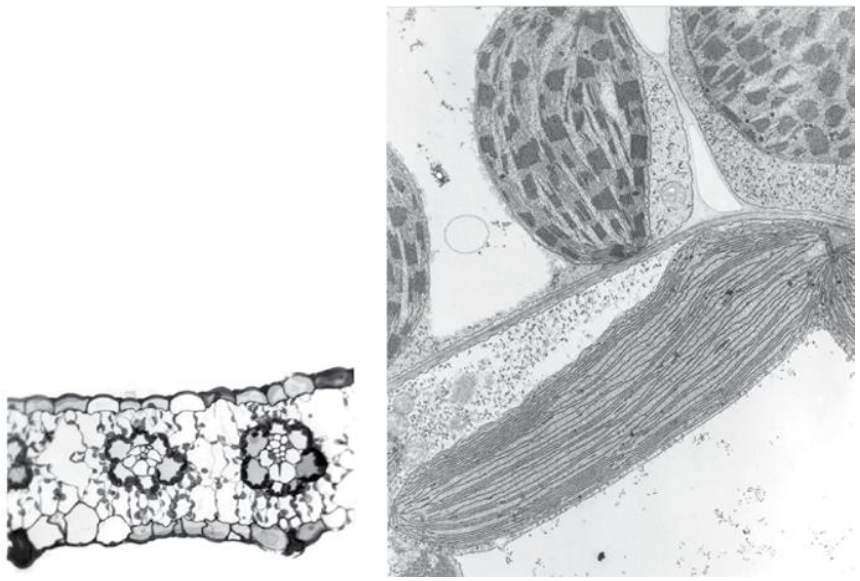


FIGURE 12.43 *Leaf (Kranz) anatomy of C_4 plants. (A) Electron micrograph showing the leaf anatomy of maize (*Zea mays*). The closely spaced vascular bundles are surrounded by large bundle sheath cells. (B) Electron micrographs comparing the chloroplasts of a bundle sheath cell (bottom) and a mesophyll cell (top) in sorghum. The chloroplast morphologies reflect their biochemical functions. The bundle sheath chloroplasts lack stacked thylakoids and contain little PSII. In contrast, the mesophyll chloroplasts contain all the transmembrane complexes required for the light reactions of photosynthesis but little or no Rubisco. Source*: (A, B) Newcomb, University of Wisconsin, Madison; previously unpublished.

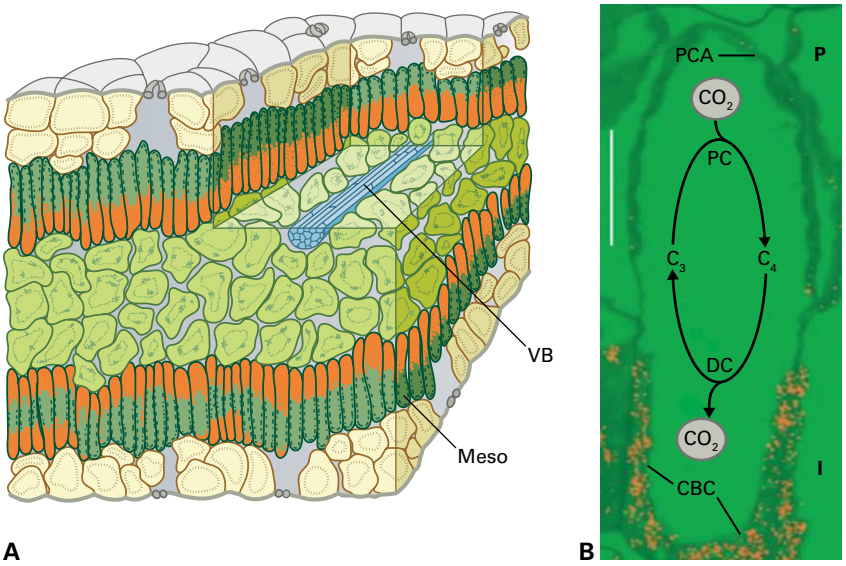


FIGURE 12.44 *Leaf anatomy of single-cell C4 plants. (A) Three-dimensional drawing of the leaf anatomy of* Borszczowia aralocaspica, *a single-cell C_4 plant. Meso, mesophyll; VB, vascular bundles. Note the lack of differentiation in the cells. (B) Immunolocalization of Rubisco at the internal region (I) of a photosynthetic cell from* Borszczowia aralocaspica. *Red chloroplasts containing the Calvin–Benson cycle (CBC) are functionally equivalent to C_4 bundle sheath chloroplasts. Chloroplasts containing PPDK, which are functionally equivalent to C_4 mesophyll chloroplasts, are situated at the peripheral region (P) where they contribute to the photosynthetic carbon assimilation (PCA). PC and DC refer to the initial carboxylation catalyzed by PEPCase and the decarboxylation of C_4 acids, respectively.*

12.10.4 The C_4 pathway increases the concentration of CO_2 in internal compartments close to vascular tissues

The C_4 pathway of CO_2 fixation requires a complex interaction between two different compartments and involves the following steps (Fig. 12.45):

1. Primary carboxylation: fixation of HCO_3^- by PEPCase in the outer compartment (for example, mesophyll cells) to yield OAA.
2. Transformation of OAA into another four-carbon acid (malate or aspartate) and transport of the four-carbon acids from the outer to the internal compartment (e.g., bundle sheath cells)
3. Decarboxylation: release of CO_2 from the four-carbon acid.
4. Secondary carboxylation: subsequent refixation of the CO_2 by Rubisco and the Calvin–Benson cycle.
5. Transfer of the three-carbon intermediates (pyruvate or alanine) resulting from decarboxylation of the four-carbon acids back to the outer compartment.

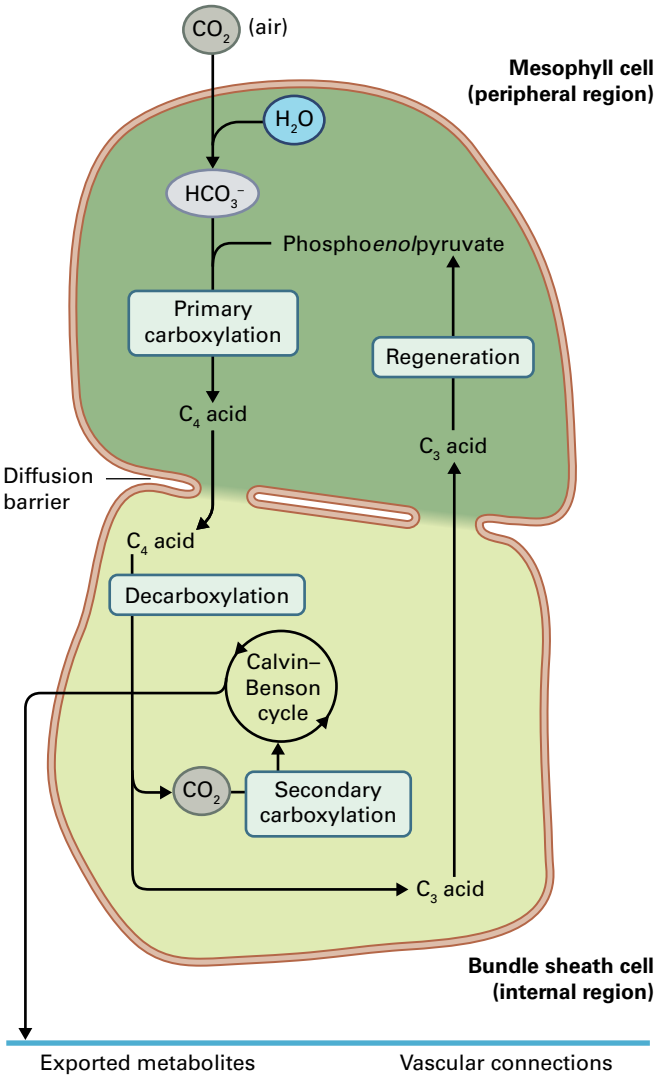


FIGURE 12.45 *General aspects of the C_4 pathway. Atmospheric CO_2 enters the peripheral region and is converted to HCO_3^- for reaction with PEP, yielding OAA (primary carboxylation). OAA is transformed to a second C_4 acid (malate or aspartate) that flows across a diffusion barrier to the internal region. There, the C_4 acid is decarboxylated, yielding CO_2 and a C_3 acid (pyruvate or PEP) (decarboxylation). The released CO_2 is fixed by Rubisco in the Calvin–Benson cycle (secondary carboxylation) and converted to carbohydrate for export to other parts of the plant. The remaining C_3 acid is transported back to the external region to regenerate PEP (regeneration).*

6 Conversion of the three-carbon intermediates to PEP to reinitiate the fixation of HCO_3^-.

Biochemical fractionation analyses have shown that OAA is generated from HCO_3^- and PEP in the cytosol of the outer compartment (i.e., mesophyll cells), whereas enzymes unique to the Calvin–Benson cycle are located only in chloroplasts of the internal compartment (i.e., bundle sheath cells). In accordance with distinct functions, electron micrographs of bundle sheath and mesophyll chloroplasts (see Fig. 12.43) show structural differences: chloroplasts of (internal) bundle sheath cells lack stacked membranes and exhibit little PSII activity, whereas chloroplasts of (peripheral) mesophyll cells have retained stacked membranes as well as PSII and PSI activities (see Fig. 12.43B). Significantly, the function of chloroplasts in the internal and peripheral compartments of single-cell C_4 species (*B. sinuspersici*) is analogous to that of land plants showing Kranz anatomy.

In the context of the two-cell C_4 pathway, all carbon fixation begins in the cytosol of mesophyll cells, where carbonic anhydrase catalyzes the conversion of atmospheric CO_2 into HCO_3^- (Reaction 12.26) for subsequent β-carboxylation of PEP to yield OAA, catalyzed by PEPCase (Reaction 12.27). Use of HCO_3^- but not CO_2, as the one-carbon substrate for PEPCase has two advantages for a more efficient initial fixation step: First, the aqueous equilibrium of these two species strongly favors HCO_3^- ion over CO_2, and second, PEPCase cannot fix O_2, which has a structure similar to that of CO_2 but not to HCO_3^-.

Reaction 12.26: Carbonic anhydrase

$$CO_2 + H_2O \leftrightarrow HCO_3^- + H^+$$

Reaction 12.27: Phospho*enol*pyruvate carboxylase (PEPCase)

$$PEP + HCO_3^- \leftrightarrow OAA + P_i$$

12.10.5 Three different types of C_4 photosynthesis are known

Three types of C_4 photosynthesis are known, differing both in the four-carbon acids transported between mesophyll and bundle sheath cells, and the mechanism of decarboxylation in the bundle sheath cells (Table 12.10). These variants are

TABLE 12.10 *Variations in C_4 photosynthesis.*

C_4 acid transported to bundle sheath cells	C_3 acid transported to mesophyll cells	Decarboxylase	Plant examples
Malate	Pyruvate	NADP-ME	*Zea mays* (maize), *Saccharum officinarum* (sugarcane)
Aspartate	Alanine	NAD-ME	*Panicum miliaceum* (millet)
Aspartate	Alanine, PEP, or pyruvate	PEPCK	*Panicum maximum* (Guinea grass)

named on the basis of the enzymes employed for decarboxylation (Reactions 12.28, 12.29, 12.31, Fig. 12.45). Although the intracellular compartmentation and energetic requirements for each of these three types differ, in all cases the CO_2 released in the bundle sheath cell is refixed by the Rubisco localized within the chloroplasts of the same cells.

In **NADP-malic enzyme (ME) C_4 photosynthesis**, OAA is transported from the cytoplasm of mesophyll cells to the chloroplasts for reduction to malate by $NADP^+$-malate dehydrogenase (Fig. 12.46A). Malate leaves the mesophyll chloroplasts for the bundle sheath chloroplasts, where NADP-ME catalyzes the oxidative decarboxylation of malate to CO_2 and pyruvate (Reaction 12.28). CO_2 is refixed by Rubisco via the Calvin–Benson cycle, and pyruvate is transported back to mesophyll cells and taken up into mesophyll chloroplasts for regeneration of PEP. The phosphorylation of pyruvate is catalyzed by pyruvate-phosphate dikinase (PPDK, Reaction 12.29), and mesophyll chloroplasts release PEP into the cytosol to start a new cycle of CO_2 fixation.

Reaction 12.28: $NADP^+$-dependent malic enzyme (NADP-ME)

$$\text{Malate} + NADP^+ \rightarrow \text{Pyruvate} + CO_2 + NADPH + H^+$$

Reaction 12.29: Pyruvate-phosphate dikinase (PPDK)

$$\text{Pyruvate} + ATP + P_i \rightarrow PEP + AMP + PP_i$$

In **NAD-ME C_4 photosynthesis** (Fig. 12.46B), cytosolic aspartate aminotransferase in mesophyll cells converts OAA to aspartate, using glutamate as donor of the amino group (Reaction 12.30). Aspartate moves to the mitochondria of bundle sheath cells, where it is converted back to OAA by aspartate aminotransferase. The mitochondrial NAD-malate dehydrogenase reduces OAA to malate, which is oxidatively decarboxylated by mitochondrial NAD-ME (Reaction 12.31). CO_2 is refixed by the Calvin–Benson cycle in the bundle sheath chloroplasts, and the newly formed pyruvate leaves the mitochondria for conversion to alanine in the cytosol of bundle sheath cells by alanine aminotransferase (Reaction 12.32). Alanine returns to the mesophyll cells, where it is deaminated to pyruvate by the alanine aminotransferase. Pyruvate regenerates the acceptor PEP in the chloroplasts of mesophyll cells as described for NADP-ME C_4 plants. The aspartate/alanine shuttle between mesophyll and bundle sheath cells ensures an adequate balance not only of organic carbon, but also organic nitrogen.

Reaction 12.30: Aspartate aminotransferase

$$\text{OAA} + \text{glutamate} \leftrightarrow \text{aspartate} + \text{2-oxoglutarate}$$

Reaction 12.31: NAD^+-dependent malic enzyme (NAD-ME)

$$\text{Malate} + NAD^+ \rightarrow \text{Pyruvate} + CO_2 + NADH + H^+$$

Reaction 12.32: Alanine aminotransferase

$$\text{Pyruvate} + \text{glutamate} \leftrightarrow \text{alanine} + \text{2-oxoglutarate}$$

PEP carboxykinase (PEPCK) C_4 photosynthesis is more complex than the other two types, because two complementary cycles shuttle C_4/C_3 metabolites between mesophyll and bundle sheath cells (Fig. 12.46C). Some of the OAA is converted to aspartate in the cytosol of the mesophyll cells (similar to the NAD-ME type), and the aspartate is transported to the cytosol of bundle sheath cells and converted to OAA by transamination. The decarboxylation of OAA catalyzed by PEPCK yields CO_2, using ATP provided by mitochondrial respiration (Reaction 12.33). The CO_2 is fixed by the Calvin–Benson cycle in the chloroplasts of bundle sheath cells. PEP, the other product of the PEPCK reaction, returns to the mesophyll cells for a new round of CO_2 fixation. In addition to the pathway shown, some of the OAA enters the chloroplast, where NADP-malate dehydrogenase catalyzes the reduction to malate. The malate is transported from mesophyll cells to bundle sheath cells and is converted to pyruvate and CO_2 in the mitochondria (similar to NADP-ME type). CO_2 diffuses to chloroplasts of bundle sheath cells, where it is assimilated by the Calvin–Benson cycle. The pyruvate leaves the mitochondria and is converted to alanine by transamination; the alanine is transported back to mesophyll cells and converted to pyruvate by transamination. Pyruvate yields PEP in chloroplasts for another cycle of CO_2 assimilation.

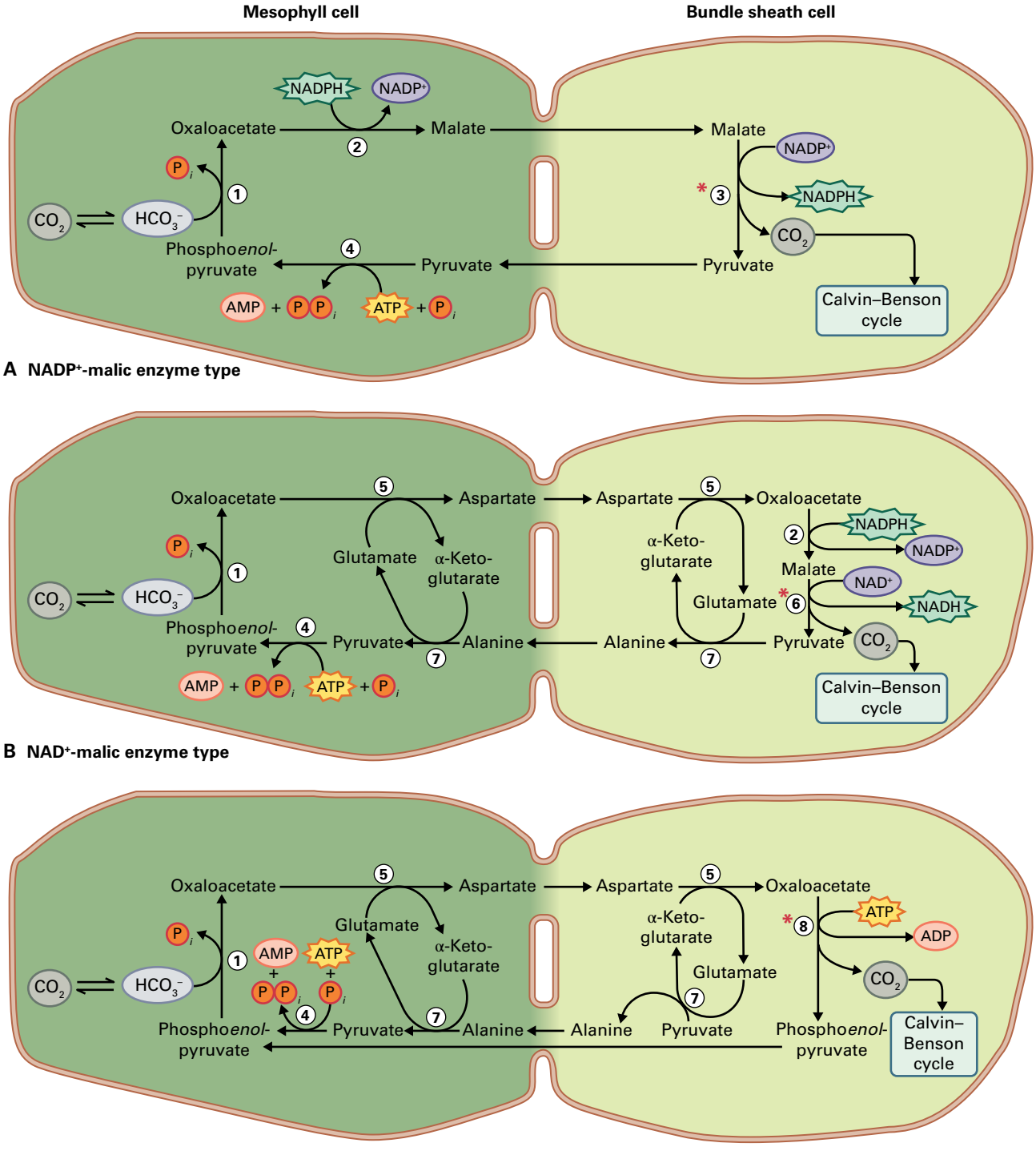
Reaction 12.33: PEP carboxykinase (PEPCK)

$$\text{OAA} + ATP \rightarrow PEP + ADP + CO_2$$

The NAD-ME and PEPCK types of C_4 photosynthesis, but not the $NADP^+$-ME pathway, use mitochondrial NAD-ME to decarboxylate malate (Fig. 12.46B,C). The flow of carbon through the bundle sheath mitochondria in the NAD-ME type of C_4 photosynthesis is much greater than that of the respiratory and the photorespiratory pathways in C_3 plants. This unique capacity of plant mitochondria reflects the evolution of the central organelle of heterotrophic metabolism to support autotrophy in photosynthetic eukaryotes.

12.10.6 The C_3 and C_4 pathways have different energy costs

In C_3 plants, the Calvin–Benson cycle consumes nine ATP and six NADPH to assimilate three molecules of CO_2 into triose phosphate (3 ATP : 2 NADPH : 1 CO_2). In C_4 photosynthesis, continuous operation of the C_4/C_3 shuttle requires restitution of PEP in mesophyll cells, which consumes two additional molecules of ATP in the successive reactions catalyzed by PPDK and adenylate kinase (AMP + ATP → 2 ADP). Thus, at least five molecules of ATP and two molecules of NADPH are needed for assimilation of one molecule of CO_2 (5 ATP : 2 NADPH : 1 CO_2).



① PEP carboxylase
② NADP+-malate dehydrogenase
③ NADP+-malic enzyme
④ Pyruvate-orthophosphate dikinase (PPDK)
⑤ Aspartate aminotransferase
⑥ NAD+-malic enzyme
⑦ Alanine aminotransferase
⑧ PEP carboxykinase

FIGURE 12.46 *Three types of C_4 photosynthetic plants: (A) NADP-malic enzyme-type, (B) NAD-malic enzyme-type, and (C) phosphoenolpyruvate carboxykinase-type. All types start with the initial fixation of HCO_3^- by PEPCase in the cytosol of mesophyll cells. However, the transformation of the C_4 dicarboxylic acid OAA proceeds through different organelles and biochemical pathways (see Section 12.10.5 for a description of the organelles in which the indicated reactions take place). The three types of C_4 plants show different mechanisms for the shuttle C_4 (amino)-acid/C_3 (amino)-acid between mesophyll and bundle sheath cells and the decarboxylation of the C_4 acid. Asterisks mark the enzyme that identifies the C_4 type.*

C_4 photosynthesis evolved to minimize energetically wasteful photorespiration; however, avoidance of photorespiration came with a penalty for photosynthetic efficiency. Flow of metabolites across membranes requires establishment and maintenance of a thermodynamic disequilibrium among different compartments, which demands continuous input of energy. In keeping with an increased metabolic flux across the envelope membranes of C_4 chloroplasts, substrate-specific transporters of these membranes are more abundant in C_4 than in C_3 plants.

12.10.7 Critical enzymes of the C_4 pathway are also regulated by light

Light-mediated regulation of enzymes coordinates the activities of mesophyll and bundle sheath cells to ensure that four-carbon acids are available for CO_2 fixation in bundle sheath cells. In C_4 photosynthesis, regulation of Calvin–Benson cycle enzymes by light is similar to C_3 plants. In addition, light also controls the C_4 cycle enzymes NADP-malate dehydrogenase, PEPCase, and PPDK: Light activation of NADP-malate dehydrogenase involves the ferredoxin–thioredoxin system (see Fig. 12.39), while PEPCase and PPDK are regulated by allosteric effectors and protein phosphorylation.

PEPCase is essentially inactive in the dark; it is not phosphorylated and so has a low affinity for PEP and is inhibited by low concentrations of malate (Fig. 12.47A). In the light, PEPCase-kinase catalyzes phosphorylation of PEPCase, rendering the enzyme less sensitive to malate. The kinase is regulated by light at the level of the gene via a complex signal transduction chain involving phospholipases C and D. When dark returns, PEPCase is converted back to the nonphosphorylated form by protein phosphatase 2A; in parallel, PEPCase-kinase is deactivated by an unknown mechanism.

PPDK catalyzes the phosphorylation of pyruvate by ATP and phosphate to yield PEP, pyrophosphate and AMP (see Reaction 12.29). A regulatory protein (PPDK-RP) regulates PPDK through dark-induced phosphorylation (deactivation) and light-promoted phosphorolysis (activation) of a threonine residue in the active site of PPDK (Fig. 12.48). The substrate of PPDK-RP for the phosphorylation of PPDK is ADP, not ATP [PPDK + ADP (AMP-**P**) ⇒ (PPDK-RP) ⇒ PPDK-**P** + AMP]. The absence of light suppresses ATP production and increases the concentration of ADP, promoting PPDK phosphorylation and abolishing the catalytic activity of PPDK. In the light, the concentration of ADP drops and facilitates the phosphorolysis of phosphorylated PPDK [PPDK-**P** + P_i ⇒ (PPDK-RP) ⇒ PPDK + **P**P_i], increasing the proportion of nonphosphorylated, active PPDK.

PPDK-RP is a unique regulatory enzyme because it catalyzes the phosphorylation of PPDK using ADP as phosphoryl donor, rather than ATP, and the phosphorolytic dephosphorylation of the (PPDK)–Thr–O–P with formation of pyrophosphate, rather than the hydrolysis employed by most protein phosphatases.

12.10.8 CAM photosynthesis involves the temporal separation of CO_2 capture and carbon fixation

Another modification of the C_3 pathway occurs in plants utilizing Crassulacean acid metabolism (CAM). Named after the *Crassulaceae* family of succulent plants, this pathway has evolved mechanisms for maximizing carbon uptake under

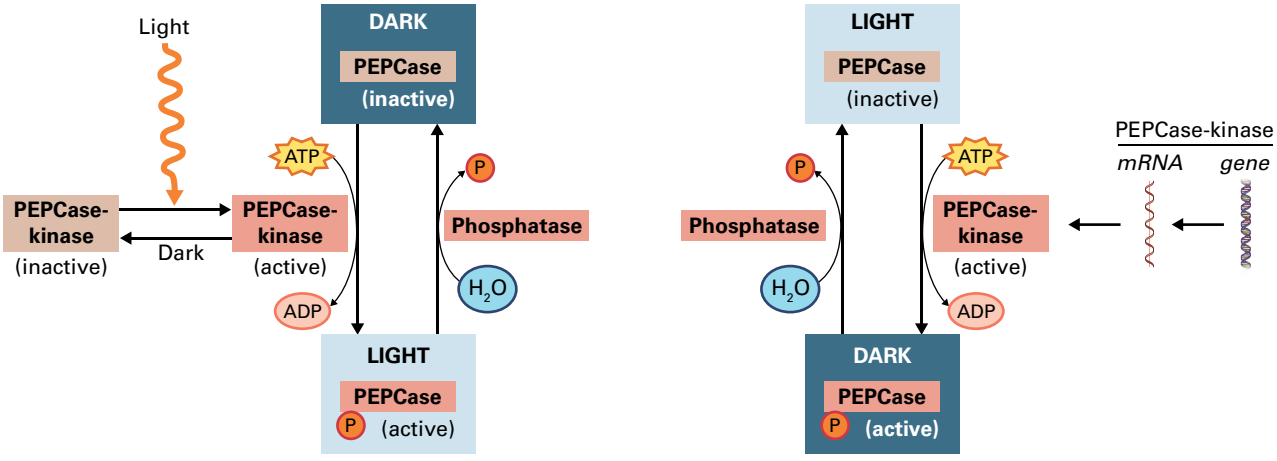


FIGURE 12.47 *Regulation of PEP carboxylase (PEPCase). Phosphorylated PEPCase is catalytically more active and less sensitive to inhibition by malate than the nonphosphorylated form. PEPCase-kinase catalyzes the phosphorylation of PEPCase. (A) C_4 plants. Diurnal phosphorylation of PEPCase regulates incorporation of HCO_3^- into PEP. Light stimulates PEPCase-kinase activity, but in the dark, PEPCase returns to the inactive form because PEPCase-kinase is inactivated and a phosphatase releases the phosphoryl group from PEPCase. (B) CAM plants. Nocturnal phosphorylation of PEPCase controls primary carboxylation. PEPCase-kinase transcripts accumulate during the night, controlled by the circadian oscillator and metabolites.*

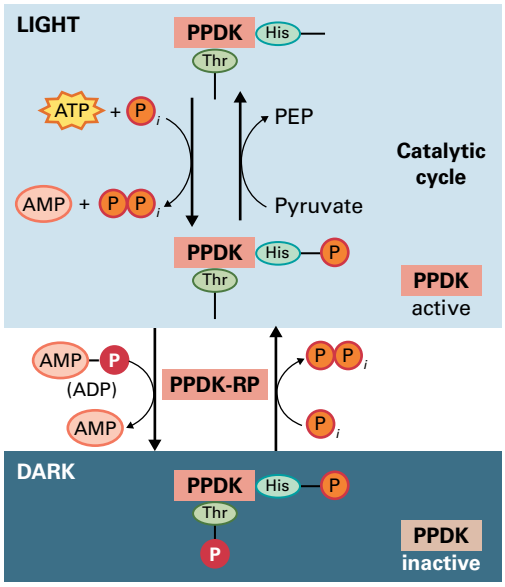


FIGURE 12.48 *Catalytic activity of PPDK and its phosphoregulation by the PPDK-regulatory protein (PPDK-RP). The phosphorylation of an essential histidine residue shown in black [PPDK–(His-P)–(Thr)] during catalysis predisposes PPDK to reversible inactivation by PPDK-RP via the ADP-dependent phosphorylation of a specific threonine residue shown in red [PPDK–(His-P)–(Thr-P)]. PPDK-RP catalyzes the reactivation of PPDK through the phosphorolytic cleavage of the phosphorylated Thr (P_i-dependent/PP_i-forming).*

environmental conditions that limit productivity, such as high temperature or shortage of water. Thus, CAM photosynthesis is commonly associated with plants that inhabit arid environments (e.g., succulents, including cacti and some commercially significant plants, such as pineapple and agave). To enhance water conservation, these plants have evolved anatomical and morphological structures, such as thick cuticles, that prevent water loss. They have also evolved mechanisms for ensuring a high concentration of CO_2 at the active site of Rubisco to minimize photorespiration.

The biochemical pathway of CO_2 fixation in terrestrial CAM plants is similar to the C_4 pathway, but instead of a spatial separation of the two carboxylations necessary for CO_2 fixation, terrestrial CAM plants use a temporal separation of the initial fixation reaction from the assimilation by Rubisco (Fig. 12.49). At night, when it is cold and leaf stomata are open, CO_2 is fixed initially into OAA and then malate via PEPCase and NADP-malate dehydrogenase. The malic acid is stored in vacuoles, where it can reach high concentrations. During the day, stomata close to prevent the loss of water, and malic acid is transported out of the vacuole. At this stage, NADP-ME catalyzes the decarboxylation of malate, yielding CO_2 and pyruvate, and the released CO_2 is fixed by Rubisco via the Calvin–Benson cycle, while pyruvate is used to form starch. The starch confined to photosynthesizing tissues of terrestrial CAM plants, named **transitory starch**, is broken

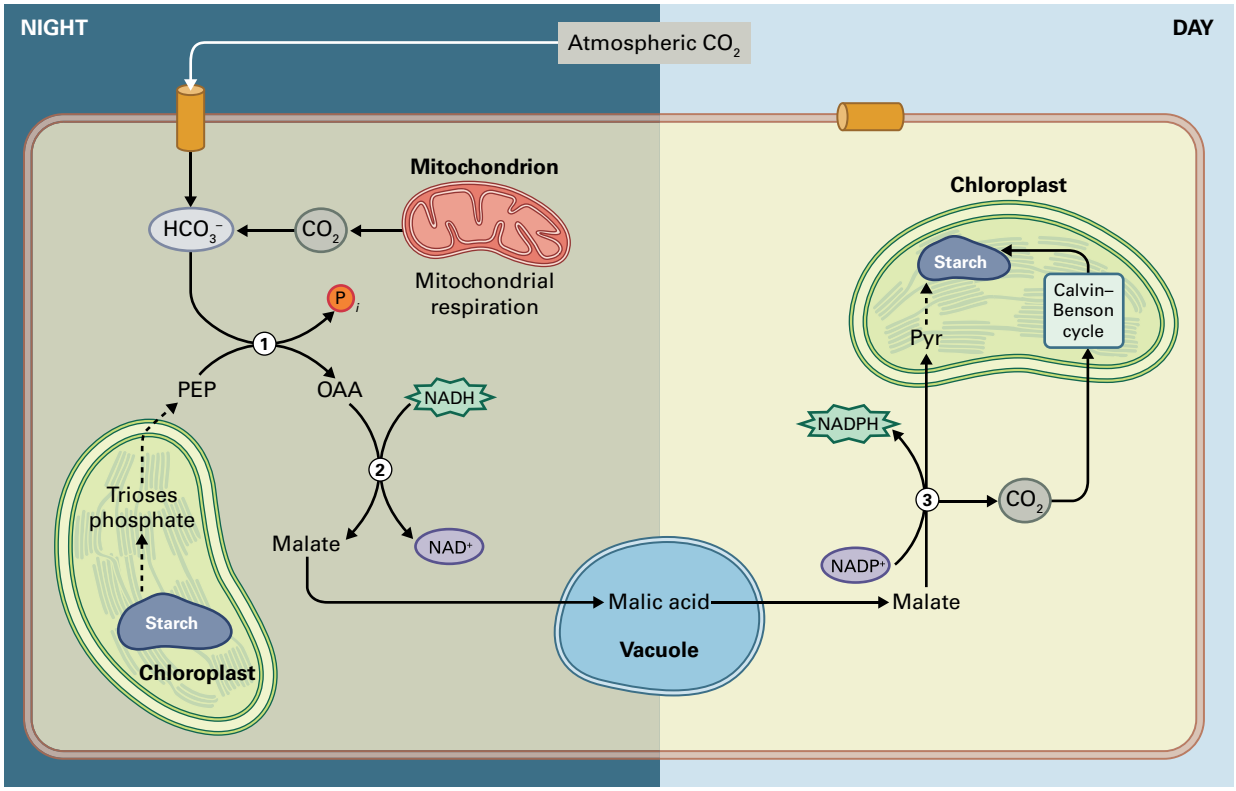


FIGURE 12.49 *Crassulacean acid metabolism (CAM). At night, both atmospheric and respiratory CO_2 provide HCO_3^- for carboxylation of PEP catalyzed by PEPCase (reaction 1). NAD-malate dehydrogenase catalyzes the reduction of the C_4 organic acid—oxaloacetic (OAA)—to malate (reaction 2). Malate is stored in the vacuole overnight. During the day, the stored malate is decarboxylated by NAD(P)-ME yielding NAD(P)H, pyruvate, and CO_2 (reaction 3). In the chloroplast, pyruvate and CO_2 are used for synthesis of carbohydrates via gluconeogenesis and the Calvin–Benson cycle, respectively.*

down at night via glycolysis and serves as a source of PEP for the fixation of CO_2 via PEPCase. In this circadian rhythm, the opening/closing of stomata, variations of organic acids and storage carbohydrates, and the activities of carboxylation and decarboxylation enzymes modulate the proportion of CO_2 taken up via PEPCase at night and Rubisco during the day.

A notable feature of terrestrial CAM plants is the alternation between stomatal opening and closing. Stomata remain open during the cool and relatively humid night, allowing uptake of atmospheric CO_2 while sustaining minimal water loss. During the heat and dryness of the day, the stomata close, preventing not only water loss but also the entry of atmospheric CO_2. Malate becomes the internal source of CO_2 in leaves. The decarboxylation of malate raises the concentration of CO_2 to high levels because CO_2 cannot escape through the closed stomata. These high concentrations of CO_2 further increase the efficiency of Rubisco as a carboxylase. The Calvin–Benson cycle is regulated as in C_3 plants.

For aquatic plants, water is readily available, but the concentration of CO_2 is low for some that exhibit CAM photosynthesis. Freshwater CAM plants (*Isoetes*, *Littorella*, *Crassula*, *Sagitaria*, *Vallisneria*) lack stomata and capture CO_2 24 hours a day. Generally, the concentration of HCO^-_3 in most freshwaters exceeds that of CO_2; however, CO_2 is the preferred source of inorganic carbon of submerged CAM plants because it is more readily taken up. More importantly, respiratory CO_2 makes a substantial contribution to the nocturnal uptake of carbon through CAM when dissolved levels of CO_2 are depleted. Freshwater CAM plants thus capture CO_2 derived from both the surrounding milieu and respiration for transformation to HCO_3^- used in the primary fixation catalyzed by PEPCase. In short, aquatic CAM photosynthesis maximizes carbon uptake in plants that prosper in water with a highly variable supply of inorganic carbon by (i) concentrating CO_2 released in the decarboxylation reaction and (ii) preventing the loss of respiratory carbon.

12.10.9 CAM PEPCase is active in the dark

CAM photosynthesis provides a fascinating example of enzyme regulation. CAM PEPCase must function at night and reduce its activity during the day, so the mechanisms that inhibit its activity in dark-treated C_4 plants do not operate here. Endogenous circadian rhythms, rather than exogenous light–dark signals, mediate PEPCase activation at night and deactivation during the day (see Fig. 12.47B). Conversions between nocturnal and the diurnal forms correlate with the cessation and onset of malate accumulation. Malate, which is present at high concentrations when it leaves the vacuole, inhibits the diurnal form of the enzyme, whereas the nocturnal form is insensitive to malate, thereby allowing the accumulation of this metabolite.

The regulation of the nocturnal and the diurnal forms of CAM PEPCase also involves protein phosphorylation by PEPCase-kinase and dephosphorylation by phosphatase 2A. The activity of PEPCase-kinase is high in the nocturnal period when PEPCase is phosphorylated, and low during the light period when PEPCase is dephosphorylated. Complementary experiments showed the functioning of PEPCase-kinase at night requires RNA and protein synthesis, indicating that the nocturnal phosphorylation of CAM PEPCase is largely controlled by a circadian oscillator at the level of protein synthesis and degradation (Fig. 12.47B).

Summary

Photosynthesis produces organic compounds from inorganic carbon by using the energy of sunlight. These redox processes are carried out in plants, algae, and various bacteria. In all cases, the photosynthetic reactions may be divided into two phases: the light reactions and the carbon reactions. In eukaryotic organisms, photosynthesis takes place in the chloroplast. This organelle is surrounded by a double membrane and contains (i) a complex internal membrane system, the thylakoid membranes, and (ii) a soluble fraction called the stroma. The two phases of photosynthesis occur simultaneously but take place in different regions of the chloroplast, with the light reactions being localized to the thylakoid membranes and the carbon reactions to the stroma.

The light reactions of photosynthesis involve the photosynthetic pigments, the photosynthetic electron transport chain, and the ATP synthesis machinery. Light is absorbed by pigments localized in pigment–protein complexes (photosystems) within the thylakoid membrane. This light energy can be transferred from antenna pigments to special pigment–protein complexes, known as reaction centers, where the light energy is converted into chemical products (photochemistry). Within the reaction center, a special chlorophyll undergoes oxidation, with the transfer of an electron to an electron acceptor during the primary reaction of photosynthesis.

Oxygenic photosynthetic organisms contain two reaction centers and two photosystems, PSII and PSI. In plants the two photosystems are spatially separated: PSII is localized in appressed thylakoids, and PSI is localized in stroma-exposed thylakoids. During noncyclic electron transfer, the two photosystems cooperate in the transfer of electrons from water to $NADP^+$ via a series of redox reactions that are mediated by both mobile and integral thylakoid membrane components of the photosynthetic electron transfer chain. During these reactions,

PSII oxidizes water and produces molecular oxygen within the thylakoid lumen. The concerted action of PSII and PSI are tuned to meet the demands of downstream metabolism. These reactions provide the O_2 for aerobic forms of life.

In addition to O_2, reduced ferredoxin, and NADPH, the noncyclic electron transfer reactions are coupled to the formation of ATP. ATP synthesis is driven by a proton gradient established across the thylakoid membrane in the transport of electrons from water to ferredoxin. During electron transport, the lumen becomes acidified by protons that are either translocated from the stroma during electron transport or released by water oxidation. Use of this electrochemical gradient as an energy source requires the ATP synthase complex. This enzyme is composed of two components—one intrinsic to the membrane and involved in transporting protons through the membrane, and the second, extrinsic, functional in the actual conversion of ADP and P_i into ATP. The synthesis of ATP appears to be accompanied by complex conformational changes in ATP synthase, driven by the movement of protons through the enzyme.

In addition to the noncyclic mechanism for ATP synthesis, chloroplasts synthesize ATP via two cyclic pathways that involve only PSI. Cyclic electron transport generates a proton gradient that is used for the synthesis of ATP, but does not yield O_2 or NADPH. In both pathways, the buildup of the proton gradient and the ensuing synthesis of ATP are enhanced by operation of the Q-cycle.

The reduction of CO_2 to carbohydrates requires the reduced ferredoxin, NADPH, and ATP that are synthesized by the photosynthetic light reactions. All plants employ the C_3 photosynthetic pathway (Calvin–Benson cycle) to fix CO_2, using the enzyme Rubisco to convert CO_2 and RuBP into the C_3 product, 3-PGA. This multienzyme cycle occurs in three phases—carboxylation, reduction, and regeneration—and requires three ATP and two NADPH molecules per molecule of CO_2 fixed. Reactions of the Calvin–Benson cycle reactions are catalyzed by soluble enzymes localized in the chloroplast stroma. Regulation of the cycle is linked to multiple light-dependent mechanisms, including the active removal of Rubisco inhibitors, changes in pH and Mg^{2+}, and disulfide redox transitions catalyzed by the ferredoxin–thioredoxin system.

Variants of C_3 photosynthesis exist in many plants. In one variation, the C_4 pathway, plants fix CO_2 into a C_4 acid in mesophyll cells, and transport this fixed CO_2 to anatomically distinct bundle sheath cells, where the CO_2 is released, refixed, and assimilated by Rubisco and other enzymes of the Calvin–Benson cycle. This sequence of reactions enhances the productivity of C_4 plants by (i) providing a higher concentration of CO_2 for Rubisco in the bundle sheath cell, and (ii) decreasing the oxygenase activity of Rubisco—a reaction that competes with the fixation of CO_2 in C_3 chloroplasts. In another variant, CAM metabolism, CO_2 is fixed at night into malate, which is decarboxylated during the day to provide CO_2 for Rubisco. CAM photosynthesis aids in the retention of water and enables plant to grow in arid environments. Several photosynthetic enzymes in C_4 and CAM plants are regulated to ensure efficient interaction of the CO_2-concentrating mechanisms with the Calvin–Benson cycle.

13



Carbohydrate Metabolism

Samuel C. Zeeman

Introduction

Plants are carbohydrate specialists. They are autotrophs and synthesize carbohydrates through **photosynthesis**, then use them to create biological macromolecules. Plant-derived carbohydrates (e.g., cellulose) dominate the biosphere and serve as a key sink for atmospheric carbon dioxide (CO_2). They also dominate animal nutrition, including our own (e.g., sugars and starch). Thus, the global importance of plant carbohydrate metabolism cannot be overstated.

Although many of the reactions involved in carbohydrate metabolism are similar in most organisms, plants have evolved enzymes and pathways that are not found in other organisms. Some distinguishing features of plants help explain their unique metabolic configuration.

- **Plants are photosynthetic.** Apart from a few parasitic species, plants harness light energy and use it to convert simple nutrients such as CO_2, water, and inorganic ions into all the intermediates required for their autotrophic lifestyle. The primary use of the captured energy is the fixation and reduction of CO_2 via the **Calvin–Benson cycle** (see Chapter 12). The resulting triose phosphates are used by photosynthetic cells for the biosynthesis of nucleic acids, proteins, lipids, and polysaccharides, as well as coenzymes and a wealth of secondary metabolites (natural products). Assimilated carbon is also converted to sugars (principally sucrose) or sugar alcohols (e.g., sorbitol) for export to other parts of the plant. Thus, plant carbohydrate metabolism simultaneously feeds many anabolic pathways (Fig. 13.1). Other activities associated with the capture of light energy include nitrite and sulfate reduction, ammonia assimilation, and numerous other biosynthetic pathways that are supplied with reducing equivalents and ATP from photosynthesis (Fig. 13.2).

  Because photosynthesis and the processes associated with light absorption are diurnal, plants must cope with major variations in the supply of energy and assimilated nutrients. At night, photosynthetic carbon assimilation stops, and energy and reducing power must be produced, as it is in nonphotosynthetic organisms, through respiration of stored carbohydrates (Fig. 13.3). Consequently, this imposes a need for flexibility in the pathways and regulation of metabolism in plants that is not seen in other organisms.

- **Plants contain plastids. Plastids** are organelles found only in plants and algae. They can occur as several different types that fulfill different, specialized roles in various plant tissues (see Chapter 1). Plastids are intimately involved in carbohydrate metabolism, and they perform many of the essential biosynthetic reactions that occur in plant cells, including photosynthesis in chloroplasts. Some metabolic pathways are duplicated; they occur in both the cytosol and plastids by the presence of distinct isoforms of each enzyme in the two compartments. To coordinate plastid metabolism with that of the rest of the cell, the plastid envelope contains a suite of transporters that shuttle metabolic intermediates between the two compartments (Fig. 13.4). The complement of transporters differs between plastid types and depends on the specific functions of the plastid. Besides linking cytosolic and plastid metabolism, these transporters also play an important role

Biochemistry & Molecular Biology of Plants, Second Edition. Edited by Bob B. Buchanan, Wilhelm Gruissem, and Russell L. Jones.
© 2015 John Wiley & Sons, Ltd. Published 2015 by John Wiley & Sons, Ltd.
Companion website: www.wiley.com/go/buchanan/biochem

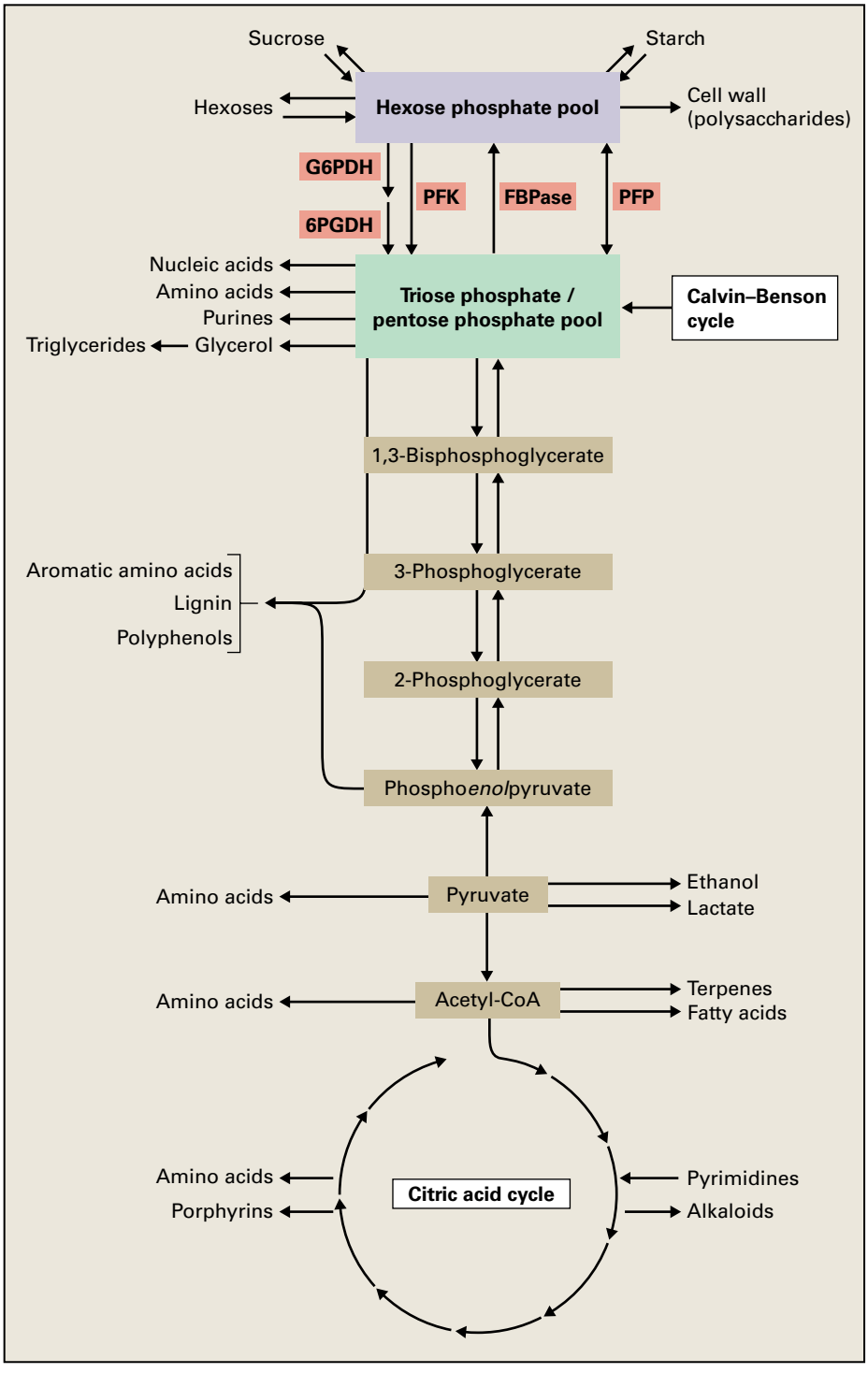


FIGURE 13.1 *Central role of carbohydrate metabolism and respiratory pathways in the supply of carbon skeletons for biosynthetic reactions. G6PDH, glucose-6-phosphate dehydrogenase; 6PGDH, 6-phosphogluconate dehydrogenase; PFK, ATP-dependent phosphofructokinase; FBPase, fructose-1,6-bisphosphatase; PFP, pyrophosphate-dependent phosphofructokinase.*

in metabolic regulation by communicating changes in metabolites levels in one compartment to another. The segregation of biosynthetic reactions into different cellular compartments also means that the required energy (ATP) and reducing power (NAD(P)H) must be transported between them (Fig. 13.5).

- **Not all plant cells are photosynthetic.** Many cell types lack chlorophyll and so are heterotrophic. Subterranean roots, for example, have no photosynthetic cells and rely on sugars translocated from the shoot. Even within a green leaf there are many cells (e.g., epidermal cells) that rely on their neighboring photosynthetic cells for

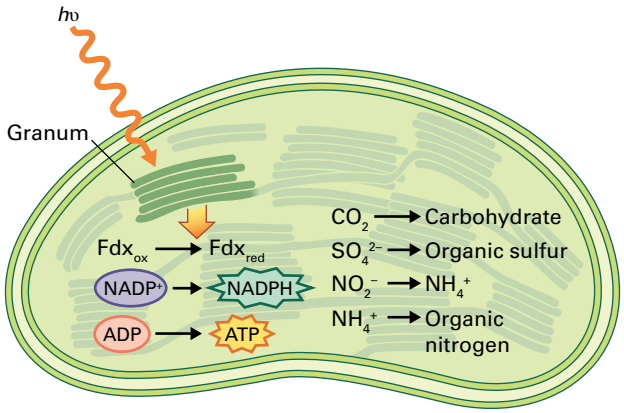


FIGURE 13.2 *Photosynthetic electron transfer generates ATP and energy-rich reductants that are used to assimilate carbon, nitrogen, and sulfur. Fdx, ferredoxin.*

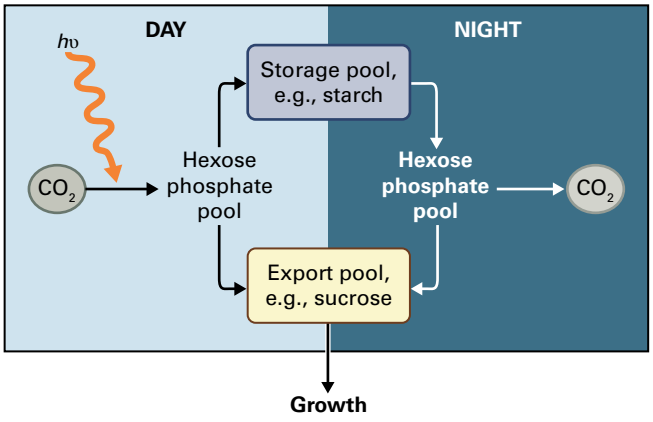


FIGURE 13.3 *During the day, carbon dioxide (CO_2) is assimilated through photosynthesis. Some is used for growth, and some is stored. At night, stored carbohydrate is used to support respiration and continued growth.*

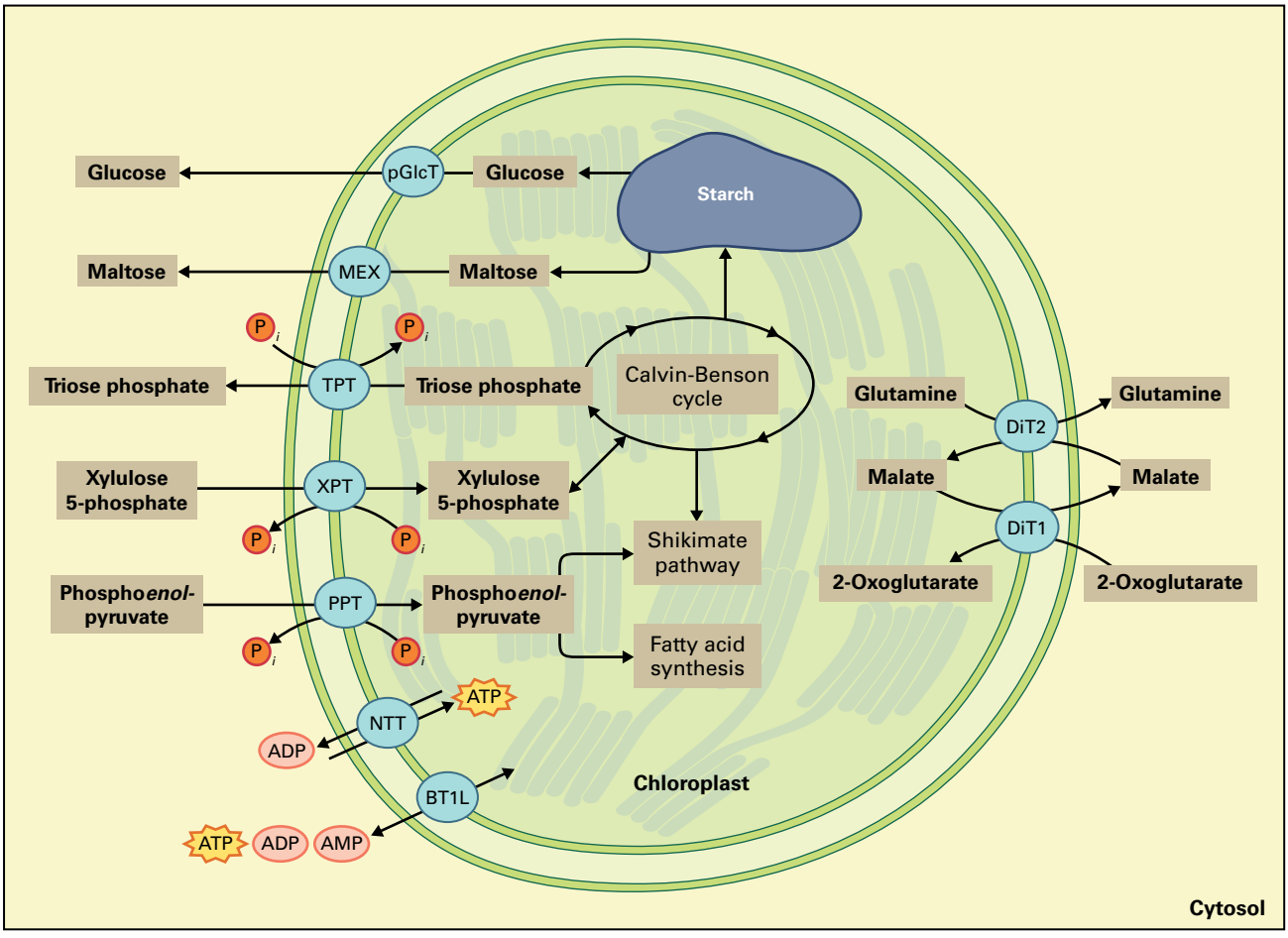


FIGURE 13.4 *Transporters located in the inner envelope membranes of plastids exchange metabolites between the cytosol and the plastid stroma. In the transport processes illustrated here, photosynthetic chloroplasts export triose phosphate in exchange for inorganic phosphate (P_i); this is a major flux in photosynthesis. Transporters also exchange pentose phosphates and phosphoenolpyruvate for P_i, and nonphotosynthetic plastids also have transporters mediating the movement of hexose phosphates (not shown). Adenylate cofactors can also be transported across the chloroplast envelope, as can maltose and glucose (the products of starch breakdown) and intermediates involved in nitrogen assimilation. All the transporters are reversible, and the direction of transport depends on the concentrations of metabolites on each side of the envelope.*

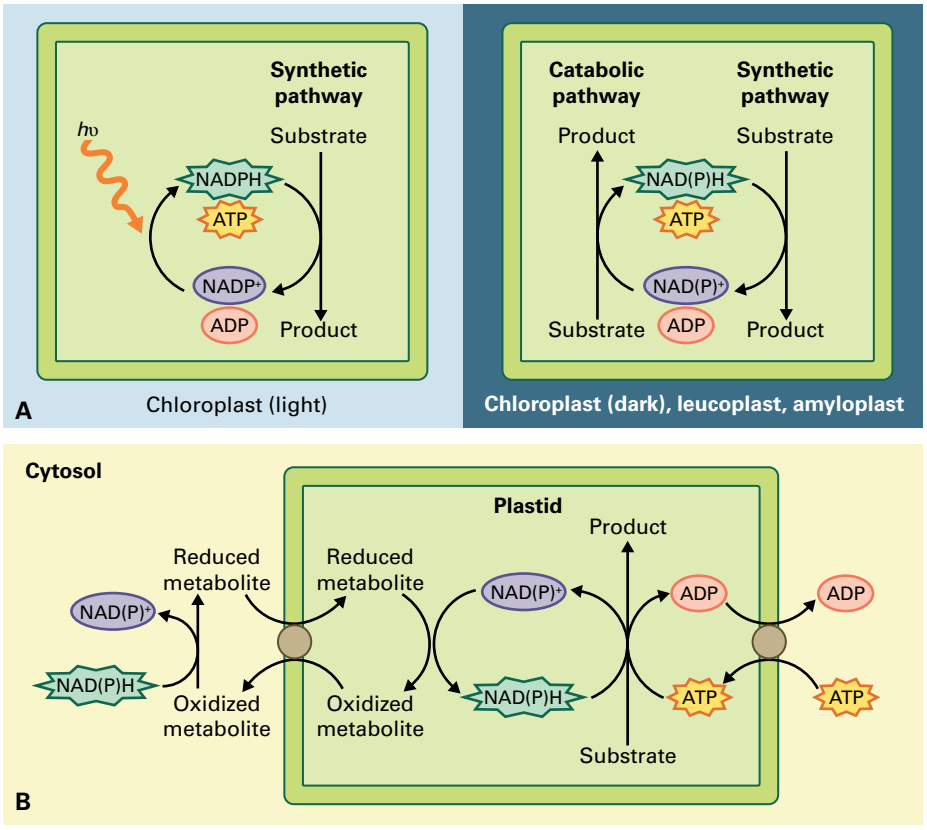


FIGURE 13.5 *Mechanism for supplying cofactors to plastids. Cofactors such as NADPH or ATP are required for biosynthetic pathways. (A) Cofactors can be generated within the plastid using light energy (hν) in the case of the chloroplast or via catabolic pathways located in the organelle. (B) A simple shuttle system for the transfer of reducing equivalents into a plastid. Cofactors may be imported from the cytosol either by direct transport (e.g., exchange of ADP for ATP) or indirectly via shuttles, as shown here.*

carbohydrates. Consequently, fluxes through the pathways of carbohydrate metabolism may differ significantly even in adjacent cells.

In other ways, all cells in a plant are alike. For example, each cell is surrounded by a **cell wall** composed primarily of carbohydrates (**cellulose**, **hemicellulose**, and **pectin**; see Chapter 2). Synthesis of these polysaccharides and other cell wall components (e.g., lignin) represents a major sink for carbohydrates, and their production can account for 30% or more of cellular carbohydrate metabolism. That said, cell wall biosynthesis for a cell may be limited to a defined phase of growth and expansion, and once the cell is fully expanded, other metabolic pathways dominate.

- **Plants are sessile organisms.** Terrestrial plants are unable to move to a new location when faced with physical or chemical stress. They must tolerate herbivory and adapt to changes in temperature and in the availability of light, water, and nutrients. This sessile nature renders plants potentially vulnerable to environmental changes. To ensure survival in unforgiving circumstances, plant metabolism is flexible, and changes in chemical composition form an important part of their acclamatory or adaptive responses. For example, when subject to herbivory, plants expend considerable resources in the production of defensive compounds to deter the herbivores.

Combined, these features mean that plant carbohydrate metabolism is complex, flexible, and subject to precise regulation.

13.1 The concept of metabolite pools

Carbohydrate metabolism is frequently depicted in terms of discrete anabolic and catabolic pathways. While this can help in grasping the basic elements of each pathway, it inevitably simplifies the true picture of metabolism, in which many pathways are interconnected and share intermediates. Parts of metabolism where pathways converge, and where intermediates are maintained near to equilibrium with each other by reversible enzyme reactions, can be viewed as "pools" of metabolic intermediates (Fig. 13.6). This concept allows the pathways to be simplified and their connections to be emphasized. Metabolites can be added to or withdrawn from these pools to serve the needs of various biochemical and metabolic pathways.

The direction of flow through a pool depends on the requirements and activities of the cell. For example, in photosynthetic tissues, carbon fluxes through pathways are largely governed by whether cells are in light or darkness. Thus, the directions of flux through a given pool might be reversed between day and night. Metabolite pools can also occur in different subcellular compartments (e.g., the plastid stroma and the cytosol). Equilibration between these pools depends on whether they are linked by the activities of **metabolite transport** proteins (Fig. 13.7). One important metabolite pool in plants is composed of hexose **phosphates** (see Section 13.2), and another is composed of **pentose phosphate pathway** intermediates and the **triose phosphates** glyceraldehyde 3-phosphate and dihydroxyacetone phosphate (see Section 13.8) (Fig. 13.7; see also Fig. 13.1).

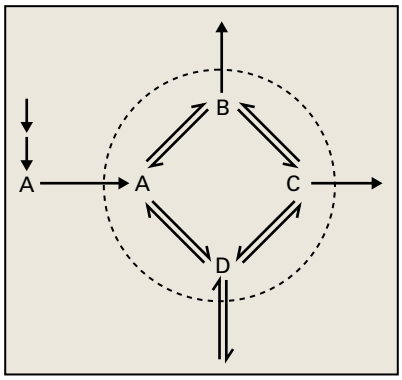


FIGURE 13.6 *A metabolic pool with four metabolites close to equilibrium. Flow through this pool is dictated by the addition of specific metabolites (A), or withdrawal of intermediates (B and C). In many cases, the metabolic status of the cell determines whether a particular compound (D) enters or leaves the pool.*

13.2 The hexose phosphate pool: a major crossroads in plant metabolism

13.2.1 Three interconvertible hexose phosphates make up the hexose phosphate pool

The **hexose phosphate pool** consists of three metabolic intermediates: **glucose 6-phosphate**, **glucose 1-phosphate**, and **fructose 6-phosphate** (Fig. 13.8). These three metabolites are kept in equilibrium through the action of phosphoglucomutase (Reaction 13.1) and **glucose-6-phosphate isomerase**

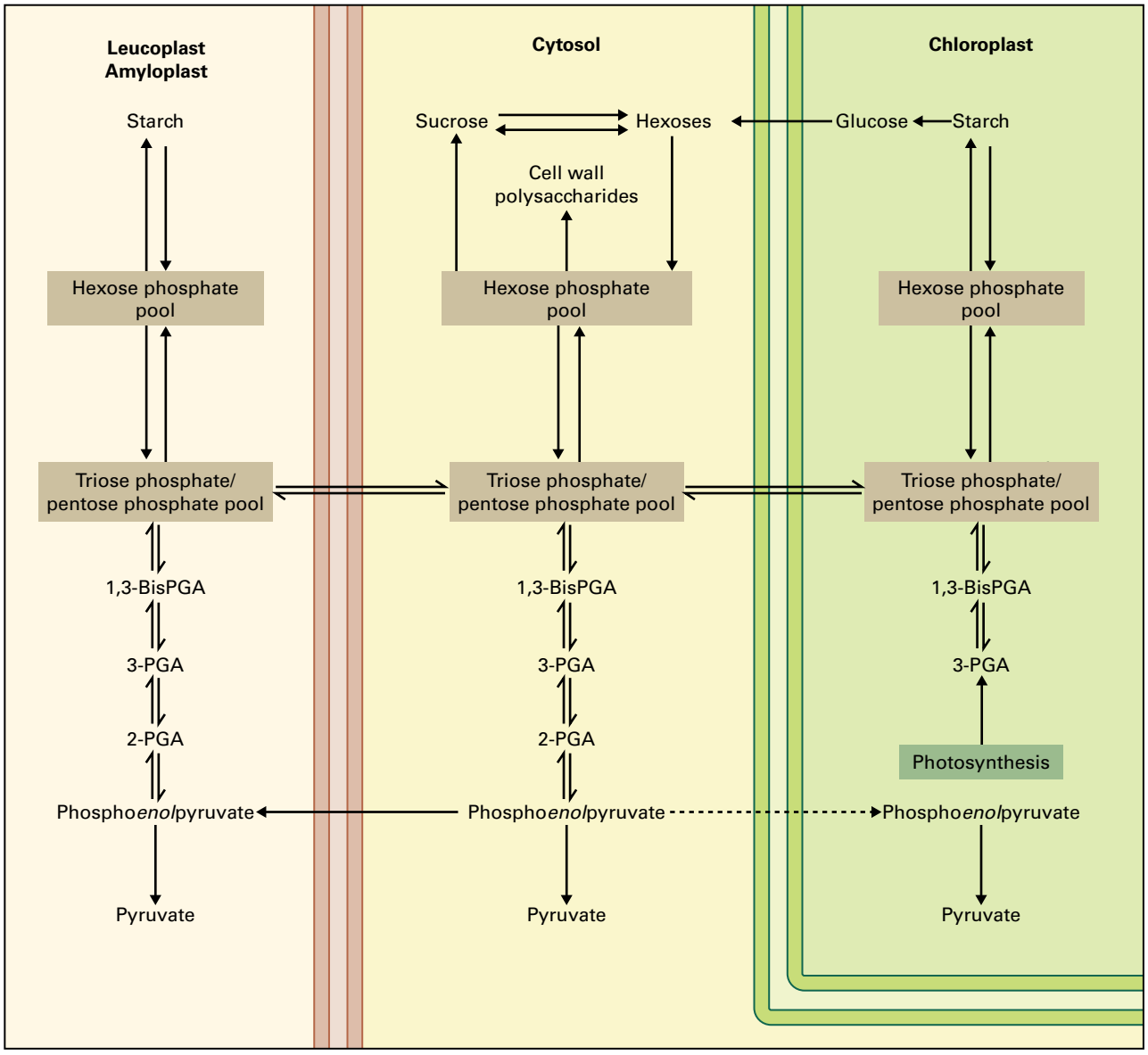


FIGURE 13.7 *Duplication of metabolic pathways between the plant cell cytosol and the stroma of photosynthetic chloroplasts and nonphotosynthetic plastids. Pathways are shown in a simplified form.*

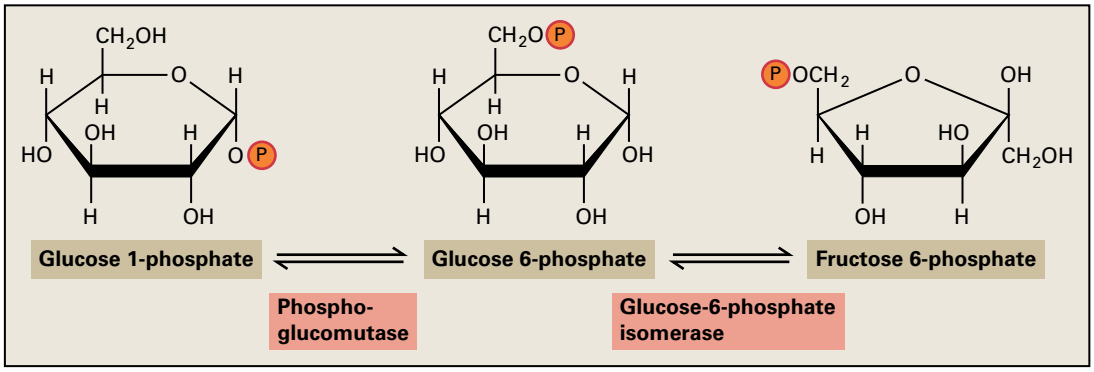
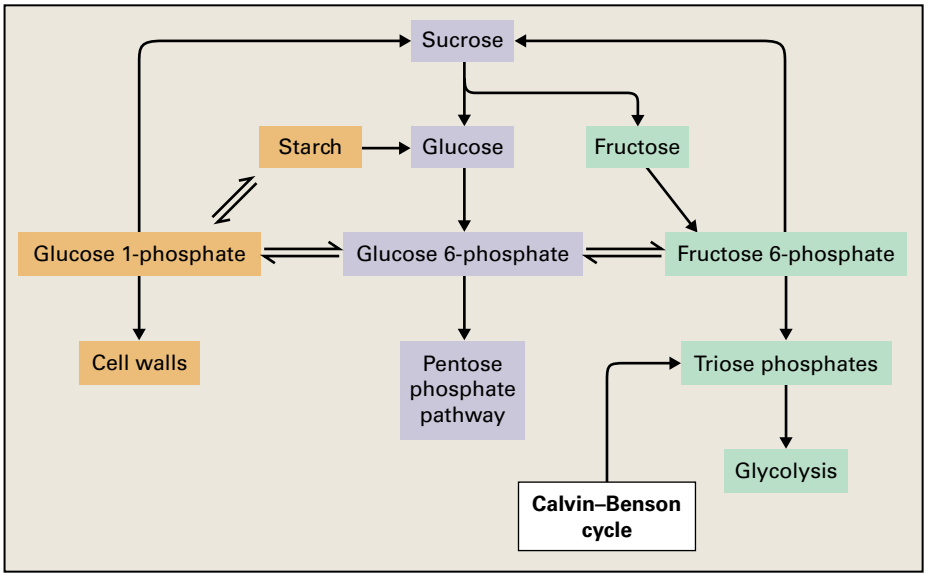


FIGURE 13.8 *Intermediates of the hexose phosphate pool are interconverted by two enzymes, phosphoglucomutase and glucose-6-phosphate isomerase.*

FIGURE 13.9 *The hexose phosphate pool contributes intermediates to glycolysis and the oxidative pentose phosphate pathway as well as to many biosynthetic processes.*



(**phosphoglucose isomerase**; Reaction 13.2). Both reactions are readily reversible and remain close to equilibrium *in vivo*.

Reaction 13.1: Phosphoglucomutase

Glucose 1-phosphate ↔ Glucose 6-phosphate

Reaction 13.2: Glucose-6-phosphate isomerase

Glucose 6-phosphate ↔ Fructose 6-phosphate

Fructose 1,6-bisphosphate, another hexose phosphate present in plant cells, is not considered part of the hexose phosphate pool, because most organisms interconvert **fructose 1,6-bisphosphate** and **fructose 6-phosphate** by means of regulated, irreversible reactions catalyzed by ATP-dependent **phosphofructokinase** (PFK) and fructose 1,6-bisphosphatase. In plants, however, these metabolites can also be interconverted by a reversible reaction catalyzed by **pyrophosphate-dependent phosphofructokinase** (PFP), an enigmatic enzyme whose role in metabolism is not fully understood (see Section 13.6.1).

Carbon can enter and leave the hexose phosphate pool in a number of different ways (Fig. 13.9). It can enter the pool during photosynthesis, when the triose phosphates produced are converted to hexose phosphates, and it can leave the pool for starch and sucrose synthesis and cell wall formation. An additional pathway for the production of hexose phosphates observed in germinated oilseeds is **gluconeogenesis**, by which storage lipids are converted to sugars (see Chapters 1 and 14). At night, when no photosynthesis occurs, or in heterotrophic tissues, carbon can enter the hexose phosphate pool through the phosphorylation of free hexoses derived from the degradation of sucrose (see Section 13.4), or from storage carbohydrates, such as starch (see Section 13.7). Other major drains on the hexose phosphate pool in the absence of photosynthesis are the respiratory pathways of **glycolysis** and the oxidative reactions of the pentose phosphate pathway, which provide energy and reducing power for the cell, respectively (Fig. 13.9).

13.2.2 Hexose phosphate pools exist in both the cytosol and the plastid stroma

The plant cytosol and plastids both contain hexose phosphate pools; depending on the plastid type, however, the capacity for the transport of hexose phosphates across the envelopes differs.

Most leaf chloroplasts have a low capacity for hexose phosphate transport, and their hexose phosphate pools are used in metabolic pathways distinct from those in the cytosol. Instead, carbohydrate exchange between these compartments is primarily by transport of the three-carbon intermediates **dihydroxyacetone phosphate**, **3-phosphoglycerate**, and **phospho*enol*pyruvate**, and the five carbon intermediate **xylulose 5-phosphate**. Phosphorylated intermediates are exchanged for **inorganic phosphate** via **antiporters** (see Chapter 3) that belong to the same family of integral membrane proteins. The counter-exchange mechanism is strictly coupled, and there is little transport of phosphate in the absence of an exchangeable substrate. Indeed, the major protein in the chloroplast inner membrane is the triose phosphate translocator (TPT; see Fig. 13.4), which is responsible for the export of the products of the Calvin–Benson cycle (see Chapter 12). The nonphosphorylated sugars derived from starch breakdown (see Section 13.7), glucose and maltose, can also cross the chloroplast envelope, but without exchange for phosphate (see Fig. 13.4).

Other plastid types, including colored **chromoplasts** and colorless, starch-storing **amyloplasts**, possess another antiporter, the **glucose-6-phosphate/phosphate translocator** (GPT). This protein can transport glucose 6-phosphate across the plastid envelope, as well as triose phosphates and xylulose 5-phosphate, in exchange for inorganic phosphate (P_i). The presence of the GPT implies a direct interaction between the cytosolic and plastid hexose phosphate pools. Chloroplasts in some cells or tissues (e.g., in guard cells, in the cells adjacent to the leaf vasculature, or in developing fruit) also possess the GPT. These chloroplasts likely perform specialized functions, and their metabolism differs from that of chloroplasts performing photosynthetic carbon assimilation. Under exceptional circumstances, such as drought or artificial feeding of leaves with high concentrations of sucrose, expression of a chloroplast hexose phosphate translocator can also be induced, and this is associated with major changes in metabolic fluxes within the leaf mesophyll cells.

13.3 Sucrose biosynthesis

Sucrose is a major product of photosynthesis in green leaves and accounts for much of the CO_2 fixed during photosynthesis. It also serves as the principal long-distance transport compound in most plants and as a storage compound in some [including sugar beet (*Beta vulgaris*), sugar cane (*Saccharum* sp.), and carrot (*Daucus carota*)]. Sucrose is suited to its transport role: By joining the carbonyl carbons of glucose and fructose in a stable glycosidic bond, sucrose formation prevents these groups from becoming oxidized through nonenzymatic reactions with other cellular components. For this reason, sucrose is described as a nonreducing sugar (Fig. 13.10).

Sucrose synthesis occurs exclusively in the cytosolic compartment of plant cells using carbon from the hexose phosphate pool. During the day, carbon enters this pool via the gluconeogenic flux from triose phosphates, which are exported from the chloroplast. This flux is regulated at the step of **fructose-1,6-bisphosphatase** (FBPase; see Section 13.6). During the night, hexose phosphates for sucrose synthesis are derived from other sources, such as by catabolism of transitory starch stored in the chloroplast. In this case, carbon exported from the chloroplast as free glucose or maltose is metabolized to hexose phosphates in the cytosol (see Section 13.7).

13.3.1 Glucose 1-phosphate can be reversibly converted to UDP-glucose

Uridine diphosphate-glucose (**UDP-glucose**; Fig. 13.11) is one of the two substrates required for sucrose synthesis (the other is fructose-6-phosphate; see Section 13.3.2). UDP-glucose is also a substrate for other anabolic reactions, including cell wall synthesis (see Chapter 2). The enzyme **UDP-glucose pyrophosphorylase** generates UDP-glucose and **pyrophosphate** (PP_i) from glucose 1-phosphate and UTP (Reaction 13.3).

Reaction 13.3: UDP-glucose pyrophosphorylase

$$\text{Glucose 1-phosphate} + \text{UTP} \leftrightarrow \text{UDP-glucose} + PP_i$$

The reaction catalyzed by UDP-glucose pyrophosphorylase is readily reversible, and whether carbon enters or leaves the hexose phosphate pool depends on the concentrations of the respective metabolites. During sucrose synthesis, the flux through this step is driven by the consumption of UDP-glucose. Interestingly, cytosolic concentrations of pyrophosphate remain relatively constant in plants. In this way, plant metabolism differs from that of animals. The cytosol of animal cells contains a **pyrophosphatase** that rapidly hydrolyzes any PP_i produced during biosynthetic reactions; the metabolism of PP_i in the plant cell cytosol, however, is coupled with other metabolic processes (see Box 13.1).

13.3.2 Sucrose is synthesized from UDP-glucose and fructose 6-phosphate

The principal route of sucrose synthesis involves the reactions catalyzed by two enzymes, **sucrose-phosphate synthase** and **sucrose-phosphate phosphatase** (Fig. 13.12).

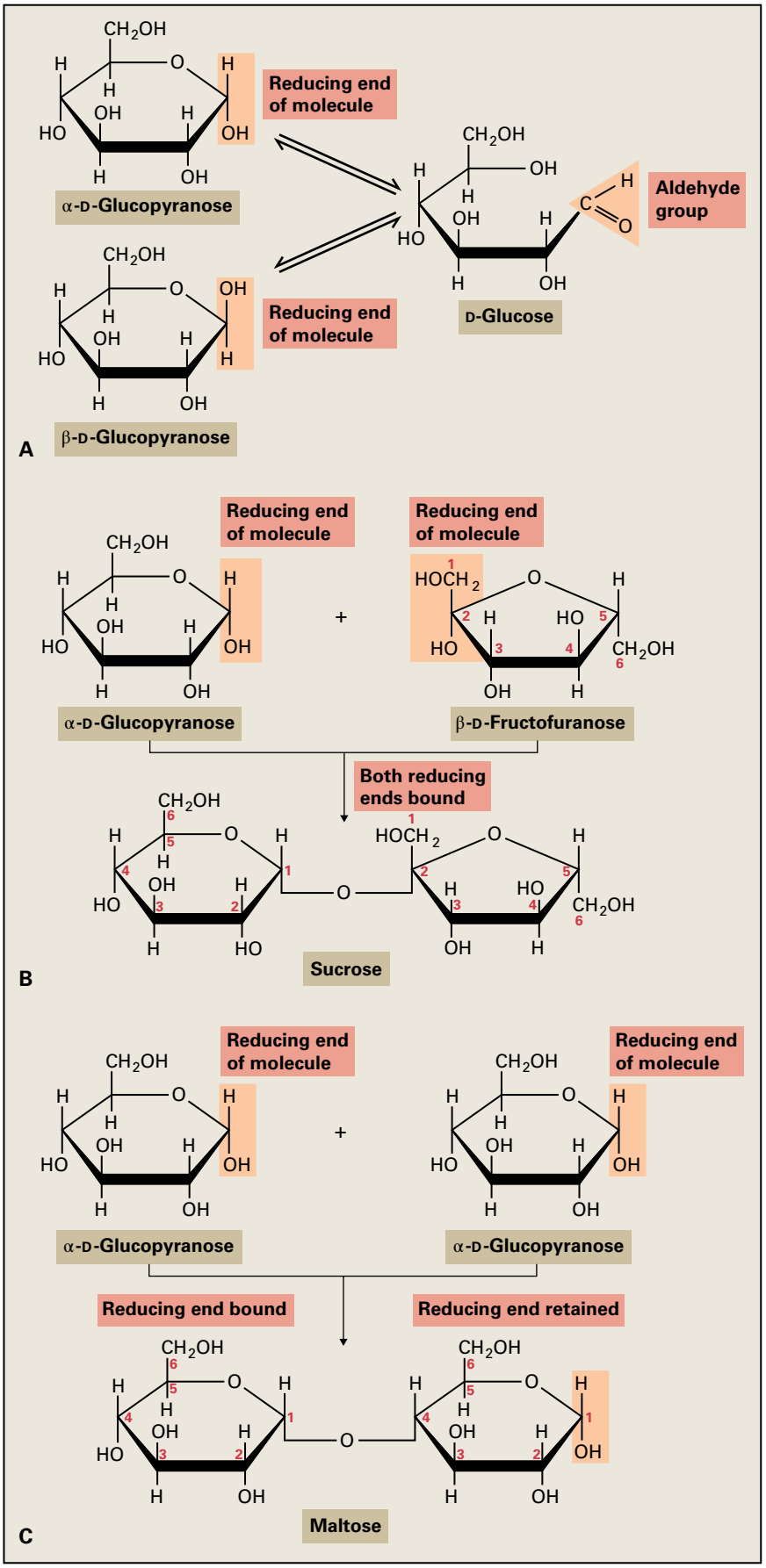


FIGURE 13.10 *Some sugars can act as reductants. (A) Glucose undergoes a conversion at the anomeric carbon (C-1) that yields an aldehyde (D-glucose) and two hemiacetal isomers (α-D-glucopyranose and β-D-glucopyranose). The aldehyde group can react with (reduce) organic and inorganic substrates and is, therefore, described as the reducing end of the molecule. (B) During sucrose synthesis, the anomeric carbon of fructose (C-2) is joined to the anomeric carbon of glucose (C-1) by a glycosidic bond. This bond protects the reducing ends of both monomers, and defines sucrose as a nonreducing sugar. (C) In the disaccharide maltose, one of the anomeric carbons of glucose remains unbound and reactive. For this reason, maltose is a reducing sugar. In trehalose, also a disaccharide of glucose, the two anomeric carbons are bound, rendering it a nonreducing sugar (not shown).*

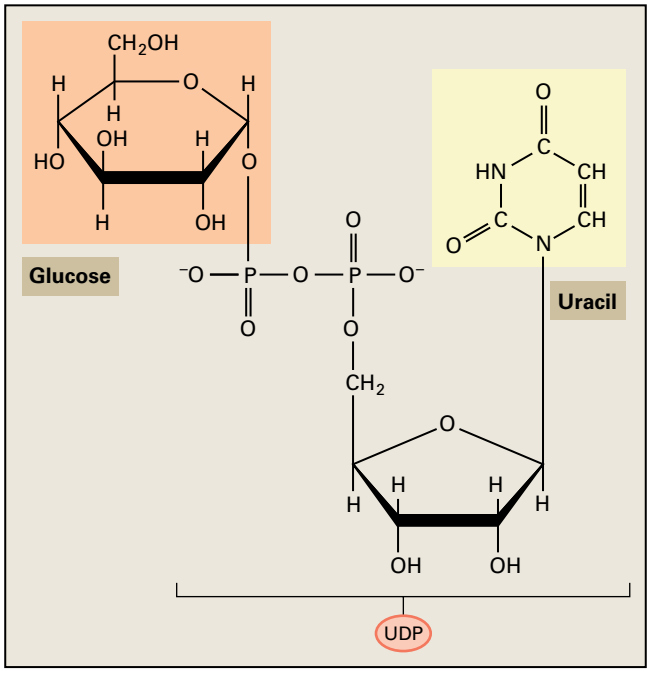


FIGURE 13.11 *Structure of uridine diphosphate-glucose (UDP-glucose).*

Reaction 13.4: Sucrose-phosphate synthase

$$\text{UDP-glucose} + \text{fructose 6-phosphate} \leftrightarrow \text{Sucrose 6-phosphate} + \text{UDP}$$

Reaction 13.5: Sucrose-phosphate phosphatase

$$\text{Sucrose 6-phosphate} + H_2O \rightarrow \text{Sucrose} + P_i$$

Sucrose-phosphate synthase transfers the glucosyl moiety of UDP-glucose to fructose 6-phosphate, yielding sucrose 6-phosphate, and the subsequent hydrolysis of sucrose 6-phosphate by sucrose-phosphate phosphatase yields sucrose and phosphate. Overall, the formation of sucrose by this route has a large negative free energy change ($\Delta G^{o\prime} = -25$ kJ mol^{-1}), which renders this sequence of reactions essentially irreversible in vivo. This is primarily due to the large negative free energy change ($\Delta G^{o\prime} = -16.5$ kJ mol^{-1}) associated with the dephosphorylation of sucrose; the preceding steps (the formation of UDP-glucose and of sucrose 6-phosphate) have relatively small negative free energy changes ($\Delta G^{o\prime}$ of -2.88 kJ mol^{-1} and -5.7 kJ mol^{-1}, respectively).

BOX 13.1 Pyrophosphate is a mysterious player in plant metabolism

Pyrophosphate (PP_i) is generated in many biosynthetic reactions (e.g., the synthesis of nucleotide sugars, such as UDP-glucose and ADP-glucose, the activation of amino acids for protein synthesis, and the polymerization of nucleic acids). In animals and many microorganisms, hydrolysis by pyrophosphatase removes the pyrophosphate produced in these reactions, and the large change in free energy ($\Delta G^{o\prime}$ of –33.4 kJ mol^{-1}) drives otherwise energetically unfavorable reactions in the direction of synthesis.

The stroma of plastids, the site of many biosynthetic reactions in plants, also contains a pyrophosphatase, but the plant cytosol, where sucrose and cell wall biosynthesis take place, can accumulate a substantial concentration of PP_i (up to 0.3 mM). This cytosolic PP_i pool is important; overexpression of a cytosol-localized bacterial pyrophosphatase in transgenic tobacco (*Nicotiana tabacum*) significantly inhibits growth. However, the way in which PP_i metabolism is linked to other cellular processes is not fully understood.

The discovery of this cytosolic PP_i pool followed the discovery of one of the enzymes that can metabolize it: the PP_i-dependent phosphofructokinase (PFP; see Section 13.6). PFP can remove or produce PP_i while interconverting fructose 1,6-bisphosphate and fructose 6-phosphate in a reversible reaction. Its presence is an enigma because it acts alongside two other cytosolic enzymes catalyzing similar, yet irreversible reactions. The conversion of fructose 6-phosphate to fructose 1,6-bisphosphate is a principal regulatory step in glycolysis in other organisms. However, regulation differs in plants due to their autotrophic nature, and it has been proposed that PFP serves other functions, including:

- maintenance of a stable pyrophosphate concentration in the cell
- generation of pyrophosphate required for the breakdown of sucrose by way of the sucrose synthase pathway (see Section 13.4)
- bypass of PFK during times of phosphate starvation, when the amounts of ATP may be insufficient for the PFK reaction (see Box 13.5)
- stimulation of carbon flow in glycolysis during anaerobic conditions
- equilibration of the hexose and pentose phosphate/triose phosphate pools during increased biosynthetic activity.

PFP has been repressed or mutated in a range of species. In general, such plants appear normal, but examination of the metabolite levels and fluxes reveals differences in each case, including minor reductions in starch content of potato (*Solanum tuberosum*) tubers, increases in the sucrose content of sugar cane (*Saccharum* sp.) stems, slight inhibition of glycolysis, and changes in the balance of hexose phosphates to triose phosphates. These studies suggest PFP influences fluxes between the hexose phosphate and triose

phosphate pools, but it is not an essential enzyme. Thus, its function remains unresolved. It may be that, under normal laboratory or greenhouse conditions, the enzyme enhances growth and fitness by a margin that is too small to measure, but large enough to ensure conservation of the enzyme during evolution. Alternatively, the enzyme may be important only under certain conditions not tested in the laboratory.

Another player in PP_i metabolism is the proton-pumping pyrophosphatase located in the tonoplast (see Chapter 3). Energy released by pyrophosphate hydrolysis drives the pump, acidifying the vacuole and generating an electrochemical gradient used to power transmembrane transport. This H^+-pyrophosphatase may participate in removing cytosolic pyrophosphate produced during biosynthesis. Analysis of *Arabidopsis* mutants deficient in this pump supports this idea: *Arabidopsis* seedlings convert storage lipids in their cotyledons into sucrose via gluconeogenesis, and pump-deficient mutants have reduced sucrose content and stunted growth due to accumulation of inhibitory levels of PP_i.

Despite these discoveries, we still do not fully understand how or why plant cells maintain a stable pool of cytosolic PP_i.

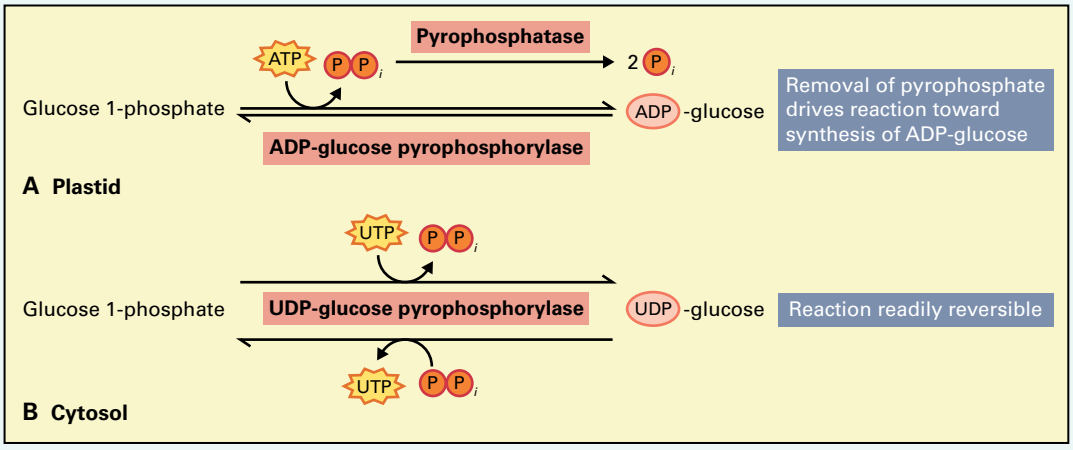
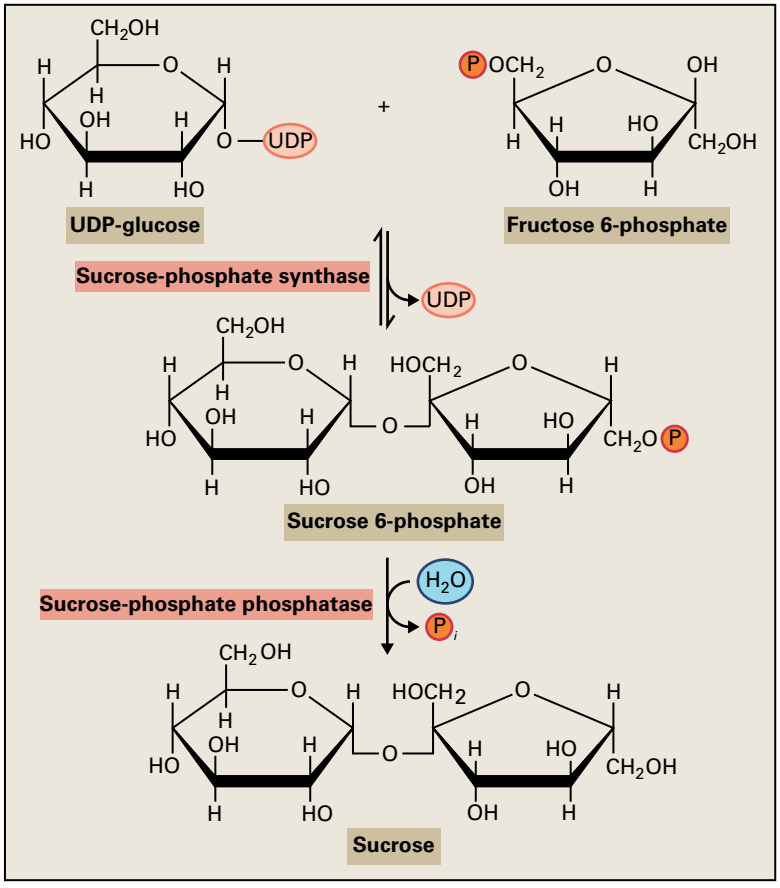


FIGURE 13.12 *Sucrose synthesis by sucrose-phosphate synthase (SPS) and sucrose-phosphate phosphatase.*



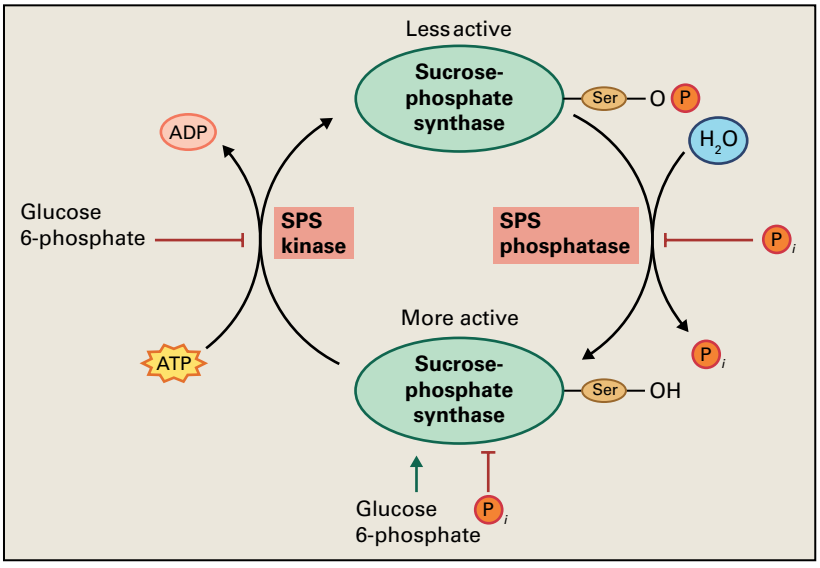


FIGURE 13.13 *Regulation of sucrose-phosphate synthase (SPS). SPS is regulated by both allosteric effectors and phosphorylation/dephosphorylation of a serine residue in the enzyme. The active enzyme is dephosphorylated and can be activated further, allosterically, by glucose 6-phosphate. SPS is inhibited by inorganic phosphate and possibly by sucrose. In addition, glucose 6-phosphate inhibits the SPS-kinase, and inorganic phosphate inhibits the SPS-phosphatase. As a result, a high ratio of glucose 6-phosphate to inorganic phosphate maintains the enzyme in its active form, whereas a low ratio inhibits the enzyme and promotes its conversion to the inactive form.*

There is evidence, mainly from work on spinach (*Spinacia oleracea*) in the 1990s, that sucrose synthesis is regulated by mechanisms that coordinate the activity of sucrose-phosphate synthase with the status of the hexose phosphate pool (Fig. 13.13). First, sucrose-phosphate synthase is subject to **allosteric modulation** by glucose 6-phosphate, which activates the enzyme, and by P_i, which inhibits it. When hexose phosphates are abundant, the enzyme is activated. Furthermore, a decrease in free P_i, which generally accompanies high concentrations of hexose phosphates, lifts inhibition. Second, sucrose-phosphate synthase is regulated by multisite, reversible protein phosphorylation. One kinase that phosphorylates Ser^{158} and downregulates sucrose-phosphate synthase activity is itself inhibited by glucose 6-phosphate. The phosphatase that upregulates the activity of sucrose-phosphate synthase is inhibited by high concentrations of P_i. Sucrose-phosphate synthase is also phosphorylated at other sites. Phosphorylation at Ser^{229} allows interaction with 14-3-3 proteins, which also inhibits its activity. By contrast, phosphorylation at Ser^{424}, which can occur during osmotic stress, can activate the enzyme. The effects of allosteric and post-translational modifications combine to provide sensitive control of sucrose synthesis. There is also evidence that sucrose levels can feed back on sucrose-phosphate synthase activity, preventing overproduction; the mechanism of this feedback, however, is not understood.

While such biochemical findings have laid the foundation for understanding the control of sucrose synthesis, the situation is likely more complex. Multiple conserved genes encode various isoforms of both sucrose-phosphate synthase and sucrose-phosphate phosphatase, and the properties of each of these isoforms have not been rigorously investigated (see Box 13.2). This may complicate the interpretation of some biochemical studies in which a uniformity of enzyme activity or activation state is assumed. For instance, one class of sucrose-phosphate synthase isoforms found in wheat (*Triticum aestivum*) and other monocotyledonous Poaceae lack the phosphorylation sites associated with 14-3-3 protein binding and osmotic stress activation, and their regulatory features are unknown.

13.4 Sucrose metabolism

After its production in source tissues, sucrose is transported within the plant via the phloem to sink tissues, where it can enter destination cells by two routes. In most cells, it moves by **symplasmic transport**, diffusing through the **plasmodesmata**. In this case, the sucrose is broken down in the cytosol or sequestered in the vacuole to maintain passive import. In some tissues, however, sucrose is unloaded from the phloem into the **apoplast** and must cross the plasma membrane to enter the destination cell, often against a concentration gradient. This **apoplastic pathway** is particularly important to developing embryos, which have no direct cytoplasmic connections to the tissues of the maternal plant. The sucrose can be either transported into these cells directly, or is first hydrolyzed to glucose and fructose in the apoplast. The potential significance of the various means of sucrose transport and degradation is receiving more attention, given that carbohydrates, in addition to being intermediates in metabolism, play a role in regulating the expression of many genes. Thus, the form of carbohydrate taken up may influence the activity of the cell (see Chapters 8 and 16).

Sucrose can be degraded by either **sucrose synthase** (Fig. 13.14) or **invertase** (Fig. 13.15):

BOX 13.2 Why plants have multiple genes that encode the same enzyme is not fully understood

Genome sequencing has revealed that multiple conserved genes frequently encode particular metabolic enzymes. In some cases, this is because the enzyme is required in different cellular compartments. For example, some enzymes of glycolysis are present in both the plastid and the cytosol, and each protein is encoded by a separate gene. This subfunctionalization offers advantages over mechanisms for dual-targeting of the same gene product to multiple compartments, as each enzyme can evolve different kinetic and regulatory properties that confer advantages to the plant.

In some cases, however, targeting to different cellular compartments cannot explain these gene duplications. For example, sucrose-phosphate synthase and sucrose-phosphate phosphatase are cytosolic enzymes, each encoded by small gene families. Here, the significance of the multiple isoforms is unknown, but different patterns of expression could mean that each isoform is responsible for synthesizing sucrose in a different tissue. In some cases, there is even greater gene replication: The *Arabidopsis* genome encodes 17 putative invertase genes, with multiple isoforms targeted to each of four cellular (and extracellular!) compartments.

Such revelations from genome sequencing define one of the challenges for molecular geneticists and biochemists today, who must work to explain the functions of these different genes. The answers may often be surprising. Studies of the β-amylase gene family in *Arabidopsis*, which has nine members, have confirmed the enzymes' supposed role in starch catabolism in chloroplasts (see Section 13.7). They have also revealed the existence of apparently noncatalytic isoforms acting in an undefined role alongside them. Furthermore, two members of the protein family are targeted to the nucleus, where they act as transcriptional regulators. Such neofunctionalization allows proteins that originate from metabolic enzymes to take on new roles, such as metabolic sensors.

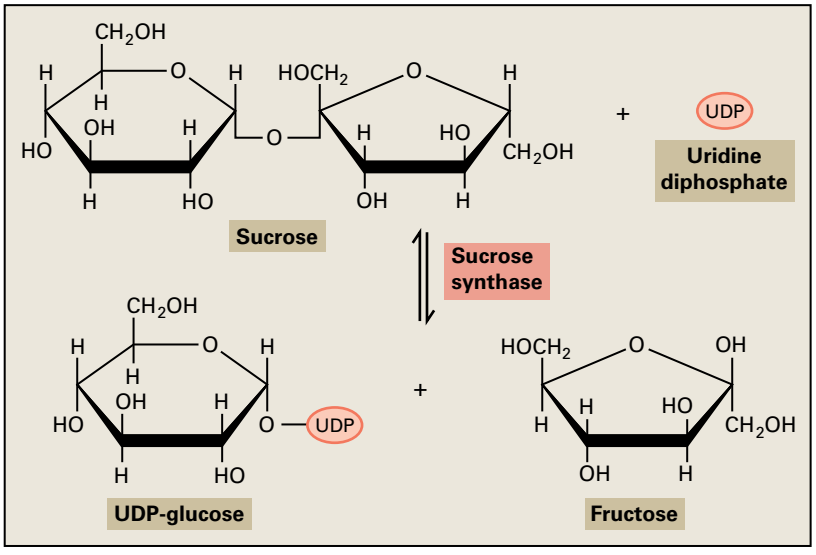


FIGURE 13.14 *Sucrose synthase catalyzes a reversible reaction that can synthesize or degrade sucrose. In plant cells, this enzyme is associated primarily with sucrose degradation.*

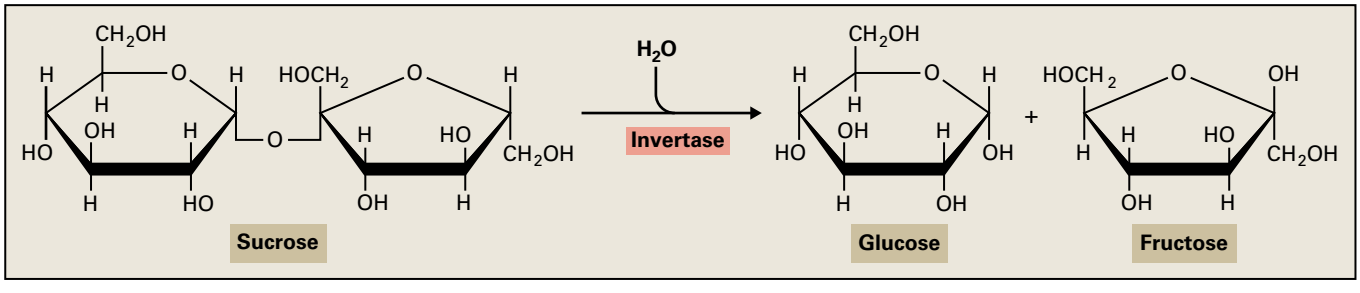


FIGURE 13.15 *Degradation of sucrose by invertase.*

Reaction 13.6: Sucrose synthase

$$\text{Sucrose} + \text{UDP} \leftrightarrow \text{UDP-glucose} + \text{fructose}$$

Reaction 13.7: Invertase

$$\text{Sucrose} + H_2O \rightarrow \text{Glucose} + \text{fructose}$$

The name sucrose synthase can be confusing. The enzyme is capable of catalyzing both sucrose synthesis and degradation; however, the activity of sucrose-phosphate synthase (see Reaction 13.4) is high in tissues that synthesize sucrose, indicating that it is the dominant enzyme for sucrose biosynthesis. In contrast, sucrose synthase is present in higher activities in sucrose-utilizing tissues (e.g., developing seeds) than in sucrose-exporting tissues (e.g., photosynthetic leaves and germinated oil seeds). Thus, the principal role of sucrose synthase is thought to be sucrose catabolism. The reaction catalyzed by invertase is irreversible and so leads only to sucrose degradation.

A difference between these two sucrose-degrading enzymes lies in the energy status of the products in relation to the cytosolic hexose phosphate pool. Invertase produces free hexoses that must be phosphorylated at the expense of ATP. By contrast, sucrose synthase generates UDP-glucose, which can react with pyrophosphate to produce glucose 1-phosphate and uridine triphosphate (UTP). Thus, sucrose synthase, combined with UDP-glucose pyrophosphorylase (see Reaction 13.3), can provide an ATP-independent pathway for hexose phosphorylation (Fig. 13.16).

The precise roles of invertase and sucrose synthase in sucrose breakdown are not well understood. Both enzymes often appear in the same tissues. In addition, both sucrose synthase and invertase occur as multiple isoenzymes, each of which probably functions in a specific tissue or cellular compartment (e.g., in *Arabidopsis* six genes encode sucrose synthase, and 17 encode different invertase isoforms; see Box 13.2).

In potato (*Solanum tuberosum*) tubers, invertase activity is too low to account for the required rate of sucrose breakdown, implicating sucrose synthase in that role. In addition, repressing the major sucrose synthase gene expressed in tubers decreases starch content and tuber growth. Comparable findings have been made in pea (*Pisum sativum*) and maize (*Zea mays*), where mutation of sucrose synthase genes results in decreased starch synthesis in developing embryos and endosperm, respectively. Studies like these have led to the concept that sucrose synthase activity tends to be associated with the utilization of sucrose for the biosynthesis of nonstructural carbohydrate polymers like starch, and of structural carbohydrate polymers like cellulose and callose. Models have been proposed that suggest direct interaction between sucrose synthase with the cellulose synthase complex, which could allow direct channeling of the UDP-glucose produced by sucrose synthase to the active site of cellulose synthase.

Invertases are often defined as either acid invertases (acidic pH optima) or alkaline invertases (neutral or alkaline pH optima). These forms operate in different cellular compartments: Acid invertases are present in both the vacuole and the apoplast, whereas alkaline invertases are present in the cytosol and plastid. Vacuolar invertase probably hydrolyzes sucrose stored in the vacuole, with the subsequent transport of the free hexoses to the cytosol for metabolism. High levels of vacuolar invertases are observed in tissues accumulating hexoses, such as developing fruits, and in rapidly growing tissues, such as the elongation zones of roots and hypocotyls. The apoplastic form of invertase is bound firmly to the cell wall matrix and hydrolyzes apoplastic sucrose delivered to sink tissues. This is particularly important in plant reproductive tissues. Repression of cell wall invertases interferes with pollen development, causing male sterility and decreased seed size in important crops like maize (*Zea mays*) and rice (*Oryza sativa*). Cytosolic invertases are also important for plant growth, particularly roots, as demonstrated through the analysis of mutants of *Arabidopsis*, *Lotus japonicus,* and rice.

Plants also possess proteinaceous invertase inhibitors that interact with the acid invertases of the apoplast and the vacuole. These inhibitors likely repress invertase activity, although

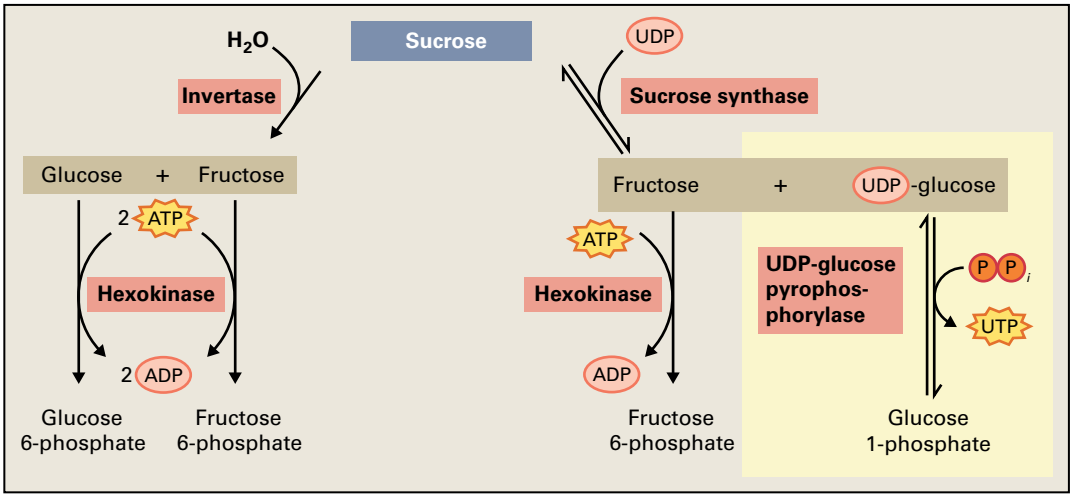


FIGURE 13.16 *Hexokinase uses ATP to phosphorylate glucose and fructose, the products of invertase. Sucrose synthase and UDP-glucose pyrophosphorylase act together to generate hexose phosphate by an ATP-independent pathway, highlighted here in yellow.*

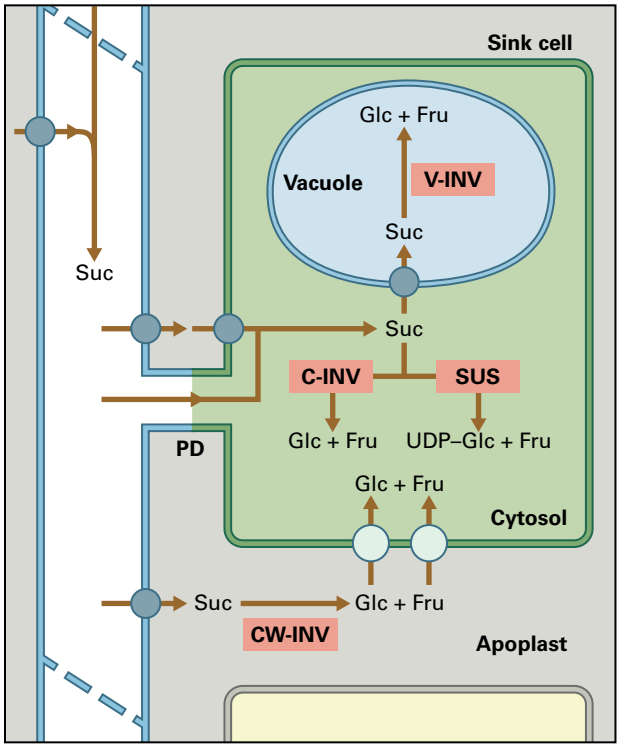


FIGURE 13.17 *Schematic diagram of invertase-mediated or sucrose synthase-mediated sucrose degradation in heterotrophic tissues. Phloem unloading of sucrose (Suc) in sinks may occur apoplastically into the cell wall matrix or symplasmically through plasmodesmata (PD). In the former case, unloaded sucrose can be hydrolyzed by cell wall bound invertase (CW-INV) into glucose (Glc) and fructose (Fru) before being taken up by membrane hexose transporters (light-blue circles). Symplasmically imported sucrose, or that taken up by membrane bound sucrose transporters (dark-blue circles), can be hydrolyzed by cytoplasmic invertase (C-INV). In some tissues, cytosolic sucrose enters the vacuole or the plastid, where it is hydrolyzed by vacuolar invertase (V-INV) or plastid invertases (P-INV) (latter not shown). Both CW-INV and V-INV are subject to posttranslational inhibition by proteinaceous inhibitors (not shown). The intracellular Glc and Fru may be respired, stored in the vacuole, or used for biosynthesis of sugar polymers (e.g., starch and cellulose). Sucrose can also be metabolized by sucrose synthase (SUS) in the cytosol.*

little is known about their precise roles. Their existence adds an additional layer of complexity onto an already complex process (Fig. 13.17). However, this is not surprising, considering the central role sucrose plays in plant metabolic biology.

13.5 Starch biosynthesis

Not all the carbohydrate assimilated in leaves is immediately used for sucrose biosynthesis and growth; some is stored for later use, when photosynthesis is not possible (see Fig. 13.3). Carbohydrate can be stored in several forms, including vacuolar sucrose or **fructans**, but the most common storage form is **starch**. In leaves, starch is synthesized during the day in chloroplasts and stored temporarily until the night, when it is degraded again. In storage tissues, such as tubers or seeds, it is synthesized in amyloplasts and stored for much longer periods.

Starch is an important plant product, accounting for half of humankind's caloric intake. Consequently, much research has been focused on its metabolism, both in crops and model species. The analogous storage compound to starch in other organisms is glycogen. In animals and fungi, glycogen is synthesized in the cytosol from UDP-glucose, while in bacteria it is synthesized from ADP-glucose. Starch and glycogen share some structural similarities (both are composed of polymers of glucose), but glycogen has a more branched structure. The biosynthesis of starch is more complex than that of glycogen.

Starch is a remarkable substance that takes the form of massive, insoluble semicrystalline granules (Fig. 13.18). By linking thousands of glucose monomers into a small number of molecules that then partially crystallize, starch represents a compact, stable, osmotically inert form of carbohydrate storage. If a comparable number of hexose units accumulated in the plastid as sucrose, the stromal solution would contain too many solute particles, and water from the cytosol would flood in by osmosis, causing the plastid to swell and burst.

13.5.1 Starch synthesis in plants begins with ADP-glucose

In the chloroplast, the Calvin–Benson cycle can feed carbon directly into the stromal hexose phosphate pool and then the starch biosynthetic pathway (Fig. 13.19). Thus, starch biosynthesis is supplied by a different pool than sucrose synthesis.

Fructose 6-phosphate can be converted to glucose 1-phosphate by the sequential action of the plastid isoforms of phosphoglucomutase and glucose-6-phosphate isomerase (see Reactions 13.1 and 13.2). The first committed step in the starch biosynthetic pathway is the production of **ADP-glucose** by **ADP-glucose pyrophosphorylase** (Reaction 13.8). Genetic studies in *Arabidopsis* and other species have demonstrated that this is the major pathway of starch synthesis in leaves, as mutants deficient in each of these three enzymes have greatly reduced starch content.

Reaction 13.8: ADP-glucose pyrophosphorylase

$$\text{Glucose 1-phosphate} + \text{ATP} \leftrightarrow \text{ADP-glucose} + \text{PP}_i$$

In amyloplasts, carbon for starch synthesis is derived from the metabolism of sucrose translocated from source tissues (see Chapter 15 and Section 13.4). Substrates for ADP-glucose production must be imported from the cytosol, usually in the form of glucose 6-phosphate (Fig. 13.19). This is illustrated by the *rugosus3* mutant of pea (*Pisum sativum*), which lacks the plastid phosphoglucomutase. It cannot convert glucose 6-phosphate into glucose 1-phosphate in the amyloplasts of its embryos and so cannot synthesize starch (see Box 13.3). In the **endosperm** of maize (*Zea mays*) and other cereal seeds, however, a second form of ADP-glucose pyrophosphorylase

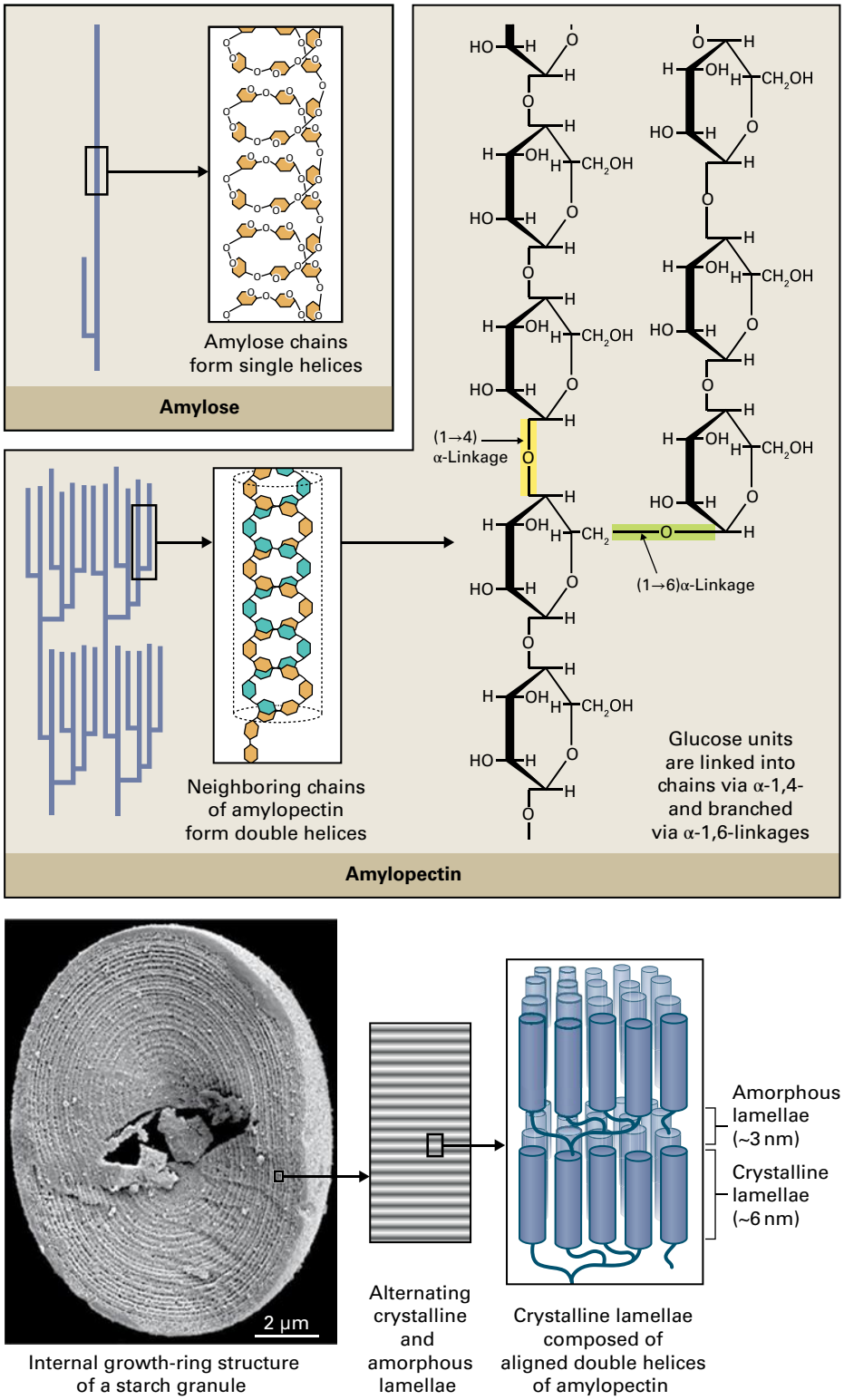


FIGURE 13.18 *Starch is a remarkable substance. Although composed almost exclusively of the two glucose polymers, amylose and amylopectin, it takes the form of massive, insoluble, semi-crystalline granules. Amylopectin is the major polymer responsible for the granule structure. It has a nonrandom branching pattern resulting in clusters of unbranched chain segments. Left-handed double helices with six glucose units per turn form between these linear segments (middle). Amylose is linear or only slightly branched. It forms single helical structures (top left). The double helices of amylopectin arrange into ordered crystalline lamellae. Crystalline lamellae alternate with amorphous lamellae (containing the branch points) with 9 nm periodicity (bottom right). A higher-order structure, with a periodicity of hundreds of nanometers is visible with light or scanning electron microscopy (bottom left). These are often referred to as growth rings, owing to the similarity in appearance to the growth rings of a tree. However, starch granule growth rings are probably a structural feature rather than representing periodic phases of growth.*

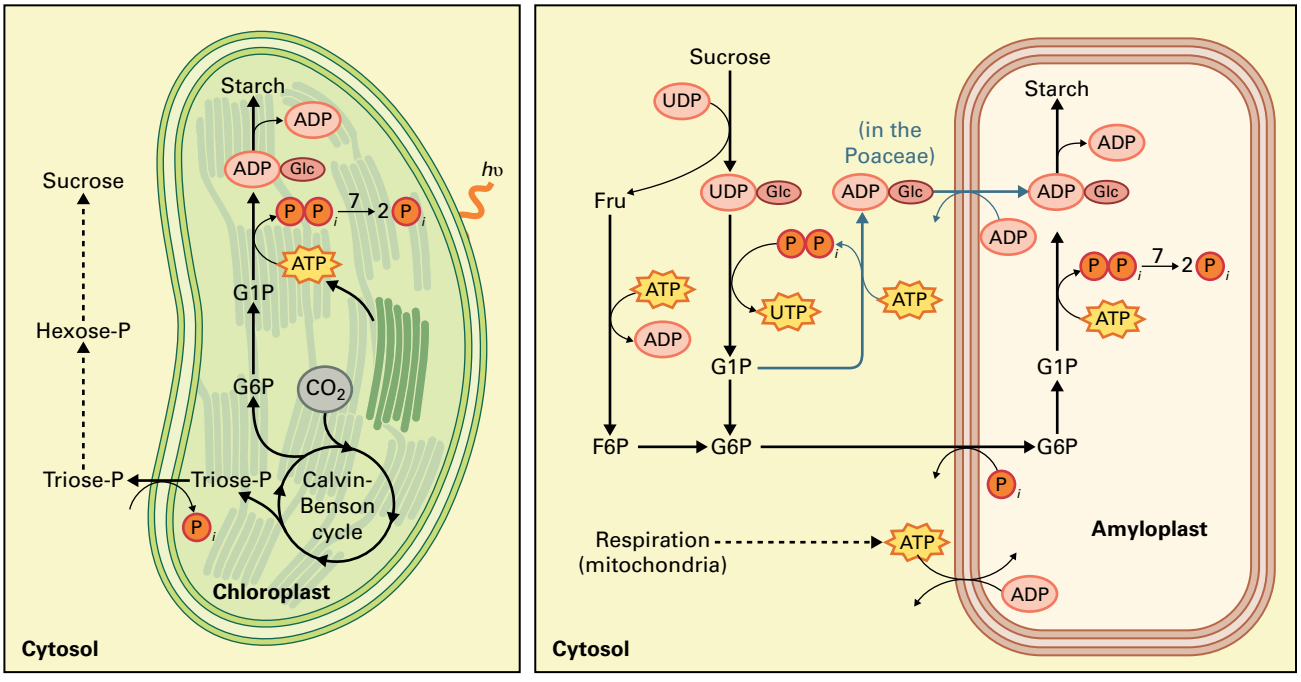


FIGURE 13.19 *Schematic representation of the pathway of starch biosynthesis and its subcellular compartmentalization in leaves (A) and heterotrophic tissues (B). Energy and substrates for starch synthesis in leaves are derived from photosynthesis, while in heterotrophic tissues they are derived from the metabolism of imported sucrose. Cereal crops have the capacity to generate ADP-glucose in the cytosol and translocate it into the amyloplast (highlighted in blue), as well as the plastid-localized pathway. This ability appears to be restricted to members of the Poaceae.*

exists in the cytosol in addition to the one in the amyloplast. A transporter specific to these monocotyledonous plants can import ADP-glucose directly into the amyloplasts in exchange for ADP (Fig. 13.19). This cytosolic route, rather than the plastid one, appears to be the major source of ADP-glucose in the cereal endosperm. Mutations affecting the cytosolic isoform of ADP-glucose pyrophosphorylase or the ADP-glucose transporter reduce starch accumulation by about 75%.

13.5.2 ADP-glucose pyrophosphorylase is a multisubunit, highly regulated enzyme

Almost all ADP-glucose produced in the plastid is directed to starch synthesis, and ADP-glucose pyrophosphorylase (Reaction 13.8) is regarded as the major regulated enzyme of the pathway. This contrasts with cytosolic **UDP-glucose pyrophosphorylase**, which provides **UDP-glucose** for multiple biosynthetic pathways (e.g., sucrose synthesis and cellulose synthesis) and so is poorly suited as a regulatory step. Another key difference is the presence of an active pyrophosphatase in the plastid stroma, but not in the cytosol. The hydrolysis of pyrophosphate renders the production of ADP-glucose in the plastid essentially irreversible.

ADP-glucose pyrophosphorylase is a heterotetramer of two large and two small subunits (Fig. 13.20), which have a common ancestry. The small subunits are catalytically active, while the large subunits have little or no activity. However, the large subunits influence the activity and regulatory properties of the small subunits in the native enzyme. Multiple isoenzymes of both subunits exist, which may be expressed on a tissue-specific basis or under different environmental conditions. The large subunit, in particular, is present in multiple copies that have diverged more in sequence over time than the small subunits. Although the function of these isoenzymes is not fully understood, different combinations of large and small subunits may yield enzymes with distinct kinetic and regulatory properties in different tissue or cell types.

In photosynthetic tissues, ADP-glucose pyrophosphorylase is activated by 3-phosphoglycerate and inhibited by P_i in a regulatory mechanism that links enzyme activity with the supply of photosynthate (Fig. 13.20). Increasing levels of the Calvin–Benson cycle intermediate 3-phosphoglycerate indicate an abundance of fixed carbon. P_i levels decrease as phosphorylated intermediates of metabolism accumulate (e.g., in the light). Consequently, the levels of the activator and inhibitor are linked and change in a reciprocal manner (Fig. 13.21). Thus, relatively small changes in the P_i:3-phosphoglycerate ratio have a large impact on ADP-glucose pyrophosphorylase activity. When photophosphorylation slows or ceases altogether (e.g., in the dark), the P_i concentration in the chloroplast rises, and starch synthesis is repressed.

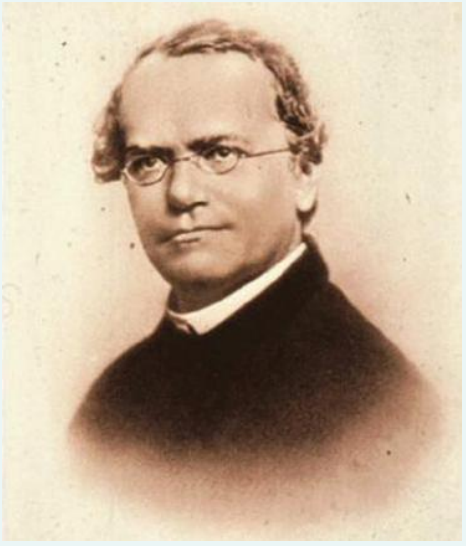
In leaves, starch synthesis occurs concurrently with sucrose synthesis, with the fine allosteric control of the pathways influencing each other (see Section 13.6.2). ADP-glucose pyrophosphorylase is also regulated by reversible redox activation (see Fig 13.20). The formation of a covalent intermolecular disulfide bridge between two cysteine residues on each of the small subunits deactivates the enzyme.

BOX 13.3 Mendel's round and wrinkled peas reflect different alleles of a starch-branching enzyme

A century before the structure of DNA was discovered, an Austrian monk named **Gregor Mendel** bred peas in the monastery garden in the town of Brno. Mendel crossed round peas with wrinkled peas and followed these traits through a series of generations. He concluded that a pair of factors (now called genes), passed from parent to offspring, governed the appearance of the seeds. Mendel published his observations in 1865, initiating the discipline of classical genetics.

In 1990, modern molecular biology revealed the molecular basis of the round and wrinkled pea phenotypes. The mutation Mendel followed was due to a transposon-like insertion into the gene encoding one of two isoforms of starch-branching enzyme. In these mutants, this loss of function is not fully compensated by the presence of the second isoform, and starch production falls by ≈30%. Carbon that would have been stored as starch instead accumulates as sucrose, lowering the osmotic potential of the developing seed and causing it to swell with fluid. On drying, the loss of the additional water results in the seed having a wrinkled appearance. The subsequent study of other wrinkled-seeded (or *rugosus*) peas helped establish other critical steps in the starch biosynthetic pathway.

Source: (right) Cover photograph for Cell 60 (1), by Bhattacharyya.





This bridge can be broken by reduction, whereupon the enzyme becomes active. In illuminated chloroplasts, reduction is mediated by **thioredoxin** (Trx), using electrons derived from the photosynthetic electron transport chain (see Chapter 12). This provides an additional link between the light reactions of photosynthesis and starch synthesis. At night, ADP-glucose pyrophosphorylase is primarily in the oxidized, inactive form, minimizing starch biosynthesis. However, the enzyme can also be activated in the dark by NTRC (see below) to an extent that depends on the level of NADPH, reflecting available sucrose. ADP-glucose pyrophosphorylase can thus link both light and sugar availability to the synthesis of starch.

In amyloplasts and other nonphotosynthetic plastids, the mechanism and importance of ADP-glucose pyrophosphorylase regulation are less clear. The potato (*Solanum tuberosum*) tuber enzyme is also redox-regulated and sensitive to the same allosteric regulation as the leaf enzyme. Redox activation is still possible, with the electrons from sucrose-derived NADPH, either via the sequential actions of **ferrodoxin-NADP reductase** and **ferrodoxin-thioredoxin reductase**, or via the plastid-localized protein **NADP-thioredoxin reductase C** (NTRC, which contains a Trx-like domain) (see Fig. 13.20). The latter enzyme has been implicated in the light-independent, sucrose-dependent reductive activation of ADP-glucose pyrophosphorylase in *Arabidopsis* chloroplasts, as well as in the activation of the amyloplast enzyme in roots. The inhibition of ADP-glucose pyrophosphorylase by phosphate is also understandable, because nonphotosynthetic plastids synthesize starch from glucose phosphate, which is imported into the plastid by a hexose phosphate/P_i antiporter. High concentrations of P_i, therefore, indicate that hexose phosphate supply from the cytosol is limiting (see Fig. 13.19). Activation of this enzyme by 3-phosphoglycerate in amyloplasts is more difficult to comprehend, though it may signal a sufficient carbohydrate supply. Interestingly, not all amyloplast-localized forms of ADP-glucose pyrophosphorylase display this regulatory characteristic.

The importance of ADP-glucose pyrophosphorylase in the regulation of starch biosynthesis has been demonstrated by the expression of an unregulated bacterial ADP-glucose pyrophosphorylase in different plant tissues. The presence of this enzyme boosts the amount of starch by up to 60%, suggesting that in wild-type plants, the amount of this enzyme, or its regulation, limits starch formation. In tissues that already contained high starch, however, this increased flux of carbon into starch is matched by the induction of starch degradation enzymes, and starch levels do not increase. This reveals a remarkable sensitivity of the plant to its own metabolic status.

Other factors may also be important in controlling the rate of starch synthesis, particularly membrane transport steps. For example, transgenic potato (*Solanum tuberosum*) plants with an increased capacity for ATP transport across the plastid envelope accumulate more starch in their tubers. Likewise, in cereal endosperm, the activity of the amyloplast ADP-glucose transporter might limit starch production.

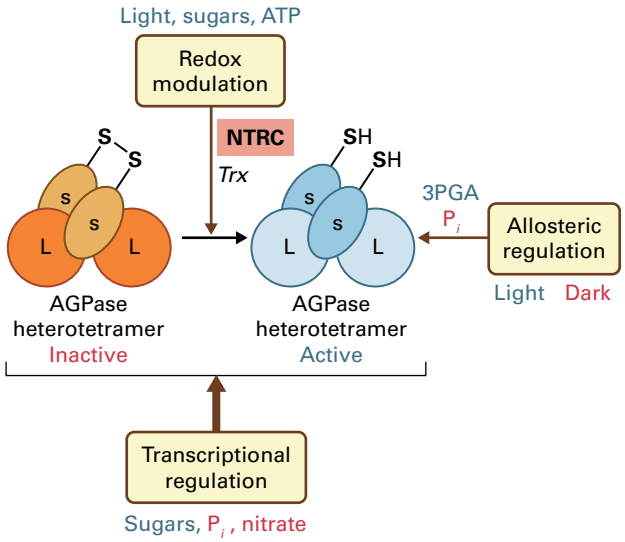


FIGURE 13.20 *Structure and regulation of plastid ADP-glucose pyrophosphorylase. Multiple mechanisms of regulation allow starch synthesis to respond to physiological and environmental stimuli. The enzyme is a heterotetramer of two large (L) and two small (S) subunits. Allosteric regulation by 3-phosphoglycerate (3-PGA) and inorganic phosphate (P_i) can rapidly adjust the rate of starch synthesis to the availability of substrates. Redox regulation via reversible disulphide bond formation between the small subunits occurs in response to light and sugar signals. Redox regulation involves thioredoxin (Trx) and a special type of NADP-dependent thioredoxin reductase (NTRC) and its associated thioredoxin found in plastids. The enzyme is more active in the reduced state (thiol groups) and less active in the oxidized state (black sulfur atoms). Transcriptional regulation in response to changes in carbon and nutrient supply allows more gradual changes in AGPase activity, which may require some days to develop. Red indicates inhibition, blue indicates activation.*

13.5.3 Starch granules contain two distinct glucose polymers, amylose and amylopectin

Starch consists of two molecules, **amylose** and **amylopectin** (see Fig. 13.18), both of which are homopolymers of α-1,4-linked glucose. Amylopectin molecules typically contain over 100,000 glucose residues and account for 70% or more of the starch. It is a branched molecule, with 4–5% of the linkages being α-1,6-bonds (branch points). The branching pattern of amylopectin is not random; the combination of branch frequency, branching pattern, and α-1,4-linked chain lengths underlie the semi-crystalline nature of starch (see Fig. 13.18). Extensive hydrogen bonding between the hydroxyl groups of the glucose residues in adjacent chains promotes the formation of double helices. These pack together into ordered crystalline layers that alternate with amorphous layers containing the branch points. Amylose is smaller than amylopectin. It typically contains around 1,000 glucose residues and accounts for 30% or less of the starch. In contrast to amylopectin, amylose has very few branch points. The proportions of amylose to amylopectin, together with the size and structure of starch granules, determine the properties of extracted starch that are

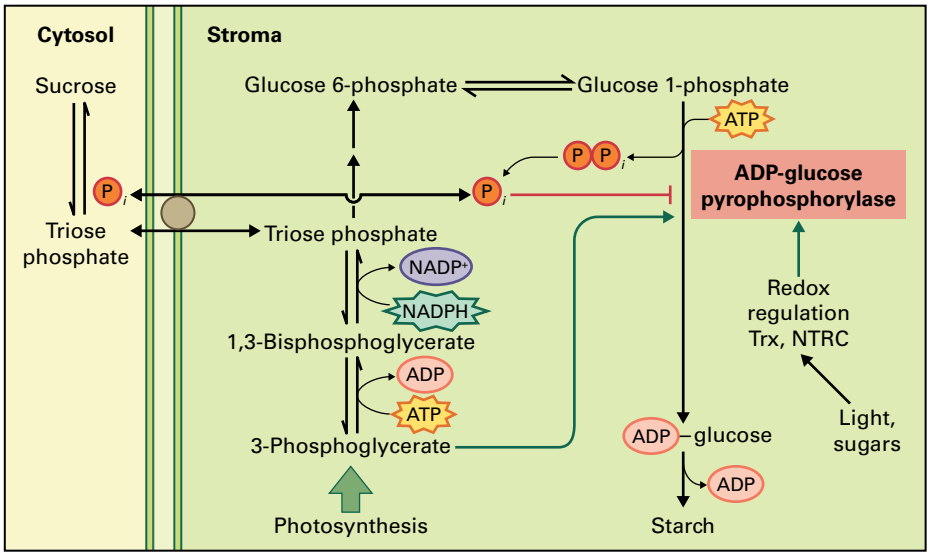


FIGURE 13.21 *Regulation of starch synthesis in chloroplasts. When 3-phosphoglycerate is abundant, signifying the availability of photoassimilates, ADP-glucose pyrophosphorylase is activated. Inorganic phosphate, which generally changes in a reciprocal manner to phosphorylated intermediates, inhibits the enzyme. Redox regulation in response to light or sugar signals increases the enzyme's sensitivity to 3-phosphoglycerate and decreases its sensitivity to phosphate.*

BOX 13.4 Starch has properties that make it useful both in cooking and in industry

Starch is the major nutritive component of our staple crops (e.g., cereals, tubers, roots, seeds). Its unique properties affect the texture of the food we eat and make it useful for other, nonfood applications.

When heated in water (e.g., during cooking), starch suspensions thicken. The granules absorb water and swell, disrupting the semi-crystalline structure and separating amylose from amylopectin. On cooling, a gel is produced as hydrogen bonds reform between amylose and amylopectin molecules, trapping water in the network. These thickened suspensions and coagulated starch gels form the basis of many a fine recipe (sauces, puddings).

When such starchy foods are frozen or cooled for long periods, however, the amylose molecules associate more closely, forming dense crystals, a process called **retrogradation**. The resulting watery, unappetizing mess can be rescued to some extent by re-heating. Similar changes occur in old bread, which loses its texture and becomes stale, not necessarily because it loses moisture, but because the amylose molecules, which disperse when the bread is baked, crystallize. Stale bread can be revived by dampening and heating to disperse the amylose (perhaps why some restaurants serve bread warm).

Food manufacturers use starches with different structures or composition. A commonly used starch comes from the waxy mutant of maize (see Chapter 7), which lacks granule-bound starch synthase and so produces only amylopectin. The kernels of this mutant have a waxy appearance, hence the name. With no amylose to crystallize out of the gel, foods produced from waxy starch can be frozen and thawed with minimal loss of texture. Mutations affecting granule-bound starch synthase and resulting in waxy-type starches are known for several crops. In the laboratory, transgenic approaches have been used to modulate multiple starch biosynthetic enzymes simultaneously, creating plants that synthesize starches with unique properties.

Many nonfood industries also use starch as a raw material. Starch finds its way into biodegradable plastics and packaging materials, into paints as a thickener, into building materials as an adhesive, into paper and textiles as a coating and sizing agent, and into pharmaceuticals and cosmetics as an inert carrying agent, to name but a few. In many cases, the native starches are chemically modified after extraction to optimize their properties for each application. Starch is also used extensively for the production of bioethanol, particularly in the United States, where over a third of the maize (*Zea mays*) crop is used for this.

important in both food and nonfood industries. These characteristics vary depending on the species and the organ used for starch storage, but can also be influenced using biotechnology by producing plants with altered amounts of the starch biosynthetic enzymes (see Box 13.4).

Starch granules range in size, from less than 1 μm in diameter to more than 100 μm and, in some cases, have distinctive morphologies. In fact, archaeologists have been able to determine the crops used by ancient civilizations through examination of the residual starch grains stuck to their cooking utensils. The transitory starch granules in leaves tend to be smaller than those in storage organs like tubers and seeds, reflecting the fact that they are synthesized over a much shorter time (a single day) and subsequently degraded at night.

13.5.4 Starch synthesis involves chain elongation, branching, and debranching reactions

Three enzymes are responsible for the synthesis of starch from ADP-glucose: **starch synthases** (Reaction 13.9), starch **branching enzymes** (Reaction 13.10) and, surprisingly, starch **debranching enzymes** (Reaction 13.11).

Reaction 13.9: Starch synthase

$$\text{ADP-glucose} + \alpha\text{-D-glucan}_{(n)} \rightarrow \alpha\text{-D-glucan}_{(n+1)} + \text{ADP}$$

Reaction 13.10: Starch branching enzyme

$$\text{Linear } \alpha\text{-1,4-D-glucan} \rightarrow \text{branched } \alpha\text{-1,6-}\alpha\text{-1,4-D-glucan}$$

Reaction 13.11: Starch debranching enzyme

$$\text{Branched } \alpha\text{-1,6-}\alpha\text{-1,4-D-glucan} + H_2O \rightarrow 2\times\text{Linear } \alpha\text{-1,4-D-glucans}$$

Starch synthase forms new α-1,4-bonds by adding individual glucose molecules from ADP-glucose to the nonreducing ends of an amylose or amylopectin chain (because the glucose residues are not symmetrical, the glucans in starch have both reducing and nonreducing ends; see Fig. 13.10). Five distinct isoforms of starch synthase are present in plants, each with a distinct biochemical function. The first to be characterized was **granule-bound starch synthase** (GBSS), which differs from the others as it is exclusively bound to starch and becomes buried within the granule as it grows. GBSS is responsible for amylose synthesis, and mutants lacking it produce amylose-free starch

(such as the waxy mutant of maize; Box 13.4). GBSS synthesizes long chains by acting in a processive way on the same substrate, using ADP-glucose that diffuses into the starch granule matrix. The embedding of GBSS may be a prerequisite for amylose production, as its product is protected from the activity of branching enzymes present in the plastid stroma.

The remaining four starch synthase isoforms are soluble in plastid stroma and partially bound to the starch granule. They contribute to the formation of amylopectin, each preferentially elongating chains of different lengths. Single isoform mutants can still synthesize starch, but usually with an altered amylopectin structure (Fig. 13.22).

Starch branching enzyme produces the α-1,6 branches in starch (see Fig. 13.18). This **glucanotransferase** cleaves an α-1,4 linkage, then joins the reducing end of the severed fragment to the side of the same or an adjacent chain, thereby forming an α-1,6 linkage. Most plants contain two isoforms of branching enzyme (class I and II), which differ in specificity. The two forms have different substrate preferences, and class I enzymes transfer longer **glucan chains** than class II enzymes. Partial loss of branching enzyme can lead to an inhibition of starch synthesis and an increase in the proportion of amylose in starch, such as in the *rugosus* mutant of pea (*Pisum sativum*; see Box 13.3). A total loss of branching enzyme (achieved using reverse-genetic methods in *Arabidopsis*) abolishes leaf starch synthesis altogether; the plant can only synthesize linear glucan chains that are rapidly degraded into fragments, such as the disaccharide **maltose**.

Although starch synthases and branching enzymes are probably sufficient for amylopectin biosynthesis, the process normally involves a degree of debranching as well. Mutants in several species that are deficient in a specific class of debranching enzyme (isoamylase 1) accumulate a highly branched soluble polymer more akin to glycogen than amylopectin (thus called phytoglycogen; Fig. 13.23). Debranching may promote crystallization by removing misplaced branches that interfere with the formation of higher-order structures within amylopectin molecules. This represents an interesting evolutionary innovation, where an enzyme associated with degradation has, through gene duplication and functional specialization, been recruited to a biosynthetic role. Other classes of debranching enzymes in plants mediate branch point hydrolysis during starch breakdown (see Section 13.7.2).

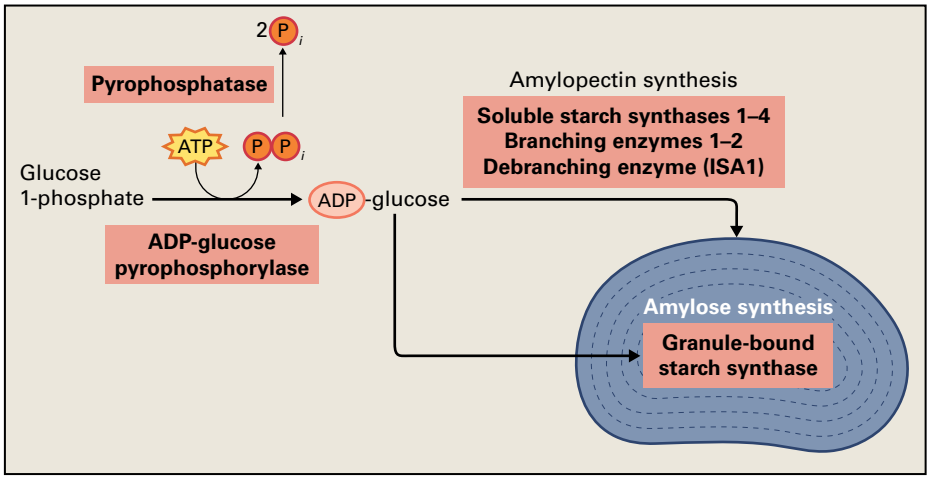


FIGURE 13.22 *Starch synthesis in the plastid stroma involves the production of branched amylopectin through the concerted actions of four isoenzymes of soluble starch synthases, two of branching enzymes, and a specialized debranching enzyme, all acting at the granule surface. The resulting amylopectin forms a semi-crystalline matrix, entrapping granule bound starch synthase, which synthesizes amylose using ADP-glucose, which diffuses into the amylopectin matrix.*

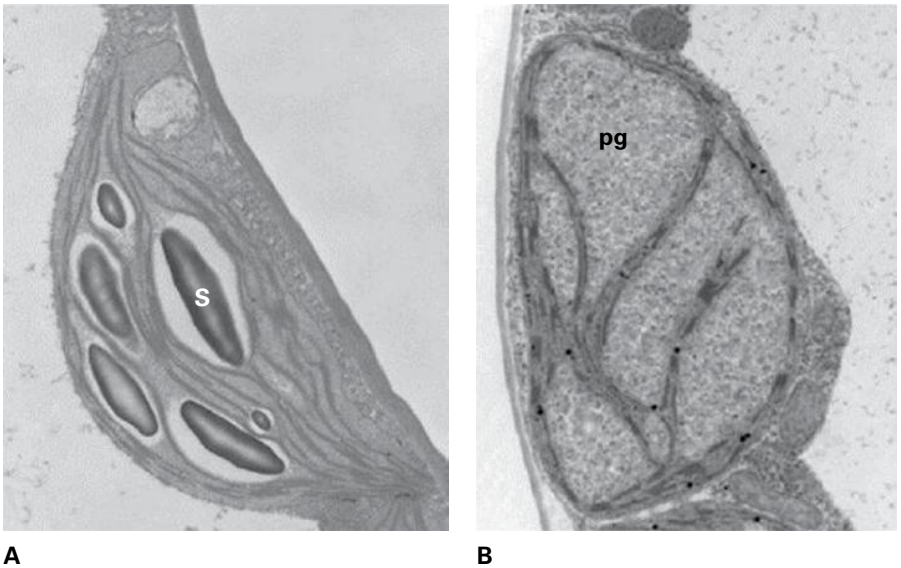


FIGURE 13.23 *Evidence that debranching enzymes participate in starch biosynthesis. Mutants of* Arabidopsis *lacking a specific class of debranching enzyme (B) synthesize less insoluble starch (S) than wild-type plants (A) and instead produce a soluble branched glucan called phytoglycogen (pg) in their chloroplasts. Each panel shows a single chloroplast approximately 5 μm in length.*

13.6 Partitioning of photoassimilates between sucrose and starch

In the leaves of most plants, sucrose and starch represent the major products of photosynthesis, and the **partitioning** between these two products depends on the species and environmental conditions. There is increasing evidence that these biosynthetic pathways are influenced by several cellular signaling processes, including light perception, the circadian clock, and metabolic signals. These inputs are integrated to optimize the allocation of assimilates into growth or storage. Not all of these regulatory mechanisms are understood, but some enzymes in the biosynthetic pathways have been identified as important control points.

13.6.1 The interconversion of fructose 6-phosphate and fructose 1,6-bisphosphate in the cytosol involves three enzymes

A critical step in central metabolism is the interconversion of fructose 6-phosphate and fructose 1,6-bisphosphate in the cytosol. This step has been studied for many years, yet numerous questions remain. This is partly because three enzymes are involved (PFK, PFP, and fructose-1,6-bisphosphatase; Fig. 13.24), each with a different mechanism of regulation. Furthermore, isoforms of PFK and fructose-1,6-bisphosphatase also occur in the plastid, which has complicated experiments designed to investigate the cytosolic step. Nevertheless, during photosynthesis, control at this point operates in conjunction with that applied to other steps discussed above (namely sucrose phosphate synthase in the cytosol and ADP-glucose pyrophosphorylase in the chloroplast). Together, these control mechanisms help to determine the distribution of photosynthate into the different biosynthetic pathways. Metabolites play an important part in this regulation by acting as allosteric effectors, while the **triose phosphate translocator** communicates changes in metabolite levels between the cytosol and the chloroplast stroma.

Reaction 13.12: ATP-dependent phosphofructokinase (PFK)

$$\text{Fructose 6-phosphate} + \text{ATP} \rightarrow \text{Fructose 1,6-bisphosphate} + \text{ADP}$$

Reaction 13.13: Fructose-1,6-bisphosphatase (FBPase)

$$\text{Fructose 1,6-bisphosphate} + \text{H}_2\text{O} \rightarrow \text{Fructose 6-phosphate} + \text{P}_i$$

Reaction 13.14: Pyrophosphate-dependent phosphofructokinase (PFP)

$$\text{Fructose 6-phosphate} + \text{PP}_i \leftrightarrow \text{Fructose 1,6-bisphosphate} + \text{P}_i$$

PFK catalyzes the C-1 phosphorylation of fructose 6-phosphate, an essentially irreversible reaction under cellular conditions. It is a glycolytic enzyme, working in the opposite direction to the flux during sucrose synthesis. The enzyme

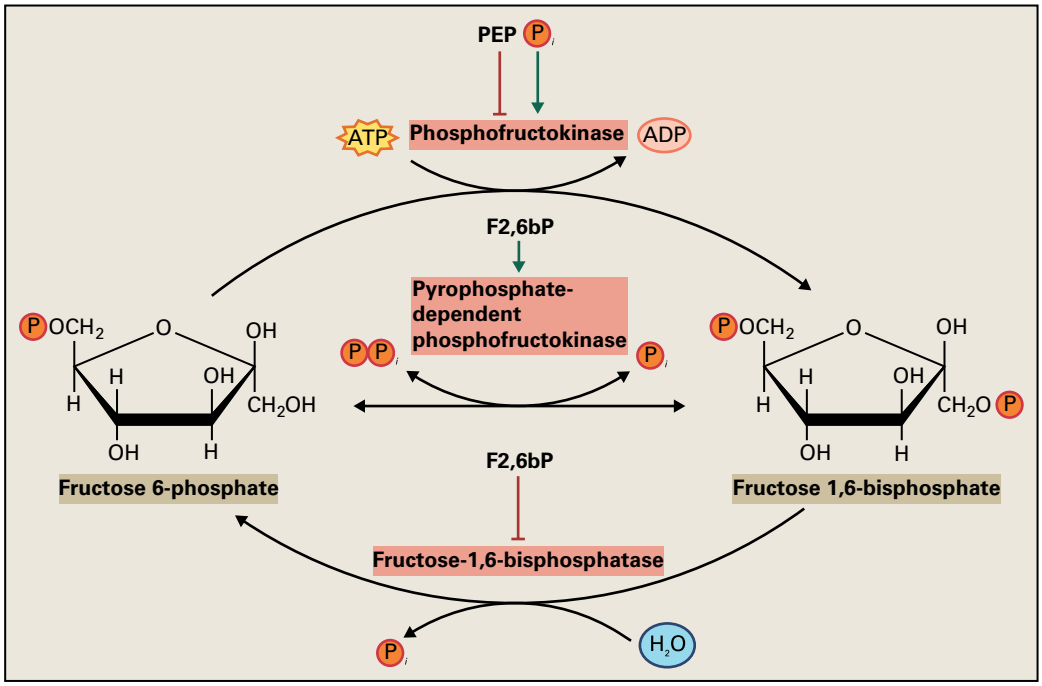


FIGURE 13.24 *Interconversion of fructose 6-phosphate and fructose 1,6-bisphosphate by ATP-dependent phosphofructokinase (PFK), PP_i-dependent phosphofructokinase (PFP), and fructose-1,6-bisphosphatase. PEP, phosphoenolpyruvate; F2,6bP, fructose 2,6-bisphosphate.*

has been studied in detail in systems other than plants, and it is viewed as a principal regulated step controlling the glycolytic flux.

In plants, both plastid and cytosolic PFK isoenzymes are strongly activated by P_i and inhibited by phospho*enol*pyruvate and other 3-carbon metabolites of the glycolytic pathway. Consequently, this early step in glycolysis is sensitive to energy demand (indicated by P_i levels) and to negative feedback from downstream intermediates in the pathway (Fig. 13.24). During photosynthesis, free phosphate levels are low due to photophosphorylation and metabolite buildup in the chloroplast, while carbon export from the chloroplast as triose phosphate is high. Thus, the cytosol is supplied with ample substrates for the reactions of glycolysis, resulting in PFK inhibition. In contrast, at night and in nonphotosynthetic tissues, P_i levels are higher and carbon supply is primarily in the form of hexose phosphates derived from starch or sucrose metabolism; thus, PFK is activated to meet respiratory and biosynthetic demands.

FBPase catalyzes the hydrolytic cleavage of phosphate from the C-1 position of fructose 1,6-bisphosphate to form fructose 6-phosphate and P_i. This gluconeogenic enzyme supports the flux of carbohydrate from the triose phosphate pool to the hexose phosphate pool in the cytosol. An isoenzyme is also present in chloroplasts, where it is part of the Calvin–Benson cycle, but it is typically absent in nonphotosynthetic plastids. FBPase is also included as a reaction of the oxidative pentose phosphate cycle (see Section 13.9).

Cytosolic FBPase is strongly inhibited by **fructose 2,6-bisphosphate**, as is the enzyme from animals. In plants, the concentration of cystosolic fructose 2,6-bisphosphate is controlled in part by the status of the triose phosphate pool, and in part by the status of the hexose phosphate pool. Consequently, the level of this inhibitor, and hence cytosolic FBPase activity, is sensitive to carbon supply from the chloroplast and the utilization of hexose phosphates for biosynthesis (see Section 13.6.2). In contrast, the plastid FBPase is regulated differently, via a redox mechanism linking its activity to the light reactions of photosynthesis (see Chapter 12).

The third enzyme, PFP, is something of an enigma. Animals and most other eukaryotes do not have it and, in contrast to PFK and FBPase, PFP catalyzes a readily reversible reaction. In many tissues, PFP is present at higher activities than PFK.

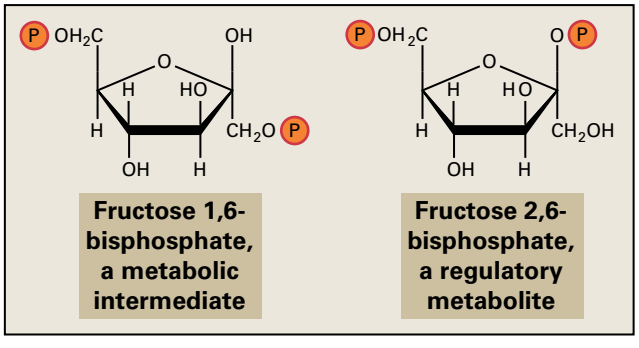


FIGURE 13.25 *Structures of fructose 1,6-bisphosphate and fructose 2,6-bisphosphate. The regulatory metabolite and the metabolic intermediate differ in the position of one phosphate group.*

Although many roles have been postulated for PFP, none has been conclusively verified (see Box 13.1). PFP is powerfully activated in the direction of fructose 1,6-bisphosphate formation by fructose 2,6-bisphosphate, the same **signal metabolite** that inhibits cytosolic FBPase (Fig. 13.25).

13.6.2 Fructose-2,6-bisphosphate is a signal metabolite that regulates the partitioning between sucrose and starch synthesis

Knowledge of the kinetics and regulation of the enzymes described in the preceding sections has allowed the development of a model explaining how starch synthesis might serve as an overflow mechanism that allows storage of any excess carbohydrate produced during photosynthesis. This is needed when sucrose synthesis starts to exceed the capacity of the leaf to export or store it. Carbon stored as starch can then be utilized to support respiration and continued sucrose biosynthesis during darkness, when photosynthesis cannot occur. Some plants, such as tobacco (*Nicotiana tabacum*), store a large fraction of photoassimilate as starch. Almost half of the total sucrose export from the leaf occurs during the night and is derived from starch synthesized during the preceding day. Other species, such as pea (*Pisum sativum*), synthesize less starch and store more sucrose in the vacuole.

Partitioning between sucrose and starch is not a binary on/off mechanism; rather, it represents continuous monitoring of the status of the various pools of metabolites in the cytosol and chloroplast. Central to this model is fructose-2,6-bisphosphate, which is found only in the cytosol and inhibits the activity of cytosolic FBPase (see Section 13.6.1). Fructose-2,6-bisphosphate is a signal metabolite. It is not part of a part biochemical pathway or cycle, but is synthesized from fructose 6-phosphate by **fructose-6-phosphate 2-kinase** and converted back to fructose 6-phosphate by **fructose-2,6-bisphosphatase** (Fig. 13.26). The inhibitory effect on cytosolic FBPase means that changes in the concentration of fructose 2,6-bisphosphate have a powerful effect on the flow of carbon from triose phosphates into the hexose phosphate pool. Thus, to understand partitioning between sucrose and starch, it is essential to understand the factors that control fructose-2,6-bisphosphate levels (Fig. 13.27).

Fructose-6-phosphate 2-kinase is activated by P_i and strongly inhibited by triose phosphates; in contrast, fructose-2,6-bisphosphatase is inhibited by P_i. Hence, the concentration of fructose-2,6-bisphosphate is in part controlled by the increase in the triose phosphate to P_i ratio occurring during photosynthesis. The levels of these regulators are communicated between the stroma and cytosol via the strict counter exchange mechanism of the TPT, linking the production of triose phosphates in the chloroplast and their consumption in the cytosol, with P_i release in the cytosol and reincorporation by photophosphorylation.

The concentration of fructose-2,6-bisphosphate is also affected by the hexose phosphate pool which, in mature leaves, primarily reflects the status of sugar export form

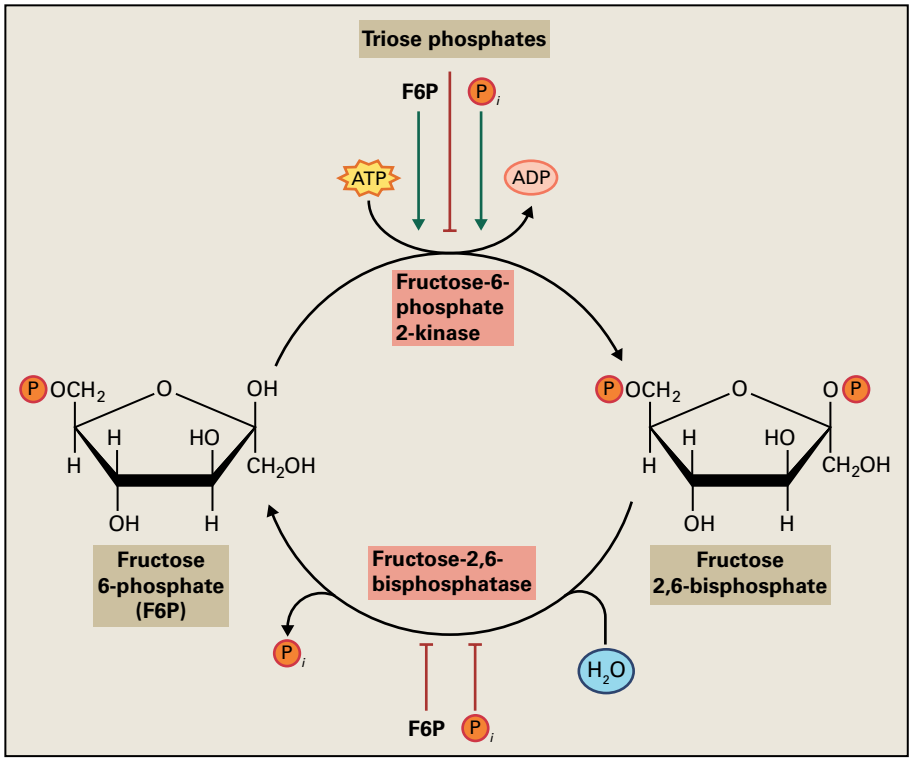


FIGURE 13.26 *Formation and degradation of fructose 2,6-bisphosphate by fructose-6-phosphate 2-kinase and fructose-2,6-bisphosphatase. Regulation by inorganic phosphate (P_i), triose phosphates, and fructose 6-phosphate is indicated.*

the leaf. When sucrose production exceeds export, sucrose accumulates and its synthesis is inhibited (possibly by inhibition of SPS, Fig.13.13), and the hexose phosphate concentration increases. One of the hexose phosphates, fructose 6-phosphate, is also a regulator of fructose-2,6-bisphosphate levels; it activates fructose-6-phosphate 2-kinase and inhibits fructose-2,6-bisphosphatase, thereby increasing the fructose 2,6-bisphosphate concentrations (see Fig. 13.26). Hence, the concentration of fructose 2,6-bisphosphate integrates both a feedforward signal (the supply of photosynthate from the chloroplast) and a feedback signal (demand for substrates for sucrose biosynthesis) to control the capacity for gluconeogenic flux.

Triose phosphate concentrations not only influence the formation of fructose 2,6-bisphosphate, but also determine the concentration of fructose 1,6-bisphosphate available as substrate for FBPase. Under standard conditions, at pH 7.0, the equilibrium position of the aldolase reaction favors the formation of fructose 1,6-bisphosphate. The equilibrium position is defined by Equation 13.1:

$$K_{eq} = \frac{[\text{glyceraldehyde 3-phosphate}][\text{dihydroxyacetone phosphate}]}{[\text{fructose 1,6-bisphosphate}]} \qquad \text{(Eq. 13.1)}$$

Because the two triose phosphates are rapidly interconverted by triose-phosphate isomerase, this equation shows that the concentration of fructose 1,6-bisphosphate is determined by the square of the triose phosphate concentration ([triose phosphate]^2), making the aldolase reaction very sensitive to the triose phosphate concentration. That is, the concentration of fructose 1,6-bisphosphate increases exponentially with a linear increase in triose phosphate concentrations. Thus, the equilibrium of the aldolase reaction and the regulation of the fructose 2,6-bisphosphate concentration by triose phosphates and P_i, are complementary mechanisms to relate the rate of sucrose synthesis to the amount of photosynthate exported from the chloroplast (Fig. 13.27).

13.6.3 Sucrose synthesis coordinates with photosynthate supply at the start of the day

At the start of the light period, photosynthesis begins and triose phosphates accumulate in the chloroplast. This causes the TPT to exchange triose phosphate for P_i. Triose phosphates accumulate in the cytosol, while P_i concentrations decline. Consequently, fructose-6-phosphate 2-kinase is rapidly inhibited, and fructose-2,6-bisphosphatase is activated. As a result, fructose 2,6-bisphosphate concentrations quickly decline, relieving the inhibition of fructose-1,6-bisphosphatase. This, combined with the impact of the equilibrium effect of the aldolase reaction, allows the carbon to flow into the cytosolic hexose phosphate pool, once the concentration of triose phosphate reaches a threshold value. In turn, the increased concentration of glucose 6-phosphate activates sucrose-phosphate synthase, allowing the synthesis of sucrose (see Fig. 13.13). Enhancing this effect will be the stabilization of sucrose-phosphate synthase in the active, nonphosphorylated state by the low concentration of phosphate and the high concentration of glucose 6-phosphate (Fig. 13.13). Hence, these two feed-forward mechanisms activate the flow of photosynthate

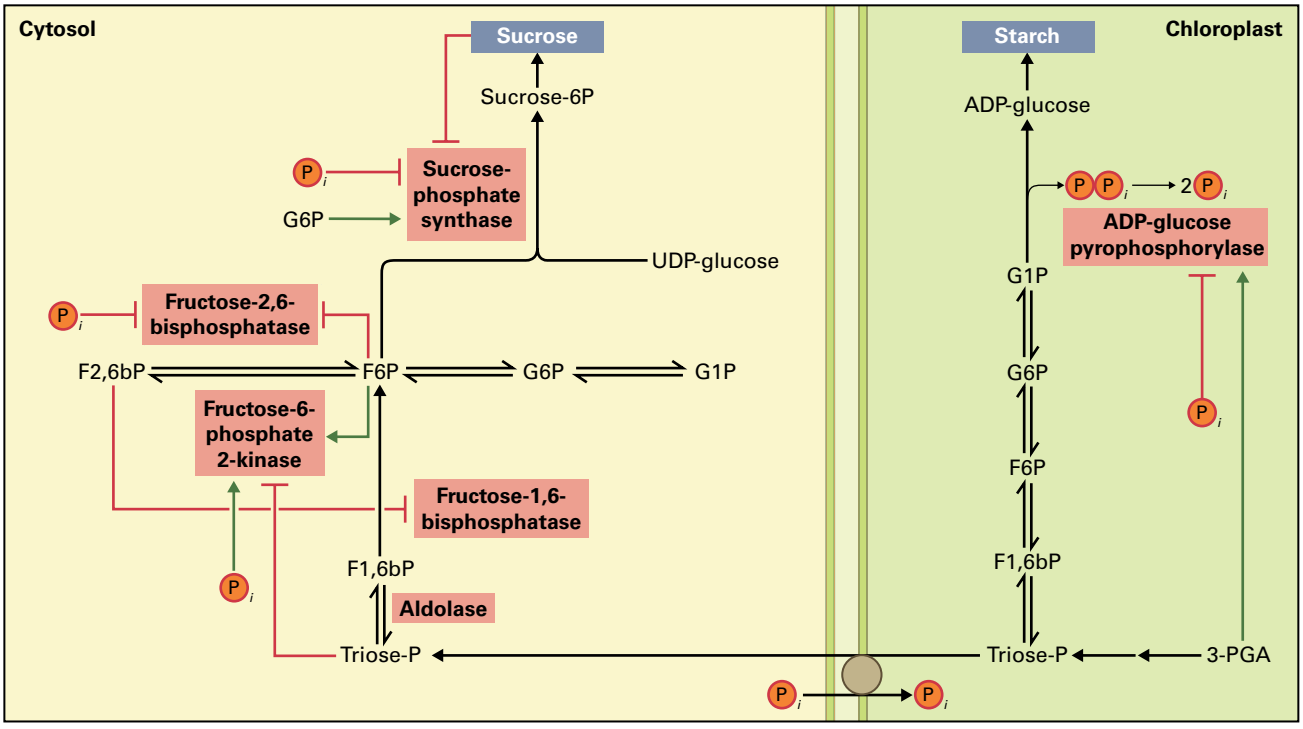


FIGURE 13.27 *Regulation of the interconversion of starch and sucrose. This interconversion provides an example of how metabolite levels are constantly monitored in the leaf cell, and how pathways are both activated and inhibited to keep them balanced.* Early daylight: *The onset of photosynthesis causes the accumulation of triose phosphates in the chloroplast. These triose phosphates are exported to the cytosol in exchange for inorganic phosphate (P_i). The triose phosphates inhibit fructose-6-phosphate 2-kinase, while the removal of cytosolic P_i weakens the activation of this enzyme and relieves inhibition of fructose-2,6-bisphosphatase and sucrose-phosphate synthase. As a result, fructose 2,6-bisphosphate (F26,bP) concentration drops, inhibition of cytosolic fructose-1,6-bisphosphatase is relieved, and carbon flows into the hexose phosphate pool. The increasing concentration of glucose 6-phosphate (G6P) activates sucrose-phosphate synthase, resulting in sucrose synthesis.* Midday: *the model postulates that sucrose-phosphate synthase is deactivated by negative feedback from sucrose accumulation, but this has not been confirmed. In any case, diminished sucrose-phosphate synthase activity results in accumulation of its substrate fructose 6-phosphate (F6P), which inhibits fructose-2,6-bisphosphatase and activates fructose-6-phosphate 2 kinase. The resulting increase in the concentration of F2,6bP leads to inhibition of fructose 1,6-bisphosphatase. Because the aldolase reaction is reversible, triose phosphates accumulate in the cytosol, preventing export of triose phosphates from the chloroplast. This results in accumulation of 3-phosphoglycerate (3-PGA), which activates ADP-glucose pyrophosphorylase and promotes starch synthesis.* Onset of darkness: *As the light intensity falls during the evening, photosynthesis progressively declines. The synthesis of 3-PGA stops, activation of ADP-glucose pyrophosphorylase is lost, and starch synthesis declines. P_i accumulates in the chloroplast, further inhibiting ADP-glucose pyrophosphorylase, which also becomes deactivated through oxidation. Although this presents the situation in the leaf as a series of distinct events, metabolite levels are constantly monitored to adjust the rates of starch and sucrose syntheses, which are kept in step with the rate of photosynthesis at all times.*

to sucrose once the threshold level of triose phosphate is reached (Fig. 13.27).

13.6.4 Partitioning shifts towards starch when sucrose synthesis exceeds sucrose export

At midday, under high light conditions, the rate at which chloroplasts supply **photosynthate** may exceed either the demand for sucrose in sink tissues or the ability of the leaf to export it. Under these conditions, starch is synthesized from the excess carbon.

When sucrose accumulates in the leaf cell, it reduces the rate of its synthesis, which increases the size of the hexose phosphate pool. The inhibition of sucrose synthesis is probably due to inhibition of sucrose-phosphate synthase, although the mechanism by which this happens is still unclear. The increase in fructose 6-phosphate both activates fructose-6-phosphate 2-kinase and inhibits fructose-2,6-bisphosphatase (see Fig. 13.26), and this dual action overrides the feedforward effect of triose phosphates. As the concentration of fructose 2,6-bisphosphate increases, it inhibits fructose-1,6-bisphosphatase and slows the flow of carbon into the hexose phosphate pool. As cytosolic triose phosphate levels increase, their export from the chloroplast is inhibited. The increase of triose phosphate in the chloroplast, in turn, causes an increase in the plastid concentrations of 3-phosphoglycerate, which activates ADP-glucose pyrophosphorylase (see Fig. 13.21). Hence, carbon flow is diverted from sucrose to starch (Fig. 13.27).

This mechanism for controlling the flow of carbon into sucrose reflects both the supply of and demand for photosynthate. Central to this mechanism are the TPT and P_i. The TPT controls carbon flow between the chloroplast and the cytosol, communicating the changes in one compartment to the other. P_i plays a major role in the fine regulation of this overflow mechanism by affecting a number of the key regulated enzymes, usually in an antagonistic way to one of the phosphorylated metabolic intermediates (i.e., components of the hexose phosphate and triose phosphate pools). As P_i levels generally change in a reciprocal manner to these intermediates, small changes in absolute amounts represent a larger change in the ratio of the effectors, with a more pronounced regulatory impact on enzyme activity. This mechanism monitors constantly the status of the various metabolic pools so that the partitioning between sucrose and starch is optimized for the particular environmental conditions of the plant.

13.6.5 The overflow model for leaf starch synthesis cannot fully explain assimilate partitioning

Plants have a way of making even the most elegant model seem inadequate. For example, the overflow model described above suggests that, on a cloudy day when the light intensity is low, the rate of photosynthesis should never meet the demand for sucrose, so no starch should be made. In reality, however, some starch is made under these conditions, albeit in lower amounts. This suggests the presence of an underlying mechanism that ensures some carbon assimilated during the day is stored in preparation for the coming night. Furthermore, partitioning responds to the **photoperiod**, such that in short days a greater proportion of assimilated carbon is stored as starch. This change is controlled—either directly or indirectly—by the **circadian clock**, which allows the plant to predict that a long night accompanies a short day, hence the need for additional starch. The rate of starch degradation is also controlled at night such that the starch reserves are depleted gradually and last the entire night (Fig. 13.28).

Studies of mutant plants also revealed a surprisingly high degree of adaptability in the pathways of photosynthetic carbon metabolism. Some naturally occurring mutants of the Florida weed "Yellowtop" (*Flaveria linearis*) have no detectable cytosolic FBPase, although the chloroplast enzyme is present. Similar laboratory-generated *Arabidopsis* plants have also been produced that grow more or less normally and produce sucrose and starch in their leaves with near-normal efficiency. Furthermore, potato (*Solanum tuberosum*), tobacco (*Nicotiana tabacum*), and *Arabidopsis* plants lacking the TPT have also been generated, which also grow well in the laboratory.

How can plants survive without these proteins, which are supposedly central to photosynthetic carbon metabolism? The answer appears to be that these atypical plants first make starch in their chloroplasts, but break it down simultaneously during the day, generating free sugars maltose and glucose (wild-type plants only break down starch at night). Consequently, carbon is not exported from the chloroplasts of these mutants as triose phosphate. Separate transporter proteins exist for both glucose and maltose, which can be metabolized in the cytosol to form hexose phosphates (see Section 13.7.3). This alternative pathway circumvents the need for the TPT and the cytosolic FBPase steps. Plants of this type demonstrate the remarkable flexibility of plant metabolism (Box 13.5).

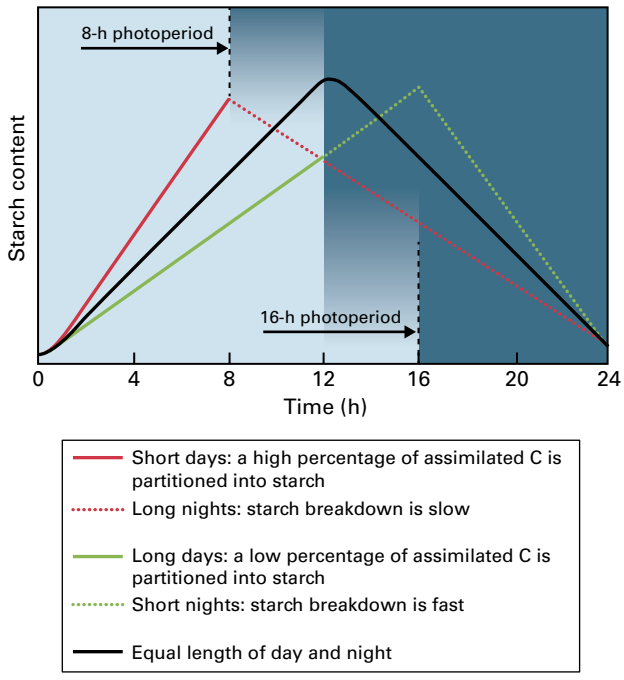


FIGURE 13.28 *Pattern of starch accumulation and utilization in* Arabidopsis *leaves during different diurnal regimes. The black line represents the near-symmetrical pattern observed under 12 h light/12 h dark conditions. The rates of starch synthesis and starch degradation respond in complementary ways to short day (red) or long day (green) conditions.*

13.6.6 At night, leaf starch reserves are broken down to support respiration and metabolism

At dusk, light intensity declines, and the supply of photosynthate decreases and eventually ceases. Many processes in plant metabolism continue, however, fueled by the remobilization of stored reserves, such as starch; energy and reducing power are provided by the respiratory pathways (**glycolysis**, the **citric acid cycle**, and the **oxidative pentose phosphate pathway**).

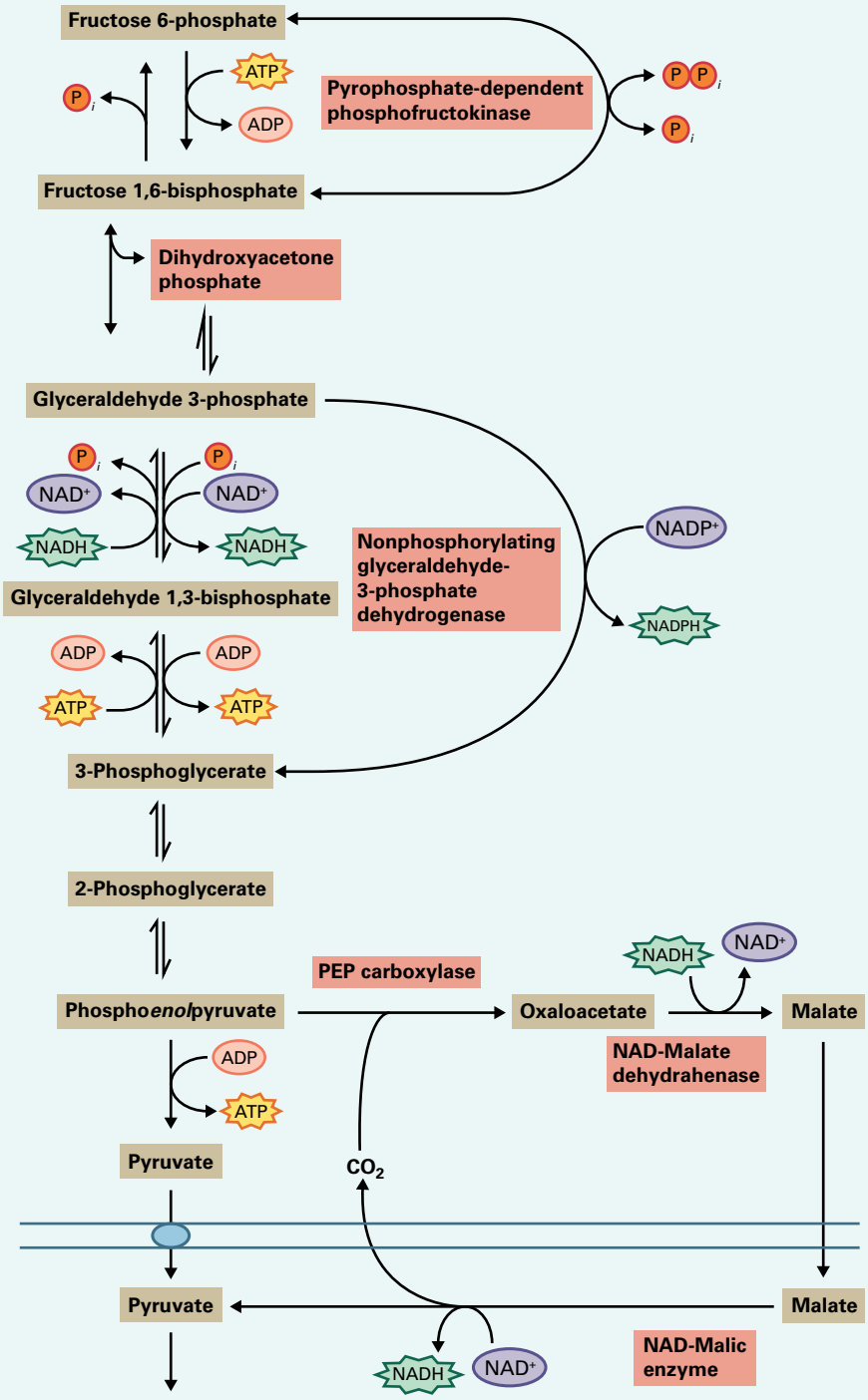
Under artificial, laboratory growth conditions, abruptly turning off the lights can cause a rapid drop in leaf sucrose levels; sucrose synthesis stops, while its export and metabolism continue. Then, after a short delay, starch degradation

BOX 13.5

Bypass reactions give plants metabolic flexibility

Because they are sessile, plants are subjected to whatever the environment has to offer. To survive, they have developed a flexible metabolism that helps them accommodate to environmental changes (for example, plants often have more than one enzyme capable of catalyzing a specific reaction).

Some enzymes of plant carbohydrate metabolism are not found in animals or in most other eukaryotic organisms. Examples include PFP, which bypasses the reaction catalyzed by fructose-1,6-bisphosphatase, and the nonphosphorylating glyceraldehyde-3-phosphate dehydrogenase that produces only NADPH and 3-phosphoglycerate. The function of these bypasses is not fully understood. They may provide the plant with an ability to withstand phosphate starvation, a common condition. Indeed, in some plants, PFP activity increases when plants are starved of phosphate. Under these conditions, concentrations of adenylate nucleotides (ATP and ADP) are reduced, and reactions requiring them may be inhibited. PFP uses pyrophosphate, an alternative energy source, thereby conserving ATP. The nonphosphorylating glyceraldehyde-3-phosphate



dehydrogenase also bypasses reactions that require ADP as a substrate, thereby allowing carbon to pass through glycolysis without the need for ATP synthesis.

Such flexibility in plant metabolism is frequently illustrated when genetic engineering is used to knock out supposedly critical enzyme activities. For example, transgenic tobacco (*Nicotiana tabacum*) plants lacking cytosolic pyruvate kinase in their leaves appear nearly normal, whereas in other organisms, the lack of this enzyme retards growth. However, it appears that reactions bypassing pyruvate kinase (e.g., a combination of phospho*enol*pyruvate carboxylase, malate dehydrogenase (see Chapter 14), and malic enzyme) can convert sufficient phospho*enol*pyruvate to pyruvate to maintain growth. A second example is plants lacking the TPT, which is required for the export of triose phosphates produced during photosynthesis; these plants reroute metabolism, synthesizing and degrading starch simultaneously to generate glucose and maltose that can be exported to the cytosol via distinct transporters. Plants lacking pyruvate kinase or the TPT, while growing relatively well in the laboratory, would almost certainly be at a disadvantage compared to their wild-type counterparts in their native habitats. The loss of some of their metabolic flexibility would take its toll. The continued study of performance of such plants may help scientists understand why plant metabolism is configured as it is.

begins and sucrose levels rise again. Under natural conditions (which can be simulated in the laboratory using a sinusoidal light regime), the changes in light intensity are more gradual, and plant metabolism can adapt.

As light intensity and photosynthesis decline, the rates of sucrose and starch synthesis also decline, and as a result, sucrose export exceeds the rate of sucrose synthesis. The associated decrease in the concentrations of hexose phosphates results in a decreased concentration of fructose 2,6-bisphosphate, relieving fructose-1,6-bisphosphatase inhibition. This, then, allows free flow from triose phosphate to the hexose phosphate pool in the cytosol. Triose phosphate is exported from the chloroplast in exchange for P_i, so the activation of ADP-glucose pyrophosphorylase by 3-phosphoglycerate is lost, while P_i inhibits it. Thus, as photosynthesis slows, partitioning is shifted away from starch in favor of sucrose synthesis. Gradually, however, the carbon assimilation rate drops below the rate necessary to support sucrose biosynthesis, and eventually it stops altogether. During this time, starch degradation is triggered, allowing sucrose synthesis to continue into the night. Much progress has been made in the last decade in understanding the pathway of starch degradation in leaves, although the trigger to initiate it and the way the rate is controlled are still not fully understood.

13.7 Starch degradation

Starch is the most widespread storage carbohydrate in plants, and it accumulates in many different tissues and organs, including the chloroplasts of leaf cells. However, it is more typically associated with plant storage organs, such as seeds, roots, and tubers, which represent staple crops. Much knowledge about **starch degradation** has been derived from biochemical analyses done on germinating cereal grain, such as barley (*Hordeum vulgare*) and wheat (*Triticum aestivum*), and this thirst for knowledge was driven by the importance of starch breakdown in the production of malt and flour for industry. It led to the discovery of hydrolytic enzymes known as amylases, several different types of which are now known.

The remobilization of starch from the endosperm of cereal grain is, however, an unusual example of starch breakdown in plants (see Box 13.6). In developing cereal grain, starch is made in the amyloplasts of the endosperm cells, which die upon seed maturation. This leaves a large starch-rich matrix surrounded by a specialized outer layer of living endosperm cells, the aleurone layer. After germination, degradative enzymes are secreted from the aleurone layer and the embryo, and starch degradation occurs extracellularly within the endosperm. This pathway differs in several important ways with the process that occurs inside chloroplasts.

13.7.1 Glucan phosphorylation modifies the starch granule surface

The semi-crystalline lamellar structure of the starch granule, which results from the packing of the double helices of adjacent amylopectin chains (see Fig. 13.18), represents a difficult structure for the enzymes of starch degradation to attack. The first step in starch degradation inside chloroplasts is the phosphorylation of a small proportion of the glucosyl residues of amylopectin by two enzymes: **glucan, water dikinase** (GWD) and **phosphoglucan, water dikinase** (PWD). GWD binds to the surface of the starch granule and introduces phosphate groups at the C-6 position of glucosyl residues (Reaction 13.15). PWD then binds to the prephosphorylated starch and introduces phosphate groups at the C-3 position of another glucosyl residue (Reaction 13.16).

Reaction 13.15: Glucan, water dikinase

$$1,4\text{-}\alpha\text{-P-glucan} + \text{ATP} \rightarrow 1,4\text{-}\alpha\text{-D-glucan 6-P} + P_i + \text{AMP}$$

BOX 13.6 Starch degradation in the endosperm a germinating cereal grain is an unusual example of starch breakdown in plants

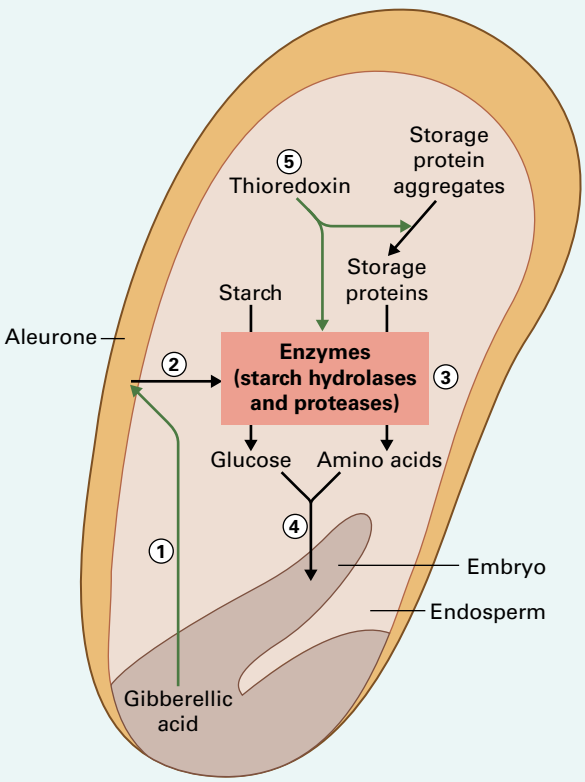
The starch-rich cereal grains represent a cornerstone of human nutrition. In addition, they have been used for thousands of years to brew beer, because fermentable sugars are generated in large amounts from the starch upon germination.

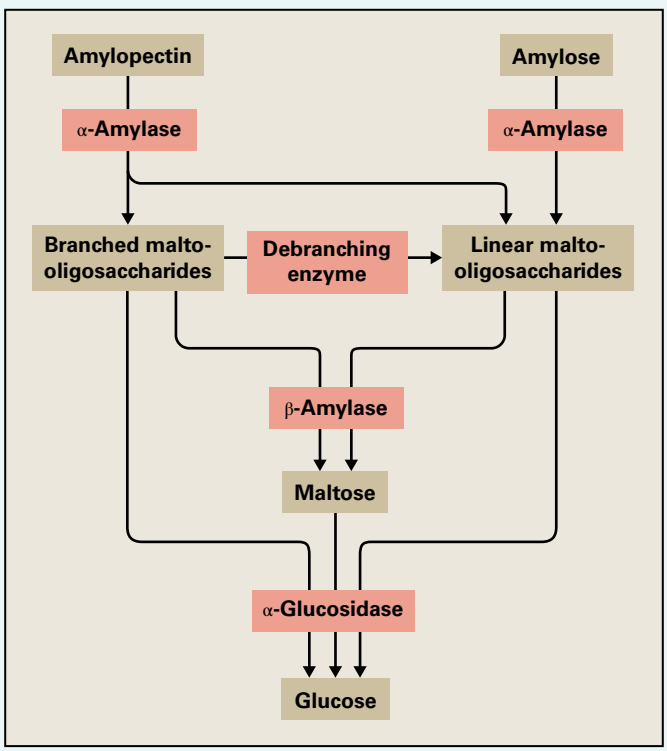
The embryo represents only a small fraction of the cereal grain volume; the rest is mostly occupied by the starch-rich endosperm. The starchy endosperm cells die upon seed maturation and desiccation, but the tissue retains the capacity for some metabolic processes, including a redox system that is important for germination.

During germination, the release of the hormone gibberellic acid from the embryo (1) triggers the secretion of enzymes from the living aleurone layer surrounding the starchy endosperm (2) and from the scutellum (the specialized cotyledon of the embryo). Three types of starch-degrading enzymes are released: α-amylase, the debranching enzyme limit dextrinase, and α-glucosidase (also called maltase). Proteases for degrading storage proteins are also secreted. In addition, secreted proteases activate a preformed β-amylase stored within the endosperm through limited proteolysis of its carboxyl terminus. Together, these enzymes hydrolyze the starch to glucose and the proteins to free amino acids (3), all of which are taken up by the embryo (4) to support seedling establishment and growth.

There is no evidence that the enzymes involved in chloroplast starch degradation, such as glucan water dikinase and phosphoglucan phosphatases, are involved in the breakdown of endosperm starch. Rather, α-amylase is thought to initiate granule degradation, acting at specific sites (pores in the starch granule surface) and leading to a characteristic 'pitting' of the granule. The combination of limit dextrinase and β-amylase can degrade the branched and linear oligosaccharides released by α-amylase to maltose and maltotriose, both of which can be hydrolyzed to the constituent glucose monomers by α-glucosidase. The glucose liberated by starch breakdown in the endosperm can be taken up by the scutellum, phosphorylated by hexokinase and converted to sucrose for transport within the germinated seedling.

The endosperm also contains an h-type thioredoxin (Trx h) (see Chapter 12), which is reduced by NADPH and NADP-thioredoxin reductase (see Chapter 14). In turn, Trx h reduces critical disulfide (S–S) groups of enzyme inhibitor proteins and storage proteins of the endosperm (5), facilitating the breakdown of starch and stored





protein to nourish the developing seedling. Following reduction to SH, the storage proteins become more soluble and susceptible to endogenous proteases, enhancing the formation of nitrogen-containing nutrients. Furthermore, the proteins with disulfide bonds that inhibit the enzymes degrading starch and storage protein are inactivated by reduction, allowing the degradative enzymes to become active and function during seedling establishment. Though not fully understood, Trx h also appears to serve as a means by which the embryo and aleurone sense the redox state of the endosperm during germination.

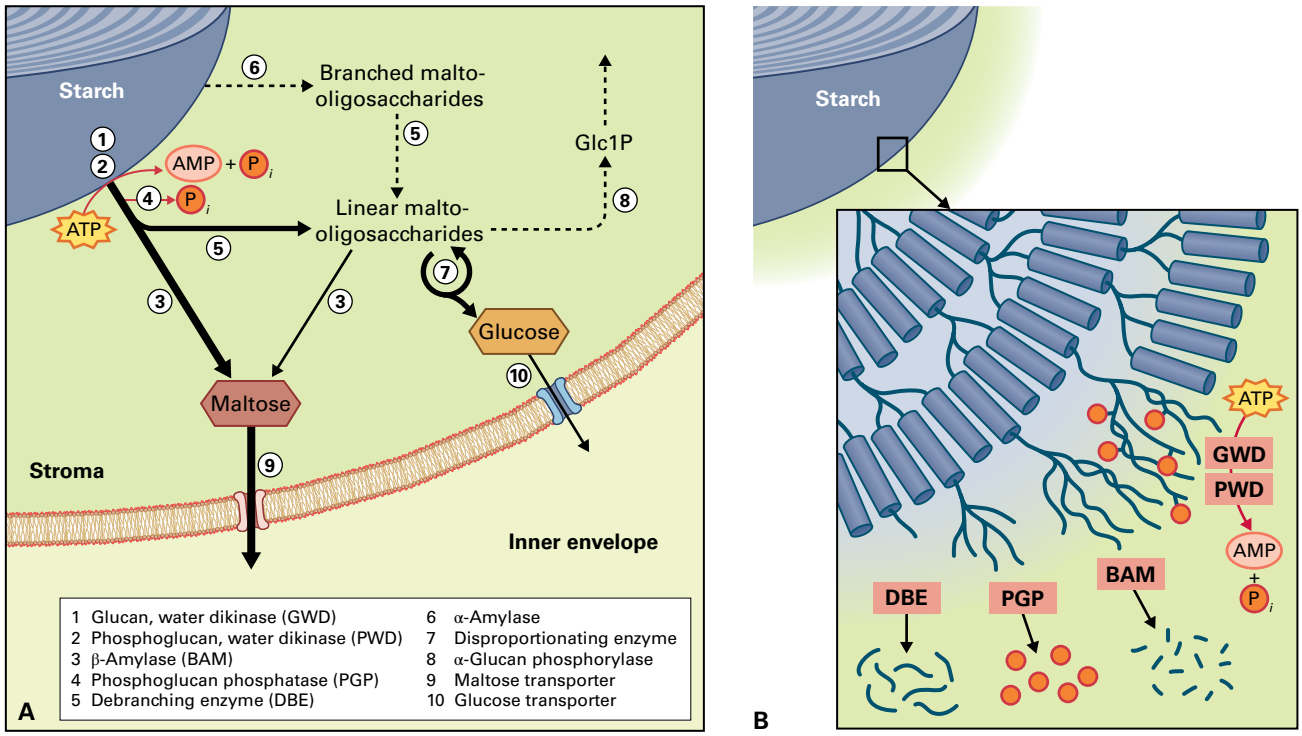


FIGURE 13.29 *Pathway of starch degradation in chloroplasts. Maltose and malto-oligosaccharides are released from the surface of the insoluble starch granule during degradation. Malto-oligosaccharides are metabolized in the stroma, and maltose and glucose are exported to the cytosol. Estimated fluxes are indicated by relative arrow size, with dashed arrows representing minor steps in* Arabidopsis. *Inset is a model depicting the role of phosphorylation by glucan, water dikinase (GWD) and phosphoglucan, water dikinase (PWD) in disrupting the packing of amylopectin double helices (gray boxes). This allows the release of maltose and malto-oligosaccharides (blue lines) by β-amylases (BAM) and debranching enzymes (DBE). Phosphate (red dots) is released concomitantly by phosphoglucan phosphatases (PGPs) to allow complete degradation.*

Reaction 13.16: Phosphoglucan, water dikinase

$$1,4\text{-}\alpha\text{-P-glucan} + \text{ATP} \rightarrow 1,4\text{-}\alpha\text{-D-glucan 3-P} + \text{P}_i + \text{AMP}$$

Phosphorylation alters the properties of the granule surface. The hydrophilic phosphate groups disrupt the packing of the double helices, perhaps even destabilizing the double helices themselves. This renders the exposed glucan chains more susceptible to the set of enzymes that can degrade the glucosidic bonds. The key role of glucan phosphorylation is illustrated by the phenotypes of GWD-deficient mutant or transgenic plants. The phosphate content of the starch is reduced and starch degradation is inhibited leading to the accumulation of high levels of leaf starch, a starch-excess (*sex*) phenotype.

13.7.2 Starch degradation yields maltose, glucose, and glucose 1-phosphate in chloroplasts

A number of enzymes participate in the subsequent degradation of starch, including β-**amylase**, debranching enzymes, **phosphoglucan phosphatases**, α-**amylase**, **disproportionating enzyme**, and starch phosphorylase. This results in a network of reactions rather than a linear pathway (Fig. 13.29). Some steps appear to be more impactful than others, as judged by the severity of the starch-excess phenotype resulting when the respective gene is mutated in *Arabidopsis*.

The linear chains of amylopectin and amylose are degraded primarily to maltose by β-amylase, which catalyzes a hydrolysis reaction that is irreversible under cellular conditions. β-Amylase gets its name from the fact that after hydrolysis, the hydroxyl group at the reducing end of the liberated maltose is in its β-anomeric form (Reaction 13.17). β-Amylase is an **exoamylase**, which acts processively from the nonreducing ends of the glucan chains until its progression is blocked by an α-1,6-branch point or a phosphate group. At branch points, β-amylase leaves short residual chains, two or three glucose residues in length. These are removed, again via an irreversible hydrolysis reaction, by one of two debranching enzymes (**isoamylase 3** or **limit dextrinase**; see Reaction 13.11). These enzymes are distinct from the **isoamylase 1-type debranching enzyme** that helps to achieve the correct structure of amylopectin (see Section 13.5.4). When β-amylase progression is blocked by a phosphate group, the phosphate is removed by one of two phosphoglucan phosphatases (Reaction 13.18). Thus, glucan phosphorylation and dephosphorylation proceed concurrently with glucan degradation.

Reaction 13.17: β-Amylase

$$1,4\text{-}\alpha\text{-D-glucan}_{(n)} + H_2O \rightarrow 1,4\text{-}\alpha\text{-D-glucan}_{(n-2)} + \text{maltose}$$

Reaction 13.18: Phosphoglucan phosphatase

$$1,4\text{-}\alpha\text{-D-glucan-P} + H_2O \rightarrow 1,4\text{-}\alpha\text{-D-glucan} + P_i$$

Chloroplasts also contain α-amylase, an **endoamylase** capable of hydrolyzing exposed internal α-1,4-glucosidic bonds (Reaction 13.19). α-Amylase can release a spectrum of linear and branched **malto-oligosaccharides** from the granule surface.

Reaction 13.19: α-Amylase

$$1,4\text{-}\alpha\text{-D-glucan}_{(n)} + H_2O \rightarrow 1,4\text{-}\alpha\text{-D-glucan}_{(x)} + \text{maltose}_{(y),(x+y=n)}$$

Thus, during starch degradation, the combined actions of α-amylase, β-amylase, and debranching enzymes can generate maltose and a mixture of short linear and branched malto-oligosaccharides in the chloroplast stroma (Fig. 13.29). Branched malto-oligosaccharides can be debranched in the stroma by debranching enzymes, and malto-oligosaccharides longer than three glucosyl residues (maltotriose) are further degraded by β-amylase. However, maltotriose is too short to be a substrate for β-amylase; it is metabolized by an α-1,4-glucanotransferase reaction catalyzed by disproportionating enzyme (D-enzyme, DPE1; Reaction 13.20). This versatile enzyme takes a part of a donor malto-oligosaccharide and transfers it to an acceptor molecule. For example, when acting on two maltotriose molecules, it transfers a maltosyl moiety from one to the other, generating glucose and maltopentaose (a chain of five glucose residues). The longer chains that it generates can again be attacked by β-amylase so, when working together, these two enzymes effectively form a cycle that converts maltotriose to maltose and glucose. Interestingly, DPE1 does not use or generate maltose, which means that any maltose generated is exported to the cytosol.

Reaction 13.20: α-1,4-Glucanotransferase (D-enzyme DPE1)

$$2\text{-Maltotriose} \rightarrow \text{Maltopentaose} + \text{glucose}$$

Maltose and, to a lesser extent, glucose are the major products of starch breakdown inside chloroplasts. This is supported by analyses of the sugars exported from isolated chloroplasts incubated in the dark, and by genetic evidence (i.e., considering the severity of the starch-excess phenotypes of mutants lacking the aforementioned enzymes). Both maltose and glucose can be exported to the cytosol via distinct transporters in the chloroplast inner envelope that facilitate their diffusion across the membrane. However, chloroplasts also possess **α-glucan phosphorylase** (also called **starch phosphorylase**), an enzyme that cleaves individual glucose residues from the nonreducing end of glucan chains by phosphorolysis, generating glucose 1-phosphate (Reaction 13.21).

Several enzymes functional in starch degradation in chloroplasts are activated by reduced Trx—namely, glucan-water dikinase, phosphoglucan phosphatase (SEX4), β-amylase1, and α–amylase3. The implication of these findings is not understood, since starch degradation takes place primarily at night, when chloroplast Trxs are mainly in an oxidized state (see Chapter 12). Moreover, Trx is considered to deactivate, rather than activate, enzymes of carbohydrate degradation. It is possible that, in this case, NTRC, which can be reduced at night by NADPH, is involved in the regulation of the enzymes (see Section 13.5.2).

Starch phosphorylase is homologous to glycogen phosphorylase, an important enzyme of glycogen degradation in animals. The animal enzyme is subject to complex allosteric and posttranslational regulation important in the control of glucose metabolism. By contrast, the precise role of phosphorylase in starch metabolism is unclear. The reaction it catalyzes is reversible and, given a glucan substrate, the net reaction direction depends on the respective concentrations of glucose 1-phosphate and P_i. Generally, estimates of these concentrations for the plastid stroma favor glucan degradation, particularly at night, when P_i levels rise and hexose phosphate levels decline. Unlike maltose and glucose released by hydrolysis, however, the glucose 1-phosphate liberated by starch phosphorylase probably serves to support plastid metabolism (i.e., the plastid oxidative pentose phosphate pathway and glycolysis). Alternative roles for starch phosphorylase have been proposed, such as the production of malto-oligosaccharides to prime starch synthesis, but conclusive genetic evidence is missing and further research is needed.

Reaction 13.21: α-Glucan phosphorylase

$$\alpha\text{-D-glucan}_{(n)} + P_i \leftrightarrow \alpha\text{-D-glucan}_{(n-1)} + \text{glucose 1-phosphate}$$

13.7.3 Maltose and glucose are metabolized in the cytosol to produce hexose phosphates

Maltose metabolism in the cytosol at night is only partially understood. A second **disproportionating enzyme** (DPE2; Reaction 13.22) catalyzes a glucosyl transferase reaction, releasing glucose and transferring the other glucosyl moiety to an acceptor molecule, the nature of which is poorly defined (Fig. 13.30). It is suspected to be a soluble heteroglycan, a polymer of relatively low abundance that contains mixed sugar residues, including arabinose, galactose, rhamnose, and glucose. The glucosyl residues transferred onto the heteroglycan by DPE2 can be removed again by a cytosolic isoform of α-glucan phosphorylase (see Reaction 13.21), which is encoded by a separate gene and has properties distinct from the plastid isoform.

Little is known about the structure, biosynthesis, and functional significance of this heteroglycan pool. It may represent a transient buffer that accommodates fluctuations in the rate of carbon supply from the chloroplast at night with its utilization in the cytosol. The combined actions of DPE2 and cytosolic α-glucan phosphorylase convert half the carbon in maltose to glucose 1-phosphate, which can equilibrate with other components of the hexose phosphate pool. The other half is released as free glucose which, together with that exported directly from the chloroplast, is phosphorylated via the action of the cytosolic hexokinase (Reaction 13.23).

Reaction 13.22: α-1,4-Glucosyltransferase (D-enzyme DPE2)

$$\text{Maltose} + \text{heteroglycan}_{(n)} \rightarrow \text{Glucose} + \text{heteroglycan}_{(n+1)}$$

Reaction 13.23: Hexokinase

$$\text{Hexose} + \text{ATP} \rightarrow \text{Hexose 6-phosphate} + \text{ADP}$$

There is also little understanding of how the enzymes in the pathway of starch degradation are regulated, despite good evidence that the overall rate of degradation is carefully controlled (e.g., it lasts the length of the night in different photoperiods; see Fig. 13.28). In plants that accumulate a lot of starch in their leaves, precise control of starch turnover is important. Premature depletion of starch reserves would result in starvation during the night, while incomplete utilization of starch would mean that assimilates that could have been exported for new root, shoot or seed production languishes unused in the chloroplast. The apparent importance of glucan phosphorylation and dephosphorylation in facilitating leaf starch degradation suggests that regulation might be applied to these enzymes, rather than the downstream hydrolytic enzymes.

Many other tissues in which starch is degraded have received far less attention than either leaves or the cereal endosperm. It is likely that in nonphotosynthetic tissues such as roots and tubers, where starch is degraded in amyloplasts, a pathway similar to that described for the chloroplast operates, although the relative importance of the different steps might not be the same as in *Arabidopsis* leaves. However, in other tissues, such as the cotyledon of pea (*Pisum sativum*), a terminal and senescing tissue, there are indications that amyloplast integrity is lost and starch degradation occurs in the cytosol or in the vacuole. It is also possible that under conditions such as carbon starvation, starch may be degraded together with other cellular components via autophagy. In such cases, one can only speculate as to the exact pathway and enzymes involved.

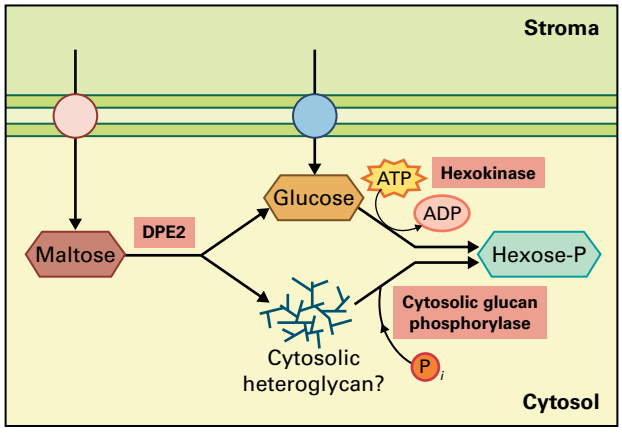


FIGURE 13.30 *Maltose and glucose metabolism in the cytosol. The disproportionating enzyme DPE2 transfers one glucosyl moiety from maltose to an acceptor molecule, probably a cytosolic heteroglycan, the exact nature of which is not known.*

13.8 The pentose phosphate/triose phosphate pool

Earlier in this chapter, triose phosphates were only considered as products of the Calvin-Benson cycle and intermediates in the synthesis of the major products of photosynthesis: sucrose in the cytosol and starch in the chloroplast stroma. However, triose phosphates are, in fact, part of a larger pool of interconvertible metabolites often referred to as the **triose phosphate/pentose phosphate pool**. This pool includes a diverse set of sugar intermediates: **ribulose 5-phosphate**, **ribose 5-phosphate**, xylulose 5-phosphate, **dihydroxyacetone phosphate**, **glyceraldehyde 3-phosphate**, **sedoheptulose 7-phosphate**, **erythrose 4-phosphate**, and **fructose 1,6-bisphosphate**. Fructose 6-phosphate, usually considered part of the hexose phosphate pool, is also linked to this pool, as it is a substrate for the enzymes **transaldolase** and **transketolase** (Fig. 13.31).

13.8.1 The pentose phosphate/triose phosphate pool integrates several key biosynthetic pathways

These sugar phosphates are components of metabolite pools that participate in several different pathways, and this emphasizes the fact that each pathway is actually a route within a

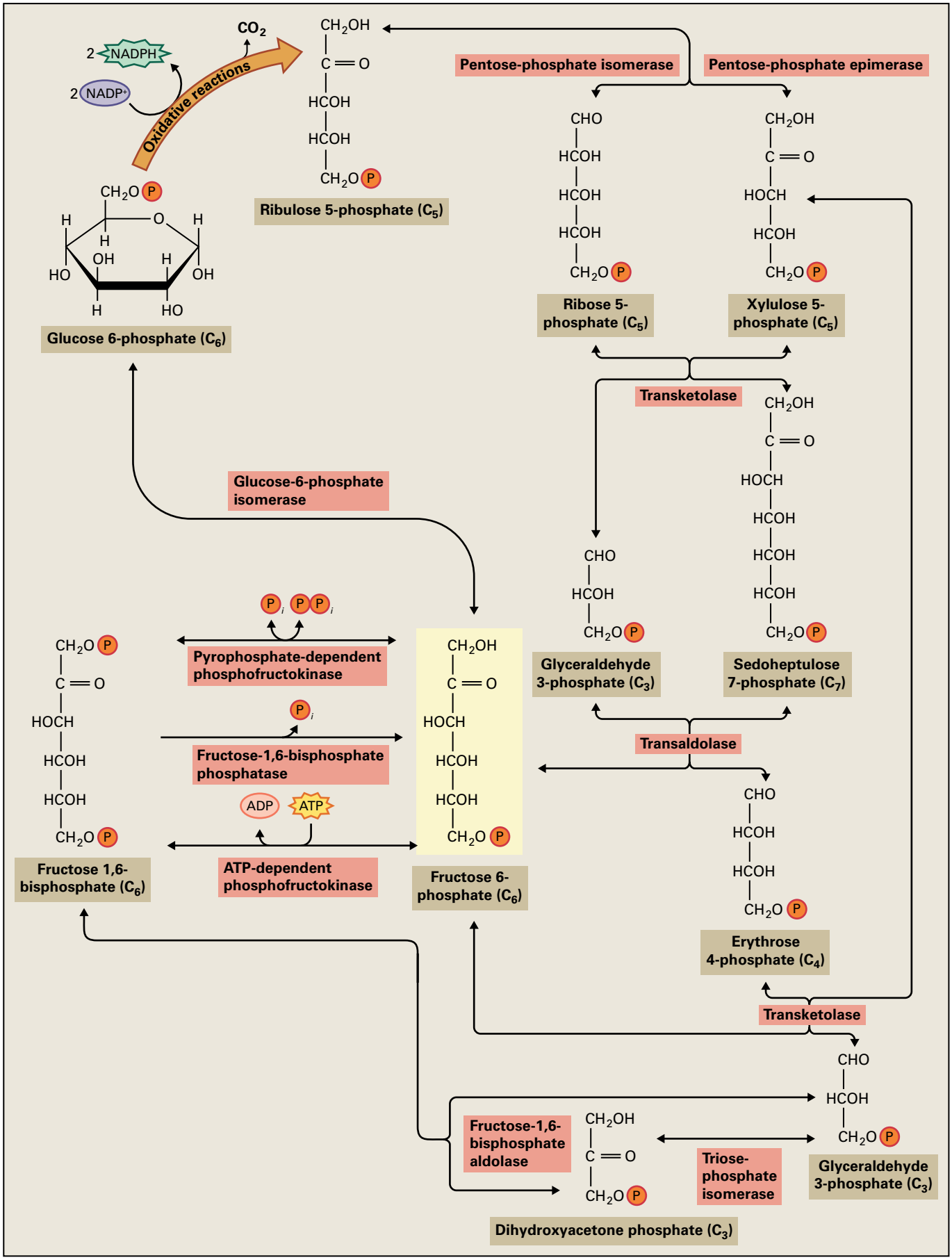


FIGURE 13.31 *The pentose phosphate pathway consists of irreversible oxidative reactions that generate NADPH and reversible reactions that equilibrate intermediates of the pentose phosphate/triose phosphate pool. In some tissues, the principal function of this pathway is to generate NADPH to be used in synthetic pathways such as fatty acid synthesis. In this case, the product of the NADPH-generating reactions, ribulose 5-phosphate, can be converted back to glucose 6-phosphate by a series of reversible reactions. In the majority of tissues, this pathway also provides carbon intermediates for several pathways (see Figure 13.32).*

much larger metabolic network. Glycolysis is usually depicted as a linear sequence of reactions that starts with hexose phosphate and ends with pyruvate (see Fig. 13.1), yielding a small net gain in ATP and NADH (most is supplied by the tricarboxylic acid cycle and electron transport in the mitochondrion). Similarly, the oxidative pentose phosphate pathway is depicted as a cyclic process in which glucose 6-phosphate is oxidized to ribulose 5-phosphate, with the concomitant formation of NADPH for use in biosynthesis, and the subsequent multistep regeneration of glucose 6-phosphate (see Section 13.9). In plant cells, however, these two pathways are actually linked by their shared intermediates, and both pathways operate interactively.

The various sugar phosphates of the glycolytic and pentose phosphate pathways occur both in plastids and in the cytosol, and there is communication between the pathways across the plastid envelope (see Fig. 13.4). Furthermore, plants use both pathways not only to produce energy-rich cofactors, but also to generate carbon skeletons required for biosynthetic reactions. In short, glycolysis, the pentose phosphate pathway, and various biosynthetic pathways are integrated by their relationship to the pentose phosphate/triose phosphate pool.

Thus, fluxes through the routes in metabolism differ considerably, depending on the prevailing conditions. For example, the direction of flux through the sugar phosphate pools in a leaf mesophyll cell differs when it is illuminated and engaged in light-driven biosynthetic processes, and when it is darkened and generating its energy and reducing power via respiratory pathways. Fluxes within cells also differ, depending on the major metabolic activities; a heterotrophic starch-storing cell has lower fluxes through the triose phosphate pool than a heterotrophic lipid-storing cell. This is because all the acetyl-CoA needed for lipid synthesis is derived from the triose-phosphate pool, whereas the carbon for starch synthesis is taken from the hexose phosphate pool. Measurement of such fluxes is arguably one of the most important, yet most difficult undertakings in the study of plant carbohydrate metabolism (see Box 13.7).

BOX 13.7 Metabolic fluxes tell the truth about metabolism

Modern research into **metabolism** has an impressive array of tools: **transcriptome** and **proteome** profiling to give a system-wide overview, methods for selective gene silencing or upregulation to investigate the importance of an enzyme in vivo, the recombinant expression of enzymes to study their properties in vitro. Methods have also been developed for **metabolomics**—the simultaneous measurement of many metabolites—that are based on techniques such as gas or liquid chromatography linked with mass spectrometry, and on nuclear magnetic resonance. This has improved the capacity for the acquisition of large metabolite datasets. Challenges remain because metabolites have different chemical properties to each other, are present in different quantities, and in some cases are sometimes unstable. Thus, even with a range of extraction and analytical methods, it can still be difficult to measure every metabolite in a pathway, even in major pathway such as the Calvin–Benson cycle.

However, even metabolomics and the large metabolite datasets it yields do not give a complete picture of metabolism, because metabolite levels do not necessarily reflect fluxes. Hypothetically, when the flux through a pathway increases, the levels of metabolites in that pathway might be expected to increase. However, this does not always happen. Furthermore, increases in the same metabolites could also occur if a reaction at the end of the pathway is downregulated, which would decrease the pathway flux. Thus, metabolite levels should be regarded with caution, and fluxes should be regarded as the truth about metabolism.

In some cases, measuring fluxes is relatively simple (e.g., nutrient uptake by the root, net carbon fixation during photosynthesis, or the accumulation of an end product like starch). However, in the heart of carbohydrate metabolism, fluxes are difficult to measure and require integrated approaches that employ theoretical, experimental, and analytical methods.

Defining the pathways in a metabolic network is a prerequisite to measuring fluxes. This theoretical step can be aided or refined using genome sequence information and transcriptome data to define the enzymes within a given plant tissue. As a starting point, networks allow the modeling of metabolism, which can then be directly tested by experimentation. Experiments typically involve supplying an isotopically labeled compound (e.g., ^{13}C- or ^{14}C-labeled CO_2 to photosynthesizing leaves; ^{13}C-labeled glucose to heterotrophic cell cultures). There are different ways in which distribution of the isotope throughout metabolism can then be measured over time. Together with the network model, this redistribution can be used to calculate flux maps or compared against the theoretical metabolic models. While research in this area is experiencing a renaissance, the complexity of plant metabolism, the duplication and subcellular compartmentalization of pathways, and the presence of multiple cell types in plant organs means there is much to learn.

13.8.2 Pentose phosphate/triose phosphate pool metabolites are kept at equilibrium by numerous reversible enzymatic reactions

In glycolysis, after the conversion of fructose 6-phosphate to fructose 1,6-bisphosphate, the reactions catalyzed by fructose-1,6-bisphosphate aldolase and triose-phosphate isomerase are reversible. Similarly, apart from the initial oxidative reactions, the steps of the pentose phosphate pathway catalyzed by ribulose-5-phosphate epimerase, ribose-5-phosphate isomerase, transketolase, and transaldolase are also reversible. This keeps the cytosolic and plastid-localized triose phosphate/pentose phosphate pool metabolites in equilibrium (Fig. 13.31).

There are three major drains on the triose phosphate/pentose phosphate pool of metabolites (Fig. 13.32). First, the triose phosphates are utilized in the reactions of the energy-conserving reactions of glycolysis (see Section 13.9). These compounds can also be transported across the envelope of the plastid by the TPT. Second, the **shikimate pathway** uses **erythrose 4-phosphate** for the formation of lignin, polyphenols, and amino acids (see Chapters 8 and 24). Third, **ribose 5-phosphate** is required for nucleic acid synthesis. As metabolites are drained from this pool, the reversible reactions adjust to allow production of the metabolite that is being depleted. Because the reactions are reversible, metabolites can flow in either direction. The oxidative reactions of the pentose phosphate pathway, which are not reversible, are regulated and operate only when reducing power (i.e., NADPH) is needed (see Section 13.9).

Fructose-1,6-bisphosphate aldolase has already been mentioned in the context of sucrose synthesis (see Section 13.6.2). It catalyzes the reversible aldol cleavage of fructose 1,6-bisphosphate to glyceraldehyde 3-phosphate and dihydroxyacetone phosphate (Reaction 13.24). The standard free energy change of this reaction indicates the equilibrium favors fructose 1,6-bisphosphate; the actual equilibrium position, however, is determined by the concentrations of all three reactants. Fructose 1,6-bisphosphate accumulates only when its cleavage products achieve a threshold concentration. Aldolases occur in nature as two distinct forms: Class I (in plants and animals) and Class II (in fungi and prokaryotes), resulting from convergent evolution. In plants, the gene family encoding Class I aldolase can be subdivided into two groups, one containing cytosolic isoenzymes, and the other containing plastid isoenzymes.

Reaction 13.24: Fructose-1,6-bisphosphate aldolase

Fructose 1,6-bisphosphate ↔ Dihydroxyacetone phosphate + glyceraldehyde 3-phosphate

Triose-phosphate isomerase, isoenzymes of which occur in both the cytosol and plastids, catalyzes the interconversion of glyceraldehyde 3-phosphate and dihydroxyacetone phosphate and is one of the most active enzymes known (Reaction 13.25). The reaction it catalyzes is readily reversible, although the equilibrium favors dihydroxyacetone phosphate by ≈14:1, making this compound the principal triose phosphate in the cell. The effect of both the aldolase and triose-phosphate isomerase equilibria is to keep the concentration of glyceraldehyde 3-phosphate low. However, the glycolytic reactions that consume glyceraldehyde 3-phosphate can proceed because they are energetically favorable and

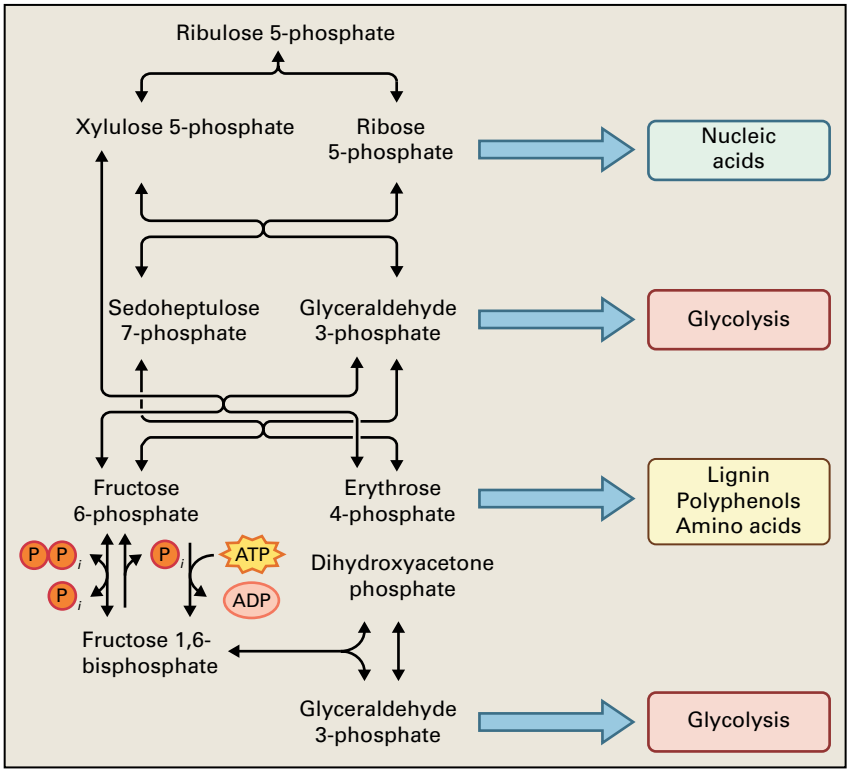


FIGURE 13.32 *Three metabolic pathways, both anabolic and catabolic, drain the pentose phosphate/triose phosphate pool. Glycolysis partially oxidizes triose phosphates to organic acids. Ribose is utilized in nucleotide synthesis. Erythrose 4-phosphate enters the shikimate pathway and contributes to the production of lignin, polyphenols, and some amino acids.*

shift aldolase and triose-phosphate isomerase equilibriums toward glyceraldehyde 3-phosphate production (see Section 13.8).

Reaction 13.25: Triose-phosphate isomerase

Glyceraldehyde 3-phosphate ↔ Dihydroxyacetone phosphate

The enzymes ribulose-5-phosphate epimerase, ribose-5-phosphate isomerase, transketolase, and transaldolase all catalyze reversible reactions that keep the sugar phosphates of the pentose phosphate pathway close to equilibrium.

Reaction 13.26: Ribulose-5-phosphate epimerase

Xyulose 5-phosphate ↔ Ribulose 5-phosphate

Reaction 13.27: Ribose-5-phosphate isomerase

Ribulose 5-phosphate ↔ Ribose 5-phosphate

Reaction 13.28: Transketolase

Sedoheptulose 7-phosphate + glyceraldehyde 3-phosphate ↔
Xylulose 5-phosphate + ribose 5-phosphate

Reaction 13.29: Transaldolase

Glyceraldehyde 3-phosphate + sedoheptulose 7-phosphate ↔
Erythrose 4-phosphate + fructose 6-phosphate

These enzymes occur in various types of plastids, but studies on different plants and tissues have yielded conflicting reports about their presence in the cytosol. Genome sequence information now suggests that some enzymes, notably transketolase and transaldolase, may be absent from the cytosol in most plants, while genes predicted to encode cytosolic forms of ribulose-5-phosphate epimerase and ribose-5-phosphate isomerase are present. The absence of some cytosolic enzymes for the reversible reactions of the pentose phosphate pathway is accommodated by the presence of transporters in the plastid inner envelope that are capable of transporting pentose and triose phosphates and, in some cases, hexose phosphates in exchange for P_i (see Fig. 13.4). Furthermore, this exchange of metabolites means that NADPH production and the withdrawal of precursors for biosynthesis can occur independently in each compartment (see Section 13.9).

13.9 Energy and reducing power for biosynthesis

In photosynthetic cells, light can supply much of the energy and reducing power needed for the biosynthetic reactions. However, in the dark and in nonphotosynthetic cells, light energy cannot be used and plants need to respire. Reducing power in the form of NADPH is produced by two oxidative reactions of the pentose phosphate pathway. Most of the ATP is produced by aerobic respiration of pyruvate in the mitochondrion (via the citric acid cycle; see Chapter 14), but some is also produced in energy-conserving reactions of glycolysis as hexose phosphates are converted to pyruvate.

13.9.1 Two pentose phosphate pathway enzymes oxidize glucose 6-phosphate to ribulose 5-phosphate and NADPH

Glucose-6-phosphate dehydrogenase catalyzes the oxidation of glucose 6-phosphate to 6-phosphoglucono-D-lactone, with the concomitant formation of NADPH from NADP+ (Reaction 13.30 and Fig. 13.33). The plant enzymes cannot use NAD^+ as an electron acceptor.

Reaction 13.30: Glucose-6-phosphate dehydrogenase

Glucose 6-phosphate + $NADP^+$ →
6-Phosphoglucono-D-lactone + NADPH + H^+

High activities of glucose-6-phosphate dehydrogenase have been found in all plant materials studied, and genome analyses reveal multiple genes encoding cytosolic and plastid-localized isoenzymes. Although reduction of the product 6-phosphoglucono-D-lactone is thermodynamically feasible, the lactone is unstable and spontaneously decomposes to form 6-phosphogluconate, making the oxidative reaction essentially irreversible. A **lactonase**, again with isoenzymes encoded by multiple genes, further increases the rate of 6-phosphogluconate formation.

The cytosolic isoenzyme of glucose-6-phosphate dehydrogenase has no allosteric regulatory properties, which is surprising considering its important role in supplying NADPH. However, the enzyme is strongly inhibited by one of its products, NADPH, consistent with the idea that the function of the enzyme is to provide NADPH for biosynthetic reactions. In contrast, the plastid isoenzymes are regulated and can occur in reduced and oxidized forms, the latter being the active form. The dithiol–disulphide interconversion between two highly conserved regulatory cysteine residues relates the enzyme's activity to the redox state of the Trx pool and the availability of light. During photosynthesis, $NADP^+$ can be reduced by the photosynthetic electron transport chain (see Chapter 12), which makes the oxidative steps of the pentose phosphate pathway superfluous. Under these conditions, plastid-localized glucose-6-phosphate dehydrogenase is deactivated by photoreduced Trx, rendering the complete pathway inoperative.

Phosphogluconate dehydrogenase (Reaction 13.31) catalyzes the irreversible oxidative decarboxylation of 6-phosphogluconate to ribulose 5-phosphate and carbon dioxide, with the concomitant reduction of $NADP^+$ (see Fig. 13.33).

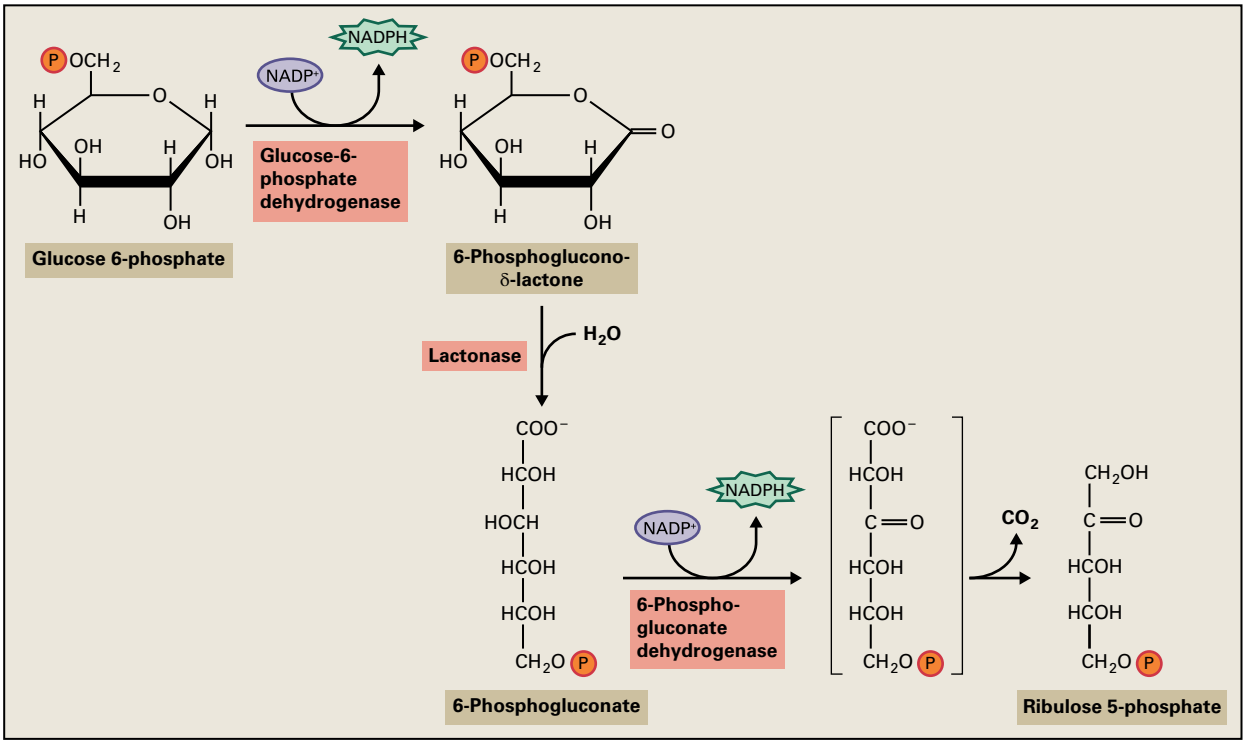


FIGURE 13.33 *The oxidative reactions of the pentose phosphate pathway convert glucose 6-phosphate to ribulose 5-phosphate, generating NADPH in the process.*

Reaction 13.31: 6-Phosphogluconate dehydrogenase

$$\text{6-Phosphogluconate} + \text{NADP}^+ \rightarrow \text{Ribulose 5-phosphate} + \text{CO}_2 + \text{NADPH} + \text{H}^+$$

As with the preceding enzymes, plants have several distinct cytosolic and plastid isoforms of this enzyme. No regulatory properties of the enzyme have been described, and its activity is probably determined by the availability of 6-phosphogluconate generated by glucose-6-phosphate dehydrogenase.

13.9.2 The reactions in the lower half of glycolysis conserve energy

In the reactions of the lower half of glycolysis, triose phosphate molecules are oxidized to form pyruvate and energy is conserved in high-energy phosphate compounds that can be used to synthesize ATP from ADP. These high-energy compounds are generated by two enzymes, **glyceraldehyde-3-phosphate dehydrogenase**, which forms the mixed acid anhydride **1,3-bisphosphoglycerate** (Reaction 13.32), and **enolase**, which generates a phosphate ester linked to the enol form of pyruvic acid, phospho*enol*pyruvate (Fig. 13.34; see also Section 13.9.3). Because the instability of the enol form of pyruvate gives the phosphate ester a high negative free energy of hydrolysis, the phosphate group can be transferred to ADP, yielding ATP.

Glyceraldehyde-3-phosphate dehydrogenase (Reaction 13.32) catalyzes a reaction in which the oxidation of the substrate (**glyceraldehyde 3-phosphate**) is linked directly to its phosphorylation and to the reduction of **NAD**$^+$ to **NADH**. The product, 1,3-bisphosphoglycerate, is a high-energy compound capable of donating its C-1 phosphate to ADP. This example of substrate-level phosphorylation was considered the model for all cellular ATP formation until the chemiosmotic scheme for ATP synthesis was accepted (see Chapters 3, 12, and 14).

Reaction 13.32: Glyceraldehyde-3-phosphate dehydrogenase

$$\text{Glyceraldehyde 3-phosphate} + \text{NAD}^+ + \text{Pi} \leftrightarrow \text{1,3-Bisphosphoglycerate} + \text{NADH} + \text{H}^+$$

The glyceraldehyde-3-phosphate dehydrogenase reaction is readily reversible, although the equilibrium position favors glyceraldehyde 3-phosphate over 1,3-bisphosphoglycerate by approximately 10:1. The subsequent phosphoglycerate kinase reaction pulls the glyceraldehyde-3-phosphate dehydrogenase reaction in favor of the products. In the cell, the equilibrium position is also determined by the NAD$^+$:NADH ratio, because these molecules bind competitively to the enzyme. The concentration of NAD$^+$ in the cell is generally around 10 times the concentration of NADH, again favoring 1,3-bisphosphoglycerate formation.

During the glyceraldehyde-3-phosphate dehydrogenase reaction, glyceraldehyde 3-phosphate oxidation is concomitant with the reduction of NAD$^+$. The 3-phosphoglyceric

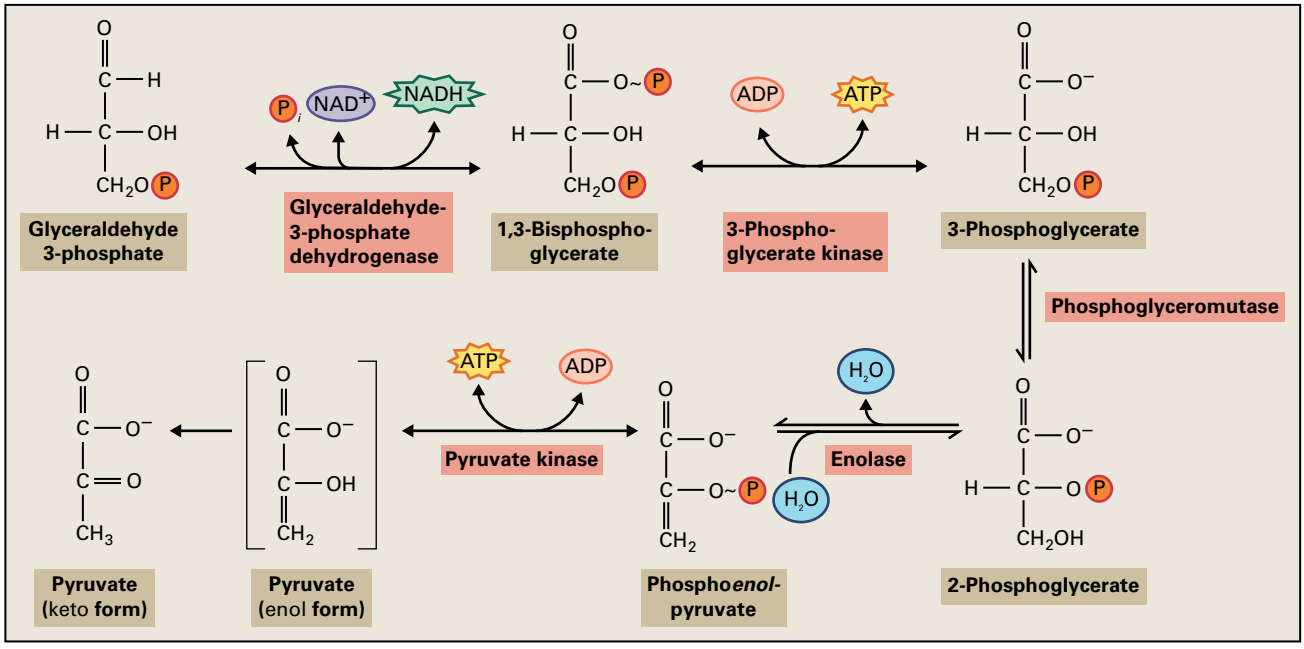


FIGURE 13.34 *Oxidative and ATP-forming reactions of the glycolytic pathway, showing the relationship between the oxidation of the three-carbon molecules of the lower half of glycolysis and the creation of phosphate compounds with high negative free energies of hydrolysis (~).*

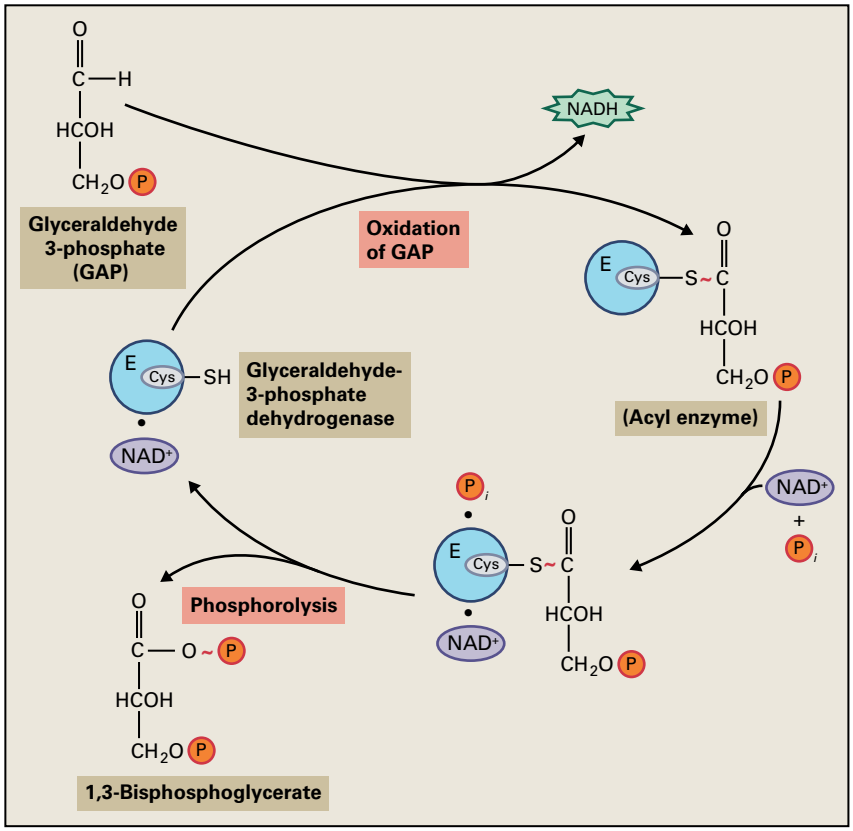


FIGURE 13.35 *Substrate-level phosphorylation by glyceraldehyde-3-phosphate dehydrogenase. In this reaction, a thioester bond is formed between a phosphoglyceric acid (derived from GAP) and a cysteine residue in the enzyme. The phosphorolysis of this bond in which the phosphate forms a mixed acid anhydride with phosphoglyceric acid (i.e., 1,3-bisphosphoglyceric acid) is accompanied by a high release of free energy. Like the thioester, the mixed acid anyhdride bond is reflective of a high negative free energy of hydrolysis and is designated by a tilde (~). In the subsequent reaction catalyzed by phosphoglycerate kinase (not shown), this phosphate group is transferred to ADP to form ATP.*

acid formed remains covalently bound to the enzyme through an energy-rich thioester bond to an active site cysteine residue. Hence, the energy made available by the oxidation of glyceraldehyde 3-phosphate is conserved, both through the formation of NADH from NAD^+ and the formation of the thioester bond. In the second half of the reaction, P_i binds to the active site and is transferred to the 3-phosphoglyceric acid moiety. This phosphorolysis reaction yields 1,3-bisphosphoglycerate (Fig. 13.35).

Three distinct forms of glyceraldehyde-3-phosphate dehydrogenase exist in plants. In addition to the cytosolic NAD^+-dependent enzyme, there is a related $NADP^+$-dependent

isoform in the chloroplast that is involved in photosynthesis (see Chapter 12). The third enzyme has a different evolutionary origin and is a nonphosphorylating, $NADP^+$-dependent glyceraldehyde-3-phosphate dehydrogenase. It is present in the cytosol and generates 3-phosphoglyceric acid instead of 1,3-bisphosphoglycerate. Thus, the enzyme does not conserve as much energy as the other isoforms and catalyzes an essentially irreversible reaction in the cell. The nonphosphorylating enzyme is upregulated during phosphate starvation in *Arabidopsis* and has been proposed to allow carbon flow through the pathway to continue when the concentrations of ADP are too low for the synthesis of ATP from 1,3-bisphosphoglycerate to proceed (see Box 13.5). It has also been proposed that the enzyme works in conjunction with the TPT and the reductive reactions of the Calvin-Benson cycle to indirectly export NADPH from the chloroplast to the cytosol.

Phosphoglycerate kinase (Reaction 13.33) catalyzes the formation of 3-phosphoglycerate from 1,3-bisphosphoglycerate, transferring the phosphate group from the 1-position to ADP, forming ATP. Both cytosolic and plastid forms of this enzyme exist, and both have properties similar to those from other organisms.

Reaction 13.33: 3-Phosphoglycerate kinase

$$\text{1,3-Bisphosphoglycerate} + \text{ADP} \leftrightarrow \text{3-Phosphoglycerate} + \text{ATP}$$

The equilibrium strongly favors the products of the reaction, because the mixed acid anhydride bond of 1,3-bisphosphoglycerate is unstable and has a high free energy of hydrolysis. Consequently ATP is generated during glycolysis. At a high ATP:ADP ratio, however, the reverse reaction can occur. For example, during photosynthesis, the enzyme is involved in the reductive reactions of the Calvin-Benson cycle, using ATP derived from photophosphorylation.

13.9.3 Phosphoglyceromutase and enolase are present in the cytosol and in heterotrophic plastids

Phosphoglyceromutase catalyzes the interconversion of 3-phosphoglycerate and 2-phosphoglycerate—a readily reversible reaction (Reaction 13.34). The enzyme moves the phosphate group from the 3-position to the 2-position, such that subsequent dehydration by enolase produces a high-energy compound, phospho*enol*pyruvate (Reaction 13.35).

Reaction 13.34: Phosphoglyceromutase

$$\text{3-Phosphoglycerate} \leftrightarrow \text{2-Phosphoglycerate}$$

Reaction 13.35: Enolase

$$\text{2-Phosphoglycerate} \leftrightarrow \text{Phospho}\textit{enol}\text{pyruvate} + H_2O$$

The dehydration of 2-phosphoglycerate generates phosphopyruvate in the enol configuration. Because this configuration is unstable, the phosphate attached to the 2-position of pyruvate has a high free energy of hydrolysis, allowing transfer of the phosphate group to ADP in the subsequent reaction catalyzed by pyruvate kinase.

Although plastid-targeted isoforms of phosphoglyceromutase and enolase are encoded in the genomes of plants, the enzymes appear to be absent in chloroplasts. This may be because 3-phosphoglycerate is the initial product of CO_2 fixation in the Calvin–Benson cycle, and the presence of these enzymes would draw carbon from this cycle into plastid glycolysis. The enzymes are present in colorless plastids from seeds and roots, where their activities are generally positively correlated with the level of biosynthetic activity of the tissue.

13.9.4 Pyruvate kinase produces ATP in the cytosol and the plastid

Pyruvate kinase (Reaction 13.36) catalyzes the transfer of the phosphate group from phospho*enol*pyruvate to ADP with the formation of ATP and pyruvate. The reaction is virtually irreversible because the initial product of the reaction is the enol form of pyruvate (see Fig. 13.34). In phospho*enol*pyruvate, the enol form is stabilized by the phosphoester bond. Removal of the phosphate group allows the resulting enol form of pyruvate to convert to the more stable keto form, removing a product from the reaction and driving the reaction forward.

Reaction 13.36: Pyruvate kinase

$$\text{Phospho}\textit{enol}\text{pyruvate} + \text{ADP} \rightarrow \text{Pyruvate} + \text{ATP}$$

Several related isoenzymes of pyruvate kinase exist in both the plastid and cytosol. In *Arabidopsis*, for example, 14 genes encode pyruvate kinase proteins. Unlike other enzymes of glycolysis, the plastid form is present in all plant tissues studied thus far. The enzyme has been reported to occur as a homo- or heteromultimer of related subunits. Interestingly, pyruvate kinase from several sources is inhibited by amino acids, such as glutamate and glutamine (Fig. 13.36). This couples the activity of the enzyme to the supply of carbon skeletons for nitrogen assimilation and amino acid biosynthesis. This form of regulation of the enzyme is related to the autotrophic nature of plants, which requires that a large amount of carbon be directed into biosynthetic activity. Furthermore, pyruvate kinase is activated by metabolites such as dihydroxyacetone phosphate (Fig. 13.36), which signals a supply of substrates.

Plant pyruvate kinases, however, appear not to share the regulatory properties of the well-studied mammalian liver enzyme. Specific sites on this enzyme are subject to phosphorylation and dephosphorylation; the phosphorylated enzyme is inactive. None of the plant enzymes appear to undergo comparable phosphorylation. Pyruvate kinase in animals and most other organisms is also allosterically activated by

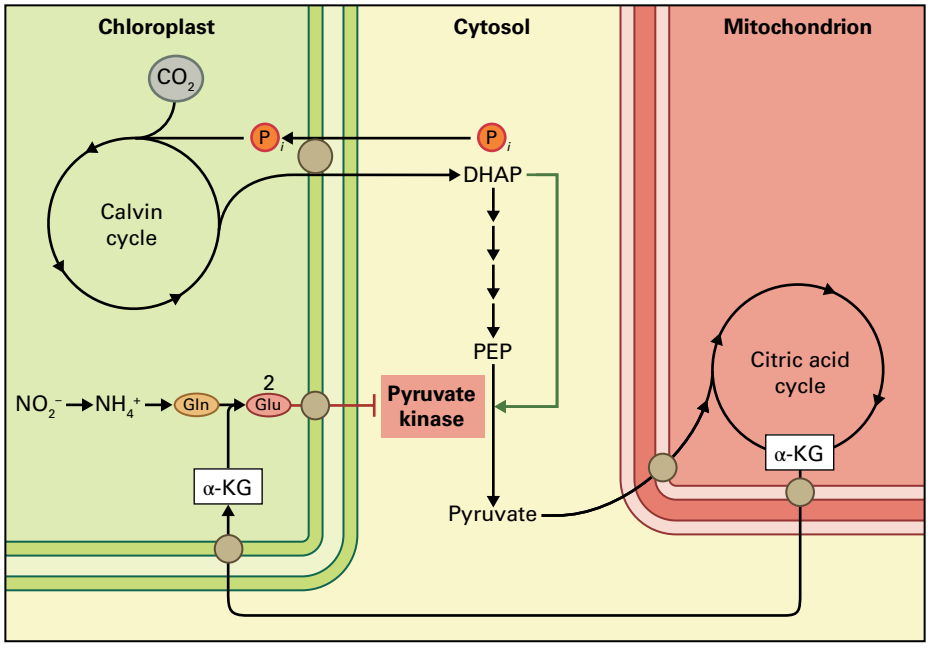


FIGURE 13.36 *Regulation of cytosolic pyruvate kinase and its relationship to nitrogen assimilation in the chloroplast. Pyruvate kinase activity in the cytosol is inhibited by amino acids such as glutamate. It is proposed that this influences the rate of production of synthesis of α-ketoglutarate (α-KG), an intermediate of the citric acid cycle, but also the carbon skeleton used in nitrogen fixation in the chloroplast. Gln, glutamine; Glu, glutamate; DHAP, dihydroxyacetone phosphate; PEP, phosphoenolpyruvate.*

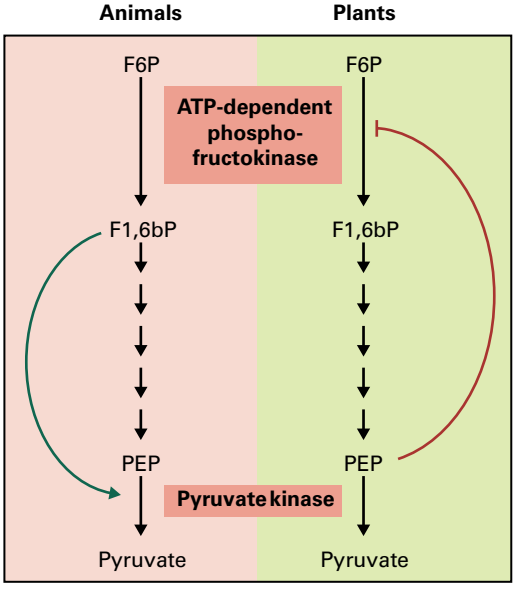


FIGURE 13.37 *Regulation of glycolysis in plant and animal cells. In animals there is a "top-down" regulation through the activation of the PFK, producing fructose 1,6-bisphosphate (F1,6bP). This activation does not occur in plants. Instead there is a "bottom-up" regulation through the inhibition of PFK by phosphoenolpyruvate (PEP). Pyruvate kinase is differently regulated, reflecting the autotrophic nature of plants.*

fructose 1,6-bisphosphate (Fig. 13.37), linking its activity to that of PFK by a feedforward loop. Although sequences similar to the fructose 1,6-bisphosphate activation site do occur in the plant enzyme, no evidence has been found for any feedforward regulation. Rather, plant glycolysis appears to be regulated upstream, through the inhibition of PFK (Fig. 13.37; see also Section 13.6).

13.9.5 Carbon import and plastid respiration support biosynthesis in nongreen plastids

The plastid enzymes of the oxidative pentose phosphate pathway and lower part of glycolysis are important in the supply of both carbon skeletons and cofactors for biosynthesis, especially in nonphotosynthetic plastids. Plastid-localized anabolic pathways, such as starch synthesis, fatty acid synthesis, and aromatic amino acid synthesis, can consume large amounts of energy (in the form of ATP) and reducing power (in the form of reduced Fdx and NAD(P)H). Chloroplasts can produce the cofactors needed via photosynthesis, but in nonphotosynthetic plastids, the cofactors must be generated another way.

Plastids do have an adenylate transport system that exchanges ATP for ADP, and this is particularly important for starch biosynthesis in potato (*Solanum tuberosum*) tuber amyloplasts. Although no known transport system exists for the direct import of NADH or NADPH, reducing equivalents can be imported or exported by one or more shuttle systems (see Fig. 13.5). For example, in castor seed (*Ricinus communis*) endosperm, a tissue that synthesizes large amounts of storage lipids, the most effective substrate for fatty acid biosynthesis (by isolated colorless plastids) is malate, which is produced in the cytosol by PEP carboxylase and malate dehydrogenase and then imported into the plastid. Within the plastid, it is oxidatively decarboxylated by **malic enzyme** (Reaction 13.37), generating NADPH and pyruvate. The subsequent oxidative decarboxylation of pyruvate by a plastid-localized pyruvate dehydrogenase complex generates acetyl-CoA for fatty acid biosynthesis and the reducing agent NADH.

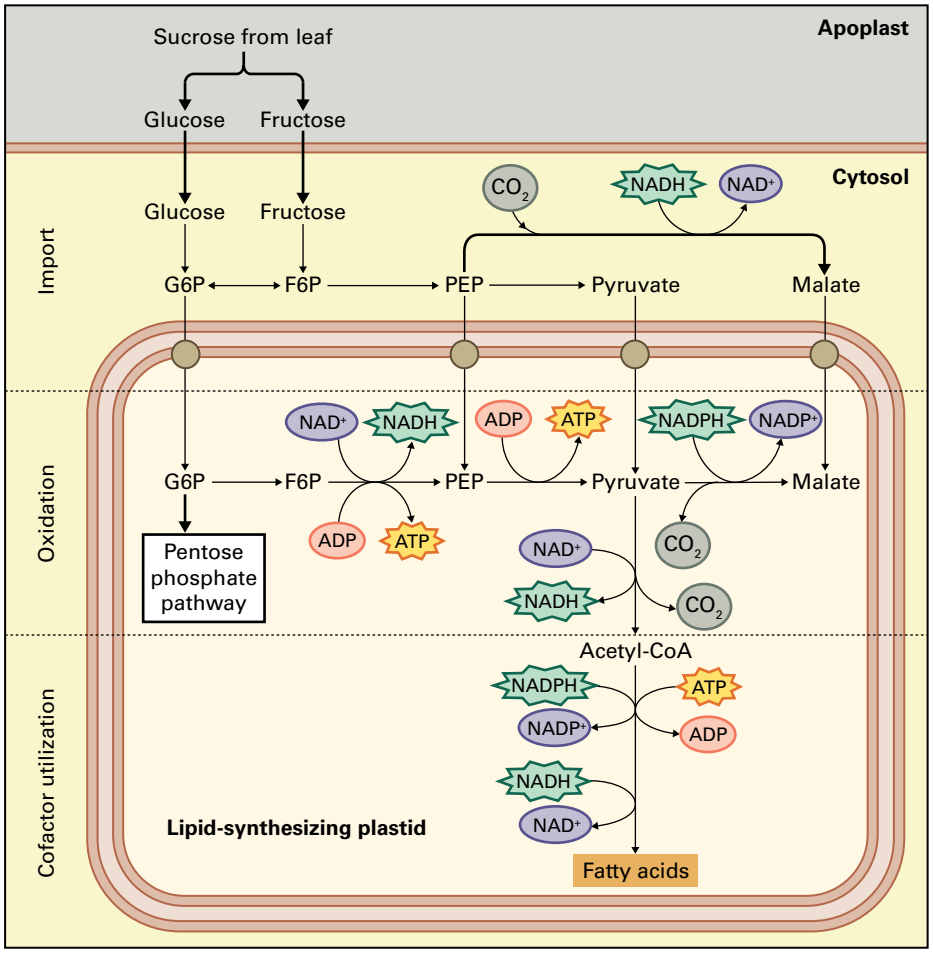


FIGURE 13.38 *Use of photoassimilate by lipid-storing seeds to generate cofactors for fatty acid synthesis in a lipid-synthesizing plastid. In a colorless plastid, glycolytic enzymes, NADP-dependent malic enzyme, and the pyruvate dehydrogenase complex not only provide carbon for fatty acid biosynthesis, but also cofactors such as ATP and NADPH required for this biosynthetic pathway. G6P, glucose 6-phosphate; F6P, fructose 6-phosphate; PEP, phosphoenol*pyruvate.

Reaction 13.37: Malic enzyme

$$\text{Malate} + \text{NADP}^+ \rightarrow \text{Pyruvate} + \text{NADPH} + \text{CO}_2$$

In most plastids, cofactors can also be generated within the organelle by respiration. In other oilseeds, such as rapeseed (canola, *Brassica napus*), isolated plastids import hexose phosphates and phospho*enol*pyruvate. These plastids have the glycolytic and the oxidative pentose phosphate pathway enzymes to metabolize hexose phosphate. The latter pathway generates significant amounts of NADPH, which are required for fatty acid chain elongation. The operation of pyruvate kinase supplies ATP as it converts the imported phospho*enol*pyruvate to pyruvate for acetyl-CoA production. Hence, both the cofactors and the acetyl CoA substrate consumed in fatty acid biosynthesis are generated within the organelle (Fig. 13.38). Because all biosynthetic pathways require reducing power and energy, respiratory pathways are needed to provide cofactors, whether the principal product of the plastid is amino acids or secondary metabolites, rather than fatty acids.

In some species, including rapeseed (*Brassica napus*), the fatty acid-synthesizing plastids are actually green and capable of limited photosynthesis via the light that filters through the wall of the seed pod. Interestingly, these plastids also contain active Rubisco. However, in this tissue the enzyme is not part of the Calvin–Benson cycle. Instead, it is supplied with substrates through the nonoxidative reactions of the pentose phosphate pathway, and its activity captures some of the CO_2 lost from pyruvate upon acetyl-CoA production. When coupled with energy derived from photosynthesis, this pathway makes the process of fatty acid biosynthesis more carbon efficient.

13.10 Sugar-regulated gene expression

Metabolites can act as allosteric regulators of enzyme activities. In addition to their role in metabolism and metabolic regulation, sugars can also act as signals, controlling cellular activities such as gene transcription, protein stability, and protein kinase activity. This is important for coupling cell or organ growth with metabolism and carbohydrate availability.

Sugar sensing has been extensively studied in simpler biological systems. For example, in *E. coli*, the presence of lactose in the growth medium results in the expression of genes required for lactose metabolism. In the yeast *Saccharomyces cerevisiae*, the presence of glucose in the growth medium represses the expression of genes required for the metabolism of other carbon sources. In plants, the situation is more

complicated, as sugars are generated internally through photosynthesis. Consequently, it is not only growth in developing tissues, but also photosynthesis in mature tissues that must respond to sugar availability.

13.10.1 Photosynthesis is regulated by sugars, with hexokinase 1 serving as a glucose sensor

Early studies of sugar sensing in plants focused on the repression of photosynthesis by excess sugars. Supplying exogenous sugars, or preventing the export of photosynthate, causes sugar accumulation in fully expanded source leaves. This results in a decrease in chlorophyll content and a reduction in the activities of the Calvin–Benson cycle enzymes, but also an accumulation of starch. Analysis of gene expression revealed that as photosynthetic genes were repressed by high sugars, genes involved in carbon storage were induced. Subsequent genome-wide studies have revealed that changes in sugar levels play a major role in regulating thousands of genes. Several sugar-sensing mechanisms have now been proposed, although much remains to be discovered about the sugar receptors and the subsequent signal transduction pathways. One major difficulty when researching sugar sensing is the fact that primary signaling events (that is, the sensing of changing levels of a particular sugar) can be confused with the metabolic consequences of altered sugar levels, which might also affect cellular activities via other downstream mechanisms. Ideally, these two different effects need to be dissociated from each other.

One approach has been to use the responses of *Arabidopsis* to high levels of exogenous sugars as the basis for genetic screens. For example, high levels of glucose repress seedling development after germination. The isolation of glucose-insensitive (*gin*) or glucose oversensitive (*glo*) mutants, having reduced or enhanced growth repression respectively, helped identify proteins involved in sugar perception and signal transduction (Fig. 13.39). These screens have also emphasized the degree of integration between sugar signaling and plant hormone signaling (e.g., auxin, ABA and ethylene; see Chapter 17), as several hormone response mutants also show altered responsiveness to sugars.

A good candidate for direct glucose perception is hexokinase 1 (HXK1), whose enzymatic function is to phosphorylate glucose and fructose using ATP (see Reaction 13.23). Mutants lacking HXK1 have a *gin* phenotype which could either result from the loss of signaling, or from the loss of the ability to metabolize glucose. However, three pieces of evidence suggest that HXK1 is a genuine signaling protein. First, *hxk1* mutants still have hexokinase activity provided by other isoenzymes. Second, the introduction of a catalytically inactive hxk1 forms into the *hxk1* mutant restores glucose sensitivity, showing that glucose sensitivity and glucose phosphorylation can be uncoupled. Third, a small proportion of HXK1 protein can be found 'moonlighting' in the nucleus, associated in a multiprotein complex with transcriptional regulators.

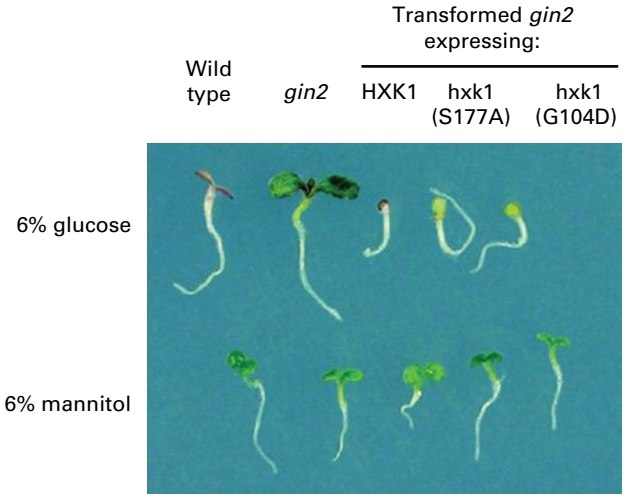


FIGURE 13.39 *Use of exogenous sugars to discover sugar-sensing mechanisms. Supplying 6% glucose to* Arabidopsis *seedlings causes a developmental arrest after germination and cotyledons fail to green (left). Using this phenotype as the basis of a genetic screen led to the discovery of glucose-insensitive (*gin*) mutants that still develop green cotyledons in the presence of 6% glucose. The* gin2 *mutant lacks hexokinase 1 (HXK1), the enzyme that uses ATP to phosphorylate glucose to glucose 6-phosphate. Transforming the* gin2 *mutant with the wild-type HXK1 proteins or mutant versions of the protein that lack catalytic activity, restores glucose sensitivity. This shows that the protein itself, rather than its catalytic activity is responsible for glucose signaling. Mannitol cannot be used by seedlings and thus served as a control. Source*: Adapted from Moore et al. (2003). Science 300:332–336.

There is evidence that sugars other than glucose are sensed in plants (sucrose and fructose, for instance), as are different nutrients and metabolite classes. Furthermore, multiple signaling mechanisms may exist for a specific sugar, as indicated by that fact that HXK1-signaling cannot explain all of the responses to glucose. Besides hexokinase, other types of proteins have been proposed as candidate receptors for **sugar signaling**. These include other enzymes, membrane receptors and specialized sugar transporters localized at the plasma membrane that activate cytosolic signaling pathways. Nuclear proteins containing both DNA-binding domains and enzyme-like domains have also been proposed to control gene expression directly in response to sugars (see Box 13.2).

13.10.2 Trehalose 6-phosphate is a signal metabolite involved in growth control

Sucrose may be sensed directly, but also indirectly through the synthesis of the signal metabolite **trehalose 6-phosphate** (Fig. 13.40). Trehalose, a disaccharide of α-1,1-linked glucosyl moieties (see Fig. 13.10), is widespread in nature, being a major sugar in many bacteria, fungi, and invertebrates. In plants, trehalose biosynthesis was initially thought to be restricted to a limited number of xerophytic species, where its

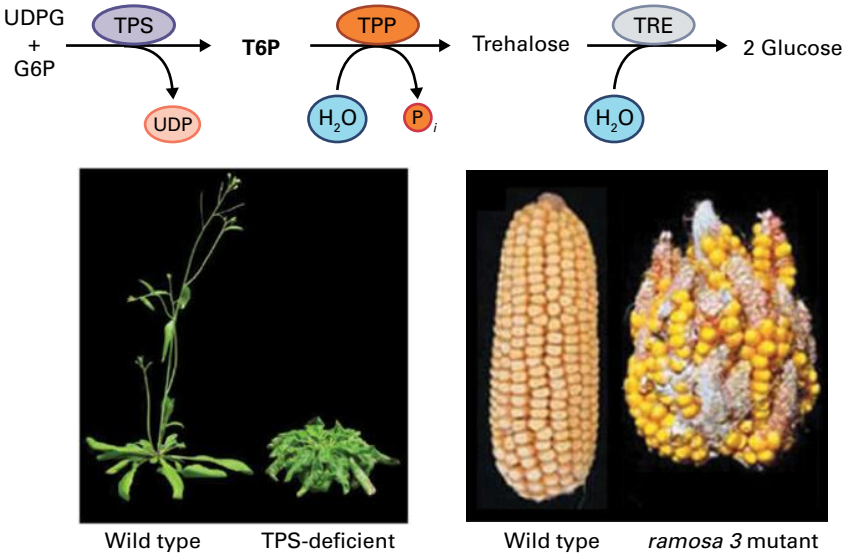


FIGURE 13.40 *Trehalose metabolism and signaling in plants. Trehalose is synthesized from UDP-glucose and glucose 6-phosphate via the enzymes trehalose-phosphate synthase (TPS) and trehalose-phosphate phosphatase (TPP). Trehalose can be hydrolyzed back to its constituent glucose monomers by trehalase (TRE). In recent years, evidence has mounted that trehalose 6-phosphate is an important signal affecting plant development, exemplified by the inflorescence phenotype of the* ramosa 3 *mutant of maize (*Zea mays*), which lacks a TPP isoform (bottom right), and the late-flowering phenotype of* Arabidopsis *plants deficient in TPS activity (bottom left).* *Source:* Adapted from Ponnu et al. (2011). Frontiers Plant Sci. 2:70; Satoh-Nagasawa et al. (2006). Nature 441:227–230.

accumulation to high levels helps to confer anhydrobiosis, the ability to withstand prolonged periods of desiccation. However, it is now clear that many if not all plants have the ability to synthesize and degrade trehalose, and that the biosynthetic intermediate trehalose 6-phosphate rather than trehalose itself is the biologically active signaling compound.

The pathway of trehalose synthesis is similar to that of sucrose synthesis (Fig. 13.40) in that it occurs in the cytosol and utilizes UDP-glucose and hexose phosphate as substrates (glucose 6-phosphate rather than fructose 6-phosphate used for sucrose biosynthesis). The enzyme **trehalose phosphate synthase** produces trehalose 6-phosphate, which is then dephosphorylated by **trehalose phosphate phosphatase**. Trehalose can be hydrolyzed back to glucose by trehalase. In most plant tissues studied, trehalose 6-phosphate levels are very low, but in general reflect sucrose levels, and may serve as a proxy for sucrose itself.

Disruption of trehalose metabolism has major impacts on plant growth and development. This is most clearly illustrated in *Arabidopsis tps1* mutants, which lack the ability to produce trehalose 6-phosphate. Seeds homozygous for *tps1* exhibit a developmental arrest in embryogenesis, despite ample carbohydrates available for growth. This phenotype can be rescued by expression of the TPS1 gene on a chemical-inducible promoter, but removal of the inducer from the growing rosette strongly affects growth and delays flowering (Fig 13.40). Another striking example is the effect of mutations at the *RAMOSA3* locus of maize (*Zea mays*), which encodes an isoenzyme of trehalose phosphate phosphatase. Mutant plants exhibit marked abnormalities in their inflorescence architecture when flowering (Fig. 13.40).

Researchers are still discovering the mechanisms by which trehalose 6-phosphate mediates its effects, but some may operate via inhibition of a conserved class of eukaryotic protein kinases. The SnRK1 protein kinase in plants is homologous to the Snf1 (Sucrose nonfermenting 1) protein kinase in yeast and the AMP-activated protein kinase (AMPK) in mammals, which are vital regulators of metabolism and energy homeostasis. In plants, SnRK1 controls energy consuming processes by phosphorylating and deactivating enzymes of central metabolism (e.g., 3-hydroxymethyl-3-methylglutaryl-CoA reductase, sucrose phosphate synthase, and nitrate reductase). It also orchestrates transcriptional reprogramming to repress genes involved in biosynthetic reactions while inducing those involved in nutrient mobilization.

The area of sugar signaling, or nutrient sensing in general, continues to be at the front line of research and, in the coming years, will improve our appreciation of the links between photosynthesis, mineral nutrient acquisition, and growth.

Summary

Some of the complexities and unique aspects of plant carbohydrate metabolism are presented in this chapter, with emphasis on photosynthetic metabolism and its primary products, sucrose, and starch. Given the diversity of the plant kingdom, any such chapter will be incomplete. For example, the leaves of some plants do not make any starch in their chloroplasts, but instead accumulate fructans in their vacuole. Unfortunately, not all pathways can be covered here.

A vital difference between carbohydrate metabolism in plants and that in other organisms stems from the fact that plants metabolize carbohydrates in both the cytosol and plastid, with most of the biosynthetic activity occurring in the latter compartment. This characteristic of

plant cells has a major impact on the organization and regulation of the carbohydrate metabolism pathways. That said, carbohydrate metabolism in the cytosol and plastid is connected by a series of metabolite transporters in the plastid envelope. Furthermore, while all plant tissues have plastids, they are themselves diverse in function, and each plastid type has a different metabolism and complement of membrane transporters, reflecting the nature of its biosynthetic activity. The overall regulation of carbohydrate metabolism is linked to the activity of these transporters. For example, the triose-phosphate translocator—the major protein of the chloroplast envelope, which catalyzes an enormous efflux of carbohydrate during photosynthesis—connects the cytosol with the plastid stroma in the middle of glycolysis. It is, therefore, not surprising that the regulation of glycolysis differs significantly in plants compared with animals.

Though metabolism is depicted as independent pathways, these pathways are intimately linked. Pools of metabolic intermediates are frequently shared by several pathways, and the direction of metabolite flow is determined by the needs of the cell, which can change dramatically (e.g., according to the availability of light in a leaf). There is also a tendency to regard plant tissues as homogeneous, whereas in fact they contain many distinct cell types, all of which differ metabolically. Perhaps only one third of the cells in a leaf are large photosynthetic palisade or spongy mesophyll cells, with most being smaller cells in the vasculature and the epidermis. A nice example of the contrast possible from cell to cell is the starch metabolism in chloroplasts of palisade cells and of stomatal guard cells. In the palisade cells, starch is made during the day from assimilated carbon and degraded at night, whereas in the chloroplasts of the guard cell the reverse is true: Starch is degraded during the day to provide solutes to increase cell turgor and help open the stomatal pore. Later, starch is made again, which may help to sequester these solutes and aid stomatal closure.

Another key feature of plant metabolism is its degree of flexibility—something that can sometimes make plant metabolism research difficult and perplexing, but ultimately fascinating. A major driver in the evolution of this flexibility is the fact that plants are sessile and must withstand extreme changes in the external environment. This might explain why several different enzymes sometimes catalyze a single step in a pathway and why plants can bypass some of the principal reactions of carbohydrate metabolism.

Considerable opportunities for future discovery await those who read this chapter and wish to pursue a better understanding of plant carbohydrate metabolism, its regulation, and metabolic signaling pathways. The possibilities today to study plants using combinations of genetic, biochemical, cell-biological and systems-level methods will tell us how plants make the products on which society depends.



14

Respiration and Photorespiration

A. Harvey Millar, James N. Siedow, and David Day

Introduction

Chapters 12 and 13 described how plants use light energy to assimilate carbon into sugars and starch, and how these molecules are subsequently broken down and converted into organic acids and other compounds. In this chapter, we address aerobic respiration—the further oxidation of these compounds to carbon dioxide (CO_2) and water (H_2O) in the mitochondrion—and review the mechanisms by which the energy released during respiration is conserved as ATP, a process called oxidative phosphorylation. We examine how plants can minimize ATP production while maintaining respiration rates, a mitochondrial attribute that may affect plant responses to environmental stress. We also describe how mitochondria and other cellular compartments interact by means of substrate shuttles across the inner mitochondrial membrane.

In addition to aerobic respiration, another respiratory process takes place in the leaves of many plants. This process, photorespiration, is the light-dependent uptake of O_2 and release of CO_2. The O_2 uptake occurs in the chloroplast as a result of the oxygenase reaction of ribulose-1,5-bisphosphate carboxylase/oxygenase (Rubisco), which leads to production of phosphoglycolate. Metabolism of phosphoglycolate involves a complex interaction among chloroplasts, peroxisomes, and mitochondria and leads to release of CO_2. Although photorespiration drains carbon from plants and adversely affects growth, it seems to be an unavoidable side reaction of CO_2 fixation in most plants. Some plants, however, have evolved anatomical and biochemical features that minimize the oxygenase reaction. These C_4 plants and Crassulacean acid metabolism (CAM) plants (see Chapter 12) demonstrate very low rates of photorespiration.

14.1 Overview of respiration

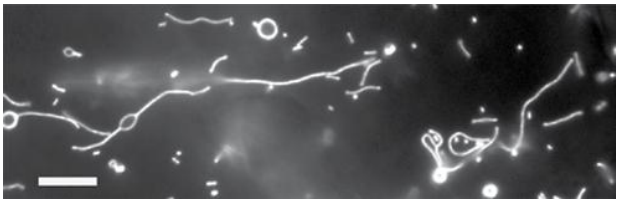
Aerobic respiration, a process common to almost all eukaryotic organisms, involves the controlled oxidation of reduced organic substrates to CO_2 and H_2O. Numerous compounds can serve as substrates for respiration, including carbohydrates, lipids, proteins, amino acids, and organic acids. Respiration releases a large amount of free energy, which is conserved in ATP molecules. This chemical bond energy can be used to drive metabolic reactions involved in the growth, development, and maintenance of the plant. In addition, the primary pathways of respiration provide metabolic intermediates that serve as substrates for the synthesis of nucleic acids, amino acids, fatty acids, and many secondary metabolites. Although the general process of respiration in plants is the same as in other eukaryotes, several features are unique to plants. These modifications apparently evolved to cope with the environmental and metabolic circumstances commonly faced by plants.

Biochemistry & Molecular Biology of Plants, Second Edition. Edited by Bob B. Buchanan, Wilhelm Gruissem, and Russell L. Jones.
© 2015 John Wiley & Sons, Ltd. Published 2015 by John Wiley & Sons, Ltd.
Companion website: www.wiley.com/go/buchanan/biochem

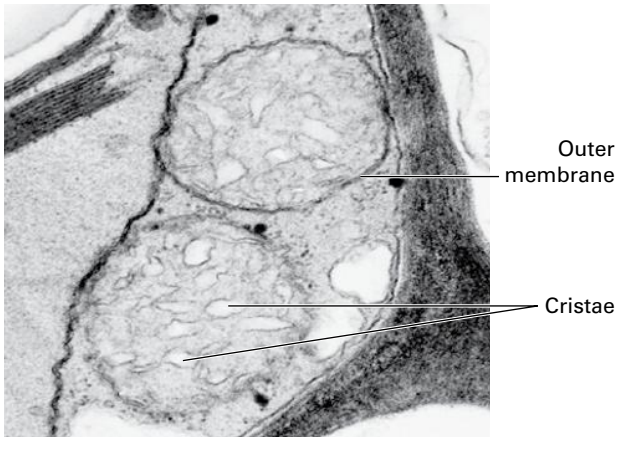
14.1.1 Plant mitochondria contain an outer and an inner membrane that separate the organelle into four functional compartments

The **mitochondrion** is the principal organelle of eukaryotic respiration. In electron micrographs, plant mitochondria appear as spherical or rod-shaped entities 0.5–1.0 μm in diameter and 1–3 μm in length, but in live cells fluorescently tagged mitochondria often appear as 10 μm or longer structures that frequently undergo fusion and fission as a discontinuous network (Fig. 14.1A). The number of mitochondria per plant cell varies and is related primarily to the metabolic activity of the tissue. The concentration of mitochondria per unit volume of cytoplasm, however, usually remains similar during different developmental stages of the same cell type. For example, the small cells of the root cap of maize seedlings contain approximately 200 mitochondria each, whereas the much larger mature root tip cells may have 2,000 or so mitochondria per cell. In very active cells such as phloem companion cells, secretory cells, and transfer cells, up to 20% of the volume of the cytoplasm may be occupied by mitochondria. On the other hand, some unicellular algae such as *Chlamydomonas* contain only a few mitochondria per cell. With a few exceptions (e.g., the very active cell types mentioned above), the density of mitochondria in plant cells is lower than in animal cells, but the respiratory rates of isolated plant mitochondria are generally higher than in those isolated from animals.

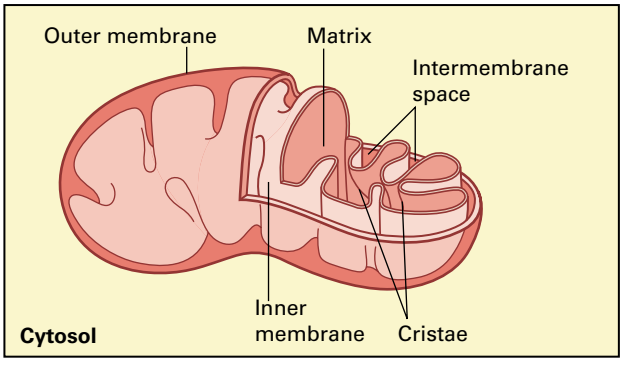
Mitochondria contain two sets of membranes that divide the organelle into four compartments: the **outer membrane**, the region between the two membranes (**intermembrane space**), a highly invaginated **inner membrane**, and the aqueous phase contained within the inner membrane (mitochondrial **matrix**) (Fig. 14.1B). Invaginations of the inner membrane give rise to **cristae**, which appear as sac-like structures under the electron microscope (Fig. 14.1C). The membranes of cristae (cristael membranes) are specialized in their structure and protein composition; points of contact with the rest of the inner membrane are referred to as junction points (Fig. 14.1D). The marked impermeability of the inner membrane necessitates the presence of carriers to facilitate the movement of metabolites between the cytosol, the intercristael space, and the mitochondrial matrix**.** By contrast, the outer membrane is permeable to solutes of molecular mass less than 10 kDa. This permeability is associated with the presence of pore-forming proteins known as **porins**. In some species, porin channels are gated by voltage and termed voltage-gated anion channels (VDAC) (see Chapter 3).



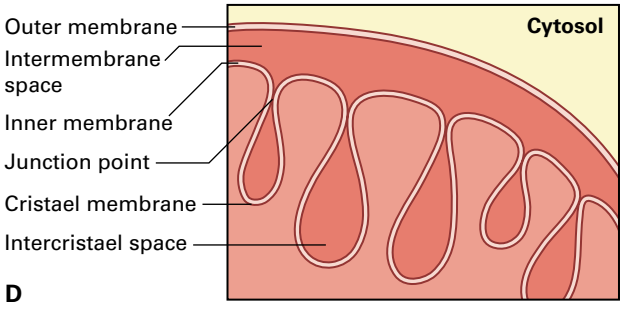
A



C



B



D

FIGURE 14.1 *Structural organization of the mitochondrion. (A) Fluorescence image of GFP-tagged mitochondrial structures in* Arabidopsis *leaf epidermis. (B) Diagram of the membrane organization of a plant mitochondrion. The outer membrane is permeable to molecules of 10 kDa or less because it contains a pore-forming protein called porin. The highly invaginated inner membrane, which contains the components of the mitochondrial electron transport chain and ATP synthase, serves as the primary permeability barrier for the organelle. The space between the two membranes is called the intermembrane space. The mitochondrial matrix, the region bounded by the inner membrane, contains the mitochondrial genome, the enzymes associated with the citric acid cycle, and the machinery required for mitochondrial protein synthesis. (C) Thin-section electron micrograph of a plant mitochondrion, showing the highly folded inner membrane structures (cristae) and the surrounding outer membrane. (D) Details of the mitochondrial outer and inner membranes.*
Source: (A) Logan, Université d'Angers, France; unpublished. (C) Wiser, University of Wisconsin, Oshkosh; unpublished.

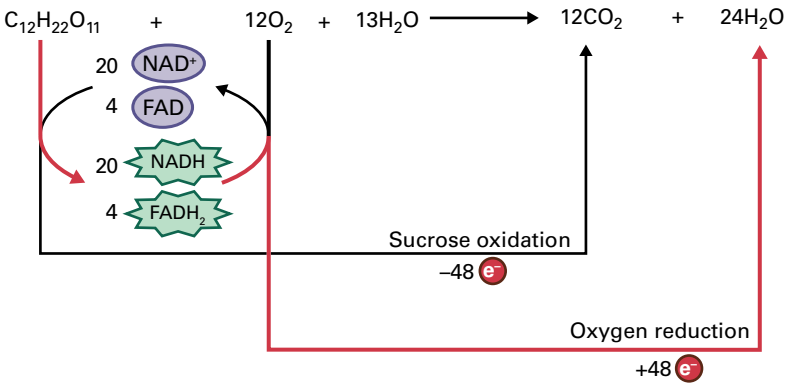


FIGURE 14.2 *Redox reactions of respiration. The oxidation of carbohydrate to carbon dioxide (CO_2) is coupled to the reduction of oxygen (O_2) to water (H_2O). The free energy released during this process is linked to the synthesis of ATP.*

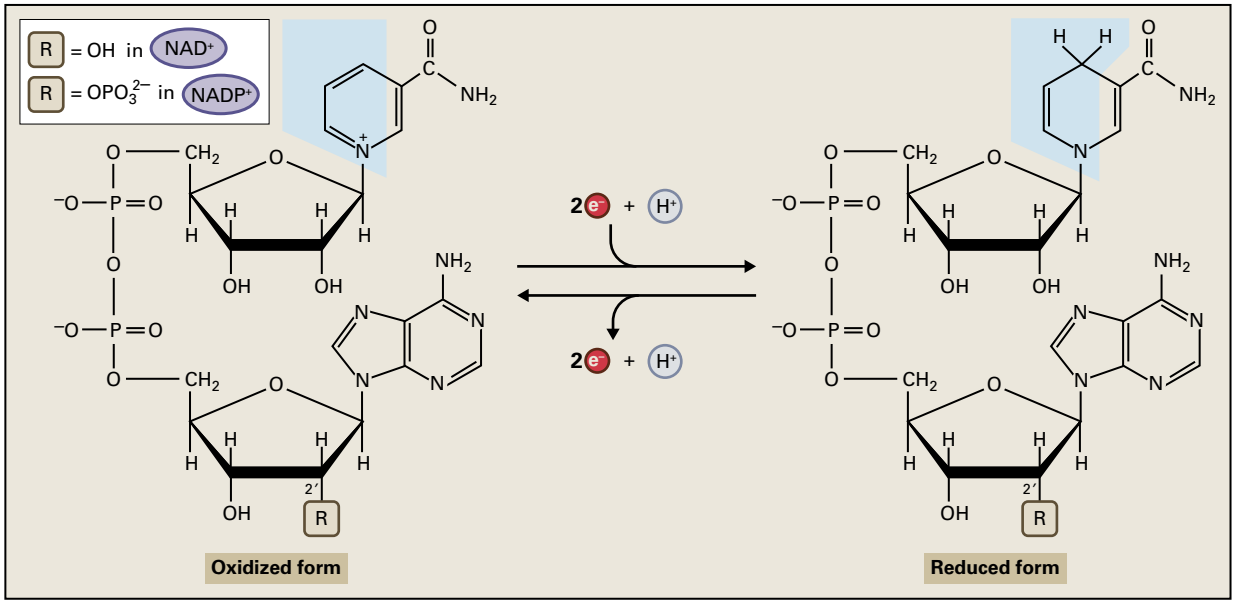


FIGURE 14.3 *Structure and redox chemistry of nicotinamide adenine dinucleotide (NAD^+) and nicotinamide adenine dinucleotide phosphate ($NADP^+$). The nicotinamide moiety of the oxidized species NAD^+ gains two electrons and a proton to produce the reduced species NADH. The related coenzyme $NADP^+$ differs from NAD^+ by the addition of a phosphate group attached to the 2′-hydroxyl of the ribose sugar moiety (variable group R in the diagram).*

The evolutionary origins of mitochondria, their semiautonomous status as organelles possessing DNA genomes and synthesizing some of their constituent proteins, and mitochondrial division are discussed in Chapter 1.

14.1.2 The principal products of respiration are CO_2, H_2O, and free energy conserved as ATP

Although respiration can oxidize many compounds, the principal substrates provided by photosynthesis for plant respiration are sucrose and starch. Using sucrose as an example of a respiratory substrate, one can represent the overall process of aerobic respiration as follows:

Reaction 14.1: Aerobic respiration of sucrose

$$C_{12}H_{22}O_{11} + 12O_2 + 13H_2O \rightarrow 12CO_2 + 24H_2O$$

This reaction scheme is the reverse of photosynthesis, and it represents a coupled pair of redox reactions in which sucrose is completely oxidized to CO_2, while O_2, the terminal electron acceptor, is reduced to H_2O (Fig. 14.2). The standard free energy change ($\Delta G^{\circ\prime}$) for this exergonic reaction, −5764 kJ mol^{-1}, provides the thermodynamic driving force for the production of ATP.

The three stages of respiration—**glycolysis**, the **citric acid cycle**, and **electron transfer/oxidative phosphorylation**—take place in different subcellular locations. Glycolysis involves a series of soluble cytosolic enzymes that oxidize sugars to organic acids. In the reaction above, one sucrose molecule is broken into two hexoses, which are then converted by glycolysis to four molecules of the three-carbon (C_3) compound pyruvate. This partial oxidation of sucrose also produces the reduced cofactor NADH (Fig. 14.3), as well as 65 ATP. The reactions of the citric acid cycle occur within the mitochondrial matrix and can completely oxidize pyruvate to CO_2; the electrons are transferred to NAD^+ and another cofactor, FAD

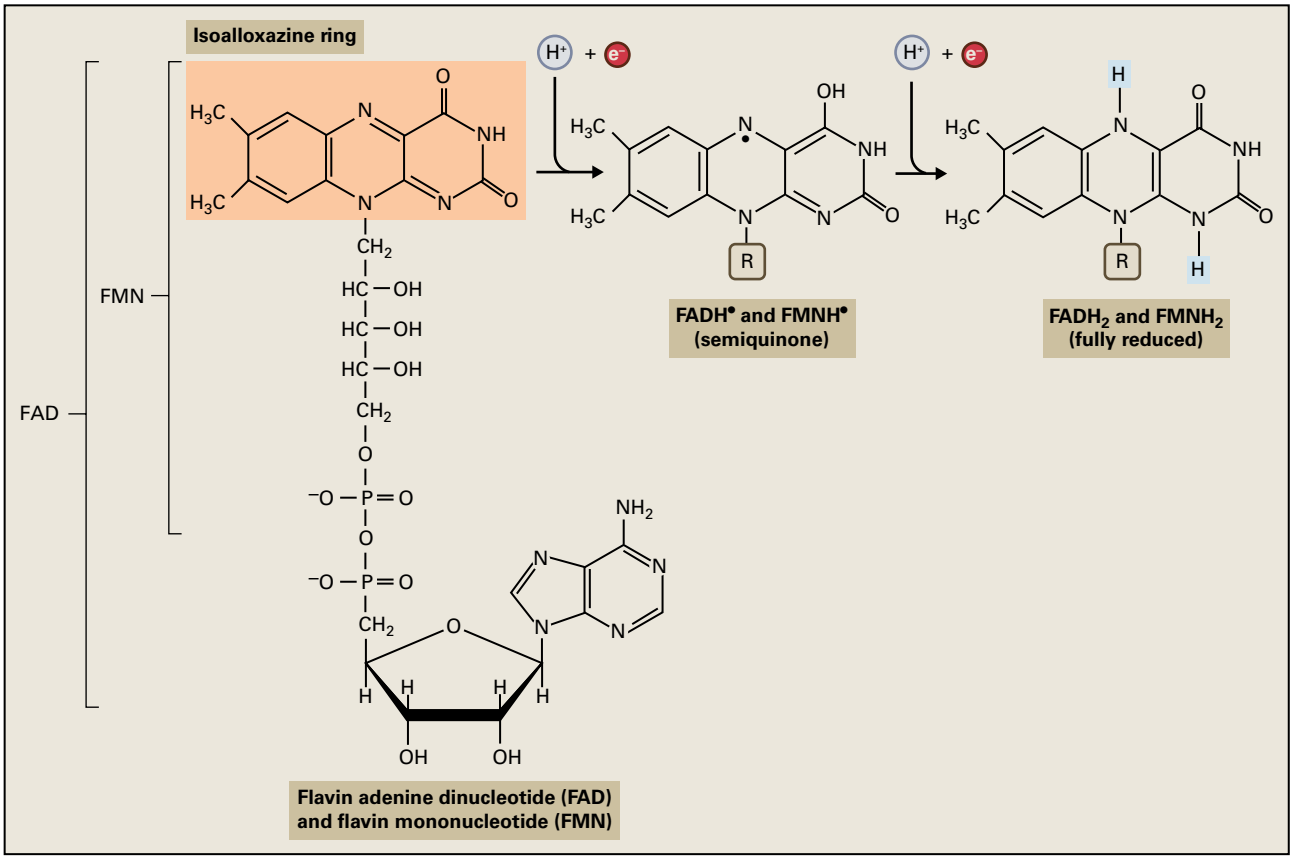


FIGURE 14.4 *Structure and redox chemistry of the flavin coenzymes, flavin adenine dinucleotide (FAD) and flavin mononucleotide (FMN). FAD and FMN differ in the nature of the substituent R-groups attached to the redox-active isoalloxazine ring system common to both coenzymes. The fully oxidized form (FAD or FMN) gains one electron plus one proton in each of two sequential reactions, forming first a semiquinone ($FADH^{\cdot}$ or $FMNH^{\cdot}$) and then the fully reduced species ($FADH_2$ or $FMNH_2$).*

(Fig. 14.4), yielding NADH and $FADH_2$. The citric acid cycle also phosphorylates ADP directly (Fig. 14.5 and Table 14.1). Finally, in the inner mitochondrial membrane, the reduced cofactors generated during glycolysis and the citric acid cycle are oxidized by a set of electron transfer proteins that ultimately donate the electrons to O_2, producing H_2O. The large amount of free energy released during this electron transfer is used to drive the formation of a proton gradient across the inner mitochondrial membrane, and the energy stored in this electrochemical gradient subsequently drives the conversion of ADP and P_i to ATP by a process known as oxidative phosphorylation (Fig. 14.5 and Table 14.1). Not every molecule of sucrose or C_6 unit of starch metabolized via glycolysis and the citric acid cycle, however, is completely oxidized in this manner; many intermediates from these two pathways are diverted along the way to provide the primary carbon building blocks for other important cellular compounds (Fig. 14.6).

14.2 Citric acid cycle

Known by several names, including the tricarboxylic acid cycle and Krebs cycle (after its discoverer, Hans Krebs), the citric acid cycle oxidizes organic acids to produce CO_2 and transfers the resulting electrons to reduce the redox cofactors NAD^+ and FAD, forming NADH and $FADH_2$.

14.2.1 Cytosolic reactions generate products that are transported into the mitochondria to feed the citric acid cycle

The nature of the end product of the glycolytic reactions in the cytosol of plants is determined by the relative activities of the three enzymes that can utilize phospho*enol*pyruvate (PEP) as a substrate. Both pyruvate kinase and PEP phosphatase form pyruvate; PEP carboxylase generates oxaloacetate (OAA) (Fig. 14.7). Pyruvate is transported directly into the mitochondrion. OAA is either transported directly into the mitochondrion or first reduced to malate by cytosolic malate dehydrogenase. The reduction of OAA in the cytosol can provide an extramitochondrial, nonfermentative mechanism for oxidizing NADH formed by glyceraldehyde-3-phosphate dehydrogenase during glycolysis (see Chapter 13).

The mitochondrial inner membrane contains separate carriers by which malate and pyruvate are taken into the mitochondrial matrix (see Section 14.7.1). Once in the

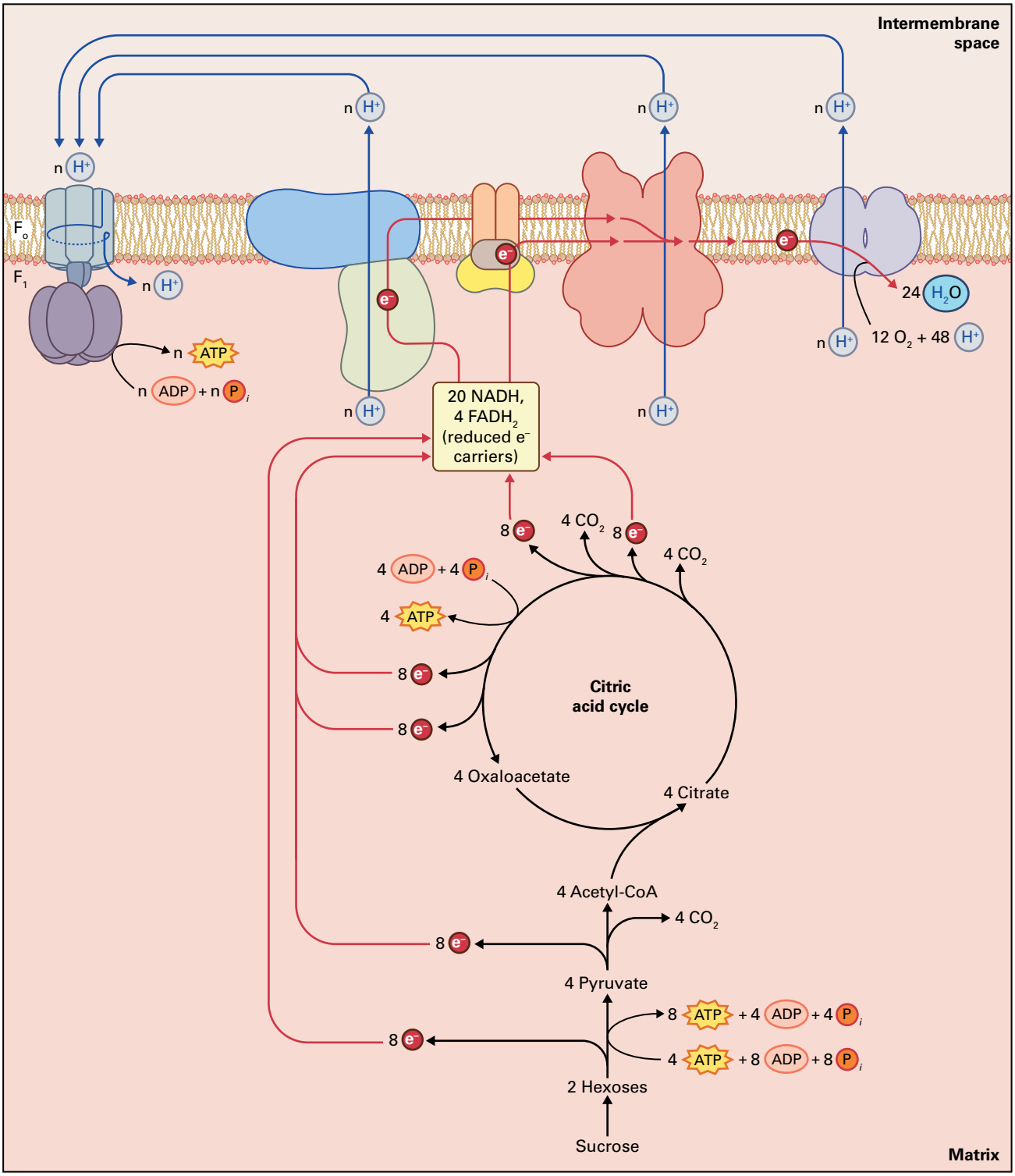


FIGURE 14.5 *General mechanism of oxidative phosphorylation in mitochondria. Electrons released during the oxidative steps of glycolysis and the citric acid cycle produce 20 molecules of NADH and 4 molecules of $FADH_2$. These reduced coenzymes are subsequently oxidized by the mitochondrial electron transport chain. The free energy released during mitochondrial electron transfer is coupled to the translocation of protons across the inner mitochondrial membrane (from the matrix into the intermembrane space), which generates a proton electrochemical gradient ($\Delta\mu H^+$) across the inner membrane. As protons move back across the inner membrane through the F_o proton channel of the ATP synthase complex, the free energy released is used by the complex's F_1 component to catalyze conversion of ADP and P_i to ATP in the mitochondrial matrix. The efficiency of net H^+ transfer and ATP synthesis can vary (n), see Table 14.1 and Section 14.4.3 for details.*

TABLE 14.1 *Net stoichiometry of sucrose oxidation.*

Metabolic pathway	Substrates	Products	ATP yield, number of molecules
Glycolysis			
	1 Sucrose	4 Pyruvate	
	4 ADP + 4 P_i	4 ATP	4
	4 NAD^+ (cytosolic)	4 NADH (cytosolic)	
Citric acid cycle			
	4 Pyruvate	12 CO_2	
	4 ADP + 4 P_i	4 ATP	4
	16 NAD^+ (mitochondrial)	16 NADH (mitochondrial)	
	4 FAD	4 $FADH_2$	
Oxidative phosphorylation			
	12 O_2	24 H_2O	
	4 NADH (cytosolic)	4 NAD^+ (cytosolic or mitochondrial)[a]	6–10*†
	16 NADH (mitochondrial)	16 NAD^+ (mitochondrial)	40†
	4 $FADH_2$	4 FAD	6†
Cumulative ATP yield			60–64*†

*Oxidation of cytosolic NADH by external NADH dehydrogenase (see Section 14.3.4) supports the same level of ATP synthesis as oxidation of mitochondrial $FADH_2$. However, if cytosolic NADH is imported into the mitochondrion via the malate–aspartate shuttle (see Fig. 14.36), it can support the same level of ATP synthesis as oxidation of mitochondrial NADH.
†Assuming oxidation of 1 mitochondrial NADH supports the synthesis of 2.5 ATP and that oxidation of $FADH_2$ supports the synthesis of 1.5 ATP (see Section 14.4.3).

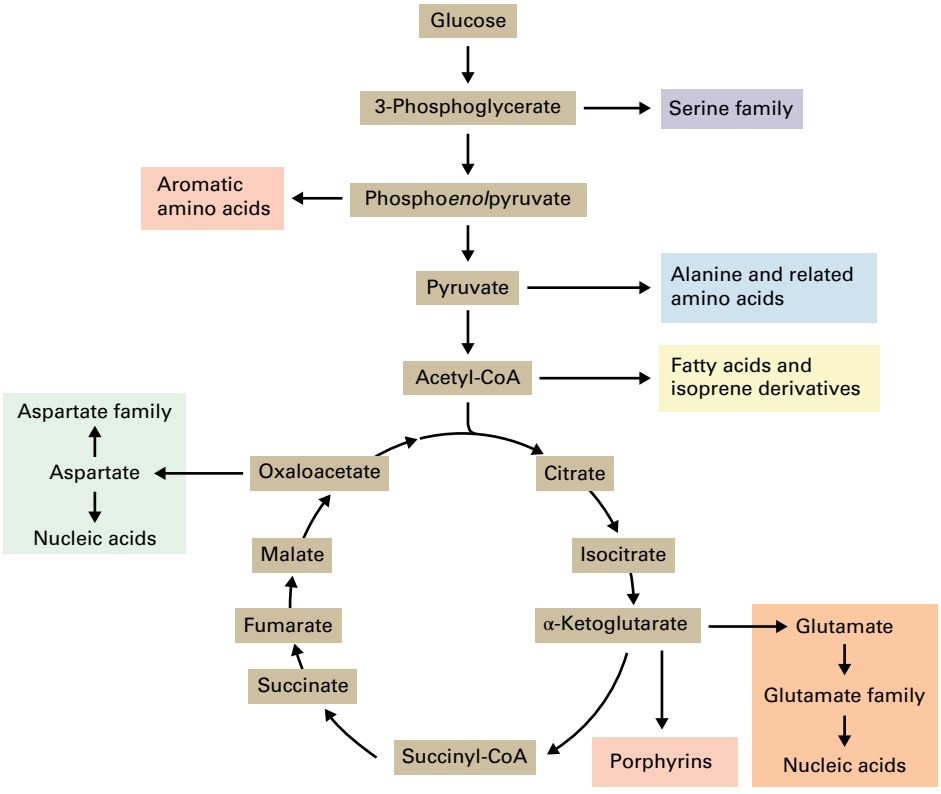


FIGURE 14.6 *Intermediates produced during the reactions of glycolysis and the citric acid cycle serve as substrates for numerous plant biosynthetic pathways. The primary intermediates for the production of amino acids, lipids, nucleic acids, cell wall sugars, and many other essential components of the plant cell are derived from compounds that originate from glycolysis or the citric acid cycle.*

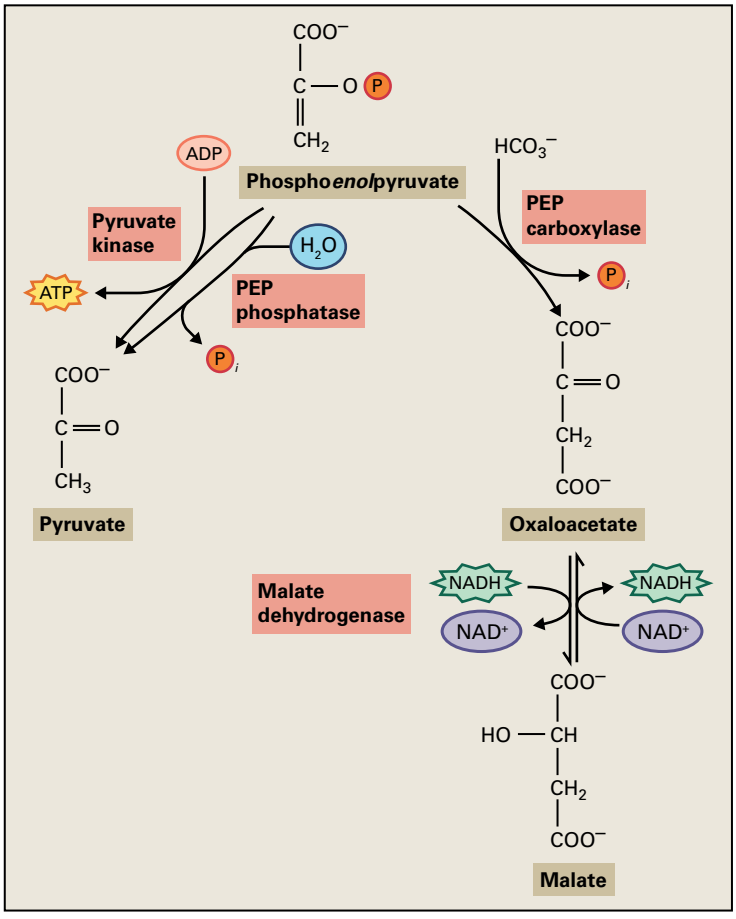


FIGURE 14.7 *Conversion of phosphoenolpyruvate (PEP) to pyruvate or malate during plant respiration. The conversion of PEP to pyruvate by the enzyme pyruvate kinase is coupled to phosphorylation of ADP. PEP phosphatase can bypass this ATP synthesis step, releasing P_i. Alternatively, PEP can react with bicarbonate ion (HCO_3^-) via the enzyme PEP carboxylase, releasing P_i and producing the C_4 product, oxaloacetate (OAA). OAA is commonly reduced to malate by NADH through the action of malate dehydrogenase. Both pyruvate and malate can be readily transported into mitochondria via carriers located in the inner mitochondrial membrane (see Fig. 14.36).*

matrix, malate can be oxidized by either of two enzymes: a mitochondrial isoenzyme of malate dehydrogenase that yields OAA and NADH, or an NAD^+-linked malic enzyme that generates pyruvate, CO_2, and NADH (Fig. 14.8). Therefore, uptake of malate from the cytosol effectively transfers reducing equivalents into the mitochondrion. The operation of both malate dehydrogenase and NAD^+-linked malic enzyme increases metabolic flexibility, allowing plants to regulate specific portions of the citric acid cycle in different tissues.

14.2.2 Pyruvate enters the citric acid cycle through the action of the pyruvate dehydrogenase complex

Before entering the citric acid cycle proper, pyruvate is oxidized and decarboxylated by the pyruvate dehydrogenase complex to form CO_2, acetyl-CoA, and NADH. The pyruvate dehydrogenase enzyme complex, which requires the bound cofactors thiamine pyrophosphate (TPP), lipoic acid, and FAD as well as free coenzyme A (CoASH) and NAD^+, links glycolysis to the citric acid cycle. The complex contains three separate enzymes: pyruvate dehydrogenase, dihydrolipoyl transacetylase, and dihydrolipoyl dehydrogenase (Fig. 14.9).

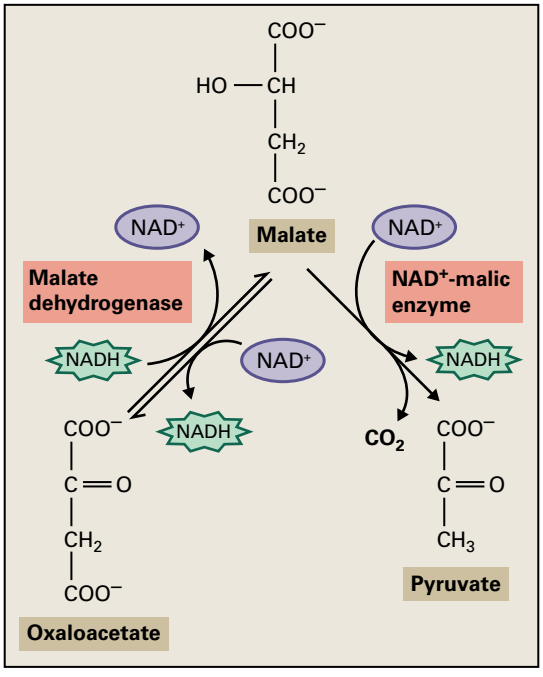


FIGURE 14.8 *Alternative routes for the oxidation of malate in plant mitochondria. Once transported into the mitochondrion, malate can be acted on by malate dehydrogenase, which couples the oxidation of malate to the reduction of NAD^+ to produce OAA and NADH, or by NAD^+-malic enzyme, which catalyzes the oxidative decarboxylation of malate to pyruvate and CO_2 and the concomitant reduction of NAD^+ to NADH. Both enzymes are located in the mitochondrial matrix.*

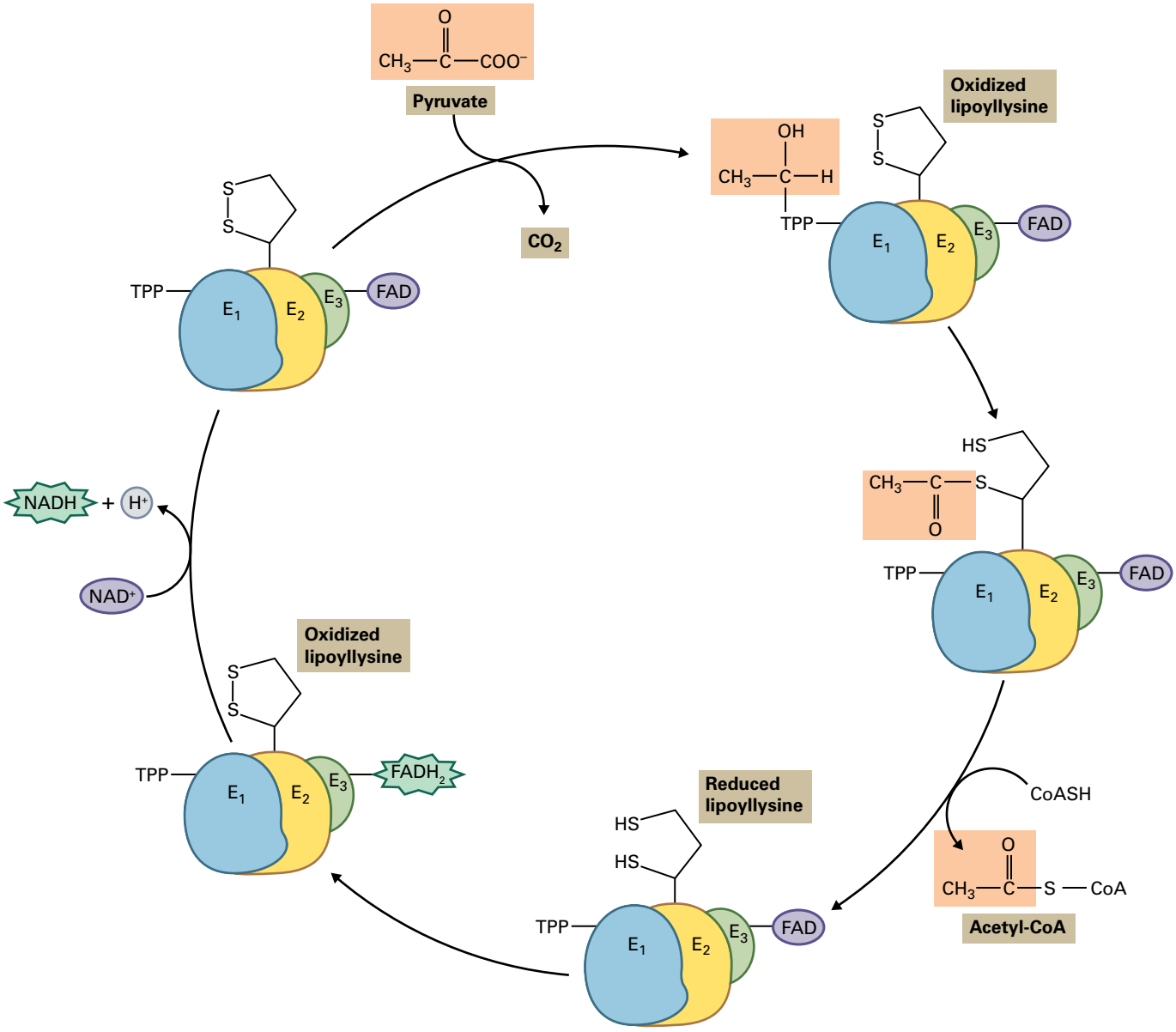


FIGURE 14.9 *Reaction sequence catalyzed by the pyruvate dehydrogenase complex. The overall reaction catalyzed by this complex involves the oxidative decarboxylation of pyruvate and leads to the formation of acetyl-CoA, CO_2, and NADH. The enzyme pyruvate dehydrogenase (E_1) initially catalyzes the decarboxylation of pyruvate to produce acetaldehyde, a C_2 product that reacts with bound thiamine pyrophosphate (TPP) to form hydroxyethyl-TPP. The hydroxyethyl derivative is transferred to the oxidized lipoamide group of dihydrolipoyl transacetylase (E_2), forming the acetyl thioester of reduced lipoic acid. E_2 then transfers the acetyl unit to the thiol moiety of coenzyme A (CoASH) to give acetyl-CoA and a fully reduced lipoamide group on the dihydrolipoyl transacetylase. Dihydrolipoyl dehydrogenase (E_3) then catalyzes the transfer of two electrons and two protons from the reduced lipoamide group of E_2 to the bound FAD of E_3, oxidizing the lipoamide and producing $FADH_2$. In the final reaction of the series, E_3 transfers two electrons and a proton to NAD^+, yielding NADH.*

Sophisticated regulatory mechanisms control the activity of the pyruvate dehydrogenase complex. In addition to feedback inhibition by its products, NADH and acetyl-CoA, pyruvate dehydrogenase activity is regulated by a kinase/phosphatase couple. ATP-dependent phosphorylation catalyzed by pyruvate dehydrogenase kinase inhibits the complex, and removal of the phosphate by pyruvate dehydrogenase phosphatase restores activity (Fig. 14.10). Pyruvate inhibits the kinase, ensuring that the dehydrogenase is active when substrate is plentiful. Ammonium ions (NH_4^+) activate the kinase (see Section 14.7.6).

14.2.3 The citric acid cycle generates reducing equivalents, CO_2, and ATP

As the citric acid cycle proper begins, acetyl-CoA and OAA condense to form the C_6 molecule citrate and free CoASH (Fig. 14.11) in a reaction catalyzed by citrate synthase. Aconitase then isomerizes citrate to isocitrate. Next, NAD^+-linked isocitrate dehydrogenase oxidatively decarboxylates isocitrate to form CO_2, α-ketoglutarate, and NADH. The α-ketoglutarate is oxidized further to succinyl-CoA, CO_2, and

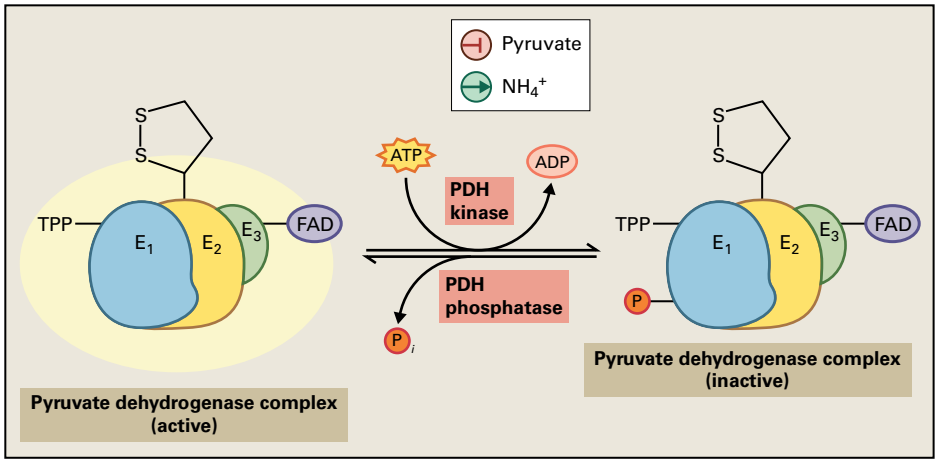


FIGURE 14.10 *Regulation of the pyruvate dehydrogenase (PDH) complex by phosphorylation/dephosphorylation. PDH kinase inactivates the PDH complex by catalyzing the phosphorylation of E_1. Reactivation involves subsequent dephosphorylation by a PDH phosphatase. Pyruvate and ammonium ions (NH_4^+) are allosteric modifiers that regulate the activity of PDH kinase.*

NADH in a reaction catalyzed by the α-ketoglutarate dehydrogenase enzyme complex. The structure of this enzyme complex is similar to that of the pyruvate dehydrogenase complex, and the reaction catalyzed is chemically analogous to the formation of acetyl-CoA from pyruvate (see Fig. 14.9). The reaction mechanisms are very similar: for example, lipoamide participates in the α-ketoglutarate dehydrogenase reaction, and dihydrolipoyl dehydrogenase is the same in both complexes.

Succinyl-CoA synthetase catalyzes the conversion of succinyl-CoA to succinate, with the concomitant phosphorylation of ADP to ATP; this is the only citric acid cycle reaction that conserves energy directly by forming ATP. In plants, this enzyme differs from its animal counterpart in being specific for ADP rather than GDP. Succinate dehydrogenase, which catalyzes the oxidation of succinate to fumarate, is the only membrane-associated enzyme of the citric acid cycle and represents the catalytic component of complex II of the respiratory electron transport chain (see Section 14.3.2).

Fumarase reversibly hydrates fumarate to form malate, and malate dehydrogenase catalyzes the final step of the citric acid cycle, oxidizing malate to OAA and producing NADH. The reaction is freely reversible, but the equilibrium in vitro strongly favors the reduction of OAA. In vivo, however, the products are consumed rapidly; OAA condenses with acetyl-CoA to produce citrate, and NADH is oxidized by the respiratory electron transport chain. This shifts the malate dehydrogenase steady state toward product formation. Malate dehydrogenase is inhibited by its product, NADH, and by acetyl-CoA.

Whereas most citric acid cycle enzymes are NAD^+-linked, $NADP^+$-dependent isoforms of isocitrate dehydrogenase and malate dehydrogenase also exist. The NADPH produced by these enzymes has many possible fates. The electron transport chains of plant mitochondria can oxidize matrix NADPH (see Section 14.3.5), and several mitochondrial reactions use NADPH as an electron donor. These include reduction of dihydrofolate to tetrahydrofolate, a substrate for the C_2 photorespiratory cycle (see Section 14.9); production of reduced glutathione, which protects against reactive oxygen species (ROS) generated during mitochondrial electron transfer (see Section 14.3.7); and reduction of thioredoxin (see Section 14.3.6).

Overall, during the pyruvate dehydrogenase reaction and one subsequent turn of the citric acid cycle proper, the three carbon atoms of pyruvate are released as CO_2, one molecule of ATP is formed directly, and four NADH and one $FADH_2$ molecules are produced (Fig. 14.11). This stoichiometry assumes the $NADP^+$-dependent isoforms of isocitrate and malate dehydrogenase do not participate in the reaction.

14.2.4 The citric acid cycle can oxidize amino acids, but fatty acid oxidation normally occurs in the peroxisome

Pyruvate, malate, and OAA from glycolysis are typically the most prevalent mitochondrial substrates in vivo, especially in the dark or in nonphotosynthetic tissues. However, other compounds are also metabolized in the mitochondrial matrix and interact with the citric acid cycle. Glycine produced during photorespiration is a special case, discussed later in detail (see Section 14.9.2), but other amino acids also serve as substrates for mitochondrial respiration in some tissues, particularly in seeds rich in stored protein. Amino acid oxidation may be preceded by a transamination reaction that generates a citric acid cycle intermediate, or the oxidation may occur directly. One example of direct oxidation within the mitochondrion involves glutamate dehydrogenase, which catalyzes a reversible reaction:

Reaction 14.2: Glutamate dehydrogenase

$$\text{Glutamate} + NAD^+ + H_2O \leftrightarrow \alpha\text{-ketoglutarate} + NADH + NH_4^+$$

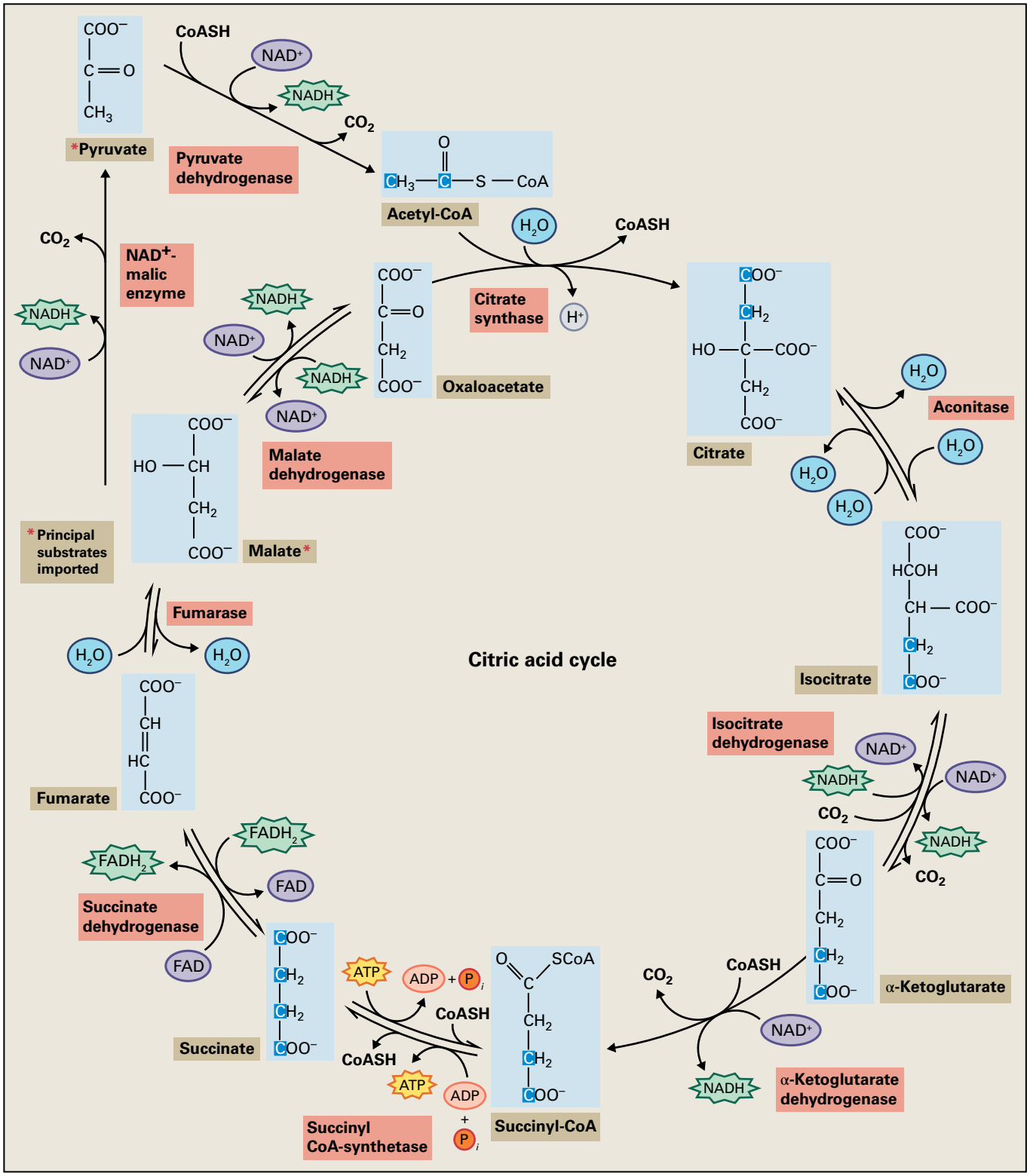


FIGURE 14.11 *Reaction sequence of the citric acid cycle. In a reaction catalyzed by citrate synthase, acetyl-CoA formed by the pyruvate dehydrogenase complex combines with OAA to produce the C_6 tricarboxylic acid citrate. In the overall cycle, the citrate is oxidized to produce two molecules of CO_2 in a series of reactions that leads to the formation of one OAA, three NADH, one $FADH_2$, and one ATP. The resulting OAA reacts with another molecule of acetyl-CoA to continue the cycle. The oxidative decarboxylation of pyruvate yields an additional CO_2 and NADH. Thus the citric acid cycle brings about the complete oxidation of pyruvate to 3 CO_2 plus 10 electrons, which are stored temporarily as 4 NADH and 1 $FADH_2$. Malate, which can be an alternative product of glycolysis in plants (see Fig. 14.7), is converted to pyruvate, CO_2, and NADH by the action of NAD+-malic enzyme. The irreversible reactions of the cycle are identified with solid arrows. The two carbons donated by acetyl-CoA are highlighted through the first symmetrical intermediate, succinate, at which point they become randomized and can no longer be traced.*

The role of this enzyme is not apparent in all plant tissues. In cotyledons of some legumes (e.g., pea and soybean), glutamate dehydrogenase and mitochondrial aspartate aminotransferase participate in the degradation of stored protein, oxidizing glutamate as a source of energy. The NH_4^+ released by this catabolic reaction is typically reassimilated (see Chapter 7). In leaves, glutamate dehydrogenase has been proposed to operate in the reverse direction as an ancillary enzyme in the reassimilation of NH_4^+ released during photorespiration, although screens for photorespiratory mutants of barley (*Hordeum vulgare*) and *Arabidopsis* did not identify plants deficient in glutamate dehydrogenase (see Chapter 7).

β-Oxidation of fatty acids to acetyl-CoA occurs in animal mitochondria; however, most fatty acid oxidation in plants takes place in peroxisomes (see Chapter 9). Mitochondria do participate in gluconeogenesis, a specialized interaction that enables plants to convert lipids to sugars (see Section 14.7.4), whereas animals lack this synthetic capability.

14.3 Plant mitochondrial electron transport

The mitochondrial electron transport chain conserved among eukaryotes consists of four membrane-bound, multiple-subunit protein complexes, commonly referred to as complexes I–IV (Fig. 14.12). These protein complexes catalyze the multistep transfer of electrons from NADH and $FADH_2$ to O_2, forming H_2O and translocating protons from the matrix to the intermembrane space. In this way, an **endergonic** (energy-consuming) reaction—proton pumping—is driven by the **exergonic** (energy-releasing) transfer of electrons from strong reducing agents to a strong oxidant. The reduction of $½O_2$ by two electrons from NADH involves a reduction potential difference ($\Delta E°'$) of 1.14 V (Fig. 14.13). This translates to 219.2 kJ of free energy released for every mole of NADH oxidized. If NADH or $FADH_2$ reduced O_2 directly, the heat released would not be biologically useful. The electron transport chain facilitates several modestly exergonic redox reactions, rather than a single explosive one, and conserves energy through proton translocation. The F_oF_1–ATP synthase (sometimes called complex V) does not have electron transfer activity, but it provides a path for proton diffusion into the matrix and uses the free energy released by this spontaneous diffusion to drive the phosphorylation of ADP.

14.3.1 The electron transport chain contains both peripheral and integral membrane proteins and a lipid-soluble quinone

The standard electron transport chain conserved among all aerobic eukaryotes is also sometimes called the cytochrome pathway, and contains four complexes (complexes I–IV) with

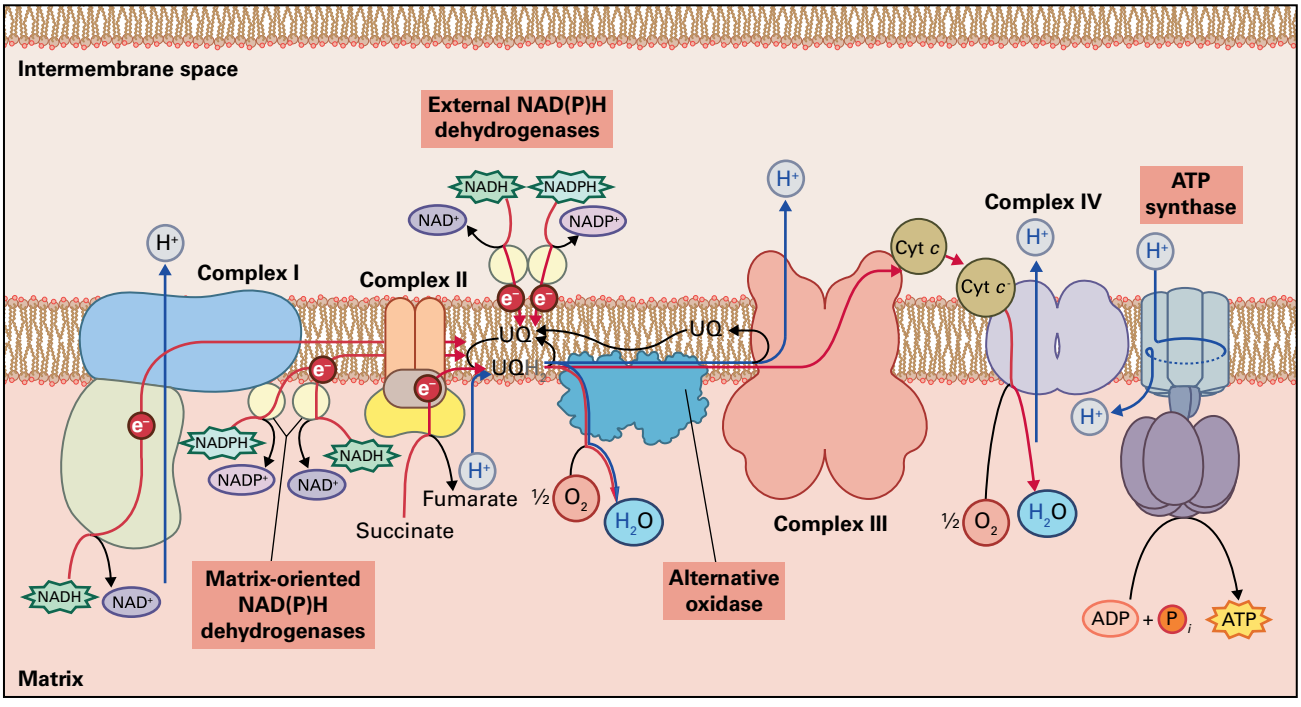


FIGURE 14.12 *Organization of the plant mitochondrial electron transport chain and ATP synthase in the inner mitochondrial membrane. Electron transfer complexes I–IV, ATP synthase, alternative NAD(P)H dehydrogenases, and the alternative oxidase (AOX) are diagrammed, incorporating what is currently known about their topological orientation in the inner membrane. Red lines indicate electron transfer pathways. A large pool of oxidized ubiquinone (UQ) and reduced ubiquinol (UQH_2) freely diffuses within the inner membrane and transfers electrons derived from the dehydrogenases to either complex III or the AOX. Blue arrows designate the direction of proton translocation at complexes I, III, and IV. Transmembrane proton movement generates a proton electrochemical gradient that drives the synthesis of ATP from ADP and P_i via the ATP synthase.*

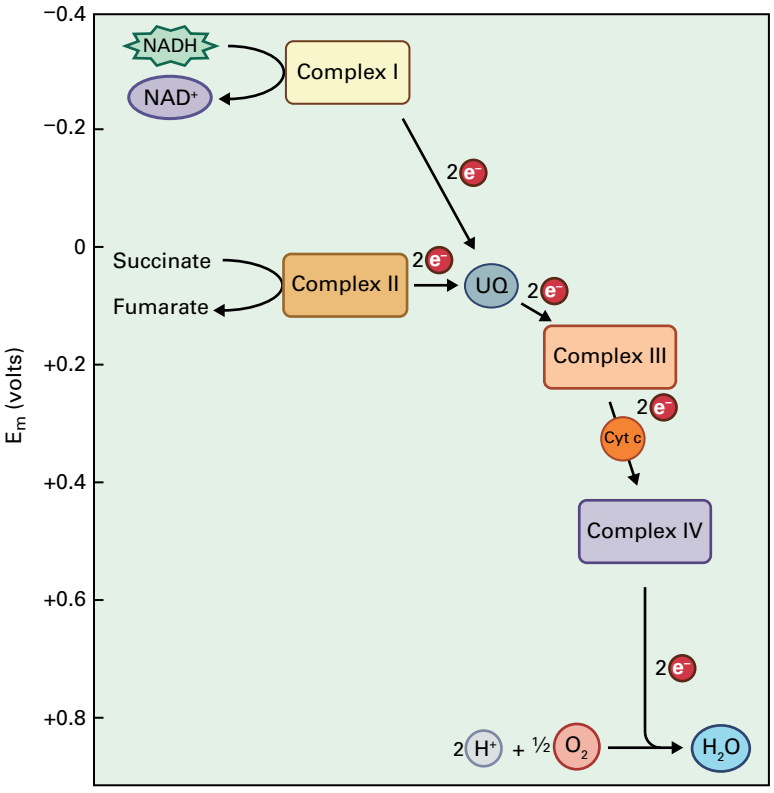


FIGURE 14.13 *Approximate positions of the components of the respiratory chain on the redox potential scale. Release of energy drives proton translocation at three sites on the chain: between complex I and ubiquinone (UQ); between UQ and cytochrome c; and between cytochrome c and complex IV.*

multiple protein subunits, as mentioned above. Some of these protein subunits are encoded by mitochondrial genes, and others by nuclear genes. Complex I is an NADH dehydrogenase that oxidizes the NADH generated in the mitochondrial matrix by citric acid cycle activity, regenerating NAD^+. Complex II (succinate dehydrogenase), which is also a component enzyme of the citric acid cycle, oxidizes succinate to fumarate. Both complex I and complex II transfer electrons to ubiquinone, an abundant, mobile electron transfer cofactor that consists of a substituted *p*-benzoquinone head group and a C_{45} to C_{50} prenyl side chain (Fig. 14.14). Ubiquinone can carry one or two electrons. Both fully oxidized ubiquinone and fully reduced ubiquinol molecules are highly hydrophobic and capable of transverse and lateral movement within the inner membrane. A free pool of ubiquinone, present at concentrations far in excess of the proteins with which it interacts, shuttles electrons from complexes I and II to complex III.

Complex III transfers electrons from ubiquinol to cytochrome *c*, the only protein in the electron transport chain not tightly associated with an integral membrane protein complex (see Fig. 14.12). Cytochrome *c*, a small (12.5 kDa), peripheral membrane protein located on the outer surface of the inner membrane and exposed to the intermembrane space, carries one electron at a time from complex III to complex IV (cytochrome-*c* oxidase), the terminal electron carrier in the electron transport chain. For every four molecules of cytochrome *c* oxidized, one molecule of O_2 is reduced to two molecules of H_2O.

Numerous electron transport cofactors are associated with the proteins of the electron transport chain. These include bound FAD and FMN molecules (see Fig. 14.6), hemes (Fig. 14.15), iron–sulfur (Fe–S) centers (Fig. 14.16), and copper atoms.

Proteomic analysis using peptide mass spectrometry has revealed the electron transfer complexes of the cytochrome pathway in plants include unique proteins. While 85% of the proteins in these complexes are clear homologs of proteins found in the same complexes in most other eukaryotes, approximately 15% of the proteins are either plant specific or are shared among plants and algae but are absent from yeast and animals. The roles of most of these unique proteins have not yet been clarified.

In addition to the cytochrome pathway, plant mitochondria also possess dehydrogenases on each face of the inner membrane that can oxidize NAD(P)H, and an alternative oxidase that can reduce O_2 without pumping protons (see Fig. 14.12). The free energy released as electrons flow through them is lost as heat, however, and cannot be used for ATP synthesis.

14.3.2 Three of the four respiratory complexes located in the inner mitochondrial membrane participate in proton translocation

Complex I is a large multisubunit complex of approximately 45 polypeptides. Depending on the species, the plant mitochondrial genome may encode as many as nine complex I components. The plant mitochondrial complex I is similar to

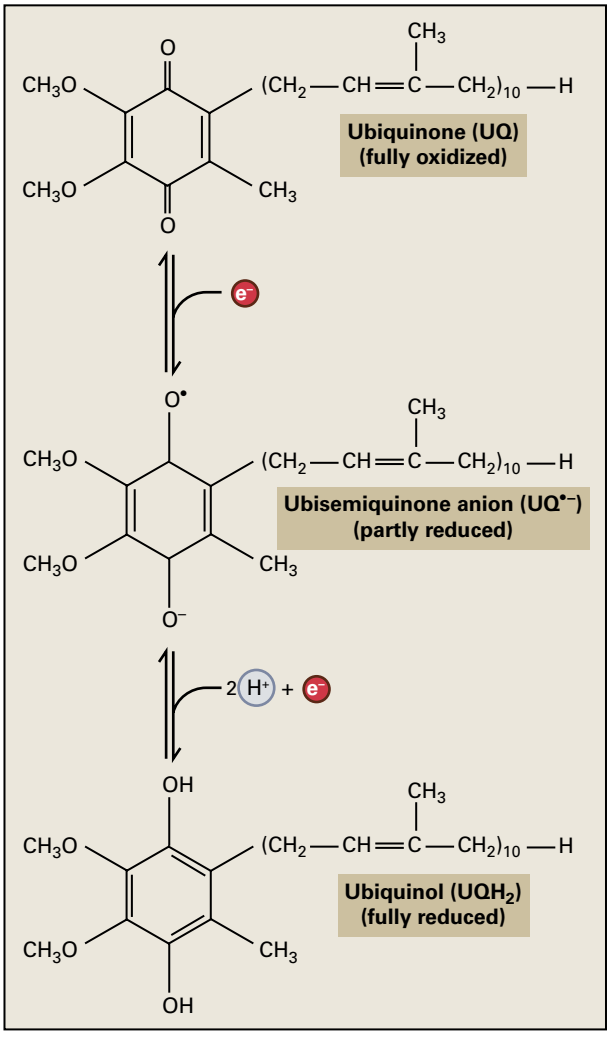


FIGURE 14.14 *Structure and redox reactions of ubiquinone. Reduction of oxidized ubiquinone (UQ) with one electron forms the ubisemiquinone anion ($UQ^{\bullet -}$). The second reduction step involves the addition of an electron and two protons to give the fully reduced ubiquinol (UQH_2). The hydrophobic prenyl side chain, which in plants commonly contains 45 or 50 carbons, retains UQ near the center of the inner membrane, between adjacent leaflets of the phospholipid bilayer.*

the mammalian and fungal NADH dehydrogenase complexes, but it contains a number of plant-specific components. Electron microscopic analysis of purified complex I from *Arabidopsis* indicates the complex has a pronounced L-shape, just like the complex in the bread mold *Neurospora crassa* and bovine heart and the X-ray structure of the bacterial enzyme (Fig. 14.17B).

Complex I oxidizes NADH produced by the reactions of the citric acid cycle and by other NAD^+-linked enzymes in the matrix. The transfer of electrons from NADH to UQ by complex I leads to long-range conformational changes in four antiporter domains in the membrane arm of the complex that propagate the translocation of protons across the membrane (Fig. 14.17A). Complex I is inhibited specifically by the plant-derived flavonoid rotenone (a rat poison) and its analogs, which appear to act at or near the site of ubiquinone reduction (Fig. 14.18).

Complex II, the smallest of the four electron transfer complexes, consists of four proteins of sizes 70, 27, 15, and 13.5 kDa (Fig. 14.19A,B). In gymnosperms and angiosperms, complex II contains no mitochondrial products, making this the only respiratory complex encoded entirely by nuclear genes. However, the mitochondria of the liverwort *Marchantia polymorpha* encode the two smaller polypeptides, and in the red alga *Chondrus crispus*, only the largest subunit is encoded in the nucleus. Unlike complex I, complex II does not translocate protons, so succinate oxidation is linked to the synthesis of less ATP than is NADH oxidation. Malonate, an analog of succinate, is a strong competitive inhibitor of succinate dehydrogenase activity (see Fig. 14.18). The crystal structure of porcine heart complex II shows the protein environments around prosthetic groups with their unique midpoint redox potentials; two ubiquinone binding sites have been identified by inhibitor binding (Fig. 14.19).

Complex III, also known as the cytochrome bc_1 complex, includes a 42-kDa cytochrome with two *b*-type hemes (named b_{566} and b_{560} for the wavelengths of their α-band absorbance peaks), a 31-kDa cytochrome c_1, a 27-kDa Rieske-type Fe–S protein, and five additional polypeptides (Fig. 14.20). The largest polypeptides in complex III are known as core proteins; in the plant complex these range in size from 51 to 55 kDa. Complex III has two quinone-binding sites, one that oxidizes ubiquinol (Center P) and one that reduces ubiquinone (Center N). These binding sites and the electron transport cofactors described above participate in a proton translocation mechanism known as the Q cycle (see Section 14.3.3). The widely utilized inhibitor antimycin A binds to Center N to block reduction of ubiquinone, and myxothiazol, another commonly used inhibitor of complex III in mitochondria, blocks the oxidation of ubiquinol at Center P (see Fig. 14.18).

The final complex of the standard respiratory chain is complex IV, cytochrome-*c* oxidase. As its name implies, this complex accepts an electron from reduced cytochrome *c* on the cytosolic side of the inner membrane and eventually donates it to O_2 on the matrix side of the membrane. The complex contains 13 polypeptides in animals and at least as many in plants, the largest three of which are encoded by the mitochondrial genome in most plants. The redox-active species of complex IV include two *a*-type hemes and two copper-containing centers. All four redox centers are located within mitochondrion-encoded subunits I and II (Fig. 14.21A). The elucidation of a high-resolution crystal structure for the mammalian cytochrome-*c* oxidase has confirmed many predictions of the structure–function features of this complex (Fig. 14.21B). Like complex I, cytochrome-*c* oxidase translocates protons across the inner membrane during electron transfer, but while the crystal structure has highlighted several routes that could facilitate the passage of protons across the membrane, it has not yet revealed the proton-pumping mechanism. Inhibitors of complex IV, which include cyanide (CN^-), azide (N_3^-), carbon monoxide (CO), and nitric oxide (NO), compete with O_2 for electrons (see Fig. 14.18).

Direct inhibition of mitochondrial function with inhibitors of the cytochrome pathway, such as antimycin A (an inhibitor

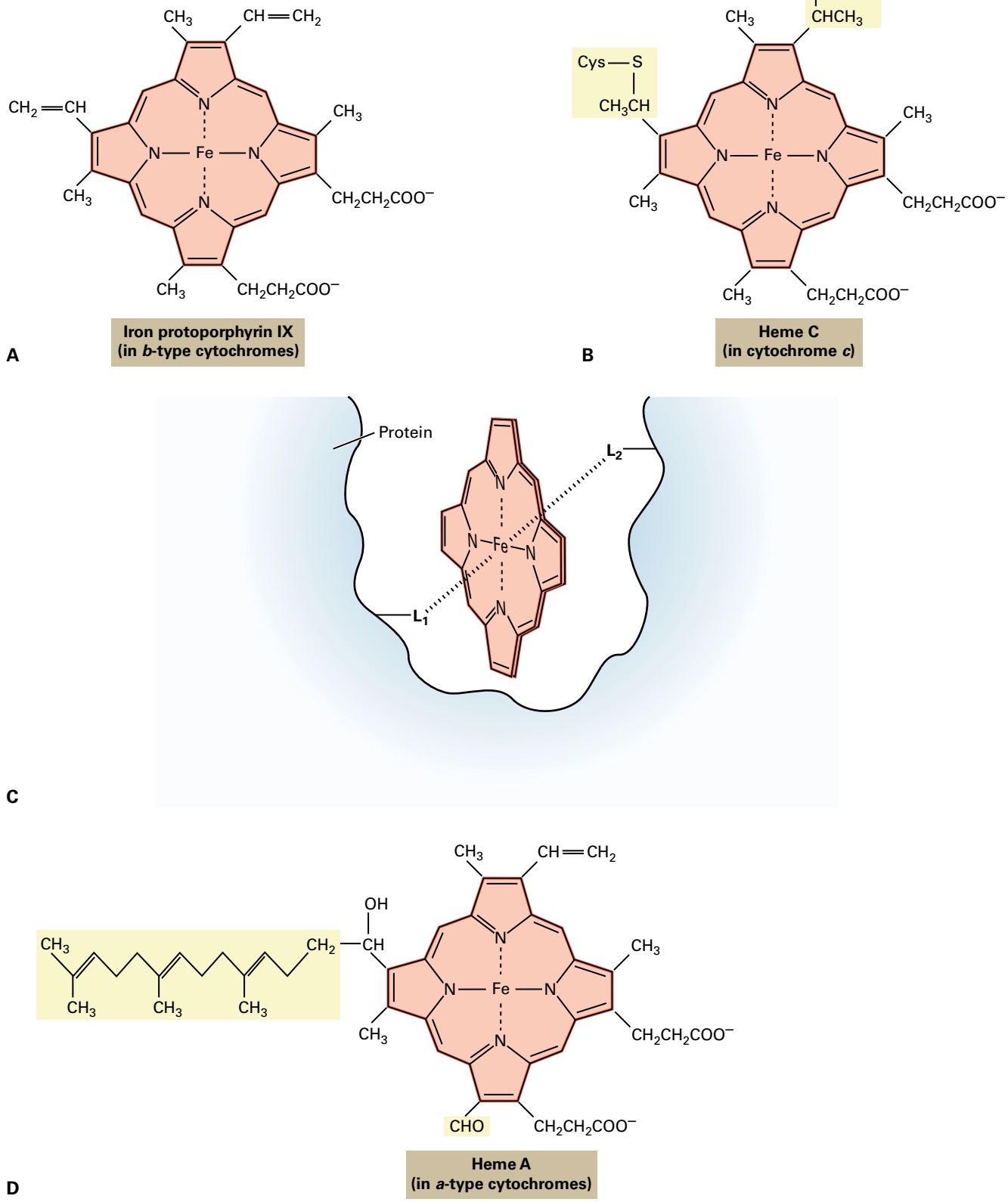


FIGURE 14.15 *Structure of the heme prosthetic groups found in cytochromes. These porphyrin prosthetic groups contain four pyrrole rings linked in a macrocyclic ring system surrounding a central iron atom coordinated to the four pyrrole nitrogen (N) atoms. Both* b*-type (A) and* c*-type (B) cytochromes contain iron protoporphyrin IX, with the iron–porphyrin complex bound to the protein through iron-binding "axial" ligands on either side of the plane of the porphyrin ring system (C). In* c*-type cytochromes, in addition to the axial ligands, the porphyrin is covalently bound to the protein via thioether bonds between the vinyl (-CH=CH$_2$) side chains of the porphyrin and one or two cysteine residues of the protein. The* a*-type cytochromes contain heme A (D), which has a C_{15} isoprenoid tail attached to one of the pyrrole rings and is noncovalently bound to the protein through one or two axial ligands. The cytochromes are located in complexes of the mitochondrial inner membrane: complex III (*b*- and* c*-types) and complex IV (*a*-type).*

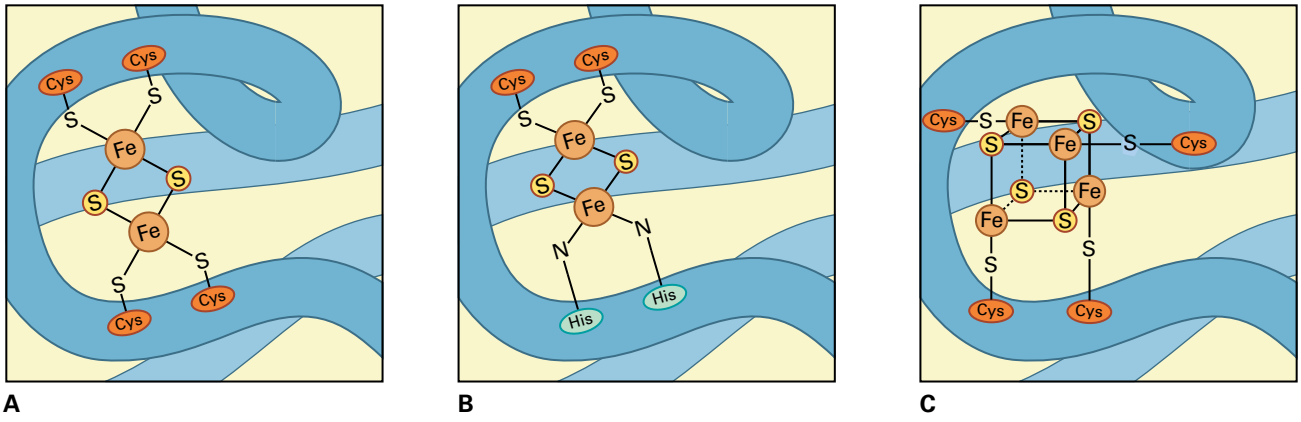


FIGURE 14.16 *Structure of the metal clusters found in iron–sulfur (Fe–S) proteins. Fe–S proteins associated with complexes I and II of the mitochondrial electron transport chain contain both 2Fe–2S clusters and 4Fe–4S clusters. A Rieske Fe–S protein is located in complex III. Four cysteine residues serve as ligands to the Fe atoms of the low-redox potential 2Fe–2S centers (A), whereas the high-redox potential Rieske 2Fe–2S centers are attached to the protein by two cysteine residues and two histidine residues (B). The irons in the 4Fe–4S centers also are bound to the protein through four cysteine ligands (C).*

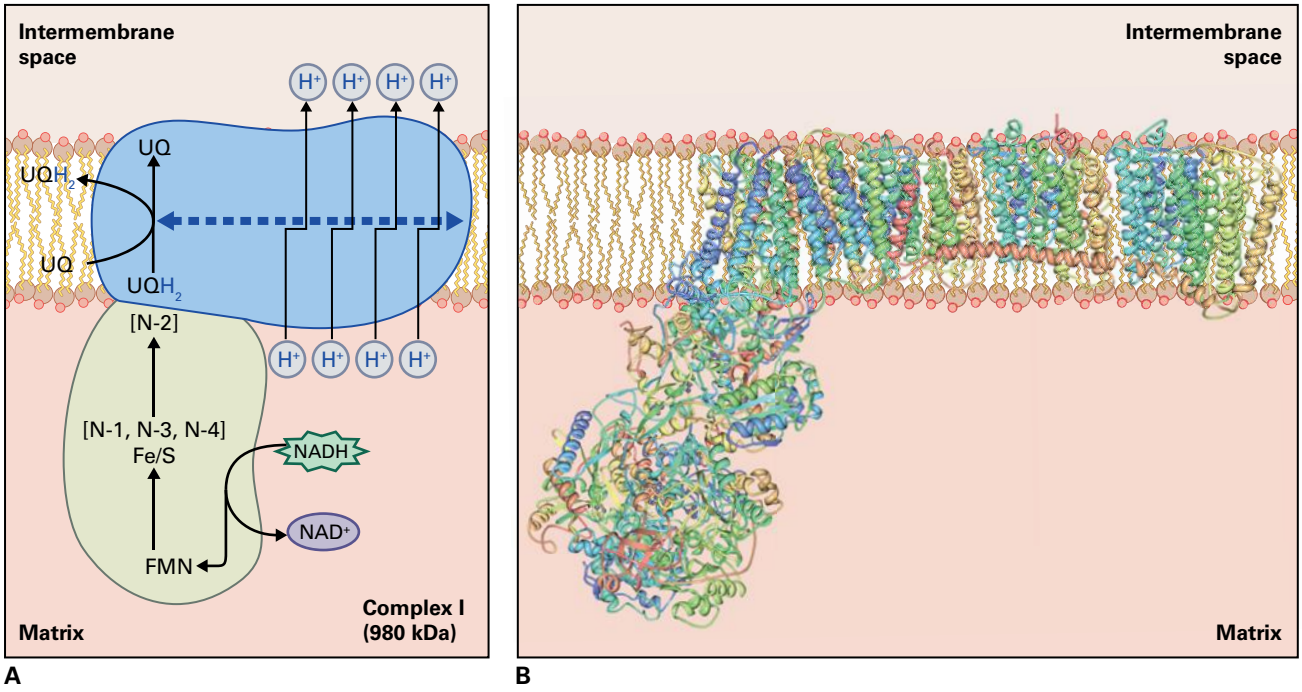
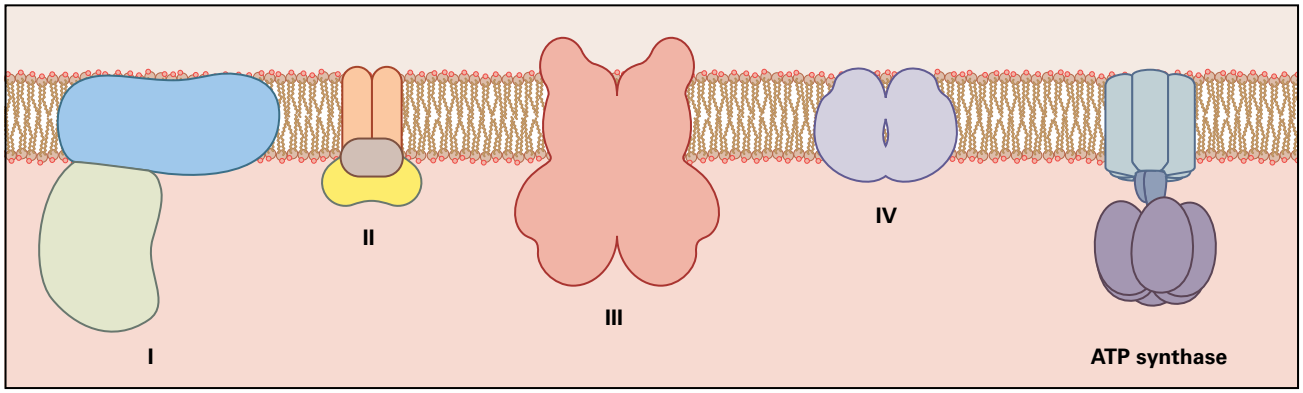


FIGURE 14.17 *Proposed structure and membrane topography of mitochondrial complex I (NADH:UQ oxidoreductase). (A) Complex I transfers electrons from matrix NADH to ubiquinone. This transfer involves FMN and four Fe–S centers (N1–N4). The $H^+/2e^-$ ratio is four, with each H^+ taken across the inner membrane by an antiporter domain in the membrane arm. The complex is readily broken into two smaller complexes, one of which (blue) is very hydrophobic and contains almost all of subunits encoded in the mitochondrion and the antiporter domains. The other arm of the complex (green) protrudes into the matrix and is composed mainly of nucleus-encoded subunits. (B) Structure of the complete complex I from Thermus thermophiles based on PDB entry 4HEA.*

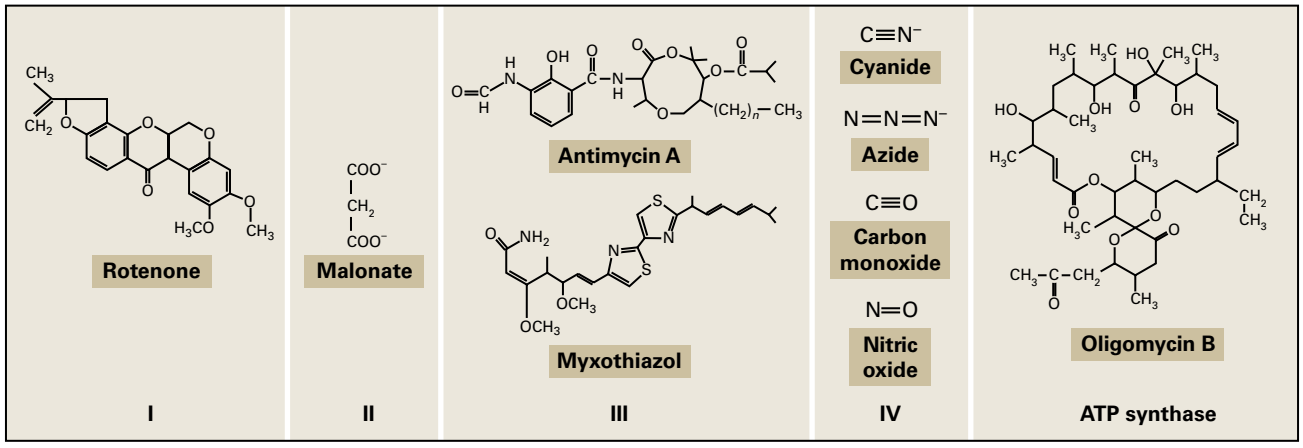
of complex III) and rotenone (an inhibitor of complex I), causes changes in gene expression similar to those seen during aluminum and cadmium stress, viral infection, and cell death induced by H_2O_2 treatment. This indicates the plant stress response is at least in part mediated by mitochondria through mitochondrial–nuclear communication pathways.

14.3.3 Proton pumping at complex III is accomplished by the Q cycle

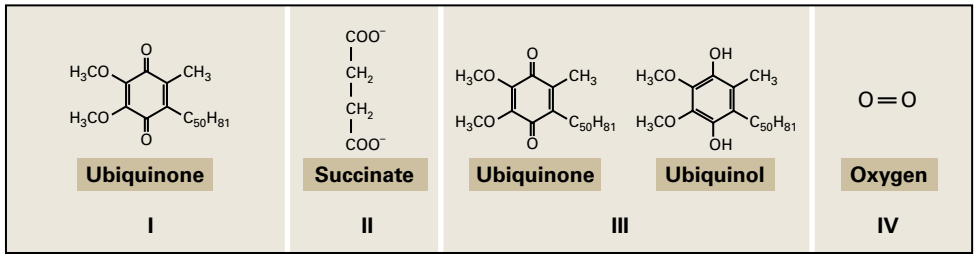
At complex III, transfer of one electron pair from ubiquinol to cytochrome *c* is accompanied by the translocation of four protons across the inner membrane (Fig. 14.22). This



Complex



Inhibitor



Substrate

FIGURE 14.18 *Inhibitors of the mitochondrial electron transport chain and ATP synthase. Specific inhibitors of each of the mitochondrial complexes are shown, as are the substrates with which the inhibitors are thought to compete.*

mechanism, called the Q cycle, presents the best case in which proton translocation by the electron transport chain is largely understood. During the Q cycle, ubiquinone is reduced to ubiquinol on the matrix side of the inner membrane. Three electron transport chain sites can reduce ubiquinone: one each at complexes I and II, and one at Center N on complex III (see Figs. 14.17, 14.19, and 14.20). The reduction is accompanied by the uptake of two protons from the mitochondrial matrix, regardless of which ubiquinone reduction site is utilized. Ubiquinol then diffuses to the outer face of the membrane and binds to Center P, the ubiquinol oxidation site on complex III (Fig. 14.22). Once bound to Center P, the ubiquinol is oxidized; one electron reduces the Rieske Fe–S center, the other reduces cytochrome b_{566}, and two protons are released into the intermembrane space. The electron on the Rieske Fe–S center is subsequently transferred to cytochrome c_1 and then to cytochrome *c*. The electron residing on cytochrome b_{566} is transferred to cytochrome b_{560}, which donates electrons to ubiquinone at Center N.

During operation of the Q cycle, two protons are translocated across the inner membrane for each electron that reduces cytochrome *c*. This stoichiometry occurs because every two ubiquinols oxidized at Center P release four protons

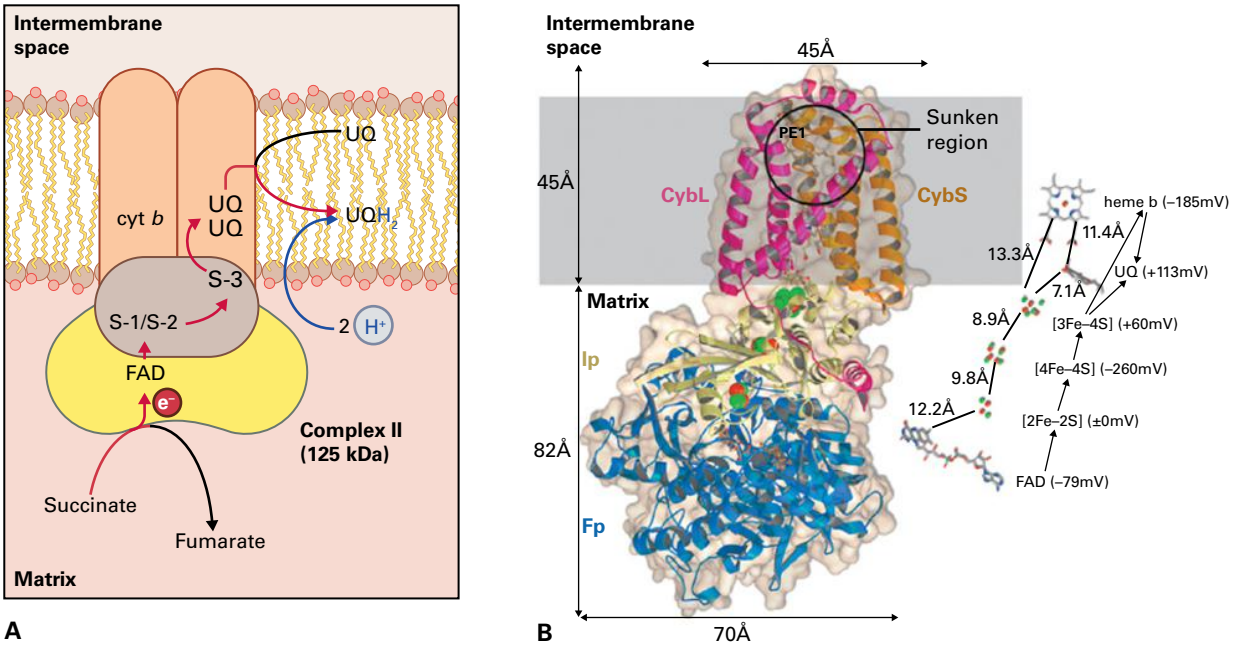


FIGURE 14.19 *Proposed structure and membrane topography of mitochondrial complex II (succinate:ubiquinone oxidoreductase). (A) The two large hydrophilic peripheral subunits that make up succinate dehydrogenase—F_p (flavin protein, yellow), which covalently binds FAD, and I_p (iron protein, brown), which covalently binds Fe–S clusters S-1, S-2, and S-3—are attached to the inner membrane through two small, hydrophobic membrane-spanning subunits (orange) that contain one* b*-type cytochrome and a ubiquinone (UQ) pair, the exact locations of which are uncertain. The proposed path of electron flow is succinate → FAD → S-1/S-2 → S-3 → cyt* b *→ the UQ pair → a UQ molecule from the mitochondrial UQ pool. (B) Ribbon diagram of mitochondrial respiratory complex II based on the crystal structure PDB entry 1ZP0. F_p is shown in blue, iron-sulfur protein (Ip) is shown in cream. The putative membrane region is shaded in gray. On the right side, the prosthetic groups constituting the electron transfer pathway (FAD, [2Fe–2S], [4Fe–4S], [3Fe–4S], and heme* b*) are shown together with ubiquinone (UQ), along with their edge-to-edge distances and midpoint redox potentials. The electron transfer flow at the Qp site is indicated by arrows.*

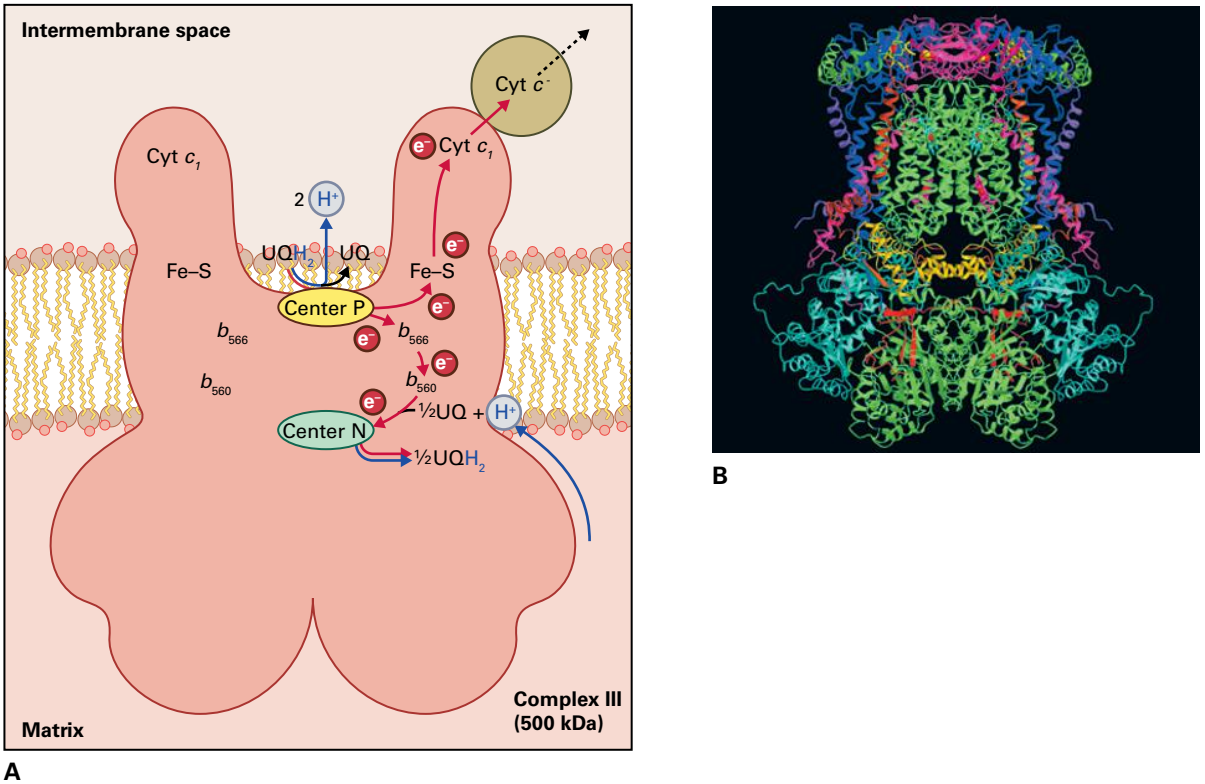
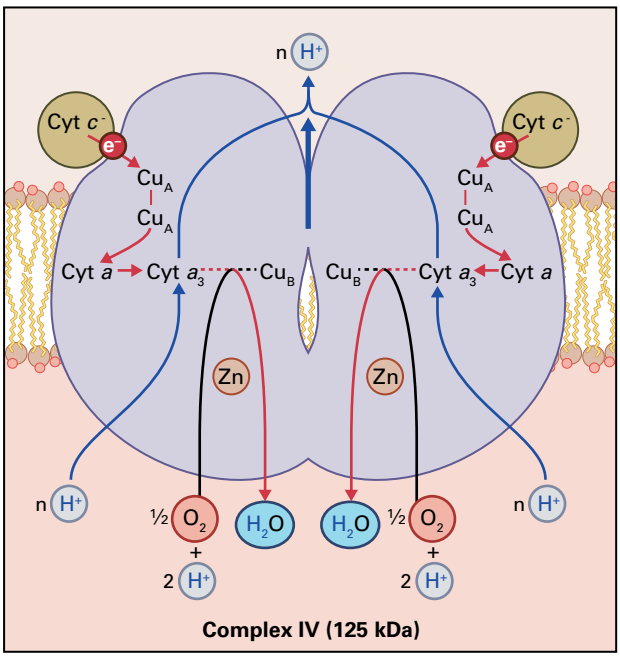
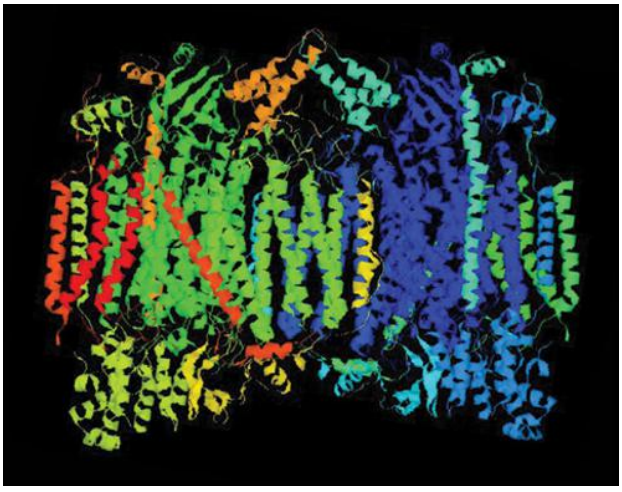


FIGURE 14.20 *Proposed structure and membrane topography of mitochondrial complex III, the cytochrome* bc_1 *complex (ubiquinone:cytochrome-*c *oxidoreductase). (A) The complex is a dimer, with each monomer containing multiple subunits. Ubiquinol (UQH_2) is oxidized at Center P, while ubiquinone (UQ) is reduced at Center N in a two-step process (see Section 14.3.3). The two electrons from UQH_2 take divergent paths, one being transferred to mobile cytochrome* c *via a Rieske Fe–S center and cytochrome* c_1*, the other reaching Center N via two* b*-type cytochromes. The inhibitory sites of antimycin and myxothiazol are at Centers N and P, respectively. (B) Crystal structure of a dimeric mammalian cytochrome* bc_1 *complex based on PDB entry 1BGY.*



A



B

FIGURE 14.21 *Proposed structure and membrane topography of mitochondrial complex IV (cytochrome-c oxidase). (A) The electron transfer center that initially oxidizes reduced cytochrome* c, *Cu_A, contains two copper atoms and resides in subunit II of the complex. All other electron carriers in cytochrome-c oxidase are found on subunit I. From cytochrome* c, *electrons flow initially to Cu_A, and then sequentially to cytochrome* a *and the coupled binuclear metal center formed by cytochrome* a_3 *and Cu_B. The a_3–Cu_B center is the site of O_2 reduction; inhibitors of cytochrome-c oxidase, such as cyanide, also act at this site. The pathway for proton translocation is an active research area and may differ between the bacterial and eukaryotic enzyme, the Zn atom can affect the entry and the exit pathways for protons in the enzyme. (B) Cytosolic view of the crystal structure of the cytochrome-c oxidase from bovine heart based on PDB entry 1OCC.*

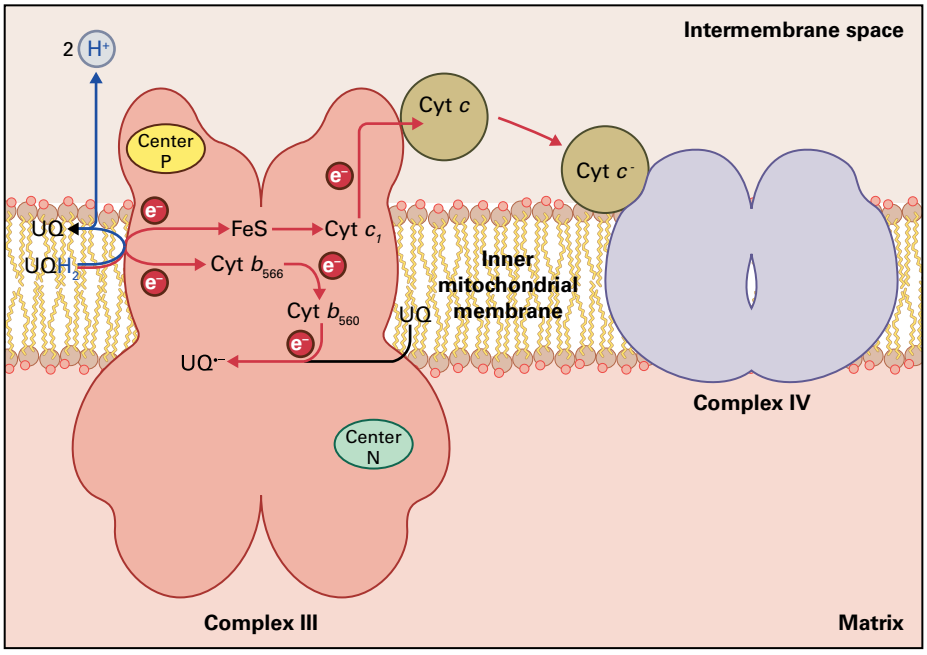
into the intermembrane space, but only two of the four electrons proceed down the electron transport chain to reduce cytochrome *c*. The other two electrons are recycled through the *b*-type hemes to re-reduce one ubiquinone to ubiquinol at Center N (Fig. 14.22).

14.3.4 The electron transport chain is physically organized in supercomplexes of respiratory complexes

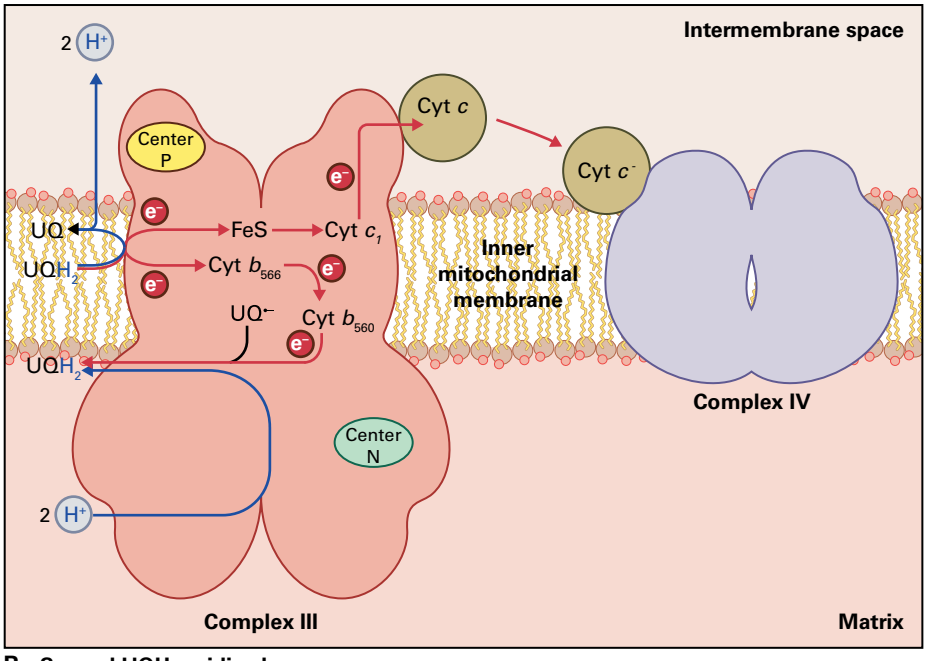
Dissolving the mitochondrial membrane using mild detergents has revealed that the respiratory complexes can form higher order supercomplexes, also called **respirasomes**. The tightest binding members of the respirasome in plants are a monomer of complex I with a dimer of complex III, forming a 1.5-megadalton (MDa) supercomplex; however, there is also strong evidence for other supercomplexes exceeding 1.5 MDa in size that contain complexes I, III, and IV. This higher-order structure may facilitate metabolic channeling during respiratory activity and could help establish and maintain the stable stoichiometries among respiratory complexes that are usually observed in animal and plant mitochondria (Fig. 14.23).

14.3.5 Plant mitochondria contain alternative NAD(P)H dehydrogenases that can oxidize NAD(P)H at both faces of the inner membrane

In addition to the NADH dehydrogenase activity associated with complex I, plants contain external and matrix-oriented NAD(P)H dehydrogenases (Fig. 14.24; see also Fig. 14.12). These NAD(P)H dehydrogenases can be distinguished from complex I by their insensitivity to the inhibitor rotenone, and they are often referred to collectively as the alternative or rotenone-insensitive bypass. This bypass transfers electrons from NAD(P)H to the ubiquinone pool, but it does not translocate protons across the inner membrane and so does not contribute to oxidative phosphorylation. As a result of the bypass, addition of rotenone does not fully inhibit oxidation of $NAD(P)^+$-linked substrates by isolated plant mitochondria, but it does lower the ADP/O values associated with substrate oxidation, that is, the theoretical number of ADP molecules phosphorylated per atom of oxygen reduced (Fig. 14.25). This bypass has substantially less affinity for NADH than does complex I and consequently operates only when matrix concentrations of NADH are high.



A **First UQH_2 oxidized**



B **Second UQH_2 oxidized**

FIGURE 14.22 *Operation of the Q-cycle during electron transfer through complex III. (A) Ubiquinol (UQH_2) binds at Center P in a pocket formed by cytochrome* b *and the Rieske Fe–S protein. Initially, one electron is transferred to the Rieske protein, and two protons are released into the intermembrane space. The resulting ubisemiquinone ($UQ^{\cdot -}$) transfers the remaining electron to the low-potential cytochrome* b_{566}*. The electron transferred to the Rieske protein is subsequently transferred to cytochrome* c_1 *and then onto cytochrome* c*. The electron on cytochrome* b_{566} *is transferred to the high-potential cytochrome* b_{560}*, which is oriented toward the matrix side of the inner membrane and is associated with a second UQ binding site in complex III, Center N. Oxidized ubiquinone (UQ) binds to Center N and is reduced by one electron, forming a relatively stable ubisemiquinone anion ($UQ^{\cdot -}$). (B) After a second round of electron transfer from cytochrome* b_{566} *to cytochrome* b_{560}*, the $UQ^{\cdot -}$ is further reduced to UQH_2 in a reaction that includes the uptake of two protons from the mitochondrial matrix. This UQH_2 dissociates from Center N, enters the UQ pool in the inner mitochondrial membrane, and diffuses across the membrane to Center P to initiate the reaction sequence again. As a result of the Q-cycle, four protons are translocated from the matrix to the intermembrane space for every two electrons transferred from complex III to cytochrome* c.

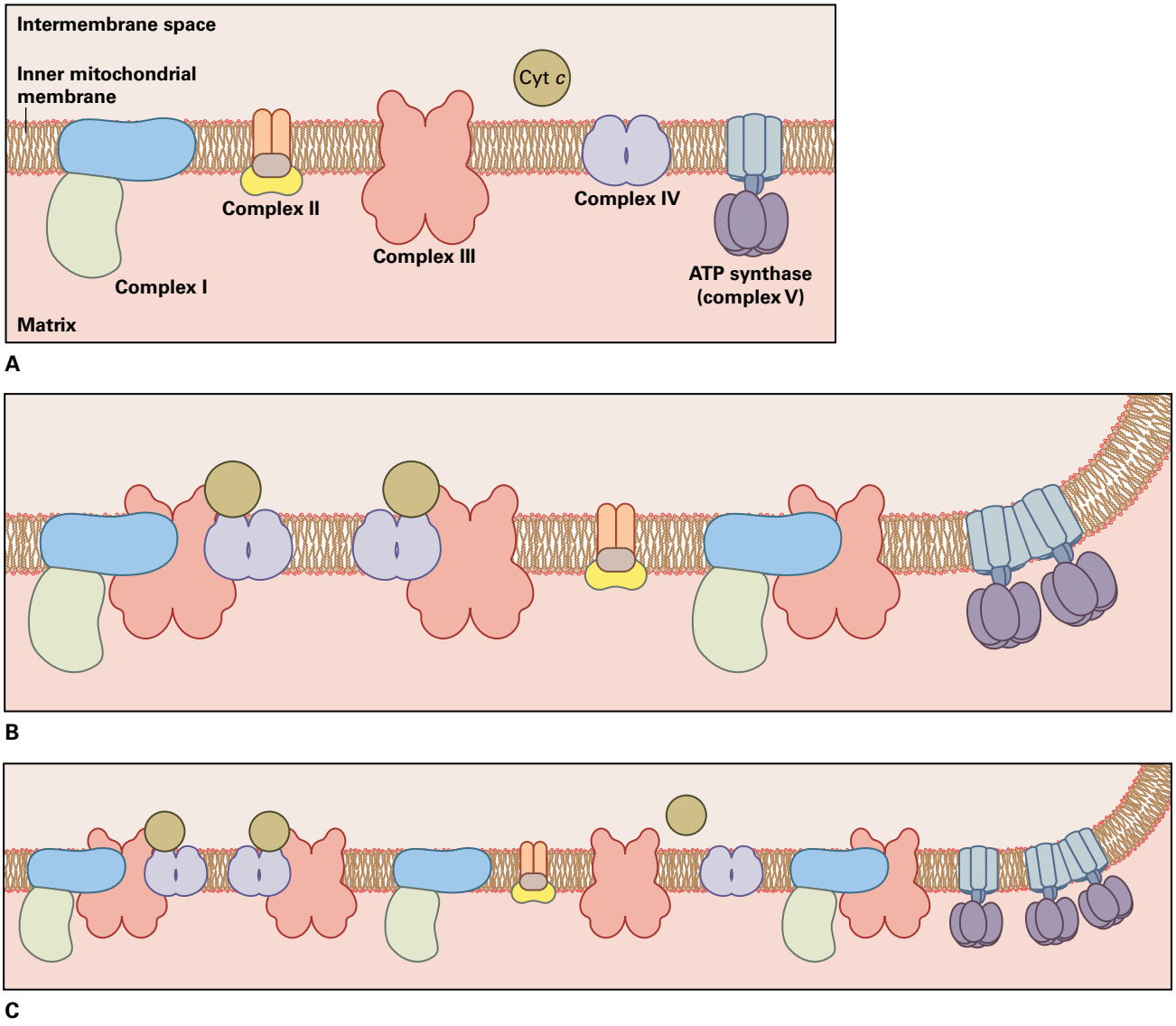


FIGURE 14.23 *Model of the mitochondrial oxidative phosphorylation system incorporating the classical model (A), the newly described respiratory supercomplexes (B), and an integrated model of the system (C). Abbreviations: M, matrix; IM, inner mitochondrial membrane; IMS, mitochondrial intermembrane space.*

In vitro activity of the external dehydrogenases depends strongly on the presence of calcium, but their regulation has not been elucidated in vivo. However, these dehydrogenases have the potential to influence the redox balance of the cytosolic pyridine nucleotide pools—that is, the ratio of $NAD(P)^+$ to NAD(P)H—and therefore may influence many cytosolic reactions.

14.3.6 Plant mitochondria have an alternative, cyanide-resistant oxidase that transfers electrons to O_2

In addition to nonphosphorylating pathways for oxidation of NAD(P)H, plant mitochondria contain a pathway for transfer of electrons from ubiquinol to O_2 that bypasses cytochrome *c* oxidase (Fig. 14.12). This nuclear-encoded alternative oxidase (AOX) is found in plants, many algae and fungi, and some protozoa. Electron flow through the AOX is insensitive to classic inhibitors of cytochrome *c* oxidase (CN^-, N_3^-, CO, and NO) and of complex III (antimycin-A, myxothiazol); however, the AOX can be specifically inhibited by salicylhydroxamic acid (SHAM) and *n*-propylgallate (Fig. 14.26). All plant species examined to date possess genes for the AOX; however, AOX activity in any given tissue varies, depending on the level of gene expression and the activation status of the oxidase (see below). Often, AOX expression is greatly enhanced in response to an environmental stress. The AOX is tightly bound to the inner membrane and diverts electrons from the standard electron transport chain at the level of the ubiquinone pool, transferring electrons from ubiquinol to O_2 and generating H_2O as the product.

BOX 14.1 Some electron transport chain components in the mitochondria resemble comparable complexes in the chloroplast

The mitochondrial electron transport chain shares several striking structural similarities with the photosynthetic electron transport chain. In the thylakoid membranes of the chloroplast (see Chapter 12), three large multisubunit protein complexes (Photosystem II, the cytochrome b_6f complex, and Photosystem I) are linked by a membrane-associated quinone (plastoquinone) and a small mobile protein (plastocyanin). Although the photosystems perform a light-harvesting function that has no mitochondrial parallel, the electron transport cofactors of the cytochrome b_6f complex mirror those of complex III: two *b*-type cytochromes, a *c*-type cytochrome (cytochrome *f*), and a Rieske Fe–S protein. The cytochrome b_6f complex interacts with plastoquinone in a Q cycle that translocates protons from the stroma to the thylakoid lumen. Furthermore, both plastocyanin and cytochrome *c* are membrane-associated soluble metalloproteins that can be reduced by a cytochrome complex and carry one electron. The redox active metal that gives plastocyanin its name and blue color is copper, not iron, but some algae grown in copper-limiting medium can replace plastocyanin with a soluble *c*-type cytochrome. The similarity of the electron transport chains and ATP synthases present in these organelles may derive from a common prokaryotic heritage.

Both organelles also contain alternative respiratory enzymes, notably the single polypeptide quinol oxidase, IMMUTANS, in plastids that participates in chlororespiration and cyclic electron transport, and the alternative oxidase in mitochondria that participates in nonphosphorylating respiration.

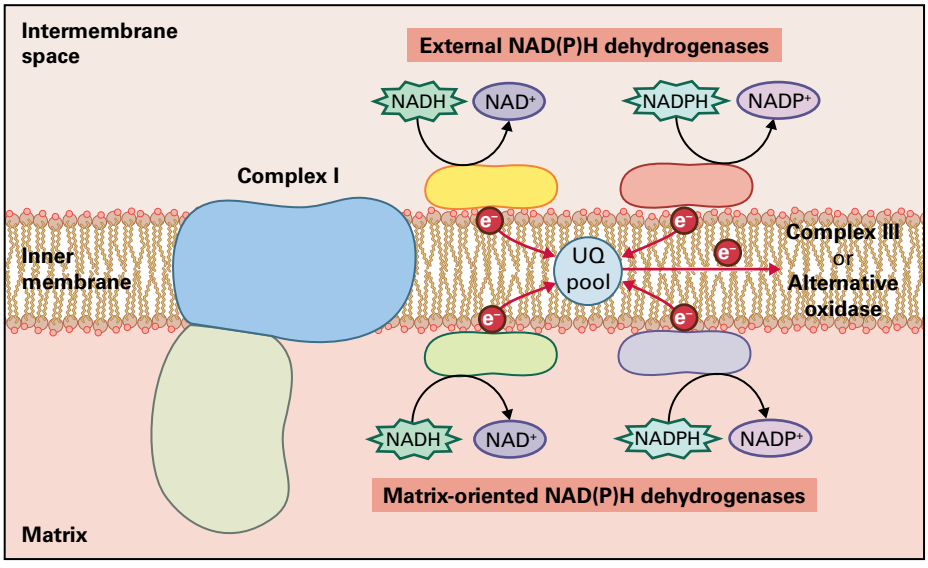
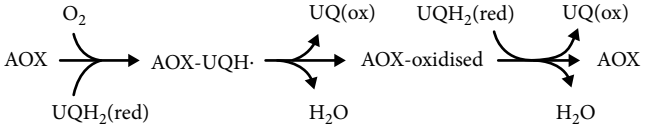


FIGURE 14.24 *Alternative NADH and NADPH dehydrogenases of the inner mitochondrial membrane. In addition to complex I, plant mitochondria possess simpler (single polypeptide) dehydrogenases on both surfaces of the mitochondrial inner membrane. These do not pump protons and are insensitive to complex I inhibitors such as rotenone. In* Arabidopsis, *seven genes encoding putative alternative dehydrogenases have been identified; however, only four activities have been described in isolated mitochondria. The two external dehydrogenases are thought to oxidize cytosolic NAD(P)H and feed electrons into the UQ pool. The two matrix-oriented enzymes provide additional routes for oxidation of the NADH and NADPH formed in the matrix.*

Reaction 14.3: Alternative oxidase

$$O_2 + 2UQH_2 \longrightarrow 2H_2O + 2UQ$$



AOX oxidises O_2 to H_2O using four electrons by binding and oxidising two molecules of UQH_2 in succession, first to form an AOX-ubiquinone radical and release one molecule of H_2O and then reduce a second UQH_2 to yield a second H_2O and regenerate the AOX active site ready for a new catalytic cycle.

Because no proton pumping results from the electron transfer between ubiquinol and O_2, all the free energy released

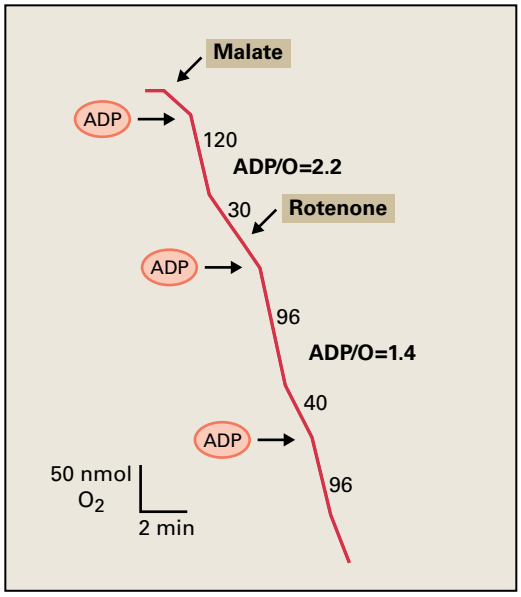


FIGURE 14.25 *Operation of the rotenone-insensitive bypass of complex I in plant mitochondria. The diagram shows an oxygen electrode recording obtained with isolated mitochondria oxidizing malate in a reaction medium containing an excess of inorganic phosphate. Oxidation of the malate within the matrix generates NADH, which, in turn, is oxidized by the respiratory chain, leading to O_2 consumption. Addition of a small amount of ADP stimulates the rate of O_2 uptake by allowing the ATP synthase to operate, dissipating the proton motive force across the inner mitochondrial membrane. When all added ADP has been phosphorylated, O_2 uptake reverts to a slow resting rate. These rate changes allow researchers to calculate an* ***ADP/O ratio*** *(the amount of ADP phosphorylated per oxygen atom consumed), which is an indication of the number of proton-translocating sites. The ratio before addition of rotenone was >2, indicating operation of three translocation sites. Addition of rotenone blocks electron flow through complex I and redirects electrons to the alternative NADH dehydrogenase on the inner surface of the inner membrane; this enzyme does not pump protons, and the ADP/O ratio decreases accordingly. Note the resting rate of O_2 consumption is a little higher when electrons bypass proton-pumping complex I.*

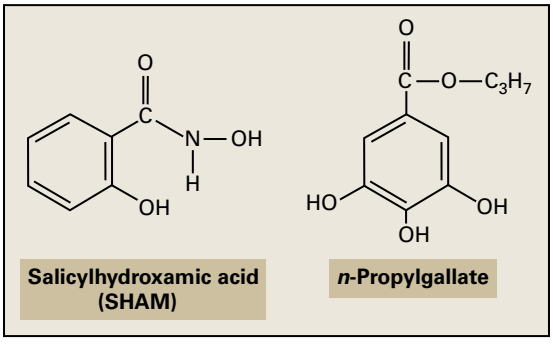


FIGURE 14.26 *Structures of salicylhydroxamic acid (SHAM) and* n*-propylgallate, inhibitors of the AOX. SHAM is thought to act as a competitive inhibitor of ubiquinol (UQH_2).*

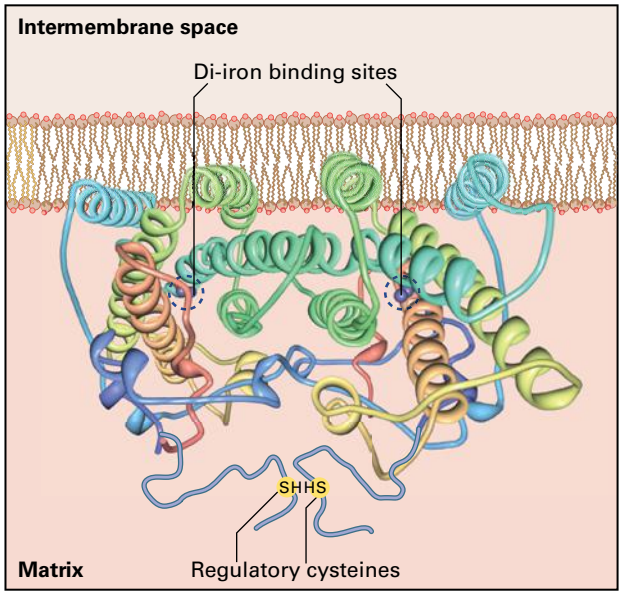


FIGURE 14.27 *Structure and membrane topography of the AOX dimer in plants, as deduced from the structure defined in a protozoan with the plant specific N-terminal extensions added that contain the regulatory cysteines. The AOX exists as a dimer partially embedded in the membrane. The dimeric structure is maintained by protein–protein interactions regardless of whether the intermolecular disulfide bond is oxidized. Each monomer is anchored to the inner mitochondrial membrane by the embedding of two α-helices. Two large hydrophilic domains flank the embedded helices and extend into the mitochondrial matrix. The amino acids that make up the di-iron center are located in the hydrophilic domain.*

during electron flow through the AOX is lost as heat and cannot be used for ATP synthesis. Thus, when electrons from NADH oxidation flow through the AOX, at least two of the three sites of proton translocation are bypassed, the resulting proton motive force is diminished, and fewer molecules of ATP are synthesized (see Section 14.4.1).

A structure for the AOX has been obtained from a protozoan and the conservation of key residues in cDNA sequences from numerous plants and fungi show that it is a good model for this enzyme across species (Fig. 14.27). The enzyme exists in the inner mitochondrial membrane as a homodimer in which two 32 kDa monomers interact non-covalently to form a dimer. In plants and fungi, an extra extension on the monomers exists which contains a conserved cysteine that undergoes reversible intermolecular disulfide bonding via thioredoxin (Trx) that is reduced by NADPH via $NADP^+$-thioredoxin reductase (Reaction 14.4).

Reaction 14.4: $NADP^+$-thioredoxin reductase

$$\underset{(-S-S-)}{NADPH + H^+ + Trx_{ox}} \rightarrow \underset{(-SH\,HS-)}{NADP^+ + Trx_{red}}$$

The AOX active site in each monomer contains a di-iron metal center with a hydroxo-bridge. AOX shares structural features with other di-iron proteins like ribonucleotide

reductase, but the iron atoms are coordinated by carboxylates from amino acid residues in AOX, which is unusual for a di-iron protein. It is noteworthy that both ribonucleotide reductase and many of the AOXs interact with reduced thioredoxin, which serves as a substrate for ribonucleotide reduction by the former enzyme and as an activator of the latter (see Section 14.6.1).

14.3.7 An antioxidant defense system removes reactive oxygen species generated by the electron transport chain

The mitochondrial electron transport chain generates superoxide ($O_2^{\cdot-}$) mainly as a result of the reaction of O_2 with components of the electron transport chain. Detoxification of $O_2^{\cdot-}$ is essential to avoid peroxidation of lipid membranes or oxidation of mitochondrial proteins and nucleic acids. A manganese-dependent superoxide dismutase in the mitochondrial matrix converts $O_2^{\cdot-}$ to hydrogen peroxide (H_2O_2), which is degraded to H_2O via a series of mitochondrial reactions that can be catalyzed by Trx-dependent peroxiredoxins, the ascorbate-glutathione cycle (see Fig. 20.37), or glutathione-dependent peroxidases that have been reported in plant mitochondria from some species.

14.4 Plant mitochondrial ATP synthesis

The mitochondrial electron transport chain translocates protons from the matrix side of the inner membrane to the cytosolic side, concentrating them in the intermembrane space. Protons diffuse back into the matrix through the F_oF_1–ATP synthase complex, which catalyzes the conversion of ADP and P_i to ATP. Numerous inner membrane transporters facilitate this process.

14.4.1 The electron transport chain couples oxidation of reducing equivalents to formation of a proton electrochemical gradient

As its name suggests, the proton electrochemical gradient ($\Delta\mu_{H^+}$) formed by the action of the electron transport chain comprises two potentials, one electrical and the other chemical (see Chapter 3). This difference in free energy, which can also be calculated in volts as proton motive force (Δp), represents the sum of the electrical component ($\Delta\psi$, negative inside the mitochondrial matrix) and the chemical component (ΔpH):

Equation 14.1: Proton electrochemical gradient

$$\Delta\mu_{H^+} = \Delta\psi + \Delta pH$$

Equation 14.2: Proton motive force

$$\Delta p = \Delta\mu_{H^+}/96.5\ \text{kJ V}^{-1}\text{mol}^{-1}$$

The concept of coupling two reactions through a proton electrochemical gradient forms the basis of the chemiosmotic theory. In mitochondria, including those from plants, the principal contributor to $\Delta\mu_{H^+}$ is $\Delta\psi$ (−150 to −200 mV); the intermembrane space pH is only 0.2 to 0.5 units lower than that of the matrix. Typical $\Delta\mu_{H^+}$ values for plant mitochondria are −200 to −240 mV in the resting state (i.e., in the absence of ADP). In chloroplasts, by contrast, ΔpH represents most of the total $\Delta\mu_{H^+}$ because chloroplasts are more permeable to some ions and contain gated ion channels that are not present in mitochondria.

14.4.2 The F_oF_1–ATP synthase complex couples dissipation of the proton electrochemical gradient with ATP formation

F_oF_1–ATP synthase is a multisubunit complex that spans the inner membrane. Although mitochondrial function is commonly associated with proton diffusion coupled to ATP synthesis, in some circumstances the F_oF_1 complex can hydrolyze ATP to ADP and P_i and drive proton translocation from the matrix into the intermembrane space.

F_oF_1–ATP synthase is composed of two major components (Fig. 3.5). The integral membrane protein complex, F_o, functions as a proton pathway through the inner membrane and consists of as many as eight or nine separate polypeptides, with three primary subunits in a ratio of $a_1b_2c_{10-12}$. The peripheral membrane protein complex, F_1, extends into the matrix space on a stalk anchored at its base to the F_o complex (Fig. 14.28). The F_1 complex contains at least five separate polypeptides, α through ε, in a stoichiometry of $\alpha_3\beta_3\gamma\delta\varepsilon$. The catalytic sites for ATP synthesis are localized primarily on the β subunits. Four of the F_o polypeptides (ATP4, ATP6, ATP8, ATP9) and one of the F_1 polypeptides (α subunit, ATP1) are commonly encoded by plant mitochondrial DNA. The F_1 stalk includes the γ-polypeptide and several other subunits, one of which is known as the oligomycin-sensitivity-conferring protein (OSCP) because it binds the antibiotic oligomycin. Binding of oligomycin to OSCP prevents proton translocation through the F_o complex, inhibits ATP synthesis, and limits mitochondrial O_2 uptake (see Section 14.5.2).

In the "binding change" reaction mechanism proposed for ATP synthase, the free energy input from proton diffusion is not required to phosphorylate ADP directly, rather it induces a conformational change that releases tightly bound ATP

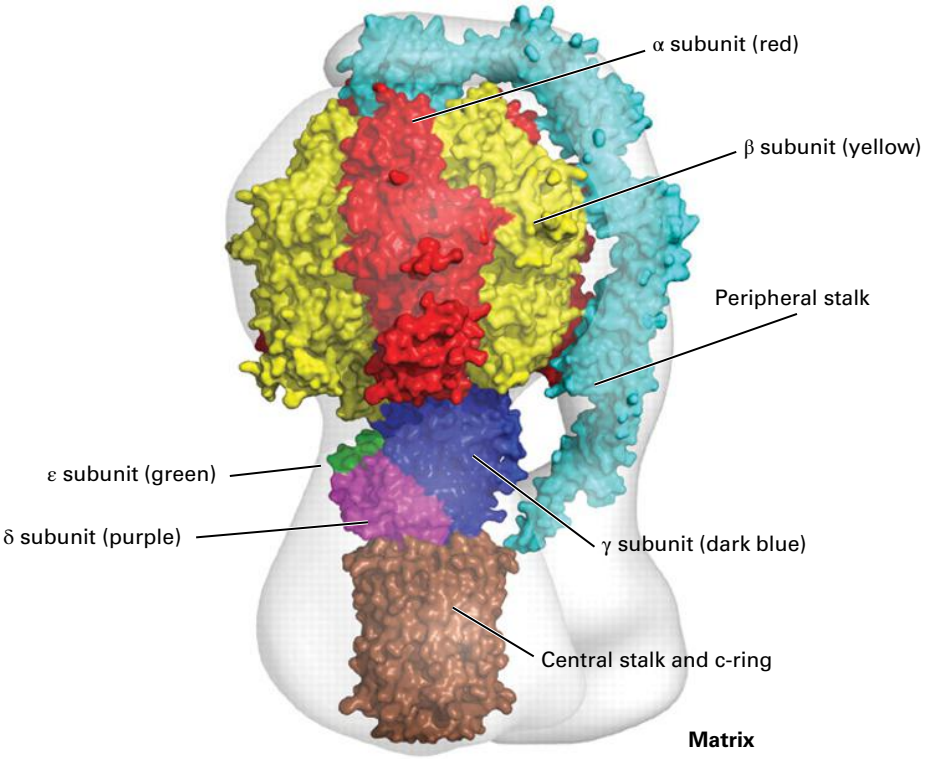


FIGURE 14.28 *Mosaic structure of the F_oF_1-ATPase from bovine mitochondria. The components of the structure were docked into a structure of the intact enzyme by electron cryomicroscopy. The extrinsic region consists of the spherical catalytic domain made up of three α subunits and three β subunits of the membrane shown in red and yellow, respectively. The γ-, δ- and ε subunits of the F_1 central stalk are shown in blue, purple and green, respectively. The central stalk and F_o c-ring shown in brown constitute the rotor. The peripheral stalk (cyan) penetrates the membrane domain and links provide a connection to the catalytic domain. The complex is an integral membrane-spanning complex that acts as a proton channel, providing the pathway for movement of protons across the inner membrane into the matrix.*

from one of the three F_1 active sites (see Chapter 3, Fig. 3.6). The $\alpha_3\beta_3$ subunit stoichiometry of the F_1 complex is consistent with this model, and the high-resolution crystal structure for the F_1 complex from mammalian mitochondria demonstrates structural and nucleotide (i.e., ATP and ADP) binding features that support this mechanistic scheme.

14.4.3 Movement of ATP, ADP, and phosphate into and out of plant mitochondria is also driven by the electrochemical proton gradient

The exact number of protons translocated per pair of electrons transferred from NADH to O_2 remains controversial, since the mechanisms that couple proton translocation to electron flow have not been clearly elucidated for complexes I and IV. However, measurements with isolated mitochondria from different sources give a value of 10 protons translocated per NADH oxidized by the cytochrome pathway. Given the free energy required for ATP synthesis and that available from the measured $\Delta\mu_{H^+}$, thermodynamic considerations indicate three protons are needed per ATP molecule synthesized. When the energy costs of transporting adenine nucleotide and phosphate across the inner membrane are taken into account, however, the H^+/ATP ratio increases (Fig. 14.29). Unlike the chloroplast, where ATP synthesis and consumption both take place in the stroma, the mitochondrion must expend free energy to import ADP and inorganic phosphate (P_i) and export ATP across the inner membrane. One ATP^{4-} is exported from the mitochondrion in exchange for one ADP^{3-} from the cytosol, and one hydroxide ion (OH^-) from the mitochondrial matrix is exchanged for one cytosolic P_i. Hydroxyl transport equates to the net movement of one proton from the intermembrane space back into the matrix. Adding this proton to the three protons needed to synthesize one ATP from ADP and P_i at the measured values of $\Delta\mu_{H^+}$ gives a value of four protons translocated per ATP synthesized.

Including the energy cost of nucleotide and P_i transport in calculations of mitochondrial efficiency lowers the ADP/O values associated with substrate oxidation. If four protons are needed to transport ADP and P_i into the mitochondrion and to synthesize ATP, then the ADP/O ratio is 2.5, rather than the 3 previously assumed. In this context, careful measurement of ADP/O ratios in isolated mitochondria often yields values close to 2.5 during oxidation of NAD^+-linked substrates. Oxidation of succinate by the bound FAD of complex II or of NAD(P)H by the rotenone-insensitive dehydrogenases drives the synthesis of only 1.5 molecules of ATP per $\frac{1}{2}O_2$ reduced, because these reactions utilize only two of the three proton translocation sites.

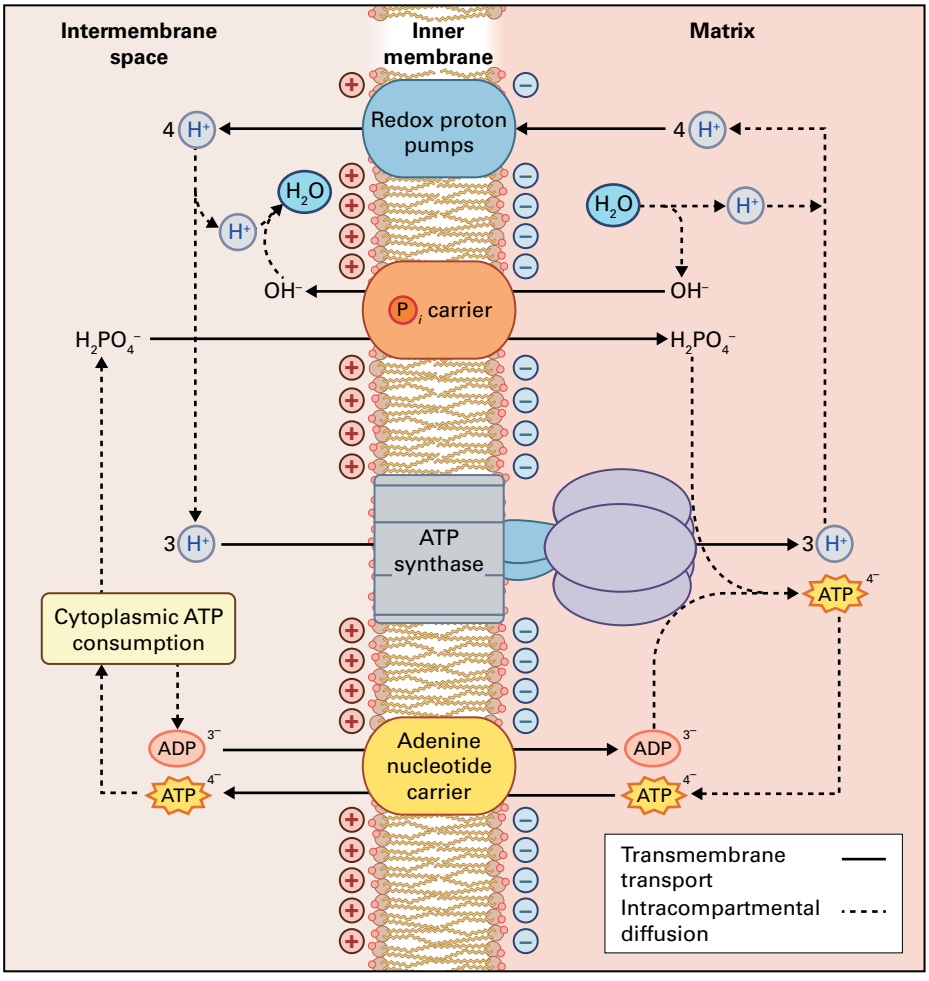


FIGURE 14.29 *The adenine nucleotide carrier and the phosphate carrier expend electron motive force to supply ATP synthase with substrate. The adenine nucleotide carrier catalyzes the electrogenic exchange of cytosolic ADP^{3-} for mitochondrial ATP^{4-}. The net negative charge on the matrix side of the membrane ($\Delta\psi$) drives ATP export against a large concentration gradient and supports a high ATP/ADP ratio in the cytosol. In addition, the outer face of the carrier has a high affinity for ADP and therefore can import ADP to maintain oxidative phosphorylation even at low cytosolic ADP concentrations. The P_i carrier catalyzes an electroneutral exchange of negatively charged phosphate for OH^- and thus balances the electrogenic adenine nucleotide exchange by dissipating the equivalent amount of ΔpH.*

14.5 Regulation of the citric acid cycle and the cytochrome pathway

14.5.1 In vegetative tissues, expression of many respiratory enzymes is largely constitutive

Expression experiments comparing different stages of plant development and different tissues consistently show most genes for mitochondrial enzymes are expressed in most organs at relatively constitutive levels, but transcript abundance is dramatically enhanced in floral organs. Interestingly, genes encoding proteins of the cytochrome pathway and the citric acid cycle are remarkably nonresponsive to environmental stresses, though signals such as light, sucrose, and the nitrogen status of the cell do affect the expression of components of the pyruvate dehydrogenase complex and the cytochrome pathway. Genes encoding the alternative oxidase (AOX) and some of the alternative NAD(P)H dehydrogenases, on the other hand, are very sensitive to environmental stress.

14.5.2 Regulation of respiratory activity in isolated mitochondria depends on availability of ADP and P_i

In isolated mitochondria, the rate of electron transfer and, therefore, the rate of O_2 uptake, are controlled primarily by the availability of ADP and P_i, a phenomenon described as **respiratory control**. In the absence of ADP or P_i, the F_o proton channel of the ATP synthase is blocked, and $\Delta\mu_{H^+}$ builds until it exerts a back pressure that restricts further proton translocation across the inner membrane. Because electron

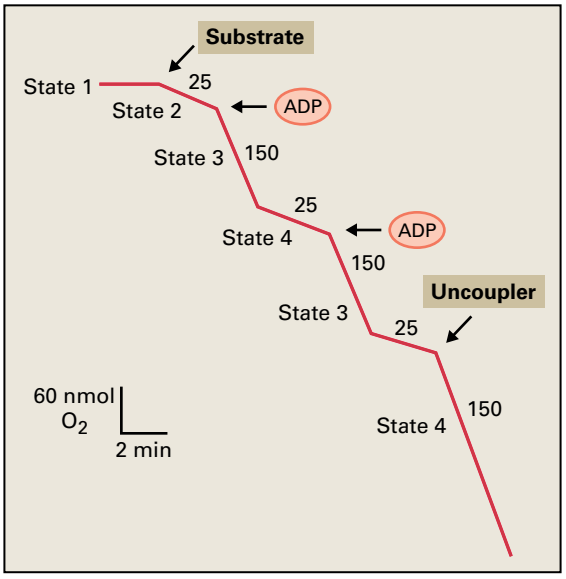


FIGURE 14.30 *Respiratory control and the impact of uncouplers on the ADP/O ratio. The rate of O_2 uptake is described by four respiratory states. State 1 occurs when no oxidizable substrate is present; O_2 consumption (O_2 nmol min^{-1} mg^{-1} of total mitochondrial protein) in state 1 is insignificant. Some O_2 is reduced (consumed) when substrate alone is added (state 2), but O_2 uptake is stimulated dramatically by adding ADP (state 3). When all ADP has been consumed, the O_2 uptake rate again decreases (state 4). The state 3 to state 4 ratio for rates of electron transfer, termed the* ***respiratory control ratio****, indicates how tightly ADP phosphorylation and electron transport are coupled. Chemical uncouplers collapse the proton gradient and release respiratory control, increasing O_2 consumption to state 3 rates.*

transport is obligately linked to proton translocation, a large $\Delta\mu_{H^+}$ also restricts the rate of O_2 uptake (Fig. 14.30). In steady state, the rate of electron transfer is determined by the rate at which protons in the intermembrane space flow back into the matrix. When ADP and P_i are available, the backflow of protons via the ATP synthase is rapid; in the absence of ADP or P_i, or both, the protons leak slowly across the inner membrane.

The proton leak can be dramatically stimulated by some compounds that act as protonophores (ion-binding, lipid-soluble molecules that allow protons to cross membranes) or proton channels. Such compounds are referred to as **uncouplers** since they disconnect electron transport from ATP synthesis by equilibrating the proton gradient across the membrane and dissipating the $\Delta\mu_{H^+}$ as heat. Uncouplers stimulate O_2 uptake, but because no $\Delta\mu_{H^+}$ is established, no ATP is formed. Mitochondria from both animals and plants contain uncoupling proteins that facilitate proton movement across the membrane in a regulated fashion. Certain plants take advantage of the heat released under conditions that do not yield ATP to promote flowering (Box 14.2). Interestingly, a similar phenomenon is observed in infants that use mitochondria rich in brown fat for warming. However, the primary role of uncoupling proteins in plants appears to be the maintenance of mitochondrial electron transport when adenylate charge is high, thus preventing the over reduction of the ubiquinone pool that can lead to oxidative damage.

14.5.3 Substrate supply, organic acids, ADP, and matrix NAD(P)H may each serve to regulate respiratory metabolism in intact tissues

In vivo respiratory rates are generally accepted as being at least somewhat linked to the energy demands of the plant cell. However, the controlling factors may be dictated by tissue-specific and environmental factors and are difficult to ascertain. Mitochondria usually do not operate at full respiratory capacity in vivo. In many tissues, the respiration rate is controlled by the rate at which mitochondrial substrates are supplied, which slows if carbohydrate reserves are low or if glycolysis is downregulated by metabolic effectors (e.g., ATP). In tissues where substrate supply is plentiful, respiration can be limited by the rate of ATP turnover. In isolated mitochondria, the respiration rate is controlled by adding ADP. In vivo, respiration is also influenced by the cytosolic ATP/ADP ratio, which depends on both the concentration of ADP and the cellular rate of ATP utilization. The mechanisms of citric acid cycle regulation in plants have not yet been fully resolved, but current data suggest cycle activity is controlled by the energy status of the cell, through its impact on mitochondrial matrix concentrations of NADH, ATP and acetyl-CoA, which inhibit various dehydrogenases through binding to substrate and allosteric sites and with certain enzymes, through redox changes via thioredoxin. Therefore, the citric acid cycle turnover rate in vivo depends on the rate of NADH reoxidation by the respiratory electron transport chain and on the cellular rate of ATP utilization. The rate at which plastid and cytosolic pathways provide citric acid cycle substrates may also be important. For example, in some leaves, which undergo large diurnal shifts in carbohydrate content, respiratory rates are proportional to the concentration of carbon substrates in the leaf cells, being very low at the end of the night and increasing substantially during the day as photosynthesis replenishes carbon reserves.

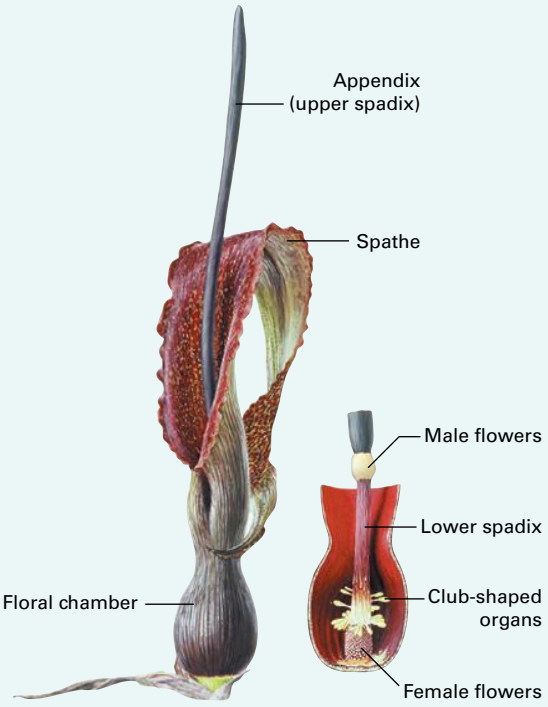
14.6 Integration of the cytochrome pathway and nonphosphorylating pathways

When nonphosphorylating respiratory pathways contribute to O_2 uptake, the extent to which respiration rates are regulated by the cytosolic ATP/ADP ratio is decreased. Because these enzymes are not involved in proton translocation across the inner mitochondrial membrane, they do not sense

BOX 14.2 The alternative oxidase and uncoupling proteins are active during thermogenesis in some flowers

The AOX and uncoupling proteins participate in thermogenesis during flowering in a few plants, mostly members of the family Araceae. These plants, which include skunk cabbage and voodoo lily, produce a club-like structure (called an appendix) on the developing floral apex. The outer layers of the appendix contain more mitochondria than most plant tissues. During anthesis (pollen release), mitochondria in the appendix use the AOX and uncoupling proteins to respire at very high rates. The free energy released as heat raises tissue temperatures 10°C to 25°C above ambient conditions and volatilizes odorous compounds that attract pollinators. In some cases, this mechanism can mimic the scent of rotting flesh and is used to deceive insects that lay their eggs.

It is unlikely that the AOX and uncoupling proteins promote thermogenesis in other plant tissues, because plants are not generally thermogenic. Observed rates of respiration in most plant organs are simply too low to generate significant amounts of heat, even if all electron flow were to be shunted through the AOX and even if uncoupling proteins completely prevented limitation of the electron transfer rate by dissipating the mitochondrial membrane potential.



Source: Benstead, Fife, Scotland, UK; previously unpublished.

the $\Delta\mu_{H^+}$ and, therefore, are not restricted by oxidative phosphorylation. This results in faster rates of respiration in the resting state. Given the ramifications of operating an energetically wasteful pathway in an organelle that functions primarily in energy conservation, it is important to understand how the nonphosphorylating NAD(P)$^+$ dehydrogenases and AOX are regulated and how they interact with the cytochrome pathway.

14.6.1 Regulation of the alternative oxidase is complex

Both the expression and activity of the AOX are subject to regulatory controls. In most plants, two or more AOX proteins encoded by separate genetic loci are expressed in a tissue-specific manner. In soybean, for example, one isoform appears to be expressed mainly in photosynthetic tissues. In both soybean (*Glycine max*) and *Arabidopsis*, one out of several AOX isoforms is expressed strongly in response to environmental stresses. In many, but not all, plants tissues, AOX expression and activity are very low until a stress is applied.

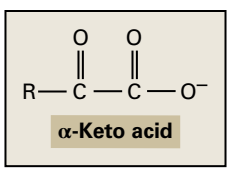


FIGURE 14.31 *Structure of an α-keto acid.*

Factors that can induce AOX synthesis include low temperature, drought, generation of $O_2^{\cdot -}$ or H_2O_2, certain herbicides, inhibitors of mitochondrial protein synthesis or electron transfer, and ripening in some fruits. In most cases, induction involves increased amounts of AOX mRNA. In cultured tobacco (*Nicotiana tabacum*) cells, addition of citrate to the growth medium also triggers AOX synthesis, suggesting a link between carbon metabolism and regulation of AOX gene transcription.

Research on mutants with elevated AOX protein levels and on plants under environmental stress has shown that regulation of AOX activity is complex and not just dependent on protein abundance. AOX activity is strongly enhanced by α-keto acids (Fig. 14.31), such as pyruvate and glyoxylate. In addition, the AOX is a target of thioredoxin (Fig. 14.32). When the intermolecular disulfide bond that can covalently link the two monomers is reduced to two sulfhydryl groups

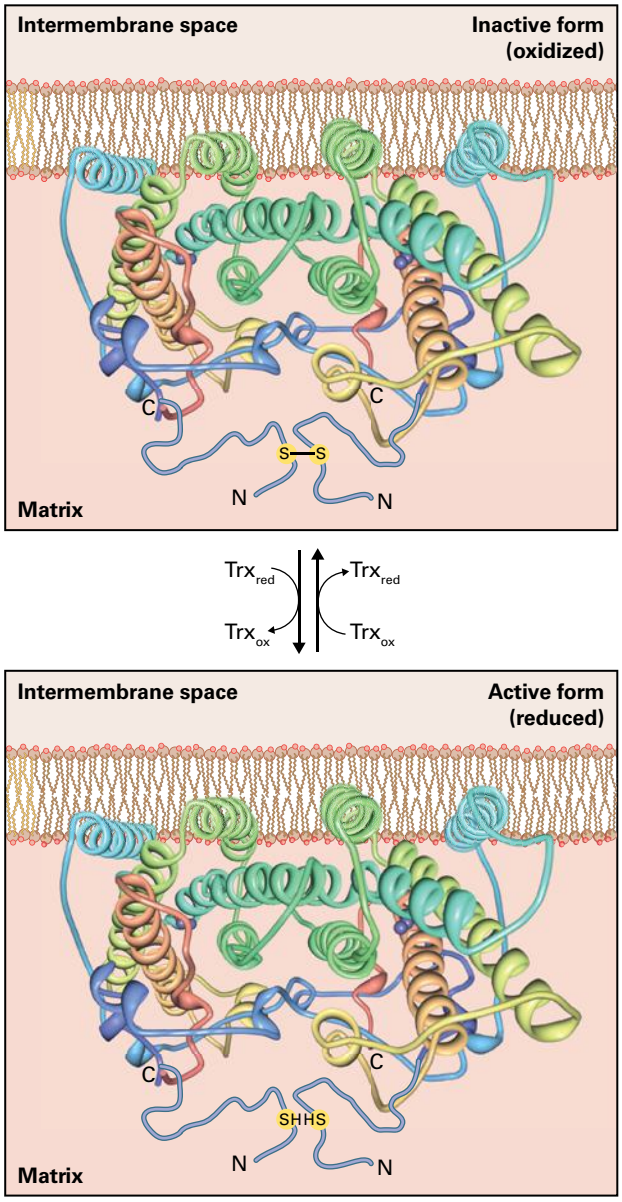


FIGURE 14.32 *Proposed regulation of the AOX through action of a redox-active regulatory sulfhydryl/disulfide system. Reduction of an intermolecular disulfide bond increases the sensitivity of the AOX dimer to activation by α-keto acids. The reduced thioredoxin would be oxidized with O_2 possibly via a peroxiredoxin (see Chapter 12).*

by thioredoxin, AOX activity significantly increases in the presence of pyruvate. In the oxidized, less active state, the AOX dimer is markedly less sensitive to stimulation by α-keto acids.

Reduction of the regulatory disulfide bond can be induced by applying citrate or isocitrate to isolated mitochondria and may involve NADPH generated in the matrix by $NADP^+$-linked isocitrate dehydrogenase. This system seems to constitute a link between the redox poise of the mitochondrial matrix and the oxidation state of the regulatory cysteine residues in the AOX whose redox state is linked to NADH (see Reaction 14.4). Because citrate can also activate AOX expression, both

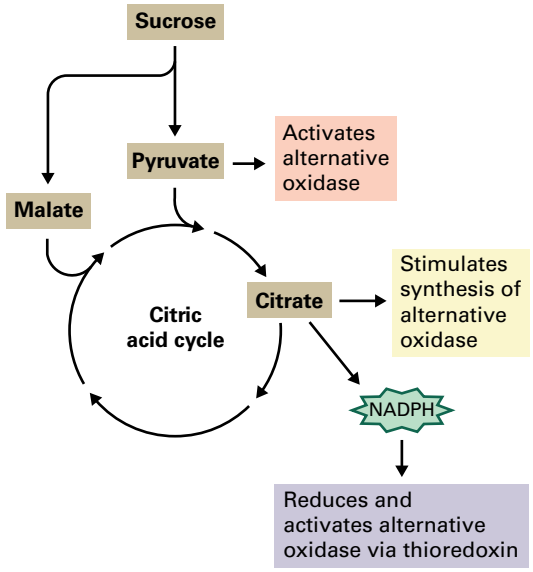


FIGURE 14.33 *Impact of sugar metabolism on AOX activity. Activation and synthesis of the AOX are linked to the carbon status of the cell. When carbon flux to the mitochondrion exceeds the capacity of the electron transport chain to accept electrons, carbon intermediates such as pyruvate and citrate accumulate and the matrix NAD(P) pool becomes highly reduced. Accumulation of citrate leads to synthesis of more AOX protein, whereas accumulated pyruvate and NADPH activate the enzyme via thioredoxin. This feed-forward control ensures the potentially wasteful AOX is active only when the carbon supply in the cell is plentiful. Activation of AOX prevents overreduction of other respiratory chain components, thereby decreasing the production of harmful active oxygen intermediates.*

the activity and synthesis of the AOX are integrated with the carbon and energy status of the cell (Fig. 14.33).

The impact of α-keto acids and disulfide bond reduction on AOX activity reveals a clearer picture of respiratory regulation. Several factors restrict electron flow though the cytochrome pathway, including increase in the cytosolic ATP/ADP ratio, decrease in cytosolic ADP concentration, and environmental stresses such as low temperature. These enhance the reduction state of the matrix $NAD(P)^+$ pool to inhibit the rate of citric acid cycle activity, thereby increasing the concentration of mitochondrial pyruvate. Both responses may feed forward to activate the AOX: pyruvate activates AOX directly, and increased matrix NAD(P)H levels act indirectly by increasing the amount of reduced thioredoxin available. Once activated, the AOX could compete effectively with the cytochrome pathway for electrons from the ubiquinone pool, allowing the plant to maintain a greater rate of aerobic respiration than if the AOX were not present. This respiratory activity may prevent damage associated with the formation of ROS (see Section 14.3.7) or with fermentative metabolism (see Chapter 22). Finally, in addition to the mechanisms shown to control AOX abundance and activity in isolated mitochondria, other regulatory mechanisms may operate in intact tissues to regulate the partitioning of respiration between the two oxidases. The effect of altering respiratory efficiency on metabolism can be substantial, and sophisticated control is to be expected.

14.6.2 Alternative oxidase regulation and ubiquinone pool redox status influence electron flow through the cytochrome and alternative pathways

In the past, the AOX was believed to function simply in an electron overflow capacity. According to this scheme, AOX activity was significant only when >40–60% of the ubiquinone pool was reduced. With the cytochrome pathway at or near saturation, ubiquinol would divert electrons to the AOX. As a consequence, AOX activity was measured by the extent to which AOX inhibitors such as SHAM inhibited respiration. This approach assumed that the cytochrome pathway was already saturated and could not compensate for the inhibited alternative pathway. Thus, any observed decrease in the respiration rate would reflect how active the AOX had been in the absence of the inhibitor. This model is now considered out of date.

It is now understood that activation by α-keto acids and thioredoxin-mediated reduction allows the AOX to compete for electrons with the cytochrome pathway even when ubiquinol concentrations are low (Fig. 14.34). If the cytochrome pathway is unsaturated, increased electron flow through it can mask inhibition of the alternative pathway; therefore, respiration rates measured in the presence and absence of SHAM do not quantify AOX activity. Instead, researchers directly measure the respiratory rate of plant tissues and simultaneously measure concentrations of ^{18}O consumed. Both plant mitochondrial respiratory oxidases discriminate against O_2 containing the ^{18}O isotope, so ^{18}O accumulates as a percentage of the O_2 in a closed respiring system over time. Owing to a measurable difference in the discrimination value of cytochrome oxidase and the AOX in plants, such measurements can be used to accurately determine the proportion of O_2 consumption by each oxidase in an intact plant tissue.

The ubiquinone pool kinetic model (Fig. 14.34) recognizes ubiquinone and uniquinol as substrates or products of both the electron transport chain's ubiquinone-reducing enzymes (complexes I and II and the rotenone-insensitive bypass), and uniquinol-oxidizing enzymes (complex III and the AOX). Partitioning between the cytochrome and nonphosphorylating pathways thus depends on both the ubiquinone redox poise and the kinetic properties of each of these enzymes.

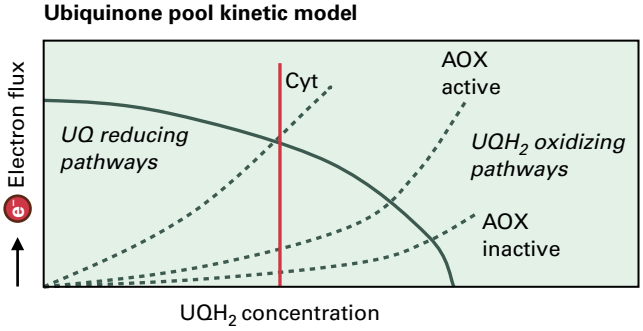


FIGURE 14.34 *The ubiquinone pool kinetic model for engagement of Cyt pathway and AOX. A plot of the rate of electron transport (y-axis) as a function of the degree of UQ reduction (x-axis) describes the kinetics of both UQ-reducing pathways (complex I, SDH, and alternative NADH dehydrogenases) as well as the two UQ-oxidizing pathways (cytochrome chain and the AOX). For the UQ-reducing pathways, the maximum rate occurs when the UQ pool is oxidized, and the rate decreases as the UQ pool becomes more reduced (i.e. UQH_2 concentration increases). Alternatively, for the oxidizing pathways, the reaction rate is zero when the UQ pool is fully oxidized, but it increases as UQ is further reduced. The intersection of the UQ-reducing and -oxidizing kinetics indicates the steady-state UQ reduction state that occurs for the given electron transport chain rate. The plot demonstrates how the cytochrome pathway dominates electron flux at lower UQH_2 levels (red line), as well as how AOX becomes more dominant when UQH_2 level rises in response to either increases in UQ reducing potential or a blockage in the cytochrome pathway.*

14.6.3 Nonphosphorylating bypasses represent a unique aspect of plant respiratory metabolism, but their role is not well understood

The existence of the alternative NAD(P)H dehydrogenases and the AOX suggests respiring plant mitochondria might be able to shunt electrons solely through these nonphosphorylating bypasses and completely eliminate ATP synthesis, the function most commonly associated with mitochondria. It is unlikely a plant would experience this extreme state, but the presence of these non-energy-conserving bypasses raises obvious questions about the role they play in plant metabolism.

One hypothesis postulates enhanced bypass performance under unfavorable circumstances. Because the alternative NAD(P)H dehydrogenases and the AOX are far less complex than their proton-translocating counterparts, these simpler proteins might function more effectively under stress than the standard electron transport chain. If so, diversion of electrons through these bypasses in response to stress might maintain higher respiration rates than the cytochrome pathway could support. The alternative internal NAD(P)H dehydrogenases may also play a role in maintaining respiration rates during stress by modulating matrix concentrations of NAD(P)H and consequently influencing carbon flow through the citric acid cycle (see Section 14.5.3). Oxidation of cytosolic NADH by the alternative external NADH dehydrogenase would provide the NAD^+ required to maintain glycolysis, and the AOX would continue to support aerobic respiration. Although ATP production would be restricted, the plant could avoid shifting to fermentative metabolism.

Microarray studies have shown that expression of genes encoding the AOX and internal and external alternative NAD(P)H dehydrogenases is induced under various stresses. This lends support to the hypothesis that these alternative pathway components are important for avoiding or

minimizing generation of ROS by the electron transport chain when environmental conditions inhibit plant respiration. In animal mitochondria, if the mitochondrial quinone pool becomes highly reduced, $O_2^{\cdot -}$, H_2O_2, and hydroxyl radical ($OH^{\cdot}$) are generated by the autoxidation of ubiquinol. Interestingly, $O_2^{\cdot -}$ induces synthesis of AOX in fungal cells, as does H_2O_2 in plant cells.

If stress causes an inhibition of the plant mitochondrial electron transport chain at a site downstream from the ubiquinone pool, then pyruvate, citric acid cycle intermediates, and reduced pyridine nucleotides will accumulate and activate the AOX through thioredoxin (Fig. 14.32). This activation would attenuate the inhibitory effects of the stress on respiration and thereby prevent high levels of reduction of the ubiquinone pool to minimize production of ROS. Activation of the alternative NAD(P)H dehydrogenases may also help prevent ROS production at complex I, while allowing NAD(P)H turnover for maintenance of glycolysis and citric acid cycle activity.

Studies with transgenic tobacco (*Nicotiana tabacum*) cell cultures in which AOX has been repressed or overexpressed have confirmed that AOX helps minimize ROS production. Studies with *Arabidopsis* have shown plants lacking AOX are more sensitive to high temperature and high light conditions. These studies support the notion of an antioxidant role for AOX; by maintaining the ubiquinone pool in a relatively oxidized state, less ROS is produced. This helps prevent oxidative damage of the mitochondria and affects signaling pathways involved in coordination of other stress-related genes, perhaps explaining how AOX helps prevent programmed cell death in plant cells.

By modulating cellular redox poise and ROS levels, the alternative NAD(P)H dehydrogenases and the AOX aid the homeostasis of the cell.

14.7 Interactions between mitochondria and other cellular compartments

In addition to synthesizing ATP, plant mitochondria generate biosynthetic precursors and carry out reactions that are linked to other metabolic pathways, including gluconeogenesis during oil seed germination, C_4 photosynthesis, Crassulacean acid metabolism (CAM), and photorespiration (see Sections 14.8 to 14.10). These processes are facilitated by an extensive array of membrane transport proteins.

14.7.1 Movement of metabolites into and out of plant mitochondria is regulated by a series of specific transporters

The inner membrane of the mitochondrion is selectively permeable. Gases and H_2O move rapidly across the membrane, as do a few other uncharged molecules, such as the protonated species of small or lipophilic organic acids (e.g., acetic acid). However, since mitochondrial chemiosmotic energy conservation is supported primarily by $\Delta\bar{\mu}_{H^+}$, movement of charged molecules across the inner membrane must be controlled so as to not dissipate the $\Delta\bar{\mu}_{H^+}$.

Charged compounds enter or leave the mitochondrion via selective carriers that are regulated by $\Delta\mu_{H^+}$. The types of movements that can occur are summarized in Figure 14.35. Transport can be linked to the membrane potential ($\Delta\psi$), the pH gradient (ΔpH), or both ($\Delta\bar{\mu}_{H^+}$); this last case applies when proton cotransport in one direction creates a charge imbalance in an exchange reaction. The $\Delta\bar{\mu}_{H^+}$ can drive transport directly or can be harnessed indirectly by coupling the transport of one species to another. **Electrogenic transport** involves the net movement of charge across the membrane, whereas **electroneutral transport** results in no net charge transfer. When an ion moves unaccompanied, the transport is termed uniport and is linked directly to $\Delta\psi$. Alternatively, one ion can move with another, either in the same direction (**symport**), or in exchange for an ion of like charge (**antiport**). Symport and antiport can be linked to either the ΔpH, if the other ion is H^+ or OH^-, or to $\Delta\psi$ if the combined transport is electrogenic. For example, the exchange of ATP^{4-}_{out}/ADP^{3-}_{in} results in electrogenic movement of a negative charge out of the mitochondrion and is driven directly by $\Delta\psi$. The P_i and pyruvate carriers, on the other hand, catalyze electroneutral exchange of an anion for OH^-, utilizing ΔpH. Because transporters such as the dicarboxylate carrier exchange a dicarboxylate anion for P_i, they too are dependent on maintenance of a ΔpH across the inner membrane.

Plant mitochondria interact in many ways with a variety of cellular metabolic processes and, therefore, require numerous transporters that exchange metabolites across the inner mitochondrial membrane (Fig. 14.36). Transport proteins provide numerous paths by which carbon and cofactors can be shipped to and from the mitochondria. The dicarboxylate, pyruvate, and amino acid carriers import substrates to the mitochondria, whereas di- and tricarboxylate carriers may export citric acid cycle carbon intermediates (see Section 14.7.2).

Plant mitochondria also contain specific transporters for the net uptake of NAD^+, CoASH, and TPP, all of which are essential cofactors for operation of the citric acid cycle. These transporters were discovered because isolated plant mitochondria lose these cofactors during prolonged storage and become unable to oxidize substrates such as malate and pyruvate. The carrier proteins were identified by complementation of yeast mutants lacking the transport of specific compounds with genes for plant carriers. Adding back these cofactors restores respiratory activity. Although slower than those involved in transport of other metabolites across the mitochondrial inner membrane, these transporters can facilitate accumulation of substantial cofactor concentrations. In vivo, they are presumably involved in mitochondrial biogenesis; organelle division would dilute and eventually deplete these cofactors if they were not imported.

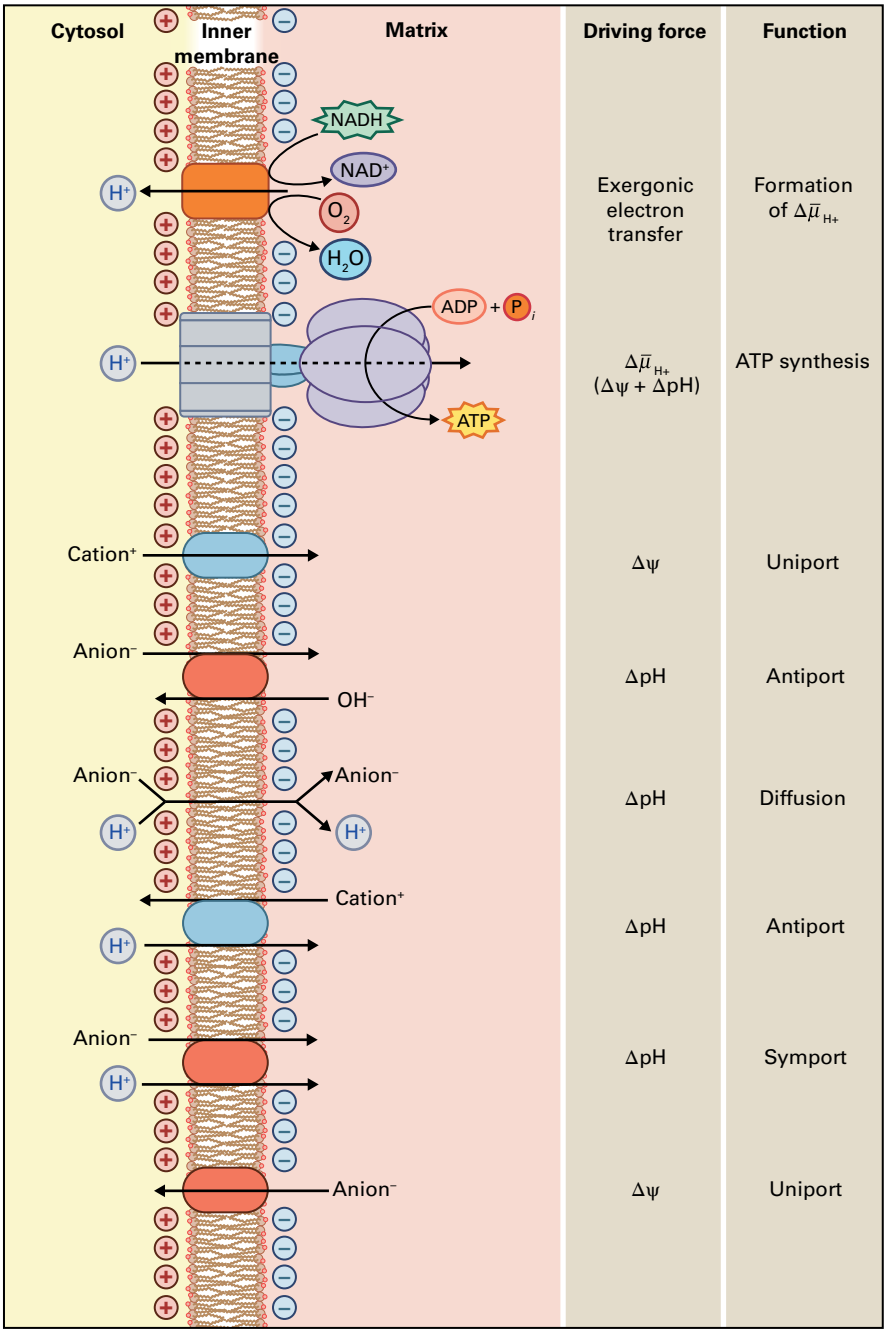


FIGURE 14.35 *The proton motive force ($\Delta\bar{\mu}_{H^+}$) established by proton pumping of the respiratory chain can drive ion transport across the inner mitochondrial membrane. Electrogenic transport involves the net movement of charge across the membrane; transport without net charge transfer is termed electroneutral. Inner membrane carriers that move only one ion (uniporters) are linked directly to Δψ. Two chemical species may be cotransported in the same direction by symporters, or in opposite directions by antiporters. In the mitochondrial membrane, such coupled transport may be driven by the ΔpH, if one of the ions is H^+ or OH^-; by Δψ, if the combined transport is electrogenic; or by a combination of ΔpH and Δψ ($\Delta\bar{\mu}_{H^+}$).*

14.7.2 Metabolite shuttles transfer carbon and reducing equivalents between mitochondria and other cellular compartments

One of the major challenges in plant mitochondrial research is developing an integrated view of mitochondria in the context of cell metabolism. Understanding how various carriers of the inner membrane interact to supply substrates for both mitochondrial and cytosolic processes is a crucial step toward this goal.

The α-ketoglutarate carrier is thought to operate with the glutamate/aspartate carrier in a substrate cycle known as the malate/aspartate shuttle (Fig. 14.37A). This shuttle, which can be demonstrated in isolated plant mitochondria, imports cytosolic reducing equivalents (NADH) into the mitochondrion in the form of malate. Reducing equivalents imported

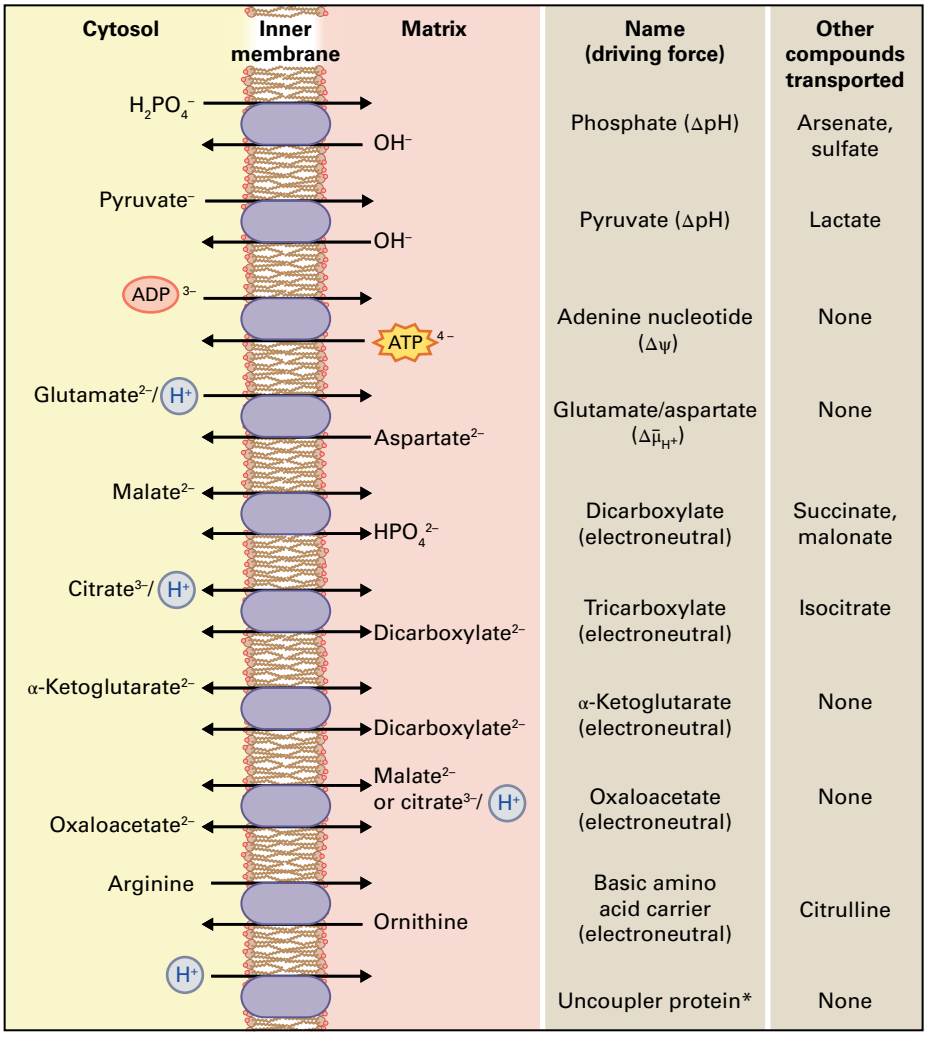


FIGURE 14.36 *Carriers (substrate transporters) of the inner mitochondrial membrane. All of these secondary active transporters are indirectly linked to the $\Delta\bar{\mu}_{H^+}$ across the membrane and are capable of accumulating substrates inside the mitochondrial matrix. Uptake of pyruvate and P_i in exchange for OH^- is linked to the ΔpH. The resulting P_i gradient can then be used to drive uptake of dicarboxylate anions via exchange on the dicarboxylate carrier. Dicarboxylates in turn can exchange for α-ketoglutarate or tricarboxylates; in the latter exchange, electroneutrality is maintained by cotransport of a proton with the citrate. This is also true for the exchange catalyzed by the OAA transporter. Exchanges of ADP for ATP and glutamate for aspartate are electrogenic and driven by the Δψ across the inner membrane. Note that glutamate exchange is coupled to cotransport of a proton to cause a charge imbalance that is thought to be important for the operation of the malate/aspartate shuttle (see Fig. 14.37). Arginine transport is important for its degradation during germination. The uncoupling protein is activated under certain circumstances and can dissipate the Δψ across the inner membrane.*

via the malate/aspartate shuttle can supply complex I, so oxidation of imported NADH is associated with greater ATP synthesis than is oxidation of cytosolic NAD(P)H by the nonphosphorylating external dehydrogenases of the respiratory chain. The glutamate/aspartate exchange is electrogenic in nature: glutamate and one proton are imported from the cytosol, and aspartate is exported from the matrix. Transporting a negative charge out of the mitochondrion ensures that this shuttle is unidirectional in respiring mitochondria, because the $\Delta\psi$ across the inner membrane (negative inside the matrix) drives aspartate out of the mitochondrion. However, the malate/aspartate shuttle can function only when the NADH/NAD^+ ratio is higher in the cytosol than the matrix. The malate/aspartate shuttle may be involved in glyoxysome–mitochondrion interactions in oil seeds (see Section 14.7.4).

Plant mitochondria also possess an OAA carrier that exchanges malate or citrate for OAA. This simpler shuttle, which has been demonstrated in isolated mitochondria, is readily reversible and can transfer reducing equivalents into or out of the mitochondrion (Fig. 14.37B). The direction of the shuttle likely depends on the concentration of the participant metabolites on either side of the mitochondrial inner membrane. In leaves, the malate/OAA shuttle is thought to participate in the photorespiratory cycle. The reducing equivalents formed by glycine oxidation in the mitochondrial

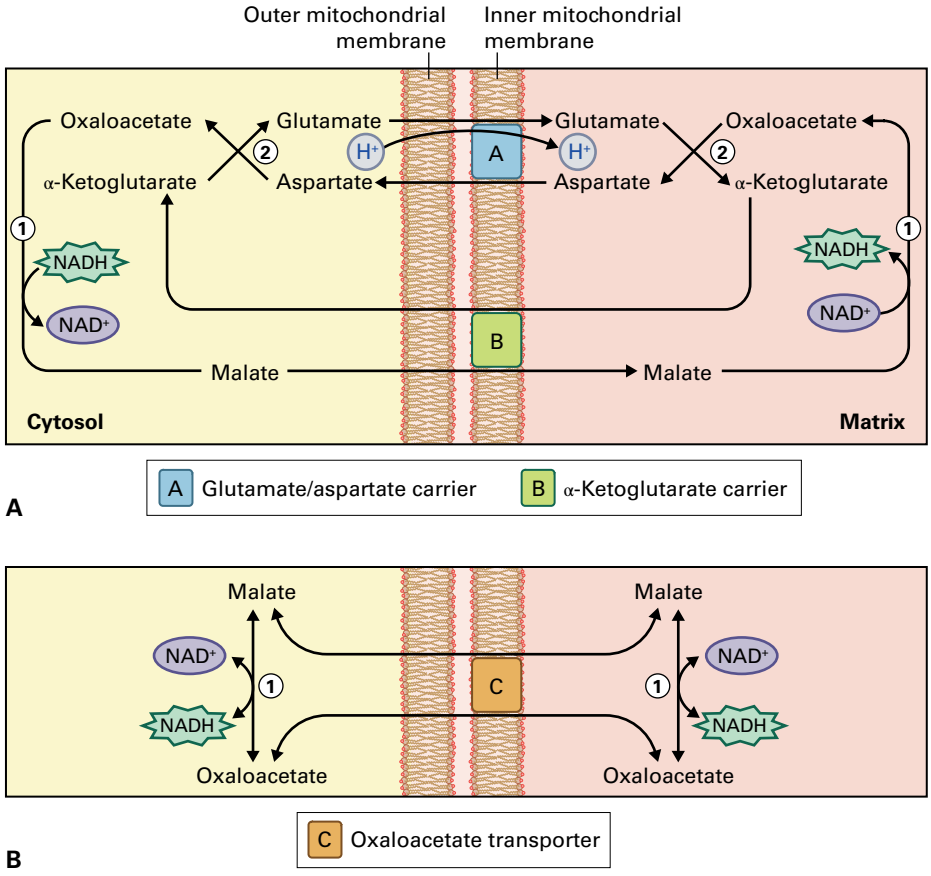


FIGURE 14.37 *Examples of mitochondrial metabolite shuttles: substrate shuttles in plant mitochondria. Plants can transfer reducing equivalents from cytosolic NAD(P)H to the mitochondrial matrix by means of substrate shuttles across the inner membrane. Two such shuttles, which have been demonstrated in isolated mitochondria, are shown. (A) Malate/aspartate shuttle. Isoenzymes of malate dehydrogenase (MDH, 1) and aspartate aminotransferase (2) are found on both sides of the mitochondrial membrane. OAA reduction in the cytosol oxidizes NADH (or NADPH) and produces malate, which moves into the mitochondrion. In the mitochondrion, the reverse reaction occurs, liberating NADH in the matrix that can be oxidized by the respiratory chain to drive ATP synthesis. Transamination of the OAA formed in the matrix prevents product inhibition of MDH. The aspartate and α-ketoglutarate formed are transported out of the mitochondrion in exchange for glutamate (carrier A) and malate (carrier B), respectively. Electrogenic glutamate/aspartate exchange is driven by $\Delta\bar{\mu}_{H^+}$, thereby providing directionality to the shuttle (i.e., reducing power is transferred into the mitochondrion only). (B) Malate/OAA shuttle. Here MDH isoforms on either side of the mitochondrial membrane are linked by malate/OAA exchange on the OAA carrier (carrier C). This shuttle is readily reversible in isolated mitochondria when sufficient MDH is added to the reaction medium.*

matrix are exported as malate to the peroxisome, where malate oxidation provides NADH to reduce hydroxypyruvate (see Section 14.9.1).

14.7.3 The citric acid cycle provides carbon skeletons for ammonia assimilation and amino acid synthesis

An important ancillary function of mitochondria in all tissues is the production and export of α-ketoglutarate for ammonia assimilation or transamination reactions in the cytosol and plastids. Ammonia assimilation requires α-ketoglutarate (see Section 14.9.2 and Chapters 7 and 16); the only net source of this α-keto acid is the citric acid cycle. In addition, mitochondria in some roots may export citric acid cycle intermediates such as malate and citrate, which are secreted into the rhizosphere to solubilize cations and facilitate plant uptake of Fe^{3+} and other mineral nutrients (see Chapter 23).

Export of citric acid cycle intermediates requires the mitochondrial import of substrates that can generate both acetyl-CoA and OAA. If pyruvate were provided as the only carbon source, export of citric acid cycle intermediates would prevent regeneration of OAA and bring the citric acid cycle to a halt. This need for anaplerotic reactions that replenish pools of citric acid cycle intermediates may explain why plant mitochondria possess relatively large amounts of NAD^+-linked malic enzyme (see Fig. 14.8).

The α-ketoglutarate, OAA, and citrate carriers of the inner mitochondrial membrane may function in the export of α-ketoglutarate and citrate. Various schemes can be drawn for this carbon export, but it has not yet been determined which

pathway operates in vivo. For example, acting in concert with the pyruvate carrier, the OAA carrier may promote the uptake of OAA and pyruvate into the mitochondrial matrix, where they can be used to synthesize citrate for subsequent export (Fig. 14.38A). There is also a cytosolic isoform of isocitrate dehydrogenase, so the exported citrate can be used to generate α-ketoglutarate for ammonia assimilation or transamination. Alternatively, malate/α-ketoglutarate exchange on the α-ketoglutarate carrier, or malate/citrate exchange on the tricarboxylate carrier, could be involved in a more complex scheme, in which NADH is transferred into the mitochondrion and more energy is generated from matrix NADH via the respiratory chain (Fig. 14.38B). When provided with the necessary extra-mitochondrial enzymes, isolated plant mitochondria are able to catalyze all of the exchanges required for both schemes.

14.7.4 Some plant tissues can convert lipids to sugars through gluconeogenesis

Most plant tissues store and respire carbohydrates. An important exception to this occurs in oil seeds, such as castor bean (*Ricinus communis*) and soybean (*Glycine max*), which store and respire lipids. Castor bean endosperm and soybean cotyledons contain substantial lipid reserves stored as triglycerides in specialized organelles called oil bodies (see Chapters 1 and 8). Utilization of these triglycerides involves their conversion to sucrose, which is then translocated to other organs in the growing seedling.

The interconversion process involves four cellular compartments: oil bodies, **peroxisomes** specialized in glyoxylate cycle and fatty acid β-oxidation (sometimes referred to as glyoxysomes) the cytosol, and mitochondria (Fig. 8.65). Triglycerides are hydrolyzed to glycerol and free fatty acids via lipases in the oil bodies (see Fig. 8.61). The glycerol is converted to triose phosphates used to synthesize sucrose in the cytosol (see Chapter 13). Fatty acids exported from the oil bodies undergo β-oxidation to NADH and acetyl-CoA (see Fig. 8.65) in the peroxisome. There, the acetyl-CoA is converted to succinate and malate by the glyoxylate cycle, in which two enzymes, isocitrate lyase and malate synthase, bypass the oxidative phase of the citric acid cycle. By preventing the complete oxidation of organic acids to CO_2, the glyoxylate cycle diverts carbon skeletons toward sugar biosynthesis. Some of the malate exported by the peroxisomes is oxidized, decarboxylated, converted to fructose-1,6-bisphosphate by reversing the reactions of glycolysis, and ultimately used to make sucrose in the cytosol (Fig. 8.65).

Mitochondria participate in gluconeogenesis because peroxisomes lack the enzymes to process succinate, which is transported to the mitochondria and converted to OAA via the last two enzymes of the citric acid cycle. Furthermore, peroxisomes lack the mitochondrial electron transport chain, so NADH formed during fatty acid oxidation is transported to the mitochondria via the malate/aspartate shuttle. Thus, aspartate aminotransferase in the mitochondrion interconverts OAA and glutamate to aspartate and α-ketoglutarate, which are transported to the peroxisomes, where the reverse reactions occur to form OAA. Conversion of this OAA to

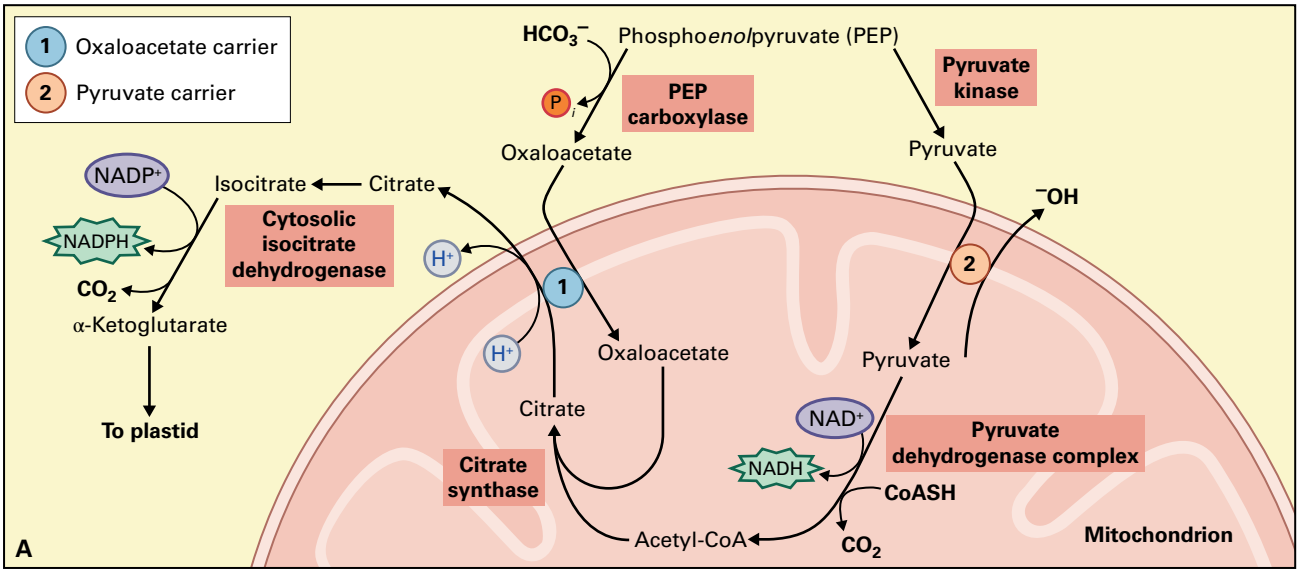


FIGURE 14.38 *Export of organic acids from the mitochondrion for support of NH_3 assimilation in the plastid. Two possible substrate shuttles in the mitochondrion have been proposed: scheme A is the simpler of the two, but scheme B has the potential to generate more ATP because more NADH is generated in the matrix. The NADH/NAD⁺ and NADPH/NADP⁺ ratios in the cytosol may determine which scheme operates by regulating the activity of cytosolic MDH and NADP⁺-isocitrate dehydrogenase, respectively. (A) OAA and pyruvate enter the mitochondrion and are used to generate citrate, which is exported from the mitochondrion (in exchange for OAA) and is converted to α-ketoglutarate in the cytosol by NADP⁺-linked isocitrate dehydrogenase. (B) Two molecules of malate enter the mitochondrion and are oxidized via MDH and NAD⁺-linked malic enzyme to produce OAA and pyruvate in the matrix, which are subsequently converted to either citrate or α-ketoglutarate. The latter compounds exchange for malate via either the α-ketoglutarate or tricarboxylate carriers.*

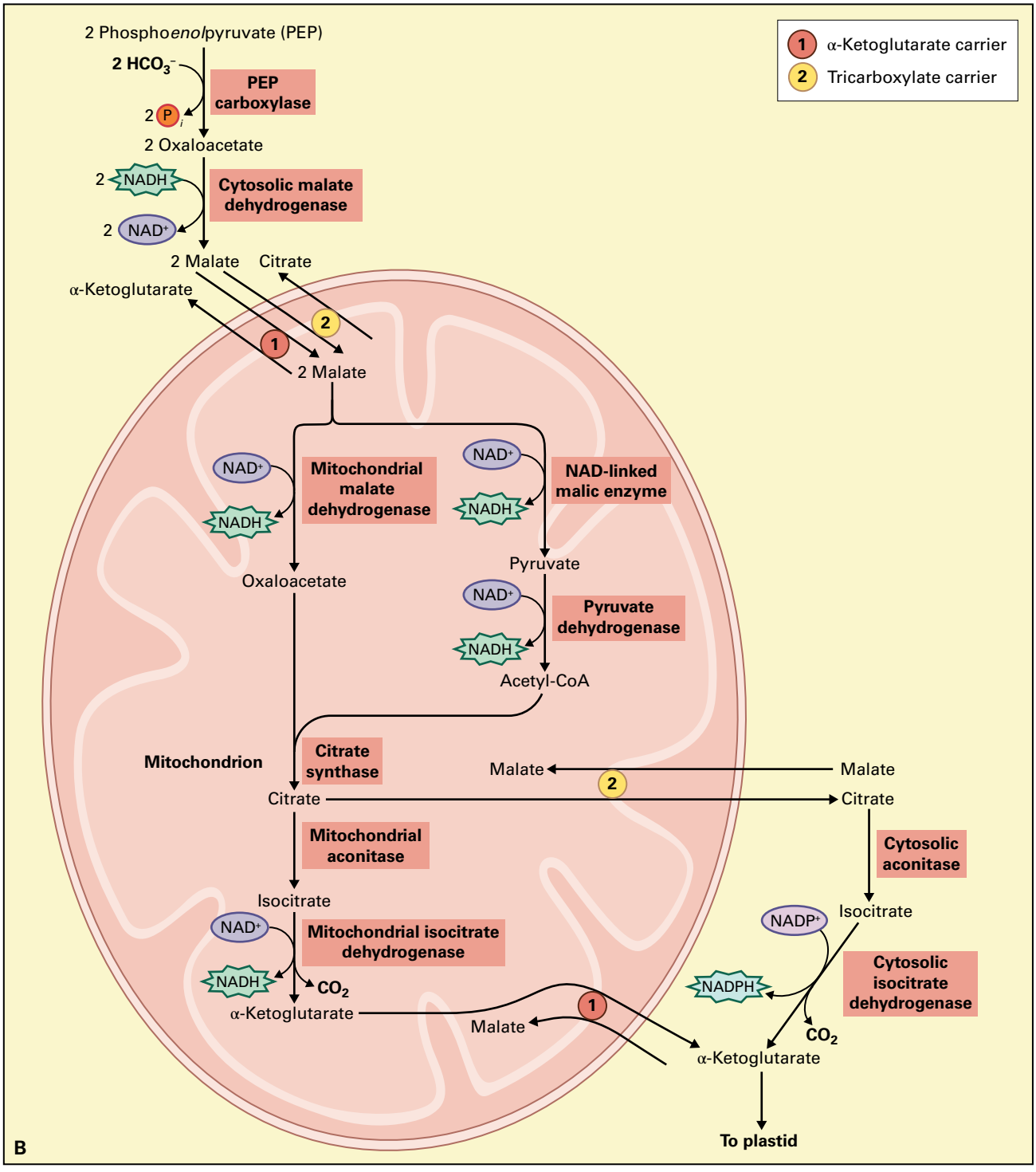


FIGURE 14.38 (*Continued*)

malate oxidizes the excess NADH in the peroxisome. The malate is recycled to the mitochondria to complete the shuttle, and the reducing equivalents released by mitochondrial malate oxidation drive ATP synthesis via the respiratory chain.

Operation of a malate/aspartate shuttle, rather than the simpler malate/OAA shuttle, has been proposed because isolated castor bean endosperm mitochondria do not transport OAA readily and the equilibrium of the malate dehydrogenase reaction does not favor OAA formation. Amination of OAA, therefore, helps drive oxidation of malate in the mitochondria. During respiration, the driving force for malate oxidation would be provided by the demand by the citric acid cycle for OAA, but during gluconeogenesis, carbon must be returned to the peroxisome to provide substrate for further sugar production. The ATP needed for gluconeogenesis is provided by mitochondrial respiration (see Fig. 8.65).

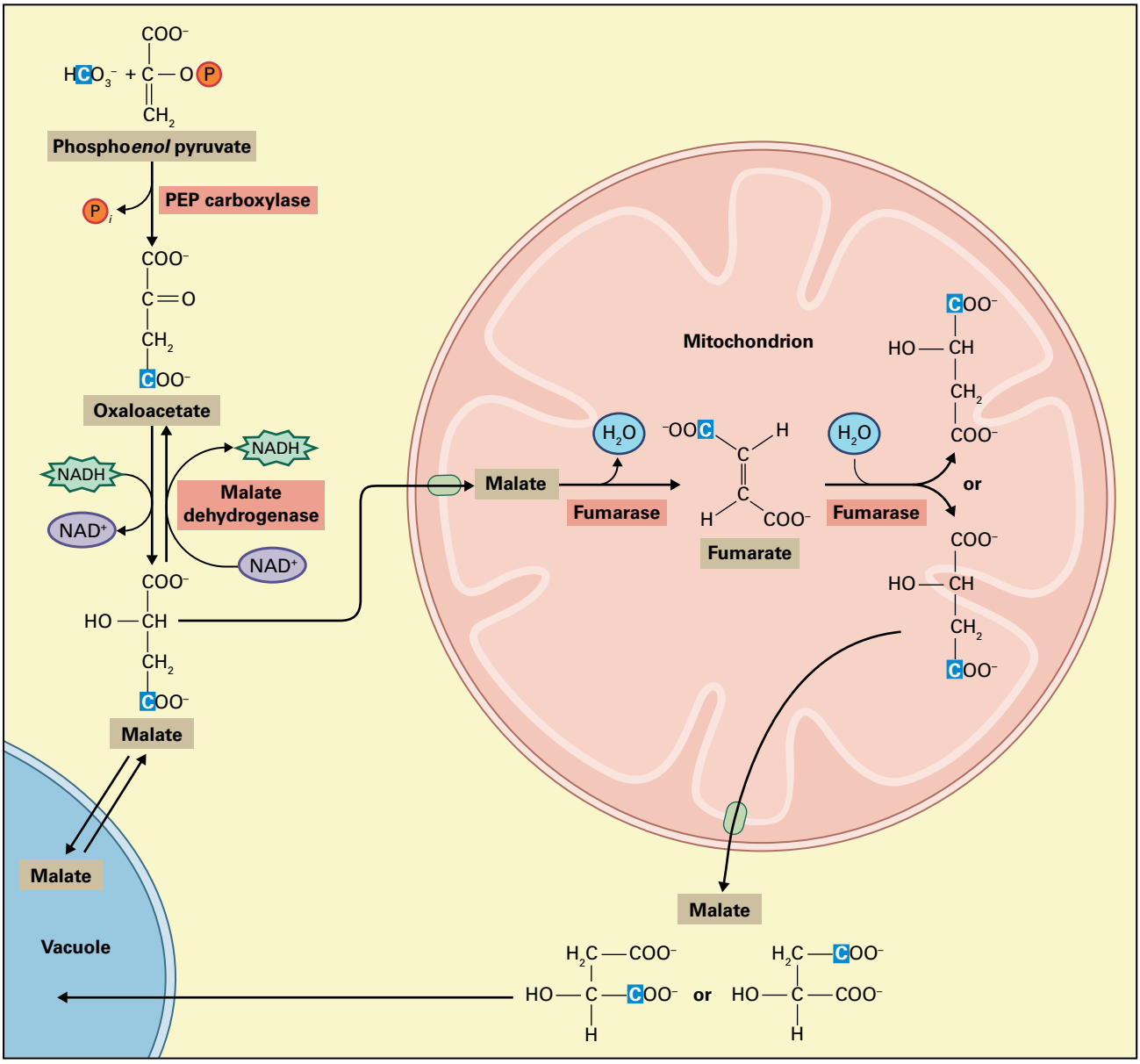


FIGURE 14.39 *Randomization of label in PEP carboxykinase-type CAM plants suggests a considerable amount of flux through the mitochondria takes place at night after CO_2 uptake. The reaction of ^{13}C-labeled HCO_3^- with PEP catalyzed by PEP carboxylase results in malate labeled exclusively at the C-4 position, but the vacuole contains large amounts of malate labeled in the C-1 position, suggesting the malate moves through the mitochondria. The carbon atoms at the C-1 and C-4 positions of malate are scrambled by the action of the citric acid cycle enzyme fumarase, which converts malate to the symmetrical molecule fumarate. When the resulting fumarate is converted back to malate, fumarase is equally likely to hydroxylate C-2 or C-3; therefore, the labeled carbon (previously C-4) can be at either the C-1 or C-4 position in the resynthesized malate molecule.*

14.7.5 Some C_4 and CAM plants use mitochondrial reactions to concentrate carbon dioxide for photosynthesis

Mitochondrial reactions are incorporated in the photosynthetic pathways of some C_4 plants and many species carrying out CAM. These reactions are unique to plant mitochondria and reflect the extent to which the central organelle of heterotrophic metabolism has evolved to support autotrophic carbon fixation.

The C_3 photosynthesis observed in most plants yields a three-carbon compound as its first stable product (see Section 14.8). C_4 photosynthesis (see Chapter 12) takes advantage of an aqueous equilibrium that favors bicarbonate ion (HCO_3^-) over CO_2 gas. In mesophyll cells, PEP carboxylase incorporates HCO_3^- into a four-carbon organic acid, which is then transported to bundle sheath cells, the site of CO_2 fixation by Rubisco. The C_4 acid is decarboxylated in the bundle sheath cells, thereby concentrating CO_2 and minimizing O_2 fixation by Rubisco.

The three different C_4 photosynthesis pathways—$NADP^+$-malic enzyme, NAD^+-malic enzyme, and PEP carboxykinase—

are each named for the bundle sheath enzyme that releases CO_2 (see Fig. 12.46). Whereas the $NADP^+$-malic enzyme pathway does not require mitochondrial activity, the NAD^+-malic enzyme and PEP carboxykinase C_4 pathways both utilize mitochondrial NAD^+-malic enzyme to decarboxylate malate and, consequently, the bundle sheath mitochondria process an enormous amount of carbon to supply the chloroplast. The photosynthetic rates attained by NAD^+-malic enzyme plants suggest carbon flux through the bundle sheath mitochondria is 10- to 20-fold greater than standard respiratory carbon flux, and several fold greater than the flux of glycine through mitochondria during photorespiration in C_3 plants.

In PEP carboxykinase plants, the situation is more complex. Although mitochondrial NAD^+-malic enzyme is active in this pathway, cytosolic PEP carboxykinase is thought to provide most of the CO_2 fixed by Rubisco (see Fig. 12.46C). Why are both enzymes required? One possible role for NAD^+-malic enzyme might involve oxidative phosphorylation. PEP carboxykinase converts OAA to PEP and CO_2 in a reaction that consumes one ATP. If the NADH generated by NAD^+-malic enzyme is utilized for ATP synthesis, the predicted stoichiometry would be roughly two malate molecules oxidized per five molecules of PEP produced.

CAM, a variation on the C_4 theme, allows plants to conserve H_2O (see Chapter 12). In CAM plants, HCO_3^- uptake by PEP carboxylase takes place at night, while stomata are open. The resulting C_4 acid, typically malate, is stored in the vacuole. Malate decarboxylation and CO_2 fixation by Rubisco take place in the same cell during the next day, with the stomata closed to prevent H_2O vapor from escaping (see Fig. 12.45). As with C_4 plants, subtypes of CAM photosynthesis are named for the decarboxylating enzyme. Malic enzyme CAM plants use both cytosolic $NADP^+$-malic and mitochondrial NAD^+-malic enzyme to decarboxylate malate. By contrast, PEP carboxykinase CAM plants contain low concentrations of malic enzyme. This does not preclude mitochondrial participation in photosynthesis by PEP carboxykinase CAM plants, because respiration may still provide ATP for the PEP carboxykinase reaction in these plants. Furthermore, PEP carboxykinase CAM plants transfer a considerable amount of label from the C-4 to the C-1 position of malate after uptake of $^{13}CO_2$. This suggests a large flux of malate into and out of the mitochondria probably occurs during the dark period, because this redistribution of label requires interconversion of malate and the symmetrical compound fumarate, a reaction catalyzed by the citric acid cycle enzyme fumarase (Fig. 14.39).

14.7.6 In photosynthetic tissues, operation of the citric acid cycle is inhibited by light

Although plant mitochondria clearly participate in light-based metabolism (e.g., photorespiration, C_4 photosynthesis, CAM), the extent to which illuminated photosynthetic tissues engage in respiration remains unclear. It is extremely difficult to measure respiration in the light, because the large amount of O_2 release and CO_2 uptake by chloroplasts mask the opposite processes in mitochondria. Photorespiration further complicates these measurements. Rates of aerobic respiration in darkened leaves are generally only 5–10% of maximum photosynthetic rates; however, all nonphotosynthetic tissues respire, and the entire plant respires during the night. Because of this, some plants may respire as much as 50–70% of carbon fixed daily by photosynthesis, depending on growth conditions.

It has long been thought that photosynthesis, particularly photophosphorylation, must poise the cytosolic ATP/ADP ratio at such high levels that respiratory control would restrict respiration severely. Indirect measurements of CO_2 output from intact leaves, combined with assessment of the external CO_2 concentration at which photosynthetic CO_2 uptake equals respiratory CO_2 release so that net photosynthetic CO_2 exchange is zero (the **CO_2 compensation point**) suggest nonphotorespiratory CO_2 release is inhibited in the light. This may indicate light slows the rate of carbon flux through the citric acid cycle by approximately 50%. The inhibitory mechanism is not known but may involve downregulation of pyruvate dehydrogenase, α-ketoglutarate dehydrogenase, and malic enzyme activities. Ammonia produced during photorespiration could stimulate PDH kinase, leading to inactivation of pyruvate dehydrogenase (see Fig. 14.10). Thioredoxin interacts with several enzymes of the citric acid cycle, but its effect on activity is yet to be determined.

On the other hand, the participation of glycolytic and citric acid cycle intermediates in many important biosynthetic pathways argues that some aerobic respiration must take place in illuminated green cells. Several observations indicate actively photosynthesizing tissues do respire. The nonphosphorylating pathways of mitochondrial electron transfer provide a mechanism by which plant mitochondria, at least in theory, can oxidize NADH without having to synthesize ATP and without being subject to respiratory control when cellular ADP concentrations are low (see Section 14.6.3). Furthermore, rapid fractionation of organelles from wheat leaf protoplasts has demonstrated cytosolic concentrations of ADP are no different in the light than in the dark, indicating photosynthesis does not appreciably deplete the pool of ADP available for oxidative phosphorylation. Mitochondrial ATP production appears necessary for maintaining high photosynthetic rates, probably because sucrose synthesis requires high amounts of cytosolic ATP.

14.8 Biochemical basis of photorespiration

14.8.1 Photorespiration is associated with light-dependent O_2 uptake and CO_2 evolution in green plant tissues

In the 1920s, the biochemist Otto Warburg (Nobel Laureate, 1931) discovered that increasing the external O_2 concentration inhibited photosynthesis in the green alga *Chlorella*. In most C_3 plants, photosynthetic rates decline as much as 50% when the O_2 concentration is doubled from the ambient value of 21%. Conversely, photosynthesis is stimulated as much as twofold by decreasing the O_2 concentration to <2%. The connection

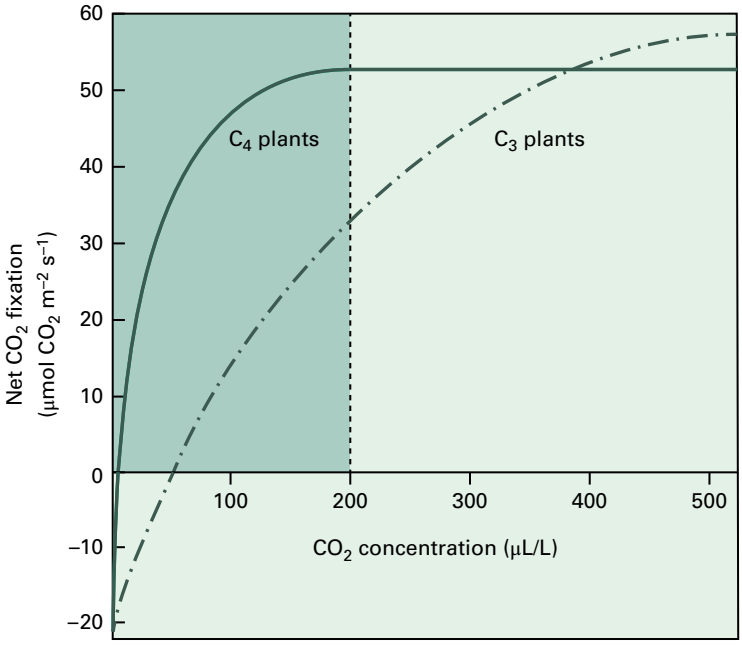


FIGURE 14.40 *Effect of CO_2 concentration on the CO_2 fixation rate. As the ambient concentration of CO_2 is increased in the presence of saturating light, net CO_2 uptake during photosynthesis increases in a roughly linear fashion, saturating at a relatively low CO_2 concentration (150 μL L^{-1}) in C_4 plants and only beginning to show signs of saturation at ambient CO_2 levels (360–375 μL L^{-1}) in C_3 plants. The concentration at which net change in CO_2 is 0 defines the CO_2 compensation point and reflects the CO_2 concentration at which the rate of gross photosynthetic CO_2 uptake exactly equals the respiration rate. The total respiration rate comprises both mitochondrial-linked (dark) respiration and photorespiration. That the CO_2 compensation point for C_3 plants (20–50 μL L^{-1}) is greater than for C_4 plants (0–5 μL L^{-1}) is associated with the presence of photorespiration in C_3 plants and its virtual absence in C_4 plants.*

between O_2 concentration and photosynthesis was strengthened by the proportional relationship between the ambient O_2 concentration and the CO_2 compensation point (Fig. 14.40; see also Section 14.7.6). The CO_2 compensation point increases with increasing O_2 concentration, suggesting competition between O_2 and CO_2 during photosynthesis. In addition, actively photosynthesizing tissues release a burst of CO_2 immediately after illumination ceases. The amount of CO_2 evolved during this **post-illumination burst** is directly proportional to the external O_2 concentration. These observations ultimately revealed a novel pathway. Whereas almost all plants are capable of photosynthesis, in which light stimulates CO_2 uptake and O_2 evolution, most also perform **photorespiration**, a light-stimulated process that consumes O_2 and evolves CO_2.

High rates of photorespiration are restricted to C_3 plants (see Chapter 12). The majority of plants fall into this category, although certain plants (i.e., C_4 and CAM plants) have evolved relatively sophisticated biochemical mechanisms that limit photorespiration by concentrating CO_2 at the site of carbon fixation. Many oxygenic photosynthetic organisms living in aquatic environments, including algae, cyanobacteria, and some plants, have also developed mechanisms for concentrating CO_2 or HCO_3^- in cells and transporting it to the chloroplast, thus minimizing the rate of photorespiration. Both photorespiration and its consequences for plants have been linked inextricably to changes in the ratio of CO_2 to O_2 in the earth's atmosphere that have taken place since life appeared. Since the beginning of the 20th century, large-scale anthropogenic CO_2 emissions have accompanied an increase in global atmospheric CO_2 concentrations that might impact and inhibit photorespiration, thereby altering existing competitive relationships among many plant species.

14.8.2 Oxygenase activity of Rubisco catalyzes the initial step of photorespiration

The origin of photorespiration is found in the kinetic properties of Rubisco, the enzyme that catalyzes the carboxylation of ribulose 1,5-bisphosphate (RuBP) to form two molecules of 3-phosphoglycerate (3-PGA), the first stable intermediate in the C_3 reductive photosynthetic carbon cycle (see Chapter 12). However, Rubisco is also capable of catalyzing an oxygenase reaction, in which a molecule of O_2 reacts with RuBP to produce one molecule of 3-PGA plus one molecule of 2-phosphoglycolate.

The Rubisco reaction mechanism (Fig. 12.38) involves the initial binding of RuBP to the enzyme, followed by formation of a 2,3-enediolate intermediate. Either CO_2 or O_2 can react directly with this enediolate species, producing, respectively, an unstable C_6 or C_5 intermediate that breaks down to the final products rapidly and irreversibly. As a result of this mechanism, CO_2 and O_2 act as competitive substrates for Rubisco, with O_2 inhibiting RuBP carboxylation and CO_2 inhibiting RuBP oxygenation. The ratio of carboxylase to oxygenase activity is a function of the relative amounts of each gas present.

14.8.3 The relative carboxylase and oxygenase activities of Rubisco depend on kinetic properties of the enzyme

The ratio of RuBP carboxylase to RuBP oxygenase activity (v_c/v_o) is an important determinant of photosynthetic efficiency and can be expressed as a function of the kinetic parameters of the two competing reactions:

Equation 14.3: Ratio of carboxylase activity to oxygenase activity

$$v_c/v_o = \left(\left[V_c/K_c\right]/\left[V_o/K_o\right]\right)\cdot\left[CO_2\right]/\left[O_2\right]$$

where V_c and V_o are the maximal velocities (V_m), and K_c and K_o are the Michaelis–Menten constants (K_m), for the carboxylase and oxygenase reactions, respectively. This formula assumes CO_2 and O_2 are each present at a concentration lower than its apparent K_m. The ratio V_m/K_m defines the pseudo second-order rate constant for each reaction, so the set of kinetic constants $[V_c/K_c]/[V_o/K_o]$ constitutes a **specificity factor** that represents the ratio of the carboxylation and oxygenation rates when the two gaseous substrates are present in equal amounts. Among land plants, Rubisco demonstrates an average specificity factor of 100, with values ranging between 80 and 130. In today's atmosphere, the air-equilibrated concentrations of the two substrates are approximately 8 μM CO_2 (0.038%) and 250 μM O_2 (21%) at 25°C. Therefore, a specificity factor of 100 gives a v_c/v_o ratio of 3.2.

14.9 The photorespiratory pathway

Given a specificity factor of 100 for Rubisco, the ratio of carboxylase to oxygenase activity is approximately 3 to 1 under present atmospheric conditions. Therefore, an appreciable amount of RuBP is converted to 2-phosphoglycolate, a compound that cannot be utilized by the C_3 reductive photosynthetic carbon cycle (Calvin–Benson cycle). A second cycle, known as the **C_2 oxidative photosynthetic carbon cycle** or photorespiratory carbon oxidation cycle, salvages this carbon so it is not lost to photosynthetic metabolism. During the C_2 cycle, two molecules of phosphoglycolate are converted to one CO_2 and one molecule of 3-PGA, which can return to the C_3 cycle. The C_3 and C_2 cycles operate together in an integrated fashion (Fig. 14.41).

14.9.1 Photorespiratory reactions occur in three organelles: chloroplast, peroxisome, and mitochondrion

The C_2 cycle (Fig. 14.42) is initiated in the chloroplast with the formation of 2-phosphoglycolate, which is subsequently converted to glycolate and P_i by the action of phosphoglycolate

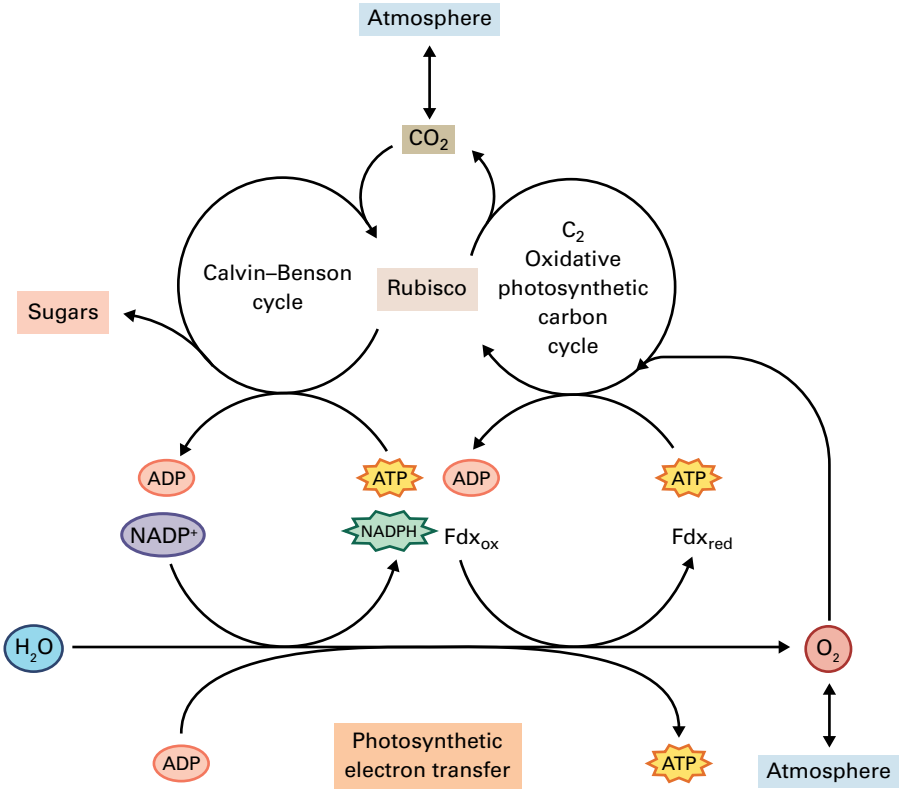


FIGURE 14.41 *Diagram of the relationship between the reductive photosynthetic (C_3 or Calvin–Benson cycle) and the oxidative photosynthetic (C_2) carbon cycles. Rubisco initiates both the Calvin–Benson cycle and photorespiration (the C_2 cycle). In both cases, photosynthetic electron transport provides energy-rich substrates (ATP and NADPH for photosynthesis, ATP and reduced ferredoxin (Fdx_{red}) for photorespiration and reassimilation of the resulting NH_3). One of the substrates of the C_3 cycle, CO_2, is a product of the C_2 cycle; in turn, the substrate of the C_2 cycle, O_2, is a product of C_3 photosynthesis. The same atmospheric pools provide gaseous substrates for and receive gaseous products from both processes.*

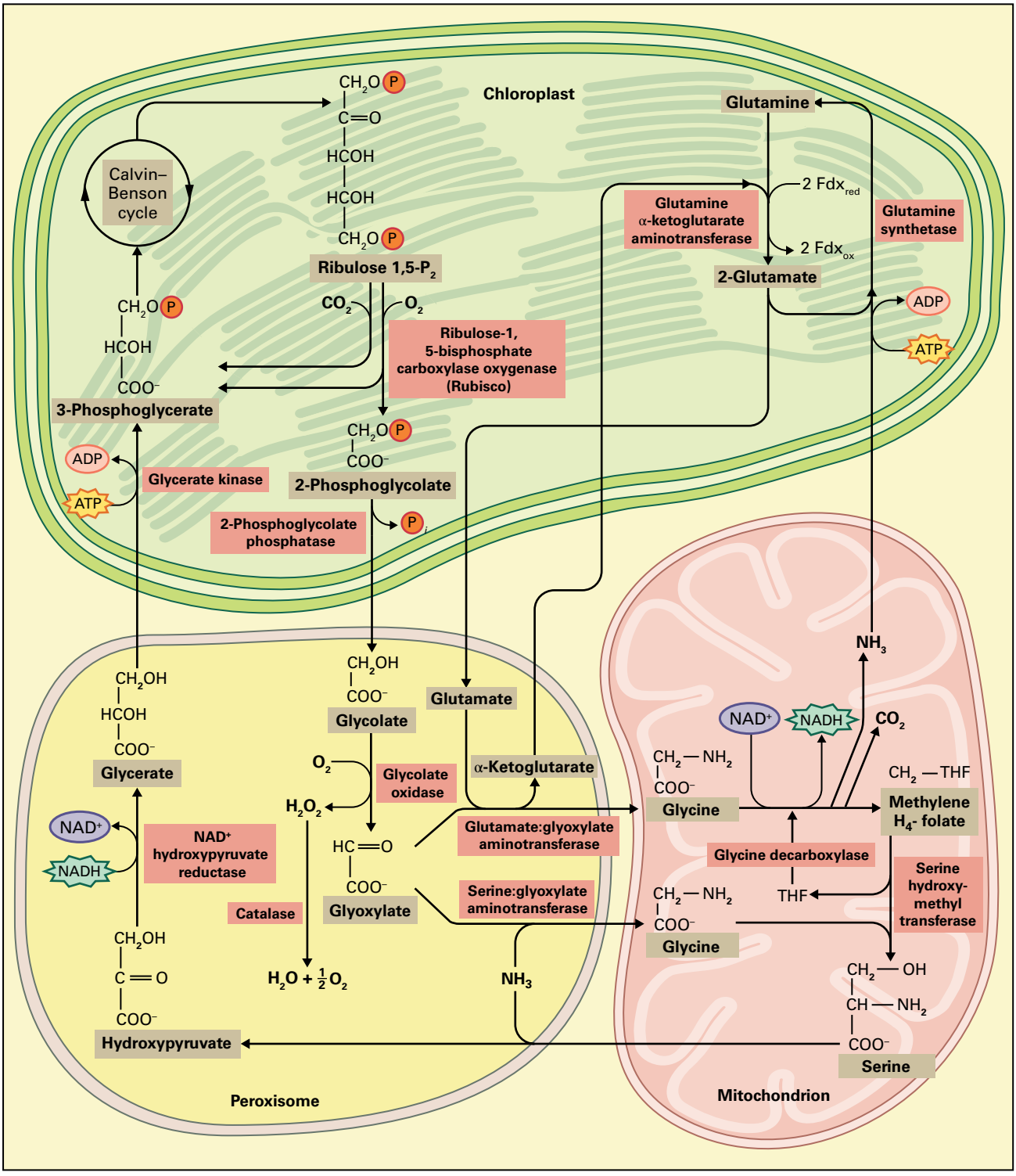


FIGURE 14.42 *Operation of the oxidative photosynthetic carbon (C_2) pathway involves cooperative interaction among three separate subcellular organelles: chloroplasts, peroxisomes, and mitochondria. The pathway is initiated in the chloroplast when Rubisco catalyzes the oxygenation of ribulose 1,5-bisphosphate to produce one molecule of 3-phosphoglycerate (3-PGA) and one molecule of 2-phosphoglycolate. The reactions of the C_2 pathway bring about the metabolic interconversion of two molecules of 2-phosphoglycolate to salvage one molecule of 3-PGA, which can be used in the operation of the C_3 cycle. Additionally, conversion of two 2-phosphoglycolate to one molecule of 3-PGA requires uptake of a third molecule of O_2 and the release of one molecule of NH_3. Reassimilation of the NH_3 requires the net input of two reducing equivalents (e.g., one molecule of NAD(P)H or two molecules of Fdx_{red}) plus one molecule of ATP. The final step in the formation of 3-phosphoglycerate also requires a molecule of ATP.*

phosphatase. The glycolate exits the chloroplast through a glycolate transporter on the inner membrane of the chloroplast envelope and then enters a peroxisome, possibly by diffusion. In the peroxisome, glycolate reacts with O_2 to produce glyoxylate and H_2O_2. This reaction is catalyzed by a peroxisomal flavin mononucleotide (FMN)-containing enzyme, glycolate oxidase. Two molecules of glyoxylate are aminated to form glycine in a peroxisomal reaction catalyzed by serine:glyoxylate aminotransferase and glutamate:glyoxylate aminotransferase. Both enzymes must function for the continued operation of the C_2 cycle (see Section 14.10.2). The H_2O_2 is removed by abundant catalase present in the peroxisome; two molecules of H_2O and one of O_2 are formed for every two molecules of phosphoglycolate that enter the C_2 cycle. As one O_2 enters the cycle, there is no net change in O_2 at this stage.

The glycine produced in the peroxisome then moves into the mitochondrion. Glycine decarboxylase, an abundant, complex enzyme with a reaction mechanism reminiscent of pyruvate dehydrogenase (see Fig. 14.9) and α-ketoglutarate dehydrogenase, catalyzes the oxidative decarboxylation of glycine to produce CO_2, ammonia, NADH, and methylene tetrahydrofolate (Fig. 14.43). Serine hydroxymethyltransferase joins the methylene tetrahydrofolate to a second molecule of glycine, producing the C_3 amino acid serine in a reaction that requires pyridoxal phosphate as a cofactor. These enzymes are virtually absent from mitochondria of heterotrophic plant tissues. Leaves maintained in the dark demonstrate low activities of these two enzymes, but expression of the enzymes is stimulated on exposure to light to process the large flux of glycine that accompanies the onset of photorespiration.

For every two molecules of glycine that enter the mitochondrion, one molecule each of serine, CO_2, and ammonia are produced, and one NAD^+ is reduced to NADH. This means one CO_2 is produced for every two molecules of O_2 taken up by the action of RuBP oxygenase.

The serine produced in the mitochondrion is transported back into the peroxisome, where it is deaminated by serine:glyoxylate aminotransferase to form hydroxypyruvate. Another peroxisomal enzyme, hydroxypyruvate reductase, catalyzes the reduction of hydroxypyruvate to glycerate, using NADH as an electron donor. The glycerate exits the peroxisome and is imported into the chloroplast by the same transporter that exports glycolate. Once inside the chloroplast stroma, glycerate is phosphorylated by ATP, yielding 3-PGA and ADP. This reaction, catalyzed by the enzyme glycerate kinase, completes the conversion of two molecules of phosphoglycolate to one of 3-PGA, which can now enter the C_3 cycle.

The phenotypes associated with mutations in genes that encode the C_2 cycle enzymes support the cycle's proposed function in recycling 2-phosphoglycolate produced by the oxygenase reaction. Such mutants die under normal atmospheric conditions that promote photorespiration (21% O_2, 0.038% CO_2) but grow normally when placed in a high CO_2 atmosphere (>0.2%), where the oxygenase activity of Rubisco is minimal. An *Arabidopsis* mutant lacking phosphoglycolate phosphatase was among the first plants reported to demonstrate this phenotype, but additional mutations have now been found in peroxisomal catalase, serine:glyoxylate aminotransferase, glycine decarboxylase, serine hydroxymethyltransferase, and chloroplast-localized isoenzymes of glutamine synthetase and ferredoxin-dependent glutamine:α-ketoglutarate aminotransferase (see Section 14.9.2).

14.9.2 Production of ammonia during photorespiration requires an ancillary cycle for its efficient reassimilation

During operation of the C_2 cycle, glycine decarboxylation releases ammonia inside the mitochondrion. To avoid toxic ammonia accumulation while preventing N loss through volatilization, photorespiring plant cells must reassimilate this ammonia efficiently. Reassimilation takes place in the chloroplast through the sequential action of glutamine synthetase (GS) and glutamine:2-oxoglutarate aminotransferase (GOGAT; see Chapters 7 and 16).

Reaction 14.5: Net reaction of GS/GOGAT enzyme couple

$$\alpha\text{-ketoglutarate} + NH_3 + ATP + 2e^- \leftrightarrow \text{glutamate} + ADP + P_i$$

The reducing equivalents for the GOGAT reaction are provided by the reduced ferredoxin (Fdx_{red}) formed during photosynthetic electron transfer, whereas the ATP consumed by the GS reaction is produced by photophosphorylation (see Chapter 12).

The need to reassimilate the ammonia produced during the operation of the C_2 cycle helps explain why two different aminotransferases are required in the peroxisome for the conversion of glyoxylate to glycine (see Fig. 14.42). For every two glyoxylates that pass through the C_2 cycle, only one serine is produced in the mitochondrion. The conversion of this serine to 3-PGA requires that serine:glyoxylate aminotransferase catalyze the deamination of the serine to produce hydroxypyruvate. This reaction aminates one of the two glyoxylates and generates glycine. Amination of the second glyoxylate is associated with reassimilation of photorespiratory ammonia. The molecule of glutamate formed during ammonia assimilation must be deaminated to regenerate the GOGAT substrate α-ketoglutarate. If glutamate is allowed to accumulate, ammonia assimilation will be inhibited by excess product and insufficient substrate. Glutamate:glyoxylate aminotransferase provides a mechanism for converting glutamate back to α-ketoglutarate. The photorespiratory N cycle and the two peroxisomal glyoxylate aminotransferases ensure that movement of N into and out of the C_2 cycle remains in balance.

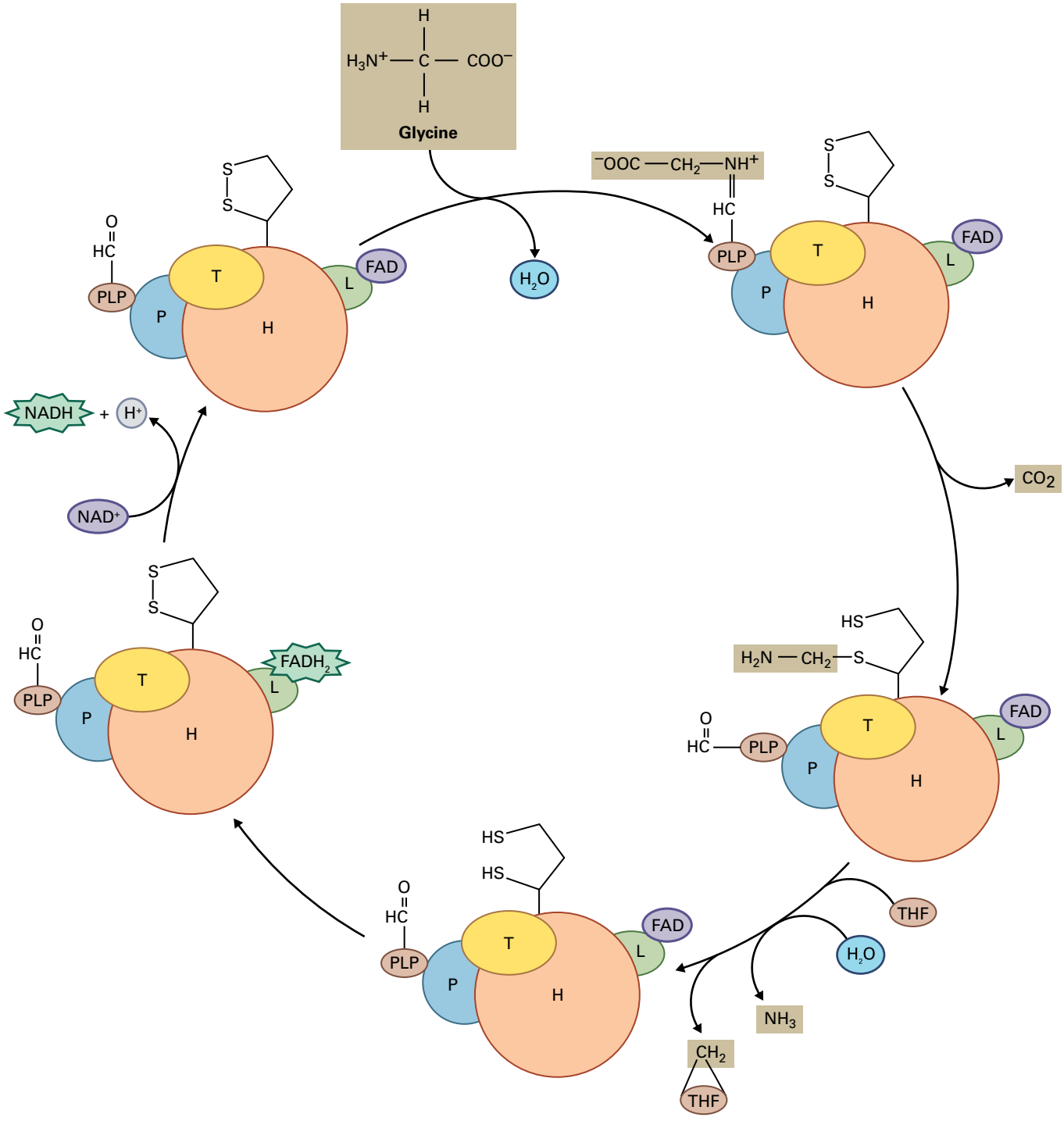


FIGURE 14.43 *Reaction mechanism of the glycine decarboxylase complex. The complex consists of four enzymes, including a pyridoxal phosphate (PLP)-containing protein (P-protein), a lipoamide-containing protein (H-protein), a protein that interacts with tetrahydrofolate (T-protein), and an FAD-containing lipoamide dehydrogenase (L-protein). The reaction sequence is initiated by formation of a Schiff's base between glycine and the PLP on the P-protein. The P-protein catalyzes an oxidative decarboxylation of the glycine and transfers the reducing equivalents and the remaining methylamine to the lipoamide moiety on the H-protein. While not entirely the same, the remaining mechanistic features of the glycine decarboxylase resemble those found in the pyruvate dehydrogenase (see Fig. 14.9) and α-ketoglutarate dehydrogenase reactions of the citric acid cycle. The same L-protein is used in all three complexes.*

14.9.3 Photorespiration increases the energy costs associated with photosynthesis

The stoichiometry associated with the C_2 cycle is not straightforward. Oxygenation of two RuBPs generates two molecules of 3-PGA and two molecules of 2-phosphoglycolate. The net reaction that converts the latter to one molecule of 3-PGA is:

Reaction 14.6: The C_2 cycle

$$2\,\text{RuBP} + 3\,O_2 + 2\,Fdx_{red} + 2\,ATP \rightarrow 3\,\text{3-PGA} + CO_2 + 2\,Fdx_{ox} + 2\,ADP + 2\,P_i$$

In photosynthesis, the relationship of O_2 evolved to CO_2 taken up is 1:1. In photorespiration, by contrast, 3 O_2 are taken up for every CO_2 evolved. Salvaging phosphoglycolate by converting it to phosphoglycerate requires a net input of two Fdx_{red} (i.e., one NAD(P)H equivalent) and two ATPs. The reducing equivalents and one ATP molecule are consumed during photorespiratory ammonia reassimilation. The remaining ATP is used to phosphorylate glycerate. Whether this exact stoichiometry operates in vivo is less certain. No endogenous source of NADH exists in the peroxisome, so the reducing equivalents needed for hydroxypyruvate reductase reaction must be imported. This probably involves malate, which can generate NADH via the peroxisomal malate dehydrogenase, forming OAA as a product.

As discussed in Section 14.7.2, malate and OAA can be exchanged between the mitochondrial matrix and the cytosol through the operation of the OAA carrier. This malate/OAA shuttle provides a convenient mechanism for moving the NADH produced by mitochondrial glycine decarboxylase reaction to the peroxisome, where it can provide electrons for the reduction of hydroxypyruvate. If this mitochondrial shuttle operates, there is no need for the mitochondrial electron transport chain to function in conjunction with the C_2 cycle, and the stoichiometry cited above would hold. However, chloroplasts also possess an OAA transporter and may utilize a malate/OAA shuttle to transfer reducing equivalents to the peroxisome. If the chloroplast-localized malate/OAA shuttle is used and all the NADH produced during glycine decarboxylation is oxidized through the mitochondrial electron transport chain, operation of the C_2 cycle would consume two NAD(P)H equivalents and actually produce one ATP for every two CO_2 evolved.

If each NADH can produce 2.5 ATPs during oxidative phosphorylation (see Section 14.4.3), the net energy cost of the operation of the C_2 cycle per CO_2 evolved is 4.5 ATP equivalents, regardless of which pathway or combination thereof operates in vivo. The cost of converting the resulting 3-PGA to 0.6 RuBP via the C_3 reductive photosynthetic carbon cycle adds an additional 4 ATP equivalents (i.e., 1 NADPH + 1.5 ATP) to the total. However, operation of the C_2 cycle also leads to loss of one CO_2, and the cost of refixing this CO_2 is another 8 ATP equivalents (i.e., 2 NADPH + 3 ATP). Assuming C_3 plants fix three molecules of CO_2 for every molecule of O_2 fixed by the C_2 cycle, the cost of fixing three molecules of CO_2 is 32.25 ATP equivalents in a C_3 plant—but only 30 ATP equivalents in many C_4 plants (Table 14.2).

TABLE 14.2 *Energy costs of photorespiration and photosynthesis.**

1 O_2 fixed by Rubisco	
C_2 cycle	2.25 ATP equivalents
Calvin–Benson cycle (regenerating RuBP from 3-PGA)	2 ATP equivalents
Recapturing 0.5 CO_2 released by C_2 cycle	4 ATP equivalents
Total	8.25 ATP equivalents
1 CO_2 fixed by Rubisco (C_3 plant)	
Calvin–Benson cycle	8 ATP equivalents
Total	8 ATP equivalents
1 HCO_3^- incorporated into C_4 acid (C_4 plant)	
C_4 cycle	2 or 3 ATP equivalents†
Calvin–Benson cycle	8 ATP equivalents
Total	10 or 11 ATP equivalents†

*Assuming a cost of 2.5 ATP per NAD(P)H oxidized.
†2 ATP equivalents for NAD^+- or $NADP^+$-malic enzyme plants, 3 ATP equivalents for PEP-carboxykinase plants.

The C_2 cycle clearly constitutes a major energy drain that lowers the efficiency of CO_2 uptake during C_3 photosynthesis. This point is emphasized when we consider that C_4 plants can make up for using additional ATP during photosynthesis by minimizing photorespiration. Plants that have evolved mechanisms to minimize photorespiration are thus at a definite advantage under recent atmospheric CO_2 concentrations, but anthropogenic CO_2 emissions may shift this advantage in the future (see Section 14.10.3).

14.10 Role of photorespiration in plants

14.10.1 The rate of photorespiration can represent an appreciable percentage of the photosynthetic rate

Under current atmospheric conditions, and given a specificity factor of 100, the rate of carboxylation to oxygenation should be approximately 3 to 1. Because each oxygenation reaction produces only 0.5 CO_2, the rate of photorespiratory

CO_2 evolution should be equivalent to 16% of the rate of gross photosynthetic CO_2 uptake (i.e., 0.5 CO_2 released per oxygenation × 1 oxygenation per 3 carboxylations). Considering the number of carbon atoms metabolized through the C_2 cycle, the rate of carbon flux through the C_2 cycle at any given time can be estimated at approximately 65% of the photosynthetic rate (4 carbon atoms metabolized through the C_2 cycle per molecule of photorespiratory CO_2 evolved × 16% of photosynthetic CO_2 uptake). Experimental measurements using oxygen isotopes to discriminate between photosynthetic CO_2 uptake and photorespiratory CO_2 efflux indicate the rate of photorespiratory CO_2 release ranges from 18% to 27% of the photosynthetic carbon fixation rate. These data conform to the theoretical calculations above; in fact, the latter value suggests the flux of carbon through the C_2 cycle can exceed the rate of photosynthetic CO_2 fixation.

The values given above clearly illustrate the inhibitory effects of photorespiration on photosynthesis. However, the inhibition of photosynthesis by photorespiration is not associated solely with the evolution of CO_2 during the operation of the C_2 cycle. For every CO_2 released during the operation of the C_2 cycle, two molecules of O_2 react at the Rubisco active site and prevent CO_2 from being fixed. We can hypothesize, therefore, that if photorespiratory CO_2 flux equals 20% of the photosynthetic CO_2 uptake, then replacing these two oxygen molecules with CO_2 would increase the rate of photosynthesis by an additional 40% (see Fig. 14.42 and Reaction 14.5). Thus, abolishing RuBP oxygenation and the resulting C_2 cycle would enhance photosynthetic CO_2 fixation not by 20%, but by 60%. This premise is supported by experimental evidence: When net photosynthetic rates in C_3 plants are under 1% to 2% O_2, increases of 50% to 70% are commonly observed. Likewise, growth under high CO_2 or low O_2 (relative to that found in the normal atmosphere) enhances production of dry biomass, further demonstrating the energy costs of the C_2 cycle.

14.10.2 The oxygenase activity of Rubisco is consistent with the enzyme's anaerobic origins

The initial appearance of the enzyme Rubisco in ancient photoautotrophic bacteria is thought to have preceded the build up of free O_2 in the Earth's atmosphere by at least 10^9 years. For a long time, therefore, the environment apparently did not select against the oxygenase activity inherent in Rubisco's catalytic mechanism. After the appearance of free atmospheric O_2, the selective pressure to minimize oxygenase activity must have been great, even though the early aerobic atmosphere contained less O_2 and more CO_2 than the air we breathe today. As recently as 100 million years ago, during the Cretaceous period, CO_2 accounted for approximately 0.3% of the atmosphere, almost an order of magnitude greater than the current CO_2 content.

The consequence of this selective pressure can be seen in the range of kinetic specificity factors (see Section 14.8.3) displayed by different photosynthetic organisms. Specificity factor values as low as 15 are seen in bacteria that photosynthesize in anaerobic environments. These prokaryotes could not grow under current aerobic conditions: even if able to tolerate O_2, they would fix more O_2 than CO_2. Cyanobacteria have specificity factors of 50–60, but can augment this with transport systems that concentrate CO_2 at the site of fixation to minimize oxygenase activity. A specificity factor of 100, average for terrestrial plants, appears to reflect the best that evolutionary selective pressure can accomplish with Rubisco alone, given its oxygenase activity has been selected against for a very long time. The Ice Ages in particular must have penalized RuBP carboxylation—CO_2 concentrations dropped well below current levels (0.038%) to values less than 0.030%. It is noteworthy that, despite the costs of photosynthetic O_2 fixation, the Calvin–Benson pathway is the only CO_2 assimilation cycle that can function in today's atmosphere. The other five carbon cyclic pathways capable of supporting autotrophic growth are restricted to bacteria occurring in habitats with little or no O_2.

The deleterious impact of photorespiration apparently led to the evolution of C_4 plants, which developed complex biochemical pathways for concentrating CO_2 near Rubisco, in lieu of evolving a more efficient enzyme. The intricate biochemical, physiological, and structural relationships that make up C_4 photosynthesis suggest that photorespiration will not be overcome by manipulating one or even several genes. Whether genetic engineering of Rubisco can accomplish what more than a billion years of intense selection pressure have not remains to be seen. However, recent work in genetically engineering a recycling pathway for the products of ribulose-1,5-bisphosphate (RuBP) oxygenation within the chloroplast of C3 plants shows that productivity gains can be made by reducing the losses and transport costs of the photorespiratory pathway.

14.10.3 Photorespiration has become an interdependent process in C_3 plant metabolism linked to a variety of benefits

Although photorespiration can restrict overall photosynthetic efficiency, it is strongly integrated with the leaf cell's carbon and nitrogen metabolic pathways and under certain conditions may be beneficial. Side reactions stemming from the photorespiration may help optimize metabolic function in C_3 plants. Most such benefits relate to nitrogen metabolism or stress tolerance. Photorespiration stimulates nitrate assimilation in C_3 plant roots, probably by increasing NADH availability in the cytosol. So, photorespiration can be positively correlated with growth under nitrogen limitation. Photorespiration is not a fully closed cycle: a small proportion of serine from photorespiratory flux is siphoned off for methionine and cysteine synthesis and is thus needed for optimal amino acid synthesis in C_3 plants. Photorespiration can enhance C_3 plant tolerance to drought, salinity and chilling. The mechanisms are still under investigation but may relate to the ability of photorespiration to dissipate

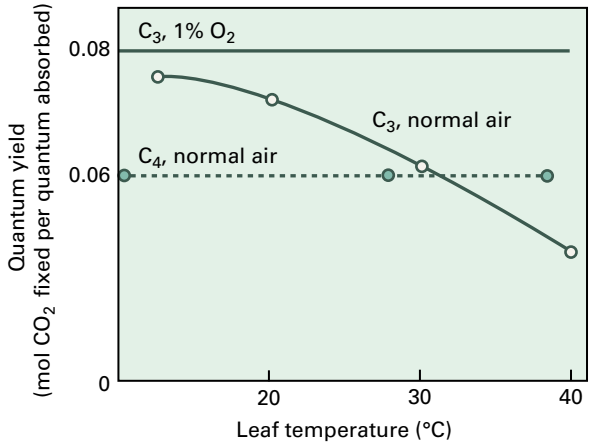


FIGURE 14.44 *Effect of leaf temperature on quantum yield in C_3 and C_4 plants. In C_3 plants, the rate of photorespiration increases with increasing temperature to a greater extent than does the rate of gross photosynthesis. The enhanced relative operation of the C_2 cycle at higher temperatures leads to a greater energy cost per net CO_2 fixed, which is reflected in a decrease in the quantum yield (moles of CO_2 fixed per photon of light absorbed). When C_3 photosynthesis is carried out in the presence of decreased (1%) O_2, photorespiration is effectively eliminated and the resulting quantum yield remains constant with increasing temperature. Plants having the C_4 pathway show a constant quantum yield with increasing temperature, thus reflecting the absence of photorespiration; instead, C_4 plants concentrate CO_2 at the site of CO_2 fixation in the bundle sheath cells. The lower quantum yield for C_4 plants than for C_3 plants in 1% O_2 reflects the fact that, although both lack photorespiration, C_4 plants retain the added energy cost (2 ATP per CO_2 fixed) needed to operate the C_4 pathway. At lower temperatures, C_3 plants have a higher quantum yield than C_4 plants even in normal air, reflecting the energy tradeoffs of having a lower rate of photorespiration but not incurring the cost of operating the C_4 pathway.*

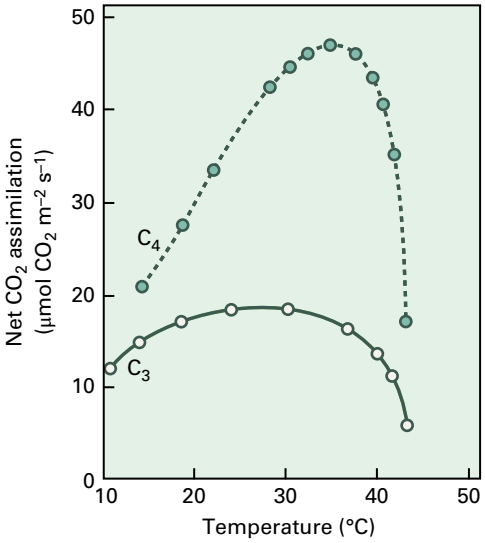


FIGURE 14.45 *Effect of ambient temperature on CO_2 assimilation in C_3 and C_4 plants. In C_3 plants the increase in the relative contribution of photorespiration to net photosynthetic CO_2 uptake as temperature increases leads to a lower optimum temperature than that for C_4 plants, where the absence of photorespiration shifts the optimum temperature for net CO_2 fixation to higher temperatures. The steep decline in photosynthetic rates at temperatures above 40°C is common to both C_3 and C_4 plants and reflects an irreversible thermal denaturation of components of the photosynthetic apparatus at high temperatures.*

over-reduction of the chloroplast that leads to photoinhibition, and also to photorespiratory ROS production, stimulating stress signaling gene expression in C_3 plants.

14.10.4 Photorespiration may influence response of C_3 plants to future climatic events

As temperature rises, changes in Rubisco's kinetic constants decrease the value of the selectivity factor, increasing oxygenase activity relative to carboxylation. Increasing temperature also decreases the aqueous solubility of dissolved CO_2 more than it does that of dissolved O_2, lowering the ratio of CO_2 to O_2 in air-equilibrated solution. Both of these effects enhance the rate of photorespiration relative to photosynthesis as the ambient temperature increases. As a result, in C_3 plants the quantum yield (see Chapter 12) for photosynthesis decreases continually as temperature increases, and the light-saturated optimum for net photosynthesis generally lies somewhere between 25°C and 35°C. In C_4 plants, which have a CO_2-concentrating mechanism that effectively eliminates photorespiration, the relative quantum yield for photosynthesis remains roughly constant with increasing temperature, and temperature optima for photosynthesis are higher (30°C to 40°C) than those of most C_3 plants. When the atmospheric fraction of O_2 is low (<2%), the photosynthetic quantum yield for a typical C_3 plant is greater than that of a C_4 plant and remains constant with increasing temperature (Figs. 14.44 and 14.45).

The projected doubling of atmospheric CO_2 concentration sometime in this century could have significant consequences for photosynthesis. Given the direct competition between CO_2 and O_2 for Rubisco-bound RuBP, higher concentrations of CO_2 would enhance carboxylation over oxygenation, even when the overall rate of photosynthesis is not controlled by Rubisco or RuBP availability. The theoretical ratio of carboxylase to oxygenase activity could increase from present value of ≈3 to >10, which should lead to an increase in net photosynthesis in C_3 plants. C_4 plants that lack measurable rates of photorespiration would not experience this photosynthetic enhancement and might be put at a selective disadvantage relative to C_3 neighbors. Such a change might assist agriculture because many of the world's most pernicious weeds are C_4 plants.

Although the efficiency of photosynthesis will increase with greater CO_2 concentrations, the absolute rate of photosynthesis may not. Numerous studies indicate that many plants acclimate to continuous exposure to high CO_2, such

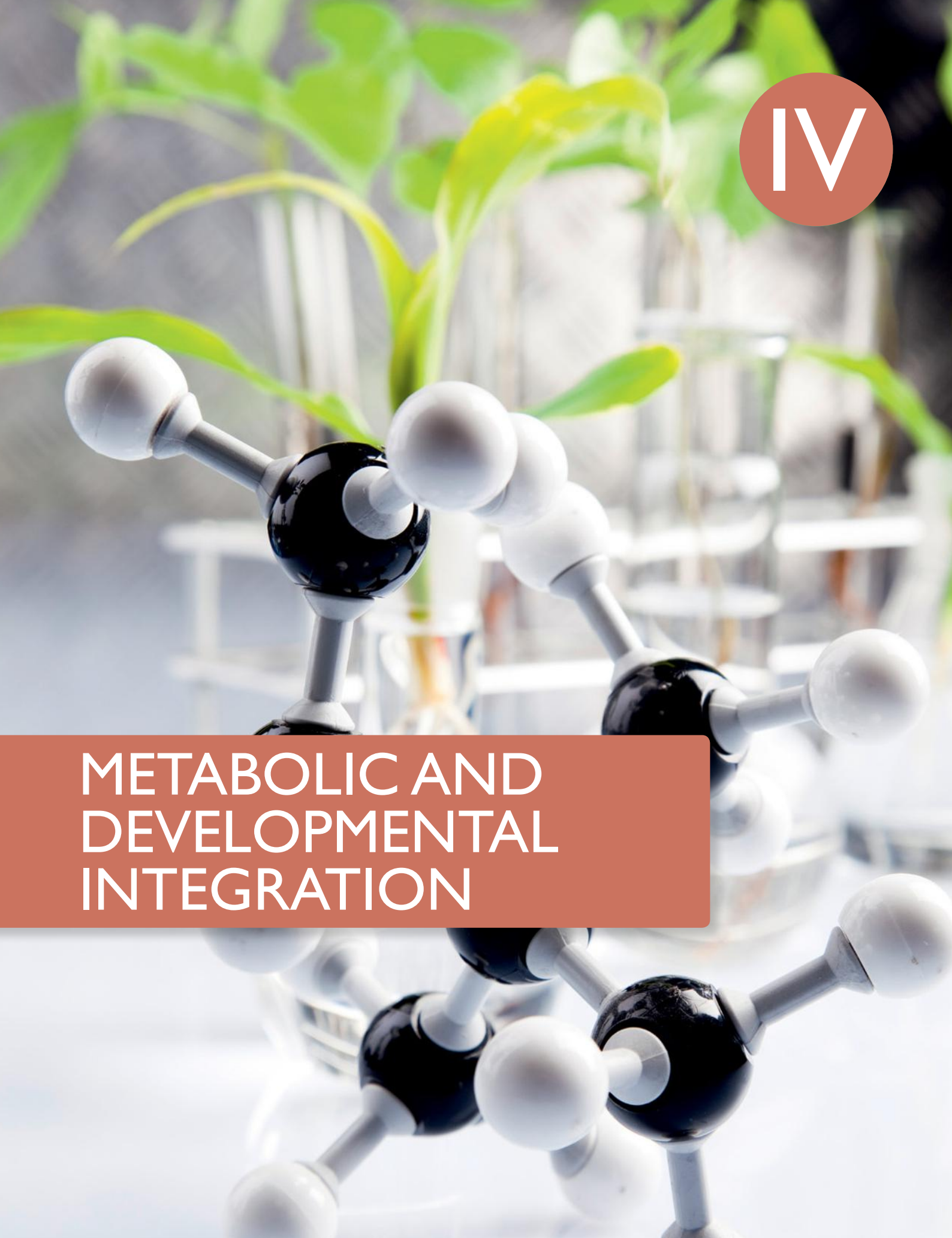
that their photosynthetic rates eventually resemble those of plants grown under current conditions. Reasons for this response include diminished amounts of Rubisco in plants grown in high-CO_2 and feedback inhibition of photosynthesis as a result of the inability to utilize all the additional carbohydrate initially produced in high-CO_2 conditions. Regardless of this acclimation effect, increased atmospheric CO_2 may impact the balance of photosynthetic and photorespiratory reactions in many plants, with consequences that are at present unknown.

Summary

Aerobic respiration involves the controlled oxidation of reduced organic compounds to CO_2 and H_2O. Much of the free energy released during respiration is conserved in the formation of ATP. In glycolysis, the first stage of respiration, carbohydrates are oxidized to organic acids in the cytosol. The organic acids produced during glycolysis are completely oxidized to CO_2 in the mitochondrial matrix via the citric acid cycle. The electrons released during the operation of the citric acid cycle are transferred through a series of multiprotein complexes located in the inner mitochondrial membrane, ultimately reducing O_2 to H_2O. The free energy released during mitochondrial electron transfer is used to generate a proton electrochemical gradient across the inner membrane. The energy available in the proton gradient is subsequently used by another protein complex, ATP synthase, to synthesize ATP from ADP and P_i. Mitochondrial respiration is regulated by the availability of ADP and P_i and by the presence of additional electron transfer complexes that allow respiration to proceed without forming a proton gradient.

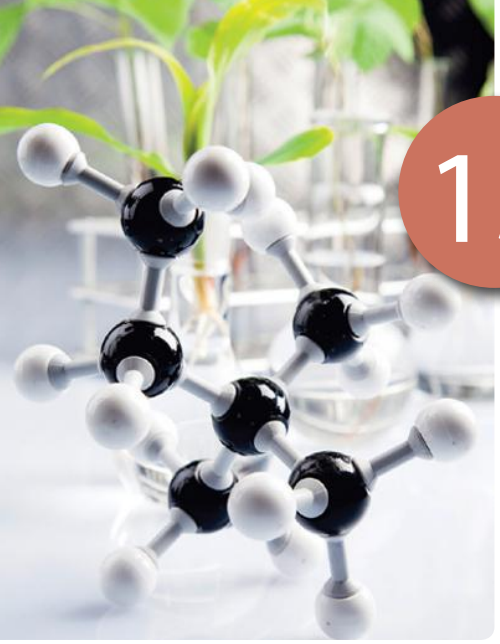
Plant mitochondria participate in several metabolic processes besides respiration, including providing reducing equivalents to other cellular compartments and carbon skeletons for amino acid biosynthesis. Plant mitochondria also participate in the biosynthesis of sugars from lipids in some germinating seeds and in the decarboxylation reactions associated with photosynthesis in some C_4 and CAM plants. The movement of metabolites into and out of mitochondria requires specific transporters in the inner mitochondrial membrane, some of which are regulated by the proton gradient.

Photorespiration involves the light-dependent uptake of O_2 and evolution of CO_2 during photosynthesis in green plant tissues. The first step in photorespiration is associated with the oxygenase activity of the photosynthetic enzyme Rubisco. Phosphoglycolate formed during the oxygenase reaction is metabolized through the photorespiratory carbon cycle to save 75% of the carbon in the form of phosphoglycerate; the remaining 25% is lost as CO_2. The reactions of the photorespiratory carbon cycle occur in three organelles: chloroplasts, peroxisomes, and mitochondria. The loss of CO_2 during photorespiration can represent an appreciable percentage of the carbon fixed during photosynthesis, decreasing the overall efficiency of photosynthesis especially in C_3 species but it can positively influence aspects of nitrogen metabolism and stress tolerance in plants. Photorespiration reflects the evolutionary origin of Rubisco in an anaerobic environment and may influence the competitiveness of some plants in response to future changes in atmospheric CO_2 concentrations.



IV

METABOLIC AND DEVELOPMENTAL INTEGRATION



15

Long-Distance Transport

John W. Patrick, Stephen D. Tyerman, and Aart J.E. van Bel

Introduction

Long-distance transport systems are integral to successful functioning of land plants. Here we focus on angiosperms, in which these transport systems are most advanced evolutionarily. Vascular plants are characterized by vascular systems composed of two specialized tissues, xylem and phloem. Xylem and phloem occur together and extend throughout the entire plant body (Fig. 15.1). Xylem transports water and soil-borne nutrients from roots to transpiring leaves, where photosynthesis forms organic carbon compounds (photoassimilates). Phloem transports water, mineral elements, amino nitrogen compounds, and photoassimilates (resources) from fully expanded leaves or storage organs (sources, net resource exporters) to meet the nutrient (carbon, nitrogen, and mineral) requirements of heterotrophic growth or storage organs (sinks, net resource importers). Xylem transport is incapable of serving this function, as sink organ transpiration is too low to drive resource transport through xylem at sufficient rates to meet sink metabolic demand. In addition to transport of resources, xylem and phloem also conduct signals that coordinate defence responses as well as homeostatic and developmental functions between plant organs. Mechanisms responsible for transporting macromolecular signals have been hijacked by pathogens, in particular viruses, to aid their systemic spread throughout the plant body.

We begin with an analysis of long-distance transport by examining requirements for specialized cell designs to support high fluxes of resources. Short-distance transport through specialized parenchyma cells is interconnected with axial flows by loading and unloading the system. Short-distance transport processes include transport across plasma membranes, tonoplasts, and through plasmodesma. Much progress has been achieved in discovering the biophysical principles of xylem transport, while more remains to be understood about mechanisms for xylem loading (repair) and phloem transport. Understanding mechanism provides the platform for discovering how flows of resources and signals are regulated as well as how transport of macromolecules, viruses, and bacteria occur. Such an exercise is at the very heart of the key principles governing whole plant productivity and concludes our review of long-distance transport. Boxes 15.1 and 15.2 provide a brief introduction to the biophysical and biochemical theory that underpins current understanding of long-distance transport.

15.1 Selection pressures and long-distance transport systems

15.1.1 Intercellular transport can occur along apoplastic, symplasmic, and transcellular routes

A number of options exist for intercellular transport between cells. The water-filled spaces of cell wall matrices (5–20 nm diameter) and lumens of xylem tracheary elements (10–300 μm diameters) are collectively referred to as the apoplast and provide one pathway for intercellular transport (pathway 1,

Biochemistry & Molecular Biology of Plants, Second Edition. Edited by Bob B. Buchanan, Wilhelm Gruissem, and Russell L. Jones.
© 2015 John Wiley & Sons, Ltd. Published 2015 by John Wiley & Sons, Ltd.
Companion website: www.wiley.com/go/buchanan/biochem

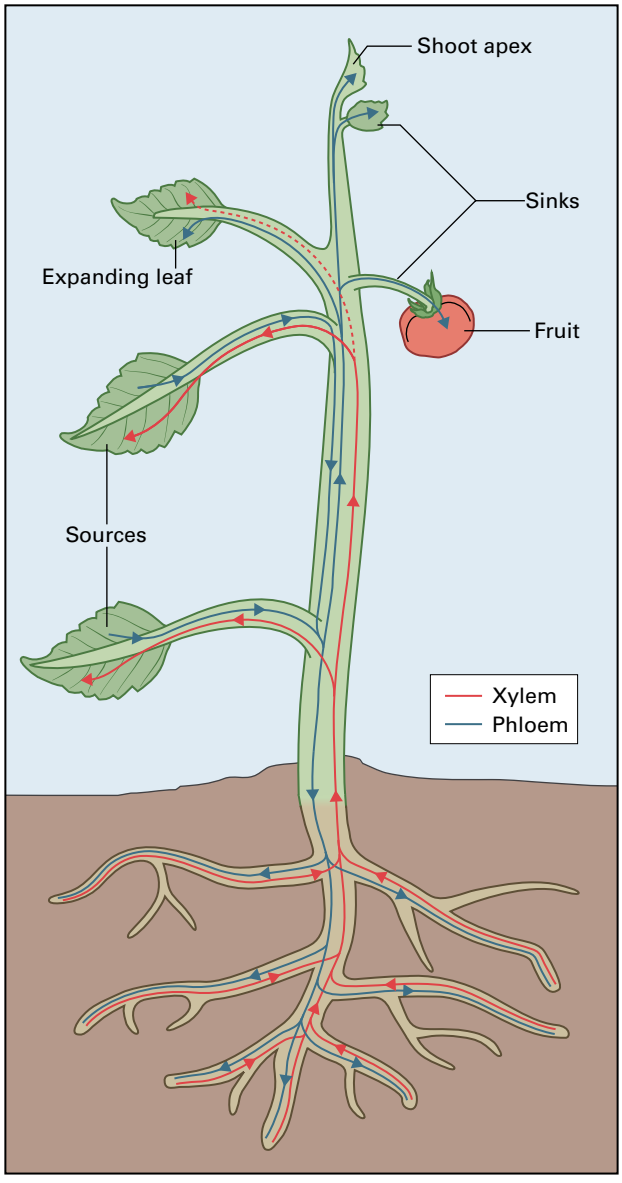


FIGURE 15.1 *Diagram showing patterns of xylem and phloem transport. Movement in xylem is upwards from roots to mature leaves, primary sites of transpiration and photosynthesis. A very small amount of xylem transport (broken line) supplies growth sinks (e.g., expanding leaves) and even less is directed to shoot apices and storage sinks (e.g., developing fruit), both of which have low transpiration rates. Movement in the phloem proceeds from sites of photoassimilate production, primary mature leaves, to sites of utilization in growth or storage sinks. Phloem transport can be bidirectional within a single internode but is unidirectional within a given vascular bundle. In lower and upper internodes, movement tends to be unidirectional downward or upward respectively.*

Fig. 15.2). In many instances, cells are highly interconnected by plasmodesmata (see Section 15.1.2), fine cytoplasmic threads that form a continuous cytosolic compartment through which intercellular transport may occur (pathway 2, Fig. 15.2). Such interconnected cytosols are referred to as symplasm (*sym* – joined together). In some cases, such as radial transport of water across roots, a transcellular pathway may be followed. Here, for each cell layer, plasma membrane and tonoplast are crossed twice to enter and exit each cell and its vacuole (pathway 3, Fig. 15.2). It is difficult to quantify the contributions of transcellular and symplasmic pathways, so generally these are taken together as a cell-to-cell pathway for water movement.

15.1.2 Plasmodesmata form an interconnected symplasm to support intercellular transport

It has been 60 years since electron microscopy visualized plasmodesmata as plasma membrane-lined cytoplasmic canals, 20–50 nm in diameter interconnecting adjacent cells. The canals contain a rod of central endoplasmic reticulum (ER) that is continuous with ER strands on either side of the shared cell wall (Fig. 15.3). The ER rod is covered with spirally arranged macromolecules from which spokes extend to protein complexes associated with plasma membrane inside the plasmodesmal canal. Openings of plasmodesmata (orifices or cytoplasmic sleeves) often exhibit constrictions (neck regions), indicating a potential for plasmodesmal closure.

Originally, plasmodesmata were considered to act as intercellular passageways for small molecules, since microinjected fluorescent dye molecules greater than 1 kDa (≈0.5–1.0 nm in diameter) were excluded (Fig. 15.4). Subsequent studies found that molecular exclusion limits of plasmodesmata depended on developmental state, tissue type, and physiological conditions. For example, plasmodesmata between meristematic cells in roots allow passage of macromolecules up to about 65 kDa. Recently, a variety of proteins, including actin and myosin, involved in macromolecular trafficking have been detected inside the plasmodesmal canals.

Plasmodesmal numbers (densities) indicate a potential for intercellular trafficking. Whether symplasmic transport occurs depends on the open state of plasmodesmata. For instance, despite high plasmodesmal numbers located at bases of leaf hairs, a functional symplasmic barrier occurs due to plasmodesmal closure (Fig. 15.4). At symplasmic barriers (no plasmodesmata or all plasmodesmata closed), resources are released through plasma membranes into adjacent cell walls, diffuse through their aqueous pores (apoplastic transport), and are absorbed via the plasma membranes of adjoining cells.

15.1.3 Resource distribution in terrestrial environments requires long-distance transport

For multicellular plants to function effectively in terrestrial environments, a strong selection pressure existed for them to extract resources from both soil and air. Soil is the primary source for water and mineral nutrients, and light energy can be captured only from aerial environments at sufficient

BOX 15.1

Fundamentals of transport

Molecules and ions move down free energy gradients that reflect differences in concentration, temperature, pressure, voltage (for electrolytes), or combinations of these. The effective motive force for movement differs for different distance scales. Molecules dissolved in a solution are subject to bulk flow (convection) of solution driven by pressure gradients, and they can be carried along in the flow over large distances. Over short distances, molecular diffusion dominates. Total flux of a molecule (J_{total}, units: mol m^{-2} s^{-1}) is the combination of bulk flow and diffusion:

$$J_{total} = J_{bulk-flow} + J_{diffusion} = vc - D_i \Delta c/\Delta x \qquad \text{(Eq. 15.B1)}$$

Bulk-flow flux is given by concentration (c) times velocity (v). Diffusive flux is determined by concentration gradient ($\Delta c/\Delta x$) and diffusion coefficient (D_i).

Diffusion

Fick's first law of diffusion describes this movement as a flux (J, units: mol m^{-2} s^{-1}) of a population of molecules of type i (J_i) that is proportional to their concentration gradient ($\Delta c_i/\Delta x$):

$$J_i = -D_i \frac{\Delta c_i}{\Delta x} \qquad \text{(Eq. 15.B2)}$$

The *diffusion coefficient* (D_i, units: m^2 s^{-1}) is unique for each diffusing element and molecule and medium through which diffusion is occurring. Examples of D for solutes in water (25°C) are sucrose 0.52×10^{-9} m^2 s^{-1}, and glucose 0.67×10^{-9} m^2 s^{-1} (note increase with decrease in molecular size).

Diffusion theory predicts that diffusion time increases with the distance squared (x^2), and a useful relationship describes the time required for 37% of the initial concentration in a plane to spread a distance (x) as:

$$t_{37\%} = \frac{x^2}{4Di} \qquad \text{(Eq. 15.B3)}$$

Bulk flow

Within xylem and phloem, flow is thought to be analogous to laminar flow along a pipe. Laminar flow is where a smooth parabolic profile of velocity occurs across a pipe's radius with higher velocities towards the center and slowed velocities adjacent to surfaces due to friction. Volume flow rate (J, units: m^3 s^{-1}) of bulk flow in a pipe is derived explicitly from the Hagen–Poiseuille law as:

$$J = \frac{\pi r^4 \Delta P}{8\eta l} \qquad \text{(Eq. 15.B4)}$$

where ΔP is the pressure gradient over length l, r is pipe radius, and η is dynamic viscosity (units: Pa s). This equation can be arranged to give an effective resistance to fluid flow for a unit pressure gradient or to predict the pressure gradient ($\Delta P/l$) required for an observed volume flow rate (J). Resistance will increase 16-fold by halving pipe diameter.

Hydraulic conductance/conductivities

The volume flow rate (J) is proportional to pressure gradient times hydraulic conductance (L_0) derived from the Hagen–Poiseuille equation as:

$$L_o = \pi r^4/8\eta l \qquad \text{(Eq. 15.B5)}$$

Conductance depends on flow-path length, and to take this factor out for comparison between systems, conductance can be multiplied by path length to determine conductivity. Conductances and conductivities are normalized to various dimensions of particular flow pathways. For water transport across a surface (a cell or a root), conductance is generally normalized to surface area to give what is also termed hydraulic conductivity (L_p, units: m s^{-1} MPa^{-1}). Note velocity of flow equals L_p multiplied by pressure gradient, and for a pipe, velocity or volume flux (units: m s^{-1}) equals $r^2\Delta P/8\eta l$ (Equation 15.B1). Leaf hydraulic conductance is generally measured as flux (units: mmol s^{-1}) divided by water potential gradient and leaf surface area to give units of mmol m^{-2} s^{-1} MPa^{-1}.

Water potential and water potential gradients

In discussing flow properties above, driving force was simply considered as the pressure gradient or concentration difference (for diffusion). To encompass all driving forces, we consider total free energy gradient on water, quantified as water potential (Ψ_w, units of pressure) and comprising the additive potentials of pressure (Ψ_P), osmotic components (Ψ_π), matric components (Ψ_m), and gravitation (Ψ_g):

$$\Psi_w = \Psi_P + \Psi_\pi + \Psi_m + \Psi_g \qquad \text{(Eq. 15.B6)}$$

water potential is a measure of free energy per unit volume (units: Joules m^{-3} or Pa). Pressure potential (Ψ_P) is equivalent to hydrostatic pressure (P), and it should be noted that this can be negative. In a pipe or porous plant cell wall, water flow is driven only by differences in pressure potential. Gravitational potential accounts for changes in free energy with height (0.01 MPa m^{-1}). This term is not relevant for tissues or cells, but is significant for flow through xylem or phloem over tens of meters in trees. Differences in osmotic potential become effective in driving water flow across a membrane that is selectively more permeable for water. Dissolved solutes decrease

free energy of water (decreases Ψ_π component) and this is numerically equivalent to, though opposite in sign, to osmotic pressure (π) determined by total osmotic concentration of all dissolved solutes. Sometimes a matric component is identified to indicate lowering of free energy of water in a thin film adhering to a surface. This effect is more important in soil, and within a plant, the effect is incorporated within P and π components. Given the above considerations, Equation 15.B6 can be simplified as:

$$\Psi_w = \Psi_P + \Psi_\pi \text{ or } \Psi_w = P - \pi \qquad \text{(Eq. 15.B7)}$$

where P can be positive (hydrostatic pressure) or negative (tension) with the appropriate sign. The turgor pressure of a cell (TP) is the difference between inside hydrostatic pressure and outside hydrostatic pressure across the plasma membrane and cell wall, which at equilibrium (i.e., when inside Ψ_w = outside Ψ_w) will equal the difference in internal minus external osmotic pressure: $TP = \pi_i - \pi_o$.

BOX 15.2

Intercellular transport across membranes and through plasmodesmata

Solute diffusion across a biological membrane may occur through the lipid phase or via specialized transmembrane proteins that speed diffusion (facilitated diffusion). Facilitated solute or water diffusion may occur through protein channels, or by solute interacting with a protein carrier to form a solute–protein complex that undergoes conformation change and in doing so transports the solute from one side to the other.

Diffusion across a membrane begins with the element or molecule partitioning from surrounding solution into the membrane, then diffusing across the membrane, and finally partitioning back out to solution on the other side. This may occur across both lipid and transmembrane proteins, the proportion depending on the type of element/molecule and specialized transmembrane proteins present. This process is embodied within the *permeability coefficient* (P_s, units: m s^{-1}). Thus, a diffusion flux (J_s, units: mol m^{-2} s^{-1}) driven by a concentration gradient (ΔC_s) of an uncharged molecule (s), across a membrane is given by:

$$J_s = P_s \times \Delta C_s \qquad \text{(Eq. 15.B8)}$$

P_s is unique for a particular element/molecule in a particular membrane. Diffusion through membrane channels conforms to Equation 15.B8 except that P_s is much higher. For instance, P_s for water movement across a lipid membrane can increase 500 fold when water channels (aquaporins) are functioning.

For electrolytes, diffusion rates and direction are modified by membrane potential differences (for more details see Chapter 3).

Rates (R_v, units: mol s^{-1}) of facilitated diffusion mediated by a carrier across a membrane can be modeled as a solute-saturable component described by Michaelis–Menten kinetics combined with a non-saturable component obeying first order kinetics as:

$$R_v = [V_{max} \cdot C/(K_m + C)] + kC \qquad \text{(Eq. 15.B9)}$$

where V_{max} (units: mol s^{-1}) is maximal velocity, K_m (mol m^{-3}), Michaelis–Menten constant, C, solute concentration, and k (units: m^3 s^{-1}) a first order rate constant.

Work must be done to transport solutes across membranes against their chemical (nonelectrolytes) or electrochemical (electrolytes) gradients. In most cases (see Chapter 3) this is achieved by proton-coupled solute transport, organized in symport or antiport configuration, with protons returning down their electrochemical gradients (proton motive force, *pmf*, units: mV) given by:

$$pmf = (E_i - E_o) + 59(pH_o - pH_i) \qquad \text{(Eq. 15.B10)}$$

where $(E_i - E_o)$ is membrane potential difference, and $(pH_o - pH_i)$ the pH difference across the membrane.

Assuming a sucrose/H^+ stoichiometry of one, a derivative of the Nernst equation predicts difference between intracellular (Ci) and external (Co) sucrose concentrations at which sucrose/H^+ symport reverses for a given *pmf* by:

$$\text{Log}_{10}(Ci) = Log_{10}(Co) - [(E_i - E_o) + 59(\text{pH}_o - \text{pH}_i)]/59 \qquad \text{(Eq. 15.B11)}$$

Plasmodesmal transport

A permeability coefficient can be derived for plasmodesmal transport (Equation 15.B8). The diffusion component is largely determined by plasmodesmal substructure (Equation 15.B2). Similar comment applies to bulk flow through plasmodesmata (Equation 15B.5).

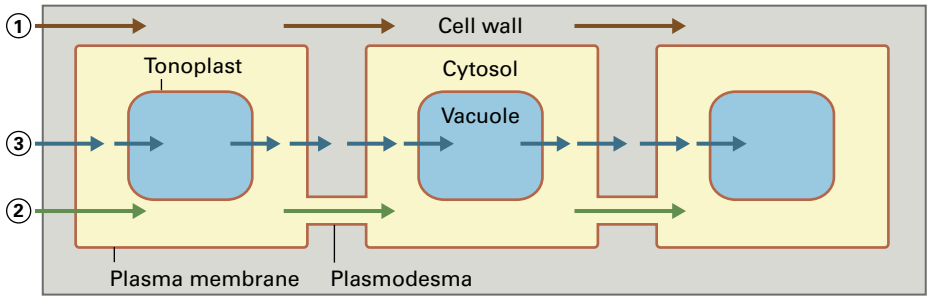
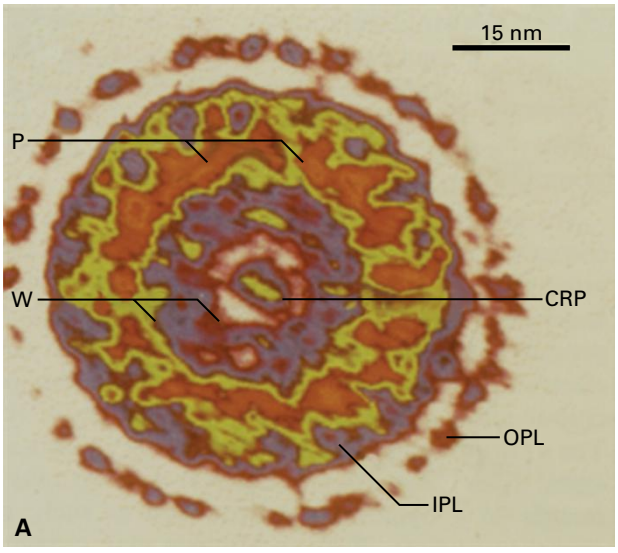
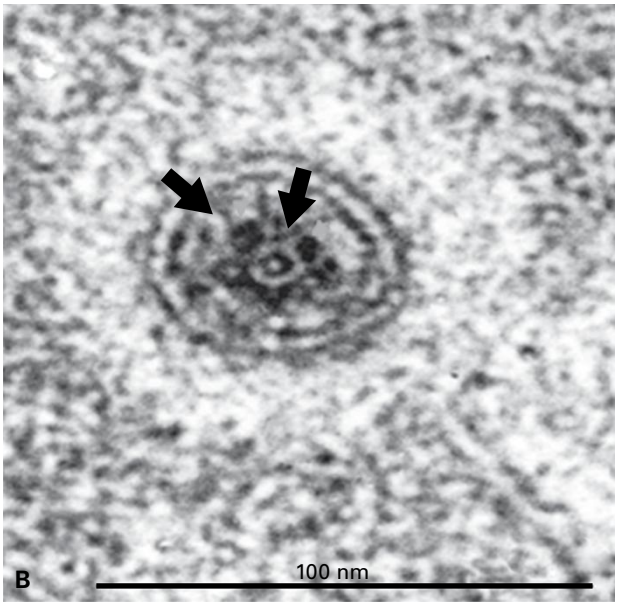


FIGURE 15.2 *Illustration of apoplast/symplasm concept and transport pathways. Resources may move from cell-to-cell by way of: (1) Apoplastic transport through their cell walls (brown arrows). Alternatively, resources may enter a cell across the plasma membrane and then move from cell-to-cell by; (2) Symplasmic transport through interconnecting plasmodesmata (green arrows) or; (3) Transcellular transport via the vacuole across the tonoplast followed by exit across the plasma membrane before regaining entry to the adjacent cell through the plasma membrane (mainly for water; blue arrows).*





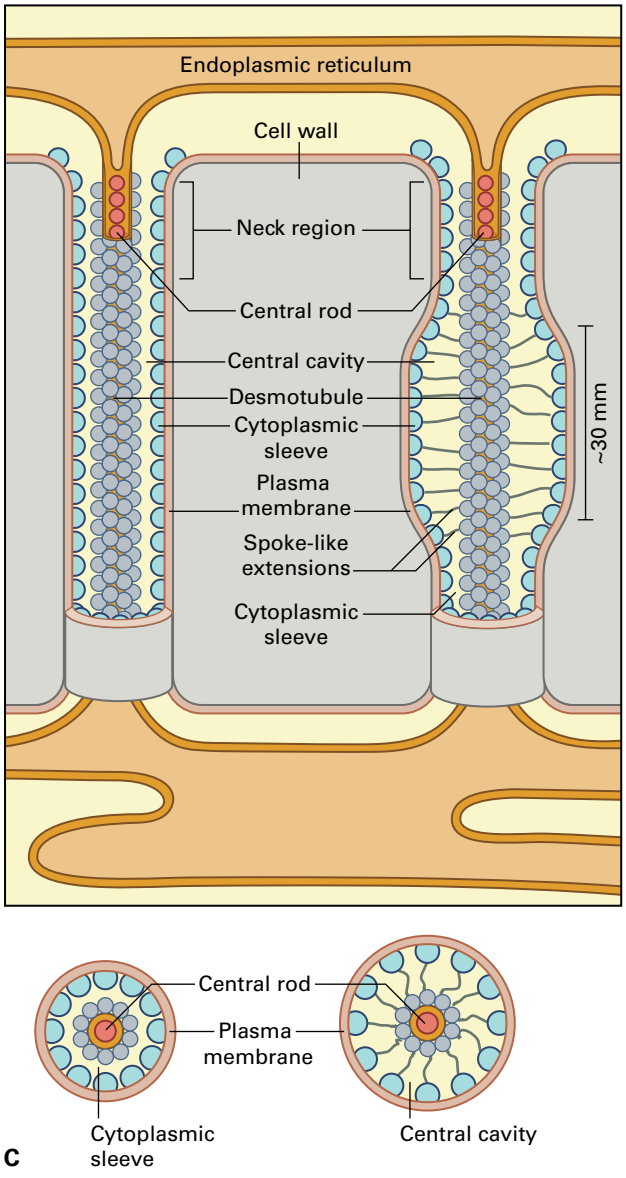


FIGURE 15.3 *Substructure of plasmodesmata. (A) A digital false-color computer-enhanced image identifies outward (OPL) and inward (IPL) leaflets of plasma membrane traversing the cell wall, a protein layer attached to the IPL (violet), attached to IPL, from which protein spokes (P, red) arise to connect with proteins (W, violet ring delimited by the two lines) spirally arranged around a central ER rod (CRP) or desmotubule. (B) Electron micrograph (EM) of a transverse section of a plasmodesma demonstrating spokes (arrows) between the plasma membrane double-layer and desmotubule. (C) Models of plasmodesmata between young (left) and mature cells (right) based on EM-images (such as A, B). Plasma membrane and ER are continuous cell to cell, with the latter tightly furled to form the desmotubule. A sleeve of cytoplasm occupies the gap between plasma membrane and desmotubule. In the mature plasmodesma (right), the sleeve has been enlarged to form a cavity. Much of the cytoplasmic sleeve is occupied by proteinaceous particles partially embedded in the plasma membrane and desmotubule. Gaps between these particles evidently represent the physical basis for molecular sieving properties of symplasmic transport. Within the central cavity, spoke-like structures extend across the cytopalsmic sleeve; their presence in the neck region is still unclear. Source*: (A) Botha et al. (1993). Annals of Botany 72:255–261. (B) R. Kollmann, University of Kiel, Germany.

energies to drive photosynthesis. A consequence is the spatial separation of two assimilatory organs (roots and leaves) that are resource interdependent. Hence, there is an obligatory requirement for long-distance transport of resources between roots and leaves (Fig. 15.1).

15.1.4 Diffusion constrains intercellular transport of resources over long distances

The simplest mechanism for intercellular transport is diffusion via an apoplastic or symplasmic pathway. As an example, applying diffusion theory (Equation 15.B3) to sucrose transport, with a diffusion coefficient in water of 0.52×10^{-9} m^2 s^{-1}, predicts that 4.8 s is required for sucrose to reach 37% of its equilibrium concentration over 100 µm, a typical cell length. However, sucrose diffusion over a distance of 1 mm (about 10 cells arranged end-to-end and interconnected by plasmodesmata) takes 8 min, and raising this distance to 1 cm increases the time to 5.6 days. Thus, for distances exceeding 1 mm, sucrose movement by diffusion alone becomes increasingly problematic for supporting metabolic demands.

Constraints imposed by diffusion can be relieved partially by cytoplasmic streaming (i.e., bulk flow; see Box 15.1). This limits the rate of intercellular sucrose transport to diffusion through plasmodesmata, which nevertheless offers a higher transport capacity than transport through a transcellular pathway (Fig. 15.5). This does not necessarily pertain to water flow, where membrane transport has an extremely high capacity conferred by aquaporins.

A plasmodesmal sucrose flux of 2×10^{-4} mol m^{-2} s^{-1} will satisfy the metabolic demand of heterotrophic cells. A sucrose concentration drop of 33 mM across each adjoining cell wall interface (predicted using Equation 15.B8) will generate this flux through plasmodesmata with maximum permeability coefficients of 6×10^{-6} m s^{-1}. Assuming a 1 M sucrose concentration at the start of the transport pathway, this arrangement would support transport across a maximum of 30 cell walls arranged in series. For an average cell length of 100 µm, this translates into a transport distance of 3 mm before sucrose available for onward transport is depleted. Overall for land plants, this exercise demonstrates that a strong selection pressure existed to evolve a long-distance transport system to deliver sucrose and other resources at rates sufficient to support plant growth.

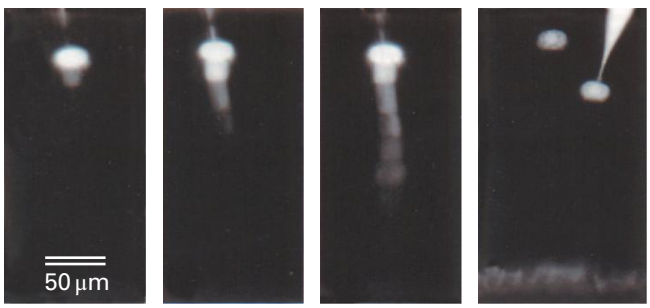
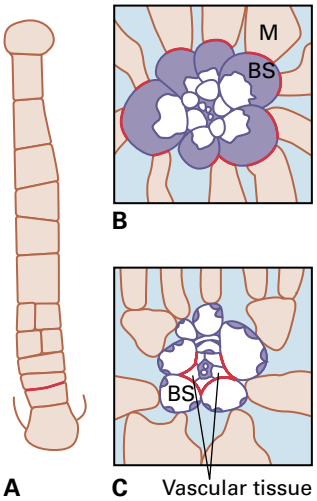


FIGURE 15.4 *Mobile and immobile fluorescent probes in the* Abutilon *nectary trichome (for a drawing of the trichome, see Fig. 15.5). (A–C) F-Glu (536 Da) movement after injection into the tip cell. The frequently observed 'stair-step' distribution of fluorescence results from diffusion within cells being relatively more rapid when compared with cell-to-cell movement. (D) The slightly larger F-Trp-Phe (739 Da) shows no sign of movement after 60 seconds. Source*: (A–D) Terry & Robards (1987). Planta 171:145–157.

15.1.5 Harnessing bulk flow through low-resistance conduits removes constraints on plant size

In contrast to diffusion, bulk flow (Equation 15.B4) has a high capacity to transport resources over long distances. Gradients in pressure potential are generated through different means to drive bulk flow in opposite directions through xylem (tension) and phloem (hydrostatic pressure) (Fig. 15.6). Since plasmodesmata (see Fig. 15.4), membranes (plasma membranes and tonoplasts; see Fig. 15.2), and cell walls (see Fig. 15.5) are bottlenecks for intercellular transport, not surprisingly the



	Transport system (red indicates the transport interface)	Superiority factor[a]
A	*Abutilon* nectary trichome (nectary secretion rate)	1,600–16,000
B	C_4 mesophyll–bundle sheath interface (photosynthesis rate, which is dictated by transport rates of C_4 and C_3 acids)	100–1,000
C	C_3 bundle sheath–vascular tissue interface (translocation rate)	30–300

[a]Actual solute flux compared with the highest known fluxes for plant membranes (1 to 10×10^{-8} mol m^{-2} s^{-1})

FIGURE 15.5 *Fluxes of cell-to-cell nutrient movement across transport interfaces between cells are much higher than expected for transmembrane transport implicating plasmodesmata as the pathway for movement. In these three examples, the transport interface for movement measured is indicated in red. BS, bundle sheath; M, mesophyll.*

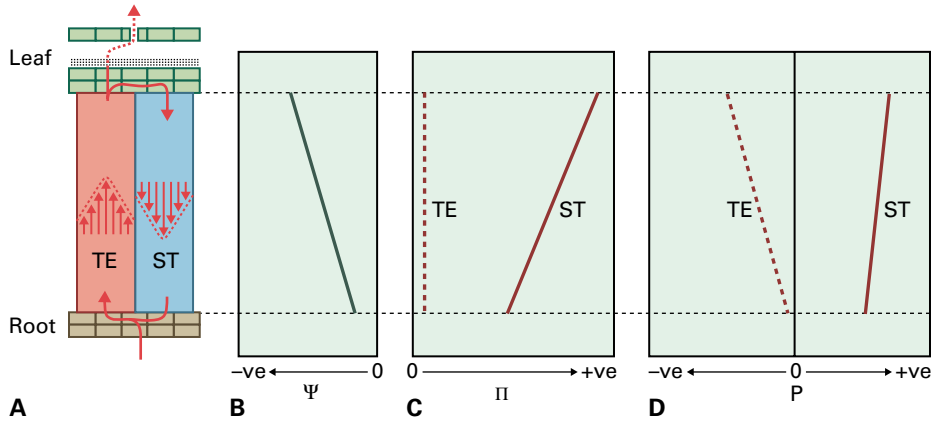


FIGURE 15.6 *Patterns of xylem and phloem transport and driving forces accounting for water flows in opposite directions in xylem and phloem during transpiration. (A) Diagram of water flows within and between longitudinal arrays of xylem tracheary elements (TE) and phloem sieve tubes (ST) interconnecting roots and fully-expanded leaves. Note that TEs (tracheids or vessel elements) in this diagram are simplified to represent the complete network. Water movement within TEs and STs is considered to be analogous to laminar flow where a smooth parabolic profile of velocity occurs across a pipe's radius with higher velocities towards the center and slowed velocities adjacent to surfaces due to friction (indicated by vertical arrows). A large component of the upward water flow from roots is lost through transpiration from leaves. (B) Xylem sets the water potential gradient of the pathway to shoots, and water approaches near equilibrium between adjacent xylem and phloem tissues. Hence their water potential (Ψ) gradients are essentially identical along axial vascular paths interconnecting roots and leaves. (C) Nutrient concentrations in TE sap are low, so TE sap osmotic pressure (π) is low and taken as constant with path length. In contrast, high sugar and nutrient concentrations present in ST saps generate high π that dominate ST sap Ψ. Osmotic pressure of ST sap decreases from leaf to root as a result of nutrient loss along the axial pathway. (D) Hydrostatic pressure (P) gradients are the sum of Ψ and π (Equation 15.B7). TE Ψ is determined by transpiration-induced tension (negative P) that drives bulk flow upwards from roots to leaves. In contrast water intake by STs, proportional to their osmotic content, creates a corresponding positive P gradient for leaf to root.*

conducting elements of the phloem, sieve elements (SEs) and those of the xylem, tracheary elements (TEs), underwent considerable evolutionary change to enhance their conductances for bulk flow (Equation 15.B5). These changes included circumventing membrane transport and widening plasmodesmal pores to eventually give rise to sieve tubes (STs), or removing end cell walls and membranes to give rise to xylem vessels (see Section 15.2).

15.2 Cell biology of transport modules

15.2.1 Vascular cells arise from (pro) cambial progenitors

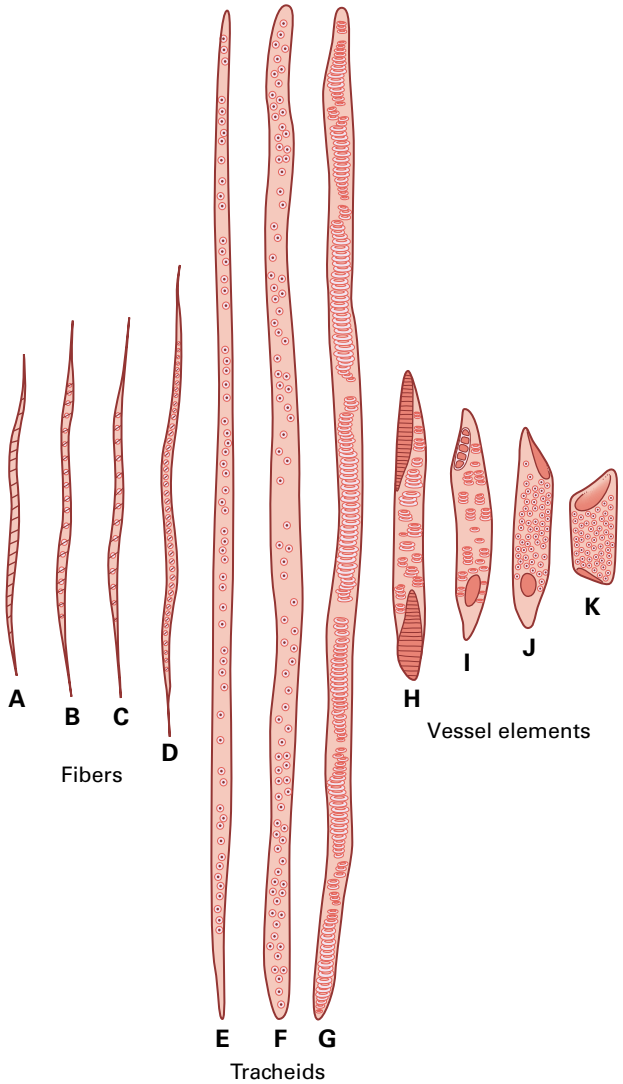
SEs function as a cellular complex with modified phloem parenchyma cells called companion cells (CCs). TEs, SE/CC complexes, and ancillary vascular cells each have specialized functions for loading, axial flow, and unloading of resources.

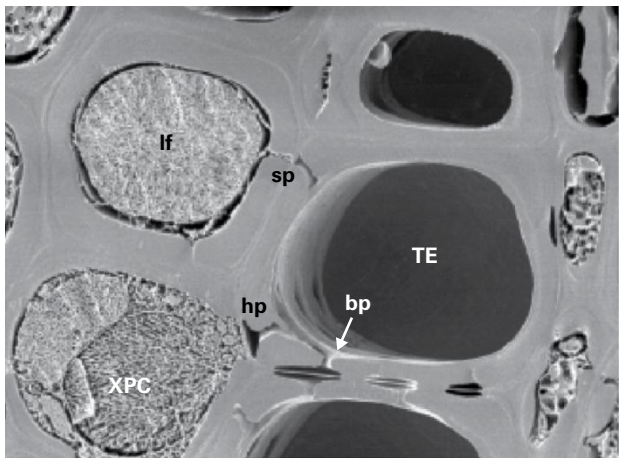
Primary phloem and primary xylem differentiate as bundles in procambial strands arising from stem cells located in root and shoot apical meristems. In eudicots, a circumferential strip of procambial cells remains undifferentiated between primary phloem and xylem to become a dividing meristematic layer (vascular cambium). In most eudicots, initials arising from divisions of vascular cambia produce secondary phloem to the outside and secondary xylem to the inside. In monocots, procambium strands completely differentiate into primary phloem and xylem without a vascular cambium.

15.2.2 Cell designs facilitate xylem transport functions

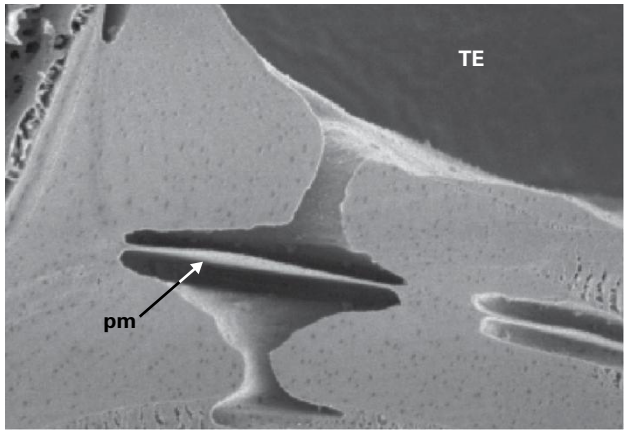
TEs are hollow tubes that have undergone elongation, secondary cell wall thickening, and lignification. Lignin is impermeable to water and solutes, and it is deposited by living protoplasts before programmed cell death and loss of plasma membrane (see Chapter 20). There are two kinds of TEs: vessel elements and tracheids (Fig. 15.7). Tracheids are the only TEs in almost all gymnosperms, while angiosperms may have both tracheids and vessel elements. A vessel is a series of vessel elements joined end-to-end. End walls between vessel elements, remnants of which are referred to as perforation plates, are dissolved to various degrees during late stages of cell maturation. Vessel elements evolved from tracheids in early angiosperms, and trends have been towards increased vessel width accompanied by decreased length, and opening of perforation plates.

The selective advantage of not having lipid membranes in TEs is illustrated by comparing the hydraulic conductance of a file of cells with and without membranes. For 10 cells end to end with dimensions of a typical xylem vessel element (200 μm long and inside diameter of 50 μm), hydraulic conductance (L_o, Equation 15.B6) is 7.7×10^{-8} m^3 s^{-1} MPa^{-1}. Hydraulic resistance is the inverse of conductance at 1.3×10^7 s MPa m^{-3}. For each membrane face, conductance of one circular piece of membrane (50 μm in diameter) with a high L_p of 3×10^{-6} m s^{-1} MPa^{-1} (indicative of aquaporin activity) is 5.9×10^{-15} m^3 s^{-1} MPa^{-1} (hydraulic resistance 1.7×10^{14} s MPa m^{-3}). Summing the 20 membrane faces in series gives a resistance for the file of cells of 3.4×10^{15} s MPa m^{-3}, a value 260 million times the





L



M

FIGURE 15.7 *Components of xylem tissue in angiosperms. Xylem fibers (A to D) are narrow elongated cells with very thick secondary cell walls specialized for support and provide strength to wood. Xylem tracheids (E, F, G) are highly elongated tapered cells that conduct water. Pits may be seen along cells where transfer of water occurs between tracheids. Xylem vessel elements (H to K) are less elongated but wider than tracheids. Their end cell walls (perforation plates) may be partially (H) or fully open (K). Vessel elements are connected end to end to form a xylem vessel. (L) Bordered pit pairs (bp) interconnect tracheary element (TE) lumens, and half bordered pits (hp) connect TE lumens to xylem parenchyma cells (XPC). A simple pit (sp) on the libriform fiber (lf) side, at the TE side is a small-bordered pit with an extended pit corridor. (M) Detail of bordered pit pair showing pit membrane (pm) in high magnification (length of pm is 3.7 μm).*
Source: (A–K) Bailey & Tupper (1918). (L, M) Micrograph provided by Dr J. Nijsse, Wageningen University; from De Boer and Volkov (2003). Plant Cell Environ. 26:87–101.

hydraulic resistance of the open tube. This means that to achieve the same flow rate with living cells, there would have to be a 260 million times greater pressure gradient!

Diameters of vessels between species range over an order of magnitude (15–300 μm), depending on age and location within a plant. This confers a much larger variation in resistance (Equation 15.B5). However, end walls account for 60–80% of the hydraulic resistance, suggesting vessel length is an important determinant of their water transport efficiency. Tracheids are generally of smaller diameter (10–50 μm) and longer (6–11 mm) than vessel elements (50–100 μm) such that both their smaller diameter and substantial increased end wall number per unit length contribute to their much lower water transport efficiency compared to vessels. Vessels, composed of many vessel elements stacked end to end, can range from several centimeters to meters in length. Water flow occurs from one tracheid or vessel to another along aligned sections of adjacent cell walls over a relatively large portion of their lengths, and not just at their very ends. Here, water passes through small porous holes in their lignified cell walls called pits.

Dome-shaped pits are aligned (pit pairs) in secondary cell walls of adjacent tracheids or vessels (Fig. 15.7L,M). The compound middle lamella is exposed in pit pairs of adjacent conduits and consists of cellulose microfibrils and a pectin/hemicellulose matrix with countless small pores. This becomes a "membrane" in the sense that water and dissolved solutes can pass relatively unimpeded, but air entry is impeded because of the small pore diameters (5–20 nm in eudicots).

The pectin in pit membranes may respond like a hydrogel to alterations in ion concentrations of xylem fluid; higher K^+ concentrations increase hydraulic conductance, possibly by shrinking the hydrogel matrix and widening pores in pit membranes. This may be an important regulatory mechanism for diverting water flow to different plant organs and for diurnal changes in stem hydraulic conductances.

Lignification of the cell walls of TEs serves two purposes: to waterproof and strengthen the walls against collapse from the large tensions developed within. In elongating stems, spiral and hoop patterns of lignification allow stretching of vessels. TEs have been shown to collapse under excessive tension, and TEs of mutants defective in lignin synthesis have reduced mechanical strength. Cell wall thickness seems to be constrained by developmental processes – smaller diameters confer increased strength, resulting in an apparent conflict between strength versus conducting efficiency. In wood comprising vessels, tracheids, and fibers, vessels function as water conduits, with the structural role taken by tracheids and fibers. Fibers are highly lignified, thin elongated cells with a small ratio of diameter to cell wall thickness that provides high strength (Fig. 15.7A–D). Vessel diameter can, therefore, be larger with concomitant increase in hydraulic conductance.

Xylem parenchyma cells are living cells associated with TEs. They have the high metabolic activity required for loading and unloading water and nutrients from TEs as well as lignin polymerization, nutrient transfer between phloem and xylem, storage of carbohydrate, and repair of xylem. They have an analogous role to phloem CCs, except linkage to TEs is transmembrane rather than via plasmodesmata. Since TEs are lignified except at pit pores, transport of nutrients and water is essentially confined to small areas of half pits where plasma membranes of xylem parenchyma cells border TEs (Fig. 15.7L). Xylem parenchyma cells that border conduits often have cell wall invaginations under pit membranes that increase the plasma membrane surface area for increased transport capacity. Transporters are highly active in xylem parenchyma cells (see Section 15.3.4).

15.2.3 Many aspects of conducting cell design enhance key phloem functions

During evolution, certain longitudinal cell arrays gradually lost their cell contents to evolve phloem conduits (Table 15.1). During SE ontogeny, the nucleus gradually disintegrates, as do the tonoplast and several other cellular components. What finally remains is the plasma membrane, a thin layer of parietal cytoplasm (mictoplasm) composed mostly of stacked ER, a few, often dilated, mitochondria, phloem-specific plastids, and SE proteins (Figs. 15.8 and 15.9).

Unequal longitudinal divisions of axial arrays of procambium cells produce SEs and CCs, and following division, the daughter cells are symplasmically isolated, probably to enable divergent differentiation to proceed (Fig. 15.8). After completing development, symplasmic contacts are restored via plasmodesmata (pore–plasmodesma units, PPUs), with a single canal at the SE side and a branched canal at the CC side (Fig. 15.8E), to form a genetic and metabolic unit (SE/CC complex). Support of cellular functions by metabolically active CCs, via unique symplasmic interconnection offered by PPUs, probably evolved as SEs lost their metabolic capability (Table 15.1).

A peculiarity of SEs and CCs is the structural diversity of their plasmodesmal connections. In (pro)cambial cells, all interfaces are connected by unbranched plasmodesmata (Fig. 15.8A–C). During differentiation into SE/CCs, plasmodesmata are transformed into sieve pores between SEs and into PPUs at SE/CC interfaces, but they remain unchanged between CCs and phloem parenchyma cells (Fig. 15.8E).

TABLE 15.1 *Ultrastructural features of sieve elements in groups of land plants reflecting their evolutionary development.*

	Mosses	Vascular cryptogams	Conifers	Angiosperms
Plasma membrane	Present	Present	Present	Present
Nucleus	Degenerate	Nuclear remnants	Nuclear remnants	Absent
Tonoplast	Small vacuoles filled with fibrillar material	Absent	Absent	Absent
Ribosomes	Not observed	Absent	Absent	Absent
Mitochondria	Intact	Intact	Few, degenerate	Few, degenerate
Endoplasmic reticulum	Smooth parietal nets and stacks	Smooth parietal nets and stacks	Smooth parietal nets and stacks	Smooth parietal nets and stacks
Cytoskeleton	Micotubuli, no microfilaments	Absent?	Absent?	Absent?
Golgi apparatus	Absent	Absent	Absent	Absent

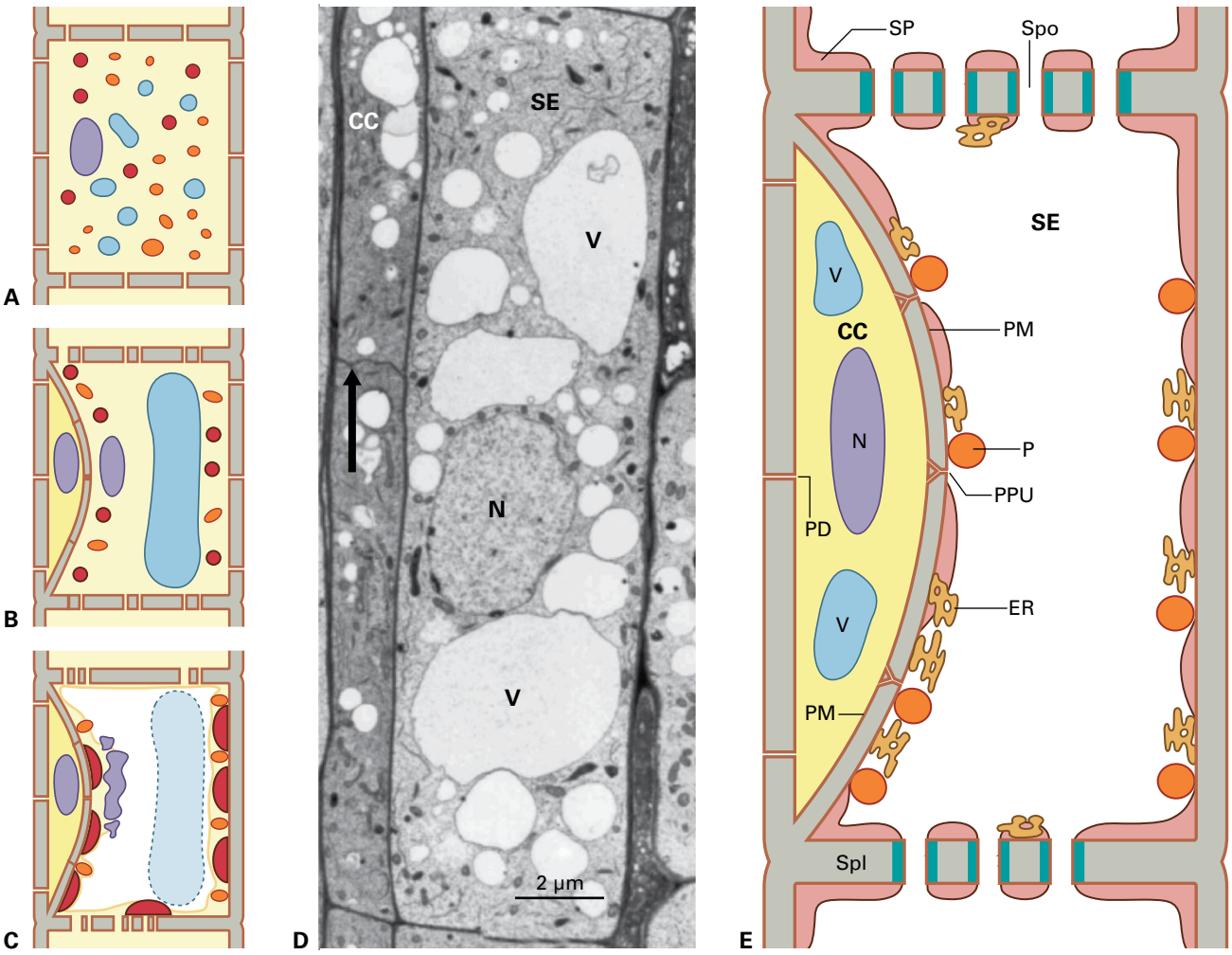


FIGURE 15.8 *Ontogeny of a sieve element/companion cell (SE/CC) complex in the transport phloem. (A) Both cell types originate from the same (pro)cambial cell characterized by a dense cytoplasm and many simple plasmodesmata. (B) After a longitudinal division, the daughter cells follow different developmental patterns. A dense cytoplasm remains in the narrower CC while the SE forms a large central vacuole (blue) and conspicuous protein bodies (red) and plastids (orange) develop. (C) The nucleus (violet), ribosomes, Golgi apparatus and vacuole membrane (tonoplast) of the SE (shown in B) degrade. The developing CC often divides transversely. (D) Electron micrograph of a longitudinal section of a differentiating SE/CC complex from a* Ricinus communis *stem. SE is highly vacuolated (V), nucleus (N) is starting to disintegrate, and SE-protein bodies and plastids are beginning to appear. In the CC, the thin transverse wall (arrowhead) indicates a recently completed cell division and cytoplasm is much denser than in the SE. Sieve pores and pore-plasmodesma units (PPUs) are yet to form. (E) Following cell elongation, only a plasma membrane (PM), a parietal ER-net (light brown), SE plastids (P) and, in eudicots, phloem-specific, structural proteins (SP) remain in SEs. CCs retain their full complement of organelles. Their nuclei (N) lie in a dense cytoplasm, numerous vacuoles (V) are present and mitochondria possess many cristae (not shown). Plasmodesmata (PD) of young SE/CC complexes undergo specific changes depending on the particular cell interface. PDs at SE/CC interfaces transform into PPUs that are branched on the CC side. PDs in longitudinal walls of SEs become truncated. PDs in transverse walls of SEs change into sieve pores (Spo, up to 1 µm in diameter) lined by callose deposits (aqua green) to form a sieve plate (SPl). Simple PDs connect CCs with adjacent phloem parenchyma cells. Note that for diagrammatic space-saving purposes the length of the SE/CC complexes has been strongly reduced compared to the width and the shared SE/CC wall is strongly curved into the SE. In reality, CCs "bulge" into the SEs to a lesser extent.*

Source: (D) A Schulz, University of Copenhagen, Denmark.

Why did SEs retain a minimal cellular organization in contrast to dead TEs (see Section 15.2.2)? Complete removal of cell contents would have been more advantageous to optimize hydraulic conductivity (see Sections 15.1.5 and 15.2.2). Strong selection pressures must have led to partial retention of their cellular contents. The most important reason is that bulk flow through STs is driven by hydrostatic pressure differences generated and regulated by membrane transport (Fig. 15.6C,D); consequently, plasma membrane integrity is essential for SE transport function.

The SE/ER may serve as a Ca^{2+} store for Ca^{2+}-dependent occlusion (see Section 15.6.4) and as a track for local movement of macromolecules (see Section 15.6.5). A principal function of structural SE proteins (Fig. 15.9D–G) may be Ca^{2+}-dependent occlusion of sieve pores (see Section 15.6.4). To prevent sieve pore occlusion by ER stacks, plastids,

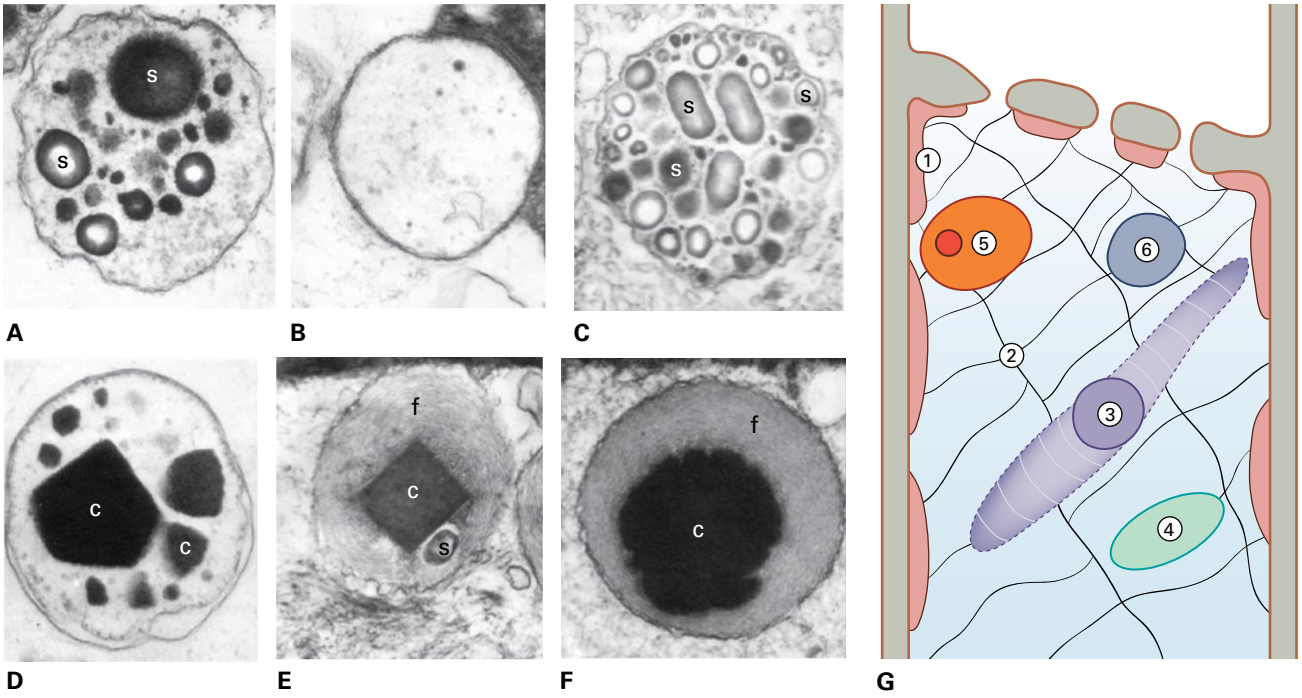


FIGURE 15.9 *Sieve element plastids and phloem-specific protein bodies located in the SE parietal cytoplasm and tethered to the plasma membrane. (A–F) Electron micrographs of different SE plastids of (A)* Aconitum, *(B)* Peperomia, *(C)* Austrobaileya, *(D)* Saruma, *(E)* Macarthuria, *and (F)* Monococcus, *approx. 1 μm in size. They have either no inclusions (B), starch grains (A, C), protein crystals (D), both protein crystals, protein filaments and starch grains (E) or protein crystals together with protein filaments (F); s, starch grains; c, protein crystals; f, protein filaments. (G) Diverse phloem-specific proteins in SEs occur in varying compositions. 1. Parietal protein clots; 2. Filamentous protein nets; 3. Dispersive protein bodies; 4. Nondispersive protein bodies; 5. Protein inclusions in SE plastids; 6. Soluble proteins are dissolved in the ST sap and translocated by mass flow.*
Source: (A–F) Behnke (1993). ALISO 3:167–182.

mitochondria, and protein aggregates that could be dragged along by bulk flow, these components are anchored to each other and to the plasma membrane. Despite the ubiquitous occurrence of SE plastids in angiosperms (Fig. 15.9A–F), their roles are not known.

15.3 Short-distance transport events between xylem and nonvascular cells

15.3.1 Xylem delivers water, nutrients, and signals to shoots at variable rates

Water flow depends largely on transpiration. However, water derived from phloem unloading in root tips and fruits may be recycled via xylem. Some plants deliver sufficient nutrients to shoots without transpiration, relying only on root pressure to force sap to the shoot. Xylem flow velocity varies during the day and is lower at night, contrasting to more constant phloem sap velocity. Peak xylem flow velocities of 40 mm s^{-1} have been recorded in plants with large vessels, but typical velocities are 0.4–1.0 mm s^{-1}. Variable velocity means nutrients and signals may be delivered to shoots at different rates. Most water is delivered to fully expanded leaves, yet these leaves have less demand for nutrients (e.g., calcium) compared to the growing shoot. This requires tuning the xylem loading of nutrients and water in roots to the resource requirements of shoots and the velocities of water flow. Transfer between xylem vessels in stems and between xylem vessels and phloem is important in this context.

15.3.2 Xylem loading of water and nutrients in roots involves multiple cellular pathways and transporters

Water moves radially across roots into xylem TE (Fig. 15.10). The stele is the central part of the root containing the pith (if present), vascular tissue, and pericycle, and occurs on the inside of the endodermis. At strategic locations (endodermis and sometimes exodermis), the root apoplast is blocked by Casparian bands composed of lignin deposited in cell walls. Some endodermal and exodermal cells have conspicuous absence of lignin and suberin lamellae and are referred to as passage cells.

Water movement through the root apoplast is driven only by pressure gradients, while transport across a membrane-delimited pathway (transcellular; see Section 15.1.1) involves pressure and osmotic gradients. During transpiration,

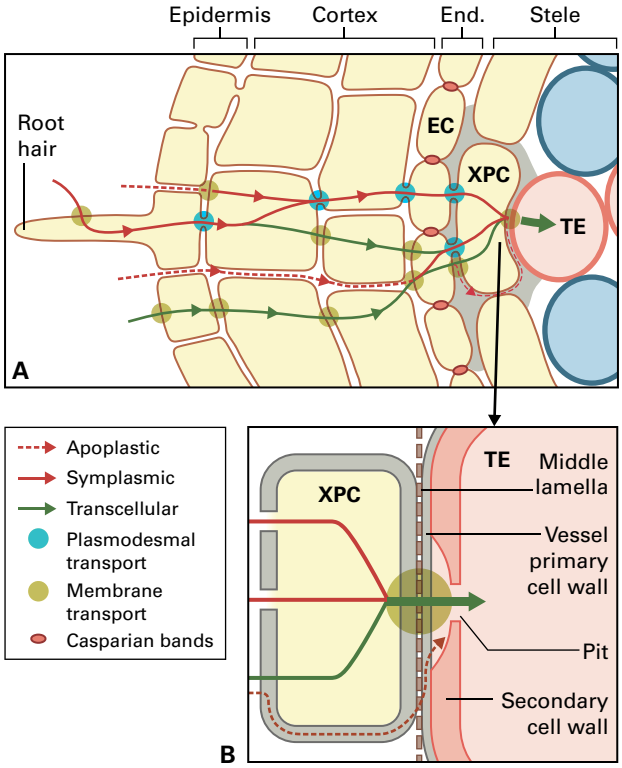


FIGURE 15.10 *Pathways of xylem loading of nutrients and water. (A) Stylized transverse section of a root showing root hair, epidermis, cortex, endodermis (End.) and stele. Pathways of nutrient and water movement across the root are indicated as well as key transport steps through plasmodesmata and plasma membranes. At the endodermis, Casparian bands block apoplastic nutrient transport. Hence nutrient movement must cross plasma membranes of each endodermal cell (EC) and pass to the stele via the symplasm or transcellularly, or once effluxed from endodermal cells via the apoplast. (B) Xylem parenchyma cells (XPC) load xylem tracheary elements (TE) through half-bordered pits where there is a concentration of membrane transporters.*

pressure gradients dominate due to large tensions in the xylem. When transpiration rate is reduced, osmotic flow may dominate because without large pressure-driven flow solutes actively loaded into the stele are not diluted, creating an osmotic gradient. Depending upon genotype and environmental conditions, 30–80% of water flow across roots occurs via the cell-to-cell pathway (symplasmic plus transcellular, Fig. 15.2). For example, apoplastic barriers tend to develop more in roots subjected to dry soil, where a greater proportion of flow occurs via the cell-to-cell pathway. Genotype comparisons show that wheat (*Triticum aestivum*) and barley (*Hordeum vulgare*) roots have a greater degree of tension-driven flow via the cell-to-cell pathway than those of lupine (*Lupinus angustifolius* L. and *Lupinus luteus* L.). Furthermore, wheat roots take up most water near their apices, while lupine roots take up water along a greater proportion of the root.

In the radial flow pathway, water flow per unit area increases toward the stele, since the same volume of flow must occur at the outer surface of the root and surface of the stele (water is incompressible). This is compensated for by a progressive increase in membrane hydraulic conductivity, probably due to greater activity of aquaporins (Fig. 15.11). At interfaces between xylem parenchyma cells and TEs, concentrated flows are linked with high expression levels of aquaporins (Fig. 15.11D,E). The central role of aquaporins in radial water transport is well illustrated by antisense suppression of *NtAQP1* expression in *Nicotiana tabacum*, which results in halving of root hydraulic conductivity.

Nutrients are taken up into the symplasm mostly at the root surface (root hairs and epidermal cells) and within the cortex. Endodermal cells retrieve nutrients swept along with water in the root apoplast (Fig. 15.10). Some nutrients and salt (NaCl) may leak around the apoplastic barriers ("bypass flow") in the endodermis and are directly swept to the xylem. This can occur where apoplastic barriers are not well developed or where lateral roots emerging from the stele cause breaks in these barriers. Mutants compromised in endodermal barrier development have decreased ability to maintain potassium supply to the shoot.

Unloading of symplasmic nutrients occurs in the stele from endodermal or xylem parenchyma cells. Different transporters and channels are located in the stele compared to cortex and epidermis (Fig. 15.12). Whereas cortical and epidermal transporters take up nutrients at very dilute concentrations, those in xylem parenchyma cells need to release nutrients. An exception is where phloem delivers nutrients, such as K^+, within the stele. These nutrients are taken up by xylem parenchyma cells, released into TEs, and transported back to the shoot. Amino-N and K^+ are recycled in this fashion, with about 30% of the K^+ delivered to the xylem originating from phloem. Another exception is the transport of sodium from the xylem to prevent excessive movement to the shoot. This can be the basis of salt tolerance in some plants.

In xylem parenchyma cells, anions such as NO_3^- and Cl^- are released passively into TEs by a variety of anion channels, while both highly selective and nonselective cation channels may release ions such as K^+ and Na^+. The release of Na^+ and Cl^- into the xylem is a focus in salinity research because reduced xylem loading of both these ions could prevent salt damage to shoots. For both reabsorption and xylem loading of ions, the proton efflux pump (H^+-ATPase) is critical (Fig. 15.12A). This pump establishes voltage and proton gradients that drive passive transport of ions (voltage gradients) and transport of other molecules and ions coupled to the flow of protons (see Box 15.2 and Chapter 3). TE sap pH also signals soil water stress to shoots.

Total osmolality of xylem sap is usually less than 40 mosmol kg^{-1}, or about –0.1 MPa osmotic potential, a relatively small component of total water potential. Nutrient concentrations of TE sap vary with soil nutrient composition, water flow rates, and plant nutritional status; for example, depending on conditions, NO_3^- may be reduced to organic N in parenchyma cells of roots or shoots, thus contributing to variable NO_3^- levels in xylem saps (Table 15.2).

In some cases, the roles of transporters in xylem loading have been established from gene silencing techniques. The SKOR protein is expressed in xylem parenchyma and pericycle cells and is a K^+ efflux channel (Fig. 15.12A). Knockout of the

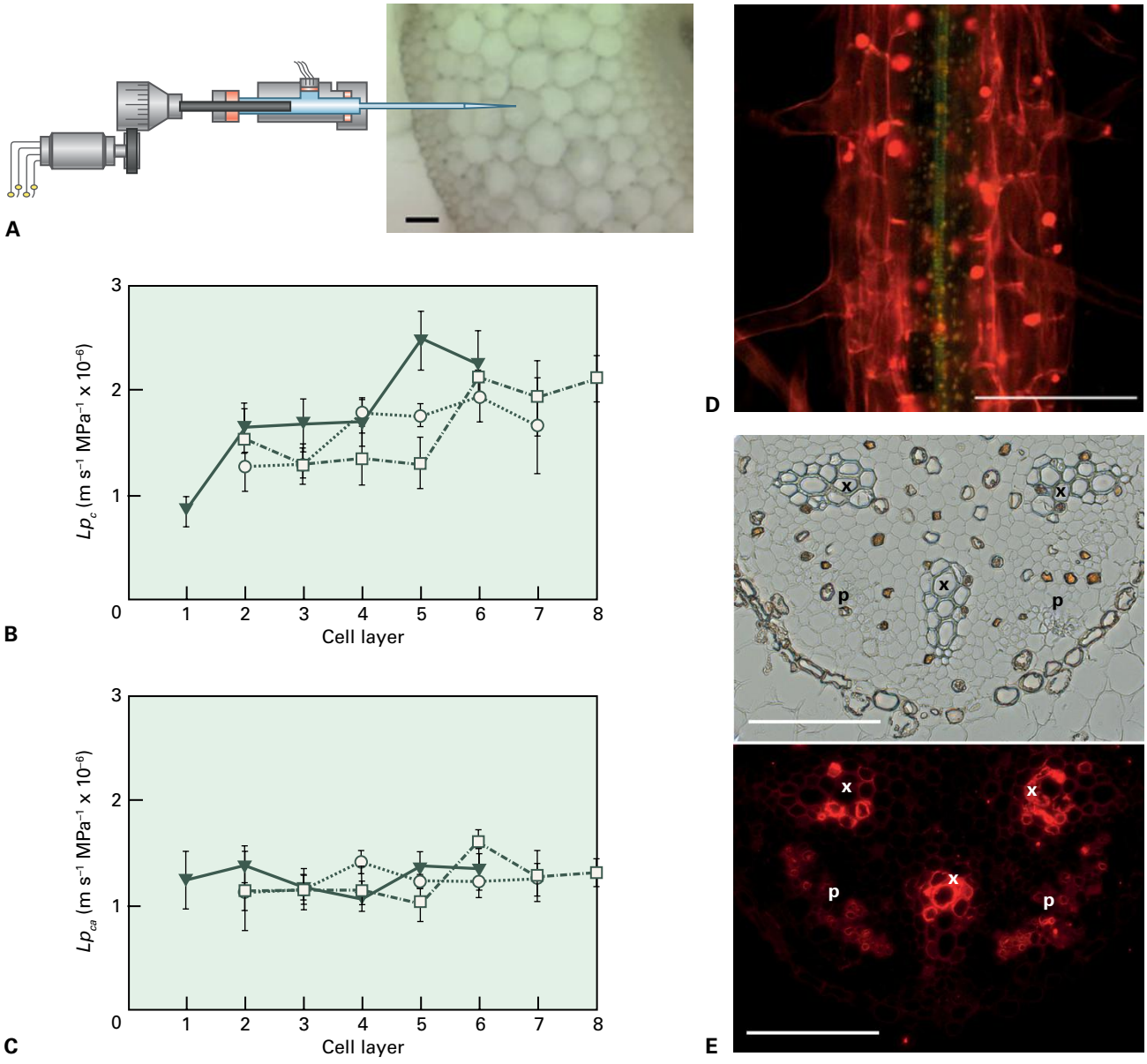


FIGURE 15.11 *Water transport across roots and loading into xylem is characterized by an increased inward radial flux of transport towards the center of the root. (A) Cell pressure probe measuring hydraulic conductivities (Lp and see Box 15.2) of cells at different positions across the root. Scale bar = 50 µm. (B) For three contrasting plant species (indicated by different symbols) cell membrane Lp_cs are similar and increase radially towards the root center. (C) When cell Lp_{ca} are scaled to the progressively reduced total cell membrane surface area across the root, effective Lp is constant across the respective cell layers. This indicates that Lp compensates for increased flux of water flow towards the root center. (D, E) In the stele, aquaporin expression is often highly concentrated around TEs to accommodate increased flux of water flow at this point. (D) Confocal micrograph of an* Arabidopsis *root from plants expressing a GFP-*AtPIP2;3 *construct stained with propidium iodide (cell walls red). Expression of the aquaporin* AtPIP2;3 *is closely associated with a TE and is visualized by the green signal from the GFP promoter fusion. (E) Immunolocalization of PIP1 protein in a grapevine (*Vitis vinifera*) root. Light micrograph of a stele cross-section (upper image) and fluorescent image below with intense (red) staining showing localization of PIP1 adjacent to xylem (X) and phloem (P) (in lower image). Scale bars = 100 µm. Source*: (A–C) Bramley et al. (2009). Plant Physiology. 150(1):348–364. (D) Wang; (E, F) Vandeleur et al. (2008). Plant Physiology.

SKOR gene with a T-DNA insertion results in 50% decline in K^+ transport to shoots. Similarly, when zinc pumps HMA2 and HMA4 are knocked out, the double mutant accumulates zinc in roots and displays zinc deficiency in shoots. Transporter asymmetries across root cells indicate a highly directional nutrient transport. Rice silicon transporters Lsi1 and Lsi2 are located at different faces of epidermal and endodermal cells (Fig. 15.12B); Lsi1, which is related to aquaporins, acts as a passive channel allowing silicon entry on the outside face of cells, while Lsi2 actively extrudes silicon from cells into the root apoplast.

Xylem loading is under control of hormones and other signals from shoots (Fig. 15.12A). Xylem loading of K^+ is related to shoot K^+ status, and phloem import of K^+ from shoots may function in this role. The plant hormone abscisic acid (ABA), recycled from shoots in the phloem, affects SKOR efflux activity and represses SKOR expression. ABA

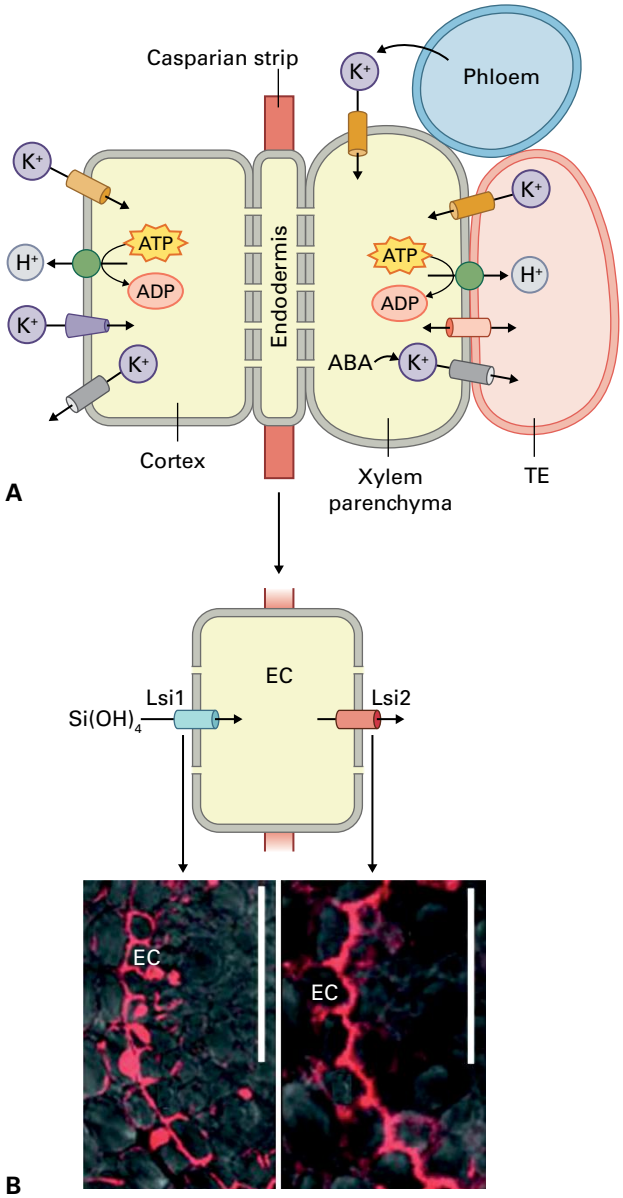


FIGURE 15.12 *Directional transport to the xylem occurs by a combination of specialized transporters in certain cells and different transporters on different sides of the same cell. (A) Directional transfer of K^+ to the xylem by different types of transporters located in epidermal/cortical versus xylem parenchyma cells. Common to all cells are H^+-ATPases (green) that energize membranes for both nutrient uptake and xylem loading. In the stele, phloem unloads K^+, a large proportion of which is reloaded into the xylem. K channels that load the TEs are also regulated by abscisic acid (ABA). (B) Directional transfer also is mediated by transporter asymmetry within a single cell type as illustrated by two silicon transporters (Lsi1 and Lsi2) in endodermal cells (EC), immunolocalized with antibodies raised against Lsi1 and Lsi2. Scale bars = 100 μm.*
Source: De Boer and Volkov (2003). Plant Cell and Environment 26:87–101; De Boer (1999). Plant Biology 1:36–45.

also downregulates release of anions via an anion channel located in the stele. ABA accumulates under water stress, so that decreased xylem loading of ions allows roots to accumulate solutes under water stress, helping to maintain their turgor pressure and growth (see Chapter 22). This analysis accounts for the independence of xylem loading of nutrients and delivery rate to shoots of water flow.

TABLE 15.2 *Concentration of major solutes in the xylem sap of three plants.*

Solute/Species	Concentration (mM)		
	Poplar	Banksia	Sunflower
NO_3^-	1–3	0.01	5–15
$H_2PO_4^-$	0.5–1.5	0.11	0.2–0.7
SO_4^{2-}	0.2–2	0.25	nM
Cl^-	0.2–0.8	2.92	nM
K^+	2–6	2.39	2–8
Ca^{2+}	0.5–1.5	0.48	0.3–1.2
Mg^{2+}	0.4–1.2	0.55	0.2–0.8

mM, millimolar; nM, nanomolar.

15.3.3 Concentrations of substances in the xylem are regulated during flow to their destination

In the axial pathway through roots/stems to transpiring leaves, water, nutrients, and hormones are able to exchange with xylem parenchyma cells to facilitate transfer between TEs, and between phloem and TEs. Concentrations of nutrients and toxic ions may be modified, depending on where TEs deliver their contents. Some plants can retrieve Na^+ from TE sap within their stems or woody trunks.

Nitrogen (N) in TE saps flowing to growing shoots is enriched by xylem-to-xylem transfer of organic N (amino acids) rather than NO_3^- between leaf traces in nodes. Similarly, xylem-to-phloem transfer enriches organic N content of phloem sap exported from leaves. This transfer diverts N supply from fully expanded leaves and enhances N delivery to growing regions.

15.3.4 Unloading of water and nutrients in leaves involves specific cellular pathways and transporters

A network of major and minor veins distributes water and nutrients to all parts of a leaf (see Section 15.4.3), such that any cell in a leaf is no more than a few cell layers from a minor vein. Minor veins are often encased in a layer of distinct cells referred to as a bundle sheath. Just as in roots, water and nutrients may flow from xylem to sites of evaporation via apoplastic or symplasmic pathways. Membrane-impermeant polar dyes loaded into petioles of transpiring leaves have shown that

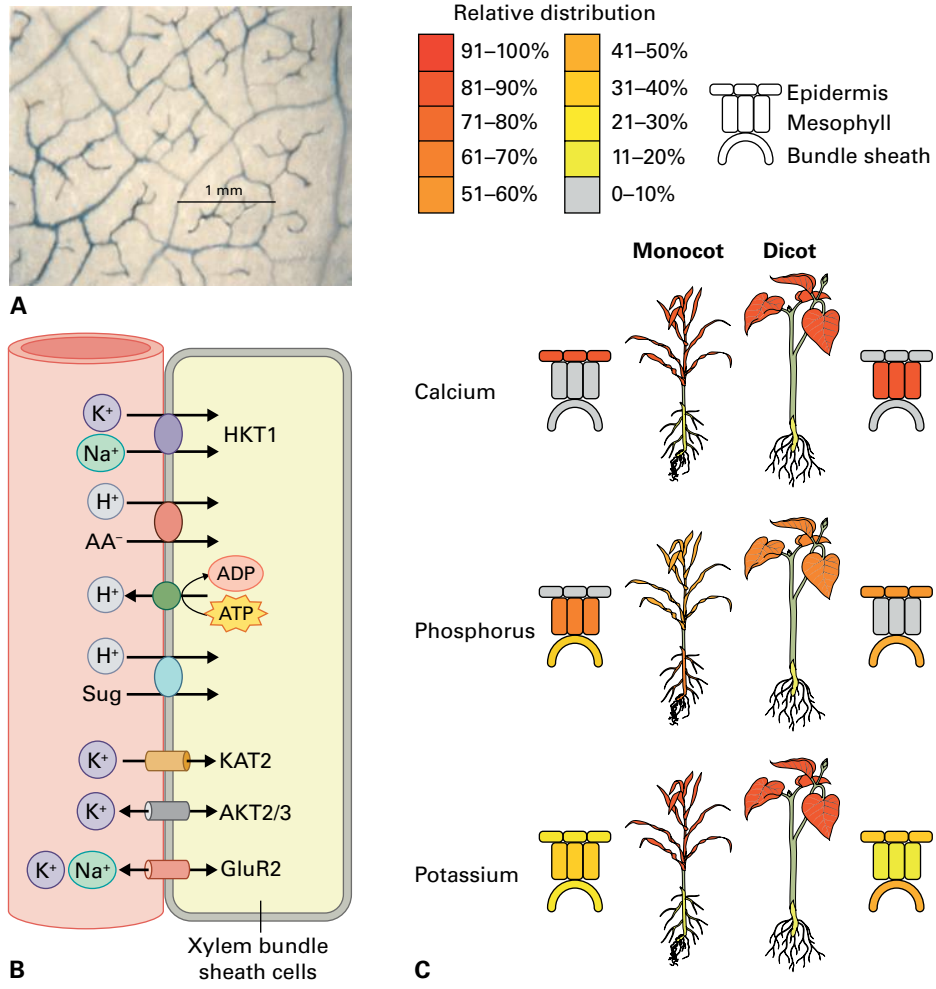


FIGURE 15.13 *Xylem unloading in leaves involves symplasmic transport and directional membrane transport. (A) As the transpiration stream exits minor veins, xylem-borne solutes that are unable to move with water into the symplasm are left behind in the minor vein apoplast as shown by the distribution of Evans Blue introduced into the xylem transpiration stream of a detached castor bean (*Ricinus communis*) leaf. (B) Xylem bundle sheath cells have a variety of transporters that control unloading and redistribution of nutrients. Note that as for root loading, H^+-ATPases energize membranes to run secondary active transporters [e.g., HKT1 Na^+ transporter, amino acid transporters (AA), sugar transporters (sug)] and channels (KAT2 and AKT2/3 K^+ channels and a nonselective GluR2 channel). This is only a small selection of transporters expected to function in xylem unloading. (C) Relative accumulation profiles of selected elements Ca, P, K at the organ level and cell-specific levels within the leaf. Model monocot (left side of each figure) and eudicot (right) shown with shoot and root concentrations. Stylized leaf cross-section shown for both monocot and eudicot represented as a heat map showing relative proportion of [ion] within the leaf. Note that the concentrations of Ca and P are reciprocal in the mesophyll and epidermis and have opposite profiles between monocots and eudicots, however there are exceptions to this allocation. The Ca distribution is positively associated with the distribution in different cell types of CAX type Ca transporters on the vacuolar membrane.*
Source: (A) D. Fisher, Washington State University, Pullman; previously unpublished.

apoplastic movement is blocked as soon as the dyes exit xylem vessels in minor veins at the bundle sheath interface (Fig. 15.13A). Thereafter, water and nutrients enter xylem parenchyma/bundle sheath cells to follow a symplasmic pathway. A membrane transport step in the water-unloading pathway is consistent with light-dependent hydraulic conductance of leaves correlating with aquaporin expression. An exception is Ca^{2+}, which moves predominately through the apoplast to the sites of storage in specific cell types in the leaf (see below).

Specific transporters are involved in xylem unloading (Fig. 15.13B). For example, AtHKT1, located in plasma membranes of leaf xylem parenchyma cells, protects leaves from Na^+ stress by recirculating Na^+. Disrupting AtHKT1 expression increases Na^+ concentrations in TE sap and decreases them in ST sap. An iron-nicotianamine transporter (AtYSL1) expressed in leaf xylem parenchyma cells is implicated in iron and nicotianamine (an iron chelate) redistribution. There are other examples of specific transporters located more or less exclusively to xylem parenchyma cells.

Nutrients are targeted to different cell types in leaves in phylogenetically distinct patterns of ion accumulation (Fig. 15.13C). For instance, Ca^{2+} accumulates in the epidermal cells but not mesophyll or bundle sheath cells of most grasses. In contrast, eudicots accumulate Ca^{2+} in palisade or spongy mesophyll, but not epidermal cells. Nutrient concentrations in leaf apoplasts also appear to be highly regulated and have been implicated in turgor pressure regulation of leaf cells and in stomatal control.

15.4 Short-distance transport events between phloem and nonvascular cells

15.4.1 Phloem can be divided into three sequential functional sectors

Angiosperm phloem comprises three sequential sectors, each of which has a specific function (Fig. 15.14). Photoassimilates produced by mesophyll cells, and minerals plus amino N compounds arriving in the transpiration stream from roots (see Section 15.3.4), together with water, are loaded into **collection phloem** (phloem loading) located within minor veins of fully expanded leaves (sources – net resource exporters). Loaded resources are translocated by the **transport phloem** through the main veins of source leaves, petioles, and ultimately stem and/or root axes (phloem transport) to be distributed between sinks (net resource importers). Resources delivered to **release phloem** are unloaded (phloem unloading) into expanding or storage cells of sink organs.

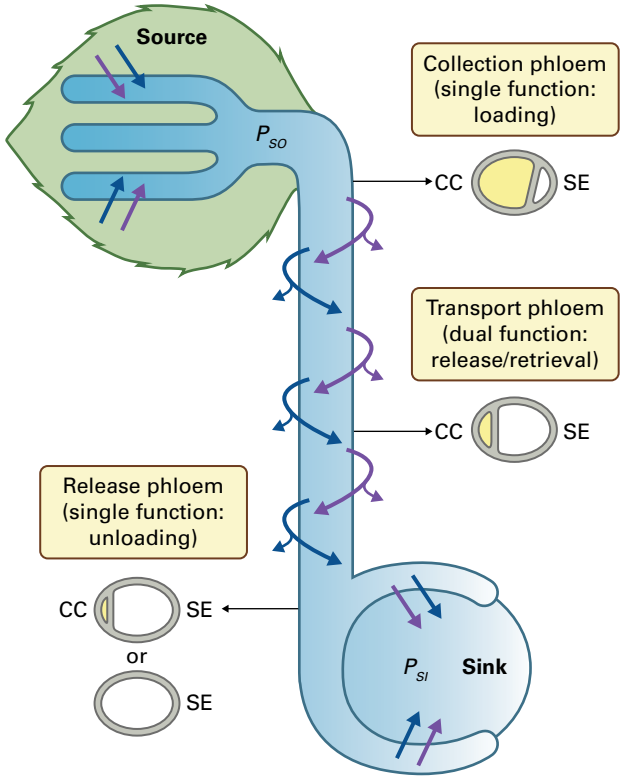


FIGURE 15.14 *Phloem includes three functional zones: collection, transport and release phloem. These functions may be associated with size ratios (oval insets represent cross-sections of SE/CCs with CC sections in yellow) between CCs and SEs that progressively decrease from source to sink. Uptake and release of photoassimilates (violet arrows) into/from SEs are accompanied by concurrent fluxes of water (blue arrows) along the phloem pathway. Influx and efflux of water are responsible for hydrostatic pressure (P) differences between ST ends in source (P_{so}) and sink (P_{si}) regions. Note that bulk flow continues into sink cells thus locating P_{si} at these sites. The blue gradient represents the presumptive hydrostatic pressure drop.*

15.4.2 Collection phloem is the site of SE loading

Photosynthetic source leaves are the principal organs supporting phloem loading. **Phloem loading** includes all transport processes responsible for transferring resources from their cellular sites of acquisition and storage to SE/CC complexes. The ultimate step of resource transfer into SE/CCs is referred to as **SE loading** and may follow an apoplastic or symplasmic route (Fig. 15.15).

15.4.3 Nutrients move symplasmically from mesophyll to bundle sheath or phloem parenchyma cells of collection phloem located in minor veins

Functional leaf design, and in particular venation patterns, optimize photoassimilate transport from mesophyll cells to SE/CC complexes. In eudicots, vein systems are mostly reticulate, with branching extending from two to seven orders (Fig. 15.16A). Veins with the highest order of

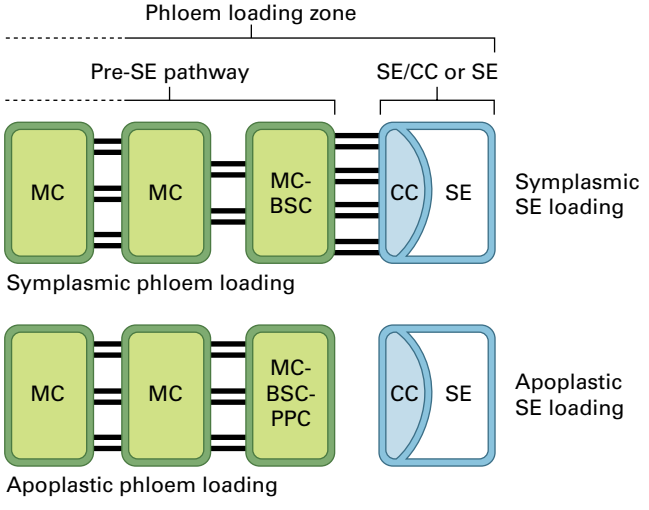


FIGURE 15.15 *Modes of phloem loading and associated terminology. Phloem loading comprises a series of transport processes within a phloem-loading zone. Loading into SE/CC complexes is called SE loading and is preceded by nutrient transport through a pre-SE pathway. If SE/CC complexes are symplasmically coupled to MCs and phloem loading is not reduced by membrane transport inhibitors (see Fig. 15.18B, C), SE loading is defined as being symplasmic. If SE/CC complexes are symplasmically isolated and phloem-loading rate is slowed by membrane-transport inhibitors (see Fig. 15.18D, E), SE loading is defined as being apoplastic. Various combinations of cell types can border the SE/CC complexes. MC, mesophyll cell; BSC, bundle sheath cell; PPC, phloem parenchyma cell; CC, companion cell; SE, sieve element. Paired horizontal lines represent plasmodesmata.*

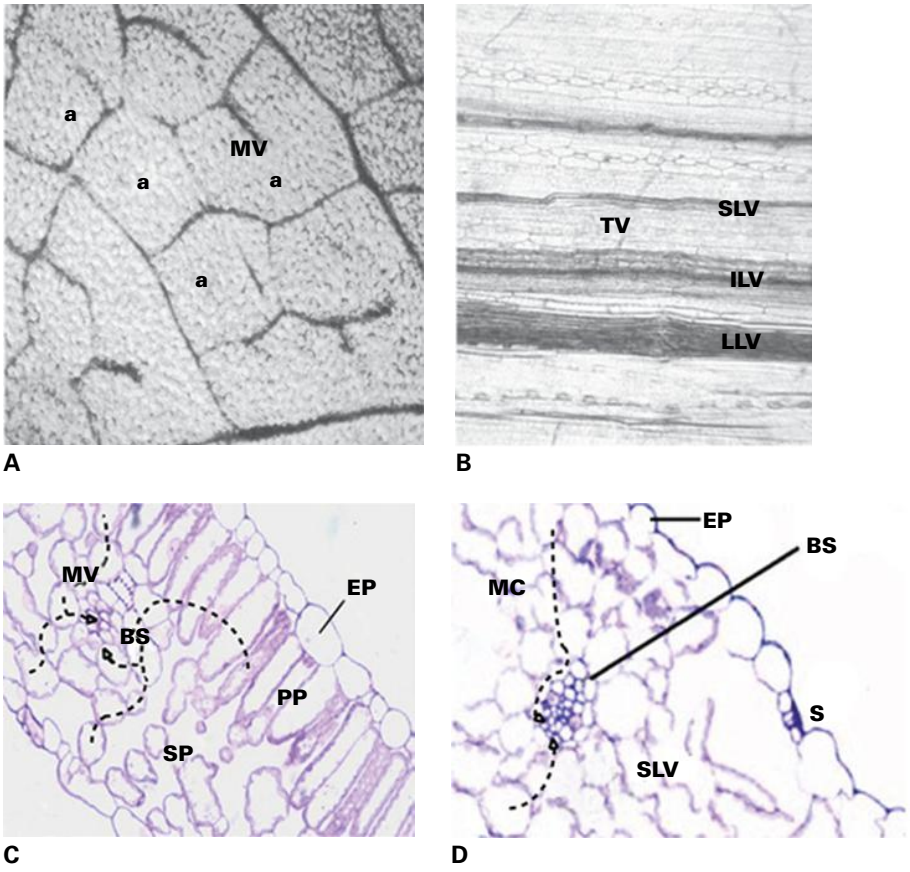


FIGURE 15.16 *Leaf structure in relation to phloem loading and export. (A, B) Light micrographs of venation patterns in whole leaf segments bleached to remove chlorophyll and visualize their vasculatures. (A) Branched venation in the leaf of fava bean (*Vicia faba*); a eudicot. Phloem loading occurs into minor veins (MV), but small veins around leaf areoles (a) also may be involved. Lower-order (i.e., larger) veins export nutrients. (B) Parallel venation in the leaf of barley (*Hordeum vulgare*); a monocot. Parallel-oriented small (SLV), intermediate (ILV) and large (LLV) longitudinal veins are connected by transverse veins (TV). Phloem loading occurs into SLVs and ILVs, ILVs and LLVs export nutrients. (C, D) Cross-sections of a tomato (*Solanum esculentum*) and barley leaves. (C) Photoassimilates are transported (dashed arrows) symplasmically from palisade (PP) and spongy (SP) mesophyll cells through bundle sheath (BS) cells towards phloem parenchyma cells in minor veins (MV) where photoassimilates are loaded into the phloem. EP, epidermis. SE loading may occur symplasmically or apoplastically (see Fig. 15.15). (D) Photoassimilates are transported symplasmically (dashed arrows) from mesophyll cells (MC) through BS cells towards phloem parenchyma cells of small longitudinal veins (SLV). Sieve-element loading may occur symplasmically or apoplastically (see Fig. 15.15). Stomata (S) in epidermis (EP). Source*: K. Ehlers, University of Giessen, Germany.

branching—minor veins—contain one or a few TEs and one or a few SE/CC complexes. Thus, by generating a large catchment area for photoassimilates in intimate contact with mesophyll cells, minor vein networks form the major site for phloem loading (Fig. 15.16A,C). Vein systems of monocot leaves comprise parallel small, intermediate, and large vascular bundles (Fig. 15.16B). Transverse veins interconnect longitudinal veins. Small and intermediate longitudinal veins (Fig. 15.16B,D) collect photoassimilates, while transverse veins transfer photoassimilates from small to large veins for export from leaves.

The densities of plasmodesmal interconnections infer photoassimilates move symplasmically from mesophyll to bundle sheath or phloem parenchyma cells of minor veins (Fig. 15.15; 15.16C,D). A *Z. mays* (maize) mutant (*sucrose export defective1—sxd1*) provides compelling evidence for symplasmic transport. The lesion results in structurally deformed plasmodesmata located between bundle sheath and phloem parenchyma cells of small longitudinal veins, and this deformation causes a pronounced reduction in photoassimilate export.

15.4.4 Composition of sieve tube sap identifies compounds loaded into the phloem

A handicap in collecting ST sap for analysis is that STs occlude in response to damage (see Section 15.6.4). However, a few plant species continue exuding ST sap after excision. Included among these are *Ricinus communis*, many palms, some lilies, and several cucurbits. Given the restricted number of exuding species, alternative methods for ST sap collection have been designed. For example, Ca^{2+} chelators such as EDTA prolong exudation of ST sap by preventing Ca^{2+}-induced sieve-plate occlusion (see

Section 15.6.4), but a disadvantage of organ excision is the potential contamination by nonphloem sap compounds. The most sophisticated method is to collect ST exudates from cut aphid stylets inserted into STs. Damage inflicted by the thin (1 μm in diameter) stylet tips does not induce sieve plate occlusion (see Box 15.3), and pure phloem sap can exude for up to 24 hours in monocotyledons.

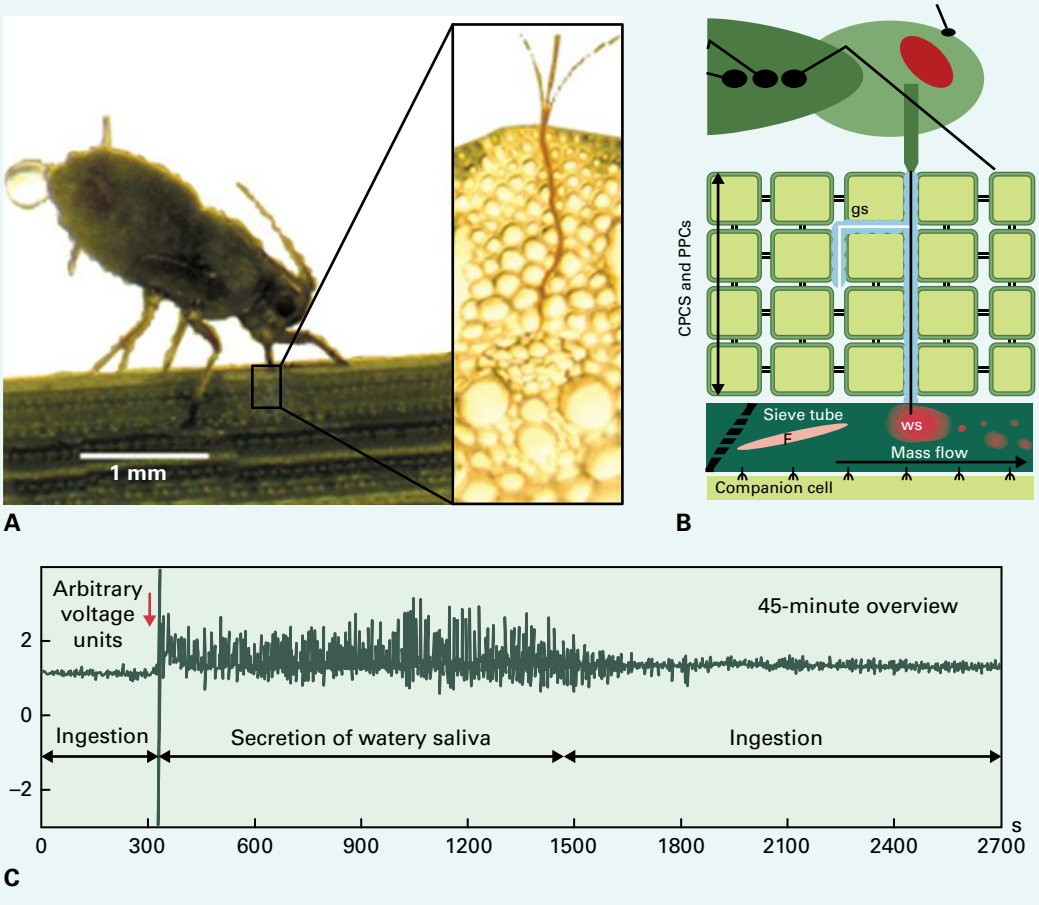
ST sap contains 10–12% dry matter and 88–90% water, rendering water the most abundant transported substance. Dissolved in ST sap are nonreducing sugars, amino N compounds, organic acids, inorganic ions, hormones, RNAs, proteins, and a wide range of plant-specific secondary metabolites. These substances collectively buffer ST sap at pH 7.0–7.5 and generate high osmotic potentials (Ψ_π of –1.4 to –2.0 MPa; Table 15.3, Fig. 15.6C).

Sugars account for up to 80% of sap osmotic content. Most herbs translocate sucrose; two groups of plants have other sugar profiles in their ST sap, but both still contain a proportion of sucrose. One group translocates sugar alcohols or polyols (principally mannitol or sorbitol), and the other translocates sugars belonging to the raffinose family oligosaccharides (RFOs, Fig. 15.17).

BOX 15.3 Aphid feeding and collection of ST exudates

Aphids feed from nutrient-rich ST content and have developed navigation mechanisms to track STs. Aphids insert their mouthparts (stylet) into shared cell walls between epidermal cells and steer them through cortex parenchyma (CPCs) and phloem parenchyma (PPCs) cells towards STs (A,B). It is almost certain that their navigation depends on continuously probing cell contents. During this stage, aphids excrete gel saliva (gs, B), which promptly hardens into a tubule through which their soft and flexible stylet is driven forward (B). Tubules can be stained to visualize the stylet path (inset A).

Upon puncturing a SE, aphids change their behavior by suddenly secreting masses of watery saliva (ws, B). During this stage, stylets can be separated from the aphid body by microcautery. Hydrostatic pressure in STs propels phloem sap through cut stylets and drops of pure ST sap can be collected. However, stylets are often occluded by phloem-specific proteins, particularly in



eudicots. Hence, the method is mainly applied for collection of ST sap from monocots over relatively short periods (<24 hours).

Electropenetrogram studies record electrical currents produced by muscular movements of aphids and membrane potentials of impaled cells (C). They demonstrate that secretion of watery saliva is followed by a regular pattern coincident with alternating uptake of ST sap driven by pressure flow and delivery of small amounts of watery saliva.

One function of watery saliva was discovered recently. Burning (red arrow in C) a broad bean (*Vicia faba*) leaf of an intact plant triggers an electric potential wave along STs initiating a massive Ca^{2+} influx into STs causing forisomes to disperse to block sieve pores (and see Section 15.6.6). Such an event deprives aphids of their food supply. As a response, aphids located several centimeters away on a main vein subjected to burning switch abruptly from ingestion to saliva secretion (C). After an extended period of secretion (≈20 min, C), the ingestion pattern is resumed. Coincidence between ST occlusion and intensified saliva secretion is interpreted as a mechanism to unblock the phloem pathway. Since ST occlusion is Ca^{2+} dependent, salivation could act to bind Ca^{2} as it contains several Ca^{2+} binding proteins and other proteins that may be involved in detoxifying plant defense compounds.

TABLE 15.3 *Sugar and amino acid concentrations in specified cellular compartments of leaves. Barley (monocot) and spinach (eudicot) transport sucrose as the principal sugar. In addition to sucrose, common plantain and celery transport the polyols, sorbitol and mannitol respectively.*

Plant spp.	Transported compound	Concentration (mM) in		
		Mesophyll cytosol	Leaf apoplast	Phloem sap
Barley	Sucrose	232	1.5	1030
	Total amino acids	275	3.1	830
Spinach	Sucrose	53	1.3	830
	Total amino acids	86	3.24	192
Common plantain	Sorbitol	133	5.5	422
	Sucrose	12	0.3	645
Celery	Mannitol	100	6.7	732
	Sucrose	86	1.2	389

A broad spectrum of amino acids and other nitrogenous compounds (ureides, citrulline, allantoin, allantoic acid) are also present in ST saps. Abundance of amide/amino acid couples of glutamine/glutamate and asparagine/aspartate is particularly striking.

For inorganic compounds and elements, K^{+} is the only species that makes a major contribution to osmotic potential of ST sap (60–100 mM). Mg^{2+} and H_2PO4^{-} occur at considerably lower concentrations; concentrations of Na^{+}, Fe^{2+}, Mn^{2+}, Cl^{-}, SO_4^{2-} and several microelements are even lower. NO_3^{-} and Ca^{2+} levels are present in the low nanomolar range.

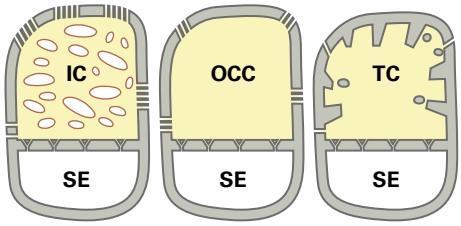
Secondary metabolites are transported in STs including a range of terpenes, alkaloids and nitrogenous substances that act as deterrents or poisons against herbivores (see Section 15.4.10). Vitamins occur in appreciable concentrations. For instance, vitamin C (ascorbic acid) and glutathione play central roles in detoxifying oxygen radicals. Indeed, a complete antioxidative capacity exists in STs.

Signaling molecules, detected at physiological concentrations in ST sap, include fatty acids, hormones, putrescine, and cyclic AMP. A portion of phloem-specific proteins may be engaged in long-distance communication along with a cohort of RNA species (see Section 15.6.5).

15.4.5 SE loading requires an intricate interplay between cell structure and metabolism

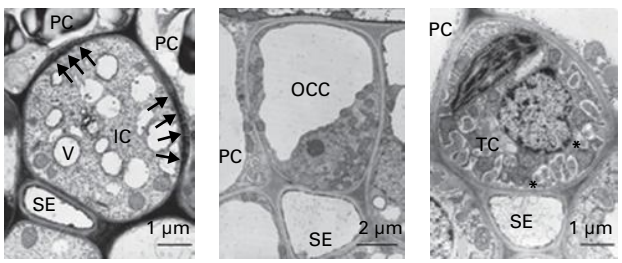
Plants can be subdivided into groups depending on their principal form of translocated sugar (Fig. 15.17). This has a bearing on SE loading mechanisms for sugars as outlined below.

Plasmodesmal frequencies interconnecting SE/CCs to adjacent bundle sheath/phloem parenchyma cells and CC ultrastructure have been used to erect hypotheses for putative



Number of plasmodesmata at the PC/CC interface	Type 1	Type 2a	Type 2b
	>10 μm^{-2}	10–0.1 μm^{-2}	<0.1 μm^{-2}
Uphill sugar gradient	Gentle	None to steep	Steep
Predominant transport sugar	Sucrose, galactosyl-oligosaccharides (RFO sugars)	Sucrose, sugar alcohols, RFO sugar	Mainly sucrose

A



B C D

FIGURE 15.17 *Relationship between minor vein CC ultrastructure and mode of phloem loading in eudicots. (A) Three types of CCs are distinguished by plasmodesmal (parallel groups of lines) densities interconnecting with phloem parenchyma (PC) or bundle sheath (BSC) cells, sugar gradient steepness from mesophyll cells (MC) to SE/CC complexes and transported sugar species. (B) Intermediary cells (ICs) characterized by numerous cytoplasmic vesicles (V) and many branched plasmodesmata at wall interfaces between PCs and ICs (arrows indicate plasmodesmal fields), load raffinose family oligosaccharides (RFOs) and sucrose. (C) Ordinary companion cells (OCCs) lack distinguishing structural features. This heterogeneous group exhibits varying densities of plasmodesmata at BSC/OCC or PC/OCC interfaces and loads a variety of sugars. (D) Companion cells modified with a transfer cell (TC) architecture, characterized by cell wall invaginations (asterisks) to increase their plasma membrane surface areas, have few plasmodesmata at PC/CC interfaces. Sucrose is the principal transported sugar. SE, sieve element.*
Source: (B, D) Oparka & Turgeon (1999). Plant Cell 11:739–750. (C) Reidel et al. (2009). Plant Physiol. 149:1601–1608.

pathways of SE loading (Fig. 15.17A). Minor vein configurations can be separated into two broad types based on apparent symplasmic continuities. Type 1 species, putative symplasmic loaders, have an "open" configuration with numerous plasmodesmal connections between CCs and bordering parenchyma cells. Their CCs invariably exhibit an intermediary cell ultrastructure (Fig. 15.17A,B). Type 2 species exhibit configurations with moderate to low PD densities between CCs and adjacent cells. They fall into two groups. The first group (Type 2A) possesses CCs lacking wall invaginations (Fig. 15.17C) and may include both symplasmic and apoplastic loaders. The second group (Type 2B) exhibit a transfer cell morphology (Fig. 17.17D) and are exclusively apoplastic loaders.

A routine test for apoplastic SE loading is to determine the sensitivity of photoassimilate export to inhibition of plasma membrane transport (in general) with a membrane-impermeant sulfhydryl reagent, para-chloromercuribenzenesulfonic acid (PCMBS), and concurrently test for any confounding effect on leaf photosynthesis. Using these approaches, responses consistent with apoplastic SE loading of sucrose and polyols are found for a wide range of plant species with Type 2 minor vein configuration, particularly those with an herbaceous habit, including many crop species (Fig. 15.18).

PCMBS-insensitive export of photoassimilate from source leaves (Fig. 15.18B,C) indicates symplasmic phloem loading. SE/CC complexes of these responders exhibit plasmodesmal frequencies greater than 1 μm^{-2} (i.e., Type 1 and Type 2a—Fig. 15.17A–C). However, several species with Type 2a configuration function as apoplastic loaders, indicating that structure alone does not determine SE loading pathway. Moreover, vein anatomy and physiological evidence indicate that different loading paths can coexist; for instance, some Type 1 species also have CCs with or without wall ingrowths in the same minor veins (Fig. 15.19).

15.4.6 Apoplastic SE loading is determined by the cellular location and transport function of membrane-bound proteins

All apoplastic loaders verified to date translocate sucrose and/or polyols. Apoplastic loading includes two transmembrane steps: sugar release into the vein apoplast and subsequent uptake by SE/CC complexes (Fig. 15.15).

Until recently, membrane transport mechanism(s) responsible for sugar release to the vein apoplast eluded discovery. This gap in understanding was breached by cloning a novel class of sugar transporters, SWEETs (Sugar Will Eventually be Exported Transporters). These function as sugar facilitators capable of transporting sucrose and glucose in an efflux mode (see Chapter 3). Consistent with serving a major role in phloem loading, AtSWEET11 and 12 localize to the collection phloem and their double mutant caused carbohydrates accumulation in source leaves and photoassimilate export to be slowed.

The mode of sucrose uptake by SE/CC complexes is well understood. Here, a H^+-symport mechanism loads sucrose or polyols into SE/CC complexes (Fig. 15.20 and Equation 15.B9; see also Chapter 3) to reach higher concentrations than in the surrounding leaf apoplast and mesophyll cytosol (Table 15.3). Several clades of sucrose/H^+ symporters (SUTs or SUCs) localize to plasma membranes of minor vein SE/CCs to participate in apoplastic loading. High-affinity SUT1 isoforms (apparent K_m values of 0.5–2 mM; Equation 15.B9), depending upon plant species, are exclusively localized to SEs

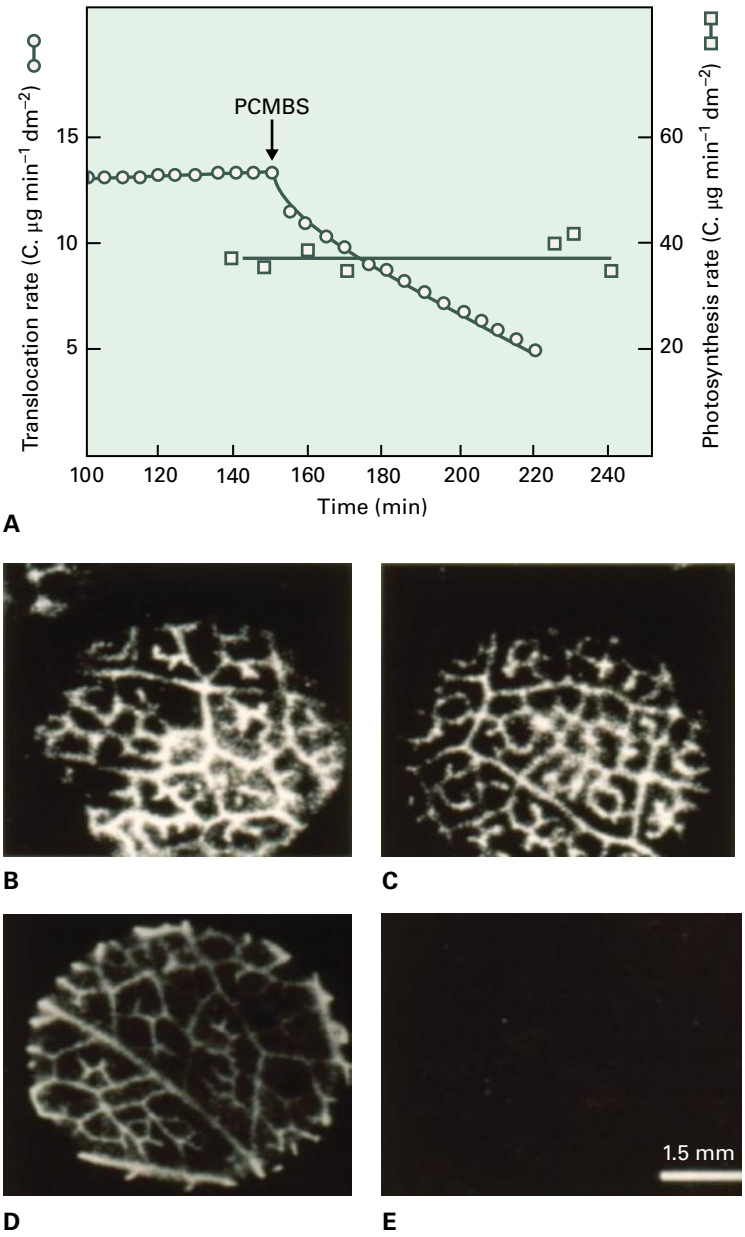


FIGURE 15.18 *Apoplastic and symplasmic phloem loading detected by exposing a leaf to a membrane-impermeant sulfhydryl reagent (PCMBS) that inactivates plasma membrane transporters. (A) PCMBS treatment of a leaf immediately slowed phloem export but had no effect on photosynthesis demonstrating that PCMBS had not entered leaf cells and had reacted exclusively with sulfhydryl groups on the outer surfaces of their plasma membrane. (B–E) Autoradiographic images of leaf discs of* Ipomea *(B, C) and* Pisum sativum *(pea) (D, E) floated on a solution containing [^{14}C]sucrose in the absence (B, D) or presence (C, E) of PCMBS. Without PCMBS, ^{14}C accumulated (white areas) by leaf discs was located in their collection phloem. In* Ipomea *leaves, phloem loading was unaffected by PCMBS (C) indicating a symplasmic loading pathway. In contrast, phloem loading was eliminated in pea leaves (E) exposed to PCMBS indicative of an apoplastic pathway of phloem loading. Source*: (B, C) Madore & Lucas (1987). Planta 171:197–204; (D, E) Turgeon & Wimmers (1988). Plant Physiol. 87:179–182.

or CCs (Figs. 15.21 and 15.22B). Consistent with a mixed apoplastic and symplasmic loading system, a SUT1 localizes to SEs and OCCs but not to intermediary cells (ICs) of *Alonsoa meridionalis* leaves. Low-affinity SUT2 and SUT4 isoforms (apparent K_m values of ca. 10 mM) colocalize with SUT1 to minor vein SEs of solanaceous species. However, in other eudicot species SUT2 occurs in SEs and SUT1 localizes to CCs (Fig. 15.22B), while SUT4 targets to tonoplast of mesophyll cells. In leaves of *Plantago major*, two high-affinity polyol/H^+ transporters, PmPLT1 and PmLT2, colocalized to CCs of minor veins and concentrate polyols in SEs (Table 15.3).

Reverse genetics demonstrate that SUT1s play key roles in apoplastic SE loading, as shown by downregulated *SUT1* expression causing substantial reductions of photoassimilate export. In contrast, knockdown of plasma membrane localized SUT4 in potato elevated rates of photoassimilate export (Table 3.5) perhaps reflecting a post-translational control of SUT1 transporter activity. However, in those species where

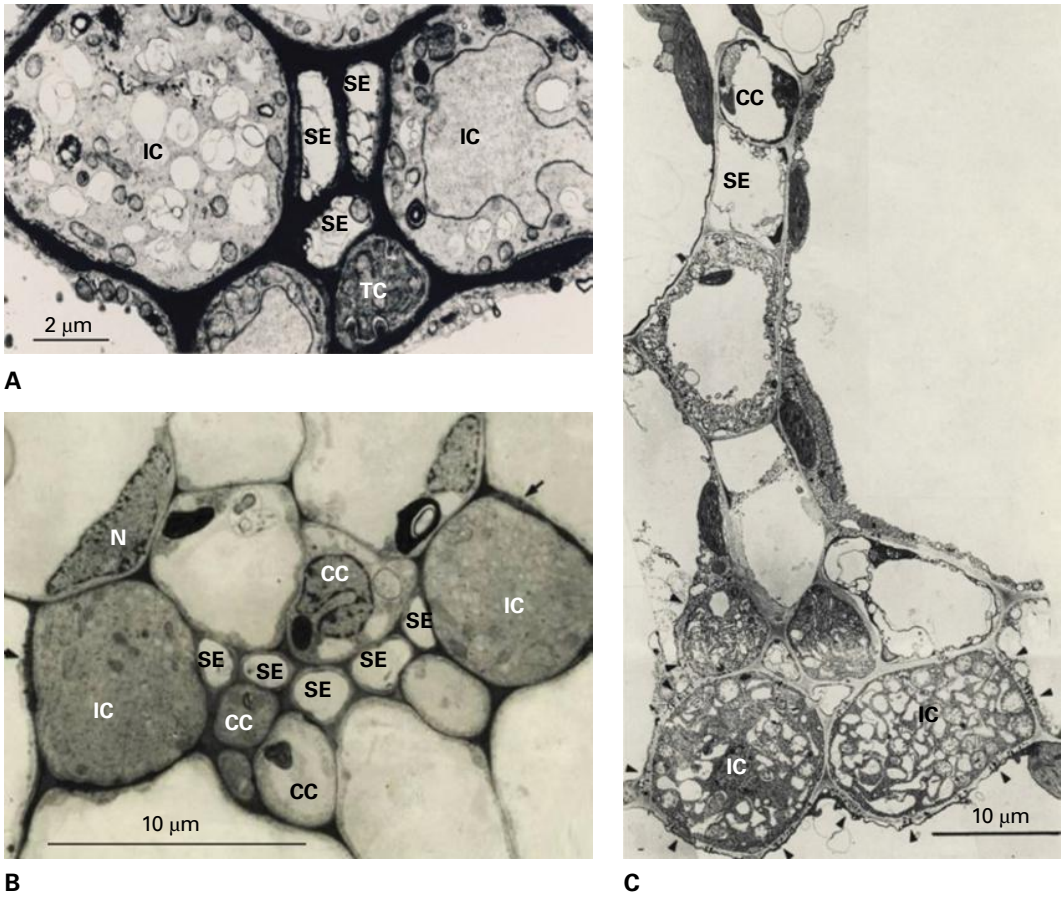


FIGURE 15.19 *Different SE/CC configurations occur in one minor vein indicating that phloem-loading modes operate in parallel in some species. Transverse EM sections show that (A) Minor veins of* Acanthus mollis *contain two SEs each flanked by an IC and one central SE accompanied by a TC. (B) Minor veins of* Coleus blumei *possess two SEs flanked by ICs and several central SEs accompanied by ordinary CCs. (C) Minor veins of* Cucumis sativus *show two IC/SE complexes at the bottom and a SE with an ordinary CC at the top. IC, intermediary cell; TC, companion cell modified to a transfer-cell morphology. Arrows and arrowheads point to pit fields of plasmodesmata.*
Source: (A) van Bel et al. (1992). Planta 186:518–525. (B) Fisher (1986). Planta 169:141–152. (C) Schmitz et al. (1987). Planta 171:19–27.

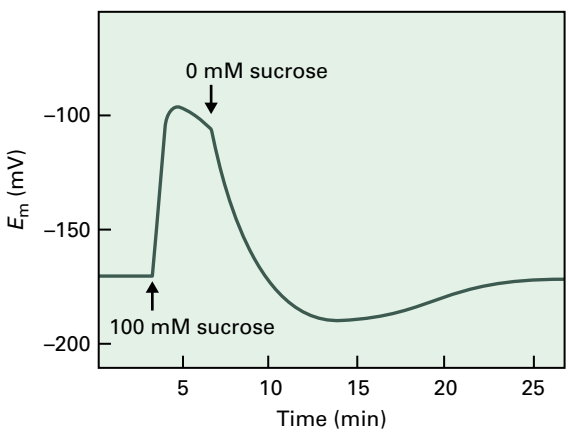


FIGURE 15.20 *Supplying sucrose causes a sharp depolarization of ST membrane potential suggesting a sucrose/H⁺ symport mechanism for phloem loading. An exuding aphid stylet was used to measure ST membrane potential in a strip of phloem from a willow* (Salix exigua) *branch. Introducing a 100 mM sucrose solution bathing the surface was followed several minutes later by a sucrose-free solution.*

SUT4 localizes to the tonoplast, SUT4 knockdowns inhibited phloem loading consistent with SUT4 functioning to release vacuolar-stored sucrose to buffer cytoplasmic sucrose pools for export.

Sugar symporters colocalize with H^+-ATPases in minor veins. The proton extrusion activities generate *pmf*s to drive sucrose/H^+ symport into SE/CC complexes (Equation 15.B10 and Fig. 15.20). This function has been verified by suppressed expression of an H^+-ATPase causing lowered sucrose content of ST exudates (Table 15.4).

Phloem loading of amino acids and amides depends upon a complex series of relationships. These include root/leaf localization of nitrate reductase (see Chapter 16), extent of xylem–phloem exchange along the transport phloem, and degree of leaf senescence (see Chapter 20), or exposure to abiotic stress (see Chapter 22), during which peptides also can be loaded. Comparison of amino acid concentrations in mesophyll cells and ST exudates (Table 15.3) demonstrates that an active phloem loading mechanism must operate. Based on expression and localization studies, a broad range of amino acid and amide transporters have been implicated in phloem

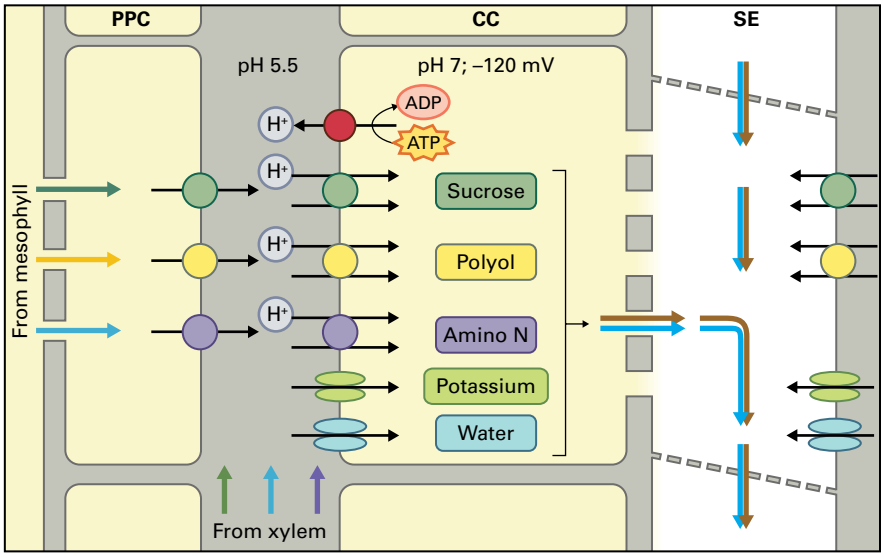


FIGURE 15.21 *Diagram illustrating cellular localization of transporters responsible for apoplastic phloem loading. Sugars and amino acids are delivered symplasmically from mesophyll and released to the phloem apoplast from phloem parenchyma cells (PPCs) by an unknown set of transporters (question marks). Amino acids are delivered to the phloem apoplast directly from the xylem transpiration stream along with K^+ and water. Plasma membrane H^+-ATPases, localized to CCs, generate a steep* pmf *used to drive proton co-transport of sucrose, polyols and amino acids into SE/CC complexes. K^+ channels retrieve K^+ and sustain SE/CC membrane potentials. Water flows into SE/CC via aquaporins.*

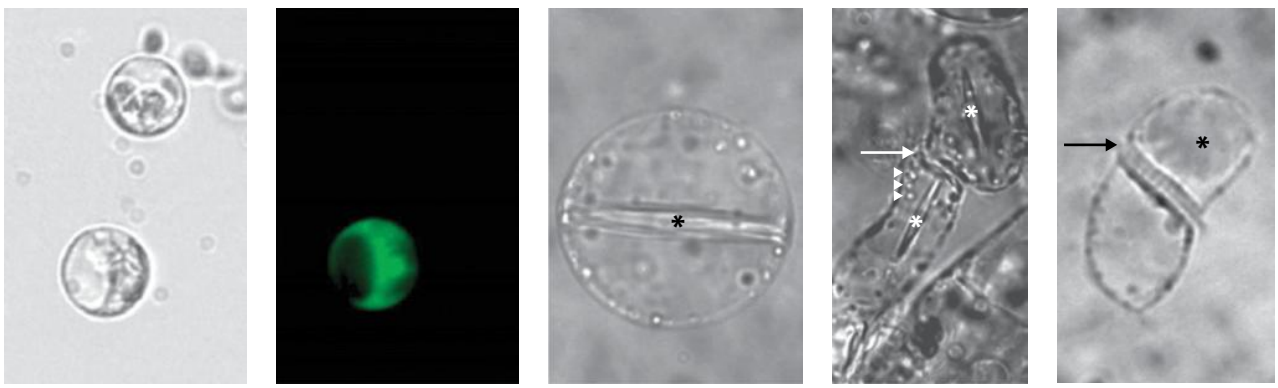


FIGURE 15.22 *Companion cell and sieve element protoplasts. (A, B) Light-microscopic (A) and fluorescence-microscopic (B) images of the same set of protoplasts. CC protoplasts of* Arabidopsis *SUC2:GFP transformants (SUC2-promoter is CC-specific) are distinguished from other protoplasts by their green GFP-fluorescence (B). (C–E) SE protoplasts from broad bean (*Vicia faba*). (C) SE protoplasts of legumes identified by presence of spindle-like protein bodies (forisomes, asterisk). Magnification 1390x. (D) "Twin SE protoplasts" at either side of a sieve plate (arrow, sieve plate; asterisk, forisome; arrowhead, SE plastids). Magnification 570x. (E) "Twin SE protoplasts" with sieve plate (arrow) and a dispersed forisome (asterisk). Magnification 1066x.*
Source: (A, B) Ivashikina et al. (2003). Plant J. 36:931–945. (C, D, E) Hafke et al. Plant Physiol. 145:703–711.

TABLE 15.4 *Impact of downregulated expression of sucrose symporters,* SUT1 *and* SUT4*, and a CC-specific H^+-ATPase,* pma4*, on relative rates of photoassimilate export from source leaves.*

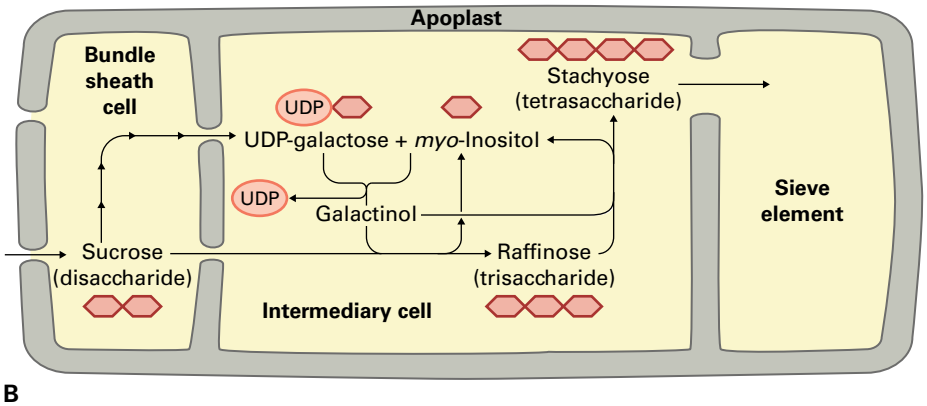
Plant spp	Suppressed expression of:	Relative rate of photoassimilate export (% wild type)
Tobacco	*NtSUT1*	18
Arabidopsis	*AtSUT1*	51
Potato	*StSUT4*	306
Tobacco	*pma4*	38

loading including those functioning in release to the vein apoplast (e.g. AtSIARS1, AtBAT1) and uptake into SE/CC complexes (e.g. AAPs, AtCAT6 and 9, AtProT1; see Chapter 3). For instance, overexpressing *PsAAP1* targeted to SE/CC complexes in the collection phloem enhanced phloem loading in pea (*Pisum sativum*).

Ions are delivered to leaves in the transpiration stream (see Section 15.3.4) and can load directly from the vein apoplast into SE/CC complexes as illustrated for K^+ (Fig. 15.21). Inward rectifying K^+ channels, detected in protoplasts derived from CCs and SEs (Fig. 15.22), may account for loading of K^+ to high concentrations (60–100 mM). With an increasing interest in food quality, phloem transport of transition elements such as iron (Fe) and zinc (Zn) have received recent attention.

Cell type	Osmotic potential (MPa)	Concentration (mM) of: Raffinose	Stachyose
Mesophyll	–0.8	0.1	67
Bundle sheath	–0.8	ND	ND
Intermediary	–4.4	0.2	334

A



B

FIGURE 15.23 *Symplasmic loading of RFO sugars occurs in Type 1 minor vein configurations (Fig. 15.17A, C). (A) RFO sugar concentrations and osmotic potentials in mesophyll, bundle sheath and intermediary cells (ICs) of a cucurbit leaf. ND, no data. (B) 'Polymer trap' model for symplasmic phloem loading. Sucrose (and in some plants, galactinol) moves symplasmically into ICs and is used to synthesize RFOs, raffinose and stachyose. These sugars can diffuse from ICs into SEs through large-diameter PPUs but their molecular size excludes backward diffusion through small plasmodesmal orifices connecting ICs with bundle sheath cells.*

15.4.7 During symplasmic SE loading, a trapping mechanism concentrates sugars in SEs

In view of an unlikely active transport through plasmodesmata, accumulating RFOs in SE/CC complexes (Fig. 15.23A) has presented a perplexing challenge. For these species, a "polymer trap" model accounts for this phenomenon, whereby sucrose, synthesized in mesophyll cells, diffuses down a concentration gradient via plasmodesmata to ICs in minor veins (Fig. 15.23B). There, sucrose is used to synthesize the larger RFO molecules raffinose and stachyose. Synthesis of these sugars maintains the concentration gradient to drive diffusion of sucrose from mesophyll cells to ICs. The larger size of RFOs prevents them from moving symplasmically back from ICs to mesophyll cells, but they can pass through the much larger PPUs to SEs. This model is consistent with RFO synthesis in ICs, where their concentrations are much higher than in mesophyll cells. In addition, suppression of RFO synthesis by downregulating two galactinol synthase genes reduced photoassimilate export from leaves.

In several Type 2A species, which translocate mostly non-RFO sugars, total osmotic concentrations are similar in mesophyll cells and minor vein SE/CC complexes. These observations suggest sugars move by bulk flow through an uninterrupted symplasm from mesophyll cells to STs. This phenomenon may be more ubiquitous than previously thought, especially in woody species. In these cases, phloem loading is passive and does not depend upon expenditure of metabolic energy.

15.4.8 In collection phloem, water flows accompany phloem loading of nutrients

Apoplastic loading of sucrose and polyols and symplasmic loading of RFOs generate steep concentration and osmotic gradients between phloem parenchyma and SE/CC complexes. These gradients induce large water fluxes across the plasma membranes of SE/CC complexes in the range of 7×10^{-10} m^3 m^{-2} s^{-1}, which require osmotic water permeability values of 40–200 μm s^{-1} corresponding to those expected for membranes containing high densities of aquaporins. Indeed, aquaporins have been detected in minor vein CCs. Water entering SE/CC complexes is drawn from minor vein apoplasts and replenished by the transpiration stream (Fig. 15.21). Simultaneous measurements of hydrostatic and osmotic pressures of ST sap sampled by stylectomy (Box 15.3) estimate ST sap water potentials to be –1.0 to –1.5 MPa (Table 15.5). These values are more negative than those of TE sap in hydrated transpiring leaves of herbaceous plants (≈ –0.5 MPa) and leaves entering incipient wilting (ca. –1.4 MPa). Thus, ST sap water potentials are more negative than those of the surrounding apoplastic fluid, allowing phloem loading of water under most conditions. For those symplasmic loading species, in which total osmotic concentrations are similar in mesophyll cells and minor vein SE/CC complexes, water inflow would be expected to occur along the entire phloem-loading pathways.

TABLE 15.5 *Minimum and maximum hydrostatic pressures (P) in, and sap osmotic potentials (π) of, sieve tubes.*

		Potential (MPa)	
Plant spp.	**Water relation parameter**	**Minimum value**	**Maximum value**
Barley	Hydrostatic pressure	+0.8	+1.4
	Osmotic potential	–1.9	–2.6
	Water potential	–1.1	–1.2
Sow thistle	Hydrostatic pressure	+1.0	+1.5
	Osmotic potential	–2.0	–3.0
	Water potential	–1.0	–1.5

Measurements of well-watered barley and sow thistle plants using aphid stylectomy. Estimates of ST sap water potentials (Ψ) are derived from these measurements (see Equation 15.B7).

15.4.9 Transport phloem is an underestimated, but important transport player

Transport phloem translocates resources and signals from collection phloem to release phloem. Whereas collection and release phloem zones are commonly a few hundred microns long, transport phloem covers large distances from source leaves to root and shoot apices, distances of 0.1–3 m (small to large herbs; shrubs) up to 100 m (tall trees).

The impact of transport phloem on nutrient transport and distribution is much greater than has been attributed by the pressure flow hypothesis of phloem translocation, which treats the transport phloem as an inert and impermeable pipe. Emerging evidence shows that transport phloem sustains onward longitudinal flux by buffering ST sap concentrations (and hence hydrostatic pressures) to deliver resources and signals to adjacent nonvascular cells and exert a pronounced influence on ST sap composition. Such dynamic functions are attributable to SE-associated cells (CCs, phloem parenchyma cells), since SEs possess a limited metabolic capacity (see Section 15.2.3).

15.4.10 Transport phloem function relies in interaction between SEs, CCs, and phloem parenchyma cells

During their lifetime, which can last for 30 years, CCs remain functionally competent to produce or process metabolites needed by SEs. In addition to supplying energy substrates (Fig. 15.24), CCs probably execute turnover of structural macromolecular components channeled to SEs via their PPUs (see Section 15.6.5). This intricate interrelationship between SEs and CCs hampers assessment of their individual contributions to their collective functioning, though future studies using CC and SE protoplasts may discriminate between their individual functions.

Phloem parenchyma cells are probably of paramount importance for phloem physiology. Given their location, it is plausible they act as sites for temporary carbohydrate storage (Fig. 15.25A). In transport phloem, plasmodesmal frequency between CCs and adjacent phloem parenchyma cells is generally low, indicative of restricted capacity for lateral symplasmic exchange of molecules along transport phloem. ST-limited translocation of membrane-impermeant fluorochromes shows these plasmodesmata are closed under conditions in which sink demand exceeds source supply (source-limiting conditions) (Fig. 15.25B); when source supply exceeds sink demand, plasmodesmata at this interface gate open (Fig. 15.25C).

Phloem parenchyma cells also function in plant defense. For instance, in solanaceous plants, phloem parenchyma cells produce the protein prosystemin. In response to an unknown signal, polypeptide systemin is cleaved from prosystemin and released into SEs. Upon arrival in sink organs, systemin triggers production of proteinase inhibitors that block protein digestion by herbivorous insects. A spectacular example of interactive phloem cell biology is the division of labor between SE/CCs and phloem parenchyma cells in producing benzylisoquinoline alkaloids abundant in latificers of opium poppy (*Papaver somniferum*). The morphinian pathway enzymes are absent from latex but reside in SEs, with their transcripts localized to CCs. This suggests trafficking of transcripts and secondary metabolites via plasmodesmata and PPUs and subsequent transport to laticifers.

15.4.11 Lateral exchange of nutrients occurs from transport phloem

Release along transport phloem supplies nutrients for storage and supports secondary growth and cell maintenance. Mature petioles, stems, and roots (axial sinks) function as short-term

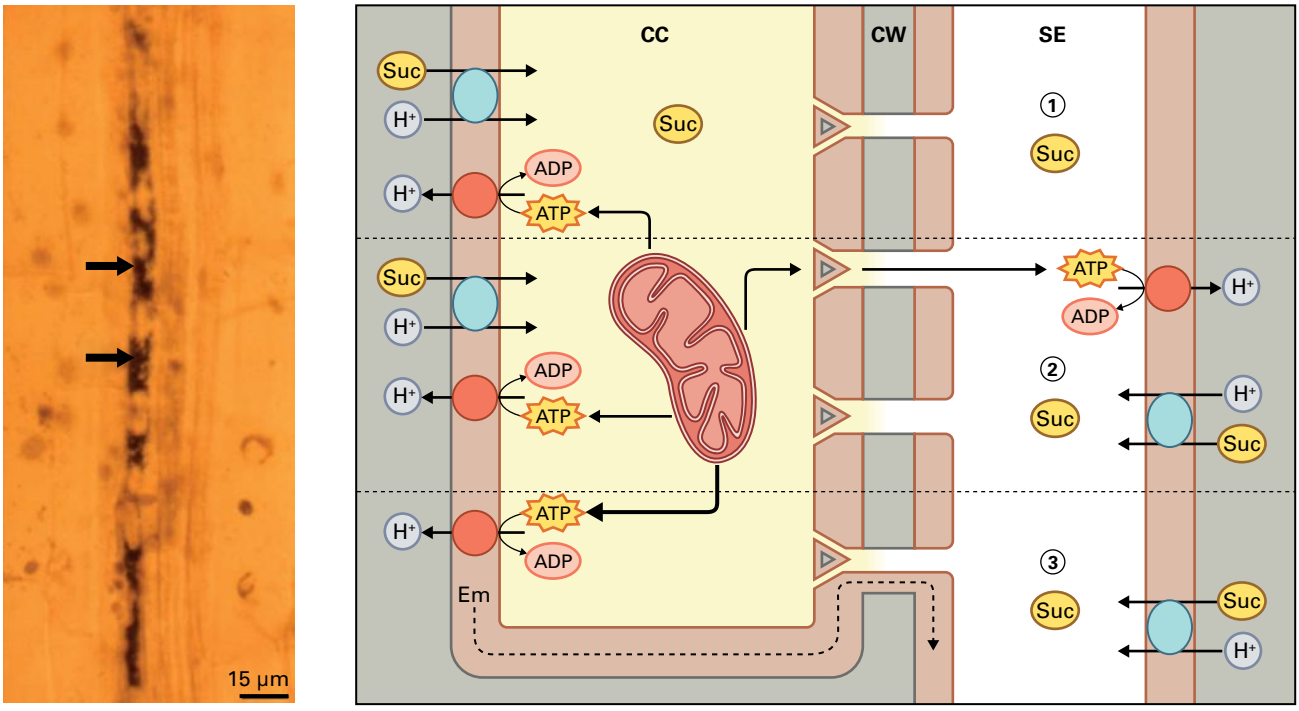


FIGURE 15.24 *Sieve element function depends on genetic and metabolic contributions by companion cells. (A) Absence of metabolic machinery in SEs (Table 15.1) is compensated by high densities of mitochondria (dark areas indicated by arrowheads) in CCs. (B) Potential energy transfer between SEs and CCs. There are three potential ways to maintain sugar concentrations in SEs. (1) Sucrose (SUC) retrieved by sucrose/H^+-symporters energized by CC-generated* pmf *and transferred to SEs via PPUs in their common cell wall (CW). (2) ATP produced by CC mitochondria moves via PPUs to SEs and energizes proton pumps in energy-deficient SEs. The* pmf *drives sucrose symporters in SE plasma membranes. (3) Electrogenic potential generated by proton pumps in CC partly propagates via plasma membranes to SEs via PPUs. There, the electrogenic potential contributes to* pmf *fuelling sucrose symporters in SEs. Deployment of sucrose/H^+-symporters on CC- or SE-plasma membranes can account for retrieval of sucrose. Not shown, the electrogenic component of the pmf, generated by the proton pump, can be augmented or replaced by K^+ release through AKT2 channels located on the SE/CC plasma membranes – the so-called K^+ battery.*
Source: (A) van Bel & Kempers (1991). Planta 183:69–76.

reservoirs for nutrients released from transport phloem that are ultimately reloaded and translocated to other (terminal) sinks (Fig. 15.25); residence times extend from seconds to months.

A high-turnover sucrose pool resides in the transport phloem apoplast, which is fed by large passive fluxes from SE/CC complexes that are driven by substantial outward gradients in sucrose concentrations across the plasma membranes. For instance, in bean (*P. vulgaris*) plants, STs lose 6% of photoassimilates per centimeter of stem, and two-thirds of this is retrieved. The phloem apoplastic pool buffers photoassimilate concentrations and, hence, hydrostatic pressures of STs through a continuous cycle of release and retrieval of photoassimilates by sugar/H^+ symport (Figs. 15.24B, 15.25A).

Apoplastic sucrose concentrations in stems range from 3 to 70 mM. Consistent with this concentration range, retrieval by transport phloem involves a complex of low- and high-affinity sugar transporters localized to SE/CC complexes. In fact, qualitative profiles of SUT clades and their cellular localization in collection phloem (see Section 15.4.6) are reproduced in transport phloem. This finding applies equally to amino N carriers and K^+ channels. Collectively these transporters function in retrieving nutrients leaked to phloem apoplast back into SE/CC complexes. However, competition for sugars leaked to phloem apoplast between SE/CC retrieval and allocation to lateral storage pools is likely as suggested by localization of a mannitol symporter to SEs, CCs, and phloem parenchyma cells of celery (*Apium graveolens*) petioles.

In some monocot stems a suberin band, deposited in walls of bundle sheath cells, blocks radial transport through the stem apoplast, and a symplasmic path is essential at least for this component of the unloading pathway. Indeed, the entire phloem-unloading pathway follows a symplasmic route in wheat and rice stems during storage product accumulation (Fig. 15.26A,C). Here, sucrose symporters located in SE/CC complexes (Fig. 15.26B,D) likely retrieve sucrose leaked to the phloem apoplast. Interestingly, a switch to an apoplastic loading step occurs at SE/CCs coincident with remobilization of stem reserves to support grain filling. Radial transport in eudicot stems also can switch reversibly between apoplastic and symplasmic routes (Fig. 15.25).

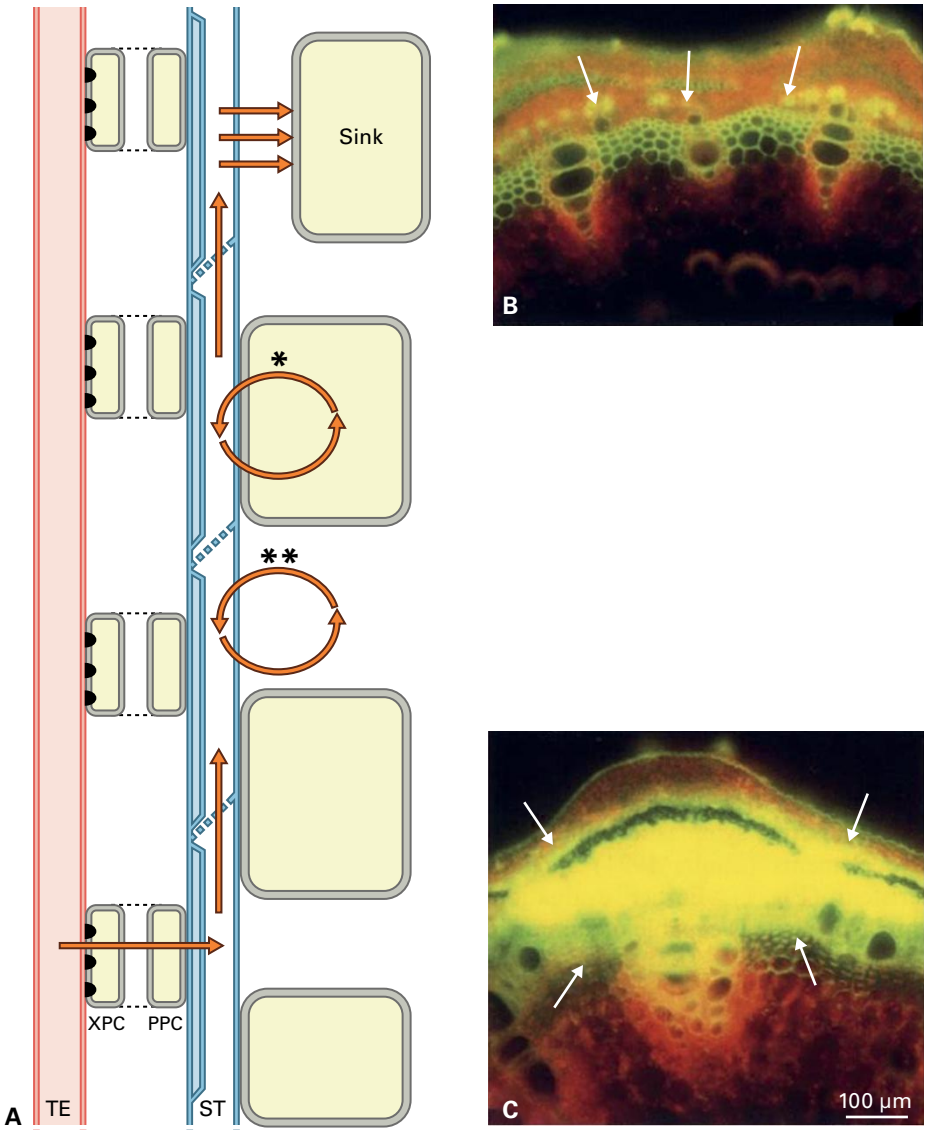


FIGURE 15.25 *Nutrient exchange between transport phloem and surrounding tissues. (A) Diagrammatic representation of nutrient exchanges with transport phloem (P). Nutrients (amino N compounds and mineral elements), retrieved from TEs by xylem parenchyma cells (XPC, mostly with cell wall invaginations – black circles) are transported along a radial pathway (dashed lines) and loaded via phloem parenchyma cells (PPC) into STs for delivery to sinks. During movement through the transport phloem, nutrients are reversibly exchanged (circular arrows) with surrounding tissues into long-term (*) or short-term (**) storage pools. Long-term (days to months) storage of nutrients occurs in PPCs and nonvascular cells. Under lowered source/sink ratios, these substances are re-mobilized and loaded into the transport phloem. Short-term (minutes to hours) storage occurs in the axial apoplast. Rapid bi-directional exchanges of nutrients across plasma membranes of SE/CC complexes act to buffer their hydrostatic pressures and sap nutrient concentrations. (B–C) Source-sink ratios influence the cellular pathway of lateral nutrient exchange as indicated by distribution of a membrane-impermeant fluorescent dye, carboxyfluorescein (CF), loaded into source leaf phloem. (B) Fluorescent micrograph of a free-hand cross section of a bean (*P. vulgaris*) stem, pruned to a low source/sink ratio, showing CF (arrows; bright yellow fluorescence), restricted to SE/CC complexes of transport phloem demonstrating these are symplasmically isolated from surrounding cells. (C) Fluorescent micrograph of a free-hand cross section of a P. vulgaris stem, pruned to high source/sink ratio, showing CF has moved from SE/CC complexes into surrounding cells (arrows; bright yellow fluorescence) indicating symplasmic continuity between transport phloem and surrounding cells.*
Source: (B, C) Patrick & Offler (1996). J. Exp. Bot. 47:1165–1178.

15.4.12 Release phloem mediates phloem unloading

Phloem unloading describes the intercellular transport of resources from SEs to sink cells. Components of this pathway include **SE unloading** arranged in series with subsequent intercellular transport through vascular and nonvascular cells (**post-SE transport**) (Fig. 15.27). Resources may be unloaded from primary or secondary phloem (see Section 15.2.1) depending upon sink type. Unloading occurs from protophloem in **growth sinks** and from primary (metaphloem) or secondary phloem in **storage sinks**.

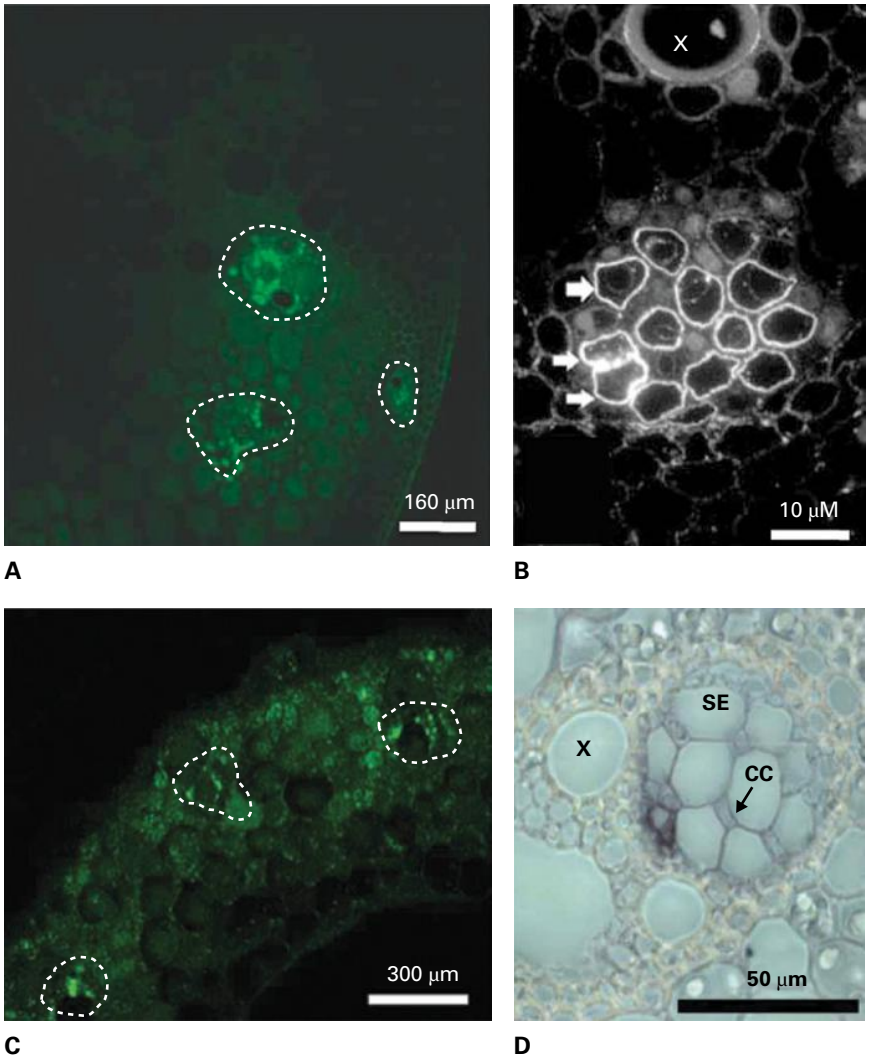


FIGURE 15.26 *Transport phloem in stems of wheat (A, B) and rice (C, D) showing escape of fluorescent carboxyfluorescein from phloem (broken white outline) into surrounding ground tissues (A, C) illustrating presence of a symplasmic unloading route. Sucrose/H^+ symporters were immunolocalized localized to SEs in wheat (B; arrows, strong fluorescence of a bound SUT1 antibody labeled with a fluorescent secondary antibody) and SE and CCs in rice (D; arrow, grey-blue immunocytochemical staining of cell walls catalyzed by a phosphatase conjugated secondary antibody labeling a bound SUT1 antibody). X = xylem.*
Source: (A, B) Aoki et al. (2004). Planta 219: 176–184. (C, D) Scofield et al. (2007). J. Exp. Bot. 58:3155–3169.

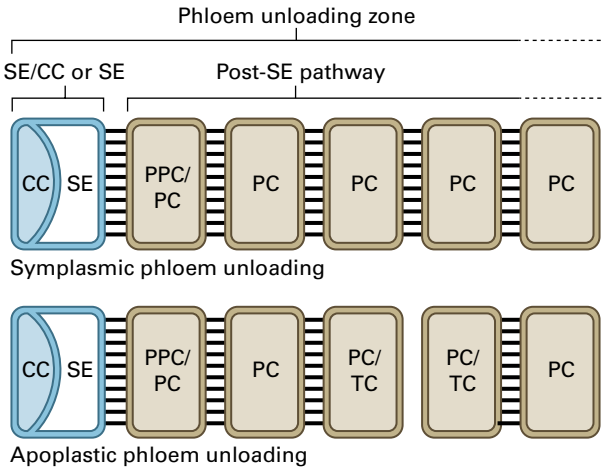


FIGURE 15.27 *Phloem unloading comprises a series of transport processes located in an array of cells (SE with or without CC; PPC, phloem parenchyma cell; PC, parenchyma cell; TC, transfer cell) designated as the phloem-unloading zone. Phloem loading and unloading are defined by similar principles (see Fig. 15.18) with one modification. Phloem unloading is defined as apoplastic if an apoplastic step occurs in the post-SE unloading pathway (lower row). SE unloading is predominantly symplasmic (see Table 15.6).*

15.4.13 Phloem sap exit from SEs is commonly symplasmic

For most sinks, SE unloading follows a symplasmic route, and only a small fraction of nutrients unloaded from SE are released directly to the phloem apoplast. Apoplastic routes are constrained by the limited plasma membrane surface areas of protophloem SEs and metaphloem SE/CC complexes and, hence, the transporter densities required to support efflux of nutrients (Table 15.6).

A major fraction of SE unloading likely occurs by bulk flow through plasmodesmata connecting SEs or SE/CC complexes with adjacent phloem parenchyma cells. The flow is driven by large hydrostatic pressure differences across this interface (Fig. 15.28). The canal diameters of these plasmodesmata could be as high as 8 nm, conferring a substantial increase (50- to 256-fold) in hydraulic conductivity over plasmadesmata of 2–3 nm in diameter (Equation 15.B5), which are found in other tissues. Thus, both hydrostatic pressure differences and plasmodesmal hydraulic conductances favor bulk flow (Equation 15.B4).

TABLE 15.6 *Putative plasma membrane (10^{-8} mol m^{-2} membrane surface area s^{-1}) and plasmodesmal (10^{-4} mol m^{-2} plasmodesmal cross-sectional area s^{-1}) fluxes of sucrose from protophloem SEs or metaphloem SE/CCs in a selection of growth and storage sinks.*

	Potential plasma membrane flux		Plasmodesmal fluxes between:		
Sink	**Putative**	**% contribution**	**SE or SE/CC–PPC**	**PPC–PPC**	**PPCvNVC**
Barely root protophloem (no CCs)	700	1.4	77	ND	ND
Elongating bean stem					
Protophloem	43	23	No PD connections with protophloem SEs		
Metaphloem	56	18	47	0.5	6
Mature bean stem	7	100	20	2	6
Developing seeds					
Wheat grain	553	1.8	16	10	10
Broad bean seed	194	5.2	23	7	14
Tomato fruit					
*Symplasmic	290	3.4	14	4	34
†Apoplastic	11.3	89	0.1	0.2	660

Putative sucrose fluxes estimated from dry weight gains, accounting for respiratory losses, of each importing organ. In addition, each flux estimate is derived on the grounds that all sucrose moves through the specified membrane or interconnecting plasmodesmatal cross sectional areas measured from histological sections.
Percentage maximal contribution to total membrane flux capped by maximal capacity for facilitated membrane transport of 10×10^{-8} mol m^{-2} s^{-1}. For example, % contribution of the plasma membrane flux for barley root protophloem is $(10/700 \times 100) = 1.4\%$. In contrast, the putative plasma membrane flux across the phloem of a mature stem of 7×10^{-8} mol m^{-2} s^{-1} is within the maximal capacity for facilitated membrane transport of 10×10^{-8} mol m^{-2} s^{-1} and hence the contribution of membrane transport is 100%. Reported range of plasmodesmal sucrose fluxes – 2 to 84×10^{-4} m^{-2} plasmodesmal cross-sectional area per second.
PPC, phloem parenchyma cell; NVC, nonvascular cell; ND, no data.
*Pre-maximal phase of sugar accumulation.
†Maximal phase of sugar accumulation.

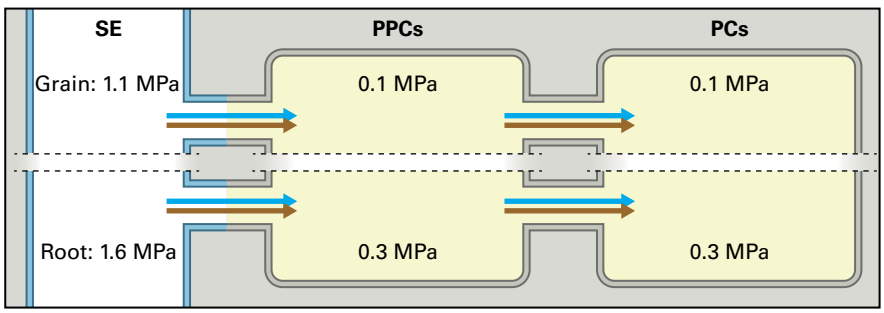


FIGURE 15.28 *Hydrostatic pressures of symplasmic unloading routes. Measured (SEs in grain and roots; PCs, root ground cells) or estimated (PPC, phloem parenchyma cell of grain and roots; PCs, maternal cells of grain) hydrostatic pressures in root apices and coats of developing wheat grains respectively show pronounced pressure differences (1.0–1.3 MPa) between SEs and adjoining cells (PPC; PC). In contrast, intercellular hydrostatic pressure differences along post-SE unloading pathway (see Fig. 15.27) tend to be minimal. Arrows indicate anticipated flows of nutrients (brown) and water (blue).*

15.4.14 For post-SE transport, a symplasmic route is the common but not universal pathway

Structural precedents exist for symplasmic unloading in all sink types, as indicated by plasmodesmata connecting SEs through to sink cells (Fig. 15.27). This pathway is characterized by a putative symplasmic constriction (i.e., low plasmodesmal densities) located at SE/ or SE-CC/phloem parenchyma cell boundaries causing the steep osmotic gradients across these boundaries (Table 15.6). These interconnecting plasmodesmata are transport-capable, as shown by passage of phloem-imported, membrane-impermeant fluorochromes.

During development, shifts between apoplastic and symplasmic routes occur in root apices, tubers, and fleshy fruits

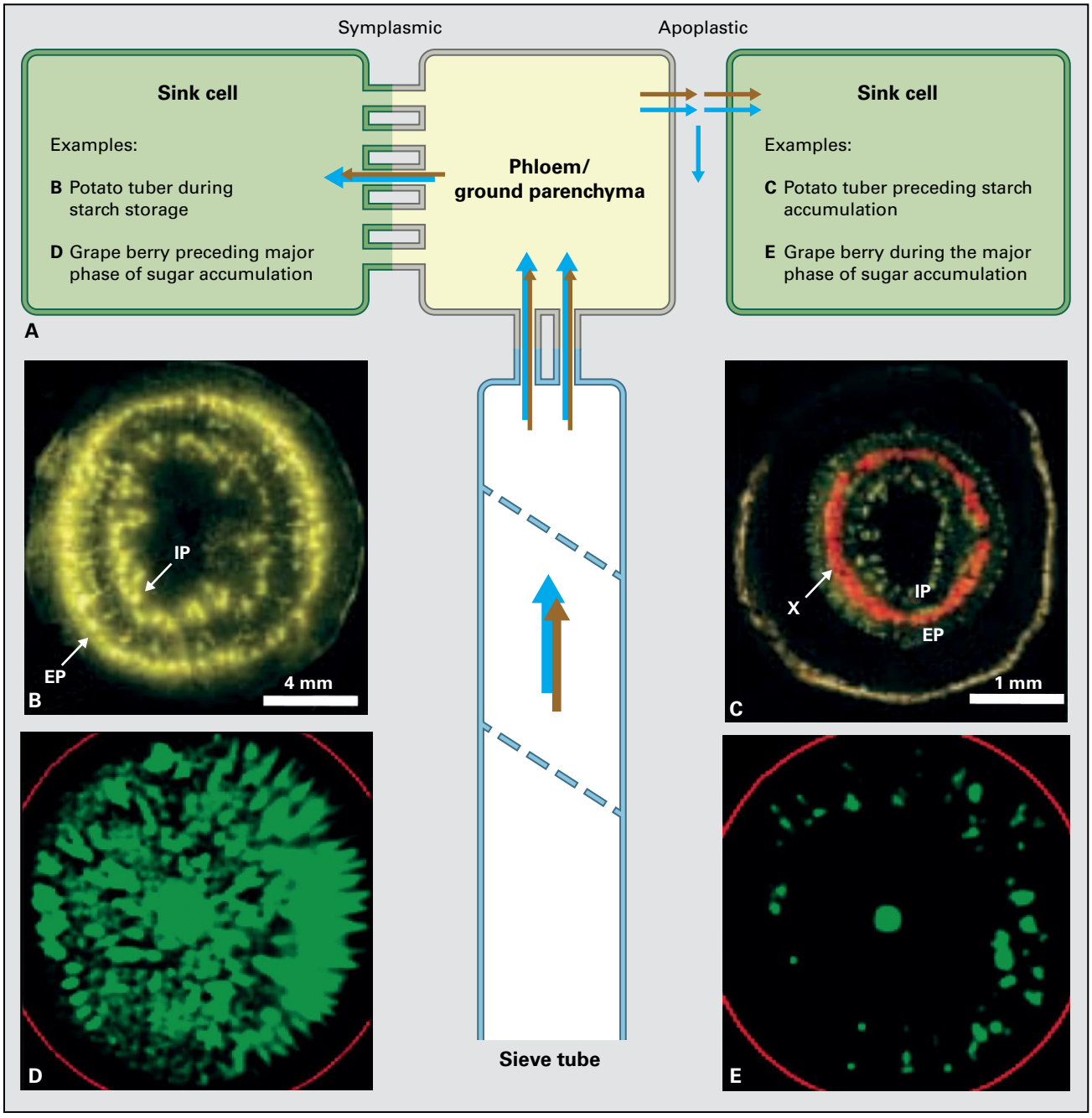


FIGURE 15.29 *Developmentally programmed plasmodesmal gating in phloem unloading pathways. (A) Phloem-delivered water (blue arrows) and dissolved nutrients (brown arrows) are unloaded symplasmically from SEs into phloem parenchyma cells by bulk flow that may continue into ground parenchyma cells. Post-SE flows may be symplasmic (A, left) or include an apoplastic step (closed plasmodesmata) (A, right). Water may flow into expanding sink cells (horizontal blue arrow) or be re-cycled to the mature plant body through the xylem (vertical blue arrow). (B–E) Histological cross-sections showing distribution of phloem-imported carboxyfluorescein (CF) in: (B, C) Developing potato tubers prior to (C), and following (B), onset of starch accumulation during which time CF was restricted to (B), or disbursed from (C), internal (IP) and external (EP) phloem respectively. Xylem (X) is C stained with Texas Red dextran. (D, E) Developing grape berries (*Vitis vinifera*) prior to (D), and during (E), their major phase of sugar accumulation during which CF moved symplasmically from (D), or was retained by (E), berry vascular bundles. Source*: (B, C) Viola et al. Plant Cell 13:385–396. (D, E) Zhang et al. (2006). Plant Physiol. 142:220–232.

(Fig. 15.29A). Before tuber initiation in potato stolons, plasmodesmata are closed and nutrient unloading from SE/CC complexes is apoplastic (Fig. 15.29C). Coincident with tuber swelling, internal and external phloem strands of tubers commence to unload symplasmically (Fig. 15.29B). Developing tomato (*Solanum lycopersicum*) fruit and grape (*Vitis vinifera*) berries exhibit a reverse behavior, with phloem unloading switching from symplasmic to apoplastic pathways (Fig. 15.29D,E). Thus, symplasmic unloading is linked to polymer formation and apoplastic unloading with elevated intracellular sugar levels. Collectively, plasmodesmal gating along unloading pathways confers flexibility in regulating nutrient fluxes as sink function alters across development.

15.4.15 Nutrient movement occurs by a combination of diffusion and bulk flow through symplasmic pathways during post-SE unloading

A concentration gradient of a major osmotic solute translates into an osmotic pressure gradient. Thus, post-SE symplasmic unloading of nutrients includes diffusion and bulk flow components (Box 15.1). Their relative contributions depend upon the path conductances and driving forces for each transport mechanism.

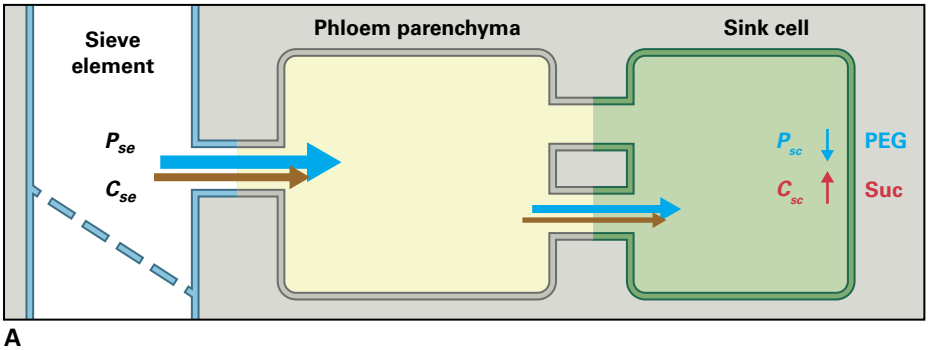
Nutrient unloading by diffusion may be linked to sink cell metabolism and intracellular compartmentation, as these processes determine nutrient concentrations in the cytosol and concentration gradients from SEs to sink cells. A similar linkage is predicted for bulk flow in growth and polymer storage sinks, where metabolic interconversion to nonosmotic species maintains a low cell osmotic and hydrostatic pressure (Fig. 15.30A).

Consistent with diffusion contributing to unloading, photoassimilate import rates into root tips and stems immersed in sucrose solutions are inversely related to bath sucrose concentrations. Similarly, photoassimilate import responds inversely to alterations in sink cell hydrostatic pressures of developing seeds, root tips, and stems (Fig. 15.30B).

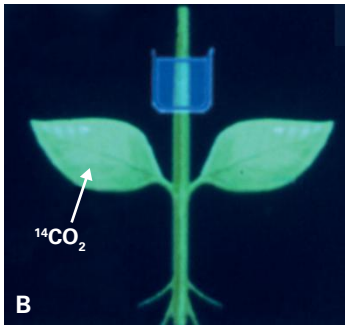
15.4.16 An apoplastic step occurs in certain post-SE unloading pathways

Nutrients traversing post-SE unloading pathways encounter symplasmic discontinuities at the interfaces between maternal seed coat and filial endosperm/embryo of developing seeds, in fleshy fruits, and in biotrophic relationships such as those formed between plant hosts and mycorrhizal or pathogenic fungi.

Once sugar accumulation commences in developing tomato fruit and grape berries, a symplasmic discontinuity develops at



A



Unloading responds to alterations in $C_{se} - C_{sc}$ (↑) or $P_{se} - P_{sc}$ (↓)

	Localized stem treatments		
	Sorbitol	Sucrose	PEG
^{14}C photoassimilate (dpm/2-cm stem)	1641	211	4699

FIGURE 15.30 *Symplasmic phloem unloading may be mediated by a combination of intercellular differences in hydrostatic pressure (bulk flow; $P_{se} - P_{sc}$) and/or sucrose concentrations (diffusion; $C_{se} - C_{sc}$ and see Equation 15.B1). (A) This proposition can be tested experimentally by increasing intracellular sucrose (C_{sc}) concentrations in, or lowering hydrostatic pressure (P_{sc}) of, sink cells by exposing these respectively and separately to solutions containing sorbitol, sucrose or polyethylene glycol (PEG; 8 kDa) at identical osmolalities. Sucrose is readily taken up thus increasing intracellular sucrose concentration in sink cells (C_{sc}) and hence lowering differences in sucrose concentration between SEs and sink cells ($C_{se} - C_{sc}$). A molecular size of 8 kDa prevents PEG from penetrating cell walls. Hence PEG exerts a local effect on the outermost cell layer by osmotically withdrawing cellular water. Consequently hydrostatic pressures (P_{sc}) are lowered thus increasing the hydrostatic pressure difference between SEs and sink cells (i.e., $P_{se} - P_{sc}$). A sorbitol solution of identical osmotic concentration is used to control for extracellular osmotic effects of sucrose. Both molecules permeate the stem apoplast resulting in no change in hydrostatic pressure difference between SEs and outermost cells (i.e., $P_{se} - P_{sc}$). Increasing C_{sc} would slow photoassimilate unloading by diffusion while decreasing P_{sc} would accelerate photoassimilate unloading by bulk flow. Arrows indicate movement of sucrose (brown) and water (blue) through a symplasmic unloading-pathway. (B) Experimental test of model proposed in (A) using accumulation of ^{14}C-labelled photoassimilates in bean* (Phaseolus vulgaris) *stems as a measure of phloem unloading. Bath solution containing sucrose, sorbitol or PEG held in wells positioned around the treated stems. Following several hours for equilibration with bath solutions, a source leaf is exposed to a pulse of $^{14}CO_2$ (left hand panel). Levels (dpm, disintegrations per minute) of ^{14}C-photoassimilates (i.e. primarily transported as sucrose) accumulated in treated stem portions provide measures of phloem unloading. The findings show increasing C_{sc} inhibits photoassimilate accumulation consistent with unloading by diffusion (cf. sorbitol treatment). In contrast, decreasing P_{sc} caused elevated photoassimilate accumulation (cf. sorbitol) indicating bulk flow drove unloading under these conditions.*
Source: (B) Patrick & Offler (1996). Journal of Experimental Botany 47:1165–1178.

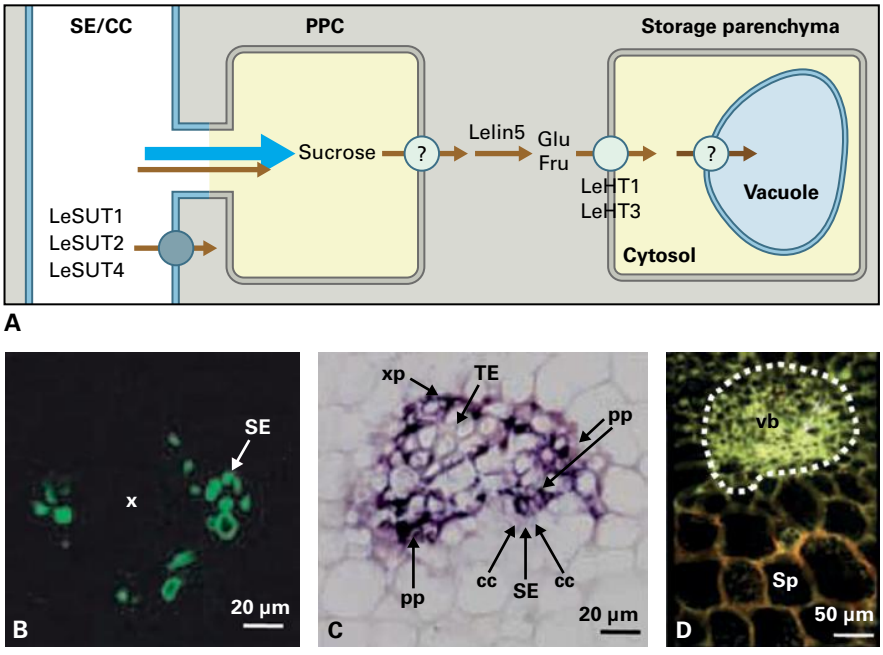


FIGURE 15.31 *Pathway of phloem unloading and sugar transporter localization in developing tomato fruits. (A) Diagrammatic representation of the cellular pathway of phloem unloading. Sucrose efflux to fruit apoplast could occur by reversal of SUTs on SEs (see text) or through yet to be identified transporters in phloem parenchyma cells following symplasmic transport from SE/CC complexes by bulk flow (sucrose brown arrow; water blue arrow). An extracellular invertase (Lelin5) hydrolyzes released sucrose. Resulting hexoses are accumulated from the fruit apoplast into storage parenchyma cells by hexose/H^+ symport mediated by LeHT1 and LeHT3. Vacuolar compartmentation of hexoses is mediated by proton antiport across the tonoplast possibly by a tonoplast monosaccharide transporter. (B–D) Cellular localization of key sugar transport proteins and an extracellular invertase. (B) Immunolocalization of LeSUT1 to SEs (green fluorescence). (C)* In situ *hybridization detected* LeLin5 *transcript in phloem parenchyma cells (pp). xp, xylem parenchyma. (D)* In situ *hybridization detected* LeHT3 *transcript colocalized to storage parenchyma cells (Sp and note orange signal) with H^+-ATPase to create the* pmf *to drive hexose symport. These transporters were absent from vascular bundles (vb and delimited by a white broken line) suggesting nonenergized unloading of sugars to the fruit apoplast.*
Source: (B) Hackel et al. (2006). Plant J. 45:180–192. (C) Jin et al. (2009). Plant Cell 21:2072–2089. (D) Dibley et al. (2005). Funct. Plant Biol. 32:777–785.

the vascular bundle/storage parenchyma interface in tomato (Fig. 15.31) and SE/CC complex/phloem parenchyma cells in grape (Fig. 15.29E). Symplasmic isolation of vascular and sink tissues ensures that elevated hydrostatic pressures or sugar concentrations in sink cells (e.g., 1 M hexoses in grape berries) do not compromise hydrostatic pressure or concentration differences driving photoassimilate import into these sinks. Dye-coupling experiments show that symplasmic continuity exists between importing SEs and nonphloem tissues in coats of developing seeds, but a symplasmic discontinuity exists at their coat/embryo interfaces (Fig. 15.32A). As a consequence in all examples described above, two plasma membrane transport steps are recruited: nutrient release into, followed by retrieval from the sink apoplast.

15.4.17 Nutrient release into and retrieval from the sink apoplast may occur during passage through post-SE unloading pathways

Simple diffusion, facilitated diffusion, and energy-coupled transport (see Box 15.2) have been proposed as mechanisms for nutrient release across efflux cell plasma membranes to sink apoplasts.

Predicted membrane fluxes by simple diffusion (Equation 15.B8) account for 50% of the observed sucrose flux direct from SE/CCs of tomato (*Solanum lycopersicon*) fruit, but less than 25% of the total membrane flux of sucrose from bean (*Phaseolus vulgaris*; *V. faba*) seed coats (Table 15.7). The unaccounted portion of these membrane fluxes must be facilitated (Equation 15.B9). In this context, SUTs and SUFs (sucrose facilitators) localize to efflux cells of fleshy fruits and inner coat cells of developing seeds (Figs. 15.31 and 15.32, respectively). If potential energy of the transmembrane sucrose concentration difference exceeds that of the *pmf,* sucrose/H^+ symporters can function in an efflux mode (Equation 15.B11). For example, in developing seeds and fleshy fruit containing extracellular invertase activity (Figs. 15.31 and 15.32), sucrose concentrations in their apoplastic saps are 1 mM or less, and efflux cells have *pmf*s of –100 mV. Using these values in Equation 15.B11 predicts a cytosolic sucrose concentration of 48 mM, at which a SUT would reverse to facilitate sucrose efflux. Thus, under these conditions, SUT reversal is plausible as ST sap concentrations are an order of magnitude higher.

In sinks lacking extracellular invertase activity (e.g., storage phase grain legume and temperate cereal grain) or sinks importing polyols not hydrolyzed by invertase (e.g., apple fruit), sugar symporter reversal is an unlikely unloading mechanism. In these cases, predicted intracellular sugar

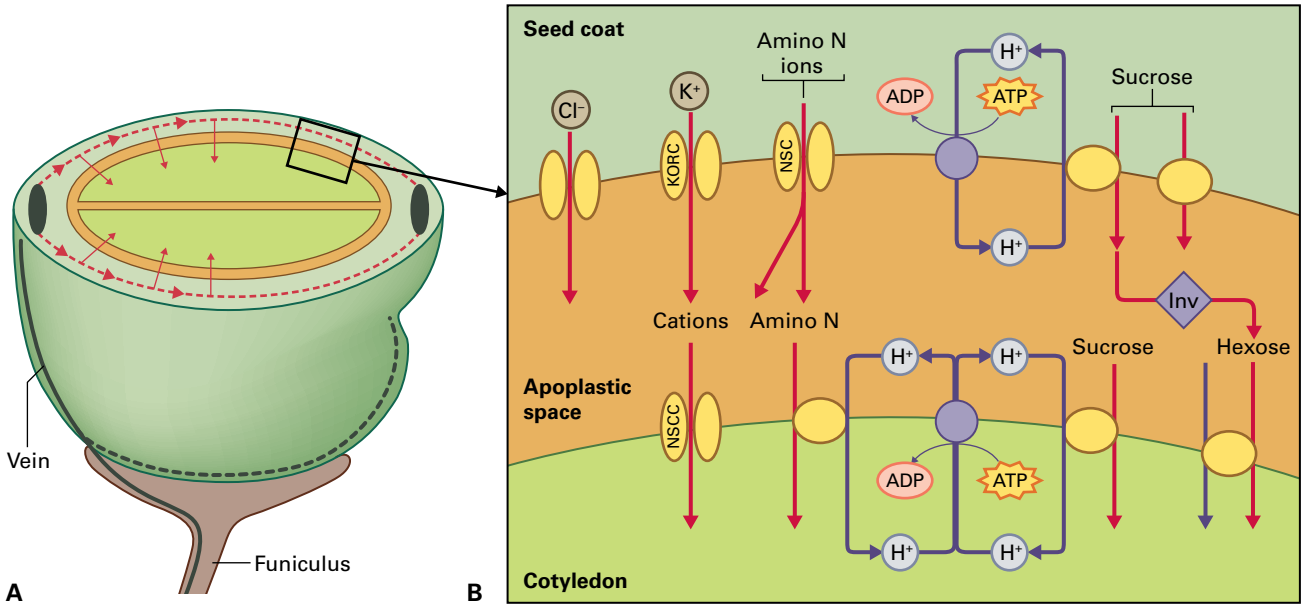


FIGURE 15.32 *Nutrient movement to, and membrane transporters operating at, coat/embryo interface of developing legume seeds. (A) Diagrammatic representation of a broad bean (*Vicia faba*) seed showing chalazal (gray solid line) and smaller lateral (gray broken line) veins, continuous with the parental vasculature entering through the funiculus, forming a single vascular ring around the seed coat equatorial region. Phloem-imported nutrients are unloaded symplasmically and spread circumferentially around the seed coat (red broken line) before moving radially inward to the apoplastic space between seed coat and cotyledon (red arrows). (B) Diagram illustrating known membrane transporters (yellow symbols) responsible for exchanging phloem-imported nutrients from seed coat to cotyledons. Membrane transport to, and from, seed apoplastic space occurs in specialized cells that in some species exhibit transfer cell morphologies. Both maternal and filial transport cells are energized by H^+-ATPases (purple symbols) that generate the* pmf *to drive sucrose/H^+ antiport from seed coats, and proton-coupled symport of amino N compound and sugars into cotyledons. Sucrose facilitators are present in unloading cells of seed coats along with ion channels including ones exhibiting specificities for K^+ (K outward rectified channel – KORC) and chloride as well as a nonselective channel (NSC) capable of transporting large molecular weight compounds. A nonselective cation channel (NSCC) occurs in cotyledon loading cells. An extracellular invertase (Inv) is only present during the pre-storage phase of seed fill.*

TABLE 15.7 *Predicted* and estimated† fluxes of sucrose across plasma membranes of putative unloading cells to the sink apoplast in developing seeds and fleshy fruit.*

Sink organ and unloading cell types	Transmembrane concentration difference (mM)	*Predicted flux by simple diffusion (10^{-8} mol m^{-2} s^{-1})	†Estimated flux (10^{-8} mol m^{-2} s^{-1})
Wheat grains			
Nucellar projection transfer cells	50	0.5	2.2
French bean seed coats			
Ground parenchyma cells	10	0.1	8.8
Broad bean seed coats			
Thin-walled parenchyma transfer cells	40	0.4	7.0
Tomato fruit			
SE/CCs	500	5.0	11.1
PPCs	100	1.0	10.4

*Predicted sucrose flux by simple diffusion = membrane permeability coefficient × transmembrane concentration difference. Lipid membrane permeability coefficient for sucrose ≈10^{-10} m s^{-1}.
†Estimated membrane fluxes determined from measurements of total plasma membrane surface areas and rates of sucrose import computed from biomass gains and respiratory losses.

concentrations (Equation 15.B11) required to reverse symporter activity are nonphysiologically high. In this context, AtSWEET, 11, 12, and 15 sucrose effluxers account for a proportion of sucrose released from seed coats. The remaining sucrose flux might be energized by sucrose/proton antiport. In addition to sucrose, large quantities of mineral nutrients, notably K^+ and Cl^-, are released through membrane channels from legume seed coats to the seed apoplast (Fig. 15.32B).

Similar to apoplastic phloem loading (see Section 15.4.6), much more is known about nutrient retrieval from sink apoplastic spaces. In developing seeds, high densities of membrane transporters, together with H^+-ATPases, colocalize to the outermost cell layers of their filial tissues (endosperm; embryo) that abut sites for nutrient release in coats (Fig. 15.32B). Reverse genetics demonstrate that amino acid and sucrose/H^+ symporters play a crucial role in biomass gain by seeds. For example, knockdown of *OsSUT1* expression resulted in a shriveled grain phenotype in rice. Overexpression of a potato sucrose/H^+ symporter (*StSUT1*) in *Pisum sativum* cotyledons enhanced rates of sucrose influx and biomass gain. Similarly, overexpression of *PsAAP1* in *P. sativum* seeds resulted in higher seed protein levels.

15.4.18 Phloem unloading also includes a flow of water

For growth sinks, imported phloem sap is the principal source of water for cell expansion, providing a direct link between phloem import and growth.

For storage sinks in which expansion growth has ceased, imported phloem water is recycled back to the mature plant body through the xylem following membrane exchange to the sink apoplast, possibly via aquaporins (Fig. 15.33). Such a system necessitates separation of nutrient and water flows at some point. Where ST saps are unloaded symplasmically, imported water could be exchanged to the sink apoplast along phloem unloading routes while imported nutrients are retained in the sink symplasm. Separation of water and nutrient flows are more critical in sinks in which an apoplastic step occurs in post-phloem unloading pathways (Figs. 15.31 and 15.32). Here, several strategies prevent imported nutrients released to sink apoplasts from being swept back to the parent plant body in water recycled to the xylem (Fig. 15.33).

15.5 Whole-plant organization of xylem transport

15.5.1 The cohesion-tension mechanism accounts for the ascent of sap

During transpiration, water evaporates from moistened cell walls lining the gas-filled spaces in leaves and then diffuses out of the leaf as vapor via open stomata. Surface tension in micropores of cell walls places water under tension. For a capillary of diameter 0.01 μm, such as those existing in leaf mesophyll cell walls, a tension of –15 MPa can occur. This is transmitted to water in TEs and down to root surfaces and soil solution. Thus, ascent of TE sap results from water being pulled along a continuous liquid pathway to leaf cell walls. This continuous unbroken file of water is aptly named the soil–plant–atmosphere continuum.

Air gaps in TEs cannot support large tensions necessary to counteract gravity and drive flow. Even the smallest diameter TEs (10 μm) can only maintain a height of 3 m by capillarity. Continuous water columns can only maintain a tension by virtue of cohesion through hydrogen bonding between water molecules. Centrifugation of water-filled capillaries and other measurements demonstrate that water can maintain tensions to –21 MPa, adequate to counteract gravity in tall trees.

Tensions within TEs and a continuous water column are crucial requirements of the cohesion–tension mechanism. Experimental observations have sometimes challenged these requirements but may suffer from disturbance of xylem tensions during measurement. The consensus is these tensions exist consistent with the cohesion–tension theorem, and controversy over the theorem relates more to the magnitude of the tensions rather than whether they exist, which is not in question. Recently an "artificial" tree was constructed using synthetic hydrogels to simulate microporous membranes in roots and leaves, connected by a microfluidic system with pore diameters between 11 and 73 μm and lengths up to 35 cm, similar to that of xylem vessels. Bulk flow through this system was demonstrated with tensions established in the "leaf" of up to –1.0 MPa (Fig. 15.34).

15.5.2 Cavitation is the Achilles heel of the cohesion–tension mechanism

TEs must remain filled with liquid water for sap ascent. Tension of continuous, water-filled TEs is in a metastable state that can rapidly switch to a different state if a gap is created consisting of water vapor in equilibrium with the remaining liquid water. This sudden reversal to vapor state is referred to as cavitation. Eventually air leaks into cavitated TEs, and pressure rises to atmospheric to cause an embolism. As TEs are progressively embolized, those that remain filled may be placed under increased tension because there are fewer available to supply water.

The initial sudden release of tension can be recorded as an acoustic event (AE) (Fig. 15.35), and the accumulative sum of AEs correlate with loss of hydraulic conductance. A sigmoidal curve generally describes cumulative AEs and loss of conductance with xylem tension. These xylem vulnerability curves can be used to define pressures at which 50% loss of hydraulic conductance (50% percentage loss of conductance, PLC) occurs as a measure of cavitation vulnerability. Species exhibit different values of xylem pressure at 50% PLC, reflecting water potential ranges encountered in the environment (Fig 15.35C) or different strategies of stomatal regulation (isohydric, where water potential at midday is maintained relatively constant

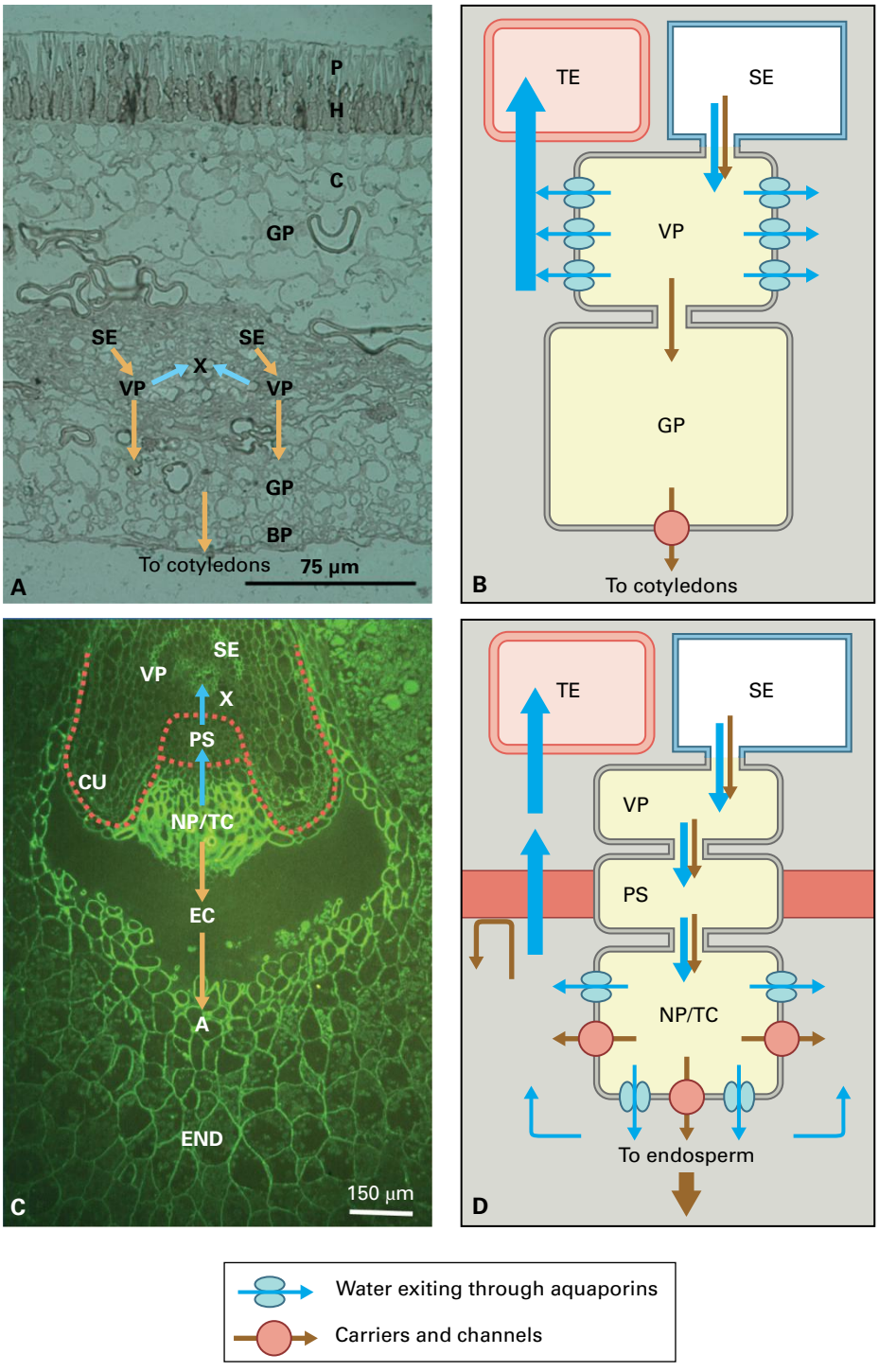


FIGURE 15.33 *Strategies to separate phloem-imported water from nutrient movement to embryo/endosperm of developing seeds and return water to xylem for re-export. (A, B) Water (blue arrows) and nutrient (brown arrows) flows in coats of developing* P. vulgaris *seeds. (A)* In situ *localization of* PvPIP2,3 *(aquaporin) expression in vascular (VP) and ground (GP) parenchyma (radially inward of vascular bundle only) cells with strongest expression in VP as indicated by darkened cytoplasms (compare with GP above VP). BP, branch parenchyma; C, chlorenchyma; H, hypodermis; P, palisade layer; SE, sieve element; X, xylem elements. (B) Model of post-phloem nutrient and water flows. Symplasmic unloading from SE to VP by bulk flow (blue arrows alongside brown arrows). Water exits from VP through aquaporins and returns to xylem TEs down a water potential gradient for re-export. Nutrients diffuse to GP for release to seed apoplast through carriers and channels for onward movement to enclosed cotyledons (see Fig. 15.31B). (C, D). Water (blue arrows) and nutrient (brown arrows) flows in developing wheat grains. (C) Immunohistochemistry of sucrose transporters by treating section with a generic SUT antibody demonstrating these transporters are localized to sieve elements (SE), vascular parenchyma (VP), nucellar projection transfer cells (NP/TC) and aleurone (A). Dotted red line demarcates location of a water-permeable apoplastic barrier deposited in cell walls of the cuticular layer (CU) and pigment strand (PS). The apoplastic barrier separates crease vascular bundle (comprised of SE; VP, vascular parenchyma cells) from an apoplastic compartment containing NP/TC, the endosperm cavity (EC) and endosperm (END). The endosperm accumulates imported sucrose as starch (note large starch grains in END). (D) Model of post-phloem nutrient and water flows. Symplasmic unloading from SEs to VP by bulk flow that possibly extends through the PS to NP/TC. Here water and nutrients exit via aquaporins and nutrient transporters respectively. Water returns to xylem TEs down a water potential gradient for re-export to the parent plant through a water-permeable, but nutrient impermeable, apoplastic barrier deposited in walls of PS and CU cells (dark red). Source*: (A) Zhou et al. (2007). Plant Cell Environ. 30:1566–1577. (C) Bagnall et al. (2000). Aus. J. Plant Physiol. 27:1009–1020.

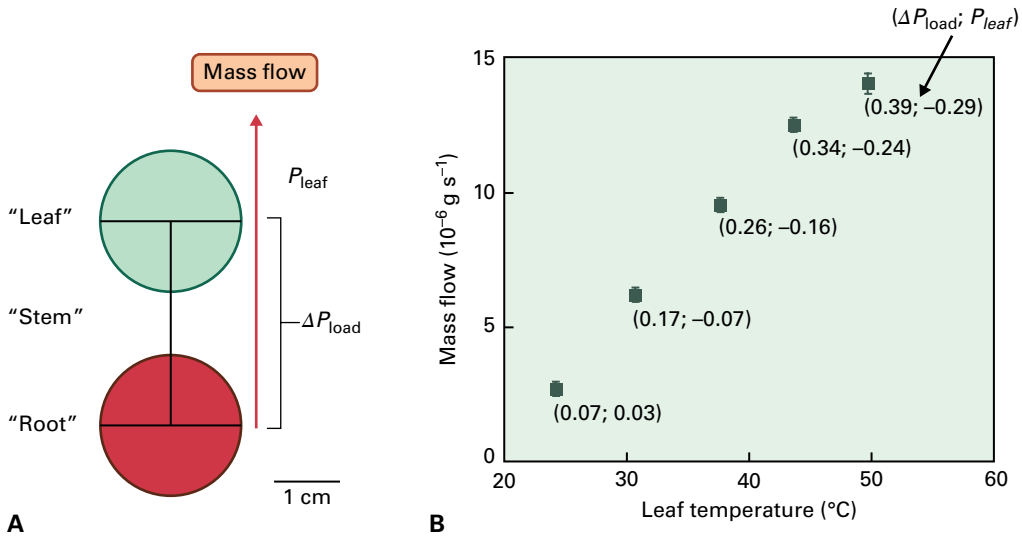


FIGURE 15.34 *A synthetic tree demonstrating bulk flow and substantial tensions in "leaves" and "conduits". (A) Synthetic tree comprising a leaf and root network (pHEMA hydrogel, colored in the diagram green and red respectively). Veins consist of 80 parallel channels of varying length arranged to form a circle (for both "leaf" and "root") and are connected by a single "stem vessel" (internal diameter ≈10 μm). (B) Bulk flow as a function of temperature applied to the "leaf". As temperature is elevated there is greater transpiration from the "leaf" and greater bulk flow through the system. Shown against each point is the pressure difference in MPa across the "Stem" (ΔP_{load}) and negative pressure (P_{leaf}) that develops at the entrance to the leaf vein network.*

with falling soil water content versus anisohydric, where water potential at midday is allowed to decline with falling soil water content). Emboli decrease TE hydraulic conductance and ultimately limit carbon gain because stomata close to prevent further cavitation and leaf desiccation.

Freeze–thaw cycles also cause cavitation. Dissolved air can come out of solution during freezing and, when thawing occurs and tensions develop in TEs, air bubbles expand to form embolisms. Plants that grow in freezing environments must refill TEs or have new TEs produced by vascular cambia.

15.5.3 Cavitation occurs by "air seeding"

Cavitation can be initiated either by pulling air into TEs through their walls or by vaporizing water within conduits. Evidence supports the first mechanism, termed "air seeding," in which surface tension in the largest cell wall pores is overcome by tension within TEs to draw minute bubbles into the conduit. Air seeding can be simulated by increasing the air pressure in a collar around a piece of stem. As predicted by the air-seeding mechanism, externally applied pressure has the same effect on embolism formation as the equivalent xylem tension (Fig. 15.35A,C).

The most likely place for air entry is via pit membranes. Pore sizes in pit membranes are normally small enough to prevent air entry, but large tensions may distort pit membranes and cause damage to increase their pore size.

Bordered pits can act as valves that shut when there is a substantial pressure gradient across the pit (Fig 15.35D). In torus-margo pits, a central torus of lignified wall is pushed against the opening of the pit cavity (border), thereby sealing off the pit. This occurs when an embolized TE is adjacent to a functioning TE causing the torus to be appressed against the bordered pit of the functioning TE. This prevents air seeding of the functioning TE; however, under large tensions, the torus may be displaced across the opening and allow air to enter (Fig. 15.35D).

15.5.4 Embolized xylem can be repaired

TEs cavitate on a regular basis (Fig 15.35B) and must be refilled to allow transpiration to continue. Refilling appears to occur in some plants while transpiration proceeds, indicating that pressures in functioning TEs may be negative while refilling occurs. The mechanism is difficult to understand because physical principles dictate that the pressure must increase to force gas in bubbles back into solution. The gas must then diffuse from TEs driven by a gas concentration gradient. Pressures in gas bubbles will be above zero and higher positive pressures will increase the concentration gradient for diffusion. Models have demonstrated that gas bubbles can dissolve provided xylem pressures are more positive than about –0.1 MPa.

During the night, when transpiration slows or stops, significant positive pressure can develop in root xylem. This occurs by pumping ions into TEs to achieve lower water potential in TE sap than in surrounding soil. Water enters down the water potential gradient and increases TE pressures. Pressures of around 0.1 MPa can be measured for a detached distal segment of root connected to a pressure probe. These pressures are enough to force water up stems to heights of 10 m and could dissolve air in embolized TEs. This is an important mechanism for refilling TE in shrubs and herbs. It is not clear if trees use this mechanism.

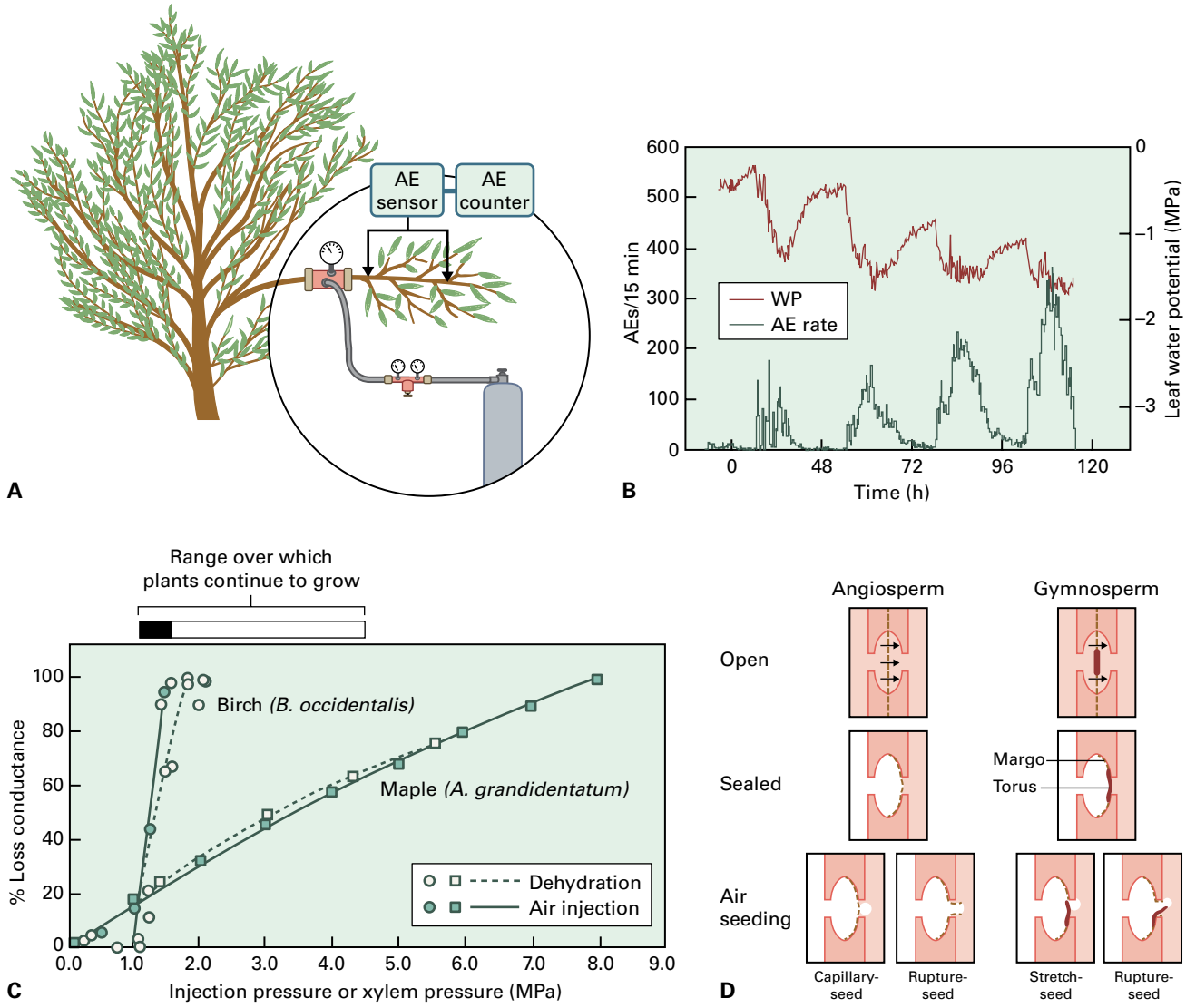


FIGURE 15.35 *Cavitation occurs by air seeding and is likely to occur through pit membranes. (A) Induction of cavitation by air injection. Air under positive pressure applied in a sealed collar around the branch causes cavitation identical to xylem tensions. Acoustic emission (AE) sensors and counters monitor progress of cavitation. (B) AE sensors monitor increasing cavitation frequencies in the petiole of a leaf during daylight as a plant is progressively drought stressed. As leaf water potential (WP) became more negative acoustic signals increase in frequency. (C) Xylem vulnerability curves for birch* (Betula) *and maple* (Acer)*. As branches dehydrate during drought and xylem tensions increase, cavitation causes a progressive loss of xylem function. The relationship between xylem tension and loss of xylem function differs between species, affecting conditions under which they can grow. This range is indicated by the solid bar for birch, and by the open bar for maple located above the graph. Xylem vulnerability curves developed by application of positive external pressures (see A) are similar to vulnerability curves caused by xylem tension. (D) Cavitation likely occurs through pit membranes. Angiosperms and gymnosperms differ in their pit architecture. Circular bordered pits are shown in transverse median section. Top: open configuration. Mid: sealed configuration where the embolized conduit is on the left. Bottom: Air seeding where a bubble escapes through damaged pit membrane (left) or via displacement of the torus from the pit opening (right).*

For refilling to occur during transpiration, there needs to be a local increase in pressure in embolized TEs. Evidence indicates a requirement for metabolic energy and a supply of water from the phloem for refilling to occur. It is clear from computer tomography images of refilling xylem that xylem parenchyma adjacent to vessels have a role in refilling. Four hypotheses have been put forward to account for local refilling: cell membrane osmosis, pit membrane osmosis, tissue pressure, and membrane asymmetry. All hypotheses evoke mechanisms for building pressure in embolized TEs, and all but the pit membrane osmosis mechanism envision an active role for xylem parenchyma cells in solute secretion and water movement into embolized TEs and a requirement that embolized TEs are hydraulically isolated from other conducting TEs under tension. Again properties of pits and pit membranes appear to be central, as these must be sites of hydraulic blockade so that pressure can be elevated in embolized TEs. Aquaporins have been implicated in the refilling process, since increased aquaporin gene expression in xylem-associated cells occurs when TEs are refilled after winter.

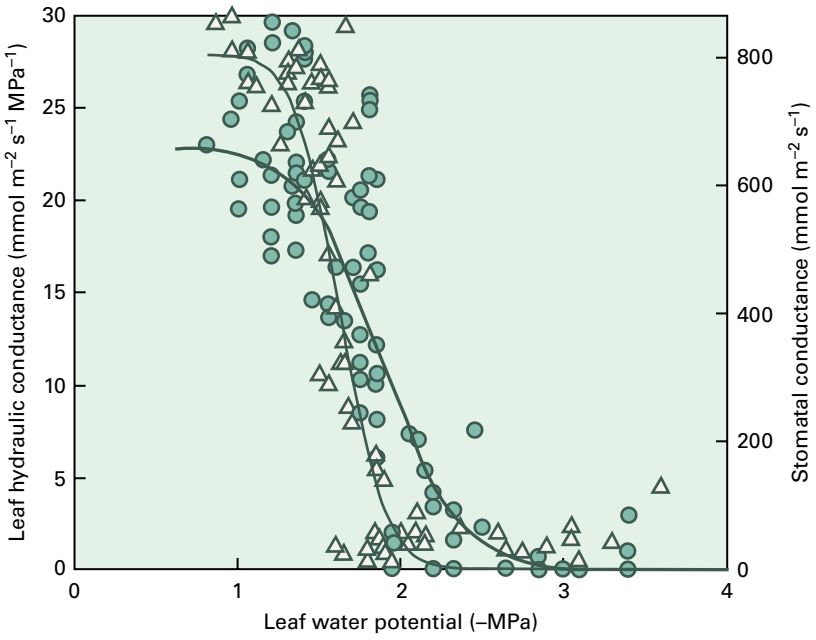


FIGURE 15.36 *Stomatal closure pre-empts significant loss of leaf hydraulic conductance as leaf water potential declines. Stomatal closure occurs during initial phases of leaf xylem cavitation. Stomatal conductance (triangles thin line) is a surrogate measure of stomatal aperture. Leaf hydraulic conductance (circles-bold line) includes leaf veins and pathways to sites of evaporation within leaves. Cavitation of veins results in loss of leaf hydraulic conductance. Data are from a tropical legume species.*

15.5.5 Cavitation can act as a hydraulic fuse and amplify water stress impacts in leaves

Although cavitation decreases TE xylem conductivity, it is not necessarily always deleterious. This is because cavitation tends to occur in xylem pathway extremities (i.e., in leaves and small branches), reducing transpirational water loss and protecting against dehydration of critical pathways such as stems and major roots. To some extent, a greater tendency towards cavitation in smaller branches might be anticipated, because xylem pathway termini have the lowest water potentials and these are magnified by increases in TE resistances toward these sites. Hydraulic resistances of leaves can account for 30–80% of whole plant hydraulic resistance. TE cavitation in leaves can cause rapid leaf dehydration and stomata seem to be highly responsive as judged by a close association between leaf xylem vulnerability to cavitation and stomatal closure (Fig. 15.36).

Sensitivity of leaf water status to carrying capacity of petiolar xylem is demonstrated by the pea *ramosus2* (*rms2*) branching mutant where wilting occurs under high evaporative demand. This phenotype is due to reduced diameters of TEs in their petioles where the Hagen–Poiseuille law indicates a drastic reduction in hydraulic conductivity (Equation 15.B5 and Fig. 15.37A,B). Under high evaporative demand, decreased petiole conductivity requires a much lower leaf water potential to drive water flow, and this low leaf water potential reduces leaf turgor pressure, as evidenced by a lowered relative water content and wilting compared to wild-type plants (Fig. 15.37C).

15.5.6 Integration of conductivities and xylem efficiencies enhance water transport

Decreased TE susceptibility to cavitation is one of several factors allowing plants to maintain water balance. Others include stomatal response, leaf abscission, root–soil interactions, and patterns of seasonal growth. Strategies may differ in different environments and, even in the same environment, different strategies may achieve the same goal. An example of some of the trade-offs that may occur is evident in xylem vulnerability curves shown for maple (*Acer*) and birch (*Betula*) (Fig. 15.35C). Both species grow in moist environments, but maple also can grow in drier conditions. As xylem tension increases in birch, stomata must close promptly after cavitations begin if rapid loss of xylem function is to be avoided. This stomatal behavior has been observed, and birch xylem remains more than 90% functional in the field. In maple, stomata remain open to much lower water potentials without fully losing xylem function; in drier sites, 50% of maple xylem may be embolized.

Coordination of conductances between roots and shoots is also important to keep stem and leaf water potentials within acceptable ranges. If roots are unable to supply water demanded by shoots, stem water potentials decrease and could trigger excessive cavitation and wilting. Counterintuitively, this can occur after water logging in soil, which starves roots of oxygen. Oxygen starvation decreases cytosolic pH in root cells, and as a result, most plasma membrane aquaporins close. Sudden reductions in root hydraulic conductivity starve shoots of

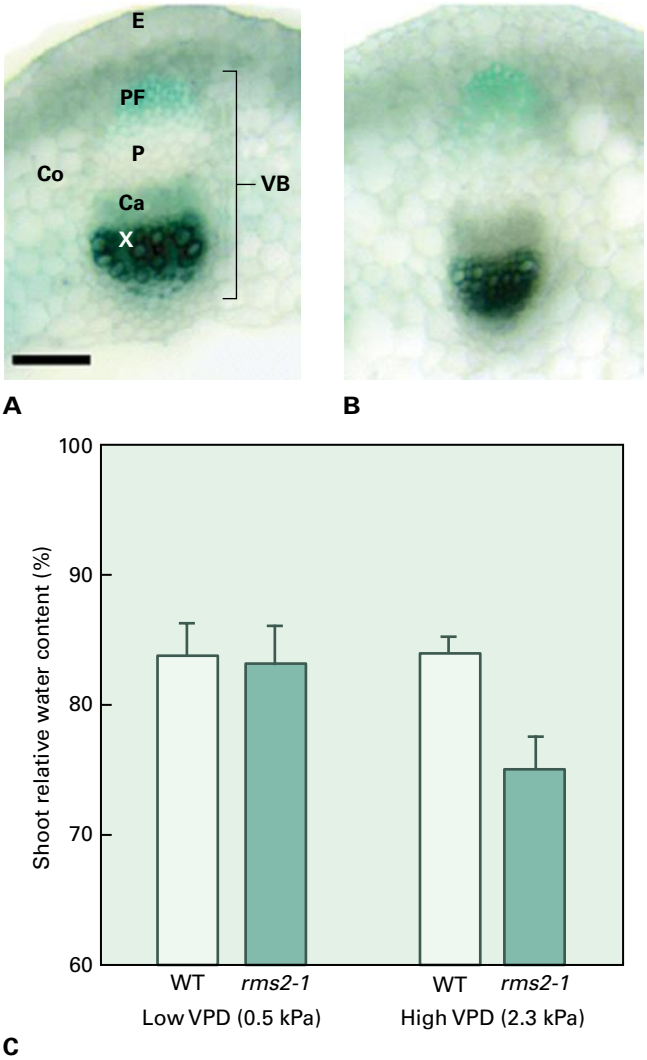


FIGURE 15.37 *Petiole hydraulic conductance can restrict water flow to leaves and cause increased sensitivity to water stress. The* rms2-1 *mutant of pea has increased branching but also shows transient wilting when plants are exposed to high vapor pressure deficits (VPD) that increase evaporation rates from leaves. (A,B) Petiole cross-sections from uppermost-expanded leaf stained to visualize xylem vessels (dark green) of (A) Wild type and (B)* rms2-1 *mutant plants. Total xylem area and TE diameter is reduced in* rms2-1 *petioles, resulting in a substantial decrease in hydraulic conductance. Bar = 100 μm. Ca, cambium; Co, cortex; E, epidermis; P, phloem; PF, phloem fibers; VB, vascular bundle; X, xylem. (C) Relative water content of shoot apices of WT and rms2-1 plants under low and high vapor pressure deficits. A decrease in relative water content occurs when water loss exceeds water uptake and leaves wilt.*
Source: Dodd et al. (2008). Plant Cell Physiol. 49:791–800.

sufficient water supply, causing plants to quickly wilt. Root-to-shoot signaling involving ABA transport in xylem can signal stomata to close under soil conditions not conducive to efficient water uptake by roots. Likewise, there appear to be shoot-to-root signals that match transpirational demand to the ability of roots to conduct water (Fig. 15.38). Clearly, this is a complex topic that cannot be pursued in detail here.

15.6 Whole-plant organization of phloem transport

15.6.1 The pressure-flow mechanism of phloem transport involves bulk flow between sources and sinks

In 1930, Ernst Münch published the first coherent concept of phloem transport in his outstanding book, *Die Stoffbewegungen in der Pflanze*. He advanced the pressure-flow hypothesis that phloem translocation occurs as a bulk flow driven by differences in hydrostatic pressure (P) between ST ends located in photoassimilate sources (P_{so}) and heterotrophic sinks (P_{si} and Fig. 15.39).

Fierce opposition to the pressure-flow hypothesis arose when EM observations found deposits occluding sieve pores. These deposits were considered to impose sufficiently low hydraulic conductances to prevent bulk flow accounting for observed rates of phloem transport. Subsequent and more refined studies showed sieve pore deposits to be artifacts of tissue fixation, and opposition to the pressure-flow hypothesis crumbled.

Bulk flow (see Box 15.1) through STs has been demonstrated using a number of experimental approaches, including concurrence between propagation velocities of heat (solvent) and transport of radiolabeled photoassimilates (solute). Recently, real-time transit imaging of phloem-mobile fluorochromes and monitoring displacement of water molecules by nuclear magnetic resonance have provided conclusive evidence that phloem transport occurs through STs by bulk flow (Fig. 15.40).

Although the pressure flow hypothesis has become an established concept, a number of caveats remain. For example, STs are shorter than the plant axis and flow between consecutively arranged STs must occur through lateral sieve plates. To what extent their sieve pore geometries and accompanying deposits of proteins and ER impact hydraulic conductances (Equation 15.B5) is uncertain but broadly are considered not to hinder bulk flow (see Section 15.6.3).

15.6.2 Water flows and equilibrium states within and beyond the phloem are crucial to nutrient translocation

Water flows into collection phloem through aquaporins and along water potential gradients that are generated by active nutrient loading of SE/CC complexes (see Section 15.4.8). The resulting elevated hydrostatic pressure drives longitudinal flows of phloem sap through the STs (Fig. 15.39).

Water inflow into collection and transport phloem is not affected by considerable diurnal fluctuations in leaf/stem water potentials (Fig. 15.41), suggesting collection and transport phloem maintain a constant water potential difference with surrounding tissues to ensure this steady inflow. Consistent

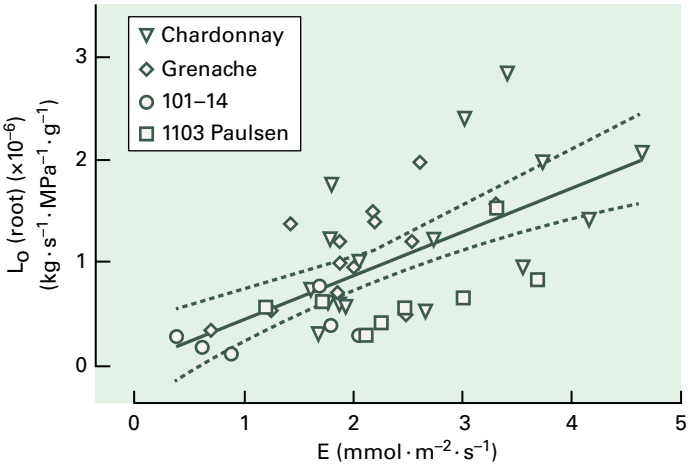


FIGURE 15.38 *Root capacity to import water from the soil as measured by root hydraulic conductance (L_o, y-axis) that is matched to shoot demand (transpiration, E, x-axis). This implies that signals are transmitted from shoot to root to coordinate water conductances. Root hydraulic conductance is normalized to root dry weight and measured using a flow meter attached to cut stumps of grapevine (*Vitis vinfera*) cultivars (listed to the right of graph) grown in pots. Immediately before measuring root conductances, transpiration rates of fully expanded leaves were recorded. Further measurements showed that root conductance was dependent on expression of aquaporins.*

with this proposition is the observation that collection and transport phloem is capable of hydrostatic pressure homeostasis, which it achieves through osmoregulation of nutrient loading from the phloem apoplast, which interchangeably relies on K^+ or sucrose transporters).

The rates at which SE unloads water and nutrients must match those of bulk flow through the transport phloem. Since diffusion of water and each nutrient species occurs independently at rates driven by their concentration gradients and diffusion coefficients (see Box 15.1), it is problematic that rates of diffusive water and nutrient unloading from these STs could be organized to match the rates of bulk flow into STs of release phloem. In contrast, symplasmic unloading by bulk flow ensures rates of import into and unloading from STs are matched. In addition, unloading STs by bulk flow into the larger cell volumes (ca. 10-fold) of surrounding phloem parenchyma cells allows hydrostatic pressure heads in STs to be dissipated (in analogy to gas laws $P_1V_1 = P_2V_2$) (Fig. 15.28). Overall, these considerations point to bulk flow being the likely mechanism for symplasmic unloading of SEs.

15.6.3 Sites of overall regulation along the transport pathway predicted by the Münch flow concept can be deduced from the variables determining bulk flow

Potential sites of regulation of phloem transport can be deduced from the variables determining bulk flow (see Box 15.1 and Fig. 15.39). Such an analysis identifies structural (ST hydraulic conductances; ST numbers in path cross-section) and physiological (hydrostatic pressure; nutrient concentration) properties of STs that could regulate rates of nutrient transport. Phloem path cross-sectional areas have attracted considerable interest based on an apparent limit to which nutrient fluxes could be supported (Fig. 15.39). However, for herbaceous plants, phloem path conductance (n L_0) does not exert a strong influence over nutrient translocation rates as illustrated by an experiment using *R. communis* (Fig. 15.42). The study also highlighted substantial regulation of phloem transport by sink hydrostatic back-pressures that, upon their dissipation by sink removal, caused considerable increases (10- to 20-fold) in phloem transport fluxes (Fig. 15.42A,B vs. C). Low plasmodesmal densities interconnecting SEs and phloem parenchyma cells of release phloem (Table 15.6) contribute to their correspondingly low hydraulic conductances. These in turn regulate symplasmic unloading, as reflected by large hydrostatic pressure differences located at these interfaces (Fig. 15.28). Thus, transport phloem can be thought of as a high-pressure manifold in which the hydrostatic pressure head is maintained by hydrostatic pressure-regulated loading of nutrients in collection and transport phloem. As a consequence, partitioning of nutrients between competing sinks is primarily controlled by hydraulic conductances of plasmodesmata linking SE/CC complexes with phloem parenchyma cells determining rates of phloem unloading (Fig. 15.43 and see Section 15.7.5).

Maintenance of a hydrostatic pressure difference between collection phloem and symplasmically connected sink cells focuses attention on phloem loading and unloading of major osmotic species to respectively raise and lower osmotic differentials between their cells and surrounding apoplasts (Fig. 15.39 and Equation 15.B7). In contrast, minor osmotic species have little influence on hydrostatic pressures and volume fluxes of water flowing through the transport pathway. Thus, for a given volume flux set by major osmotic species, phloem transport rates of minor osmotic species are solely determined by their concentration in ST sap arising from phloem loading and retrieval activities (Fig. 15.39). This is clearly illustrated by strong correlations found between concentrations of amino acids in ST saps and rates of amino N transport (Fig. 15.44).

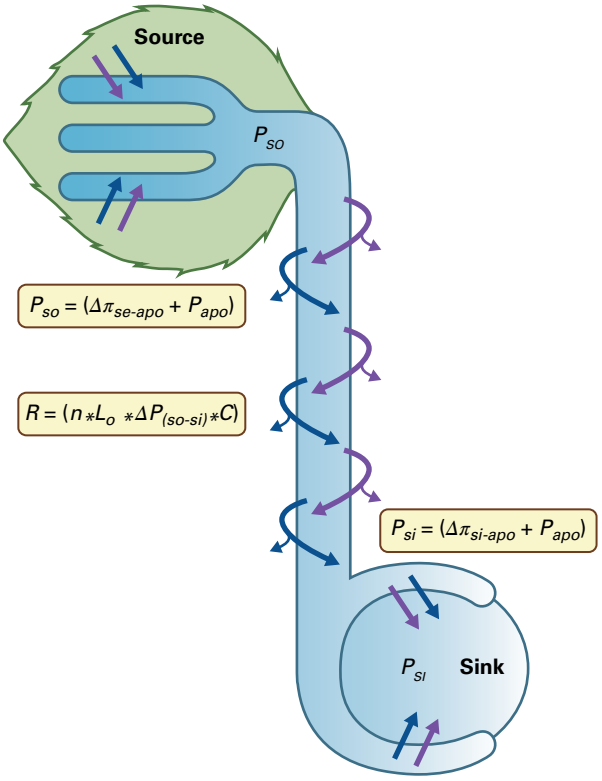


FIGURE 15.39 *Generation of pressure flow through sieve tubes. Driving force for bulk flow is determined by hydrostatic pressures (P) differences between source (P_{so}) and sink (P_{si}) ends of the transport pathway (i.e. ΔP_{so-si}). Since water approaches near equilibrium between SEs or sink cells and their surrounding apoplasts (apo), water potential of each cell is determined by the difference in P and osmotic pressures (π) as shown for SEs: $P_{se} - \pi_{se} = P_{apo} - \pi_{apo}$ (see Equation 15.B7) and hence $P_{se} = [(\pi_{se} - \pi_{apo})] + P_{apo}] = (\Delta\pi_{se-apo} + P_{apo})$. In source leaves, major osmotic species are loaded into STs to high concentrations so that π_{se} offsets transpiration-induced tensions in the leaf apoplast (P_{apo}) to drive water uptake and hence generate P_{so}. At sinks, exit of ST sap from STs occurs by bulk flow through plasmodesmata and, as a consequence, P_{si} is located in the post-SE unloading pathway (see Fig. 15.27). Since growth and storage sinks are hydraulically isolated from the remaining plant body, P_{si} is predominantly determined by $\pi_{si} - \pi_{apo}$ with P_{apo} exerting little influence. Thus phloem loading and unloading set the magnitude of $P_{so} - P_{si}$. Volume flow rate ($m^3\ s^{-1}$) of ST sap (see Equation 15.B4) is modulated by pathway hydraulic conductance (L_o and see Equation 15.B5) summed over number (n) of conducting units in a path cross-section. Radii of sink plasmodesmal canals are major determinants of L_o. Bulk flow rate (R) of a nutrient species is then a function of volume flow rate and concentration (C) of the transported nutrient.*

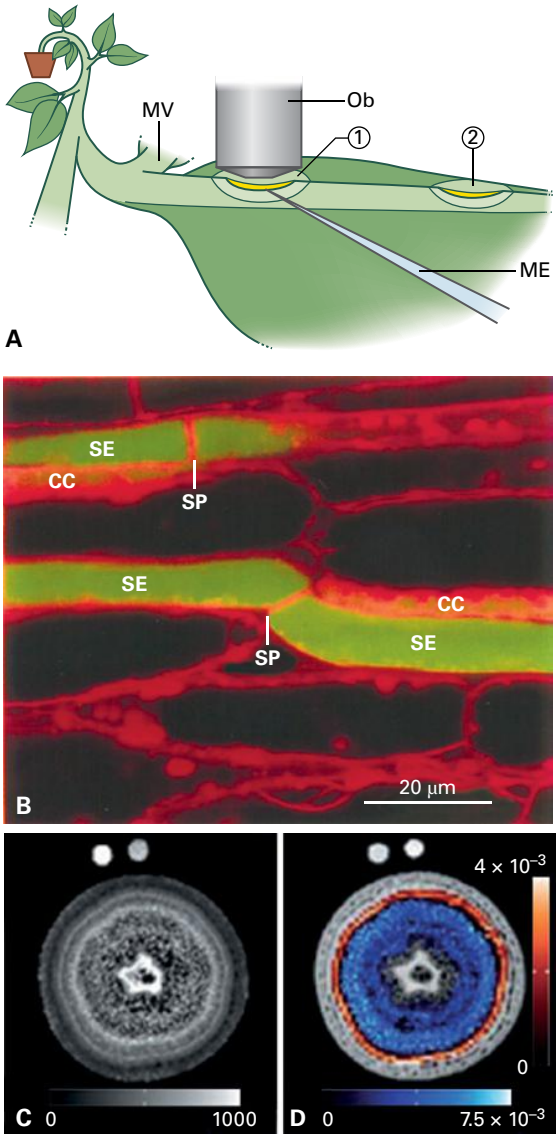


FIGURE 15.40 *Methods for assessing phloem as a translocation pathway and for monitoring bulk flow velocities. (A, B). Use of fluorescent phloem-mobile dyes in broad bean leaves. (A) Application of fluorochromes to a paradermal cut (2) made at the lower side of the main vein (MV) enables detection of fluorescence at an observation window (1) downstream of dye application by confocal laser scanning microscopy (Ob). (B) Strong fluorescence (green) in SEs of* Vicia faba *demonstrates these cells form the pathway for phloem transport. Longitudinal uniformity of fluorescence intensity is consistent with bulk flow and its retention across sieve plates (SP) shows that these structures or any deposits on them do not inhibit bulk flow. Fluorochromes (yellow) accumulate in CC vacuoles. (C, D) Nuclear magnetic resonance (NMR) records nuclear magnetic spin resonance of water molecules moving in phloem and xylem as illustrated for a cross-section of poplar hypocotyl. (C) A microscopic control cross-section. (D) Presented is a velocity flow (i.e., volume flux; see Equation 15.4B) map derived from water flowing downward through phloem (orange/yellow, 0.1–0.3 mm s^{-1}) and upward through xylem (blue, 0.3–0.8 mm s^{-1}). These measured velocities greatly exceed predicted velocities for diffusion over distances greater than several mm (see Equation 15.B3). The color scaling on the horizontal and vertical bars depict flow velocities. Source*: (A, B) Knoblauch & van Bel (1998). Plant Cell 10:35–50. (C, D) Windt et al. (2006). Plant Cell Environ. 29:1715–1729.

15.6.4 Sieve pore occlusion is a sophisticated surveillance system that prevents phloem sap loss from mechanically damaged SEs

Effective sieve-plate occlusion in response to wounding may have been a key factor in the evolutionary success of angiosperms. Occlusion prevents leakage of photoassimilates from

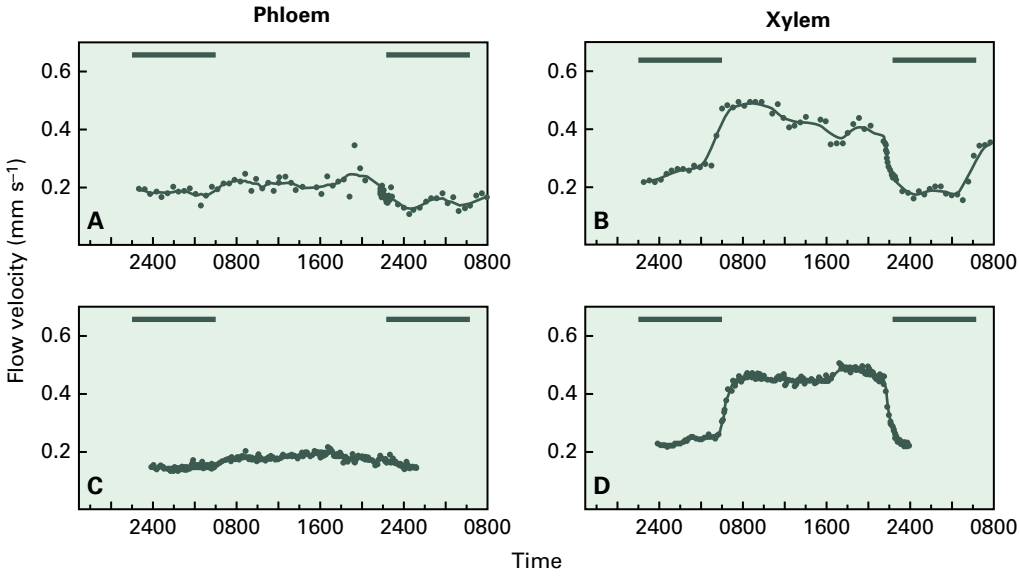


FIGURE 15.41 *Phloem transport velocities (A, C) are unaffected by the marked diurnal changes in transport velocities through the xylem (B, D). The* in situ *velocity measurements were made using NMR of* Ricinus *stems (see Fig. 15.40C). The dark period is indicated by black horizontal bars.*

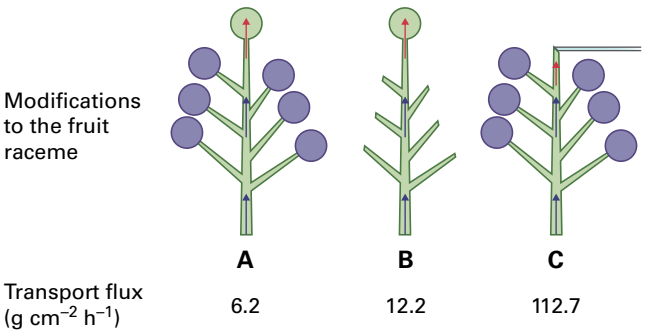


FIGURE 15.42 *Demonstration of spare transport capacity of transport phloem using castor bean (*Ricinus communis*) plants; ST sap bleeders (see Section 15.4.4). Bulk flow rates of ST sap were expressed as transport fluxes through the transport phloem ST cross-sectional area (red arrows) at a site immediately below insertion of the most apical fruit (green circle) in the fruit cluster. Nutrient import by remaining fruits (purple circles) is depicted by purple arrows. In configurations A and B, transport fluxes were determined by dry weight increase of the most apical fruit across a set interval of days in which respiratory losses were accounted for (40–50% of imported carbon). In C, transport flux was determined as the dry weight of ST sap exuded from the cut stump immediately below the excised apical fruit and collected into a microcapillary across an interval of hours. Transport flux through transport phloem to the apical fruit in (A) of an intact fruit cluster and (B) in a cluster in which all other fruit development was prevented by excising flowers at anthesis. (C) Transport flux through transport phloem exuding through a cut stump with remaining fruit attached. Transport flux (R_t) = path conductivity (L_p) × pressure difference (source-sink) ($P_{source} - P_{sink}$) × nutrient concentration (C). Path conductivity (see Box 15.1) and nutrient concentrations are identical across the three treatments. If path conductivity were limiting bulk flow, then fruit removal should have proportionally increased flow to the remaining terminal fruit in B as spare phloem became available. Thus the observed doubled flux is less than an expected ca. sixfold increase if path conductivity was limiting flow. Rather sink hydrostatic back-pressure is operating through a plasmodesmal controlled release from*

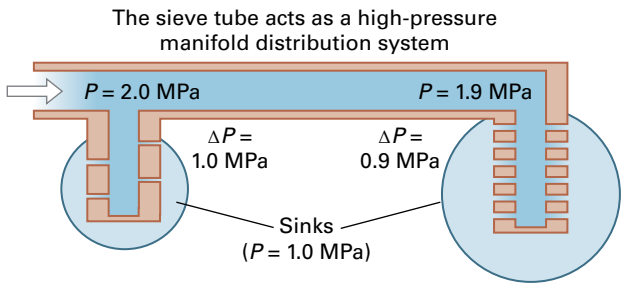


FIGURE 15.43 *Symplasmic unloading of resources from SEs are constrained by a limited plasmodesmal connectivity (i.e., hydraulic conductivity) between SE/CCs and adjacent phloem parenchyma cells. As a consequence, large differences in hydrostatic pressure develop across SE/CC/phloem parenchyma cell interfaces far exceeding hydrostatic pressure differences between source and sink ends of the STs. Thus phloem functions as a high-pressure manifold distribution system in which hydrostatic pressure differentials between source and sink ends of STs are similar for different sink types. This highlights the role plasmodesmata interconnecting SE/CCs with phloem parenchyma cells play in regulating pressure differentials between STs and sink cells that in turn determine nutrient distribution patterns between sinks.*

herbivore-severed SEs and is also a mechanical barrier against invasion by phytopathogens.

The plasmodesmal origin of sieve pores may shed some light on how occlusion evolved. Parenchyma cells react to abrupt turgor loss of neighboring cells—as happens with wounding—by plasmodesmal closure maintained by callose deposition at the PD orifices. Sieve pores have perfected this

FIGURE 15.42 (*Continued*) *the fruit phloem terminus as demonstrated by fruit excision in C where plasmodesmal control is removed. Hydrostatic pressure at the exuding stump is zero thus drastically increasing $P_{source} - P_{sink}$ by a magnitude commensurate with the 18-fold increase in flux. This outcome demonstrates transport phloem has spare transport capacity.*

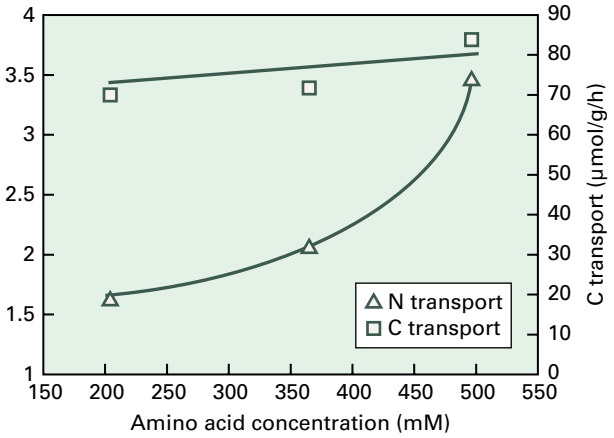


FIGURE 15.44 *Distinction between how major and minor osmotic species determine their rates of phloem transport. Carbon and amino N import rates into developing seeds of three* Brassica *genotypes plotted as a function of total amino acid concentrations in ST sap. Each point represents a data point for a genotype. Note strong concentration dependence of amino N import rate while that of carbon is independent. In these studies, amino N compounds contributed approximately 20% to osmotic content of the ST sap.*

damage response strategy through an instantaneous influx of Ca^{2+} initiating callose deposition around sieve pores (Fig. 15.45A–D). In addition, sieve plates are often plugged by SE proteins, which are probably Ca^{2+} reactive. For instance, PP1 protein in cucurbit STs has Ca^{2+}-binding properties that may apply to many structural SE proteins, in particular to forisomes. These large protein bodies occur in *Fabaceae* SEs, where they disperse in response to Ca^{2+} supply and turgor shocks (Fig. 15.45E–G). Isolated forisomes show a reversible dispersion/contraction in the presence/absence of Ca^{2+}.

15.6.5 Macromolecular signals are transmitted through the phloem

Phloem functions as a long-distance transport conduit for macromolecular signals integrating homeostasis and development of spatially separated organs. The presence of proteins and RNA species in ST sap (see Section 15.4.4) has been linked to systemic signaling by grafting experiments (Fig. 15.46). Functional junctions formed between stock and scion of intergeneric grafts between family members (e.g., tomato on potato plants; Fig. 15.46D) are generated by plasmodesmal bridges developed between vascular cells (Fig. 15.46A–C). Studies on long-distance signaling require intergeneric grafts of individuals with (slightly) different genomes to detect a systemically transported gene product through the graft junction in the scion/rootstock.

Intergeneric grafts have established that proteins, mRNAs and sRNA species (including siRNAs and miRNAs) engaged in transcriptional and posttranscriptional regulation are transported systemically and effect gene expression at sites remote from their point of origin (Fig. 15.46E–J). Hence, inter-organ responses can be coordinated through phloem-

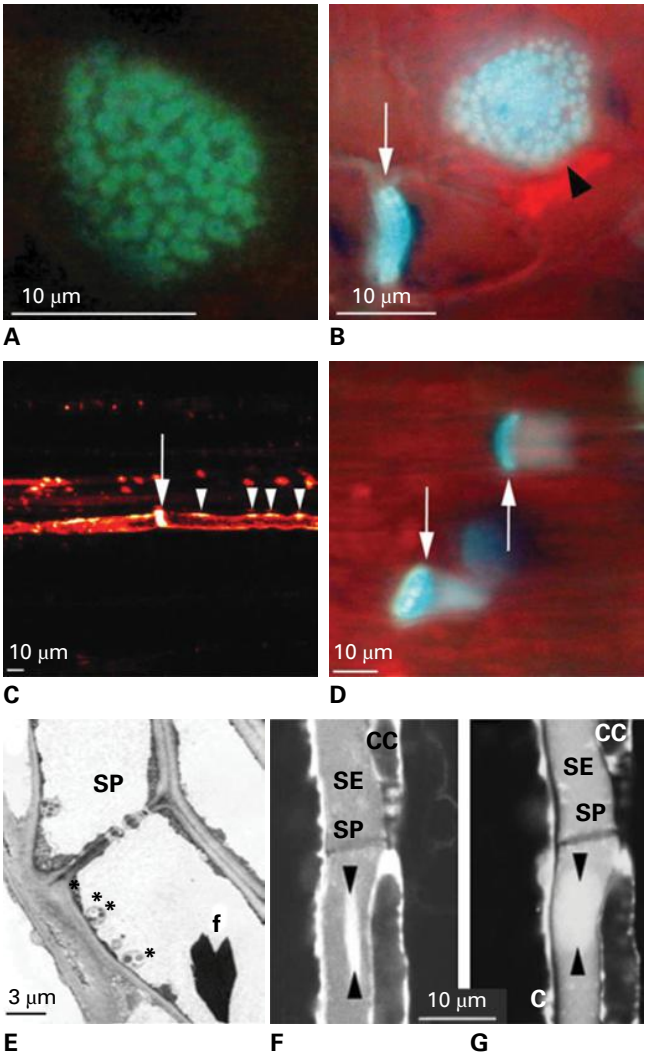


FIGURE 15.45 *Occlusion of sieve plates. (A) Surface view of a sieve plate of* V. faba*; callose collars (green) around sieve pores. (B) Transverse section of a normal sieve plate (white arrow) with thick callose deposits (stained by aniline blue) and a surface view of a lateral sieve plate (black arrowhead) in a longitudinal wall between two STs. (C) Aniline blue staining of callose collars around sieve pores (white arrows) and PPUs (arrowheads). (D) Callose deposits (white arrows) and protein plugs (fading blue haze) in* V. faba *STs. (E) Electron micrograph of an intact SE (SP, sieve plate) of* V. faba *containing a forisome (f) and SE plastids (asterisks). (F, G) Confocal microscopic images of sieve plate (SP) occlusion by forisomes in* V. faba*. Fluorescence-labeled condensed forisome (between the arrowheads) in SE (F) disperses (G) after impalement by a microcapillary (not visible in G). SE, sieve element, CC companion cell.*
Source: (A–D) A. Furch, University of Giessen, Germany. (E) Ehlers et al. (2000). Protoplasma 214:80–92. (F, G) Knoblauch et al. (2001). Plant Cell 13:1221–1230.

translocated macromolecular signals. This is of paramount importance in orchestrating defense responses against fungal infection or herbivory. Furthermore, spatially separated developmental events are coordinated by macromolecular signals. For instance, floral initiation is under remote control of fully expanded leaves sensing day length changes, the signals (in this case, a CC-synthesised protein) for which are transmitted to shoot apices via the phloem (see Chapter 19).

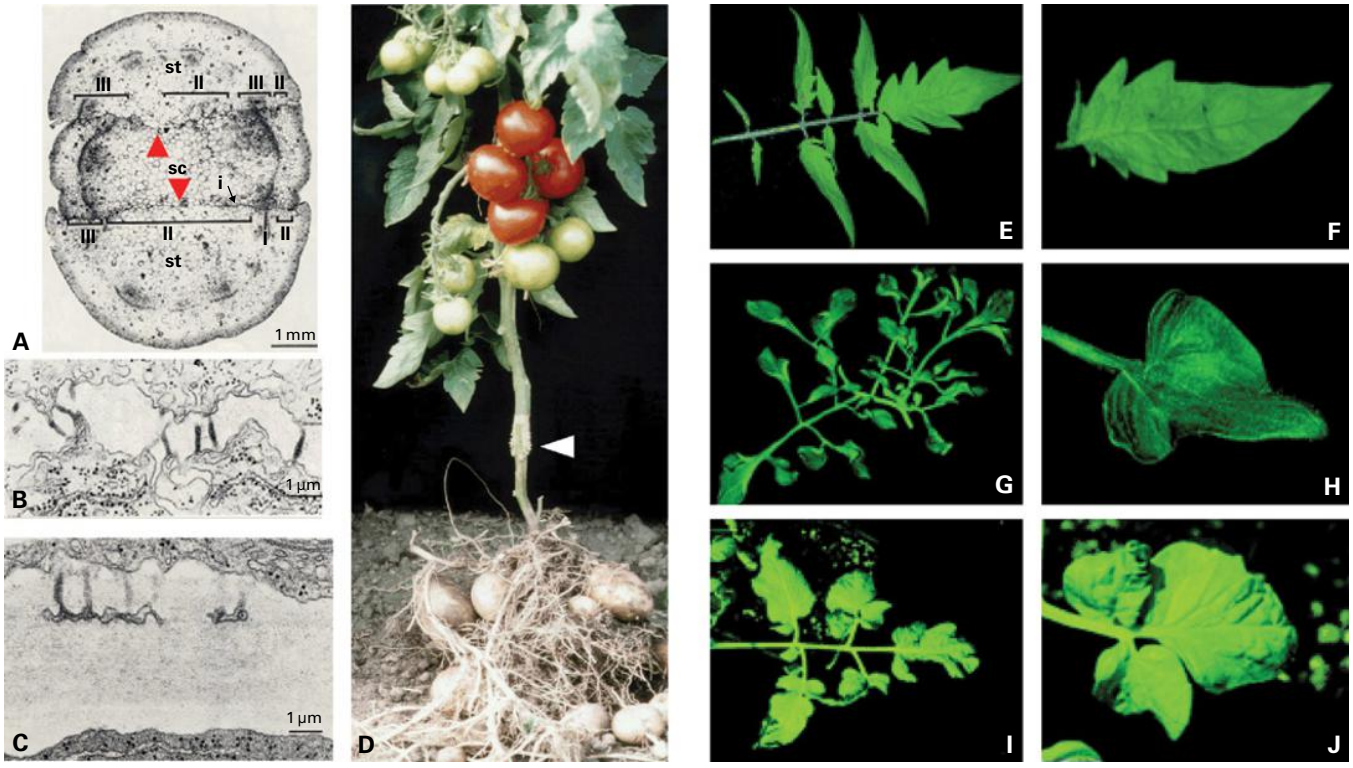


FIGURE 15.46 *Graft unions and experimental use of graft constructs. (A) Transverse section of a graft interface of an* Impatiens walleriana *scion (shoot explant) and an* Impatiens olivieri *root stock. To obtain a functional graft, the scion (sc) must be placed onto the stock (st) so that their vascular areas align (I). In other areas (II aligned parenchymatous tissue; III mismatching tissues), cells are unable to interconnect via plasmodesmata; a prerequisite for functional coupling of scion and stock. Demarcation of scion and stock (i) is visible as a dark zone (red arrowheads). (B) Only in vascular areas (I; see A) are newly formed plasmodesmata able to coalesce. (C) In other zones, plasmodesmata fail to coalesce. (D) A heterograft of tomato (scion) and potato (stock) plants showing recovery of xylem and phloem functioning needed to produce tomato fruits and potato tubers. Graft union is marked with an arrowhead. (E–J) Grafting scions on stocks of tomato with differing genotypes shows that a mutation in the rootstock is phenotypically expressed in the scion. This demonstrates that mutant mRNA must be transported from root to shoot putatively in the phloem. (E) Leaf of* Xanthophyllic *(*Xa*, yellowish leaf) mutation, (F) Xa leaflet, (G)* Mouse ear *(*Me*) mutant leaf, (H)* Me *leaflet, (I)* Xa *heterografted scion with Me-like morphological traits such as altered leaf shape, increased leaf subdivision, trichomes in the middle region of developing leaves and a more intense green color, (J)* Xa *heterografted leaflets. Results indicate that genetic information for increased leaflet production and chlorophyll expression is translocated through the graft junction to the scion.*
Source: (A–C) Kollmann et al. (1985). Protoplasma 126:19–29. (D) R. Kollmann, University of Kiel, Germany. (E–J) Kim et al. (2001). Science 293:287–289.

Recently, macromolecules also have been found in TE sap as part of a likely long-distance system that confers resistance against biotic and abiotic stresses.

Macromolecular messages are transcribed and translated in CCs (or phloem parenchyma cells), released into SEs, and carried by bulk flow to their sites of action. How macromolecular signals are released into SEs is a matter of debate. A prominent model (Fig. 15.47A) envisions that endogenous macromolecular complexes are formed in CCs and contain proteins with sites for plasmodesmal recognition, plasmodesmal docking, and for their unfolding. Actin filaments, in conjunction with ER, may function as tracks for macromolecular complex delivery to plasmodesmata, whether or not enclosed in membrane vesicles (Fig. 15.47B). Spirally arranged macromolecules on plasmodesmal ER-rods (Fig. 15.3C) may be actin filaments that enable transfer of macromolecular complexes through plasmodesmata (Fig. 15.47B). These trafficking mechanisms are presumably analogous to those operating for symplasmic trafficking between parenchyma cells (see Section 15.1.2). In addition, less selective passage mechanisms exist. For instance, GFP (Fig. 15.22B) complexed with additional peptides up to molecular sizes of 65 kDa and expressed in CCs is released into SEs. It seems unlikely that such foreign proteins pass through PPUs using specific trafficking mechanisms.

At least some SE proteins are retrieved by CCs and re-enter STs, thereby seeming to progress by "hopping" along the transport phloem. Re-entry of macromolecules into CCs may be crucial for long-distance signaling. For instance, signal amplification requires that macromolecules return into CCs along the pathway. Furthermore, macromolecular messages tagged by "zip codes" appear to find their way to specific recipient cell types, a phenomenon requiring selective entry and exit mechanisms.

Despite macromolecule abundance in ST sap, identities of macromolecules involved in long-distance signaling are largely unknown (Table 15.8), including those compounds involved in systemic acquired resistance (SAR). It is expected that a loose

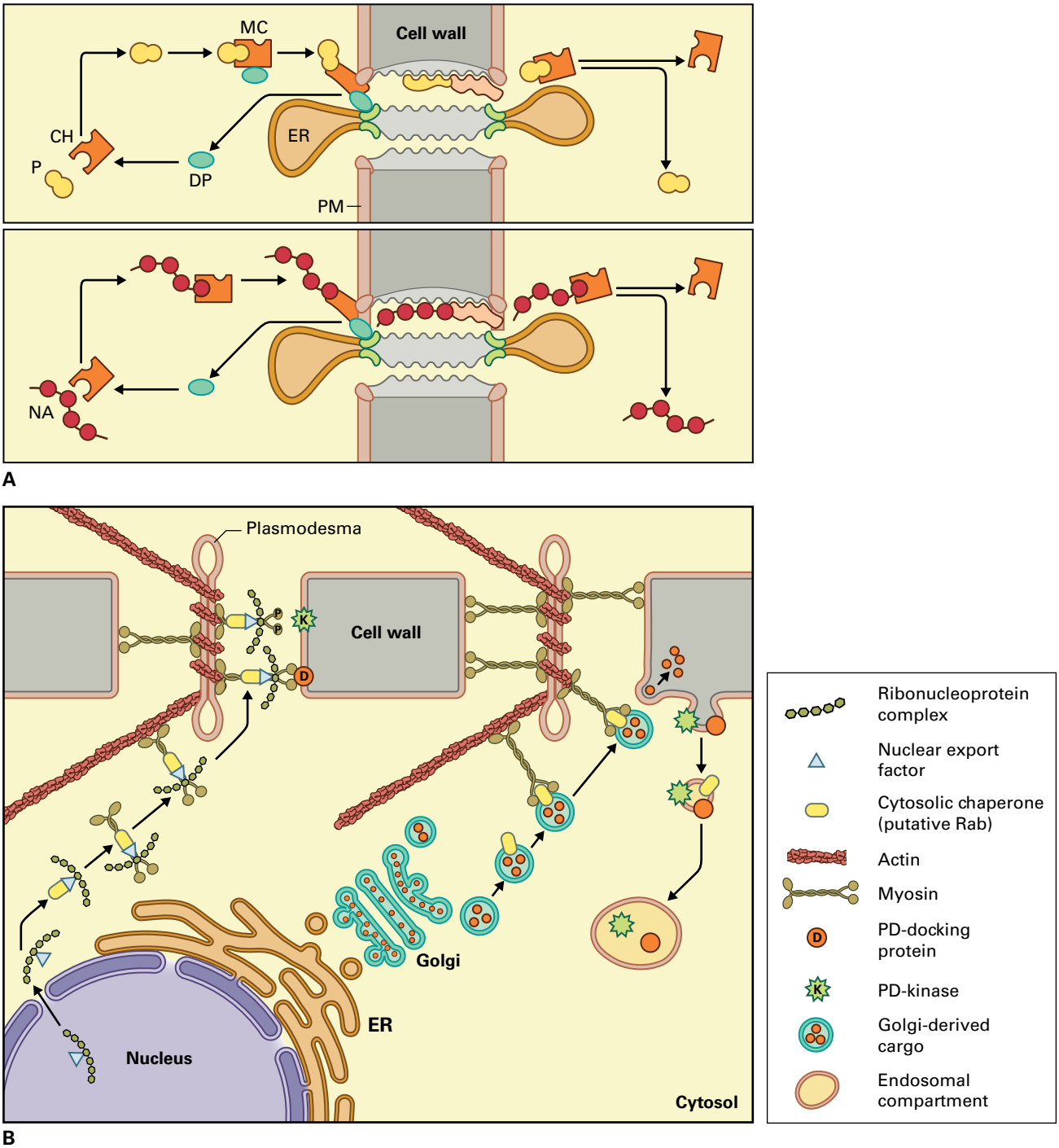


FIGURE 15.47 *Hypothetical models of macromolecular trafficking to, and through, plasmodesmata. (A) Upper cartoon: Only specific proteins (P) are picked up by chaperone (CH) and docking (DP) proteins to form macromolecular complexes (MC). This complex is recognized and processed by a protein structure at plasmodesmal orifices. After uncoupling of the docking protein, the P–CH complex is trafficked through plasmodesmata in an unfolded state and released at the other side, where the protein is released. Lower cartoon: In a similar way, innate RNA and viral RNA (NA) are trafficked through plasmodesmata. Viral movement proteins (see Fig. 15.48) possess similar functions to the chaperones in plasmodesmal trafficking of viral RNA. (B) Alternative models of intra- and intercellular transfer of macromolecules towards and through plasmodesmata. Left side: Myosin-bound macromolecular complexes are carried along actin filaments, most likely at interfaces between actin filaments and ER tubules, towards the recognition, docking and processing sites at the plasmodesmal orifices. Subsequent active trafficking of macromolecular complexes through plasmodesmata depends on interaction between myosin and actin. Right side: Golgi vesicles may be directed in a similar way towards the plasmodesmata and excreted by exocytosis in the vicinity of the plasmodesmal orifices.*

TABLE 15.8 *Transcriptomics of sieve tube sap.*

RNA	Function	Plant species
BEL-1	Tuber development	*Solanum tuberosum*
CmGAIP	Leaf development	*Cucurbita maxima*
CmNACP	Meristem maintenance	*Cucurbita maxima*
CmPP16	RNA transport	*Cucurbita maxima*
DELLA-GAI	Leaf development	*Arabidopsis thaliana*
PFP-LeT6	Leaf development	*Solanum lycopersicum*

Some mRNAs found thus far in ST saps shown to be potential long-distance carriers of genetic information.

maze of numerous intertwining reactions, spanning SEs, CCs, and phloem parenchyma cells, is responsible for SAR.

Plant viruses have hijacked nucleic acid replication machinery and mechanisms for trafficking macromolecules through plasmodesmata of host plants, and they rely on bulk flow through the phloem for long-distance transmission. Viral infections often spread from leaves by entering minor veins to be exported through STs (Fig. 15.48A). Viral multiplication and spread are characterized by efficient use of their small genomes. For example, the tobacco mosaic virus genome, which comprises only four open reading frames, encodes a 183-kD protein that enables breakdown of the host genome into macromolecular complexes and multiplies by subsequent rearrangement of nucleic acid units. A 126-kD protein is likely responsible for intracellular transfer of viral RNA and docking to plasmodesmata. Movement proteins carry viral complexes through plasmodesmal sleeves. Having arrived in CCs, capsid proteins are expressed. Similar to RNA–movement protein–capsid protein complexes are trafficked through PPUs to minor vein SEs as demonstrated by cucumber mosaic virus. There, movement proteins are uncoupled and viral genomes are enveloped in capsid proteins (Fig. 15.48B).

Aphids transmit numerous viruses (see Box 15.3). Some of these viral groups (luteoviridae, geminiviridae) are unable to escape from SE/CCs and multiply solely in CCs. Confinement of these viral particles to SE/CC-complexes illustrates the dissimilar nature of phloem parenchyma/CC and SE/CC plasmodesmata.

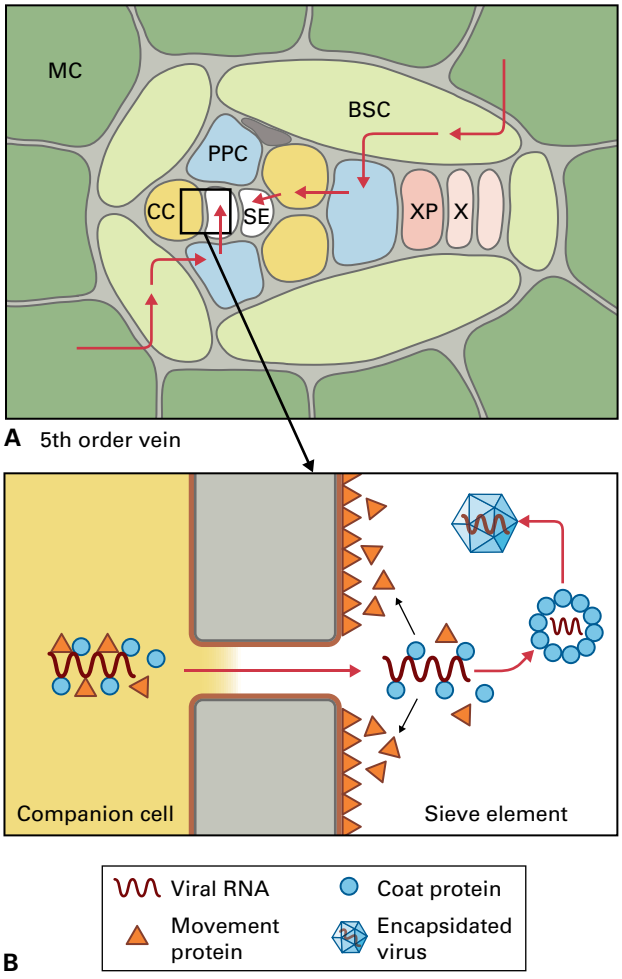


FIGURE 15.48 *Phloem transport events in viral spread. (A) Viral infection in a source leaf spreads by intercellular movement of viruses into the vasculature and is usually phloem transported. To enter phloem of a minor vein, a virus must travel through mesophyll cells (MC), bundle sheath cells (BSC) and possibly phloem parenchyma cells (PPC) before entering CC, and finally SE. It is unclear from which cell type, BSC or PPC, viruses move to enter CC and how this is achieved. (B) For mesophyll cell-to-SE viral transfer, movement proteins are involved. Movement proteins, mostly in cooperation with other viral proteins, are responsible for trafficking through plasmodesmata (see Fig. 15.47). In SE, viruses are often encapsidated (viral RNA encapsulated by coat protein monomers) during or after passage of a viral RNA/protein complex through PPUs into SEs following uncoupling of movement proteins. X, xylem vessel; XP xylem parenchyma.*

15.6.6 Sieve tubes conduct electrical signals

Apart from chemical messages, STs also conduct electrical signals as electrical potential waves. Two types of electrical potential waves have been observed: one is designated an action potential, the other a wound or variation potential. Generally, action potentials are of shorter duration and move more quickly than variation potentials; amplitudes of variation potentials are commensurate with stimulus strength, while those of action potentials are not. Stimuli such as touch, light pulses, or abrupt temperature changes induce action potentials, whereas variation potentials arise from mechanical damage. Severe wounding by burning probably causes combined action and variation potentials.

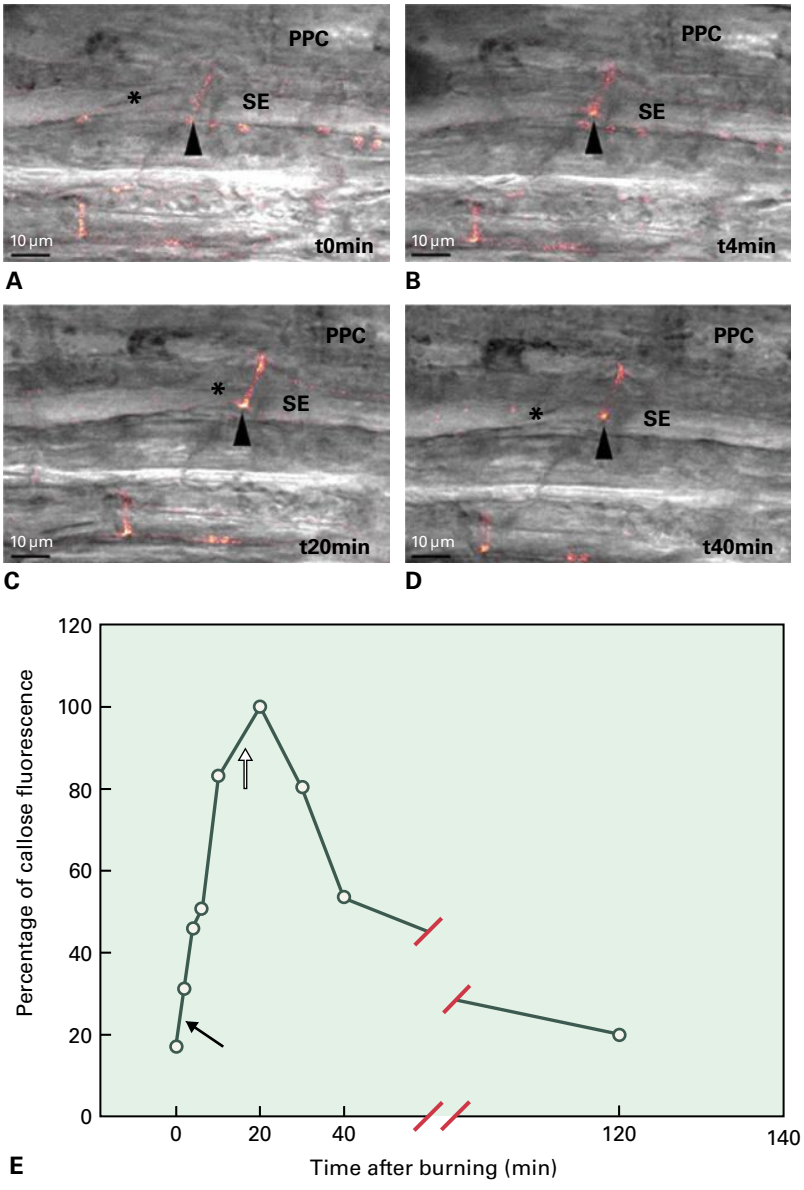


FIGURE 15.49 *Induction of sieve-plate closure by a remote burning stimulus. (A–D) Real-time overlays of light microscope and multiphoton confocal laser scanning microscope images of forisome dispersion/contraction (asterisk), and callose deposition/degradation (demonstrated by aniline blue staining visible as red fluorescence) in SEs after burning of* V. faba *leaf tips (at a distance of 3 cm from the observation window). The forisome is dispersed in (B) and therefore not visible (PPC, phloem parenchyma cell). Relative fluorescence in images A–D was quantified at the sieve plate (arrowhead). (E) Time-correlated comparison of forisome dispersion (solid arrowhead)/contraction (open arrowhead) and callose deposition/degradation. Forisome re-contracted before callose deposition reached its maximum. Callose degradation to ground levels is completed after 2 hours. Source*: (A–D) Furch et al. (2007). J. Exp. Bot. 58:2827–2838.

An initial Ca^{2+} influx followed by a massive Cl^- efflux and subsequent K^+ influx trigger propagation of electrical potential waves, mainly along STs, which impact remote organ functions. For instance, electrical potential waves stimulate expression of genes encoding enzymes that interfere with insect feeding and digestion. Electrical potential waves also influence photosynthesis and other physiological processes in distant leaves.

Remarkable is the remote electrical potential wave effect on sieve plate occlusion. In *V. faba* STs, the Ca^{2+} influx that accompanies the passage of electrical potential waves leads to a sudden dispersion of forisomes (Fig. 15.49B). When forisomes have recontracted, callose is deposited around sieve pores and slowly degraded during the next few hours (Fig. 15.49C–E). Thus, severe wounding exerts remote control on ST closure by a two-step occlusion mechanism characterized by rapid plugging of sieve pores with proteins followed by callose deposition ensuring longer-term occlusion (Fig. 15.49E). If damage does not affect SE functioning, membrane-located pumps expel Ca^{2+} ions from SEs to restore sieve-plate conductivity.

15.7 Communication and regulation controlling phloem transport events

15.7.1 Source/sink limitations control solute flow in the phloem

Flux control analysis demonstrates that all phloem sectors contribute to regulating transport. The balance between resource supply and resource demand by heterotrophic sink organs modulates the degree of control imposed by any transport process located along the transport pathway. Source limitation, and hence control, is imposed under conditions where resource supply does not meet potential demand for resources by sinks. Conversely, sink limitation is imposed when potential resource supply exceeds sink demand. Source- or sink-limited flow is vulnerable to environmental conditions and alters during plant development. For example, transport to meristems tends to be source limited whereas flows to expanding and storage sinks are sink-limited.

Signals can exert coarse control by determining absolute quantities of transport structures (plasmodesmal numbers; plasma membrane areas; transporter densities) and/or fine control mediated through reversibly adjusting their capacities (plasmodesmal conductances; post-translational regulation of transporter kinetic properties).

15.7.2 Leaf photosynthesis and sugar metabolism/storage regulate photoassimilate export

Leaf photosynthesis provides feed-forward control of phloem transport under source-limiting conditions as demonstrated by top-down flux control analysis (see Section 15.7.1) of plants raised under low light levels. Here, some 80% of the control of photoassimilate transport from source to sink was deduced to be located in photosynthetic leaves. This state reflects photosynthetic rates determining concentrations of sugars available for phloem loading (Equation 15.B9) as well as possibly functioning as signals to regulate processes contributing to phloem loading, as outlined below.

Collectively, current photosynthesis, sucrose biosynthesis, and remobilization of stored leaf sugars determine the instantaneous sizes of the leaf sugar pool available for export. If photosynthetic rates fall below sink demand, depletion of leaf sugar pool sizes is ameliorated by balancing carbon flows into and from leaf storage pools. Carbon flows into the cytosolic sucrose pool of mesophyll cells are controlled by sugar-regulated expression of key photosynthetic enzymes (see Chapter 12), sucrose biosynthetic enzymes (see Chapter 13), and membrane transporters contributing to carbon exit from chloroplasts and vacuolar exchange (Fig. 15.50).

15.7.3 Nutrient flows through transport phloem are regulated by buffering supplies from adjacent storage pools

Radial resource exchange between transport phloem and the surrounding apoplast provides short-term buffering to longitudinal flow through the transport phloem when the balance between source supply and sink demand shifts. This buffering phenomenon is demonstrated by imposing a cold block to a stem. Downstream of the cold block, photoassimilate release is accelerated, while upstream retrieval of photoassimilates is enhanced to generate hydrostatic pressures favorable for driving phloem transport to and away from the cold block (Fig. 15.51). Apoplastic pools of sucrose are relatively small and have a half-life of minutes. If a downward shift in source/sink balance is sustained over hours, then buffering longitudinal flow increasingly depends upon remobilizing stem storage reserves (Fig. 15.25). Indeed, for some grain crops, remobilizing stem-stored carbohydrates contributes substantially to final grain yield, especially under drought conditions.

15.7.4 Sink demand for nutrients is communicated through signals that activate remote regulatory responses

Photoassimilate export from leaves of a source-limited system (see Section 15.7.1) does not respond rapidly if at all to an increase in sink demand. In contrast, alterations to demand in a sink-limited system (see Section 15.7.1) elicit substantial and rapid (minutes to hours) responses in rates of photoassimilate export (Fig. 15.52). These rapid responses indicate a close coupling between sink demand, and phloem loading can occur under sink limitation.

Alterations in sink demand of major osmotic species can be transmitted instantly to source leaves as changes in hydrostatic pressure of SE/CC complexes. Pressure regulation of H^+-ATPase activity changes the *pmf* across plasma membranes of SE/CC complexes, providing a common mechanism for controlling apoplastic phloem loading by proton-coupled transport mechanisms.

Changes in steady-state balances between source supply and sink demand also can be sensed by upward and downward alterations in apoplastic sucrose contents in collection phloem. For example, transcript and protein levels of a sucrose/H^+ symporter (*BvSUT1*) in CCs of excised sugar beet (*Beta vulgaris*) leaves were selectively and rapidly repressed in response to transpiration-delivered sucrose. Consistent with a regulatory system, these effects were reversed rapidly upon lowering apoplastic sucrose levels. How sucrose is sensed is not certain, but the signal transduction pathway includes a protein phosphorylation cascade (Fig. 15.53).

Changes in demand for minor osmotic species rely on altering their rates of phloem loading (Fig. 15.39 and associated text). Hence demand must be communicated from sink to source; likely candidates are hormone signals that undoubtedly interact with sugar-signaling pathways.

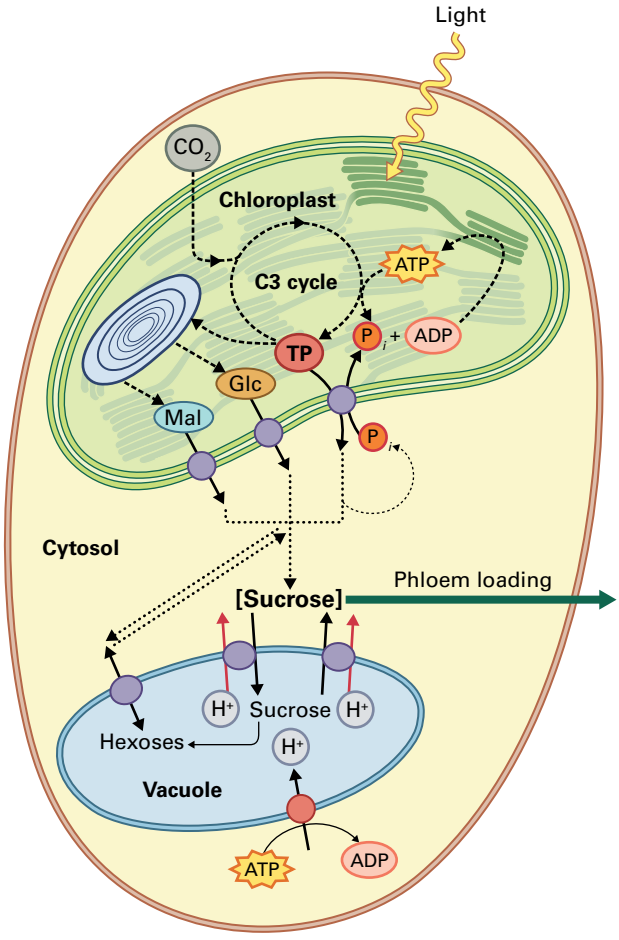


FIGURE 15.50 *Biochemical and membrane transport processes contributing to the cytoplasmic sucrose pool available for phloem loading. Mesophyll cell with chloroplast and vacuole. Maltose (Mal) and glucose (Glc), products of starch hydrolysis in chloroplast stroma, along with C3-generated triose-phosphate (TP), are exported across chloroplast envelopes by transporters. Within mesophyll cytosols these substrates are rapidly interconverted into sucrose. Sucrose and hexoses in excess of those required for phloem loading may be sequestered into mesophyll vacuoles respectively by sucrose/H^+ antiport energized by a tonoplast localized proton-pumping ATPase and by hexose carriers functioning by facilitated diffusion. Release from vacuolar storage is by sucrose symporters (e.g., SUT4) and hexose carriers. P_i, inorganic phosphate.*

15.7.5 Plasmodesmal conductances exert a greater influence over transport rates compared to sink metabolism/compartmentation

A direct relationship between rates of cellular metabolism/compartmentation and phloem unloading infers that phloem unloading rates can be regulated by intercellular concentration or hydrostatic pressure gradients generated by metabolism/compartmentation. However, large concentration or osmotic differences (0.7–1.3 MPa) (Fig. 15.28) between SEs and sink cells attenuate the influence that changes in sink cell nutrient concentration or osmotic pressure can exert on these differences. For example, the sucrose concentration expected in sink cell cytosol ranges from 10 to 100 mM, and a minimal SE sucrose concentration is 350 mM (Table 15.3). Thus, the concentration and osmotic differences that are available between SEs and sink cells for regulating phloem unloading range from 250 to 340 mM sucrose. Control exercised by metabolism/compartmentation in sink cells governing the concentration/osmotic gradient could at best alter unloading rates by 36% (i.e., 340/250). Experimental observations are consistent with this conclusion. For example, rates of phloem import into elongating roots are independent of differences in hydrostatic pressures as well as concentration of key osmotic compounds between phloem and ground tissue (Table 15.9). Applying diffusion and bulk flow equations to this finding (see Box 15.1), leads to the deduction that plasmodesmal conductance exercises major control over nutrient fluxes unloaded through symplasmic pathways (Fig. 15.43).

Plasmodesmal control will exert greatest impact on nutrient transport rates along symplasmic unloading pathways at points of their lowest conductance. In a range of sink types, these points are located at SE/phloem parenchyma cell boundaries, as reflected by estimates of plasmodesmal fluxes (Table 15.6) and the largest differences in sucrose concentration and hydrostatic pressure (Fig. 15.28). Hence, considerable control of phloem unloading is probably exercised by altering conductances of plasmodesmata connecting SE/CC complexes with surrounding phloem parenchyma cells. For instance, hormones are implicated in regulating plasmodesmal conductances to control symplasmic phloem unloading in stems (Fig. 15.54).

Overall, these observations suggest that sinks modulate conductance of strategically located plasmodesmata to regulate nutrient unloading rates to levels commensurate with their metabolic and growth demands.

15.7.6 Apoplastic unloading requires communication of sink demand across two adjoining plasma membranes at the apoplastic step

Apoplastic steps located in post-SE unloading pathways of developing seeds and fleshy fruits (Figs. 15.31 and 15.32) impose a requirement for communication of the demand by recipient sink tissues across two membranes: one responsible for nutrient release and the other for nutrient uptake. Feedback control, generated by nutrient demand, involves transmission of regulatory signal(s) from sites of metabolism/compartmentation within sink tissues to control nutrient transport processes. For major osmotic species, the following

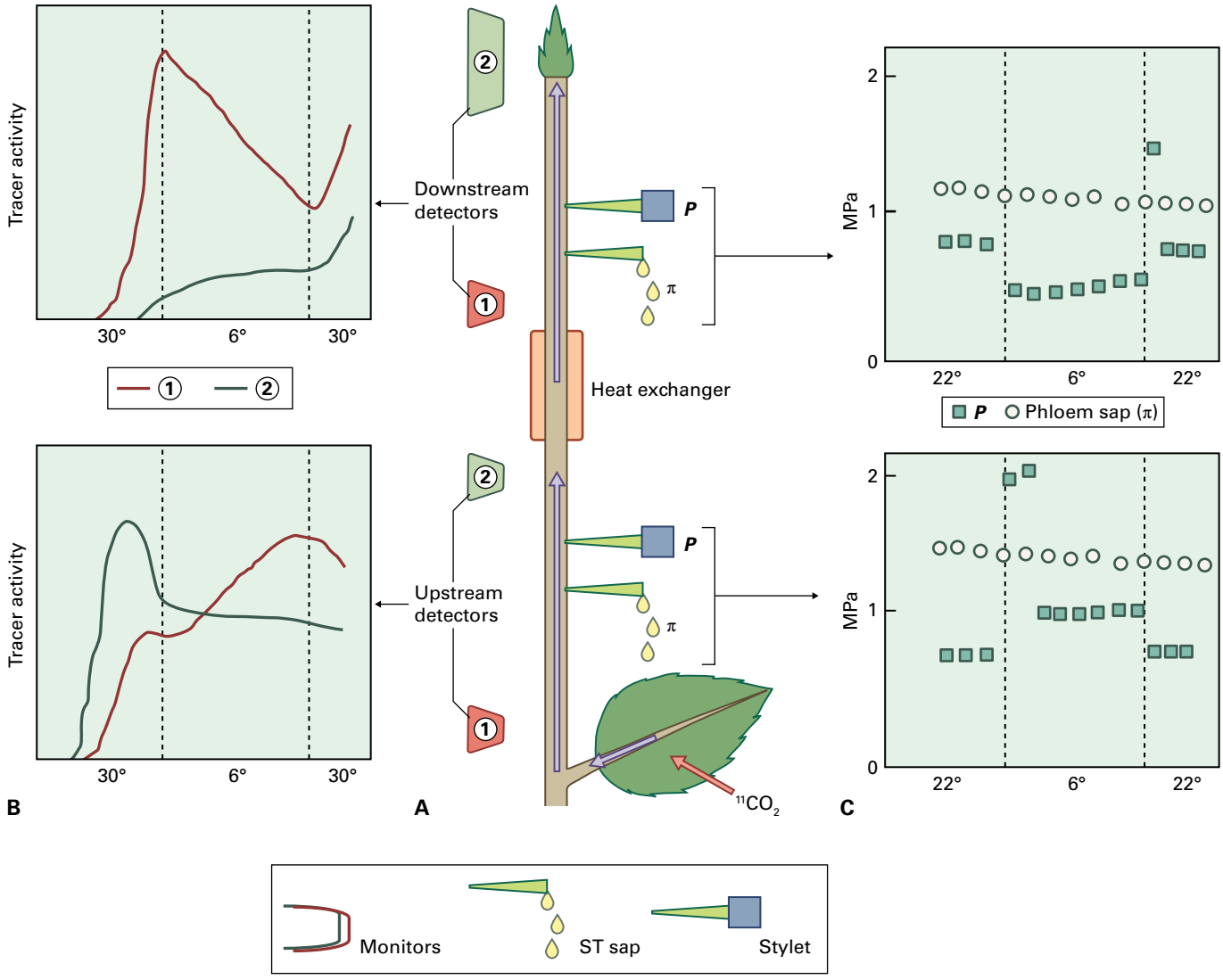


FIGURE 15.51 *Rapid buffering of axial transport by radial water and solute exchange demonstrated using a cold block to interrupt axial transport. (A) Experimental set up. Continuous real-time measurement of photoassimilate transport using the strong gamma emitting carbon isotope C^{11} introduced by exposing a source leaf to $^{11}CO_2$. Transport of ^{11}C-photoassimilate (gray arrows) detected by monitors located at points up- or downstream of a stem portion enclosed within a heat exchanger. Cut aphid stylets, located up- and downstream of the heat exchanger, were used to collect ST sap for osmotic (π) determinations. SE hydrostatic pressure (P) was measured using a pressure transducer glued to each stylet. (B) Continuous recordings of ^{11}C-photoassimilate levels in a stem at selected sites along the axial pathway following exposure of a source leaf to $^{11}CO_2$. Transport was blocked by chilling a portion of a stem to 6°C. Axial transport continued both up- and downstream of the block. (C) Time-course measurements of P within SEs and ST sap π. P rapidly adjusted to altered stem temperature with an elevation upstream and a decline downstream of the temperature block. These adjustments account for photoassimilate flow being maintained either side of the temperature block. Since sap π was temperature independent, P changes must result from a coupled exchange of water and nutrients across SE/CCs with surrounding phloem apoplast. Net radial exchanges were in the opposite directions with net reloading upstream and net unloading downstream of the temperature block.*

closed-loop control applies in developing legume seeds. Depletion of sucrose pools by increased rates of polymer formation in cotyledons ease substrate-regulated repression of *SUT1* expression and, as a result, increase sucrose uptake from the seed apoplast (Fig. 15.55C). Resulting decreases in apoplastic sap osmolality stimulate an efflux of nutrients from seed coats that is regulated by a turgor pressure–homeostat mechanism (Fig. 15.55B). Under these conditions, the hydrostatic pressure of unloading cells acts as a key modulator to link demand for major osmotic nutrients by cotyledons to nutrient supply from seed coats. This, in turn, links demand to rates of phloem import (Fig. 15.55A), which are possibly augmented through regulating plasmodesmal conductance in some as yet to be determined mechanism (see Section 15.7.5).

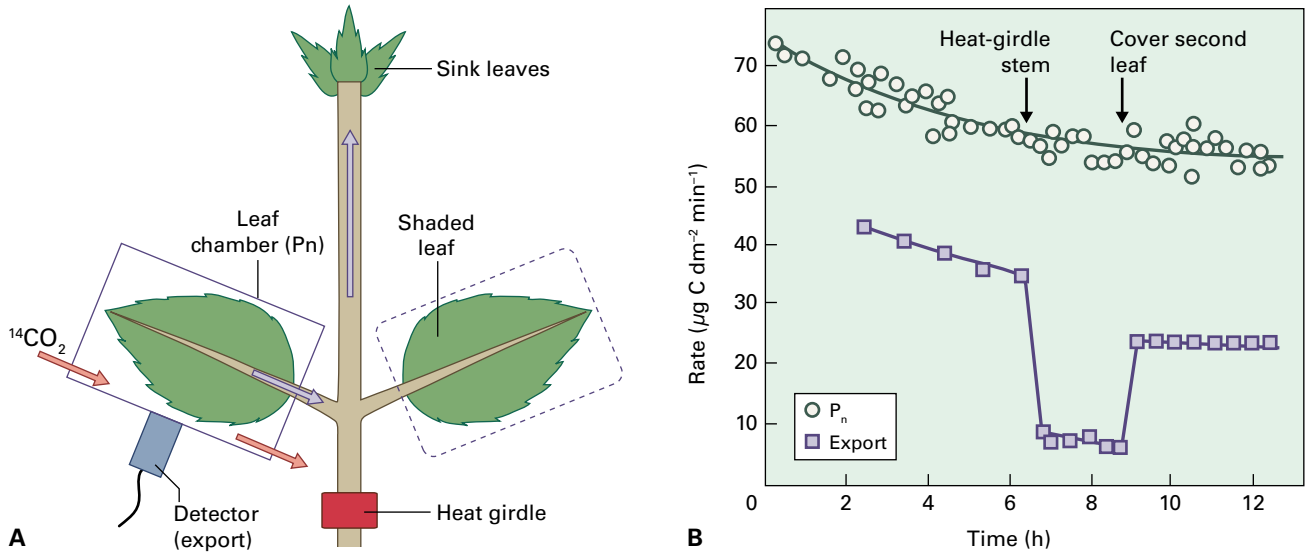


FIGURE 15.52 *Rapid responses of photoassimilate export to changes in source supply or sink demand. (A) To concurrently monitor photosynthesis of, and export from, a source leaf, a source leaf is enclosed in a chamber and air containing constant specific activity $^{14}CO_2$ is passed through the chamber and ^{14}C export is monitored along with net photosynthetic rate* (Pn *determined by infrared gas analysis). Export rate is the difference between* Pn *and retention of carbon within the leaf (monitored by a GM detector). Also illustrated are the stem site of heat girdling to block phloem transport to roots and darkening of the remaining source leaf. (B) Real time measurements record impacts of altering source/sink ratios of a bean* (Phaseolus vulgaris) *plant on* Pn *and photoassimilate export. Source/sink ratios were altered by sequentially heat girdling the stem preventing flow to the root sink (increased source/sink ratio) and shading the remaining primary leaf (decreased source/sink ratio). Irrespective of the direction in which source/sink ratio was shifted there was an immediate response of export rate while leaf photosynthesis remained largely unaltered.*

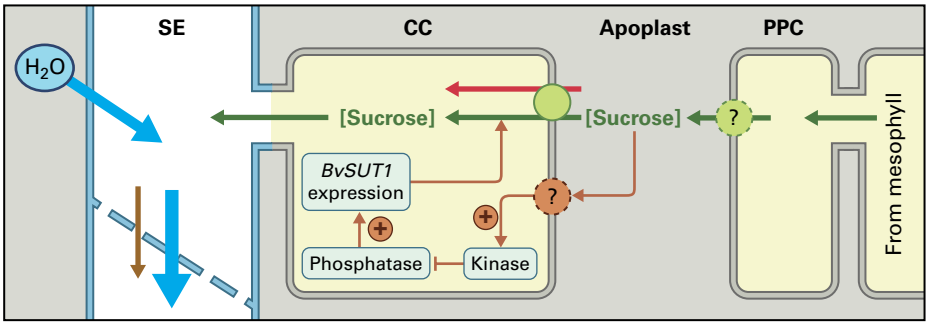
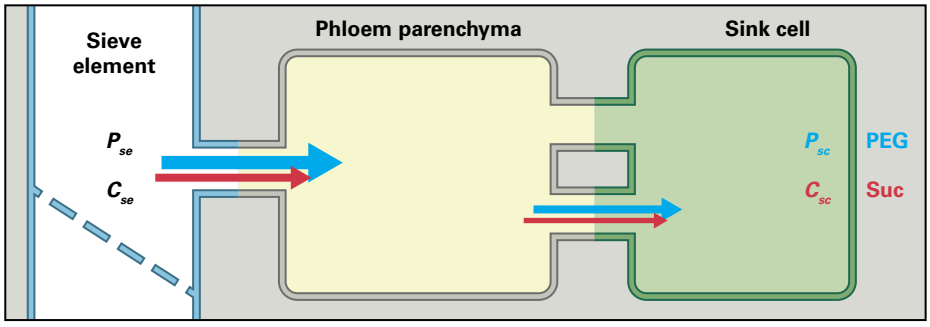


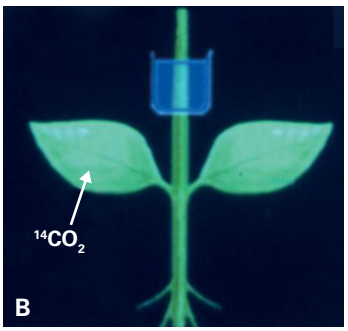
FIGURE 15.53 *Sucrose repression of sucrose symporter activity in apoplastically loading leaves coordinates photosynthetic sucrose supply with sink sucrose demand. Dynamic changes in apoplastic sucrose concentrations balance sucrose demand with supply from the mesophyll. An unknown sucrose sensor unrelated to the hexokinase pathway is hypothesized to activate a protein kinase that in turn inhibits a phosphatase thus de-repressing expression of* BvSUT1 *transporter transcript.*

TABLE 15.9 *Relationship between instantaneous relative import rates of carbon-11 into, and cortical cell hydrostatic pressures* (P) *and intracellular nutrient concentrations at, specified intervals along the primary root axis of maize across which phloem* P *remains invariant at 1.4 MPa. Import of carbon-11 relative to total carbon-11 levels detected in the entire root.*

Distance from root tip (mm)	Relative import of carbon-11	Cortical cell *P* (MPa)	Concentrations (mM) of:		
			Potassium	Sucrose	Hexose
0–5	0.18	0.66	95	12	90
5–10	0.09	0.66	51	1	150
10–15	0.02	0.61	ND	ND	ND

ND, no data.





Hormones act on plasmodesmal conductance of the phloem unloading pathway as shown by clamping $C_{se} - C_{sc}$ or $P_{se} - P_{sc}$

Manipulation of diffusion and bulk flow	^{14}C photosynthate (dpm/2cm stem) Control	GA_3 + kinetin
Sucrose	211	971
PEG	4669	8182

FIGURE 15.54 *Plant hormones regulate conductance of symplasmic phloem unloading pathways. Experimental model of symplasmic phloem unloading in which sucrose concentration ($C_{se} - C_{sc}$) and hydrostatic pressure ($P_{se} - P_{sc}$) differences were clamped by exposing bean (*Phaseolus vulgaris*) stems to solutions containing 300 mosmol kg^{-1} of sucrose or polyethylene glycol (PEG; 8 kDa). Arrows indicate movement of sucrose (red) and water (blue) through a symplasmic unloading pathway. For more details see Fig. 15.30. (B) Bath solutions containing sucrose or PEG solutions $\pm 10^{-5}$ M GA_3 + kinetin held in wells attached to stems. Following equilibration with bath solutions for several hours, a source leaf was exposed to a pulse of $^{14}CO_2$ (left hand panel). Levels (dpm, disintegrations per minute) of ^{14}C-photoassimilates (primarily transported as sucrose) accumulated in treated stem portions provide measures of phloem unloading. Stimulation of ^{14}C-photoassimilate accumulation by plant hormones, when $C_{se} - C_{sc}$ or $P_{se} - P_{sc}$ are clamped can only result from their action on pathway (plasmodesmal) conductance for diffusion (see Equation 15.B8) and bulk flow (see Equation B.5) respectively.*

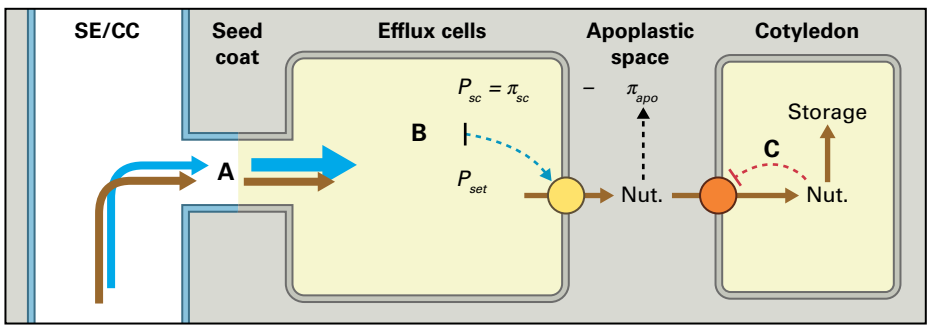


FIGURE 15.55 *A mechanistic model describing how nutrient import to, and within, developing legume seeds is integrated. Phloem-imported nutrients are unloaded as a bulk flow (A; nutrients brown arrow, water blue arrow). Transporter-mediated efflux (brown arrow over yellow circle) from seed coat (sc) to apoplastic space (apo) is regulated by a turgor-homeostat (B). Changes in nutrient withdrawal from the seed apoplastic space by cotyledons causes an immediate osmotic change ($\pi_{sc} - \pi_{apo}$) in seed-coat turgor (P_{sc}). Any deviation in P_{sc} from a turgor set-point (P_{set}) produces a pressure error signal (broken blue line) that alters effluxer activity to match change in rates of nutrient uptake by cotyledons. Transporter-mediated uptake of nutrients from the seed apoplast by cotyledons (brown arrow over orange circle) is coupled to rates of conversion of nutrients into storage compounds (C). Here metabolically induced changes in intracellular nutrient pool sizes regulate activities of plasma membrane transporters by de-repressing transporter gene expression (broken line in C).*

Summary

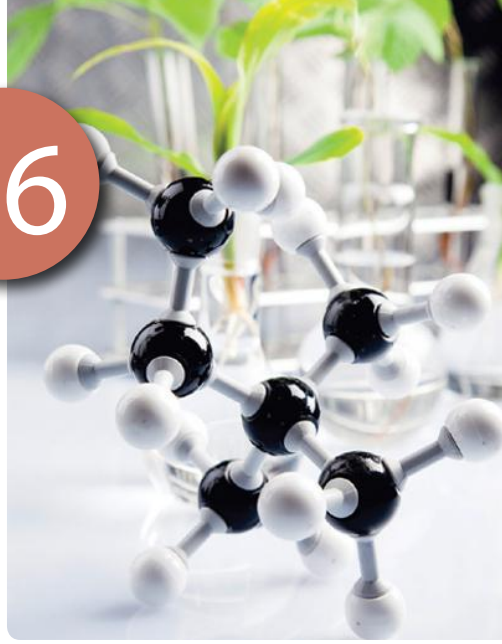
Long-distance transport of resources and signals in vascular plants follows two functionally distinct pathways, xylem and phloem, which closely parallel each other throughout the plant body. Volume flow in xylem is primarily driven by tensions resulting from transpirational water losses. Substances in xylem move to sites of transpiration, whereas movement in phloem is metabolically directed.

Xylem TEs and phloem SEs are structurally modified to form pathways of relatively high hydraulic conductivity. Such design features also accommodate other requirements, such as narrow TEs for strength and rapid sealing to prevent embolism spread. Similarly, proteins in SEs have the potential to impede bulk flow, but major control on transport appears to be exercised at the sink end of phloem pathways. Rapid sealing mechanisms prevent sap loss from damaged SEs.

Long-distance transport of resources and signals involves loading into, axial transport through, and unloading from vascular conduits. Loading and unloading depend upon short-distance transport processes that collectively determine overall fluxes of resources and signals. Plasma membrane (from and to the apoplast) and plasmodesmal (symplasmic) transport both play central roles in resource loading and unloading. Key to TE loading and unloading are efflux from and retrieval by xylem parenchyma cells, respectively. Xylem parenchyma cells also control the diversion of nutrients and toxic ions to different plant regions. These cells also are implicated in repair of embolized TEs after cavitation. Loading SE/CC complexes may be entirely symplasmic or include an apoplastic step at SE/CC/phloem parenchyma or bundle sheath cell interfaces. The concentrating step for symplasmic loading depends upon synthesis of large molecular weight sugar species (RFOs) in CCs that exceed plasmodesmal molecular exclusion limits preventing their back leakage to mesophyll cells. In contrast, apoplastic loaders depend on activities of membrane symporters to load sucrose into SE/CC complexes. These symporters also function along the transport phloem to buffer onward sap transport in tandem with regulated plasmodesmal gating to control nutrient fluxes to and from SEs.

Macromolecular signals, synthesized in CCs, are transferred through PPUs to SEs along with hormones and signals mediating systemic acquired resistance. Viruses have hijacked these transport mechanisms for systemic spread throughout their host plants. In most sinks, nutrients exit STs as a bulk flow of solution via plasmodesmata. This step has a low hydraulic conductance and is accompanied by a large hydrostatic pressure drop, making it effectively irreversible. Plasmodesmata in post-phloem unloading pathways have molecular exclusion limits of at least 30 kDa, presumably an important factor for accommodating high-solute fluxes. In certain circumstances, an apoplastic step is present and may contribute to a sink's capacity to accumulate osmotically active compounds to high concentrations.

Loading, axial transport, and unloading are highly regulated to deliver resources and signals at required levels. For phloem, transport rates are governed by loading of major osmotic species, principally sugars, to generate hydrostatic pressure. Pressure signals transmitted from sinks along phloem conduits function to regulate loading activities. Transport phloem has spare transport capacity but buffers transport fluxes against variation in source outputs. Control of resource partitioning is localized to recipient sink organs where plasmodesmal conductance appears to play an important role. For xylem, transport rates are more variable, being dependent on transpiration, but nutrient transport can be uncoupled from water transport through TE loading. Some nutrients are recycled from phloem to xylem, and K^+ recycling from phloem to xylem in roots is likely to be a component of signaling shoot K^+ status to regulate TE loading.



16

Nitrogen and Sulfur

Sharon R. Long, Michael Kahn, Lance Seefeldt, Yi-Fang Tsay, and Stanislav Kopriva

Introduction

The essential elements **nitrogen** and **sulfur** are acquired by plants primarily through interaction with solutions in the soil (Fig. 16.1). Uptake and use of nitrogen- and sulfur-containing ions occur through highly evolved morphological, physiological, and biochemical mechanisms. Nitrogen and sulfur are often present in soil in oxidized forms that must be reduced for the element to be used in metabolism. These conversions take place in highly reducing environments (characterized by low $E°$ values) and link nitrogen and sulfur assimilation with pathways that generate reducing potential. Nitrate and sulfate reduction are compartmentalized and regulated to facilitate integration with other cellular metabolism. A combination of biochemical and molecular genetic approaches is further elucidating these pathways.

16.1 Overview of nitrogen in the biosphere and in plants

Nitrogen (N) is the fourth most abundant element in living organisms. While nitrogen constitutes less than 0.1% of the earth's crust, it makes up about 80% of the atmosphere, mostly as **dinitrogen** (N_2). Despite the disparity in content, the large mass of the earth's crust means the number of N atoms below ground is about 50 times greater than in the entire atmosphere. Most of this nitrogen is trapped in igneous rocks, and weathering of those rocks does not release much nitrogen to the living world.

The cycling of N between geochemical and biochemical states is quite complex (Fig. 16.2), given the many oxidation states the N atom can occupy in inorganic and organic compounds (Table 16.1). Most of the N taken up by organisms is recycled from a pool of nitrogenous compounds that have been used by other organisms. New inputs to this pool are generated during chemical reactions that accompany natural events (e.g., fire and lightning) or human activity (e.g., use of internal combustion engines and application of **chemical fertilizers**).

The main input to the nitrogen pool in natural ecosystems is from reduction of atmospheric and dissolved N_2 to **ammonia** (NH_3) through the biological process of **nitrogen fixation** (Table 16.2). Nitrogen fixation is carried out only by prokaryotes, including both eubacteria and archeae. The NH_3 produced by nitrogen fixation is usually assimilated into amino acids and thence to protein and other N-containing compounds. NH_3 released from organisms or added as fertilizer may be converted to **nitrite** (NO_2^-) and **nitrate** (NO_3^-) ions by nitrifying bacteria. In turn, NO_3^- enters metabolism through reduction to the **ammonium ion** (NH_4^+) and subsequent assimilation to amino acids by bacteria, fungi, and plants, or it can serve as an electron acceptor for denitrifying bacteria when oxygen is limiting. Losses from the nitrogen compound pool occur physically, when nitrogen (especially NO_3^-) is leached into inaccessible domains in the soil, and chemically, when **denitrification** or the anaerobic ammonium oxidation (**anammox**) reactions release N_2 (Fig. 16.2).

Plants can synthesize the suite of nitrogenous compounds common to all living organisms, as well as numerous molecules found only in plants (Fig. 16.3). The largest requirement for N is the synthesis of amino acids (see Chapter 8), the

Biochemistry & Molecular Biology of Plants, Second Edition. Edited by Bob B. Buchanan, Wilhelm Gruissem, and Russell L. Jones.
© 2015 John Wiley & Sons, Ltd. Published 2015 by John Wiley & Sons, Ltd.
Companion website: www.wiley.com/go/buchanan/biochem

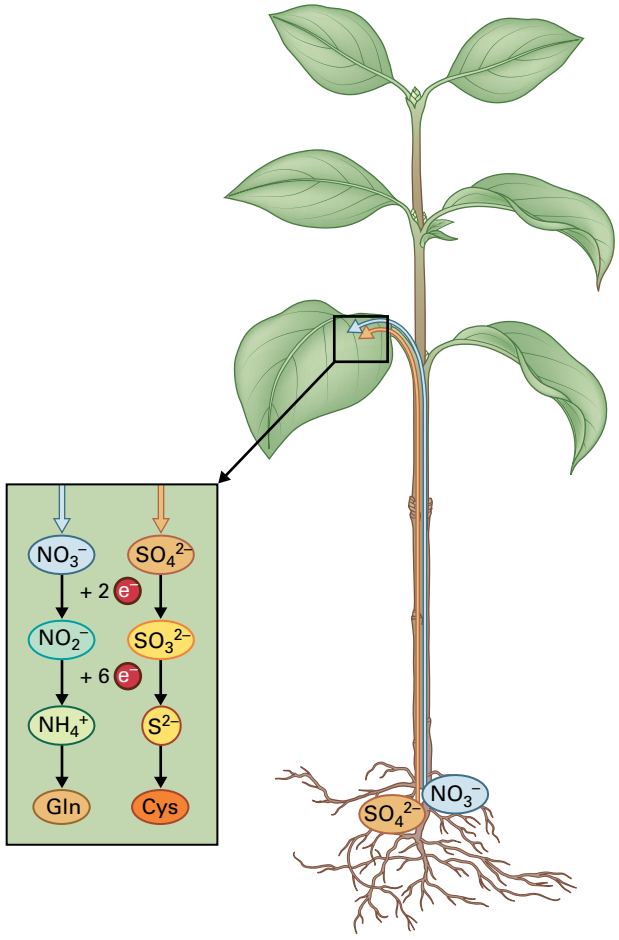


FIGURE 16.1 *Nitrogen and sulfur cycles in plants. Nitrogen and sulfur are both taken up by roots from the soil solution, and both undergo major changes in oxidation state as they are converted from inorganic to biochemically available forms. Nitrogen is converted from nitrate (NO_3^-; oxidation +5) to ammonium (NH_4^+; –3) before being further converted to other compounds through the intermediate amino acid glutamine (Gln). Sulfur is converted from sulfate (SO_4^{2-}; –6) to sulfite (SO_3^{2-}, oxidation +3 and then to sulfide (S^{2-}) and sulfhydryl compounds (R-SH; –2), such as the amino acid cysteine (Cys).*

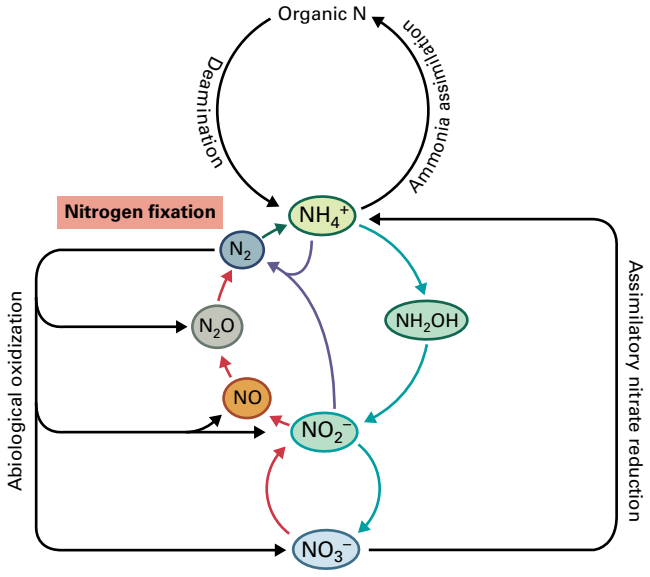


FIGURE 16.2 *The nitrogen cycle. Organic N compounds (top), which are constituents of all living organisms, are released into the environment by death and decay and are excreted as waste by some animals. Microorganisms deaminate organic nitrogen, utilizing the carbon as a food source and liberating ammonium (NH_4^+) in the process. Plants and microorganisms can take up nitrate (NO_3^-) (bottom) and reduce it to NH_4^+ for subsequent assimilation into organic N-containing compounds. Many biological processes that change the oxidation state of nitrogen are catalyzed exclusively by prokaryotes. These include nitrification (blue-green arrows; NH_4^+or nitrite, NO_2^-, is oxidized and the energy released is used to fix inorganic carbon), denitrification (red; nitrogen serves as a terminal electron acceptor and is reduced during anaerobic respiration), annamox (purple; the anaerobic production of molecular nitrogen from $NH_4^+$and NO_2^-), and nitrogen fixation (green; dinitrogen gas, N_2, is reduced to NH_4^+).*

TABLE 16.1 *Inorganic nitrogen compounds.*

Compound	Oxidation state of N	Name
N_2	0	Dinitrogen (nitrogen gas)
NH_3	–3	Ammonia
NH_4^+	–3	Ammonium ion
N_2O	+1	Nitrous oxide
NO	+2	Nitric oxide
NO_2^-	+3	Nitrite
NO_2	+4	Nitrogen dioxide
NO_3^-	+5	Nitrate

building blocks of proteins and precursors to many other compounds. Nitrogen is also an essential component of nucleic acids (see Chapter 6), cofactors, and other common metabolites, and is a major component of chlorophyll (see Chapter 12). The characteristic yellow color of nitrogen-starved plants (chlorosis) reflects their inability to synthesize adequate amounts of green chlorophyll under N-limited conditions (Fig. 16.4). Several plant hormones contain N or are derived from nitrogenous precursors (see Chapter 17). Plants synthesize diverse nitrogenous **secondary compounds**, most prominently the alkaloids (see Chapter 24). Although flavonoids and other plant phenolics do not contain N, they are derived from phenylalanine (see Chapter 24), which means their synthesis is linked to amino acid metabolism. The most important step in assimilating inorganic N into these organic metabolites is the condensation of ammonia and glutamate to form glutamine; this reaction is catalyzed by **glutamine synthetase**, an enzyme subject to extensive regulation in all plants (see Chapter 8).

Plants may acquire nitrogen through NH_4^+ uptake and incorporation into organic compounds, NO_3^- uptake and reduction to NH_4^+, or, in the case of plant hosts for nitrogen-fixing bacteria, acquisition of fixed N from bacterial **endosymbionts** (from the Greek: "living together within").

TABLE 16.2 *Rates of natural and anthropogenic nitrogen fixation.*

Source	Amount of N fixed (Tg/year)*
Lightning	<10
Biological N-fixation in terrestrial systems†	90–140
Biological N-fixation in marine systems	30–300‡
N fertilizer chemical synthesis	100
Fossil fuel combustion	>20

*The standard unit of measure is the teragram, Tg (10^{12} g), equal to 10^6 metric tons.
†This estimate includes both natural ecosystems and agricultural nitrogen fixation.
‡Estimates differ because of variable data.

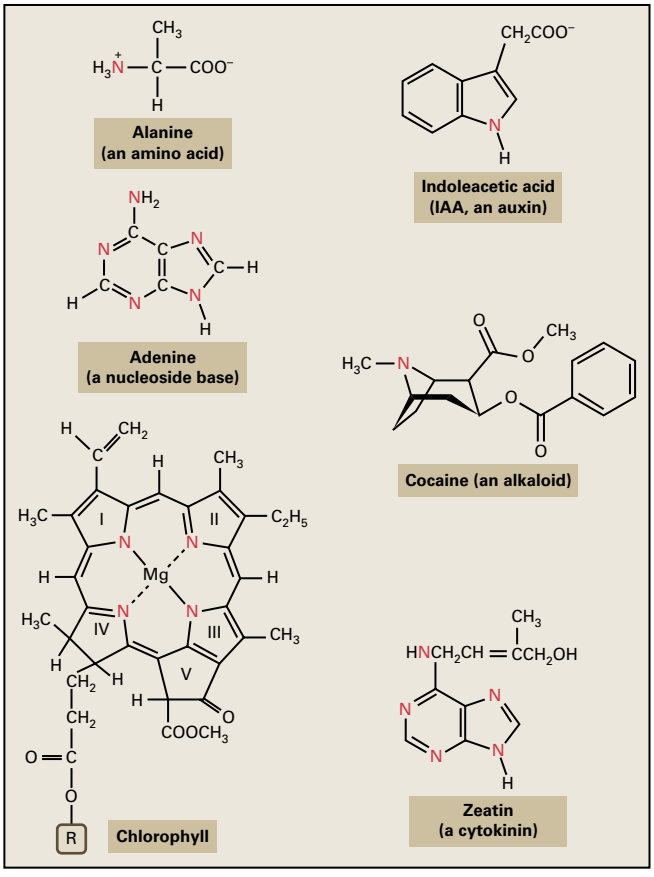


FIGURE 16.3 *Selected organic nitrogenous compounds of biological importance. Though some, such as amino acids and nucleoside bases, are found in all living organisms, chlorophyll is found only in plants and other photosynthetic organisms. Alkaloids such as cocaine are often unique to plants, and hormones such as zeatin and IAA are found in plants and certain plant-interactive microbes.*

Plants display diverse strategies in acquiring nitrogen, as is evident both in comparisons of different species with one another and in comparison of individuals of a given species that are grown in different environments (Fig. 16.5). For



FIGURE 16.4 *Nitrogen deficiency phenotype in wheat plants. Compared to well-nourished plants (left), N deficiency (right) is associated with diminished growth and yellowing (chlorosis) of older leaves.*
Source: From CIMMYT gallery; International Maize and Wheat Improvement Center http://www.flickr.com/photos/cimmyt/5083622155/.

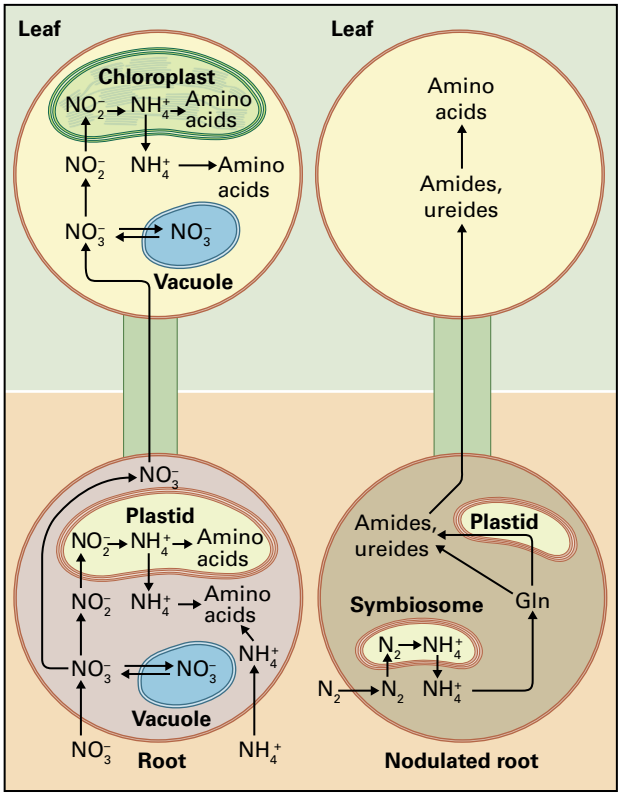


FIGURE 16.5 *Schematic overview of N uptake from mineral nutrition (left) and by a nodulated legume with N-fixing symbionts (right). Plant roots can import nitrate (NO_3^-), ammonium (NH_4^+), and other nitrogenous compounds from the soil. For use in synthesis of amines, NO_3^- must be reduced to NO_2^- and then to NH_4^+. Nitrate reduction in the cytosol and storage in the vacuoles can occur in either the roots or the leaves. Nodulated plants are able to take up nitrogen from the soil (not shown), and generate NH_4^+ also by reducing N_2 through the action of symbiotic bacteria. The NH_4^+ from nitrogen fixation is assimilated into amino acids and ultimately incorporated into amide amino acids (glutamine or asparagine) or ureides for export to the leaves (see Section 16.4.9 and Figs. 16.25 and 16.26).*

BOX 16.1

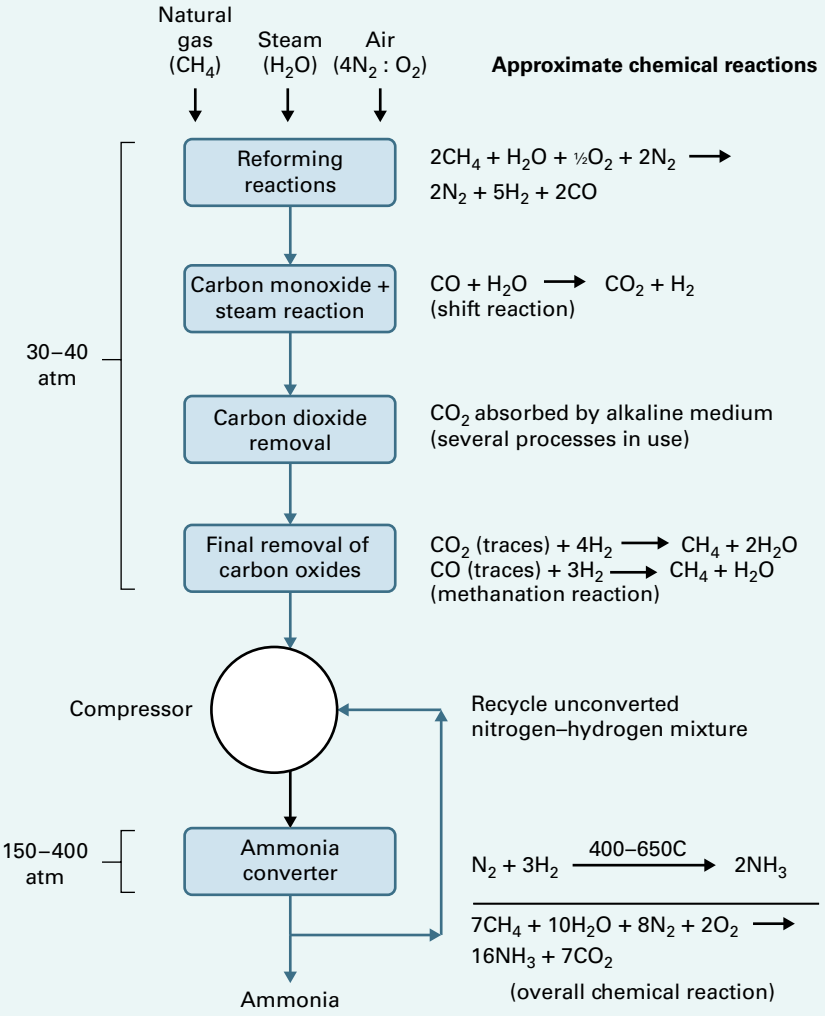
Nitrogenous soil amendments have a long history

The use of soil amendments to enhance plant growth appears to have been widespread in many cultures, according to unwritten tradition and later written records. Farmers rotated crops and applied manure or simple minerals with little quantitative rigor until the 18th to 19th centuries, when chemical analysis of soils and study of plant growth requirements became more defined. By the early 19th century, nitrogen fertilizer was applied on a larger scale, both in the form of manures, including guano, and as mineral nitrates. However, the use of nitrogen supplies for fertilizer had to compete with the demand for these chemicals as components of explosives and gunpowder.

Production of ammonia (NH_3), initially a byproduct of the coking of coal, was transformed in 1913 by the work of Fritz Haber and Carl Bosch in Germany, who developed a complete practical synthesis of NH_3 from N_2 and H_2 in the presence of an iron catalyst at high temperature and pressure. The reaction of dinitrogen with hydrogen gas is actually exothermic (ΔH_f° for $NH_3(g)$ is –46.1 kJ mol^{-1}), but the activation energy for the reaction is very high because of the triple bond in dinitrogen:

$$N_2(g) + 3H_2(g) \rightarrow 2NH_3(g)$$

At room temperature the reaction is favored but very slow, and at very high temperature the equilibrium favors reactants, not products. K_{eq} is 6.0×10^5 at 298 K, 2.1 ($\times 10^0$) at 450 K, and 4.4×10^{-5} at 800 K. The industrial **Haber–Bosch** process that takes hydrogen from methane to make ammonia is a compromise, using pressures ranging from 150 to 400 atmospheres, temperatures ranging from 400°C to 650°C, and metal catalysts; ammonia is removed as it is formed (see figure). Agricultural practices based on inputs of NH_3-based nitrogen fertilizers (see Table 16.2) require large amounts of fossil fuel (usually methane), which may become a serious limitation as energy costs rise. **Industrial nitrogen fixation** uses about 5% of world natural gas production to produce over 100×10^{12} g N/yr (see Table 16.2).



example, NO_3^- taken up by roots may be reduced and assimilated in the root ($NO_3^- \rightarrow NH_4^+ \rightarrow$ glutamine), or it may be transported to the shoot as NO_3^- and then assimilated. NO_3^- may also be stored in vacuoles in root or shoot cells. Plants able to establish symbioses control the formation and function of the required symbiotic structures in response to their nutritional environment. For example, legume plants grown in the presence of NO_3^- preferentially use this as a source of nitrogen for nutrition and do not form symbiotic nodules (see Section 16.4.2) or allow invasion of bacterial endosymbionts such as *Rhizobium*. Acquisition of nitrogen occurs in a context that is physiological, developmental, and environmental. A comprehensive investigation of nitrogen assimilation requires the study of genes and gene expression, of protein structure and activity, and of root development and physiology.

As photoautotrophs, plants are typically limited in their growth by the availability of nutrients other than carbon. They need relatively large amounts of nitrogen, and because usable nitrogen can be lost from the rhizosphere by leaching or microbial transformation, nitrogen availability frequently limits plant productivity. As a result, widespread application of nitrogenous **fertilizer** has been a key factor in improving agricultural yields during the 19th and 20th centuries (Box 16.1). As the human population grows and the demand for agricultural products increases, it becomes all the more important to understand the mechanisms of plant nitrogen acquisition.

16.2 Overview of biological nitrogen fixation

16.2.1 Some prokaryotes can reduce nitrogen gas to ammonia using the enzyme nitrogenase

N_2 constitutes about 80% of the earth's atmosphere, but the stability of its triple bond renders it inert and metabolically inaccessible to most organisms. Eukaryotes cannot use N_2, but some microbes called **diazotrophs**, which include many different eubacteria as well as some methanogenic archaea, are able to catalyze the enzymatic reduction of this compound to ammonia (NH_3) using the enzyme nitrogenase (Reaction 16.1, see Section 16.3). Unlike the Haber–Bosch process (see Box 16.1), such biological nitrogen fixation occurs at ambient temperatures and atmospheric pressure.

Reaction 16.1: Nitrogenase

$$N_2 + 16\,ATP + 8e^- + 8H^+ \rightarrow 2NH_3 + H_2 + 16\,ADP + 16P_i$$

Diazotrophs are represented by free-living microbes as well as a few species of bacteria that are able to establish symbiotic associations with plants. Much of what we know about the genetics and biochemistry of nitrogen fixation has been determined by studying free-living eubacteria such as ***Clostridium, Klebsiella, Azotobacter***, and ***Anabaena***, and results from these investigations have provided detailed information about factors that constrain all nitrogen-fixing systems. These free-living nitrogen-fixing microbes must obtain their energy from outside sources, for example, by oxidizing decaying or decomposing materials in the soil. By contrast, nitrogen fixed by bacteria in symbiosis is exchanged for carbon fixed by the plant, and nitrogen fixation is more efficient because the plant environment provides optimized physiological conditions. This support can overcome constraints that often limit nitrogen fixation by nonsymbiotic bacteria (see Section 16.4).

16.2.2 Nitrogen fixation is sensitive to oxygen

Nitrogen fixation is a unique biochemical reaction that consumes energy-rich compounds while requiring strong biological reductants (see Reaction 16.1). Because nitrogenase and some of the proteins that supply it with reductant are sensitive to oxygen, many nitrogen-fixing bacteria are anaerobes. Neither fermentation nor anaerobic respiration oxidizes reduced carbon compounds as efficiently as aerobic respiration, so anaerobic bacteria must process large quantities of substrate to generate the large amount of ATP required for N_2 fixation. In contrast, aerobes and microaerobes can take advantage of the increased ATP production from aerobic metabolism but must contend with the oxygen sensitivity of nitrogenase.

In some cases, free-living nitrogen-fixing organisms use mechanical, temporal, or biochemical barriers to keep oxygen away from the biological catalysts of nitrogen fixation. In other cases, the nitrogen fixation machinery is segregated spatially into specialized structures. For example, some **filamentous cyanobacteria** generate **heterocysts,** thick-walled cells that fix nitrogen but cannot complete all the reactions of oxygenic photosynthesis. Heterocysts produce the ATP needed for nitrogen fixation using cyclic photophosphorylation, a light-dependent process that does not create oxygen gas (see Chapter 12). Some nonfilamentous cyanobacteria segregate photosynthesis from nitrogen fixation temporally, performing oxygenic photosynthesis in the light, and nitrogen fixation in the dark.

16.3 Enzymology of nitrogen fixation

Nitrogenase is a complex, metal-containing enzyme. At least three distinct classes of nitrogenase are known that differ in their metal composition, but the best-studied nitrogenase is the **molybdenum** (Mo)-dependent enzyme (Fig. 16.6).

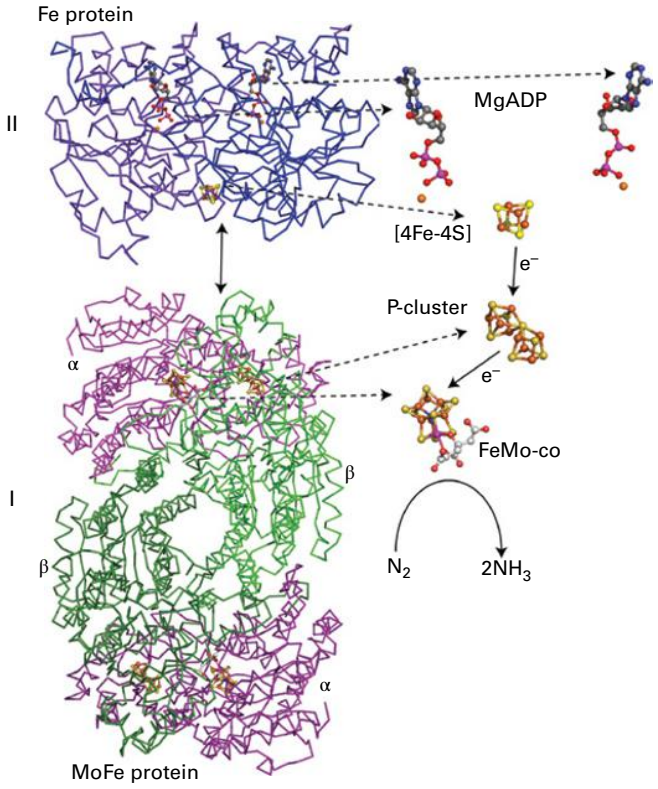


FIGURE 16.6 *Structures of MoFe (Component I, nitrogenase; lower figure) and Fe (Component II, nitrogenase reductase; top of figure) proteins of nitrogenase, and electron flow through the two enzymes. The Fe protein is encoded by* nifH, *and it accepts electrons from a carrier, such as ferredoxin or flavodoxin. The identity of the carrier varies, depending on the biological system involved. The Fe protein, with net hydrolysis of ATP, transfers single electrons at very negative potential to P-clusters in the MoFe protein. The MoFe protein, an* $\alpha_2\beta_2$ *heterotetramer of subunits encoded by* nifD *and* nifK, *accepts electrons at the FeMo cofactor and binds* H^+ *ions and* N_2 *molecules in a stepwise cycle, ultimately leading to the production of* H_2 *and ammonia.*

16.3.1 Nitrogenase is composed of two component proteins

Nitrogenase is a complex consisting of the **MoFe protein** (**dinitrogenase** or component I) a heterotetramer, and the **Fe protein** (**dinitrogenase reductase** or component II) a homodimer. The reduction of N_2 by nitrogenase involves a complicated interplay between these two components. The MoFe protein houses the active site metal cluster where N_2 binds, whereas the Fe protein delivers electrons to the MoFe protein component in a reaction coupled to the hydrolysis of MgATP. Enzymatic reduction of N_2 by nitrogenase also requires the reduction of two protons to form H_2, so the reaction uses eight protons and eight electrons and hydrolyzes 16 MgATP to 16 MgADP and 16 P_i (see Reaction 16.1). Why nitrogenase evolves H_2 during N_2 reduction is not well understood.

Part of the complexity of the interactions between these two proteins is dictated by the fact that the Fe protein can only transfer one electron at a time to the MoFe protein. This transfer is coupled to the hydrolysis of two MgATP molecules to yield two MgADP and two P_i. After it has donated an electron to the MoFe protein, the oxidized Fe protein dissociates and another reduced Fe protein takes its place. Thus, the complete reduction of one N_2 molecule requires that Fe proteins associate and dissociate from the MoFe protein at least eight times in order to accumulate sufficient electrons to achieve N_2 and proton reduction and generate ammonia. The oxidized Fe proteins released from the MoFe protein are reactivated for the cycle by being reduced using a small electron carrier protein (i.e., ferredoxin or flavodoxin), with electrons coming from metabolism; the two MgADP are exchanged for two MgATP molecules.

Two similar nitrogenase classes (often called alternative nitrogenases) contain **vanadium** (V) or Fe in place of the Mo. Far less is known about how these enzymes reduce N_2, but it is thought they follow the same basic reaction sequence outlined above for the Mo-dependent nitrogenase system. Related, but distinct genes code for the alternative nitrogenase classes. The metal content of the active sites are similar between the classes, with the key difference being the presence of a single Mo or V, or an additional Fe atom in the active site of the cofactor (see Section 16.3.2).

16.3.2 The MoFe protein binds N_2 at a unique metal cofactor

The MoFe protein houses the active site where N_2 binds and is reduced. The protein is a $(\alpha\beta)_2$ heterotetramer, with each αβ dimer representing a functioning catalytic unit (Fig. 16.6). Each MoFe protein is, therefore, composed of two catalytic units, with each unit having a site for associating with an Fe protein.

Each αβ dimeric unit of the MoFe protein contains two unique metal cluster assemblies, or cofactors. One cofactor, called the **FeMo cofactor** or FeMoco (fee-moh-koh), is composed of Mo, Fe, sulfur (S), carbide (C), and the organic acid ***R*-homocitrate** that are arranged in a complex metal cluster with an overall stoichiometry of [1Mo–7Fe–9S–1C–1homocitrate] (Fig. 16.7). FeMoco can be viewed as a [4Fe–3S] cube linked by three sulfides (S^{2-}) to a [1Mo–3Fe–3S] cube. The organic acid *R*-homocitrate binds to the Mo on one end of the cofactor using two of its oxygen atoms. The cofactor is covalently bound to the protein through a cysteine (Cys) amino acid side chain ligand to a specific Fe on one end and through a histidine (His) side chain ligand to the Mo on the other end. A high-resolution X-ray structure of the MoFe protein shows an additional carbon atom (C) at the center of the FeMoco cage, an extraordinary configuration for a single carbon.

FeMoco is the site of N_2 binding and reduction, but exactly where N_2 binds to this metal cluster during the reaction is not yet established. Growing evidence suggests some substrates,

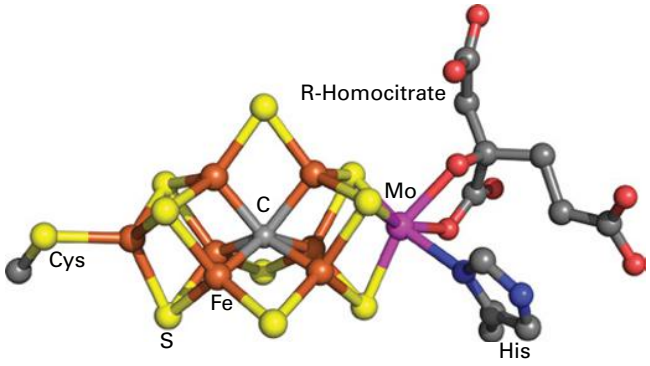


FIGURE 16.7 *Molecular model of iron-molybdenum cofactor (FeMo cofactor). Carbon is shown in gray, iron in rust, sulfur in yellow, oxygen in red, nitrogen blue, and molybdenum in magenta. The atom at the center of FeMo-co is a carbide (C^{4-}) atom C. The Mo-type of nitrogenase is present in all symbiotic bacteria, including* Rhizobium *and* Bradyrhizobium.

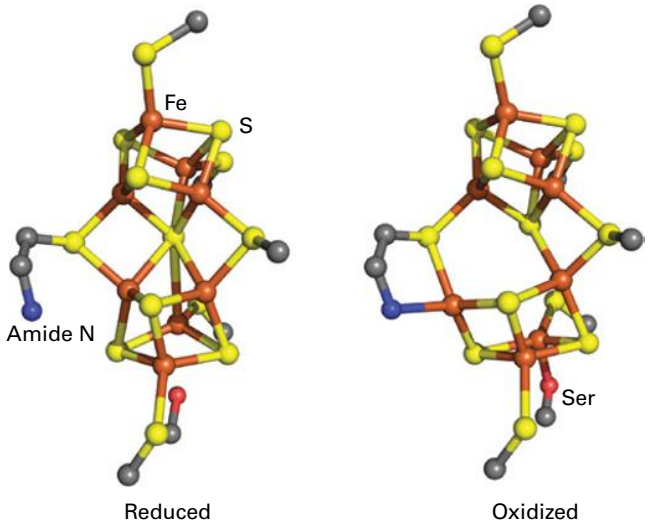


FIGURE 16.8 *Structure of the P-clusters of the MoFe protein. Reduced and oxidized conformations are shown. Iron atoms are shown in rust, sulfur atoms in yellow.*

including N_2, bind to one or more of the Fe atoms in the central region. These studies have taken advantage of the fact that nitrogenase can reduce several nonphysiological substrates, small molecules that contain double or triple bonds. The classic alternative substrate for nitrogenase is the alkyne **acetylene** ($HC{\equiv}CH$), which is reduced to the alkene ethylene ($H_2C{=}CH_2$). Because ethylene is easily measured using gas chromatography, the reduction of acetylene by nitrogenase is commonly used as a test for nitrogenase activity, both in the field and with the purified enzyme.

Each αβ dimer of the MoFe protein contains a second metal cluster called the **P-cluster** (see Figs. 16.6 and 16.8). This cluster contains Fe and S with a stoichiometry of [8Fe-7S], arranged in an overall structure that can be viewed as a [4Fe–4S] cube bridged by an S at one corner to a [4Fe–3S] cube (Fig. 16.8). In addition to the usual binding of the P-cluster to the protein through cysteine residues, the P-cluster is also linked to the protein in certain oxidation states through the O side chain of a serine and an amide from the protein backbone. The cluster rearranges as it is oxidized or reduced, but the function of this rearrangement remains unknown. The P-cluster likely accepts each electron donated by the Fe protein, and it transfers one or more electrons to the FeMo-cofactor to support substrate reduction. How many electrons accumulate on the P-cluster and the order of the electron flow through the P-cluster during the complete catalytic cycle remain to be firmly established.

16.3.3 The Fe protein is a reductase that also hydrolyzes MgATP

The Fe protein functions as a reductase, delivering electrons to the MoFe protein, and it is constructed from two identical protein subunits (γ_2). These two subunits are covalently linked to each other through a single [4Fe–4S] cube cluster that is bound by two cysteine amino acids from each subunit (see Fig. 16.6). The [4Fe–4S] cluster is located at one end of the Fe protein. Each protein subunit also contains a nucleotide-binding site, which is located on the end of the protein away from the [4Fe–4S] cluster.

The binding of two MgATP molecules, one to each subunit, changes the overall structure of the Fe protein. Important consequences of this protein conformational change include changes to the properties of the [4Fe–4S] cluster. The reduction midpoint potential of the [4Fe–4S] cluster changes from –300 mV to –420 mV when MgATP binds. Since the nucleotide-binding site is located some distance away from the [4Fe–4S] cluster, this change in potential must be accomplished through protein conformational changes. The more negative reduction potential of the [4Fe–4S] cluster associated with ATP binding promotes electron transfer from the Fe protein to the MoFe protein. The MgATP-induced protein conformational change also increases the affinity for docking of the Fe protein to the MoFe protein. Thus, the MgATP-bound state of the Fe protein favors association with the MoFe protein and subsequent electron transfer.

This feature has been exploited to trap a stable Fe protein–MoFe protein complex by using a MgATP analog. The complex was examined by X-ray crystallography, revealing the location of Fe protein docking to the MoFe protein (see Fig. 16.6). This arrangement suggests an electron transfer chain that starts at the [4Fe–4S] cluster of the Fe protein, goes to the P-cluster of the MoFe protein, and finishes at the MoFe-cofactor of the MoFe protein. The initial transfer of a single electron from the [4Fe–4S] cluster of the Fe protein is activated by the hydrolysis of the two bound MgATP molecules. The reactions of the Fe protein and of the MoFe protein can be viewed as two joined cycles (Fig. 16.9), with the Fe protein cycle driving the stepwise progression of the MoFe protein cycle.

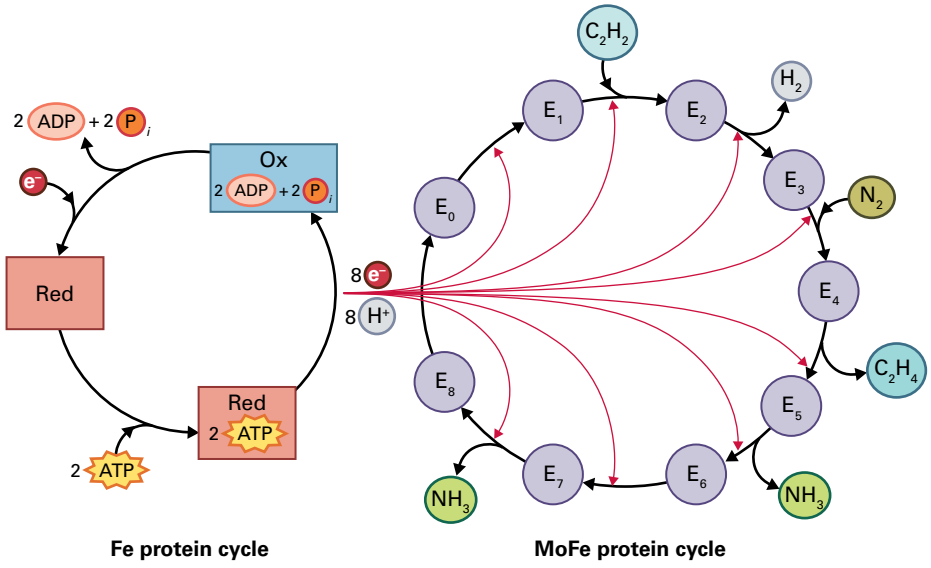


FIGURE 16.9 *The Fe and MoFe enzyme cycles. E_n represents the redox state of the MoFe protein enzyme after it has accepted n electrons, and red arrows illustrate the transfer of a single electron and association of a proton. In the initial steps of the reaction, H_2 may evolve without productive binding of N_2, essentially wasting the ATP and reductant invested in creating these intermediates. Dinitrogen (N_2) can bind to the enzyme by displacing H_2 from either the E_3 or E_4 forms; thus, formation of molecular hydrogen is an obligatory step in the enzymatic reduction of N_2. Treatment of later complexes with acid releases ammonia, which suggests the N atoms in these complexes are associated with more than one H.*

Multiple electrons must be accumulated within the MoFe protein, where they are distributed between the P-cluster, the FeMo cofactor, and partially reduced substrates. The MoFe protein must accumulate a minimum of eight electrons to complete the N_2 reduction catalytic cycle. The stepwise reduction of the MoFe protein is conveniently represented by designating the protein as being in an E_n state, where n is the number of electrons that have accumulated within the MoFe protein. In this nomenclature, E_0 represents the MoFe protein in its resting state, while each subsequent reduced state is designated as E_1, E_2 through E_8. Different substrates bind to different E states of the MoFe protein. For example, acetylene is proposed to bind to the E_2 state, while N_2 is proposed to bind to the E_3 and E_4 states.

For proton and acetylene reduction in the absence of N_2, only the E_0–E_2 states need to be accessed, as these reactions are only two-electron reductions. For the reduction of N_2, all eight E states would be accessed. The intermediates that exist during the reduction of N_2 are not known, but it is assumed N_2 stays bound to FeMo-cofactor during the complete reaction, existing as partially reduced intermediates that stay bound to FeMo-cofactor until ammonia is released. Based on the reduction of N_2 with small metal compounds, it is reasonable to assume partially reduced intermediates bound to FeMo-cofactor occur at the levels of reduction of diazene (HN=NH) and hydrazine (H_2N–NH_2). The actual intermediates involved, the site of intermediate binding, and the distribution of electrons within the MoFe protein during catalysis must be established in future studies to gain a better understanding of the mechanism of this complex enzyme.

Reduced ferredoxin (or, in some organisms, flavodoxin) is thought to donate electrons to dinitrogenase reductase in many free-living nitrogen-fixing bacteria. The enzyme pyruvate **ferredoxin (flavodoxin) oxidoreductase** can transfer electrons to oxidized ferredoxin (flavodoxin) from pyruvate. Some organisms, including rhizobial symbionts, may have alternative, electron transport-coupled methods of generating the low-potential electrons required to reduce these electron carrier proteins.

16.4 Symbiotic nitrogen fixation

In natural terrestrial ecosystems, 80–90% of the nitrogen available to plants originates from biological nitrogen fixation, and of that total, approximately 80% is produced in symbiotic associations. Symbiotically fixed nitrogen can increase plant growth and yield considerably, as seen in comparisons of plants grown on nitrogen-poor soils with or without effective symbiotic bacteria (Fig. 16.10). The benefits of nitrogen fixation, however, are not without cost: if all plant resources required to establish **nodules** (specialized structures where nitrogen fixation takes place; see Section 16.4.2), fix nitrogen, and transport the resulting ammonia throughout the plant are taken into account, obtaining nitrogen through symbiosis consumes 12–17 g of carbohydrate per gram of nitrogen fixed. Predictably, legumes have mechanisms to suppress nodule formation and function if nitrate or ammonia is available as an alternate source of nitrogen. Improved understanding of plant and bacterial genes used in symbiosis may allow plant breeders and microbiologists to provide better-functioning host bacteria for agricultural systems.



FIGURE 16.10 *Legumes depend on effective rhizobia. At right, soybean provided with an effective rhizobial inoculum; at left, soybean grown with an ineffective native rhizobial resident in the soil.*
Source: Vessey (2004) Crop Management doi:10.1094/CM-2004-0301-04-RV.

Quantitative isotope ratio measurements are used to assess the contribution of nitrogen fixation to total nitrogen in plants. Atmospheric nitrogen is essentially all $^{14}N_2$, and soil often contains greater amounts of the stable isotope ^{15}N. A plant that obtains fixed nitrogen from the atmospheric pool through nitrogen-fixing symbiosis will have less ^{15}N in its total nitrogen than if it obtains nitrogen only from soil sources. The best controls for this measurement are plants of the same species grown in the same soil but without symbiotic bacteria. **Rhizosphere** (root zone) and other associations of plants with some free-living nitrogen-fixing bacteria (e.g., *Azospirillum, Azoarcus,* and *Herbaspirillum*) increase yield in crops including sugar cane (*Saccharum* spp.) and sorghum (*Sorghum* spp.). The microbes enhance plant growth by producing plant hormones and other compounds, but the contribution of nitrogen fixation to this growth increase is not clear.

16.4.1 Diverse vascular plants establish nitrogen-fixing symbioses

Nitrogen-fixing symbioses are not restricted to vascular plants. Hosts for nitrogen-fixing bacteria include fungi (lichens) and animals ranging from marine corals to terrestrial termites. In the case of vascular plants, three major groups of prokaryotes establish morphologically developed N_2-fixing symbioses.

The first group of symbioses exists between cyanobacteria, such as ***Anabaena***, and diverse plants, including cycads, ferns, liverworts, hornworts, and one angiosperm genus, ***Gunnera***. These hosts elaborate specialized structures to accommodate the cyanobacteria. For example, *Gunnera* is infected in glands at the base of leaf petioles, cycads produce specialized "coralloid" roots, and ***Azolla,*** a water fern that associates symbiotically with the cyanobacterium *Anabaena,* harbors the bacteria in a leaf cavity. The *Azolla–Anabaena* pair is used as a cocrop with **rice (*Oryza sativa*)**; it produces sufficient fixed nitrogen to allow continuous and sustainable rice cultivation.

A second type of symbiosis occurs between members of a Gram-positive **actinomycete** genus (***Frankia***) and a diverse group of dicots from over 20 genera in eight or more families within the **Rosid I lineage** of dicotyledonous plants (Fig. 16.11). The hosts include trees or woody shrubs such as alder (*Alnus*), myrtle (*Myrica*), *Casuarina*, and *Ceanothus.* These symbiotic associations play a significant role in the nitrogen economies of forests and other natural ecosystems. The *Frankia* symbionts group taxonomically as a few closely related clades, with no apparent transfer to distantly related actinomycetal species. The taxonomy of these *Frankia* groups correlates with that of the host plants.

Symbiotic *Frankia* and their hosts establish nodules, unique structures within the host roots in which nitrogen fixation occurs. *Frankia* penetrate the plant root with filamentous bacterial hyphae, either through root hairs or by means of intercellular penetration along contiguous cell walls. Within plant cells, the bacterial hyphae form branches, establishing a large bacterial surface area in intimate contact with plant cell membranes. The form of the invading bacteria differs between host plants, from simple or swollen branches to septate vesicles. The plant accommodates the invading bacteria by constructing a peripheral capsule rich in cell wall-like materials, and the body of the root nodule forms by new divisions of cortical and hypodermal cells. Plant hormone changes are associated with nodule formation and infection: auxin-dependent promoters, for example, show enhanced activity in infected host cells of actinorhizal nodules. The plant also differentiates by expressing nodule-specific genes encoding proteases, cell wall proteins, hemoglobin, cell division functions, and metabolic enzymes. At the molecular level, some genes required for legume symbiosis (see Section 16.4.3) have sequence and functional homologs in *Frankia* hosts (see Box 16.2).

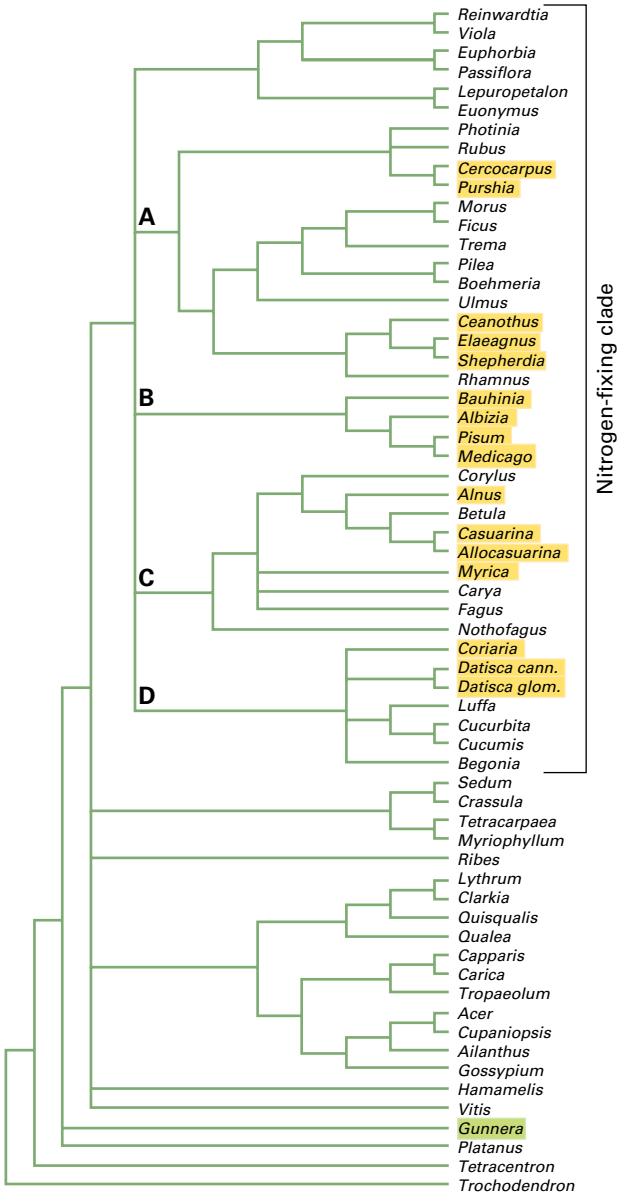


FIGURE 16.11 *Phylogenetic analysis of 99* rbcL *genes (encoding the large subunit of Rubisco) from genera representing the subclass Rosidae and additional angiosperm taxa. Taxa that engage in nodular nitrogen-fixing symbioses are highlighted in yellow.* (Gunnera*, which hosts cyanobacterial endosymbionts, is marked in green.) Note that a single clade includes all the nodule-forming genera included in the tree. Subclades A, C, and D include actinorhizal symbiotic hosts; the legume family (Fabaceae) falls into subclade B.*

A third group of symbioses involves rhizobia, which are Gram-negative bacteria that infect numerous **legumes** (Fabaceae) and one known nonlegume, ***Parasponia*** (Ulmaceae). These plants are also in the Rosid I lineage (Fig. 16.11, see Section 16.4.2). Rhizobial endosymbionts contribute nitrogen to commercially important seed legumes such as peanut (***Arachis hypogaea***), soybean (***Glycine max***), lentil (***Lens culinaris***), bean (***Phaseolus vulgaris***), pea (***Pisum sativum***), cowpea (***Vigna unguiculata***), and forage crops, such as clover (***Trifolium*** spp.) and alfalfa (***Medicago sativa***). Rhizobial symbioses are also important in plants used for land stabilization and reclamation, and in natural environments.

Taxonomic analyses group most of the rhizobial bacteria into distinct major clusters within the α-proteobacteria (including ***Rhizobium***, ***Sinorhizobium***, ***Azorhizobium***, ***Mesorhizobium***, and ***Bradyrhizobium***), and β-proteobacteria (***Burkholderia*** and ***Cupravidius***). These genera do not form single clades within either the alpha or beta groups. Symbioses between groups of plant hosts and particular bacterial species, or biovars, display various levels of specificity (Table 16.3). Host specificity does not correlate strictly with bacterial phylogeny; disparate genera of bacteria may nodulate a single type of host plant. Host specificity does, however, correlate with the structures of bacterial signal molecules, the **Nod factors** (see Section 16.4.4), and with corresponding bacterial ***nod* genes**.

16.4.2 Legumes develop root nodules to house rhizobial symbionts

In the presence of compatible rhizobial species, legume hosts also form **root nodules** (Fig. 16.12), in which environments conducive to nitrogen fixation are established, especially the microaerobic conditions needed for bacteria to synthesize ATP and stabilize nitrogenase. Plant metabolism in the nodule generates organic acids, some of which are catabolized by the rhizobial symbionts to fix nitrogen. The bacteria release the resulting ammonia to the plant, which assimilates it into **amides** or **ureides**. These compounds are used to transfer fixed (reduced) nitrogen to the rest of the plant. Few rhizobia fix nitrogen outside the plant host. Bacterial nitrogen fixation is most useful to the plant when it has no other nitrogen sources; both nodule formation and function are subject to downregulation by host plants that are provided with nitrate or ammonia.

Root nodules are constructed by the plant in response to bacteria. Briefly, the rhizobia, attracted to molecules released by the host legume's roots (see Section 16.4.3), attach to the host's root hairs. The rhizobia produce chemicals called Nod factors (see Section 16.4.4) that cause the colonized root hairs to curl, trapping the rhizobia, which then penetrate the root hairs and typically form a tubular structure called an infection thread. Once the bacteria reach the root itself, they stimulate cortical cell division, leading to the formation of the nodule (see Sections 16.4.5–8). As the nodule develops, the rhizobia are released inside the plant cells that form the nodule, still surrounded by a plant-derived membrane. The bacteria within these plant membranes have weak cell walls and form large, irregularly shaped branching cells called bacteroids, at which point they depend entirely on the host legume for their energy needs (see Section 16.4.9).

The molecular signals and mechanisms underlying nodule formation have been studied by combining genetics with analysis of cell behavior, biochemical function, and gene expression.

BOX 16.2 Nodulation shares features of signaling pathways involved in other symbioses

Nod factors are structurally similar to chitin fragments, which are components and breakdown products of fungal cell walls that elicit plant defense reactions. It is intriguing that legumes detect a bacterial signal resembling a pathogenic elicitor, and that the plant inducers of bacterial *nod* genes are flavonoids, a chemical family employed in legumes as phytoalexin defense molecules in response to pathogens. The pattern of signaling in which an organism first evolves to tolerate a toxic molecule and then to respond to its presence is a classic paradigm of coevolution.

Recruitment of existing pathways for new uses is also suggested by the fact that some host genes required for rhizobial symbioses are also used for other plant symbioses. A *Casuarina* gene required for *Frankia* symbiosis is homologous to *SYMRK* and can complement a legume SymRK-deficient mutant. Some legume genes required for nitrogen fixing symbiosis—SymRK, ion channel, and CCAMK—are also required for vesicular–arbuscular mycorrhizal infection of those same plants. Mycorrhizal cultures produce lipochitin oligosaccharide (LCO)-like chitin-oligomers that resemble Nod factors and can cause legume Ca^{2+} spiking. Ca^{2+} spiking can be triggered by unmodified chitin as well. It remains to be discovered whether the chemical modifications of mycorrhizal LCOs confer added information, such as host range and the ability to trigger unique functions to support mycorrhizal infection and differentiation.

Further evidence for the evolutionary relatedness of mycorrhizae and rhizobial symbioses comes from study of ***Parasponia***, the only nonlegume nodulated by *Rhizobium*. In this plant, a single protein appears to act as receptor for both mycorrhizal and rhizobial signals. The ancient and widespread occurrence of **mycorrhizal symbioses** suggests the genes governing these associations may have been co-opted during coevolution to enable the more recent *Frankia* and *Rhizobium* symbioses.

TABLE 16.3 *Examples of rhizobia-plant host range.*

Bacterial species*	Frequently studied host plants†
Sinorhizobium meliloti	*Medicago* (alfalfa, barrel-medic)
Rhizobium leguminosarum bv viciae *R. leguminosarum* bv trifolii	*Vicia* (vetch) *Pisum* (pea) *Trifolium* (clover)
Mesorhizobium loti	*Lotus* (trefoil) *Lupinus* (lupine)
Bradyrhizobium japonicum	*Glycine* (soybean) *Macroptilium* *Vigna* (cowpea)

*Previous taxonomic schemes classified many of these genera as *Rhizobium*.
†Only the genus of the host plants is indicated. The list of host plants is not comprehensive, particularly for broad host-range bacteria.
bv, biovar.

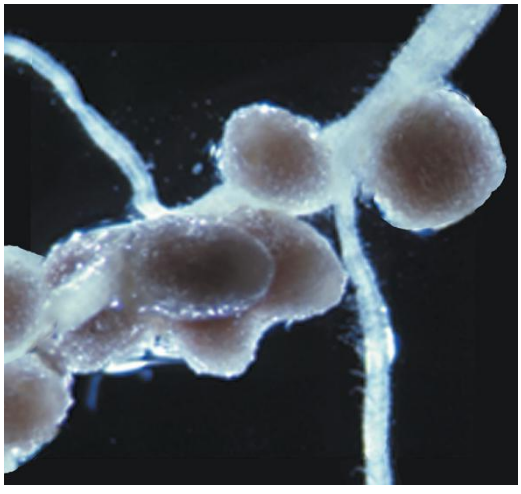
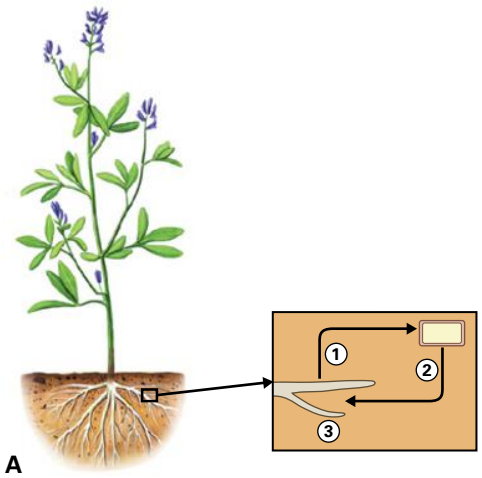


FIGURE 16.12 *Photo of root nodules on pea* (Pisum sativum). *Source*: Long, Stanford University, Palo Alto, CA; previously unpublished.

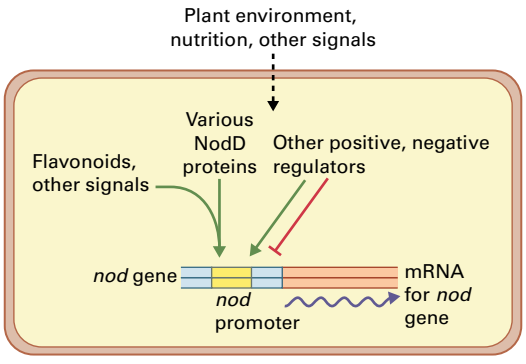
16.4.3 Plant flavonoids activate rhizobial transcription

Accurate mutual recognition in legume-rhizobia systems is accomplished by exchange of biochemical signals. Molecules released by the host plant induce bacterial gene expression (Fig. 16.13), and this leads to production of bacterial signal molecules and proteins that modify plant metabolism and development.

Specific bacterial genes are involved in the sequential stages of symbiosis. The rhizobial genes responsible for early nodule formation are termed *nod* genes (see Section 16.4.4), and expression of these genes typically depends on a chemical signal from the plant (the inducer) and on a bacterial transcription

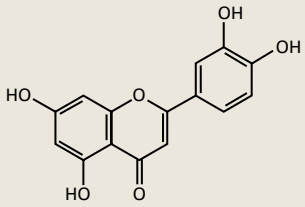
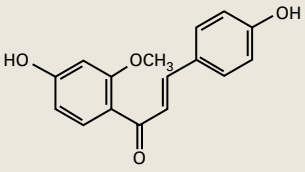
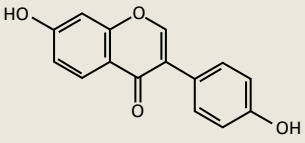
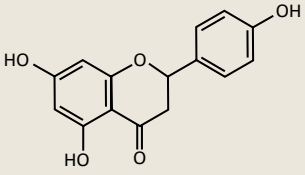


A



B

Host compounds that actively induce *nod* gene expression

Flavonoid inducers Category	Name/activity	Specific structure
Flavone	Luteolin, a flavone inducer from *Medicago* spp., active on *S. meliloti*	
Chalcone	4,4′-Dihydroxy-2′- methoxychalcone, a chalcone inducer from *Medicago*	
Isoflavone	Daidzein, an isoflavone active on *B. japonicum*	
Flavanone	Naringenin, a flavanone active on *R. leguminosarum* bv. *viciae*	

C

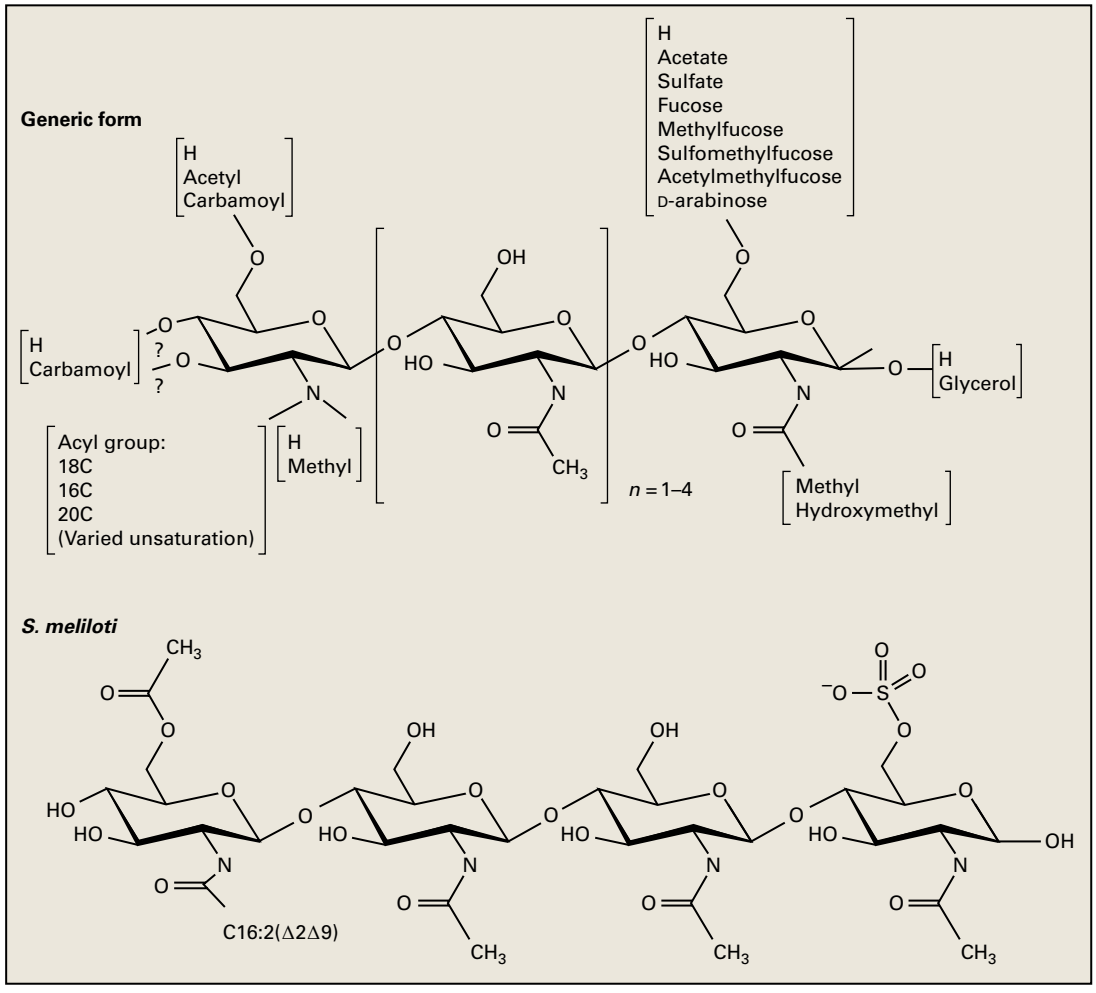
FIGURE 16.13 *Signals in early nodule development. (A) Plant and bacteria exchange molecular signals. In many cases, step 1 is plant production of a root-derived flavonoid, and step 2 is recognition of the flavonoid and production of a bacterial Nod factor, which triggers responses in the plant (step 3). (B) In the bacterium, the transcriptional activator NodD interacts with a plant inducer and the transcriptional machinery of the bacterium to induce expression of bacterial* nod *genes. The circuits for* nod *gene activation may also respond to environmental cues and as yet unknown signals from the plant. (C) Flavonoids, the prominent inducers of rhizobial* nod *gene expression. The plant compounds that most actively induce expression of nodulation genes vary among different plant-symbiont systems. A bacterium's* nodD *genotype is a primary determinant of the preferred inducer structure.*

activator, NodD (Fig. 16.13B). The plant signals that induce *nod* gene expression are commonly flavonoids (Fig. 16.13C; see also Chapter 24), and their diverse structures provide initial recognition for plant–bacteria communication.

Genetic and biochemical data indicate rhizobial **NodD proteins** interact directly with the signals generated by the plants. Plant pathways for inducer biosynthesis (see Chapter 24, Fig. 24.59) respond to bacterial signals; the **flavonoid** profile of **root exudates** changes in response to inoculation with rhizobia. The pattern of inducer and inhibitor production by the plant implies developmental and environmental regulation: for example, inducer release is most concentrated near the root tip, and flavonoid pathway enhancement in response to rhizobia is similarly localized. Additional negative and positive regulators of ***nod* gene** expression include bacterial proteins that respond to nutritional status and other environmental signals.

16.4.4 Bacteria synthesize molecular signals that control plant development

Symbiotic rhizobia also produce various molecular signals that trigger nodulation-related changes in the host plant, including **oligo-** and **polysaccharides** and proteins. Many rhizobial *nod* genes, for example, encode enzymes that direct the synthesis of Nod factors, bacterial products that act as nodule morphogens. Nod factors are **lipooligosaccharides**, fatty acid derivatized oligomers of chitin [β-1,4-linked ***N*-acetylglucosamine** (GlcNAc)] (Fig. 16.13D). The core Nod factor structure is a chitin backbone of three to five GlcNAc residues with an *N*-acyl substitution on the nonreducing end GlcNAc residue. This basic structure is constructed by three proteins common to all Nod factor-producing strains: NodA, NodB, and NodC. Other enzymes, which differ among bacterial species, decorate



D

FIGURE 16.13 (*Continued*) *(D) Structures of Nod factors, the N-acylated chito-oligosaccharides produced by bacteria. Nod factors are synthesized by enzymes encoded in the bacterial* nod *genes (B) and exported from the bacteria to the plant (step 2 in A). Plants respond to Nod factors with changes in ion flux, calcium spiking, morphogenesis, and transcription (step 3 in A). Top: all known Nod factors have a linear backbone of β-1,4-linked* N*-acetylglucosamine. Modifications to the reducing and nonreducing ends differ according to bacterial strain or species. The Nod factor modifying groups determine which host plant(s) will display nodulation-like reactions to the factor. Bottom: the Nod factor synthesized by* Sinorhizobium meliloti *and active on* Medicago *species. The 6-O-sulfonyl modification on the reducing end residue (right) and the modifications on the nonreducing end (6-*O*-acetyl and* N*-acyl) affect activity and host specificity of the molecule.*

this core structure with various C-6 modifications on the reducing and nonreducing ends, N-methylation or O-carbamoylation of nonreducing end residues, and other O-substitutions on the inner GlcNAc residues. The pattern of these modifications determines which hosts the bacteria will nodulate, and it is assumed this recognition is mediated by the detailed structure of the Nod factor receptors in the host plant (see Section 16.46). Broad host-range rhizobia appear to produce multiple Nod factor structures. Enzymes made by *nod* genes may also form or modify other compounds that play a role in symbiosis, such as lipids and carbohydrates.

Additional types of specific extracellular polysaccharides are required to invade many host plants. For example, *S. meliloti* mutants with defects in the structure or processing of extracellular polysaccharides (EPSs) are unable to infect *Medicago*: infection thread growth after infection by these mutants is feeble and aborts early. Prominent rhizobial extracellular carbohydrates include loosely associated **EPSs** (e.g., **succinoglycan**; Fig. 16.14A); **lipopolysaccharides** that extend from the lipid-A anchor in the bacterial outer membrane; K-antigens, unusual EPSs that contain keto-deoxyoctanoic acid; neutral cyclic beta-glucans; and cellulose. The roles played by various EPSs in symbiosis may differ from one host-rhizobial symbiotic pair to another.

Finally, in some broad host-range bacteria, **Type III/Type IV secretion systems** appear to play a major role in determining which plants can be nodulated (Fig. 16.14B). Such secretion complexes presumably deliver effector molecules to the extracellular environment or directly to the host cell. The processes of invasion and release, which require coordinated activity of the bacterial and plant cells, may also require specialized transfer of signals and material at the plant–bacterial interface.

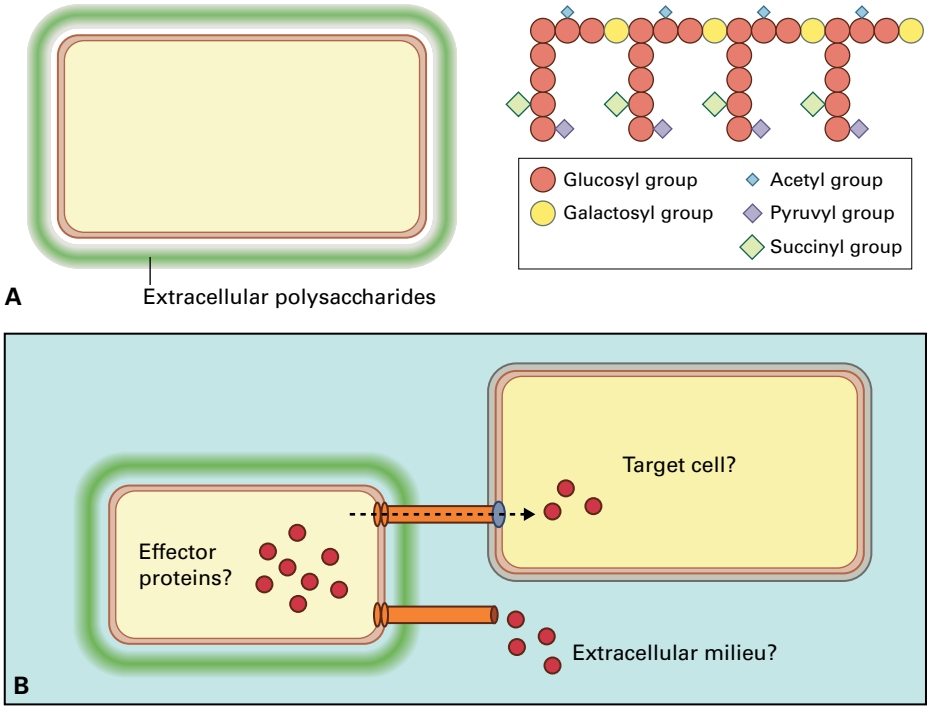


FIGURE 16.14 *Extracellular molecules are important for rhizobial infection of some plant hosts. (A) Some rhizobial species, here exemplified by* Sinorhizobium meliloti, *produce extracellular polysaccharides (EPS), which are required for host invasion. Left: schematic of Gram-negative bacterium with capsular and exopolysaccharides exterior to the outer membrane. Right: structure of the well-studied EPS-I (succinoglycan) of* S. meliloti. *The repeating unit of the EPS is an eight-sugar branched oligomer, consisting of a backbone of four residues [→4)β-Glc-(1→4)β-Glc-(1→4)β-Glc-(1→3)β-Gal-(1→] and a four-residue side chain of mixed β1→3 and β1→6 Glc. The backbone and side chain are modified by acidic derivatization. The EPS contains hundreds of these eight-residue repeats, of which four are shown here. (B) In some broad host-range rhizobial strains such as* Sinorhizobium fredii *NGR234 and* Mesorhizobium loti, *Type III or IV secretion systems are required for symbiosis on some host plants. The secretion systems export proteins; in principle, these may be introduced into other bacterial cells, into plant cells, or into the medium.*

16.4.5 Nodule development requires the interplay between molecular and developmental signals

In many cases, bacterial infection begins in the root hair initiation segment of the root. Cellular and molecular assays reveal multiple responses and altered root hair function following exposure to Nod factor (Table 16.4). These responses, which include altered ion fluxes and **Ca^{2+} spiking**, likely signal developmental changes in the root hair, such as its growth into the curled structure known as the "shepherd's crook," which traps one or more bacteria against the developing cell wall (Fig. 16.15A).

Over a period of hours to days, this wall deforms and extends into the root hair, leading to a tube-like structure known as the **infection thread**. As rhizobia grow and divide and the adjacent plasma membrane and infection thread wall expand, the bacteria push farther into the root (Fig. 16.15Bi). The bacteria interact with the underlying root tissues while remaining within a plant-derived membrane. Infection threads filled with dividing bacteria penetrate one or more root layers to meet dividing plant cells. The matrix (lumen) of infection threads contains a number of secreted bacterial and plant proteins and extracellular products, exemplified by a specific plant **arabinogalactan** protein in the **extensin** family. At least one molecular mechanism for the change in cell wall activity is a plant pectin hydrolase. During this process, subepidermal and cortical plant cells display active reorganization of cytoskeleton, cytoplasm, and membrane systems that resemble predivision phragmoplasts. How infection threads exit a plant cell is not known, but it must involve fusion of the infection thread membrane with the cytoplasmic membrane and subsequent rhizobial penetration of cell wall spaces.

TABLE 16.4 *Root hair cellular responses to bacterial Nod factor.*

Response	Timing
Membrane potential depolarization Ion currents Tip flux of Ca^{2+} ion	Observed in root hairs within 1 minute of NF application
Ca^{2+} spiking in and around root hair cell nucleus	Begins within ~10 minutes after NF exposure
Root hair growth perturbation: pause in growth, reinitiation of polar growth, curling	Occur over a period of hours
Reduction in rate of **reactive oxygen** production	Sustained for at least 1 hour; followed by ROS increase

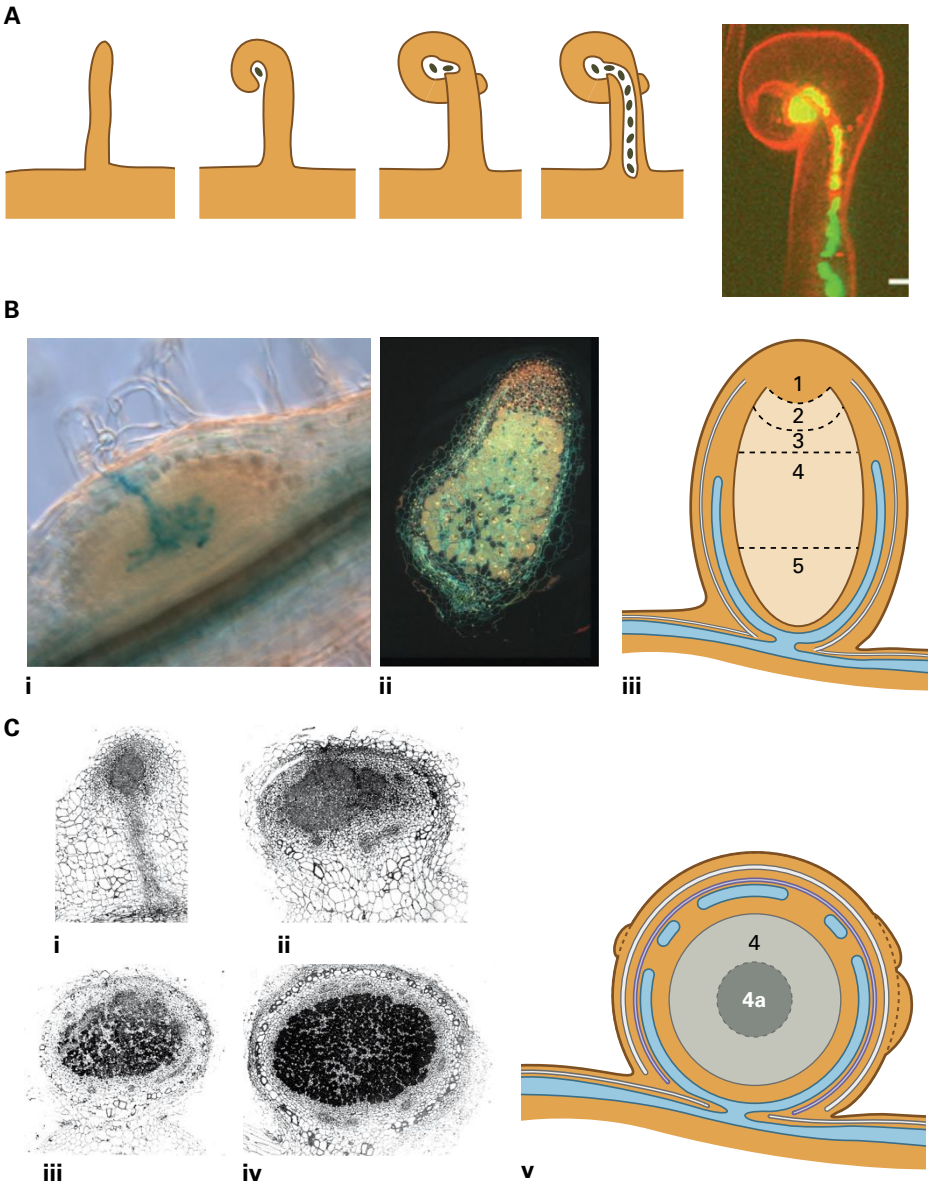


FIGURE 16.15 *Formation of nitrogen-fixing nodules. (A) Diagrammatic representation of root hair invasion (left) and photograph of an infected root hair (right) from alfalfa (*Medicago sativa*). In the photograph, bacteria fluoresce green and yellow, and the plant cell fluoresces red. Root hair growth is perturbed so the hair deforms and curls as it elongates; bacteria trapped in the curl form an infection thread and proliferate as they invade. (B) Nodule morphogenesis for an indeterminate (cylindrical, meristematic) nodule, such as that generated by alfalfa (*Medicago*), pea (*Pisum*), and clover (*Trifolium*). The first cell divisions occur in the inner cortical layer of the root and continue as the infection thread penetrates (i); bacteria in the infection thread are stained blue from a LacZ marker. A nodule meristem forms and persists so that newly divided, uninfected plant cells are continuously formed at the distal (from the root) nodule tip. An elongated nodule, formed by activity of a persistent meristerm, has zones of uninfected, infected, and senescent cells along a distal to proximal axis of the nodule. The nodule is stained with DAPI (labeling DNA and cell wall) and acridine orange (labeling RNA orange and DNA green) (ii). Numbers in diagram (iii) correspond to the following structures: 1, nodule meristem; 2, infection thread growth and cell penetration; 3, expanding infected cells; 4, mature bacteroid-containing tissue; 5, senescent bacteroid-containing tissue. (C) Nodule morphogenesis for a determinate (spherical) nodule, such as that produced by soybean (*Glycine*), trefoil (*Lotus*), and bean (*Phaseolus*). (i) Initial cell divisions are observed in the root outer cortex, followed by invasion of bacteria into plant cells; (ii–iv) many rounds of host and bacterial cell division give rise to zones of infected and uninfected cells in a spherical, stable nodule. Bars = 250 μm. (v) Schematic diagram of the zones of the fully formed determinate nodule: 4, mature bacteroid-containing tissue; 4(a), zone where senescence starts in determinate nodules. Mature determinate nodules lack meristematic tissues. Source*: (A) Gage; (B) Long & Haney; © ASM press; (C) Long & Dudley Dudley © Springer citation Planta volume.

The nodule body forms through division of cortical cells that dedifferentiate and re-enter the cell cycle. Overall developmental features of root nodules may differ, but two well-studied forms are **determinate** (spherical) and **indeterminate** (cylindrical, meristematic) **nodules** (Fig. 16.15Bii, iii, and C). Development and morphogenesis involve major plant hormone pathways as described below.

Alternative invasion mechanisms have been observed. For example, in crack invasion, Nod factor-producing bacteria take advantage of breaks in the epidermis, and cortical cells accessed

in this way are then invaded using a short infection thread. A variant on this is found in some ***Bradyrhizobium*** species that lack genes for Nod factor synthesis but can still promote infection and nodule development by a Nod factor-independent mechanism. These bacteria appear to penetrate roots through epidermal cracks and enter host cells by an endocytosis-like interaction with the intercellular wall and matrix. This type of entry may represent an ancestral mechanism for bacterial infection leading to symbiosis.

16.4.6 Molecular genetics and biochemical analyses have revealed plant genes and proteins required for nodulation

The molecular genetics of nodule development has been revealed by combining biochemical analyses, such as study of extracted protein or RNA species, with the use of plant or bacterial mutants. Plant mutants that form no nodules (Nod$^-$ phenotype) or nonfixing nodules (Fix$^-$ phenotype) are often characterized by analyzing molecular and cellular behaviors (Table 16.4) in responding roots, notably in the model systems ***Lotus japonicus*** and ***Medicago truncatula***. Key insight has come from using such phenotypes to define the defects in plant mutants that fail to form nodules. For example, various Nod$^-$ plant mutants can be distinguished by observing which early nodulation events they complete before the process fails. These combined data have led to identification of genes and gene products that contribute to symbiotic behavior across various developmental stages.

Proteins that interact with Nod factor have also been found in tissue culture, seeds, and roots through direct biochemical assay. Low- and high-affinity binding proteins have been described in roots and cell cultures from several legume species, and some purified lectins also bind Nod factor. Among other possible functions, these proteins may function directly in signaling or play a role in delivering, sequestering, or degrading Nod factor.

Multiple plant receptors are involved in Nod factor perception. Legume nodulation genes encoding receptor-like proteins have been identified in both *Lotus japonicus* and *Medicago truncatula*. In each species, distinct genes encode an inferred "**entry**" **receptor** and a "**signaling**" **receptor**. Mutations in either gene cause a severe nodulation defect: the plants do not form nodules, and they exhibit little or no response to bacteria or Nod factor.

Each of these two proteins is a membrane spanning receptor-like protein with an extracellular portion bearing several LysM domains (Fig. 16.16). Originally identified in bacterial and bacteriophage proteins, the **LysM motif** is an amino acid sequence of 44–65 residues that establishes a chitin-binding domain. It has been identified in plant proteins that bind chitin as part of a fungal detection program. Chitin constitutes the oligomeric backbone of Nod factor. The two LysM-bearing proteins are proposed to be the Nod factor receptors. Direct binding of the two LysM-type receptor proteins to Nod factor has not been demonstrated, but their membrane localization has been confirmed by cellular assays. Swapping extracellular LysM domains between the signaling receptors of two species can change their ability to partner

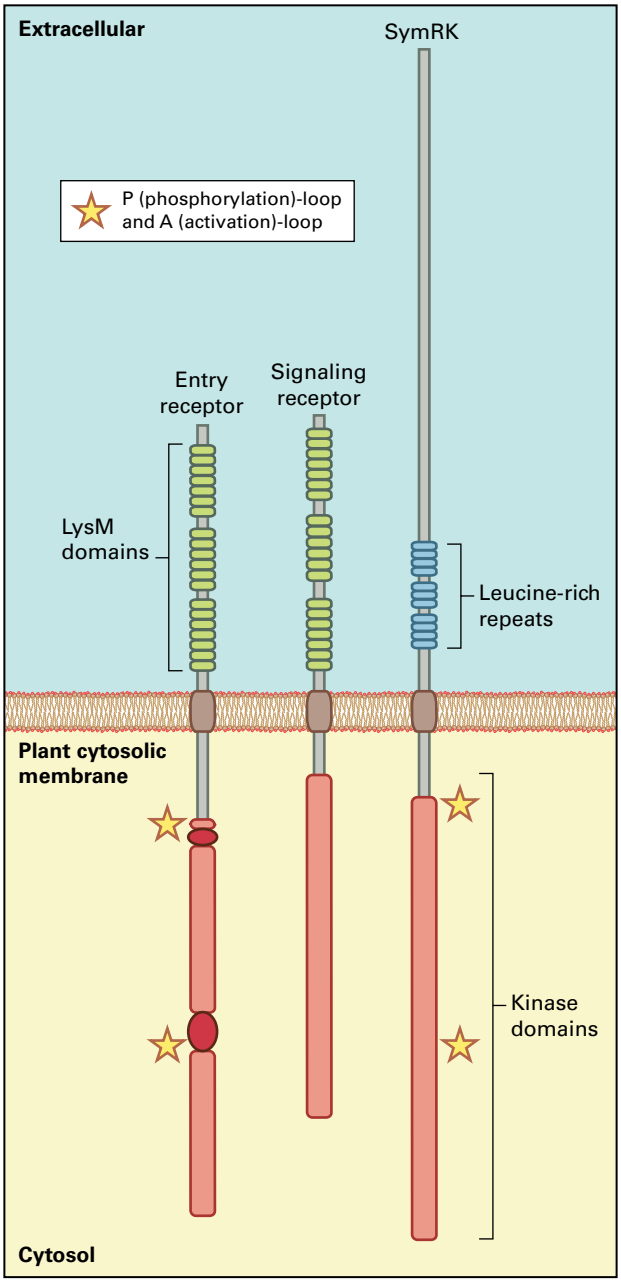


FIGURE 16.16 *Required plant nodulation genes encode proteins with receptor-like features. The entry receptor (exemplified by LjNFR1 and MtLYK3) has three extracytoplasmic LysM domains resembling protein elements that bind chitin and chitin-like molecules. The cytoplasmic domain of the entry receptor includes a kinase domain with several common kinase elements such as the P (phosphorylation) and A (activation) loops (shown by stars). The signaling receptor similarly has three extracytoplasmic LysM domains but lacks the kinase features found in the entry receptor. The signaling receptor (for example, MtNFP and LjNFR5) is required for any host response to NF. An entry receptor (for example, MtLYK3 and LjNFR1) is required for infection. The symbiosis receptor kinase, SymRK, which is exemplified by MtDMI2, LjSYMRK, and inferred gene products in pea (*Pisum sativum*) and soybean (*Glycine max*), has three extracellular leucine-rich repeat domains in a large N-terminal segment. The cytoplasmic portion has a kinase domain that includes the conserved activation loop. Mutations in these residues eliminate in vitro autophosphorylation activity and generate a* Nod$^-$ *phenotype in vivo.*

with distinct rhizobial inocula, implying a direct role for the signaling receptor in species-specific Nod factor perception.

The entry receptor, exemplified by LjNFR1 and MtLYK3, includes a cytoplasmic domain showing the elements of a typical kinase (Fig. 16.16): a conserved glycine-rich P (phosphorylation) loop; a catalytic domain; an activation loop that, when phosphorylated, changes conformation to assist correct docking of the kinase and its substrate; and an Asp-Phe-Gly (DFG) triplet that is near to the activation loop and plays a role in its phosphorylation. The entry receptor autophosphorylates with γ-^{32}P-ATP and is postulated to transfer the phosphoryl group to a target signal transduction protein. The signaling receptor protein, however, lacks some sequence features that are usually present in active kinases; the C-terminal cytoplasmic domain has the catalytic domain characteristic of a kinase, but is missing the P-loop and activation loop, and it does not autophosphorylate. The signaling receptor may interact with other proteins to transmit a signal via kinase activity.

A candidate partner kinase for the signaling and entry receptors is the **symbiosis receptor kinase**, SymRK (Fig. 16.16). This receptor is required both for symbiosis with rhizobia and for establishing a symbiosis with broad host-range mycorrhizal fungi that enhances plant mineral uptake and drought resistance. The *SYMRK* gene predicts an extracellular domain with **leucine-rich repeats**, a membrane-spanning domain, and an intracellular kinase. The kinase domain is capable of autophosphorylation and can act as a kinase on target proteins in vitro.

The signaling and entry receptors affect some early root hair cell behavior (Table 16.4, Rows 1–3) even in the absence of SymRK, and it is inferred they influence ion channels and cytoskeletal elements. Biochemical and imaging analyses indicate the entry receptor protein interacts with E3-ubiquitin ligase and membrane-associated proteins, such as flotillins and remorins. It is presumed the receptors communicate with other signal transduction pathways in the root hair cell, perhaps by co-opting systems that are in place for other plant cell functions. Pharmacological studies indirectly point to phosphoinositide signaling; direct confirmation of secondary signaling mechanisms may come from definition of more host genes that transduce Nod factor receptor binding into subsequent cell activities.

Other plant proteins required for nodulation include **nuclear membrane** components, which are required downstream of the receptors. These include proteins that have sequence similarity to a K^+ ion transporter in the archaeal species *Methanobacterium thermoautotrophicum*. These channel proteins localize to the nuclear membrane (Fig. 16.17) and are required for subsequent Ca^{2+} spiking (see Section 16.4.7). Genetic studies imply that these proteins mediate flux of K^+ or similar monovalent cations and that the C-termini play a role in modulating channel function. It is possible that an ion flux mediated by these channels plays a role in the dynamic behavior of Ca^{2+} in the nucleus.

Other required genes encode homologs of conserved nucleoporin proteins included in the ring complex, which is located in the cytoplasmic and nuclear faces of yeast or mammalian nuclear pores (Fig. 16.17). Nuclear pores are generally permeable to small molecules but play a more selective role in protein and mRNA transport. In animal cells, the ring complex is also implicated in phosphorylation events linked to the cell cycle, and it may play a role in spindle assembly and alignment in cell division. The localization of the symbiosis-related ion channel and nuclear pore proteins in the nuclear membrane implies a dynamic cytoplasm–nucleus interaction during Nod factor signaling.

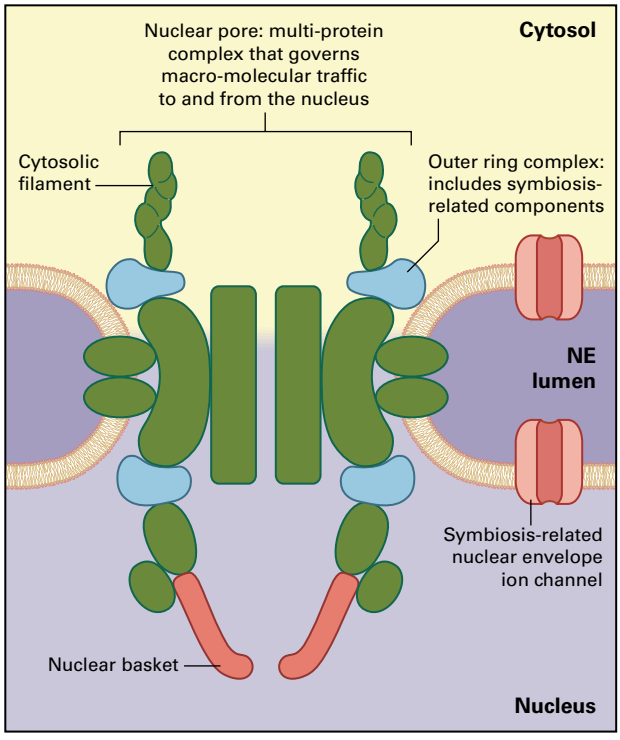
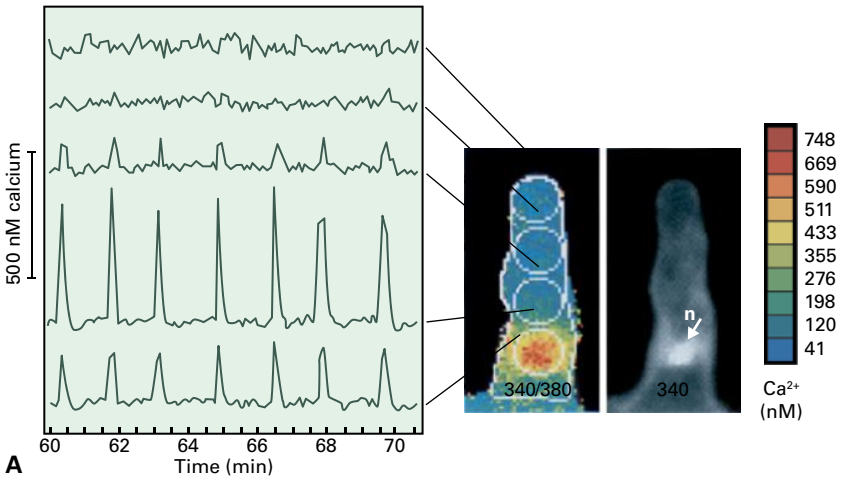
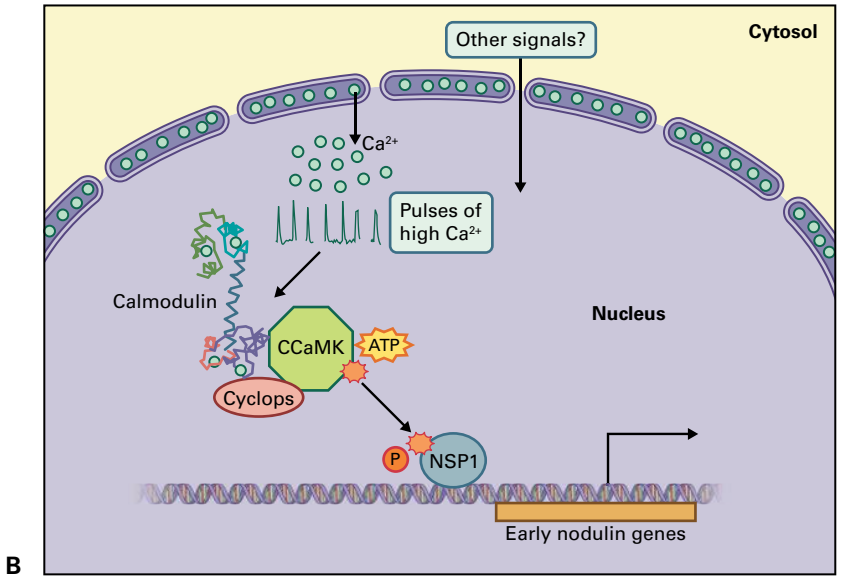


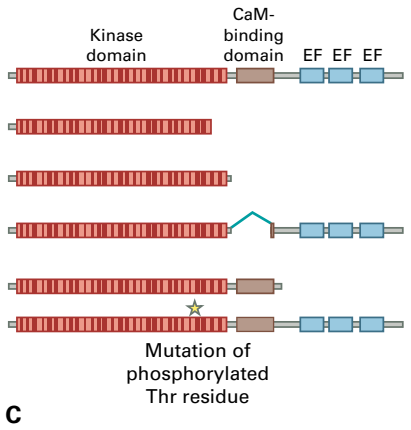
FIGURE 16.17 *Elements of a nuclear pore are required for effective symbiosis signaling. Here, the cytoplasmic face of the membrane is at the top of the illustration, and the nuclear volume is at the bottom. Several required legume symbiosis genes are homologous to mammalian genes encoding components of the nuclear pore's ring complex. These proteins localize to the Nup107 complex (shown in blue), a part of the ring structure on both the cytoplasmic and nuclear sides of the membrane. Signaling also requires nuclear membrane proteins predicted to be ion channels (pink); it is not known whether these are on the inner or outer face of the nuclear membrane.*

16.4.7 Calcium spiking and a calcium-calmodulin-dependent protein kinase are elements of a central regulatory point in Nod factor signaling

Nod factor treatment causes root hairs to display "calcium spiking," transient, periodic increases and decreases in Ca^{2+} ion levels (Fig. 16.18A). This behavior depends on the upstream receptors and nuclear membrane components described above. The spiking occurs in the nuclear and







Form nod in response to nod factor?	Phosphorylates substrate protein?	Forms spontaneous nodules in absence of bacteria?
Yes	Yes; CCaM-dependent	No
No	40% of WT; CCaM-independent	
No	30% of WT; CCaM-independent	
No	30% of WT; CCaM-independent	Yes
No	Inactive	No
Yes	Loses auto-phosphorylation; retains partial CCaM-dependent kinase activity	Yes

FIGURE 16.18 *(A) Calcium spiking in root hairs responding to* Rhizobium *nodulation factors. Nod factor may elicit this plant cell behavior by influencing calcium-specific pumps and channels. Cytoplasmic calcium was imaged using fluorescent calcium-sensitive dye and was quantified on the basis of the ratio of fluorescence observed at 340 and 380 nm. The single-wavelength image at right (340 nm) shows the nucleus (n), where calcium spiking is most prominent. (B) Within the plant nucleus, calcium-activated calcium- and calmodulin-dependent protein kinase (CCaMK) phosphorylates transcription factor NSP1. Activated NSP1 and a similar factor NSP2 are able to bind the promoters of genes for early nodulins, such as ENOD11, and for downstream regulators ERN and NIN. (C) CCaMK is a master regulatory switch for nodule development, and functional domains of wild-type CCaMK include: an N-terminal kinase domain, C-terminal EF-hand domains that bind Ca^{2+} directly, and a domain that binds Ca^{2+}-calmodulin (CaM). The wild-type protein (top) displays Ca^{2+}-and CaM-dependent in vitro activities: Ca^{2+} binding stimulates autophosphorylation, and CaM binding stimulates transfer of phosphate to a target protein. The activity of CCaMK is negatively autoregulated by a region adjoining the kinase domain. Plants carrying the wild-type CCaMK gene form nodules in the presence of homologous rhizobia. Deletions or certain point mutations in the autoregulatory domain in the* Lotus *and* Medicago *alleles of CCaMK result in proteins with constitutive activity. Plants carrying these deregulated forms of CCaMK form spontaneous nodules in the absence of bacteria.*

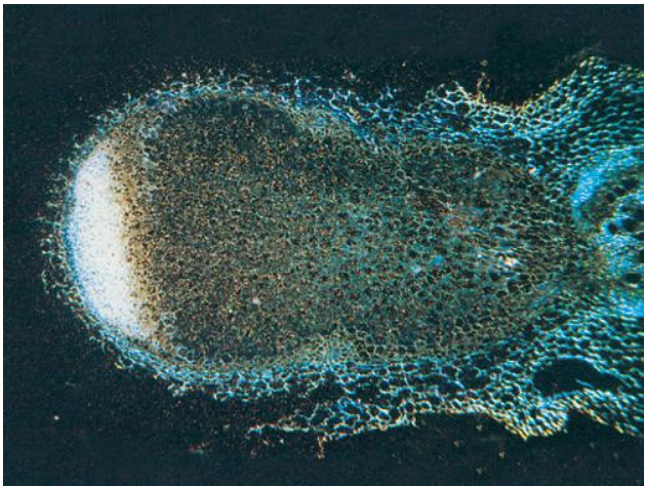


FIGURE 16.19 *Patterns of early nodulin (*ENOD*) gene expression in developing nodules vary according to each gene. For example,* ENOD12 *is expressed in the early infection zone of pea nodules (compare Figure 16.15C), as shown in this in situ hybridization. photographed in dark-field illumination. Silver grains from probe hybridization scatter light and, therefore, appear bright against the dark background.*
Source: Scheres et al. (1990). Cell 60:281–294.

perinuclear regions within the root hair. Ca^{2+} spiking is a prominent signal transduction motif in some animal cell responses, such as T-lymphocyte responses to antigen and Sonic Hedgehog (Shh) signaling in vertebrate neuron development. Empirical studies and modeling analyses show that Ca^{2+} spiking behaviors must involve at least two components: (1) a channel that releases Ca^{2+} from a reservoir, and (2) an energy-dependent Ca^{2+} pump for reuptake of Ca^{2+} into the reservoir to restore the starting level of ion. The two components typically have a feedback system that sustains or attenuates the behavior. In animal systems, feedback mechanisms include secondary signals or Ca^{2+}- or other ion-induced effects. In the case of root hairs, the reservoir is believed to be the nuclear membrane lumen. Pharmacological evidence points to the involvement of phosphoinositide signaling and a Type IIA Ca^{2+}-pump.

Downstream of Ca^{2+}-spiking, a **calcium–calmodulin-activated protein kinase** (CCaMK) (Fig. 16.18B) is required for subsequent nodule development. This protein is structurally and functionally homologous to a previously characterized lily (*Lilium*) CCaMK. In response to Ca^{2+} ion, the symbiosis CCaMK autophosphorylates at a site in the N-terminal domain, thereby inhibiting activity of the C-terminal kinase domain. Deleting or mutating the autoinhibitory N-terminal domain of the symbiotic CCaMK protein creates a constitutively active protein that triggers spontaneous formation of root nodules in the absence of bacteria (Fig. 16.18C). CCaMK thus appears to be a central coordinating switch point for early steps in the signaling pathway. Symbiotic effectiveness of CCaMK requires a companion protein, CYCLOPS, which is likewise localized in the nucleus.

16.4.8 Nodulins are nodule-specific proteins synthesized by the plant

Nodules are distinct organs that express dozens to a few hundred nodule-specific, plant-synthesized proteins, or **nodulins.** Correspondingly, transcriptomic studies indicate that novel RNA sequences are expressed at various stages of nodule development. For the first 24 hours after inoculation, pure Nod factor and live bacterial cultures elicit equivalent transcriptional responses. After this point, a full plant response is seen only with live bacteria.

Plant genes expressed early, or in the absence of bacterial infection, are termed "early nodulins" (encoded by *ENOD* genes). In emerging nodules, some nodulins may be limited to a distinct cell type or nodule zone (Fig. 16.19). The functions of the *ENOD* gene products, and the significance of their expression patterns, are likely to be revealed through combined genetic and biochemical analysis. These can also serve as useful developmental markers for the successive stages of the plant response to bacteria, and as reporters for dissecting the effects of distinct microbial signals in early symbiosis.

Some *ENOD* genes are transcribed in root hairs as soon as 4 hours after adding bacteria or Nod factor. Induction requires the signaling pathway described above, plus proteins encoded by *NSP1* and *NSP2*, members of the plant-specific GRAS family of transcription activators. NSP1- and/or NSP1–NSP2 protein complexes bind to promoters of a well-studied early nodulin, ENOD11 (Fig. 16.20). More transcription factors, such as NIN and ERN, act later in symbiosis. Nodule gene expression is subject to additional control mechanisms: for example, microRNA (miRNA) controls a nodule meristem-associated transcript, MtHAP.

The most prominent late nodulins are the leghemoglobins (Lb), which are required to establish an appropriate oxygen environment with high O_2 flux and low free O_2 tension (see Section 16.4.9). Other late nodulin proteins are involved in metabolizing carbon and nitrogen or in transporting compounds across the symbiosome membrane (see Sections 16.4.5–16.4.9). Some nodulins may mediate signal transduction or cellular response pathways required for the differentiation of plant and bacterial cells to accomplish nitrogen fixation. In some cases, selective gene expression is observed in uninfected host cells; functions for such genes include specialized metabolic steps and possible regulatory proteins. Bacteria likewise differentiate, most prominently by transcribing the genes for nitrogenase and for allied functions, including electron transport and metabolic pathways.

16.4.9 Plant hormones play a role in nodule development

Molecular and developmental studies imply roles for various plant hormones, including auxin, cytokinin, jasmonic acid, abscisic acid, and ethylene in the coordination of nodule

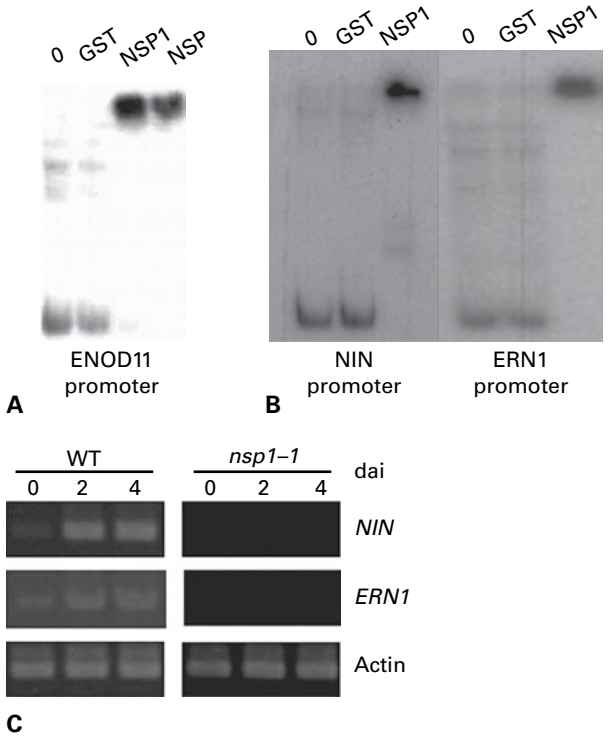


FIGURE 16.20 *Transcription factors are required for expression of early nodulins and other regulators. (A) Electrophoretic mobility shift assay showing binding of the NSP1 protein to the promoter of ENOD11, a well-characterized early nodulin. Binding specificity is shown by competition with unlabeled promoter DNA fragments. (B) NSP1 binds to the promoters of genes NIN and ERN1 which encode transcription factors required for downstream nodulation responses. (C) The NIN and ERN1 genes are transcribed in wild-type nodules (left), but not in response to rhizobial inoculation in roots of* nsp1 *or* nsp2 *mutants. dai: days after inoculation.*
Source: Hirsch et al. (2009). Plant Cell 21:545–557.

morphogenesis. The effects of these hormones may overlap or compete, and the hormones may have distinct actions in different cell types (epidermal vs. cortical) and at different stages of nodule development (early signal transduction, nodule formation, and nodule growth and maturation).

Cytokinins are linked to nodule development through several lines of experimentation. Cytokinin content increases in roots exposed to compatible rhizobia, and the expression levels of cytokinin-responsive genes increase. Applying cytokinin-producing *E. coli* to the roots of some legumes causes the development of pseudonodules (bacteria-free organs that are similar to nodules in form and that express nodule-specific proteins). Nonfunctional mutant forms of the cytokinin receptor (MtCre1 or LjLHK1, both homologous to *Arabidopsis AtCre1*) can severely limit nodule formation, indicating cytokinin responsiveness is required for nodule primordia formation. Furthermore, constitutive overexpression of LjLHK leads to spontaneous nodule-like growths in the absence of bacteria or Nod factor. Taken together, these data imply that cytokinins promote nodule morphogenesis. Genetic analyses suggest that cytokinins act downstream of the Nod factor signaling pathway; it is also possible they act in parallel with other molecular controls of cell division.

The role of ethylene is complex, as indicated by plant mutant analyses, by inhibitor studies, and by the pattern of expression of ethylene biosynthesis genes in nodule tissues (Fig. 16.21). Ethylene diminishes plant sensitivity to Nod factor: responses such as calcium spiking and early nodulin transcription require higher Nod factor concentration as ethylene concentration goes up. Mutants unable to respond to ethylene (e.g., defects in the legume genes homologous to AtEIN2) form excessive numbers of nodules. On the other hand, ethylene may play a positive role in infection thread formation and some other responses.

Auxin transport is altered in plants undergoing nodulation, and auxin transport inhibitors (ATIs) can induce phenocopies of nodule development. By using the strength of auxin-dependent promoters to indicate auxin availability and activity, it is inferred that early nodule development, such as establishment of the primordium, is characterized by low auxin levels, but that later nodule growth is accompanied by increases in auxins. Specific members of auxin transporter gene families may play distinct roles in nodule development. The pathways for auxin, ethylene, and cytokinin interact with each other and with control mechanisms for other hormones including ABA, jasmonic acid, and salicylic acid.

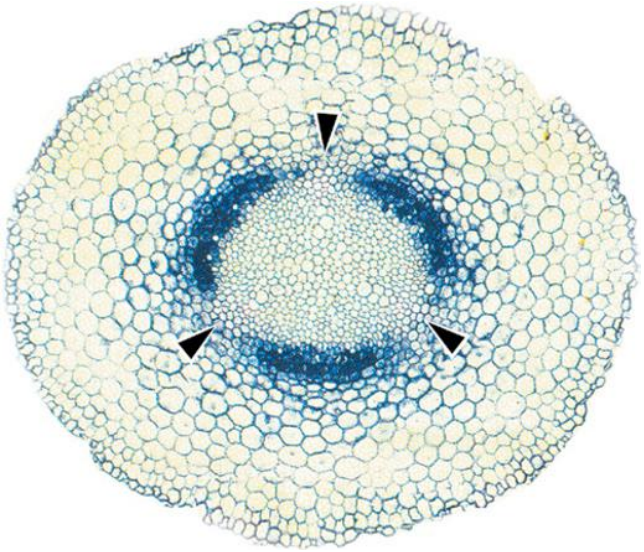


FIGURE 16.21 *Expression of a gene involved in ethylene biosynthesis, 1-aminocyclopropane-1-carboxylic acid (ACC) oxidase, in roots responding to rhizobia. In this cross-section of the pea root, hybridization of a probe for ACC oxidase transcripts is visualized as dark signal against the cleared root segment. The position of ACC oxidase expression correlates with the phloem elements of the root vasculature. Nodule primordia tend to form in the zones shown by arrowheads, representing the cortical cells just outside the xylem poles. This implies that nodule primordia are unlikely to form in zones adjacent to ethylene production.*
Source: Heidstra et al. (1997). Development 124:1781–1787.

16.4.10 Local and systemic molecules play a role in regulating nodule formation and differentiation

In addition to hormones, other intercellular signals play a major role in regulating nodulation and nodule number. In particular, regulation of nodule number occurs via signals exchanged between roots and shoots, and grafting studies show that the root and shoot genotypes both play a role. The ability to regulate nodule number is controlled by a number of genes. Among these, a homolog of CLAVATA-1 acts in the shoot: plants with a mutation in this gene (*LjHar1*, *MtSUNN,* and soybean *NTS*) form abnormally high numbers of nodules. In turn, several nodule-active CLV3-like peptides (CLE category) act in roots to downregulate nodule formation. The ability of these peptides to decrease nodule number requires downstream *SUNN* (*NTS1*, *HAR1*). Thus, root CLE peptides—or a subsequent signal that they control—appear to interact with shoot receptor kinases to generate a second, shoot-produced signal that subsequently reduces formation of new nodules.

16.4.11 Rhizobia and their plant hosts interact to create a microaerobic nodule environment that enables nitrogen fixation

After the infection thread traverses one or more layers of host cells, or after the bacteria penetrate layers via intercellular spaces, the bacteria are released into infected cells. This endocytosis-like process generates cytoplasmic organelles called **symbiosomes** (Fig. 16.22), which contain the rhizobia within a plant-derived membrane. In the symbiosomes, rhizobia differentiate into nitrogen-fixing **bacteroids**, which in some plant hosts are morphologically distinct from the free-living bacterial forms (Fig. 16.22A,B). In some cases, bacteria duplicate their genomes without cellular division and appear to be terminally differentiated.

The symbiosome membrane is thought to mediate the flow of nutrients and energy between the plants and the bacteria (Fig. 16.22C). Some plant proteins are uniquely expressed in infected cells and are delivered to or across the symbiosome membrane. These proteins have distinct targeting peptides, which implies the symbiosome is a unique cell compartment. In some legumes, a specific plant signal peptidase is required for bacterial differentiation. This complex is localized to the endoplasmic reticulum and processes host precursor proteins, yielding mature forms that display differentiation-controlling effects on bacteria in culture, and when expressed transgenically in other host plants. A bacterial transporter, BacA, is also required for bacterial differentiation and nitrogen fixation and may participate in the process of plant–bacterial signal exchange.

The nodule provides a compartment where bacteria can fix nitrogen in amounts useful to the plant. Because the nitrogenase enzyme is oxygen sensitive, it is a physiological challenge to supply the enzyme with large amounts of ATP and low potential reductant simultaneously. Thus, a major feature of the nitrogen-fixing nodule is that it establishes a microaerobic environment that can stably support aerobic respiration and ATP synthesis, while also being compatible with the sensitivity of nitrogenase. The microaerobic conditions are generated by interaction between the two symbionts.

Three factors are important in maintaining low O_2 concentrations in nodules (Fig. 16.23). First, entry of O_2 into the nodule is controlled by a variable-permeability barrier in the nodule parenchyma. Experimentally induced increases or decreases in external O_2 concentration cause changes in the cellular O_2 content, but these changes are sensed and reversed by an unknown compensation mechanism that restores the O_2 concentration to its previous value.

Second, the O_2-binding plant protein Lb plays an active role in regulating and delivering O_2 in the infected cells. Both apoprotein and heme are made by the plant cell. Legume leghemoglobin genes are similar to other genes that encode O_2-binding proteins in widely diverse plant families, but their promoters are distinct. A high level of Lb expression is found only in nodules, where Lb is present at millimolar concentrations. Lb protein is a monomer with a single heme moiety, and despite its name, it is more analogous to myoglobin; it does not display the cooperative O_2-binding behavior found in animal hemoglobins. The affinity of Lb for oxygen can be influenced by pH and organic acids, but whether Lb is regulated by small molecules within the nodule is not known. Leghemoglobin increases the flux of O_2 moving through the plant cytoplasm to the bacteroids while controlling the concentration of free O_2. Although Lb-bound O_2 diffuses more slowly than O_2, O_2 is far less soluble (≈25 μM) than the Lb:O_2 complex. As an O_2-binding protein, Lb can also act as a buffer to moderate changes in O_2 concentration that result from fluctuations in the rate of respiration or the permeability of the diffusion barrier.

Finally, bacterial respiration is the major O_2 sink (Fig. 16.23). Whereas the free-living rhizobia typically have a cytochrome oxidase with a K_m for O_2 of around 50 nM, the bacteroid cytochrome oxidase has a much lower K_m for O_2, about 8 nM (by contrast, K_m values for plant mitochondrial cytochrome oxidases are near 100 nM O_2). Highly expressed by bacteria within the nodule, this type of high-affinity cytochrome oxidase is required for nitrogen fixation. Because bacterial respiration is more effective than plant respiration at low O_2 concentrations, most nodule respiration is thought to occur in the bacteroids. However, plant mitochondria often have a more peripheral location in infected cells, which may give them better access to O_2 diffusing through the intercellular spaces.

Nodule physiology is vulnerable to oxygen-related compounds, such as peroxide, superoxide, and hydroxyl radicals, and although the oxygen concentration in nodules is low, the

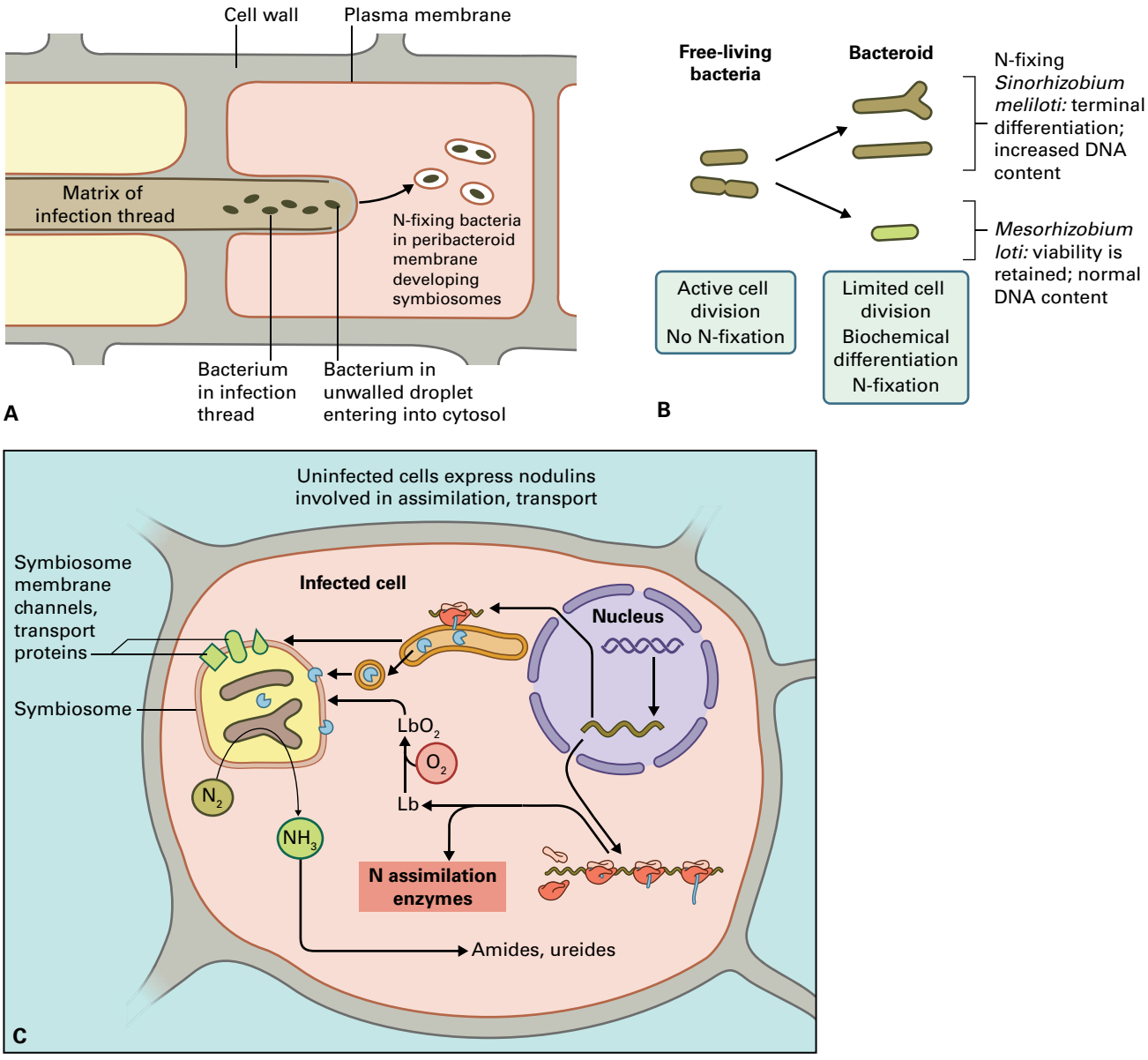


FIGURE 16.22 *Events that lead to nitrogen-fixing cells. (A) The infection thread releases bacteria into a target cell, which envelopes them in host plasma membrane. The bacteria then undergo limited cell division (indeterminate nodules) or extensive rounds of cell division accompanying host cell division (determinate nodules). (B) After release, bacteria differentiate to form morphologically distinct bacteroids. Different plant-bacterial combinations yield distinct bacteroid forms. (C) In the plant nucleus, a series of genes (late nodulins) are expressed only during later stages of nodule development, in response to bacterial differentiation. Some of these transcripts are specific to infected or uninfected cells. The plant-encoded products include the oxygen-binding protein leghemoglobin, specialized membrane proteins targeted to the symbiosome membrane, and enzymes that catalyze ammonia assimilation and synthesis of molecules used to carry N to the rest of the plant. Bacterial genes are also expressed during this period.*

abundance of iron (Fe) proteins can lead to significant amounts of these reactive compounds. Plant cells and bacteroids each have active systems to detoxify these molecules; inhibiting these cellular defenses impairs nodule metabolism and nitrogen fixation.

The low O_2 concentration within the nodule is a key element in regulating bacteroid expression of nitrogenase. In some rhizobial species, the O_2-sensitive hemoprotein kinase FixL controls a regulatory cascade that activates transcription of nitrogen fixation genes (Fig. 16.24). Part of a two-component regulatory system, FixL phosphorylates its partner FixJ, which once phosphorylated, activates transcription of other regulatory proteins. Two of these proteins, NifA and FixK, control expression of diverse *nif* and *fix* genes (*nif* genes are those that are required for nitrogen fixation for which similar genes exist in free-living diazotrophs; *fix* genes are those that are required for fixation in otherwise normal nodules). The bacteroids express nitrogenase (*nifHDK*) and the associated proteins required for reduction of dinitrogen to ammonia only in the correct context of a

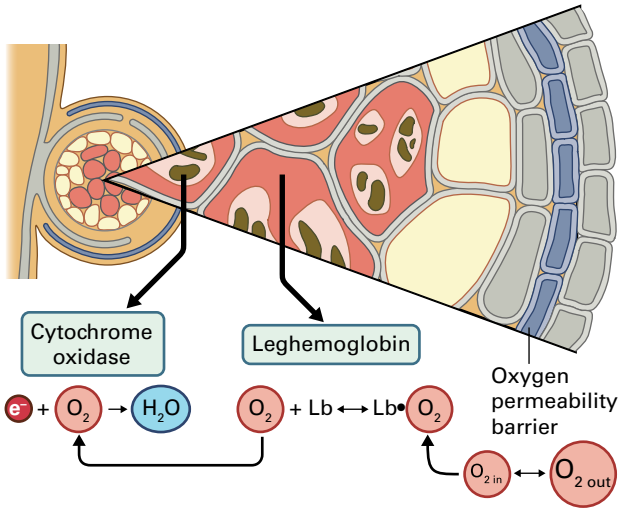


FIGURE 16.23 *In nitrogen-fixing nodules, mechanisms that maintain ATP production in an appropriately low O_2 environment include a high-affinity cytochrome oxidase, the oxygen-binding protein leghemoglobin, and a variable-permeability barrier that controls gas exchange at the nodule periphery. The "empty" cells around the central region are thought to contain the permeability barrier that limits the flow of oxygen to the leghemoglobin-containing central region of infected host cells.*

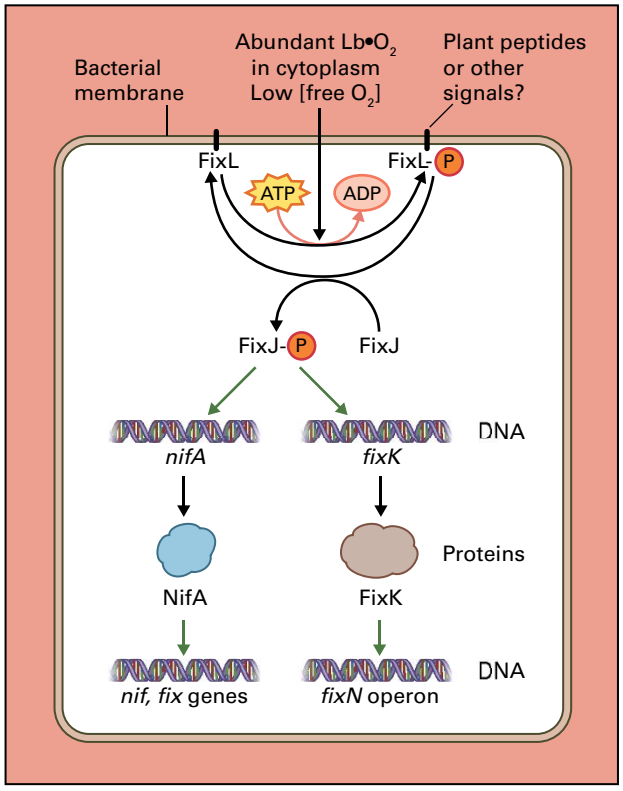


FIGURE 16.24 *In response to a low-O_2 environment, the FixL/FixJ signal cascade activates expression of bacterial genes required for nitrogen fixation. The FixL heme-containing protein is anchored in the bacterial plasma membrane. In the absence of O_2, FixL is phosphorylated and in turn phosphorylates the soluble FixJ response regulator, which can bind to DNA and activate transcription of the genes needed for nitrogen fixation. Binding of oxygen to the FixL heme inhibits the protein's histidine kinase activity, repressing the expression of these genes under conditions where nitrogenase would be unstable. In addition to this O_2-sensing system, bacterial differentiation is affected by plant nuclear-encoded peptides that are processed by the endoplasmic reticulum.*

developed, microaerobic nodule. Specific ferredoxins and the high affinity cytochromes described above are examples of proteins encoded by the *fix* genes that are needed for fixation to occur in nodules. The plant can also contribute directly to the formation of an active nitrogenase by providing the bacteria with homocitrate, a component of its FeMoCo cofactor.

16.4.12 Host plants provide carbon to the bacteroids as dicarboxylic acids

Although photosynthate enters the nodule as sucrose, genetic and biochemical evidence show that bacteroids do not need to catabolize mono- or disaccharides to fix nitrogen effectively. Instead, sugars are converted to organic acids before the carbon is made available to the bacteria, probably by using pathways more often associated with fermentation than oxidation (Fig. 16.25).

Some evidence indicates phospho*enol*pyruvate (PEP) is converted to oxaloacetate by PEP carboxylase, and NAD^+ is regenerated by reducing oxaloacetate to malate (see Chapters 13 and 14). Intact nodules rapidly incorporate $^{14}CO_2$ label into malate and aspartate, and tissue concentrations of PEP carboxylase and malate dehydrogenase are increased by the synthesis of nodule-specific isoforms of these enzymes. Transport activities further support an important role for organic acids in symbiotic carbon metabolism. The symbiosome membrane can transport dicarboxylic acids but not sugars, and most bacterial mutants with defects in dicarboxylic acid transport are ineffective. Amino acid transport may also be needed, because some symbiotic rhizobia, which do not require branched chain amino acids when growing as free-living bacteria, depend on plant-derived branched-chain amino acids in symbiosis.

In the nodule, dicarboxylic acids are used in both catabolic and anabolic processes. Some of these acids are fed to bacteroids, which oxidize them and transfer the electrons to O_2 by way of electron transfer chains that terminate at the high-affinity cytochrome oxidase. This respiration ultimately provides ATP for nitrogen fixation; however, the mechanism by which reductant destined for nitrogenase is generated and transferred to nitrogen fixation has not yet been defined. In another major role, dicarboxylic acids provide the carbon backbones for the nitrogen-containing transport compounds, such as asparagine and glutamine, which are exported from the nodule to carry nitrogen to other parts of the plant (Fig. 16.25).

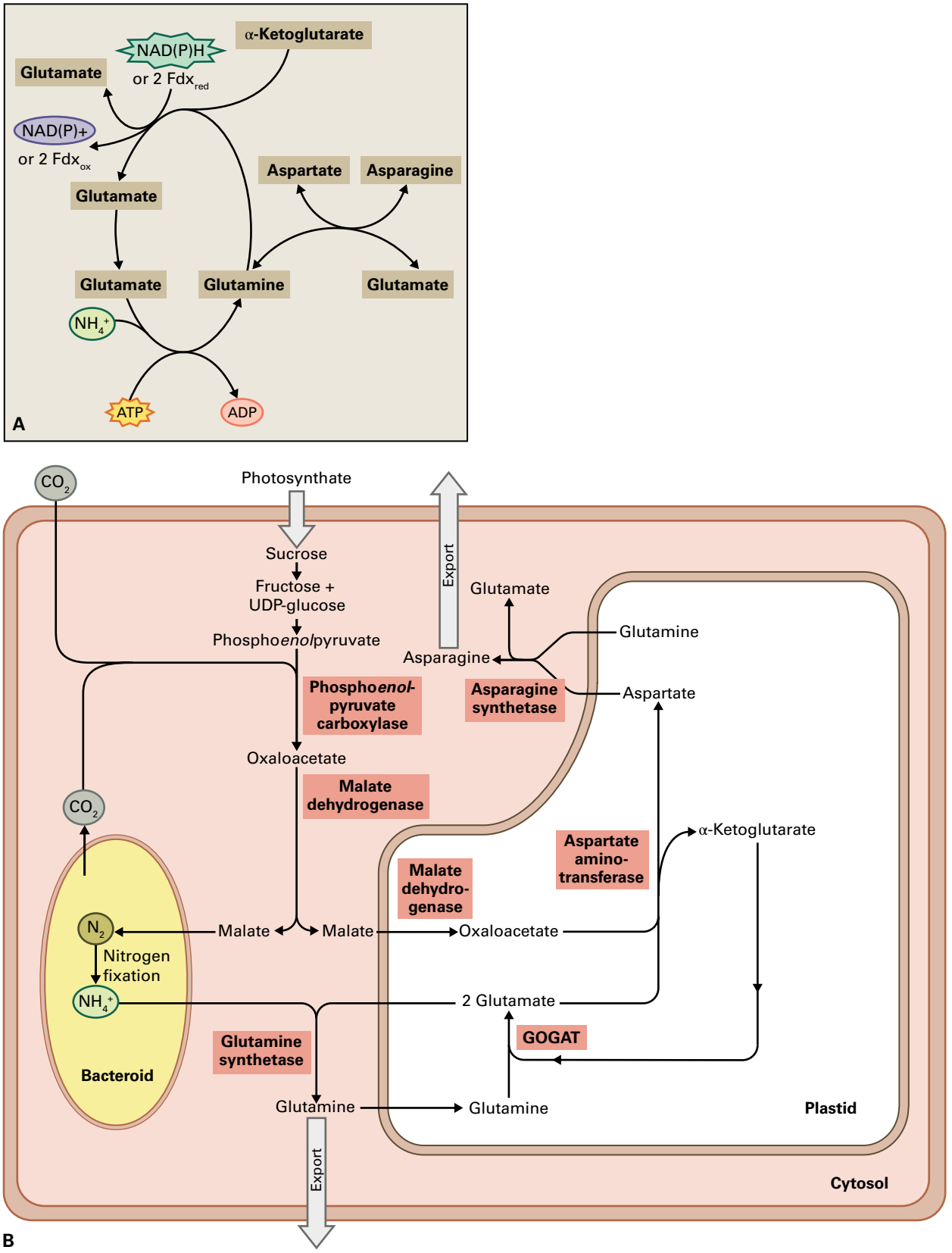


FIGURE 16.25 *Primary nitrogen assimilation pathways in nodules of pea, alfalfa, and other species that export amides. (A) The GS-GOGAT cycle, in which ammonium (NH_4^+) is combined with glutamate to yield glutamine in an ATP-dependent reaction. Reaction of glutamine with α-ketoglutarate and a reductant yields two molecules of glutamate, one of which is used to regenerate the cycle, and the other to deliver amino groups to general metabolism. (B) Plant carbon metabolism produces dicarboxylic acids, which are used to generate the ATP and reductant needed for nitrogen fixation in the bacteroids. The reduced nitrogen released is assimilated in the plant cytoplasm and plastids to produce glutamine and asparagine, which are transported through the xylem to the rest of the plant.*

16.4.13 Plant gene products assimilate ammonia and export nitrogen from the nodules

Unlike free-living bacteria, which assimilate the nitrogen they fix, bacteroids release nitrogen to the plant, primarily as ammonia (see Fig. 16.22C). Ammonia may traverse the symbiosome membrane by facilitated diffusion; in soybean (*Glycine max*), this transport is thought to be mediated by the NOD-26 aquaporin-related channel. Ammonia assimilation occurs in the plant cytosol and organelles. Plant glutamine synthetase (GS) and NADH-dependent glutamate synthase (NADH-GOGAT) are responsible for the initial assimilation of ammonia into organic compounds (Fig. 16.25A; see also Chapter 7). In some plants, a nodule-specific GS is expressed, whereas in others, synthesis of a vegetatively expressed GS is upregulated. GS can bind NOD-26, and this may increase the efficiency of ammonia assimilation.

After assimilation of ammonia into glutamine, its fate depends largely on the nitrogenous transport compounds used by the plant host. In one major class of legumes that includes alfalfa and pea, nodules export ammonia as **amides**, namely glutamine and asparagine (Fig. 16.25B), which are easily generated from citric cycle intermediates (see Chapter 14). Nodules contain active aspartate aminotransferases, which may be located in plastids at the periphery of infected cells. A nodule-induced asparagine synthetase produces asparagine from aspartate using glutamine as an amide donor (Fig. 16.25A). In trefoil (*Lotus*), an asparaginase that is usually active in roots is repressed during nodule development, and this repression may facilitate export of intact asparagine from the nodule. The amides can be metabolized in leaves by transamination and transamidation reactions similar to those used in their synthesis (see Chapter 7).

A second major group of legumes that includes soybean (*Glycine*) and cowpea (*Vigna*) also exports nitrogen from the nodules as the **ureides** allantoin and allantoic acid. The biosynthesis of these compounds involves multiple compartments, as purines are synthesized in the infected cells and then oxidized in neighboring uninfected cells (Fig. 16.26). In the leaves of nodulated plants, the allantoin is catabolized using allantoin amidohydrolyase to yield ammonia, rather than by hydrolysis of allantoin to generate urea with subsequent degradation of the urea using urease. The ammonia is then assimilated by GS and ferredoxin-dependent GOGAT.

16.5 Ammonia uptake and transport

For plants dependent on mineral nitrogen, ammonium (NH_4^+) and nitrate (NO_3^-) are the major sources. Though nitrate levels in soil are generally higher than ammonium levels, substantial levels of NH_4^+ ion may occur in acidic or anoxic soils, where rates of nitrification are low. For example, ammonium is a major nitrogen source for rice plants grown in flooded paddy soil. Excess ammonium is toxic, however, and plants have evolved mechanisms to regulate its uptake and expel it actively in an energy-dependent process.

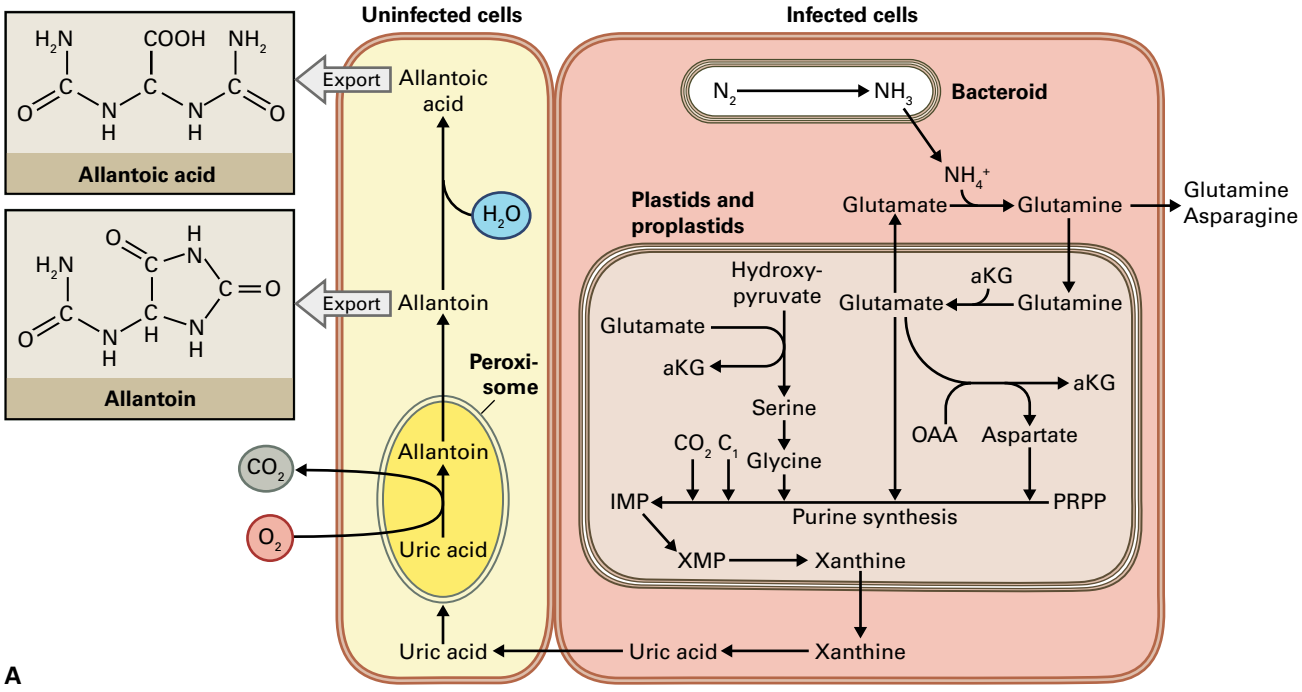
For **ammonium uptake** from the soil, plants use two separate transport systems: a nonsaturable, low-affinity system and a saturable, high-affinity system (Fig. 16.27A). The high-affinity ammonium uptake system involves transporters in the **AMT/Rh** family. *Arabidopsis* has six *AMT* genes: *AMT1;1–5* and *AMT 2;1*. Four of these, *AMT 1;1, AMT 1;3, AMT 1;5* (expressed in the rhizodermis), and *AMT 1;2* (cortex and endodermis; Fig. 16.27B), account for ≈30, ≈20, ≈30, and ≈10%, respectively, of the total high-affinity ammonium influx in *Arabidopsis* roots. Most organisms have *AMT* /Rh genes, but unlike the prokaryotic AMT transporter and human erythrocyte rhesus-associated glycoprotein Rh (both of which function as NH_3 channels), plant AMT transporters function as NH_4^+ uniporters. The proteins involved in the low-affinity system have not yet been identified, but potassium channels, nonselective cation channels, or aquaporins are potential candidates.

Plant AMT transporters are regulated at both the transcriptional and posttranslational levels. Transcript levels for *AMT1;1–3* and *1;5* are upregulated under nitrogen-deficient conditions, and AMT1.1 and AMT1.2 proteins are regulated by allosteric transactivation. Crystal structures of the *E. coli* and archaeal ammonium transporters reveal a trimer with a substrate-conducting channel in each monomer (Fig. 16.28). Homology models, suppressor screening, and phosphoproteomic studies suggest the cytosolic C-terminus of plant AMT transporters, which contains two conserved short α-helices, interacts with the cytosolic surface of a neighboring subunit. Phosphorylation of a threonine residue (460 in AMT1.1 and 472 in AMT1.2) in the C-terminus of a single monomer leads to a conformational change that leads to the cooperative closure of all three pores in the trimer (Fig. 16.28). This provides a rapid shut-off mechanism that prevents toxic accumulation of ammonium.

Ammonium can accumulate in the vacuole, and the *Arabidopsis* **tonoplast intrinsic proteins** TIP2;1 and TIP2;3 transport NH_3 when expressed in yeast or oocytes. These tonoplast intrinsic aquaporins may be involved in loading NH_3 into the acidic vacuole, where it is then trapped as the NH_3 protonated form, NH_4^+ (Fig. 16.29). In sum, membrane potential is a driving force for the high-affinity ammonium uptake across plasma membranes mediated by AMT transporters, while vacuolar acidification could be the main factor for accumulating ammonium in the vacuole (Fig. 16.29).

16.6 Nitrate uptake and transport

Nitrate serves as both nutrient and signal, and it has pronounced effects on plant metabolism and growth. Nitrate is a major soil nitrogen source, and plants devote significant



A

Reaction	Enzyme	Location
Purine nucleotide synthesis		
↓		Proplastids of infected cells
Inosine monophosphate[a] (IMP)		
↓ NAD⁺ → NADH	IMP dehydrogenase	Plastids of infected cells or cytosol
Xanthosine monophosphate		
↓ Ribose, P_i	Nucleotidase or Nucleosidase	Proplastids of infected cells
Xanthine		
↓ NAD⁺ → NADH	Xanthine dehydrogenase	Cytosol
Uric acid		
↓ O_2, CO_2	Urate oxidase (= uricase)	Peroxisomes in uninfected host cells
Allantoin		
↓ H_2O	Allantoinase	Endoplasmic reticulum in uninfected host cells
Allantoic acid		

[a] An alternative possibility is conversion of inosine monophosphate to hypoxanthine, which is then oxidized to xanthine by xanthine dehydrogenase.

B

FIGURE 16.26 *Complex cellular and subcellular compartmentation of ureide biosynthesis enzymes in plants such as soybean and cowpea. (A) In tropical legumes such as cowpea and soybean, nitrogenous compounds in addition to glutamine and asparagine are exported from infected cells. A substantial fraction of the fixed nitrogen is exported to adjacent uninfected cells as uric acid, a decomposition product of purines. In the uninfected cells, uric acid is degraded to allantoin and allantoic acid, which are then transported through the xylem to the rest of the plant. The uricase reaction which produces allantoin is especially interesting because it depends on oxygen, which is in limited supply. (B) The purine degradation pathway in nodules, showing the relevant enzymes and their locations.*

carbon and energy reserves to its uptake and assimilation. Plants detect nitrate and integrate its assimilation with photosynthesis and overall carbon/nitrogen metabolism. This allows plants to control growth rates, root architecture, carbon/nitrogen ratios, reductant levels, and ionic and pH balances under diverse environmental conditions.

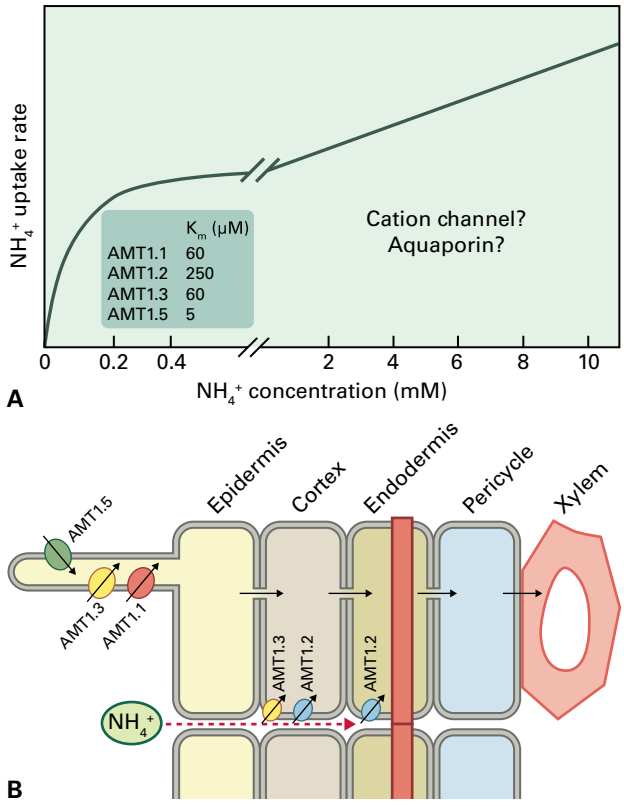


FIGURE 16.27 *Ammonium uptake. (A) Uptake by the high-affinity system demonstrates Michaelis–Menten kinetics, and uptake by the low-affinity systems demonstrates nonsaturating kinetics. In* Arabidopsis, *four ammonium transporters (AMT1.1, AMT1.2, AMT1.3, and AMT1.5) are involved in high-affinity uptake. The proteins required for low-affinity uptake have not been identified. (B) Schematic illustration of spatial expression pattern of* Arabidopsis *ammonium transporters in roots.*

Nitrate assimilation begins with its transport across the plasma membrane (Fig. 16.30). Usually, nitrate is taken up from the soil solution by root epidermal, cortical, and endodermal cells, though primary uptake can also occur in leaves. Uptake by leaves is important during foliar application of fertilizer, as well as for epiphytes. Once within the symplasm, nitrate can be transported into the vacuole, where storage of high concentrations (>20 mM) is possible. Major storage organs for nitrate include the roots, stems, and leaf midribs, but nitrate can also be loaded into the xylem for long-distance transport to the shoot. Diverse physiological, genetic, and environmental factors determine how nitrate is allocated and stored.

Two types of **symporters** (NRT1 and NRT2) and one **antiporter** (CLC) are involved in nitrate transport in plants. NRT1 and NRT2 function in nitrate uptake and transport across both the plasma membrane and tonoplast, whereas CLC functions primarily in transport across the tonoplast.

16.6.1 Plants use both low- and high-affinity transport systems for nitrate uptake from the soil

Usable nitrate concentrations in the soil can vary by over four orders of magnitude, from micromolar to millimolar. To cope with this wide range of concentrations while avoiding both deficiency and toxicity, plants use two nitrate uptake systems: a high-affinity system with $K_m \approx 50$ μM and a low-affinity system with $K_m \approx 5$ mM (Fig. 16.31). Both are mediated by active H^+-coupled mechanisms, using the H^+ gradient generated by the H^+-ATPase as the driving force for nitrate import.

These two uptake systems involve two nitrate transporter families, NRT1 and NRT2. In *Arabidopsis*, two NRT1 transporters (AtNRT1.1 [CHL1] and AtNRT1.2), and four NRT2 transporters (AtNRT2.1, AtNRT2.2, AtNRT2.4 and AtNRT2.5) are assisted by one NAR2 protein (AtNAR2.1) for nitrate uptake. AtNRT2.1 and AtNRT2.2 are both nitrate-inducible, high-affinity nitrate transporters, whereas AtNRT1.2 is a

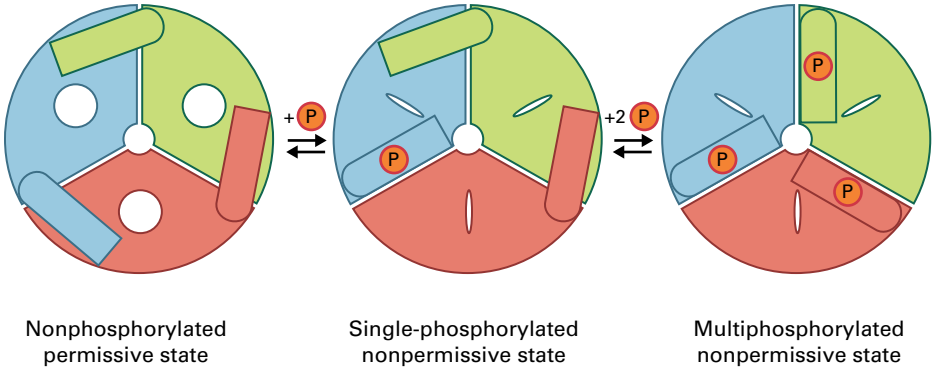


FIGURE 16.28 *Schematic representation of the allosteric regulation of the ammonium transporter AMT. Ammonium transporters exist as homotrimers, and each monomer contains an independent pore for ammonium. The cytosolic C-terminus of a single monomer is proposed to interact with the neighboring monomer. Posttranslational phosphorylation of the C-terminus of a single monomer (indicated by red phosphate) is proposed to lead to a conformational change, resulting in cooperative closure of all three pores in the complex.*

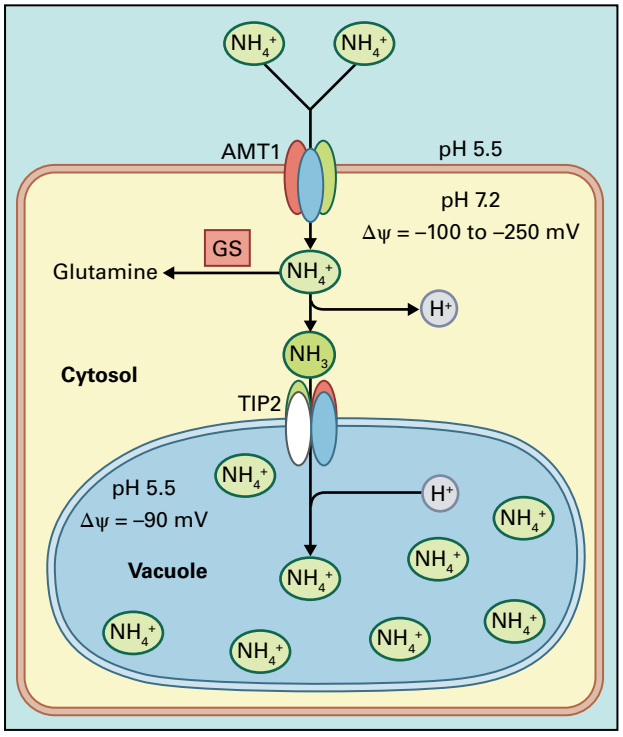


FIGURE 16.29 *Ammonium uptake across the plasma membrane is mediated by ATMs, and membrane potential is the driving force. Ammonium transport across the tonoplast may be mediated by TIP2 aquaporins, and vacuolar acidification could be the main factor for accumulation of ammonium in vacuole.*

constitutively expressed low-affinity transporter. AtNRT1.1 (CHL1) is a dual-affinity transporter involved in both high- and low-affinity uptake (Fig. 16.31).

AtNRT1.1 (CHL1) was the first member of the NRT1 family identified by genetic studies selecting for chlorate resistance. Chlorate is a chlorine analog of nitrate that becomes toxic when it is imported by nitrate uptake systems and reduced to chlorite by nitrate reductase (Fig. 16.32). One of the chlorate-resistant mutants, *chl1*, is defective in uptake. CHL1 contains 12 transmembrane domains, with the six N-terminal and six C-terminal transmembrane domains separated by a large hydrophilic loop (see Fig. 16.31). Functional studies of the protein expressed in *Xenopus* oocytes showed it is a H^+-coupled nitrate transporter with a H^+/NO_3^- ratio larger than one. The *Arabidopsis* genome includes 53 NRT1 (PTR) transporter genes; some of the proteins encoded by these genes (**NRT PTR family**) transport dipeptides, but not nitrate. Likewise, most NRT1 homologs isolated from cellular organisms are dipeptide transporters (e.g., DtpT from *E. coli*, PepT1 from human, and PTR2 from *Saccharomyces cerevisiae*). It is thought that nitrate transport activity evolved from an ancient dipeptide transporter.

The two modes of AtNRT1.1 activity are regulated by phosphorylation and dephosphorylation of the threonine 101 residue (Fig. 16.31). AtNRT1.1 is a high-affinity nitrate transporter when T101 is phosphorylated, whereas the dephosphorylated form of AtNRT1.1 is a low-affinity nitrate transporter. The switch in phosphorylation is triggered by changes in external nitrate availability. This allows transporter function to adapt to available resource levels in the root environment.

NRT2 transporters are high-affinity H^+-coupled nitrate transporters that also have 12 transmembrane domains (Fig. 16.31), but they share no significant sequence similarity with NRT1 transporters. The first member of the NRT2 family identified was *crnA* from *Aspergillus*, and subsequently several *NRT2* genes were isolated from bacteria, yeast, mosses, algae, and plants. In algae and plants, an additional component, NAR2 (NRT3), is required for the high-affinity nitrate transport of NRT2. NAR2, which contains two transmembrane domains, plays a role in targeting AtNRT2.1 to the plasma membrane. *Arabidopsis* has seven *NRT2* genes and two *NAR2* (*NRT3*) genes; one of the NRT2 proteins, AtNRT2.7, is involved in vacuolar nitrate transport in seeds (see Fig. 16.30 and Section 16.6.2).

Consistent with their roles in uptake, expression of AtNRT1.1, 1.2, and 2.1 in *Arabidopsis* is restricted to the outer cell layers of the root, including the epidermis, cortex, and endodermis (Fig. 16.33). AtNRT2.1 is expressed mainly in the basal part (oldest portion) of the root, while AtNRT1.1 (CHL1) is expressed more in the young root. In addition, expression levels of the NRT1 and NRT2 genes are differentially regulated by nitrate, nitrogen starvation, and reduced forms of nitrogen. The relative contribution of these transporters in nitrate uptake depends on the age and nitrogen status of plants.

16.6.2 Transporters responsible for vacuolar storage and xylem loading have also been identified

Once inside the cell, a major part of free nitrate is stored in vacuoles, where concentrations can reach 20–70 mM. When plants are shifted to nitrate-depleted or nitrate-sufficient media, vacuolar nitrate concentrations may vary considerably, even while cytosol nitrate concentration is kept constant. The homeostasis of cytosolic nitrate is determined by the balance between uptake, efflux, nitrate reductase activity, and vacuole storage and remobilization (see Fig. 16.30).

Arabidopsis AtCLCa is a $2NO_3^-/1H^+$ antiporter involved in **nitrate homeostasis**. Located in the tonoplast and predominantly expressed in leaf laminae, it is responsible for nitrate accumulation in the vacuole (see Fig. 16.30) and belongs to the **large chloride channel (CLC) family**. Some members of the CLC family are H^+-gated anion channels (e.g., mammalian ClC-0 and ClC-1), while others are Cl^-/H^+ antiporters (e.g., mammalian lysosomal ClC7 and *E. coli* ClCec-1). Unlike these CLCs, however, AtCLCa has much higher permeability for nitrate than chloride. *Arabidopsis* has seven CLC genes.

Different plant tissues may employ distinct transporters, as illustrated by nitrate relations in developing *Arabidopsis* seeds. One of the tonoplast-localized transporters, AtNRT2.7 (see Fig. 16.30), is expressed mainly during the later stages of

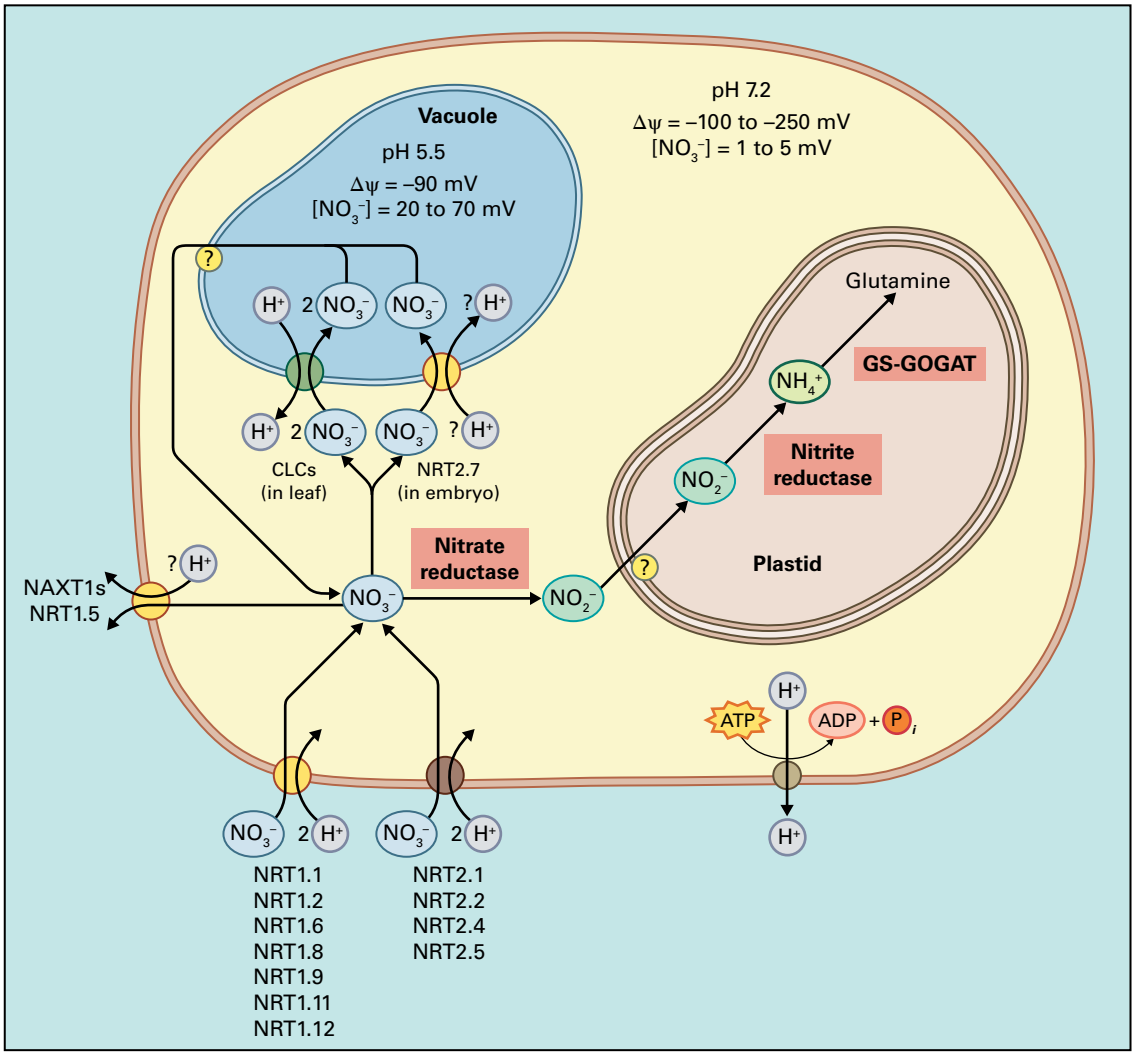


FIGURE 16.30 *Nitrate assimilation by plant cells involves transport of nitrate across the plasma membrane and then reduction to ammonia in a two-step process. Nitrate can be stored in and remobilized from the vacuole. A H⁺-ATPase maintains the electrochemical gradient that drives cellular uptake of nitrate. The values shown for electrical potentials and intracellular nitrate concentrations are typical, but can vary significantly.*

seed development. Lower seed nitrate content in an *nrt2.7* mutant suggests AtRNT2.7 mediates nitrate loading into the vacuole during seed maturation. By contrast, the plasma membrane-localized transporter AtNRT1.6 is expressed in the funiculus at the early stages of embryo development. Increased seed abortion rate and embryo abnormality in an *atrnt1.6* mutant indicate nitrate is important for early embryo development.

Root-to-shoot nitrate transport is mediated by the xylem. For **xylem loading**, nitrate must be transported out of the parenchymal cells that are close to the xylem. According to electrochemical gradients, nitrate should undergo passive transport out of a plant cell, likely through a channel. However, two NRT1 transporters (NAXT1 and AtNRT1.5) mediate **nitrate export**, and AtNRT1.5 expressed in pericycle cells next to root xylem is responsible for nitrate xylem loading (see Fig. 16.30 and 16.33). Root-to-shoot nitrate transport is not completely eliminated in *atnrt1.5* mutants, suggesting additional genes or mechanisms are involved in xylem loading.

16.7 Nitrate reduction

Nitrate itself is not incorporated into organic compounds, but is first reduced to ammonium in a two-step process (see Fig. 16.30). Nitrate is first reduced to nitrite by **nitrate reductase** (NR, Reaction 16.2), then nitrite is reduced to ammonium by **nitrite reductase** (NiR, Reaction 16.3) in a reaction involving reduced **ferredoxin** (Fdx_{red}). During this eight-electron transfer, the oxidation state of nitrogen drops from +5 to –3. The subsequent reactions that assimilate ammonium into amino acids also consume organic carbon (see Chapter 7). Plants reduce nitrate and nitrite in both root and shoot tissues.

Reaction 16.2: Nitrate reductase

$$NO_3^- + NAD(P)H + H^+ \rightarrow NO_2^- + NAD(P)^+ + H_2O$$

Reaction 16.3: Nitrite reductase

$$NO_2^- + 6Fdx_{red} + 8H^+ \rightarrow NH_4^+ + 6Fdx_{ox} + 2H_2O$$

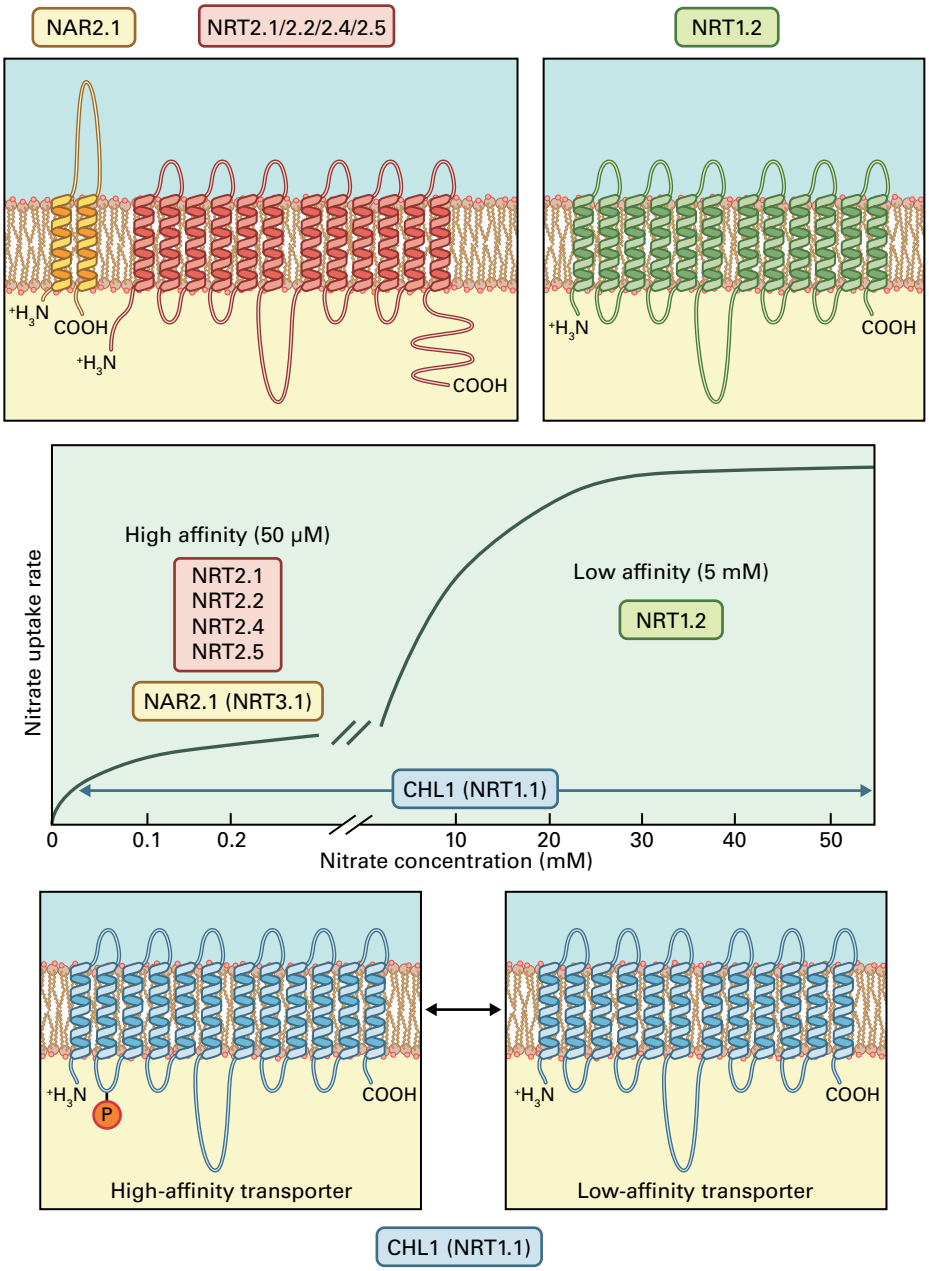


FIGURE 16.31 *Kinetics of nitrate uptake. Nitrate uptake displays two saturated phases, with K_m in the micromolar range for the high-affinity system and in the mM range for the low-affinity system. In* Arabidopsis, *CHL1 (AtNRT1.1; shown in blue) is a dual-affinity nitrate transporter involved in both high- and low-affinity uptake, with the two action modes switched by phosphorylation/dephosphorylation of T101. AtNRT2.1 and AtNRT2.2 (shown in red) associated with AtNAR2.1 (shown in yellow) are involved in high-affinity uptake, while AtNRT1.2 (shown in green) participates in low-affinity uptake.*

In the reduction of nitrate to nitrite (Reaction 16.2), NADH or NADPH serves as the reductant and a proton is consumed in the reaction. This reaction is catalyzed by NR, a complex metalloenzyme that forms homodimers (Fig. 16.34) and homotetramers. NR has binding sites for NAD(P)H and for nitrate, and three cofactors—**FAD**, **heme-Fe**, and the **molybdenum cofactor** (**MoCo**, Fig. 16.35)—provide the redox centers that facilitate the chain of electron transfer reactions. In the native enzyme, the midpoint potentials ($E'°$) for FAD, heme-Fe, and MoCo are −272, −160, and −10 mV, respectively. Each NR subunit is almost 1,000 amino acids long and contains all three cofactors. Most forms of plant NR use NADH, but some are bispecific and can use either NADPH or NADH.

16.7.1 NR subunits contain three distinct regions, each associated with a specific electron transport cofactor

Within the NR holoenzyme, each cofactor is a redox center associated with a distinct functional and structural region of the protein. Partial proteolysis of the enzyme produces

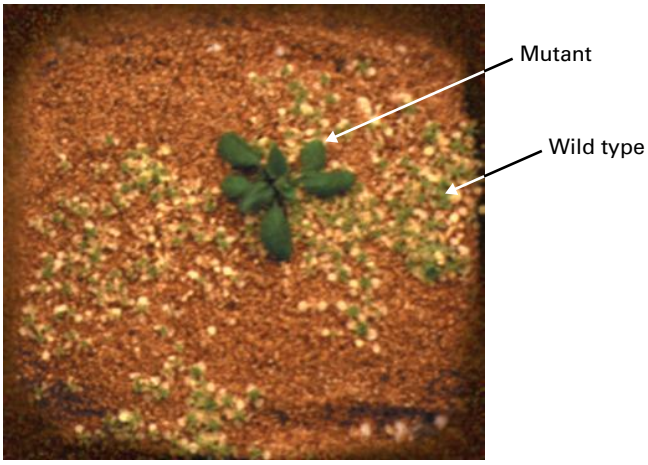


FIGURE 16.32 *Nitrate uptake mutants can be selected by treating plants with chlorate. Wild-type plants take up chlorate and reduce it to the toxic product chlorite, resulting in chlorosis. Nitrate uptake mutants are unable to import chlorate and so remain green.* *Source*: Crawford, University of California–San Diego, La Jolla, CA, previously unpublished.

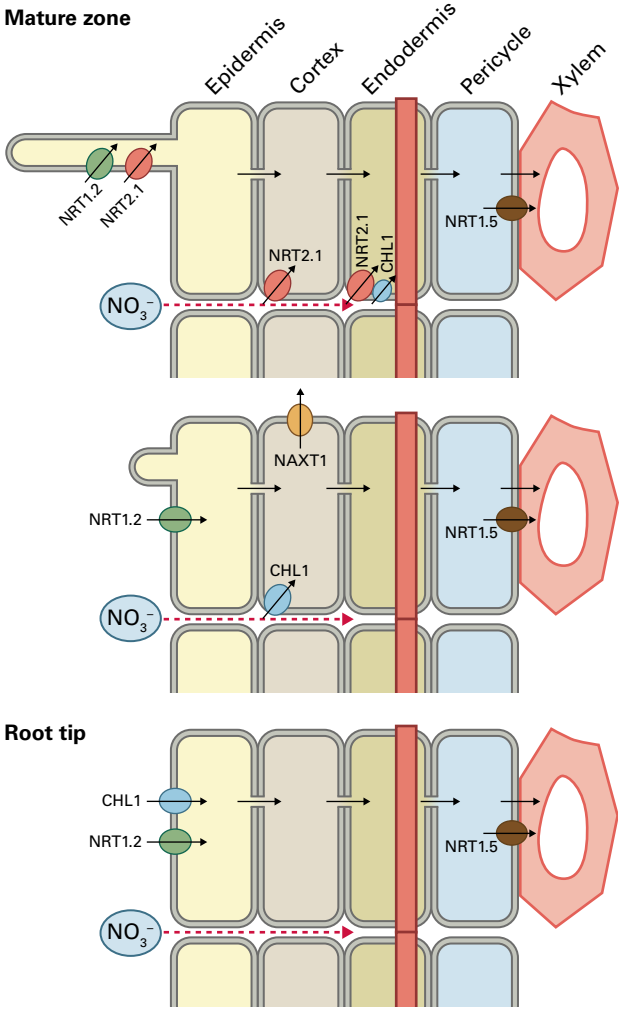


FIGURE 16.33 *Schematic presentation of spatial expression pattern of* Arabidopsis *nitrate transporters in different zones of root tissue. Bottom: cross-section of root near the tip, in which the epidermal cells have not begun to form a hair extension. Center: cross-section of a root with emerging root hair. Top: more mature part of the root in which a root hair is fully formed. CHL1 (AtNRT1.1), AtNRT1.2, AtNRT2.1, and AtNRT2.2 are involved in uptake, and AtNRT1.5 is involved in xylem loading.*

discrete fragments that display partial enzymatic activity. One fragment binds FAD and can use NADH to reduce ferricyanide, an artificial electron acceptor. A second fragment contains MoCo and heme-Fe and can reduce nitrate in the presence of methyl viologen, an artificial electron donor. The partial activities associated with NR fragments are consistent with the structural evidence for discrete functional regions.

The spatial arrangement of functional regions, inferred from cDNA sequences, are as follows: the **MoCo domain** is near the N-terminus, the **heme-Fe domain** is in the middle, and the **FAD domain** is at the C-terminus (see Fig. 16.34). The three functional regions are connected by two hinges, one of which contains a regulatory site that is phosphorylated and binds 14-3-3 proteins, which modulate NR activity (see Section 16.7.4 and Chapters 3 and 18). Figure 16.34B shows a model for the structural and functional relationship of the domains.

Each functional region of NR is an independent unit that belongs to a distinct protein family. The FAD-binding region (260–265 amino acids) is similar to the **ferredoxin-NADP$^+$ reductase** (**FNR**) family of flavin oxidoreductases, which includes FNR, cytochrome P450 reductase, nitric oxide synthase, and cytochrome b_5 reductase. The crystal structure of the FAD region reveals two domains, each forming a lobe separated by a cleft (see Fig. 16.34B): the N-terminal lobe binds FAD, and the C-terminal lobe binds the substrate NAD(P)H. In the C-terminal lobe, a cysteine provides a thiol group that interacts with the NAD(P)H and is thought to position the NAD(P)H to facilitate electron transfer to FAD. Although this cysteine is invariant in the FNR family of flavoproteins, it is not required by NR; a serine substitution for the cysteine renders NR less active but still able to bind NADH and reduce FAD.

The central heme domain of 75–80 residues is similar to that of the **cytochrome b_5 family** of heme proteins. These proteins share certain properties: they can oxidize cytochrome *c* and have a characteristic cytochrome *b*-type fold that binds the heme moiety noncovalently. Proteins in the cytochrome b_5 family may be soluble or membrane bound, and they often associate with flavoproteins. The axial ligands of the NR heme-Fe are thought to be histidines provided by the NR protein.

The large N-terminal domain containing the MoCo (360–370 amino acids) belongs to a special class of MoCo-binding proteins. Of the enzymes that contain a MoCo, including **xanthine oxidase**, **biotin sulfoxide reductase**, **dimethyl sulfoxide** (DMSO) **reductase**, and **sulfite oxidase** (Section 16.14.5), only sulfite oxidase has significant sequence similarity to NR. Like NR, sulfite oxidase has an attached cytochrome b_5 heme domain, although this heme domain is N-terminal to the MoCo-binding region in sulfite oxidase

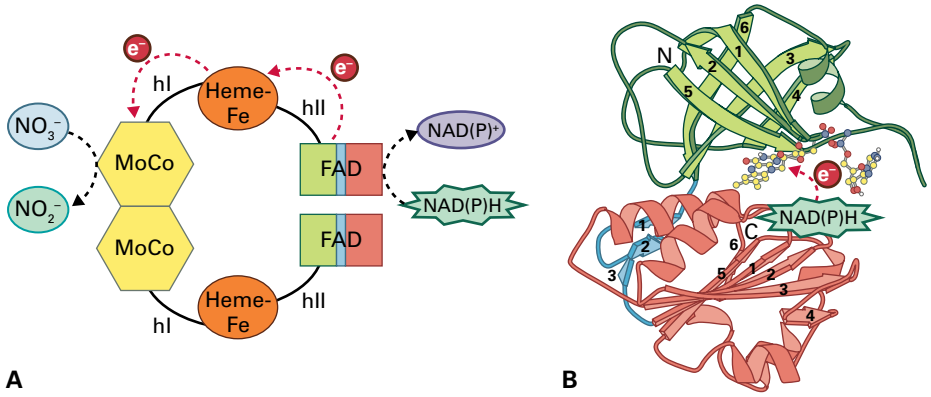


FIGURE 16.34 *(A) Domain structure of nitrate reductase. An NR monomer has three major domains that bind molybdenum cofactor (MoCo), heme, and FAD respectively. The FAD-binding region receives electrons from NAD(P)H, and the heme domain shuttles electrons to the MoCo-binding region, which transfers electrons to nitrate. Hinge 1 and 2 (hI and hII) which separate the functional domains. (B) Crystal structure of the FAD-binding domain of NR. The C-terminal fragment of NR, showing the N-terminal lobe of the fragment (green), a linker domain (blue), and the C-terminal lobe (red). The N-terminal lobe is bound to FAD, whereas the C-terminal lobe binds NAD(P)H.*

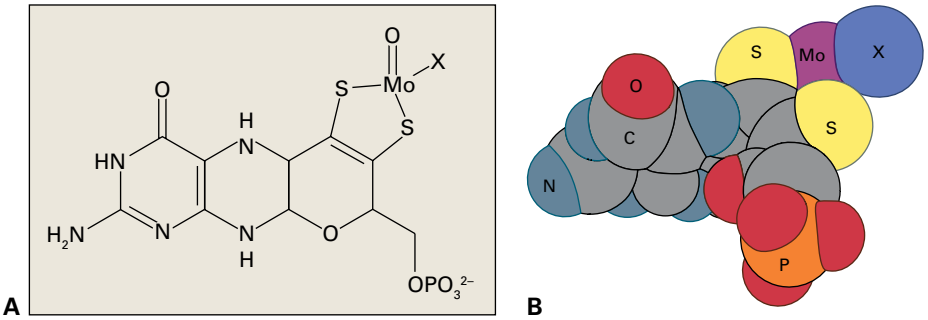


FIGURE 16.35 *Molybdenum cofactor (MoCo) of NR. (A) Chemical structure. (B) Space-filling model.*

and C-terminal to the MoCo region in NR. These alternative arrangements of functional protein units imply domains have been shuffled in different configurations to form new enzymes during the course of evolution. Compared to sulfite oxidase, the substrate funnel of the NR MoCo domain narrows to an elongated slot wide enough for the planar nitrate molecule, but not for the bulkier sulfate molecule. This may explain why nitrate inhibits sulfite oxidase, but sulfate does not inhibit NR.

16.7.2 Nitrate is reduced in the cytosol of root and shoot cells

NR and nitrate reduction occur in the cytosol of cells throughout the vegetative organs of the plant. In most species, NR is found in both shoots and roots, and its distribution depends on environmental conditions. However, some species [e.g., cranberry (*Vaccinium macrocarpon*), white clover (*Trifolium repens*), and young chicory (*Cichorium intybus*)] localize almost all their NR in roots, whereas others (e.g., cocklebur (*Xanthium* spp.)) express NR almost exclusively in leaves.

Within a specific organ, NR shows cell type-specific localization. At low external nitrate concentrations, NR is found primarily in epidermal cells and cortical cells close to the root surface. At higher external nitrate concentrations, activity is also detected in cells of the cortex and vascular system. In maize (*Zea mays*), a C_4 plant, NR is located in the mesophyll, but not in **bundle sheath cells**—a finding consistent with the far greater capacity of mesophyll chloroplasts to generate reductant by way of noncyclic photosynthetic electron transfer (see Chapter 12).

16.7.3 NR gene transcription is regulated by diverse signals

Green tissues have much more NiR activity than NR activity, and this ensures that nitrite does not accumulate to toxic levels. Thus, NR is thought to catalyze the rate-limiting step in the conversion of nitrate to ammonium. Plants use several mechanisms to adjust the concentration and activity of NR in response to such diverse signals as nitrate abundance, nitrogen metabolites (especially glutamine), CO_2, carbon metabolites (especially sucrose), cytokinins, and light.

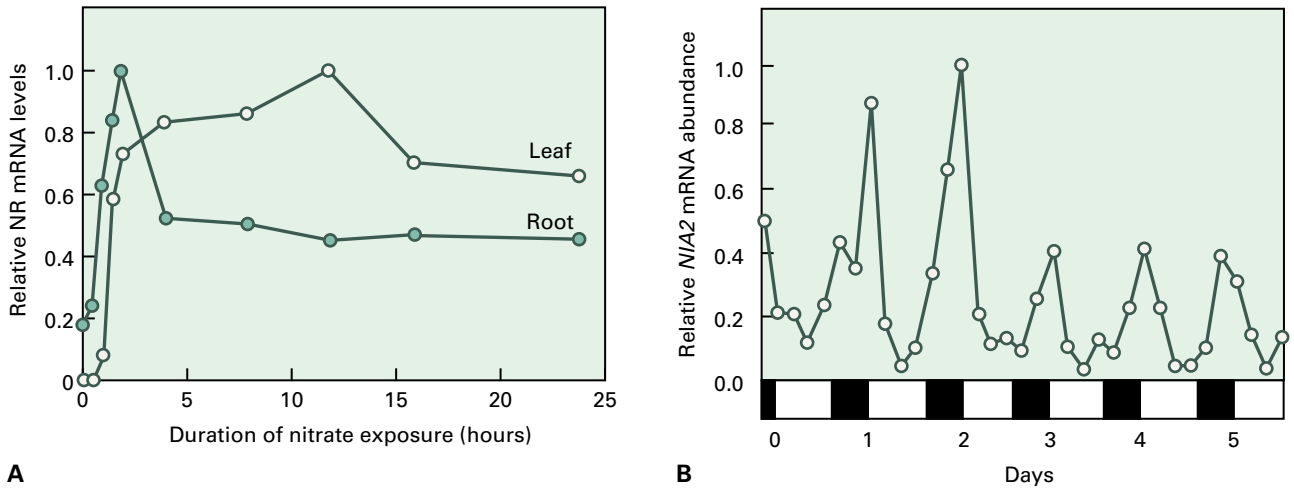


FIGURE 16.36 *Regulation of NR gene expression. (A) Transcription of NR mRNA levels in roots and leaves is influenced by the availability of nitrate. Seven day old barley seedlings grown in the absence of nitrate were treated with 15 mM nitrate at time zero. RNA was extracted from roots and leaves at the indicated times, and relative NR mRNA levels were determined. (B) In plants grown in the presence of nitrate, NR mRNA levels demonstrate a diurnal cycle. RNA was extracted from leaves of tomato plants at the indicated times, and relative NR mRNA levels were determined.*

TABLE 16.5 *Signals that influence the transcription and activity of NR.*

	Effect on NR	
Signal	**Transcription**	**Enzyme Activity**
Glutamine	↓	
Nitrogen starvation	↓	
Circadian rhythm	Modulates, depending on time of day	
Nitrate	↑	
Cytokinin	↑	
Sucrose	↑	
Light	↑	↑
Darkness	↓	↓
High [CO_2]		↑
Low [CO_2]		↓
Oxygen		↑
Anoxia		↓

Expression of the NR gene is substrate inducible in many plants (Fig. 16.36A and see Section 16.9), and in leaves, NR induction also requires functional, genetically intact chloroplasts. This coordinated regulation of a cytosolic enzyme by plastid signals probably prevents nitrite production in cases where a chloroplast defect renders NiR activity is deficient.

In addition to the primary signal, nitrate, NR mRNA quantities respond to other signals that link nitrate reduction to photosynthesis, carbon metabolism, and diurnal cycles. For maximal induction of NR mRNA, plants require light or a source of reduced carbon. Genetic and physiological data imply **phytochrome** (see Chapter 18) mediates this light-induced enhancement of NR mRNA concentrations. Light regulation is most dramatic in etiolated seedlings, but also occurs in green tissues. Once the NR gene is induced, NR mRNA quantities cycle in a diurnal rhythm driven by circadian clocks (Fig. 16.36B). A downstream metabolite may act as a signaling molecule that controls NR activity. Several lines of evidence suggest that glutamine can repress expression of NR genes (Table 16.5). During diurnal cycling, glutamine concentrations increase as NR transcript concentrations decrease in wild-type plants; further, in NR mutant plants, glutamine concentrations are always high and NR mRNA concentrations low.

In summary, key regulatory mechanisms control NR gene expression so that nitrate reduction is coordinated with the demand of the shoots for nitrogen, the availability of nitrate and light (reduced carbon), and proper chloroplast function.

16.7.4 Phosphorylation-dependent binding of 14-3-3 proteins post-translationally modulates NR activity in response to endogenous and environmental signals

Post-translational mechanisms control NR protein concentration and activity in response to certain physiological conditions. For example, NR protein levels decrease when plants are

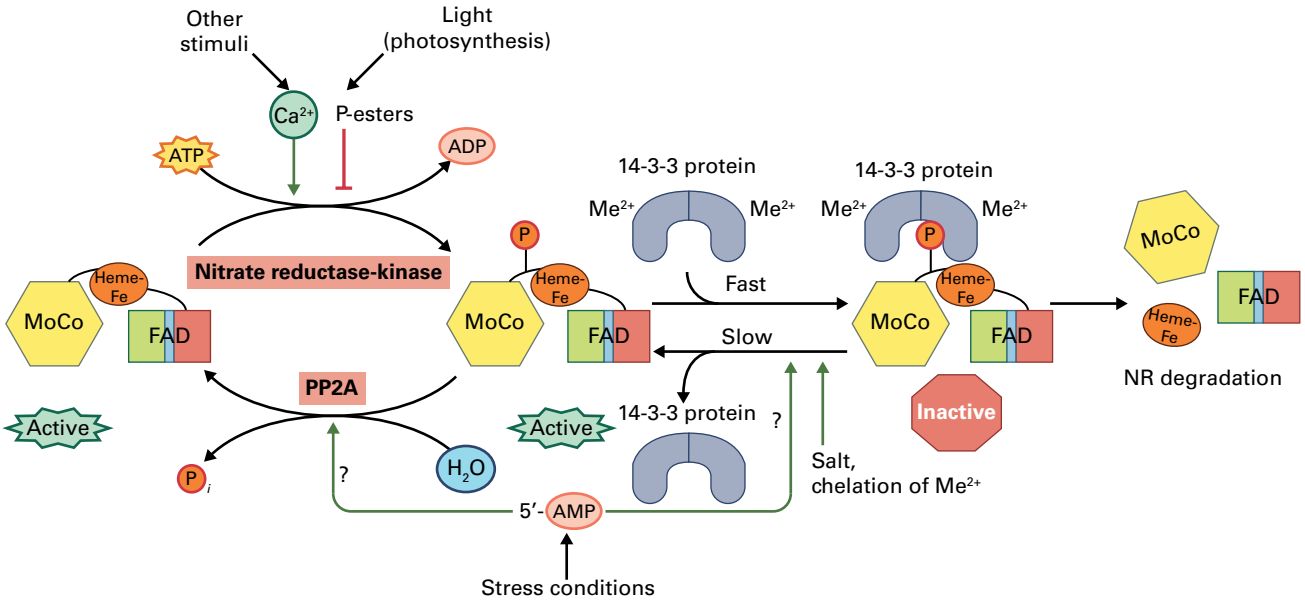


FIGURE 16.37 *Proposed model for regulation of nitrate reductase activity by phosphorylation/dephosphorylation and reversible binding of 14-3-3 protein. NR is phosphorylated by protein kinases on a serine residue in hinge 1. Phosphorylated NR is still active but is bound by 14-3-3 dimers, which inactivate NR. NR in 14-3-3 complexes is more rapidly degraded than free NR and not a substrate for phosphatases. If NR is released from 14-3-3 proteins, the regulatory phosphate can be removed by protein phosphatase PP2A.*

deprived of nitrogen or light for several days, even while amounts of NR mRNA remain high. A more rapid and reversible inhibition of NR activity occurs when plants are held in darkness or exposed to low concentrations of CO_2. Under these conditions, NR inhibition occurs within minutes, resulting from the phosphorylation of a conserved serine in the hinge 1 region (see Fig. 16.34) by calcium-dependent protein kinases, followed by Mg^{2+}- or Ca^{2+}-dependent binding of **14-3-3 proteins** (Fig. 16.37). A type 2A protein phosphatase (PP2A) reactivates NR by dephosphorylating the hinge 1 serine, which prevents 14-3-3 proteins from binding. The reactions that inhibit and reactivate NR are modulated by Ca^{2+}, 5′-AMP, and P_i, which may act as secondary messengers. The kinase/14-3-3 inhibition mechanism allows rapid and reversible inhibition of NR activity when conditions do not favor nitrate assimilation.

The regulation of both NR transcription and enzyme activity allows plants to fine-tune the amount of nitrate reduction. Light (or its photosynthetic product, sucrose) induces NR transcription, particularly in etiolated plants. Probably serving as a feed back regulatory loop, light also increases the concentration of glutamine, which suppresses NR transcription (see Chapter 8). Once induced, however, NR transcription in photosynthetic tissues demonstrates a cyclic pattern, so that maximal transcript values are achieved just before the appearance of light (see Fig. 16.36B). NR protein in photosynthetic tissues is reversibly inhibited by conditions that prevent photosynthetic carbon reduction, such as darkness or CO_2 deprivation. Upregulation of NR transcription has the potential to enhance nitrite production. Thus when NiR activity is low, as in darkness, NR activity must also be downregulated to prevent accumulation of toxic concentrations of nitrite. A list of signals influencing NR transcription and activity is provided in Table 16.5.

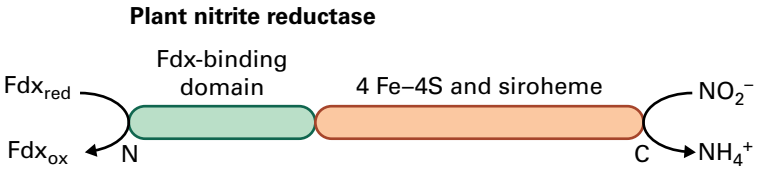
16.8 Nitrite reduction

After nitrate reduction, the next step in nitrate assimilation is the reduction of nitrite to ammonia, which is catalyzed by **NiR** (Reaction 16.3). Six electrons are transferred in this step, and the source of electrons is reduced ferredoxin (Fdx_{red}), produced in chloroplasts by noncyclic (linear) photosynthetic electron transfer. Nitrite reduction also uses Fdx_{red} in the plastids of nonphotosynthetic tissues such as the root. In such colorless plastids, NADPH from the oxidative pentose phosphate pathway (Chapter 13) reduces ferredoxin in a reaction catalyzed by **ferredoxin-NADP$^+$ reductase** (Reaction 16.4). Significantly, the ferredoxin in nonphotosynthetic plastids is more electropositive (by ca. 70 mV) than its chloroplast counterpart, thereby facilitating its reduction by NADPH.

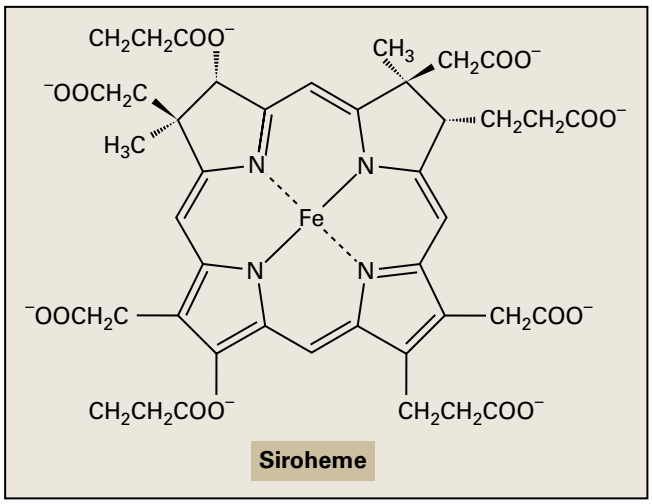
Reaction 16.4: Ferredoxin-NADP$^+$ reductase

$$NADPH + 2Fdx_{ox}(Fe^{3+}) \rightarrow NADP^+ + 2Fdx_{red}(Fe^{2+}) + H^+$$

NiR is a nuclear-encoded protein with an N-terminal transit peptide that is cleaved from the mature enzyme as it is translocated into the plastid. The enzyme, a monomer of 60–70 kDa, has two functional domains and cofactors that shuttle electrons from Fdx_{red} to nitrite (Fig. 16.38A). The N-terminal half of the enzyme is thought to bind ferredoxin. The C-terminal half, which shares sequence homology with bacterial NADPH-sulfite reductases, contains the binding site for nitrite, as well as two redox centers, a 4Fe–4S center, and a **siroheme** (Fig. 16.38B). These two prosthetic groups are in close proximity, bridged by a sulfur ligand. Four cysteines located in two clusters provide both the bridging ligand and sulfur ligands for the 4Fe–4S cluster. Mutations that place bulky side chains next



A



B

FIGURE 16.38 *(A) Structure of nitrite reductase from higher plants. The N-terminal region oxidizes ferredoxin. The C-terminal region, which binds an Fe_4S_4 center and a siroheme group, reduces nitrite to ammonium. (B) Structure of siroheme prosthetic group.*

to two of these cysteine residues result in diminished NiR activity and can change the spectra of the siroheme in NiR protein, supporting a role for these cysteines in cofactor binding.

NiR is regulated transcriptionally, usually in coordination with NR. Because nitrite is toxic, cells must contain sufficient NiR to reduce all the nitrite produced by NR. Thus, plants maintain an excess of NiR activity whenever NR is present by inducing NiR gene expression in response to light and nitrate. If NiR concentrations are diminished, either by mutation or antisense expression, plants accumulate nitrite and are chlorotic. The regulatory mechanisms that control NR activity are thought to assist in preventing nitrite accumulation.

16.9 Nitrate signaling

In addition to being a nutrient, nitrate acts as a signal molecule that regulates its own uptake and assimilation. Nitrate induces transcription of nitrate transporters, NR, and NiR as well as the production of the reducing equivalents needed for nitrate assimilation. This rapid transcriptional regulation, termed primary nitrate response, can be triggered within 10 minutes by addition of as little as 100 nM nitrate and does not require de novo protein synthesis. Nitrite, the product of nitrate reduction, also acts as a potent signal to upregulate expression of the genes needed for nitrate uptake and assimilation; however, organic nitrogen compounds like glutamate (see Table 16.5) repress these genes as a mechanism of negative feedback regulation.

In roots, the levels of nitrate-induced expression of primary nitrate response genes in roots display two saturable phases involving the dual-affinity nitrate transporter NRT1.1 (CHL1; see Section 16.6.1), which also acts as a nitrate sensor. Using dual-affinity binding and a phosphorylation switch regulated by protein kinase CIPK23, NRT1.1 (CHL1) senses changes in nitrate concentration and induces a different level of transcriptional responses (Fig. 16.39).

In addition to mediating transcriptional responses in plants, nitrate also regulates seed dormancy, leaf expansion, and root architecture. Nitrate stored in the seed or applied exogenously relieves seed dormancy, and ABA and AtNRT1.1 (CHL1) are involved in this signaling pathway. **Root architecture** is also regulated by nitrate in a complicated way; for example, localized application of nitrate can stimulate primary and lateral root growth, while high nitrate concentrations cause a systemic inhibition of root development. Such regulation could allow plants to seek sufficient nitrogen sources and optimize their nitrogen uptake. ABA, auxin, nitrate transporters NRT2.1 and NRT1.1 (CHL1), transcription factor ANR1, and miRNA167 and its target ARF8 participate differently in the regulatory and signaling pathways mediating root adaptation to nitrate supply.

16.10 Interaction between nitrate assimilation and carbon metabolism

To coordinate the production of the carbon skeletons needed for amino acid synthesis, nitrate also upregulates genes involved in carbon metabolism. Plants exposed to nitrate redirect carbon from starch synthesis to the production of amino acids and organic acids, such as malate, by controlling

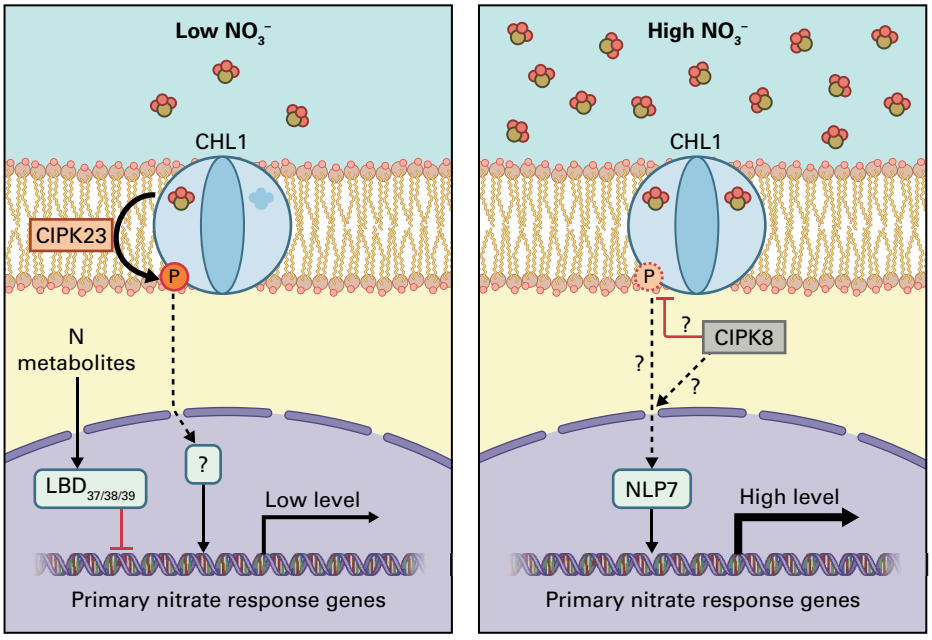


FIGURE 16.39 *Schematic representation of signaling pathways for nitrate-regulated transcriptional responses in* Arabidopsis. *Low external nitrate stimulates phosphorylation of the nitrate transceptor CHL1, which induces a low level of primary nitrate response gene expression; high external nitrate represses CHL1 phosphorylation and leads to high levels of gene expression. Under low-nitrate conditions, CIPK23 phosphorylates CHL1, and CIPK8 is involved in high-nitrate responses. NLP7 and the lateral organ boundary domains (LBDs) are transcription factors regulating nitrate-related genes.*

the synthesis and activity of key enzymes. For example, **PEP carboxylase** (which catalyzes the synthesis of oxaloacetate, a citric cycle intermediate readily converted to α-ketoglutarate) is upregulated by high nitrate. In contrast, **ADP glucose pyrophosphorylase**, which is required for starch biosynthesis, is downregulated in response to treatment with high concentrations of nitrate. These regulatory events are expressed most dramatically in NR^- mutants, which cannot reduce, but instead accumulate nitrate. Thus, nitrate acts as a signal that directs plants to redirect carbon flow into compounds that support nitrogen assimilation into amino acids.

On the other hand, expression of genes involved in nitrate uptake and assimilation is induced by light and sugars. Repression of these genes in the dark can be prevented by providing high concentrations of reduced carbon, such as sucrose. However, unlike other sugar responses in which hexokinase functions as a sugar sensor independently of its metabolic activity, glucose 6-phosphate is the sugar signal, and the catalytic activity of hexokinase is required for the induction of nitrate uptake transporters NRT1.1 and NRT2.1 by sucrose. Coordinated regulation between nitrate metabolism and carbon metabolism ensures efficient utilization of these two nutrients to allow maximum plant growth.

16.11 Overview of sulfur in the biosphere and plants

Sulfur is an essential macronutrient for all living organisms, and it occurs in nature in various oxidation states as part of inorganic and organic compounds. All these oxidation states can support growth of various bacteria and archaea. The major inorganic form of sulfur is **sulfate** (SO_4^{2-}), which is found in many minerals (e.g., gypsum) and at a high concentration in the oceans (ca. 26 mM or 2.8 g L^{-1}). Natural organic sulfur compounds include gases such as hydrogen sulfide and dimethylsulfide, which are emitted to the atmosphere both by geochemical processes and by action of the biosphere.

Sulfur deficiency in plants is associated with reduced yield and quality of crops and increased susceptibility to disease. While sulfur inputs from the atmosphere or soil are typically adequate, recent decreases in atmospheric sulfur availability have resulted in sulfur deficiency in many growing regions. Sulfur deficiency triggers multiple changes in plant metabolism, and these molecular responses to sulfur starvation have been extensively studied by a variety of genetic and genomics technologies. As a result, plant sulfur physiology has become an excellent model for plant systems biology.

Sulfate enters a plant primarily through the roots by way of an active uptake mechanism (Fig. 16.40). Although roots can assimilate sulfate, most sulfate is translocated to the shoot. In photosynthetic cells, sulfate can be transported either into the vacuoles for storage, or into the chloroplasts for assimilation. There are two major assimilation pathways: one in which sulfate is reduced to **sulfide** and incorporated into cysteine, and another in which sulfate is activated to **3′-phosphoadenosine 5′-phosphosulfate** (**PAPS**) and added to organic molecules. Sulfate can be linked to an oxygen atom to form a sulfate ester, to a nitrogen atom to form a sulfamate, or to a carbon atom to form a sulfonic acid; further metabolism of thiols produces thioethers, methylsulfonium compounds, and sulfoxides (Table 16.6 and Figure 16.40).

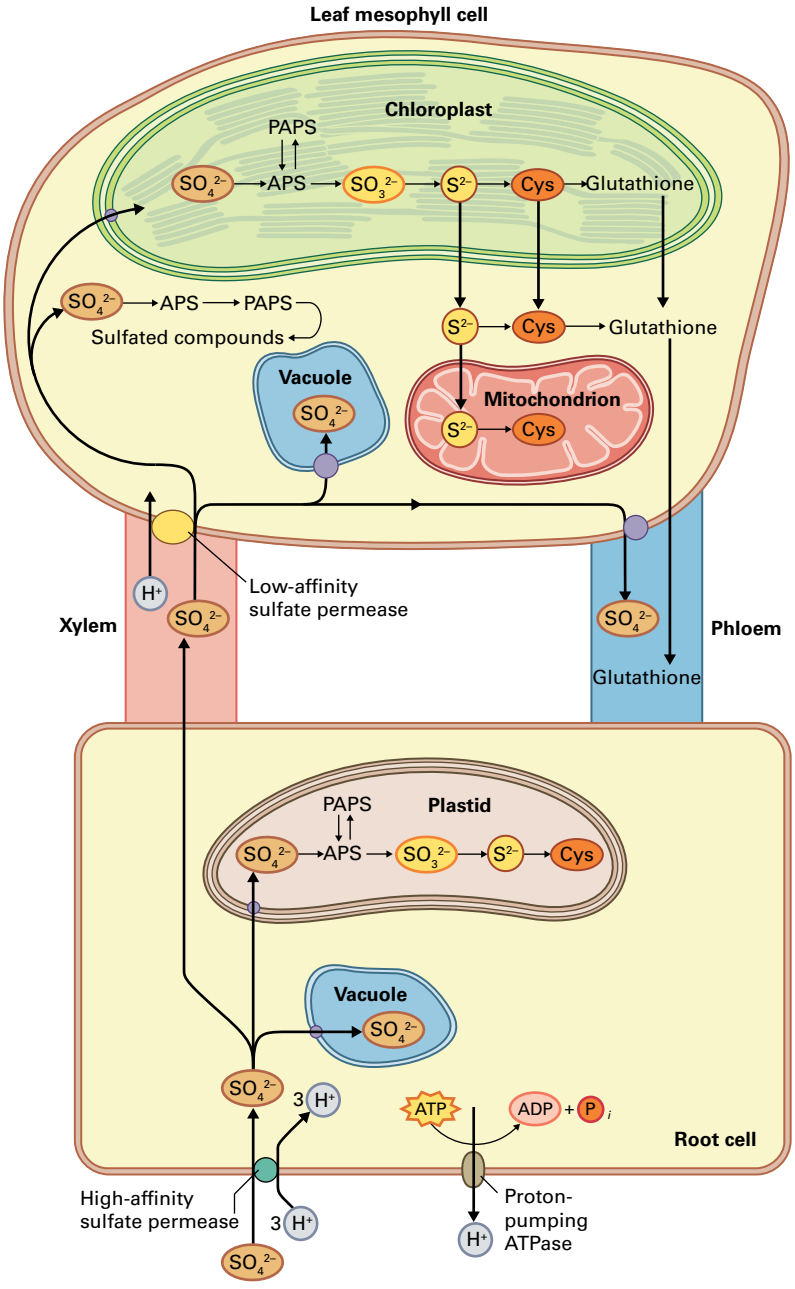


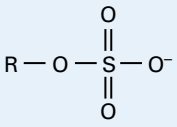
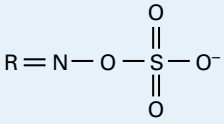
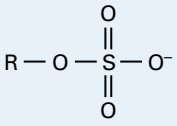
FIGURE 16.40 *Overview of sulfur uptake, reduction, and transport in plants. Like nitrate, sulfate uptake across the plasma membrane is energized by an electrochemical gradient that is maintained by a proton-pumping ATPase. Part of the sulfate is stored in vacuoles. Reduction of sulfate takes place in the plastids of root and leaf cells. Cysteine synthesis occurs in the cytosol, plastids, and mitochondria, while glutathione can be synthesized in the cytosol and plastids. The assimilation of sulfate into sulfated compounds takes place in the cytosol*

16.12 Sulfur chemistry and function

16.12.1 Cysteine, the sulfur donor in methionine synthesis, is essential for protein synthesis

Cysteine and methionine are the two sulfur-containing amino acids used in protein synthesis. In plants, cysteine is the primary product of sulfate assimilation and a starting point for synthesis of methionine in a reaction series known as transsulfuration (Fig. 16.41, see Chapter 7). Cysteine is particularly important for the structural and catalytic functions of proteins. The thiol groups of two cysteine residues can be oxidized to form a covalent disulfide bond, which is the most important linkage for establishing tertiary and, in some cases, quaternary protein structures. These disulfide bonds can be also reversed by reduction, a property crucial for controlling activity of proteins. The redox state of the cysteines that can form disulfide bonds (reduced or oxidized) is ultimately controlled by cellular processes and reactions that generate biological reducing agents (e.g., noncyclic electron transfer and the oxidative pentose phosphate pathway). The activities of some chloroplast enzymes functioning

TABLE 16.6 *Structures and examples of sulfur-containing compounds formed by plants.*

Compound	Generic structure	Examples
Thiols (mercaptans)	RSH	L-Cysteine, coenzyme A
Sulfides or thioethers	RSR_1	Hydrogen sulfide (H_2S), L-methionine
Sulfoxides	$RSOR_1$	Allicin
Methylsulfonium compounds	$(CH_3)_2S^+R$	*S*-Adenosyl-L-methionine, *S*-methylmethionine, DMSP, dimethylsulfonic hydroxybutyrate
Sulfate esters		Phenol sulfates, polysaccharide sulfates
Sulfamates		Aryl sulfamates, mustard oil glycosides
Sulfonic acids		Glucose-6-sulfonate, cysteic acid, taurine, sulfoquinovosyl diacylglycerol

DMSP, dimethyl sulfoniopropionate.

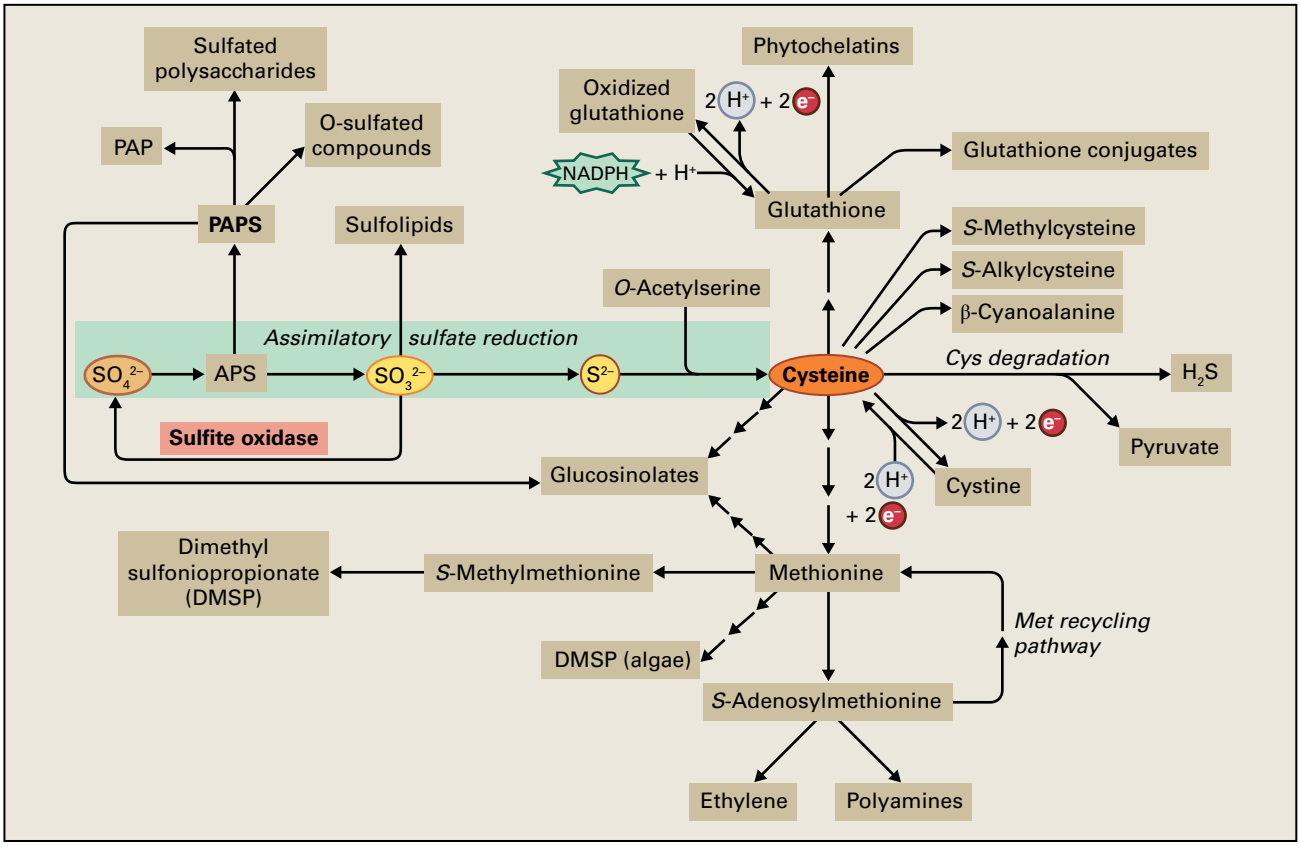


FIGURE 16.41 *Sulfur assimilation in plants. Sulfate is incorporated into a wide range of compounds. Most sulfate is first reduced to sulfide and subsequently incorporated into cysteine, which functions as a sulfur donor in many reactions. Some sulfur is incorporated in the oxidized form to sulfated compounds in an early branch in the pathway. Some metabolites, like glucosinolates, contain both reduced and oxidized sulfur. The sulfo- group in sulfolipids is derived from sulfite. APS, adenosine 5′-phosphosulfate; PAPS, 3′-phosphoadenosine-5′-phosphosulfate; PAP, adenosine 3′,5′-bisphosphate.*

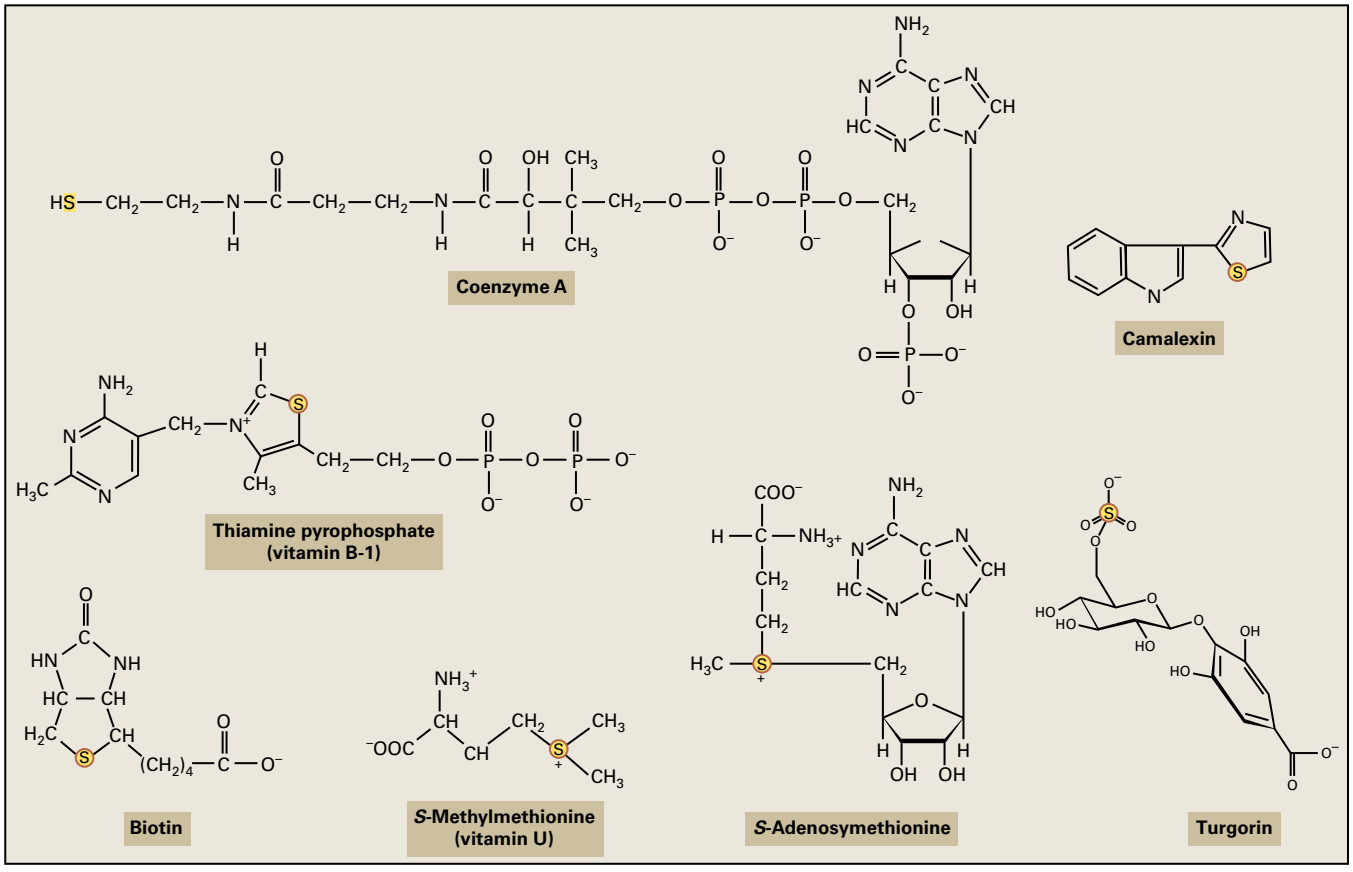


FIGURE 16.42 *Structures of representative sulfur-containing compounds: group-transfer cofactors, signaling molecules, and phytoalexins.*

in carbon metabolism are regulated by reversible disulfide bond formation, which is mediated by proteins (e.g., **thioredoxin**, **glutaredoxin**) and the nonprotein tripeptide, glutathione (see Section 16.15).

16.12.2 Many plant products, including coenzymes, lipids, and secondary metabolites, contain sulfur

Plants contain a wide variety of sulfur compounds, some with important functions in primary and natural product (secondary) metabolism, and others for which no function has been established. Several group-transfer coenzymes and vitamins, including coenzyme A, *S*-adenosyl-L-methionine (SAM), thiamine, biotin, lipoic acid, and *S*-methylmethionine contain functionally important sulfur moieties (Fig. 16.42). Chloroplast membranes contain a **sulfolipid**, **sulfoquinovosyldiacylglycerol** (see Chapter 10). Some signaling molecules contain sulfur as a key component, including the sulfated lipooligosaccharides that function as Nod factors (see Fig. 16.13D), and turgorin (Fig. 16.42), a sulfated derivative of **gallic acid** responsible for thigmotactic movement in leaves of the sensitive plant (*Mimosa pudica*). Several **peptide hormones**, such as **phytosulfokines**, require sulfation of their tyrosine residues for biological function.

Sulfur-containing compounds play a particularly important role in plant stress defense. The major component of various defense systems is glutathione (described in detail in Section 16.15). In addition, many sulfur-containing **phytoalexins**, such as **camalexin** (Fig. 16.42), are produced by members of the Brassicaceae in response to pathogen attack. Thioredoxin is also emerging as a defense protein with certain pathogens. Some plants deposit elemental sulfur in their stems as a potent fungicide, but perhaps the best known sulfur-containing defense compounds are the **alliins** in onion and garlic and **glucosinolates** in Brassicaceae, which are also responsible for the flavor and smell of the corresponding vegetables and provide health benefits (see Chapter 24).

16.12.3 Sufficient sulfur in agricultural soils is important for the yield and quality of crops

Animals, including humans, require dietary sources of methionine because they are unable to reduce sulfur. The value of crop plants, therefore, is influenced by their methionine and cysteine content, and so sulfur availability and sulfur content have a significant impact on plant productivity and utilization. Seed proteins of some crop plants, particularly legumes, have low **methionine content**; as a result, food



FIGURE 16.43 *Aerial photograph of two* Brassica napus *fields, one fertilized with sulfate (foreground), the other not (background).* B. napus*, an oilseed variety, must be fertilized with sulfur to maximize yield. The difference in abundance of blooms between the sulfur-fertilized and the unfertilized fields is evident.*
Source: Schnug & Haneklaus (1994). Voelkenrode Sonderh. 144:14–21.



FIGURE 16.44 *Loaves of bread baked from (left to right) low-, high-, and excess-sulfur wheat. Limitations in sulfur availability cause a shift in the expression profile of seed storage proteins in wheat. In grain from wheat plants grown under S-limiting conditions, proteins with fewer cysteines predominate. The low-cysteine proteins are unable to form abundant disulfide bonds and adversely affect the baking quality of wheat flour.*
Source: Byers et al. (1987). Aspects Appl. Biol. 15:337–344.

derived from legumes must be supplemented with foods rich in this amino acid. Improving the nutritional index by altering the amino acid composition of seed storage proteins is a goal for many biotechnological projects.

Sulfur was long considered a nonlimiting nutrient for agriculture, but recent curbs on emission of sulfurous air pollutants, such as sulfur dioxide, have resulted in lower sulfur soil content. Many agricultural areas, especially in northern Europe, must be fertilized with sulfate to maintain crop yields and quality (Fig. 16.43). Sulfur deficiency adversely affects the yield of oilseed *Brassica* species and the baking quality of wheat flour (Fig. 16.44). Sulfur deficiency is also a cause of increased **acrylamide** contents in many bakery products. Acrylamide is formed during baking by a reaction between reducing sugars and asparagine. Sulfur-deficient plants accumulate large quantities of free amino acids, thereby increasing the potential for acrylamide formation. In addition, sulfur deficiency is associated with increased susceptibility of crops to attack by insects and fungi, consistent with the prominence of some sulfur-containing compounds and proteins in plant defense against pathogens.

16.12.4 Plants play a major role in the global biogeochemical sulfur cycle

The interconversion of oxidized and reduced sulfur species on Earth is known as the biogeochemical sulfur cycle (Fig. 16.45). Although the burning of fossil fuels is the greatest contributor to atmospheric sulfur content, a large amount of atmospheric sulfur is derived from marine algae, many of which produce **dimethylsulfoniopropionate** (**DMSP**), a tertiary sulfur analog of the quaternary nitrogen compounds known as **betaines** (Fig. 16.46A). DMSP has many functions, including roles as osmoprotectant, cryoprotectant, and repellant against planktonic herbivores. When released from algae, DMSP is degraded to **dimethyl sulfide** (**DMS**), which is volatilized into the atmosphere and subsequently oxidized to DMSO, sulfite, and sulfate (Fig. 16.46B). Atmospheric sulfate acts as a nucleus for formation of water droplets and is associated with the formation of clouds. The link between oceanic algae and cloud formation has been proposed as a climate-regulating mechanism.

16.13 Sulfate uptake and transport

Sulfate transport into root cells, like that of nitrate, is driven by active proton cotransport (see Fig. 16.40). Because plant roots contain multiple transporters with differing affinities for sulfate, the rate of sulfate uptake into roots is multiphasic over a range of sulfate concentrations (Fig. 16.47). Sulfate uptake is generally inhibited by **selenate**, **molybdate**, and

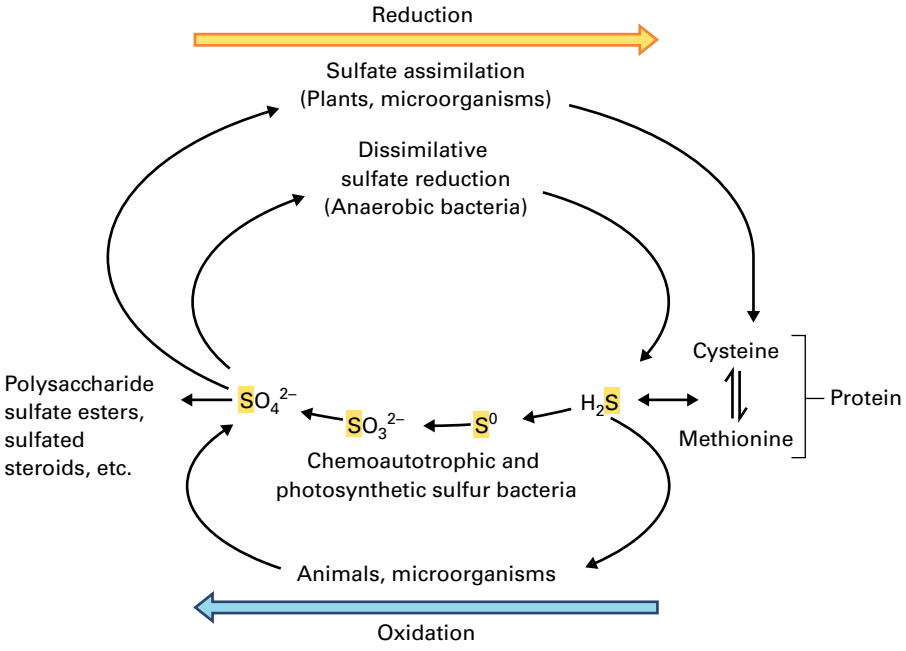
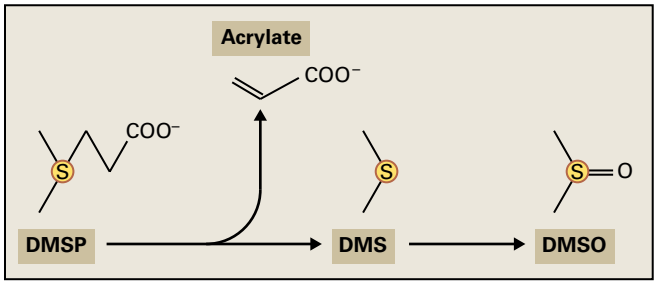
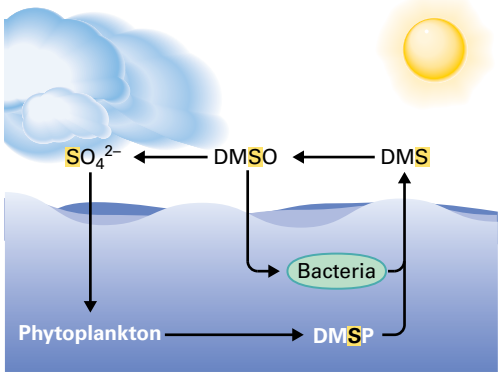


FIGURE 16.45 *The biogeochemical sulfur cycle. Plants and microorganisms reduce sulfate to sulfide for assimilation into cysteine. Some anaerobic bacteria use sulfate as a terminal electron acceptor much as aerobic organisms use oxygen. This process, known as dissimilation, generates H_2S. Oxidation of reduced sulfur to sulfate completes the cycle. Oxidation occurs through aerobic catabolism of sulfur compounds, which is carried out by animals, microorganisms, and plants or by bacteria that use reduced sulfur compounds as electron donors for chemosynthetic or photosynthetic reactions. Reduced sulfur is also oxidized geochemically when oxygen is present.*



A



B

FIGURE 16.46 *The phytoplankton-climate connection. (A) Phytoplankton produce DMSP, which is broken down by bacteria to DMS and acrylate. (B) DMS volatilizes and is oxidized to DMSO and sulfate, which nucleates water droplets, leading to cloud formation. Sulfate is returned to the sea dissolved in rain. Because cloud cover reduces the growth of phytoplankton and is accompanied by atmospheric cooling, phytoplankton may serve as a homeostatic climate regulation mechanism. The extent to which phytoplankton regulate climate is still debated.*

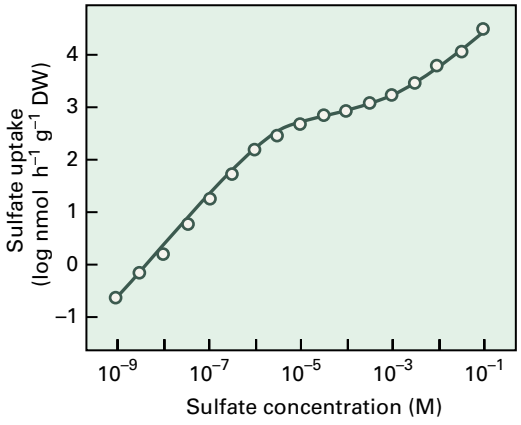


FIGURE 16.47 *Uptake of sulfate by barley roots. The graph shows the multiphasic rate of sulfate uptake by barley roots incubated with a range of sulfate concentrations. DW, dry weight.*

chromate anions, which compete with sulfate for binding to the transporters. Plants possess gene families encoding 12–16 sulfate transporters that fall into four groups. Individual transporters have different kinetic properties and distinct expression patterns and regulation, indicating specialized functions of the groups as well as of individual members within the groups.

Sulfate-uptake systems can be classified as either sulfate permeases or facilitated transport systems. Plant **sulfate permeases** are similar to fungal and mammalian H^+/SO_4^{2-} cotransporters. They consist of a single polypeptide chain with the 12 transmembrane domains characteristic of cation/solute transporters. These plant transporters can functionally complement a mutant strain of yeast lacking sulfate permease. A second mechanism, ATP-dependent transport, is exemplified by a system in cyanobacteria that includes a

multiprotein complex of three cytoplasmic membrane components (CysA, CysT, and CysW) and a sulfate-binding protein (SbpA) in the periplasmic space (SulT family transporter). This is the predominant type of sulfate transporter in bacteria, and it mediates sulfate transport into plastids in *Chlamydomonas*.

Despite progress in characterization of plant sulfate transport, the transporter responsible for the major flux of sulfate across the tonoplast into the vacuole remains to be identified.

16.14 The reductive sulfate assimilation pathway

The reduction of sulfate to sulfide is an energy-intensive process that consumes 732 kJ mol^{-1}. In contrast, nitrate and carbon assimilation require less energy (347 and 478 kJ mol^{-1} respectively). In plant tissues, the energy for **sulfate assimilation** is largely met by the ATP and reductant derived from photosynthesis. In nonphotosynthetic tissues, the reducing power for sulfate assimilation is probably generated by the oxidative pentose phosphate pathway, and the energy (ATP) for sulfate assimilation by respiration.

Sulfate assimilation is divided into three steps: activation of inorganic sulfate, reduction to sulfide, and incorporation of sulfide into cysteine. Plastids are the only compartment that contains the entire pathway for cysteine biosynthesis from inorganic sulfate. The activation step can take place in the cytosol as well as plastids, and cysteine synthesis occurs in all compartments capable of protein synthesis (i.e., cytosol, plastids, and mitochondria).

16.14.1 Sulfate activation is catalyzed by ATP sulfurylase

Sulfate is chemically inert, and to enter the assimilatory pathway, it must be activated by the enzyme ATP sulfurylase (EC 2.7.7.4), as depicted in Figure 16.48 and Reaction 16.5. The resulting compound, **adenosine 5′-phosphosulfate** (**APS**; sometimes referred to as 5′-adenylylsulfate), contains a phosphoric acid–sulfuric acid anhydride bond that enables the sulfuryl moiety to undergo modification in subsequent metabolic reactions.

Reaction 16.5: ATP sulfurylase

$$SO_4^{2-} + MgATP \leftrightarrow MgPP_i + APS$$

APS is a central branch-point intermediate that feeds two pathways: sulfate reduction and sulfation. The free energy of APS formation ($\Delta G^{\circ\prime}$) is estimated to be +41.8 kJ mol^{-1}, which favors ATP formation. Therefore, at equilibrium, APS can accumulate only to approximately 10^{-7} M. The forward reaction is driven by efficient removal of APS and PP_i, and at least two plant enzymes, **APS kinase** and **APS reductase**, metabolize APS while inorganic pyrophosphatase hydrolyzes PP_i (see Chapter 13).

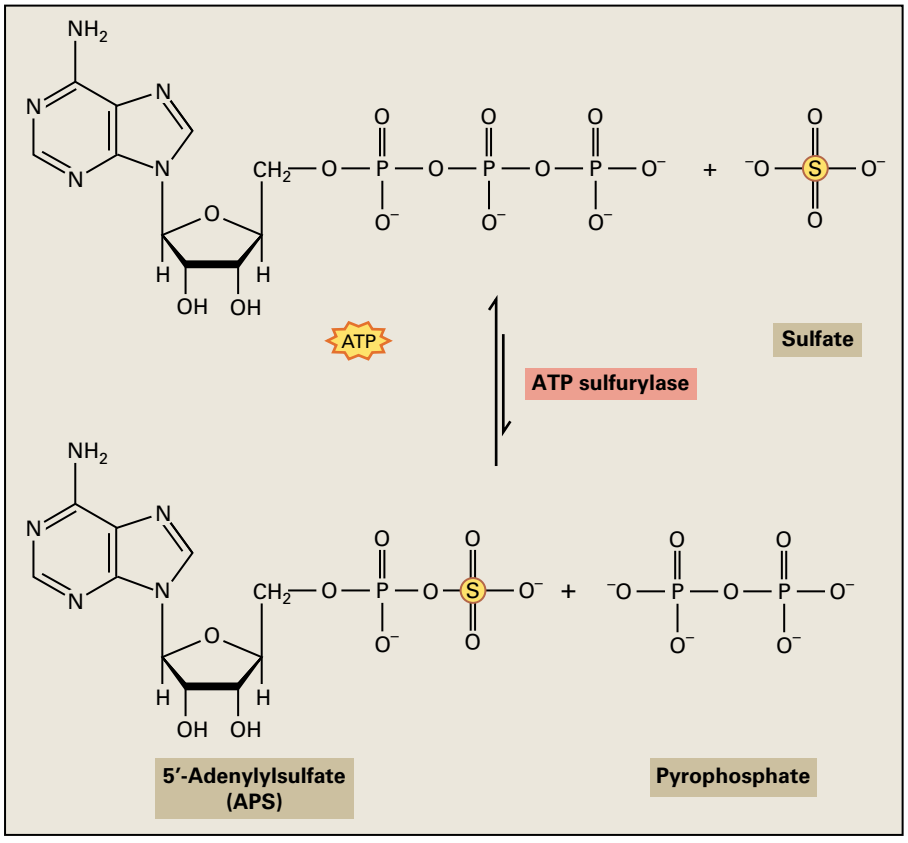


FIGURE 16.48 *Reaction catalyzed by ATP sulfurylase.*

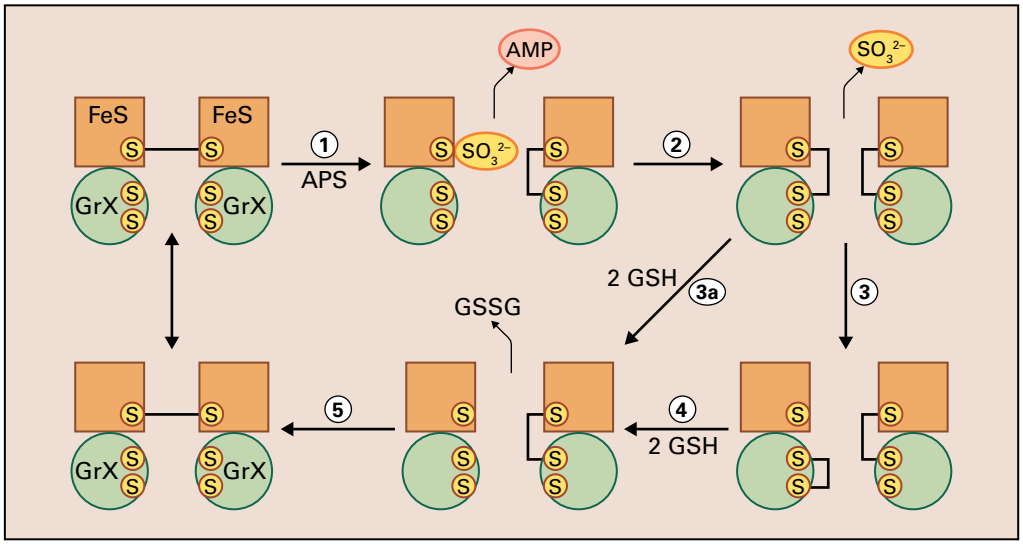


FIGURE 16.49 *Possible reaction mechanism of APS reductase (APR). The N-terminal, iron-sulfur cluster (Fe-S) containing the APR domain is represented as a square, and the C-terminal glutaredoxine-like domain (Grx) is shown as a circle. In its resting state, APR is a dimer held together by a disulfide bridge between the N-terminal Fe-S-containing domains, formed by Cys-248. The active center in the Grx domain is reduced. When APR reacts with APS (1), a stable intermediate with sulfite bound to Cys-248 is formed, and AMP is released. A thiolate of the Grx domain reacts with the sulfocysteine, releasing sulfite; a disulfide bond between the Grx domain and Cys-248 forms (2). The second Cys in the Grx domain can then attack the disulfide bond, transferring it to the Grx active site (3), or glutathione (GSH) can reduce the Grx-Cys248 bond directly (3a); the preferred reaction is not known. The Grx active site/Grx-Cys248 bond is then reduced by GSH, releasing GSSG (4). The disulfide bond between Cys-248 is re-established through an intra molecular reaction (5).*

Plant ATP sulfurylase is a homotetramer of 52–54 kDa polypeptides, and its substrates bind in an ordered and synergistic manner, with MgATP binding before sulfate. This enzyme activity is present predominantly in plastids (85–90% of total activity), with the remainder in the cytosol. In *Arabidopsis*, chloroplast ATP sulfurylase activity decreases during plant growth, while cytosolic activity increases. Plant ATP sulfurylase is encoded by small multigene families in all plant species analyzed to date. In many species, distinct plastidic and cytosolic isoforms can be identified, whereas in *Arabidopsis*, the four genes that encode ATP sulfurylase all contain a plastid-targeting peptide.

The contribution of ATP sulfurylase to the regulation of sulfate assimilation in plants is unclear. In some plants, steady-state ATP sulfurylase mRNA and enzyme activity both increase in response to sulfate starvation and are repressed by feeding of reduced sulfur compounds, such as cysteine and glutathione. Thus, in these species ATP sulfurylase gene expression is regulated by the demand for pathway end products. In other plants, including *Arabidopsis*, ATP sulfurylase is not regulated to such a great extent, and the control of the pathway resides elsewhere. Even in this latter case, disruption of ATP sulfurylase results in accumulation of sulfate. ATP sulfurylase transcripts are targeted and cleaved by microRNA (see Section 16.17.1). Overexpression of ATP sulfurylase in Indian mustard (*Brassica juncea*) results in greater accumulation of various metals and increased tolerance to selenate. These plants thus have a potential use for **phytoremediation** of soils contaminated with selenium.

16.14.2 APS reductase reduces activated sulfate to sulfite

APS is reduced to sulfite (SO_3^{2-}) by APS reductase (EC 1.8.4.9), with glutathione as the physiological electron donor (Reaction 16.6).

Reaction 16.6: APS reductase

$$\mathrm{APS} + 2\,\mathrm{glutathione}_{red} \rightarrow \mathrm{SO_3^{2-}} + \mathrm{glutathione}_{ox} + \mathrm{AMP} + 2\mathrm{H^+}$$

APS reductase is localized in the plastids of plants and algae, with the notable exception of the sulfate reducing center found in the mitochondria of *Euglena gracilis*. The plant enzyme occurs as a dimer of 45-kDa subunits, each of which contains a reductase and a glutaredoxin-like domain. The N-terminal reductase domain possesses an atypical diamagnetic and asymmetric [Fe_4S_4] iron–sulfur cluster, while the C-terminal domain interacts with the electron donor, glutathione, and is so equivalent to the thioredoxin cofactor needed for PAPS reduction in bacteria and fungi. Accordingly, the reduction of APS to sulfite can be divided into three distinct steps (Fig. 16.49).

Plants contain multiple APS reductase genes (*Arabidopsis* possesses three isoforms), and the enzyme is regulated by multiple environmental conditions, generally according to the demand for reduced sulfur. Transcript levels and enzyme activity increase under conditions of sulfur starvation and are

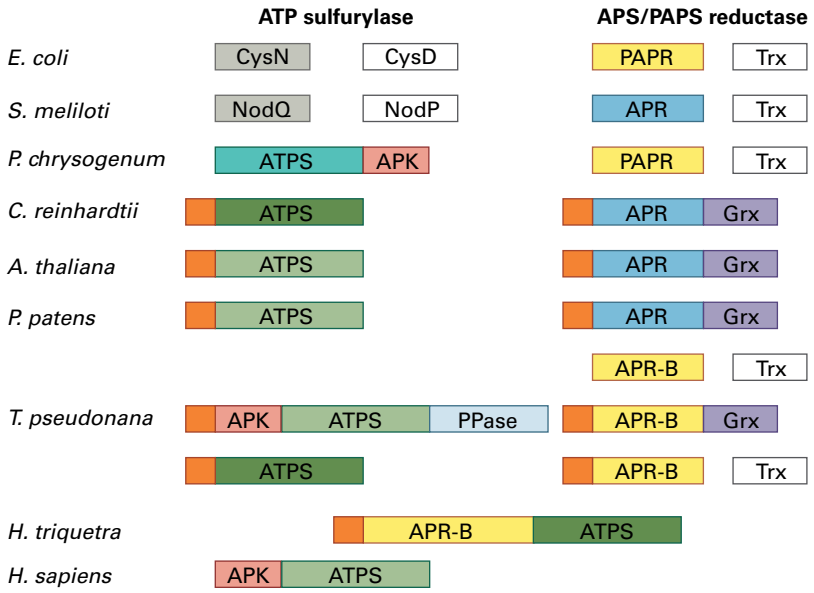


FIGURE 16.50 *Forms and fusions of ATP sulfurylase and APS or PAPS reductase found in various organisms. Depicted are enzymes from* Escherichia coli, Sinorhizobium meliloti, Penicillium chrysogenum, Chlamydomonas reinhardtii, Arabidopsis thaliana, Physcomitrella patens, Thalassiosira pseudonana, Heterocapsa triquetra, *and* Homo sapiens. *Note the different origin of ATP sulfurylase in plants and green algae and similarity of the plant and animal genes. Isoforms of ATPS are shown in varied shades of green. [Fe_4S_4] cluster binding domains are depicted in blue, the cofactor-independent PAPS reductase/APR-B is yellow, the glutaredoxin domains (Grx), sometimes referred to as Trx/Grx domains, are purple, while free thioredoxin necessary for the enzyme reaction is white. Orange rectangles represent N-terminal plastid-targeting peptides.*

repressed when plants are treated with reduced forms of sulfur. In *Arabidopsis*, flux control analysis revealed APS reductase controls 90% of the reduction of internal sulfate into thiols and proteins. Control is shared with the sulfate uptake system. Disruption of the *Arabidopsis* APR2 isoform of APS reductase reduces flux through the pathway and increases accumulation of sulfate. In addition, overexpression of APS reductase in plants increases the amounts of compounds containing reduced forms of sulfur and may result in cellular damage when the activity is too high.

16.14.3 Sulfite reduction is catalyzed by ferredoxin-dependent sulfite reductase

Plant **sulfite reductase** (EC 1.8.7.1) adds six electrons to free sulfite, forming sulfide (S^{2-}, Reaction 16.7). Reduced ferredoxin is the source of electrons.

Reaction 16.7: Sulfite reductase

$$SO_3^{2-} + 6\,Fdx_{red} \rightarrow S^{2-} + 6\,Fdx_{ox}$$

Plant sulfite reductase is a monomeric 65-kDa hemoprotein found in plastids. Like NiR (see Section 16.8 and Reaction 16.4), sulfite reductase contains one siroheme (see Fig. 16.38) and one [Fe_4S_4] iron–sulfur cluster. The amino acid sequence of the plant enzyme is also homologous to NiR, indicating sulfite and nitrite reductases emerged as a result of a gene duplication event. In fact, purified sulfite reductase from spinach (*Spinacia oleracea*) can reduce nitrite, although its affinity for nitrite is two orders of magnitude lower than for sulfite, its physiological substrate.

Unlike ATP sulfurylase and APS reductase, the enzyme activity and transcript levels of sulfite reductase are not affected appreciably by sulfur nutrition. Sulfite is a toxic anion that would damage cells if accumulated, so presumably sulfite reductase activity is maintained in excess. Significantly lower levels of sulfite reductase lead to a substantial reduction of plant growth.

16.14.4 Enzymes of sulfate assimilation exist in different forms in various organisms

Although the individual reactions of sulfate assimilation are common among plants, fungi, and prokaryotes, the enzymes catalyzing these reactions are often diverse (Fig. 16.50). For example, a new isoform of APS reductase isoform, APR-B, found in the moss ***Physcomitrella patens*** and other basal plants, is more similar to bacterial PAPS reductases because it does not require the [Fe_4S_4] cofactor and does not possess the glutaredoxin-like domain (Fig. 16.50). In this case, Trx serves as the reductant, as in bacteria. In addition, the APS reductase of many prokaryotes is similar to the N-terminal domain of plant APR instead of **PAPS reductase**. Further diversity within eukaryotes has been revealed within

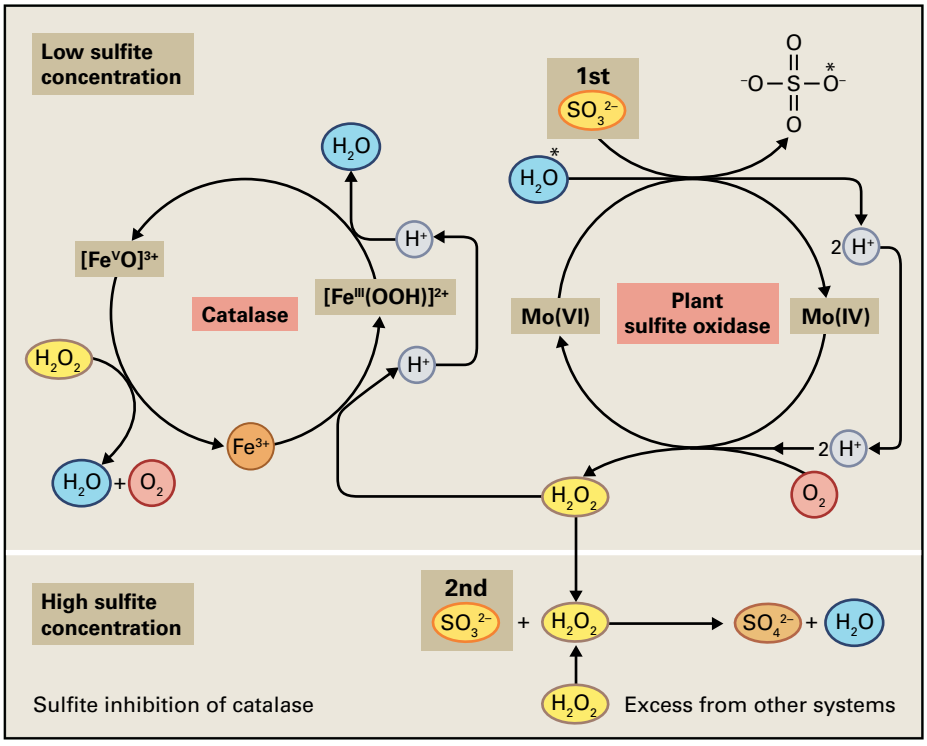


FIGURE 16.51 *Model of interaction between plant sulfite oxidase (SO) and catalase. During each catalytic cycle, plant SO oxidizes one molecule of sulfite and generates one molecule of H_2O_2. At low sulfite concentrations, all H_2O_2 formed is immediately degraded by peroxisomal catalase. At high sulfite concentrations, however, catalase is inhibited by sulfite, and the H_2O_2 molecule generated by plant SO nonenzymatically oxidizes a second molecule of sulfite. The oxygen introduced by the sulfate produced from H_2O is identified with an asterisk.*

genome sequences. The genomes of eukaryotic microalgae originating from secondary or tertiary endosymbiotic events, such as diatoms and haptophytes, are especially valuable sources of new variants and gene fusions (Fig. 16.50). Interestingly, the sequenced genomes of eukaryotic microalgae possess only APR-B-like genes. The APR-B class of APS reductase seems to be the predominant form among the marine phytoplankton, where it might represent adaptation to iron-limited environments. These new genes may potentially be used to improve efficiency of sulfur metabolism of crop plants.

16.14.5 Sulfite oxidase protects plants against surplus of SO_2

Sulfite-oxidizing enzymes have been known in animals and microorganisms for years, but their presence in plants has been revealed only in the last decade. Sulfite oxidase (EC 1.8.3.1) belongs to a family of molybdoenzymes possessing a **dioxomolybdopterin cofactor**. The protein occurs as a dimer of 45-kDa subunits, is localized in peroxisomes, and exhibits constitutive expression in a variety of tissues. The enzyme catalyzes the oxidation of sulfite to sulfate, with molecular oxygen as an electron acceptor (Reaction 16.8). Hydrogen peroxide (H_2O_2), the other reaction product, can either be metabolized by catalase or can nonenzymatically oxidize another sulfite molecule (Fig. 16.51).

Reaction 16.8: Sulfite oxidase

$$SO_3^{2-} + H_2O + O_2 \rightarrow SO_4^{2-} + H_2O_2$$

The role of **sulfite oxidase** in plants is not clear, as the enzyme actually catalyzes a reaction that acts against the direction of sulfate assimilation. A futile cycle between sulfate reduction to sulfite and reverse oxidation by sulfite oxidase is prevented by compartmentalization of the two processes in **plastids** and **peroxisomes**, respectively. Plants deficient in sulfite oxidase are more sensitive to treatment with bisulfite or to fumigation with SO_2, while overexpression of the gene leads to increased protection. Thus, the function of sulfite oxidase in plants is most probably protection against excess sulfite.

16.15 Cysteine synthesis

16.15.1 The combined activities of serine acetyltransferase and *O*-acetylserine (thiol) lyase convert serine to cysteine

The final step in the **reductive sulfate assimilation** pathway is the synthesis of cysteine by condensation of ***O*-acetylserine** (**OAS**) and **sulfide**. OAS is formed from serine and acetyl-CoA in a reaction (Reaction 16.9 and Fig. 16.52) that is catalyzed by serine acetyltransferase (EC 2.3.1.30) and is

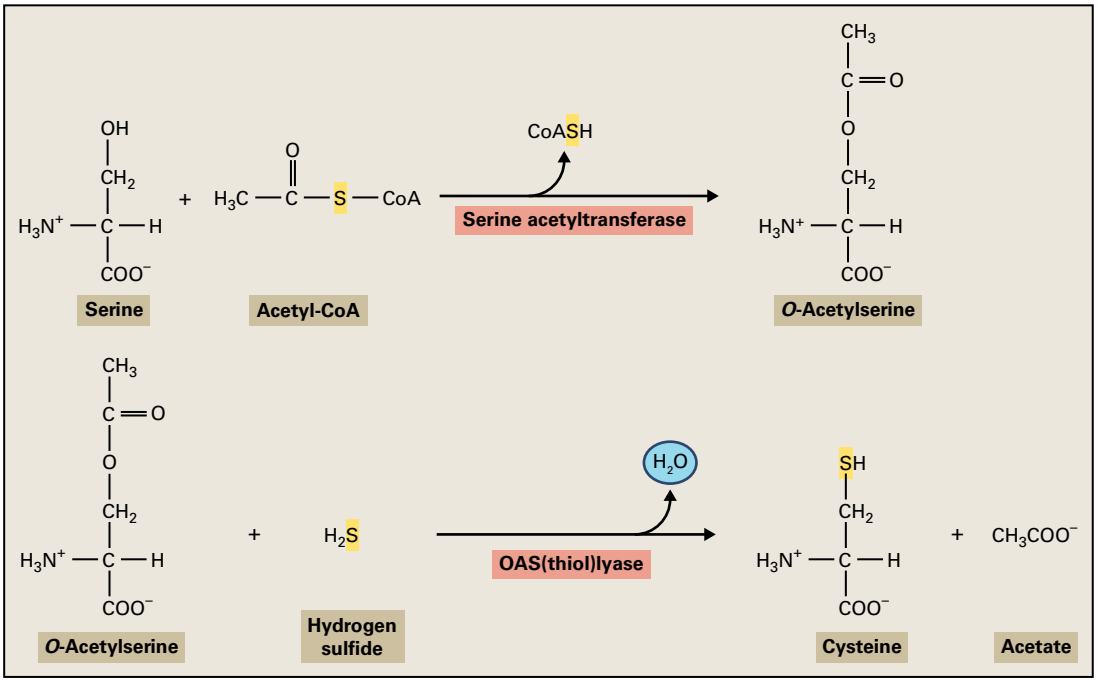


FIGURE 16.52 *Reactions responsible for assimilation of reduced sulfur into cysteine.*

specific to cysteine biosynthesis. OAS and the sulfide ion then react to form cysteine (Reaction 16.10 and Fig. 16.52) in a reaction catalyzed by **OAS(thiol)lyase** (EC 2.5.1.47), a pyridoxal phosphate-containing enzyme.

Reaction 16.9: Serine acetyltransferase

$$\text{Serine} + \text{acetyl-CoA} \rightarrow \textit{O}\text{-acetylserine} + \text{CoA}$$

Reaction 16.10: O-acetylserine (thiol)lyase

$$\textit{O}\text{-acetylserine} + S^{2-} \rightarrow \text{cysteine} + \text{acetate}$$

Serine acetyltransferase and OAS (thiol)lyase are localized in the cytosol, plastids, and mitochondria, and accordingly, both enzymes are encoded by small multigene families.

All plant species analyzed to date possess at least three **serine acetyltransferase** (***SERAT***) genes. The *Arabidopsis* SERAT isoforms differ significantly in their kinetic properties, and they also display different sensitivity to feedback inhibition by cysteine. Plant species differ in the localization of cysteine-sensitive serine acetyltransferases: in *Arabidopsis* the cytosolic SERAT1;1 and 3;2 are inhibited by cysteine, and in pea (*Pisum sativum*) it is the plastidic isoform. Analysis of *Arabidopsis* plants with multiple *SERAT* genes disrupted by T-DNA insertions revealed that each isoform can support plant growth, even when the total enzyme activity is less than 1% that of wild-type plants. The enzyme activity is nonetheless indispensable for plants, as disruption of all *SERAT* genes leads to embryo lethality. Significant reduction of the mitochondrial isoform may cause growth retardation depending on conditions. Altogether, it seems that mitochondria are the major site of SERAT activity and of OAS synthesis.

OAS (thiol)lyase belongs to the family of β-substituted alanine synthases (BSAS) in the superfamily of pyridoxal phosphate-dependent enzymes. BSAS enzymes are encoded by nine genes in *Arabidopsis* and eight in rice (*Oryza sativa*), and evolutionarily basal plants possess at least four genes. In addition to cysteine synthase activity, BSAS isoforms catalyze the synthesis of β-cyanoalanine from cysteine and HCN and *S*-sulfocysteine from OAS and thiosulfate. As with the *SERAT* gene family, there is some functional redundancy among the individual BSAS isoforms, but some isoforms have specialized functions. Disruption of individual *BSAS* genes does not yield any obvious phenotypic changes under normal growth conditions, with the exception of the mitochondrial *AtBSAS2;2*, which results in a slightly lower biomass accumulation. The total enzyme activity was, however, strongly reduced in plants lacking the cytosolic or plastidic forms of OAS (thiol)lyase, BSAS1;1 or BSAS2;1, respectively. **β-Cyanoalanine synthase** activity may be the primary activity of mitochondrial BSAS3;1, which thus functions in detoxification of cyanide. It appears the major site of cysteine synthesis is the cytosol, and this process utilizes OAS primarily synthesized in mitochondria and sulfide produced in the plastids.

In contrast to the enzymes involved in activating and reducing sulfate, *SERAT* and *BSAS* genes are highly similar to those from microorganisms and do not show great diversity. All OAS (thiol)lyase and serine acetyltransferase mRNAs are expressed in both leaves and roots, and in general, the steady state levels of these mRNAs are not responsive to sulfate starvation. Attempts to increase cysteine synthesis and, consequently, various cysteine metabolites by overexpression of serine acetyltransferase and OAS (thiol)lyase have yielded mixed results. Overexpression of OAS (thiol)lyase in plastids

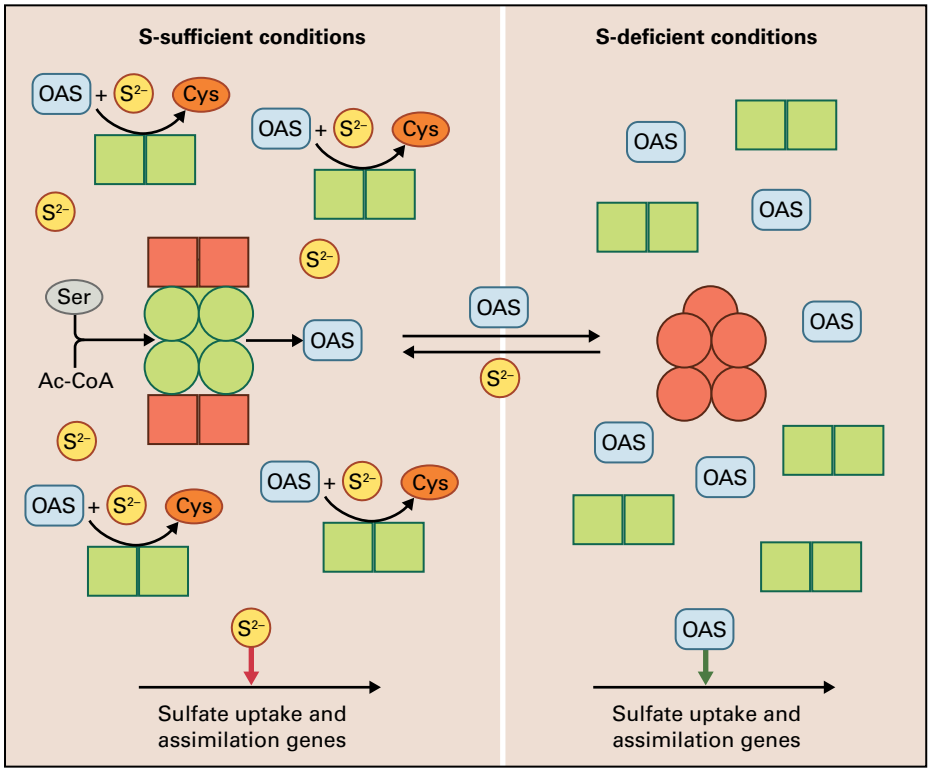


FIGURE 16.53 *Regulation of cysteine synthesis by OAS and thiol compounds. Active forms of enzymes are green, inactive states are presented in red. Squares represent OAS (thiol)lyase dimers, which are present in excess over the serine acetyltransferase (SERAT) hexamers indicated as circles. During sulfur sufficient conditions, sulfide promotes formation of the complex, thereby stimulating OAS production. OAS is used by free OAS (thiol)lyase to synthesize cysteine. Sulfate uptake and assimilation genes are repressed by compounds containing reduced sulfur. In sulfur-deficient conditions, OAS accumulates because of an insufficient production of sulfide. The complex is destabilized by OAS, inactivating serine acetyltransferase. OAS accumulation induces expression of genes involved in sulfate uptake and assimilation. Sulfide inhibits expression of these genes.*

or the cytosol of different plant species has only a small effect on cysteine and glutathione content, but these plants are often more tolerant to various stress conditions that cause increased demand for reduced sulfur. Overexpression of serine acetyltransferase does lead to increased cysteine and glutathione levels, and the extent of the increase depends on the subcellular compartment and cysteine sensitivity of the expressed isoform. The two enzymes together form an enzyme complex named cysteine synthase.

16.15.2 The cysteine synthase multienzyme complex displays a novel regulatory mechanism in control of sulfate assimilation

The cysteine synthase complex of serine acetyltransferase and OAS (thiol)lyase does not facilitate substrate channeling in the enzymatic reaction. Instead, the protein–protein interaction plays a regulatory role. The active complex is composed of a hexamer (dimer of trimers) of serine acetyltransferase and two dimers of OAS (thiol)lyase. The protein–protein interaction in the complex greatly increases the catalytic activity of serine acetyltransferases, but OAS (thiol)lyase is inactive in the complex (Fig. 16.53). The two proteins are not expressed to the same levels in plants; OAS (thiol)lyase is much more abundant. The ratio among the enzymes varies widely in the different compartments, with about 300-fold surplus of OAS (thiol)lyase in plastids and threefold surplus in mitochondria. Therefore, in vivo only a small fraction of the total OAS(thiol)lyase actually associates with serine acetyltransferases, leaving sufficient free enzyme for cysteine synthesis.

The binding properties of the two proteins are strongly affected by concentrations of OAS and sulfide: OAS dissociates the complex, whereas sulfide promotes complex formation (Fig. 16.53). The concentration of OAS causing 50% dissociation of the complex (58 μM) is well within the range of physiological OAS concentration; therefore, relatively small fluctuations of OAS levels may have large effects on the rates of OAS and cysteine synthesis. This regulatory mechanism complements the transcriptional regulation of sulfate transporters and APS reductase during sulfur deficiency, which may include OAS as a signal, thereby allowing fine-tuning of pathway control. Experiments with *Arabidopsis* mutants reveal that complex formation in chloroplasts is indirectly linked to noncyclic electron transport through a **cyclophilin**—a protein foldase whose activity is enhanced by reduced thioredoxin (see Chapter 12).

16.16 Synthesis and function of glutathione and its derivatives

As a major end product of the reductive sulfate assimilation pathway, the tripeptide glutathione is the major nonprotein thiol in plants. It is present in millimolar concentrations that far exceed the low micromolar concentrations of cysteine. Glutathione and its derivatives are involved in storage and long-distance transport of reduced sulfur, in signal transduction pathways, in scavenging hydrogen peroxide and other reactive oxygen species (see Chapter 22), in detoxifying xenobiotics (e.g., herbicides; see Chapter 3), in activating and conjugating phenylpropanoids and hormones, and in serving as substrate for phytochelatin synthesis. Glutathione also plays a major role in maintaining redox balance of the cell.

16.16.1 Glutathione is synthesized enzymatically in two ATP-dependent steps

Two enzymes make up the **glutathione** biosynthetic pathway (Fig. 16.54). First, γ-glutamylcysteine synthetase (EC 6.3.2.2) catalyzes the formation of a peptide bond between the γ-carboxyl group of glutamate and the α-amino group of cysteine (Reaction 16.11). Next, glutathione synthetase (EC 6.3.2.3) catalyzes the formation of a peptide bond between the cysteinyl carboxyl group of γ-glutamylcysteine and the α-amino group of glycine (Reaction 16.12). ATP is hydrolyzed in each reaction.

Reaction 16.11: γ-Glutamylcysteine synthetase

$$\text{Glutamate} + \text{cysteine} + \text{ATP} \rightarrow \gamma\text{-glutamylcysteine} + \text{ADP} + P_i$$

Reaction 16.12: Glutathione synthetase

$$\gamma\text{-Glutamylcysteine} + \text{glycine} + \text{ATP} \rightarrow \text{glutathione} + \text{ADP} + P_i$$

Some plants produce tripeptides related to glutathione. Species in the order Fabales synthesize **homoglutathione** (in which β-alanine replaces glycine), and species in the Poaceae (grass family) generate **hydroxymethylglutathione** (in which serine replaces glycine). A third class (in which glutamate replaces glycine) is found in maize (*Zea mays*). However, all these plant species also form glutathione. In the legumes, homoglutathione is synthesized by a specific homoglutathione synthetase (EC 6.3.2.23) that evolved from a recent duplication of a glutathione synthetase gene. The two thiols are essential for formation and function of nodules. Specific functions of glutathione homologs have not been established.

Glutathione is present in all plant cell compartments, but it is synthesized only in plastids and the cytosol. The γ-glutamylcysteine synthetase was originally found in both compartments; however, the enzyme was subsequently shown to be exclusively targeted to the plastids, at least in the Brassicaceae. In *Arabidopsis*, for example, both the plastidic and cytosolic forms of glutathione synthetase are encoded by a single gene that produces two transcripts, one with and one without the plastid-targeting peptide, by using alternative transcript initiation sites. Complete disruption of the γ-glutamylcysteine synthetase gene is embryo lethal; seeds of plants lacking glutathione synthetase do germinate, but do not survive beyond a seedling stage even if glutathione is supplied externally. This phenotype can be complemented by targeting the enzyme solely to the cytosol. Thus, glutathione synthesis and distribution in *Arabidopsis* rely on multiple transport steps. Not only must glutathione be transported into mitochondria and plastids, to ensure its synthesis in the cytosol, the intermediate γ-glutamylcysteine must be exported from the plastids; this exchange across plastid membranes is facilitated by orthologs of the *Plasmodium* chloroquine-resistance transporter.

The γ-glutamylcysteine synthetase enzyme shows great diversity among different organisms. Although it can complement a γ-glutamylcysteine synthetase mutant of *E. coli*, the plant enzyme shares little sequence similarity with proteins from *E. coli,* fungi, or mammals. Plant γ-glutamylcysteine synthetase is feedback-inhibited by glutathione and regulated by changes in cellular redox homeostasis. The crystal structure of the protein from *Brassica juncea* shows two cysteine pairs that form disulfide bonds (Fig. 16.55). One of these disulfides is conserved among all plant γ-glutamylcysteine synthetases and is responsible for redox regulation. This feedback inhibition mechanism may be important for preventing accumulation of high (nonphysiological) concentrations of glutathione if the supply of precursor amino acids becomes too large. Details of the mechanism for reduction of the oxidized enzyme under physiological conditions are not known.

Manipulation of glutathione synthetase has only a limited effect on glutathione levels, but γ-glutamylcysteine synthetase is an important determinant of glutathione concentration in the cell. Transgenic plants overexpressing the bacterial gene for this enzyme show increased GSH levels that often correlate with higher resistance to abiotic stress. The rate of glutathione synthesis also appears to depend on the availability of cysteine and glycine (a product of photorespiration; see Chapter 14). *Arabidopsis* γ-glutamyl cysteine synthetase mutants all contain significantly lower glutathione levels and typically exhibit compromised tolerance to various stresses. The *cad2* mutant, for example, is sensitive to the heavy metal cadmium, *pad2* is sensitive to pathogens, and *rax1* is impaired in chloroplast-nucleus signaling and constitutively expresses stress-inducible genes. One mutant with very low glutathione levels, *rml1*, lacks a root meristem and is unable to develop primary roots. Glutathione-controlled redox homeostasis is also important for auxin transport and signaling in root tips.

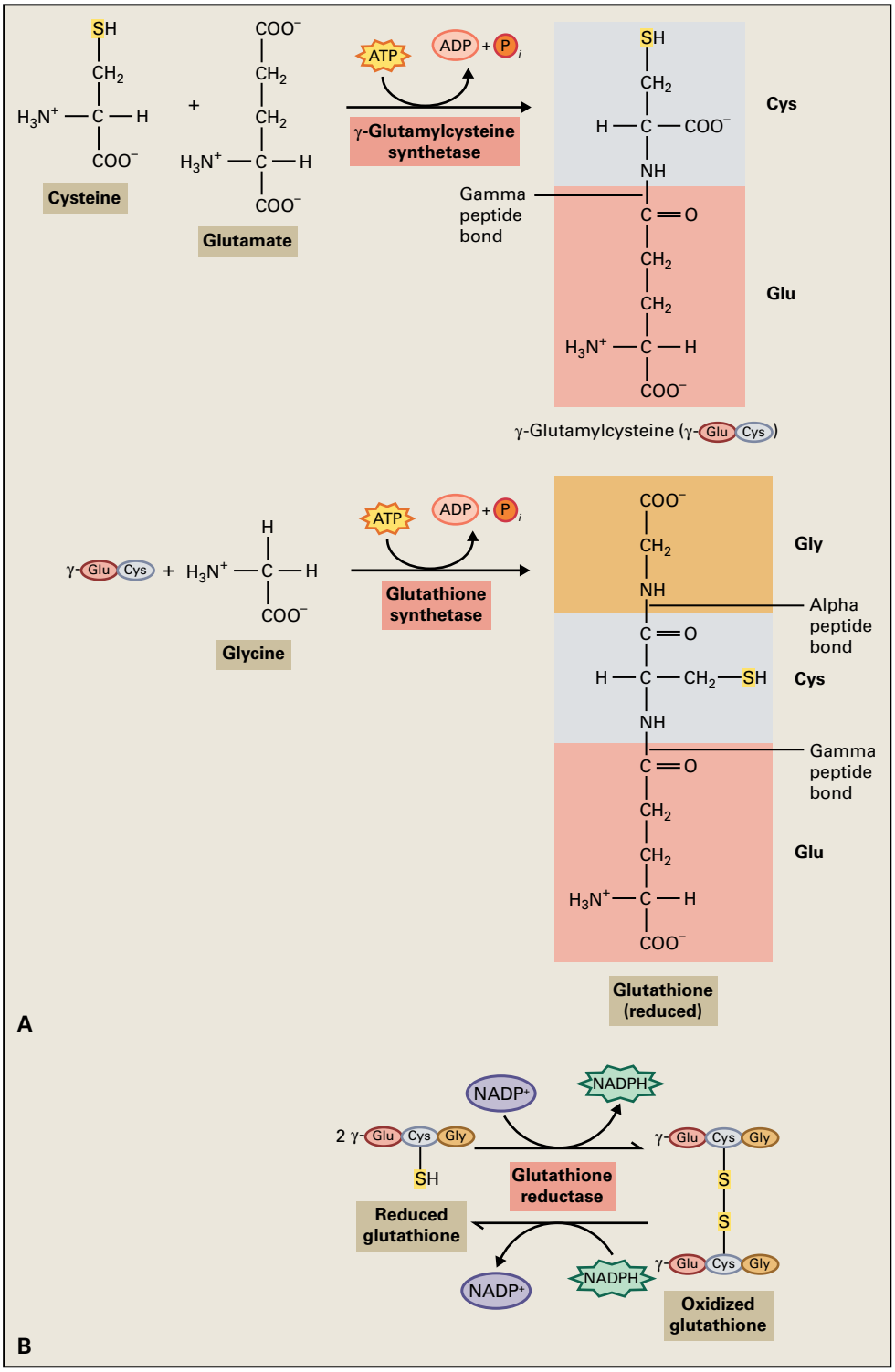


FIGURE 16.54 *Reactions responsible for glutathione (A) biosynthesis and (B) redox homeostasis.*

16.16.2 Glutathione is the precursor of phytochelatins

Phytochelatins are small cysteine-rich oligopeptides with the general structure $(\gamma\text{-Glu-Cys})_n$ Gly ($n = 2–11$). They bind heavy metals and are found in plants, fungi, and other organisms upon exposure to metals, such as cadmium (Cd^{2+}), or high concentrations of micronutrients, such as copper (Cu^{2+}).

Phytochelatins are synthesized enzymatically from glutathione by the enzyme phytochelatin synthase (EC 2.3.2.15). In this transpeptidation reaction, which requires the presence of metal ions, γ-Glu-Cys dipeptides from

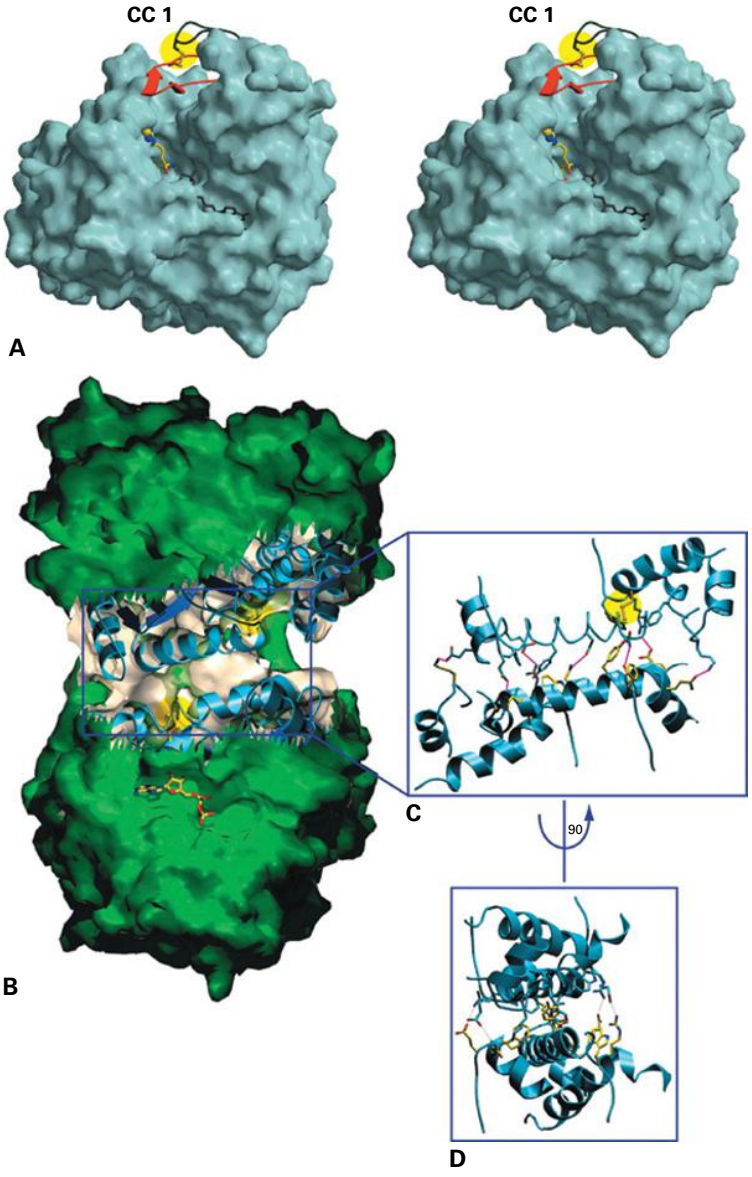


FIGURE 16.55 *Redox regulation of γ-glutamylcysteine synthetase from* Brassica juncea *(BjGCL) is implemented via two intramolecular disulfide bonds. (A) Stereo view of oxidized BjGCL (gray surface) indicating the relative position of a β-hairpin motif (in red). The disulfide bond CC1 (in yellow) may function as a loaded spring that fixes the hairpin over the substrate-binding sites. The inhibitor buthionine sulfoximine bound in the active site is shown in bond representation (in yellow) along with ADP (in black), whose position has been inferred from the* E. coli *structure (PDB ID: 1VA6). The side chain of* rax1-1 *R220 is shown as a space-filling model. (B) Surface view of the dimer found in crystals grown under nonreducing conditions. Redox regulation of BjGCL occurs via dimer-to-monomer transition. At the level of the dimer interface, the surface has been removed to show the contributing helical elements (in blue). The disulfide bond CC2 in both molecules is highlighted in yellow, and a molecule of ADP is shown in the nucleotide-binding site. (C) Enlarged view of the dimer interface in the same orientation as seen in B and D, following a 90° rotation. Seven salt bridges (in magenta) with bonding distances smaller than 3.1 Å and three conserved aromatic residues at the surface of each molecule contribute to interface stabilization.*
Source: Hothorn et al. (2006). J. Biol. Chem. 281:27557–27565.

glutathione are transferred onto an elongating phytochelatin oligopeptide (or another molecule of glutathione) (Fig. 16.56 and Reaction 16.13).

Reaction 16.13: Phytochelatin synthase

$$\gamma\text{-Glu-Cys-Gly} + (\gamma\text{-Glu-Cys})_n\text{-Gly} \rightarrow (\gamma\text{-Glu-Cys})_{n+1}\text{-Gly} + \text{Gly}$$

Plant phytochelatin synthase is composed of a conserved N-terminal and variable C-terminal domain. Cyanobacteria possess a truncated protein lacking the variable domain. Phytochelatin synthase belongs to a superfamily of Cys proteases, such as papain. In accordance with the papain reaction mechanism, phytochelatin synthase also transfers a γ-Glu-Cys unit from glutathione (bound to metal) onto a catalytic cysteine residue before it transfers this onto the N-terminus of glutathione or phytochelatin. Phytochelatin synthase also degrades glutathione conjugates.

Phytochelatins serve as a mechanism for detoxification of heavy metals by vacuolar sequestration, an example of one type of biomineralization (Fig. 16.57). As such, phytochelatins are important for plant tolerance to heavy metals, in particular Cd and arsenic (As). Mutations or complete lack of phytochelatin synthase result in cadmium sensitivity in *Arabidopsis cad1* (*Cd-sensitive*) mutants or in the Bryophytes, respectively. Overexpression of phytochelatin synthase or of γ-glutamylcysteine synthetase leading to increased glutathione content generally increases tolerance to Cd and As. Such increased potential to synthesize phytochelatins leads to greater metal accumulation in plant tissues, and such plants may be good candidates for use in phytoremediation.

16.16.3 Glutathione plays an important role in detoxification of xenobiotics

Plants can detoxify or inactivate many substances, including endogenously produced toxins and hormones and **xenobiotic** chemicals such as herbicides, by forming conjugates

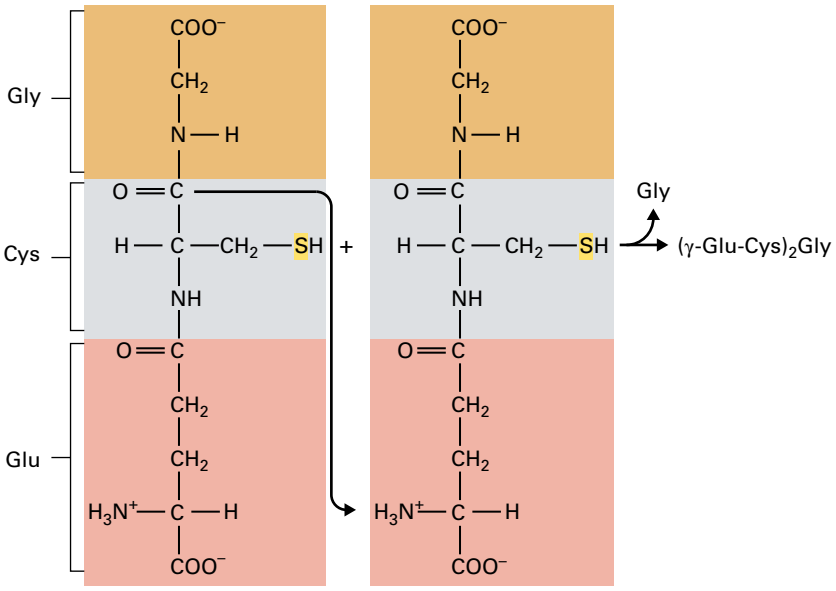


FIGURE 16.56 *Phytochelatin synthase catalyzes the transpeptidation reaction of glutathiones to produce* $(\gamma\text{-Glu-Cys})_n$ *Gly (n = 2-11). Initially, the glycine moiety of one glutathione is removed and a new peptide bond is formed with the residual cysteine and the amino group of the glutamate on a second molecule of glutathione. This reaction is repeated to form the phytochelatin oligomers.*

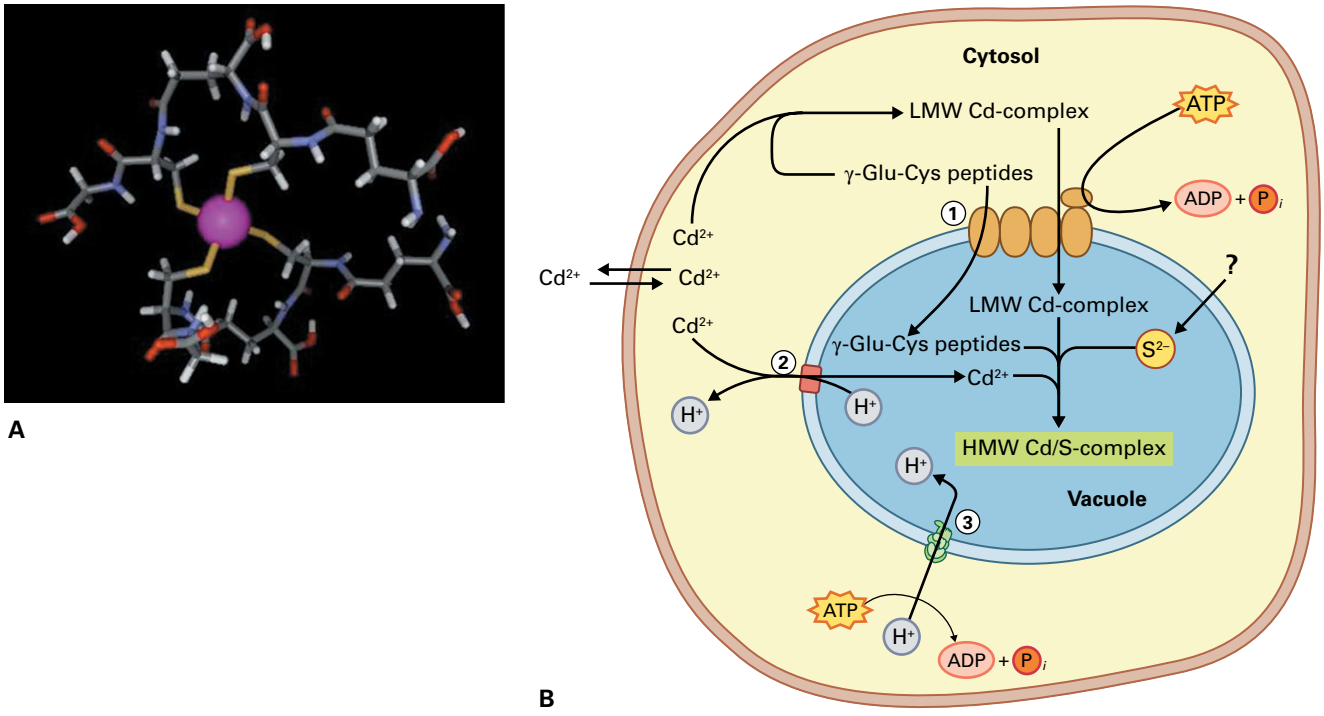


FIGURE 16.57 *Two molecules [*$(\gamma\text{-Glu-Cys})_2$ *Gly] coordinated with a cadmium ion. (A) By binding toxic heavy metal ions, phytochelatins remove them from the cellular machinery. It is thought the thiol groups of phytochelatins serve as the ligand for heavy metal ions. (B) A model for the mechanism of CdS mineralization and sequestration in plant cells mediated by phytochelatins. Both phytochelatins and low-molecular-weight (LMW) phytochelatin-Cd complexes formed in the cytosol enter the vacuole by way of an ABC transporter (1). Cd ions enter the vacuole by way of an antiporter in exchange for protons (2). HMW, high molecular weight. The electrochemical gradient across the tonoplast is maintained by a proton-pumping ATPase (3). The end product is a CdS crystallite.*

with glutathione. This reaction is catalyzed by glutathione *S*-transferase, which links the reactive thiol group of cysteine to the xenobiotic (Fig. 16.58; see also Fig. 3.14 in Chapter 3). The conjugates are then transported into vacuoles by an ABC-type glutathione translocator. Within the vacuole, detoxification is completed as glutathione conjugates are hydrolyzed to cysteine conjugates.

Plant glutathione transferases (EC 2.5.1.18) are encoded by a large and diverse gene family, such as the 48-member family in *Arabidopsis*. The enzymes are usually localized in the cytosol, where they catalyze the detoxification of xenobiotics and reduction of the organic hydroperoxides formed during oxidative stress. In addition, glutathione transferases facilitate transport of natural products into the vacuole and

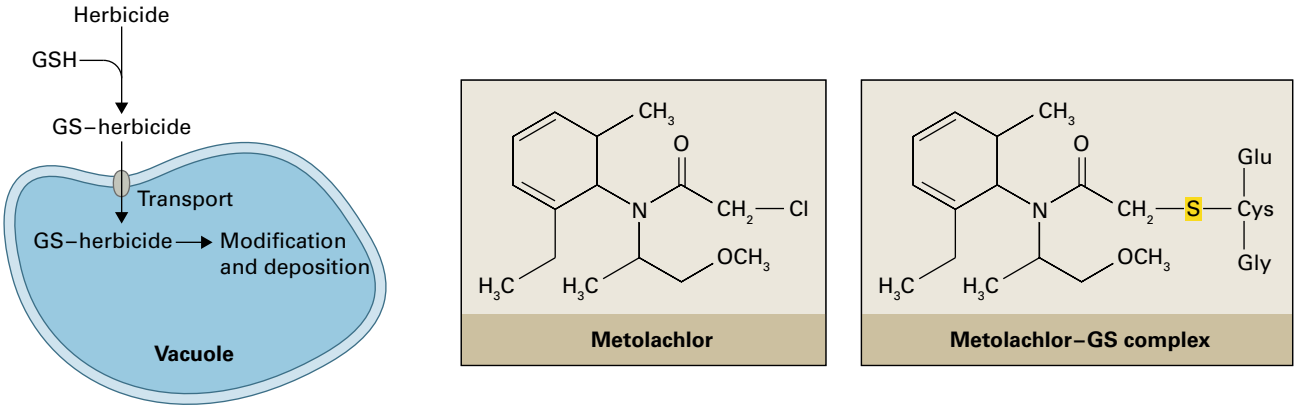
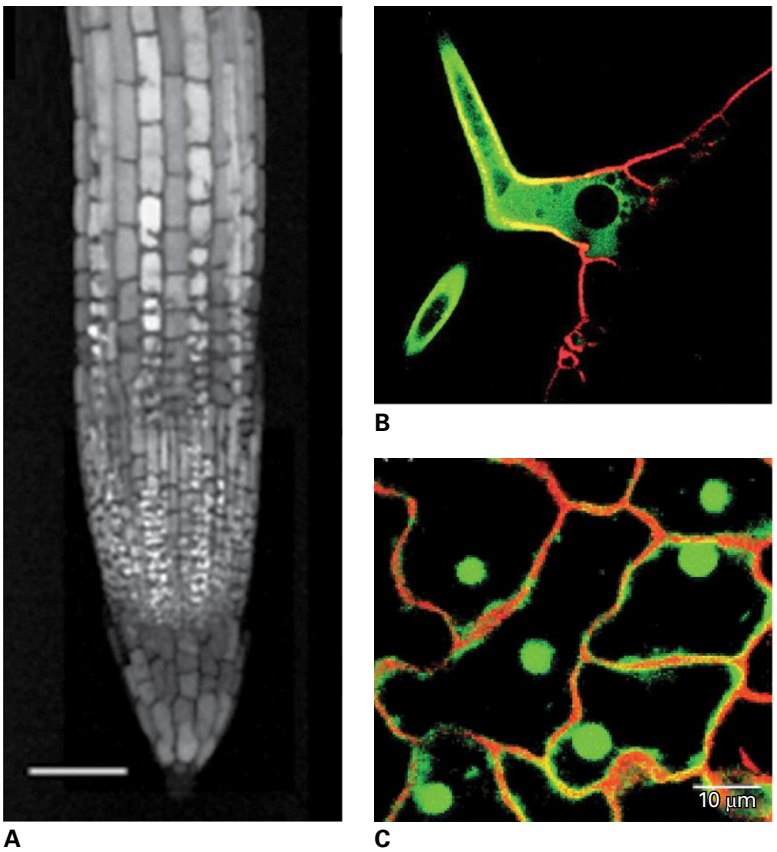


FIGURE 16.58 *Detoxification of a herbicide (e.g., Metolachlor) by conjugation to glutathione. The conjugate is then transported into the vacuole.*

FIGURE 16.59 In situ *localization of glutathione. The tissue was infiltrated with 100 µM monochlorobimane, which after conjugation to glutathione produces a fluorescent product, and in (B) and (C) additionally with 50 µM propidium iodide, staining cell walls in red, and 5 mM sodium azide to prevent transport of the conjugate into the vacuoles. (A) Black and white image of* Arabidopsis *roots, showing higher glutathione concentration (represented by brightness) in atrichoblasts than in trichoblasts. (B)* Arabidopsis *leaf epidermis showing a strong labeling of glutathione (green) in trichomes. (C) Poplar* (Populus) *leaf upper epidermis showing glutathione labeling in cytosolic strands and nucleus.*
Source: Combined from (A) Fig. 6A from J. Microsc. (2000). 198(3):162–173. (B) Fig. 2D from Proc. Natl. Acad. Sci. USA (2000). 97(20):11108–11113. (C) Fig. 1A from Plant Cell Environ. (2003). 26(6):965–975.



are involved in various stress-signaling pathways. While individual isoforms bind specific substrates, the general structure of the proteins is conserved.

This mechanism for **herbicide** detoxification has been applied successfully to agriculture by identifying the substances that stimulate expression of glutathione *S*-transferase and the vacuolar transporter, or that result in an increased rate of glutathione synthesis. These substances, termed **safeners**, are used to increase the resistance of crop plants to herbicide.

The conjugation of glutathione to xenobiotics has also been exploited for in vivo glutathione imaging. Since conjugation requires catalysis by a glutathione transferase, the measurement is specific for the cytosolic glutathione pool. This enables quantitative measurement of cytosolic glutathione in a noninvasive, cell-specific manner using confocal laser scanning microscopy (Fig. 16.59). Using this method, the cytosolic glutathione concentration in cells of root epidermis was estimated to be 3 mM, but marked differences in glutathione concentration are evident between different cell types in plant organs (Fig. 16.59). Glutathione redox potential can also be visualized using modified, redox-sensitive fluorescent proteins targeted to individual cell compartments.

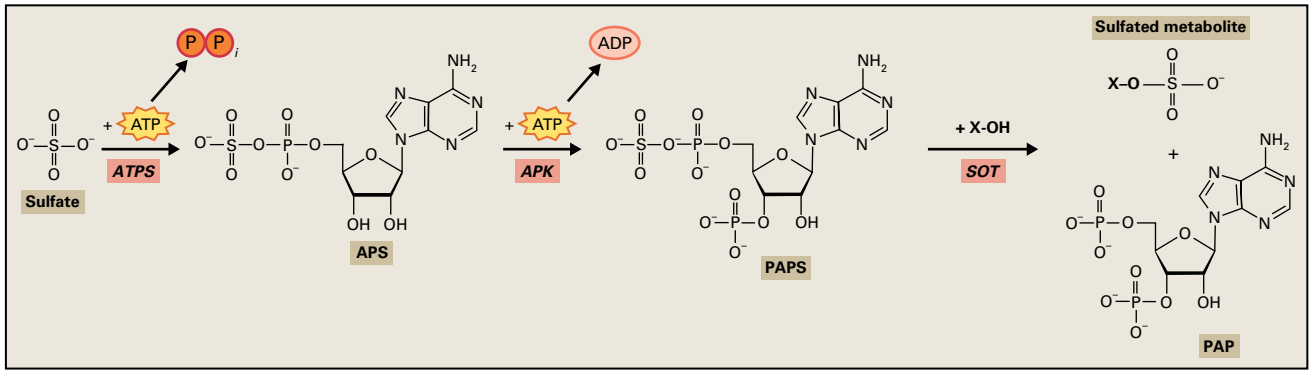


FIGURE 16.60 *Sulfate assimilation into sulfated metabolites. Sulfate is activated by adenylation to adenosine 5′-phosphosulfate (APS) in an ATP-dependent reaction catalyzed by ATP sulfurylase (ATPS). APS is further phosphorylated by APS kinase (APK) to 3′-phosphoadenosine 5′-phosphosulfate (PAPS). PAPS is the sulfate donor for sulfation of hydroxylated precursor (X-OH) by sulfotransferase (SOT) to form sulfated metabolite and adenosine 3′,5′-bisphosphate (PAP).*

16.17 Sulfated compounds

Most of the sulfate that enters plant cells is metabolized by the sulfate reduction pathway, but some is converted to PAPS and incorporated in various sulfated compounds. Many of the known sulfated plant metabolites play roles in defense against biotic and abiotic stress. The glucosinolates are the best-characterized group of such sulfated secondary compounds (see Chapter 24), and another large group of sulfated compounds are sulfated flavonoids, which are important in medicine. Present in more than 250 species, where they are involved in detoxifying reactive oxygen species and regulating plant growth, sulfated flavonoids also possess an anticoagulant activity and inhibit platelet aggregation and may be used for prevention of thrombosis. Several other sulfated compounds participate directly in plant defense against pathogens, such as sulfated derivates of jasmonic acid and sulphated β-1,3-glucan and fucan oligosaccharides, the latter inducing salicylic acid defense signaling. In addition, sulfated compounds are involved in seismonastic movements of *Mimosa*, and small sulfated peptides, such as phytosulfokines and PS1, are important regulators of plant growth.

16.17.1 APS kinase is the enzyme at the interface between primary and secondary metabolism

To be incorporated into sulfated compounds, sulfate is activated in two steps. As mentioned in Section 16.14.1, sulfate is first activated by ATP sulfurylase, which adenylates the sulfate to generate the intermediate APS (see Reaction 16.5). In the second step, APS is further phosphorylated by APS kinase to PAPS, the activated form of sulfate for all sulfation reactions (Reaction 16.14, Fig. 16.60).

Reaction 16.14: APS kinase

$$\text{APS} + \text{ATP} \rightarrow \text{PAPS} + \text{ADP}$$

PAPS is synthesized in the plastids and cytosol, the two compartments where APS is also produced. Plant APS kinases show strong sequence conservation with their homologs from bacteria, fungi, and animals and are encoded by a small gene family. *Arabidopsis*, for example, possesses one cytosolic and three plastidic isoforms, but the plastidial and cytosolic PAPS pools are interchangeable and connected by specific envelope-localized PAPS transporters.

Consistent with the function of sulfated compounds in plant stress response, APS kinase transcript levels are regulated by oxidative stress and by compounds involved in stress signaling. Disruption of two plastidic APS kinase isoforms, APK1 and APK2, reduces levels of glucosinolates and other sulfated compounds. The reduced synthesis of these secondary metabolites results in redirection of sulfur flux into primary assimilation, and the plants accumulate glutathione. In addition, similar to other enzymes of the pathway, APS kinase is redox regulated.

16.17.2 Sulfotransferases catalyze the transfer of sulfo-group to various metabolites

Transfer of the functional sulfo-group to hydroxylated substrates, that is, sulfation, is catalyzed by sulfotransferases in a reaction that requires PAPS as the sulfate donor and a compound with an available hydroxyl group as an acceptor. Advanced eukaryotes encode multiple sulfotransferase isoforms that accommodate the structural diversity of the biological acceptors of the sulfate group. The sulfotransferase family in *Arabidopsis* includes 18 members, but substrate specificities and biological functions are known for fewer than half of these. Sulfotransferases SOT16, SOT17, and SOT18 catalyze the final step of glucosinolate biosynthesis, sulfation of desulfoglucosinolates. Accordingly, these have broad substrate specificity (see Chapter 24). By contrast, *Arabidopsis* SOT15 specifically catalyzes sulfation of 11- and 12-hydroxyjasmonate. Consistent with the potential role of sulfated compounds in plant defense, mRNA levels of several

sulfotransferase isoforms increase upon treatment with jasmonate or salicylic acid and upon interaction with bacterial pathogens and elicitors. Several additional sulfotransferases have been isolated, cloned, and characterized from other species, including flavonol sulfotransferases from *Flaveria chloraefolia* and *F. bidentis*, and a sulfotransferase from *Mimosa putida* that catalyzes synthesis of turgorin. No sulfotransferases were found in the moss *Physcomitrella patens* or green alga *Chlamydomonas reinhardtii*, implying a late evolutionary origin for these enzymes.

16.18 Regulation of sulfate assimilation and interaction with nitrogen and carbon metabolism

16.18.1 Glutathione plays an important role in demand-driven regulation of sulfate assimilation

Sulfate assimilation is regulated according to the physiological need for reduced sulfur. Demand for sulfur increases when its supply becomes limited (sulfate starvation). It also increases during stress because of the involvement of glutathione and other sulfur-containing compounds in stress response. Glutathione levels can be depleted experimentally by inhibition of γ-glutamylcysteine synthetase with buthionine sulfoximine. Conversely, demand is reduced for plants that are supplied with reduced sulfur, which can be achieved by fumigation with sulfur dioxide or hydrogen sulfide, or by treatments with thiols. According to the demand-driven model of regulation of sulfate assimilation, sulfate uptake and the flux through the pathway increase when demand is high and decrease when the demand is low (Fig. 16.61). Because the activities of APS reductase and sulfate transporters are regulated by changes in demand for reduced sulfur, they possess the highest control over the flux. These treatments and environmental conditions each affect glutathione level, and it is likely the plant senses and responds to fluctuations in glutathione.

Sulfate assimilation pathway components show parallel regulation at the levels of enzyme activity, protein accumulation, and mRNA levels, pointing to a straightforward transcriptional regulation of the pathway. A sulfur-starvation response *cis* element, SURE, and a transcription factor, SLIM1, are involved in regulating expression of genes involved in sulfate assimilation. SLIM1 belongs to the ethylene-insensitive-like family of transcription factors and plays a central role in plant response to sulfur starvation. SLIM1-deficient plants are unable to induce sulfate transporters during low sulfur availability, resulting in significant growth defects

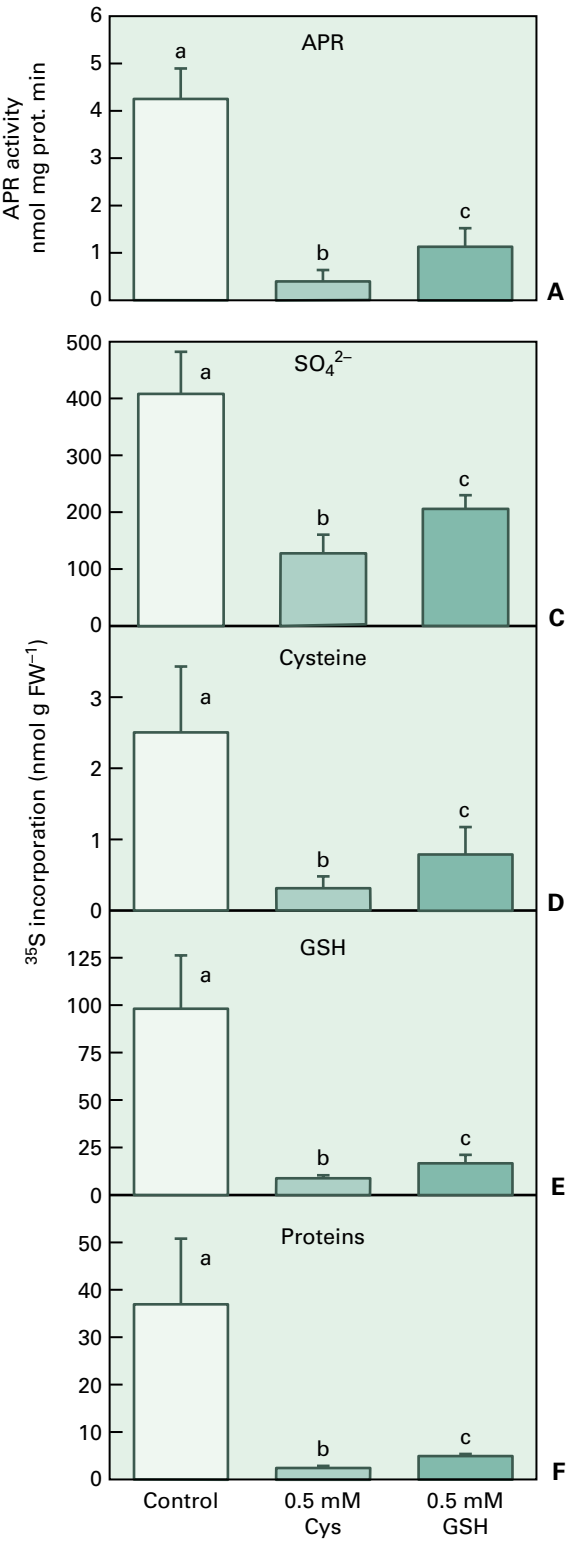


FIGURE 16.61 *Feedback regulation of flux through sulfate assimilation.* Arabidopsis thaliana *root cultures were supplemented with 0.5 mM cysteine or 0.5 mM glutathione (GSH) for 20 hours. Radioactive [^{35}S] sulfate was then added, and the cultures were further incubated for 4 hours. APS reductase activity (APR) and incorporation of radioactivity from [^{35}S]sulfate into sulfate (a measure of sulfate uptake), cysteine, glutathione, and proteins were measured. Controls were cultivated without additions.*

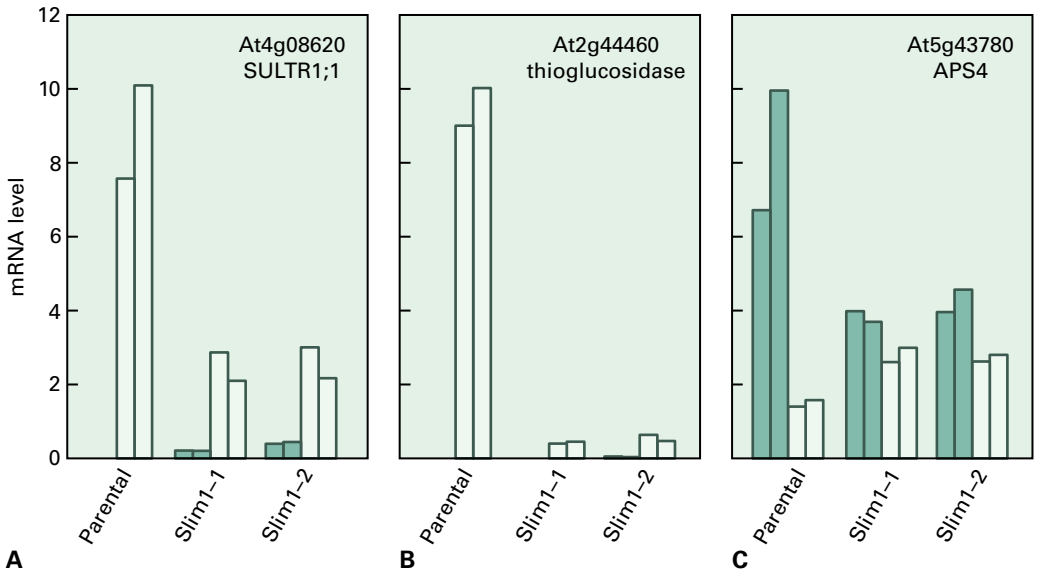


FIGURE 16.62 *SLIM1 is a central regulator of plant sulfur deficiency response.* Arabidopsis *plants were grown at 1,500 μM sulfate (green bars) or 15 μM sulfate (white bars). Transcript levels of two genes induced by sulfate deficiency (At4g08620 and At2g4460) and one gene repressed (At5g43780) by S deficiency were measured in two independent RNA preparations from wild-type plants, and two alleles of* slim1 *mutants by quantitative real-time PCR. (A) SULTR1;1 is a high-affinity sulfate transporter; (B) Thioglucosidase; (C) APS4 is a form of ATP sulfurylase. Data were normalized using ubiquitin as an internal standard.*

under such conditions (Fig. 16.62). Other regulatory mechanisms are involved in fine-tuning the plant response to environmental cues, including post-translational inhibition of APS reductase and γ-glutamylcysteine synthetase by glutathione, feedback inhibition of serine acetyltransferase by cysteine, and modulation of OAS (thiol)lyase and serine acetyltransferase binding by OAS and sulfide. The response of mRNA levels to changes in sulfur demand may be uncoupled from the changes in corresponding enzyme activity: such post-transcriptional regulation has been described for sulfate transporters and APS reductase.

One such post-transcriptional mechanism uses the microRNA miR395, which is induced by sulfur starvation. It accumulates to high levels in roots and shoots of sulfur-starved plants in a SLIM1-dependent manner, and it targets three isoforms of ATP sulfurylase and the low-affinity SULTR2;1 sulfate transporter. This microRNA enables efficient transport of sulfate to the shoots under sulfur-deficient conditions by restricting *SULTR2;1* expression to xylem parenchyma cells of the roots and limiting sulfate assimilation in the roots. Accordingly, ectopic expression of miR395 results in sulfate accumulation in the leaves.

16.18.2 Sulfur starvation response is a frequent model for systems biology

Sulfur deficiency broadly affects general plant metabolism, as shown by transcript and metabolite profiling of plants grown under normal and sulfur-depleted conditions. Numerous sulfate assimilation genes show increased expression, while genes involved in glucosinolate biosynthesis are strongly reduced. Corresponding metabolite analyses show glucosinolates are degraded during sulfur-deficient conditions, and they serve as an alternative sulfur source. Network analysis of combined transcript and metabolite data revealed novel regulators and several new genes involved in glucosinolate synthesis. Sulfur deficiency leads to accumulation of free amino acids, particularly of OAS, and to increased mRNA levels of sulfate transporters, APS reductase, and many other genes that respond to sulfate starvation. At least some of these genes are directly induced by OAS. Sulfur deficiency also affects expression of genes involved in jasmonate and auxin biosynthesis and those in major metabolic pathways, such as the Calvin–Benson cycle, glycolysis, and lipid synthesis.

Components of the sulfur starvation signal transduction pathway have been identified in the green alga *Chlamydomonas reinhardtii*. Mutations in **sulfur acclimation (*sac*) genes** result in a lack of response to sulfur limitation: *sac*1 mutants lack both general and specific responses to sulfur starvation, including the effects on photosynthesis, whereas *sac*2 and *sac*3 mutants are deficient only in sulfate uptake and assimilation. The *Sac*1 gene encodes a protein homologous to ion channels, one inferred to be a sulfate sensor, *Sac3* encodes an Snf1-like kinase (its disruption leads to derepression of **arylsulfatase** expression), and *Sac2* is involved in post-transcriptional regulation of APS reductase, but has not been identified. Another Snf1-like kinase epistatic to *Sac3* is indispensable for eliciting the sulfur starvation response in the alga. It is not known whether land plants employ similar regulatory mechanisms and components.

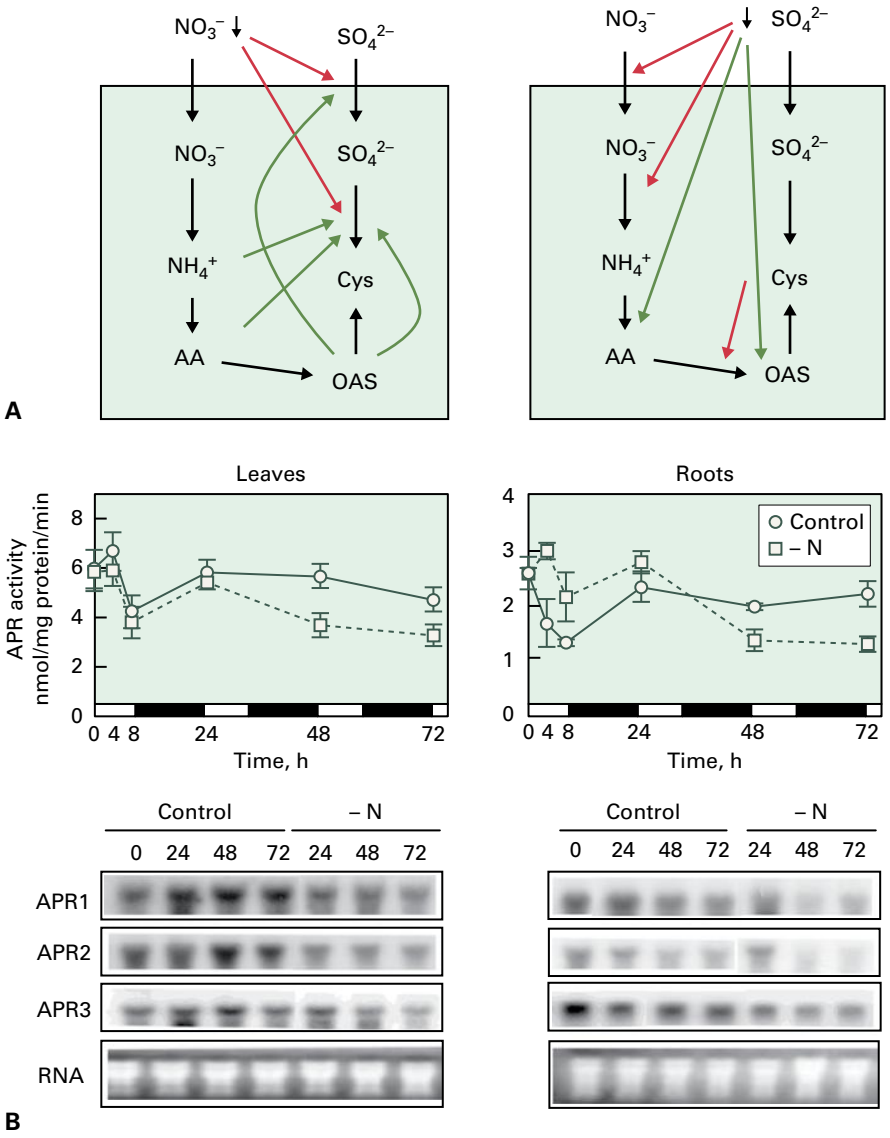


FIGURE 16.63 *Regulatory interaction of sulfate and nitrate assimilation. (A) Green arrows represent upregulation, and red arrows denote repression by nitrogen (left) or sulfate (right) deficiency. (B) Reduction in APR activity (upper panel) and mRNA levels (lower panel) in shoots and roots of* Arabidopsis *plants subjected to nitrogen deficiency for 72 hours.*
Source: (B) Adapted from Plant Physiol. (2000). 122(3):737–746.

16.18.3 Sulfate assimilation is closely linked with carbon and nitrogen metabolism

Synthesis of cysteine connects the three major pathways of primary metabolism—carbon fixation, nitrate assimilation, and sulfate assimilation. Accordingly, the pathways are well coordinated. Sulfate uptake and APS reductase activity decrease during nitrogen and carbon starvation (e.g., in low CO_2 atmosphere). Sulfate starvation leads to reduction of nitrate uptake and nitrate reductase activity, chlorophyll degradation, and reduced photosynthesis (Figs 16.63 and 16.64). APS reductase, in parallel with nitrate reductase, displays a diurnal rhythm in activity and transcript levels, and it is induced by light and carbohydrates (Fig. 16.64). Flux through the sulfate reduction pathway is far greater in the light than in the dark and is increased by addition of reduced nitrogen sources and carbohydrates. Recently, the transcription factor LONG HYPOCOTYL5 (HY5) was identified as important for light induction of APS reductase and its regulation by OAS and nitrogen availability.

Phytohormones also affect sulfate assimilation. The genes of sulfate assimilation and glucosinolate synthesis are coordinately upregulated by jasmonic acid. APS reductase, the key enzyme in the pathway, is upregulated by other phytohormones involved in stress signaling, namely salicylate and ethylene. Interestingly, abscisic acid promotes synthesis of cysteine and glutathione but has a negative effect on APS reductase. Cytokinins, which are strongly connected with nitrogen and phosphate nutrition, regulate sulfate assimilation as well. The upregulation of sulfate transporters by sulfur starvation is partially dependent on cytokinin signaling. The regulation of sulfate assimilation is thus complex, involving and coordinating many signals and effectors.

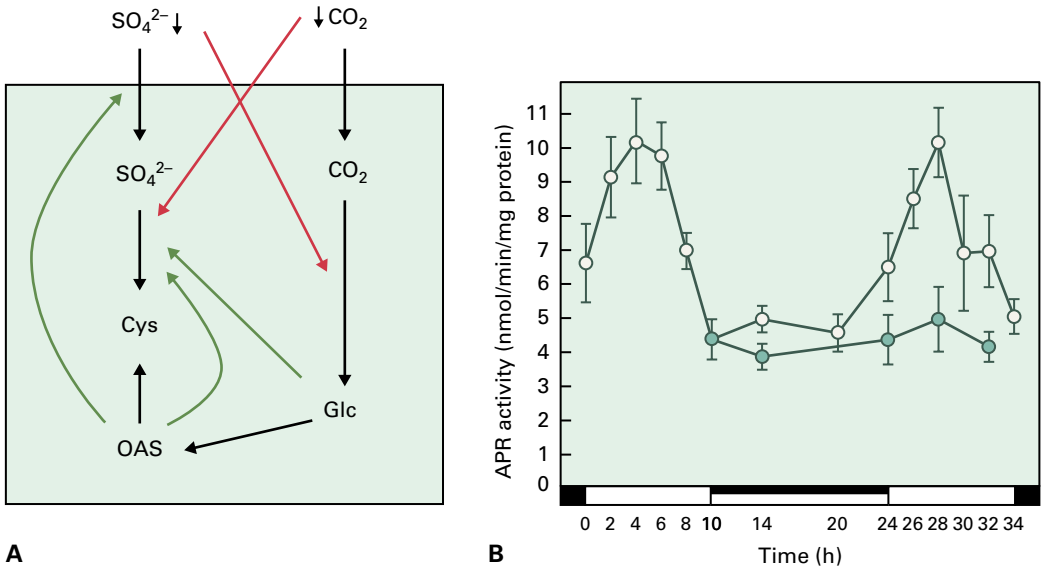


FIGURE 16.64 *Regulatory interaction of sulfate and carbon assimilation. (A) Green arrows represent upregulation, red arrows denote repression by CO_2 or sulfate deficiency. (B) Diurnal rhythm of APR activity at normal day/night rhythm (full symbols) and constant light (open symbols).*

Summary

Plants are major players in the geochemical cycles of both sulfur and nitrogen. The inorganic forms of these elements are incorporated into carbon-bonded molecules using reducing power derived from photosynthesis. The reduction and assimilation reactions are integrated into general plant metabolism: For example, they are regulated by light and carbon availability, plant growth, hormones, and other factors. Nitrogen and sulfur are required for protein synthesis, and each is essential for making multiple types of other small and macromolecules. Nitrogen or sulfur assimilation functions are sometimes compartmentalized within plant cells or located in specific tissues or organs.

The biochemically useable state of nitrogen is ammonia (NH_3). Biochemically useful nitrogen can also be derived from the reduction of nitrate (NO_3^-) or by bacterial nitrogen (N_2) fixation. The key catalyst of nitrogen fixation, nitrogenase, has two functional component proteins. Dinitrogenase is the enzyme that actually reduces molecular N_2. It contains unusual metal clusters including one type that generally includes Fe, S, and either Mo or V. Dinitrogenase reductase uses ATP to lower the potential of reductants obtained from metabolism to a level where electrons can reduce the dinitrogenase clusters.

Some plants, including agriculturally and ecologically important legumes, can enter into symbiosis with nitrogen-fixing bacteria to acquire bacterially produced ammonium in exchange for plant carbon from photosynthesis. The cellular and developmental functions underlying legume symbiosis include signal exchange and specific gene expression to accomplish metabolic exchange. The nitrogen-fixing forms of the bacteria, termed bacteroids, are surrounded by a plant-derived membrane that controls the exchange of nutrients between the bacteroid and the plant cytoplasm.

A mature nodule is organized to support the energy-intensive nitrogen fixation reaction by delivering oxygen and carbon sources to the bacteroids at low concentrations of free O_2 in order to protect nitrogenase, a notoriously oxygen-sensitive enzyme. Ammonium released by bacteroids is first assimilated in the plant by glutamine synthetase and other enzymes, sometimes employing nodule-specific isozymes. Assimilated nitrogen leaves the nodule as either amides or ureides, depending on the host species, which leads to distinct patterns of gene expression, compartmentation, and regulation of these final steps in different hosts.

Plant use of environmental ammonium and nitrate begins with high- and low-affinity transporters that are subject to various levels of regulation. High-affinity ammonium transporters in the AMT/Rh family appear to act as uniporters and are regulated at the transcriptional level and by posttranslational phosphorylation. Nitrate transporters include the symporters NRT1 and NRT2, which function at both the plasma membrane and

tonoplast, along with the tonoplast antiporter CLC protein. To adapt to environmental nitrate availability, which can vary over four orders of magnitude, the NRT1/2 transporters participate in both high- and low-affinity transport using active proton-coupled mechanisms. The various forms are subject to tissue-specific and environmentally regulated expression and to posttranslational modification. Nitrate loading into cellular vacuoles may employ distinct transporters.

To be assimilated, nitrate is reduced to nitrite and subsequently to ammonia, overall an eight-electron transfer. To avoid build up of toxic nitrite, NR activity is highly regulated and NiR is not limiting. NR gene expression is regulated by diverse signals, including nitrate levels, light, carbon availability, and hormones. The NR polypeptide includes three domains, each binding a specific cofactor and associated with separable partial activities: an N-terminal molybdenum cofactor (MoCo)-binding domain, a central heme-binding domain similar to cytochrome b_5 family, and a C-terminal FAD-binding region that also binds the substrate NAD(P)H. The three functional regions are joined by hinge segments that participate in posttranslational regulation of activity, such as phosphorylation-dependent 14-3-3 protein binding. NR is localized in the cytoplasm and in some cases shows cell type-specific localization.

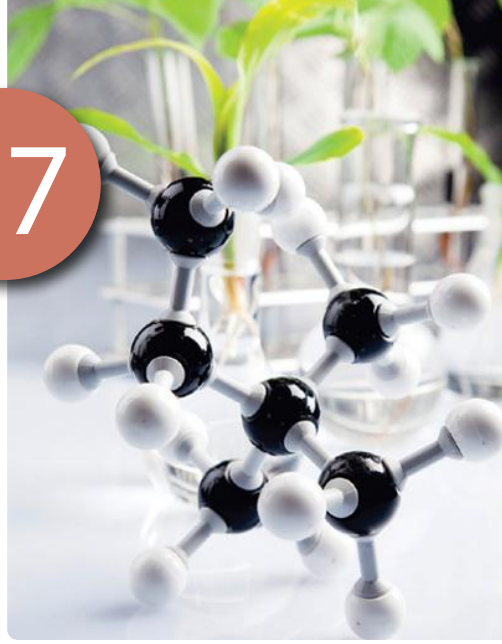
Ferredoxin (Fdx) provides the reducing power for plastid-localized NiR to catalyze conversion of nitrite to ammonia, a six-electron transfer. Fdx_{red} is produced in the chloroplasts of green tissues by noncyclic electron transport; in nonphotosynthetic cells a more electropositive Fdx is reduced via ferredoxin-$NADP^+$ reductase, using NADPH from the oxidative pentose phosphate pathway.

Sulfur is required in all organisms for synthesis of proteins and cofactors. Sulfur is used in plants for additional unique structures and functions, such as the sulfoquinovosyl-diacylglycerol lipids in chloroplast membranes. As the primary producers of organic sulfur compounds, plants play a key role in the global sulfur cycle by coupling photosynthesis to the reduction of sulfate, assimilating sulfur into cysteine and metabolizing this amino acid to form methionine, glutathione, and other compounds; this, in turn, is the source of reduced sulfur for animals.

The sulfate ion is taken up into plants via active proton cotransporters in root cells. Permeases and facilitated transport systems accomplish sulfate transport between organs, cells, and subcellular compartments. Multigene families encode these transporters, which display different kinetics and expression patterns to accomplish sulfate distribution across the plant.

For assimilation, sulfate is first activated by reaction with ATP to form adenosine 5′-phosphosulfate (APS), a reaction catalyzed by ATP sulfurylase. The S atom in APS can be reduced first to sulfite by APS reductase and then to sulfide by sulfite reductase. Reduction of sulfate is highly energy-intensive. It can be carried out in plastids of many cell types, but a preponderance of sulfate reduction occurs in green tissues, and it is more active in the light than the dark. Cysteine is synthesized by condensation of sulfide with *O*-acetylserine; enzymes for production of *O*-acetylserine and cysteine are encoded by multigene families and are localized in all compartments that carry out protein synthesis. Cysteine is the donor of reduced sulfur for synthesis of other sulfur-containing metabolites, such as methionine and glutathione.

Alternatively, APS is further activated by APS kinase to form PAPS (phospho-adenosyl phosphosulfate), which is the molecular source for sulfate used in sulfated polysaccharides, glucosinolates, and other metabolites. Sulfate uptake and assimilation are regulated by demand, and at multiple levels from transcription to activity. This regulation integrates factors including growth, light, and sulfur availability, and these functions are an appealing target for systems analysis.



17

Biosynthesis of Hormones

Gerard Bishop, Hitoshi Sakakibara, Mitsunori Seo, and Shinjiro Yamaguchi

Introduction

Plant hormones are signal molecules, present in trace quantities. Changes in hormone concentration and tissue sensitivity mediate a range of developmental processes in plants, many of which involve interactions with environmental factors. This chapter is concerned with the biosynthetic, catabolic, and conjugation pathways that together control plant hormone homeostasis. Attention will be focused on the so-called "classic," first five plant hormones discovered—gibberellins, abscisic acid, cytokinins (CKs), indole-3-acetic acid and ethylene—and more recently investigated compounds that have regulatory roles in plant development, such as brassinosteroids, polyamines, jasmonic acid, salicylic acid, and strigolactones (Fig. 17.1). Each of these hormones has its own particular properties, so the pathways regulating their production and degradation are diverse and have been elucidated by synergistic use of many disciplines, including chemistry, biochemistry, plant physiology, genetics, and more recently molecular genetics. Mutant plants that are unable to catalyze an enzymatic reaction leading to the formation or degradation of a bioactive hormone have been powerful tools in plant hormone research. Such mutants have been invaluable in hormone analysis studies and in phenotypic rescue experiments using intermediates in the biosynthetic pathway. They also provide the essential material for cloning of genes that encode biosynthetic enzymes. In addition, inhibitors of plant hormone biosynthesis have been used to dissect reactions for which relevant mutants have not been identified. More recently, transgenic technology has provided insights into pathways by altering the expression of genes involved in biosynthesis or catabolism of hormones. In summary, each hormone biosynthetic pathway has been elucidated using similar techniques with biases towards certain methodologies according to the nature of the biosynthetic pathway and the availability of mutants.

17.1 Gibberellins

Gibberellins (GAs) were first isolated from the fungus *Gibberella fujikuroi* in 1926 by the Japanese scientist Eiichi Kurosawa, who was investigating the causative agent of *bakanae*, the "foolish seedling" disease of *Oryza sativa*, which was frequently responsible for major reductions in grain yield. Diseased *O. sativa* seedlings exhibited excessive shoot elongation and yellowish-green leaves (Fig. 17.2). Those that survived to maturity were taller than their healthy counterparts and seeds were either absent or poorly developed. Kurosawa demonstrated that diseased *O. sativa* plants were infected with a fungal pathogen, *G. fujikuroi*, which secreted a factor that increased the rate of shoot elongation. He also noted that the active factor promoted the growth of *Zea mays*, *Sesamum indicum*, *Pennisetum glaucum*, and *Avena sativa* seedlings. In the 1930s, the fungal growth-inducing factor was crystallized and named gibberellin. At about the same time, scientists in the West were actively investigating hormonal regulation of plant growth by auxin (see Section 17.4). They either failed to appreciate the significance of the Japanese work on GAs or were unaware of its existence, despite the availability of English translations. Not until the early 1950s did GA research became

Biochemistry & Molecular Biology of Plants, Second Edition. Edited by Bob B. Buchanan, Wilhelm Gruissem, and Russell L. Jones.
© 2015 John Wiley & Sons, Ltd. Published 2015 by John Wiley & Sons, Ltd.
Companion website: www.wiley.com/go/buchanan/biochem

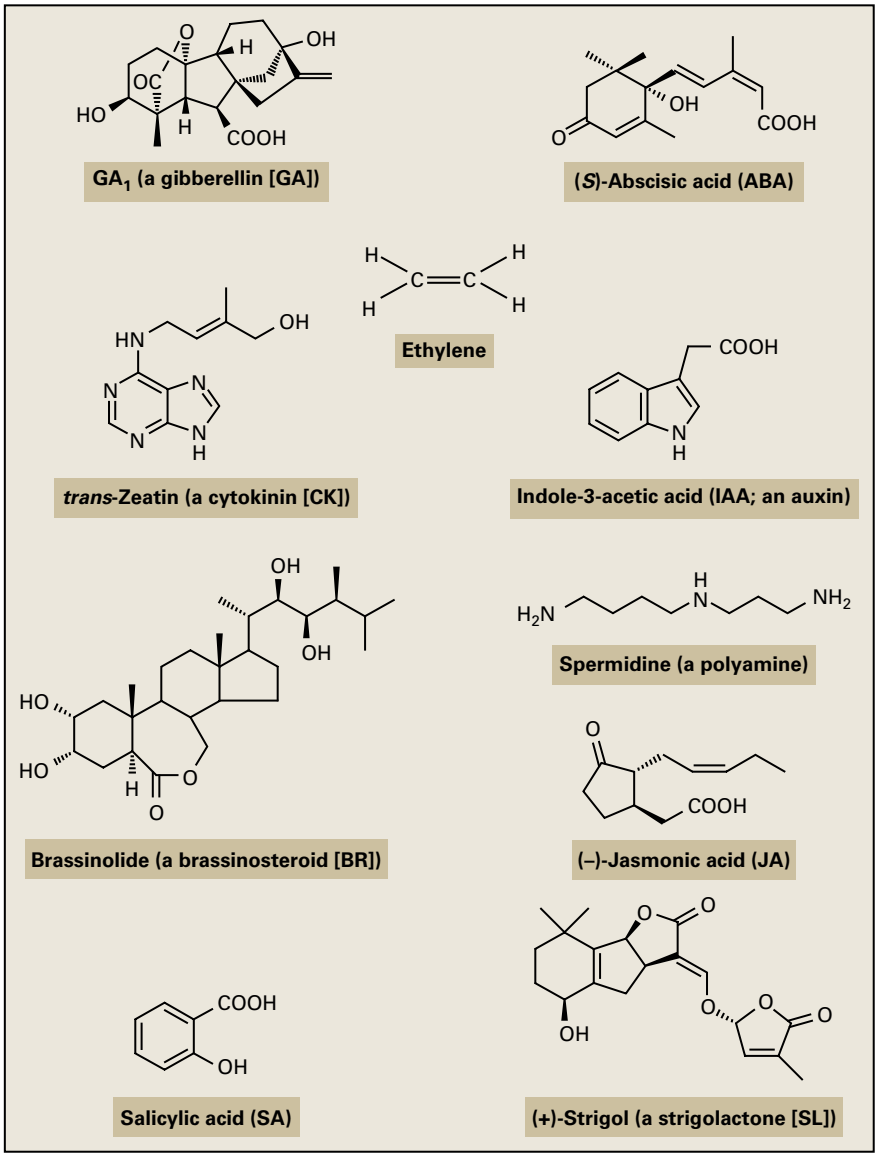


FIGURE 17.1 *Structures of representatives from the 10 types of plant hormones discussed in this chapter.*

international in scope when groups from the US and UK initiated their own studies with *G. fujikuroi*. The British isolated gibberellic acid and the Americans gibberellin X. The compounds proved to be identical, and the structure of gibberellic acid, now known as GA_3, was elucidated in 1956. Shortly thereafter, GAs were shown to be endogenous components of plants, and it became apparent that they were not merely an interesting group of fungal metabolites but endogenous regulators of many aspects of higher plant growth and development.

17.1.1 Among more than 100 GAs identified from plants, only a few act as bioactive hormones

The GAs are a group of tetracyclic diterpenes. At the time of writing, 136 different GAs had been characterized. To avoid confusion, the nomenclature GA_1 to GA_{136} has been adopted, and the numbers GA_{136} to GA_n will be allocated sequentially as further GAs are characterized. Among more than 100 GAs identified from plants, only a few function as bioactive hormones. Many nonbioactive GAs present in plants are biosynthetic precursors of bioactive forms or are inactivated metabolites. The most commonly found bioactive GAs in plants are GA_1 and GA_4, both of which have a hydroxyl group on C-3β, a carboxyl group on C-6, and a γ-lactone between C-4 and C-10 (Fig. 17.3). The recent identification of a soluble GA receptor, GIBBERELLIN INSENSITIVE DWARF 1 (GID1), from *O. sativa* and its homologs in *Arabidopsis* and *Hordeum vulgare* has demonstrated that these structural requirements for bioactive GAs are reflected in their affinity for the GID1 receptor. GA_1 has been identified frequently in a variety of plant species, suggesting that it acts as a widespread bioactive hormone. However, GA_4 also exists in most species and is considered to be the major bioactive GA in *Arabidopsis* and some Cucurbitaceae. GA_3 and GA_7, 1,2-double bond analogs of GA_1 and GA_4, respectively, are also active per se in plants (Fig. 17.3).



FIGURE 17.2 O. sativa *seedling infected with* Bakanae *(foolish seedling) disease caused by the fungal pathogen,* Gibberella fujikuroi.

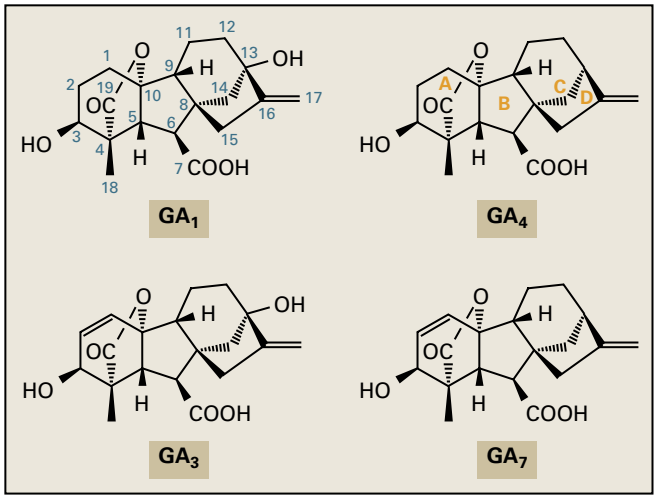


FIGURE 17.3 *Structures of bioactive GAs in plants.*

17.1.2 Bioactive GAs affect many aspects of plant growth and development

GAs are best known for their influence on stem elongation (Fig. 17.4) and leaf growth (Fig. 17.5), but they also affect other developmental processes in a wide range of plants. In some species, GAs stimulate fruit growth without fertilization of ovules (parthenocarpy). In flowering plants that require one or more long days to flower or that require a cold treatment, GA application often can substitute for the environmental signal. GAs can stimulate seed germination in many plant species. *Arabidopsis* and *Solanum lycopersicum* mutants that are severely



FIGURE 17.4 *Effect of GA_3 on stem elongation of dwarf* P. sativum *seedlings: (left) control plants, (right) plants seven days after treatment with 5 μg of GA_3.*
Source: A. Crozier, University of Glasgow, UK; previously unpublished.

defective in GA synthesis are nongerminating, and their germination can be induced by GA treatment. GA-induced de novo synthesis of α-amylase and other enzymes in the aleurone layer of cereal grains has been used extensively in studies of GA action. Because of this effect, GA_3 is used widely in the malting industry to speed up and regularize malt production. In general, vegetative tissues contain low nanogram or sub-nanogram quantities of GAs per gram fresh weight, whereas GAs occasionally accumulate at much higher levels in some reproductive organs such as anthers and developing seeds.

17.1.3 GA biosynthesis starts in the plastid

The initial steps in biosynthesis of GAs involve formation of isopentenyl diphosphate and its conversion to geranylgeranyl diphosphate (GGDP), a common precursor for various terpenoids, such as carotenoids and phytol (Fig. 17.6). Plants have two distinct pathways for biosynthesis of isopentenyl diphosphate: the mevalonate pathway in the cytosol, and the methylerythritol phosphate (MEP) pathway in plastids (see Chapter 24). Metabolism studies using isotope-labeled precursors in *Arabidopsis* seedlings showed that the MEP pathway in plastids provides the majority of isopentenyl diphosphate to GAs, whereas only a minor contribution is from the cytosolic mevalonate pathway.

Three different classes of enzymes are required for GA biosynthesis from GGDP in plants: terpene synthases (cyclases), Cytochrome P450 monooxygenases, and 2-oxoglutarate-dependent dioxygenases (see Sections 17.1.4–17.1.6).

FIGURE 17.5 *Promotion of Tanginbozu dwarf* O. sativa *(d35) leaf sheath elongation 3 days after treatment with GA_3: (left) control; (center) 100 pg of GA_3 per seedling; (right) 1 ng of GA_3 per seedling.*
Source: A. Crozier, University of Glasgow, UK; previously unpublished.



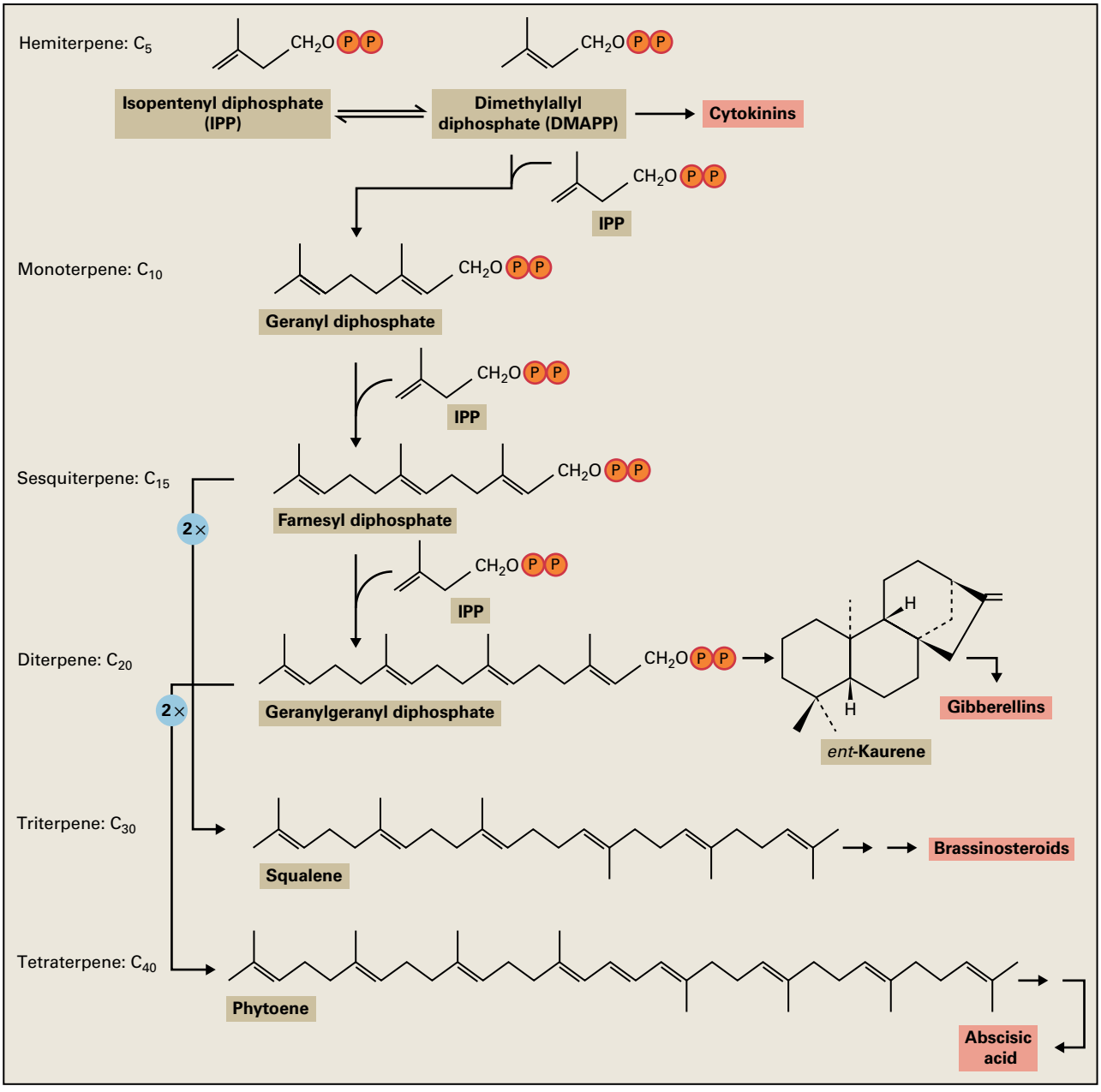


FIGURE 17.6 *Terpenoid biosynthesis pathway, showing biosynthetic origins of GAs as well as CKs, BRs, and ABA.*

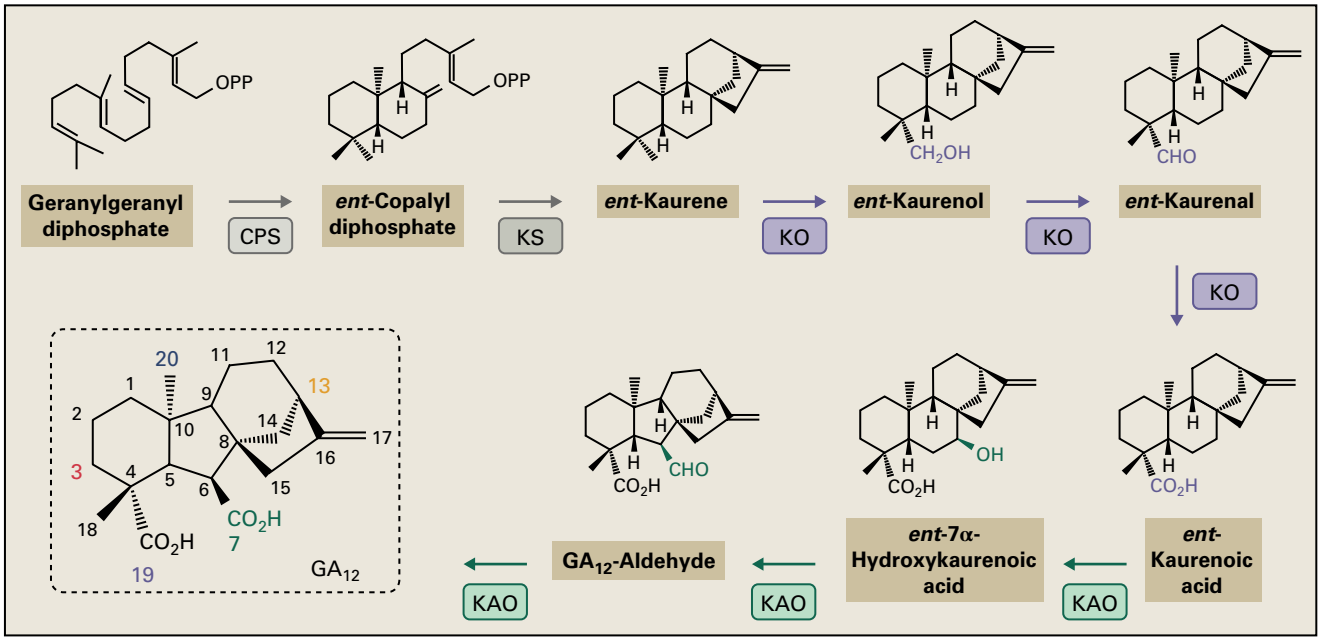


FIGURE 17.7 *Early stages of plant GA biosynthesis. CPS,* ent*-copalyl diphosphate synthase; KS,* ent*-kaurene synthase; KO,* ent*-kaurene oxidase; KAO,* ent*-kaurenoic acid oxidase. Colored carbon atoms on* GA_{12} *are oxidized for the synthesis of* GA_1 *(see also Fig. 17.9).*

17.1.4 In plants, the synthesis of *ent*-kaurene from geranylgeranyl diphosphate is catalyzed by two distinct enzymes

Synthesis of *ent*-kaurene from GGDP is catalyzed by two distinct terpene synthases, *ent*-copalyl diphosphate synthase (CPS) and *ent*-kaurene synthase (KS) (Fig. 17.7). CPS catalyzes conversion of GGDP to a partially cyclized product, *ent*-copalyl diphosphate. This reaction does not involve the removal of the diphosphate group and is initiated by addition of a proton to the terminal olefin bond of the substrate. KS catalyzes formation of *ent*-kaurene, a tetracyclic hydrocarbon, from *ent*-copalyl diphosphate. This cyclization reaction is initiated by elimination of the diphosphate group. A gene encoding CPS was first identified as the causal gene of the *Arabidopsis ga1-3* mutant, an extreme dwarf resulting from GA deficiency. A cDNA clone encoding KS was initially isolated based on partial amino acid sequences of a purified enzyme from immature pumpkin seeds, a rich source of GA biosynthesis enzymes. Evidence suggests that both CPS and KS have an amino-terminal plastid-targeting signal, and that *ent*-kaurene synthesis occurs in plastids.

17.1.5 Cytochrome P450 monooxygenases convert *ent*-kaurene to GA_{12}

ent-Kaurene is oxidized to GA_{12} by NADPH-dependent, membrane-bound CYP450 monooxygenases: *ent*-kaurene oxidase (KO, CYP701A) and *ent*-kaurenoic acid oxidase (KAO, CYP88A) (Fig. 17.7). KO catalyzes the three-step oxidation on C-19 to synthesize *ent*-kaurenoic acid. KAO also is a multifunctional enzyme that catalyzes the three-step conversion of *ent*-kaurenoic acid to GA_{12}, including the conversion of *ent*-7α-hydroxy-kaurenoic acid to GA_{12}, which involves contraction of the B-ring from a C_6 to a C_5 structure. The nitrogen-containing heterocyclic compounds paclobutrazol, uniconazole, tetcyclasis, and ancymidol retard plant growth by inhibiting KO (see Fig. 17.8) However, these compounds are not specific inhibitors of GA biosynthesis because they also affect other CYP450 enzymes, including those involved in the biosynthesis of brassinosteroids and the catabolism of abscisic acid (see Section 17.6.4). Several GA-deficient dwarf mutants, including *lh* (*P. sativum*), *d35* (*dx*) (*O. sativa*), and *ga3* (*Arabidopsis*), have defective KO activity. A gene encoding KAO was first identified as a causative gene of the *H. vulgare grd5* mutant, a GA-responsive dwarf. Experiments using enzymes fused to green fluorescent protein (GFP) suggest that KO is present in the outer membrane of the plastid, whereas KAO is located in the endoplasmic reticulum.

17.1.6 Conversion of GA_{12} to bioactive GAs involves two pathways: one in which C-13 is hydroxylated early, and one in which C-13 is not hydroxylated

The multistep conversion of GA_{12} to bioactive GAs proceeds via one of two pathways, one where C-13 is hydroxylated producing GA_{20} and GA_1, the other where hydroxylation at C-13 does not occur producing GA_9 and GA_4 (Fig. 17.9). Although a soluble, 2-oxoglutarate-dependent 13-hydroxylation activity

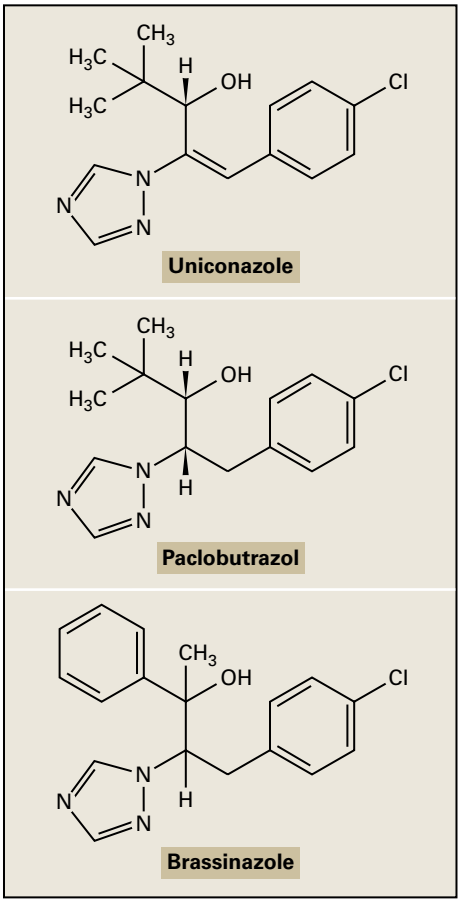


FIGURE 17.8 *Structures of uniconazole, paclobutrazol, and brassinazole. Uniconazole and paclobutrazol are triazoles that inhibit KO (see Fig. 17.7). However, uniconazole is not specific and also suppresses BR biosynthesis. The structurally related compound, brassinazole, is a strong BR inhibitor, blocking at least one CYP450 mediated step in the BR biosynthesis pathway (see Fig. 17.58). Its effect on GA biosynthesis is undetermined.*

has been detected in cell-free extracts from *Spinacia oleracea* leaves, the 13-hydroxylase activity identified in *Cucurbita* spp. endosperm, developing *H. vulgare*, and *P. sativum* embryos are all monooxygenases.

In either pathway, GA 20-oxidase and GA 3-oxidase, both soluble 2-oxoglutarate-dependent dioxygenases, are responsible for the production of bioactive GAs (Fig. 17.9). GA 20-oxidase catalyzes the sequential oxidation of C-20, including the loss of C-20 as CO_2 and the formation of γ-lactone. The subsequent introduction of a 3β-hydroxyl group by GA 3-oxidase converts inactive precursors (GA_{20} and GA_9) to bioactive forms (GA_1 and GA_4). Some GA 3-oxidases have minor catalytic activity to synthesize GA_3 from GA_{20} via GA_5, a 1,2-double bond analog of GA_{20} (Fig. 17.9). The subcellular localization of GA 20-oxidase and GA 3-oxidase has not been demonstrated experimentally, but they are considered to be cytosolic enzymes because they lack obvious targeting sequences.

In both *Arabidopsis* and *O. sativa,* enzymes catalyzing early steps of GA biosynthesis are encoded by one or two genes, and mutants defective in these enzymes typically exhibit severe dwarfism. In comparison, GA 20-oxidase and GA 3-oxidase are each encoded by multigene families, and mutants defective in a GA 20-oxidase or GA 3-oxidase isoform display a moderately dwarfed phenotype. In *P. sativum*, a major GA 3-oxidase that controls internode elongation is encoded by the *Le* gene, originally described by Gregor Mendel in his breeding experiments with tall and dwarf peas.

17.1.7 Bioactive GAs are rendered inactive via multiple metabolic routes in plants

GAs are inactivated in several different ways in plants. The best-characterized inactivation reaction is oxidation on C-2, catalyzed by GA 2-oxidase, a 2-oxoglutarate-dependent dioxygenase (Fig. 17.10). Initially identified GA 2-oxidases utilized bioactive GAs (GA_1 and GA_4) and their immediate precursors (GA_{20} and GA_9) as substrates. Later, a new type of GA 2-oxidase was discovered, which accepts only earlier intermediates, GA_{12} and GA_{53}. Thus, many GAs in the biosynthesis pathway are targets of GA 2-oxidation. Genes encoding GA 2-oxidases were first identified through functional screening of a cDNA expression library.

A study on a tall mutant of *O. sativa*, *elongated uppermost internode* (*eui*), led to the discovery of a new GA inactivation mechanism. The *eui* mutant accumulates large amounts of bioactive GAs in internodes. The *Eui* gene encodes a CYP450 monooxygenase, CYP714D1, which inactivates GAs by epoxidation of the 16,17-double bond of various GAs, including GA_4, GA_9, and GA_{12} (Fig. 17.10). The 16,17-epoxides are hydrolyzed to give 16,17-dihydrodiols either in vivo or during purification. The occurrence of GA 16,17-dihydrodiols in many plant species suggests that 16,17-epoxidation may be a widespread GA inactivation mechanism. More recent work has shown that *Arabidopsis* GAMT1 and GAMT2 catalyze methylation of the C-6 carboxyl group of GAs using *S*-adenosyl-L-methionine (SAM) as a methyl donor (Fig. 17.10). As seen for GA 2-oxidase and EUI, both GAMT1 and GAMT2 use a variety of GAs as substrates, and produce the corresponding methyl esters. Whether methylation of GAs is a common inactivation reaction in other plants has yet to be investigated.

GAs can be converted into conjugates in plants. Conjugation of GAs to glucose takes place either through a hydroxyl group of GA to give a GA-*O*-glucosyl ether or through the 6-carboxyl group to give a GA-glucosyl ester. Genes encoding enzymes that catalyze the formation of GA conjugates have not been identified.

17.1.8 There are remarkable differences in GA biosynthesis pathways and enzymes between plants and fungi

Recent identification of fungal genes encoding GA biosynthesis enzymes from *G. fujikuroi* and a species of *Phaeosphaeria* uncovered substantial differences in GA biosynthesis genes and

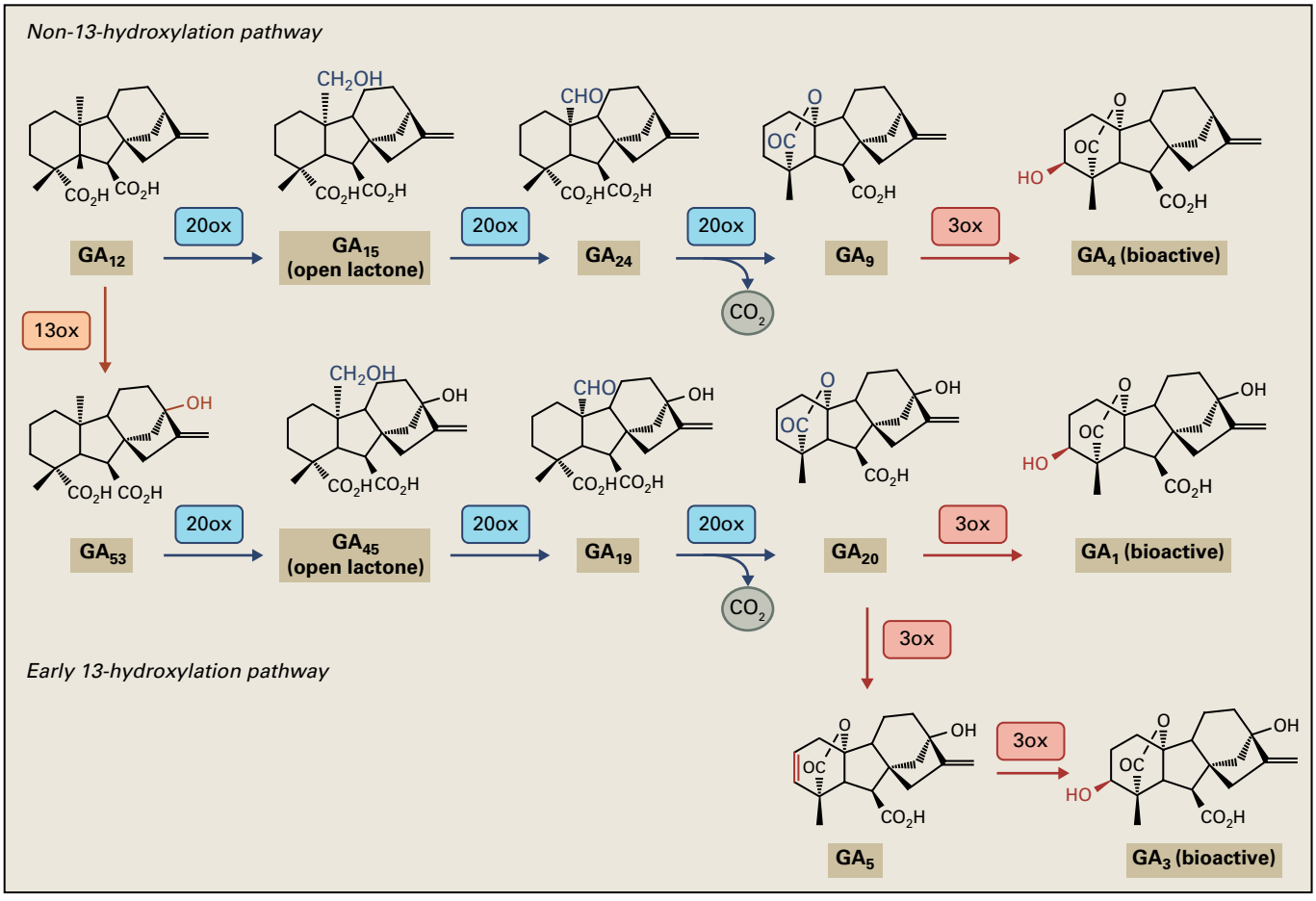


FIGURE 17.9 *Conversion of GA_{12} to bioactive GAs in plants. 20ox, GA 20-oxidase; 3ox, GA 3-oxidase; 13ox, GA 13-oxidase.*

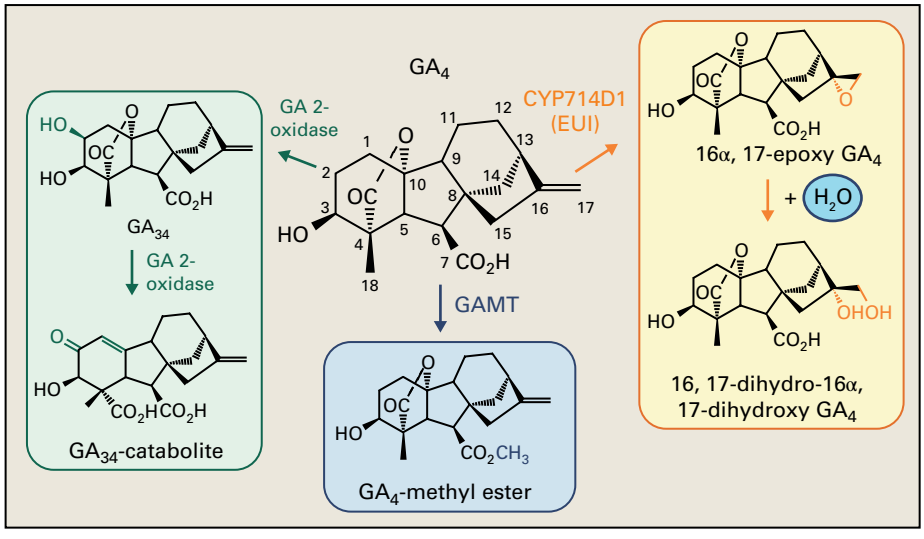


FIGURE 17.10 *GA_4 inactivation pathways. Inactivation by GA 2-oxidase introduces a 2β-hydroxyl group. In some cases, further metabolism occurs to form GA-catabolites, in which C-2 is oxidized to a ketone and the lactone is opened with the formation of a double bond. 16α,17-epoxy GAs produced by CYP714D1 (EUI) are hydrolyzed to give 16,17-dihydrodiols either in plants or during purification. GAMT catalyzes methylation of the C-6 carboxyl group. GAs are also converted into various glucose conjugates in plants (not shown).*

enzymes between plants and fungi. In plants, two separate terpene synthases, CPS and KS, are involved in the synthesis of *ent*-kaurene from GGDP (see Fig. 17.7), whereas these two steps are catalyzed by a single bifunctional enzyme in *G. fujikuroi* and *Phaeosphaeria*. *G. fujikuroi* has a CYP450 monooxygenase (CYP68A) that plays a similar role to that of KAO in plants, but this enzyme also catalyzes 3β-hydroxylation to produce GA_{14}, 3β-hydroxylated GA_{12}. GA_{14} is converted to GA_4 by

another CYP450 monooxygenase (CYP68B) that exhibits GA 20-oxidase activity. Thus, unlike in plants, 3β-hydroxylation and 20-oxidation are catalyzed by CYP450 monooxygenases in *G. fujikuroi*. Notably, GA biosynthesis genes are clustered on a single chromosome in fungi, whereas they are randomly located on chromosomes in plants. These significant differences in genes and enzymes suggest that plant and fungi evolved their GA biosynthesis pathways independently.

17.1.9 Some enzymes that participate in GA biosynthesis are feedback-regulated

The concentration of bioactive GAs in plants is under homeostatic control via feedback regulation. A link between GA biosynthesis and action was first suggested by the presence of abnormally high concentrations of GAs in certain GA-insensitive dwarf mutants, such as *Rht3* (*Triticum* spp.), *D8* (*Z. mays*), and *gai* (*Arabidopsis*). Transcript analysis in a number of plant species showed that the effect of GA concentration is targeted to late biosynthesis enzymes, GA 20-oxidase and GA 3-oxidase, and the GA inactivating enzyme, GA 2-oxidase: Expression of genes encoding GA 20-oxidase and GA 3-oxidase is highly elevated in GA-depleted plants, whereas they are down-regulated after GA application (Fig. 17.11). Such changes in transcript levels usually occur within 1-3 hours of GA application, before a growth response is discernible. By contrast, expression of genes encoding GA 2-oxidase are downregulated in GA-deficient plants, but upregulated upon GA treatment (Fig. 17.11). Thus, GA homeostasis in plants is likely to be maintained at least in part through coordinated regulation of biosynthesis and inactivation genes.

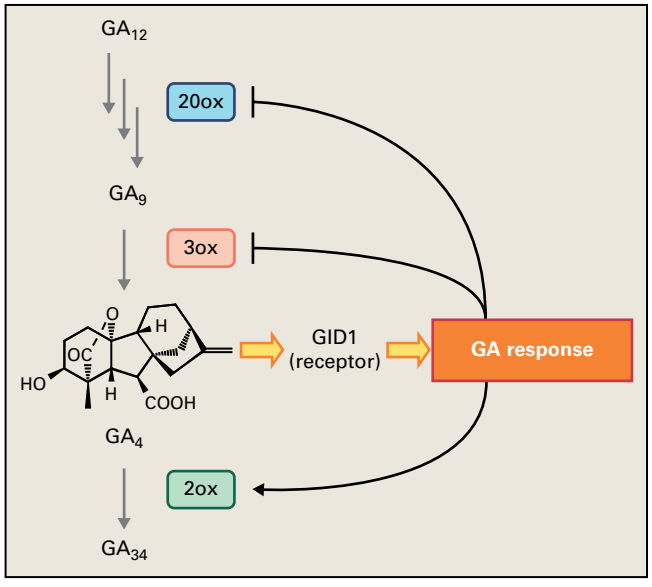


FIGURE 17.11 *Feedback regulation of GA biosynthesis and inactivation pathways. T-bars and black arrow depict negative and positive regulation, respectively. Gray arrows indicate metabolic conversions. 20ox, GA 20-oxidase; 3ox, GA 3-oxidase; 2ox, GA 2-oxidase.*

17.1.10 GA mediates light-induced germination of lettuce seeds

Evidence suggests that in some cases, bioactive GAs function as key mediators between perception of environmental signals and the resulting growth responses. Seed germination can be controlled by light in plants such as *Lactuca sativa* and *Arabidopsis* where the effect of light is primarily mediated by phytochrome.

A clear link between GA metabolism and phytochrome has been established in the case of red light (RL)-induced germination of photodormant Grand Rapids *L. sativa* seed. In a typical phytochrome-mediated response, RL induces germination and this effect is reversed by a subsequent treatment with far red light (FRL) (see Chapter 18). Following a pulse of RL, germination is preceded by elevated GA 3-oxidase expression and an increase in the GA_1 content (Fig. 17.12). When RL treatment is followed by a pulse of FRL germination is not induced, the GA_1 pool size does not increase, and GA 3-oxidase transcription remains unaltered (Fig. 17.12). Germination in darkness occurs only after treatment with GA.

The amounts of the GA_1 precursors GA_{19} and GA_{20} are not affected by RL and FRL treatments (Fig. 17.12). Whether RL and FRL control the turnover rates for these compounds is unclear. Of the two GA 20-oxidase genes cloned from *L. sativa* one is light regulated, its expression repressed by RL and enhanced by FRL, whereas the other is light-independent. Under all light regimes, however, *L. sativa* seeds contain far more GA_{20} than GA_1, so GA 20-oxidase activity and the rate of GA_{20} synthesis do not limit the amount of substrate available for GA_1 production (Fig. 17.12). These results together indicate that RL-inducible GA 3-oxidase gene expression and the increase in GA_1 concentration plays a critical role in regulating seed germination in *L. sativa*.

17.1.11 Mutations in the GA pathway led to major advances in agriculture

In the 1960s, the introduction of semi-dwarf cultivars of cereal crops, including *O. sativa* and *Triticum* spp., in combination with increased fertilizer use, led to a dramatic increase in food production worldwide. The impact of these advances in agriculture was termed the "green revolution". The major semi-dwarfing gene of *O. sativa, sd-1*, originally derived from the Chinese cultivar Dee-Geo-Woo-Gen, produced *O. sativa* cultivars with short, thick culms and improved lodging resistance without affecting grain quality. Since the 1960s, *sd-1* has been the predominant semi-dwarfing gene introduced into *O. sativa* cultivars and shown to encode a defective GA 20-oxidase. Because GA 20-oxidases are encoded by small gene families, members of which have redundant functions, the loss-of-function GA 20-oxidase mutants are only mildly GA-deficient (Fig. 17.13). Interestingly, in *Triticum* spp., a semi-dwarfing gene that contributed to the green revolution was defective in GA signaling. These instances highlight the important role of GAs in regulating developmental processes that are critical in agriculture.

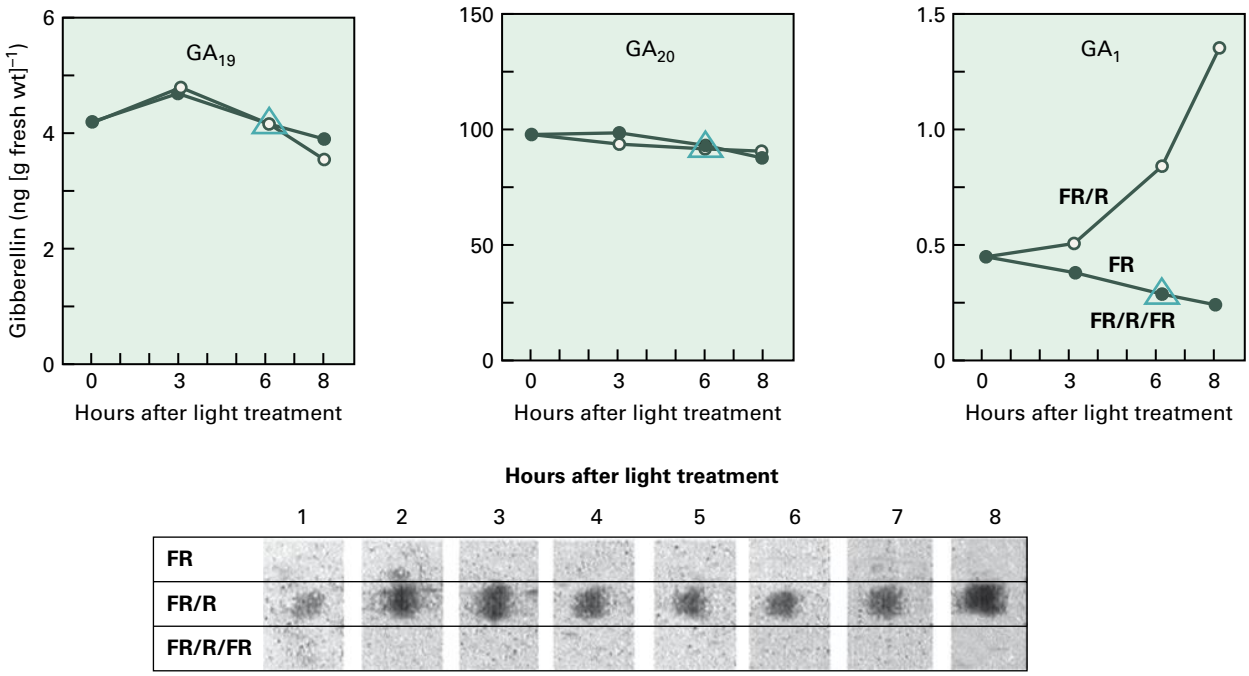


FIGURE 17.12 *Regulation of GA in Grand Rapids* L. sativa *by red (R) and far-red (FR) light. (Upper panels) Effects of R and FR light on GA levels. Note that phytochrome-mediated, R light induced seed germination is associated with increased GA_1 content. (Lower panels) Hybridization of a GA 3-oxidase cDNA clone to northern blots containing 50 μg of total RNA extracted from* L. sativa *seed after treatment with R and FR light. Source*: Electrophoretograms: Toyomasu et al. (1998). Plant Physiol. 118: 1517–1523.



FIGURE 17.13 *A semi-dwarf* O. sativa *cultivar carrying the* sd-1 *gene (dee-geo-woo-gen, left) and its tall isogenic line (woo-gen, right).*

17.2 Abscisic acid

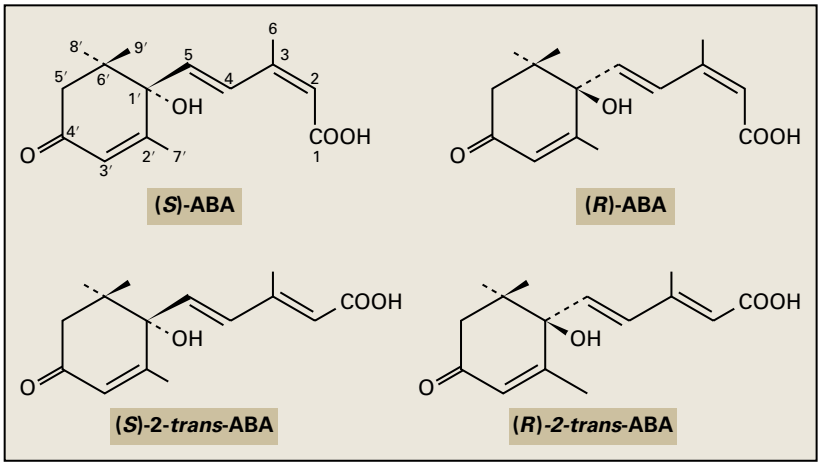
Growth-inhibiting compounds were isolated from plants in the early 1950s. Acidic compounds separated by paper chromatography were tested for their ability to promote growth in oat coleoptile, but instead these experiments detected compounds that inhibited coleoptile elongation, referred to as the β-inhibitor complex. Subsequent investigations correlated high β-inhibitor levels with suppression of *Solanum tuberosum* tuber sprouting, abortion of *Lupinus arboreus* pods, and bud dormancy in deciduous trees, such as *Acer pseudoplatanus* and *Betula pubescens*. In the early 1960s, US scientists isolated an abscission-accelerating compound called "abscisin II" from young *Gossypium hirsutum* fruits and simultaneously researchers in the UK isolated a dormancy-inducing factor called "dormin." The structure of abscisin II, later called **abscisic acid** (ABA), was determined in 1965 and dormin was subsequently shown to be ABA.

ABA has a single chiral center at C-1′. Only the (*S*)-enantiomer occurs in nature (Fig. 17.14). In contrast, synthetic ABA is a racemic mixture although stereospecific synthesis of both (*S*)-ABA and (*R*)-ABA have been reported. The 2-*cis* double bond of both enantiomers is isomerized by light to the 2-*trans* isomers, (*S*)-2-*trans*-ABA and (*R*)-2-*trans*-ABA (Fig. 17.14). For convenience, the term ABA hereafter will refer to the naturally occurring (*S*)-enantiomer.

17.2.1 Contrary to its name, ABA does not induce abscission

As its name indicates, ABA was originally thought to induce abscission, however, abscission is regulated by ethylene rather than ABA. Moreover, increased internal concentrations of ABA are unlikely to impose dormancy of *S. tuberosum* tubers or

FIGURE 17.14 *Structures of ABA enantiomers. (S)-ABA is naturally occurring form.*



resting buds of deciduous trees. Studies with ABA-deficient mutants of *Z. mays* have provided no support for conjecture that asymmetric distribution of ABA is involved in the negative geotropic response of roots. Accumulation of ABA during seed development, however, has been associated with maturation of the seed, development of desiccation tolerance, and suppression of vivipary (Fig. 17.15). Certain types of seed dormancy are linked to high concentrations of ABA, and rapid increases in ABA lead to water stress-induced closure of stomata (Fig. 17.16).



FIGURE 17.15 *Precocious germination (vivipary) of immature* Z. mays *seeds homozygous for* vp1. *The color-less* vp1 *kernels lack anthocyanins in the aleurone layer, and germinate before maturity because of ABA insensitivity. The seed is viable if transplanted directly from immature ears.*
Source: S. McCormick, University of California, Berkeley; previously unpublished.

17.2.2 Many fungi, including fungal pathogens of the genera *Cercospora* and *Botrytis*, synthesize ABA from farnesyl diphosphate

Although ABA is a relatively simple C_{15} compound, its biosynthetic pathway proved difficult to define—in part, because of poor incorporation of label from putative precursors, even in water-stressed leaves that were synthesizing ABA rapidly. By the early 1970s, two pathways leading to ABA had been proposed. The "direct C_{15}" route envisaged ABA production from the C_{15} precursor farnesyl diphosphate, while the "indirect C_{40}" route postulated oxidative cleavage of a putative C_{40} intermediate, such as violaxanthin, to yield a C_{15} intermediate of ABA (Fig. 17.17; also see Fig. 17.6).

Although the first pathway was initially favored, evidence for its operation was scant. Suggestions that ABA might originate from a xanthophyll were based on reports that exposure to light or lipoxygenase could convert violaxanthin to xanthoxin, a C_{15} compound similar in structure to ABA. Xanthoxin is present in plant tissues in trace quantities, and metabolism of [^{14}C]xanthoxin to ABA was demonstrated in tomato and bean (*Phaseolus* sp.) plants. Nevertheless, conclusive evidence that endogenous ABA originated from xanthoxin was lacking, and it remained to be established whether xanthoxin was formed in vivo from a C_{40} precursor or more directly from farnesyl diphosphate (Fig. 17.17).

In 1977, investigators discovered that the plant pathogen *Cercospora rosicola* produced large amounts of ABA, well in excess of the levels found in plants. In a simple synthetic liquid medium, *C. rosicola* cultures grown for 20 days accumulate up to 30 mg of ABA per liter. Unlike plants, the fungus incorporated labeled acetate, farnesol, and other intermediates into ABA and 1′-deoxyABA. When fed to *C. rosicola*, [^{14}C] 1′-deoxyABA was metabolized to ABA, indicating that 1′-hydroxylation is the final step in the fungal ABA biosynthesis pathway. Figure 17.18 illustrates possible biosynthesis pathways for ABA in fungi. Note that the pathway may be slightly different among species and genera. Nonetheless, it is evident that a direct C_{15} ABA biosynthesis pathway operates in fungi.

17.2.3 Gas chromatography–mass spectrometry showed that plants synthesize ABA from a C_{40} precursor

Experiments with mutants and with inhibitors of carotene synthesis were keys to understanding ABA biosynthesis. Carotenoid-deficient *Z. mays* mutants, for instance, had reduced ABA content and ABA content was depleted in wild-type *H. vulgare* and *Z. mays* after treatment with fluridone,

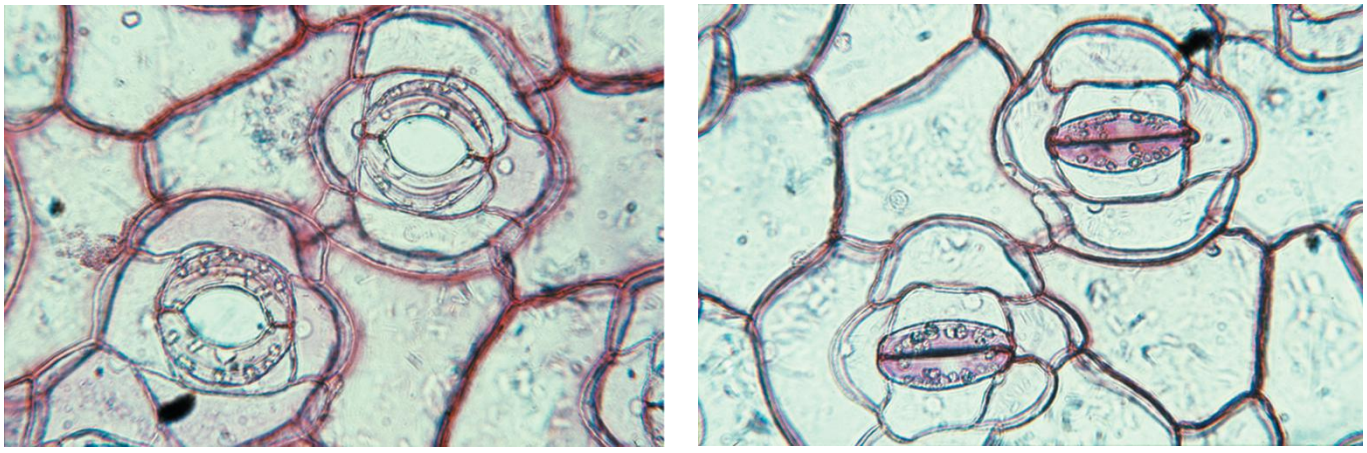


FIGURE 17.16 *ABA-induced stomatal closure. Epidermal strips of* Commelina communis *L. incubated in buffer (10 mM Pipes, pH 6.8) containing 50 mM KCl and supplied with CO_2-free air. The stomata are open after two to three hours (A). When transferred to the same solution plus 10 μM ABA, the pores close within 10 to 30 minutes (B).*
Source: J. Weyers, University of Dundee, UK; previously unpublished.

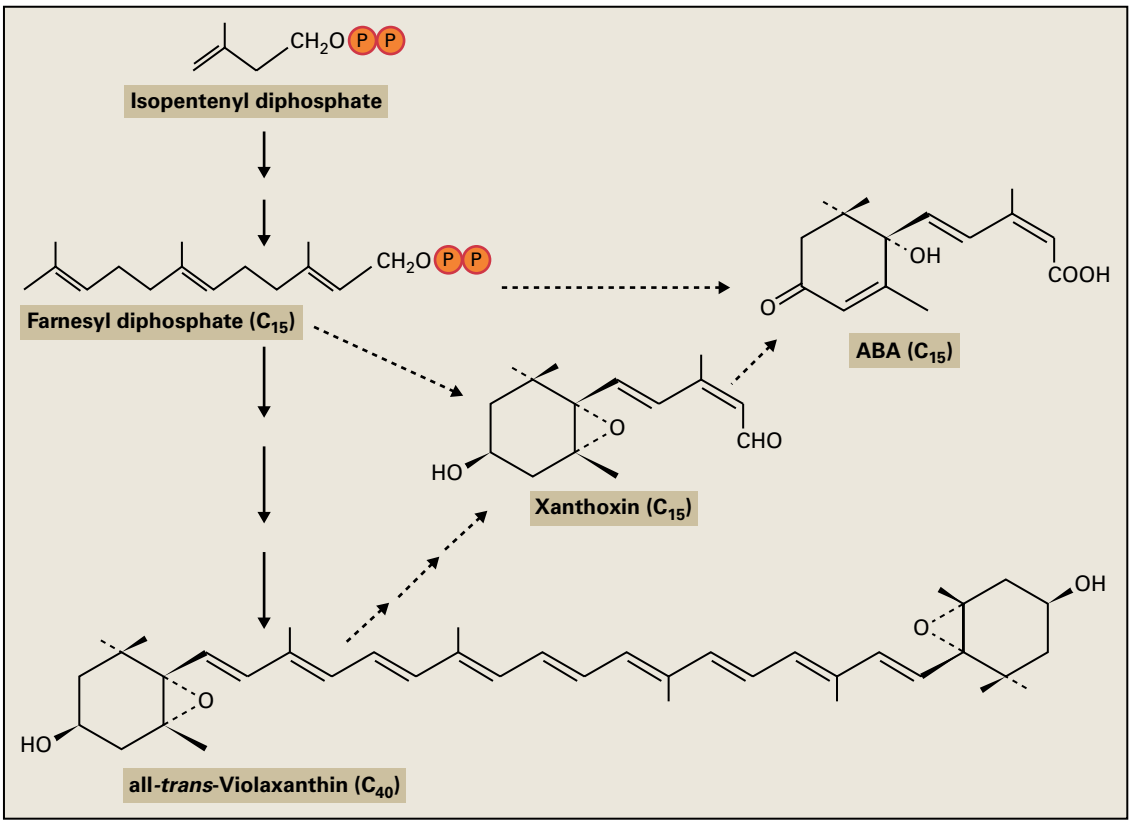


FIGURE 17.17 *Summary of two possible ABA biosynthetic routes. In the direct C_{15} pathway, farnesyl diphosphate is modified to yield ABA. Alternatively, in the indirect C_{40} pathway, a carotenoid, 9-*cis*-violaxanthin, is cleaved to form a C_{15} ABA precursor, xanthoxin.*

which inhibits β-carotene synthesis by blocking the conversion of phytoene to phytofluene (see Fig. 17.19). Firm evidence that C_{40} xanthophylls are intermediates in ABA biosynthesis was obtained in 1984. Water-stressed *P. vulgaris* and *Xanthium* leaves were incubated in $^{18}O_2$, reasoning that if 1′-deoxy-ABA were the immediate precursor of ABA in plants, as it is in *C. rosicola*, one ^{18}O atom would be associated with the hydroxyl group incorporated into ABA ring at the 1′-position (Fig. 17.20A). Gas chromatography (GC) was used to separate the $^{18}O_2$-labeled metabolites, which were then characterized by mass spectrometry (MS). (See Chapter 2, Box 2.2, for a discussion of analytical techniques that utilize MS.) GC-MS revealed that no ^{18}O was incorporated into the ABA ring. Instead, one labeled atom appeared in the

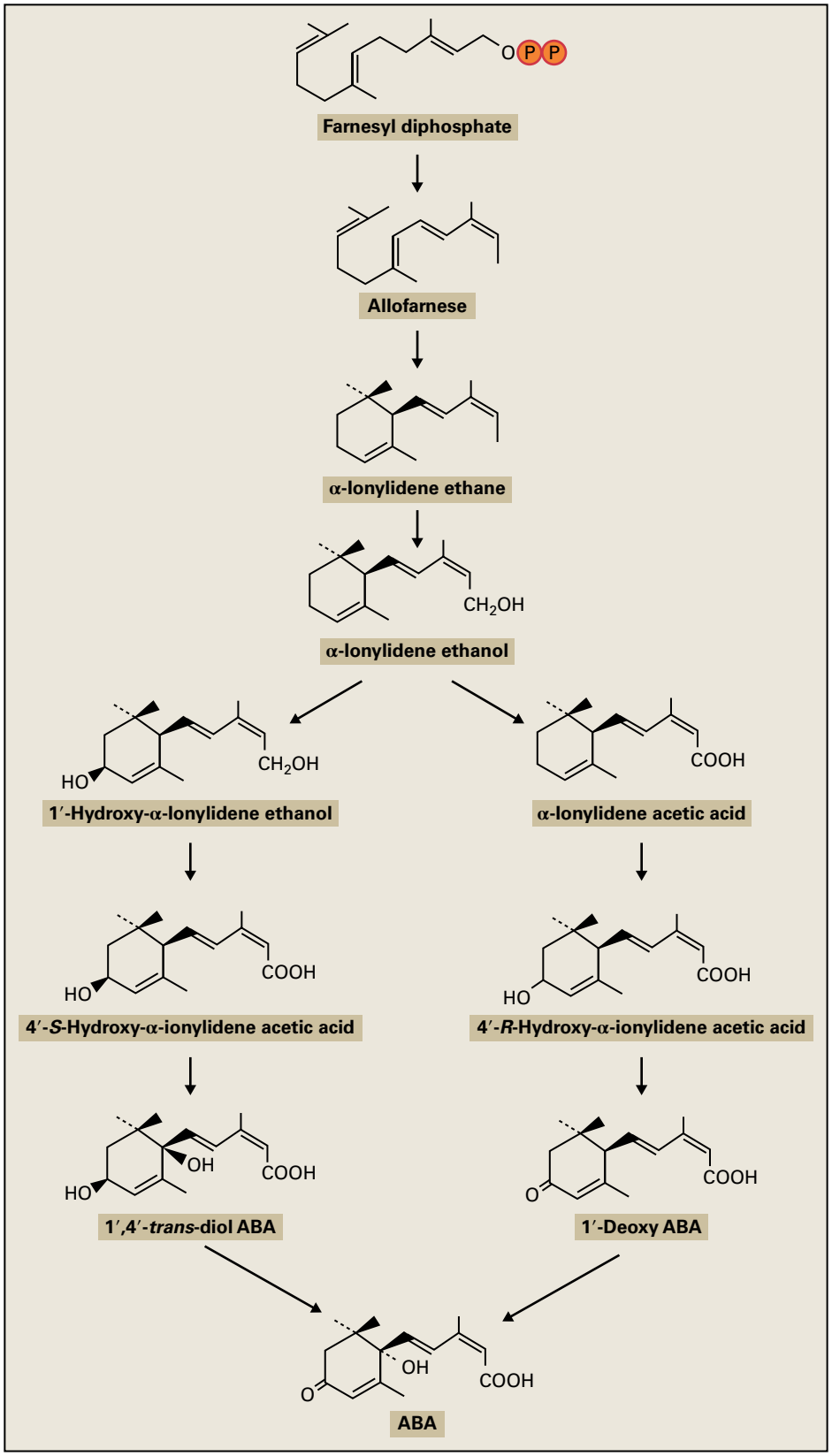


FIGURE 17.18 *Possible fungal C_{15} ABA biosynthesis pathways.*

side chain carboxyl group, demonstrating that 1′-deoxy-ABA was not the immediate ABA precursor in water-stressed leaves. These results indicated that ABA was synthesized from a preformed precursor with oxygen atoms at the 1′ and 4′ positions. This was consistent with a C_{40} pathway to ABA, with $^{18}O_2$ cleaving violaxanthin to form xanthoxin labeled at the 1-CHO group, followed by oxidation of the labeled xanthoxin to yield ABA with one ^{18}O atom in the carboxyl group (Fig. 17.20B).

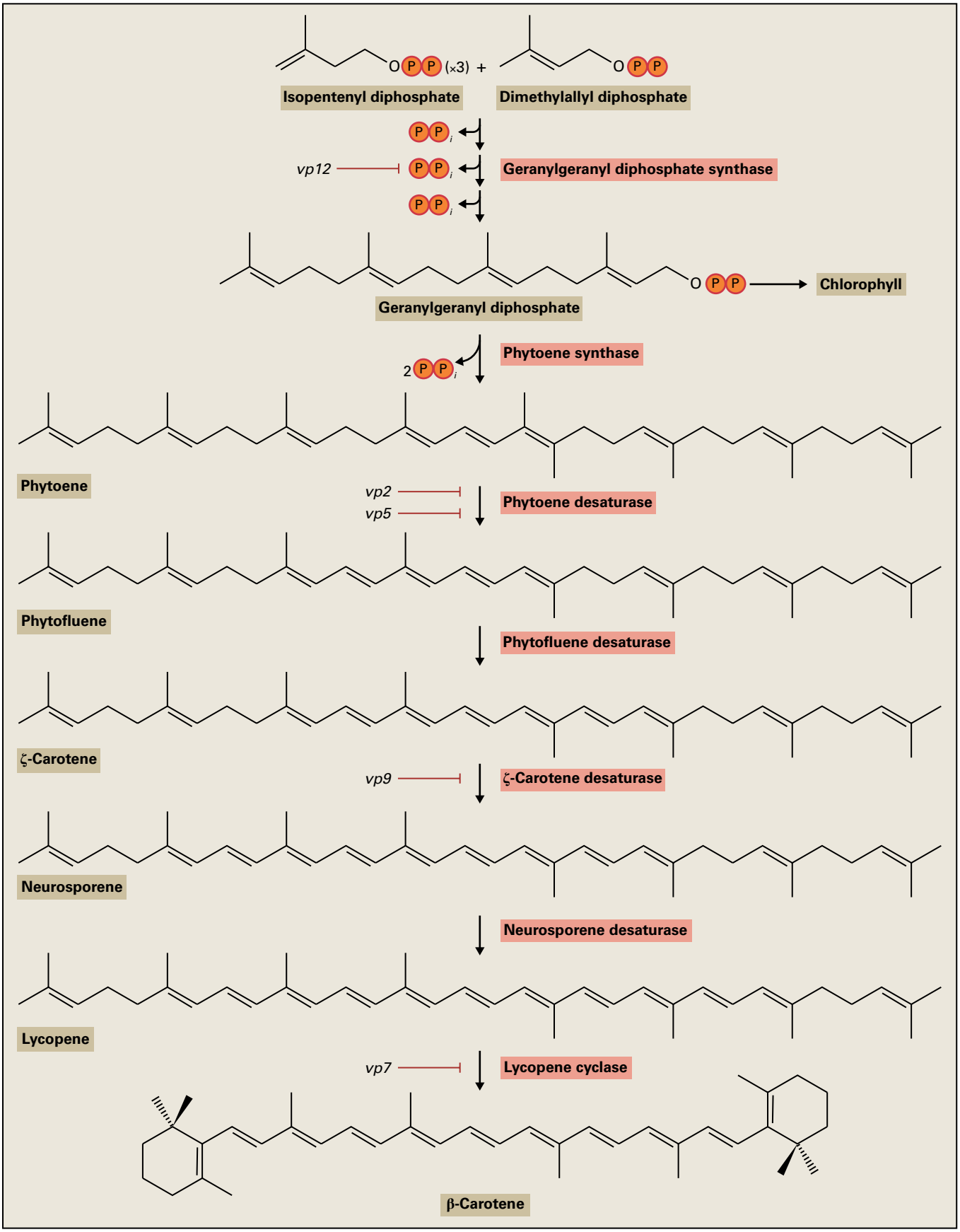


FIGURE 17.19 *Early stages in the indirect C_{40} ABA biosynthesis pathway: production of geranylgeranyl diphosphate (GGDP) and synthesis of β-carotene. Enzymes deficient in* Z. mays vp *mutants are indicated. The chemical inhibitors fluridone and norflorazon block conversion of phytoene to phytofluene (not shown).*

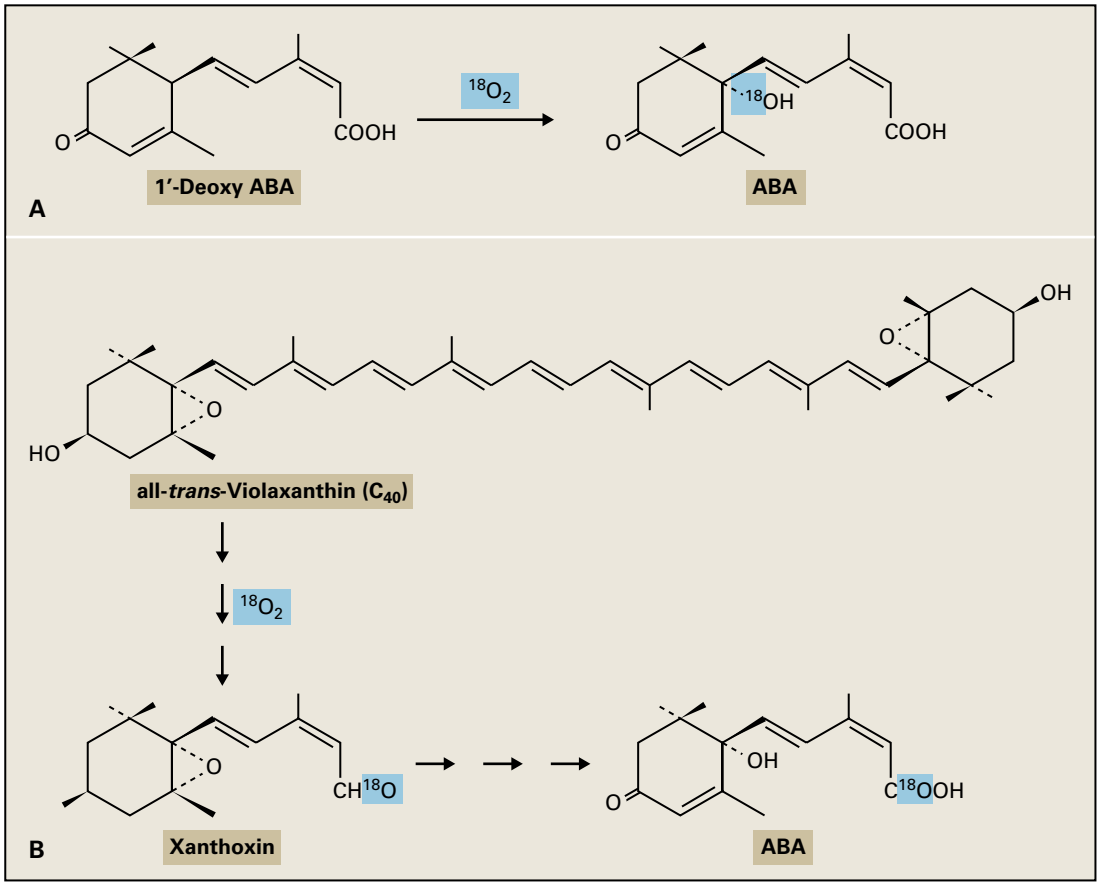


FIGURE 17.20 *Isotopic labeling experiments confirmed the existence of an indirect C_{40} plant ABA biosynthetic pathway. GC-MS revealed that ABA synthesized by plant tissues in the presence of $^{18}O_2$ was not labeled at the 1′-hydroxyl group, as would be expected if ABA were generated directly from 1′-deoxy-ABA (A). However, the appearance of label in the ABA carboxyl group was consistent with oxidative cleavage of all-*trans*-violaxanthin and subsequent conversion of xanthoxin to ABA (B).*

17.2.4 ABA synthesis is regulated by a cleavage reaction that generates the first C_{15} intermediate

Many ABA-deficient viviparous (*vp*) mutants of *Z. mays* are blocked at various points in the terpenoid and carotenoid biosynthesis pathways (see Fig. 17.19). GGDP synthase, a key enzyme in the terpenoid pathway, catalyzes the three successive condensations with isopentenyl diphosphate that convert dimethylallyl diphosphate to the C_{20} compound GGDP. As a consequence of GGDP deficiency, seedlings of the *vp12* mutant have low chlorophyll content and reduced capacity for synthesis of carotenoids and ABA. Like the chemical inhibitor fluridone, the *vp2* and *vp5* mutations block the conversion of phytoene to phytofluene. Available evidence implies that the *vp9* mutant cannot synthesize neurosporene from ζ-carotene; the *vp7* lesion restricts the conversion of lycopene to β-carotene.

Following the conversion of β-carotene to zeaxanthin, two epoxidation reactions catalyzed by zeaxanthin epoxidase convert zeaxanthin to all-*trans*-violaxanthin via antheraxanthin (Fig. 17.21). Both epoxidation steps are blocked in the ABA-deficient *aba1* mutant of *Arabidopsis* and the *aba2* mutant of *Nicotiana plumbaginifolia*. The *ABA2* gene encodes a chloroplast-imported 72.5-kDa protein that shares sequence similarities with bacterial oxidases. ABA2 catalyzes the two-step conversion of zeaxanthin to all-*trans*-violaxanthin in vitro. *ABA1* was shown to be orthologous to *ABA2*.

All-*trans*-violaxanthin is converted to 9′-*cis*-neoxanthin or 9-*cis*-violaxanthin. In *Arabidopsis* ABA-deficient *aba4* mutants, endogenous levels of 9′-*cis*-neoxanthin and all-*trans*-neoxanthin are reduced, whereas those of all-*trans*-violaxanthin and 9-*cis*-violaxanthin are increased. *ABA4* encodes a protein with a predicted chloroplast-targeting peptide. Mature ABA4 protein has a predicted molecular mass of 17.0 kDa and four transmembrane domains. ABA4 is thought to function as a neoxanthin synthase or as part of components required for neoxanthin synthesis. To date, no mutant defective in isomerization of all-*trans*-violaxanthin or all-*trans*-neoxanthin has been isolated.

The first committed step in the ABA biosynthesis pathway, oxidative cleavage of 9′-*cis*-neoxanthin and/or 9-*cis*-violaxanthin, yields the first C_{15} intermediate, xanthoxin. Studies with *vp14*, an ABA-deficient viviparous *Z. mays* mutant generated by transposon tagging, have successfully cloned the gene encoding 9-*cis*-epoxycarotenoid dioxygenase that catalyzes this conversion. The derived amino acid sequence of VP14 is

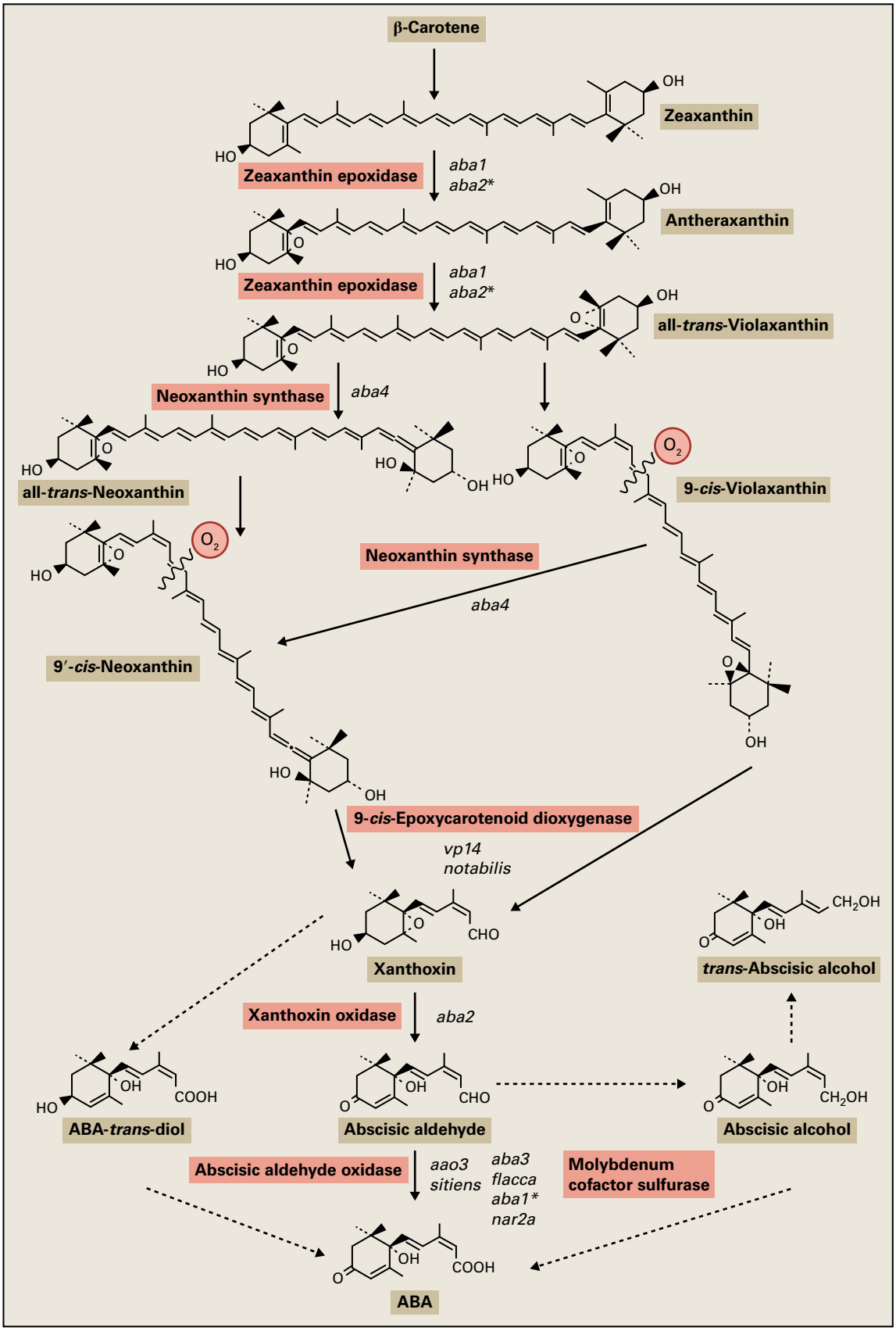


FIGURE 17.21 *Later stages in the indirect C_{40} ABA biosynthesis pathway: β-carotene to ABA. Biosynthetic steps blocked in the following mutants are indicated.* Arabidopsis *mutants:* aao3, aba1, aba2, aba3, aba4; H. vulgare: nar2a; S. lycopersicum *mutants: flacca, notabilis, sitiens; N. plumbaginifolia mutants: aba1*, aba2*; Z. mays mutant: vp14*

similar to sequences of bacterial lignostilbene dioxygenases, which catalyze a reaction resembling the oxidative cleavage of 9′-*cis*-neoxanthin. Recombinant VP14 protein catalyzes the in vitro conversion of both 9-*cis*-violaxanthin and 9′-*cis*-neoxanthin to xanthoxin, while the corresponding *trans* isomers are not cleaved. Production of xanthoxin from 9-*cis*-epoxycarotenoids is also blocked in the wilty *S. lycopersicum* mutant *notabilis*. 9-*cis*-epoxycarotenoid dioxygenase is encoded by a multigene family. In *Arabidopsis*, a 9-*cis*-epoxycarotenoid dioxygenase encoded by *AtNCED3* gene is responsible for ABA production upon water stress, while *AtNCED6* and *AtNCED9* gene products are involved in ABA production in seeds. This conversion appears to be a rate-limiting step in ABA biosynthesis; ABA accumulation in response to water stress correlates well with 9-*cis*-epoxycarotenoid dioxygenase mRNA and protein levels, and overexpression of this gene resulted in ABA overproduction. Characterization of this control point is likely to provide intriguing insights into regulation of seed dormancy, drought resistance, and cold hardening.

The penultimate step of the ABA biosynthesis pathway converts xanthoxin to abscisic aldehyde. This reaction involves oxidation of the 4′-hydroxyl group to a ketone, desaturation of the 2′-3′ double bond and opening of the 1′-2′ epoxide ring. No intermediates have been detected. Chemical oxidation of the 4′-hydroxyl group facilitates quantitative conversion of xanthoxin to abscisic aldehyde, suggesting that the reaction in vivo may result from a single enzymatic step and subsequent rearrangements. The *Arabidopsis aba2* mutant was shown to have a defect in this reaction. The *ABA2* gene encodes a protein, xanthoxin oxidase, that belongs to a family of short-chain dehydrogenase/reductases. Recombinant ABA2 protein catalyzes the conversion of xanthoxin to abscisic aldehyde in the presence of NAD. Oxidation of the 1-CHO group of abscisic aldehyde, catalyzed by abscisic aldehyde oxidase, leads to formation of ABA (Fig. 17.21). There are many mutants defective in conversion of abscisic aldehyde to ABA, including *sitiens* and *flacca* in *S. lycopersicum*, *nar2a* in *H. vulgare, aba3* and *aao3* in *Arabidopsis,* and *aba1* in *N. plumbaginifolia*. *flacca*, *aba3* and *aba1* mutants lack the activities of xanthine dehydrogenase in addition to that of aldehyde oxidase.

FLACCA and *ABA3* encode Mo cofactor sulfurase, which catalyzes the final step of Mo cofactor synthesis required for aldehyde oxidase and xanthine dehydrogenase activities (Fig. 17.21). The *nar2a* mutant has a defect in nitrate reductase activity in addition to aldehyde oxidase and xanthine dehydrogenase activities, indicating that the corresponding gene encodes an enzyme responsible for an earlier step of Mo cofactor synthesis. The *Z. mays* viviparous mutants *vp10*/*vp13* and *vp15* are also impaired in earlier steps of Mo cofactor synthesis. On the other hand, the *sitiens* and *aao3* mutants are impaired specifically in abscisic aldehyde oxidase activity. The *AAO3* gene encodes abscisic aldehyde oxidase that functions as a dimer of the 147-kDa protein containing non-heme iron, FAD, and Mo as prosthetic group. The activity to produce ABA from xanthoxin via abscisic aldehyde is not increased following the onset of water stress, albeit the expression of *AAO3* and *ABA3* is induced in this condition. These two final conversions do not appear to limit the rate of ABA biosynthesis, as foliar levels of xanthoxin and abscisic aldehyde are invariably very low compared to ABA.

The *S. lycopersicum flacca* and *sitiens* mutants and *aba3* in *Arabidopsis* convert abscisic aldehyde to abscisic alcohol and accumulate *trans*-abscisic alcohol. A shunt pathway from abscisic alcohol to ABA, representing a minor source of ABA in most plants, allows these mutants to synthesize low amounts of ABA. Wild-type *S. lycopersicum* and the *flacca* and *sitiens* mutants all contain ABA-1′,4′-*trans*-diol and convert [^{2}H]ABA-1′,4′-*trans*-diol to ABA (Fig. 17.21). However, the origins of the diol have not been established, and its relationship to ABA in vivo remains to be clarified.

17.2.5 ABA is metabolized to several compounds, including phaseic acid, dihydrophaseic acid, and glucose conjugates

ABA metabolism is summarized in Figure 17.22. The main route involves hydroxylation of the 8′ carbon, spontaneous rearrangement of the resulting 8′-hydroxy-ABA to form phaseic acid (PA), and reduction to dihydrophaseic acid and *epi*-dihydrophaseic acid. Dihydrophaseic acid undergoes conjugation at the 4′-position to form dihydrophaseic acid-4′-*O*-*β*-glucoside. Because of its rapid conversion to PA, 8′-hydroxy-ABA has rarely been isolated, but its formation has been inferred by the presence of the conjugate 8′-*O*-(3-hydroxy-3-methylglutaryl)-8′-hydroxyABA. The alternative routes in ABA metabolism involve conversion to 7′- and 9′-hydroxy-ABA, as well as conjugation to form ABA-β-glucosyl ester and ABA-1′-*O*-glucoside. *P. sativum* seedlings convert ABA to ABA-1′,4′-*trans*-diol; in *S. lycopersicum*, however, the diol is an ABA precursor rather than a catabolite.

ABA 8′-hydroxylase is a membrane bound CYP450 monooxygenase classified as *CYP707A*. Single or multiple mutants defective in these genes contain elevated endogenous ABA levels, and exhibit enhanced stress resistance and increased seed dormancy. Conversely, constitutive expression of a *CYP707A* gene results in reduced ABA content, demonstrating that 8′-hydroxylation is the predominant pathway for ABA catabolism.

Numerous bioassays have indicated that the biological activity of ABA is dependent on the presence of a free 1-carboxyl group, a 2-*cis*,4-*trans*-pentadienoic side chain, a 4′-keto group, and a 2′-3′ double bond. Except for 8′-*O*-(3-hydroxy-3-methylglutaryl)-8′-hydroxyABA, ABA metabolites and conjugates formed from ABA do not possess all of these features and are probably deactivation products (Fig. 17.22). In theory, ABA β-glucosyl ester and ABA-1′-*O*-β-glucoside could act as storage products that can be hydrolyzed to release free ABA. Genes encoding enzymes that catalyze β-glucosidation of ABA and hydrolysis of ABA β-glucosyl ester in vitro have been isolated but their physiological importance remains to be determined.

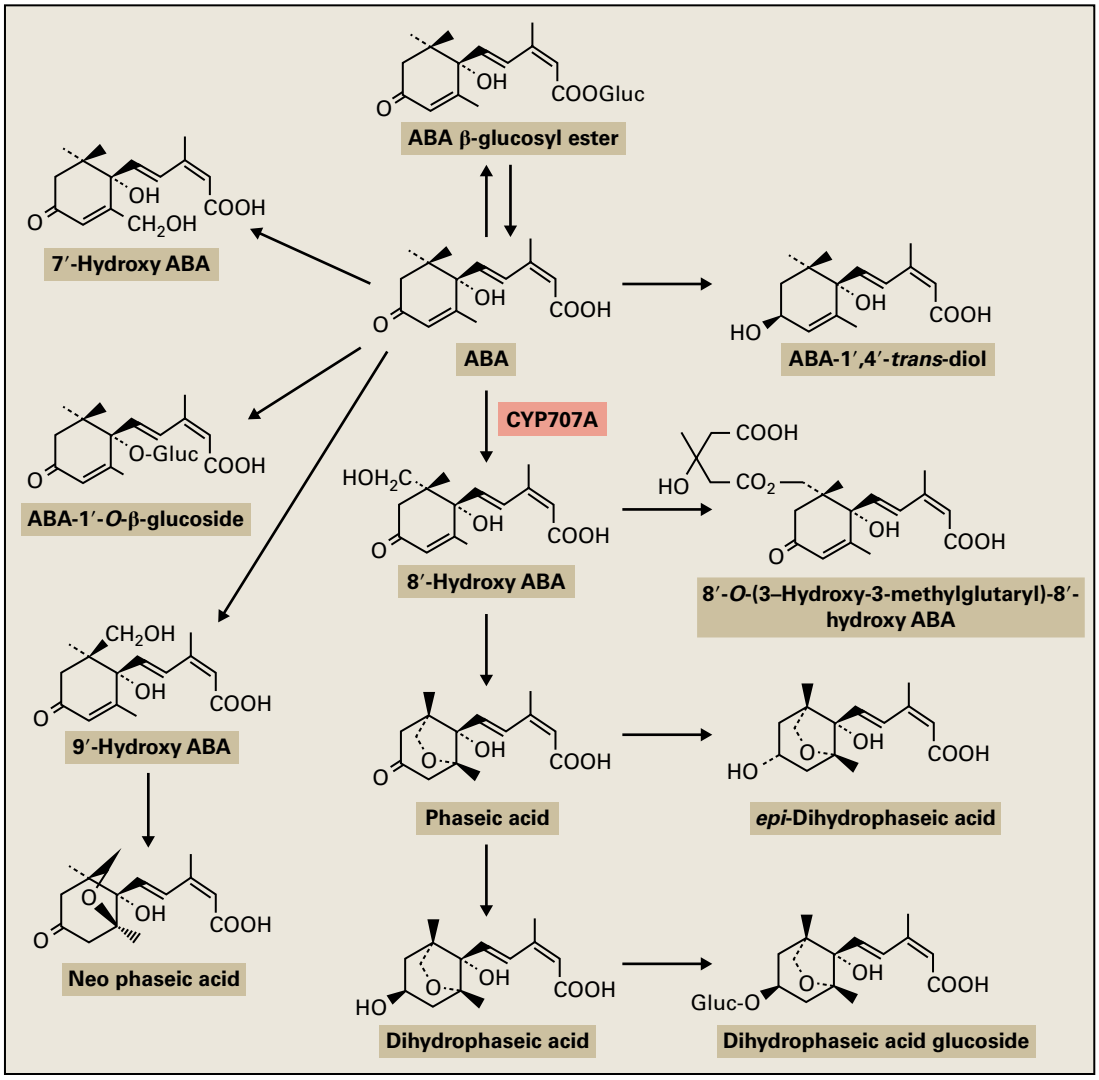


FIGURE 17.22 *ABA metabolism pathways. The major route proceeds by way of 8′-hydroxy ABA, which is rapidly converted to phaseic acid; this in turn, is reduced to* epi*-dihydrophaseic acid and dihydrophaseic acid. Dihydrophaseic acid undergoes conjugation to yield dihydrophaseic acid -4′-O-glucoside. ABA can also be conjugated, forming ABA β-glucosyl ester and ABA-1′-O-β-glucoside.*

17.3 Cytokinins

The discovery of CKs has its roots in the 1930s quest for chemical factors that would allow the culturing of plant tissues in synthetic media. In the 1950s, a substance that strongly stimulated cell proliferation in *Nicotiana tabacum* tissue culture was first purified and crystallized from autoclaved herring sperm DNA extracts. This growth-stimulating compound N^6-furfuryl aminopurine was named kinetin (Fig. 17.23). Kinetin has not been found in living plants and is believed to be an artificial by-product of DNA breakdown. Kinetin, in combination with auxin, was found to promote the initiation and maintenance of cell division in cultured *N. tabacum* parenchyma. A naturally occurring kinetin-like substance was first isolated from immature *Z. mays* endosperm in the early 1960s and named zeatin (*trans*-zeatin, tZ; Fig. 17.23). Usage of the term "cytokinins" for kinetin-like compounds was defined

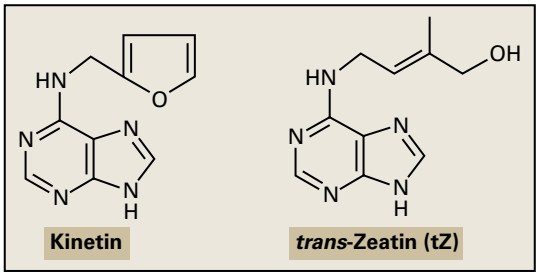


FIGURE 17.23 *CK structures. The first CK identified was the synthetic compound Kinetin. The first plant CK isolated was* trans*-Zeatin.*

as a "generic name for substances which promote cell division and exert other growth regulatory functions in the same manner as kinetin." Endogenous plant CKs have been isolated, all of which are adenines that have a substituted N^6 terminus on either an isoprene-derived side chain (greater abundance), or an aromatic derivative side chain (less abundant).



FIGURE 17.24 Arabidopsis *callus production is induced by auxin (IBA) and CK (tZ). Callus subcultured on auxin medium produces only roots (left); but on medium containing a high ratio of CK to auxin produces shoots (right).*
Source: T. Kakimoto, Osaka University, Japan; previously unpublished.

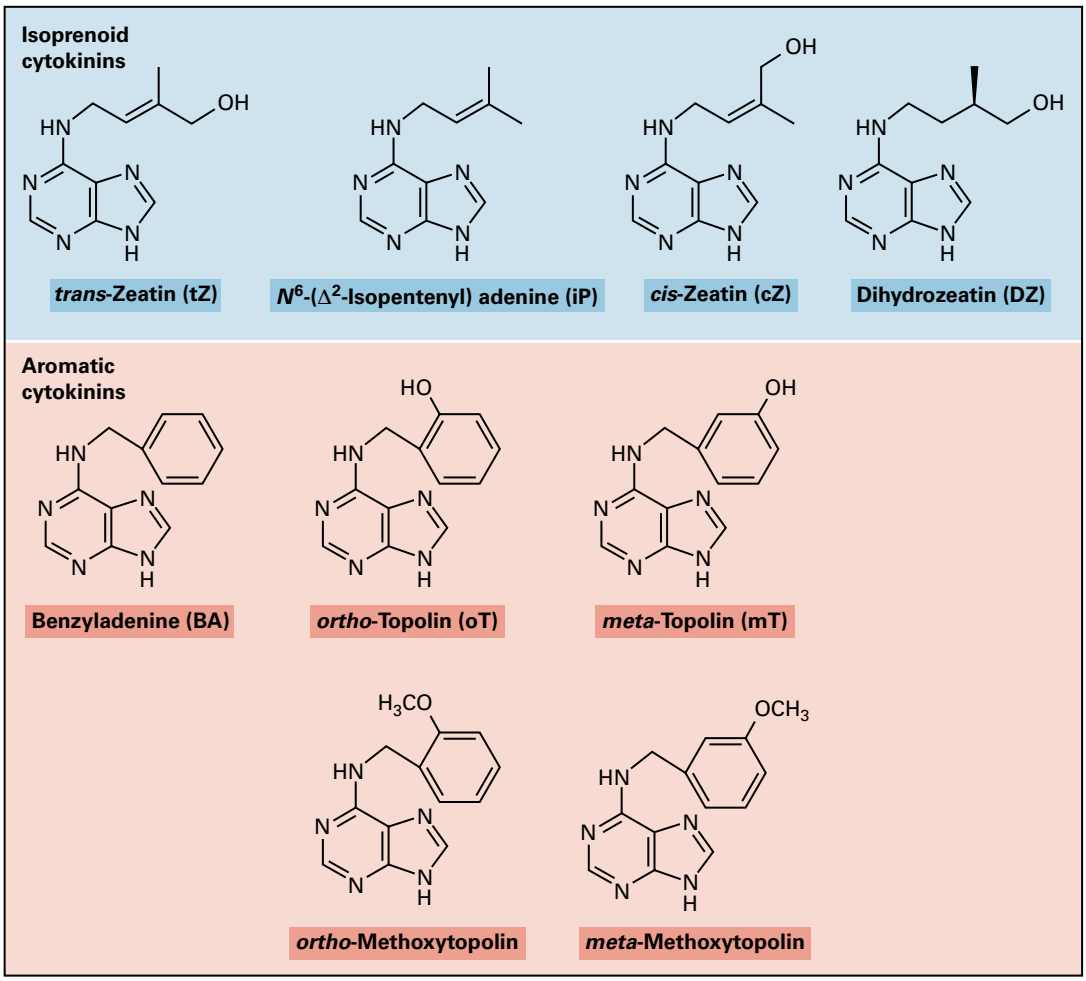


FIGURE 17.25 *Structures of naturally occurring CKs. In general, isoprenoid CKs are in greater abundance than aromatic CKs. Aromatic CKs have been described in only some plant species. Benzyladenine is found in* P. patens.

Although CKs were first identified as activators of cell proliferation, it is now known that they are involved in a wide variety of plant growth and development processes, usually in close cooperation with one or more of the other plant growth regulators. For instance, a high CK to auxin ratio promotes shoot differentiation from callus in culture, whereas auxin alone initiates root formation (Fig. 17.24), and intermediate ratios promote largely undifferentiated callus. CKs are also

involved in the regulation of apical dominance, retardation of leaf senescence, and competence of reproductive organs.

17.3.1 Structural variations occur in the side chains of CKs

Isoprenoid CKs have an isoprene-derived side chain and the common active forms include isopentenyladenine (iP; N^6-(Δ^2-isopentenyl)adenine), *trans*-zeatin (tZ), *cis*-zeatin (cZ), and dihydrozeatin (DZ) (Fig. 17.25). There are differences in their activity, abundance, and stability in vivo, but as yet there is no widely accepted view of the physiological relevance of these variants. In general, iP and tZ are active, and their derivatives are abundant, but they are susceptible to degradation by CK oxidase (CKX). cZ is thought to be less active and relatively more stable than tZ and iP because of its low affinity for CKX. cZ and its conjugates are more abundant than tZ- and iP-type CKs in *Z. mays*, *O. sativa*, chickpea (*Cicer arietinum*) and a moss (*Physcomitrella patens*). DZ appears to be biologically stable because of its resistance to CKX and is generally found in small quantities except for some legumes.

The aromatic CKs, which have aromatic derivative side chains, have been described in only a few plant species, including poplar (*Populus* × *robusta*), white lily (*Zantedeschia aethiopica*), *Arabidopsis*, and *P. patens*. Aromatic CKs are found as *ortho*-topolin and *meta*-topolin, as hydroxylated benzyladenines, and *ortho*-methoxytopolin, and *meta*-methoxytopolin (Fig. 17.25). It is not clear whether the aromatic forms are common in plants.

17.3.2 CKs are present as conjugates

CKs are present in plants as nucleoside, nucleotide, and glycosidic conjugates (Fig. 17.26), implying that there is a metabolic network for their interconversion. Glucosylation of CK occurs at the *N3, N7,* or *N9*-positions of the purine moiety to form *N*-glucosides (Fig. 17.26). In tZ, DZ, and cZ, glycosylation can occur at the hydroxyl group of the side chain to form *O*-glucosides or *O*-xylosides, with *O*-glucosylation being more common than *O*-xylosylation, found only in *Phaseolus* sp. Conjugation generally greatly reduces biological activity but increases stability. Conjugates are a storage form of CK, and as such are generally in greater abundance than their more biologically active cognate CK.

Amino acid conjugates of CK have also been isolated from some organisms. Lupinic acid, which was first found in lupine seedling, is an alanine conjugate of tZ at the *N9* position of the adenine moiety (Fig. 17.27) and is more stable but less active. In the slime mold *Dictyostelium discoideum*, discadenine (Fig. 17.27) has been found to be an inhibitor of spore germination. Lupinic acid has been found in several plant species, such as *Z. mays* and *P. sativum*, but discadenine appears to be restricted to *Dictyostelium*.

17.3.3 The initial step of isoprenoid CK biosynthesis is catalyzed by adenosine phosphate-isopentenyltransferase

The major isoprenoid CK biosynthesis step in plants is conjugation of adenine nucleotide and the prenyl-moiety of dimethylallyl diphosphate (DMAPP), catalyzed by adenosine phosphate-isopentenyltransferase (IPT) (Fig. 17.28). This reaction requires a divalent metal ion, such as Mg^{2+}. Plant IPTs predominantly use ATP or ADP rather than AMP as a prenyl-acceptor. In plants, *IPT* is encoded by a small multigene family, members of which are differentially expressed according to tissue. Expression patterns of *IPT* in *Arabidopsis* indicate that the initial step of CK biosynthesis occurs in various parts of plant body, such as phloem of roots and shoots, immature seeds and lateral root primordia. *IPT* mutants of *Arabidopsis* show severely decreased levels of iP and tZ-type CKs, suggesting that IPTs are responsible for the bulk of iP and tZ-cytokinin synthesis. The biosynthetic pathway of aromatic CKs is poorly characterized and the enzymes are yet to be cloned.

17.3.4 *trans*-Hydroxylation in tZ biosynthesis is catalyzed by a CYP450 monooxygenase

In *Arabidopsis* the *trans*-hydroxylation of the prenyl side chain in tZ biosynthesis is catalyzed by CYP450 monooxygenases CYP735A1 and CYP735A2 (Fig. 17.28). CYP735A predominantly hydroxylates iPRMP or iPRDP, rather than iPRTP, and does not hydroxylate iP or iPR. Expression of *CYP735A1* and *CYP735A2* is upregulated by CK itself and downregulated by auxin or ABA, indicating that the two hormones cooperatively and negatively regulate tZ formation by repressing *CYP735A*.

17.3.5 There are two pathways for formation of active CKs

To become biologically active, iP and tZ nucleotides are converted to a nucleobase. There are two pathways for active CK formation: a two-step pathway and a direct pathway (Fig. 17.28). In the two-step pathway, dephosphorylation from a CK nucleotide to a nucleoside is catalyzed by 5′-ribonucleotide phosphohydrolase (5′-nucleotidase), and the deribosylation step is catalyzed by adenosine nucleosidase. These enzymes have been characterized in several plant species from partially purified preparations, but corresponding genes have not been identified. In both steps, the enzymes are not specific to CK nucleotides and nucleosides, but they have a higher affinity for adenine nucleotide and adenosine than for the corresponding N^6-substituted compounds. Thus,

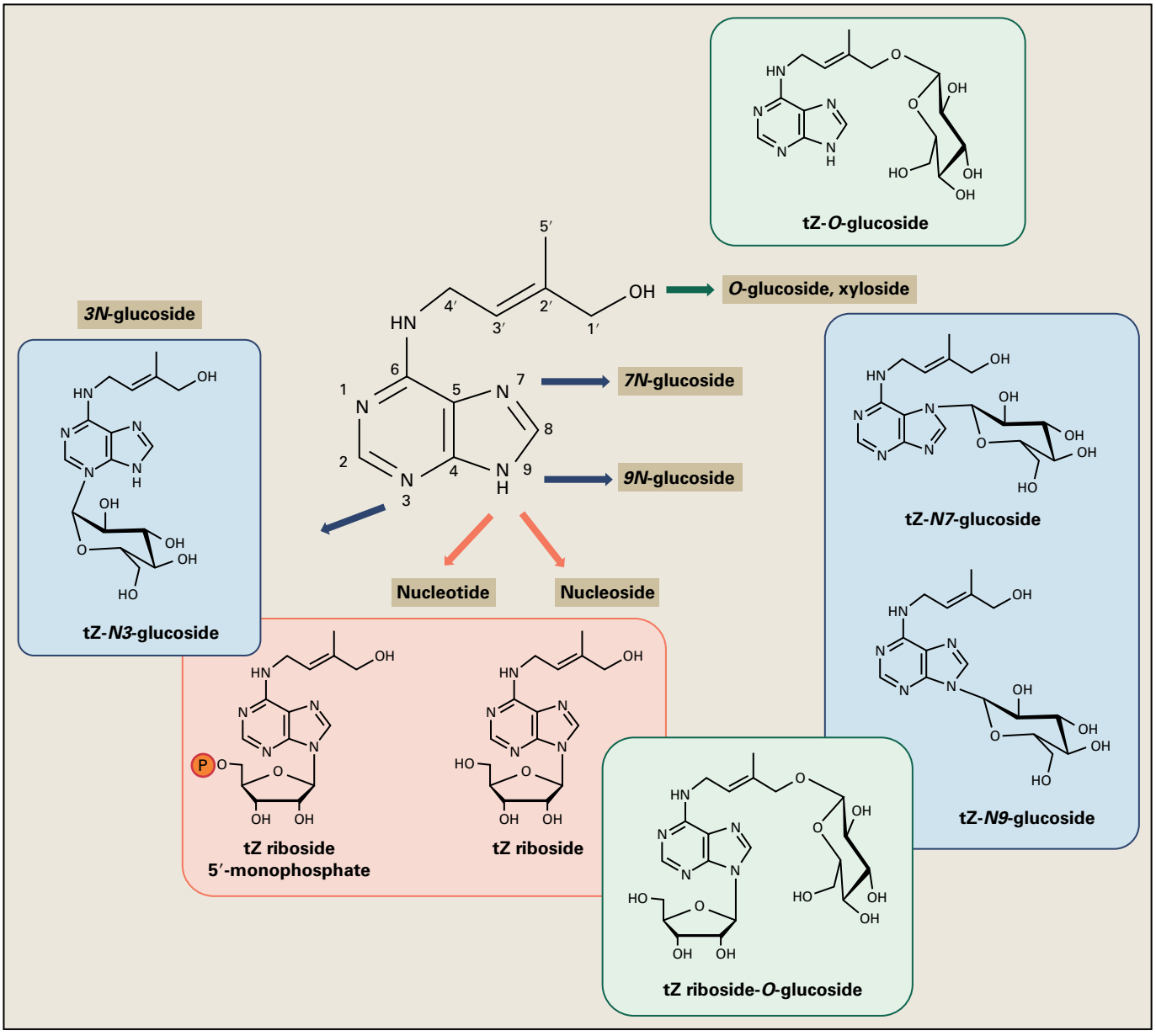


FIGURE 17.26 *Conjugates of tZ. Only representative structures are shown. Conjugation of iP, cZ, and DZ occurs in the same manner, but iP conjugates do not include* O*-glycosides because they lack a hydroxyl group at the end of the side chain.* P *represents a phosphate group.*

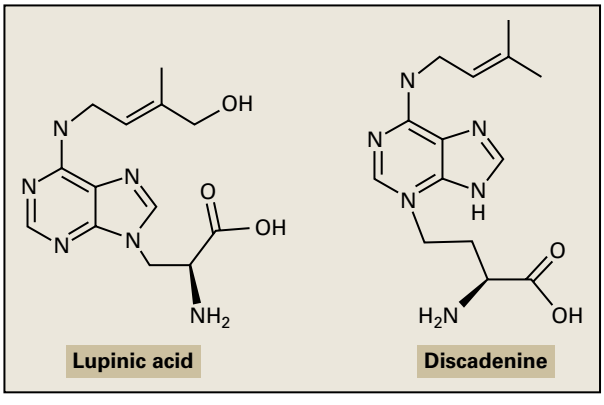


FIGURE 17.27 *Structures of amino acid CK conjugates. Discadenine is only found in slime molds.*

the two-step pathway is thought to be a part of the purine metabolic pathway.

17.3.6 LONELY GUY catalyzes the direct activation pathway

The direct pathway mediates release of a CK nucleobase from the corresponding nucleotide in a one-step reaction, which is catalyzed by CK riboside 5′-monophosphate phosphoribohydrolase (Fig. 17.28). This enzyme is defective in the *O. sativa lonely guy* (*log*) mutant that has abnormal shoot apical

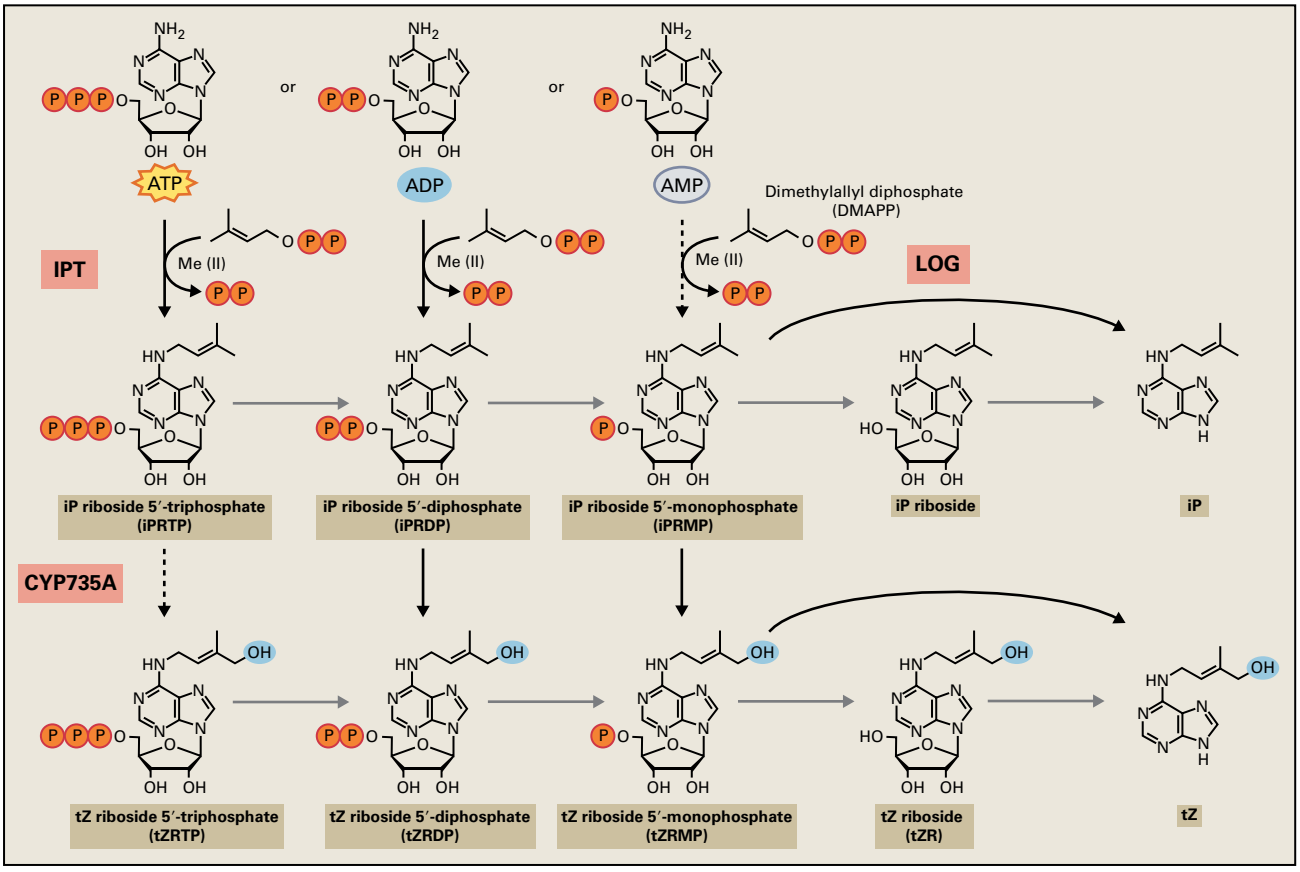


FIGURE 17.28 *Plant CK de novo biosynthesis pathway. Plant IPTs preferably utilize ATP or ADP as isoprenoid acceptors to form iPRTP and iPRDP, respectively. CYP735A preferentially utilizes iPRMP and iPRDP as substrate. Synthetic route indicated by gray arrows are not well characterized at the genetic level. For enzymes involved in the two-step pathway, see Fig. 17.33. P, phosphate group. Me (II), a divalent metal ion.*

meristems. LOG only metabolizes CK nucleotides (5′-monophosphate) and not AMP, indicating that it is a specific enzyme for CK metabolism. Similar to *IPT*, *LOG* is encoded by a small multigene family with members exhibiting distinct patterns of expression. At present, it is not clear whether there is a functional difference between the two-step pathway and the direct pathway.

17.3.7 *Agrobacterium* IPT has distinct substrate specificity

Some plant pathogenic bacteria utilize CKs to influence plant growth. *Agrobacterium tumefaciens* infects eudicots as well as some monocots and induces the formation of crown galls (Fig. 17.29) by integrating the T-DNA (Transfer-DNA) region of the Ti-plasmid into the plant nuclear genome. Ti-plasmids commonly contain an *IPT* (*Tmr*) within the T-DNA and nopaline-forming Ti-plasmids contain another *IPT* gene (*Tzs*) in a region that is not transferred to the host plant. Tmr and Tzs are structurally related to higher plant IPTs, but differ in their substrate specificity. Tmr and Tzs can utilize



FIGURE 17.29 *Three-month-old crown gall tumor on a* Rosa *spp. stem inoculated with wild-type Agrobacterium tumefaciens.*

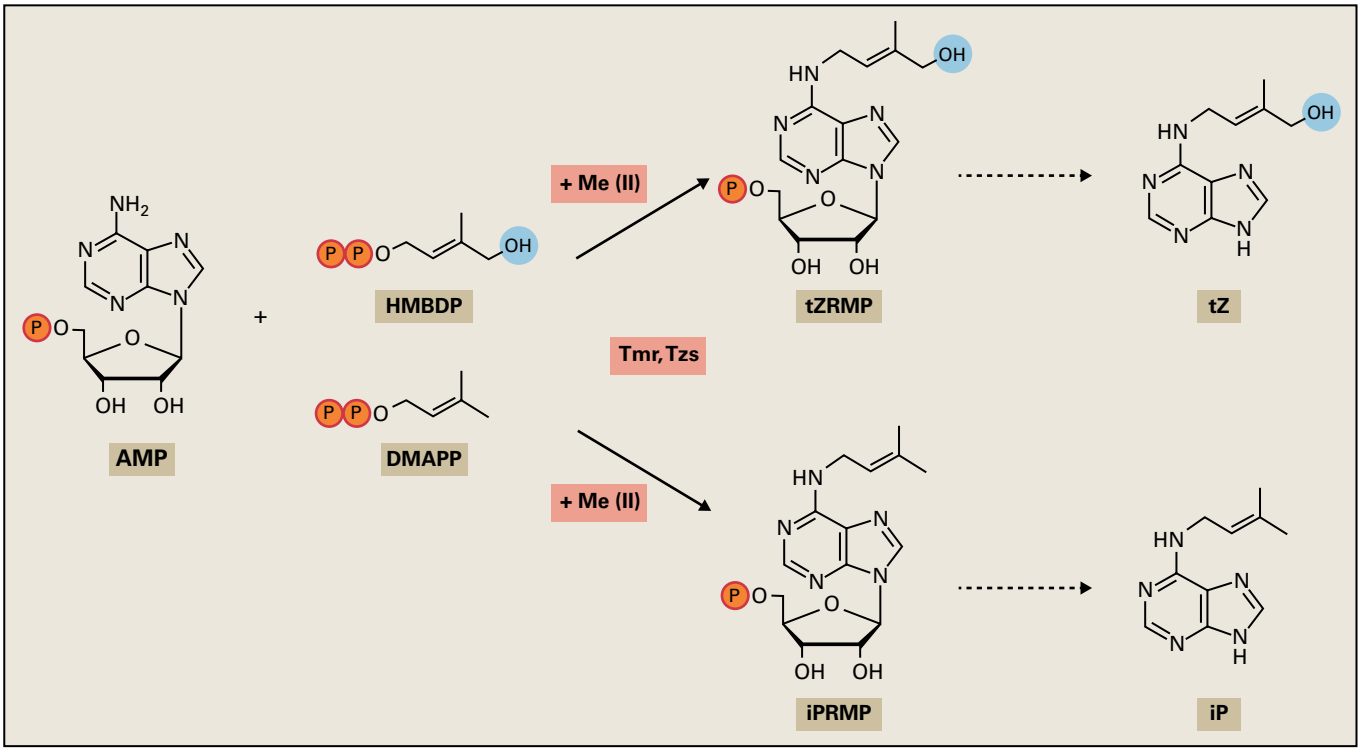


FIGURE 17.30 *CK biosynthesis pathway catalyzed by* Agrobacterium *IPT.* Agrobacterium *IPTs, Tmr and Tzs, exclusively utilize AMP as an isoprenoid acceptor and can utilize HMBDP or DMAPP as the donor. In* Agrobacterium*-infected cells, Tmr preferentially utilizes HMBDP and produces tZRMP in plastids.* P *represents a phosphate group. Me (II), divalent metal ion.*

DMAPP and 1-hydroxy-2-methyl-2-(*E*)-butenyl 4-diphosphate (HMBDP) as prenyl-donor substrates to produce iP nucleotide and tZ nucleotide, respectively, and exclusively use AMP as the prenyl acceptor (Fig. 17.30). HMBDP is a metabolic intermediate in the methylerythritol phosphate (MEP) pathway, which occurs in plastids and in many prokaryotes (see Chapter 24). *Agrobacterium* IPTs can synthesize tZ nucleotide directly in the absence of host plant CYP735A when HMBDP is the substrate.

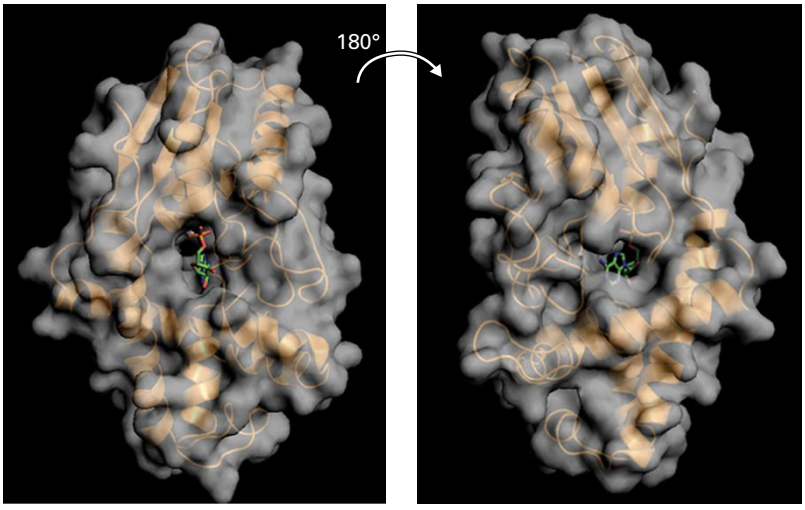
17.3.8 *Agrobacterium* IPT creates a bypass of direct tZ-type CK synthesis in host plastids

In *Agrobacterium*-infected plant cells, Tmr and Tms, encoded on the T-DNA, overproduce CK and auxin, respectively, resulting in hypertrophic and hyperplastic cell growth. Although Tmr utilizes DMAPP and HMBDP in vitro, crown galls and *Tmr*-overexpressing transgenic plants almost exclusively contain tZ-type CKs. Recent studies have demonstrated that Tmr is targeted to and functions in plastids of infected host plant cells, although it does not contain a typical transit peptide for plastid import. In plastid stroma, Tmr allows the cell to synthesize CK from HMBDP without CYP735A-mediated hydroxylation. This bypass enables *A. tumefaciens* to produce large amounts of tZ in order to induce gall formation.

After infection of olive (*Olea europaea*), oleander (*Nerium* sp.), and privet (*Ligustrum* sp.), *Pseudomonas savastanoi* produces large amounts of CKs and auxin, most of which are tZ and tZR, leading to the formation of unorganized galls. Plasmids of *Ps. savastanoi* have the *Ptz* gene, which encodes an IPT, and *Tms*. Although these genes have substantial homology to the corresponding genes in *A. tumefaciens*, *Pseudomonas* tumors involve no transfer of genetic material. So, it is not clear whether Ptz utilizes HMBDP produced in the plastids of infected host plant cells or not.

17.3.9 Structural studies reveal the molecular mechanism of the initial step in CK biosynthesis

The crystal structure of Tzs indicated that the initial step of CK biosynthesis, a carbon–nitrogen-based prenylation, proceeds via the SN2-reaction mechanism (Fig. 17.31). Tzs has a solvent-accessible channel that serves as the reaction center. In the reaction, the carboxylate group of an aspartate residue (Asp33 in Tzs) serves as a general base to deprotonate the N^6-amino group of AMP. The resulting nucleophile attacks the carbon (C^1) of DMAPP. Collapse of the penta-covalent transition state yields iP riboside 5′-monophosphate and diphosphate as products. Threonine and arginine residues (Thr10 and Arg138 in Tzs) stabilize the penta-covalent transition state.



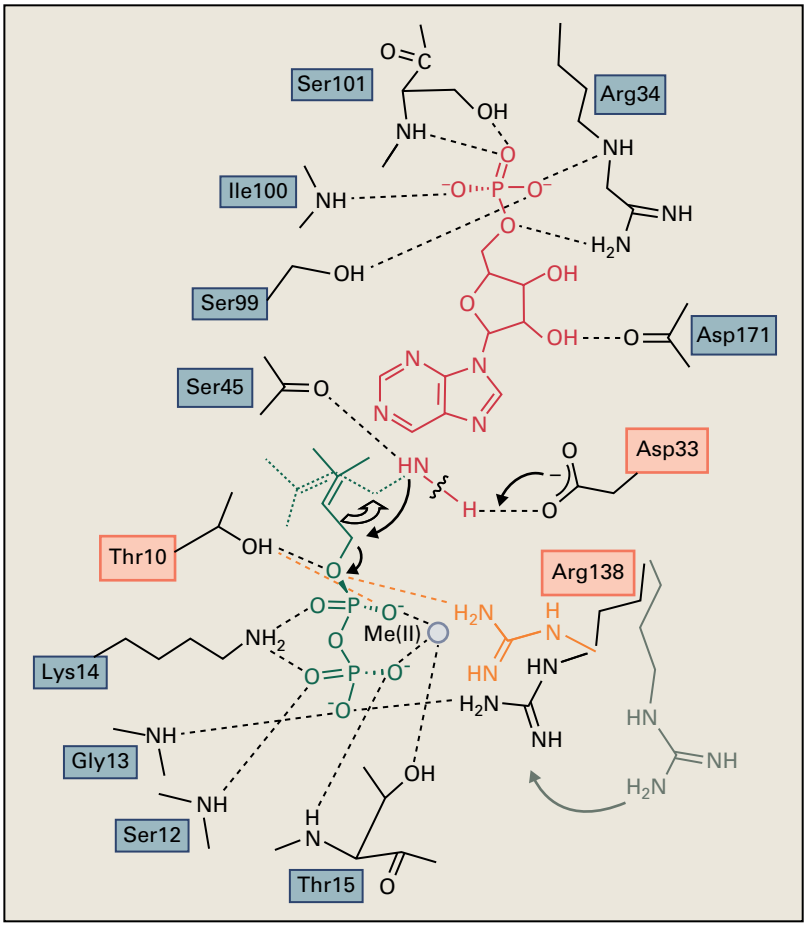


FIGURE 17.31 *Structure of an* Agrobacterium *IPT, Tzs (upper), and proposed reaction mechanism of prenyl transfer (lower). Arg-138 in the absence of divalent metal ion [Me(II)] is shown in orange, and in the absence of prenyl-donor substrate in gray. Dashed line indicates hydrogen-bonding network among substrates and amino acid residues. Highlighted amino acid residues are important for reaction process.*

17.3.10 CKs are also produced through degradation of tRNA

In addition to prenylation of adenine nucleotide by IPT, plants can produce CK through degradation of tRNA. Organisms such as mammals and bacteria, in addition to plants, contain prenylated adenine in a subset of tRNA species. Degradation of tRNA thus can release CKs. Several CK species derived from tRNA-degradation have been reported, such as iP riboside (iPR), *cis*-zeatin riboside (cZR), tZR and their 2-methylthio derivatives (Fig. 17.32). The first step of modification is catalyzed by tRNA-isopentenyltransferase (tRNA-IPT) with DMAPP as a prenyl-donor, and further modifications produce the other CKs. *Arabidopsis* and *O. sativa* have two *tRNA-IPT* genes, one of which is similar to eukaryotic genes and the other is like its prokaryotic counterparts. In *Arabidopsis*, a *tRNA-IPT* double mutant lacks tRNAs with isopentenyl or *cis*-hydroxylated side chains, but also cZ-type CKs, strongly suggesting that cZ-type CKs arise from tRNA degradation in *Arabidopsis*. It is

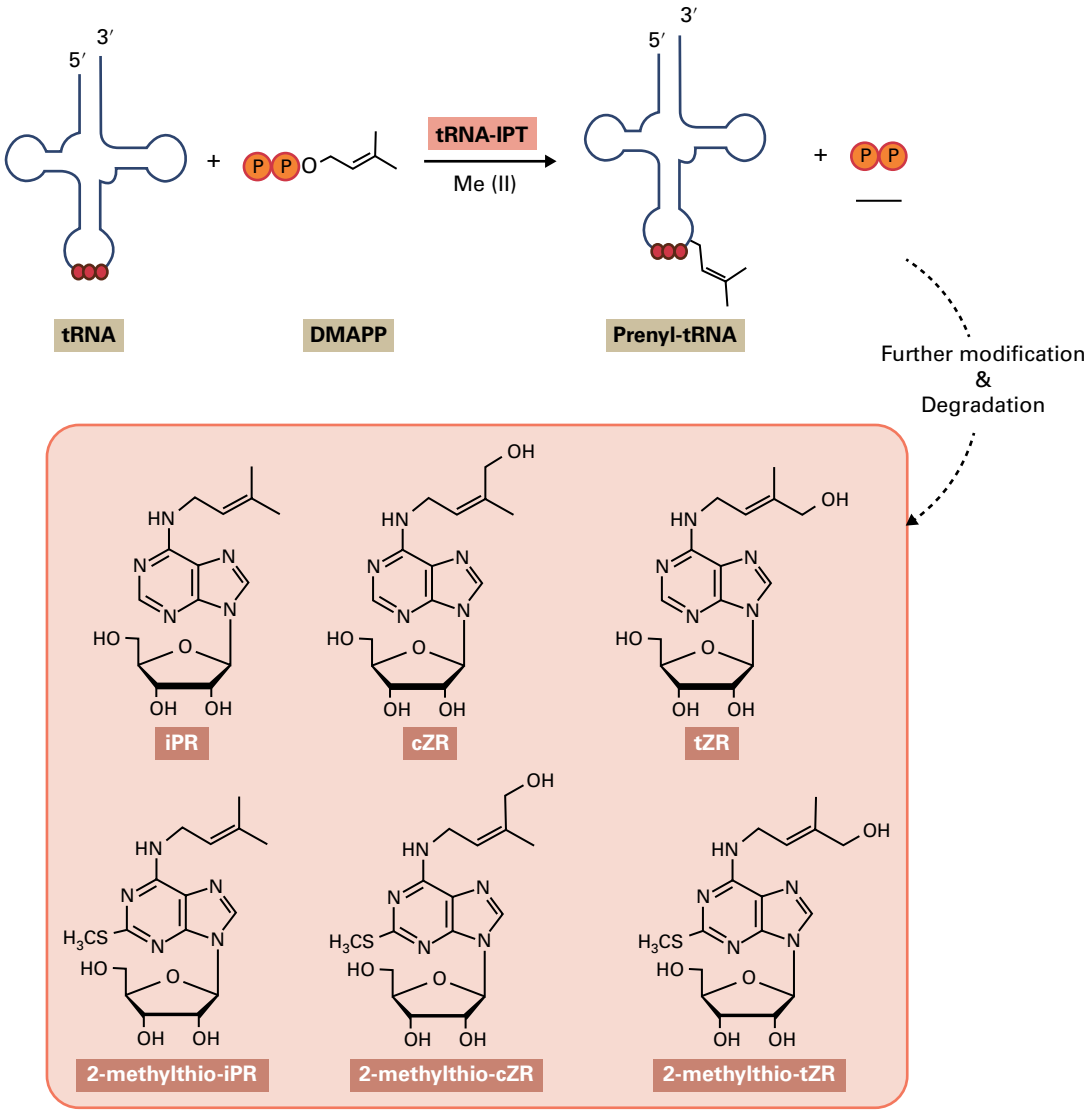


FIGURE 17.32 *CK production by tRNA degradation. tRNA-IPT conjugates DMAPP to adenine in a subset of tRNA species. Further modification and degradation results in the release of CKs. Structures of CKs derived from tRNAs are shown.*

still unclear whether all cZ-type CKs are derived from tRNA degradation in cZ-abundant plant species, such as *O. sativa*.

17.3.11 The initial step of CK biosynthesis occurs in multiple subcellular compartments using DMAPP from different origins

DMAPP is produced through the MEP and mevalonate (MVA) pathways (see Chapter 24). In general, the MEP pathway is found in bacteria and plastids, and the MVA pathway in the cytosol of eukaryotes. IPTs are localized in multiple subcellular compartments. In *Arabidopsis*, IPT1, IPT3, IPT5, and IPT8 are located in plastids, and the relative expression levels of *IPT3* and *IPT5* are higher than the other *IPTs*. A selective labeling experiment in *Arabidopsis* seedlings demonstrated that side chains of iP and tZ-type CKs originate predominantly from the MEP pathway. On the other hand, IPT4 and IPT7 localize in cytosol and mitochondria, respectively. Application of lovastatin, an inhibitor of the MVA pathway, leads to a decrease in tZ-type CK accumulation in tobacco BY-2 cell cultures, suggesting that the MVA pathway can be the predominant origin of tZ-type CKs at other developmental stages and under different conditions. A majority of cZ-type CK side chains have also been shown to come from the MVA pathway.

17.3.12 tZ can be converted to DZ and cZ

The double bond of the tZ side chain can be enzymatically reduced to DZ by a zeatin reductase and this enzyme has been isolated from immature embryos of *Phaseolus vulgaris*. Zeatin reductase, which requires NADPH as a cofactor, uses tZ as substrate, but not cZ, tZR, iP, or tZ-*O*-glucoside.

In addition to degradation of tRNA, cZ-type CKs can be formed by isomerization of tZ, a reaction that is catalyzed by zeatin *cis-trans* isomerase. The isomerase was partially

purified from immature seeds of *P. vulgaris*, and catalyzes isomerization of zeatins in both directions in favor of cZ to tZ. Since the *Arabidopsis tRNA-IPT* double mutant lacks cZ-type CKs, *trans* to *cis* isomerization is a minor factor in cZ production in *Arabidopsis*. At present, the physiological significance of CK reduction and isomerization is not well understood. The genes responsible for side chain-modifying reactions have not been identified.

17.3.13 Interconversion of CK nucleobase, nucleoside and nucleotide are partially shared with the purine salvage pathway

Exogenously applied CK nucleobase and nucleoside are rapidly metabolized to the corresponding nucleotide, and then further converted to other forms, suggesting that nucleotide formation plays a key role in metabolizing exogenous CKs. It is currently accepted that some of the enzymes in the purine salvage pathway catalyze the interconversion of CK nucleobase, nucleoside and nucleotide (Fig. 17.33).

Adenine phosphoribosyltransferase (APT) should catalyze the conversion from CK nucleobase to the corresponding nucleotide, as well as adenine. A reduction in metabolic conversion of exogenously applied CK nucleobase in an *APT Arabidopsis* mutant supports this idea. Adenosine kinases phosphorylate CK nucleosides in vitro. Adenosine phosphorylase can also convert CK nucleobase to its corresponding nucleoside. As is the case with 5′-nucleotidase and nucleosidase, these enzymes have a higher affinity for adenine and adenosine than for the N^6-substituted compounds, indicating that these conversions are side reactions of the purine salvage pathway.

These pathways, via the purine nucleoside phosphorylase/adenosine kinase pathway and the APT pathway, could play a role in regulating CK activity in vivo. However, the extent of any physiological contribution to endogenous CK metabolism has not yet been well defined.

17.3.14 Degradation by CKX plays a key role in regulating cytokinin activity

In addition to biosynthesis and activation, deactivation is an important step in controlling active CK levels. CKX mediates irreversible CK degradation by cleaving the side chain of an unsaturated isoprenoid side chain (Fig. 17.34). Among the naturally occurring CKs, iP, iPR, tZ, tZR, cZ, cZR, *N*-glucosides, and *N*-alanyl conjugates can be in vitro substrates, but generally CKX has a higher affinity for iP, tZ, and their nucleosides than others. Aromatic CKs are resistant to CKX. CKX is a flavoprotein, a member of an FAD-dependent oxidoreductase superfamily, and reacts more efficiently as a dehydrogenase with an electron donor other than oxygen.

Like *IPT* and *LOG*, *CKX* is encoded by a small multigene family. Among the *Arabidopsis CKXs*, there are significant differences in gene expression patterns, subcellular localization, and substrate specificity, perhaps because of functional differentiation among the CKX enzymes. Overexpression of *CKX* decreases CK content and retards shoot development due to a large reduction in cell proliferation rates within the shoot meristem (Fig. 17.35). Conversely, overexpression enhances root growth and the size of root meristems. Thus, CKs play opposite roles in regulating shoot and root meristem development. On the other hand, reduction of *CKX2* expression by natural variation increases CK levels in *O. sativa* (Fig. 17.36), indicating that control of CK activity in shoot apical meristems at the degradation step is important for agricultural productivity.

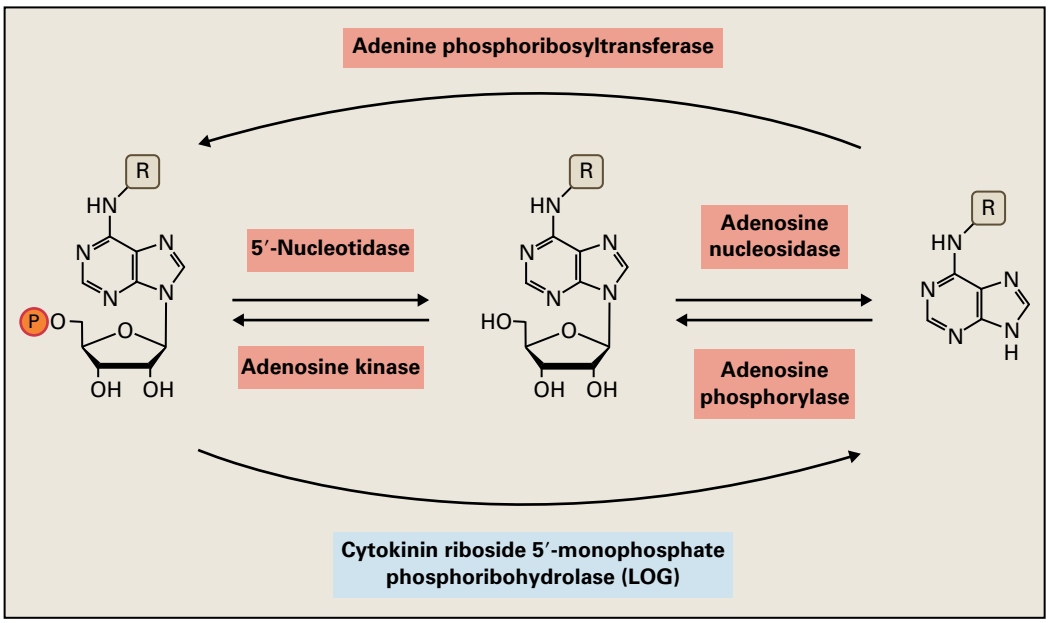


FIGURE 17.33 *Possible interconversion of CK nucleobases, nucleosides, and nucleotides. LOG is a specific enzyme for CK metabolism, but others are not.*

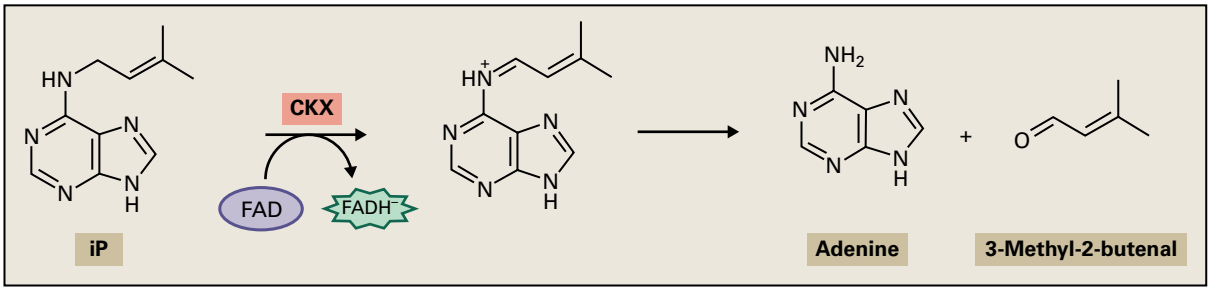
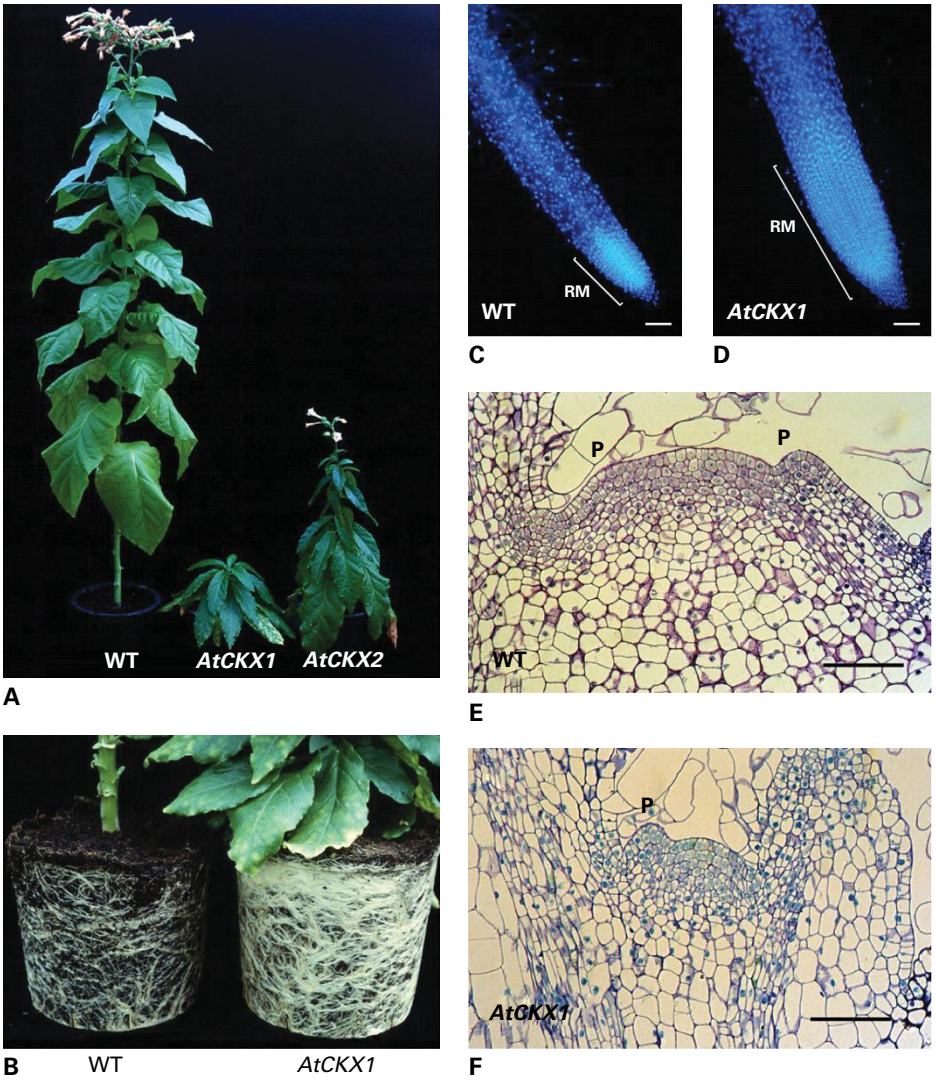


FIGURE 17.34 *CKX removes the side chain from CK molecules. CKX catalyzes the oxidation of the secondary amine group on the side-chain of the adenine ring. The resulting imine product is nonenzymatically hydrolyzed, producing adenine and an aldehyde.*

FIGURE 17.35 *Opposite phenotypes resulting from reduction of CKs in* N. tabacum *shoot and root. (A) Shoot phenotype of wild-type (WT) and transgenic lines overexpressing two different constructs of the* Arabidopsis *CKX genes:* AtCKX1 *and* AtCKX2. *(B) Root phenotype of WT and* AtCKX1. *(C), (D) Root apices of WT and* AtCKX1 *stained with DAPI. (E, F) Longitudinal section through shoot apical meristem (SAM) of WT and* AtCKX1. *The SAM is reduced in CK-deficient plants (*AtCKX1*). RM, root meristem; P, leaf primordia. Bar represents 100 μm.*



17.3.15 Local CK metabolism plays an important role for regulating apical dominance

The mutual regulation of auxin and CKs plays a central role in the control of axillary bud outgrowth and dormancy (Fig. 17.37). This regulatory system consists of the auxin-dependent expression of *CKX* and *PIN*, which is a component of auxin polar transport, and repression of *IPT* by auxin. In an intact plant, basipetal transport of auxin from shoot apices represses *IPT* and maintains *CKX* and *PIN* expression in the stem, resulting in a reduction of steady-state CK levels and maintenance of auxin transport. After meristem decapitation, defects in auxin polar transport in the stem induces *IPTs* and represses *CKX*, resulting in the accumulation of CKs in the nodal stem. The de novo CKs promote development of axillary buds into new shoot apices. After new shoot apices are established, basipetally transported auxin represses *IPT* and upregulates *CKX* to reduce CK activity to pre-decapitation levels.

17.3.16 Glucosylation of the side chain hydroxyl group is catalyzed by zeatin *O*-glucosyltransferase

O-glucosylation of zeatins (i.e., tZ, cZ and DZ) is catalyzed by zeatin *O*-glucosyltransferase with UDP-glucose as the donor substrate. The zeatin *O*-glucosyltransferase identified in *P. lunatus* and *Arabidopsis* preferentially uses tZ over cZ, DZ, or tZR. On the other hand, *Z. mays* zeatin *O*-glucosyltransferases predominantly utilize cZ over tZ. Although the role of *O*-glucosides in metabolic homeostasis is not fully understood, these glucosylated compounds can be reactivated by β-glucosidase to release active CKs. A possible CK β-glucosidase gene, *Zm-p60.1*, was isolated from *Z. mays*, although its physiological relevance remains unresolved.



FIGURE 17.36 O. sativa CKX *gene mutation increases grain number. Panicles of Koshihikari (left) and Habataki (right). Natural variations within the Habataki* CKX2 *gene reduce expression levels in shoot meristems, resulting in increased grain numbers.*

17.3.17 *N*-Glucosylation of the purine moiety is catalyzed by *N*-glucosyltransferase

Glucosylation of CKs occurs at the 3, 7, and 9 positions of the purine moiety, and modification at the 7 and 9 positions results in inactivation. In *Arabidopsis*, CK *N*-glucosyltransferase, UGT76C1 and UGT76C2, conjugates glucose to CK nucleobases at the *N7*- or *N9*-position of the adenine moiety, but *N3*-glucosides are rarely found in planta and the biochemical nature of glucosyltransferases acting at the *N3*-position is not known. Since Zm-p60.1 does not hydrolyze *N7*- and *N9*-glucosides, the *N*-glucosides are thought to be irreversibly inactivated forms.

17.4 Auxins

During the 19th century, Theophili Ciesielski studied the geotropic responses of plants, and Charles Darwin and his son Francis investigated phototropism as well as geotropism. These investigations laid the groundwork for Fritz Went, who in 1926 obtained from oat coleoptiles a diffusible growth-promoting factor subsequently named "auxin." The primary auxin present in most plants was eventually identified as **indole-3-acetic acid** (IAA) (Fig. 17.38). Indole-3-butyric acid (IBA), 4-chloroindole-3-acetic acid, and phenylacetic acid, which are also known as auxins, naturally

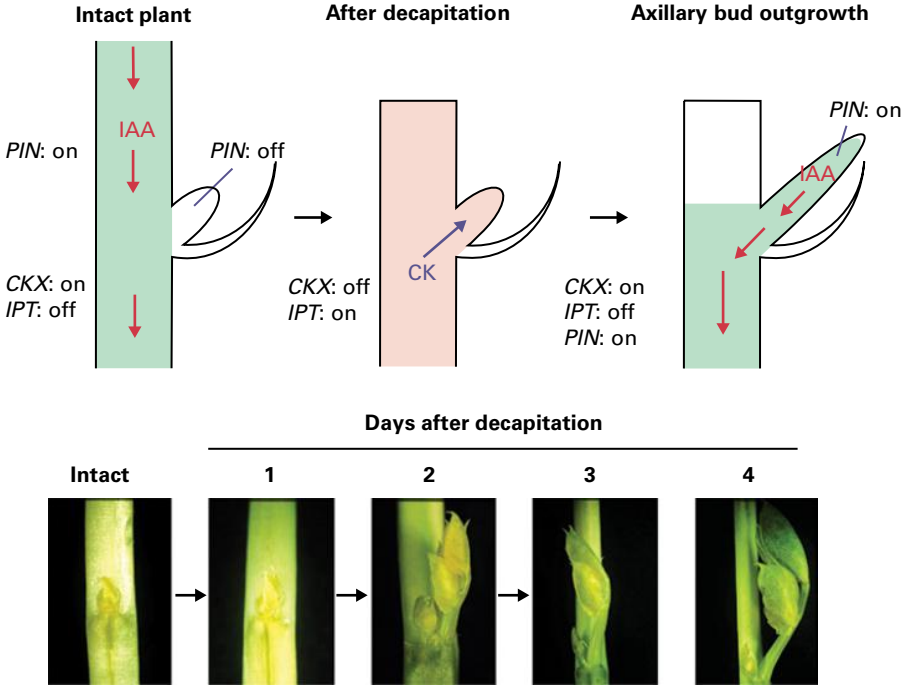


FIGURE 17.37 *A model of the interactions between auxin and CKs in controlling apical dominance. In an intact plant, auxin derived from the shoot apex maintains* PIN1 *and* CKX *expression and represses* IPT *expression. Since CK level is kept lower, axillary bud outgrowth does not occur. After decapitation (1 day after decapitation in photo), the auxin level in the stem decreases, resulting in the release of repression of* IPT *expression and down-regulation of* CKX *and* PIN1 *expression. The de novo synthesized CK in the stem is transported into dormant axillary buds and initiates their outgrowth. After axillary bud outgrowth (2 day and after in photo), de novo synthesized IAA from the new shoot apex again represses* IPT *expression and induces* CKX *and* PIN1.

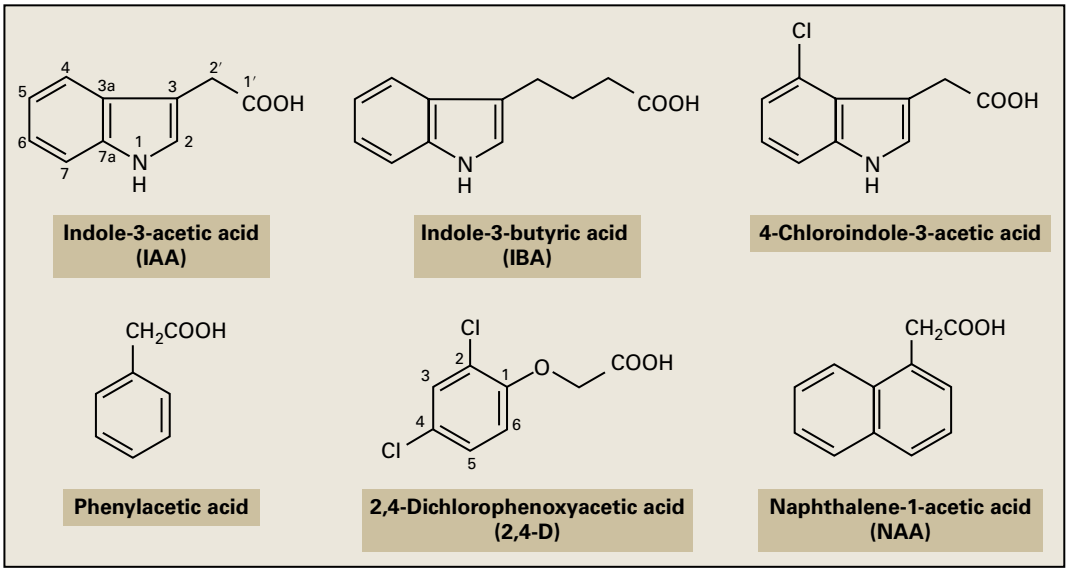


FIGURE 17.38 *Structures of auxins. IAA is the most widely distributed plant auxin. IBA, 4-chloroindole-3-acetic acid, and phenylacetic acid also naturally occur, but are less prevalent. 2,4-D and NAA are synthetic auxins.*

occur in plants but are less prevalent than IAA. Auxins are involved in regulation in a wide variety of physiological processes, including apical dominance, tropisms, phyllotaxis, shoot elongation, induction of cambial cell division, and root initiation. Synthetic auxins such as 2,4-dichlorophenoxyacetic acid (2,4-D) and naphthalene-1-acetic acid (NAA) (Fig. 17.38) are used extensively in horticulture to induce rooting and to promote the set and development of fruit. At high concentrations the synthetic auxins are effective herbicides against broad-leaved plants.

The auxin activity in plants is primarily regulated by control of IAA content via several processes: de novo biosynthesis, and inactivation by various conjugation and catabolic pathways. There are two de novo IAA biosynthesis pathways, one of which is dependent on the amino acid precursor L-tryptophan and the other is L-Trp-independent, although the L-Trp-dependent pathway is likely to be dominant. Hydrolysis of IAA conjugates also releases active auxin. IAA content in individual tissues can also be influenced by basipetal polar transport that results in the downward movement of IAA from apical meristems and young leaves towards the root system.

17.4.1 Multiple routes are employed in the L-Trp-dependent auxin biosynthesis

In plants, multiple routes have been identified in L-Trp-dependent IAA biosynthesis: their first products are indole-3-pyruvic acid and tryptamine (Fig. 17.39). Indole-3-pyruvic acid is formed by Trp aminotransferase, followed by conversion to IAA by YUCCA, a flavin-containing monooxygenase. Tryptamine is produced by decarboxylation of L-Trp, catalyzed by Trp decarboxylase (Fig. 17.39). Tryptamine is then converted to indole-3-acetoaldehyde, and then to IAA.

Indole-3-ethanol and its conjugates are produced in a side shunt from indole-3-acetaldehyde. These compounds may have a storage role, given that they can be rapidly reconverted to indole-3-acetaldehyde and used as a substrate for IAA biosynthesis.

IBA has been found in a number of plants. It has auxin activity and is used to induce root formation on cuttings. IAA is converted to IBA in *Z. mays* and *Arabidopsis* (Fig. 17.39). In vitro studies with *Z. mays* have demonstrated that IBA synthase uses acetyl-CoA and ATP as cofactors, and exogenous IBA is conjugated rapidly by plants. Conversion of IBA to IAA has also been reported. Whether IBA is an auxin per se, or its biological activity results from conversion to IAA, is not clear.

17.4.2 YUCCAs play a key role in auxin biosynthesis and plant development

Although plants have multiple routes for the L-Trp-dependent pathway, several lines of evidence from studies on gain-of-function and loss-of-function mutants demonstrates a key role for YUCCAs in auxin biosynthesis. *Arabidopsis yuc-1D*, a gain-of-function mutant of *YUCCA*, contains increased concentrations of free IAA and shows characteristic phenotypes found in auxin overproduction mutants. Transgenic rice (*O. sativa*) and *Petunia*, overexpressing *YUCCA* homologs, also display an auxin overproducing phenotype with increasing IAA concentrations. *YUCCA* is encoded by a small multigene family, members of which are differentially expressed according to tissue. The expression of *YUCCAs* is temporally and

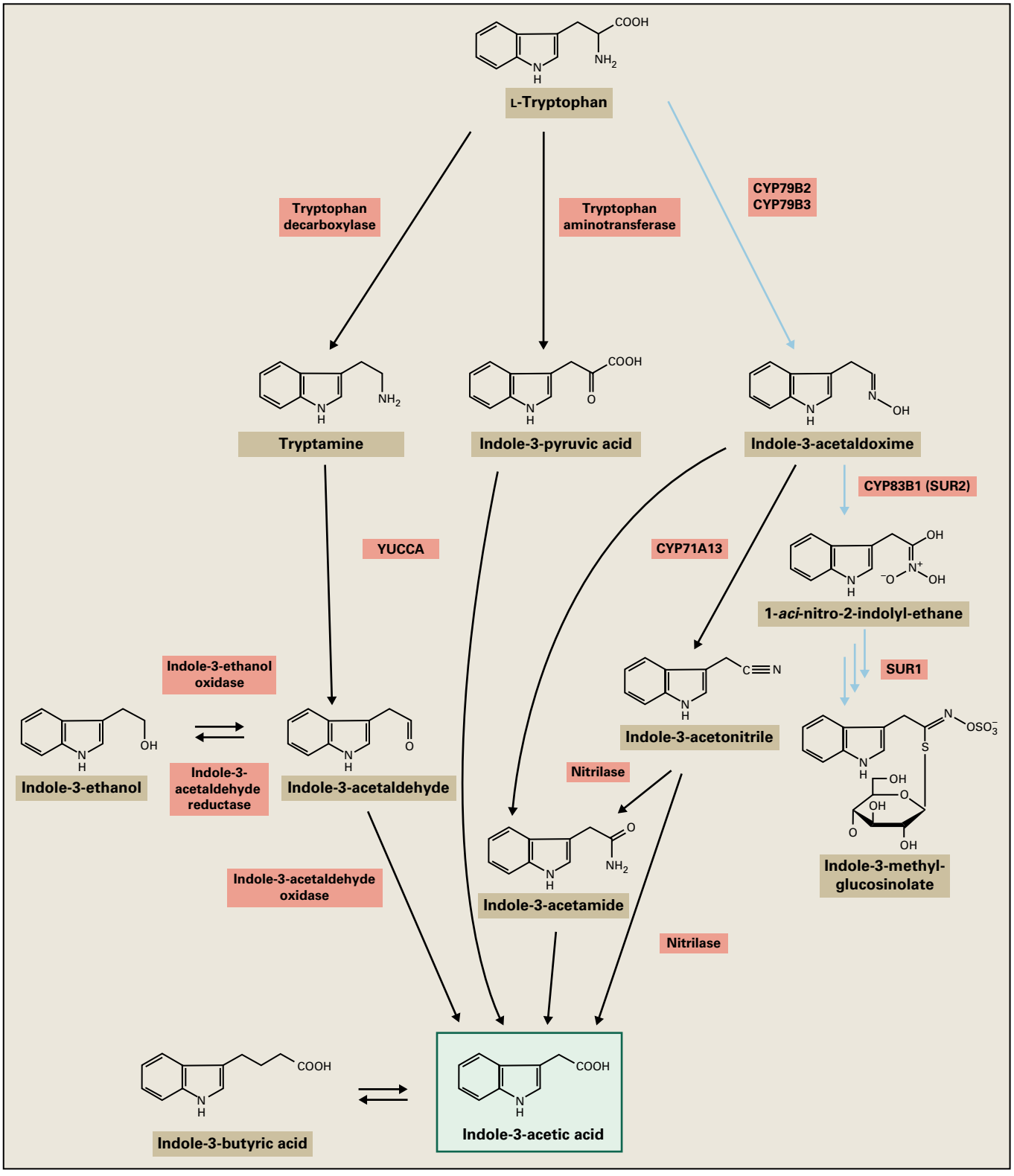


FIGURE 17.39 *L-Trp-dependent auxin biosynthesis pathway. Blue arrows indicate metabolic pathway shared with glucosinolate biosynthesis.*

spatially restricted and they are expressed in shoot and inflorescence apices, cotyledon tips in mature embryos, stamen, pollen, and stipules. Double and quadruple mutants of YUCCA exhibit various auxin-deficient phenotypes. *Arabidopsis yuc1yuc4* double mutants make less vascular tissue, fail to produce normal flowers and are sterile, and *yuc1yuc4yuc10yuc11* quadruple mutants produce seedlings lacking a hypocotyl and a root meristem. Thus, de novo IAA biosynthesis mediated by YUCCA has a crucial role in the formation of floral organs and vascular tissues.

17.4.3 IAA biosynthesis pathway is shared with glucosinolate biosynthesis pathway in a few plant families

Some plant families, such as Brassicaceae and Caricaceae, contain glucosinolates, a class of sulfur-containing secondary metabolites derived from glucose and amino acids. In the biosynthesis of indole glucosinolates, L-Trp is successively converted to indole-3-acetaldoxime by CYP79B2 or CYP79B3, to 1-*aci*-nitro-2-indolyl-ethane by CYP83B1 (SUR2), and to indole-3-methylglucosinolate (Fig. 17.39). SUR1 is involved in the conversion of 1-*aci*-nitro-2-indolyl-ethane to indole-3-methylglucosinolate. In these plant families, the IAA biosynthesis pathway is shared with the glucosinolate synthesis pathway. Indole-3-acetaldoxime is converted to IAA via indole-3-acetonitrile or indole-3-acetamide. CYP71A13 catalyzes conversion of indole-3-acetaldoxime to indole-3-acetonitrile, and nitrilase catalyzes conversion from indole-3-acetonitrile to indole-3-acetamide or IAA. Recent work in *Arabidopsis* establishes conversion of indole-3-acetaldoxime to IAA via indole-3-acetamide but the catalytic enzymes have not been characterized. The physiological relevance of this pathway in IAA biosynthesis is evidenced by increased concentrations of IAA in *Arabidopsis* seedlings of CYP79B2 overexpression lines and decreased concentrations of IAA in *cyp79B2cyp79B3* double mutants. In either *sur1* or *sur2 Arabidopsis* mutants, auxin is overaccumulated probably because indole-3-acetaldoxime could not be used for glucosinolate biosynthesis but is channeled into IAA biosynthesis.

17.4.4 TAA1s also play a role in auxin biosynthesis and plant development and are required for shade avoidance

Identification of genes for Trp aminotransferase (TAA1) in *Arabidopsis* revealed that auxin biosynthesis via indole-3-pyruvic acid is involved in shade avoidance responses and in ethylene–auxin interactions. The *TAA1* allele is a causal gene of *shade avoidance* mutants, which are unable to elongate in simulated shade. *TAA1* was also identified as a causal gene of *weak ethylene insensitive* mutants, which show root-specific decrease in sensitivity to ethylene. *TAA1* encodes a small family of aminotransferases with strong similarity to C-S lyase. Multiple mutants of this family of genes show severe auxin-related phenotypes, such as defects in root gravitropism, vasculature organization, and shoot and flower development. Since any defects in shade-induced hypocotyl elongation are not seen in multiple YUCCA mutants (*yuc3yuc5yuc7yuc8yuc9*), YUCCAs may not be required for shade avoidance.

17.4.5 Tryptophan-independent IAA biosynthesis was demonstrated, but the biological importance remains unclear

Evidence for IAA biosynthesis independent of L-Trp has been obtained with the orange pericarp (*orp*) mutant of *Z. mays*, a Trp auxotroph (Fig. 17.40). The *orp* phenotype results from mutations in two genes that encode the β-subunit of Trp synthase, which catalyzes the condensation of L-Ser and indole (Fig. 17.41; see also Chapter 7). Seeds of the *orp* mutant contain increased concentrations of two L-Trp precursors, anthranilate and indole (Fig. 17.41). Seeds germinate and form shoots normally, but seedlings die at the four- to five-leaf stage unless supplemented with L-Trp. Despite their diminished capacity for L-Trp synthesis, *orp* mutants are rich in IAA. Although *orp* seedlings contain roughly one-seventh the L-Trp present in wild-type *Z. mays*, IAA contents are increased 50-fold. Furthermore, labeling with $^{2}H_{2}O$ has indicated that isotopic enrichment of the *orp* IAA pool was much greater than in the L-Trp pool. [^{15}N]L-Trp does not label the IAA pool significantly in either wild-type or *orp* seedlings, but [^{15}N]anthranilate is incorporated into IAA to a similar extent in both tissues. These findings suggested the existence of L-Trp-independent IAA biosynthesis in *Z. mays*. The IAA precursor is probably an indolic intermediate of Trp biosynthesis, downstream from anthranilate and upstream from L-Trp. The conversion of indole-3-glycerol phosphate to

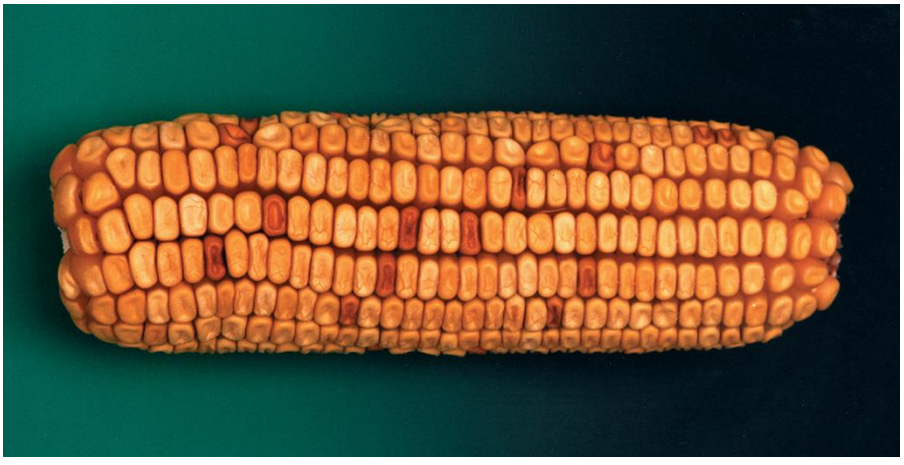


FIGURE 17.40 Z. mays *ear segregating kernels for the two-gene recessive trait orange pericarp* (orp)*; the orange kernels are homozygous for both mutant genes.*
Source: J. Cohen, University of Minnesota, MN, and A.D. Wright, University of Missouri, Columbia; previously unpublished.

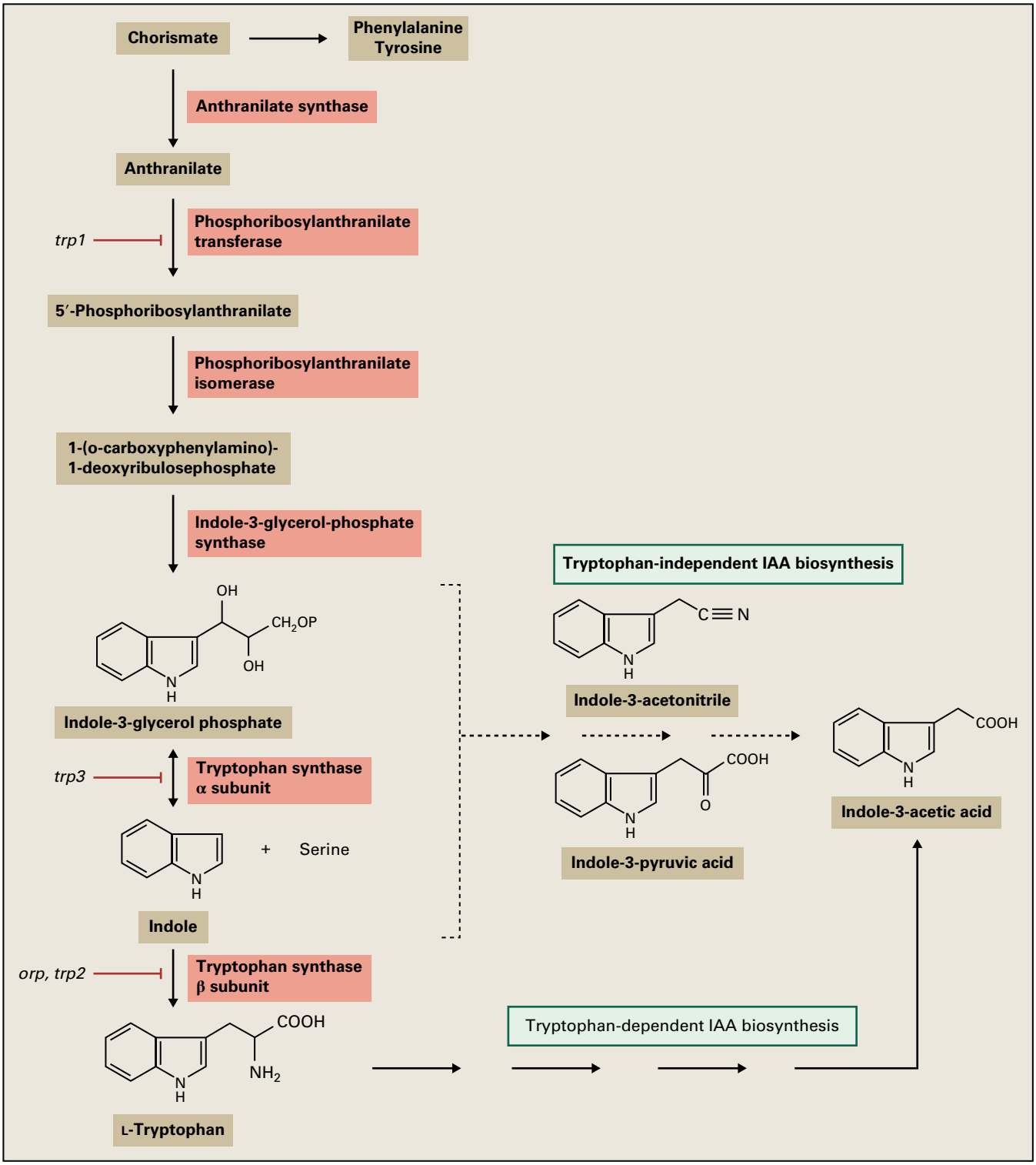


FIGURE 17.41 *Biosynthesis of* L*-Trp and* L*-Trp dependent and independent IAA biosynthesis. The enzymes affected in* Z. mays orp *and* Arabidopsis trp1, trp2, *and* trp3 *mutants are indicated.*

indole is reversible, and the available data suggest that either of these compounds could be the branch point for IAA biosynthesis (Fig. 17.41).

Although the experimental data in *Z. mays orp* appear robust, and there are several reports suggesting a dominant role of Trp-independent pathway for IAA synthesis, subsequent studies indicate that L-Trp-dependent IAA synthesis is the predominant route for auxin biosynthesis, and that the independent pathway plays only a minor role. ^{13}C-labeled precursor feeding experiments in a *Z. mays* kernel culture

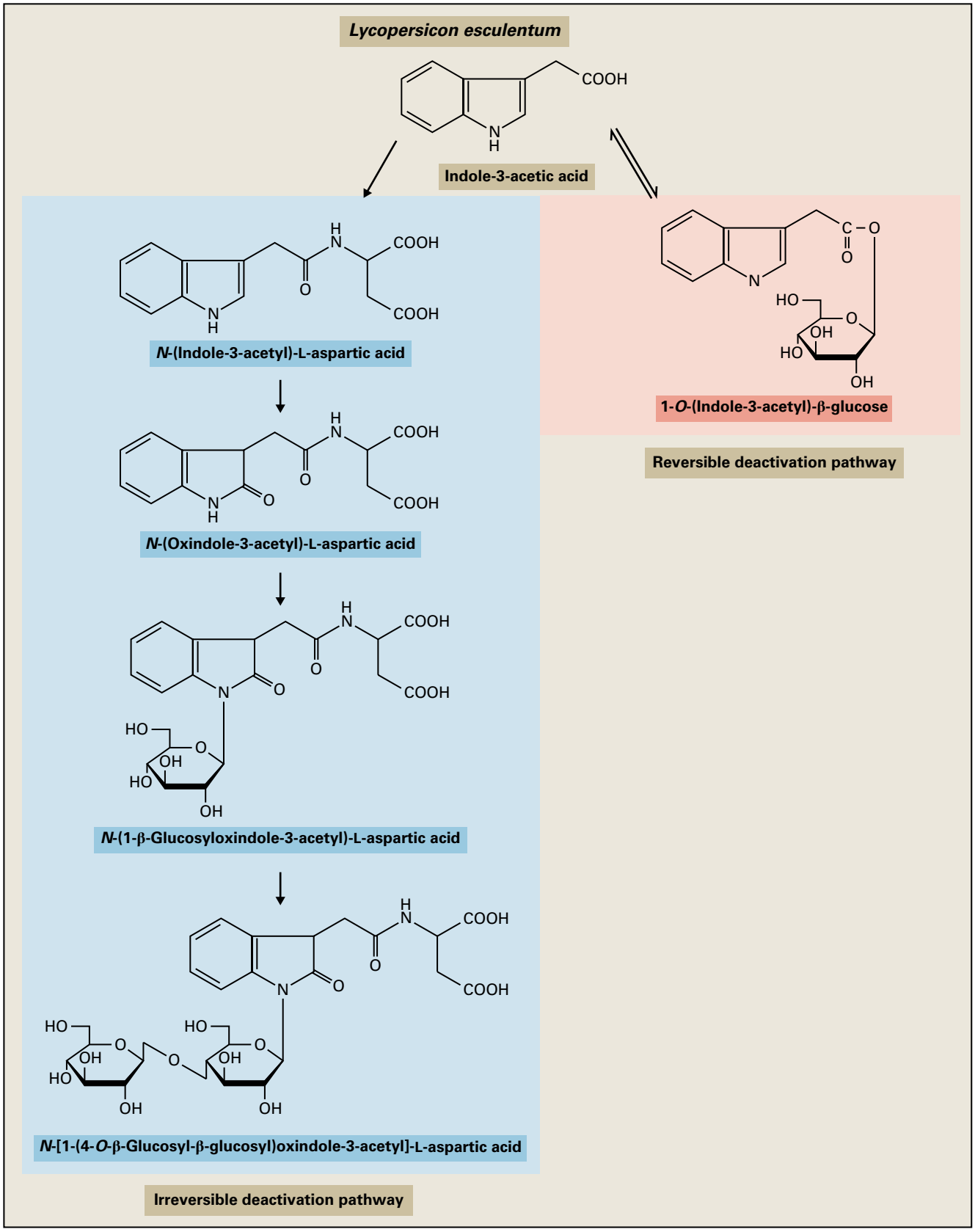


FIGURE 17.42 *Nondecarboxylative catabolism and conjugation of IAA in* S. lycopersicum *pericarp discs.* N-*(1-β-Glucosyloxindole-3-acetyl)-L-aspartic acid and* N-*[1-(4-*O*-β-glucosyl-β-glucosyl)oxindole-3-acetyl]-L-aspartic acid are permanently deactivated IAA conjugates formed in both green and red* S. lycopersicum *fruits, whereas the 1-*O*-(indole-3-acetyl)-β-glucose formed by red pericarp tissues can be converted back to IAA.*

showed that [3,3′-^{13}C]tryptophan was efficiently incorporated into IAA with retention of the 3,3′ bond, excluding the possibility that absorbed Trp is degraded to indole which then serves as an IAA precursor. Furthermore, in an evaluation of the metabolic origin of the IAA carbon skeleton by feeding [U-$^{13}C_6$]glucose the possibility that IAA was synthesized by way of indole-3-glycerol phosphate was also excluded.

Although occurrence of a Trp-independent pathway was also suggested with *Arabidopsis trp1*, *trp2*, and *trp3* mutants all conditional Trp auxotrophs, experiments with *trp3* and labeled precursors ([^{2}H]$_5$-L-Trp and [^{15}N] anthranilate) suggested a minor role of the independent pathway, if any, in the biosynthesis.

17.4.6 Several pathways for IAA conjugation and catabolism have been elucidated

IAA catabolism results in loss of auxin activity and irreversibly decreases the size of the IAA pool. Catabolism can proceed by decarboxylative or nondecarboxylative pathways, and in either case can involve oxidation of the indole ring. As with CKs, catabolism of IAA sometimes involves conjugation reactions. While some conjugated IAA species appear to be permanently inactive, others can be cleaved to yield active free hormone (see Section 17.4.8).

Peroxidase-catalyzed decarboxylation of IAA has been studied in vitro with a variety of plant materials. The action of peroxidase (frequently referred to as IAA oxidase) results in the production of either decarboxylated oxindoles or decarboxylated indoles. For many years, the decarboxylative catabolism was thought to represent the major IAA degradation pathway in plant tissues. However, evidence obtained with *Z. mays*, tomato and pea indicates that peroxidases have only a minor role in the regulation of endogenous IAA pools. IAA–amino acid conjugates that were once perceived as storage products have been identified as intermediates in nondecarboxylative catabolic pathways that deactivate IAA irreversibly.

The principal IAA deactivation pathway in green *S. lycopersicum* fruits converts IAA to *N*-(indole-3-acetyl)-L-aspartic acid (IAA-Asp). The indole ring of IAA-Asp is oxidized to form *N*-(oxindole-3-acetyl)-L-aspartic acid (OxIAA-Asp), which is subjected to successive glycosylations at the indole nitrogen (Fig. 17.42). An IAA to OxIAA-Asp deactivation pathway also operates in *Dalbergia*, but instead of *N*-glycosylation, the indole ring of OxIAA-Asp is hydroxylated at C-3 or C-4. A parallel pathway in *Dalbergia* forms similar products that are conjugated to Glu rather than Asp. Additional nondecarboxylative IAA degradation pathways that involve conjugation reactions have been identified in *Vicia faba* and *Z. mays* seedlings (Fig. 17.43).

17.4.7 IAA ester conjugates serve as storage products in *Z. mays* seeds

The conjugation reactions discussed above, including aspartylation or glutamylation of the 1′ carboxyl, *N*-glycosylation of the indole ring, and glycosylation of either the 3 or 7 hydroxyl groups, appear to permanently deactivate IAA. However, *O*-glycosylation of the 1′ carboxyl is typically reversible, so IAA–ester conjugates may function as storage products (see Fig. 17.42).

In *Z. mays*, IAA-ester conjugates are formed primarily in the liquid endosperm of developing seeds. IAA is first converted to 1-*O*-(indole-3-acetyl)-β-glucose (1-*O*-IAA-glucose) in a reaction catalyzed by IAA glucosyltransferase (Fig. 17.44). Isomers of 1-*O*-IAA-glucose can be formed by nonenzymatic reactions. Two of these isomers, 4-*O*-IAA-glucose and 6-*O*-IAA-glucose, can be cleaved by 6-*O*-IAA-glucose-hydrolase to release active IAA. A second enzyme that liberates active hormone, 1-*O*-IAA-glucose hydrolase, also can transfer IAA from 1-*O*-IAA-glucose to glycerol. However, the major pathway from 1-*O*-IAA-glucose involves its conversion to 2-*O*-(indole-3-acetyl)-*myo*-inositol, which is further conjugated to 2-*O*-(indole-3-acetyl)-*myo*-inositol arabinoside and 2-*O*-(indole-3-acetyl)-*myo*-inositol galactoside (Fig. 17.44). During the first days of germination, the *Z. mays* embryo derives most of its IAA from these three conjugates. However, the supply of hydrolyzable IAA conjugates declines as the seedling grows, and the young plant rapidly develops the capacity to synthesize IAA.

In *Z. mays* and *Arabidopsis*, genes for IAA glucosyltransferase, *iaglu*, and *UGT84B1*, respectively, have been identified. In vitro studies show that UGT84B1 reacts with IAA as well as indole-3-butyric, indole-3-propionic, and cinnamic acids. Surprisingly, the closest *Arabidopsis* homolog of *iaglu*, UGT75D1, showed no activity toward IAA.

17.4.8 Amino acid conjugation of IAA is catalyzed by enzymes of the GH3 family and together with IAA-amido hydrolases are involved in IAA homeostasis

Studies in *Arabidopsis* identified a subset of GH3 family proteins as IAA-amido synthetase, which catalyzes amino acid conjugation of IAA in the presence of ATP and Mg^{2+}. GH3.2 to GH3.6 and GH3.17 conjugate various L-amino acids, such as L-Ala L-Asp, L-Glu, L-Met, and L-Tyr to IAA in vitro, and can utilize indole-3-pyruvic acid, indole-3-butyric acid, phenyl acetic acid, and naphthalene-1-acetic acid as substrates. Most of the IAA-amido synthetase genes are responsive to auxin treatment, suggesting that plants use feedback regulation to control the amounts of active auxin. Genes for IAA-amido hydrolases were identified in *Arabidopsis* and are encoded by a small multigene family. The

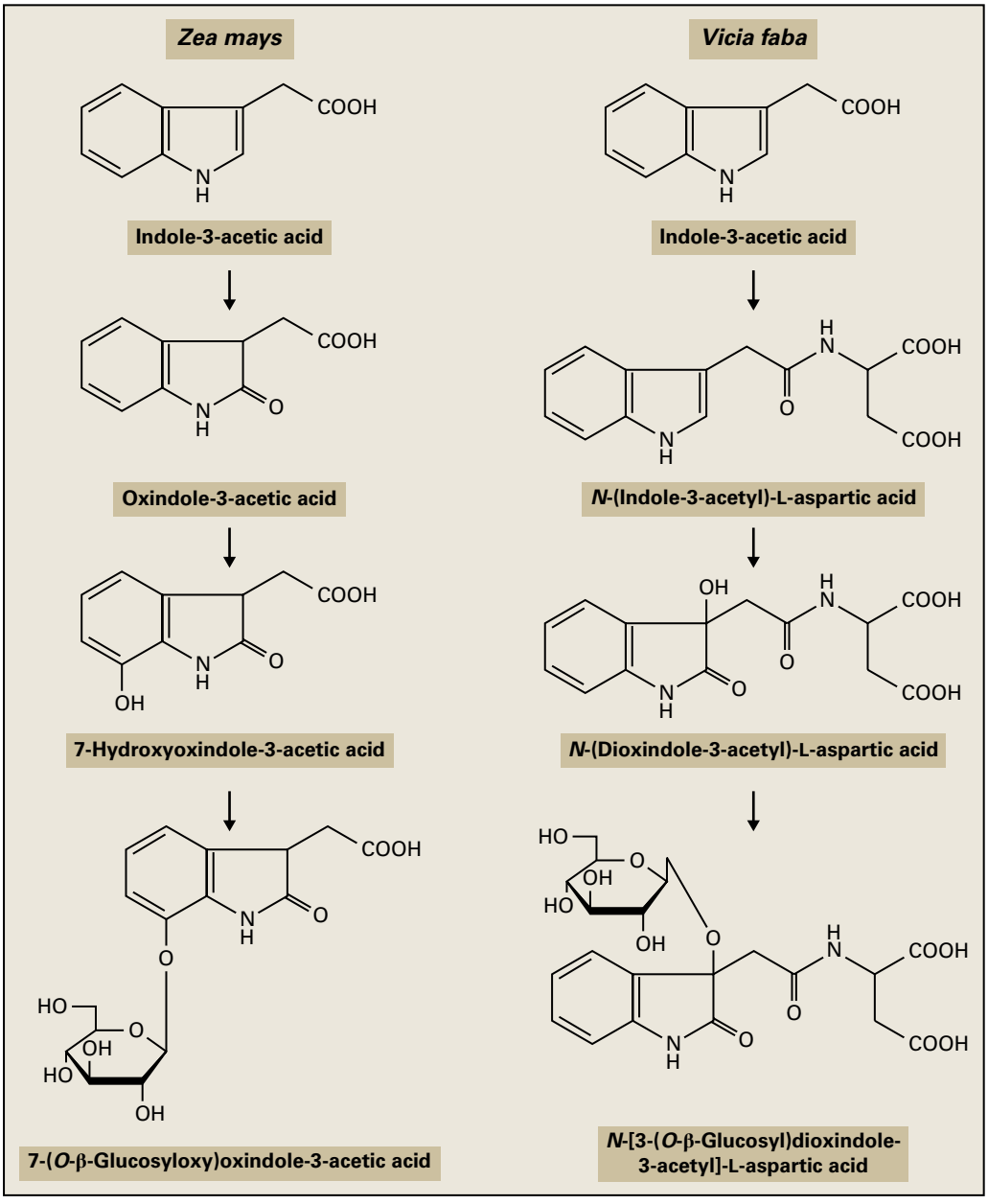


FIGURE 17.43 *Nondecarboxylative catabolism and conjugation of IAA in seedlings of* Z. mays *and* Vicia faba.

IAA-amido synthetases and hydrolases play a complementary role in the maintenance of IAA homeostasis (Fig. 17.45).

17.4.9 Some bacterial pathogens encode novel IAA synthesis and conjugation pathways

As described in Section 17.3.7, some bacterial enzymes catalyze the production of plant hormones. The enhanced synthesis of IAA in *A. tumefaciens*-induced galls and tumors (see Fig. 17.29) results from expression of two bacterial genes that are transferred to the plant when the T-DNA integrates into the host genome. These genes are associated with a unique two-step Trp-dependent pathway to IAA. The *iaaM* gene encodes Trp monooxygenase, which converts L-Trp to indole-3-acetamide. The product of the *iaaH* gene, indole-acetamide hydrolase, catalyzes the conversion of indole-3-acetamide to IAA. Cognate genes with similar functions occur in the plant pathogen *Ps. savastanoi*. A third *Ps. savastanoi* gene, *iaaL*, encodes IAA-Lys synthase. When expressed in the cells of the plant host, IAA-Lys synthase conjugates IAA and L-Lys to form ε-*N*-(indole-3-acetyl)-L-Lys, which is metabolized further to α-*N*-acetyl-ε-*N*-(indole-3-acetyl)-L-Lys (Fig. 17.46).

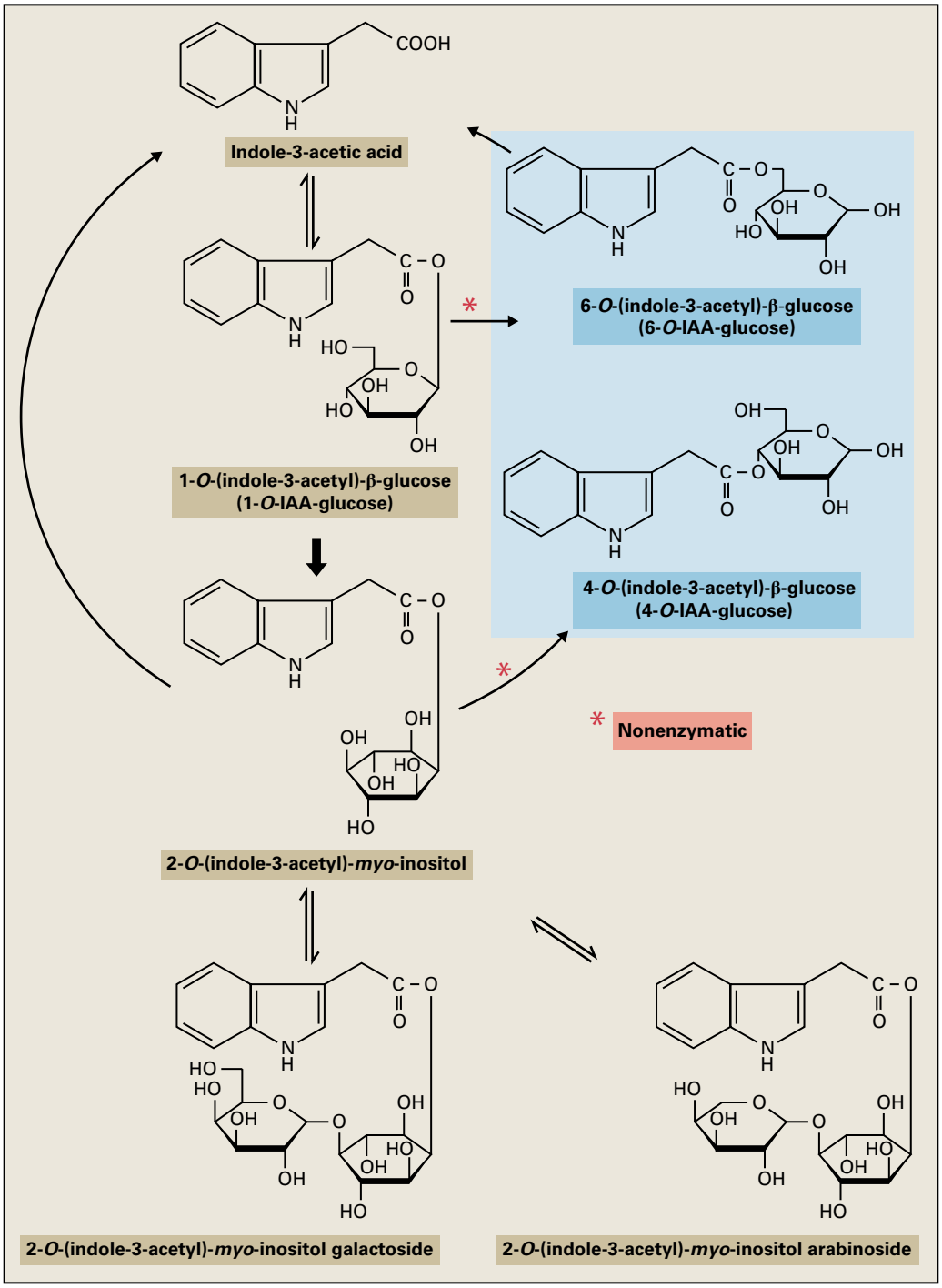


FIGURE 17.44 *Biosynthesis and hydrolysis of IAA ester conjugates in* Z. mays.

17.4.10 Transgenic plants expressing IAA biosynthesis genes have been used to study the effects of excess amounts of endogenous IAA

Transgenic plants expressing the *A. tumefaciens* IAA biosynthesis genes have been produced in several laboratories. Weak coexpression of the *iaaH* and *iaaM* genes in transgenic tobacco (*N. tabacum* cv. Petit Havana SR1) results in a marginal increase in endogenous IAA. Depending on the tissue, there is a two- to threefold increase in the amount of IAA conjugates—primarily IAA-Asp and IAA-Glu, with smaller amounts of 1-*O*-IAA-glucose. Transgenic plants exhibited no obvious changes in vegetative phenotype, but their flowers were heterostylous and pollen production was impaired, resulting in infertility. Thus, when IAA production is enhanced, conjugation

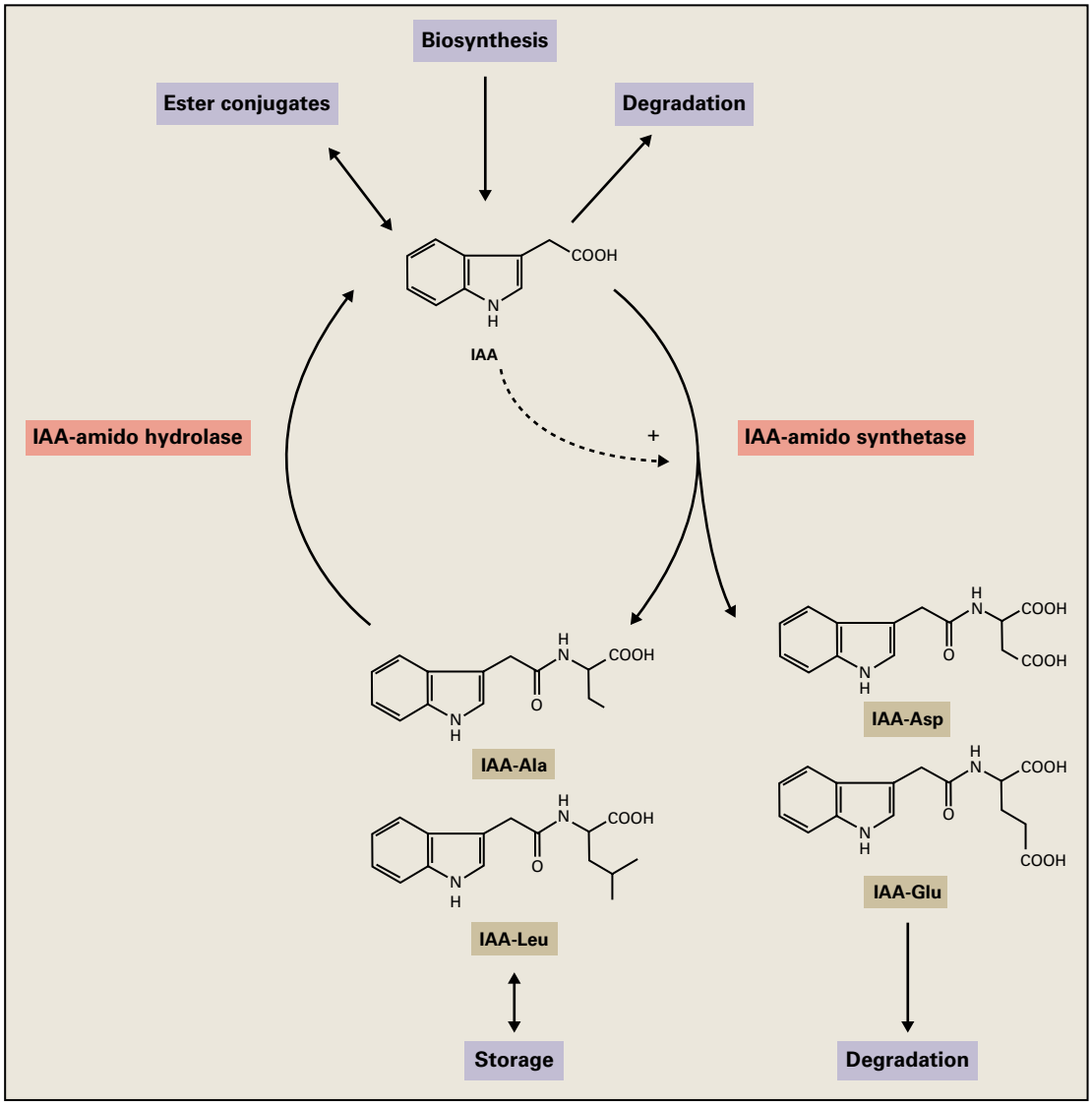


FIGURE 17.45 *Metabolic homeostasis regulating IAA concentration by IAA-amido synthetases and hydrolases. Dotted arrow shows transcriptional activation for several IAA-amido synthetase genes.*

appears to play a key role in regulating the size of the endogenous IAA pool and maintaining an almost normal phenotype. However, strong *iaaH*/*iaaM* expression driven by the CaMV 35S promoter increased the concentration of free and conjugated IAA in stems by 10- and 20-fold, respectively, whereas foliar IAA and IAA conjugates increased three- to fivefold. This increased IAA content was accompanied by major phenotypic effects, including pronounced apical dominance, dwarfism, excess adventitious root formation, increased phloem and xylem formation, excess lignification, leaf epinasty, and abnormal flower production (Fig. 17.47). Similar phenotypes have been observed in several transformed plants that overproduce IAA, including *Petunia* and *Arabidopsis*.

High concentrations of IAA are typically accompanied by an increased rate of ethylene biosynthesis, and it was not initially possible to determine whether the phenotypic effects of IAA overproduction were a direct result of IAA or a consequence of increased ethylene levels. To investigate these possibilities, investigators crossed IAA-overproducing transgenic *N. tabacum* cv. Samsun plants with plants expressing a bacterial ACC deaminase that catalyzes the breakdown of the ethylene precursor ACC and thereby reduces ethylene concentration (see Section 17.5.2). With cv. Samsun (Fig. 17.48) the phenotypic effects of IAA-overproduction are not as severe as with the Petit Havana SR1 transformant (see Fig. 17.47), although inhibition of stem growth, leaf epinasty, and reduced apical dominance are still evident. The phenotype of the Samsun double-transformants, in which IAA overproduction is not accompanied by increased ethylene biosynthesis, shows that apical dominance and leaf epinasty are controlled primarily by IAA, whereas reduced stem elongation is an indirect consequence of high ethylene concentrations (Fig. 17.48).

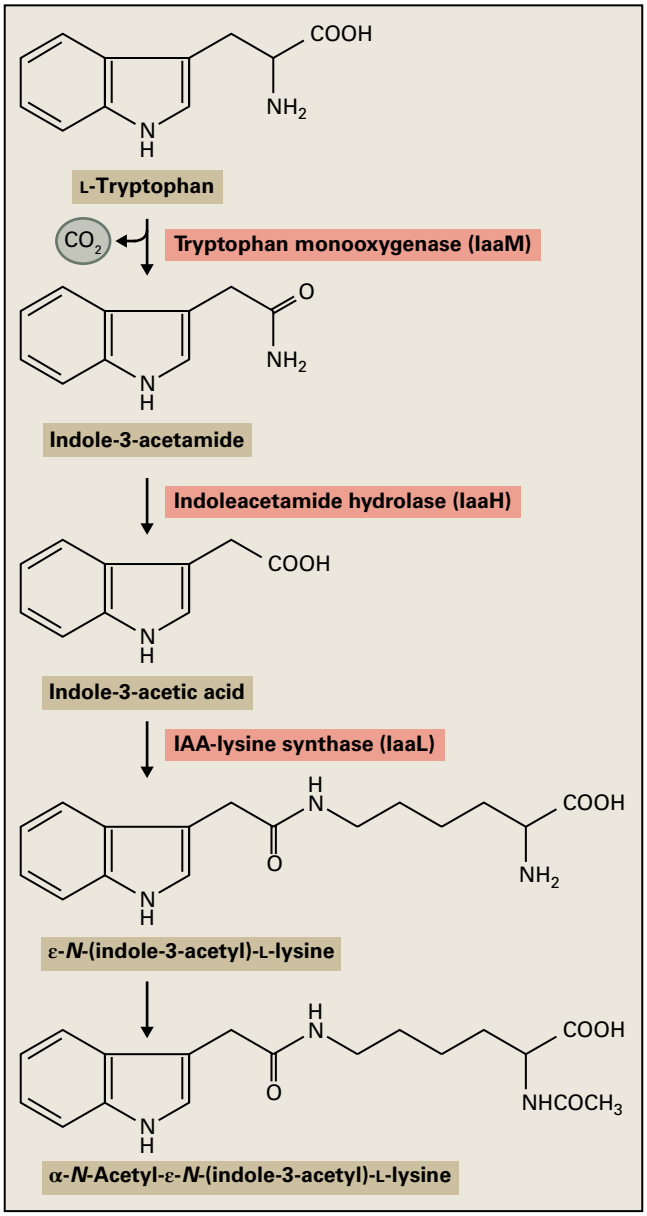


FIGURE 17.46 *IAA biosynthesis and conjugation pathways in* A. tumefaciens *and* Pseudomonas savastanoi. *IaaL does not occur in* A. tumefaciens.

17.4.11 GAs increase IAA pools, whereas CKs may down-regulate IAA synthesis and turnover

Application of GA_3 to Little Marvel dwarf pea seedlings enhances shoot growth with a concomitant eightfold increase in IAA content of elongating tissues. Conversely, the size of the endogenous IAA pool is reduced in the Alaska pea seedlings dwarfed by treatment with uniconazole, a GA biosynthesis inhibitor (see Section 17.1.5). The effects of uniconazole on both internode growth and IAA content are counteracted by GA_3 treatment.



FIGURE 17.47 *Eight-week-old tobacco plants,* N. tabacum *cv. Petit Havana SR1: wild-type plant (left); IAA-overproducing plant expressing* A. tumefaciens iaaH *and* iaaM *genes under the control of the CaMV 35S promoter (right). Note the severe stunting associated with production of IAA at about 500% of wild-type concentrations. Source*: Adapted from Nilsson et al. (1993). Plant J. 3:681–689.



FIGURE 17.48 *Uncoupling of auxin and ethylene effects in eight-week-old transgenic* N. tabacum *cv. Samsun. (Left) An ethylene-deficient plant expressing a* Pseudomonas *ACC deaminase gene under the control of the figwort mosaic virus 19S promoter. The phenotype is indistinguishable from wild-type plants. (Middle) A double transformant with increased IAA content and decreased ethylene production. (Right) An IAA-overproducer expressing the* A. tumefaciens iaaM *gene under the control of the CaMV 35S promoter. The phenotype indicates that apical dominance and leaf epinasty are primarily controlled by IAA, whereas ethylene is partially responsible for the inhibition of stem elongation observed in IAA-overproducing plants. Source*: Romano et al. (1993). Plant Cell 5:181–189.



FIGURE 17.49 *The triple response to ethylene of six-day-old etiolated* P. sativum *seedlings and four-day-old etiolated* Vigna radiata *bean seedlings. (A) Untreated control* P. sativum *seedlings (0) and* P. sativum *seedlings grown for two days in air supplemented with ethylene at 0.1, 1.0, and 10 µl/ml. Note the concentration-dependent effects of ethylene on diageotropism, inhibition of epicotyl elongation, and lateral enlargement of the epicotyl. (B) Control* V. radiata *seedlings (0) and* V. radiata *seedlings grown for two days in air supplemented with 1 and 10 µl/ ml ethylene, which induces a concentration-dependent inhibition of hypocotyl elongation, lateral enlargement of the hypocotyl, and extreme bending of the apical hook. (C) Magnification of ethylene-treated etiolated* V. radiata *seedlings.*
Source: (A–C) H. Mori, Nagoya University, Japan; previously unpublished.

Little is known about the mechanism by which GA_3 increases endogenous IAA concentrations in peas. One proposal postulates that D-Trp is converted to IAA more effectively than its L-isomer and acts as an intermediate between L-Trp and indole-3-pyruvic acid in the IAA biosynthesis pathway; moreover, GA_3 treatment supposedly enhances the activity of the racemase that regulates the conversion of L- to D-Trp, thereby increasing the rate of IAA biosynthesis.

In contrast to GA_3, CK reduce the size of endogenous IAA pools. Transgenic tobacco plants that express the *A. tumefaciens ipt* gene overproduce CKs. Compared with wild-type plants, these transgenics contain significantly lower concentrations of free IAA and in most cases IAA conjugates. Rates of IAA biosynthesis also are reduced, as determined by ^2H_2O incorporation studies, and exogenous [$^{13}C_6$]IAA is degraded more slowly in the *ipt*-transformed plants. Thus, elevated amounts of CKs, primarily tZ, tZR, and tZRMP, not only reduce the size of the endogenous IAA and IAA conjugate pools but also appear to lower the rate of IAA turnover.

Just as CK overexpression antagonizes IAA synthesis, IAA overexpression appears to downregulate CK production. IAA-overproducing tobacco plants that express *iaaH* and *iaaM* (see Fig. 17.47) contain lower concentrations of endogenous tZ and related CKs than wild-type plants. Since IAA represses expression of *IPT* and *CYP735A* (see Sections 17.3.4 and 17.3.15), an action point of auxin for downregulating CK production is the early step of CK biosynthesis.

17.5 Ethylene

In 1886, while a graduate student in St. Petersburg, Dimitry Nikolayevich Neljubow noticed that etiolated pea seedlings grew horizontally in laboratory air, and vertically in air from outside the laboratory. After an extensive study to exclude cultural practices, light, and temperature as causative agents, he showed that **ethylene**, in the gas used for lighting, induced this abnormal growth. Many of ethylene's physiological effects on plant growth and development, including its impact on seed germination, root and shoot growth, flower development, senescence and abscission of flowers and leaves, and the ripening of fruit, were discovered prior to 1940. Subsequent work has since shown that ethylene also participates in the modulation of plant responses to a range of biotic and abiotic stresses.

When investigators in the 1930s proposed that ethylene was both an endogenous plant growth regulator and a fruit-ripening hormone, their hypothesis was met with skepticism by their contemporaries, many of whom considered ethylene to be an unimportant product of the paramount plant hormone, auxin. This prejudice hampered research on ethylene while attention focused on auxin, GAs, and CKs.

Initial ethylene quantification was cumbersome and insensitive, and some relied on bioassays based on leaf epinasty or the growth of etiolated *P. sativum* and *Vigna radiata* seedlings (Figs. 17.49A,B). Gas chromatography and the development of the flame ionization detector increased ethylene detection by a factor of 10^6. This major development led to rapid advances in ethylene research and ethylene was quickly established as an endogenous plant growth regulator.

17.5.1 Ethylene is synthesized from *S*-adenosyl-L-methionine via the intermediate 1-aminocyclopropane-1-carboxylic acid (ACC)

Synthesis of ethylene from its immediate precursor 1-aminocyclopropane-1-carboxylic acid (ACC) is catalyzed by ACC oxidase (ACO). ACC is produced from SAM in a

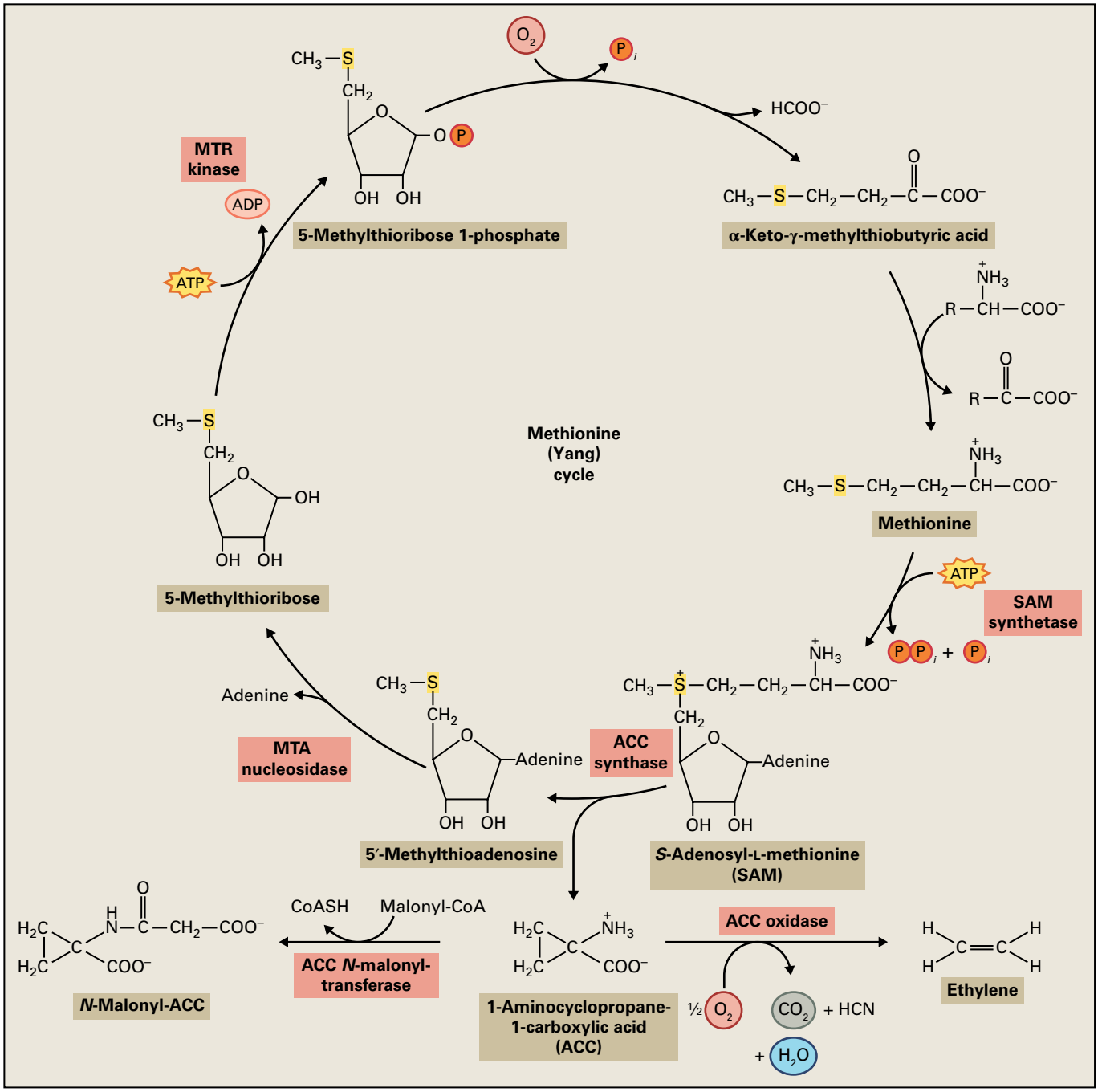


FIGURE 17.50 *The Met cycle and ethylene biosynthesis. Ethylene is synthesized from Met by way of SAM and ACC. The enzymes that catalyze these three steps are SAM synthase, ACC synthase (ACS), and ACC oxidase (ACO). 5′-Methylthioadenine, a product of the ACO reaction, is salvaged for the resynthesis of Met through the methionine cycle (see Chapter 7). If the methylthio-group from SAM were not recycled, Met availability and ethylene biosynthesis would probably be restricted by sulfur availability. By converting ACC to N-malonyl-ACC instead of to ethylene, plants can deplete the ACC pool and thereby reduce the rate of ethylene production.*

reaction catalyzed by ACC synthase (ACS). These reactions are part of the methionine cycle or Yang cycle named after S. F. Yang, who carried out the early work in elucidating the pathway (Fig. 17.50). In addition to its role in ethylene biosynthesis, SAM is involved in the biosynthesis of polyamines (PA) (see Section 17.7) and a wide range of methylation reactions.

ACS, which cleaves SAM to form the ethylene precursor ACC and 5′-methylthioadenosine (Fig. 17.50), was first characterized in a semi-purified preparation from *S. lycopersicum* pericarp. The enzyme has subsequently been isolated from a number of plant tissues following induction by factors that include exogenous IAA, wounding, lithium chloride stress, and climacteric fruit ripening. ACSs have been cloned from

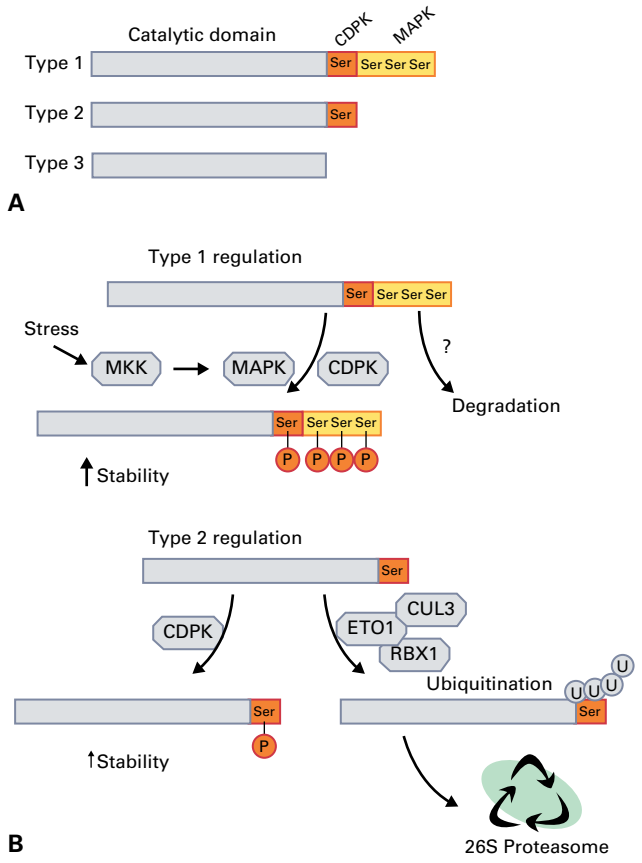


FIGURE 17.51 *ACS types and mechanisms of protein regulation. (A) ACS proteins fall into three major classes according to their C-terminal sequences. Type 1 have three conserved Ser residues (yellow) that can be phosphorylated by a MAPK and a single conserved Ser (red) that can be phosphorylated by a CDPK. Type 2 are slightly truncated and have a Ser that can be phosphorylated by a CDPK. Type 3 lack any conserved C-terminal Ser residues. (B) Type 1 regulation: CDPK and MAPK phosphorylation of C-terminal region increases ACS stability. The MAP kinase (MKK), induces MAPK activity when stimulated by stress e.g. wounding or pathogen attack. Unphosphorylated protein is removed by a yet to be defined mechanism. Type 2 regulation: CDPK phosphorylation of C-terminal Ser increases ACS stability by preventing binding of the ETO protein. Unphosphorylated ACS undergoes ETO binding and this facilitates the formation of a RING E ligase complex that includes a Cullin3 (CUL3) protein and a RING Box 1 protein (RBX1). The E3 ligase adds ubiquitin (U) moieties to the ACS protein thereby targeting it for degradation by the 26S proteasome.*

numerous species and the highly conserved sequences include a lysine (Lys) residue that reacts with SAM and pyridoxyl 5′-phosphate at the active site. Plants typically contain several isoforms of ACS that are differentially expressed in response to wounding, ripening, and various stresses. In *Arabidopsis* three major groups of ACSs have been classified according to C-terminal sequences that play a role in protein turnover (Fig. 17.51). Type 1 enzymes have three conserved C-terminal serine (Ser) residues that can be phosphorylated by a mitogen-activated protein kinase (MAPK) and a single conserved Ser as a substrate for calcium-dependent protein kinases (CDPKs). Type 2 enzymes only have the CDPK site and the C-terminus is shorter. Type 3 enzymes lack both types of phosphorylation sites.

17.5.2 ACSs are major regulators of ethylene biosynthesis

ACSs catalyze the rate-limiting step in ethylene biosynthesis and their levels are controlled by transcription and protein stability. Increased ethylene production, associated with germination, ripening, flooding, and chilling, is invariably accompanied by increased ACC production due to induction or activation of ACS. The enzyme requires pyridoxal phosphate for activity and is sensitive to inhibitors of pyridoxal phosphate, especially aminoethoxy-vinyl glycine and amino-oxy acetic acid. These inhibitors allow investigators to distinguish between the effects of ACS and ACO. The naturally occurring isomer of SAM, (–)-*S*-adenosyl-L-methionine, is the preferred substrate for ACS, while (+)-SAM is an effective inhibitor. However, incubating the enzyme with high concentrations of (–)-SAM can irreversibly modify and inhibit ACS. This "suicide inactivation" involves covalent linkage of a fragment of the SAM molecule to the active site of the enzyme. This substrate-dependent inactivation may be a contributory factor in the rapid turnover of ACS in plant tissues.

Transcriptional control

Ethylene biosynthesis rates are influenced by other plant hormones and by ethylene itself. Auxins promote ethylene synthesis by enhancing the rate of ACC production. Transcript analysis showed that auxin application results in increased levels of certain ACS mRNAs, indicating transcriptional control, and the respective ACS genes have been shown to have *cis*-acting auxin-response elements. Transcriptional control of ACS levels is also observed during *S. lycopersicum* fruit development and ripening. Unripe developing fruits have autoinhibitory ethylene production and certain ACS genes are transcribed. During ripening ethylene can promote (autocatalyze) its production and different ACS genes are transcribed.

Control via protein turnover

Early observations indicated that ACS stability in *S. lycopersicum* fruits varied between ripe and unripe fruits. More recent experiments have shown that ACS turnover plays an important role in regulating ethylene production and that the C-terminal regions of the ACS protein act in regulating this turnover. The stability of ACS proteins is influenced by their phosphorylation status at C-terminal regions with the phosphorylated forms being more stable. Type 1 ACS proteins are phosphorylated by a MAPK in response to stress, for example, pathogen and wounding, and by a CDPK. Phosphorylation increases protein stability whereas unphosphorylated proteins are degraded by an undefined mechanism. Type 2 ACS proteins are phosphorylated by a CDPK and this prevents binding of the ETO (**Et**hylene **o**verproducing)

gene product that is part of an E3 ligase required for ubiquitination of proteins. ETO1 binds ACS and also CUL3 (Cullin3 another part of E3-ligase) that can catalyze the addition of ubiquitin to ACS. The E-ligase complex associated with ACS degradation is the RING ligase that is composed of an E2 conjugating enzyme, a cullin, RBX1 (Ring Box 1), and an adaptor protein(s) (Fig. 17.51). Once ACS is ubiquitinated it is targeted for proteolysis by the 26S proteasome. See Chapter 18 for more details on ubiquitination and proteasome degradation.

17.5.3 ACC oxidase resisted biochemical characterization and was cloned using molecular techniques

The conversion of ACC to ethylene is catalyzed by ACO, previously referred to as "ethylene-forming enzyme" (see Fig. 17.50). The ACO reaction can be summarized in Reaction 17.1:

$$\mathrm{ACC} + \mathrm{O_2} + \text{ascorbate} \xrightarrow{\mathrm{Fe^{2+}}} \mathrm{C_2H_2} + \mathrm{CO_2} + \text{dehydroascorbate} + \mathrm{HCN} + 2\mathrm{H_2O}$$

ACO is activated by one of its products, carbon dioxide. The cyanide generated by the reaction is detoxified by conversion to β-cyanoalanine, which is further metabolized to Asn or γ-glutamyl-β-cyanoalanine.

ACO, which is extremely unstable, proved difficult to purify by conventional techniques. A cDNA clone (pTOM13) of the enzyme was identified using a differential screen of cDNAs in tomato fruit. pTOM13 antisense tomato plants have reduced ethylene production (Fig. 17.52) and confirmation that pTOM13 encodes an ACO was shown in yeast expressing pTOM13. Recombinant yeast were able to convert ACC to ethylene and the recombinant 35-kDa protein met all criteria for authentic ACO activity, including inhibition by Co^{2+}.

All plant tissues appear to contain ACO, as measured by the rate of ethylene evolution in the presence of a saturating concentration of ACC. Under stress conditions, in response to ethylene, and at selected stages of development (e.g., fruit ripening), ACO activity increases markedly. Both senescence and ripening-induced increases in ACO activity are a result of increased transcription.

17.5.4 When supply of available SAM is low, ethylene and polyamine biosynthetic pathways may compete for this shared substrate

Biosynthesis of both ACC (see Fig. 17.50) and PAs (see Fig. 17.63) involves the incorporation of the aminopropyl group from SAM. Under certain conditions, competition for SAM may restrict rates of ethylene or PA production. Inhibition of ACC synthesis by aminooxyacetic acid results in increased PA production. Conversely, inhibition of PA biosynthesis leads to increased concentrations of ACC and ethylene. This implies that one SAM-dependent pathway is stimulated when the other is blocked. When competition for the available SAM is circumvented by low demand for PAs, or when ACC levels are increased by upregulation of 5′-methylthioribose-recycling enzymes (see Fig. 17.50), ethylene and PA production will not directly interact. Whether ACC/PA interactions represent a



FIGURE 17.52 *Effect of antisense ACO genes on ripening and spoilage of* S. lycopersicum *cultivar Ailsa Craig fruit picked three weeks after onset of ripening and stored at room temperature for three weeks. (Left) Fruits from the descendants of the original TOM13-antisense plants, which generate about 5% of the normal amount of ethylene. They ripen fully but do not overripen and deteriorate. (Right) Fruits from wild-type plants grown and stored under identical conditions. They produce normal amounts of ethylene and consequently exhibit severe signs of over-ripening.*
Source: D. Grierson, University of Nottingham, UK; previously unpublished.

widespread means for controlling ethylene production remains an open question.

17.5.5 Most hormones must be catabolized, but volatile ethylene can be released as a gas

Prior to 1975, ethylene metabolism by plants was considered to be an artifact, caused by bacterial contamination. However, there is now evidence from plants grown in sterile conditions that [^{14}C]ethylene is oxidized to [^{14}C]CO_2 or converted to [^{14}C]ethylene oxide and [^{14}C]ethylene glycol. Ethylene metabolism exhibits a very high K_M indicative of a chemical reaction rather than a physiological process. In peas, the concentration of ethylene yielding a half-maximal rate of ethylene metabolism is ≈1,000 times the concentration required for half-maximal response in the pea growth test illustrated in Figure 17.49A. It is likely that ethylene metabolism is largely a consequence of artificially elevated ethylene levels. The major route by which plant tissues lose ethylene is probably diffusion to the surrounding atmosphere.

17.5.6 Repression of ethylene biosynthesis can delay over-ripening in fruit, and represents an important field of biotechnological research

There is a great deal of interest in downregulating ethylene biosynthesis, since elevated levels can trigger ripening and subsequent over-ripening of climacteric fruits such as bananas, apples and tomatoes. Two different biotechnological strategies have been employed to generate transgenic tomato fruit that resist over-ripening. One, the overexpression of a *Pseudomonas* gene encoding ACC deaminase, reduces ethylene levels in fruits by catalyzing the conversion of ACC to α-ketobutyric acid and NH_3. The second approach to limiting ethylene biosynthesis involves use of antisense gene constructs against either ACO or ACS. Analysis of transgenic fruit produced by these procedures has demonstrated a direct correlation between the level of ethylene inhibition and rate of ripening.

The phenotype of transgenic tomato fruit expressing antisense ACO has been studied in most detail. In these fruit, ethylene production is inhibited by about 95% during ripening. ACO antisense fruit grow normally and begin to change color, losing chlorophyll and accumulating lycopene, at the same stage of development as nontransformed fruit. However, transgenic fruit exhibit reduced reddening and an increased resistance to over-ripening and shriveling when stored at room temperature for prolonged periods (Fig. 17.52). Transgenic fruit do not soften as readily and can be left on the plant longer to ripen more fully. Biotechnological manipulation of ethylene production for improved crop yield and less spoilage is possible in other climacteric fruits, such as melons, pears (*Pyrus* sp.), kiwi (*Actinidia deliciosa*) fruit, apples (*Malus* sp.), nectarines (*Prunus* sp.), avocados (*Persea americana*), and a range of tropical fruit that are rarely seen outside their country of origin because they over-ripen and spoil readily. The same technology can also be used to delay the senescence of flowers and enhance the longevity of cut blossoms.

17.6 Brassinosteroids

In the early 1960s, researchers hypothesized that the rapid germination and growth of pollen grains was associated with the presence of a growth promoter. A crude extract of pollen from *Brassica napus* (rape) induced rapid elongation of *P. vulgaris* (pinto bean) internodes distinct from GA-mediated stem elongation. This early work led to the isolation and identification of brassinolide (BL) the first steroidal plant growth regulator (Fig. 17.53). A second plant steroid, castasterone (CS; Fig. 17.53) was isolated from insect galls of chestnut (*Castanea*). Since these reports, a number of related steroidal compounds have been isolated from a variety of plant sources, and collectively called **brassinosteroids** (BRs)

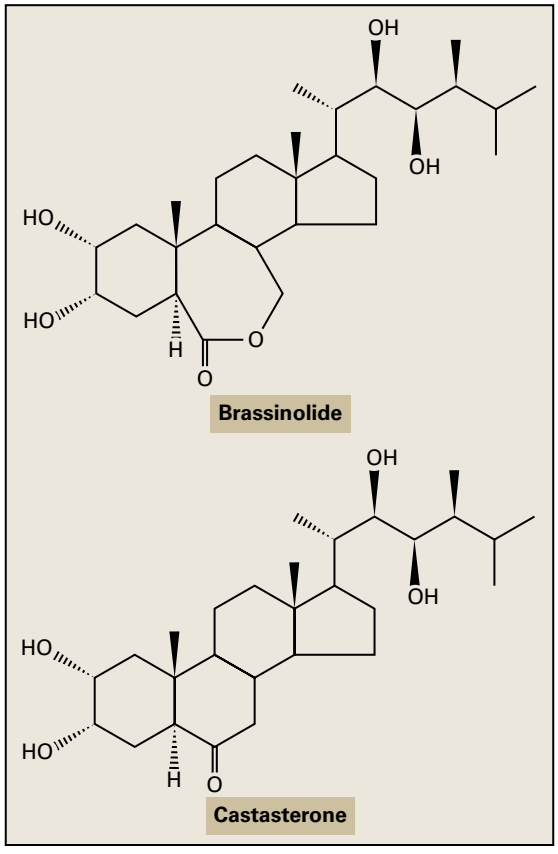


FIGURE 17.53 *Structures of brassinolide and castasterone.*

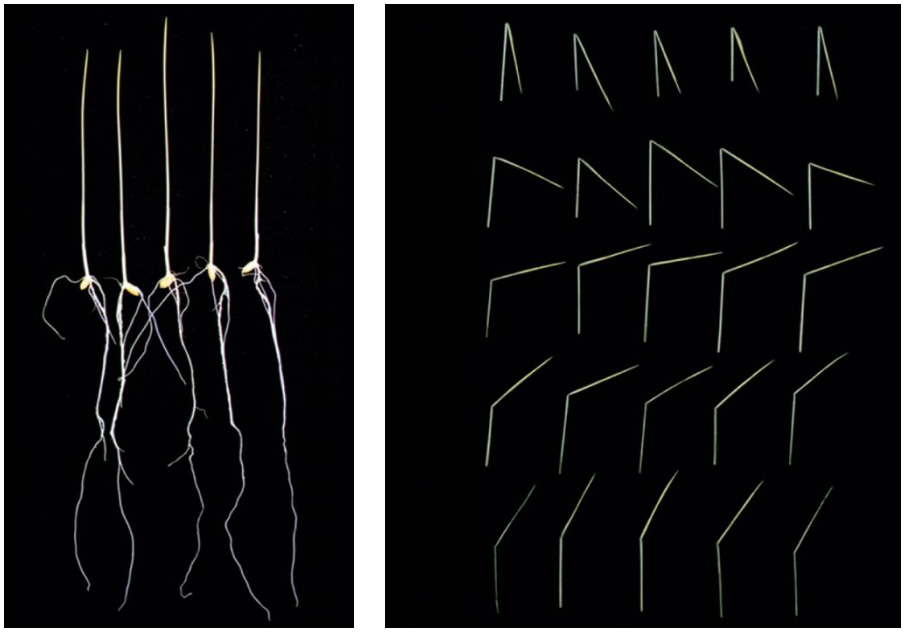


FIGURE 17.54 *Etiolated* O. sativa *seedlings used to obtain excised leaf lamina (left) and the effects of increasing concentrations of BL on the rice lamina inclination bioassay (right). BL and other BRs induce a dose-dependent swelling of the adaxial cells of the joint between the leaf's blade and sheath. This bioassay is very sensitive and is used in studies on BR structure–activity relationships as well as for screening fractionated plant extracts for BR activity.*
Source: T. Yokota, Teikyo University Utsunomiya, Japan; previously unpublished.

that exhibit significant biological activity in the *O. sativa* lamina inclination assay (Fig. 17.54).

BRs occur in algae, ferns, gymnosperms and angiosperms but have not been detected in microorganisms. More than 40 BRs have been identified and, structurally, they are C_{27}-, C_{28}-, and C_{29}-steroids with different functional groups on the A- and B-rings and side chain (Fig. 17.55). Brassinolide, a C_{28}-BR, has the highest biological activity of the BRs and is distributed widely in the plant kingdom, along with biosynthetically related compounds. The biosynthesis of BL from campesterol has been studied most extensively using normal and transformed cells of *Catharanthus roseus* (Madagascar periwinkle).

17.6.1 BRs affect a range of morphological characteristics

Application of BRs induces a broad spectrum of responses, including increased stem elongation, pollen tube growth, unrolling of grass leaves, bending of grass leaves at the sheath/blade joints, proton pump activation, reorientation of cellulose microfibrils, xylogenesis, and enhanced ethylene production. The existence of dwarf mutants of *Arabidopsis*, *P. sativum*, *O. sativa* and *S. lycopersicum* defective in BR biosynthesis or signaling indicates that BRs promote the growth or elongation of plant cells. *Arabidopsis* mutants grown in light have dark green leaves with reduced cell size, reduced apical dominance and diminished male fertility (Fig. 17.56). Curiously, when grown in dark, these mutants do not etiolate and share some characteristics with light grown plants. When BL is applied to BR biosynthesis mutants these phenotypic abnormalities are reversed.

17.6.2 The plant sterol campesterol is a precursor of brassinolide

All plant sterols are synthesized from cycloartenol (Fig. 17.57), which is derived from squalene by way of 2,3-epoxysqualene; cholesterol biosynthesis in animals, in contrast, proceeds from lanosterol. A characteristic feature of plant sterols is alkylation at C-24 with C1 or C2 substituents. Cholesterol, however, a widely distributed minor sterol in plants, is not alkylated at C-24 (Fig. 17.57). Common sterols found in plants include sitosterol (C_{29}), stigmasterol (C_{29}), campesterol (C_{28}), 24-epicampesterol (or 22-dihydrobrassicasterol) (C_{28}), and cholesterol (C_{26}). One of the rarer sterols includes 24-methylene-25-methylcholesterol, and sterol biosynthesis intermediates such as 24-methylenecholesterol (C_{28}) and isofucosterol (C_{29}) are also present in some species (Fig. 17.57). Except for stigmasterol, all these compounds are thought to be BR precursors, with the parent sterol and the BR derivative sharing the same C-24 and C-25 substituents.

Sitosterol is the most abundant sterol and comprises 50–80% of the total sterol content of many plants, but it appears not to be a preferred precursor for BR biosynthesis. In many plants, BL and biosynthetically related compounds are the major BRs, indicating that campesterol is utilized preferentially for biosynthesis. Analysis of mutants defective

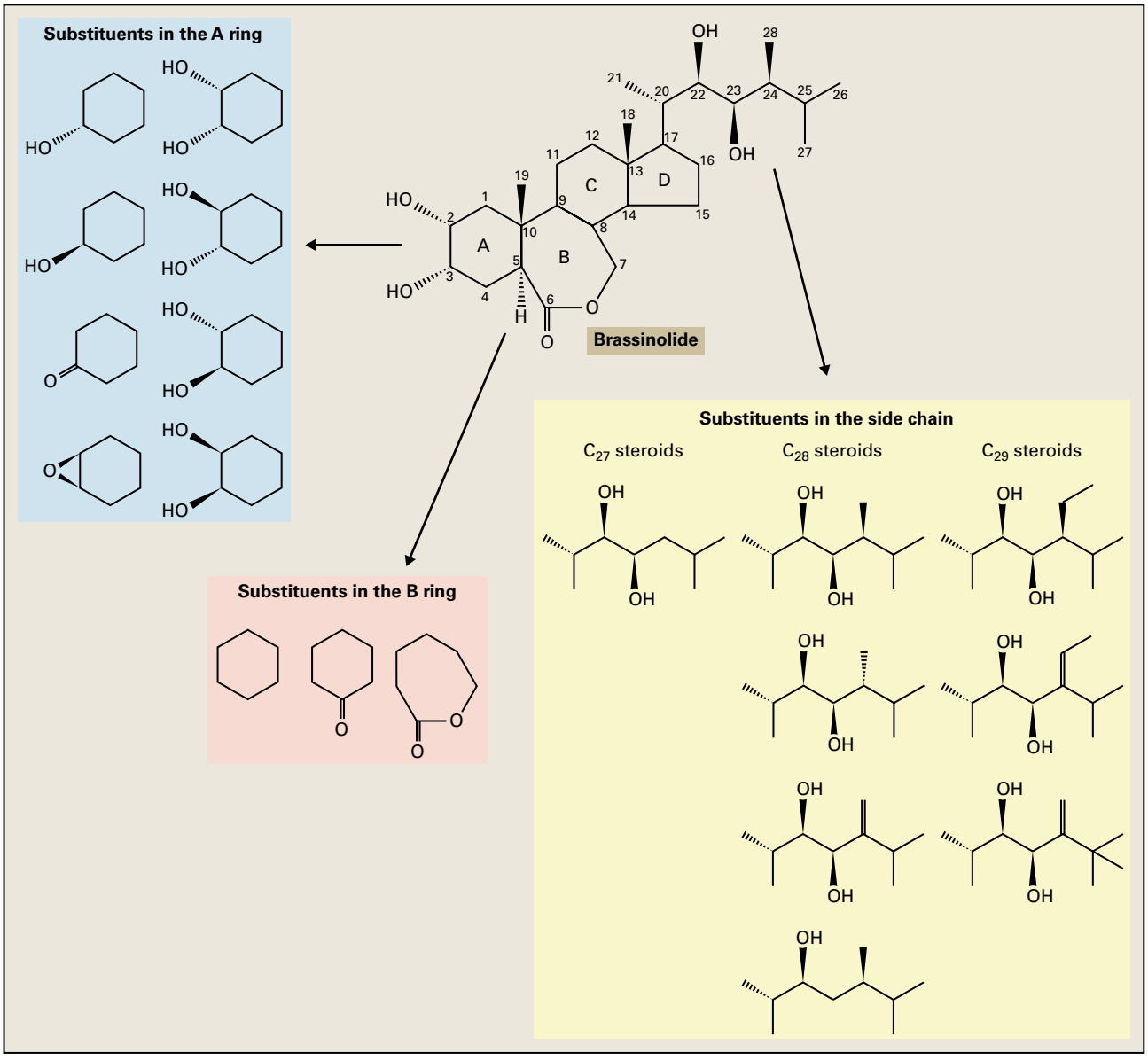


FIGURE 17.55 *Functional groups in the A ring, B ring, and side chain of natural BRs. BL is the most biologically active BR.*



FIGURE 17.56 *Sixteen-day-old* Arabidopsis *seedlings: wild-type (left), BL-deficient det2 mutant (center), BL-deficient dim mutant (right). Source*: T. Yokota, Teikyo University, Utsunomiya, Japan; previously unpublished.

in sterol biosynthesis indicates that synthesis of sitosterol and campesterol utilize the same enzymes.

17.6.3 The synthesis of BL from campesterol

The biosynthetic pathways leading to production of BL was initially established in cultured cells of *C. roseus* through feeding labeled substrates and following their metabolism. Phenotypic rescue experiments and analysis of endogenous BR levels of mutants defective in BR synthesis provided novel tools to further characterize the pathway. The presence of many C-6-deoxo intermediates led to the generation of the early and late C-6 oxidation pathways. Subsequently BL synthesis has been proposed to occur via a "metabolic grid" in which the order of oxidation at certain C atoms is arbitrary. Analysis of recombinant

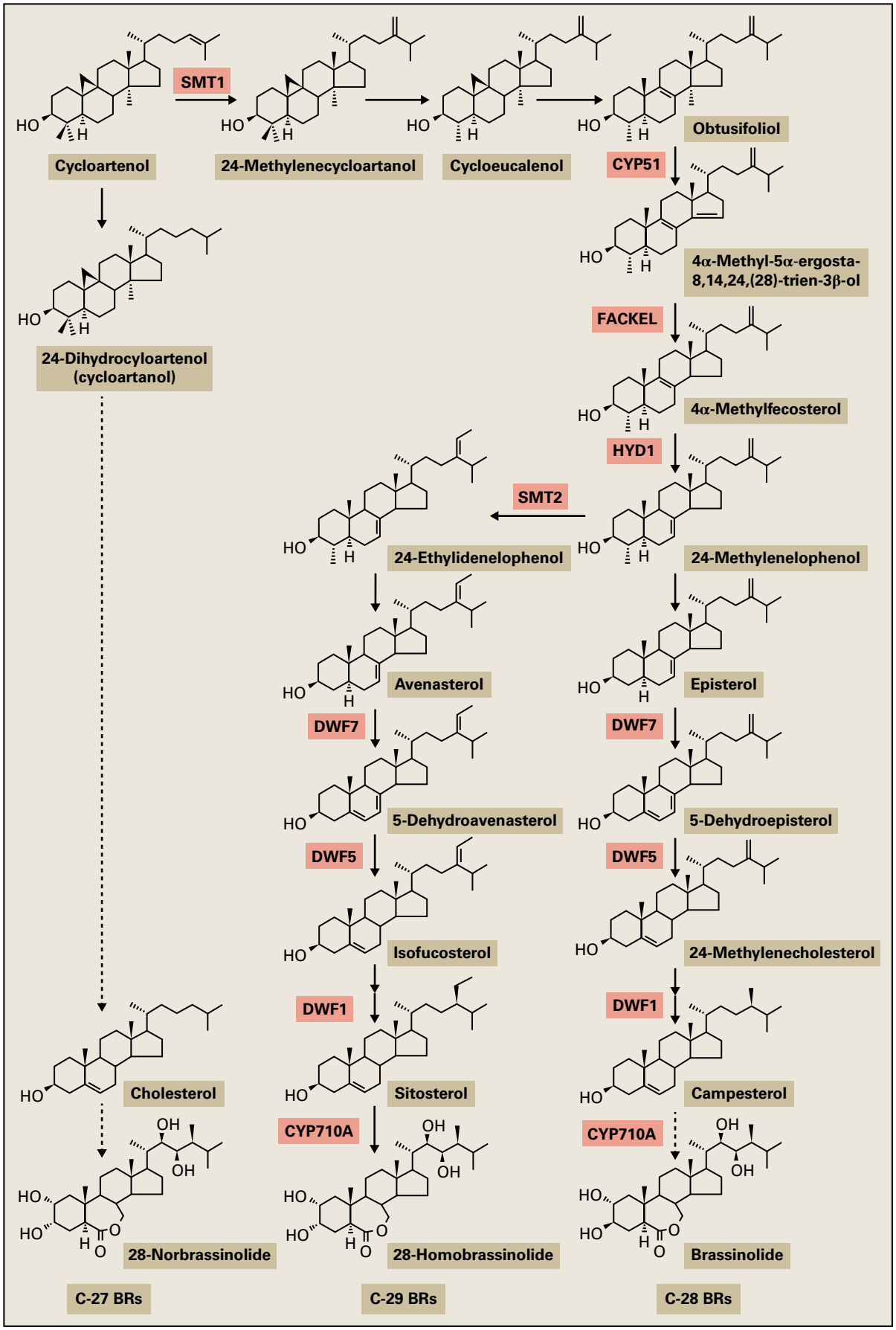


FIGURE 17.57 *Biosynthesis of sterols in vascular plants and biosynthetic lesions in* Arabidopsis *mutants. The biosynthesis of sterols in vascular plants is not fully understood, especially the synthesis of cholesterol. Broken lines indicate multiple steps. Sites where* Arabidopsis *gene products act on the pathway are indicated: CYP51; CYP710A; DWF1, DWARF1; DWF5, DWARF5; DWF7, DWARF7, FACKEL; HYD1, HYDRA1; SMT1, STEROL METHYLTRANSFERASE1; SMT2, STEROL METHYLTRANSFERASE2.*

enzymes and affinity for different substrates are also providing novel insights into the order of reactions. A consensus is emerging that there is no single definitive route to BL synthesis, however the most likely route is via the late C-6 oxidation of BRs as described in the following sections.

The first step

The first step in the synthesis of BL is conversion of campesterol to its 22-hydroxylated product (22S)-22-hydroxy-campesterol (Fig. 17.58). The *Arabidopsis DWARF4* gene encodes a CYP450 enzyme, CYP90B, and this more readily hydroxylates campesterol rather than campestanol, which therefore places it as the first reaction in the conversion of campesterol to BL. (22S)-22-hydroxy-campesterol is then converted to the C-2 ketone by CYP90A1 and the keto moiety is a substrate for the 5α-reductase activity of DEETIOLATED2 (DET2). The reduction of the D4 bond is impaired in the *det2* dwarf mutant of *Arabidopsis* and this reaction is analogous to the conversion of testosterone to dihydrotestosterone in animals. The amino acid sequence deduced from the *DET2* gene shares 40% homology with a mammalian steroid 5α-reductase, which catalyzes the NADPH-dependent conversion of testosterone to dihydrotestosterone.

C-23 hydroxylation

Previously CYP90A encoded by the *Constitutive photomorphogenic and dwarfism* (*Cpd*) gene was thought to be the C-23 hydroxylase in BL synthesis. This is no longer the case and CYP450s, CYP90C, and CYP90D catalyze C-23 hydroxylation of BRs (Fig. 17.58). In *Arabidopsis* these enzymes have redundant function as only *cyp90C* and *cyp90D* double mutants have a strong dwarfing phenotype. Recombinant enzyme assays indicate that both CYP90C1 and CYP90D1 are able to convert (22S,24R)-22-hydroxyergost-4-en-3-one,(22S,24R)-22-hydroxy-5α-ergostan-3-one, and 3-*epi*-6-deoxocathasterone to their C23-hydroxylated products. But they showed limited conversion of (22S)-22-hydroxycampesterol and 6-deoxocathasterone. This indicates a new preferred synthesis route leading to the production of BL that shortcuts the need to synthesize intermediates such as 6-deoxocathasterone and 6-deoxoteasterone that were present in previous pathways (Fig. 17.58).

C-6 oxidation

The *S. lycopersicum Dwarf* gene was cloned by transposon tagging and found to encode a CYP450 enzyme CYP85A1. This enzyme catalyzed the conversion of 6-deoxocastasterone to castasterone (CS). CYP85A3 in *S. lycopersicum* is a CYP85A1 homolog that is fruit specific and can convert 6-deoxocastasterone to BL. In *Arabidopsis* CYP85A1 and CYP85A2 exhibit overlapping function, with single loss of function mutations having weak or no phenotype. Biochemical analysis indicates CYP85A1 can synthesize CS whereas CYP85A2 can make both CS and BL.

Transcriptional feedback regulation of BL synthesis

Transcripts encoding CYP85A1, CYP85A2, CYP90B1, CYP90C1, and CYP901 from *Arabidopsis* are downregulated by bioactive BRs. Feedback regulation requires a functional BRASSINOSTEROID-INSENSITIVE1 (BRI1) receptor as mutants lacking the receptor have defective feedback regulation with very high P450 transcript levels and BR accumulation observed. Binding of the BRASSINAZOLE RESISTANT1 (BZR1) transcription factor, a transcription factor involved in BR signaling (see Chapter 18), has identified a specific BR-response element to which BZR1 binds as a repressor. This response element has also been identified in the promoters of the other P450 genes in BR synthesis indicating coordinated repression of BR synthesis genes.

17.6.4 Chemical inhibitors have been used to dissect pathways of BR biosynthesis

The use of inhibitors of plant hormone biosynthesis complements studies with biosynthetic mutants in helping to elucidate metabolic pathways. They also provide phenotypic evidence for the role the hormone plays in growth and development in species for which mutants are difficult to generate. Triazoles, such as uniconazole and paclobutrazol (see Fig. 17.8), inhibit *ent*-kaurene oxidase, a CYP450 involved in GA biosynthesis (see Fig. 17.7). Modification of uniconazole in which the *tert*-butyl group is replaced by a phenyl group generated brassinazole, a strong inhibitor of BR synthesis (Fig. 17.8). Treatment of plants with brassinazole generates phenotypes similar to BR-synthesis mutants by inhibiting the C-22 hydroxylase reaction catalyzed by CYP90B.

17.6.5 BR metabolism routes have been identified

Mutants and genes

Both molecular genetic and chemical approaches have helped elucidate mechanisms of BR metabolism. Activation tagged mutants leading to over expression of CYP734A1 and CYP72B1 generates phenotypes similar to the BR-deficient dwarf mutants. CYP734A1 overexpression mutants accumulate C-26 hydroxylated BRs and the recombinant enzyme has been shown to have C-26 hydroxylase activity. CYP72B1 overexpression mutants do not accumulate C-26 hydroxylated BRs and its function is yet to be defined. CYP734A1 transcript levels are under positive feedback regulation by BRs whereas CYP72B1 transcription does not seem to be affected.

Molecular genetic techniques have also revealed the importance of glycosylation and sulfonation in BR metabolism. Analysis of UDP-glycosyltransferases (UGTs) has shown that plant steroids can act as substrates, and in *Arabidopsis* 23-*O*-glucosylation of BL and CS is observed. Transgenic plants overexpressing UGT73C5 contained reduced amounts of BRs and displayed BR-deficient phenotypes that can be rescued by exogenous application of BRs. Sulfonation of BRs by recombinant plant steroid sulfotransferase has been observed although the substrate range of these enzymes is limited and BR-sulfates have not been observed in plants.

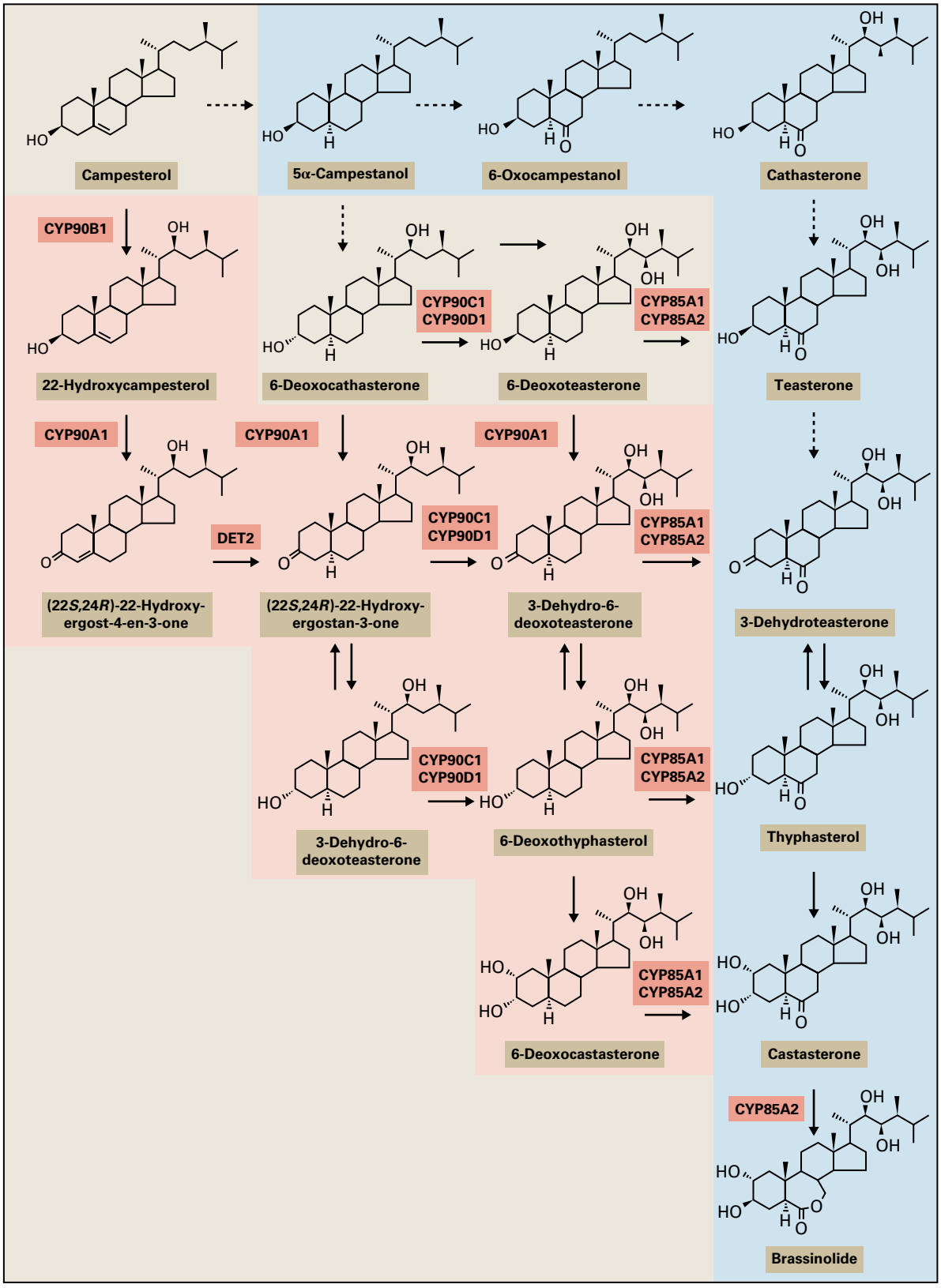


FIGURE 17.58 *Biosynthesis of BL from campesterol. Intermediates with turquoise background are those originally observed as the early C-6 oxidation pathway. Intermediates with pink background indicate most likely synthesis route. Location and class of CYP450 enzymes are provided: 85A1, C-6 oxidase (nonlactonizing); 85A2, C-6 oxidase (lactone – BL formation); 90B, C-22 hydroxylase; 90C/D, C-23 hydroxylase; DET2, DEETIOLATED2 = 5α-reductase; CYP90A1, C-3 oxidation. Broken arrows indicate probable multienzyme catalyzed reaction with other intervening intermediates, solid arrows indicate single step.*

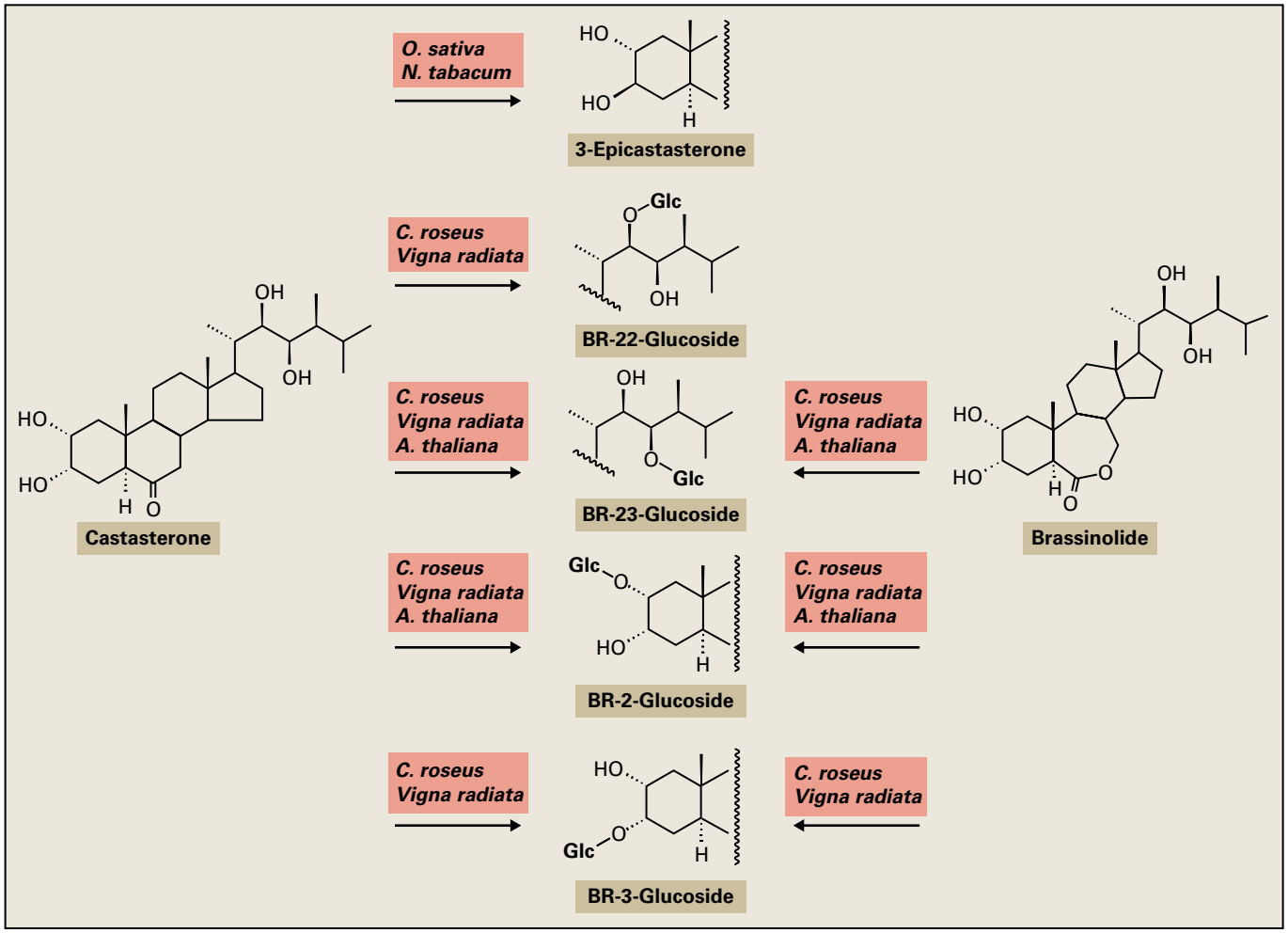


FIGURE 17.59 *Metabolism of castasterone (CS) and BL. In addition to the metabolites indicated, water-soluble metabolites are formed from CS and BL, but their structures have not been determined.*

Analysis of metabolites

Molecular genetic approaches are complemented with experiments focused on chemical analysis of metabolism products of BRs including CS and BL. This has provided further mechanisms of BR deactivation (Fig. 17.59) although many water-soluble metabolites with undetermined structures are also formed. Metabolism of 24-epicastasterone and 24-epibrassinolide, though rare in plants, has been investigated in most detail (Figs. 17.60 and 17.61). From these studies, four basic reaction sequences have been identified, the type of metabolism observed being dependent on plant species and BR used.

Epimerization of the 2- and 3-hydroxyls, followed by glucosylation or esterification

The α-hydroxyls on the A-ring often epimerize to form β-hydroxyls. 3-Epicastasterone is found as a minor metabolite of CS in tobacco and rice seedlings (see Fig. 17.59). 3-Epimerization has also been observed following application of 24-epicastasterone and 24-epibrassinolide to cell cultures of *S. lycopersicum* and serradella (*Ornithopus sativus*) (Figs. 17.60 and 17.61). 2-Epimerization is observed when *Cucumis sativus* seedlings metabolize 24-epibrassinolide (Fig. 17.61). Because 2-epicastasterone, 3-epicastasterone, and 2,3-diepicastasterone are major endogenous BRs in *P. vulgaris* seeds, and all are less active biologically than CS, epimerization of the 2- and 3-hydroxyls appears to be a general deactivation reaction.

After 3-epimerization, the resulting 3β-hydroxyl group is esterified with lauric, myristic, or palmitic acids in *Ornithopus* cells (Figs. 17.60 and 17.61). Lily (*Lilium* sp.) pollen contains teasterone-3-*O*-esters conjugated with lauric and myristic acids. However, no acyl conjugates of typhasterol, CS, and BL are known to occur naturally, suggesting that only the 3β-hydroxyl is susceptible to conjugation with fatty acids. In *S. lycopersicum* cells, 3-epimerization is not followed by esterification but with glucosylation of either the 2α- or the 3β-hydroxyl group. Accordingly, 3-epimerization to form a 3β-hydroxyl group precedes further conjugation.

Hydroxylation of C-20 and successive side chain cleavage

Hydroxylation of C-20 has been observed after application of 24-epicastasterone and 24-epibrassinolide to *Ornithopus* cells

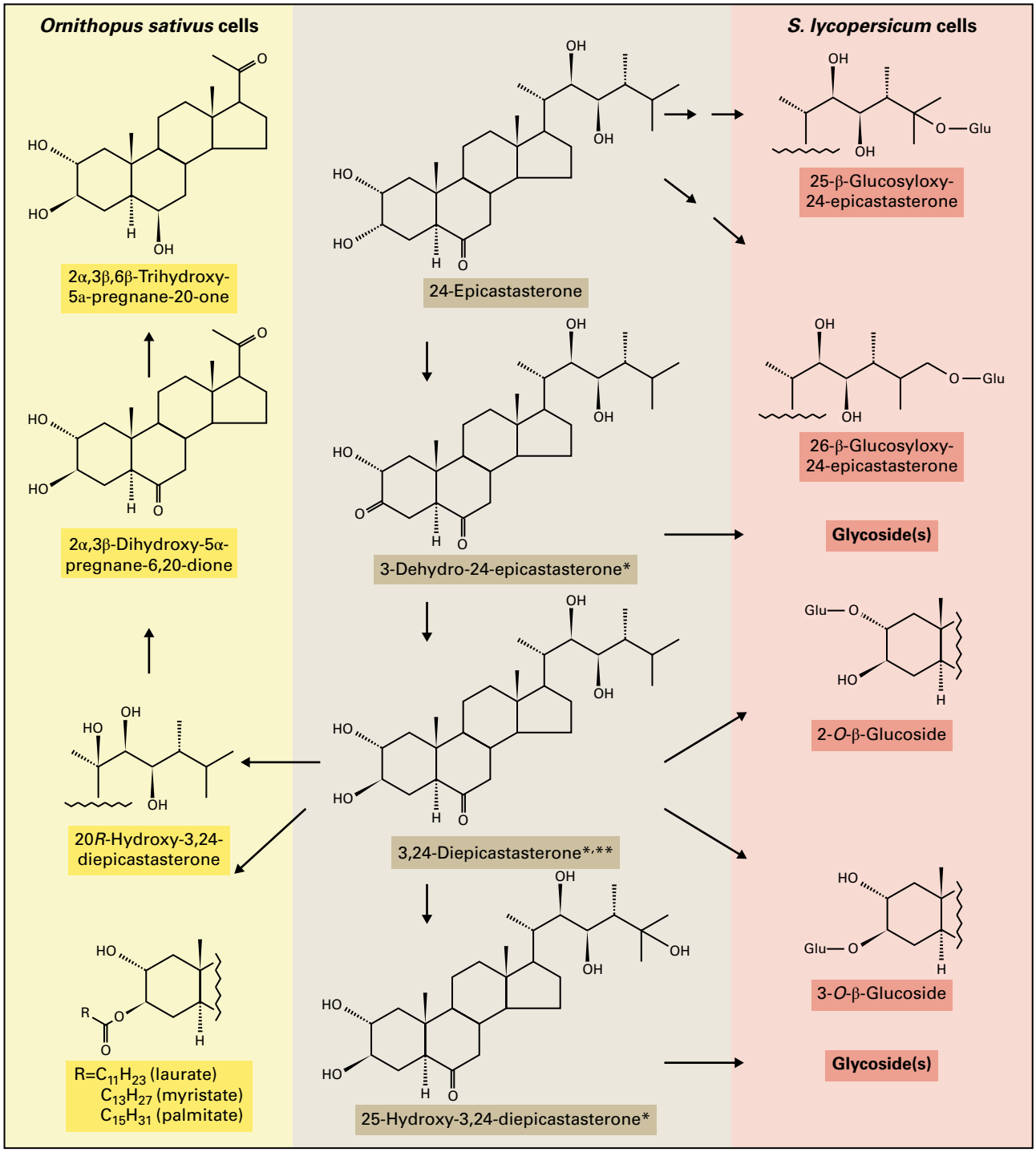


FIGURE 17.60 *Metabolism of 24-epicastasterone. *Present as glycoside(s) in* S. lycopersicum *cells. **Identified as the free form in* Ornithopus *cells.*

(Figs. 17.60 and 17.61). 20-Hydroxylation probably occurs after 3-epimerization and is followed by cleavage of the bond between C-20 and C-22, which yields pregnane derivatives. A pregnane-6,20-dione derived from 24-epicastasterone undergoes further reduction of the 6-keto group to form a 6β-hydroxyl moiety.

Glucosylation of C-23 hydroxyl group

In *Vigna radiata* cuttings, BL is converted almost exclusively to its 23-*O*-glucoside, while CS is converted to nonglycosidic metabolites (see Fig. 17.59). 23-*O*-glucosides of 25-methyldolichosterone and its 2-epimer are endogenous components in immature seeds of *P. vulgaris*. 23-*O*-glucosylation, therefore, appears to be an important deactivation step in some legumes.

Hydroxylation of C-25 and C-26 and subsequent glucosylation

In cultured cells of *S. lycopersicum*, 24-epimers of CS and BL are not metabolized to 23-*O*-glucosides. Instead, the C-25 or

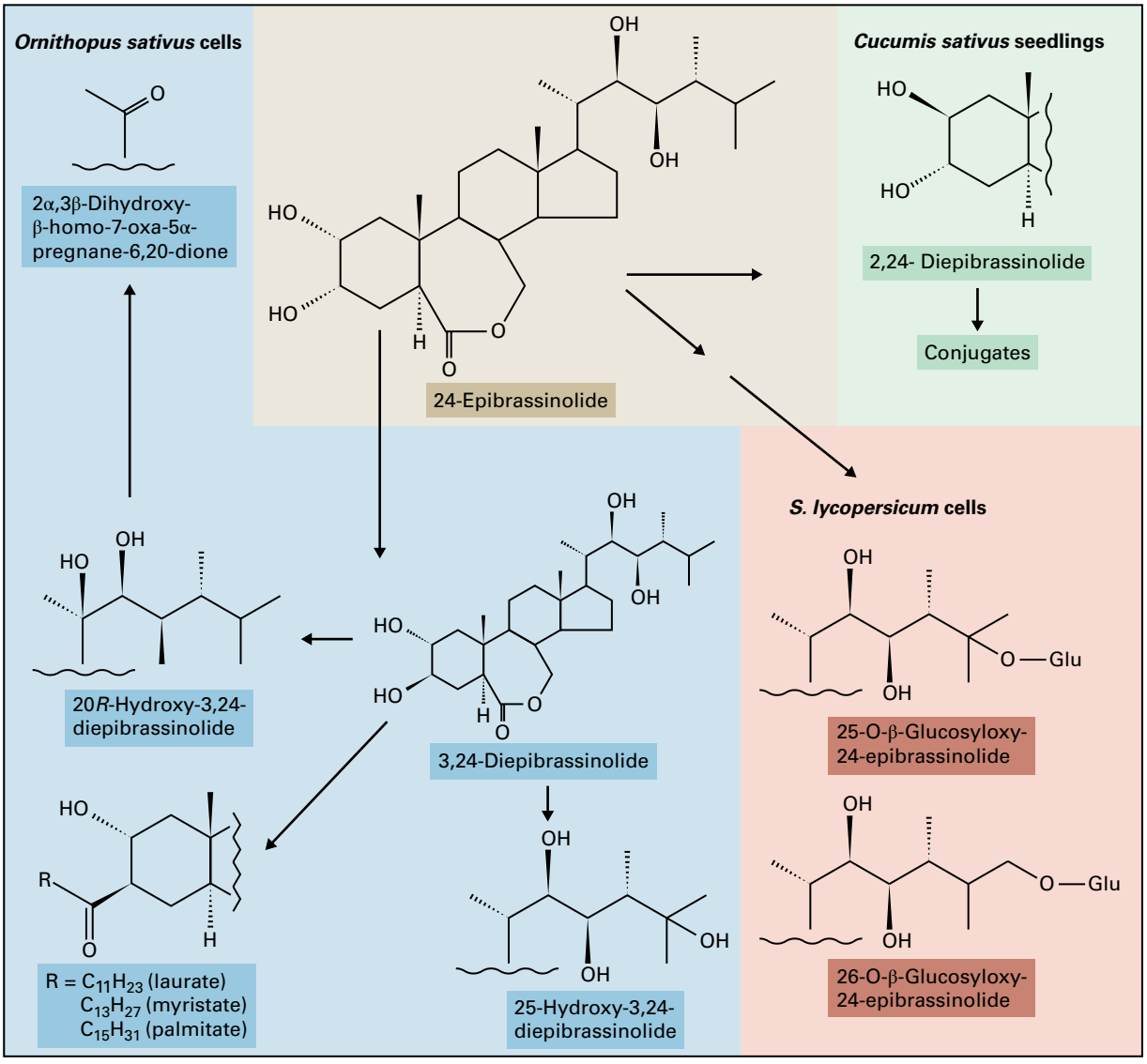


FIGURE 17.61 *Metabolism of 24-epibrassinolide.*

C-26 positions are subjected to hydroxylation followed by glucosylation (Figs. 17.60 and 17.61). Thus, modification of the BR side chain may be determined by whether there is a 24α- or 24β-methyl group present. Other possibilities cannot be ruled out, however, as metabolism of the α- and β-isomers have not been examined in the same plant species. 25-Hydroxy-3,24-diepicastasterone is derived from 24-epicastasterone in *S. lycopersicum* cells, while 25-hydroxy-3,24-diepibrassinolide is produced from 24-epibrassinolide in *Ornithopus* cells.

In the *O. sativa* lamina inclination assay (see Fig. 17.54), 25-hydroxylation increases biological activity of 24-epibrassinolide 10-fold, whereas 26-hydroxlation reduces activity. 25-Hydroxy BRs are inactive when applied to *Arabidopsis* BR-mutants. 25-Hydroxy-BL has not been detected in plants and among the naturally occurring BRs, BL exhibits the most biological activity.

17.7 Polyamines

Polyamines (PAs) are organic polycations commonly found in both prokaryotes and eukaryotes. Because of their polycationic nature, PAs have a high affinity for anionic constituents such as DNA, RNA, phospholipids, and acidic proteins, as well as anionic groups in membranes and cell walls. PAs stimulate many reactions involved in the synthesis of DNA, RNA, and proteins, and are essential for the growth and development of living cells. PAs elicit diverse physiological responses in plants, including cell division, tuber formation, root initiation, embryogenesis, flower development, fruit ripening, and stress tolerance. Because PAs are much more abundant in plants than other hormones, and because millimolar concentrations of PAs are required to induce a biological response, PAs may not have a truly hormonal role. Instead, as is the case in animals, they appear to participate, directly or indirectly, in

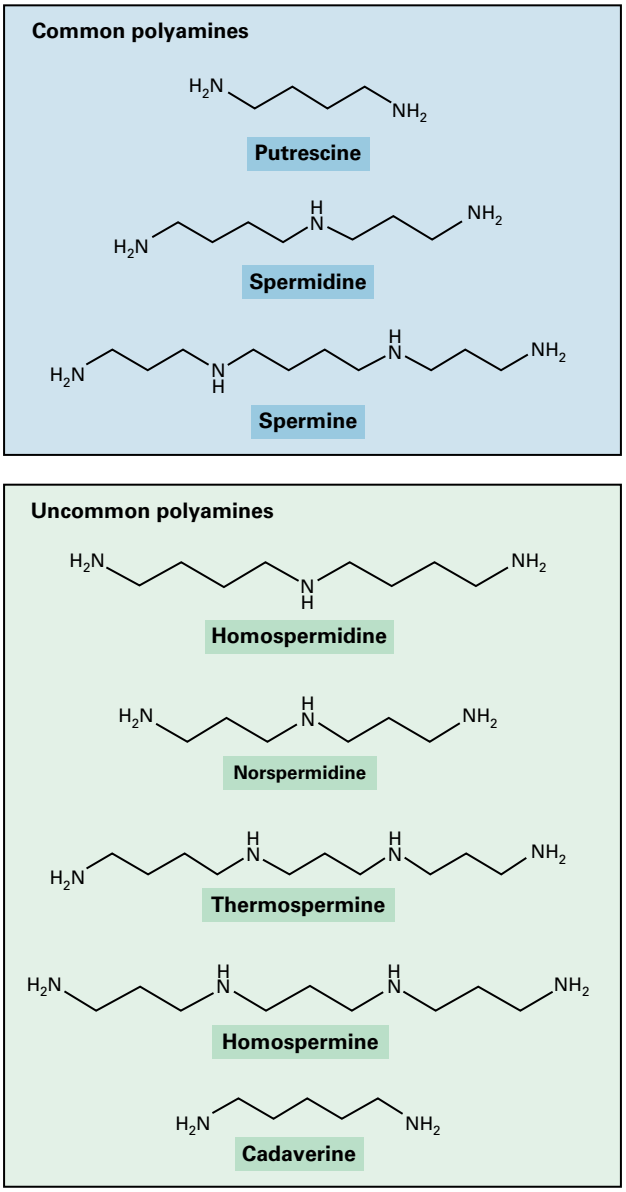


FIGURE 17.62 *Structures of PAs. Putrescine, spermidine, and spermine are commonly found in plants.*

several key processes and metabolic pathways, which are essential for normal growth and development.

The PAs found most frequently in plants and other organisms are putrescine, spermidine, and spermine (Fig. 17.62). In addition, several uncommon PAs, such as homospermidine, norspermidine, norspermine, thermospermine, and cadaverine, have been found in plants. Although cadaverine is present at lower concentrations than the other PAs, it is a common constituent of legumes. Plant PAs occur both as free amines and as amide conjugates of hydroxycinnamic acids such as *p*-coumaric, ferulic, and caffeic acids. These conjugates represent a significant portion of the total PA pool. Participation of conjugates in various cellular processes is seen in the association between hydroxycinnamic acid amide accumulation and flowering, seed and fruit development, and hypersensitive responses to viral and fungal infections.

17.7.1 The first step of polyamine synthesis is decarboxylation of arginine or ornithine

The first step of PA biosynthesis is decarboxylation of the amino acids Arg or ornithine (Orn), which is catalyzed by Arg decarboxylase (ADC) or Orn decarboxylase (ODC) (Fig. 17.63). Putrescine synthesis from Arg requires three enzymatic steps catalyzed by ADC, agmatine iminohydrolase, and *N*-carbamoylputrescine amidohydrolase, but putrescine can also be directly made by Orn decarboxylation. Since ODC in plants is usually less active than ADC, Arg decarboxylation is the major pathway for putrescine synthesis. In *S. lycopersicum* roots, expression pattern of *ODC* is different from *ADC* in terms of response to sucrose, CK, and auxin, suggesting a differentiation of physiological role between the two pathways. On the other hand, there are two *ADC* genes (*ADC1* and *ADC2*) but no *ODC* gene in *Arabidopsis*, indicating that PAs are exclusively produced via ADC in *Arabidopsis*. Seeds from an *ADC* double mutant are abnormal and fail to germinate.

Despite some conflicting evidence, ODC enzymes from *H. vulgare*, jute (*Corchorus* spp.), and *S. lycopersicum* generally exhibit end-product inhibition in the presence of putrescine, spermidine, or spermine. However, ADC enzymes from *A. sativa, O. sativa, C. sativus,* and *Lathyrus sativus* are inhibited by agmatine but are relatively insensitive to PAs. Environmental stresses increase ADC activity, upregulating putrescine production. Abiotic stresses, such as low temperatures, high salt, and dehydration, as well as ABA treatment, induce expression of *ADC1* or *ADC2* in *Arabidopsis*. The potent enzyme inhibitors α-difluoromethylarginine and α-difluoromethylornithine irreversibly inhibit ADC and ODC, respectively.

17.7.2 Putrescine is converted to spermidine and spermine

Spermidine synthase catalyzes the conversion of putrescine to spermidine, and spermine synthase converts spermidine to spermine (Fig. 17.63). Both enzymes transfer an aminopropyl group from decarboxylated *S*-adenosyl-L-methionine (dSAM) to their respective substrates. *S*-Adenosyl-L-methionine decarboxylase (SAM decarboxylase) converts SAM to dSAM. The synthesis of dSAM is inhibited by spermidine but increases in response to increasing putrescine. Because SAM is also a precursor of ethylene, and because PAs and ethylene inhibit each other's biosynthesis, control of the fate of SAM may significantly influence plant growth (see Section 17.5.4).

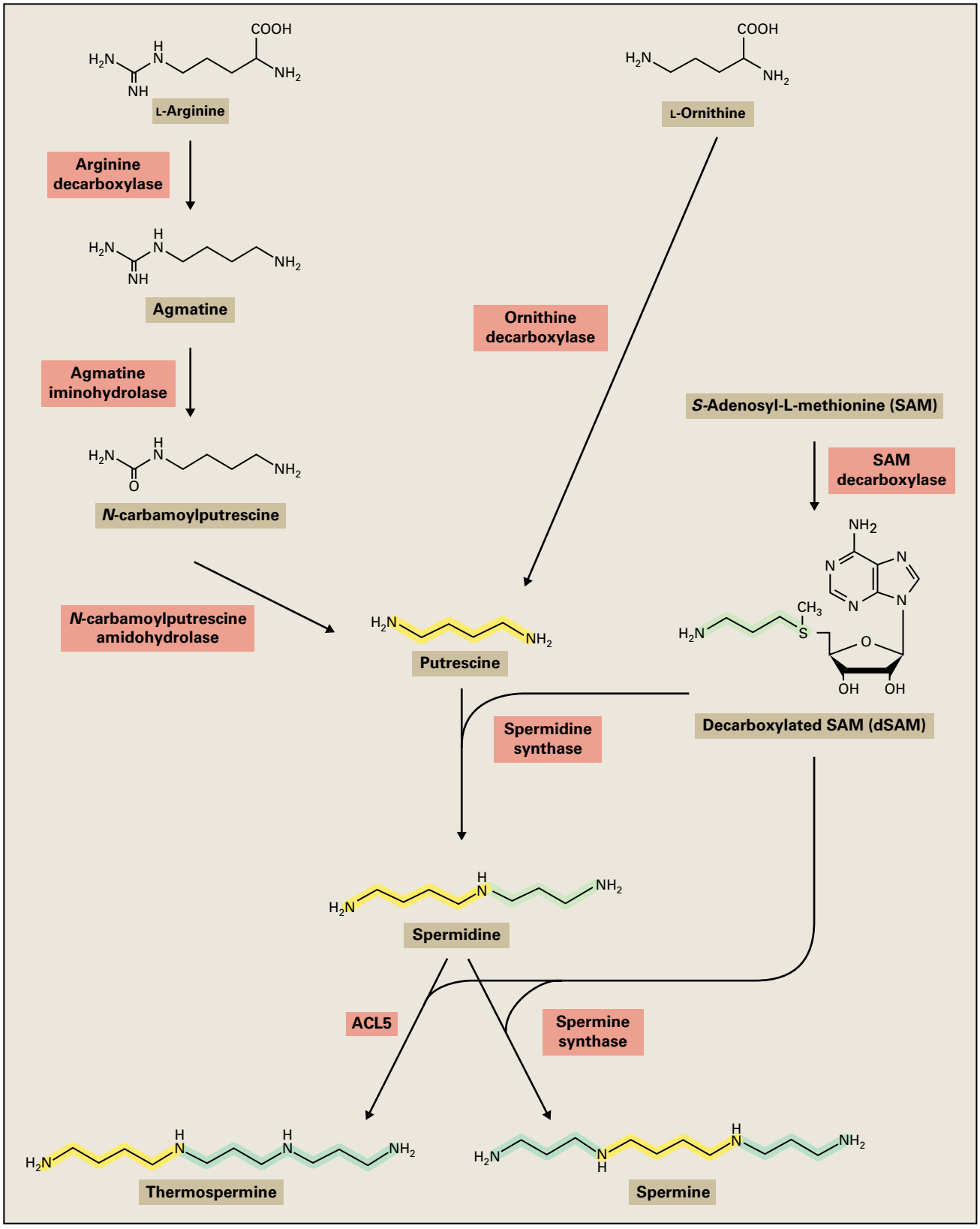


FIGURE 17.63 *Biosynthesis of putrescine, spermidine, and spermine. In most plants, arginine decarboxylase is more active than ornithine decarboxylase. Thermospermine could be synthesized in some plant species.*

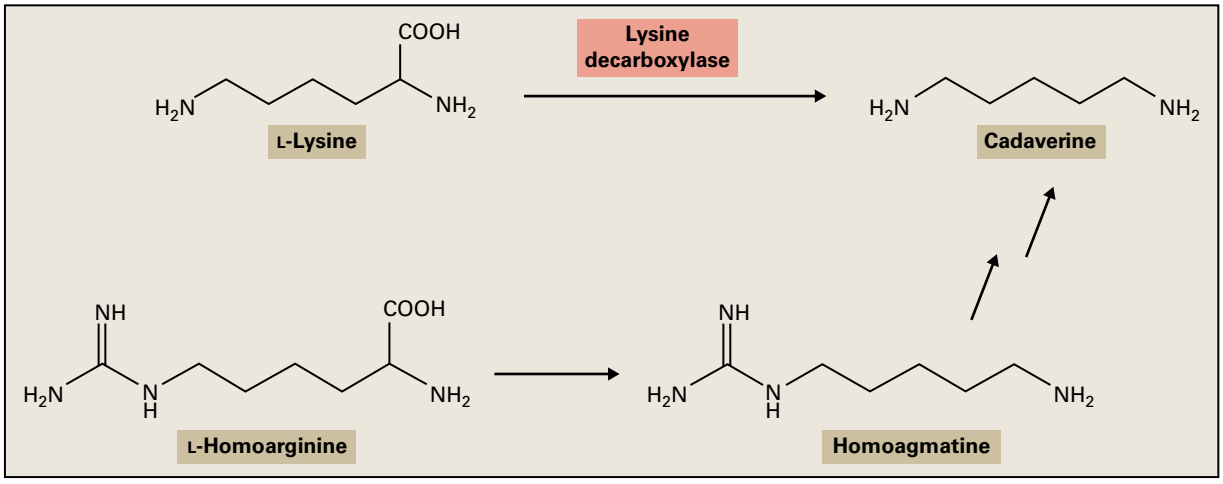


FIGURE 17.64 *Biosynthesis of cadaverine. The responsible genes for cadaverine synthesis have not been identified in plants.*

In *Arabidopsis*, there are two genes for spermidine synthase (*SPDS1* and *SPDS2*) and two for spermine synthase (*ACL5* and *SPMS*). Recent studies have demonstrated that ACL5 catalyzes synthesis of thermospermine rather than spermine. A loss-of-function mutant of *ACL5* has severe defects in stem elongation, but exogenous application of thermospermine, but not spermine, rescues the phenotype, indicating that thermospermine is required for normal stem elongation in *Arabidopsis*.

17.7.3 Cadaverine is synthesized from Lys or L-homoarginine

Cadaverine synthesis from L-Lys is catalyzed by Lys decarboxylase (Fig. 17.64). Lys decarboxylase activity is low in most plant tissue but in some leguminous species Lys decarboxylase activity increases with the accumulation of quinolizidine alkaloids, which are synthesized from cadaverine. In *L. sativus*, cadaverine is produced either from Lys or from L-homoarginine by way of homoagmatine (Fig. 17.64). Both conversions are catalyzed by a single decarboxylase that is distinct from Arg decarboxylase and Lys decarboxylase. The genes encoding cadaverine synthesis have not been identified in plants.

17.7.4 Polyamines are degraded by oxidative deamination

PAs are catabolized by oxidative deamination catalyzed by diamine oxidase and polyamine oxidase (Fig. 17.65). Diamine oxidase, a copper-containing enzyme, has a high affinity for diamines such as putrescine and cadaverine. The terminal (primary) amino groups are subjected to oxidative deamination, resulting in the co-production of aminoaldehyde, hydrogen peroxide, and ammonia. The aminoaldehydes derived from putrescine and cadaverine cyclize spontaneously to yield 1-pyrroline and 1-piperidine, respectively. PAs are precursors of various important alkaloids, and diamine oxidases participate in the biosynthesis of alkaloids containing a heterocyclic ring.

A second class of plant flavin enzymes, polyamine oxidases, catabolize spermidine and spermine, by oxidation of secondary amino groups, forming hydrogen peroxide, 1,3-diaminopropane, and aminoaldehydes. The aminoaldehydes derived from spermidine and spermine are 4-aminobutyraldehyde and 4-(3-aminopropyl)aminobutyraldehyde, respectively. A part of PA degradation appears to occur in the apoplast, as polyamine oxidase activity is detected in the cell wall fraction. Hydrogen peroxide generated by these oxidases may be involved in lignifying cell walls.

There are five *Arabidopsis* genes for polyamine oxidase (*PAO1* to *PAO5*). PAO1 and PAO4 convert spermine to spermidine, and PAO3 converts spermine to spermidine and spermidine to putrescine. These lines of evidence indicate an involvement of these polyamine oxidases in back-conversion pathways, which have been demonstrated in mammals. In addition, PAO2, PAO3, and PAO4 are localized in peroxisomes, suggesting a novel role for peroxisomes in PA metabolism. The hydrogen peroxide produced by these oxidases is unlikely to play a specialized role in cell function because peroxisomes efficiently eliminate hydrogen peroxide.

17.8 Jasmonic acid

Jasmonic acid (JA) and related compounds, often referred to as jasmonates collectively, were initially isolated as inhibitors of plant growth. Later, they have been shown to regulate various physiological processes in plants, including development of flowers and defense responses against herbivores and fungal pathogens. Jasmonates are similar structurally to prostaglandins, autacoidal hormones that exhibit various biological activities in mammals (Fig. 17.66). Both jasmonates and prostaglandins are derived from fatty acids.

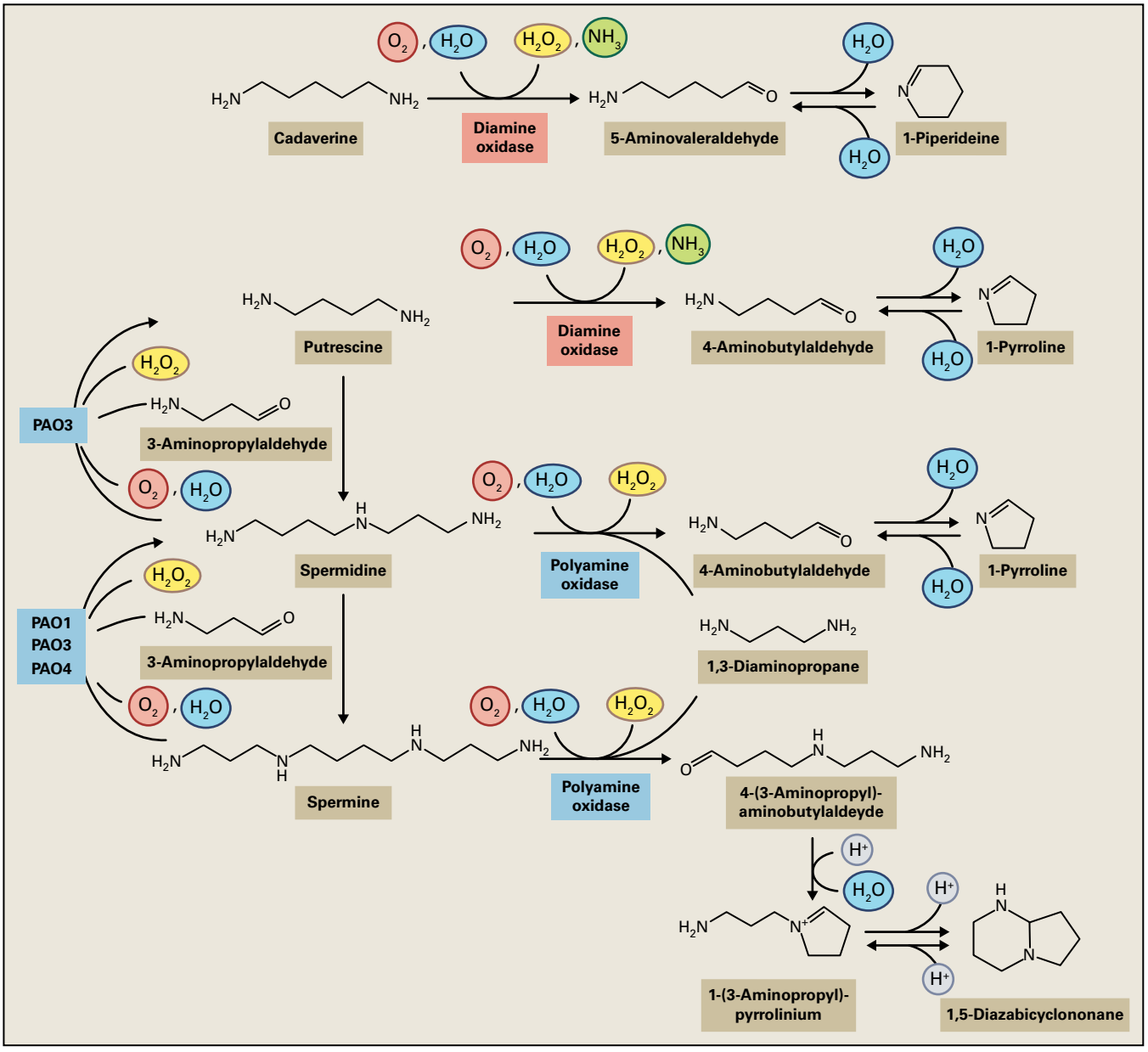


FIGURE 17.65 *Catabolism of PAs by diamine oxidases and polyamine oxidases. Some* Arabidopsis *polyamine oxidases (PAO1, PAO3, PAO4) may be involved in PA back-conversion pathways.*

Methyl jasmonate is well known in the perfume industry as a fragrant component of the essential oils of jasmine (*Jasminum grandiflorum*).

In 1971, JA was isolated from culture filtrates of a fungus, *Botryodiplodi theobromae*, as a plant growth inhibitor. Cucurbic acid (Fig. 17.66) was isolated from immature pumpkin (*Cucurbita* sp.) seeds in 1977 and identified as a new type of growth inhibitor, different from ABA. In the early 1980s, JA and methyl jasmonate were detected as senescence-promoting or growth-retarding substances in many plant species, including *Artemisia absinthium* (wormwood), *Vicia faba*, *P. vulgaris*, *Dolichos lablab*, and *Castanea crenata*. In 1989, the 12-*O*-β-glucoside of tuberonic acid (12-hydroxy-(+)-7-isojasmonic acid; Fig. 17.66) was characterized as a potato tuber-inducing factor.

(−)-JA and methyl (−)-jasmonate are the major jasmonates isolated from plant tissues. Their naturally occurring stereoisomers, (+)-7-isojasmonic acid and methyl (+)-7-isojasmonate, also appear to be active agents in planta because they exhibit higher biological activity in some, but not all, test systems. In vitro, (+)-7-isojasmonic acid is unstable and is isomerized by treatment with acid, base, or heat to form a 9:1 equilibrium mixture of (−)-JA: (+)-7-isojasmonic acid, because the carbonyl group at C-6 can tautomerize to an enol by utilizing the proton from C-7. To what extent this chemical process is involved in conversion of (+)-7-isojasmonic acid to (−)-JA in plants is unclear. Whether (−)-JA occurs naturally or is an artifact derived from (+)-7-isojasmonic acid has been the subject of debate. However, identification of the *trans*-alkyl compound, 6-*epi*-7-isocucurbic acid (which does not

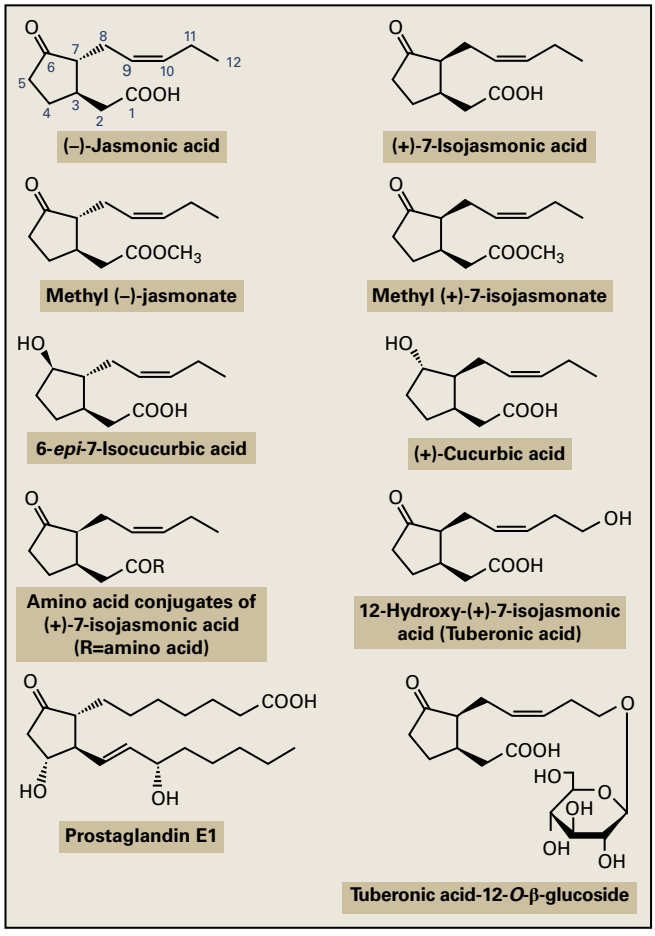


FIGURE 17.66 *Structures of JA and its derivatives. The structure of prostaglandin E1, a mammalian autacoidal hormone, is also shown.*

possess the C-6 carbonyl group; Fig. 17.66), in plant extracts supports the view that (–)-JA is an endogenous constituent of plant tissues.

17.8.1 Jasmonates inhibit growth processes in many tissues and are essential for reproductive development and pathogen resistance

Exogenous JA was first reported to inhibit the growth of *O. sativa*, *T. aestivum*, and *L. sativa* seedlings; it was subsequently shown to inhibit seed and pollen germination, retard root growth, and promote the curling of tendrils. JA content is high in vegetative sink tissues, and the compound regulates accumulation of vegetative storage proteins during seed development in *Glycine max* and *Arabidopsis*.

Arabidopsis mutants severely defective in JA biosynthesis or response are male sterile. Fertility of such JA synthesis mutants can be rescued by exogenous JA treatment. In *Arabidopsis* JA-deficient mutants, anther filaments do not elongate sufficiently to a position above the stigma, suggesting that JA plays a role in coordinating the timing of growth and development of floral organs. In addition, anther dehiscence does not occur at the time of flower opening and the majority of mutant pollen grains are not viable in JA-deficient mutants.

JA plays an important role in plant resistance to insects and necrotrophic pathogens. Plants accumulate JA and its derivatives when they are wounded or treated with pathogen-derived elicitors (oligosaccharides). Exogenous treatment with JA activates expression of hundreds of defense-related genes. Changes in gene expression result in upregulation of synthesis of defense-related proteins and metabolites, including antifungal proteins, antifeedants, phytoalexins, and volatiles that attract predatory insects. JA treatment also downregulates expression of genes encoding enzymes involved in growth and primary metabolism, including photosynthesis, so that resources can be used for defense.

17.8.2 Jasmonates are synthesized from α-linolenic acid

The first step of JA biosynthesis is release of α-linolenic acid, a C_{18} poly-unsaturated fatty acid, from plastid membrane lipid by lipase (Fig. 17.67). This enzyme was first discovered using the *Arabidopsis defective in anther dehiscence 1* (*dad1*) mutant, defective in flower development due to JA-deficiency. α-Linolenic acid is converted to 13-hydroperoxylinolenic acid by 13-lipoxygenase, and then allene oxide synthase (AOS) catalyzes the formation of 12,13*(S)*-epoxylinolenic acid. AOS is a plastid-localized CYP450 enzyme with several unusual characteristics. Unlike the majority of CYP450 enzymes which act as monooxygenases, AOS does not require oxygen and is therefore not an oxidase, nor does it require NADPH or P450 reductase. 12,13*(S)*-epoxylinolenic acid, the product of AOS, is rapidly cyclized by the enzyme allene oxide cyclase (AOC), yielding 12-oxo-*cis*-10,15-phytodienoic acid (OPDA), a cyclopentanone derivative. AOC also is a plastid-localized enzyme carrying an amino-terminal plastid-targeting sequence.

The second stage of JA biosynthesis occurs in the peroxisome, suggesting that OPDA produced in the plastid is first exported from this organelle and then imported into the peroxisome for subsequent metabolic conversions. The mechanism for this export is not understood, whereas import into peroxisomes of *Arabidopsis* is partly dependent on the ATP-cassette transporter PXA1/CTS. In the peroxisome, OPDA is first converted to 3-oxo-2-(*cis*-2′-pentenyl) cyclopentane-1-octanoic acid (OPC-8:0) by OPDA reductase (OPR) (Fig. 17.67). This enzyme was first purified from *Corydalis sempervirens*. Subsequent reverse genetic studies in *Arabidopsis* showed that a specific isoform encoded by the *OPR3* gene participates in JA synthesis. OPC-8:0 is activated by a carboxyl-CoA ligase, which is encoded by the *OPCL1* gene in *Arabidopsis*, and then converted to (+)-7-isojasmonic acid by three rounds of β-oxidation (see Fig. 17.67 and Chapter 8.8.5). β-Oxidation in plants is catalyzed by

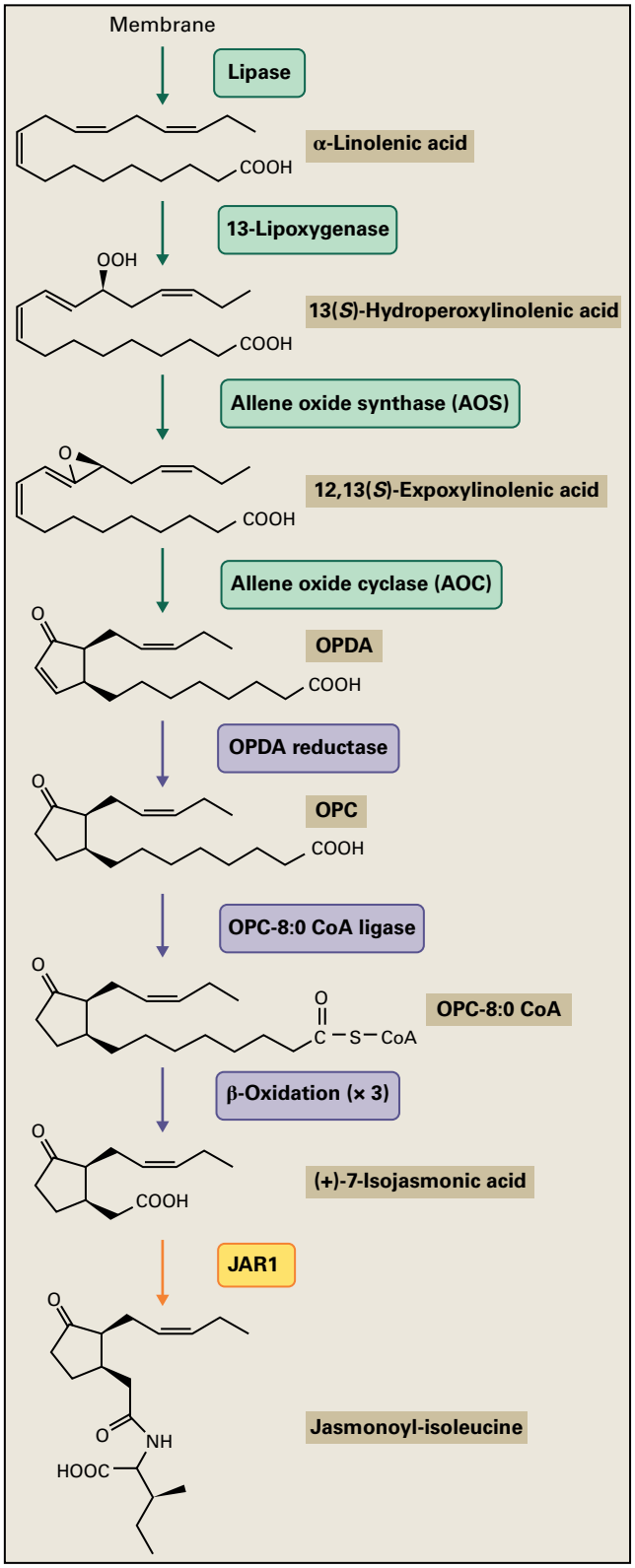


FIGURE 17.67 *Biosynthesis of jasmonoyl-isoleucine in plants. The first step of jasmonoyl-isoleucine biosynthesis is release of α-linolenic acid from plastid membrane lipid. Enzymes and metabolic conversions that occur in the plastid and the peroxisome are shown in green and blue, respectively. Subcellular localization of JAR1 has not been determined experimentally, but it is thought to be a cytosolic enzyme because of a lack of any apparent organelle targeting sequence. OPDA, 12-oxo-cis-10,15-phytodienoic acid; OPC, 3-oxo-2-(cis-2′-pentenyl)-cyclopentane-1-octanoic acid.*

acyl-CoA oxidase, a multifunctional protein (which exhibits its 2-*trans*-enoyl-CoA hydratase, L-3-hydroxyacyl-CoA dehydrogenase, D-3-hydroxyacyl-CoA epimerase, and $\Delta^3\Delta^2$-enoyl-CoA isomerase activities), as well as a L-3-ketoacyl-CoA thiolase.

17.8.3 Jasmonoyl-isoleucine is an active hormone in the jasmonate signaling pathway

JA is subjected to an amide-linked conjugation to isoleucine (Ile) and other amino acids to yield jasmonoyl-isoleucine (JA-Ile) and other jasmonoyl-amino acid conjugates, respectively (Fig. 17.67). In *Arabidopsis*, these conjugation reactions are catalyzed by an enzyme encoded by the *JAR1* (*JASMONATE RESISTANT 1*) locus. *JAR1* belongs to a large gene family encoding enzymes that adenylate a carboxyl group of the substrate followed by an exchange with a second substrate, which, in the case of JAR1, is an amino acid. Similar reactions are catalyzed by a subset of GH3 family proteins for synthesis of amino acid conjugates of IAA (see Section 17.4.8).

jar1 mutants were isolated because of their resistance to exogenous JA in a root growth inhibition assay. The *jar1* phenotype suggests that conversion of JA to JA-Ile is required to activate the JA signaling pathway. Recently, researchers have found that JA-Ile stimulates binding of the F-box protein CORONATINE-INSENSITIVE 1 (COI1) to jasmonate ZIM domain (JAZ) proteins, a class of negative regulators of JA signaling. The COI1-JAZ interaction triggered by JA-Ile promotes the ubiquitination-dependent degradation of JAZ proteins by the 26S proteasome. Studies with *coi1* mutants have shown that COI1 is required for most, if not all, JA responses. Taken together, these results indicate that COI1 is a critical perception component of the JA signal. Unlike JA-Ile, other jasmonate compounds, including (–)-JA, methyl (–)-jasmonate and OPDA are unable to activate COI1-JAZ interaction in vitro. These findings indicate that JA-Ile, as well as other JA-amino acid conjugates that also promoted COI1-JAZ interactions, act as active hormones in the JA signaling pathway.

Evidence suggests that JA-Ile synthesis is under positive feedback regulation. Many genes that encode JA-Ile biosynthesis enzymes are positively regulated by JA treatment, including 13-lipoxygenase, AOS, AOC, OPDA reductase (OPR3), and JAR1 (Fig. 17.67).

17.8.4 Coronatine is a bacterial toxin that activates jasmonate signaling

Coronatine (CO) is a phytotoxin produced by some plant pathogenic bacteria. There is evidence that CO exerts its virulence effects by activating JA signaling in host plants. The structural similarity of CO to JA-Ile supports the idea that

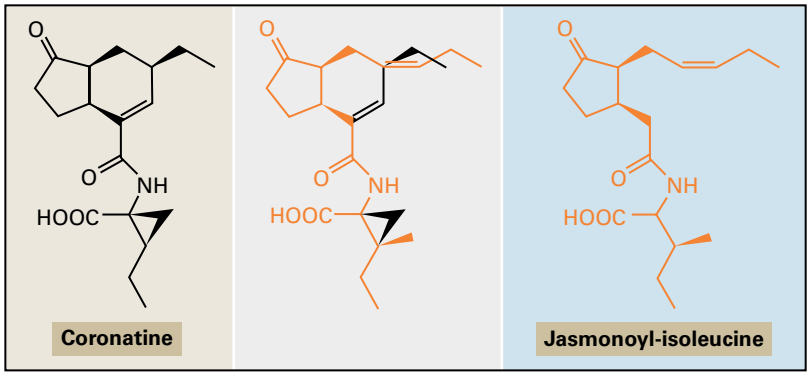


FIGURE 17.68 *Structural similarity between coronatine, a bacterial toxin (left) and jasmonoyl-isoleucine (right). To highlight the similarity, these structures are superimposed (center).*

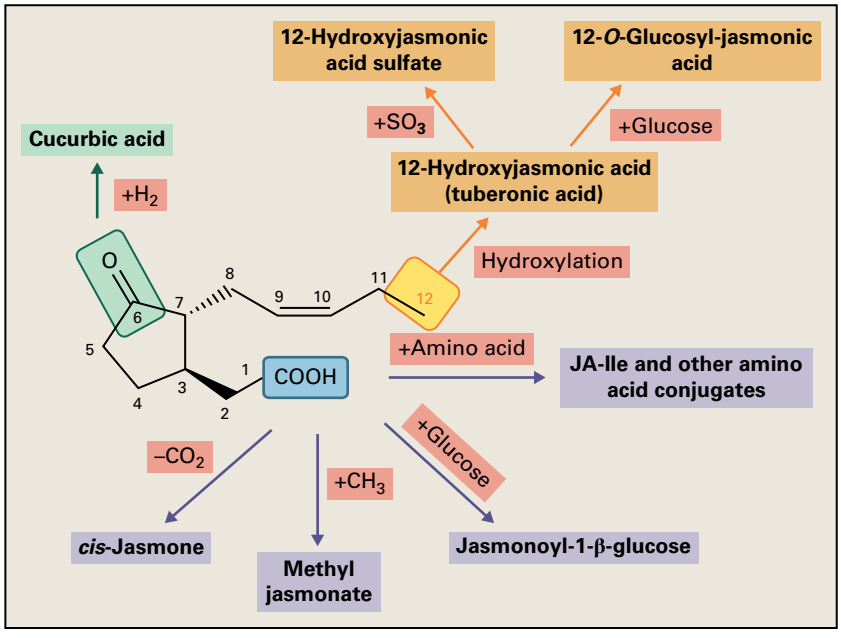


FIGURE 17.69 *Metabolism of JA in plants. JA is metabolized through modification of the carboxyl group (blue), C-12 oxidation (orange) or the reduction of C-6 ketone (green). 12-Hydroxy-(+)-7-isojasmonic acid is further metabolized to conjugates.*

this toxin acts as a molecular mimic of JA-Ile (Fig. 17.68). This hypothesis has been proven by recent experiments showing that CO binds directly to COI1-JAZ complexes in vitro even more effectively than does JA-Ile. CO appears to reduce the effectiveness of salicylic acid-dependent disease resistance responses by activating the JA signaling pathway.

17.8.5 JA is metabolized to various products via multiple pathways

Besides being converted to amino acid conjugates, JA can undergo several other modification reactions (Fig. 17.69). So far, only a few enzymes involved in these reactions have been identified, and the biological roles of these modifications are not fully understood. JA is converted to volatile methyl jasmonate by an SAM-dependent carboxyl methyltransferase. Methyl jasmonate is thought to act as an airborne signal in interplant communication, being released in response to wounding and other abiotic stresses. Another volatile compound, *cis*-jasmone, is synthesized from JA by decarboxylation (Fig. 17.69), but the enzyme responsible for this reaction has not been clarified. Gene expression profiling of *cis*-jasmone-regulated genes in *Arabidopsis* revealed a unique and more limited set of genes upregulated by *cis*-jasmone treatment in comparison with methyl jasmonate treatment, suggesting a unique role of *cis*-jasmone in defense responses. The carboxyl group of JA can also be modified through conjugation with glucose to give jasmonoyl-1-β-glucose in cell cultures of tobacco and tomato.

12-Hydroxy-(+)-7-isojasmonic acid is also known as tuberonic acid (see Fig. 17.66) because of its tuber-inducing activity in potato, whereas its glucoside appears to be the transport form. Systematic investigation of the biochemical functions of *Arabidopsis* sulfotransferases identified an enzyme, designated as AtST2a, that catalyzes sulfonation of 12-hydroxy-(+)-7-isojasmonic acid using 3′-phosphoadenosine 5′-phosphosulfate as a sulfate donor (Fig. 17.69). Recent survey of 12-hydroxy-(+)-7-isojasmonic acid and its sulfonated and glucosylated derivatives demonstrated that these compounds are constituents of various organs of many plant species. Thus, 12-hydroxylation of JA and subsequent glucosylation and sulfonation appears to be a widespread JA metabolic route in plants. Reduction of the C-6 keto group of the cyclopentanone ring leads to the formation of cucurbic acid.

17.9 Salicylic acid

Salicylic acid (SA) (see Fig. 17.1) is far better known for its medicinal properties (Box 17.1) than for its regulatory roles in plants. Although many physiological effects of SA application have been reported, only a few have been shown to be physiologically important in plants, for example, the regulatory role of SA in thermogenesis of various species and in the response of plants to pathogens.

17.9.1 Salicylic acid can retard senescence of petals and induce flowering

Soluble aspirin tablets disintegrate rapidly in water, and the acetylsalicylic acid is converted to SA. Adding aspirin to a vase of water containing cut flowers will retard senescence of petals and make flowers last longer. This is probably a consequence of reduced rates of ethylene biosynthesis, in light of reports that SA blocks the conversion of ACC to ethylene. SA also induces flowering in the duckweeds *Lemna gibba*, *Spirodela polyrrhiza*, and *Wolffia microscopia* when these long-day plants are grown under a noninductive short day photoperiod (Chapter 19). This effect is not specific, however, and related phenolics also can stimulate flowering in these and other species. Furthermore, because SA concentrations are similar in vegetative and induced tissues, the compound is unlikely to be an endogenous flower-inducing signal.

17.9.2 Salicylic acid regulates thermogenesis in voodoo lily

Clear evidence linking endogenous SA with a regulatory role in plants was first obtained during studies on thermogenesis in flowers of voodoo lily (*Sauromatum guttatum*). During thermogenesis, much of the electron flow in mitochondria is

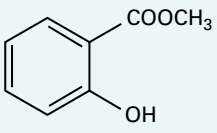
BOX 17.1

Salicylic acid has been used as an analgesic for more than 2,000 years

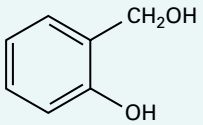
Since the 4th century BC, plants such as willow, myrtle, poplar and meadowsweet have been used to relieve pain caused by a variety of conditions, including diseases of the eye, rheumatism, childbirth and fever. The active component remained unknown until the 19th century when SA and related compounds, such as methyl salicylate, saligenin, and their glycosides, were isolated from willow and other plant sources. Oil of wintergreen extracted from the American plant, *Gaultheria procumbens*, was an especially rich source of methyl salicylate and was a widely used analgesic during the mid-19th century.

In 1858, salicylic acid was chemically synthesized in Germany, and its commercial production began in 1874 at one tenth the cost of making wintergreen oil. However, the sharp bitter taste and gastric irritation associated with SA made long term use difficult. This problem was overcome in the 1890s, when clinical tests carried out by the German pharmaceutical company Frederick Bayer and Co. showed that these side effects could be avoided by replacing SA with its acetylated derivative. In 1898, acetylsalicylic acid was given the trade name aspirin. Within one year of its launch, aspirin began to be manufactured in tablet form, rather than as a powder, and sales soon swelled to amazing proportions.

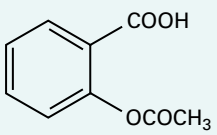
More than 100 years later, aspirin tablets are still sold widely as a ready remedy for many conditions, including the common cold, headache, fevers, and rheumatoid arthritis. Aspirin is also increasingly used to prevent and treat heart attacks and cerebral thrombosis. The beneficial effects ascribed to acetylsalicylic acid include retarding production of prostaglandins, which promote blood clotting. Moreover, a growing number of discerning airline passengers are taking a precautionary aspirin tablet prior to departure to lessen the risks, albeit relatively small, of blood clots and coronary problems associated with long flights. The current world production of aspirin is many thousands of tons per year, and average consumption in developed countries is about 100 tablets per person per annum.



Methyl salicylate



Saligenin



Acetylsalicylic acid

diverted from the cytochrome respiration pathway to the cyanide-insensitive nonphosphorylating electron transport pathway unique to plant mitochondria (Chapter 14). Also, the glycolytic pathways and Krebs cycle enzymes, which provide substrates for alternative oxidase, are activated. Energy released by electron flow through this alternative respiratory pathway is not conserved as chemical energy but is released as heat. The flower of *S. guttatum* develops from a corm and can reach more than 70 cm in height (see Box 14.2). On the day of anthesis, the spathe unfolds and shortly afterwards the upper spadix begins to generate heat, volatilizing pungent amines and indoles that attract insect pollinators. The temperature of the spadix can increase to 14°C above ambient by early afternoon but falls to normal values by evening. A second burst of thermogenicity begins in the lower spadix in late evening and ends early next morning after an increase in temperature of more than 10°C (Fig. 17.70). In 1937 it was proposed that thermogenesis in *S. guttatum* was initiated by "calorigen," a water-soluble substance produced in the staminate flower primordia positioned between the upper and lower spadix. In 1987, calorigen was identified as SA when it was shown that treating immature spadix sections with as little as 0.12 μg of SA per gram fresh weight caused their temperatures to rise by as much as 12°C. Large increases in endogenous concentrations of SA occur immediately prior to onset of thermogenicity in both upper and lower spadix.

17.9.3 Salicylic acid production is associated with disease resistance

More widespread interest in SA was generated when it was closely linked to the hypersensitive response, a disease resistance mechanism in which plants restrict spread of fungal, bacterial or viral pathogens by producing necrotic lesions around the initial point of penetration (Fig. 17.71). This localized cell death often is associated with changes in healthy, distant parts of plants that enhance resistance to secondary infection by a broad range of pathogens. Increased resistance, which develops over a period of several days to a week following initial pathogen invasion, is referred to as systemic acquired resistance (SAR). Associated with hypersensitive response and SAR is synthesis of five or more families of serologically distinct, pathenogenesis-related (PR) proteins. Two of these families encode the hydrolytic β-1,3-glucanases and chitinases. While the precise function of other families of PR proteins is not well understood, their expression is associated with resistance to a large number of viral, fungal, and bacterial pathogens.

The indication that SA was involved in plant defense against disease came with the finding that SA treatment of the leaves of Tobacco Mosaic Virus (TMV)-susceptible tobacco (*N tabacum* cv. Xanthi *n*) induced the accumulation of PR proteins and enhanced resistance to TMV infection. It has now been shown that SA treatment also induces SAR against many pathogens in a variety of plants. In the TMV-resistant tobacco cultivar Xanthi-*nc*, but not the susceptible Xanthi-*n*, the endogenous SA pool increases about 40-fold in TMV-inoculated leaves and about 10-fold in uninfected leaves of the same plant. The steep rise in SA content parallels or precedes induction of PR protein gene expression in both inoculated and uninoculated leaves of TMV-resistant plants. Endogenous SA, therefore, appears to play a key role in signal transduction leading to activation of genes encoding PR proteins and in establishing the hypersensitive response and SAR. Studies with *C. sativus* and *S. tuberosum*, and other species indicate that involvement of SA in these responses is not unique to *N. tabacum*.

Despite arguments that SA acts as the primary long distance signal translocated in the phloem from the site of pathogen invasion to uninfected leaves where it initiates

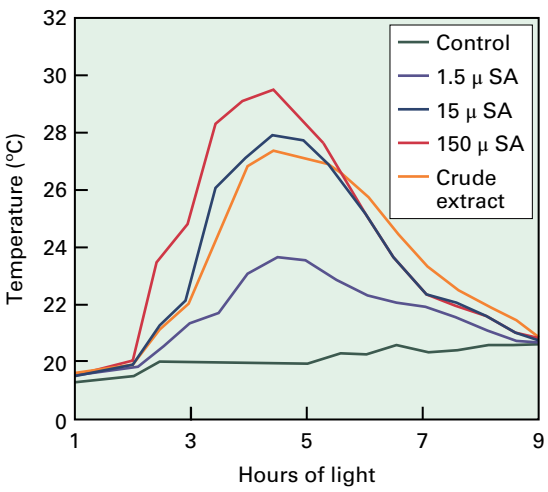


FIGURE 17.70 *The response of the* Sauromatum guttatum *appendix (upper spadix) to application of SA or a crude extract of male flowers of the same species. Both exogenous treatments result in a marked increase in appendix temperature.*

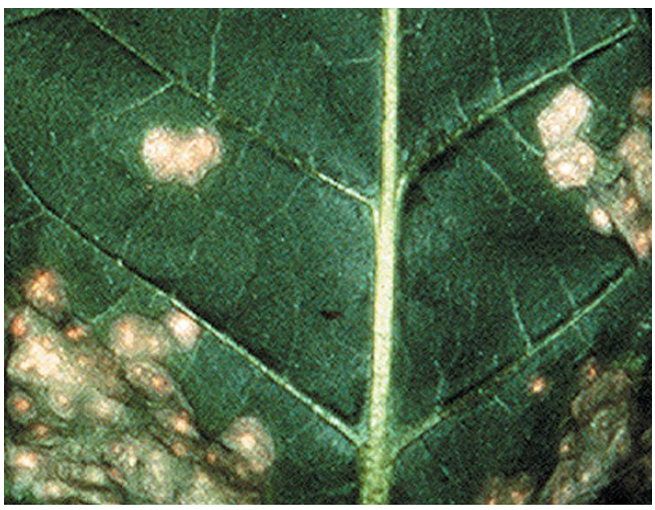


FIGURE 17.71 *Necrotic lesions on the leaf of resistant* Nicotiana tabacum *formed in response to infection with TMV.*
Source: J. Draper, University of Wales, Aberystwyth, UK; previously unpublished.

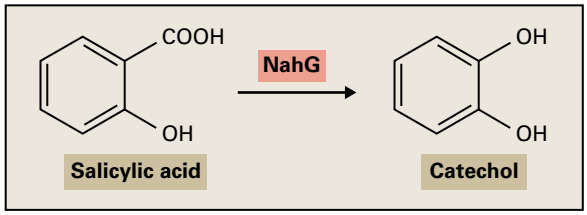


FIGURE 17.72 *The* Pseudomonas putida nahG *gene product catalyzes the metabolism of SA to catechol.*

development of the SAR response, grafting studies with wild-type and TMV-susceptible transgenic Xanthi-*nc* tobacco plants have refuted this hypothesis. Accumulation of SA is prevented in transgenic plants expressing the *Ps. putida nahG* gene, the product of which catalyzes the conversion of SA to catechol (Fig. 17.72). This research indicates that local infection leads to the production of an unidentified mobile signal that is transported to distal tissues, where it initiates the accumulation of SA required for induction of SAR.

17.9.4 Two distinct pathways exist for the biosynthesis of salicylic acid in plants

In 1993, SA biosynthesis in *N. tabacum* was proposed to involve a side branch of the phenylpropanoid pathway, which converts *trans*-cinnamic acid to benzoic acid (BA), the latter undergoing 2-hydroxylation to form SA (Fig. 17.73). It was suggested that after TMV-inoculation, a large pool of benzoic conjugate (100 μg/g fresh weight) is hydrolyzed, releasing BA, which activates BA 2-hydroxylase (BA2H), responsible for catalyzing the conversion of BA to SA. BA2H has been partially purified and shown to have characteristic features of NADPH-dependent CYP450 monooxygenases, with the exception of being a soluble protein, unlike typical P450 enzymes that are membrane bound. No gene encoding BA2H has been identified. More recent work has suggested that the rate-limiting step in SA biosynthesis is the conversion of *trans*-cinnamic acid to BA, involving a β-oxidation pathway in which *trans*-cinnamoyl-CoA is the first of four intermediates (Fig. 17.73). Indirect evidence supports involvement of *trans*-cinnamic acid as a key intermediate in SA biosynthesis: TMV inoculation of leaves of transgenic Xanthi-*nc* plants, in which phenylalanine ammonia lyase activity is suppressed, exhibit a four-fold lower increase in SA than do inoculated leaves of wild-type plants.

SA is produced as a biosynthetic precursor of a siderophore (iron-chelating compound) by some bacteria, where SA is synthesized from chorismate. In bacteria, chorismate is first converted to isochorismate by isochorismate synthase (ICS), which is then converted to SA and pyruvate by isochorismate pyruvate lyase (IPL). There is evidence that a large fraction of SA in *Arabidopsis* is synthesized from isochorismate as in bacteria: the *ics1/sid2* mutant defective in ICS has been shown to accumulate only 5-10% of SA of wild type after pathogen infection (Fig. 17.73). So far, no IPL activity has been reported in plants. The discovery of the isochorismate pathway in *Arabidopsis* poses the question of relative contributions of the BA- and isochorismate-dependent pathways. The two pathways may operate under different conditions, although this is not likely to be the case in *Arabidopsis* as the *ics1/sid2* mutant fails to accumulate SA in response to various SA-inducing environmental cues. The relative contribution of the two pathways might differ in plant species. In SA synthesis upon exposure to ozone in *N. tabacum*, radiolabeled BA is incorporated into SA and the *ICS* gene (unique in the genome) is not expressed, suggesting the operation of the BA-dependent pathway. By contrast, in *Arabidopsis* the same ozone treatment led to an induction of the *ICS1* gene.

17.9.5 Methyl salicylate may play a role as a mobile signal in systemic acquired resistance

In both healthy and infected tobacco leaves, the main SA metabolites are SA 2-*O*-β-glucoside (SAG) and SA β-glucosyl ester (SGE), with the latter occurring transiently and in smaller quantities than the former (Fig. 17.73). UDP glucose-dependent glucosyltransferases that catalyze the formation of SAG and SGE have been identified in *N. tabacum* and *Arabidopsis*. SGE is readily converted back to SA by SA β-glucosidase, which has been partially characterized in *N. tabacum* leaves.

The carboxyl group of SA is methylated to form methyl salicylate (MeSA) by a carboxyl methyltransferase that uses SAM as methyl donor (Fig. 17.73). This enzyme has been identified in several plant species, including *Arabidopsis, N. tabacum*, and *Clarkia breweri*. MeSA is converted back to SA by MeSA esterase, SABP2, which was initially purified as a high-affinity SA binding protein from *N. tabacum*. The amino acid sequence of the SABP2 protein indicates that it is a member of the α/β hydrolase superfamily, which shares a conserved α/β core domain and catalyzes hydrolysis of different substrates. Analysis of the crystal structures of SABP2, alone and in complex with SA, revealed an active site typical of α/β hydrolases, with Ser, His, and Asp residues as the catalytic triad. SA is bound in the active site and acts as a potent product inhibitor of catalysis. An amino acid substitution of Ala^{13} to Leu of SABP2 (A13L) results in loss of SA-binding activity without losing its catalytic function as MeSA esterase. Thus, this mutant version of SABP2 is insensitive to product inhibition by SA.

Using the *A13L* mutant of *SABP2*, evidence has been provided that MeSA esterase activity of SABP2 is required for SAR signaling in systemic *N. tabacum* leaves. In transgenic *N. tabacum* plants with elevated MeSA esterase activity in infected leaves, MeSA concentrations do not increase in infected leaves, phloem exudates and systemic leaves. Furthermore, SAR is blocked when SA methyl transferase

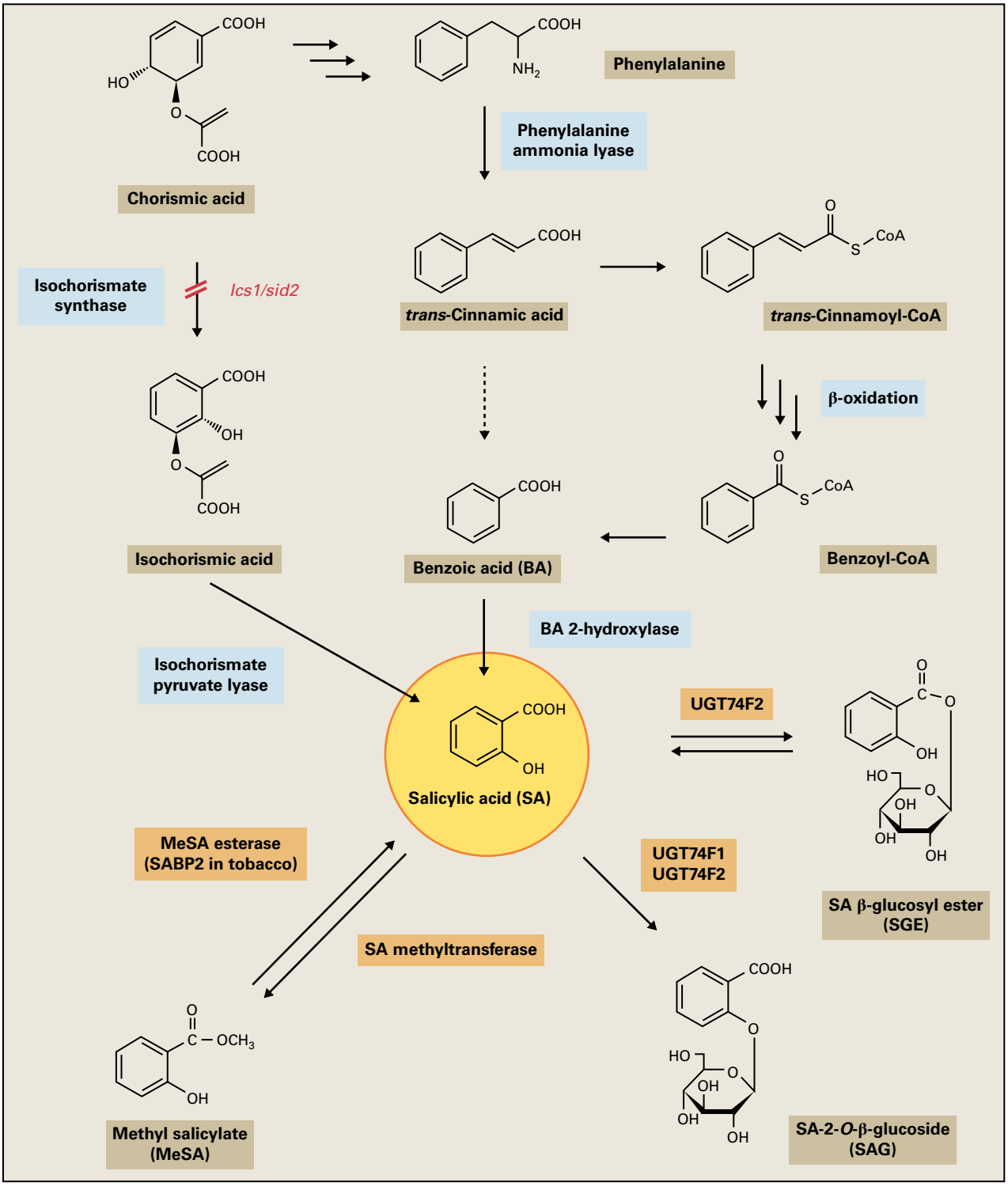


FIGURE 17.73 *Proposed SA biosynthesis and metabolism pathways in plants. Current evidence suggests trans-cinnamic acid is converted to BA by way of the β-oxidation pathway. A CoA-independent route for the conversion of* trans*-cinnamic acid to BA may also exist (dashed arrow). In* Arabidopsis*, studies using mutants defective in isochorismate synthase (ics1/sid2) demonstrate that the majority of SA is synthesized by way of isochorismic acid. For the conversion of chorismic acid to phenylalanine, see Chapter 7. In Arabidopsis, UDP-glucose- dependent glucosyl-transferases, designated as UGT74F1 and UGT74G2, catalyze the formation of SA β-glucosyl ester (SGE) and SA-2-O-β-glucoside (SAG).*

(which converts SA to MeSA) is silenced in infected leaves, and MeSA treatment of lower leaves induced SAR in upper untreated leaves. Therefore, MeSA has been proposed to be an essential part of the SAR signal in tobacco. However, more recent work has shown that *Arabidopsis* mutants defective in expression of a SA methyltransferase gene are devoid of pathogen-induced MeSA accumulation but still show increased SA concentrations in systemic leaves and develop

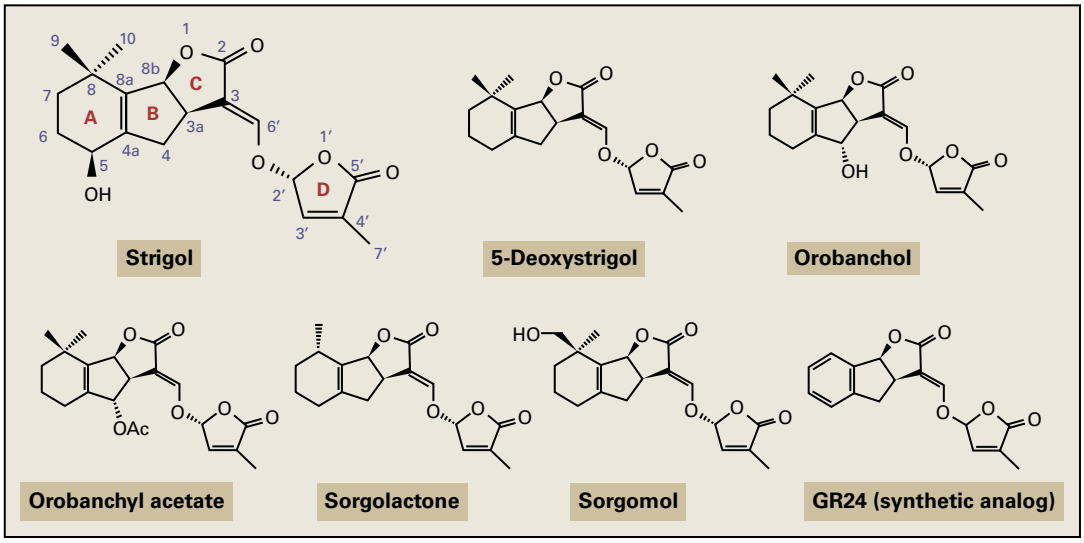


FIGURE 17.74 *Structures of naturally occurring strigolactones (SLs) and a synthetic SL analog, GR24.*

SAR upon local inoculation of a pathogen, suggesting that MeSA is dispensable for SAR in *Arabidopsis*. Thus, whether MeSA is a common mobile signal for SAR in plants is still under debate and requires further investigations.

17.10 Strigolactones

Parasitic plants of the *Striga*, *Orobanche*, and *Alectra* genera (Orobanchaceae) are root parasites that cause losses in crop yields in many parts of the world. Control of these parasitic plants is difficult because they produce a huge number of seeds that remain viable in soil for many years until they detect germination stimulants released from host roots. A pure crystalline germination stimulant of *Striga* seeds was isolated in 1966 from cotton root exudates. This stimulant, termed strigol, has a characteristic chemical structure, including two lactone rings linked via an enol ether bridge (Fig. 17.74). Later, diverse strigol-related compounds, collectively called **strigolactones (SLs)**, were isolated as germination stimulants of parasite seeds in root exudates of various plant species (Fig. 17.74).

Until recently, a biological function of SLs in host plants was unknown. It was discovered in 2005 that SLs are plant-derived signals that induce hyphal branching of arbuscular mycorrhizal fungi (AM fungi), a phenomenon that is observed at the initial stage of colonization (Fig. 17.75). This symbiotic interaction is observed in more than 80% of terrestrial plants. Since AM fungi facilitate the uptake of water and mineral nutrients such as phosphate and nitrate by host plants, it is considered that plants evolved to produce SLs to enable AM fungi to colonize their roots. Parasitic plants are thought to abuse these chemical signals to recognize the vicinity of a potential host plant (Fig. 17.75). Studies using various SLs and their synthetic analogs suggest that the structure of the CD rings of SLs is crucial for their biological activity.

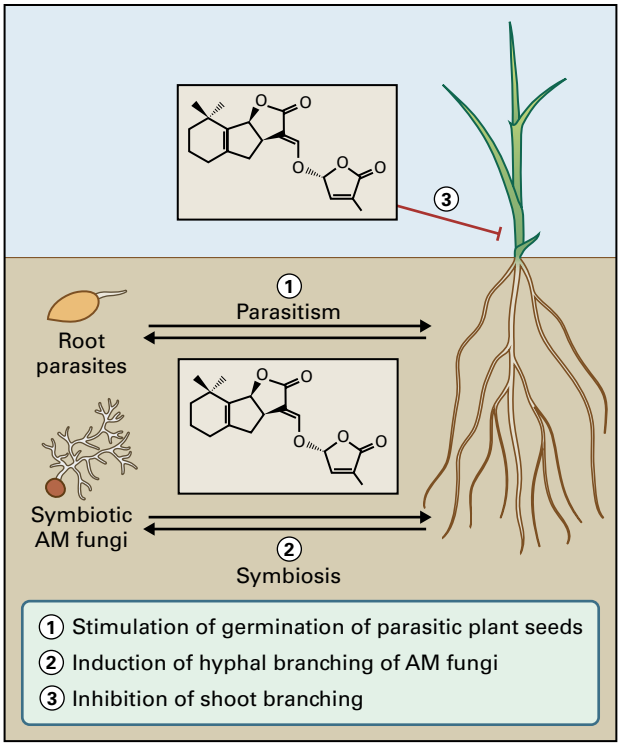


FIGURE 17.75 *SLs are released from roots and act as chemical signals in communication with root parasite seeds and arbuscular mycorrhizal (AM) fungi in the rhizosphere. They also act as endogenous regulators of shoot branching in plants.*

Extensive survey of SLs revealed their occurrence in root exudates of a wide variety of plant species, including non-hosts of AM fungi (e.g., brassicaceae, of which *Arabidopsis* is a member). These findings suggested that SLs might have unidentified role(s) in plants. In 2008, it became apparent that SLs were not just chemical signals in the rhizosphere but also endogenous regulators of shoot branching.

17.10.1 Genetic studies suggested a novel carotenoid-derived signal inhibits shoot branching

Shoot branching involves the formation of axillary buds in the axils of leaves and subsequent outgrowth of the buds. In many species, only a small proportion of buds grow to form branches, with both the timing and extent of bud activation being tightly regulated by endogenous and environmental factors. The participation of auxin and CK in the regulation of axillary bud activity has long been known (see Fig. 17.37). Besides these two hormones, studies with excessive shoot branching mutants suggested the involvement of a novel hormone-like compound in inhibiting outgrowth of axillary buds. These mutants include *ramosus* (*rms*) of *P. sativum*, *decreased apical dominance* (*dad*) of *Petunia, more axillary growth* (*max*) of *Arabidopsis* and particular *dwarf (d)* mutants of *O. sativa*. Grafting experiments suggest that some of these mutations affect genes required for synthesis of this hormone, while others are required for perception or transduction of the signal. For example, the excessive shoot branching phenotype of *max1*, *max3*, and *max4* mutants is rescued when grafted onto wild type rootstock, while the *max2* scion on wild-type rootstock still produces excessive branching (Fig. 17.76). These results suggest that *MAX1*, *MAX3*, and *MAX4* are required for the synthesis of a root-derived graft-transmissible signal that inhibits axillary bud outgrowth, while MAX2 is involved in perception or transduction of this signal in shoots. Since a *max4* rootstock does not cause excessive branching in wild type scion, the shoot branching inhibitor synthesized in the scion (shoot) is also sufficient to prevent excessive shoot branching (Fig. 17.76).

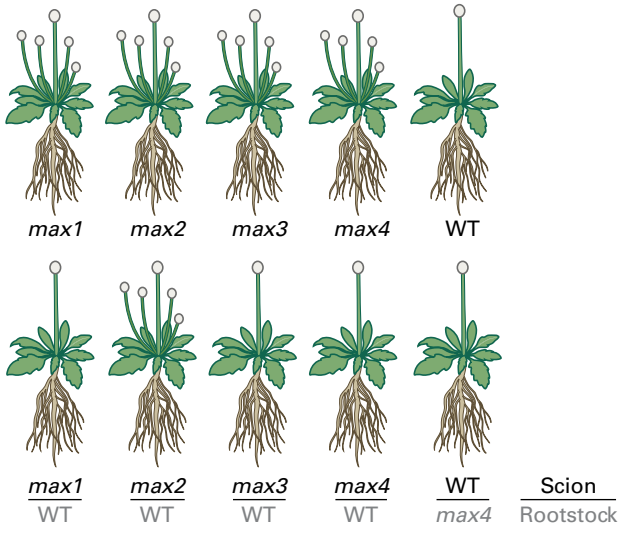


FIGURE 17.76 Arabidopsis max *mutants produce more branches in comparison with wild type (WT) (upper panel). The branching phenotype of* max1, max3 *and* max4 *shoots, but not that of* max2 *shoots, are rescued when grafted onto a WT rootstock (lower panel).*

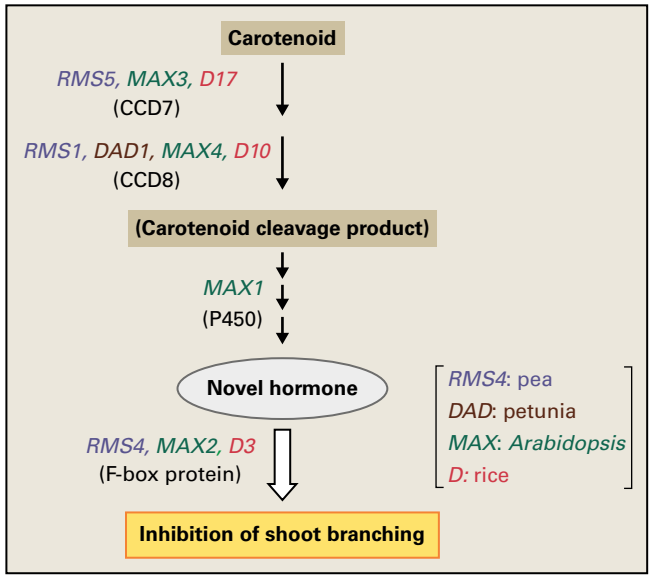


FIGURE 17.77 *A hypothetical pathway for the novel shoot branching inhibitor hormone. Carotenoid cleavage dioxygenases (CCDs) and a CYP450 are required for synthesis, whereas an F-box protein is probably involved in perception or transduction of the hormonal signal.*

This idea was supported by the molecular identification of *Arabidopsis MAX* genes and several *RMS*, *DAD*, and *D* loci in *P. sativum, Petunia*, and *O. sativa*. *MAX3*, *RMS5*, and *D17* encode carotenoid cleavage dioxygenase 7 (CCD7), while *MAX4*, *RMS1*, *D10*, and *DAD1* encode another subclass of CCDs designated as CCD8 (Fig. 17.77). *MAX1* encodes a protein in the CYP450 monooxygenase superfamily, of which members are typically involved in metabolism of lipophilic small molecules, as discussed earlier. These findings are consistent with the idea that MAX1, MAX3 and MAX4 participate in biosynthesis of a carotenoid-derived hormone-like compound. MAX2, RMS4, and D3 are orthologous members of the F-box protein family, which are known to function as substrate recognition subunits of SCF ubiquitin E3 ligase for proteasome-mediated proteolysis. Some members of this protein family include TIR1, GID2/SLY1 and COI1, all of which are components of hormone perception or signaling (see Chapter 18), suggesting that *max2*, *rms4* and *d3* mutants are defective in a response to the novel hormone.

17.10.2 Strigolactone inhibits shoot branching

Recently, SLs have been shown to inhibit shoot branching in the proposed RMS/DAD/MAX/D pathway (Fig. 17.78). Two lines of evidence support this idea. First, SL concentrations in root exudates and in roots are significantly decreased in the *ccd7* and *ccd8* mutants of *P. sativum* and *O. sativa*. Second, axillary bud outgrowth in *ccd7* and *ccd8* mutants of *P. sativum*, *O. sativa* and *Arabidopsis* is inhibited by exogenous SL.

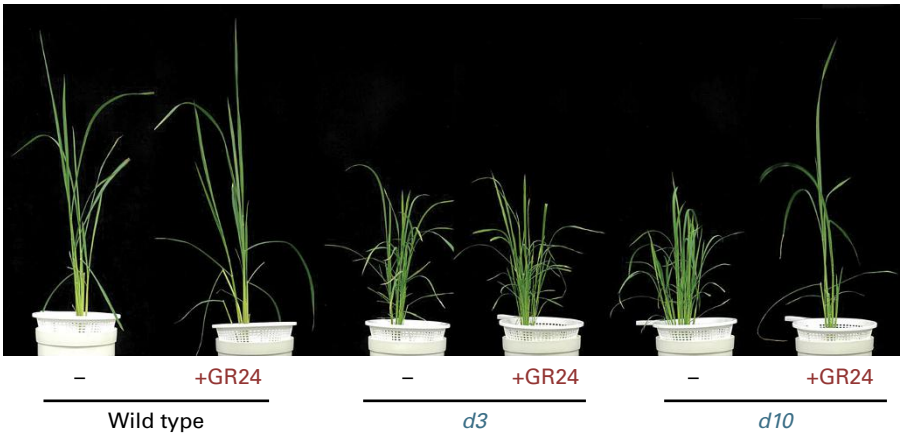


FIGURE 17.78 *The excessive branching (tillering) and semi-dwarf phenotypes of the* O. sativa *d10 mutant are fully complemented by exogenous GR24, a synthetic SL analog (supplied at 1 μM in the hydroponic culture media). In contrast, the d3 mutant is insensitive to GR24.*

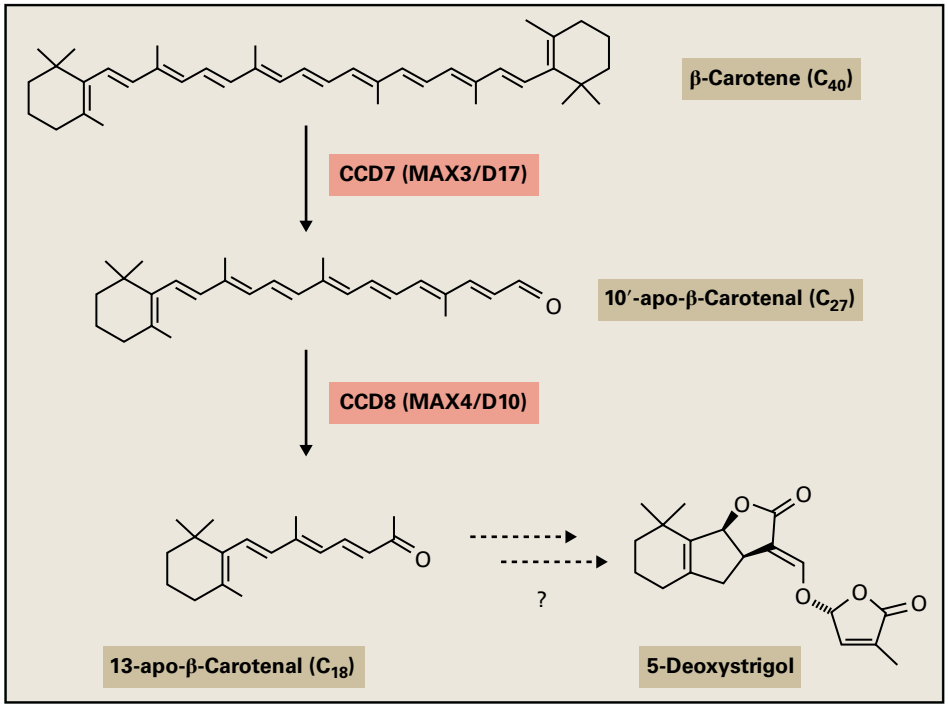


FIGURE 17.79 *Oxidative cleavage reactions catalyzed by recombinant CCD7 and CCD8 proteins in vitro or in bacterial cells using β-carotene as a substrate. Note that CCD7 can use other carotenoids as substrates and the exact reactions catalyzed by these CCDs in planta has not been conclusive.*

Figure 17.78 illustrates the branching phenotype as well as plant height of the *O. sativa ccd8/d10* mutant that was nearly fully complemented by including GR24 in culture media. In contrast, *P. sativum* and *O. sativa* branching mutants characterized as lacking a response to the branching inhibitor (*rms4*, *max2*, and *d3*, see Fig. 17.77) were insensitive to exogenous GR24 (Fig. 17.78), and were not deficient in SLs. These results indicate that the inhibitory effect of SLs on shoot branching is specific to the proposed RMS/D pathway. It is not known whether SL itself is an active form of this hormone class, because application of an SL analog might be metabolized in plants and converted to an active compound. Together, current data indicate that SLs act as a new class of branch-inhibiting hormones or their biosynthetic precursors.

17.10.3 Strigolactone biosynthesis pathway remains to be elucidated

Until recently, the biosynthetic origin of SLs was unknown, although their chemical structures suggested that they are terpenoids. In recent studies using chemical inhibitors and mutants of *S. lycopersicum* and *Z. mays,* SLs were shown to be derived from carotenoids. This is consistent with the discovery that carotenoid cleavage dioxygenases, CCD7 and CCD8, participate in SL biosynthesis. Recombinant CCD7 and CCD8 proteins from *Arabidopsis* and *O. sativa* sequentially cleave β-carotene, forming a C_{18} apocarotenoid in vitro and in bacterial cells (Fig. 17.79). However, CCD7 could also use other carotenoid substrates, and the exact reactions catalyzed

by these CCDs in planta have not been identified. MAX1, a CYP450 monooxygenase named CYP711A1 potentially catalyzes a later step of SL biosynthesis, although its substrate and product are unknown. Considering the chemical structure of SLs, more enzymes are likely to be required for their biosynthesis from a carotenoid-cleavage product.

17.10.4 Strigolactone biosynthesis is under feedback regulation

In *O. sativa, P. sativum*, and *Petunia*, genes encoding CCD8 are highly upregulated in the SL-deficient and -insensitive mutant backgrounds, suggesting feedback regulation of CCD8 expression. Consistent with this, *CCD8/D10* gene expression is downregulated by SL treatment in *O. sativa*. Furthermore, SL levels are substantially increased in the SL-insensitive *O. sativa d3* mutant in comparison with wild type. These results indicate that there is a link between SL action and biosynthesis in these plant species, as previously recognized for other plant hormones.

17.10.5 Strigolactone production is elevated under mineral nutrient deficiency

The amounts of SLs released from roots are drastically increased under deficiency of phosphate or nitrate in hosts of AM fungi. This is thought to be an adaptive response of plants under nutrient deficiency in order to maximize the symbiotic interaction with AM fungi, which assist the uptake of mineral nutrients by the host plant. This idea is supported by the observation that *Lupinus albus* (white lupin), a nonhost of AM fungi, does not increase SL production in response to phosphate deficiency, unlike the mycotrophic *Trifolium pratense*. These results indicate that SL production is closely related to the strategy of plants for mineral nutrient acquisition.

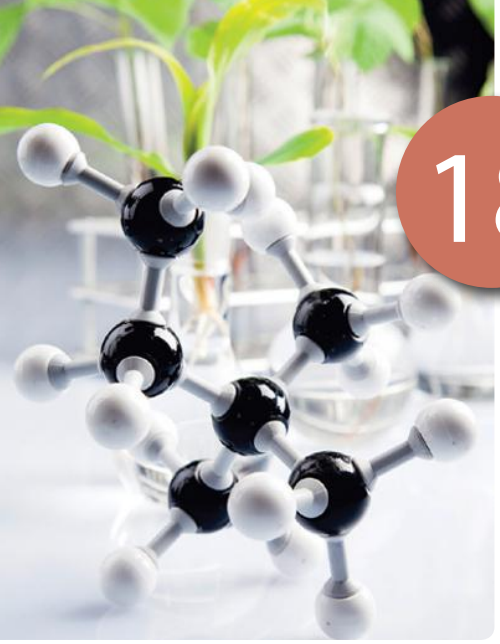
Summary

A battery of endogenous hormones regulate plant growth and responses to environmental stimuli, including GAs, ABA, CKs, IAA, ethylene, BRs, PAs, JA, SA, and SLs. Most of these compounds are present in plant tissues at low concentrations (nanogram or subnanogram per gram fresh weight) and pool sizes are tightly controlled by various biosynthetic, catabolic, and conjugation pathways. To date, the major biosynthesis routes for these hormones have been elucidated and most of the genes encoding enzymes in these pathways have been identified. Combinations of different experimental approaches, including chemistry, biochemistry, molecular biology, and genetics, have contributed to these achievements. The use of hormone-deficient and -overproduction mutants has been particularly powerful in the isolation of new genes, as well as in understanding the biochemical function of gene products.

Although these hormones are diverse in their chemical structures, there are some common features in their biosynthetic and catabolic pathways. Members of the CYP450 monooxygenase superfamily are frequently involved in the biosynthesis and/or deactivation of various hormones, including GAs, ABA, CKs, IAA, BRs, JA, and SLs. Methylation of a carboxyl group by SAM-dependent methyl transferases also participates in homeostasis of multiple hormones discussed in this chapter. With the exception of ethylene, conjugation with glucose or an amino acid commonly occurs in many hormone metabolism pathways. However, in all cases, hormone conjugation is only one of many routes for deactivation. At least in some cases, hormone conjugates are thought to function as a storage form, from which a free, bioactive hormone can be released upon hydrolysis. It has long been assumed that hormone conjugates are not bioactive per se in plants. However, a recent finding that JA-Ile (and some other amino acid conjugates of JA) might act as an active signal in the JA response pathway provides a new view regarding the role of hormone conjugation.

Studies have shown that the major part of hormone biosynthetic and catabolic pathways are conserved in diverse plant species, but in some cases, species-specific biosynthesis routes have been found, including one of the IAA pathways in *Arabidopsis*, which relates to the production of indole glucosinolates as secondary metabolites in this species. Increasing evidence suggests that many hormones, if not all, function as intermediates between the perception of environmental signals and resulting alterations in growth and developmental patterns. Examples include light-regulation of GA_1 concentrations in lettuce seeds, an increase in ABA concentrations under water stress, and JA accumulation in response to wounding. In addition, hormone concentrations are regulated by the action of other hormones.

There is emerging evidence suggesting that hormone concentrations in plants are determined as a consequence of multiple layers of regulation. For example, in both GA and BR pathways, negative feedback regulation involves a change in accumulation of particular mRNAs encoding biosynthesis and inactivating enzymes. However, as shown for ACS in ethylene biosynthesis, hormone homeostasis can also be controlled by turnover of the enzyme through protein modification. Advances in hormone biosynthesis research have started to expand our understanding of how plants utilize multiple classes of hormones to regulate their growth and development under changing environmental conditions.



18

Signal Transduction

Ottoline Leyser and Stephen Day

Introduction

Plant cells detect a wide range of signals that originate either within the plant or the surrounding environment, and they use this information to regulate their behavior. In all cases, the responses of cells rely on **signal transduction**—the process by which information is transferred from the site(s) of perception to the site(s) of response. Investigations over recent years have provided detailed molecular descriptions for several intracellular signal transduction pathways, tracing the interactions that link signal perception to cellular responses. In addition, the research reveals how combinations of pathways interact to allow cells to integrate multiple sources of information.

18.1 Characteristics of signal perception, transduction, and integration in plants

18.1.1 Plant cells monitor a continuous, complex stream of information

Plants regulate their biology in accordance with diverse environmental and internal cues. In the physical environment, plant cells detect gravity, temperature, local distributions of soil nutrients and water, and mechanical forces such as wind, the pressure between the root and soil, and internal tension or compression. They also sense the concentrations of gases such as carbon dioxide, oxygen, and ozone as well as the intensity, direction, and spectral quality of light; indeed, through the perception of light and temperature, they sense the time of day and the time of year. In the biotic environment, cells sense the presence of pathogens, herbivores, neighboring plants, and symbiotic bacteria and fungi. Internally, plants monitor their developmental stage, health, and water, nutrient, and photosynthate status. In addition, signaling interactions between cells in developing regions of the plant determine patterns of cells, tissues, and organs, while long-range signals control larger patterns of development. Somehow, plants organize appropriate local and systemic responses to each of these signals (Fig. 18.1).

Plant responses to these diverse categories of information interact and feed back on each other. For example, at the vegetative shoot apex, local cell-to-cell signaling first determines the pattern of leaf initiation and then, within each developing leaf, controls the arrangement of cell types. These patterning processes need no external help, since isolated shoot apices or individual leaf primordia can produce normal, if small, shoots and leaves in tissue culture. In real life, however, developing regions such as the shoot apex are in continuous communication with the rest of the plant through long-range signals carried in the vascular tissue. This allows the plant to modulate larger patterns of development, such as the balance of shoot to root growth, or the decision to flower. As each region of the plant responds to such signals, it may alter its own signaling patterns; the transition of an axillary bud from dormancy to growth, for example, is linked to the initiation of auxin export from the bud into the main stem.

Biochemistry & Molecular Biology of Plants, Second Edition. Edited by Bob B. Buchanan, Wilhelm Gruissem, and Russell L. Jones.
© 2015 John Wiley & Sons, Ltd. Published 2015 by John Wiley & Sons, Ltd.
Companion website: www.wiley.com/go/buchanan/biochem

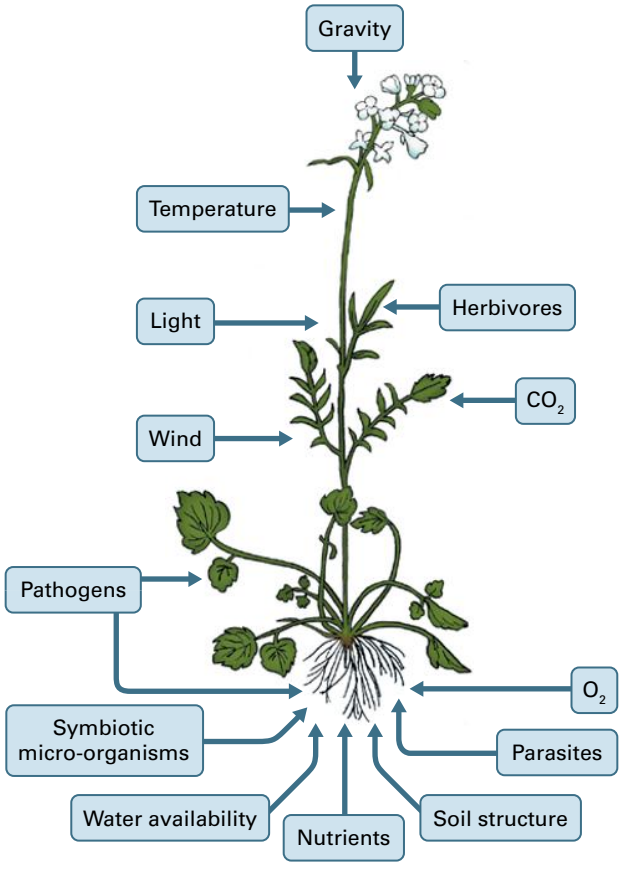


FIGURE 18.1 *External information that affects plant physiology, defense, and development comes from many aspects of the plant's physical and biological environments. Almost all external signals can vary in intensity, sometimes from minute to minute.*

Regardless of how complex they become, all plant responses to internal and environmental signals begin at the level of the individual cell. This chapter, therefore, considers signal perception, transduction, and integration from the cellular perspective. This section discusses the characteristics of signaling mechanisms operating in eukaryotic cells, plant cells in particular. Subsequent sections consider specific plant signaling pathways and examples of intracellular signal integration in detail.

18.1.2 Chains of signal-transducing molecules connect perception to response

Plants perceive environmental information that is both physical (e.g., light intensity and temperature) and chemical (e.g., water availability and nutrient concentration). Signals operating within and between plant cells are mostly chemical, although exceptions can be made for electrical events at membranes and physical forces generated by tissue growth.

Regardless of signal type, plant cells perceive most environmental information and most intercellular signals at dedicated **receptor proteins**. Signal perception results in a change in receptor protein activity, typically to regulate an

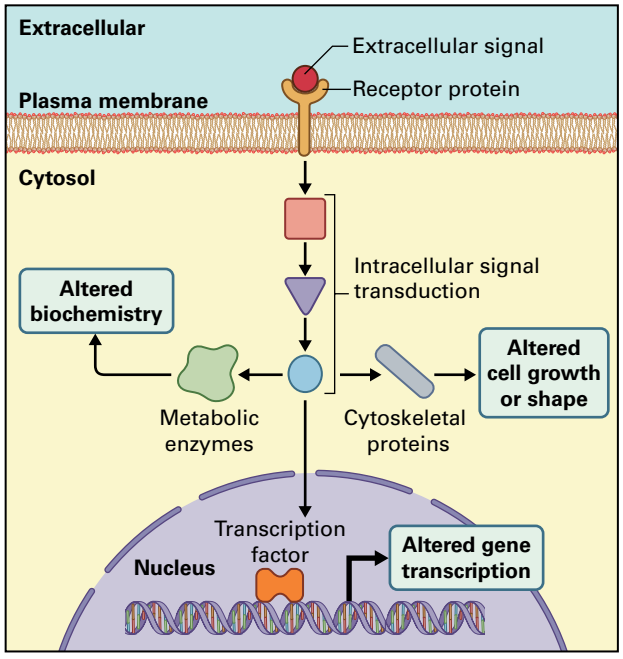


FIGURE 18.2 *Plant signal perception, transduction, and response. An extracellular signal is shown binding to a plasma membrane receptor protein. The receptor controls the activity of an intracellular transduction pathway that regulates cell responses to the signal. Overall, information inherent to the signal is transferred from the site of perception to sites of response within the cell. Note that the cell wall is not shown for clarity.*

intracellular signal transduction pathway (Fig. 18.2). Operation of the transduction pathway then depends on interactions between its component signal-transducing molecules, which often result in covalent modifications and/or allosteric changes. For example, some receptor proteins respond to signal perception by activating intracellular protein **kinases**, enzymes that phosphorylate proteins. Phosphorylation typically causes an allosteric change in the target protein that can change its activity to induce either a change in cell behavior or downstream signaling. Interactions within a transduction pathway often also lead to movement of signaling molecules within the cell, for example through release of a signaling protein from an anchoring complex or opening of ion channels. In such ways, transduction pathways transfer information inherent to the perceived signal through the cell to the sites of response.

Many pathways also eventually regulate the synthesis, activity, or stability of **transcription factors**, proteins that regulate gene transcription. This may reflect a central role for transcriptional control in establishing overall patterns of cellular behavior. Research has, however, focused on transcriptional regulation; gene expression is also regulated at other levels, and not all cellular responses require changes in gene activity.

Some transduction pathways also act on cytoplasmic or membrane components, often leading to very rapid responses. For example, germinating pollen tubes grow at tens to hundreds of nanometers per second, and they are steered through the style to the ovule by signals perceived by

plasma membrane receptors. The receptors induce a cytoplasmic signal transduction pathway responsible for aligning the cytoskeleton at the tube tip and, hence, determining the direction of growth. Similarly, changes in guard cell osmotic potential and, therefore, turgor can open or close stomata over a period of minutes—a process mediated by the regulation of ion flux via plasma membrane channels in response to factors such as light, the hormone abscisic acid (ABA), and carbon dioxide concentration (see Section 18.9).

18.1.3 Signal transduction in plant cells evolved from ancient signaling mechanisms

The classes of signaling molecules and types of signaling interactions present in plant cells also exist, with varying degrees of overlap, in prokaryotes, animals, and fungi. Intracellular signal transduction mechanisms are, therefore, evolutionarily ancient. In contrast, most of the molecules that carry intercellular signals within a plant are unique to the plant kingdom, reflecting independent evolution of multicellularity in the different eukaryotic kingdoms.

The diversity of extracellular signals and conservation of intracellular transduction mechanisms are reflected in the structure of receptor proteins. For example, receptor proteins in the plasma membrane often possess an extracellular **ligand-binding domain** that captures the signal, a transmembrane domain that anchors it within the membrane, and an intracellular **effector domain** that interacts with downstream signaling components. Ligand-binding domains have diverse structures, reflecting the wide range of extracellular signals, whereas effector domains are typically highly conserved within and between species. Transferring receptor proteins between kingdoms can demonstrate this. For example, the yeast (*Saccharomyces cerevisiae*) receptor protein SLN1 is required for osmoregulation, and loss-of-function mutations in the receptor are lethal. Mutant yeast can be rescued by transformation with the *Arabidopsis* gene for the cytokinin receptor, CRE1, but only if they are also given a cytokinin supply to activate the receptor (Fig. 18.3). CRE1 and SLN1 are both histidine kinases that act through the two-component system (see Section 18.5), and despite responding to very different external signals, their effector domains (represented by the kinase receiver domain, see Section 18.5) are sufficiently similar for CRE1 to interact with the necessary downstream signaling pathway in yeast.

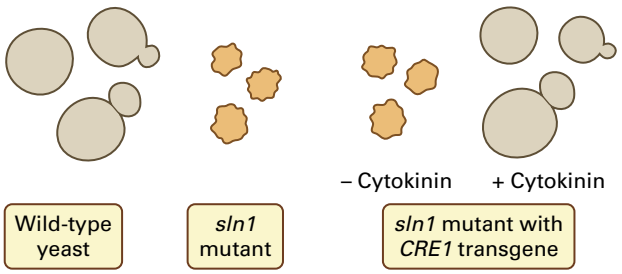


FIGURE 18.3 *CRE1, a plant cytokinin receptor, can substitute for the yeast receptor SLN1, which is required in yeast for osmoregulation. Yeast* snl1 *mutants lacking SLN1 die, and mutants expressing a* CRE1 *transgene survive, but only if cytokinin is present to activate the CRE1 receptor.*

The same phenomenon occurs at the level of individual cells within a species: diverse extracellular signals activate similar intracellular signal transduction pathways. Combined with the ancient origin of intracellular signaling mechanisms, this has led to the concept of **signaling cassettes**, modular signal transduction mechanisms that are frequently conserved within and between diverse organisms and that process a wide range of upstream signals to trigger a wide range of downstream responses. Examples discussed in this chapter include kinase cascades and two-component mechanisms.

18.1.4 Diverse transduction pathways share common characteristics

A huge variety of signal transduction pathways occur in plant cells. They display diversity both in their molecular constituents and in the interactions that occur between those constituents. There are, however, some common themes.

Signals are almost always progressively amplified as information travels along a pathway. An individual kinase, for example, can phosphorylate many copies of its target protein, and opening of a single membrane calcium channel allows flux of multiple calcium ions. In a special case of signal amplification, large-scale activation of gene transcription is often achieved through the activity of **transcriptional cascades**. For example, the perception of light as a seedling emerges from the soil leads to the accumulation of a handful of master transcription factors (see Section 18.7.3). These then induce transcription from genes encoding secondary transcription factors, which may induce transcription from other transcription factor genes. Collectively, the transcription factors in the cascade regulate the expression of thousands of downstream genes required for the seedling's growth as an autotroph.

Transduction pathways can continue after the initiating signal has ended, with the duration of signaling tightly regulated by inactivating mechanisms such as dephosphorylation of phosphorylated proteins. In contrast, if the initiating signal persists, feedback mechanisms often reduce the activity of the associated transduction pathway, leading to desensitization of the cell to the signal.

When a component of a pathway has several downstream targets, the pathway branches and a single perceived cue leads to diverse responses that may occur in different compartments of the cell. The complexity of the intracellular signaling network is also greatly increased by the fact that many signaling components are encoded by multigene families. Often, family members have similar, but nonidentical activities, and cellular responses are modulated by differential expression of genes within a family. The phytochrome light receptors

provide a clear example. As described in Section 18.7, phytochromes are divided into two subgroups: light-labile phytochrome (phyA, the concentration of which falls in the light) and light-stable phytochrome (phyB–E, which have similar concentrations in light and darkness). Accumulation of light-labile phyA in dark-grown seedlings gives cells an extreme, but transient sensitivity to light that is not seen in mature shoots, in which lower levels of light-stable phytochromes predominate.

Cell-to-cell variation in the expression of receptors and signaling intermediates may help explain one of the abiding puzzles in the study of plant signal transduction—that a small group of classical plant hormones mediates a huge range of processes in plant development, physiology, and defense. For example, auxin functions in mechanisms that establish the polarity of the embryo, initiate and maintain the apical meristems of the shoot and root, determine sites of leaf initiation and the pattern of vascular development, mediate tropic movements, regulate the degree of shoot branching and the balance of shoot to root growth, and initiate regeneration after wounding. For such diverse functions to occur in response to individual signals, different cell types must respond in different ways. In a simple example, treatment with indole-3-acetic acid (IAA, the major naturally occurring plant auxin) at concentrations of about 10^{-7} M stimulates elongation of cells in the shoot, but inhibits elongation of cells in the root. Cell-to-cell or temporal variations in the expression of the signal transduction network also likely underlie the phenomenon of **competence**, the ability of a cell (or tissue or organ) to respond to a signal with a particular development outcome.

18.1.5 Interactions between transduction pathways allow signal integration

Signaling pathways initiated by different cues interact with each other. Indeed, few, if any, discrete pathways exist in plant cells. Instead, most known pathways interact with other pathways in ways that both regulate cellular responses and feed back onto the structure and behavior of the signaling network.

Signal transduction pathways may interact because they converge onto the same signaling intermediates, or onto the same response molecules, to regulate a common process. For example, in the control of stomatal aperture, intracellular signals initiated by light and ABA converge to regulate guard cell plasma membrane proton pumps, the activities of which regulate membrane polarization and form a key step in the transduction of both signals. In this case, the two signals have conflicting effects on the pump: light upregulates the activity of the pump to promote stomatal opening, whereas ABA blocks the pump to induce stomatal closure (see Section 18.9).

Pathways also interact through the regulation of one pathway by a component of another. Considering stomata once more, light activates the proton pump by causing its phosphorylation. This pathway is inhibited by ABA signaling through a mechanism that appears to require the ABA signaling intermediate, hydrogen peroxide; ABA signaling both regulates the proton pump directly and interferes with the transduction pathway that links light perception to pump activity. In a conceptually similar manner, the response to a signal can include changes in the synthesis, perception, or transduction of one or more other signals. For example, auxin and ethylene mutually stimulate each other's synthesis.

Through interactions such as these, signals perceived by different receptors, and representing different information acquired by the cell, are integrated while being processed by a complex and continually adjusting signal transduction network. This allows cells to integrate multiple sources of information rapidly, for example, to modulate their response to local environmental cues (such as guard cell light exposure) according to intercellular signals relating to the status of the plant as a whole (such as ABA as an indicator of water stress).

The convergence of signal transduction onto common signaling intermediates and response molecules allows signal integration but also risks loss of **specificity**, the extent to which distinct signals are able to induce distinct responses. For example, as discussed in Section 18.3, calcium ions (Ca^{2+}) are signaling intermediates downstream of a wide range of different receptors. This raises the question of how the cell achieves the appropriate response to each perceived cue when it is using identical signaling components in multiple contexts.

Part of the answer is through the compartmentalization of signaling pathways coupled to rapid inactivation of signaling components. A signal transduction pathway may be restricted to the cytosol, to a particular class of organelle, or to the nucleus. When this is the case, damaging interactions can be avoided if those signaling intermediates that can diffuse between compartments are inactivated rapidly relative to the rate of diffusion. A similar phenomenon occurs on a smaller physical scale through the regulated binding of signaling components to scaffold proteins, facilitating interactions between components within a transduction pathway while limiting interactions between pathways. This is believed to occur in **mitogen-activated protein kinase** (MAPK) **cascades** , where it is thought to help divide the multitude of possible cascades into defined signaling cassettes (see Section 18.3.2).

18.1.6 Signaling mechanisms in plant cells can be grouped according to multiple criteria

Descriptions of intracellular signaling in plants may be organized according to cellular location and the class of signaling mechanism, or they may be arranged signal by signal or discussed with respect to particular cellular responses. This chapter uses all three approaches according to which best suits the available data. Section 18.2 considers signal perception at the plasma membrane, including research on

the perception of brassinosteroids, bacterial flagellin, CLE peptides, ABA, and mechanical forces. Section 18.3 then considers the functions of second messengers and kinase cascades in signal transduction and integration.

Sections 18.4 to 18.7 consider the perception and transduction of individual signals; they discuss how cells respond to the hormones ethylene, cytokinin, and auxin and how signal transduction follows light perception by phytochromes. These are among the best understood transduction pathways in plant cells. Signaling by gibberellins is discussed in Section 18.8 in relation to signal integration by DELLA proteins during seedling responses to light. Section 18.9 then considers the integration of light, ABA-, and CO_2 signaling in the control of stomatal aperture. This is far from an exhaustive survey of signal transduction in plant cells, but hopefully it provides a framework for understanding related areas of research.

18.2 Overview of signal perception at the plasma membrane

18.2.1 The plasma membrane is a major site of signal perception

Plant cells have two routes by which they are able to communicate with one another: the **apoplast**, formed by the interconnected cell walls of the plant, and the **symplast**, the cytoplasmic continuum created by strands of cytoplasm connecting neighboring cells via plasmodesmata. Molecular transport through the apoplast and symplast is discussed in detail in Chapter 15. With respect to intercellular signaling, the apoplast is associated with the transmission of signals such as the plant hormones and signal peptides, which require conventional receptor proteins. In contrast, signaling via the symplast allows regulated movement of RNAs and transcription factor proteins, which can induce responses in the receiving cell more directly.

For signals arriving at the cell through the apoplast, the plasma membrane is a major site of perception; indeed, large and hydrophilic molecules that lack a membrane import channel can only be perceived by plasma membrane receptors. Receptors at the membrane also perceive some physical signals, for example mechanical force (see Section 18.2.4) and blue light (via phototropins, see Box 18.2).

Plasma membrane receptors are divided into three major groups distinguished by how they interact with intracellular signaling components: receptor kinases, G protein-coupled receptors, and ion channel receptors. The receptor kinases are by far the largest group of membrane receptors in plants, and they transduce extracellular signals through phosphorylation of intracellular targets (see Section 18.2.2). G protein-coupled receptors regulate trimeric GTP-binding proteins (**G proteins**) located on the inner surface of the membrane (see Section 18.2.3). Lastly, ion channel receptors regulate membrane ion channels and, thus, ion fluxes into or out of the cell (see Section 18.2.4).

Despite the importance of signal perception at the plasma membrane, it should be noted that small, lipophilic molecules can cross the membrane and be perceived in the cytoplasm or nucleus. This is the case for ethylene, which is detected by receptors on the endoplasmic reticulum membrane (see Section 18.4), and for the hormones auxin and gibberellin, which are perceived by soluble receptors that interact with the cell's protein degradation machinery (see Sections 18.6 and 18.8). Similarly, the plasma membrane is no barrier to many physical cues; the phytochrome and cryptochrome families of photoreceptors, for example, are intracellular, having both cytoplasmic and nuclear locations, depending on the light conditions and the particular family member (see Section 18.7, see Box 18.2).

18.2.2 Signaling by the largest group of membrane receptor kinases can involve both receptor heterodimerization and receptor endocytosis

Phosphorylation is the most common posttranslational modification used by cells to regulate protein activity. Catalyzed by **kinases**, phosphorylation can alter protein stability, subcellular location, binding properties, enzyme activity, and susceptibility to subsequent modifications. Furthermore, single proteins may be phosphorylated at multiple amino acid residues, sometimes by different kinases and with different effects, enabling integration of separate signal transduction pathways. Consequently, it is not surprising that kinases and **phosphatases** (which dephosphorylate proteins) play vital roles in signal transduction in all organisms.

In plants, signal perception appears to rely heavily on plasma membrane **receptor-like kinases** (RLKs), a family of over 600 proteins in *Arabidopsis* and over 1,100 in rice (*Oryza sativa*) that typically phosphorylate target proteins on serine and threonine residues. RLKs possess an extracellular domain that provides potential ligand-binding sites, a transmembrane domain, and an intracellular kinase domain. They act in a wide range of processes, including hormone perception, development, defense, symbiosis, and pollen tube germination and guidance. The best understood of the signal transduction mechanisms mediated by RLKs is the perception of brassinosteroids (BRs). RLKs also function in the perception of **CLE peptides** (CLAVATA3/ENDOSPERM SURROUNDING REGION, Box 18.1).

BRs are a group of steroid hormones that function in a variety of cellular and developmental contexts, such as promotion of cell elongation during etiolation of dark-grown seedlings. Research on the RLKs required for BR perception and on other, closely related RLKs has revealed multiple,

BOX 18.1

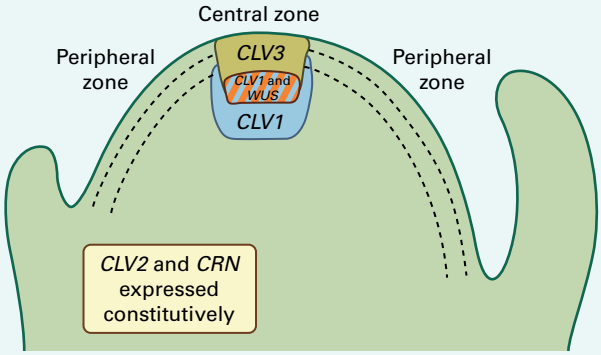
CLE peptide signals act in several developmental contexts

The **CLE peptides**, named after CLAVATA3 (CLV3)/ENDOSPERM SURROUNDING REGION (ESR), were discovered through research on the control of the size of the *Arabidopsis* shoot apical meristem (SAM). The SAM is composed of a central zone (CZ) and a peripheral zone (PZ) (panel A). Cells in the CZ act as stem cells for shoot development; they divide to supply cells to the PZ, in which cells both divide and differentiate to initiate the structures of the shoot.

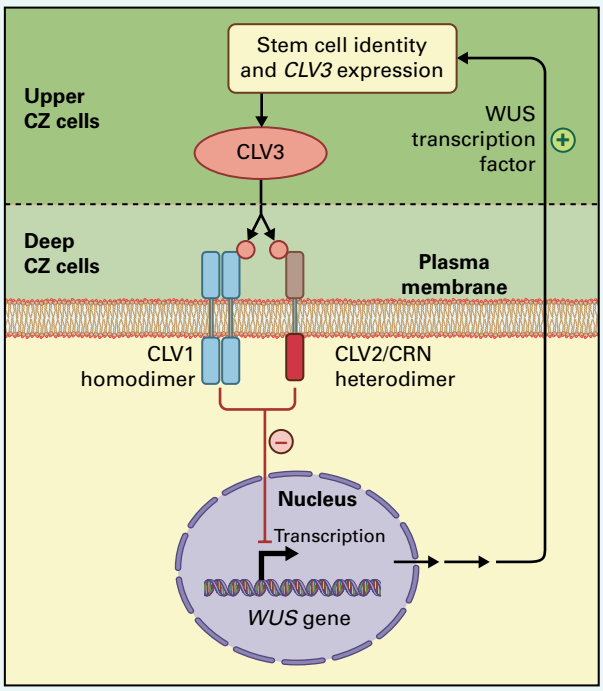
The size of the CZ and, therefore, of the whole SAM is regulated by a feedback loop acting on the genes *WUSCHEL* (*WUS*) and *CLAVATA3* (*CLV3*). *WUS* is expressed in a small group of cells deep in the CZ and is required for the production of a signal that confers stem cell identity throughout the CZ. At least in part, this signal consists of the WUS protein—a transcription factor that is transported between meristem cells via plasmodesmata (see Section 11.5.1).

In the upper CZ layers, WUS activates transcription from *CLV3*, which encodes a small protein that is processed to produce a secreted, 13 amino acid CLE peptide. The CLV3 CLE peptide acts as a short-range signal perceived by cells deeper in the CZ (panel B; cell wall not shown). In the current model, perception of the CLV3 CLE peptide occurs at two receptors: a homodimer of the CLV1 protein, and a heterodimer consisting of the CLV2 and CORYNE (CRN) proteins. CLV1 is a LRR-receptor-like kinase (see Section 18.2.2), and CLV2 and CRN are related proteins. CLV2 resembles CLV1 but lacks an intracellular kinase domain. In contrast, CRN possesses a kinase domain but lacks a full extracellular domain. The CLV2/CRN heterodimer therefore has the necessary domains for signal perception and transduction. Signals from the CLV1 and CLV2/CRN receptors converge to down regulate *WUS* expression. This completes the feedback loop and creates a mechanism in which SAM size is determined by the balance of *WUS* expression, which acts to promote CZ identity and hence SAM growth, and CLV3 signaling, which limits *WUS* activity.

In total over 30 genes encoding proteins likely to produce secreted CLE peptides have been identified in *Arabidopsis*. The genes are expressed in a variety of tissues, and CLE peptides have been implicated in the regulation of root apical meristem activity and in vascular differentiation. Although *CLV1* expression is confined to the SAM, *CLV2* and *CRN* are both expressed in a wide range of tissues. Therefore, the CLV2/CRN receptor may function beyond the CZ of the SAM and in the perception of other CLE peptides. Supporting this, both *crn* and *clv2* mutants have defects in stamen and anther development.



A



B

pairwise interactions between RLKs. The results of such research also indicate receptor endocytosis may have a key role in the regulation of signal transduction from RLKs.

BRs bind to the extracellular domain of the BR receptor BRASSINOSTEROID INSENSITIVE1 (BRI1) (Fig. 18.4). BRI1 is a member of the largest subgroup of RLKs, those in which the extracellular domain contains leucine-rich repeats (LRRs), which consist of a series of repeated motifs of 20–29 amino acid residues rich in leucines, thought to function in protein–protein interactions. As steroid molecules, BRs are unlikely targets for a LRR; in BRI1, however, the LRR is interrupted by a 70-amino acid 'island domain' that is likely the site of BR binding.

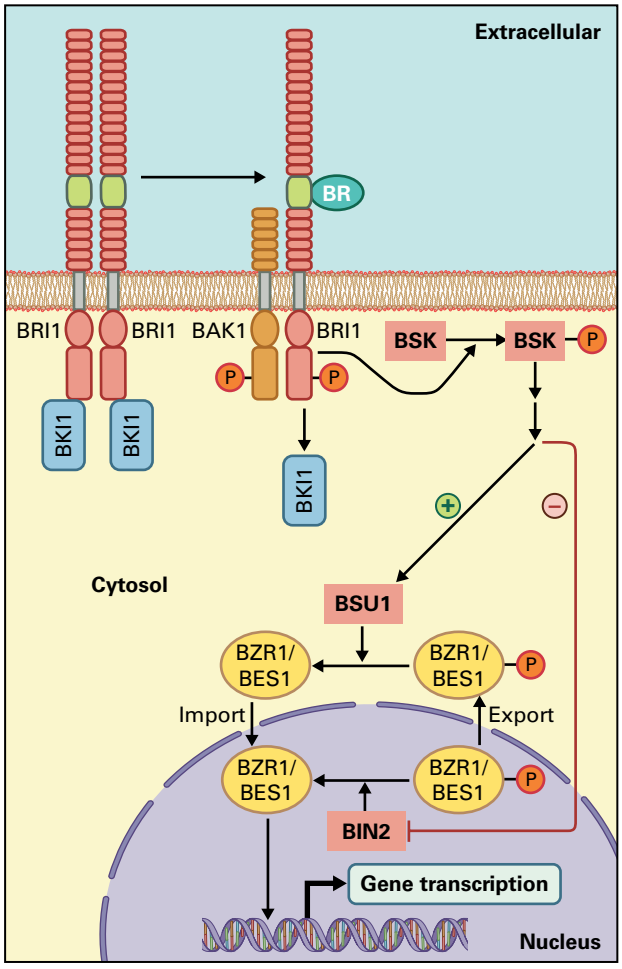


FIGURE 18.4 *Brassinosteroids (BR) bind to the BRI1 receptor, causing dissociation of the inhibitor BKI1 and heterodimerization and reciprocal phosphorylation of BRI1 and BAK1. BRI1 phosphorylates BSKs, inducing signal transduction pathways that lead to accumulation of unphosphorylated forms of the BZR1 and BES1 transcription factors in the nucleus and consequent changes in gene transcription. Note that the cell wall is not shown for clarity.*

BRI1 exists in the plasma membrane as a homodimer associated with the inhibitory protein BKI1 (BRI1 KINASE INHIBITOR1). BR binding induces the dissociation of BKI1 from the receptor, probably induced by phosphorylation of BKI1 by BRI1, and leads to the loss of BKI1 from the plasma membrane. Freed from BKI1 inhibition, BRI1 phosphorylates downstream targets. In addition, the BRI1 homodimer splits, and BRI1 forms heterodimers with another LRR-RLK called BAK1 (BRI1-ASSOCIATED KINASE1). Reciprocal phosphorylation within the heterodimer—of BAK1 by BRI1 and then of BRI1 by BAK1—subsequently enhances signaling from BRI1. BAK1 has a truncated extracellular domain containing only a short LRR domain and no island domain, and it does not appear to have a ligand-binding function.

The signal transduction pathway downstream of BRI1 is not fully known. In the current model, BRI1 phosphorylates and activates a small family of kinases (BSK1, BSK2, and BSK3) that induce downstream BR responses through their own kinase activities. The targets of the BSKs are unknown; however, downstream responses are mediated through the regulation of a family of transcription factors that includes BZR1 and BES1. The activity of these transcription factors is downregulated through phosphorylation by the kinase BIN2 and upregulated through dephosphorylation by the phosphatase BSU1. Phosphorylation inhibits the activity of BZR1 and BES1 by multiple mechanisms, including the retention of the two transcription factors in the cytoplasm, an increase in their rate of degradation, and a reduction in their DNA binding ability. Following BR perception, BIN2 is inhibited and BSU1 is stimulated, leading to accumulation of unphosphorylated BZR1 and BES1 in the nucleus and regulation of BR-responsive genes (e.g., the inhibition of transcription from the *DWF4* gene).

The tomato (*Solanum lycopersicum*) homolog of BRI1 acts both as the BR receptor and as the receptor for the defense signal **systemin**, an 18 amino acid peptide produced by tomatoes and other Solanaceae in response to insect attack and that acts as a systemic signal capable of inducing defense-related genes. The ability of tomato BRI1 to bind two different signals raises the question of how specificity is maintained to differentiate responses to BRs and to systemin. One possibility is that systemin binding induces interaction with an LRR-RLK other than BAK1.

BRI1 is likely to signal from both the plasma membrane and endosomes (intracellular vesicles created by endocytosis; see Chapter 1). Both BRI1 and BAK1 are removed from the plasma membrane into endosomal membranes and then cycled back to the plasma membrane via transport vesicles budding off from recycling endosomes (Fig. 18.5). BRI1 cycling is constitutive and is not affected by either BR binding or the loss of *BAK1* function. Treatment with brefeldin A, an inhibitor of endosomal trafficking, causes accumulation of BRI1 in endosomes and increases signaling through the BR pathway, suggesting a role for signaling from endosomal BRI1. The use of endosomes for signal transduction from plasma membrane receptors increases the membrane area available for signaling interactions. Furthermore, for typical elongated, differentiated plant cells in which the central vacuole occupies most of the cell volume, receptor endocytosis may help ensure even signaling strengths from different regions of the plasma membrane. As the resultant endosomes are circulated around the cell by cytoplasmic streaming, receptors activated at all parts of the plasma membrane are brought into the proximity of the nucleus.

Moving away from BR signaling, research on other functions of BAK1 suggests multiple interactions between pairs (at least) of plasma membrane RLKs. In addition to BRI1, BAK1 associates with the receptor for bacterial flagellin, an LRR-RLK called FLS2 (FLAGELLIN-SENSITIVE2). FLS2 induces a range of defense responses after flagellin binding. Similar to the case for BRI1, ligand binding to FLS2 induces association of FLS2 with BAK1, which promotes signaling by the receptor. Unlike BRI1, however, FLS2 is not constitutively cycled through endosomes. Instead, FLS2 endocytosis

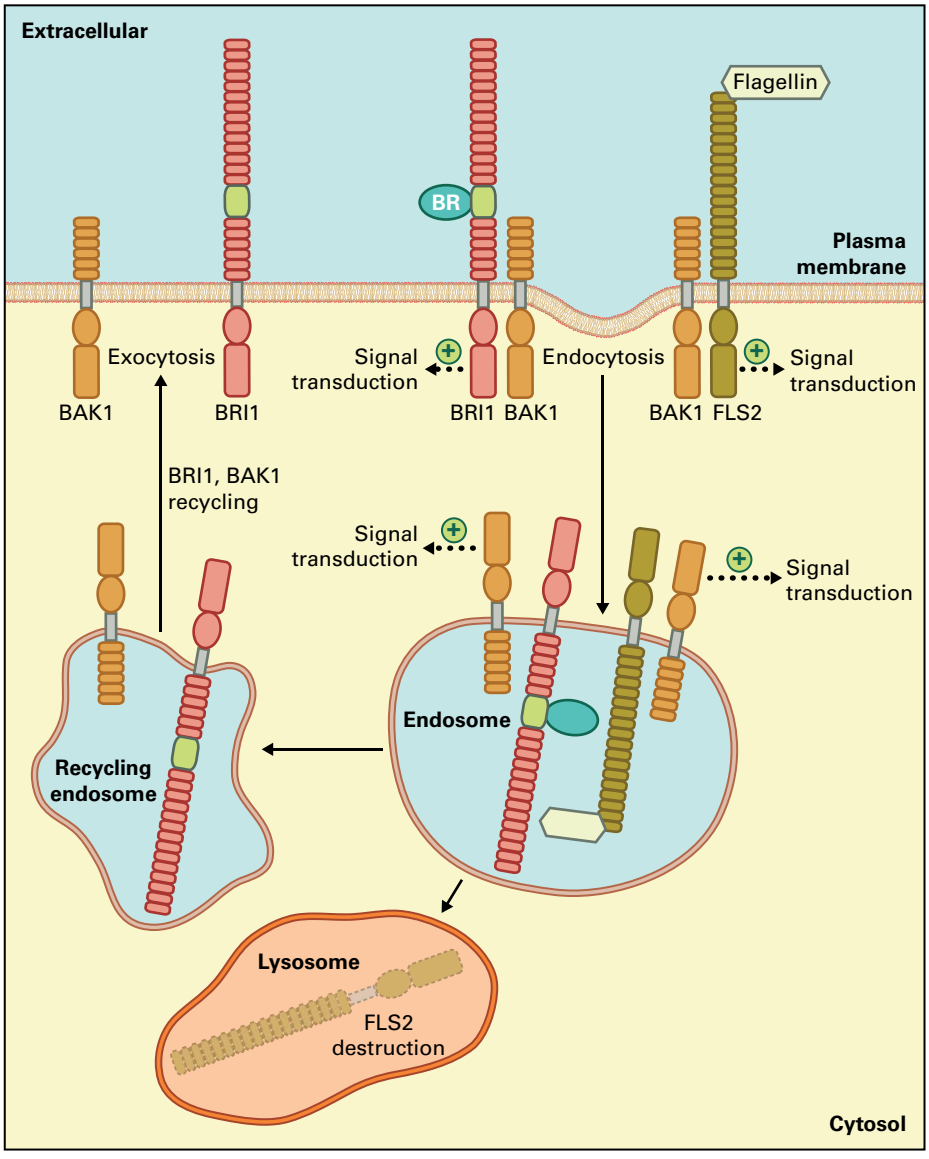


FIGURE 18.5 *BRI1 and FLS2 receptors activated by binding to BR and flagellin, respectively, signal from both the plasma membrane and, after endocytosis, endosomal membranes. Following endocytosis of both the inactive (not shown) and activated forms of BRI1, endosomal BRI1 is recycled to the plasma membrane. In contrast, only active FLS2 undergoes endocytosis, and endosomal FLS2 is targeted for destruction in lysosomes. Note that the cell wall is not shown for clarity.*

is induced by flagellin binding, and although FLS2 is also believed to signal from endosomes, the receptor is not recycled; instead endosomal FLS2 is eventually destroyed (Fig. 18.5).

The functions of kinases closely related to BAK1 demonstrate further levels of complexity (Fig. 18.6). BAK1 is a member of a family of five LRR-RLKs called SERKs (SOMATIC EMBRYOGENESIS RECEPTOR-LIKE KINASEs). BAK1 is SERK3. SERK1 acts redundantly with BAK1 as a co-receptor for BRI1. However, SERK1, together with SERK2 also functions in the development of microspores in the anther, a process that does not appear to require BAK1. Lastly, mutational analysis shows that with SERK4, BAK1 has a BR-independent role in controlling the cell death response. The functions of SERK5 are unknown.

In addition to RLKs, plants possess histidine kinase receptors. These include the receptors for ethylene and cytokinin and constitute a separate group of kinases derived from bacterial two-component systems. Histidine kinase receptors are discussed in detail in Sections 18.4 and 18.5.

18.2.3 Plant cells possess a small group of putative G protein-coupled receptors

G protein-coupled receptors (GPCRs) regulate the activity of trimeric GTP-binding proteins (**G proteins**) (Fig. 18.7). These consist of Gα, Gβ, and Gγ subunits, and as trimers, they are inactive and bound at the Gα subunit by a molecule

of GDP. GPCRs possess an extracellular ligand-binding domain, a transmembrane domain composed of seven hydrophobic helices, and an intracellular domain that interacts with inactive G protein trimers. Ligand binding by the receptor induces the Gα subunit of the trimer to release its bound GDP molecule and bind a molecule of GTP instead. This activates the G protein, which uncouples from the receptor and dissociates into the Gα subunit and a Gβ/Gγ dimer.

Gα and Gγ both have short, covalently attached lipid tails that anchor them to the inside of the plasma membrane so that Gα and the Gβ/Gγ dimer diffuse on the membrane to activate downstream signaling proteins. A single ligand-bound GPCR can amplify a signal by activating multiple G proteins. Signaling is terminated by the hydrolysis of bound GTP to GDP by Gα (which has GTPase activity), and this process is stimulated by **GTPase activating proteins** (GAPs). GDP-bound Gα reassociates with the Gβ/Gγ dimer to form an inactive trimer, which then binds a GPCR to complete the cycle.

The alternation of Gα between an active GTP-bound and an inactive GDP-bound form is a general feature of the GTP-binding protein superfamily. The superfamily includes GTP-binding initiation and elongation factors that act in protein synthesis, and also the **small** or **monomeric G proteins**, whose functions include signal transduction, organellar trafficking, and cytoskeleton assembly. The regulation of

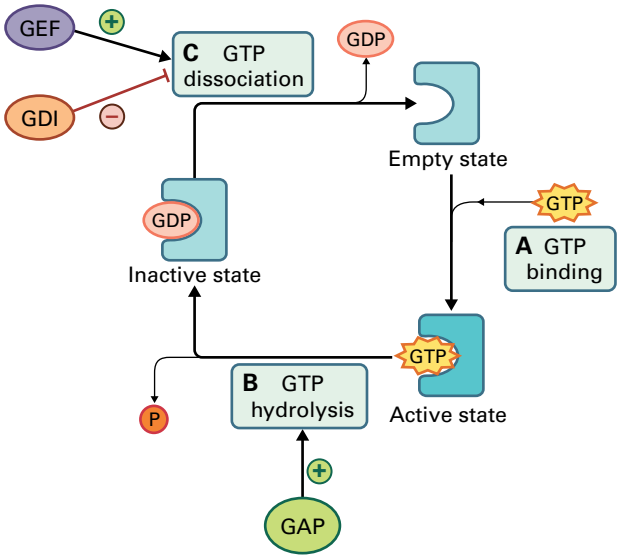


FIGURE 18.8 *(A) Monomeric G proteins are converted from an empty state to an active state by GTP binding. (B) They are inactivated by GTP hydrolysis, which is stimulated by a GTPase activating protein (GAP). (C) GDP release, which is inhibited by GDP dissociation inhibitors (GDIs) and stimulated by guanine nucleotide exchange factors (GEFs), returns the G protein to its empty state and allows reactivation.*

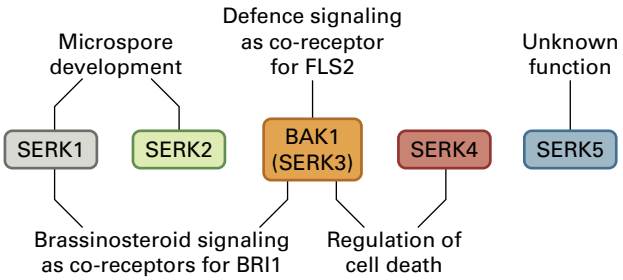


FIGURE 18.6 *The SERK family of LRR-RLKs have multiple and overlapping functions.*

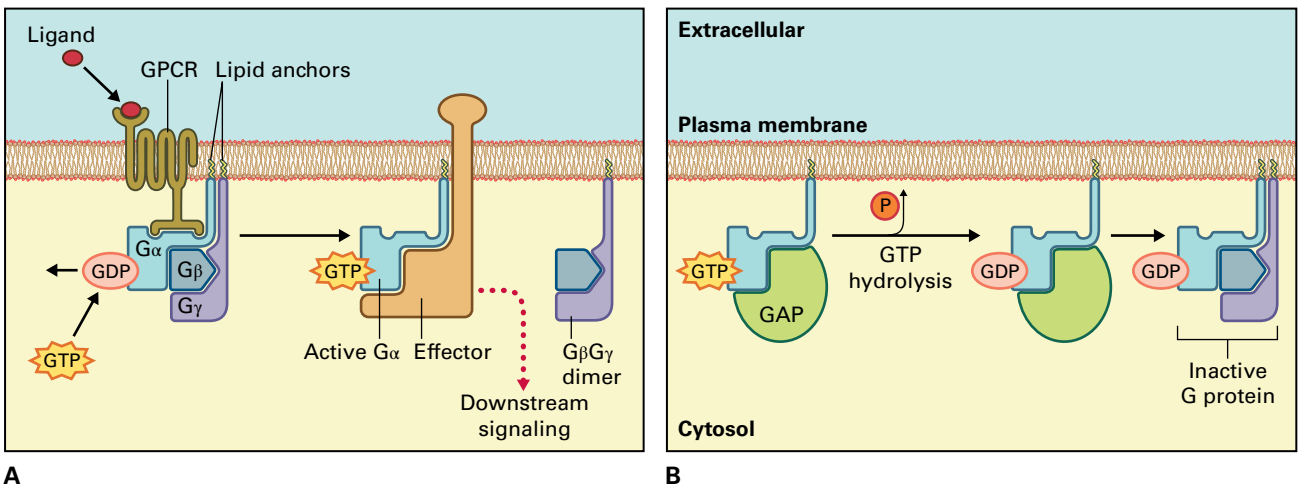


FIGURE 18.7 *Regulation of heterotrimeric G proteins. (A) Ligand binding by a G protein-coupled receptor (GPCR) induces the Gα subunit of the heterotrimeric G protein to exchange GDP for GTP. This leads to the dissociation of the G protein into active Gα and Gβ/Gγ subunits that regulate the activity of downstream effector proteins (Gβ/Gγ activity not shown). (B) Gα is inactivated by the hydrolysis of bound GTP to GDP, which is stimulated by a GTPase activating protein (GAP). Inactive Gα binds to the Gβ/Gγ dimer, reconstituting the inactive heterotrimeric G protein. Note that the cell wall is not shown for clarity.*

monomeric G proteins has parallels with the regulation of Gα activity (Fig. 18.8). Monomeric G proteins are activated by **guanine nucleotide exchange factors** (GEFs), which induce the exchange of GDP for GTP, a function equivalent to that of GPCRs. As is the case for regulation of Gα activity, the hydrolysis of GTP to GDP by monomeric G proteins is stimulated by GAPs. Lastly, **GDP dissociation inhibitors** (GDIs) prevent the spontaneous release of GDP by monomeric G proteins, a role played by the Gβ/Gγ dimer in trimeric G proteins.

A sharp contrast exists between the extent of GPCR signaling in plants and animals. Mammals possess between 500 and 1,000 GPCRs, depending on the species, together with multiple copies of the G protein subunits and a wide range of G protein-regulated signal transducing proteins, including kinases, ion channels, and enzymes involved in the production or destruction of second messengers such as cyclic nucleotides. In contrast, analysis of the *Arabidopsis* genome has identified only a handful of putative GPCRs. Unequivocal roles for the function of these GPCRs are currently lacking. Furthermore, *Arabidopsis* possesses only one Gα-, one Gβ-, and two Gγ-encoding genes. The nature of the signaling proteins acting downstream of Gα and the Gβ/Gγ dimer in plants is uncertain.

18.2.4 Ion channel receptors can perceive mechanical stimuli

Ion channels are water-filled pores created by conformational changes in multisubunit, membrane-spanning proteins. They allow inorganic ions to flow across membranes, down their electrochemical gradients. Pore diameter and the charges on the amino acid residues that line the pore determine which ions are able to use a channel (see Chapter 3 for more details).

Ion channels can be regulated by binding either extracellular or intracellular ligands and by changes in voltage across the membrane or by mechanical force. In the plant plasma membrane, no identified ion channel proteins function as receptors for extracellular ligands; mechanosensing calcium ion channels, however, play a role in plant responses to physical forces.

Plants display developmental responses to gravity, touch, soil pressure, wind, and the stresses imposed by their own weight and tissue growth. Mechanical stimulation results in an immediate and transient increase in cytosolic calcium ion concentration. Though this suggests the existence of mechanosensing ion channels, the identity of such channels has yet to be confirmed. One candidate is the MID1 COMPLEMENTING ACTIVITY1 (MCA1) protein of *Arabidopsis*. MCA1 is believed to be a plasma membrane calcium ion channel that responds to mechanical stimulation, and the roots of *mca1* loss-of-function mutants are unable to penetrate harder agar growth media, implying an abnormal response to pressure.

18.3 Intracellular signal transduction, amplification, and integration via second messengers and MAPK cascades

18.3.1 Second messengers act as diffusible signals within the cell

Second messengers are diffusible, intracellular signals that are typically synthesized or released in a transient, but concentrated pulse following primary signal perception. They provide a means of rapidly relaying signals to downstream transduction components. Second messengers include small molecules and mineral ions that diffuse through the cytosol, as well as lipid-based signaling molecules that diffuse within membranes. Here, we consider two cytosolic second messengers: cyclic nucleotides and calcium ions (Ca^{2+}).

The term second messenger was first used to describe **cyclic 3′,5′-adenosine monophosphate** (cAMP) after the discovery in the late 1950s that cAMP mediated signal transduction in response to a number of animal hormones. In the canonical pathway, hormone perception by an animal G protein-coupled receptor (see Section 18.2.3) leads to activation, via the G protein's Gα subunit, of a plasma membrane **adenylyl cyclase**. This enzyme catalyzes the conversion of ATP to cAMP (Fig. 18.9), which in turn diffuses to activate cytosolic **cAMP-dependent protein kinase** (PKA). PKA phosphorylates downstream target proteins to activate appropriate transduction pathways. Animal cells also use **cGMP** as a second messenger; it is produced by **guanylyl cyclase** and activates **cGMP-dependent protein kinase** (PKG). In addition to activating PKA and PKG, cyclic nucleotides in animal cells act by opening plasma membrane **cyclic nucleotide-gated ion channels** (CNGCs), which allow nonselective influx of the Ca^{2+}, K^+, and Na^+ cations. The cyclic nucleotide signal is terminated by the conversion of cAMP and cGMP into their noncyclic forms by phosphodiesterases.

Cyclic nucleotides have more restricted roles in plant cells than in animal cells. Importantly, no plant homologs of PKA or PKG have been found, and cyclic nucleotide signaling in plant cells may, therefore, be limited to the regulation of CNGCs. Like those found in animal cells, plant CNGCs are nonspecific cation channels. They have been implicated in various processes, including gibberellic acid (GA) and phytochrome signaling, pollen tube growth, cell cycle control, and stress and defense signaling. For example, pathogen infection induces rapid cAMP production and the influx of Ca^{2+} into plant cells, which is believed to occur through CNGCs. Spikes in cytosolic Ca^{2+} concentration are associated with a variety of defense responses, such as the expression of defense-related genes and the induction of programmed cell death.

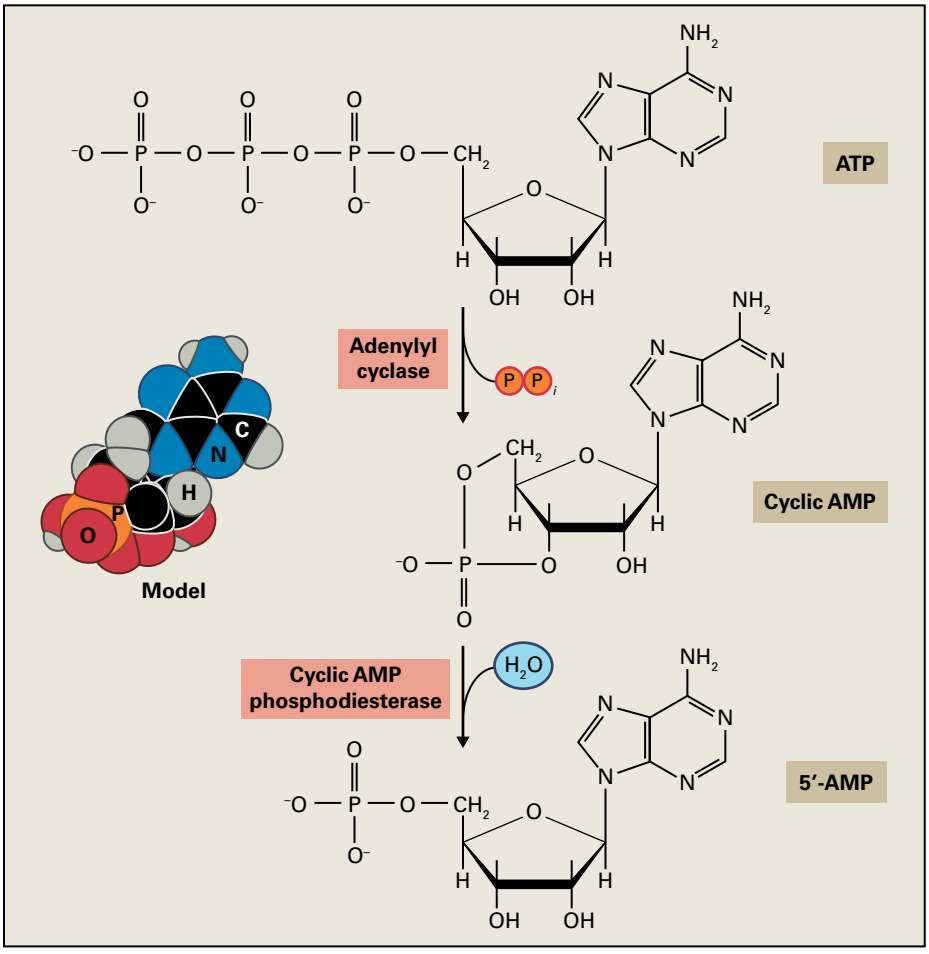


FIGURE 18.9 *Synthesis and degradation of cyclic 3′,5′-AMP by adenylyl cyclase and cyclic AMP phosphodiesterase. cAMP is shown as a structural formula and as a space-filling model.*

Ca^{2+} is a far more significant second messenger in plant cells than are the cyclic nucleotides. Cells maintain very low resting cytosolic Ca^{2+} concentrations $[Ca^{2+}]_{cyt}$ of around 100–350 nM while sustaining large Ca^{2+} stores in the vacuole and endoplasmic reticulum (ER) at concentrations of about 1–2 mM (Fig. 18.10). In the cell wall, Ca^{2+} concentration is estimated at about 0.5–1 mM. $[Ca^{2+}]_{cyt}$ is measured using cells transformed to produce Ca^{2+}-responsive luminescent or fluorescent dyes. This approach has shown spikes of $[Ca^{2+}]_{cyt}$ reaching approximately 1 μM can occur in response to a huge range of biotic and abiotic stimuli including pathogen infection (as above), nodulation factors, the hormones GA and ABA, red and blue light, UV-B radiation, low and high temperature, touch, wind, changes in the gravity vector, and anaerobic, drought and salt stress.

$[Ca^{2+}]_{cyt}$ spikes result from the opening of Ca^{2+}-permeable channels in the plasma membrane, ER membrane, or vacuolar membrane (tonoplast). Reflecting the complexity of stimuli that induce $[Ca^{2+}]_{cyt}$ spikes, there are several Ca^{2+}-permeable channels, which are gated by mechanical stimuli (see Section 18.2.4), by changes in the membrane electrical potential, or by ligands such as cyclic nucleotides (for the plasma membrane CNGCs), and the second messengers inositol trisphosphate (IP_3) and cyclic ADP-ribose (for channels on internal membranes).

$[Ca^{2+}]_{cyt}$ regulation of downstream signaling is largely mediated by Ca^{2+}-sensitive protein kinases. Plant cells contain kinases that bind Ca^{2+} directly as well as kinases that are regulated by the Ca^{2+}-binding **calmodulin** proteins (CaMs) and by binding to both Ca^{2+} and CaMs. The Ca^{2+} signal is terminated by membrane Ca^{2+} pumps (Ca^{2+} ATPases) and proton/calcium exchangers (antiports) that return $[Ca^{2+}]_{cyt}$ to its resting level (Fig. 18.10).

Ca^{2+} signaling illustrates one of the main questions facing research on second messengers, the problem of signal specificity (see Section 18.1.4). With so many stimuli leading to $[Ca^{2+}]_{cyt}$ spikes, and the large number of Ca^{2+}- and/or CaM-regulated kinases activating diverse downstream pathways, how does Ca^{2+} signaling link each stimulus to its appropriate response? There are several possibilities.

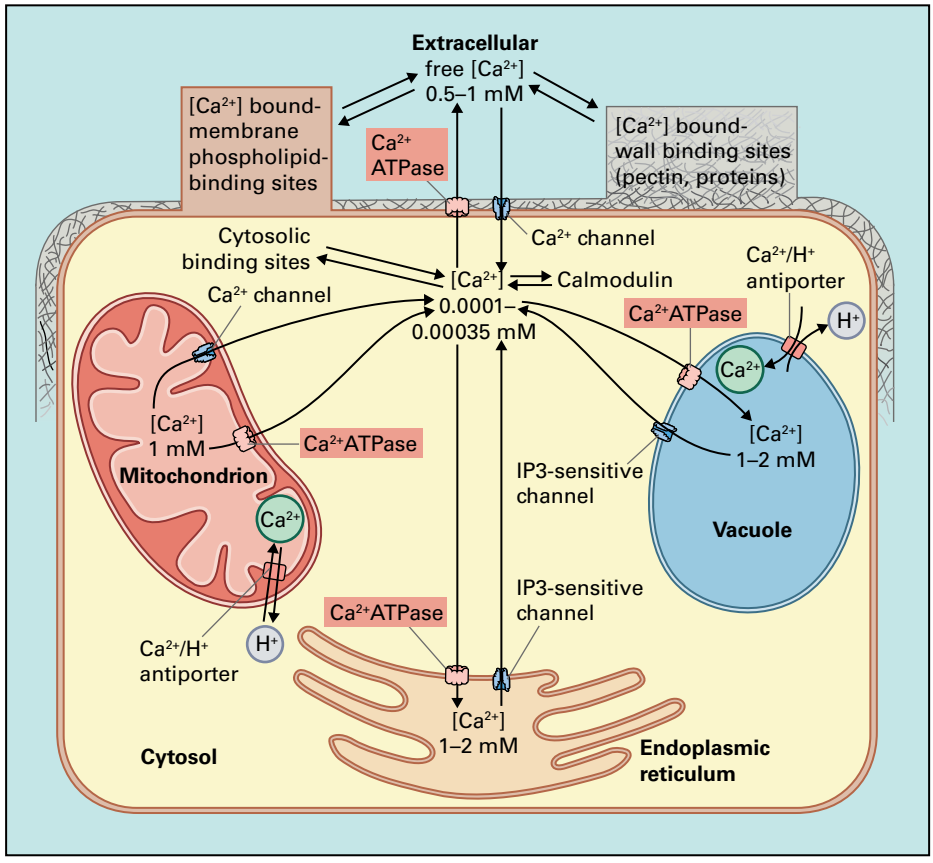


FIGURE 18.10 *Interactions of intracellular and extracellular Ca^{2+} in cell signaling. The concentration of free Ca^{2+} is much lower in the cytosol than in the cell wall or organelles. When the cell is signaled, channels in various organelles and/or the plasma membrane open to allow Ca^{2+} to enter the cytosol by diffusion down its electrochemical gradient. Ca^{2+} ATPases (Ca^{2+} pumps) and Ca^{2+}/H^+ antiports return the cytosolic concentration to its resting value.*

First, responses may depend on the spatial pattern of the Ca^{2+} signal. As a result of Ca^{2+} uptake by organelles and Ca^{2+} binding by proteins, the rate at which Ca^{2+} diffuses in the cytoplasm is at least two orders of magnitude below that of Ca^{2+} diffusing in a simple solution. This allows spatial segregation of $[Ca^{2+}]_{cyt}$ changes, for example in the formation of standing gradients of $[Ca^{2+}]_{cyt}$, which are important in directing the growth of root hairs and pollen tubes (Fig. 18.11).

Next, information may also be encoded in the temporal pattern of $[Ca^{2+}]_{cyt}$ changes. During the regulation of stomatal aperture, for example, $[Ca^{2+}]_{cyt}$ oscillates, and the correct period of oscillation is required for signaling (see Section 18.9). In some cases, an increase in $[Ca^{2+}]_{cyt}$ may be necessary, but is insufficient for a response, which means the presence or absence of other signaling molecules determine whether the response occurs.

Lastly, it is unlikely that all cells produce all components of the Ca^{2+} signal transduction machinery at all times. Signal specificity may depend in part of the subset of the Ca^{2+}-related signaling apparatus that is expressed by the individual cell.

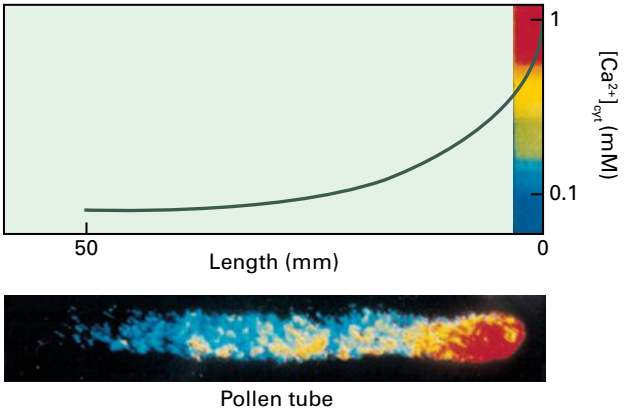


FIGURE 18.11 *Pollen tubes maintain a standing gradient of cytosolic $[Ca^{2+}]$ in their tip region. The standing gradient is essential for growth and results from a tip-associated cluster of Ca^{2+} channels. Pollen tubes can be loaded with $[Ca^{2+}]$-sensitive fluorescent dyes such as indo-1 or fura-2 for quantification of free $[Ca^{2+}]$ by fluorescence microscopy.*

18.3.2 MAPK cascades function in diverse signal transduction pathways

MAPK cascades exist in all eukaryotic cells and represent a classic example of a signaling cassette, a conserved modular transduction mechanism that processes multiple upstream signals to trigger multiple downstream responses. The core cascade consists of a series of three kinases: a MAPK, a **MAPK kinase** (MAPKK), and a **MAPKK kinase** (MAPKKK) (Fig. 18.12). MAPKKK phosphorylates and activates MAPKK, which in turn phosphorylates and activates MAPK. The active MAPK may translocate to a different part of the cell and phosphorylate downstream transduction components, such as other kinases, metabolic enzymes, or transcription factors to regulate their activity. Signaling through the cascade is induced by activation of the MAPKKK, which can occur by a variety of mechanisms, for example, phosphorylation by an upstream kinase or binding by a monomeric G protein. Signaling is attenuated by the appropriate phosphatases.

In plants, MAPK cascades have been implicated in diverse processes, including jasmonic acid (JA) and ABA signal transduction, formation of the division plate during cell division, regulation of asymmetric divisions during embryogenesis and stomatal patterning, and cellular responses to abiotic stresses and pathogens. Underlying these numerous functions is a complex network of kinases, consisting in *Arabidopsis* of about 60 MAPKKKs, 10 MAPKKs, and 20 MAPKs. This gives the potential for thousands of MAPK cascade-forming combinations. Individual upstream signals can activate multiple MAPK cascades, and individual kinases can be activated by multiple upstream signals, indicating the network handles both diverging and converging transduction pathways. There is an "hourglass" pattern to the number of kinases existing at each level: a large number of MAPKKKs activate a much smaller number of MAPKKs, which in turn activate a somewhat larger number of MAPKs.

A good example of divergent signaling through the network of MAPK cascades is provided by the response to bacterial flagellin. As discussed in Section 18.2.2, flagellin detection by the cell surface receptor FLS2 induces a variety of defense mechanisms in *Arabidopsis*. These are mediated in part through MAPK cascades that result in increases in the activity of at least three MAPKs (MPK3, MPK4, and MPK6), each with different effects on downstream signaling (Fig. 18.13). For example, MPK3 phosphorylates and activates the transcription factor VIP1, causing VIP1 to translocate from the cytoplasm to the nucleus, where it activates defense-related genes. Inactive MPK4 exists as a nuclear complex with the transcription factor WRKY33. Active MPK4 phosphorylates a substrate protein called MKS1, leading to an MKS1/WRKY33-containing complex that dissociates from MPK4, allowing WRKY33 to induce transcription from a distinct set of defense-related genes. Lastly, MPK6 phosphorylates and stabilizes ACS6, an enzyme in the ethylene biosynthetic pathway, which leads to increased ethylene production.

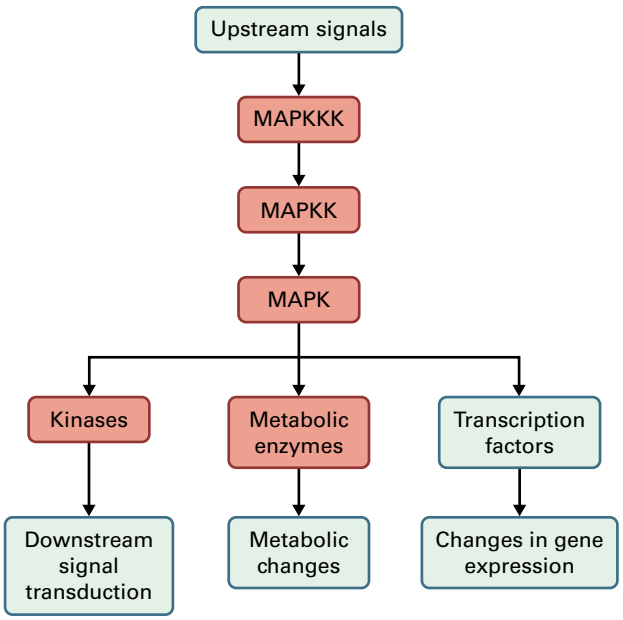


FIGURE 18.12 *Mitogen-activated protein kinase (MAPK) cascades are signaling modules found in all eukaryotic cells. Upstream signals activate a MAPK kinase kinase (MAPKKK), which phosphorylates and activates a MAPK kinase (MAPKK). In turn, the MAPKK phosphorylates and activates a MAPK, which may phosphorylate a variety of downstream targets.*

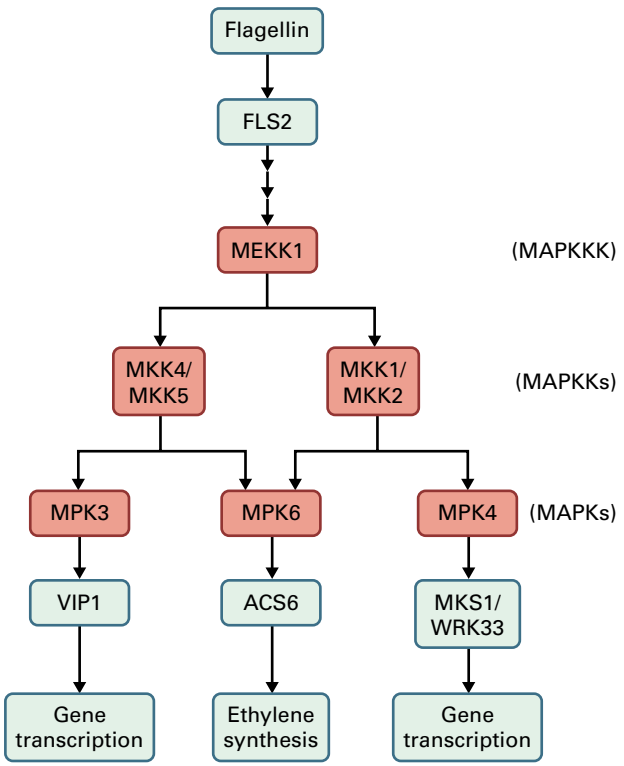


FIGURE 18.13 *Divergent signaling in response to flagellin. Flagellin binding to the cell surface receptor FLS2 leads to the activation of the MAPKKK MEKK1. Signaling through MKK1, MKK2, MKK4, and MKK5, MEKK1 activity results in that activation of three MAPKs—MPK3, MPK4, and MPK6—with different effects on downstream signaling (see text).*

MPK6 illustrates well the extent of signal convergence through MAPK cascades. In addition to the flagellin response, changes in MPK6 activity have been reported in response to hydrogen peroxide, ozone, cold, drought, touch, wounding, JA, and ABA. Furthermore, MPK6 (with MPK3) is activated downstream of the MAPKKK YODA, which functions in embryogenesis and stomatal patterning. Reflecting this convergence of signals, MPK6 can functionally interact with at least five MAPKKs.

These data suggest MAPK cascades form a signaling network in which individual kinases have multiple inputs and outputs. As discussed in Section 18.1.4, this raises the question of how signal specificity is maintained. Specificity may be improved through selective colocalization of kinases into cascade-forming combinations to restrict the extent of kinase interactions. There are several examples in yeast and animal cells of specific cascades formed by the binding of the appropriate kinases to cellular scaffold proteins. Another mechanism may be selective repression of some cascades by phosphatases to allow only certain transduction pathways to operate. Phosphatases that target particular MAPKs have been identified in *Arabidopsis*.

Finally, interactions between kinase cascades may allow cells to integrate the information they receive and so tailor responses to their individual circumstances. For example, in tobacco (*Nicotiana tabacum*), the MAPKs WIPK (homologous to *Arabidopsis* MPK3) and SIPK (homologous to MPK6) activate a variety of defense mechanisms in response to wounding and pathogens. Transcription of the *WIPK* gene is promoted by the activity of SIPK, leading to accumulation of WIPK protein and an increase in WIPK activity. Hence, signaling through the MAPK cascade network can feed back to modulate network structure, in this case providing the cell with a mechanism to ramp up defense-related signaling.

18.4 Ethylene signal transduction

18.4.1 Ethylene participates in stress responses, developmental transitions, and patterning events

Ethylene (C_2H_4) can be synthesized throughout the plant, and its production increases rapidly following abiotic or biotic stresses, such as physical force, wounding, drought, flooding, herbivory, and disease. Responses to stress-induced ethylene include changes in growth habit, strengthening of cell walls, and expression of defense-related genes. Ethylene production is also developmentally regulated, and ethylene signaling can trigger developmental transitions. For example, increased ethylene synthesis promotes senescence and abscission of leaves and flowers, and in many species, fruit ripening. Lastly, ethylene plays a role in pattern formation in developing organs; in the *Arabidopsis* root, for example, ethylene influences the size of the meristematic zone and the arrangement of root hairs.

Research on ethylene signal transduction has largely focused on the responses of dark-grown *Arabidopsis* seedlings to the gas. These include tightening of the seedling apical hook, reduction in hypocotyl elongation, and increased hypocotyl thickness, a combination called the **triple response** (Fig. 18.14). The triple response has provided researchers with a clear phenotype to use in screens for mutations and treatments that affect ethylene signaling. In the natural environment, the triple response enhances the seedling's ability to grow through compacted soil, which both stimulates ethylene production by mechanical force and inhibits ethylene diffusion.

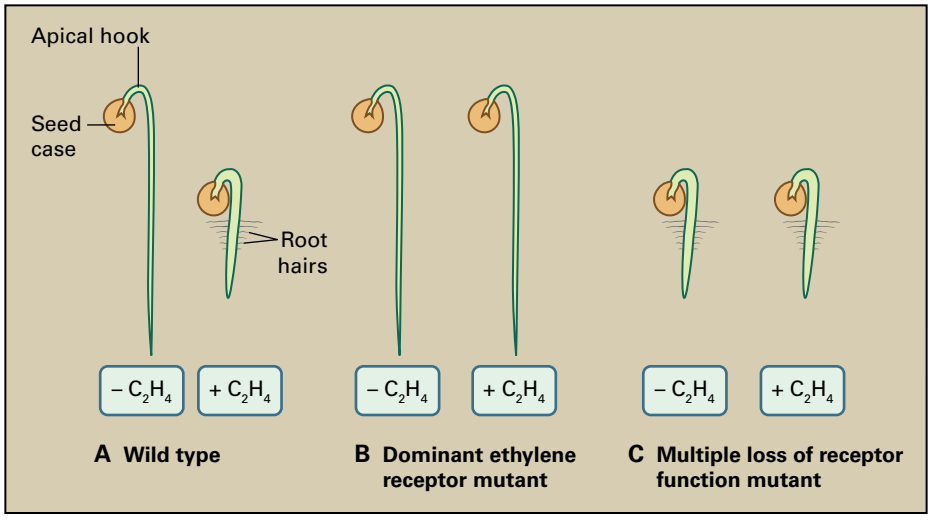


FIGURE 18.14 *Dark-grown* Arabidopsis *seedlings showing the induction of the triple response by ethylene. (A) Ethylene treatment reduces shoot elongation, increases shoot thickness, and causes a tightening of the apical hook. (B) Dominant mutations in ethylene receptor genes cause ethylene insensitivity. (C) In contrast, mutants with loss of function of multiple ethylene receptors show a constitutive ethylene response.*

18.4.2 Ethylene is perceived by receptor complexes at the endoplasmic reticulum

As a small, nonpolar, gaseous molecule, ethylene can diffuse from cell to cell both in solution and through air spaces. It is also possible that vascular transport of the immediate precursor to ethylene, 1-aminocyclopropane-1-carboxylic acid (ACC), can transmit the ethylene signal over long distances.

In *Arabidopsis*, ethylene perception depends on five related receptors located at the ER membrane: ETHYLENE RESPONSE1 and 2 (ETR1 and ETR2), ETHYLENE RESPONSE SENSOR1 and 2 (ERS1 and ERS2), and ETHYLENE INSENSITIVE4 (EIN4). These receptors were identified by single dominant mutations that reduce ethylene binding and result in the loss of ethylene responses by the plant (Fig. 18.14). This is a surprising result, since each ethylene-insensitive mutant still possesses four genes encoding wild-type receptors. Furthermore, recessive, null mutations in any one receptor have no phenotypic effect, showing that the ethylene receptors are functionally redundant. However, loss of the function of multiple receptors leads to a constitutive ethylene response, the opposite phenotype to that induced by the dominant mutations (Fig. 18.14).

Together, these data suggest a counterintuitive model for ethylene perception in which the receptors are active in the absence of ethylene and are inactivated by ethylene binding (Fig. 18.15). The dominant mutations prevent ethylene binding and so lock a receptor in its active state, producing a constitutive 'no ethylene' signal and, hence, a loss of ethylene response. In contrast, multiple null mutants have significantly reduced receptor activity even in the absence of ethylene, resulting in constitutive ethylene responses.

The ethylene receptors exist as homo- and heterodimers and bind to ethylene via a copper cofactor. They have homology to histidine kinase receptors that act in bacterial two-component systems; however, histidine kinase activity does not appear to be necessary for ethylene signaling. Section 18.5 discusses two-component systems with reference to cytokinin signaling and gives details of the structures and subtypes of the ethylene receptors in that context.

The ethylene receptors form complexes at the ER membrane with the downstream signaling protein CONSTITUTIVE TRIPLE RESPONSE1 (CTR1). CTR1 was defined by loss-of-function mutations that cause a constitutive triple response, indicating CTR1 inhibits ethylene responses. Both the presence of CTR1 at the ER and its ability to suppress ethylene responses depend on binding between CTR1 and the receptors. Mutated CTR1 that cannot bind to receptors is cytosolic and inactive, resulting in a constitutive triple response. These data suggest that in the absence of ethylene, ethylene receptors activate bound CTR1, which acts to prevent ethylene responses. Ethylene binding, however, prevents the receptors from activating CTR1 and so allows ethylene responses to occur (Fig. 18.15).

The precise mechanism of ethylene signal transduction after perception at the ER membrane by receptor–CTR1 complexes is uncertain. CTR1 is homologous to mammalian RAF kinases, MAPKKKs that initiate MAPK signaling cascades (see Section 18.3.2), and mutations that abolish CTR1 kinase function result in constitutive ethylene responses, indicating kinase activity is required for CTR1 to inhibit ethylene signaling. This suggests a MAPK cascade functions in ethylene signaling, but conclusive evidence is lacking.

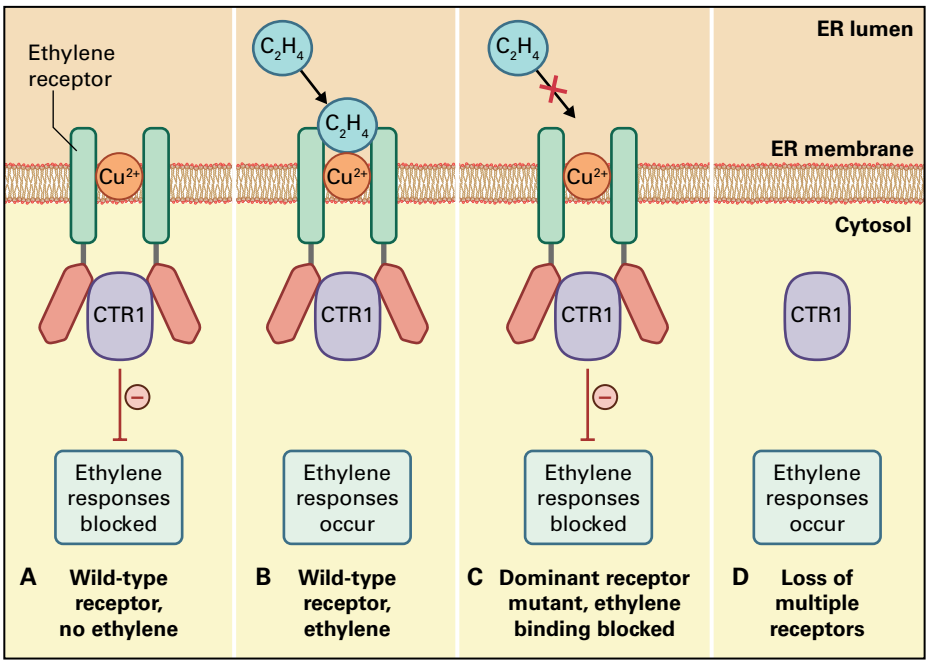


FIGURE 18.15 *Ethylene signal transduction by receptor-CTR1 complexes. (A) In the absence of ethylene, ethylene receptors at the ER membrane activate bound CTR1, which inhibits ethylene responses. (B) Ethylene binding prevents the receptors from activating CTR1, allowing ethylene responses to occur. (C) Dominant receptor mutants are unable to bind ethylene, resulting in constitutive CTR1 activity and suppression of ethylene responses. (D) Loss of multiple receptors reduces binding and activation of CTR1, resulting in permanent ethylene responses.*

18.4.3 Ethylene responses depend on the EIN3 family of transcription factors

Mutant analysis has identified positive regulators of ethylene responses downstream of CTR1, notably the EIN2 and EIN3 proteins (Fig. 18.16). Loss of EIN2 function results in complete ethylene insensitivity, demonstrating EIN2 is absolutely required to induce ethylene responses. EIN2 is an ER-tethered protein the phosphorylation of which is dependent on CTR1. Ethylene results in its dephosphorylation and cleavage, and the resulting C-terminal cleavage product translocates to the nucleus, where it can activate EIN3.

EIN3 is a transcription factor that induces gene expression in response to ethylene signals transduced through EIN2. Together with the related proteins EIN3-LIKE1 (EIL1) and EIL2, it appears necessary for the induction of most transcriptional responses to ethylene. For example, double mutants lacking functional EIN3 and EIL1 display virtually no changes in gene transcription after ethylene treatment. Among the genes induced by EIN3 and the EILs are more transcription factors (e.g., ERF1) that induce other ethylene responsive genes, allowing rapid amplification of the ethylene signal and activation of hundreds of genes in response to ethylene perception (Fig. 18.16).

EIN3 activity is controlled through the regulation of EIN3 protein stability. EIN3 is bound by F-box proteins (see Section 18.6) EBF1 and EBF2, which prevent its activity by targeting it for destruction. Ethylene signaling prevents EBF1 and EBF2 from inducing EIN3 destruction, leading to accumulation of EIN3 and induction of ethylene-responsive genes. One mechanism by which this may be achieved is by destruction of the EBF1 and EBF2 mRNAs through action of the EIN5 protein (also called XRN4), an exoribonuclease required for full ethylene response. EIN3 stability may also be regulated by phosphorylation of EIN3, and EIN3 can be phosphorylated at two sites, one that increases and another that decreases its half-life.

Interestingly, one of the genes directly induced by EIN3 encodes EBF2, creating a negative feedback cycle in which EIN3 promotes its own destruction. It is tempting to speculate this mechanism enables ethylene signaling to switch off rapidly once ethylene is no longer present. An effective off-switch could be particularly important for ethylene signal transduction because ethylene appears to bind tightly to its receptors. For example, the half-life of ethylene dissociation from the ETR2 receptor as measured in transgenic yeast is approximately 10 hours.

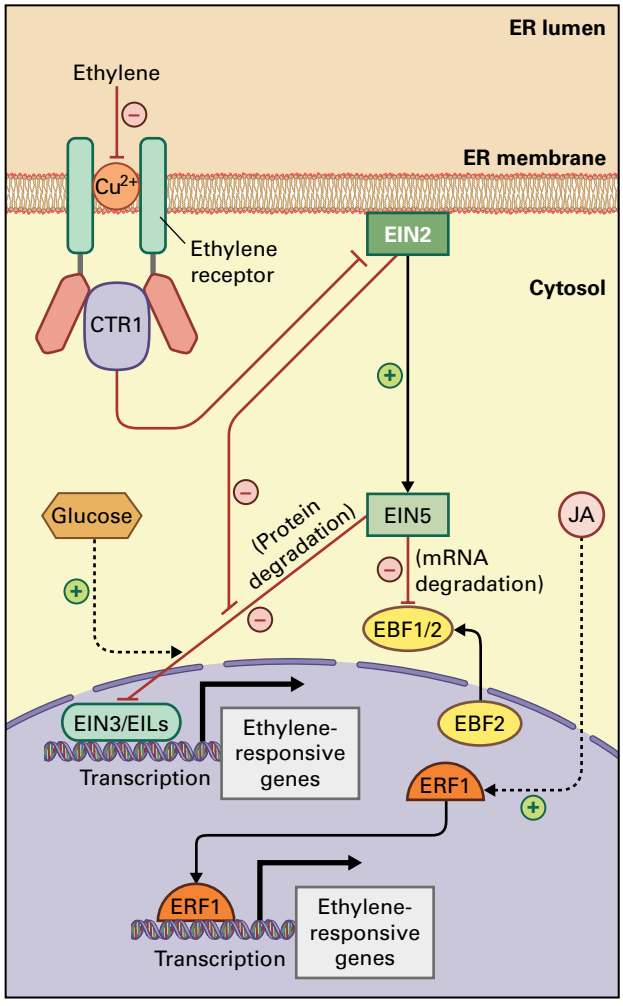


FIGURE 18.16 *Ethylene signal transduction. Ethylene binding prevents ethylene receptors from activating CTR1, thus preventing CTR1 from inhibiting the activity of downstream components, such as EIN2. The transduction of the inhibitory signal from CTR1 to EIN2 may involve a kinase cascade. EIN2 promotes the activity of EIN3 and EIL transcription factors by preventing protein degradation induced by EBF1 and EBF2. This may occur in part by activation of EIN5, which degrades EBF1 and EBF2 mRNAs. EIN3 and EILs promote the expression of ethylene responsive genes, including downstream transcription factors such as ERF1, and the negative regulator EBF2. Glucose signaling enhances EIN3 degradation. Jasmonic acid (JA) signaling promotes the expression of* ERF1. *Lines ending in an arrow head indicate positive regulation. Lines ending in a bar indicate negative regulation.*

18.4.4 Ethylene signaling interacts with other signaling mechanisms

Points of interaction have been identified between ethylene signal transduction and other signaling mechanisms in the plant (Fig. 18.16). For example, whereas ethylene promotes EIN3 stability, glucose promotes EIN3 destruction. The mechanism by which glucose affects EIN3 stability is unknown, but the glucose-induced signals may counteract ethylene responses. Since ethylene signaling commonly leads to a reduction in both plant stature and leaf size, this provides a means by which abundant glucose produced by photosynthesis could promote plant growth.

Immediately downstream of EIN3, the ERF1 transcription factor provides another point of interaction. As described above, expression of the *ERF1* gene is directly induced by EIN3. *ERF1* is also activated by signals induced by JA, a hormone involved in regulating plant defense against herbivores. Ethylene and JA are synergistic in their activation of *ERF1*, and since the synthesis of both hormones is induced by wounding from herbivores, they combine to amplify the plant's response.

In addition to interactions during ethylene signal transduction, cross-regulation between ethylene and other hormones occurs at the level of hormone synthesis. The best-understood case is the interaction between ethylene and auxin. As stated above, the immediate precursor of ethylene is ACC. Auxin promotes the expression of ACC synthase and in doing so induces ethylene production. Similarly, ethylene promotes transcription of genes required for auxin biosynthesis in *Arabidopsis* roots. Therefore, some of the effects of auxin and ethylene on the plant may be due in part to the mutual induction of each other's synthesis.

18.5 Cytokinin signal transduction

18.5.1 The cytokinin signal is transduced by proteins derived from bacterial two-component systems

Cytokinins are signaling molecules related to adenine that function in a range of processes including seed development and germination, development at the shoot and root apical meristems, vascular patterning, shoot branching, leaf senescence, circadian rhythms, stress responses, and interactions with pathogens and nodulating bacteria. Cytokinin signal transduction involves a mechanism derived from the bacterial **two-component system**, a major signal transduction module that regulates responses to a wide range of physical and molecular stimuli in prokaryotes.

The basic two-component system consists of two proteins, a **histidine kinase** and a **response regulator** (Fig. 18.17). The

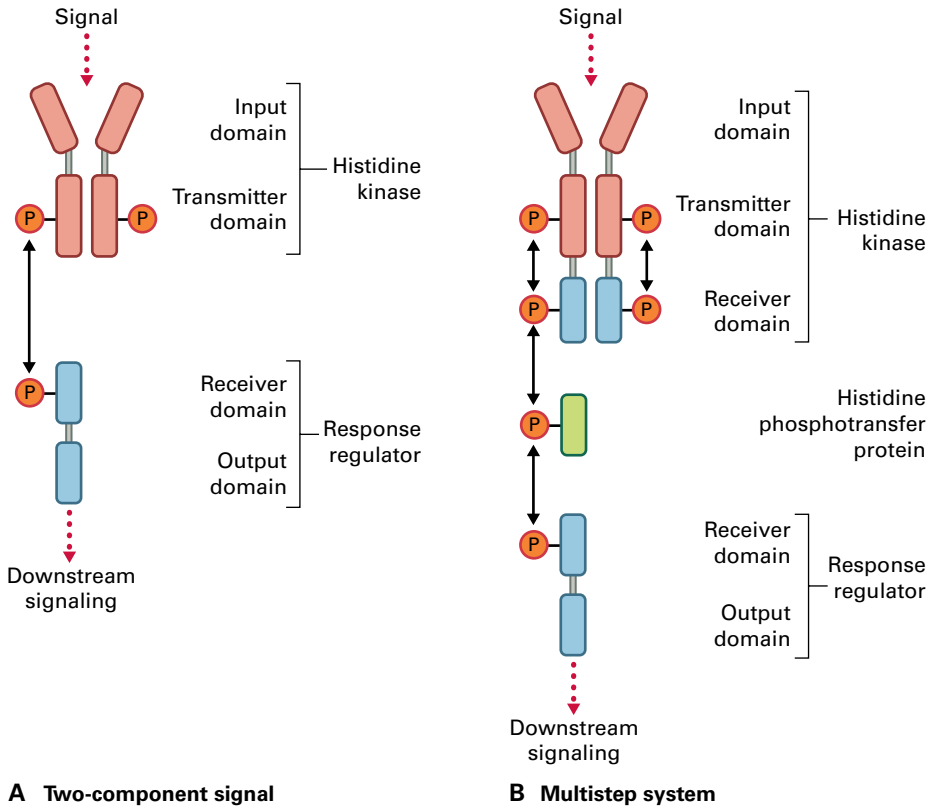


FIGURE 18.17 *The two-component system and its multistep derivative. (A) The two-component system consists of a histidine kinase and response regulator. On activation of the input domain by ligand binding or other processes, the histidine kinase autophosphorylates a histidine residue in the transmitter domain. This phosphoryl group is then transferred to a conserved aspartate residue in the receiver domain of the response regulator, resulting in the activation of the neighboring output domain. (B) In the multi-step derivative, the histidine kinase often contains its own receiver domain, and phosphotransfer to the response regulator is mediated by a histidine phosphotransfer protein. The phosphoryl group moves from the transmitter domain to the receiver domain of the histidine kinase, then to a histidine phosphotransfer protein, and then to the response regulator. All phosphotransfers in the two systems can also occur in the reverse direction.*

histidine kinase exists as a dimer and may be membrane spanning or soluble. Each kinase monomer possesses two domains: an input domain and a transmitter domain. The input domains of the two monomers are responsible for signal perception, following which the monomers reciprocally phosphorylate a histidine residue in each other's transmitter domain. Therefore, signal perception leads to autophosphorylation of the histidine kinase.

The response regulator also contains two domains, a receiver domain and an output domain. Phosphoryl groups are transferred from autophosphorylated histidine kinases to an aspartate residue in the receiver domain of response regulators. This activates the output domain of the response regulator, leading to onward signaling (e.g., induction of gene transcription by response regulators that act as transcription factors).

Though this basic system is only found in prokaryotes, an evolutionary derivative consisting of a multistep phosphorelay with three components occurs in prokaryotes, plants, and fungi, but not animals (Fig. 18.17). In the multistep system, the histidine kinase often contains its own receiver domain, to which the phosphoryl group is transferred after autophosphorylation. Rather than the phosphoryl group then moving directly from the kinase to the response regulator, this phosphotransfer occurs via an intermediate called a **histidine phosphotransfer protein** (HPt). HPts share similarities with the transmitter domain of the histidine kinase, indicating the multistep system evolved using protein domains already present in the basic system. In both the basic and multistep systems, all phosphotransfers can occur in both directions (e.g., from the response regulator to the histidine kinase in the basic system). Signal transduction, therefore, depends on the balance of 'forward' and 'reverse' phosphotransfers.

18.5.2 Cytokinin is one of several signals tranduced by two-component systems in *Arabidopsis*

Genome analysis reveals *Arabidopsis* has 11 putative histidine kinases, five functional HPts (*Arabidopsis* histidine-containing phosphotransfer factors, **AHPs**), and 23 response regulators (*Arabidopsis* response regulators, **ARRs**). Three of the histidine kinases, all AHPs, and virtually all ARRs have been implicated in cytokinin signaling (Fig. 18.18).

The three cytokinin receptors of *Arabidopsis*, ARABIDOPSIS HISTIDINE KINASE2 and 3 (AHK2 and AHK3) and CYTOKININ RESPONSE1 (CRE1, also called AHK4), are plasma membrane histidine kinases. Each has an extracellular input domain that binds cytokinins, a transmitter domain, and a receiver domain. Cytokinin binding induces autophosphorylation. Phosphoryl groups are then transferred via the receiver domain to AHPs, inducing AHP movement from the membrane into the nucleus and the subsequent transfer of phosphoryl groups to the "type-B" subfamily of ARRs. *Arabidopsis* also produces a pseudo-AHP, called AHP6, which lacks the histidine residue required to receive a phosphate group transferred from a cytokinin receptor. AHP6 acts as an inhibitor of cytokinin signaling, perhaps by competing with genuine AHPs for access to the receptors.

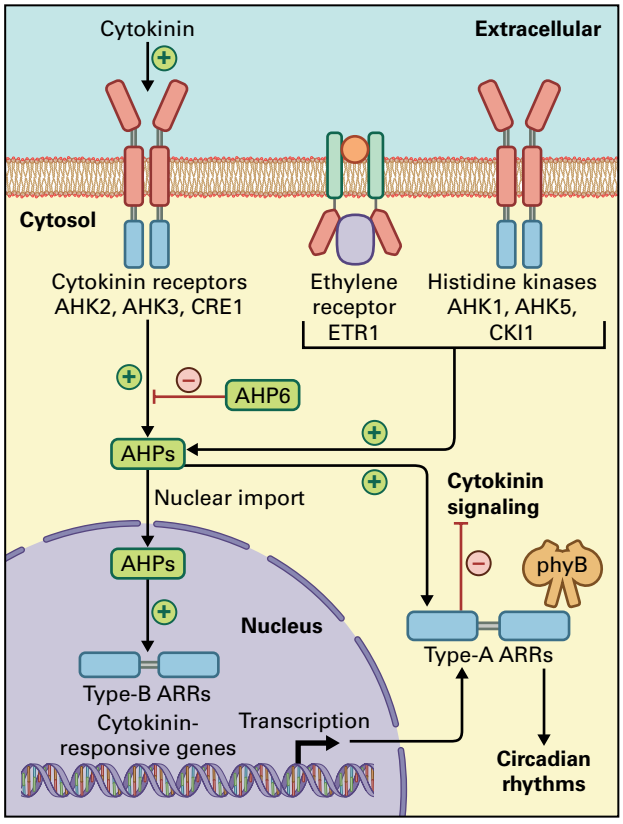


FIGURE 18.18 *Signaling mediated by two-component-derived proteins in* Arabidopsis. *During cytokinin signaling, histidine kinase receptors bind cytokinins and initiate a phosphorelay that activates type-B ARRs, which induce transcription of cytokinin-responsive genes. Signal transduction is inhibited by AHP6, a pseudo-AHP that is thought to compete with genuine AHPs for access to the receptors. Other histidine kinases (ETR1, AHK1, AHK5, and CKI1) probably also signal through the phosphorelay mechanism. Type-A ARRs are activated by the phosphorelay initiated by cytokinin receptors, are induced at the level of transcription by type-B ARRs, and in some cases are stabilized by cytokinin signaling (not shown). Type-A ARRs inhibit cytokinin signaling by an unknown mechanism, resulting in negative feedback. Some type-A ARRs also interact with phyB and mediate phyB's input into circadian rhythms. Note that cell wall is not shown for clarity.*

Type-B ARRs are transcription factors, and in response to phosphorylation by AHPs, they function in a partially redundant fashion to induce transcription from cytokinin-responsive genes. In addition to type-B ARRs, *Arabidopsis* possesses type-A ARRs, which are unable to bind DNA and do not induce transcription. Type-A ARRs are activated as direct targets of phosphotransfer from AHPs, and in response they act as negative regulators of cytokinin signaling. The biochemical mechanism of type-A ARR action is unknown. Interestingly, type-B ARRs induce transcription from type-A *ARR* genes in response to cytokinin, and cytokinin signaling also increases the half-life of some type-A ARR proteins. Therefore, cytokinin promotes both the activity and abundance

of type-A ARRs, creating a negative feedback loop that dampens cytokinin signaling (Fig. 18.18).

Apart from the three cytokinin receptors, five of the remaining eight putative histidine kinases in *Arabidopsis* are the ethylene receptors (ETR1, ETR2, ERS1, ERS2, and EIN4, see Section 18.4). These have a membrane-spanning input domain that binds ethylene via a copper cofactor and a histidine kinase transmitter domain; however, the histidine kinase domain is only functional in two ethylene receptors (ETR1 and ERS1). In addition, mutant analysis indicates kinase activity in ETR1 and ERS1 is not needed for ethylene signaling. The picture is further complicated by the fact that only three of the five receptors (ETR1, ETR2, and EIN4) possess a receiver domain of the two-component type. Hence ETR1, but no other ethylene receptor, has both histidine kinase activity and a receiver domain. This may allow ETR1 to interact with the downstream two-component-derived elements—AHPs and through them, ARRs—but currently the extent and role of such signaling are unclear.

The final three histidine kinases in *Arabidopsis* are AHK1, AHK5, and CKI1. All possess a functional input domain, histidine kinase, and receiver domain and are, therefore, likely to signal through AHPs and ARRs, creating possible interactions with cytokinin (and ETR1) signaling (Fig. 18.18). CKI1 is required for megagametophyte development, and AHK1 and AHK5 both appear to mediate stress responses: AHK1 acts as a positive regulator of drought and salt responses, while AHK5 regulates stomatal closure (see Section 18.9) in response to hydrogen peroxide, which is produced following a variety of stresses.

Finally, two-component-derived proteins also transduce signals that are not perceived by histidine kinases. Phytochrome B (phyB, see Section 18.7) interacts with ARR3 and ARR4 (type-A ARRs) in *Arabidopsis* (Fig. 18.18). These mediate the input of phyB into the circadian oscillator in a manner independent of cytokinin signaling. Double mutants lacking ARR3 and ARR4 function also have circadian abnormalities under blue light and continual darkness, conditions in which phyB is inactive. Hence, the two response regulators likely have additional roles in regulating circadian rhythms. Interestingly, the central oscillator of the clock involves pseudo-response regulators, proteins related to ARRs but lacking the ability to accept a phosphoryl group from AHPs.

18.6 Integration of auxin signaling and transport

18.6.1 Complex patterns of auxin flux and accumulation direct key events in plant development

Auxin was discovered in the early 20th century through investigations into seedling phototropism. The predominant auxin in plants is **IAA**, and the list of its known functions now includes numerous other aspects of plant development. In addition to acting in the regulation of tropisms, auxin functions in patterning the embryo, controlling development at both the root and shoot apical meristems, and coordinating regeneration after wounding. Over a larger scale, auxin acts in the control of both lateral root initiation and bud outgrowth and forms part of the mechanism that coordinates root and shoot growth.

The developmental roles of auxin rely on complex patterns of intercellular auxin transport and accumulation. During embryogenesis in *Arabidopsis*, for example, auxin transport from the basal to the apical cell of the two-cell embryo created by zygotic division is thought to direct the apical cell towards the formation of the embryo proper, while most derivatives of the basal cell form a supporting, nutritive structure called the suspensor. Later, specification of root development requires a shift in the direction of auxin transport to create an auxin flux running from the presumptive embryonic shoot apex down through the embryo into the suspensor.

Unique among plant hormones, auxin moves between cells by a dedicated transport system composed of an intricate network of transmembrane proteins. This network is regulated by auxin signaling to generate multiple levels of feedback between auxin signal transduction and auxin transport. Together with local synthesis and degradation, such feedback helps to generate both stable and dynamic patterns of auxin flux and accumulation that are required for development. Auxin transport is also regulated by developmental information and environmental cues in ways that coordinate development with internal and external information.

The following sections consider auxin signal transduction, intercellular auxin transport, and the feedback between the two.

18.6.2 Transduction of intracellular auxin is mediated by targeted protein degradation

Auxin enters cells by both passive movement and active transport (see Section 18.6.4). Within the cell, auxin is perceived by a small family of soluble, nuclear receptors that act in protein complexes involved in targeting proteins for degradation (Fig. 18.19).

In eukaryotic cells, proteins are tagged for destruction by sequential conjugation with the small protein **ubiquitin** to attach a poly-ubiquitin chain. Once tagged in this way, proteins can be recognized and destroyed by the **26S proteasome**, a large complex of proteolytic enzymes. Addition of ubiquitin is a multistep process. First, a high-energy thioester bond is formed between ubiquitin and an **E1 ubiquitin-activating enzyme** by a mechanism that requires ATP hydrolysis. The ubiquitin is then transferred to an **E2 ubiquitin-conjugating enzyme**, to which it also attaches via a thioester bond. The ubiquitin-carrying E2 and the target protein are then brought together by an **E3 ubiquitin-protein ligase**, which catalyzes the transfer of the ubiquitin molecule to the target.

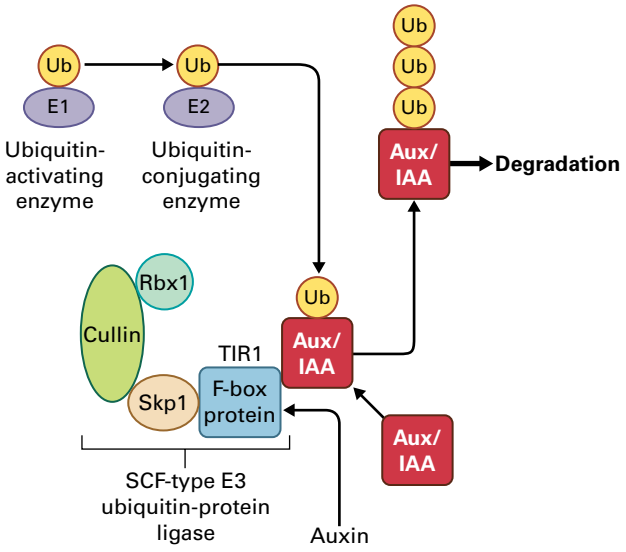


FIGURE 18.19 *Targeted protein degradation mediates auxin signal transduction. Auxin binding to the F-box protein TIR1 enhances interaction between TIR1 and Aux/IAA proteins. This allows polyubiquitination of Aux/IAA proteins through the sequential actions of E1, E2, and E3 enzymes and so targets Aux/IAAs for degradation. Ub, ubiquitin.*

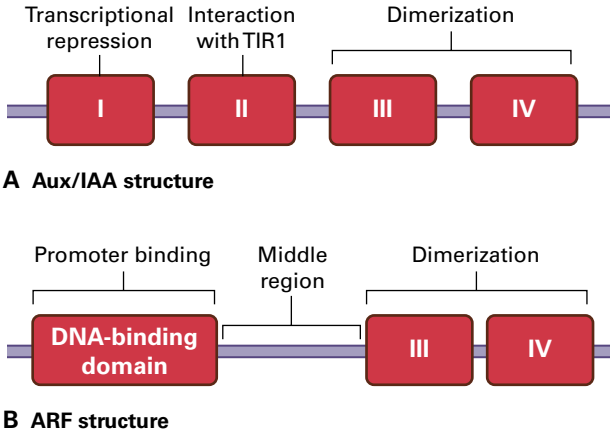


FIGURE 18.20 *Structure of Aux/IAAs and ARFs. (A) Aux/IAAs possess a transcriptional repressor domain (I), a domain required for interaction with TIR1 and the AFB proteins (II), and two dimerization domains (III and IV). (B) ARFs possess a DNA-binding domain, a middle region, and dimerization domains related to those in Aux/IAAs.*

Plants possess multiple E3 enzymes, which occur in distinct families. With respect to auxin signal transduction, the E3 enzymes of interest are multiprotein **SCF complexes** (named after three of their major constituents: a **Skp1** protein, a **Cullin** protein, and an **F-box** protein). A fourth subunit called **Rbx1** forms a dimer with Cullin, and the Cullin–Rbx1 dimer transfers the ubiquitin to the target protein (see Section 10.6). The target protein associates with the complex via the F-box protein, while Skp1 acts as a scaffold to connect the other subunits (Fig. 18.19). Therefore, the F-box protein is what gives an SCF complex its specificity for target proteins.

Intracellular auxin signal transduction involves the binding of auxin to members of a small family of F-box proteins that function as auxin receptors. The family consists of TIR1 (TRANSPORT INHIBITOR RESISTANT1) and related AUXIN SIGNALING F-BOX PROTEINs AFB1, AFB2, and AFB3. These are among about 700 F-box proteins in the *Arabidopsis* genome. In addition to the auxin receptors, these include the **zeitlupe** photoreceptors, which function in the regulation of the circadian clock (Box 18.2), proteins that act in signal transduction of gibberellins (see Section 18.8) and the defense-related hormone JA.

Of the auxin receptors, TIR1 has been studied in the most detail. A soluble, nuclear protein, TIR1 brings a group of short-lived transcriptional repressors called Aux/IAAs to the SCF complex for polyubiquitination. The association between TIR1 and Aux/IAA occurs at a region of LRRs (see Section 18.2.2) in TIR1. The interaction is enhanced by auxin, which binds to a hydrophobic pocket within the LRR region to increase the size of the binding surface for the Aux/IAA, which docks onto TIR1 directly over the auxin molecule. Inositol hexakisphosphate is a possible cofactor in the interaction. Because of its mode of action, auxin has been described as molecular glue that helps Aux/IAAs stick to TIR1. As a consequence, auxin increases the rate at which Aux/IAAs are targeted for ubiquitination and degradation. Hence, increases in auxin concentration reduce the half-life of Aux/IAA proteins (Fig. 18.19).

Aux/IAAs contain four conserved domains (Fig. 18.20). Domain I, at the amino terminus, is a potent transcriptional repressor. Domain II is responsible for the interaction with TIR1 and is required for auxin-induced degradation of Aux/IAAs. The carboxyl-terminal domains III and IV are dimerization domains that mediate the formation of Aux/IAA dimers. Domains III and IV are also present in a group of transcription factors called **Auxin response factors** (ARFs, Fig. 18.20) and mediate the formation of both ARF–ARF and ARF–Aux/IAA dimers. Within a cell there is, therefore, a complex pattern of dimerization within and between the Aux/IAA and ARF families, and changes to this pattern are thought to be crucial to auxin signal transduction.

The simplest example arises from the interaction between Aux/IAAs and a group of ARFs that act as transcriptional activators (Fig. 18.21). ARFs contain an amino-terminal DNA-binding domain, which can also mediate ARF–ARF dimerization and is separated from the carboxyl-terminal dimerization domains by a middle region (Fig. 18.20). The 22 ARFs in the *Arabidopsis* genome are classified into subgroups according to the composition of the middle region, and a group of five ARFs characterized by a glutamate-rich (Q-rich) middle region act as transcriptional activators. ARFs bind to the promoters of auxin-inducible genes. At low auxin concentrations, the ARFs form heterodimers with Aux/IAAs, and the repressor domain of the Aux/IAA prevents gene transcription (Fig. 18.21). Since Aux/IAAs lack a DNA-binding domain, they require an ARF to bring them to a promoter region to repress transcription. Auxin reduces Aux/IAA concentration, freeing the Q-rich ARFs from repression

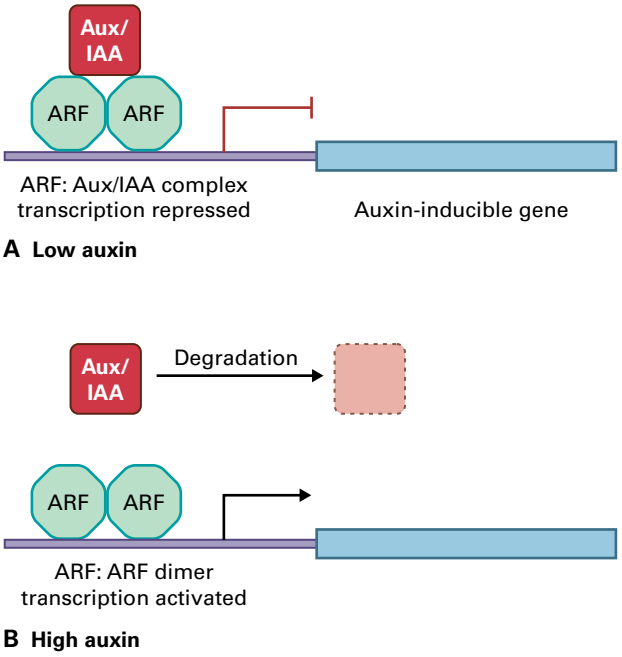


FIGURE 18.21 *Auxin-responsive genes are activated by the Q-rich sub-family of ARF proteins. (A) Activation is blocked at low auxin concentration by the formation of an ARF:Aux/IAA complex. (B) High auxin concentrations induce Aux/IAA degradation and so activate transcription.*

thereby activating gene transcription. *Aux/IAA* genes are among those induced by this mechanism, as are *GH3* genes which encode auxin-conjugating enzymes responsible for reducing free auxin levels. Therefore, auxin signal transduction includes at least two negative feedback loops that dampen the auxin response.

Unlike the Q-rich ARFs, at least some members of other ARF subgroups act as transcriptional repressors, suggesting auxin responses mediated by Aux/IAAs and ARFs are more complex than simple gene induction. Aux/IAAs also have diverse properties. For example, the half-lives of the 29 *Arabidopsis* Aux/IAAs can vary by an order of magnitude. These data suggest the effects of auxin signaling depend on the particular combinations of ARF and Aux/IAA expressed in individual cells.

18.6.3 Cells may perceive extracellular auxin

In addition to the perception of intracellular auxin by TIR1 and AFBs, there is evidence for a receptor for extracellular auxin. A candidate is a membrane-associated protein called AUXIN-BINDING PROTEIN1 (ABP1).

ABP1 is localized both at the plasma membrane and the ER; however, ABP1 only binds auxin efficiently at extracellular pHs, suggesting it associates with auxin on the outer face of the plasma membrane. Evidence that ABP1 may act as a receptor for extracellular auxin comes, among other things, from research on the auxin response of protoplasts (tissue-cultured cells lacking a cell wall).

In some contexts, auxin treatment induces very rapid (<1 minute) changes in plasma membrane ion fluxes. In protoplasts, the result is a shift in osmotic potential that causes water intake and protoplast swelling. This effect can be mimicked in the absence of auxin if protoplasts are treated with antibodies that bind to the ABP1 auxin binding site, but can be blocked by antibodies that bind to ABP1 elsewhere. These results support the hypothesis that ABP1 is an auxin receptor. Antibodies bound to the auxin binding site might trigger signal transduction leading to changes in ion fluxes, whereas antibodies binding elsewhere might prevent either auxin binding or subsequent signaling by ABP1.

18.6.4 Auxin signaling regulates the machinery of auxin transport

The polarized flow of auxin through tissues and organs requires auxin movement into and out of successive cells, and this involves both active and passive movement of auxin across the plasma membrane (Fig. 18.22). Active transport of auxin is mediated by at least three classes of membrane transporter proteins: the **AUX1/LIKE AUX1 (AUX/LAX)** family, which act as auxin influx carriers, **ABCB proteins**, which mediate both auxin influx and efflux depending on the protein, and **PIN proteins**, which are believed to function as auxin efflux carriers. In addition, the pH difference between the apoplast (pH 5.5) and the cytoplasm (pH 7) is thought to drive passive movement of auxin into the cell. IAA is a weak acid and exists in both its protonated and ionized forms in the acidic conditions of the wall. Uncharged, protonated IAA can move across the plasma membrane, but once in the neutral cytoplasm, it ionizes and is unable to move back out. Therefore, whereas auxin influx occurs by both passive flow and active transport, the movement of auxin out of the cell is necessarily mediated by efflux carriers.

The polarity of intercellular auxin flux depends largely on the asymmetric distribution of the auxin membrane transport proteins, in particular the PIN proteins. *Arabidopsis* has eight PIN proteins (PIN1–8), several of which are associated with mutant phenotypes that suggest disrupted auxin transport. For example, *pin1* mutants are defective in organ initiation at the shoot apical meristem, a process that requires the auxin flux-driven formation of localized auxin concentration maxima (see below). Techniques such as immunolocalization or the fusion of PIN proteins to reporter proteins demonstrate that PIN polarization in auxin-transporting cells corresponds to the predicted direction of auxin flux. A major feature of auxin movement in the plant, for example, is the transport of auxin synthesized by young leaves in a shoot-to-root direction through xylem parenchyma cells and the vascular cambium.

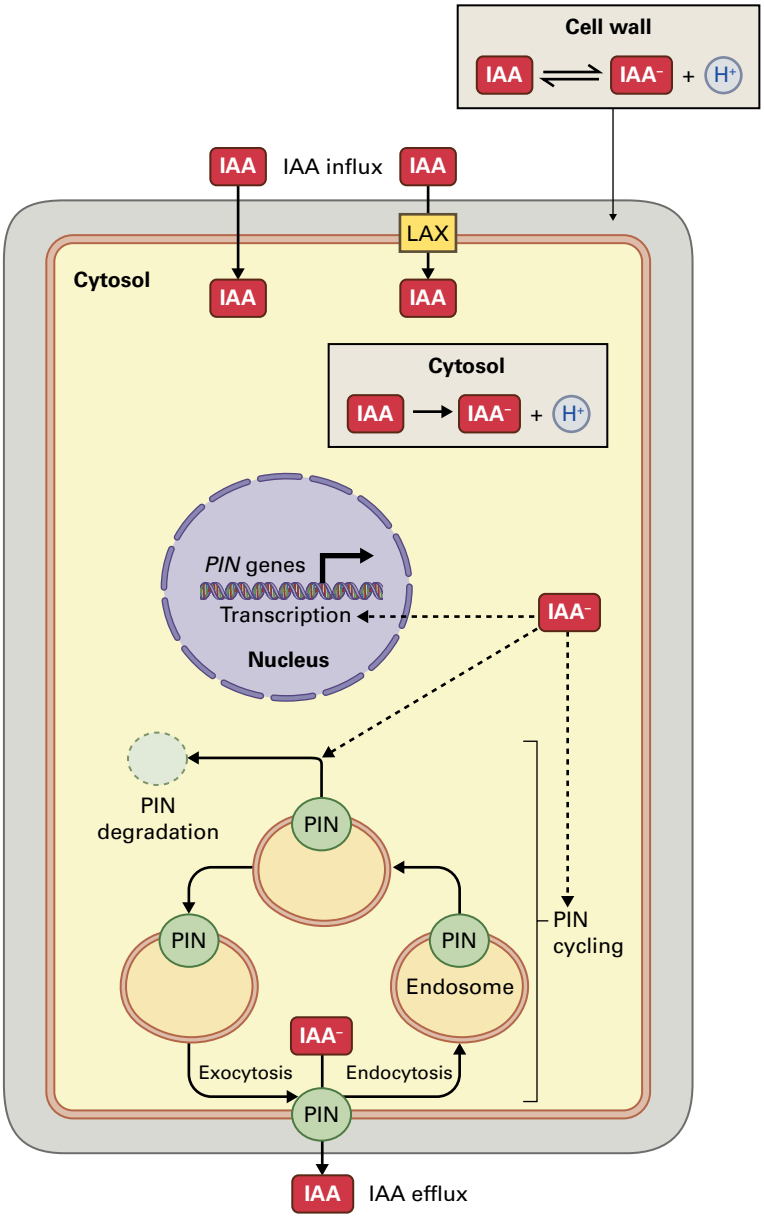


FIGURE 18.22 *Auxin (IAA) influx occurs by passive diffusion and by active transport via LAX proteins. Auxin efflux occurs by active transport by PIN proteins, and the distribution of PIN proteins is thought to determine the direction of intercellular auxin flux. Feedback between auxin signaling and auxin transport occurs at multiple levels. For example, auxin signaling regulates the transcription, cycling, and degradation of PIN proteins. Auxin influx and efflux are also mediated by ABCB proteins (not shown).*

This auxin flow is known as the **polar transport stream** and is associated with the polarization of PIN1 to the basal (root-facing) membrane of the transporting cells. Auxin is also transported from the shoot to the root by bulk flow through the phloem,

Several levels of interaction have been identified that link the auxin transport machinery to auxin signaling. Auxin treatment induces expression of *PIN* genes and leads to the accumulation of PINs, a mechanism by which increased auxin concentration in a cell could increase auxin efflux activity. In some contexts, however, auxin treatment also reduces the stability of PIN proteins; therefore, the overall effect of auxin concentration on PIN abundance can be complex.

Auxin signaling also affects the mechanism determining PIN polarization. In some cell types PIN proteins undergo continual cycling between the cell membrane and endosomes (Fig. 18.22). Over the short term, auxin treatment inhibits endocytosis of PIN proteins and so may lead to accumulation of PINs at the plasma membrane and, therefore, promotion of auxin export from the cell. In contrast, longer term auxin treatments can increase PIN internalization. As with PIN abundance, therefore, auxin signaling appears to interact with

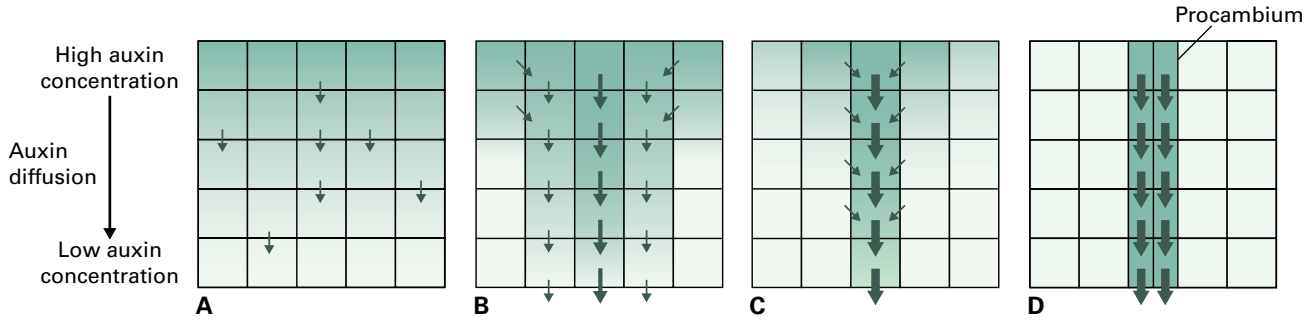


FIGURE 18.23 *Canalization hypothesis. (A) Cells between an auxin source (top) and sink (bottom) begin to transport auxin in the direction of auxin flux. (B, C) Positive feedback between auxin transport and the capacity for auxin transport causes the channeling of auxin flux into narrow strands of increasingly polarized cells. (D) When auxin concentration rises above a threshold, cells in such strands differentiate into vascular tissue.*

PIN cycling in a complex manner that includes both positive and negative regulation.

Auxin also induces transcription from *PINOID* (*PID*), a gene encoding a protein kinase that regulates PIN polarization. PID is a serine/threonine kinase that appears to regulate the position of PIN proteins with respect to the apical-to-basal (shoot-to-root) axis of the plant. Loss of PID function leads to a consistent shift of apically localized PIN proteins to the basal face of cells. In contrast, constitutive expression of a PID transgene can cause basally localized PIN proteins to move to the apical face of cells. PID has been shown to phosphorylate PIN proteins directly. Therefore, an intuitive explanation for the data is that PIN proteins phosphorylated by PID are targeted to the apical face of the cell, whereas unphosphorylated PINs are directed to the basal face.

In addition to control by auxin signaling, auxin transport is also regulated by cell type and environmental information. For example, epidermal cells at both the root and shoot tips display different auxin transport characteristics to cells in underlying tissues. This is discussed below with respect to leaf initiation. A clear example of environmental influence on auxin flux occurs in tropisms, in which environmentally responsive redirection of auxin transport leads to localized auxin concentration-dependent changes in cell expansion, and causes tropic curvature.

18.6.5 Feedback between auxin signaling and transport is required for both vascular patterning and leaf initiation

The regulation of PIN distribution and concentration by auxin suggests feedback between auxin signaling and auxin transport. A major function of such feedback is in development, which requires robust, partially self-organizing mechanisms for creation of patterns of cells, tissues, and organs. Two well-studied examples of auxin-mediated development are the patterning of vascular tissue and leaf initiation.

The **canalization hypothesis** proposes a positive feedback mechanism that links vascular development to auxin flux (Fig. 18.23). According to this hypothesis, polarized auxin transport by a cell induces an increase in both the polarization and activity of that cell for subsequent auxin transport. With a limited auxin source and a defined auxin sink, this creates competition between cells for auxin and progressive channeling of auxin flux into a narrow file of highly polarized cells that connect the source to the sink. The hypothesis further proposes that, at a certain threshold of auxin concentration, cells in the strand are induced to differentiate into vascular tissue. Monitoring PIN distribution, for example, through use of PINs fused to green fluorescent protein (PIN–GFP), shows canalization in action. In a variety of contexts, vascular differentiation is preceded by the gradual formation cell files expressing increasingly high PIN levels localized according to the predicted direction of auxin flux. These files subsequently differentiate into vascular strands.

In contrast to the stable routes for auxin transport generated during vascular development, organ initiation at the shoot apical meristem depends on repeated changes in auxin flux and accumulation (Fig. 18.24). This is shown by the development of naked pin-like structure at the shoot apex following disruption of auxin flow by auxin transport inhibitors, or in the *pin1* mutant (it was this that gave the PIN genes their name). Leaves can be induced to develop on such pins by local auxin application, suggesting that leaves and other organs are initiated at sites of high auxin concentration.

The pattern of auxin flux in untreated, wild-type meristems has been investigated by real-time imaging of PIN-GFP and by PIN immunolocalization. The results of these studies have led to the proposal that cells in the meristem's epidermal layer distribute PIN proteins such that each cell transports auxin toward the neighbor in the layer with the greatest auxin concentration. The result is a feedback mechanism that generates a convergence of auxin flux to create a local auxin concentration maximum in the epidermis. Cells at this site initiate a leaf. In subepidermal layers at the site of initiation, PIN proteins eventually relocate to the basal cell face and direct auxin flux towards deeper tissues (where it is involved in vascular differentiation in the developing leaf). These fluxes drain

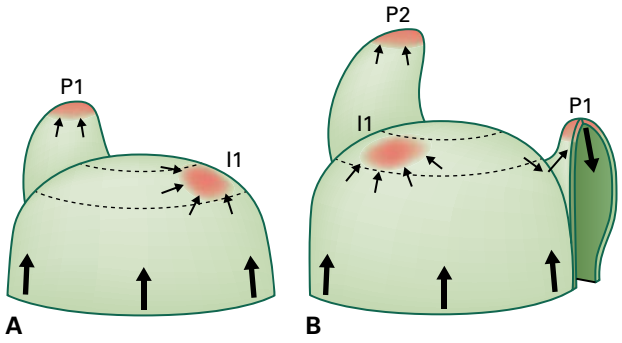


FIGURE 18.24 *Leaf initiation. Auxin concentration is shown in red, and polar auxin transport is indicated by arrows. (A) In the meristem epidermis, auxin is transported up its concentration gradient, leading to localized auxin accumulation that defines the leaf initiation site (I1). (B) As the leaf initiates (P1), auxin is transported from epidermis at the leaf tip into subepidermal layers. This drains auxin from the surrounding epidermis, causing redistribution of auxin transport towards the next initiation site.*

auxin away from surrounding epidermal cells and so inhibit leaf initiation in the vicinity of the new primordium.

As each leaf is initiated, the change in the pattern of auxin concentration in the epidermis causes a shift in PIN polarization in epidermal cells such that auxin is directed towards the next leaf initiation site. This generates the regular pattern of leaves around the apex (the phyllotaxy). Note that the mechanism requires auxin to be retained in the epidermal layer, which is achieved by the localization of AUX/LAX influx carriers to the epidermal cells.

The hypothesized mechanisms of vascular patterning and leaf initiation show how complex interactions between auxin, its transport, and its signaling can create patterns that regulate plant development. Both the parameters of the interactions and their outcome depend on developmental context. Furthermore, the core mechanisms may be regulated by additional local and long-range signals.

18.7 Signal transduction from phytochromes

18.7.1 A major function of phytochromes is to distinguish between red and far-red light

Phytochromes are present in all green plants, several bacterial groups, and some fungi. They were discovered through investigation into the phenomenon of **red/far-red photoreversibility**. For example, in many species germination is promoted by short exposure to red light (wavelengths of 620–700 nm) but is inhibited if this is followed immediately by exposure to far-red light (wavelengths of about 700–800 nm).

Photoreversibility arises from the interconversion of phytochromes between two isomers with different light-absorbing properties (Fig. 18.25). Phytochromes are synthesized as an inactive, red light-absorbing isomer called $\mathbf{P_R}$. Light absorption by P_R converts it to an active, far-red-absorbing isomer called $\mathbf{P_{FR}}$ (**photoconversion**). Similarly, light absorption by P_{FR} converts it back to P_R. Hence, red light promotes phytochrome responses by converting inactive P_R into active P_{FR}, while far-red light inhibits the same responses by converting P_{FR} back to P_R. In addition to photoconversion, P_{FR} can revert spontaneously to P_R. Although such reversion occurs in light and darkness, it is measured by the fall in P_{FR} concentration in the dark, and so is known as **dark reversion** (Fig. 18.25).

Phytochromes act with other plant photoreceptors to modulate physiology and development (Box 18.2). Photoconversion between P_R and P_{FR} allows phytochromes to provide information about the ratio of red to far-red light (R:FR ratio) in the plant's environment. This is biologically relevant because leaves absorb most red light, whereas they transmit most far-red light. Therefore, a low R:FR ratio indicates shading from competitors, which has a variety of developmental effects, depending on the species. In weedy plants such as *Arabidopsis*, low R:FR inhibits seed germination and induces shade escape responses during plant growth. Phytochrome-mediated responses also include seedling photomorphogenesis, flowering, and control of the circadian clock.

Phytochromes are soluble proteins and are dimers in which each subunit is bound to a molecule of phytochromobilin, a linear tetrapyrrole that functions as the light-absorbing chromophore (Fig. 18.25). Light absorption by phytochromobilin causes its isomerization and subsequent changes to both the absorption spectrum of the chromophore and the conformation of the phytochrome protein. Although the absorption peaks of P_R (about 660 nm) and P_{FR} (about 730 nm) are in the red and far-red regions of the spectrum respectively, both isomers absorb some light at all wavelengths from UV-B to far-red (Fig. 18.26). Therefore, no wavelength of illumination fully drives phytochromes into existing purely as P_R or P_{FR}.

Plants produce several different phytochromes. *Arabidopsis*, for example, contains five different phytochromes (phyA–E) that possess identical chromophores and show the same absorption spectra in their P_R and P_{FR} forms, but have different apoproteins and display overlapping, but distinct functions. The main functional distinction is between **light-labile** and **light-stable** phytochromes; in *Arabidopsis*, only phyA is light labile, and the other four phytochromes are light stable.

Light-labile phytochromes are the predominant form in imbibed seeds and in seedlings kept in continual darkness. Tests on *Arabidopsis* show that in these circumstances, the *PHYA* gene is strongly expressed, resulting in the accumulation of high concentrations of the phytochrome's P_R isomer (P_RA). This causes extreme light sensitivity, because even very low light exposures generate sufficient $P_{FR}A$ to induce responses. This is true across the entire P_R absorption spectrum. Hence, after several days in darkness, imbibed *Arabidopsis* seeds germinate following brief exposures to even UV-B or far-red light. Obviously, these responses do not show photoreversibility (Fig. 18.26).

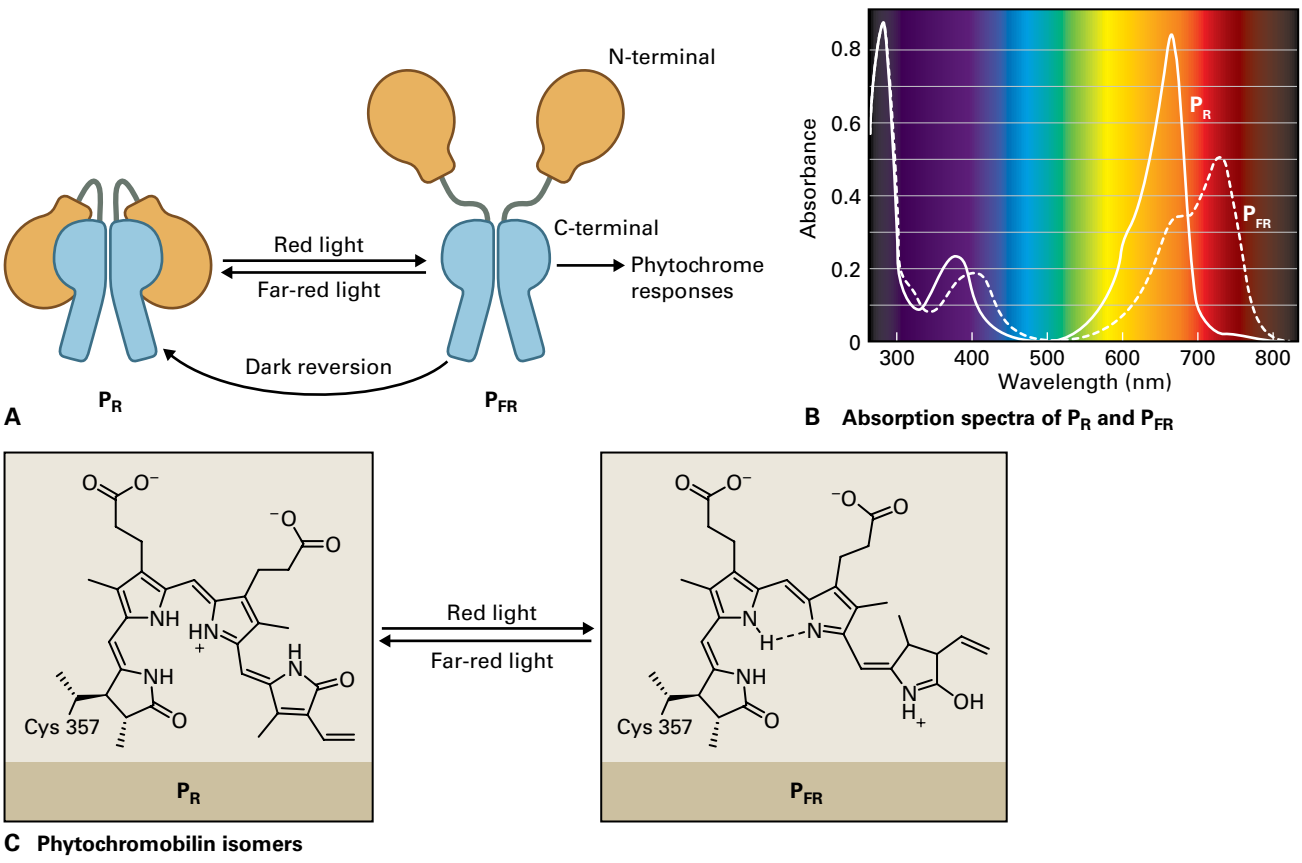


FIGURE 18.25 *Phytochromes exist as dimers and undergo photoconversion between inactive P_R and active P_{FR}. (A) P_{FR} also reverts in a light-independent manner to P_R (dark reversion). When P_R converts to P_{FR}, phytochromes undergo a conformational change that is believed to involve the unfolding of the N-terminus from the C-terminus. (B) Absorption spectra for P_R and P_{FR} show peaks for red (around 660 nm) and far-red (around 730 nm), respectively. (C) The phytochrome chromophore is a linear tetrapyrrole called phytochromobilin that undergoes light-induced isomerization.*

BOX 18.2 Plant photoreceptors

The **action spectra** of light-regulated responses demonstrate plants are highly sensitive to UV-B radiation (wavelengths from about 280 nm to 320 nm), UV-A radiation (from about 320 nm to 380 nm), blue light (from about 380 nm to 500 nm), red light (from about 620 nm to 700 nm), and far-red light (from about 700 nm to 800 nm). It is, therefore, at these wavelengths that plant photoreceptors are most sensitive. UV-B radiation is detected by the UV RESISTANCE LOCUS 8 (UVR8) protein. UV-A and blue wavelengths are detected by **cryptochromes**, **phototropins**, and the recently discovered **zeitlupes**. Responses to red and far-red light are mediated by **phytochromes**. It has also been proposed that plants may possess receptors for green light (wavelengths from about 500 nm to 600 nm); however, responses to green light are often subtle and are sometimes mediated by cryptochromes and phytochromes, both of which display a degree of sensitivity to this region of the spectrum.

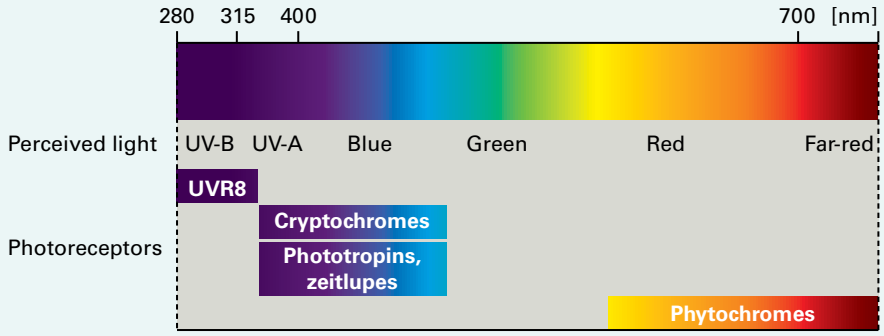
Most photoreceptors consist of proteins bound to light-absorbing pigments called chromophores, which give a photoreceptor is spectral sensitivity. In response to light absorption by the chromophore, the photoreceptor protein regulates downstream signaling. Phytochromes and cryptochromes are both soluble receptors that function primarily in the nucleus to regulate the activity of transcription factors (see Section 18.7). These two classes of photoreceptor combine to regulate developmental responses to light intensity, such as the de-etiolation (photomorphogenesis) of seedlings on reaching the soil surface. As described in Section 18.7, phytochromes also mediate responses to variations in the spectral quality of light that indicate shading by other plants.

Zeitlupes are light-responsive F-box proteins (see Section 18.6.2) that target proteins that function in the circadian clock and the photoperiodic regulation of flowering for degradation. Both the circadian clock and the initiation

of flowering are also regulated by signaling initiated by cryptochromes and phytochromes. UVR8 is a **β-propeller protein** (characterized by a propeller-like domain of flat 'blades' around a central channel). In the absence of UV-B, UVR8 exists as a homodimer. On UV-B absorption, the dimer dissociates and UVR8 monomers interact with nuclear proteins to induce UV acclimation and morphological responses such as reduced hypocotyl elongation.

Phototropins are plasma membrane-associated protein kinases responsible for regulating phototropism and light-induced chloroplast movement. They also function in the control of stomatal aperture (see Section 18.9) and in the regulation of hypocotyl and leaf expansion. Light absorption by phototropins causes their autophosphorylation and induces signal transduction pathways that lead to the redistribution of PIN auxin efflux carriers necessary for directional growth (see Section 18.6.3) and to the changes in plasma membrane ion fluxes that regulate guard cell turgor (see Section 18.9.2).

Signal transduction pathways from different photoreceptors interact, allowing integration of information from the light environment. For example, although phototropism is primarily mediated by phototropins, the amplitude of phototropic bending is modulated by cryptochrome and phytochrome signaling. As discussed in Section 18.7.3, the plasma membrane-associated protein PKS1 interacts with both phyA and phototropin1 and may allow phytochrome signaling to influence phototropic responses. There are also direct and indirect interactions between phytochromes and cryptochromes. For example, phytochromes phosphorylate cryptochromes in vitro, and both phytochromes and cryptochromes inhibit the activity of the protein COP1, which acts as a negative regulator of light responses (see Section 18.7.3). UVR8 also interacts with COP1. In contrast to the action of phytochromes and cryptochromes, however, this leads to COP1 accumulation, which promotes UV-B induced responses.



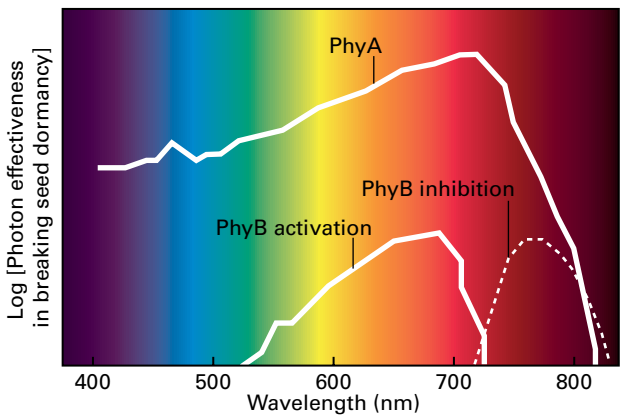


FIGURE 18.26 *Action spectra for the phyA- and phyB-induced germination of* Arabidopsis *seeds. The action spectrum for phyB was determined with seeds imbibed in water for very short periods and is reversible by exposure to far-red light. The action spectrum for phyA was determined using seeds imbibed in water for 2 days in darkness. phyA-induced germination is extremely light-sensitive and does not display photoreversibility.*

Prolonged light exposure and the conversion of P_RA to $P_{FR}A$ cause phyA concentration to drop approximately 100-fold. This occurs partly because the $P_{FR}A$ protein is rapidly degraded and partly because light inhibits *PHYA* transcription in a process that is itself mediated by phytochrome signaling. Despite the fall in concentration, phyA still functions in light-grown plants. In contrast to phyA, the light-stable phytochromes (phyB–E) have about the same concentrations in both light and darkness and are the major group found in mature plants.

18.7.2 Phytochromes in the P_{FR} form are translocated into the nucleus

Because phytochromes are synthesized in the inactive, P_R form, this is the only isomer present in seedlings germinated in continual darkness. Immunolocalization and the use of fluorescently-labeled phytochromes suggest that, under these

conditions, phytochromes are exclusively cytosolic. However, exposure to light and the conversion of P_R to P_{FR} causes movement of phytochromes from the cytosol into the nucleus.

Research on *Arabidopsis* indicates that the kinetics and mechanism of this process differ between phyA and phyB (Fig. 18.27). Phytochromes are too large to diffuse passively through nuclear pores and so require active transport across the nuclear membrane. In the case of phyB, this is conceptually simple. PhyB possesses a nuclear localization sequence (NLS) that is believed to be uncovered by the conformational change occurring as P_RB converts to P_{FR}B. This allows binding by nuclear import proteins and trafficking of phyB across the nuclear membrane in a process that takes place over a period of hours. In contrast, phyA lacks a NLS, and P_{FR}A depends on the proteins FHY1 and FHL for nuclear import. These act redundantly to bind specifically to P_{FR}A and, via their own NLSs, traffic it into the nucleus. Nuclear import of P_{FR}A is extremely rapid, detectible within minutes of light exposure.

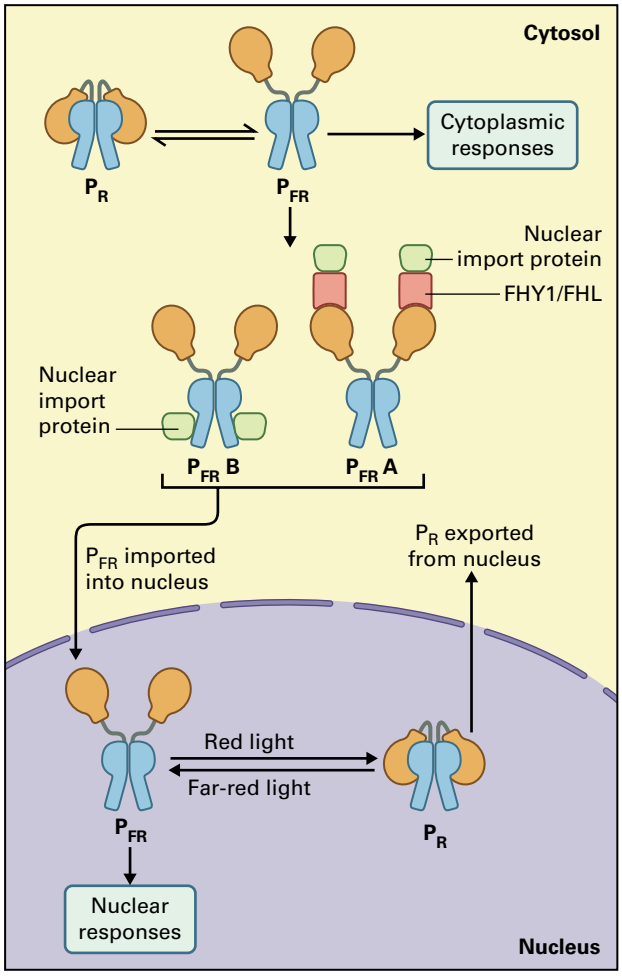


FIGURE 18.27 *Conversion of cytoplasmic P_R to P_{FR} induces movement of phytochromes into the nucleus. Nuclear import of P_{FR}B is mediated by import proteins binding to the phyB nuclear localization sequence. In contrast, phyA lacks a nuclear localization sequence, and nuclear import of P_{FR}A requires the proteins FHY1 and FHL. Conversion of nuclear P_{FR} to P_R induces translocation of phytochromes back to the cytoplasm.*

Furthermore, because of the high concentration of phyA in dark-grown seedlings, both red and far-red light produce sufficient P_{FR}A for its accumulation in the nucleus to be observed.

Within the nucleus, both phyA and phyB accumulate in a speckled pattern, which has led to the hypothesis that phytochromes act in the nucleus as components of large signaling complexes. Consistent with this, the speckles—usually called **nuclear bodies** (NBs)—associated with P_{FR}B disappear upon exposure to far-red light and, hence, the conversion of P_{FR} to P_R. Furthermore, NBs have a circadian pattern: they disappear at night and re-form shortly *before* dawn, indicating regulation by the circadian clock and suggesting a point of integration between light- and clock-signaling. Lastly, the reversion of P_{FR}B to P_RB by exposure to far-red light also causes phyB to be exported from the nucleus, suggesting that, while cytosolic P_{FR} is imported into the nucleus, nuclear P_R is exported back to the cytosol. Notice that, because photoconversion is extremely rapid relative to phytochrome trafficking, both forms are present in both the cytosol and the nucleus of light-grown plants.

18.7.3 Phytochromes regulate transcription factor stability

Some phytochrome-mediated responses are extremely rapid and almost certainly depend on signal transduction within the cytoplasm. For example, phytochrome-induced cytoplasmic streaming in *Vallisneria* (eelgrass) has been recorded within 2.5 seconds of light exposure. Phytochromes have serine/threonine kinase activity and may, therefore, initiate cytoplasmic signal transduction through phosphorylation of downstream signaling proteins. A candidate effector is PKS1, a plasma membrane-associated protein of unknown biochemical function that is phosphorylated by phytochromes and is required for normal phyA-induced responses. PKS1 also interacts with the photoreceptor phototropin1, which is required for phototropism (Box 18.2). This may form part of the mechanism by which phytochrome signaling modulates the extent of phototropic curvature.

Despite evidence of cytoplasmic signal transduction, mutations that prevent nuclear import of a phytochrome also block most responses mediated by that phytochrome. For example, movement of phyA into the nucleus is completely blocked in the *fhy1/fhl* double mutant of *Arabidopsis*. Mutant seeds lose the phyA-induced germination response, and mutant seedlings lose phyA-mediated de-etiolation responses, indicating these are mediated by nuclear signaling. Consistent with a primarily nuclear role for phytochromes, phytochrome signaling is associated with extensive changes in gene expression. In the most dramatic case, phytochrome signaling changes the expression of over 10% of the *Arabidopsis* transcriptome during the initial exposure of seedlings to light.

Phytochrome-mediated changes in gene expression appear to depend largely on modulation of transcription factor stability. In brief, phytochrome signaling both promotes the

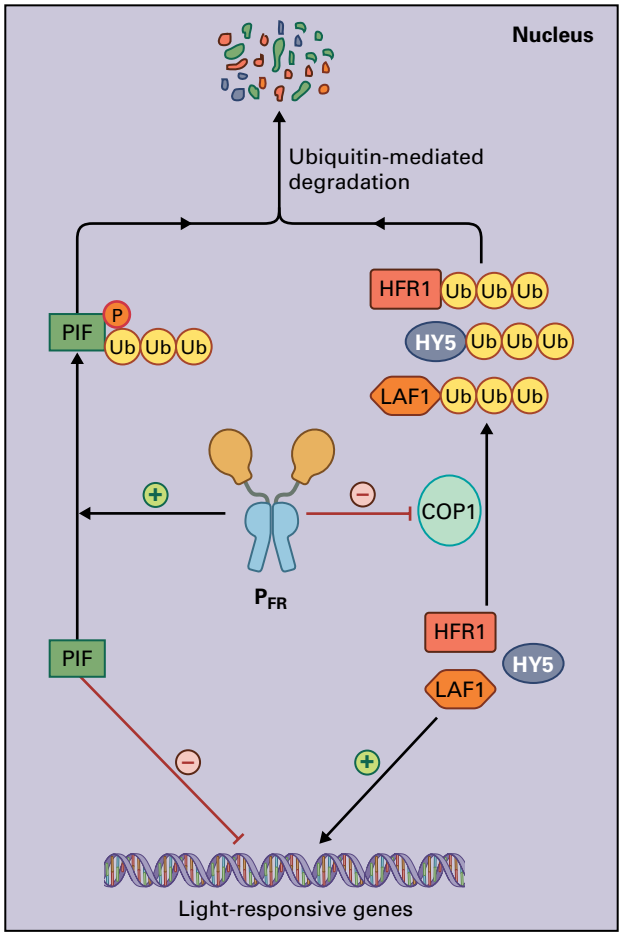


FIGURE 18.28 *Phytochromes regulate the stability of transcription factors in the nucleus. In the P_{FR} form, phytochromes induce phosphorylation and ubiquitin-linked degradation of PIFs, transcription factors that inhibit light responses. P_{FR} also inhibits the activity of COP1, which ubiquitinates the transcription factors HFR1, HY5, and LAF1, which promote light responses. In doing so, P_{FR} increases the stability of HFR1, HY5, and LAF1, leading to induction of light-responsive genes.*

degradation of transcription factors that act as negative regulators of light responses and stabilizes the transcription factors that act as positive regulators (Fig. 18.28).

The main class of negative regulators is the phytochrome-interacting factors (PIFs), which bind specifically to P_{FR}. PIFs are basic helix–loop–helix (bHLH) transcription factors. In *Arabidopsis*, they consist of a family of 15 proteins, of which at least six function in phytochrome signaling with overlapping, but varied roles. PIF3 was the first PIF identified and has been studied in detail. It promotes etiolation in dark-grown seedlings by inducing expression of etiolation-related genes. Upon light exposure, PIF3 colocalizes with phytochromes in NBs and is subsequently degraded, resulting in the inhibition of etiolation and promotion of photomorphogenic development. PIF3 degradation correlates with the phosphorylation of PIF3 and depends on its ubiquitination and subsequent targeting to the 26S proteasome (see Section 18.6.2). One model of phytochrome action is that phytochromes induce PIF phosphorylation to direct PIFs to an E3 ubiquitin protein ligase for ubiquitination (see Section 18.6.2). Phytochromes can phosphorylate PIFs in vitro.

While promoting ubiquitination of PIFs, phytochrome signaling inhibits ubiquitination of the transcription factors HY5, LAF1, and HFR1, which promote expression of light-inducible genes (Fig. 18.28). In darkness, HY5, LAF1, and HFR1 are ubiquitinated by the E3 enzyme COP1 and are, therefore, degraded by the 26S proteasome. Interestingly, COP1-dependent ubiquitination is also responsible for phyA degradation in the light. Phytochromes bind to COP1 and inhibit its activity, partly by causing exclusion of COP1 from the nucleus. The consequence is accumulation of HY5, LAF1, and HFR1 and the induction of light-responsive genes.

Phytochrome activity is affected by phosphorylation. Phytochromes autophosphorylate and do so more actively in the P_{FR} than P_R form. They are also phosphorylated by other, unknown kinases. The consequence of phosphorylation appears to be a decrease in P_{FR} activity through changes in phytochrome stability and in the affinity of phytochromes for interacting partners, such as PIF3. Phytochromes can be dephosphorylated by a type 5 protein phosphatase (PAPP5). The combination of phytochrome phosphorylation and dephosphorylation may, therefore, provide cells with a means of controlling the amplitude of the phytochrome signal.

18.8 Gibberellin signal transduction and its integration with phytochrome signaling during seedling development

Gibberellins (GAs, gibberellic acid) are a group of tetracyclic, diterpenoid hormones that function in a wide range of developmental processes, including germination, stem elongation, leaf expansion, the initiation of flowering, and floral development. GAs are synthesized in many parts of the plant and, in general, promote developmental transitions and growth. Mutants with reduced GA synthesis and plants or seeds treated with GA biosynthesis inhibitors display poor germination, are dwarfed, and flower late (Fig. 18.29). This section describes GA signal transduction and then considers the integration of gibberellin- and phytochrome-signaling during seedling development.

18.8.1 Gibberellin signal transduction depends on degradation of DELLA proteins

In a striking parallel with auxin signal transduction (see Section 18.6), GA signaling is mediated by the ubiquitination-dependent degradation of proteins that function as negative

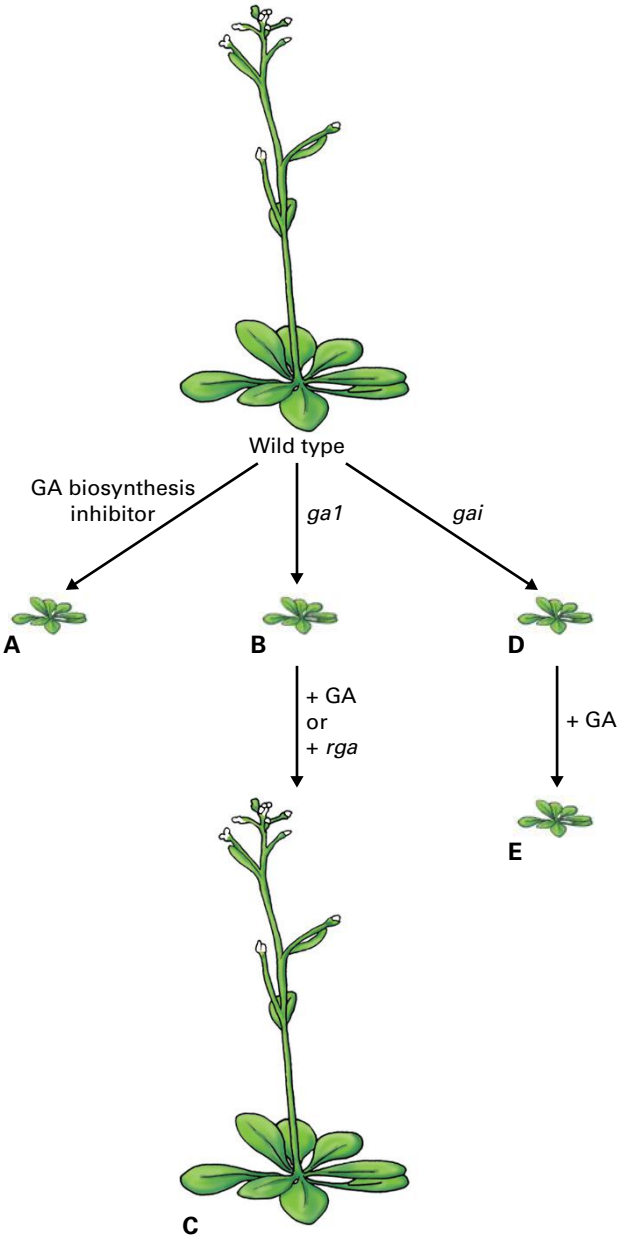


FIGURE 18.29 Arabidopsis *mutants with altered gibberellin (GA) synthesis or response. Chemical inhibition of GA synthesis (A) and disruption of GA biosynthesis by the* ga1 *mutation (B) both result in dwarf, late-flowering plants.* ga1 *mutants are rescued by addition of GA or by DELLA loss-of-function mutation* rga *(C). The* gai *mutation results in constitutive DELLA activity that causes a dwarf phenotype (D) that is not rescued by GA treatment (E).*

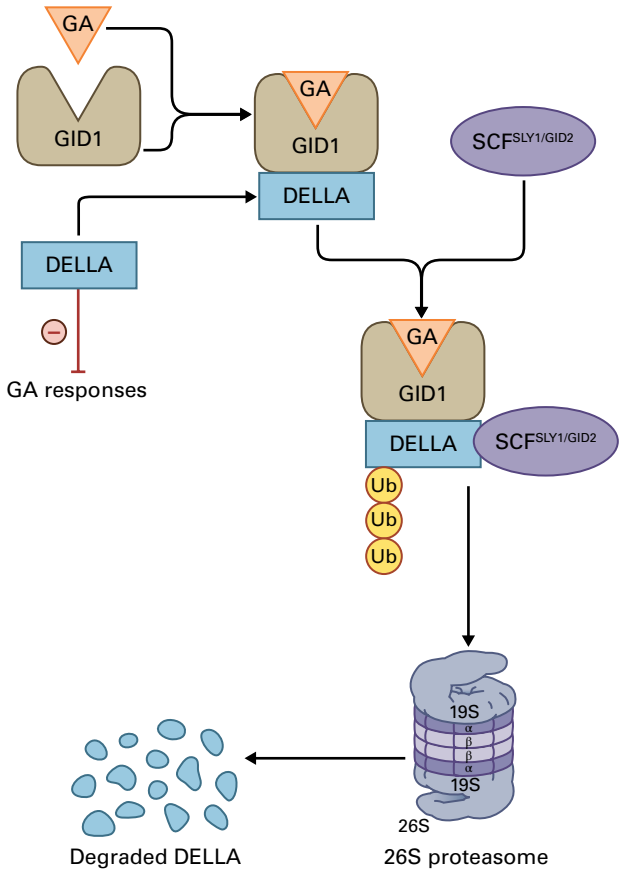


FIGURE 18.30 *GA-mediated degradation of DELLA proteins relieves DELLA inhibition of GA responses. GA-binding by the receptor GID1 promotes binding between GID1 and DELLAs, which favors interaction between DELLAs and SCF complexes containing the F-box protein SLY1/GID2 (SCF$^{SLY1/GID2}$). SCF$^{SLY1/GID2}$ ubiquitinates DELLA proteins and so targets them for destruction by the 26S proteasome.*

regulators of growth, in this case, the **DELLA proteins** (DELLAs). GA is perceived by soluble GA-insensitive dwarf1 proteins (**GID1 proteins**, Fig. 18.30), originally identified through the *gid1* mutant of rice (*Oryza sativa*). The *Arabidopsis* genome encodes three functionally redundant GA receptors, GID1a–c. GID1 proteins bind GA, and this enhances their interaction with DELLAs. In turn, the GID1-DELLA interaction promotes association between DELLAs and a family of F-box proteins related to SLEEPY1 (SLY1) in *Arabidopsis* and its homolog GID2 in rice. This leads to ubiquitination of DELLA proteins by SLY1/GID2-containing SCF complexes and the subsequent degradation of the DELLAs by the 26S proteasome (Fig. 18.30). For details of F-box proteins, SCF complexes, and ubiquitination-mediated protein degradation, see Section 18.6.2.

The function of DELLA proteins as negative regulators of GA signaling and inhibitors of plant growth is demonstrated by the phenotype of loss-of-function mutations in DELLA genes (see Fig. 18.29). For example, the GA biosynthesis mutant *ga1* (*gibberellic acid1*) of *Arabidopsis* has severely reduced GA levels and a dwarf, late-flowering phenotype. However, *ga1* mutants are partially rescued by loss of function of the DELLA gene *RGA* (*REPRESSOR-OF-ga1-3*). These data can be explained by assuming that RGA acts to repress growth and delay flowering, and that RGA function is inhibited by GA.

DELLAs are soluble, nuclear proteins that belong to the GRAS family (from GAI [see later], RGA, and SCARECROW) of plant regulatory proteins. They share a C-terminal GRAS domain with other members of the family but possess a unique N-terminal DELLA domain (Fig. 18.31), named after

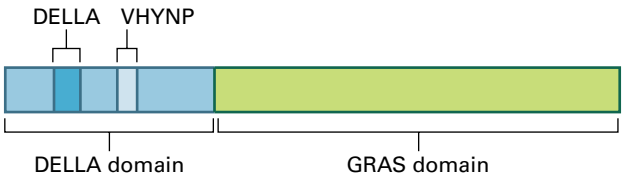


FIGURE 18.31 *DELLA protein structure. DELLA proteins belong to the GRAS family of plant regulatory proteins. The C-terminal GRAS domain is the functional domain determining DELLA activity. The N-terminal DELLA domain contains the conserved DELLA and VHYNP motifs (named after the first five amino acids in each), which are essential for interaction with GID1 and, therefore, for GA-induced DELLA protein degradation.*

a conserved amino acid sequence near the N-terminus (D E L L and A are the single-letter abbreviations of the first five amino acid residues in this sequence). The DELLA domain also contains a conserved VHYNP sequence, and both the DELLA and VHYNP sequences are required for the interaction between DELLA proteins and GID1s. Mutations that disrupt either sequence cause a dominant, GA-insensitive dwarf phenotype due to the inability of GA to induce degradation of the mutant DELLA protein. Study of such mutations led to the identification of the first known DELLA protein, GAI (GA-insensitive) of *Arabidopsis* (see Fig 18.29). A similar mutation in the wheat (*Triticum aestivum*) DELLA gene *Reduced height1* is responsible for the semi-dwarf wheat varieties that enabled the yield gain underlying the "green revolution" of the 1960s and 1970s.

The rice genome encodes only a single DELLA protein (SLR1). In contrast, *Arabidopsis* encodes five DELLA proteins (RGA, GAI, RGA-LIKE1 (RGL1), RGL2, and RGL3), and analysis of the interaction between DELLA loss-of-function mutations and the *ga1-3* extreme GA-biosynthetic mutant has revealed some specialization of function within the *Arabidopsis* DELLA family. For example, there is a clear distinction between the roles of GAI and RGA and that of RGL2. *ga1-3* mutants do not germinate without GA treatment, and they grow into extremely dwarfed, late-flowering plants with abnormal floral development. Combined loss of *GAI* and *RGA* functions rescues the dwarf and late-flowering aspects of the *ga1-3* phenotype but does not enable GA-independent germination. In contrast, loss of *RGL2* permits *ga1-3* seeds to germinate without added GA but does not rescue vegetative growth or flowering time. These and other experiments indicate GAI and RGA are the main repressors of vegetative growth and flowering, whereas RGL2 is the primary repressor of germination.

18.8.2 DELLAs have a dual function in the nucleus

DELLA proteins appear to act in two distinct ways in the nucleus: they promote transcription from target genes and inhibit the activities of at least some phytochrome-interacting factors (PIFs, see Section 18.7.3). The interaction between DELLAs and PIFs is considered in Section 18.8.3. Here, we

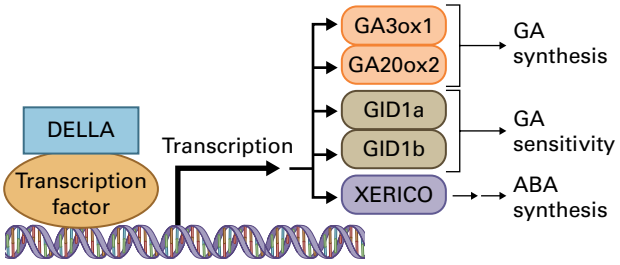


FIGURE 18.32 *Induction of transcription by DELLA proteins. In the current model of DELLA protein action, DELLAs induce transcription by binding to and activating a separate transcription factor. Genes induced by DELLAs include those encoding GA biosynthetic enzymes (*GA3ox1 *and* GA20ox2*), GA receptors (*GID1a *and* GID1b*), and* XERICO*, which promotes ABA synthesis.*

discuss the role of DELLA proteins in enhancing gene transcription, in particular genes involved in GA signaling.

The use of an inducible DELLA transgene (encoding a GA-insensitive version of RGA) has led to the identification of 14 genes from which transcription is rapidly promoted by DELLA activity in *Arabidopsis*. Supporting a role for DELLAs in inducing transcription is the observation that the DELLA protein associates with the promoters of eight of these genes. DELLA proteins, however, lack an identified DNA-binding domain, so it is likely DELLAs promote gene expression by associating with a separate DNA-binding protein or transcription factor (Fig. 18.32).

Interestingly, among the genes identified as DELLA targets are two GA biosynthetic genes (*GA3ox1* and *GA20ox2*) and two GA receptor genes (*GID1a* and *GID1b*). By promoting the expression of these genes, DELLAs increase both GA synthesis and GA sensitivity, creating a negative feedback loop in which DELLA activity increases GA signal transduction and, therefore, leads to DELLA degradation (Fig. 18.32). This is consistent with other evidence for feedback in GA signaling. For example, in *Arabidopsis*, GA treatment or increased GA signaling due to mutation cause a decrease in transcription from genes encoding GA biosynthetic enzymes and the upregulation of genes encoding enzymes that inactive GAs. In contrast, GA deficiency or mutations that inhibit GA signaling have roughly the opposite effect.

Putative DELLA targets also include the *XERICO* gene, which is thought to promote ABA synthesis. This represents a point of interaction in the generally antagonistic relationship between GA and ABA signaling (Box 18.3).

18.8.3 DELLAs and PIFs act antagonistically during seedling photomorphogenesis

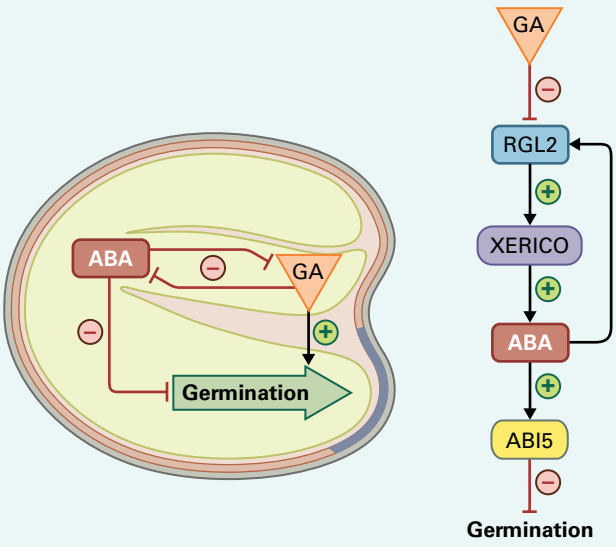
In flowering plants, seedlings grown in continual darkness display **etiolation**, a developmental program characterized by reduced root growth, a rapidly elongating stem (hypocotyl or epicotyl) that ends in an apical hook, and folded, unexpanded

BOX 18.3 Antagonistic regulation of germination and stress responses by GA and ABA

GA and ABA often act antagonistically. For example, germination in many species requires biosynthesis of gibberellins and subsequent GA signaling. In contrast, ABA inhibits germination and mutations that cause ABA deficiency can rescue the nongerminating phenotype of GA-deficient mutants.

In both the seed and in growing plants, ABA and GA reciprocally suppress each other's synthesis and promote each other's degradation. Hence, seeds of GA deficient *ga1* mutants of *Arabidopsis* accumulate higher concentrations of ABA, while in the ABA-deficient mutant *aba2*, seeds contain higher levels of GA. This suggests a model for the control of germination in which GA and ABA are responsible for two competing positive feedback loops. Initially, ABA signaling dominates over GA signaling, with high ABA levels and low GA levels maintained by the ABA effects on GA synthesis and degradation. Subsequently, germination is induced by factors that create a switch to dominance by GA signaling, with high GA levels and low ABA levels maintained by the GA effects on ABA metabolism (A).

The antagonism between GA and ABA during germination is reflected in the functions of the *Arabidopsis* DELLA protein RGL2 (see Section 18.8 and (B)), which acts to suppress germination in part by promoting ABA synthesis. RGL2 is thought to induce transcription from the gene *XERICO* which encodes an E3 ubiquitin ligase (see Section 18.6.2). Overexpression of *XERICO* leads to increased concentrations of ABA, suggesting the XERICO protein targets an inhibitor of ABA synthesis for ubiquitination and, therefore, degradation. Hence, by inducing XERICO synthesis, RGL2 increases ABA concentration in the seed, whereas by inducing RGL2 degradation (see Section 18.8), GA depresses ABA levels. Interestingly, an increase in ABA concentration in the seed leads to an increase in both RGL2 mRNA and protein, suggesting positive feedback between ABA and RGL2. Downstream of RGL2, ABA promotes expression of the *ABI5* gene, which encodes a transcription factor that inhibits germination. Interestingly, the antagonistic effects of ABA and GA on germination are recapitulated during plant responses to adverse conditions such as salt stress, drought, and extremes of temperature. These abiotic stresses lead to an adaptive reduction in growth rate that appears to depend largely on the action of DELLA proteins. For example, salt stress leads to a reduction in GA levels and a consequent increase in DELLA concentrations. Furthermore, mutants such as *ga1* with reduced GA synthesis or *gai* with constitutive DELLA activity have increased salt tolerance. In contrast, mutants with loss of DELLA function do not restrain growth fully in response to salt and have reduced survival rates during salt stress. Salt stress also promotes ABA synthesis. ABA induces stress-related genes independently of GA-signaling. In addition, however, ABA induces DELLA accumulation by inhibiting GA synthesis.



leaves or cotyledons around an inactive shoot apical meristem. This pattern of development maximizes upward growth to bring the seedling shoot to the soil surface. Once in the light, seedlings display **photomorphogenesis** (de-etiolation). Stem elongation slows rapidly, the apical hook unfolds, the leaves or cotyledons expand and develop chloroplasts, the shoot apical meristem becomes active, and root growth accelerates (Fig. 18.33).

Comparing germination and photomorphogenesis, it is clear that there is a change in the effects of light on GA-regulated processes. Consider an *Arabidopsis* seed and seedling. During germination, light-promoted GA synthesis and signaling lead to cell elongation in the embryonic root and hypocotyl. In contrast, in an etiolated seedling, light exposure reduces GA synthesis and signaling in the hypocotyl, reducing cell elongation. The situation in other organs is more complex; for example, cotyledon expansion is promoted by light and GAs, but largely occurs in the photomorphogenic seedling rather than during germination.

Another difference between germination and photomorphogenesis is that whereas light-induced germination is primarily mediated by phytochromes, seedling photomorphogenesis is induced by light perceived at both phytochromes and cryptochromes (UV-A/blue light receptors, Box 18.2).

In both cases, light perception inhibits the activity of the E3 ubiquitin ligase COP1, which results in accumulation of transcription factors such as HY5, LAF1, and HFR1 (see Section 18.7.3). These transcription factors then induce expression of light-responsive genes. At the same time, phytochromes induce ubiquitination and destruction of PIF transcription factors, which act in darkness to promote expression of etiolation-related genes (see Section 18.7.3).

The change in the effect of light on GA signaling between germination and photomorphogenesis occurs largely at the level of GA metabolism. Light promotes GA synthesis in the seed but inhibits GA synthesis in the etiolated seedling (Fig. 18.34). For example, blue light inhibits the GA biosynthetic genes *GA3ox1* and *GA20ox1* and promotes expression of the GA-inactivating gene *GA2ox1* in *Arabidopsis* seedlings. Similarly, light causes a rapid reduction in the concentration of bioactive GA in etiolated pea (*Pisum sativum*) seedlings; consistent with this finding, GA-deficient seedlings display a partially photomorphogenic phenotype in darkness.

In addition to the effect of light on GA concentration, recently it has been discovered that phytochrome and GA signaling have antagonist effects on PIF activity in the seedling (Fig. 18.34). DELLA proteins bind both PIF3 and PIF4 in *Arabidopsis*, which prevents the PIFs from binding the promoters of their target genes and, hence, prevents PIF-induced etiolation. In darkness, however, high GA levels promote etiolation by leading to the degradation of DELLAs, which permits PIF3 and PIF4 activity. In the light, the fall in GA concentration leads to the accumulation of DELLAs, which block PIF3 and PIF4. In combination with the phytochrome-mediated destruction of PIFs, this induces the switch from etiolation to photomorphogenesis.

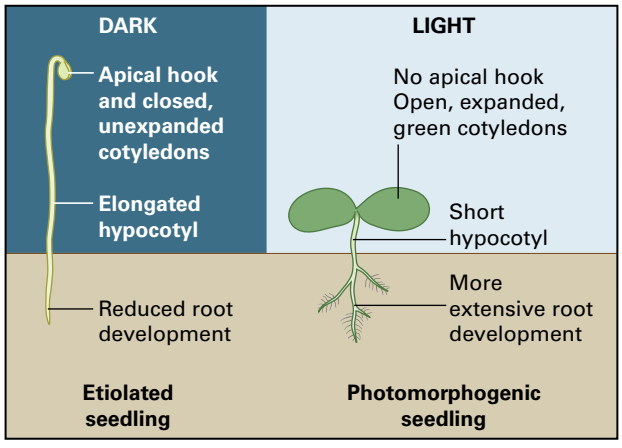


FIGURE 18.33 *Characteristics of etiolated and photomorphogenic seedlings.*

18.8.4 The GA signal transduction pathway evolved in stages

The GA signal transduction pathway and the antagonistic roles of DELLAs and GA in regulating growth are conserved across angiosperms (flowering plants) and gymnosperms (conifers). Stages in the evolution of GA signal transduction have been revealed by research on interactions between GID1 homologs and DELLA proteins in the moss *Physcomitrella patens* and in the lycophyte *Selaginella kraussiana*.

Mosses are nonvascular plants that evolved approximately 430 million years ago, whereas lycophytes are primitive vascular plants and appeared about 400 million years ago (Fig. 18.35). Genome analysis shows that both *P. patens* and *S. kraussiana* possess GID1 homologs and DELLA proteins; however, GA signaling appears to be absent in moss and highly limited in *Selaginella*.

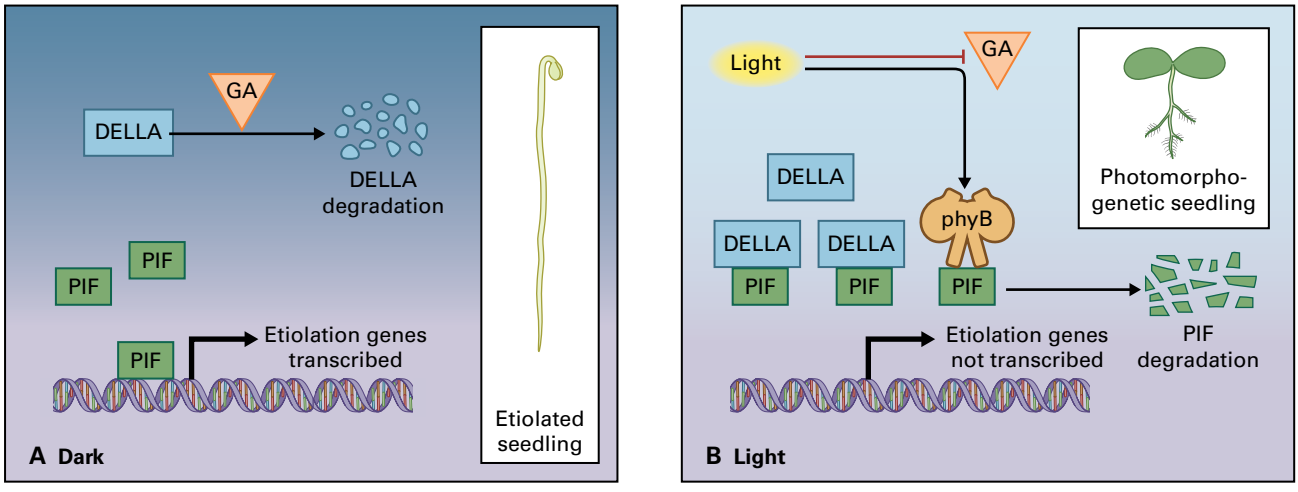


FIGURE 18.34 *Direct interactions between DELLAs and PIFs during seedling photomorphogenesis. (A) In darkness, high gibberellin (GA) levels lead to the degradation of DELLA proteins, allowing PIF transcription factors to induce transcription from etiolation-related genes. (B) Light causes a fall in GA concentration in the seedling, resulting in accumulation of DELLA proteins in the nucleus. DELLAs bind directly to PIFs to prevent PIF-induced gene transcription. In addition, light induces movement of phytochromes into the nucleus and phytochrome-mediated degradation of PIF proteins. As a result, the seedling switches from etiolation to photomorphogenesis.*

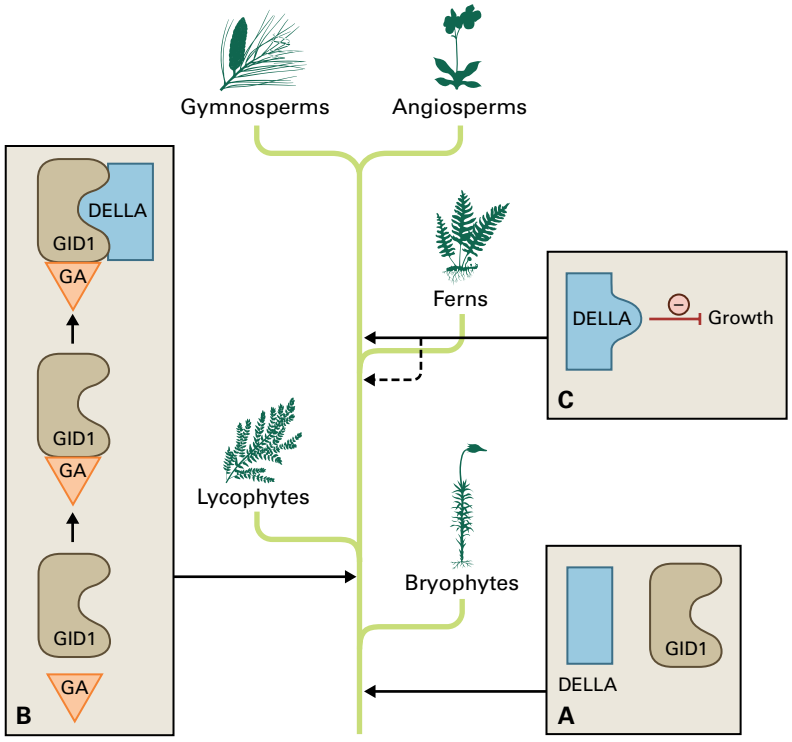


FIGURE 18.35 *Evolution of the GID1/DELLA interaction and of DELLA function.(A) DELLAs and GID1-like proteins evolved before the divergence of bryophytes, but in bryophytes they do not interact. (B) Subsequently, but before the evolution of lycophytes, GA synthesis, GID1-GA binding, and GA-promoted GID1/DELLA interaction arose. (C) Before the evolution of seed plants (gymnosperms and angiosperms), and perhaps before the evolution of ferns, DELLAs gained a growth-suppressing function.*

Moss produces no known bioactive GAs and has no clear response to exogenously applied GAs. Consistent with this, there is no interaction between GID1-like proteins and DELLA homologs in moss, which lack the required DELLA and VHYNP sequence (see above). It is likely that moss does not perceive GA and lacks a GA signal transduction pathway; the moss GID1 homologs and DELLA proteins must, therefore, have (unknown) GA-independent functions.

GID1 and DELLA proteins in *S. kraussiana* do interact, and their interaction is promoted by GA. Therefore, the initial steps of GA signal transduction in lycophytes are similar to those in flowering plants. Furthermore, GA treatment downregulates transcription from the *GID1* gene of *S. kraussiana*, paralleling the negative feedback observed in GA signal transduction in *Arabidopsis* (see Section 18.8.2). Unlike the case in flowering plants, however, GA does not stimulate the growth of lycophytes, and it is thought that DELLA proteins do not inhibit lycophyte (or moss) growth. It is currently unclear what function(s) GA has in lycophytes.

Interestingly, DELLA genes from both *P. patens* and *S. kraussiana* can suppress growth when expressed in *Arabidopsis*. This indicates the evolution of growth suppression by DELLAs depended on changes in downstream interacting components such as PIFs and DELLA-regulated genes rather than on changes in the structure of the DELLAs themselves. In a similar vein, DELLAs from both *Arabidopsis* and *S. kraussiana* can interact with a GID1-like protein from moss, showing the evolution of this interaction depended largely on changes in DELLA structure rather than GID1 structure. Nonetheless, a change in GID1 structure was required between the evolution of mosses and the evolution of vascular plants to allow GA binding by GID1 and, therefore, GID1's function as a receptor.

These experiments suggest the following model for the evolution and of the GID1/DELLA interaction and its consequences (Fig. 18.35). In moss, GA signal transduction is absent, but GID1 homologs and DELLAs are present and presumably have other functions. Prior to the evolution of lycophytes, GID1 gained the ability to bind GA, DELLA proteins gained the ability to bind GID1, and GA stimulation of the GID1/DELLA interaction arose. The growth-restraint function of DELLAs appeared after the divergence of lycophytes but before the evolution of seed plants (gymnosperms and angiosperms). It remains unclear at what point in this series the ubiquitination of DELLAs by F-box proteins—and its promotion by GA—evolved.

18.9 Integration of light, ABA, and CO_2 signals in the regulation of stomatal aperture

18.9.1 An intricate signal transduction network regulates stomatal aperture

Stomata allow diffusion of both carbon dioxide into the leaf for photosynthesis and water out of the leaf, driving the transpiration stream. The size of the stomatal pore is governed by

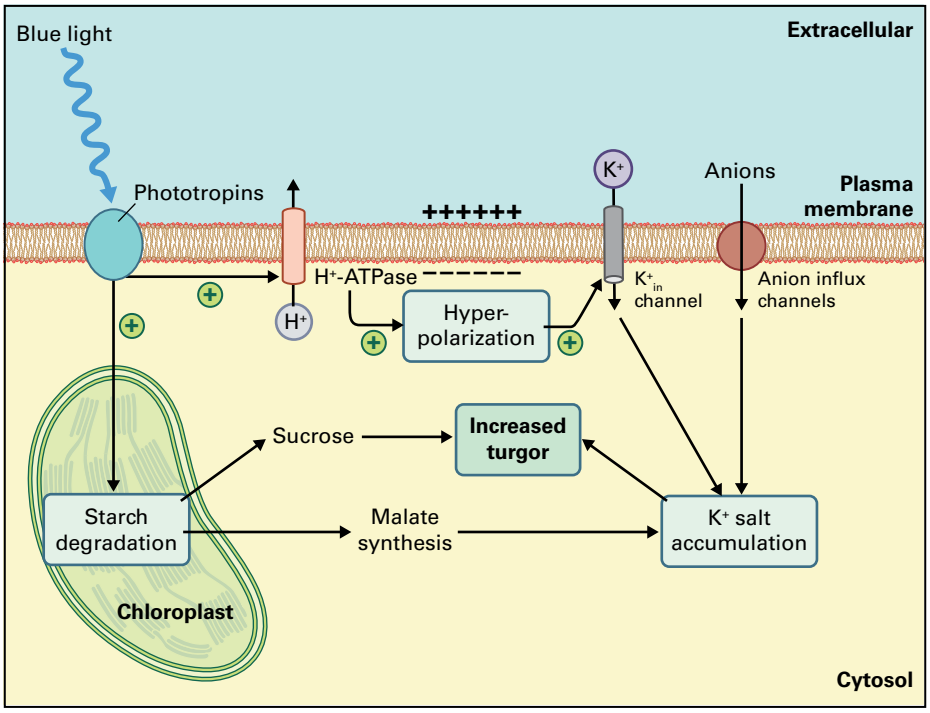


FIGURE 18.36 *Blue light induces an increase in guard cell turgor. Blue light absorption by phototropins results the activation of a plasma membrane H^+-ATPase, leading to membrane hyperpolarization and consequent activation of voltage-sensitive K^+_{in} channels. K^+ influx is balanced by anion influx and synthesis, causing accumulation of K^+ salts and increased turgor. In the afternoon, sucrose replaces K^+ salts as the osmoticum. Note that the cell wall is not shown for clarity.*

a combination endogenous and environmental factors including light, carbon dioxide, humidity, hormones (in particular ABA), temperature, ozone, and the plant's internal clock and water status. These combine to regulate stomatal aperture in a way that provides a compromise between CO_2 uptake and excessive water loss.

The stomatal pore varies in size because of turgor changes in the two, flanking guard cells. Owing to the pattern of microfibrils in guard cell walls, an increase in turgor causes guard cells to elongate and forces them to bend outwards, which opens the pore. Conversely, a decrease in turgor shortens guard cells and closes stomata. These changes are accompanied by substantial variation in guard cell volume and require extensive vesicle trafficking between the cytoplasm and the plasma membrane to increase or decrease plasma membrane surface area.

There has been much research into the mechanisms that regulate guard cell turgor and into the signal transduction network that ties these mechanisms to endogenous and environmental signals. Here we consider the integration of signal transduction in response to light, ABA, and CO_2 concentration.

18.9.2 Light-induced stomatal opening depends on phototropin signaling

In most species, stomata open in response to light. Action spectra and mutational analysis demonstrate this depends on blue/UV-A wavelengths perceived by phototropins (Box 18.2). On absorbing light, guard cell phototropins initiate a signal transduction pathway that activates plasma membrane proton pumps (H^+-ATPases) that pump protons out of the cytosol and into the apoplast (Fig. 18.36). This increases the potential difference between the cytosol and apoplast, causing hyperpolarization of the plasma membrane, which activates membrane-spanning, voltage-gated potassium intake channels (K^+_{in}), triggering an influx of potassium ions (K^+) down their electrochemical gradient from the apoplast into the cytosol. The increase in cytosolic K^+ concentration is balanced by the accumulation of malate and anions such as Cl^-, and NO_3^-, which are imported across the plasma membrane. Malate is also synthesized within the guard cells from starch. For a detailed discussion of ion transport, see Chapter 3.

Plasma membrane ion fluxes are matched by ion fluxes across vacuolar membranes. This leads to the accumulation of potassium salts in the cytosol and vacuoles and, therefore, an overall lowering of the guard cell's water potential. Consequent water uptake increases the guard cell's turgor and causes stomatal opening. Under natural conditions, accumulated potassium salts are replaced during the morning by sucrose, which is responsible for maintaining guard cell turgor through the day.

The transduction pathway that links light perception by phototropins to the activation of the H^+-ATPase is currently incompletely understood (Fig. 18.37). In response to blue light, the H^+-ATPase is phosphorylated on serine and threonine residues in its C-terminus. This is followed by the binding of a 14-3-3 protein to the same domain. 14-3-3 proteins can cause changes in target protein activity or protein relocation, and can also act as a scaffold to allow protein–protein interactions. Binding by the 14-3-3 protein in response to H^+-ATPase phosphorylation is absolutely required for induction of proton pumping.

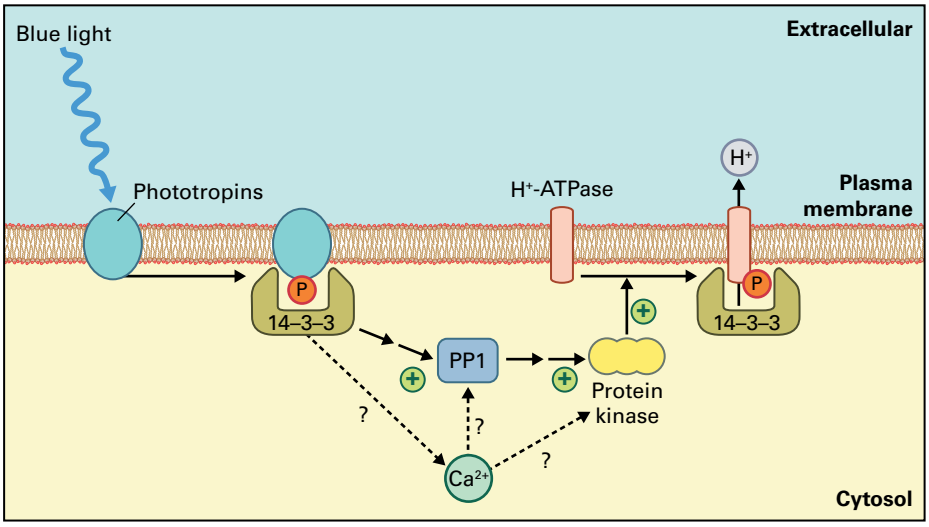


FIGURE 18.37 *Signal transduction from phototropins to the H⁺-ATPase in the guard cell. Absorption of blue light induces phototropin autophosphorylation and association with a 14-3-3 protein. This initiates a signal transduction pathway that includes a type 1 protein phosphatase (PP1), and a protein kinase that phosphorylates the H⁺-ATPase. Phosphorylation induces binding of a 14-3-3 protein and activation of the H⁺-ATPase. Phototropin signaling may also involve an increase in cytosolic calcium concentration. Note that the cell wall is not shown for clarity.*

Phototropins are membrane-associated kinases, and their kinase activity is stimulated by light absorption causing autophosphorylation that initiates downstream signaling. There is no evidence that phototropins directly phosphorylate the H⁺-ATPase; therefore, other signaling components must transduce the signal from phototropins to the proton pump. Interestingly, these include a 14-3-3 protein that binds to phototropin after the photoreceptor autophosphorylates. Given binding between a 14-3-3 protein and the H⁺-ATPase, this raises the possibly of the formation of a complex containing phototropin, 14-3-3 proteins, and the H⁺-ATPase.

A type 1 protein phosphatase (PP1) is also implicated in the transduction pathway. Chemical inhibition of PP1 activity suppresses blue light-induced phosphorylation of the H⁺-ATPase and stomatal opening. Similarly, light-induced opening is reduced in plants expressing a dominant, inactive form of PP1. These experiments suggest that PP1 acts as a positive regulator of the pathway linking phototropins to activation of the proton pump. The transduction pathway may also involve changes in cytosolic Ca^{2+} concentration (see Section 18.9.4). Ultimately, signaling from phototropins must lead to activation of the protein kinase responsible for phosphorylating the H⁺-ATPase.

18.9.3 An ABA-induced rise in cytosolic Ca^{2+} concentration induces stomatal closure

ABA acts as a signal to induce stomatal closure. Synthesized in water-stressed leaves, ABA is also produced in roots in response to soil dryness and may be transported to the shoot in the transpiration stream. Grafting experiments between wild-type plants and ABA-deficient mutants, however, indicate ABA synthesis is required only in the shoot for root water stress to induce stomatal closure. This suggests water-stressed roots transmit an ABA-independent signal that induces ABA synthesis in the shoot and consequent stomatal closure. It has been proposed that the root-to-shoot signal could be drought-induced changes in hydraulic force in the xylem. Such changes transmit very rapidly from the root to xylem capillaries in the leaf and could be detectible by mechanosensitive ion channels in leaf cells.

ABA causes stomata to close by reversing the accumulation of potassium salts in guard cells and inducing the conversion of sugars into starch. The resulting fall in solute concentration leads to loss of water from the guard cell into the apoplast by osmosis, a fall in guard cell turgor, and closing of the stomatal pore.

ABA signaling in guard cells is largely mediated through the second messenger Ca^{2+} (Fig. 18.38). Acting through an incompletely understood network of signaling intermediates, ABA induces release of calcium ions from internal stores such as the ER and activates plasma membrane Ca^{2+} influx channels. The consequent rise in Ca^{2+} concentration in the guard cell cytosol, $[Ca^{2+}]_{cyt}$, inactivates the plasma membrane H⁺-ATPase and, therefore, prevents proton pumping out of the cell. Increased $[Ca^{2+}]_{cyt}$ also activates plasma membrane anion efflux channels, and these two effects combine to depolarize the membrane. Membrane depolarization closes voltage-sensitive K^+_{in} channels but opens K^+_{out} channels. In addition, K^+_{in} channels are inhibited directly by the rise in $[Ca^{2+}]_{cyt}$. Overall, therefore, the increase in $[Ca^{2+}]_{cyt}$ causes the net efflux of anions and K^+ from the cell, leading to a fall in guard cell turgor.

Despite a clear role for $[Ca^{2+}]_{cyt}$ in the guard cell response to ABA, not all guard cells display measurable increases in $[Ca^{2+}]_{cyt}$ after ABA treatment. This suggests ABA may induce stomatal closure by both Ca^{2+}-dependent and Ca^{2+}-independent

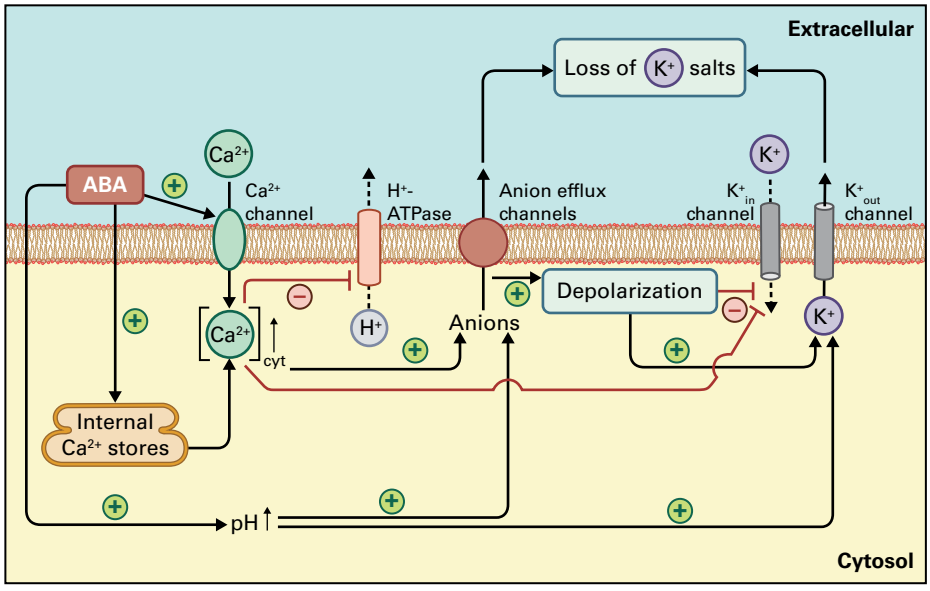


FIGURE 18.38 *ABA induces efflux of K^+ salts from the guard cell. ABA activates Ca^{2+} influx channels and induces Ca^{2+} release from internal stores, leading to a rise in cytosolic Ca^{2+} concentration, $[Ca^{2+}]_{cyt}$. This inhibits the H^+-ATPase and activates anion efflux channels leading to membrane depolarization. Depolarization inhibits K^+_{in} channels and activates K^+_{out} channels. K^+_{in} channels are also inhibited directly by Ca^{2+}. In addition, ABA causes an increase in cytosolic pH, which promotes anion efflux- and K^+_{out} channels. Note that for clarity the cell wall is not shown.*

pathways, and also that the significance of the two pathways may vary between guard cells. The proposed Ca^{2+}-independent pathway may involve ABA-induced changes in cytosolic pH (Fig. 18.38). ABA causes an alkalization of the guard cell cytosol, increasing the pH by 0.1–0.3 units. This promotes activity both of plasma membrane anion efflux channels and K^+_{out} channels, and so should also induce a loss of guard cell turgor. A role for a change in pH is supported by the fact that ABA-induced stomatal opening is blocked by treating guard cells with the weak acid sodium butyrate to prevent alkalinization of the cytosol.

Comparing the effects of ABA and blue light suggests that the respective signal transduction pathways compete for control of guard cell turgor via their antagonistic effects on plasma membrane ion transport proteins and plasma membrane polarization. In addition, ABA inhibits signal transduction between phototropins and the H^+-ATPase, countering blue light-induced phosphorylation and activation of the proton pump. This inhibition appears to depend on the production of hydrogen peroxide (H_2O_2) in response to ABA.

18.9.4 Oscillations in cytosolic calcium ion concentration are associated with both ABA and CO_2 signaling in guard cells

Although a simple ABA-induced increase in $[Ca^{2+}]_{cyt}$ is sufficient to cause stomatal closure, the mechanism of $[Ca^{2+}]_{cyt}$ signaling over the longer term is more complex. Prolonged ABA exposure induces slow oscillations of $[Ca^{2+}]_{cyt}$ in guard cells, and combining long-term monitoring of $[Ca^{2+}]_{cyt}$ by fluorescent indicators with experimental manipulation of $[Ca^{2+}]_{cyt}$ through alteration of external ion concentrations shows these oscillations are required to keep stomata closed. A sustained high $[Ca^{2+}]_{cyt}$ does not maintain closure, whereas slow $[Ca^{2+}]_{cyt}$ oscillations do (Fig. 18.39). The optimal oscillation rate measured in *Arabidopsis* is about one peak in $[Ca^{2+}]_{cyt}$ per 10 minutes, pointing to a dynamic component in the downstream interpretation of Ca^{2+} concentration.

Understanding calcium signaling in the guard cell is further complicated by the effect of CO_2 concentration on $[Ca^{2+}]_{cyt}$ oscillations (Fig. 18.39). High CO_2 is associated with a slow rate of $[Ca^{2+}]_{cyt}$ oscillation (measured at about one peak per 10 minutes), and this is linked to stomatal closure. However, low CO_2 concentration is associated with more rapid $[Ca^{2+}]_{cyt}$ oscillations (measured at about two peaks per 10 minutes), and this is associated with stomatal *opening*. Therefore, $[Ca^{2+}]_{cyt}$ oscillations appear able to induce stomata to open, to close, or to stay closed depending on the rate of oscillation and the upstream signal.

The induction of slow $[Ca^{2+}]_{cyt}$ oscillations by ABA or high CO_2 in *Arabidopsis* requires the *GROWTH CONTROLLED BY ABA2 (GCA2)* locus (Fig.18.39). Loss-of-function *gca2* mutants have reduced stomatal closure in response to both ABA and high CO_2, and this is associated with impaired regulation of $[Ca^{2+}]_{cyt}$ oscillations. In contrast, the HT1 protein kinase functions in CO_2 signal transduction but not in ABA signaling. Stomata of loss-of-function *ht1* mutants close in both high and low CO_2 but are still responsive to ABA. This indicates HT1 acts as a negative regulator of CO_2-induced stomatal closure. The mechanism by which plant cells perceive CO_2 concentration has yet to be discovered.

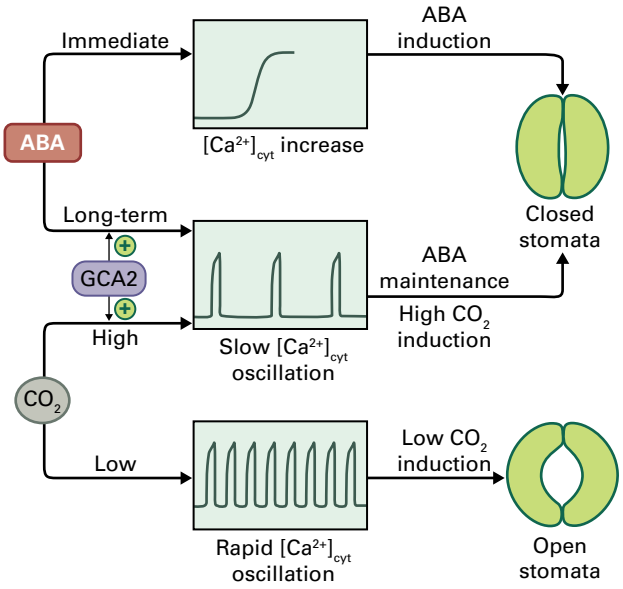


FIGURE 18.39 *Effects of ABA and CO_2 on Ca^{2+} concentration in the guard cell cytosol, $[Ca^{2+}]_{cyt}$. ABA induces an immediate rise in $[Ca^{2+}]_{cyt}$ which is associated with ABA-induced stomatal closure. ABA also induces a long-term pattern of slow $[Ca^{2+}]_{cyt}$ oscillations, which are required for ABA maintenance of stomatal closure. Slow $[Ca^{2+}]_{cyt}$ oscillations are also induced by high CO_2 and are associated with high CO_2-induced stomatal closure. In contrast, low CO_2 causes rapid $[Ca^{2+}]_{cyt}$ oscillations, and these are associated with low CO_2-induced stomatal opening. GCA2 is required for ABA and high CO_2 to induce slow $[Ca^{2+}]_{cyt}$ oscillations.*

Finally, blue light absorption by phototropin in *Arabidopsis* and tobacco seedlings causes a transient increase in $[Ca^{2+}]_{cyt}$, and inhibition of calcium signaling in guard cells by calmodulin antagonists (see Section 18.3.1) inhibits blue-light-induced proton pumping and stomatal opening. Therefore, it is possible $[Ca^{2+}]_{cyt}$ also induces stomata to open in response to blue light.

For calcium signaling to lead to either an increase or a decrease in guard cell turgor, individual ion channels must display different responses to different patterns of $[Ca^{2+}]_{cyt}$ changes. To help explain how this could be achieved, it has been proposed that the Ca^{2+}-sensitivity of key signal transduction components may be regulated according to prior signaling patterns in the guard cell. In support of this idea, activation of plasma membrane anion efflux channels in guard cell protoplasts by elevated $[Ca^{2+}]_{cyt}$ requires pre-exposure of the protoplasts to a high external Ca^{2+} concentration.

18.10 Prospects

In recent years there have been several successes in the hunt for core mechanisms by which plant cells perceive and transduce individual signals. This work will continue, not least because new intercellular signaling molecules continue to be discovered. Alongside research on individual transduction pathways, however, knowledge of signaling mechanisms in plant cells has become sufficiently sophisticated to allow development of models that describe interactions between signaling pathways and also the modulation of signaling networks over time.

As increasing numbers of signaling components and interactions between them are taken into consideration, the systems being described will become too complex for intuitive understanding. At that stage, investigating the properties of a signaling system will require formal modeling accompanied by computer simulation. This has already begun in a few cases. Computer simulation allows models to be tested by comparing the behavior of the theoretical system with its real life counterpart. Models that faithfully reproduce the behavior of the living system can then be subjected to novel constraints or perturbations to develop hypotheses and suggest experiments.

Most recent advances in our understanding of signal transduction in plants have come from model species such as *Arabidopsis thaliana*. The application of this knowledge to less laboratory friendly but more agriculturally significant species may have practical benefits, for example in areas such as drought tolerance. Increasing the number of species studied also allows evolutionary insights into signaling mechanisms. This has already been achieved with respect to the evolution of some individual signaling components; for example, revealing different domain structures and signaling mechanisms of phytochromes in plants, bacteria and fungi and also showing patterns of evolution of the phytochrome family within plants. Comparisons between taxa can also reveal differences in signaling interactions, for example the stepwise evolution of the GID1/DELLA interaction and of DELLA-mediated growth suppression in land plants (see Section 18.8.4). As research into signal transduction networks progresses, it should be possible to extend results such as these to encompass the evolution of larger signaling systems and also to map more accurately the timing of signaling innovations during plant evolution.

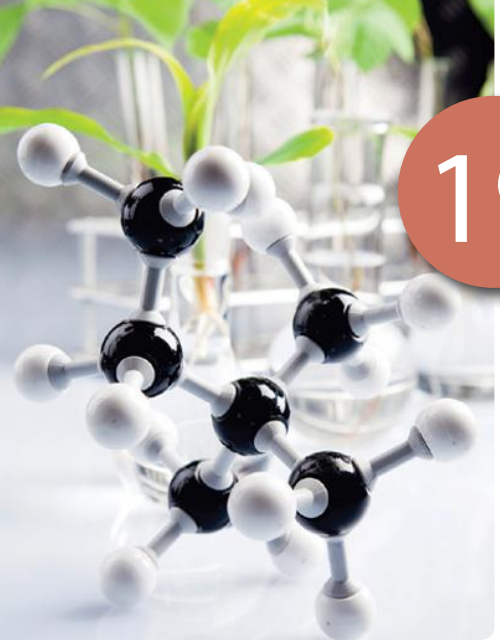
Summary

Plant development, physiology, and defense are flexible processes regulated by numerous internal and external cues. At the cellular level, detection of physical and chemical signals by receptor proteins initiates intracellular transduction pathways that control cell behavior. In addition, transduction pathways initiated by separate signals and perceived by distinct receptors interact to form a signaling network that integrates the

acquired information. Above the cellular level, short- and long-range intercellular signaling coordinates the activity of tissues, organs, and the plant as a whole. Cellular and intercellular aspects of signaling are tightly coupled, feeding back on each other as cells regulate the synthesis of hormones and other intercellular signals in accordance with the signals they receive.

Recent years have seen rapid advances in our understanding of intracellular signal transduction in plants, with mechanisms of perception, transduction, and response identified for several signals. Of particular interest is the widespread role of the regulation of protein degradation: for example, as mediated by phytochromes and by the auxin and GA receptors, and also functioning in the modulation of ethylene signaling. Given that over 5% of the *Arabidopsis* genome encodes proteins with homology to known mediators of ubiquitination-dependent proteolysis, it is probable that targeted protein degradation acts in many other signal transduction pathways. By a similar argument, it is likely that the more than 600 RLKs encoded by the *Arabidopsis* genome have a major, although currently poorly understood, role in signal perception.

There has also been progress in understanding the mechanisms by which responses to different signals are integrated, for example via the network of MAPK cascades, during the integration of GA and light signals, or in the regulation of stomatal aperture. Fewer details, however, are available on how signal integration is achieved without the loss of signal specificity, the ability of a particular signal to induce a particular response. Perhaps the most famous example of this is the convergence of signaling mechanisms on the regulation of cytosolic Ca^{2+} concentration. Here it is thought specificity may emerge from the temporal and spatial patterns of Ca^{2+} concentration (see Sections 18.3.1 and 18.9.4). The twin problems of explaining signal integration and signal specificity are likely to become increasingly important as models of intracellular signaling networks grow more complex.



19

Molecular Regulation of Reproductive Development

Ueli Grossniklaus

Introduction

Flower and seed formation represents an important phase in the life cycle of plants (Fig. 19.1). Flowers contain the reproductive organs producing the gametes that are central to sexual propagation, which culminates in the formation of seeds. A strict control of flowering time ensures the formation of as many seeds as possible, which is critical for the competitive advantage of a plant in its natural habitat, as well as in an agricultural setting. The importance of plant reproduction is demonstrated by the agricultural importance of fruit and seed crops, with cereals contributing as much as 80–90% of the world's calorie supply.

This chapter describes how the plant integrates external and internal signals to decide when to flower. It also explains how flower morphogenesis is controlled, how gametes are formed in the reproductive floral organs, and how the gametes unite to form the next generation, the developing embryo. While other plant species are considered, this chapter focuses on genetic studies in the model species *Arabidopsis thaliana*, through which much of the molecular basis of plant reproductive development has been unravelled.

19.1 The transition from vegetative to reproductive development

19.1.1 The first step in sexual plant reproduction is the decision to flower

The decision to flower marks the transition from vegetative to reproductive growth and is a key decision in the life cycle of plants. While growing vegetatively, the shoot apical meristem produces leaves with axillary meristems, which can form indeterminate secondary shoots. During the transition to flowering, the apical meristem is reprogrammed to an inflorescence meristem, which produces floral meristems on its flanks. The floral meristems, in turn, produce floral organs that form a single flower and are, therefore, determinate because they form a defined number of organs. This shift in meristem identity represents a major developmental change.

Precise timing of the decision to flower is crucial to guarantee reproductive success. It not only ensures that conditions

Biochemistry & Molecular Biology of Plants, Second Edition. Edited by Bob B. Buchanan, Wilhelm Gruissem, and Russell L. Jones.
© 2015 John Wiley & Sons, Ltd. Published 2015 by John Wiley & Sons, Ltd.
Companion website: www.wiley.com/go/buchanan/biochem

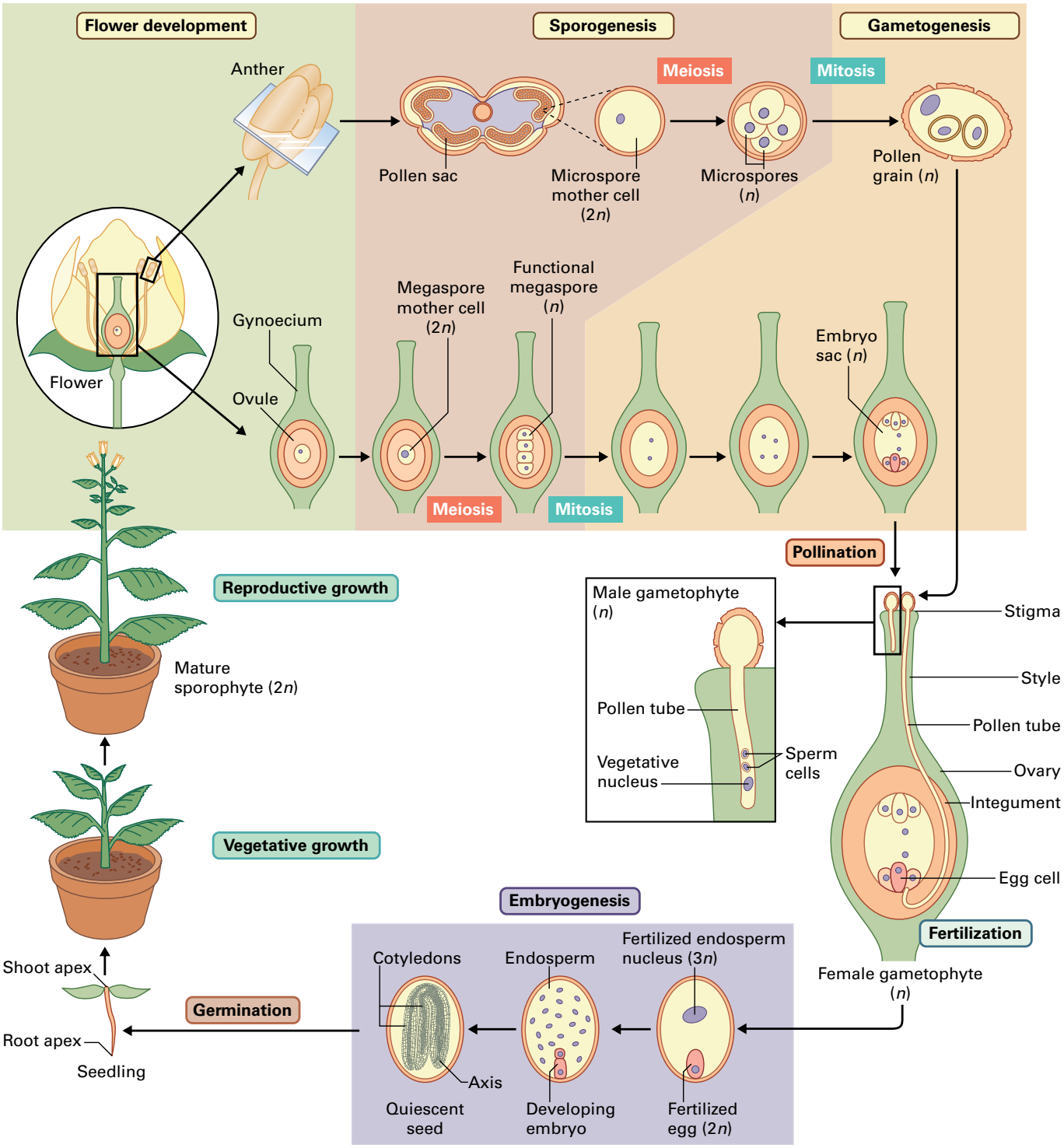


FIGURE 19.1 *The life cycle of a flowering plant, which involves the alternation of haploid (gametophytic) and diploid (sporophytic) generations. The haploid meiotic products produced in anthers (microspores) and ovules (megaspores) undergo several division cycles to form multicellular gametophytes, the pollen grain (male gametophyte) and embryo sac (female gametophyte), respectively.*

are favorable for reproduction, it also optimizes the availability of mating partners. A good example of this is the synchronous flowering of some cactus species, which open their flowers only for a few hours in a short time window. Synchronous flowering both enhances the chance for cross-pollination and reduces the proportion of seeds lost to predators. Moreover, the manipulation of flowering time through breeding has expanded the cultivation range and yield of many crops. For example, winter varieties of wheat (*Triticum aestivum*) and canola (*Brassica napus*) are sown in autumn and then overwinter in the vegetative phase. The extended vegetative growth period leads to yields that,



FIGURE 19.2 *Winter and spring varieties of crop plants. The same variety of wheat either sown in autumn (left) or spring (right) illustrates the advantage of an extended vegetative growth period.*
Source: http://www.islandgrains.com/whats-the-difference-between-spring-wheat-and-winter-wheat/.

depending on crop and cultivar, can be 50–100% higher than those of varieties sown in spring (Fig. 19.2). It is not surprising, then, that the timing of the decision to flower is under several levels of control.

19.1.2 Induction of flowering integrates external and internal cues

Before a plant starts to flower, it must accumulate enough resources to sustain seed development, and it must ensure that the environmental conditions are favorable for reproductive success. The plant must first generate enough leaves to produce sufficient photosynthate to support seed formation, which requires a significant amount of metabolic resources. In addition, flowering should be optimized with respect to environmental conditions, such as light, temperature, and the availability of water. Thus, plants must integrate environmental cues with internal conditions, and this requires complex gene regulatory networks.

Indeed, a large number of mutants have been identified that alter flowering time in *Arabidopsis*, and the physiological, genetic, and molecular analyses of these mutants have shown that flowering time is influenced by day length (**photoperiod**), light quality, ambient temperature, exposure to long periods of cold (**vernalization**), as well as developmental and hormonal signals. For example, studies with *Arabidopsis* mutants and natural varieties (accessions) uncovered the roles of both photoperiod and vernalization in the control of flowering time. Plants exposed to long days (16 hours of light) rather than short days (8 hours of light) flower much earlier, and mutations that disrupt the response to photoperiod cause plants to flower late under long days, but they have no effect under short days (Fig. 19.3). Some *Arabidopsis* accessions flower early if they are vernalized. This is particularly true for accessions that grow farther north (at higher latitudes), while accessions from more southern regions do not require vernalization, indicating that this is an adaptation to cold climates. However, *Arabidopsis* plants eventually flower even under short days and without vernalization, a response that requires the genes of the autonomous pathway. Plants with mutations affecting this branch of regulation flower later under both long and short days but respond to vernalization (Fig. 19.3). Finally, flowering time in *Arabidopsis* is also controlled by ambient temperature and the phytohormone gibberellin, which promotes flowering, particularly under short day conditions.

Together, genetic analyses in *Arabidopsis* have identified five distinct but interconnected pathways that regulate flowering time: the photoperiod, vernalization, autonomous, thermosensory, and gibberellin pathways.

19.1.3 Photoperiod is an important regulator of floral induction

At moderate to high latitudes, photoperiod is a reliable indicator of the season, so it is not surprising that most plants use day length as a cue for flowering. At the beginning of the 20th century, scientists found that certain varieties of tobacco (*Nicotiana tabacum*) flower during the short days in the southern United States but fail to flower in the longer days farther north. In contrast, ryegrass (*Lolium perenne*) only flowers under long days. Similar experiments showed that photoperiod regulates flowering time in a wide variety of plants, and three major behaviors in response to day length (photoperiodism) could be distinguished (Fig. 19.4).

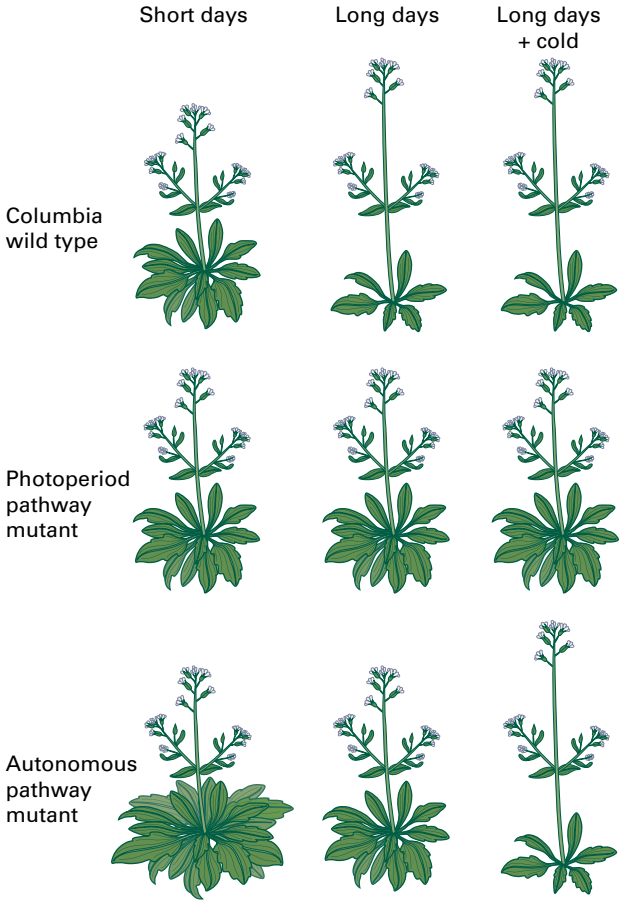


FIGURE 19.3 *Response of* Arabidopsis *plants to environmental conditions. Columbia wild-type plants flower late under short days and early under long days, a response not affected by vernalization. Plants with mutations affecting the photoperiod pathway are indistinguishable from the wild type under short day conditions, but flower late under long days, irrespective of vernalization. In contrast, plants with mutations affecting the autonomous pathway flower later than the wild type under both short and long days but this phenotype is overcome by vernalization.*

Long-day plants, such as clover (*Trifolium pratense*) and oat (*Avena sativa*) are induced to flower after exposure to long days and short nights, and the opposite is true for **short-day plants**, for example, coffee (*Coffea arabica*) and hemp (*Cannabis sativa*), which flower under short days and long nights. **Day-neutral plants**, such as tomato (*Solanum lycopersicum*) and cucumber (*Cucumis sativus*), flower regardless of the photoperiod. As mentioned above, many species, including *Arabidopsis* and snapdragon (*Antirrhinum majus*), eventually flower even under noninductive photoperiods (facultative long- and short-day plants), whereas others, such as clover, have an absolute photoperiod requirement (obligate long- and short-day plants). Finally, some plants have a complex requirement for a specific combination of long and short days to induce flowering.

In most cases, plants measure the duration of the night (dark) rather than the day (light). This was demonstrated by breaking the night with a short period of light. In cocklebur (*Xanthium strumarium*), a short-day plant, breaking the dark period for as little as 5 minutes with light is enough to prevent flowering. Most long-day plants are less sensitive to a break in the dark period, but many will flower under short days with a light period of 30–60 minutes during the night (Fig. 19.4). In addition to photoperiod, flowering time is also modulated by the quality of light.

19.1.4 Phytochromes and cryptochromes detect photoperiod

Plants have a variety of photoreceptors, and two types, phytochromes (red light receptors) and cryptochromes (blue light receptors), are required for photoperiodism. The *Arabidopsis* genome encodes five phytochromes (PHYA to PHYE), whose functions are distinct but also overlap. Phytochromes absorb red and far-red light and control various developmental processes, including germination, internode elongation, shade avoidance, entrainment of the plant's circadian clock, and flowering (see Chapter 18). *Arabidopsis* has two cryptochromes (CRY1and CRY2) that, besides being involved in floral induction, also play a role in the entrainment of the circadian clock and phototropism.

The discovery that floral induction in short-day plants could be prevented by a short disruption of the dark period with light allowed an investigation into the wavelengths of light that are perceived by the plant. Disruption with red light blocked the transition to flowering, but this effect could be reversed by following exposure to red light with exposure to far-red light. This reversible behavior implied an involvement of phytochromes in the control of flowering time. Indeed, *Arabidopsis phyA* mutants flower somewhat later than the wild type and do not respond to disruption of the dark period. The situation, however, is complex: While *PHYA* seems to promote flowering, *PHYB* delays it, as evidenced by the early flowering phenotype of *phyB* mutants, and other phytochromes also contribute to the repression of flowering. Cryptochromes are also involved in photoperiodism: *Arabidopsis cry2* mutants flower later than the wild type under inductive long days. Thus, in *Arabidopsis* and its relatives, both *PHYA* and *CRY2* promote flowering, whereas in other plants this role is taken by *PHYA* alone; for example, mutants that lack *PHYA* in pea (*Pisum sativum*), a long-day plant, are insensitive to photoperiod and flower at the same time under long- and short-day conditions.

19.1.5 Mobile signals control floral induction

The discovery of photoperiodism opened the door to many experimental manipulations and the physiological dissection of the transition to flowering. Since floral induction leads to a reprogramming of the shoot apical meristem, an important

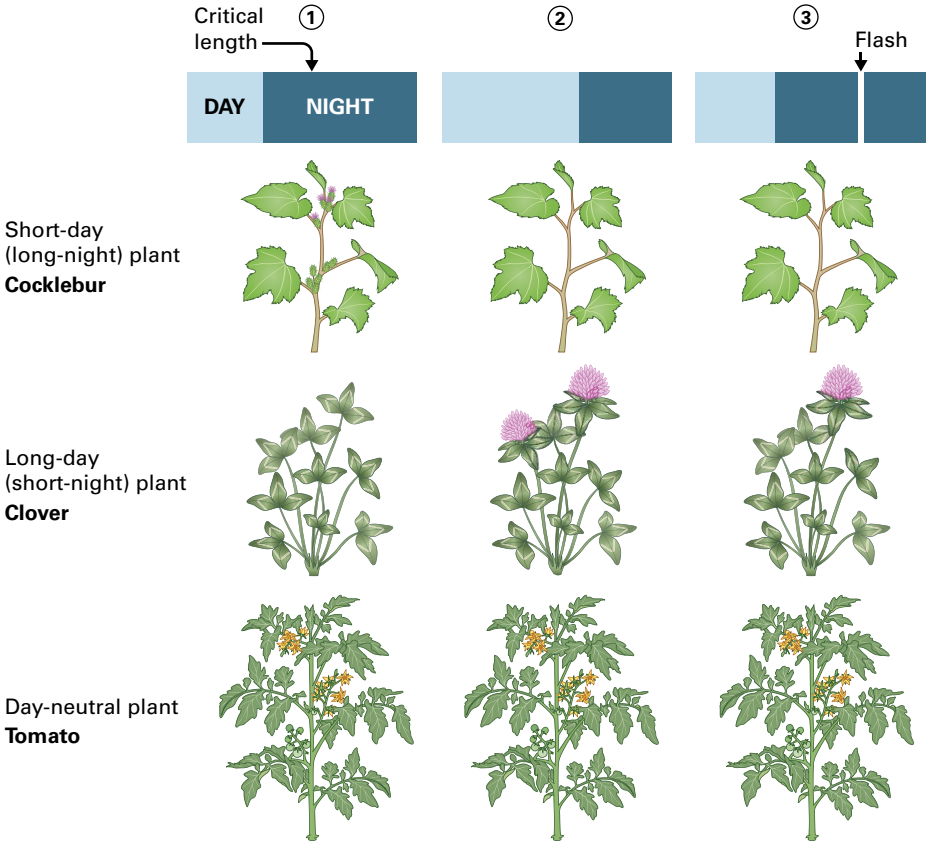


FIGURE 19.4 *Plant responses to different photoperiods (1–3). A short-day day plant requires a dark period of more than 12 hours, while a long-day plant requires one of less than 12 hours. A long-day plant can be induced to flower if the long night is interrupted by a light flash. A day-neutral plant flowers irrespective of photoperiod.*

question to address was whether day length is sensed directly in the shoot apex or in other parts of the plant. In experiments with spinach (*Spinacia oleraceae*), a short-day plant, exposure of only the leaves to the inductive photoperiod induced flowering, whereas exposure of the shoot apex to short days did not. These results indicated the photoperiod was measured in the leaves, but how does this lead to the reprogramming events in the shoot apex?

A series of grafting experiments addressed this question. Grafting a single leaf of a beefsteak plant (*Perilla crispa*) that was exposed to the inducing photoperiod onto an uninduced stock causes the plant to flower (Fig. 19.5). Thus, a mobile signal, referred to as **florigen**, is transported from the induced leaf to the uninduced shoot apex through the phloem. The same leaf can be sequentially grafted onto other vegetative rootstocks and induce flowering in six to seven plants. This suggests that, once induced, the leaf continuously produces the mobile signal that controls the flowering status of the plant.

The molecular identity of florigen was not unveiled for decades until molecular genetic experiments in *Arabidopsis* identified the protein encoded by *FLOWERING LOCUS T* (*FT*) as a major component of the mobile signal that induces flowering. FT contains a phosphatidylethanolamine-binding domain, which in mammals is involved in kinase signaling and appears to mediate protein–protein interactions. In *Arabidopsis*, FT is synthesized in the leaf upon floral induction and moves to the shoot apex (Fig. 19.6). There, it interacts with a bZIP transcription factor encoded by *FLOWERING LOCUS D* (*FD*) to regulate target genes that mediate the reprogramming of the meristem to produce flowers.

19.1.6 Photoperiod controls the activity of CONSTANS

To measure the length of the day, the plant must compare it with an internal standard. Many physiological processes follow a circadian rhythm, an oscillatory behavior with a period of approximately 1 day. This allows an organism to anticipate periodic changes in the environment and adjust its physiological activities accordingly. In plants, up to 60% of genes are regulated by the circadian clock, which influences many aspects of development, such as flower opening, leaf movements, stomatal opening, and many other processes, including the decision to flower.

It was proposed that flowering is induced when a rhythmic process under the control of the circadian clock is sensitive to light at a particular time of the day, in other words when exposure to light and this process coincide (**external coincidence model**). Indeed, many mutations in *Arabidopsis* affect the photoperiod pathway; they delay flowering under long but not under short days, and are interlinked with the circadian clock; they either affect its entrainment, are components of the clock itself, or are regulated by it. The last one is true for *CONSTANS* (*CO*), a key regulator of flowering whose mRNA

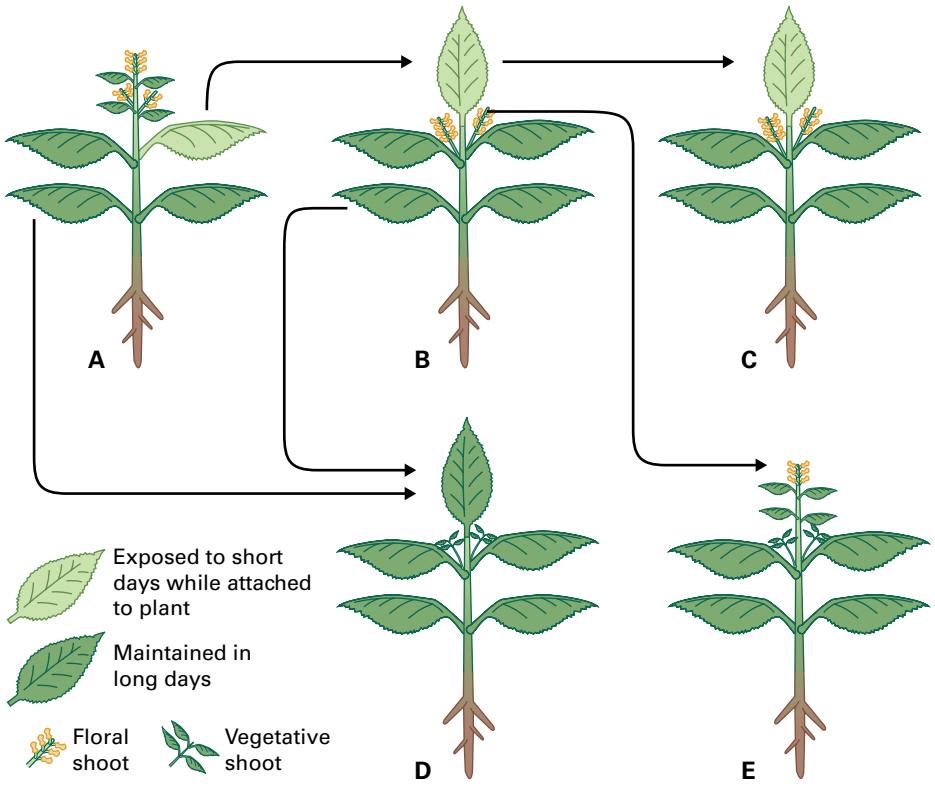


FIGURE 19.5 *Permanent photoinduction by leaves of the beafsteak plant (*Perilla crispa*). (A) Induction of a single leaf by short days (light green) can induce flowering. (B) If the same leaf is grafted onto a plant that was kept under noninductive conditions, it can induce flowering of that plant, indicating the production of a flower promoting, mobile signal in the induced leaf. (C) The grafting process can be repeated with the same effect, indicating the induction of the mobile signal is permanent. Grafting of (D) a noninduced leaf or (E) a flowering apex does not induce flowering of the host plant.*

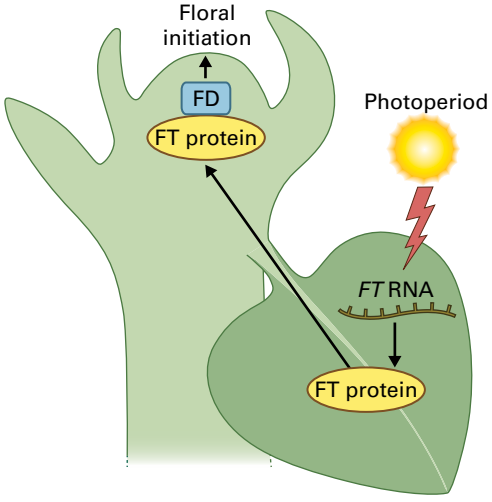


FIGURE 19.6 *FT protein is the florigen. FT is produced in the leaf under an inductive photoperiod. It is transported via the phloem to the shoot apex where it forms a heterodimer with FD to regulate target genes that control the reprogramming into an inflorescence meristem.*

starts to accumulate at dusk and reaches a maximum during the dark period under short days (Fig. 19.7).

CO transcription is not only under the control of the circadian clock, but is also regulated by a blue light-dependent complex involving GIGANTEA (GI) and the FLAVIN-BINDING, KELCH REPEAT, F-BOX1 (FKF1) protein, the last one mediating protein degradation. Accumulation of the GI-FKF1 complex in the late afternoon leads to degradation of CYCLING DOF FACTOR1 (CDF1), a repressor of *CO*, thereby activating *CO* expression at dusk. In the dark, however, CO protein is unstable and fails to accumulate. In contrast, under long days, *CO* mRNA reaches a peak at the end of the day and is translated in the light. Exposure to blue and far-red light, which promotes flowering in *Arabidopsis* via CRY2 and PHYA, stabilizes the CO protein, which thus accumulates under long days and activates its target gene *FT* (Fig. 19.7). *CO* expression and consequently the activation of *FT* occur in the companion cells of the phloem, through which the FT protein is subsequently transported to the shoot apex. As a consequence, *Arabidopsis* flowers only when *CO* transcription and translation coincide with exposure to light as it occurs under long days. The rhythmic accumulation of the CO protein and its sensitivity to light thus provide the molecular basis for the external coincidence model.

Orthologs of *CO* and *FT*, *Heading date 1* (*Hd1*) and *Heading date 3a* (*Hd3a*), also control flowering in rice (*Oryza sativa*), despite rice being a short-day plant. While *Hd1* regulates the expression of *Hd3a* in rice as do *CO* and *FT* in *Arabidopsis*, the molecular mechanisms differ. Hd1 acts as transcriptional repressor of *Hd3a* under long days, and as an

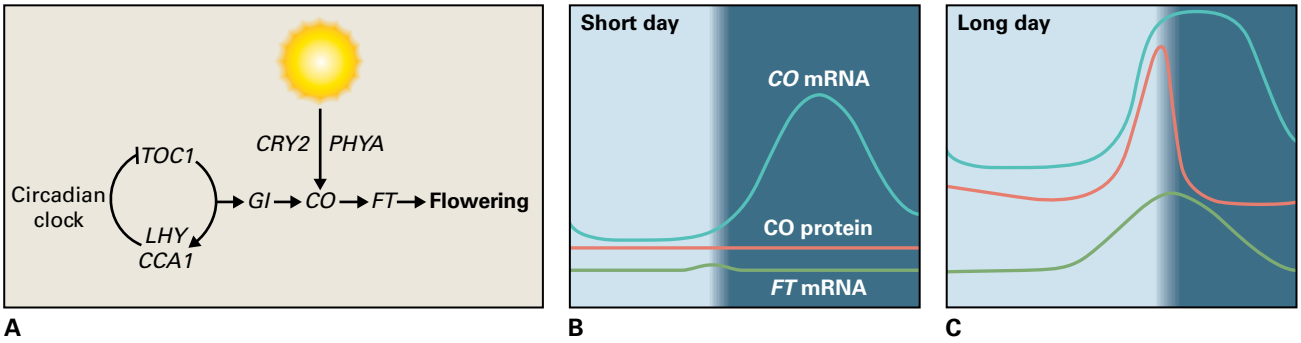


FIGURE 19.7 *CO is a central regulator of the photoperiod pathway. (A) CO is regulated through output of the circadian clock and the photoreceptors PHYA and CRY2. (B) Under short days, CO mRNA accumulates in the dark but the protein is degraded such that it does not accumulate to activate FT. (C) Under long days, CO mRNA accumulation occurs during the light and the CO protein is stabilized by the activity of the photoreceptors such that FT transcription is activated.*

activator of *Hd3a* under short days. Thus, *Hd3a*, the *FT* ortholog inducing flowering, is only produced under short days in rice.

19.1.7 The vernalization and autonomous pathways converge on the regulation of *FLOWERING LOCUS C*

Many plants growing at higher latitudes require vernalization, a 4- to 12-week exposure to cold that usually occurs during winter. Vernalization ensures that plants do not flower prematurely in late summer, when the photoperiod may be inductive for flowering but seed formation could be compromised by frost. However, even *Arabidopsis* accessions that require vernalization eventually flower in the absence of the cold treatment (flowering in these cases is promoted by the autonomous pathway), whereas other plants, such as some varieties of cabbage (*Brassica oleraceae*), have an absolute vernalization requirement (Fig. 19.8).

Once an annual plant undergoes vernalization, it "remembers" the cold treatment throughout its life (through many mitotic cell divisions). This is demonstrated in experiments with pennycress (*Thlaspi arvense*), where leaves can be removed after vernalization and used to regenerate plants in vitro. The regenerated plants show a flowering behavior as if they had been vernalized; their progeny, however, do not flower, indicating that the following generation requires vernalization. Thus, the memory of vernalization is maintained over many mitotic divisions, but not through meiosis.

Unlike photoperiod, which is detected in leaves, vernalization relies on events in the shoot apex. This can be shown by specifically treating the shoot apex or leaves of celery plants (*Apium graveolens*) with cold. Only when the shoot apex is subjected to cold does the plant show a typical vernalization response.

The genetic basis of vernalization was first dissected in *Arabidopsis* by crossing winter-annual accessions (germinate in autumn and require vernalization to flower in spring) with summer annual accessions (germinate in spring and flower in the same season without vernalization). The vernalization-requiring accessions had active alleles of the *FRIGIDA* (*FRI*) and *FLOWERING LOCUS C* (*FLC*) loci, whereas summer-annuals had inactive alleles of these genes. The *FLC* gene encodes a transcription factor of the MADS domain family (see Chapter 9), and its expression is regulated by FRI. Mutations in *FRI* cause reduced *FLC* expression and early flowering, as do mutations in other regulators of *FLC*, for instance *FRIGIDA LIKE1* (*FRL1*), *FRIGIDA ESSENTIAL1* (*FES1*), *SUPPRESSOR OF FRI4* (*SUF4*), and *FLC EXPRESSOR* (*FLX*). These regulatory proteins form a multisubunit activator complex that recruits the general transcription machinery and chromatin modification factors (see Section 19.1.8) to the *FLC* locus. *FLC* is a potent repressor of flowering: plants with high levels of *FLC* expression, for instance winter-annuals with active *FLC* and *FRI* alleles, flower late. Vernalization reduces *FLC* expression and thus results in earlier flowering (Fig. 19.9).

The response of *FLC* to cold exposure is gradual: the longer the cold treatment, the greater the reduction in *FLC* expression. This explains why vernalization is quantitative, with short exposures to cold promoting flowering less than long exposures. However, *FLC* is not only downregulated by vernalization, also the autonomous pathway affects *FLC* expression. With increasing age of the plant, *FLC* expression levels drop gradually, such that they eventually are low enough to allow flowering.

In conclusion, a range of external and internal signals converge on *FLC* and regulate its expression, which ultimately controls the transition to flowering.

19.1.8 *Arabidopsis* mutants allowed dissecting the molecular basis for the cellular memory of vernalization

The stable transmission of vernalization through mitotic divisions implies that a cellular memory mechanism allows cells to remember the exposure to cold. In fact, once *FLC* has been downregulated by vernalization, its expression level remains low even after the plant has been returned to a warm



FIGURE 19.8 *Vernalization requirements in cabbage. The plant on the left is a 5-year-old winter variety that has not been exposed to cold and thus never flowered. In contrast, the summer variety shown by the child flowers without vernalization.*
Source: R. Amasino, University of Wisconsin-Madison; previously unpublished.

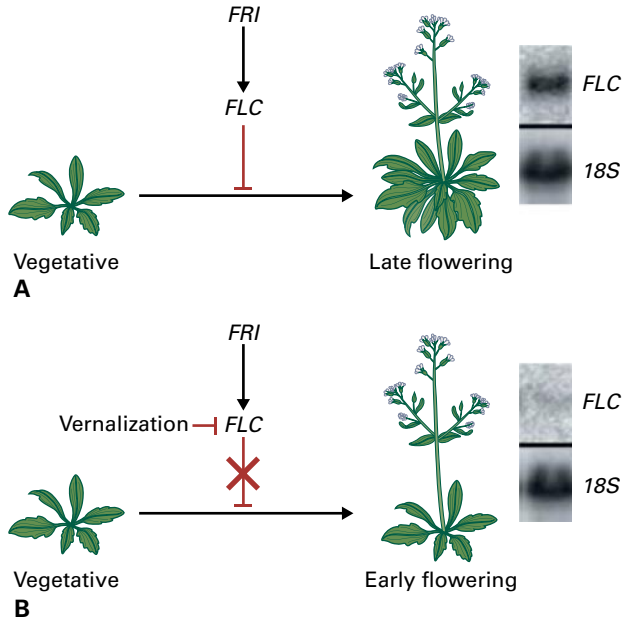


FIGURE 19.9 *FLC is repressed by vernalization. (A) FLC is a strong repressor of flowering that is activated by FRI and shows high expression in the absence of a cold treatment as shown in the Northern blot on the right. (B) Vernalization represses FLC (see Northern blot) so that the plant initiates flowering.*

temperature. Since the low expression state of *FLC* is maintained over many cell divisions even in the absence of the cold stimulus, this can be viewed as an epigenetic phenomenon.

Genetic screens for *Arabidopsis* mutants that flower late even after vernalization allowed the dissection of the molecular basis of this process. In one mutant, *vernalization insensitive3* (*vin3*), *FLC* expression is not reduced during vernalization, and this gene is required for initiating *FLC* repression during cold exposure. Indeed, expression of *VIN3* increases during the cold (i.e., it is vernalization induced), but it is insufficient to cause vernalization when overexpressed. Other mutants, including *vernalization2* (*vrn2*), do not affect downregulation of *FLC* itself but its maintenance, as *FLC* levels increase again after returning *vrn2* mutants to warm temperature. Thus, *VRN2* can be viewed as part of the cellular memory system.

The molecular characterization of these genes revealed that they affect histone modifications that lead to a silenced chromatin organization (see Chapter 9). *VIN3* encodes a plant homeodomain (PHD) domain, which is often found in proteins modifying chromatin. VRN2 is a homolog of *Drosophila* Suppressor of zeste 12, a component of the highly conserved ***Polycomb* repressive complex 2** (PRC2). The PRC2 complex is conserved between animals and plants and has histone H3 lysine 27 trimethylation (H3K27me3) activity that is mediated by homologs of the *Drosophila* histone methyltransferase Enhancer of zeste [E(Z)] (Box 19.1).

19.1.9 Integration of signals controls expression of meristem identity genes

In addition to the photoperiod, vernalization, and autonomous pathways, ambient temperature and gibberellins also control flowering. Ultimately, all these activities lead to a reprogramming of the vegetative apical meristem to an **inflorescence meristem**.

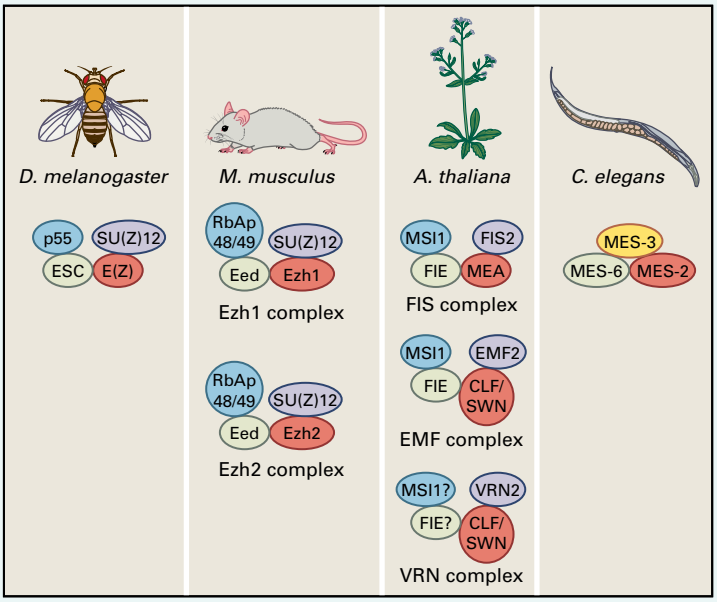
For this to occur, all the activities of the different flowering pathways must be integrated in the shoot apex. This is achieved by regulation of floral integrator genes, which are targets of multiple floral pathways. For instance, *FT* is

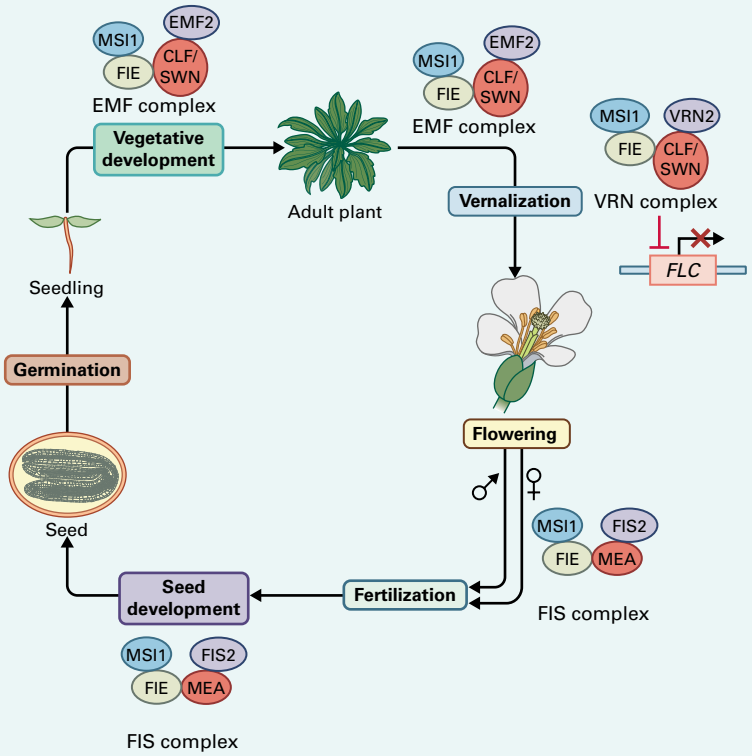
BOX 19.1

Polycomb complexes occur in both plants and animals

PRC2 complexes are highly conserved during evolution and are found in vertebrates, invertebrates, and plants. They consist of four conserved core subunits and some variably associated proteins. PRC2 maintains target genes in a repressed state through its histone methyltransferase activity, which is mediated by *Drosophila* E(Z) and its homologs. In plants, there are three E(Z) homologs, CURLY LEAF (CLF), MEDEA (MEA), and SWINGER (SWN), and at least three different PRC2 complexes have been identified through their function in distinct developmental processes.

For instance during vernalization, the VRN-PRC2 complex containing the core subunits VRN2, FERTILIZATION INDEPENDENT ENDOSPERM (FIE), MULTISUPPRESSOR OF IRA1 (MSI1), and the histone methyltransferases CLF or SWN place H3K27me3 marks on the *FLC* locus, thereby silencing its expression (see below). A dimer of the two PHD domain proteins VRN5 and VIN3, the latter being induced by cold, enhances VRN-PRC2 activity and stably represses the *FLC* locus. At some point during the reproductive cycle, however, the repressive H3K27me3 histone marks have to be erased, as the progeny of a vernalized plant does not flower early. This erasure occurs during early embryogenesis, but the molecular mechanisms involved are currently not well understood.





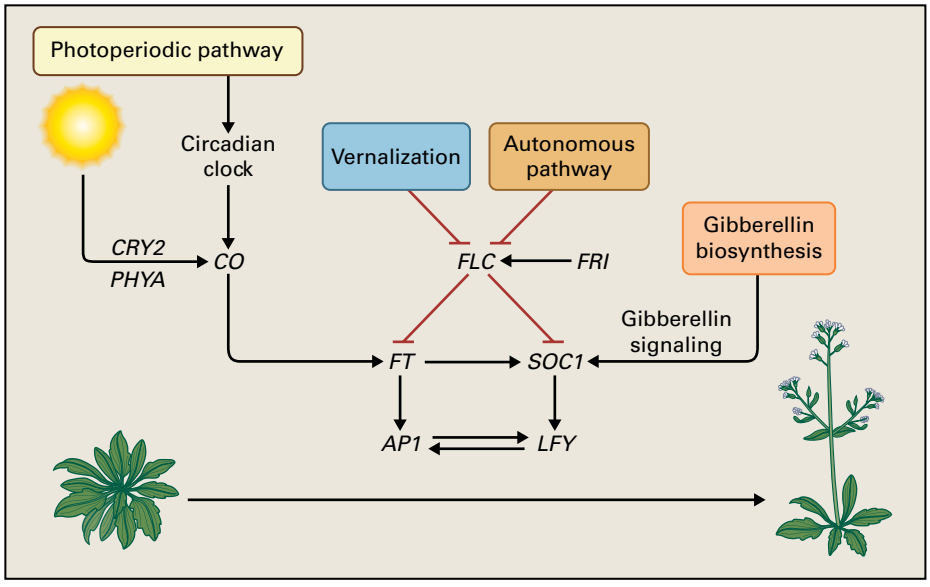


FIGURE 19.10 *Integration of the various flowering pathways. The transition from vegetative to reproductive growth is controlled by four major pathways whose activities are integrated through the regulation of FT and SOC1 that, in turn, activate the meristem identity genes AP1 and LFY.*

activated by CO, but at the same time, it is repressed by FLC and regulators of the thermosensory pathway. Similarly, the MADS box gene *SUPPRESSOR OF OVEREXPRESSION OF CONSTANS1* (*SOC1*) is repressed by FLC but activated by FT and the gibberellin pathway (Fig. 19.10). In this way, information from the different pathways is integrated and leads to the reprogramming of the shoot meristem through the activation of specific genes in the apex, including *LEAFY* (*LFY*) and *APETALA1* (*AP1*). Both these genes are activated by FT and SOC1 and ultimately confer floral identity to the primordia produced by the meristem. They encode transcription factors of the MADS domain and LFY-FLO family, respectively, and mutations in them cause partial transformation of flowers to shoots.

19.2 The molecular basis of flower development

The development of flowers is one of the most intensively studied developmental processes. Although work in various plants, including snapdragon (*A. majus*), rice (*O. sativa*), tobacco (*N. tabacum*), and petunia (*Petunia hybrida*), has contributed to our understanding of the molecular genetic basis of flower development, most of the molecular work has been performed using *Arabidopsis*.

19.2.1 Inflorescence architecture is determined by *LEAFY*

Once the vegetative meristem has been reprogrammed into an inflorescence meristem, it produces new meristems that give rise to either secondary inflorescences or flowers (Fig. 19.11). An inflorescence is indeterminate if it continues to produce flowers throughout the life of the plant; it is determinate if the apical meristem produces a certain number of flowers and then converts into a floral meristem itself, thereby terminating the inflorescence. In its extreme form, as in tulips (*Tulipa gesneriana*) and many other Liliaceae, the reproductive meristem produces only a single, terminal flower.

The identity of the floral meristem is determined by the function of two closely related genes that encode the AP1 and CAULIFLOWER (CAL) transcription factors. Whereas *ap1* mutants have phenotypes that reveal aspects of the gene's function as both a meristem and floral organ identity gene, *cal* single mutants look like the wild type. In an *ap1 cal* double mutant, however, the function of both genes in determining floral meristem identity is dramatically revealed: instead of producing floral meristems, the apical meristem of the double mutant produces inflorescence meristems, which in turn produce inflorescence meristems again, giving rise to a mass of inflorescence meristems, but no flowers (Fig. 19.12). Such apices look like tiny cauliflowers and, indeed, cauliflower and romanesco broccoli are two of the cultivated forms of *B. oleracaea* that have a similar phenotype.

Whether a primordium produces a flower depends on the action of another transcription factor, LFY, which is encoded by a highly conserved gene that controls floral meristem identity in angiosperms and possibly also in gymnosperms (expression of *LFY* homologs is induced in their reproductive cones). In an *lfy* mutant, the cells that should produce a flower meristem instead form a shoot that produces leaves. Conversely, constitutive overexpression of *LFY* transforms the apical meristem into a floral meristem after the transition to flowering, resulting in the formation of a single, terminal flower. A similar phenotype is observed in *terminal flower1* (*tfl1*) mutants. In this mutant, *LFY* is expressed in the inflorescence meristem, causing its conversion into a floral meristem. LFY controls the expression of

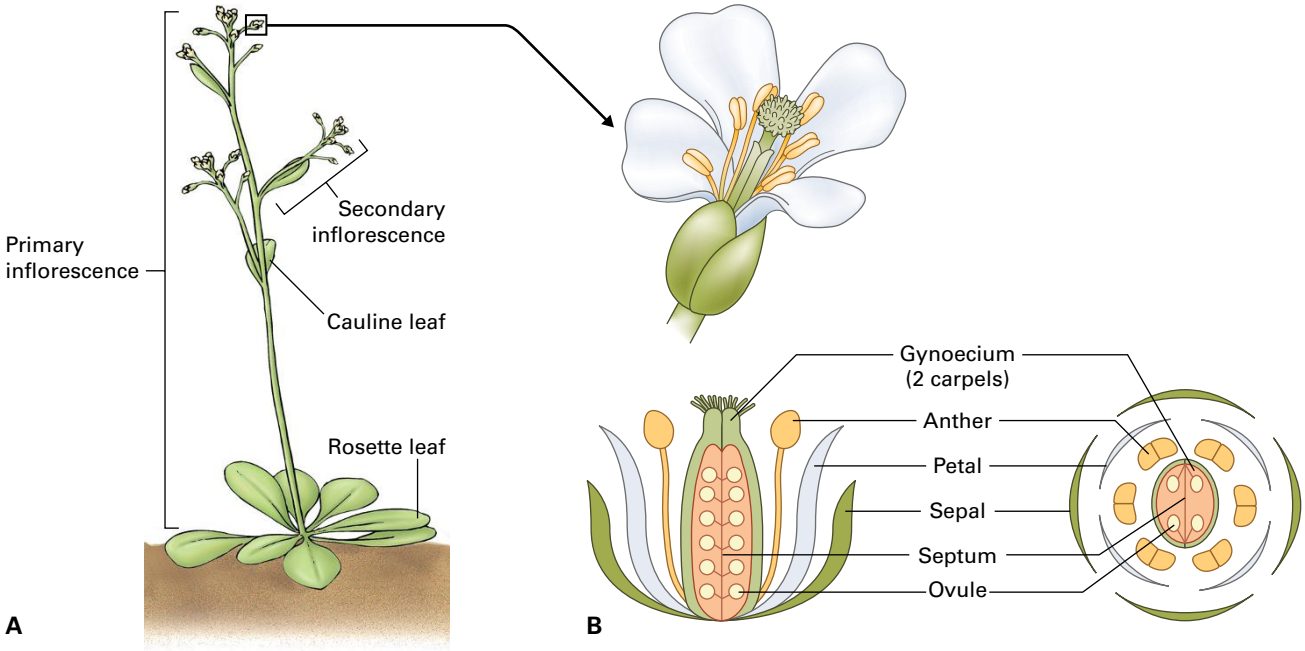


FIGURE 19.11 *Diagram of an* Arabidopsis *plant and flower. (A) Before flowering, the vegetative meristem produces rosette leaves. After floral induction, the primary inflorescence meristem produces cauline leaves with secondary inflorescences emerging from their axils, and flowers. (B) Schematic representation of flower with longitudinal and transverse sections. The first and second whorls produce sterile floral organs, the sepals and petals. The third and forth whorls produce reproductive organs, the stamens and carpels.*



FIGURE 19.12 *Meristem identity genes control inflorescence development. (A) shows an* Arabidopsis *wild-type inflorescence, while two redundant floral meristem identity genes are mutated, both in the ap1 cal double mutant of* Arabidopsis *(B) and in cauliflower (C). Source*: A. Bolanos, S. Hofstetter and H.P. Schöb, University of Zurich; previously unpublished.

regulatory genes that are required for flower formation, including *AP1* and *CAL*, and it is expressed very early in the cells that form a floral meristem. The regulatory interactions, however, are complex, and *LFY* itself is activated through the redundant function of AP1, CAL, and FRUITFUL (FUL), resulting in a positive feedback loop.

In an indeterminate wild-type inflorescence meristem, *LFY* is only expressed in the cells that will form a floral meristem but not in the apex, where it is normally repressed by TFL1 (Fig. 19.13). This explains why mutations disrupting *TFL1* or the constitutive expression of *LFY* both lead to the formation of terminal flowers. A change in expression of *LFY* and/or *TFL1* may give rise to a variety of inflorescence architectures by altering the determinacy of inflorescence meristems.

19.2.2 Diverse floral morphologies have a common body plan

There is tremendous diversity of floral morphologies, and the abrupt appearance and rapid diversification of flowering plants in the mid-Cretaceous led to Charles Darwin's metaphor of the "abominable mystery." This enormous and beautiful diversity, however, is solely based on variations of a common theme: all flowers, as diverse as they may appear, have a common body plan and develop in very similar ways.

All plants have the same arrangement of floral organs, namely (from outside to inside) sepals, petals, stamens, and carpels, and all arranged in concentric whorls, starting at the periphery of the floral meristem and moving towards its

center (see Figs. 19.11 and 19.14). Once a group of cells is determined to form a floral meristem, floral organs are sequentially formed. In *Arabidopsis*, four **sepals** are formed in the outermost whorl (whorl 1), followed by four **petals** in whorl 2. Sepals and petals are sterile organs and together make up the **perianth**, which is often specifically shaped and colored to attract pollinators and protects the reproductive organs in the center of the flower. In *Arabidopsis*, the reproductive organs are represented by the six **stamens**, which develop in whorl 3, and the two **carpels** that originate from the innermost whorl (whorl 4) and fuse to form the **gynoecium**, which harbors the ovules (see Fig. 19.11). As the floral meristem produces a more or less defined number of organs in the four whorls and the production of new cells stops thereafter, it is a determinate meristem. Consistent with this, the *WUSCHEL* (*WUS*) gene, which is required for stem cell maintenance in meristems, becomes repressed in the floral meristem once the primordia of the reproductive organs are formed.

Flowers can also lack organs, however, or the organs may be modified to look more like another organ of the flower. For instance, in many members of the Liliaceae, the sepals are colorful and petal-like, so the organs of the perianth look alike and are often referred to as tepals (Fig. 19.15). Even in grasses, which do have unusual flowers, the typical arrangement of the floral organs can still be seen. The **lodicules** occupy the position of the petals, whereas two dimorphic organs, the **palea** and **lemma**, can be viewed as the equivalents of sepals (Fig. 19.15).

This extraordinary conservation of the floral body plan suggests that the underlying molecular mechanisms are also shared. Accordingly, the genes controlling floral organ identity are highly conserved, and differences in their regulation can explain the morphological variety seen in flowers.

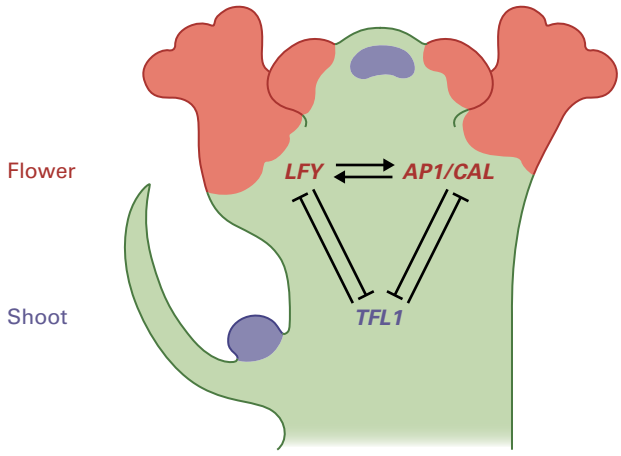


FIGURE 19.13 *Regulatory interactions between genes conferring identity to inflorescence and floral meristems. LFY and AP1/CAL are expressed in floral meristems and positively regulate each other. TFL1 is expressed in the apex of the inflorescence meristem and engages in negative regulatory interactions with the floral meristem identity genes LFY and AP1/CAL, preventing the termination of the shoot apex in a flower.*

19.2.3 The ABC model determines organ identity

The genes controlling floral organ identity were identified through studies of homeotic mutations, which transform one organ into another and are, thus, involved in determining the identity of these organs. A well-known homeotic mutation, which has attracted the attention of horticulturists, leads to the replacement of the reproductive organs by perianth organs, thereby forming a filled or double flower (Fig. 19.16). The first such double flower mutant of *Arabidopsis* was described in 1873, and consistent with the highly conserved organization of flowers, mutations with similar phenotypes in *Arabidopsis* and snapdragon affect homologous genes.

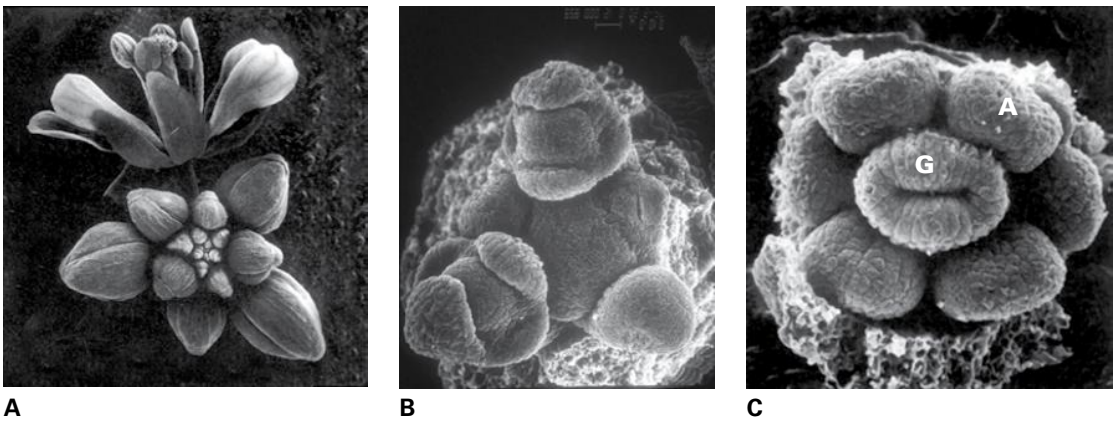


FIGURE 19.14 *Flower development in* Arabidopsis *as seen by scanning electron microscopy. (A) Top view of a primary inflorescence showing the spiral arrangement of the floral buds. (B) Higher magnification of the shoot apex showing the spiral initiation pattern of floral meristems. In contrast, the floral meristems initiate the primordia of floral organs (here sepals) in centric whorls. (C) A close-up of a flower meristem at a later stage. Sepal and petal primordia have been removed to reveal the concentric primordia of stamens and two carpels that have fused to form a gynoecium. A, anther; G, gynoecium.*
Source: (A, C) Smyth et al. (1990). Plant Cell 2:755–767. (B) J. Bowman, Monash University; previously unpublished.

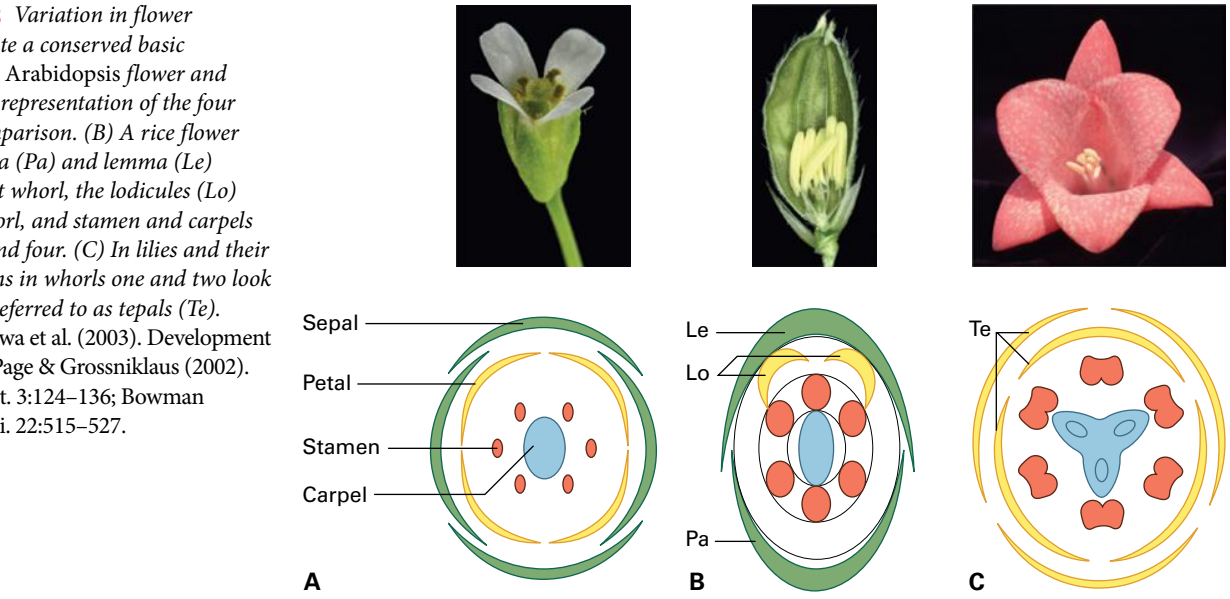


FIGURE 19.15 *Variation in flower structure despite a conserved basic body plan. (A)* Arabidopsis *flower and diagrammatic representation of the four whorls for comparison. (B) A rice flower where the palea (Pa) and lemma (Le) occupy the first whorl, the lodicules (Lo) the second whorl, and stamen and carpels whorls three and four. (C) In lilies and their relatives, organs in whorls one and two look alike and are referred to as tepals (Te).* *Source*: Nagasawa et al. (2003). Development 130:705–718; Page & Grossniklaus (2002). Nat. Rev. Genet. 3:124–136; Bowman (1997). J. Biosci. 22:515–527.

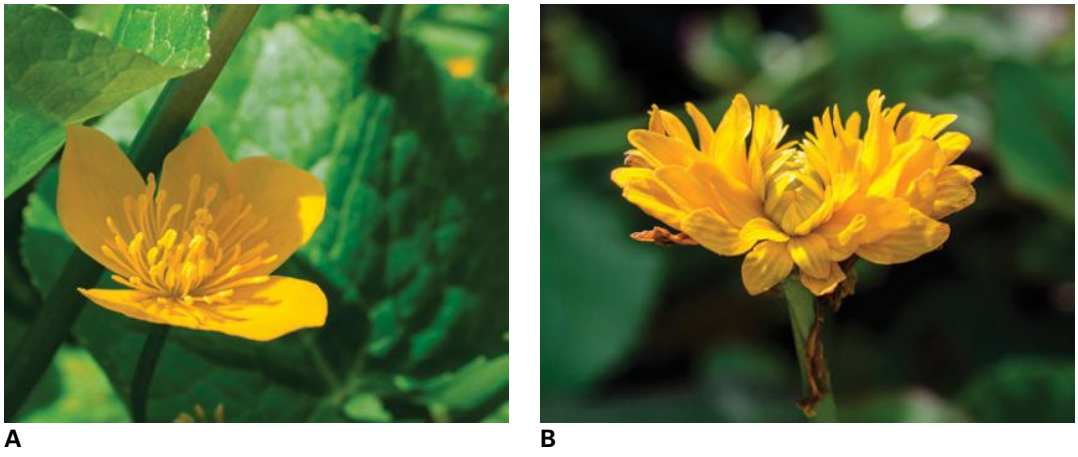


FIGURE 19.16 *Double flowers in the marsh marigold (*Caltha *spp.). The reproductive organs of whorls three and four in the wild-type flower (A) are replaced by sterile organs in this mutant (B), which has an agamous-like phenotype with indeterminate flowers.* *Source*: A. Hedhly, University of Zurich; previously unpublished.

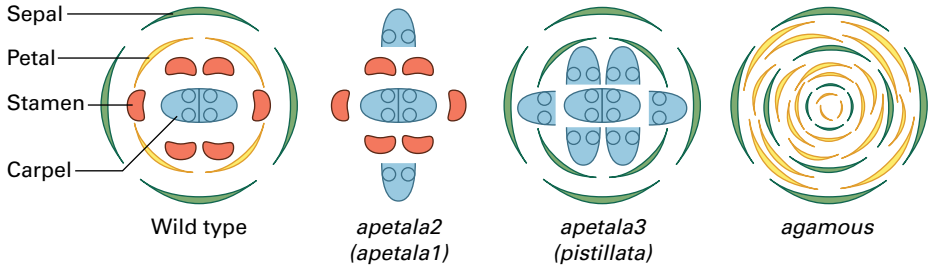


FIGURE 19.17 *The original ABC mutants. Each mutant shows homeotic transformations, that is the transformation of one organ into another. The B-class mutants ap3 and pi look identical, while the A-class mutant ap1 has a floral meristem identity phenotype in addition to the homeotic phenotype shown here for ap2. The C-class mutant ag affects floral meristem determinacy in addition to organ identity. The organs are color-coded: sepals, green; petals, yellow; stamens, red; carpels, blue.*

Homeotic mutants in *Arabidopsis* always affect two adjacent whorls. For instance, in *agamous* (*ag*), the mutation producing double flowers, the sepals in whorl 3 are replaced by petals, and the gynoecium in whorl 4 is replaced by another *ag* flower, so the pattern sepals–petals–petals is reiterated several times (Fig. 19.17). This phenotype shows that *AG* not only controls floral organ identity, but is also responsible for the determinate nature of the flower. In an *ag* mutant, *WUS* is not

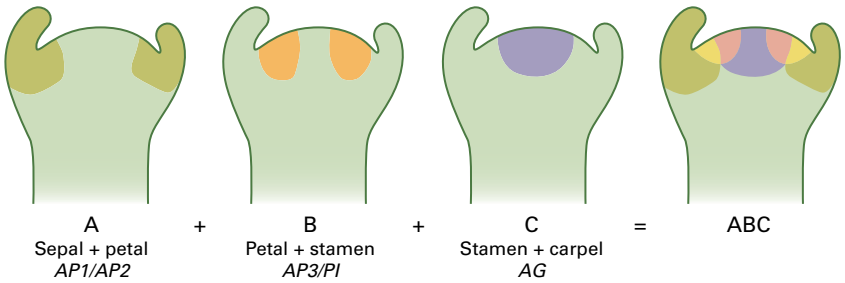


FIGURE 19.18 *ABC model for floral organ specification. Functional domains of the A- (dark green), B- (orange), and C-class (purple) genes encompass two whorls and their specific combinations specify organ identity in each of the four whorls.*

repressed after the initiation of floral primordia in the inner whorls, and thus the stem cell pool in the floral meristem is maintained and produces additional organs. Also the homeotic mutants *pistillata* (*pi*) and *apetala3* (*ap3*), which have identical phenotypes, affect two whorls: petals in whorl 2 are replaced by sepals, and stamens in whorl 3 by carpels. Finally, the two outermost whorls are affected in the homeotic mutants *ap1* and *apetala2* (*ap2*) (Fig. 19.17).

In addition to determining inflorescence meristem identity, *AP1* also plays a role in specifying floral organ identity. While the sepals in *ap1* mutants are converted to leaf-like organs that produce secondary and tertiary flowers in their axils, the petals are usually missing and occasionally replaced by stamens or mosaic organs. In *ap2* mutants, sepals in whorl 1 are converted to carpels and stamens replace the petals in whorl 2 (Fig. 19.17). In addition, *ap2* flowers have often fewer organs than wild-type flowers and sometimes all organs in whorl 2 are missing. This phenotype indicates that *AP2* not only determines the identity of floral organs, but also specifies the number of organ primordia that are formed.

Based on the organ identity phenotypes observed in these homeotic mutants, the original **ABC model** for flower development (Fig. 19.18) was formulated. In this model, the genes controlling floral organ identity are subdivided into three classes: A-class genes (*AP1*, *AP2*) are active in whorls 1 and 2, B-class genes (*PI*, *AP3*) in whorls 2 and 3, and C-class genes (*AG*) in whorls 3 and 4. The domains in which each class of homeotic genes is active partially overlap, such that each whorl has a unique combination of activities that determines the identity of the organs it usually forms. Class A alone determines sepal identity, classes A and B together specify petal identity, classes B and C confer stamen identity, while class C alone is needed to form carpels. Moreover, classes A and C act antagonistically, that is they repress each other's activity. Thus, if C class activity is missing in whorls 3 and 4, A-function extends into these whorls and vice versa.

This simple model for the combinatorial function of the A-, B-, and C-class genes can explain the observed phenotypes in single mutants and faithfully predicts those of double mutants (Fig. 19.19). For instance, if A-function is lost, then C-function extends into whorls 1 and 2, such that carpels are formed in whorls 1 and 4, which now only express the C-function gene *AG*, while stamens are formed in whorls 2 and 3, which express both C- and B-function. If both A- and B-function are removed, only the C-function is expressed in all four whorls, leading to the formation of a flower with carpels in all whorls. Using combinations of homeotic mutants and transgenic plants that overexpress a homeotic gene in all four whorls, any floral organ can be made in any position in a predictable way. For example, if an A-class mutant is combined with a transgene that leads to overexpression of the B-class genes throughout the flower meristem, flowers with only stamens develop, controlled by the combination of C- and B-class genes now present in all four whorls (Fig. 19.19).

Some phenotypes, however, cannot be predicted on the basis of the ABC model. A triple mutant that expresses neither A-, nor B-, nor C-class genes produces flowers that have leaf-like organs in all whorls, illustrating that floral organs are modified leaves. The ABC model also does not make predictions for the phenotype of a double mutant affecting A- and C-class genes, as B-class genes usually act in combination with either A- or C-class genes. It turns out that such mutants have leaf-like organs in whorl 1, which does not express any of the homeotic genes, and leaf-like organs with stamenoid characters in whorl 2, because it expresses B-class genes that are involved in stamen formation. This pattern is then reiterated as the flower meristem loses its determinacy in the C-class mutant *ag*.

Although subsequent molecular analyses have added layers of complexity to the original ABC model, the model has proven robust in predicting phenotypes of (multiple) mutants and transgenic lines and explaining the diversity of floral morphologies found in nature. For example, the model predicts that in tulips and other Liliaceae, which have petal-like organs in whorls 1 and 2, the B-function extends into whorl 1. Indeed, B-class genes in tulips are expressed in whorl 1, such that petal-like organs form in this whorl under the control of A- and B-class genes.

19.2.4 Organ specification is explained by the molecular quartet model

The homeotic genes described above all encode transcription factors, which is consistent with their function in specifying organ identity. It is thought that each combination of A-, B-,

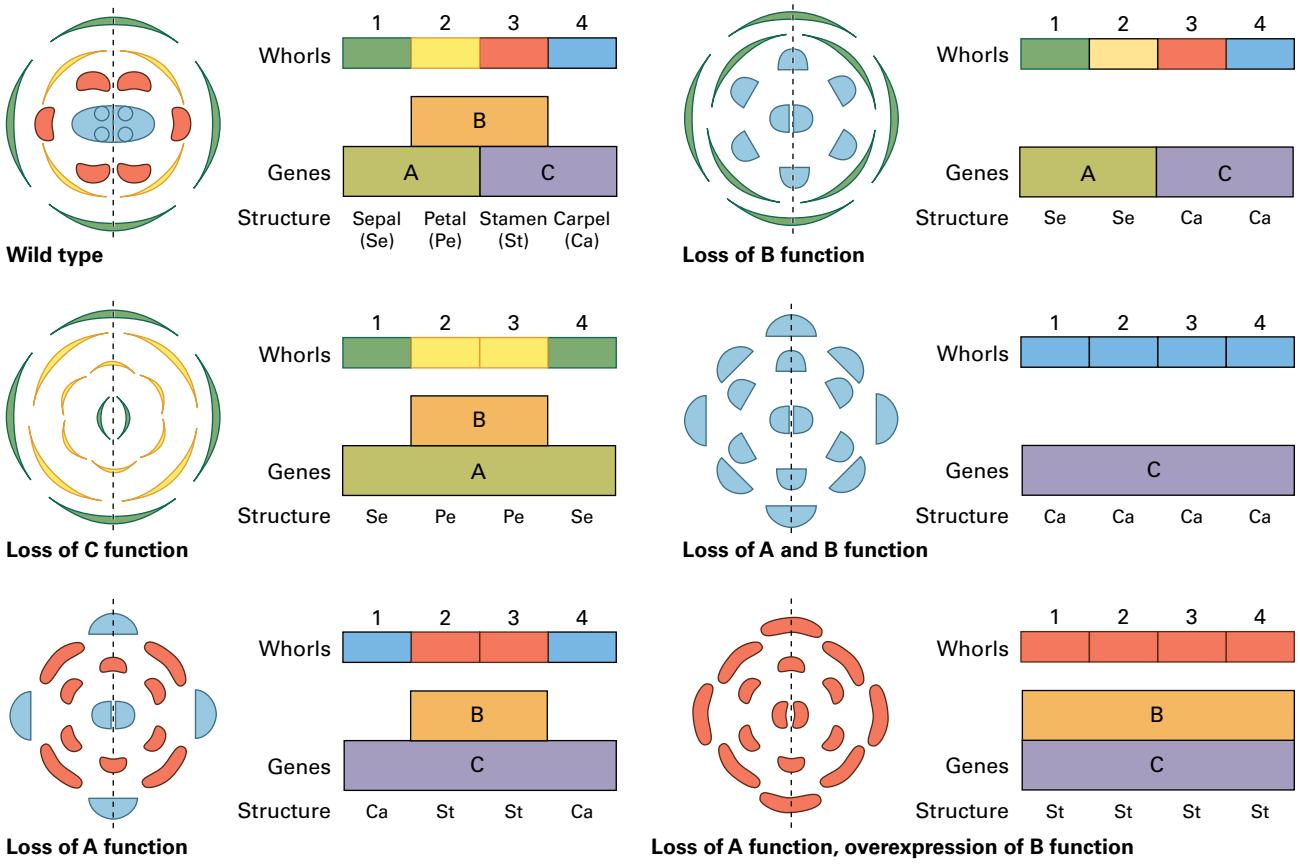


FIGURE 19.19 *Mutant phenotypes of single and multiple mutants based on the ABC model. The ABC model postulates that A and C functions are antagonistic. When C-function is missing, A-function expands into whorls 3 and 4 leading to the formation of petals in whorl 3, where B-function is present, and sepals in whorl 4. Conversely, if A-function is lost, C-function extends into whorls 1 and 2, leading to the formation of carpels and stamens. Based on the ABC model, double mutant phenotypes can be accurately predicted as described in the text. However, additional functions of the homeotic genes can lead to modified phenotypes, e.g. combinations with ag have indeterminate flowers and ap2 mutants often lack organs in whorl 2.*

or C-class transcription factors regulates a set of target genes required for the development of the corresponding organ.

All homeotic genes except *AP2* encode MADS-domain transcription factors (see Chapter 9), which are characterized by a highly conserved, N-terminal DNA-binding domain. The 56–60 amino acid MADS-domain occurs in plant, animal, and fungal proteins and binds DNA sequences with similarity to the CC[A/T]$_6$GG motif, also known as CArG-box (Fig. 19.20). *AP2* differs from the others in that it was the founding member of a transcription factor family unique to plants that contains an AP2 DNA-binding domain. The MADS-domain proteins bind DNA as multimeric complexes; for example, AP3 and PI proteins can bind to a CArG-box only if both proteins are part of the multimeric complex, providing a molecular explanation for why the corresponding mutants have identical phenotypes.

The molecular and genetic characterization of plant homeotic genes revealed that they function similarly to the homeotic genes in animals. In both cases, specific combinations of transcription factors specify the identity of organs or segments, respectively. In the case of animals, all homeotic genes encode homeodomain transcription factors, whereas plant homeotic genes encode transcription factors belonging to the MADS-domain or AP2 DNA-binding domain family. The floral organ identity genes are conserved throughout angiosperms, and homologs with corresponding functions have been identified in many plants.

With the exception of *AP2*, which is expressed in all four whorls, floral organ identity genes are expressed in the domains predicted by the ABC model. For example, the B-class genes *PI* and *AP3* are expressed in whorls 2 and 3, and C-class gene *AG* in whorls 3 and 4 (Fig. 19.21). This correspondence of function and expression domains suggests that homeotic genes are primarily regulated at the transcriptional level.

The difference between the expression pattern of *AP2* and its functional domain can be explained by the expression of microRNA *miR172* in whorls 3 and 4 (see Chapter 6). This microRNA targets *AP2* mRNA and prevents its translation into a protein (Fig. 19.22), such that the AP2 protein is present only in whorls 1 and 2, in a pattern complementary to that of the AG protein as expected based on the ABC model. A refined analysis of the *AP2*, *AG*, and *miR172* expression patterns has shown that *AP2* accumulates mostly in whorls 1 and 2 and only partially overlaps with *miR172* in the center of the flower. Also, *AP2* never completely expands into the

center of *ag* mutant flowers. Thus, the original ABC model must be further modified so that *AP2* and *AG* do not act in a mutually exclusive fashion; instead, the decision to form petals or stamens may depend on their relative abundance in whorls 2 and 3.

While the manipulation of homeotic genes changes floral organ identity, A-, B-, and C-class genes are insufficient for converting a leaf into a floral organ. However, when they are expressed together with the *SEPALATA* genes (*SEP1*, *SEP2*, *SEP3*), vegetative and cauline leaves are converted into floral organs, their identity depending on which combination of A-, B-, and C-class genes are co-expressed with *SEP1/2/3*. The *SEP* genes are redundant, and only the triple *sep1/2/3* mutant produces flowers in which all organs are converted into sepals. Thus, *SEP1/2/3* are required for the normal development of petals, stamens, and carpels, and are referred to as E-class genes (the D-class is involved in ovule identity, see Section 19.4.1). During early flower development, *SEP1* and *SEP2* are expressed in all four whorls, while *SEP3* is only expressed in whorls 2, 3, and 4.

Like most other homeotic genes, the *SEP* genes encode MADS-domain transcription factors that interact with other MADS-domain proteins. To explain the known combinatorial interactions, it was suggested that they form complexes consisting of four proteins ("floral quartets"). Each quartet consists of a set of MADS-domain proteins specifying a particular organ and controls a set of target genes required for its formation (Fig. 19.23). For instance, the quartet directing petal development would contain the A-class protein AP1, the B-class proteins PI and AP3, and a SEP protein. In whorl 4, however, two SEP proteins would form a quartet with two AG proteins, which specify carpel development. Indeed, the existence of multimeric protein complexes as proposed in the floral quartet model was demonstrated in planta.

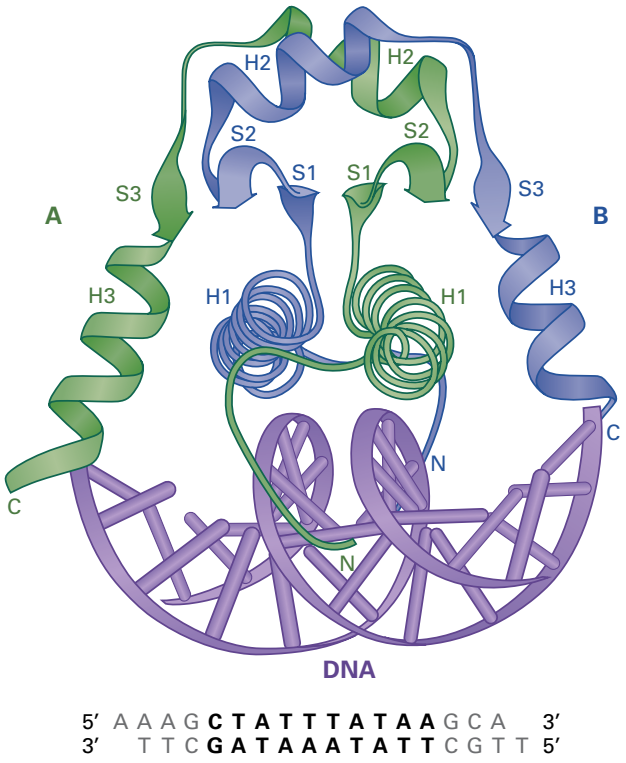


FIGURE 19.20 *MADS-domain proteins bind DNA. Structure of a dimer formed by two MADS-domains binding to a CArG-box on DNA.*

19.2.5 A number of factors regulate the expression of floral homeotic genes

Most of the flower organ identity genes are expressed in specific domains of the floral meristem that give rise to the organs they control. The homeotic genes are activated by LFY and AP1, which are, therefore, important for both specifying the identity of the flower meristem and activating organ identity genes during the early stages of flower development. During these early stages, however, both *AP1* and *LFY* are expressed throughout the floral meristem, while their B- and C-class target genes are only expressed in specific domains. Therefore, other factors must be involved in controlling the specific expression domains of the homeotic genes.

For instance, LFY activates the C-class gene *AG*, but this requires the homeodomain transcription factor WUS

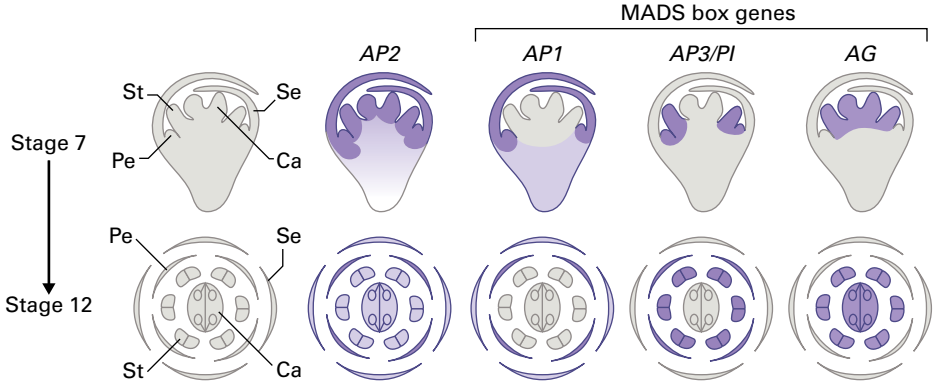


FIGURE 19.21 *Expression patterns of floral homeotic genes. The MADS-box genes AP1, AP3, PI, and AG are expressed in two adjacent whorls as expected based on the ABC model. AP2, however, is expressed in all four whorls throughout flower development. This raises questions regarding the function of AP2, which was predicted to act antagonistically to AG and, based on the original ABC model, should not be coexpressed with AG in whorls 3 and 4.*

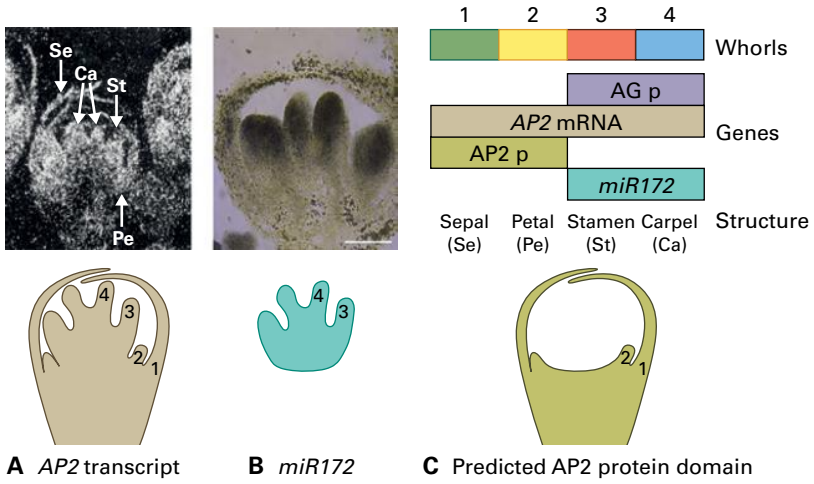


FIGURE 19.22 *AP2 is regulated by a microRNA. AP2 is expressed in all four whorls (A), although it supposedly acts antagonistically with AG and should thus repress AG in whorls 3 and 4. This conundrum is resolved by the expression of miR172 in whorls 3 and 4 (B), where it prevents the translation of AP2. Thus, the AP2 and AG proteins do not co-occur in whorls 3 and 4, and act antagonistically as expected (C).*
Source: Steimer et al. (2004). Curr. Opin. Plant Biol. 7:11; Jofuku et al. (1994). Plant Cell 6:1211; X. Chen, University of California - Riverside; previously unpublished.

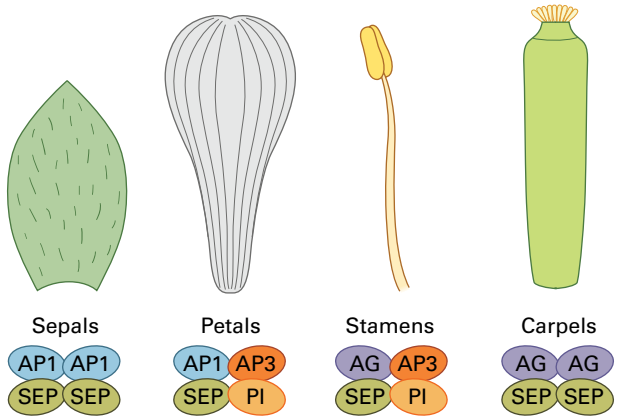


FIGURE 19.23 *Quartet model for floral organ identity. The homeotic proteins form tetrameric complexes that involve between two and four distinct proteins. In each whorl, a specific combination of proteins forms a quartet, which regulates specific target genes that are required to form the specified organ.*

(see Chapter 11) as co-factor. *WUS* is expressed early during flower development, prior to *AG*. LFY and WUS activate *AG* in whorls 3 and 4 by binding to *cis*-regulatory elements in the second intron of the *AG* gene. However, *AG* is also regulated by A-class genes, as A- and C-class act antagonistically. While mutations in *AP1* do not affect *AG* expression, *AG* is misexpressed in whorls 1 and 2 of *ap2* mutants, leading to homeotic transformations. Thus, AP2 controls the spatial expression pattern of *AG*. Genes that are involved in regulating the spatial expression domain of homeotic genes are referred to as **cadastral genes**; therefore, *AP2* is both a homeotic and a cadastral gene. Since *AP1* expression expands into whorls 3 and 4 in an *ag* mutant, *AG* has three functions: It is a homeotic, cadastral, and floral determinacy gene.

Once floral homeotic gene expression patterns have been established through the action of the floral meristem identity and cadastral genes, they must be maintained, and this is achieved by *Polycomb* group (PcG) and *trithorax* group (TrxG) genes. PcG genes encode a heterogeneous group of proteins that form repressive multiprotein complexes. In *Drosophila*, they were originally defined through their requirement for maintaining homeotic genes in a repressed state. TrxG genes, on the other hand, are required to maintain their active state of gene expression. In a *curly leaf* (*clf*) mutant, for instance, repression of *AG* in whorls 1 and 2 is not maintained later during flower development, and *AG* is expressed ectopically in leaves. *CLF* encodes a homolog of the *Drosophila* histone methyltransferase E(Z) and is part of the PRC2 complexes (see Chapter 11 and Box 19.1) that regulate homeotic gene expression (EMF-PRC2) and the floral repressor *FLC* (VRN-PRC2). Interestingly, in mutants of *ATX1*, an *Arabidopsis* gene similar to *Drosophila trithorax*, the expression of floral homeotic genes is reduced. *ATX1* also encodes a histone methyltransferase, but it is responsible for the trimethylation of histone H3 lysine 4 (H3K4me3), which is associated with active chromatin and acts antagonistically to H3K27me3. Thus, PcG and TrxG proteins are required to maintain homeotic genes in a repressed or active state of expression in both animals and plants.

These highly conserved multiprotein complexes must have an ancient origin that predates the separation of the plant and animal lineages. However, multicellularity and, therefore, the function of homeotic genes evolved separately in animals and plants, suggesting that PcG and TrxG regulatory modules were recruited independently to regulate homeotic genes in these two lineages (Fig. 19.24). This is an example of convergent evolution, as PRC2 complexes have not only been recruited to regulate homeotic genes in animals and plants, but also regulate genomic imprinting in both lineages (see Section 19.10).

In animals, another complex consisting of PcG proteins, ***Polycomb* repressive complex 1** (PRC1), is required to stabilize the silenced state of PRC2 target genes through the monoubiquitylation of histone H2A. Only a few of the genes encoding components of *Drosophila* PRC1 are conserved in plant genomes. Among them are the RING-finger proteins

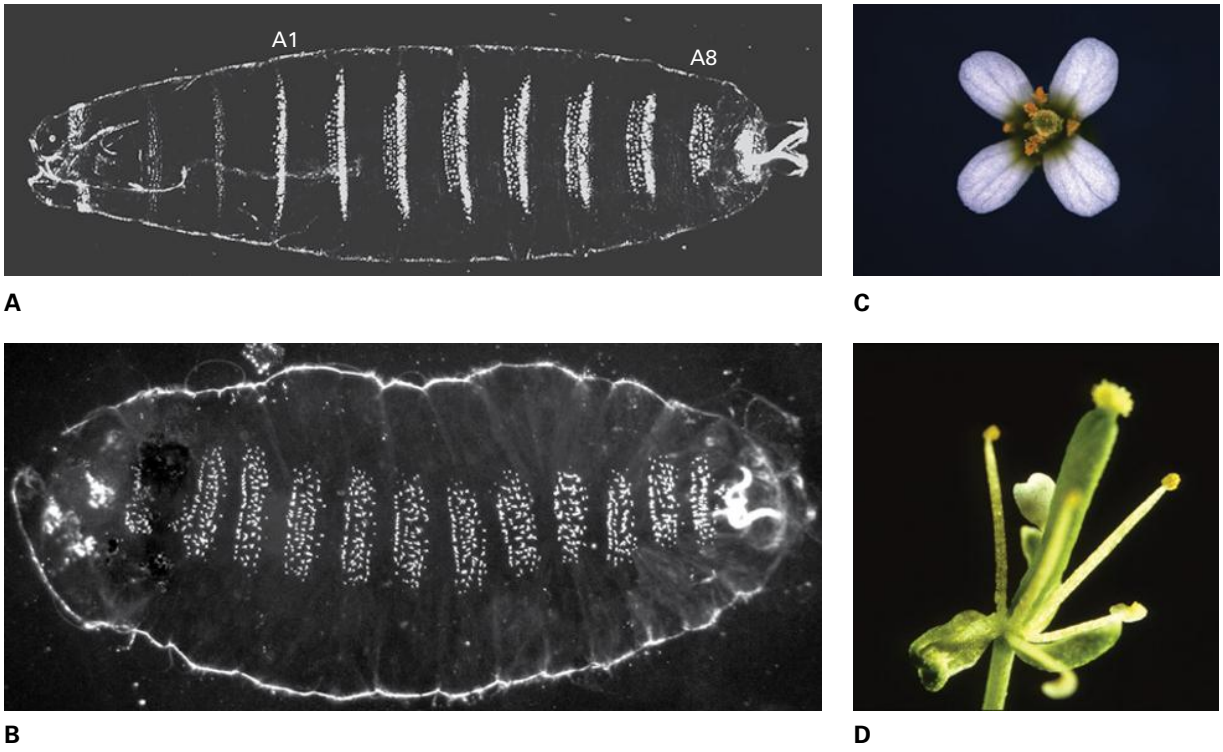


FIGURE 19.24 *Homeotic phenotypes in PcG mutants. PcG proteins are highly conserved and play similar roles in plants and animals where they have been independently recruited to regulate homeotic genes. (A)* Drosophila *wild type larvae where each abdominal segment (A1–A8) has a distinct cuticle pattern. (B)* Drosophila *su(z)12 larvae where all segments are homeotically transormed and have A8 identity. (C)* Arabidopsis *wild-type flower. (D)* Arabidopsis *clf flower with homeotic organ transformations.*
Source: (A, B) Birve et al. (2001). Development 128:3371. (C) A. Herrmann, University of Zurich; previously unpublished. (D) J. Goodrich, University of Edinburgh; previously unpublished.

RING1A and RING1B, which mediate H2A monoubiquitination and, when disrupted, show phenotypes similar to those observed in PRC2 mutants. This suggests that, in addition to PRC2, which is highly conserved, complexes with functions similar to those of PRC1 also exist in plants.

19.3 The formation of male gametes

19.3.1 Gamete development in plants is strikingly different from that in animals

Once the plant has produced flowers, a key event in plant reproduction takes place in the floral reproductive organs (the anthers and ovules): the transition from the diploid **sporophytic** to the haploid **gametophytic** generation.

There are many striking differences in the reproduction of animals and plants. In plants, meiosis produces **spores**, whereas in animals meiosis is intimately connected to gamete production. In fact, the spore-producing sporophyte represents the dominant phase of the life cycle in flowering plants, while the gamete-producing **gametophytes** consist of only a few cells, and their development depends on resources from the sporophyte (see Fig. 19.1). However, this is not true for all plants. In mosses and liverworts, for example, the gametophytes are free-living, photosynthetically active organisms that represent the dominant phase of the life cycle (Fig. 19.25). What is common to all gametophytes, however, is that they are multicellular, form from haploid spores through mitotic divisions, and only subsequently produce the gametes. This is in contrast to animals, where the meiotic products differentiate directly into gametes.

In plants, there is no early separation of soma and germline. Rather, any sporophytic cell can give rise to a gametophyte and so somatic mutations can sometimes be inherited. The first cells to eventually give rise to a gamete are the archespores that differentiate in the anther and ovule. Thus, these cells can be viewed as the first cells of the plant equivalent of the germline, which is only established late in development and independently in each reproductive organ.

19.3.2 During anther development, cells are set aside that eventually give rise to pollen

The stamen, the male reproductive organ of flowering plants, typically consists of a stalk-like filament and an anther. Formation of the haploid microspores (**microsporogenesis**) and pollen development (**microgametogenesis**) take place within the anther. The development of anthers and male gametophytes is highly conserved among angiosperms, with

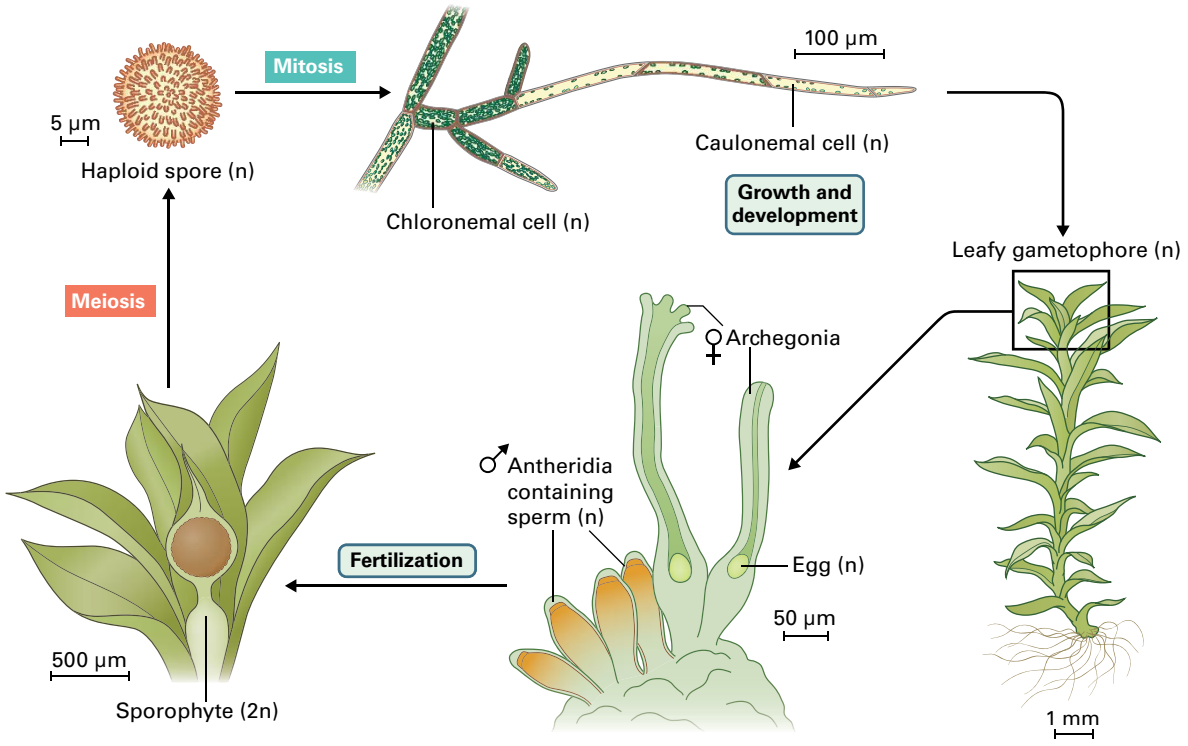


FIGURE 19.25 *Life cycle of the moss* Physcomitrella patens. *Gametophytes are free-living organisms that produce gametes in specialized reproductive organs. Fertilization of the egg cell by a motile sperm forms a zygote, which develops into a sporophyte that is dependent on the gametophyte. Sporogenesis produces spores that initiate the gametophytic generation.*

only minor differences among certain plant families. Therefore, the molecular insights into male reproductive processes gained from model species can be directly translated to crop plants, a fact that has been exploited in several biotechnological applications. Male sterile mutants are useful in the production of hybrid seeds, which are widely used in agriculture because crosses involving a male sterile parent, serving as the female, are much easier to conduct on a large scale.

During anther development, cells are set aside that will eventually give rise to pollen. The first step in this process is the specification of four subepidermal cells into archespores, which eventually form the four-lobed anthers typical of flowering plants. The subepidermal cells can be traced back to the L2 layer of the shoot meristem, which is thus the layer that gives rise to the germline in plants. In *Arabidopsis* the *SPOROCYTELESS/NOZZLE (SPL/NZZ)* gene is required for archespore formation in both male and female reproductive organs. *SPL/NZZ* is a direct target of AG and encodes a transcription factor with similarities to MADS-domain proteins.

Each archespore divides to form a primary parietal and a primary sporogenous cell. The primary sporogenous cell divides again to produce the **microsporocytes** (also referred to as microspore or pollen mother cell), and it serves as an organizing center in the formation of the pollen sac (microsporangium), in which pollen development takes place. Induced by signals from sporogenous cells, the primary parietal cell divides to form an outer endothecial and an inner secondary parietal cell, which divides once more to form the cells of the middle and tapetum layer that is in direct contact with the microsporocytes (Fig. 19.26).

The tapetum encloses the pollen sac that contains the microsporocytes. Tapetal cells produce diverse compounds, such as phenolics, flavonols, and proteins that contribute to the formation of the intricate outer wall of the pollen, the exine. The tapetal cells eventually undergo programmed cell death, and some of their cellular components are incorporated into the pollen coat that lines the surface of the mature pollen grain's exine layer (Fig. 19.27). The pollen coat plays a central role in pollen recognition at the stigma surface (see Section 19.5.2). In fact, many mutations that result in male sterility (lack of pollen production) primarily affect the tapetum, indicating that the tapetum plays an essential, noncell autonomous role for pollen development.

19.3.3 Complex cell–cell communication events underlie microsporogenesis

As mentioned in the previous section, during anther development, the two daughter cells of the archespore adopt different fates: the primary sporogenous cells form the microspore mother cells and, thus, the gametes, whereas the primary parietal cells form the sporophytic tissues of the pollen sac. Using mutants in both *Arabidopsis* and rice (*Oryza sativa*), it

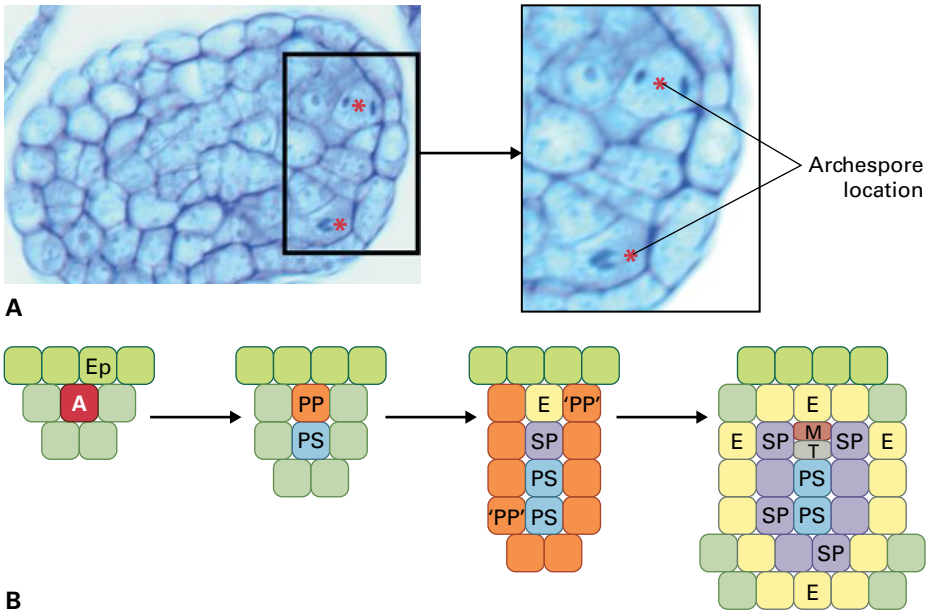


FIGURE 19.26 *Development of the pollen sac. (A) A cross section of a young anther primordium showing two of the four enlarged archespores. (B) Asymmetric division in the anther. An archespore (A) differentiates underneath the epidermis (Ep). An asymmetric division forms the primary parietal (PP) and the primary sporogenous (PS) cells. The PS divides to form a pool of microspore mother cells and induces neighboring cells to adopt a PP-like fate ('PP') and PP cells to divide and form endothecial (E) and secondary parietal (SP) cells. The 'PP' cells then undergo the same asymmetric division to form E and SP cells. The 'PP' cells then undergo the same asymmetric division to form E and SP cells, which eventually divide to form the middle (M) and tapetal (T) cell layers surrounding the PS cells (only one cell is shown that already underwent this division). Source*: Scott et al. (2004). Plant Cell 16:S46.

was shown that this cell fate decision is governed by several signaling cascades.

In the *extra sporogenous cells* (*exs*)/*excess microsporocytes1* (*ems1*) mutant of *Arabidopsis,* too many microsporocytes are formed at the expense of tapetal cells. This phenotype might be explained if cells that give rise to the tapetal layer adopted instead a microsporocyte fate. *EXC*/*EMS1* encodes a leucine-rich repeat receptor-like kinase (LRR-RLK; see Chapter 18) that is expressed in the parietal cell lineage. Mutations in another gene, *TAPETAL DETERMINANT1* (*TPD1*), give rise to the same phenotype as *exs*/*ems1* mutants, but *TPD1* is predominantly expressed in microsporocytes and encodes a secreted protein that interacts with EXC/EMS1. This suggests that TPD1 is a ligand produced in the sporogenous lineage that is recognized by EXC/EMS1 in the parietal lineage to organize the formation of the pollen sac. The same holds true for the rice orthologs of these two genes. Finally, a double mutant affecting another pair of RLKs, the *SOMATIC EMBRYOGENESIS RECEPTOR-LIKE KINASE1* and *2* (*SERK1, SERK2*), shares the same phenotype, illustrating the complexity of cell–cell communication events that regulate this important cell fate decision.

Once the microsporocytes are formed, they undergo two meiotic divisions to produce four haploid microspores. Progression through meiosis requires a suite of genes, many of which are conserved between yeast, animals, and plants. Many sterile mutants in plants are the result of mutations affecting meiosis, and most of these affect both sexes, although a few are sex specific. At the end of meiosis, a tetrad of microspores encased in a callose wall is formed. Individual microspores are released through digestion of the callose by a tapetum-derived enzyme (callase) (Fig. 19.27).

The free microspore marks the beginning of the gametophytic phase, during which the mature male gametophyte is formed inside the pollen sac. But microspores are surprisingly plastic and, under appropriate conditions, they can form embryos (**androgenesis**) that are haploid. Doubling their chromosomes, which can happen spontaneously or after treatment with colchicine, results in diploid plants with a uniformly homozygous genome. Such an immediate route to homozygosity is of great interest for plant breeders because it circumvents time-consuming, repeated self-fertilization to generate homozygous plants through inbreeding (Box 19.2).

19.3.4 Microgametogenesis involves two rounds of mitosis

Initially, the free microspores are apolar, with a centrally located nucleus surrounded by small vacuoles. Then the microspore expands in a process that is accompanied by the formation of a large vacuole. This results in the formation of a polarized, unicellular microspore, which divides asymmetrically during pollen mitosis I (PM I) to form a bicellular microspore consisting of a large vegetative cell and a small generative cell (Fig. 19.28). The generative cell detaches from the pollen cell wall and becomes internalized, harbored within the cytoplasm of the vegetative cell ("cell within a cell" configuration).

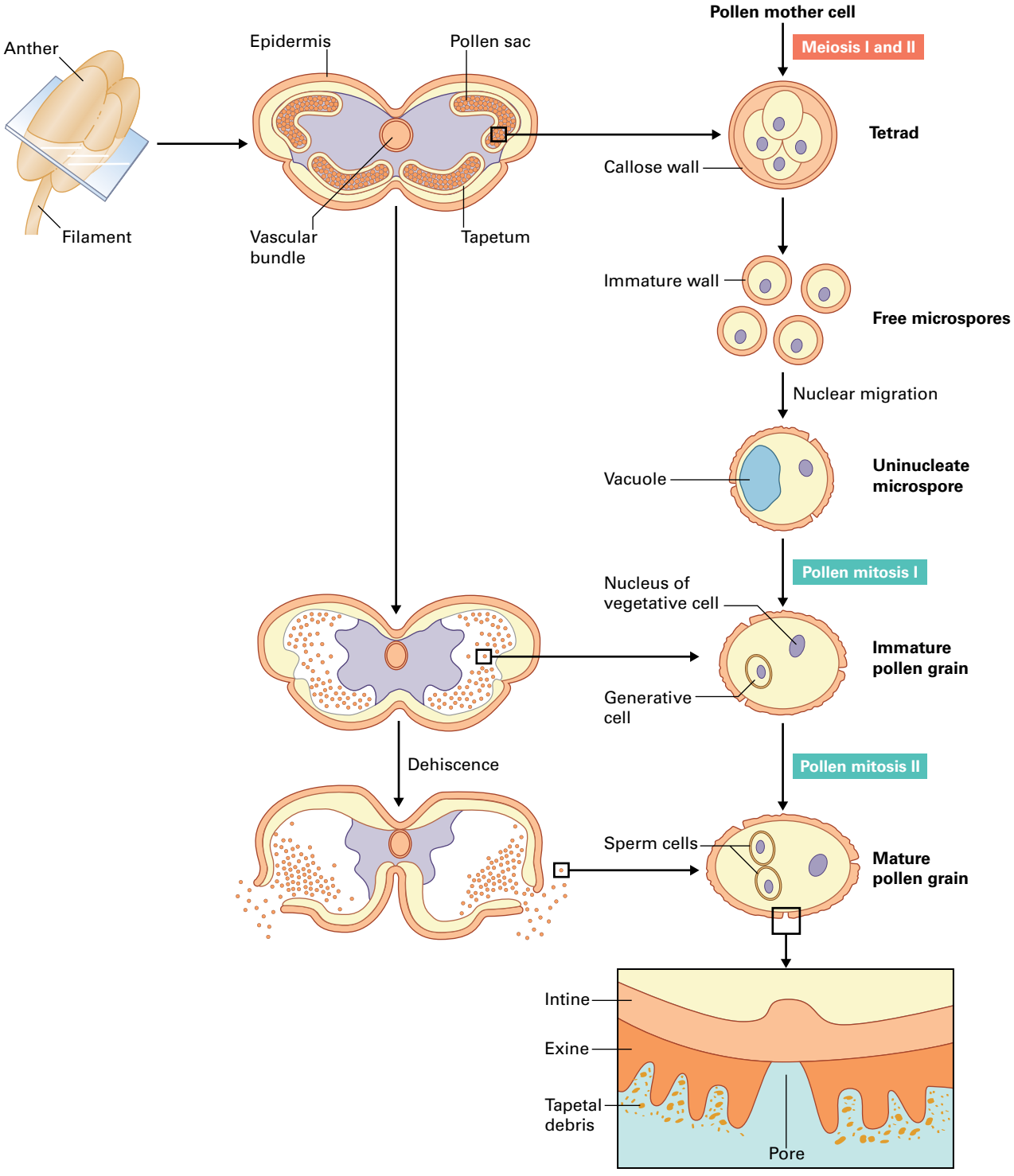


FIGURE 19.27 *Diagram of pollen development. Meiosis occurs in the pollen sacs of the anther and produces a tetrad of microspores. Callase digestion releases free microspores that initiate microgametogenesis. The microspore polarizes and undergoes an asymmetric division (PM I) to form a large vegetative and a small generative cell that gets internalized. The generative cell divides once more (PM II) to form the two sperm cells.*

As in many other developmental processes in animals and plants, the asymmetric PM I marks the beginning of the distinct developmental fates of the daughter cells. Only the generative cell undergoes pollen mitosis II (PM II) to form the two sperm cells, which contribute to the next generation. The chromatin in the generative cell nucleus is more condensed than that of the vegetative nucleus and finally reaches the highly condensed state typical of sperm cells (Fig. 19.28). In contrast, the vegetative cell does not divide further, but is responsible for bringing the sperm cells to the female gametes, carrying them in its cytoplasm as cargo. The vegetative cell stores a large variety of mRNAs and proteins that allow an

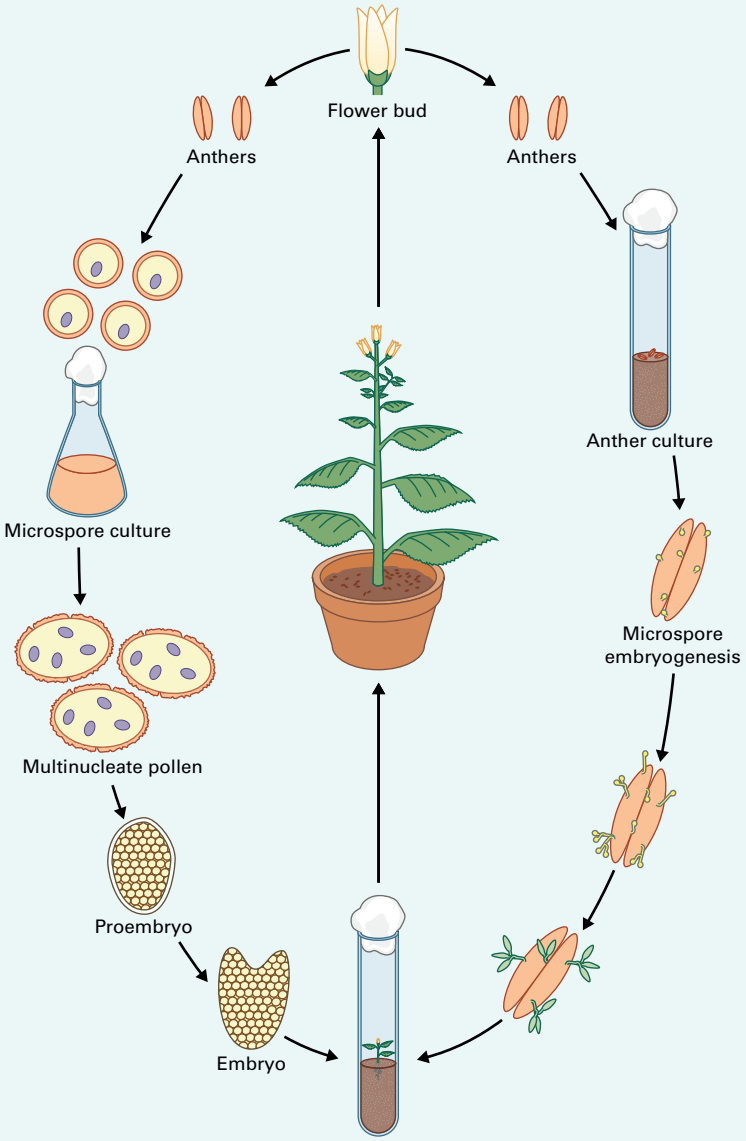
BOX 19.2

Microspore culture can revert the gametophytic developmental program to a sporophytic program, yielding haploid plants

Cultured anthers or microspores can be used to generate haploid plants. This technique is of interest to plant breeders because doubling the chromosome number of the resulting haploid plants, either spontaneously or by chemical treatment, can generate homozygous diploids.

Flower buds at the appropriate developmental stage are collected and the microspores isolated and cultured. For some plants, microspore culture (left pathway) is inefficient, and the anthers must be cultured instead (right pathway). The sporophytic anther tissue is thought to provide factors required for the development of microspore-derived embryos. Formation of embryos is typically induced by a stress treatment. In some cases, whole plants are grown under stress conditions (such as low temperatures or nitrogen starvation). In other cases, anthers are excised or microspores isolated from a nonstressed plant; after the isolated tissues or cells are subjected to a stress treatment (e.g., heat shock or starvation for nitrogen and sucrose), they are transferred to a medium containing sucrose and nitrogen to promote further development of microspore-derived embryos.

After stress treatment, microspore embryos arise by one of two developmental pathways. In the first pathway (shown on the left), the vegetative cell of a binucleate pollen grain continues to proliferate, forming a multinucleate pollen grain and eventually an embryo. In the second, the uninucleate microspore undergoes a symmetrical cell division, giving rise to two equal-sized cells that both continue to divide (not shown). Both pathways involve a release of the cell cycle arrest that the vegetative cell undergoes during normal pollen development.



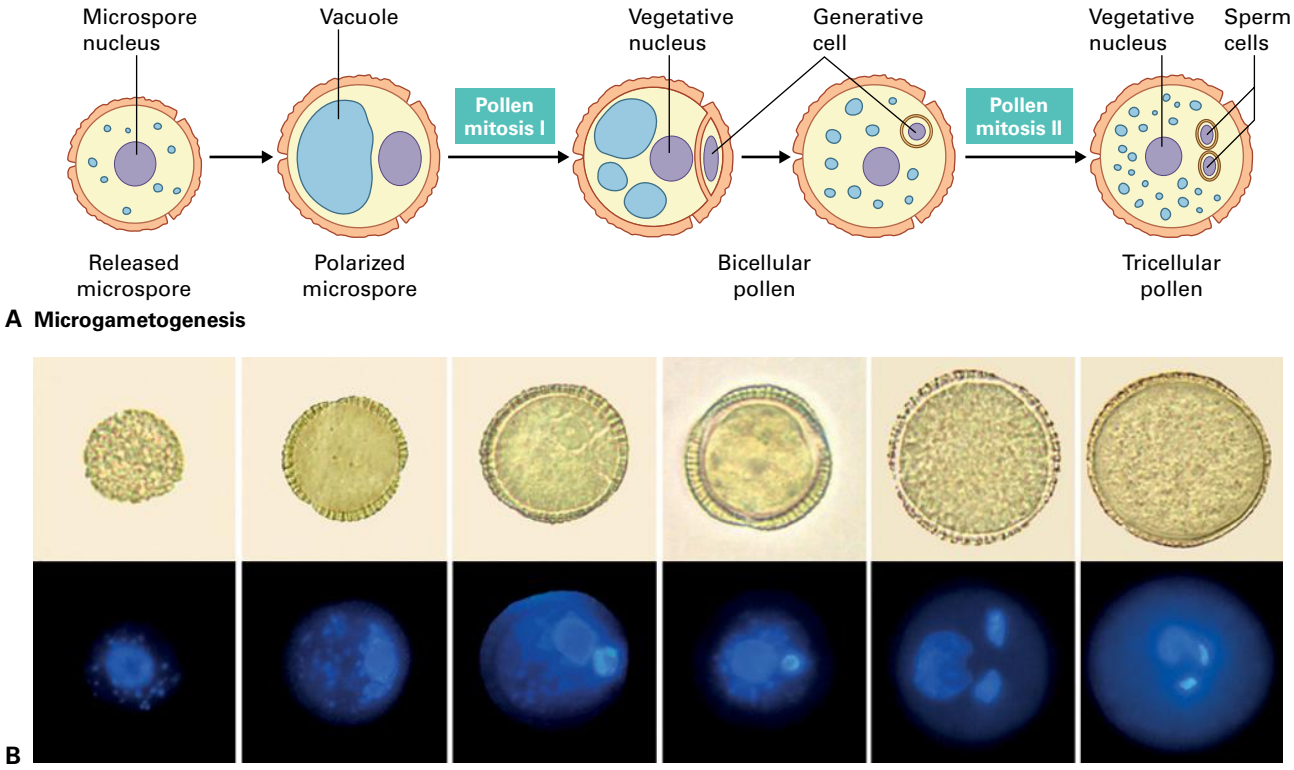


FIGURE 19.28 *Microgametogenesis in* Arabidopsis. *Diagramatic (A), light (B) and fluorescent microscopical (C) representation of the developmental progression through male gametogenesis (see main text for details). The fluorescent pictures show DAPI-stained pollen. The large vegetative nucleus and the two small sperm nuclei with highly condensed chromatin are clearly visible in tricellular pollen. Source*: (B) D. Twell, University of Leicester; previously unpublished.

immediate response upon pollination, for example, rapid germination and fast initial pollen tube growth through the female reproductive tissues (see Section 19.5.3). The timing of PM II varies between species: in some plants, like *Arabidopsis*, PM II occurs prior to the release of pollen from the anthers (**anthesis**) such that tricellular pollen is released, but in most plants, like maize (*Zea mays*) and tobacco (*N. tabacum*), PM II takes place after pollen germination on the stigma, and the pollen released at anthesis is bicellular.

The many known male sterile mutations are usually recessive mutations affecting the diploid sporophyte, most often anther development and meiosis. The identification of mutants that affect the haploid phase of development has proven more difficult because even a fully penetrant mutant that affects microgametogenesis produces 50% normal pollen, so these plants appear fully fertile. With the development of efficient insertional mutagenesis systems, however, it became possible to perform large-scale screens for mutants affecting both male and female gametophyte development (Box 19.3).

Characterizations of gametophytic mutants have provided insights into the diverse developmental processes controlling microgametogenesis. For example, in *Arabidopsis* mutations in the A-type cyclin-dependent kinase gene *CDKA;1* (see Chapter 11) or the *F-BOX-LIKE 17* (*FBL17*) gene (see Chapter 18) lead to the formation of pollen with a single sperm-like cell, although this cell can divide later during pollen tube growth. FBL17 targets the CDK inhibitory proteins KRP6 and KRP7 (see Chapter 11) for degradation by the ubiquitin–proteasome pathway (see Chapter 10). While these two CDK inhibitors are expressed in both daughter cells after PM I, *FBL17* is only transiently expressed in the generative cell, where it leads to the cell type-specific degradation of KRP6/7, allowing the generative cell to proceed to S-phase. In contrast, CDKA;1 activity remains inhibited by KRP6/7 in the vegetative cell, thereby blocking cell cycle progression and enforcing the vegetative cell fate (Fig. 19.29).

Mutations in the *RETINOBLASTOMA-RELATED* (*RBR*) gene, which encodes a central regulator of the G1/S transition (see Chapter 11), result in a phenotype opposite that of *cdka;1* and *fbl17*: The vegetative and sometimes the generative cell undergo additional division cycles. As this phenotype depends on CDKA;1 activity, RBR acts downstream of the KRP6/7-mediated inhibition of CDKA;1, enforcing cell cycle exit and thus differentiation of the vegetative cell, while promoting cell cycle progression in the generative cell (Fig. 19.29). Mutations disrupting the *DUO POLLEN* (*DUO*) genes also produce bicellular pollen. *DUO1* encodes R2R3 MYB transcription factor (see Chapter 9) specifically expressed in the generative and sperm cells. It is required for the activation of gamete differentiation as well as the progression to the G2/M phase, thereby integrating differentiation and cell cycle control to ensure the production of a pair of fully differentiated sperm cells (Fig. 19.29).

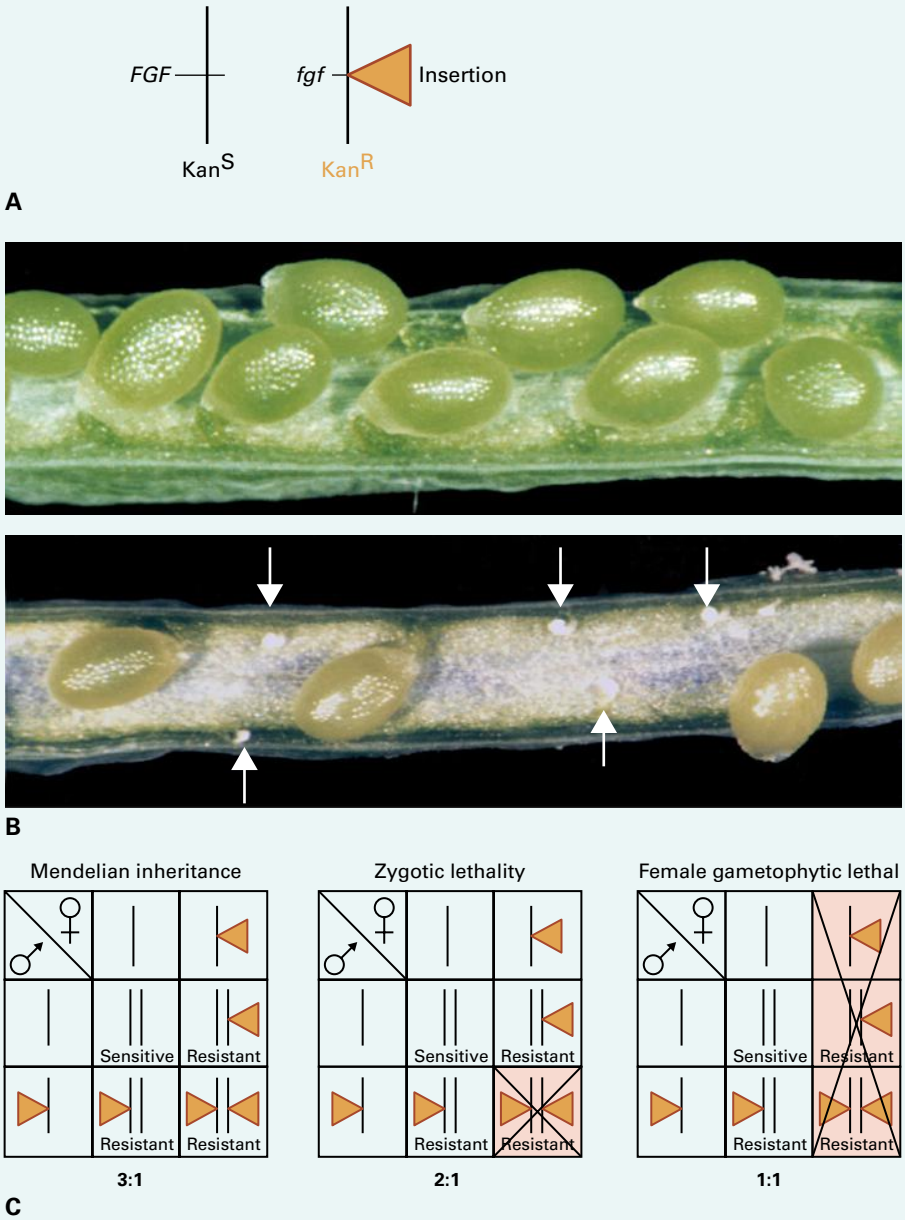
Pollen and sperm cells harbor a complex complement of mRNAs and small RNAs, including microRNAs and natural antisense RNAs (see Chapter 6). For instance, silencing of

BOX 19.3

Gametophytic mutations can be identified by segregation ratio distortion

Because mutants that are essential for the male or female can only be maintained as heterozygotes, their identification has proven difficult. Heterozygous male gametophytic mutants produce 50% wild-type pollen and appear fully fertile due to the large excess of pollen produced. Female gametophytic mutants also produce 50% normal female gametophytes, leading to apparently normal fruit development because half of the ovules develop into seeds. That half of the ovules remain unfertilized (arrows in B) and that the plant is thus semisterile can only been seen if the fruits are opened. Because chemical mutagenesis leads to a strong reduction of fertility, it was only possible to use this characteristic phenotype once insertional mutagenesis, be it through transposons or T-DNA, became possible. If an insertion disrupts a *FEMALE GAMETOPHYHTE FACTOR* (*FGF*) (A), required for the development or function of the female gametophyte, it will cause semisterility (B). However, semisterility can be due to other causes, such as chromosomal translocations, partially penetrant sporophytic mutants, or poor growth conditions. Because mutant gametophytes do not pass on the insertion to their progeny, gametophytic mutations are further characterized by segregation ratio distortion (C). A fully penetrant gametophytic mutation that only affects one sex is expected to segregate 1:1 among the progeny, instead of the Mendelian 3:1 ratio. Because insertions usually carry a dominant marker (e.g. conferring kanamycin resistance, Kan^R), their segregation can easily be followed. Segregation ratio distortion is a hallmark lethal mutations and its degree can be used to identify zygotic lethal (2:1) and sex-specific gametophyte lethal (1:1) mutants.

Source: U. Grossniklaus, University of Zürich; previously unpublished.



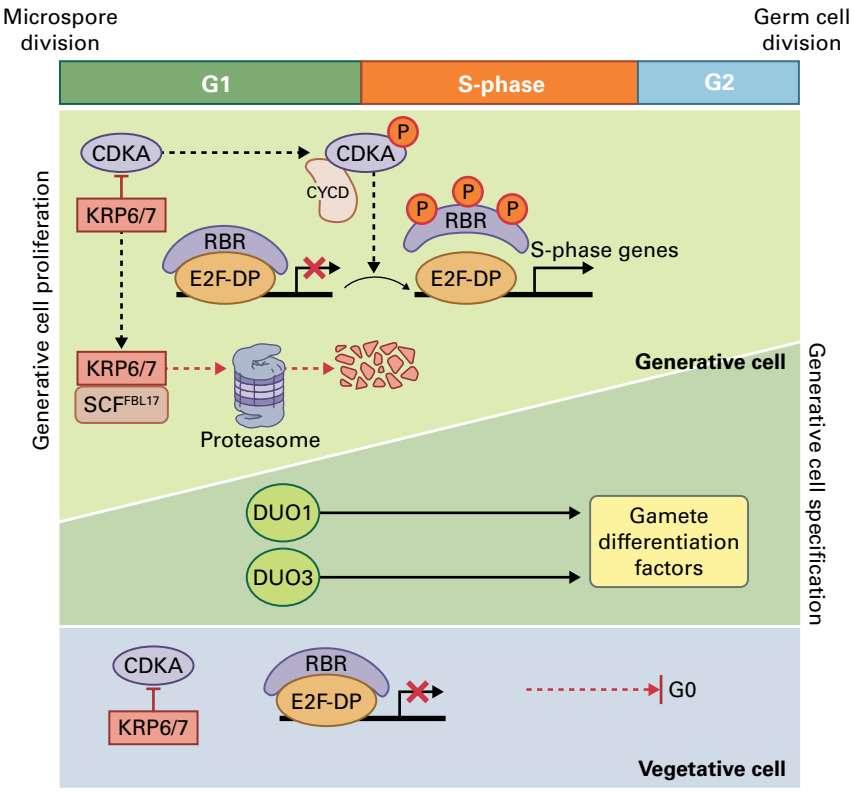


FIGURE 19.29 *Relationship between cell cycle progression and cell specification during pollen development. In the vegetative cell, which does not undergo pollen mitosis II, KRP6/7 inhibits CDKA such that RBR remains complexed with E2F/DP inhibiting genes required for the initiation of S-phase. In the generative cell, the FBL17-SCF ubiquitin ligase complex ubiquitinylates KRP6/7 targeting it for degradation and thus releasing the inhibition of CDKA. CDKA can now form a complex with cyclin D (CYCD), which phosphorylates RBR, leading to its release from E2F/DP and the activation of S-phase genes. Concomitantly, the transcription factors DUO1 and DUO3 activate genes required for gamete differentiation.*

transposable elements is lost specifically in the vegetative nucleus, leading to the formation of short interfering 21 nucleotide RNAs (21nt siRNA) from the *Athila* retrotransposon. Although produced in the vegetative cell, these 21nt siRNAs preferentially accumulate in the sperm cells, where they may stably silence these transposons from generation to generation. Although the exact mechanisms are unclear, this finding indicates that vegetative and generative cells communicate with each other, possibly through the action of small RNAs.

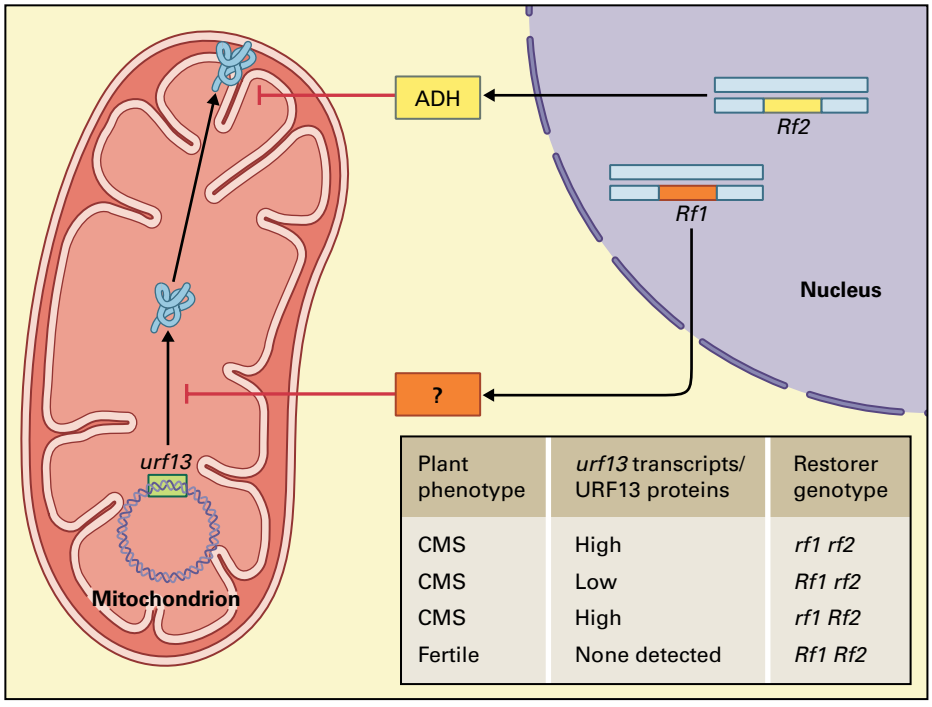
19.3.5 Cytoplasmic male sterility is caused by mitochrondrial defects

Another type of male sterility is caused by mutations in the mitochondrial, rather than the nuclear genome. In most angiosperms, mitochondria are inherited from the cytoplasm of the egg cell. Therefore, such mutations are called cytoplasmic male sterility (CMS) mutations, and they show a purely maternal inheritance that does not conform to Mendel's rule of segregation. CMS is common in wild plant populations and has been reported in more than 150 species, including maize, rice, and bean (*Phaseolus vulgaris*). CMS is of great commercial interest because it facilitates the production of hybrid seeds: If the female parent used to generate F1 hybrids is male sterile (nuclear or CMS), its labor-intensive emasculation can be avoided. However, due to its particular inheritance properties, the progeny of a CMS female is expected to be male sterile, which is detrimental to agricultural use. Therefore, male sterility in F1 hybrids must be suppressed, and this is achieved by using a male parent that carries a so-called *Restorer of fertility* (*Rf*) gene that is encoded in the nucleus.

In all naturally occurring CMS cases studied, sterility has been traced back to the production of an aberrant protein in the mitochondria, but the exact protein affected depends on the species. Although all cells of the plant carry the same mitochondria, CMS causes defects only in the anther or the pollen, depending on the species or type of CMS. How these aberrant proteins affect male reproductive development is not really understood; however, many *Rf* genes reduce the production of the aberrant mitochondrial protein, thereby restoring fertility.

The first commercially used CMS in maize, CMS-T, was used for hybrid seed production starting in the 1950s, and by 1970 85% of the maize F1 hybrids grown in the USA carried CMS-T. CMS-T, however, was particularly susceptible to the fungus that caused Southern corn leaf blight (*Bipolaris maydis*), which ravaged the USA in 1969–1970, causing tremendous losses in corn yields. For this reason, CMS-T is not used anymore in hybrid seed production. This tragedy illustrates the danger of depending on a small variety of genotypes in agriculture.

The aberrant mitochondrial protein specific to CMS-T is URF13, and it is encoded by a chimeric gene. How it affects tapetum function is unknown. Restoration of CMS-T requires both *Rf1* and *Rf2*, which together abolish the production of the aberrant URF13 protein to restore fertility (Fig. 19.30). The molecular nature of *Rf1* is unknown, but *Rf1* greatly decreases the abundance of *urf13* transcripts, while *Rf2* has no effect on *ufr13* transcript accumulation. *Rf2* encodes an



Plant phenotype	*urf13* transcripts/ URF13 proteins	Restorer genotype
CMS	High	*rf1 rf2*
CMS	Low	*Rf1 rf2*
CMS	High	*rf1 Rf2*
Fertile	None detected	*Rf1 Rf2*

FIGURE 19.30 *The CMS-T system of maize. The toxic effect of the URF13 protein (encoded by the mitochondrial genome) is suppressed by the nuclear-encoded Restorer proteins Rf1 (which reduces urf13 transcripts) and Rf2, an alcohol dehydrogenase (ADH) thought to detoxify the compound induced by the URF13 protein.*

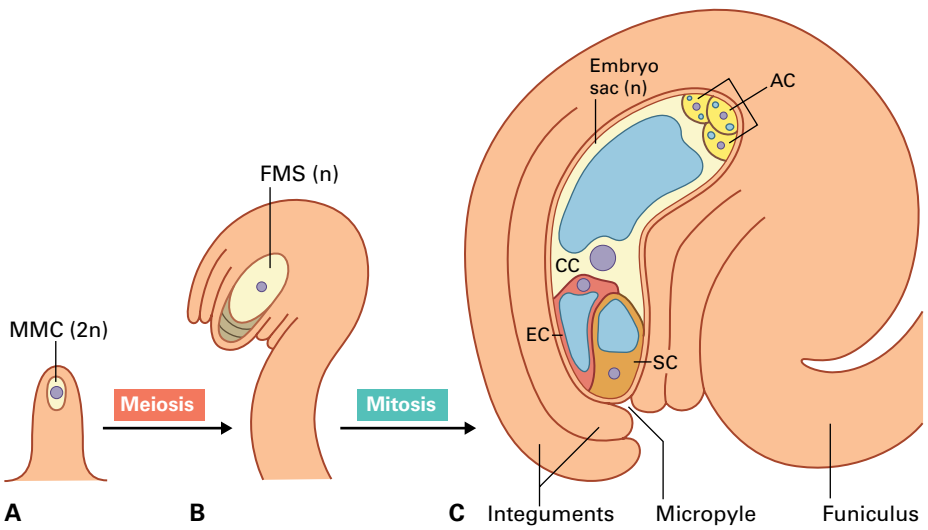


FIGURE 19.31 *Ovule development is coordinated with megasporogenesis and megagametogenesis. (A) From the nucellus tissue at the tip of the young ovule primordium a subepidermal cell differentiates into the megaspore mother cell (MMC). (B) The nucellus is enveloped by two integuments, and the ovules bend into an anisotropic shape. The surviving functional megaspore (FMS) initiates embryo sac development. (C) The mature ovule has two fully developed integuments that enclose the mature embryo sac with its four cell types: two synergid cells (SC) of which only one is shown, egg cell (EC), central cell (CC), and three antipodal cells (AC).*

aldehyde dehydrogenase, and it may be involved in the detoxification of toxins whose production or accumulation is caused by the URF13 protein.

19.4 The formation of female gametes

Female gametes are produced by the embryo sac (haploid female gametophyte), which develops inside the ovule in a coordinated manner with the sporophytic integuments that enclose it. Female gamete formation involves two subsequent developmental processes: **megasporogenesis** generates the haploid spores, and it is followed by **megagametogenesis**, which forms the mature embryo sac through mitotic divisions of one of these spores.

19.4.1 Ovule development has characteristics of shoot development

Inside the carpels, ovules form as finger-like protrusions from the placenta, and three distinct regions can be distinguished in early ovule primordia (Fig. 19.31): the nucellus region at the apex from which germline cells differentiate, the chalazal region that gives rise to the integuments, and the funicular region that connects the ovule to the placenta. The integuments grow and enclose the nucellus, leaving a small opening, the micropyle, through which the pollen tube enters to effect fertilization (see Section 19.5.5).

After fertilization, the integuments develop into the seed coat, which provides protection for the next generation. The funiculus provides the connection to the mother plant, through which resources required for seed development are transported.

In *Arabidopsis*, ovule identity is conferred on developing primordia through the redundant function of three MADS-box genes. In triple mutants disrupting the *SHATTERPROOF1* and *2* (*SHP1*, *SHP2*) and *SEEDSTICK* (*STK*) genes, ovules are converted to carpels. The same phenotype is observed in petunia if the MADS-box genes *FLORAL BINDING PROTEIN 7* and *11* (*FBP7*, *FBP11*) are downregulated. Overexpression of *FBP11* under a strong constitutive promoter leads to ovule formation on the surfaces of sepals and petals, demonstrating its function as an ovule identity gene (Fig. 19.32). Because these genes only determine the identity of ovules, they are sometimes referred to as D-class genes.

Some *Arabidopsis* mutants exhibit abnormal integuments. In most sporophytic ovule mutants, development of the embryo sac is arrested, suggesting that events occurring in the integuments are required for normal megagametogenesis, possibly through signals that are noncell autonomous. Conversely, ovules lacking an embryo sac may appear normal, though effects on gene expression in sporophytic tissues of the ovule have been detected. This suggests communication between the sporophytic and gametophytic generation during ovule development.

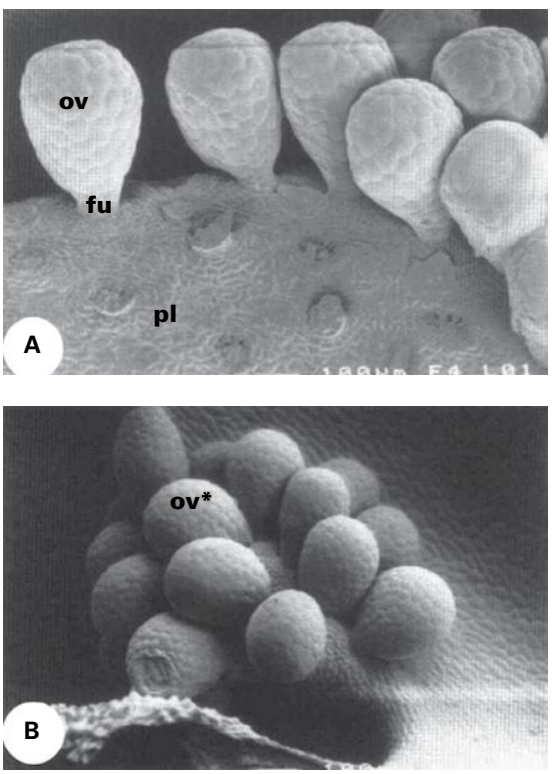


FIGURE 19.32 *D-class genes specify ovule identity. (A)* Petunia *ovules (ov) normally form the placenta (pl) connected by a funiculus (fu). (B) Ectopic ovules (ov*) induced on sepals by overexpression on the petunia D-class gene FBP11.*
Source: Colombo et al. (1995). Plant Cell 7:1859.

Molecular genetic characterizations of genes involved in ovule development revealed patterning principles that act in both the shoot meristem and the ovule primordium. Indeed, leaf primordia and integuments both form from the flanks of an apex and have a distinct abaxial–adaxial polarity. These similarities are also reflected at the molecular level. For example, *WUS*, which is required for stem cell maintenance in the shoot apex through a noncell autonomous mechanism (see Chapter 11), is also expressed in the nucellus. Lack of *WUS* activity results in a failure to initiate leaves or integuments, indicating that the same signaling module is used to influence adjacent groups of cells. Furthermore, a suite of genes (or their close homologs) plays a role in the establishment of polarity in both integuments and leaves (Fig. 19.33). These include transcription factors of the HD-ZIPIII class of homeodomain proteins on the adaxial side, and of the KANADI (KAN) and YABBY class on the abaxial side. For instance, the *YABBY* gene *INNER NO OUTER* (*INO*) is only expressed in the abaxial region of the outer integument, and *ino* mutations completely abolish the outgrowth of the outer integument.

19.4.2 During megasporogenesis, the diploid megaspore mother cell undergoes meiosis to give rise to four haploid megaspores

Early during ovule development, a single archespore enlarges and differentiates into the **megaspore mother cell** (MMC), which undergoes two meiotic divisions to form a tetrad of haploid megaspores. This process requires many of the same meiotic genes that also function during microsporogenesis. In most flowering plants, only a single megaspore, the functional megaspore (FMS), survives and forms the embryo sac (monosporic development), whose cells thus share the same genotype.

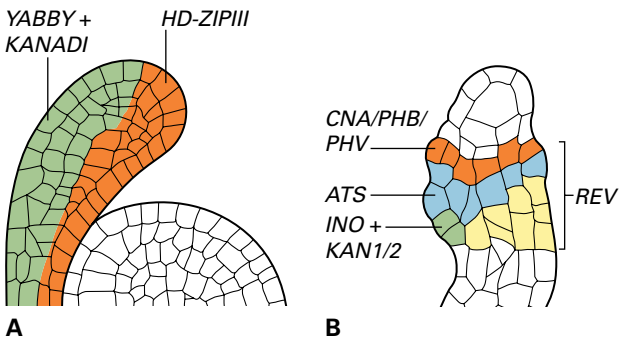


FIGURE 19.33 *Establishing polarity of leaves and integuments is based on similar molecules. (A) Leaf polarity is determined by transcriptions factors specifically expressed in the abaxial (KAN and YABBY family) and adaxial (HD-ZIPIII family) parts of the primordium. (B) The polarity of integuments is patterned similarly, involving the YABBY factor INO and KAN1/2 on the abaxial side and the HD-ZIPIII factors PHABULOSA (PHB), PHAVOLUTA (PHV) and CORONA (CNA) on the adaxial side. Other factors involved in integument patterning are REVOLUTA (REV) and ABERRANT TESTA SHAPE (ATS).*

Formation of the MMC requires the SPL/NZZ gene product also involved in microspore formation (see Section 19.3.2), and usually only a single subepidermal cell from the L2 layer acquires this fate. However, in some mutants, such as *multiple archesporial cell 1* (*mac1*) in maize and *multiple sporocyte 1* (*msp1*) in rice, multiple L2 cells differentiate into an MMC and sometimes even initiate meiosis. This observation suggests that the MMC usually blocks other cells from adopting the same fate through **lateral inhibition**. Lateral inhibition plays an important role in many developmental decisions in animals and plants, and it relies on cell–cell communication. *MSP1* encodes an RLK that binds the peptide TAPETUM DETERMINANT-LIKE 1A, and downregulation of this gene results in a phenotype similar to that of *msp1*.

Recent work in *Arabidopsis* has shown that signaling by small RNAs also plays a role in limiting the number of germline cells. Mutations in *ARGONAUTE 9* (*AGO9*) (see Chapter 6), as well as mutations in two other genes involved in small RNA biogenesis or function (*RDR6* and *SGS3*), produce multiple enlarged cells in the nucellus. The same is true for mutations in *MNEME* (*MEM*), which encodes an RNA helicase and may also contribute to this pathway (Fig. 19.34). However, unlike in *mac1* and *msp1* mutants, the enlarged cells in *ago9* and *mem* mutants express FMS-specific markers and are able to initiate gametophyte development without prior meiosis. Thus, these mutants show aspects of apospory, one of the elements of apomixis (see Section 19.4.5).

19.4.3 During megagametogenesis, the FMS divides mitotically to form the embryo sac

Once the haploid FMS is specified, it divides mitotically to form the female gametophyte. Another ARGONAUTE protein, AGO5, seems required to initiate this process of megagametogenesis, and neither *AGO5* nor *AGO9* are expressed in the cells that show a phenotype, suggesting noncell autonomous effects. About 70% of flowering plants form an eight-nucleate, seven-celled embryo sac of the *Polygonum* type, though a wide variety of other morphologies have also been described.

In *Arabidopsis* and maize, a *Polygonum* type embryo sac is formed through three mitotic divisions in a syncytium, which are followed by cellularization once eight nuclei have been formed. After the first division, the two nuclei migrate to opposite poles, where they divide two more times in synchrony, separated by a large central vacuole. This yields four

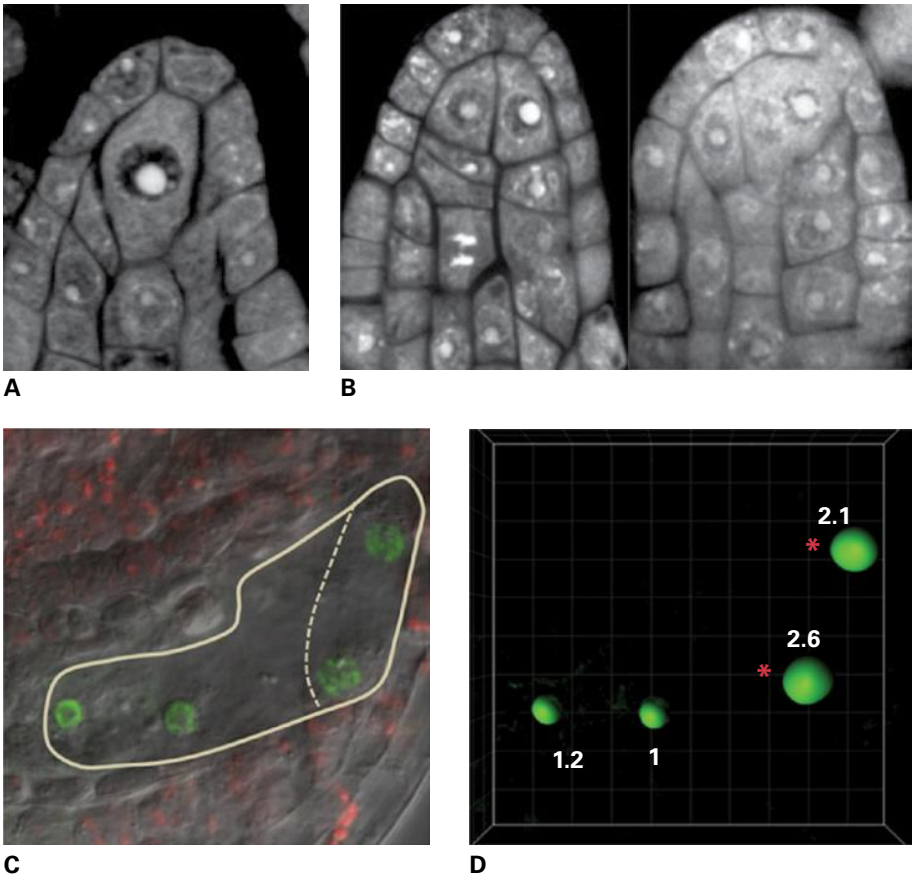


FIGURE 19.34 *The plant germline is specified by a small RNA pathway. (A) In an* Arabidopsis *wild-type plant, a single subepidermal cell enlarges and differentiates into a MMC. (B) In ago9 mutants, two or three enlarged cells form, and some of these can directly give rise to an embryo sac. (C) Two 2-nucleate embryo sacs in the mem mutant. (D) Measuring DNA content of the nuclei in (C) shows that one is derived from the normal FMS (1n), the other from an unreduced, enlarged cell (2n).*
Source: Olmedo-Monfil et al. (2010). Nature 464:628–632 and Schmidt et al. (2011). PLoS Biol. 9(9):e1001155.

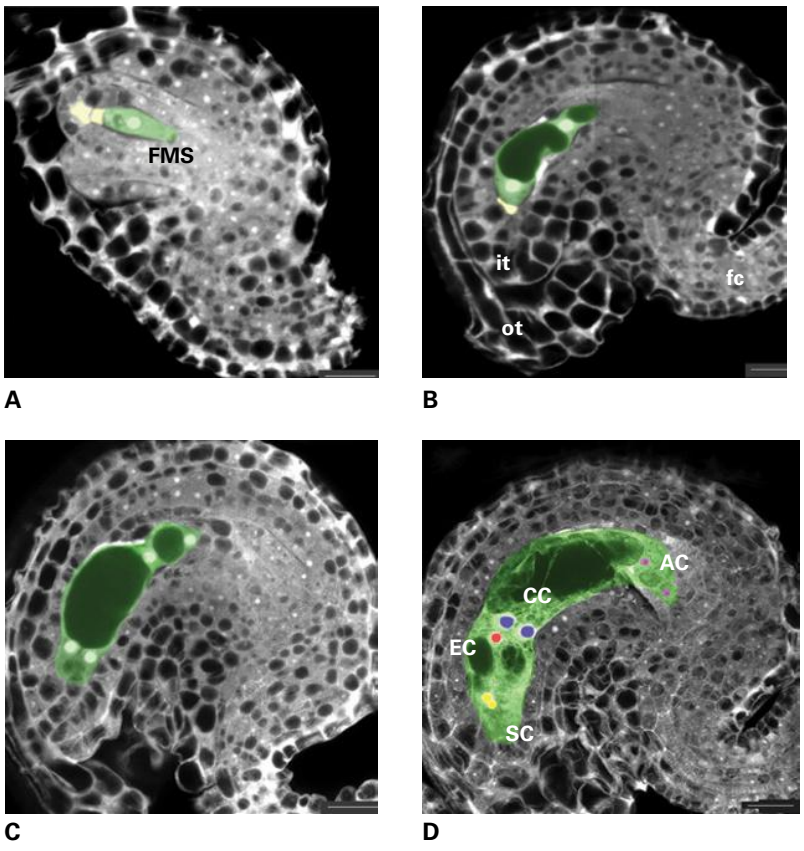


FIGURE 19.35 *Confocal optical sections illustrating embryo sac development in* Arabidopsis. *(A) The functional megaspore (FMS) initiates embryo sac development. (B) Two-nucleate embryo sac with a large central vacuole. (C) Four-nucleate embryo sac. (D) Mature embryo sac with differentiated synergid cells (SC, yellow nuclei), egg cell (EC, red nucleus), central cell (CC, blue unfused polar nuclei), and antipodal cells (AC, only two of the three purple nuclei are visible). it, inner integument; ot, outer integument; fc, funiculus. Source*: Yang et al. (2010). Annu. Rev. Plant Biol. 61:89.

nuclei at each pole, two of which (the polar nuclei) migrate towards each other and fuse prior to or during fertilization, depending on the species (Fig. 19.35). Concomitantly, cellularization forms seven cells: two gametes and five accessory cells. The accessory cells at the micropylar pole are the two synergids that play a crucial role in fertilization, and at the chalazal pole the three antipodals whose function is not well understood. Next to the synergids is the egg cell, which after fertilization gives rise to the embryo, and in the center, the homodiploid central cell will get fertilized to form the endosperm.

As with pollen development, the use of novel strategies for genetic screens (see Box 19.4) led to the identification of many mutations that disrupt embryo sac development. Gametophytes are haploid, so many of the mutations affect general functions, and mutants arrest during the mitotic phase. Therefore, most molecular analyses have focused on mutants with late phenotypes that either affect cell specification or interfere with fertilization (see Sections 19.5.5 and 19.5.6). Many of the other mutants, however, have provided important insights into basic cellular processes, such as cell cycle regulation, that, due to redundancy, have not been easy to study in other contexts. For example, mutations in proteins affecting DNA replication, licensing of origins of replication, degradation by the ubiquitin–proteasome pathway, chromatin remodeling, and histone acetylation all block mitotic progression through gametogenesis. Mutations in *RBR* lead to extra mitotic divisions in the embryo sac and a failure to express cell type-specific makers, thus connecting cell cycle control and differentiation processes. *RBR* plays a similar role during male gametophyte development (see Fig. 19.29).

19.4.4 Cell fate determination in the embryo sac relies on positional information and cell–cell communication

The polar nature of the embryo sac and its small number of distinct cell types make it an ideal system for studying fundamental aspects of plant development, such as cell specification and differentiation (Fig. 19.36). Although our understanding of cell fate determination in the female gametophyte is still fragmented, a number of mutants in *Arabidopsis* have provided important insights.

Prior to cellularization, the eight nuclei in the syncytial embryo sac adopt a distinct size that predicts their fate. This observation prompted the hypothesis that the nuclei sense positional information within the embryo sac that ultimately determines their specification. Indeed, cell fates are affected in several mutants with altered positioning of the nuclei. For example, in some embryo sacs of the *eostre* mutant in *Arabidopsis*, only one nucleus occupies the micropylar pole, while two are positioned more centrally, a pattern opposite to that observed in the wild type. Indeed, both nuclei in the more central region can differentiate into egg cells and are competent for fertilization. It was proposed that an auxin gradient specifies cell fates in the embryo sac; however, recent experiments

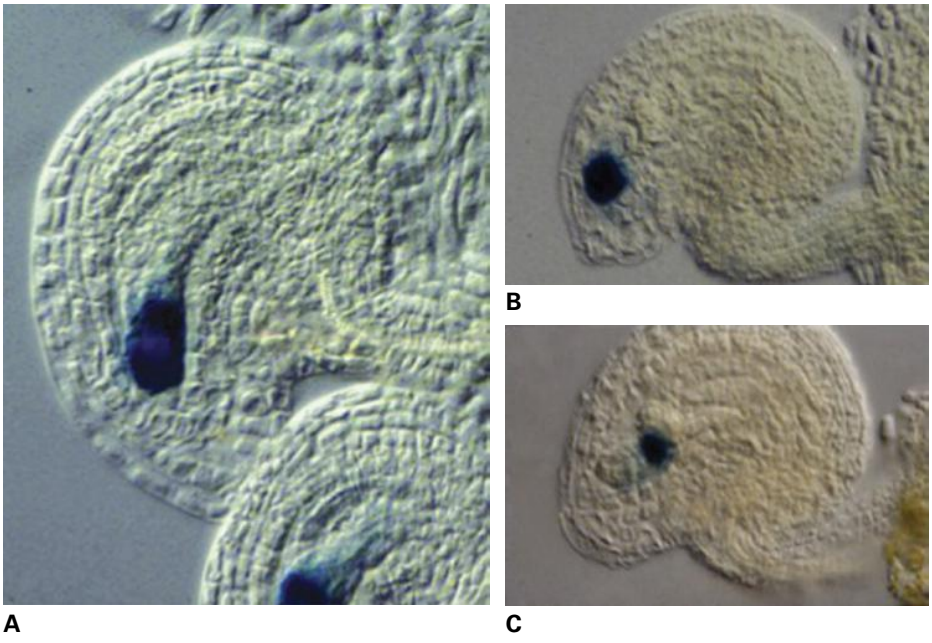


FIGURE 19.36 *Cell type-specific markers expressed in the* Arabidopsis *embryo sac. Enhancer trap lines expressed in (A) the egg apparatus (egg cell and synergids), (B) the synergids, and (C) the egg cell.*
Source: U. Grossniklaus, University of Zurich; previously unpublished.

could not detect auxin activity inside the female gametophyte. Thus, the molecules that provide this positional information are still unknown.

The analysis of another set of *Arabidopsis* mutants, *lachesis* (*lis*), *clotho* (*clo*), and *atropus* (*ato*), revealed the importance of non-cell autonomous signaling events in preventing accessory cells from adopting a gametic fate. In these mutants, synergid and central cells express egg cell characteristics while losing attributes of their original fate. Moreover, the antipodal cells show aspects of central cell specification. Thus, all cells of the embryo sac can potentially acquire a gametic fate. *LIS* is mainly expressed in the egg and central cell, suggesting that gametic cells prevent accessory cells from adopting this fate through a lateral inhibition mechanism.

LIS, *CLO*, and *ATO* encode components of the core splicing machinery. It is, therefore, likely that their role in lateral inhibition is indirect. *LIS* activity is only required in the egg cell, which thus serves as an organizing center orchestrating cell specification in the embryo sac through non-cell autonomous signals. In maize, ZmEAL1, a secreted protein of the defensin-like class and expressed in the egg cell, also affects this process, revealing the role of peptide signals in cell specification.

In summary, studies of mutants affecting specification and differentiation of the cell types in the female gametophyte have uncovered an important role of cell–cell communication and revealed an unexpected developmental plasticity that allows these cells to respond to altered signals.

19.4.5 Apomixis: asexual reproduction through seeds

Sexual reproduction produces new combinations of genotypes and, therefore, genetically and phenotypically variable progeny. Some plants can also produce seeds that are exact copies of the mother plant through **apomixis**, asexual reproduction through seeds.

Apomixis has great potential for agriculture, because apomictic seeds are clonal and preserve the genotype of the mother. Thus, apomixis can potentially be used to maintain **hybrid vigor** over many generations. Many crops are cultivated as F1 hybrids, produced by crossing two inbred parental lines. Hybrids have higher productivity, but their seeds cannot be stored to be planted in the next year because recombination and segregation break down their uniform, but highly heterozygous genotype. Thus, hybrid seeds must be generated every year, an obstacle that would be circumvented if apomixis could be induced in F1 hybrids.

Apomixis occurs in 500–600 species that belong to about 40 plant families and so is thought to have arisen multiple times during evolution. Consequently, there are also many different ways a clonal seed can be produced. In some species, such as citrus varieties and mango (*Magnifera indica*), an embryo is formed directly from a sporophytic cell of the integuments and invades the embryo sac, competing with the sexually produced embryo. In such **sporophytic apomixis**, a diploid cell gives rise to the next generation, thereby maintaining the maternal genotype. Because this can occur alongside sexual reproduction, sporophytic apomicts often produce a mix of clonal and sexual progeny.

In **gametophytic apomixis**, on the other hand, a female gametophyte is formed from an unreduced cell, thereby preserving the genotype of the mother. Because no meiosis occurs, this is referred to as **apomeiois** (Fig. 19.37). This can occur in various ways that are broadly classified as diplospory and apospory, which for instance occur in dandelion (*Taraxacum officinale*) and hawkweed (*Hieracium* spp.), respectively. In diplospory, meiosis of the MMC is omitted or aborted, resulting in formation of two unreduced spores, one of which forms the female gametophyte. This is in contrast to

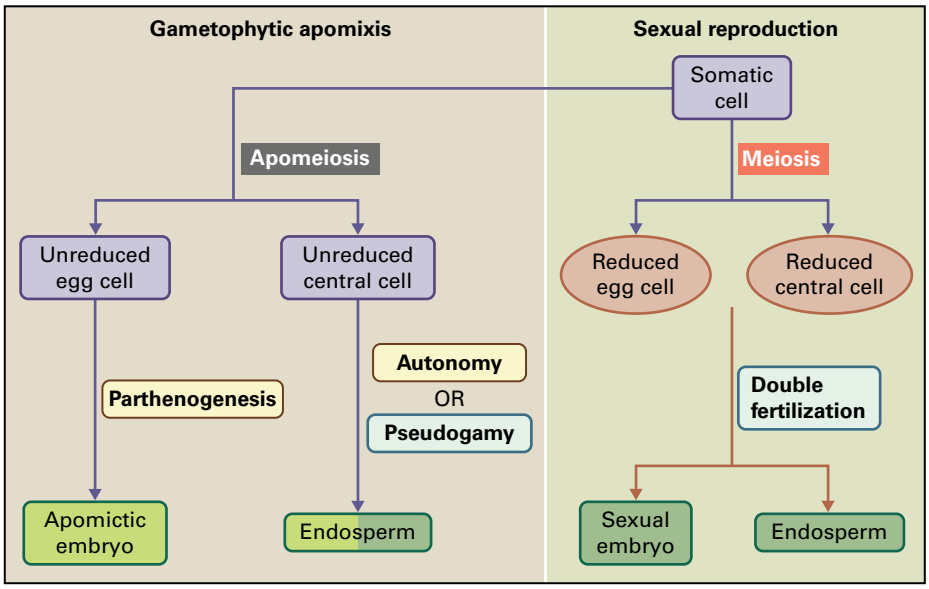


FIGURE 19.37 *Schematic representation of gametophytic apomixis and sexual reproduction. In gametophytic apomixis three developmental steps are altered such that meiosis is prevented (apomeiosis), the embryo can develop without fertilization (parthenogenesis), and functional endosperm is formed (autonomy or pseudogamy).*

apospory, where a nucellar cell other than the MMC forms the embryo sac. However, to form the next generation, the unreduced egg cell of this embryo sac must also form an embryo in the absence of fertilization (**parthenogenesis**). Finally, seed development cannot proceed normally without the formation of endosperm, the second product of double fertilization in sexual angiosperms. This can either occur through **pseudogamy,** where the endosperm is formed by fertilization, or by **autonomous** endosperm formation, in the absence of fertilization. Both modes of endosperm development in apomicts require developmental adaptations, however. Thus, at least three developmental processes are altered during apomixis in comparison to sexual reproduction: the initiation of embryo sac development from an unreduced cell (apomeiosis), the activation of embryogenesis without fertilization (parthenogenesis), and the production of functional endosperm (Fig. 19.37).

Little is known about the molecular basis of apomixis, but it is under genetic control and often influenced by the environment. In many species, apomeiosis and parthenogenesis are regulated by two independent, dominant loci. Often, these loci are in large blocks of the genome that do not recombine, making map-based cloning approaches difficult. However, screens in *Arabidopsis* and maize have identified mutants that show aspects of apomixis. Various *Arabidopsis* mutants affecting small RNA biogenesis and function (*ago9*, *rdr6*, *sgs3*, and possibly *mem*; see Section 19.4.2) can form unreduced embryo sacs in a process similar to apospory. Other mutants, for example *dyad* and a triple mutant of genes involved in meiosis (the 'mitosis instead of meiosis' line *MiMe*), resemble diplospory and form unreduced embryo sacs.

While true apomixis, which does not depend on a specific pollen donor, has not yet been achieved in *Arabidopsis*, a cross of *dyad* or *MiMe* with a special haploid inducer line generates clonal offspring. Similar haploid inducer lines, which eliminate the paternal genome after fertilization through unknown mechanisms, also exist in maize and have been used for decades to generate maternal haploid progeny. If the chromosome set of such haploid plants is doubled, for example by treatment with colchicine, a homozygous inbred plant is generated. As an alternative to microspore culture (see Box 19.2) this approach is often used in breeding programs.

19.5 Pollination and fertilization

19.5.1 Plants use a variety of strategies to bring sperm and egg cells together

Once gametes are produced, they must fuse to generate the next sporophytic generation. In bryophytes and pteridophytes, the sperm cells produced by antheridia are motile, and fertilization depends on the availability of water. In contrast, seed plants (spermatophytes) produce pollen, which germinates to form a pollen tube that transports the sperm to their target cells. In cycads and ginkgo (*Ginkgo biloba*), the sperm are flagellated and motile, and once released from the pollen tube into an integument-enclosed space, they swim to fertilize the egg cell. In all other seed plants, the sperm cells are not motile and depend on the pollen tube (vegetative cell) for their transport. In gymnosperms, germination and growth of the pollen tube can take months or even years, whereas in angiosperms, pollen tube germination and growth are extremely rapid, which may have contributed to the evolutionary success of the angiosperms. In fact, pollen tubes are the fastest growing cells known, with growth rates as fast as 650 µm per minute in chicory (*Cichorium intybus*).

In angiosperms, many of the processes that lead to successful fertilization require an exchange of signals between the pollen and the female tissues. This starts with the

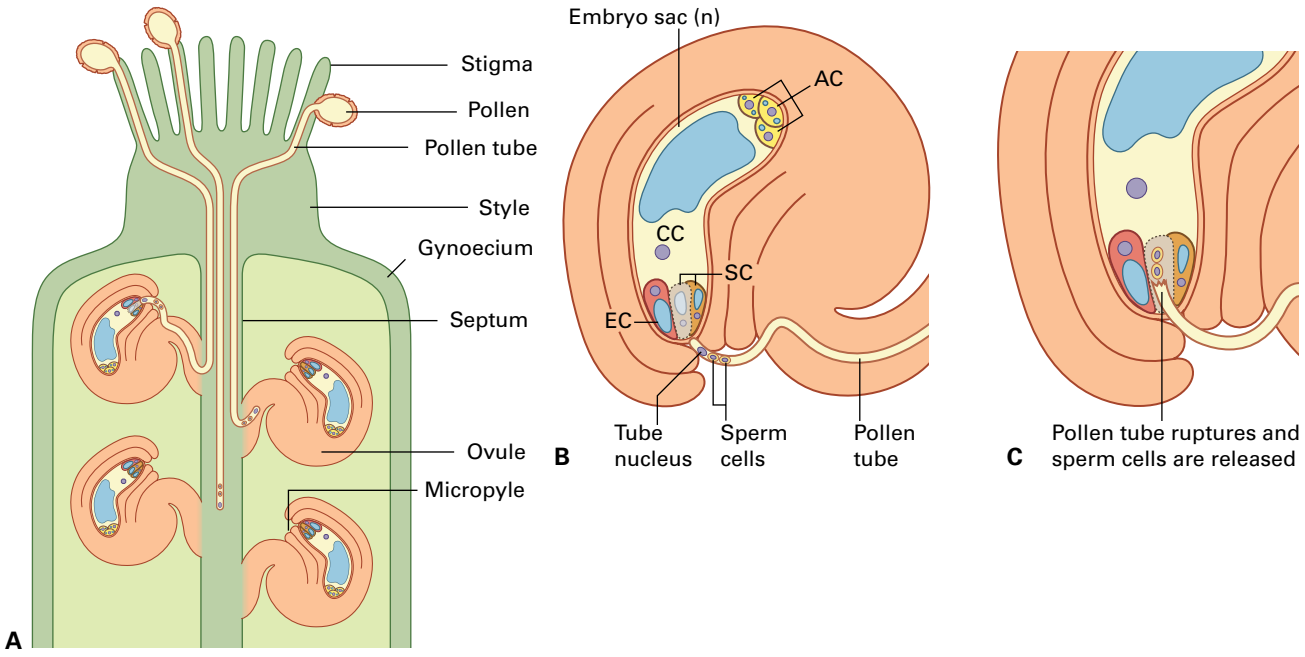


FIGURE 19.38 *Path of the pollen tube from pollination to fertilization. (A) Pollen germinates and grows a pollen tube through the style into the transmitting tract in the septum of the gynoecium, from where it emerges and is guided to the micropyle. (B) As the pollen tube arrives at the micropyle, one of the synergids (SC) starts to degenerate. (C) During pollen tube reception, the pollen tube penetrates the degenerating synergid, where it ruptures and releases the sperm cells to fertilize the egg (EC) and central cell (CC). AC, antipodal.*

recognition on the stigma surface (see Section 19.5.2), is followed by directed growth through the transmitting tract (see Section 19.5.3), guidance of the pollen tube into the micropyle (see Section 19.5.4), and pollen tube reception by the female gametophyte (see Section 19.5.5), and concludes with double fertilization whereby one sperm fuses with the egg and the other with the central cell to form the zygote and endosperm, respectively (see Section 19.5.6) (Fig. 19.38).

19.5.2 Pollen grains adhere to the stigma, where they must hydrate before they can germinate

After their formation in the pollen sac, pollen grains are released from the anther in a desiccated state (anthesis or anther dehiscence). Depending on the plant's reproductive strategy, the pollen is transported by wind, insects, birds, or even fruit bats to other flowers, where it adheres to the stigma, the receptive tip of the carpel(s) that form the gynoecium. This initial contact can be crucial for subsequent interactions and can determine whether a compatible interaction occurs. Often, pollen from other species cannot germinate on the stigma, or self-pollen is rejected through a self-incompatibility system to prevent inbreeding (see Section 19.6).

Some species, for example *Arabidopsis* and sunflower (*Helianthus annuus*), have dry stigmas, and adherence of pollen to the stigmatic papillar cell is mediated by components of the pollen exine. This adhesion is strong, but much weaker with pollen of other plant families, although the underlying chemical interactions are unknown. After this initial contact, the pollen coat, a matrix of long- and short-chain lipids with a small set of proteins, flows onto the papillar cell at the contact site. This contact seems to change the properties of the underlying membrane and enables the flow of water from the papillar cell to the pollen grain, allowing it to hydrate. This process may be mediated by aquaporins (see Chapter 3) in the membrane of the papillar cell.

The pollen coat plays a crucial role in pollen hydration, as was demonstrated by the *eceriferum* mutants in *Arabidopsis*. These mutations affect the biosynthesis of long-chain lipids and waxes, and the mutants are male sterile under dry conditions. If grown under high humidity, however, the male sterile phenotype is suppressed. Hydration activates pollen metabolism and, using the resources stored during pollen development, the pollen germinates and rapidly grows a pollen tube.

In species with wet stigmas, such as tomato, petunia, and lily (*Lilium longiflorum*), water is present in the stigma exudates, so water release may not be as tightly controlled as on a dry stigma. The exudate contains proteins, lipids, polysaccharides, and pigments that support pollen tube growth. In part, however, the lipid-rich exudate may substitute for the function of the pollen coat. Mutants lacking the secreted matrix are female sterile, but sterility can be suppressed by addition of exogenous lipids onto the stigma, which is sufficient for pollen hydration and germination. Thus, also in a wet stigma, access of the pollen to water seems to be regulated and influenced by lipids.

19.5.3 Following germination, the pollen tube grows to reach the embryo sac

Following germination, the pollen tube must grow fast through the stigma and style to reach the embryo sac, where it delivers the two sperm cells to effect double fertilization. As there is usually an excess of pollen over ovules, there is intense competition between growing pollen tubes. Pollen tubes grow only at their tips, and as they grow, their cytoplasm remains in the area behind the tip and callose plugs are formed at regular intervals to seal off the part of the tube left behind. These callose plugs are produced by callose synthase, the exact positioning of which depends on cortical microtubules. The pollen cell wall is unusual and can be divided into an outer cell wall, consisting mainly of pectins, and an inner cell wall, containing callose and cellulose that, however, only gets deposited at some distance from the tip.

Tip growth of the pollen tube depends on turgor pressure, loosening of the cell wall to allow expansion, and a constant supply of cell wall and membrane materials for incorporation at the tip. Vesicle trafficking also provides positional information by delivering specific proteins and lipids to localized membrane domains. For example, when the pollen tube changes growth direction, the delivery of vesicles must be retargeted and membrane homeostasis adjusted. Thus, vesicle and endomembrane trafficking are regulated to allow a dynamic control of polarized tip growth.

Small GTPases (see Chapter 18) transduce signals from the cell membrane to the cytoskeleton in yeast and animal cells. In plants, the ROP GTPases (see Chapter 5) also affect the dynamics of actin polymerization at the tip of the pollen tube, which is required for the appropriate targeting and fusion of vesicles. Moreover, other target proteins regulated by ROP GTPases are more directly involved in vesicle fusion, for example through controlling a complex that tethers vesicles to the membrane. ROP signaling also affects the levels of intracellular calcium and reactive oxygen species (ROS), which in turn can influence the activity of calcium channels, the actin cytoskeleton, and vesicle trafficking (Fig. 19.39).

Ion fluxes and a calcium gradient at the tip are required for tip growth, and this is consistent with the large number of ion transporters and channels that are expressed in pollen tubes. When pollen tubes alter their growth direction, a reorientation of the maximum of the calcium gradient is the first change that can be detected. Interfering with this calcium gradient blocks tip growth. Later during pollen tube growth, calcium and proton gradients oscillate, and these oscillations are strongly correlated with oscillations in pollen tube growth activity.

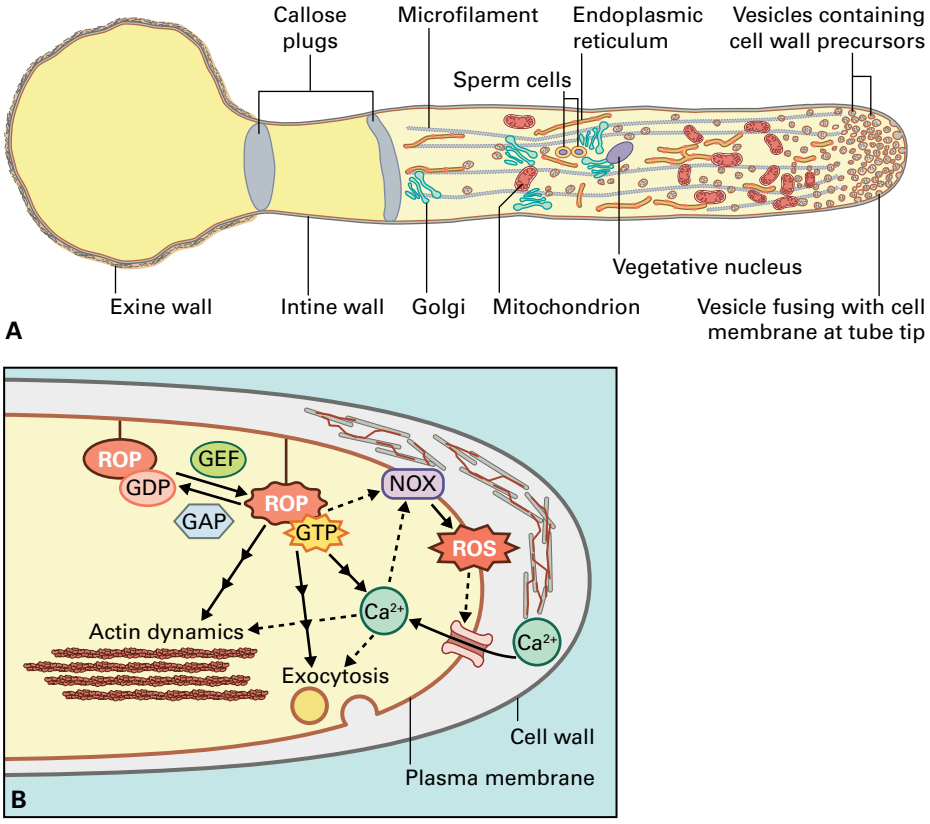


FIGURE 19.39 *(A) Schematic representation of a growing pollen tube. (B) Signaling events at the tip of a growing pollen tube. The ROP GTPase cycles between a GDP- and GTP-bound state, mediated by the GDP exchange factor GEF and the ROP-GTP activating protein GAP. Activated ROP leads to the production of reactive oxygen species (ROS) by NADPH oxidases (NOX) and calcium influx, and regulates exocytosis and actin dynamics that are central to tip growth.*

19.5.4 Pollen tube guidance requires interaction and communication with the female tissues

Pollen tube growth must be directed towards the female gametophyte, and this path requires various interactions with female tissues that provide directional cues. In both lily and *Arabidopsis*, copper-binding proteins known as plantacyanins provide this initial chemotactic guidance. In lily, plantacyanins are secreted by the cells lining the transmitting tract of the wet stigma and can reorient pollen tube growth in vitro, indicating they act as a chemotactic signal. *Arabidopsis* mutants harboring mutations in homologs have normal pollen tube growth likely due to genetic redundancy; however, overexpressing plantacyanin in the stigmatic papillar cells results in a loss of directional growth, and many pollen tubes grow around the papillar cell, unable to find the transmitting tissue. This suggests that plantacyanin overexpression may mask the normal gradients of chemotactic signals and causes pollen tubes to lose their orientation.

In *Arabidopsis*, the pollen tube grows between the cells of the transmitting tissue, present in the septum separating the two carpels, towards the base of the gynoecium. The pollen tubes eventually leave the transmitting tissue at seemingly random positions to grow on the surface of the placental tissue inside the carpel cavity, from where they grow along the funiculus of an ovule to enter the micropylar opening (see Fig. 19.38). In wild-type plants, this process is precise, with every ovule receiving only one pollen tube. This precision is thought to be regulated by several signals that direct pollen tube growth. First, a long-range signal directs pollen tube growth along the funiculus towards the micropylar opening; then, a short-range signal guides the pollen tube inside the micropyle, where it makes contact with the female gametophyte.

Once fertilization has occurred, no other pollen tubes are attracted, suggesting the existence of a repulsive signal. The growth direction of in vitro growing pollen tubes is affected by nitric oxide (NO), a gas with signaling function in both animals and plants. However, whether NO is a repulsive signal also in planta is not known. The combination of attracting and repulsing signals ensures that only one pollen tube enters a micropyle, thereby preventing the release of more than two sperm, which could cause polyspermy.

In *Arabidopsis* the chemotactic signals are produced by the embryo sac: pollen tube guidance is disrupted in mutants in which the female gametophyte is either absent or arrested. The source of the guidance signal was dissected using a semi-in vitro system with ovules of the wishbone flower (*Torenia fournieri*). In these ovules, the micropylar part of the embryo sac is not enclosed by integuments, so synergids, egg, and part of the central cell are exposed. If such ovules are placed on growth medium, pollen tubes can detect the guidance signals and target the filiform apparatus, a structure secreted by the synergids (Fig. 19.40). However, only pollen tubes that have grown through a stigma, which was cut and placed on the medium so they can grow onto it, are properly guided, whereas pollen tubes germinated in vitro are not. This finding suggests that pollen tubes must be activated through unknown interactions in the stigma, such that they are competent to respond to the guidance cues.

Laser ablation of the cells in the female gametophyte demonstrated that the synergids are the source of the guidance signal. Subsequently, an analysis of genes expressed in the synergids of the wishbone flower identified secreted CRPs with similarities to antimicrobial defensins that are able to attract pollen tubes. Downregulation of two of these CRPs showed that they are required for pollen tube attraction in the semi-in vitro system described above. Thus, these CRPs, named LURE1 and LURE2, serve as guidance signals in this system.

Another micropylar signaling molecule was identified in maize. The *ZmEA1* gene, expressed in the synergids and egg cell, encodes a small protein with a putative transmembrane domain that is cleaved, such that a part of the protein can diffuse into the micropyle. Downregulation of *ZmEA1* in transgenic plants by RNAi interferes with micropylar guidance, demonstrating its importance in this signaling process. How these guidance molecules are perceived by the pollen tube, however, is currently unknown.

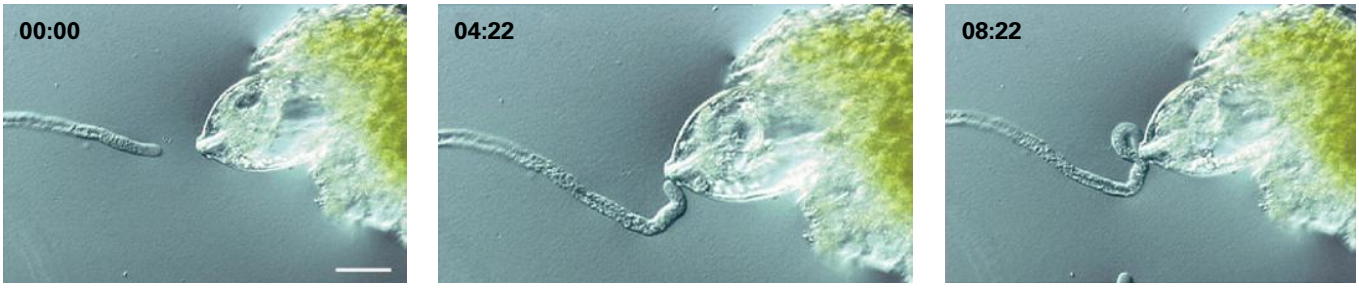


FIGURE 19.40 *(A–C) Pollen tube guidance in a semi-in vitro system. The exposed embryo sac of* Torenia fournieri *secretes an attractant that guides the pollen tube towards the filiform apparatus between the two synergid cells. The pollen tube targets and penetrates the synergid.*
Source: Higashiyama et al. (2008). Sex. Plant Reprod. 21:117.

19.5.5 Pollen tube reception requires active communication between male and female gametophytes

Once the pollen tube enters the micropyle, it penetrates one of the synergid cells and ruptures to release the two sperm cells. Subsequently, one sperm fuses with the egg, and the other fuses with the central cell to initiate seed development. The receptive synergid cell initiates a programmed degeneration process, possibly to reduce its turgor pressure and make other cellular adjustments that allow pollen tube discharge. The timing of this degeneration process varies between species: it can start shortly after pollination, which implies the existence of a long-range signal that controls this process, or only once the pollen tube enters the micropyle, as in *Arabidopsis*.

For many years, the rupture of the pollen tube in the synergid cell was considered a purely mechanical process caused by an environment of drastically different osmolarity leading to pollen tube lysis. Identification of the allelic gametophytic *Arabidopsis* mutants *feronia* (*fer*) and *sirène*, however, showed it to be under the control of the female gametophyte. In these mutants, wild-type pollen tubes are attracted to and enter the female gametophyte, but instead of stopping their growth and rupturing to release the sperm cells, they continue to grow inside the embryo sac. This showed that pollen tube reception requires active communication between the male and female gametophytes. *FER* encodes an RLK (see Chapter 18) that is expressed in the synergid cells in which it accumulates in the region around filiform apparatus (Fig. 19.41). Although the putative ligand for FER is unknown, it is likely that it is either secreted or present on the surface of the pollen tube.

Several other mutants with a *fer*-like phenotype have been identified, including *nortia* (*nta*) and *turan* (*tun*), which like *FER* were named after Etruscan goddesses of fertility, and *lorelei* (*lre*). The molecular characterization of these genes suggests that complex signaling events occur at the synergid membrane. Whereas *LRE* encodes a putative glycophosphatidylinositol-anchored protein and NTA belongs to the MLO (MILDEW RESISTANCE LOCUS O) family of seven transmembrane proteins (see Chapter 21), *TUN* encodes a putative UDP-glycosyltransferase superfamily protein, which may be required for glycosylation of the membrane proteins involved in pollen tube reception (see Chapter 4).

The molecular nature of *NTA* revealed interesting parallels between pollen tube reception and fungal infection (see Chapter 21). The first member of the MLO family to be identified was a powdery mildew resistance gene in barley (*Hordeum vulgare*). The wild-type allele is required for a successful penetration of the epidermis by tip-growing fungal hyphae, a function conserved across plant species that in *Arabidopsis* is shared by three redundant MLO proteins (see Chapter 21). This raised the question of whether similar molecular processes are involved in plant defense and plant reproduction. While *NTA* is expressed rather specifically in synergid cells, *FER* is detected in most plant tissues and shows strong expression in epidermal cells. Indeed, homozygous *fer* mutants are resistant to powdery mildew infection,

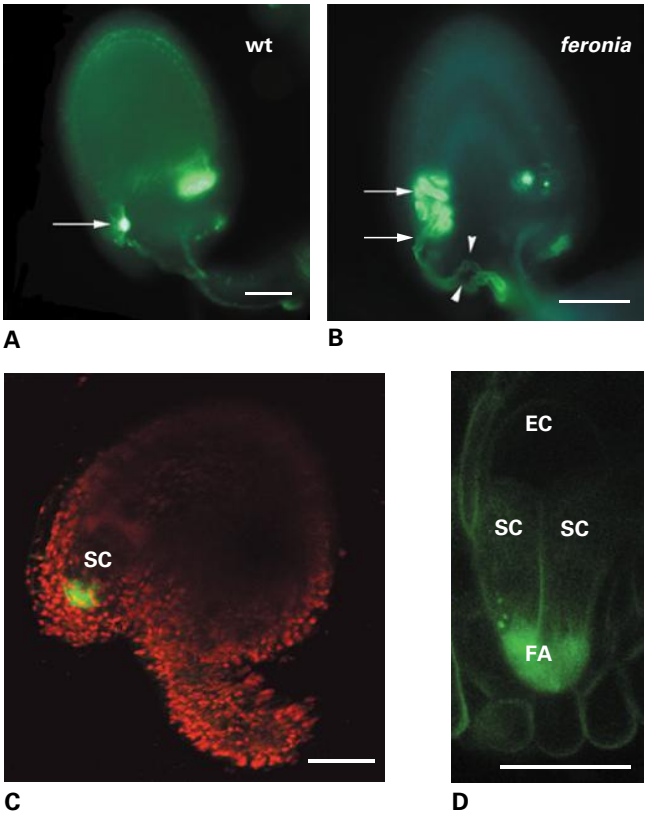


FIGURE 19.41 *Pollen tube reception in* Arabidopsis *requires the FERONIA receptor-like kinase. (A, B) Ovules stained with aniline blue to visualize the pollen tubes. In the wild type (A), the pollen tube enters the micropyle and penetrates the synergid where it ruptures. In fer mutant female gametophytes (B), the pollen tube fails to rupture and continues to grow inside the embryo sac. In this image, two pollen tubes entered the micropyle. (C, D) The FER-GFP fusion protein (green) expressed under the FER promoter is visible at high levels in the synergid cells (SC) (C), where it accumulates at the micropylar pole around the filiform apparatus (FA). EC, egg cell. Source*: Escobar-Restrepo et al. (2007). Science 317:656.

suggesting that in leaves, FER, together with the three redundant *Arabidopsis* MLO proteins, confers susceptibility to the invading fungus, while in the synergid FER, together with NTA, is required for successful pollen tube reception. Similarities with defense-related processes have also been found for other aspects of plant reproduction. For instance, CRPs that have similarities to defensins serve as signaling molecules in pollen tube guidance, pollen tube rupture, and self-incompatibility (see Section 19.6).

Successful fertilization also relies on the precise timing of pollen tube rupture, which involves the two closest *Arabidopsis* homologs of FER, the redundant ANXUR (ANX1/2) RLKs, both of which are exclusively expressed in pollen. In *anx1/2* double mutants, pollen tubes can germinate in vitro, but they burst soon after germination, while in planta they can grow into the style but only rarely reach the gyneocium. Thus, it appears that *ANX1/2* are required to prevent premature rupture of the pollen tube, and a putative ligand may relieve this repression once it has entered the synergid cell.

Moreover, pollen tube rupture depends on ion transporters, possibly changing the pollen tube's osmolarity and lead to

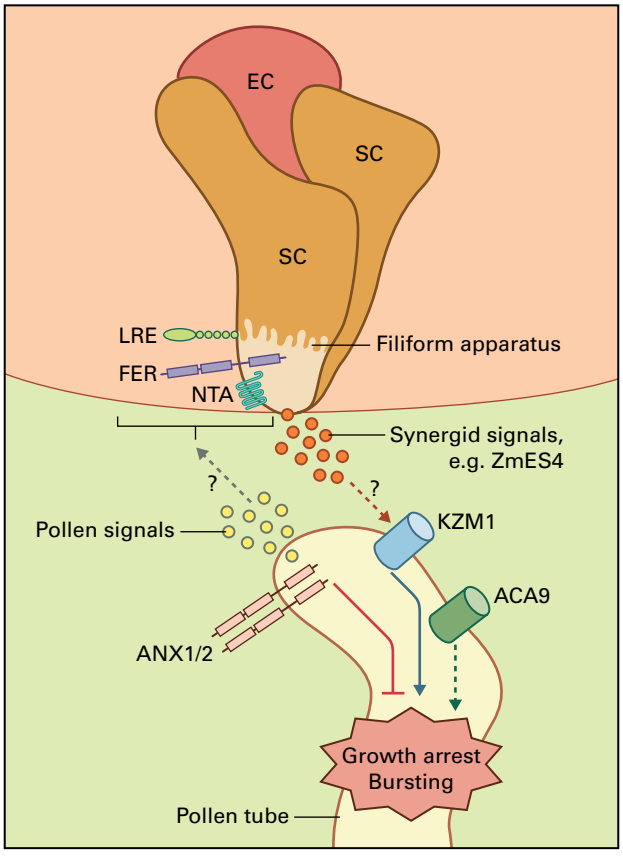


FIGURE 19.42 *Signal exchange during pollen tube reception. In the synergid cells (SC), the membrane proteins FER, NTA and LRE are involved in the perception of a putative ligand produced by the arriving pollen tube. The rupture of the pollen tube is prevented by ANX1/2, the closest homologs of the FER receptor-like kinase. Rupture is presumably induced by secreted signals from the synergids; in maize this is ZmES4 that eventually activates KZM1. See text for details.*

lysis. In *Arabidopsis*, pollen tubes of mutants affecting the autoinhibited Ca^{2+} ATPase *ACA9* gene can enter the micropyle but fail to burst and discharge their contents, suggesting that Ca^{2+} transport plays an important role in this process (Fig. 19.42). Recent studies in maize have shown that in vitro application of the ZmES4 defensin-like CRP leads to the opening of the inward-rectifying K^+ channel KZM1. *ZmES4* is specifically expressed in the embryo sac and its downregulation leads to a failure of pollen tube discharge but leaves guidance unaffected. Together with the fact that ZmES4 acts in a species-specific manner, these observations suggest that ZMES4 serves as a female gametophyte-derived signal that induces pollen tube rupture upon normal reception, releasing the sperm cells to effect double fertilization.

19.5.6 Double fertilization involves two gametic fusion events

When the pollen tube ruptures to release its contents, the two sperm cells remain together and rapidly reach a position between the egg and central cell. The sperm cells remain

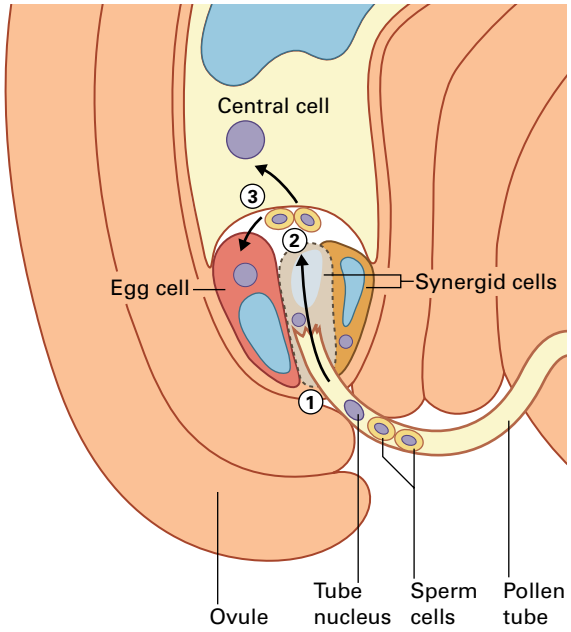


FIGURE 19.43 *Sequential steps during double fertilization. (1) The pollen tube penetrates the degenerating synergid, (2) the sperm cells are discharged as the pollen tube ruptures and localize next to egg and central cell, and (3) one sperm cell fuses with the egg and the second with the central cell, followed by karyogamy of maternal and paternal nuclei.*

immobile for several minutes before they separate and fertilize the egg and central cell to initiate seed development (Fig. 19.43).

In the male gametophytic *generative cell specific1/hapless2* (*gcs1/hap2*) mutant of *Arabidopsis*, the rapid movement of the sperm cells is normal, but they remain in the position between egg and central cell and do not fuse with the female gametes, indicating that the GCS1 gene product is required for gamete fusion. Interestingly, *GCS1* is highly conserved and plays a similar role in gamete fusion in the unicellular green alga *Chlamydomonas reinhardtii* and the malaria parasite *Plasmodium falciparum*.

In an in vitro system using isolated sperm and egg cells from maize, fusion of the gametes triggers Ca^{2+} influx at the site of fusion, and a Ca^{2+} wave subsequently spreads throughout the egg in a manner similar to that in animals. Artificial Ca^{2+} influx caused by the addition of Ca^{2+} ionophores to the egg cell triggers some aspects of egg activation, such as the secretion of cell wall components, indicating that the Ca^{2+} increase is functionally important.

A longstanding question is whether the two sperm cells of flowering plants are functionally equivalent. In the wild leadwort (*Plumbago zeylandica*), for example, the two sperm cells are dimorphic and differ in size and the number of organelles, and the smaller sperm cell always fertilizes the egg cell. This raises the question whether the two sperm cells in other species may not be equivalent either, even though they may not differ in morphology. *Arabidopsis* mutants have shown that its isomorphic sperm cells are functionally equivalent. Some mutants, such as *eostre* and *rbr* (see Section 19.4.4), sometimes produce two egg cells, both of which may be fertilized. Some male gametophytic mutants, on the other hand, produce only one sperm-like cell

that can fertilize either the egg or the central cell. These observations indicate that there is no a priori distinction between the two sperm cells, and this was confirmed in an experiment with a photoconvertible fluorescent protein expressed in the sperm cells, which allowed the differential marking of the two sperm cells in the pollen tube. Observing double fertilization showed that the two sperm fuse randomly with either female gamete, demonstrating their functional equivalence.

The fact that both sperm cells have the potential to fuse with either the egg or the central cell raises the question why polyspermy (events where both sperm cells fuse with the same female gamete) does not occur in plants. In animals, a fast block, relying on membrane depolarization and Ca^{2+} influx, and a slow block, involving the fusion of secretory vesicles and modification of the extracelluar matrix, prevent polyspermy. In plants, it is not clear whether similar mechanisms exist, even though a Ca^{2+} wave has been observed after in vitro fertilization. However, the central cell can be fertilized by multiple sperm. In many apomicts, where the egg cell develops parthenogenetically and is not fertilized, the central cell fuses with both sperm cells delivered by the pollen tube to ensure normal endosperm development (see Section 19.7). Therefore, at least the central cell has no fast block to prevent polyspermy.

Such a block may not be necessary if it can somehow be ensured that the two sperm cells fuse with distinct female gametes. Because only a single pollen tube usually enters the micropyle, opportunities for fusion with multiple sperm cells are extremely rare. Indeed, plants limit access of sperm to the embryo sac by preventing the attraction of multiple pollen tubes. In wild-type plants, gene expression in the persisting synergid cell gets rapidly downregulated upon pollen tube reception, and likely also the expression of the pollen tube attractant. However, in *fer* and other *Arabidopsis* mutants that affect pollen tube reception, two or even three pollen tubes can enter the micropyle. This seems to be caused by continued gene expression in the persisting synergid cells of these mutants. Thus, pollen tube rupture or sperm release is required to downregulate gene expression in synergid cells and stop the continued production of the attractant. Fertilization itself causes this downregulation, suggesting noncell autonomous signaling events between the female gametes and the synergid cells. In *gcs1* and *duo1* mutants, in which pollen tubes discharge occurs but the sperm cells do not fuse with the female gametes, additional pollen tubes are attracted to and penetrate the persisting synergid cell. If these additional pollen tubes are wild-type, they can rescue ovules that received defective sperm cells, thereby maximizing reproductive success.

19.6 The molecular basis of self-incompatibility

Plant stigmas are exposed to many types of pollen, and if pollen from a different species fertilizes the egg cell, this usually leads to inviable progeny. In most cases, foreign pollen does not germinate or, if it does, it cannot interpret the signals that should guide it to the micropyle. If the pollen is from a closely related species, however, it may overcome these prefertilization barriers to interspecific hybridization and eventually reach the degenerating synergid cell.

At this step, however, fertilization can also be blocked if the signals required for pollen tube reception cannot be properly interpreted. For example, in crosses between *A. thaliana* and *A. lyrata*, almost all ovules are targeted by an *A. lyrata* pollen tube, but in about half of them, the pollen tube fails to rupture, showing a phenotype similar to that observed in the *fer* mutant. Fertilization occurs in the remaining half of the ovules, illustrating that sometimes the complex signals can successfully be exchanged if the species are sufficiently close (*A. thaliana* and *A. lyrata* diverged 5–10 million years ago). These hybrid seeds, however, usually abort if they are not rescued through ovule culture, a method that is often used to facilitate wide crosses in breeding programs.

Plants have not only evolved mechanisms to prevent interspecific hybridization, but most species can also prevent self-fertilization. Self-fertilization can lead to inbreeding depression, the counterpart to hybrid vigor, because inbreeding leads to high levels of homozygosity, including that of deleterious alleles. Of course, self-fertilization can also be advantageous because no partner is required for reproduction. Thus, many pioneer plants are self-fertilizing. Based on phylogenetic evidence, however, most self-fertilizing species are evolutionarily "young," and this mode of reproduction has negative effects for the long-term survival of a species.

Most species rely on a mechanism to prevent self-pollination. For example, the timing of anther dehiscence and stigma receptivity may not coincide (**dichogamy**), preventing germination of self-pollen on the stigma. Alternatively, anther and stigma can be spatially separated to reduce self-pollination (**herkogamy**) (Fig. 19.44). An extreme version of spatial separation is the formation of distinct male and female flowers, either on the same individual as in maize (**monoecy**), or on different individuals (**dioecy**), as in hemp (*C. sativa*) or willow (*Salix alba*). Another mechanism for preventing self-pollination is a **self-incompatibility** system that allows the distinction of self and non-self pollen on the same stigma.

19.6.1 The genetics of self-incompatibility can be complex

Biochemical self-incompatibility systems rely on molecular recognition processes that allow discrimination of self and non-self pollen. Conceptually, such a system must involve at least one pollen factor and one stigma factor. If the factors match, for example, in a molecular interaction that is similar to ligand-receptor recognition, self-fertilization is prevented.

The genetic investigation of self-incompatibility, which was discovered about 200 years ago in early plant hybridization studies, began soon after the rediscovery of Mendel's laws of inheritance. In the 1920s, self-incompatibility was found to be caused by a single locus, now referred to as the



FIGURE 19.44 *Heterostyly in* Primula veris. *The thrum morph (left) has the anthers at the top of the tube near the corolla and the stigma in the middle of the tube. In the pin morph (right), the position of anthers and stigma are reversed.*
Source: R. Ganz, B. Keller and E. Conti, University of Zurich; previously unpublished.

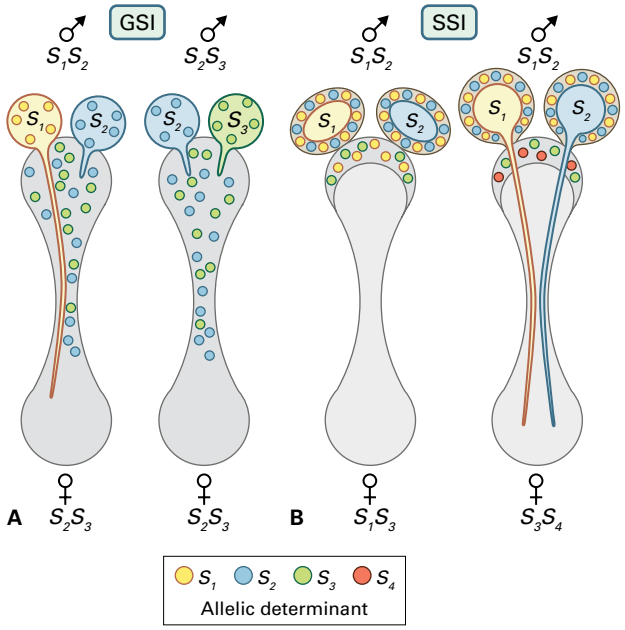


FIGURE 19.45 *Genetic basis of self-incompatibility. (A) In gametophytic self-incompatibility (GSI), pollen grains that have S-alleles different from those of the female are successful, i.e. the genotype of the male gametophyte matters. On an S_2S_3 stigma, for example, S_1 pollen grows through the style but S_2 and S_3 pollen tubes are arrested. (B) In sporophytic self-incompatibility (SSI), all pollen derived from a male sharing any S-allele with the female fail to germinate, i.e. the genotype of the male sporophyte matters. Because the pollen factor is present in the pollen coat, neither S_1 nor S_2 pollen can germinate on an S_1S_3 stigma, while they are successful on a S_3S_4 stigma.*

Sterility, or *S*-locus in most species. The *S*-locus has numerous alleles (S_1, S_2, S_3, etc.), and incompatibility results whenever both crossing partners carry the same allele. Thus, the *S*-locus must be highly polymorphic, with every allele of the *S*-locus differing in sequence from all others; wild cabbage (*B. oleracea*), for example, has more than 50 *S*-alleles.

Each *S*-locus allele consists of at least the genes encoding the pollen and the stigma factor, respectively. To prevent the breakdown of self-incompatibility, genes coding male and female factors must be inherited together as a single unit. Therefore, recombination between the two components of the *S*-locus must be suppressed. How recombination at the *S*-locus is prevented is not well understood, but the chromosomal rearrangements that characterize different alleles of the *S*-locus may contribute to this suppression of recombination.

Based on genetic behavior, self-incompatibility can be subdivided into two types. In **gametophytic self-incompatibility** (GSI), self-recognition depends on the genotype of the *S*-locus carried by the haploid pollen grain, the male gametophyte. If that pollen *S*-allele matches one of the two *S*-alleles expressed in the diploid stigmatic tissues, the pollen is rejected (Fig. 19.45). GSI systems are widespread and have been described in over 60 plant families, including the Solanaceae, Rosaceae, and Papaveraceae. In these systems, incompatible pollen tubes usually germinate, but their growth is inhibited in the style before they reach the ovules. In **sporophytic self-incompatibility** (SSI), pollination is usually interrupted early, at pollen hydration or pollen tube germination. The *S*-locus genotype of the diploid pollen parent, the sporophyte, determines whether pollination is successful. If any of the two *S*-alleles in the male parent is shared with the female parent, the cross is incompatible (Fig. 19.45). SSI is less common, occurring in the Asteraceae and Brassicaceae, but it includes one of the best-studied examples at the molecular level (*Brassica* spp.).

Although most self-incompatibility systems are controlled by genes within a single *S*-locus, the situation can be more complex. In rye (*Secale cereale*), for example, the two gametophytically acting loci *S* and *Z* control self-incompatibility, and in the tall buttercup (*Ranunculus acris*) self-incompatibility relies on at least four different loci. In the systems we describe in the following sections, however, genes encoded at a single *S*-locus determine success or failure of pollination, but the underlying molecular mechanisms differ greatly.

19.6.2 Sporophytic self-incompatibility in *Brassica* is mediated by a receptor-like kinase

In the Brassicaceae, the SSI system relies on interactions between the pollen grain and a stigmatic papillar cell. The self-incompatibility reaction is rapid, established within

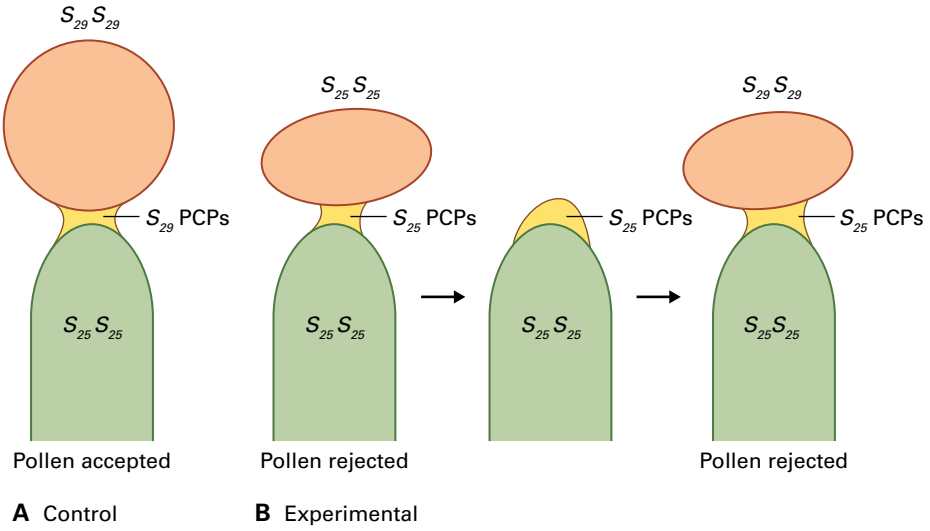


FIGURE 19.46 *The pollen factor is present in the pollen coat. Plants homozygous for an S-allele are shown for simplicity. After adhesion of the pollen on the papillar cell, the pollen coat containing pollen coat proteins (PCPs) flows partly onto the stigmatic papillar cell. PCPs can be deposited onto a papillar cell by placing and then removing a pollen grain on it with a micromanipulator. (A) A compatible cross between pollen from an $S_{29}S_{29}$ plant and a $S_{25}S_{25}$ female can be made into (B) an incompatible cross by first placing pollen from an $S_{25}S_{25}$ plant onto the point of adhesion, thus depositing the PCPs that initiate the self-incompatibility response. The same can be achieved by depositing biochemical fractions enriched for 6–8 kDa PCPs onto the papillar cell.*

minutes, and is localized on the surface of the papillar cell. This is illustrated by placing pollen grains on individual papillar cells using a micromanipulator. When self-compatible and -incompatible pollen grains are deposited next to each other on a single papillar cell, the incompatible grain does not hydrate, but the compatible grain germinates. Thus, the interaction must be localized to a small region of the papillar cell's surface and does not involve a response of the whole cell. Furthermore, if the nonhydrated pollen is subsequently placed onto a compatible stigma, it can effectively participate in pollination. Therefore, unlike in the systems described below, the SSI system in Brassicaceae does not cause cell death of incompatible pollen.

Once a pollen grain lands on the stigma, a part of the pollen coat flows onto the papillar cell (see Section 19.5.2). The pollen coat contains the pollen factors that determine the specificity of the self-incompatibility interaction. This can be demonstrated by placing a compatible pollen grain on to the same spot where an incompatible pollen grain was placed and then removed. The compatible pollen cannot germinate because the pollen coat material that was left behind initiated an incompatible reaction (Fig. 19.46). The presence of pollen factors in the pollen coat explains the sporophytic nature of the self-incompatibility system in Brassicaceae. The pollen coat contains molecules that were produced by the tapetum. Since the tapetum is diploid, it usually expresses both *S*-alleles of the pollen parent, such that two distinct pollen factors encoded by the two *S*-alleles are expected to be present in the pollen coat.

The self-incompatibility response is mediated by the interaction of an RLK expressed in the papillar cell and a secreted ligand in the pollen coat (Fig. 19.47). The *S*-locus receptor kinase (SRK) is a single-transmembrane serine/threonine kinase that is localized to the plasma membrane of the papillar cell. It binds and recognizes the pollen factor, a small CPR of the defensin class, which is referred to as *S*-locus cysteine-rich protein (SCR) or *S*-locus protein 11 (SP11). Both SRK and SCR/SP11

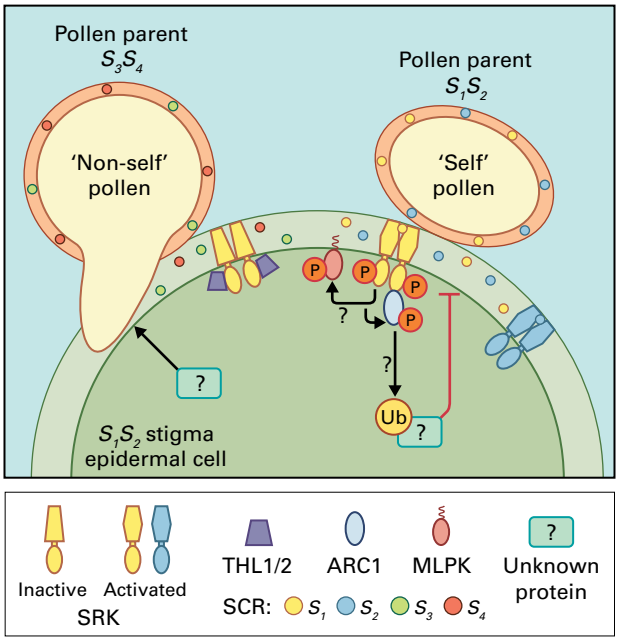


FIGURE 19.47 *Model for SSI in Brassica spp. Left, a compatible interaction is shown where SRK is not activated. Right, an incompatible interaction where the SCR/SP11 ligand induces a signaling cascade in the papillar cell. See text for details. Ub, ubiquitin.THL, thioredoxin h-like protein; ARC1, Armadillo repeat-containing protein 1; MLPK, M-locus protein kinase.*

are polymorphic as expected, and at the amino acid level their sequences can differ by as much as 35% for SRK and 70% for SCR/SP11. In fact, several biochemical, genetic, and molecular biological approaches to identify the pollen factor failed, and a genomics approach brought the breakthrough by looking for an anther-expressed polymorphic gene closely linked to *SRK*.

The specific interaction of SRK and SCR/SP11 variants encoded by the same *S*-allele prevents pollen hydration. That

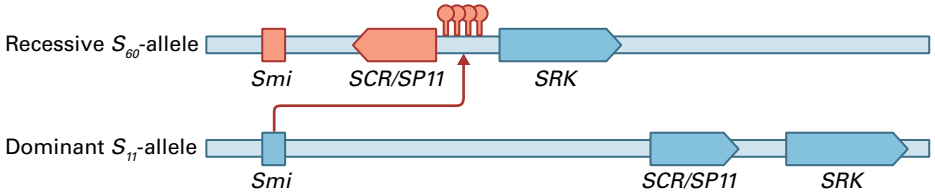


FIGURE 19.48 *Model for the dominant/recessive S-alleles in Brassica rapa. The dominant S_{11} allele contains the Smi gene, which produces a small RNA that is complementary to a sequence in the promoter of the SCR/SP11 gene of the recessive S_{60} allele. The small RNA leads to the silencing of SCR/SP11 on the recessive allele by DNA methylation. Blue genes: expressed, red genes: not expressed.*

these two proteins are solely responsible for determining the specificity of the interactions has been shown by both loss-of-function and gain-of-function approaches. Downregulation of *SRK* in transgenic plants leads to the breakdown of self-incompatibility in an allele-specific fashion. Conversely, expression of an additional *SRK* or *SCR/SP11* allele confers an additional specificity to stigma or pollen, respectively.

The two proteins are not only required, but sufficient for self-incompatibility, because the transfer of corresponding *SRK* and *SCR/SP11* alleles from *A. lyrata* to *A. thaliana*, which became self-fertilizing less than one million years ago, shows that they are still functional. Although self-fertilization in *A. thaliana* has multiple independent origins, 95% of the European accessions share an inversion in the *SCR/SP11* gene, suggesting a rapid, recent spread of this allele. Thus, the signal transduction components acting downstream of *SRK* all function in self-fertilizing *A. thaliana*. This is consistent with the recent evolution of self-fertilization in this species but also with the fact that these downstream components may also be essential for signaling processes other than self-incompatibility.

While much work has been done to understand the evolution and function of the determining pollen and stigma factors, less is known about the signal transduction cascade induced by binding of SCR/SP11 to SRK. SRK forms homodimers in the absence of its ligand, but these are kept in an inactive state by two thioredoxin *h*-like proteins (THL1/2) through a mechanism that is not well understood. Interaction of SRK with SCR/SP11 relieves this inhibition, leading to autophosphorylation of SRK. This allows interaction with the Armadillo repeat-containing protein 1 (ARC1), which binds only the phosphorylated form of the intracellular SRK kinase domain. How this interaction leads to the inhibition of pollen germination is unknown, but the localization of ARC1 to the proteasome indicates an involvement in protein degradation. Finally, the *M*-locus protein kinase (MLPK), mutations in which render plants self-compatible, is also involved in signal transduction through an unknown mechanism. MLPK is putatively myristoylated and thus likely membrane bound (Fig. 19.47).

Most *S*-alleles are co-dominant but some show dominant/recessive interactions. For example, the *Brassica rapa* S_{11}-allele is dominant over the S_{60}-allele in the pollen, so pollen produced by a $S_{11}S_{60}$ plant can germinate on a stigma expressing the S_{60}-allele. These dominant/recessive interactions may be complex and can differ between the stigma and the pollen. The dominance of the S_{11}-allele in pollen depends on an epigenetic mechanism. The recently discovered *Smi* gene of the S_{11}-allele encodes a small RNA that acts in *trans* on the *SCR/SP11* gene of the S_{60}-allele, leading to the methylation of its promoter via the RNA-dependent DNA methylation pathway. DNA methylation leads to the silencing of the pollen factor gene *SCR/SP11* of the S_{60}-allele and thus its recessive behavior in pollen (Fig. 19.48).

19.6.3 Gametophytic self-incompatibility in poppy: a signaling cascade leads to cell death of the pollen tube

While the SSI system in *Brassica* spp. acts early during the pollen–stigma interaction, gametophytic systems (GSI) lead to the death of the pollen tube after it germinates. In the field poppy (*Papaver rhoaes*), for example, pollen tubes germinate but die shortly after they penetrate the stigma. The signaling events of the self-incompatibility response in poppy have been characterized in detail, since the response can be recreated in an in vitro system, and stigmatic extracts from poppy can efficiently inhibit growth of incompatible pollen tubes. Therefore, the requirements for the self-incompatibility reaction and associated signaling events can be studied by comparing pollen tubes in the presence of stigma extracts from either compatible or incompatible plants.

The ligand that induces cell death in the growing pollen tube is a low-abundance glycoprotein of about 15 kDa that is secreted by stigmatic cells. This stigma factor, referred to as PrsS (*Papaver rhoaes* stigma *S*), is polymorphic and inhibits pollen tube growth in an allele-specific manner. Although it has no obvious similarity to known ligands, its secreted nature and small size suggest that it is detected by a putative receptor on the pollen tube in an allele-specific manner. This receptor, PrpS (*Papaver rhoaes* pollen *S*) encodes a novel transmembrane protein of about 21 kDa. As expected, *PrpS* and *PrsS* are polymorphic, and the proteins interact through an extracellular loop of PrpS. Downregulation of *PrpS* alleviates pollen tube growth inhibition in an allele-specific manner, demonstrating the crucial role of PrpS in the recognition process. A second integral membrane protein, the S-protein binding protein (SBP), may facilitate the interaction between ligand and receptor. It binds PrpS, but not in an allele-specific manner, and enhances the effect of PrpS to inhibit pollen tube growth in the in vitro system.

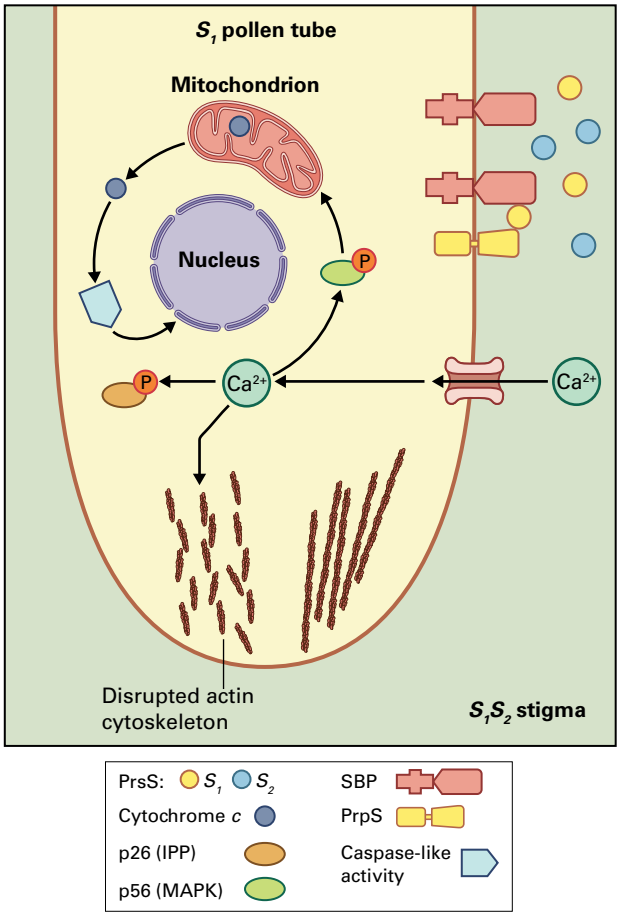


FIGURE 19.49 *Model for GSI in* Papaver rhoaes. *Binding of the stigma factor PrsS to the pollen membrane protein PrpS activates a signaling cascade that leads to the arrest of pollen tube growth by the depolymerization of actin and, ultimately, to programmed cell death. See text for details.*

The first response observed after receptor–ligand binding is an influx of Ca^{2+} into the pollen tube, which alters the tip-focused Ca^{2+} gradient that is required for growth (see Section 19.5.3). This increase in Ca^{2+} also disrupts the actin cytoskeleton and induces the Ca^{2+}/calmodulin-dependent phosphorylation of target proteins. Among these are a 26 kDa inorganic pyrophosphatase (p26, IPP) and a 56 kDa mitogen-activated protein kinase (p56, MAPK). Activation of the MAPK cascade eventually leads to the initiation of programmed cell death, characterized by leakage of cytochrome *c* from mitochondria, activation of caspase-like proteases, and degradation of nuclear DNA (Fig. 19.49).

19.6.4 A widespread gametophytic self-incompatibility system involves stylar ribonucleases

A different gametophytic self-incompatibility system that occurs in several families, including Solanaceae, Rosaceae, and Scrophulariaceae, is based on nonspecific ribonucleases, the *S*-locus ribonucleases (S-RNAses), which represent the stigma factors of this system. Incompatible pollen tubes germinate, but their growth is typically arrested in the upper third of the style. The growth of these pollen tubes is slowed, they show abnormal membranes and organelles, and their tips swell and sometimes burst. This is the effect of the abundant S-RNAses, which are excreted into the extracellular matrix of the wet stigmas that are characteristic for these families.

Although the S-RNAses are nonspecific and degrade diverse RNA molecules, they do this exclusively in self pollen. S-RNAses are polymorphic and have two hypervariable regions that are responsible for their *S*-allele specificity. If compatible and incompatible pollen tubes grow in the same style, only incompatible pollen tubes are stopped on their way to the ovules. To explain this allele-specific behavior, it was proposed that only the self S-RNAse is taken up into the pollen tube by an allele-specific transporter. This idea was rejected when it was shown that S-RNAses are nonspecifically taken up by both self and non-self pollen tubes and, thus, that the processes leading to the allele-specific growth inhibition must take place after the S-RNAses entered the pollen tubes. Although the S-RNAses were the first factors of any self-incompatibility system to be identified at the molecular level in the late 1980s, it took almost 30 years to understand how this specific action of S-RNAses is achieved.

The pollen factor of violet-flowered petunia (*P. inflata*) was isolated in searches for polymorphic genes that were closely linked to the stigma factor, the *S*-RNAse gene. These searches identified the *S*-locus F-box (SLF) protein, which belongs to a cytoplasmic protein family whose members are part of E3 ubiquitin ligase complexes. F-box proteins provide specificity to E3 ubiquitin ligase complexes by binding to specific substrates and targeting them for proteolysis through the ubiquitin–proteasome pathway (see Chapter 10). Indeed, SLF binds to subunits of the E3 ligase complex and also interacts with S-RNAses. Although this interaction is not allele-specific, SLF interacts more strongly with non-self S-RNAses than with its self S-RNAse. The fact that proteasome inhibitors block the growth of compatible, but not incompatible pollen tubes lends further support to the idea that degradation of the S-RNAse is required to allow normal pollen tube growth. Based on these observations, it was proposed that all non-self S-RNAses are degraded via the proteasome pathway through interactions with SLF, thereby allowing growth of compatible pollen tubes. In contrast, SLF would not interact with the self S-RNAse, which would remain active and inhibit the growth of self-pollen tubes.

This model requires the pollen factor SLF to recognize a large number of different S-RNAses, except for the one encoded by the same *S*-allele. This is problematic because the degree of polymorphism of *SLF* genes is limited (only 0–15% among nine *SLF* alleles analyzed, much lower than that of the corresponding *S*-RNAse genes, which is 20–60%). Moreover, *S*-RNAse and *SLF* genes do not show the signatures of coevolution expected for the pollen and stigma factors of a self-incompatibility system. Although SLF could be clearly linked to pollen specificity, the fact that the SLF proteins encoded by the S_7- and S_{19}-alleles of the white moon petunia (*P. axillaris*) are identical in amino acid sequence, despite their genetically distinct behavior in crossing experiments, showed that additional

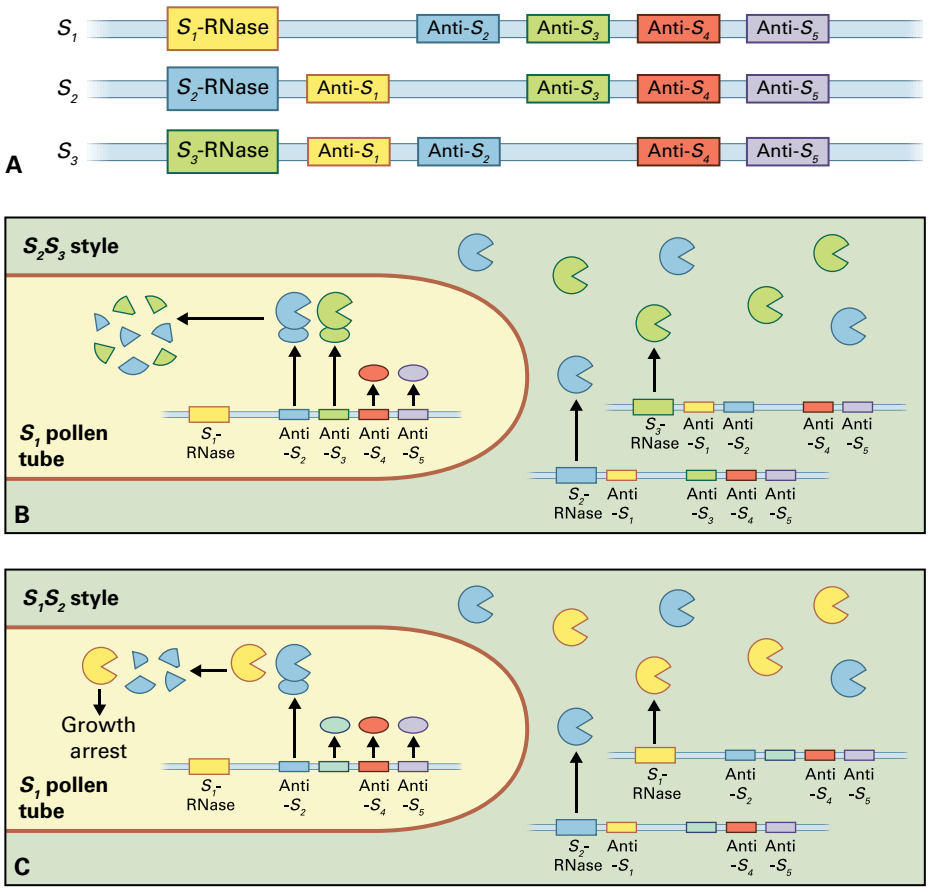


FIGURE 19.50 *Model for GSI in Petunia spp. (A) Various S-alleles have a single S-RNAse gene encoding the stigma factor but several SLF genes with distinct specificities (anti-S_1, anti-S_2, etc.) that collectively represent the pollen factor. (B) A compatible and (C) an incompatible interaction where no anti-S_1 SLF is present in the pollen such that S_1-RNAse is not degraded and arrests pollen tube growth. See text for details.*

factors must be involved. The discovery that multiple *SLF* genes are encoded by each *S*-allele suggested that they are collectively required to recognize the many different S-RNAses. Thus, each SLF must interact only with a small number of non-self S-RNAses, but collectively they can recognize a large number (Fig. 19.50).

How and where the S-RNAses are degraded is still not well understood, and this process may involve the subcellular compartmentalization and dynamic release of S-RNAses. Non-self S-RNAses are not degraded after their uptake; rather, they are sequestered into endomembrane vesicles together with a 120-kDa glycoprotein. During subsequent pollen tube growth, these vesicles break down and release the S-RNAses in self-pollen tubes but remain intact in non-self pollen tubes. Loss of HT-B, factor 4936, or the 120-kDa glycoprotein, which suppresses the self-incompatibility response, also prevents the breakdown of these vesicles. Thus, cell biological processes, such as subcellular compartmentalization, and biochemical mechanisms including protein degradation, must be integrated to achieve a functional self-incompatibility response.

19.7 Seed development

Following the fusion of sperm and egg cells, the next sporophytic generation begins its development. This occurs within the protective covers of the developing seed, which forms from the ovule after fertilization. Seeds are enclosed in the developing fruit derived from the gynoecium. Fruits are the major means by which plants disperse their seeds, and many plants depend on animals for their dissemination.

19.7.1 Seed development involves coordination of different compartments

In angiosperms, the fertilized egg (the diploid zygote) develops into the embryo, while the fertilized central cell forms the endosperm, a terminal tissue that nourishes the embryo during its development. In gymnosperms, in contrast, the large multicellular female gametophyte, which is formed prior to fertilization, serves as the embryo-nourishing tissue.

For more than a century, two competing theories have been put forth to explain the evolution of endosperm, but its evolutionary origin is still unclear. The formation of female gametophytes that do not become fertilized in gymnosperms is energetically costly. It was, therefore, proposed that their formation became dependent on fertilization to prevent this waste of energy. In this scenario, the endosperm's evolutionary origin is of gametophytic nature. The second theory suggests the endosperm is of zygotic origin, and that initially a second embryo was formed, which then evolved into endosperm to support the development of its genetic twin. Indeed, although double fertilization was considered a defining feature of angiosperms, two zygotes are formed in Mormon tea (*Ephedra nevadensis*) and paddy oats (*Gnetum gnemon*), both gymnosperms. Thus, double fertilization

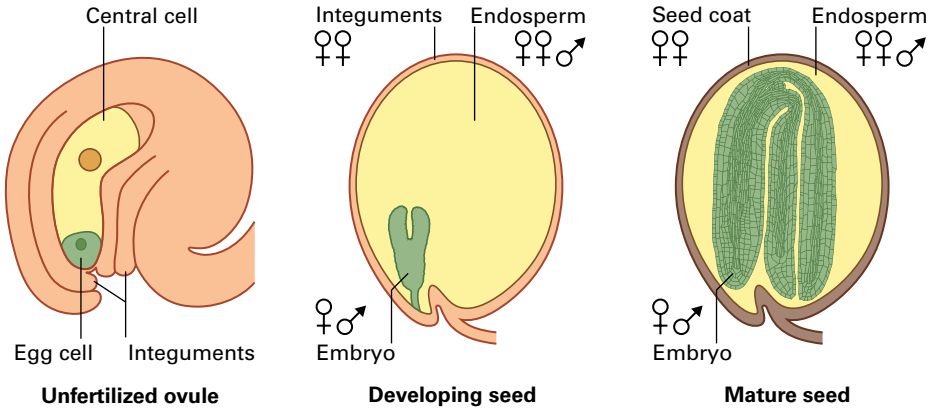


FIGURE 19.51 *Schematic representation of seed development. Origin and genetic contribution of the maternal and paternal parents to the embryo, endosperm, and seed coat are indicated.*

is not unique to angiosperms, but because it is unclear whether it is a derived or primitive feature, this does not allow a decision regarding the evolutionary origin of endosperm.

The embryo and endosperm depend on each other and develop in a coordinated fashion. In addition, they are enclosed in the seed coat, a tissue of maternal origin, which also influences their development (Fig. 19.51). To achieve normal development, the three compartments of the seed must exchange signals and coordinate their development, but little is known about the molecular basis of these interactions. Whereas the endosperm is of great importance for the later phase of embryo development, it does not seem to be absolutely required early on. For instance, if RNA polymerase II is downregulated in the egg and central cell, the embryo develops to the globular stage (see below), while endosperm development is blocked. Similarly, in the *glauce* mutant of *Arabidopsis*, no endosperm is formed but the embryo can develop normally to the globular stage. Thus, during its early development, the embryo does not seem to depend on signals or products from the endosperm.

Important interactions between the seed coat and the endosperm, however, occur both before and after fertilization. For example, seed coat development is repressed by PcG proteins (see Chapter 9) prior to fertilization. Relief of this repression requires fertilization of the central cell, as it is not observed in autonomous endosperm mutants (see Section 19.7.4) that do not affect the maternal tissues. Following fertilization, other pathways control seed coat development. For example, mutants of the *miniseed* (*mini*) and *haiku* (*iku*) class produce small seeds in which endosperm proliferation is reduced. These genes encode components of a signal transduction pathway involving an LRR–RLK (IKU2), a WRKY class transcription factor (MINI3), and a plant-specific VQ-motif protein (IKU1). Although these genes are only expressed in the endosperm, they affect cell elongation in the integuments of the seed coat, suggesting the signals from the endosperm control seed coat development and are important to control seed size. Conversely, another WRKY transcription factor, TRANSPARENT TESTA GLABRA2 (TTG2), functions in the integuments and promotes cell elongation, allowing endosperm proliferation and seed growth. In contrast to TTG2, the transcription factors AP2 and AUXIN RESPONSE FACTOR2 (ARF2) restrict cell proliferation in the integuments, thereby physically restricting seed size. Collectively, these interactions illustrate the interdependence of maternal and zygotic tissues during seed development.

19.7.2 Parental effects on seed development can be of sporophytic or gametophytic origin

Parental effects play an important role in seed development. All the compartments of the seed are interdependent, so a mutation affecting a gene with activity in the maternal seed coat can potentially affect the development of either of the two fertilization products. Such a mutation results in a **sporophytic maternal effect** on seed development. Seeds from homozygous mutant mothers would be defective even with a wild-type pollen donor; if the cross were performed in the other direction, however, the seeds would develop normally. This difference in the outcome of reciprocal crosses is the hallmark of a maternal (or paternal) effect mutation.

The gametes themselves may also lack gene products that are important during the later steps of seed development. In this situation, a mutation affecting an activity in the gametophyte leads to aberrant seed development through a **gametophytic maternal effect**. A female gametophyte lethal mutation that blocks the development or function of the embryo sac results in ovules that do not become fertilized and fail to develop into seeds. In a gametophytic maternal effect mutation, however, the female gametes participate in fertilization, and the defect becomes apparent only later on, for example if it leads to seed abortion (Box 19.4). Thus, in a heterozygous gametophytic maternal effect lethal mutation, half of the seeds abort regardless of the contribution of the male; in the reciprocal cross, no phenotype is observed.

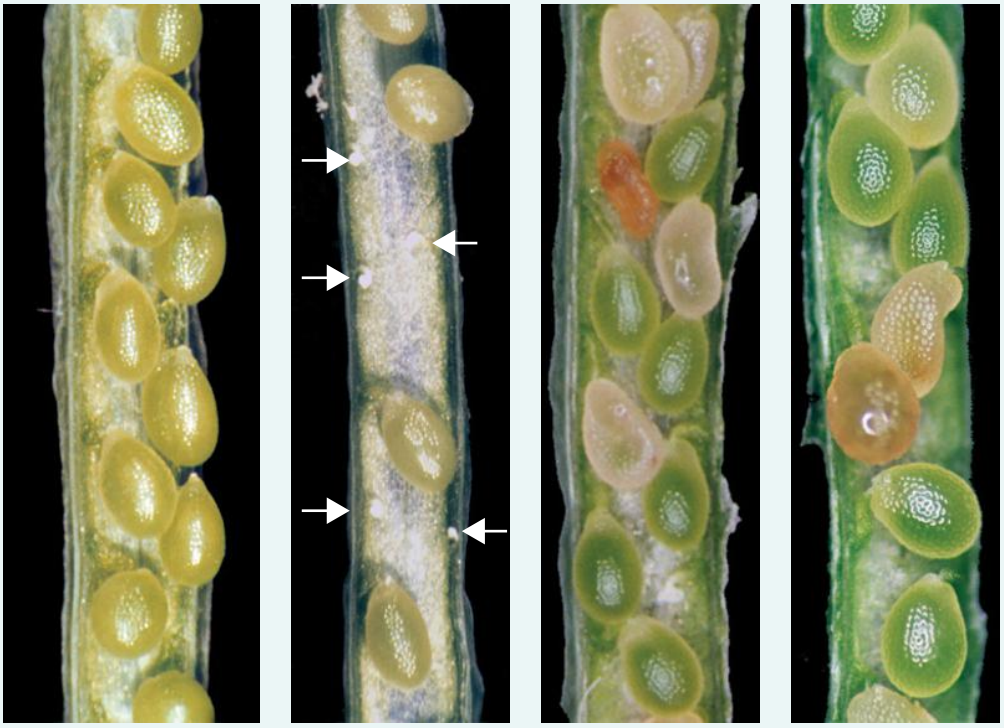
The mechanistic basis for a gametophytic maternal effect on seed development can be diverse. First, such a mutation may be **haploinsufficient** in the endosperm; reciprocal crosses with the wild-type result in different genetic compositions of the triploid endosperm with one or two wild-type alleles. If one wild-type allele is not sufficient to sustain normal seed formation, this

BOX 19.4

Phenotypic classes of reproductive mutants

Different classes of female reproductive mutants can be identified by the phenotypes they display in opened, developing siliques. In the wild type (A) nearly 100% of the seeds develop normally (green seeds). In contrast, ovules carrying a mutant allele of a female gametophyte lethal mutation (B) do not develop into seeds. Consequently, in a plant heterozygous for such a mutation only half of the seeds develop normally, whereas the remaining ovules did not get fertilized and are visible as shriveled, white ovules (arrows). In a gametophytic maternal effect mutation (C), ovules carrying mutant gametophytes will get fertilized but the seeds abort later during development, such that 50% of the seeds are normal (green) and 50% abort (white or brown seeds). This is in contrast to a zygotic embryo lethal mutation (D) where only homozygous embryos abort, resulting in 25% aborting seeds (white or brown seeds).

Source: U. Grossniklaus, University of Zurich; previously unpublished.



results in a maternal effect on seed development. Second, either one or both of the female gametes may lack a gene product that is deposited and stored, but required only after fertilization. If the lack of this gene product cannot be compensated for by the paternal genome, a gametophytic maternal effect on seed development results and is sometimes referred to as a maternal effect of **cytoplasmic nature**. This situation is typical of maternal effects in many animals, where the large egg cell carries all required products for the initial division cycles of the zygote. Finally, the female gametes may carry specific epigenetic modifications in their genome that result in differential expression after fertilization, sometimes referred to as a maternal effect of **chromosomal nature**. For example, a maternal allele may carry a mark that renders it active after fertilization while the paternally inherited allele remains silent. Thus, the embryo is functionally hemizygous for this locus. Such parent of origin-dependent effects on gene expression are referred to as **genomic imprinting** (see Section 19.7.5).

The maternal seed coat plays a role in seed dormancy and germination, and maternal effects on seed color and seedling physiology have also been described, but maternal effects were considered unimportant with respect to development. This view was largely based on the fact that plant cells can give rise to embryos in culture, indicating that neither the specialized cytoplasm of the egg cell nor a particular epigenetic configuration of its genome is required for embryogenesis. The discovery of *medea* (*mea*), a gametophytic maternal effect mutation in *Arabidopsis* that is required for normal embryo and endosperm development changed this perception. Seeds that inherit a mutant allele of *mea* through the

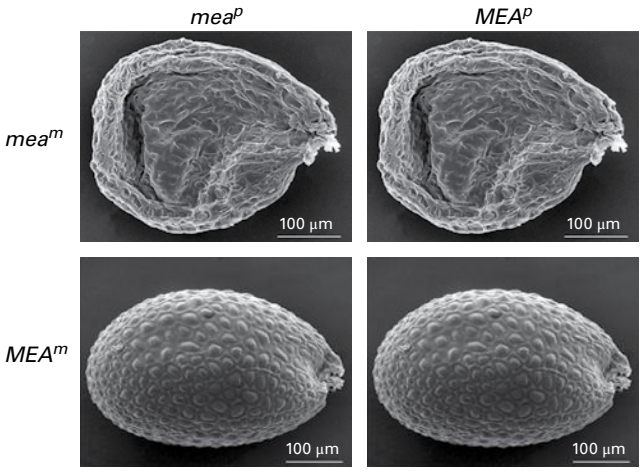


FIGURE 19.52 *Genetic behavior of the* Arabidopsis *maternal effect mutation medea in reciprocal crosses. Seeds derived from mutant female gametophytes (i.e. those inheriting a mutant maternal mea^m allele) abort irrespective of the paternal contribution. In contrast, all seeds inheriting the wild-type MEA^m allele are normal, even if they inherit a mutant paternal mea^p allele.*
Source: Baroux et al. (2002). Adv. Genet. 46:165.

female gametophyte abort regardless of the contribution of the father (Fig. 19.52). Subsequently, it was found that about half of all mutants that have a gametophytic inheritance pattern (see Box 19.3) show embryo or endosperm phenotypes after fertilization. Thus, maternal effects are widespread and, in contrast to the situation in culture conditions, zygotic embryogenesis seems to require extensive maternal input.

Conceptually, defects in the sperm cells could also lead to paternal effects of cytoplasmic or chromosomal nature. Plant sperm cells contain a diverse set of transcripts, so it is feasible that some of these transcripts are delivered to the zygotic products upon fusion with the female gametes. The *Arabidopsis SHORT SUSPENSOR* (*SSP*) gene is transcribed in the sperm cells, but is only translated after delivery to the female gametes. In the zygote, SSP activates the YODA (YDA) MAPK pathway, which regulates the elongation of the zygote and its first asymmetric division. In *ssp* or *yda* mutants, zygote elongation does not occur, and the first division is nearly symmetric. While only homozygous *yda* embryos show this phenotype, *spp* is a paternal effect mutation and the phenotype is only observed if *ssp* is inherited from the father. The dependence of zygote elongation on paternal *SSP* activity provides mechanism to ensure that this event only occurs after successful fertilization.

19.7.3 Embryogenesis establishes the main axis of the sporophyte

While gametophytic parental effect mutations clearly show that some input for early development comes from the parents, many more genes are required for embryogenesis, and their mutation can result in embryo lethality (see Box 19.4).

When the zygotic genome becomes active after fertilization is a matter of intense debate. Various lines of evidence suggest that the maternal contribution is important and zygotic genome activation is a gradual process as it was described for animals. Depending on the locus, several division cycles may be required until maternally and paternally inherited genomes are fully active. On the other hand, some genes are active soon after fertilization, and there are examples where both parental genomes seem to be fully active as early as the two-cell stage of embryogenesis. More studies are needed to determine how the timing of zygotic genome activation is controlled and how plant species differ in this regard.

The major function of embryogenesis is to set up the stem cell populations in the embryonic root and shoot meristems. In *Arabidopsis*, the cell divisions during embryogenesis follow a stereotypic pattern, such that it is highly predictable which cells divide and how the division planes will be oriented (Fig. 19.53). However, in many plant species the embryonic cell divisions do not follow a predictable pattern. This suggests that the fate of an embryonic cell is not determined by its lineage, but rather is influenced by its neighbors: cells adopt a fate based on their position in the embryo.

A substantial amount of evidence indicates this is also true in *Arabidopsis,* and that cell specification is flexible during development. In *Arabidopsis*, as in all plants studied to date, the zygote elongates along the micropylar–chalazal axis of the ovule and then divides asymmetrically to form a large, basal cell and a small, apical cell. The apical cell divides further to form the embryo proper, while the basal cell forms the suspensor, connecting the embryo proper to the ovule (Fig. 19.53). Given that the first asymmetric division establishes the apical–basal polarity of the embryo, much effort has gone into understanding the control of this process.

Parental and zygotic factors are both required for zygote elongation and division. Members of the WUSCHEL-RELATED HOMEOBOX (WOX) transcription factor family play an important role at this stage. Transcripts of *WOX2* and *WOX8* are present in both the egg cell and zygote but become restricted to the apical and basal cell, respectively. After division of the zygote, *WOX8*—together with its close homolog *WOX9*—regulates the development of the basal lineage but also, through the noncell autonomous activation of *WOX2*, the apical lineage (Fig. 19.54). Neither single nor multiple mutations in these genes affect the asymmetric division, so the role of these mutations in this process remains obscure.

WOX8 and *WOX9* are directly activated in the zygote by the transcription factor WRKY2. In *wrky2* mutants, the egg cell is formed, but the zygote fails to reorganize the polar distribution of the cytoplasm after fertilization, does not elongate properly, and divides symmetrically. These defects are partly overcome when *WOX8* is expressed in the egg cell and early embryo, providing a link between the polarization of the zygote and early embryonic pattern formation (Fig. 19.54). This partial rescue and the fact that *wox8/9* double mutants have a normal zygotic division suggest that additional, yet unknown factors also contribute to this process.

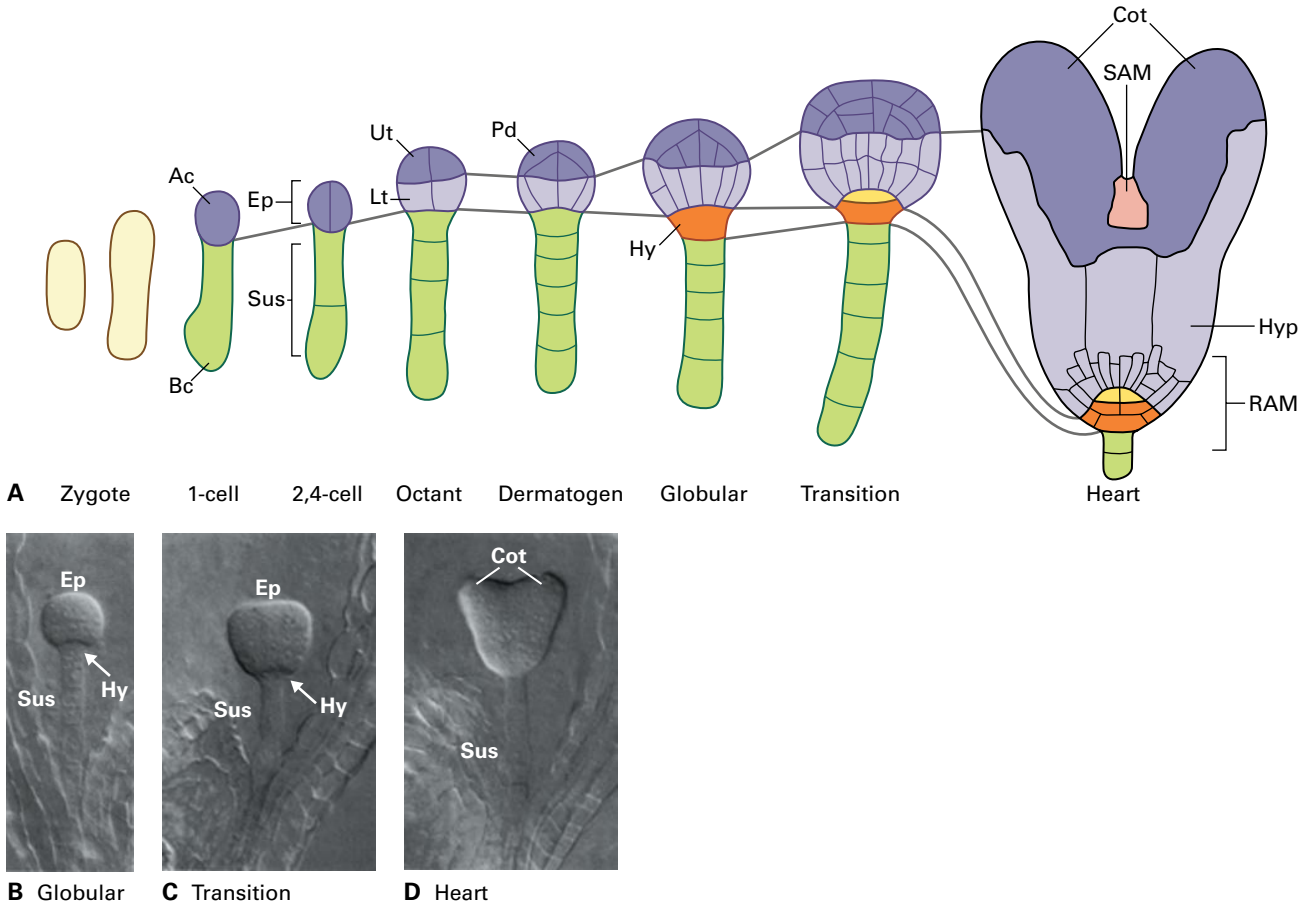


FIGURE 19.53 *Embryogenesis in* Arabidopsis. *(A) Schematic representation of development from the zygote to the heart stage, where the main elements of the embryo, i.e. shoot apical meristem (SAM), root apical meristem (RAM), cotyledons (Cot) and hypocotyl (Hyp) are already determined. Lineages of the suspensor (Sus) as well as the upper (Ut) and lower tier (Lt) of the embryo proper (Ep) are indicated. (B–D) Cleared specimen of selected stages. Ac, apical cell; Bc, basal cell; Pd, protoderm; Hy, hypophysis.*
Source: (B–D) Yadegari et al. (1994). Plant Cell 6:1713–1729.

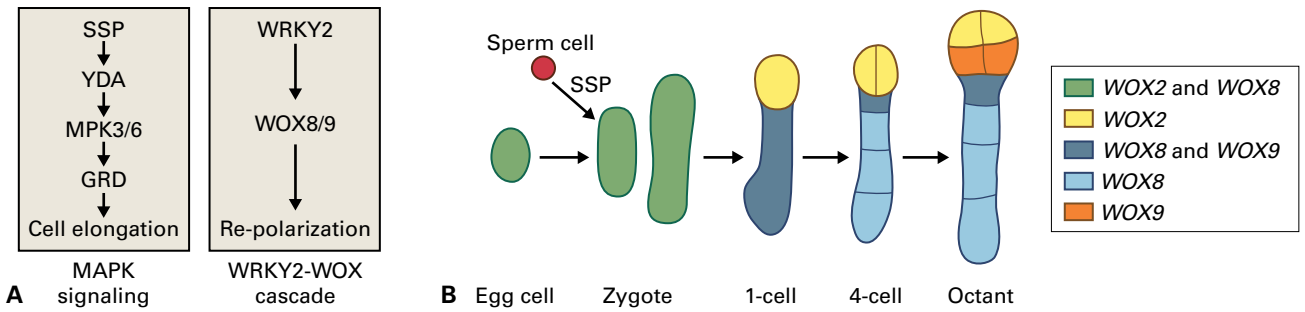


FIGURE 19.54 *Control of the asymmetric division of the* Arabidopsis *zygote. (A) Zygote elongation and asymmetric division is controlled by the parallel WOX and YDA pathways. (B) The YDA pathway is activated by the SPP protein, whose RNA is delivered via the sperm cells. WOX homeobox genes show distinct expression patterns along the apical–basal axis of the embryo.*

The *YDA* MAPK pathway mentioned above, which is triggered by paternal *SSP* supplied by the sperm, also regulates the first asymmetric division. How the two pathways interrelate is not yet entirely clear, but insights have come from the characterization of GROUNDED (GRD), a transcription factor of the RKD family, which is required for *YDA* signaling but is not a target of the *YDA* MAPK cascade. However, *grd* and *wox8/9* mutants show a strong synergistic interaction: triple mutants arrest as zygotes or early embryos without apparent polarity, suggesting they act independently to regulate zygote polarity and elongation (Fig. 19.54).

Once the asymmetric division is achieved, the apical–basal axis of the embryo must be consolidated and reinforced. These subsequent patterning processes depend on the plant hormone auxin. Although auxin is apparently not involved in the first division of the zygote, it rapidly accumulates in the apical cell, once it has formed, as a consequence of polar auxin transport. Members of the PIN-FORMED (PIN) plasma

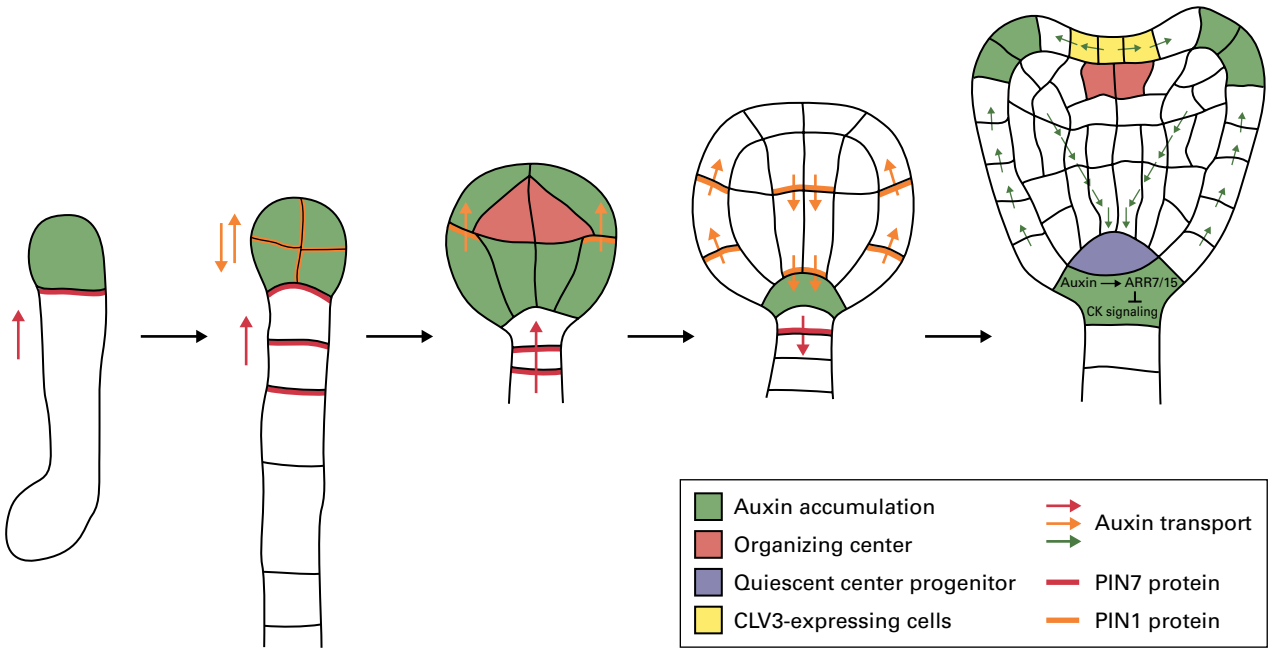


FIGURE 19.55 *Formation of the embryonic root and shoot meristems. Patterning along the apical-basal axis involves the local accumulation of auxin first in the apical cell and its descendants, and then in the hypophysis, which forms the root meristem. Expression of WUS and CLV3 in the young embryo establishes the shoot meristem. See text for details.*

membrane protein family function as efflux transporters of auxin (see Chapter 18).

PIN7 is localized at the apical membrane of the basal cell—and initially in the suspensor cells derived from the basal cell—and thus transports auxin into the apical cell (Fig. 19.55). After the first division of the apical cell, PIN1 accumulates at the inner surface of the cells of the embryo proper, leading to the uniform distribution of auxin in the lineage forming the embryo proper. At the early globular stage, a dynamic reorganization of the PIN transporters occurs, such that PIN1 and PIN7 become localized at the basal membrane of embryonic and suspensor cells, respectively. This leads to the accumulation of auxin in the hypophysis, the top-most cell of the suspensor. The hypophysis is the only cell derived from the basal lineage that contributes to the embryo and plays an important role in organizing the embryonic root meristem (Fig. 19.55). This relocalization of the PIN proteins depends on GNOM, a guanine nucleotide exchange factor for adenosyl ribosylation factors (ARF-GEF), which is involved in the directional delivery of PIN proteins to the plasma membrane. This explains the gross patterning defects in *gnom* mutants, which were isolated in a seminal screen for mutants affecting embryonic pattern formation in *Arabidopsis*. In *gnom* mutants, PINs remain unpolarized and the apical–basal axis of the embryo cannot properly be formed.

The hypophysis not only accumulates auxin, it also shows a high level of cytokinin signaling. The asymmetric division of the hypophysis forms a lens-shaped apical cell, in which cytokinin signaling remains high, and a larger basal cell with high auxin levels. In this cell auxin directly activates the *ARABIDOPSIS RESPONSE REGULATOR* genes *ARR7* and *ARR15*, which are repressors of cytokinin signaling. Thus, the antagonistic interaction of auxin and cytokinin establish the identity of the lens-shaped cell, which gives rise to the quiescent center cells that organize the embryonic root meristem.

The shoot meristem is formed independently through the establishment and successive refinement of expression domains of regulatory factors. The root and shoot fates of the basal and apical domains in the embryo are determined by complementary master regulators, the PLETHORA and HD-ZIPIII transcription factors, respectively. Ectopic expression of these regulators in the appropriate genetic background can convert a shoot into a root, and *vice versa*. For example, expression of the HD-ZIPII factor *REVOLUTA* in the basal region of the embryo can convert the root into a second shoot. The stem cell niche for the shoot meristem is set up after transverse divisions at the octant stage have formed outer (protoderm, the precursor of the epidermis) and inner cells of the embryo proper. The four apical inner cells begin to express *WUS* and give rise to the organizing center of the embryonic shoot meristem (Fig. 19.55). Slightly later, at the transition stage, when globular embryos loose their radial symmetry and form a bilateral heart stage embryo, *CLAVATA3* (*CLV3*) is expressed in the same area. *CLV3* is required to maintain the meristem's stem cell population though a feedback loop with *WUS* (see Chapter 11). Specifying the embryonic shoot meristem between the emerging cotyledons involves many factors, including auxin and the transcription factors SHOOT MERISTEMLESS and CUP SHAPED COTYLEDON1/2, which regulate each other in a complex way.

The embryo is not only patterned along the apical–basal axis, but the division that forms the protoderm also initiates patterning along the radial axis, eventually forming an epidermal layer, multilayered ground tissue, and the vasculature

in the center. At the heart stage, the body plan of the embryo is fully established: both root and shoot meristems are defined, and the cotyledon primordia and various radial tissues have been set up. What follows are growth and expansion of the cells forming the cotyledons and the hypocotyl to form a torpedo and finally a mature embryo, where the cotyledons and the hypocotyl are approximately of the same length. In *Arabidopsis*, the entire morphogenetic phase starting with the zygote and ending with the fully grown embryo is completed within a week, followed by another week of seed maturation, which is dedicated to processes that prepare the seed for dispersal and germination.

19.7.4 Endosperm development is controlled by maternal and zygotic factors

The second product of fertilization, the endosperm, produces proteins and carbohydrates to support embryogenesis and germination. In many angiosperms, the endosperm is transient in nature: it proliferates during the early phase of seed formation, but is absorbed by the embryo during its growth. This process likely involves some form of programmed cell death and leaves only one or a few cell layers that surround the embryo, including the epidermal layer of the endosperm (**aleurone**). In these cases (including tomato, tobacco, and *Arabidopsis*), the endosperm does not serve a major storage role, rather the embryo itself stores the resources required for germination. In other species, especially the cereals, the endosperm is persistent, contributes up to 80% of the seed mass, and provides the resources required for germination and survival until the seedling is established. Persistent endosperm is one of the most important resources used for food, feed, biofuel, and other industrial materials.

Though many studies have addressed the biosynthesis and mobilization of food reserves in the endosperm, we still know relatively little about the molecular basis of its development. There are two major forms of endosperm development. In some species, for instance in the orange jewelweed (*Impatiens capensis*) and the pukeweed (*Lobelia inflata*), the fertilized endosperm divides to form daughter cells at each division, similar to what occurs during embryogenesis. This cellular type of endosperm development, however, is rare.

Most species have nuclear endosperm development, where the initial divisions of the endosperm occur in a syncytium. Thus, in nuclear endosperm development, as in that of the female gametophyte, the nuclei divide in the absence of cytokinesis (Fig. 19.56). The fertilized central cell nucleus (secondary endosperm) divides prior to the first division of the zygote, and rapid subsequent divisions form the syncytial endosperm (**coenocyte**). The initial divisions are synchronized, but the nuclei in distinct endosperm regions later divide at different rates, forming mitotic domains that correspond to the micropylar, peripheral, and chalazal endosperm (Fig. 19.56). The free nuclear division cycles are followed by cellularization of the endosperm. In *Arabidopsis*, cellularization occurs at the heart stage of embryo development, starting

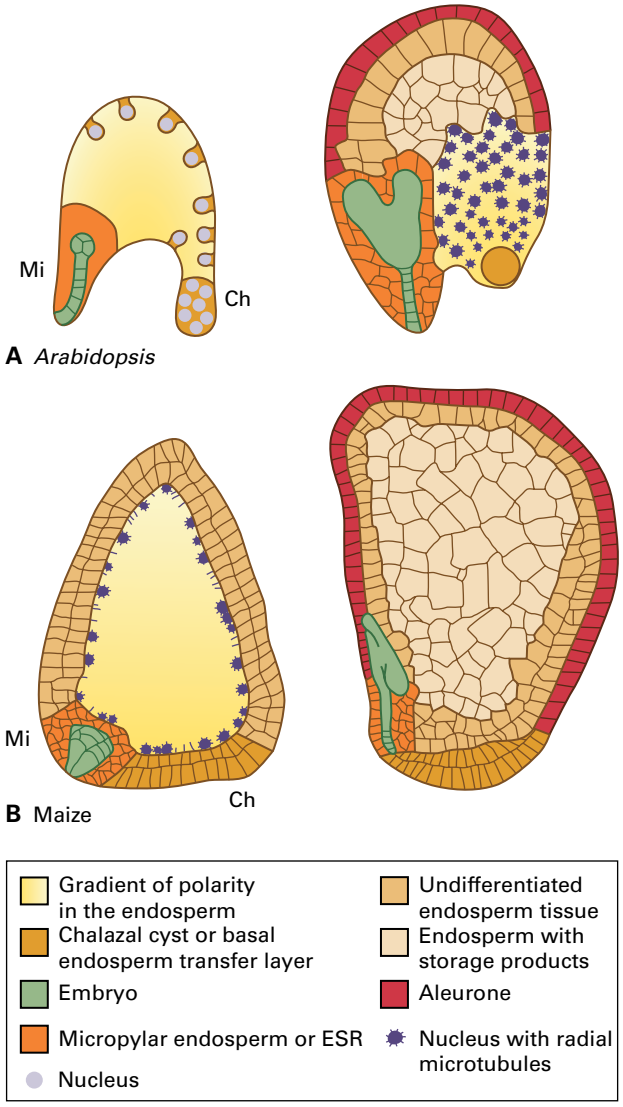


FIGURE 19.56 *Endosperm development in* Arabidopsis *(A) and maize (B). Although the endosperm of oil seeds and cereals are anatomically distinct, equivalent domains can be distinguished at the micropylar pole (Mi) around the embryo, at the chalazal pole (Ch), and in between. Endosperm cellularization initiates around the embryo in* Arabidopsis *and then spreads around the periphery towards the chalazal pole, while in maize, cellularization starts at the periphery and progresses to the center. Peripheral nuclei in dense cytoplasmic domains form a radial microtubule network to organize cell wall formation around them.*

in the micropylar embryo-surrounding region (ESR) and progressing toward the chalazal pole. In the cereal coenocyte, cellularization starts at the periphery and advances towards the center of the seed until the endosperm cavity is filled. Also in the cereal endosperm, regions with distinct cell fates can be identified: ESR, aleurone, starchy endosperm in the center, and the basal endosperm transfer layer (BETL), which corresponds to the chalazal endosperm of *Arabidopsis* (Fig. 19.56).

Endosperm cellularization is followed by differentiation of specific tissues within the endosperm and, finally, by maturation. During the latter phase, the bulk of the cereal endosperm synthesizes and stores starch and proteins,

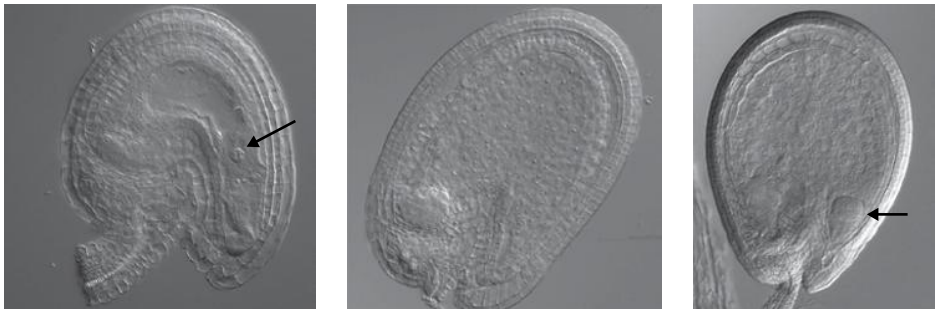


FIGURE 19.57 *Fertilization-independent endosperm development in the fis class mutants. (A) In unpollinated pistils of the wild type, the central cell (arrow points to its nucleus) is arrested until fertilization occurs, while (B) in mea embryo sacs, it proliferates in the absence of fertilization but no embryo forms. (C) A wild-type seed from a pollinated pistil with developing embryo (arrow) and endosperm for comparison.*
Source: Köhler et al. (2003). EMBO J. 22:4804.

while the aleurone accumulates proteins and lipids that are important for germination. Here, only one of these specialized endosperm tissues is discussed, the micropylar endosperm or ESR, which is important for embryogenesis.

The ESR of *Arabidopsis* and cereals is characterized by regionally restricted gene expression. ESR-expressed genes include the sucrose transporter gene *AtSUC5*, which is involved in reserve accumulation in the embryo, and also genes encoding secreted peptides, indicating that signaling is important for ESR function. Indeed, in *Arabidopsis* the endosperm breaks down to provide nutrients and space for the growing embryo. This primarily concerns the ESR and may involve communication between embryo and endosperm. Although the embryo does not appear to influence ESR degeneration (which occurs even in the absence of normal embryo growth, at least in cereals), the endosperm has a strong effect on embryo development. Plants carrying mutations affecting the basic-HLH transcription factor ZHOUPI (ZOU), which is specifically expressed in the ESR, endosperm is persistent and embryos are small and have an abnormal epidermis. Thus, *ZOU* regulates two distinct processes: ESR degradation and the non-cell autonomous signals for the formation of the embryonic epidermis. The latter is mediated by activating the ESR-expressed *ABNORMAL LEAF SHAPE1* (*ALE1*) gene encoding a subtilisin protease. Such proteases may play a role in the processing of peptide ligands, several of which are expressed in the ESR. Thus, the formation of the embryonic epidermis seems to require an unknown peptide ligand, whose production in the ESR depends on *ZOU* and *ALE1*. The transmission of this signal requires the function of the embryo-expressed RLKs GASSHO1 and GASSHO2, mutations in which also lead to defects in the embryonic epidermis. These examples illustrate the importance of cell–cell communication processes between seed compartments.

The production of endosperm is energetically costly and should be tightly controlled and coordinated with embryo development. Thus, endosperm proliferation is repressed in the absence of fertilization through the action of PcG proteins (see Chapter 9). The FIS–PRC2 complex plays a predominant role in the regulation of female gametophyte and seed development (see Box 19.1). It contains the histone methyltransferase MEA and the core subunits FERTILIZATION-INDEPENDENT SEED2 (FIS2), FIE, and MSI1. Mutations in any of these four genes, collectively referred to as *fis* class mutants, lead to autonomous endosperm formation in the absence of fertilization (Fig. 19.57). Thus, as in animals where their deregulation can lead to cancer, PRC2 complexes regulate cell proliferation also in plants.

This autonomous, diploid endosperm, however, does not develop normally and fails to cellularize, because the type I MADS-domain transcription factor AGL62 fails to be downregulated in *fis* class mutants. In wild-type seeds, the expression of *AGL62* drops just prior to cellularization, and in *agl62* mutants the endosperm cellularizes precociously, suggesting that *AGL62* is important to maintain the syncytial state of the endosperm. Thus, the FIS–PRC2 complex controls the developmental transition from nuclear to cellular endosperm.

Normally, endosperm proliferation is triggered by fertilization, which releases repression by the FIS–PRC2 complex, but the signaling events involved in this release are unknown. In addition to its role prior to fertilization, the FIS–PRC2 complex also plays a role after fertilization. If *fis* class mutants are fertilized by wild-type pollen, all seeds start to develop but abort later during seed development. Both embryo and endosperm show abnormal proliferation, producing enlarged heart stage embryos and overgrowth of the chalazal endosperm. As embryo and endosperm have identical genotypes, however, it is not easy to determine whether the FIS–PRC2 plays a role in both fertilization products, as indicated by the phenotype and mRNA expression patterns of the *FIS* genes, or whether the embryonic defects are a consequence of endosperm failure. In all *fis* class mutants, seed abortion depends solely on the genotype of the embryo sac, thus representing a typical gametophytic maternal effect.

19.7.5 Genomic imprinting involves DNA methylation and PRC2-based repression

Genomic imprinting is the parent-specific marking of a chromosome or gene. This term was coined to describe the observation that paternal X-chromosomes are specifically eliminated during embryogenesis in sciarid flies (*Sciara coprophila*). Thus, these chromosomes must carry a mark, or

imprint, that distinguishes them from maternal chromosomes. The first demonstration of parent-of-origin-dependent behavior for a single gene, rather than an entire chromosome, was made for the *R1* (*colored1*) locus in maize (see Chapter 9). The *R1* locus controls anthocyanin pigmentation in the aleurone, and its alleles show different phenotypes depending on the direction of the parental cross. Inheritance of the *R1* allele from the mother results in full pigmentation of the kernel, whereas inheritance from the father produces kernels with a mottled phenotype, where most aleurone cells fail to express *R1*. A series of genetic experiments performed in the 1960s demonstrated that the *R1* phenotype depends only on parental origin, in other words that *R1* is regulated by genomic imprinting.

In molecular terms, genomic imprinting results in the differential expression of an allele, depending on which parent it is inherited from. Although maternal and paternal alleles of imprinted loci may not differ in sequence and are present in the same nucleus, they are differentially expressed. Thus, they must differ with respect to imprinting marks that were established according to the sex of the parent while the alleles were separated. In plants, this must occur after the lineages for male and female reproductive organs separate, but before fertilization.

Recent work on the mechanisms of imprinting in plants has highlighted several similarities with mammals, in particular the role of DNA methylation and PRC2-based repression. Given that imprinting evolved independently in these lineages, this is a remarkable example of convergent evolution, where similar molecular modules are recruited for the differential regulation of genes. Much of what is known about the molecular basis of imprinted expression comes from the study of a small set of genes in *Arabidopsis*, mainly the maternally expressed *MEA*, *FIS2*, and *FLOWERING WAGENINGEN* (*FWA*) loci, and the paternally expressed *PHERES1* (*PHE1*) gene. Two of the major regulators of imprinted expression are METHYLTRANSFERASE1 (MET1), a maintenance DNA methyltransferase that re-establishes methylation in the CG context after replication, and DEMETER (DME), a DNA glycosylase that removes methylated cytosines from DNA. Imprinting of *FIS2* and *FWA*, a homeobox gene without apparent function in seed development, is regulated by these two factors. Methylation of cytosines in their 5′-regulatory regions is maintained by MET1 during sporophytic development, where both alleles are methylated. This is also true during male gametophyte development; paternal alleles in the sperm cells are methylated and not expressed. In the female gametophyte, however, methylation is presumably removed from the maternal alleles by DME, which is expressed predominantly in the central cell of the embryo sac. Indeed, *FWA* and *FIS2* are expressed strongly in the central cell, and the maternal alleles are subsequently also active in the endosperm while the paternal alleles are not (Fig. 19.58). Thus, the presence or absence of methylation in the promoters of these genes seems to determine their imprinting status. Indeed, when allele-specific methylation is analyzed 7–8 days after pollination, the parental alleles in the endosperm are differentially methylated.

When exactly the maternal alleles are demethylated is unclear, but the expression of *DME* in the central cell suggests

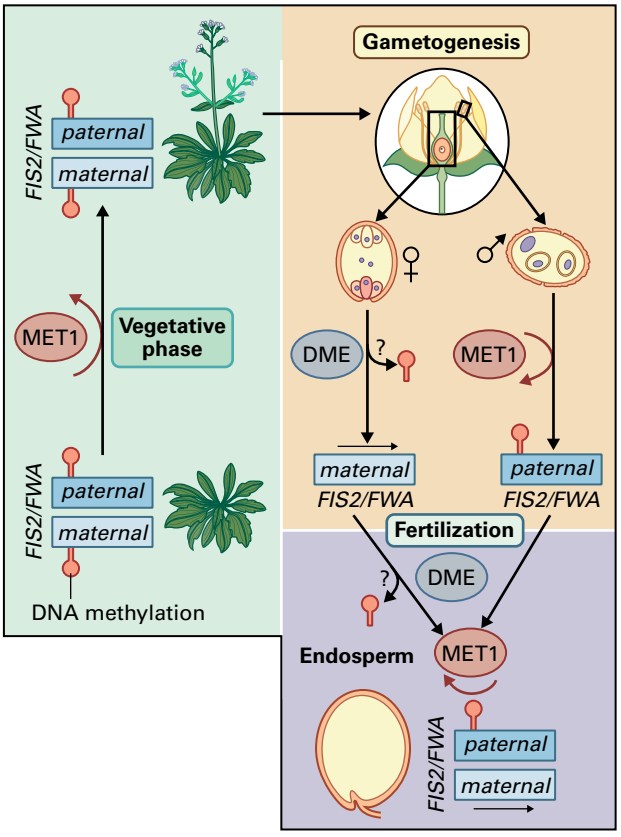


FIGURE 19.58 *Model for the regulation of genomic imprinting by DNA-methylation. The MET1 DNA methyltransferase maintains methylation at the FIS2 and FWA loci throughout sporophytic and pollen development. In the central cell, either before or after fertilization, the DNA glycosylase DME removes the methylcytosines, leading to the differential marking and eventually expression of maternal and paternal alleles in the endosperm. See text for details.*

that this may occur prior to fertilization. A recent analysis of DNA methylation at the *FWA* locus directly in the central cell showed, however, that it is still methylated. This suggests that DME acts only after fertilization and it is unclear how maternal and paternal alleles are marked, causing differential demethylation. A similar situation was described for the *ZmFie2* locus in the endosperm and the *Maternally expressed in embryo1* (*Mee1*) locus in the embryo of maize. In both cases, allele-specific DNA methylation or demethylation, respectively, occurs only after fertilization, and methylation status and expression do not correlate. Thus, at least in some cases, differential DNA methylation does not seem to be the imprint that is inherited from the parents, as it is only established after fertilization, possibly as a consequence of transcription.

The regulation of *MEA* and *PHE1* is more complex and, in addition to DNA methylation, involves repression by the FIS–PRC2 complex. In a *dme* mutant, the maternal *MEA* allele fails to be expressed, suggesting that DME-mediated demethylation plays a similar role as it does for *FWA* and *FIS2*. However, if DNA methylation is removed paternally, as in a *met1* mutant, the paternal allele is still silent, while maternal *fis* mutations lead to some expression from the paternal *MEA* allele. These findings suggest the maternally produced FIS–PRC2 complex

represses the paternal *MEA* allele after fertilization in an autorepressive fashion. A more detailed analysis, however, showed that a short piece of the *MEA* promoter devoid of DNA methylation can confer imprinted expression to a reporter gene. This suggests that the role of *DME* is indirect, perhaps by regulating higher order chromatin structure (chromatin loops), and that it is not differential methylation that specifically marks the maternal allele. Furthermore, if both known regulators of the paternal allele, paternal *MET1* and the maternal FIS–PRC2 complex, are lacking, the two parental alleles are still differentially expressed, suggesting that additional, unknown factors are involved in establishing the imprints that mark the parental alleles (Fig. 19.59).

PHE1 was isolated as a direct target gene of MEA, which specifically represses the maternal *PHE1* allele. Thus, the FIS–PRC2 complex is involved in allele-specific repression, a function that was also demonstrated in mammals, where PRC2 represses the paternal alleles of selected imprinted genes. The regulation of *PHE1* is more complex, however, as methylation of repeats that are downstream of the locus is required for efficient repression of the paternal allele by the FIS–PRC2 complex. In the active paternal allele, in contrast, these repeats are methylated. Given that sequences both upstream and downstream of *PHE1* are involved in its regulation, it is possible that they interact by forming a chromatin loop, as has been suggested for the *MEA* locus (Fig. 19.59).

Several hundred additional loci that are candidates for imprinting have been identified in *Arabidopsis*, maize, and rice following advances in sequencing technologies, which allow the profiling of mRNAs in an allele-specific manner. Such profiling approaches have identified genes that show differential expression of the parental alleles in the endosperm. While these are excellent candidates for further studies, different steady-state levels of paternal and maternal transcripts are not sufficient to demonstrate imprinting. The same difference could come about by producing and storing an mRNA in the egg cell

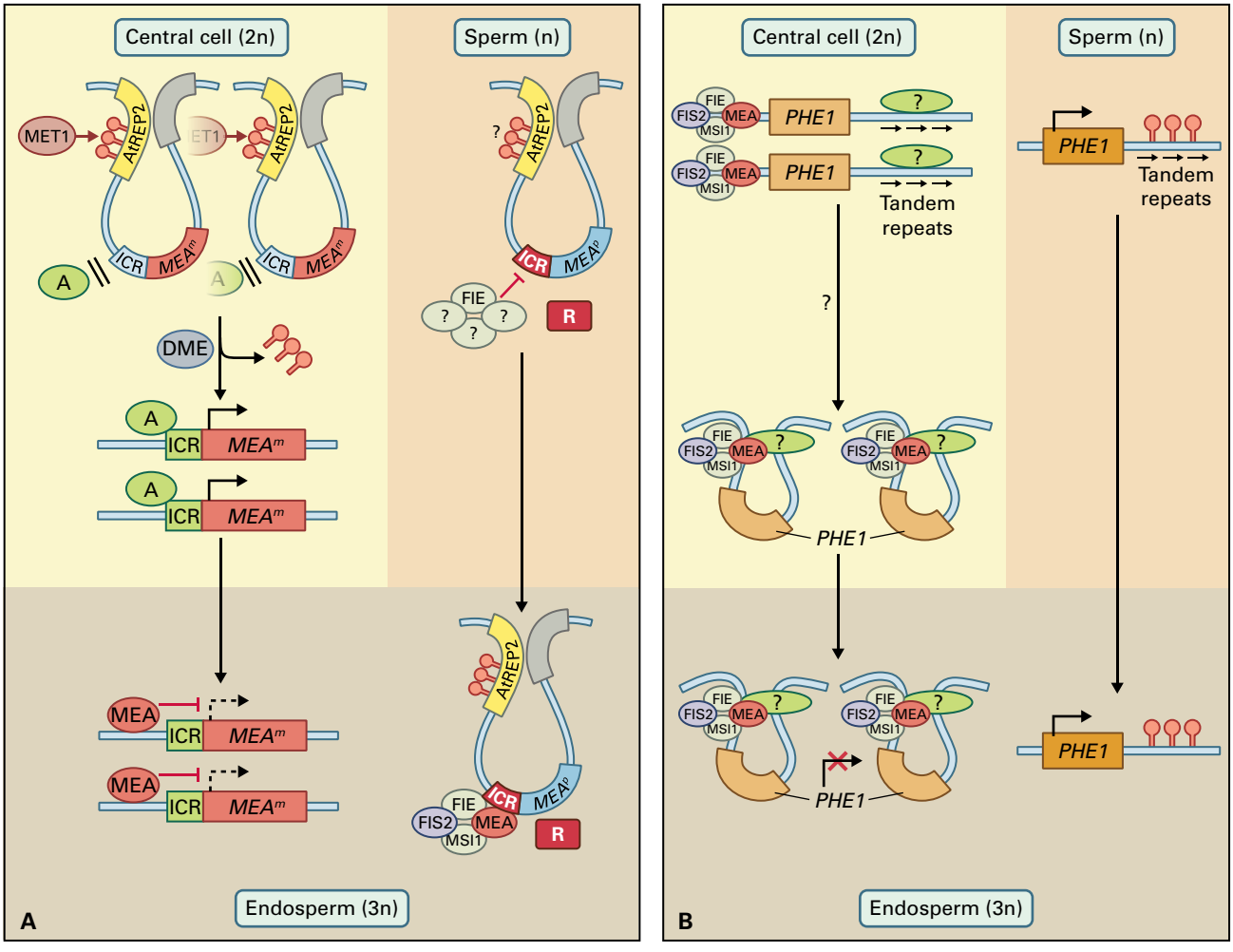


FIGURE 19.59 *Model for the role of higher order chromatin organization in the regulation of genomic imprinting. At the MEA and PHE1 loci, chromatin looping has been proposed to play a role in imprinting. (A) Maternal copies of MEA are in a loop making them inaccessible to activating imprinting factors. Removal of methylcytosines by DME in the central cell opens the loop, allowing access to unknown factors (A) marking the active allele. The paternal copy remains in a loop and is kept silenced by the FIS–PRC2 and additional, unknown repressors (R) in the endosperm. Autorepression of MEA reduces expression of the maternal allele after fertilization. (B) At PHE1 the loops are maintained on the maternal copies, a process involving the FIS–PRC2 and tandem repeats located downstream of PHE1 that have to remain unmethylated. The paternal PHE1 allele, where these repeats are methylated, does not form a loop and is active in the endosperm.*

or by delivering it to the zygote via the sperm. It is, therefore, important to show that the gene is either not expressed in the gametes or that one parental allele only is actively transcribed after fertilization, an experimentally challenging task.

Genomic imprinting is generally considered to occur in the endosperm, but there are also a few genes that appear to be imprinted in the embryo. The best studied is *Mee1*, a gene of unknown function, which is maternally expressed in maize embryos only after fertilization. However, quite a few more differentially expressed genes in the embryo have been identified and about a dozen were recently shown to show imprinted expression in the *Arabidopsis* embryo. Finally, little is known about the role of imprinted genes, in either endosperm or embryo, as the function of only a handful of imprinted genes is known (see above).

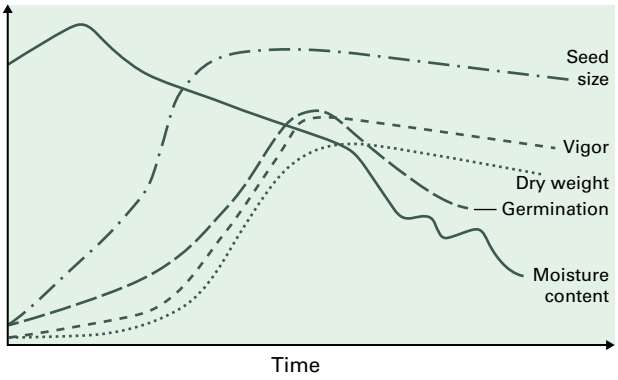


FIGURE 19.60 *Physiological changes during seed development. Note the loss in moisture content that occurs during seed maturation and the reduced ability to germinate, which reflects the establishment of seed dormancy at the end of seed maturation.*

19.7.6 Seed maturation prepares the seed for dispersal and germination

Seed development is not complete when the embryo and endosperm are formed. In fact, seed maturation, the period that follows the morphogenetic phase of seed formation, encompasses many steps that are required to prepare the seed for dispersal (Fig. 19.60).

Seed maturation involves mainly the accumulation of storage products, such as starch, lipids, and proteins, and is followed by seed desiccation. The synthesis of nutrients stored in the seed is crucial for germination and seedling establishment. These resources bridge the period required for the seedling to become photosynthetically active and to be able to acquire nutrients from the soil. The fact that the embryo must survive long periods without water requires extensive changes in its physiology, as it loses up to 90% of the water content. A large number of chaperones, including the family of LATE EMBRYO ABUNDANT (LEA) proteins, play a crucial role in the desiccation process of seeds and pollen, both of which are dispersed in a dry state. The storage of nutrients and the establishment of desiccation tolerance are crucial for seed dispersal and the evolutionary success of land plants.

During seed maturation, dormancy is also established. Mature seeds are dormant for a period of time that is specific to the plant species. When dormant, seeds cannot germinate, even under conditions that favor germination. The onset of dormancy during seed maturation and the release of dormancy during germination are both under the control of the phytohormones gibberellin and abscisic acid (ABA). ABA promotes dormancy and prevents germination, whereas gibberellin is required for germination. In mutants deficient for ABA biosynthesis, dormancy is not established and the seeds germinate precociously on the ear or in the seedpod (**vivipary**). Eventually, the balance of these two hormones regulates when a seed germinates.

Germination and seedling establishment are followed by vegetative growth of the plant, which then switches to reproductive growth under the appropriate internal and external conditions. The return to the reproductive phase of development and the formation of flowers closes the circle.

Summary

Plant reproduction is a central process in the plant's life cycle. Flowering, pollination, and fertilization culminate in the formation of seeds, which ensure the propagation of the species but are also the main output of agricultural production. Reproductive success involves interconnected signaling events that control the optimal time for flowering, depends on intricate gene regulatory networks that control floral morphogenesis, necessitates a complex series of cell–cell communication mechanisms to achieve fertilization, and relies on epigenetic regulation to form seeds, the final product of plant reproduction. Tremendous progress has been made over the last decade in deciphering the molecular mechanisms underlying these diverse developmental processes, chiefly through experiments using *Arabidopsis* as a model system but also through work on other plants.

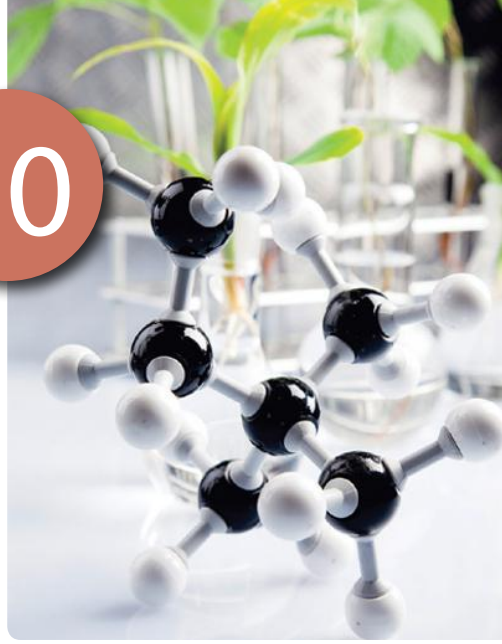
External and internal signals are integrated to tightly control flowering time, ensuring the formation of as many seeds as possible. Best understood at the molecular level are the regulatory cascades that control two key transcriptional regulators: *CO* by the photoperiod pathway and *FLC* by the vernalization and autonomous pathways. The stable maintenance of repression at *FLC*, and thus the memory of the exposure to cold, relies on

Polycomb complexes, epigenetic regulators conserved from plants to mammals. *CO* and *FLC* integrate various signals and coordinately regulate *LFY* and *AP1*, which mediate the transition from vegetative to inflorescence meristem identity.

The formation of flowers is one of the best-studied processes in plant development, largely governed by transcriptional networks that regulate organ-specific gene expression. The combinatorial action of homeotic genes, mostly transcription factors of the MADS-domain family, specifies floral organ identity. Expression of these transcription factors is regulated by the meristem identity factors LFY and AP1. In turn, the products of homeotic genes form multimeric quartet complexes that regulate downstream genes involved in the development of the different floral organs. Much of floral diversity can be explained by the altered expression patterns of floral homeotic genes, leading to a change in flower morphology.

Because male and female gametophytes develop deeply enclosed in the reproductive organs of the flower, the molecular mechanism controlling their development has long been elusive. Recent advances, however, show that a tight integration of cell cycle control and cell specification is central to male gametophyte development, while signaling via small, secreted proteins seems to be involved in patterning the female gametophyte. Cell–cell communication involving various secreted peptides—many of which belong to the defensin family of cystein-rich proteins—and cell surface receptors, is even more prominent during pollination and fertilization. Many plant species evolved self-incompatibility systems, allowing them to discriminate self from non-self pollen. The molecular nature of these systems are diverse but well understood at the molecular and cell biological level. After pollen germination, a complex series of cell–cell communication events during pollen tube growth, guidance, and reception ensures successful fertilization.

Finally, double fertilization initiates the formation of seeds, a highly coordinated process that involves interactions of three partners: the maternal seed coat, the embryo, and the endosperm. During embryogenesis, the plant hormone auxin plays a crucial role in setting up the apical–basal axis of the young embryo, which forms the main axis with the root and shoot apical meristems. Normal development of the embryo depends on the formation of endosperm, the second product of fertilization, which provides nutrients and signals to the developing embryo. Endosperm development serves as a paradigm for epigenetic regulation in plants, as it is the major site of genomic imprinting and its proliferation depends on *Polycomb* group complexes. Once the embryo is formed, complex physiological changes ensure that the seeds becomes dormant and can survive in a dry state, allowing long-distance seed dispersal.



20

Senescence and Cell Death

Howard Thomas, Helen Ougham, Luis Mur, and Stefan Jansson

Introduction

Selective death of cells, tissues and organs is an essential feature of plant development and survival. The controlled death and elimination of parts strongly influences plant shapes, habits, environmental interactions, and adaptations (Fig. 20.1). We see this clearly in the deciduous behavior of temperate trees, for example. The general term for the biological mechanisms underlying terminal events in the lives of plants and their parts is **programmed cell death (PCD)**. PCD includes any process by which protoplasm dies, with or without elimination of the associated cell wall, as part of a genetically determined developmental or adaptive event in the plant life cycle. PCD plays such important roles in plant differentiation and adaptation that the diverse forms and functions of the world's flora could not have evolved without it. Examples include:

- development of unisexual flowers in which cells destined to form male or female parts are selectively deleted
- pollen and egg cell production and post-meiotic development of micro- and megasporophytes
- degeneration of suspensor cells during embryo differentiation
- development of starchy endosperm in cereal grain maturation and death of aleurone cells during germination
- formation of xylem, sclerenchyma, and other specialized cell and tissue types such as epidermal hairs, oil glands, and abscission layers
- generation of complex organ forms, for example, the degeneration of strips of cells (called lorae) resulting in the fan-like shape of palm leaves
- senescence of organs, including leaves, roots, flower parts, and the tissues of ripening fruits
- reactions to abiotic stresses, for example aerenchyma formation under anaerobic conditions
- responses to biotic stresses, including the hypersensitive response, in which infection by a pathogen triggers defensive cell death in the host.

20.1 Types of cell death

Although the term PCD usefully encompasses all the ways by which a cell may die in the interests of plant development or survival, it does not tell us anything about mechanisms. In this chapter we survey the range of ways in which plants and their parts initiate, execute, and regulate the processes that lead to cell death.

20.1.1 Modern research on eukaryotic cell death has its roots in animal science

The recent upsurge in the study of cell death in eukaryotes was sparked in the early 1970s by research investigating how animal cells die. Two major types of cell death were identified by

Biochemistry & Molecular Biology of Plants, Second Edition. Edited by Bob B. Buchanan, Wilhelm Gruissem, and Russell L. Jones.
© 2015 John Wiley & Sons, Ltd. Published 2015 by John Wiley & Sons, Ltd.
Companion website: www.wiley.com/go/buchanan/biochem

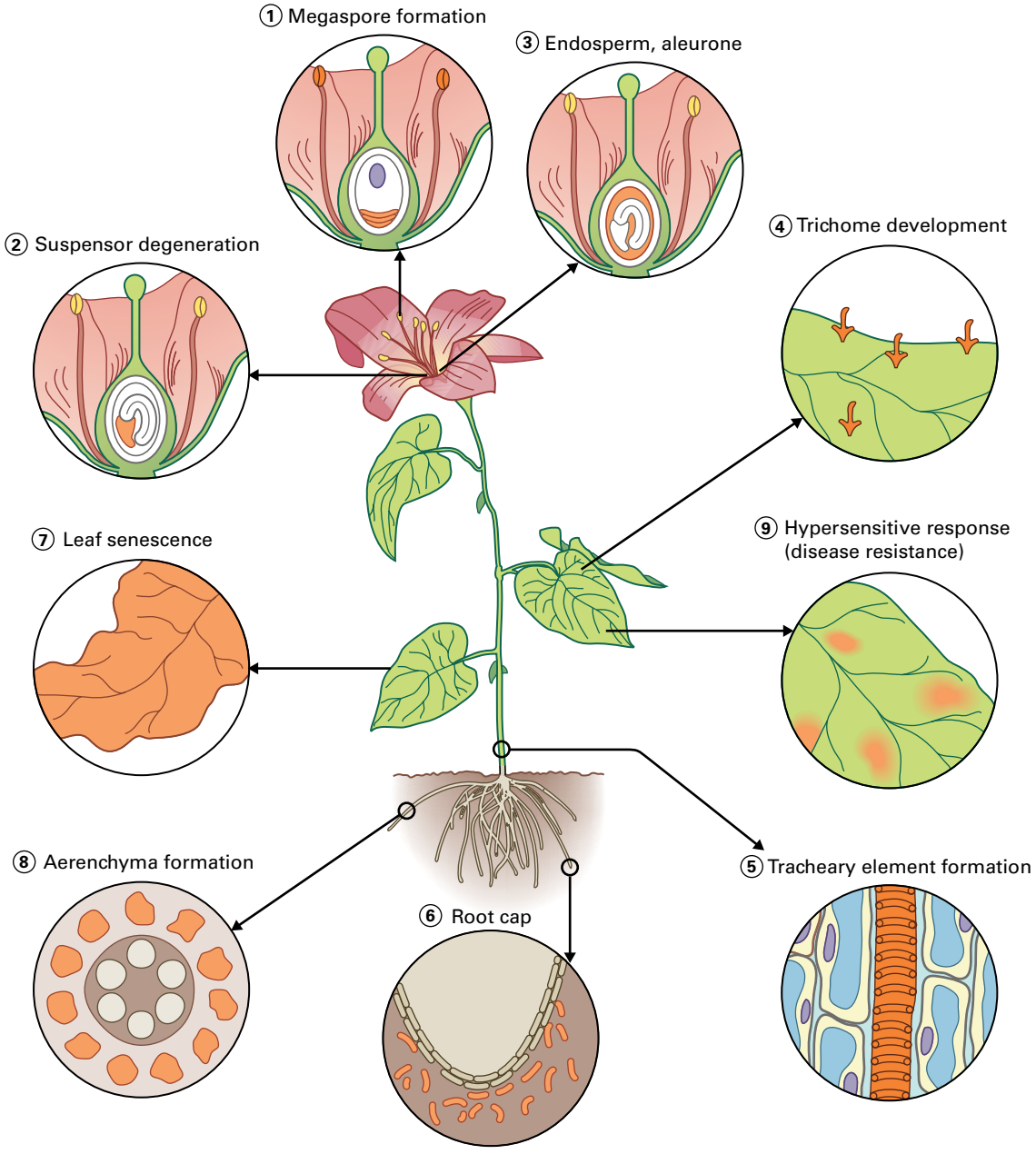


FIGURE 20.1 *Programmed cell death (PCD) occurs in many plant cells and tissues and is involved in numerous developmental and adaptive processes, including gamete formation (1); embryo development (2); degeneration of tissues in the seed and fruit (3); tissue and organ development (4 through 6); senescence (7); and responses to environmental signals and pathogens (8 and 9).*

this work: **apoptosis**, a highly regulated, energy-dependent process; and **necrosis**, which results from trauma (Fig. 20.2).

Cells undergoing apoptosis shrink and the cytoplasm condenses, although plasma membrane and organellar integrity are retained. The nuclear DNA also condenses and is cleaved into fragments of approximately 50 kbp. Nuclear DNA is often, but not always, further digested by endogenous Ca^{2+}-dependent endonucleases into oligonucleosomal sized fragments. These can be visualized on a gel as a ladder of DNA with fragments of multiples of around 180 bp (Fig. 20.3). Nuclei in which DNA has been attacked by endonucleases may be detected by terminal dUTP nick end labeling (**TUNEL**; Fig. 20.4). Fragmentation of nuclear DNA results in the breakdown of chromatin structure and is characteristic of some, but not all, forms of apoptosis. At the same time, the nucleus breaks up and the cell itself is converted into **apoptotic bodies**, small membrane-bound structures containing nuclear debris. These bodies migrate to the margin of the cell and are taken up by adjacent cells through the process of phagocytosis.

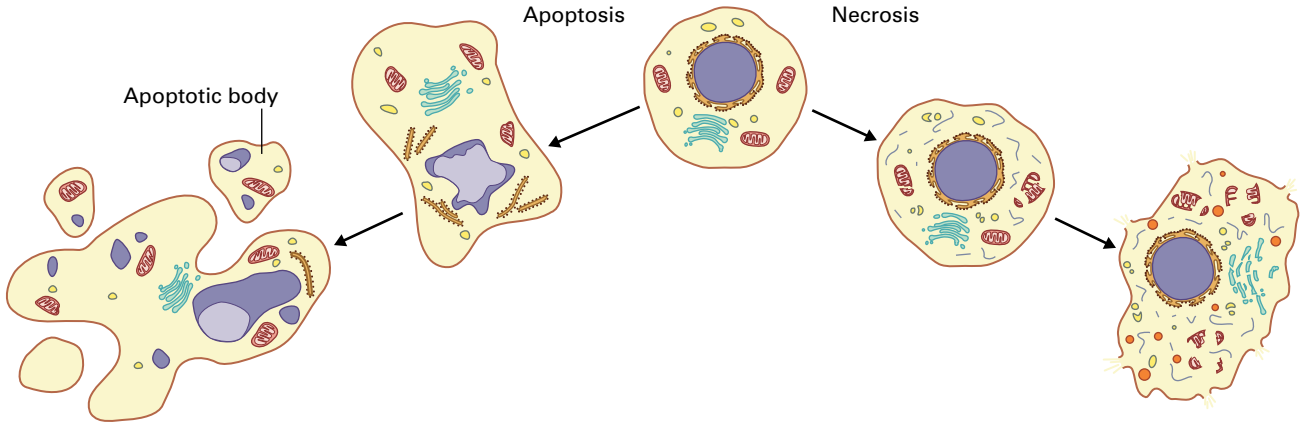


FIGURE 20.2 *Two types of cell death identified in animal cells. Apoptosis is a form of PCD in which chromatin condenses, the nuclear and plasma membranes bleb, and apoptotic bodies are formed that are eventually engulfed by neighboring phagocytes. Necrosis often occurs when cells are physically damaged; it results in rupture of membranes, release of cellular contents, and tissue inflammation.*

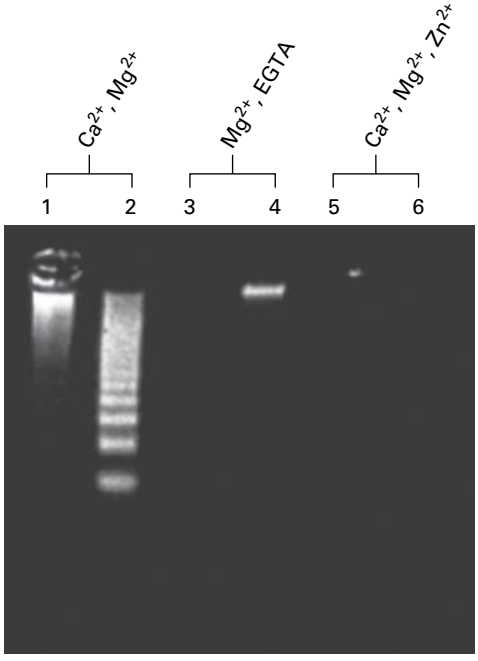


FIGURE 20.3 *DNA degradation in nuclei of rat thymocytes (lanes 1, 3, and 5) and lymph node cells (lanes 2, 4, and 6) as catalyzed by endogenous Ca^{2+}- and Mg^{2+}-dependent nuclease activity. In the presence of Ca^{2+} and Mg^{2+}, DNA laddering is observed (lanes 1 and 2). Adding the Ca^{2+} chelator EGTA (lanes 3 and 4) or Zn^{2+} (lanes 5 and 6) inhibits DNA degradation.*
Source: Peitsch et al. (1993) EMBO J. 12(1):371–377.

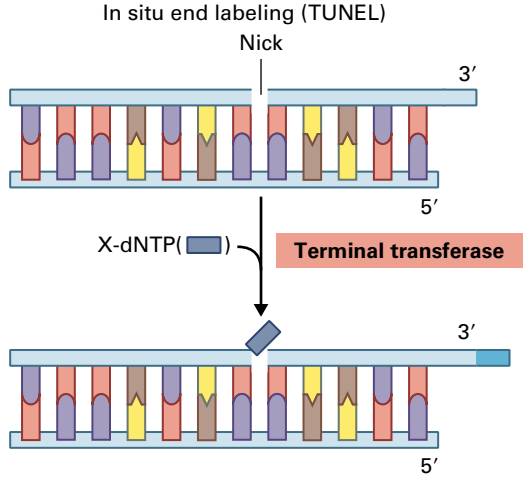


FIGURE 20.4 *In the TUNEL assay, terminal deoxynucleotidyl transferase is used to estimate the extent of DNA cleavage, based on the labeling of free 3′-OH ends of DNA with fluorescein-labeled deoxyuridine (X-dNTP) or some other fluorescently labeled nucleotide triphosphate. Note that the TUNEL method estimates only the extent of DNA cleavage and does not provide information on the size of the cleaved product.*

Additional markers for apoptosis include the formation of mitochondrial permeability transition pores (PTP) and the proteolysis of the DNA-repair enzyme poly (ADP)-ribose polymerase (PARP). PTP formation disrupts mitochondrial function and allows the release of proteins into the cytoplasm, of which **cytochrome *c*** appears to be particularly important. In human cells, cytochrome *c* interacts with a molecular chaperone (Apaf-1) and a procaspase. **Caspases** are a family of **c**ysteine proteases that cleave at specific **asp**artate-containing sites. They participate in both the initiation of apoptosis and the disassembly of cellular contents. Interaction of cytochrome *c*–Apaf-1–procaspase multimers leads to the formation of a wheel-like super-complex known as the **apoptosome**. The procaspase is cleaved into a mature form in an ATP-dependent process, leading to activation of additional caspases and a caspase-dependent nuclease, cleavage of PARP,

and digestion of structural nuclear proteins and several cytoskeletal components.

Animal cells that suffer physical damage die by necrosis, which is a fundamentally different process from apoptosis and which results in rupture of the plasma membrane and endomembranes causing hydrolytic enzymes and other materials to be rapidly released (see Fig. 20.2). Most cellular debris is engulfed by specialized phagocytes. Release of enzymes following trauma results in inflammation, whereas cells that die by apoptosis do not rupture, and therefore do not cause inflammation.

The term apoptosis, although frequently used as a synonym for PCD, has a specific meaning, and its use beyond its well-established context in animal development and pathology should be avoided. Nevertheless, the apoptosis model has influenced concepts of cell and tissue death across all organisms, and established some basic principles recognized in virtually all forms of PCD:

- Non-necrotic cell death is an active process, requiring the orderly operation of metabolism dependent on sources of biological energy.
- Cell death programs in general comprise specific genes that can be modified with predictable consequences for the course of terminal metabolic and cellular events.
- Execution of the program is characterized by cascade processes in which activation of a specific step propagates by turning on downstream actions which in turn invoke further activities and so on.

A terminal PCD process in plants that exhibits these characteristics is sometimes called "apoptosis-like," but this should not be taken to mean that true apoptosis in the strict sense occurs in plants.

20.1.2 Specific lytic processes dispose of cytoplasm and its components during PCD in plants

Chromatin condensation and DNA laddering do not accompany most types of PCD observed in plants. The presence of the cell wall precludes phagocytosis, by neighboring plant cells, of any structures equivalent to apoptotic bodies. Moreover, no gene sequences with convincing homology to caspases have been reported in plants. There are reports of plant proteases with caspase-like characteristics, for example, endopeptidases of the **vacuolar processing enzyme** (VPE) group, but these so-called "**metacaspases**" have yet to find an agreed physiological role. Metacaspase activity has been measured during some PCD events in plants, including tracheary element formation, pollen death resulting from self-incompatibility, and the hypersensitive response. Inhibitors against mammalian caspases can be effective in suppressing some of these processes.

In the absence of phagocytosis, how do plants eliminate unwanted cytoplasm or whole cells during PCD? The general term for the dissolution of cytoplasm within the cell wall through the action of the cell's own catabolic machinery is **autolysis**. As described in subsequent sections, plants employ several different kinds of autolytic process during development and adaptation. One way that some plant cells can dispose of their cellular contents is through **autophagy**, a death process in which the cell "eats itself" from within. Vesicles are produced that engulf portions of the cytosol, including intact organelles. These vesicles, called **autophagosomes**, are taken up by the central vacuole of the cell (Fig. 20.5A), or in some cases fuse with lysosomes (lytic vesicles; Fig. 20.5B), and are broken down by hydrolases. Blocking the action of proteolytic enzymes by treatment with inhibitory chemicals such as E-64 or concanamycin A (CMA), disrupts autophagic pathways and results in accumulation of autophagic bodies (Fig. 20.5A,B). Autophagosomes have been observed in senescing corolla cells of Japanese morning glory (*Ipomoea tricolor,* Fig. 20.5C) and during sucrose starvation of cultured *Nicotiana tabacum* BY-2 cells (Fig. 20.5D shows autophagic bodies in the vacuole of a CMA-treated cell).

Mechanistically, autophagy involves distinctive stages: (i) vesicle induction; (ii) vesicle expansion; (iii) tonoplast docking and fusion; and (iv) digestion. Molecular components regulating autophagy have been particularly well described in yeast, but homologs of most of these **autophagic genes** (*ATG*) are also present in *Arabidopsis* (Table 20.1) and other plant species. Initiation of autophagy is regulated by a target of rapamycin (TOR) kinase. Under normal conditions TOR kinase phosphorylates ATG1 kinase and accessory proteins, leading to their inactivation. To initiate autophagy, TOR kinase is inactivated, allowing ATG1 to interact with several ATG proteins, leading ultimately to the formation of a vacuolar-sorting complex that includes a phosphatidylinositol 3-kinase (PI3-K) protein. This is a key vesicle nucleation step in which tubular **pre-autophagic structures** (PASs) are formed, possibly from the endoplasmic reticulum (ER). PASs coalesce to form a cage that captures a portion of the cytoplasm. This late expansion phase is aided by many ATG proteins, with a key event being the linking of the vesicle to cytoskeletal microtubules via an ATG8 conjugate to a lipophilic phosphatidylethanolamine moiety allowing targeting to the vacuole.

Another important feature is the addition to the autophagosome of a protein complex consisting of ATG5, ATG12, and ATG16. The exact function of this complex is unknown, but it is required for vesicle expansion. Docking/fusion involves formation of a receptor complex including VT11, a **v**esicle-located **S**oluble ***N***-ethylmaleimide-sensitive factor **A**daptor protein **RE**ceptor (v-SNARE, see Chapter 4), coming together with a vacuolar membrane syntaxin protein, VAM3. Once within the vacuole (Fig. 20.5), breakdown involves several enzymes that in plants include VPE-type metacaspases (see Section 20.7.1).

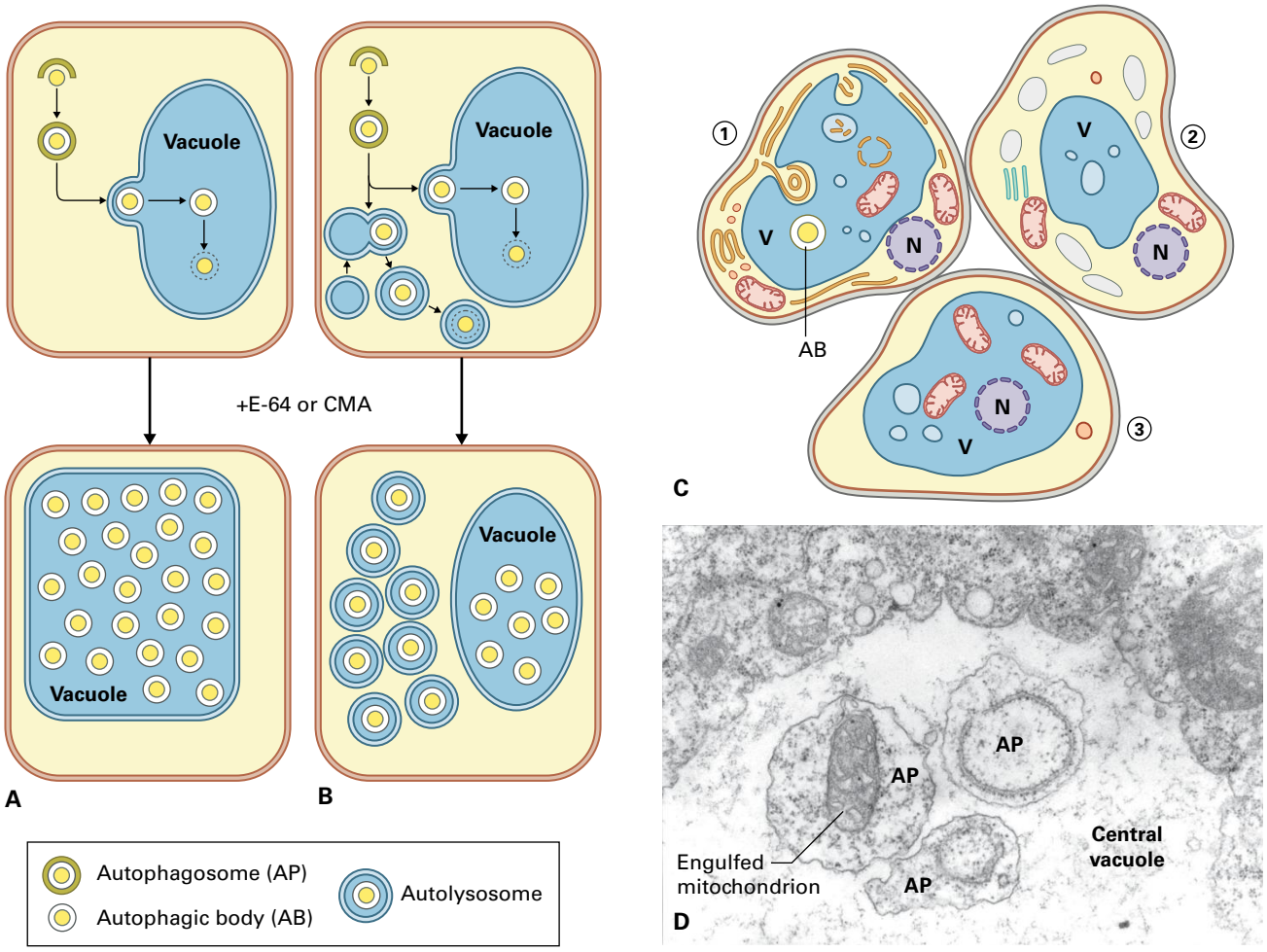


FIGURE 20.5 *Autophagy pathways in plant cells. (A) Induction of autophagy in* Arabidopsis *and many other species results in formation of a double-membrane autophagosome around a portion of cytoplasm. The outer membrane fuses with the tonoplast and the inner membrane and contents enter the lumen of the vacuole (Vac) and are degraded (upper panel). Treatment with inhibitors of vacuolar proteases (E-64, CMA) results in accumulation of autophagic bodies inside the vacuole (lower panel). (B) In tobacco (*Nicotiana *spp.) an additional autophagy pathway operates, in which autophagosome contents are degraded by fusion with small lysosomes (upper panel). Treatment with E-64 or CMA leads to accumulation of autolysosomes in the cytoplasm as well as autophagic bodies in the vacuole (lower panel). (C) Autophagy in some dying senescing corolla cells of* Ipomoea tricolor. *The three cells shown represent different stages of PCD, 1 being the earliest, and 2 and 3 later stages of autophagy. AB, autophagic body; N, nucleus; V, vacuole. (D) Transmission electron micrograph of part of a sucrose-starved cell from a culture of the tobacco (*Nicotiana tabacum*) cell line BY-2 (bright yellow-2) treated with CMA, showing autophagosomes accumulated in the central vacuole, one of which has engulfed an entire mitochondrion.*
Source: Bassham (2007). Curr. Opin. Plant Biol. 10: 587–593.

TABLE 20.1 Arabidopsis *proteins with functions in autophagy.*

Complex/process	Proteins	Potential function
PI-3 kinase complex	ATG6, VPS15, VPS34	Autophagosome formation
Ubiquitin-like conjugation	ATG5, 7, 10, 12	Conjugation of ATG12 and ATG5
Ubiquitin-like conjugation	ATG3, 4, 7, 8	Conjugation of ATG8 to phosphatidylethanolamine
ATG9 complex and localization	ATG9, 2, 18	Membrane recruitment to autophagosome
Regulation	TOR, ATG1, 13	Initiation of autophagy
SNARE	VTI12	Fusion of autophagosomes with the vacuole

Source: Bassham (2007). Curr. Opin. Plant Biol. 10:587–593.

20.1.3 Plant cells remain viable during most of the developmental program that leads to cell death

An understanding of PCD requires a clear distinction to be made between processes that lead to death, during which time cells are viable, and the final act of death. In some cases the phase preceding death can be arrested or even reversed. Senescence of green (mesophyll) cells of leaves is a case in point. Mesophyll cells remain viable until almost all of the leaf's resources have been exported. While their plastids and other organelles are salvaged, senescing leaves remain turgid, indicating the continued integrity of membranes, cell compartments, and water relations. Wilting as a result of loss of cellular turgor and consequent cell death is a late event in leaf senescence. In comparison to the time-scale of the senescence phase, the terminal autolytic process of declining viability itself is probably very rapid.

Cell death in plants permits developmental and biochemical plasticity. Almost all phases of the plant life cycle are influenced by PCD. The following sections will describe some instances of PCD that occur during plant development, starting with seed germination and proceeding through vegetative and reproductive development.

20.2 PCD during seed development and germination

The seeds and fruits of many species are albuminous, that is, they store reserve materials to support germination in endosperm, the product of the second fertilization event when one of the two pollen grain nuclei fuses with the polar nuclei of the female gametophyte. Cereal endosperm comprises two cell types: **starchy endosperm** and **aleurone**. Aleurone cells are derived from maternal tissue, and studies of maize (*Zea mays*) mutants and transgenics show that their identity is determined by their peripheral location at the surface of the starchy endosperm. Both starchy endosperm and aleurone undergo developmentally regulated PCD but follow distinctly different routes. In mature grain, the starchy endosperm is dead, but unlike almost all other eukaryotic cells that undergo PCD, the contents of these cells are not broken down but are preserved, in a desiccated or mummified state. When grain germinates, hydrolytic enzymes are secreted by the scutellum and aleurone layer, and the entire starchy endosperm is degraded. PCD processes during the development of endosperm and aleurone in albuminous seeds of eudicots and other monocots are similar to those described below for cereals.

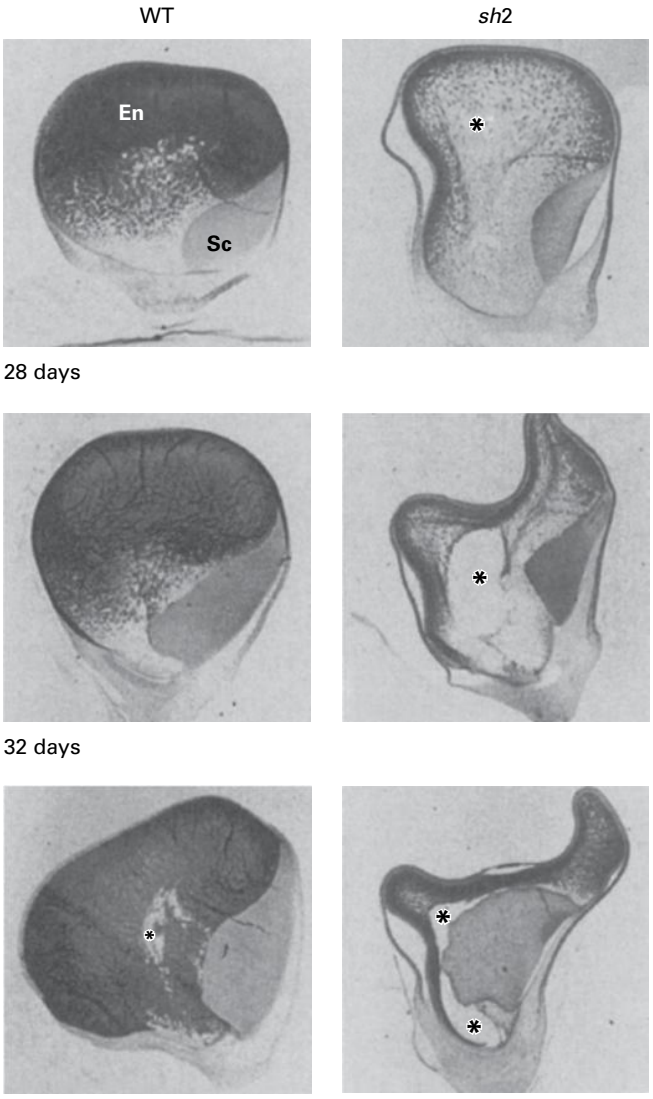


FIGURE 20.6 *Endosperm (En) development in wild-type and* shrunken2 *(*sh2*) maize genotypes. The* sh2 *mutant undergoes premature degradation of the starchy endosperm to yield cavities (*). Shown are kernels of wild type (WT) and* sh2 *mutant plants at 28 days, 32 days, and 40 days after pollination. The starch is stained with iodine-potassium iodide. Sc, scutellum/embryo.*
Source: (A–F) Young et al. (1997). Plant Physiol. 115:737–751.

20.2.1 During cereal seed development, the contents of starchy endosperm cells undergoing PCD are preserved

Mutations have been identified in maize in which the normal pattern of endosperm development and endosperm cell death is altered. The *shrunken2* (*sh2*) mutation results in premature death of starchy endosperm cells and degradation of their walls and contents (Fig. 20.6). Laddering of DNA occurs during PCD of *sh2* starchy endosperm cells. Furthermore, unlike

normal starchy endosperm cells, those of *sh2* mutants become autolyzed, which causes endosperm to deform and produces aberrant, shrunken kernels.

An interesting aspect of cell death in starchy endosperm of maize concerns the role of ethylene, a hormone frequently associated with senescence (see Section 20.11.2). Ethylene production is much higher in kernels of *sh2* mutants relative to wild type, and treatment of developing wild-type kernels with ethylene brings about an increase in cell death and production of aberrant kernels (Fig. 20.7). Additional evidence that ethylene might be an important player in regulating PCD in maize kernels comes from experiments with ethylene biosynthesis inhibitor aminoethoxyvinylglycine (AVG). AVG reduced the extent of DNA fragmentation in *sh2* starchy endosperm cells and decreased the size of the central cavity formed in aberrant kernels (see asterisks in Fig. 20.6).



FIGURE 20.7 *Ethylene can cause kernel deformation in wild-type maize kernels. Shown are a control kernel of wild-type maize (A) and an ethylene-treated kernel (B) 32 days after pollination. The arrow points to dead cells in the scutellum. The starch is stained with iodine-potassium iodide. En, endosperm; Sc, scutellum/embryo. Source*: (A, B) Young et al. (1997). Plant Physiol. 115:737–751.

20.2.2 Gibberellic acid and abscisic acid are important regulators of cell death in cereal aleurone

Unlike cells of the starchy endosperm, aleurone cells remain alive until germination and endosperm mobilization are complete, whereupon they undergo autolysis and die (see Fig. 20.8). **Gibberellic acid** (GA) and **abscisic acid** (ABA) tightly regulate this process. Whereas GA stimulates onset of PCD in aleurone layers of barley (*Hordeum vulgare*) and wheat (*Triticum aestivum*), ABA postpones PCD (Fig. 20.9). The effects of ABA on cell death in barley aleurone are dramatic. ABA-treated aleurone protoplasts can be kept alive for more than 6 months, whereas GA treatment of protoplasts brings about death of most cells in 5–8 days.

The **protein storage vacuoles** (PSVs) of aleurone cells become acidic, lytic compartments within the first few hours following GA treatment. Aleurone cells contain PSVs that have a luminal pH of around 7, but after 3–4 hours of GA treatment the lumen reaches a pH of 5.5. The vacuoles of GA-treated cells also accumulate a spectrum of acid hydrolases, including several aspartic and cysteine proteases, as well as nuclease activities. Vacuoles in ABA-treated cells that do not undergo PCD lack these enzyme activities and maintain a pH near neutrality. The function of PSVs in GA-treated aleurone cells resembles that of vacuoles in senescing photosynthetic cells (see Section 20.7.1). The vacuoles of both kinds of tissue contain similar lytic enzymes and, in contrast to the PCD process in tracheary elements for example (see Section 20.3.2), they retain an intact tonoplast throughout the period of macromolecule breakdown and export. During GA-induced PCD, aleurone DNA is not degraded by laddering but instead is cleaved directly into small fragments that are not resolvable by electrophoresis (Fig. 20.10) or TUNEL.

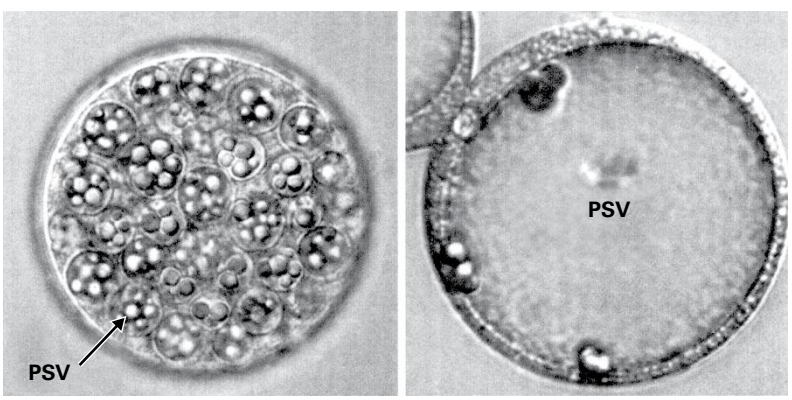


FIGURE 20.8 *PCD in the cereal aleurone is accompanied by an autolytic process during which there is extensive vacuolation of the cytoplasm without rupture of membranes or the formation of autophagic vacuoles. In the barley (*Hordeum vulgare*) aleurone cell (left) small protein storage vacuoles (PSV) lose their stored protein and fuse to form one large central vacuole (right). Membrane integrity is maintained until death ensues. Source*: P. Bethke & R. Jones, University of California, Berkeley; previously unpublished.

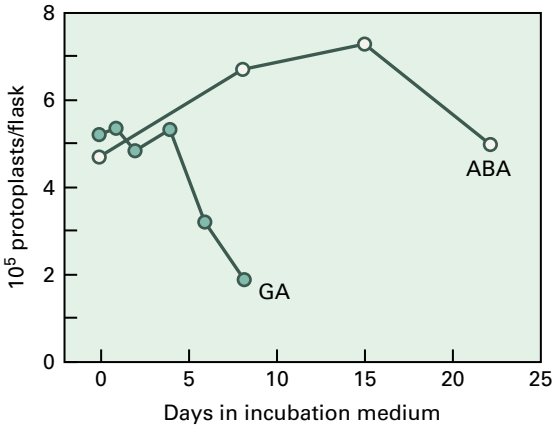


FIGURE 20.9 *Gibberellic acid (GA) promotes PCD and abscisic acid (ABA) delays PCD in barley aleurone cells. Aleurone cells were incubated in a medium containing 5 μM GA or 25 μM ABA; cell death was monitored by counting the number of live cells.*

20.2.3 In cereal aleurone, cyclic GMP and nitric oxide may participate in the signaling pathway that leads to PCD

The signal transduction cascade leading to GA-induced synthesis and secretion of hydrolases has been extensively studied and is known to include cytosolic free Ca^{2+}, cytosolic pH, cyclic GMP, and calmodulin (CaM) as well as protein kinases and protein phosphatases. In contrast, much less is known about the signaling components that promote GA-induced death in cereal aleurone cells. Evidence in favor of an important role for protein phosphorylation comes from experiments in which aleurone cells have been treated with inhibitors and synthetic substrates. Blocking a cGMP-linked GA-signaling pathway reduces expression and secretion of α-amylase and prevents GA-induced increases in nuclease activities, DNA degradation, and cell death. This makes cGMP a likely candidate for the GA signal transduction pathway that leads to cell death in aleurone cells.

Recently nitric oxide (NO) has become recognized as a significant player in PCD processes in plants. NO donors such as sodium nitroprusside delay GA-induced cell death in barley aleurone, and NO scavengers accelerate the process. Aleurone tissue is able to make NO nonenzymatically from nitrite. The mechanism by which cells perceive NO and how this relates to signaling pathways for aleurone PCD are not clear. NO is known to react with heme-containing proteins, such as guanylyl cyclase, which is activated by NO to generate cGMP. NO also nitrosylates proteins containing exposed thiol groups, causing reversible conformational changes. NO is a potent antioxidant too. Any or all of these properties may turn out to be critical in the regulation of PCD in aleurone and other tissues.

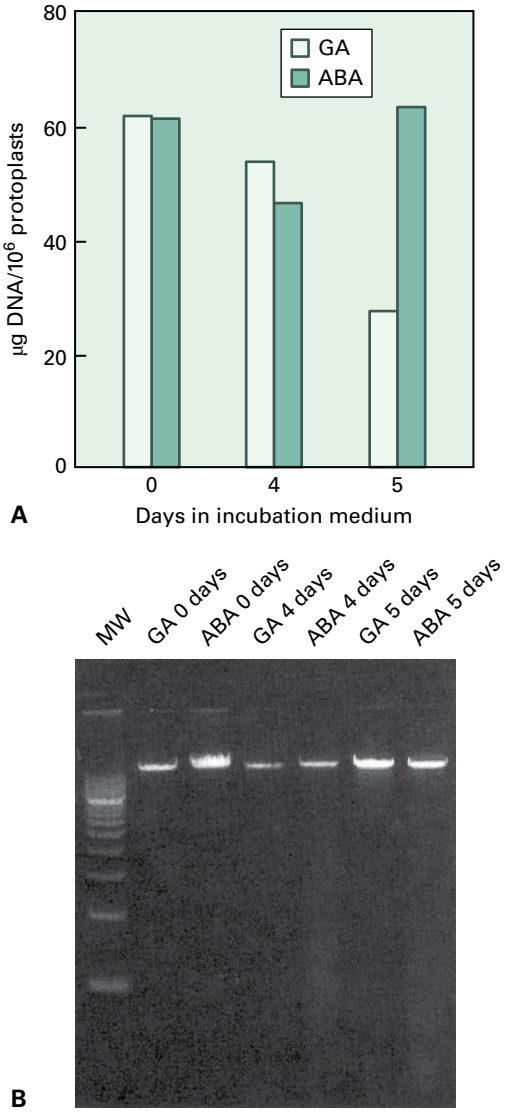


FIGURE 20.10 *DNA degradation is a late event in aleurone PCD. (A) Aleurone cells begin to lose DNA only after they become committed to die. (B) DNA breakdown is not accompanied by formation of the 180-bp ladders characteristic of apoptosis (see Fig. 20.3 for comparison). MW, molecular mass markers; GA, gibberellic acid; ABA, abscisic acid.*
Source: Bethke et al. (1999). Plant Cell 11:1033–1045.

20.3 Cell death during the development of secretory bodies, defensive structures and organ shapes

During embryogenesis in animals, structures are often formed by cell migrations (gastrulation). Generation of morphological and anatomical structures by gastrulation-type cell movement is not possible in plants because plant cells are locked in place by their rigid walls. Instead, plants typically

rely on localized cell death to regulate volume-to-surface-area ratios and develop spaces for transport and secretion.

Botanists use the term **lysigeny** to refer to the disintegration of cells that occurs when new structures are differentiated in this way. Lysigeny, with or without cell separation (**schizogeny**), is responsible for the differentiation of secretory ducts, cavities, and canals in many species. Cell and cytoplasm elimination processes similar to lysigeny and schizogeny in outcome are widely deployed by plants to sculpt external and internal structures into well-adapted configurations necessary for efficient function and survival. A developmental PCD process, with similarities to lysigeny, that is universal among higher plants is formation of the thick-walled cells lacking protoplasm that are essential components of vascular and supportive tissues. Examples of the sculptural roles of PCD in morphology and anatomy are discussed in subsequent sections.

20.3.1 Localized cell death during the differentiation of secretory structures occurs by lysigeny and schizogeny

Oil glands on the surfaces of citrus fruit develop because a group of subepidermal cells undergoes **schizolysigeny**, a combination of lysigenous and schizogenous PCD, forming a cavity that fills with essential oil (Fig. 20.11). Mucilaginous canals found in the bud scales of *Tilia cordata* (small-leaf linden, small-leaf lime) arise exclusively by lysigenous cell death, whereas air spaces in *Avicennia marina* (mangrove) leaves are schizolysigenous in origin. The resinous secretory ducts in the phloem of plants of the sumac family (Anacardiaceae) develop schizogenously and are the source of urushiol, the severe allergen in the sap of poison oak and poison ivy (*Toxicodendron* spp.).

Many trichomes, thorns or spines on the surfaces of leaves and stems are dead at maturity. Extreme examples of this are seen in cacti, in which green stems functionally replace leaves, and leaves are reduced to spines. Localized cell death during foliar development is also responsible for indentations and holes found in leaves of some species of the families Araceae and Aponogetonaceae (Box 20.1).

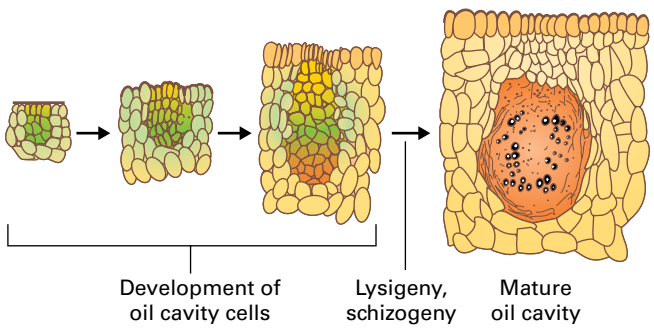


FIGURE 20.11 *Formation of an oil gland in citrus peel occurs by a combination of lysigeny, the death and dissolution of the protoplast and cell wall, and schizogeny, wall separation to produce an intercellular space. The resulting cavity becomes filled with essential oils secreted from cells surrounding the cavity.*

The extent to which lysigeny, autophagy and the other kinds of autolytic PCD process have common mechanisms of regulation and biochemical execution has not been established by systematic comparative studies.

20.3.2 PCD during tracheary element formation is studied in vitro using cultured *Zinnia elegans* mesophyll cells

Xylogenesis (wood formation) is a type of developmentally regulated PCD initiated during embryogenesis and continued throughout the life of the plant. Xylem typically contains tracheary elements (TEs), the vessel elements and tracheids of the water-conducting system (Fig. 20.12). During the final stages of differentiation, TEs undergo secondary cell wall thickening, followed by autolysis of protoplasm and cell death. All that remains of the cell in its final differentiated form is the cell wall with its characteristic secondary thickenings. Connected end to end, these hollow tubes form the vessels through which water is conducted.

Differentiation of TEs normally takes place from procambium and cambium but the process can be reproduced in vitro using cultured zinnia (*Zinnia elegans*) mesophyll cells, isolated from intact leaves. When isolated cells are incubated in a culture medium containing an auxin and cytokinin as many as 40–60% dedifferentiate and then re-differentiate into TEs in the absence of cell division (Fig. 20.13). Differentiating TEs develop secondary cell wall thickenings characteristic of those found during differentiation in vivo. Shortly after the secondary wall thickenings become visible, the tonoplast ruptures. This may be the committed step to death, as it is followed by breakdown of the remaining organelles and ultimately the loss of cell contents. Breakdown of protoplasm is paralleled by an increase in activity of degradative enzymes including DNases, RNases, and proteases.

In vitro induction of TE differentiation provides an ideal system for studying the development of cells in which programmed death is essential for final form and function. A large population of cells can be induced to undergo the process synchronously, allowing biochemical and molecular analyses of the events that accompany differentiation. This differs from most in vivo systems, where only a few cells differentiate at once, and those are embedded within other tissues.

20.3.3 Events during in vitro formation of zinnia tracheary elements comprise three stages

In the zinnia in vitro system, the process of TE formation occurs in 4 days and has been divided into three distinct stages—(1) dedifferentiation, (2) restriction of developmental

BOX 20.1 How PCD can modify leaf morphology

A freshwater plant popular with aquarists, the lace plant (*Aponogeton madagascariensis*, Aponogetonaceae) undergoes an unusual form of leaf sculpting that creates a delicate latticework. Starting early in leaf development, regions of cells experience PCD so that perforations form as the lamina expands. As in the case during differentiation of tracheary elements, the tonoplast membranes of lace plant cells rupture early in the PCD process, releasing the vacuolar contents. In contrast, the nuclei retain their integrity until late in the process, and although the genomic DNA becomes fragmented, it does not exhibit the laddering pattern seen in apoptosis. In addition to the cell contents, the walls of dying cells are also degraded during PCD, with cellulases acting early in the development of perforations and pectinases active throughout the whole period of lace plant leaf development. Later, the walls of living cells surrounding the perforations become modified by deposition of suberin (see Chapter 24), which may prevent the further spread of PCD and protect the cells from invasion by microbes.

Of the other plants that use PCD to create holes and indentations in their leaves, the best known is the Swiss cheese plant, *Monstera deliciosa* (Araceae). Unlike the lace plant, in *Monstera* the targeted leaf cells do not undergo cell wall degradation. Early in development, the leaf blade forms distinctive perforations as discrete patches of cells die. These initially minute perforations increase by about 10,000-fold in area as the leaf expands. The occurrence of PCD over a short period of time rather than throughout leaf development results in a relatively small number of holes or interruptions to the leaf surface.

In contrast to the lysigeny-like origin of holes in the leaves of *Aponogeton madagascariensis* and *Monstera deliciosa*, the dissected, fan-like leaves of palms arise by cell separation (schizogeny). Corrugations (plications) are formed through intercalary growth, followed by dissection of the initially simple leaf blade through an abscission-like process of leaflet separation. Phylogenetic analyses of the diversity of mechanisms employed during development of perforated and dissected foliage indicate that recruitment of cell death and cell separation programs for sculpting leaves has occurred independently several times during plant evolution.

Source: A.N.D. Dauphinee, Dalhousie University, Canada.



potential, and (3) TE-specific development. The expression patterns of many genes change as these stages progress (Fig. 20.14). Genes expressed during dedifferentiation (stage 1) include those involved in wound responses in plants, such as the protease inhibitor genes *ZePI-1* and *ZePI-2*, the pathogenesis-related gene *ZePR*, and those involved in protein synthesis, such as ribosomal protein (RP) and elongation factor (EF) genes. Different transcripts for genes involved in phenylpropanoid metabolism (see Chapter 24 and Section 20.6.3) are present at various stages, with phenylalanine ammonia lyase (PAL) and cinnamic acid 4-hydroxylase (C4H) expressed in both stages 1 and 3 and cinnamyl alcohol dehydrogenase (CAD) accumulating in stages 2 and 3. Tubulin (*Tub*) genes are expressed during all three stages. Onset of stage 2, during which the cultured cells commit to TE formation, is characterized by the appearance of tracheary element differentiation-related (TED) transcripts.

Secondary cell wall thickenings are laid down during stage 3 of zinnia cell culture. Immunocytochemistry has shown that arabinogalactan- and extensin-like proteins as well as novel glycoproteins accumulate in the TE cell wall. After secondary walls have been laid down, the protoplast degenerates. Electron microscopy indicates that autolysis of cell contents is

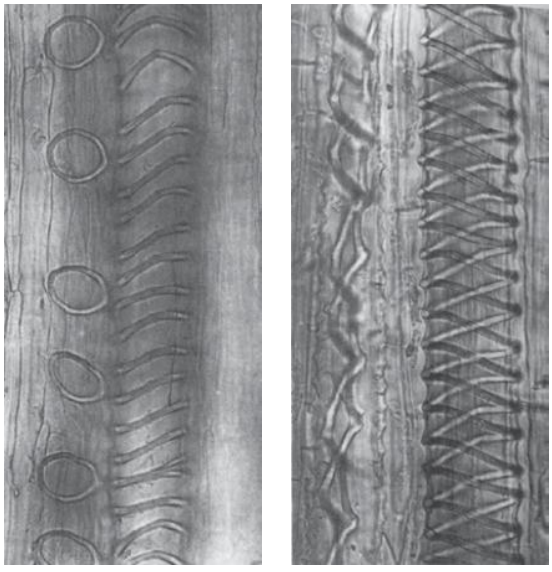


FIGURE 20.12 *TE in the primary xylem of castor bean (*Ricinus communis*) showing annular (A) and double helical (B) thickenings in the cell walls of vessel elements.*
Source: A. Raven et al. (1999). In Biology of Plants, W.H. Freeman, New York.

brought about when the tonoplast ruptures and releases lytic vacuolar enzymes into the cytosol.

Genes encoding lytic enzymes (e.g., proteases and nucleases) are expressed during late stage 2 and early stage 3. Genes for cysteine proteases and an S1-type nuclease (ZEN1) have been cloned, and biochemical evidence confirms localization of these gene products in differentiating TE. Transient suppression of *Zen1* expression has shown ZEN1 to be the key nuclease in degradation of nuclear DNA. In addition to cysteine proteases, at least three serine proteases are found in zinnia TE. One of the serine proteases may be a secreted enzyme that is involved in regulating TE differentiation. There is evidence for a regulatory role for cysteine proteases and the proteasome (see Chapter 10) in initiating the death program. For example, when inhibitors of cysteine protease are added to zinnia cells before the start of secondary wall thickening, further TE differentiation is blocked. Inhibitors of proteasome activity also lead to arrest of TE formation. However, no specific protease has so far been shown to be indispensable for TE PCD. It appears that lignification continues following PCD, using precursors provided by adjacent cells.

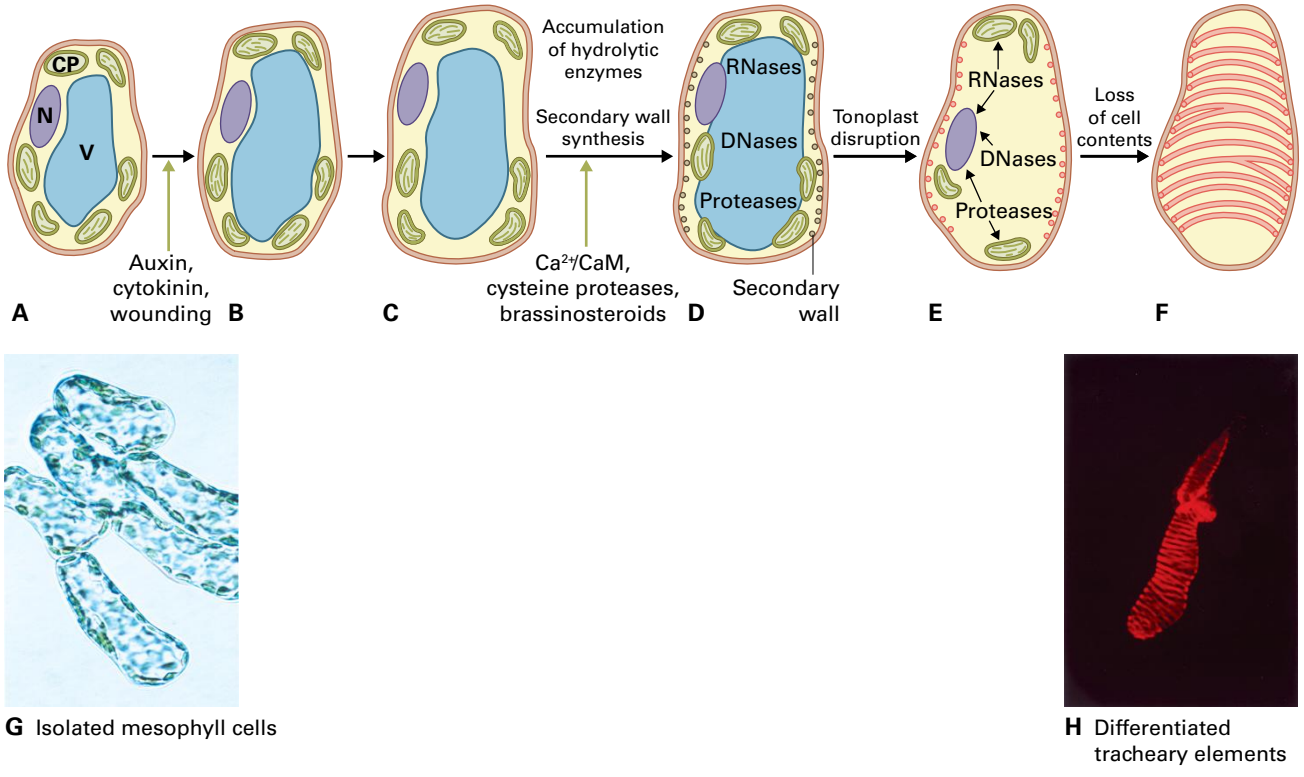


FIGURE 20.13 *The redifferentiation of cultured zinnia mesophyll cells into TE involves PCD. (A) A cultured mesophyll cell with its complement of cellular organelles. After induction by modification of the hormone content of the culture medium, the cell dedifferentiates (B), then differentiates to form sequentially a TE precursor cell (C), an immature TE with characteristic secondary cell wall thickenings (D), a maturing TE, in which lysis of the vacuole is followed by total degradation of the cellular contents (E), and finally a mature, dead, empty TE (F). (G) Cultured mesophyll cells, under normal light microscopy, in which small, green chloroplasts can be seen at the outer periphery of the cytoplasm. (H) Mature TE generated from a cultured mesophyll cell. This empty cell is stained with fluoroglucinol, which fluoresces in the presence of lignin and highlights the banded secondary cell wall. CaM, calmodulin.*
Source: (G, H) A. Groover, University of North Carolina, Chapel Hill; previously unpublished.

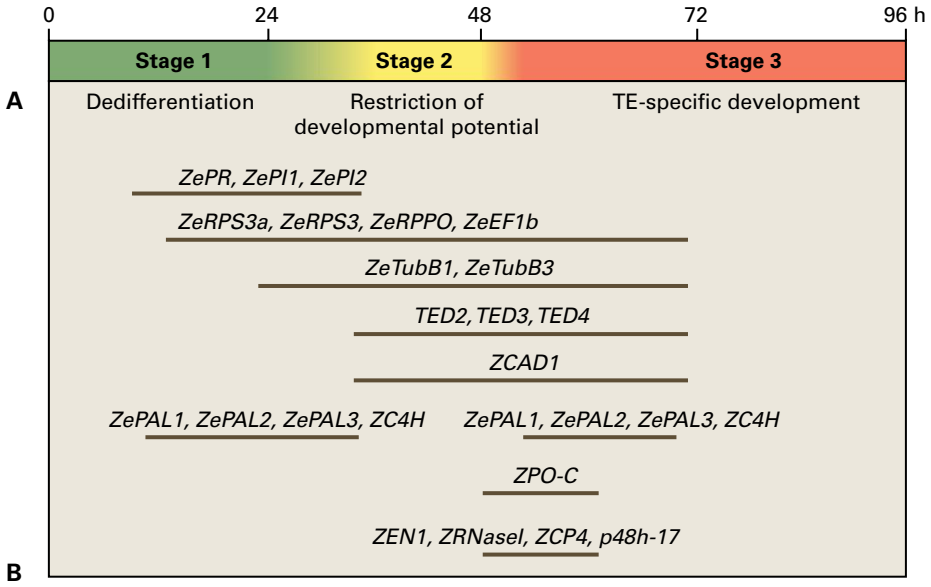


FIGURE 20.14 *Stages of gene expression during zinnia mesophyll redifferentiation. TE differentiation has been divided into three stages totaling about 96 hours. The identities of most of the genes expressed during these stages are discussed in Section 20.3.3. Among the genes not named in the text are* ZPO-C *(a peroxidase gene),* ZRNaseI, *and* ZCP4 *and* p48h-17 *(possible cysteine proteases).*

20.3.4 In addition to auxin and cytokinin, Ca^{2+} and proteases appear to promote PCD in zinnia TE

PCD in zinnia lacks the hallmark cellular events associated with apoptosis. Rupture of the tonoplast is accompanied by changes in the organization of cellular organelles and cell wall (Fig. 20.15). Lignification of the cell wall occurs after the tonoplast breaks, and the plasma membrane remains intact until almost all recognizable organelles have disappeared. This form of PCD may be particularly suited to the disposal of all cellular materials required to provide a clear pathway for water movement in the TE.

Auxins and cytokinins are required for zinnia TE differentiation, but other putative signaling molecules also play important roles in this process. Ca^{2+} and CaM have been shown to be likely players in signaling pathways leading to TE differentiation. For example, removal of Ca^{2+} from culture medium reduced TE formation from 50% to less than 10%, and Ca^{2+} channel blockers are effective in inhibiting TE differentiation when applied at any time during the first 48 hours of culture. Differentiation of TE can also be blocked by applying CaM antagonists to the culture medium. Ca^{2+} may be an important player in the cell death stages of TE formation as Ca^{2+} channel blockers can prevent cell death in differentiating TEs. There is also compelling evidence linking other molecules (NO, for example) to the initiation of cell death in zinnia TEs.

A secreted serine protease that accumulates in the incubation medium of cultured zinnia has also been shown to have an effect on PCD of TEs. Several types of experiments have shown that this serine protease may play a role in PCD of cultured zinnia cells. First, addition of soybean (*Glycine max*) trypsin inhibitor to TE culture media inhibited cell death and arrested TE differentiation. The soybean inhibitor also inhibited the activity of a 40-kDa serine protease that accumulated in the medium coincident with cell death. Second, proteolytic enzymes such as trypsin or papain dramatically accelerate cell death of TEs when added to culture media. Effects of added trypsin on TE PCD can be reversed by lowering the Ca^{2+} concentration of the incubation medium or by adding Ca^{2+} channel blockers. These data were interpreted as showing the involvement of Ca^{2+} in protease-mediated PCD during TE formation.

20.3.5 TE formation has also been studied in *Arabidopsis* and *Populus*

Cell death in TEs has been analyzed in model systems in addition to zinnia. *Arabidopsis* has been used to study gene expression patterns during TE differentiation in vivo and to identify mutants affected in TE PCD. Several *Arabidopsis* homologs to zinnia TE-specific genes have been identified. Functional evidence for roles of such genes in TE PCD has been provided only for a paralogous pair of vacuolar cysteine proteases, XYLEM CYSTEINE PROTEASE1 (XCP1) and XCP2, and for an S1-type ZINNIA ENDONUCLEASE1 (ZEN1). ZEN1 was shown to promote nuclear DNA degradation in the zinnia tracheary elements in vitro, while a detailed immunolabeling analysis showed that XCP1 and XCP2 participate in clearing of TE cell contents. Studies in *Arabidopsis* have also addressed whether TE PCD is controlled as an independent process or is an inevitable fate following deposition of secondary cell walls. Transgenic *Arabidopsis* plants overexpressing *NAC SECONDARY WALL THICKENING*

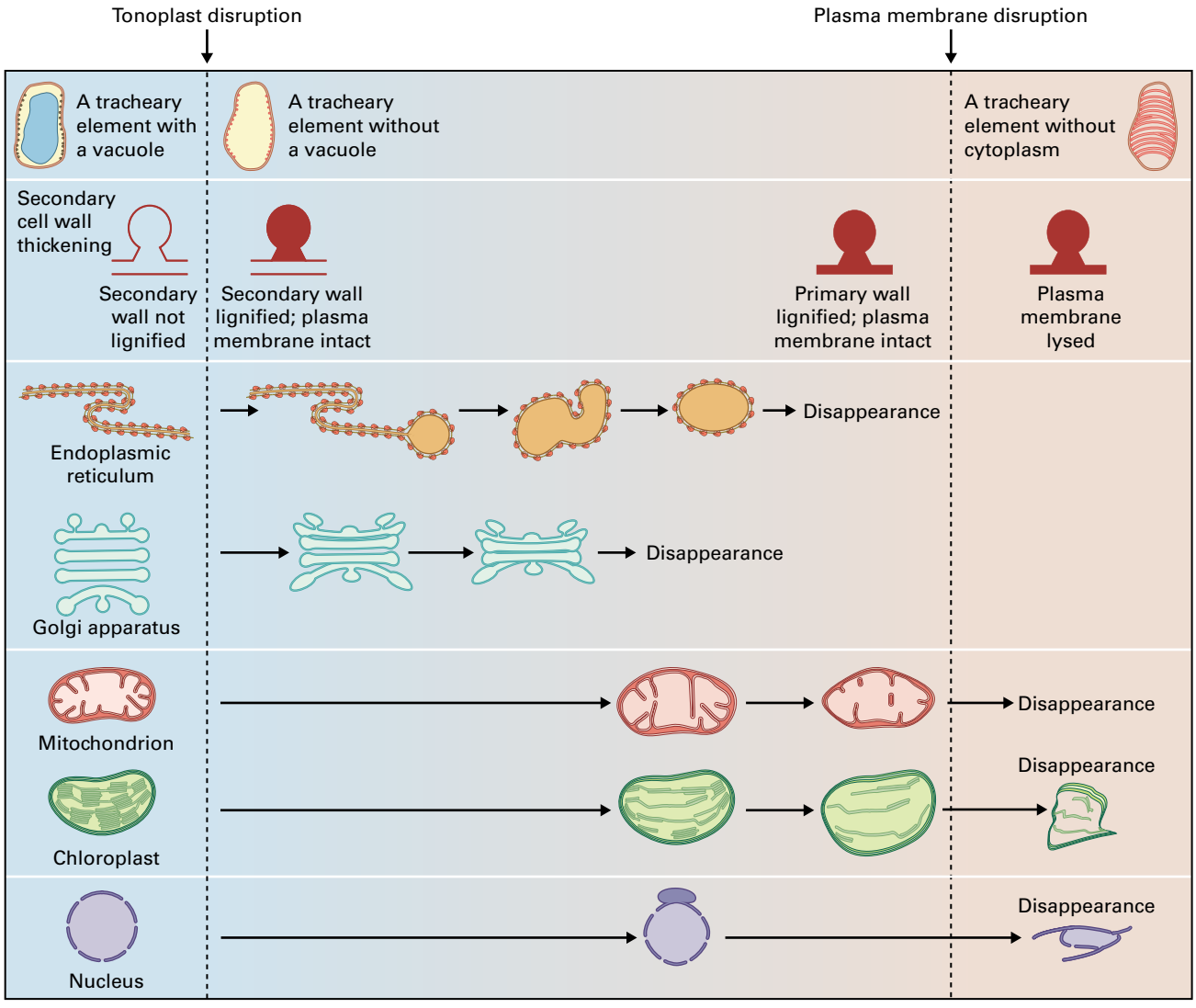


FIGURE 20.15 *Structural changes in the organelles of differentiating zinnia TE. The sequence of organellar changes is shown in relation to the status of the tonoplast and plasma membrane.*

PROMOTING FACTOR1, 2 and *3* (*NST1-3*) display ectopic deposition of secondary cell wall thickenings in parenchyma cells without concomitant cell death. Conversely, *gapped xylem* (*gpx*) mutant plants display PCD without apparent secondary cell wall formation, demonstrating that secondary cell wall formation and PCD can be independent of each other.

The large size of tree trunks enables separation of discrete cell layers by tangential sectioning, and the availability of extensive genomics resources for the model genus *Populus* allows patterns of gene expression to be localized by transcriptional profiling. Figure 20.16 shows a micrograph of a section of the woody tissue of hybrid aspen (*Populus tremula* × *tremuloides*) in which the age-gradient of xylem at increasing distance from the cambium represents stages in cell death. Expression of cell death-related genes across the gradient is represented by a **heat-map** (a matrix in which intensity of expression is color-coded). Among the genes highly expressed are homologs of *Arabidopsis* genes encoding XCP2, VPE isoforms α and γ, and METACASPASE9 (AtMC9), all of which are implicated in control of TE PCD or other PCD processes in plants. It is notable that xylem fibers of hybrid aspen undergo a cell death program differing significantly from that of TEs. PCD in xylem fibers proceeds slowly, involving gradual degradation of cytoplasmic contents. Upregulation of several autophagy-related genes in fibers, but not in TEs, suggests that cytoplasmic lysis in fibers is an autophagic process (Fig. 20.16).

20.4 PCD during reproductive development

As Figure 20.17 illustrates, PCD occurs throughout reproductive development, a topic discussed in detail in Chapter 19. This section focuses on the role of PCD in floral organ and gamete formation, pollination, and early embryo development.

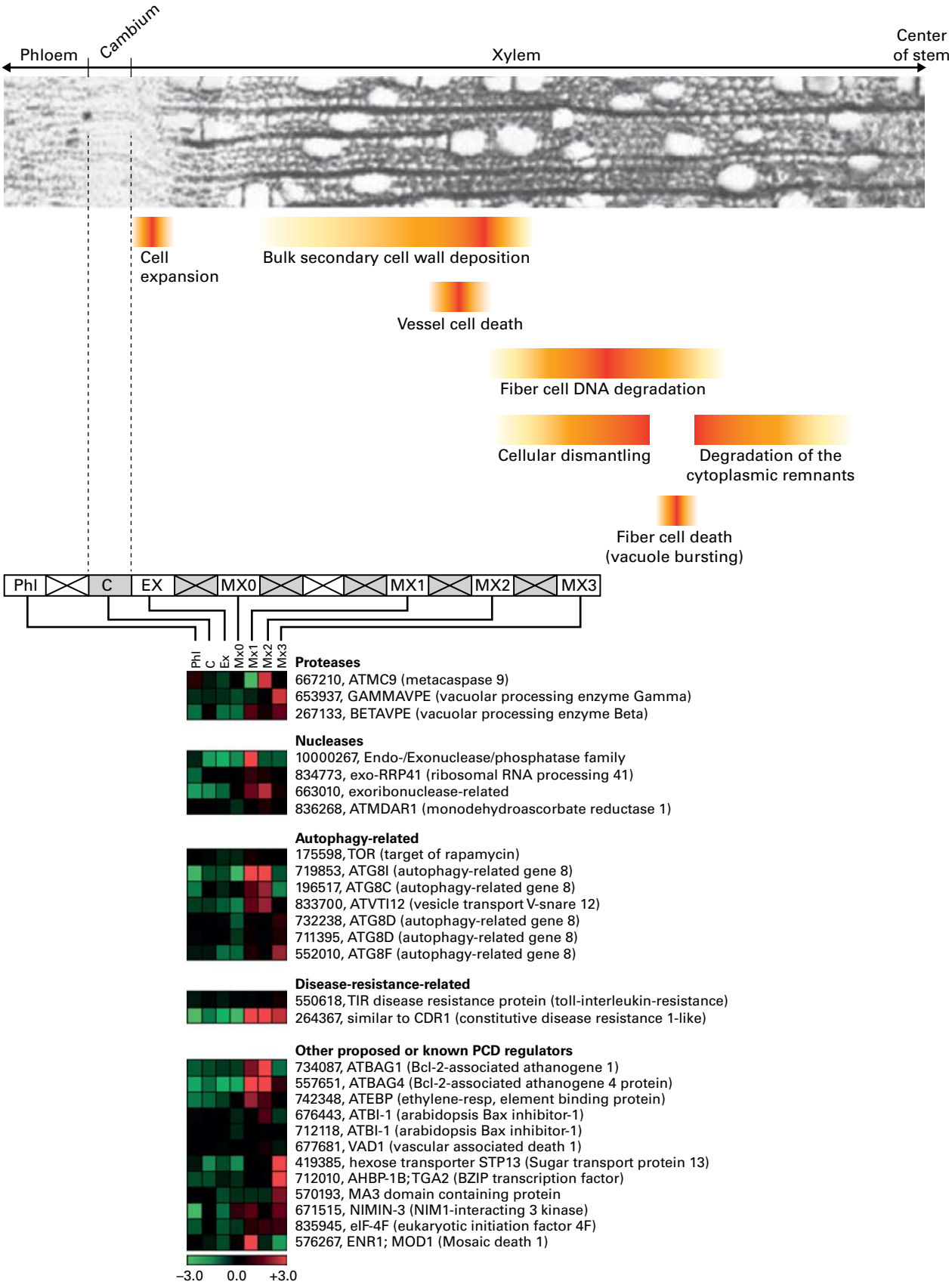


FIGURE 20.16 *Gene expression during xylem development in the woody tissues of hybrid aspen (*Populus tremula × tremuloides*) stem. Samples were collected from the trunks of* Populus *trees by cryosectioning 50-μm sections in the tangential plane. The lower part of the figure is a heat map representation of expression levels for* Populus *genes that show statistically significant upregulation during the late stages of xylem development and are homologous to known regulators of cell death or autophagy-related genes in* Arabidopsis*; the annotation given for each* Populus *gene corresponds to the name of the most similar* Arabidopsis *gene. Expression values are derived from a microarray analysis and are shown as relative values in* $\log_2$ *scale.*

Source: Courtois-Moreau et al. (2009). Plant J. 58:260–274.

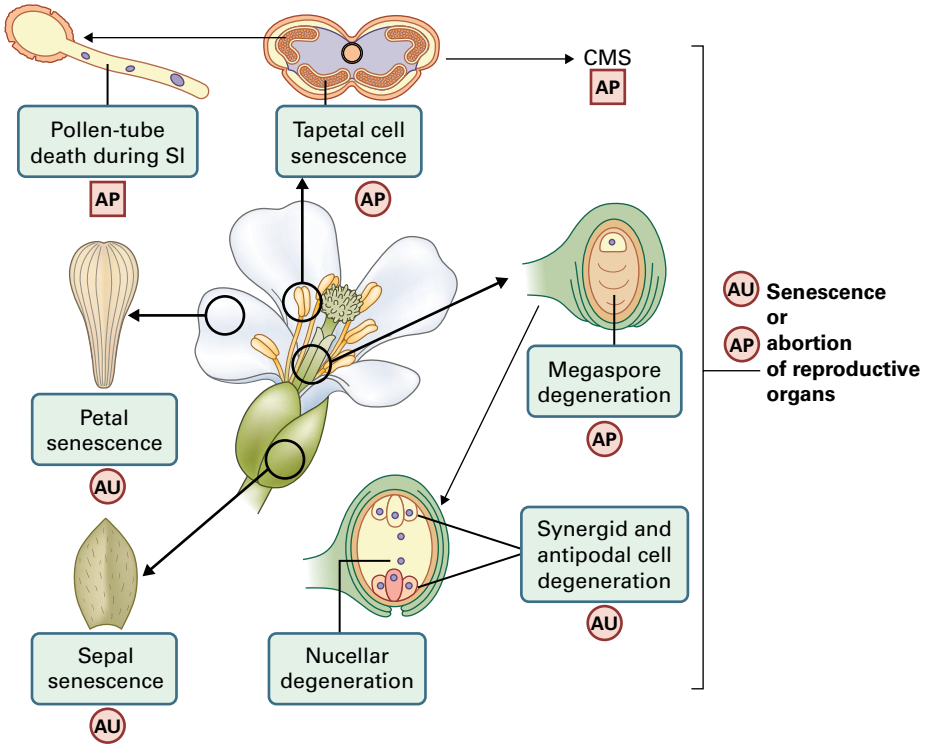


FIGURE 20.17 *PCD events in floral organs. SI, self-incompatability; CMS, cytoplasmic male sterility; Strong evidence for a PCD mechanism—apoptosis-like (AP) or autophagy-like (AU)—is denoted by a square, weak evidence by a circle.* *Source*: Rogers (2006). Ann. Bot. 97: 309–315.

20.4.1 Selective death of male or female floral parts occurs during development of unisexual flowers

Flower development is radically affected by PCD of selected cells or groups of cells. In most plants that have unisexual flowers, the developing flower initially contains primordia for both male and female organs. At early stages, male and female flowers are indistinguishable. During flower formation, at a developmental stage that varies with plant species, either male or female parts cease growing and are eliminated via a cell death program. For example, in maize the male inflorescence (tassel, Fig. 20.18A) is spatially separate from the female inflorescence (ear). Young flowers in the tassel contain primordia for both stamens and gynoecium, but as the flowers develop, gynoecial cells stop growing and dividing, and organelles, including the nucleus, break down. In *tasselseed 2* mutants, however, arrest and degeneration of gynoecia do not occur, and female flowers are produced in tassels (Fig. 20.18B). Thus, *TASSELSEED 2* (*TS2*) is required for death of developing female organs in tassels. *TS2* is expressed in gynoecial cells in tassels just before the start of gynoecial degeneration. *TS2* encodes a product with similarity to hydroxysteroid dehydrogenases, raising the possibility that it may regulate cell death by generating a steroid-like molecule that acts as a signal in the cell death pathway. *TS2* is also expressed in pistils of female spikelets, but primary pistils do not undergo *tasselseed*-mediated cell death because its action is suppressed by another gene, *SILKLESS 1* (*SK1*). *TS2* and *SK1* are among a group of genes that control the sexual identity of maize flowers by selectively promoting or inhibiting cell death in different tissues (Fig. 20.18C).

20.4.2 Cell death is an essential part of gametogenesis

Haploid tissues are also influenced by cell death programs. During megagametogenesis in angiosperms, three of four megaspores formed after meiosis of the megaspore mother cell undergo PCD, leaving one megaspore that gives rise to the egg and other components of the embryo sac.

In microsporogenesis, the tapetum that surrounds the microsporocytes dies and disintegrates. Cell shrinkage, condensation of chromatin, swelling of the ER, and the persistence of mitochondria has been observed. Towards the end of the unicellular stage of pollen development, DNA laddering occurs, and the nuclei of tapetal cells and tissues of the anther wall become TUNEL-positive. Release of cytochrome *c* from mitochondria, a characteristic of animal apoptosis, has been also reported. Blocking death of *Arabidopsis* tapetal cells by expressing early in microsporogenesis a transgene that encodes a suppressor of apoptosis results in pollen abortion. Development of viable pollen is also prevented if the tapetum undergoes PCD too early in microsporogenesis. This is a possible explanation for cytoplasmic male sterility (CMS), a phenotype in which pollen abortion is determined by the mitochondrial genome. Many kinds of CMS can be corrected by nuclear restorer genes, reflecting the importance of crosstalk between mitochondria and nucleus in microsporogenesis. One way in which plant

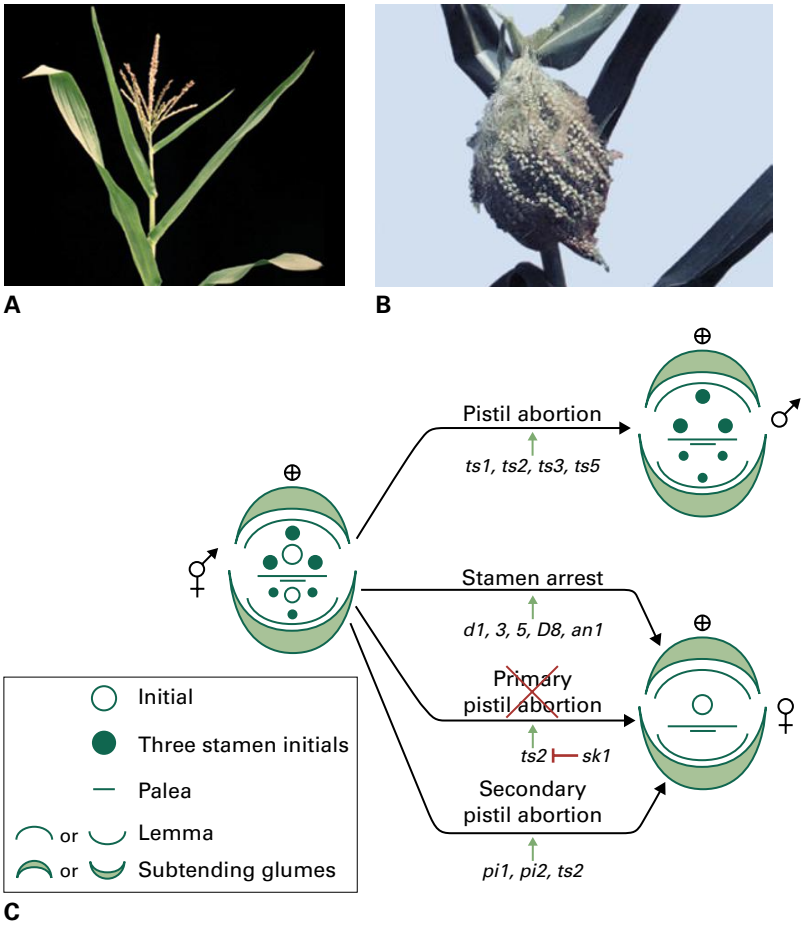


FIGURE 20.18 *The inflorescences of maize contain flowers that are initially bisexual, but PCD results in the death of male or female tissues to give rise to a female inflorescence (ear) or male inflorescence (tassel, A), respectively. In the* tasselseed2 (ts2) *mutant (B), female tissues in the tassel do not undergo PCD, and the resulting tassel flowers are mostly pistillate. (C) Maize floral diagrams showing an immature spikelet (left) with two perfect (bisexual) floral meristems, each with a central pistil initial, three stamen initials, a palea, lemma, and subtending glumes. The transition to paired staminate spikelets in the tassel (top right) and to solitary pistillate spikelets in the ear (bottom right) is depicted. Secondary pistils also abort in ear florets (indicated by asterisk). The* tasselseed (ts) *genes are required for pistil abortion in the tassel and in the secondary ear florets. The* silkless1 (sk1) *gene protects primary ear pistils from tasselseed-mediated cell death. Stamen arrest in ear spikelets and in* ts2 *mutant tassel spikelets requires* dwarf (d) *and* anther ear 1 (an1) *genes; pistillate* (pi) *genes are required for E2 pistil abortion.*
Source: (A) Neuffer et al. (1997). Mutants of Maize. Cold Spring Harbor Laboratory Press; (B) L. Jesaitis, University of California, Berkeley; previously unpublished. (C) Kim et al. (2007). Genetics 177: 2547–2551.

mitochondria contribute to CMS is by releasing cytochrome *c*. We may conclude that the onset of PCD in tapetum is signaled through a relatively narrow developmental window at around the tetrad stage of microsporogenesis and is an example of timely and selective cell death as an essential event in normal differentiation.

20.4.3 Cell death during incompatibility reactions prevents self-pollination

Many plant species employ a self-incompatibility strategy to ensure outcrossing. In *Papaver rhoeas*, the field poppy, the pistil self-incompatibility locus encodes low-molecular-weight S proteins that trigger a Ca^{2+}-dependent signaling network in incompatible pollen. The consequence is a rapid arrest of pollen tube growth, depolymerization of actin, and activation of a MAP kinase cascade. These events in turn promote PCD during which cytochrome *c* leaks into the cytosol, DNA is fragmented, and metacaspases are activated.

Following fertilization in most angiosperms, the first mitotic division of the zygote gives rise to two cells. One produces the embryo. The other develops into the suspensor, which may undergo a few rounds of mitosis but eventually undergoes PCD. DNA laddering has been observed in maize kernels during degeneration of the suspensor and differentiation of the scutellum, coleoptile, and root cap.

20.5 Senescence and PCD in the terminal development of leaves and other lateral organs

Senescence and subsequent death are the terminal phases of development in all plant organs, including leaves, stems, roots, and flowers. During senescence, plants dispose of unneeded cells and tissues while simultaneously reclaiming valuable resources, especially nitrogen and phosphorus. Senescence generally follows organ maturity and occurs without growth or morphogenesis. It can be dramatically influenced by environmental and endogenous (e.g., hormonal) perturbations. Sometimes senescence is rapid: the petals of *Ipomoea tricolor* senesce after the flower has been open for only one day (Fig. 20.19). In other cases, senescence is not initiated for months or even years. For example *Pinus longaeva*

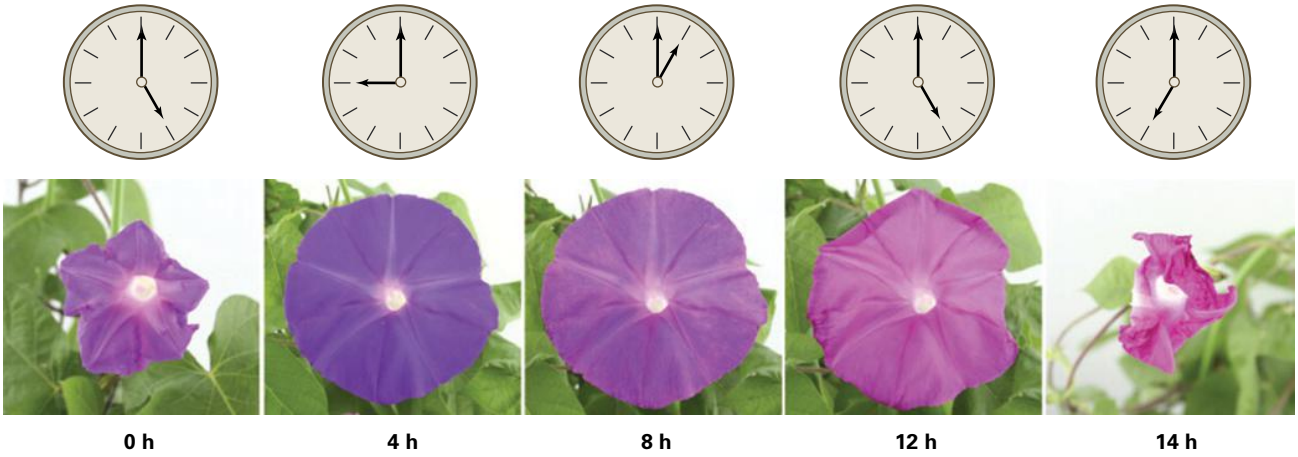


FIGURE 20.19 *Senescence in the* Ipomoea tricolor *corolla is very rapid. Flowers begin to open at around 05:00 to 06:00 hours (stage t0) and remain open until 1300 to 1400 (t8) the same day. At that time, the corolla begins to curl and the flower changes color from blue to purple (t12). Curling continues during the day until reaching the final stage (t14), where the corolla has completely curled inward.*
Source: Shibuya et al. (2009). Plant Physiology 149:816–824.



FIGURE 20.20 *Leaves of the extraordinary South African desert plant* Welwitschia mirabilis *can live for decades or even centuries.*
Source: http://www.biologie.uni-hamburg.de/b-online/earle/we/welwitschiaceae.htm.

(bristlecone pine) leaves reportedly have a lifespan of 45 years, and the large strap-like leaf of the desert plant *Welwitschia mirabilis* (Fig. 20.20) has been estimated to survive for up to 1,000 years or more.

We do not know how various cellular senescence programs are integrated during the development and life history of organs or whole plants. There may be a "die now" signal constantly present to which a cell, tissue or organ becomes competent to respond at a time dictated by its individual developmental program. Alternatively, there may be cell-specific die-now stimuli that invoke senescence or death programs in their targets. The phenotypes of some genetic variants, including certain "stay-greens" (see Section 20.5.3) and disease-lesion mimics (see Section 20.10.3), appear to reflect mutations in genes regulating the timing or location of normal senescence and PCD. Analyzing these genes gives important insights into how selective cell death is deployed in plant differentiation. Sections **20.5** through **20.8** discuss senescence in detail.

20.5.1 Senescing cells undergo internal reorganization and are metabolically active

During senescence, new metabolic pathways are activated and others turned off. A scheme outlining likely steps in the pathway leading to leaf senescence is shown in Figure 20.21. In this scheme, signal transduction cascades linked to various triggers such as hormonal or environmental stimuli lead to an initiation phase involving the activation and inactivation of many genes and the transition to a phase of controlled redifferentiation of cell structures and remobilizing of materials. Finally a termination phase ensues, in which many features of generalized PCD can be recognized. The integrity of organellar membranes and compartmentation of biochemical pathways are preserved until late in the terminal phase.

Leaf and fruit senescence are characterized by dramatic changes in major organelles:

- Chloroplasts of leaf mesophyll cells and green immature fruits respectively redifferentiate into gerontoplasts and chromoplasts (Fig. 20.22).
- As discussed in Section 20.2.2, protein storage vacuoles of germinating (i.e., senescing) aleurone cells form a large central vacuole that maintains the integrity of the tonoplast (see Fig. 20.8); this also occurs in eudicot endosperm and storage cotyledons.
- Oil bodies (**oleosomes**) of cotyledons and endosperm are lost during senescence, and lipid metabolism in these storage tissues is associated with a specialized type of peroxisome (originally referred to as **glyoxysome**), which plays

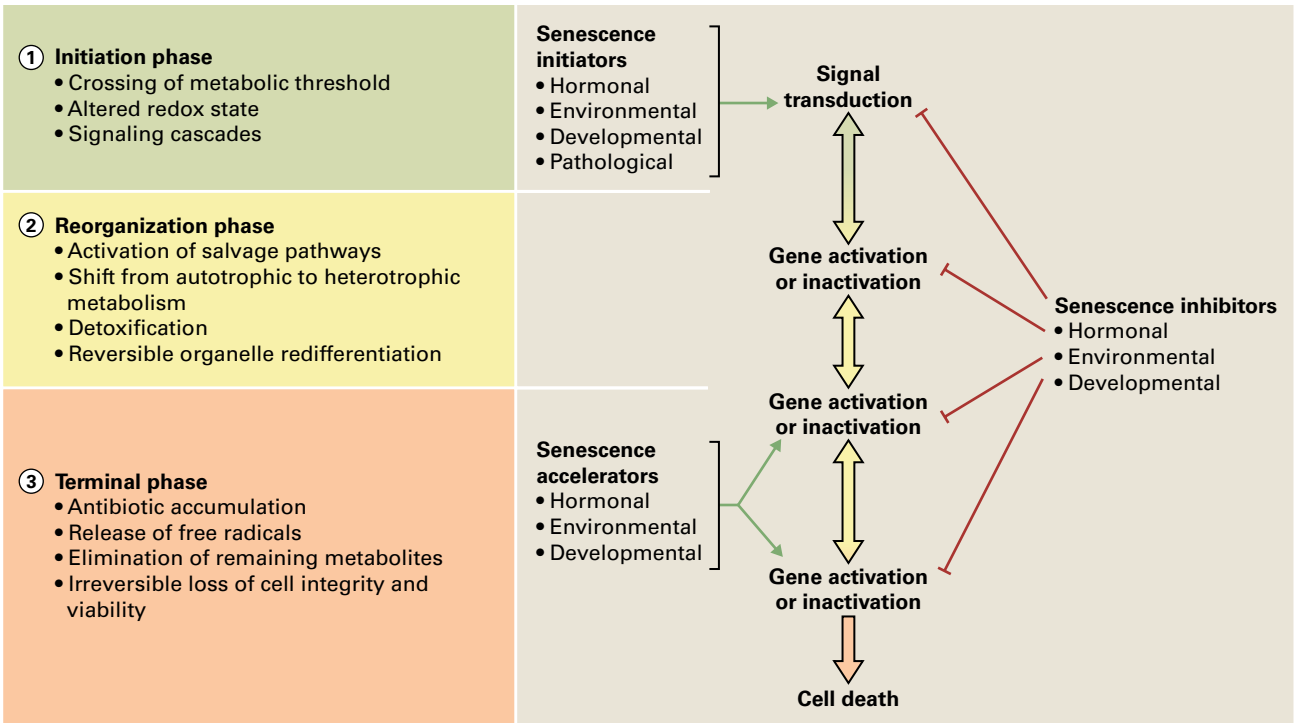


FIGURE 20.21 *A proposed scheme showing steps in the process of leaf senescence from the initiating signal to cell death.*



FIGURE 20.22 *During senescence, chloroplasts in leaves are converted to yellow gerontoplasts, while the chloroplasts of green fruit redifferentiate into yellow, orange, or red chromoplasts during ripening.*

an important role in gluconeogensis (see Section 20.8.1, Chapter 1, and Chapter 8).

- Likewise, the peroxisomes of senescing photosynthetic tissues in many species become specialized for gluconeogenesis (see Fig. 8.65).

These changes in cellular compartmentation distinguish differentiation from deterioration and emphasize that senescence is a programmed process and not a form of necrosis.

Ultrastructural changes in senescing leaf cells are accompanied by biochemical conversions, notably degradation of chlorophyll and storage proteins accompanied by reconfiguration of primary and secondary metabolism. Much of the biochemical activity in a senescing plant cell is directed towards salvage and redistribution of metabolites and structural materials, particularly reserves of nitrogen and phosphorus. However, other physiological imperatives also influence senescence. Declining photosynthesis means that energy demands of remobilization and other processes are met from heterotrophic sources, a trend associated with modifications to respiratory and oxidative metabolism. Further changes can involve secondary metabolites, which may influence interactions with both pests and beneficial organisms.

Because fertilized flowers would compete with those that have yet to attract pollinators, floral parts tend to have shorter lifespans than leaves (particularly post-pollination), and senescence in these organs is usually irreversible and comparatively insensitive to abiotic environmental influences. As in leaves, senescence of floral parts involves macromolecule breakdown, nutrient salvage and modification of organelle structure and function. Differential PCD occurs either by lysigeny or by an apoptosis-like route.

20.5.2 Applying the tools and resources of plant genomics gives new insights into the nature and control of senescence

DNA microarrays and other high-throughput techniques for gene-expression profiling have generated a wealth of information on gene expression during senescence. The general picture that has emerged is that there is no universal senescence gene expression pattern to be found. Although the overall patterns of gene expression during senescence seem to be similar in most plants, different senescence-inducing treatments in a single species yield unique gene expression profiles. However, entry into senescence is always accompanied by a massive shift in gene expression: numerous genes highly expressed in nonsenescent leaves are turned off, while others—including more than 800 described so far in *Arabidopsis*—are turned on. Many of the genes upregulated in senescence have putative roles in degradation of cellular components. The nomenclature of these genes varies from species to species, including *See* (**S**enescence **E**nhanced **E**xpression) from maize, *LSC* (**L**eaf **S**enescence **C**lone) from *Brassica napus*, *SAG* (**S**enescence-**A**ssociated **G**ene) from *Arabidopsis*, *SENU* (**Sen**escence **Up**regulated) from tomato (*Solanum lycopersicum*), and *PAUL* (***P****opulus* **Au**tumn **L**eaf) from *Populus tremula*. Here we will use *SAG*s as a general designation for genes that are upregulated during senescence. Table 20.2 is a representative list of *SAG*s, compiled from studies of a range of species.

A variety of expression patterns have been observed for *SAG*s (Fig. 20.23). Some are expressed early in senescence, others late. Some appear in natural senescence of attached tissue but not in detached tissue. Gene expression profiles during senescence partially overlap with expression patterns induced by treatment with salicylic acid (SA), jasmonic acid, or ethylene, but distinguishing between primary and secondary events is not a straightforward task, and no clear pattern has emerged that fits a simple model for regulation of gene expression during senescence. Microarray studies can, however, provide much information concerning the classes of genes induced during senescence, including those responding differentially to particular treatments or mutations. Although increased mRNA abundance does not necessarily result in increased protein abundance, it is likely that in most cases higher expression of genes encoding enzymes in a given pathway indicates an increased flux through that pathway. For example, many genes coding for proteases are induced during senescence (Table 20.2). Other *SAG*s encode enzymes involved in remobilization of proteins and amino acids, lipid catabolism, β-oxidation of fatty acids, and gluconeogenesis. Numerous genes encoding metallothioneins (see Chapter 16), perhaps involved with protection against oxidative damage or with ion storage and transport, are likewise highly expressed during senescence. Antifungal proteins, pathogenesis-related (PR) proteins and chitinases (see Chapter 21) are also encoded by *SAG*s in a number of species (Table 20.2). The multitude of factors influencing leaf senescence is illustrated by the characterization of *ore* mutants of *Arabidopsis***.** Mutations in genes encoding a plastid ribosomal protein, a cytokinin receptor, and an F-box protein, among others, are linked to delayed senescence in *ore* mutant plants.

Nuclear genes encoding photosynthetic proteins are by and large turned off as leaves enter into senescence (see Fig. 20.21), and indirect evidence suggests that gene expression in plastids is massively suppressed. Not surprisingly, several genes relating to synthesis of photosynthetic pigments (chlorophylls and carotenoids) are also downregulated, while some flavonoid biosynthesis genes may be induced.

Genes encoding transcription factors show large alterations in mRNA abundance during senescence, and overexpression or downregulation of many of these have resulted in senescence phenotypes. However, causal relationships have been hard to elucidate, as all processes that influence the growth rate or wellbeing of a leaf can potentially delay or accelerate senescence. Nevertheless, *Arabidopsis WRKY53* (see Sections 20.8.2 and 20.11.3) and *AtNAP* are promising candidates. *WRKY53* interacts with more than 60 genes of various kinds, including genes for other transcription factors and for SAG12, a vacuolar cysteine protease in the aleurain family that is a recognized marker for senescence in *Arabidopsis*.

Similarities and contrasts between leaf and petal cell senescence are apparent in the complement of genes expressed in the two organs. Transcriptome analysis in *Arabidopsis* indicates that senescing leaves and petals have about 25–30% of expressed genes in common, possibly reflecting the evolutionary origin of petals as modified leaves. A systematic comparison of leaf and petal senescence in wallflower (*Erysimum linifolium*) (Fig. 20.24) identified upregulation in both tissues of remobilization-related genes, such as that encoding an aleurain-like cysteine protease similar to SAG12. By contrast, expression of chitinase and glutathione S-transferase defense genes remained constant or fell with age in leaves, whereas they were strongly activated in petals. This suggests that defenses against pathological infection are enhanced during senescence of floral tissues to safeguard healthy development and dispersal of seeds.

20.5.3 Mutant and variant senescence genes have been mapped to specific genomic locations, and some have been isolated by positional cloning

Genetic investigation of senescence has a long history: cotyledon color in peas (*Pisum sativum*) was studied by Gregor Mendel, the father of modern genetics. Plants homozygous for the recessive allele *i* are deficient in chlorophyll degradation (see Section 20.6.1), which results in green cotyledons and delayed yellowing of leaves during senescence**.** Mendel's gene for cotyledon senescence was recently isolated using a combination of gene mapping, comparative genomics, and functional analysis (Fig. 20.25).

TABLE 20.2 *Cloned genes that show increased transcription during senescence.*

Gene name	Function	Class*	Plant	Other information†
SAG2	Cysteine protease		*Arabidopsis*	Oryzain γ-like
See1	Cysteine protease	5	Maize	Oryzain γ-like
LSC7	Cysteine protease	7	*Brassica napus*	Oryzain γ-like
See2	Cysteine protease	5	Maize	Vacuolar processing
SAG12	Cysteine protease	5	*Arabidopsis*	Widely-used senescence marker
LSC790	Cysteine protease	10	*B. napus*	
LSC760	Aspartic protease	7	*B. napus*	
UBC4	Ubiquitin carrier protein		*Nicotiana sylvestris*	
UBI7	Polyubiquitin		Potato	
RNS2	Ribonuclease		*Arabidopsis*	Senescing petals
MS	Malate synthase	6	Cucumber	Glyoxysomal enzyme
ICL	Isocitrate lyase	6	Cucumber	Glyoxysomal enzyme
pBPCK-7A	Phospho *enol* pyruvate carboxykinase	6	Cucumber	Cotyledons
gMDH	NAD^+-malate dehydrogenase	6	Cucumber	
LSC101	Fructose-1,6-bisphosphate aldolase	10	*B. napus*	
LSC540	Glyceraldehyde-3-phosphate dehydrogenase	10	*B. napus*	
See3	Pyruvate, orthophosphate dikinase	10	Maize	
LSC2C$_2$13	Pyruvate, orthophosphate dikinase	5	*B. napus*	
pTIP11	β-Galactosidase	10	Asparagus	Postharvest
PLD	Phospholipase D		Castor bean	Detached leaf
LSC8	NADH:ubiquinone oxidoreductase	10	*B. napus*	
Atgsr2	Glutamine synthetase	7	*Arabidopsis*	
	Glutamine synthetase		Radish	
	Glutamine synthetase		Rice	
LSC460	Glutamine synthetase	7	*B. napus*	
pTIP12	Asparagine synthetase	9	Asparagus	Postharvest

(*continued*)

TABLE 20.2 (*continued*)

Gene name	Function	Class*	Plant	Other information†
SGR	Stay-green		*Festuca*	Chlorophyll degradation
LSC54	Metallothionein I	5	*B. napus*	
JET12-like	Metallothionein		*Sambucus*	Leaf abscission
LSC2C$_2$10	Metallothionein II	7	*B. napus*	
rgMT	Metallothionein II		Rice	Stress-induced
LSC30	Ferritin	7	*B. napus*	
LSC680	ATP sulfurylase	9	*B. napus*	
GSTII-27	Glutathione *S*-transferase	5	Maize	
LSC650	Catalase	7	*B. napus*	
LSC550	Cytochrome P450	9	*B. napus*	
LSC2C$_2$60	Cytochrome P450	9	*B. napus*	
LSC2C$_2$26	Cytochrome P450	5	*B. napus*	
LSC94	PR1a	8	*B. napus*	
LSC2C$_2$22	Chitinase	5	*B. napus*	
LSC2C$_2$12	Antifungal protein	7	*B. napus*	
TOM13	ACC oxidase	5	Tomato	Fruit ripening
TOM75	MIP membrane channel		Tomato	Fruit ripening, water stress
AtNAP			*Arabidopsis*	Transcription factor
NAM-B1			*Triticum*	Regulates nutrient mobilization
WRKY53			*Arabidopsis*	Regulates senescence and stress responses

*Classes 1 through 10 correspond to the expression patterns indicated in Fig. 20.23.
†Indicates type of enzyme or any other situations where induced expression of the gene has been detected.
PR, pathogenesis related; ACC, 1-aminocyclopropane-1-carboxylic acid; MIP, major intrinsic protein.

The mutant gene *stay-green* (*y*), which confers unlimited foliar greenness in the pasture grass *Festuca pratensis* (Fig. 20.25A), was identified by conventional Mendelian analysis. Chlorophyll metabolism in the *F. pratensis* mutant shows similar biochemical abnormalities to Mendel's green cotyledon line. Grasses of the genera *Festuca* and *Lolium* readily form interspecific hybrids, and recombination between their genomes occurs at high rates. The stay-green locus *y* was introgressed from *F. pratensis* into *Lolium perenne* (perennial ryegrass; Fig. 20.25A), where it could be located in the genome by genetic mapping using *Festuca*-specific molecular markers. *L. perenne* is an agriculturally significant temperate pasture species for which a good genetic linkage map has been established, and comparative studies have shown that much of the *L. perenne* map is co-linear with that of the model monocot, rice (*Oryza sativa*). By using common molecular markers, it is possible to "read across" from a region of the *L. perenne* map to the corresponding map location in rice. When this was done for the map position of the introgressed stay-green gene (on the short arm of *L. perenne* chromosome 5), it identified a region of rice chromosome 9 (Fig. 20.25B) where several research groups had previously located a quantitative trait locus (QTL) governing yellowing in rice leaf senescence. It seemed likely that the *F. pratensis* and rice loci represented the same gene.

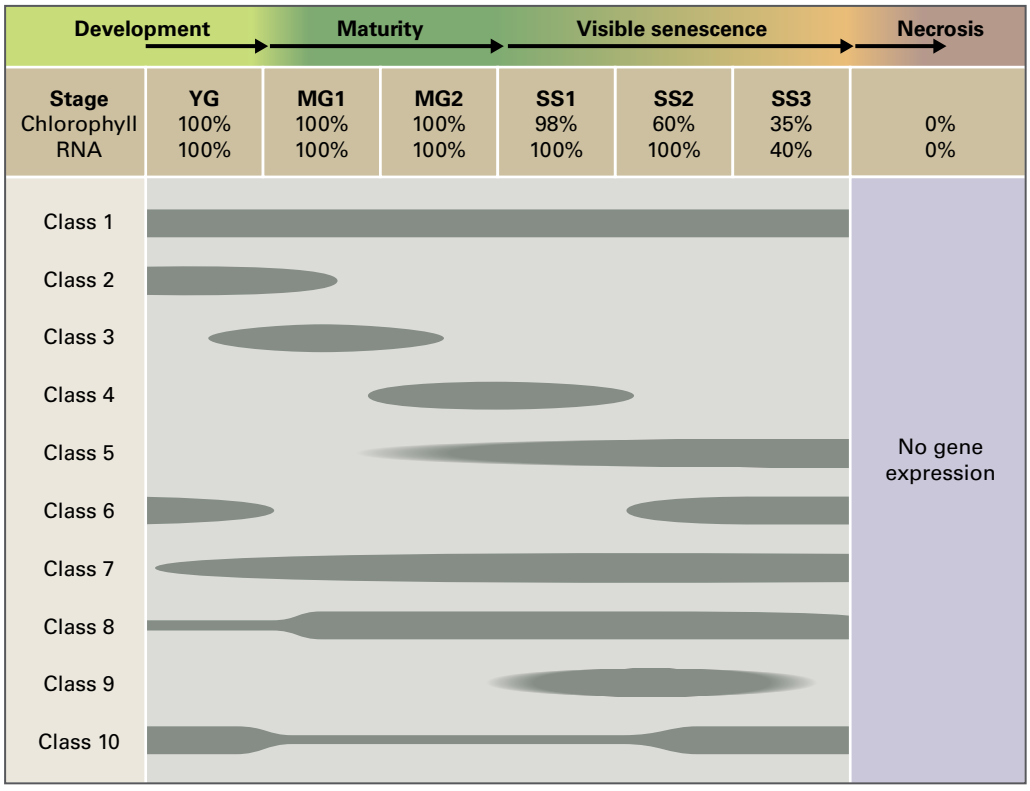
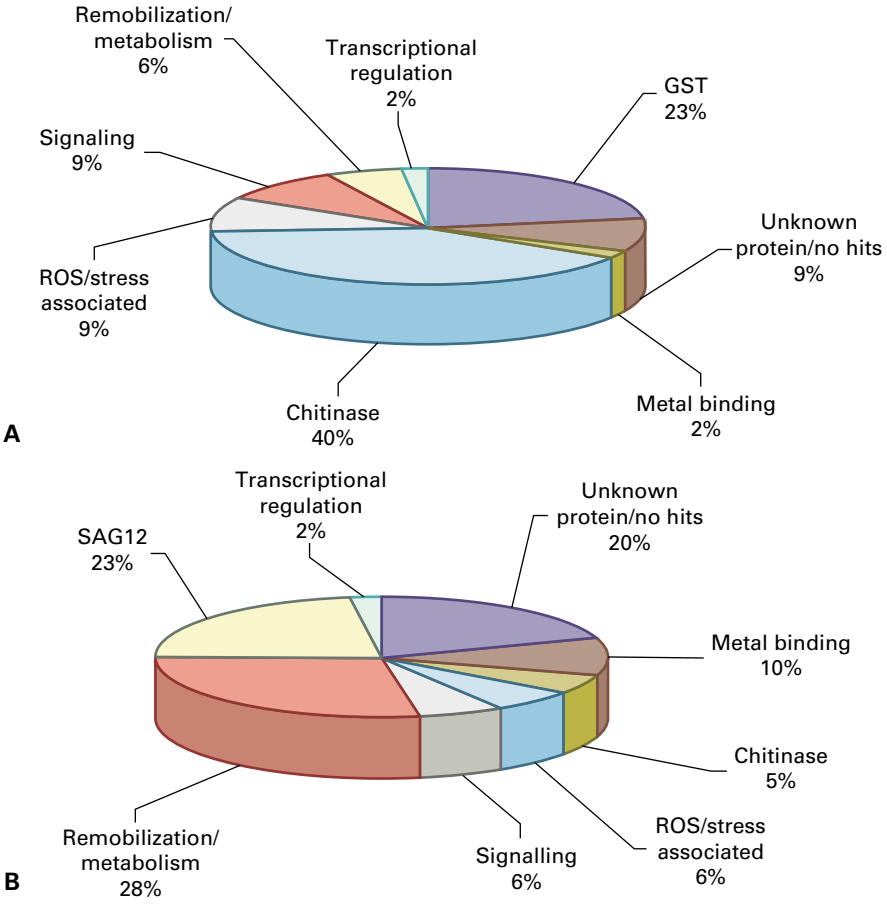


FIGURE 20.23 *Stages in* Brassica napus *leaf senescence. SAGs are divided into 10 classes according to their temporal patterns of expression (see Table 20.2). Concentrations of chlorophyll and RNA are quantified as percentages of the concentrations of chlorophyll and RNA present in a mature, expanded leaf. YG, fully expanded leaf; MG1, leaves from flowering plants; MG2, leaves from plants with developing siliques; SS1, SS2, and SS3, visibly senescing leaves.*

FIGURE 20.24 *Microarray analysis was used to assess expression of genes in senescing leaves and petals in wallflower (*Erysimum linifolium*). (A) Genes upregulated in senescing petals but expressed stably or downregulated in senescing leaves, as grouped by putative functional class. (B) Groups of genes upregulated in both senescing petals and leaves. Source*: Price et al. (2008). Plant Physiol. 147:1898–1912.



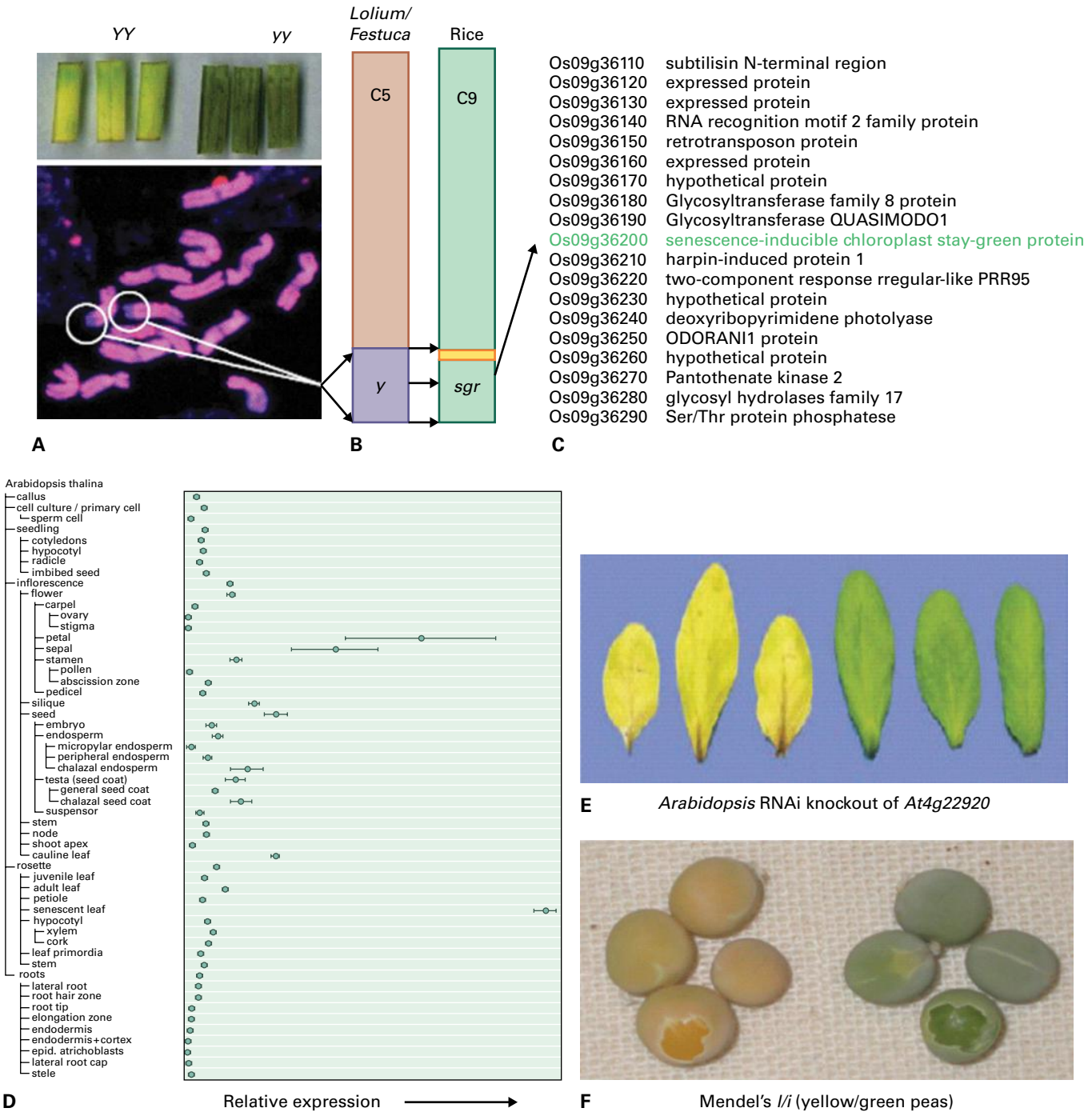


FIGURE 20.25 *Isolation of a senescence gene by map-based cloning. (A) The recessive* stay-green *mutation* (y) *introgressed from* F. pratensis *into* L. perenne *is located in a terminal segment of each of a pair of* L. perenne *chromosomes. (B) Molecular mapping places the Y locus in a sector of* Lolium/Festuca *chromosome 5 syntenic with a region of rice chromosome 9, corresponding to* sgr, *a major QTL for rice leaf senescence. (C) The number of candidate genes is narrowed down to about 30 on a single rice BAC. (D) One sequence,* Os09g36200, *is homologous with* Arabidopsis At4g22920, *which shows very clearly the expected senescence-associated expression pattern. (E) The phenotype of an RNAi knockout of* At4g2290 *in* Arabidopsis *is identical to that of the* F. pratensis *phenotype. (F) Allelic variation in* SGR *is responsible for the phenotypes of Mendel's green and yellow pea cotyledons.*
Source: Jones et al. (2009). New Phytol. 183:935–966.

Bacterial artificial chromosome (BAC) libraries of the rice genome are available in which each individual genomic clone has been related to a specific region of the rice genetic map. By reading across from the map position of the stay-green locus to the rice physical map based on BAC alignments, the gene was narrowed down to a relatively small number of candidates on a few BACs. Further fine mapping in *Lolium-Festuca* introgression lines finally

focused on a single BAC carrying fewer than 20 genes (Fig. 20.25C).

Researchers now turned to *Arabidopsis*, in which sophisticated genomics tools allow putative genes to be rapidly evaluated and characterized. The expression profiles of *Arabidopsis* versions of each of the candidates on the rice BAC were examined, and one stood out as being strongly upregulated in leaf senescence (Fig. 20.25D). Expression of this gene (of unknown function at the time) was targeted for suppression in *Arabidopsis* using the RNA interference technique, and the resulting plants exhibited a stay-green phenotype identical to that of the original *F. pratensis* mutant (Fig. 20.25E). Finally, a combination of mapping and gene characterization showed that this gene, now called *SGR* (***S**tay-**GR**een*) is responsible for the green/yellow cotyledon trait observed by Mendel in pea (Fig. 20.25F). *SGR* has a highly conserved structure and has been identified not only in angiosperms but also in mosses, unicellular green algae, and prokaryotic cyanobacteria. *SGR* functions in the disassembly of thylakoid photosystem complexes, making chlorophyll and protein available to their respective degradation pathways.

The technique of positional cloning within a QTL has also identified an agriculturally important regulatory senescence gene in cereal species. Wild emmer (*Triticum turgidum* ssp. *dicoccoides*) is an ancestor of durum (pasta) wheat, *T. turgidum* ssp. *durum*. Inbred lines of durum wheat in which chromosome 6 was substituted with emmer chromosome 6 have higher grain protein content (GPC) than nonrecombinant durum wheat. This is associated with more rapid leaf senescence and mobilization of foliar nitrogen in emmer. Molecular mapping narrowed down the region of chromosome 6 responsible for high GPC to a single QTL and finally to a single gene encoding a transcription factor with close sequence similarity to the *Arabidopsis* protein NO APICAL MERISTEM (NAM). The *Triticum* spp. gene was designated *NAM-B1*. The *NAM-B1* alleles of durum wheat and hexaploid bread wheat (*T. aestivum* ssp. *aestivum*) are nonfunctional as a consequence of sequence changes that became fixed during cereal domestication. The effect of the *NAM-B1* emmer allele on senescence and GPC in durum wheat is partially moderated by redundancy at two other *NAM* loci in the genome. When transcript levels of all *NAM*s were reduced in hexaploid wheat by applying the RNA interference technique, leaf senescence was delayed by a remarkable 24 days and GPC reduced by 5.8%. Grain of delayed senescence lines was also deficient in Zn and Fe (30% and 24% respectively). This study identifies a critical role for *NAM* genes in regulating cereal leaf senescence and determining the partitioning of nitrogen and minerals between the grain and crop residue.

20.5.4 Delayed senescence has agricultural implications

A survey of stay-green genetic variants, in which senescence has been visibly modified, reveals two broad classes of *SAG*s. Members of the first group, exemplified by *SGR*, encode enzymes or effectors of the metabolic pathways activated in senescence. *NAM-B1* is an example of genes in the second class, which regulate initiation of senescence programs or their rate of progress. *SAG*s in both classes have considerable agronomic importance. For example, the record yield of grain maize, achieved in 1985 on a farm in Illinois, is almost 24 t ha^{-1}. The factors contributing to this extraordinary productivity (over 70% of theoretical maximum) are complex, but it is significant that the variety used was FS854, a stay-green line. In the semi-arid tropics, stay-green is a vital character in the struggle to feed populations living under harsh economic and environmental circumstances. *Sorghum* spp. and *Pennisetum* spp. (millet) lines exhibiting the stay-green phenotype often show enhancement of other desirable characters such as disease and insect resistance, wide environmental adaptiveness, appropriate time to maturity, good tillering, reasonably good grain yield, juiciness, palatability, and digestibility.

Stay-green would seem to be such a desirable trait that it is reasonable to ask why it does not occur in all plants. One group of plants—evergreen shrubs and trees—have adopted this strategy as a fitness attribute for the particular ecological niches they occupy, often related to need for low rates of internal nitrogen recycling in nutrient-poor environments. We have seen that nonfunctional alleles of the *NAM* family confer extended greenness on the durum and bread wheat compared with their wild relatives. Protection of such crop species from consequent competitive and environmental pressures is largely achieved through agricultural practices including control of weeds and pests, water availability and fertilizer supply. Otherwise it seems that stay-greens pay a fitness penalty and are poor survivors in most ecosystems.

Plant breeding has traditionally brought about crop improvement incrementally by empirically selecting more favorable alleles associated with genetic loci specifying agronomically significant traits. A detailed understanding of the molecular basis of plant senescence combined with high-precision tools for mapping and modifying specific genes can make breeding increasingly efficient and targeted.

20.6 Pigment metabolism in senescence

Color change is a characteristic symptom of senescence, ripening, and programmed death in plants. Studying the genetic and biochemical regulation of pigment metabolism gives insights into the mechanisms and adaptive significance of senescence processes. Visible loss of green over time is the clearest symptom of senescence in leaves (Fig. 20.26). Color changes during foliar senescence are directly related to regulation of nutrient mobilization and resorption from leaf cells, often under conditions of biotic and abiotic stress. The colors of flowers and ripe fruits are invitations to pollinating and seed-dispersing animals, respectively. Some pathways of pigment metabolism, such as chlorophyll breakdown and anthocyanin synthesis,

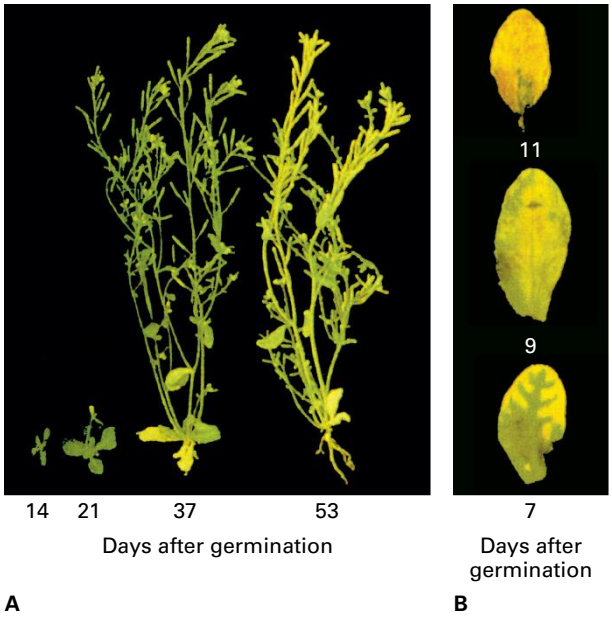


FIGURE 20.26 *Senescence in* Arabidopsis thaliana. *(A) Development of* Arabidopsis *plants is shown at various times after germination. Photographs show plants at 14, 21, 37, and 53 days after germination (left to right). Note the yellowing of shoots of the 53-day-old plant. (B) Age-related changes in rosette leaves of* Arabidopsis *7, 9, and 11 days after leaf expansion had ceased. Note the progressive yellowing of leaves, beginning farthest from the major veins.*
Source: (A, B) Bleecker & Patterson (1997). Plant Cell 9:1169–1179.

are specifically turned on during senescence. In other cases existing pigments are unmasked or their light-absorption properties are altered as a result of chemical modification.

20.6.1 Chlorophyll is degraded by way of a complex enzymatic pathway involving several subcellular compartments

Figure 20.27 illustrates chlorophyll catabolism. The first step is release of chlorophylls from their association with pigment-binding proteins in the thylakoid membrane, a reaction in which SGR plays a critical role (Fig. 20.27 reaction 1). The Mg of chlorophyll *a* is removed, resulting in the production of pheophytin *a* (Fig. 20.27 reaction 3). It is not clear whether the loss of Mg is catalyzed by an enzyme or a low molecular weight chelating substance. Pheophytin *a* is hydrolyzed by the enzyme pheophytinase to yield pheophorbide *a* (Fig. 20.27 reaction 4). The other product of pheophytinase action is phytol, which usually accumulates in the **plastoglobules** (lipid droplets) of gerontoplasts (see Fig. 20.22), largely in the form of esters. Chlorophyll *b* must be converted to chlorophyll *a* before it can be metabolized by the breakdown pathway. The enzyme responsible, chlorophyll *b* reductase (Fig. 20.27 reaction 2), is activated during senescence. Both pheophytin and pheophorbide retain an intact tetrapyrrole ring structure and are olive-green in color.

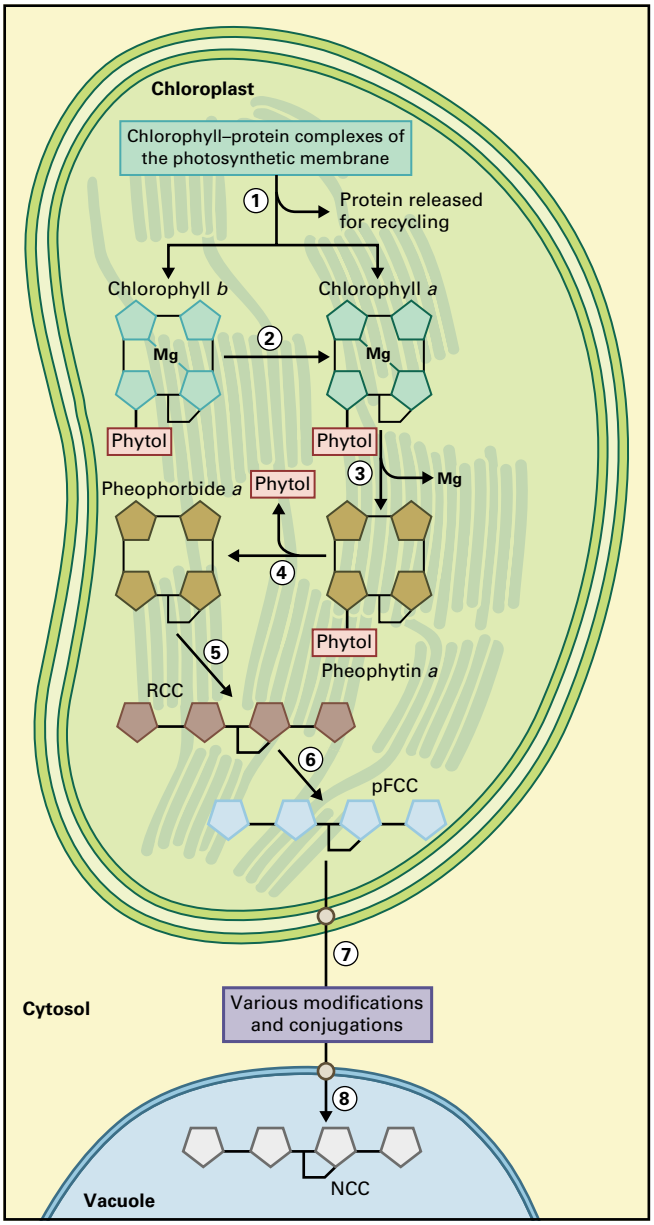


FIGURE 20.27 *The pathway and subcellular organization of chlorophyll breakdown during senescence. Enzymes and activities are identified as follows: 1, SGR; 2, Chlorophyll b reductase; 3, Dechelation reaction; 4, Pheophytinase; 5, Pheophorbide a oxygenase; 6, RCC reductase; 7, ATP-dependent catabolite transporter; 8, ABC transporter.*
Source: Thomas (2010). McGraw Hill 2010 Yearbook of Science and Technology, pp. 211–214.

The ring of pheophorbide is opened to generate a colorless straight-chain tetrapyrrole. Two enzymes are responsible, the first of which is pheophorbide *a* oxygenase (PaO; Fig. 20.27 reaction 5). The PaO reaction requires O_2 and involves Fe, which operates in a redox cycle driven by reduced ferredoxin. PaO uses pheophorbide *a* but not pheophorbide *b* as a substrate. The PaO reaction generates a red chlorophyll catabolite (RCC) that does not normally accumulate in plants but is immediately metabolized further by RCC reductase

(Fig. 20.27 reaction 6). This enzyme catalyzes the ferredoxin-dependent reduction of a double bond in the pyrrole system of RCC to produce an almost colorless tetrapyrrole with a strong blue fluorescence (primary fluorescent chlorophyll catabolite, or pFCC).

RCC reductase converts pheophorbide *a* to one of two possible epimers of pFCC, differing in stereochemistry around carbon atom 1. Substituting valine for a phenylalanine in the RCC reductase active site changes the product of enzymic reaction from pFCC-1 to pFCC-2. The role of RCC reductase in chlorophyll catabolism has been confirmed by genetically engineering the RCC reductase gene in *Arabidopsis*, a pFCC-1 forming species. Changing the active site resulted in the accumulation of terminal catabolites with the alternative stereochemisty.

Studies of the subcellular location and interactions of the enzymes of chlorophyll catabolism have established that they form a complex associated with the thylakoid membrane. SGR is thought to stabilise the complex and mediate in its docking with thylakoidal chlorophyll-proteins. Integrity of the complex is necessary to avoid leakage of phototoxic chlorophyll catabolites. In *SGR* knockout mutants, the complex fails to assemble and chlorophyll remains undegraded.

FCC is exported from the gerontoplast to the cytosol by an ATP-dependent transporter located in the plastid envelope (Fig. 20.27 reaction 7) and enters the vacuole through ABC transporters in the tonoplast (Fig. 20.27 reaction 8; see Chapter 3). En route to the vacuole, pFCC is hydroxylated and may be conjugated—malonyl and β-glucosyl derivatives have been identified—or otherwise modified. The end-products of these modifications are a range of nonfluorescent chlorophyll catabolites (NCCs) that vary greatly in number and type depending on the species. Once in the acidic environment of the vacuole, NCCs may undergo nonenzymic tautomerization and further alterations. All carbon and nitrogen in the chlorophyll molecule ends up in vacuoles: there is no evidence for transport out of the cell, which means that dismantled chlorophyll is simply abandoned when the senescing cell progresses into the death phase. This is the price the plant pays for getting access to the large reserves of mobilizable nitrogen tied up in the proteins of thylakoid membrane pigment complexes.

20.6.2 During senescence carotenoid pigments and their derivatives are unmasked, and in some cases their production can be upregulated

In leaves of some species chlorophyll loss is accompanied by decreases in carotenoids, but foliage of deciduous trees and many other plants develops striking colors before being shed. Fruits also become brightly colored during ripening. In such cases, the loss of chlorophyll reveals underlying carotenoids, which provide a yellow or orange background against which new pigments accumulate.

New carotenoids are synthesized by the terpenoid pathway (see Fig. 17.19). Geranylgeranyl diphosphate (GGPP) synthase makes the basic C_{20} unit from which all carotenoids are constructed. Phytoene synthase condenses two molecules of GGPP into the C_{40} carotenoid phytoene, and phytoene desaturase (PDS) activity leads to the formation of lycopene, the red pigment of tomato, bell pepper (*Capsicum*), and similar fruits. The activities of GGPP synthase and PDS increase markedly during ripening of pepper. Carotenoids may be further metabolized to so-called apocarotenoids, compounds with important roles in diverse biological processes including synthesis of vitamins, production of volatile attractants, antifungal defenses, and regulation of development and senescence. For example, production of the apocarotenoid hormone ABA is generally upregulated during senescence (see Section 20.11.5). Apocarotenoids are products of the activities of carotenoid cleavage oxygenases. CCD8 is a cleavage dioxygenase that operates in a reaction sequence leading to the production of 13-apo-β-carotenone (C_{18}) and a C_9 product. It is currently unresolved whether either product functions as the biologically active inhibitor of branching or its precursor. The CCD8 gene is strongly expressed in tissues undergoing developmental cell death such as xylem, cork, and senescing leaves. Mutants with loss of CCD8 function show delayed senescence as well as increased branching.

The carotenoids synthesized in plastids of ripening fruit concentrate in structures variously described as fibrils, crystals, or globules, which become increasingly numerous as chloroplasts redifferentiate into chromoplasts or gerontoplasts. Specific proteins called **fibrillins** are associated with the carotenoid bodies of ripening fruit tissues. Fibrillins have also been detected on the surface of plastoglobules of gerontoplasts. Fibrillin genes are strongly expressed in fruits, floral parts, and senescing leaves. Plastoglobule-like lipid bodies occur throughout the plant and bacterial kingdoms, and fibrillin gene homologs are correspondingly widely distributed. Fibrillin proteins function in lipid storage, in transporting newly synthesized or modified carotenoids, and in stabilizing plastid structure in fruits, leaves, and other colored organs.

20.6.3 Senescence can also alter phenylpropanoid metabolism

Other pigments and secondary compounds that accumulate in senescing and ripening tissues are products of phenylpropanoid metabolism. Many of the striking pigments of autumnal foliage are red and purple anthocyanins and yellow flavanoids, water-soluble phenylpropanoid derivatives that accumulate in vacuoles. This diverse group of phytochemicals also includes phenolics, tannins, flavonoids, and lignins (see Chapter 24). Phenylpropanoid pathways are complex, branched metabolic sequences with several control points (Fig. 20.28). Wounding, ethylene treatment, exposure to ozone, and other stimuli that invoke senescence- or PCD-like pathological responses also commonly increase the rate and pattern of phenolic product synthesis. Among the important compounds derived from phenylpropanoid metabolism is SA, a significant factor in the regulation of disease resistance and associated PCD events (see Section 20.11.3 and Chapters 17 and 21).

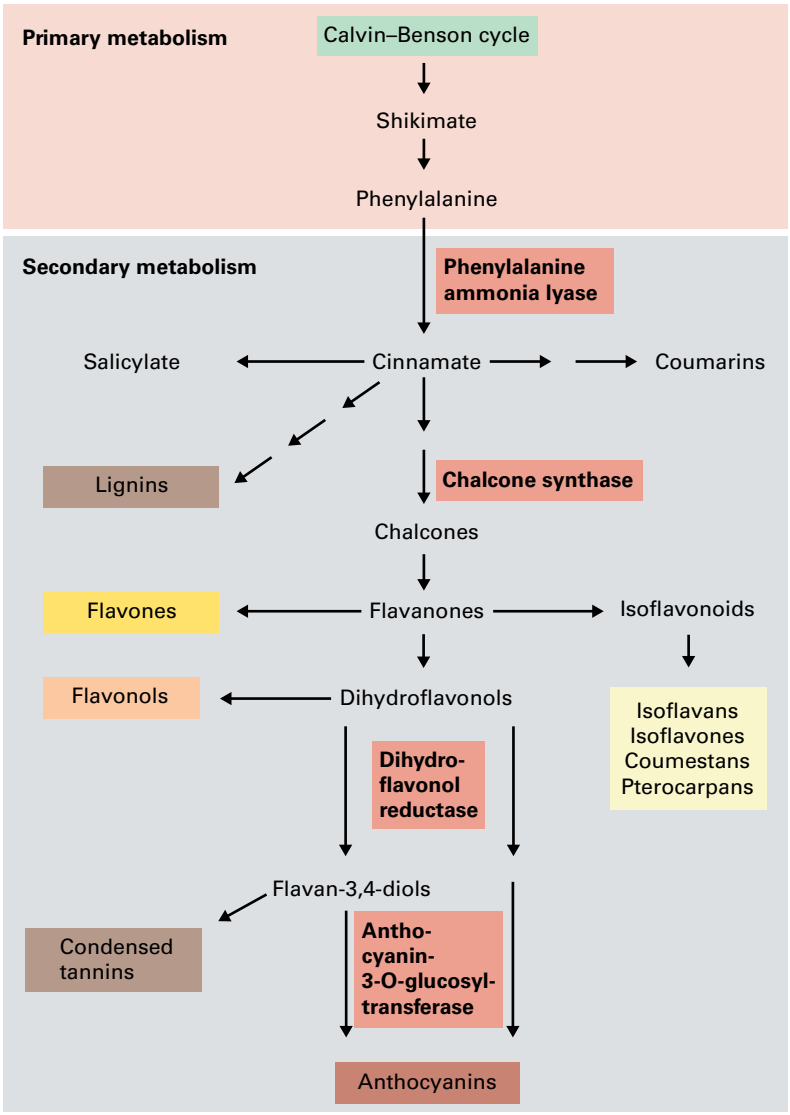


FIGURE 20.28 *Phenylpropanoid metabolism. Phenylalanine, a product of the shikimate pathway (see Chapter 7), enters secondary metabolism by way of the reaction catalyzed by phenylalanine ammonia lyase. Among the phenylpropanoid end products important in senescence and PCD are salicylate, which is implicated in PCD-like resistance to pathogen infection (see Chapters 17 and 21); lignins and tannins, which accumulate as tissues age (see Chapter 24); isoflavonoid phytoalexins, which have antipathogen properties (see Chapters 21 and 24); and anthocyanins (see Chapter 24), which are responsible for some of the vibrant pigments of ripening fruits and senescing leaves. Anthocyanin production depends on dihydroflavonol-4-reductase, a developmentally regulated enzyme that is active during the ripening of strawberry fruit.*

Anthocyanins are of adaptive value to plants both in stress responses and in signaling to beneficial or predatory animals, and there is an extensive literature on the significance of the range of possible anthocyanin functions in senescing leaves. By contrast with carotenoids, which are highly hydrophobic and confined to the lipophilic environment of plastid membranes and plastoglobules, anthocyanins and other flavonoids are water-soluble and accumulate in vacuoles. The behavior of the two classes of pigment during senescence is indicative of the state of their respective organelle compartments. Anthocyanins and proanthocyanins account for the colors of some ripe fruits, such as strawberry (*Fragaria* spp.). Expression of the branch-point enzyme dihydroflavonol reductase (DFR, Fig. 20.28) varies during strawberry fruit development. DFR is active in early development as condensed tannins accumulate, is subsequently downregulated, and then comes on again strongly as fruit color develops.

The anthocyanin responsible for the red color of autumn leaves is commonly cyanidin-3-glucoside. The final step in its synthesis is catalyzed by anthocyanidin-3-*O*-glucosyltransferase. Its gene is strongly upregulated in senescence. C1, a transcriptional regulator of genes in the anthocyanin pathway, is expressed more strongly as leaves age and floral parts develop. C1 is also upregulated during developmental cell death in xylem and cork. Unlike carotenoids, which are ubiquitous in plants, animals, and bacteria, anthocyanins are restricted to conifers and angiosperms, and their participation in programs for senescence and cell death has evolved relatively recently.

20.7 Macromolecule breakdown and salvage of nutrients in senescence

Light and CO_2 are not usually limiting for plant growth, but in many ecological and agricultural situations water and nutrients, particularly nitrogen and phosphorus, are. Plants are generally economical with nitrogen and phosphorus, recycling these and other macro- and micronutrients from

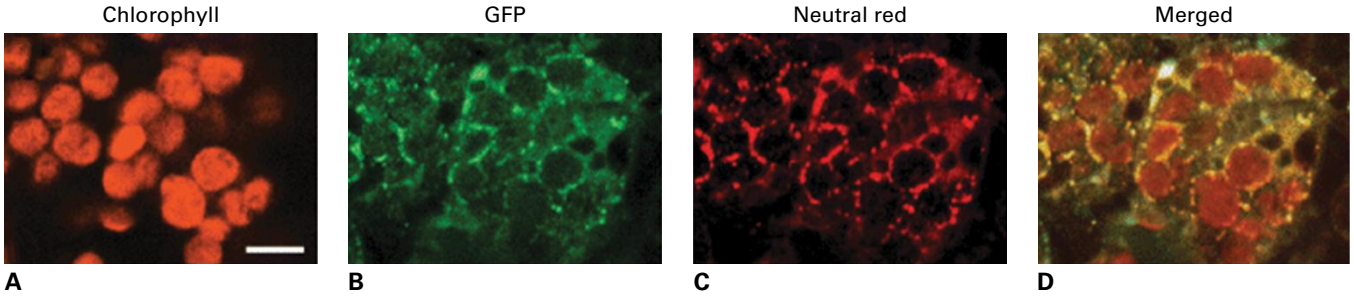


FIGURE 20.29 *Confocal images through the mesophyll of a senescing* Arabidopsis *leaf. The transgenic plant expresses a SAG12-GFP fusion protein which co-localizes with neutral red dye, indicating that SAG12 is targeted to the vacuole. Bar = 10 μm.*
Source: Otegui et al. (2005). Plant J. 41: 831–844.

older organs or from developing tissues undergoing PCD, like xylem. Much of the nitrogen and phosphorus of mature cells is tied up in proteins and nucleic acids and must be released from these macromolecules by activating specific metabolic pathways. A major function of the genetic programs for senescence and cell death is to regulate the efficient salvage of nitrogen and phosphorus and ensure their transfer to growing or storage tissues.

20.7.1 The expression of many protease genes is upregulated during senescence

In green cells, most protein is located in chloroplasts, so these organelles are the source of most organic nitrogen salvaged from senescing tissues. The most abundant proteins are Rubisco, located in the soluble stroma phase of the chloroplast, and the chlorophyll-binding light-harvesting proteins (LHCP) of the thylakoid membranes. Many studies have demonstrated that the progress of leaf senescence, measured as yellowing or as declining rates of photosynthesis, is broadly in step with decreasing amounts of these and other plastid proteins. Despite the scale of the process and the relative ease with which the substrates can be analyzed by sensitive methods such as immunoblotting, knowledge about the location, regulation, and enzymology of plastid protein breakdown during senescence is incomplete.

Among the many proteolytic activities present in plastids, ATP-dependent proteases of the Clp class are promising candidates for a key role in plastid proteolysis during senescence. At least 15 different Clps have been identified in plastids, the genes for two of which (Clp3 and ClpD) are strongly upregulated during senescence. Another class of proteases, the FtsH group, is also of interest, since genes encoding FtsH7 and FtsH8, two of the nine different enzymes of this class, are also highly expressed in senescing leaves. Whether any or all of these proteases play a part in the net loss of Rubisco and other plastid proteins during senescence and ripening remains an unanswered question.

Export of proteins from plastids for degradation elsewhere has been considered as a possible mechanism, and vacuoles would be an obvious destination. Most researchers agree that proteolysis, especially the critical first stages, occurs within the plastid, but the application of new microscopy techniques is disclosing a more complex picture of vesicle traffic within senescing cells that may explain how proteases and substrates get together. By tagging the vacuolar protease SAG12 with green fluorescent protein, it can be located within the cell by confocal microscopy (Fig. 20.29). Fluorescence of the tagged protein is coincident with signal from a vacuole-specific dye revealing the presence of lytic vesicles in the cytosol.

SAG12 is one of a number of cysteine endopeptidases specifically expressed during leaf senescence in many species. These enzymes have none of the structural motifs characteristic of proteins imported into the plastid. Indeed, many are clearly targeted to the ER or vacuole (see Chapter 4) and are closely related to proteases expressed during seed germination (see Chapter 19). For example, SEE1, a cysteine protease from senescing maize leaves, is similar in structure to the aleurains and oryzains of germinating barley and rice respectively (Fig. 20.30). There are at least 15 members of the family of aleurain-like cysteine endopeptidases in *Arabidopsis*. Association of cysteine proteases with plant senescence has a suggestive parallel with involvement of caspases in apoptosis. However the two types of protease have very different structures and enzymic properties and are only distantly related. One feature that aleurain-type endopeptidases do share with caspases is post-translational activation. In general these proteins are synthesized as pre-pro enzymes. The newly synthesized protein has a 10–26 amino acid signal peptide (pre-domain) that directs it into the lumen of the ER. It also has a 38–150 amino acid pro-domain that blocks the enzyme's active site and facilitates correct protein folding. Activation of the enzyme requires removal of the pre-pro extensions by proteolysis.

The major cleavage-activated proteases of plants are vacuolar processing enzymes, asparagine-specific cysteine endopeptidases of the legumain class. VPEs have been identified as active participants in a wide range of senescence and PCD processes. Like aleurains, VPEs are synthesized in an inactive pre-pro form. Activation takes place in the vacuole and involves the autocatalytic removal of N- and C-terminal peptides. SEE2 is a maize legumain, the gene for which is activated during leaf

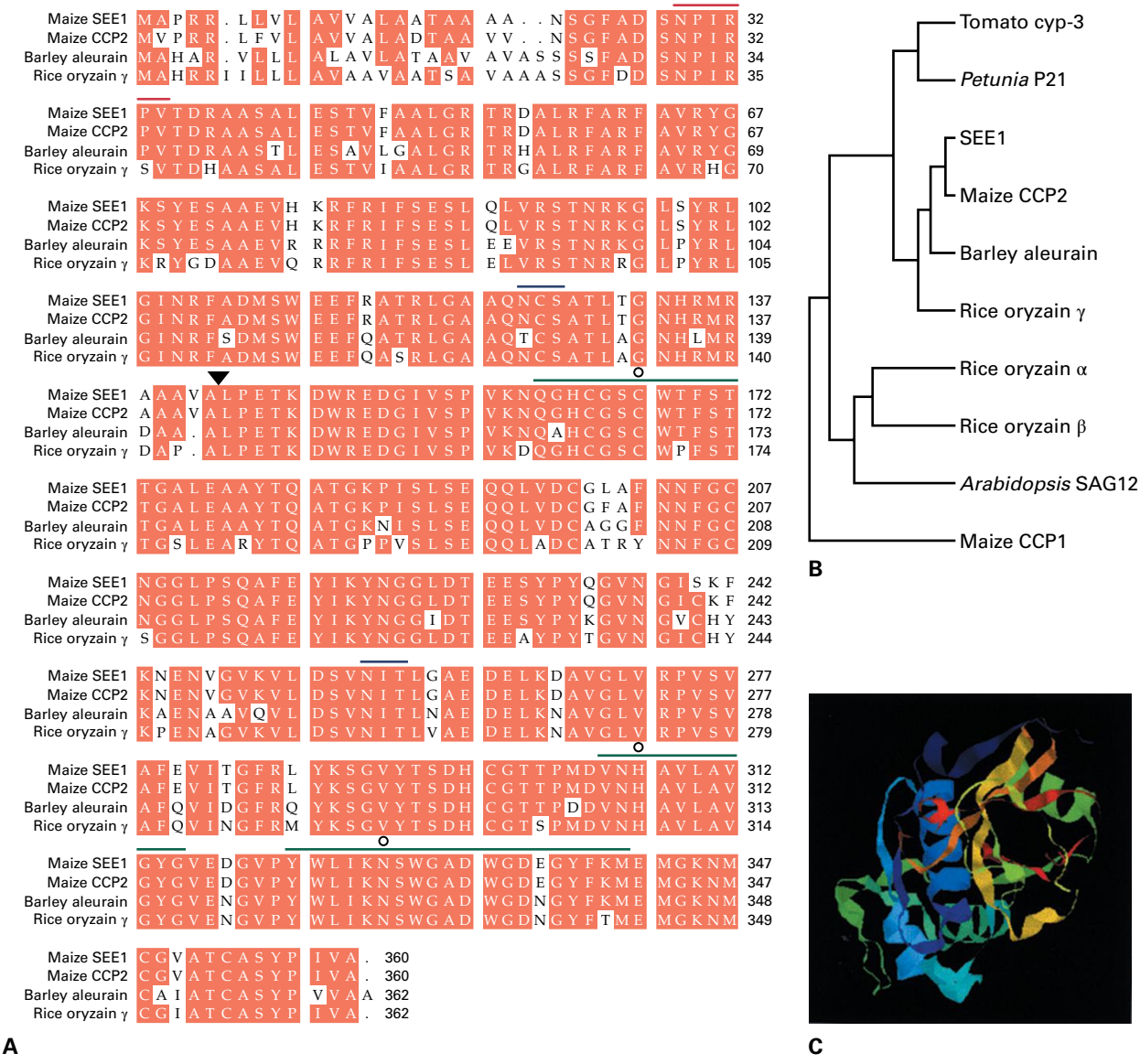


FIGURE 20.30 *Comparison of the foliar senescence-associated protease* SEE1 *from maize with other cysteine endopeptidases. (A) The amino acid sequence inferred from* See1 *cDNA aligned with the sequences of other proteases from the same family. Conserved structural features include a putative vacuole sorting motif (residues 29 through 34; red line), potential glycosylation sites (125 through 127, 256 through 258; blue lines), and the probable cleavage point that removes the prodomain (between 142 and 143; arrowhead). Open circles indicate the cysteine-histidine-asparagine triad of the active site, and the green lines identify the surrounding conserved regions. (B) Dendrogram locating* SEE1 *in the same subfamily as the cereal germination proteases aleurain and oryzain. Note that* SAG12 *of* Arabidopsis *is comparatively distantly related to* SEE1. *(C). The degree of conservation of cysteine protease structural motifs in* SEE1 *allows a three-dimensional model to be devised.*

senescence. Preventing expression of the *SEE2* gene by transposon mutagenesis has a range of morphological and physiological effects, including delaying senescence (Fig. 20.31). This is evidence that legumain-dependent proteolytic cascades may have both direct and indirect influence on developmental senescence in whole plants and their parts.

As in leaf cells, aleurain-like proteases and VPEs of the legumain family (possibly with a metacaspase function) are upregulated during petal senescence. Vesicles containing a cysteine protease have been observed in senescent daylily (*Hemerocallis* spp.) petals. It is thought that they release their contents into the cytosol, initiating rapid protein degradation. Loss of tonoplast integrity and leakage of water, electrolytes, and hydrolases from vacuoles results in wilting, further degradation of macromolecules, and final loss of petal cell viability.

20.7.2 Plastid rRNA is an important source of phosphorus remobilized during senescence, but how nucleases access this substrate is not known

In many ways, nucleic acid degradation and its control in senescence resemble protein mobilization. Genes encoding catabolic enzymes are activated, hydrolytic activities increase,

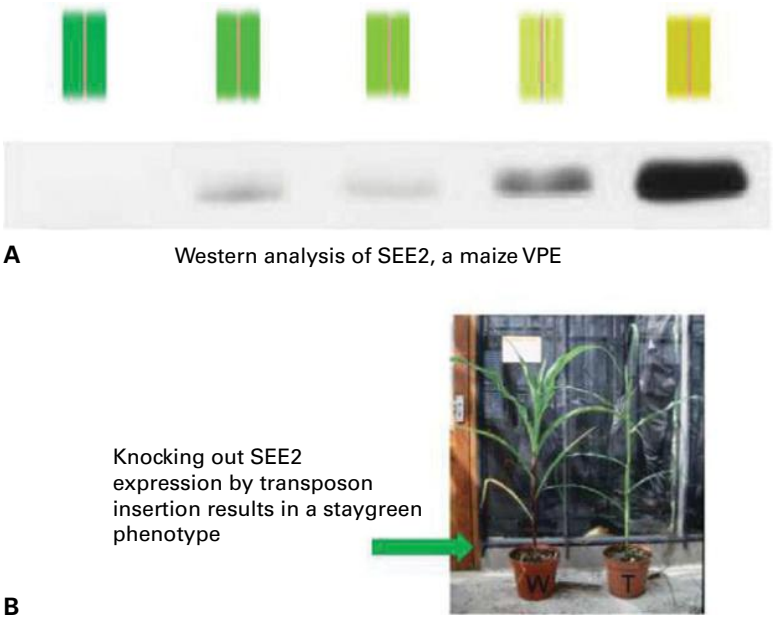


FIGURE 20.31 *Expression of* SEE2, *a VPE-type proteinase, in relation to leaf senescence in maize. (A) SEE2 protein detected by immunoblotting increases during leaf yellowing. (B) A genotype in which a transposon insertion has knocked out* SEE2 *expression exhibits a delayed senescence (stay-green) phenotype.*
Source: Donnison et al. (2007). New Phytol. 173:481–494.

and amounts of their presumed in vivo substrates decline correspondingly. However, locations of known enzymes do not correspond to principal sites of degradation. Quantitatively the largest nucleic acid fraction contributing to phosphorus remobilization is the RNA of plastid ribosomes. Ribonuclease (RNase) cleavage rapidly breaks RNA down to low-molecular-weight products with little accumulation of large intermediate fragments. Some RNases, particularly those associated with self-incompatibility (see Chapter 19), are extracellular in location, but others have ER and/or vacuole targeting motifs (see Chapter 4). BFN1 (**Bi**Functional **N**uclease **1**) is an *Arabidopsis* RNase that is strongly expressed in senescing leaves and also petals and stamens. It is highly similar to ZEN1, a nuclease associated with PCD during tracheary element development (see Fig. 20.14) and DSA6, a nuclease from ephemeral flowers of the daylily. Transcriptional regulation of BFN1 has been analyzed by fusing its promoter to a reporter gene and transforming the construct into *Arabidopsis* and tomato. The promoter was observed to be active in senescent leaves and floral organs; differentiating xylem; the abscission zones of leaves, flowers, and fruit; at anthesis; and during seed development. This is consistent with a function for BFN1 in senescence and PCD throughout the plant and the life-cycle.

20.7.3 The products of macromolecule breakdown are further metabolized before export from senescing cells

The proportions of different amino acids present in the phloem connecting senescent leaves with young developing tissues are quite divergent from the amino acid profile of total leaf protein. Although there is evidence that amino acids can be modified during transport, extensive metabolism of the products of proteolysis occurs before they are loaded into the phloem.

Typically the amides glutamine and asparagine are prominent among the organic nitrogen exports derived from breakdown of protein during leaf senescence (Fig. 20.32). Assimilatory and catabolic formation of glutamine occurs by addition of a second amino group to pre-existing glutamate. The enzyme responsible is glutamine synthetase, which catalyses the ATP-dependent reaction between glutamate and ammonium (NH_4^+). The other major amide, asparagine, is made by transamidation from glutamine to aspartate. In senescence a major source of NH_4^+ for amide synthesis is thought to be deamination promoted by glutamate dehydrogenase. Deaminases may also release NH_4^+ from other amino acids. Glutamate is a key intermediate in amide formation, acting as both NH_4^+ donor and acceptor. Plant tissues contain a range of transaminases that catalyze reactions between particular amino acids and α-ketoglutarate to produce glutamate and potentially respirable α-keto acids (see Section 20.8.1 and Chapter 14).

Proteins are major sources of remobilizable sulfur as well as nitrogen. Organic sulfur is translocated mainly as homoglutathione. Growth under low nitrogen supply promotes both nitrogen and sulfur remobilization from senescing leaves, but sulfur insufficiency has a much less pronounced effect on sulfur redistribution. This suggests that the internal sulfur cycle is regulated via protein nitrogen cycling (see Chapter 16).

Much of the organic phosphorus in leaves is in the form of nucleic acids. A fundamental chemical difference between phosphorus and nitrogen in organic combination within cells is that the former does not bond directly to carbon but instead exists as ester-linked phosphate. Phosphate esters have high negative free energies of hydrolysis. Phosphatases are ubiquitous and especially active during senescence. Conditions during senescence are thus both energetically and enzymically favorable for the release of phosphate from organic molecules. Phosphate is the form in which phosphorus is readily moved

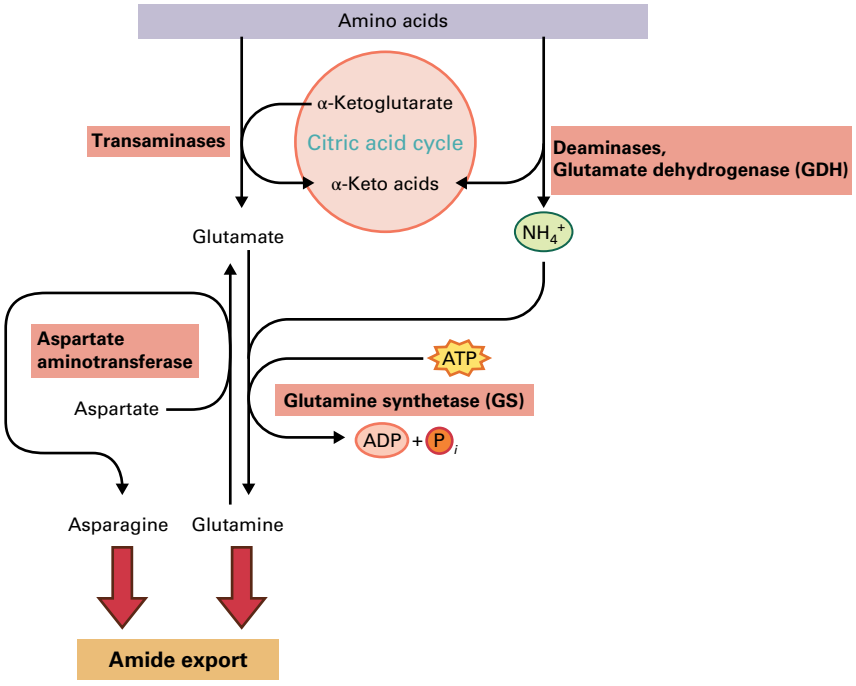


FIGURE 20.32 *Glutamate has a central role in the interconversions undergone by amino acid products of proteolysis. Ammonium, the product of deaminases and of glutamate dehydrogenase, reacts with glutamate to make glutamine in a reaction catalyzed by glutamine synthetase. Glutamine and asparagine are major mobile forms of remobilized protein nitrogen.*

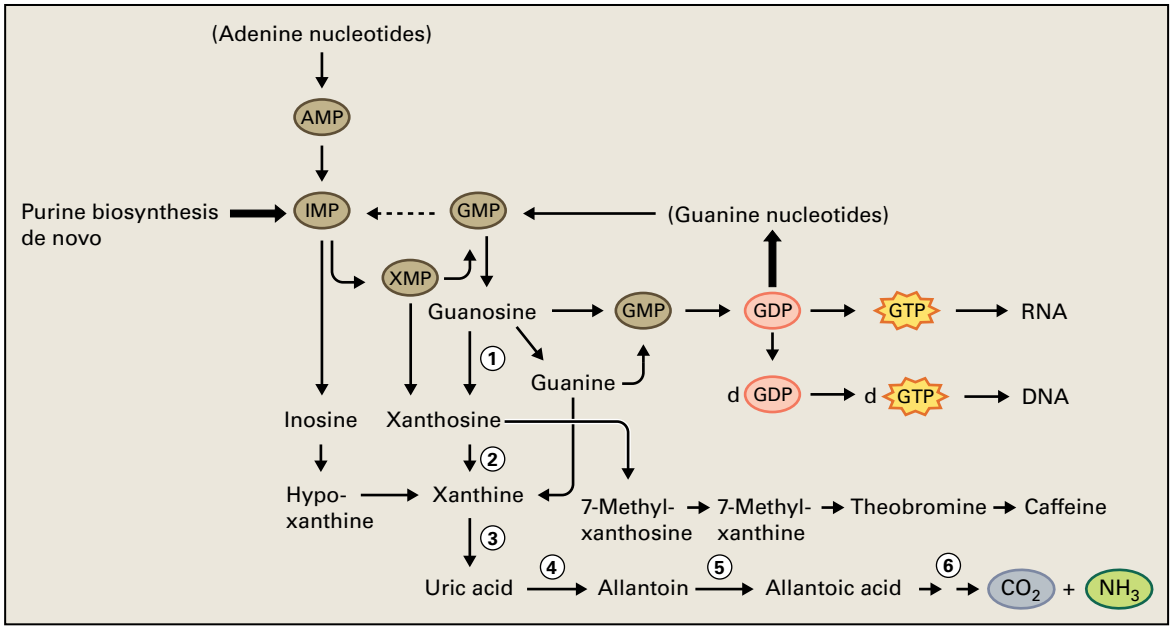


FIGURE 20.33 *Possible pathway for guanosine metabolism in plants. During senescence, guanosine and other nucleotides are broken down to yield CO_2 and NH_3. Among the enzymes that participate in guanosine catabolism are (1) guanosine deaminase, (2) nucleosidase, (3) xanthine dehydrogenase, (4) uricase, (5) allantoinase, and (6) allantoicase.*

around in the phloem. Nucleoside products of nuclease and phosphatase action are cleaved into sugars, purines and pyrimidines. Pathways leading to the catabolism of guanosine are shown in Figure 20.33. Expression of genes for xanthine oxidase-dehydrogenase, uricase, and allantoinase (glyoxysomal enzymes in the pathway that catabolizes adenine and guanine to ammonia and CO_2) is strongly activated in senescing leaves. Transcripts of the gene for allantoinase in *Arabidopsis* are also abundant in cells of xylem and cork tissues, indicating a role for this enzyme in terminal PCD processes.

20.7.4 Macromolecule salvage is regulated by substrate availability as well as the abundance of recycling enzymes

Making or activating new proteolytic activities is one way in which net protein breakdown can be initiated and sustained in senescence. Alternatively, or additionally, the degradative enzymes may already be present in pre-senescent tissues, but their substrates may have to undergo a change in structure or

subcellular location to become available for hydrolysis. How senescing cells retain structural and functional integrity of critical enzymes in a cellular environment where proteolysis and other lytic processes predominate is only beginning to be understood.

There are several ways in which differential stability may be ensured. One is to allow enzymes to be more or less equally exposed to degradation but to activate expression of selective genes so that some are continuously replenished. Another mechanism is compartmentation. Although their organelles undergo structural changes, the cells of senescing tissues retain a high degree of internal organization and compartmentation until late in PCD. Chlorophyll degradation illustrates the way in which controlled traffic between organelles is necessary for the orderly progress of senescence. The pathway includes highly localized actions in the thylakoid membranes, stroma, plastid envelope, cytosol, tonoplast, and vacuolar sap. It may seem strange to consider chlorophyll as a toxin, but free chlorophyll is a potent photosensitizer capable of killing any cell that accumulates it. To gain access to a major source of salvageable amino acids in the pigment–protein complexes of the chloroplast, it is necessary to remove chlorophyll and rapidly metabolize it by the general route used for dangerous compounds.

Compartmentation of enzyme isoforms can influence their stability. For example, plastids, mitochondria, peroxisomes, and cytosol each contain different isoforms of aspartate aminotransferase. During leaf senescence, total activities of aminotransferases and glutamine synthetase decline, but cytosolic isoforms remain unaffected or even increase in activity. Loss during senescence of plastid isoforms of several of the enzymes of primary carbon and nitrogen metabolism strongly suggests that proteolysis is compartmentalized. In addition, the plastid isoforms of some enzymes, for example, alanine aminotransferase, are intrinsically less resistant to proteolytic attack than the cytosolic forms. Thus the mechanisms that direct senescence programs include biochemical regulation as well as control of gene expression.

Experiments carried out on the lability of isolated enzymes indicate how the presence and absence of substrates, cofactors, and allosteric effectors may influence the integrity of protein structure and function within senescing cells. If an enzyme (e.g., the cytosolic form of glutamine synthetase) has its catalytic and allosteric sites occupied by the appropriate balance of metabolic effectors and substrates, it can be comparatively resistant to attack by proteases (Fig. 20.34). This implies that if an enzyme is gainfully employed in an active metabolic pathway, it is less likely to be proteolyzed than if it is operating below capacity. Thus if energy supply for photosynthesis declines and flux through the Calvin–Benson cycle decreases, as happens in senescence, one can see how enzymes of the cycle might be preferentially degraded compared with, for example, amino-acid-metabolizing enzymes that are fully occupied in processing the products of protein breakdown.

The notion that a cofactor can control degradation of a particular protein through its influence on conformational state explains other aspects of senescence. For example, the chlorophyll–protein complexes of thylakoid membranes are highly resistant to attack by proteases, but without pigments present in the correct stoichiometric ratios, chlorophyll-binding proteins cannot fold properly and are susceptible to proteolytic attack. Thus removal of chlorophyll by degradation via PaO is necessary before proteins of the thylakoid complexes can be broken down in senescence. Mutants that lack PaO activity (see Fig. 20.25) not only retain chlorophyll but also have much reduced breakdown of pigment-binding thylakoid proteins.

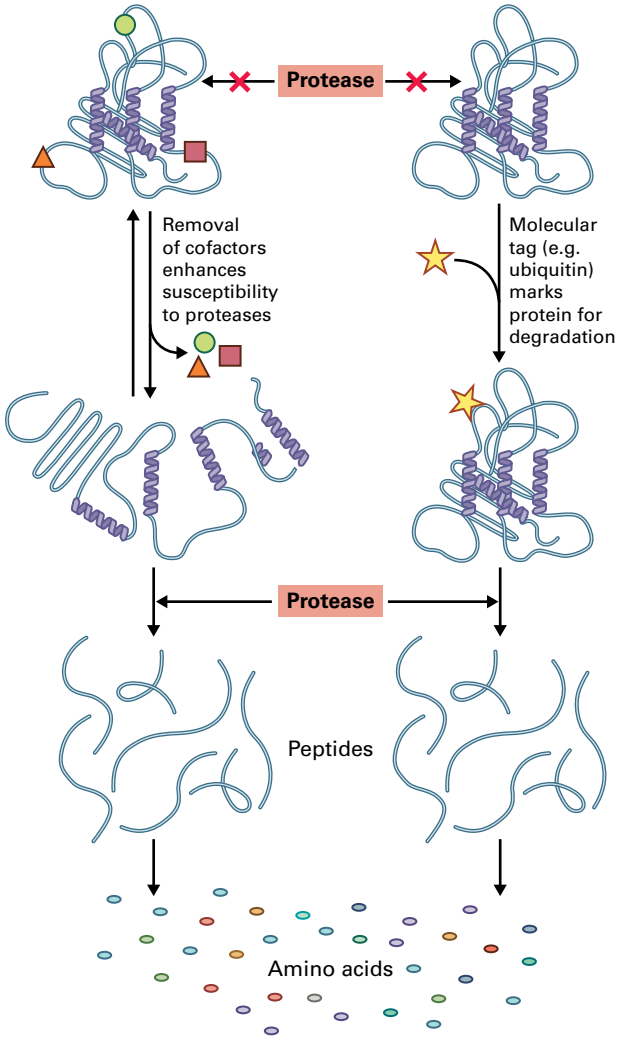


FIGURE 20.34 *Senescence may be associated with increasing susceptibility of proteins to breakdown. Two possible mechanisms are illustrated. In one case (left side of figure), occupation of binding sites by cofactors (e.g., enzyme substrates) or allosteric effectors locks the protein into a conformation resistant to proteolysis, so that the equilibrium between resistant and susceptible protein conformations is determined by the abundance of these ligands. In the other case (right side), the protein is marked for degradation by the addition of a tag such as ubiquitin and is thereby made available for proteolysis. Both the ubiquitin system and the influence of chlorophyll on the stability of some chloroplast proteins are discussed in Chapter 10.*

Another way in which proteolysis may be activated is by structural modification of an intrinsically stable protein substrate (Fig. 20.34). For example, Rubisco is actively broken down following exposure to reactive oxygen species. The ubiquitin system (which regulates protein lifespans in a wide range of cell processes, see Chapter 10) is another mechanism for activation followed by proteolysis that has been suggested to play a part in PCD. Genes encoding polyubiquitin; ubiquitin extension protein; activating, conjugating, and ligase enzymes of the ubiquitin cycle; and components of the proteasome have been cloned from a variety of plant sources. Some of these genes have been isolated from senescing tissues, and mRNAs for polyubiquitin and conjugating enzyme are abundant in senescing tobacco (*Nicotiana tabacum*) leaves. Experiments with promoter–reporter gene fusions indicate that the polyubiquitin promoter is more active in senescent than young leaves. Biochemical evidence for a specific role of the ubiquitin system in protein remobilization during senescence is meager, but a function for the pathway in stress responses is well established. It may be that the ubiquitin system is not a causative agent in senescence, but rather is upregulated in response to the stress-like conditions that develop during PCD.

20.8 Energy and oxidative metabolism during senescence

Senescence is an active process and requires a supply of energy to power metabolic and transport activities. Photosynthesis supplies the needs of early events in the senescence program, but respiration becomes increasingly significant as light interception and CO_2 fixation decline. The reactive oxygen species (ROS) that are generated during plant metabolism can damage and even kill cells; ROS often increase in abundance with tissue age. Specific enzyme systems and gene regulation mechanisms control, and are controlled by, the redox status of the cell. The loss of viability in the final stages of PCD is often the result of unconstrained oxidation and propagation of ROS and free radical cascades.

20.8.1 Senescence both modifies and is influenced by the state of energy metabolism in plastids, peroxisomes, and mitochondria

The rate of photosynthesis in leaves and other green tissues such as pericarp declines during senescence. Estimates of gas exchange show that photosynthetic capacity diminishes roughly in parallel with other indices such as chlorophyll or protein content. The precise nature of the rate-determining metabolic step that accounts for falling photosynthetic capacity is probably different in different species and under different developmental or environmental conditions. Often, declining efficiency of photosystem II (measured by chlorophyll fluorescence) is the limitation. In other circumstances the capacity of the cytochrome b_6f electron transport complex or the CO_2-fixation activity of Rubisco may set the pace for falling rates of photosynthesis as leaves senesce. The time of onset and rate of decrease in photosynthetic capacity are important senescence parameters that place a limit on the net contribution of assimilate the leaf makes to whole-plant carbon economy (Fig. 20.35). For this reason, delaying

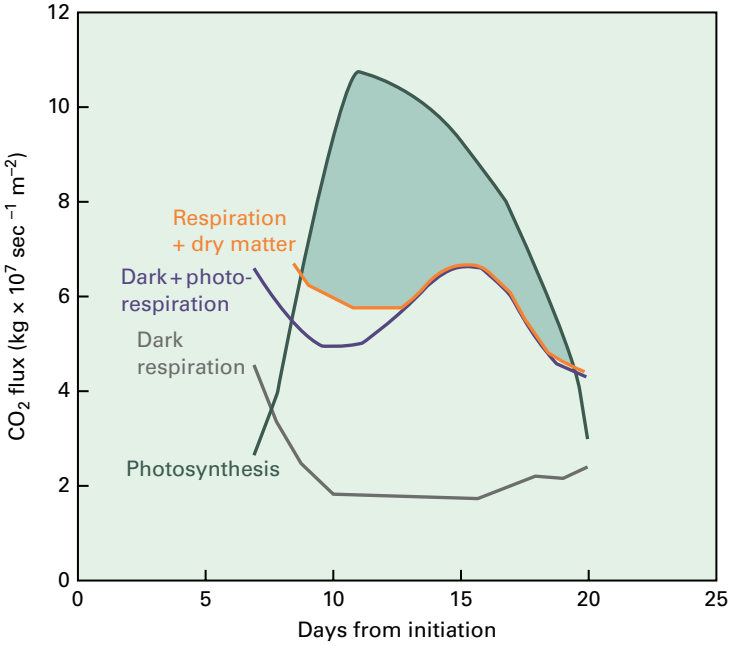


FIGURE 20.35 *Over the life of a* Phaseolus vulgaris *leaf, the carbon it assimilates through photosynthesis can be respired, converted into leaf material (dry matter), or exported to support growth elsewhere in the plant. Leaf senescence, which begins about 10 days following leaf initiation, sets a limit on the leaf's carbon export capacity.*
Source: Thomas (1984). In Cell Ageing and Cell Death (eds. I Davies, DC Sigee), pp. 171–188. Cambridge: Cambridge University Press.

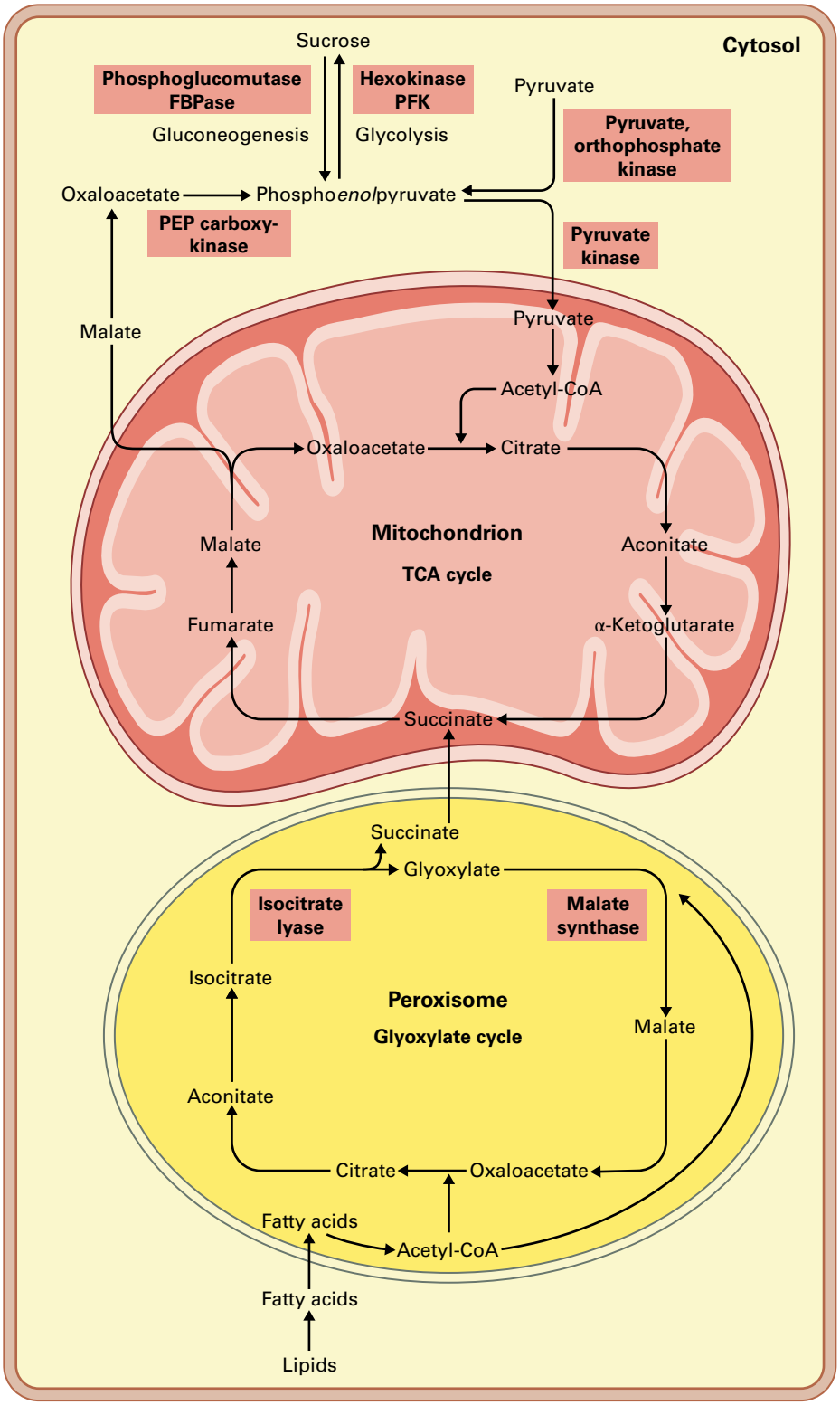


FIGURE 20.36 *Gluconeogenesis in senescing leaf cells. The glyoxylate cycle is activated in peroxisomes during senescence and allows the carbon (acetyl-CoA) from lipolysis and β-oxidation to be routed around the two CO_2-liberating steps of the citric acid cycle. Malate synthase and isocitrate lyase are the key activities in this sequence. The carbon salvaged from lipid can then be converted into transportable sucrose by the reversible steps of glycolysis, provided the irreversible pyruvate kinase reaction can be bypassed. This may be achieved by converting an organic acid to a glycolytic intermediate upstream from pyruvate [e.g., decarboxylation of oxaloacetate to phosphoenolpyruvate (PEP) by PEP carboxykinase]. Another type of pyruvate kinase bypass involves using an alternative route from pyruvate to PEP, such as the reaction catalyzed by pyruvate, orthophosphate dikinase, the gene for which is activated during maize leaf senescence.*

senescence is often an agricultural objective to ensure high productivity (see Section 20.5.4).

During leaf senescence, particularly in crop species that have been bred for highly efficient transfer of fixed carbon from vegetative tissues to grain, the conversion of lipid to sugar via gluconeogenesis is activated (Fig. 20.36). The key feature of gluconeogenesis is a bypass through which acetyl-CoA from the β-oxidation of fatty acids is diverted from the two CO_2-generating reactions of the citric acid cycle and is instead converted to organic acids. The glyoxylate bypass is characterized by two distinctive enzymes, isocitrate lyase and malate synthase, which become activated as senescence proceeds. Malate, oxaloacetate, and pyruvate are readily interconverted and represent entry points for carbon into the glycolytic pathway. Reversing the reactions of glycolysis leads to hexose and subsequently sucrose synthesis. There is, however, one essentially irreversible step in glycolysis, namely pyruvate kinase, which converts phosphoenolpyruvate (PEP) to pyruvate. If gluconeogenesis is an important pathway in mobilizing leaf reserves, one or more of the enzymes that bypass the pyruvate kinase reaction would be expected to be active, or even induced, during senescence. PEP carboxykinase, which catalyzes the formation of PEP from oxaloacetate, is thought to be the bypass enzyme active during oilseed germination, but generally declines in activity and protein abundance with leaf age. Another candidate for the bypass role in gluconeogenesis is pyruvate orthophosphate dikinase. The mRNA encoding this enzyme has been observed to be more abundant in senescing than pre-senescent maize leaves. There is also evidence of a further role for pyruvate orthophosphate dikinase in amino acid metabolism and export during senescence.

Activation of gluconeogenesis in leaf senescence is associated with functional transformation of peroxisomes. The transition has been studied in detail in cucumber (*Cucumis sativus*) cotyledons. Here the enzyme complement of peroxisomes responsible for lipid mobilization during seed germination is replaced by that of the photorespiratory organelles as cotyledon cells become photosynthetic, and subsequently reverts to a gluconeogenesis profile during cotyledon senescence. Elegant immunomicroscopy established that the glyoxylate cycle marker enzymes malate synthase and isocitrate lyase and the peroxisome marker glycolate oxidase coexist in the same particle during the changeover from one function to the other. Consistent with the reworking of protein complement within the organelle is the observation of specific endo- and exopeptidases, some of which are particularly active in senescence.

Senescence is an energy-demanding process and respiratory poisons such as the uncoupling agent dinitrophenol are very effective at halting its progress. Among the many ATP-consuming reactions that become active in senescence are chlorophyll catabolism; amide synthesis, transport and loading activities; reversal of glycolysis in gluconeogenesis; and de novo protein synthesis. Declining photosynthesis and continued active export of sugars combine to make senescing tissues increasingly carbon starved, so new sources of respirable energy are required to meet metabolic and transport demands. Amino acids derived from proteolysis are an important source of carbon skeletons (see Section 20.7.3). One hypothesis for why amides are the most common form of organic nitrogen transported out of senescing tissues is that carbon starvation favors a carbon skeleton carrying two amino moieties (such as asparagine or glutamine) rather than just one (see Chapter 7 or 16).

In tomatoes, peaches (*Prunus persica*), and many other fruits, ripening is associated with the **climacteric**, a characteristic burst of respiration. The reason for a respiratory climacteric in such species is still poorly understood. All other aspects of ripening in nonclimacteric fruit such as citrus, strawberry, or grape, proceed in the absence of the respiratory climacteric. The respiratory climacteric is closely followed by the more or less total conversion of starch into sucrose. In unripe banana (*Musa* spp.), for example, starch accounts for about 20% of the fresh weight; up to 5% of carbohydrate is lost as respiratory CO_2 during sucrose accumulation. Glycolytic flux and mitochondrial respiration are enhanced and generate ATP for the conversion of starch to sucrose and carbon skeletons needed for transamination reactions and other metabolic processes in fruit tissue.

The respiratory climacteric is usually associated with an increase in ethylene production, which is itself an ATP-demanding process. Ethylene in turn exerts autocatalytic control over its own biosynthesis and acts as a transcriptional regulator of metabolism, including respiration, during senescence and ripening (see Section 20.11.2).

20.8.2 Senescence is sensitive to cellular redox conditions

Oxidative metabolism is a central feature of senescence at the cellular level. Some signaling pathways that regulate senescence may include redox-sensing components. For example, the expression of genes encoding fibrillins (see Section 20.6.2) is sensitive to oxygen. Induction of fibrillin biosynthesis by drought, wounding, or ABA involves a signaling pathway in which hydrogen peroxide (H_2O_2), or the superoxide anion ($O_2^{\cdot -}$) from which it is generated, is a key component. H_2O_2 is a product of normal enzymic reactions in peroxisomes, glyoxysomes, chloroplasts, and other cell compartments. Defenses against accumulation of H_2O_2 and $O_2^{\cdot -}$ include catalase (CAT), superoxide dismutase (SOD), and the antioxidant ascorbate, which with a second antioxidant, glutathione, participates in a cycle driven by ascorbate peroxidase (APX), monodehydroascorbate reductase, dehydroascorbate reductase and glutathione reductase (Fig. 20.37; see also Chapter 22). The activities of peroxisomal CAT2 and cytosolic APX1 decrease during bolting of *Arabidopsis*, before any measurable loss of chlorophyll. Levels of H_2O_2 increase at this time, then begin to fall as the stress-inducible CAT3 isoform is activated and APX1 activity restored. Finally, H_2O_2 increases as senescence proceeds to completion. These observations suggest a simple model of the control of ROS during senescence based on the timing and

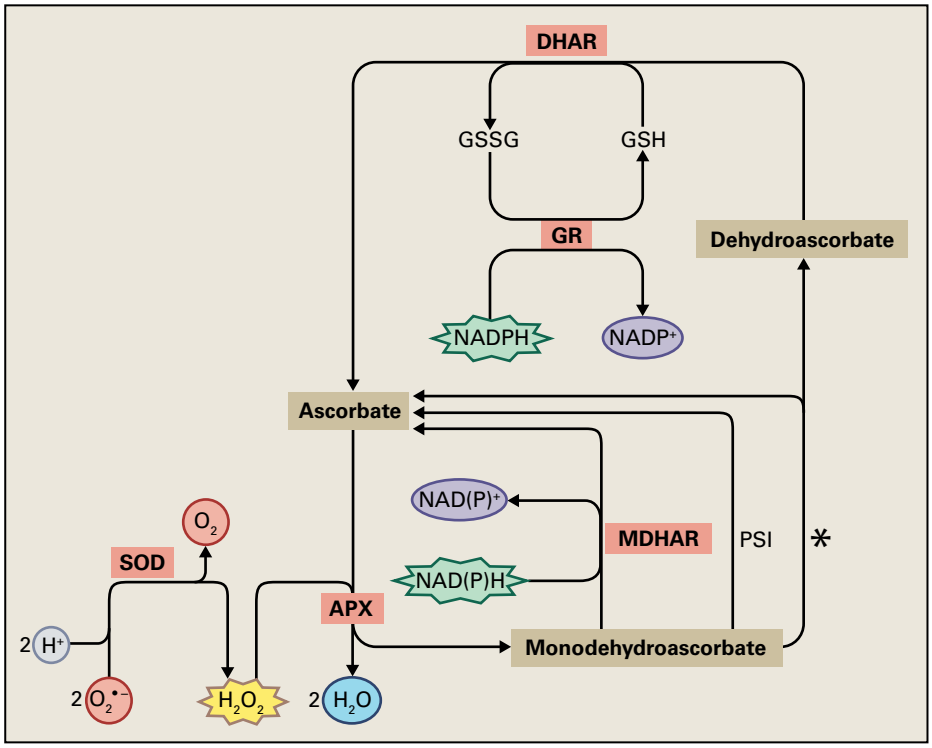


FIGURE 20.37 *The ascorbate–glutathione redox cycle in senescence. Ascorbate is regenerated from oxidized forms by a cycle catalyzed by ascorbate peroxidase (APX), monodehydroascorbate reductase (MDHAR), dehydroascorbate reductase (DHAR), and glutathione reductase (GR). Superoxide dismutase (SOD) is one of the enzymatic defenses against the buildup of reactive oxygen species. In mature leaves, photosynthetic electron transfer generates NADPH, which donates electrons to ascorbate by way of reduced glutathione (GSH). In senescing leaves, NADPH production decreases, resulting in increased ratios of oxidized glutathione (GSSG) to GSH and of dehydroascorbate to ascorbate. These relatively subtle changes can result in substantial changes in cellular redox conditions and signal new patterns of gene expression. PSI, Photosystem I; *, nonenzymatic reaction.*

interaction of CAT and APX activities (Fig. 20.38). The shifting balance between ROS production and ROS removal and the resulting shifts in cellular redox state alter gene expression. In this context, the redifferentiation of peroxisomes into glyoxysomes could be of special significance in senescence, since the transition is clearly associated with an altered profile of superoxide-producing and antioxidant enzymes.

The transcription factor WRKY53 (see Section 20.5.2) participates in a complex signaling network by which redox status regulates senescence. WRKY53 is induced by H_2O_2 and autoregulates its own synthesis by feedback inhibition. The many senescence-related genes with which WRKY53 interacts include *CAT1*, *2*, and *3* and *NPR1* (***N**on-expressor of **P**athogenesis **R**elated genes **1***), a redox-sensitive, stress-activated transcriptional cofactor that participates in transduction of SA signaling during both senescence and plant defense responses. SA and jasmonic acid, whose roles in senescence are discussed in Section 20.11, control WRKY53 functions in senescence and resistance to pathogens via the regulatory protein ESR (**E**pithiospecifying **S**enescence **R**egulator). Thus WRKY53 is a critical node in a complex signaling network by which redox status regulates senescence.

It should be emphasized that ROS are considered here to act as part of a subtle signaling mechanism in coherent, viable

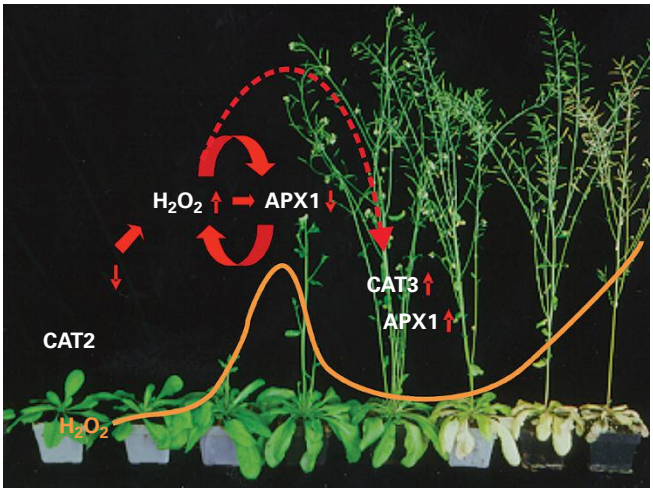


FIGURE 20.38 *A peak in H_2O_2 production occurs during bolting of* Arabidopsis. *The diagram illustrates a possible model to explain this peak. CAT2 is downregulated, leading to an increased H_2O_2 level that may inactivate APX1. Declining APX1 activity allows further increases in H_2O_2 that ultimately induce CAT3 expression and activity, which removes H_2O_2 and thereby restores APX1 activity.*

Source: Zimmerman et al. (2006). Plant Cell Environ. 29: 1049–1060.

cells. In excess they are capable of rapidly destroying the cell through the propagation of free radical cascades, and such a process certainly leads to death in some pathological conditions (see Chapters 21 and 22). But this kind of unregulated, catastrophic mechanism is likely to contribute only to the most terminal phase of normal senescence.

20.9 Environmental influences on senescence and cell death I: Abiotic interactions

Seasonal or otherwise, predictable environmental cues can trigger senescence as part of an adaptive strategy, as is observed in trees that respond to declining day length through mass leaf senescence in the autumn. Senescence is also a tactic deployed when an unpredictable stress is experienced, such as aerenchyma development as a response to oxygen limitation. The relationship between environmental stimuli and senescence can be complex. For instance drought invokes premature foliar senescence in many species, but water limitation during senescence will slow development of yellowing and other symptoms. Frequently the speed and severity of a developing stress overruns the capacity of tissues to invoke and execute the comparatively slow senescence program, with the result that cells divert more or less directly to the more rapid PCD pathways characteristic of physiological or pathological events such as the hypersensitive response (see Section 20.10).

20.9.1 Plant adaptation and acclimation often requires senescence to be cued by environmental factors

At latitudes away from the tropics, change in day length over the course of the year is a reliable reference that permits plants that can sense it to prepare for seasonal stresses. Foliar senescence is a prominent developmental event in flora of these regions. Proper timing of leaf senescence is critical for a plant, and can be described in general terms as a trade-off between the carbon and nitrogen demands of the plant, since the loss of photosynthetic carbon acquisition that results from degradation of leaf photosynthetic pigments and proteins is balanced by recovery of nitrogen and other nutrients from senescing leaves. This can most easily be illustrated by the highly coordinated autumnal senescence that deciduous trees undergo in temperate regions. In aspen (*Populus tremula*) (Fig. 20.39), initiation of autumn senescence is strictly controlled by photoperiod. A particular aspen tree will always

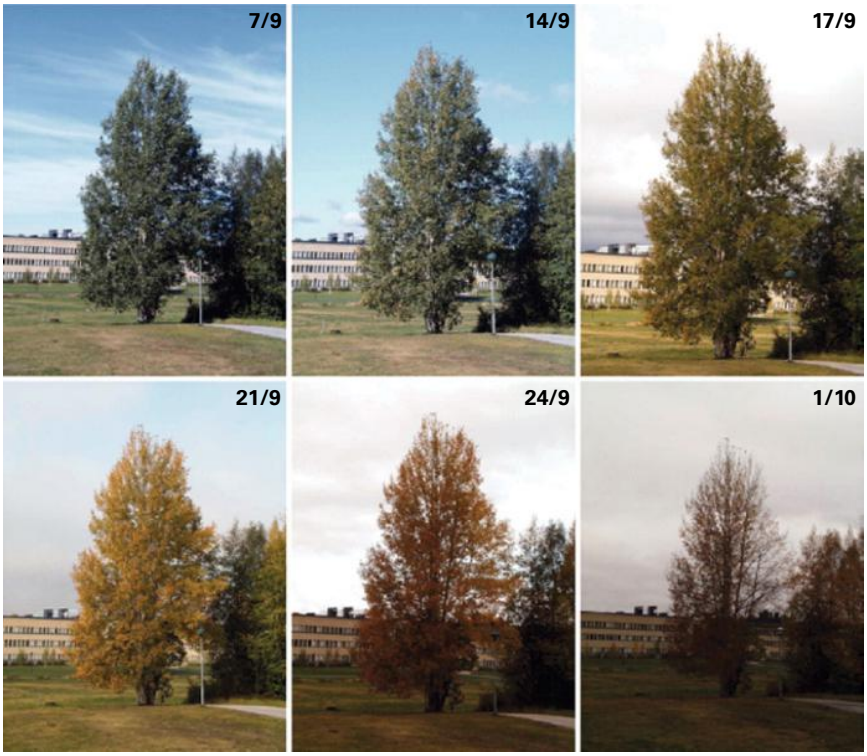


FIGURE 20.39 *Autumn senescence in an aspen tree, observed from September 7 to October 1 in Umeå, Sweden. The highly synchronized physiologies of a given individual's leaves makes aspen a convenient model for studies of senescence in free-growing tree species. The timing of the onset of senescence is set by day length, whereas the rate of senescence once initiated is largely determined by temperature.*
Source: Bhalerao et al. (2003). Plant Physiol. 131:430–442.

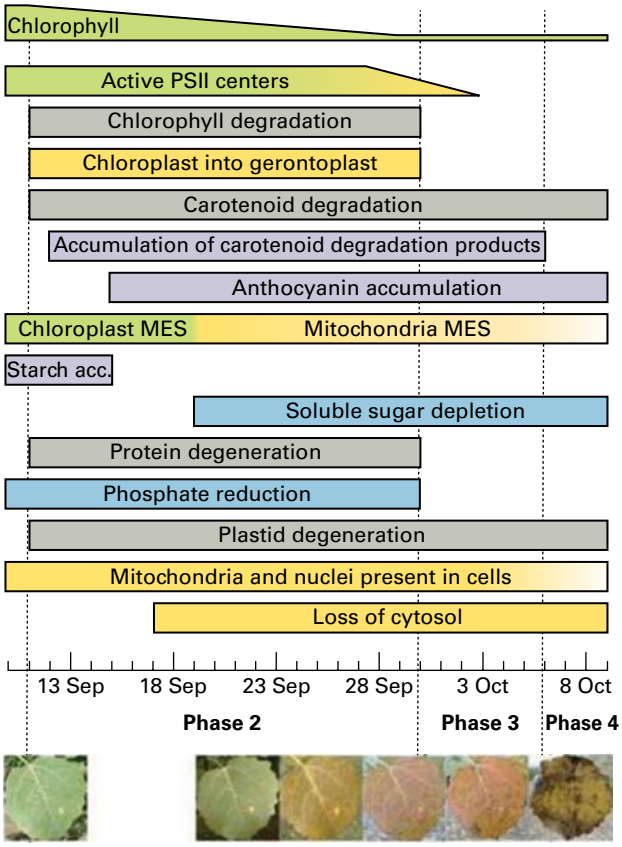


FIGURE 20.40 *A timetable detailing cellular events during autumnal senescence in aspen. Four phases are identified, based on physiological, biochemical and microscopical analyses. The pre-senescent Phase 1 is followed by Phase 2, during which chloroplasts are converted to gerontoplasts, major pigmentation changes occur, N and P are mobilized and sugars metabolized. During Phase 2 the major energy source (MES) switches from chloroplasts to mitochondria. By Phase 3 less than 5% of original chlorophyll remains, cell contents are severely depleted but metabolism continues and viability is sustained in some cells. Phase 4 is the stage at which cell death is complete and few structures are recognizable within residual cell walls.*
Source: Keskitalo et al. (2005). Plant Physiol. 139:1635–1648.

start autumn senescence at more or less the same date every year without any obvious influence of temperature. Many stresses, such as attack by pathogenic fungi or herbivorous insects, can induce localized leaf senescence prematurely, but when autumn senescence is triggered, the whole crown starts to senesce in a coordinated fashion, according to a predictable timetable of cellular events (Fig. 20.40).

Initiation of senescence is set by day length, but once the process is underway, changes in autumn coloration are controlled by temperature. The rate of chlorophyll degradation is enhanced by low temperature, probably via increased photooxidative stress, so that the time from initiation of senescence until leaves start to yellow (when about two-thirds of the chlorophyll has been degraded; see Fig. 20.40) can differ by 1 to 2 weeks, depending on severity of the decrease in temperature. Anthocyanin production is also stimulated by low temperature. The combined effects of decreased chlorophyll and increased anthocyanin levels make autumn splendor more pronounced in years when the critical weeks represented by Phase 2 (Fig. 20.40) are colder. There is often a very large natural variation between trees of the same species: two aspens growing in the same stand can differ in timing of senescence by three weeks. Photoperiodic control of initiation of senescence is beneficial for trees growing at high latitudes. In these forests, nitrogen availability is typically a limiting factor for growth, and many trees sacrifice weeks of potential photosynthetic carbon gain in order to ensure that sudden frost will not kill leaf cells before remobilization has occurred, leading to losses of large amount of nitrogen and other nutrients in falling leaves. Since these climates are often characterized by rapid and unpredictable temperature changes in autumn, photoperiodic cues predict the approach of winter better than temperature. In addition, daily change in photoperiod is much greater at higher latitudes, allowing for a precise setting of the calendar. There is growing evidence for the importance of phytochrome (see Chapter 18) in day length perception and autumnal responses in *Populus tremula*, but how the signal to trigger senescence is transduced from photoreceptors is not known. Transcription factors have an important regulatory role integrating autumnal senescence with growth, flowering, and dormancy. For example, constitutive expression in transgenic poplar of a MADS homeotic gene known to induce early flowering in birch (*Betula pendula*) and apple (*Malus* x *domestica*) resulted in delayed bud dormancy and senescence and retention of photosynthetic activity, chlorophyll, and proteins in leaves under winter conditions. It should be noted that apple, pear (*Pyrus* spp.), and some other woody members of the family Rosaceae are unusual in being temperate deciduous winter-dormant trees that are photoperiod insensitive. It appears that chilling is the major triggering factor for the autumn syndrome in these species.

20.9.2 When environmental challenges exceed the plant's adaptive capacities, senescence becomes a stress response

As sessile organisms, plants cannot escape environmental stresses such as drought or flooding. Senescence is one of the responses employed by plants to deal with suboptimal environmental conditions, and senescence-related genes are frequently identified amongst those upregulated in response to abiotic stresses (see Chapter 22). For example, patterns of tissue senescence and death are responsive to temperature and CO_2, and the changes induced in plant tissues by ultraviolet radiation include enhanced expression of genes associated with senescence.

The development of **aerenchyma** in plant roots subject to flooding illustrates how plants deploy PCD in response to stressful environmental conditions. During aerenchyma formation in most species, cells are removed from mature roots

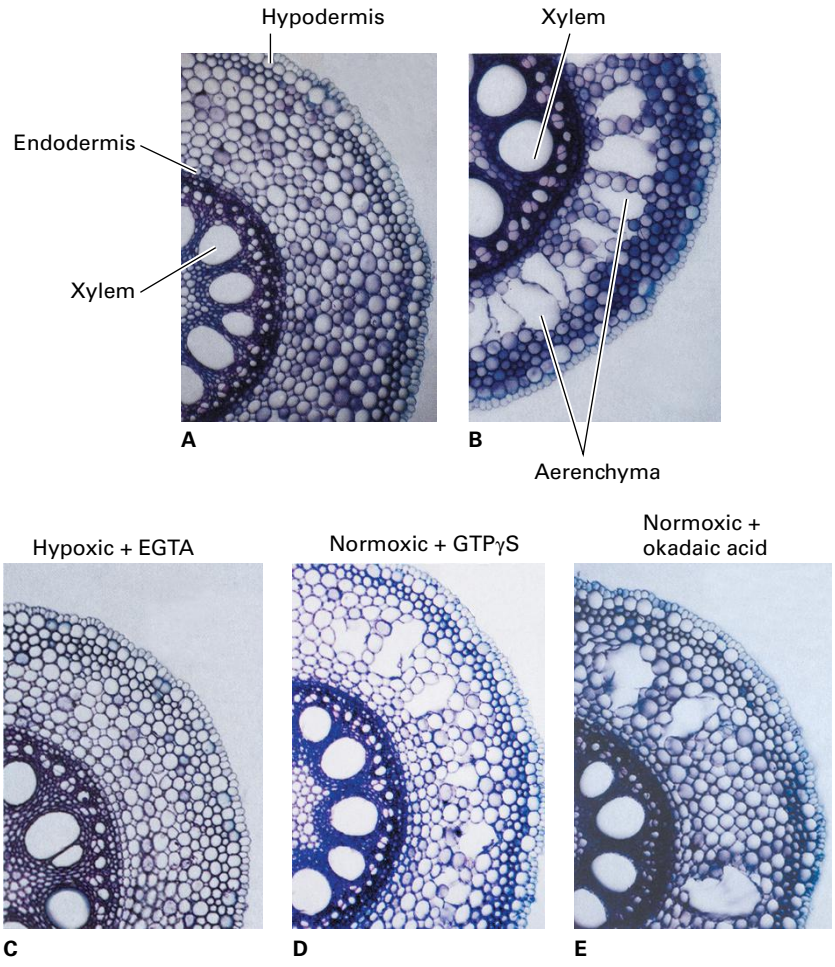


FIGURE 20.41 *Aerenchyma formation in maize roots in response to hypoxia. Roots were grown under aerobic (A) and hypoxic (B) conditions. Under low-oxygen conditions, cortical cells between the endodermis and hypodermis undergo lysigeny to form air spaces that are continuous throughout the root, allowing submerged roots to access atmospheric gases obtained by above-ground tissues. Aerenchyma formation is influenced by agonists and antagonists of signal transduction pathways. The Ca^{2+} chelator EGTA prevents aerenchyma in maize roots under hypoxic conditions (C), whereas the G-protein activator GTPγ-S (D) and the protein phosphatase inhibitor okadaic acid (E) induce aerenchyma formation under aerobic conditions.*
Source: (A–E) He et al. (1996). Plant Physiol. 112:463–472.

by lysigeny, creating channels through which air can diffuse from shoot to root (Fig. 20.41A,B). In a few species, aerenchyma is schizogenous in origin; air spaces are formed by cell separation but no cells are lost. Because of the adverse effects of flooding and poor aeration on yield, much research on aerenchyma has been carried out on crop species, particularly rice and maize. More recently the important processes of root responses to hypoxia have been replicated in the model plant *Arabidopsis,* allowing the application of genomics to analysis of aerenchyma development.

The formation of aerenchyma in roots of plants that are not adapted to wetland conditions is triggered by oxygen deficiency. Aerenchyma formation has been extensively studied in maize roots in response to oxygen-limiting conditions as well as other environmental stresses, including the depletion of nitrogen and phosphorus. Aerenchyma results from PCD of a specific group of root cortical cells located between the endodermis and hypodermis. This response to hypoxia or anoxia can be rapid and results in removal of whole cortical cells including cell walls (Fig. 20.41A,B).

Concentrations of ethylene and its precursor 1-aminocyclopropane-1-carboxylic acid (ACC) are elevated in roots grown under low oxygen. There is strong evidence that ethylene regulates aerenchyma formation. Inhibitors of ethylene synthesis, such as aminoethoxyvinylglycine (AVG), or of ethylene action, such as silver ions, can prevent formation of aerenchyma under oxygen-limiting conditions. Conversely, exogenous ethylene can bring about aerenchyma formation under aerobic conditions.

Microarray profiling of transcript abundance during low-oxygen-induced aerenchyma formation in *Arabidopsis* roots reveals significant alterations in expression of genes involved in glycolysis and fermentation pathways, ethylene synthesis and perception, calcium signaling, nitrogen utilization, trehalose metabolism, and alkaloid synthesis. Among the activities induced in maize roots by low oxygen or ethylene treatment are several cell-wall-modifying enzymes, including cellulase. The large increase in cellulase activity in hypoxic (4% O_2) conditions compared with the normoxic (21% O_2) control is strongly correlated with levels of ACC synthase, a key enzyme in ethylene biosynthesis (Fig. 20.42).

Cytosolic Ca^{2+} is part of a signal transduction pathway linking both anoxia and ethylene to PCD in maize cells. Under anoxic conditions, removing Ca^{2+} from the medium surrounding roots by using the Ca^{2+} chelator EGTA prevents aerenchyma formation (see Fig. 20.41C) and inhibits the rise in cellulase activity. Use of specific inhibitors has shown that G-proteins, protein kinases and protein phosphatases are also likely to be involved in regulating aerenchyma formation in response to both oxygen and ethylene in maize roots. GTPγS,

which locks G-proteins into the active state, and okadaic acid, which inhibits protein phosphatase activity, each promote the formation of cellulase and aerenchyma in roots under aerobic conditions (see Fig. 20.41D,E). On the other hand, an inhibitor of protein kinase activity prevents formation of aerenchyma in roots under hypoxia. Taken together, these data implicate cytosolic Ca^{2+} and CaM in a signaling cascade that could activate protein kinase and protein phosphatase activities to promote modification of proteins involved in PCD. In maize roots incubated under low oxygen conditions, or treated with ethylene, TUNEL-positive nuclei develop in the cortex within hours, whereas there is little or no staining in normoxic controls (Fig. 20.43). This suggests that fragmentation of DNA is a factor in the mechanism of PCD in aerenchyma formation.

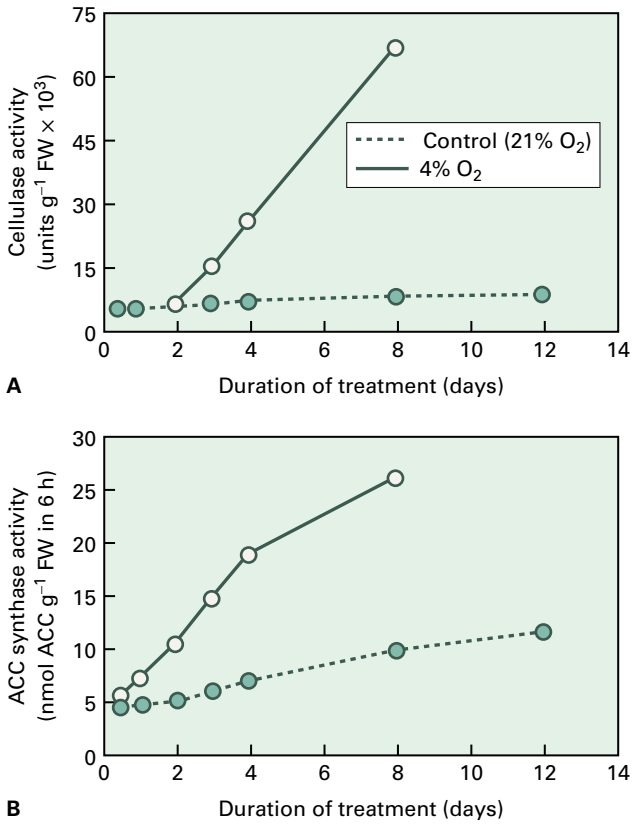


FIGURE 20.42 *Increases in the activities of cellulase (A) and of a rate-limiting enzyme in ethylene biosynthesis, ACC synthase (B), accompany aerenchyma formation in hypoxic maize roots. Both enzymes increase with the duration of hypoxia.*

20.10 Environmental influences on senescence and cell death II: PCD responses to pathogen attack

Plants are continuously under attack from armies of microorganisms and pests such as insects. To survive they have evolved highly efficient defenses that, unlike the immune responses of humans and other animals, are mostly confined to the site of attempted invasion. Defense is often associated with cell death. Conversely, some pathogens actively induce cell death or senescence-like symptoms to promote disease development. Different strategies are employed by different pathogens, and it is prudent not to overgeneralize from observations made in a single species or from a small number of plant–pathogen interactions.

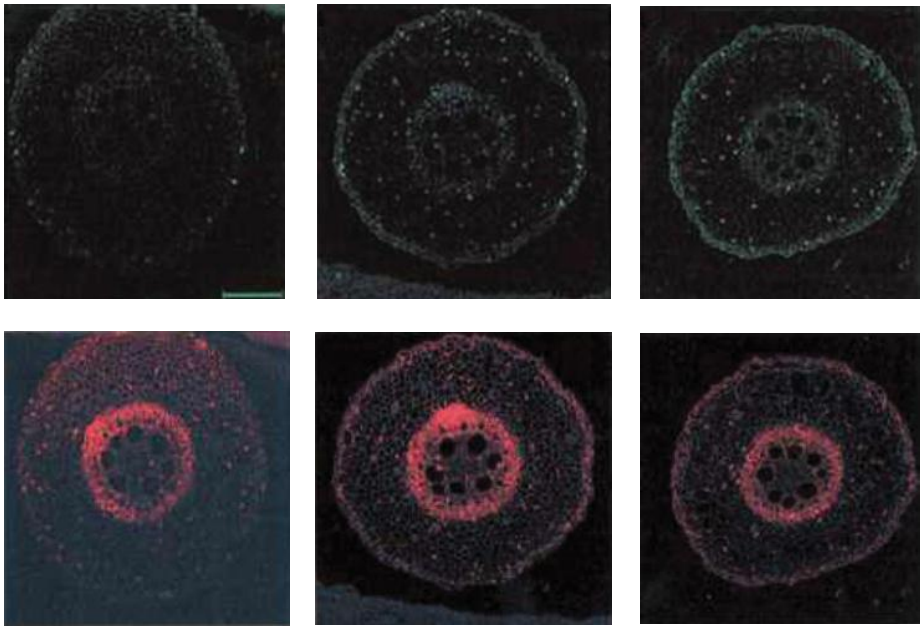


FIGURE 20.43 *TUNEL staining (see Fig. 20.4, Section 20.1.1) in maize root transverse sections. (Top row, from left to right) The cortex of roots grown under normoxic (21% O_2) conditions reveals no DNA fragmentation (green fluorescence), but roots subjected to hypoxia (3% O_2) or treated with exogenous ethylene (1 μL L^{-1} C_2H_4) stain positive for fragmented DNA. (Bottom row) Root sections stained with the DNA-binding agent propidium iodide (red fluorescence) are included for comparison. The scale bar is 250 μm.*
Source: Gunawardena et al. (2001) Planta 212:205–214.

20.10.1 Cell death is a common response to attack by pathogens

Plant cell death has perhaps been most intensively studied within the context of interaction with pathogens. In plants, cell death linked to resistance is known as the **hypersensitive response** (HR), a phrase coined following a microscopic examination of rust interactions with cereal species, cells of which were described as responding hypersensitively. HR has been linked with the organism's attempts at confining and neutralizing the threat of infection. Even after many years of study, however, it is unclear whether HR is required for, or is a consequence of, resistance.

The size of the area affected by HR may vary but it is always associated with the pathogen at the site of attempted infection. The phenotype of HR can be greatly influenced by the infection strategy of the pathogen. Tobacco Mosaic Virus (TMV) moves rapidly between infected cells so that when HR forms in resistant genotypes, large areas (about 0.5 cm diameter) of cell death are seen (Fig. 20.44A). In other cases, HR occurs as a necrotic fleck. A single pathogen can elicit flecks of different sizes on two distinct plant genotypes (Fig. 20.44B). Necrotic flecks and single cell HR (Fig. 20.44C) are usually elicited by fungal or bacterial pathogens. Although varying in phenotype, HR has some common features. Cell death in HR is often rapid, in many cases being complete within a day of first infection. Microscopic examination of cells undergoing PCD frequently reveals cytoplasmic clumping and vesiculation (Fig. 20.44D), and ultimately HR cell walls become reinforced with a variety of phenolic compounds so that they fluoresce under UV light (Fig. 20.44E). Early work using metabolic and protein synthesis inhibitors quickly showed that HR was dependent on the plant's biochemistry and therefore represented an example of PCD.

It is thought that in HR a common death mechanism (or small number of mechanisms) is triggered by multiple stimuli (e.g., different species of pathogen). Following pathogen attack, the genetic program associated with the HR is likely to involve three types of genes: (i) genes that respond to triggers that initiate death; (ii) genes involved in limiting the extent of death and that may suppress PCD in the absence of infection; and (iii) genes that integrate the death mechanism with other plant defenses. Identifying genes of each class has been a major objective for molecular plant pathologists.

Many genes involved in initiating HR have been studied for many years and are well-characterized. These genes were named **resistance (*R*) genes** by plant breeders who found them to be important sources of crop resistance against pathogens. Groundbreaking work in the 1940s demonstrated that initiation of the HR required the interaction of a single resistance gene product with a single product encoded by the pathogen, called an **avirulence (*avr* gene)**. *R–avr* interactions can be considered as triggers of PCD; they are discussed in detail in Chapter 21. Beyond *R* genes, plant molecular biologists have sought to elucidate HR mechanisms by (i) seeking parallels with better characterized mammalian forms of PCD; (ii) generating and screening mutant lines that exhibit alterations in cell death; and (iii) investigating the roles of ROS and reactive nitrogen species that are generated on a large scale during HR. Each approach has made major contributions to our knowledge of HR.

20.10.2 Mechanisms of HR PCD have similarities with, but significant differences from, both autophagy and apoptosis

As researchers have compared HR with other forms of PCD in animals and plants, they have identified aspects of autophagy that are linked to HR, as well as some similarities between HR and apoptosis. Recent molecular breakthroughs have shown that autophagy (see Section 20.1.2) plays complex roles in HR. When the effects of suppressing *ATG* genes were assessed in *Nicotiana benthamiana*, reduced expression of *ATG6* (also known as *Beclin1*) resulted in a spreading HR following challenge with either TMV or bacterial pathogens (Fig. 20.45). *ATG6* is involved in the nucleation stage of vesicle formation, and consistent with this, suppression of the PI3-K-containing vacuolar sorting complex also leads to spreading cell death. Such observations suggest that autophagy is important in confining the extent of HR cell death.

Additional results show that VPEs (see Section 20.7.1), thought to be terminal components in autophagic body processing (see Fig. 20.5), play an active role in the cell death process. As with many forms of HR, the response induced by TMV in tobacco can be suppressed by the application of mammalian caspase inhibitors (Fig. 20.46A). However, VPE inhibitors but not general cysteine (E-64) or serine protease inhibitors (PMSF; phenylmethanesulphonylfluoride) can also inhibit HR. In a major advance, suppression of VPE gene expression in *N. benthamiana* was shown to abolish HR (Fig. 20.46B–E), measurable caspase-like activity, and DNA laddering. Furthermore, an *Arabidopsis* γVPE knockout mutant exhibited a significant reduction in cell death and caspase activity when challenged with an HR-eliciting bacterial pathogen. Such data suggest that VPEs are the source of HR-associated caspase-like activity and implicate vacuolar processing as a key feature of the HR cell death mechanism. The in vivo targets of VPE activity remain to be defined but are likely to be key triggers in the cell death process.

20.10.3 Cell death mutants are powerful tools for dissecting plant responses to pathogens

Basic to the concept of PCD is that the program is primarily genetic, so a common experimental approach is to search for mutants that display altered forms of death. Mutants that exhibit the abolition or reduction of cell death in situations where it would be expected are likely to be altered in genes

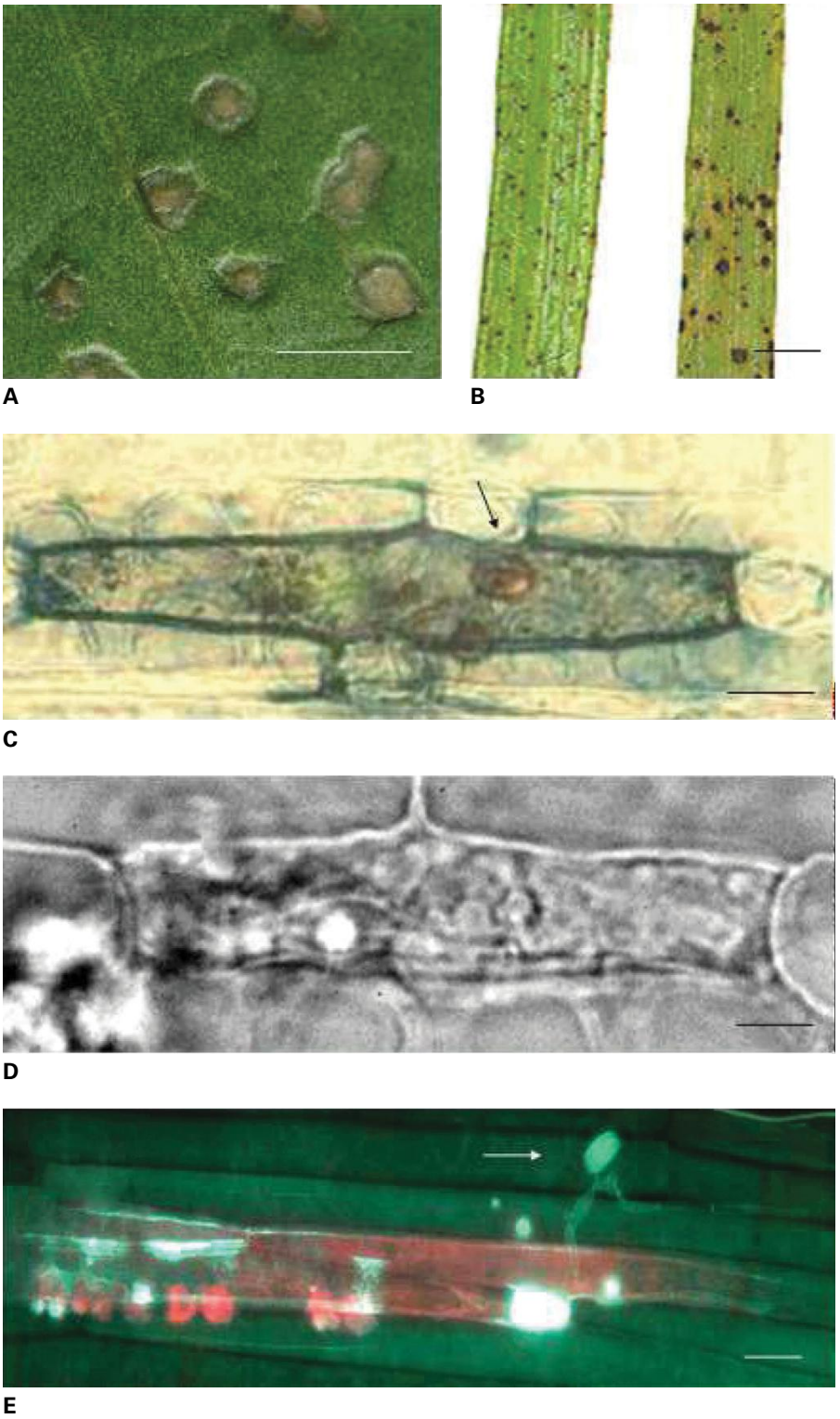


FIGURE 20.44 *Cell death during the HR. (A) HR elicited by tobacco mosaic virus (TMV) on resistant tobacco at 4 days after infection. Bar = 1cm. (B) HR-flecks on* Brachypodium distachyon *ecotypes ABR5 and ABR2 at 3 days following inoculation with the rice blast pathogen* Magnaporthe grisea *strain Guy-11. A dying* B. distachyon *ABR5 cell attacked by* M. grisea *Guy11 is shown, either (C) dyed with the vital stain trypan blue (infecting fungus arrowed) or (D) unstained to highlight disruption of cytoplasmic structure. Bars = 10 mm. (E) Increased autofluorescence in and around a HR exhibited by a single barley cell at 48 h following attack by the powdery mildew fungus* Blumeria graminis *(arrowed). Bars = 10 mm.*
Source: (B–D) Routledge et al. (2004). Mol. Plant Pathol. 5:253–265.

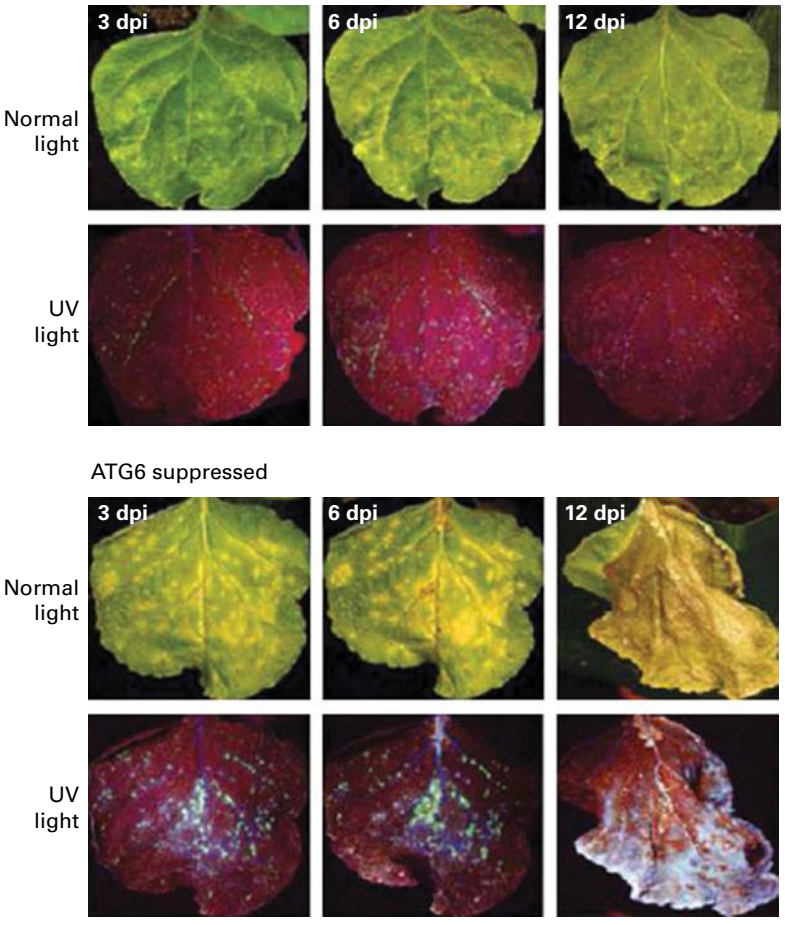


FIGURE 20.45 *Expression of the gene* ATG6 *(also known as* Beclin1*) confines the hypersensitive response. TMV-induced PCD was assessed in nonsilenced control and* ATG6/Beclin1*-silenced plants. Representative photographs of TMV were taken under visible and UV light. Note the spreading necrosis and green fluorescence under UV seen with the* ATG6*-silenced lines. The red color under UV arises from chlorophyll autofluorescence. Infection foci in leaves 12 days post inoculation (dpi) appear white under UV light due to cell death.*
Source: Liu et al. (2005). Cell 121:567–577.

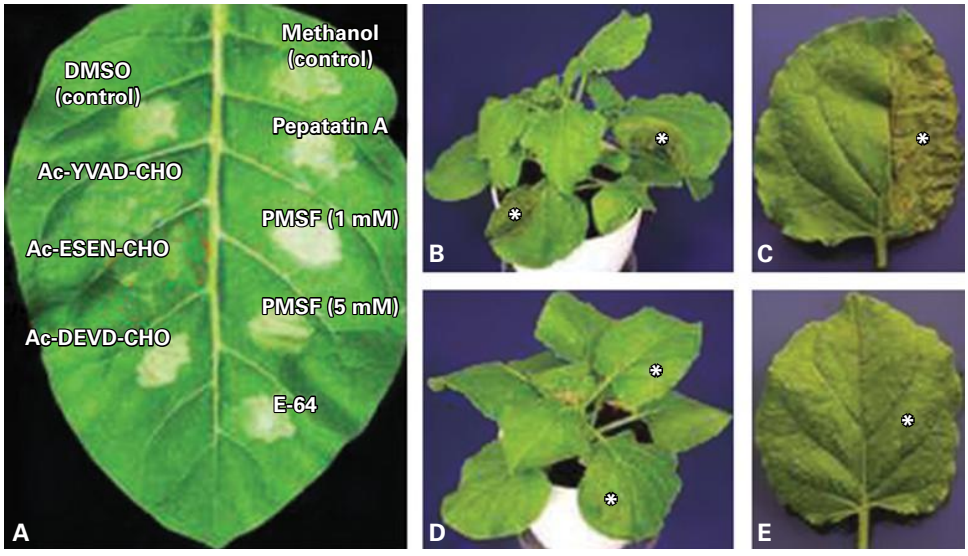


FIGURE 20.46 *The role of vacuolar processing enzymes (VPEs) in the initiation of the HR, shown by the effect of treatment with specific inhibitors and by gene silencing. (A) The HR induced by TMV in* N. tabacum *leaves is inhibited by a caspase-1 inhibitor (Ac-YVAD-CHO) and a VPE inhibitor (Ac-ESEN-CHO). The photograph was taken 24 hours after infection. (B,C) Nonsilenced and (D,E) VPE-silenced* N. benthamiana *plants were infected with TMV on halves of their leaves (*). The photographs of the plants and their leaves were taken 24 hours after inoculation.*
Source: Hatsugai et al. (2004). Science 305:855–858.

whose products are components of the killing process. Alternatively, mutants that display unexpected cell death are probably altered in genes that normally suppress cell death (Fig. 20.47).

Spontaneous cell death lesions have often been noted in crop species, such as maize where there are some 32 examples known. One is **l**ethal **l**eaf **s**pot 1 (*lls1*), which exhibits developmental and light-dependent cell death. Cloning and characterization of *lls1* shows that it encodes pheophorbide *a* oxygenase, a protein involved in cleaving the chlorophyll catabolite, pheophorbide (see Section 20.6.1). Damaging singlet oxygen may be generated when the intact tetrapyrrole ring of pheophorbide is excited by light. The *lls1* mutant accumulates pheophorbide because of the blockage at PaO, leading to cell damage and spontaneous light-induced lesions.

Some spontaneous lesion mutations are of great practical importance. In rice, spontaneous cell death was first associated with the Sekiguchi lesion (*sl*) mutant. The mutation underlying the *sl* phenotype has not been determined but this has not prevented its exploitation in agriculture, as it confers resistance against the devastating disease rice blast, caused by the fungus, *Magnaporthe grisea*. The *mlo* mutation of barley can lead to a tendency to form necrotic flecking on plants but it is widely used in spring barley cultivars as it confers long-lasting field resistance against powdery mildew.

It is, however, in *Arabidopsis thaliana* that the greatest efforts have been made to generate and characterize cell death mutants (Table 20.3). These are classified as either reduced cell death (RCD) or spontaneous death (SD) mutants. There are relatively few RCD mutants that exhibit greatly compromised cell death. Other RCD mutants have been isolated, but these are not listed in Table 20.3 as they have been linked either to an altered *R* gene or to situations where components immediately downstream of the *R* gene are abolished, such as *ndr1, pad4* and *eds1* (see Chapter 21). Such mutants still undergo non-HR forms of cell death, however, suggesting that only the triggering of the death program, rather than the program itself, is compromised.

Some SD mutants have likewise been linked to (presumably malfunctioning) *R* genes. For example, the *Rp1* gene in maize encodes resistance to the rust fungus *Puccinia sorghi*. Several alleles linked to a SD phenotype map to the *Rp1* locus. Further evidence for rogue *R* genes initiating cell death was found following a comprehensive crossing program involving large numbers of wild ecotypes of *Arabidopsis thaliana*. About 2% of these intraspecific crosses displayed a SD phenotype, and in at least one case the phenotype was linked to a disease resistance gene homolog interacting with a specific allele at a second locus.

Of the RCD mutants in which the killing components of the cell death program may be compromised, the *defense-no-death* (*dnd1, dnd2*) class (Table 20.3) are the best characterized. These are mutated in cyclic nucleotide gated channels located in the plasma membrane. These heterotrimeric ion channels facilitate cation fluxes of Ca^{2+}, K^+, or Na^+. The *dnd* class of mutants also exhibit highly activated defense responses but recent genetic analyses have indicated that

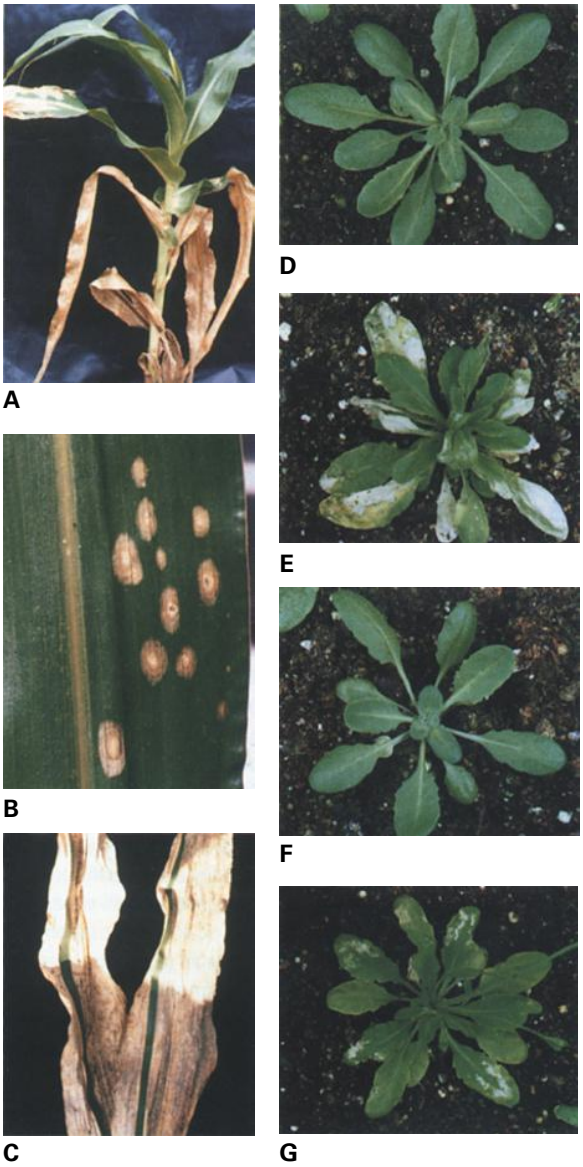


FIGURE 20.47 *Lesion-mimic mutants spontaneously develop areas of dead tissue, indicating a misregulation of the functions that control cell death. Lesion mimics have been identified in a wide range of plants, including maize (e.g.,* lls1*, left panels) and* Arabidopsis *(e.g.,* lsd *mutants, right panels). (A) Expression of the* lls1 *phenotype is developmentally regulated. Older leaves on the lower part of the plant are more severely affected, while younger leaves at the top are much less lesioned. (B)* lls1 *lesions can be triggered by mechanical wounding, such as pinpricks.* lls1 *is a propagation type of lesion mimic, which means that, once initiated, the lesion continues to spread across the leaf. The amount of cell death seen on this leaf exceeds that directly caused by the mechanical damage. (C) Revertant sectors remain green in this* lls1 *plant, showing that* Lls1 *function is cell-autonomous. (D)* lsd1-1*, a conditional lesion-mimicking mutant, remains healthy when grown under permissive conditions. (E) When shifted to nonpermissive conditions,* lsd1-1 *develops areas of dead tissue. Like* lls1*,* lsd1 *is a propagation type of lesion-mimicking mutant; the tissue death spreads out from the point of initiation until the whole leaf is dead. The mutant* lsd3 *is also conditional, as shown under permissive (F) and nonpermissive (G) conditions.* lsd3 *is an initiation type of lesion mimic, which means the lesions are determinate in size; once formed, they do not enlarge.*
Source: (A–G) Dangl et al. (1996). Plant Cell 8:1793–1807.

TABLE 20.3 *Lesion mimic and other cell death mutants of* Arabidopsis, *showing the range of genes, cell functions and signaling factors (where known) implicated in the corresponding PCD phenotypes.*

					Main associated signals					
		Allele	Gene product (where known)	Role (where known)	Ca^{2+}	ROS/$^1O_2$	Salicylic acid	Jasmonates	Ethylene	Sphingolipids
Reduced cell death (RCD) mutants		*dnd1*	AtCNGC2	Cyclic nucleotide-regulated ion channels			+	+	+	
		dnd2	AtCNGC4		+		+	+	+	
		executer1/2	Nuclear protein	Required for singlet oxygen-dependent death		+				
		Atrboh D/F	Plasma membrane component of NADPH oxidase	Generation of electron flow across membrane leading to ROS formation		+				
Spontaneous death (SD) mutants	Initiation class	*acd5*	Lipid kinase	—			+			+
		acd6	Ankyrin protein with transmembrane region				+			
		flu	Negative regulator of tetrapyrrole biosynthesis	Regulates Glu tRNA reductase, the first committed steps in tetrapyrrole biosynthesis		+				
		lsd2 to *lsd7*	—	—			+			
		cpr5	Transmembrane transporter	—			+	+	+	
		hrl1	—	—			+	+	+	
		cet1 to *cet4*	—	—				+		
		cpr22	Fusion of AtCNGC11/AtCNG12	Cyclic nucleotide-regulated ion channels	+		+			
		lin2	Coproporphyrinogen III oxidase	Chlorophyll biosynthesis		+				

(*continued*)

TABLE 20.3 (*continued*)

	Allele	Gene product (where known)	Role (where known)	Main associated signals					
				Ca^{2+}	ROS/$^1O_2$	Salicylic acid	Jasmonates	Ethylene	Sphingolipids
Propagative class	*acd1*	Pheophorbide *a* oxygenase	Chlorophyll catabolism		+				
	acd2	Red chlorophyll catabolite reductase	Chlorophyll catabolism		+				
	lsd1	Zn finger protein	Transcriptional activator		+				
	acd11	—	Sphingosine transfer protein						+
	vad1		Gram domain-containing protein			+		+	

these are not the cause of the failure to initiate cell death. Within the context of a HR, ion fluxes are crucial early events. Biochemical analyses have shown that the first indication of HR is the initiation of a H^+/K^+ exchange across the plasma membrane leading to alkalinization of the leaf apoplast. The importance of H^+/ K^+ exchange to initiation of cell death was shown when expression of a bacterial proton pump, *bO,* in transgenic plants initiated cell death. Ca^{2+} fluxes across the plasma membrane and from the ER and organelles into the cytoplasm represent a complex but important initiatory cell death pathway. Application of a range of Ca^{2+} inhibitors, coupled with imaging of Ca^{2+} in transgenic plant lines, has shown that cell death can be suppressed if Ca^{2+} fluxes are perturbed. One key effect of Ca^{2+} fluxes is to initiate the generation of ROS that can be directly toxic as well as having signaling roles.

SD mutants have also been called lesion-mimic mutants on the assumption that plants are acting as though under attack by pathogens to produce lesions analogous to the HR. Although this may be the case, cell death may also arise through loss of homeostatic function. In this context, it is relevant that HR is unaltered in many SD mutants. The SD category can be subdivided into mutants in which necrotic flecking does not spread and mutants that exhibit runaway cell death. Clearly, the former class could be altered in factors that suppress initiation of cell death (initiation class) while the latter could also be perturbed in factors that normally confine HR to the site of infection (propagative class). Unfortunately, molecular characterization of SD has revealed rather a diverse set of mutated loci that currently cannot be easily consolidated into a common mechanism (Table 20.3). Greater insights may be afforded from a consideration of defense signaling pathways that are active in each genotype. Mutants of the initiation class often display activation of SA, jasmonate, or ethylene-mediated signaling pathways, all of which are associated with HR. Activation of one or more of these pathways could be a key initiatory event. *vascular associated death1* (*vad1*) of *Arabidopsis* (Table 20.3) is a possible example of a propagative SD mutant, in which necrosis develops from the leaf veins. The *vad1* mutation has been mapped to a membrane-associated protein that is also induced during HR, and may represent a link between developmental and pathogen-induced cell death.

SD mutants of the *acd* class (Table 20.3) are characterized by their ***a**ccelerated **c**ell **d**eath* phenotype. The observation that a lipid, possibly ceramide, kinase is altered in *acd5* SD could be a mechanistic clue. In mammalian apoptosis, the accumulation of the sphingolipid ceramide is an important initiatory event that acts, in part, by perturbing mitochondrial function. In contrast, phosphorylated sphingolipids have anti-apoptotic roles so that a mutation in a lipid kinase protein could lead to a deficiency of phosphoceramides resulting in cell death. The identification of a sphingolipid transfer protein as a propagative class SD mutant (*acd11*) underlines the importance of this class of lipids in plant cell death. However, it should be noted that HR in the *acd5* mutant is apparently normal.

A well-characterized propagative cell death mutant in *Arabidopsis* is *lesions simulating disease 1* (*lsd1*; Fig. 20.48). Mutant plants exhibit a sensitized HR that is initiated at lower levels of inoculation with a wide variety of pathogens. The LSD1 protein is a Zn-finger protein that acts as a transcriptional activator and is known to regulate the expression of Cu/Zn superoxide dismutase and *CAT* genes; hence abolition of LSD1 function increases levels of ROS. LSD1 also physically interacts with LSD-ONE-LIKE 1 (LOL1) protein, which promotes cell death via an unknown mechanism. In line with a role for LOL1 in HR PCD, overexpression of *LOL1* in transgenic plants augments HR.

Also within the propagation class of mutants are *acd1* and *acd2* (Fig. 20.48), which are mutated in genes encoding two enzymes involved in the breakdown of chlorophyll catabolites (see Section 20.6.1). *acd1* is the *Arabidopsis* equivalent of maize *lls1*, being mutated in PaO, while the next enzyme in the catalytic pathway, RCC reductase, is perturbed in *acd2.* Both mutants resemble maize *lls1* in accumulating free photosensitizing tetrapyrroles in the chloroplast stroma, leading to production of harmful singlet oxygen in light. Similarly, abnormal overproduction of free tetrapyrroles, such as occurs in the SD mutant *flu* (*fluorescent*), leads to cell death. In this case, singlet oxygen cell death requires the participation of at least two nuclear proteins, EXECUTER 1 and 2, the products of RCD class genes (Table 20.3). The mechanism through which either EXECUTER protein acts is unknown.

20.10.4 ROS are triggers and participants in the HR death program

An early response to HR-eliciting pathogens is the generation of reactive oxygen species (ROS), consisting mainly of superoxide ($O_2^{\cdot -}$), hydrogen peroxide (H_2O_2) and the hydroxyl radical ($HO^{\cdot}$). Each species can act as an oxidant, causing significant damage to macromolecules and thus affecting cell viability. Unsurprisingly, the **oxidative burst**, a surge in ROS production that often occurs within hours of infection, has been implicated as initiating HR and cell death. Central to establishing this theory was the observation that cell cultures or intact plant tissue respond to exposure to $O_2^{\cdot -}$ or H_2O_2 by initiating an HR-like cell death. Further, the application of the ROS scavenging enzymes CAT or SOD could suppress HR. However, even after many years of investigating, the relative importance of either $O_2^{\cdot -}$ or H_2O_2 to initiation of HR remains debatable.

A series of ROS-generating complexes has been implicated as contributing to the oxidative burst; their relative importance and roles are still debated by plant scientists (Fig. 20.49). Most often ROS generation has been linked to an NADPH oxidase complex, which exhibits homology to membrane-associated components of NADPH oxidases in human neutrophils. This complex uses NADPH as an electron donor to generate $O_2^{\cdot -}$. Some mutants in NADPH oxidase genes in *Arabidopsis* (e.g., respiratory burst oxidase homolog, *Atrboh*;

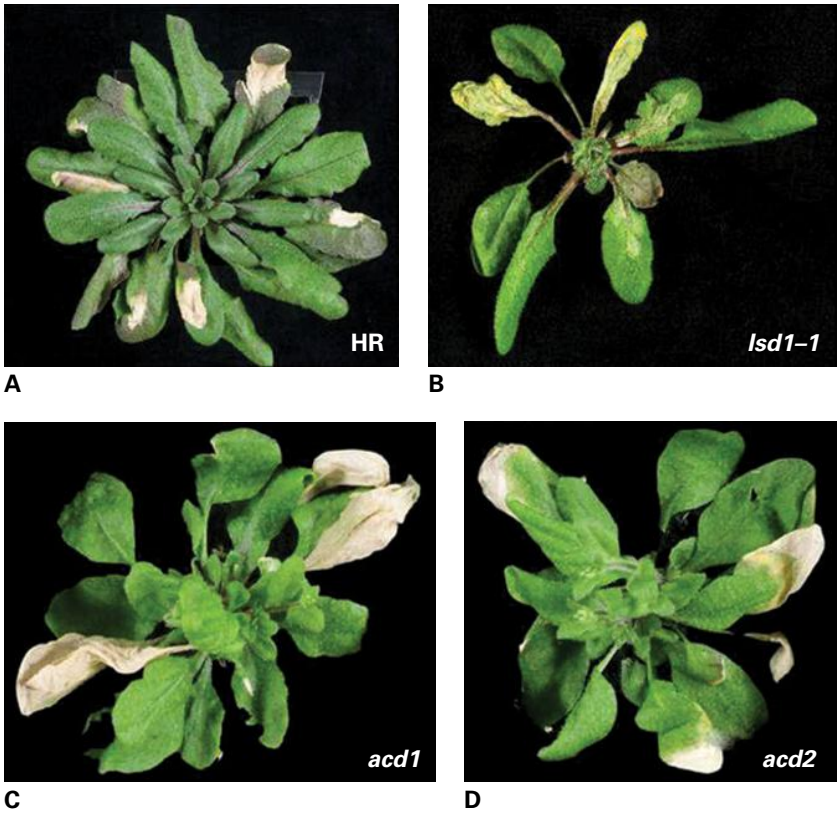


FIGURE 20.48 *HR and lesion mimic mutants of* Arabidopsis. *Lesion-mimic mutants spontaneously develop areas of dead tissue, indicating a misregulation of the functions that control cell death. Cell death in lesion mimics resembles that in the HR, and yields genetic insights into the regulation of the latter. (A) A HR initiated in* Arabidopsis *at 48 hours following infiltration with* Pseudomonas syringae *pv.* tomato *DC3000* avrRpm1. *(B) Spontaneous cell death in* lsd1-1, *which has been shown to influence the expression of antioxidant and cell death-promoting genes and to interact with metacaspase proteins which can either promote (AtMC1) or suppress cell death (AtMC2). (C)* acd1 *is a lesion in the gene encoding PaO (see Section 20.6.1). In* acd1 *pheophorbide builds up, which initiates cell death through the generation of singlet oxygen* $^1O_2$. *(D) RCC is reduced to form primary fluorescent chl catabolite (pFCC) by red chlorophyll catabolite reductase encoded by* ACD2. acd2 *null mutants exhibit cell death phenotypes through the accumulation of RCC and the generation of* $^1O_2$.

Table 20.3) have apparently reduced HR. Equally, however, such investigations have revealed ROS to have roles in cellular signaling not associated with cell death.

In neutrophils, the main role of NADPH oxidases is to increase the internal pH of hydrolytic vesicles called phagosomes within which invading pathogens have been phagocytosed. Similarly, the NADPH oxidase in plants may initiate the oxidative burst by changing the chemical environment to favor the activity of another demonstrated source of ROS, high-pH activated peroxidase. Other sources of ROS are the organelles: disruption of electron transport in mitochondria and/or chloroplast leads to the generation of ROS.

There are many mechanisms through which ROS could initiate cell death. One that has received much attention is lipid peroxidation. In this process hydrophilic moieties are introduced into lipid bilayers, leading to their disruption and the leakage of cytoplasmic contents. Indeed, increased electrolyte leakage is a widely used early marker for HR. Additionally, several of the breakdown products of bilayer phospholipid-derived products exhibit plant cell toxicity. There are a number of reports of significant lipid peroxidation during HR but there is considerable debate whether this occurs through oxidative damage or the activity of lipoxygenase (see Section 20.11.4). For example, suppression of lipoxygenase gene expression in *N. benthamiana* resulted in reduced cell death following challenge with *Phytophthora parasitica* var. *Nicotianae*.

In considering mechanisms by which ROS kill cells, the contribution of NO cannot be ignored. As well as an emerging role in various senescence and cell death processes in plants (see Sections 20.2.3 and 20.11.2), NO has now an established role in HR and may act in concert with ROS in cell death. NO may also act to suppress cell death, with these very different modes of action being dependent on the concentration of NO. A range of approaches has been used to measure NO production and has shown increased production to coincide with the oxidative burst, consistent with its supposedly supportive role in lipid peroxidation, Besides such correlative evidence, addition of NO scavengers or mammalian inhibitors of nitric oxide synthase (NOS) suppresses HR cell death in range of plant–pathogen interactions. Genetic evidence for a role for NO in HR was provided through the expression of a nitric oxide dioxygenase (NOD) in transgenic *Arabidopsis*. NOD catalyses the dioxygenation of NO to nitrate, and in NOD-expressing transgenic lines

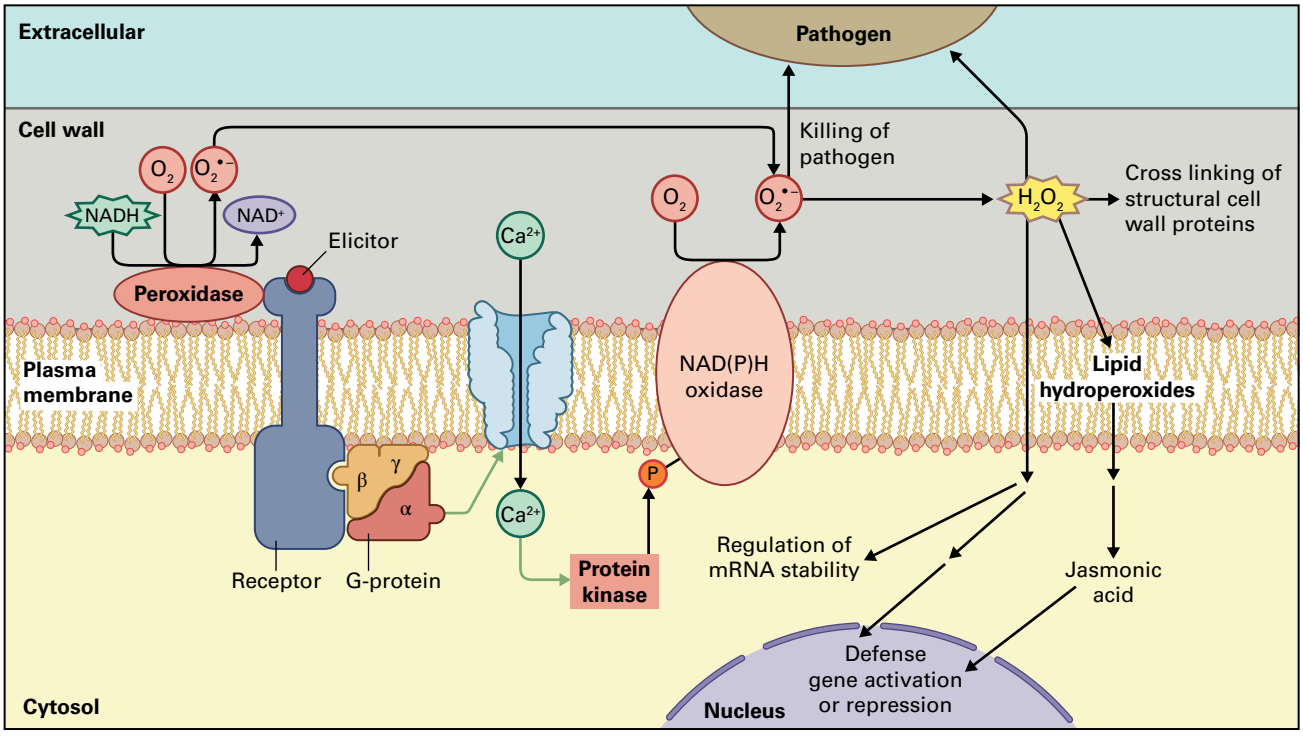


FIGURE 20.49 *Model postulating the relationship between pathogen attack and the production of ROS. Pathogen-derived elicitors interact with a receptor to initiate extracellular generation of ROS. Pathways to ROS generation are indicated. The receptor can activate NADH-dependent cell wall peroxidase, which reduces molecular oxygen (O_2) to superoxide ($O_2^{\cdot-}$) via an as yet poorly defined mechanism. Alternatively, the receptor may activate a heterotrimeric G-protein to initiate an influx of Ca^{2+}, which in turn stimulates protein kinase activity to turn on an NAD(P)H oxidase. Using NAD(P)H as a reductant, the NADPH oxidase generates $O_2^{\cdot-}$. $O_2^{\cdot-}$ can contribute towards killing the pathogen or else, in a low pH environment, forms H_2O_2. H_2O_2 can also aid in killing the pathogen or may be used as a cofactor in oxidative crosslinking of cell wall proteins, thereby restricting pathogen penetration of the host. H_2O_2, particularly if further reduced to form hydroxyl ($^{\cdot}OH$) radicals, will initiate membrane lipid peroxidation. This could be a step inducing the formation of the defense hormone, jasmonic acid. Equally, H_2O_2 can migrate through the membrane to act as an oxidative signal regulating defense gene expression.*

HR elicited by a bacterial pathogen showed reduced NO production and, crucially, delayed cell death. One important outstanding question is the mechanism through which NO is generated. Although mammalian NOS inhibitors can suppress NO production no plant NOS has been isolated. The NADPH-dependent reduction of nitrite by nitrate reductase is a likely alternative mechanism but nonenzymatic reduction of nitrite is also a potential source of NO (see Section 20.2.3).

20.10.5 Some plant pathogens cause necrosis of the host plant tissue

HR is not the only form of cell death associated with pathogenic challenge. In the case of attack by necrotrophic pathogens, which feed on dead tissue, host cell death and maceration is intrinsic to their pathogenic mechanisms. One such necrotrophic pathogen is the causal agent of grey mold, *Botrytis cinerea*, which is highly virulent on soft fruits (Fig. 20.50A) and a major source of reduced soft fruit yields. *B. cinerea* attacks not only the fruit but also the leaves of plants (Fig. 20.50B).

It may be surprising that necrotrophic pathogens induce PCD given that cell death in HR is often a mechanism to limit the spread of pathogens. It is clear, however, that initiation of HR actually aids *B. cinerea* pathogenesis. Indeed, microscopic examination shows that cells infected with *B. cinerea* exhibit cytoplasmic vesiculation and coagulation, a feature of HR (compare Fig. 20.44D with Fig. 20.50C). In necrotrophic attack, cell death is initiated not through recognition of an avirulence gene product, but through the action of a pathogen-derived toxin or enzyme. *B. cinerea* produces a series of botrydial and botcinolide toxins that, when applied to plants, cause chlorosis and light-dependent death. However, more important for *B. cinerea* are enzymes that degrade the cuticle. These serve two functions: to aid in host penetration and to induce the host to generate an oxidative burst elicited through cell wall fragments. Hence, the pathogen tricks the host into killing itself. However, *B. cinerea* must still withstand effects of ROS generation. Here it is likely that SOD plays a role, as knockouts in the *BcSOD1* gene exhibit reduced virulence. As cells start to die, a cocktail of pectolytic enzymes produced by the fungus helps macerate host tissue via non-PCD necrotic mechanisms as well as by supplying further PCD elicitors.

In other necrotrophic pathogens, toxins play a much more active role in initiating host cell death. A particularly well-characterized toxin, victorin, is produced by *Cochliobolus victoriae*. *C. victoriae* is the cause of Victoria blight in oats



A B



C

FIGURE 20.50 *Infection of plants with* Botrytis cinerea. *(A) Strawberry fruits at 7 days and (B)* Arabidopsis *leaves at 3 days following inoculation with* Botrytis cinerea. *Bar = 1cm. (C) Trypan blue vital staining of an infected* Arabidopsis *epidermal cell at 24 hours following infection. Bar = 50 mm. Source*: Photographs from L. Mur's own work, taken by T. Pugh.

(*Avena sativa*), and its pathogenicity is absolutely dependent on the production of victorin. Victorin is a host-selective toxin in that it requires interaction with an oat *Vb* allele. Application of victorin alone to *Vb* oats is an effective inducer of chlorosis and ultimately cell death and has become a well-characterized model for PCD (Fig. 20.51). Initial studies established that victorin binds to and inhibits the 100-kDa protein of glycine decarboxylase (GDC), an enzyme of photorespiration (see Chapter 14). Victorin also initiates proteolytic cleavage of Rubisco by an unidentified protease, making a return to normal carbon fixation impossible and encouraging the initiation of senescence. More exhaustive analyses have demonstrated that victorin induces many features classically associated with PCD, including DNA fragmentation and the initiation of PTP formation within mitochondria. PTP formation allows the entry of victorin to inhibit GDC as well as dissipating the mitochondrial membrane potential leading to a collapse in ATP generation. Crucially, the use of inhibitors has established that a key trigger for these victorin effects is the activation of host Ca^{2+} and ethylene signaling. Taken together, victorin appears to trigger host PCD in a manner that also includes facets of a senescence program. The next section considers further interplay between senescence and pathogenesis-related PCD in terms of the role of plant hormones.

20.11 Plant hormones in senescence and defense-related PCD

It is notable that initiation of a senescence-like chlorosis response is a feature common to many plant diseases. In the well-characterized bacterial pathogen *Pseudomonas syringae* pathovar (*P.s.* pv.) *tomato,* which can attack *Arabidopsis*, chlorosis is dependent on the toxin coronatine. Coronatine acts by exactly mimicking the action of jasmonates, which, although having a role in defense, can also contribute to initiation of chlorosis. Related bacterial phytopathogenic species provide

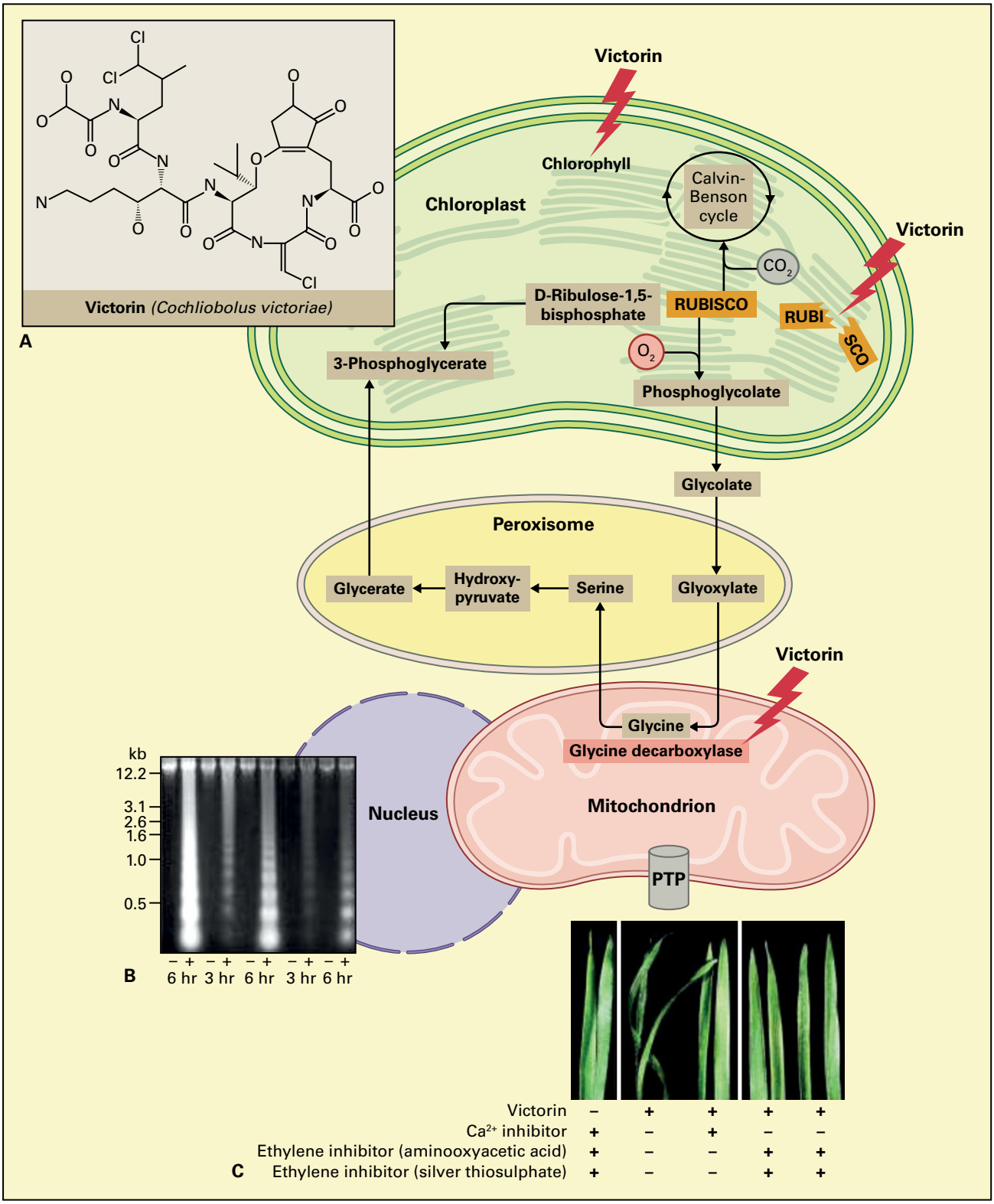


FIGURE 20.51 *Mechanism of victorin-induced PCD. The toxin victorin (A) is produced by the oat fungal pathogen* Cochliobolus victoriae. *(B) Treatment with victorin will cleave RUBISCO, initiate proteolytic chlorophyll catabolism and disrupt photorespiration by inhibiting glycine decarboxylase. Mitochondria are perturbed through the initiation of PTPs, leading to a dissipation of proton motive force. Within the nucleus, victorin initiates DNA laddering. (C) Victorin-initiated PCD can be suppressed by calcium and ethylene inhibitors.*
Source: Navarre & Wolpert (1999). Plant Cell 11:237–249.



FIGURE 20.52 *Wildfire disease and senescence in tobacco. (A) Wildfire disease symptom at seven days after infection caused by* Pseudomonas syringae *pathovar* tabaci. *The original site of infection, by this stage a necrotic area, is shown (arrowed 1). Note the spreading necrosis proceeding along the central vein, and large area of chlorosis (2). (B) A senescent tobacco leaf also displaying necrotic and chlorotic symptoms.*

other examples of toxins. In *Phaseolus vulgaris* pathogen *P. s.* pv. *phaseolicola*, chlorosis is elicited through the action of a tetrapeptide toxin, phaseolotoxin. This acts by inhibiting carbamoyltransferase within the ornithine cycle to block arginine biosynthesis. With the wildfire pathogen of tobacco, *P. s.* pv. *tabaci,* chlorosis is initiated by tab-toxin, a dipeptide that inhibits glutamine synthase resulting in a buildup of ammonia that disrupts photosynthesis and destroys thylakoid membranes. If wildfire symptoms on tobacco are compared with senescence in the same species, phenotypic similarities are immediately apparent (Fig. 20.52). Hence, current thinking suggests that pathogenic attack establishes a new sink within plants so that infected plant cells become a source of photoassimilates. Upon infection, there is a rapid reduction in photosynthetic electron flow but an increase in the production of hexose sugars, possibly arising from the mobilization of starch. There are also increases in cell wall invertase activities, which could supply sugars to pathogens located in the apoplast.

Equally, it is counterintuitive that, during the senescence phase of their life cycles, plants would offer a feast to potential invaders when resources should be allocated elsewhere, for example in seed filling. This may explain why bona fide senescence in plants is often associated with the initiation of plant defense, and why certain hormones to which senescence has been shown to be responsive, for example, jasmonates or salicylates, are also well-established mediators of resistance against pathogens. Here we discuss the roles of the major classes of plant growth regulators in senescence, PCD and pathogenesis.

20.11.1 Cytokinins act as senescence antagonists

Cytokinins appear to play a major role in regulating senescence by inhibiting the senescence process. Two lines of evidence initially suggested that cytokinins might function in blocking senescence. First, levels of endogenous cytokinins



FIGURE 20.53 *Green islands in leaf of* Prunus*, caused by infection with the necrotrophic fungus* Cercospora. *Original photograph by John L Stoddart and Howard Thomas.*

decrease in most senescing tissues. Second, exogenous application of cytokinins can cause a delay in senescence in most tissues. The effect of cytokinins varies with the age and type of tissue treated as well as from species to species. The ability of cytokinins to delay senescence has been exploited by some plant pathogens that infect leaves. Increased cytokinin levels in a zone surrounding the infection site causes delayed senescence in this tissue, producing "green islands," areas of green tissue in a background of senescing, yellowing leaf (Fig. 20.53). It is not clear whether the pathogen generates cytokinin directly or induces the plant to produce it.

Molecular techniques have been used to examine the role of cytokinins at various stages of plant development, including senescence. The *ipt* gene from *Agrobacterium tumefaciens* encodes the enzyme isopentenyltransferase, which catalyzes a limiting step in cytokinin biosynthesis (see Chapter 17). This bacterial gene has been used to generate transgenic plants that overproduce cytokinins. The *ipt* gene has been fused to a variety of promoters to enhance tissue-specific expression and produce localized areas with high concentrations of cytokinins. In all cases, delayed senescence was seen in the parts of the plant that had highest cytokinin levels. Elevated levels of cytokinin caused by the overexpression of the transgene led to other phenotypic

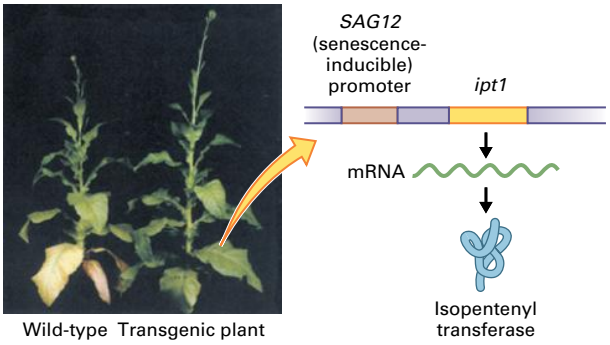


FIGURE 20.54 *Autoregulated expression of a cytokinin biosynthesis gene in tobacco results in delayed leaf senescence in the transgenic plant (right) in comparison with the wild-type plant (left). The* Agrobacterium tumefaciens *gene encoding isopentenyltransferase* (ipt1)*, an enzyme that catalyzes the synthesis of cytokinin, was fused to the promoter of* SAG12*, a gene specifically expressed in senescing tissue. Expression of this fusion gene in transgenic tobacco is induced when a leaf begins to senesce. The resulting increase in cytokinin content blocks leaf senescence.*
Source: Gan & Amasino (1997). Plant Physiol. 113:313–319.

abnormalities as well, making it difficult to determine if the delay in senescence was due directly to high cytokinin levels or to some secondary effect. When plants containing the *ipt* gene fused to a heat shock promoter were given a heat treatment to induce transgene expression delayed leaf senescence correlated with elevated levels of cytokinins. These results are somewhat complicated by the fact that the heat treatment required to induce expression via the heat shock promoter is in itself a form of stress that may affect the senescence program.

In an elegant refinement of these experiments, *ipt* was fused to the promoter of *SAG12*, a gene specifically expressed in senescing *Arabidopsis* leaf tissue. Tobacco (*Nicotiana tabacum*) plants transformed with the *SAG12* promoter-*ipt* fusion produce cytokinin in an autoregulated fashion (Fig. 20.54). As tissue starts to senesce, the transgene is induced, and cytokinins are produced. Cytokinins inhibit senescence, which in turn decreases expression of the transgene. Cytokinin is produced only in senescing tissue, and only in the amount needed to block senescence. Plants expressing *SAG12-ipt* have no significant morphological differences from the untransformed plants but do show a significant delay in leaf senescence, with older leaves retaining photosynthetic activity longer than leaves of control plants lacking the transgene (Fig. 20.54). These experiments have been repeated in many plant species, including food crops, and demonstrate that production of cytokinins in leaves can result in delayed senescence. One consequence of longer photosynthetic life span of leaves on these plants is a concurrent increase in the number of seeds produced. Remarkable improvements in drought tolerance have also been observed. The practical implications for agriculture are obvious.

One possible explanation for the senescence-delaying effects of cytokinin is their enhancement of sink activity. Tissues with the highest cytokinin levels are the strongest metabolic sinks, thus the majority of nutrients are directed to them. Cytokinins are normally produced in roots and transported to leaves. One hypothesis to explain leaf senescence post-flowering suggests that, in many plants, cytokinins from the root are redirected into the developing seed instead of into leaves. The seed, therefore, becomes a stronger sink and nutrients are diverted from leaves into seeds, triggering leaf senescence. Extracellular invertase, which is associated with apoplastic phloem unloading, is of particular significance for source–sink interactions in cytokinin function. Inhibiting extracellular invertase also results in the inhibition of cytokinin-mediated delay of leaf senescence.

Recent work has identified an important role for a cytokinin receptor, the histidine kinase AHK3, in controlling the response of leaf senescence and other developmental processes to cytokinin. A loss-of-function mutant of *AHK3* in *Arabidopsis* is alone among the known cytokinin receptors in conferring reduced sensitivity of leaf senescence to applied cytokinin, but the timing of natural leaf senescence is not affected. On the other hand, the gain-of-function *AHK3* *Arabidopsis* mutant *ore12-1* (see Section 20.5.2) shows delayed leaf senescence. The action of AHK3 is mediated by phosphorylation of ARR2 (**A**rabidopsis **R**esponse **R**egulator 2), which is essential for determining leaf longevity.

Cytokinin may influence the course of senescence by repressing the expression of key *SAG*s. Among a group of genes observed to be upregulated when *Petunia hybrida* callus cultures are transferred to low-cytokinin medium is a gene encoding a cysteine protease and one encoding a peroxidase. Expression of these two genes is strongly enhanced in senescing leaves. Upregulation of the protease gene *See1* in maize and *Lolium multiflorum* has also been shown to be suppressed by cytokinin treatment. It seems likely, therefore, that cytokinins act at two levels: at a distance by promoting differentiation and strong sink activity, and locally in senescing cells by mediating the launch of the senescence program.

The dual action of cytokinins is seen most dramatically in regreening (Fig. 20.55). At flowering the lowest, oldest leaves of a mature plant of *Nicotiana rustica* are almost completely yellow. If the shoot is cut off just above the lowest node and the plant kept in dim light, leaves will gradually regain their green color. This process is greatly accelerated if the leaf is treated with cytokinin solution. During regreening, expression of *SAG*s is suppressed, genes for plastid assembly are turned on, gerontoplasts of the yellow leaf redifferentiate into chloroplasts and photosynthetic activity returns. Not only is this a demonstration of the potency of cytokinin as an anti-senescence factor, it shows that leaf senescence is potentially reversible to an advanced stage and thus fundamentally distinct from other PCD processes.

20.11.2 Ethylene acts primarily as a promoter of senescence

Among the known plant hormones, ethylene is typically the strongest promoter of senescence. Treatment with exogenous ethylene can induce senescence of leaves and flowers and

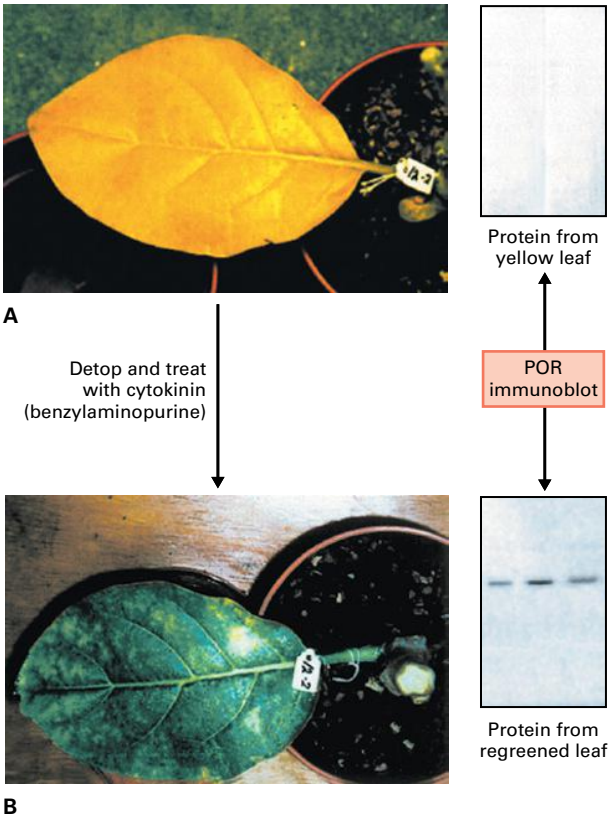


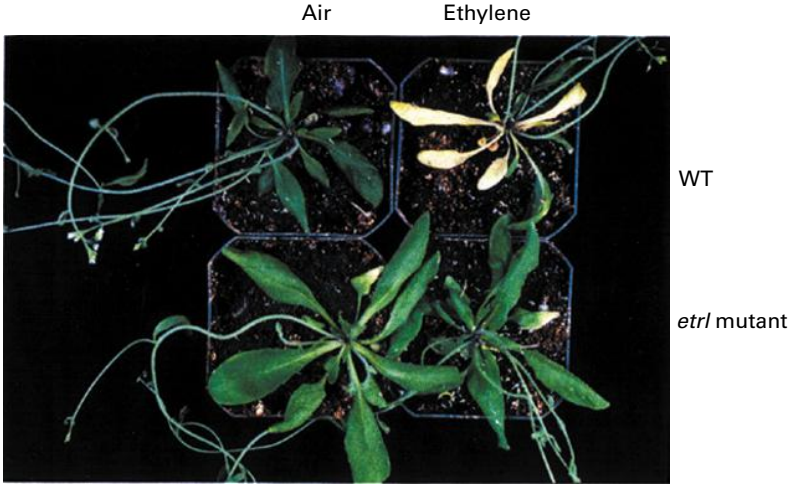
FIGURE 20.55 *Regreening in tobacco. Nothing illustrates the fundamental distinction between senescence and many other kinds of PCD better than reversibility. (A) The most basal (oldest) leaf on a flowering* Nicotiana rustica *shoot has lost nearly all measurable chlorophyll. However, the leaf can recover full greenness (B) if the stem is removed at the node, particularly if the leaf is treated with the synthetic cytokinin benzylaminopurine. Even terminally senescent tobacco leaf cells can redifferentiate their gerontoplasts into functional chloroplasts. Proteins characteristic of chloroplast assembly in very young cells—such as the chlorophyll synthesis enzyme protochlorophyllide oxidoreductase—are re-expressed.*
Source: Zavaleta-Mancera HA (2000) Regreening of senescing *Nicotiana* leaves. PhD Thesis, University of Wales.

ripening of fruits in many, but not all, plants. For example, treatment of *Arabidopsis* leaves with ethylene causes changes that parallel those seen in naturally senescing leaves (Fig. 20.56). Leaves begin to yellow, and there is a corresponding decrease in expression of photosynthesis-related genes along with an increase in expression of *SAG*s. Furthermore, endogenous ethylene levels correlate with leaf senescence. As leaves get older, or are induced to senesce by dark treatment, they produce more ethylene.

For many plants, pollination triggers floral senescence. Ethylene production in *Petunia hybrida* can be detected within 20 minutes of pollination, preceding penetration of the stigma by the pollen tube (Fig. 20.57). Thus, the recognition of pollen by stigma may be sufficient to induce ethylene production. In contrast, there are also cases in which normal flower senescence is essentially insensitive to ethylene. Lilies of the genus *Alstroemeria,* widely used as cut flowers, are among the best-known examples of ethylene-insensitive floral senescence.

Because of its economic importance, much of the work on ethylene regulation of senescence has been done in the context of fruit ripening. During normal development of climacteric fruit such as tomato there is a developmentally regulated burst of respiration and ethylene production, followed by an increase in the expression of specific genes encoding enzymes such as polygalacturonidase that contribute to the softened-tissue phenotype associated with ripening. Linked to this are changes in fruit color and flavor that characterize ripening. The effectiveness of exogenous ethylene as a ripening agent has been known for over a century, and controlled exposure to ethylene is still a major factor in the successful marketing of many fruits. Further evidence for the critical role of ethylene in senescence comes from experiments designed to test whether ethylene perception is required for senescence. The *Arabidopsis etr1* mutant (see Fig. 20.56) and tomato *never ripe* (Fig. 20.58) are insensitive to ethylene due to mutations in an ethylene receptor protein. These plants show delayed leaf senescence and, in the case of tomato, normal senescence of floral organs is delayed as well. *never ripe* fruits do not fully ripen, giving the tomato mutant its name.

FIGURE 20.56 *Ethylene promotes leaf senescence in wild-type (WT)* Arabidopsis*, but not in the ethylene-insensitive* etr1 *mutant.*
Source: Bleeker, University of Wisconsin, Madison; previously unpublished.



Experiments to reduce ethylene production in plants have provided more evidence for the role of ethylene in senescence. Chemical inhibitors of ethylene biosynthesis or action have been shown to inhibit fruit ripening and leaf senescence. Similar results have been obtained with plants engineered to produce reduced levels of ethylene. ACC synthase and ACC oxidase catalyze the last steps in ethylene biosynthesis in plants. Tomato plants expressing these genes in the antisense orientation exhibit greatly reduced ethylene levels. When these plants are grown in air, their fruit never completely ripen and leaf senescence is delayed, but they show normal senescence and ripening when treated with exogenous ethylene (Fig. 20.59).

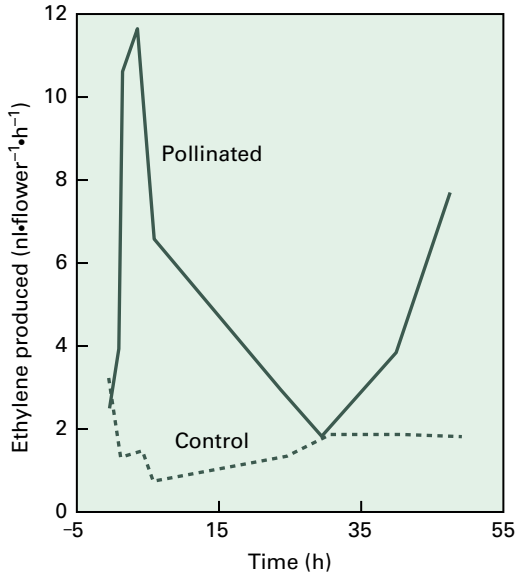


FIGURE 20.57 *Ethylene production by unpollinated control and pollinated* Petunia hybrida *flowers. Note the burst of ethylene synthesis that rapidly follows application of pollen.*

It should be noted that the role of ethylene can be somewhat different in different organs, even within the same plant. In ethylene-insensitive mutants of *Arabidopsis* and tomato, leaf senescence is delayed, but leaves eventually senesce even in the absence of ethylene perception. However, fruits of ethylene-insensitive tomato mutants never fully ripen. Therefore, ethylene promotes but is not essential to senescence in leaves, whereas it is an absolute requirement for tomato ripening. Finally, ethylene does not act alone to promote senescence. Age-related factors not yet identified are also important in regulating senescence, and treatment of leaves, flowers and fruits with ethylene is effective in inducing the senescence program only if various organs have reached the appropriate developmental stage. In addition, tomato plants engineered to overproduce ethylene show no altered leaf senescence phenotype, again suggesting that ethylene alone is not sufficient to trigger senescence.

Ethylene effects on senescence are antagonized by NO. In unripe strawberry and avocado (*Persea americana*) NO levels are high and ethylene levels low, a condition which is reversed during ripening. Transgenic *Arabidopsis* expressing a NO-degrading dioxygenase (NOD) exhibit a senescence-like phenotype with associated increases in many senescence-associated and ethylene biosynthesis genes. If NOD plants were gassed with NO, the senescence phenotype was suppressed. A possible mechanism through which NO could suppress ethylene synthesis was revealed by a proteomic study focusing on protein S-nitrosylation, where NO is covalently attached to cysteine thiol groups. Among the S-nitrosylated proteins identified was *S*-adenosylmethionine (SAM) synthetase that forms part of the ethylene biosynthetic cycle. S-nitrosylated SAM synthetase exhibited suppressed enzyme activity and therefore, in presence of NO, ethylene production is likely to be reduced.

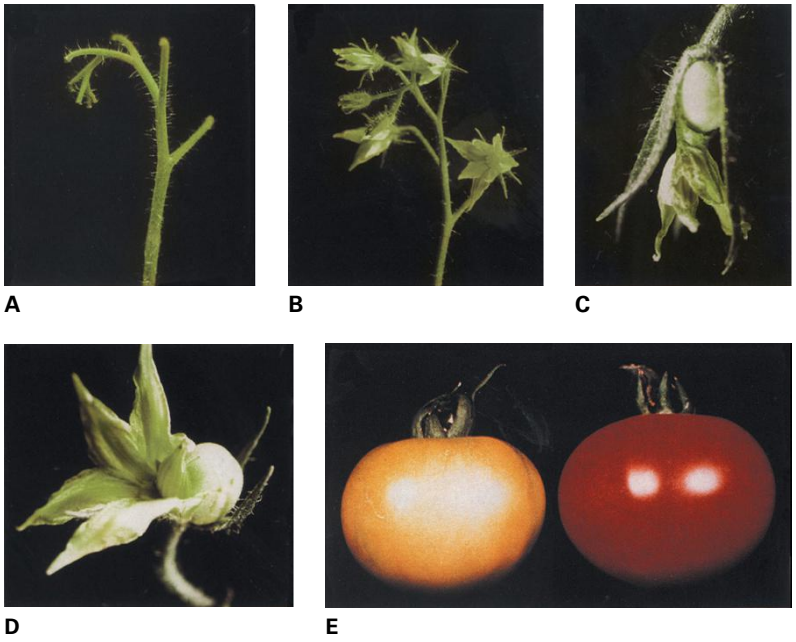


FIGURE 20.58 *In wild-type tomato, treating the inflorescence with ethylene causes the flowers to senesce and abscise (A). An ethylene receptor mutant,* never ripe*, is insensitive to ethylene, so that treatment of a* never ripe *inflorescence does not trigger senescence and abscission (B). In untreated wild-type flowers, floral senescence follows pollination (C), whereas* never ripe *flowers do not senesce after pollination but instead remain intact, even as the fruits begin to develop (D). As the name implies, fruits of the* never ripe *mutant do not ripen, as illustrated by* never ripe *and wild-type tomato fruits of approximately the same age and grown under the same conditions (E). Thus, in tomato ethylene is a key signal in inducing floral senescence after pollination as well as fruit ripening.*
Source: (A–E) Lanahan et al. (1994). Plant Cell 6:521–530.

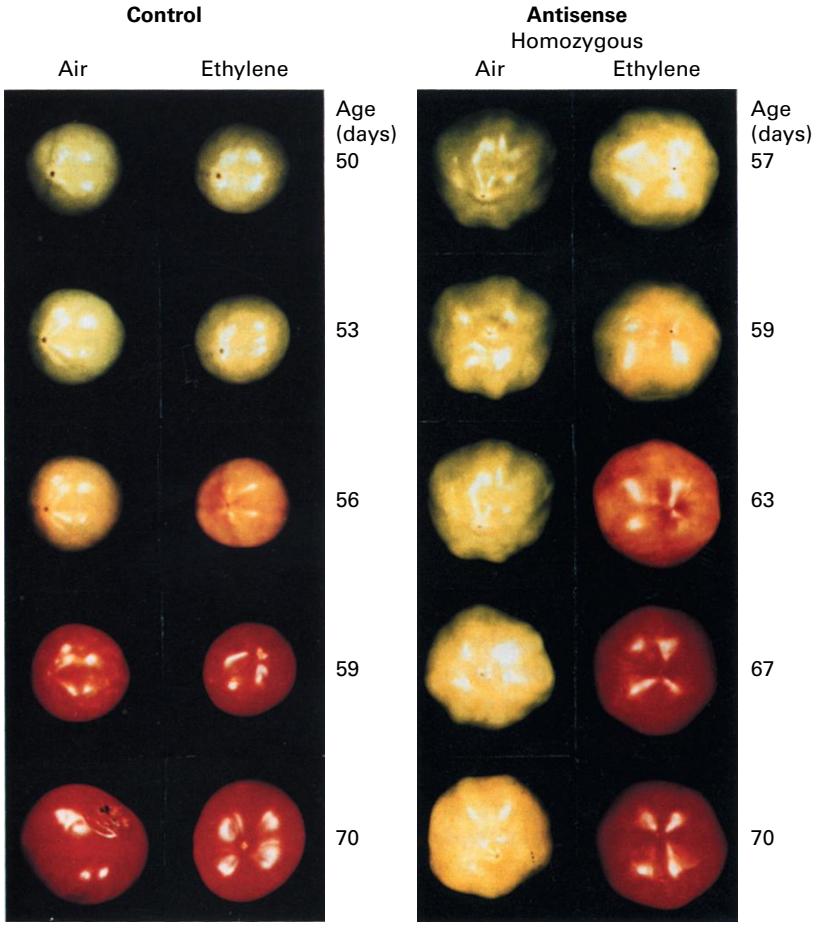


FIGURE 20.59 *Tomato fruits require both ethylene and unknown age-dependent factors for normal ripening. Fruits from wild-type control plants (left panel) maintained in air or in air supplemented with ethylene ripen at roughly the same time. Tomato plants expressing the ACC synthase gene in the antisense orientation (right panel) produce markedly less ethylene than do wild-type plants, and their fruits do not ripen when maintained in air but do ripen normally when kept in air with added ethylene. These results demonstrate two points. First, ethylene is necessary for tomato fruit ripening. In the plants that produce little ethylene, the fruit do not ripen unless they are treated with exogenous ethylene. Second, ethylene alone is insufficient to induce ripening. For example, ethylene does not induce ripening in fruits from wild-type plants that are less than 59 days old.*
Source: Theologis et al. (1993) Dev. Genet. 14:282–295.

20.11.3 Salicylic acid is a key component of signaling pathways in some forms of PCD

The hormone SA was first described as an important mobile signal in establishing systemic acquired resistance to pathogen attack within days of the initial hypersensitive response (HR; see Section 20.10). Subsequently it has become clear that SA may not be the most important systemic signal, but it has emerged as playing a major role in setting the kinetics of HR and also in conferring tolerance to heat stress and suppressing plant growth in response to chilling. The expression of many genes has been shown to be influenced by SA, including those encoding acidic forms of PR proteins and the class of small molecular weight heat shock proteins. The PR protein gene *PR1* has been particularly useful for mapping the SA signaling pathway. In particular, characterization of the non-PR expressing mutant *npr1-1* (see Section 20.8.2) has revealed a key transcriptional regulator of SA-mediated effects. Under nonstressed conditions *NPR1* exists in the cytoplasm in oligomeric form, but with oxidative stress *NPR1* monomers are liberated, aided by thioredoxins. *NPR1* monomers are targeted to the nucleus where they interact with activators of *PR1* gene expression. *NPR1* also binds to *WRKY53*, an important transcriptional regulator of senescence.

Interaction of SA with oxidative stress is essential for its action. Moreover SA acts to augment oxidative stress. Such potentiation of the oxidative burst by SA has been shown to occur during pathogen-elicited HR and responses to heat stress. In both cases the SA-ROS interaction is essential for full resistance/tolerance to be exhibited. The mechanism(s) of SA-augmented oxidative stress remain to be defined completely, but they include disruption of mitochondrial electron transport.

SA also has a role in leaf senescence. In a microarray experiment comparing senescence in wild-type *Arabidopsis* to that in *npr1* and in a transgenic line expressing *NahG* (a bacterial gene which degrades SA to catechol), expression of many *SAG*s, including *SAG12*, is suppressed (Fig. 20.60). Phenotypically, *NahG* transgenic plants and *npr1* mutants show delayed yellowing and reduced necrosis, indicating that SA acts mainly in the death phase of senescence.

20.11.4 Some evidence suggests roles for jasmonates in senescence

Jasmonates, a large group of signal molecules that includes jasmonic acid (JA) and related compounds (see Chapter 17), are derived from the acyl chains of membrane phospholipids. Lipoxygenase enzymes catalyze the dioxygenation of

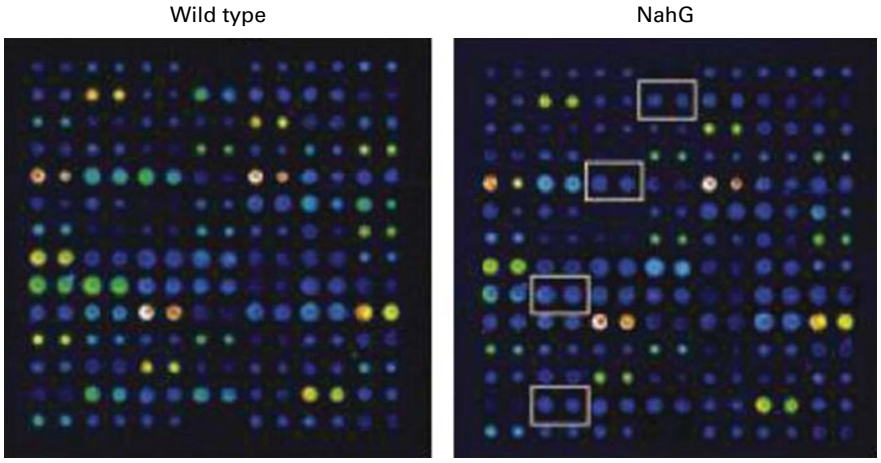


FIGURE 20.60 *cDNA microarrays illustrate the impact of salicylic acid (SA) on senescence-related gene expression in wild-type* Arabidopsis *and a transgenic line expressing the bacterial* NahG *gene, whose product degrades SA to catechol. cDNAs for senescence-enhanced and control genes were spotted onto glass slides and probed with first-strand cDNA made from RNA isolated from wild-type or* NahG *plants. Intensity of fluorescence correlates to levels of expression, with white the highest, followed by red, orange, yellow, green, turquoise, bright blue, and dark blue. Most genes are expressed at the same level in both plants, but some* SAGs *are suppressed in the* NahG *plants (see boxes).*
Source: Buchanan-Wollaston et al. (2003) Plant Biotechnol. J. 1:3–22.

polyunsaturated fatty acids in lipids, leading to the formation of oxylipins, the group of biologically active derivatives to which jasmonates belong. Oxylipins in general, and jasmonates in particular, came to prominence when it was established that they play a central role in defenses against insects. There is growing evidence in favor of many developmental functions for oxylipins, including regulation of senescence. For example, suppression of phospholipase or acyl-hydrolyase activity has been shown to delay senescence, and increases in lipoxygenase activity are characteristic of senescence. The role of jasmonates themselves in senescence is unclear. Levels of JA increase during senescence in detached *Arabidopsis* leaves, and senescence is perturbed in the JA-insensitive mutant *coi1*, which is altered in a key signaling component. On the other hand, normal developmental senescence is unaffected in *coi1*. Further work is required to clarify the role of jasmonates in senescence.

20.11.5 Additional hormones influence defense responses and senescence

ABA acts in most situations as a promoter of senescence. While leaf abscission is clearly related to senescence, and exogenous ABA can often cause yellowing in leaves, there is no consistent correlation between endogenous ABA levels and tissue senescence. During senescence there is generally an increase in expression of genes encoding enzymes of ABA biosynthesis, including 9-*cis*-epoxycarotenoid dioxygenase and aldehyde oxidase, and of the ABA-inducible receptor-like kinase gene *RPK1*.

Some of the possible links between ABA and senescence appear contradictory. ABA is reported to promote accumulation of H_2O_2 in leaf tissues, though it is not clear whether this is a cause or effect of accelerated senescence. At the same time, ABA has also been observed to enhance gene expression and enzyme activity for SOD, APX, and CAT. Furthermore, ABA induction of senescence was suppressed in transgenic lines where the activity of phospholipase was reduced. This suggests that membrane perturbation, which may or may not depend on oxidative stress, is important for the action of ABA on senescence. A known interaction between ABA and ROS has been revealed in the tomato ABA mutant *sitiens*. In this mutant, compromised ABA signaling leads to increased H_2O_2 generation, cell death and resistance following attack by the necrotrophic pathogen *Botrytis cinerea*. This suggests a role for ABA in suppressing defense—including cell death—against pathogens. Similarly, in the case of *Pseudomonas syringae*, a bacterial virulence effector, *AvrPtoB*, is delivered into the cytoplasm and specifically activates ABA signaling, again to suppress defenses. In short, ABA effects are strongly context-specific. For example, the capacity of ABA to immortalize isolated aleurone cells (Section 20.2.2) suggests a function in regulating the balance between the maintenance of viability during senescence and the subsequent onset and execution of terminal PCD processes.

Other hormones have been shown to contribute to senescence. Gibberellins (GAs) usually retard senescence, but this is by no means a universal response. For example, in *Arabidopsis* GA has been noted to repress the effects of the anti-senescence hormone cytokinin. This may be mediated by the gene *SPINDLY* (*SPY*) because *spy* mutants, besides exhibiting a constitutive GA phenotype, do not respond to exogenously applied cytokinin by delaying senescence. In most cases, treatment with exogenous auxins delays senescence, but there are also species in which such treatments promote senescence. Attempts to correlate levels of endogenous auxin or GA with senescence have been inconclusive.

Summary

Mechanisms of senescence and cell death in plants share some features with PCD processes in other organisms, but the ways in which they are regulated, integrated into development and responsive to the environment are distinctive. The fate of most plant cells is sooner or later to undergo autolysis, following one of several possible routes. These routes include lysigeny (with or without schizogeny), autophagy, transdifferentiation, hypersensitive cell death, or necrosis. There are common factors between these different outcomes, for example, activation of macromolecular hydrolysis and oxidative metabolism, but also many nonoverlapping functions. These provide plants with versatile options for dealing with the challenges of a sedentary lifestyle.

Despite rapid advances in our understanding of plant PCD, many major unknowns remain. To what extent is the picture established for model species, notably *Arabidopsis*, applicable to plants in general (and crop species in particular)? How are cell death and senescence processes switched on at the molecular level? What are the biochemical and regulatory mechanisms of nutrient recycling? To what extent are PCD, senescence, maturation, ripening, lifespan and ageing related and can understanding such relationships offer the prospect of controlling these critical biological processes? Among the new approaches that are being employed to answer these questions are the tools of Systems Biology, the study of micro-RNAs and epigenetics and the application of modeling techniques and phenology. The objectives of the next period of research effort will include breaking down PCD and senescence into subprocesses and quantifying their contributions to development, fitness, and productivity. This will involve physiological, biochemical, and "omics" analyses and comparative studies to establish read-across between plant models and other species. Ultimately the practical aim is to pinpoint the genes that will make a difference when manipulated, allowing development, longevity, fitness, and crop performance to be predicted and controlled.



V

PLANT ENVIRONMENT AND AGRICULTURE



21

Responses to Plant Pathogens

Kim E. Hammond-Kosack and Jonathan D. G. Jones

Introduction

Plants must defend themselves continuously against attack from bacteria, viruses, viroids, fungi, oomycetes, protists, mycoplasmas, invertebrates, and even other plants. In vertebrate immune systems, specialized cells devoted to defense are rapidly mobilized to the infection site, where they either kill the invading organism or limit its spread. In contrast, plant cells have both preformed and inducible defenses, and these cell-autonomous plant defenses prevent most infections. Indeed, in wild plant populations, most plants are healthy most of the time; if disease does occur, it is usually restricted to only a few plants and affects only a small amount of tissue. Disease, the outcome of a successful infection, rarely kills a plant. Natural selection likely acts to curtail pathogen lethality; those pathogens that keep a host species alive longer may achieve more reproduction.

Interactions between plants and pathogenic organisms have been the subjects of intensive research for at least five main reasons. First, a detailed understanding of plant–pathogen interactions should provide sustainable solutions for the control of crop diseases. Crop monocultures are vulnerable to severe disease epidemics that can lower both crop yield and quality and diminish the safety of our food supply (Fig. 21.1 and Box 21.1). Disease control using agrochemicals increases energy consumption, environmental pollution, and the cost of production. Second, studies of plant–pathogen interactions can reveal signaling mechanisms by which plant cells cope with biotic stresses. For example, do defense signaling mechanisms triggered by pathogen invasion differ from those provoked by wounding, low or high temperature, high salinity, desiccation, or waterlogging? Third, studying plant–microbe interactions in general reveals how organisms from different kingdoms communicate with one another. What type of messages do they exchange, how and where do these exchanges occur, and how are appropriate responses on both sides activated? Fourth, understanding plant–pathogen interactions leading to disease can illuminate how other organisms co-exist within a plant without causing damage, and how symbiotic organisms establish beneficial interactions with plants. Fifth, host–parasite and host–symbiont interactions provide fascinating insights into evolution.

This chapter examines the molecular mechanisms by which plants defend themselves from attack by microbial and viral pathogens and invertebrate pests. It also covers how pathogenic organisms may have evolved and the strategies they use for invasion of plant tissue.

21.1 Pathogens, pests, and disease

Pathogens and pests have coevolved with plant hosts since long before the domestication of crop plants. A **plant pathogen** is any organism that completes a part or all of its life cycle inside the plant, often with detrimental effects. A **plant pest**, on the other hand, is a herbivorous insect, nematode, mammal, or bird that eats vegetative tissue, fruits, and seeds.

Biochemistry & Molecular Biology of Plants, Second Edition. Edited by Bob B. Buchanan, Wilhelm Gruissem, and Russell L. Jones.
© 2015 John Wiley & Sons, Ltd. Published 2015 by John Wiley & Sons, Ltd.
Companion website: www.wiley.com/go/buchanan/biochem



FIGURE 21.1 *The floral tissues of hexaploid wheat (*Triticum aestivum*) severely infected with the ascomycete fungus* Fusarium graminearum *and other cereal-attacking* Fusarium *species. Referred to as* Fusarium *head blight,* Fusarium *ear blight, or head scab, this disease is a threat to global wheat crops. Wheat spike infections take place at crop anthesis if wet weather prevails, leading to premature bleaching and senescence of floral tissues (left). Infected wheat grains are small, shriveled, and show a pink coloration (lower right) compared to the plump grains recovered at harvest from a healthy wheat ear (upper right). Several mycotoxins produced by cereal-infecting* Fusarium *species are harmful to both human and animal consumers. Source*: Beacham et al. (2009). The Biologist 56:98–105.

Three scenarios can explain the origin of pathogens. First, when plant ancestors emerged onto the land from the oceans, they may have brought parasites with them. Second, ocean-dwelling species, upon arrival on dry land, may have evolved from a free-living existence to a pathogenic lifestyle. Third, the arrival of the new land-dwelling species and the emergence of non-motile, plant-based communities may have provided new niches for existing pathogenic species to either switch or expand their host range. These evolutionary steps occurred many millions of years ago and resulted in a continuum of intimate associations between land plants and other species (Fig. 21.2).

The onset of agriculture approximately 10,000 years ago shifted the relationship between the few (<30) domesticated species and their pests and pathogens. During crop domestication, agricultural practices became more mechanized and intensive. The size, density, and genetic uniformity of crop populations expanded, as yields and product quality increased to meet rising human and domestic animal needs. Today, on the 10.5% of the planet's surface where crop agriculture is practiced, large areas are occupied by **monocultures** of millions of genetically identical crop plants. These monocultures favor the selection of genetic variants of pathogens and pests that can overcome the defense mechanisms of the host genotype. When a genetic variant arises that can overcome resistance, either through mutation, genetic recombination, or acquisition of new genetic information by **horizontal gene transfer** from another species, it can reproduce rapidly and cause massive crop losses.

21.2 An overview of immunity and defense

The interactions between organisms from different kingdoms can be represented as consisting of three phases, referred to as a "zig-zag-zig" scheme (Fig. 21.3A).

Most microorganisms carry molecules called pathogen- or microbe-associated molecular patterns (PAMP/MAMPs), which are often cell wall components that can be recognized by cell surface **pattern recognition receptors** (PRRs) in plants. This recognition by PRRs activates plant defenses, resulting in pattern (or PRR)-triggered immunity (PTI) (Fig. 21.3A,B). PTI in plant cells places selective pressures on potentially pathogenic species to produce proteins or other **effector** molecules, which interfere with and suppress these defense mechanisms or their activation (Fig. 21.3B). This is known as **effector-triggered susceptibility** (ETS). PTI selects also for P/MAMP variants that trigger less PTI.

Successful plant colonization mediated by specialist pathogen effector molecules places selective pressure on the plant population for recognition of these effector molecules and consequent activation of defense. These variant plants have alleles of **resistance (*R*) genes** that recognize either the effector molecules or the effects of these effectors on host proteins. This form of defense is known as ***R* gene-mediated defense**, or **effector-triggered immunity** (ETI; Fig. 21.3A,B). Defense mechanisms triggered during ETI are usually stronger than

BOX 21.1

Plant diseases have plagued agriculture throughout history

Throughout history, a number of plant diseases have plagued agriculture, some resulting in dramatic crop losses and devastating societal consequences.

Perhaps the most notorious of these was the Irish potato famine of the 1840s. The result of late blight disease (A), caused by the oomycete pathogen *Phytophthora infestans*, the famine reduced the population of Ireland from 8 to 5 million in just 3 years through starvation and emigration.

Black stem rust, which results from infection by the basidiomycete *Puccinia graminis* f. sp. *tritici* (B), caused the collapse of production of the North American wheat (*Triticum* spp.) crop in the 1950s. Through the development of new wheat varieties able to resist infection, this problem was alleviated. The disease has since returned in Africa, however, with the emergence of Ug99, a new and highly virulent strain that is not controlled by resistances in most wheat varieties. Wheat productivity has decreased in all the African regions affected by Ug99. It is spreading across Africa and the Middle East and may soon reach the Punjab in India.

Global banana (*Musa* spp.) production is under threat from black Sigatoka disease, caused by the ascomycete fungus *Mycosphaerella fijiensis*. The disease leads to the premature ripening of fruit, which are then difficult to export and often causes yield losses of over 50%. It is a constant threat to banana productivity because a single highly susceptible variety called Cavendish, bred over 80 years ago, is now grown globally in monoculture.

In addition to mass food shortages, plant diseases have cultural impacts. In the 1870s, the rust *Hemileia vastatrix* decimated coffee (*Coffea* spp.) production of Sri Lanka and led to the adoption of tea as the caffeinated drink of choice in Britain.



A



B

Worldwide, 25 to 35% of crop yield is lost each year because of pests and pathogens, necessitating a USD 30 billion/year agrochemical industry. Diseases on the harvested grain, fruits, seeds, and roots may also cause blemishes that can severely reduce market value. Some pathogenic species attack plant material after harvest, during transport and storage and cause post-harvest losses.

(A) The rapid development of late blight disease in a potato crop caused by the oomycete pathogen *Phytophthora infestans*. Left top to bottom, development of a late blight epidemic in a Scottish potato field crop over a two-week period destroys plants in the entire field. Top right, multiple late blight lesions on a potato (*Solanum tuberosum*) leaf. When lesions are formed on the same leaf by the two different mating types A1 and A2, mating and oospore formation can occur. Bottom right, a close up of the white asexual sporangia and sporangiospores emerging from the lower leaf surface under high humidity around the margins of the leaf lesion.

(B) Black stem rust disease on wheat caused by the basidiomycete *Puccinia graminis f. sp. tritici*. Left, an infected wheat (*Triticum aestivum*) tiller with pustules of urediniospores erupting onto the plant surface. The spores are subsequently dispersed either by the wind or during grain harvest (center). Wheat yield losses caused by black stem rust are often severe (50–70%), and individual fields can be destroyed. The fungus also develops teliospores on wheat plants that grow and following sexual mating produce a secondary spore, the basidiospore. Basidiospores infect an alternate host, the common barberry plant (*Berberis vulgaris*). On barberry leaves and stems a further spore stage, the aeciospore, is produced (right), and these wind-dispersed spores re-infect the wheat crop. Elimination of barberry from areas of wheat cultivation prevents sexual reproduction in the fungus and slows the evolution of new resistance-breaking strains.

Source: Image numbers 24472, 24478, 24525, 528370 and Blight 4, Source - David Cooke The James Hutton – all unpublished images, UDSA –web source barberry, UDSA fact sheet.

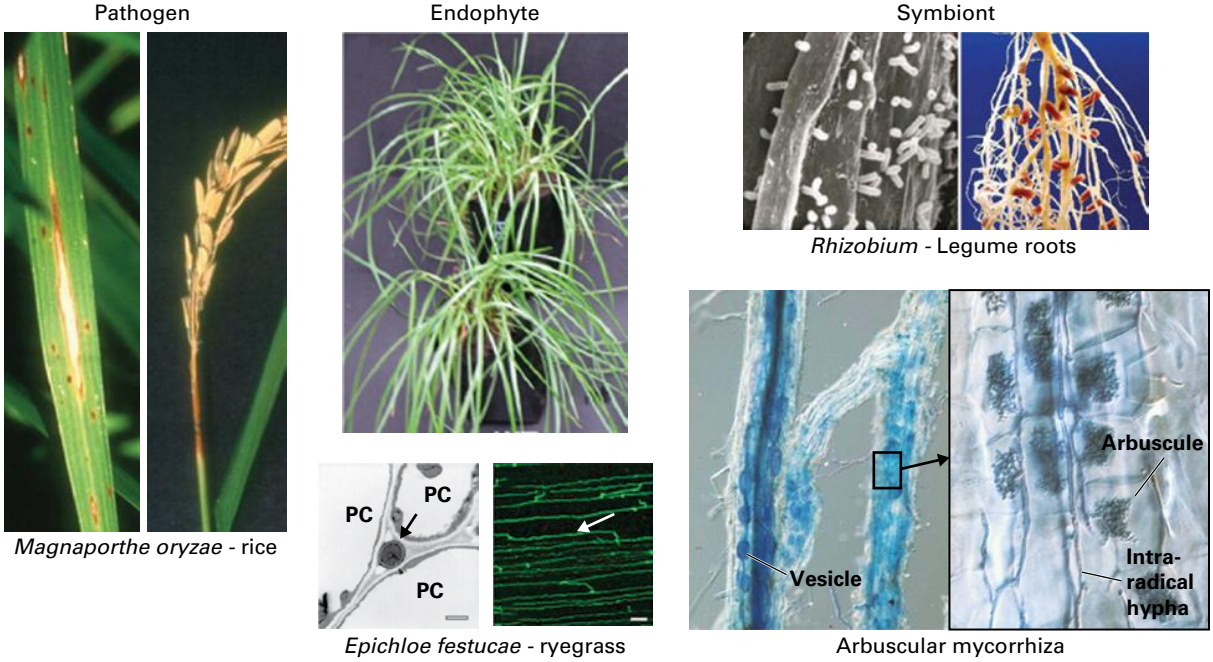
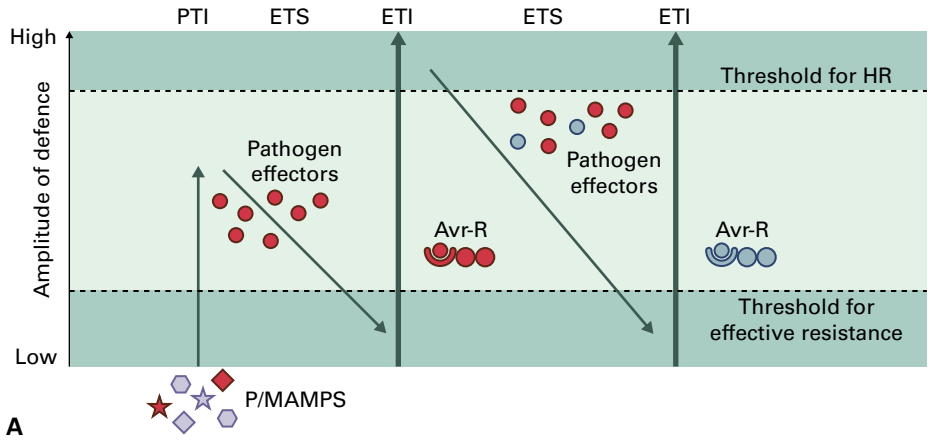


FIGURE 21.2 *Pathogens, endophytes, and symbionts: the continuum of microbe–plant interactions. Numerous microbial species have evolved the ability to infect plants in order to grow, develop, and complete their life cycle, but the outcomes are diverse. Pathogens (left) enter and colonize plants in different ways, feed on plant cells, adversely alter plant metabolism, cause a range of detrimental disease symptoms, and lower yields. For example, the fungus* Magnaporthe oryzae *causes rice blast disease and is a serious threat to global rice production. In contrast, endophytes (center) enter and live within plants for at least part of their life without causing apparent disease. Some endophytic infections protect plants by improving tolerance to abiotic or biotic stresses, but others cause detrimental effects. For example,* Epichloe festucae *is an endophytic fungus that infects cool season grasses of the subfamily Pooideae. Infection causes no symptoms to the plant, but causes health problems to foraging farm animals and wild mammals because the fungal hyphae that grow between the plant cells (PC, see arrows in bottom panels) produce various toxic indole-diterpene metabolites. Symbionts (right) form intimate associations with plants that greatly benefit plant growth and development. Numerous species of* Rhizobium *bacteria, for example, infect roots of different legume species, induce nodule formation, and fix nitrogen for the plant. Endomycorrhizae are specialist fungi that infect plant roots and invade cells to form arbuscules. The plant and fungal plasma membranes surrounding the arbuscules contain special transporter proteins across which nutrients can be exchanged. Sugars move from the plant to the fungus as a carbon source for fungal growth, and minerals, especially phosphate, move from the fungus to the plant. Fungal hyphae extend from the infected root into the surrounding soil beyond the regions that can be exploited by root hairs. Arbuscular mycorrhiza associations benefit numerous plants, especially tree species, by acquiring phosphate from nutrient poor soils.*
Source: Rice blast - APS website – *Magnaporthe oryzae*. Epichloe: Takemoto et al. (2006). Plant Cell 18:2807–2821. Rhizobium – Todar's Online textbook of bacteriology, http://textbookofbacteriology.net/Impact_2.htm. Arbuscularmycorrhiza - Prof Martin Parniske.



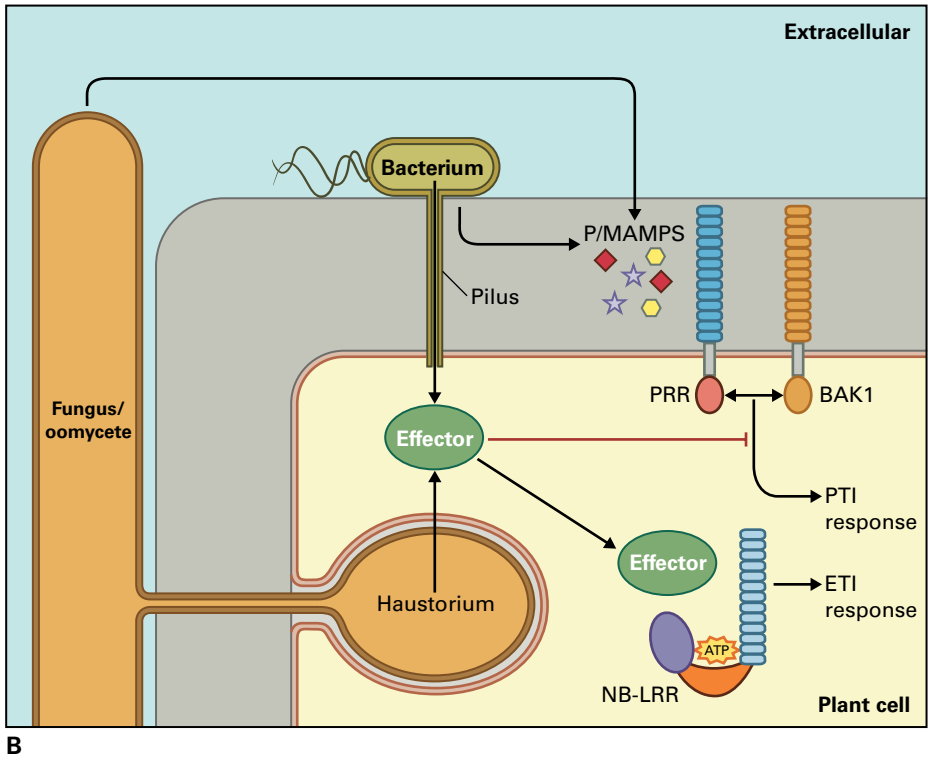


FIGURE 21.3 *The principles of plant immunity. (A) Zig-zag-zig plant defense response model, showing the amplitude of the defense response elicited by various stages of infection. P/MAMP, pathogen- or molecule-associated molecular patterns; PTI, pattern-triggered immunity; ETS, effector-triggered susceptibility; ETI, effector-triggered immunity; Avr-R, interaction of the recognized effector (avirulence or* avr *gene) and the host resistance gene (the* R *gene); HR, hypersensitive cell death response. (B) The various cellular locations where pathogen–host communication occurs. Bacterial plant pathogens propagate in the extracellular spaces of plant tissues. Most fungal and oomycete pathogens also extend hyphae into this space, although many also form specialized feeding structures, haustoria, that penetrate host cell walls but not the plasma membrane. Other fungi extend invasive hyphae into plant cells, but again do not breach the host membrane. Molecules released from the pathogens into the extracellular spaces, such as lipopolysaccharides, flagellin, and chitin (pathogen- or molecule-associated molecular patterns, P/MAMPs) are recognized by cell surface pattern recognition receptors (PRRs) and elicit P/MAMP-triggered immunity (PTI). Many PRRs consist of an extracellular leucine-rich repeat (LRR) domain (mid-blue), and an intracellular protein kinase domain (red). Many PRRs interact with the related protein BRASSINOSTEROID INSENSITIVE 1-ASSOCIATED KINASE 1 (BAK1) to initiate the PTI signaling pathway. Bacterial pathogens deliver effector proteins into the host cell by a type-III secretion pilus, whereas fungi and oomycetes deliver effectors from haustoria or other intracellular structures by an unknown mechanism. These intracellular effectors often act to suppress PTI; however, many are recognized by intracellular nucleotide-binding (NB)-LRR receptors, which induce effector-triggered immunity (ETI). NB-LRR proteins consist of a carboxyl-terminal LRR domain (light blue), a central NB domain (orange crescent) that binds ATP or ADP, and an amino-terminal Toll, interleukin-1 receptor, resistance protein (TIR), or coiled-coil (CC), domain (purple oval).*

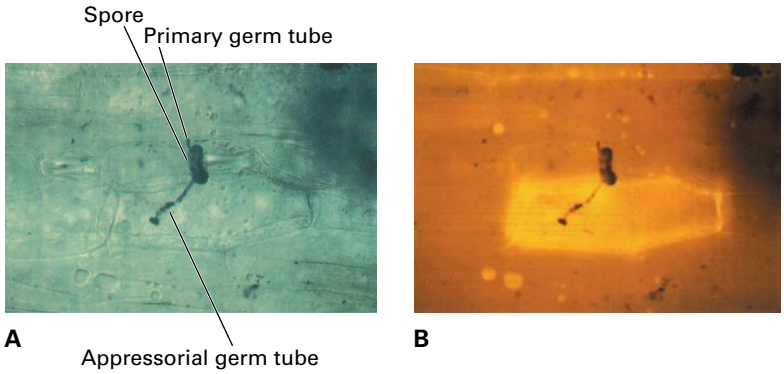


FIGURE 21.4 *The hypersensitive cell death response (HR) in resistant barley (*Hordeum vulgare*) epidermal cells to attack by germinating spores of the barley powdery mildew fungus (*Blumeria graminis *f. sp.* hordei*). (A) Image obtained by phase-contrast light microscopy showing the fungal spore and stained extracellular primary germ tube, the appressorial germ tube. (B) Whole cell autofluorescence of the same epidermal cells as seen under UV light excitation (wavelength 310 nm); only the single cell undergoing the HR exhibits autofluorescence.*
Source: Gorg et al. (1993) Plant J. 3:857–866.

those triggered by PAMPs, often culminating in a programmed cell death referred to as the **hypersensitive response** (HR) (Fig. 21.4). Though R proteins are usually cytoplasmic receptors that recognize, directly or indirectly, cytoplasmic pathogen effectors, some R proteins are cell surface receptors that recognize apoplastic effectors.

For historical reasons, many effector-encoding genes were first called **avirulence** (**Avr**) **genes**, because they are recognized by a cognate resistance gene. For example, the *Pseudomonas* AvrPto effector causes **avirulence** (lack of disease) on tomato (*Solanum lycopersicum*) lines that carry the corresponding *Pto* resistance gene.

A successful pathogen overcomes PTI and has effectors that evade R protein-mediated detection. PTI can either be evaded (or attenuated) by mutations that result in subtle changes in the P/MAMP, or suppressed using effectors. Successful pathogens that evade detection in turn impose selection for novel *R* gene variants that can recognize other pathogen effector molecules and then activate defense. In turn, an R protein that recognizes a widespread pathogen effector provides selection pressure on the pathogen for variants that can evade this new *R* gene-specified recognition. These molecular interactions result in **coevolution** between plants and pathogens.

Even during susceptibility, plant defenses are activated, though not enough to completely stop the pathogen. This is sometimes referred to as **basal defense**. Enhanced disease susceptibility (EDS) mutants are compromised in basal defense and are thus quantitatively more susceptible than wild-type plants. This basal defense activation is thought to be due to incomplete attenuation of PTI by the pathogen effector complement, and may also include some weak effector recognition and thus weak ETI.

Mammals have an innate immune system based primarily on PTI via cell surface TOLL-like receptors, and also can trigger defense via Nod-like receptors (NLRs) that resemble plant intracellular R proteins. They also carry an adaptive immune system involving somatic diversification in their antibody complement and circulating antibody-producing cells. Plants lack adaptive immunity and mobile cells, and rely entirely on cell-autonomous **innate immunity**.

Only a small proportion of plant–pathogen infections result in disease. This low rate of pathogen success may be the result of one or several of four main factors:

- the plant species attacked is unable to support the life-strategy requirements of the potential pathogen and so is considered a nonhost;
- the plant possesses preformed structural barriers or toxic compounds that confine infection to specialized pathogen species. Such preformed defenses can be important for disease resistance;
- on recognition of the attacking pathogen, defense mechanisms are induced and the invasion remains localized (Fig. 21.4);
- environmental conditions change, and the pathogen perishes before infection has reached the point at which it is no longer influenced by adverse external stresses.

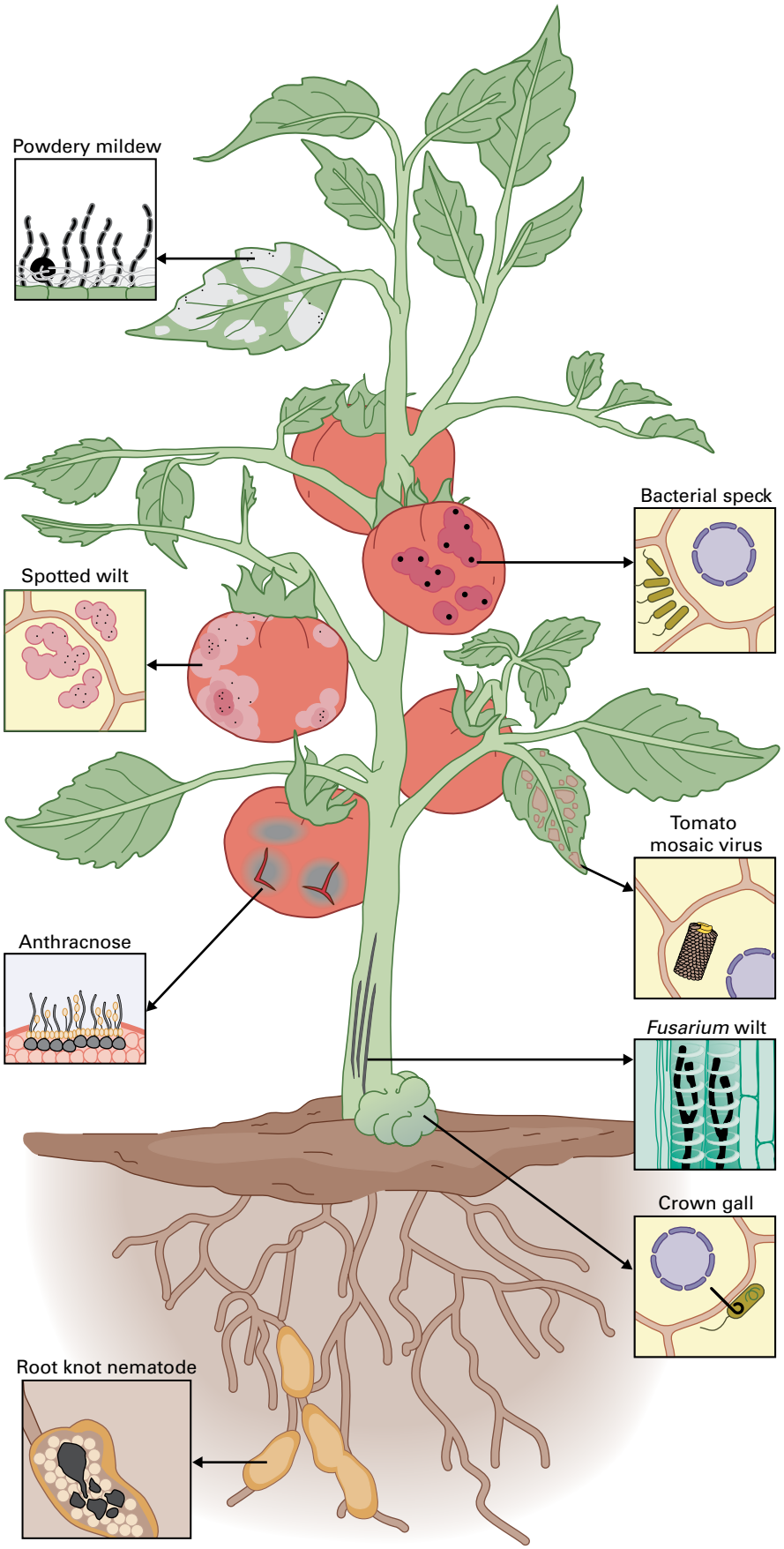
The first three interactions are said to be genetically **incompatible**, but only the third mechanism based on pathogen recognition depends exclusively on induction of defense responses to limit pathogen attack.

Induced defenses can appear rapidly (e.g., production of reactive oxygen species) or later (e.g., accumulation of antimicrobial compounds). Activation of defense in a leaf can trigger elevation of defenses in distal leaves via the movement of systemic signal molecules around the plant. The plant defense system must have enough discriminatory capacity to distinguish harmful plant pathogens from beneficial organisms such as *Rhizobium* bacteria (for legume species) and mycorrhizal fungal species (for almost all vascular plants).

21.3 How pathogens and pests cause disease

Successful pathogens must enter the host plant, grow long enough to obtain nutrients, suppress defenses, and then reproduce to continue their life cycle. Each phase requires different solutions to various problems.

FIGURE 21.5 *Most microbes attack only a specific part of the plant and produce characteristic disease symptoms, such as a mosaic, necrosis, spotting, wilting, or enlarged roots. Tomato (*Solanum lycopersicum*) plants are attacked by more than 100 different pathogenic microorganisms. The diagram illustrates symptoms caused by bacteria (bacterial speck, spotted wilt, crown gall), fungi (*Fusarium *wilt, powdery mildew, anthracnose), viruses (tomato mosaic virus), and nematodes (root-knot nematode).*



Pathogens has evolved various and specific ways to invade plants (Fig. 21.5). Some species penetrate surface layers directly using mechanical pressure or enzymatic attack, some pass through natural openings, such as stomata or lenticels, and others only enter through wounded tissue. Once inside the plant, one of three main attack strategies is deployed (Table 21.1): **necrotrophy**, where the plant cells are killed in advance of infection; **biotrophy**, where the plant cells remain alive throughout infection; and **hemibiotrophy**, where the pathogen initially keeps cells alive but at later stages of the infection, kills them.

This process of infection, colonization, and reproduction is known as **pathogenesis**. A pathogen strain that causes disease is termed **virulent**. Some of the biotrophic species can only exist in association with living plants and are termed **obligate biotrophs** (Fig. 21.6).

21.3.1 Virulent pathogens have unique survival-promoting characteristics

The success of plant pathogens can be attributed to various factors:

- a mode of pathogenesis that permits a high rate of reproduction (often with multiple cycles) during the main growing season;
- an efficient dispersal mechanism by wind, water (rain splash), or vector organisms, such as insects;
- A different type of reproduction (often sexual) toward the end of each growing season to produce a second type of structure (e.g., spore or propagule) that has long-term survival capacity (sometimes as long as 30 years);
- a high capacity to generate genetic diversity. Many pathogens have a haploid genome during the phase of greatest reproduction, which permits adaptive mutations to be immediately selected within the pathogen population. Subsequent sexual reproduction creates a novel pool of recombinant genotypes from which new epidemics can arise;
- monocultures of crop plants and well-adapted pathogen genotypes.

21.3.2 Oomycete and fungal pathogens use diverse pathogenesis strategies

Oomycetes are fungus-like organisms that belong to the *Chromalveolates*, along with brown algae and mammalian parasites, such as the malaria parasite *Plasmodium falciparum*. Both oomycetes and fungi can be biotrophic, necrotrophic, or hemibiotrophic plant pathogens; less than 2% of the ≈100,000 known fungal species, however, colonize plants and cause disease.

Necrotrophic species that produce cell wall-degrading enzymes tend to attack a broad range of plant species. For example, the oomycete *Pythium* and fungus *Botrytis* each attack over 1,000 plant species. Some necrotrophs produce host-selective toxins that are active in only a few plant species; such toxins have a specific mode of action, inactivating a single plant enzyme. For example, the **HC toxin** produced by the fungal pathogen *Cochliobolus carbonum* of maize (*Zea mays*) inhibits histone deacetylase activity (Fig. 21.7), which is involved in gene regulation (see Section 21.3.7 and Chapter 9). *Alternaria alternata* f. sp. *lycopersici* produces the AAL toxin, which activates a plant cell death program in tomato (*Solanum lycopersicum*) leaves. Two cereal-infecting fungi produce light-sensitive toxin proteins: ToxA is produced by both *Stagonospora nodorum* and *Pyrenophora tritici-repentis*, which cause glume blotch and tan spot disease, respectively, on wheat (*Triticum* spp.). Other fungi produce nonselective toxins. For example, *Fusicoccum amygdali* produces the toxin **fusicoccin**, which targets the plasma membrane H^+-ATPase in many plant species (see Chapter 3), causing irreversible opening of stomata and plant wilting, followed by cell death and fungal colonization.

Sclerotinia sclerotiorum is a necrotrophic fungus that infects over 400 plant species. It secretes the phytotoxin **oxalic acid** to assist the early phases of the infection. Oxalic acid, by manipulating the redox status of invaded plant tissues, suppresses several early plant defenses, including the oxidative burst (see Section 21.5.3) and callose deposition. Once infection is established, however, this necrotroph then induces the generation of plant **reactive oxygen species** (ROS), which lead to death of host tissue and, ultimately, pathogen growth.

Biotrophic fungi keep host cells alive and usually exhibit specialization for plant species. For example, the obligate biotroph powdery mildew fungus (*Blumeria graminis*) occurs in genetically distinct forms called *formae specialis* ('forms of a species'; f. sp.) that infect either barley (*Hordeum vulgare*) or wheat (*Triticum* spp.), but not both. When biotrophic pathogens colonize, the metabolism and development of the plant are often dramatically altered. Metabolites are lost from the host to feed the pathogen, and there are alterations in the levels of **phytohormones** involved in plant growth and development. Effects can include delayed **senescence** of the infected tissues (Fig. 21.8) and stunting or other abnormal growth patterns, resulting in yield losses.

To efficiently utilize living plant cells as a food substrate, biotrophic fungi undergo three developmental changes (Fig. 21.9). First, they usually penetrate the rigid cell wall via the formation of a specialized infection structure on the plant surface called an **appressorium**. Then, the emerging penetration peg breaches the rigid plant cell wall and provides entry into the plant cell. Finally, a **haustorium** (Fig. 21.9B) forms upon entry into the plant cell. The haustorium develops behind an invagination of the plant plasma membrane, and each haustorium becomes encased in a host **extrahaustorial membrane** (EHM). This specialized feeding structure increases surface contact between the two organisms to maximize nutrient and water flow and favor pathogen growth. The origin and constitution of the EHM remains enigmatic. Studies involving *Arabidopsis thaliana* and powdery mildew infections have shown the EHM lacks numerous host plasma

TABLE 21.1 *Strategies utilized by plant pathogens.*

	Necrotrophy	Biotrophy	Hemibiotrophy
Attack strategy	Secreted cell wall-degrading enzymes, host toxins, or both	Intimate intracellular contact with plant cells	Initial biotrophic phase
Specific features of interaction	Plant tissue killed and then colonized by the pathogen; extensive tissue maceration	Plant cells remain alive throughout infection; minimal plant cell damage	Plant cells alive only in the initial stages of infection; extensive plant tissue damage at later stages
Host range	Broad	Narrow; often only a single species of plant is attacked	Intermediate
Examples	Rotting bacteria (e.g., *Erwinia* spp.); rotting fungi (e.g., *Botrytis cinerea*)	Fungal mildews and rusts; viruses and endoparasitic nematodes; *Pseudomonas* spp. bacteria	*Phytophthora infestans* (causal agent of potato late blight disease)

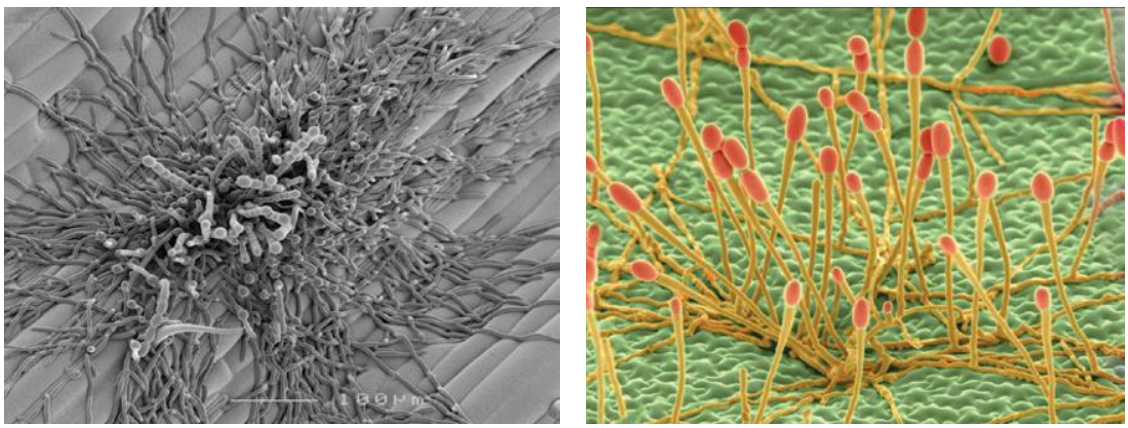


FIGURE 21.6 *Scanning electron micrographs of a powdery mildew pustule on a barley or grape vine leaf. The two fungal species infecting are* Blumeria graminis *f. sp.* hordei *on barley (*Hordeum vulgare*, left) and* Uncinula necator *on grape vine (*Vitis *sp., right). The abundant asexual mildew spores are held high above the leaf surface in preparation for wind dispersal under dry conditions.*
Source: J. Foundling, Syngenta Jealott's Hill; previously unpublished.

membrane proteins. This suggests that it originates from another membrane, such as the vacuole, from de novo assembly, or from the plasma membrane by a mechanism that excludes host proteins. Fungal rusts, powdery mildews, oomycete white rusts, and downy mildews all make haustorial associations with host plants.

Not all species require formation of an appressorium for penetration. A few biotrophic fungi (for example, the tomato leaf mold pathogen *Cladosporium fulvum*) enter through stomata and do not form haustoria. Instead, they grow within the intercellular air space (the **apoplast**), subsisting on leaked nutrients (Fig. 21.10).

Hemibiotrophic pathogens first use a biotrophic and then a necrotrophic mode of nutrition. The switch may be triggered by higher nutritional demands as pathogen biomass increases and asexual reproduction occurs. Some of the most devastating phytopathogenic species are hemibiotrophs. For example, the oomycete *Phytophthora infestans* causes late blight of potato (*Solanum tuberosum*, see Box 21.1). In this interaction, the switch from biotrophic to necrotrophic nutrition occurs within a few days. In contrast, for other nonbiotrophic species, the symptomless phase is far longer. For example, the wheat-infecting fungus *Mycosphaerella graminicola* (*Zymoseptoria tritici*) infects leaves through open stomata, but only kills plant cells after a long intercellular growth phase; the fungal biomass subsequently increases and sporulation occurs (Fig. 21.11). For the related banana-infecting *Mycosphaerella fijiensis,* the symptomless infection phase is typically around 50 days before the black Sigatoka disease symptoms (see Box 21.1) first appear.

21.3.3 Bacterial pathogens of plants and animals use similar molecular virulence mechanisms

Phytopathogenic bacteria specialize in colonizing the apoplast to cause rots, spots, vascular wilts, cankers, and blights. Most are Gram-negative rod-shaped bacteria from the genera

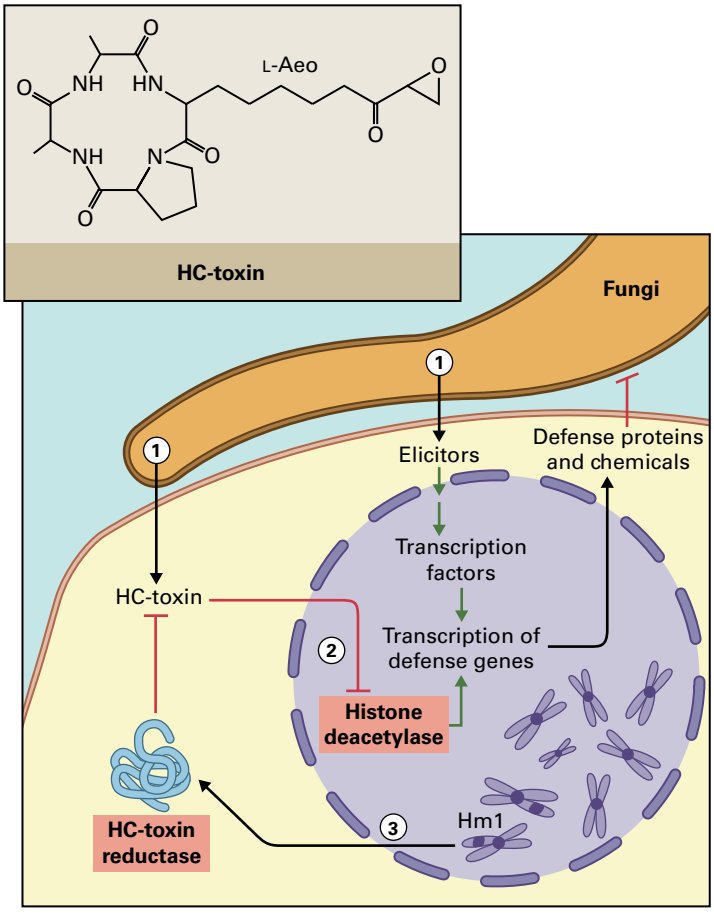


FIGURE 21.7 *Some necrotrophic fungi produce host-selective toxins. The maize pathogen* Cochliobolus carbonum *secretes HC toxin (1) and numerous nonspecific fungal elicitors that trigger plant defense responses. (2) HC toxin is hypothesized to enter the responding plant cells, where it inhibits histone deacetylase activity. Histone deacetylase is responsible for the reversible deacetylation of core histones (H3 and H4) assembled in the chromatin. Its inhibition is believed to interfere with transcription of maize defense genes to favor fungal growth and disease development. (3) Hm1-resistant maize plants produce an HC-toxin reductase (HCTR), which detoxifies HC toxin by reducing the carbonyl group of the side chain of L-Aeo (2-amino-9,10-epoxy-8-oxo-decanoic acid), an unusual epoxidated fatty amino acid.*

Pseudomonas, Agrobacterium, Xanthomonas, Dickeya, and *Erwinia/Pectobacterium*. *Agrobacterium*-mediated plant transformation is described in Box 21.2.

Three features characterize bacteria–plant relationships. First, phytopathogenic bacteria rarely enter plants by direct penetration of the cell wall. During their parasitic life, most reside within the intercellular spaces of plant organs or in the xylem (Fig. 21.12), and many damage plant tissues by secreting toxins, extracellular polysaccharides (EPSs), or cell wall-degrading enzymes. Second, bacterial toxins contribute to the production of symptoms in certain plant species, but targeted mutagenesis has shown they are often nonessential for pathogenesis. Third, the secreted EPSs, which surround the growing bacterial colony, may aid bacterial virulence, for example, by saturating intercellular spaces with water or blocking the xylem to produce wilt symptoms, but are not required for pathogenesis.

Other potential roles for bacterial toxins and factors associated with disease are receiving renewed attention. Coronatine is a toxin effector produced by the bacterium *Pseudomonas syringae* to mimic the plant hormone jasmonic acid-isoleucine (see Section 21.8.5), and this assists bacterial infection. Coronatine is involved in causing stomata to open after closing in response to PAMPs, as well as in interfering with salicylic acid (SA)-mediated defense responses. Necrotrophic bacteria that deploy pectic enzymes from the outset of infection, such as *Erwinia*, have a broad host range and cause extensive cell death and tissue maceration. The pectic enzymes cleave plant cell wall polymers either by hydrolysis (polygalacturonases) or through beta-eliminations (pectate or pectin lyases) (see Chapter 2).

Bacteria frequently deploy a "quorum-sensing" mechanism to facilitate successful colonization of plant tissue (Fig. 21.13). Virulence factors are usually not expressed until the bacterial population density is sufficient to ensure the plant cells are immediately overwhelmed by the attack. The soft rot pathogen *Erwinia carotovora* only produces cell wall-degrading enzymes when the bacterial population reaches a certain density in the host extracellular spaces. If these enzymes were produced at a low pathogen density, they might activate plant defenses (see Section 21.8.2) without the bacteria being present in sufficient numbers to resist them. Quorum sensing in *E. carotovora* is mediated by *N*-acylhomoserine lactones, small molecules released from the bacterial cells into the surrounding medium. The bacterial blight pathogen of rice (*Oryza sativa*), *Xanthomonas oryzae* pv. *oryzae*, secretes a highly conserved sulfated peptide called Ax21, which mediates quorum sensing by controlling *Xanthomonas* motility, biofilm formation, and virulence.

Some phytopathogenic bacteria depend on insects for entry into plants. These are mainly species that infect the phloem, xylem, and associated vascular tissues. During herbivore insect penetration and feeding, the mouthparts pick up

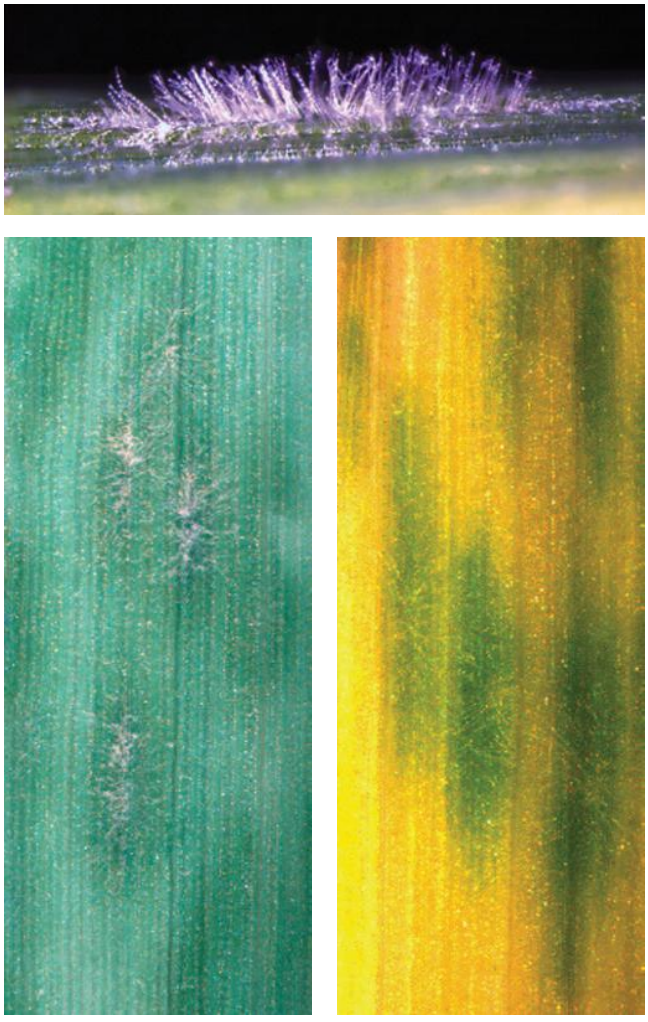


FIGURE 21.8 *Biotrophic pathogens keep plant cells alive. Post infection, biotrophs can alter the levels of phytohormones to delay senescence of the infected tissue and aid nutrient acquisition. In and around pustules of the sporulating barley mildew fungus (*Blumeria graminis *f. sp.* hordei*) (top), delayed senescence causes the formation of "green islands" (lower left), which are evident as the leaves senesce and lose their chlorophyll content more slowly from the infected regions (lower right).*
Source: P. Spanu, Imperial College; previously unpublished.

bacteria already within the tissue. These bacteria are then transmitted to a new vascular region on which the insect next feeds. For example, phytoplasmas are specialized bacteria that are obligate parasites of the phloem tissue. They are mainly spread by insects in the families Cicadellidae (leaf hoppers), Fulgoroidae (plant hoppers), and Psyllidae (jumping plant lice). The xylem-colonizing bacterium *Xylella fastidiosa* is transmitted by various species of *Homalodisca* in the family Cicadellidae.

During infection, most bacteria remain in extracellular spaces and use a specialized mechanism, the **type III secretion system** (T3SS), to deliver bacterial effector proteins into the plant cell. This mechanism is also used by many bacterial species that infect animals. The T3SS involves a protein complex that spans both the inner and outer bacterial membranes and a pilus that projects through the plant cell wall and into the host cell (Fig. 21.14). The structural components of the T3SS are encoded by the clustered **hypersensitive response and pathogenicity cluster** (*hrp*) genes. Many different types of bacterial Avr effectors delivered by type III secretion have been identified to be enzymes such as phosphatases, proteases, phosphoserine lyases, or E3 ubiquitin ligases that attenuate host defense signaling.

21.3.4 Plant pathogenic viruses move by way of plasmodesmata and phloem

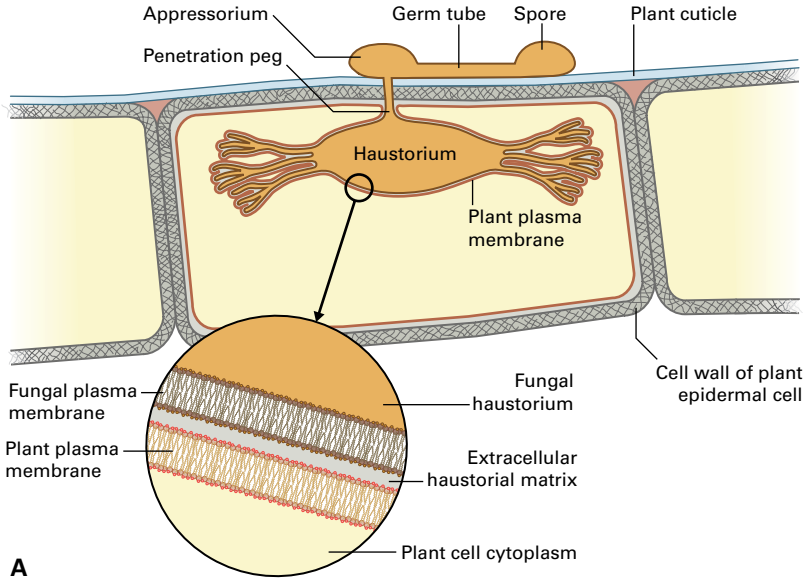
Over 40 families of DNA and RNA plant viruses exist, and most are single-strand (ss) positive-sense (+) RNA viruses (Fig. 21.15A). Symptoms of viral infection include tissue yellowing (chlorosis) or browning (necrosis), mosaics, and plant stunting. Plant viruses are biotrophs, and all species face the same three basic challenges: How to replicate in the initially infected cell, how to move into adjacent cells and the vascular system and thereby colonize the entire plant, and how to be transmitted to the next host plant.

Plant viruses have small genomes; most encode only three to 10 proteins. Each gene has one or more specific functions, as illustrated by the genome of tobacco mosaic virus (TMV) (Fig. 21.15B), which functions in replication, cell-to-cell movement, symptom development, and encapsidation. The initial major challenge was to identify the host genes required for viral replication and transmission.

When viruses enter plant cells following mechanical wounding or transmission by a vector, either viral translation or transcription followed by translation occurs to produce the proteins required for viral replication. Genome replication for ss (+) RNA viruses, ss negative-sense (–) RNA viruses, double-stranded (ds) RNA viruses, and plant pararetroviruses, such as CaMV containing partially dsDNA genomes, occurs in the cytoplasm and utilizes the virus DNA-encoded RNA-dependent RNA polymerases (RdRps). In contrast, genome amplification of ssDNA viruses, such as geminiviruses, occurs in the nucleus and involves hijacking components of host DNA replication.

The compartmentalization of viral genome replication means that replicated nucleoprotein complex or nascent genomes require transportation to the only site in the host cell where intracellular (symplastic) movement is permitted, the **plasmodesmata**. In contrast to animal viruses, there is no example of plant viruses crossing the plasma membrane of the infected plant cell. Plant virus movement proteins in association with various components of the host cell cytoskeleton, including actin filaments and microtubules, facilitate transport of nucleoprotein complexes and virus particles into adjacent cells via modified plasmodesmata.

Two mechanisms are deployed for viral movement. Tobamoviruses (ss (+) RNA genomes), such as TMV, transiently increase the size exclusion limit of plasmodesmata



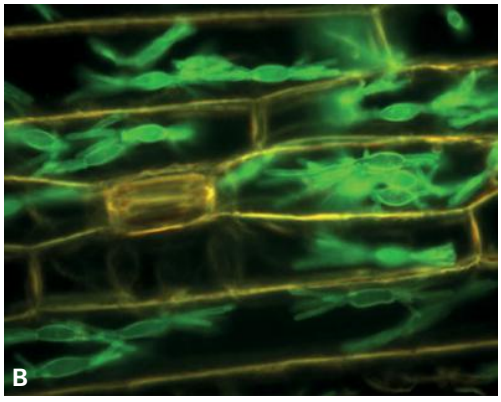


FIGURE 21.9 *Some biotrophic fungi invade host cells to extract nutrients. (A) The fungal haustorium facilitates transfer of nutrients from a living plant cell to the pathogen. The extracellular haustorial matrix contains products of both fungal and plant origin. (B) Haustoria of the biotrophic barley mildew fungus* Blumeria graminis *f.sp.* hordei *inside the epidermal cell of barley (*Hordeum vulgare*), stained with a lectin (wheatgerm agglutinin) bound to Alexa-288. Each multidigitate structure is surrounded by the perihaustorial membrane of host origin. As with other mildews, this specialized membrane is continuous with the host plasma membrane, but has different biochemical properties. In mildews, the perihaustorial membrane is thought to be where nutrients are absorbed and effectors are delivered. Source*: (B) P. Spanu, Imperial College; previously unpublished.



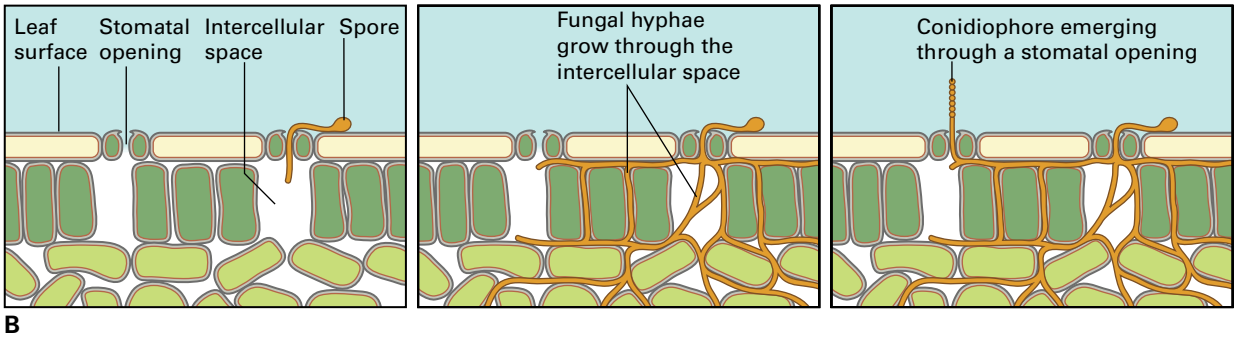


FIGURE 21.10 *Some biotrophic fungi invade their host leaf through stomata. (A) The leaf mold fungus* Cladosporium fulvum *infects through the lower surface of a tomato (*Solanum lycopersicum*) leaf, shown at 14 days after infection. This biotrophic pathogen is restricted to attacking only a few species of the genus* Solanum. *(B) The* C. fulvum *life cycle on tomato. Spores germinate on the leaf surface, hyphae grow across the surface until a stomatal opening is encountered, and hyphae enter the intercellular spaces of the leaf (left). Hyphae within the leaf grow through the intercellular spaces in the mesophyll cell layer (center). Approximately 14 days after infection, the sporulation structures (conidiophores) emerge through the stomatal openings (right). Source*: (A) K.E. Hammond-Kosack, The Sainsbury Laboratory, Norwich, UK; previously unpublished.

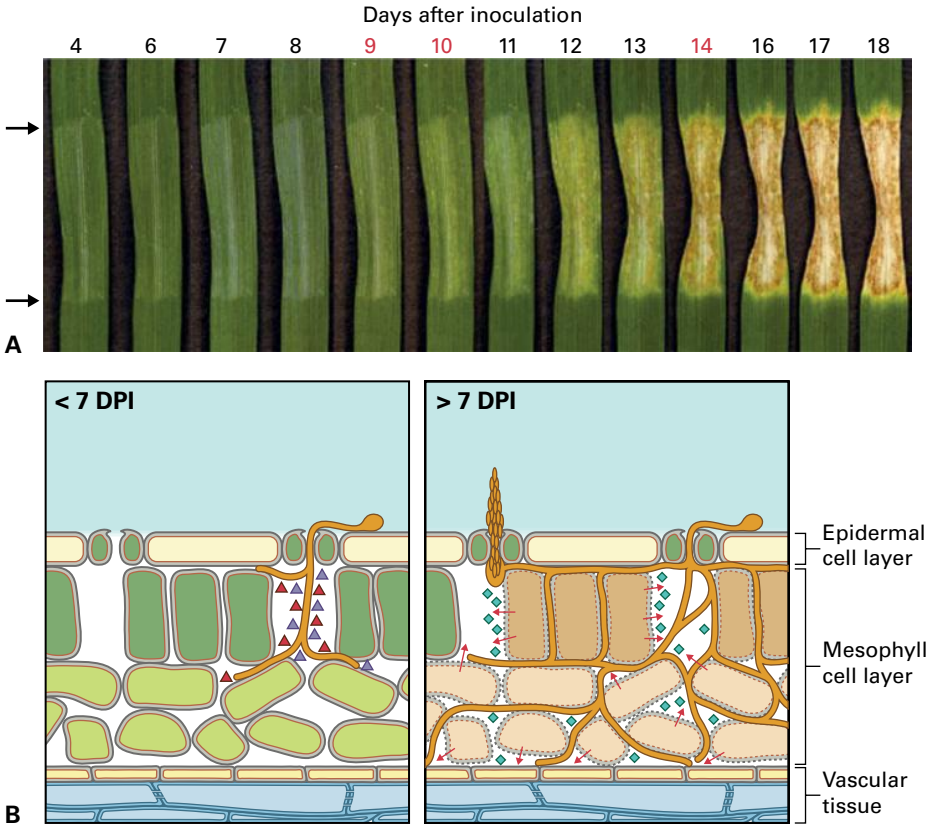


FIGURE 21.11 *Wheat leaf (*Triticum *sp.) infection caused by the hemibiotrophic fungus* Mycosphaerella graminicola *(*Zymoseptoria tritici*). This leaf blotch disease is particularly severe when cool, moist conditions prevail and can reduce wheat grain yields by as much as 30%. (A) Time course of symptom development. A representative leaf was inoculated with fungal sporidia within the region delimited by the arrows and then photographed at 24-hour intervals. For the first 8–9 days, the infection is symptomless; visible brown lesions rapidly appear by day 14 and fungal sporulation within pycnidia occurs within the lesion. (B) The infection process. (Left) Early symptomless colonization (<7 days post leaf inoculation, DPI) involves the release of plant defense-suppressing apoplastic effectors (red and blue triangles) from slow-growing intercellular hyphae (orange). (Right) After 7 days, leaf mesophyll cell death and the loss of membrane permeability allow nutrient release into the apoplast. Defense-suppressing effectors are "switched off", although other potentially toxic effectors (blue diamonds) may be produced. Extensive hyphal growth and asexual sporulation (pycnidia and pycnidiospore formation) are now supported within leaf lesions. Under high humidity, the mature pycnidiospores ooze out onto the leaf surface via the open stomata.*
Source: Keon et al. (2007) MPMI 20:178–193.

BOX 21.2

Agrobacterium-mediated T-DNA transfer, a mechanism used in pathogenesis, is also a tool for plant transformation

Agrobacterium tumefaciens is a soil bacterium that is closely related to *Rhizobium*. It causes crown-gall disease in many dicotyledonous plant species (A). *Agrobacterium* genetically transforms plant cells with a DNA fragment called the **T-DNA** (transferred DNA). The process involves DNA transfer from the bacterium into the plant cell nucleus, where it stably integrates into the plant genome (B).

Gene expression from a wild-type T-DNA results in remarkable changes in plant cell metabolism. Plant growth hormones (auxins and cytokinins) are made, leading to neoplastic growth (tumor formation). Also, within gall tissue, various amino compounds called **opines** are synthesized, which the bacteria can use as their sole carbon and nitrogen source. *Agrobacterium* strains are classified based on the types of opine production they cause (e.g., octopine and nopaline). Opine catabolism within bacterial cells requires specialized enzymes encoded by the *Agrobacterium* **tumor-inducing (Ti) plasmid**. Because neither the plant nor any other soil-dwelling microorganism can use opines, this provides a competitive advantage for Agrobacteria within the gall tissue.

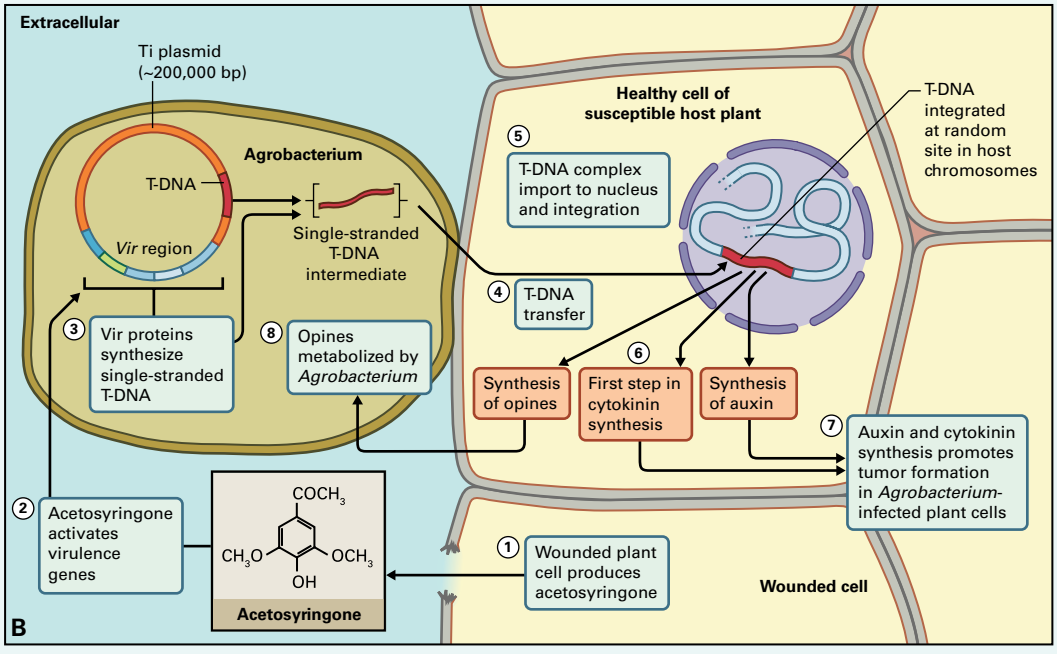
Molecular genetic studies have been the key to elucidating *Agrobacterium*–plant cell interactions. The bacterium predominantly infects plants at a wound site where damaged plant cells synthesize and secrete unusual phenolic compounds that include **acetosyringone**. A set of chromosomal virulence (*chv*) genes located on the *Agrobacterium* chromosome are involved in bacterial chemotaxis toward and attachment to the wounded plant cells. However, open stomata can sometimes be used to circumvent the physical barrier of the plant cuticle.

The subsequent binding of the bacteria to specific plant cell wall components initiates a seven-step process involving the synthesis, transfer, targeting, and insertion of the *Agrobacterium* T-DNA into the plant genome, culminating in gall formation (B). This process is controlled by genes located on the 200-kB Ti plasmid of *Agrobacterium*, either within the T-DNA itself or within a 35-kB virulence (*vir*) region, which is composed of seven major loci (*VirA* to *VirG*). For step 2, the VirA/VirG transcriptional regulators that activate all the other *vir* genes, are two-component sensor/signaling systems (see Chapter 18) widely used by bacteria to regulate both environmental and developmental mediated responses. In step 5, the proteins that transport the T-complex from *Agrobacterium* into the plant cell cytoplasm are functionally similar to those involved in bacterial plasmid conjugation. The targeting of the T-complex into the plant cell nucleus proceeds via an endogenous macromolecular transmission and targeting pathway, which appears to be analogous to that deployed by certain DNA plant viruses.

The ability of *Agrobacterium* T-DNA to integrate stably into a plant genome has led to its widespread exploitation as a vector for the genetic transformation of higher plant cells with **recombinant DNA** molecules. However, to regenerate plants with a normal appearance, the *Agrobacterium* genes specifying tumor formation had first to be eliminated. In addition, a technique called agroinfiltration is used routinely in several plant species to transiently express genes in leaf cells by infiltration into leaf panels of a high density of *Agrobacterium* cells containing defined recombinant DNA molecules.

Source: (A) M. Hammond-Kosack; previously unpublished.





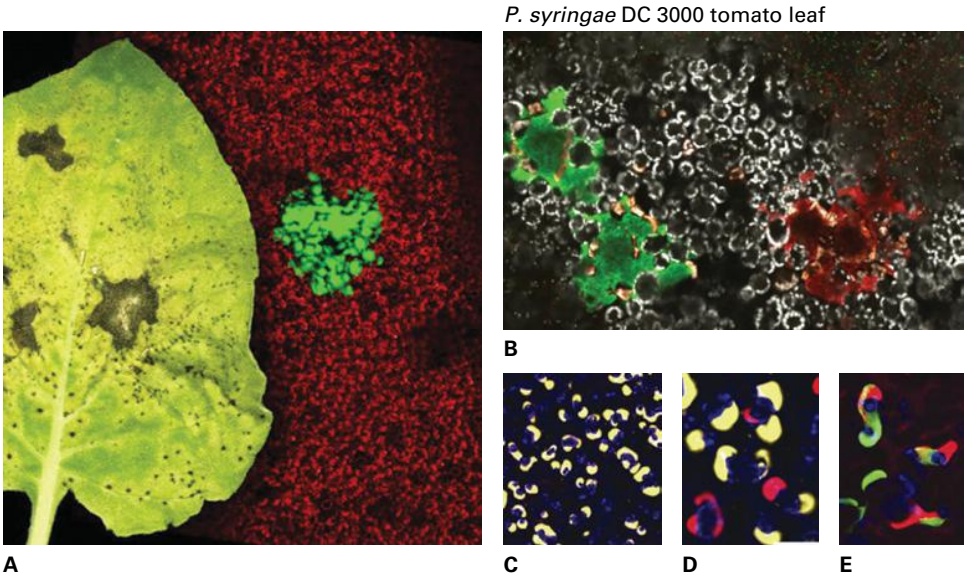


FIGURE 21.12 *Different pathovars of the bacterial pathogen* Pseudomonas syringae *infect and reside within the intracellular spaces of a range of crop plant species, including tomato (*Solanum lycopersicum*), soybean (*Glycine max*), tobacco (*Nicotiana tabacum*), and green bean (*Phaseolus vulgaris*). (A) Using a strain of* P. syringae *pv* tomato *expressing a green fluorescent protein (GFP), the localized accumulation of a bacterial population is visualized by viewing an infected tobacco leaf under UV light. (B) Two colonies of* P. syringae *pv tomato growing within the leaf mesophyll expressing either GFP (left) or the red fluorescent protein (RFP) (right). (C–E) Confocal images showing various fluorescent* Pseudomonas syringae *pv.* phaseolicola (Psp) *strains forming colonies in the apoplast of bean (*Phaseolus vulgaris*) leaf tissue. (C) Discrete colonies of a single Psp strain expressing the yellow fluorescent protein (YFP) in close contact with mesophyll cells. (D,E) Mixed inoculations with a Psp strain expressing RFP and a second strain expressing either GFP or YFP. Although both strains form individual colonies emitting one fluorescence (D), mixed colonies expressing both fluorescent proteins are also evident (E).*
Source: (A) Collmer (2012). Trends Microbiol.; (B) Collmer & Worley; previously unpublished; (C–E) Godfrey et al. (2010). MPMI 23(10): 1294–1302.

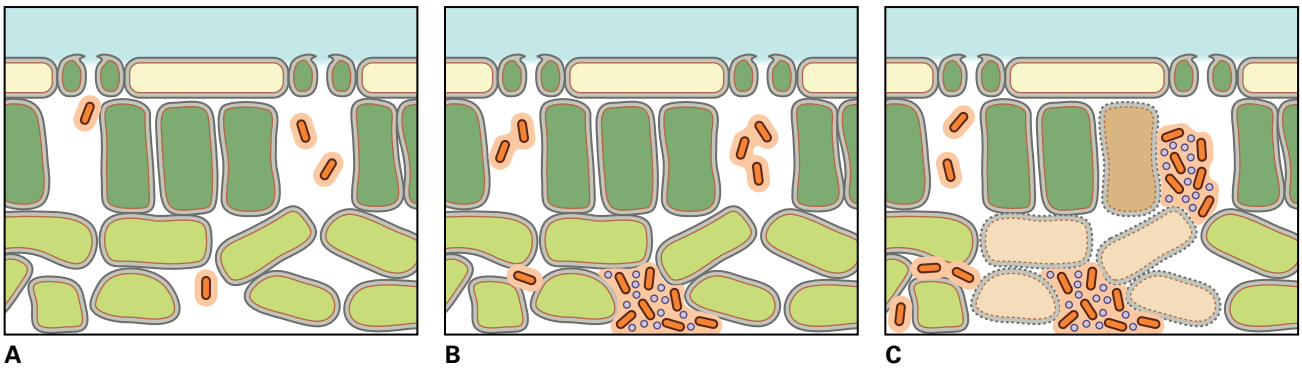


FIGURE 21.13 *Quorum sensing during growth of a pathogenic bacterium in the intercellular spaces of plant leaves. Bacteria enter the leaf through stomatal openings. (A) Early in leaf colonization, the bacterial population is sparse and only a low concentration of* N*-acylhomoserine lactone is present. (B) As the density of the bacterial population rises, elevated* N*-acylhomoserine lactone concentrations lead to expression of many different types of cell wall-degrading enzymes and other effector molecules. (C) These higher concentrations of bacteria, enzymes, and effectors result in the death of plant cells and the appearance of disease symptoms.*

10-fold to permit trafficking of the large nucleoprotein complex. Genetic studies showed that interaction of the TMV 30-K movement protein with a cell wall pectin methylesterase is required for TMV cell-to-cell movement and infection. In contrast, some dsDNA viruses, such as cauliflower mosaic virus (CaMV), orchestrate the formation of large tubular structures composed of movement proteins to facilitate the movement of encapsidated virus particles through enlarged plasmodesmata.

The second common feature of virus cell-to-cell movement is the involvement of the endoplasmic reticulum and membrane trafficking. Synaptotagmin proteins are calcium sensors that regulate synaptic vesicle exo- and endocytosis in animals and plants (see Chapter 4). In *Arabidopsis,* the synaptotagmin protein SYTA regulates endosome recycling as well as movement protein-mediated trafficking of plant virus genomes through plasmodesmata. The SYTA protein localizes to endosomes in plant cells and binds directly to the movement

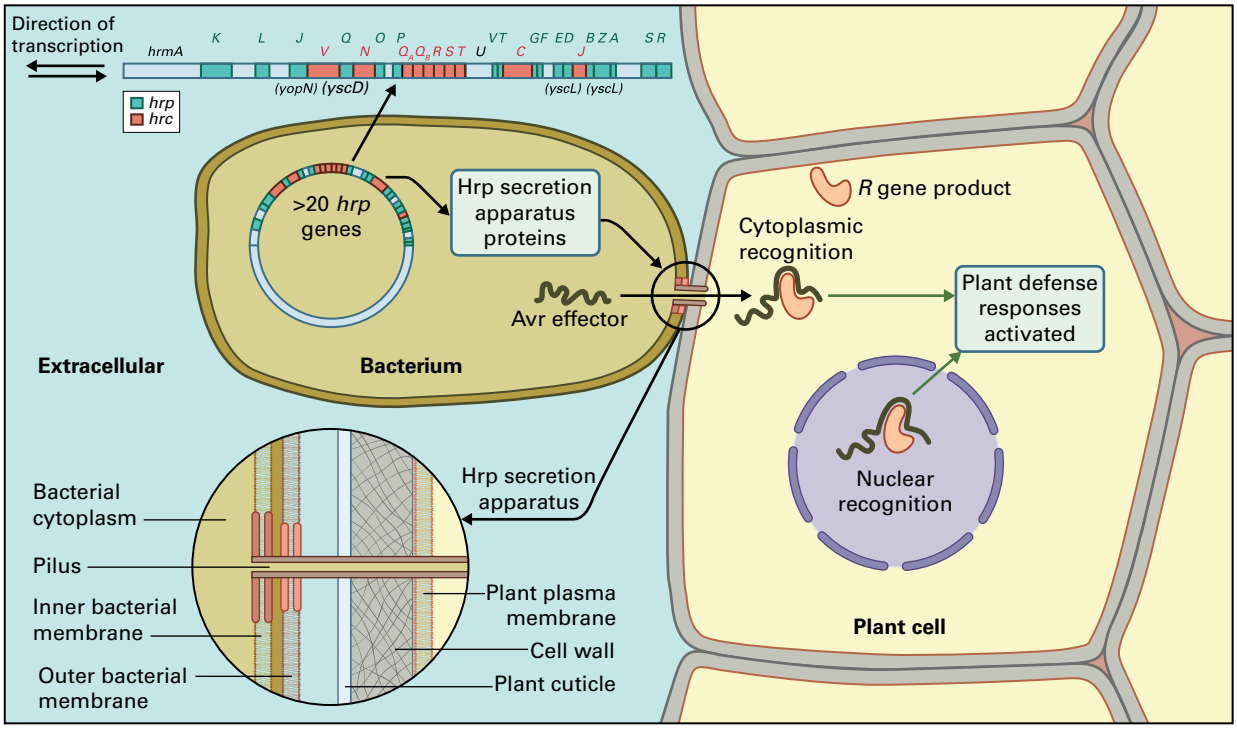


FIGURE 21.14 *Bacterial pathogens of plants and animals utilize similar secretion pathways during pathogenesis. One such system, the type III secretion system (T3SS), involves a protein complex that spans both the inner and outer bacterial membranes and a pilus that projects through the plant cell wall and into the host cell. The structural components of the T3SS are encoded by clustered* hrp *genes. Nine of the Hrp proteins of pathogenic plant bacteria are similar to components of the T3SS of animal pathogenic bacteria; consequently, members of this subset of Hrp genes are referred to as Hrc genes (hypersensitive response and conserved). Cytoplasmic R proteins activate plant defense responses only after corresponding Avr effectors have been delivered directly into the plant cytoplasm. Once Avr effectors are inside the plant cell, Hrp proteins are not needed for plant defense activation.*

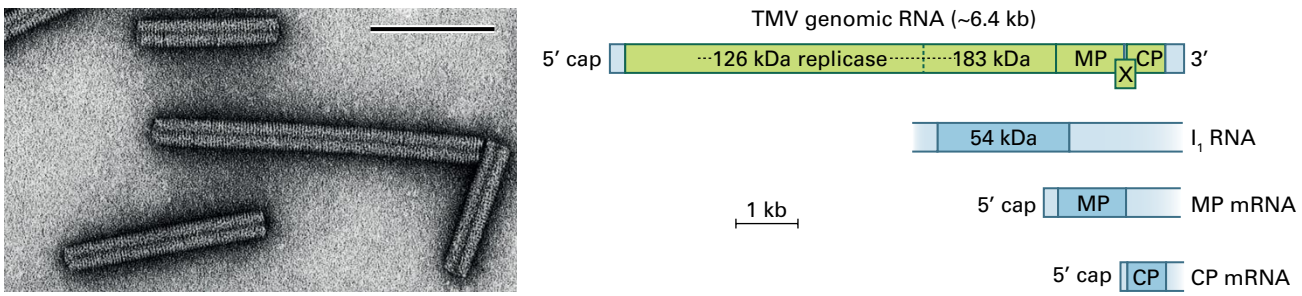


FIGURE 21.15 *The encapsidated ssRNA virus, tobacco mosaic virus (TMV). (A) Transmission electron micrograph of TMV particles. Each rod is 18 nm in diameter. (B) TMV has a single-stranded positive sense RNA genome that is 6,395 nucleotides in length, with a cap at the 5′ end and a tRNA-like secondary structure at the 3′ end. The genome encodes at least four viral proteins, the open reading frames (ORFs) of which are represented by boxes. The 183-kDa replicase protein is synthesized by readthrough of a leaky termination codon at the end of the 126-kDa replicase protein ORF. The replicase proteins are translated from the genomic RNA. The movement protein (MP, 29 kDa), which facilitates the cell-to-cell movement of viral particles via plasmodesmata and into systemic tissue, and the coat protein (CP, 17 kDa) are translated from subgenomic RNAs. An additional subgenomic RNA (I_1) encoding a putative 54-kDa protein has been detected in TMV-infected tobacco leaves, but it is not known whether this is translated to produce a protein product during TMV infection.*
Source: (A) Franki et al. (1985) Atlas of Plant Viruses, Vol. 2, CRC Press, Boca Raton, FL, p. 138.

proteins of both cabbage leaf curl virus (CaLCuV-ssDNA genome) and tobacco mosaic virus (TMV-ssRNA genome) to facilitate cell-to-cell movement. These virus movement proteins transport their cargo to the plasmodesmata in readiness for cell-to-cell spread via an endocytic recycling pathway (Fig. 21.16).

The processes controlling long-distance systemic transport of virus particles or viral nucleic acid within the phloem

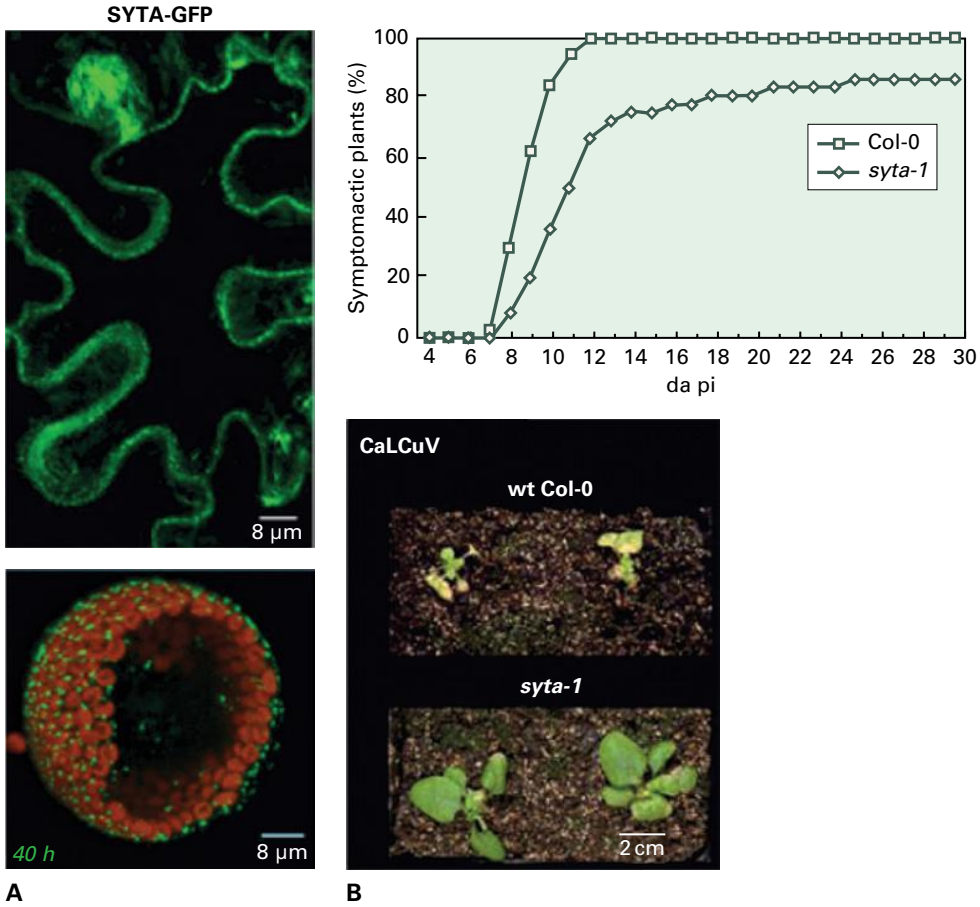


FIGURE 21.16 *The plasmodesmata protein STYA assists virus movement. (A) Endosome localization of the SYTA-GFP tagged protein in a leaf epidermal cell (top) or protoplast prepared from a leaf mesophyll cell (bottom). The STYA protein binds directly to the movement protein of both cabbage leaf curl virus (CaLCuV-ssDNA genome) and tobacco mosaic virus (TMV-ssRNA genome) and facilitates cell-to-cell movement. (B) Infection by the CaLCu virus is slower in the* syta-1 *mutant* Arabidopsis *plants (top), and the disease symptoms are less severe (bottom).*
Source: Lewis & Lazarowitz (2010). Proc. Natl. Acad. Sci. USA 107:2491–2496.

are probably distinct from those controlling movement between mesophyll cells. How viruses enter or leave the phloem is not well understood. Once inside the phloem, viruses can move at speeds of up to 1 cm/hour. Most viruses are transported in the phloem as either nucleoprotein complexes or virions, with contributions from host and virus proteins. The coat protein is necessary for this process to work efficiently for some viruses, for example TMV; for other viruses, however, it may not be involved. One challenge is to identify the host components in the phloem that interact with either the coat protein or virus particles to facilitate this rapid transport and subsequent re-entry of the virus into mesophyll cells once a new organ is reached. The interaction between the TMV 30-kDa movement protein and a specific host-encoded pectin methylesterase is one of the few mechanisms involved in vascular exit of the TMV virion or a coat protein–viral nucleic acid–protein complex into distal leaves. Some virus proteins contribute to the establishment and maintenance of systemic infection by suppressing RNA silencing-mediated degradation of viral RNA (see Section 21.9.2).

21.3.5 Some pathogenic nematodes modify the metabolism of root cells, inducing the plant to form specialized feeding structures

More than 20 genera of nematode cause plant diseases, and infections by these tiny roundworms (≈1 mm long) are nearly always confined to the plant root system. These root infections can dramatically alter plant metabolism and often result in substantial modifications to root architecture (Fig. 21.17).

All parasitic nematode species are obligate biotrophs, and all possess a hollow feeding stylet that can penetrate plant cell walls. Ectoparasitic nematodes feed exclusively at the root surface, whereas endoparasitic species invade root tissues and spend a large portion of their life cycle in intimate association with root cells. By far the most damaging nematodes are the two groups of sedentary endoparasitic species belonging to the family *Heteroderidae*: the **cyst nematodes** (genera *Heterodera* and *Globodera*) and the **root-knot nematodes**

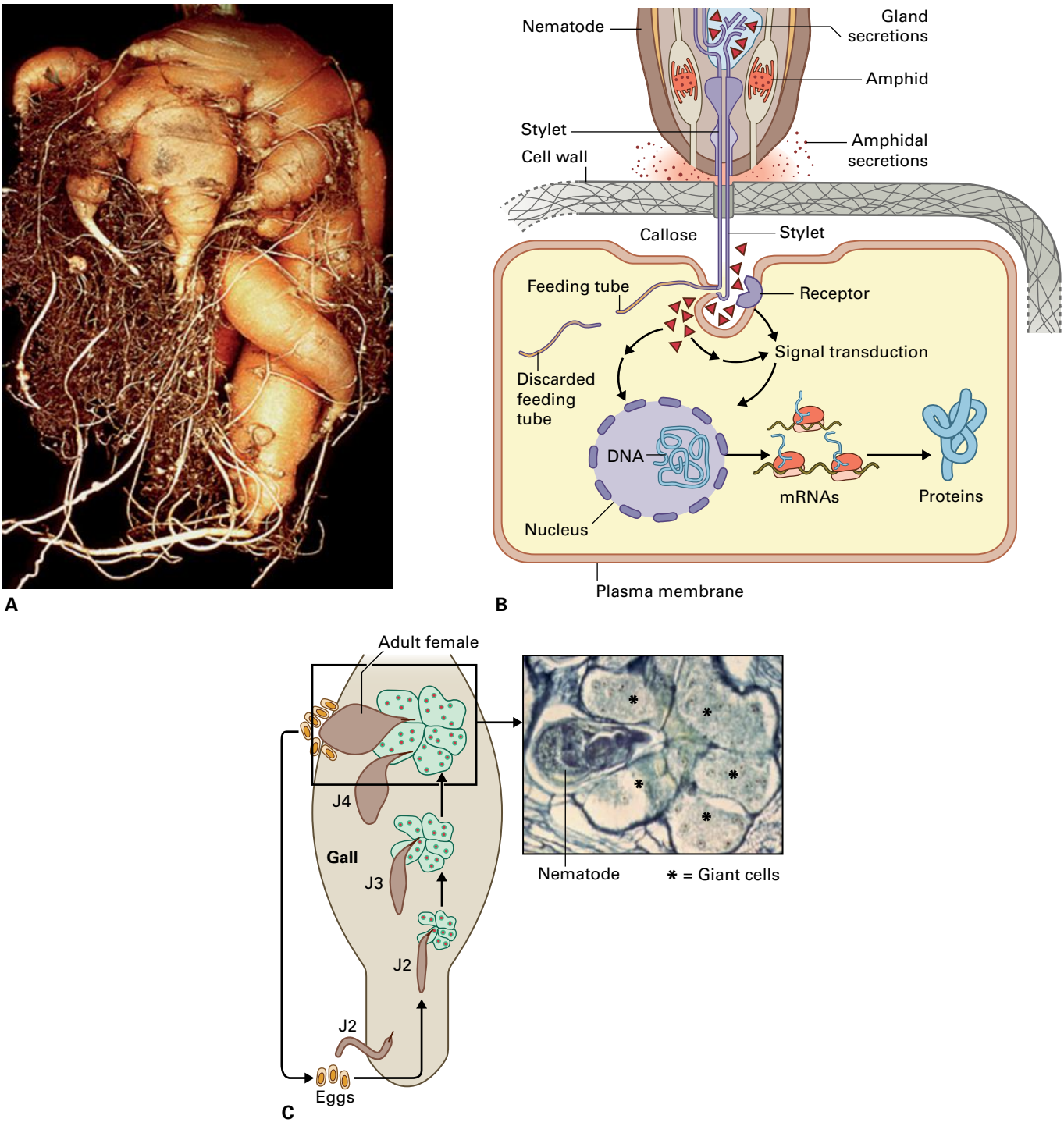


FIGURE 21.17 *Plant root–endoparasitic nematode interaction. (A) The swollen and distorted appearance of a carrot (*Daucus carota*) root caused by infection of the root-knot nematode* Meloidogyne hapla. *(B) The nematode uses a stylet at the anterior to enter a plant cell and pump secretions from the amphid glands into the plant cell. Subsequently, inside the invaded plant cell a new feeding tube is synthesized, which the nematode uses to extract nutrients specifically from the modified cell cytoplasm. In each plant cell selected, hundreds of discarded feeding tubes can accumulate. (C) Life cycle of the root-knot nematode and a stained transverse tissue section showing the giant cells induced by the feeding sedentary nematode. Nematode eggs hatch in the vicinity of the root tip. The second-stage juvenile (J2) then migrates towards the root, enters it close to the tip, migrates towards the vascular tissue, selects a single xylem parenchyma cell, loses mobility, and commences feeding. The body of the feeding sedentary nematode swells (third stage juvenile—J3), and feeding induces plant cell mitosis uncoupled from cytokinesis and DNA endoreduplication. This results in abnormal cortical cell growth and the formation of large giant cells around the J3, fourth-stage juvenile (J4) and the adult nematode. The induced giant cells facilitate nutrient removal from the vascular tissue to enhance nematode growth and facilitate the formation of hundreds of mature eggs inside the body of the female nematode.*
Source: (A) Hapla, APS website; (C) Mitchum et al. (2008). Curr. Opin.Plant Biol. 11:75–81.

(genera *Meloidogyne*). These nematodes spend 30–40 days feeding on highly modified xylem parenchyma cells, and they severely restrict plant growth and development.

The life cycle of the endoparasitic nematodes commences when dormant eggs perceive a chemical signal released by plant roots to induce the hatching of the juvenile nematode. For the potato (*Solanum tuberosum*) and soybean (*Glycine max*) cyst nematodes, the hatching factors are solanoeclepin A and glycinoeclepin A, respectively. Motile second-stage juveniles penetrate roots and then migrate to the vascular tissue just behind the root tip. Once feeding is initiated, the nematode loses motility and becomes sedentary.

To commence feeding, the juvenile cyst nematodes push their stylets through the plant cell wall, but not the plasma membrane, and release glandular secretions into the selected cell(s) (Fig. 21.17B). Molecules in the secreted fluid induce rapid modifications to the cytoplasm of the plant cell, and the metabolic activity of the plant cell increases. In addition, the nematode triggers partial dissolution of cell walls, such that the symplastic connections of the modified cell to its neighbors become more extensive, until finally protoplast fusion occurs. Eventually, as many as 200 plant cells may be recruited by the nematode to form the **syncytial feeding structure**. In contrast, the feeding of root-knot nematode juveniles induces mitosis uncoupled from cytokinesis and DNA endoreduplication (see Chapter 11). These result in abnormal cortical cell growth and the formation of a series of **giant cells** (Fig. 21.17C). In other respects, the morphology of the syncytial and giant cells is similar; both become closely associated with the phloem via transfer cell connections to ensure the entire plant is tapped for nutrients. In effect, the developing female root-knot and cyst nematode populations on the root system become powerful alternative sinks for sugars and so lower crop yields from infected plants.

Studies with mutant lines of *Arabidopsis thaliana* have revealed several plant proteins and metabolites required for nematode infection. The root-knot nematode must disrupt the plant cytoskeleton to establish a successful infection. By lowering the levels of a plant actin depolymerizing factor, the F-actin component in the cytoskeleton can be stabilized, thereby blocking giant cell maturation and reproduction of the nematode. For the beet cyst nematode, transport of auxin to the initial syncytium and the subsequent lateral redistribution of auxin are critical to ensure the radial expansion of the feeding site as the female nematode's size increases and egg maturation occurs.

One key issue in plant-sedentary nematode associations is the nature of the biochemical signals within the nematodes' glandular secretions that cause such dramatic changes in root cell architecture. Microscopic analysis has revealed a structure called a **feeding tube**, which is exclusively associated with the stylet. Unlike the stylet, the feeding tube is located within the plant cell cytoplasm (Fig. 21.17B). A new feeding tube is formed every time the nematode feeds; thus, by the time pathogenesis is complete, hundreds of feeding tubes have been made in each giant or syncytial cell. Microinjection experiments using fluorescently labeled dextrans of different molecular weights determined the size exclusion limit for molecules passing through the feeding tube is between 20 and 40 kDa. This suggests the signals of the nematodes could be relatively small molecules. The identification of the bioactive gland secretion components is currently an area of intense research (see Section 21.3.7).

21.3.6 Feeding arthropods damage plants and facilitate colonization by viral, bacterial, and fungal pathogens

Diverse insect species feed, reproduce, and shelter on plants. Two main herbivorous insect categories are recognized: those that chew and those that suck sap (Fig. 21.18).

Chewing insects cause the more spectacular plant tissue damage. For example, Colorado potato beetles (Fig. 21.18A) and locust species may defoliate an entire crop within a few days. For other chewing species, the extent of damage frequently depends on the developmental stage of both the pest and the plant. The larva of the European corn borer attacks only the leaves of young maize (*Zea mays*) plants, but as both plant and pest mature, the insect becomes a devastating stalk borer. Other chewing insects feed exclusively on roots or seeds.

The sap-sucking insects, such as adult leafhoppers, aphids (Fig. 21.18B), thrips, and plant bugs, instead cause minimal direct tissue destruction. Via a specialized mouthpart, the stylet, the phloem sieve elements are located, penetrated, and the sap removed (Fig. 21.19). Heavy infestations of sap-sucking insects cause chronic shortages of photosynthates and lead to a severe reduction of plant growth.

Plant volatiles released at the site of insect feeding can act as both attractants and deterrents to further colonization by the same or other insect species. Detailed analysis of the changes to air composition in the vicinity of feeding insects, in combination with electrophysiological experiments to explore insect neural stimulations in response to specific plant volatiles, reveal the complexity of insect–plant communication events.

The largest group of plant volatiles is the terpenes, a diverse class of secondary metabolites that includes monoterpenes (C10) and sesquiterpenes (C15) (see Chapter 24). One plant-produced sesquiterpene, (E)-β-farnesene (EBF), has been considered a potential defense against aphids, since its emission by plants causes aphids to drop off the plant or depart from the feeding site. For many aphids, EBF is the principal constituent of the aphid alarm pheromone, and the constitutive production of EBF by plants could hold promise in the control of specific aphid pests. In certain cropping habitats (e.g., tropical rainforests) the insect pressure is so great that young plant leaves emerge with different spectral and volatile properties than the mature leaves and initially remain undetected.



A



B

FIGURE 21.18 *Chewing and sap-sucking insects. (A) The stem- and leaf-chewing Colorado potato beetle (*Leptinotarsa decemlineata*). (B) Sap-sucking green peach-potato aphid (*Myzus persicae*). The green peach-potato aphids can transmit over 100 species of plant infecting viruses. Some of the most damaging diseases include potato leaf roll virus and potato virus Y to Solanaceae, beet western yellows and beet yellows viruses to Chenopodiaceae, lettuce mosaic virus to Compositae, cauliflower mosaic and turnip mosaic viruses to Cruciferae, and cucumber mosaic and watermelon mosaic viruses to Cucurbitaceae.*
Source: (A) Monsanto Co., St. Louis, MO; previously unpublished; (B) Rothamsted Research images; previously unpublished.

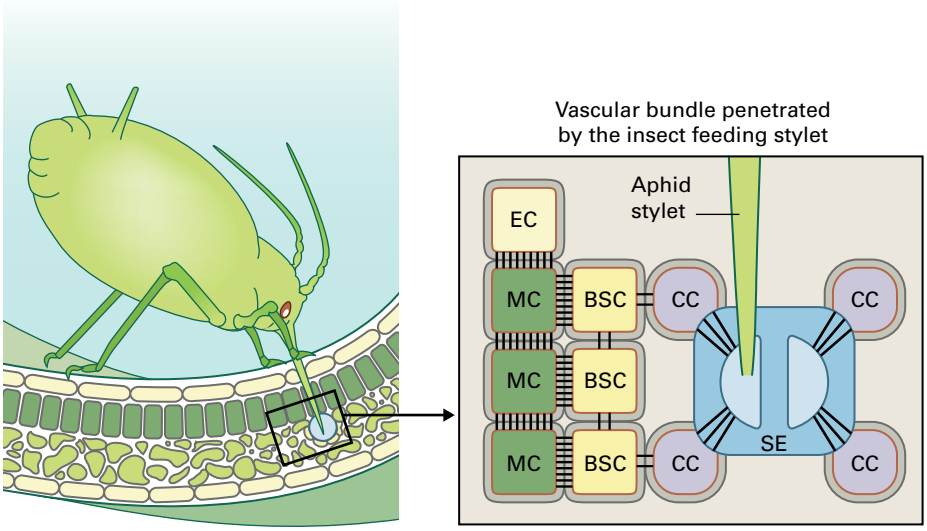


FIGURE 21.19 *Insects can be vectors for the transmission of viruses into plant cells. An aphid feeding stylet delivers viruses directly into the phloem sieve elements (SE). The virus particles then move by way of the translocation stream to other regions of the plant, where they can exit into the surrounding cells through the SE and the companion cells (CC), through the plasmodesmatal connections. BSC, bundle sheath cell; MC, mesophyll cell; EC, epidermal cell. The relative frequency of plasmodesmatal connections is indicated by the number of lines between cells.*

Many insect pest species also transmit viruses. The sap-sucking species are effective virus vectors, delivering virus particles directly into the vascular tissue, thereby permitting their rapid dissemination throughout the plant. Some virus species can also replicate and persist inside insect vectors. During subsequent feeding, the insect thus infects almost every susceptible plant. Both the barley yellow dwarf virus and potato virus Y are transmitted persistently by the green peach aphid (*Myzus persicae*) (see Fig. 21.18B). Chewing insects rarely transmit viruses, but the tissue damage caused frequently permits attack by necrotrophic fungal and bacterial species (see Sections 21.3.2 and 21.3.3).

21.3.7 Pathogen effectors promote susceptibility by diverse mechanisms

The interactions between plants and fungi, oomycetes, bacteria, nematodes, viruses, and insects reveal the range of molecules that pathogens can synthesize in an effort to gain nutrients from their host plants and, hence, reproduce to complete their life cycles. An **effector molecule** is made by a pathogen to enhance the pathogen's colonizing abilities.

Effector molecules are sometimes referred to as compatibility factors because interactions between plants and pathogens that result in disease are described as **compatible interactions**. In contrast, interactions that fail to result in disease formation are **incompatible**. Many effector molecules either singly or in specific combinations suppress host PTI or ETI (see Fig. 21.3). The isolation and characterization of effector molecules is of great interest, because nature has selected over millions of years molecules that target important host defense components. Different types of effectors are summarized in Table 21.2.

The plant cuticle and the cell walls represent significant barriers to colonization. To promote infection, many fungal and bacterial pathogens secrete enzymes, such as cutinases, cellulases, xylanases, pectinases, and polygalacturonases. Hydrolysis of the major components of the aerial surface of plants such as **cutin**, and those within the underlying plant

TABLE 21.2 *Examples of plant pathogen effectors.*

Pathogen class	Species	Effector name	Effector function
Virus	Tobacco mosaic virus (TMV)	P50	Viral replicase
Virus	Potato virus X	CP	Coat protein
Oomycete	*Hyaloperonospora arabidopsidis*	Atr1/Atr13	Contributes to pathogen virulence inside host cells by suppressing PTI
Oomycete	*Phytophthora infestans*	Avr3a	Interacts with and stabilizes the plant U-box E3 ligase CMPG1 protein, preventing INF1 triggered plant cell death during the biotrophic phase
Fungus	*Melampsora lini*	AvrL567	Haustorially expressed secreted protein translocated into plant cells; exact function in virulence unknown
Fungus	*Cladosporium fulvum*	Avr2	Inhibits multiple extracellular cysteine proteases, like Rcr3,required for ETI and basal defense
Bacterium	*Pseudomonas syringae* pv. *tomato*	AvrPto	Enhances bacterial growth and plant necrosis. Interferes with protein kinase function to suppress defenses
Bacterium	*Xanthomonas euvesicatoria*	AvrBs2	Protein containing a domain homologous to the *Escherichia* coli glycerolphosphodiesterase and the agrocinopine synthase of *Agrobacterium tumefaciens*. Required for bacterial virulence by an unknown mechanism
Bacterium	*Ralstonia solanacearum*	PopP2	PopP2 belongs to the YopJ-like family of effectors found in mammalian and plant pathogens. PopP2 has autoacetyl-transferase activity that targets a lysine residue well conserved in this effector family. Probably affects plant gene transcription to favor bacterial virulence
Root-knot nematode	*Meloidogyne incognita*	16D10	Interacts with tomato Scarecrow-like transcription factors which regulate root radial patterning. This secreted nematode peptide functions as a signaling molecule to interfere with root proliferation by targeting host transcription factors
Cyst nematode	*Heterodera schachtii*	CBP	Binds to and increases plant pectin methyl-esterase protein, thereby reducing the level of methyl-esterified pectin in cell walls. This subsequently facilitates the access of other cell-wall-modifying enzymes to cell wall polymers, which is required for syncytium formation and development
Aphid	*Acyrthosiphon pisum*	C002	Assists aphid feeding on phloem sap in sieve elements and thereby increases aphid survival rates

cell wall such as **cellulose**, **hemicelluloses**, and **pectin**, weakens these structures and facilitates pathogen entry. Most pathogens produce a diversity of **cell wall-degrading enzymes**.

Many plant pathogens also produce a range of toxins (see Section 21.3.3). Some chemicals are toxic to all plants, whereas others are toxic to only one or a few plant species (**host-selective toxins**). Regardless of type, these toxins inhibit the action of specific plant proteins. For example, the fungus causing Northern leaf blight disease of maize, *Cochliobolus carbonum*, makes a host-selective toxin called HC toxin (see Fig. 21.7). Like many other fungal toxins, the HC toxin is a cyclic

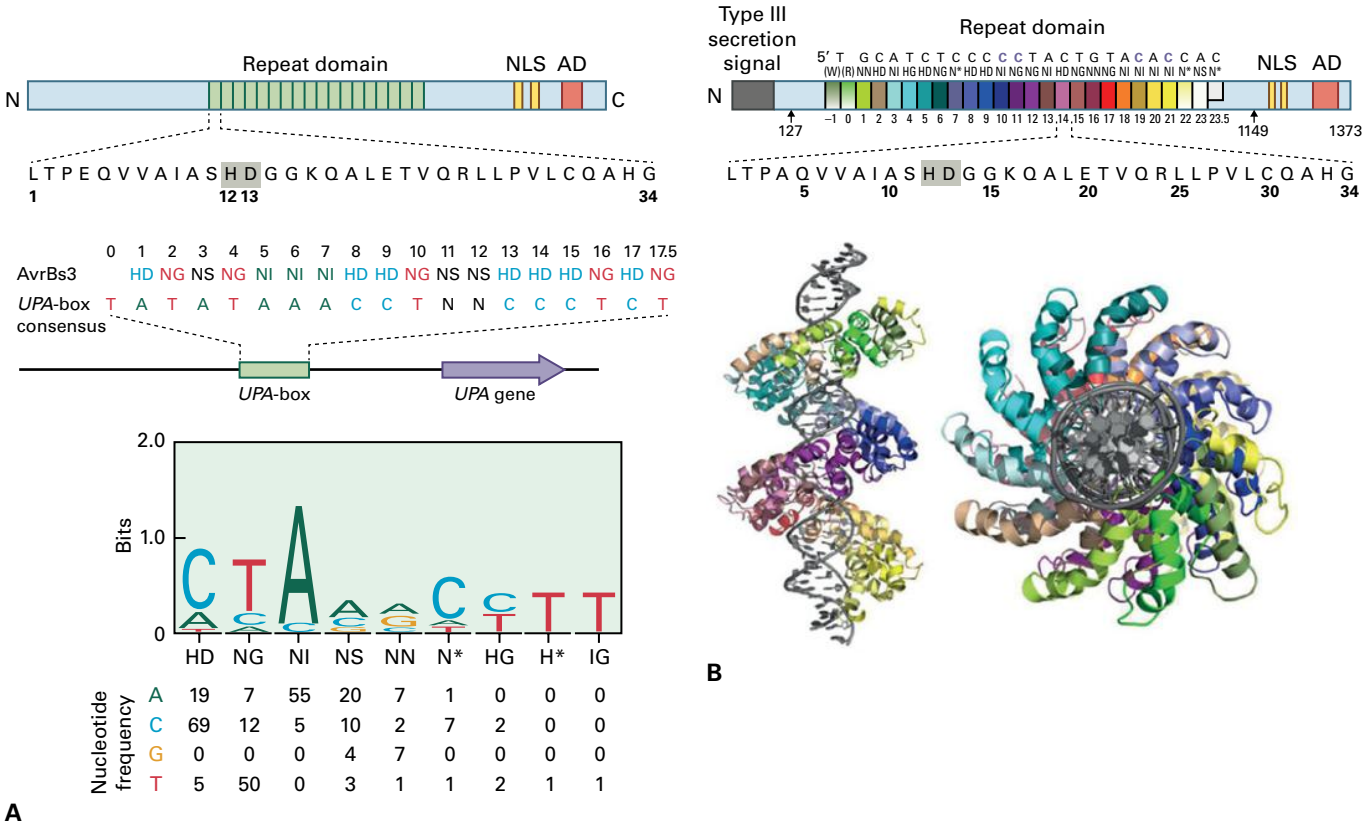


FIGURE 21.20 *Transcription activator-like effectors (TALEs) are natural type III effector proteins that are secreted by numerous species of* Xanthomonas. *(A) TALEs have an elegant code linking the central domain of TALEs with their target DNA binding site. In the example illustrated, the AvrBs3 effector acts as a transcriptional activator in the plant cell nucleus, where it directly binds to DNA in the promoters of plant genes upregulated by AvrBs3 (UPA), via the tandem repeats. The repeats in the central domain differ from each other mainly in amino acid positions 12 and 13 (repeat variable di-residues, RVDs). Computational and functional analyses have revealed a strong correlation between unique pairs of RVDs and the corresponding nucleotide in the TALE-binding site. For example, the amino acid di-residue histidine-aspartic acid (HD) binds to cytosine (C), the di-residue asparagine-glycine (NG) binds to thymine (T), the di-residue asparagine-isoleucine (NI) binds to the nucleotide adenine (A), and the di-residue asparagine-asparagine (NN) binds to guanine (G), and to a lesser degree adenine (A). The UPA-box contains the nucleotide consensus sequence in the promoter region to which the AvrBs3 effector binds and UPA-gene denotes the induced target gene. (B) The crystal structure of the* Xanthomonas oryzae *effector PthXo1 bound to its DNA target in the promoter of the rice* Os8N3 *gene. The domain organization of PthXo1 shown in the upper panel has the 23.5 repeats color-coded to match those shown in the lower panel. The RVDs that recognize the nucleotide cytosine are shown in gray box. The lower panel shows the structure of the PthXo1 DNA-binding region in complex with its target site. Each repeat forms a left-handed, two-helix bundle that presents the unique RVD-containing loop to the DNA. The repeats self-associate to form a right-handed superhelix wrapped around the DNA major groove. The first RVD forms a stabilizing contact with the protein backbone, while the second makes a base-specific contact to the DNA sense strand. Two degenerate amino-terminal repeats also interact with the DNA.*

peptide. It is synthesized continuously by two specific tetrapartite cyclic peptide synthetases (HTS1 and HTS2) and then exported outside the fungal cell. In maize (*Zea mays*) leaves, the HC toxin inhibits histone deacetylases to effect changes in host gene expression, presumably those genes involved in defense against *C. carbonum*. Mutant strains of *C. carbonum* that do not produce the HC toxin are **nonpathogenic** (do not cause disease). Maize genotypes that carry the *Hm1* gene, which encodes an enzyme that can metabolize and thereby detoxify HC toxin (see Fig. 21.7), are resistant to *C. carbonum*.

The related fungi *Stagonospora nodorum* and *Pyrenophora tritici-repentis* are necrotrophic pathogens of wheat (*Triticum aestivum*) and cause the diseases *Stagonospora nodorum* blotch and tan spot, respectively. Numerous secreted proteinaceous host-specific toxins are produced by both pathogens. These toxins trigger severe necrosis and disease in wheat lines harboring the corresponding dominant sensitive alleles of the wheat gene. The *ToxA* gene encodes a 13-kDa polypeptide and was likely transferred from *S. nodorum* to *P. tritici-repentis*. In wheat leaves, the small ToxA protein is internalized within sensitive host cells, where it localizes to chloroplasts. ToxA stimulates host cell death in a light-dependent manner: it forms oligomers and interacts with plastocyanin, a component of the photosynthetic electron transport chain (see Chapter 12). Protein sequence and

structural studies on ToxA have revealed an arginine-glycine-aspartate solvent-exposed loop is required for internalization into wheat cells. The ToxA protein has structural similarity with effectors produced by other fungal pathogens (Table 21.2)

For plant pathogenic bacteria in the genus *Xanthomonas*, TAL (transcription activator-like) effectors (Fig. 21.20) contribute to disease formation or trigger defense by binding host DNA and activating effector-specific host genes. So far, these are the only type of bacterial effectors known to regulate host cell gene expression directly. Their discovery also led to the description of a new type of DNA-binding protein. TAL effectors are delivered into plant cells by T3SS, and once inside, they activate transcription of specific plant genes that enable pathogen spread. For example, PthXo1, a TAL effector of the rice pathogen *Xanthomonas oryzae*, activates expression of the rice gene *Os8N3*, allowing *Xanthomonas* to colonize rice plants. The rice Os8N3 protein is also required for normal plant development, so the host gene cannot be inactivated or eliminated to avoid infection. Instead, there is strong selective pressure for the plant to accumulate Os8N3 promoter mutations that prevent PthXo1 binding and, as a consequence, for the *Xanthomonas* bacteria to make compensatory changes in the TAL effector's DNA-binding specificity.

The specificity of DNA binding by each TAL effector and ability to adapt to host mutations depend on a variable number of typically 34 imperfect amino acid repeats in each TAL protein. The greatest polymorphism has been observed at positions 12 and 13 in each repeat, the repeat-variable diresidue (RVD) (Fig. 21.20A). Remarkably, the amino acid residues representing the RVDs of each TAL bacterial effector protein correspond to the nucleotides in the target site plant DNA. A "one-RVD-to-one nucleotide" relationship was identified, which can be imprecise. RVDs bind their cognate nucleotides through a unique structure of the protein when it interacts with the binding site in the DNA (Fig. 21.20B). The RVD code was initially deduced through molecular genetic analyses of the interaction between AvrBs3 (the TAL effector of a *Xanthomonas* pathogen of pepper (*Capsicum* sp.)) and its target DNA sequence in the promoter of the *Bs3* resistance gene. BS3 evolved as an allele of a gene that, when transcriptionally activated by a bacterial effector, elicits defense responses. The specificity of each *Xanthomonas* effector can be predicted from the protein sequence, and the target site in the promoter DNA of the host gene can be readily identified. Different DNA binding motifs can be added to a plant promoter, and these confer TAL effector-dependent expression of reporter genes in planta. Furthermore, TAL effectors can be designed to bind any DNA sequence (see Section 21.11).

Pathogenic strains of the bacterium *P. syringae* pv. *syringae* (*Pss*) cause disease on many different plants, including brown spot disease on bean (*Phaseolus vulgaris*). Some *Pss* strains secrete syringolin A (SylA), a peptide derivative synthesized by a mixed nonribosomal peptide synthetase/polyketide synthetase encoded by a gene cluster. The effector SylA is secreted by the bacteria into the host plant cells. Strains of *Pss* engineered not to produce SylA are significantly reduced in virulence towards bean leaves (see Fig. 21.16). Once inside the cells, SylA irreversibly inhibits the proteasome (see Chapter 10).

Effectors often target host cell enzymes for inactivation. Three functions for different *C. fulvum* effectors have been defined, and each exhibits a different type and degree of sequence polymorphism (Table 21.3). The Avr2 effector inhibits tomato cysteine proteinases that are important components of plant defense. Effectors from *P. infestans* and from nematodes also inhibit this class of cysteine proteases. Avr4 inhibits plant chitinases, likely playing a crucial role at the growing hyphal tip. The Ecp6 effector contains a LysM domain, which specifically binds chitin fragments. However, unlike Avr4, Ecp6 does not inhibit plant chitinases. Instead, it functions by binding to chitin fragments, thus preventing this type of PAMP from being detected by plant cells and initiating PTI. Effectors from the rice blast fungus *Magnaporthe oryzae* and wheat blotch fungus *Mycosphaerella graminicola* also contain multiple LysM domains and bind chitin fragments to prevent PTI and assist the early biotrophic phase of the infection.

The rice blast fungus *Magnaporthe oryzae* invades rice by forming an appressorium (Fig. 21.21) in which enormous turgor pressure is created via hydrolysis of storage carbohydrate to glycerol. A septin ring assembles on the lower side of the appressorium to provide cortical rigidity and membrane curvature for the formation of a single penetration peg, which then enters the plant cell. However, unlike the powdery mildews, the penetrating *M. oryzae* hyphae do not form a haustorium to extract nutrients; instead, the hyphae invade successive living rice cells while enclosed in host-derived extra-invasive hyphal membrane. A structure called the **biotrophic interfacial complex** (BIC) accumulates fluorescently labeled effectors secreted by the invasive hyphae (Fig. 21.21). At the BIC complex, some of the accumulating *M. oryzae* effectors are translocated into the host cell cytoplasm. Other *M. oryzae* effectors do not accumulate at the BIC, but instead uniformly surround the invasive hyphae. The fungal effectors that reach the rice cytoplasm then move via plasmadesmata into uninvaded neighboring host cells, presumably preparing them before invasion.

Several effectors from the basidiomycete fungus *Melampsora lini*, which causes flax rust disease, have been identified and their crystal structures determined. They are small secreted proteins expressed exclusively in the fungal haustorium and then translocated into the host cells (Fig. 21.22A). The mechanism of AvrL567 and AvrM rust effector entry into plant cells is controversial and likely involves endocytosis (Fig. 21.22B). Residues located on the protein surface are important for recognition by the plant (see Section 21.7).

Another basidiomycete, the maize smut fungus *Ustilago maydis*, causes the formation of large tumors. During infection, *U. maydis* secretes several chorismate mutases, key enzymes of the shikimate pathway that catalyze the conversion of chorismate to prephenate, the precursor for tyrosine

TABLE 21.3 *Features of some of the Avr and ECP proteins produced by the fungus Cladosporium fulvum and secreted into the apoplast during tomato leaf infection.*

Protein	Extent/type of polymorphism	Main protein function	Role in the interaction
Avr2	Small deletions or insertions	Inhibition of plant cysteine proteases	Reduction in the effectiveness of one class of induced defense proteins
Avr4	Point mutations leading to amino-acid substitutions	Chitin-binding	Protection of fungal chitin from degradation by induced plant chitinases
Avr9	Whole gene deletions	A high-affinity Avr9 binding site (HABS) has been detected in resistant and susceptible tomato and non-host Solanaceous plants	Secreted cysteine-knot protein; unknown function
Ecp2	Point mutations leading to amino acid substitutions	Unknown function; gene sequences homologous to Ecp2 have been identified in over 100 other microbial species, including plant pathogens	Unknown function
Ecp6	Limited point mutations resulting in a total of five single-nucleotide polymorphisms (SNPs) and one amino-acid substitutions	Binding chitin fragments; functional homologs have been identified in other plant pathogens	Removal of chitin fragments detectable by plant chitin receptors; gene deletion leads to reduced virulence

and phenylalanine (see Chapter 7). The chorismate mutase Cmu1 secreted by *U. maydis* is required for plant colonization. The enzyme is taken up by plant cells, can spread to neighboring cells, and changes the metabolic status of these cells. The overall effect of Cmu1 and other secreted effectors produced by *U. maydis* is to reduce the accumulation of salicylic acids and therefore reduce the intensity of the defense response at the site of infection (see Section 21.8.2).

Effector properties of plant viral proteins and their ability to trigger disease resistance have now been clarified for many viruses and often the viral coat protein can elicit the resistance response, but the plant can evolve to recognize any viral protein. In contrast, identifying the effector molecules produced by parasitic nematodes of feeding aphids is difficult. The nematode-secreted peptide 16D10, which was first isolated from the soybean root-knot nematode *Meloidogyne incognita*, interacts with a plant regulatory protein, stimulates root growth, and binds *in planta* to two SCARECROW-like transcription factors (see Chapter 11). But how this peptide contributes to the infection process remains unclear.

21.3.8 Pathogens specialize to colonize different host tissues

Infection by each pathogen species tends to be restricted to specific plant organs and tissue types (see Fig. 21.5). The mechanisms underlying this organ and tissue specificity have not been elucidated. Conceivably, only specific plant organs can fulfil the nutritional requirements of the pathogen. Alternatively, different effector molecules may need particular conditions to be fully functional, so that effector molecules can only aid the infection process in particular regions of the plant or at specific stages of plant development.

Some obligate biotrophs, such as the fungal rusts, infect taxonomically distinct plant species to complete different phases of their complex life cycle. For example, *Puccinia graminis* var. *tritici* infects wheat stems and leaves, but subsequently infects the leaves of a dicotyledonous plant species Barberry (*Berberis vulgaris*) to complete the life cycle (see Box 21.1). Successful infection of these **alternate hosts** might require a distinct suite of effector molecules. Importantly, asexual spores are produced during growth on grass leaves, but the sexual reproductive cycle is confined to the barberry.

The downy mildew pathogen *Hyaloperonospora arabidopsidis* and the white rust pathogen *Albugo laibachii* are obligate biotroph oomycete pathogens of *Arabidopsis*, and both elaborate haustoria in infected cells. Remarkably, infections by *A. laibachii* enhance host plant susceptibility to other pathogens to which the host is normally resistant, including recognized races of *H. arabidopsidis* (Fig. 21.23). After suppression of host defense by *Albugo* infection, genetically incompatible pathogens become able to infect and sporulate. Cell death mechanisms are also suppressed. The result is a mixture of different pathogenic species successfully infecting in close proximity

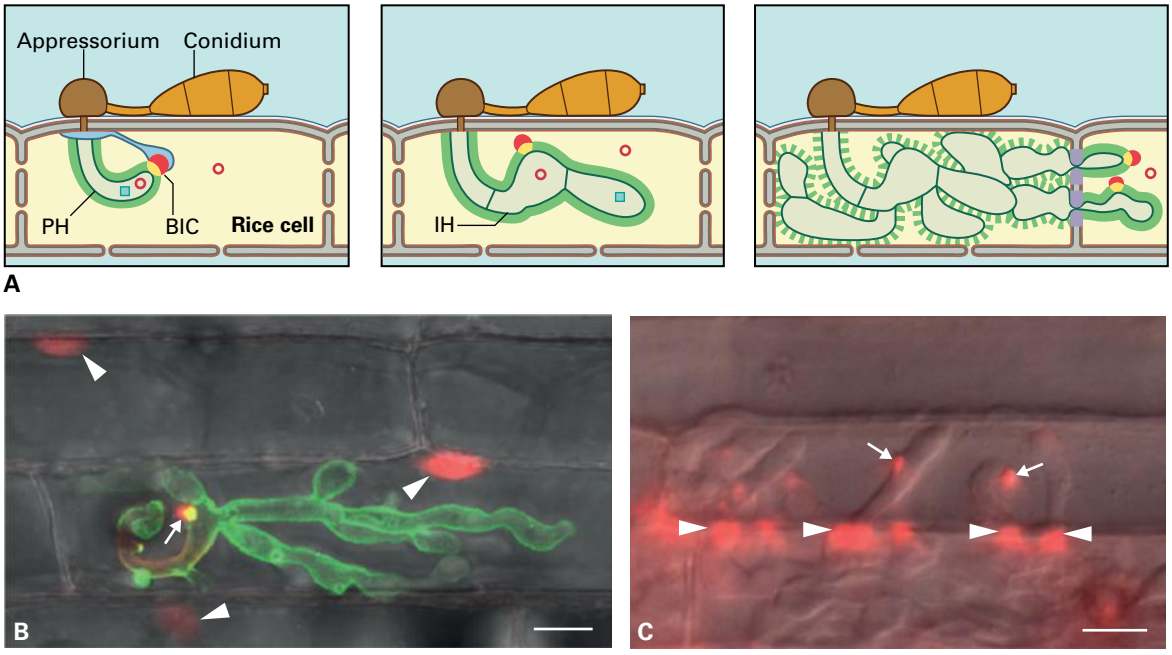
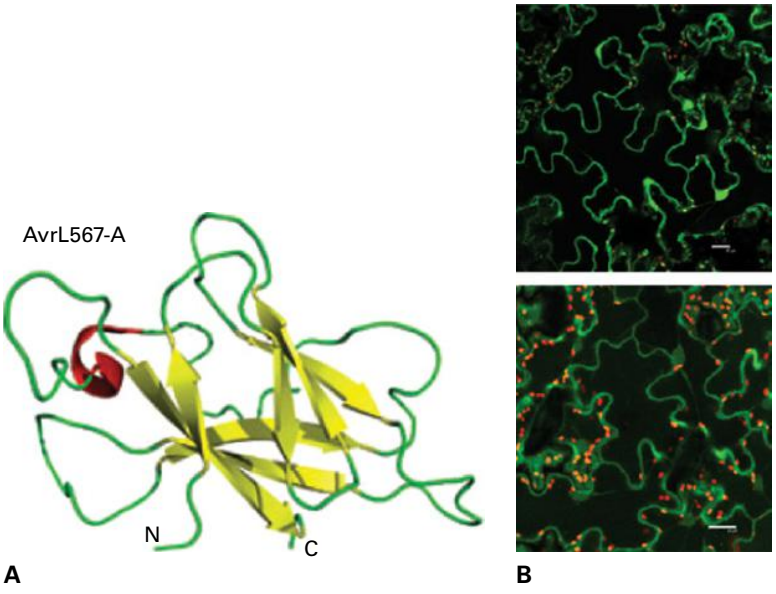
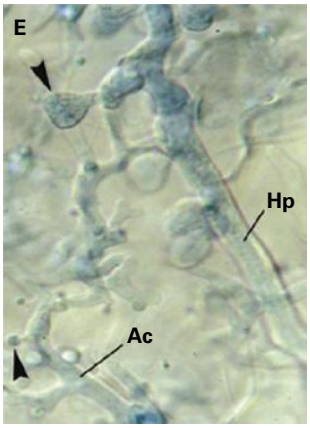


FIGURE 21.21 *Formation of the biotrophic interfacial complex (BIC) complex during* Magnaporthe oryzae *infection of rice (*Oryza sativa*) leaves. The BIC is a plant-derived, membrane-rich structure that facilitates translocation of some effector proteins into the host cell cytoplasm. (A) Schematic representation of the post-penetration differentiation of a filamentous primary invasive hypha (PH) (left, ≈22–25 hours post inoculation, hpi) into a pseudohyphal-like bulbous invasive hypha (IH) (middle, ≈26–30 hpi.) in an invaded rice cell. This differentiation occurs for each new hypha invading a living neighbor cell (right, ≈36–40 hpi). Cytoplasmic effectors (open red circles) show preferential accumulation in the BIC, which is first located in front of the growing primary hyphal tips, and then remains behind beside the first-differentiated bulbous IH cell. Other apoplastic effectors (green squares) are secreted into and retained within the extra-invasive hyphal membrane compartment surrounding the PH (green solid line). (B) A confocal projection image shows an IH (at 30 hpi) expressing the BAS4 effector fused to the fluorescent reporter protein GFP and the effector protein PWL2 fused to a different fluorescent reporter protein mCherry (red, a brighter variant of mRFP) engineered with a C-terminal viral nuclear localization signal. The fluorescently labeled PWL2 (red) preferentially accumulated in the BIC (white arrow). The nuclear targeting of the cytoplasmic effector PWL2:mCherry (red color) facilitates visualization of effector translocation through the BIC and subsequent cell-to-cell spread in advance of hyphal colonization. The apoplastic effector BAS4: EGFP (green) remains localized to the outside of the invasive hyphae within the extra-invasive hyphal membrane. (C) IH expressing cytoplasmic effector BAS2:mRFP (red). The IH were imaged after growth into a second-invaded cell at 36 hpi. The BAS2:mRFP fusion protein accumulated in BICs (arrows) and at cell wall crossing points (arrowheads, purple in right panel in A).*
Source: (B) Giraldo et al. (2013). Nat. Commun. 4:1996.

FIGURE 21.22 *Flax rust effectors. (A) Crystal structure of the flax rust effector AvrL567-A. (B) Translocation of pathogen effector proteins into the host cell cytoplasm, monitored by transient effector expression (flax rust effector AvrM -cerulean fusions) in tobacco (*Nicotiana tabacum*) leaves. Top, the cerulean tag only. Bottom, AvrM-cerulean fusion appears as bright red circles on the inside of the plant plasma membrane when viewed by UV microscopy.*
Source: (B) Rafiqi et al. (2010). Plant Cell 22:2017.




A



B

FIGURE 21.23 *(A) Preinfection (48 hours) of wild-type* Arabidopsis thaliana *with a virulent isolate of* Albugo candida *(white blister rust) suppresses host defenses and, following secondary inoculation, enables avirulent downy mildew pathogens to colonize and reproduce. (B) Juxtaposition of hyphae of* A. candida *(Ac) and* Hyaloperonospora parasitica *(Hp) in the mesophyll of a sequentially inoculated cotyledon of* Brassica juncea. *Arrowheads indicate a characteristic large, lobed haustorium of Hp compared with the much smaller, stalked haustorium of* A. candida.
Source: E. Kemen, Max-Planck-Institute, Cologne.

to each other. Such mixed infections are common in nature, though due to their complexity, less commonly investigated.

21.3.9 Genome sequencing reveals the gene complements and virulence factor repertoires of plant pathogens

Pathogen genome sequencing enables definition of the complete repertoire of predicted genes for a plant pathogenic species. Comparison of the content and organization of each genome provides researchers with a wealth of information to better understand pathogen and pest biology. Genome information also provides clues to the range of inter- and extracellular molecules (proteins and metabolites) produced by pathogens that might be detected by plant cells to prevent infection of the different types of pathogens. The genomic era began for plant-infecting pathogens with the sequencing of plant viruses and viroids, then plant pathogenic bacteria, and recently a full range of plant pathogenic fungi, oomycetes, plant parasitic nematodes, and insect pests. The first pathogenic species to be fully sequenced in each kingdom is given in Table 21.4, along with some species where the sequenced genome has given insight into the mechanisms underlying pathogenicity and host range.

Since the late 2000s, low-cost next-generation sequencing (NGS) methods and new sequence assembly algorithms have made it possible to undertake whole genome sequencing of many different strains or isolates of the same pathogenic species. By comparing closely related genomes, the candidate effector gene sets that may be responsible for key biological differences can be pinpointed and then assessed for function. In many whole genome studies, the transcribed portion (transcriptome) of the pathogen genome expressed *in planta* was also characterized, in an attempt to identify the putative effector sequences and induced metabolic pathways. Today, the genome sequences of hundreds of pathogenic species are available, with the number of species with full genomic sequence information predicted to rise to several thousands in the near future.

What has this wealth of genomic sequencing revealed so far? Particularly striking is the discovery that the genomes of taxonomically closely related species often exhibit remarkable diversity in genome size and architecture (Fig. 21.24 and Table 21.5). Reciprocally, common genome features, such as the clustering of effector genes in specific regions of the genome, can be found in phylogenetically unrelated species. For example, within the genomes of many plant pathogenic bacteria resides a cluster of genes that encode the type 3 secretion system (T3SS) (Fig. 21.25). The genomes of plant pathogens often show similarities to their free-living relatives.

In summary, the availability of full genome sequences for hundreds of pathogenic species from a wide range of taxa is revealing the gene complements and virulence factor repertoires of plant pathogens.

21.4 Preformed defenses

Most healthy plants synthesize a range of secondary metabolites with antimicrobial properties (see Chapter 24). These compounds either exist in biologically active forms or are stored as inactive precursors and converted by host enzymes to active forms in response to pathogen attack or tissue damage. In general, these preformed inhibitors are sequestered in vacuoles or organelles in the outermost layers of plant cells. Therefore, the mode of pathogen attack influences the concentrations of inhibitors it encounters: Necrotrophs invariably cause the release of high levels of inhibitors, while haustoria-forming biotrophic fungi may never encounter them. Two well-characterized classes of preformed inhibitors are the saponins and the glucosinolates (see Chapter 24); a third class are the benzoxazinoid acetal D-glucosides.

Saponins are glycosylated triterpenoid compounds related to sterols. The chemical structure of the triterpenoid saponin **avenacin A1**, found in oat (*Avena sativa*) roots, is illustrated in Figure 21.26. The wheat root pathogen *Gaeumannomyces graminis* var. *tritici* is extremely sensitive to avenacins. As a consequence, the root-debilitating disease called "take all" caused by *G.g. tritici* occurs on wheat and barley, but never in

TABLE 21.4 *The history of model species and plant pathogen genome sequencing.*

Date	Species	Estimated gene number	Comments
1977	Bacteriophage φX174	11	First replicating agent (virus) genome
1995	*Haemophilus influenzae*	1,740	First prokaryote (bacterial) genome
1996	*Saccharomyces cerevisiae*	6,000	First eukaryote (yeast) genome
1998	*Caenorhabditis elegans*	20,000	First invertebrate (nematode) genome
2000	*Drosophila melanogaster*	14,000	First insect genome
2000	*Arabidopsis thaliana*	25,500	First plant genome
2000	*Xylella fastidiosa*	2,900	First bacterial plant pathogen genome
2002	*Magnaporthe grisea*	11,100	First fungal plant pathogen genome
2002	*Oryza sativa*	37,500	Rice. First cereal crop. Draft sequences 2002, completed 2005
2003	*Pseudomonas syringae*	5,800	Model bacterial plant pathogen
2008	*Meloidogyne hapla*	14,200	First plant pathogenic nematode genome
2009	*Phytophthora infestans*	14,000	Potato blight pathogen – Oomycete genome
2010	*Acyrthosiphon pisum*	34,000	First aphid genome
2010 onwards	Parallel sequencing of multiple isolates per species		Predominantly use NGS approaches and the reference sequenced genome as the scaffold

oat (Fig. 21.26). *G.g. avenae* carries a saponin-detoxifying enzyme (avenacinase) that is required for pathogenesis on oats. Tomato plants produce tomatine, a compound that is closely related to avenacin. Only certain pathovars of the fungal pathogen *Septoria lycopersici* can cause disease on tomatoes, and these pathovars produce a glucosidase that can detoxify tomatine.

Glucosinolates are sulfur-containing glucosides produced by *Brassicacae*, including *Arabidopsis thaliana*. Glucosinolates are divided into three classes, depending upon the nature of their side chains, which are derived from aliphatic, indolyl, or aralkyl α-amino acids (see Chapter 24). Defenses based on glucosinolates can be preformed or induced. Some glucosinolates become biologically active only in response to tissue damage via the activity of the enzyme myrosinase (a thioglucosidase) (Fig. 21.27). In healthy plant cells, subcellular compartmentalization separates myrosinase from the glucosinolate substrate, either in specialized myrosin cells in the phloem parenchyma or in stomatal cells. The unstable aglycone intermediate generated by myrosinase enzyme activity is converted into various products, including volatile isothiocyanates (mustard oils) (Fig. 21.27). Genetic variation exists for the glucosinolate profiles in oilseed rape plants (*Brassica napus*). An elevated proportion of butenyl glucosinolates, via the elimination of the pentenyl type, decreases leaf tissue palatability to unspecialized *Brassicae* pests, such as rabbits, pigeons, and slugs, whereas it increases susceptibility to specialized insect pests, such as adult flea beetles (*Psylliodes chrysocephala*). Glucosinolates active against insects and necrotrophs are usually preformed, but some antimicrobial glucosinolates are induced (see Section 21.5.6).

The benzoxazinoid acetal D-glucosides are a class of nitrogen-containing compounds produced by maize, wheat, and rye (*Secale cereale*). Resistance to various insect species is strongly correlated with the presence of some of these compounds. For example, in maize, resistance to the European corn borer (*Ostrinia nubilalis*) is strongly correlated with the presence of DIBOA and DIMBOA (see Chapter 7). The biosynthetic pathway required for their production has been elucidated for maize (Fig. 21.28). In chloroplasts, indole is synthesized and then exported to the cytoplasm for metabolism by cytochrome P450 enzymes located in the endoplasmic reticulum. The benzoxazinoids formed are then glucosylated by the transfer of glucose from UDP-glucose, and the resulting glucosides are stored in the vacuole. These glucosides are nontoxic. Within maize chloroplasts, specific glucosidases cleave

TABLE 21.5 *Key features of plant pathogen genomes.*

Pathogen type/species	Genome features	Function
Gram-negative bacteria/*Pseudomonas, Xanthomonas, Ralstonia, Erwinia, Pectobacterium*	Multiple genomic islands: clusters of genes coding for type III secreted effectors (T3SE)	T3SE are either species-specific or common to multiple species, and many contribute to the infection process
	Horizontal gene transfer between distantly related bacterial species	Acquiring new disease-causing abilities or expanded host ranges
Gram-positive bacteria/*Leifsonia xyli* subsp. *xyli*	Large fraction of pseudogenes (13%) and genome shrinkage (i.e., loss of specific gene types)	Adaptation to a specific plant niche—for this species, the xylem
Obligate biotrophs/*Blumeria formae speciales*	Large genomes (120–150 Mb) with a high proportion of repetitive DNA (65–75%); both lineage-specific expansion and contraction of specific gene families	Restricted gene set for nitrate assimilation and sulfate assimilation reflects the reliance on plant metabolism for pathogen nutrition
Hemibiotrophic and necrotrophic ascomycetes	Majority have genome sizes of 35–45 Mb; small to large gene families for CWDE and small secreted proteins (SSPs); many possess secondary metabolism gene clusters	Gene gain/loss or gene family expansion/reduction associated with particular infection lifestyles; many SSPs are species-specific and may assist infection of specific plant hosts
Biotrophic basidiomycete smut fungi/*Ustilago maydis* and *Sporisorium reilianum*	Smaller genomes (≈19–21 Mb), small clusters of genes coding for secreted proteins, and a reduced set of genes encoding plant cell wall hydrolytic enzymes	To assist the long biotrophic lifestyle and tumor formation on the different host plants
Oomycetes/*Phytophthora*	Large genomes (≈220–280 Mb) of the *Phytophthora* species; a proliferation of repetitive DNA and, in particular transposable elements (TEs); RXLR and Crinkler effector genes embedded within long stretches of repetitive DNA	Repetitive DNA frequently coincides with a breakdown in the overall macro and micro order of the genes (synteny) between closely related species; within these syntenic breakpoint regions, effector and other genes evolve at accelerated rates compared to genes residing elsewhere in the genome
Obligate biotrophic oomycetes/*Albugo* and *Hyaloperonospora*	Smaller genomes (≈40–100 Mb), reduced set of genes encoding plant cell wall hydrolytic enzymes	Restricted gene sets reflect reliance on plant metabolism for pathogen nutrition
Root-knot nematodes/*Meloidogyne*	*M. hapla* – 54 Mb, *M. incognata* – 86 Mb Large gene families for plant cell wall-degrading enzymes (PCWD), including cellulases, xylanases, arabinases, pectinases, and expansins; many genes acquired by horizontal gene transfer from soil bacteria or from plant hosts; many species-specific sequences in the predicted secretomes	Adaptation to a specific plant niche and specific plant taxa
Phloem-feeding specialist insect/pea aphid (*Acyrthosiphon pisum*)	Large genome (≈464 Mb); many expanded gene families include those involved in sugar transport; many of the genes encoding immune system components are absent	The reduced immune capabilities of aphids could facilitate the acquisition and maintenance of bacterial symbionts, which provide essential amino acids that are absent or rare in the sugar-rich phloem sap

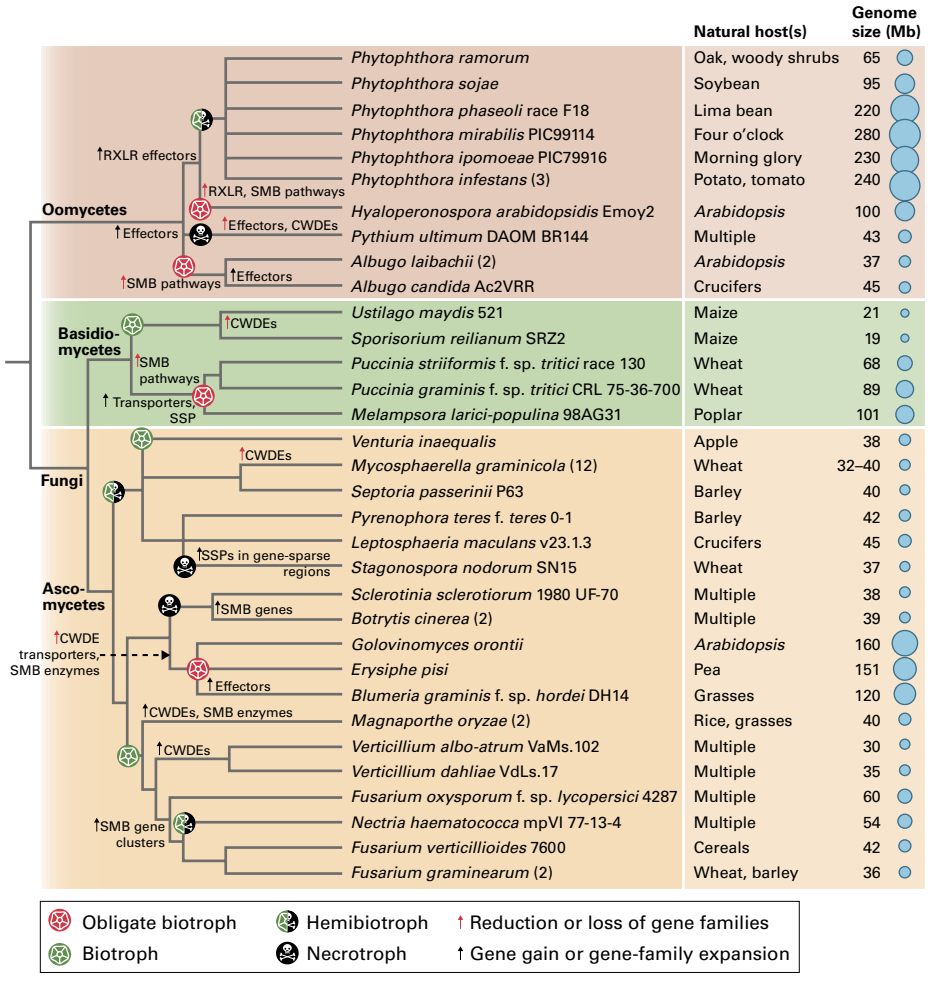


FIGURE 21.24 *Evolution and genome sizes of sequenced filamentous plant pathogen genomes. Filamentous eukaryotic plant pathogens belong to either the fungi or the stramenopiles (oomycetes). The representative phylogeny was generated using Interactive Tree Of Life (iTOL) with National Center for Biotechnology Information (NCBI) taxonomy identifiers (branch lengths are arbitrary). Isolate identifier, or the number of isolates sequenced, is indicated next to the species name. Pathogen lifestyles and major variations in gene families are indicated along the tree branches. The principal host plants and genome size, main insights gained from genome comparisons, are shown next to the tree branches. CWDE, cell wall-degrading enzyme; RXLR, arginine–any amino acid–leucine–arginine; SMB, secondary metabolites biosynthesis; SSP, small secreted protein.*

the glucosides to release the free benzoxazinoids. The benzoxazinoid DIMBOA, which is toxic to insects, only accumulates when the plant cell is damaged and permits the mixing of the vascular and chloroplast contents.

21.5 Induced defense

As explained in Section 21.2, defense is induced either by recognition of relatively conserved P/MAMPs by cell-surface pattern recognition receptors (PRRs), resulting in P/MAMP- (or PRR-) triggered immunity (PTI), or by recognition of effectors (directly or indirectly) by intracellular NB-LRR receptors leading to effector-triggered immunity (ETI). The following section explains how the recognition process then triggers signaling pathways that lead to the induction of various defense mechanisms.

21.5.1 PTI is one mechanism of induced defense

Pathogen molecules that can trigger PTI are shared by many different pathogenic species because they have conserved functions, such as **chitin** and other **glucans** that are essential for rigid fungal cell wall formation, the protein **flagellin** of the flagellum that is required for bacterial movement, and elongation factor-Tu (EF-Tu) of bacterial ribosomes.

Specialized PRRs have been identified in plants that recognize distinct P/MAMPs (Fig. 21.29). In *Arabidopsis*, the flagellin-sensing FLS2 protein detects a 22 amino acid peptide (flg22) derived from the N-terminal fragment of flagellin; this part of the protein is highly conserved across bacterial species. The *Arabidopsis* EF-Tu receptor EFR protein perceives an acetylated N-terminal 18 amino acids (elf18) of elongation factor-Tu. FLS2 and EFR have a similar

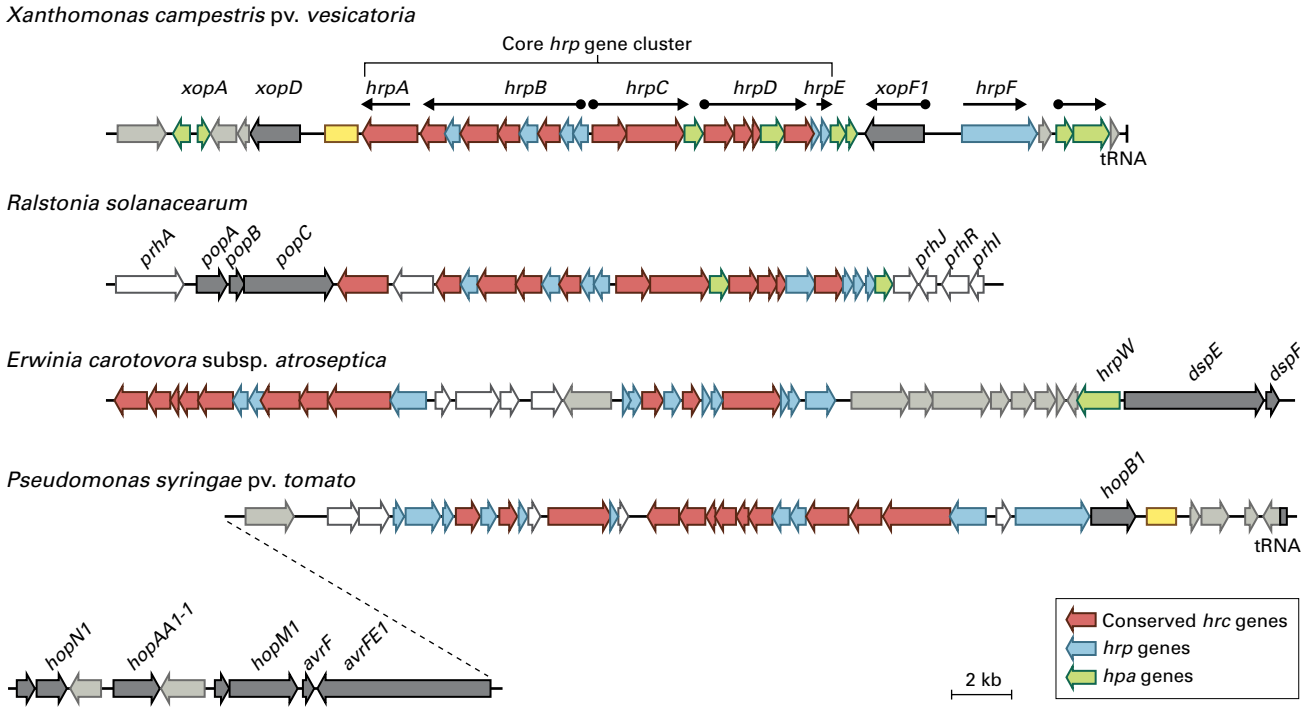


FIGURE 21.25 *Bacterial virulence gene islands. Schematic overview of the hypersensitive response and pathogenicity (*hrp*) regions from four different sequenced plant pathogenic bacteria. The* hrp *clusters of* Xanthomonas campestris *pv.* vesicatoria *strain 85–10,* Ralstonia solanacearum *strain GMI1000,* Erwinia carotovora *subsp.* atroseptica *strain SCRI1043, and* Pseudomonas syringae *pv.* tomato *strain DC3000 are shown. Red arrows indicate* hrc *(*hrp *conserved in plant and animal infecting bacteria) genes, blue arrows indicate* hrp *genes, green arrows indicate* hpa *(*hrp *associated) genes that contribute to, but are not essential for the pathogenic interaction with the plant, black arrows indicate type III effector genes, gray arrows indicate genes coding for proteins of unknown or other functions, and white arrows indicate genes encoding regulators of type three secretion system (T3SS) expression. Yellow boxes denote insertion sequences (IS) elements, acquired by horizontal gene transfer from other plant pathogenic bacteria. Arrows above the* Xanthomonas *sequence indicate the operon structure and the black dots highlight the* HrpX*-regulated genes which contain in their promoter region a plant-inducible promoter box (PIP box).*

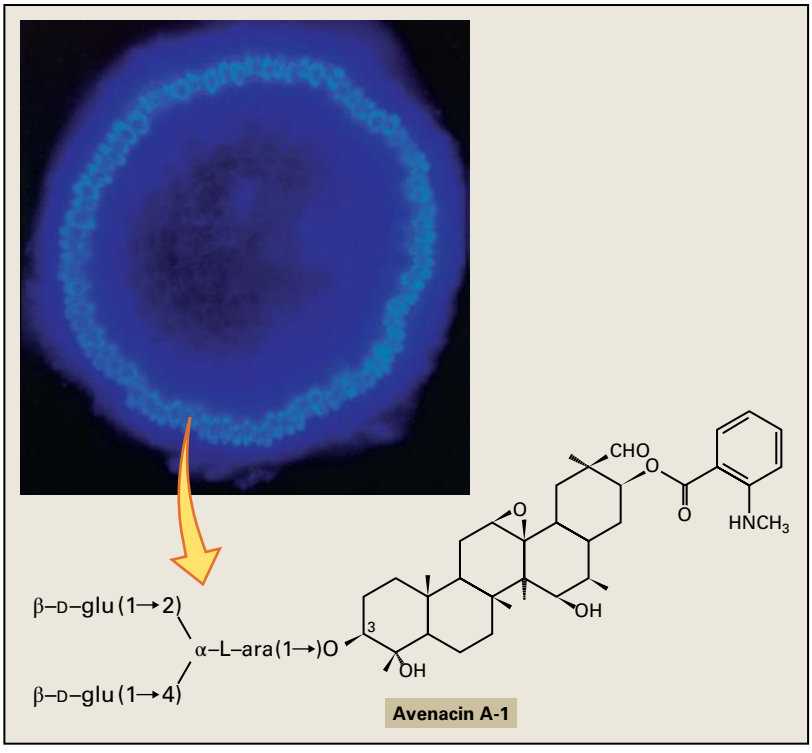


FIGURE 21.26 *Avenacin A-1 is a preformed defense saponin produced in the roots of oat (*Avena sativa*) but not in wheat (*Triticum *spp.) or barley (*Hordeum vulgare*). The epidermal location of avenacin in healthy oat roots is revealed when root sections are viewed under UV fluorescence. The root-infecting take-all fungus* Gaeumannomyces graminis *var.* tritici *is extremely sensitive to avenacin A-1, whereas a closely related species,* G. g. *var.* avenae, *carries a saponin-detoxifying enzyme that removes the 1 → 2- and 1 → 4-linked terminal* D*-glucose (glu) sugar molecules, rendering the avenacin A-1 nontoxic.*
Source: Osbourn (1999). Fungal Genet. Biol. 26:163–168.

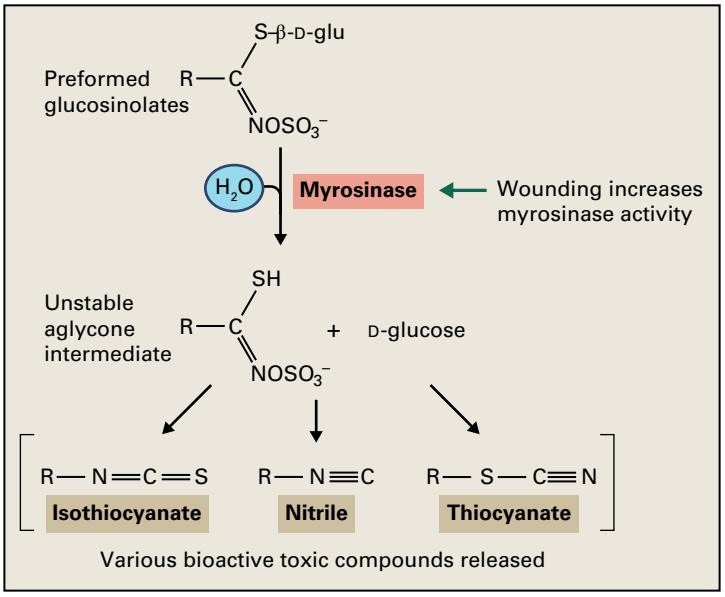


FIGURE 21.27 *Some glucosinolates are preformed defense compounds. Glucosinolates contain two sulfur atoms, one forming the link between a central carbon atom and the sugar group, the other in a sulfite (SO_3^-) group. When plant tissue is damaged, hydrolysis of these stored, preformed glucosinolates leads to the formation and release of numerous bioactive toxic compounds. Wounding activates myrosinase enzyme activity and also causes cellular decompartmentalization, which brings the activated myrosinase enzyme into contact with the glucosinolate substrates. Myrosinase cleaves the sugar–sulfur bond to release the sugar. The resulting compound spontaneously decays to produce sulfate (SO_4^{2-}) and toxic isothiocyanates, nitriles and thiocyanates.*

overall protein structure, and their activation triggers a rapid association with LRR kinase BAK1, which participates in subsequent signal initiation (Fig. 21.29).

Plant PRRs that recognize fungal chitin fragments (chitin oligomers) have been isolated from rice (*Oryza sativa*), wheat (*Triticum* sp.), and *Arabidopsis*. CEBiP (chitin elicitor binding protein) and CERK1 (chitin elicitor receptor kinase 1) both span the plasma membrane only once and possess extracellular domains that contain a different number of LysM motifs that bind chitin fragments. The CERK1 protein possesses an intracellular protein kinase domain that is involved in downstream signaling (Fig. 21.29; see also Fig. 21.41), whereas CEBiP does not. *Arabidopsis* CERK1 is also involved in recognition of bacterial peptidoglycan, a polysaccharide that carries a repeating *N*-acetylglucosamine unit.

The sequence of events activated during PTI is summarized in Figure 21.30. The microbial elicitor is recognized by a PRR in the plant plasma membrane. Recognition results in the rapid influx of calcium (Ca^{2+}) ions into the cell and production of ROS, such as superoxide anions ($O_2^{\cdot -}$) and hydrogen peroxide (H_2O_2). When ROS are produced at locally high concentrations, they have direct antimicrobial properties, while at lower concentrations ROS act as signaling molecules. These early events activate a signaling pathway that involves a series of specific protein kinases. BIK1 (and several related proteins) are receptor-like cytoplasmic protein kinases that are required for full FLS2 or EFR signaling, and they are targeted by some pathogen effectors (see Section 21.3).

21.5.2 Protein kinase signaling in plant defense involves MAPKs and CDPKs

Upon elicitation, at least two classes of protein kinases are activated: the **mitogen-activated protein kinases** (MAPKs; see Chapter 18) and **calcium-dependent protein kinases** (CDPKs). The CDPK class of protein kinases is absent from mammals, whereas the MAP kinases participate in signaling in all eukaryotes. In response to PAMP recognition and the rapid influx of Ca^{2+} ions, there is post-translational and sequential activation of a MAPKK kinase (MAPKKK), a MAPK kinase (MKK), and four different MAP kinases, as well as simultaneous activation of CDPKs (Fig. 21.30).

The expression of some genes is also induced rapidly. These genes typically encode other signaling proteins, such as protein kinases and regulatory proteins, such as transcription factors, which increase signaling complexity and further enhance plant defense activation. Later-expressed genes often encode proteins responsible for targeting other proteins for degradation via the **proteasome** (see Chapter 10). Such degradation may promote defense via removal of negative regulators of defense, or enable the defense response program to be reset so that subsequent pathogen challenges can be recognized and responded to. Protein inactivation is often achieved by the addition of ubiquitin molecules to certain sites on the protein (ubiquitination), thereby marking it for proteasome degradation (see Chapter 10).

The MAP kinases MPK3, MPK4, and MPK6 have roles in defense. MPK3, MPK6, and MPK11 have been linked to PTI. MPK4 was originally reported as a negative regulator of plant immunity because the *mpk4* mutant has a severely dwarfed growth phenotype, accumulates high levels of SA, and constitutively expresses several defense related genes. The *P. syringae* HopAI1 effector is a phosphothreonine lyase that irreversibly inactivates MPK3, MPK6, and MPK4, thereby preventing defense responses that would otherwise inhibit bacterial growth.

The best-studied in vivo substrate of MPK4 activity is MPK4 substrate 1 (MKS1). MKS1 forms a nuclear complex with MPK4 and the WRKY33 transcription factor (see Section 21.5.5). Following P/MAMP perception and MPK4 activation, phosphorylation of MKS1 leads to its exit from complexes with MPK4, thereby releasing the WRKY33 transcription factor, which is then available to bind to the cognate W box in the promoters of various target genes. For

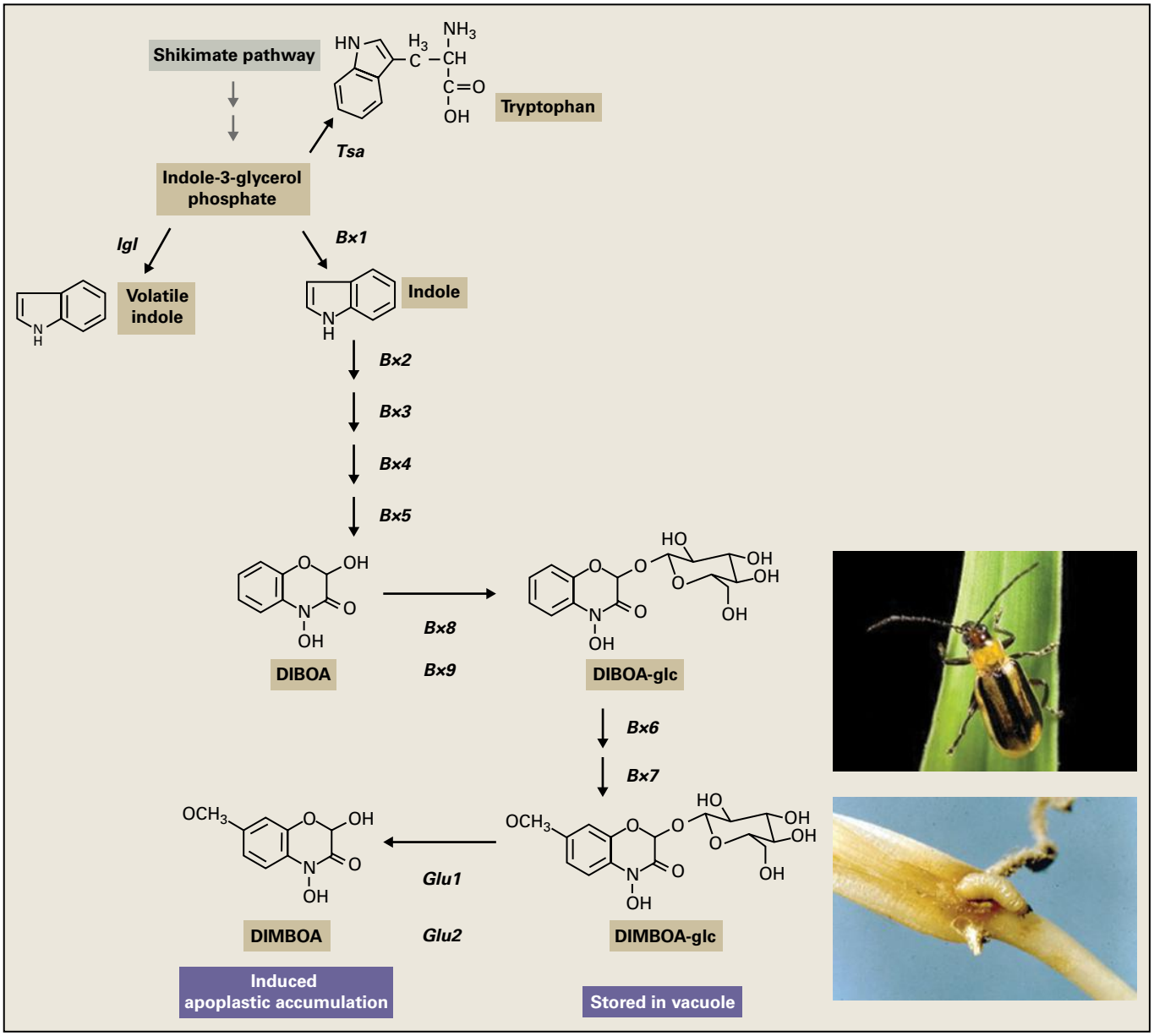


FIGURE 21.28 *Synthesis and storage of benzoxazinoid (Bx) secondary metabolites in grass species. The first step in Bx biosynthesis, the production of indole, occurs in the chloroplast by the conversion of indole-3-glycerol phosphate, an intermediate in the pathway to tryptophan synthesis, into indole. In maize (*Zea mays*), this reaction is catalyzed by either BENZOXAZINELESS1 (Bx1) or INDOLE GLYCEROL PHOSPHATE LYASE (Igl). The* Bx1 *gene is under developmental control and is mainly responsible for Bx production, whereas the* Igl *gene is inducible by stress signals, such as wounding, herbivory, or jasmonates. In maize leaves, the indole is exported to the cytosol, where it undergoes reactions catalyzed by various Bx enzymes associated with the endoplasmic reticulum. In many grass species Bx biosynthesis is mostly under developmental control and leads to accumulation of inactive Bx-glucosides that are stored in the vacuole. In rye (*Secale cereale*) and wild barley (*Hordeum vulgare*), 2,4-dihydroxy-2H-1,4-benzoxazin-3(4H)-one (DIBOA) is the dominant Bx, whereas in wheat and maize, the methoxy derivative, 2,4-dihydroxy-7-methoxy-2H-1,4-benzoxazin-3(4H)-one (DIMBOA) is more prevalent. DIMBOA accumulates in the apoplast, whilst inactive DIMBOA glucoside is stored in the vacuole. With the exception of Bx9, which is on maize chromosome 1, all* Bx *genes are located in a small segment of maize chromosome 4, spanning a genetic distance of only 6 cM. Lines of maize with high levels of DIMBOA in their roots are less damaged by the larvae of the Western Corn rootworm (*Diabrotica virgifera virgifera*) than lines with lower DIMBOA levels.*
Source: Ahmad et al. (2011). Plant Physiol. 157(1):317–327.

example, WRKY33 induces transcription of *PHYTOALEXIN DEFICIENT3* (*PAD3*), which encodes the cytochrome P450 monooxygenase required for synthesis of the antimicrobial phytoalexin camalexin (see Section 21.5.6). MPK3 and MPK6 can also directly phosphorylate WRKY33. Therefore, both MPK4 and MPK3/MPK6-mediated signaling are involved in WRKY33-induced *PAD3* expression, indicating dual control of PAD3 regulation in response to pathogen perception.

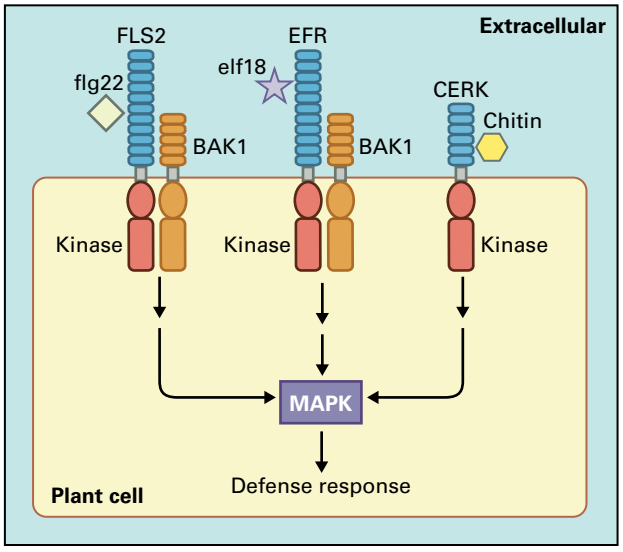


FIGURE 21.29 *Plants activate defense via cell surface pattern-recognition receptors (PRRs) upon recognition of conserved pathogen molecules (P/MAMPs), resulting in pattern-triggered immunity (PTI). In* Arabidopsis*, the flagellin-sensing FLS2 protein detects an N-terminal fragment of flagellin (flg22) that is highly conserved in pathogenic bacterial species. A second* Arabidopsis *PRR, the EF-Tu receptor EFR perceives an acetylated N-terminal 18 amino acids (elf18) of bacterial elongation factor-Tu. FLS2 and EFR have a similar overall protein structure. Both span the plasma membrane only once and possess an extracellular leucine-rich repeat (LRR) domain that recognizes and binds the cognate PAMP, and both carry an intracellular protein kinase domain. Activation of FLS2 or EFR triggers a rapid association with a second LRR kinase, BAK1, which participates in subsequent signal initiation. A third* Arabidopsis *PRR, the chitin receptor CERK1 (chitin elicitor receptor kinase 1) contains extracellular domains that contain LysM motifs that bind chitin fragments. The CERK1 protein possesses an intracellular protein kinase domain that is involved in downstream defense signaling, and does not require BAK1 for signaling. Note that the cell wall is not shown for clarity.*

21.5.3 Synthesis of reactive oxygen species (ROS) involves two mechanisms

The synthesis of ROS during the oxidative burst involves at least two separate mechanisms: NADPH oxidase and extracellular peroxidases.

The plasma membrane-spanning **NADPH oxidase** transfers an electron from NADPH within the cell across the plasma membrane and uses this to convert extracellular oxygen to the superoxide anion ($O_2^{\cdot -}$) (Fig. 21.31). The superoxide anions are then rapidly converted to hydrogen peroxide (H_2O_2), either spontaneously or through the action of **superoxide dismutase.** In *Arabidopsis,* NADPH oxidases are encoded by 10 respiratory burst oxidase homolog (*Atrboh*) genes. Two of the proteins, AtrbohD and F, are required for production of ROS in response to flg22 and during genetically incompatible host–pathogen interactions involving the oomycete *Hyaloperonospora arabidopsidis* and the bacterium *P. syringae*. Activation of NADPH oxidases involves the combined action of CDPKs and other protein kinases.

Two extracellular (apoplastic) peroxidase enzymes (PRX) are also sources of ROS production leading to the arrest of pathogen growth. *Arabidopsis* lines with diminished PRX33 and PRX34 expression have reduced ROS production and callose deposition in response to the P/MAMPs flg22 and elf18. The *prx33* mutant line is more susceptible to infection by a virulent strain of *P. syringae* than either the *AtrbohD* or *AtrbohF* mutant lines. The ROS generated by the extracellular peroxidases likely have role(s) as antimicrobial agents and in crosslinking specific polymers to the cell wall to improve rigidity.

21.5.4 Cell wall fortification is another induced defense response

Minute **papillae** often form directly beneath the attempted penetration site of biotrophic fungi (Fig. 21.32). These papillae are primarily composed of **callose** (a β-1,3 glucan polymer) and **lignin** (a highly complex phenolic polymer; see Chapter 2), and they are thought to block fungal penetration into plant cells. Induced callose deposition within plasmodesmata also likely blocks virus cell-to-cell movement.

Extracellular basic **hydroxyproline rich glycoproteins** (HRGPs) contribute to fortifying the cell wall in two ways. Preformed HRGPs crosslink rapidly to the wall matrix via the tyrosine in the repeated motif PPPPY that reacts with H_2O_2. The later de novo HRGP synthesis initiates additional lignin polymerization to further reinforce cell walls (see Chapter 2). These localized reinforcements make the plant cell wall more refractory to microbial penetration and enzymatic degradation.

Another class of defense-related extracellular proteins are **polygalacturonase-inhibiting proteins** (PGIPs), which carry a leucine rich-repeat (LRR) motif (see Section 21.6.2). These inhibit a specific subclass of necrotrophic pathogen cell wall-degrading enzymes called polygalacturonases. PGIPs likely retard polygalacturonase function, which would result in elevated levels of **oligogalacturonides** with chain length of >8 units (sometimes referred to as damage-associated molecular patterns or DAMPs) that are detected by PRRs (Fig. 21.33). Thus, PGIPs prevent complete hydrolysis of pectin so that oligogalacturonides persist long enough to activate these PRRs.

21.5.5 WRKY transcription factors contribute to plant defense responses

WRKY proteins are a large class of WRKY domain-containing, sequence-specific, DNA-binding transcription factors found almost exclusively in plants. WRKY domains comprise an almost invariant WRKYGQK sequence followed by a zinc-finger motif. *Arabidopsis* contains over 70 WRKY proteins that have been classified into three main groups and various subgroups. More than 70% of the *Arabidopsis WRKY* gene family members are

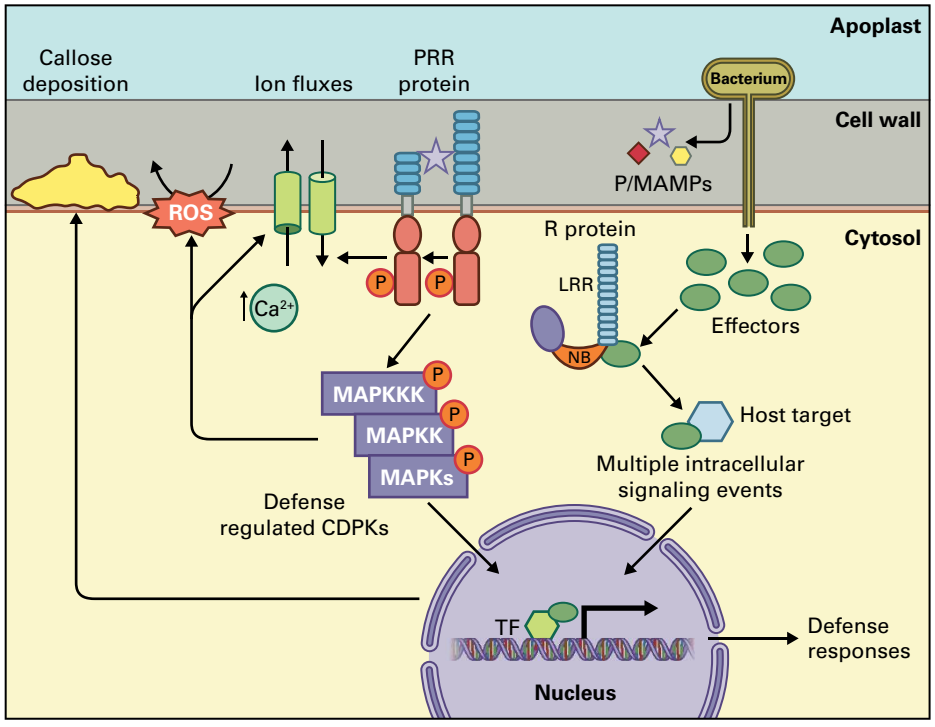


FIGURE 21.30 *Pattern-triggered immunity (PTI) and effector-triggered immunity (ETI) activation of early defenses. Following bacterial infection, detection of P/MAMPS by cell surface pattern-recognition receptors (PRRs) and detection of specific bacterial effectors delivered into the plant cell cytoplasm by resistance proteins (R) results in the rapid activation of numerous plant responses. These coordinated responses include alterations in ion fluxes at the plasma membrane, a local rise in cytoplasmic free calcium ion concentrations, the generation of various reactive oxygen (ROS) species at the cell surface, induction of cytoplasmic signaling cascades involving mitogen activated protein (MAP) kinases and calcium-dependent protein kinases (CDPKs), protein phosphorylation (P), induction of the expression of a first set of genes that encode regulatory and signaling proteins, and localized callose deposition to strengthen the cell wall. Collectively, these plant responses create a local environment that is unfavorable for bacterial growth and multiplication.*

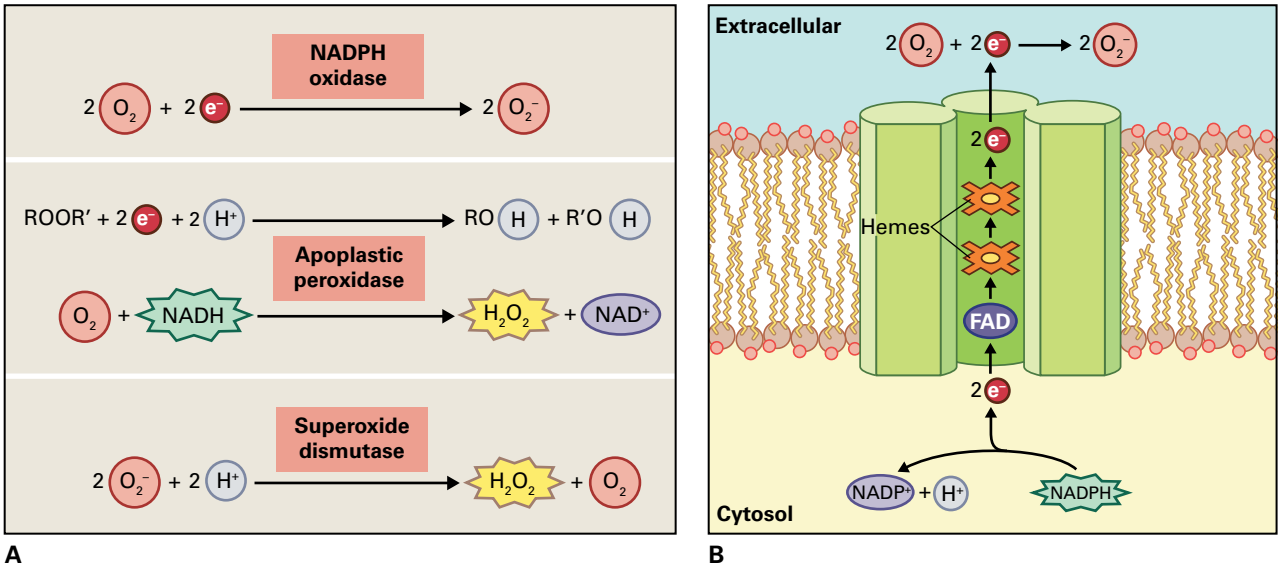


FIGURE 21.31 *Production of various reactive oxygen species. (A) Three routes are depicted: conversion of oxygen to superoxide (O_2^-) by the plasma membrane NADPH oxidase, generation of hydrogen peroxide (H_2O_2) by an apoplastic peroxidase, and conversion of O_2^- to hydrogen peroxide by the intracellular enzyme superoxide dismutase. (B) Activity of the NADPH oxidase. Electrons from intracellular NADPH are donated to extracellular oxygen to form superoxide, via electron carrying FAD and heme groups in the membrane-spanning enzyme.*

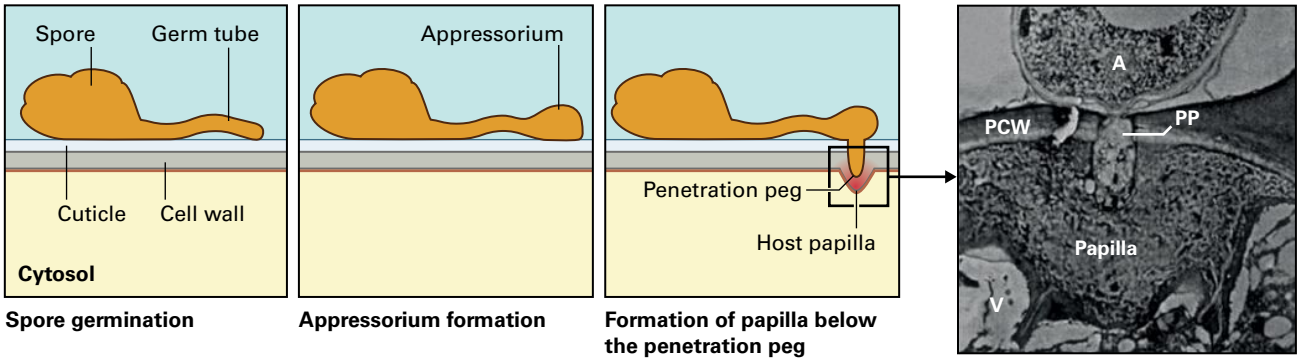


FIGURE 21.32 *A mildew fungus spore germinates and, after a short distance of growth over the leaf surface, forms an appressorium (A) structure for attachment. Subsequently, a fungal penetration peg (PP) is produced that passes through the plant cuticle and epidermal cell wall. Papillae frequently form on the inner surface of the cell wall, directly beneath the invasion site, to prevent further ingress of hyphae. In some pathosystems, however, this localized reinforcement of the cell wall is thought to anchor an invading hypha by forming a tight seal between the neck of the haustorium and the plasma membrane of the epidermal cell invaded. A transmission electron microscope image of the point of penetration. PCW, plant cell wall; V, vacuole.*
Source: (photo) Hammond-Kosack & Jones (1996). Plant Cell 8:1773–1791.

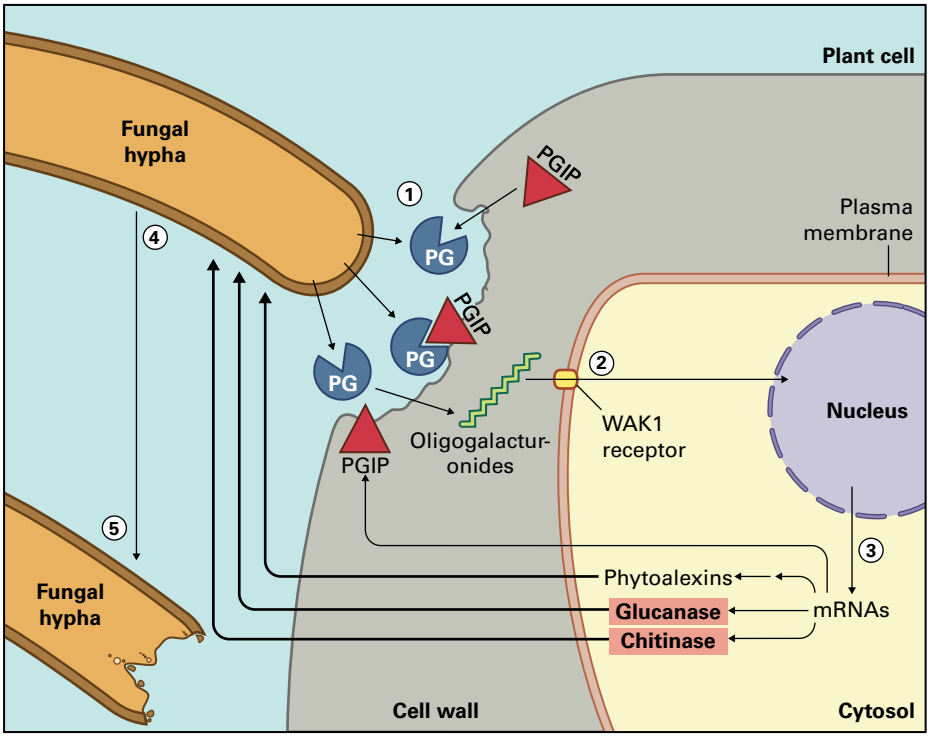


FIGURE 21.33 *PG–PGIP model. (1) Polygalacturonases (PG) secreted by the fungal hyphae interact with secreted polygalacturonase-inhibiting proteins (PGIP) in the plant cell wall. (2) PGs release from the plant cell wall various oligogalacturonides that interact with the plant receptor of oligogalacturonides (in* Arabidopsis*, the wall-associated kinase 1, or WAK1 receptor). (3) Transduction of the oligogalacturonide signal results in the expression of plant defense proteins, including PGIPs. (4) Chitinases, glucanases, and phytoalexins are secreted by the plant and (5) damage the fungal hyphae.*

responsive to pathogen infection or salicylic acid treatment, and some *WRKY* genes are also induced by abiotic stress (see Chapter 22).

In *Arabidopsis*, WRKY proteins contribute to the regulation of a wide range of biological functions, including hormone signaling, growth, secondary metabolism, response to various abiotic stresses, seed germination, leaf senescence, and the synthesis of phytoalexin and other defenses against pathogens. Despite this functional diversity, almost all the analyzed WRKY proteins recognize and bind to the core W box sequence TTGACC/T in the promoter of the responsive plant genes. Different WRKY proteins interact with each other and with other plant proteins.

21.5.6 Phytoalexins are antimicrobial compounds that accumulate at sites of incompatible pathogen infection

Phytoalexins are low molecular weight, lipophilic antimicrobial compounds that accumulate rapidly at sites of incompatible pathogen infections. They are derived from primary metabolites that are used for novel biosynthetic pathways. For example, phenylalanine is a substrate for the synthesis of various flavonoid and isoflavanoid phytoalexins via **phenylalanine ammonia lyase** (PAL), which controls a key branch point in the phenylpropanoid biosynthetic pathway (see

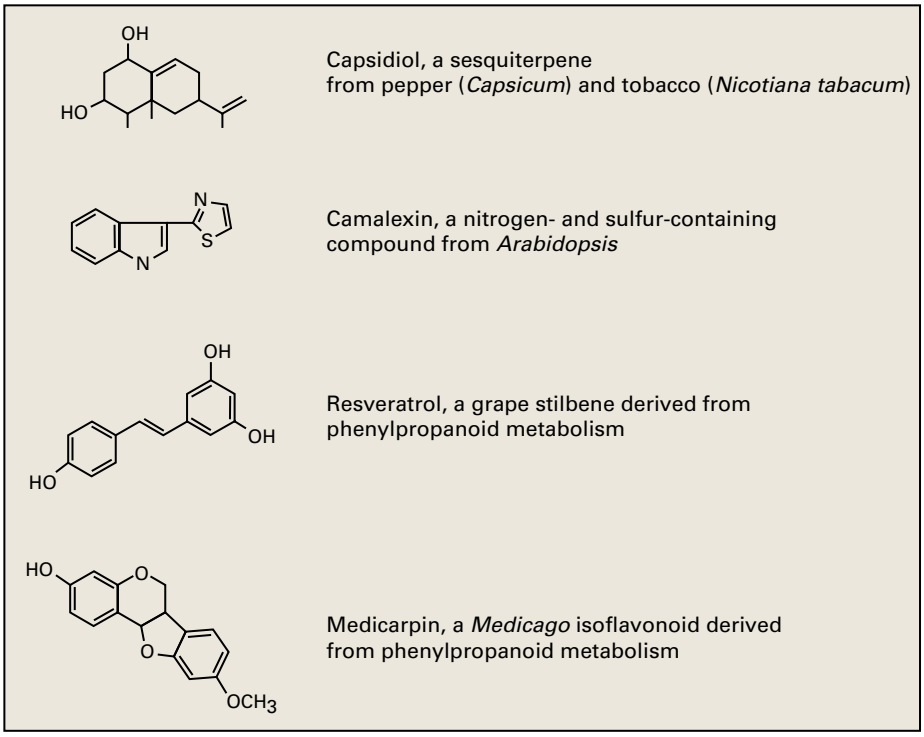


FIGURE 21.34 *Structures of a selection of phytoalexins.*

Chapter 24). Other phytoalexins, for example, capsidiol and rishitin, accumulate rapidly in tobacco (*Nicotiana tabacum*) and potato (*Solanum tuberosum*) in response to pathogen attack.

Different plants make chemically distinct phytoalexins (Fig. 21.34), and the synthesis of most phytoalexins involves the activities of many biosynthetic enzymes, requiring highly coordinated signal transduction and regulation of gene expression. Coordination is likely achieved via a common DNA sequence element within the promoters of genes that encode enzymes of phytoalexin synthesis. In the case of flavonoid biosynthesis in parsley (*Petroselinum* sp.), this appears to involve an H-box (CCTACC(N)7CT) and a G-box (CACGTG).

Definitive genetic and biochemical proof of the role of phytoalexins in disease resistance has come from mutants that are deficient in phytoalexin production. The phytoalexin deficient (*pad*) mutants of *Arabidopsis* fail to synthesize a UV-fluorescent compound camalexin. The *pad3* mutant, which lacks the cytP450 required for camalexin biosynthesis, is more susceptible to the necrotroph *Alternaria brassicicola*, but has an unaltered response to other pathogens, such as the bacterium *P. syringae*.

In *Arabidopsis*, PTI induces production of indole glucosinolates, which provide broad-spectrum control of fungal pathogens. PTI and fungal pathogen entry into epidermal tissue induces several specific cytochrome P450 enzymes, and this leads to accumulation of the indole glucosinolate 4-methoxyindol-3-ylmethylglucosinolate (4M13G). *Arabidopsis* PEN2 encodes a peroxisome-associated myrosinase and is induced upon infection and by P/MAMPs (see Section 21.4). The atypical PEN2 myrosinase then converts the indole glucosinolate 4M13G into toxic compounds that are exported from the plant cell via the ABC transporter encoded by PEN3 to the sites of fungal infection (Fig. 21.35).

21.5.7 Salicylic acid biosynthesis is required for local defense signaling

Salicylic acid (SA) is a phenolic compound (see Chapter 24) that accumulates to high levels as both free and glucoside conjugates in the vicinity of incompatible infection sites. SA is derived from the phenylpropanoid pathway, and numerous roles for them in plant defense have been proposed (Fig. 21.36).

The requirement for SA in some incompatible pathogen interactions has been demonstrated using transgenic plants that constitutively express a bacterial *nahG* gene. This gene encodes the enzyme salicylate hydroxylase, which converts SA to catechol and thus dramatically reduces SA levels. Reduced SA accumulation in the *nahG*-expressing plants correlates with a weakening of several *R*-gene-mediated resistance phenotypes, for example *N*-mediated resistance to TMV, and also abolishes the induction of various defense genes. SA-mediated defenses are especially important in conferring resistance to pathogens that are either obligate biotrophs or have an initial phase of biotrophic colonization.

Two distinct biosynthetic pathways to SA have been identified in both *Arabidopsis* and tobacco (*Nicotiana tabacum*): the isochorismate (IC) and the phenylalanine ammonia-lyase (PAL) pathway (Fig. 21.37). Both originate from chorismate, the end product of the shikimate pathway (see Chapter 7). *Arabidopsis* appears to synthesize SA primarily

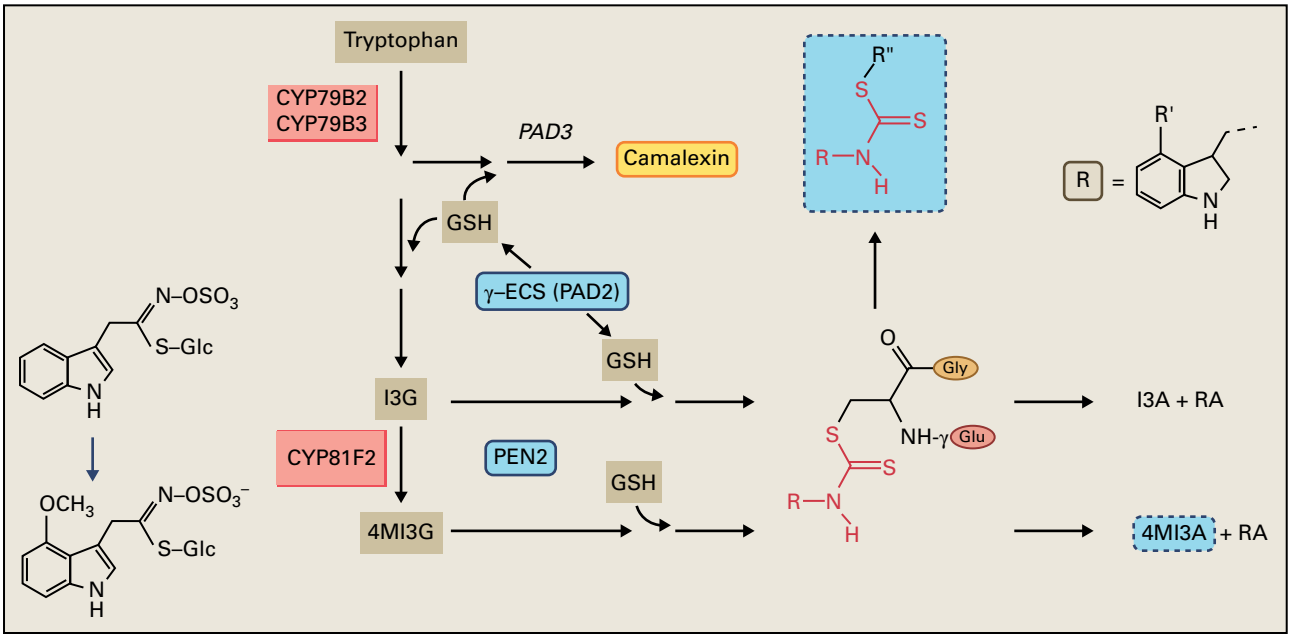
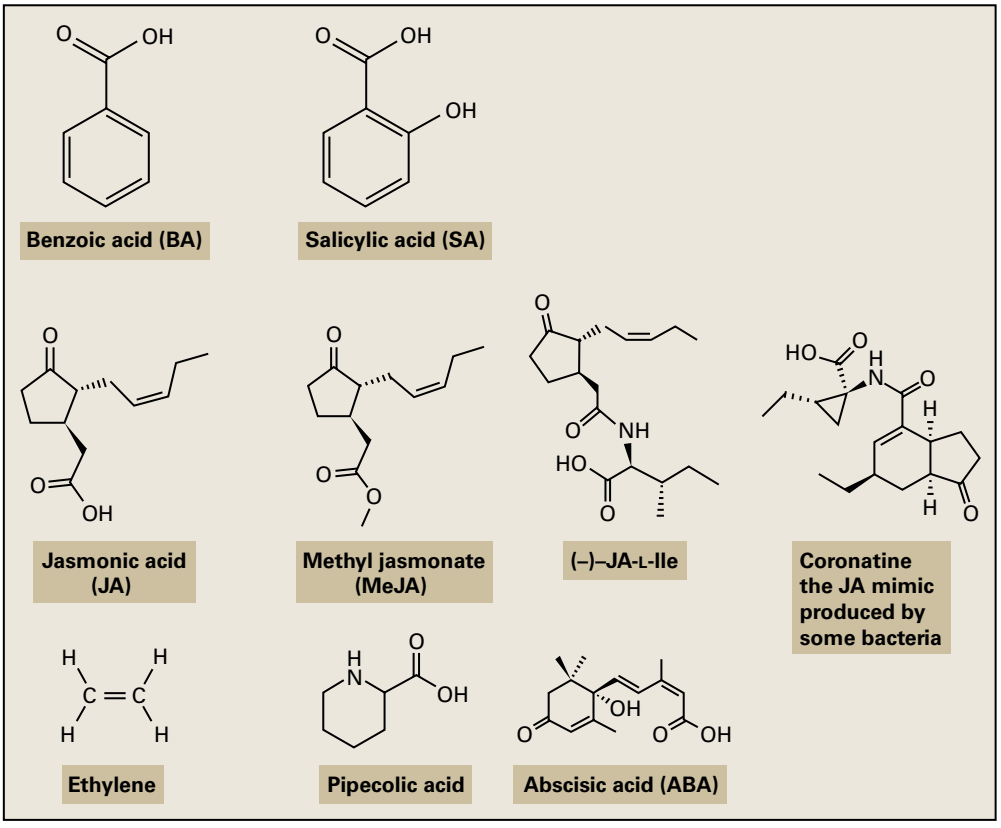


FIGURE 21.35 *An inducible tryptophan-derived indole glucosinolate pathway in plant cells mediates broad-spectrum antifungal defense. The CYP81F2 gene encodes a P450 monooxygenase that is essential for the pathogen-induced accumulation of 4-methoxyindol-3-ylmethylglucosinolate (4MI3G), which in turn is activated by the atypical PEN2 myrosinase (a type of β-thioglucoside glucohydrolase) for antifungal defense. This pathway is active in living cells and enables the recruitment of indole glucosinolates into PAMP-triggered immunity (PTI). Other tryptophan-derived metabolites are involved in* Arabidopsis *defense against powdery mildews, including the phytoalexin camalexin. Components critical for termination of pre- and post-invasive fungal growth are highlighted with blue and orange frames, respectively. The matching structure fragments of the isothiocyanate-glutathione adduct and some of the Brassicaceae phytoalexins are highlighted in red. GSH, glutathione; I3G, indol-3-ylmethylglucosinolate; I3A, indol-3-ylmethylamine; PEN2, penetration 2 gene; γ-ECS, gamma-glutamylcysteine synthetase; PAD3, phytoalexin deficient 3 gene; RA, raphanusamic acid; 4MI3A, 4-methoxyindol-3-ylmethylamine.*

FIGURE 21.36 *Some of the key plant signaling molecules involved in the local and systemic activation, modulation, and amplification of plant defense responses.*



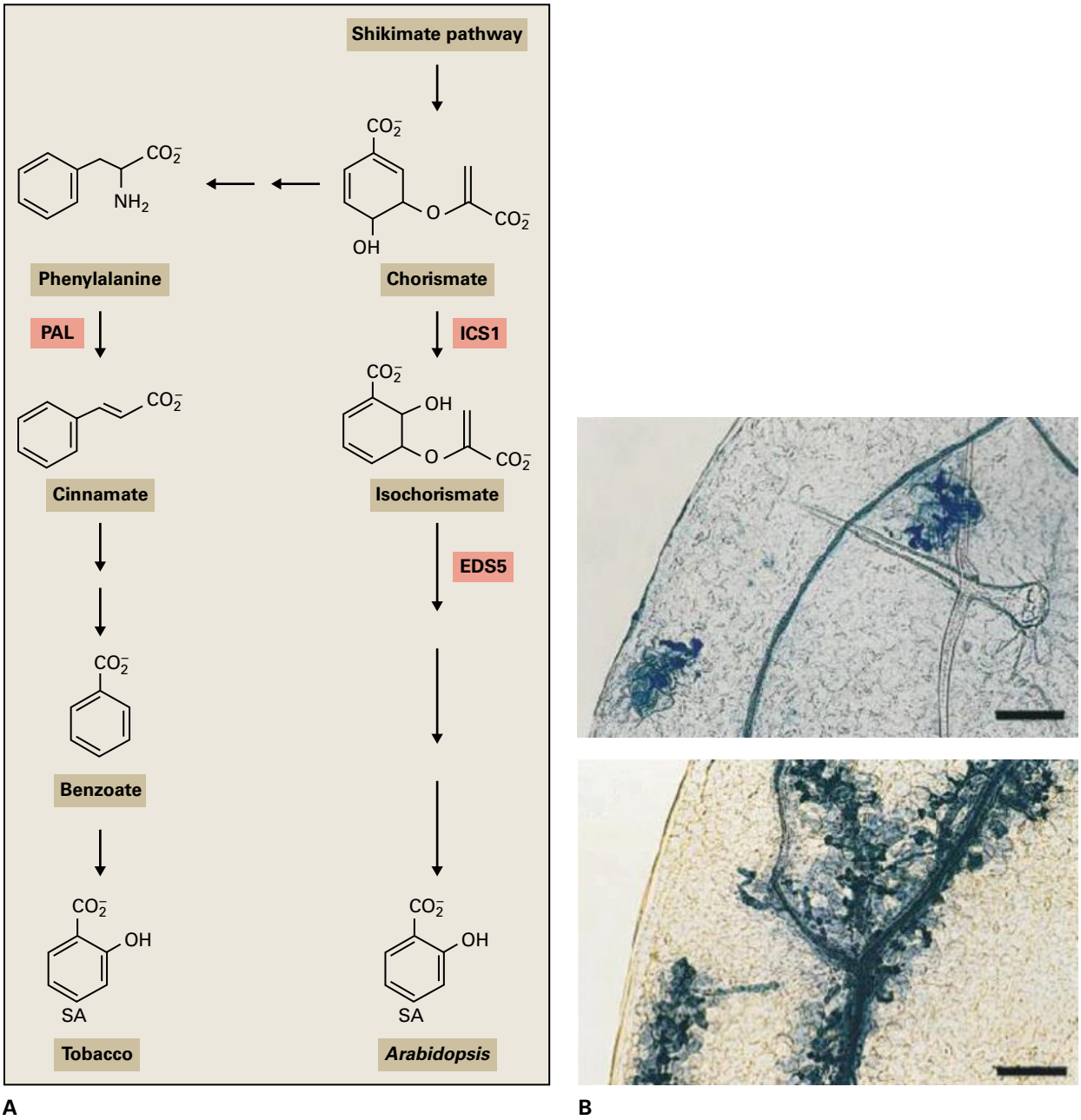


FIGURE 21.37 *Biosynthesis of salicylic acid (SA) in plants. (A) SA in* Arabidopsis *is predominantly produced from isochorismate. Isotope feeding experiments suggest that other plants synthesize SA from cinnamate produced by PAL. The importance of the enzymes phenylalanine ammonia lyase (PAL) and isochorismate synthase (ICS) in SA accumulation has been demonstrated in experiments using mutants, gene silencing, and chemical inhibition. EDS5, ENHANCED DISEASE SENSITIVITY 5, a MATE transporter of unknown function. (B) Resistance response of* Arabidopsis *wild-type (Col-0) and ics1 mutants to incompatible isolates of the oomycete, the downy mildew* Hyaloperonospora arabidopsidis. *Top, Col-0 with blue staining of typical HR reaction. Bottom, ics1 mutant with blue staining of hyphae with trailing necrosis. Bars = 25 μm. Source*: (B) Nawrath & Métraux (1999). Plant Cell 11:1393–1404.

via isochorismate in the chloroplast, whereas in tobacco, SA biosynthesis may occur primarily via benzoic acid in the cytosol. In some plant species, such as rice (*Oryza sativa*) and poplar (*Populus* sp.), SA synthesis is not dramatically induced by pathogen infection; instead, the SA and SA-derived compounds are present at high levels in uninfected plants already, typically higher than those levels found in pathogen-induced *Arabidopsis* leaves. *Arabidopsis* salicylate-deficient mutations *sid1* and *sid2* cannot make SA and show enhanced disease susceptibility. *SID1* encodes a MATE transporter and *SID2* encodes isochorismate synthase. These genes are weakly induced during PTI but strongly during ETI.

During the local response, SA has been proposed to act synergistically in a signal amplification loop with ROS to drive the local HR at the point of initial pathogen infection. Low doses of both exogenous H_2O_2 and pathogen facilitate SA accumulation, leading to enhanced local ROS production. Also, SA accumulation can inhibit heme-containing ROS scavenging

systems, such as catalases and ascorbate peroxidases, thereby increasing overall ROS levels following pathogen recognition.

21.5.8 Some pathogen infections activate jasmonic acid (JA) and ethylene biosynthesis and signaling

The biosynthesis of **jasmonic acid** (JA) and ethylene (see Fig. 21.36) are described in detail in Chapter 17. In response to P/MAMPs, JA and ethylene biosynthesis is initiated. Ethylene is produced by *Arabidopsis* within 10 minutes in response to flg22, while JA levels rise more slowly. The subsequent signaling processes are complex because they reflect the balance of processes initiated by SA, JA, and ethylene. The output of the combination of these signaling molecules is different from the sum of each alone, owing to extensive crosstalk between the various signaling processes (see Section 21.8.5). Additional functions of both signaling molecules are described in Chapters 17 and 18.

21.5.9 Many defenses activated in PTI are also activated in ETI

PTI leads to cell wall fortification and the induction of genes that encode antimicrobial proteins or enzymes in pathways leading to the synthesis of antimicrobial compounds and ROS induction. Many of the responses are shared with ETI (see Section 21.6), although how the activation of these mechanisms converges after PTI and ETI is not understood. ETI is usually stronger than PTI (see Fig. 21.3A and Fig. 21.4) and often culminates in the hypersensitive response (HR). These induced defense responses result in the creation of unfavorable conditions for pathogen growth and reproduction, while at the same time the responding cells detoxify and impair the spread of harmful enzymes and toxins produced by the pathogen.

21.6 Effector-triggered immunity, a second level of induced defense

Plant breeders rely on genetic variation for disease resistance in their selection of superior crop varieties. Such genetic variation, however, usually maps to genes that are not specifically involved in PTI. This section reviews how analysis of such variation led to the discovery of receptors that recognize pathogen effectors.

21.6.1 Plants show extensive and heritable variation for disease resistance

Variation in disease susceptibility in the wild is widespread. Following the rediscovery of Mendel's work, plant breeders in the early 1900s recognized that resistance to plant pathogens was often inherited as a single dominant or semi-dominant trait. Cereal plant pathologists working in the 1910s to 1930s realized that pathogen populations could shift from season to season and between regions, as new wheat, barley, and oat varieties were locally introduced. Therefore, pathologists began to propagate different strains of pathogens in pure form and found that not all races could grow on the same host variety.

Research in the 1930s and 1940s on the interaction between flax and the flax rust fungus *Melampsori lini* clarified the inheritance of plant resistance and pathogen virulence, resulting in the **gene-for-gene model** (Fig. 21.38). This model predicts that plant resistance only occurs when a plant has a **dominant resistance** (*R*) **gene** and the pathogen expresses the complementary **dominant recognized effector** (*Ree*), previously referred to as an avirulence (*Avr*) gene. The model holds true for most biotrophic and many hemibiotrophic plant–pathogen interactions. Within the model shown in Figure 21.3A, the pathogen *Avr* genes encode effectors that are recognized by the products of *R* genes.

Virulence of pathogens that deploy host-selective toxins for successful pathogenesis involves a different mechanism. In this case, virulence is dominant when the pathogen produces a functional toxin or enzyme to cause disease (see Fig. 21.7). Plant resistance is then a recessive trait when the toxin target has been lost or altered. For example, in wheat the interaction between the *Tsn1* gene product and the *ToxA* gene product of the fungus *Stagonospora nodorum* (see Section 21.3.8) causes disease in wheat genotypes possessing a functional copy of the *Tsn1* gene. In contrast, the maize *Hm1* gene, which encodes a reductase that can detoxify the *C. carbonum* HC toxin (see Fig. 21.7), confers resistance as a dominant trait.

Disease-tolerant plants restrict symptom development even though they are heavily infected, but they can still be an important source of pathogen spores that can infect fully susceptible plants.

Following the realization that disease resistance can be heritable, 20th century plant breeders developed breeding programs to identify resistant germplasm in wild relatives of crop plants and then introgress (breed) the corresponding resistance (*R*) genes into elite cultivars. The discovery that plants have centers of origin, where the greatest genetic diversity for both the plant and its pathogens resides, greatly assisted the collection of novel germplasm for breeding. Considerable early success was achieved in disease control using such resistant cultivars. Within a few years of an *R* gene being introduced into commercial production, however, pathogen races often evolved to overcome the *R* gene, and severe disease epidemics frequently recurred. This **boom and bust cycle** has a simple underlying molecular explanation (Fig. 21.39). Some *R* genes have, however, given excellent disease control for over 25 years in large-scale commercial production. For example, the tomato *Cf-9* gene-mediated resistance to the fungus *Cladosporium fulvum* has remained effective since the early 1980s. The various molecular and biochemical explanations underlying these **durable resistances**

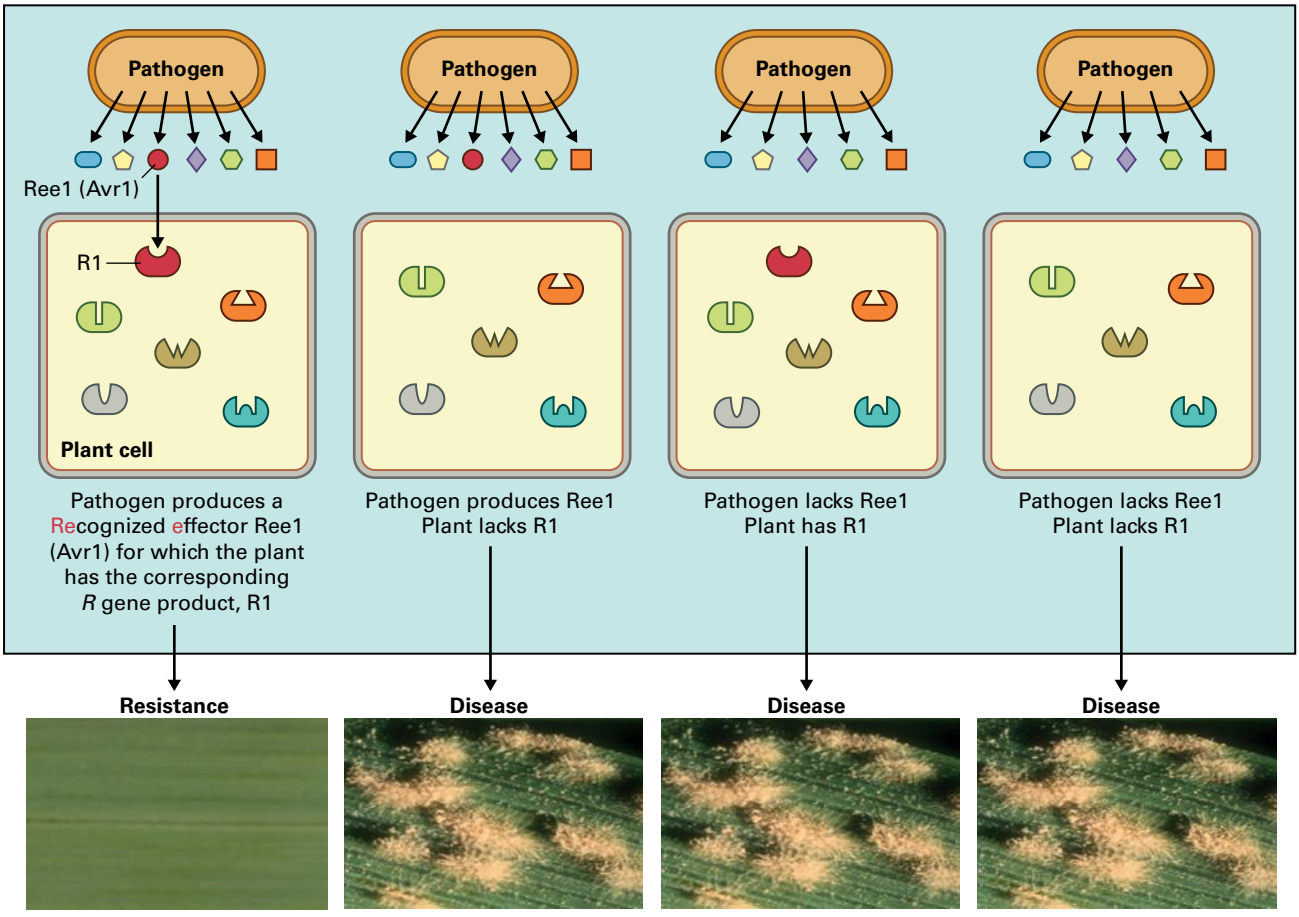


FIGURE 21.38 *The gene-for-gene model. The four strains of a pathogen (top) each produce a distinct repertoire of effector molecules. Two of the four carry the avr1 gene and so produce the effector molecule Avr1 (red). The four genotypes of the host each have a repertoire of R genes, and two of the four have the R1 gene, which encodes the R1 protein that enables the plants to recognize the pathogen Avr1 effector. Therefore Avr1 can also be called the recognized effector (Ree1). A plant is resistant to the pathogen only when a pathogen carrying the avr1 gene infects a plant carrying the R1 gene, thus triggering R gene-mediated defense mechanisms (left). In all other cases, the plant is unable to recognize the pathogen and thus is susceptible to infection and disease. The photographs show resistant and susceptible outcomes following inoculation of barley leaves (*Hordeum vulgare*) with the barley mildew fungus (*Blumeria graminis *f. sp.* hordei*).*

are of great interest. Because many *R* genes are not durable, agrochemical control of disease is widespread.

21.6.2 Plant disease resistance proteins share common motifs

The majority of predicted R proteins that mediate **race-specific resistance** and trigger ETI (see Fig. 21.3A) have diagnostic structural motifs (Table 21.6). This suggests the different R protein classes use a limited range of biochemical mechanisms to fulfill two basic functions: first, they directly or indirectly recognize the presence of the effector, and second, following recognition, they activate downstream signaling leading to rapid induction of various defense responses. During normal plant growth and development, most *R* genes conferring race-specific resistance are constitutively expressed at low levels. Likewise, R protein levels are low in healthy plants.

The common structural motifs found in R proteins conferring race-specific resistance are illustrated in Figure 21.40. A nearly ubiquitous feature is the reiterated LRR motif, which contains several leucine or other hydrophobic amino acids at regular intervals over a stretch of 23 or 24 amino acids (Fig. 21.41). This part of the repeat forms a structure within the protein called a **parallel β-sheet**. Within this structure, the hydrophobic leucine sequence is in the interior of the protein, and the other residues are exposed to the solvent, where they form a surface capable of interacting with other proteins. Different interacting surfaces can be generated via single amino acid changes, and this permits the evolution of specific interactions (Fig. 21.41B).

LRR motifs mediate protein–protein and receptor–ligand interactions in many organisms, and in plant R proteins they likely participate in effector perception. This LRR motif also predominates in the extracellular domain of several P/MAMP receptors, for example FLS2 (see Fig. 21.29) and in some downstream components of the activated defense response, for example, the polygalacturonase-inhibiting proteins

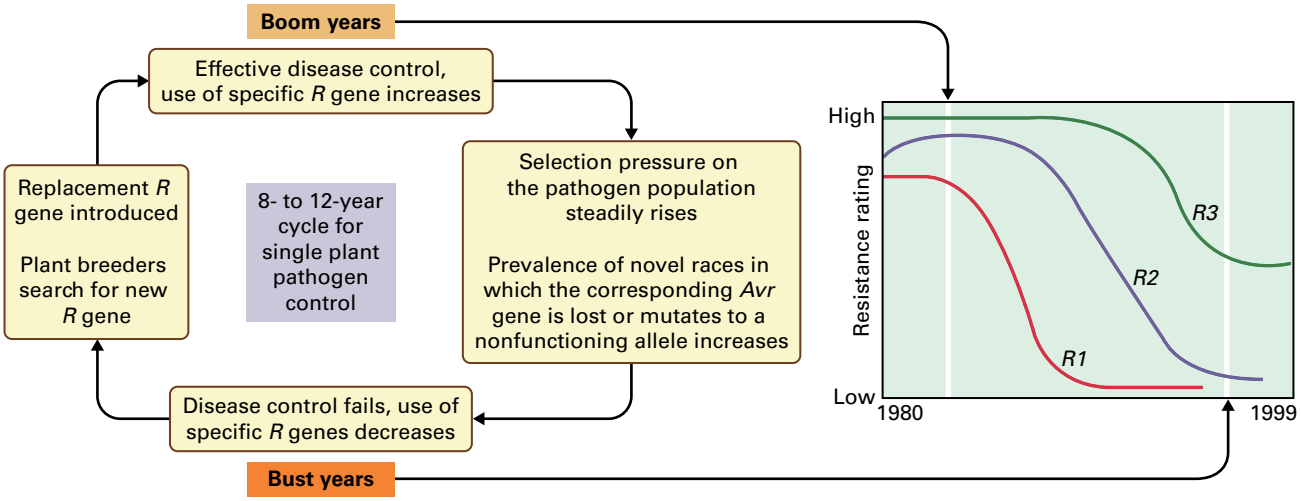


FIGURE 21.39 *The boom and bust cycle. Plant breeders often achieve initial success in disease control through breeding new disease resistant cultivars. However, within a few years of the introduction of an* R *gene into commercial production, the gene may cease to protect the crop from disease, and severe epidemics occur (left). This boom and bust cycle of disease resistance results because effective disease control (the boom years) occurs only when the pathogen population consists entirely of races that express the corresponding functional* Avr *gene (i.e., the recognized effector gene). Once an* avr *mutant race of the pathogen appears, disease control fails (the bust years). Introgression of another* R *gene allele typically initiates another boom and bust cycle, as illustrated by the disease rating curves for* R2 *and* R3 *(right). The cyclic nature of the disease control achieved with many* R *gene alleles sustains demand for agrochemicals to provide an alternative solution.*

TABLE 21.6 *Diagnostic structural domains and motifs in the intracellular immune receptors.*

Protein domain or motif	Feature(s)	Function(s) in plant defense
CC domain	Coiled-coil structure—a repeated heptad sequence with interspersed hydrophobic amino acid residues	Protein–protein interactions and protein dimerization; CC domain of barley MLA10 interacts with WRKY1/2 transcription factor
TIR domain	Sequence similarity to the cytoplasmic domain of the Toll and IL-IR proteins	Avr-dependent TIR–TIR interactions required for tobacco N protein oligomerization
NB-ARC domain	Nucleotide binding domain shared by APAF1, certain R proteins and CED-4. Contains a P-loop NTPase fold, an ARC1 motif, which consists of four-helix bundles, and an ARC2 motif that adopts a winged-helix fold	Binds and hydrolyzes ATP, a molecular switch that performs reversible intra- and intermolecular protein phosphorylation and autophosphorylation
LRR domain	Intracellular or extracellular; concatenated repeats of 23 or 24 amino acids in length; inner beta-sheet surface with buried leucines and solvent-exposed x residues in LxxLxL	Protein–protein interactions; controls direct or indirect recognition of specific pathogen races. Interactions between LRR and NB-ARC domain contribute to recognition specificity
Serine-threonine kinase domain	Intracellular	Protein phosphorylation and autophosphorylation

(PGIPs, see Section 21.5.4). LRR protein kinases are also important in other aspects of plant growth and development: The *Arabidopsis* LRR-kinase protein CLAVATA 1 is required for maintenance of the shoot apical meristem and recognizes the peptide CLAVATA 3 (see Chapter 11), and BRI1 is required for brassinosteroid perception (see Chapter 18).

The majority of intracellular LRR-containing R proteins possess a nucleotide-binding site (NB). The NB is part of a larger NB-ARC domain that is shared between R proteins and the human apoptotic protease-activating factor 1 (APAF1) and the *Caenorhabditis elegans* cell death protein CED-4. Many conserved motifs can be recognized in the NB-ARC domain (Fig. 21.42), including the NB motif (which forms a P-loop NTPase fold), the ARC1 motif (which consists of four-helix bundles), and the ARC2 motif (which adopts a winged-helix fold). A nucleotide-binding pocket forms at the interface of these three motifs, where the most conserved motifs in the NB-ARC domain occur.

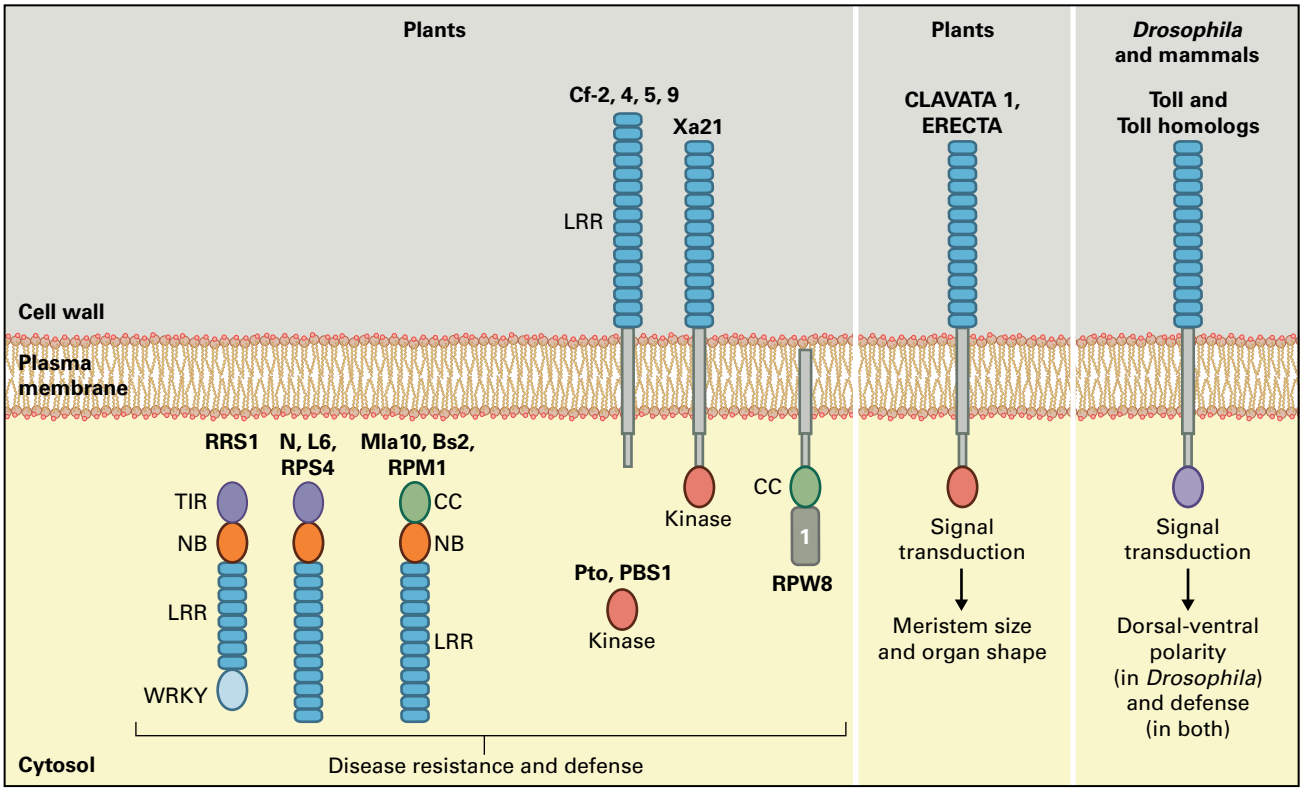


FIGURE 21.40 *Schematic diagram illustrating several plant resistance proteins and other LRR-containing proteins (left). Structurally related proteins that are involved in various aspects of plant development, as well as other eukaryotic proteins that coordinate development and the induction of the immune response in animals, are included for comparison (right). The predicted protein domains and motifs include: CC, coiled-coil domain; TIR, Toll, Interleukin 1 receptor, Resistance protein-like motif; NB, nucleotide binding site; LRR, leucine-rich repeat, WRKY, a motif characteristic of some plant transcription factors and domain 1 that lack significant homology to known proteins. The plant R proteins depicted from left to right are* Arabidopsis *RRS1 and RPS4 resistance to* Pseudomonas syringae *strains expressing AvrRps4, tobacco N resistance to tobacco mosaic virus, L6 flax rust resistance 6; Mla10 resistance to* Blumeria graminis *f.sp.* hordei *expressing Avra10,* Arabidopsis *RPM1 resistance to* Pseudomonas syringae *pv.* maculicola *expressing AvrRpm1 or AvrB; pepper Bs2 resistance to* Xanthomonas euvesicatoria *strains expressing AvrBs2; tomato Cf-2, Cf-4, Cf-5 and Cf-9 for resistance to* Cladosporium fulvum *races expressing, respectively, Avr2, Avr4 Avr5 and Avr9; tomato Pto resistance to strains of* Pseudomonas *bacteria expressing AvrPto,* Arabidopsis *PBS1 a serine/threonine protein kinase required by the NB-LRR R protein RPS5 for resistance against strains of* Pseudomonas *bacteria expressing AvrPphB; rice Xa21 resistance to* Xanthomonas oryzae *pv.* oryzae *and* Arabidopsis *RPW8 resistance to several powdery mildew species, including* Golovinomyces orontii.

The activity of these multidomain R proteins depends on their ability to bind and hydrolyze nucleotide triphosphates; mutations that alter key residues within the binding pocket abolish or derepress R protein function. The activation of R proteins is tightly regulated because they frequently trigger cell death. This balance between R protein autoinhibition and activation seems to be achieved by intramolecular interactions between the various domains. It is likely that the ATP-bound form activates defense, and recognized effectors may stabilize this ATP-bound form.

The N-termini of NB-LRR proteins are structurally diverse. Some possess a domain similar to the cytoplasmic signaling domain of the *Drosophila* Toll and mammalian interleukin-1 receptor (IL-1R) proteins, and these are called TIR domains (see Fig. 21.40). Interestingly, these animal proteins are crucial to innate immunity. The non-TIR-NB-LRR R proteins are often referred to as CC-NB-LRRs or CNLs, because many possess a coiled coil region (CC) between the N-terminus and the NB domain. CC domains are implicated in protein homo- and heterodimerization (see Table 21.6). Interestingly, the TIR-NB-LRR class is absent from the genomes of cereal species and from the Lamiales. Evolutionary studies suggest CNLs are likely the more ancient subclass of *R* gene. Structural studies suggest both CC and TIR domains are capable of homo- or heterodimerization.

Some R proteins that recognize apoplastic effectors are receptor-like proteins (RLPs) that have an extracellular LRR domain, a single transmembrane domain, and a short cytoplasmic tail that lacks a C-terminal protein kinase domain (see Fig. 21.40). For example, the tomato *Cf* genes confer race-specific resistance against the extracellular colonizing fungus *Cladosporium fulvum*. *Cf-9* confers resistance to

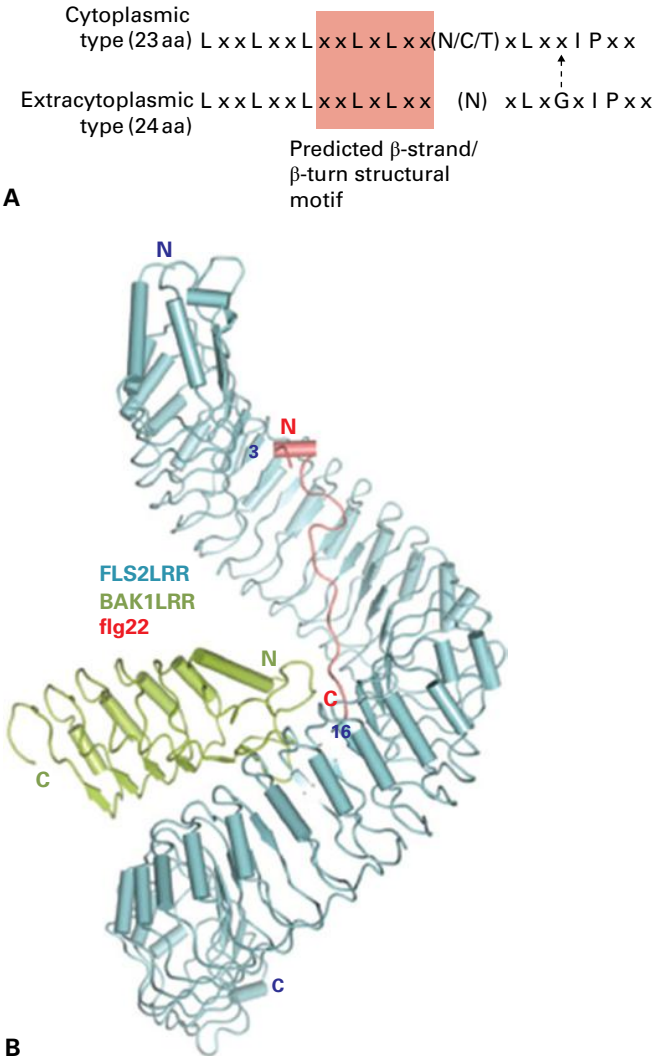


FIGURE 21.41 *Structure of leucine-rich repeat (LRR) containing proteins. (A) LRRs of cytoplasmic and extracytoplasmic plant R proteins, which contain leucine or other hydrophobic amino acids at regular intervals over a 23 or 24 amino acid length, respectively. The boxed area indicates the leucine residues within the β-strands/β-turn structure which are predicted to project into the hydrophobic core of the protein while the side chains of the flanking x amino acids are exposed to solvent. R gene sequence comparisons indicate the x amino acids in the xxLxLxx region are hypervariable and have ratios of nonsynonymous to synonymous substitutions significantly greater than one. There is a selective advantage when a protein possesses a high amino acid diversity in this region, which in some cases has evolved to detect variation in interacting ligand molecules including pathogen-derived effectors. (B) Two plant LRR proteins forming a defense immunity complex in which both LRR proteins interact with the P/MAMP flg22. The LRR-rich ectodomains mediate flg22-induced heterodimerization of the immunity receptors FLS2 and BAK1. The overall structure of the FLS2LRR-BAK1LRR immunity complex with the P/MAMP flg22 (red) shows that flg22 is positioned between LRR3 and LRR16 in the FLS2 protein (indicated by blue numbers). BAK1 recognizes the C-terminal side of the FLS2-bound flg22. N, N terminus; C, C terminus.*

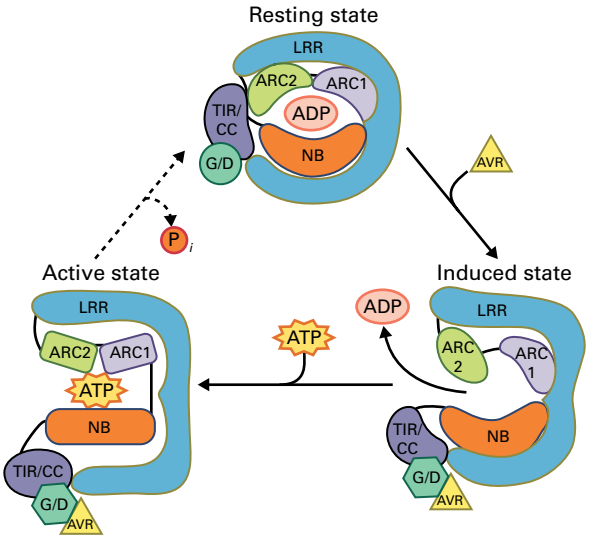


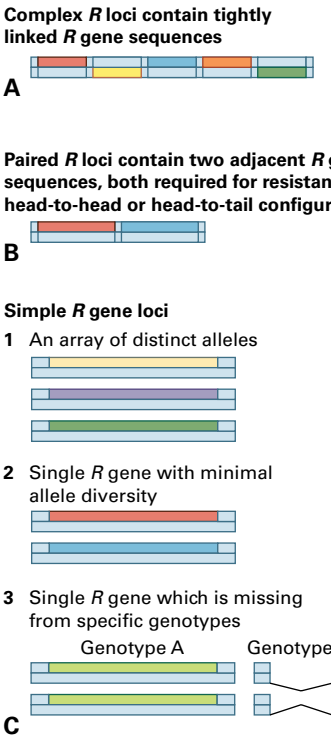
FIGURE 21.42 *Model for NB-LRR protein activation. In the absence of a pathogen, an NB-LRR protein resides in its resting (ADP) state, in which the LRR stabilizes the closed conformation. The recognition platform for the AVR protein (triangle) is provided by the C-terminal part of the LRR together with the TIR/CC domain and the latter could be bound to an interactor (referred to as the guardee or decoy, G/D). Perception of the AVR (directly or via the G/D) changes the interaction surface between the N-terminal part of the LRR and the ARC2 subdomain, thereby releasing the auto-inhibition conferred by the LRR. Subsequently, nucleotide exchange triggers a conformational change, altering the interactions of the NB-ARC domain with the CC and LRR domains (induced state). In the activated state the NB subdomain is accessible to interaction with downstream signaling partners. Hydrolysis of ATP returns the NB-LRR protein to its resting state.*

races of *C. fulvum* carrying *Avr9*, while *Cf-4* confers recognition of *C. fulvum* races carrying *Avr4*. The proteins encoded by *Cf-9* and *Cf-4* are closely related (90% identical), and small differences in their LRRs specify whether Avr9 or Avr4 is recognized.

21.6.3 Allelic variation occurs at some *R* gene loci

To overcome individual *R* gene alleles, plant pathogens can mutate their recognized effector genes to a form that is not detected; natural selection then favors these novel virulent races (see Fig. 21.39). Therefore, plants must evolve novel R protein variants to detect either the modified Avr determinant or another pathogen component (see Fig. 21.3A). The most informative clue as to the evolution of this diversity is the genomic organization of *R* genes.

Genetic and molecular analysis of various *R* loci revealed the existence of two main types of *R* locus (Fig. 21.43). First, many *R* genes are members of multigene families arranged in clustered arrays to form **complex loci**. Sometimes these loci extend genetically over several centimorgans and contain numerous *R* gene alleles. Examples include the maize *Rp1*



Examples		Number of *R* homologs at locus
Tomato	*Cf-9*	5
Tomato	*Cf-2*	3
Tomato	*Pto*	5
Arabidopsis	*RPP5*	8–10
Flax	*M*	15
Arabidopsis	*RPS4/RRS1*	few
Arabidopsis	*RPP2A/RPP2B*	few
Rice	*RGA4/RGA5*	few
Flax	*L*	13 alleles
Arabidopsis	*RPS2*	2 alleles
Arabidopsis	*RPM1*	2 alleles

FIGURE 21.43 *Main types of plant resistance* (R) *locus organization: (A) complex* R *loci, (B) paired* R *loci and (C) various simple* R *loci.*

rust resistance locus, the flax *M* rust resistance locus, and the potato *R2* and *R3a* loci for *P. infestans* resistance. Some alleles may confer resistance to several different fungal species, as is the case for the maize *Rp1* locus. Some complex loci, such as *Xa21* in rice, do not exhibit alleles other than for presence and absence of the *R* gene. The tomato *Pto* gene is linked to five other *Pto* homologs at the *Pto* locus, but only two haplotypes have been characterized physically and genetically. At the tomato *Cf-9* locus, three haplotypes have been described in Cf9, Cf4, or near-isogenic Cf0 tomato, carrying 5, 5, or 1 *Cf-9* homologous genes (Fig. 21.40), several of which individually confer *Cf*-resistance gene function. A second type of *R* locus consists of a single copy gene at a **simple locus**, which can also exhibit an array of distinct alleles, as at the flax *L* locus (Fig. 21.43). Alternatively, simple *R* loci can carry *R* gene sequences that either exhibit no allelic diversity, or simply vary for the presence or absence of the functional gene.

How then do novel R protein variants arise from complex and simple *R* loci? For complex loci, the linked and homologous *R* gene sequences provide the DNA homology for recombination events leading to the evolution of novel specificity through mispairing, intra- and intergenic recombination, and gene duplication, as shown in Figure 21.44. However, there is no evidence to suggest that plants evolved a special mechanism to generate novelty at *R* loci. For *R* genes at simple loci with an array of distinct alleles, in addition to spontaneous mutations, unequal intragenic recombination or slipped alignment during replication, facilitated by direct DNA repeats within the LRR coding sequence, may generate *R* gene allelic diversity. For solitary *R* genes, the possibilities to generate novelty are more limited, but can still enable substantial allelic diversity, as found in flax L6.

21.6.4 Recognition of pathogen effectors is direct or indirect

Each *R* gene product is envisaged to have two functions: recognition of the corresponding effector and activation of downstream signaling pathways to activate defense. How does recognition occur?

The most simple scenario is one in which R proteins directly recognize the corresponding Avr protein. For example, all flax rust *R* genes cloned to date encode intracellular TIR-NB-LRR proteins, and several of these bind the cognate Avr effectors. Following effector detection, a hypersensitive response at the haustorial formation site prevents further infection. Eleven allele variants at the flax *L* locus confer different recognition specificities, mostly specified by the sequence coding for the LRR domain. Domain swap experiments involving different *L* alleles have confirmed that the LRR domain is important for determining R-Avr recognition specificity. The most variable amino acids in the different L proteins lie in the concave β-sheet surface (see Fig. 21.41) and, therefore, could participate in R–Avr interactions. By altering specific surface-exposed amino acid residues, these rust Avr effector proteins escape recognition, rendering the

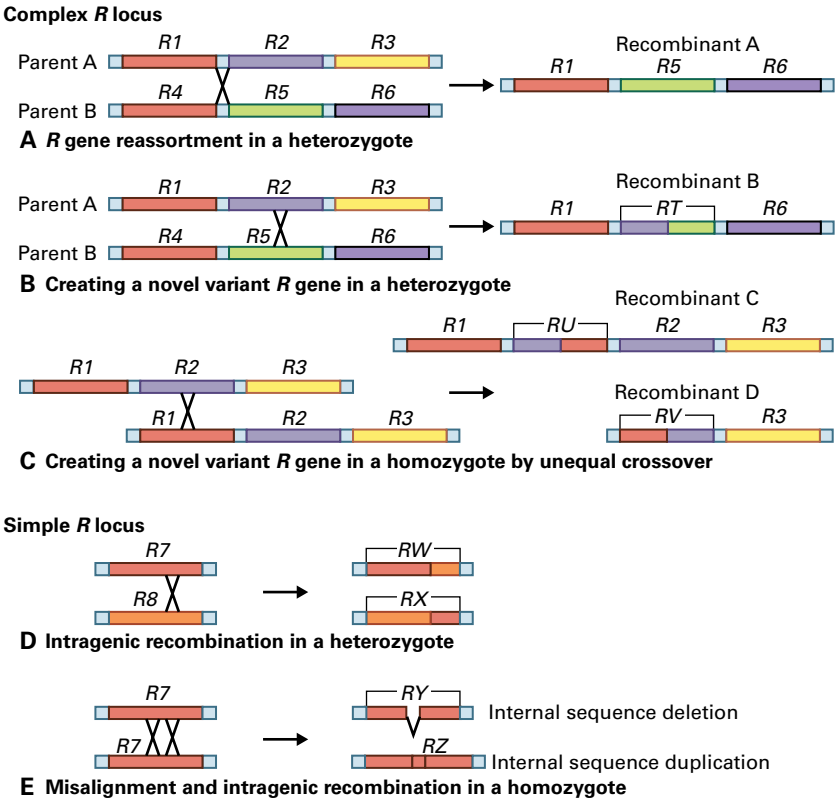


FIGURE 21.44 *New* R *alleles can be generated by several different mechanisms, but the likelihood of their occurrence depends on whether the plant species is maintained as an outbreeding (cross-pollinating) population (A,B) or an inbreeding (self-pollinating) population (C,D,E). The evolution of resistance in plants appears to occur primarily at the single-gene level so that novel specificities that arise by intergenic recombination between similar genes (C) are rare. The variant* R *alleles eventually selected encode proteins with increased effectiveness or confer a novel recognition capacity. RT, RU, RV, RW, RX, RY, and RZ represent different recombination products.*

plant susceptible. Similarly, the polymorphic barley mildew A (MLA) *R* locus encodes allelic receptors of the CC-NB-LRR type. MLA alleles share >90% sequence identity, but each recognizes a different race of powdery mildew. The recognition specificity of distinct MLA alleles is conferred by their LRR domains.

Only a few of the first-discovered R proteins directly bind the cognate effector. Many R proteins recognize the effects of pathogen effectors on host proteins (Fig. 21.45) rather than the effectors directly. As described in Section 21.2.4, plants respond to pathogens by activating PTI, and in turn, some pathogens can overcome these defenses by producing effector molecules to modify or suppress host responses. Each R protein might act as a guard of a host component (the "guardee"). When the pathogen effector molecule modifies this component, the modification is recognized by the R protein and ETI is activated.

This guard hypothesis predicts that multiple pathogen effector proteins may interact with a common host target that can be guarded by more than one R protein. The CC-NB-LRR R proteins RPS2 and RPM1 recognize AvrRpt2, or AvrRpm1 and AvrB, respectively. The *Arabidopsis* RIN4 protein is targeted by these three effectors, which are delivered into plant cells via the bacterial type III secretion system (Fig. 21.46). RIN4 is a 211 amino acid plasma membrane-associated protein, which interacts with the nonrace-specific disease resistance 1 protein NDR1 that triggers SA production. The AvrB and AvrRpm1 proteins cause phosphorylation of RIN4, whereas the AvrRpt2 protein is a protease that degrades it. *Arabidopsis* plants that carry the *RPM1* gene are

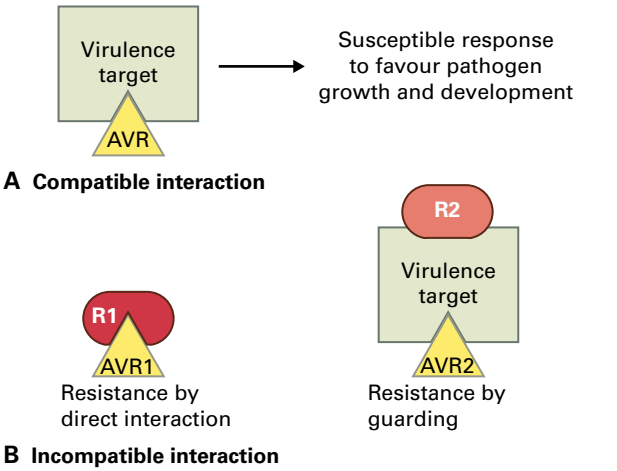


FIGURE 21.45 *Guarding of pathogen virulence targets by plant R proteins. (A) A virulence target exists in a susceptible host plant. Upon pathogen infection, the Avr effector binds to its cognate virulence target, resulting in modifications to the target. These modifications lead to pathogen virulence and host susceptibility, thereby generating a compatible interaction. (B) Incompatible interactions conferred by a resistant host plant can arise in two ways. (Left) The R1 protein directly recognizes the Avr1 effector itself. An example of this type of interaction occurs between rice blast Avr-Pita and rice Pi-ta. (Right) The R2 protein is a guard protein, recognizing the modified plant virulence target caused by the earlier binding of the Avr2 effector. An example of this type of interaction occurs between AvrB/AvrRpm1 (Avr), RIN4 (the virulence target) and RPM1 (R2). Direct recognition by R1 may be circumvented by alterations of the Avr1 effector without modifying its virulence function. By contrast, recognition mediated by the guarding R2 protein cannot be circumvented by alterations of the Avr2 effector without affecting its virulence function.*

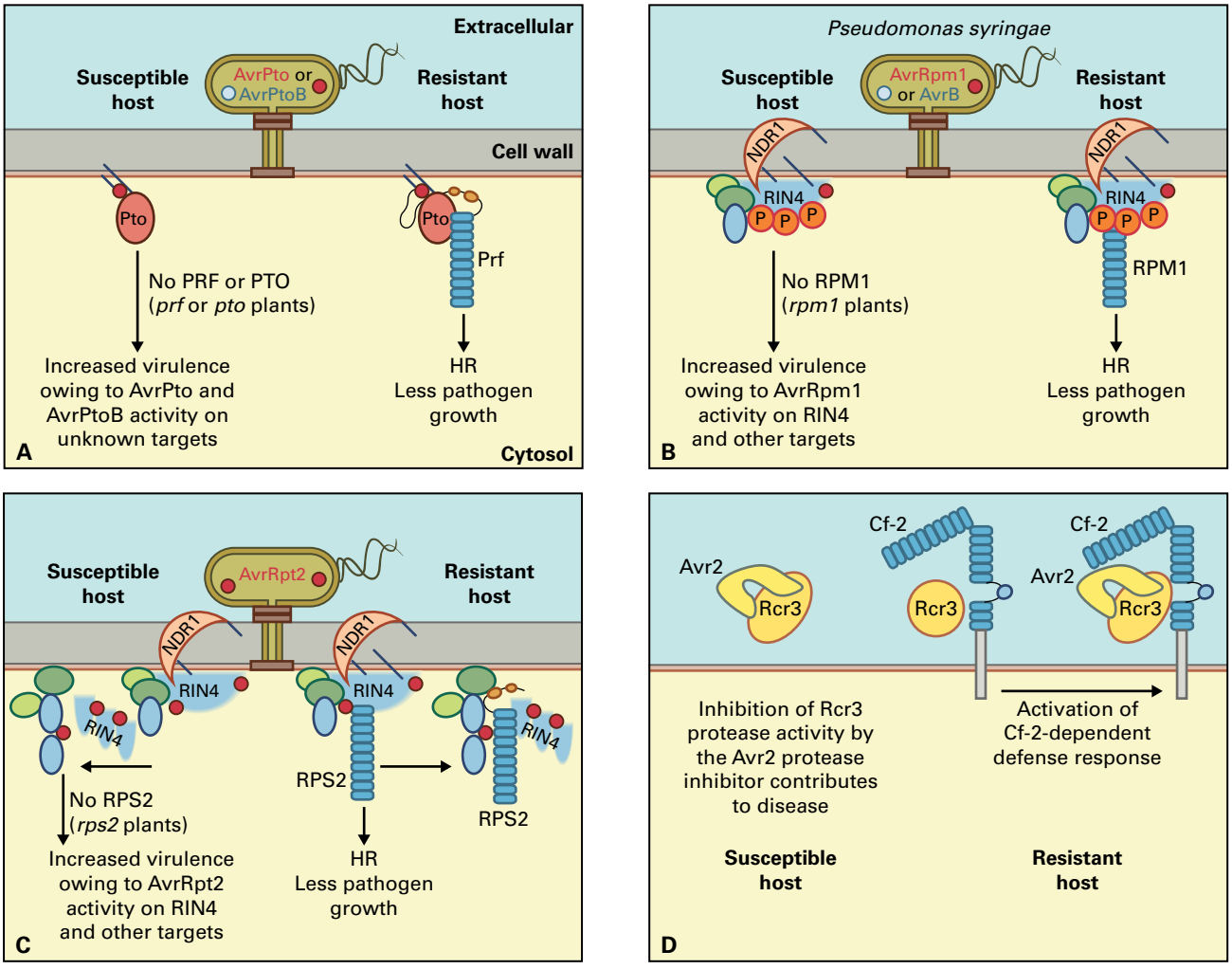


FIGURE 21.46 *Direct and indirect recognition of pathogen effectors triggers plant defenses. (A) Pto is a tomato serine/threonine protein kinase that requires the NB-LRR protein Prf. The two proteins form a molecular complex in which Prf guards Pto. Pto is the target of two unrelated* P. syringae *effectors, AvrPto and AvrPtoB, delivered into the cell by the type III secretion system (T3SS; brown and green syringe). Each effector contributes to pathogen virulence. (B)* Arabidopsis *RPM1 is a peripheral plasma membrane NB-LRR protein. It is activated by either the AvrRpm1 or the AvrB effector proteins. AvrRpm1 enhances the virulence of some* P. syringae *strains on* Arabidopsis *as does AvrB on soybeans. AvrRpm1 and AvrB are modified by eukaryote-specific acylation once delivered into the cell by the T3SS and are thus targeted to the plasma membrane. The biochemical functions of AvrRpm1 and AvrB are unknown, although they target RIN4, which becomes phosphorylated (+P), and activate RPM1. In the absence of RPM1, AvrRpm1 and AvrB presumably act on RIN4 and other targets to contribute to virulence. Light blue unlabeled ovals in this and subsequent panels represent unknown proteins. (C) RPS2 is a plasma membrane NB-LRR protein. It is activated by the AvrRpt2 cysteine protease type III effector from* P. syringae. *AvrRpt2 is a third effector that targets RIN4. Cleavage of RIN4 by AvrRpt2 leads to RPS2-mediated ETI. In the absence of RPS2, AvrRpt2 presumably cleaves RIN4 and other targets as part of its virulence function. (D) The transmembrane R protein Cf-2 guards the extracellular cysteine protease Rcr3. Cf-2 recognizes the* C. fulvum *extracellular effector Avr2, which encodes a cysteine protease inhibitor. Avr2 binds and inhibits the tomato Rcr3 cysteine protease. Mutations in Rcr3 result in the loss of Cf-2-dependent recognition of Avr2. Hence, Cf-2 seems to monitor the state of Rcr3 and activates defense if Rcr3 is inhibited by Avr2. Remarkably, a nematode effector also targets Rcr3 and triggers Cf-2-dependent resistance. Note that in D the plant cell wall is not shown for clarity.*

resistant to infection by *P. syringae* strains carrying the *avrRpm1* or *avrB* genes, because RPM1 recognizes phosphorylated RIN4. RPM1 then activates a signaling pathway that leads to defense activation. Similarly, *Arabidopsis* plants that carry *RPS2* are resistant to infection by *P. syringae* carrying *avrRpt2*. RPS2 is normally found in a complex with RIN4, and degradation of RIN4 by the AvrRpt2 protease releases RPS2, rendering the R protein capable of activating a defense response. Thus, the guarding of RIN4 by at least two different R proteins assures continuous monitoring of the RIN4 protein status.

The tomato Mi-1.2 protein also belongs to the CC-NB-LRR class of R proteins, but is extended at the C-terminus with a Solanaceae-specific domain. Remarkably, *Mi-1.2* confers resistance to the root-knot nematode *Meloidogyne incognita*, the potato aphid *Macrosiphium euphorbiae*, the sweet potato white fly *Bemisia tabaci*, and the tomato psyllids insect *Bactericerca cockerelli*. These diverse resistances conferred by

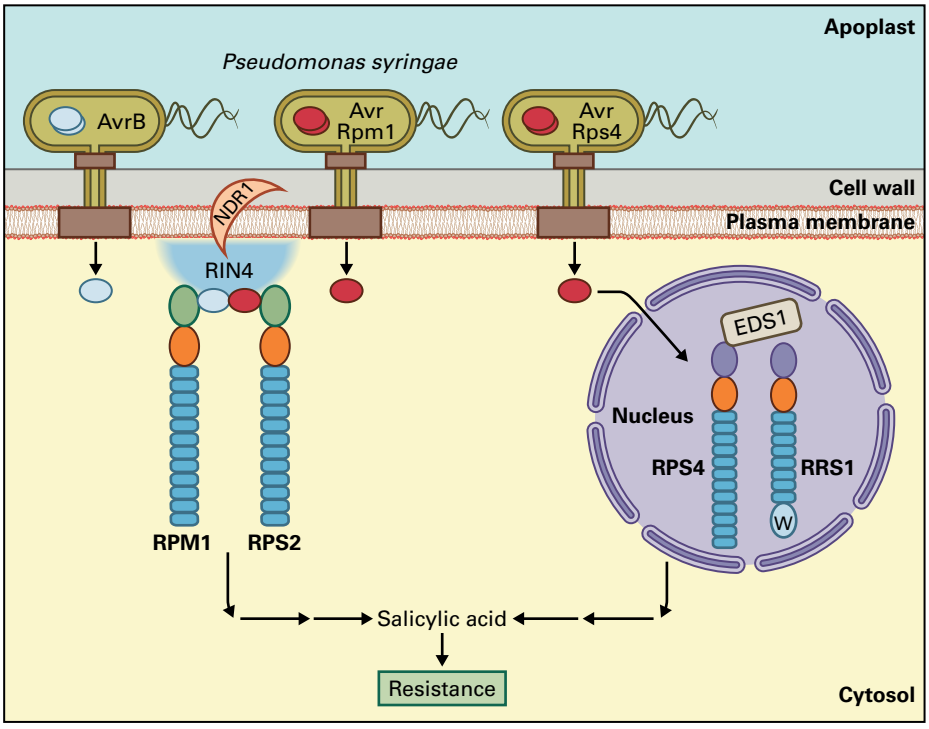


FIGURE 21.47 *The NONRACE-SPECIFIC DISEASE RESISTANCE 1 protein (NDR1) and the ENHANCED DISEASE SENSITIVITY 1 protein (EDS1) mediate, respectively, the defense signaling abilities of CC-NB-LRR and TIR-NB-LRR disease resistance proteins. (Left) NDR1 spans the plasma membrane and interacts with the RIN4 protein that resides in the cytoplasm in close proximity to the plasma membrane. RIN4 is targeted by three bacterial effectors delivered into plant cells via the type III secretion system. The guarding of RIN4 by at least two different R proteins (RPM1 and RPS2) assures continuous monitoring of the RIN4 protein status. RPM1 or RPS2 then activate a signaling pathway that leads to defense activation. (Right) EDS1 is required for resistance mediated by the TIR-NB-LRR class of R proteins (RPS4 and RRS1) as well as basal defense against many virulent pathogens. EDS1 is a lipase-like protein that always functions in association with either of two other lipase-like proteins, PAD4 or SAG101. Both the cytoplasmic and nuclear pools of EDS1 are required to activate defense signaling. At least two bacterial effectors interact with the WRKY domain of the RRS1 protein. Both RRS1 and RPS4 cooperate to activate plant defenses. Although the NDR1 and EDS1 proteins function in two different signaling pathways, these must later converge, because all these resistances require the induction of salicylic acid synthesis.*

one *R* gene might be due to each invertebrate targeting a shared guardee that is guarded by Mi-1.2.

The Prf protein (a NB-LRR protein) from tomato (*Solanum lycopersicum*) may recognize the direct interaction between Pto and AvrPto. The Pto protein kinase confers resistance in tomato to strains of *Pseudomonas* bacteria that express *AvrPto*. Bacteria deliver AvrPto protein into the plant cell cytoplasm via a T3SS (see Section 21.3.3). When AvrPto interacts with the Pto kinase, both proteins are directed to the plasma membrane via an N-terminal myristoylation site. The direct interaction between the Pto and AvrPto proteins is recognized by Prf, which then activates various downstream defense responses (Fig. 21.46A). The discovery of the direct Pto–AvrPto interaction was important because cytoplasmically localized protein kinases were previously unknown to function as receptors in any organism and the same domain in the Pto kinase confers both recognition and signaling capacity. Another example of R protein guarding is provided by the tomato Cf-2 protein. Originally identified as mediating resistance to specific races of the fungus *C. fulvum* expressing the effector Avr2 (Table 21.3), Cf-2 also confers resistance to the cyst nematode *Globodera rostochiensis*. Cf-2 enables the plant to recognize binding of the Avr2 proteinase inhibitor (PI) of *C. fulvum* to the plant apoplastic protease Rcr3 (Fig. 21.46D), which then triggers defense responses. The presence of Cf-2 also senses binding of the venom allergen-like effector protein Gr-VAP1 of *G. rostochiensis* to the Rcr3 protease. In the absence of Cf-2, variants of Rcr3 encoded by specific alleles increase susceptibility of tomato plants to *G. rostochiensis*, revealing a key role for Rcr3 as a virulence target for this cyst nematode species. Some alleles of Rcr3 trigger Cf-2-dependent defense, even in the absence of Avr2, suggesting that selection must constrain guardee alleles to avoid inadvertent R protein-dependent defense activation.

The TIR-NB-LRR class of R proteins can confer resistance to biotrophic fungi, bacteria, and viruses. How might they signal? The presence of the conserved TIR domain has raised the possibility that immune responses in plants, mammals, and invertebrates utilize an ancient, conserved mechanism, or arose via convergent evolution (see Fig. 21.40). Intriguingly, the protein kinases PELLE and IRAK that function downstream of the *Drosophila* Toll and human IL-1R receptors, respectively, show strong homology to the PTO resistance protein (Fig. 21.46, see also Fig. 21.40).

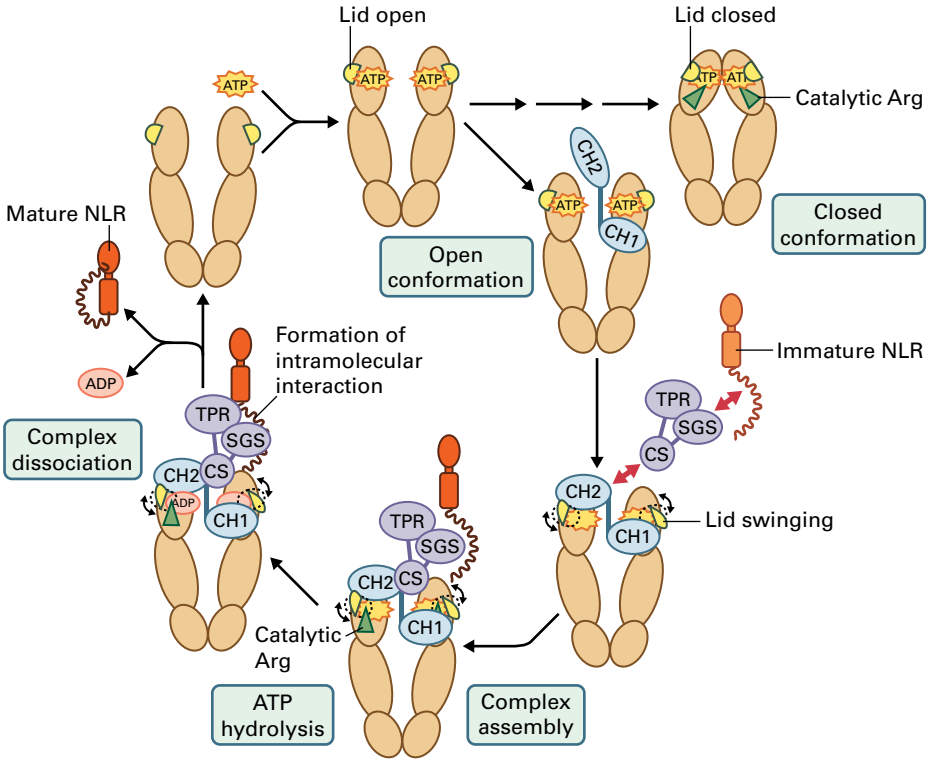


FIGURE 21.48 *A proposed model for NB-LRR (NLR) protein maturation by the HSP90–SGT1–RAR1 ternary complex. The three proteins are HEAT SHOCK PROTEIN 90 (HSP90, brown), SUPPRESSOR OF THE G2 ALLELE OF SKP1 (SGT1, purple), and REQUIRED FOR MLA12 RESISTANCE 1 (RAR1, blue). This model shows HSP90 as the central protein of the cycle that involves the following interacting domains: the N-terminal domain of HSP90 containing the ATP-binding site (yellow half-circle), the TPR, SGS and CS domains of SGT1, and cysteine- and histidine-rich domain 1 and 2 (CH11 and CH2) of RAR1. In this model, interactions occur sequentially in a clockwise direction. Upon ATP binding, the lid segments of the HSP90 dimer form a closed conformation to create an active ATPase enzymatic site with the key arginine in the catalytic (green triangle). When the RAR1 CH1 domain binds to one of the ATP-loaded HSP90 lids this prevents the formation of the lid-closed conformation. Binding of the RAR1-CH1-domain then facilitates the interaction of the RAR1 CH2-domain with the other HSP90 lid of the dimer. The bound RAR1 CH-domains promote the formation of the HSP90 complex with SGT1 and an immature NLR protein (orange). The stable HSP90-RAR1-SGT1-NLR ternary complex then triggers the hydrolysis of ATP by the catalytic Arg to facilitate the intramolecular reorganization of the NLR protein. After release of the ADP, the RAR1-SGT1-NLR complex dissociates from HSP90 and releases the mature NLR protein (red).*

21.6.5 Other plant proteins are required for R protein action

Mutagenesis of resistant plant lines carrying an *R* gene followed by screening for disease-sensitive mutants has revealed other plant genes required for disease resistance.

In *Arabidopsis*, mutations in the *EDS1* (*ENHANCED DISEASE SENSITIVITY 1*) gene eliminate race-specific resistance mediated by the TIR-NB-LRR class of R proteins, and also reduce basal defenses against many virulent pathogens. EDS1 is required for many (but not all) *RPP* gene-mediated resistances to various races of the downy mildew oomycete (*Hyaloperonospora arabidopsidis*), and for RPS4- and RRS1-mediated resistance to *P. syringae* carrying AvrRps4. EDS1 is a member of a family of proteins that carry an atypical lipase motif, and has been located to both the nuclear and cytoplasmic compartments. EDS1 likely functions as a heterodimer with either of two related proteins PAD4 and SAG101. PAD4 mutants are also more disease-susceptible. Although mutations in EDS1 and NDR1 (see section 21.6.4) compromise function of TIR-NB-LRR and CC-NB-LRR signaling, both proteins are required for SA production, indicating that the signal transduction pathways involving these proteins later converge (Fig. 21.47 and see Section 21.8.4).

In barley and *Arabidopsis*, mutations in either *RAR1* (required for Mla-mediated resistance 1) or *SGT1* (suppressor of the G2 allele of *skp1*) result in susceptibility to powdery mildew fungi or downy mildew, respectively, even when the plant genotypes carry functional copies of various race-specific *R* genes and the fungal races express the correct cognate Avr effector. These two proteins, in conjunction with HSP90 (heat shock protein 90) (Fig. 21.48), are required for resistance mediated by multiple R proteins recognizing viral, bacterial, oomycete, or fungal pathogens.

RAR1 contains two highly conserved zinc-binding domains called CHORD-I and CHORD-II (cysteine- and histidine-rich domain). The CHORD-I domain binds to the molecular chaperone HSP90. Both RAR1 and HSP90 stabilize certain NB-LRR proteins and thereby ensure the R proteins can assume a conformation that is competent to receive

pathogen signals. Both RAR1 and HSP90 bind to SGT1 (Fig. 21.48), which is required for the function of R proteins of the TIR-NB-LRR class, the CC-NB-LRR class, the eLRR class, and RPW8. SGT1 contains three distinct domains: a tetratricopeptide repeat domain (TPR), the CS motif (present in CHP and SGT1 proteins), and the SGS motif (an SGT1-specific sequence). The CS motif of SGT1 is sufficient to bind to the ATPase domain of HSP90 as well as interact with the CHORD-II domain of RAR1.

The structure of the HSP90–SGT1–RAR1 complex has been elucidated, and a dynamic model for the interaction of the three components proposed (Fig. 21.48). Overall, this HSP90–SGT1–RAR1 chaperoning complex is proposed to maintain the steady state levels of different R proteins and ensure that R proteins are correctly folded and maintained in a recognition-competent state in the appropriate cellular compartment. It may be required for the conformational changes involved in resistance activation. Misfolded R proteins can inappropriately activate defense and therefore must be immediately inactivated and degraded. This chaperon complex is structurally and functionally conserved in other eukaryotes.

Some NB-LRR proteins require other NB-LRR proteins to function. The *N REQUIRED GENE 1* (*NRG1*) is required for function of the tobacco TIR-NB-LRR protein N, which confers resistance against TMV through recognition of the TMV p50 protein. NRG1 is a CC-NB-LRR type R protein. Similarly, the TIR-NB-LRR protein RPS4 also requires the TIR-NB-LRR-WRKY protein RRS1 for its function (and vice versa) (see Section 21.5.5). In some CC-NB-LRRs, the CC domain resembles that present in the atypical *Arabidopsis* R protein RPW8 (see Section 21.6.3). This is referred to as the CC_R domain. CC_R-NB-LRR-encoding genes are present in most plants; examples include the *Nicotiana benthamiana* NRG1 protein and the *Arabidopsis* activated disease resistance gene 1 (ADR1) protein. CC_R domains are sufficient for the induction of defense responses, and this activity is SGT1-independent. Both CC_R domain genes are unique to genomes that carry TIR-NB-LRR genes, suggesting CC_R domain proteins may be required for signaling by TIR-NB-LRR R proteins.

21.6.6 Many *R* genes can function in heterologous plant species

Most *R* gene sequences confer resistance when introduced into a susceptible genotype of the original host or a closely related species. For example, the tobacco *N* gene is active in tomato, where it restricts TMV infections to localized necrotic lesions, as it does in tobacco. Thus, Avr-dependent R protein signaling cascades are conserved between related plant species.

Pto, Cf-9, and Bs2 from Solanaceous plants do not confer recognition of their corresponding effectors in *Arabidopsis*. However, barley Mla can confer function in *Arabidopsis*, and *Arabidopsis* RPS4 and RRS1 can function in Solanaceae. Overexpression of some *R* genes in heterologous plants results in necrotic symptoms in the absence of pathogen attack, or plants with altered development.

These data highlight how finely tuned the relationship is between R proteins and signaling partners in their native species. The evolution of *R* gene sequences is most likely constrained not only by selection for pathogen recognition, but also for functional interactions with guardee proteins, and for avoidance of recognition of related endogenous plant proteins that control plant development.

21.7 Other sources of genetic variation for resistance

21.7.1 A few plant R proteins are unique

A few *R* genes provide broad-spectrum resistance to multiple pathogenic species, and functional homologs of these *R* genes have not been reported in other plants. Potentially each R protein could provide a plant species-specific function, but it is more likely that the corresponding *R* gene needs to be formally identified in other plant species.

RPW8.2 from *Arabidopsis* confers broad-spectrum resistance to several powdery mildew species, including *Golovinomyces orontii.* RPW8 proteins feature an N-terminal transmembrane domain and one or more coiled-coil (CC_R) domains (homologous to the ADR1/NRG1 subclass of CC-NB-LRR proteins), and they lack an LRR domain.

The wheat *Lr34* gene provides durable adult plant resistance to the basidiomycetes *Puccinia triticina* and *P. striiformis*, which respectively cause leaf rust and stripe rust, and to the ascomycete powdery mildew species *Blumeria graminis* f. sp *tritici*. Through plant breeding, the *Lr34* gene is now present in most wheat cultivars globally. The *Lr34* gene sequence encodes a putative adenosine triphosphate binding cassette (ABC) transporter that may translocate toxic compounds stored in plant cells (possibly in the vacuole) to the point of fungal ingress, arresting growth.

Two major quantitative loci, *rhg1* and *Rhg4*, control root infections in soybean (*Glycine max*) crops caused by the cyst nematode *Heterodera glycines*. Roots of plants carrying the *Rhg* genes are penetrated by infective juvenile nematodes, but the feeding nematodes die before reaching adult stages (see Section 21.1.5). The *Rhg4* locus encodes a serine hydroxymethyltransferase, an enzyme that is ubiquitous in nature and structurally conserved across kingdoms. It is responsible for interconversion of serine and glycine and essential for one-carbon metabolism. Transcriptional and metabolic profiling studies indicate the syncytial feeding cells support a demand for folate one-carbon metabolism. Nematodes, like other animals, acquire folate from their diet; therefore, impaired folate production at induced feeding site may lead to a nutritional deficiency that starves the nematode.

21.7.2 Insensitivity to host-selective toxic proteinaceous effectors and metabolites is important in plant defense against necrotrophs

Two closely related necrotrophic fungal pathogens, *Stagnospora nodorum* and *Pyrenophora tritici-repentis*, produce host-selective toxins that induce susceptibility only in wheat genotypes that harbor the corresponding toxin sensitivity gene *Tsn1*. The Tsn1 protein has several R protein-like features, including serine-threonine kinase, NB, and LRR domains, which are required for ToxA sensitivity and disease susceptibility. Wheat genotypes that are insensitive to ToxA lack the entire gene sequence, and Tsn1 does not seem to directly bind the ToxA effector. These findings suggest that necrotrophic pathogens may subvert the resistance mechanisms acquired by plants to combat other pathogen types by making molecules that provoke cell death, and have also evolved ways to thrive in environments that would be detrimental to biotrophic pathogens.

21.7.3 Recessively inherited resistance genes provide resistance against bacteria, fungi, and viruses in cereal and noncereal species

Recessively inherited resistance is rarely reported to control either bacterial or fungal infections. However, this mode of inheritance is more frequently encountered in the successful control of plant viruses. Some of the different types of recessive resistance (*r*) genes and how they function are described below and in Table 21.7.

Resistance to some bacteria involves sequence variation in proteins targeted by virulence effectors. In rice, nine of the 30 documented resistance genes against the bacterial blight pathogen *Xanthomonas oryzae* pv. *orzyae* are recessively inherited. The *xa13* gene occurs as a series of natural alleles of *Os-8N3*, whose expression is induced by strains of *Xanthomonas oryzae* pv *oryzae* carrying the gene *pthXo1*, which encodes the transcription activator-like (TAL) effector PthXo1 described in Section 21.3.8. The *xa13* alleles are unresponsive to PthXo1, and plants with *xa13* are resistant to strains of the pathogen that rely solely on PthXo1 as the essential effector for virulence. Os-*8N3* encodes a member of the NODULIN3 gene family of SWEET proteins that transport sugar.

Recessive (*mlo*) alleles of the *Mlo* locus in barley, *Arabidopsis*, tomato, and pea confer broad spectrum resistance to various powdery mildew species. The deduced MLO ≈60-kDa gene product is predicted to be anchored in the plasma membrane by a conserved seven membrane-spanning-domain protein. Two *mlo* mutant alleles are deployed commercially to reduce the risk of mildew infection in barley (*Hordeum vulgare*).

Recessively inherited resistance against viruses often confers non-HR immunity, as opposed to an HR-associated defense. Virus genomes are small and code for just a few functional proteins (see Section 21.3.4; see Chapter 10). To complete their life cycle, viruses rely on host plant proteins involved in DNA replication, transcription, and translation. Therefore, recessive antiviral resistance genes are frequently mutant alleles of genes that encode plant host proteins required at specific steps in the virus life cycle. For example, mutations in the eukaryotic translation initiation factor 4E (eIF4E) or its isologs eIF(iso)4E occur in many cereal and noncereal plant species, where they confer resistance primarily against RNA viruses belonging to the *Potyviridiae* family (Fig. 21.49). These viruses encode VPg, a small protein that is attached to the 5′ end of the viral RNA genome. VPg is a likely functional equivalent of the eukaryotic mRNA cap structure, which is important for translation initiation and recruitment of ribosomes via interaction with eIF4E or eIF(iso)4E (see Chapter 10). Both the potyviral VPg protein and the eIF4E/eIF(iso)4E proteins are multifunctional and are involved in processes other than initiation of protein synthesis. The exact purpose of the VPg–eIF4E interaction has still to be discovered; however, specific mutations in the host *eIF4E* gene lead to a failure of the potyvirus to complete their life cycle (i.e., translation, replication, or cell-to-cell trafficking), which results in resistance without HR formation.

21.8 Local and systemic defense signaling

Within minutes of pathogen, insect, or nematode attack, plant defense responses are activated locally, and within hours, defense responses are elaborated in tissues distant from the invasion site and even in neighboring plants. Remarkably, the type of induced systemic response is determined by the identity of the initial attacking organism. As shown in Figure 21.50, induced systemic responses to fungi, bacteria, and viruses are distinct from those to insects. Nematodes appear to induce a mixture of the two. The adaptive significance to plants of orchestrating systemic responses is enormous. They ensure that distant plant tissues can deal more effectively with subsequent attackers.

21.8.1 Plants activate systemic responses to pathogens

Fungi, bacteria, and viruses systemically activate a defense response known as **systemic acquired resistance** (SAR). For SAR to occur, the initial infection must result in formation of necrotic lesions, either as part of the HR or as a symptom of disease. SAR is induced strongly by ETI and weakly by PTI, and during SAR, a specific subset of pathogenesis-related (PR) genes (described later) is activated in the plant tissues distant to the initial pathogen infection site. SAR activation

TABLE 21.7 *Recessively inherited resistance genes.*

Gene	Plant	Pathogen(s)	Infection type/organ/ cell layer attacked	Protein type	Proposed/known protein function	Race specific?
edr1	*Arabidopsis*	Enhanced resistance to *Pseudomonas syringae*, *Hyaloperonospora arabidopsidis*, powdery mildew *Golovinomyces cichoracearum*, but enhanced susceptibility to *Colletotrichum higginsianum* and the necrotrophic *Alternaria brassicicola*	Various extracellular and intracellular lifestyles on leaves	A Raf-like mitogen-activated protein kinase kinase kinase (MAPKKK)	Mutation creating a premature stop codon eliminates the kinase domain. Proposed to be a negative regulator of plant defense	No
eIF4E or its isologs *eIF(iso)4E*	Multiple cereal and noncereal species	RNA viruses mostly belonging to the *Potyviridiae* family	Systemic intracellular infections throughout the plant	Eukaryotic translation initiation factor. Multifunctional and involved in processes other than the initiation of protein synthesis	Mutations result in abolition of interaction with the viral Vpg protein attached to 5′ end of the viral RNA genome. As a result, virus fails to hijack various host processes to complete its life cycle	Mostly yes
mlo	Barley (*Hordeum vulgare*), *Arabidopsis* and tomato	Various powdery mildew fungal species	Obligate biotroph/ multiple organs/ epidermal specific	Plant-specific seven transmembrane helices protein	Negative regulator of plant defense and/or PCD	No
RRS1-R	*Arabidopsis*	Bacterial blight pathogen *Ralstonia solanacearum*	Extracellular/multiple organs/all tissue layers	TIR-NB-ARC-LRR-WRKY	Upon physical interaction with bacterial effector Pop2, RRS1 cooperates with another TIR-NB-LRR protein RPS4 to activate defense	Yes
xa5	Rice (*Oryza sativa*)	Bacterial blight pathogen *Xanthomonas oryzae* pv. *oryzae*	Extracellular/multiple organs/all tissue layers	Subunit of the general transcription factor TFIIA required by RNA polymerase II	The mutant xa5 protein, which has only two residue changes, retains its basic transcription factor function and may possess enhanced ability to interact with the bacterial effector Avrxa5	Yes
xa13 (Os-8N3)	Rice	Bacterial blight pathogen *Xanthomonas oryzae* pv. *oryzae*	Extracellular/multiple organs/all tissue layers	A member of the NODULIN3 gene family of SWEET proteins that transport sugar	*xa13* alleles are unresponsive to the TAL effector PthXo1	Yes

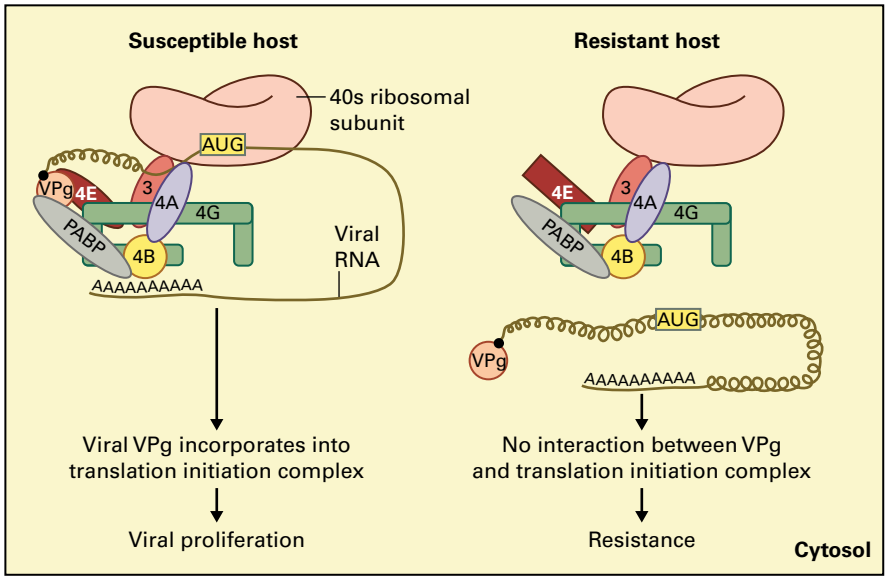


FIGURE 21.49 *R proteins and defense activation. Recessive resistance to potyviruses is conferred by mutant alleles of a eukaryotic translation initiation factor 4E (eIF4E). Initiation of translation in plants (and other eukaryotes) uses a multi-protein complex consisting of initiation factors 3, 4A, 4B, 4E, 4G, poly(A)-binding proteins (PABPs), 40S ribosomal subunit and several other minor components. An interaction between the mRNA cap structure (m7GpppG) and eIF4E is required for efficient translation. Potyviruses produce a small protein called VPg, which is covalently attached to the 5′-end of their RNA genomes and is likely to play a role similar to the mRNA cap structure during translation initiation (left). Some naturally occurring structural variants of eIF4E confer resistance to potyviruses in many plant species, probably because of their inability to bind potyviral VPg and recruit potyviral RNA into the translation initiation complex (right).*

also leads to a significant reduction in disease symptoms after subsequent infection by many different pathogen species. For example in tobacco, *N*-gene mediated resistance against TMV protects the plant against later infection by most, but not all, tobacco pathogens, including an identical TMV strain. SAR can convert normally genetically compatible plant–pathogen interactions into incompatible ones. Therefore, by understanding how SAR works, it may be possible to engineer broad-spectrum disease control into crops (see Section 21.10).

A requirement for SA in SAR activation was demonstrated by expression of the bacterial NahG SA hydroxylase in tobacco and *Arabidopsis* plants. These plants do not accumulate free SA and are incapable of activating SAR. So is SA the translocated signal?

In vivo ^{14}C-SA labeling studies revealed that, following TMV infection on N tobacco, as much as 70% of the SA increase in uninfected tissue results from its translocation from the infected leaves; a series of grafting experiments between wild-type and NahG plants, however, indicated that SA is only needed in the distal plant organs for SAR to be induced (Fig. 21.51). Therefore, SA is probably not the mobile signal in tobacco. Grafting experiments using tobacco showed that SA methyltransferase activity, which converts SA into methylsalicylic acid (MeSA), is required in the tissue that generates the mobile signal. Conversely, MeSA esterase activity, which converts MeSA back to SA is required for signal perception in the distal tissues. However, in *Arabidopsis*, SA is required for SAR, whereas MeSA is dispensable for SAR. Thus, MeSA may have a signaling role for SAR induction in tobacco, but not in all plant species.

SA induces or potentiates many plant defense responses and induces a set of pathogenesis-related (PR) proteins. Seventeen families of PR proteins have been classified (Table 21.8), and the same types of PR protein families occur in most plant species. Transcripts of *PR* genes accumulate within minutes to hours of pathogen attack and PTI or ETI activation, and they are also induced in compatible interactions, but much more weakly and slowly. Induction of PR proteins distal to the initial site of infection frequently occurs. Several PR proteins are also induced as plants start to flower or experience abiotic stress.

Some PR proteins function as chitinases and glucanases, degrading fungal cell wall structural polysaccharides and impairing fungal growth. SA regulates the transcriptional activation of many *PR* genes. Also, ethylene and SA can act synergistically, enhancing *PR* gene expression even further. Other PR defense proteins, such as lipoxygenase, may contribute to defense by generating secondary signal molecules, such as jasmonic acid (JA) and lipid peroxides, and by producing an array of toxic volatile and nonvolatile secondary metabolites with antimicrobial activity.

Various synthetic chemicals induce SAR. Two of the most potent are 2,6-dichloroisonicotinic acid (INA) and benzo(1,2,3) thiodiazole-7-carbothionic acid *S*-methyl ester (BTH). Both compounds act as SA mimics and activate SAR when applied to NahG plants.

To understand the molecular and biochemical basis of SAR, mutagenesis screens using *Arabidopsis* revealed the SAR-deficient mutant *dir1-1* (*defective in induced resistance*). The *dir1-1* mutant plants can activate defenses locally,

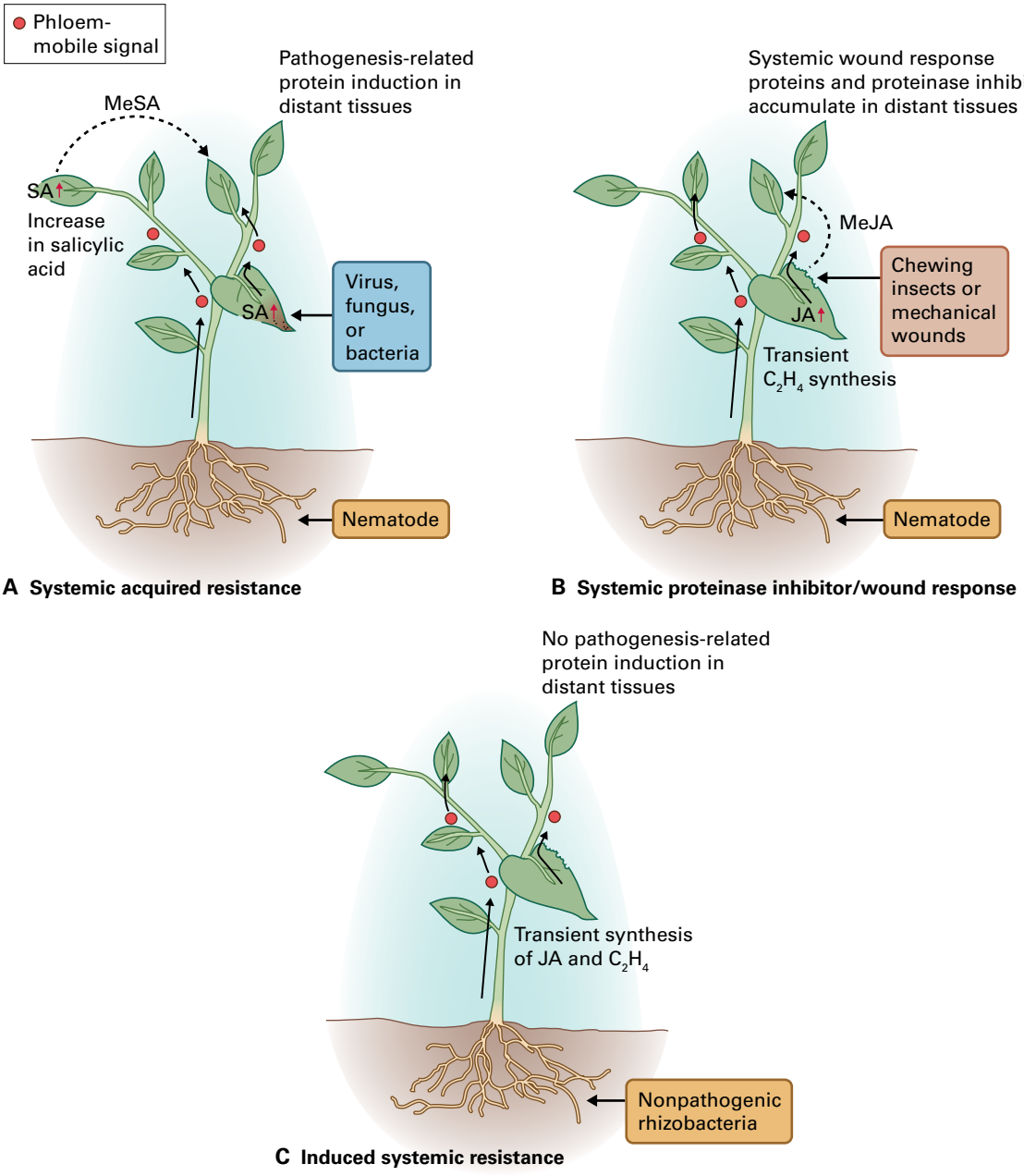


FIGURE 21.50 *Systemic responses to plant pathogens. (A) Viruses, fungi, and bacteria activate systemically a subset of defense responses in a phenomenon known as systemic acquired resistance (SAR), in which local necrosis formation at the initial site of pathogen invasion triggers both a local increase in salicylic acid (SA) and formation of a phloem-mobile signal. Subsequently, in distal plant tissue, SA concentrations increase and volatile methyl-SA (MeSA) is released. Together, these signals induce synthesis of various pathogen-related proteins in non-invaded parts of the plant. (B) In contrast, attack by chewing insects or mechanical wounding activates a different protective response, the systemic PI/wound response, wherein initial tissue damage causes a transient increase in the synthesis of ethylene and jasmonic acid (JA). Volatile methyl jasmonate (MeJA) and another phloem-mobile signal called systemin then activate the systemic responses, which include the accumulation of proteinase inhibitors (PIs) and other systemic wound response proteins (SWRPs). Root-attacking nematodes appear to induce a mixture of both the SAR and systemic PI/wound responses. (C) Induced systemic resistance (ISR) caused by soil-inhabiting nonpathogenic rhizobacteria colonizing plant roots. ISR requires both JA- and ethylene-mediated signaling to induce protective defense responses in the distant leaf tissue. This form of defense does not involve accumulation of pathogenesis-related (PR) proteins or require SA.*

indicating DIR1 is only required for the systemic responses. DIR1 is predicted to encode an apoplastic lipid-transfer protein, and this protein was detected in the vascular exudates of wild-type plants after localized pathogen inoculation. Therefore, the DIR1 protein has a role in either the generation of the systemic signal or transport of another lipid-based signal to distal tissues.

A mutant impaired in the biosynthesis of glycerol 3-phosphate (G3P) also fails to activate SAR. The SAR response can be rescued by the addition of either G3P or vascular exudates from

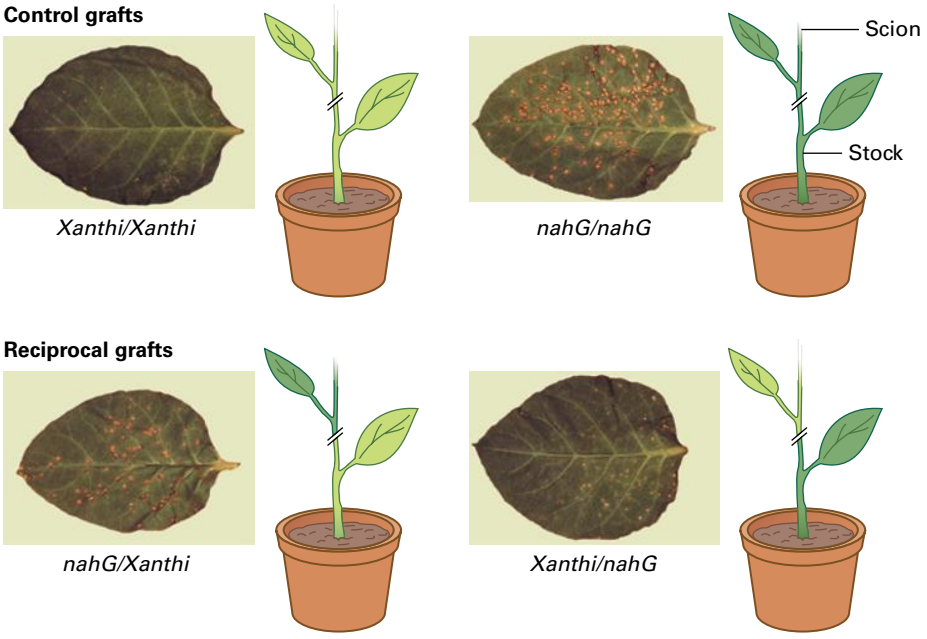


FIGURE 21.51 *Grafting experiments demonstrate that salicylic acid (SA) is unlikely the phloem-mobile signal that activates SAR. An absolute requirement for SA in systemic acquired resistance (SAR) was demonstrated using transgenic tobacco (*Nicotiana tabacum*) and* Arabidopsis *expressing the bacterial* nahG *gene, in which the NahG SA hydroxylase degrades SA to catechol, CO_2, and water. These plants did not accumulate free SA and were incapable of activating SAR. Then a series of grafting experiments between wild-type and transgenic nahG-expressing plants revealed that, to induce SAR, SA only needed to be present in the distal plant organs. Reciprocal and control grafts were generated using two types of tobacco plants, which expressed either the N resistance gene alone (cultivar* Xanthi*) or the N gene in combination with the nahG transgene to remove inducible SA (nahG). The four types of grafted plants were inoculated with TMV on the lower rootstock leaves; 7 days later, the same TMV isolate was inoculated onto the upper scion leaves. The photographs show the infection types on the scion leaves five days after the second TMV inoculation. The nahG scions grafted onto the* Xanthi *rootstocks (nahG/*Xanthi*) were unable to mount an SAR response. In contrast,* Xanthi *scions grafted onto nahG rootstocks (*Xanthi*/nahG) demonstrated SAR responses similar to those of the control* Xanthi/Xanthi *grafts not expressing the nahG transgene. The nahG/nahG grafts lacking SA were unable to mount an SAR response.*
Source: (Photos) Vernooij et al. (1994). Plant Cell 6:959–965.

induced wild-type plants to the distal tissues. Thus, G3P may also be a signaling molecule in SAR that requires DIR1. In addition, analysis of vascular exudates revealed azelaic acid as a mobile signal capable of inducing SAR. Application of azelaic acid leads to induction of the *AZI1* (*AZELAIC ACID-INDUCED 1*) gene, which is predicted to encode a secreted lipid-transfer protein. Reciprocal application of vascular exudates from wild-type and *azi1* mutant plants show that AZI1 is involved in the production or translocation of a mobile signal. Together, these studies reveal that multiple mobile signals are transported through the vasculature to systemic, uninfected parts of the plant, where they induce the accumulation of SA, a signal molecule for SAR. These mobile signals in *Arabidopsis* and their roles and potential interplay are depicted in Figure 21.52.

21.8.2 NPR1, NPR3, and NPR4 mediate SA induction of *PR* genes

A key protein in SAR is NPR1 (NONEXPRESSOR OF PATHOGENESIS-RELATED GENES 1) (Fig. 21.53). *Arabidopsis npr1* mutant plants fail to induce *PR* genes upon treatment with chemical inducers, such as SA and INA, and are compromised in SAR. The *npr1* mutant does, however, show a stronger HR and greater SA accumulation in response to genetically incompatible pathogens, whereas NPR1 overexpressing *Arabidopsis* lines exhibit a weaker HR. Therefore NPR1 is a positive regulator of SAR but a negative regulator of effector triggered HR (ETI). NPR1 encodes an ankyrin repeat protein that positively regulates SA signaling and is a member of a small gene family that includes NPR3 and NPR4 (see later). Similar ankyrin repeats are found in numerous eukaryotic proteins involved in protein–protein interactions.

In healthy plant cells, NPR1 is retained in an oligomeric form in the cytoplasm by intermolecular disulfide bridges, and S-nitrosylation by nitric oxide (NO) facilitates NPR1 oligomerization. The NO moiety becomes covalently attached to the thiol side chain of cysteine, resulting in protein S-nitrosylation (NPR1 oligomer). Upon pathogen infection, thioredoxins also located in the cytoplasm counteract the S-nitrosylation of NPR, leading to monomer release and migration of this transcription cofactor to the nucleus (NPR1 monomer). SA affects cellular redox state and NPR1 nuclear translocation. Once inside the nucleus, NPR1 binds to TGA (TGACG-motif binding) transcription factors, enhancing

TABLE 21.8 *Recognized families of pathogenesis-related proteins.*

Family	Type member	Properties
PR-1	Tobacco PR-1a	Unknown
PR-2	Tobacco PR-2	β-1,3-glucanase
PR-3	Tobacco P, Q	Chitinase type I,II,IV,V,VI,VII
PR-4	Tobacco 'R'	Chitinase type I,II
PR-5	Tobacco S	Thaumatin-like
PR-6	Tomato Inhibitor I	Proteinase-inhibitor
PR-7	Tomato P_{69}	Endoproteinase
PR-8	Cucumber chitinase	Chitinase type III
PR-9	Tobacco "lignin-forming peroxidase"	Peroxidase
PR-10	Parsley "PRI"	Ribonuclease-like
PR-11	Tobacco "class V" chitinase	Chitinase type I
PR-12	Radish Rs-AFP3	Defensin
PR-13	*Arabidopsis* THI2.1	Thionin
PR-14	Barley LTP4	Lipid-transfer protein
PR-15	Barley OxOa (germin)	Oxalate oxidase
PR-16	Barley OxOLP	Oxalate-oxidase-like
PR-17	Tobacco PRp27	Unknown

their binding to SA-responsive promoters. This then leads rapidly to the transcriptional activation of a wide repertoire of defense responses and pathogen resistance.

The NPR1 protein carries a Broad-complex, Tramtrack, and Bric-a-brac BTB domain, also found in various proteins that make E3 ligase complexes with CULLIN3 (see Chapter 10). In addition, once within the nucleus NPR1 is phosphorylated on two serine residues, and this facilitates the interaction between NPR1 and CULLIN to enhance NPR1 degradation. NPR1 protein turnover (degradation) by the 26S proteasome is required for full induction of the NPR1-induced genes, the mechanism of which is still under investigation. It is hypothesized that NPR1 turnover facilitates the "refreshment" of the transcription initiation complex. NPR1 is responsible for heightening defense responses in SAR-induced plants during subsequent pathogen attacks.

Two receptors for SA have been identified in *Arabidopsis*: the low-affinity NPR3 protein and the high-affinity NPR4 protein. At the site of infection, NPR1 must be degraded in the nucleus via interaction with NPR3 to allow PCD and ETI to occur. In a healthy plant, if NPR1 enters the nucleus, it is degraded by NPR4, whose interaction with NPR1 does not require SA. At a distance from the site of infection, NPR4 functions in conjunction with NPR1 and promotes defense gene induction without host cell death. In *npr3npr4* double mutant plants, local NPR1 levels remain high and no SAR occurs.

Both NPR3 and NPR4 proteins have two functions, as SA receptors and as adaptor proteins that link the NPR1 protein to CULLIN3. Upon binding SA, NPR3 promotes the NPR1–NPR3 interaction, whereas NPR4 disrupts the NPR1–NPR4 interaction. At the high SA concentrations typically induced locally at the sites of initial pathogen infection, the low-affinity NPR3 receptor mediates degradation of the cell death suppressor NPR1, thereby permitting activation of ETI and cell death to occur. In contrast, at the lower SA concentrations typically found in distal tissues, SA is unable to bind to NPR3, and cell death is blocked. In these distal tissues, SA instead binds to the high-affinity

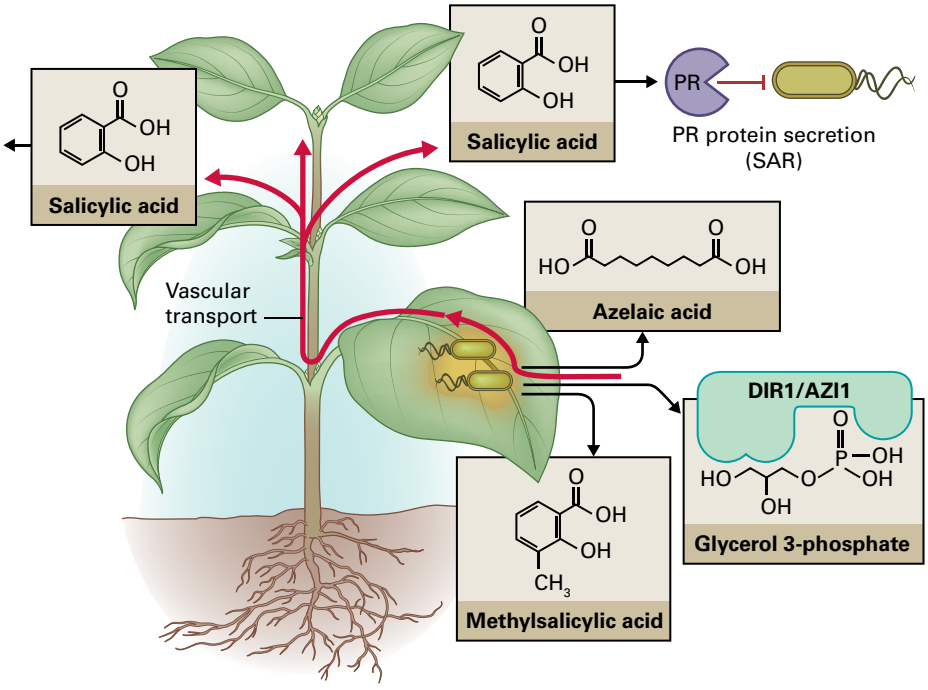


FIGURE 21.52 *Systemic activation of plant defense responses. Several proteins and metabolites with various functions are required to establish and maintain the systemic acquired resistance (SAR) response. DIR1 and AZI1 are predicted to be apoplastic lipid-transfer proteins that have a role in either generation of the systemic signal or transport of various systemic signals to distal tissues. The metabolites glycerol 3-phosphate (G3P) and azelaic acid are two systemically mobile signals that accumulate in vascular exudates in activated plants. When the mobile signals reach the systemic tissues, accumulation of salicylic acid (SA) occurs and induces or potentiates many plant defense responses, including the induction of a set of pathogenesis-related (PR) proteins. The induced volatile metabolite methylsalicylic acid (MeSA) may have a SAR signaling role in tobacco, but not in all plant species.*

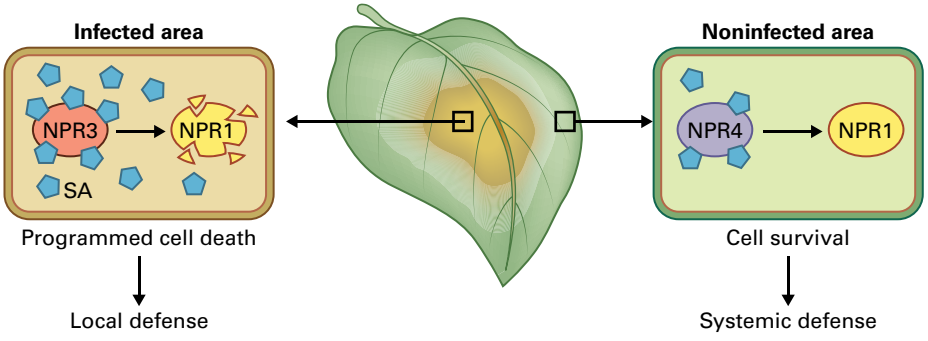


FIGURE 21.53 *SA-mediated control of plant cell death and survival. Upon microbial infection, SA levels increase, its concentration decreasing gradually with increasing distance from the site of infection. At high SA concentrations—typically found in infected areas of the plant—the receptor NPR3, which binds SA with low affinity, mediates degradation of the cell-death suppressor NPR1 (left), thereby favoring programmed cell death and local effector-triggered immunity. However, at the lower SA concentrations typically found in cells distant from the infection site, SA cannot bind to the low-affinity receptor NPR3, so cell death is blocked. In these cells, SA instead binds to the high-affinity receptor NPR4 (right), blocking degradation of NPR1, thereby favoring cell survival and expression of genes associated with activation of systemic defenses.*

receptor NPR4, blocking the degradation of NPR1 to favor cell survival and the expression of genes associated with SAR (Fig. 21.53).

21.8.3 Systemic responses to mechanical wound and insect attack occur in plants

Many herbivorous insects mechanically wound plant tissue while feeding and induce the rapid accumulation of proteinase inhibitors (PIs) and other systemic wound response proteins (SWRPs) throughout the plant (see Fig. 21.50). The systemic response to chewing insects is frequently referred to as the **wound response**, because similar molecular and biochemical events are triggered after plant tissue is mechanically wounded. In tomato, although high concentrations of oligogalacturonides released from damaged plant cell walls induce PI and SWRP genes locally, these oligogalacturonides do not move systemically. Instead an 18 amino acid polypeptide called **systemin** (see Chapter 17) is the mobile systemic signal.

Systemin can initiate defense responses at a few femtomoles (10^{-15} moles) per plant. It is synthesized by cleavage from the C-terminus of pro-systemin, a 200 amino acid precursor protein, in the cytoplasm at the site of wounding. Systemin is released from damaged cells, moves throughout the damaged

leaf within 30 minutes, and is transported via the phloem to upper unwounded leaves within 60–90 minutes.

The importance of systemin to plant defense against insect attack has been demonstrated using transgenic tomato plants that produce either continuously high or lower than normal systemin levels in response to wounding. When systemin levels are high, the tomato plants constitutively express defense mechanisms even in the absence of wounding, and are more resistant to herbivory by larvae of the tobacco hornworm *Manduca sexta*. When systemin production is lower than normal, plants have a severely reduced systemic induction of defense mechanisms and are more susceptible to *M. sexta* larvae.

Once systemin reaches the target tissue in tomato plants, its perception activates several signaling pathways that lead to expression of various defense mechanisms. One pathway is similar to that elicited by P/MAMPs, involving ion fluxes across the membrane, an oxidative burst, and the activation of MAP kinases (see Fig. 21.30). This activates a lipid-based signaling cascade and JA production (see Chapter 17). JA induces transcription of PI and other SWRP genes; however, for JA induction of PI genes to occur, a third signal molecule is required, the gaseous hormone **ethylene**.

Ethylene transiently accumulates within 30–120 minutes of systemin addition to the translocation stream. When ethylene synthesis is blocked pharmacologically or by reverse genetics using transgenic plants expressing an antisense ACC oxidase gene (see Chapter 17), neither wounding nor systemic or JA treatments can induce PI gene expression. A tomato mutant in JA biosynthesis called *defenseless 1* (*def1*) has a compromised insect defense response (Fig. 21.54). SA inhibits both the octadecanoid pathway and ethylene biosynthesis. The SA inhibition of the wound response explains why PI and SWRP genes are not induced during SAR to pathogens, when high levels of SA accumulate.

Some, but not all, features of the defense response to wounding are conserved across plant species. For example, in both *Arabidopsis* and tomato, JA signaling plays a crucial role in initiation of the wound response; however, the systemin signaling pathway is found only in the Solanaceae. *Arabidopsis* has no genes that encode proteins resembling prosystemin; therefore, in *Arabidopsis*, JA is most likely the signal that directly induces the systemic wound response.

21.8.4 Insect herbivores induce production of proteinase inhibitors

In addition to activating the systemic wound response, attacking insect herbivores activate synthesis of a different group of defense proteins to microbial pathogens that interfere with the insect digestive system. They include serine, cysteine, and aspartyl PIs and polyphenol oxidases. These proteins interact with proteins and proteinases in the herbivore gut and inhibit proteolysis of the ingested food. The result is reduced availability of essential amino acids, which either retards herbivore growth and development or kills them. Nematodes induce PI accumulation, which results in similar adverse effects.

21.8.5 Jasmonic acid and ethylene mediate resistance to necrotrophs

Plant **defensins** are defense-related proteins with antimicrobial activity. This growing family of basic cysteine-rich peptides with a molecular mass below 7 kDa is of particular

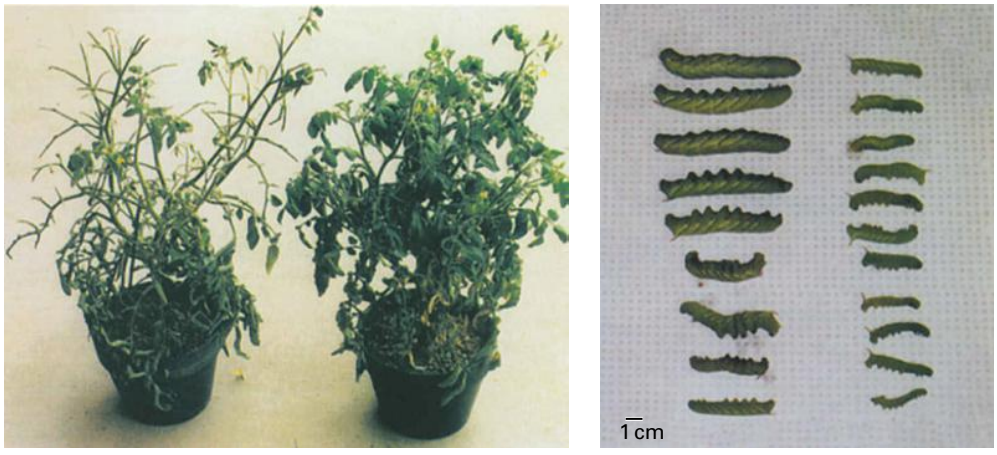


FIGURE 21.54 *The tomato mutant* defenseless *(def1, A, left) is deficient in the biosynthesis of the octadecanoid pathway-derived signal, jasmonic acid. The* defenseless *plant has a compromised systemic wound response compared with that of the wild-type plant (A, right). When larvae of the tobacco hornworm insect (*Manduca sexta*) feed on* defenseless *plants (B, left), their growth rate is faster than when feeding on wild-type tomato plants, which can systemically synthesize PI and other systemic wound response proteins in response to feeding by larvae (B, right).*
Source: Howe et al. (1996). Plant Cell 8:2067–2077.

interest for three reasons. First, unlike SA-mediated defense responses, plant defensin accumulation in vegetative plant tissues is controlled by a combination of JA and ethylene. Second, JA levels rise in systemic tissues. Third, insects, birds, and mammals produce structurally and functionally similar defensin peptides following microbial attack. For example, the fruit fly *Drosophila melanogaster* produces a peptide called drosomycin that resembles plant defensins from radish. Both peptides exhibit potent antifungal activity (Fig. 21.55). This conserved structure/function relationship indicates an ancient conserved defense strategy against microbial attack involving extracellular peptide production.

Necrotrophic fungal, oomycete, and bacterial pathogens, as well as insects, trigger defense responses that are mediated by JA in combination with ethylene (Fig. 21.56). In *Arabidopsis*, the thionin gene *Thi2.1* and plant defensin gene *PDF1.2* are locally and systemically activated after infection with a necrotizing pathogen or exogenous application of ethylene and **methyl jasmonate,** but not after the leaves have been treated with SA. Coronatine is the toxin effector produced by the bacterium *P. syringae* to mimic JA and thereby assist infection (see Section 21.3.3). JA can become conjugated to different amino acids. In particular, JA-isoleucine is the JA derivative that is recognized by COI1, and is crucial for JA signaling.

Most JA responses are mediated by the F-box protein COI1 (CORONATINE INSENSITIVE 1). In *Arabidopsis*, JA-insensitive *coi1* mutants are more susceptible to necrotrophic pathogens, such as *Alternaria brassicicola* and *Botrytis cinerea*.

A key regulator of JA responses in plant–pathogen interactions is the basic helix–loop–helix transcription factor AtMYC2. In addition, JAZ (JASMONATE ZIM-domain-containing) proteins in *Arabidopsis* negatively regulate JA signaling by binding AtMYC2. In the presence of JA-Ile, these JAZ proteins interact with the COI1 protein, promoting ubiquitination of the JAZ proteins and leading to their degradation by the 26S proteasome, releasing AtMYC2 to activate the JA-responsive genes (Fig. 21.56). The crystal structure of the *Arabidopsis* JA receptor has revealed the JA responses are mediated by a complex formed between COI1 and JAZ proteins that requires the presence of both the signal JA-Ile and inositol 6-phosphate (see Chapter 17).

JA and ethylene signaling molecules often work in combination during the defense response. Ethylene is frequently synthesized during both compatible and incompatible interactions. In *Arabidopsis*, the ethylene signal is perceived by five ethylene receptors, each of which contains a protein kinase domain (see Chapter 18). These receptors are negative regulators of ethylene signaling and interact with another negative regulator, CTR1, which negatively regulates downstream components of the ethylene-signaling pathway and is inactivated by ethylene. This inactivation by ethylene abolishes negative regulation of the downstream ethylene-signaling components EIN2 and EIN3. EIN2 is a membrane protein

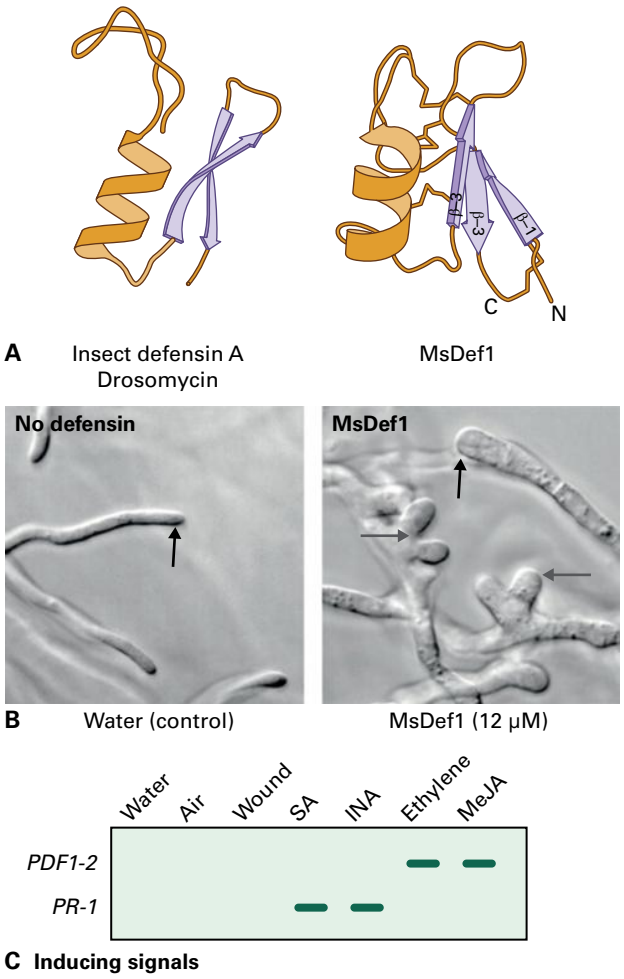


FIGURE 21.55 *Plant defensins are small, cysteine-rich peptides that accumulate at the periphery of the plant plasma membrane and are frequently found in dry plant seeds. They are induced during the defense response in growing plants. Plant defensin peptides are structurally and functionally similar to those produced by insects, birds, and mammals after a microbial attack. (A) The* Drosophila *drosomycin defensin peptide (left) resembles MeDef1 a 45 amino acid protein from the seed of* Medicago sativa *(right). (B) MsDef1 inhibits in vitro growth of a filamentous fungus,* Fusarium graminearum*, at micromolar concentrations (right). It prevents normal filamentous hyphal growth; instead, only a few short and highly swollen hyphae form. (C) In* Arabidopsis*, induction of the defensin PDF1-2 gene transcript is regulated by defense signaling cascades that require ethylene and methyl jasmonate (MeJA). Application of either of these two signaling molecules does not induce the pathogenesis-related PR-1 gene, which is activated by salicylic acid (SA) or dichloroisonicotinic acid (INA). Source*: (B) Sagaram et al (2011). PLoS One 6(4):e18550.

with a C-terminal domain that is released by proteolysis upon activation of ethylene signaling, and leads to elevated levels of EIN3, a short-lived transcription factor protein that accumulates in the nucleus after ethylene levels rise. EIN3 regulates the expression of many ethylene target genes, for example ERF1 that encode ethylene-response element binding (AP2/EREBP) transcription factors involved in defense against

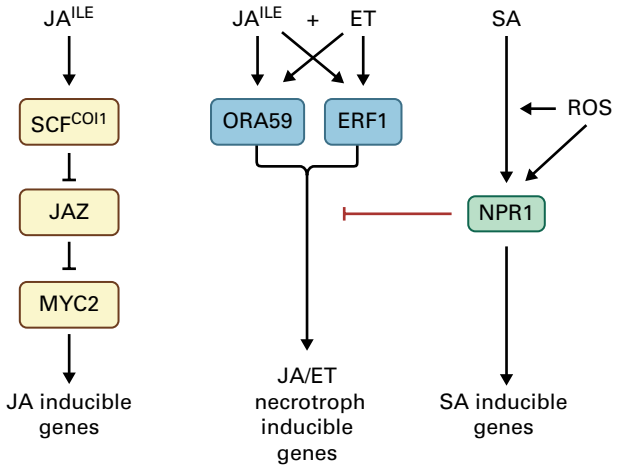


FIGURE 21.56 *Comparison of the three main defense signaling pathways locally activated following pathogen infection or pest attack. The signaling pathways are activated by jasmonic acid-isoleucine (JA^{ILE}) (left), a combination of JA^{ILE} and ethylene (ET) (center), and salicylic acid (SA) and reactive oxygen species (ROS) (right). The JA^{ILE} and combined JA^{ILE}/ET response pathways are important for defense against necrotrophic fungal, oomycete, and bacterial pathogens as well as insects. In contrast, the SA defense pathway is crucial for defense against biotrophic and hemibiotrophic pathogens. (Left) Most JA responses are mediated by the F-box-containing CORONATINE INSENSITIVE 1 protein (COI1). COI1 functions as a jasmonate receptor and forms Skp1/Cullin1/F-box protein COI1 (SCF^{COI1}) complexes. In* Arabidopsis, *key regulators of JA that mediate defense activation are the basic helix-loop-helix transcription factor AtMYC2 and JAZ proteins (JASMONATE ZIM-domain-containing), which bind to AtMYC2 and negatively regulate JA signaling. When JA^{Ile} levels rise, the JAZ proteins interact with the COI1 protein, promoting ubiquitination of the JAZ proteins and their degradation by the 26S proteasome. The released AtMYC2 transcription factor goes on to activate the JA-responsive genes. (Center) The crosstalk and integration of the JA^{ILE} and ET signals in plant defense requires two members of the ETHYLENE RESPONSE FACTOR (ERF) family of transcription factors, namely ORA59, which contains an APETALA2/ERF domain and ERF protein 1 (ERF1). Cooperation between ORA59 and ERF1 activates the expression of several defense-related genes, including plant defensins (for example* PDF1.2*) and basic chitinases (for example* ChiB*). (Right) SA mediated defense signaling can be further enhanced when reactive oxygen species levels are elevated. SA signaling requires the protein NONEXPRESSOR OF PATHOGENESIS-RELATED GENES 1 (NPR1). NPR1 is an ankyrin repeat protein that exists in healthy plants in the cytoplasm in an oligomeric form. Upon pathogen infection, due to a change in redox status, monomers of NPR1 are released and migrate to the nucleus (see Section 21.8.2). Once inside the nucleus, NPR1 binds to TGA (TGACG-motif binding) transcription factors, enhancing their binding to SA-responsive promoters. This in turn leads to the activation of multiple defense-related genes, including the pathogenesis-related proteins (for example PR1). In certain situations, the SA defense signaling pathway can suppress the JA^{ILE}/ET signaling pathway. Plant defense signaling can also be influenced by the plant hormones gibberellic acid and abscisic acid.*

necrotrophs. Overexpression of ERF1 enhances resistance against *Botrytis cinerea* and increases susceptibility to the hemibiotroph *P. syringae* pv. *tomato*.

21.8.6 Salicylic acid and jasmonic acid/ethylene are mutually antagonistic signals and also intersect with other signaling pathways

SA signaling triggers resistance to biotrophic and hemibiotrophic pathogens, whereas a combination of JA and ethylene activates defense against necrotrophic pathogens. These two pathways are mutually antagonistic: elevated SA levels and resistance to biotrophs are often correlated with increased necrotroph susceptibility, and elevated levels of resistance to necrotrophs are often correlated with enhanced susceptibility to biotrophs. This classical view requires revision because other hormones contribute to pathogen virulence and to plant defense. A complex crosstalk influences the levels of these induced hormones, and the eventual biological outcomes are influenced by both pathogen lifestyle and plant genetics.

Gibberellic acid (GA) signaling is regulated by the DELLA proteins (see Chapter 18). In *Arabidopsis*, loss of DELLA proteins results in increased resistance to *P. syringae* pv. *tomato*, and this is associated with increased SA biosynthesis and signaling. DELLAs can also interact with the JA signaling pathway by interacting with the JAZ proteins that prevent AtMYC2 activation; DELLAs thus promote JA signaling. This explains why *Gibberella fujikuroi*, the rice necrotrophic fungal pathogen and cause of "foolish seedling" disease, makes gibberellin: removal of DELLAs attenuates JA signaling. The binding of GA to the DELLA proteins leads to their degradation and enables JAZ proteins to reimpose suppression of AtMYC2. This also explains the increased resistance of the DELLA mutants to biotrophs and hemibiotrophs.

In summary, plant signaling molecules such as SA, JA, ethylene, and GA can influence the balance and level of activation of different facets of the plant defense response via complex mechanisms that remain an active topic of investigation. It is also clear from pathogen genome sequencing projects and targeted biochemical studies that certain pathogenic species produce some of these plant hormones and can, therefore, influence this crosstalk.

21.9 Plant gene silencing confers virus resistance, tolerance, and attenuation

Neither the HR nor the SAR is responsible for limiting the systemic spread of viruses through the plant vascular system. Thus, other defense mechanisms must be responsible for controlling virus infections.

21.9.1 The systemic long-distance spread of viruses is restricted

Arabidopsis mutants have provided genetic evidence for the involvement of specific host genes in controlling vascular movement of a tobamovirus or a potyvirus. At least three loci, *RTM1* (restricted TEV movement 1), *RTM2*, and *RTM3*, are required for restriction of long-distance tobacco etch virus (TEV) movement in the *Arabidopsis* ecotype Col-0. The RTM1 protein is similar to the lectin jacalin. The RTM2 protein contains several domains, including an N-terminal region with similarity to plant small heat shock proteins and a C-terminus that includes a predicted transmembrane spanning domain. These two proteins of the RTM system function within the phloem sieve elements to restrict long-distance movement of TEV.

21.9.2 RNA silencing is important for resistance to many virus species

Plants infected with some viruses can recover and produce new shoots that do not show viral disease symptoms (Fig. 21.57). This is because plants can attenuate the accumulation of many virus species by a mechanism called **RNA silencing** (see Chapter 6). Although plant viruses are highly diverse in sequence, morphology, genome organization, protein production, and host range, all virus species accumulate viral RNA as a part of their life cycle. Accumulation of viral RNA, particularly double-stranded viral RNA (dsRNA), provides the signal that activates the silencing mechanism. The formation of dsRNA can be part of the normal virus replication process, the result of an inverted repeat sequence within the single-strand RNA (ssRNA) that folds into a hairpin structure, or through the presence of a complementary RNA product from overlapping bidirectional transcription.

RNA silencing is an effective defense mechanism that has three main characteristics. First, it is homology-dependent and, therefore, specific to viral RNA. It is driven by small inhibitory RNAs (siRNAs) derived from a double-stranded form of the viral RNA; host-encoded RNAs are not affected by the viral RNA-induced silencing mechanism. Second, there is enormous potential for amplification, because siRNAs can serve as primers for production of secondary long viral dsRNAs from ssRNA templates by plant-encoded RNA-dependent RNA polymerases (see Chapter 6). Third, siRNAs also function as a mobile signal that moves ahead of or with the advancing virus. This signal ensures the virus is not able to escape the effects of silencing by movement between cells or in the phloem.

To counter this efficient RNA silencing mechanism, many plant viruses encode proteins that act as suppressors of RNA silencing. Silencing suppressors from different virus species are mostly unrelated in sequence or structure. Under the strong selection pressure of RNA silencing, several different mechanisms appear to have evolved independently that fulfill the same function. This is an example of **convergent evolution**. Suppressor proteins often provide the virus with additional, unrelated roles in virus replication, and their ability to suppress RNA silencing has evolved as an additional feature. The P19 protein of tomato bushy stunt virus binds siRNAs, and this prevents formation of an active RISC (see Chapter 6). In contrast, the 2b protein of cucumber mosaic virus appears to inhibit the endonuclease activity of Argonaute (see



FIGURE 21.57 *RNA silencing is a general antiviral plant defense mechanism. The bottom leaves of a tobacco plant were inoculated with tobacco ringspot virus (TRSV). By 23 days post inoculation, strong ringspot symptoms developed on the lower leaves; there is, however, a gradual decline in the development of ringspot symptoms on the upper leaves, and the top leaves appear normal and are virus free. The virus causing the initial symptoms activated RNA silencing, which inhibited spread of the infection into the upper leaves and also caused them to be immune to secondary infection by the same virus. Source*: Wingard (1928). J. Agric. Res. 37:127–153.

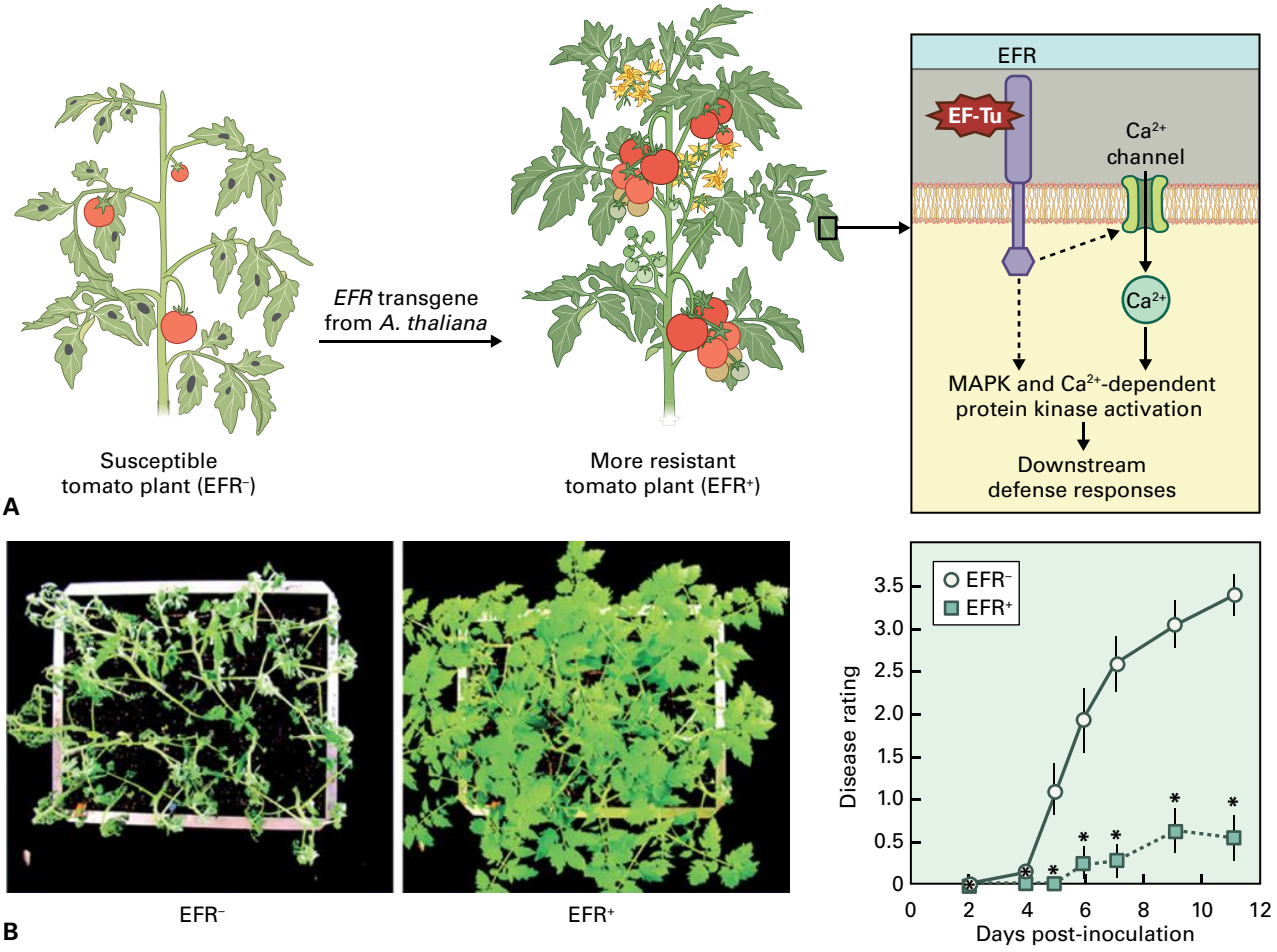


FIGURE 21.58 *Transfer of a pattern-recognition immune (PTI) receptor to a crop confers resistance to several bacterial pathogens. (A) Engineering broad-spectrum resistance in tomato, a member of the Solanaceae, by transferring a pattern-recognition receptor from* Arabidopsis *(family Brassicaceae). Elongation factor Tu receptor (EFR; purple) is absent from the solanaceous species* N. benthamiana *and tomato, and these plants are normally susceptible to infection by phytopathogenic bacterial from different genera. Transgenic expression of* Arabidopsis *EFR increases resistance to these bacterial pathogens, presumably by activating a signaling cascade that confers resistance to a range of bacteria expressing its cognate P/MAMP, elongation factor Tu (EF-Tu; orange). This interfamily transfer of EFR-mediated disease resistance suggests* N. benthamiana *and tomato contain the components necessary for EFR signaling other than the receptor. MAPK, mitogen-activated protein kinase. (B) Wild-type (EFR⁻; left) and transgenic plants expressing EFR (EFR⁺; middle) tomato plants infected with a virulent isolate of* Ralstonia solanacearum. *The time course of disease symptom formation (right) reveals the dramatic reduction in disease severity in the transgenic ERF plants.*
Source: (B) Lacombe et al. (2010). Nat. Biotechnol. 28:365–369.

Chapter 6). The formation of some virus disease symptoms, especially plant stunting and abnormal development, may be the result of interference by viral suppressor proteins in siRNA and microRNA processing.

21.10 Control of plant pathogens by genetic engineering

Exciting opportunities exist to use plant PRRs, plant *R* and other genes, and pathogen *Avr* and effector genes to improve crop disease resistance. In addition, processes required for pathogenesis can be targeted for novel plant-specified inhibitory mechanisms.

21.10.1 Pattern-recognition receptors can elevate pathogen resistance in plants

Pattern-recognition receptors (PRRs) detect microbes by recognizing conserved pathogen/microbe-associated molecular patterns (P/MAMPs, see Section 21.5). However, different plant families carry distinct repertoires of PRRs that perceive distinct P/MAMPs.

The *Arabidopsis* PRR protein EFR perceives the acetylated N-terminus of the bacterial elongation factor-Tu (EF-Tu) (Section 21.5.1), but bacterial EF-Tu is not perceived in the

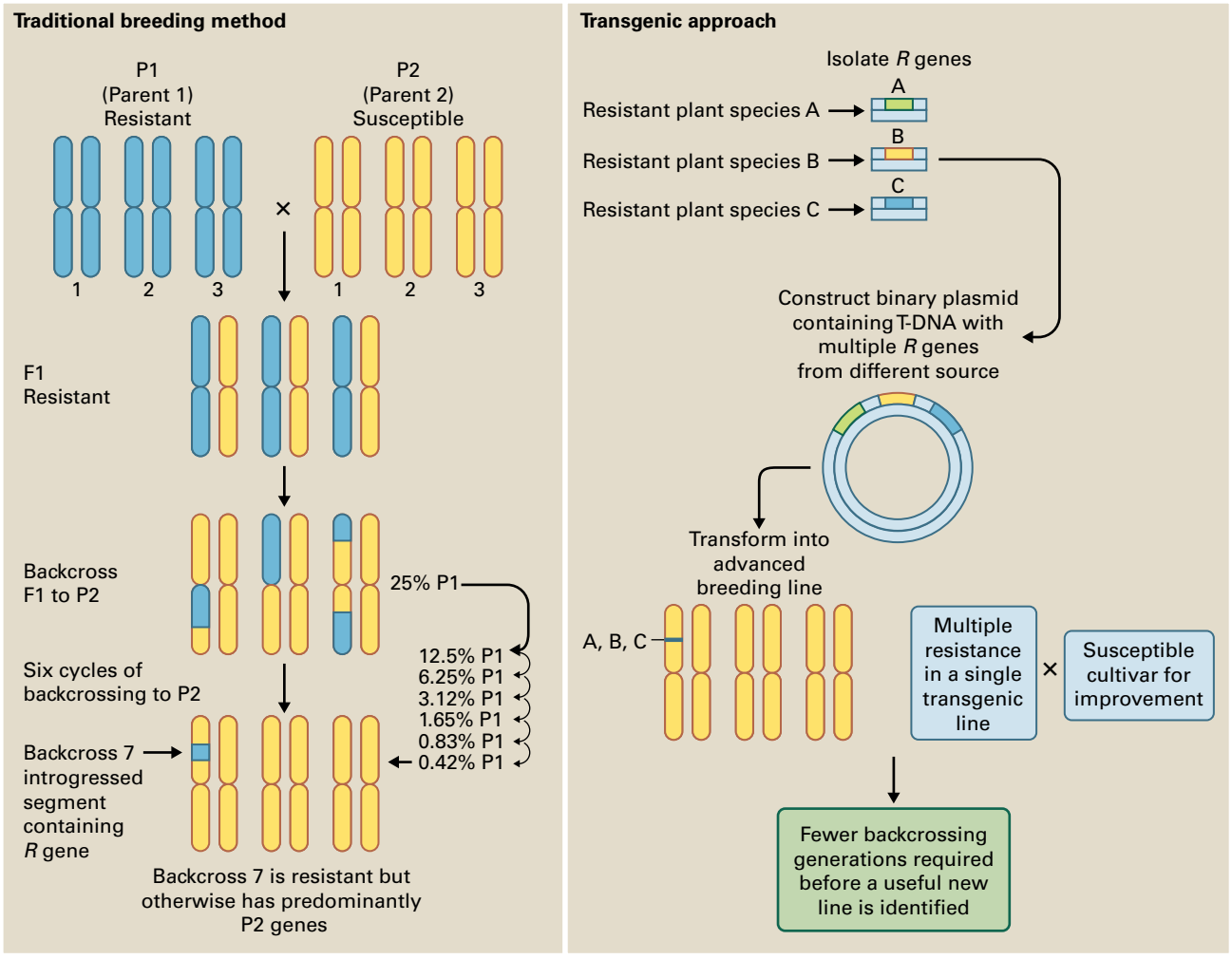


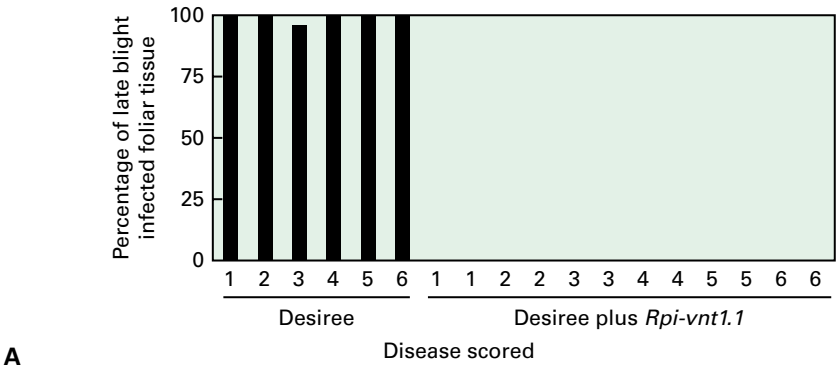
FIGURE 21.59 *Traditional breeding compared with transformation technology approaches to introgress desirable genes into commercial crop plants. In a traditional breeding method (left), as much as 0.4% of the genome complement from each donor parent can remain in the seventh backcross generation along with the R gene of interest (originally from parent 1). In the transgene transformation approach, multiple R genes from several initial sources are first assembled into a single Ti plasmid. After T-DNA integration into the plant genome, these R genes co-segregate in all subsequent breeding steps, greatly simplifying the subsequent backcrossing program for introducing multiple new traits into a cultivar. When the transgenic transformation approach is used, the entire sequence of the introduced DNA is known, whereas in the traditional breeding program, neither the total extent of the introgressed DNA nor its sequence identity is known.*

Solanaceae. Transfer of EFR from *Arabidopsis* into tobacco (*Nicotiana benthamiana*) and tomato (*Solanum lycopersicum*) confers responsiveness to EF-Tu and elevates resistance to phytopathogenic bacteria from different genera, including *A. tumefaciens*, *P. syringae*, *Ralstonia solanacearum*, and *Xanthomonas perforans* (Fig. 21.58). These results suggest that extending the P/MAMP recognition repertoire of crop plants can elevate their pathogen resistance.

21.10.2 *R* genes can confer broad-spectrum resistance

Traditionally plant breeders have introgressed, via lengthy breeding programs, novel *R* genes from wild relatives of crop species into elite commercial cultivars to control diseases (Fig. 21.59 and also see Fig. 21.39, Section 21.6.1). During breeding, the *R* gene must be recombined away from any linked unwanted alleles of other genes that reduce crop performance (linkage drag). The availability of cloned *R* genes opens the possibility of their direct transfer into elite lines by genetic transformation (see Box 21.2).

Genetic transformation enables transfer of several different *R* genes that may be effective against a single pathogen species in a "cassette" of linked genes that cannot be separated by recombination (Fig. 21.59). This should slow pathogen evolution to overcome resistance, because the various *R* genes could only be overcome if, in a single pathogen isolate, several effector genes were simultaneously mutated. The introduction of *R* genes by transformation also means that interplant species fertility barriers can be crossed, thereby increasing the repertoire of plant species from which useful novel resistance sources can be obtained.



A



B

FIGURE 21.60 *Comparison of severity of late blight disease caused by* Phytophthora infestans *in* Rpi-vnt1.1*-transgenic and non-transgenic var. Desiree potato plants. (A) Percentage of late blight infected leaf tissue during the vegetative growing stage. (B) Photograph of the control Desiree (left) and transgenic (right) plants almost one month after first symptoms of infection on Desiree plants were observed. No symptoms of late blight were present on transgenic plants during the growing season or as the crop matured.*
Source: (B) Jones et al. (2014). Phil. Trans. R. Soc. Ser. B 369:doi:10.1098/rstb.2013.0087.

R genes that confer resistance to all or most races of a pathogen species are attractive candidates for interspecies transfer, because they may confer the same broad-spectrum resistance as occurs in their native genomes. For example, most accessions of the wild diploid potato species *Solanum bulbocastanum* are resistant to all known races of *Phytophthora infestans*. Using map-based cloning the resistance gene *RB/Rpi-blb1* was isolated. Transgenic cultivated potato plants (*Solanum tuberosum*) expressing the *RB* gene show a high level of resistance to nearly all *P. infestans* isolates, including a European "super race" that can overcome all 11 known *R* genes in cultivated potato. Two other *R* genes conferring broad-spectrum resistance to *P. infestans* have been isolated: *Rpi-blb2* from *S. bulbocastanum* and *Rpi-vnt1.1* from *S. venturii*. Transgenic cultivated potato lines expressing both *Rpi-blb1* and *Rpi-blb2* provided durable control of late blight disease in several years of field trials in the United Kingdom and mainland Europe (Fig. 21.60).

Isolating *R* genes from wild relatives and introducing them into elite lines, whether by breeding or transformation, is laborious; therefore, it is important to prioritize those *R* genes that are most likely to be durable, and analysis of pathogen effector complements can help. If an *R* gene recognizes an effector that is conserved in all known races of a pathogen, it is more likely to be durable than an *R* gene that recognizes an effector that is absent from many races of the pathogen. Some effectors are essential for full virulence of the pathogen (see Box 21.3). Emerging knowledge of differences in the effector complement between pathogen races can thus be helpful for choosing *R* genes for prioritization. Already useful in the potato/*P. infestans* interaction, these approaches are deployed to identify durable resistance genes against the Ug99-derived races of the wheat stem rust fungus *Puccinia graminis* f. sp. *tritici*, which threatens wheat harvests in Africa and Asia (see Box 21.3 and Box 21.1). Tomato and banana are susceptible to the closely related leaf mold (*Cladosporium fulvum*) and black Sigatoka (*Mycosphaerella fijiensis*) diseases, respectively. Homologs of *C. fulvum* Avr4 and Ecp2 effectors are present in *M. fijiensis*. Since tomato Cf-4 confers recognition of Avr4 homologs from both pathogens, it may prove useful for *M. fijiensis* resistance in banana.

To control the wheat glume blotch pathogen *Stagonospora nodorum,* the ToxA and other related toxins recovered from fungal culture filtrates have been used globally to screen both existing commercial elite wheat germplasm and potential donor breeding lines for the lack of a necrotic response. This

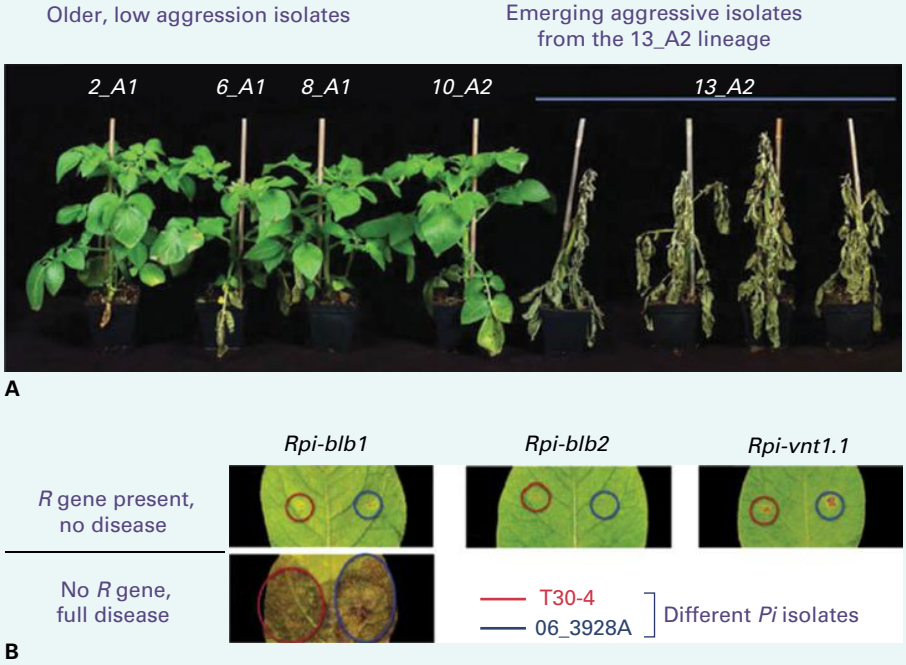
BOX 21.3

Effector-guided *R* gene deployment

Effector-guided *R* gene deployment is a disease control strategy based on the identification of core pathogen effectors that lack sequence polymorphism. It is currently being used in potato (*Solanum tuberosum*) to mitigate the impact of the late blight pathogen *Phytophthora infestans*. This pathogen undergoes major population shifts in agricultural systems via the successive emergence and migration of asexual lineages (A). A new aggressive lineage in the European *P. infestans* population termed 13_A2 is rapidly displacing other older lineages. Comparative whole-genome and transcriptome sequencing (see Chapter 9) of *P. infestans* pathogen races has revealed the core RXLR effector repertoire found in isolates from the new aggressive lineage of *P. infestans* 13_A2 and two older European *P. infestans* isolates. All three *P. infestans* isolates carry intact and in planta induced *Avrblb1*, *Avrblb2*, and *Avrvnt1* effector genes that trigger resistance in potato lines carrying the corresponding disease resistance genes *Rpi-blb1*, *Rpi-blb2*, and *Rpi-vnt1.1* (B). *R* gene stacking can be achieved by conventional plant breeding with marker-assisted selection or by plant genetic engineering with T-DNA cassettes containing the desired *R* gene combinations. This core effector-guided approach helps to exclude any *R* genes from the elite potato germplasm improvement scheme that are already defeated by the pathogen because the cognate core effectors contain sequence polymorphisms that evade plant recognition.

(A) Disease-causing abilities of historic and current *Phytophthora infestans (Pi)* isolates. (B) The conserved core effectors *Avrblb1, Avrblb2* and *Avrvnt1* are present in all *Pi* isolates. These are recognized when the corresponding *R* genes *Rpi-blb1*, *Rpi-blb2,* and *Rpi-vnt1.1* are expressed in the host plant.

Source: Cooke et al. (2010). PloS Pathog. 8(10):e1002940.



ensures that the corresponding *Tsn* locus, which confers *S. nodorum* disease susceptibility, is eliminated from all commercial wheat breeding programs.

Some *R* genes confer resistance to all races of a single pathogenic species, for example the recessive barley *mlo* resistance gene. Other *R* genes confer resistance to multiple unrelated pathogenic species, for example the tomato *Mi* gene, which confers both nematode and whitefly and psyllid resistance. Certain *R* genes confer resistance to different but taxonomically closely related fungal species, for example the wheat *Lr34* gene, which confers resistance to leaf rust and stripe rust fungal pathogens (see Section 21.7.1). By analyzing the increasing amount of genome and transcriptome sequence information available for crop species, highly homologous *R* gene sequences can be isolated and tested for their ability to confer broad-spectrum resistance spectrum in different crop plant species.

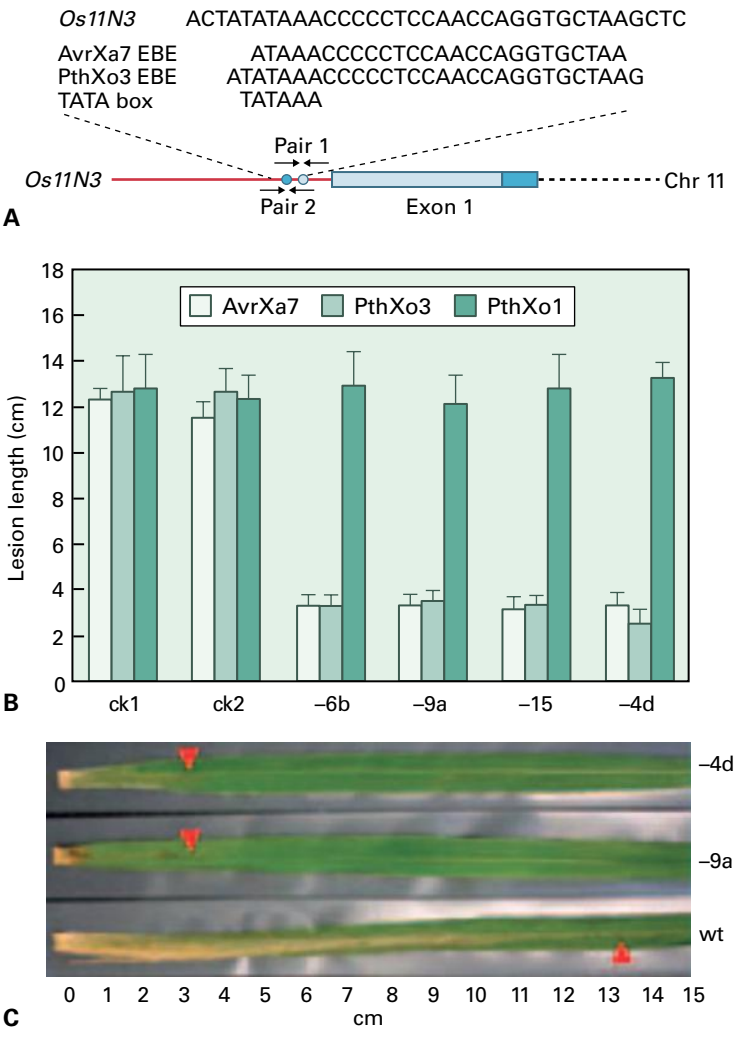


FIGURE 21.61 *TALEN technology has been used to edit a specific pathogen susceptibility (S) gene in rice to thwart the virulence strategy of* Xanthomonas oryzae *pv.* oryzae *(Xoo) and engineer heritable genome modifications for resistance to bacterial blight. The rice bacterial blight susceptibility gene Os11N3 (also called OsSWEET14) was targeted for TALEN-based disruption. (A) The Os11N3 promoter contains an effector-binding element (EBE) for AvrXa7, overlapping with another EBE for PthXo3 and with the TATA box. Two pairs of designer TALENs (pair 1 and pair 2) were independently deployed to induce mutations in these overlapping EBEs of the Os11N3 promoter and thereby interfere with the virulence function of AvrXa7 and PthXo3, but not the developmental function of Os11N3. Each designer TALEN contained 24 repeat units for recognition of a specific set of 24 contiguous nucleotides at the target sites. (B) Severity of disease damage to wild-type and transgenic rice plants caused by AvrXa7-, PthXo3-, and PthXo1-dependent Xoo strains. Lengths of leaf lesions in wild-type plants (ck1), a nontransgenic plant (ck2) and transgenic plants homozygous for Os11N3 promoter mutations of 6 bp (–6b), 9 bp (–9a), 15 bp (–15) and 4 bp (–4d) deletions, respectively, measured 14 days post inoculation with different Xoo strains expressing three different TAL effectors. (C) Resistance phenotype displayed to Xoo (avrXa7) by two transgenic rice plants (carrying either the –4d or –9a deletion constructs) compared with the disease susceptibility phenotype of a wild-type plant (wt). Leaves were inoculated at the left end and the extent of visible disease symptom formation is indicated by the red arrowheads.*
Source: Ting Li et al. (2012). Nat. Biotechnol. 30(5):390.

Many race-specific R proteins are temperature-sensitive. For example, *N* gene-mediated tobacco mosaic virus (TMV) resistance fails at temperatures above 30°C and permits the virus to spread systemically throughout the plant. With climate changes now being experienced in many global regions, *R* genes that fail at higher temperatures may give inconsistent pathogen control. A lack of correct R protein folding or incorrect cellular localization may explain this phenomenon.

21.10.3 TAL effectors can be used for engineering resistance

Transcription activator-like (TAL) effectors of *Xanthomonas oryzae* pv. *oryzae* (*Xoo*) contribute to pathogen virulence by transcriptionally activating specific rice disease-susceptibility (*S*) genes (see Section 21.1.8). TAL effector nucleases (TALENs) are fusion proteins that combine the DNA recognition repeats of native or customized *Xoo* TAL effectors and the DNA cleavage domains of FokI nuclease. These TALENs are useful for precise genome engineering.

For example, to engineer rice plants (*Oryza sativa*) resistant to *Xanthomonas* bacterial infection, the promoter of the rice bacterial blight susceptibility gene *Os11N3* (also called *OsSWEET14*) was targeted for TALEN-based disruption. This gene encodes a member of the SWEET sucrose-efflux transporter family. The *Xoo* TAL effectors AvrXa7 or PthXo3 activate this gene and thus divert sugars from the plant cell to the bacteria. The promoter of *Os11N3* contains binding sites for both TAL effectors near the TATA box. TALENs were designed to mutate DNA sequences required for TAL effector binding, but not the development function of *Os11N3*. The modified *Os11N3* gene was no longer inducible when the rice plants were infected by pathogenic *Xoo* strains that could deliver either the AvrXa7 or PthXo3 TAL effectors into the rice cells. The stable TALEN-modified plants showed strong (though recessive) resistance to infection by the AvrXa7- or PthXo3-dependent *Xoo* strains, but not the PthXo1-dependent pathogenic *Xoo* strain (Fig. 21.61). So far, natural polymorphisms in the *Os11N3* gene that would prevent induction by AvrXa7- and PthXo3-dependent *Xoo* strains and also confer disease resistance have not been identified in rice germplasm. By using TALENs to edit a rice gene



A B

FIGURE 21.62 *Papaya ringspot virus (PRSV) is a limiting factor in the production of papaya worldwide. By constitutively overexpressing the coat protein of this virus in papaya, several highly resistant varieties are now in commercial use in Hawaii and elsewhere. (A) Transgenic papaya line (left) showing resistance to PRSV compared to infected non-transgenic papaya (right). (B) Aerial view of transgenic papaya test field in Hawaii, showing a block of healthy transgenic papaya plants surrounded by severely infected non-transgenic papaya.*
Source: Gonsalves, AgBioForum 7(1 & 2), http://www.agbioforum.org/v7n12/v7n12a07-gonsalves.htm.

required for *Xoo* susceptibility, desirable alleles conferring resistance can be obtained that can then be used in rice breeding programs.

21.10.4 Virus sequences can induce resistance to virus infection

Virus sequence-induced resistance was based on the concept that a transgenic plant engineered to express viral proteins could interfere with the normal pathogenicity program of the virus. Coat protein (CP)-mediated resistance was proposed to operate through high CP levels, which inhibit disassembly of the virus particles in the initially infected cells, whereas the overexpression of a nonfunctional mutant movement protein (MP) was proposed to lead to competition for plasmodesmatal binding sites between the nonfunctional and the wild-type MP of the infecting virus. However, molecular analysis of transgenic CP or MP plants has revealed that resistance is RNA-mediated and sequence-specific, and likely functions by post-transcriptional silencing of viral gene expression (see Section 21.9.2).

CP sequence-induced virus resistance was one of the early success stories of plant genetic engineering and led to the development of virus-resistant papaya and squash cultivars for commercial production. For example, papaya crops in Hawaii derived from transgenic lines carrying the CP gene of papaya ringspot virus (PRSV) provide effective control of this virus (Fig. 21.62).

21.10.5 Genetically engineered disease control is a knowledge-based approach

The transgenic disease control options described above have each taken immediate advantage of fundamental discoveries that had significantly advanced our overall understanding of host–pathogen interactions. In each example, a target of potential pathogen vulnerability was exposed through the acquisition of new knowledge, various intervention options were proposed and tested in the laboratory, growth room, or glasshouse, and only the best solutions went on to rigorous field testing and, finally, commercial release. In addition, many of the single gene-engineered disease control solutions that failed to make the grade, either in early testing or later when tested under field conditions, have provided considerable useful and novel insight into the importance of other plant components and information on the ways in which pathogens can rapidly evolve to overcome plant defenses.

Summary

Plants are resistant to most plant pests and pathogens. Every plant cell can defend itself from attacking pathogenic microorganisms and invertebrates. Some defenses, such as antimicrobial secondary metabolites, are constitutive and located in specific cellular compartments ready to be released upon cell damage. Other defense responses, such as those induced by pathogen invasion, require detection of the pathogen by the plant. Defense activation is correlated with rapid activation of defense-related genes and often culminates in the hypersensitive response that causes localized cell death to impair pathogen spread.

Plant resistance to pathogens can be mediated by dominant resistance (*R*) genes in plants that are complementary to avirulence (*Avr*) genes in pathogens. Avr effector proteins exhibit extensive sequence diversity, and their function in the pathogen and in the host plant is still poorly understood. In contrast, plant R proteins are strikingly similar in structure, sharing such motifs as leucine rich repeats (LRRs), a nucleotide binding or a serine/threonine protein kinase domain, among others. R proteins both detect pathogens and initiate signal transduction to activate defense mechanisms. In addition, *R* loci/genes can evolve new *R* gene specificities to keep pace with the evolution of virulence in pathogen populations.

By investigating the genomes of numerous pathogens and pests, the full repertoires of effector genes thought to function either in the suppression or inactivation of plant defenses have been predicted and their specific roles experimentally tested.

Plant defense reactions involve complex biochemical pathways and multiple signal molecules, including ROS, NO, SA, JA, and ethylene, to provoke the induction of proteins, secondary metabolites, and often cell wall fortification reactions—both at the infection site and systemically throughout the attacked plant. Specialist defenses against plant viruses include post-transcriptional gene silencing (PTGS); those against insects involve proteinase inhibitor proteins. Many aspects of induced plant defense appear to be conserved in other eukaryotes, perhaps indicating the existence of an ancient defense strategy that evolved early against pathogen attacks.

The genetic engineering of plants has started to achieve broad-spectrum and durable pest and pathogen control in crops. However, a better understanding of the factors and mechanisms involved in plant–pathogen interactions is still needed and better resistance strategies still need to be deployed to reduce crop losses.

22

Responses to Abiotic Stress

Kazuo Shinozaki, Matsuo Uemura, Julia Bailey-Serres, Elizabeth A. Bray, and Elizabeth Weretilnyk



Introduction

Plants are frequently exposed to environmental **stress**, external conditions that adversely affect growth, development, or productivity. Stress can be **biotic**, imposed by other organisms (Chapter 21), or **abiotic**, arising from an excess or deficit in the physical or chemical environment. Environmental conditions that cause damage to plants include flood, drought, high or low temperatures, excessive soil salinity, inadequate mineral nutrients, and excess or insufficient light. Phytotoxic compounds, such as ozone, can also damage plant tissues.

Stress triggers a wide range of plant responses, from alterations in gene expression and cellular metabolism to changes in growth rate and crop yield. The duration, severity, and rate at which a stress is imposed all influence how a plant responds. Several adverse conditions in combination can elicit a response that is different from that caused by a single stress. A response can be triggered directly by a stress, such as drought, or result from stress-induced injury, such as loss of membrane integrity. Moreover, resistance and sensitivity to stress vary according to species, genotype, developmental stage, and organ or tissue type (Fig. 22.1).

The molecular mechanisms underlying plant responses to abiotic stress, including changes in gene expression and cellular signal transduction, have been analyzed extensively, and various transcription factors and signaling molecules are now known to play important roles in cellular homeostasis under stress conditions. The functions of these factors are described in this chapter.

22.1 Plant responses to abiotic stress

22.1.1 Plant stress diminishes crop yield

As human populations grow, agricultural systems must feed more people while competing with urban development for premium arable land. This increasing demand, coupled with shrinking resources, has fueled research into elucidating mechanisms by which plants respond to stress and manipulating these mechanisms to enhance plant productivity in suboptimal environments.

The impact of the environment on plant productivity becomes apparent when record yields are compared to average yields. If record yields are assumed to represent plant growth under ideal conditions, then the losses associated with biotic and abiotic stress can reduce average productivity by 65–87%, depending on the crop. Successful application of biotechnological and classical breeding techniques may lead to stress-tolerant crop plants that enhance world food supplies and provide considerable economic benefit. These crops may promote survival during periods of intense or prolonged stress or maintain high plant productivity under conditions of moderate environmental stress.

Biochemistry & Molecular Biology of Plants, Second Edition. Edited by Bob B. Buchanan, Wilhelm Gruissem, and Russell L. Jones.
© 2015 John Wiley & Sons, Ltd. Published 2015 by John Wiley & Sons, Ltd.
Companion website: www.wiley.com/go/buchanan/biochem

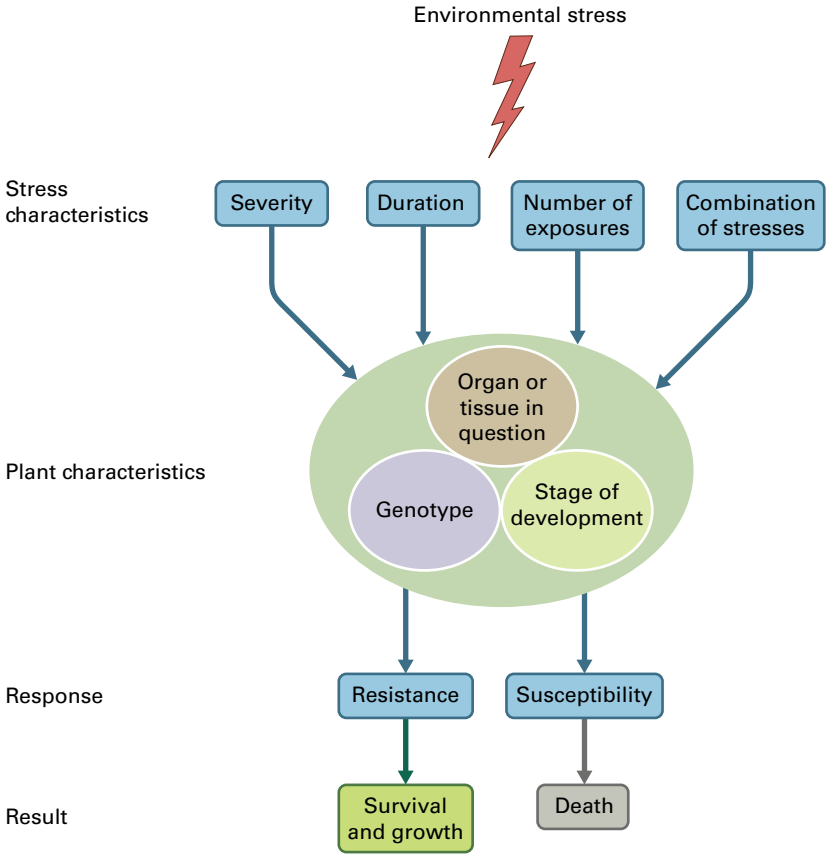


FIGURE 22.1 *Many factors determine how plants respond to environmental stress: the genotype and developmental conditions of the plant, the duration and severity of the stress, the number of times the plant is subjected to stress, and any additive or synergistic effects of multiple stressors. Plants respond to stress through a variety of mechanisms. Failure to compensate for severe stress can result in plant death.*

22.1.2 Resistance mechanisms allow organisms to avoid or tolerate stress

Stress resistance mechanisms can be grouped into two general categories: **avoidance** mechanisms, which prevent exposure to stress, and **tolerance** mechanisms, which enable the plant to withstand stress (Fig. 22.2). Many desert plants are xerophytic—tolerant of water deficits—because their morphological characteristics facilitate survival under arid conditions. A drought-avoidance mechanism—deep roots—provides another class of plants (phreatophytes) with improved access to groundwater. In contrast, desert ephemerals evade drought by germinating and completing their life cycles while adequate water is available. Sunken stomata, light-reflective spines, and deep roots are among the constitutive, genotypically determined traits for stress resistance that are expressed whether the plants are stressed or not. They constitute **adaptations**, evolutionary improvements that enhance the fitness of a population of organisms.

Other resistance mechanisms are achieved through **acclimation**, the adjustment of individual organisms in response to changing environmental factors. During acclimation, an organism alters its **homeostasis**, its steady-state physiology, to accommodate shifts in its external environment. A period of acclimation before stress is encountered may confer resistance to an otherwise vulnerable plant. For example, during the summer, trees in the northern latitudes cannot withstand freezing but many can acclimate and eventually withstand freezing in winter. Whether based on acclimation or adaptation, successful mechanisms for stress resistance support survival under lethal conditions or maintain productivity under circumstances that impair crop yields.

22.1.3 Gene expression patterns often change in response to stress

Stress-induced changes in metabolism and development can often be attributed to altered patterns of gene expression. A stress response is initiated when a plant recognizes a stress at the cellular level. Stress recognition activates signal transduction pathways that transmit information within individual cells and throughout the plant (Fig. 22.3). Ultimately, changes in gene expression are integrated into a response by the whole plant that modifies growth and development and that may even influence reproductive capabilities. The duration and severity of the stress dictate the scale and timing of the response.

Little is known about how plants recognize stress. Our best insights come from yeast and bacterial proteins that initiate signal transduction in response to abiotic stress, such as low osmotic potential. Though plants likely contain similar proteins, comparable functions have not yet been demonstrated. The intricate signaling pathways that are assumed to participate in altering plant gene expression in response to stress have yet to be elucidated; however, there is considerable

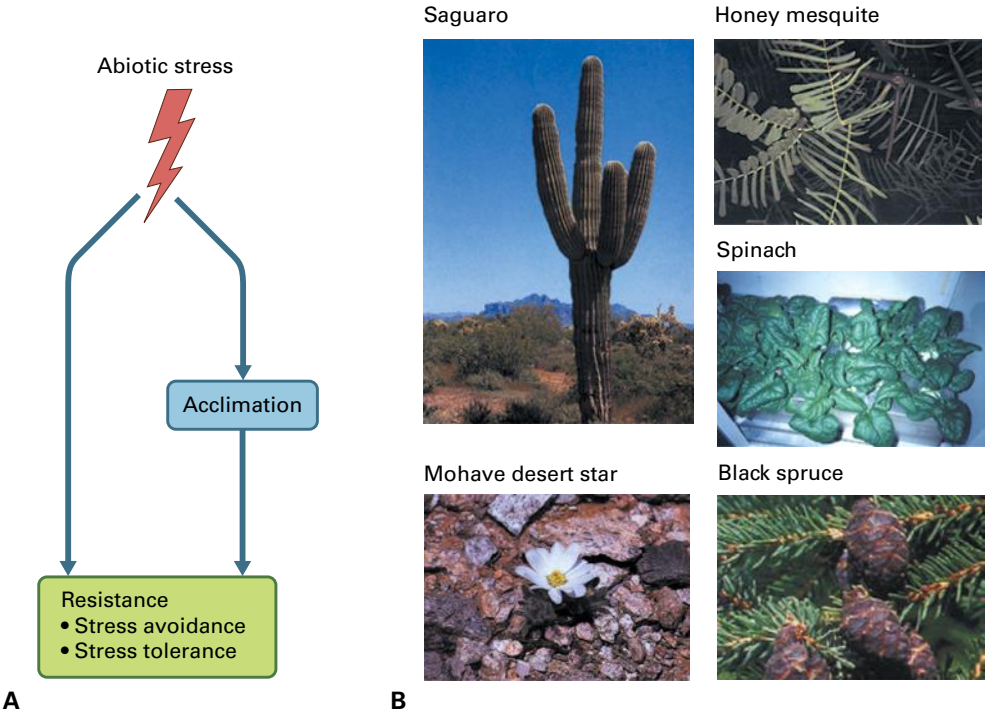


FIGURE 22.2 *Stress resistance can involve tolerating or avoiding the stressful condition. (A) Some resistance mechanisms are constitutive and active before exposure to stress. In other cases, plants exposed to stress alter their physiology in response, thereby acclimating themselves to an unfavorable environment. (B) Examples of constitutive mechanisms of drought resistance include the succulent, photosynthetic stem of the saguaro cactus* Cereus giganteus, *a drought-tolerant species; the deep roots of the honey mesquite* Prosopis glandulosa *var.* glandulosa, *a drought-avoiding species; and the wet-season life cycle of the Mohave desert star,* Monoptilon bellioides. *Examples of acclimation mechanisms include osmotic adjustment (see Section 22.2.3) in plants such as spinach (*Spinacia oleracea*) and freezing tolerance (see Section 22.4) in cold-hardy trees such as black spruce,* Picea mariana *Mill.*
Source: Epple & Epple (1995). A Field Guide to the Plants of Arizona. Falcon Press Publishing, Helena, MT.

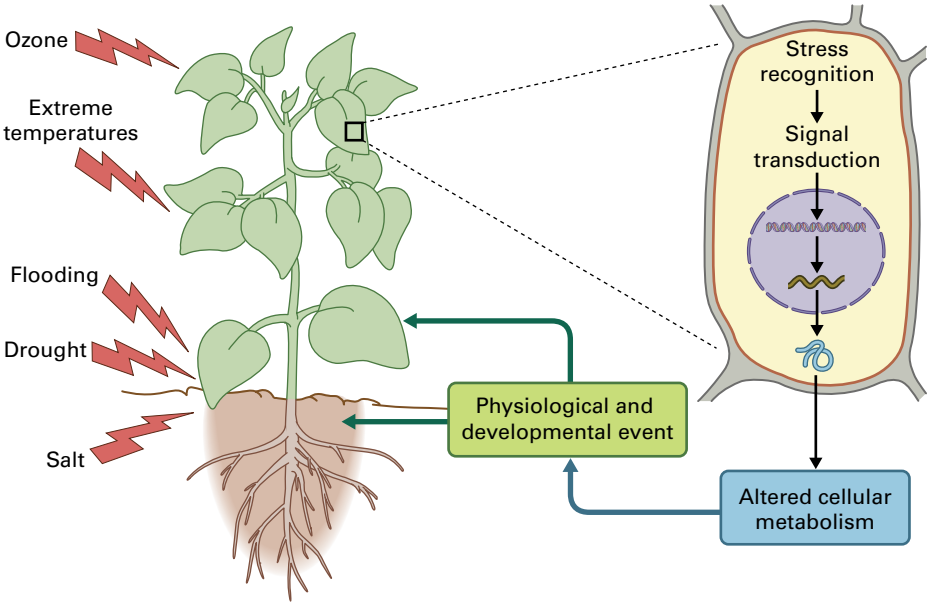


FIGURE 22.3 *Plants respond to stress both as collections of cells and as whole organisms. Stressors constitute environmental signals that are received and recognized by the plant. After stress recognition, the signal is communicated within cells and throughout the plant. Transduction of environmental signals typically results in altered gene expression at the cellular level, which in turn can influence metabolism and development of the whole plant.*

evidence that regulation of plant stress responses involves hormones—especially abscisic acid (ABA), jasmonic acid (JA), and ethylene—and secondary messengers such as Ca^{2+} (see Chapters 17 and 18).

In response to stress, some genes show increases in expression, while others are repressed. Protein products of stress-induced genes often accumulate in response to unfavorable conditions. The functions of these proteins and the mechanisms that regulate their expression are currently a central topic of research in stress physiology. Although most studies have focused on transcriptional activation of gene expression, accumulation of gene products may also be

influenced by post-transcriptional regulatory mechanisms that increase levels of specific protein-coding mRNAs or noncoding regulatory RNAs, enhance translation, stabilize proteins, and alter protein activity by various types of modifications.

Using molecular genetic techniques, researchers have dissected plant responses associated with exposure to specific abiotic stress. The stresses addressed in this chapter include water deficit, low and high temperatures, hypoxia, and environmental oxidants. Other sources of abiotic stress described elsewhere in this text include nutrient deficiencies and toxic concentrations of aluminum (see Chapter 23), cadmium (see Chapter 16) or other metals. Plant responses to these disparate stresses can incorporate similar or even overlapping strategies, such as the activation or repression of gene expression, production of proteins or compatible solutes, activation of transport activity, etc. In addition, plants are often exposed to simultaneous or sequential abiotic stresses, such as heat and drought, or flooding followed by drought. Interactions between different types of stress, whether synergistic or antagonistic, likely influence the success in coordinating the activity of many genes that together increase abiotic stress survival in crops.

22.2 Physiological and cellular responses to water deficit

22.2.1 Many environmental conditions can lead to water deficit

Water-related stress results if the environment contains excess water or if the quantity or quality of water available is insufficient to meet basic needs. Though periods of little or no rainfall can lead to drought, water deficit can also occur in environments in which water is not limited. In saline habitats, for example, high salt concentrations make it more difficult for plant roots to extract water from the environment. In addition, low temperatures can also result in water stress; exposure to freezing temperatures, for example, can lead to cellular dehydration as water leaves the cell and forms ice crystals in intercellular spaces (see Section 22.4). Occasionally, even plants that have been watered well show periodic signs of water deficit, such as a transient loss of turgor at midday. In this case, wilting indicates that transpirational water loss has exceeded the rate of water absorption. Many factors can affect the response of a plant to water deficit, including the duration of water deficiency, rate of onset, and possible acclimation to water stress by previous exposure. The response of a plant to water deficit can be complex and incorporate many of the strategies and mechanisms of tolerance and resistance used in response to other types of stress; therefore it is addressed first.

22.2.2 Two parameters that describe the water status of plants are water potential and relative water content

Water can be described thermodynamically in terms of its free energy content, also known as its chemical potential. Plant physiologists use a related parameter, **water potential** (Ψ_w; see Chapter 15, Box 15.1, for a more quantitative discussion of this topic). Such measurements can be used to evaluate the extent to which a cell, organ, or whole plant is "hydrated."

Equation 22.1: Water potential

$$\Psi_w = \Psi_s + \Psi_p + \Psi_g + \Psi_m$$

The Ψ_w of a plant equals the sum of various component potentials. **Solute potential**, Ψ_s, is dictated by the number of particles dissolved in water. Water potential decreases as solute concentration increases. **Pressure potential**, Ψ_p, reflects physical forces exerted on water by its environment. When water is subjected to negative pressure (tension), Ψ_p is less than 0 MPa (megapascals) and Ψ_w is diminished. (Note that water potential is typically defined in units of pressure rather than energy.) In contrast, water potential is increased by positive pressure (turgor, $\Psi_p > 0$ MPa). **Gravitational potential**, Ψ_g, can have a substantial effect when water is transported over vertical distances greater than 5–10 meters, but this term can be omitted when describing transport between cells or within small plants. A fourth factor, **matric potential**, Ψ_m, accounts for how solid surfaces (e.g., cell walls and colloids) interact with water and depress Ψ_w. Because Ψ_m values are small and difficult to measure, however, its impact on plant water potential is usually ignored. For conditions under which Ψ_g and Ψ_m are insignificant, the water potential equation is frequently simplified as follows:

Equation 22.2: Water potential (simplified)

$$\Psi_w = \Psi_s + \Psi_p$$

Water potential can be used to predict the movement of liquid water into or out of a plant cell. The difference in water potential across a membrane determines the direction of flow: water moves spontaneously from regions of high water potential to adjoining regions of low water potential.

Physiological or metabolic changes detected in water-stressed plants are not always correlated with changes in plant Ψ_w measurements. To address these issues, a second parameter frequently used to assess water status—**relative water content** (RWC)—is often reported in conjunction with plant Ψ_w measurements.

Equation 22.3: Relative water content

$$\text{RWC} = \left[\left(\text{fresh wt.} - \text{dry wt.}\right) / \left(\text{turgid wt.} - \text{dry wt.}\right)\right] \times 100$$

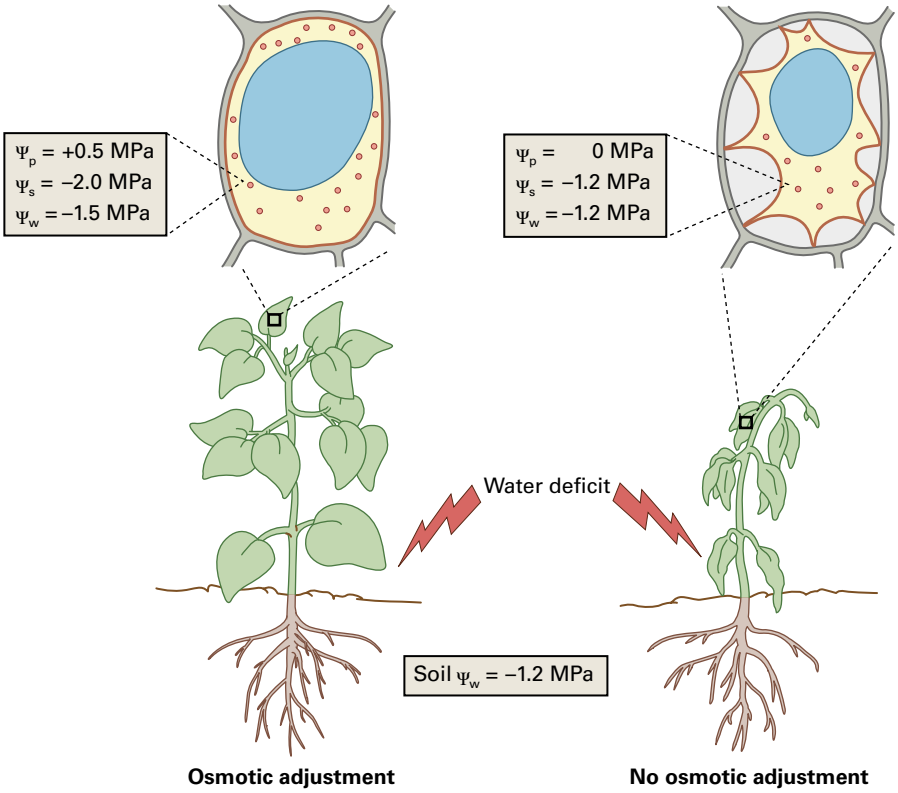


FIGURE 22.4 *Osmotic adjustment occurs when the concentrations of solutes within a plant cell increase to maintain positive turgor pressure within the cell. As the cell actively accumulates solutes, Ψ_s drops, promoting the flow of water into the cell. In cells that fail to adjust osmotically, solutes are concentrated passively, but turgor is lost.*

When water uptake by roots closely matches water loss by leaves, the RWC of transpiring leaves typically ranges from 85% to 95%. If the RWC for an organ drops below a critical value, tissue death follows. The value for critical RWC varies among species and tissue types, but it is frequently less than 50%.

22.2.3 Osmotic adjustment is a biochemical mechanism that helps plants acclimate to dry or saline soil

While some plants are highly sensitive to water stress and wilt (dehydrate), others can endure dry or saline conditions without evident loss of turgor. To extract water from the soil, a plant root must establish a water potential gradient so that water flows toward the root surface from the soil (i.e., the water potential must be lower in the root than in the surrounding soil). Many drought-tolerant plants regulate their solute potential (Ψ_s) to compensate for transient or extended periods of water stress. This process, called **osmotic adjustment**, results from a net increase in the number of solute particles in the plant cell. The osmolalities achieved through osmotic adjustment exceed those from passive concentration of solutes by dehydration. By decreasing plant Ψ_s, osmotic adjustment can drive root Ψ_w to values lower than soil Ψ_w, thereby allowing water to move from soil to plant down a potential gradient (Fig. 22.4). Osmotic adjustment is believed to play a critical role in helping plants acclimate to conditions of drought or high salinity.

22.2.4 Compatible solutes and aquaporins play roles in osmotic adjustment

One mechanism for osmotic adjustment is the accumulation of **compatible solutes**, or **compatible osmolytes**, a chemically diverse and highly soluble group of organic compounds that do not interfere with cellular metabolism, even at high concentrations (Fig. 22.5).

Synthesis and accumulation of these compounds are widespread in plants, but their distribution varies among species. For example, whereas one such compatible solute, the amino acid proline, is accumulated by a taxonomically diverse set of plants, the quaternary ammonium compound β-alanine betaine appears to be confined to representatives of a few genera of Plumbaginaceae (Leadwort). Stress can trigger the irreversible synthesis of these compounds (for example, glycine betaine; see Section 22.3.4), alter the balance between their synthesis and catabolism (e.g., proline), or trigger their release from polymeric forms (e.g., monomeric sugars like glucose and fructose can be released from their polymeric forms, starch and fructans). Once the stress is removed, these monomers can be repolymerized to facilitate rapid and reversible osmotic adjustment, or they can be metabolized to produce primary metabolites or energy.

Unlike many inorganic solutes, which may become toxic at high concentrations, the organic character of compatible solutes greatly diminishes their potential toxicity. Many ions found in cells adversely affect metabolic processes at high concentrations, possibly by binding to and altering the

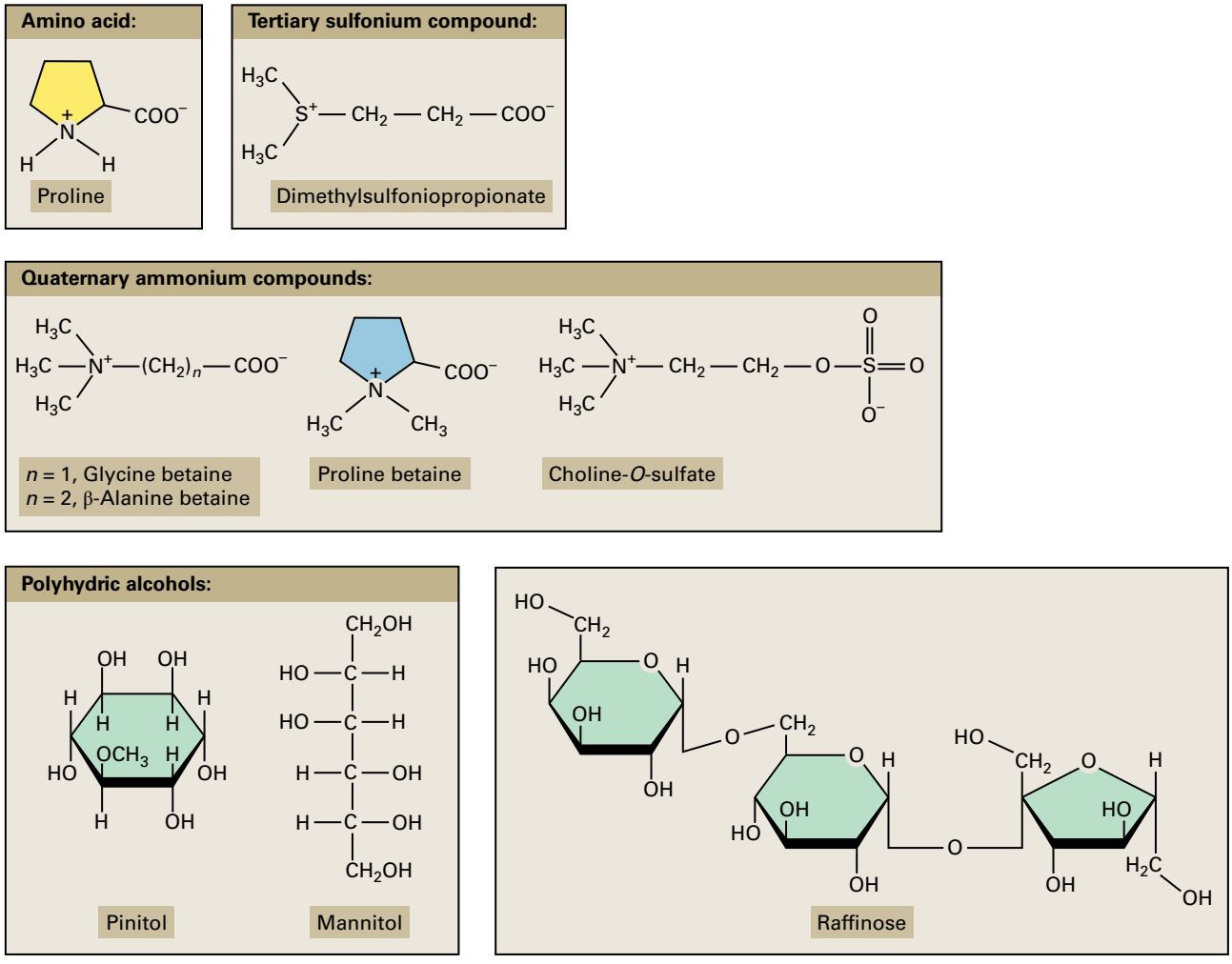


FIGURE 22.5 *Chemical structures of several important compatible solutes (osmolytes) that accumulate in plant cells in response to water deficit. The organic character and nonionic or zwitterionic nature of compatible solutes greatly diminishes their potential toxicity.*

properties of cofactors, substrates, membranes, and enzymes. Furthermore, many ions can enter the hydration shells of a protein and promote its denaturation. In contrast, compatible solutes tend to be neutrally charged at physiological pH, either nonionic or **zwitterionic** (dipolar, with spatially separated positive and negative charges), and are excluded from hydration shells of macromolecules (Fig. 22.6).

In addition to stereotypical charge characteristics, compounds active in osmotic adjustment show distribution patterns that support water potential equilibria among the various membrane-bound compartments of the cell. Vacuoles tend to accumulate charged ions and solutes that would perturb metabolism if present in the cytoplasm. Compatible solutes in the cytoplasm, however, allow the cytosol to achieve osmotic balance with the vacuole.

Another possible mechanism for osmotic adjustment is increasing movement of water into the cell. The hydrophobic nature of the lipid bilayer presents a considerable barrier to the free movement of water into the cell and between intracellular compartments. However, plasma membranes and tonoplasts can be rendered more permeable to water by proteinaceous transmembrane water channels called **aquaporins** (see Chapter 3). Water movement through aquaporins can be modulated rapidly, and evidence suggests these channels may facilitate water movement in drought-stressed plant tissues and promote rapid recovery of turgor upon watering. The abundance of aquaporin mRNA is correlated with turgor changes in leaves subjected to osmotic stress. Higher transcript levels, enhanced translation, and activation of existing proteins may constitute multiple mechanisms for regulating aquaporin abundance and activity, which may be advantageous for plants coping with water deficit.

22.2.5 Some compatible solutes may have protective functions in addition to osmotic adjustment

The role that compatible solutes play in osmotically stressed plants is often defined as "**osmoprotection**"—solute accumulation is believed to have a protective function against water

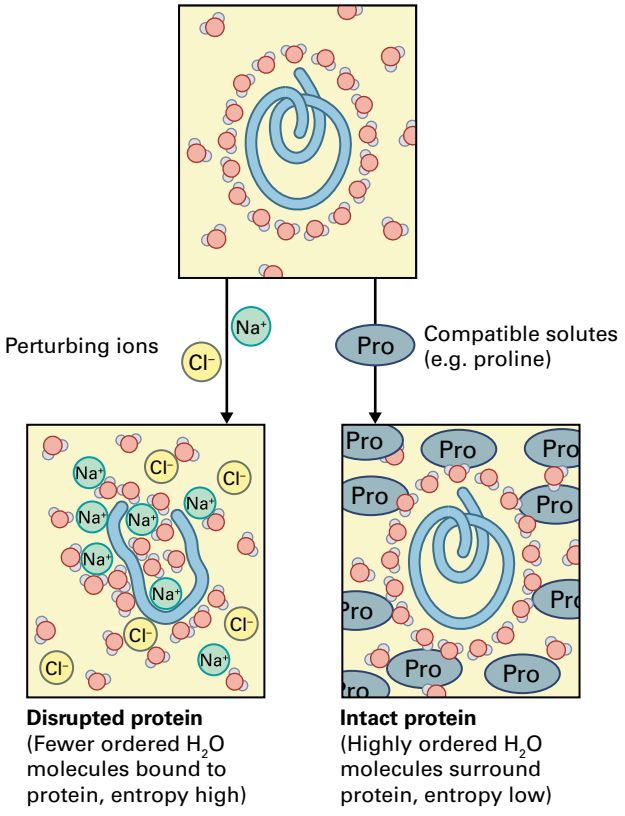


FIGURE 22.6 *Hydration shells of macromolecules are not disrupted by compatible solutes. Depicted is a protein with a hydration shell (i.e., surrounded by ordered H_2O molecules). Ions such as Na^+ and Cl^- can penetrate these shells and interfere with the noncovalent interactions that maintain the structure of the protein. Unlike ions, compatible solutes, such as proline and glycine betaine, do not penetrate the protein's hydration shell, so protein and solute do not come into direct contact. The hydration shells of the ions and compatible solutes are not shown.*

deficit. However, this term should be applied with discretion. Historically, direct physiological evidence for osmoprotection has been obtained for bacteria, but not for plants. Salt-sensitive bacteria, such as *Escherichia coli*, can be induced to grow in high-salt media supplemented with specific compounds, including the osmolytes shown in Figure 22.5. Therefore, the presence of concentrated compatible solutes in drought-tolerant and halophilic ("salt-loving") plants has been taken as compelling, albeit indirect, evidence for the role of osmolyte in plant osmoprotection.

Compatible solutes that accumulate in plants may also act as antioxidants to minimize the impact of abiotic stress in plants. In vitro, many of these compounds directly offset the deleterious, perturbing effects of ions. For example, glycine betaine prevents salt-induced inactivation of Rubisco and destabilization of Photosystem II (PSII). Sorbitol, mannitol, *myo*-inositol, proline, and raffinose can also scavenge hydroxyl radicals in vitro, though glycine betaine cannot. This antioxidant activity suggests a protective role for these compounds in osmotic stress tolerance distinct from osmotic adjustment.

22.2.6 Genetic engineering provides an opportunity to test the adaptive significance of compatible solutes

Drought- or salt-sensitive plants can be transformed with genes encoding enzymes that are critical for the synthesis of a putative osmoprotectant. Transformed plants can then be assayed for enhanced accumulation of compatible solutes and ability to adjust osmotically to conditions of drought and high salinity. In fact, biotechnological approaches for enhancing drought tolerance typically involve dissection of the biosynthesis pathways of specific osmolytes and subsequent manipulation of enzymes operating in those pathways. Among the compounds studied to date are proline, glycine betaine, oligosaccharides such as raffinose, and polyhydric alcohols, including mannitol and pinitol. The results from these studies indicate a role for these compounds not only in responses to water and salinity stress, but to other types of abiotic stress as well.

Upon exposure to abiotic stress, many plants accumulate carbohydrates such as mannitol, trehalose, *myo*-inositol, fructan, galactinol, and raffinose. These metabolites not only serve as energy storage but are thought to play roles in balancing osmotic strength, stabilizing macromolecules, and preserving the membrane. Genetic manipulations of key enzymes involved in the biosynthetic pathways of these carbohydrates can improve abiotic stress tolerance in transgenic plants. Metabolite profiling using different types of mass spectrometry has revealed that various types of metabolite, including proline and branched chain amino acids such as valine, leucine, and isoleucine, accumulate in response to abiotic stress and serve a protective function in cells (see Fig. 22.6). The mechanisms that facilitate proline accumulation in response to environmental conditions are discussed in Chapter 7.

Glycine betaine (*N,N,N*-trimethylglycine, GB) is synthesized under various types of environmental stress and functions as a major osmoprotectant. It stabilizes the quaternary structures of the PSII protein-pigment under high salinity and maintains the ordered state of membranes at extreme temperatures. GB is synthesized mainly from choline via betaine aldehyde (BA), with the first and second steps in the pathway catalyzed by choline monooxygenase (CMO) and betaine aldehyde dehydrogenase (BADH), respectively (Fig. 22.7). A wide variety of plant species accumulate GB, but *Arabidopsis*, rice (*Oryza sativa*), and tobacco (*Nicotiana*) are considered "nonaccumulators." Genetic engineering to introduce GB-biosynthetic pathways into nonaccumulator species is a promising approach to increase abiotic stress tolerance. Transgenic rice plants overexpressing the barley *BADH* gene convert applied BA into GB more efficiently than wild-type plants and exhibit significant tolerance to salt, cold, and heat stress.

Raffinose family oligosaccharides (RFOs), such as raffinose and stachyose and their precursor galactinol, play important roles in drought stress tolerance in plants and seeds. RFOs are important for reducing **reactive oxygen species** (ROS) that accumulate and cause oxidative stress under conditions of

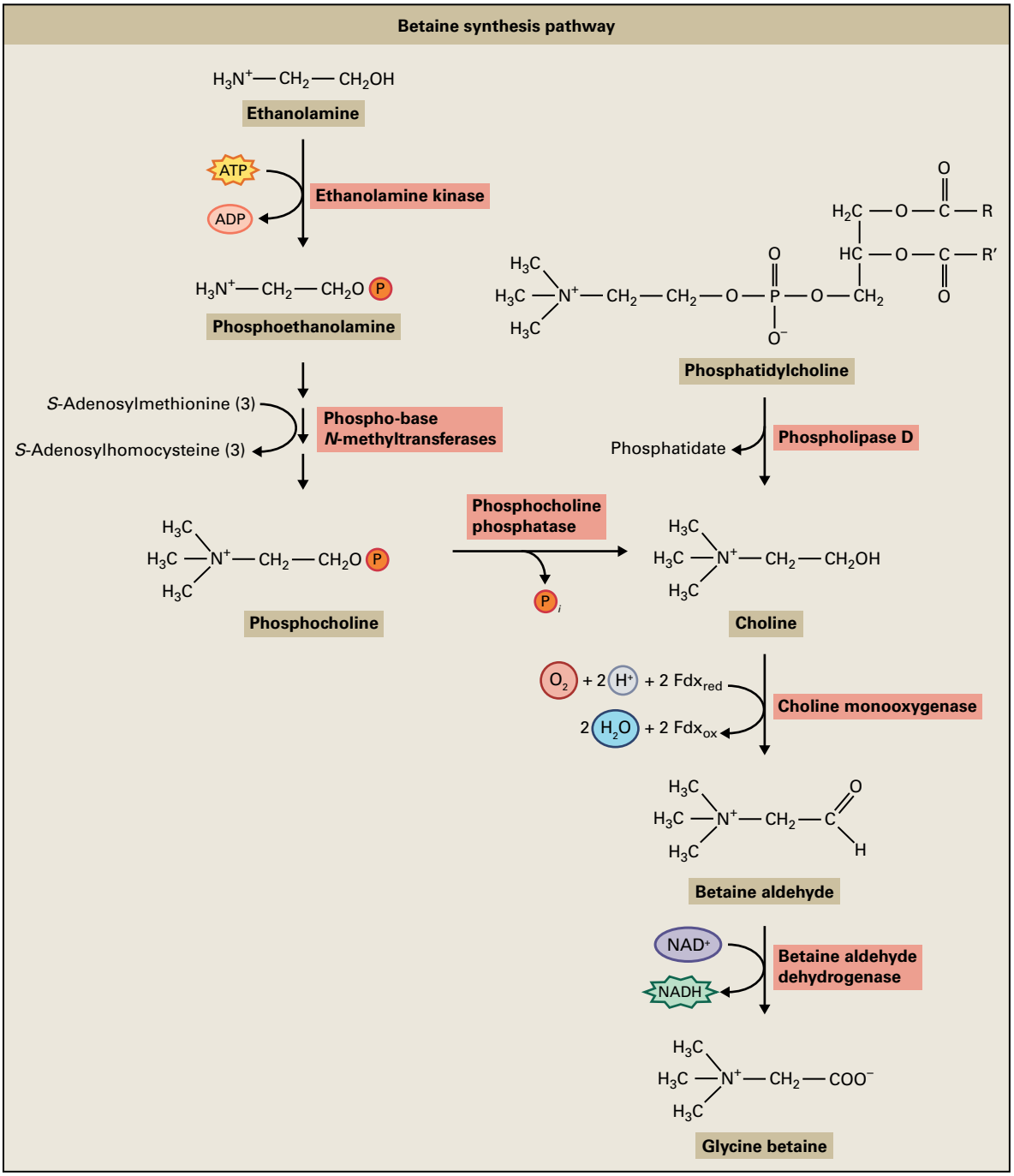


FIGURE 22.7 *Proposed biosynthetic pathways of glycine betaine from choline. Introduction of such pathways into nonaccumulator species is a promising approach for increasing abiotic stress tolerance.*

abiotic stress. They are synthesized from UDP-galactose (Fig. 22.8), which is converted into galactinol by galactinol synthase (GolS). Raffinose synthase then produces raffinose from the galactinol. Both raffinose and galactinol accumulate in *Arabidopsis* in response to drought, high salinity, and cold stress. These stressors induce expression of the genes for GolS and raffinose synthase, resulting in the production of RFOs. Overexpression of the stress-inducible GolS gene improves drought tolerance by activating the accumulation of galactinol and raffinose in transgenic *Arabidopsis* plants.

22.2.7 Some proteins protect macromolecules and membranes against damage

Large numbers of proteins, such as late embryogenesis abundant (LEA) proteins and heat shock proteins (HSPs), protect plant cells directly against water or osmotic stress damage. They exert their protective effects either as highly hydrophilic proteins that retain water or as molecular

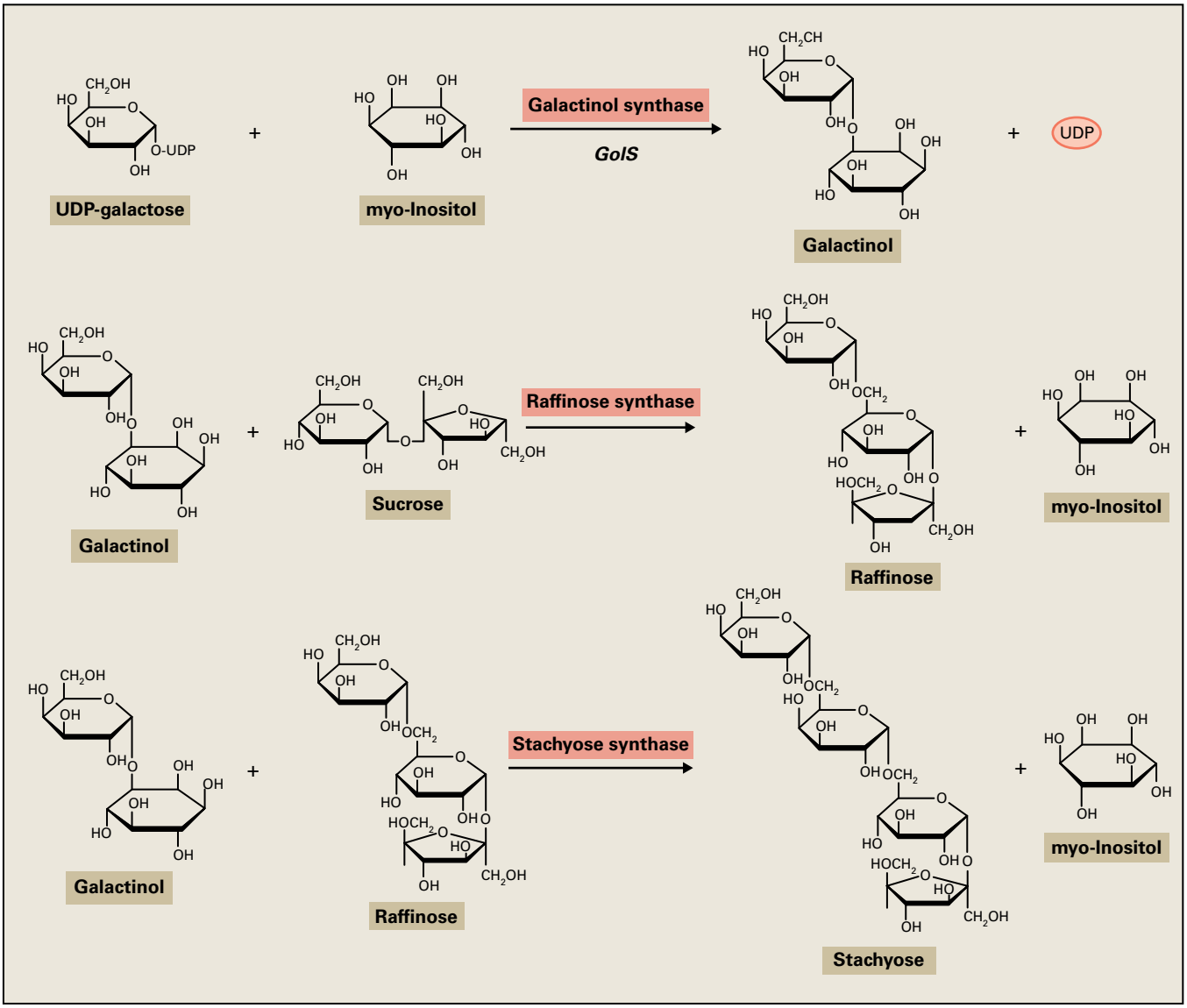


FIGURE 22.8 *Biosynthetic pathway for raffinose family oligosaccharides (RFOs). RFOs are osmolytes that also reduce reactive oxygen species that cause oxidative stress.*

chaperones that prevent denaturation of macromolecules and protect membranes. Plants exposed to abiotic stress usually express or accumulate higher levels of these proteins, suggesting they are necessary in plant abiotic stress protection in general.

LEA proteins were first reported as a group of proteins produced in abundance during late embryogenesis, with maximum expression during seed desiccation. Their genes have been identified and their mRNAs shown to accumulate during the seed maturation process. Some LEA family genes are also induced by cold, osmotic stress, or exogenous ABA.

Although their precise functions remain unknown, LEA proteins accumulate in stressed plants and are thought to be protective molecules that confer stress tolerance. They are associated with desiccation tolerance in seeds, pollen, and anhydrobiotic plants and may be essential for the survival of plant cells under such conditions. LEA proteins may function in an unstructured state, with folding and conformational changes induced under conditions of water deficit. LEA proteins become more folded and develop a significant α-helical component when dried. Another hypothesis is that LEA proteins may decrease the collisions between partially denatured proteins, thereby reducing aggregation of exposed hydrophobic domains.

Drought conditions may also induce accumulation of HSPs, which accumulate in plants in response to high temperature stress (see Section 22.7); some genes encoding HSPs are also induced by drought or osmotic stress. HSPs are molecular chaperones with important roles in the folding and assembly of proteins, stabilization of proteins and membranes, protein refolding, and removal of nonfunctional and degraded proteins under conditions of stress. Manipulation of HSP gene expression not only enhances thermotolerance of transgenic plants, but also increases water stress tolerance.

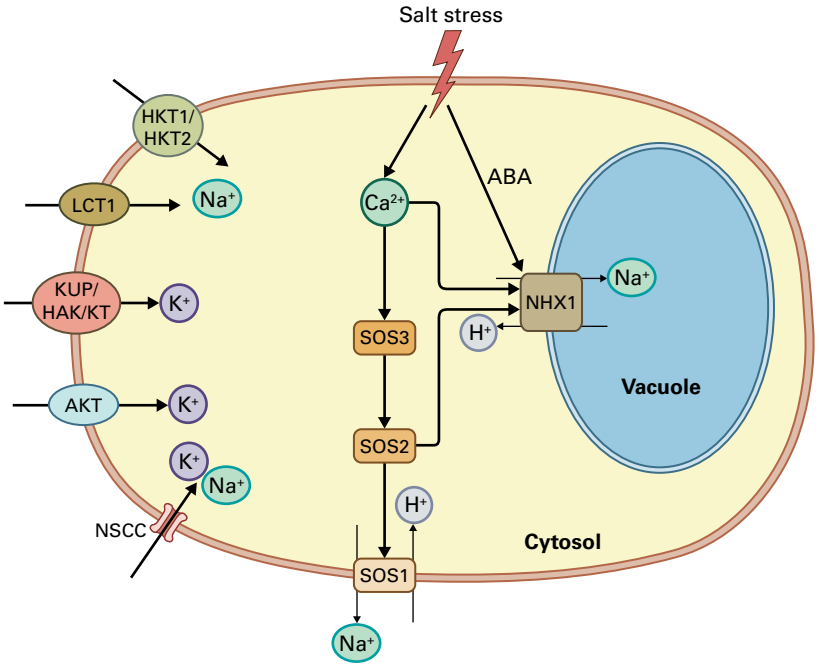


FIGURE 22.9 *Ion channels and transporters help maintain ionic homeostasis under conditions of salt stress. Salt treatment increases the activity of Na^+/H^+ antiporters, which then move Na^+ either out of the cell or into the vacuole. For example, salt stress triggers changes in Ca^{2+}, which regulate SOS3, which then regulates SOS2 protein kinase to activate the plasma membrane SOS1 Na^+/H^+ antiporter. Changes in ABA levels also regulate the NHX1 Na^+/H^+ antiporter and other ion transporters. Other transporters that mediate Na^+ transport into the cell include non-selective cation channels (NSCC) and HKT1/HKT2, the low-affinity cation transporter (LCT1), and K^+ transporters of the KUP/HAK/KT and AKT families. Note that the cell wall is not shown for clarity.*

22.2.8 Water deficit and salinity affect transport across membranes

Drought and salt stress both involve acclimation to low water potential; however, plants growing under high salinity must also cope with potentially toxic amounts of specific ions. Although ion uptake may provide a means of osmotic adjustment, high cytosolic concentrations of some ions such as Na^+ perturb metabolism. Thus, regulating the concentration, composition, and distribution of ions within the cell can be an essential feature of tolerance to osmotic stress.

Plants or cultured cells exposed to high NaCl concentrations tend to accumulate Na^+ as a result of Na^+ influx through channels and transporters (Fig. 22.9). Electrophysiological studies have indicated that nonselective cation channels (NSCCs) mediate primary influx of Na^+ under saline conditions, but no definitive candidate molecules have been identified. Other Na^+ transporters identified in plants include the high-affinity K^+ transporter HKT1, which controls the internal Na^+ distribution between the root and the shoot under saline conditions, and HKT2, which plays a role in primary Na^+ uptake under K^+ deprivation. Transporters such as the low-affinity cation transporter 1 (LCT1) and K^+ transporters of the K^+ uptake permease/high-affinity K^+ uptake/K^+ transport (KUP/HAK/KT) and *Arabidopsis* K^+ transporter (AKT) families may also participate in Na^+ uptake. Na^+ inhibits a variety of biological processes, including K^+ absorption. Under conditions of salt stress, therefore, plants exclude Na^+ and accumulate K^+ in shoots to maintain a high cytosolic K^+/Na^+ ratio, especially in leaves.

Cytoplasmic Na^+ accumulation is partially prevented by the active export of cytosolic Na^+ across the plasma membrane to the extracellular space and across the tonoplast into the vacuole. In the vacuole, it can accumulate to concentrations that would otherwise have a marked effect on the osmotic balance of plant cells. Salt treatment increases the activity of vacuolar Na^+/H^+ antiporters in several plant systems, such as sugar beet (*Beta vulgaris*) cultures and barley (*Hordeum vulgare*) roots. Operation of these carriers requires an electrochemical potential gradient across the tonoplast, usually generated through the action of H^+ pumps such as the plasma membrane H^+-ATPase and vacuolar H^+-ATPase and H^+-pyrophosphatase (H^+-PPase) (see Chapter 3).

Arabidopsis SALT OVERLY SENSITIVE 1 (SOS1) is a plasma membrane Na^+/H^+ antiporter that mediates the passive transport of H^+ into and active transport of Na^+ out of the cell (Fig. 22.9). *Arabidopsis sos1* mutants show an NaCl-hypersensitive phenotype, whereas overexpression of *SOS1* improves salt stress tolerance. Transgenic plants treated with increasing Na^+ concentrations show significant salt tolerance compared to wild-type controls, and this tolerance is due to reduced accumulation of Na^+.

Na^+ compartmentalization into vacuoles is another mechanism of avoiding high Na^+ toxicity, and the vacuolar Na^+/H^+ antiporter Na^+/H^+ exchanger 1 (NHX1) is important in this process (Fig. 22.9). Transgenic plants overexpressing *NHX1* show increased Na^+ transport into vacuoles and can grow in salty water. Overexpression of *NHX1* in transgenic *Arabidopsis* improves salinity stress tolerance, allowing transgenic plants to grow and produce seeds even in the presence of 200 mM NaCl hydroponic solution (control plants in the same solution die). *NHX* overexpression confers salt tolerance in a wide range of plant species.

22.2.9 The hormone ABA plays an important role in plant response to water deficit

In addition to its roles in seed maturation and germination, the plant hormone abscisic acid (**ABA**) also plays important roles in plant responses to water deficit (see Chapter 17). ABA

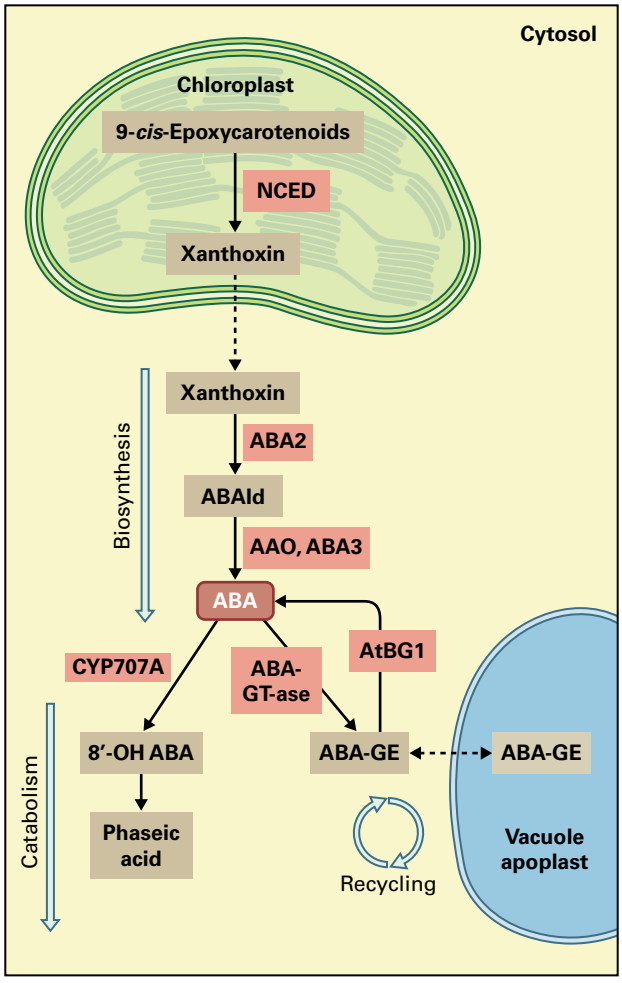


FIGURE 22.10 *ABA biosynthesis and degradation in response to abiotic stress. In the final process of the ABA biosynthetic pathway, xanthoxin is cleaved from 9-cis-epoxycarotenoids by NCED and released from the chloroplast into the cytoplasm. Then, ABA is produced through abscisic aldehyde (ABAld) formation. In ABA catabolism, the major pathway seems to be an oxidative pathway that is triggered by ABA 8′-hydroxylation catalyzed by the CYP707A family. There are other pathways for ABA inactivation, such as glucosylation. Red letters indicate drought stress-responsive regulation. CYP707As are shown in orange, which indicates dehydration and rehydration-responsive regulation. For more details on ABA metabolism see Chapter 17. NCED, 9-cis-epoxycarotenoid dioxygenase; ABA2, short-chain dehydrogenase/reductase; AAO, abscisic aldehyde oxygenase; ABA3, molybdenum cofactor sulfurase; CYP707A, ABA 8′-hydroxylase; ABA-GTase, ABA glucosyltransferase; AtBG1, β-glucosidase; ABA-GE, ABA glucosyl ester.*

is produced in response to water deficit and is involved in stomatal closure, which is required to prevent water loss from leaves under conditions of dehydration. The responses of stomata to water deficit have been studied extensively (see Chapter 3). ABA production is also essential for the cellular accumulation of various metabolites and proteins that have protective roles in water deficit resistance. Moreover, accumulated ABA induces a number of stress genes, the products of which are important for plant responses and tolerance to dehydration. Endogenous ABA levels—determined by the balance between ABA biosynthesis and catabolism—increase significantly in response to drought or high salinity.

ABA is primarily synthesized de novo in response to drought and high salinity, and the genes involved in ABA biosynthesis and catabolism have been identified mainly through genetic and genomic analyses (see Chapter 17). Xanthoxin, a C_{15} precursor of ABA, is produced by direct cleavage of C_{40} carotenoids by 9-*cis*-epoxycarotenoid dioxygenase (NCED) in plastids. This step is critical for ABA stress responses (Fig. 22.10, see Chapter 17). NCED is encoded by a multigene family, and the stress-inducible *NCED3* gene plays a key role in ABA biosynthesis under stress conditions. In *Arabidopsis*, overexpression of *NCED3* increases endogenous ABA levels and improves drought stress tolerance, whereas disruption results in defective ABA accumulation under drought stress and impairs drought stress tolerance.

At least two regulatory pathways exist for ABA catabolism: the oxidative pathway and the sugar conjugation pathway. The oxidative pathway is catalyzed by ABA C-8′ hydroxylase to produce phaseic acid. This enzyme belongs to a class of cytochrome P450 monooxygenases, the CYP707As (Fig. 22.10), of which there are four members in *Arabidopsis*. Among the four CYP707As, CYP707A3 is a major enzyme for ABA catabolism during the osmotic stress response. The *CYP707A3* gene is induced by rehydration after exposure to conditions of dehydration, and *CYP707A3* knockout mutants show increased endogenous ABA and dehydration tolerance. In the sugar conjugation pathway, ABA is inactivated in sugar-conjugated forms, such as ABA glucosyl ester, and stored in vacuoles or apoplastic pools (Fig. 22.10). Under conditions of dehydration, ABA is released from the glucosyl ester form by β-glucosidase. Regulation of the genes involved in ABA synthesis and catabolism by transgenic technology can improve drought tolerance.

ABA transport is also thought to be important for plant responses to abiotic stress. *NCED3* is mainly expressed in vascular tissues, and endogenous ABA is mainly synthesized in vascular tissue of leaves. ATP binding cassette (ABC) transporters function as ABA transporters in both the export and import of ABA. Regulation of ABA transport is important for both inter- and intracellular signaling in plants.

22.3 Gene expression and signal transduction in response to dehydration

Water deficit or dehydration can induce or repress the expression of thousands of plant genes with diverse functions. Many products of dehydration-inducible genes function in stress tolerance and responses at the cellular level, and their overexpression can improve stress tolerance, indicating important functions in plant responses and adaptation to dehydration or drought.

22.3.1 Microarray and other techniques provide insights into the expression of dehydration-inducible genes and their predicted functions

Microarray technology employing cDNAs or oligonucleotides (Chapter 9) is a powerful tool for analyzing the gene expression profiles of plants exposed to abiotic stress. Using this technology, many stress-inducible genes have been identified in various plants, and most of these are common among different plants, indicating their general roles in plant stress responses. Analysis of their functions is important for understanding the molecular mechanisms governing plant stress responses and tolerance. Moreover, basic knowledge regarding their functions is useful for enhancing stress tolerance in crops through transgenic technology.

Microarrays and more recently RNA sequencing technologies have been used to identify genes in *Arabidopsis* that are differentially expressed in various organs under various growth conditions, including stress conditions and phytohormone treatment. In addition, coexpression analysis of different transcriptome datasets provides a new method for the discovery of genes with similar expression profiles based on bioinformatics analysis; such genes often have similar functions, and this facilitates elucidation of stress-induced genes of unknown function. Results from these investigations show that many dehydration-inducible genes are also induced by high salinity and ABA treatment, suggesting significant crosstalk between the drought, high-salinity, and ABA response pathways. In contrast, only a small number of drought-inducible genes are also induced by cold stress.

The products of the dehydration-inducible genes identified through recent microarray analyses can be classified into two major groups:

- proteins and enzymes that function in abiotic stress tolerance, such as chaperones, LEA proteins, osmotin, antifreeze proteins, RNA-binding proteins, key enzymes for osmolyte biosynthesis, water channel proteins, sugar and proline transporters, detoxification enzymes, and various proteases
- regulatory proteins, such as protein factors involved in further regulation of gene expression and signal transduction. These include transcription factors, protein kinases, protein phosphatases, enzymes involved in phospholipid metabolism, other signaling molecules, and factors involved in posttranscriptional regulation, such as RNA-processing enzymes.

Many transcription factor genes are stress inducible, suggesting that various transcriptional regulatory mechanisms may function in regulating dehydration, cold, or high-salinity stress signal transduction pathways. These transcription factors control expression of stress-inducible genes, either cooperatively or independently, and may constitute regulatory networks.

Transcriptome analyses at the whole-genome level have also been carried out using high-throughput DNA sequencing and genome tiling arrays (see Chapter 9), and novel mechanisms of transcriptional regulation by noncoding RNAs or micro-RNAs have been reported. Micro-RNAs are involved in post-transcriptional regulation in abiotic stress responses by regulating mRNA stability (see Chapter 6). Sense and antisense RNAs for stress-responsive mRNAs have been reported to function in stress responses. Moreover, gene expression driven by stress often depends on DNA methylation or posttranslational histone modification. Modifications of DNA or histones may play important roles in gene expression and plant growth under stress conditions. Therefore, in addition to gene expression, epigenetic regulation (see Chapter 9) may play an important role in plant adaptation to abiotic stress.

22.3.2 Water deficit triggers changes in gene expression at the transcriptional level

Various transcription factors are important regulatory factors in stress-responsive gene expression. Several act as master switches for the expression of various sets of downstream genes through specific binding to the ***cis*-acting elements** in their promoters. Corresponding transcription factors have been isolated that bind to *cis*-elements and initiate transcription of target genes. This type of transcription unit is called a "**regulon.**" Analysis of the expression mechanisms of osmotic and cold stress-responsive genes has revealed multiple regulons in transcription. Many plant transcription factors, such as AP2/ERF, bZIP, MYB, MYC, Cys2His2 zinc-finger, and NAC, constitute multigene families involved in stress-responsive gene expression.

Dehydration triggers de novo production of ABA, which in turn induces expression of stress-related genes (see Section 22.2.7). There is evidence for both ABA-dependent and -independent regulatory systems governing stress-inducible gene expression. Many dehydration- and salinity-inducible genes can also be activated by exogenous ABA treatment, but a number of genes are also unaffected by ABA treatment. Promoter regions of dehydration-inducible genes have been analyzed extensively to identify regulatory *cis*-acting elements. Both *cis*- and *trans*-acting regulatory elements functioning in ABA-independent and -dependent gene expression induced by water deficit have been studied in detail.

22.3.3 Endogenous ABA accumulation under dehydration stress also controls gene expression

Analysis of ABA-responsive promoters has revealed a diverse range of potential *cis*-acting regulatory elements, but most ubiquitous *cis*-elements share the (C/T)ACGTGGC

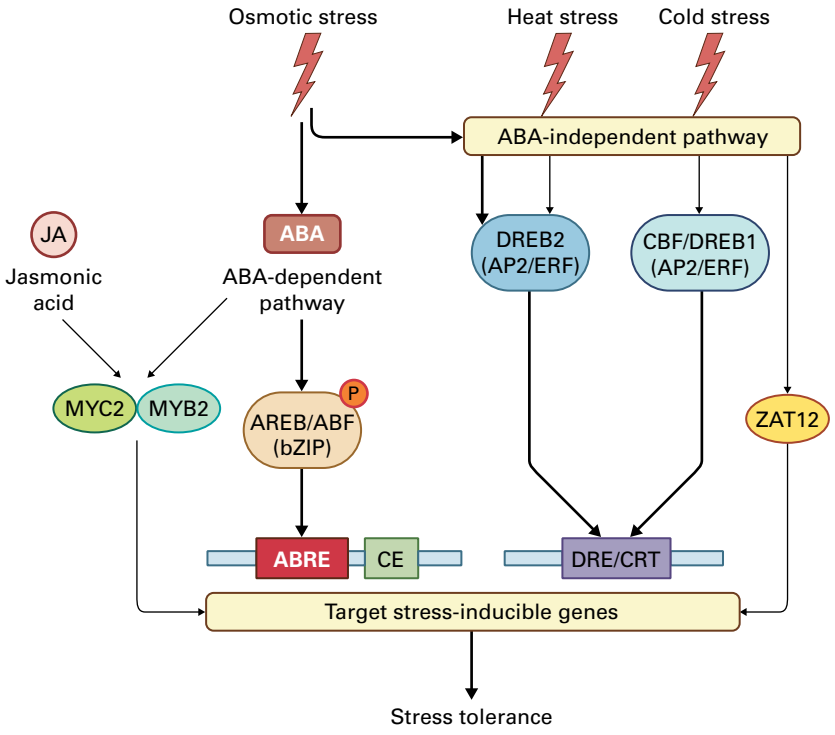


FIGURE 22.11 *Overlapping transcriptional regulatory networks in plant responses to osmotic, heat, and cold stress. Transcription factors and* cis*-acting elements are shown in ovals and boxes, respectively. ABA-dependent pathway (shown in red): ABRE is a key cis-acting element of genes regulated by ABA-dependent stress responses. The coupling element (CE) is necessary for ABA-dependent transcription. AREB/ABF are major transcription factors in the ABA response, and are phosphorylated for their activation (see Fig. 22.12). MYC2 is not only regulated by ABA, but also by jasmonic acid (JA) and functions in crosstalk between ABA and JA responses (see Section 22.8). MYB2 is induced by ABA and functions in cooperation with MYC2 in dehydration-inducible gene expression. Other transcription factors have been identified in abiotic stress response but are not shown. ABA-independent pathways (shown in blue): DRE/CRT is a key* cis*-acting element of genes regulated by ABA-independent stress responses. CBF/DREB1s are major transcription factors in the cold stress response, whereas DREB2 is mainly regulated by osmotic and heat stress. CBF/DREB1 is explained in Section 22.4.7. The roles of ZAT12 in the cold stress response and DREB2 in the heat response are described in Sections 22.4.7 and 22.7.5, respectively.*

consensus sequence, the **ABA-responsive element** (ABRE; PyACGTGGC). ABRE is a major *cis*-acting element in ABA-responsive gene expression (Figs. 22.11 and 22.12) that requires another *cis*-acting element, the **coupling element** (CE), for function. The basic leucine zipper (bZIP) transcription factors AREB and ABF can bind to the ABRE *cis*-acting element to activate ABA-dependent gene expression.

The AREB and ABF transcription factors require an ABA-mediated signal for activation, as indicated by their reduced activity in the ABA-deficient *aba2* and ABA-insensitive *abi1* mutants and their enhanced activity in the ABA-hypersensitive *era1* mutant of *Arabidopsis*. This is due to the ABA-dependent phosphorylation of AREB and ABF proteins by the SNF1-related protein kinases SnRK2s (Fig. 22.12 and see Section 22.3.5). Transgenic plants expressing an active form of AREB1 with multi-site mutations show induction of many ABA-responsive genes without application of exogenous ABA. These observations indicate an important role of protein phosphorylation in the activation of AREB and ABF transcription factors in response to increased levels of endogenous ABA under osmotic stress conditions. In addition to the AREB and ABF bZIP transcription factors that function as key regulators of ABA-dependent gene expression, various transcription factors with MYB2, MYC2 (bHLH), NAC, HD-ZIP, HD, HB, AP2, and B3 domains are involved in ABA responses under osmotic stress conditions (see Section 22.8). Among them, MYB2 and MYC2 are involved in stress-regulated gene expression after the accumulation of ABA. MYC2 is also important in jasmonic acid (JA)-regulated gene expression (see Fig. 22.11).

22.3.4 ABA-independent pathways can also influence the abiotic stress response and DREB2 transcription factors

The promoters of genes such as *RD29A* and *COR15*, which induced by dehydration, high salinity, and cold, contain two major *cis*-acting elements, ABRE and DRE (**dehydration-responsive element**)/CRT (**C-RepeaT**), both of which are involved in stress-inducible gene expression (Figs. 22.11 and 22.12). Whereas ABRE functions in ABA-dependent pathways, DRE/CRT functions in ABA-independent gene expression in response to abiotic stress (Fig. 22.12); it also contains the conserved *cis*-acting promoter motif A/GCCGAC.

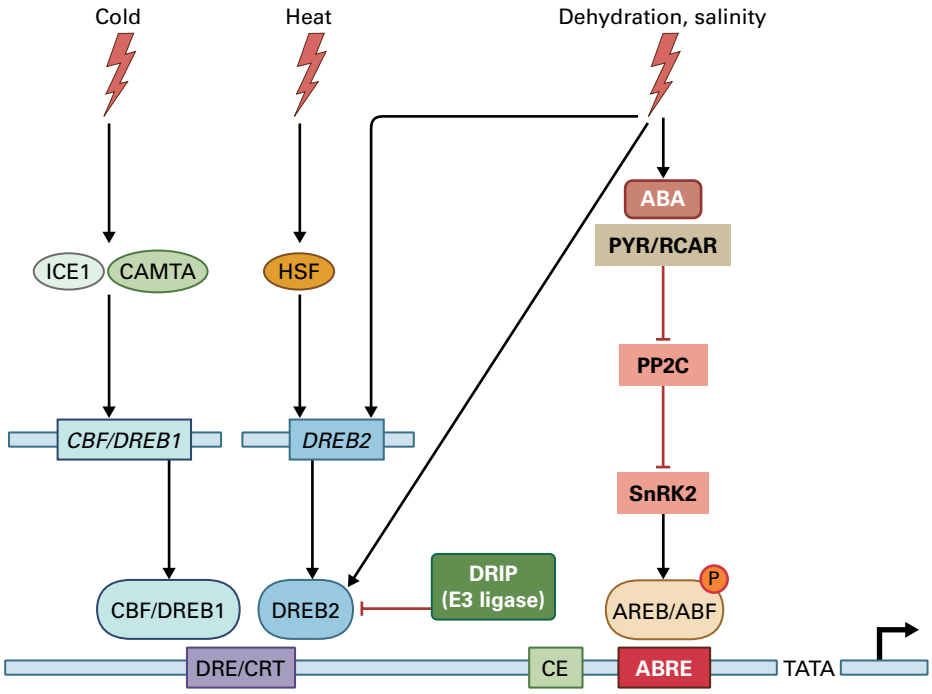


FIGURE 22.12 *Function of* cis*-acting elements DRE/CRT and ABRE in ABA-independent and -dependent induction of* RD29A*, respectively. AP2/ERF transcription factors CBF/DREB1 and DREB2 bind DRE/CRT in response to different types of stress: CBF/DREB1 functions in cold-inducible gene expression, and their genes are regulated by the transcription factors ICE1 and CAMTA (see Section 22.4.7). DREB2 is involved in dehydration- and salinity-inducible gene expression and is activated by protein stabilization. AREB/ABFs are bZIP transcription factors that bind ABRE/CE and mediate ABA-dependent gene expression (see Fig. 22.11). Major ABA signaling cascades (involving ABA receptors PYR/RCARs, PP2C phosphatases, and SnRK2 protein kinases) function upstream of AREB/ABF transcription factors (see Section 22.8). The function of CBF/DREB 1 in cold response is also described in Section 22.4.7, and the function of DREB2 in heat response is also described in Section 22.7.5.*

Two transcription factors belonging to the AP2/ERF family, CBF/DREB1 and DREB2, bind to the DRE/CRT element. The genes encoding CBF/DREB1 are rapidly and transiently induced by cold stress, and their products activate expression of target stress-inducible genes (see Section 22.4.7); expression of DREB2, on the other hand, is mainly induced by dehydration, high salinity, and heat stress.

Overexpression of CBF/DREB1 in transgenic plants increases tolerance to drought, freezing, and salt stress, suggesting the CBF/DREB1 proteins function in the development of cold stress tolerance without posttranslational modification (Fig. 22.13A). Overexpression of DREB2 in transgenic *Arabidopsis* plants, though, does not improve stress tolerance, which suggests the involvement of post-translational activation of DREB2 proteins.

Deletion of a region of 30 amino acids adjacent to the AP2/ERF DNA binding domain, named the DREB2A negative regulatory domain (NRD), transforms DREB2A into the constitutively active form DREB2A-CA, which interacts with an E3 ubiquitin ligase (DRIP: DREB2 interacting protein 1). Posttranslational regulation may be necessary for stabilization of the DREB2A protein. *Arabidopsis* DREB2A target genes are induced to a significantly greater extent by dehydration stress than by cold stress (see Fig. 22.12).

Preference of DNA-binding activities has been compared between the DREB2A and DREB1A protein. Whereas DREB2A binds preferentially to the sequence ACCGAC, DREB1A shows affinity for the A/GCCGACNT sequence. These data indicate that the function of the DREB2-type transcription factor in the drought stress response is different from that of the DREB1 protein involved in the cold stress response (Fig. 22.13B). DREB2A is also involved in responses to heat and drought stress, as discussed in Section 22.8.

Transgenic plants that overexpress various transcription factors have more abiotic stress tolerance. For example, overexpression of the rice (*Oryza sativa*) NAC transcription factor SNAC1 improves drought tolerance of transgenic rice and induces expression of a large number of stress-regulated genes. Another good example involves the NF-Y transcription factor family; transgenic maize (*Zea mays*) plants overexpressing ZmNF-YB2 exhibit tolerance to drought based on various stress-related parameters including chlorophyll content, stomatal conductance, leaf temperature, reduced wilting, and maintenance of photosynthesis. Moreover, maize plants overexpressing *ZmNF-YB2* have better grain yield under conditions of drought stress (Fig. 22.14). Constitutive or conditional expression of transcription factors has great potential for the development of drought-tolerant crops.

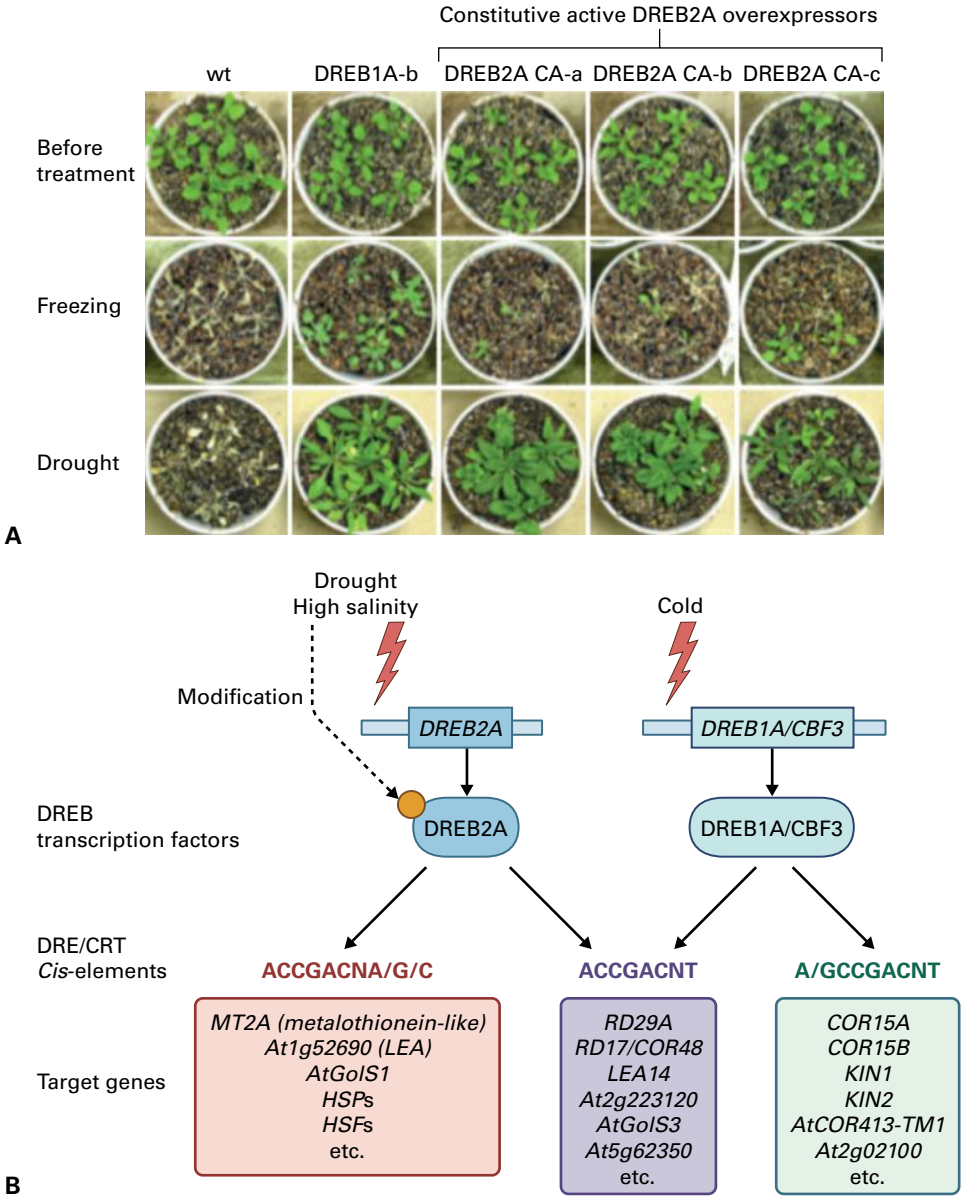
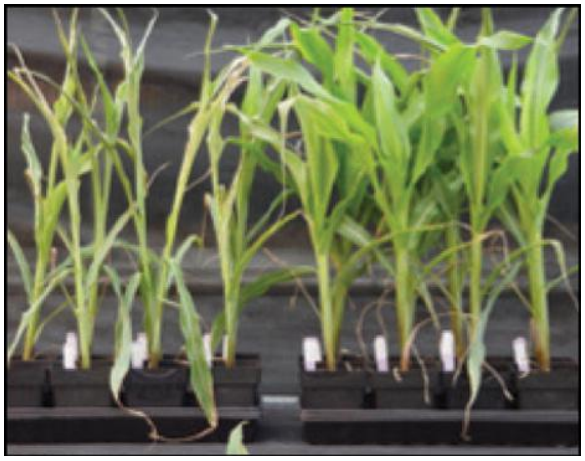


FIGURE 22.13 Arabidopsis *CBF/DREB1 and DREB2 mediate overlapping and unique pathways of resistance to freezing, drought, and salt stress. (A) Transgenic* Arabidopsis *plants that overexpress DREB1 or the constitutively active form of DREB2 (DREB2-CA) show tolerance to both drought and freezing stress. (B) Model of the induction of genes regulated by DREB1 and DREB2A under drought, salinity, and cold stress. The genes downstream of DREB1 and DREB2A are categorized into three groups. The center group contains genes shared by DREB1A and DREB2A, and the other groups consist of DREB1A- and DREB2A-specific genes.*
Source: Sakuma et al. (2006). Plant Cell 18:1292–1309.

22.3.5 Osmotic stress triggers various signaling pathways in plants

Though changes in transcriptional regulation in response to osmotic stress have been analyzed extensively, their cellular signal transduction pathways are not yet fully understood. Our current understanding of cellular signal transduction in the osmotic stress response has been based largely on knowledge obtained from analysis of yeast and other microorganisms. Protein kinase homologs have been identified based on their functions in stress signaling pathways (Fig. 22.15). Genetic screening of mutants showing abnormal responses to abiotic stress, either resistance or sensitivity, has been performed to isolate factors involved in stress responses and signaling pathways.

Stress signaling involves modification of regulatory proteins through phosphorylation and dephosphorylation, ubiquitination, and calcium binding. These groups of regulatory proteins are modified or activated to fulfill their functions quickly. Although the complexity of this signal transduction network is still not completely understood, several types of protein kinase and calcium-sensing proteins have been characterized, and their functions have also been investigated in transgenic plants.



A



B

FIGURE 22.14 *Transgenic maize (*Zea mays*) plants that overexpress* ZmNF-YB2 *(plants at right) grown in a greenhouse (A) and a test field (B) show significantly improved drought tolerance. The rice (*Oryza sativa*) actin gene promoter was used to overexpress* ZmNF-YB2 *cDNA.*

Osmotic stress sensors have been analyzed in bacteria and yeast. In yeast, the **His-Asp phosphorelay system** functions in sensing osmotic stress. The membrane-bound histidine kinase Sln1p functions as an osmosensor, and the *Arabidopsis* histidine kinase AHK1 can complement a yeast *sln1* mutant, indicating AHK1 also functions as an osmosensor in yeast. In addition, AHK1 protein functions as a positive regulator in water deficit and osmotic stress signaling in plants (Fig. 22.15). Transcriptional profiling analysis of *ahk1* knockdown mutants has revealed that some target genes of AREB1, ANAC, and DREB2A transcription factors are downregulated in the mutant. In contrast, transgenic *Arabidopsis* overexpressing *AHK1* driven by its own promoter show markedly improved drought stress tolerance. The response regulator-like factors (ARRs) are thought to function downstream of AHK1 in osmotic stress signaling pathways like the yeast His-Asp osmosensing phosphorelay system Sln1p-Ypd1p-Ssk1p.

The **mitogen-activated protein kinase (MAPK)** cascade functions in various cell signaling cascades (see Chapter 18), including osmotic stress responses in eukaryotes. It is characterized by a three-step phosphorylation relay by MAPK, MAPK kinase (MAPKK), and MAPKK kinase (MAPKKK) on conserved threonine, tyrosine, and serine residues (see Chapter 18). In yeast, the HOG1 pathway (Ssk2/22p-Pbs1p-Hog1p) is a MAPK cascade that functions downstream of Sln1p-Ypd1p-Ssk1p. In plants, MAPK cascades are rapidly activated by various environmental stresses and pathogen infection. The *Arabidopsis* MEKK1-MKK2-MPK4/MPK6 cascade is activated by salinity and also cold stress, and plays a role in cellular stress signaling pathways (Fig. 22.15). These observations suggest that MAPK cascades function in abiotic as well as biotic stress signaling. However, the upstream signaling components in plants have yet to be determined.

ROS are produced in response to reduced metabolic activities of chloroplasts and mitochondria in biotic and abiotic stress responses (see Section 22.6). Factors involved in signal transduction pathways may function as ROS sensors to control downstream events. ROS regulate transcription factors, such as the heat shock factors (HSFs) involved in the heat stress response (see Section 22.7) and NPR1 involved in disease resistance. Protein kinases such as SOS2 and ANP1 and heterotrimeric G proteins are also regulated by ROS. Therefore, ROS can modulate abiotic stress signaling pathways and function in crosstalk in stress signaling (see Section 22.8).

Of the many second messengers involved in cell signaling pathways, Ca^{2+} is the most ubiquitous (see Chapter 18). In plants, Ca^{2+} levels increase transiently in response to various stimuli, including water deficit. Osmotic stress can trigger rapid and dynamic oscillations in cytosolic Ca^{2+} levels that are mediated by various Ca^{2+} channels and transporters (Fig. 22.15). The Ca^{2+}-dependent stress signaling pathway is important in plants and is mediated by calcineurin B-like (CBL) proteins and their downstream CBL interacting protein kinases (CIPK). CBL proteins bind Ca^{2+} via a helix–loop–helix structure motif (the EF hand), and function as Ca^{2+} signal sensors under conditions of stress in plants. The specific interactions of different CBLs with CIPKs can transmit signals to downstream proteins such as transcription factors by protein phosphorylation to activate the plant stress response. The major component in this signaling pathway is SOS3/CBL4 and its interactive partner SOS2/CIPK24. Disruption of either or both of these genes results in the severe "salt overly sensitive" (SOS) phenotype, suggesting an important role of the SOS3-SOS2 protein kinase cascade in salinity stress signaling pathways (see Fig. 22.9).

Calcium-dependent protein kinases (CDPKs) are well characterized and are also of particular interest in plant calcium-mediated signal transduction (Fig. 22.15). CDPKs have both a kinase domain and a calmodulin-like domain in a single protein. CDPKs phosphorylate their respective substrates to transduce perceived signals, and binding of calcium can stimulate their protein kinase activity.

The identification of protein kinases that activate AREB and ABF transcription factors is important for understanding

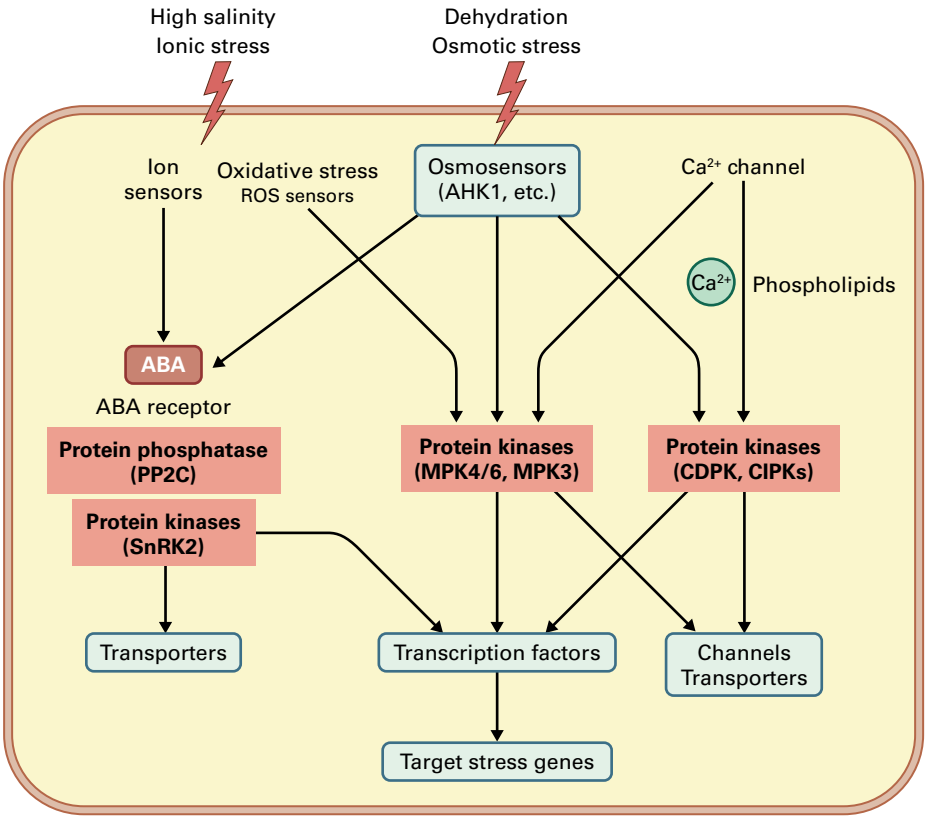


FIGURE 22.15 *Cellular signal transduction cascades in response to high salinity and water deficit. Osmotic change, ionic stress, cold stress (not shown) and reactive oxygen species trigger stress responses, and many stress sensors have been identified. ABA is an important mediator of stress signals, and Ca^{2+} and phospholipids are second messengers in stress signaling pathways. Protein phosphorylation plays important roles in stress and ABA signal transduction pathway, and involves a number of different protein kinases, including SnRK2 in the ABA response, and MAP kinase, calcium-regulated protein kinases, and two-component histidine kinase in the osmotic stress response. Transcriptional regulation is most important for the regulation of stress genes, whose products function in both stress response and stress tolerance. In addition, the activities of various types of transporters are required for homeostasis during stress conditions.*

upstream ABA signaling pathways. One ABA-activated SnRK2 protein kinase (OST1/SRK2E/SnRK2.6) functions in the ABA signal transduction pathway controlling stomatal closure (Fig. 22.15). SnRK2 is a member of the SNF1-related protein kinase family, which contains ten members in *Arabidopsis* and rice. SnRK2s are activated by dehydration, salinity, and ABA. Several SnRK2s of various plants can phosphorylate AREB and ABF or related proteins in vivo and in vitro, indicating that SnRK2s are upstream factors of AREB and ABF. A triple loss-of-function mutant of *Arabidopsis* SnRK2.6, 2.2, and 2.3 exhibits a strong growth defect, which is related to ABA responses such as germination, stomatal closure, and root growth. These three SnRK2 proteins are repressed by ABI1-related PP2C protein phosphatases, which are major negative components in the ABA signaling pathway. The ABI1-related PP2Cs directly and negatively regulate the activities of these three SnRK2 via dephosphorylation.

The pyrabactin resistance (PYR)/PYR-related (PYL)/regulatory component of ABA receptor (RCAR) family of ABA receptors (**PYR/PYL/RCAR protein family**) have ABA-binding activity and inhibit PP2C activity by ABA-mediated interaction (Fig. 22.16). Furthermore, ABA-activated SnRK2 protein kinases are inhibited in loss-of-function mutants of PYR/PYL/RCARs. A signaling complex of PYR/PYL/RCAR, PP2C, and SnRK2 is important for ABA perception and the initial signal transduction process. PYR/PYL/RCARs function as cytoplasmic ABA receptors and inhibit PP2C-mediated inactivation of SnRK2 in an ABA-dependent manner (Fig. 22.16). Under normal growth conditions without ABA, PP2C inhibits SnRK2 by direct binding and dephosphorylation of SnRK2. In response to abiotic stress, endogenous ABA is synthesized and binds to the PYR/PYL/RCAR receptor, and ABA-bound PYR/PYL/RCAR inhibits PP2C activity. This activates SnRK2, which then phosphorylates its target proteins, such as AREB/ABF bZIP transcription factors and ion transporters. The structure of the ABA-PYR/PYL/RCAR-PP2C complex was determined by X-ray diffraction (Fig. 22.17). An ABA-bound receptor is capable of competitively inhibiting the phosphatase activity of PP2C. Perception of ABA and its stream signal transduction are fully understood at the molecular level to illustrate the precise molecular switch of ABA signaling (Fig. 22.16).

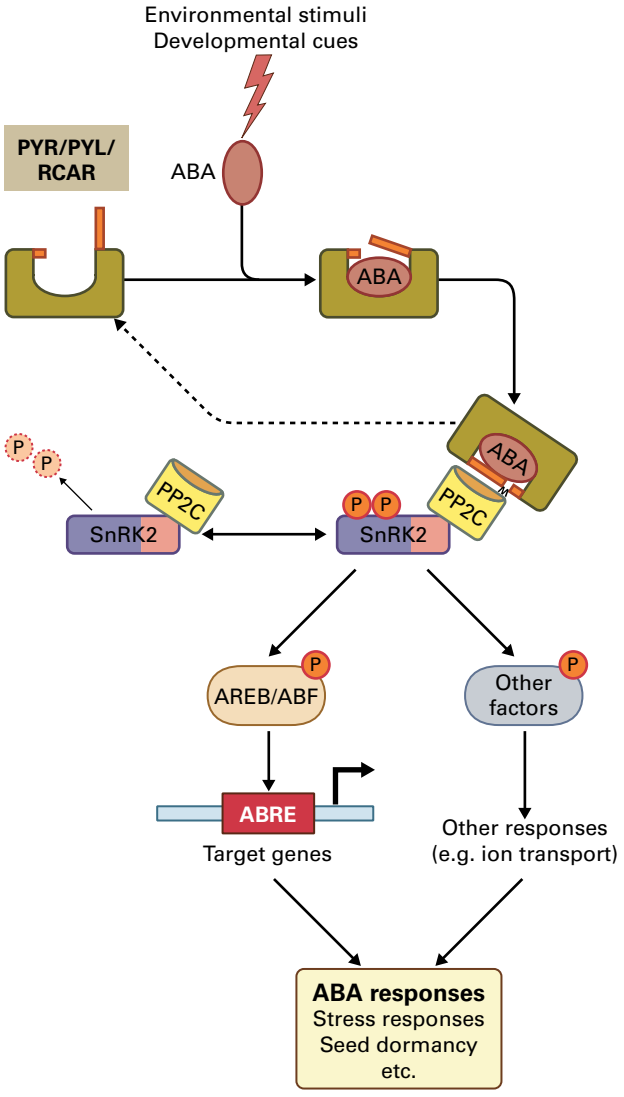


FIGURE 22.16 *Proposed model of the early process of ABA perception and signal transduction. PYR/PYL/RCAR functions as an ABA receptor, and PYR/PYL/RCAR, PP2C phosphatase and SnRK2 protein kinase form a signaling complex. In the absence of ABA, PP2C binds to and inactivates SnRK2. In the presence of ABA under abiotic stress conditions, PYR/PYL/RCAR binds to ABA and inhibits PP2C activity. Then, SnRK2 is released from the inhibition by PP2C and activated to phosphorylate downstream transcription factors, including AREB/ABFs and transporters. These activated proteins then function in cellular and molecular responses to abiotic stress in an ABA-dependent manner.*

22.3.6 Genetic screens have identified stress signaling proteins

Genetic analyses have also revealed genes involved in the signal transduction pathways that control stress-responsive gene expression. Various mutants with tolerance to abiotic stressors have been isolated and some of the mutant genes have been identified. For example, SOS mutants were isolated by screening salinity-hypersensitive mutants with root response to salinity stress, and the gene encoding a CIPK/SnRK3 protein kinase was identified (see Section 22.3.5). In addition, genetic screens have been carried out using various reporter gene constructs to identify mutants with altered expression of stress-induced genes (see Box 22.1).

22.4 Freezing and chilling stress

22.4.1 Freezing and chilling stress have both similarities and differences

Freezing and chilling stress impose both direct and indirect effects on plant health. Direct effects include solidification of membrane lipids and reductions in enzymatic reaction rates, and these occur over a relatively short time. Indirect (or secondary) injury symptoms, on the other hand, appear gradually over time and include solute leakage from cells, respiration and photosynthesis imbalance, ATP depletion, accumulation of toxic substances, and wilting by water loss (see Chapter 8).

Both freezing and chilling stress are associated with some form of cellular injury caused by the direct effects of low temperature; however, freezing stress has several additional indirect effects due to ice crystal formation and growth in extracellular compartments that can damage plants at the whole-plant, tissue, and cellular levels. In addition, freezing of water in the extracellular spaces results in osmotic dehydration and, therefore, increases in solute concentrations inside the cell. These damaging effects together markedly affect plant performance, and susceptible plants will die. Another difference between the two forms of temperature is the time effect: while chilling injury occurs some time after exposure of plants to the stress (the period differs between plants, organs, tissues, and developmental stage), freezing injury may be visible instantly after freezing occurs. Thus, these two low-temperature stressors must be considered distinct and analyzed individually with suitable methods.

22.4.2 Chilling stress causes membrane destabilization and metabolic dysfunction

Membrane lipids maintain a fluid (liquid crystalline) phase at normal, warm temperatures, which ensures maintenance of cellular function (see Chapter 8). When the temperature decreases, however, lipids with high melting temperatures begin to solidify (gel phase) and become phase-separated within the membrane. Membranes become leaky or otherwise dysfunctional, intracellular water and solutes are lost, and membrane-associated reactions such as carrier-mediated transport, enzyme-mediated processes, and receptor function are inactivated.

Although low temperature affects plant cells in many different ways, one of the most important is its effect on photosynthesis. Low temperature markedly impairs the electron transport chain while showing little effect on

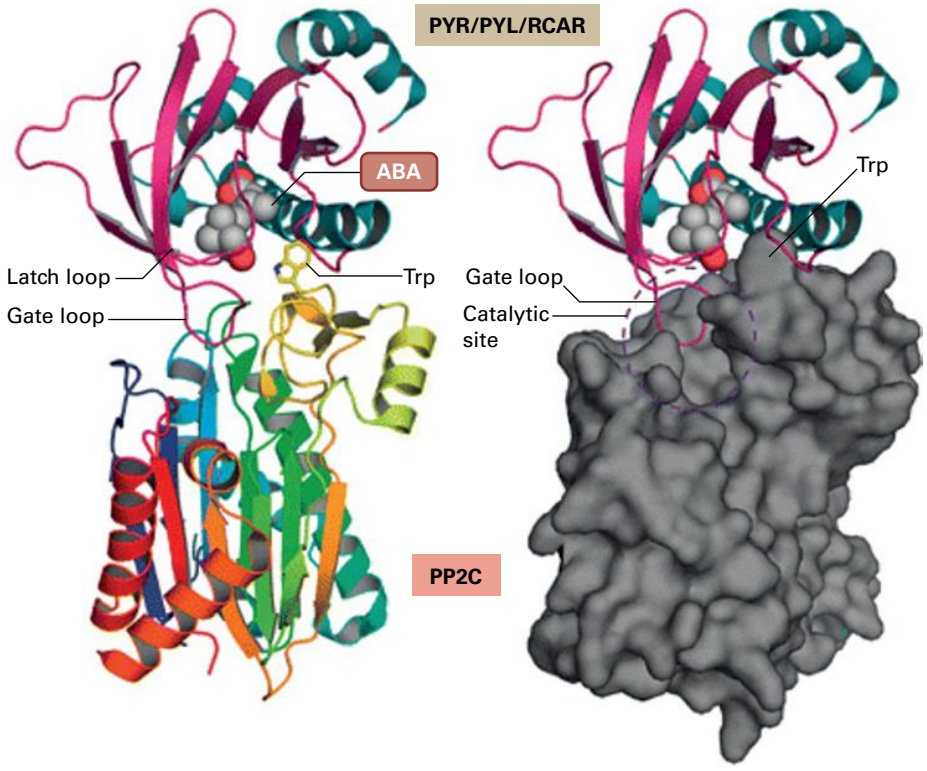


FIGURE 22.17 *Three-dimensional structure of the complex of ABA-bound PYR/PYL/RCAR (ABA receptor) and ABI1 (PP2C). PP2C is represented by both a ribbon (left) and surface (right) model. ABA-bound PYL1 can competitively inhibit the phosphatase activity of PP2C using the gate loop like a plug.*

photoenergy reception. As a result, chloroplasts are exposed to excess excitation energy, and photoreduction of oxygen molecules occurs with concomitant production of ROS (see Section 22.7). The resultant oxidative stress with increased free radical levels damages membrane lipids and proteins as well as macromolecules in chloroplasts.

The development of injury symptoms sometimes becomes more apparent after a return to normal temperatures. At low temperature, the development of symptoms requires a long time, and injury may not advance due to the slow rate of the dysfunctional process. Several studies have shown that chilling injury occurs due to the lack of or impaired cellular recovery functions. Although the D1 protein, a major component of the PSII reaction center, is affected at low temperature, the major cause of chilling injury to the PSII is the lack of recovery from damage caused by ROS after returning to warmer temperatures. ROS scavengers such as glycine betaine, a compatible solute (Figure 22.5), may increase the efficiency of PSII metabolic turnover during the recovery process from abiotic stressors. This hypothesis is supported by genetic engineering studies that indicate overexpression of ROS-scavenging enzymes improves low temperature tolerance.

22.4.3 Freezing also causes membrane destabilization and damage due to osmotic and mechanical stress

As explained in Section 22.4.1, freezing has a marked impact on cellular water and causes a type of water deficit stress that distinguishes it from the effects of chilling. The chemical potential of ice is lower than that of unfrozen water. In addition, the vapor pressure of extracellular ice is lower than that of the water in the cytoplasm or vacuole. As ice forms in extracellular compartments, the cellular water moves down the water potential gradient, across the plasma membrane and toward the extracellular ice (Fig. 22.18). As a result, cell volume decreases and intracellular solute concentration increases; extracellular ice formation also distorts the shape of cells. These types of stress persist as long as freezing continues, and they even increase when temperature decreases, causing further injury to plant cells.

The plasma membrane is the primary site of freezing-induced injury, and much of the damage involves membrane destabilization caused by cellular dehydration. Membrane structures and interactions are altered when freezing-induced dehydration brings the plasma membrane into close apposition with the membranes of organelles, such as the chloroplast, leading to membrane destabilization. Membrane destabilization results in distinct forms of injury in some plants, such as expansion-induced lysis, loss of osmotic responsiveness associated with lamellar-to-hexagonal II phase transition in less tolerant (nonacclimated) cells, and loss of osmotic responsiveness associated with fracture-jump lesion in more tolerant (cold-acclimated) cells (Fig. 22.19).

Membrane destabilization also results from the osmotic and mechanical stress imposed during freeze–thaw cycles. Osmotic dehydration increases solute concentrations in the cytoplasm and other intracellular compartments, and this can inactivate membrane-associated enzyme and transporter activities. Direct interaction of solutes with the membrane results in dissociation of membrane proteins due to changes in electrostatic and hydrophobic interactions. In addition,

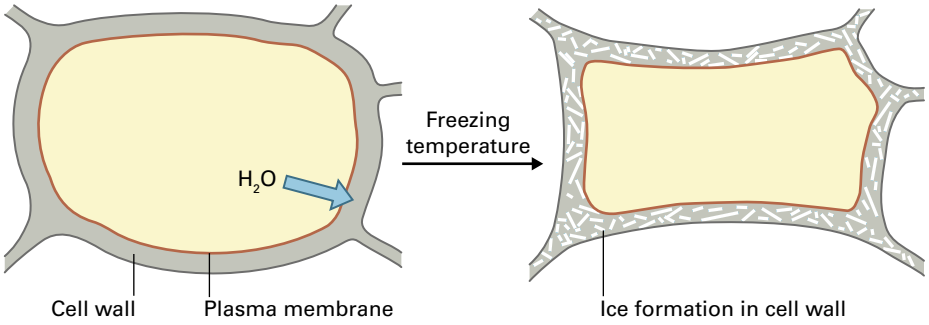


FIGURE 22.18 *Exposure of plants to freezing temperatures causes a cellular water deficit as water travels down its potential gradient, crossing the plasma membrane into the cell wall and intercellular spaces. When the rate of freezing is sufficiently slow to prevent formation of ice crystals in the cytoplasm, the cell dehydrates and freezing occurs in the apoplast.*

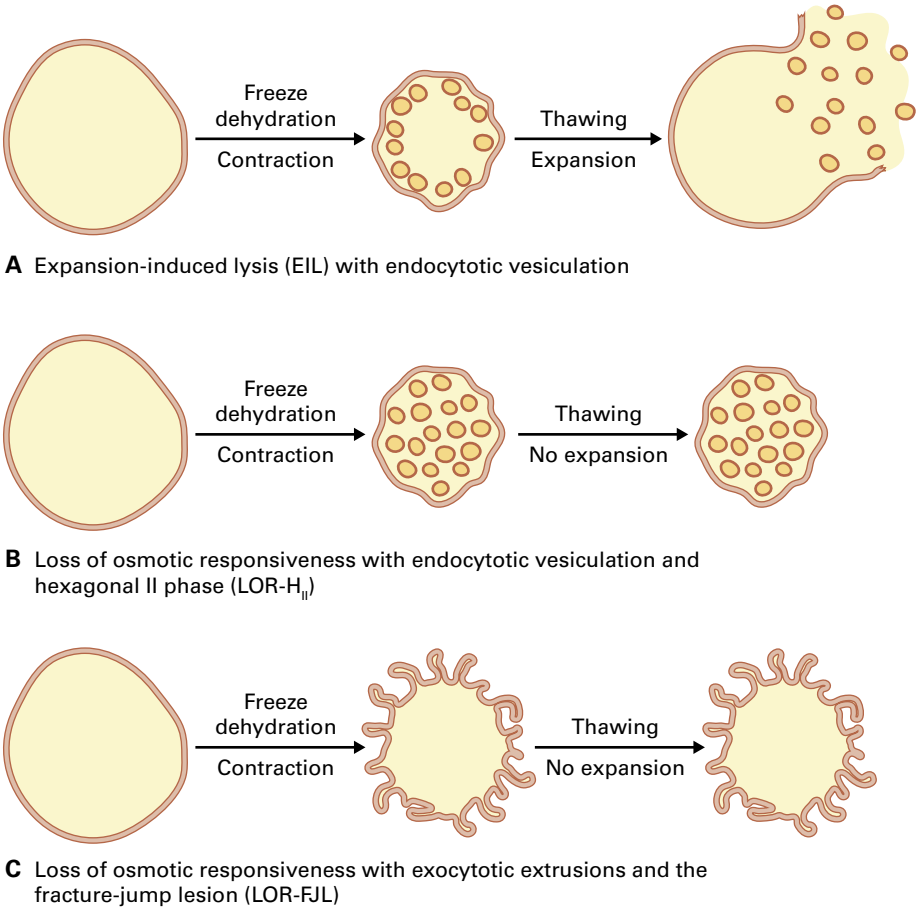


FIGURE 22.19 *Freezing-induced lesions associated with the plasma membrane in isolated protoplasts. (A) When a suspension of protoplasts isolated from nonacclimated plants is frozen, freezing-induced dehydration occurs in the protoplast, gradually reducing protoplast volume. To maintain membrane tension, the plasma membrane must be removed from the surface of the protoplast, and this is accomplished through formation of endocytotic vesicles that are not continuous with the plasma membrane. Under mild but injurious dehydration conditions, the protoplasts cannot expand during thawing due to the lack of the plasma membrane materials, resulting in expansion-induced lysis. (B) When severe freezing-induced dehydration occurs at lower temperature, the plasma membrane of the protoplast is brought into close apposition to endomembranes, ultimately resulting in irreversible ultrastructural changes of the lipid bilayers (such as lamellar-to-hexagonal II phase transition) due to membrane–membrane interactions. Consequently, the protoplast does not respond osmotically when thawed (loss of osmotic responsiveness). (C) In protoplasts isolated from cold-acclimated plants, freezing-induced dehydration results in the reduction of their volume, but the plasma membrane forms exocytotic extrusions that are continuous with the plasma membrane. No lysis occurs upon thawing of protoplasts that were frozen at any temperature. Membrane–membrane interactions occur when the protoplast is subjected to severe freezing-induced dehydration, but a distinct structure associated with the plasma membrane, the fracture-jump lesion (FJL), occurs. The FJL is a result of membrane–membrane fusion and is manifested as a jump of the fracture plane from one membrane to the other in freeze-fracture electron micrographs. Consequently, the protoplast does not respond osmotically when thawing (loss of osmotic responsiveness associated with the fracture-jump lesion, but not with the hexagonal II phase formation).*

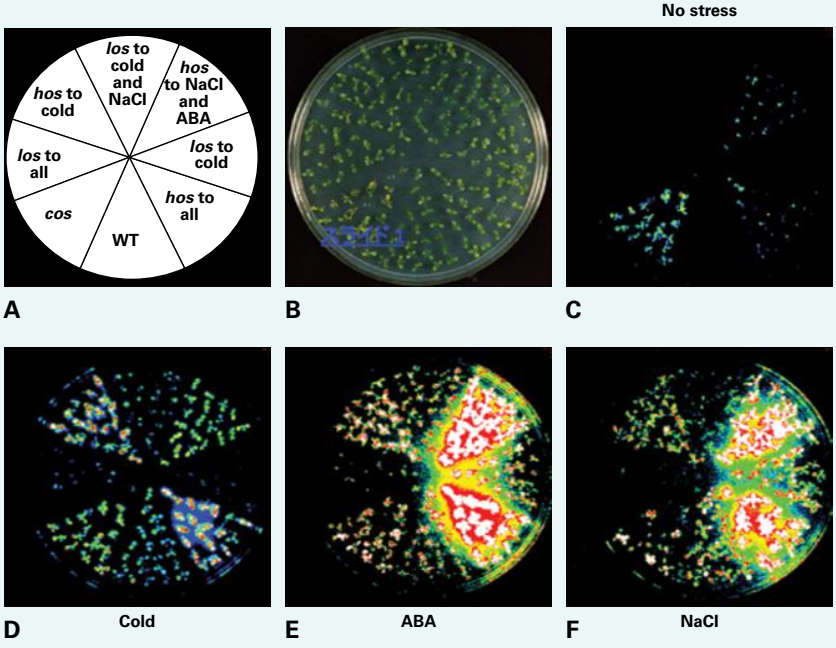
BOX 22.1

A genetic screen was used to identify mutants with altered *RD29A* gene expression in response to abiotic stress

Genetic screens have been used to identify genes involved in the plant abiotic stress response. *Arabidopsis* plants were transformed with the firefly luciferase gene fused to the *RD29A* promoter, which is induced by drought, cold, and ABA treatment. *Arabidopsis* plants containing the *RD29A* promoter-luciferase (*LUC*) transgene were then mutated by EMS or T-DNA insertion for mutant screening. Mutants were isolated that exhibited constitutive expression (cos), high expression (hos), or low expression (los) of luciferase in response to cold and salt stress treatments (see figure). The proteins encoded by the mutated genes function not only as transcription factors upstream of RD29A gene activation, but also in posttranscriptional regulation of the transcription factors.

Many factors involved in stress signaling were identified among the mutants isolated. For example, LOS5 and LOS6 were identified as ABA3 (encoding molybdenum cofactor sulfurase) and ABA1 (encoding zeaxanthin epoxidase), respectively. These are involved in ABA biosynthesis. One of the *HOS* genes, named *FRY1* (*FIERY 1*), encodes inositol polyphosphate 1-phosphatase, which is involved in inositol-1,4,5-triphosphate signaling. FRY1 functions as a negative regulator of ABA and stress signaling, suggesting the involvement of phospholipids in stress signaling pathways. Another *HOS* gene, *HOS15* encodes a WD40 repeat protein similar to TBL1, which is associated with histone deacetylation in mammals. HOS15 is likely involved in histone H4 deacetylation to regulate stress tolerance through chromatin remodeling. Repressor of silencing (ros) has been identified in other mutants. *ROS1* encodes a DNA glycosylase that demethylates DNA by base excision repair and can counteract RNA-dependent DNA methylation. ROS3 contains an RNA recognition motif and may direct sequence-specific demethylation by ROS1 and related DNA demethylases. Therefore, this mutant screening approach provides a powerful tool not only for analysis of upstream signal transduction pathways, but also for studies of post-transcriptional regulation of gene expression and chromatin regulation.

Source: Ishitani et al. (1997). Plant Cell 9:1935–1949.



*Luminescence images of wild-type (*RD29A *promoter:*LUC *transgenic* Arabidopsis *plant) and mutants (*hos, los, *and* cos*) under cold, osmotic, and ABA stress. (A) Arrangement of the wild-type (WT) and mutant lines. Clockwise: wild-type* RD29A-LUC *transgenic parent;* cos*, mutants with constitutive* RD29A *expression;* los *to all, mutants with reduced responses to cold, ABA, and osmotic stress;* hos *to cold, mutants with enhanced response to cold;* los *to cold and NaCI, mutants with reduced responses to cold and osmotic stress;* hos *to NaCI and ABA, mutants with enhanced response to ABA and osmotic stress;* los *to cold, mutants with reduced response to cold stress;* hos *to all, mutants with enhanced response to cold, ABA, and osmotic stress. (B) Morphology of the seedlings of WT and mutants. (C) Luminescence from plants before stress and ABA treatments. Note the constitutive luminescence of the* cos *mutant. (D) Luminescence from plants exposed to cold conditions for 2 days. (E) Luminescence from plants after ABA treatment. The plants were placed at room temperature (20–22°C) for 2 days to allow the luminescence to drop to pre-cold treatment levels before spraying with 100 μM of ABA and imaging 3 hours later. (F) Luminescence from plants under osmotic stress. Three days after ABA treatment, luminescence from the plants dropped to pretreatment levels. The plants were then treated with high salt for 5 hours by flooding the plate with 300 mM NaCI. Some of the* cos *mutant seedlings died after cold and ABA treatment and so did not emit luminescence upon NaCI treatment.*

solute concentration affects lipid phase behavior due to the electrostatic interactions with charged headgroups of bilayer lipid molecules. Mechanical stress is another factor that destabilizes the membrane; ice formation in the extracellular space results in deformation of the cell, and ice crystals can directly damage the plasma membrane.

Freezing stress also causes other types of damage in cells. Cell wall–plasma membrane interactions are altered due to freezing; for example, in some plants, survival of intact cells is less than that of isolated protoplasts, which do not have a cell wall. This is because the presence of the cell wall can add extra stress from extracellular ice crystals on cells. Further, several specific proteins become detached from the plasma membrane when intact cells with a cell wall are frozen, suggesting the physicochemical interactions between the cell wall and the plasma membrane occurring during freezing cause extra damage to the plasma membrane. Freezing leads to acidification of the cytoplasm, probably as a result of disturbance of H^+-transport systems associated with the vacuolar membrane (tonoplast). This acidification markedly affects metabolic reactions in the cytoplasm. Taken together, these observations indicate that freezing exposes cells to very complex multifaceted stress, and the rate of freezing and the temperature and rate at which ice crystals form can strongly affect the extent of damage to the cell.

22.4.4 Plants have multiple low-temperature sensing systems

To adapt to low temperature, plants must first perceive changes in temperature. The cyanobacterium *Synechocystis* PCC6803 has a putative low-temperature sensor, the histidine kinase Hik33. Low temperature activates Hik33 by signals mediated by changes in membrane fluidity, leading to autophosphorylation and subsequent phosphate transfer to the response regulator Rre26. Microarray data have shown that HiK33 regulates the expression of 21 of 36 cold-regulated genes. Thus, Hik33 is considered a low temperature regulator that activates expression of the majority of cold-regulated genes, in addition to another temperature-sensing pathway involved in cellular responses of the cyanobacterium to low temperature. Although no *Hik33* orthologs have been found in higher plants, two-component systems like the combination of His and Rre are involved in responses to some phytohormones (see Chapter 18). The participation of these two-component systems in low temperature sensing in plants remains to be determined.

There are a number of candidate low temperature sensors in plants, although these have not been confirmed. For example, changes in **membrane fluidity** are considered to play a role in sensing a temperature drop outside the cell. Alterations in membrane fluidity of alfalfa cells using treatments with dimethylsulfoxide as a membrane fluidizer and benzyl alcohol as a membrane stabilizer result in changes in both freezing tolerance and cold-induced gene expression. Calcium influx and cytoskeleton organization are also affected under these conditions, so changes in membrane fluidity may act as sensors and induce a series of signal transduction events at low temperatures.

22.4.5 Plants can acclimate to freezing by increasing membrane stability

The ability to survive temperatures below freezing is genotype-specific. Whereas many important crop plants, including corn (*Zea mays*), tomato (*Lycopersicon esculentum*), and rice (*Oryza sativa*), are unable to withstand freezing temperatures, many temperate and sub-arctic plants can survive freezing temperatures, and some can even survive temperatures below –40°C. However, these plants are not tolerant to freezing throughout the growing season.

Freezing tolerance develops in a process known as cold acclimation, a response to low but nonfreezing temperatures that occur before freezing. As an example, *Arabidopsis* can normally survive temperatures as low as –5°C, but after exposure to temperatures in the range of 1°C to 5°C for one to seven days, it can survive much lower temperatures of –8°C to –13°C. This makes *Arabidopsis* a good model for studying the mechanisms underlying freezing tolerance. A number of seemingly disparate responses occur during cold acclimation, including alterations in membrane composition and accumulation of compatible solutes, but these changes ultimately contribute to protection of the plasma membrane, the primary site of freezing injury in plants.

The most notable changes in the plasma membrane after cold acclimation are the increase in proportion of plasma membrane phospholipids (see Chapter 8), which is widely observed in various herbaceous and woody plants, and concomitant decrease in the proportion of glucocerebrosides. These cold-induced changes in lipid composition improve water retention at the membrane surface, which can prevent thermotropic and lyotropic lipid phase alterations in the membrane bilayers during freezing. Comprehensive lipid analysis, however, does not support the suggestion that there is a single lipid component that predominantly affects maintenance of plasma membrane integrity during freeze–thaw cycles. Rather, altered lipid–lipid (or lipid–protein) interactions after cold acclimation should contribute to the increased plasma membrane stability against freezing stress.

Plasma membrane proteins and microdomains also respond dynamically to cold acclimation. Cold-responsive proteins in the plasma membrane include osmotic and other stress-related proteins, proteolysis-associated proteins, and membrane trafficking proteins. Plasma membrane microdomains are enriched in glucocerebrosides and sterol lipids, and the proportions of both lipids change after cold acclimation. Cold acclimation also results in changes in microdomain proteins, such as those associated with membrane transport, membrane trafficking, and cytoskeleton–plasma membrane interactions. Thus, microdomain analysis is a promising

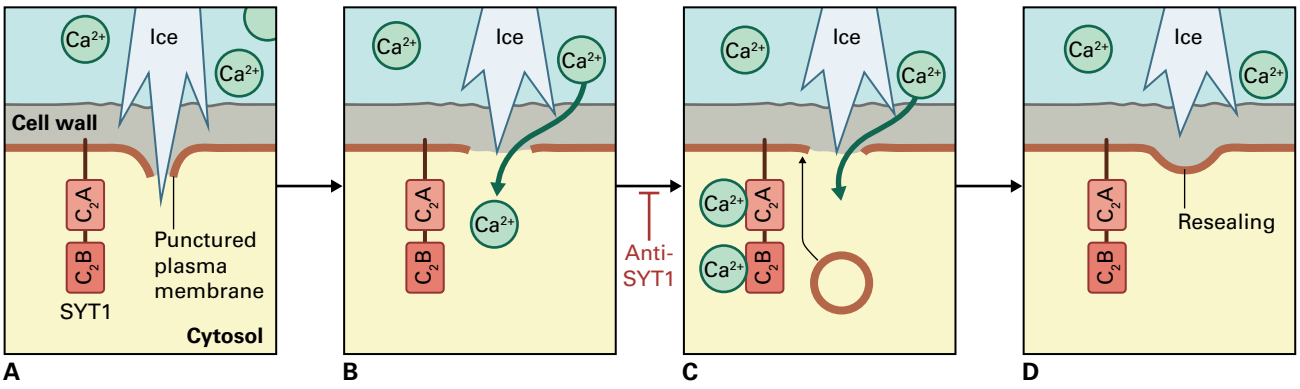


FIGURE 22.20 *Model for Ca^{2+}- and SYT1-induced membrane resealing occurring during freeze/thawing. (A) The plasma membrane is mechanically punctured by ice crystals, and (B) Ca^{2+} moves from the extracellular space into the cytoplasm through the damaged sites. (C) Endomembranes may then fuse at the site of the damaged plasma membrane via Ca^{2+} binding SYT1. (D) The damaged site is resealed.*

means of determining the molecular and functional responses of the plasma membrane to low temperature and freezing tolerance in plants.

Although not analyzed in detail, some cold-responsive proteins in the plasma membrane do affect freezing tolerance. Phospholipases influence freezing tolerance probably through alterations in the plasma membrane lipid composition and phospholipid-mediated signaling. In *Arabidopsis*, antisense suppression of phospholipase Dα1 (PLDα1), the most abundant plant phospholipase, increases freezing tolerance. The difference in freezing tolerance is probably because suppression of PLDα1 inhibits an increase in the proportion of phosphatidic acid that promotes destabilizing phase transition of the membrane bilayers. In contrast, *Arabidopsis* phospholipase Dδ (PLDδ) knockout lines show reduced freezing tolerance, and overexpressors show increased freezing tolerance. PLDδ modifications do not change the proportion of major phospholipids in the plasma membrane during freezing but selectively increase molecular species of phosphatidic acid, suggesting that specific phosphatidic acid species act as signal transducers of low temperature.

Another plasma membrane-associated protein that affects freezing tolerance is SYNAPTOTAGMIN1 (SYT1). Synaptotagmins are a family of membrane-trafficking proteins that function as calcium sensors in plasma membrane vesicle fusion processes mediated by the SNARE protein complex. The level of *Arabidopsis* SYT1 increases rapidly in the plasma membrane in parallel with the development of freezing tolerance during cold acclimation. As *Arabidopsis* freezing tolerance is enhanced by exogenous application of calcium, and both *Arabidopsis SYT1*-RNAi lines and T-DNA insertion mutants clearly have less freezing tolerance than wild-type plants, SYT1-dependent membrane resealing in the presence of calcium is considered a vital component of plant freezing tolerance (Fig. 22.20). Genetic screens for mutants showing enhanced osmotic sensitivity have also identified SYT1 as an important component in osmotic tolerance.

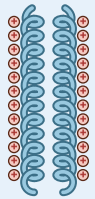
22.4.6 Cold-induced changes in metabolite profiles have important roles in cold acclimation

Compatible solutes, such as simple sugars (sucrose, glucose, fructose, raffinose, and stachyose), proline, and glycine betaine, accumulate in conjunction with the development of freezing tolerance in many plant species. The deduced molecular functions of compatible solutes in freezing stress tolerance are similar to those in osmotic and dehydration stress (see Sections 22.2.3 and 22.2.4). The *Arabidopsis* mutant *eskimo1*, which is constitutively freeze-tolerant, overproduces proline at warm temperatures. The *ESKIMO1* gene encodes a 57-kDa protein of unknown function belonging to a large gene family of DUF231 proteins. The *eskimo1* mutation alters the expression of genes that overlap with those regulated by other abiotic stressors, including salt, osmotic, and cold stress, but that are apparently independent of those mediated by CBF/DREB1 transcription factors (see Section 22.4.7). Sugars have been suggested to protect membranes and contribute to improved freezing tolerance after cold acclimation. In fact, exogenous sugar application has been used to recover the impaired increase in freezing tolerance of *Arabidopsis sensitive-to-freezing 4* (*sfr4*) mutant. However, in some cases, the accumulation of sugars alone is not sufficient for the development of freezing tolerance. Several single-gene mutants of *Arabidopsis* that are defective in freezing tolerance nonetheless accumulate sugars normally in response to low-temperature stress.

22.4.7 Freezing tolerance involves changes in gene expression

In most cases, the cold acclimation-induced alterations described above are mediated by changes in gene expression at low temperature. Since the mid-1980s, when changes in gene expression in response to cold acclimation were first

TABLE 22.1 *The five groups of LEA proteins.*

	Hypothetical structures	Representative proteins	Structural characteristics and shared motifs	Properties	Proposed function
Group 1 (D-19 family*)		Em (early methionine-labeled protein, wheat)	Most (70%) protein conformation is random coil with some predicted short α-helices Rich in charged amino acids and glycine	More hydrated than most globular polypeptides	Binds water to minimize loss of cellular water content Overexpression confers water-deficit tolerance on yeast cells
Group 2 (D-11 family*)		DHN1 (maize) D-11 (cotton)	Structure variable Includes one or more conserved lysine-rich regions that may form α-helices. The consensus sequence is EKKGIMDKIKELPG. The number of repeats per protein varies May or may not contain a poly(serine) region Contain regions of variable length rich in either glycine and threonine or glutamate and lysine	Most members localize to cytoplasm and nucleus, but also associated with plasma membrane	May stabilize macromolecules under conditions of reduced water content
Group 3 (D-7 family*)		HVA1 (*Hordeum vulgare* ABA-induced) D-7 (cotton)	Contain repeated motifs of the consensus sequence TAQAAKEKAXE Predicted to contain amphipathic α-helices Predicted to form dimers	D-7 is abundant in cotton embryos (0.25 mM) Putative dimer of D-7 may bind as many as 10 inorganic phosphates and their counterions	HVA1 promotes stress tolerance in transgenic plants
Group 4 (D-95 family*)		D-95 (soybean)	Hydropathy plots are unremarkable and slightly hydrophobic N-terminal region contains a possible amphipathic α-helix	A gene encoding a similar protein in tomato is expressed in response to nematode feeding	
Group 5 (D-113 family*)		LE25 (tomato) D-113 (cotton)	Shares sequence homology at the conserved N terminus, is predicted to form α-helix C-terminal domain is predicted to be a random coil of variable length and sequence Rich in alanine, glycine, and threonine	D-113 is abundant in cotton seeds (up to 0.3 mM)	May bind membranes or proteins to maintain structural integrity May sequester ions to protect cytosolic metabolism LE25 confers salt and freezing tolerance to yeast

*The protein families are named for seed proteins from cotton.

observed in spinach (*Spinacia oleracea*), numerous genes responsive to low temperature treatments have been identified. Unfortunately, no clear functional roles have yet been determined for many of these genes.

Several of the genes induced by low temperature are also induced by water deficit or ABA (see Section 22.3). Gene products that are hydrophilic and soluble when boiled, including Group 2 and Group 3 LEA proteins (Table 22.1) and the products of other unique genes, accumulate during cold acclimation. One such unique gene product is COR15a, a small, nuclear-encoded hydrophilic protein that is targeted to the chloroplast. When imported into the chloroplast, the protein is processed to form the mature protein, COR15am, a 9.4-kDa polypeptide. Protoplasts of nonacclimated transgenic *Arabidopsis* plants that constitutively express the *COR15a* gene show increased freezing tolerance. COR15am has been suggested to alter the intrinsic curvature of the chloroplast envelopes and protect chloroplast proteins through direct associations with each other.

As described in Section 22.3, many of the cold-regulated genes contain a DRE or CRT *cis*-acting DNA element in their promoter regions that binds CBF/DREB1 transcriptional activators (see Fig. 22.12). Three *CBF/DREB1* genes (*CBF1/DREB1b*, *CBF2/DREB1c*, and *CBF3/DREB1a*), which each contain sequences encoding a 60 amino acid DNA binding AP2/ERF domain, are present in tandem array on *Arabidopsis* chromosome 4 and are induced rapidly (within 15 minutes) upon exposure to low temperature, with peak expression after 2 hours. Constitutive or stress-induced *CBF/DREB1* expression (with constitutive CaMV 35S promoter or dehydration- and cold-inducible *RD29A* promoter, respectively) in *Arabidopsis* increases the abundance of *COR* and other DRE/CRT-containing target gene transcripts in nonacclimated plants, which in turn increases freezing tolerance.

Overexpression of the transcriptional activator *CBF/DREB1s* enhances freezing tolerance to a greater extent than overexpression of *COR15a* alone. Further, *CBF/DREB1* genes are widely conserved in plants, and the number of these genes and the extent of their expression are correlated with the degree of freezing tolerance in some plant groups. Taken together, these results suggest a role of cold-regulated genes in the development of tolerance to low temperature and have facilitated new research on protection of crop plants against freezing using overexpression of transcription factors.

Microarray analysis of plants overexpressing *CBF/DREB1* has identified its target genes. The number of direct CBF/DREB1 target genes is around 40, and about 100 genes have been assigned to the CBF/DREB1 regulon. The CBF/DREB1 regulon genes encode proteins that fall into two groups: proteins that function in stress tolerance and those that are involved in further regulation of the expression of other genes. COR proteins, along with enzymes involved in proline metabolism (Δ^1-pyrroline-5-carboxylate synthase) and raffinose synthesis (galactinol synthase, GolS), belong to the CBF/DREB1 regulon and participate in enhancement of freezing tolerance. The presence of proteins with regulatory functions in the CBF/DREB1 regulon, such as transcription factors, suggests there may be some subregulons within the CBF/DREB1 regulon. In fact, microarray experiments and subsequent bioinformatics analysis have revealed that approximately 20% of the CBF/DREB1 regulon genes do not have the core DRE/CRT sequence (CCGAC) in their promoter sequences. Thus, there must be complex, elaborate gene regulatory networks within the CBF/DREB1 regulon that control the development of freezing tolerance during cold acclimation.

The circadian system regulates the expression of *CBF/DREB1* as well as some CBF/DREB1 regulon genes. The extent to which *CBF/DREB1* transcripts accumulate upon exposure to low temperature varies with the time of day that the plants are transferred to low temperature. Cold-induced *CBF/DREB1* transcript accumulation reaches the maximum level at 4 hours and the minimum at 16 hours after subjective dawn. Accordingly, CBF/DREB1 target genes do in some cases show circadian rhythmic oscillation. This is of interest because freezing tolerance shows rhythmic changes within the day. However, the detailed mechanisms underlying the circadian rhythmicity of plant freezing tolerance remain to be determined.

The *INDUCER OF CBF EXPRESSION* (*ICE1*) gene has been identified as a regulator of *CBF3/DREB1A* gene expression. *ICE1* encodes a MYB-like basic helix–loop–helix (bHLH) transcription factor and is expressed constitutively, suggesting that cold-induced posttranslational modification is necessary to activate ICE1 for *CBF3/DREB1A* expression. *ICE1* overexpression enhances expression of the *CBF/DREB1* regulon genes and increases freezing tolerance in plants after cold acclimation (see Fig. 22.12). Thus, ICE1 functions as an upstream regulatory protein to control *CBF3/DREB1A* transcription. ICE1 also functions in the regulation of stomata numbers in leaf epidermal cell development. However, it is not involved in the cold induction of other *CBF/DREB1* genes. It has been proposed that the involvement of calcium in *CBF2/DREB1C* expression is mediated by a calmodulin-binding transcription factor (CAMTA) (see Fig. 22.12).

The CBF/DREB1 cold-responsive pathway likely plays an important role in cold acclimation in plants, but additional pathways must also be involved in activating cold-induced reactions in response to low temperature. The *eskimo1* mutant, which is constitutively freezing tolerant, does not show constitutive *CBF/DREB1* gene expression. Similarly, the *sfr4* mutant, which shows impaired freezing tolerance enhancement during cold acclimation, does not differ in *CBF/DREB1* gene expression on exposure to low temperature (see Section 22.4.5). The ZAT12 cold-responsive pathway also plays a role in cold acclimation. Overexpression of *ZAT12*, which encodes a zinc-finger transcriptional repressor protein, alters gene expression profiles and increases freezing tolerance of plants. The ZAT12 cold-responsive pathway appears to interact with the CBF/DREB1 cold-responsive pathway: some target genes are shared by the two pathways and some genes in the CBF/DREB1 pathway are downregulated by ZAT12 overexpression, which suggests complicated regulatory systems for genes associated with freezing tolerance.

22.5 Flooding and oxygen deficit

Flooding (waterlogging of soil to complete submergence) can also trigger a number of different stress responses in plants. Whereas oxygen concentrations in well drained, porous soil are nearly equal to atmospheric concentrations (20.6% oxygen, 20.6 kPa), the diffusion coefficient of oxygen in water is four orders of magnitude lower than that in air. When flooding occurs, soil gases are replaced with water, thereby reducing entry of oxygen into the soil and making it difficult for roots and other organs to carry out respiration.

Like most eukaryotic organisms, plants are obligate aerobes that derive most of their energy from mitochondrial respiration of hexose sugars to ATP. Under normal aerobic conditions, plants oxidize 1 mol of hexose sugar through glycolysis, the citric acid cycle, and oxidative phosphorylation to yield 30–36 mol of ATP (see Chapters 13 and 14). In the absence of oxygen, however, plants produce ATP mainly by glycolysis, which yields only 2–4 mol of ATP per mole of hexose sugar. The function of a noncyclic flux mode of citric acid cycle can boost the ATP output by 1 mol per pyruvate metabolized (see Section 22.5.2). Cytoplasmic ATP/ADP ratios decline as mitochondrial ATP production is inhibited. Ironically, oxygen deficit associated with flooding can also prevent plants from obtaining adequate water from the soil due to gating of root cell aquaporins; this reduces the permeability of root cells to water and limits transport of water to aerial tissue.

The supply of oxygen to root cells is influenced by several factors, including soil porosity, water content, temperature, root density, and the presence of competing algae and aerobic microorganisms. Oxygen concentrations in root tissues also vary according to root depth, root thickness, the volume of intercellular gaseous spaces, and cellular metabolic activity. Oxygen gradients exist within other organs and tissues, including meristems, tubers, and developing seeds.

Plant or cellular oxygen status can be defined as **normoxic**, hypoxic, or **anoxic** (Table 22.2). To survive short-term flooding, plants must generate sufficient ATP, regenerate $NADP^+$ and NAD^+, and avoid accumulation of toxic metabolites. Periods of oxygen deficit can trigger developmental responses that promote acclimation to hypoxic or anoxic conditions.

TABLE 22.2 *Impact of oxygen deprivation on respiratory metabolism.*

Oxygen status	Effect on metabolism
Normoxic (aerobic)	Aerobic respiration proceeds normally; almost all ATP production results from oxidative phosphorylation
Hypoxic	Partial pressure of O_2 limits ATP production by oxidative phosphorylation; glycolysis and a non-cyclic flux mode of the citric cycle account for a larger percentage of ATP yield than under normoxic conditions; metabolic and developmental changes are stimulated that result in adaptation, acclimation to a low-oxygen environment
Anoxic (anaerobic)	ATP is produced only by glycolysis and a non-cyclic flux mode of the citric cycle; cells exhibit low ATP content, diminished protein synthesis, and impaired division and elongation. If anoxic conditions persist, many plant cells die

22.5.1 Plants vary in their ability to tolerate flooding

Plants can be generally classified as wetland, flood tolerant, or flood sensitive, according to their ability to withstand periods of soil flooding or submergence (Table 22.3).

Wetland plants possess anatomical, morphological, and physiological features that permit survival in waterlogged soils and partial submergence. Growth in a wetland environment promotes formation of a thickened root hypodermis to reduce O_2 loss to the anaerobic soil. To facilitate transport of O_2 from aerial structures to submerged roots and thereby maintain aerobic metabolism and growth, some plants develop specific structures: **aerenchyma** (continuous, columnar intracellular spaces formed in root cortical tissues (Fig. 22.21; see also Section 22.5.4 and Chapter 20), adventitious roots from the hypocotyl or stem (Fig. 22.22), **lenticels** (openings in the

TABLE 22.3 *Plant species categorized by sensitivity to flooding.*

Wetland	Flood tolerant	Flood sensitive
Acorus calamus	*Arabidopsis thaliana*	*Glycine max* (soybean)
Echinochloa crus-galli (rice grass)	*Echinochloa crus-pavonis* (barnyard grass)	*Lycopersicon esculentum* (tomato)
Echinochloa phyllopogon (barnyard grass)	*Rumex acetosa* (sorrel)	*Pisum sativum* (pea)
Erythina caffra (coral tree)	*Solanum tuberosum* (potato)	
Rumex palustrus (marsh dock)	*Zea mays* (corn)	
Oryza sativa (rice)	*Triticum aestivum* (wheat)	
Phragmites australis (common reed)	*Hordeum vulgare* (barley)	

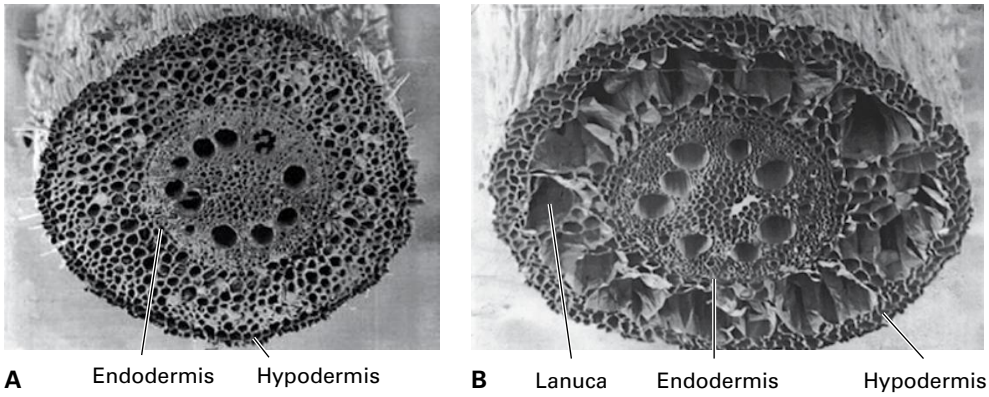


FIGURE 22.21 *Aerenchyma development in the root cortex of maize (*Zea mays *L.) after oxygen deprivation. Photomicrographs of transverse sections of maize roots maintained under aerobic conditions (A) or under 72 hours of hypoxia (B) demonstrate the formation of cortical aerenchyma in hypoxic roots. The hypodermis and endodermis remain intact, and the lacunae created by the death of the central cortical cells form columnar gas-conducting chambers.*
Source: He et al. (1996). Plant Physiol. 112:463–472.

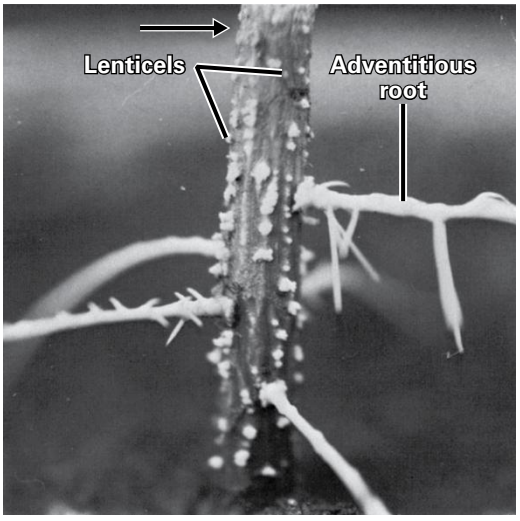


FIGURE 22.22 *Adventitious roots and prominent (hypertrophied) lenticels on the stem of young ash (*Fraxinus pennsylvanica *Marshall) after flooding. The black arrow indicates the water depth during flooding.*
Source: Kozlowski (1984) Physiological Ecology. Academic Press, New York.



FIGURE 22.23 *Pneumatophores of mangrove (*Avicennia nitida*) develop from roots submerged in estuarine mud.*
Source: Bowes (1996). A Colour Atlas of Plant Structures. Manson Publishers.

periderm that allow gas exchange, Fig. 22.22), shallow roots, and **pneumatophores** (shallow roots that grow with negative geotrophy out of the aquatic environment, Fig. 22.23). Other adaptive strategies include elongation of stems or leaf petioles towards the water surface (Fig. 22.24) and thinning of leaves to improve underwater photosynthesis. The morphological and anatomical characteristics that improve tissue aeration can be constitutive or induced by flooding.

When inundated by water, wetland species alter cellular metabolism in root and aerial organs to increase survival. Partial submergence of deepwater rice (*Oryza sativa* L. var. Indica) promotes formation of adventitious roots and accelerates internodal stem elongation, which enables stems and leaves to be maintained above the aquatic environment (Fig. 22.25). This escape strategy is associated with ATP production through active consumption of available carbohydrates coupled to glycolysis, fermentation, and a partially functioning citric acid cycle.

Rice seeds are among the few that can germinate in an anaerobic environment, and germinated rice seedlings promote coleoptile elongation towards light and oxygen over root growth. In this situation, a calcineurin B-like interacting protein kinase (CIPK) and sucrose nonfermenting 1 related

protein kinase 1A (SnRK1A) sense changes in ATP or sugar homeostasis to promote synthesis of starch catabolizing amylases. In addition, mitochondrial morphology is altered (Fig. 22.26), but functional electron transport chain complexes of the inner membrane and enzymes of the citric acid cycle in the matrix are maintained. This rapid coleoptile elongation is an escape strategy that is effective if photosynthetic activity can be established before seed starch reserves are fully consumed.



FIGURE 22.24 *The leaf petiole of* Rumex palustris *elongates in response to submergence.*
Source: Photo by Rens Voesenek.

In contrast, other wetland plants, such as the marshland monocot *Acorus calamus*, respond to flooding by downregulating their metabolism, which allows them to maintain a nearly quiescent state for several months while utilizing the starch reserves stored in their rhizomes. This **quiescence strategy**, a restriction of metabolism to survive a long and deep flood, is observed in a number of wetland species and submergence-tolerant accessions of rice.

Flood-tolerant plants can endure flooding and anoxia only temporarily. Like wetland species, these plants generate ATP through anaerobic metabolism during short-term flooding. In most cases, root elongation is inhibited, overall rates of protein synthesis are diminished, and patterns of gene expression are markedly altered. *Arabidopsis* ecotypes vary in the length of time they can endure complete submergence. Whereas *Arabidopsis* plants survive two weeks or more, young seedlings of maize, for example, can survive only 3–5 days of submergence, depending on genotype and developmental age. Survival of the low oxygen stress associated with waterlogging is prolonged if maize seedlings become hypoxic before experiencing anoxia. Hypoxia promotes formation of adventitious and nodal roots with cortical aerenchyma as an acclimation to soils with low oxygen content (see Fig. 22.22) and enhances the ability to transport lactate out of roots.

Flood-sensitive plants exhibit an injury response to anoxia. As with flood-tolerant species, flood-sensitive plants carry out anaerobic respiration; these plants, however, rapidly succumb to flooding because of cytoplasmic acidification. When deprived of oxygen, flood-sensitive species exhibit greatly diminished protein synthesis, degradation of mitochondria, inhibited cell division and elongation, disrupted ion transport, and cell death within root meristems. Typically, these plants do not develop root aerenchyma and cannot survive more than 24 hours of anoxia.

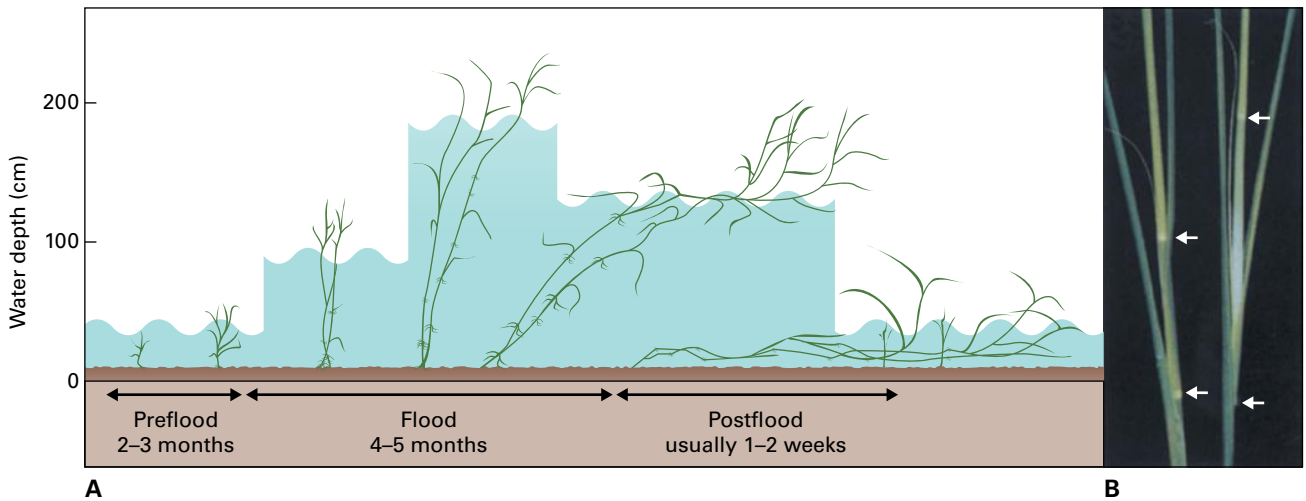
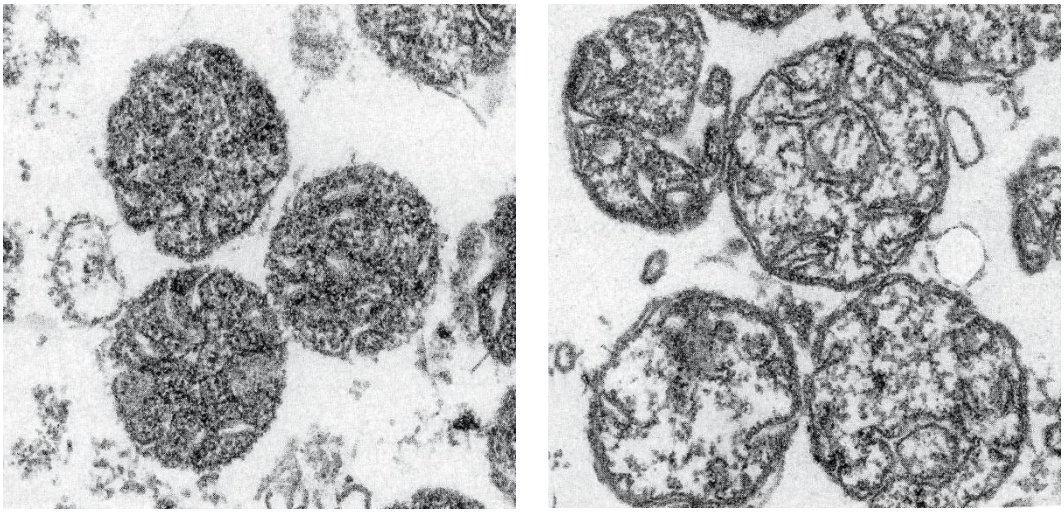


FIGURE 22.25 *Growth responses of seedlings of deepwater rice (*Oryza sativa *L. var. Indica) to flooding. (A) Seedlings are established before the annual flood. Submergence promotes rapid internodal elongation and development of adventitious roots. Once the flood waters recede, the adventitious roots grow into the soil and aerial portions of the plant grow upward. (B) Photographs comparing internode elongation in aerobic (left) and submerged (right) plants. Arrows indicate positions of nodes.*
Source: (B) Kende et al. (1998). Plant Physiol. 118:1105–1110.



A B

FIGURE 22.26 *Photomicrographs comparing mitochondria from rice (*Oryza sativa *L.) seedlings germinated aerobically and exposed to aerobic (A) or anaerobic (B) treatments for 48 hours. A mitochondrion from anoxic seedlings has well-developed cristae but its matrix is less dense. Source*: Couée et al. (1992). Plant Physiol. 98:411–421.

22.5.2 During short-term acclimation to anoxic conditions, plants generate ATP through breakdown of carbohydrates, glycolysis, and fermentation

Flooding stimulates an increase in glycolytic flux known as the **Pasteur effect**, where sucrose or glucose from the phloem is directed toward glycolysis in flooded organs. However, in some cases, flooding can restrict the translocation of photosynthate from leaves; flooded organs of some species hydrolyze stored starch (see Chapter 13) to obtain additional sugars.

The availability and mobilization of carbohydrate reserves is essential in oxygen-deprived organs. Starch is slowly hydrolyzed by amylases in rhizomes of flood-tolerant *Acorus calamus* and in germinating seeds and leaves of rice plants under oxygen constraints; however, many species must rely on soluble carbohydrate reserves for energy production under hypoxia and anoxia. Sucrose breakdown generally follows an increase in production of UDP-sucrose synthase (SUS) (Fig. 22.27). Utilizing SUS rather than ATP-dependent invertase reduces the investment in ATP to produce glucose-6-phosphate and fructose-6-phosphate. Use of pyrophosphate-dependent phosphofructokinase (PFP) by rice and other species during oxygen deprivation further maximizes glycolytic ATP output.

The energy-yielding steps of glycolysis generate low amounts of ATP while reducing NAD^+ to NADH (see Chapter 13). To support ongoing glycolysis in the absence of mitochondrial respiration, the glycolytic substrate NAD^+ must be regenerated. The principal end products of glycolysis in oxygen-deprived plant tissues are lactate and ethanol (Fig. 22.27); alanine, succinate, and γ-aminobutyrate (GABA) are also be formed. Alanine and succinate are the principal products of a noncyclic flux mode of the citric acid cycle that generates 1 additional mol ATP per mol pyruvate metabolized. This consumes 1 mol of glutamate and pyruvate to generate 1 mol alanine and 2-oxoglutarate. The 2-oxyoglutarate can be used for substrate level ATP production through conversion of succinyl CoA to succinate. Alternatively, 2-oxoglutarate is shunted to GABA. Oxaloacetate reduced to malate and then fumarate, can produce NAD^+ necessary to maintain succinyl CoA ligase. This alternative pathway of pyruvate consumption yields additional ATP. The relative abundance of specific end products varies according to the plant species, genotype, and organ as well as the duration and severity of oxygen deprivation.

Both lactate- and ethanol-producing fermentations yield NAD^+, but lactate lowers cytosolic pH, whereas ethanol does not. According to the Davies–Roberts lactate dehydrogenase (LDH)/pyruvate decarboxylase (PDC) pH-stat hypothesis, anaerobic metabolism is regulated by the activities of pH-sensitive enzymes. According to this model, LDH, an enzyme with an alkaline pH optimum, converts pyruvate, which is produced initially by glycolysis, to lactate, and the lactate produced reoxidizes NADH but also lowers the cytoplasmic pH. As the cytosol acidifies, LDH is progressively inhibited and a second enzyme, PDC, is activated. The pH optimum for PDH is lower than the normal cytoplasmic pH; therefore, the accumulation of lactate ultimately stimulates the conversion of pyruvate to acetaldehyde. Alcohol dehydrogenase (ADH) subsequently reduces the acetaldehyde to ethanol while oxidizing NADH to NAD^+.

Unlike lactate, ethanol is an uncharged molecule at cellular pH and can diffuse across plasma membranes. As a result, the switch to ethanol production stabilizes cytoplasmic pH at a slightly acidic value. Cytosolic pH may also be maintained by operation of the noncyclic flux mode of the citric acid cycle, which is coupled with production of the zwitterionic species alanine from pyruvate. In some plants, the zwitterionic species GABA is formed from pyruvate. Both alanine and GABA

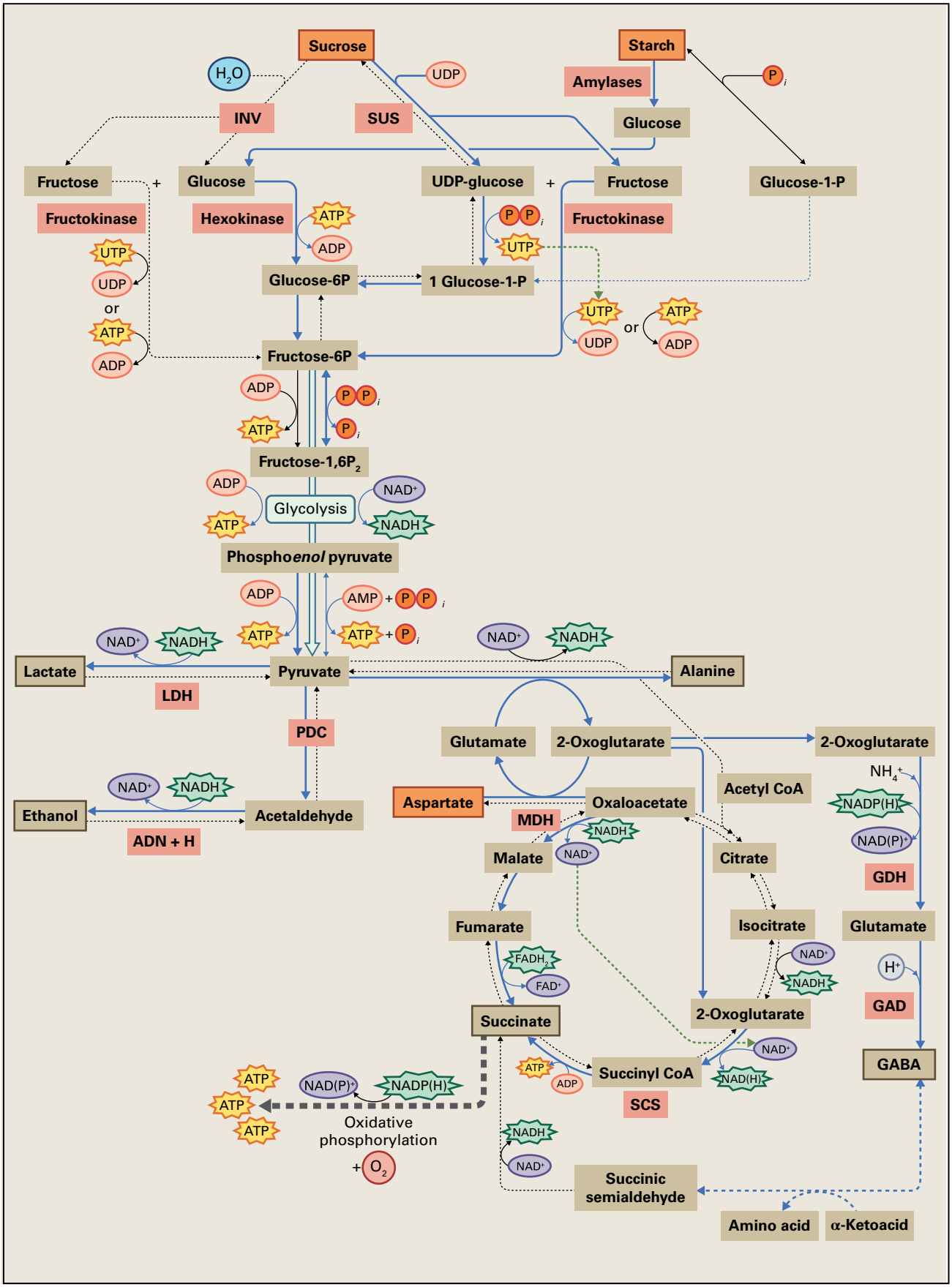


FIGURE 22.27 *Metabolic acclimation under O_2 deprivation. Plants have multiple routes of sucrose catabolism, ATP production, and NAD(P)$^+$ regeneration. These include ethanol and lactate production as well as a modified noncyclic citric acid flux mode that is both an alanine and 2-oxoglutarate shunt and a γ-aminobutyric acid (GABA) shunt. Blue arrows indicate reactions that are promoted during anaerobic stress, and gray dashed lines indicate reactions that are inhibited during the stress. Metabolites indicated in brown boxes are major or minor end products of metabolism under hypoxia. Metabolites indicated in orange boxes decrease under hypoxia. ADH, alcohol dehydrogenase; GAD, glutamic acid decarboxylase; GDH, glutamate dehydrogenase; INV, invertase; LDH, lactate dehydrogenase; MDH, malate dehydrogenase; PDC, pyruvate decarboxylase; SCS, succinyl CoA synthetase; SUS, sucrose synthase.*

can rapidly re-enter the citric acid cycle upon reoxygenation, minimizing the net loss of carbon (Fig. 22.27).

A different hypothesis predicts that concentrations of pyruvate, rather than cytoplasmic pH, regulate ethanolic fermentation. This PDC/pyruvate dehydrogenase (PDH)-stat hypothesis is based on the observation that the K_m of cytosolic PDC ranges from 0.25 to 1.0 mM pyruvate, while that of mitochondrial PDH ranges from 50 to 75 μM. Since cellular concentrations of pyruvate are usually less than 0.4 mM, an increase in pyruvate under hypoxia or anoxia stimulates PDC activity. This model is supported by several observations. First, ethanol production can be stimulated under aerobic conditions that inhibit mitochondrial PDH activity. Second, lactate production does not accompany ethanolic fermentation in certain species. Finally, roots of transgenic tobacco plants that have twice the normal activity of PDC produce more ethanol under anoxia than do wild-type roots.

The LDH/PDC pH-stat and PDC/PDH-stat hypotheses are not mutually exclusive; the regulation of the switch to ethanolic fermentation may vary according to the species, organ and the conditions of low-oxygen stress.

Plants generally increase cellular levels of PDC and ADH in response to flooding. Mutants of maize and other plants that are deficient in ADH are more sensitive to flooding than are isogenic wild-type genotypes. In maize, genotypes severely deficient in ADH1 exhibit acetaldehyde accumulation and a more rapid and sustained drop in cytoplasmic pH than does the wild-type in response to anoxia (Fig. 22.28). However, plants engineered to overproduce PDC or ADH and flood-sensitive species such as pea (*Pisum sativum*) that can rapidly and dramatically upregulate ADH activity still succumb to flooding as a result of exhaustion of carbohydrate reserves and eventual cytoplasmic acidosis.

In nature, hypoxia frequently precedes anoxia in flooded roots. If maize or rice seedlings are transferred to hypoxic conditions (3 kPa O_2) before transfer to anoxia (0 kPa O_2), their survival rates increase considerably and the ability to continue cell elongation is greatly improved. This hypoxic pretreatment promotes acclimation by increasing glycolytic flux and ATP production. An important feature of this acclimation is development of the capacity to export lactate from the cytoplasm to the surrounding medium (Fig. 22.29), a further indication that avoidance of cytoplasmic acidosis is a major factor in survival of low-oxygen conditions.

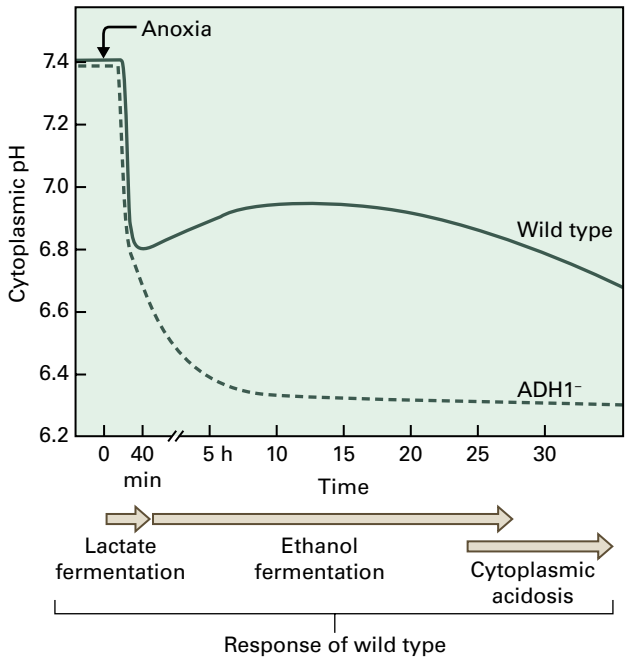


FIGURE 22.28 *Response of root tips of wild-type maize (solid line) and mutants deficient in ADH1 (dashed line) to anoxia. Wild-type root tips experience a rapid decrease in cytoplasmic pH, followed by a partial recovery; however, the wild-type root cells ultimately succumb to cytoplasmic acidosis. Root tips of ADH1-deficient seedlings show rapid cytoplasmic acidosis and cell death.*

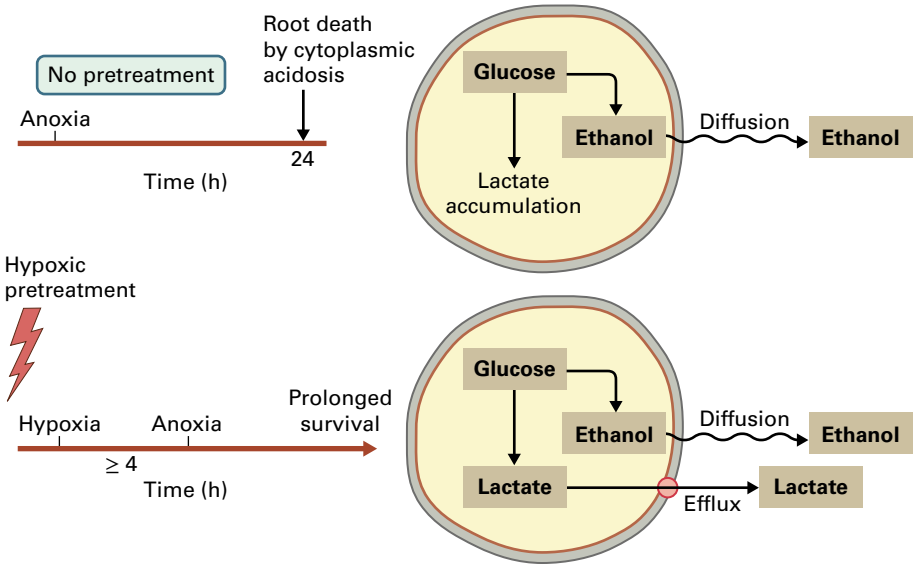


FIGURE 22.29 *Effects of hypoxic pretreatment and acclimation on survival of anoxia: avoidance of cytoplasmic acidosis by lactate efflux. Flooding typically results in hypoxia, followed by anoxia. Lactate levels and ethanolic fermentation increase in both anoxic and hypoxic cells. Exposure of maize seedlings to hypoxia for several hours before being transferred to anoxia increases the capacity of roots for lactate efflux and prolongs survival.*

22.5.3 Shifting from aerobic metabolism to glycolytic fermentation involves changes in gene expression

Generally, anoxia causes a rapid and dramatic shift in gene expression patterns, including a significant reduction in total protein synthesis. Protein synthesis is also reduced and altered under hypoxia, but to a lesser extent. Modifications in the pattern of protein synthesis observed in anoxic and hypoxic tissues result from transcriptional and post-transcriptional regulation of gene expression. Although most gene transcription is generally repressed in response to oxygen deprivation, an important subset of genes is upregulated. These include transcription factors, metabolic enzymes, and uncharacterized proteins. A number of the proteins synthesized in high amounts in hypoxic and anoxic organs are enzymes involved in sucrose and starch degradation, glycolysis, ethanol fermentation, and alanine production.

The *ADH* gene promoters of maize and *Arabidopsis* possess functional *cis*-acting elements that are required for expression in hypoxic and anoxic cells. These elements include G-box type motifs and the **anaerobic response element** (ARE), which is found in the promoter region of many genes that are transcriptionally induced by low oxygen in monocots and dicots. Transcription factors that interact with *Arabidopsis ADH1* have also been identified. Dimethyl sulfate footprinting and DNase I hypersensitivity analyses of *ADH* promoters have demonstrated both constitutive and dynamically modified DNA–protein interactions that correlate with transcriptional activity. The submergence of rice seedlings causes histone H3 lysine methylation (H3K4) in both 5′ and 3′ regions of *ADH1* that is associated with decreased chromatin compaction and increased gene transcription. Together, these observations indicate the higher-order structure of the chromatin of *ADH* genes is influenced by oxygen availability. *Arabidopsis ADH1* is also transcriptionally induced by application of ABA, dehydration, and cold stress.

Changes in gene expression cannot be attributed solely to transcriptional controls. In maize and *Arabidopsis*, many cytosolic transcripts accumulate at approximately the same amount under normal and oxygen deprivation conditions, but are poorly translated under oxygen deprivation. At least in maize, these mRNAs are constitutively transcribed. The majority of the stress-induced mRNAs, including *ADH1*, are translated efficiently in anoxic/hypoxic cells. The translation of maize *ADH1* mRNA under low-oxygen conditions depends on the presence of particular sequences in the 5′ and 3′ untranslated regions. The reduced synthesis of many normal cellular proteins reflects the failure of their mRNAs to effectively maintain initiation of translation during stress. These transcripts are limited in translation and protected from degradation by storage in an mRNA ribonucleoprotein particle, also called **stress granules** (Fig. 22.30), as a means of conserving cellular energy, as evidenced by their rapid relocation to polyribosomes upon reoxygenation. Distinctions in mRNA binding proteins and changes in translational machinery, including phosphorylation of translation factors and ribosomal proteins, may allow for discrimination in translation of cellular mRNAs in oxygen-deprived cells.

22.5.4 The plant hormone ethylene promotes long-term acclimative responses in wetland and flood-tolerant species

Flooding or submergence stimulates production and limits outward diffusion of the gaseous hormone ethylene, a key trigger for adaptive responses to submergence and low oxygen levels (<12.5–3 kPa). The levels of 1-aminocyclopropane-1-carboxylic acid (ACC) synthase and ACC oxidase, enzymes of the ethylene biosynthesis pathway, increase in response to hypoxia in maize root tips. In hypoxic roots, ethylene promotes the formation of aerenchyma in the central portion of the root cortex; anoxic roots develop fewer aerenchyma because O_2 is essential for ethylene synthesis (Fig. 22.31A; see also Chapter 17).

Aerenchyma (see Fig. 22.21) provide a conduit for gas diffusion between roots and aerial organs, and can form by cell death and dissolution (**lysigeny**), separation of cells without collapse (**schizogeny**), or a combination of lysigeny and schizogeny (**schizolysigeny**). The aerenchyma of rice and maize are lysigenous and most likely result from programmed cell death (see Chapter 20). In many wetland species, aerenchyma formation is a normal developmental process in young plants that is initiated before flooding and further promoted in response to flooding.

Plants that have aerenchyma are able to maintain synthesis of high amounts of ATP in root cells submerged in an poorly oxygenated environment. The formation of aerenchyma reduces the severity of hypoxia and facilitates growth of submerged roots in species such as rice. When flooding inhibits the growth of existing roots or causes their death in nonwetland species, new roots develop at the upper portion of the primary root, on the hypocotyl, or from internodes above the air–water/air–soil interface. These adventitious roots form aerenchyma that facilitate the transport of O_2 from aerial portions of the plant to O_2-deprived root tissues. Adventitious root formation is also an ethylene-regulated process.

The role of ethylene in aerenchyma development has been confirmed by exposing aerobic roots to inhibitors of ethylene synthesis, antagonists of ethylene action, and exogenous ethylene. Development of aerenchyma also involves a Ca^{2+}-mediated signal triggered by ethylene. At least two cell wall-degrading enzymes, cellulase and xyloglucanase, are present or synthesized in large amounts in hypoxic roots and also play a role in aerenchyma formation (Fig. 22.31B).

Ethylene is also involved in the flooding response of deepwater rice varieties that can grow in water as deep as 4 meters (see Fig. 22.25). Submergence of the young plants increases ethylene entrapment and biosynthesis, which is followed by a decrease in ABA concentration and an increase in responsiveness to the hormone gibberellin (GA)

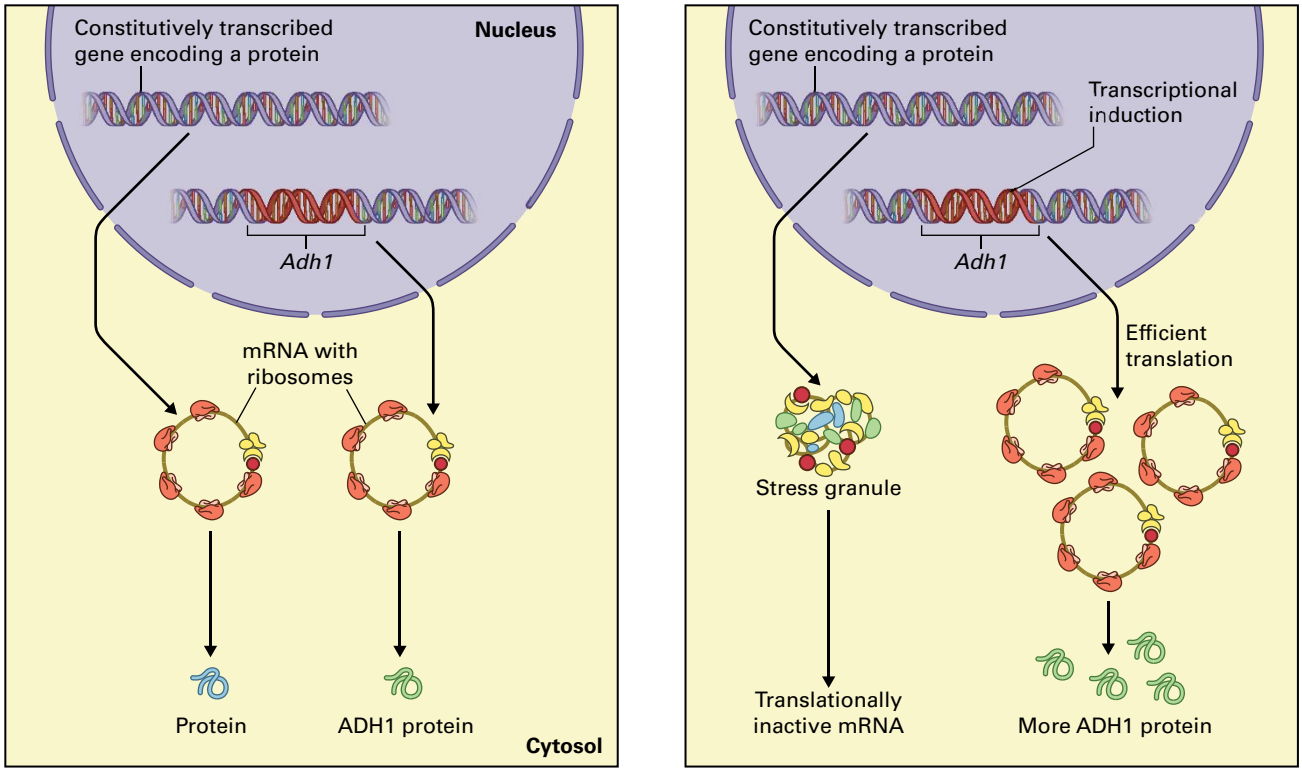


FIGURE 22.30 *Transcriptional and posttranscriptional mechanisms control gene expression in hypoxic and anoxic cells of plants. In maize, nuclear run-on experiments have shown that genes encoding a number of housekeeping proteins are constitutively, but poorly transcribed under hypoxia and anoxia. These mRNAs do not associate efficiently with ribosomes during oxygen deprivation. mRNAs encoding enzymes important for anaerobic metabolism, such as Adh1, increase in response to transcriptional induction and are efficiently translated during the stress. In* Arabidopsis, *repression of mRNA translation during hypoxia/anoxia is selective, with only about 6% of cellular mRNA displaying efficient translation. mRNAs that are poorly translated during stress are sequestered in translationally inactive messenger ribonucleoprotein complexes with similarities to stress granules. Upon reoxygenation, these mRNAs are rapidly recruited to active translation complexes (i.e., polyribosomes). In this manner, the cellular investment of energy in protein synthesis is limited during stress. Protein synthesis rapidly recovers once aerobic respiration resumes.*

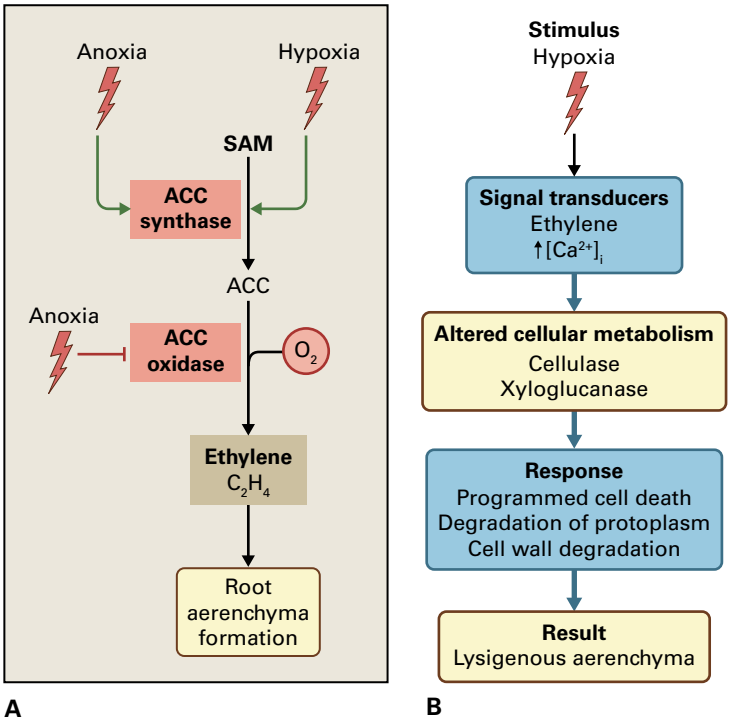


FIGURE 22.31 *Formation of aerenchyma is stimulated by hypoxia but not by anoxia. (A) Ethylene production leads to lysigenous aerenchyma in the root cortex, and the conversion of SAM and ACC to ethylene requires O_2. (B) Transduction of the signal for low O_2 in maize leads to programmed cell death during the formation of lysigenous aerenchyma (see Chapter 20). Chemicals that increase the cytosolic Ca^{2+} concentration under aerobic conditions promote aerenchyma formation, whereas compounds that block Ca^{2+} movement under anoxia inhibit aerenchyma formation.*

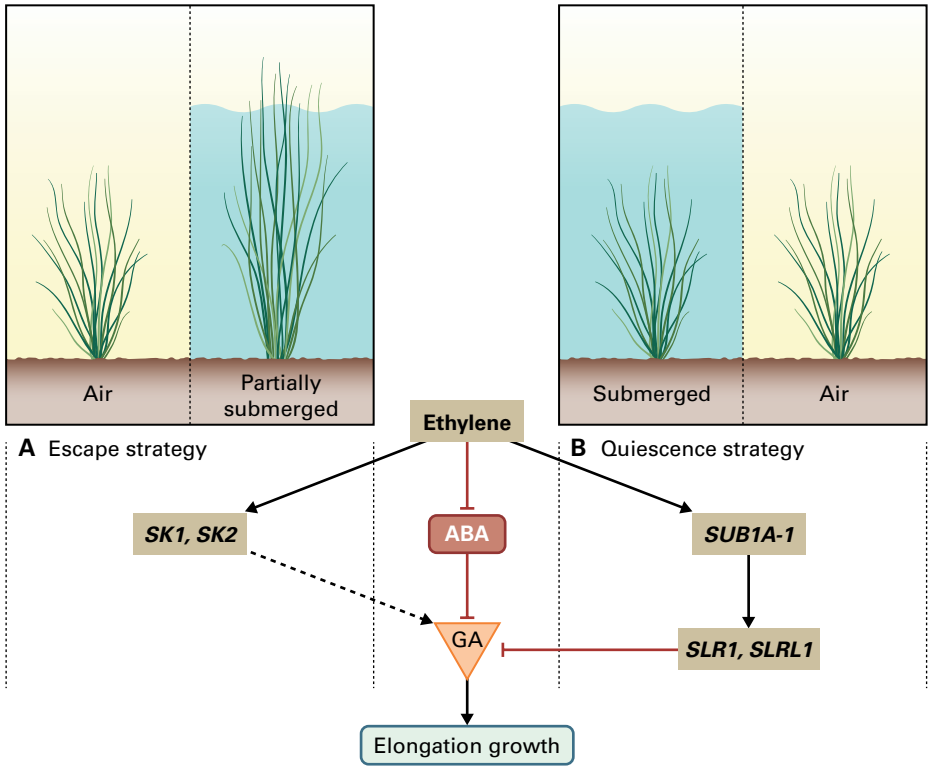


FIGURE 22.32 *Ethylene and flooding responses in rice. The elongation of stem and leaf cells is positively regulated by GA. Under normal growth conditions, ABA inhibits GA activity. When plants are submerged, cellular ethylene levels rise due to biosynthesis and entrapment by the surrounding water. This promotes the breakdown of ABA, increasing cellular responsiveness to GA, which then stimulates cell elongation. In deepwater rice (*Oryza sativa *L. var. Indica), this is accompanied by increased accumulation of bioactive GA. (A) The escape strategy of deepwater rice involves rapid stem elongation to maintain leaf tissue above the water level, in response to a slow, progressive flood. This growth is mediated by GA biosynthesis and action. Quantitative trait locus (QTL) mapping identified two closely linked ethylene responsive factor (AP2/ERF) family transcription factors, SNORKEL1 and 2 (SK1 and SK2), on chromosome 12 that drive the deepwater escape response. Ethylene accumulation in underwater stems promotes transcription of* SK1 *and* SK2*, triggering internode elongation. These genes are present in some wild rice species, but are absent or nonfunctional in non-deepwater domesticated rice. (B) In the quiescence strategy of submergence-tolerant varieties, shoot elongation is suppressed to conserve carbohydrates and increase survival under short-term complete inundation conditions. GA signaling and cell elongation are inhibited by the ethylene-induced action of SUBMERGENCE-1A (SUB1A-1 allele) on the growth-inhibition genes SLENDER RICE-1 (SLR1) and SLR LIKE-1 (SLRL1). Submergence-induced* SUB1A *is present in a cluster of two or three ERF transcription factor on rice chromosome 9 in submergence-tolerant rice accessions.*

(see Chapter 17). Subsequently, cell division in the intercalary meristem increases, as does cell elongation in the stem internodes. In the wetland species *Rumex palustrus*, ethylene entrapment within the leaf petiole inhibits the ABA biosynthetic enzyme 9-*cis*-epoxycarotenoid dioxygenase (NCED) and promotes ABA catabolism to phaseic acid (Fig. 22.10), enhancing GA-activated elongation of cells. A more pronounced elongation of cells on the adaxial side of the petiole allows leaves of plants in shallow floods to become more erect and extend above the air–water interface. The rapid elongation growth that permits escape from submergence in rice and *R. palustris* (see Fig. 22.24) is associated with increases in xyloglucan endotransglycosylase/hydrolases (XTHs) and expansins, nonenzymatic cell wall loosening proteins. Thus, ethylene accumulation in response to flooding facilitates the escape strategy that enables better photosynthate production and O_2 entry necessary for maintenance of growth.

Two major quantitative trait loci (QTL) involved in flooding responses in rice encode multiple transcription factors in the ethylene responsive factor (AP2/ERF) family that control GA-regulated elongation growth under submergence. Remarkably, these genes orchestrate opposing responses (Fig. 22.32).

The *SUB1* (*SUBMERGENCE1*) locus on chromosome 9 of rice controls tolerance of prolonged periods of submergence by limiting growth and encodes at least two related AP2/ERF genes, *SUB1B* and *SUB1C*. In rice that tolerates 14 days or more of complete submergence, this locus has a third related AP2/ERF transcription factor gene, *SUB1A*. The ethylene-induced expression of *SUB1A* during submergence limits further ethylene synthesis, the consumption of starch and soluble carbohydrates, and the responsiveness to GA, despite the decline in ABA concentration. This repression of elongation growth is manifested by SUB1A through maintenance of GRAS family transcription factors that repress GA-mediated gene expression. These include the rice DELLA domain protein SLENDER RICE-1 (SLR1) and a related protein SLR-like 1 (SLRL1) that lacks a DELLA domain (see Chapter 18).

Altogether, the submergence-induced expression of *SUB1A* invokes an energy conservation strategy that limits elongation growth and prolongs meristem viability.

Deepwater rice has three QTL responsible for promoting rapid underwater elongation growth in response to increased GA production and responsiveness. Genetic mapping identified the *SNORKEL* locus on chromosome 12, which encodes two AP2/ERF genes, *SNORKEL1* (*SK1*) and *SNORKEL2* (*SK2*), that are in the same phylogenetic subgroup as the *SUB1*s (Fig. 22.32). *SK1/SK2* genes are absent or nonfunctional in rice varieties that lack the rapid internode elongation response characteristic of deepwater rice. Both *SK*s are ethylene-regulated and highly induced in internodes upon submergence. Transfer of these genes to nondeepwater rice confers a significant increase in underwater internode elongation.

22.5.5 How do plants sense oxygen deprivation?

Plant responses to flooding include transient alterations in gene expression and metabolism, as well as long-term developmental responses. Are these responses triggered directly or indirectly by low concentrations of available O_2?

A direct sensing mechanism generates a response to a decline in O_2 used by an enzyme or other specific process. An indirect mechanism involves the diminished production of ATP, increased production of NADH, and decreased cytosolic pH that result from anaerobic respiration. Temporal and spatial changes in calcium and ROS (H_2O_2 and NO) also occur as O_2 availability diminishes. Evidence implicates Ca^{2+} as an important second messenger in transducing the low-oxygen signal, altering gene expression, and promoting aerenchyma formation. Any or all of these consequences of oxygen deprivation could participate in signal transduction processes. Plant hormones, such as ethylene and ABA, may also be involved in transducing the low-oxygen signal.

A homeostatic sensor of oxygen availability in plants is mediated by the N-end rule pathway of targeted turnover of a group of transcription factors. The N-end rule controls the degradation of proteins based on the presence of specific N-terminal residues that trigger destabilization. There are 11 N-terminal destabilizing residues in plants, but only Cys is involved in oxygen sensing. For proteins that begin Met-Cys, a methionine aminopeptidase can remove the first residue, resulting in a protein with an N-terminal Cys. This residue is susceptible to conversion to Cys-sulfinate or Cys-sulfonate through spontaneous or enzymatic oxidation. The N-terminus then becomes a substrate for an arginyl tRNA transferase, which adds an N-terminal Arg. The protein then has an N-terminus that is an N-degron, which can be recognized by a specific N-recognin E3 ligase, leading to ubiquitination at a specific Lys and degradation by the 26S proteosome.

In *Arabidopsis*, five constitutively expressed or hypoxia-induced AP2/ERF proteins are stable under oxygen deficient conditions, but degraded under oxygen replete conditions. The second amino acid of these proteins, a Cys, is necessary for their N-end rule turnover. Oxidation of the cysteine by oxygen, ROS, or NO is proposed to initiate the N-end rule turnover process of these proteins. Thus, low oxygen conditions stabilize certain AP2/ERFs that regulate the transcription of genes associated with anaerobic metabolism.

Additional plant proteins associated with signal transduction processes that control survival of low-oxygen conditions include the monomeric RHO of plant (ROP) G-proteins, CIPK, and SnRK1A. Plant hemoglobin-like proteins may also be involved in regulation of signaling or anaerobic ATP production. Despite the absence of clarity on the mechanisms governing low oxygen sensing and response, studies in several model species indicate that survival involves effective management of the reconfiguration of metabolism so that carbohydrate reserves are not rapidly exhausted under prolonged stress.

22.6 Oxidative stress

22.6.1 Oxidative stress results in production of ROS and causes severe cellular damage

Oxidative stress results from conditions that promote formation of ROS, which can damage or kill cells. Environmental factors that cause oxidative stress (Fig. 22.33) include air pollution (increased amounts of ozone or sulfur dioxide), oxidant-forming herbicides such as Paraquat (methyl viologen, 1,1′-dimethyl-4,4′-bipyridinium), heavy metals, drought, heat and cold stress, wounding, the transition to anoxia and reoxygenation, UV light, and intense light conditions that stimulate photoinhibition (see Chapter 12). Oxidative stress also occurs in response to senescence (see Chapter 20) and pathogen infection (see Chapter 21).

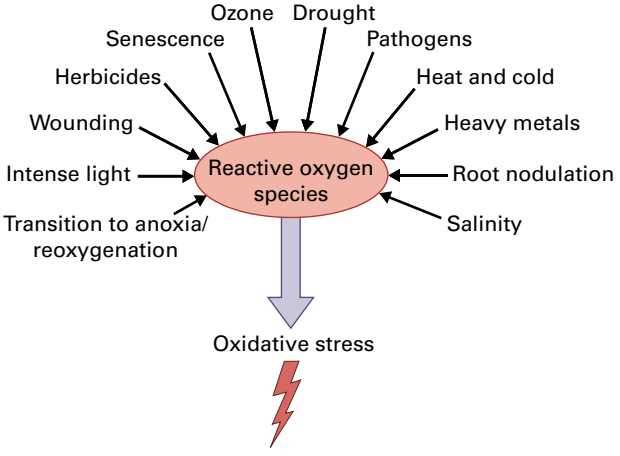


FIGURE 22.33 *Environmental factors that increase the concentrations of reactive oxygen species (ROS) in plant cells.*

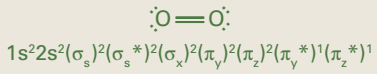
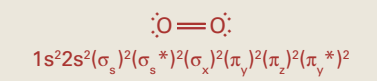
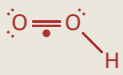
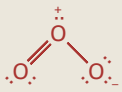
Compound	Shorthand notation(s)	Structural representation(s)	Sources
Molecular oxygen (triplet ground state)	O_2 ; $^3\Sigma$		Most common form of dioxygen gas
Singlet oxygen (first excited singlet state)	$^1O_2$; $^1\Delta$		UV irradiation, photoinhibition, photosystem II e^- transfer reactions (chloroplasts)
Superoxide anion	$O_2^{\bullet -}$		Mitochondrial e^- transfer reactions, Mehler reaction in chloroplasts (reduction of O_2 by iron–sulfur center FX of Photosystem I), glyoxysomal photorespiration, peroxisome activity, plasma membrane, oxidation of paraquat, nitrogen fixation, defense against pathogens, reaction of O_3 and OH^- in apoplastic space
Hydrogen peroxide	H_2O_2		Photorespiration, β-oxidation, proton-induced decomposition of $O_2^{\bullet -}$, defense against pathogens
Hydroxyl radical	$OH^{\bullet}$		Decomposition of O_3 in presence of protons in apoplastic space, defense against pathogens
Perhydroxyl radical	$O_2H^{\bullet}$		Reaction of O_3 and OH^- in apoplastic space
Ozone	O_3		Electrical discharge or UV radiation in stratosphere, reactions involving combustion products of fossil fuels and UV radiation in troposphere

FIGURE 22.34 *Molecular structure of reactive oxygen species (ROS) active in plants: singlet oxygen, hydrogen peroxide, superoxide anion, hydroxyl radical, and perhydroxyl radical.*

In plants, production of ROS (Fig. 22.34) such as singlet oxygen ($^1O_2$), hydrogen peroxide (H_2O_2), and superoxide ($O_2^{\bullet -}$), hydroxyl ($HO^{\bullet}$), and perhydroxyl ($HO_2^{\bullet -}$) anions is an inescapable consequence of aerobic metabolic reactions. The chloroplast electron transfer chain, for example, produces $^1O_2$ at PSII and $O_2^{\bullet -}$ at PSI and PSII. Mitochondria produce $O_2^{\bullet -}$ at complexes I and III. Peroxisomes and NADPH oxidases (respiratory burst oxidases, RBOHs) at the plasma membrane also produce $O_2^{\bullet -}$ and H_2O_2, and $O_2^{\bullet -}$, respectively. H_2O_2 is relatively stable and travels relatively long distances, but other ROS have very short half-lives and, therefore, can travel only short distances. For example, ROS produced by plastids and mitochondria are implicated in retrograde signaling to the nucleus. Although all ROS are highly reactive and can destroy lipids, nucleic acids, and proteins, some ROS such as $O_2^{\bullet -}$ and H_2O_2 are required for lignification (see Chapter 2 and 24) and function as signals in defense responses to pathogen infection (see Chapter 21) as well as in response to a number of abiotic stresses. Plants scavenge and dispose of excessive ROS through use of antioxidant defense systems (nonenzymatic and enzymatic) present in several subcellular compartments. When these defenses fail to halt the self-propagating autooxidation reactions associated with ROS, cell death ultimately results.

22.6.2 Cells have both enzymatic and nonenzymatic antioxidant defense systems

Plant antioxidant defense systems include nonenzymatic and enzymatic systems (Fig. 22.35) involving compounds and enzymes that are not distributed uniformly and that vary among subcellular compartments.

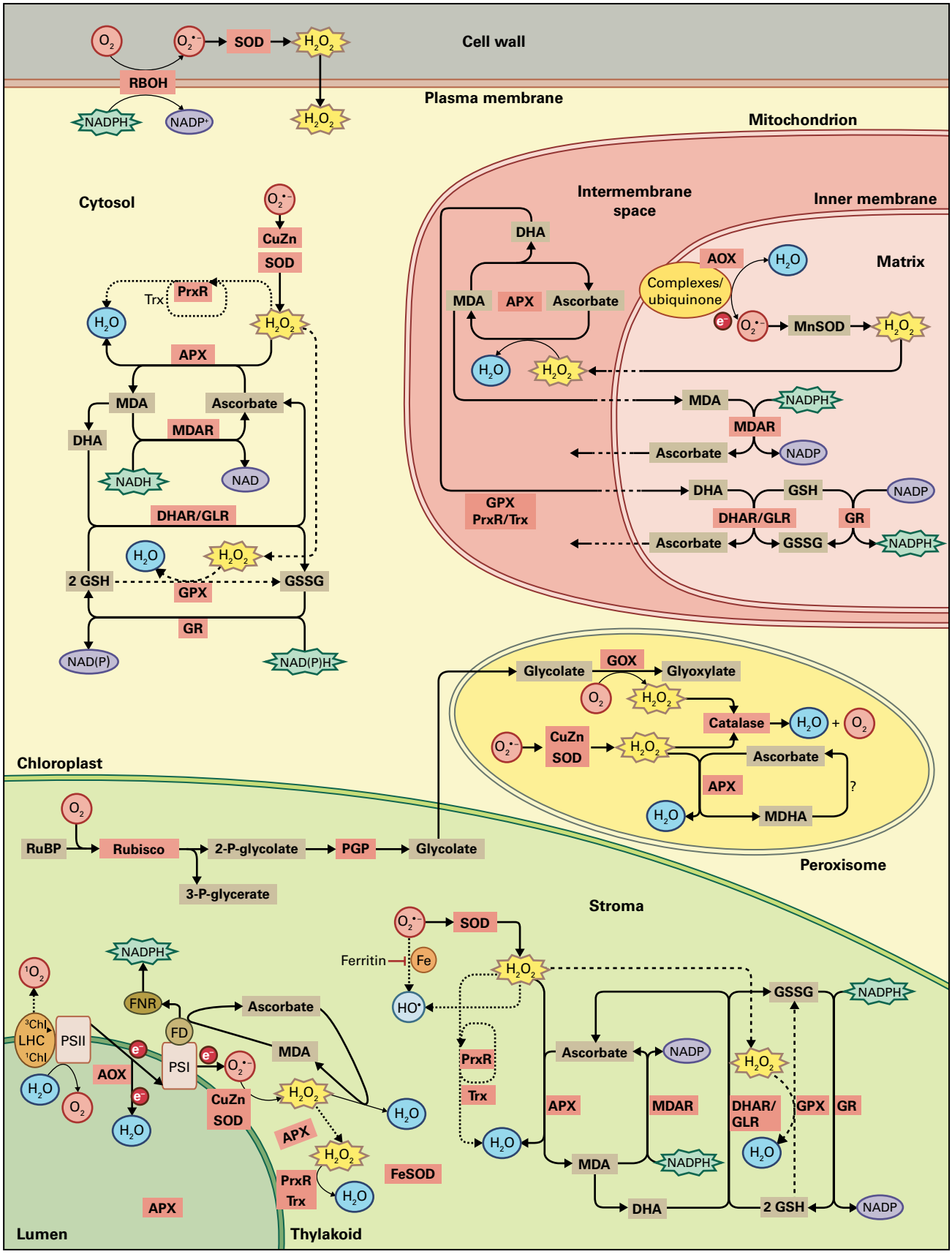


FIGURE 22.35 *Localization of reactive oxygen species (ROS) generation and scavenging pathways in plant cells. The water–water cycle detoxifies $O_2^{\cdot-}$ and H_2O_2, and alternative oxidase (AOX) reduces the production rate of $O_2^{\cdot-}$ in thylakoids [bottom left; in some plants iron superoxide dismutase (FeSOD) might replace CuZnSOD in the chloroplast]. ROS that escape this cycle or are produced in the stroma undergo detoxification by SOD and the stromal ascorbate–glutathione cycle. Peroxiredoxin (PrxR) and glutathione peroxidase (GPX) are also involved in H_2O_2 removal in the stroma (bottom right). Excited chlorophyll (Chl) in its triplet state at the light-harvesting complex (LHC) can generate $^1O_2$ when the*

The major nonenzymatic antioxidants in plants (Table 22.4) include ascorbate (vitamin C), reduced glutathione (GSH), α-tocopherol (vitamin E), and carotenoids; polyamines and flavonoids also provide some protection from free radical injury. Upon interaction with ROS, GSH is oxidized to GSSG, and ascorbate is oxidized to monodehydroascorbate and dehydroascorbate. These three oxidized compounds are then reduced back to GSH and ascorbate through the ascorbate–glutathione cycle, the major antioxidant pathway in plastids. ROS are generated in plastids as a part of normal biochemical processes that include photosynthetic electron transfer. The photosynthetic apparatus receives additional protection from oxidative damage by the exothermic production of the xanthophyll zeaxanthin (see Chapter 12).

The major enzymatic ROS scavenging systems (Table 22.5) include superoxide dismutase (SOD), catalase (CAT), and

TABLE 22.4 *Subcellular locations of antioxidants.*

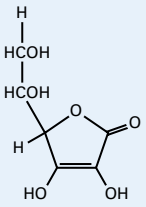
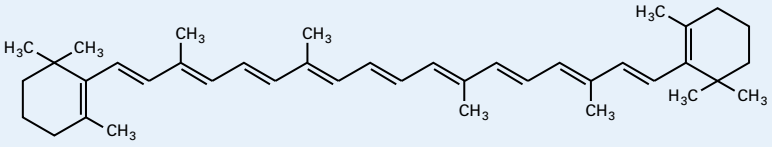
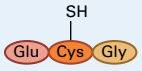
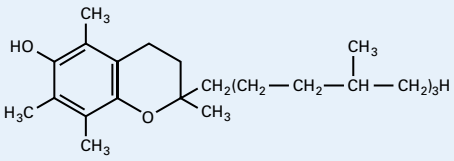
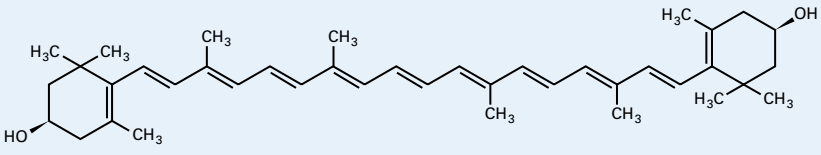
Antioxidant	Structure	Subcellular location
Ascorbate (vitamin C)		Apoplast, cytosol, mitochondrion, nucleus, peroxisome, plastid, vacuole
β-Carotene		Plastid
Glutathione, reduced (GSH)		Cytosol, mitochondrion, plastid, nucleus
Polyamines (e.g., putrescene, shown here)	$H_2N(CH_2)_4NH_2$	Cytosol, mitochondrion, nucleus, plastid
α-Tocopherol (vitamin E)		Membranes (including plastid membranes)
Zeaxanthin		Chloroplast

FIGURE 22.35 *(Continued) electron transport chain is over-reduced. ROS are produced in peroxisomes during fatty acid oxidation, photorespiration or other reactions are decomposed by SOD, catalase (CAT) and ascorbate peroxidase (APX) (middle right). SOD and other components of the ascorbate–glutathione cycle are also present in mitochondria. In addition, AOX prevents oxidative damage in mitochondria (top right). In principle, the cytosol contains the same set of enzymes found in the stroma (bottom). NADPH oxidases (respiratory burst oxidase homologs [RBOHs]) are the major producers of ROS-associated signals required in a wide range of biological activities. The enzymatic components responsible for ROS detoxification in the apoplast and cell wall are only partially known, and the ROS-scavenging pathways at the vacuole and nucleus are unknown. GPX pathways are indicated by dashed lines and PrxR pathways are indicated by dotted lines in the stroma and cytosol. Although the pathways in the different compartments are mostly separated from each other, H_2O_2 can easily diffuse through membranes and antioxidants such as glutathione and ascorbic acid can be transported between the different compartments. DHA, dehydroascrobate; DHAR, DHA reductase; FD, ferredoxin; FNR, ferredoxin NADPH reductase; GLR, glutaredoxin; GR, glutathione reductase; GOX, glycolate oxidase; GSH, reduced glutathione; GSSG, oxidized glutathione; MDA, monodehydroascorbate; MDAR, MDA reductase; PGP, phosphoglycolate phosphatase; PSI, photosystem I; PSII, photosystem II; RuBP, ribulose-1,5-bisphosphate; Rubisco, RuBP carboxylase oxygenase; Trx, thioredoxin.*

TABLE 22.5 *Subcellular locations of antioxidant enzymes.*

Antioxidant enzyme	Abbreviation	Subcellular location
Ascorbate peroxidase	APX	Cytosol, mitochondrion,plastid, peroxisome, root nodules
Catalase	CAT	Peroxisome
Dehydroascorbate reductase	DHAR	Cytosol, root nodules
Glutathione reductase	GR	Cytosol, mitochondrion, plastid, root nodules
Glutathione peroxidase	GPX	Cytosol, mitochondrion, plastid
Monodehydroascorbate reductase	MDAR	Cytosol, mitochondrion, plastid, root nodules
Peroxiredoxin	PrxR	Chloroplast, mitochondrion
Superoxide dismutase (grouped by metal cofactor)	Cu/ZnSOD	Cytosol, peroxisome, plastid, root nodules
	MnSOD	Mitochondrion
	FeSOD	Plastid

ascorbate peroxidase (APX). SODs are the first enzymes for detoxification of ROS, dismuting $O_2^{\cdot -}$ to H_2O_2 and CAT and APX subsequently convert H_2O_2 to H_2O. Glutathione peroxidase (GPX) consumes GSH to convert H_2O_2 to GSSG and H_2O. Other enzymes such as glutathione reductase (GR), dehydroascorbate reductase (DHAR) and monodehydroascorbate reductase (MDAR) are antioxidant enzymes of the ascorbate–glutathione cycle, but they do not detoxify ROS directly. Regulation of the concentrations of antioxidants and antioxidant enzymes constitutes an important mechanism for avoiding oxidative stress.

22.6.3 Ozone exposure causes severe oxidative stress in plants

One of the best-characterized oxidative stressors is exposure to high concentrations of ozone. Ozone is harmful because it is a highly reactive oxidant (Fig. 22.36), and exposure to it decreases rates of photosynthesis, growth of shoots and roots, and crop yields. It also causes leaf injury (Fig. 22.37) and accelerates senescence.

Plants vary greatly in their ability to survive in high-ozone environments, and their resistance involves both avoidance and tolerance mechanisms. Avoidance involves physically excluding the pollutant by closing stomata, the principal sites of ozone entry. Tolerance can result from biochemical responses that induce or activate the antioxidant defense system and possibly also various repair mechanisms. Resistance is also influenced by environmental factors that can cause oxidative stress (e.g., water status, temperature, and light intensity) as well as by the developmental age of the plant or plant organ. Although ozone-induced injury can increase the susceptibility of plants to pathogens, ozone exposure paradoxically can induce pathogen resistance by upregulating the antioxidant enzymes that are induced by the hypersensitive response (HR; see Chapters 20 and 21) and systemic acquired resistance (SAR; see Chapter 21).

Although the mechanisms of ozone toxicity are not completely understood, damage is likely a consequence of oxidative destruction of plasma membrane lipids and proteins and production of free radicals or other reactive intermediates (Fig. 22.38). Upon entering cells, ozone may react with ethylene and other alkenes in the apoplastic fluid to form $HO^{\cdot -}$, $O_2^{\cdot -}$, and H_2O_2, which damage cellular components. Damage to membrane lipids alters ion transport, increases membrane permeability, inhibits H^+-pump activity, collapses membrane potential, and increases Ca^{2+} uptake from the apoplast. Proteins, nucleic acids, and carbohydrates are among targets of ozone-derived ROS. The mechanism of ozone action can differ, depending on whether the exposure is acute, chronic, or repeated. The term ozone dose is used to describe the combination of duration and level of exposure. Tolerance to ozone-induced injury is inherited as a quantitative trait in many species.

Ozone exposure causes a rapid inhibition of photosynthesis, which is reflected in changes in the activity or synthesis of chloroplast proteins. In several plants (e.g., potato, radish, poplar, and wheat), chronic exposure to ozone reduces the abundance of ribulose bisphosphate carboxylase/oxygenase (Rubisco) in mature but not immature leaf tissue. This loss of Rubisco is the result of increased degradation of the protein, but it may also involve changes in transcription, accumulation, and translation of *rbcS* and *rbcL* mRNAs. In potato, induction of ethylene synthesis is followed by a decrease in *rbcS* and *rbcL* transcript levels, suggesting that gene expression may be regulated by the stress production of this phytohormone. Degradation of the large subunit of Rubisco is also

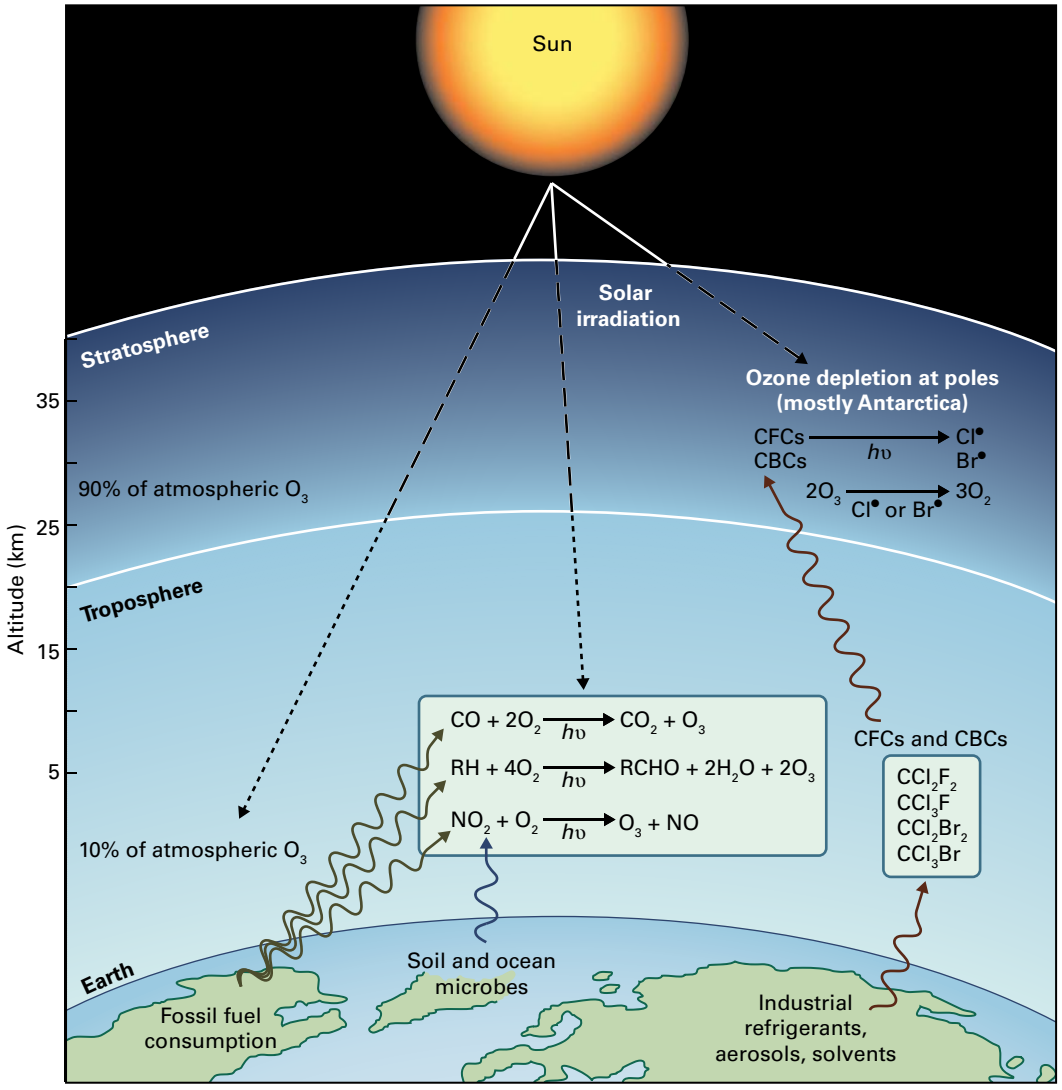


FIGURE 22.36 *Stratospheric consumption and atmospheric generation of O_3. Ninety percent of atmospheric O_3 is in the stratosphere, 10% in the troposphere. Stratospheric ozone beneficially decreases the penetration of solar radiation to the troposphere. Anthropomorphic release of chlorofluorocarbons (CFCs) leads to depletion of stratospheric ozone, especially over polar regions. The burning of fossil fuels increases the production of carbon compounds that react in sunlight with oxygen to form ozone in the troposphere.*

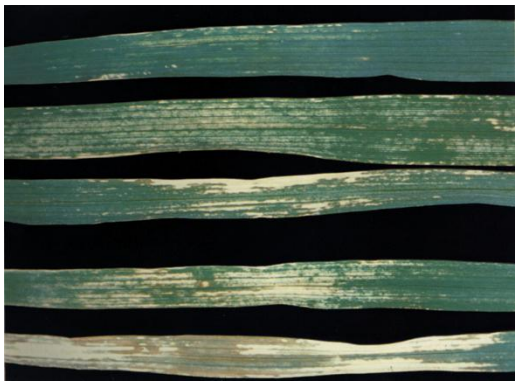


FIGURE 22.37 *Ozone-damaged oat (*Avena sativa *L.) leaves. Chlorotic lesions develop in the middle of the leaves. Leaf tips (oldest leaf cells) and leaf bases (youngest leaf cells) show the least damage.*
Source: Jacobson & Hill (1970) Recognition of Air Pollution Injury to Vegetation: A Pictorial Atlas. Air Pollution Control Association, Pittsburgh, PA.

observed in response to two other forms of oxidative stress, high-intensity light and oxidant herbicides (e.g., Paraquat). Collectively, unifying evidence links the loss of photosynthetic capacity to one or more of the following: reduced activity of PSI, PSII, or Rubisco; declining steady-state concentrations of Rubisco; increased turnover of the PSII protein D1, and possibly photoinhibition (see Chapter 12).

22.6.4 Various abiotic and biotic stressors cause oxidative stress

Various abiotic and biotic stresses also disturb the equilibrium of ROS production and scavenging to rapidly increase ROS concentrations in cells. Temperature stresses, such as excessive heat, chilling, or freezing, also increase cellular ROS

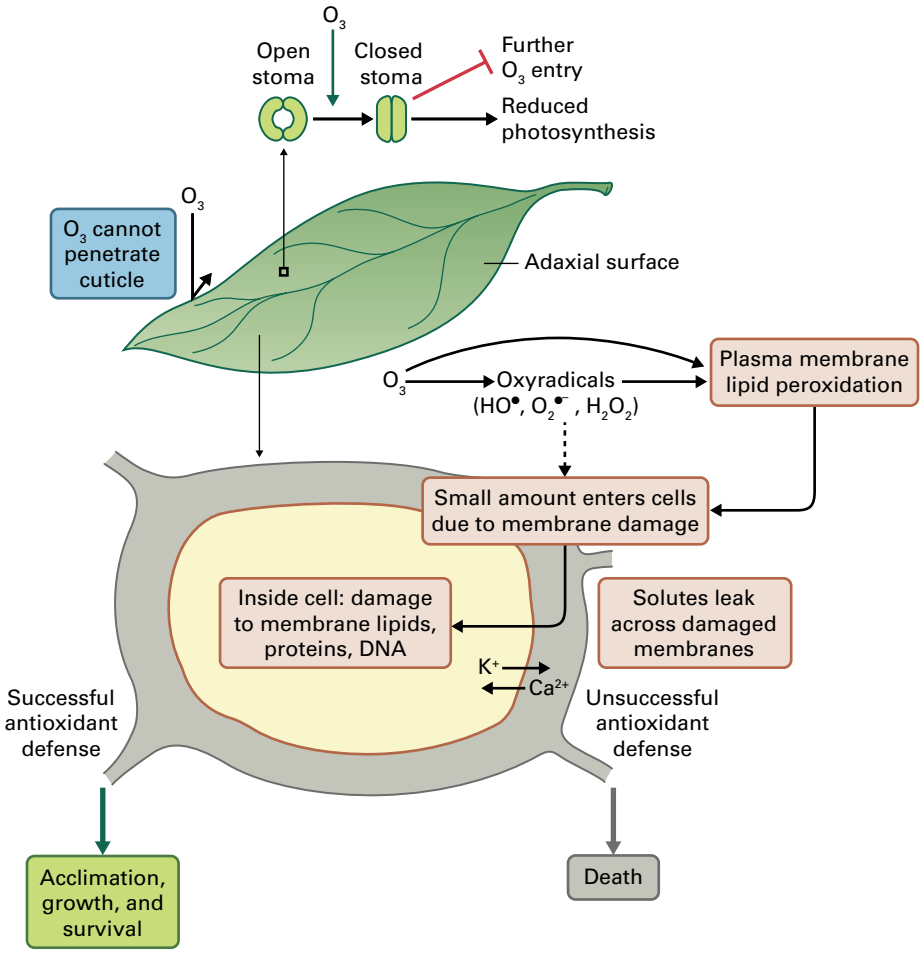


FIGURE 22.38 *Ozone action and plant responses. Because O_3 is polar and hydrophilic, it is unable to penetrate the leaf cuticle and penetrates the plasma membrane only poorly. Stomatal closure can diminish O_3 entry into the periplasmic space. Damage from O_3 occurs primarily as a result of peroxidation of plasma membrane lipids and stimulation of ROS production. Exposure to O_3 activates the antioxidant defense mechanisms within the cell. Whether antioxidant defenses are successful depends on the concentration of O_3, the duration of exposure, the age of the plant, and the genotype.*

levels and render membranes and proteins disfunctional. Heat stress impairs the mitochondrial respiratory electron transport chain, which causes oxidative damage to membrane lipids by peroxidation. Chilling stress inactivates cytochrome *c* oxidase and increases ROS production, and in chloroplasts, chilling and freezing damage the photosynthesis machinery and increase ROS concentrations. Oxidative stress during temperature stress can be further enhanced by high light; in cucumber (*Cucumis sativus*), for example, Cu/Zn SOD is the primary target of chilling stress combined with high light, which stimulate production of ROS and inactivation of PSI. Increases in ROS and ROS-associated injury are also observed in response to salinity, drought, osmotic stress, and reoxygenation following flooding.

Oxidative burst, the rapid production of ROS (primarily $O_2^{\bullet -}$ and H_2O_2) at the site of invasion, is the primary defense system of plants to pathogen attack. Plasma membrane-associated NADPH-oxidase (RBOH) and apoplastic peroxidase systems are responsible for oxidative burst, which produces reduced ROS that trigger programmed cell death to block the spread of infection (hypersensitive responses, see Chapters 20 and 21). A balance between the ROS production and scavenging under stressful conditions is clearly important for maintaining cellular activities and for cell survival.

22.6.5 Increased synthesis of nonenzymatic and enzymatic antioxidants can improve tolerance to oxidative stress

In many plants, oxidative stress can stimulate synthesis of both nonenzymatic and enzymatic antioxidants (Table 22.6). Mutants with altered nonenzymatic antioxidants, such as GSH and ascorbate, exhibit different levels of environmental stress sensitivities. As mentioned above, oxidative stress results in oxidation of GSH to GSSG, and ascorbate to monodehydroascorbate and dehydroascorbate, and these oxidized compounds can then be reduced and reformed to GSH and ascorbate through the ascorbate–glutathione cycle. Eventually, many plants increase enzyme activities (or amounts) of GSH and ascorbate biosynthesis and the ascorbate–glutathione cycle. Therefore, the balance of various nonenzymatic antioxidants must be controlled to maintain proper redox state of cells. Elevated glutathione biosynthetic capacity in the chloroplasts of transgenic tobacco plants unexpectedly causes oxidative stress. Overexpression of an enzyme (β-carotene hydroxylase) in *Arabidopsis* increases a nonenzymatic antioxidant, xanthophyll (a flavonoid), in chloroplasts and enhances oxidative stress tolerance under high light conditions.

TABLE 22.6 *Stress conditions that stimulate increased levels or activities of antioxidants and antioxidant enzymes of various species.*

Antioxidant or enzyme*	Stress conditions
α-Tocopherol (vitamin E)	Drought
Anionic peroxidases	Chilling, high CO_2
Ascorbate peroxidase	Drought, high CO_2, high light intensity, ozone, Paraquat, salinity
Catalase	Chilling
Glutathione	Chilling, drought, γ-irradiation, heat stress, high CO_2, ozone, SO_2
Glutathione reductase	Chilling, drought, high CO_2, ozone, Paraquat, salinity
Polyamines	Drought, heat, ozone, deficiency of K, P, Ca, Mg, Fe, Mn, S, or B
Superoxide dismutase	Chilling, high CO_2, high light, increased O_2, ozone, Paraquat, salinity, SO_2

*Changes in the amounts of these compounds and enzyme activities are dependent on the developmental stage of the plant and the experimental parameters.

Studies in *Arabidopsis* and other plant species have revealed redundancy of genes encoding enzymes associated with antioxidants and antioxidant enzymes. The differential expression of these genes appears to be regulated in a specific manner by different forms of abiotic or biotic stress. The over- and underexpression of genes encoding antioxidant enzymes has confirmed their roles as ROS scavenging enzymatic systems in numerous plant species. In some cases, ectopic overexpression of ROS-scavenging enzymes or transcription factors that enhance their expression has relieved susceptibility to abiotic stresses. APX overexpression decreases accumulation of H_2O_2 and increases chilling tolerance of rice, whereas knock out of cytosolic APX activity reduces tolerance to a variety of conditions with an oxidative component in *Arabidopsis*. Overexpression of pea (*Pisum sativum*) chloroplast SOD in tobacco (*Nicotiana tabacum*) increases Paraquat-induced membrane damage. Further, transgenic alfalfa (*Medicago* sp.) overexpressing tobacco Mn-SOD shows enhanced tolerance to freezing stress, and a salt-tolerant tomato (*Lycopersicon esculentum*) cultivar has higher levels of an Mn-SOD than a salt-sensitive cultivar under saline conditions.

Subcellular compartmentation influences the roles of antioxidant metabolites in detoxification; duplicate biochemical functions are often accomplished by distinct, spatially segregated antioxidant systems. For example, H_2O_2 is scavenged by both catalase (in the cytosol and peroxisomes) and ascorbate peroxidase (in the cytosol and plastids). Because compartmentation, and even location within an organelle, can be critical for function, the simple overexpression of antioxidant enzymes may not necessarily improve stress tolerance. Increased concentrations of a single antioxidant or antioxidant enzyme may not protect plant tissues if other oxidant-scavenging mechanisms are limiting or if overexpression results in increased production or reduced scavenging of ROS. In certain cases, however, overexpression of one or more antioxidant enzymes may provide protection from oxidative stress.

Oxidative stress tolerance probably depends on the successful induction of functional detoxification systems in the subcellular compartments that are exposed to high concentrations of free radicals. Overexpression of antioxidant enzymes can result in tolerance to single and multiple causes of oxidative stress, including pathogens, Paraquat, and osmotic stresses (e.g., chilling, salinity, and drought). However, increases in these compounds and enzymes are not always beneficial, most likely because of the complex compartamentalized networks involving ROS as a signaling and the antioxidants and antioxidant enzymes that control the damaging activities of ROS.

22.6.6 ROS can be signaling molecules in cells

While ROS are considered toxic byproducts of aerobic metabolic reactions that must be eliminated, they also act as signaling molecules that control a variety of cellular processes in plants, such as abiotic and biotic stress responses, programmed cell death, growth, development, pathogen defense, and stomatal responses. ROS generation in chloroplasts or mitochondria causes changes in nuclear gene expression, which indicates intracellular transmission of ROS information. ROS signals can be sensed by ROS sensors, such as two-component histidine kinase systems and redox-sensitive transcription factors and phosphatases. ROS eventually elicit changes in gene expression that modify various cellular processes.

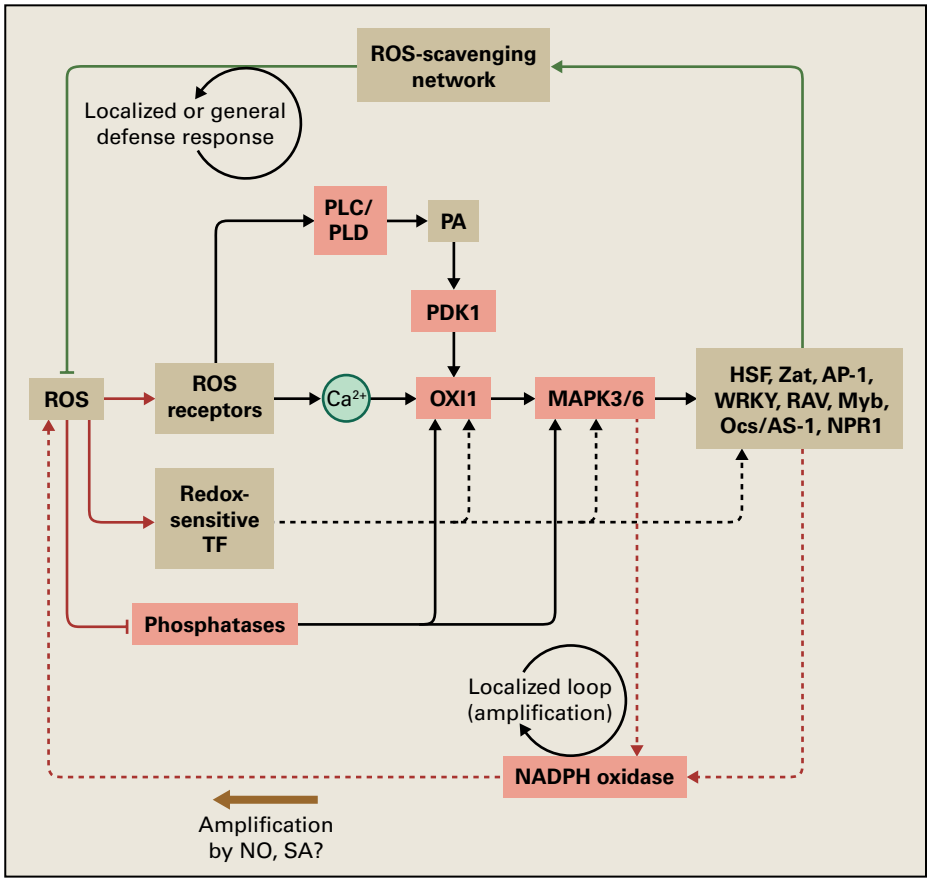


FIGURE 22.39 *Proposed model of the ROS signal transduction pathway. ROS can be detected by at least three mechanisms: ROS receptors, redox-sensitive transcription factors, and phosphatases. Detection by ROS receptors generates Ca^{2+} signals and activates phospholipase C/D (PLC/PLD) to generate phosphatidic acid (PA). PA and Ca^{2+} are thought to activate the protein kinase OXI1, which then activates a mitogen-activated-protein kinase (MAPK) cascade (MAPK3/6) to induce or activate different transcription factors that regulate the ROS-scavenging and ROS-producing pathways. Activation or inhibition of redox-sensitive transcription factors by ROS might also affect the expression of OXI1 or other kinases, and the induction of ROS-specific transcription factors. Inhibition of phosphatases by ROS might result in the activation of kinases, such as OXI1 or MAPK3/6. Two loops are involved in the ROS signal transduction pathway: a localized or general defense response (a negative feedback loop; solid green line) can be activated to suppress ROS, and a localized amplification loop (positive feedback loop; red dashed line) can be activated to enhance ROS signals via NADPH oxidases. Salicylic acid (SA) and nitric oxide (NO) might be involved in this amplification loop as enhancers. HSF, heat shock factor; PDK, phosphoinositide-dependent kinase; TF, transcription factor.*

Several components involved in ROS signaling downstream of detection have been identified (Fig. 22.39). After ROS are detected, Ca^{2+} signals involving calcium-binding proteins, such as calmodulin, are generated and phospholipases (C and D) are activated to produce phosphatidic acid. Ca^{2+} and phosphatidic acid are thought to activate a protein kinase (OXI1) and, subsequently, a mitogen-activated protein kinase (MAPK) cascade, which results in modulation of several transcription factors. ROS signals detected by redox-sensitive transcription factors are thought to affect OXI1, MAPKs, and ROS-specific transcription factors. ROS signals detected by inhibition of phosphatases may activate OXI1 and MAPKs. Ultimately, ROS signals, independent of detection systems, stimulate various ROS defense systems, such as changes in ROS-production/scavenging balance and production of ROS stress-protective proteins and compounds.

ROS (i.e., H_2O_2) application induces global alterations in gene expression in plants. In *Arabidopsis* and tobacco (*Nicotiana tabacum*), 1–2% of genes show changes in their expression levels in response to H_2O_2. ROS also alter several transcription factors, including HSFs, NPR1, WRKYs, and Myb-type transcription factors. Upregulation of these transcription factors ultimately causes changes in expression of downstream genes for kinases, peroxisome biogenesis-related proteins, antioxidant enzymes, and defense-associated proteins. Exposure to ROS also results in changes in protein profiles in subcellular compartments. In mitochondria, for example, levels of antioxidant defense proteins (such as peroxiredoxins and protein disulfide isomerase) increase, as do levels of enzymatic antioxidants (peroxidases and SOD) and enzymes associated with the ascorbate–glutathione cycle in chloroplasts.

ROS may also act on the transcriptome to induce oxidative stress by reducing antioxidant activity. Antisense lines of

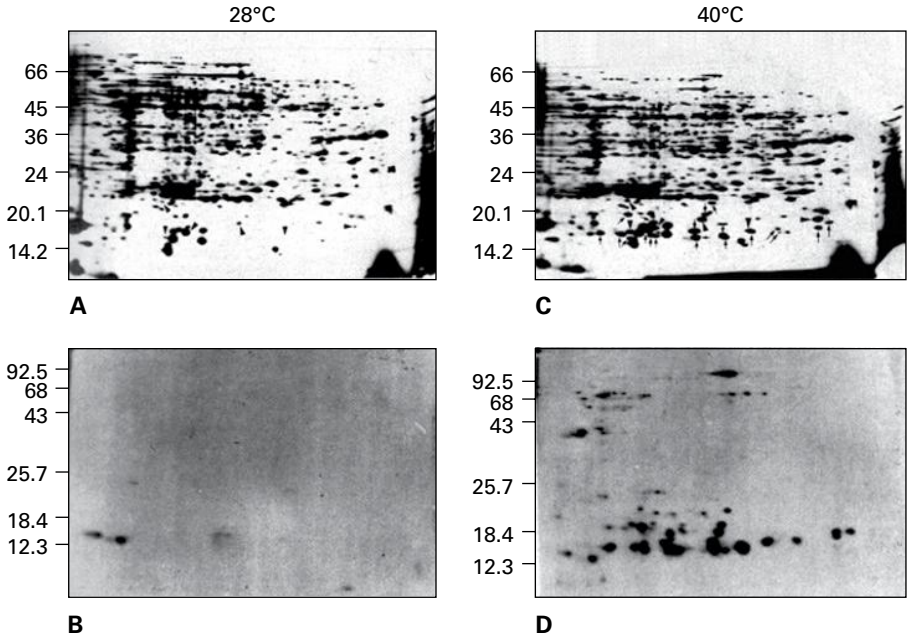


FIGURE 22.40 *HSPs, particularly those of low molecular mass (smHSPs), accumulate in soybean* (Glycine *max*) *seedlings in response to high temperatures. Total protein was extracted from seedlings that were incubated in the presence of* ^{3}H *-leucine at 28°C (A,B) or 40°C (C,D) for 3 hours, and then resolved by two-dimensional polyacrylamide gel electrophoresis. Proteins were visualized by silver staining (A,C) or by fluorography (B,D). Source*: (A–D) Mansfield & Key (1987). Plant Physiol. 84:1007–1017.

CAT and APX show elevated expression of SOD and GR, which may be compensatory mechanisms in plants to reduce oxidative stress. There is considerable interest in identifying "ROS gene network" components in plants, which requires controlling ROS toxicity by using ROS themselves as signaling molecules. In *Arabidopsis*, the ROS gene network contains approximately 150 genes that encode ROS-producing and -scavenging enzymes including CAT, APX, alternative oxidase, peroxiredoxin, and Cu-SOD. Further analyses with additional mutants and knockouts of multiple genes in the ROS gene network will enable further investigation of the roles of the network in oxidative stress responses; it may reveal crosstalk between ROS and other abiotic/biotic stress signaling pathways.

22.7 Heat stress

22.7.1 Heat stress alters cellular function

As with other abiotic stress conditions, heat stress can be chronic or long-term (as experienced in hotter habitats), or it can be more acute (as a result of seasonal or daily temperature extremes). Heat stress may occur under numerous temporal and developmental conditions, with results ranging from retarded growth to damaged organs and plant death. In the field, leaves may experience heat stress when transpiration is insufficient (i.e., when water is limiting and temperature is high) or when stomata are partially or fully closed and irradiance is high; in germinating seedlings, when the soil is warmed by the sun; in organs with reduced capacity for transpiration (e.g., fruit); and overall, from high ambient temperatures. The duration and severity of stress, susceptibility of different cell types, and stage of development all influence the ability of a particular genotype to survive heat stress.

Many features of the responses of plants to chronic heat stress are conserved in all organisms. The signature response to acute heat stress is a rapid and transient reprogramming of gene expression, including a decrease in the synthesis of normal proteins and accelerated transcription and translation of **heat shock proteins** (HSPs). This response is observed when plants are exposed to temperatures 5°C or more above their optimal growing conditions (Fig. 22.40).

In addition to altering patterns of gene expression, heat also damages cellular structures, including organelles and the cytoskeleton, and impairs membrane function. Organisms amenable to genetic manipulation, especially *E. coli*, yeast, and *Arabidopsis*, have been used to determine the cellular and metabolic changes required to survive high temperatures. Transcription factors, including HSFs involved in the expression of HSPs and other heat-inducible genes, have been identified, and their different roles in stress responses and tolerance have been investigated. There is overlap and crosstalk between heat stress and other abiotic stress signaling and response pathways, which have been analyzed using reverse genetic approaches.

22.7.2 Plants can acclimate to heat stress

Plants and other organisms can acquire thermotolerance if subjected to a nonlethal (**permissive**) high temperature for several hours before encountering normally lethal (**nonpermissive**) heat stress conditions. Acclimation to otherwise damaging high temperatures can also occur if the temperature increases gradually to the nonpermissive temperature, as may occur from morning to mid-afternoon on a hot day. *Arabidopsis* plants acclimated to survive a normally lethal 45°C treatment are shown next to nonacclimated plants in Figure 22.41. The acclimation process involves the synthesis of HSPs, some of which have been directly shown to be

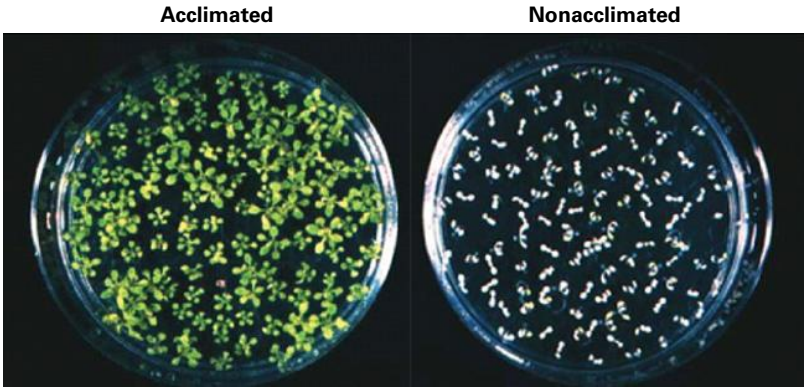


FIGURE 22.41 *Acclimation of* Arabidopsis *seedlings to high temperature. For acclimation, 10-day-old seedlings were treated for 90 min at 38°C and returned to 22°C for 2 hours before treatment at 45°C for 2 hours. Nonacclimated seedlings were directly exposed to 45°C. Seedlings were photographed after 5 days at 22°C. Nonacclimated seedlings died after treatment and did not produce more leaves.*
Source: Vierling, University of Arizona.

TABLE 22.7 *HSPs and their characteristics.*

Protein classes	Subfamilies	Size (kDa)	Major functions	Subcellular location
HSP100/Clp	Class I: ClpB, A/C, D Class 2: ClpM, N, X, Y	100–114	Protein disaggregation, unfolding, degradation (Clp protease)	Cytosol, mitochondria, chloroplast
HSP90	Hsp90	80–94	Maturation of signaling molecules, genetic buffering	Cytosol, chloroplast, mitochondria, endoplasmic reticulum
HSP70	DnaK BiP and GRP Hsp110/SSE	69–71	Prevention of aggregation, assisting refolding, protein import and translocation, signal transduction, and transcriptional activation	Cytosol, chloroplast, mitochondria, endoplasmic reticulum
HSP60/Chaperonin	Cpn60 CCT	60	Folding, assisting refolding	Chloroplast, mitochondria, cytosol
Small HSP (sHSP)		15–30	Prevention of aggregation, stabilization of nonnative proteins	Cytosol, chloroplast, mitochondria, endoplasmic reticulum, nucleus, peroxisome

required, as well as many other poorly understood changes in cellular metabolism. This type of rapid acclimation is transient, and begins to decay after 24 hours or less. Despite this capacity for acclimation, there is, of course, a limit to how much heat a plant can withstand. The relationships between this type of acclimation and overall differences in the ability of various plant genotypes and species to grow at different optimal temperatures remain to be resolved.

22.7.3 HSPs are conserved among different organisms

The rapid, high-level expression of HSPs in response to heat stress has led to significant focus on these proteins. Major classes of HSPs are conserved among all organisms, both prokaryotic and eukaryotic. These proteins function as molecular chaperones and are involved in various aspects of the folding of nascent proteins or refolding of proteins denatured by heat. Some HSPs are expressed throughout the life cycle of the plant. Indeed, some proteins designated as HSPs are not induced by heat at all, but rather are defined as HSPs according to sequence homology and possible functional similarities. The roles played by some plant HSPs have been inferred from complementation studies in yeast. For example, an HSP104 deletion mutant of yeast that is not thermotolerant can be partially rescued by a member of the *Arabidopsis* HSP100 family. However, the plant protein affords the yeast mutant less thermotolerance than the native yeast counterpart. Recently, T-DNA or Ds-tagged mutants have been used to analyze the functions of HSPs and HSFs to determine their roles in stress tolerance of plants.

22.7.4 Five major classes of HSPs function as molecular chaperones

HSPs are grouped into five distinct classes named for their approximate molecular masses (Table 22.7). HSPs are thought to work in concert for the protection of complex cellular systems. They act as a protein quality control network to promote folding and proper localization of nascent proteins,

prevent irreversible aggregation of denatured proteins, and facilitate recovery of denatured protein function. HSPs can also direct damaged proteins to the cellular degradation machinery as another way to maintain normal cellular function and promote recovery from stress. Different classes of HSPs play complementary and overlapping roles in the protection of cells from stress-mediated cellular damage.

HSP100/ClpB family proteins are members of the AAA+ family of proteins, which are ATPases that function in disaggregation of denatured proteins. Plants possess cytosol-, chloroplast-, and mitochondrion-localized HSP100/ClpB proteins. Cytosolic HSP100 is essential for heat stress tolerance in plants, but is not essential for plant growth. Genetic analysis of *Arabidopsis* HSP101 has shown that it interacts with small HSPs to resolubilize aggregated proteins after exposure to heat stress. Chloroplast Hsp100/ClpB protein plays an essential role in chloroplast development as well as the heat stress response.

Proteins of the HSP90 family are found in bacteria and in the cytosolic, nuclear, and endoplasmic reticulum (ER) compartments of eukaryotic cells. In yeast, HSP90 is essential for growth at all temperatures. HSP90 has ATPase activity and has been shown in yeast and mammalian cells to be involved in a complex cycle with other auxiliary proteins to regulate the maturation and activity of numerous signaling proteins. How this activity is related to the plant heat stress response is still under investigation, but even *Arabidopsis* has four genes encoding cytosolic Hsp90 proteins.

HSP70 proteins (known as DnaK in prokaryotes) are ATPases essential for normal cell function. Some members are expressed constitutively, whereas others are induced by heat or cold. Present in multiple compartments (e.g., the cytoplasm, ER, mitochondria, and chloroplasts), HSP70 proteins are ATP-dependent molecular chaperones that interact with many different proteins, given their involvement in protein folding, unfolding, assembly, and disassembly (see Chapters 4 and 10). The most highly conserved feature shared among HSP70 proteins is the N-terminal ATP binding domain; the C-terminus, however, varies and may determine substrate specificity. Additional proteins, termed cochaperones, including DnaJ (Hsp40 in eukaryotes) and GrpE, stimulate Hsp70 ATPase activity and facilitate interactions of HSP70 proteins and their targets. A dramatic feature of plants compared to other organisms is their very large number of DnaJ proteins, which may each have specific adaptor functions for one or more Hsp70s.

Members of the HSP60 protein family are also known as **chaperonins**, and were the first proteins defined as molecular chaperones. Chaperonins are present in the bacterial cytosol (GroEL), the mitochondrial matrix (first termed Hsp60), and the chloroplast stroma. Chaperonins are abundant even at normal temperatures; their major role is thought to be in protein folding and assembly (see Chapters 4 and 10). They share a common oligomeric structure of two seven-member rings, and require ATP for their function. In plants, the best-studied family member is chaperonin 60, a nuclear-encoded chloroplast protein that is involved in Rubisco assembly, but its expression is not increased in response to heat stress. In vitro, chaperonins prevent other proteins from aggregating at physiologically relevant temperatures and are important in protein refolding.

One unique aspect of the heat shock response in plants is the abundance of small HSPs (sHSPs). Higher plants express 11 classes of sHSP, and plants are the only organisms in which sHSPs are targeted to virtually every intracellular compartment (Table 22.7). Although sHSPs are also found in all organisms, with the exception of a few prokaryotes, the diversification of plant sHSPs occurred after the divergence of plants and animals. Furthermore, sHSPs are the most strongly induced of all the HSPs in plants. It has been suggested that sHSPs evolved in response to the multiple stressors, including heat, that plants encountered on migration to land and because unlike animals they are sessile and cannot move to a more favorable environment. The defining feature of sHSPs is a C-terminal domain that is homologous to α-crystallins, proteins of the vertebrate eye lens. Although sHSP monomers are small (≈15–22 kDa in plants), in their native state the majority form large oligomers of 12 or more subunits. The most detailed structural information for any eukaryotic sHSP comes from determination of the 3D structure of the oligomeric form of a cytosolic sHSP from wheat, which is a dodecamer (Fig. 22.42). Current models from work performed in



FIGURE 22.42 *Structure of the native, oligomeric wheat sHSP, Hsp16.9 (Protein Database accession number 1GME). (Left) The dodecameric oligomer, with six subunits in the top ring (three dimers) and six subunits in the bottom ring, each uniquely colored. The diameter of the ring is approximately 95 Å. (Right) A dimer of subunits.*

vivo in yeast and *E. coli*, and in vitro with plant and other sHSPs, indicate that sHSPs bind denatured proteins in an ATP-independent manner and make these proteins available for refolding by ATP-dependent chaperones, primarily HSP70.

22.7.5 Expression of many HSPs is controlled by HSFs that recognize a conserved promoter sequence

HSFs are transcription factors that function as terminal components in heat stress signal transduction and are activated to transcribe their target genes, including HSPs. The *cis*-acting DNA target of HSFs, the **heat shock element** (HSE), is made up of 5-bp repeats in alternating orientations with the consensus nGAAn. An HSF-regulated promoter may contain five to seven of these repeats close to the TATA box. Many HSEs contain the DNA element 5′-CTnGAAnnTTCnAG-3′. Notably, the HSF DNA binding domain and the HSE are common to all eukaryotes. HSEs were also the first *cis*-acting transcriptional control element to be described. When an HSP gene promoter containing HSEs is linked to the firefly luciferase reporter gene and expressed in plants, tightly regulated, high-level luciferase expression can be observed. The level of gene expression is proportional to the time and temperature of heating, indicating the remarkable heat-sensing mechanism involved.

Although HSFs and HSEs are conserved, plants have an unusually large number of HSFs. For example, *Arabidopsis* has 21 HSF genes, and there are three classes of plant HSF (A–C), which are distinguished mainly by the structures of their oligomerization domains. Interestingly, not all HSFs are involved in regulation of gene expression in response to high temperature; however, several HSFs constitute a regulatory network and control transcription of HSPs as well as other genes. In tomato (*Lycopersocon esculentum*), HsfA1a is a master regulator that is expressed constitutively to regulate heat shock-induced expression of HsfA2 and HsfB1. HsfA2 is the major HSF in thermotolerant tomato cells, and forms a heterooligomeric complex with HsfA1a, which functions as a nuclear retention factor and a coactivator.

The *HsfA3* gene is regulated by DREB2A, an AP2/ERF transcription factor that functions mainly in dehydration-inducible gene expression. DREB2A is regulated by heat stress as well as dehydration, indicating HSF-mediated crosstalk between heat shock and dehydration stress responses. Regulatory networks composed of transcription factor cascades are important in crosstalk between abiotic stress signaling pathways.

Similar to other HSFs, the HSF of *Arabidopsis* can only bind DNA as trimers (Fig. 22.43), and heat stress is required for trimerization. The oligomerization and DNA-binding domains of HSF are conserved among different organisms. Trimerization depends on the presence of a leucine zipper configuration of hydrophobic heptad repeats located adjacent to the DNA binding domain. The mechanism that controls trimerization is poorly understood, but recent studies have indicated that trimerization, DNA binding, and transcriptional activity are repressed in the absence of heat stress (Fig. 22.43). When the HSF is overexpressed in *Arabidopsis*, the transcription factor is not active; overexpression of HSF in heterologous systems, however, such as *E. coli, Drosophila*, and HeLa cells, results in constitutively active HSF. This indicates that the mechanism of repression is selective for homologous HSF but not heterologous HSF. The *Arabidopsis* HSF can be derepressed when it is tagged with a reporter gene and then overexpressed.

Overexpression of transcription factors may prove an efficient way to improve stress tolerance, because a single transgenic protein can induce an entire battery of coordinately regulated genes. There is considerable interest in determining whether overexpressing this HSF construct in crop plants improves heat tolerance in the field.

22.7.6 Important questions remain about heat stress sensing and signaling

Many important questions remain about heat stress responses. How is heat stress sensed and the signal transduced? Is there a central network in heat stress responses? How do HSPs recognize target proteins for refolding or degradation?

There are clearly multiple signaling pathways in the heat stress response, as well as crosstalk between heat and oxidative stress responses. This means that heat stress triggers H_2O_2 production in cells and can lead to cellular damage. Under some conditions, this oxidative burst is correlated with the induction of heat stress-inducible genes, which may be due to the direct sensing of H_2O_2 by HSFs. Mutants of two NADPH oxidases show defects in thermotolerance, suggesting the involvement of ROS in the heat response. Moreover, other signaling molecules, such as calcium, are also involved. Calcium levels transiently increase in response to heat stress, but calcium transients are often observed in response to various types of stimuli. Phytohormones, such as ABA, salicylic acid (SA), and ethylene, are also suggested to have some link with heat stress responses, as they accumulate in response to heat stress, but are not correlated with thermotolerance.

22.8 Crosstalk in stress responses

Plants have developed survival strategies to cope with various types of environmental stress. Different types of abiotic stress affect plant growth under natural environmental conditions, and different stress signaling pathways interact to allow the plant to cope with complicated stress conditions. The plant hormones ABA, JA, SA, and ethylene are produced endogenously to regulate protective responses against various stressors through synergistic and antagonistic actions. ROS also function as common stress signal factors in stress responses. Abiotic stressors regulate the expression of

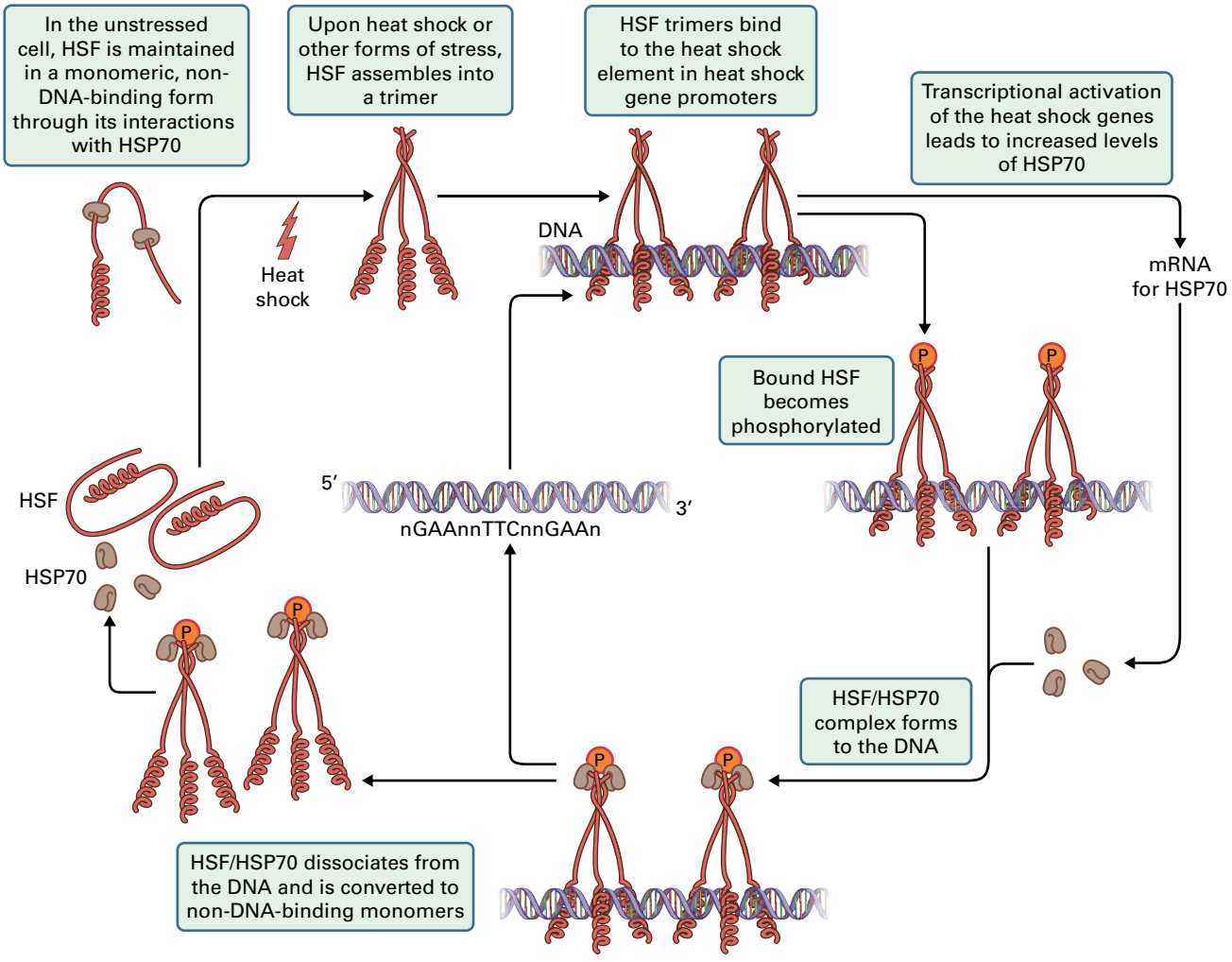


FIGURE 22.43 *Model for HSF activation of gene expression. In the unstressed cell, HSF is maintained as a monomer and cannot bind DNA. Upon heat shock, the HSF is assembled into a trimer capable of binding a specific DNA sequence. This model is mainly based on the research of bacterial HSFs.*

different but overlapping sets of genes—some are regulated differentially by plant hormones, and others are induced similarly by ROS. Thus, signaling pathways consist of complex networks with crosstalk that allow plants to respond to different types of environmental stress. Important factors involved in the points of convergence between biotic and abiotic stress signaling pathways, especially transcription factors and protein kinases, are particularly implicated in ROS and hormone signaling.

Rapid production of ROS in response to various types of stress plays a pivotal role in abiotic stress responses. To prevent cell injury or death due to excess ROS, ROS-scavenging enzymes such as SOD and APX regulate the steady-state level of ROS. Large-scale transcriptome analyses of plants subjected to various abiotic stress treatments have revealed the induction of a large set of genes encoding ROS-scavenging enzymes under these conditions. Several scavenging enzymes have been used to engineer abiotic stress-tolerant plants.

Whereas the plant hormones SA, JA, and ethylene play central roles in biotic stress signaling upon pathogen infection, ABA mediates abiotic stress signaling. However, recent studies have indicated the involvement of ABA in defense signaling via synergistic or antagonistic interactions with other hormone signaling pathways. In many cases, ABA acts as a negative regulator of disease resistance. Antagonistic interactions between the ABA and JA/ethylene pathways have also been studied in detail. Taken together with the observation that exogenous methyl jasmonate and ethylene do not affect suppression of defense gene expression induced by exogenous ABA, the ABA-mediated abiotic stress response may be a dominant process.

JA and ethylene are also involved in abiotic stress responses. Recent studies have shown that the bHLH transcription factor AtMYC2 plays a role in multiple hormone signaling pathways, suggesting that AtMYC2 is a key regulator of the crosstalk between biotic and abiotic stress responses via hormone signaling. Genetic analysis of the JA-insensitive *jin1* mutant has indicated that *JIN1* is allelic to *AtMYC2*, which was initially identified as a transcriptional activator involved in ABA-mediated drought stress signaling.

Transcriptional regulation also functions in crosstalk in stress signaling. The DREB2A transcription factor is a good example. Many heat shock-inducible genes as well as typical drought-inducible genes are upregulated by DREB2A, and transgenic *Arabidopsis* plants overexpressing the constitutively active form (CA) of DREB2A are more resistant to high temperature stress than wild-type controls. Thus, the DREB2A protein is believed to be involved in both water deficit and heat stress-responsive gene expression.

Genes regulated by the DREB2A transcription factor are categorized into three groups: those induced by drought, by heat stress, and by both drought and heat. The heat shock transcription factor gene *AtHsfA3* was identified as a target gene of DREB2A that contains at least two DRE/CRT core sequences in its promoter. It can be highly upregulated by the overproduced DREB2A-CA protein in transgenic plants even under normal conditions. Therefore, a new cascade of plant heat shock signaling has been established in which high temperature stress can rapidly induce *DREB2A* gene expression, and then DREB2A protein can bind the DRE/CRT sequence in *AtHsfA3* promoter and activate its transcription to control downstream *HSP* genes (see Fig. 22.12).

Summary

Abiotic stresses, including drought, chilling, heat, and flooding, are prevalent in nature and can substantially diminish crop yields. Plant responses to stressful environmental factors can permit the plant to withstand the stress; alternatively, such responses may be a manifestation of injury that has occurred in response to the abiotic stress. The response depends on the severity and duration of the stress, the developmental stage of the affected plant, the tissue type, and the interactions of multiple stresses. Mechanisms that permit stress survival are termed resistance mechanisms and can allow an organism to avoid or tolerate stress. Acclimation, a process that improves stress resistance, may occur in response to a mild nonlethal stress. Changes in gene expression may be involved in the mechanism of stress resistance or may be a result of injury. Recent advances in functional analyses of stress regulated genes and their products have revealed detailed molecular processes of plant responses to different types of abiotic environmental stresses. Cellular signal transduction pathways as well as gene expression in response to abiotic stresses have been extensively analyzed. Described in this chapter are the abiotic stresses arising from drought, salinity, low temperature, flooding, air pollution, and high temperature.

Stresses involving water deficit may arise from drought conditions, saline soils, or low temperature. To quantify the effect of stress on the plant, one can determine the water status of the plant by using either Ψ_w or RWC. Measuring the water status of the plant is important for determining the impact of the environmental condition. Decreases in plant water potential may be brought about by osmotic adjustment, the accumulation of compatible solutes that promote acclimation to dry or saline soils. In addition to osmotic adjustment, some compatible solutes, such as glycine betaine, mannitol, raffinose, pinole, and proline, serve other protective functions. Effects of water deficit and perturbing ions on the membrane may be minimized by the action of carriers, pumps, and channels. Various types of genes are induced by water deficit, including those that may protect the plant from abiotic stresses like LEA proteins and HSPs. The mechanisms of gene induction are regulated by specific DNA elements: two classes of elements, ABRE and DRE, have been found in many water-deficit-induced genes. Major transcription factors that control dehydration-responsive gene expression have been analyzed, and their target genes have been identified by microarray analysis. Regulatory factors including signaling factors and stress sensors have been studied extensively. Receptors and transporters of ABA were identified for further understanding of cellular and inter cellular signal transduction pathways. Application of the stress genes for molecular breeding of drought stress tolerance is now in progress by transgenic technology.

Freezing and chilling stresses cause cellular injuries in plants in different ways. Chilling stress causes membrane destabilization and metabolic dysfunction while freezing stress has several indirect damage effects due to ice crystal formation and its growth in extracellular compartments. Plants respond and adapt to low temperature stress at cellular level. Plants can acclimate to subfreezing temperatures as a result of increasing membrane stability and accumulation of specific protective metabolites and proteins. There are many genes with different functions that are induced in response to low temperature. The gene products mainly function in protection of cells from freezing. Regulation of low-temperature-induced genes has been analyzed extensively and *cis*-regulatory elements in gene promoters and transcription factors, like CBF/DREB1, have been identified for further analysis of their regulatory networks. Sensing and signal transduction in plant responses to cold stress have been analyzed to identify important signaling components.

Flooding can cause an oxygen deficit in the cell that impacts respiratory metabolism. The ability to tolerate flooding varies greatly among species and can be altered

by acclimation processes involving exposure to severe hypoxic conditions (i.e., <3 kPa oxygen). During short-term acclimation to anoxic conditions, plants generate ATP through glycolysis and fermentation; this shift from aerobic metabolism to glycolytic fermentation involves changes in gene expression. The plant hormone ethylene promotes long-term acclimative responses to waterlogging and submergence, including formation of aerenchyma and stem elongation. Some wetland genotypes are adapted to long-term flooding. QTL analysis revealed two important genes in flooding responses, *SUBMERGENCE1* (*SUB1A*) locus involved in submergence tolerance and *SNORKEL1* (*SK1*) and *SNORKEL2* (*SK2*) loci found in deepwater rice that enable submergence escape. All three of these rice genes encode related ERF transcription factors, are ethylene induced and influence GA-mediated elongation growth. But they confer opposing strategies of flooding survival. These indicate important roles of ethylene and the growth regulation it modulates during responses in rice.

Oxidative stress may arise from any abiotic or biotic stress that causes the formation of a reactive oxygen species (ROS), such as hydrogen peroxide (H_2O_2), superoxide anion ($O_2^{\cdot -}$), and hydroxyl radical ($HO^{\cdot}$), or perhydroxyl radical ($HO_2^{\cdot}$). Plants scavenge and eliminate these reactive molecules by using antioxidant defense systems including antioxidants and antioxidant enzymes, which are present in various subcellular compartments. Ozone exposure to plants can be used as a model system to determine how ROS cause oxidative damage to cellular processes. Studies in which antioxidant enzymes, such as SODs, APX, and CAT, are overexpressed in transgenic plants have emphasized the important role of subcellular compartmentation in detoxification mechanisms. ROS functions as signaling molecules to control various cellular responses to abiotic and biotic stresses. ROS signals can change gene expression to regulate downstream genes and various cellular processes. Sensing systems of ROS signals have not been elucidated, yet.

Heat stress responses are widely conserved among different organisms. Thermotolerance can be developed as plants acclimate to a nonlethal high temperature. During heat stress in plants, as in other organisms, gene expression patterns, including transcription and translation, are altered to promote the accumulation of HSPs. The five major classes of HSPs, defined according to size, are conserved among different organisms. In general, the HSPs function as chaperones to promote proper folding of proteins. Expression of HSPs is controlled by a transcription factor that recognizes a conserved DNA element, 5-nGAAn-3′, present in multiple copies in the promoter. The HSF transcription factor is active as a trimer and must be derepressed to activate gene expression. Heat sensing systems are likely to be general among various organisms.

Understanding of plant cellular responses to a variety of abiotic stress has proceeded extensively based on molecular biology and genomics. Many stress-inducible genes have been identified to function in abiotic stress responses and tolerance, which indicates importance of transcriptional regulation in plant stress response. Plants have many more transcription factors than animals. In addition to transcriptional modulation, post-transcriptional regulation and epigenetic regulation have been shown to function in plant abiotic stress responses. Plant hormones play important roles in abiotic stress responses in gene expression as well as signal transduction. Among them, ABA, ET, JA, and SA are major hormones in abiotic stress responses. These hormones also function in crosstalk between biotic and abiotic stress responses. Many genes associated with mammalian signal transduction cascades, such as protein kinases, phospholipid-related enzymes, receptor kinases, and G-proteins, are also present in plants. Functional analyses of these signaling molecules have been in progress using various mutant lines. However, numerous important questions remain unanswered. Most of the mechanisms by which higher plants perceive abiotic stresses have not been elucidated. Progress in this crucial area will advance our knowledge of stress-initiated signal perception and transduction events substantially. Crosstalk in stress signaling will provide us complex regulatory networks in response to complex environment responses of plants.



23

Mineral Nutrient Acquisition, Transport, and Utilization

Emmanuel Delhaize, Daniel Schachtman, Leon Kochian, and Peter R. Ryan

Introduction

The importance of mineral nutrients to crop production has been recognized for more than 2,000 years. Plant mineral nutrition is unique because green plants, the only multicellular autotrophic organisms, can mine inorganic elements from the environment without having to rely on high-energy compounds synthesized by other organisms. Plant nutritionists have contributed in many ways towards increasing crop yields. In the past 60–80 years the industrial scale production and distribution of mineral fertilizers has been directly correlated with higher crop production globally. This has been essential for increasing food production and meeting the needs of a growing population. The major mineral nutrients phosphorus and potassium are obtained by mining natural deposits and therefore can be viewed as limited resources. This is especially true of phosphorus where the known major deposits of high quality phosphate rock could be depleted before the end of this century. This is not a concern for nitrogen following the invention of the Haber–Bosch process that allows nitrogenous fertilizers to be produced through the fixation of nitrogen gas.

Recently, there has been an upsurge in research and a renewed interest in the field of plant mineral nutrition now that contemporary experimental approaches are being used to dissect mechanisms underlying transport and utilization of mineral ion nutrients. This resurgence is fueled by the availability of new powerful tools, including molecular techniques, complete genome sequences, the development of model plant systems, high-resolution electrophysiological methods, and sophisticated tools for studying plant physiology. These tools have allowed physiologists to move from studies on whole tissues where single transport mechanisms could not be resolved, to an era where both molecular and genetic methods have revealed underlying mechanisms for transport and utilization of mineral nutrients. The current challenge is to fit these individual pieces back together to begin to understand the molecular physiology of mineral nutrient acquisition and utilization in the intact plant.

This chapter focuses on recent findings concerning the physiology of transport in relation to two macronutrients (potassium and phosphorus), two micronutrients (copper and iron) and a toxic element (aluminum). Recent research has begun to elucidate the mechanisms involved in homeostasis of several mineral nutrients, and the central roles of microRNAs in these mechanisms are discussed. Topics related to mineral nutrition have been addressed in other chapters of this text. Plant uptake and assimilation of nitrogen and sulfur, for example, are discussed in Chapters 7 and 16. Anabolic and catabolic reactions involving the most abundant mineral nutrients—carbon, hydrogen, and oxygen—appear throughout the text and constitute the primary focus of Chapters 12 to 14. Long-distance transport of selected mineral nutrients is discussed in Chapter 15, and Chapter 3 provides the basis for understanding processes involved in the transport of ions across plant membranes.

Biochemistry & Molecular Biology of Plants, Second Edition. Edited by Bob B. Buchanan, Wilhelm Gruissem, and Russell L. Jones.
© 2015 John Wiley & Sons, Ltd. Published 2015 by John Wiley & Sons, Ltd.
Companion website: www.wiley.com/go/buchanan/biochem

23.1 Overview of essential mineral elements

Plant mineral nutritionists define **essential minerals** as ones that (a) are required to complete a plant's life cycle, and (b) are components of an essential plant metabolite or constituent. Their absence results in distinct deficiency symptoms as shown in Figure 23.1. The most common classification of the 17 essential mineral nutrients is based on the relative concentration of each in the plant when the nutrient is present in adequate concentration for normal plant function. The **macronutrients** are carbon, hydrogen, oxygen, nitrogen, potassium, calcium, magnesium, phosphorus, and sulfur. Except for the more abundant oxygen and carbon, the concentrations of macronutrients generally found in plants range from 1,000 to 15,000 µg per gram of dry weight. In contrast, the concentrations of **micronutrients** (chlorine, boron, iron, manganese,

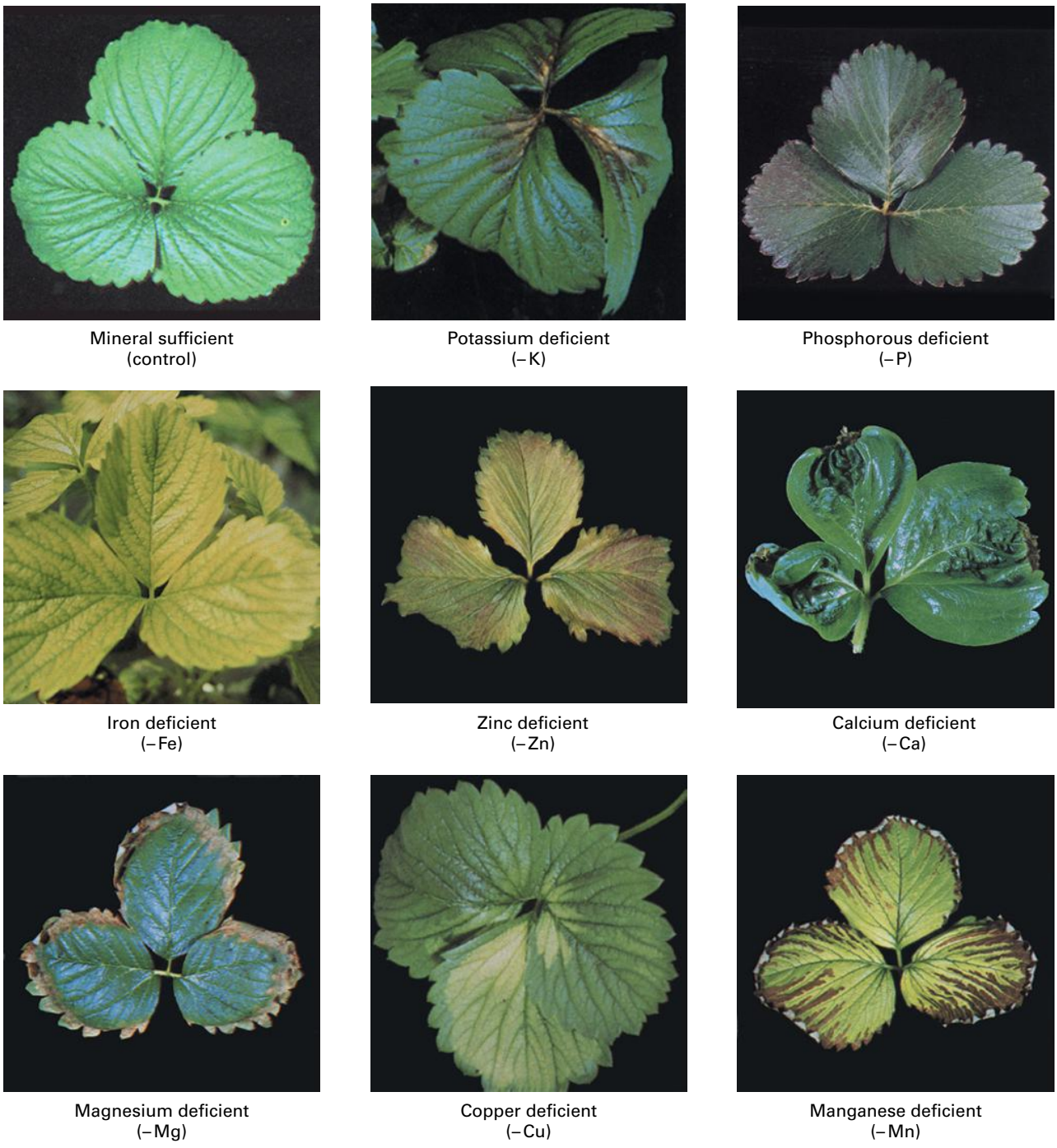


FIGURE 23.1 *Symptoms observed in leaves of strawberry plants deficient in K, P, Fe, Zn, Ca, Mg, Cu, or Mn. A leaf from a mineral-sufficient control plant is also shown.*
Source: Ulrich & Allen (1992). Agri. Exp. Station Bull. 1917. University of California Board of Regents, Division of Agriculture and Natural Resources, Davis.

TABLE 23.1 *Concentrations of essential mineral nutrients considered to be in the adequate range for plants.*

Element	Chemical symbol	Concentration in dry material ($\mu g\ g^{-1}$)	Concentration in fresh tissue*
Macronutrients			
Nitrogen	N	15,000	71.4 mM
Potassium	K	10,000	17 mM
Calcium	Ca	5,000	8.3 mM
Magnesium	Mg	2,000	5.5 mM
Phosphorus	P	2,000	4.3 mM
Sulfur	S	1,000	2.1 mM
Micronutrients			
Chlorine	Cl	100	188 μM
Boron	B	20	123 μM
Iron	Fe	100	120 μM
Manganese	Mn	50	61 μM
Zinc	Zn	20	20.4 μM
Copper	Cu	6	6.2 μM
Molybdenum	Mo	0.1	0.07 μM
Nickel	Ni	0.005	0.006 μM

*Fresh weight concentrations were calculated by assuming a 15:1 fresh weight–dry weight ratio.

zinc, copper, molybdenum, and nickel) usually found in plants are 100- to 10,000-fold less than those of the macronutrients.

Of the 17 nutrient elements determined to be essential in plants, 14 are shown in Table 23.1, and the last element listed, nickel, was shown to be essential only within the last 30 years. The three elements most abundant in plant tissues (carbon, hydrogen, and oxygen) are not included in the table. Also not listed are sodium, silicon, and cobalt, which some researchers view as beneficial but not essential.

23.2 Mechanisms and regulation of plant K^+ transport

23.2.1 K^+ transport in plants has been studied extensively

Potassium (K^+) is the most abundant cellular cation, with cytoplasmic concentrations regulated between 80 mM and 200 mM, and total tissue concentrations of approximately 20 mM. It plays roles in myriad cellular and whole-plant functions, serving as an osmoticum for cellular growth and stomatal function, balancing the charges of diffusible and nondiffusable anions, activating more than 50 plant enzymes, and participating in numerous metabolic processes, including photosynthesis, oxidative metabolism, and protein synthesis. K^+ is a very mobile nutrient and its uptake from soil and transport within cells and around the whole plant has been studied intensively for the last 50 years. Many of these studies have focused on K^+ transport in roots because roots are the primary mineral-absorbing organs and are amenable to studies of ion transport. A major contribution to our understanding of K^+ transport has also come through the study of stomatal guard cells which are probably the best characterized cells for ion transport processes in plants. Although the importance of controlling and facilitating K^+ entry into the plant at the plasma membrane of root cells and guard cells is unquestioned, other K^+ transport sites within the plant are equally important, particularly when K^+ transport and translocation at the whole-plant level are considered. K^+ recirculation within the plant is well documented, as are complex patterns of K^+ translocation between tissues and organs (see Chapter 15). In white lupine (*Lupinus albus*), about one-half of the absorbed K^+ that is translocated to the

shoot by the xylem is returned to the root by the phloem, and nearly 75% of phloem-borne K^+ returning to the root reenters the xylem stream and is again transported to the shoot. Some sites of K^+ transport are diagrammatically outlined in Figure 23.2.

K^+ enters the root symplasm following transport across the root cell plasma membrane. From these cells, K^+ can travel through the symplasm to the vascular tissues, where it is unloaded from xylem parenchyma into xylem vessels for long-distance transport to the leaves. K^+ is reabsorbed from the xylem into leaf cells. After efflux from fully expanded source leaves, it can be loaded into phloem cells for translocation to actively growing sink tissues (e.g., shoot and root apices), where it can be unloaded by way of symplasmic or apoplastic pathways. K^+ can also cross the tonoplast membrane for storage in vacuoles of both root and shoot cells. The integration and regulation of K^+ transport systems at different sites along the long-distance pathway allows the plant to regulate the partitioning and circulation of K^+. The integration of these K^+ transporters plays a central role in plant growth and development and in the allocation of mineral nutrients in response to changes in nutrient availability. Note that this model is equally relevant for all essential mineral nutrients, because a range of different transporters localized to specific cell types must function to move each essential element throughout the plant.

23.2.2 Early physiological and biochemical studies indicated the existence of multiple K^+ transporters

Prior to the application of radioisotopes and tools of molecular biology, early studies on plant K^+ transport focused on the use of excised roots. Seedlings were grown in dilute hydroponic media, typically dilute Ca-salt solutions (e.g., $CaCl_2$ or $CaSO_4$) because Ca^{2+} was needed to maintain normal membrane function. Roots of these seedlings exhibited extremely high initial rates of mineral ion absorption and thus were useful experimental material. These "low-salt roots" contain low concentrations of mineral salts, high concentrations of sugar (a replacement osmoticum for K^+ salts) and a large transport capacity all of which make it easier to measure the uptake of mineral nutrients. This experimental system is still used even after the introduction of radioisotope methods.

The availability of radioisotopes for biological research enabled new techniques for measuring transport processes to be developed. Investigators could label a solution with a radioisotope or a radioactive analog of the mineral ion of interest (e.g., $^{42}K^+$ or $^{86}Rb^+$ for K^+) to quantify the uptake, translocation, or efflux of the radioactivity administered. Pioneering work in the use of radiotracers to measure mineral ion fluxes advanced the field of ion transport (Box 23.1). Plant biologists were the first to treat mineral ion transporters as enzymes and to apply analysis from enzyme kinetics to studies of K^+ absorption by roots. When low-salt barley (*Hordeum vulgare*)

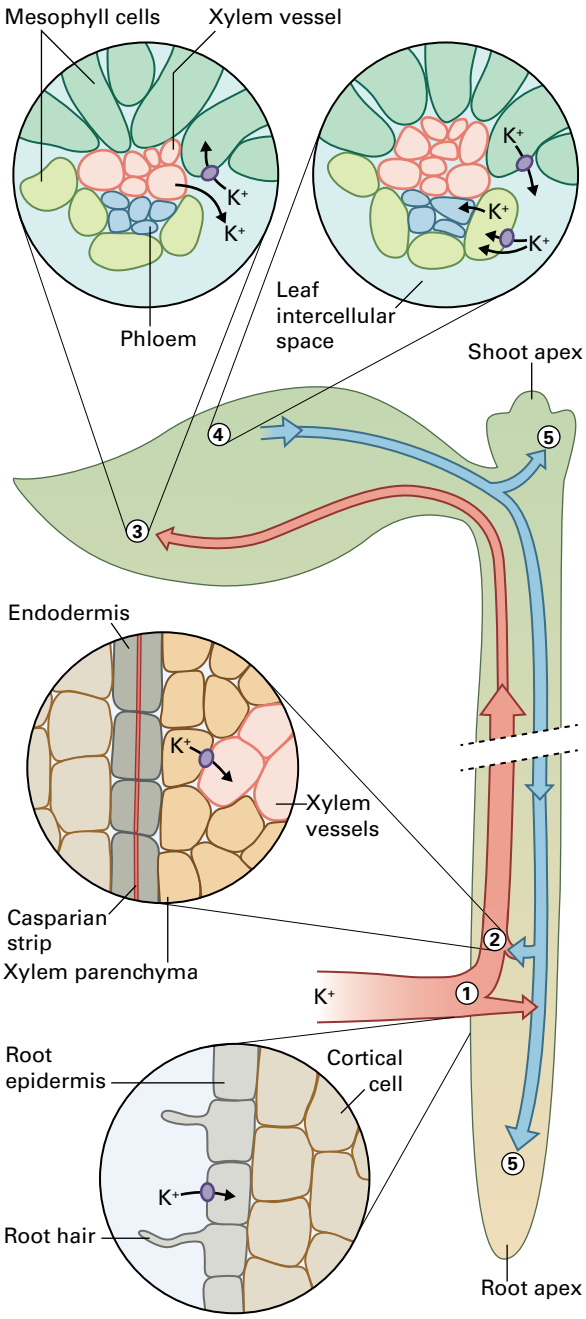


FIGURE 23.2 *Diagrammatic depiction of K^+ transport into and within the plant. K^+ is transported within the xylem (red arrows) and phloem (blue arrows). The numbers represent important transport sites along the long-distance K^+-transport pathway. For four of the five numbered sites, enlargements depict K^+ transport at the cellular level. (1) K^+ is absorbed across the root cell plasma membrane (longitudinal view). (2) K^+ is transported into nonliving, thick-walled xylem vessels by way of efflux across the xylem parenchyma plasma membrane (cross-sectional view). (3) K^+ is transported by the xylem to the shoot (leaf), moves from the xylem vessel to the apoplast surrounding the neighboring leaf cells, and is absorbed into the leaf parenchyma cells (cross-sectional view). (4) K^+ is loaded into the phloem of a fully expanded source leaf after K^+ efflux from leaf cells. Transport into the sieve tube–companion cell complex can occur by a combination of apoplastic and symplasmic routes (cross-sectional view). (5) K^+ moves through the phloem to the shoot and root apices, where it is unloaded for subsequent use.*

BOX 23.1

Radioisotopes are used to measure ion fluxes in cells

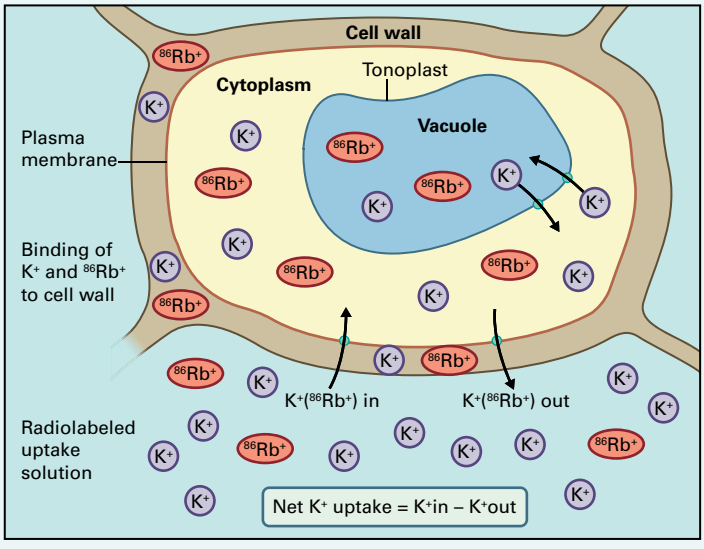
Radioisotopes have been used to monitor mineral ion transport processes in plants for almost 50 years. It is relatively easy to immerse plant roots (or other tissues such as excised leaves) for a prescribed time in an uptake solution labeled with radioisotope, wash the tissue to remove adhering radiolabeled solution, and quantify the radioisotope associated with the tissue by detecting either β- or γ-radiation. Using radioisotopes to measure ion flux accurately, however, is not easy. The difficulty arises from the anatomical characteristics of plant cells. As shown in the accompanying figure, a plant cell contains three major compartments: cell wall, cytoplasm, and vacuole. When the cell is placed in an uptake solution containing $^{42}K^+$ or $^{86}Rb^+$, cation-binding sites and pores in the cell wall are the first sites to bind or accumulate the radiotracer. As the concentration of radiotracer within the cell wall near the plasma membrane surface increases, the K^+ that is transported across the plasma membrane becomes a mixture of unlabeled ions and the radioisotope analog ion. Given longer uptake times, the radioisotopic fraction of the K^+ pool in the cytoplasm will increase. When the amount of radioisotope in the cytoplasm becomes great enough, a substantial radioisotope efflux out of the cell and influx into the vacuole will occur. This combination of efflux and influx confounds attempts to measure a unidirectional influx.

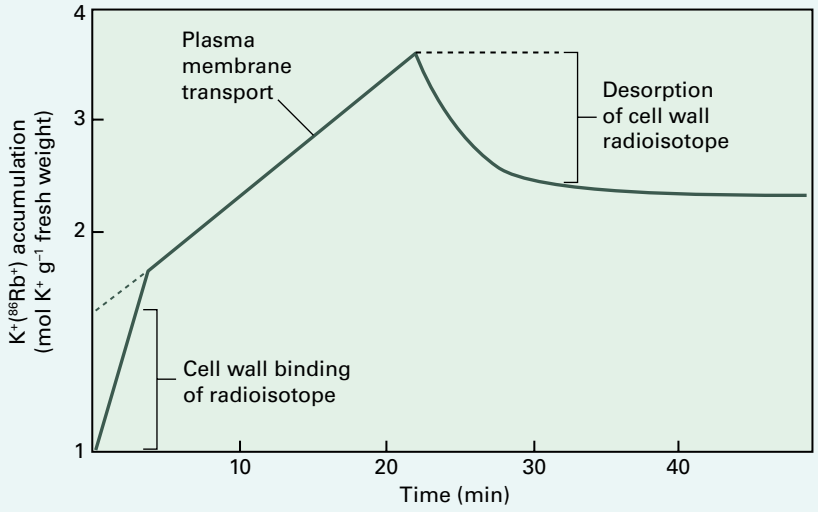
Under steady-state conditions, the entry of mineral ions into cells is a net flux consisting of unidirectional influx and efflux components. Because researchers are usually interested in the unidirectional influx of an ion, the duration of the uptake period is crucial: enough time must elapse for quantifiable concentrations of radioisotope to enter the symplasm. However, an overly long uptake period provides time for a substantial efflux of absorbed radioisotope out of the cell and can create conditions in which the entry of ions into the cell is limited by the rate of transport into the vacuole.

Because the cell wall can bind and accumulate a large amount of cationic radioisotope, a desorption regime must be developed that effectively removes the radiolabel from the cell wall. This desorption period must also be timed carefully, so that a large fraction of the cell wall label is removed but not the radioisotope that has been transported into the cytoplasm. Generally, for a monovalent cation such as K^+, unlabeled uptake solution is an effective desorption solution. Alternatively, solutions that contain high concentrations of K^+ and Ca^{2+} can be used to optimize desorption of $^{42}K^+$ or $^{86}Rb^+$ from negatively charged cell wall binding sites.

The graph shows a time course for radioisotope accumulation and subsequent desorption in plant roots. After an initial rapid phase of isotope accumulation as label equilibrates with and binds within the wall, there is a slower phase of radioisotope accumulation, resulting from unidirectional cation influx into the cytoplasm. The effect of terminating radiotracer uptake by transferring the radiolabeled roots into desorption solution is also indicated. Under ideal conditions, the desorption phase rapidly removes most of the radiolabel in the cell wall without affecting the radiolabel accumulated in the symplasm. The difference between the amount of desorbed radiotracer, and the total amount of radiotracer present in the plant tissue before desorption, represents a measure of unidirectional influx into the cytoplasm.

To obtain a reasonable measure of unidirectional K^+ influx into root cells, one effective uptake-desorption





regime for robust plant roots such as maize or barley, or for smaller roots such as those of *Arabidopsis*, utilizes a radiotracer uptake period of 10 to 20 minutes, followed by a desorption period of 10 to 20 minutes. If uptake is continued for longer periods (several hours), a third, slower phase of accumulation, caused by radiotracer efflux out of the cell or significant flux into the vacuole, is often seen. This process tends to be slower than the ion influx through the plasma membrane.

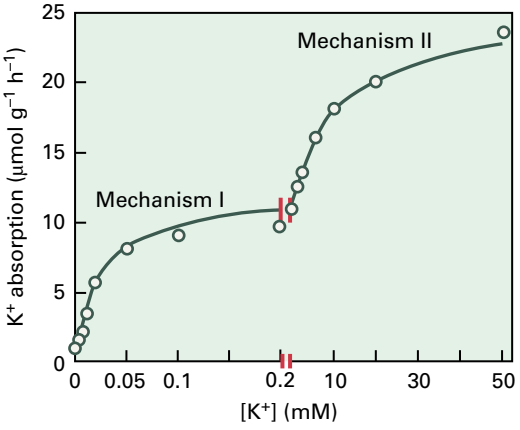


FIGURE 23.3 *Dual isotherm depicting the rate of K^+ absorption in barley roots over a wide range of K^+ concentrations in the absorption solution. Note change in the concentration scale after 0.2 mM K^+.*

roots were exposed to solutions containing low concentrations (0 to 200 μM) of the K^+ analog $^{86}Rb^+$, the resulting high-affinity uptake demonstrated saturating (Michaelis–Menten) kinetics. The high-affinity K^+ transporter, which was designated Mechanism I, was subsequently shown to transport K^+ (and Rb^+) preferentially over other alkali cations. Over a broader concentration range for K^+, the uptake kinetics of K^+ had a complex appearance that could be more clearly represented by two separate saturating curves (Fig. 23.3). It was proposed that roots also contain a low-affinity uptake system, Mechanism II, which is active at higher external concentrations of K^+. This pattern of K^+ uptake was described as the **dual isotherm** and was hypothesized to reflect the activities of two families of transporters. High-affinity K^+ transport was thought to dominate at low concentrations of K^+ in soil, whereas at higher K^+ concentrations, a low-affinity K^+ transporter operated that was less specific for K^+ over other alkali cations (such as Na^+). The concept that mineral uptake involves distinct transporters with different substrate affinities is further supported by thermodynamic evidence. At low external concentrations of K^+ (less than 100 μM), root cells often take up K^+ against the electrochemical potential gradient for the cation (see Chapter 3). Under these circumstances, uptake cannot occur by diffusion and instead must be mediated by either an ATP-driven ion pump or a transporter that is coupled to the energy stored in a transmembrane gradient of H^+ or Na^+.

Subsequent physiological studies provided evidence for separate high- and low-affinity transporters of K^+ in roots. For example, Figure 23.4 illustrates the kinetics of K^+ influx in maize (*Zea mays*) roots, investigated by studying Rb^+ as an analog of K^+. The transport kinetics are complex and appear to result from the functioning of a saturable high-affinity transporter and a low-affinity K^+ transporter that exhibits first-order kinetics. With the use of specific inhibitors such as *N*-ethylmaleimide (NEM), the high-affinity uptake could be selectively inhibited without impairing the linear transport component. In other experiments, the application of a K^+-channel blocker such as tetraethylammonium (TEA) ion selectively inhibited the linear, low-affinity transport component. Further physiological studies showed that the high-affinity K^+ uptake system exhibited increased transport activity induced by K^+ starvation, a very high affinity for K^+ (K_m = 5–30 μM), and a strong selectivity for K^+ and Rb^+ over

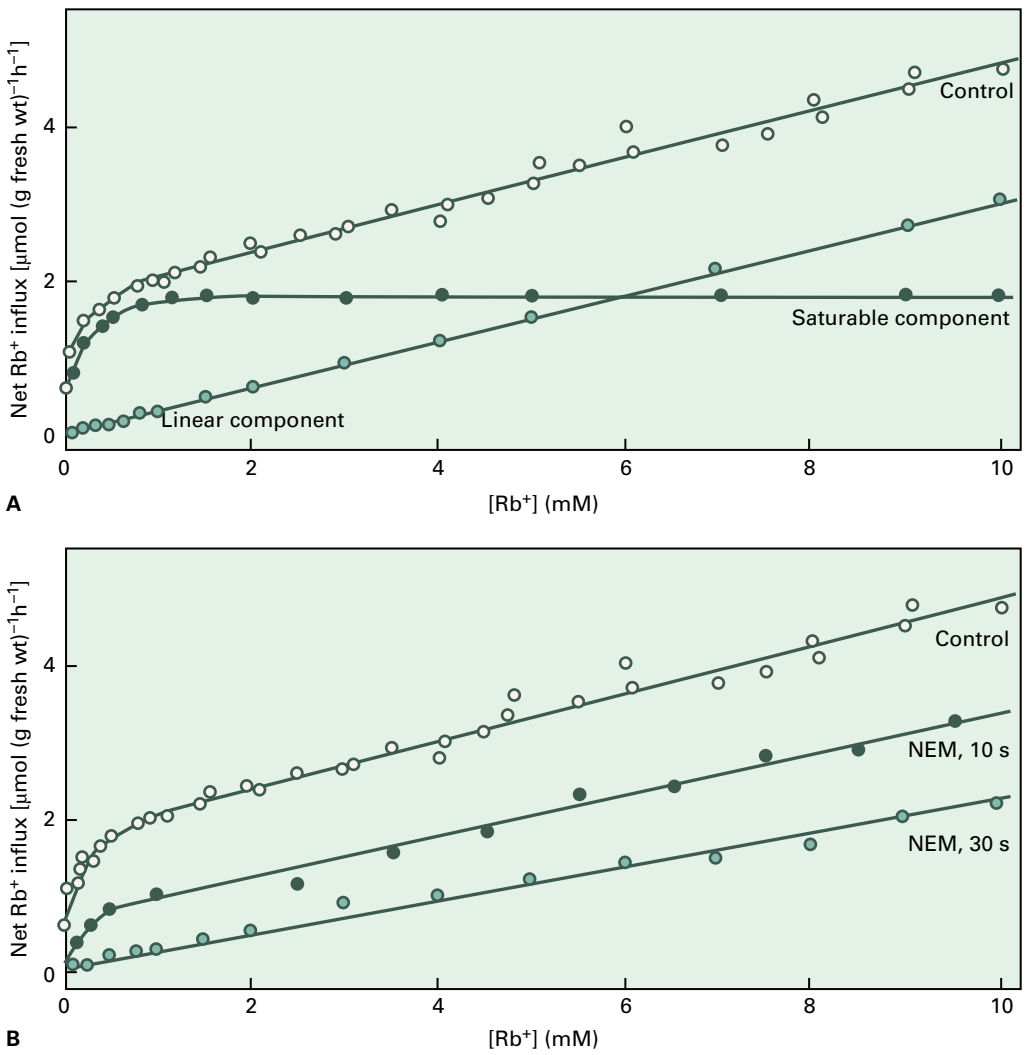


FIGURE 23.4 *Kinetics of $^{86}Rb^+$ influx into maize roots grown in high salt conditions. (A) The control curve (white) has been separated into its saturable high-affinity (dark symbols) and linear low-affinity (lighter symbols) transport components. (B) Influence of the sulfhydryl modifier N-ethylmaleimide (NEM) on $^{86}Rb^+$ influx in maize roots grown in high salt conditions. Root segments were pretreated with 0.3 mM NEM for 10 seconds (dark symbols) or 30 seconds (lighter symbols), then washed for 10 minutes in 1 mM dithioerythritol to bind and inactivate unreacted NEM before $^{86}Rb^+$ uptake. NEM inhibits the high-affinity transporter but does not affect the low-affinity transporter.*

other alkali cations. In contrast, the low-affinity K^+ transporter was found to be less selective for K^+ and Rb^+ over Na^+, and less influenced by changes in the K^+ status of the plant. However, more-definitive evidence supporting the existence of multiple K^+ transporters has been derived from the molecular and biophysical studies detailed below.

23.2.3 The carrier-kinetic approach for analyzing ion transport

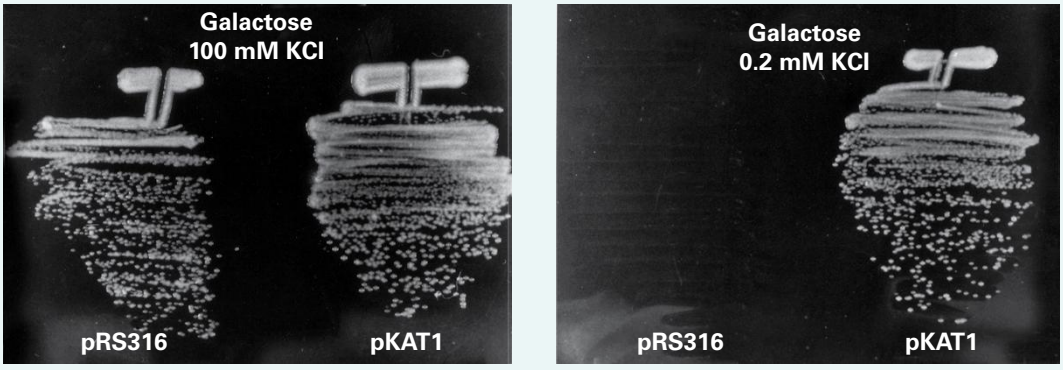
When Michaelis–Menten enzyme kinetic analysis was first applied to concentration-dependent studies of root K^+ uptake, it had a big impact on the field of ion transport. This approach gave researchers a new way to look at and analyze ion transport processes, both in plants and in a wide range of other organisms. Transport of a wide range of substrates by many plant and animal tissues was observed to involve complex kinetics. Often, ion uptake curves contained several different phases or components. From the results of the molecular cloning and genetic dissection of different plant K^+ transporters, including several different root K^+ transporters, we now know of the existence of multiple K^+ transporters operating over a range of K^+ concentrations; however, the identity and function of high- and low-affinity transporters in roots is still not fully elucidated. While there are multiple K^+ transporters that play distinct and sometimes overlapping roles in high and low affinity uptake, characterization of several of them has shown that a single transporter can yield complex kinetics which may be regulated by post-translational modifications. For example, K^+ transport by cells of *Arabidopsis* and of yeast (*Saccharomyces cerevisiae*) expressing the K^+ transporter AtKUP or studies in *Xenopus laevis* oocytes on the nitrate transporter NRT1.1 show that a single protein can mediate both high or low affinity ion uptake.

BOX 23.2 Yeast complementation: a powerful tool for plant mineral nutrition

The single-celled yeast, *Saccharomyces cerevisiae*, has proved of immense value to researchers wishing to isolate new genes encoding ion transport proteins from plants. The genome of *S. cerevisiae* is completely sequenced and routine methods allow knockout mutations to be generated in any gene. Yeast is a good model for plant cells because like plants, yeast pumps protons across its plasma membrane to generate an electrochemical gradient. This gradient in pH and electrical potential drives the flux of many ions across the plasma membrane. The characterization of ion transport processes in yeast and the isolation of the corresponding genes have typically preceded such studies in plants. The availability of yeast mutants defective in specific transport processes allows related genes to be cloned from plants by *functional complementation*. This method allows cDNAs encoding transport proteins with a particular function to be isolated from a bank or library of thousands of cDNA clones. The cDNA library is first constructed from the mRNA of the tissue of interest (e.g., roots) and cloned into a vector that will express the cDNA in yeast. Once the plasmid library has been introduced into a specific yeast mutant (e.g., a mutant for K^+ transport), the yeast can be screened on selective medium (e.g., low K^+ concentration) where the only cells that grow are those expressing the plant cDNA that complements the mutation. Many hundreds of thousands of yeast cells, each expressing a single plant cDNA, can be screened rapidly. This procedure has been instrumental in the discovery of many plant genes encoding transport proteins for K^+, phosphate, sulfate, Fe^{2+}, Zn^{2+}, Cu^+, Mn^{2+}, Ca^{2+}, and borate.

Yeast complementation can also be used to establish the function of a specific cDNA that shows sequence homology to other transport proteins. In this case the mutant yeast is transformed with a single plasmid–cDNA construct rather than a population of plasmids, and complementation of the mutation confirms the proposed function. In the example shown, the *trk1trk2* mutant of *S. cerevisiae* defective in K^+ transport shows restored growth after transformation with pKAT1 (vector containing a plant K^+ transport gene) but not with the empty pRS316 vector (control). Note that the control and the mutant expressing *KAT1* grow equally well on high-K^+ medium (100 mM; left), whereas at a low concentration of K^+ (0.2 mM), only cells expressing *KAT1* are able to grow (right). Yeast has also been used to isolate cDNAs that confer tolerance to toxic concentrations of ions and many of these encode transport proteins. Once it is demonstrated that the plant proteins function in yeast this simpler system provides enormous advantages for studying their transport properties in more detail.

Source: Anderson et al. (1992). Proc. Natl. Acad. Sci. USA 89:3736–3740.



23.2.4 Model biological systems and high-resolution molecular and electrophysiological tools have provided new insights into the mechanisms of mineral transport in plants

Over the past 30–40 years our understanding of K^+ transport systems in plants has greatly increased with the advent of new technologies and by the use of biological systems (termed heterologous systems) for cloning and characterizing the function of plant mineral ion transporters. Starting in the 1990s *Saccharomyces cerevisiae* was used very effectively as a heterologous system to clone genes encoding K^+ transporters as well as those of many other ion transporters (Box 23.2). While *S. cerevisiae* proved to be difficult for electrophysiological studies, these cells could be very easily used with radiotracers for studying substrate specificity of individual transporters. By contrast, oocytes of *Xenopus laevis* provide a high-resolution system for electrophysiological characterization (see Chapter 3.4.2). *X. laevis* oocytes are relatively large (≈1 mm diameter), single-celled structures that are readily injected and impaled with microelectrodes. Typically, the

cDNA of a transport protein to be studied is transcribed to cRNA and then injected in the oocyte. The oocyte translates the cRNA and after several days of incubation, transport function can be studied by comparison with water-injected controls. *Xenopus* oocytes allowed for high-resolution characterization of K^+ channel kinetics and substrate selectivity using sophisticated electrophysiological techniques.

The patch clamping technique developed in the 1980s for the study of membrane transport mechanisms was another important technological advance. Although the patch clamp technique was first applied to animal cells, it was quickly adapted for studies of plant cell membranes. Patch clamping was applied to plants in the study of K^+ channels in the guard cell plasma membrane (see Box 3.6). Patch clamp analysis of protoplasts derived from various cell types (e.g., root cells, guard cells, leaf cells, and cereal aleurone cells) revealed the presence of two types of K^+ channels: inward-rectifying channels, which open on hyperpolarization of the membrane potential (E_m) to facilitate K^+ uptake, and outward-rectifying channels (K^+_{out} channels), which open on depolarization of E_m and transport K^+ out of the cell. Outward-rectifying channels are involved in osmotic adjustment, stomatal function, regulation of E_m, and the unloading of salts from xylem parenchyma into xylem vessels for long-distance transport to the shoot. Plant K^+_{in} channels differ from their animal counterparts by remaining open for long periods. This property is important because they function as a major transport pathway for acquisition of K^+ from soil as well as during the slow opening and closing of stomata that require sustained fluxes of K^+ into or out of the guard cells.

Electrophysiological and molecular tools are now routinely used to resolve questions concerning plant K^+ transport. Whereas heterologous expression systems provide information about single transport molecules, electrophysiological experiments in which root cells are impaled with a single salt-filled glass microelectrode provide information about the voltage gradient across the plasma membrane (i.e., **membrane potential,** or E_m, see Box 3.2 Chapter 3). Early studies indicated that high-affinity K^+ uptake is **electrogenic** (see Chapters 3 and 14) meaning that it is associated with current flow across the membrane. More recently microelectrodes have been used together with genetic tools to dissect the function of specific K^+ channels. In *Arabidopsis*, a mutant disrupted in AKT1 (see Section 23.2.5) revealed that this K^+ channel contributed between 55 and 63% of the K^+ transport capacity of the cell when external K^+ concentration is between 10 and 1,000 μM. Initially this result was surprising because it had been thought that channels would be ineffective at absorbing K^+ from low external concentrations since they only facilitate the passive movement of ions across membranes (i.e., down their electrochemical gradient). The electrochemical gradient comprises the sum of the electrical (membrane potential) and chemical gradients (inside vs. outside concentration of K^+). It was subsequently shown that membrane potentials of root cells reach negative potentials as low as –235 millivolts, which is sufficient to drive the uptake of K^+ at these low external K^+ concentrations. Recently, double mutants of *Arabidopsis* confirmed that AKT1 and a high-affinity K^+ transporter contribute to K^+ uptake in root cells when external K^+ concentrations are very low. These findings highlight how molecular, genetic, electrophysiological, and radioactive tracer technologies can be combined to fully dissect and understand membrane transport processes in higher plants.

23.2.5 K^+ transporters are encoded by numerous plant genes

Although the physiological and biophysical studies discussed above have increased our understanding of plant K^+ transport and nutrition they do not fully describe the complexity of K^+ transport mechanisms in plant tissues such as roots. As researchers gain new information about the range of K^+ transporters present in plants along with the relationship between transporter structure, function, and regulation, they can elucidate the multiple roles K^+ transport plays in the growth and development of intact plants.

Biochemical approaches have primarily been successful for characterizing H^+-ATPases because these transport proteins are relatively abundant in the plasma membrane and tonoplast compared to channels or carrier-like transporters. Screening cDNA libraries with heterologous probes that encode K^+ transporters was unsuccessful when only animal or microbial genes were available. However, as noted above, complementation of yeast (*S. cerevisiae*) mutants has been a successful method in cloning plant K^+ transport genes as well as a range of other plant solute transporters (Box 23.2).

The first K^+ transport genes to be characterized from plants, *KAT1* and *AKT1,* were cloned by complementation of the yeast K^+ transport-defective mutant *trk1trk2* with an *Arabidopsis* cDNA library. *KAT1* and *AKT1,* which share extensive homology, were both found to encode members of the Shaker superfamily of K^+ channels (see Chapter 3) that contain distinctive structural features such as pore loops. The function of these proteins as inward-rectifying K^+ channels was established on the basis of their current-voltage properties in *Xenopus* oocytes and later confirmed in yeast and insect cells. Figure 23.5, depicting a typical current-voltage relationship for *KAT1* expressed in *Xenopus* oocytes, shows that the channel is activated by the shift of E_m to more negative voltages and then mediates a strong inward current (K^+ influx). The transport characteristics of *KAT1*- and *AKT1*-encoded proteins possess the hallmark properties of inward K^+ channels studied by patch-clamping plant cells, including their voltage dependence, selectivity for K^+ over other cations, time-dependent kinetics, lack of inactivation, and responses to the K^+ channel blockers TEA and Ba^{2+}.

For many years it was a mystery as to why the AKT1 channel could not be functionally expressed in *Xenopus* oocytes. Not all transport proteins can be studied in oocytes for reasons such as low and therefore undetectable currents, lack of protein targeting to the plasma membrane, toxicity to the

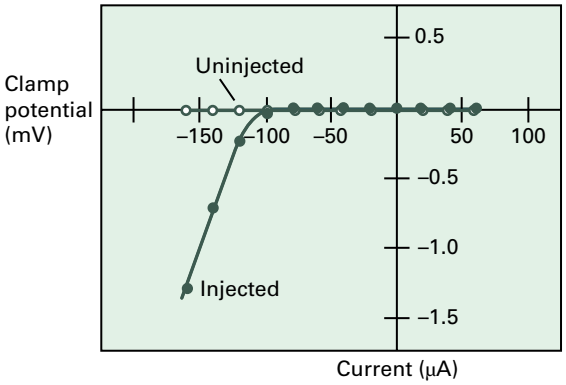


FIGURE 23.5 *Current–voltage relationship for uninjected* Xenopus *oocytes (white) and oocytes injected with* KAT1 *mRNA 4 days before this experiment (dark).* KAT1 *mRNA leads to development of inward current in response to hyperpolarizing voltages more negative than –100 mV, which is typical of an inward-rectifying K^+ channel.*

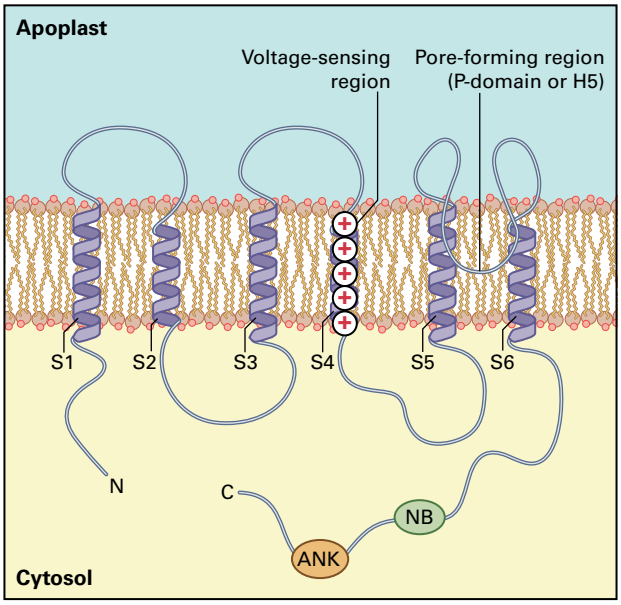


FIGURE 23.6 *Proposed structural model for AKT1, a plant K^+_{in} channel. Six membrane-spanning domains are present near the N-terminus. A nucleotide-binding sequence (NB) and ankyrin-like domains (ANK) are found near the C-terminus. The S4 region, believed to be the voltage sensor, contains several positively charged amino acids within the membrane-spanning region. The P-domain, also referred to as H5, is thought to form the mouth of the pore and to play a critical role in channel selectivity.*

oocytes, lack of post-translational modification, or missing subunits. In the case of AKT1 it was discovered that the channel must be phosphorylated for it to be functional in oocytes. A specific kinase called CIPK23 (CBL-interacting protein kinases) phosphorylates AKT1 *in planta*. The CIPK kinases are found as large families in plants (at least 25 in *Arabidopsis*) and are most similar to the sucrose nonfermenting (SNF) kinases of yeast and the AMP-dependent kinases of animals. The CIPK kinases interact with small Ca^{2+} sensors that act as downstream effectors. These small sensors are named CBLs, standing for **c**alcineurin **B**-**l**ike proteins. This CBL/CIPK/AKT1 pathway implicates Ca^{2+} signaling in the regulation of K^+ uptake. When K^+ is limiting it is likely that increases in reactive oxygen species trigger Ca^{2+} fluctuations, which in turn regulates K^+ uptake.

KAT1and AKT1 share structural features with other channels possessing P-loops (Fig. 23.6). These proteins contain six membrane-spanning domains near the N-terminus (S1–S6), a conserved voltage-sensing region within S4, and the amphipathic P-domain (also called H5) between S5 and S6. The P-domain is highly conserved in the K^+ selective P-loop and in Shaker-type channels and has been shown to form the channel pore that governs ion permeation and selectivity. The common motif that is the signature for K^+ selectivity is comprised of the core amino acid residues GYG. This motif is present in the K^+ selective channels of all organisms and is a major determinant of the selectivity of these pores. These channels are formed by four of the individual subunits shown in Figure 23.6 (see also Fig. 3.26). Carbonyl groups in each of the four filters in the channel tetramer coordinate two K^+ ions. The crystal structure of certain K^+ channels has been determined from many organisms, but not from plants. These studies have provided a detailed understanding of K^+ channel structure and the critical features that determine most aspects of their function. The structure of the channel and its interaction with the hydrated K^+ ions helps explain why the V_{max} of K^+ channels is near the diffusion limit as well as the strong discrimination against smaller cations such as Na^+. The S4 transmembrane domains contain positively charged basic amino acids at every third or fourth position that serves as the voltage sensor for the channel. Movement of this region within the membrane in response to a polarization voltage results in opening and closing of these channels.

The cloning of *KAT1* and *AKT1* led to the identification of additional related genes in *Arabidopsis* and other plant species, indicating the existence of a multigene family encoding K^+ transporters (Table 23.2, Shaker-type cation transporters). In the past 20 years as more sequence information became available and whole genomes sequenced, there have been a large number of *KAT1*- and *AKT1*-like genes identified. One explanation for the large numbers of genes in these families may be related to their localization in specific plant tissues or cell types. For example *KAT1* and its ortholog in potato (*Solanum tuberosum*), *KST1*, are expressed in guard cells and presumably encode K^+_{in} channels involved in stomatal function. AKT1, on the other hand, is localized to the root epidermis and cortex where it plays a role in plant uptake of K^+. *AKT2* (also sometimes designated *AKT3*), which shares 60% identity with *AKT1,* is expressed in leaves but not roots, suggesting that it encodes the same K^+ transport function in leaves as *AKT1* mediates in roots. The C-terminal domain of the potato K^+ channel, KST1, has been used as bait in the yeast two-hybrid system (Box 23.3) to identify proteins that associate with KST1. This approach, expected to identify proteins that regulate the channel or anchor it in the membrane, instead has led to the cloning of

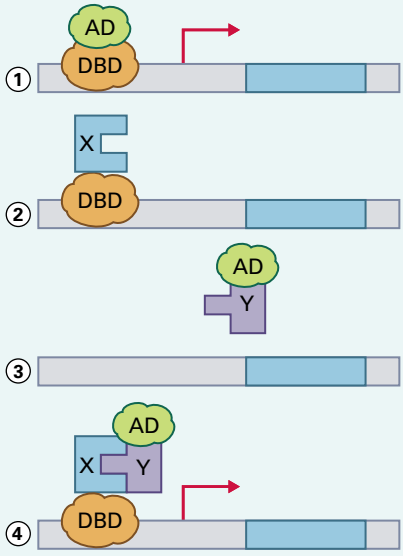
TABLE 23.2 *Number of predicted K^+ transporter genes in the genomes of* Arabidopsis, *poplar, rice, and* Chlamydomonas.

	A. thaliana	*P. trichocarpa*	*O. sativa*	*C. reinhardtii*
Cation transporters				
KcsA type	1	0	0	0
Shaker type	9	11	6	0
TPK/KCO	5	10	4/3	0
Unclassified 6TM1P	0	0	0	9
CNGC	20	12	10	0
TPC	1	1	1	0
HKT	1	2	6	0
KUP/HAK	13	28	25	3

Source: Ward, J.M., Maser, P., Schroeder, J.I. 2009. Plant Ion Channels: Gene Families, Physiology, and Functional Genomics Analyses. *Annu. Rev. Physiol.* 71: 59–82.

BOX 23.3 The yeast two-hybrid system is a genetic method that can identify protein–protein interactions within a cell

The yeast two-hybrid system is based on the modular nature of transcription factors, which generally are composed of two domains: a DNA-binding domain (DBD) and an activation domain (AD). An intact transcription factor, such as the yeast Gal4 protein, binds to specific recognition sequences within a promoter by way of the DBD. Next, the AD recruits the general transcription machinery to the promoter-activating expression of the downstream gene (1; see figure). These two domains can be separated and expressed as fusion proteins either alone or together within yeast cells. When only the DBD (fused to a protein of interest [X]) is expressed, the promoter is bound but transcription cannot be activated because the AD is lacking (2). Similarly, when the AD is fused to a second protein (Y) and expressed, the AD is unable to bind to the promoter and therefore also cannot activate transcription of the downstream gene (3). If X and Y are able to interact, however, coexpression of the two hybrid proteins brings the DBD and the AD into proximity, thereby re-forming an active transcription factor (4). If reporter genes (blue box) are used that confer an easily scoreable phenotype, such as nutrient prototrophy, the ability of X and Y to associate can be easily assessed. The two-hybrid system is widely used to identify new binding proteins, to map binding domains of known interactions, and to generate mutations that affect those interactions.



two new K^+ channel genes, *SKT1* and *SKT2*, which exhibit substantial similarity to *Arabidopsis AKT2*. Subsequent investigations have determined that the C-termini of all K^+_{in} channels contain conserved sequences that are involved in the association of K^+ channel subunits. The heteromeric composition of the K^+ channel tetramer may be another way in which subtle differences in K^+ channel function are determined.

23.2.6 Genome sequences and molecular techniques have revealed multiple gene families encoding K^+ transporters

K^+ channels and transporters control the fluxes of K^+ into and out of plant cells as well as control intracellular concentrations of K^+ in the cytoplasm and in organelles. As for animal cells, plant cells possess both inward (K^+_{in}) and outward rectifying K^+ (K^+_{out}) channels. In plant cells these channels appear to have a similar structure to each other, both having six transmembrane domains and a classical pore loop as described above. The physiological function of inward rectifying K^+ channels ranges from a critical role in the osmoregulation of guard cells to the uptake of K^+ from soils. The opening of inward rectifying K^+ channels is triggered by the hyperpolarization of the membrane potential. In the case of guard cells the inward flux of K^+ through channels leads to the swelling of guard cells and the opening of stomata. In roots, channels play a critical role in K^+ uptake over a wide range of concentrations. While outward rectifying K^+ channels were clearly measurable upon depolarization of the membrane potential in the earliest electrophysiological studies, their molecular identification came much later. One well-characterized outward rectifying channel is called SKOR, the stelar K^+ outward rectifying channel. When expression of this channel was knocked out using genetic methods xylem K^+ concentrations were decreased. This phenotype coupled to the function and localization of the channel in root stelar cells pointed to an important role of SKOR in loading K^+ into the xylem.

Using electrophysiological methods K^+_{out} channels were localized to xylem parenchyma cells. To isolate xylem parenchyma protoplasts from barley roots for patch clamping, the stele was dissected from the root, after which the cell walls were digested enzymatically. Patch clamp studies with these cells identified three types of ion channels in the xylem parenchyma plasma membrane: an inward-rectifying K^+ channel and two outward-rectifying channels—one selective for K^+ and the other a nonselective cation channel. The molecular identification and physiological characterization of this K^+ channel revealed an important mechanism that is involved in the regulation of K^+ translocation from root to shoot.

In addition to the highly selective K^+ channels with six transmembrane domains, there are two other major classes of related channels that include the CNGCs (cyclic nucleotide gated channels) and TPKs (twin-pore K^+ channels). The CNGCs have six transmembrane domains, a pore region and a C-terminus that contains a cyclic nucleotide-binding domain. The CNGCs are allosterically regulated by cyclic nucleotides and are not activated by membrane potential. Because of the structure of the pore in these channels, they are not selective for K^+ but also transport most divalent cations. The physiological roles of the CNGCs are not well defined, except for a few that have been shown to be involved in plant response to pathogens. In contrast to the nonselective nature of CNGCs, the TPKs are highly selective for K^+ over other cations. These channels contain four transmembrane and two pore domains. TPKs are also known as VKs (vacuolar K^+ channels) because they were first identified in vacuolar membranes of guard cells where they are activated by elevated concentrations of cytosolic Ca^{2+} of about 1 μM. TPK1 has two EF-hand Ca^{2+} binding domains in the C-terminus which are likely to be the basis of how the channel is regulated directly by changes in cytosolic Ca^{2+} concentrations. *Arabidopsis* mutants in which TPK1 has been disrupted lack detectable VK channel activity as measured using electrophysiological methods and exhibit slower stomatal closing in response to ABA. This suggests an important role for this channel in release of K^+ from the vacuole that is required for guard cell shrinkage and stomatal closure.

Plant, fungal and bacterial genomes all possess genes encoding a similar type of transporter that was originally named KUPs (K^+ uptake permease), but in plants they are also known as the K^+ transporters KTs and HAKs. These transporters have 10–14 predicted transmembrane domains. Whereas bacterial and fungal genomes contain only one or two genes encoding these transporters, plant genomes contain many more, with 13 in *Arabidopsis*, 25 in rice (*Oryza sativa*) and 28 in poplar (*Populus* spp.) (Table 23.2). The function of most of the KUP transporters in plants and the reason for the large number of genes encoding these transporters remains a mystery. Disruption of a few of the KUPs in *Arabidopsis* show a distinct phenotype. These include Shy3-1 (short hypocotyl in the dark) whose phenotype results from a point mutation in *AtKUP2*. The mutant *Trh1* (tiny root hair) is caused by a disruption in *AtKUP4*. Both of these phenotypes show reduced cell size and implicate the KUP family of K^+ transporters in cell expansion, one of the key roles that K^+ plays in plant nutrition. An elegant study on cotton (*Gossypium hirsutum*) fiber, one of the largest single cells in the plant kingdom, provided a temporal correlation between the expression of a member of the KUP family and elongation of the cotton fiber. This study provides additional support for the role of these KUP transporters in cell elongation that is presumably driven by the uptake of K^+. Although it is clear that AtHAK5 functions as a high affinity K^+ transporter it cannot be assumed that other members of this family function only in the high affinity mode. In fact AtKUP1 has been shown to be a dual affinity (high and low) transporter and information from fungi and bacteria show that some of the KUPs function as low affinity transporters (Fig. 23.7).

23.2.7 Sodium and sodium–potassium transporters play roles in sodium transport and salt tolerance

The founding member of the *HKT* family was cloned by complementation of the yeast *trk1trk2* K^+ transport mutant with a cDNA library isolated from K^+-starved wheat (*Triticum aestivum*) roots. The deduced amino acid sequence of HKT1 contains eight predicted transmembrane domains and four pore loops. The four pore loops in this single peptide suggest that these transporters function as monomers that resemble the

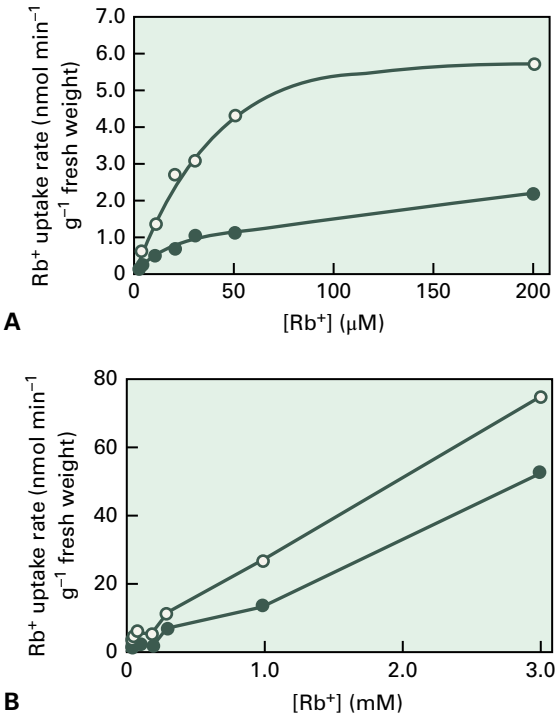


FIGURE 23.7 *Concentration-dependent kinetics of Rb^+ ($a\ K^+$ analog) uptake in transgenic* Arabidopsis *suspension cells expressing* AtKUP1. *(A) Kinetics of Rb^+ uptake from a micromolar solution by cells transformed with* 35S:AtKUP1 *(white symbols) or an empty vector (dark symbols). Here, AtKUP1 is shown to mediate high-affinity K^+ uptake. (B) Kinetics of Rb^+ uptake from a millimolar solution reveal that AtKUP1 can also facilitate low-affinity K^+ uptake.*

Shaker channels formed by four monomers that each contains a single pore loop. Initially, wheat HKT1 was characterized as a high affinity K^+ transporter, only later to be shown to function as a K^+/Na^+ cotransporter or channel. Only one gene encoding HKT is found in the *Arabidopsis* genome, but multiple genes have been found in rice and poplar (Table 23.2).

Early clues as to the function of HKT came from the localization of wheat HKT to the inner root cortex and stele, as well as to the vasculature of leaves and stems. HKTs have been functionally characterized in *Xenopus* oocytes, yeast and tobacco (*Nicotiana tabaccum*) suspension cultured cells. There appear to be multiple genes encoding two types of HKT transporters in plant genomes. One type is characterized as a Na^+ channel and the other as a K^+/Na^+ cotransporter that transports Na^+ in the absence of K^+. Although the function of these transporters has been somewhat controversial, several studies have implicated them as an important determinant that controls Na^+ transport particularly in monocots such as rice and wheat. A current model for how these transporters function in modulating Na^+ levels in leaves is that they reabsorb Na^+ from the xylem into bordering xylem parenchyma cells. It has also been suggested that the uptake of Na^+ by xylem parenchyma cells is associated with K^+ efflux as a result of depolarized cell membranes, thereby enhancing the K^+ concentrations of leaves under saline conditions.

The link between Na^+ and K^+ uptake in many plant species is well known. When plants are grown under saline conditions there is an inverse relationship between Na^+ and K^+ concentrations such that as Na^+ increases in leaves, K^+ concentrations decrease. This knowledge was used to select rice lines under saline conditions that maintained K^+ concentrations in leaves and are salt tolerant because they exclude Na^+. Genetic methods were used to map a QTL in a salt-tolerant rice line (Nona Bokra) to a gene encoding OsHKT1;5. A mutation in this gene was found in Nona Bokra rice that enhances overall Na^+ transport activity when characterized in *Xenopus* oocytes. Within the rice plant, expression of this transporter was localized to xylem parenchyma cells. Based on its localization and function, a model was proposed that OsHKT1;5 reabsorbs Na^+ from the xylem which reduces its transport and accumulation in leaves.

In wheat, two genetic loci have been identified that also lower Na^+ transport to leaves. Both loci (*Nax1* and *Nax2*) possess members of the HKT family that reduce Na^+ transport from root to shoot by removing Na^+ from the xylem and storing it in the vascular parenchyma or in the leaf sheath. *Nax2* was identified in durum wheat with an enhanced ability to exclude Na^+. A gene closely related to HKT1;5 in rice was identified as underlying the *Nax2* locus in durum wheat. Similar to results with rice, this locus in wheat resulted in a higher K^+ to Na^+ ratio in leaves. The gene underlying *Nax1* in wheat was also identified as a member of the *HKT* family and reduces the rate of Na^+ transport from root to shoot by retaining Na^+ in the leaf sheath. Overall, significant progress has been made in the last 10 years in our understanding of the transport proteins that control plant K^+ accumulation and Na^+ transport under saline conditions.

23.3 Phosphorus nutrition and transport

Phosphorus (P) is one of the most important fertilizer inputs for crop plants. P can exist in plants as both soluble inorganic phosphate anions (abbreviated as P_i), and organophosphate compounds. Unlike nitrate and sulfate, P_i is not reduced in plants during assimilation but instead remains in its oxidized state, forming phosphate esters with a wide range of organic compounds. P is an important structural component of nucleic acids and phospholipids, and plays a critical role in energy conversion in the form of high-energy phosphoester and diphosphate bonds. P is important both as a substrate and regulatory factor in photosynthesis and oxidative metabolism, it participates in signal transduction, and it regulates the activities of a diverse array of proteins by way of covalent phosphorylation/dephosphorylation reactions.

Poor P_i availability is one of the major constraints to plant growth because of its low solubility and high sorption capacity in soil. Indeed, some soils contain a high total P content but only have a small fraction that is available to plants as P_i. Soil P_i concentrations are often 1 μM or less, and P_i is rapidly

depleted from the rhizosphere by roots. The majority of P_i in the rhizosphere moves to the root by diffusion, which is a slow process in biological terms and considerably slower than the movement of other macronutrients by mass flow. Plants have evolved specialized mechanisms for obtaining P_i from the soil and roots exhibit an impressive plasticity in response to low availability of P_i.

23.3.1 Phosphate is transported into roots by an active, high-affinity mechanism

Experiments using radiolabeled $^{32}P_i$ have shown that $H_2PO_4^-$ is the primary form of P transported into root cells from the soil. Since root cells must transport this anion against a sizeable negative membrane potential and concentration gradient (low μM in the soil compared to mM in the cytoplasm) the uptake of P_i into root cells is an active process requiring expenditure of energy. This active uptake occurs by transport coupled to the transmembrane electrochemical H^+ gradient generated by the plasma membrane H^+-ATPase. This is supported by the following observations:

- Root P_i uptake is often accompanied by an alkalinization of the external media, which translates into a H^+: $H_2PO_4^-$ flux stoichiometry of between two and four protons for every P_i taken up.
- Root P_i uptake is enhanced when the pH of the uptake solution is lowered.
- Electrophysiological measurements of root P_i influx show that the process is accompanied by a transient depolarization of E_m, followed by a repolarization (and often a hyperpolarization) of E_m. This is consistent with the operation of a H^+-P_i cotransporter that transports net positive charge into the cell. The acidification of the cytoplasm stimulates the H^+-ATPase, which explains the subsequent repolarization.
- Studies using pH microelectrodes and pH-sensitive fluorescent dyes show that P_i absorption acidifies the cytoplasm.
- Protonophores such as CCCP, a molecule that collapses transmembrane H^+ gradients, abolishes root P_i uptake.

Studies using roots, leaves, and cell suspensions from different plant species and physiologically relevant concentrations of P_i (low micromolar range) show the existence of high-affinity P_i transport (K_m = 1–5 μM). This high-affinity transport is tightly regulated by plant P status. For example, if P is withheld from roots of tomato (*Solanum lycopersicum*) and barley for several days, high-affinity P_i influx is markedly stimulated in these plants. When P_i is resupplied to the roots, the influx of P_i declines within 1–2 hours. The inverse relationship between root P_i influx and plant P status can be seen in electrophysiological traces. Addition of P_i to roots of P-replete plants results in little or no depolarization of E_m, which correlates with the magnitude of P_i influx (Fig. 23.8A,B). However, in plants starved of P for 7 days (Fig. 23.8C) or 14 days (Fig. 23.8D), the membranes are depolarized in proportion to the severity of P deficiency. The relationship of root P_i uptake to P nutrition will be revisited in Section 23.3.3 when discussing molecular regulation of root P_i uptake.

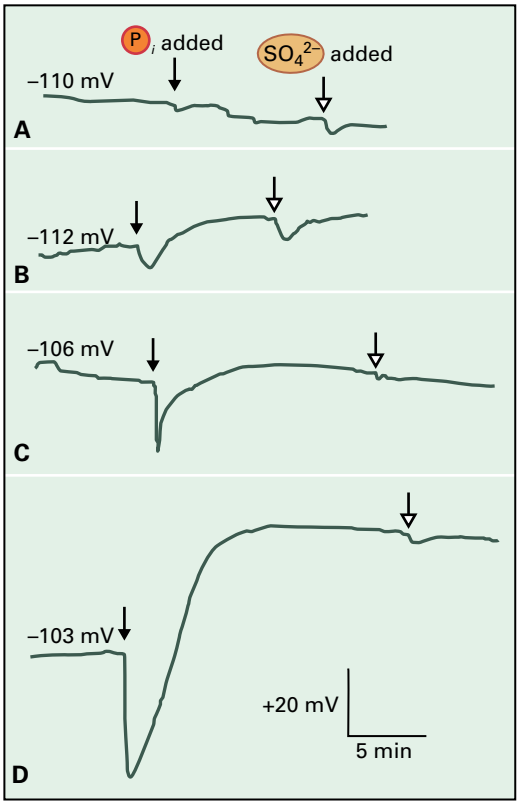


FIGURE 23.8 *Phosphate-induced transients in transmembrane electrical potential in roots of* Trifolium repens. *The solid arrows indicate the addition of 125 μM P_i to media buffered at pH 5 with MES buffer and the resulting change in the root membrane potential. The open arrows indicate the addition of 63 μM sulfate as a control for the general effect of mineral anions on the membrane potential. (A) Plant grown on P_i for the entire 29-day period; (B) P_i withheld for final day of growth; (C) P_i withheld for last 7 days of growth; (D) P_i withheld for last 14 days of growth.*

23.3.2 Roots use various mechanisms to increase the bioavailability of P in the rhizosphere

P is the macronutrient least available to plant roots, because it is readily bound to soil particles and soluble ligands. In acid soils P_i forms insoluble complexes with Fe(III) and Al cations and forms strong chemical bonds with metal oxides on mineral surfaces. In calcareous soils, similar reactions occur between P_i and calcium carbonate. Additionally, soil microbes can effectively convert P_i to organic forms of P that are not readily taken up by roots. Plants have developed an array of mechanisms to mine otherwise unavailable soil reserves of P. In response to P deficiency, the structure and function of root systems can be altered to increase the solubility of soil P and to enhance the exploration of soils by root systems. Root

characteristics that enhance the uptake of P_i under conditions of low P availability include the following:

- Associations between roots and **mycorrhizal** fungi which help plants acquire P_i from a greater soil volume.
- Alterations in root architecture and branching to allow more effective exploration of the soil.
- Increases in root hair density and length to increase the absorptive surface area of roots and to reduce the length of the diffusive pathway for P_i to reach the root surface.
- Release of organic acids and H^+ to solubilize inorganic forms of P.
- Exudation of phosphatases to release P_i from organic forms of P in the soil.
- Upregulation of high-affinity P_i transporters in the root cell plasma membrane.

Utilization of these mechanisms varies among genotypes, not only between different plant species but also between cultivars within species. This suggests that breeding and molecular approaches have the potential to enhance the ability of crops to use soil P more efficiently.

The beneficial effects of mycorrhizal associations on plant growth largely relate to the increased uptake of immobile nutrients from the soil, notably P_i. The predominant mycorrhizal associations that influence root P absorption involve the **ectomycorrhizae** and **vesicular-arbuscular mycorrhizae** (VAM; Fig. 23.9). VAM are the most abundant mycorrhizae and colonize roots of a wide range of plant species in almost all types of soils. They form extensive hyphal networks in the soil and within root cortical tissues, forming intimate associations in cells without penetrating the plasma membrane of host cells. VAM are characterized by the formation of branched haustoria (arbuscules) within the tissues of the root cortex that are the sites of solute exchange between the fungus and the host plant. Solutes that are exchanged by plant and fungi must therefore traverse the plasma membranes of both organisms. The fungal mycelium extends into the soil, and in low P soils, VAM can enhance P_i absorption by root systems two- to six-fold over nonmycorrhizal roots. The stimulation of root P_i absorption by VAM is a result of a more thorough exploration of soil P reserves. Extensive hyphal growth, similar to increased root hair growth, reduces the distance that P must diffuse to reach the sites of absorption. The relationship between fungus and plant is a symbiotic one because the movement of P_i from the fungus to the plant is exchanged for a flow of fixed carbon from the plant to the fungus. The regulation of P nutrition in plants is substantially influenced by mycorrhizal interactions with roots (see below).

In response to P starvation some plant species form cluster roots (also known as proteoid roots) that exude large quantities of organic anions. This phenomenon has been extensively studied in white lupine and members of the Proteaceae. P deficiency triggers proliferation of short secondary lateral roots that form a tight "bottlebrush-like" cluster densely covered in root hairs. These specialized root structures enable the plant to effectively extract immobile nutrients such as P_i from a limited soil volume

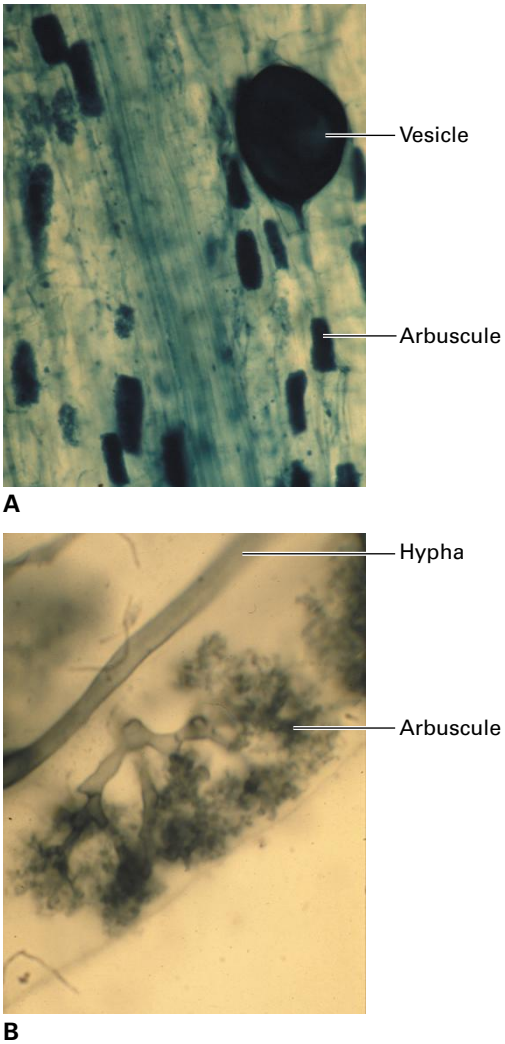


FIGURE 23.9 *Light micrographs of vesicular–arbuscular mycorrhizae (VAM, or endomycorrhizae) showing the structure of vesicles (A) and arbuscles (B).*
Source: (A) D. Redecke, University of Marburg, Germany; previously unpublished. (B) K. Wex, University of Marburg, Germany; previously unpublished.

(Figs. 23.10 and 23.11). Cluster roots release organic anions at a particular stage of development. These organic anions include citrate and malate, which are effective chelators of Al and Fe in the soil. The high concentrations of organic anions around the cluster roots solubilize mineral forms of P to increase the availability of P_i which is rapidly taken up by the dense mat of root hairs that cover the roots. White lupine can release as much as 25% of its total fixed C as organic anions into the soil illustrating the priority that plants place on obtaining scarce sources of P.

When P-deficient many plants also release phosphatases from roots. Plants synthesize a wide range of phosphatases, which are classified as alkaline or acid phosphatases based on their pH optima. The enzymes secreted from roots in response to P deficiency are acid phosphatases, which hydrolyze a wide range of P-containing substrates. These secreted phosphatases are capable of hydrolyzing esterified forms of P (e.g., ATP) *in vitro* and therefore may enhance P_i availability from soil

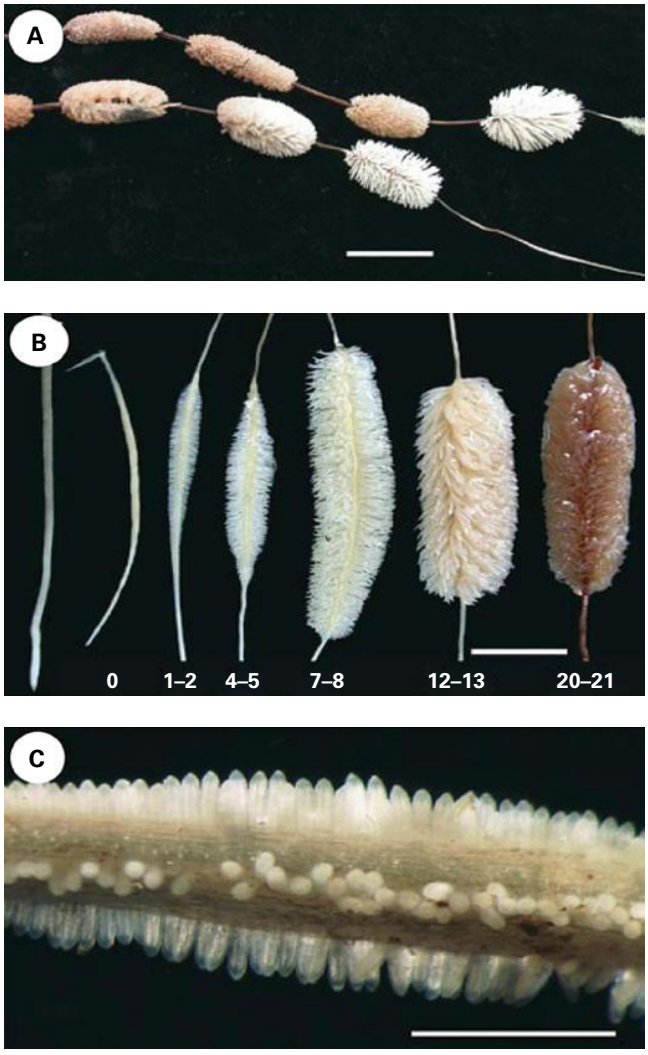


FIGURE 23.10 *Cluster roots of Australian native* Hakea *spp. grown in nutrient solution with low P_i concentration (less than 1 μM). (A) Cluster roots on* Hakea petiolaris *showing distinct "bottlebrush-like" structures separated by unbranched regions. The youngest cluster roots are on the right side of photograph. Bar = 20 mm. (B) Six stages of cluster-root development in* H. prostrata*, labeled from left to right, are arranged according to their age. The numbers indicate the days following rootlet emergence from the swollen axis (day 0) until cluster-root senescence (day 20 to 21). A noncluster root is shown on the far left. Bar = 10 mm. (C) Close up of a young cluster root of* H. prostrata *approximately 2–3 days after rootlet emergence. Thousands of densely-spaced rootlets emerge from the parental root axis in longitudinal rows. Bar = 5 mm.*

in the rhizosphere by releasing P_i from organic sources. Although many of these enzymes have been characterized, direct evidence that they play roles in P nutrition is available for only a few. For example, a mutation in the *AtPAP26* gene, a member of the secreted acid phosphatase family of *Arabidopsis*, results in mutant plants that grow more slowly than wild type in low P conditions. In addition to being secreted, a proportion of AtPAP26 resides in the vacuole and the impaired growth may be related to an inability to effectively recycle P_i within the plant as well as a reduced capacity to utilize organic P in the soil.

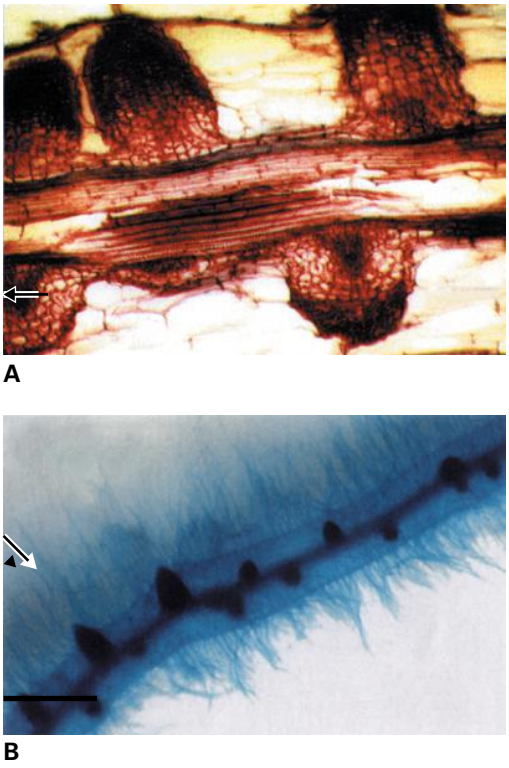


FIGURE 23.11 *(A) Longitudinal section of cluster root from a P-deficient* L. albus *plant showing the dense cluster of emerging lateral roots. Solid arrow shows a developing tertiary root meristem. (B) Secondary lateral root excised from* L. albus *plant grown without P. The root was cleared with sodium hypochlorite and stained with methylene blue. By 8 days after emergence, tertiary lateral roots are beginning to emerge through the epidermis (solid arrow). Bar = 1 mm. Source:* (A,B) Johnson et al. (1996). Plant Physiol. 112:31–41.

23.3.3 Molecular studies provide insights into the complex regulation of P acquisition and homeostasis in plants

The molecular regulation of P nutrition is being revealed by the characterization of mutants perturbed in P_i acquisition and homeostasis. Central to the homeostasis of P nutrition in plants is the regulation of P_i uptake by roots from the external medium. The *Pht1* (***Ph**osphate **t**ransporter**1***) P_i transporter genes from plants were originally cloned based on their sequence similarity to PHO84, a high-affinity P_i transporter of the yeast *S. cerevisiae*. Indeed many of these plant genes are able to complement the *pho84* yeast mutant defective in P_i uptake. Members of the Pht1 family of P_i transporters share important structural similarities (Fig. 23.12). Predicted secondary structures are characterized by six N-terminal transmembrane domains and six C-terminal transmembrane domains separated by a central hydrophilic region. Additional structural motifs that are conserved in these P_i transporters include sites for protein kinase C- and casein kinase II-mediated phosphorylation and for N-linked glycosylation.

Many Pht1 transporters function in high affinity P_i uptake when expressed in plants that is consistent with a role in P_i

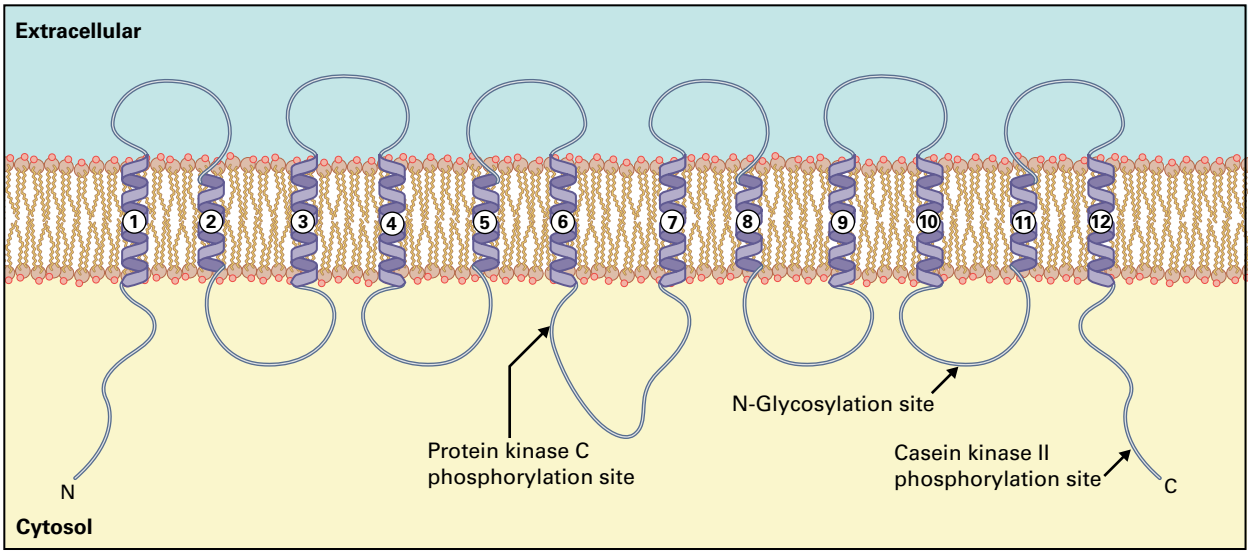


FIGURE 23.12 *Proposed structural model for plant plasma membrane high-affinity P_i transporters showing the six-loop-six motif of 12 membrane-spanning domains. The predicted sites for phosphorylation by protein kinase C and casein kinase II and for N-glycosylation are shown.*

uptake from soil. Additional evidence for this role includes: (1) their expression in root epidermal cells and root hairs, critical sites for P_i uptake; (2) regulation of their expression by plant P-status which mirrors the observed changes in P_i uptake rates (see above); (3) their localization to the plasma membrane; (4) physiology consistent with H^+-P_i cotransporter function; and (5) the reduction of P_i uptake by *Arabidopsis* plants carrying knockout mutations in certain members of the *Pht1* family.

Once P_i is taken up from the external medium, transporters are also responsible for moving P_i between and within cells. These P_i transporters are less well defined and may include members of the Pht1 family as well as three additional families distinct from Pht1. Members of the Pht2, Pht3 and Pht4 families have all been shown to be P_i transporters and are located on organelle membranes where they are thought to participate in intracellular transport between the organelles and cytosol. Two of the proteins are located on chloroplast membranes (Pht2 and Pht4) and others are located on mitochondrial (Pht3) and Golgi apparatus membranes (Pht4).

The isolation and characterization of mutants has helped unravel the regulatory mechanisms involved in P homeostasis of plants. The first P-nutrition mutants of *Arabidopsis* were isolated based on their perturbed accumulation of P in shoots. Shoots of the *pho1* (***pho****sphate****1***) mutant are P-deficient even when plants are grown on substrate that is high in P_i. The mutant is impaired in its ability to load P_i into the xylem resulting from a mutation in a membrane protein thought to transport P_i into the xylem. By contrast, the *pho2* mutant accumulates excess P_i in shoots and is clearly perturbed in a mechanism that regulates P_i uptake and homeostasis. Detailed analysis has identified a regulatory system that involves microRNAs and PHO2 in the post-transcriptional regulation of two P_i transporters of the Pht1 family (Pht1;8 and Pht1;9, Fig. 23.13A,B). The *PHO2* gene encodes an ubiquitin-conjugating enzyme (UBC) that under high P conditions is thought to target the degradation of the transporters themselves or regulators of their expression. Details on the role of UBCs in degradation of proteins by the ubiquitination pathway is discussed in Chapter 10 and summarized in Figure 10.33. Mutants lacking functional PHO2 protein accumulate excess P_i because they are unable to downregulate the two P*i* transporters even when they have sufficient P (Fig. 23.13C). *PHO*2 mRNA possesses five target sites in its 5′ UTR for binding of miR399 resulting in degradation of PHO2 transcript (see Chapter 9 for details of gene regulation by miRNAs). Expression of *MIR399* is itself upregulated under P-deficiency. Furthermore, *MIR399* is primarily expressed in shoots and the processed miRNA399 acts as a phloem-mobile signal to regulate PHO2 activity in roots. Therefore, when sufficient P is available, *PHO2* transcripts are abundant resulting in active PHO2 proteins that downregulate the activity of Pht1;8 and Pht1;9. When P-deficient, *MIR399* expression is increased in shoots and processed miRNA is translocated to roots. *PHO2* mRNA is then degraded relieving the suppression of Pht1;8 and Pht1:9 which results in enhanced P_i transport. Overexpression of *MIR399* mimics the *pho2* mutant consistent with the proposed model (Fig. 23.13D).

While this mechanism for regulating P_i uptake, with some modifications, appears to be common to many plant species, it is a subcomponent of a more complex network. The *phr1* (***ph****osphate starvation* ***r****esponse1*) mutant of *Arabidopsis* was originally identified as being impaired in a broad range of P-deficiency responses. The mutant is unable to upregulate a range of genes normally induced by P-deficiency including those encoding Pht1 transporters, RNAses and acid phosphatases. PHR1 is a transcription factor of the MYB superfamily that binds to a motif (PIBS) present in the promoters of many genes that respond to P_i starvation and acts to enhance transcription under P deficiency. The induced expression of *MIR399* is an example of a gene regulated by PHR1, and the perturbed uptake of P_i in *phr1* mutants can be attributed to an

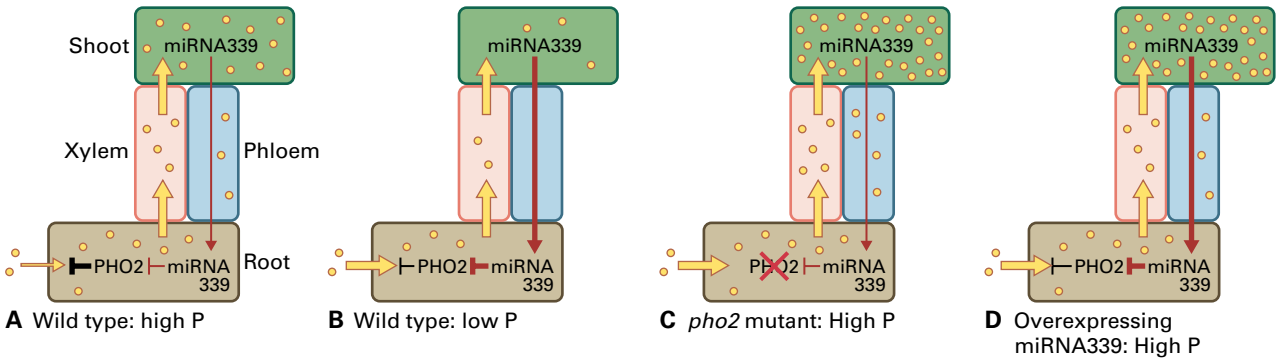


FIGURE 23.13 *Model of a module that regulates P_i homeostasis in plants. Shown is a simplified schematic of a plant comprising 4 cells: a root cell, a xylem vessel, a phloem cell and a shoot cell. The yellow arrows depict P_i transport with the thickness denoting the rate of transport. Phosphate ions are shown as small yellow circles and red lines denote the flow of microRNA (miR339) that targets PHO2 transcript. Lines terminating with a "T" junction denote suppressive action and the thickness of the lines indicate the degree of suppression. (A) When the plant has adequate P, the ubiquitin conjugase activity of PHO2 suppresses the function of phosphate transporters. (B) When P-deficient, expression of a specific microRNA (miR399) is induced primarily in shoots. miR399 is translocated via the phloem to roots where it targets the degradation of PHO2 transcript. With reduced PHO2 levels, suppression of P_i transporters is relieved and P_i uptake increases. (C) The* pho2 *mutant lacks the ubiquitin conjugase activity and is unable to downregulate P_i transport even when the plant has sufficient P resulting in P toxicity. (D) Constitutive overexpression of* MIR399 *confers the same phenotype as the* pho2 *mutant since high levels of miR399 degrade PHO2 transcripts.*

indirect effect on Pht1 transport through the PHO2/miR399 mechanism. An inability to upregulate *MIR399* expression in *phr1* mutants maintains active PHO2 and hence suppressed Pht1 transport activity.

The influence of PHR1 on P-homeostasis is more global than PHO2 as it acts on a wide range of processes involved in P-deficiency including the ability to alter metabolic pathways. PHR1 is subject to regulation and is the target of a small ubiquitin-like modifier (SUMO) E3 ligase which serves to activate PHR1. This SUMO, named SIZ1, also regulates gene expression in response to stresses other than P-deficiency. As more mutants are discovered it is becoming apparent that the regulation of P homeostasis in plants is far more complex than originally envisioned and comprises components that interact with pathways specific for maintaining P_i homeostasis and with mechanisms that serve to regulate other aspects of plant development.

Recent research on species that form effective mycorrhizal associations (e.g., *Medicago truncatula*) has identified mechanisms that regulate P_i uptake by the symbiosis between fungus and plant host. The symbiosis with VAM adds complexity to the way that P_i is taken up by plants with direct (roots and root hairs) and indirect (VAM) pathways that need to be regulated. As discussed above for nonmycorrhizal roots, P-deficiency upregulates the activity of high-affinity P_i transporters at the plasma membrane of root cells. However, when roots are infected with VAM that are actively absorbing P from the soil, these plant P_i transporters become almost inactive. Instead P_i is taken up into plants by other transporters of the same family that are specifically expressed in the infected cells. In particular, two subfamilies of the *Pht1* transporter gene family are expressed predominantly in cortical root cells colonized by VAM fungi. The promoters of these genes possess regulatory elements that respond to mycorrhizal infection by increasing their expression. These Pht1 transporters are thought to be the primary mechanism that takes up the P_i provided by VAM into plant cells, and their location in the host plasma membrane that surrounds the branches of an arbuscule is consistent with this idea. An essential role of specific Pht1 transporters in mycorrhizal symbiosis has been demonstrated by knock down of expression of these genes resulting in reduced P_i uptake by the symbiosis and in loss of effective colonization of root cells by the VAM.

23.4 The molecular physiology of micronutrient acquisition

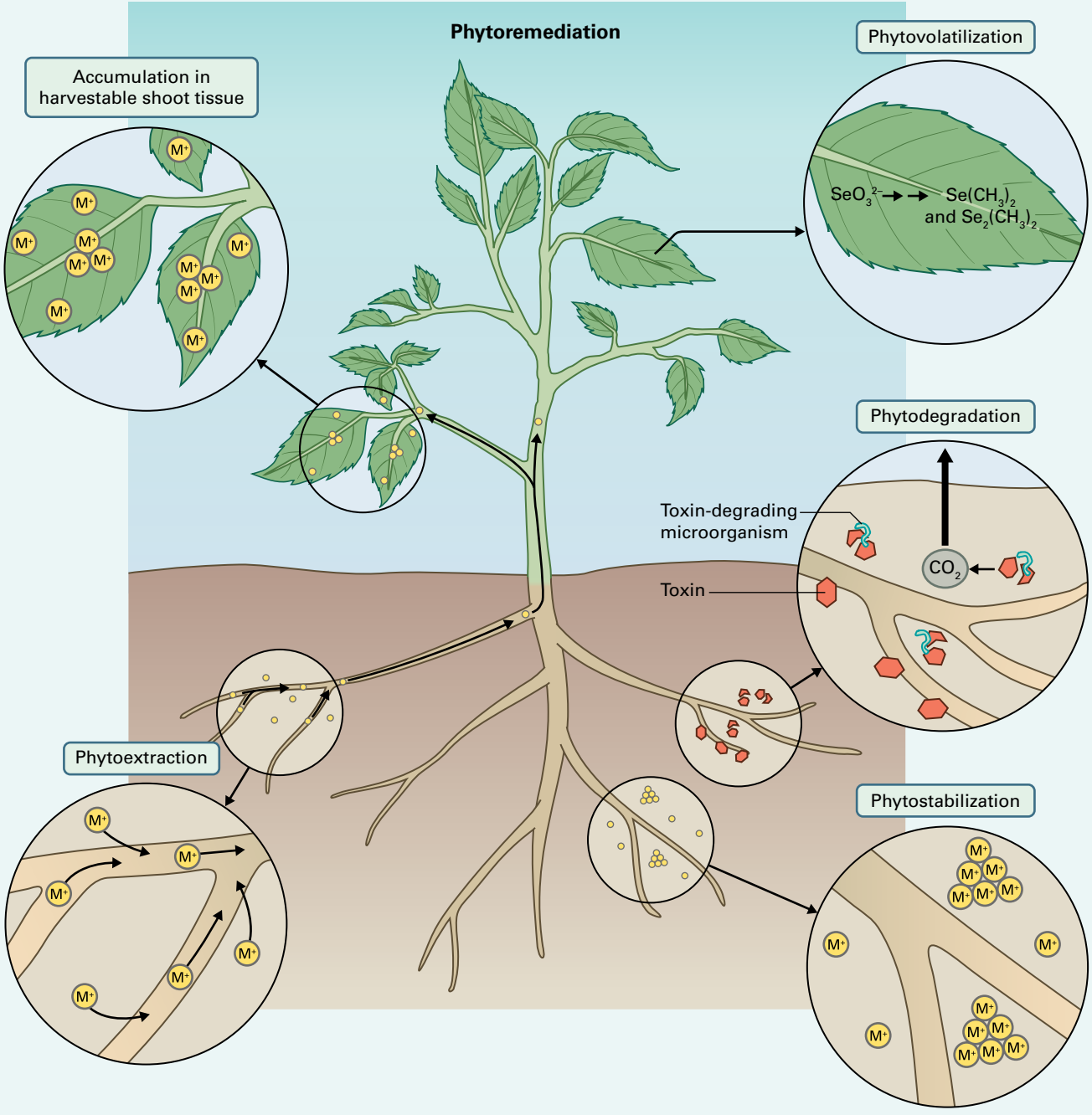
Micronutrients such as Fe, Zn, Mo, and Cu are important to agriculture because their low availability in many soils limits crop production. There is also growing interest in how the micronutrient content of foods might be modified to benefit human health and nutrition. This is especially true in developing countries where diets are often based on one major crop. Furthermore, nonessential heavy metals such as Cd can be taken up via the same transport processes that plants use to acquire essential micronutrients, providing a primary site for the entry of toxic heavy metals into the food chain. Even some essential micronutrients such as Zn and Cu are toxic if accumulated and ingested at high concentrations. Moreover, scientists have realized that terrestrial plants might constitute an inexpensive mechanism for cleaning soils contaminated with heavy metals, a technology termed **phytoremediation** (see Box 23.4).

Research into micronutrient transport and acquisition from soil is complicated by the low concentrations of these minerals in the soil and their complex chemistry. The concentrations of available (soluble) micronutrients in the soil are typically orders of magnitude less than the concentrations

BOX 23.4

The conceptual basis for phytoremediation, the use of plants to clean contaminated soils, came from identifying plants that hyperaccumulate metals

Contamination of the environment with heavy metals and radionuclides is a serious problem both for human health and agriculture. In many locations throughout the world, sizeable land areas contain surface soils contaminated with hazardous amounts of toxic heavy metals such as Cd, Zn, Pb, Cu, Cr, Hg, Ni, and U. The engineering-based technologies currently in use to remediate surface-contaminated soils (e.g., removal of topsoil for storage in landfills) can be prohibitively expensive and often disturb the landscape. As an alternative, the use of plants as an inexpensive method for remediation of soils polluted with heavy metals has attracted enormous interest. Some plant species can grow in soils that are heavily contaminated with metals and even



accumulate these metals to high concentrations in shoots. The existence of these metal hyperaccumulator species suggests that plants could be used to **bioremediate** metal-contaminated soils (i.e., to detoxify them by means of biological activity).

Phytoremediation (plant-based bioremediation) can involve **phytoextraction** (removal of toxins from soil), **phytostabilization** (complexation and immobilization of toxins within the soil), and **phytodegradation** of organic contaminants in the rhizosphere (see figure). Phytoextraction involves the use of terrestrial plants to absorb heavy metals from the soil and transport them to the shoots. Phytoextracted metals may accumulate in plant shoot tissues (e.g., Pb, Ni) or may be released as volatile species (e.g., Se). For metals that become concentrated within plant tissues, remediation involves harvesting the shoot biomass, which is reduced in volume (e.g., ashed) and then disposed of in a final repository. Moreover, for Se, the toxicity of the volatile species dimethylselenide and dimethyldiselenide is much lower than that of the soluble oxyanions, such as selenite (SeO_3^{2-}), present in soil solution.

Metal-hyperaccumulating plant species are endemic to metalliferous soils and can tolerate and accumulate high amounts of heavy metals in their shoots. Hyperaccumulators were first identified more than 100 years ago; this fascinating collection of different plants not only can grow in soils contaminated with high concentrations of a specific heavy metal, but also often have a higher tolerance for that metal. To date, hyperaccumulating plant species have been identified in nearly 400 taxa representing about 45 plant families. There is strong evidence for hyperaccumulators of Zn/Cd, Ni, and Se and some indications of plants that accumulate Co, Cu, and possibly Pb.

One well-known heavy metal hyperaccumulator is *Noccaea caerulescens*, a member of the Brassicaceae that accumulates Zn and Cd (see figure). Certain ecotypes of *N. caerulescens* have been shown to accumulate and tolerate as much as 40,000 μg of Zn per gram dry weight in their shoots (foliar Zn in hydroponically grown plants is ordinarily around 100–200 μg g^{-1}; 30 μg g^{-1} is considered sufficient). This species also accumulates high concentrations of Cd and has also been suggested to accumulate high amounts of other heavy metals. Several studies conducted with *N. caerulescens* to remediate soils contaminated with Zn and Cd have had moderate success. One drawback to using *N. caerulescens* (or most other hyperaccumulators) for phytoremediation is that the species is slow-growing and does not produce substantial shoot biomass. To maximize phytoextraction, a species should have high shoot biomass and should accumulate metals to high concentrations in their shoots. Nonetheless, the unique physiology of heavy metal transport and tolerance in *N. caerulescens* makes it an interesting experimental plant for basic research aimed at elucidating the mechanism of heavy metal hyperaccumulation, especially with the goal of transferring hyperaccumulating traits to species with a higher biomass.

of most of the macronutrients, and they rarely exist as free cations. Instead they form complexes with ligands that vary in stability, size, and charge. Consequently the study of micronutrients must address the presence of metal chelates in the rhizosphere, the forms in which the micronutrients are transported into plant cells, and the nature of the metal–chelate complexes present within cells as they are either stored or transported long distances by the xylem and phloem. The present section will focus on the physiology and molecular biology of Fe and Cu acquisition and distribution by plants.

23.4.1 How do plants acquire Fe from the soil?

Fe is an essential nutrient for plants. Although abundant in the Earth's crust, the concentration of soluble Fe in the soil is usually very low. Most Fe in the soil exists in one of two oxidation states: Fe(III) or ferric Fe has the +3 oxidation state and Fe(II) or ferrous Fe has the +2 oxidation state. The ability to change oxidation state is central to the participation of Fe in the reversible oxidation–reduction (redox) reactions essential for mitochondrial respiration and the light reactions of photosynthesis. Fe also functions as a co-factor in Fe–sulfur clusters, in the porphyrin ring of heme and as nonheme Fe. Multiple Fe–sulfur clusters are present in Complexes I and II of **oxidative phosphorylation** as well as certain **metalloproteins** such as ferredoxin.

In aerobic conditions and when soil pH is above 6.0, Fe(II) is readily oxidized to Fe(III) and exists mostly as sparingly-soluble ferric oxides. Under these conditions the concentration of soluble inorganic Fe is typically $<10^{-16}$ M, many orders of magnitude below the concentrations required for sustained plant growth. As a consequence, plants grown on alkaline or calcareous soils are especially prone to Fe deficiency. Typical symptoms of deficiency include interveinal chlorosis (yellowing, see Fig. 23.1), stunted growth and poor yields. Fe availability improves when solution pH is reduced to ≈pH 4 because the concentration of soluble Fe increases by a factor of 10^8 and more of it occurs as the reduced Fe(II) form which can be absorbed directly by some plants. Fe(II) is also more common in anaerobic conditions such as the flooded paddy fields where rice is grown.

Regardless of oxidation state, most soluble Fe in soil solution is chelated by organic and inorganic ligands. The organic ligands are a diverse range of compounds derived from soil bacteria and fungi or degraded organic matter. The concentration of soluble Fe:chelates in the soil solution remains very low and plants employ several mechanisms to acquire Fe from soil to meet their growth requirements.

23.4.2 Plants use two main strategies for absorbing Fe from the soil

In eudicots and nongrass monocots, Fe(III) chelates are reduced to Fe(II) at the root surface and Fe(II) is taken up by a transport protein located at the plasma membrane, called the Strategy I mechanism. By contrast, members of the grass family (Poaceae), release **phytosiderophores** from roots that chelate and solubilize Fe(III) to make it available for uptake, called the Strategy II mechanism. The term phytosiderophore derives from the well-characterized Fe uptake system in microorganisms that involves the release of specific Fe-chelating compounds named **siderophores** (Greek: "iron bearers") to mobilize Fe from their surroundings. These strategies are described in more detail below.

Strategy I plants respond to Fe deficiency with (1) enhanced efflux of protons (H^+) from root cells; (2) induction of a plasma membrane ferric reductase in root epidermal cells to reduce extracellular Fe(III) to Fe(II) at the root surface; and (3) induction of an Fe(II) transporter at the root-cell plasma membrane to facilitate Fe(II) uptake (Fig. 23.14). Some Fe-deficient plants also release organic anions from their roots that may increase the solubility of Fe. The increase in H^+ efflux occurs from the upregulation of a H^+-ATPase on the plasma membrane of root epidermal cells. The resulting acidification of the rhizosphere increases Fe solubility. In *Arabidopsis* the H^+-ATPase is encoded by the gene *AHA2*. The reduction of Fe(III) to the more soluble Fe(II) at the root surface is critical for Fe absorption in eudicots. This is controlled by the NADPH-dependent ferric chelate reductase, *FRO2* (Fig. 23.15), a member of a superfamily of flavocytochromes that transport electrons across membranes. *FRO2* expression in the root epidermis is enhanced during Fe deficiency, and the *Arabidopsis* mutant (*frd1*) that lacks FRO2 reductase activity rapidly becomes chlorotic. Conversely, plants engineered to overexpress *FRO2* perform better than wild-type plants when Fe supply is restricted. Additional *FRO* genes are expressed in other parts of the plant during Fe deficiency including the vasculature and shoots and these are probably involved in reabsorbing Fe from the apoplast of various tissues.

Once Fe(III) is reduced to Fe(II) it is taken up by IRT1 (**i**ron-**r**egulated **t**ransporter), a member of the ZIP (**Z**rt/**I**rt-related **p**rotein) family, localized to the plasma membrane of root epidermal cells. ZIPs occur in plants, animals, bacteria and fungi where they transport a range of metals including Fe, Zn, Mn and Cd. *IRT1* expression is enhanced in Fe-deficient

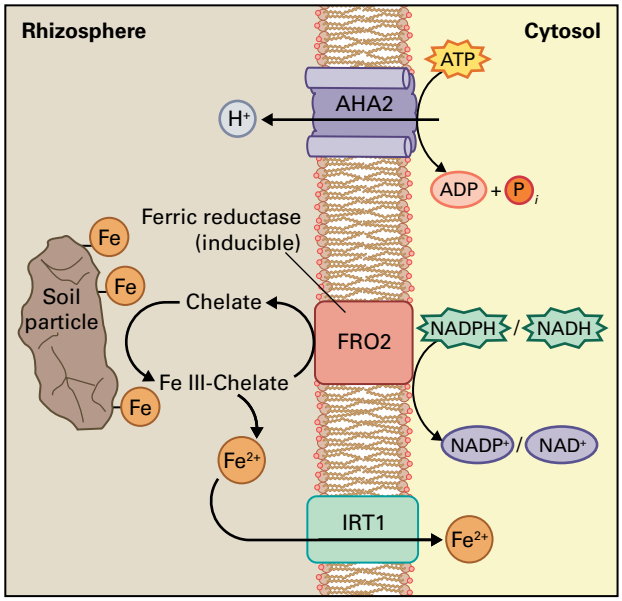


FIGURE 23.14 *Model of Fe uptake by eudicots and nongrass monocots. The model depicts the key plasma membrane-localized components that are induced in roots by Fe deficiency in* Arabidopsis. *These include a plasma membrane H^+-ATPase (AHA2) which acidifies the rhizosphere and increases Fe solubility, the ferric reductase FRO2 that reduces Fe(III) chelates in the rhizosphere releasing Fe(II), and the high-affinity transporter IRT1 which transports Fe(II) across the plasma membrane.*

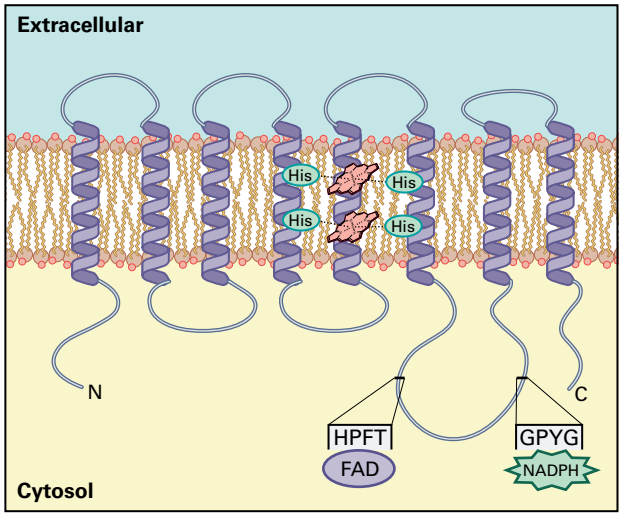


FIGURE 23.15 *Predicted protein structure for FRO2, the root plasma membrane ferric chelate reductase in* Arabidopsis. *FRO2 is predicted to include six membrane-spanning domains within the C-terminal region and two membrane-spanning domains within the N-terminal region. Four histidine residues are predicted to coordinate two heme groups localized to two of the internal membrane-spanning domains, forming a complex that may play a role in transmembrane electron transport. Near the C-terminus is a cytoplasmic loop that includes putative FAD- and NADPH-binding domains.*

Arabidopsis plants, and mutants lacking IRT1 function die before setting seed unless supplied with high levels of soluble Fe. IRT1 was first identified from its ability to complement a yeast strain (*fet3fet4*) impaired in high and low affinity Fe

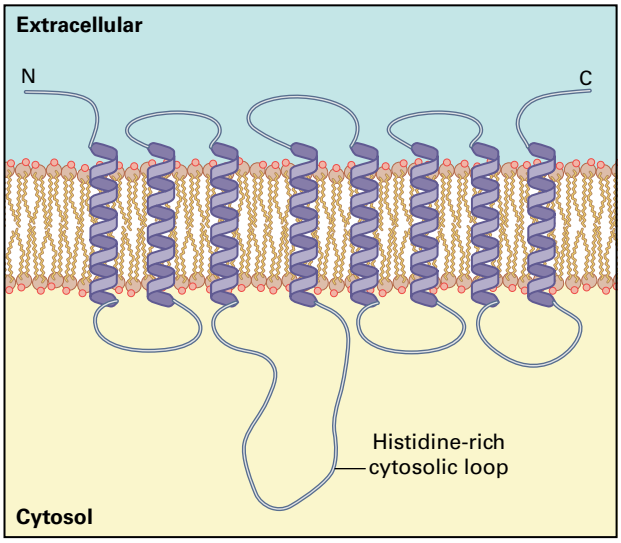


FIGURE 23.16 *Predicted protein structure of the members of the ZIP family of micronutrient transporters. The notable structural features include eight membrane-spanning domains and a cytoplasmic loop of variable length situated between the third and fourth transmembrane helices. This cytoplasmic domain contains histidine repeats that may function in metal-binding.*

uptake (see Box 23.2). IRT1 was the first member of this family of micronutrient transporters to be characterized in plants and its discovery led to the isolation of other Fe and Zn transporters in plants and yeast. IRT-type proteins are predicted to have eight membrane-spanning regions and a histidine-rich motif between the third and fourth transmembrane domains, which may act as the metal-binding site (Fig. 23.16). IRT1 can transport other micronutrients and even Cd, albeit with a lower affinity, and this can sometimes induce toxicity in Fe-deficient plants. The 16 members of the *ZIP* family in *Arabidopsis* are expressed in various tissues. While several *ZIPs* can complement the *fet3fet4* yeast mutant most do not contribute directly to Fe uptake from soil. Instead they perform similar functions transporting Fe and other metals.

Responses to Fe deficiency outlined above are regulated by members of the basic helix-loop-helix (bHLH) family of transcription factors. The role of these regulators was discovered by characterizing a tomato mutant (*fer*) defective in this gene. Plants carrying the *fer* (**Fe r**eductase) mutation are unable to induce the normal physiological responses to Fe deficiency and rapidly become chlorotic at low Fe concentrations. A gene called *FIT* performs a similar function in *Arabidopsis* and *fit* mutants also need high Fe concentrations to survive beyond the seedling stage.

Grasses differ from eudicots in their response to Fe deficiency. They do not increase H^+ excretion or ferric chelate reductase activity and they are unable to absorb Fe supplied as very stable Fe(III) chelates such as ethylenediamine-*N*,*N*′-bis(2-hydroxyphenyl)acetic acid (EDDHA). Despite these apparent limitations grasses tend to grow better than eudicots on calcareous (alkaline) soils where the concentrations of available Fe are extremely low. Grasses achieve this by releasing compounds from their roots (Strategy II) that efficiently chelate and solubilize ferric iron (Fig. 23.17). These compounds are nonprotein imino acids called phytosiderophores, the synthesis of which starts with L-methionine (Fig. 23.17). Phytosiderophore function is less affected by pH than the ferric chelate reductase activity which has an optimum below pH 7.

Fe deficiency stimulates the synthesis of many different phytosiderophores in grasses, with deoxymugineic and avenic acids being among the best characterized. Grass species such as barley that release large amounts of phytosiderophore tend to be more efficient at extracting Fe from alkaline soils than those such as rice and wheat that release smaller amounts. Deoxymugineic acid release from rice and barley is mediated by proteins belonging to the major facilitator family of transporters. The genes encoding these proteins in rice and barley are called *TOM1* and *HvTOM1*, respectively (**t**ransporter **o**f **m**ugineic acid family phytosiderophores 1) (Fig. 23.18). *TOM1* and *HvTOM1* are predominantly expressed in roots and developing seed but Fe deficiency strongly induces their expression in the vascular bundle of leaf sheaths as well as roots. Transgenic plants over-expressing *TOM1* and *HvTOM1* show enhanced deoxymugineic acid release and greater tolerance to low Fe.

Once Fe(III) is chelated by a phytosiderophore in the soil the entire complex is transported into the root cells by proton-coupled transporters belonging to the oligopeptide transporter family (OPT). The first Fe(III):phytosiderophore transporter to be characterized was named yellow-stripe 1 (YS1) because it was identified as the cause of the *yellow stripe* (*ys1*) mutation of *Z. mays* which produces distinctive interveinal chlorosis. *Yellow stripe 1-like* (*YSL*) genes are present in monocots and eudicots (18 in rice and 8 in *Arabidopsis*) but only the grasses use them for acquiring Fe from the soil. Some of these YSLs are likely to transport Fe complexes across membranes in other cells and tissues as well (see below).

Rice is unusual among the grasses because it also displays aspects of the Strategy I mechanisms for Fe uptake. In addition to releasing phytosiderophores, Fe-deficient rice roots enhance expression of an IRT-type transporter, OsIRT1, which allows Fe(II) uptake from the reducing environment common in flooded paddy fields. This extra facility to take up reduced Fe may compensate for the relatively low exudation of phytosiderophores in rice.

These responses to Fe deficiency in grasses are also regulated by basic helix–loop–helix (bHLH) transcription factors. In rice the bHLH protein OsIRO2 (**iro**n-related transcription factor**2**) regulates genes involved in phytosiderophore synthesis and Fe uptake. The expression of *OsIRO2* and many other genes involved in Fe uptake and homeostasis is controlled by IDEF1, a transcription factor from the ABI3/VP1 family that specifically binds to the Fe-deficiency responsive *cis*-acting element IDE1. A different subset of Fe deficiency-induced genes (including certain *YSLs* in rice) is upregulated by another transcription factor belonging to the NAC family called IDEF2. These findings indicate that plants have a complex network of regulatory genes to control their responses to Fe deficiency.

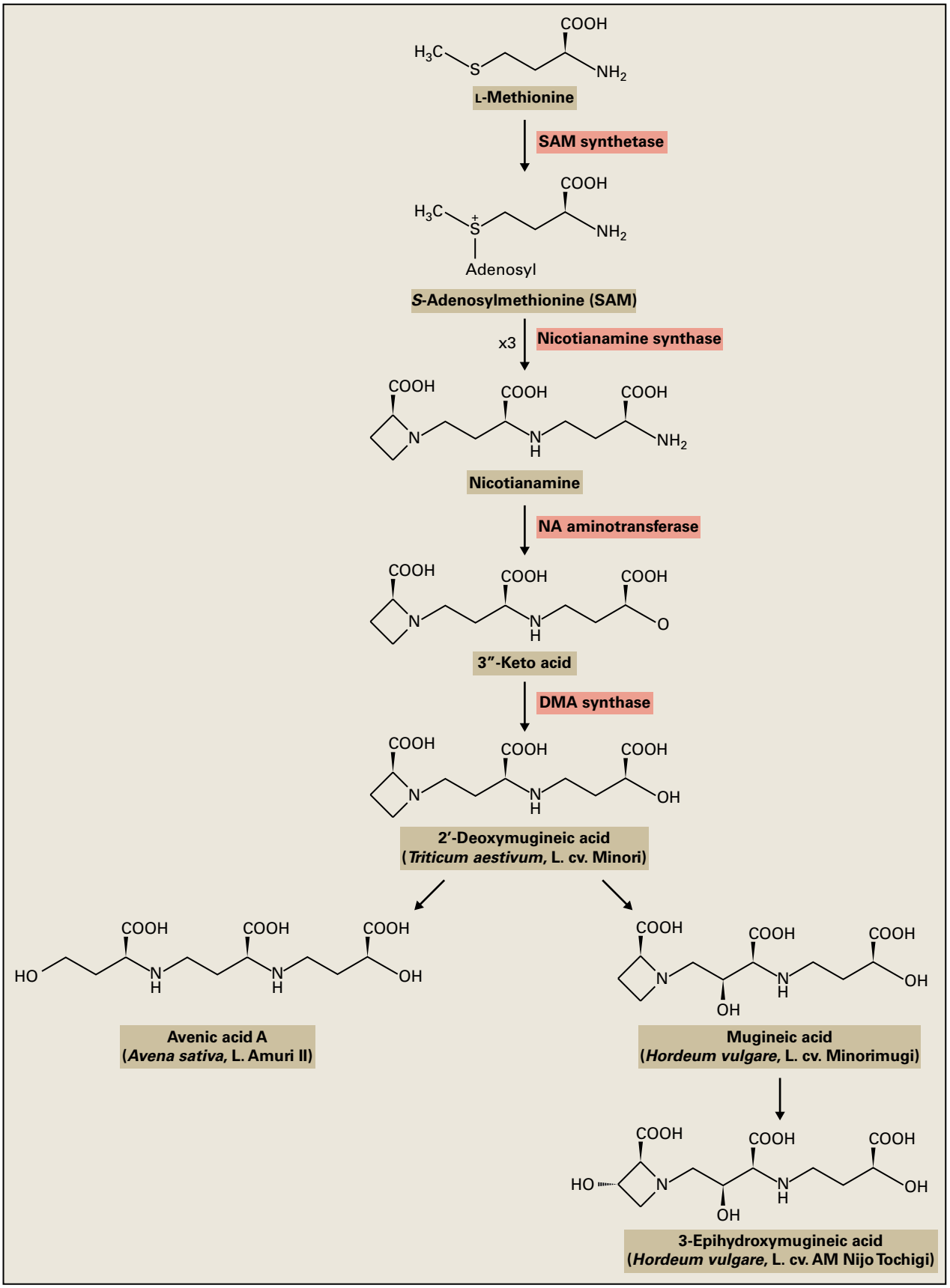


FIGURE 23.17 *Biosynthetic pathways for phytosiderophores can vary between different grass species. Here, the different phytosiderophores released by oat (*Avena sativa*) and barley share a common biosynthetic precursor, L-methionine, but are synthesized by two different pathways. The intermediate product nicotianamine is important for the transport and distribution of Fe and other micronutrients in all plants.*

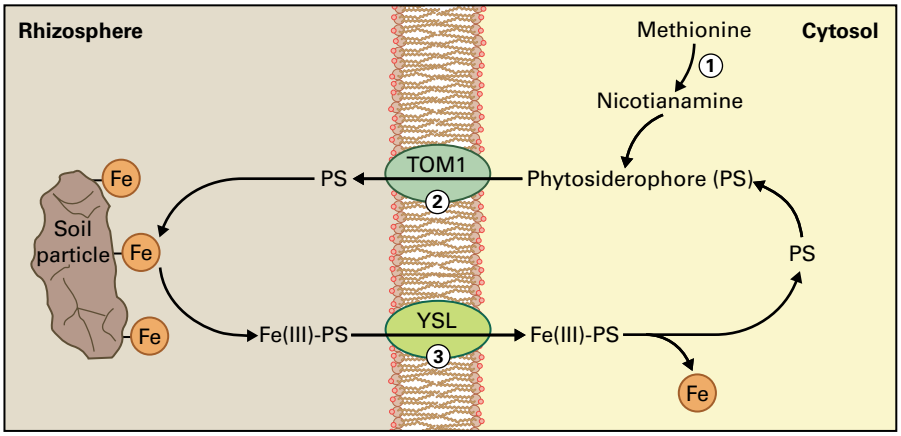


FIGURE 23.18 *Model of Fe uptake by graminaceous plants. Phytosiderophores (PS) are synthesized in the cytoplasm from methionine by way of nicotianamine (1); a transporter on the plasma membrane induced by Fe deficiency (called TOM1 in rice) releases the PS into the rhizosphere (2); and a transporter belonging to the YSL family is also induced by Fe deficiency and transports the Fe(III)-PS complex into the cytoplasm (3).*

23.4.3 Transport of Fe within the plant

Fe travels from root to shoot via the xylem. Once in the cell Fe is chelated by ligands to prevent it from precipitating at the neutral pH of the cytosol. Chelation of Fe also protects cells from the damaging effects of Fenton reactions which are catalyzed by free Fe and that generate reactive oxygen species. The compounds that chelate Fe in the cytosol are not known but an Fe:ligand complex of some type is likely to diffuse through the symplasm to the stele where it is released into the xylem (apoplast). In the xylem (pH 5.5) Fe is bound by citrate and perhaps other compounds, which chaperone Fe to shoots in the transpiration stream. In grasses, these other compounds might include phytosiderophores. The role of citrate in the movement of Fe to the shoots of *Arabidopsis* was revealed by examining a mutant called *frd3* (*ferric reductase defective3*). *frd3* mutant plants are constitutively upregulated in the Fe-deficiency responses and show typical symptoms of Fe deficiency under normal growth conditions. The *FRD3* gene underlying this mutation encodes a transport protein from the multidrug and toxic compound extrusion (MATE) family (see Chapter 3) that releases citrate into the xylem from the root pericycle and cells internal to the pericycle. The reduced citrate concentration in the xylem of *frd3* mutant plants prevents the effective retrieval of Fe from the xylem by shoot cells.

Fe is also transported throughout the plant in the phloem. Phloem is a living tissue that conducts sugars and nutrients from the leaves to other plant tissues (see Chapter 15). The phloem is particularly important in delivering nutrients to developing roots, shoots and seeds which are poorly served by the xylem due to their low transpiration rates. Since the pH of the phloem is similar to the cytosol (≈7.2) Fe must be chelated to remain soluble. In castor bean (*Ricinus communis*) most Fe in the phloem is bound to a 17-kD protein called the iron transport protein (ITP). ITP is a dehydrin protein that has a stronger binding affinity for Fe(III) than Fe(II). Nicotianamine (NA) is another compound in the phloem that forms stable complexes with Fe(II) at neutral pH. It is an intermediate of phytosiderophore synthesis and is synthesized from *S*-adenosyl L-methionine by nicotianamine synthase (NAS) (see Fig. 23.17). NA is critical for the internal transport and distribution of Fe and other micronutrients in all plants.

The involvement of NA in Fe nutrition was first revealed by characterizing the *chloronerva* (*chln*) mutant of tomato. *chln* mutants lack nicotianamine synthase (NAS) activity and develop Fe deficiency symptoms despite accumulating high concentrations of Fe in their roots and shoots. The absence of NA from the vasculature of *chln* mutant plants inhibits their capacity to retrieve Fe from the phloem and distribute it to other tissues. *Arabidopsis* has four *NAS* genes, two of which are upregulated in roots by Fe deficiency. Mutations in any one of these genes cause no discernible phenotype but the quadruple mutant generates the same interveinal chlorosis observed in *chln* mutant plants. In grasses, phytosiderophores might also assist Fe transport in the phloem.

These findings support a model in which Fe(III) moves in the phloem as a complex, perhaps with ITP, but where loading or unloading from the phloem occurs as Fe(II):NA complexes, probably via YSL transporters. An extra reductase step would also be required to reduce Fe(III) to Fe(II) prior to binding with NA. YSLs also mediate reabsorption of Fe from the xylem and from senescing leaves to the phloem for long distance transport to sink cells. For example, OsYSL2 is a phloem-localized transporter in rice critical for the translocation of Fe–NA to shoots and developing seeds.

23.4.4 Storage of Fe within cells

Mitochondria, plastids, and vacuoles are important organelles for storing intracellular Fe (Fig. 23.19). These compartments provide a buffer which maintain safe concentrations of Fe in the cytosol. This enables cells to satisfy their nutrient requirements while minimizing the risk of oxidative stress. Most Fe in leaf cells is located in chloroplasts as ferritin, a storage

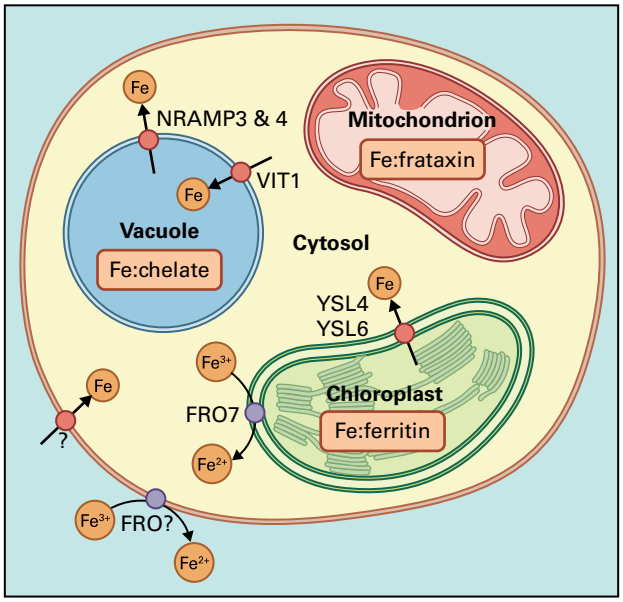


FIGURE 23.19 *Transport of Fe within plant cells. It is unclear how Fe is taken up by shoot cells but it is likely to involve similar mechanisms to those described for roots, involving a FRO-like ferric chelate reductase and a transporter. Once Fe is taken up into the cytosol, the main organelles involved in Fe homeostasis are vacuoles, chloroplasts and mitochondria, and many transport processes controlling the distribution of Fe between these compartments are yet to be discovered. In* Arabidopsis*, loading Fe into vacuoles requires the transporter VIT1 and retrieval from vacuoles involves NRAMP3 and NRAMP4. Fe is complexed in the vacuole perhaps with nicotianamine (NA), phosphate or phytate. Uptake of Fe by chloroplasts requires ferric chelate reductase activity (FRO7) and release is facilitated by YSL4 and YSL6. Fe-binding proteins ferritin and frataxin chelate Fe in the chloroplasts and mitochondria respectively.*

protein that has the ability to bind several thousand atoms of Fe. Mitochondria contain another Fe-binding protein called frataxin. Ferritin and frataxin help regulate Fe concentrations in cells especially during germination and early development. Mutant plants that are unable to synthesize ferritin are smaller, less fertile and their leaves contain higher levels of reactive oxygen species compared to wild-type plants. Chloroplasts are very sensitive to Fe deficiency. They have a high requirement for Fe due to the redox reactions occurring in thylakoids and the metabolism of photosynthetic pigments. Fe uptake by chloroplasts requires the activity of a ferric chelate reductase (FRO7) and unidentified transporters (Fig. 23.19) while efflux is mediated by members of the YSL family. In *Arabidopsis*, for example, YSL4 and YSL6 mediate Fe efflux from chloroplasts during senescence or when Fe is supplied in excess. The double mutant, *ysl4ysl6*, retains Fe in its chloroplasts and is hypersensitive to high concentrations of Fe.

Fe transport into the vacuoles of *Arabidopsis* cells is mediated by VIT1 (**V**acuolar **I**ron**T**ransporter**1**). *VIT1* expression is enhanced in vascular tissues during seed development and *vit1* mutants grow poorly when Fe supply is restricted. The Fe stored in vacuoles is chelated possibly by NA, phosphate, or even phytate. Retrieval of Fe from vacuoles involves members of the NRAMP family of transporters but other proteins may also be involved. *Nramp* genes form a diverse family in bacteria, fungi, plants, and animals which encode metal transporters with a broad range of specificity. Although the *Arabidopsis* genome contains several *Nramp* genes that can complement yeast mutants deficient in Fe uptake, the AtNRAMP3 and AtNRAMP4 proteins localize to the tonoplast of root and shoot cells and show enhanced expression during Fe deficiency. These transporters play critical roles in Fe nutrition and may also transport other transition metals such as Mn and Cd. Seedlings carrying the double mutation, *atnramp3atnramp4*, stop growing when Fe supply is restricted and are unable to retrieve Fe from vacuoles during germination, especially from the vascular tissues. Other members of this family are primarily expressed in roots and some of these (e.g., *AtNRAMP1*) may also be involved in Fe transport.

23.4.5 Interactions between Fe nutrition and other transition elements

There is considerable overlap in the mechanisms for acquiring and managing different mineral nutrients. This is especially true for the transition elements such as Fe, Mn, Cu, and Zn as well as for nonessential elements such as Cd. This overlap extends to the complexes they form in the soil and cytosol, their susceptibility to reductase activity, and to the transporters that absorb and distribute them throughout the plant. For instance, although IRT1 is more specific for Fe(II) than for other divalent cations, Fe-deficient plants sometimes enhance the uptake of other metals including Cu, Mn, Zn, Ni, Cd and Co. Furthermore the *frd3* mutant of *Arabidopsis* with disrupted Fe nutrition can also accumulate excess Mn, Zn and Cu. Transition elements can also affect plant responses to Fe deficiency. For example, the onset of Cu deficiency in *Arabidopsis* induces FRO2 activity even when Fe supply is adequate and this increases the reduction of Cu(II) to Cu(I). Conversely, high external Zn concentrations can repress the induction of *IRT1* and *FRO2* expression in Fe-deficient *Arabidopsis* plants even though reduction of Zn is not required for uptake. Similar interactions occur in grasses, an example being Zn-deficient barley plants that release phytosiderophores from their roots, enhancing the uptake of both Zn and Fe. Overexpression of NAS in transgenic plants to increase internal NA levels elevates Fe, Zn, Ni and Mn in shoots indicating that these metal ions are bound by similar compounds as they move from the root to the shoot. These complexes may also share YSL proteins to shuttle them between vasculature tissues or load and unload them from the phloem. For example, OsYSL2 in rice is important for the translocation of Fe(II):NA and Mn(II):NA to the shoots. Therefore, cells need to balance the demands of Fe nutrition with the risks of inadvertently absorbing other nonlimiting minerals to excess.

23.4.6 Copper taken up as the reactive Cu^+ ion is bound by chaperones within the cell

Copper shares the important attribute with Fe in that it exists as multiple oxidation states under physiological conditions. This allows Cu to act as an essential cofactor of enzymes involved in redox reactions. Copper metalloenzymes play important roles in photosynthesis, mitochondrial respiration, cell wall biosynthesis and superoxide scavenging. Under physiological conditions free Cu exists as Cu^{2+} or Cu^+ and these ions can rapidly disrupt cellular function by binding nonspecifically to a range of molecules. Indeed, Cu^{2+} is able to displace other ions, such as Mn^{2+} and Zn^{2+}, from their binding sites within metalloenzymes resulting in inactive proteins. Furthermore, free Cu readily generates reactive oxygen species that can cause oxidative stress within cells. For these reasons, the uptake, accumulation and delivery of Cu to target proteins are tightly regulated within plants.

Cu is generally found in trace amounts in soils with Cu deficiency being a larger problem for agriculture than Cu toxicity. Similar to Fe, Cu(II) in soil solution is first reduced to Cu(I) by the action of reductases prior to uptake by roots. As discussed above, ferric reductase activity induced by either Fe or Cu deficiency reduces Cu(II) to Cu(I) in addition to reducing Fe(III) to Fe(II). Members of the Cu transporter family of membrane proteins located on the plasma membrane transport Cu^+ from the external solution into the cytoplasm (Fig. 23.20). These proteins are known as the COPT family in *Arabidopsis,* and share considerable sequence and functional similarities to related proteins from other eukaryotes. Members of the COPT family were first identified based on sequence homology to other previously characterized Cu transporters, and by their ability to complement yeast mutants impaired in high-affinity Cu uptake. COPT proteins are predicted to possess three transmembrane domains and most possess methionine-rich domains at their amino-terminus. In yeast, Cu transporters that belong to the same family, the methionine rich domains serve to sequester Cu from an oxidizing environment allowing the metal ion to be stabilized by the thioester residues prior to transport. Subsequent transfer of Cu across the plasma membrane is thought to occur by a succession of Cu exchange reactions between binding sites within the pore of the transporter. As noted above, free Cu in the cytosol can disrupt cell function and chaperones serve to bind and sequester the Cu as required. These chaperones are small, water-soluble proteins possessing cysteine-rich motifs that provide thioester residues for complexing Cu. The loaded, chaperones then deliver the Cu to other transport proteins for uptake into organelles or to recently-synthesized Cu metalloenzymes that lack the cofactor metal (apo-form).

Other transport proteins involved in trafficking Cu include P-type ATPases that are specifically involved in the transport of heavy metals (named HMA transporters). Unlike COPT proteins, HMA transporters hydrolyze ATP as an energy source for Cu transport. The proton pump is an example of a P-type

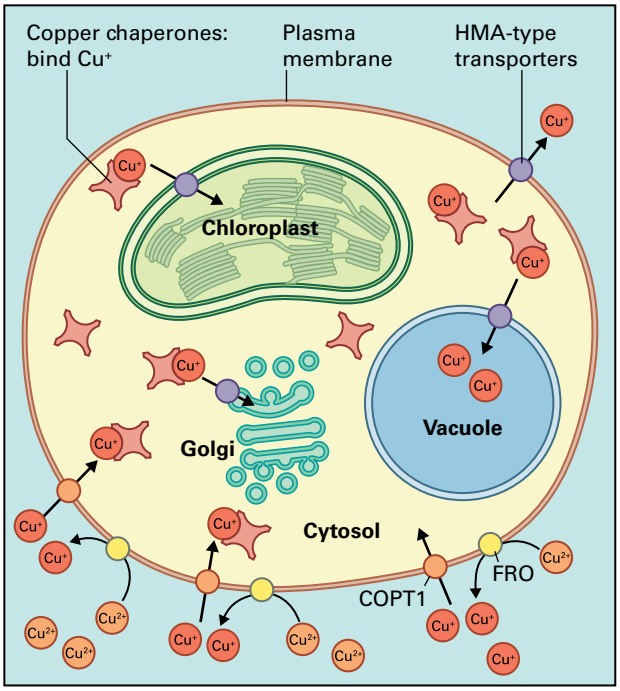


FIGURE 23.20 *Cu transport within plants cells showing the reduction of Cu^{2+} to Cu^+ at the plasma membrane by reductase activity (yellow), the role of COPT1 proteins in Cu^+ uptake, chaperones in binding reactive Cu^+ in the cytosol allowing it to be trafficked around the cell without causing damage, and HMA P-type ATPases that transport Cu into organelles or out of the cell.*

ATPase and its function is discussed in detail elsewhere (see Chapter 3). The HMA transporters share many attributes with other P-type ATPases but differ in possessing metal-binding domains in their membrane-spanning domains as well as at their termini. Members of the HMA family transport Cu into chloroplasts where it is incorporated as a metal cofactor into Cu/Zn superoxide dismutase (SOD) and plastocyanin. Other members of this family transport Cu out of the cell and serve to protect cells when Cu concentrations become excessive whereas others transport Cu into organelles such as the Golgi. Figure 23.20 summarizes the cellular processes involved in the uptake and distribution of Cu.

23.4.7 Copper homeostasis in plants involves specific transcription factors and microRNAs

The homeostasis of Cu in plants shares features in common with P_i homeostasis in that both involve microRNAs and transcription factors that respond to nutrient deficiency to regulate gene expression. When plants become Cu deficient, the expression of a range of genes is upregulated and these serve to increase the acquisition of Cu as well as redirecting Cu away from nonessential metalloproteins towards essential ones. Central to this regulation in *Arabidopsis* is the transcription factor SPL7 (**S**quamosa **P**romoter-binding **L**ike). SPL7

recognizes and binds to a GTAC core motif found as multiple copies within the promoters of genes upregulated by Cu deficiency. When *Arabidopsis* is Cu deficient, the expression of a range of genes including *COPT1*, *COPT2* (two members of the Cu transport family discussed above), *FRO3* (Fe reductase), *Fe SOD* (iron superoxide dismutase), *CCH* (a copper chaperone) and several microRNAs are all increased in wild-type plants but unaltered in an *spl7* mutant plant.

These responses serve to not only enhance the capacity of the plant to take up Cu, but also to make more efficient use of Cu within the plant. The induced miRNAs target the degradation of mRNAs encoding Cu-binding proteins considered to be nonessential thus redirecting Cu to those proteins with an essential function. Some of the proteins that decrease in abundance with Cu deficiency include Cu/Zn SOD, plantacyanin and the laccases, whereas the levels of plastocyanin, which plays an essential role in photosynthesis, are maintained. SOD activity is critical for preventing oxidative stress and the reciprocal regulation of the Cu/Zn and Fe SODs maintains this important cellular function as Cu nutrition changes. Therefore as Cu/Zn SOD activity declines in Cu deficient plants due to the action of miR398 targeting its mRNAs for degradation, an increase in Fe SOD expression maintains the overall SOD activity. The production of Cu/Zn SODs is further suppressed by miR398 because it also targets the mRNA encoding a Cu chaperone required for delivering Cu to SOD apoproteins. Therefore in Cu-deficient plants these regulatory pathways allow Cu to be retrieved from nonessential proteins and to be directed towards the essential Cu metalloenzymes (Fig. 23.21).

23.5 Plant responses to mineral toxicity

23.5.1 Aluminum toxicity is a major limitation to crop production on acid soils

Soil acidity affects 30% of total global land area and limits agricultural productivity around the world. Acid soils are especially widespread in tropical and subtropical regions where it impacts food production in many developing countries. Excessive use of ammonium fertilizers and other high-input farming practices can also accelerate soil acidification in developed countries. Liming (application of calcium carbonate) can neutralize soil acidity, but this is neither an economic option for poor farmers nor an effective strategy for alleviating subsoil acidity in the short term.

The major factor limiting plant production on acid soils is aluminum (Al) toxicity. Al is the most prevalent metal in the Earth's crust and its chemistry in soils and aqueous solutions is complex. Above ≈pH 5.5 most of the Al occurs as insoluble minerals but in more acidic conditions these minerals dissolve releasing several soluble monomeric Al species. Among these, the trivalent cation species, Al^{3+}, is most damaging to plants. Figure 23.22 illustrates the monomeric hydrolysis products of Al in solution and shows how the phytotoxic Al^{3+} dominates as pH decreases below 5.0. Monomeric Al also forms complexes with various ligands including carboxylates, sulfate, and phosphate even when these groups are in macromolecules such as proteins and nucleotides.

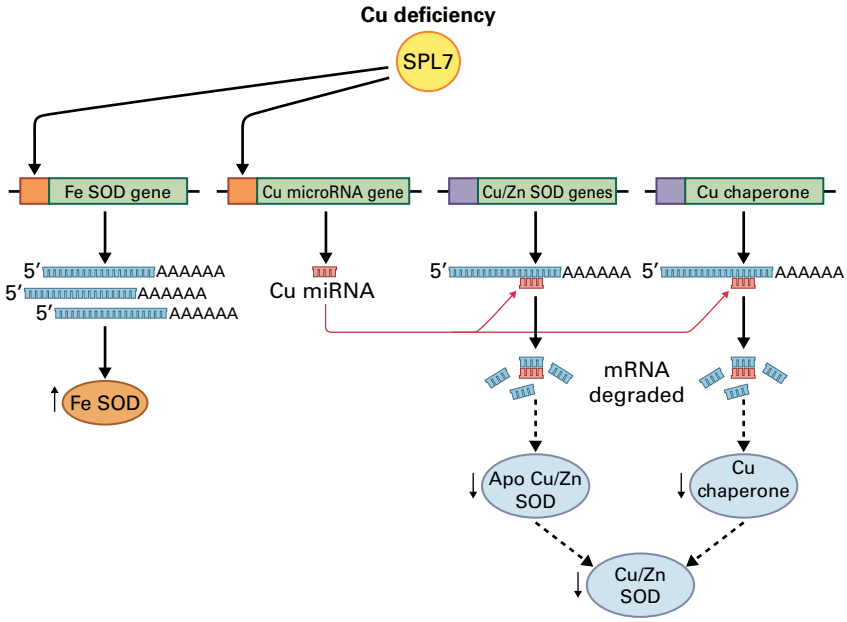


FIGURE 23.21 *Model showing the regulation of SOD activity in Cu-deficient plants. When plants sense Cu deficiency, the transcription factor SPL7 binds to gene promoters that possess core GTAC motifs and activates gene transcription. Increased expression of miRNA398 targets the degradation of mRNA for both Cu/ZnSODs and a chaperone responsible for insertion of Cu into the apo-SOD protein. Production of active Cu/ZnSOD is suppressed by both pathways and the Cu can be redirected towards the production of essential Cu metalloproteins. Another gene regulated by SPL7 encodes FeSOD. Enhanced FeSOD transcription results in increased active protein thus maintaining overall SOD activity in the cell.*

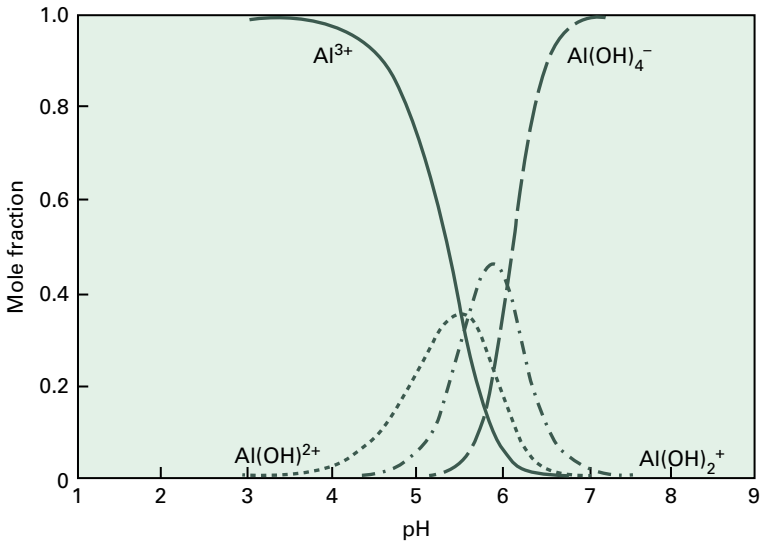


FIGURE 23.22 *Distribution of mononuclear aluminum ion species in aqueous solution, showing the mole fraction of each species as a function of solution pH. Note the predominance of phytotoxic Al^{3+} at pH 5 or lower.*

Stunted roots are the most obvious symptom of Al toxicity and this restricts the capacity of plants to access water and nutrients. Root apices are particularly sensitive and only a few millimeters need to be exposed to Al for growth to be inhibited (Fig. 23.23). Al toxicity results from multiple interactions between Al and important biological ligands in the cell wall, the plasma membrane and cytosol. For instance, Al can block Ca^{2+} and K^+ channels and inhibit Mg uptake that in the long term will induce mineral deficiencies. At the cellular level Al induces oxidative stress, destabilizes phospholipid bilayers, disrupts cytoplasmic Ca^{2+} homeostasis, and disrupts components of the cytoskeleton. This complex array of responses makes it difficult to determine which are the primary causes of toxicity and which are secondary responses to stress.

23.5.2 Al tolerance relies on exclusion and internal mechanisms

Some plant species and even genotypes within species grow better on acid soils than others and the mechanisms involved have been the focus of considerable research. Figure 23.23 shows Al-tolerant (Atlas) and Al-sensitive (Scout) cultivars of wheat grown in an acidic $CaSO_4$ solution containing Al. The inhibition of root growth and damage to root apices is more severe in Scout than Atlas whereas shoot growth is less affected by Al. Early studies established that tolerant genotypes within some species (e.g., wheat and barley) accumulate less Al in their roots than sensitive genotypes. By contrast other highly tolerant species such as tea (*Camellia sinensis*) and *Hydrangea* sp. accumulate high concentrations of Al in their root and shoot tissues. These examples illustrate the two types of tolerance mechanisms that operate in plants: ***exclusion mechanisms*** which reduce Al uptake or minimize its interaction with root cells, and ***internal mechanisms*** which enable plants to safely accommodate any Al that enters the cells. Al could be excluded from the symplasm by binding to cell walls, decreasing its permeability across the plasma membrane, chelating it with ligands released from the root, exporting it out of the cell or by increasing rhizosphere pH to reduce the local concentration of Al^{3+} near the root surface. Internal mechanisms could involve chelating Al in the cytosol or sequestering it to subcellular compartments such as the vacuole.

Al tolerance is a multigenic trait in important crops such as wheat, rice and maize. This means that more than one gene contributes to the phenotype and that their effects may be additive. Nevertheless a single genetic locus often accounts for most of the phenotypic variation in Al tolerance in wheat suggesting that many of the other loci contribute relatively low levels of tolerance. The situation in maize is more complex and at least five different loci contribute to Al tolerance. The genes underlying these loci may encode multiple physiological mechanisms.

23.5.3 Exclusion of Al relies on the efflux of organic anions from roots by ALMT and MATE transporter proteins

The exclusion of Al from wheat roots relies on the release or efflux of malate anions from roots (Fig. 23.24). Indeed, Al tolerance among a wide range of wheat genotypes is highly correlated with malate efflux from the root apices and shows a saturating dependence on the concentration of Al in the external media (Fig. 23.25). Since malate anions form a stable complex with Al^{3+} it reduces the concentration of Al^{3+} near the sensitive root apices. Subsequent studies showed similar mechanisms operate in other members of the Poaceae (e.g., maize, barley, *Sorghum* spp., *Secale cereale*) as well as species in the Araceae (e.g., taro, *Colocasia esculenta*), Polygonaceae (e.g., buckwheat, *Fagopyron esculentum*), Brassicaceae (e.g.,

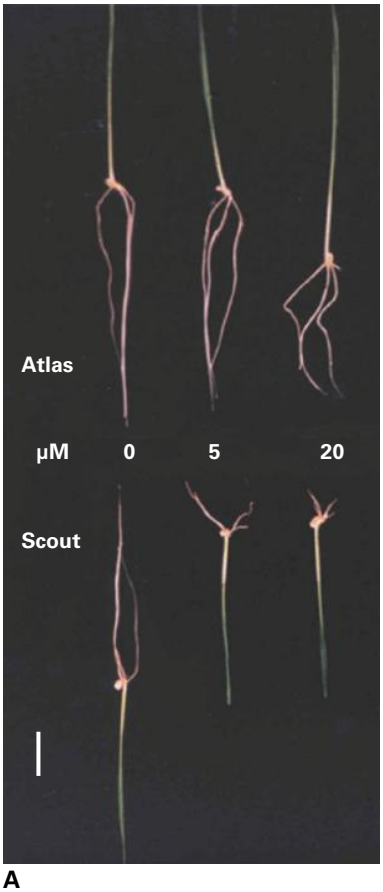


FIGURE 23.23 *Effects of Al treatment on root growth in Al-tolerant and Al-sensitive cultivars of wheat. (A) Seedlings of the Al-tolerant cultivar* Atlas *and the Al-sensitive cultivar* Scout *were grown for 4 days in 0.6 mM $CaSO_4$ solutions containing 0, 5, or 20 μM $AlCl_3$ (pH 4.5). The inhibition of root growth is significantly greater in* Scout *than* Atlas *but shoot growth is relatively unaffected. Scale bar represents 1 cm. (B) Scanning electron micrograph of root apices from Al-sensitive and Al-tolerant wheat lines grown in 5 μM $AlCl_3$ for 4 days. The sensitive plants incur greater damage than the tolerant line. Scale bar represents 0.5 mm. Source:* (A) I. Raskin, Rutgers University, NJ; previously unpublished.

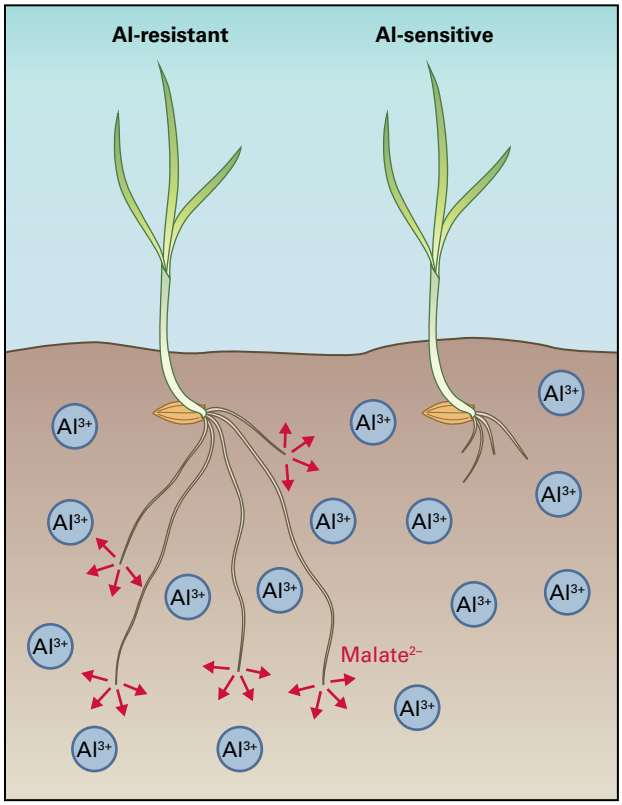


FIGURE 23.24 *Acid soils contain high concentrations of soluble Al^{3+} that can inhibit root growth. Increased tolerance to Al in wheat relies on Al-activated efflux of malate anions from root apices Malate protects the roots by chelating toxic Al^{3+} cations in the apoplast reducing Al uptake and minimizing damage to Al-sensitive root apices. Note that the malate is unlikely to diffuse far into the soil as shown diagrammatically in the cartoon. Malate efflux is facilitated by TaALMT1, a malate-permeable anion channel which is more highly expressed in root apices of Al-tolerant genotypes than sensitive genotypes. Organic anion release from roots (especially malate and citrate) is a mechanism for Al exclusion in a wide range of species. Efflux of these anions is mediated by transport proteins from the ALMT and MATE families.*

Arabidopsis, *Brassica napus*), and the Fabaceae (e.g., rice bean, *Vigna umbellata*; bean, *Phaseolus vulgaris*; soybean, *Glycine max*). The organic anions released vary from species to species. Malate and citrate are most common but oxalate efflux occurs from a few species (buckwheat, taro). All three anions form strong complexes with Al^{3+} that serves to lower the free concentration of Al^{3+} and reduce its uptake by roots.

The gene encoding the Al-activated efflux of malate in wheat is *TaALMT1* (*Triticum aestivum* aluminum-activated malate transporter). *TaALMT1* was discovered because it is more highly expressed in the root apices of Al-tolerant wheat plants than Al-sensitive plants. TaALMT is a member of a previously uncharacterized protein family with five to seven transmembrane domains in the N-terminal half of the protein and a long hydrophilic C-terminal region. TaALMT1 localizes to the plasma membrane of root cells and its higher expression in Al-tolerant genotypes is driven by tandemly repeated sequences in the *TaALMT* promoter that enhance gene transcription. Heterologous expression of *TaALMT1* in several different plant species confers an Al-activated efflux of malate and greater Al tolerance. Electrophysiological studies in *Xenopus* oocytes and suspension-cultured cells of *N.*

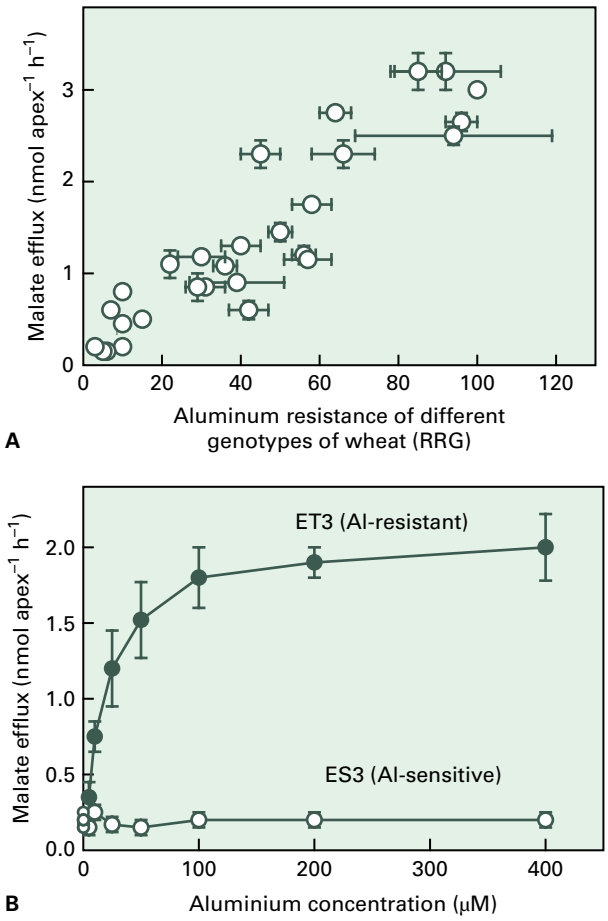


FIGURE 23.25 *Malate efflux from root apices is correlated with Al tolerance among different cultivars of wheat. (A) Malate release from excised root apices over 80 minutes was measured in 28 cultivars of wheat treated with 100 μM $AlCl_3$ and 0.2 mM $CaCl_2$ (pH 4.2). Al tolerance was estimated from measurements of relative root growth (RRG) in 0.2 mM $CaCl_2$ with 0 and 10 μM $AlCl_3$ and (pH 4.2) over 7 days. (B) External Al activates malate efflux and the response saturates at high Al^{3+} concentrations. Data are shown from the Al-tolerant and sensitive wheat cultivars ET3 and ES3, respectively.*

tabaccum are consistent with *TaALMT1* encoding a ligand-gated ion channel which facilitates malate efflux. *TaALMT1* confers the major component of Al tolerance in wheat but additional mechanisms also contribute in some genotypes.

An understanding of the genetics and physiology of Al tolerance in sorghum (*S. bicolor*) and barley led to the discovery of a second family of Al tolerance genes. Tolerance in these species is controlled by a single major genetic locus that segregates with the Al-activated efflux of citrate. Fine mapping of these genetic loci identified the *SbMATE* gene in sorghum and the *HvAACT1* (***H**ordeum **v**ulgare* **a**luminum-**a**ctivated **c**itrate **t**ransporter1) gene in barley, both of which belong to the MATE (**m**ultidrug **a**nd **t**oxic compound **e**xudation) family. The MATE family of transporter proteins is a large and diverse group present in prokaryotic and eukaryotic cells. Many MATE proteins function as cotransporters (often as antiporters with protons or sodium) to transport secondary metabolites and small organic compounds out of the cytosol. The SbMATE and HvAACT1 proteins localize to the plasma membrane of root cells and function as Al-activated transporters facilitating citrate efflux from root apices. *SbMATE* expression in *S. bicolor* is enhanced by Al treatment whereas the expression of *HvAACT1* is constitutively higher in tolerant genotypes of barley than sensitive genotypes. However, in both cases, the Al tolerance among genotypes is strongly correlated with the level of gene expression.

Members of the *ALMT* and *MATE* families confer Al tolerance in many other species as well. For example, *AtALMT1*, one of the 14 members of the *ALMT* family in *Arabidopsis*, appears to function in a similar manner to TaALMT1 in wheat even though their amino acid sequences are only 44% identical. *Arabidopsis* plants carrying a knockout mutation in *AtALMT1* (*Atalmt1*) show reduced Al-activated malate efflux and increased sensitivity to Al. Other *ALMTs* are likely to contribute to the Al tolerance of *B. napus* and *S. cereale* and *MATEs* are likely to contribute to the Al tolerance of maize and some wheat genotypes. The emerging picture from these studies is that *ALMT* genes control the release of malate anions whereas *MATE* genes control the release of citrate anions. Therefore the primary determinant for whether malate or citrate release occurs from roots is the type of transport protein expressed and not differences in metabolism.

Al activates the transport function of most ALMT and MATE proteins involved in Al tolerance. The details of this activation are not known but it is likely that Al interacts directly with the proteins themselves. This interaction may alter the tertiary structure of the proteins that then activates transport activity. The activation of organic anion efflux occurs rapidly in some species, while in others, it is delayed by several hours or even days after the addition of Al and then increases gradually through time. The rapid response (Type I) is interpreted as Al activating proteins already present in the membrane (Fig. 23.26). Examples include malate efflux from wheat and citrate efflux from barley that is consistent with the constitutive expression of the *TaALMT1* and *HvAACT1* genes in these species. The delayed response (Type II) reflects the requirement for Al to first induce gene and protein expression before function can begin (Fig. 23.26). Examples of this response include malate efflux from *Arabidopsis* and citrate efflux from maize, sorghum and rye. Regardless of whether Al induces expression of the ALMT and MATE proteins most still require external Al to activate transport function.

23.5.4 Al-tolerance genes identified by mutational analysis

Rice has a high basal level of Al tolerance compared to most cereals that cannot be explained by organic anion efflux. Some of the genes controlling Al tolerance in rice, as well as additional tolerance genes in *Arabidopsis*, were discovered by screening mutagenized seedlings for altered sensitivity to Al. These screens identified *STAR1* (sensitive to Al rhizotoxicity)

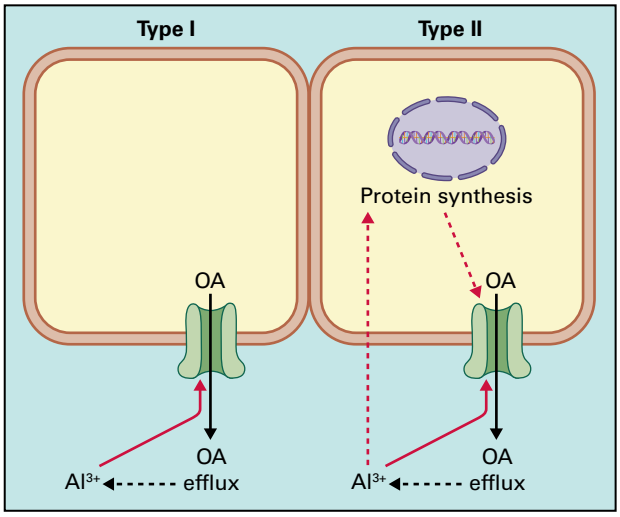


FIGURE 23.26 *Model for Al-activated efflux of organic acid anions (OA) from roots. In Type I response, Al^{3+} rapidly triggers organic anion release from root cells by activating a pre-existing transport protein on the plasma membrane (solid orange line). To date, these transporters have been shown to be members of the ALMT (malate efflux) or MATE (citrate efflux) protein families. Al is likely to interact directly with the transport proteins to activate efflux. Organic anions then chelate the Al^{3+} cations in the apoplast preventing them from damaging root cells (broken black line). In the Type II response, efflux is delayed by several hours after Al is added. In this mechanism Al first induces the expression of the transport proteins and perhaps other proteins (broken orange line). Al then activates transport function in the newly synthesized proteins in a similar manner to that described for Type I responses (solid orange line).*

in rice and *ALS1* and *ALS3* (Al sensitive) in *Arabidopsis* that encode full or partial ABC-like transport proteins. STAR1 interacts with another protein called STAR2 to form a functional ABC (**A**TP **b**inding **c**assette) transport protein. The STAR1/2 complex appears to export secondary metabolites from the cell (e.g., UDP-glucose or phenolic compounds) possibly via exocytosis of vesicles but exactly how this confers tolerance is uncertain. These exported compounds might bind with Al^{3+} in the apoplast or they could be substrates for subsequent enzyme reactions that modify cell walls to minimize Al^{3+} damage. Mutant screens also identified C2H2-type zinc-finger transcription factors encoded by *ART1* (***Al** resistance **t**ranscription factor1*) in rice and *STOP1* (***s**ensitive **to** **p**H1)* in *Arabidopsis*. *ART1* and *STOP1* are required for the induction of these ABC-type genes and many other genes involved in tolerance and therefore appear to be important regulators of plant responses to Al and pH stress.

23.5.5 The engineering of Al tolerance in plants

Some plant crop species grow well on acid soils and others can be improved by conventional breeding strategies. For important crop species that possess insufficient natural variation to breed for tolerance, biotechnology provides opportunities of increasing food production on acid soils. Once the role of organic anion efflux in Al tolerance was understood, many researchers attempted to genetically engineer this trait into model plant species. Two main strategies were employed to increase organic anion efflux from roots. The first increased the expression of genes involved in the synthesis of malate or citrate (e.g., citrate synthase, malate dehydrogenase), while the second increased the capacity for organic anion transport out of the cells. Most success has been achieved by transforming plants with the *ALMT* and *MATE*-type tolerance genes discussed above. For example, over-expression of the wheat *TaALMT1* gene in barley results in a 25-fold increase in organic anion efflux compared to controls and a significant increase in root growth in nutrient solution and soils containing toxic levels of Al.

Summary

Plants use a wide range of mechanisms and responses to acquire essential mineral nutrients from the soil and to tolerate toxic soil environments. Some of these approaches are exceptionally complex. Diverse, nutrient-specific strategies allow terrestrial plants to increase the availability of essential minerals in the soil, transport them into the root, and translocate them throughout the plant. Plants must also regulate the acquisition of potentially toxic but essential elements such as Fe and Cu to prevent both nutrient deficiency and metal toxicity.

The field of plant mineral nutrition, rooted in physiological investigations, has recently moved into a new era of discovery in which molecular research approaches are being applied to questions of mineral nutrition. A current challenge faced by plant scientists is to integrate the information gained from molecular dissections of these intricate processes with previous and current research into the physiology of mineral nutrition at the levels of cell, organ, and whole plant. The ultimate goal of this work is to further the scientific understanding of how intact plants grow, whether in a farmer's field or in a native ecosystem.



24

Natural Products

Toni M. Kutchan, Jonathan Gershenzon, Birger Lindberg Møller, and David R. Gang

Introduction

Plant secondary metabolites, also referred to as natural products or specialized metabolites, constitute an enormously rich reservoir of chemical biodiversity. More than 200,000 diverse chemical structures have been identified. In comparison with primary metabolites, which are essential to plant growth and development, secondary metabolites have internal roles in plants and also are integral to the communication of a plant with its environment. This interaction takes many forms. It can be an accumulation of pigments in flower petals, or a release of volatile chemicals by flowers to attract pollinators. It can be the release of volatiles by a leaf damaged by a grazing caterpillar to attract predatory wasps in a tritrophic interaction, or the production of bitter or toxic chemicals that serve as antifeedants. It can also be the release by roots of secondary metabolites into the rhizosphere to attract beneficial soil microorganisms.

Primary and secondary metabolites cannot be readily distinguished by their precursor molecules, chemical structures, or biosynthetic origins. For example, the diterpenes kaurenoic acid and abietic acid are formed by a similar sequence of related enzymatic reactions (Fig. 24.1); whereas the former is an essential intermediate in the synthesis of gibberellins (see Chapter 17), the latter is a resin component largely restricted to members of the Fabaceae and Pinaceae. Similarly, the essential amino acid proline is classified as a primary metabolite, whereas the C_6 analog pipecolic acid (Fig. 24.1) is considered an alkaloid and, thus, a secondary metabolite. Even lignin, the essential structural polymer of wood and second only to cellulose as the most abundant organic substance in plants, has been considered a natural product rather than a primary metabolite. In the absence of a valid distinction between primary and secondary metabolites based upon structure or biochemistry, a functional definition is used herein: primary products participate in nutrition and essential metabolic processes in the plant, and secondary products influence communication between the plant and its environment.

Organic chemists have long been interested in secondary metabolites for their practical utility as dyes, polymers, fibers, glues, oils, waxes, flavors, fragrances, drugs, insecticides, and herbicides. Scientists have investigated their chemical properties extensively since the 1850s, and these investigations stimulated development of the chromatographic separation techniques, spectroscopic methodologies, and synthetic approaches that are the foundations of contemporary organic chemistry. Today it is recognized that natural products have important ecological roles in plants, and their study has transitioned into the realm of modern biology.

Plant natural products can be divided into several major groups based on their chemical structures, with the best studied being the terpenoids, cyanogenic glucosides and glucosinolates, alkaloids, and phenolics. In this chapter, we provide an overview of the biosynthesis of these major classes of plant natural products as well as their physiological functions, human uses, and potential biotechnological applications. Overarching issues that may apply to all these classes of compounds, such as the role of multienzyme complexes (metabolons) in their biosynthesis and their storage in specialized structures and subcellular compartments (e.g., resin ducts, subcuticular sacs, and vacuoles), are presented in the sections that deal with the classes of natural product in which these topics have been best studied.

Biochemistry & Molecular Biology of Plants, Second Edition. Edited by Bob B. Buchanan, Wilhelm Gruissem, and Russell L. Jones.
© 2015 John Wiley & Sons, Ltd. Published 2015 by John Wiley & Sons, Ltd.
Companion website: www.wiley.com/go/buchanan/biochem

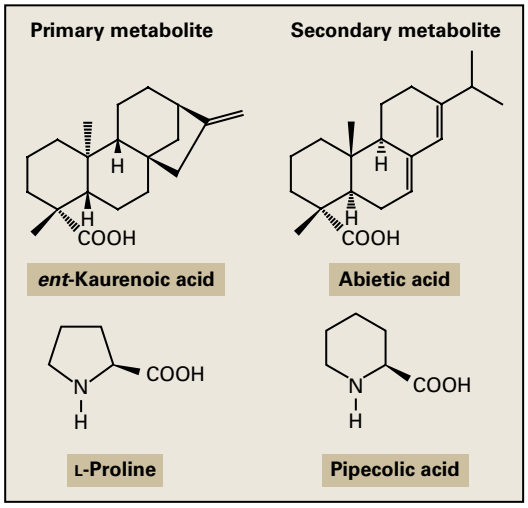


FIGURE 24.1 *Kaurenoic acid and proline are primary metabolites, whereas the closely related compounds abietic acid and pipecolic acid are considered secondary metabolites.*

24.1 Terpenoids

24.1.1 Terpenoids are classified by the number of five-carbon units they contain

Terpenoids—with over 30,000 members described to date—take the honors for being the largest class of small molecule natural products in plants. They exhibit enormous structural diversity, but are united by a common biosynthetic origin. Derived from the joining of five-carbon isopentane units, terpenoids are also referred to as isoprenoids and as terpenes. The terms "terpene" and "terpenoid" originate from the word turpentine ("terpentin" in German) because some of the first terpenes described were isolated from turpentine.

The five-carbon units from which terpenoids are formed are sometimes called isoprene units, because some terpenoids decompose to give off the gas isoprene at elevated temperatures (Fig. 24.2). The classification of terpenoids has a long history (see Box 24.2, later in the chapter). The 10-carbon terpenoids were once thought to be the smallest naturally occurring representatives of this class. Hence, these were called **monoterpenes**, and the name persists. Designating the 10-carbon terpenoids as monoterpenes (one terpene) makes it necessary to name the five-carbon terpenoids as **hemiterpenes** (half terpenes), the 15-carbon terpenoids as **sesquiterpenes** (one and one-half terpenes), the 20-carbon terpenoids as **diterpenes** (two terpenes), the 30-carbon terpenoids as **triterpenes** (three terpenes), and so on.

24.1.2 Terpenoids fulfill many different functions in plants

Although terpenoids are found in all living organisms, they reach their greatest structural and functional diversity in plants. Many terpenoids have a well-characterized function in basic plant growth and development and so can be classified as primary, rather than secondary metabolites.

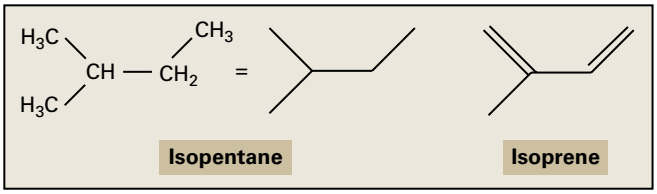


FIGURE 24.2 *The structure of the basic five-carbon (C_5) units of terpenoids. Isopentane (left) is a branched C_5 hydrocarbon, and isoprene (right) is a gas formed when certain terpenoids decompose.*

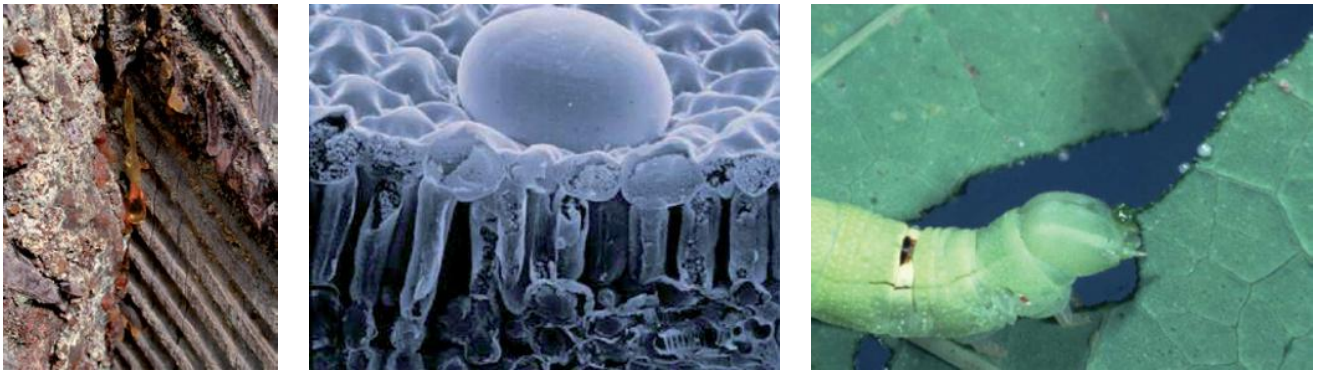
These primary metabolites include several types of plant hormones: the gibberellins (diterpenes, C_{20}, see Chapter 17), brassinosteroids (triterpenes, C_{30}, see Chapter 17), abscisic acid (see Chapter 17), and the strigolactones (see Chapter 17). The natural cytokinins (see Chapter 17) have a C_5 terpenoid side chain. While abscisic acid is formally a sesquiterpene (C_{15}) and strigolactones have 19-carbon atoms in their basic skeleton, both are actually derived by cleavage of a group of tetraterpenes (C_{40}), the carotenoids.

Carotenoids are another major group of plant terpenoids with well-understood functions. These red, orange, and yellow substances participate in the energy-transfer processes of photosynthesis (see Chapter 12), protect photosynthetic tissues from oxidation under high light conditions, and attract animals to flowers and fruits for dispersal of pollen and seeds. Sterols are triterpene derivatives that are essential components of cell membranes, which they stabilize by interacting with the phospholipids (see Chapter 1).

Chains of terpenoid five-carbon units are usually very lipophilic. When attached to other molecules, they may anchor those molecules to proteins or lipid membranes. For example, phytol, a side chain of four five-carbon units (C_{20}) helps insert chlorophyll into the photosystem complexes that are, in turn, embedded in the thylakoid membrane. The antioxidant tocopherols and electron carriers, including ubiquinones, plastoquinones, and phylloquinones, are anchored into membranes by side chains of 4–10 five-carbon units. Some plant proteins are inserted into membranes or directed into protein–protein interactions by means of 15- or 20-carbon terpenoid side chains that are added post-translationally to a cysteine residue near the C-terminus. Finally, very long terpenoid molecules known as dolichols (15–23 five-carbon units) are involved in sugar transfer reactions that take place during cell wall and glycoprotein synthesis.

24.1.3 Most plant terpenoids have important ecological roles as well as utility for humans

Most of the thousands of terpenoids produced by plants have no discernible roles in growth and development and are, therefore, secondary metabolites. Many of these are volatile compounds or constituents of essential oils, resin, latex, and



A B C

FIGURE 24.3 *Terpenoids can be used for plant defense. These compounds often form oily, sticky, or irritating mixtures that deter herbivore feeding and pathogen invasion. (A) The resin of conifers comprises mainly monoterpenes (C_{10}) and diterpenes (C_{20}). When the tree is damaged and resin ducts are severed, the smelly monoterpenes quickly evaporate from the extruded resin, leaving behind the sticky diterpenes, which become polymerized. (B) The monoterpene-rich oil of peppermint (*Mentha *sp.) is stored in glandular hairs on the surface of leaves and other organs. Shown in this cutaway view of a young leaf is a single glandular hair, about 0.5 mm in diameter, on the leaf surface. (C) Plant latex is a milky fluid that is made up of an emulsion of proteins, natural products, and other cellular constituents that often contains diterpenes, triterpenes, or higher order terpenes, including rubber. Stored in ducts known as laticifers, it is exuded after injuries, such as that caused by herbivory.*
Source: (A) Reiderer, University of Würzburg, Germany; (B, C) Wittstock & Gershenzon (2002). Curr. Opin. Plant Biol. 5:300–307.

waxes. Once thought of as metabolic waste products, these terpenoids actually serve a suite of ecological roles: they can defend against herbivores and pathogens, inhibit germination and growth of competing plants, or attract animals that disperse pollen and seeds.

Many terpenes form sticky, oily, smelly, or irritating mixtures (Fig. 24.3), so it is easy to appreciate their defensive properties. For example, the triterpene azadirachtin (Fig. 24.4) from the seed oil of the Asian neem tree (*Azadirachta indica*) is a powerful insect feeding deterrent and exerts a variety of toxic effects on insects as well. This complex, highly oxygenated terpenoid was isolated following centuries of use of neem foliage by Indian farmers to protect stored grain from pests. Because of its low toxicity to mammals, azadirachtin has considerable potential for controlling agricultural and household insect pests, and several preparations containing it are now on the market. Few terpenoids have been investigated as thoroughly as azadirachtin.

Mono- and sesquiterpenes are generally volatile compounds and are the principal constituents of herb and spice plants, such as basil, oregano, mint, bay, parsley, and dill (see Fig. 24.5). These compounds also serve as defenses against chewing herbivores. They are stored in glandular hairs or secretory cavities in leaves or fruit and are volatilized when the tissue is crushed. Terpenoids are volatilized from the foliage of nearly all plant species investigated, especially after insect feeding. For example, plants such as maize (*Zea mays*), cotton (*Gossypium hirsutum*), lima bean (*Phaseolus lunatus*), and *Arabidopsis* respond to herbivore damage by emitting a blend of monoterpenes and sesquiterpenes. These substances repel additional herbivores and attract herbivore enemies, such as parasitic wasps and predatory arthropods.

The emission of certain terpenes from plant leaves can also be independent of herbivory. The hemiterpene isoprene and several monoterpenes are emitted by many plant taxa, especially woody species, in substantial amounts and have a major impact on the levels of ozone, carbon monoxide, and other gases in the atmosphere. In the plant, isoprene and monoterpenes appear to protect against thermal and oxidative stress, perhaps by stabilizing membranes or combining directly with reactive oxygen species, such as singlet oxygen, hydroxyl radicals, and nitrous oxides.

Terpenoids also play important roles in human society. They are used as flavors and fragrances of foods, beverages, soaps, perfumes, toothpaste, and other products. Some find use as industrial materials (resins and rubber) or pigments (carotenoids), and yet others are insecticides that are of value because of their low toxicity to humans and lack of persistence in the environment (azadirachtin and pyrethrins). Many terpenoids are also of nutritional or pharmaceutical significance, including vitamins A, D, E, and K as well as some well-known drugs (see Fig. 24.4): Taxol is a diterpene from yew (*Taxus brevifolia*) that has become a blockbuster drug for the treatment of ovarian and breast cancer, artemisinin is a sesquiterpene from *Artemisia annua* used against malaria, and the cardenolides (triterpenes, such as digitoxigenin) extracted from foxglove (*Digitalis lanata*) are prescribed to millions of patients for the treatment of heart disease. Carotenoids are also becoming more popular as "neutraceuticals" (foods with health benefits) believed to help prevent cancer, heart disease, and macular degeneration.

24.1.4 Terpenoids are formed by the fusion of five-carbon "isoprene units"

The five-carbon isopentane or isoprene units that make up terpenoids are usually joined in a "head-to-tail" fashion (Fig. 24.6). This pattern was first recognized in the

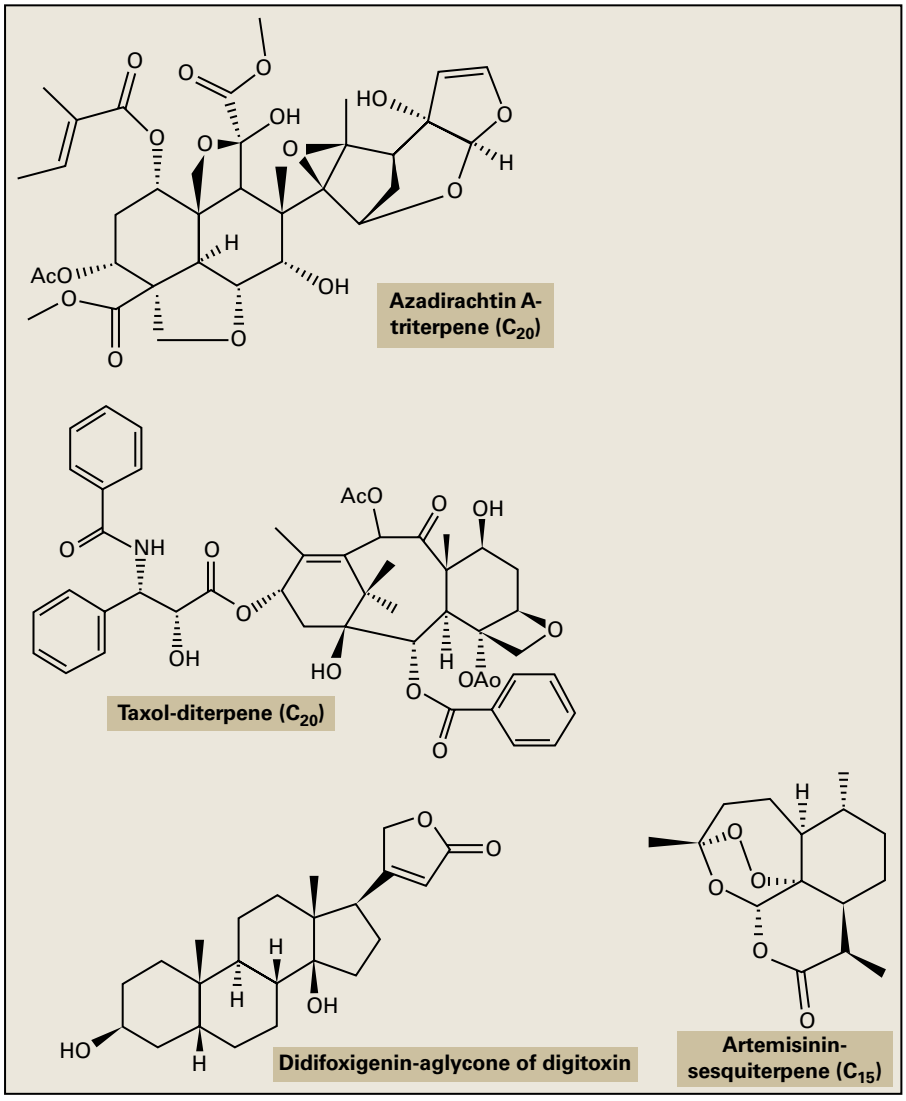


FIGURE 24.4 *Structures of some economically important terpenes. Azadirachtin is a triterpene (C_{30}) derivative from the seed oil of the Asian neem tree (*Azadirachta indica*) used in insect pest control. Taxol, a diterpene (C_{20}) derivative, is from the yew tree (*Taxus brevifolia*) and used in cancer treatment. Digitoxigenin is an aglycone of digitoxin, a steroid glycoside used to treat heart disease. Artemisinin is a sesquiterpene from* Artemisia annua *used against malaria.*

late 1800s and updated in the 1930s upon the realization that other types of reactions could occur in terpenoid formation because of the chemical mechanisms involved (Box 24.2). However, all terpenoids were proposed to be formed from a "biological" isoprene unit. These units can be joined in head-to-tail, head-to-head, and by various head-to-middle fusions, and substantial structural rearrangement can occur during biosynthesis. In such modified terpenoids, it may be difficult to discern the original organization of the isoprene units (Fig. 24.6). Nevertheless, dissection of terpenoid skeletons into isoprene units is often valuable for understanding their mode of biosynthesis.

The biosynthesis of terpenoids can be conveniently divided into four stages described in subsequent sections: (i) the synthesis of the biological five-carbon isoprene unit, (ii) repetitive condensations of the five-carbon unit to form a series of larger and larger prenyl diphosphates, (iii) conversion of prenyl diphosphates to the basic terpenoid skeletons, and (iv) further modifications to the basic skeletons, including oxidation, reduction, isomerization, conjugation, and other transformations.

24.2 Biosynthesis of the basic five-carbon unit

The basic five-carbon unit of terpenoid biosynthesis is represented by **isopentenyl diphosphate** and **dimethylallyl diphosphate**. These intermediates are synthesized in plants by two completely different routes that are spatially separated but exchange intermediates: the mevalonate pathway (see Section 24.2.1) and the methylerythritol 4-phosphate (MEP) pathway (see Section 24.2.2).

24.2.1 The mevalonate pathway converts acetyl-CoA to isopentenyl diphosphate and dimethylallyl diphosphate

The first route proceeds via the reactions of the mevalonate pathway (Fig. 24.7). Demonstrated initially in yeast and mammals, this well-characterized sequence begins with the condensation of three molecules of acetyl-CoA in two steps to

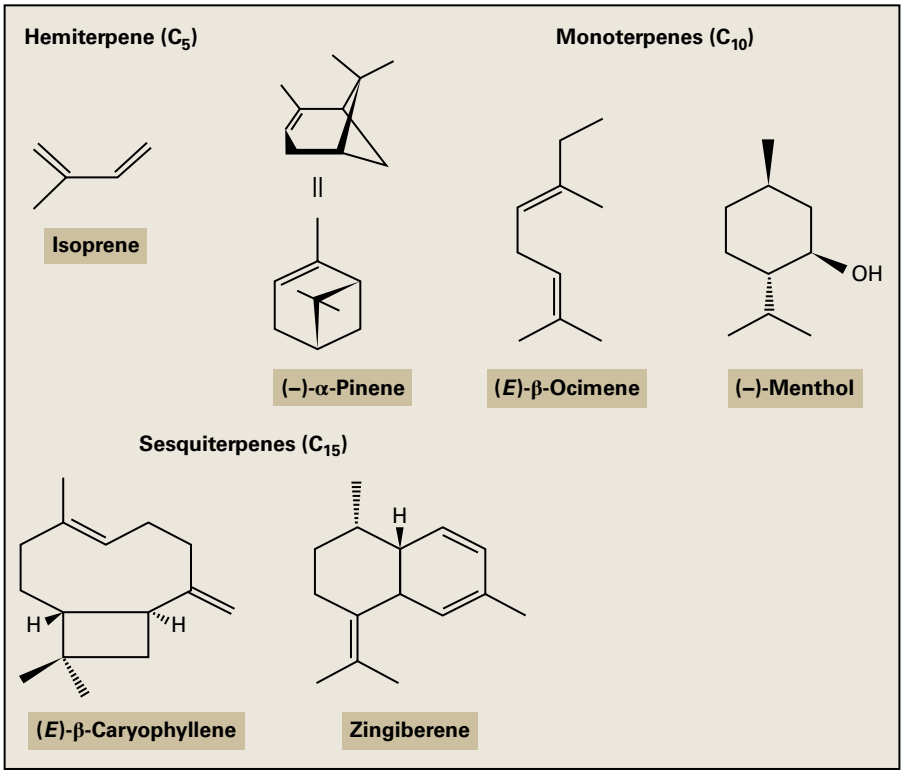


FIGURE 24.5 *Volatile terpenes are often stored in specialized structures in herb and spice plants, or are released directly as volatiles from many species of plants. Isoprene is a hemiterpene (C_5); α-pinene (conifer resin), (E)-β-ocimene, and menthol (peppermint oil) are monoterpenes (C_{10}); (E)-β-caryophyllene (an essential oil of many plants, including clove, rosemary, and hops) and zingiberene (ginger oil) are sesquiterpenes (C_{15}). The high vapor pressure of these compounds arises from their low molecular weights and lack of polar oxygen functions.*

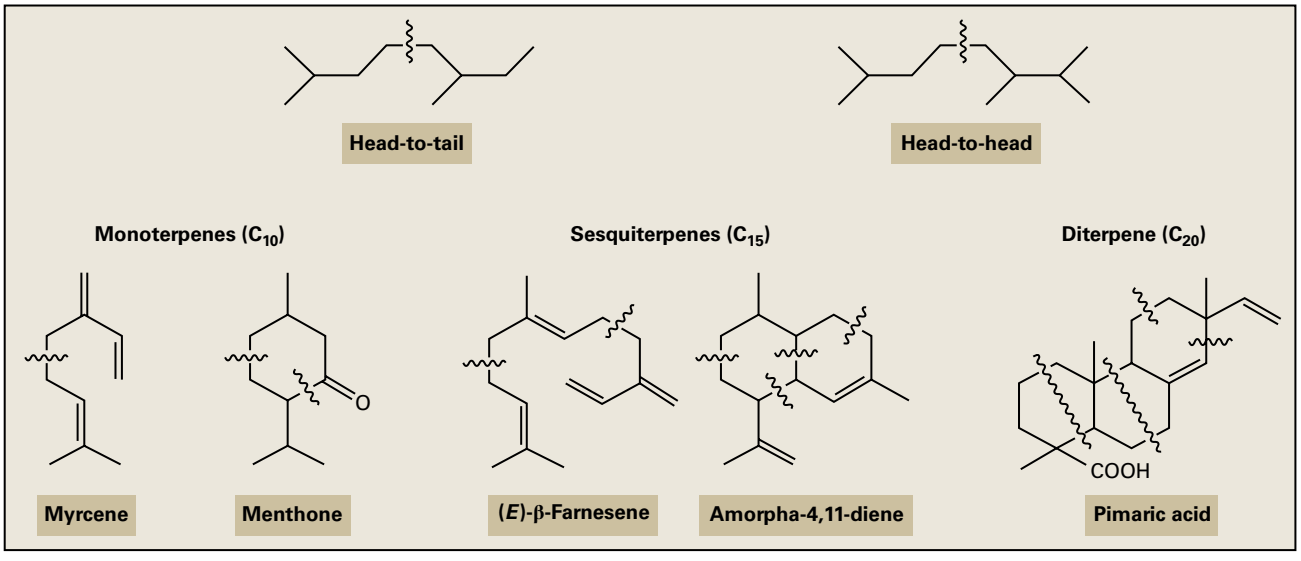


FIGURE 24.6 *Terpenoids are formed from the fusion of five-carbon isopentane units (isoprene units), which are usually joined in a head-to-tail fashion. The division of terpenoids into such units helps to visualize their biosynthetic assembly, although extensive metabolic rearrangements may complicate this task. Myrcene and menthone are monoterpenes (C_{10}—two C_5 units); (E)-β-farnesene and amorpha-4,11-diene are sesquiterpenes (C_{15}—three C_5 units); and pimaric acid is a diterpene (C_{20}—four C_5 units).*

form the six-carbon compound, 3-hydroxy-3-methylglutaryl-CoA (HMG-CoA). This intermediate is reduced by **HMG-CoA reductase** in two coupled, NADPH-requiring reactions to form mevalonic acid. Next come two sequential ATP-dependent phosphorylations that produce mevalonic acid-5-diphosphate. Finally, a decarboxylation-elimination reaction involving a third phosphorylation yields isopentenyl diphosphate, which can be isomerized to dimethylallyl diphosphate by isopentenyl diphosphate isomerase, an enzyme which also catalyzes the reverse reaction.

The third enzyme of the mevalonate pathway, HMG-CoA reductase, has been studied intensively because it catalyzes a

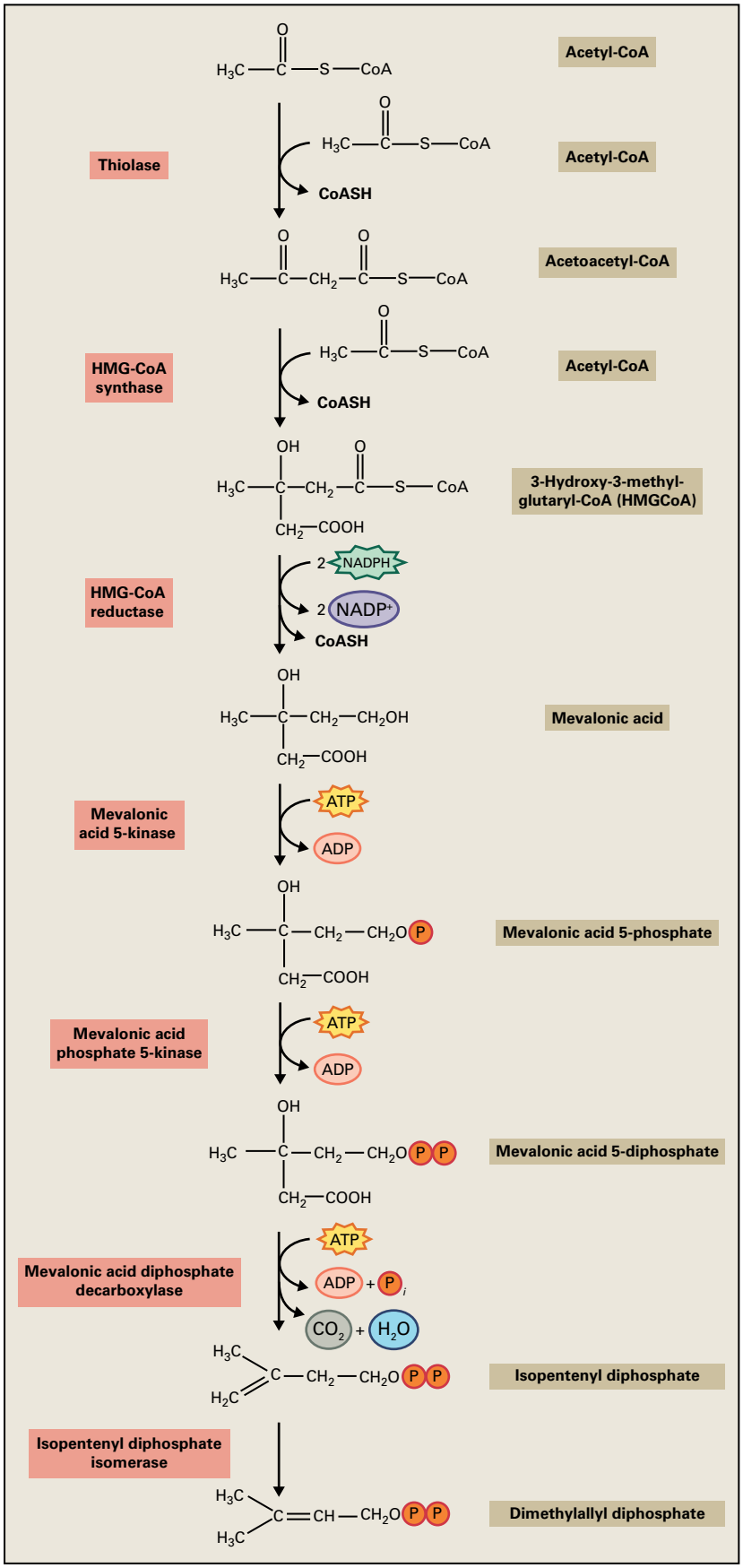


FIGURE 24.7 *The mevalonate pathway for the formation of isopentenyl diphosphate, the basic five-carbon unit of terpenoid biosynthesis. Synthesis of each isopentenyl diphosphate unit requires three molecules of acetyl-CoA. The mevalonate pathway occurs in the cytosol of plant cells.*

rate-determining step in the biosynthesis of sterols, such as cholesterol, in animals. HMG-CoA reductase in plants has been assumed to be an important regulatory step in terpenoid biosynthesis as well. In fact, many studies have reported a close correlation between changes in HMG-CoA reductase activity and alterations in the rate of terpenoid biosynthesis. The mechanism of this control may lie in part at the level of transcription, since all plants examined possess multiple HMG-CoA reductase genes exhibiting tissue-, development-, or stress-specific expression patterns. The activity of HMG-CoA reductase is also subject to posttranslational regulation by a protein kinase cascade that phosphorylates, and thereby inactivates, the enzyme.

24.2.2 The methylerythritol 4-phosphate pathway converts pyruvate and glyceraldehyde 3-phosphate to isopentenyl diphosphate and dimethylallyl diphosphate

One of the most exciting advances in plant biochemistry in recent years was the discovery of a second route for producing the basic five-carbon building blocks of terpenoid biosynthesis, a route completely distinct from the mevalonate pathway (Fig. 24.8). This route begins with pyruvate and glyceraldehyde 3-phosphate and is usually named for its second intermediate, 2*C*-methyl-D-erythritol 4-phosphate (MEP).

The existence of a second, nonmevalonate pathway to isopentenyl diphosphate in plants had been suspected for many years based on the poor incorporation of mevalonate into certain types of terpenoids. In the early 1990s, researchers found that the incorporation of ^{13}C-labeled precursors into terpenoids in plants gave a different pattern of labeling than would have been expected from the mevalonate pathway. They went on to identify the intermediates, enzymes, and genes of the pathway, an effort greatly facilitated by the presence of this pathway also in *Escherichia coli* with all its genetic and genomic resources.

The initial step of the MEP pathway is the condensation of pyruvate and glyceraldehyde 3-phosphate to form a 1-deoxy-D-xylulose 5-phosphate intermediate. This condensation is catalyzed by a thiamine pyrophosphate-utilizing enzyme that mediates C_2 transitions like the transketolases of the Calvin–Benson cycle and the oxidative pentose phosphate pathway (see Chapter 12). This intermediate is rearranged and reduced to form 2*C*-methyl-D-erythritol 4-phosphate. Next, a nucleotide-5′-triphosphate, cytidine triphosphate, is transferred followed by an additional phosphate group from ATP to give 4-diphosphocytidyl-2*C*-methyl-D-erythritol 2-phosphate. Linking of the additional phosphate group to a phosphate moiety of the nucleotide leads to formation of a cyclic diphosphate and loss of cytidyl monophosphate. The last two steps are catalyzed by iron-sulfur reductases that first convert the cyclodiphosphate to (*E*)-4-hydroxy-3-methylbut-2-enyl diphosphate via a reduction and elimination. This final intermediate is then reduced further to give isopentenyl diphosphate and its allylic isomer, dimethylallyl diphosphate, in a 5:1 ratio. Both isopentenyl diphosphate and dimethylallyl diphosphate are needed for later steps in terpenoid biosynthesis.

24.2.3 The MEP and mevalonate pathways play different roles in plant terpenoid biosynthesis

The MEP pathway is present in vascular plants, algae, cyanobacteria, eubacteria, and Apicomplexan protists; it is absent, however, in archaea, fungi, and animals, all of which use the mevalonate pathway for making terpenoids. Only plants possess both the MEP and mevalonate pathways, and the two pathways reside in separate compartments: the mevalonate pathway is localized in the cytosol, and the MEP pathway is present in plastids. Since the MEP pathway is common to cyanobacteria, this spatial separation is consistent with the presumed origin of plastids from free-living cyanobacteria that retained their terpenoid biosynthetic machinery after becoming endosymbionts.

The two pathways for producing the C_5 units of terpenoid biosynthesis do not contribute equally to the formation of all terpenoids. The plastid-localized MEP pathway supplies most or all of the substrate for formation of terpenoids whose later biosynthetic steps also take place in plastids, including C_5 (isoprene), C_{10} (monoterpenes), C_{20} (diterpenes, side chain of chlorophyll), and C_{40} (carotenoids) compounds. The mevalonate pathway supplies most of the C_5 units for the biosynthesis of C_{15} (sesquiterpenes), C_{30} (triterpenes and sterols), and larger compounds (dolichols), substances whose later steps are largely cytosolic. However, the exchange of intermediates between the pathways is well documented. The simultaneous existence of two, spatially separated pathways for making the five-carbon units of terpenoid biosynthesis may help explain how plants can produce such a wide range of terpenoid metabolites in a regulated manner.

24.3 Repetitive additions of C_5 units

24.3.1 Isopentenyl diphosphate and dimethylallyl diphosphate condense to form larger intermediates

The second stage of terpenoid biosynthesis involves fusion of the basic C_5 building blocks, isopentenyl diphosphate and dimethylallyl diphosphate, into larger prenyl diphosphates and other metabolic intermediates (Fig. 24.9). As the smallest prenyl diphosphate with an allylic double bond, dimethylallyl diphosphate is a primer to which varying numbers of isopentenyl diphosphate units can be added in sequential chain elongation steps. Thus, isopentenyl diphosphate and dimethylallyl diphosphate condense in head-to-tail fashion to form the allylic C_{10} compound, **geranyl diphosphate**. Another molecule of isopentenyl diphosphate may then condense head-to-tail with geranyl diphosphate to generate the C_{15} allylic diphosphate, **farnesyl diphosphate**. Addition of a further isopentenyl diphosphate gives the C_{20} **geranylgeranyl diphosphate**.

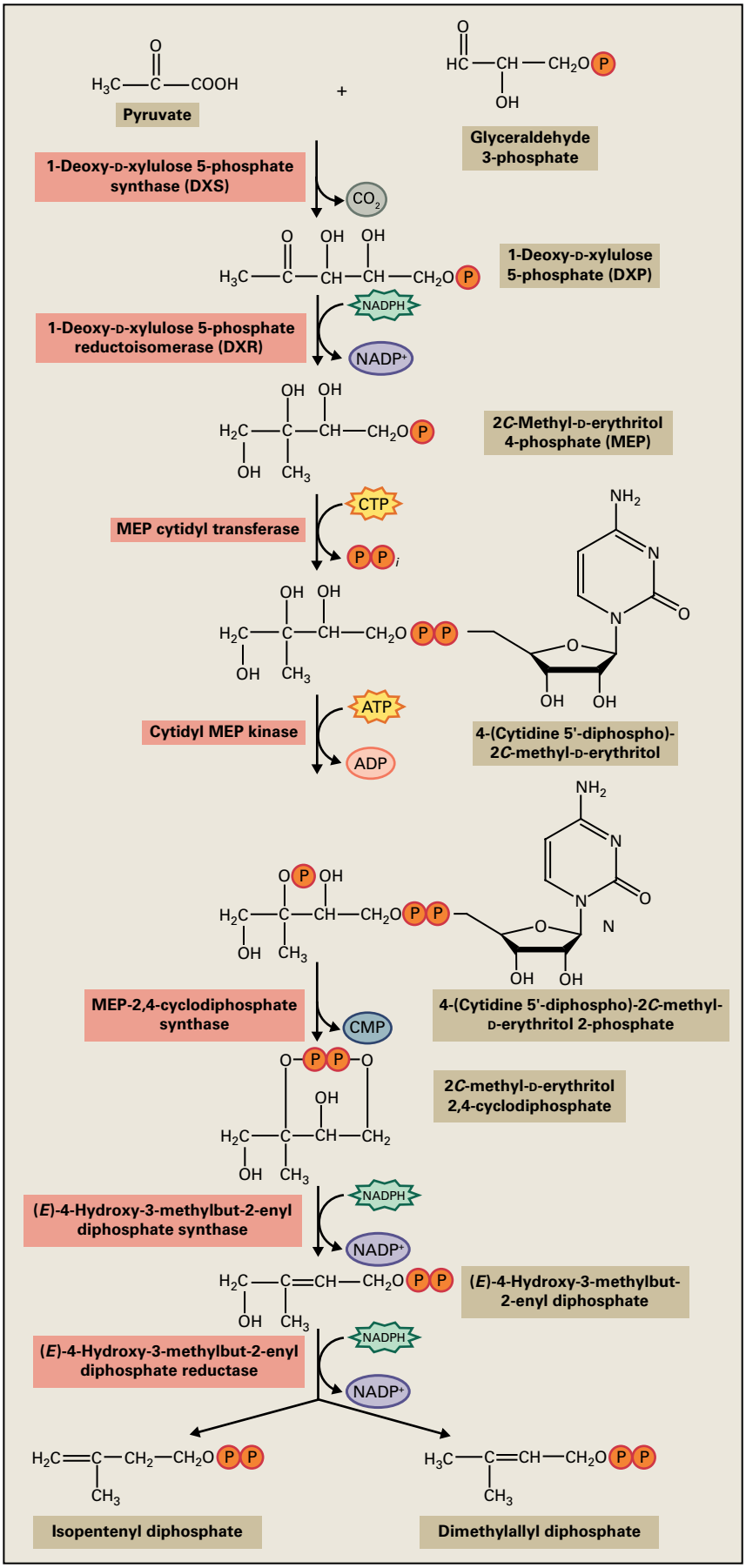


FIGURE 24.8 *The MEP pathway, a second route for the formation of isopentenyl diphosphate in plants, occurs in plastids.*

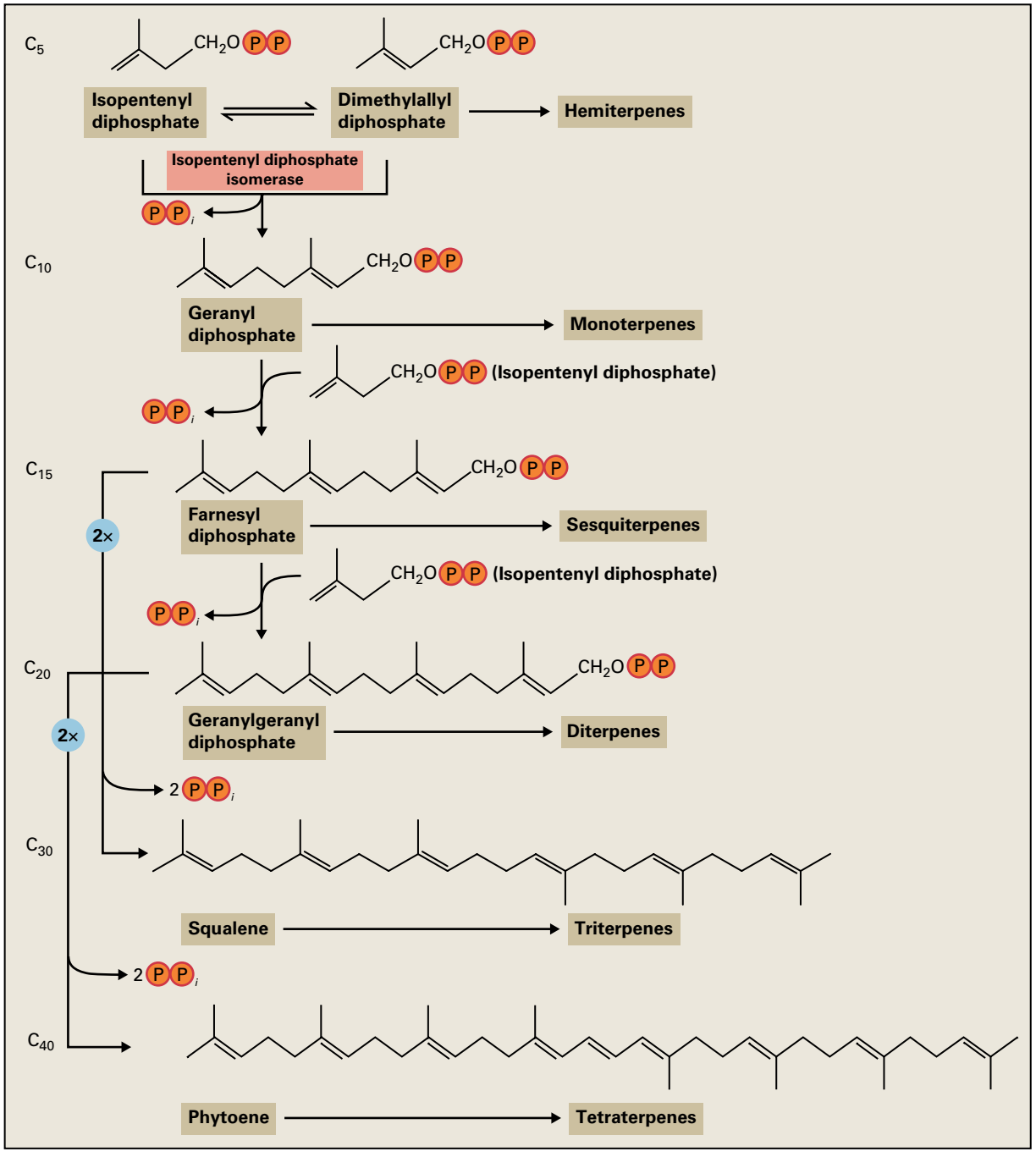


FIGURE 24.9 *The major subclasses of terpenoids are biosynthesized from the basic C_5 building blocks, isopentenyl diphosphate and its isomer, dimethylallyl diphosphate, which is formed from isopentenyl diphosphate via isopentenyl diphosphate isomerase. Reactions catalyzed by prenyltransferases condense varying numbers of isopentenyl diphosphate and dimethylallyl diphosphate units to geranyl diphosphate, the precursor of monoterpenes (C_{10}), farnesyl diphosphate, the precursor of sesquiterpenes (C_{15}), and geranylgeranyl diphosphate, the precursor of diterpenes (C_{20}). To make triterpenes (C_{30}), two farnesyl (C_{15}) units are combined, while to make tetraterpenes (C_{40}), two geranylgeranyl (C_{20}) units are joined.*

The formation of the major C_{30} and C_{40} terpenoids in plants, however, does not occur by stepwise C_5 addition. Instead, the C_{30} terpenoids (triterpenes) arise by head-to-head addition of two molecules of the C_{15} intermediate farnesyl diphosphate to produce squalene. In an analogous manner, C_{40} terpenoids (tetraterpenes) arise by head-to-head addition of two molecules of the C_{20} intermediate geranylgeranyl diphosphate producing phytoene (Fig. 24.9).

24.3.2 Condensation of prenyl diphosphates is catalyzed by prenyltransferases

The chain elongation reactions of terpenoid biosynthesis are mediated by enzymes known as **prenyltransferases**. Geranyl diphosphate, farnesyl diphosphate, and geranylgeranyl diphosphate are each formed by specific prenyltransferases

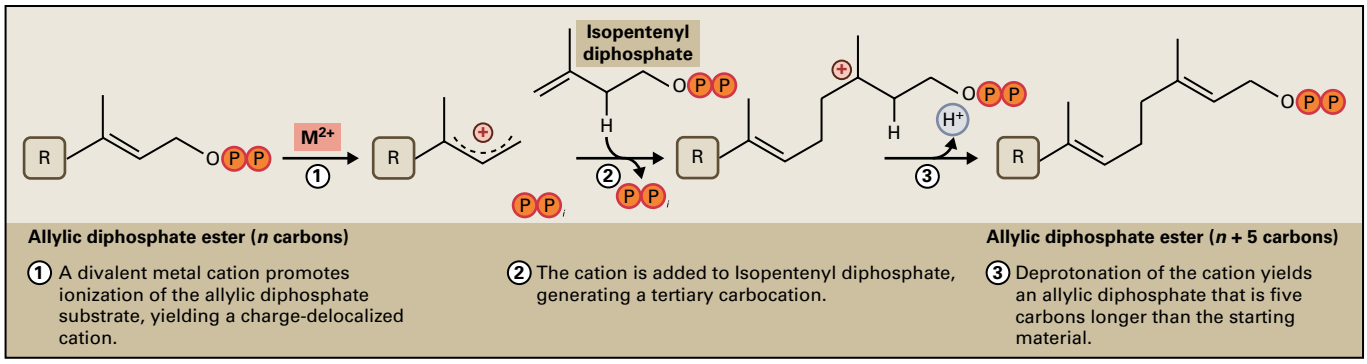


FIGURE 24.10 *The prenyltransferase reaction.*

that catalyze one, two, or three consecutive C_5 additions, respectively, starting from the allylic dimethylallyl diphosphate and the homoallylic isopentenyl diphosphate. The prenyltransferase reaction is driven by the ionization of the diphosphate moiety of the allylic substrate to form a resonance-stabilized allylic carbocation (Fig. 24.10). After addition of isopentenyl diphosphate, a proton is eliminated to form a new allylic prenyl diphosphate with five additional carbon atoms. Depending on the proton removed, the double bond can have an (*E*)- or (*Z*)-configuration. Most short-chain prenyl diphosphates that are intermediates in plant terpenoid biosynthesis have all (*E*)-double bonds.

Not all prenyltransferases make isoprenyl diphosphates. Some produce very long terpenoid polymers, such as rubber, which is formed from the head-to-tail condensation of thousands of isopentenyl diphosphate units in which the double bonds have mostly (*Z*)-configurations. Other prenyltransferases condense isoprenyl diphosphates with nonterpenoid acceptors, including chlorophyll, proteins, quinones, or other aromatic compounds to give rise to complex substances with terpenoid side chains.

24.4 Formation of parent carbon skeletons

24.4.1 Terpene synthases catalyze the conversion of prenyl diphosphates to parent terpene carbon skeletons

The prenyl diphosphates geranyl diphosphate (C_{10}), farnesyl diphosphate (C_{15}), and geranylgeranyl diphosphate (C_{20}) are the central intermediates of terpenoid biosynthesis. Under catalysis of a large family of enzymes called **terpene synthases**, they are converted to monoterpenes, sesquiterpenes, and diterpenes, respectively (see Fig. 24.9). The enzyme products of terpene synthases are usually cyclic, often have multiple ring systems, and comprise the primary representatives of each of the many diverse terpene skeletal types.

Terpene synthases employ a **carbocationic reaction mechanism** similar to that of the prenyltransferases (Fig. 24.11). The reaction is initiated by ionization of the diphosphate group, which requires a divalent metal ion, such as Mg^{2+}. The resulting enzyme-bound, allylic carbocation may then cyclize by addition of the resonance-stabilized cationic center to one of the other carbon–carbon double bonds in the substrate. Cyclization can be followed by a series of rearrangements, including hydride and alkyl shifts, and additional cyclizations, mediated through enzyme-bound carbocationic and neutral intermediates. The multiple fates of these reactive carbocations are responsible for the great diversity of terpene synthase products. The reaction cascade eventually terminates by deprotonation of the cation to form a new double bond or by capture by a nucleophile, such as water.

The typical substrates of most known monoterpene and sesquiterpene synthases, geranyl diphosphate and farnesyl diphosphate, respectively, cannot cyclize directly because of the (*E*)-geometry of their double bonds. In enzymes such as in limonene synthase (Fig. 24.11), cyclization is preceded by isomerization of the initial carbocation to an intermediate capable of cyclization. Other terpene synthases do not carry out cyclizations, and reaction involves just diphosphate ionization and termination, resulting in an alkene or alcohol with the same acyclic carbon skeleton as the parent prenyl diphosphate.

24.4.2 Terpene synthase and prenyltransferase proteins have similar mechanisms and structures

Both terpene synthases and prenyltransferases employ similar electrophilic reactions involving carbocation intermediates to form new carbon–carbon bonds. In the terpene synthase reaction, the initial cationic center and the double bond attacked reside on the same molecule leading to cyclization, whereas in prenyltransferases they are on different molecules leading to elongation. The formation of carbon–carbon bonds by such electrophilic addition is unusual in plant

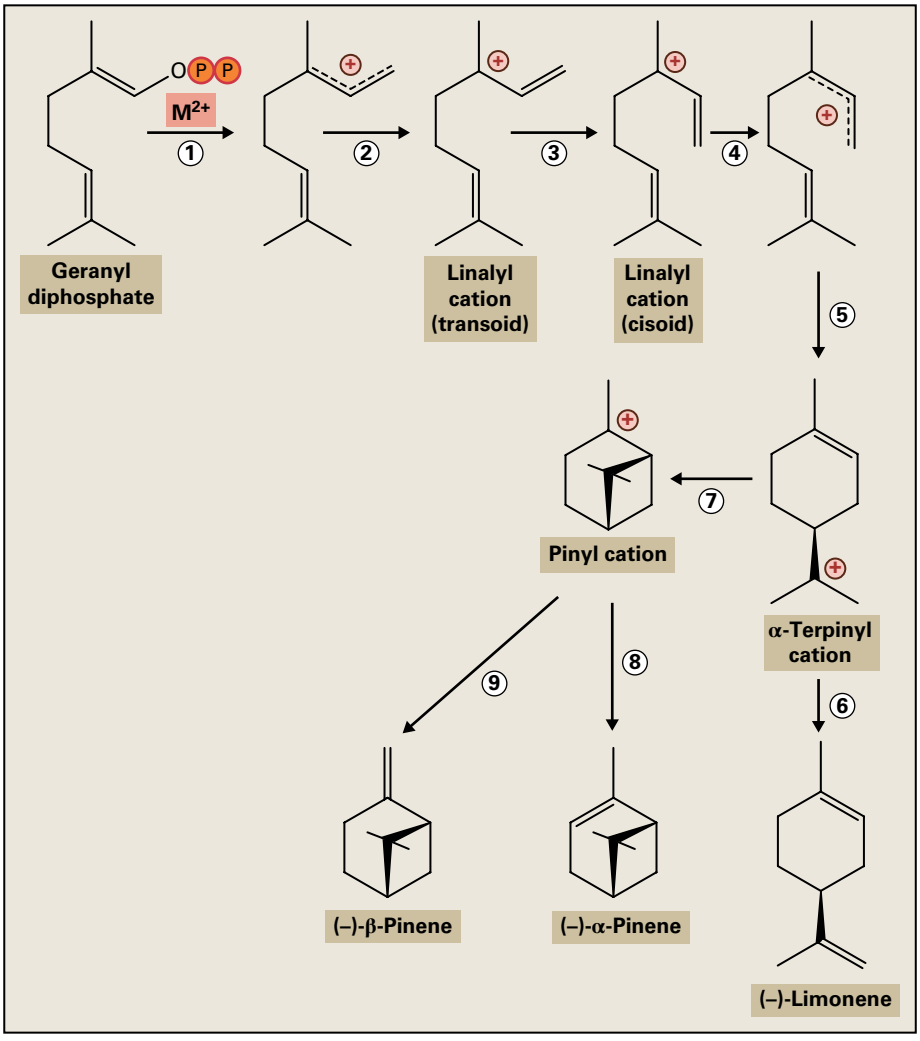


FIGURE 24.11 *A monoterpene synthase reaction. Depicted is the cyclization of geranyl diphosphate to limonene, which forms α- and β-pinene as additional products. (1) Ionization of the substrate is promoted by a divalent metal cation, yielding a charge-delocalized cation that is converted (2) to the tertiary linalyl cation. (3) Rotation around a single bond provides an intermediate capable of cyclization. In a charge-delocalized form (4), the α-terpinyl cation undergoes cyclization (5) and then deprotonation to form limonene (6). The α-terpinyl cation can undergo a second cyclization (7), involving folding of the isopropyl tail over the ring to generate the pinyl cation. This cation, in turn, can be deprotonated in two different ways (8,9) to form either α- or β-pinene.*

metabolism. The carbon–carbon bonds of most other substances, such as amino acids, carbohydrates, fatty acids, and nucleic acids, are usually constructed by nucleophilic condensation reactions involving carbonyl groups.

Crystallographic studies reveal that the structures of terpene synthases and prenyltransferases share marked similarities, even though their amino acid sequences do not have significant similarity. Both types of protein contain "terpene folds," domains made up of α-helices in which the diphosphate moieties of substrates bind to aspartate-rich regions via divalent metal ions (Fig. 24.12). The substrate is bound in an orientation that directs the reaction once the diphosphate has ionized. Small changes in the shape of the active site can change the conformation of the substrate and alter the products formed. After substrate binding, the active site is closed to the outside environment to protect the carbocationic intermediates from being quenched by water.

24.4.3 Terpene synthases are major contributors to the enormous diversity of terpene products in plants

An interesting feature of terpene synthases is the ability of a single enzyme to catalyze the formation of more than one product from a single substrate. For example, some enzymes that produce limonene also produce the bicyclic monoterpenes, α- and β-pinene (see Fig. 24.11). About half of all known terpene

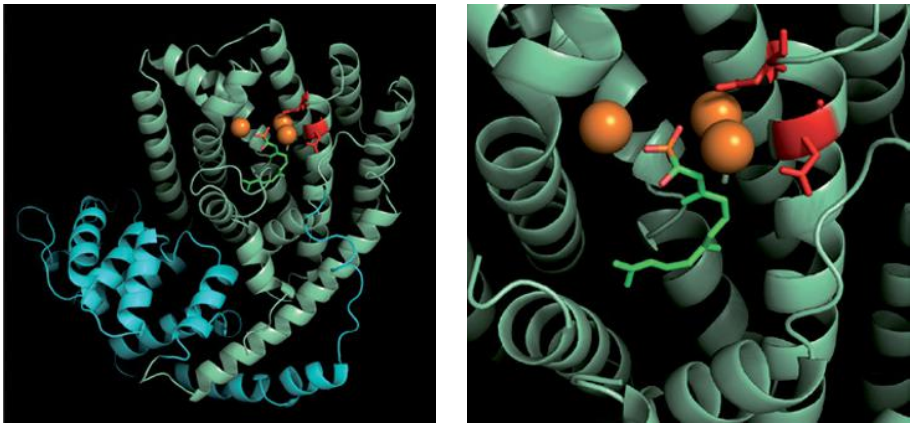


FIGURE 24.12 *Structure of SbTPS1 from sorghum (*Sorghum bicolor*), a terpene synthase that makes multiple sesquiterpenes . (A) Two domains of α-helices form the overall structure of SbTPS1. The active site cavity is located in the central part of the C-terminal domain. (B) A cross-section of the active site is depicted that contains the substrate analog, 1-hydroxyfarnesyl phosphonate, instead of the native substrate, farnesyl diphosphate. Two aspartate residues of the protein (in red as D294 and D297) are involved in binding the three Mg^{2+} ions, which in turn bind the substrate by coordinating with the diphosphate group.*

synthases form significant amounts (>10%) of more than one product, and some of these enzymes produce as many as 50 different products. Such amazing catalytic versatility can be attributed to the multiple chemical fates of the highly reactive carbocationic intermediates produced by the enzyme. The great diversity of terpene structures in plants is also a result of the large families of terpene synthase genes (40–150 members) found in all plant genomes investigated.

Among the different classes of terpenes, diversity is generated by terpene synthases in slightly different ways. Sesquiterpene synthases produce a greater variety of carbon skeletons from farnesyl diphosphate than monoterpene synthases do from geranyl diphosphate because of the additional five-carbon unit and extra double bond in the substrate. Formation of larger rings from farnesyl diphosphate can proceed without any preliminary isomerization steps.

Diterpene synthases carry out two different kinds of cyclization of their substrate geranylgeranyl diphosphate (Fig. 24.13). The first resembles the reactions catalyzed by monoterpene and sesquiterpene synthases, in which the diphosphate group is ionized and the resulting carbocation attacks one of the double bonds. In the second, however, the carbocation is generated by protonation of the terminal double bond, as exemplified by the conversion of geranylgeranyl diphosphate to copalyl diphosphate, an intermediate to many types of diterpene skeletons. The product copalyl diphosphate retains its diphosphate group and so can serve as a substrate for other diterpene synthases that employ the first kind of cyclization method. Some diterpene synthases carry out both kinds of cyclization in sequential fashion.

Triterpene synthases do not employ prenyl diphosphate substrates. After two molecules of farnesyl diphosphate (C_{15}) combine head-to-tail to produce the C_{30} intermediate squalene (see Fig. 24.9), epoxidation yields oxidosqualene. Plant triterpene cyclases use oxidosqualene as a substrate, employing a protonation-initiated cyclization to form a variety of carbon skeletons containing three to five rings (Fig. 24.14). Cycloartenol is the precursor of the sterols.

24.5 Modification of terpenoid skeletons

The parent carbon skeletons produced by terpene synthases are often modified to generate more variability in plant terpenoids. These modifications most commonly involve oxidation, reduction, isomerization, acylation, and glycosylation reactions, and their effects can be seen in such complex terpenoid end products as taxol and azadirachtin (see Fig. 24.4). Compared to other aspects of terpenoid biosynthesis, however, skeletal modifications of terpenoids are poorly studied.

Among the better known modification pathways are those leading to menthol (see Figs 24.3 and 24.5), the major component of peppermint oil, and artemisinin, an important antimalarial drug isolated from *Artemisia annua* (see Fig. 24.4 and Section 24.2.3). The pathway to the sesquiterpene artemisinin begins with the action of a prenyltransferase that forms farnesyl diphosphate from three C_5 units, followed by the action of a terpene synthase that cyclizes farnesyl diphosphate to amorpha-4,11-diene (Fig. 24.15). Skeletal modification follows, which as for other terpenes involves various oxidation and reduction reactions. Amorphadiene is first subjected to the two-step oxidation of a methyl group to an aldehyde, catalyzed by a cytochrome P450 (Box 24.1). Then, a terminal carbon–carbon double bond is reduced by an enoate reductase, and the aldehyde function is oxidized to a carboxylic acid. The resulting dihydroartemisinic acid is converted to the final product by a nonenzymatic photo-oxidation that

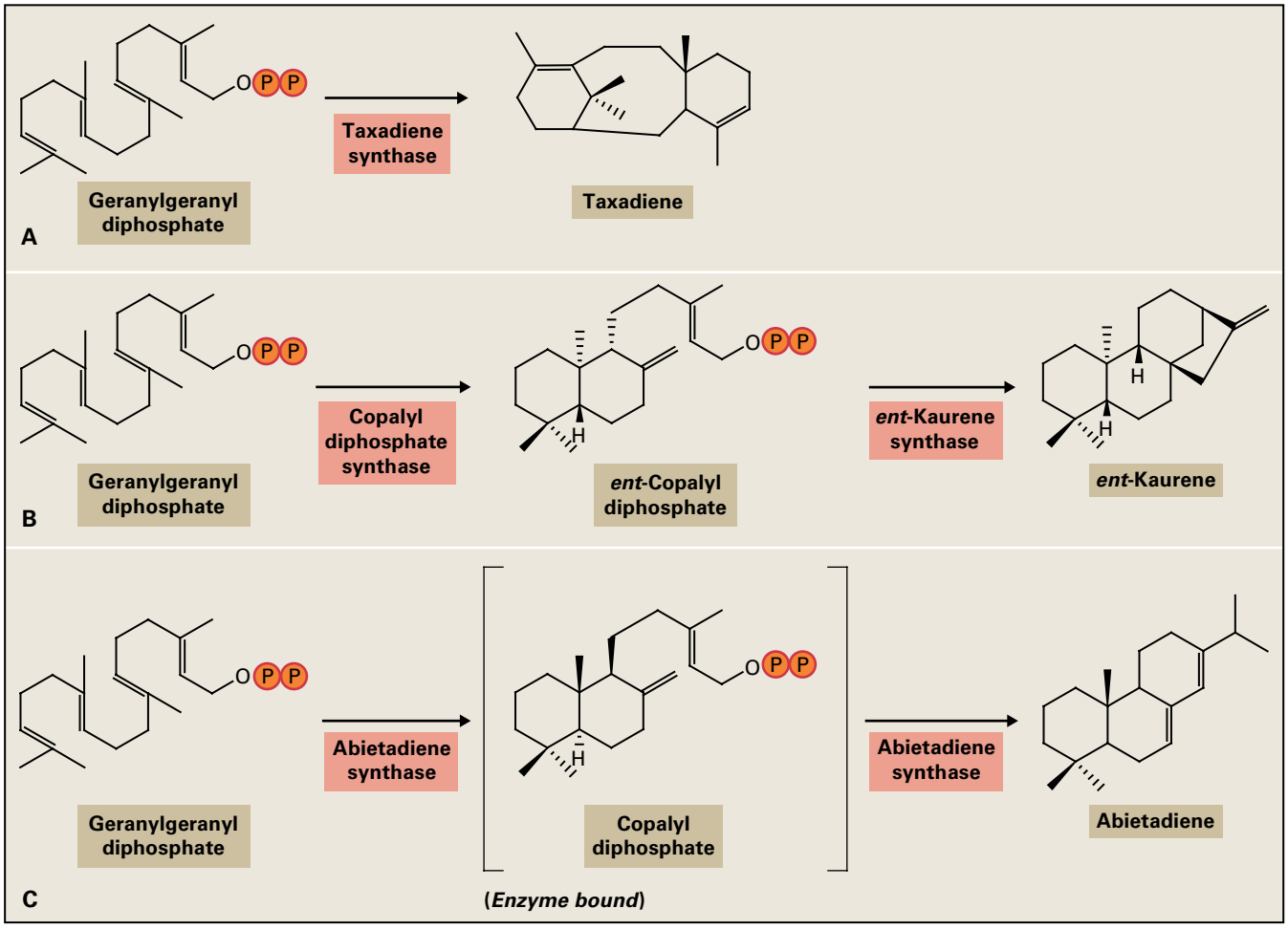


FIGURE 24.13 *Diterpene synthases use two different types of reactions. (A) In the first type, ionization of the diphosphate group leads to a carbocation that cyclizes like the carbocations formed by monoterpene and sesquiterpene synthases. (B) In the second type, protonation of the terminal double bond leads to cyclization with retention of the diphosphate group. The product of the second type can be cyclized by an ionization-initiated diterpene cyclization of the first type. (C) Some diterpene synthases carry out both types of cyclization in sequence.*

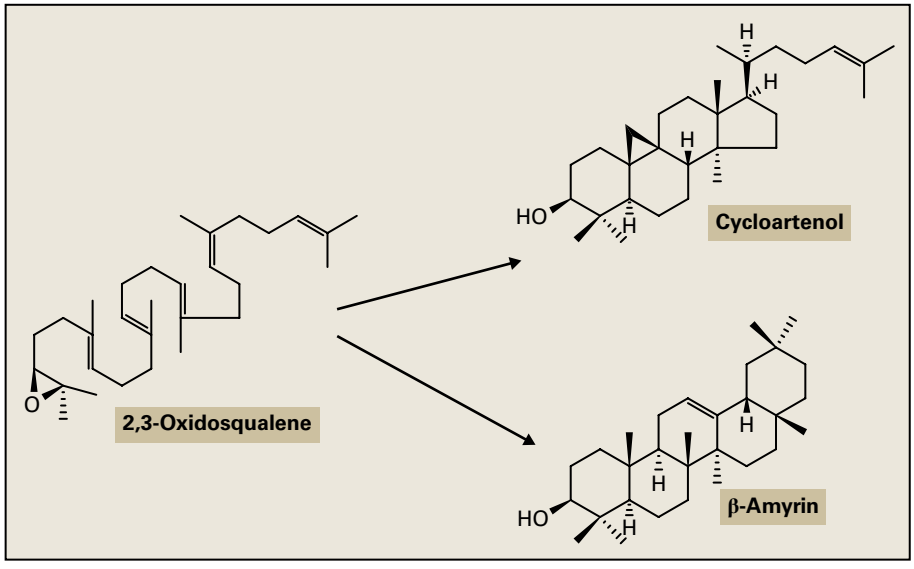


FIGURE 24.14 *Triterpene synthases employ a cyclization mechanism that begins with a proton triggering the opening of the epoxide ring. Cycloartenol is the precursor to all plant sterols, and β-amyrin is a widespread pentacyclic triterpene.*

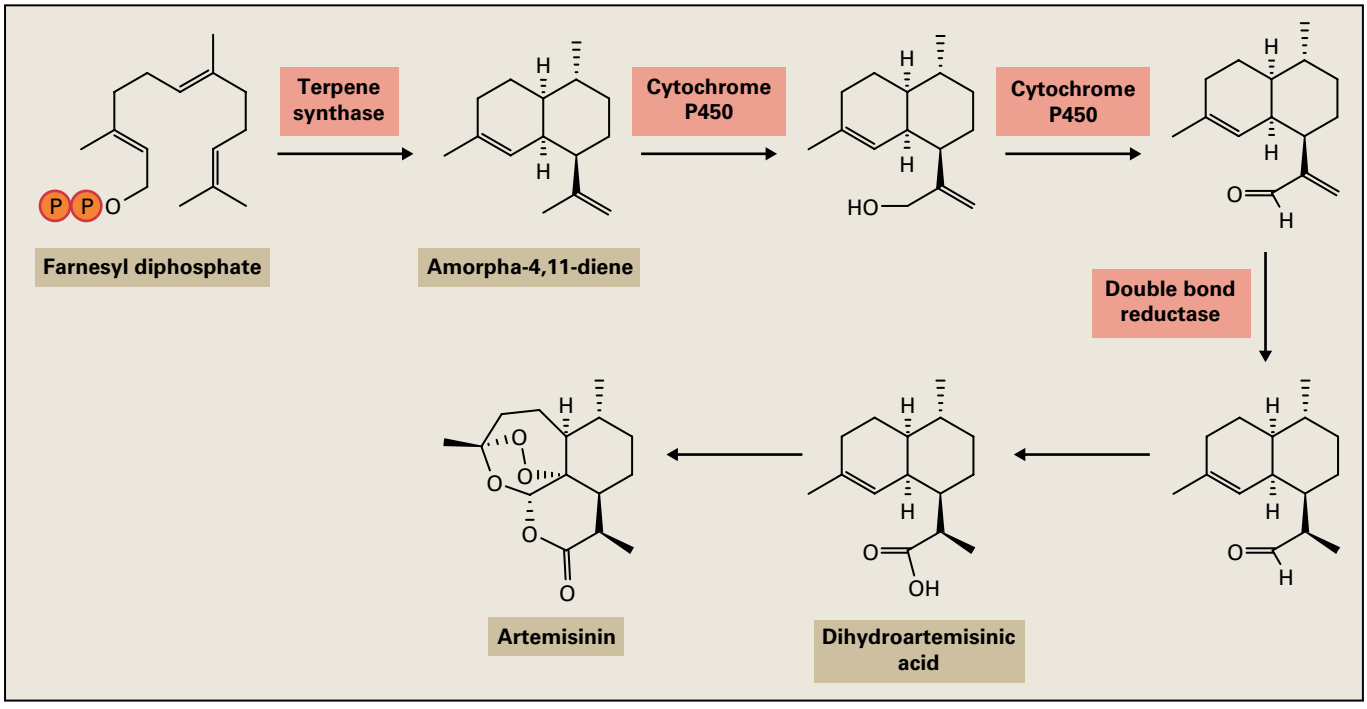


FIGURE 24.15 *Biosynthetic pathway to the antimalarial drug artemisinin in the wormwood plant (*Artemisia annua*). After formation of farnesyl diphosphate by a prenyltransferase, this acyclic C_{15} intermediate is converted to amorpha-4,11-diene by a terpene synthase. Next, skeletal modification is carried out by cytochrome P450s and a double bond reductase to yield dihydroartemisinic acid. The final step may involve nonenzymatic photo-oxidation.*

is not completely characterized. Extensive research on artemisinin has revealed much more than just the sequence of the pathway. For example, this sesquiterpene accumulates within the plant in glandular trichomes on leaves and floral parts, and its formation is regulated by a WRKY transcription factor that activates transcription of certain biosynthetic genes.

24.6 Metabolic engineering of terpenoid production

Many of the terpenoids that are in high demand as flavors, fragrances, pigments, or drugs are produced in low amounts by plants. It is also often difficult to chemically synthesize these compounds in an economic manner or to induce high levels of accumulation in plant cell or organ cultures. Therefore, enthusiasm has grown for creating transgenic plant lines capable of producing increased levels of valuable terpenoids.

Recent successes in cloning genes that encode enzymes of terpenoid biosynthesis have provided the necessary tools for this effort. A typical strategy is to overexpress one or more genes that either lead to a new terpenoid (not usually present in the plant) or that speed up the rate of biosynthesis for an endogenous terpenoid. Expression of these genes must be targeted to tissues and cells that have a sufficient supply of precursors (such as isopentenyl diphosphate), an adequate capacity for accumulating high levels of the target compound (such as cells of glandular trichomes or resin ducts), and a lack of enzymes that could cause further metabolism.

Perhaps the best-known example of terpenoid engineering in plants is the creation of "golden rice," a variety of rice (*Oryza sativa*) with increased β-carotene in its kernels (Fig. 24.16A). A vitamin A precursor, β-carotene is scarce in the staple crops of many developing countries, causing a variety of ailments, especially in children. Overexpression of enzymes from four terpenoid biosynthetic steps diverted enough geranylgeranyl diphosphate to β-carotene via phytoene to cause a 20-fold increase in carotenoids in normally white rice, turning it golden in color.

In another example, plant terpenoid genes were used to engineer microbes to produce artemisinic acid, a precursor to the antimalarial sesquiterpene artemisinin (see Fig. 24.16B). This was achieved using *E. coli* that were modified for high levels of terpenoid biosynthesis through insertion of the entire mevalonate pathway (not normally present), rather than by trying to speed up the endogenous MEP pathway, which was subject to regulatory controls.

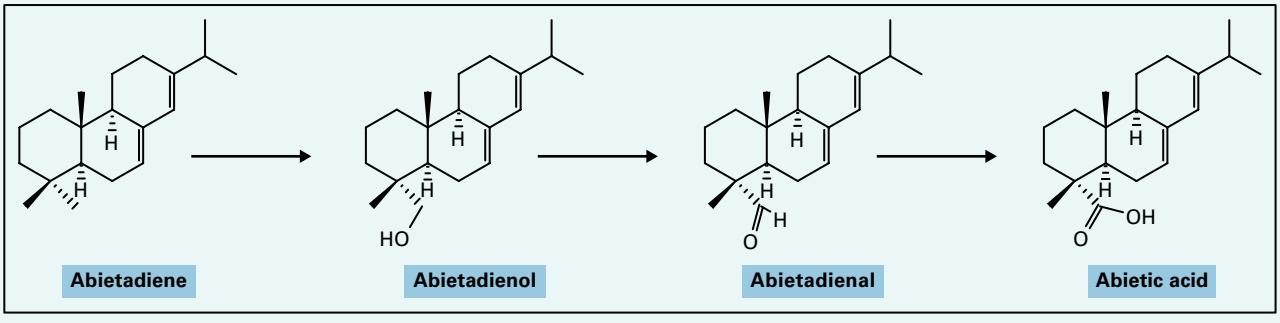
Other approaches to enhance terpenoid production include identification and transformation with regulatory genes, such as those expressing transcription factors. Attempts have also been made to increase the number of terpenoid storage structures (i.e., glandular trichomes, resin ducts, and secretory cavities). In addition, some researchers have tried to engineer specific enzymes for increased or altered product specificity. For example, certain terpene synthases that make multiple products have been modified to make a single product with only a few sequence changes.

BOX 24.1 Cytochrome P450 enzymes play a role in natural product biosynthesis

The plant cytochrome P450 (CYP) family of monooxygenases is a large gene family, and enzymes of this class are often called P450s or CYPs for short. Each is given a CYP designation, for example, CYP73A5 (*Arabidopsis* cinnamate 4-hydroxylase), that is based on sequence homology to other P450s and effectively categorizes individual enzymes into CYP subfamilies according to phylogenetic relationships. Genes with the same subfamily designation often catalyze the same or similar reactions. The moss *Physcomitrella patens* has 73 CYP subfamilies, but angiosperms typically have 55–60, 51 of which are universal to all plants (some subfamilies are clade specific and have affinities to other common subfamilies). *Arabidopsis* has 246 P450 genes.

P450 monooxygenases have diverse functions and catalyze reactions that typically involve redox state changes (oxidations, hydroxylations, epoxidations, dehydrations, etc.), carbon–carbon bond formation, or rearrangements (e.g., methylene dioxybridge formation, demethylations, isomerizations). The active site of a P450 contains a heme functional group that is held in a conformation such that its absorption spectrum contains a strong peak at ≈450 nm when it is reduced and CO (carbon monoxide) is bound, hence the name cytochrome P450. Obtaining a CO-difference spectrum is a diagnostic test for these enzymes, which are strongly inhibited by CO and ketoconazole.

Most P450s require molecular oxygen for activity, although some, such as allene oxide synthase, can utilize endogenous peroxides that are part of the substrate. Most are also membrane-bound and use NADPH as a cofactor. Some P450s, especially animal enzymes, have broad substrate preferences, and serve to act as general oxygenases, involved in elimination of xenobiotics from the body. Most plant P450s have limited or strict substrate selectivities (e.g., the signature CYP79 enzyme in cyanogenic glucoside biosynthesis (Section 24.8.1) or the P450 enzymes in the biosynthesis of the alkaloid berberine (Section 24.12.3) and are regio- and even enantiospecific. Cytochrome P450 enzymes that act on terpenoids can carry out multistep oxidations, such as the sequential conversion of a saturated carbon to an alcohol, aldehyde, and a carboxylic acid as shown in the biosynthesis of the diterpenes in conifer resins.



24.7 Cyanogenic glycosides

Cyanogenic glycosides (Fig. 24.17) are β-glycosides of α-hydroxynitriles (**cyanohydrins**). They are characterized by their ability to liberate hydrogen cyanide (HCN) when hydrolyzed by β-glycosidases; this process (cyanogenesis) typically occurs when plant tissue containing cyanogenic glycosides is disrupted, for example, when bitten, chewed, or ingested by animals or insects. Cyanogenic glycosides are important components of plant defense against generalist herbivores due to their bitter taste and release of toxic HCN upon tissue disruption (see Section 24.9.1).

Cyanogenic glycosides are derived from five protein amino acids (Val, Ile, Leu, Phe, and Tyr) and the nonproteinogenic amino acid cyclopentenyl glycine (Fig. 24.18). These core structures of cyanogenic glycosides may be further modified by single or multiple hydroxylations. The number of cyanogenic glycosides found in nature is further expanded by the structural diversity of the sugar moiety. Cyanogenic glycosides are widely distributed among more than 2,600 different species of pteridophytes, gymnosperms, and angiosperms. Whereas pteridophytes and gymnosperms contain cyanogenic glycosides derived from aromatic amino acids, angiosperms may contain cyanogenic glycosides derived from either aliphatic or aromatic amino acids (Figs. 24.18 and 24.19). Many crops, including **sorghum** (*Sorghum bicolor*), **cassava** (*Manihot esculentum*), and **barley** (*Hordeum vulgare*), are cyanogenic; understanding the roles of cyanogenic glycosides, their biosynthetic pathways, and underlying regulatory mechanisms in these species is crucial for the development of nontoxic varieties and food products.



FIGURE 24.16 *(A) Metabolic engineering of plant terpene production has yielded a variety of rice ("golden rice", here compared to ordinary rice on the left) with high levels of a vitamin A precursor, β-carotene, to help reduce vitamin A deficiency in many rice-eating countries. (B) The antimalarial drug artemisinin was originally isolated from* Artemisia annua. *Much effort has been devoted to breeding* A. annua *with higher artemisinin levels. In addition, much of the artemisinin pathway has been engineered into microbes to increase production.*
Source: (A) Golden Rice Humanitarian Board, www.goldenrice.org; (B) HarroBouwmeester, Wageningen University, The Netherlands.

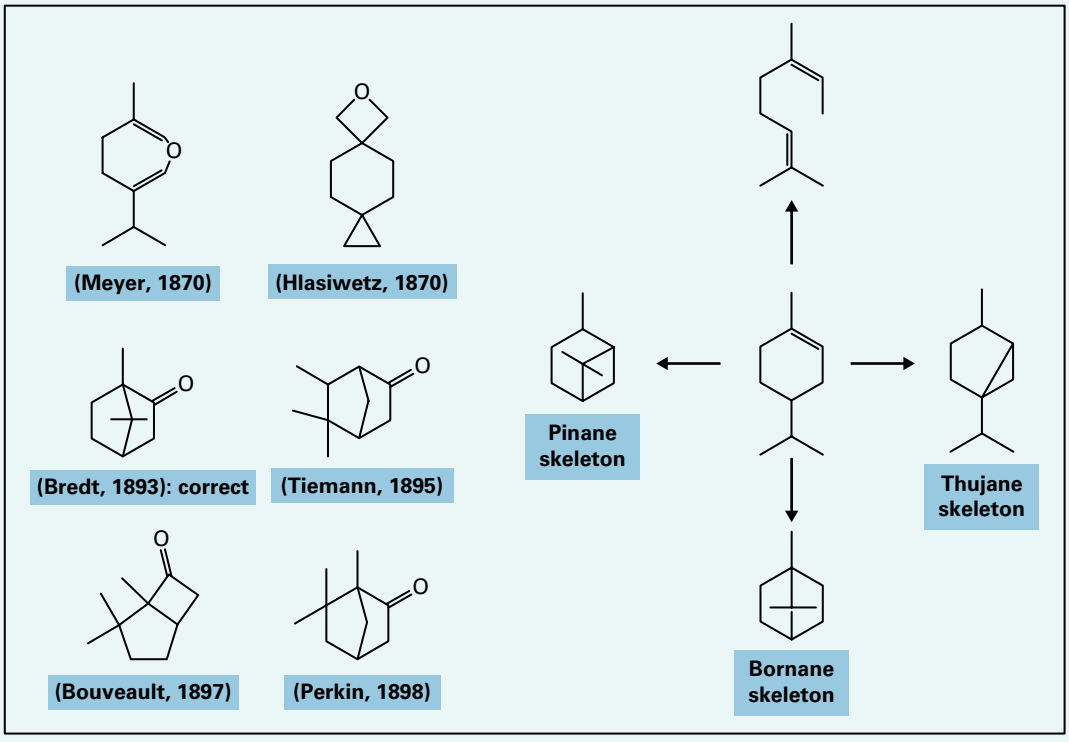
BOX 24.2

Early investigators formulated rules for identifying and classifying terpenoid structures

In the late 1800s, chemists struggled to determine the structures of monoterpenes, and these difficulties are illustrated in the numerous structures proposed for camphor (see structures at left of figure, which include the names of the proposers and the dates proposed). Chromatographic purification techniques and spectroscopic methods for structure elucidation were not available to these chemists, who relied on the preparation of crystalline derivatives to assess purity and on chemical degradation studies to determine structures. Systematic study of the monoterpenes led early investigators to recognize that many terpenoid compounds might be constructed by joining isoprene units, in a repetitive head-to-tail fashion (see pathway illustrated and Fig. 24.6) and correctly proposed the structure for camphor. This concept is known as the **isoprene rule**.

By the 1930s, faced with a bewildering array of terpenoid substances, investigators sought to develop a unifying principle that could rationalize the natural occurrence of all of the known terpenoids, even those that did not strictly fit the isoprene rule. The ingenious solution was to focus on reaction mechanisms and ignore the precise character of the biological precursor, assuming only that it had a terpenoid structure during reaction. It was hypothesized that electrophilic reactions generated carbocationic intermediates, which underwent subsequent C_5 addition, cyclization, and in some cases skeletal rearrangement before elimination of a proton or capture by a nucleophile to yield the observed terpenoid products. This proposal, called the **biogenetic isoprene rule**, can be stated simply: a compound is "isoprenoid" if it is derived biologically from an "isoprenoid" precursor, with or without rearrangements.

This concept emphasizes the biochemical origin rather than structure. The great strength of the biogenetic isoprene rule lay in its use of biosynthetic mechanism to classify the bulk of known terpenoids, including structures that did not strictly follow the original isoprene rule. Application of the biogenetic isoprene rule is illustrated by the way several of the common monoterpene skeletons can be derived from a precursor with simple head-to-tail coupling of two isoprene units (right of figure). It was found that these reactions could occur via carbocations. Note the bornane skeleton from which camphor is derived. Also note that the Bredt 1893 structure is correct.



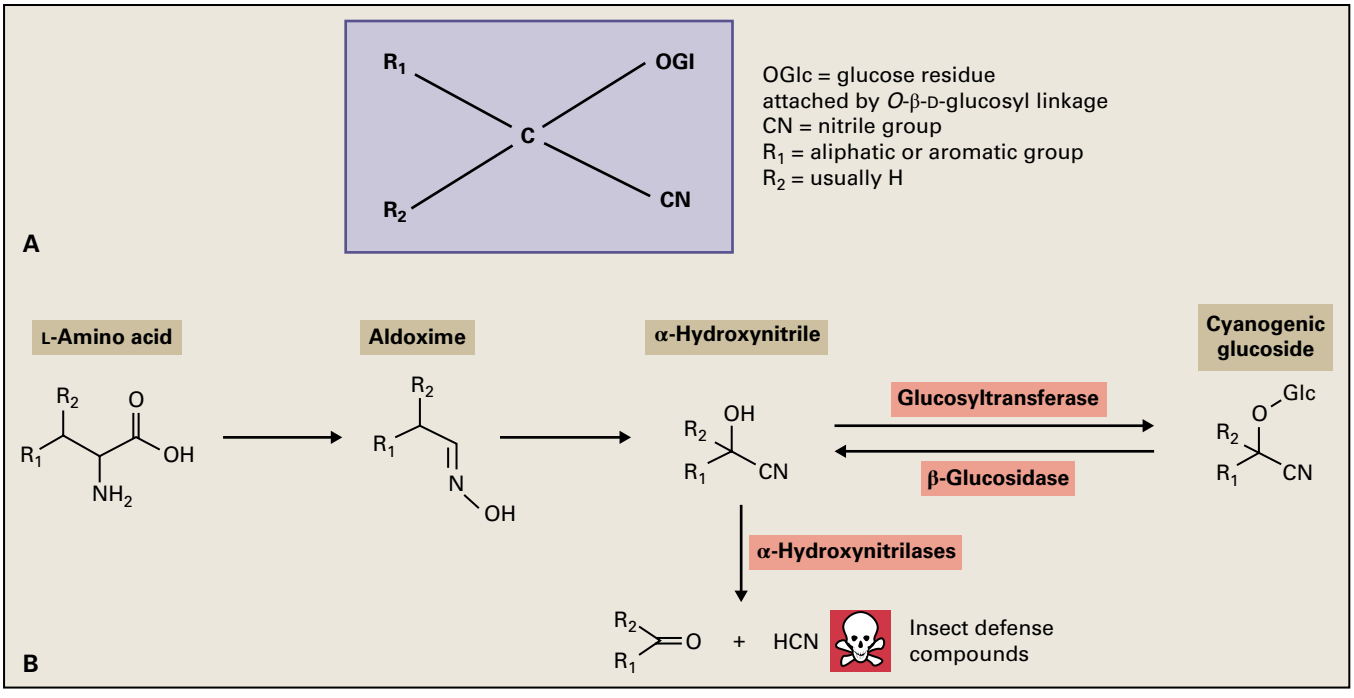


FIGURE 24.17 *(A) General structure of cyanogenic glycosides. The sugar residue is always a D-glucose that is joined by an O-β-D-glucosyl linkage (referred to more specifically, then, as cyanogenic glucosides), but additional sugars present may be different. (B) Cyanogenesis. Cyanogenic glycosides are formed from a limited number of L-amino acids and converted to cyanogenic glycosides with E-oximes and α-hydroxynitriles as key intermediates. Upon hydrolysis of the cyanogenic glycoside by the action of β-glycosidases and α-hydroxynitrilases, toxic hydrogen cyanide (HCN) and ketones or aldehydes are produced.*

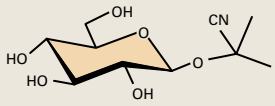
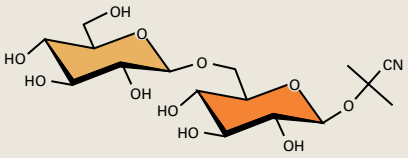
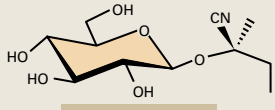
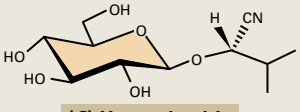
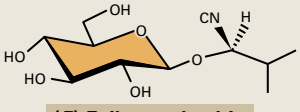
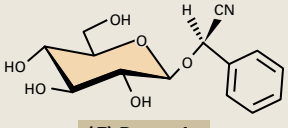
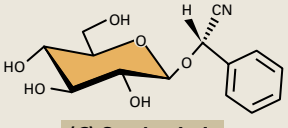
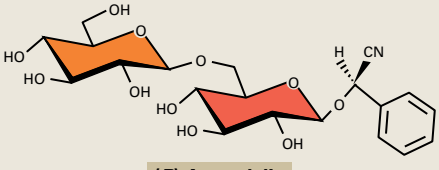
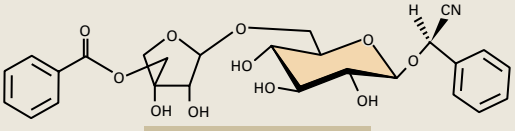
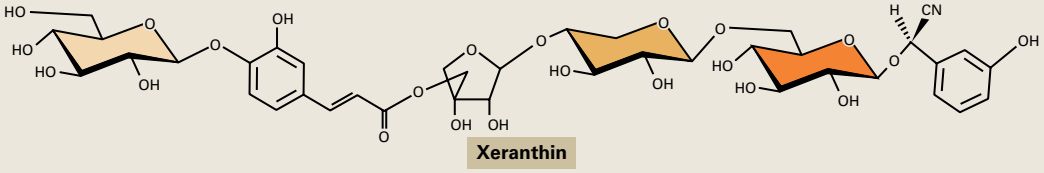
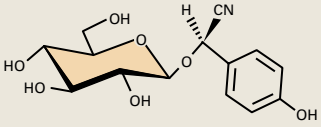
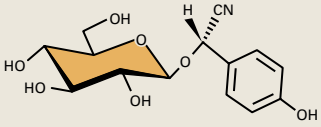
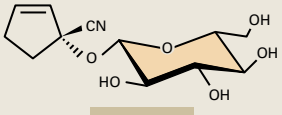
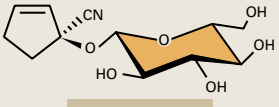
Precursor	Cyanogenic glycoside (α-hydroxynitrile glycoside)
Valine	 Linamarin  Linustatin
Isoleucine	 (*R*)-Lotaustralin
Leucine	 (*S*)-Heterodendrin  (*R*)-Epiheterodendrin
Phenylalanine	 (*R*)-Prunasin  (*S*)-Sambunigrin  (*R*)-Amygdalin  Oxyanthin 5″-benzoate  Xeranthin
Tyrosine	 (*R*)-Toxihyllin  (*S*)-Dhurrin
Cyclopentynyl glycine	 Deidaclin  Tetraphyllin A

FIGURE 24.18 *Structures of selected cyanogenic glycosides (α-hydroxynitrile glycosides).*

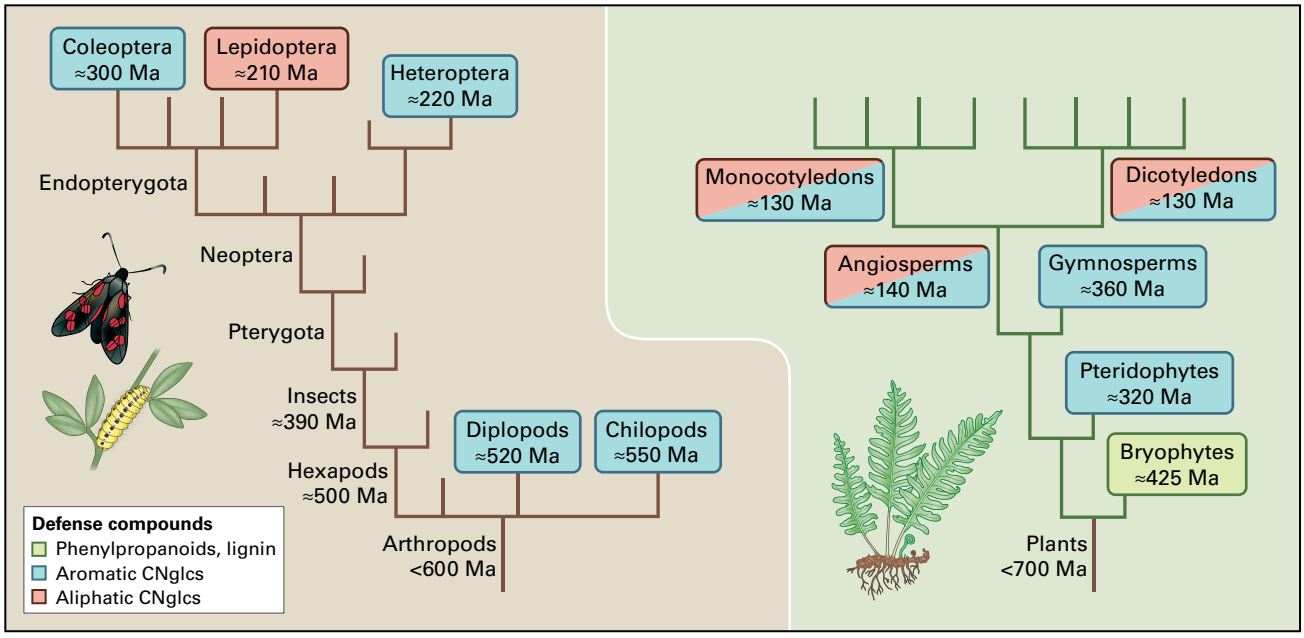


FIGURE 24.19 *Evolutionary trees depicting the evolution of arthropods and plants and the presence of different classes of defense compounds, including cyanogenic glycosides. Plants and insects have coevolved for the last ≈400 million years, and both groups of organisms produce toxic secondary metabolites like cyanogenic glucosides to defend themselves. A few arthopod families also accumulate cyanogenic glucosides, for example,* Zygaena *larvae that has evolved the ability to either sequester cyanogenic glucosides from* Lotus *plants or, if reared on acyanogenic* Lotus, *to synthesize cyanogenic glucosides de novo.*

BOX 24.3 Cyanogenesis can be used for high-throughput mutant screening

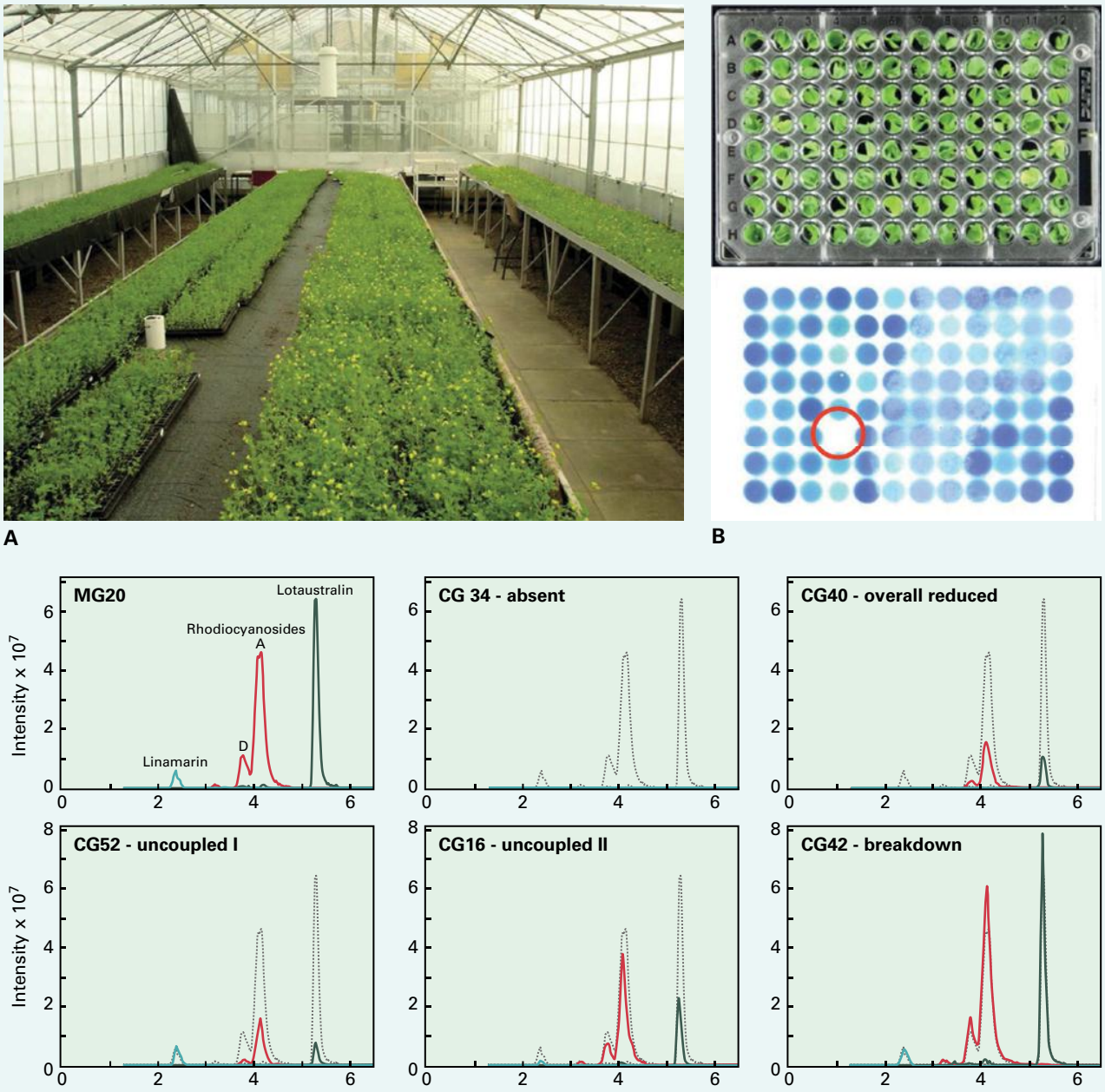
Several plant species are polymorphic with respect to **cyanogenesis**, and cyanogenic and acyanogenic plants occur together in nature. The best-studied example is white clover (*Trifolium repens*), which is polymorphic with respect to the ability to both synthesize and degrade cyanogenic glucosides. To rapidly identify individual natural variants in cyanogenic plant species among a large plant population (e.g., in white clover) and to identify mutants obtained following mutagenesis programs (e.g., in the crop plant forage sorghum and in the genetic model plant *Lotus japonicus*), a fast screening system was developed.

Tiny pieces of plant tissue stamped out using a cork borer were placed in the wells of microtiter plates covered by Feigl–Anger paper and sealed. Freeze–thawing the plates disrupted the subcellular structure of the plant tissue, resulting in cyanide release from samples containing cyanogenic glucosides as well as the β-glucosidase and α-hydroxynitrilase required for their degradation. The volatile HCN released reacted with the exposed part of Feigl–Anger paper to produce a blue area corresponding to the diameter of the well. Plants with a reduced content of cyanogenic glycosides or devoid of hydrolytic enzyme activity gave either reduced or no color reaction. The biochemical screen thereby enabled identification of mutants in biosynthetic, regulatory, or catabolic genes that could be classified into separate groups and characterized in detail using the reverse genetic technique of targeted induced local lesions in genomes (TILLING).

High water-use efficiency and tolerance to drought and elevated temperatures make sorghum an ideal cereal crop for arid and semi-arid regions of the world. The screening program identified acyanogenic mutants in forage sorghum that lacked the ability to synthesize the cyanogenic glucoside, **dhurrin** (see Fig. 24.18). These mutants were of interest because they removed the risk of cyanide intoxication of grazing animals. Sorghum mutants cyanogenic at the seedling stage but devoid of cyanogenic glucosides at the adult stage were also identified, as were mutants with an overall reduced content.

In parallel to the screening of field-grown sorghum mutants, a screening program was carried out in the model legume *L. japonicus* to identify mutants in which the synthesis of the two cyanogenic glucosides,

lotaustralin and linamarin (see Fig. 24.18), were uncoupled. The results showed that different β-glucosidases are involved in degradation of cyanogenic glucosides and that β- and γ-hydroxynitrile glucosides are also present in *L. japonicus*. The availability of the genome sequence and of an efficient transformation system makes *L. japonicus* an excellent genetic model plant for future genetic studies of cyanogenic glucoside metabolism.



(A) Lotus japonicus *M2 plants obtained following ethyl methanesulfonate treatment and grown for identification of mutants deficient in cyanogenic glucoside synthesis or catabolism. (B) Leaflets were placed in microtiter plates tightly covered by Feigl–Anger paper and subjected to freeze-thawing. Hydrogen cyanide release resulted in blue staining of the area above the well. (C) Targeted LC-MS analysis of the content of α-, β-, and γ-hydroxynitrile glucosides present in MG20* L. japonicus *wild-type and mutant plants. Some mutants are totally devoid of hydroxynitrile glucosides, whereas others show altered ratios and some have wild-type levels but have lost the ability to hydrolyze the compounds.*

24.8 Cyanogenic glycoside biosynthesis

24.8.1 Cyanogenic glycoside biosynthesis is catalyzed primarily by two groups of enzymes

The biosynthesis of cyanogenic glycosides is catalyzed by cytochrome P450 enzymes (see Box 24.1) and UDP-glycosyltransferases. Both belong to multienzyme families in which other members are involved in synthesis of other classes of bioactive natural products, including phenylpropanoids, alkaloids, and terpenoids.

The pathway for cyanogenic glycoside biosynthesis was first elucidated in sorghum (*Sorghum* sp.) using biochemical approaches. Sorghum contains the tyrosine-derived cyanogenic glucoside dhurrin, and the dhurrin biosynthetic pathway involves the intermediates *N*-hydroxytyrosine, *N,N*-dihydroxytyrosine, (*E*)- and (*Z*)-*p*-hydroxyphenylacetaldoxime, *p*-hydroxyphenylacetonitrile, and *p*-hydroxymandelonitrile (Fig. 24.20). These intermediates all contain functional groups

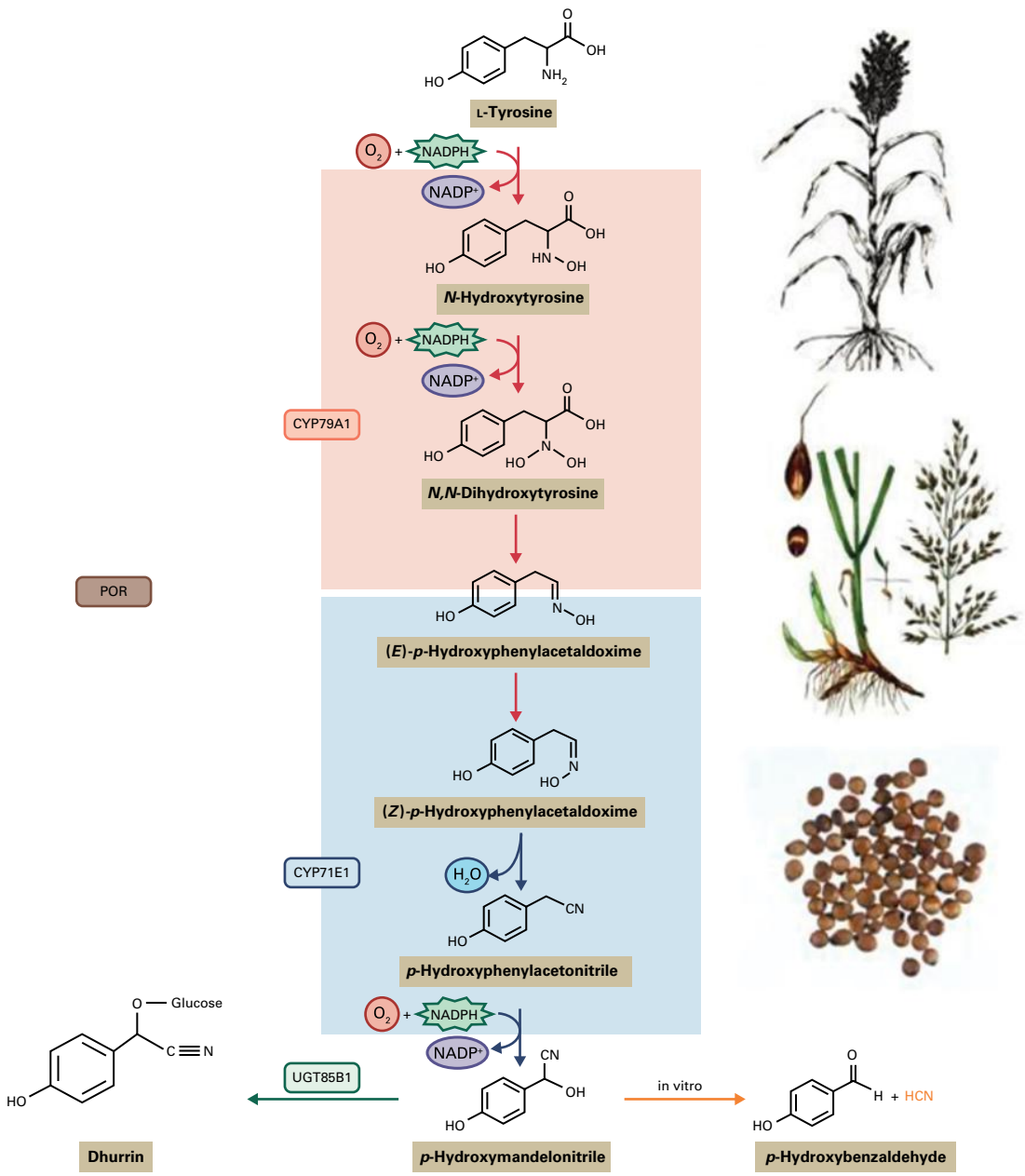


FIGURE 24.20 *Biosynthesis and degradation of the tyrosine-derived cyanogenic glycoside dhurrin in* Sorghum bicolor. *The enzymes catalyzing the different steps are shown. Each cytochrome P450 enzyme catalyzes more than one step in the pathway. These steps are indicated by red (CYP79A1) and blue (CYP71E1). Degradation of dhurrin occurs when the plant tissue is disrupted, and can proceed nonenzymatically. The NADPH cytochrome P450 oxidoreductase (POR) provides reducing power from NADPH in single electron transfer steps.*

not commonly seen in metabolites of primary metabolism. Microsomal preparations from etiolated sorghum seedlings formed the starting material for isolation of two multifunctional membrane-bound cytochrome P450 enzymes that catalyze the tyrosine-to-*p*-hydroxymandelonitrile conversion (Fig. 24.20): CYP79A1 catalyzes conversion of the amino acid L-tyrosine to *(E)*-*p*-hydroxyphenylacetaldoxime, and CYP71E1 catalyzes the conversion of *(E)*-*p*-hydroxyphenylacetaldoxime into *p*-hydroxymandelonitrile. A soluble UDP-glucosyltransferase (UGT85B1) catalyzes conversion of *p*-hydroxymandelonitrile into dhurrin. The corresponding P450 cDNA and genomic clones were also obtained.

Subsequent studies in other cyanogenic species involved metabolomics, proteomics, and transcriptomics, genome sequencing, heterologous expression of candidate genes, and natural variation and mutants. They have shown the pathway for cyanogenic glycoside biosynthesis in these species also utilizes cytochrome P450 enzymes and UDP-glycosyltransferases and follows the same sequence of transformation of intermediates as identified in sorghum. Sequence comparisons, however, indicate that the genes encoding the biosynthetic enzymes in different cyanogenic plant species are not necessarily orthologous. Independent evolution of cyanogenic glycoside biosynthesis in several higher plant lineages by gene duplication from related gene families and diversification (assumption of a totally new function) is a likely scenario. This is supported by the demonstration that some insects synthesize cyanogenic glucosides de novo using the same set of intermediates, two multifunctional cytochrome P450s, and a membrane-bound UDP-glucosyltransferase, which evolved by convergent evolution and not by horizontal gene transfer or divergent evolution (see Box 24.4).

The substrate specificity of the plant CYP79 enzymes that catalyze formation of oximes from amino acids is restricted to a single amino acid or two structurally similar amino acids. In contrast, the enzymes that catalyze the subsequent steps in cyanogenic glycoside synthesis exhibit broader substrate specificity. This promiscuity may have provided the starting point for evolution of new functions and thus, for repeated evolution of cyanogenic glycoside synthesis following the emergence of the CYP79 enzyme.

When the genes encoding the pathway for cyanogenic glycoside formation were identified in *L. japonicus*, *S. bicolor*, and cassava (*M. esculentum*), it became apparent that the genes were clustered within all three species (Fig. 24.21). This indicates a strong evolutionary mechanism promoting this type of genomic organization; however, the clusters differ substantially in size, gene density, and with respect to the additional genes present. Self-organization of biosynthetic

BOX 24.4

Reduction of cyanogenic glucoside levels in cassava requires extensive processing, but may also be accomplished through genetic engineering

The high levels of cyanogenic glycosides that accumulate in some plant species pose health hazards when the plant material is used for human consumption or as animal feed. Examples include cassava tubers, bitter almonds, and forage sorghum.

Cassava (*Manihot esculenta*) is a tropical and subtropical crop favored for its drought tolerance and high yields of starchy tubers, even on marginal soils. In rural populations, especially in sub-Saharan Africa, cassava tuber is a major staple food eaten regularly and in such quantities that it constitutes a dominant portion of the diet for millions of people. To avoid cyanide intoxication from the cyanogenic glucosides linamarin and lotaustralin, the tubers require extensive processing (see figure). The processing, however, is associated with loss of proteins, minerals, and vitamins, which decreases the nutritional value.

The biosynthesis of cyanogenic glucosides in cassava occurs mainly in young leaves, and the compounds are then transported to the tubers, as demonstrated through removal of the phloem tissue by stem girdling. *De novo* biosynthesis also takes place in the tuber peel. Using RNA interference (RNAi) technology, the level of cyanogenic glucosides can be reduced to 1% of wild-type levels in leaves. In contrast, reduction of the tuber levels to below 10% of wild-type levels is difficult, possibly reflecting the strong sink nature of the tuber tissue. In the seedling stage, cyanogenic glucosides serve as important transporters of reduced nitrogen, so RNAi seedlings have long and slender stems, long internodes, poorly developed leaves, and shorter and thicker roots (if any at all) when grown in vitro at low nitrogen. Transfer to standard media or soil restores the wild-type phenotype.

Farmed cassava is vegetatively propagated from stem cuttings, so the negative phenotype observed at the seedling stage following depletion of cyanogenic glucoside availability is not of direct practical relevance. The seedling phenotype illustrates that the presence of cyanogenic glucosides may offer specific advantages, for example at selected developmental stages or as a response to certain environmental challenges.



A



B



C



D



E



F



G

Processing cassava to remove cyanogenic glucosides and their toxic degradation products. The outer part of the cassava tuber is high in cyanogenic glucoside content and so initially removed, either with a knife (A) or by hand following soaking (B). Following grating (C), the tuber material is placed in a sack placed under stones to squeeze out the cyanide containing juice (E). The pressate may be stabilized by roasting (D, F) or simply air dried while the man is watching (G). Cassava processing is typically carried out by women.

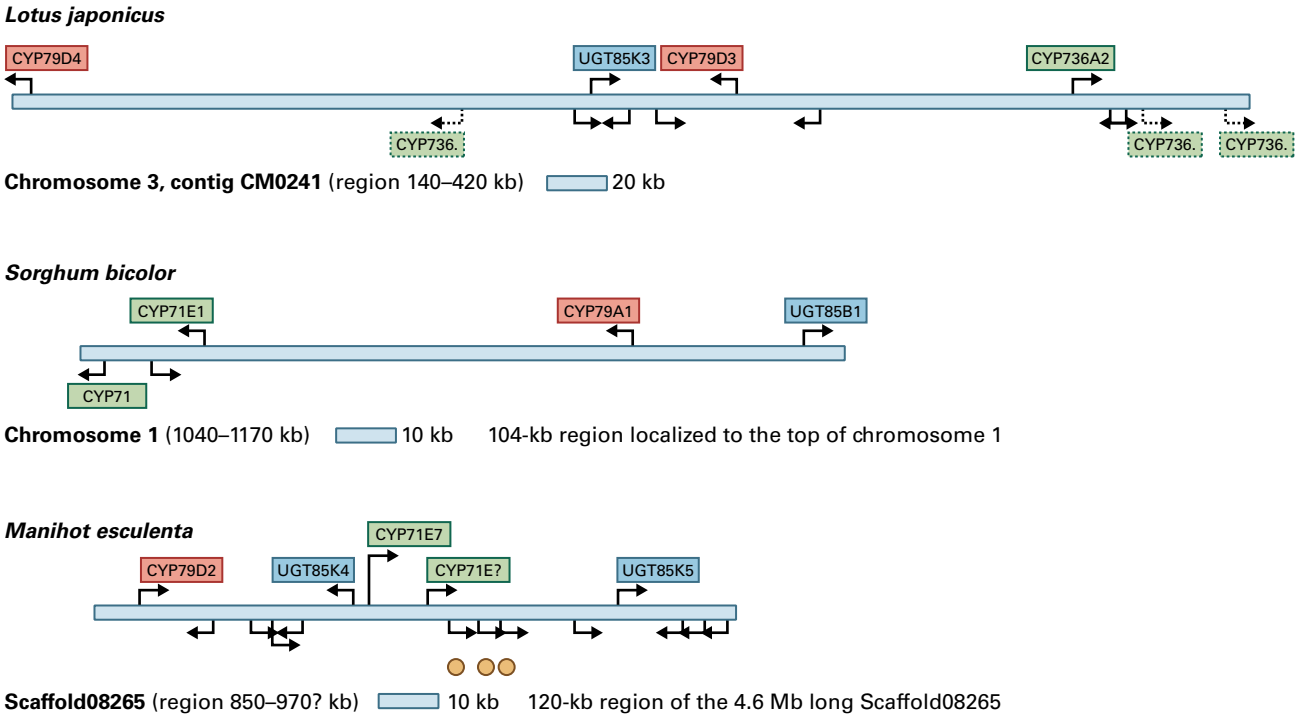


FIGURE 24.21 *Clustering of cyanogenic glucoside biosynthetic genes in the genomes of* Lotus japonicus, Sorghum bicolor, *and* Manihot esculenta. *The genes are positioned differently in the clusters and with large differences in the spacing. Arrows indicate orientation of functional genes. CYP79 genes are shown in pink, CYP71E and CYP736 genes in green, and UGT85 genes in blue.*

pathways into gene clusters may reduce the likelihood of crossover events that result in the accumulation of toxic intermediates. In a dynamic ecological contest, co-inheritance of gene clusters may favor maintenance of adaptive chemical defense polymorphisms in natural populations subjected to opposing selection pressures (see Section 24.19).

24.8.2 Metabolon formation helps regulate cyanogenic glycoside synthesis

The enzymes of cyanogenic glycoside biosynthesis are organized within a dynamic **metabolon** (macromolecular enzyme complex) (Fig. 24.22) (see Sections 24.12.4 and 24.18.4). There is precedence for metabolon participation in primary metabolism, for example in glycolysis, the tricarboxylic acid cycle, and fatty acid biosynthesis.

Metabolon formation facilitates channeling of toxic and labile intermediates (see Fig. 24.20) toward formation of the final product. The E-oxime formed by the first P450 enzyme is reactive and must be efficiently converted into the Z-isomer by the second P450 before the dehydration reaction and further conversion can take place. Likewise, rapid glycosylation of the last intermediate in the pathway, the labile α-hydroxynitrile, is required to prevent its dissociation into HCN and an aldehyde. The metabolon controls the number of products formed and protects the cell from autotoxicity.

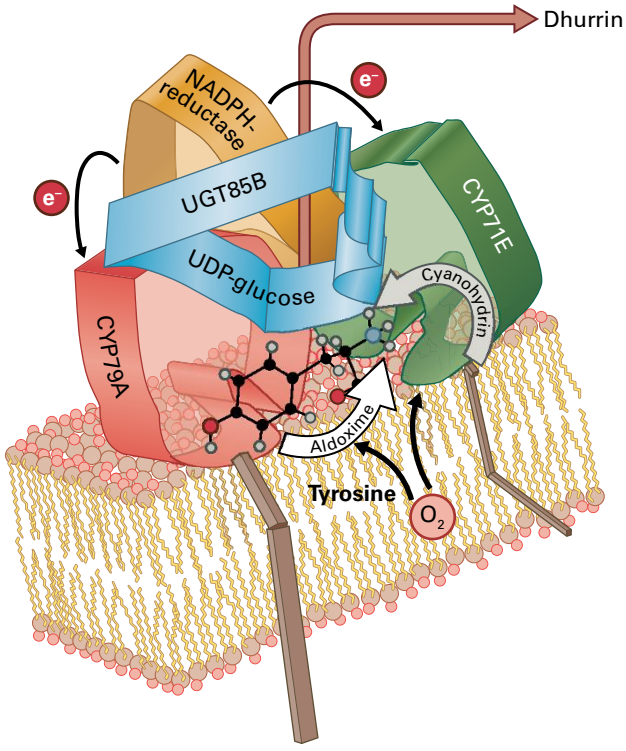


FIGURE 24.22 *Metabolon formation in cyanogenic glycoside synthesis. The two cytochrome P450 enzymes (CYP79A1 and CYP71E1) and UDP-glucosyltransferase (UGT85B1) interact to channel intermediates in the biosynthetic pathway directly into formation of dhurrin.*

Metabolon formation in cyanogenic glycoside synthesis is a dynamic process mediated by weak protein–protein interactions or controlled by the composition of the lipids in the endoplasmic reticulum interacting with the P450s. The transient nature of the metabolon affords metabolic flexibility and enables interaction with other primary and secondary metabolic processes. For example, the second P450 in the pathway is highly sensitive to oxygen, so fungal attack followed by oxygen burst may inactivate this P450 and result in the release of oximes with antifungal effects. In a similar manner, the small

BOX 24.5 Sequestering and de novo biosynthesis of cyanogenic glucosides in insects

Some specialized herbivores, especially insects, preferentially feed on cyanogenic plants. The larvae of such herbivores have acquired the ability to either metabolize cyanogenic glucosides without release of HCN or to sequester them for use in their own defense against predators.

Larvae of the burnet moth (*Zygaena filipendulae*) not only sequester the cyanogenic glucosides linamarin and lotaustralin (see Fig. 24.18) from their food plants (Fabaceae), they are able to carry out de novo synthesis of the same compounds. The larvae store these cyanogenic glucosides in cuticular cavities and secrete them upon stimulation as sticky droplets to deter potential predators. The ratio and content of cyanogenic glucosides are tightly regulated in the different stages of the *Z. filipendulae* life cycle, and the compounds play other roles in addition to defense. The transfer of a nuptial gift of cyanogenic glucosides during mating, for example, may explain why females prefer to mate with males carrying high amounts of cyanogenic glucosides. The reduced nitrogen contained in cyanogenic glucosides may be remobilized into primary nitrogen metabolism.

Linamarin and lotaustralin biosynthesis in *Z. filipendulae* share the same unusual biosynthetic intermediates as in plants. Three genes (*CYP405A2*, *CYP332A3*, and *UGT33A1*) encode the entire biosynthetic pathway. As in plants, the insect P450 enzymes are multifunctional. Phylogenetic analyses demonstrated that the ability to synthesize cyanogenic glucosides has evolved in plants and insects by convergent evolution, not from horizontal gene transfer or divergent evolution. Thus, plants and insects have independently found a way to package a cyanide time bomb to fend off herbivores and predators.



Larvae of Zygaena filipendulae *sequester the cyanogenic glucosides linamarin and lotaustralin present in their host plant* Lotus corniculatus *or synthesize the same compounds de novo from their parent amino acids. When irritated, cyanogenic glucoside-loaded defense droplets are exuded and visible on top of the black patches of the integument. When the female imago is ready to mate, she prefers males with high cyanogenic glucoside content. During the mating process, the male transfers cyanogenic glucosides to the female.*

family of CYP79-encoding genes found in many plant species not accumulating cyanogenic glycosides may be involved in controlling the release of volatile oximes or corresponding nitriles. Diurnal variations in CYP79 expression or metabolon formation may also enable release of volatile oximes. The function of volatile oximes as insect attractants has been documented in a number of moth-pollinated night-scented orchids, in which they increase the likelihood of pollination.

24.9 Functions of cyanogenic glycosides

24.9.1 Cyanogenic glycosides act as plant defense compounds

One of the most notable functions of cyanogenic glycosides in plants depends on their activation by β-glycosidases to release toxic volatile HCN, as well as a ketone or aldehyde, to fend off herbivores and pathogens (see Fig. 24.17). This is a classic example of how plant defense compounds may be stored in a nontoxic form that, upon attack, is activated to provide an immediate chemical defense response. However, whether such a defense system is able to successfully fend off an attack depends on the actual cyanogenic glycoside level and whether the rate of HCN release is high enough to block the mitochondrial electron transport chain in the attacking organism at the oxygen-binding site of cytochrome *c* oxidase. The bitterness of the cyanogenic glycoside and hydrolysis products may also prevent feeding.

Natural populations of cyanogenic plants vary greatly in their content of cyanogenic glycosides, and variation is also pronounced with respect to plant ontogeny, leaf age, and environmental conditions. Biosynthesis of cyanogenic glycosides primarily occurs in young and developing tissues, and the levels found in older plant parts generally decrease, as de novo biosynthesis proceeds at a low rate or does not keep up with the net gain in total biomass. Environmental stresses such as drought may induce cyanogenic glycoside production. This signifies that a plant that is harmless to an herbivore when grown under one set of conditions may be toxic or lethal under another. Thus, in many cases cyanogenesis provides an effective general defense system.

Cyanogenesis-based plant defense systems are estimated to be 400 million years old (see Fig. 24.19). Some fungi and herbivores have co-evolved and counteract and exploit cyanogenesis-based defenses for their own benefits. Fungal pathogens of cyanogenic plants may tolerate HCN based on their use of cyanide-resistant alternative oxidases and efficient metabolism of HCN into formamide in a reaction catalyzed by formamide hydrolyase. Hydrolysis of formamide provides the fungus with ammonia as a source of reduced nitrogen.

Some highly cyanogenic plant species are more susceptible to fungal infection than are varieties with reduced cyanide potential. This applies to the interaction between the rubber tree (*Hevea brasiliensis*) and the causative agent of rubber tree leaf blight, the fungus *Microcyclus ulei*. The main cyanogenic glycoside found in the rubber tree is linamarin (see Fig. 24.18), and *M. ulei* is tolerant of the levels of HCN released during disease development. In the highly cyanogenic rubber tree varieties, the accumulated levels of free HCN in the leaves impairs overall plant defense by inhibiting formation of the phytoalexin scopoletin and most likely also by inhibiting the activity of peroxidases and polyphenoloxidases. This illustrates that the versatile batteries of chemical plant defenses within a single plant species in some cases do not act synergistically but may be trade-offs against each other due to negative interactions at the biochemical level.

Some arthropods are also able to cope with and in some cases benefit from or even depend on the presence of cyanogenic glycosides in their host plant. Sequestration of the plant-derived cyanogenic glycosides in the arthropod or de novo synthesis of the same compounds provides the arthropod with a defense system against its own predators (see Box 24.5).

24.9.2 Cyanogenic glycosides play other roles in plants

In addition to serving as defense compounds, cyanogenic glycosides serve many other functions that afford an advantage at certain developmental stages or following specific environmental challenges.

The total cyanogenic glycoside content of a plant typically shows diurnal changes. In leaves of the rubber tree (*Hevea brasiliensis*) and in cassava, the cyanogenic glycosides are constantly degraded and resynthesized: The levels are highest at dawn, decrease rapidly upon exposure to sunlight, and are re-established after sunset and during the night. This observation prompted investigations into the operation of an endogenous turnover pathway for cyanogenic glycosides that is not accompanied by HCN release (Fig. 24.23). Using sorghum (*Sorghum bicolor*) as an experimental system, the turnover pathway was found to proceed with conversion of dhurrin to *p*-hydroxyphenylacetonitrile. The action of a heteromeric complex of nitrilases (NIT4A/B2) then catalyzes the conversion of the nitrile into *p*-hydroxyphenylacetic acid and ammonia. Hydrogen cyanide released by the classic β-glycosidase catalyzed hydrolysis of cyanogenic glycosides is converted into β-cyanoalanine by the action of β-cyanoalanine synthase with a stoichiometric consumption of cysteine. NIT4A/B1 and/or NIT4A/B2 complete the cyanide detoxification reaction by converting β-cyanoalanine into asparagine and aspartic acid.

The ability to turnover cyanogenic glycosides without release of toxic constituents provides an avenue for their use as long- and short-distance transporters of reduced nitrogen and glucose. This was first demonstrated in studies with the rubber tree (*H. brasiliensis*), where cyanogenic glycoside

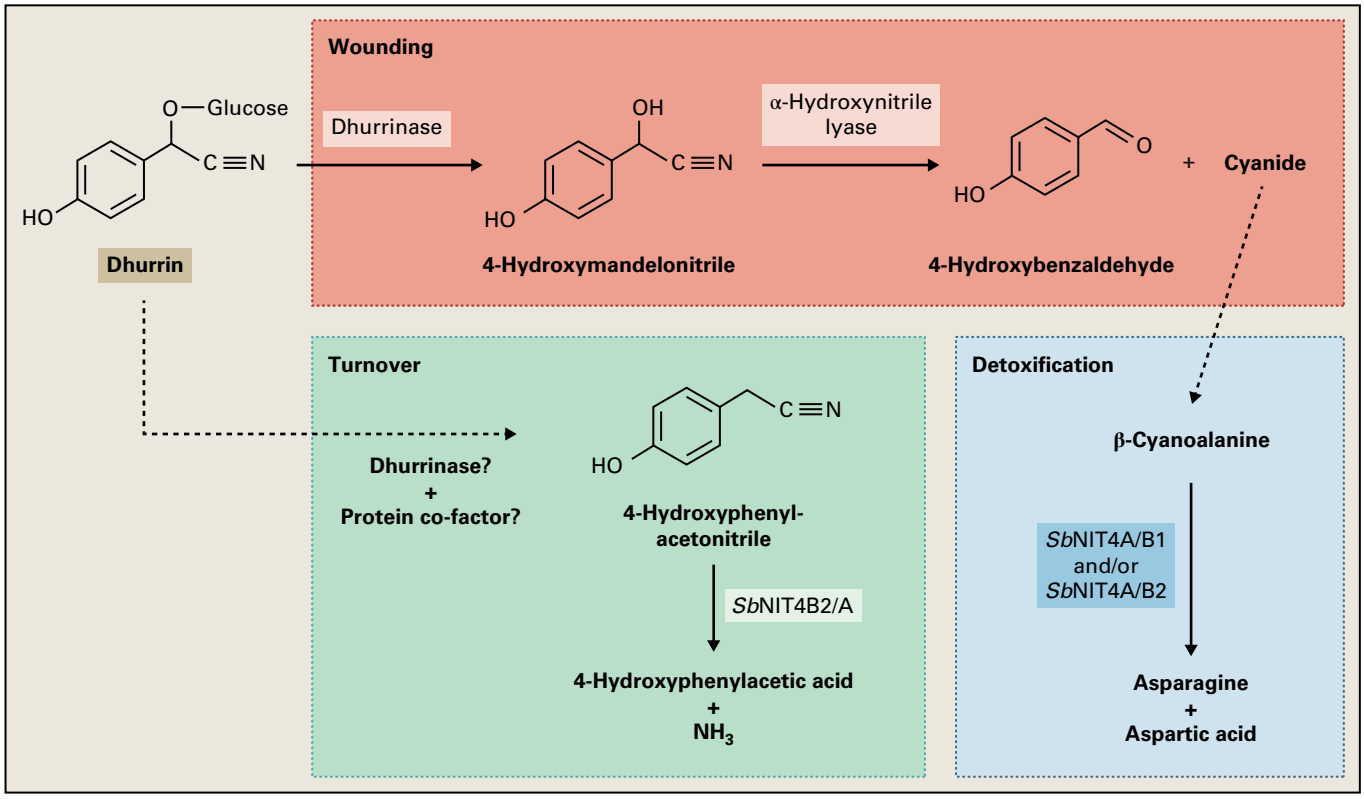


FIGURE 24.23 *Endogenous turnover pathways of the cyanogenic glycoside dhurrin in sorghum. Dhurrin can be metabolized in the plant either through wounding (i.e., herbivory) or in a diurnal rhythm. This exemplifies its role as both a defense compound, and as a transportable source of reduced nitrogen and glucose.*

transport buffers nitrogen and glucose supplies during seedling development and for the latex regeneration process following bark tapping.

In some cyanogenic plant species like white clover (*Trifoleum repens*), natural variants exist that are not cyanogenic (acyanogenic), either because they cannot synthesize cyanogenic glycosides de novo or because they cannot degrade them. The cyanogenic and acyanogenic plants coexist, but with a shift in prevalence from year to year that reflects fluctuations in the main environmental challenges. In general, cyanogenic plants dominate in seasons with heavy attack by generalist herbivores (e.g., snails) that avoid eating them, and acyanogenic plants dominate in cooler climates and profit from resource allocation trade-offs when herbivore attack is minimal. Thus, the presence of cyanogenic glycosides offers additional possibilities for fine-tuning plant metabolism and adapting to environmental stress.

24.10 Glucosinolates

24.10.1 Glucosinolates also derive their biological activity following hydrolysis

Glucosinolates are sulfur-rich, anionic β-thioglycosides. They contain a central carbon atom that is bound by a sulfur to a glycone group, and by a nitrogen to a sulfonated oxime group. In addition, the central carbon is bound to a side group (Fig. 24.24A). Different glucosinolates have different side groups as defined by the amino acids from which they are derived. The amino acid precursors include alanine, valine, isoleucine, leucine, methionine, phenylalanine, tyrosine, and tryptophan, and chain-elongated forms of methionine and phenylalanine.

Glucosinolates constitute a small class of specialty compounds that obtain their biological activity following hydrolysis by β-thioglucosidases, also known as myrosinases. The labile aglycon that is formed may rearrange in different ways to produce isothiocyanates, nitriles, epithionitriles, oxazolidine-2-thiones, and thiocyanate (Fig. 24.24B). The profile of bioactive products obtained is shaped by the glucosinolate side chain structure and the presence of modifying protein partners or specifier proteins, the presence of ferrous ions, and pH.

To prevent damage to the plant, myrosinase and glucosinolates are stored in separate subcellular compartments and come together only under conditions of stress or injury (e.g., cell disruption due to biting or chewing by herbivores).The hydrolysis products produced as a result of cell disruption are referred to as the **mustard oil bomb** and provide defense against generalist herbivores.

The natural occurrence of glucosinolates is largely restricted to the Brassicales order, including oil seed rape (*Brassica napus*), cabbage and broccoli (*Brassica oleracea*), radish (*Raphanus sativus*), horseradish (*Armoracia rusticana*), and *Arabidopsis thaliana*. Besides the structural variation

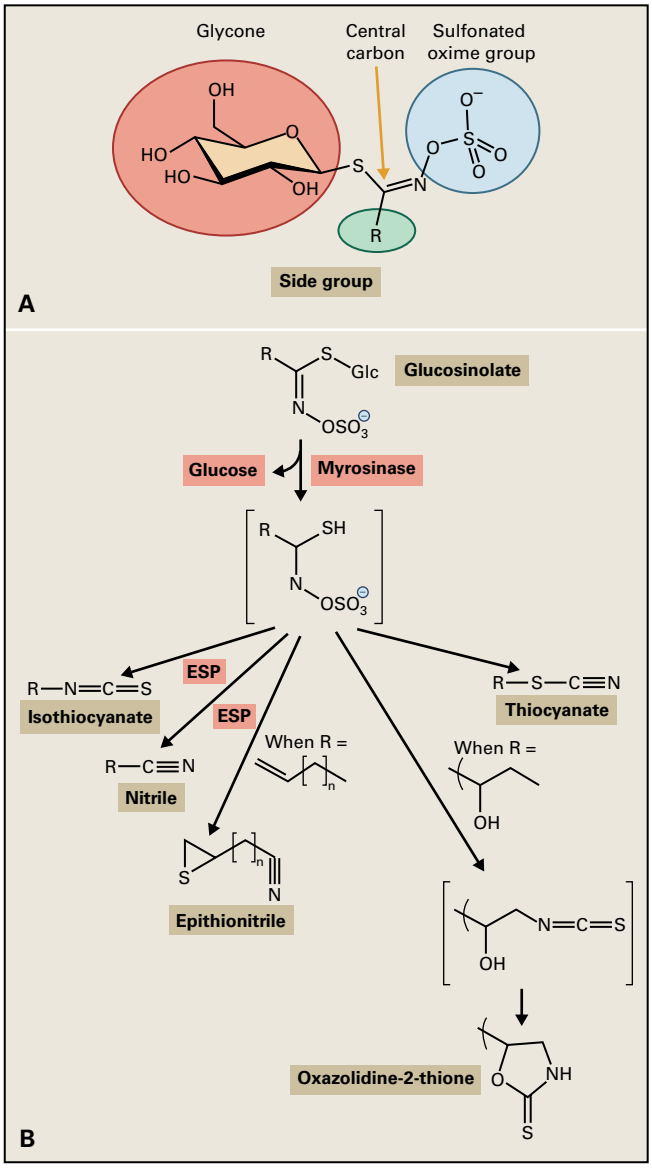


FIGURE 24.24 *(A) Core structure of a glucosinolate. Every glucosinolate contains a central carbon atom, which is bound through a sulfur linkage to the glycone group, and through a nitrogen linkage to a sulfonated oxime group. The central carbon is also bound to a side group (R); different glucosinolates have different side groups. (B) The possible products formed following hydrolysis of the thioglucosidic linkage. ESP, epithiospecifier protein.*

offered by different degrees of chain elongation of mainly Met- and Phe-derived glucosinolates, the core structure may be further modified by the activity of flavin monooxygenases and 2-oxoglutarate-dependent dioxygenases.

24.10.2 Biosynthesis of glucosinolates

Glucosinolate biosynthesis, like cyanogenic glycoside biosynthesis, begins with the conversion of the parent amino acid into an E-oxime in a reaction catalyzed by cytochrome P450 enzymes belonging to the CYP79 family (Fig. 24.25). In a second set of reactions catalyzed by cytochrome P450 enzymes belonging to the CYP83 family, the E-oxime is hydroxylated to a labile *aci*-nitro compound or nitrile oxide that is conjugated to glutathione. The conjugation reaction may proceed nonenzymatically. The GSH conjugate is then cleaved by a cytosolic γ-glutamyl peptidase, resulting in the formation of a Cys-Gly conjugate. The Gly may subsequently be removed by the action of a carboxypeptidase; alternatively, the C-S lyase SUPERROOT 1 may be able to cleave the Cys-Gly as well as the Cys conjugate to afford a thiohydroximic acid. S-glucosylation by the action of a UDPG-glucosyltransferase belonging to the UGT74 family converts the thiohydroximic acid into a desulfoglucosinolate that is converted into the glucosinolate by sulfotransferases (SOT16, 17, 18).

Structural diversity of glucosinolates also arises from the ability of some CYP79 enzymes to use chain-elongated forms of Met and Phe as substrates (see Box 24.6).

24.11 Alkaloids

24.11.1 Alkaloids have a 3,000-year history of human use

For much of human history, **alkaloid**-containing plant extracts have been used as ingredients in potions and poisons. In the eastern Mediterranean, use of the latex of the opium poppy (*Papaver somniferum;* Fig. 24.26) can be traced back at least to 1400–1200 BC. The Sarpagandha root (*Rauwolfia serpentina*) has been used in India since approximately 1000 BC. Ancient people used medicinal plant extracts as purgatives, antitussives, sedatives, and treatments for a wide range of ailments, including snakebite, fever, and insanity.

As the use of medicinal plants spread westward across Arabia and Europe, new infusions and decoctions played a role in famous events. During his execution in 399 BC, the philosopher Socrates drank an extract of coniine-containing hemlock (*Conium maculatum*; Fig. 24.27). In the last century BC, Queen Cleopatra used extracts of henbane (*Hyoscyamus*), which contains atropine (Fig. 24.28), to dilate her pupils and appear more alluring to her male political rivals. Over the centuries, however, the king of all medicinals has been opium, which was widely consumed in the form of Theriak, a concoction consisting mainly of opium, dried snake meat, and wine (see Box 24.7). Analysis of the individual components of opium led to the identification of morphine (Fig. 24.29A), named for Morpheus, the god of dreams in Greek mythology. The isolation of morphine in 1806 gave rise to the study of alkaloids.

The term alkaloid, coined in 1819 in Halle (Saale) Germany, finds its origin in the Arabic name *al-qali,* the plant from which soda was first isolated. Alkaloids were originally

defined as pharmacologically active, nitrogen-containing basic compounds of plant origin. After 200 years of alkaloid research, this definition no longer encompasses the entire alkaloid field, but in many cases it is still appropriate. Alkaloids are not unique to plants. They have also been isolated from numerous animal sources (see Box 24.8); the alkaloid morphine, for example, has been detected in mammals and is synthesized de novo in mouse (see Box 24.9). Many of the alkaloids that have been discovered are not pharmacologically active in mammals, and some are neutral rather than basic in character, despite the presence of a nitrogen atom in the molecule.

24.11.2 Alkaloid-containing plants were mankind's original "materia medica"

Alkaloid-containing plants were mankind's original "materia medica," and many are still in use today as prescription drugs (Table 24.1). One of the best-known prescription alkaloids is the antitussive and analgesic codeine from the opium poppy, *Papaver somniferum* (Fig. 24.29). Plant alkaloids have also served as models for modern synthetic drugs, such as the tropane alkaloid atropine (see Fig. 24.28) for tropicamide used to dilate the pupil during eye examinations and the indole-derived antimalarial alkaloid quinine for chloroquine (Fig. 24.30).

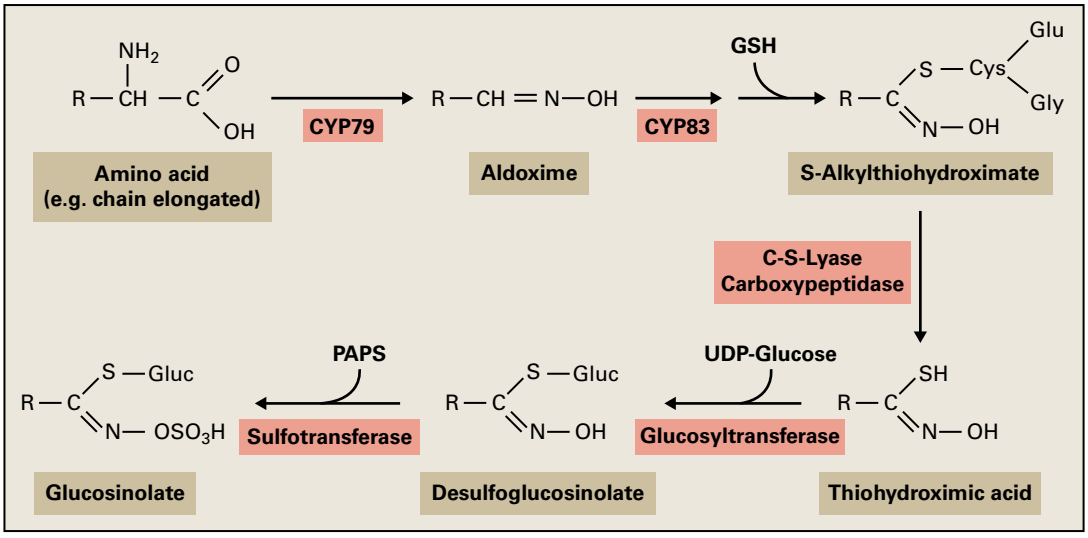


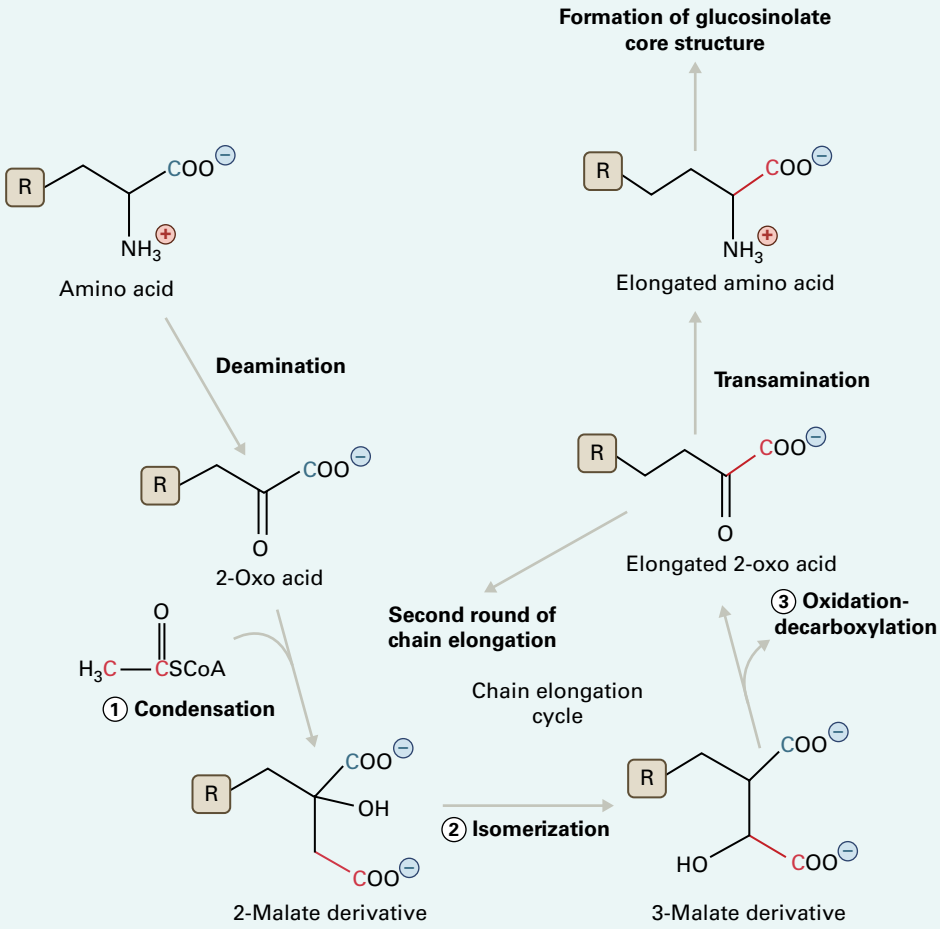
FIGURE 24.25 *Biosynthesis of glucosinolates. Cleavage of the glutathione (GSH) conjugate may be achieved by multiple routes, including action of a carboxypeptidase or the C-S lyase SUPERROOT 1 to produce the thiohydroximic acid.*

BOX 24.6

Amino acid chain elongation is a key part of glucosinolate biosynthesis

A unique and integral part of glucosinolate biosynthesis is the side chain elongation of the precursor amino acids. This is the prerequisite for much of the structural diversity within the glucosinolate family. Special enzymes are responsible for catalyzing the synthesis of different side chains of the various glucosinolates. The enzyme methylthioalkylmalate (MAM) synthase, which elongates the side chain of methionine, resembles the enzyme isopropylmalate synthase (IPMS) of the biosynthesis of the amino acid L-leucine (see Chapter 7). There are two major structural differences between MAM synthase and IPMS: the last 120 amino acids at the carboxy terminus of IPMS are absent in MAM synthase; in the active sites of the enzymes, two amino acids have been exchanged.

The evolution of MAM synthase has been a major driver in the amino acid chain elongation process in glucosinolate metabolism and illustrates how changes at the protein level may lead to the recruitment of an enzyme from primary metabolism (IPMS) to serve an important new function (MAM synthase) in the synthesis of secondary metabolites, providing yet another example of the role of gene duplication and diversification in the evolution of natural product biosynthetic pathways (see Sections 24.8.2 and 24.19).



The amino acid chain elongation reactions in glucosinolate synthesis. (1) Condensation of the 2-oxo acid and acetyl-CoA is catalyzed by MAM synthase This condensation step followed by (2) isomerization of the 2-malate derivative to the 3-malate derivative and (3) oxidative decarboxylation of the 3-malate derivative to the 2-oxo acid now elongated by one methylene (-CH_2-) group forms the elongation cycle. The elongation cycle can be repeated two to six times.

In addition to having a major impact on modern medicine, alkaloids have also influenced world geopolitics. Notorious examples include the Opium Wars between China and Britain (1839–1859) and the efforts currently underway in various countries to eradicate illicit production of heroin, a semi-synthetic compound derived by acetylation of morphine (see Fig. 24.29C), and cocaine, a naturally occurring alkaloid of the coca plant (Fig. 24.31). Because of their various pharmacological activities, alkaloids have influenced human history profoundly, both for good and ill. Of interest to plant biologists, however, is the evolutionary process in plants that has caused alkaloids to evolve and the role in communication of the plant with the environment in which these molecules participate.

24.11.3 Physiologically active alkaloids participate in plant chemical defenses

More than 20,000 alkaloids have been isolated from various organisms since the discovery of morphine. It is estimated that the number of plant genera is greater than 20,000. Approximately 9% of plant genera have alkaloid-accumulating species, and these plants occur most abundantly in genera belonging to angiosperms (flowering plants). Each species that accumulates alkaloids does so in a unique, defined pattern. Some plants, such as the periwinkle (*Catharanthus roseus*) contain more than 100 different monoterpenoid indole alkaloids. Certain alkaloids are restricted to a single species, such as (+)-tubocurarine in the liana *Chondrodendron tomentosum*, whereas other alkaloids are more widely distributed among plant families.

Why should a plant invest so much nitrogen into synthesizing alkaloids of such diverse structure? How does only one plant species evolve to produce a particular alkaloid? The role of alkaloids in plants and their evolution have been long-standing questions, but a picture is emerging that supports an ecochemical function for these compounds.

The role of chemical defense for alkaloids in plants is supported by their wide range of physiological effects on animals and by the antibiotic activities many alkaloids possess. Various alkaloids are also toxic to insects or function as feeding deterrents. For example, nicotine, found in tobacco (*Nicotiana* sp.), was one of the first insecticides used by humans and remains

one of the most effective (Fig. 24.32). Herbivory stimulates nicotine biosynthesis in wild tobacco plants. Another effective insect toxin is caffeine (Fig. 24.33), found in seeds and leaves of cocoa (*Theobroma cacao*), coffee (*Coffea arabica*), cola (family Malvaceae), maté (*Ilex paraguariensis*), and tea (*Camellia sinensis*). At a dietary concentration well below that found in fresh coffee beans or tea leaves, caffeine kills nearly all larvae of the tobacco hornworm (*Manduca sexta*) within 24 hours, primarily by inhibiting the phosphodiesterase that hydrolyzes cAMP. The steroid alkaloid α-solanine, a cholinesterase inhibitor found in potato tuber (*Solanum tuberosum*, Fig. 24.34), is the trace toxic constituent thought to be responsible for the teratogenicity of sprouting potatoes.



A B

FIGURE 24.26 *(A) Maturing capsule of the opium poppy* Papaver somniferum. *When the capsule is wounded, a white, milky latex is exuded. Poppy latex contains morphine and related alkaloids, such as codeine. When the exuded latex is allowed to dry, a hard, brown substance called opium is formed. (B) Statuette from Gazi of a goddess of sleep crowned with capsules of the opium poppy (1250–1200 BC).*
Source: (A) Kutchan, Liebnitz Institut für Pflanzenbiochemie, Halle, Germany; previously unpublished; (B) Ministry of Culture Archaeological Receipts Fund, Athens, Greece.

Two groups of alkaloids that have been well studied with respect to ecochemical function are the pyrrolizidine and quinolizidine alkaloids (Fig. 24.35). Pyrrolizidine alkaloids, frequently found in members of the tribe Senecioneae (Asteraceae) and in the Boraginaceae, render most of these plants toxic to mammals. In *Senecio* species, senecionine N-oxide is synthesized in roots and translocated throughout the plant. In species such as *Senecio vulgaris* and *S. vernalis,* 60–80% of the pyrrolizidine alkaloids accumulate in the inflorescences. Members of the *Senecio* genus are responsible for livestock poisonings and also represent a potential health hazard for humans.

Naturally occurring pyrrolizidine alkaloids are harmless but become highly toxic when transformed by cytochrome P450 monooxygenases in the liver. On the other hand, several insect species have adapted to the pyrrolizidine alkaloids that accumulate in plants and have evolved mechanisms for using these alkaloids to their own benefit. Some insects can feed on pyrrolizidine alkaloid-producing plants and effectively and efficiently eliminate the alkaloids after enzymatic modification, such as formation of N-oxide derivatives. Other insects not only feed on these plants, but also store the pyrrolizidine alkaloids for their own defense or convert the ingested pyrrolizidine alkaloids to pheromones that attract prospective mates (see Box 24.8).

The quinolizidine alkaloids occur primarily in the genus *Lupinus* and are frequently referred to as lupine alkaloids

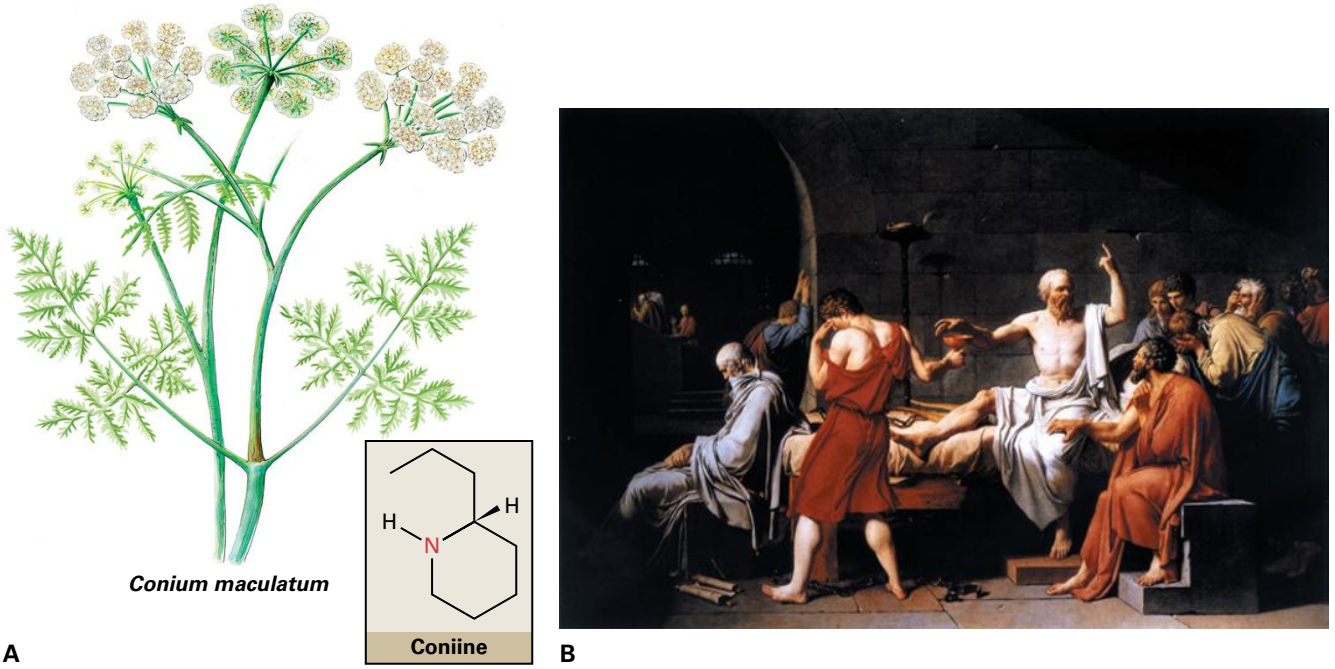


FIGURE 24.27 *(A) The piperidine alkaloid coniine, the first alkaloid to be synthesized, is extremely toxic, causing paralysis of motor nerve endings. (B) In 399 BC, the philosopher Socrates was executed by consuming an extract of coniine-containing poisonous hemlock. This depiction of the event, "The Death of Socrates," was painted by Jacques-Louis David in 1787.*
Source: (B) The Metropolitan Museum of Art, New York, NY.

(Fig. 24.35B); they are toxic to grazing animals, particularly to sheep. The highest incidence of livestock losses attributable to lupine alkaloid poisoning occurs in autumn during the seed-bearing stage of the plant life cycle—the seeds being the plant parts that accumulate the greatest quantities of these alkaloids. Because of their bitter taste, lupine alkaloids can also function as feeding deterrents. Given a mixed population of sweet and bitter lupines, rabbits and hares readily eat the alkaloid-free sweet variety and avoid the lupine alkaloid-accumulating bitter variety, indicating that lupine alkaloids can reduce herbivory by functioning both as bitter-tasting deterrents and toxins. Given this collection of examples, alkaloids can be viewed as a part of the chemical defense system of the plant that evolved under the selection pressure of predation.



Hyoscyamus niger

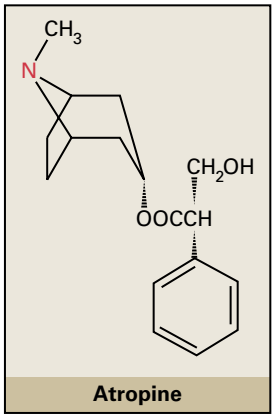


FIGURE 24.28 *Structure of the anticholinergic tropane alkaloid atropine from* Hyoscyamus niger.

BOX 24.7

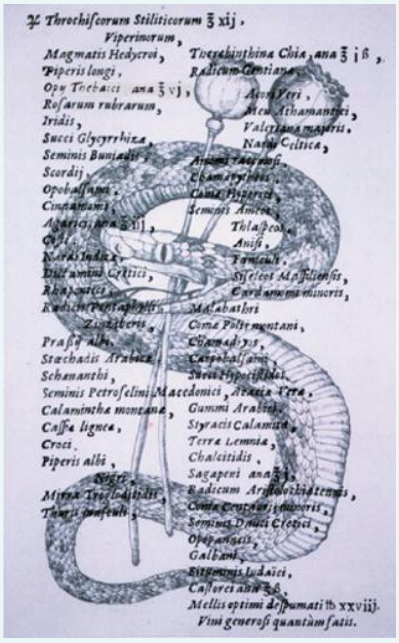
Theriak, an ancient antipoisoning nostrum containing opium, wine, and snake meat, is still used today in rare instances

One of the oldest and most long-lived medications in the history of mankind is Theriak. Originating in Greco-Roman culture, Theriak consists of mainly opium and wine with a variety of plant, animal, and mineral constituents. Panel A of the figure shows a recipe for Theriak from the French Pharmacopée Royale in 1676.

Theriak was developed as an antidote against poisoning, snake and spider bites, and scorpion stings. History has it that the Roman Emperor Nero contracted the Greek physician Andromachus to discover a medicine that was effective against all diseases and poisons. Andromachus improved the then-existing recipe to include, in addition to opium, five other plant poisons and 64 plant drugs. Another crucial component was dried snake meat, believed to act against snakebite by neutralizing the venom.

Today, Theriak is still prescribed in rare cases in Europe for pain and other ailments. Panel B shows a valuable Theriak-holding vessel made of Nymphenburg porcelain (in about 1820), which is on display in the Residenz Pharmacy in Munich, Germany.

Source: (A) French Pharmacopée Royale; photograph: Kutchan, Leibnitz Institut für Pflanzenbiochemie, Halle, Germany; previously unpublished; (B) Residenz Pharmacy, Munich, Germany; photograph: Kutchan, Leibnitz Institut für Pflanzenbiochemie, Halle, Germany; previously unpublished.



A



B

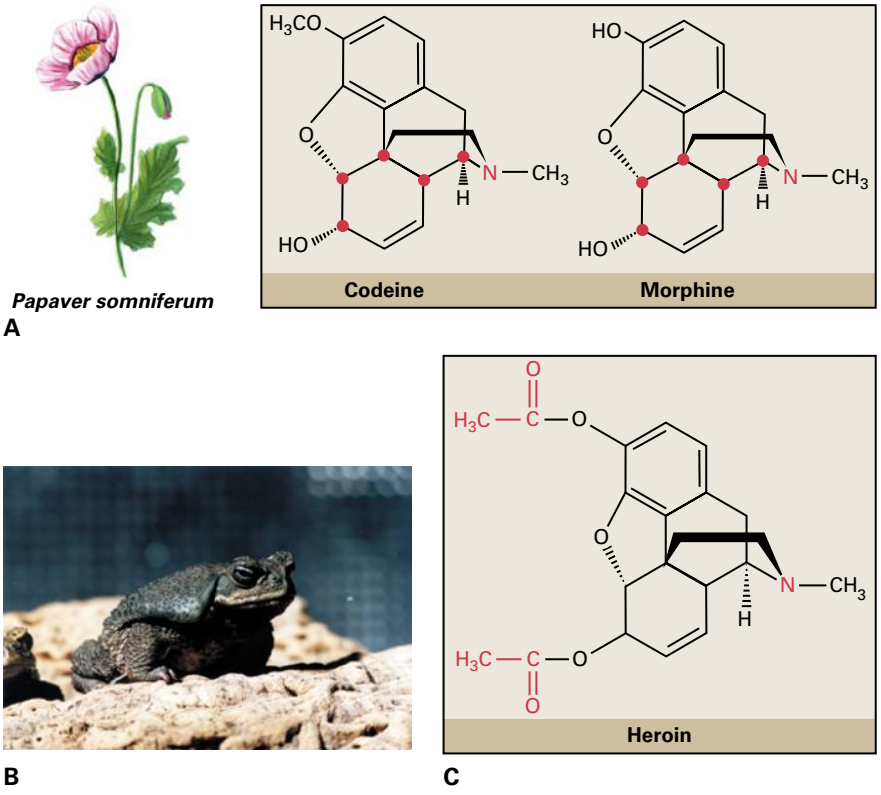


FIGURE 24.29 *(A) Structures of the alkaloids codeine and morphine from the opium poppy* Papaver somniferum. *Asymmetric (chiral) carbons are highlighted with red dots. (B) The frog* Bufo marinus *accumulates a considerable amount of morphine in its skin. (C) Structure of diacetyl morphine, commonly known as heroin.*
Source: (B) Rickl, Universität München, Germany; previously unpublished.

24.11.4 Typically considered constitutive defense compounds, some alkaloids are synthesized in response to plant tissue damage

Alkaloids are thought to be part of the direct chemical defense system of many plants, and in some cases, such as that of nicotine in tobacco (*Nicotiana tabacum*), convincing evidence has been presented that an alkaloid is involved in induced chemical defense.

Wild species of tobacco are highly toxic to the hornworm *Manduca sexta*, a tobacco-adapted species. Feeding by larvae of *M. sexta* on its host plant *Nicotiana attenuata* elicits responses from the plant that are distinguishable from mechanical simulation of the damage that results from feeding. Mechanical damage induces accumulation of the plant hormone jasmonic acid (see Chapter 17) in the wounded leaf, and that systemically results in an accumulation of nicotine in the whole plant. Feeding by the tobacco hornworm results in higher leaf jasmonic acid levels than mechanical wounding, but whole plant nicotine levels do not surpass those achieved with mechanical damage. Hornworm feeding, in particular chemicals present in hornworm regurgitant, interferes with whole plant accumulation of nicotine, and it appears that the plant hormone ethylene (see Chapter 17) is specifically elicited by hornworm herbivory. The interplay between jasmonic acid and ethylene regulates nicotine biosynthesis and accumulation that results from insect attack of the tobacco plant.

To determine whether nicotine actually functions in defense required down regulating the nicotine biosynthesis gene that encodes putrescine *N*-methyl transferase in *N. attenuata* using RNA interference (RNA*i*) technology. This reduced constitutive and inducible nicotine levels by greater than 95% in the transgenic plants. Larvae of the tobacco hornworm (Fig. 24.36) grew faster and preferred transgenic plants with reduced nicotine in choice tests. When planted in their native habitat, the low nicotine, transgenic plants were attacked more frequently and lost more leaf area to a variety of native herbivores compared to wild-type plants that contained normal levels of nicotine. Nicotine down-regulated plants were also used to demonstrate a role for this alkaloid in reproductive fitness of *Nicotiana* flowers (Box 24.10).

24.12 Alkaloid biosynthesis

24.12.1 Alkaloid biosynthesis research has been aided by the development of techniques for high-throughput sequencing of transcriptomes

Many alkaloids have complex chemical structures and contain multiple asymmetric centers. This complicates structure elucidation and has made the study of alkaloid biosynthesis

BOX 24.8

Some butterflies and moths use alkaloids for sexual signaling or for protection against predators

Alkaloid-bearing species have been found in nearly all classes of organisms, including frogs, ants, butterflies, bacteria, sponges, fungi, spiders, beetles, and mammals. Alkaloids of various structures have been isolated from a variety of marine creatures. Some animals, such as amphibians, produce an array of either toxic or noxious alkaloids in the skin or the secretory glands. Others, such as the insects described below, use plant alkaloids as a source of attractants, pheromones, and defense substances.

Some butterflies gather alkaloidal precursors from plants that are not their food sources and convert these compounds into pheromones and defense compounds. Larvae of the cinnabar moth (*Tyria jacobaea*) continuously graze their plant host *Senecio jacobaea* until the plant is completely defoliated (A). The alkaloids thus obtained by the larvae are retained throughout metamorphosis. Male Asian and American arctiid moths incorporate pyrrolizidine alkaloids into their reproductive biology by sequestering these alkaloids in abdominal scent organs called coremata, which are everted in the final stages of their courtship to release the pheromones necessary to gain acceptance by a female. The coremata of a male Asian arctiid moth (*Creatonotos transiens*) is directly proportional in size to the pyrrolizidine alkaloid content of its diet during the larval stage (B). The courtship success of these male butterflies, therefore, depends on their ingesting alkaloids from higher plants.

The larvae of a second insect group, the Ithomiine butterflies, feed on solanaceous plants and sequester the plant toxins, including tropane alkaloids and steroidal glycoalkaloids. Adult Ithomiinae, however, do not contain tropane and steroid alkaloids; they prefer to ingest plants that produce pyrrolizidine alkaloids, sequestering these bitter substances as N-oxides and monoesters. The pyrrolizidine alkaloid derivatives protect Ithomiinae butterflies from an abundant predator, the giant tropical orb spider. The spider will release a field-caught butterfly from its web, but will readily eat a freshly emerged adult that has not yet had an opportunity to feed on the preferred host plant. When palatable butterflies were painted externally with a solution of pyrrolizidine alkaloids, the spider released them from its web. In contrast, palatable butterflies treated the same way with Solanaceae alkaloids were devoured. In general, mostly male butterflies are found feeding on the pyrrolizidine alkaloid-accumulating plants; up to 50% of the pyrrolizidine alkaloids present in these males is sequestered in the spermatophores and transferred to females at mating. In some butterfly species, the protective alkaloids are then transferred on to the eggs.

Source: (A, B) Kutchan, Leibnitz Institut für Pflanzenbiochemie, Halle, Germany; previously unpublished.



A



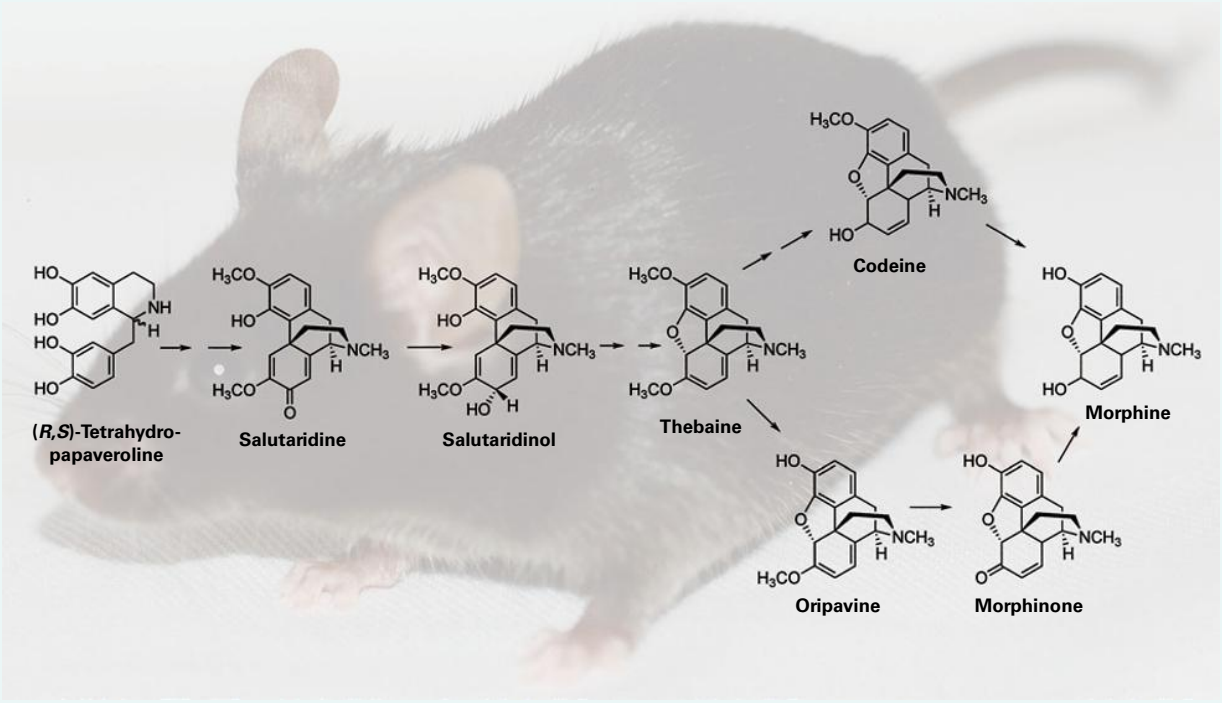
B

quite difficult. For example, although nicotine (one asymmetric center; see Fig. 24.32) was discovered in 1828, its structure was not known until it was synthesized in 1904. In addition, the structure of morphine (five asymmetric centers; see Fig. 24.29A) was not elucidated until 1952, almost 150 years after its isolation, and the enzymes involved in its biosynthesis were identified more than 200 years after it was first isolated.

Why has it been so difficult to elucidate alkaloid biosynthetic pathways? Plants synthesize natural products at a

BOX 24.9 Morphine, the opiate analgesic formed in opium poppy, is synthesized de novo in mouse

Morphine has been detected in animal tissues, such as in skin of the frog *Bufo marinus* (Fig. 24.29B), but whether the alkaloid is formed de novo in frog has not been clarified. Humans also excrete a small amount of morphine in urine, but it is not yet clear whether this morphine is of dietary or endogenous origin. The simple isoquinoline alkaloid tetrahydropapaveroline is found in human and rodent brain as well as in human urine. The structural elements suggested a potential biogenetic relationship between tetrahydropapaveroline and morphine. Studies using high-resolution mass spectrometry have shown that mice have the biosynthetic capability to convert tetrahydropapaveroline, a normal constituent of rodents, into morphine. In fact, the morphine detected in mouse urine results from de novo biosynthesis, and the medical implications of the plant alkaloid morphine also being synthesized in animals may be significant to pain research.



relatively sluggish rate, so steady-state concentrations of the alkaloid biosynthetic enzymes can be low. In addition, the large amounts of tannins and other phenolics that accumulate in plants interfere with extraction of active enzymes. Even when plants are treated with radiolabeled precursors and the resulting radioactive alkaloids are chemically degraded to identify the position of the label, the low rate of natural product metabolism can prevent the high rates of incorporation required to yield clear results. The use of polyvinylpyrrolidone and Dowex-1 in preparing protein extracts from plant tissues has helped overcome the enzyme inactivation by phenolic compounds, but isolation of the enzymes involved in natural product synthesis has had only limited success because of their very low concentrations in the plant.

Next-generation sequencing technologies (Fig. 24.37) have enhanced the study of alkaloid biosynthesis by generating deep transcriptome datasets of a rapidly increasing number of plant species. From a comparative expression analysis of transcript, either between tissues of one plant or between plant species, candidate biosynthetic genes can be selected and recombinant enzymes experimentally verified. This new transcriptomic approach circumvents problems previously encountered with whole-plant studies, such as year-round availability of plant material, and the inability of dedifferentiated plant cell cultures to synthesize certain alkaloids to any appreciable extent due to tissue-specific expression of alkaloid biosynthesis genes. An example of an alkaloid biosynthetic pathway that has been largely elucidated within a short period of time from a transcriptome dataset is that of the terpenoid-isoquinoline alkaloid emetine (Fig. 24.38), an orally active emetic and amoebicide from the Central American plant *Psychotria ipecacuanha*.

TABLE 24.1 *Physiologically active alkaloids used in modern medicine.*

Alkaloid	Plant source	Use
Ajmaline	*Rauwolfia serpentina*	Antiarrhythmic that functions by inhibiting glucose uptake by heart tissue mitochondria
Atropine, (±)hyoscyamine	*Hyoscyamus niger*	Anticholinergic, bronchodilator
Caffeine	*Coffea arabica*	Widely used central nervous system stimulant
Camptothecin	*Camptotheca acuminata*	Potent anticancer agent
Cocaine	*Erythroxylon coca*	Topical anesthetic, potent central nervous system stimulant, and adrenergic blocking agent; drug of abuse
Codeine	*Papaver somniferum*	Relatively nonaddictive analgesic and antitussive
Coniine	*Conium maculatum*	First alkaloid to be synthesized; extremely toxic, causes paralysis of motor nerve endings, used in homeopathy in small doses
Emetine	*Uragoga ipecacuanha*	Orally active emetic, amoebicide
Morphine	*Papaver somniferum*	Powerful narcotic analgesic, addictive drug of abuse
Nicotine	*Nicotiana tabacum*	Highly toxic, causes respiratory paralysis, horticultural insecticide; drug of abuse
Pilocarpine	*Pilocarpus jaborandi*	Peripheral stimulant of the parasympathetic system, used to treat glaucoma
Quinine	*Cinchona officinalis*	Traditional antimalarial, important in treating *Plasmodium falciparum* strains that are resistant to other antimalarials
Sanguinarine	*Eschscholzia californica*	Antibacterial showing antiplaque activity, used in toothpastes and oral rinses
Scopolamine	*Hyoscyamus niger*	Anticholinergic, effective against motion sickness
Strychnine	*Strychnos nux-vomica*	Violent tetanic poison, rat poison, used in homeopathy
(+)-Tubocurarine	*Chondrodendron tomentosm*	Nondepolarizing muscle relaxant producing paralysis, used as an adjuvant to anesthesia
Vincristine	*Catharanthus roseus*	Antineoplastic used to treat childhood leukemia and other cancers.



Cinchona officinalis

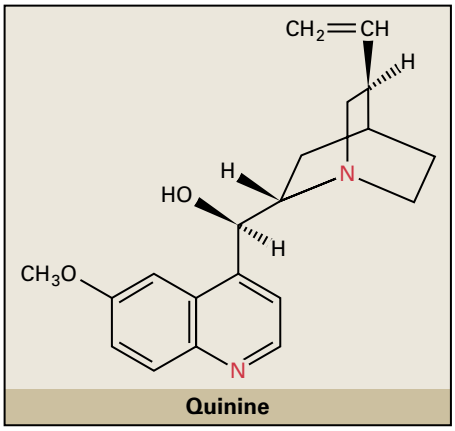


FIGURE 24.30 *Structure of the monoterpenoid indole alkaloid-derived quinine from* Cinchona officinalis. *An antimalarial quinine-containing tonic prepared from the bark of* C. officinalis *greatly facilitated European exploration and inhabitation of the tropics during the past two centuries.*



Erythroxylum coca

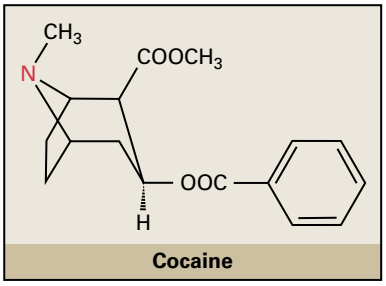
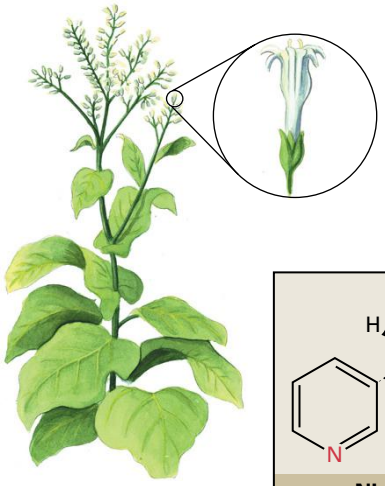


FIGURE 24.31 *Structure of the tropane alkaloid cocaine, a central nervous system stimulant derived from* Erythroxylum coca.

24.12.2 Plants synthesize alkaloids from simple precursors, using unique enzymes

Until the mid-20th century, our view of plant alkaloid biosynthesis was based on biogenic hypotheses. Pathways suggested by illustrious natural product chemists were based on projections considered feasible within the realm of organic chemistry. In the 1950s, however, alkaloid biosynthesis became an experimental science, as radioactively labeled organic molecules became available for testing hypotheses. These early precursor-feeding experiments established that alkaloids are, in most cases, formed from L-amino acids (e.g., tryptophan, tyrosine, phenylalanine, lysine, and arginine), either alone or in combination with a steroidal, secoiridoid (e.g., secologanin) or other terpenoid-type moiety. One or two transformations



Nicotiana tabacum

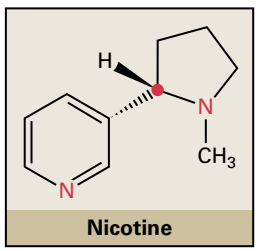


FIGURE 24.32 *Structure of nicotine from* Nicotiana tabacum.



Coffea arabica

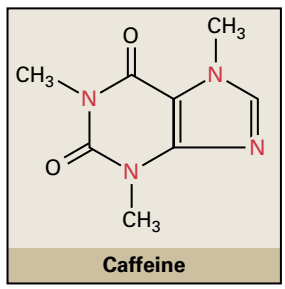
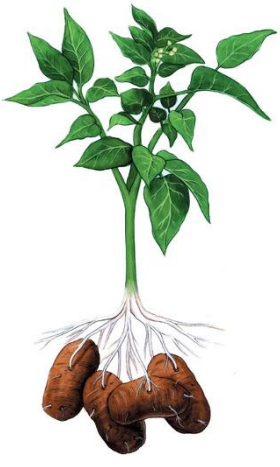


FIGURE 24.33 *Structure of the purine alkaloid caffeine from* Coffea arabica.



Solanum tuberosum

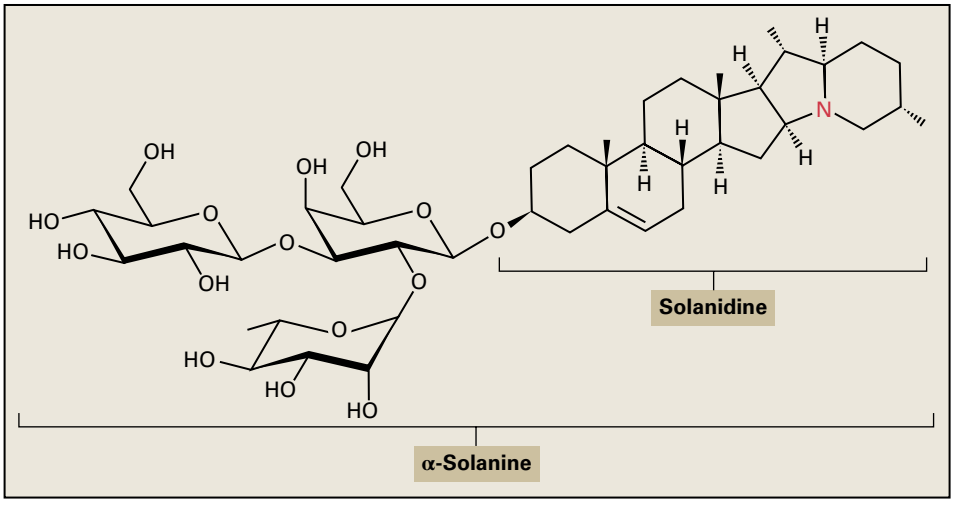


FIGURE 24.34 *Structure of the steroid alkaloid glycoside α-solanine from* Solanum tuberosum *(potato). The aglycone solanidine is derived from cholesterol.*

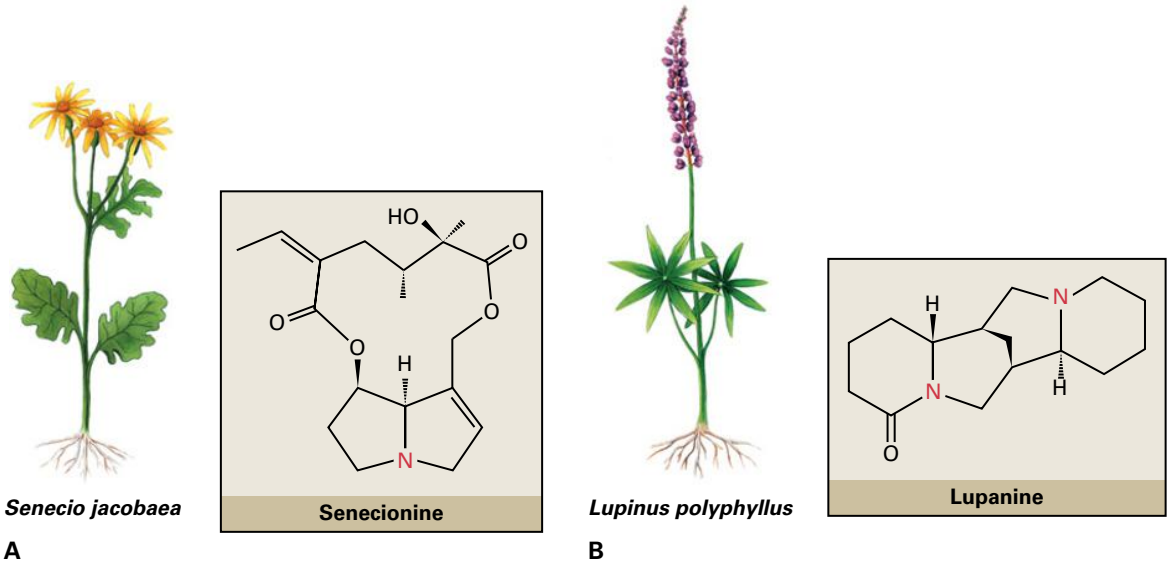


FIGURE 24.35 *Pyrrolizidine and quinolizidine alkaloids. (A) Structure of the pyrrolizidine alkaloid senecionine from ragwort (*Senecio jacobaea*). (B) Structure of the quinolizidine alkaloid lupanine from the bitter lupine* Lupinus polyphyllus. *Lupanine is a bitter compound that functions as a feeding deterrent.*



FIGURE 24.36 *The tomato hornworm (*Manduca quinquemaculata*) elicits and responds to nicotine in* Nicotiana attenuata*, just as the tobacco hornworm (*Manduca sexta*). The tomato hornworm also responded strongly to nicotine biosynthesis-silenced transgenic* Nicotiana attenuata *plants in the fields of Utah.*
Source: Ian Baldwin, Max Planck Institute for Chemical Ecology, Jena, Germany.

can convert these ubiquitous amino acids from primary metabolites to substrates for species-specific alkaloid metabolism. Although we do not thoroughly understand how most alkaloids are made by plants, several systems can serve as examples of the types of building blocks and enzymatic transformations that have evolved in alkaloid biosynthesis.

Ajmalicine (Fig. 24.39), an L-tryptophan-derived monoterpenoid indole alkaloid, was the first alkaloid for which biosynthesis was clarified at the enzyme level. In plants, the biosynthesis of ajmalicine and more than 1800 other monoterpenoid indole alkaloids begins with the decarboxylation of the L-amino acid tryptophan by tryptophan decarboxylase to form tryptamine. Then tryptamine, by action of strictosidine synthase, is stereospecifically condensed with the secoiridoid secologanin (derived in multiple enzymatic steps from geraniol) to form 3α(*S*)-strictosidine. Strictosidine can then be enzymatically permutated in a species-specific manner to form a multitude of diverse structures (Fig. 24.39). The elucidation of the enzymatic formation of ajmalicine laid the groundwork for analysis of more complex biosynthetic pathways, such as those leading to two other L-tryptophan-derived monoterpenoid indole alkaloids, ajmaline (Fig. 24.40) and vindoline.

24.12.3 The berberine synthesis pathway has been defined completely at the enzyme and gene levels

The first alkaloid for which each biosynthetic enzyme and corresponding cDNA were identified, isolated, and characterized is the antimicrobial benzylisoquinoline alkaloid, berberine, in *Berberis* (barberry). This pathway exemplifies the role of substrate-specific enzymes and compartmentalization in alkaloid biosynthesis.

The biosynthesis of tetrahydrobenzylisoquinoline alkaloids in plants begins in the cytosol with a matrix of reactions that generates the first tetrahydrobenzylisoquinoline alkaloid, (*S*)-norcoclaurine (Fig. 24.41) from two molecules of

BOX 24.10 Nicotine has a role in reproductive fitness of *Nicotiana attenuata* flowers

Flowers produce distinctive combinations (bouquets) of volatile secondary metabolites that aid reproduction by attracting pollinators. Another familiar example of a floral reproductive aid is flower color, which can attract specific pollinators, such as hummingbirds or bees. Flowers face a diverse challenge in that they must attract a pollinator, but must also repel florivores and nectar thieves, which do not contribute to pollen transfer.

The combination of the secondary metabolites nicotine and benzylacetone in flowers of *Nicotiana attenuata*, a tobacco species native to western North America, optimizes reproductive fitness. *N. attenuata* flowers attract the moth *Hyles lineata* (A) and the hummingbird *Archilochus alexandri* (B) as pollinators. Using genetic engineering, *N. attenuata* plants have been designed to lack nicotine, benzylacetone, or both nicotine and benzylacetine. When these metabolically tailored plants were tested in the wild for fitness, the plants that contained both nicotine and benzylacetone in their floral blend sired more seeds on other plants and produced larger seed capsules themselves. Benzylacetone attracts visitors to a flower, while nicotine prevents visitors from loitering while also deterring florivory by caterpillars and nectar robbing by carpenter bees. Combinations of attractants and repellents can help flowers to attract mates while avoiding predators, a pull and push strategy that optimizes a visitor's behavior.

Source: Kessler, Max Planck Institute for Chemical Ecology, Jena, Germany.



A



B

L-tyrosine. One tyrosine is decarboxylated to form tyramine or is acted on by a phenol oxidase to form L-dopa. Dopamine can then be formed by decarboxylation of L-dopa or by the action of a phenol oxidase on tyramine. Determining which of these two pathways dominates in a plant is difficult because all of the enzyme activities are present in protein extracts and *Berberis* species are not yet genetically tractable.

The benzyl moiety of (*S*)-norcoclaurine is formed by transamination of the second L-tyrosine molecule to form *p*-hydroxyphenylpyruvate, which is then decarboxylated to *p*-hydroxyphenylacetaldehyde. Dopamine and *p*-hydroxyphenylacetaldehyde are then stereoselectively condensed to form (*S*)-norcoclaurine. A series of methylation and oxidation reactions yield the branchpoint intermediate, (*S*)-reticuline (Fig. 24.42).

In *Berberis*, the *N*-methyl group of (*S*)-reticuline is oxidized to form the berberine bridge carbon C-8 of (*S*)-scoulerine (see Fig. 24.41). The specific pathway from (*S*)-scoulerine that leads to berberine proceeds with O-methylation to (*S*)-tetrahydrocolumbamine. The 3-*O*-methyl moiety of tetrahydrocolumbamine is converted to the methylenedioxy bridge of canadine by canadine synthase, a cytochrome P450 enzyme. The final step in the biosynthesis of berberine is catalyzed by (*S*)-tetrahydroprotoberberine oxidase, an enzyme with a covalently bound flavin.

The berberine bridge enzyme and (*S*)-tetrahydroprotoberberine oxidase each consumes 1 mol of O_2 and produces 1 mol of H_2O_2 per mol of berberine formed. Overall, the course of reactions from 2 mol of L-tyrosine to 1 mol of berberine consumes 4 mol of *S*-adenosylmethionine and 2 mol of NADPH.

24.12.4 Enzymes of alkaloid biosynthesis are localized to specific subcellular compartments and cell types

Alkaloid biosynthetic enzymes can be localized within a cell to different compartments. The cytochrome P450 enzymes of alkaloid biosynthesis, for example, are associated with the endoplasmic reticulum, whereas methyltransferases are found mainly in the cytosol. Strictosidine synthase of monoterpenoid indole alkaloid biosynthesis is contained within the vacuole, and the berberine bridge enzyme and (*S*)-tetrahydroprotoberberine oxidase of berberine biosynthesis are compartmentalized in vesicles thought to be derived from the smooth endoplasmic reticulum; berberine accumulates in the central vacuole of the *Berberis* cell.

Another aspect of the structural organization of an alkaloid biosynthetic pathway is the formation of a metabolon, as evidenced in morphine biosynthesis (Fig. 24.43) with the physical interaction of salutaridine reductase and salutaridinol acetyltransferase. As with cyanogenic glycoside biosynthesis (see Section 24.8.2) and the core phenylpropanoid pathway (see Section 24.18.4), the metabolon facilitates the channeling of substrates, confers protection of chemically labile intermediates, regulates flux through a pathway, and interacts with a cellular structural element or organelle (to control the localization of the biosynthetic machinery).

Alkaloids are synthesized and accumulate in specialized cell types. Knowledge gained on enzymes and genes of alkaloid formation enabled analyses of the tissue and cell types involved for several classes of alkaloid, including monoterpenoid indole and morphinan alkaloids. Multiple cell types, including leaf epidermal cells, are necessary for the formation and storage of, for example, vindoline and catharanthine in *Catharanthus roseus* (Fig. 24.44). These cell types are not adjacent, implying transport of biosynthetic intermediates. This suggests that several levels of posttranslational regulation may control alkaloid formation. For example, biosynthetic enzymes may have to associate to form a multienzyme complex; intermediates may have to be transported between cell types, in some cases over long distances within a tissue.

The development of technologies for the analysis and quantitation of the contents of single cell types has aided elucidation of alkaloid biosynthetic pathways. Laser capture microdissection, a technique by which single cells are excised under a microscope with a laser and then captured in a microtube, greatly aided the discovery of genes of alkaloid biosynthesis in *C. roseus*. The captured cells can be extracted and analyzed for natural products by mass spectrometry, or the RNA in the cells can be sequenced using next-generation sequencing to yield gene expression profiles. Even more promising and exciting in metabolite analysis of single plant cells is MALDI imaging of intact tissue. This technology uses matrix-assisted laser desorption ionization (MALDI) mass spectrometry to scan tissue in two dimensions as the mass spectrum is recorded. Current laser resolution is approximately the diameter of a plant cell, allowing for cell specific metabolite analysis across tissues.

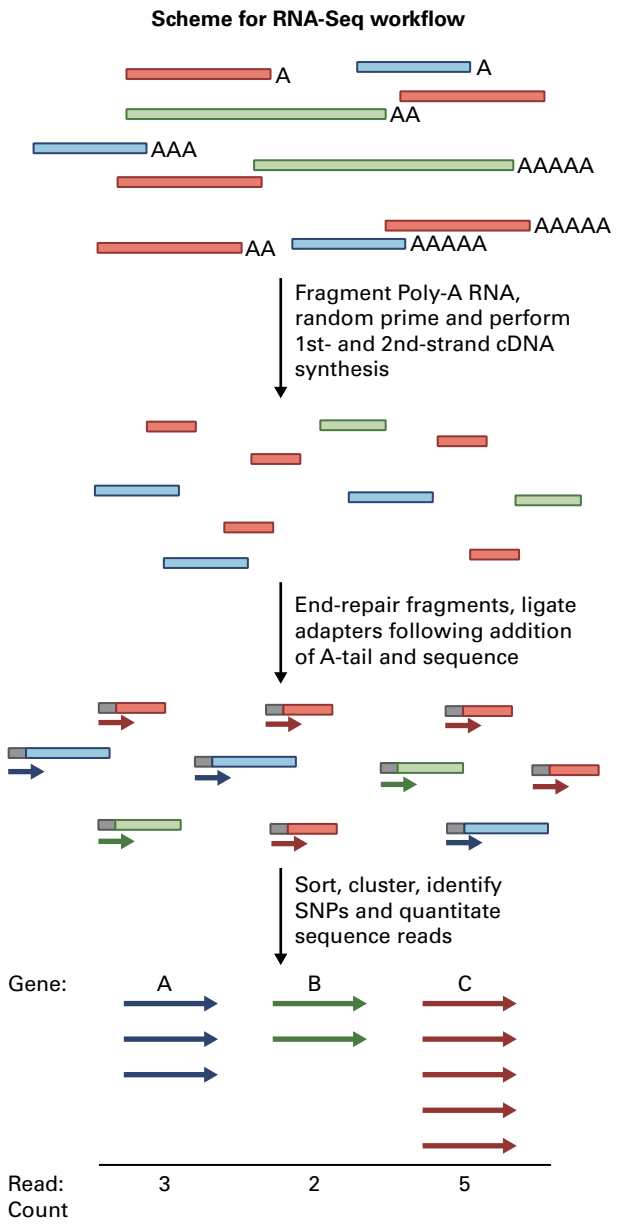


FIGURE 24.37 *Deep transcriptome sequencing using next-generation sequencing technologies yields transcript sequences and quantitation of sequence reads that provide information on differential gene expression.*

24.13 Biotechnological application of alkaloid biosynthesis research

24.13.1 Biochemical and molecular genetic techniques facilitate identification, purification, and production of useful alkaloids

The current status of the alkaloid branch of the field of natural products reflects the many advances in analytical chemistry, enzymology, and pharmacology. Only minimal quantities of a

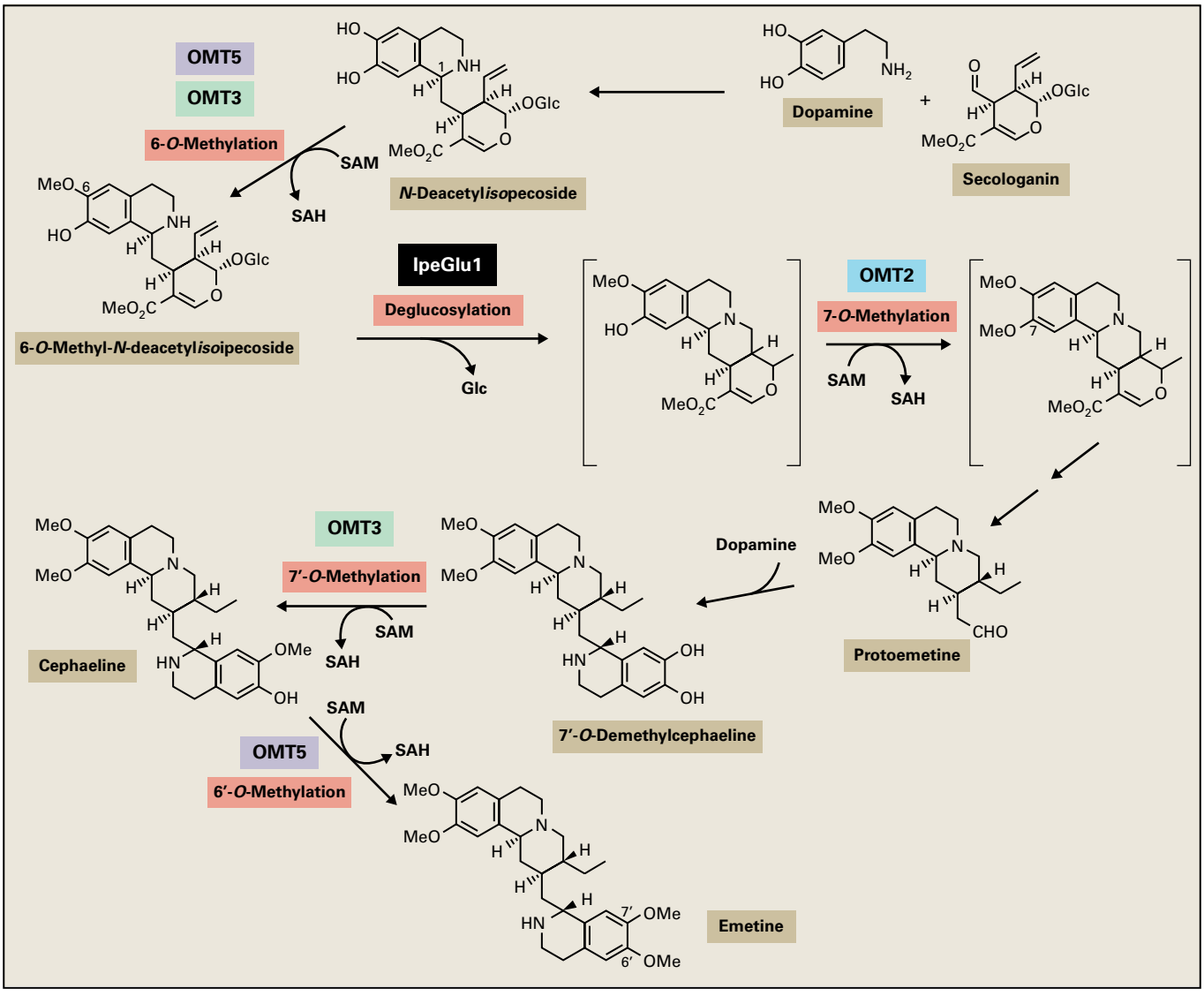


FIGURE 24.38 *Emetine formation was not well studied until the advent of transcriptome sequencing of plants. In a relatively short time, emetine biosynthesis has been nearly completely elucidated at the enzyme and cDNA levels, beginning with knowledge of the transcriptome. A hallmark of emetine formation is that permissive* O*-methyltransferases act at multiple positions along the biosynthetic pathway.*

pure alkaloid are now necessary for elucidation of a complete structure by mass spectrometric and NMR spectroscopic analyses. Absolute stereochemistry can be assigned by determining the crystal structure. The pharmacological activities of crude plant extracts or pure substances are determined by fully automated systems, such that millions of data points are collected each year in industrial screening programs. The factor that limits the number of biological activities for which we can test is the number of available target enzymes and receptors. As more of the underlying biochemical bases for diseases continue to be discovered, the number of test systems will increase.

When a small quantity of an alkaloid of complex chemical structure from a rare plant is found to be physiologically active, it must first pass animal and clinical trials. If these are successful, enough material will be needed to satisfy market demand. The following studies demonstrate how alkaloid biosynthesis has been engineered to quantitatively and qualitatively alter alkaloid accumulation.

24.13.2 Atomic structures of alkaloid biosynthetic enzymes yield information on their reaction mechanisms

The first alkaloid biosynthetic enzyme for which the atomic structure was solved was strictosidine synthase (Fig. 24.45), which is active in monoterpenoid indole alkaloid formation and initiates the biosynthetic pathways that lead to approximately 2,000 plant compounds. Synthases are a heterogeneous class of enzymes that catalyze a wide variety of reactions; strictosidine synthase stereospecifically condenses an amine and aldehyde to form a Schiff base that cyclizes to a nitrogen heterocycle in a reaction called a Pictet–Spengler reaction.

The crystal structure of strictosidine synthase in complex with its natural substrates tryptamine and secologanin represents a novel six-bladed β-propeller fold in plant proteins (Fig. 24.45). A common repetitive motif of three hydrophobic

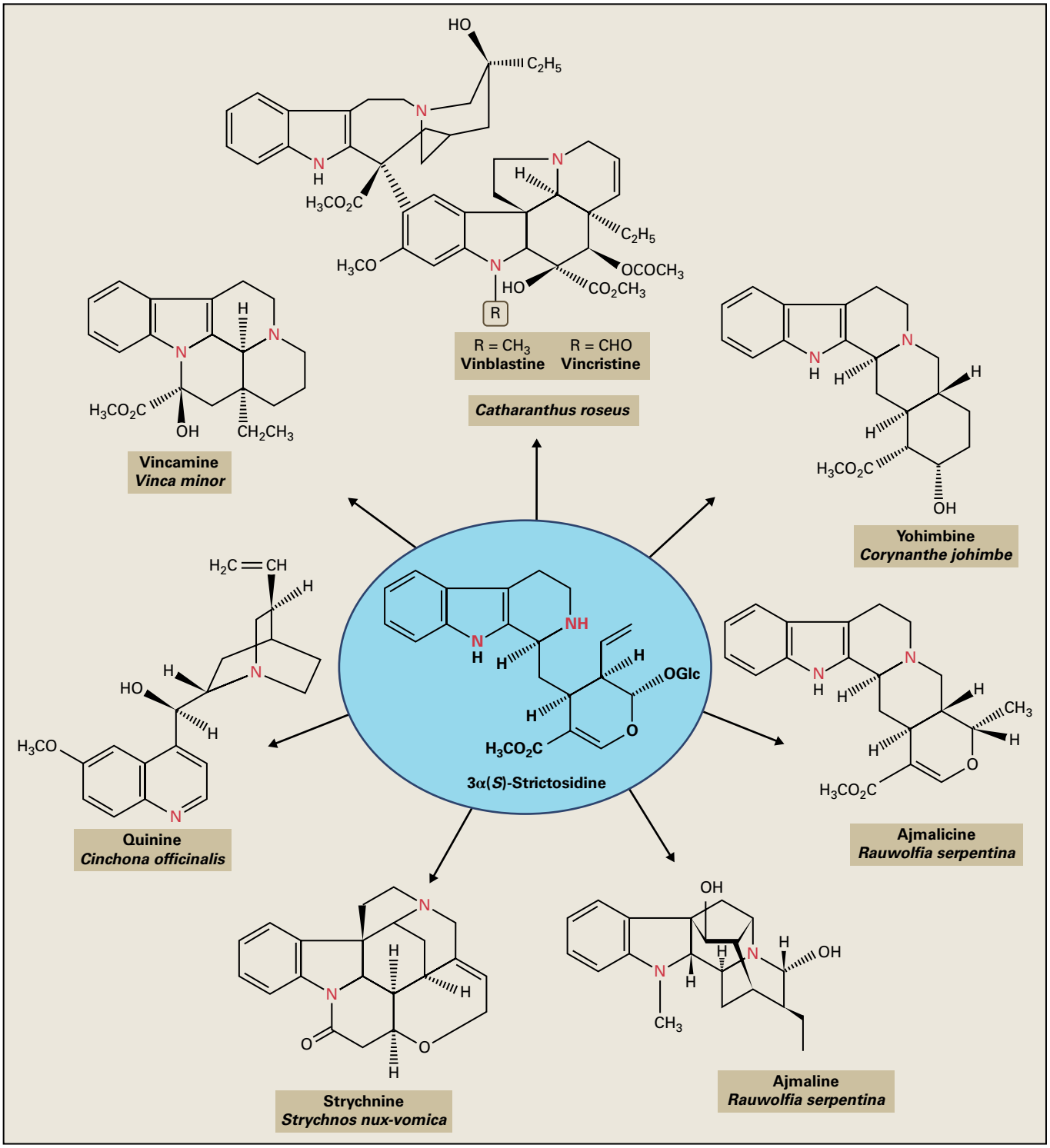


FIGURE 24.39 *Strictosidine, the product of tryptamine and secologanin, is the precursor for many species-specific alkaloids.*

residues followed by a small residue and a hydrophilic residue indicated by the structure-based sequence comparison suggests a possible evolutionary relationship between strictosidine synthase and several sequence-unrelated six-bladed β-propeller structures. The crystal structure of strictosidine in complex with its substrates has enabled the rational design of the enzyme to generate mutants that expand the natural substrate specificity. This has resulted in the production of novel derivatives of monoterpenoid indole alkaloids produced by the native enzyme.

Since the crystallization of strictosidine synthase, a number of additional alkaloid biosynthetic enzymes have had their atomic structures solved. These include strictosidine glucosidase, vinorine synthase, raucaffricine glucosidase,

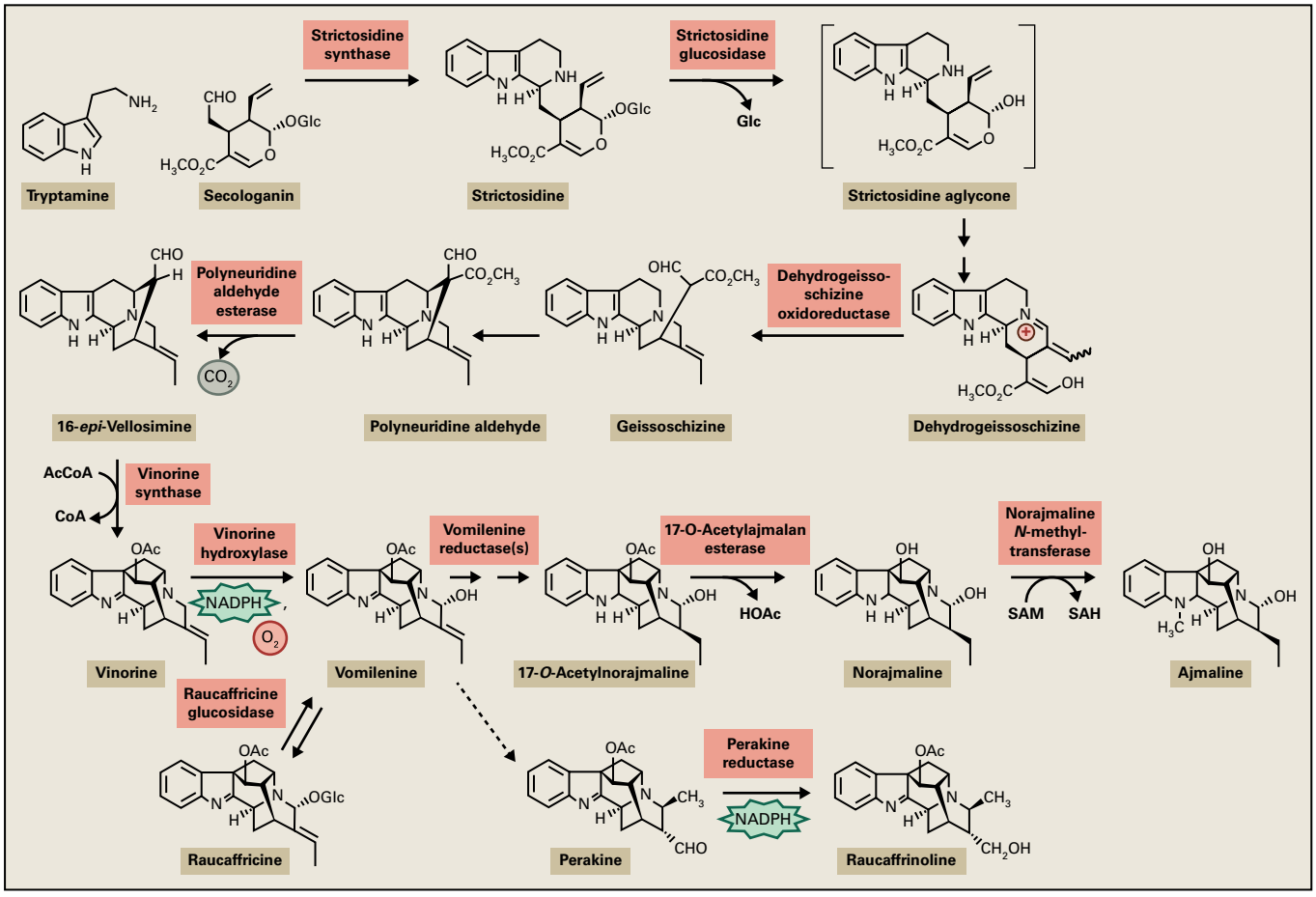


FIGURE 24.40 *The biosynthesis of the antiarrhythmic monoterpenoid indole alkaloid ajmaline in* Rauwolfia serpentina *from tryptamine and secologanin is one of the best-understood alkaloid biosynthetic pathways. Several of the enzymes have been crystallized, and their atomic structures have been determined (Section 24.13.2).*

perakine reductase, polyneuridine aldehyde esterase, and the first enzyme of morphine biosynthesis in the opium poppy to be crystallized, salutaridine reductase (Fig. 24.46).

24.13.3 Metabolic engineering of natural product pathways is the future of plant pharmaceutical biotechnology

Opium, known and used for its medicinal properties, is the air-dried latex (milky exudate) obtained by excision of *Papaver somniferum* capsules after petal fall while the capsules are still unripe (see Fig. 24.26). The exuded latex turns brown due to oxidation and can be scraped off the capsule and formed into a block of crude opium. Opium has been used for thousands of years as an analgesic, a narcotic, and a cough suppressant and has also been smoked for pleasure. Opium contains the morphinan class of alkaloids, which include the analgesic, antitussive drugs morphine and codeine (see Fig. 24.29).

In modern medicine, morphinan alkaloids, of which morphine is the main component, are purified from opium for the pharmaceutical industry. Owing to the commercial importance of morphine and the opium poppy, the biosynthesis of morphine and the ability to metabolically engineer opium poppy have been intensely investigated. Morphine biosynthesis is completely understood at the enzyme level and nearly clarified at the gene level. Opium poppy has been transformed with a number of morphine biosynthetic genes, and regenerated plants have been tested in field trials in Tasmania, a major producer of opium poppy for the pharmaceutical industry.

Synthetic biology is a new area of biological research that combines science and engineering. Although many different definitions exist, synthetic biology is seen as the design and construction of new biological functions and systems not found in nature. It has been applied to the production of isoquinoline alkaloids in bacteria and yeast. Biosynthetic pathways that lead to the central isoquinoline alkaloid biosynthetic precursor, reticuline, have been constructed in *Escherichia coli* and *Saccharomyces cerevisiae* (Fig. 24.47). Genes specific to selected classes of isoquinoline alkaloids, such as the protoberberines, benzo[*c*]phenanthridines, and morphinans, were expressed in these systems and resulted in the accumulation of specific biosynthetic precursors of berberine, sanguinarine, and morphine. Yeast has also been engineered to convert thebaine into morphine and commercially relevant derivatives.

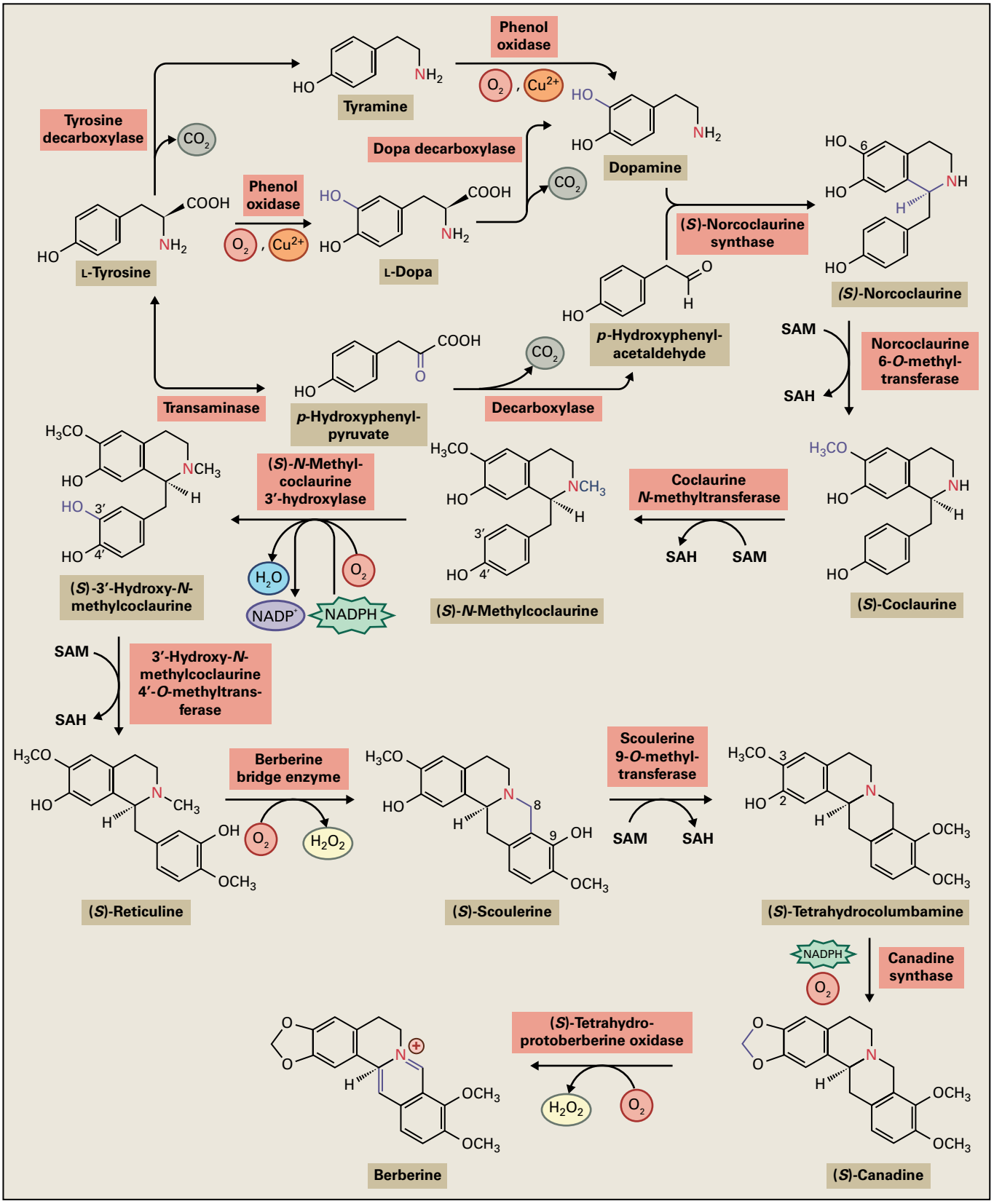


FIGURE 24.41 *Biosynthesis of berberine from two molecules of L-tyrosine. SAM, S-adenosylmethionine; SAH, S-adenosylhomocysteine. (S)-reticuline functions as a branchpoint intermediate in the biosynthesis of tetrahydrobenzylisoquinoline-derived alkaloids (see Fig. 24.42).*

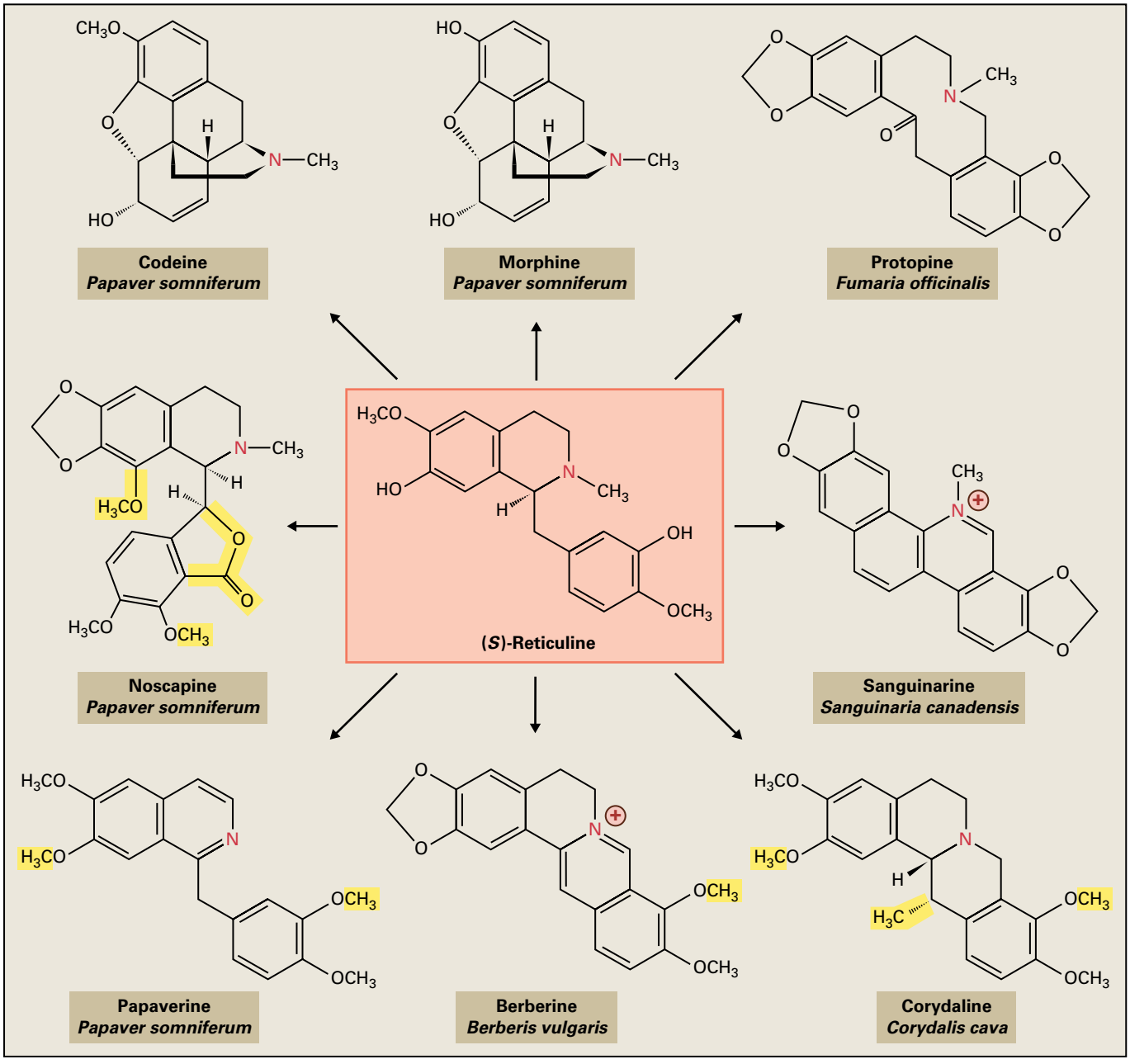


FIGURE 24.42 *(S)-Reticuline has been called the chemical chameleon. Depending on how the molecule is twisted and turned before undergoing enzymatic oxidation, a vast array of tetrahydrobenzylisoquinoline-derived alkaloids of remarkably different structures can be formed.*

Synthetic biology is certain to play an important role in the production of commercially important alkaloids in the future.

The monoterpenoid indole alkaloid family is a structurally diverse group with established therapeutic importance and complex biosynthesis. The chemotherapeutic bisindole alkaloids vinblastine and vincristine of the Madagascar periwinkle (*Catharanthus roseus*) have been targets of biosynthetic and synthetic biology studies. Many of the enzymes and genes of vinblastine and vincristine biosynthesis have been identified and characterized. Using information provided by the atomic structure of strictosidine synthase, an enzyme was engineered to accept unnatural halogenated substrates and produce halogenated monoterpenoid indole alkaloids in transgenic *Catharanthus roseus* hairy root cultures. Bacterial halogenases have been introduced into *Catharanthus roseus* cell- and hairy root cultures together with the modified strictosidine synthase to generate a synthetic system that accumulates halogenated monoterpenoid indole alkaloids of complex structure, such as 10-chloro-ajmalicine, 10-chloro-catharanthine and 15-chloro-tabersonine (Fig. 24.48).

The design of these alternative systems and optimized plants requires molecular manipulation, which in turn requires knowledge of alkaloid biosynthetic pathways at the enzyme level. Much progress has been made with selected alkaloids, but much remains to be discovered about the enzymatic synthesis of pharmaceutically important alkaloids such as camptothecin, colchicine, and quinine to name only a few examples. With the advent of next generation sequencing

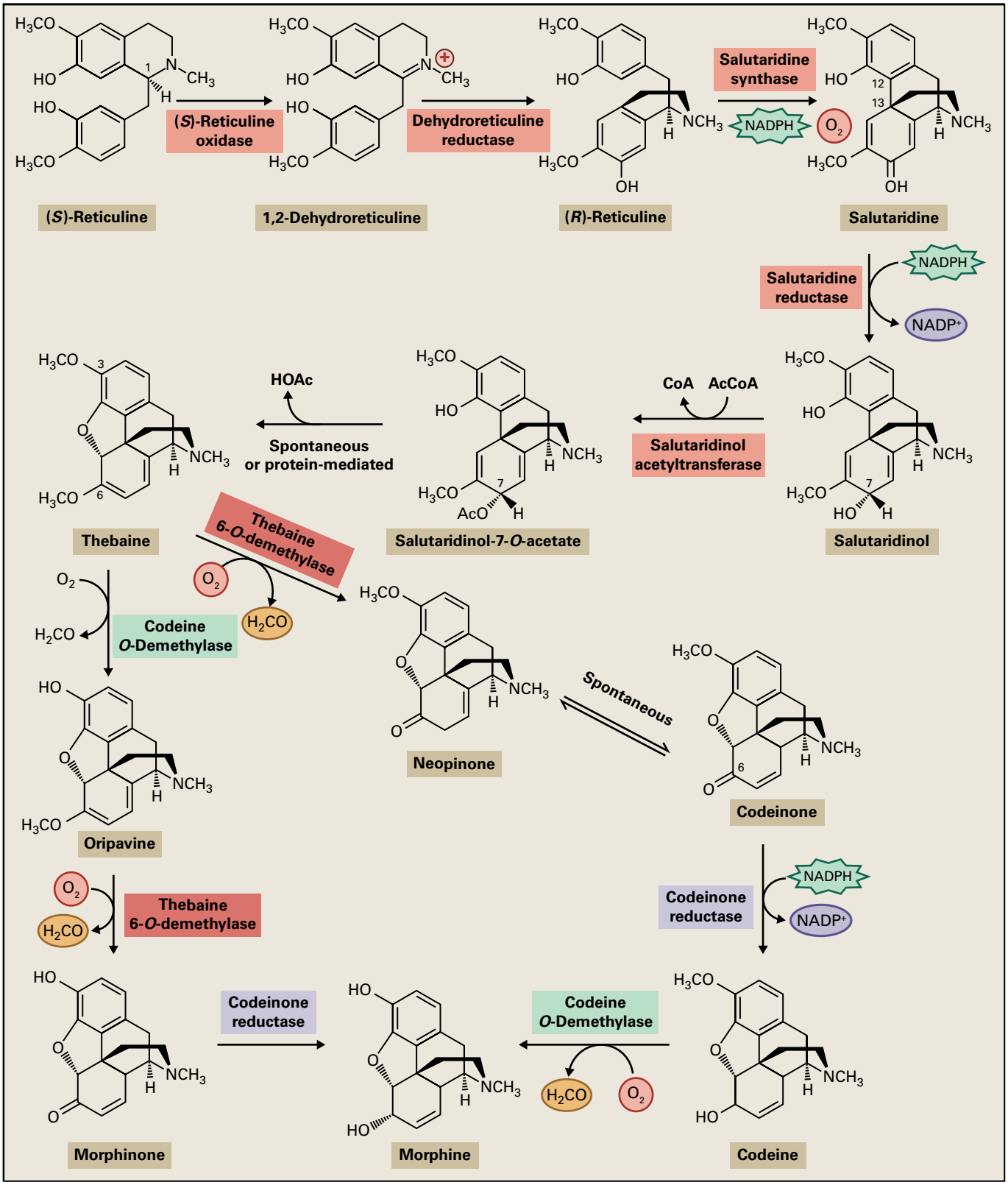


FIGURE 24.43 *The isolation and characterization of all of the enzymes of morphine biosynthesis is complete more than 200 years after the discovery of the alkaloid. Most of the cDNAs that encode enzymes of morphine biosynthesis have also been characterized. The discovery that mammals can also synthesize morphine has tremendous implications concerning the evolutionary development of the opiate receptor in animals and humans (see Box 24.9). Enzymes are color-coded to indicate that they can act at two points in the pathway, resulting in a metabolic grid between thebaine and morphine.*

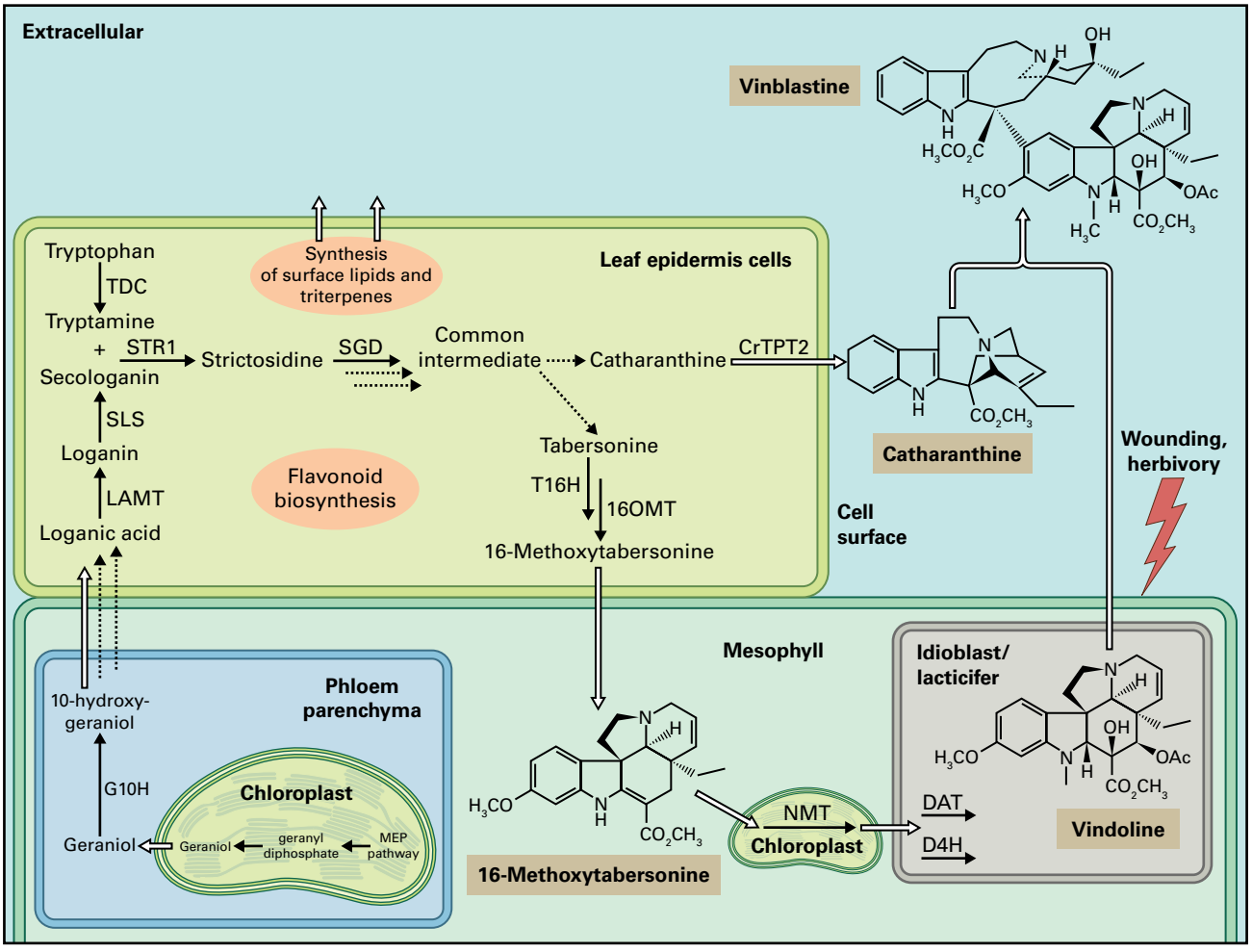


FIGURE 24.44 *The biosynthesis of monoterpenoid indole alkaloids in the Madagascar periwinkle (*Catharanthus roseus*) involves multiple subcellular compartments and cell types. The cytochrome P450-dependent enzymes in the pathway (G10H, SLS, T16H) are associated with the endoplasmic reticulum. Strictosine synthase (STR1) is vacuolar. O-Methyltransferases (such as LAMT and 16OMT) are typically localized to the cytosol, as are the acetyltransferase DAT and the oxoglutarate dependent dioxygenase D4H. The terpenoid biosynthetic intermediate geraniol is formed in the chloroplast, and the N-methyltransferase (NMT) is localized to the plastid. The biosynthetic pathway that leads to 10-hydroxgeraniol occurs in phloem parenchyma, while subsequent steps that lead to catharanthine and 16-methoxytabersonine are localized to leaf epidermal cells. Catharanthine is then transported to the cell surface by the ABC transporter CrTPT2, while 16-methoxytabersonine is transported to the mesophyll, where it is further modified and eventually transported into idioblast and laticifer cells, the sites of vindoline accumulation. The bisindole alkaloid vinblastine, which is formed by oxidative coupling of catharanthine and vindoline, is formed upon injury of leaf tissue by wounding or herbivory. G10H, geraniol 10-hydroxylase; LAMT, loganic acid O-methyltransferase; TDC, tryptophan decarboxylase; STR1, strictosidine synthase; SLS, secologanin synthase; SGD, strictosidine glucosidase; T16H, tabersonine 16-hydroxylase; 16OMT, 16-hydroxytabersonine 16-O-methyltransferase; NMT, 16-methoxytabersonine N-methyltransferase; DAT, deacetylindoline O-acetyltransferase; D4H, desacetoxyvindoline 4-hydroxylase; ABC transporter, ATP-binding cassette transporter.*

(Fig. 24.37) and single-cell analytics, the rate at which new biosynthetic genes are identified is certain to increase in the coming years.

As genes are isolated, we can anticipate that heterologous expression systems will continue to be developed in plant, bacterial, yeast, and insect cell culture systems to allow production of single enzymes and pathways for biomimetic syntheses of alkaloids. Our understanding of how the expression of alkaloid biosynthesis genes is regulated by elicitors or in specific tissues will also improve as the promoters of alkaloid biosynthetic genes are analyzed. The future will bring more genetically engineered microorganisms and eukaryotic cell cultures that produce alkaloids, metabolically engineered plants with tailored alkaloid spectra and enzymatic synthesis of novel alkaloids through combinatorial biochemistry.

24.14 Phenolic compounds

24.14.1 Plants contain a remarkably diverse array of phenolic compounds

The transition of early vascular plants to a terrestrial habitat was successful in large part because of the development and elaboration of a diverse group of compounds known generally

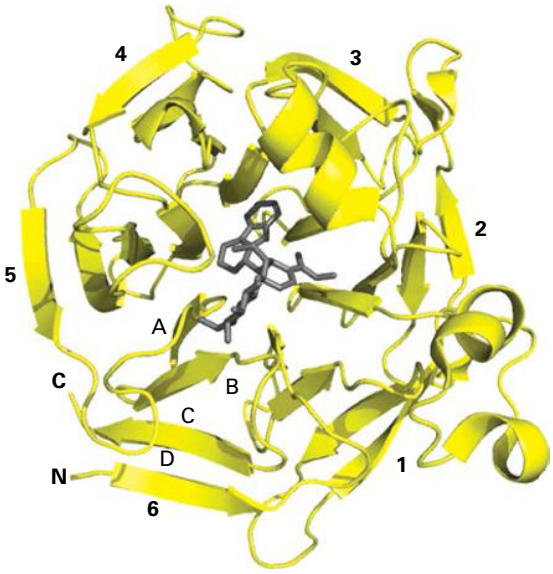


FIGURE 24.45 *The structure of strictosidine synthase (β-propeller fold) is shown in complex with strictosidine in stick presentation (gray). The six blades of the propeller are indicated by numerals, the four β-sheets of a blade by A, B, C, D, and the N- and C-termini by nitrogen and carbon. Structure-based sequence alignment reveals a common repetitive sequence motif that suggests an evolutionary relationship between strictosidine synthase and several sequence- and functionally unrelated six-bladed β-propeller structures that include diisopropylfluorophosphatase from* Loligo vulgaris*, brain tumor NHL domain, serum paraoxonase, and the low-density lipoprotein receptor YWTD domain.*

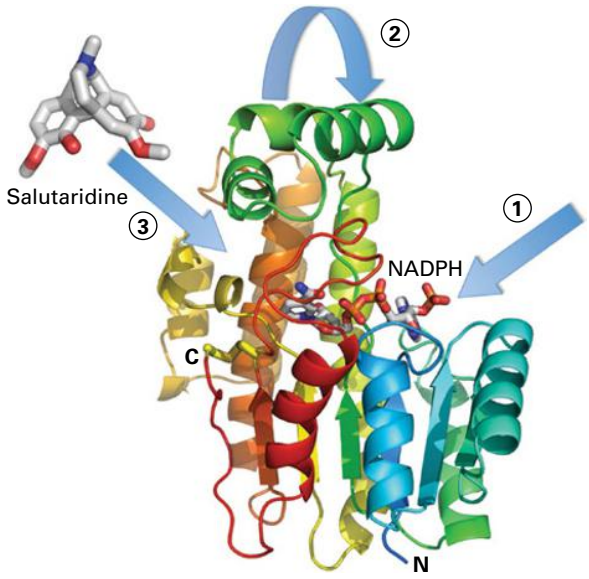


FIGURE 24.46 *The core salutaridine reductase structure is highly homologous to other members of the short chain dehydrogenase/ reductase family. The major difference is that the cofactor NADPH and the substrate-binding pocket are covered by a loop, on top of which lies a large "flap"-like domain. This configuration appears to be a combination of the two common structural themes found in other members of the short chain dehydrogenase/ reductase family. The ribbon, colored from blue to red, indicates the progression of the amino acid chain from the N- to the C-terminus. The bound NADPH is represented by a stick figure. (1) The cofactor NADPH binds to the enzyme, (2) the flap over the catalytic site changes the conformation of the enzyme, and (3) the substrate salutaridine then enters the active site and reduction of the carbonyl moiety to a hydroxyl group occurs.*

as "phenolics." Although the majority of phenolics are structural components of cell walls, a vast array are the toxins and antifeedants of plant defense, coloring agents of flowers and fruits, aroma complement of plant organs (such as flower scents and fruit flavors), and antioxidants of wood, bark, and seeds. These and other functions performed by plant phenolics are essential for the continued survival of vascular plants.

Plant phenolics vary greatly in size and complexity, but all generally possess (or are derived from compounds that once possessed) an aromatic arene (phenyl) ring with at least one hydroxyl group attached (Fig. 24.49). The phenolic hydroxyl group is acidic compared to other hydroxyl groups because it resides on an arene ring, which can readily stabilize a deprotonated oxygen substituent. As a result, plant phenolics are reactive and well suited to being the building blocks of large polymers, such as lignins or suberins, and in the generation of a large number of compounds that play important roles in many aspects of plant biology.

Phenolic compounds can be classified in various ways, for example according to the functional groups attached to the phenol, or based on the number of phenol units in the molecule. Major subclasses of phenolic compounds include the flavonoids, anthocyanidins, isoflavones, chalcones, stilbenes, coumarins and furanocoumarins, monolignols and lignans, naptha- and anthraquinones, and diarylheptanoids.

24.14.2 Evolution of phenolics helped plants overcome the challenges of a terrestrial environment

Phenolic compounds account for approximately 40% of organic carbon in plants and are derived primarily from **phenylpropanoid** and **phenylpropanoid-acetate** backbones (Fig. 24.50), although related biochemical pathways, such as those leading to "hydrolyzable" tannins, also contribute. The phenylpropanoid and phenylpropanoid-acetate pathways, discussed in more detail later in this chapter, produce products that ameliorate the challenges that faced early land plants. These challenges persist and provide selection pressure to maintain the phenylpropanoid pathway in plants (Table 24.2).

Evolution of the phenylpropanoid-acetate pathway, present in the most primitive of land plants as well as in many algae, helped overcome the first of these challenges, damaging UV irradiation, which was faced by plants even before they left the water. This pathway leads to production of a large and diverse class of compounds called **flavonoids**, which has more than 5,000 members. Flavonoids, such as quercetin

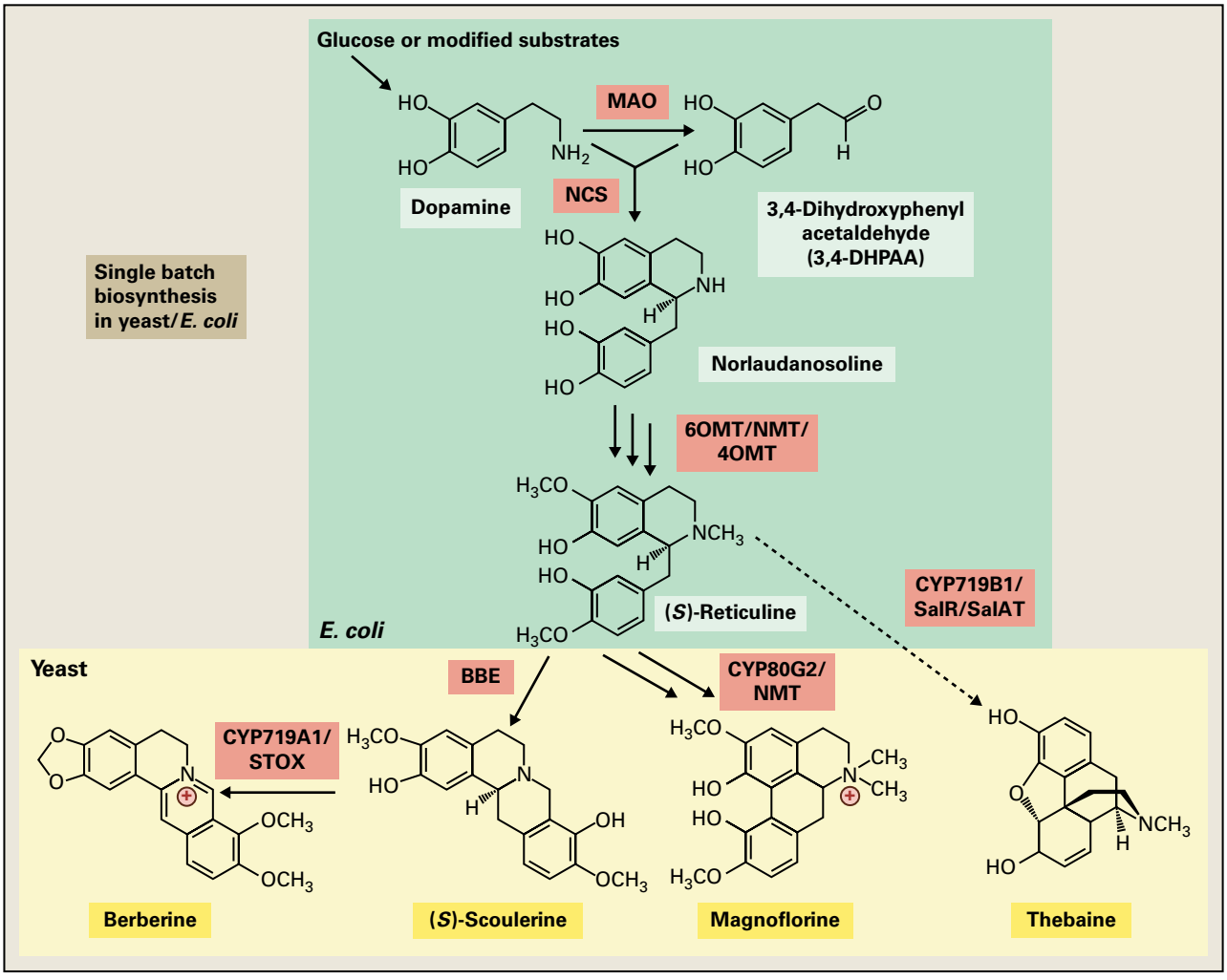
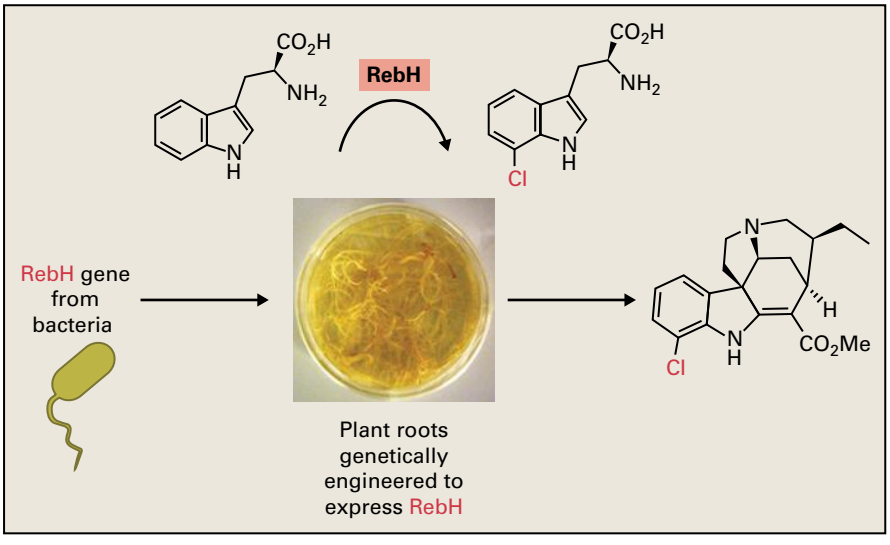


FIGURE 24.47 *Bacteria and yeast have been engineered with a combination of plant and animal genes to produce isoquinoline alkaloids, such as the protoberberine alkaloid berberine and the aporphine alkaloid magnoflorine. Microbial production of the morphine precursor thebaine has not yet been achieved, but this is an attractive target due to commercial importance in the synthesis of pharmaceutically relevant opiates. Yeast has been engineered, however, to produce morphine from thebaine. MAO, Monoamine oxidase; NCS, norcoclaurine synthase; 6OMT, norcoclaurine 6-O-methyltransferase; NMT, coclaurine* N*-methyltransferase; 4′OMT, 3′-hydroxy-*N*-methylcoclaurine 4′-O-methyltransferase; BBE, berberine bridge enzyme; CYP719A1, canadine synthase; STOX, (S)-tetrahydroprotoberberine oxidase; CYP80G2, corytuberine synthase; CYP719B1, salutaridine synthase; SalR, salutaridine reductase; SalAT, salutaridine acetyltransferase. Single batch biosynthesis here means a co-culture of yeast and the bacterium* Escherichia coli.

FIGURE 24.48 *The product of the gene* rebH *from the antitumor agent rebeccamycin biosynthetic cluster in the soil bacterium* Lechevalieria aerocolonigenes *incorporates halogen in the conversion of* L*-tryptophan into 7-chlorotryptophan.* rebH *was introduced into root cultures of the medicinal plant* Catharanthus roseus *and resulted in the generation of novel halogenated monoterpenoid indole alkaloids.*
Source: O'Connor, John Innes Centre, Norwich, UK.



(Fig. 24.50), consist of a basic three-ring core structure that is modified to produce subclasses (Fig. 24.51), such as the anthocyanins (pigments), proanthocyanidins or condensed tannins (feeding deterrents and wood protectants), isoflavonoids (active in plant defensive and signaling), and flavones and flavonols (anti-inflammatory agents in animals). The most basic flavonoids—the flavones, flavonols, and flavanones—are widespread in the plant kingdom and typically absorb damaging UV rays.

The second challenge was a desiccating environment. This was overcome not only by development of cutin and the cuticle on the epidermis (derived from fatty acid pathways, see Chapter 9), but also by the advent of the phenylpropanoid pathway and development of a class of compounds known as **suberins** (see Chapter 8), which are mixed polymers of phenolic (more hydrophilic) and aliphatic (hydrophobic) moieties. Suberin plays a critical role in the periderm of roots and in bark by providing a hydrophobic barrier to prevent water loss. A major component of cork, it also provides a physical barrier that inhibits attack by pathogens.

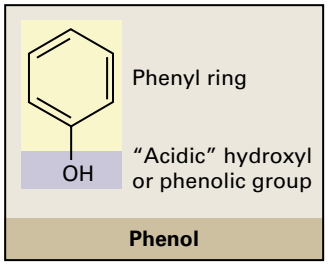


FIGURE 24.49 *Structure of phenol.*

The third challenge, the opposing forces of gravity and the need to grow taller to outcompete competitors for sunlight, was overcome by further elaboration of the phenylpropanoid pathway and development of **lignin** (see Chapter 2). Lignin is a crosslinked macromolecule made up of monolignol monomers (see Section 24.17). It provides the "cement" to cellulose's rod-like structure in specialized cell walls, such as fibers, tracheids, and vessels to enable plants to support their weight on land and transport water and minerals from roots to leaves, even in the tallest of trees.

Another challenge that plants continue to face is the need to deter herbivores and pathogens while maintaining a sessile growth habit. This has been achieved by elaboration of several other subclasses of compounds that provide a chemical defense by being antiherbivory, insecticidal, antifungal, bactericidal

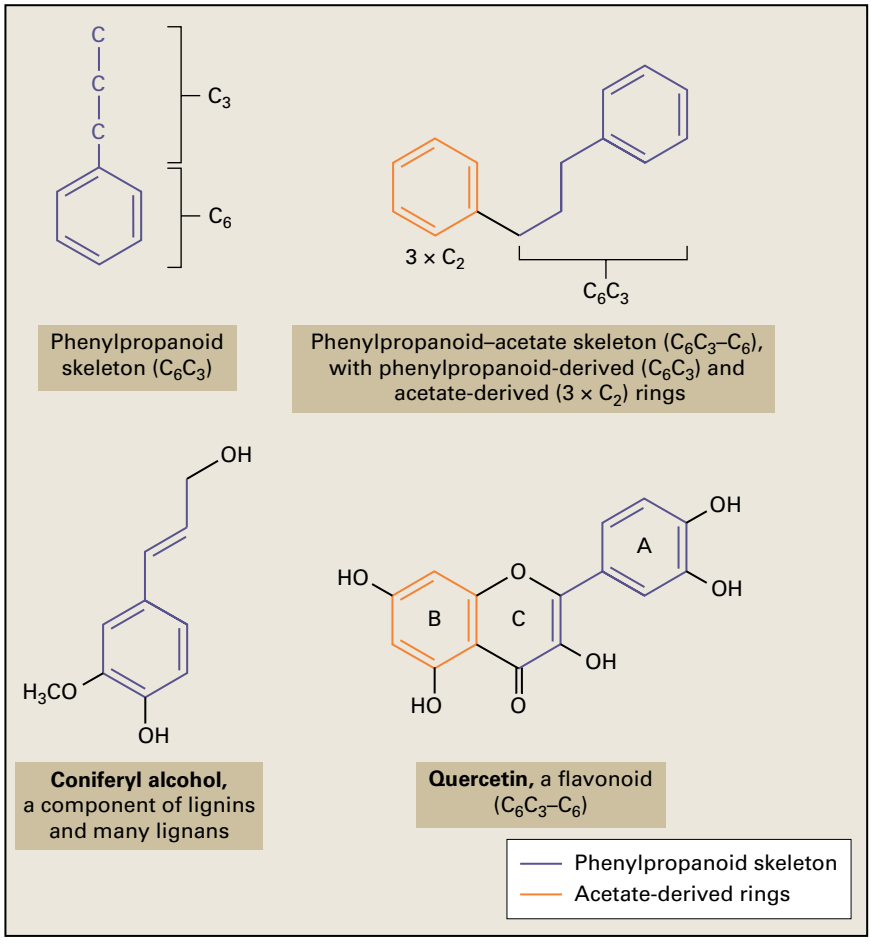


FIGURE 24.50 *Phenylpropanoid and phenylpropanoid-acetate and skeletons and representative plant compounds based on those structures. Flavonoids, such as quercetin, typically have three interconnected rings at their core, the A, B, and C rings. Modifications to the C ring are responsible for creation of new classes of compounds, whereas modifications to the A and B rings lead to diversification within the compound class.*

TABLE 24.2 *Roles of phenolics against environmental challenges.*

Challenge	Phenolic compounds	Pathway
UV irradiation	Flavonoids (anthocyanins, proanthocyanidins, condensed tannins, isoflavonoids, flavones, flavonols, etc.)	Phenylpropanoid-acetate
Desiccation	Suberins	Phenylpropanoid-fatty acid
Gravity	Lignins	Phenylpropanoid
Herbivores/pathogens	Stilbenes, coumarins, furanocoumarins	Phenylpropanoid-acetate
	Diarylheptanoids, gingerols, phenylphalenones, lignans, volatile aromatics	Phenylpropanoid-acetate
	Hydrolyzable tannins	Shikimate

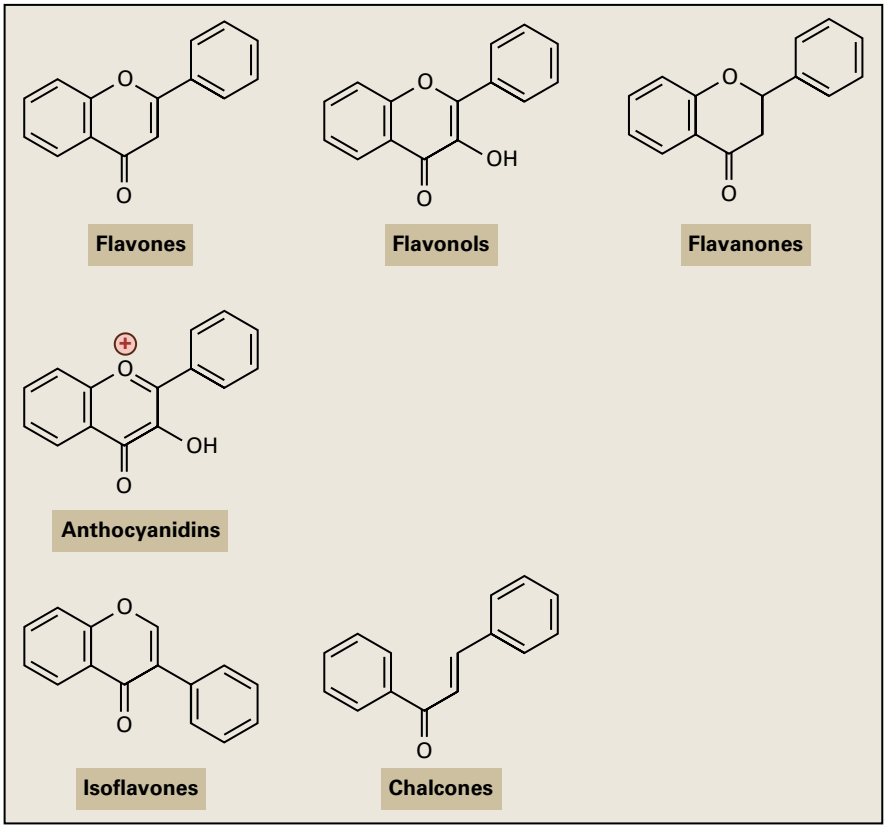
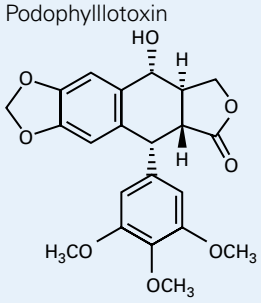
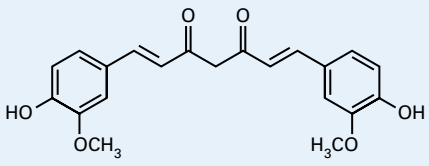
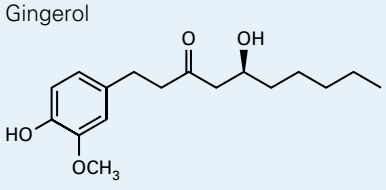
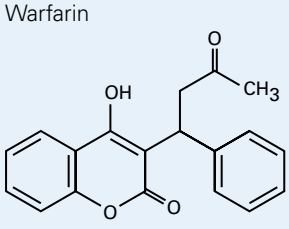
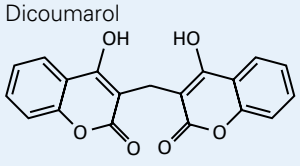
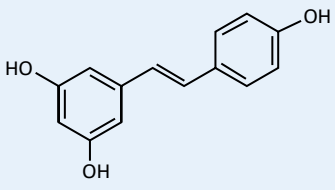


FIGURE 24.51 *Basic structures of phenylpropanoid-acetate-derived subclasses of flavonoids.*

and bacteriostatic, allelopathic, or otherwise toxic in nature. As examples, the **stilbenes**, **coumarins**, and **furanocoumarins** are phenylpropanoid-acetate-derived compounds that discourage herbivory, inhibit seed germination, or deter bacterial or fungal pathogens. Some, such as resveratrol, also have important human health-enhancing properties (see Section 24.14.3).

Other phenylpropanoid-derived compounds, such as the **diarylheptanoids** and allies such as **gingerols** and **phenylphalenones**, impart colors, organoleptic properties, and medicinal value to humans (see Section 24.14.3), but also play defensive roles or act as pollinator or seed disperser attractants in diverse groups of plants. **Lignans**, the dimers or higher order oligomers of monolignols, are not believed to share the extensive polymerization that occurs in lignins and suberins, are widespread throughout the vascular plants and serve mainly defensive roles by protecting against pathogens or acting as antioxidants in all plant tissues. **Volatile aromatics** derived from the phenylpropanoid pathway, such as phenylacetaldehyde and eugenol, function in pollinator attraction, seed dispersal, and protection from herbivory and pathogen attack. Such compounds also contribute to the aromas and flavors that make spices such highly prized plant products the world over.

TABLE 24.3 *Societal uses of plant phenolics.*

Phenolic compound	Plant source	Use
Lignans		
Podophylllotoxin 	May apple (*Podophyllum peltatum*)	Derivatized to form cancer-treating drugs
Diarylheptanoids		
Curcumin 	Turmeric rhizome (*Curcuma longa*)	Anti-inflammatory, pungent component of turmeric
Gingerol 	Ginger rhizome (*Zingiber officinale*)	Anti-inflammatory, pungent component of ginger
Coumarins		
Warfarin 	Synthetic derivative of dicoumarol	Anticoagulant
Dicoumarol 	Sweet clover (*Melilotus* sp.)	Anticoagulant produced by fermentation of sweet clover
Stilbenes		
Resveratrol 	Skins of red grapes (*Vitis* sp.)	Improves heart health, deters cancer development

(*continued*)

TABLE 24.3 (*continued*)

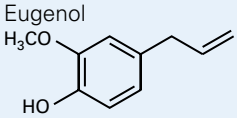
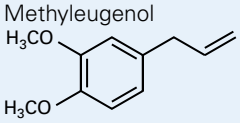
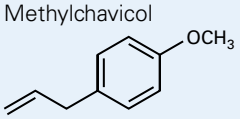
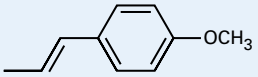
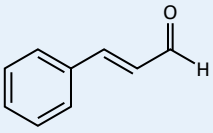
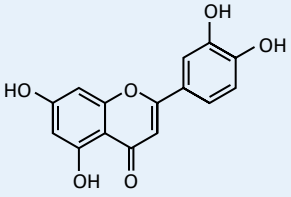
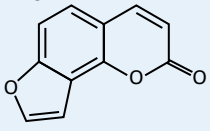
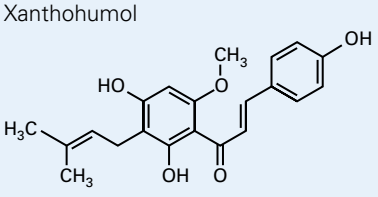
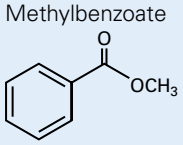
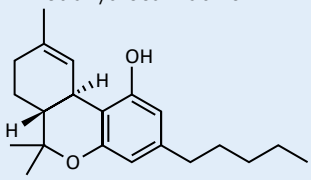
Phenolic compound	Plant source	Use
Phenylpropenes		
Eugenol 	Essential oils from cloves (*Eugenia* sp.) and other plants	Fragrance, flavoring, and bactericidal used in dentistry
Methyleugenol 	Essential oils from basil (*Ocimum basilicum*)	Fragrance and flavoring
Methylchavicol 	Essential oil from basil (*Ocimum basilicum*)	Licorice flavor
Anethole 	Star anise (*Illicium verum*)	Anise flavor
Cinnamaldehyde 	Cinnamon bark (*Cinnamomum verum*)	Spice
Flavones		
Luteolin 	Mint leaves (*Mentha* sp.)	Antioxidant
Furanocoumarins		
Angelicin 	Pitch trefoil (*Bituminaria bituminosa*)	Potential phototherapeutic, antiviral
Chalcones		
Xanthohumol 	Hops (*Humulus lupulus*)	Anticancer

TABLE 24.3 (*continued*)

Phenolic compound	Plant source	Use
Benzenoids		
Methylbenzoate 	Snapdragon flower (*Antirrhinum* sp.)	Fragrance
Polyketides*		
Δ^9-Tetrahydrocannabinol 	Marijuana (*Cannabis sativa*)	Antiemetic

*A large class of diverse polymeric compounds that are characterized by more than two carbonyl groups connected by single intervening carbon atoms.

24.14.3 Phenolics are beneficial to humans

Human societies would not exist in their present form without the properties imparted by phenolic compounds (Table 24.3). Leather, which throughout early human history enabled more rapid transportation and thereby better trade (and war), has been produced for millennia by treating raw animal hides with "tannins," either **gallate esters** or **condensed tannins** (see Section 24.16.2). The wheel was perfected because of the properties of wood, the strength and durability of which can be attributed to the lignin polymers and lignans, flavonoids, and hydrolyzable tannins. Much of the world relies on wood for building as well as a fuel to provide warmth; we are now turning to wood products as a source of lignocellulosic materials for biofuel production. As alternatives to dwindling natural resources are sought, plants, based in part on the phenolics that they contain, are among the best choices for renewable industrial feedstocks and materials.

Human health is also intimately tied to this class of compounds, as many medicinal compounds are derived or inspired by plant phenolics. Examples include the lignan **podophyllotoxin** from May apple (*Podophyllum peltatum*), which is derivatized to form teniposide, etoposide, and etophos, used to treat a number of cancers; the diarylheptanoid **curcumin** from turmeric (the curry spice), which has potent anti-inflammatory properties and is used worldwide to treat arthritis and other inflammatory diseases; and the stilbene **resveratrol** from red grapes and wine, which has been demonstrated to improve heart health and deter cancer development. The world is a healthier, more colorful, tasty, and fragrant place because of the phenolics that plants produce.

24.15 Phenolic biosynthesis

24.15.1 The phenylpropanoid and phenylpropanoid-acetate pathways share a common core phenylpropanoid pathway

As mentioned in the previous section, most phenolics originate from the phenylpropanoid and the phenylpropanoid-acetate pathways. Both the phenylpropanoid and phenylpropanoid-acetate pathways share the first three biochemical steps, the core **phenylpropanoid pathway** (Fig. 24.52). These steps begin with an L-phenylalanine precursor and end with the formation of 4-coumaroyl CoA, a reactive compound that can participate in further reactions that lead to the wealth of compounds that are the plant phenolics.

24.15.2 L-Phenylalanine is the precursor for most plant phenolics

The obvious choices for primary metabolites that might lead into these pathways are L-phenylalanine (Phe) and L-tyrosine (Tyr) (Fig. 24.53). Decades of research have established that L-Tyr, although it has a 4-hydroxyl group, is not the precursor of most plant phenolics. Numerous labeling studies, in which radiolabeled or stable isotopically labeled compounds were "fed" to plants to monitor formation of phenolics and incorporation rates of the labeled compounds, have shown that L-Phe is the preferred precursor in most cases. L-Phenylalanine is synthesized through the shikimate pathway (see Chapter 7).

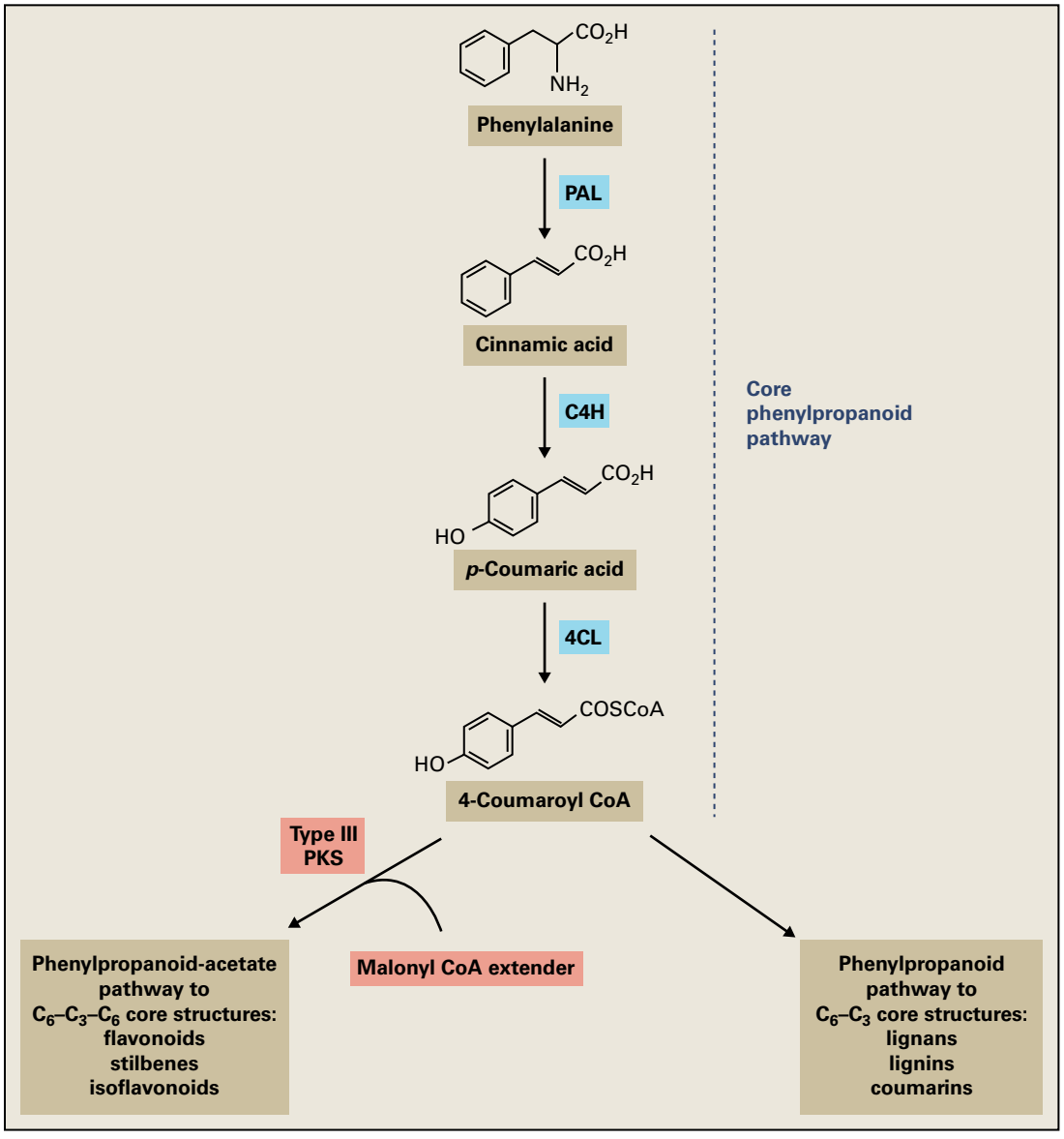


FIGURE 24.52 *Overview of the biosynthetic pathways contributing to the production of several of the major subclasses of phenolic compounds in plants. Synthesis begins with L-phenylalanine and diverges into the phenylpropanoid-acetate and phenylpropanoid pathways. Both pathways share the first three steps, the core phenylpropanoid pathway, which ends with the formation of 4-coumaroyl CoA.*

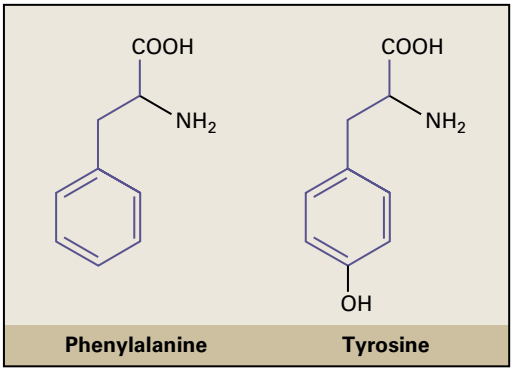


FIGURE 24.53 *The aromatic amino acids phenylalanine and tyrosine are derivatives of the shikimic–chorismic acid pathway (see Chapter 7).*

24.15.3 Phenylalanine ammonia lyase is the entry point enzyme to most plant phenolics

Phenylalanine ammonia lyase (PAL) catalyzes the first step in phenylpropanoid metabolism in which L-Phe undergoes deamination to yield ***trans*-cinnamate** and ammonia. The ammonia generated by PAL spontaneously becomes protonated in the cytosol to form NH_4^+ (Fig. 24.54).

PAL was one of the first enzymes identified, and is one of the best-studied in phenylpropanoid metabolism. The elucidation of the crystal structure of the PAL from parsley (*Petroselinum crispum*) has helped elucidate the function and regulation of this protein. A cytosolic protein, PAL belongs to

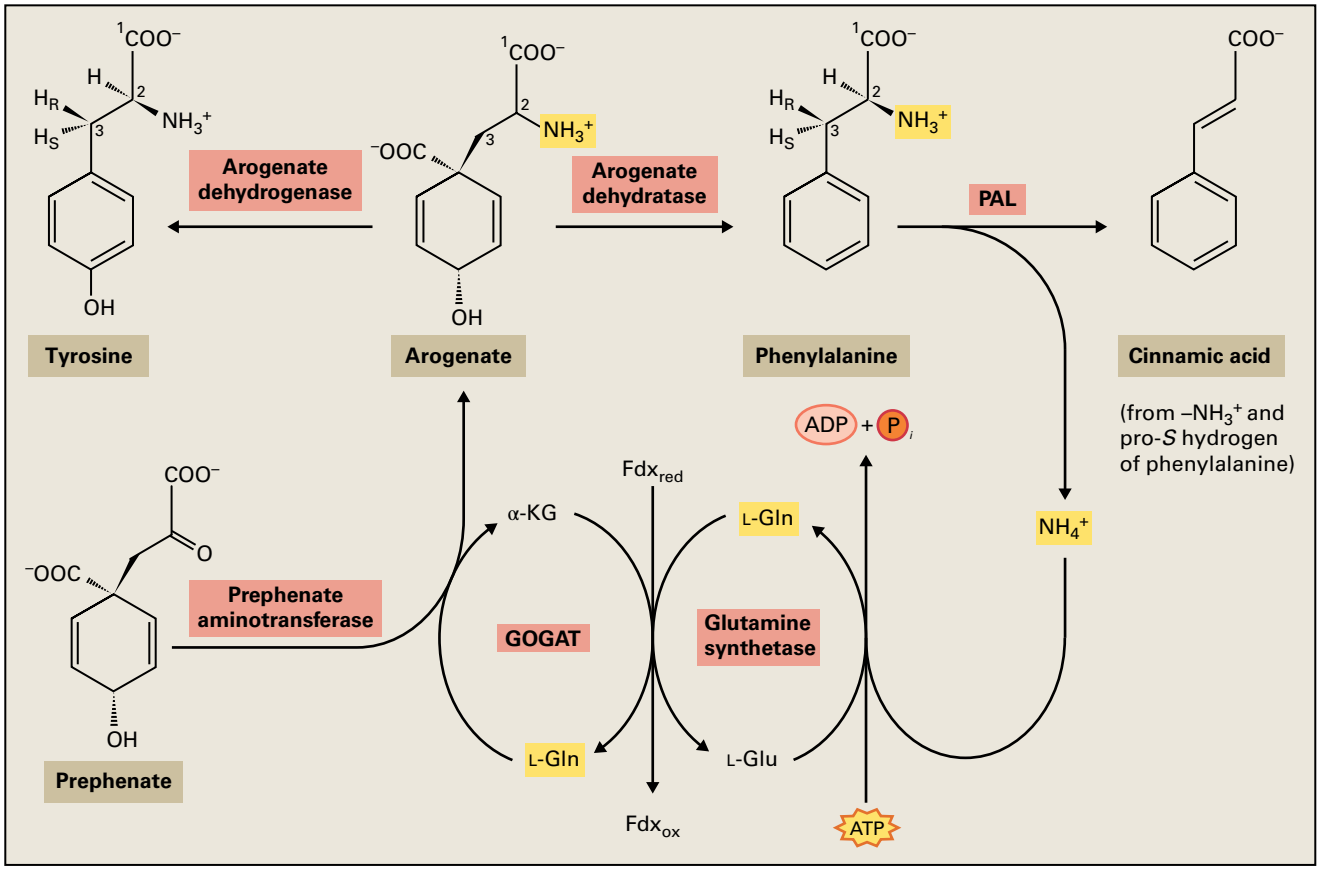


FIGURE 24.54 *The nitrogen cycle present in cells is actively engaged in phenylpropanoid-acetate/phenylpropanoid metabolism. It prevents accumulation of ammonia and eliminates the requirement for N during phenolic synthesis. GOGAT, glutamine: α-ketoglutarate aminotransferase; L-Gln, glutamine; L-Glu, glutamate; α-KG, α-ketoglutarate; Fdx_{red}, reduced ferredoxin; Fdx_{ox}, oxidized ferredoxin.*

the histidine ammonia lyase (HAL) gene family, which is widespread in plants, fungi, microbes, and animals. The enzymes in this family consist mostly of α-helices, exist as tetramers in solution, and require no exogenous cofactors.

Most PAL isoforms do not efficiently utilize any substrate other than L-Phe, supporting the role of L-Phe as the general precursor for the phenylpropanoid and phenylpropanoid-acetate pathways. Most plants have several PAL genes, ranging from four in *Arabidopsis thaliana* to close to two dozen in some rare instances, such as cultivated tomato (*Solanum lycopersicum*). These genes exist as a small gene family and are differentially expressed throughout plant development, leading to specific roles for specific PAL isoforms. In most plants, as in *Arabidopsis thaliana* and poplar (*Populus* sp.), all PAL isoforms utilize L-Phe almost exclusively, with L-Tyr being either a very poor substrate, or not a substrate. Different isoforms or gene family members appear to play different roles in the plant. For example, although PAL1, PAL2, and PAL4 from *A. thaliana* are believed to be involved in lignin biosynthesis, only PAL1 and PAL2 are thought to play a role in providing precursors for flavonoid and sinapate ester biosynthesis. PAL4 has no role in flavonoid biosynthesis; PAL3 has poor activity, and its actual role in the plant has not been established. PAL1 and PAL2 may act redundantly, or may play distinct roles under normal conditions, but they can substitute for each other when either is mutated. Single knockout mutations in either have no apparent phenotype, but a double *pal1/pal2* mutation causes severe growth defects and dramatic reduction in lignin, flavonoid, and sinapate ester formation.

24.15.4 Conversion of L-Phe into cinnamate requires a subcellular nitrogen cycle

The availability of L-Phe can determine flux into the phenylpropanoid and phenylpropanoid-acetate pathways. The phenylpropanoid pathway contributes to the deposition of a large amount of organic carbon produced from the conversion of the amino acid L-Phe into cinnamate. An equimolar amount of nitrogen is released by PAL in the form of NH_4^+ (Fig. 24.54), which is toxic at high concentrations. Moreover, production of polymers such as lignin requires a very high demand for nitrogen. A nitrogen cycle within plant cells that utilizes glutamine synthetase and glutamate synthetase (GS and GOGAT; see Chapter 7) to produce glutamate ensures that sufficient flux through L-Phe is possible.

Glutamate is the amino donor in the reaction that forms arogenate from prephenate (Fig. 24.54). NH_4^+ is released by PAL in

the cytosol, but formation of arogenate occurs in the plastid, so transport of NH_4^+ is a critical component of this cycle; the transporter involved, however, has not yet been characterized.

24.15.5 Cinnamate-4-hydroxylase (C4H) is a membrane-bound cytochrome P450 monooxygenase that produces *p*-coumarate

The second enzyme in the core phenylpropanoid pathway is cinnamate 4-hydroxylase (C4H) (see Fig. 24.52), an ER membrane-bound cytochrome P450 monooxygenase that produces 4-coumarate (***p*-coumarate**). C4H, which belongs to the CYP73A class of P450 enzymes, typically exists as a single gene in most angiosperms, although some plants have one to three additional C4H-like enzymes. *Arabidopsis* has only one C4H, whereas the moss *Physcomitrella patens* has four CYP73A genes. C4H requires molecular oxygen and a cytochrome P450 reductase for activity, and is specific for *trans*-cinnamate. C4H is regiospecific as well, with hydroxylation only occurring at the 4-position (or *para* position) on the aromatic ring.

Because the carboxylate functional groups of both cinnamate and *p*-coumarate have a pKa value of 4, these two critical pathway intermediates exist as deprotonated forms under physiological conditions (hence use of the names cinnamate and *p*-coumarate instead of cinnamic acid and *p*-coumaric acid); because they are negatively charged under physiological conditions, these otherwise hydrophobic molecules remain soluble in the aqueous environment of the cell (solubilities of ≈3 mM and 165 mM, respectively, in water), making it possible for them to accumulate to high concentrations. However, both metabolomics based and targeted metabolite analyses have demonstrated that these molecules do not accumulate in most plant tissues and, if detectable, are found only at low concentration.

C4H has a high affinity towards *trans*-cinnamate (K_m of ≈10 μM). Other enzymes that utilize this substrate have a much higher K_M, such as cinnamate carboxylmethyl transferase (125–200 μM). This differential substrate affinity effectively shunts metabolite flux toward *p*-coumarate unless or until C4H activity is reduced, thereby allowing for formation of alternative products. This type of regulation appears to be active in formation of volatile phenylpropanoids versus phenylpropanoid-acetate derived flavonoids in specific cell types, such as some glandular trichome secretory cells.

24.15.6 Coumarate CoA ligase (4CL) activates *p*-coumarate

The third enzyme of the core phenylpropanoid pathway, 4-coumarate CoA ligase (4CL, see Fig. 24.52), utilizes *p*-coumarate, ATP, and coenzyme A to form the CoA thioester derivative, ***p*-coumaroyl-CoA**, a highly activated molecule that resides at a critical position in the greater plant metabolic network (Fig. 24.55). *p*-Coumaroyl-CoA is the substrate for chalcone synthase (CHS), the first committed step in the phenylpropanoid-acetate pathway, and for hydroxycinnamoyl transferase (HCT), the first committed step in the phenylpropanoid pathway to G lignin, S lignin, selected lignans, and volatile phenylpropenes. *p*-Coumaroyl-CoA is also precursor to a suite of other phenolic compounds that result from branches of the greater network, including the diarylheptanoids, phenylphalenones, hydroxycinnamyl amides, and coumarins (see Fig. 24.52).

Availability and competition for *p*-coumaroyl-CoA determine the abundance of entire classes of phenolic compounds. Thus, *p*-coumaroyl-CoA serves the function of a metabolic hub (see Section 24.18.4). The phenylpropanoid pathway, in fact, diverges from the phenylpropanoid-acetate pathway by differential utilization of the common hub intermediate, *p*-coumaroyl-CoA (see Section 24.16).

Plants contain a small family of 4CL genes; for example, *Arabidopsis* has seven 4CL and 4CL-like genes. Depending on the species, the corresponding enzymes have various substrate selectivities. The best-studied 4CL enzymes are from tobacco (*Nicotiana tabacum*), which has uncharacterized 4CL-like genes and four known 4CL genes, with slightly differing substrate selectivity.

24.16 The phenylpropanoid-acetate pathway

The phenylpropanoid-acetate and phenylpropanoid pathways diverge through differential utilization of *p*-coumaroyl-CoA (see Fig. 24.52 and Fig. 24.55). The phenylpropanoid pathway culminates in formation of compounds with a C_6–C_3 core, hence the term phenylpropanoid (see Fig. 24.50). These compounds include the monolignols, which are then used in the synthesis of lignins and the structurally and biosynthetically related lignans (see Section 24.17). The phenylpropanoid-acetate pathway, on the other hand, culminates in the formation of products that are built up of a C_6–C_3–C_6 core structure and include the flavonoids and diarylheptanoids (Fig. 24.56). Flavonoids were most likely the first complex phenolic compounds produced by plants; the monolignols, lignans, and lignins likely evolved later.

24.16.1 Products of the phenylpropanoid-acetate pathway are called polyketides, and plant polyketide synthases (PKSs) are the catalysts of polyketide diversity

Products of the phenylpropanoid-acetate pathway are called polyketides because of the manner in which they are synthesized. The pathway originated when type-III polyketide

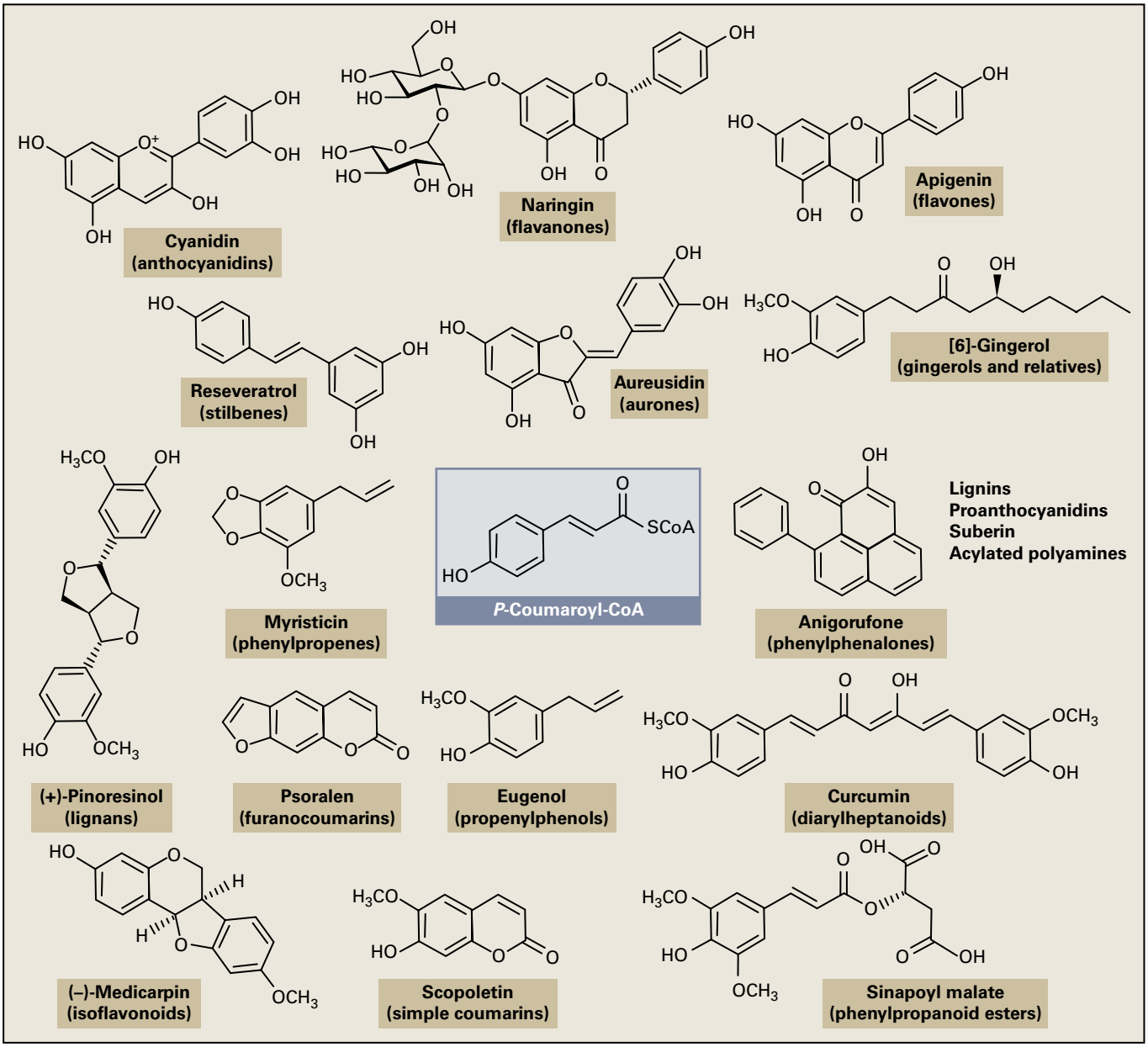


FIGURE 24.55 p-*Coumaroyl-CoA plays a central role in phenypropanoid-acetate/phenylpropanoid metabolism, as illustrated by the great diversity of phenolic compounds to which it gives rise.*

synthases (PKS) related to ketoacyl-ACP III (KAS III) of fatty acid synthesis (see Chapter 8) developed the ability to utilize a hydroxycinnamoyl-CoA ester molecule instead of acetyl-CoA. This CoA ester condensed with one or more molecules of malonyl-CoA, resulting in polyketides, which were then converted into chalcones and, ultimately, to more complex polyphenolic compounds, such as flavonoids and diarylheptanoids (see Section 24.16.2).

PKSs still utilize malonyl-CoA for elongation, as does the fatty acid synthesis pathway. The evolution of this one function, the ability to condense polyketides with an aromatic starter molecule, led to development of the UV and desiccation protection needed for plants to survive on land, and indicates how even a minor mutation can have long-reaching effects on the biosphere.

In contrast to fatty acid synthases like KAS III (see Section 8.4.4), plant type-III PKSs are relatively small homodimeric enzymes (≈42 kDa per subunit) that utilize acyl-CoA esters instead of acyl-ACPs as substrates. Plant type III PKSs are typically named for the class of compounds that they produce. Chalcone synthase (CHS) (Figs. 24.56 and 24.57) and stilbene synthase (STS) (Fig. 24.57) are the best understood, with the former likely the first type-III PKS activity to evolve in plants.

All plant lineages can produce at least the most basic of flavonoid classes, the chalcones and flavanones (Figs. 24.51 and 24.56). Although the direct synthesis of chalcones

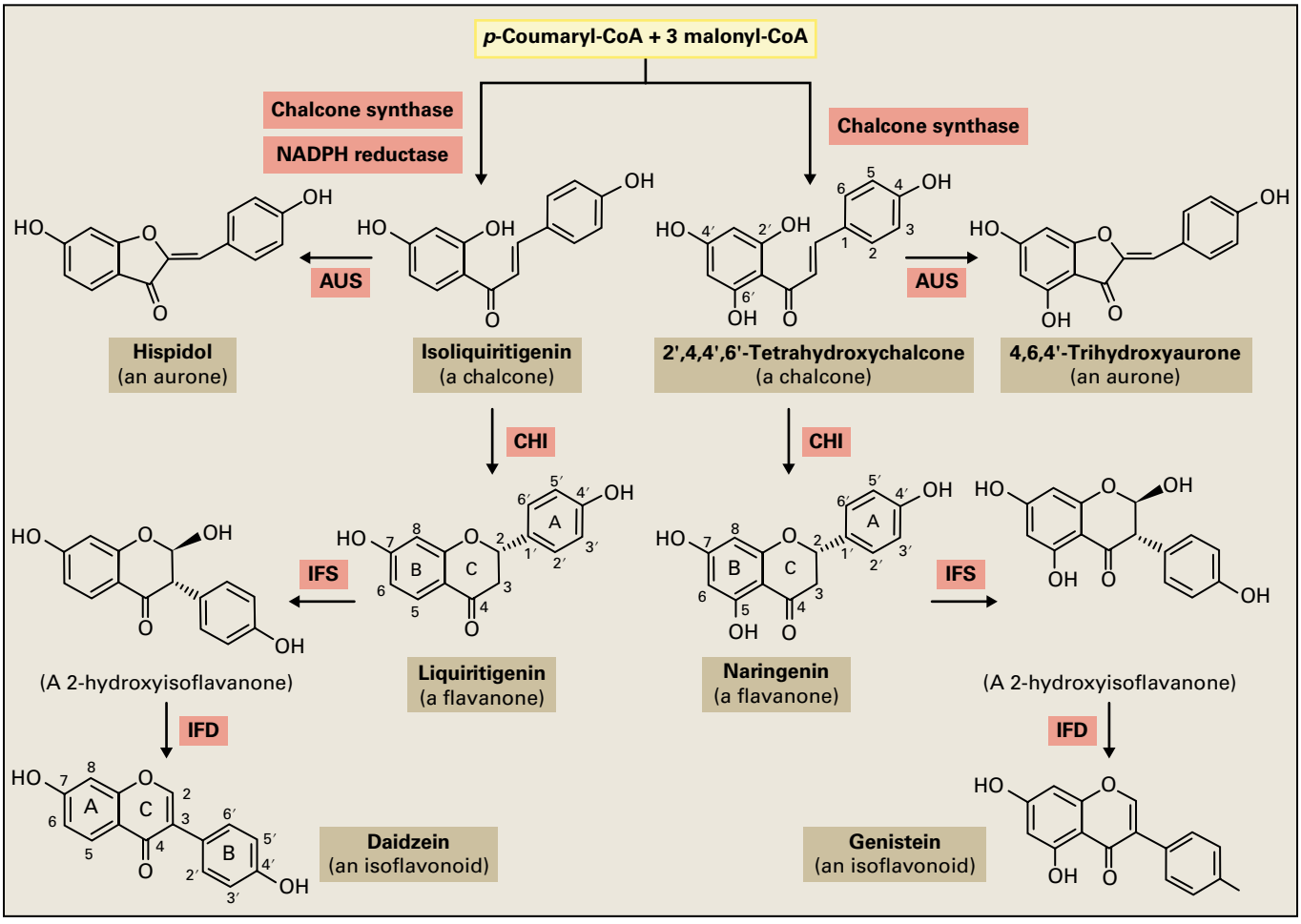


FIGURE 24.56 *Biosynthetic pathways of specific flavonoid subclasses, including the chalcones, aurones, flavanones, and isoflavones (isoflavonoids). The enzymes involved (and their cofactors) are as follows: CHI, chalcone isomerase; AUS, aurone synthase; IFS, 2-hydroxy-isoflavanone synthase (O_2, cyt. P450, NADPH); IFD, 2-hydroxyisoflavanone dehydratase.*

typically does not involve modification by other enzymes, some chalcone derivatives are reduced at specific positions in the synthesized aromatic ring (loss of hydroxyl groups), leading to deoxychalcones. In some plant groups, the coordinated action of CHS and an NADPH-dependent reductase generates a 6-deoxychalcone (**isoliquiritigenin**) as opposed to **naringenin chalcone**, which is the product of CHS working alone (Fig. 24.56). It is not known how or even if CHS and the reductase interact. Both isoliquiritigenin and naringenin chalcone can then be converted by aurone synthase, a polyphenol oxidase homolog, into **aurones,** such as **hispidol** and **aureusidin**, a subclass of flavonoids that, as their name suggests, are bright yellow in color (Fig. 24.56).

While most type-III PKSs have CHS activity, a growing number of different activities (Box 24.11) produce di-, penta-, and heptaketides and an array of compound classes such as benzalacetones, stilbene carboxylates, pyrones, chromones, C-methylated chalcones, acridone alkaloids, diarylheptanoids, and gingerol-related compounds, as well as others (Fig. 24.57).

Subsequent to polyketide formation, diverse enzymes modify the core polyketide to produce the large array of compounds derived from the phenylpropanoid-acetate pathway. These enzymes include NADPH-dependent reductases, prenyltransferases, and glycosyltransferases. The substrate specificity, with appropriate tissue-specific expression of these various enzymes, leads to the great diversity of species- and tissue-specific polyketides observed in the plant kingdom.

24.16.2 The phenylpropanoid-acetate pathway leads to synthesis of flavonoids, stilbenes, isoflavonoids, and coumarins

The flavonoids (including the isoflavonoids, catechins, condensed tannins, and other derivatives) are perhaps the best-studied group of phenylpropanoid-acetate derived compounds. They are also, along with the lignans, responsible for much of the diversity observed in compounds derived from L-Phe in the plant kingdom. Major classes of flavonoids include flavanones, flavones, isoflavones, isoflavanones, pterocarpans, dihydroflavonols, flavonols, leucoanthocyanidins (flavan-3,4-diols), anthocyanins, proanthocyanidins (including condensed tannins), phlobaphenes, and catechins (flavan-3-ols).

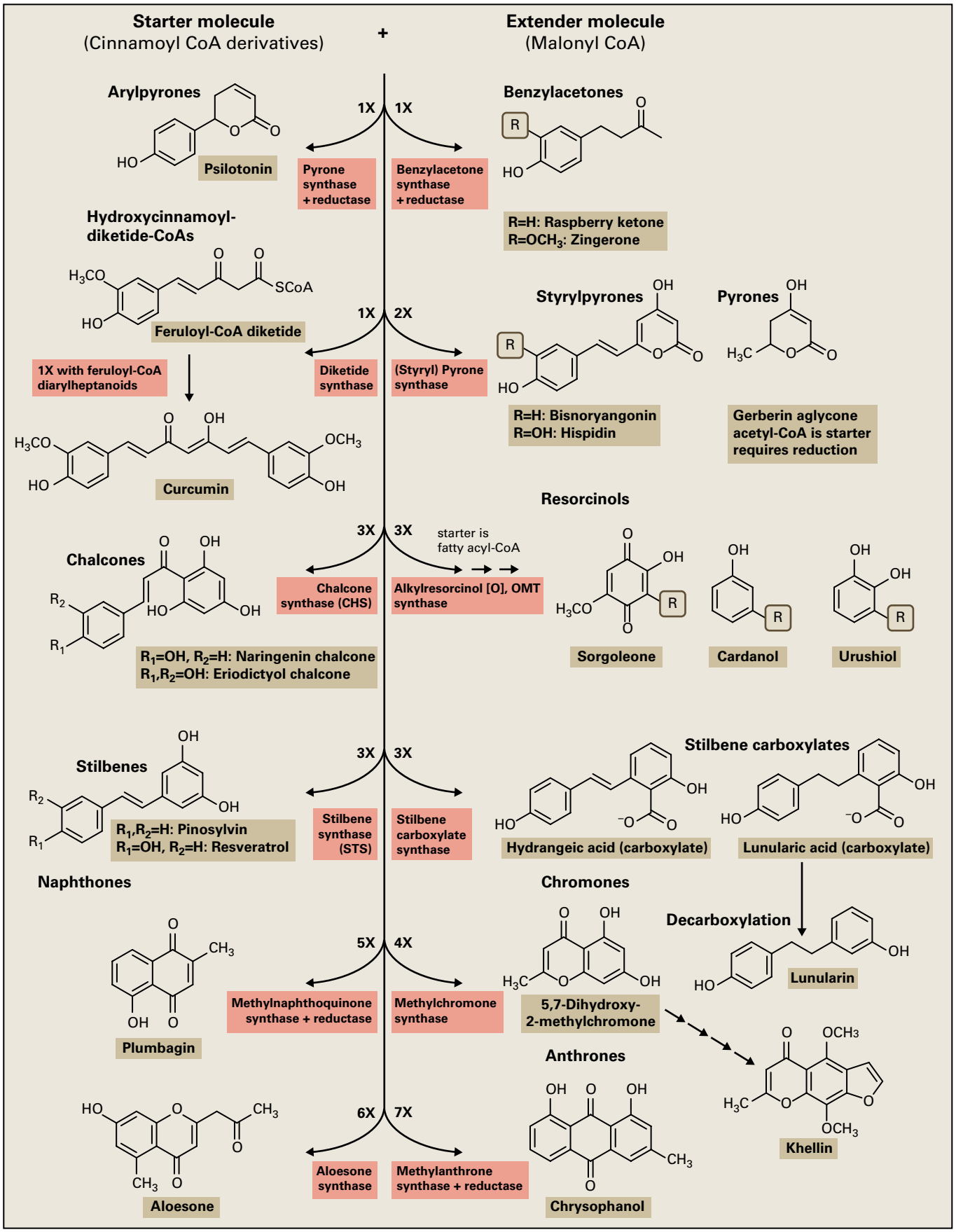


FIGURE 24.57 *Biosynthesis of polyketide classes in plants, including benzalacetones and arylpyrones, methylpyrones and styrylpyrones, stilbene carboxylates, resorcylic acids, anacardic acids, resorcinols, urushiols, and cardanols, chromones, naphthoquinones, and anthrones. The designation 1X, 2X, 3X etc., refers to the number of molar equivalents of malonyl-CoA required. Some classes utilize acetyl-CoA or fatty acyl-CoA instead of hydroxycinnamoyl-CoAs as starter molecules, but still produce phenolic products.*

BOX 24.11 Exotic polyketides result from a variety of starter molecules and condensations

Other polyketide-derived compounds are produced by type III PKS enzymes that belong to the CHS/STS family, but that differ from canonical CHS/STS enzymes in starter substrate or in the number of condensation reactions with malonyl-CoA (see Fig. 24.57). Additional modifications (such as methylations and glycosylations) lead to compound diversification within a class. Examples are given for the following classes with corresponding number of condensations: the benzylacetones and arylpyrones (e.g., **raspberry ketone**, **zingerone**, and **psilotonin**), one condensation; the methylpyrones and styrylpyrones (e.g., **gerberin aglycone**, and **hispidin**), two condensations; the stilbene carboxylates, resorcylic acids, anacardic acids, resorcinols, urushiols, and cardanols (e.g., **hydrangeic** and **lunularic acids**, **olivetolic acid**, **6-nonadecyl salicylic acid**, **sorgoleone**, **pentadecylcatechol**, and **lunularin**), three condensations; chromones (e.g., **khellin**), four condensations; possibly methylnaphthoquinones (e.g., **plumbagin**), five condensations; acetonyl-methylchromones (e.g., **aloesone**), six condensations; and anthrones (e.g., **chrysophanol**), seven condensations.

Many products of the alternative PKS pathways are physiologically active. The anacardic and resorcylic acids, urushiols, and cardanols all have allergenic properties and are the active components responsible for the contact dermatitis caused by members of the Anacardiaceae (poison ivy, poison oak and poison sumac, all *Toxicodendron* species). Such compounds are also present at high levels in the sap of the lacquer tree (*Toxicodendron vernicifluum*), which oxidizes and polymerizes in the presence of moisture to form lacquer, used to form traditional Asian lacquer wares. Some alkylresorcinols, such as sorgoleone secreted from sorghum roots, possess potent allelopathic properties.

Flavonoids typically have three interconnected rings at their core (see Fig. 24.50). The A ring is derived from a hydroxycinnamoyl-CoA precursor (typically *p*-coumaroyl-CoA) (Fig. 24.58), and the B ring is formed by the condensation reactions involving malonyl-CoA in the active site of CHS. The C ring is formed by closure of the chalcone, leading to formation of flavanones. This latter reaction occurs spontaneously in aqueous solution, but is relatively slow and produces products that are racemic at C2. Most flavanones isolated from plants, on the other hand, possess the *S* configuration at C2. Chalcone isomerase (CHI) catalyzes the rapid and stereospecific formation of *S* flavanones (see Fig. 24.56), which are important branchpoint intermediates in the flavonoid pathway. Modifications to the C ring are responsible for creation of new classes of compounds, whereas modifications to the A and B rings lead to diversification within compound class. Thus, enzymes that modify the C ring are the most important for generation of diversity within the flavonoid class. This trend is repeated in the lignans, diarylheptanoids, and other phenolic classes.

After the core flavanone structure (such as naringenin) is formed by CHS and the C ring is closed by CHI, several important modifications can take place that lead to great structural diversity. Entry into the isoflavonoid pathway occurs by action of two enzymes (see Fig. 24.56). The first is a cytochrome P450, isoflavone synthase (IFS), which catalyzes an oxygenation and an unusual C-2 to C-3 aryl migration to yield the 2-hydroxyisoflavanones. Dehydration of the 2-hydroxyisoflavanones by the second enzyme, 2-hydroxyisoflavanone dehydratase (IFD), leads to the isoflavones, such as **genistein** and **daidzein**. The isoflavones can be further metabolized, primarily in the Fabaceae, to yield isoflavanones, such as **(–)-vestitone**, pterocarpan phytoalexins, such as (–)-medicarpin in alfalfa (*Medicago sativa*) (Fig. 24.59), or rotenoids (e.g., **9-demethylmunduserone** from *Amorpha fruticosa*).

In a second major conversion, the flavanone C ring can be aromatized by the 2-oxoglutarate-dependent flavone synthase (FNS), to form an achiral class of compounds, the flavones (see Fig. 24.58). These are among the most primitive of the flavonoids, along with the dihydroflavonols and flavonols, and are found in the earliest vascular plants as well as nonvascular plants.

Another modification of flavanones involves oxygenation at position 3 (on the C ring) by a 2-oxoglutarate-dependent flavanone 3-hydroxylase (F3H) to form dihydroflavonols, such as dihydrokaempferol. The A ring can be further oxygenated by F3′5′H/CYP75A or F3′H/CYP75B to form compounds with higher orders of hydroxylation within this class (see Fig. 24.58). The C-ring keto group can be reduced by dihydroflavonol reductase (DFR) to form the leucoanthocyanidin class, which sits at another important branch point in the greater flavonoid biosynthetic network.

Leucoanthocyanidins (flavan-3,4-diols) are precursors for anthocyanins, flavan-3-ols (catechins), and condensed tannins (proanthocyanidins) (see Fig. 24.58). Anthocyanidin synthase (ANS), also called leucoanthocyanidin dioxygenase (LDOX), is a 2-oxoglutarate-dependent dioxygenase that catalyzes the formation of anthocyanidins, such as cyanidin, pelargonidin, and delphinidin (Fig. 24.60), from their leucoanthocyanidin analogs. A UDP-glucose dependent glucosyltransferase (UGT) then catalyzes the formation of the anthocyanins, colored compounds that are important constituents of flower petals, leaves, stems, and fruits and play roles in pollinator or seed disperser attraction.

In contrast to the brightly hued anthocyanins, the catechins (flavan-3-ols, see Fig. 24.58) are colorless. These compounds are thought to have human health benefits, and

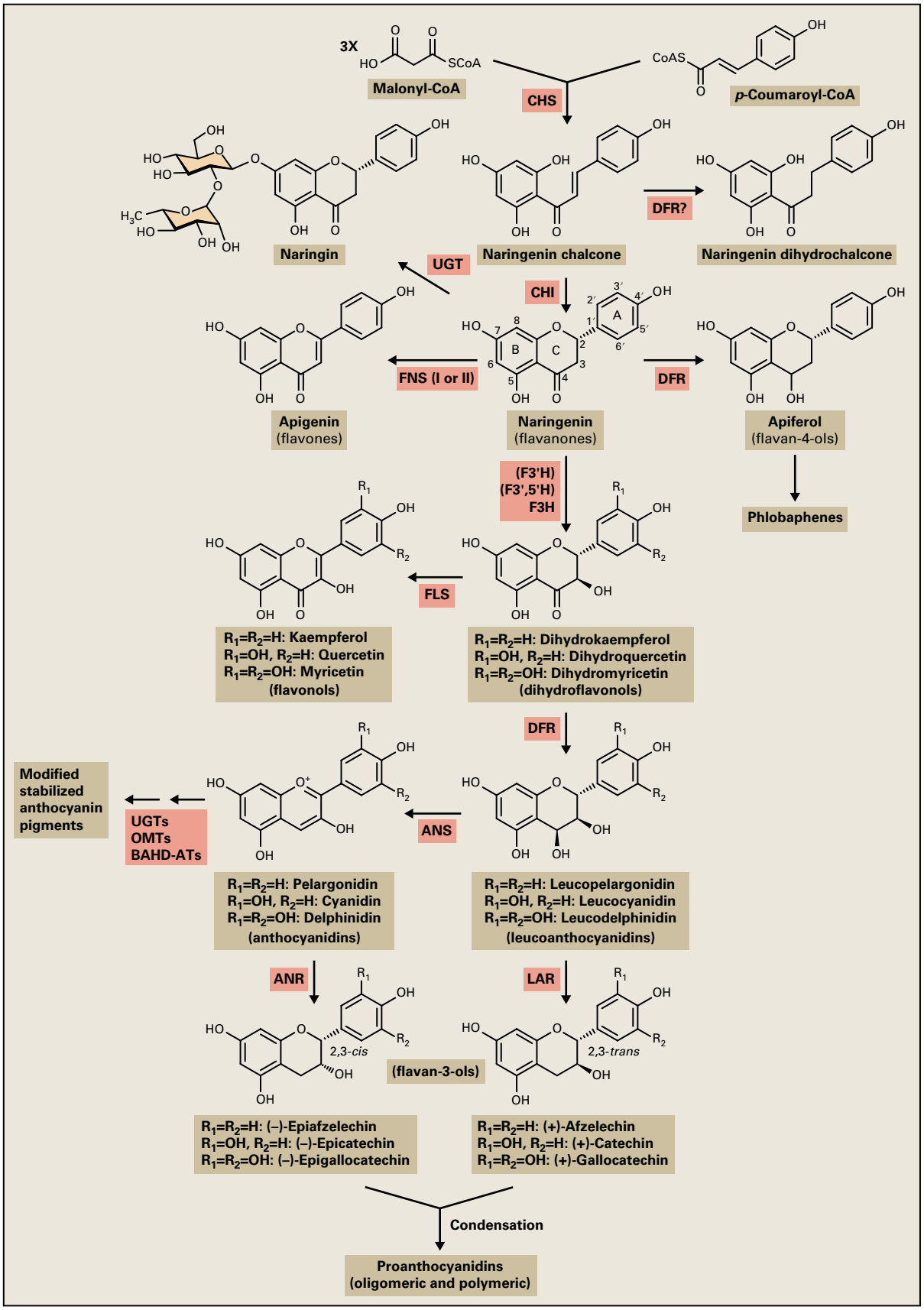


FIGURE 24.58 *The core flavonoid pathway includes two important "hub" metabolites, naringenin and apigenin, which lead to production of thousands of other metabolites in the flavone and other branches of flavonoid metabolism. Major enzymes (and their cofactors) are indicated that lead to compound class formation: FNS, flavone synthase (FNS I: 2-oxoglutarate, O_2; FNS II: O_2, cytochrome P450, NADPH); F3H, flavanone 3-hydroxylase (α-ketoglutarate, O_2, ascorbate, Fe(II)); FLS, flavonol synthase (α-ketoglutarate, O_2, ascorbate, Fe(II)); DFR, dihydroflavonol 4-reductase (NADPH); ANS, anthocyanidin synthase (α-ketoglutarate, O_2, ascorbate, Fe(II)); ANR, anthocyanidin reductase (NADPH); LAR, leucoanthocyanidin reductase (NADPH); UGT, UDP-glucose:flavonoid glucosyltransferase (UDP-glucose); OMTs, O-methyltransferases (AdoMet); BAHD-ATs, BAHD family acyltransferases. The A, B, and C rings of the flavonoid skeleton are indicated on naringenin, as is a standard numbering system.*

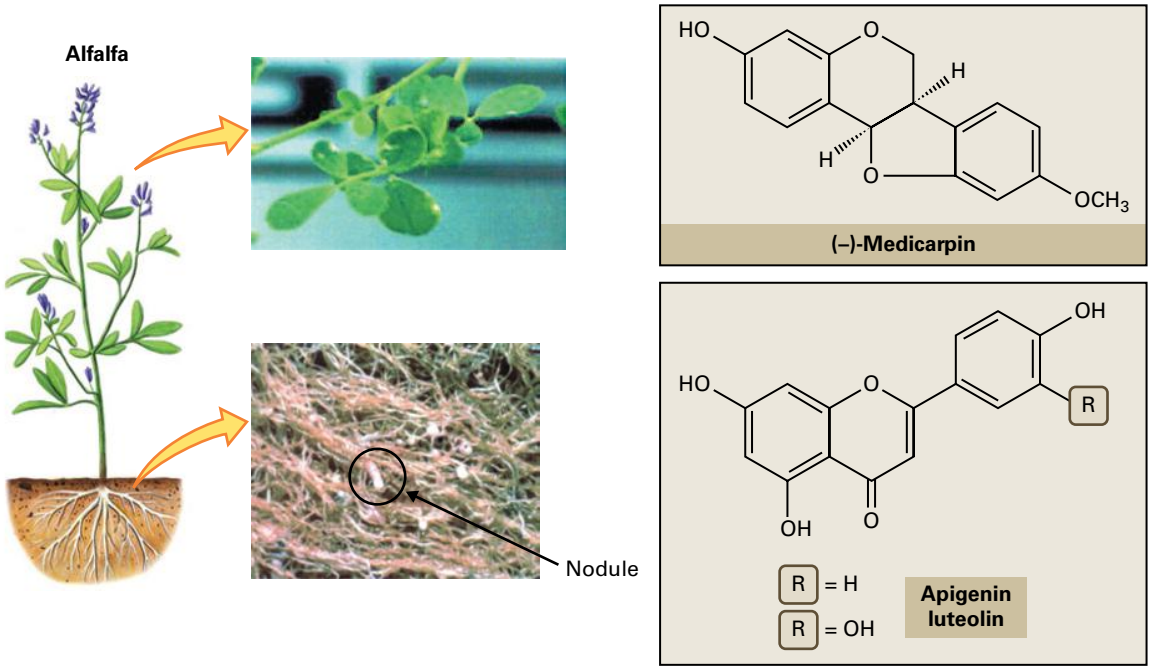


FIGURE 24.59 *Flavonoids perform diverse functions in alfalfa (*Medicago sativa*). The flavonoids apigenin and luteolin function as signaling molecules that induce* Nod *gene expression in compatible* Rhizobium *bacteria, facilitating the development of nitrogen-fixing root nodules (see Chapter 16). The phytoalexin isoflavonoid pterocarpan medicarpin participates in inducible plant defense.*
Source: Davin (alfalfa plant), M. L. Kahn (nodules), Washington State University, Pullman; previously unpublished.

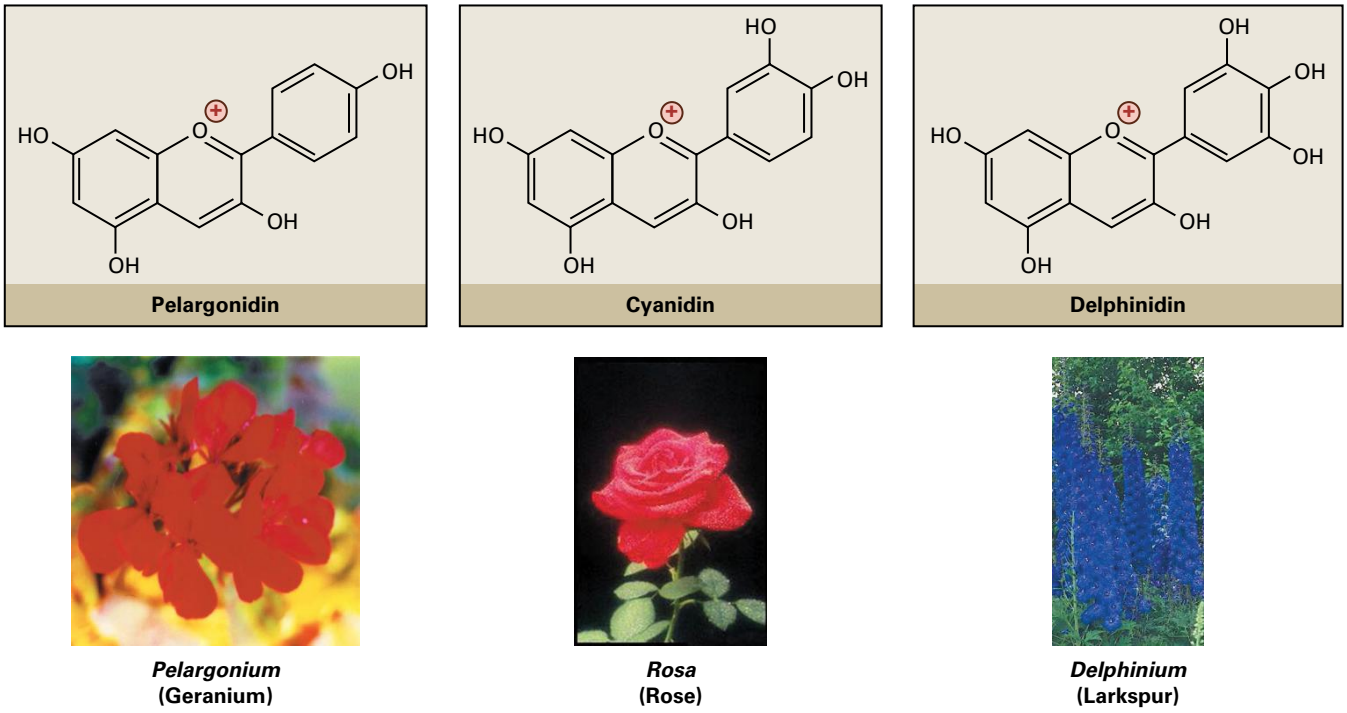
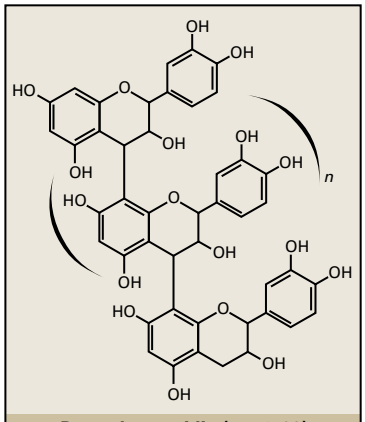


FIGURE 24.60 *Selected anthocyanin pigments: pelargonidin, cyanidin, and delphinidin from geranium, rose, and larkspur, respectively.*

to have a role in plant defense. Especially well known are *epi*-gallocatechin 3-gallate (EGCG) from green tea and *epi*-catechin from cocoa, which impart strong antioxidant properties. Leucoanthocyanidin reductase (LAR) catalyzes the conversion of 2,3-*trans*-3,4-*cis*-leucocyanidins into(+)-flavan-3-ols, such as (+)-2,3-*trans*-catechin ((+)-catechin). The catechins then serve as building blocks of the proanthocyanidins, along with the *epi*-catechins, which are formed from anthocyanidins by anthocyanidin reductase (ANR, see Fig. 24.58). The actual mechanism is yet to be determined whereby these compounds are polymerized to form the colored proanthocyanidins (condensed tannins, Fig. 24.61).



Red sorghum



Proanthocyanidin (n = 1–30)

FIGURE 24.61 *Red sorghum produces proanthocyanidin antifeedant compounds (condensed tannins) in its seed coat, which deter birds from feeding on the seed. White sorghum, which is deficient in these compounds, is rapidly consumed by birds. Similar compounds are present in many species.*
Source: Lumpkin, US Department of Agriculture, Washington State University, Pullman; previously unpublished.

Coumarins (e.g., coumarin; see Table 24.3) belong to a widespread family of plant metabolites called the benzopyranones, with more than 1,500 representatives in more than 800 plant species. Their roles in plants appear to be mainly defense-related, given their UV-screening-, germination inhibitory-, antimicrobial-, and antifeedant properties. The structures of representative simple coumarins, umbelliferone and scopoletin, are shown in Fig. 24.62. Additional families of plant coumarins (Fig. 24.63) include linear furanocoumarins (e.g., psoralen), angular furanocoumarins (e.g., angelicin), pyranocoumarins (e.g., seselin), and pyrone-substituted coumarins (e.g., 4-hydroxycoumarin). The carbons destined to form the furano- and pyrano- groups originate from a prenyl group that is attached to the simple coumarin core structure after the latter is produced from *p*-coumaroyl-CoA or feruloyl-CoA by the 2-oxoglutarate dependent dioxygenase, *p*-coumaroyl-CoA 2-hydroxylase (C2H). Again, *p*-coumaroyl-CoA serves as precursor to yet another large class of plant phenolics. Other modifications to coumarins are catalyzed by prenyltransferases, oxidases, and *O*-methyltransferases.

Coumarins present serious health threats and benefits. Ingesting coumarins from plants such as clover can cause massive internal bleeding in mammals. This discovery ultimately led to the development of the rodenticide, Warfarin (see Table 24.3) and to the use of related compounds (blood thinners) to treat and prevent stroke. These planar UV-absorbing molecules can intercalate into DNA helices, causing chromosomal breakages upon UV light activation, ultimately leading to cell death. In this manner, compounds such as the photosensitizing compound 8-methoxypsoralen, present in leaf tissue of *Heracleum mantegazzianum* (giant hogweed), can cause severe phytophotodermatitis (Fig. 24.64). Psoralen (see Fig. 24.63), on the other hand, is successfully used to treat various skin disorders (e.g., eczema and psoriasis) by combination of oral ingestion and UV-A treatment.

24.17 The phenylpropanoid pathway

The phenylpropanoid pathway diverges from the phenylpropanoid-acetate pathway by differential utilization of *p*-coumaroyl-CoA. It culminates in formation of monolignols, which are then used as intermediates in the synthesis of lignin and the structurally and biosynthetically related lignans (Fig. 24.65).

After cellulose, lignin is the most abundant biopolymer on Earth and accounts for roughly 20–30% or more of the carbon that is fixed by a plant. Lignin is a structural component of the plant cell wall. It appears that production of monolignols evolved later than phenolic compounds, produced by the phenylpropanoid-acetate pathway, as monolignols are not present in nonvascular plants.

Most plants produce only two hydroxycinnamates, *trans*-cinnamate and *p*-coumarate. It was originally believed that caffeate and ferulate were intermediates in the pathway that led to the monolignols. Caffeate and ferulate are, however, not core pathway intermediates—they are unusual phenylpropanoids that are only produced or accumulate in specific plant species, such as the mint family and the grasses, respectively.

24.17.1 The phenylpropanoid pathway culminates in formation of the monolignols

A *p*-coumaroyl-CoA molecule, destined for incorporation into compound classes such as lignins, lignans, and volatile phenylpropenes, is converted by cinnamoyl-CoA:NADPH oxidoreductase (CCR) to form *p*-coumaryl aldehyde. The latter is then transformed by cinnamyl alcohol dehydrogenase (CAD) into the monolignol, *p*-coumaryl alcohol, the precursor of H lignins, a large number of lignans, and certain volatile aromatics such as ***t*-anol**, **anethole**, and **methylchavicol** (see Section 24.17.3). CCR is a type B reductase that abstracts the pro-*S* hydride from behind the nicotinamide plane of NADPH during reduction; CAD, on the other hand, is a type A reductase that abstracts the pro-*R* hydride from in front of the nicotinamide plane (Fig. 24.66).

When other monolignols (such as **caffeyl alcohol**, **coniferyl alcohol**, **5-hydroxyconiferyl alcohol**, or **sinapyl alcohol**) are required, *p*-coumaroyl units are first transferred from *p*-coumaroyl-CoA to shikimate by hydroxycinnamoyl-CoA:shikimate hydroxycinnamoyltransferase (HCT) to form the ester, ***p*-coumaroyl-5-*O*-shikimate** (see Fig. 24.65). This is a regiospecific reaction, with only the 5-*O*-shikimate product being enzymatically formed.

HCT belongs to a subclade of the BAHD family of plant acyltransferases that includes several other hydroxycinnamoyl transferases involved in the production of secondary metabolites, such as **chlorogenic acid**, which is an ester of caffeic acid and quinate (see Fig. 24.65). Hydroxycinnamoyl-quinate transferase (HQT) functions as the chlorogenic acid synthase in plants such as apple and artichoke.

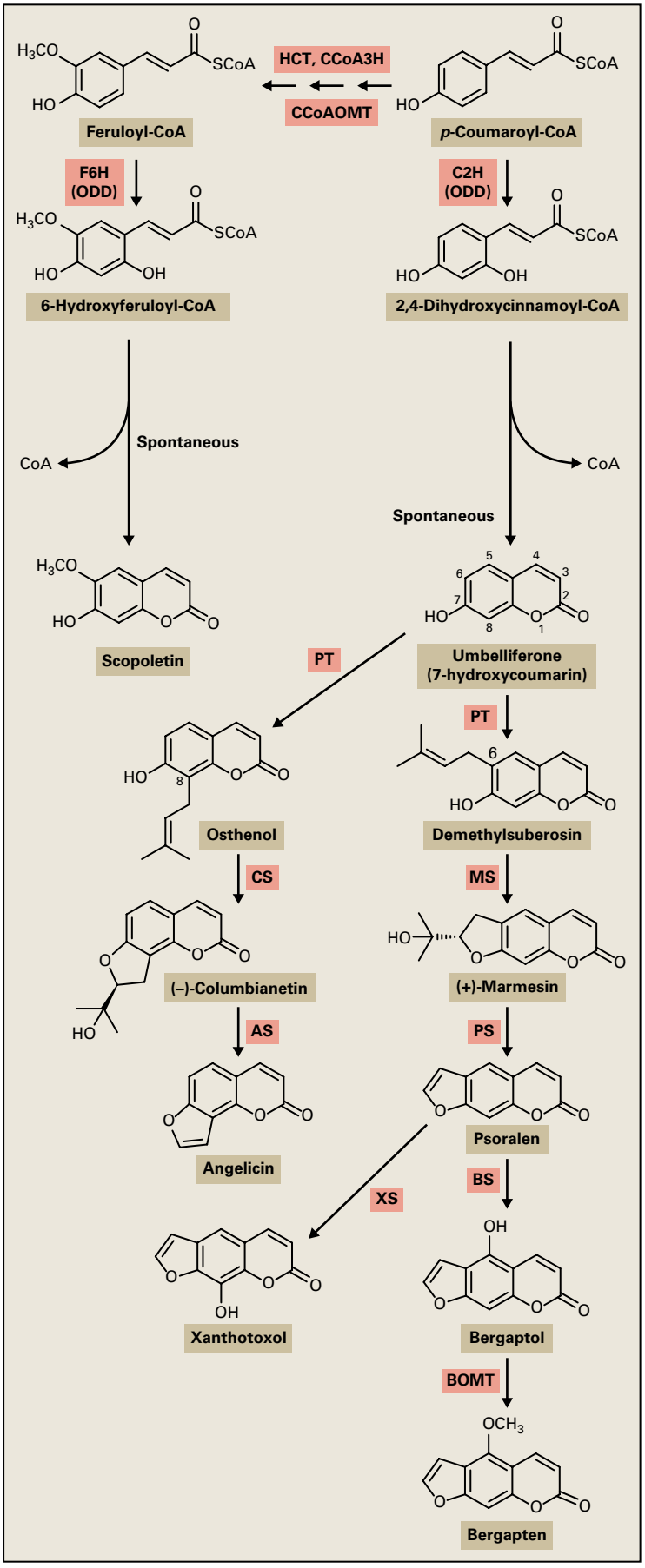


FIGURE 24.62 *Most coumarins are produced from either* p*-coumaroyl-CoA or feruloyl-CoA (although some such as coumarin are produced from cinnamoyl-CoA). Conversion of the hydroxylated product of the coumarin synthase reaction (CoA ester or carboxylate) to the coumarin is spontaneous in aqueous solution. Major enzymes (and their cofactors) are indicated: F6H, feruloyl-CoA 6-hydroxylase/coumarin synthase [α-ketoglutarate, O_2, ascorbate, Fe(II)]; C2H, p-coumaroyl-CoA 2-hydroxylase/coumarin synthase [α-ketoglutarate, O_2, ascorbate, Fe(II)]; PT, dimethylallyl prenyltransferase; MS, marmesin synthase (O_2, cytochrome P450, NADPH); PS, psoralen synthase (O_2, cytochrome P450, NADPH); BS, bergaptol synthase (O_2, cytochrome P450, NADPH); XS, xanthotoxol synthase (O_2, cytochrome P450, NADPH); BOMT, bergaptol* O*-methyltransferase (AdoMet); CS, columbianetin synthase (O_2, cytochrome P450, NADPH); and AS, angelican synthase (O_2, cytochrome P450, NADPH).*

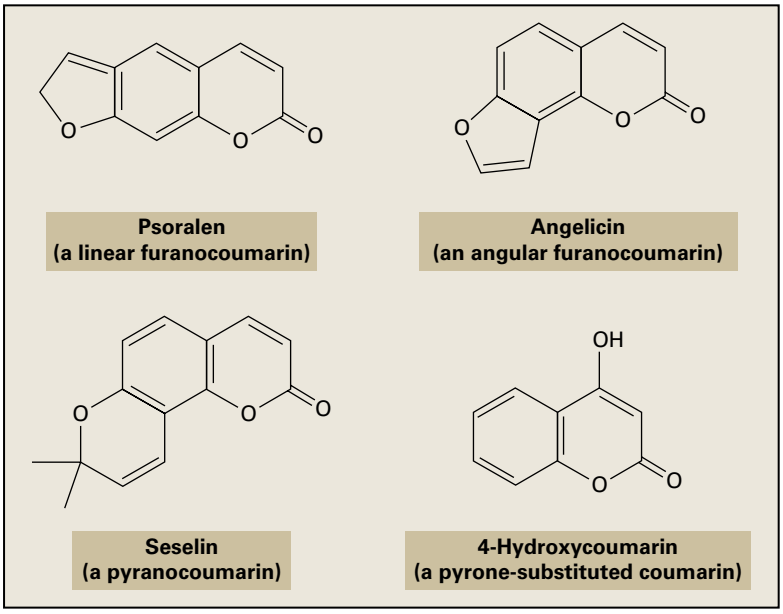


FIGURE 24.63 *Structures of the linear furanocoumarin psoralen, the angular furanocoumarin angelicin, the pyranocoumarin seselin, and the pyrone-substituted coumarin 4-hydroxycoumarin.*



Heracleum

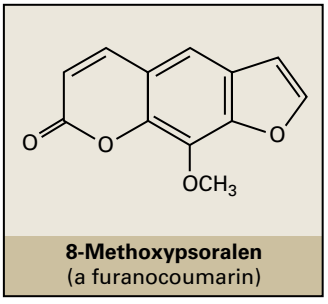




FIGURE 24.64 *A linear furanocoumarin, 8-methoxypsoralen, sensitizes human skin to UV-A light. This compound, present in external tissues of* Heracleum *species, causes severe blistering on skin contact followed by exposure to UV-irradiation.*
Source: Photographs: Towers, University of British Columbia, Vancouver, Canada; previously unpublished.

The next reaction in the pathway to the monolignols is also highly substrate selective and is catalyzed by a cytochrome P450 enzyme of the CYP98A class called *p*-coumaroyl-5-*O*-shikimate 3′-hydroxylase (C3′H, see Fig. 24.65). Genetic experiments with the *ref8* mutation (defective in the *CYP98A3* gene) and detailed characterization of the *CYP98A3* gene product from *Arabidopsis thaliana* validated involvement in production of caffeoyl-5-*O*-shikimate. HCT (or a similar acyltransferase) then transfers the caffeoyl group back to CoASH. Thus, HCT appears to play two roles in the pathway. It is curious that plants would form the unusual shikimate ester as a transient intermediate in the pathway, only to return the more oxygenated hydroxycinnamoyl moiety back to CoASH for the next step in the pathway.

24.17.2 Monolignols are primarily converted into lignans and lignins

Monolignols are primarily converted into two distinct classes of plant metabolites, the lignans (dimers formed by phenolic oxidative coupling of coniferyl alcohol monomers) and the lignins (polymers formed by phenolic oxidative coupling of hydroxycinnamyl alcohol monomers; see Chapter 2), although other products, such as volatile phenylpropenes (propenylphenols, allylphenols, and derivatives), are also derived from these intermediates. Most flux through the phenylpropanoid pathway in plants is directed to the production of lignins, which are structural components of cell walls. Free radicals participate in the reactions that produce both di- and oligomeric lignans and lignins as well as related complex plant polymers, such as those in suberized tissue.

Lignan dimers are found in ferns, gymnosperms, and angiosperms; higher oligomeric forms also occur. Lignans have a likely role in plant defense. Plicatic acid (Fig. 24.67), for example, is deposited in large quantity during heartwood formation in Western red cedar (*Thuja plicata*), thereby contributing to the color, quality and durability of this highly valued heartwood. Lignans are also used in human medicine. For example, podophyllotoxin (Fig. 24.67) is used to treat venereal warts, and its semisynthetic derivatives, teniposide, etoposide, and etophos are used in chemotherapy to treat a variety of cancers. Lignan formation favors *E*-coniferyl alcohol as the initial substrate, although other monolignols, allylphenols, and phenylpropanoid monomers can be used to a lesser extent.

Although the term **lignan** was initially coined to describe a class of dimeric phenylpropanoid (C_6C_3-C_6C_3) metabolites linked by their 8-8′ bonds, this definition has been expanded

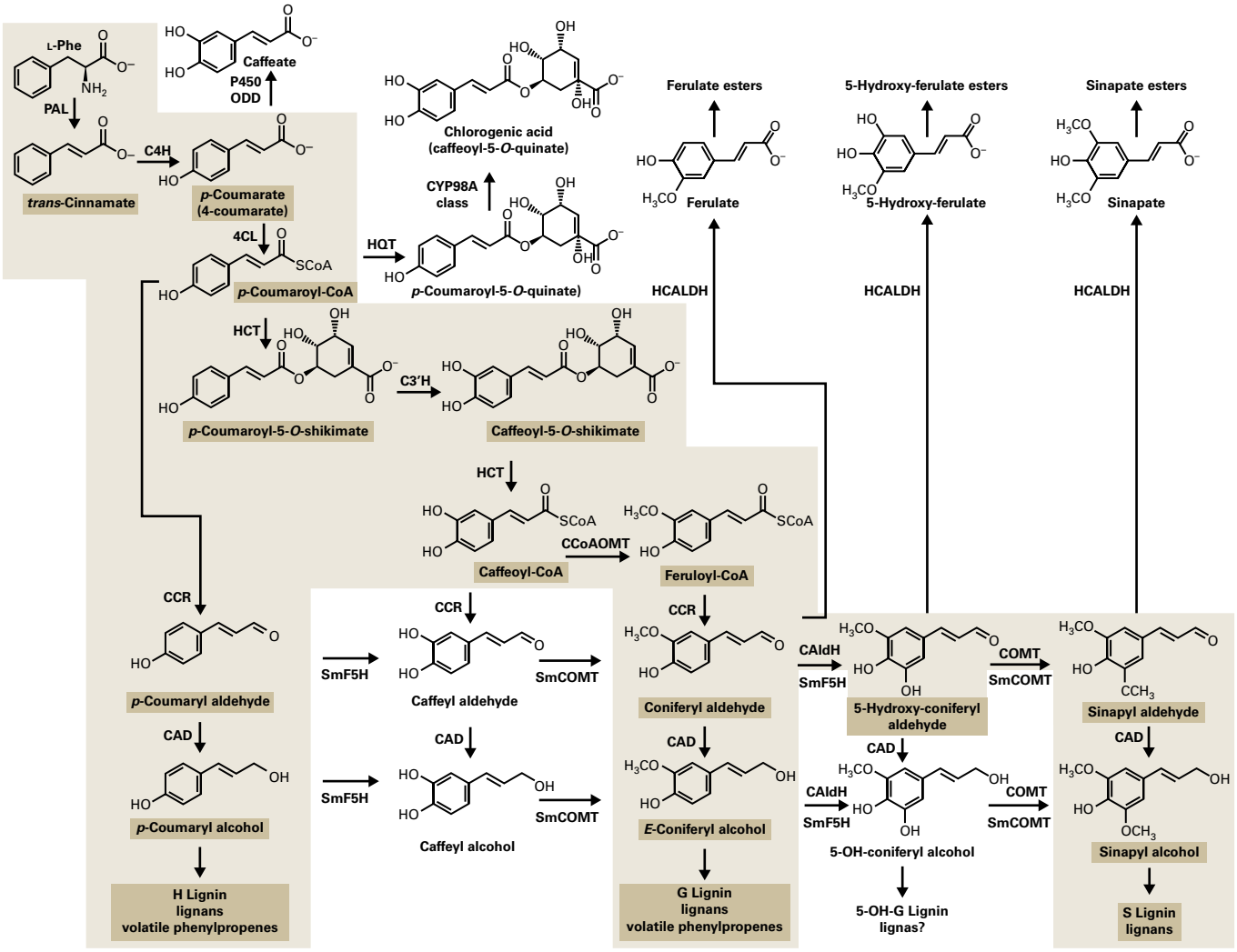


FIGURE 24.65 *Phenylpropanoid metabolism leading to production of the monolignols,* p-*coumaryl, coniferyl, and sinapyl alcohols, as well as to other (sub)classes of plant phenolics. Considerable revision of this network has taken place in the last 20 years. Instead of being a completely interconnected grid, it appears that only specific routes are available in most plant cells. Pathways not shaded are not universal, but can contribute to significant flux in certain species. Enzymes (and their cofactors) are as follows: PAL, phenylalanine ammonia lyase (MIO); cinnamate-4-hydroxylase (O_2, cytochrome P450, NADPH); 4CL, 4-hydroxycinnamoyl-CoA ligase (ATP, coenzyme A [CoASH]); HCT, hydroxycinnamoyl-CoA:shikimate hydroxycinnamoyl transferase (shikimate); C3′H, p-coumaroyl-5-*O*-shikimate 3′-hydroxylase (O_2, cytochrome P450, NADPH); CCoAOMT, caffeoyl-CoA O-methyl transferase (AdoMet); CCR, (hydroxy)cinnamoyl-CoA reductase (NADPH); CAldH, coniferyladehyde 5-hydroxylase (O_2, cytochrome P450, NADPH); CAD, (hydroxy)cinnamyl alcohol dehydrogenase (NAD^+); HCALDH, hydroxycinnamaldehyde dehydrogenase (NAD^+); COMT, "caffeic acid" O-methyltransferase (AdoMet); ODD, 2-oxoglutarate-dependent dioxygenase (α-ketoglutarate, Fe(II), ascorbate); HQT, chlorogenic acid synthase/hydroxycinnamoyl-CoA:quinate hydroxycinnamoyl transferase (quinate); CYP98A class, cytochrome P450 involved in production of chlorogenic acid, related to C3′H; SmF5H and SmCOMT, multifunctional P450 and OMT, respectively, involved in monolignol formation in the moss* Selaginella moellendorfii, *not found yet in other plants.*

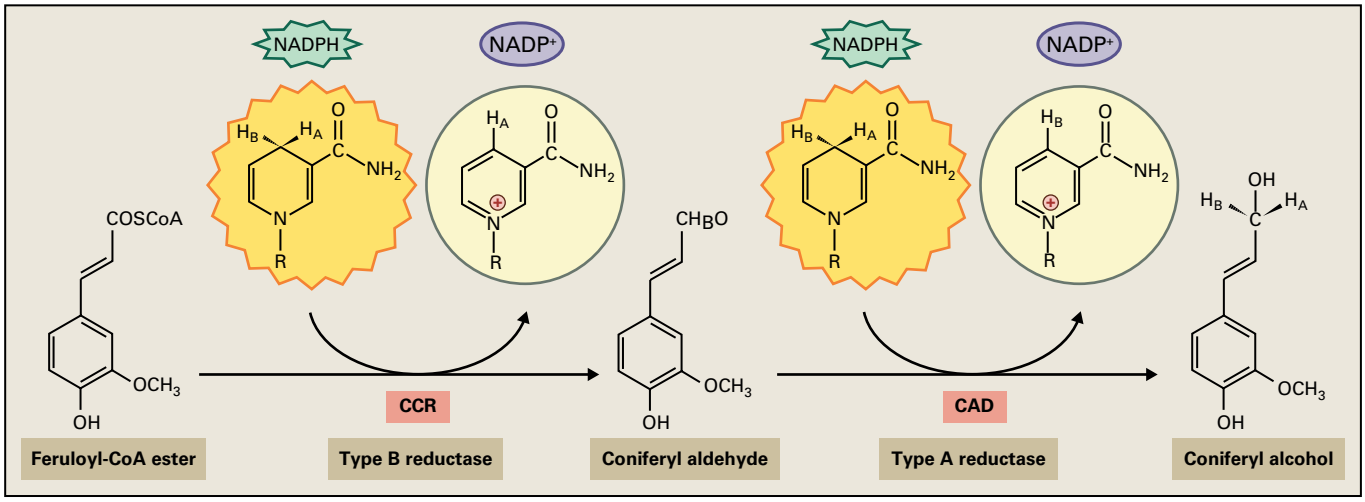
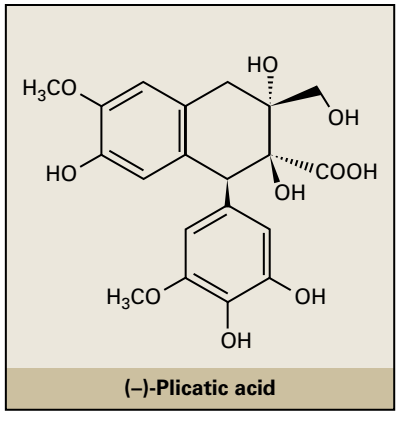


FIGURE 24.66 *The stereospecificity of a type B oxidoreductase, NADPH-dependent cinnamoyl-CoA reductase (CCR), and a type A oxidoreductase, cinnamyl alcohol dehydrogenase (CAD). H_A, pro-R (the hydrogen projecting upwards from the A-face of the nicotinamide ring, that is, out from the plane of the page); H_B, pro-S (the hydrogen projecting upwards from the B-face of the nicotinamide ring, i.e., behind the plane of the page). R, adenine nucleotide diphosphate.*



Thuja plicata

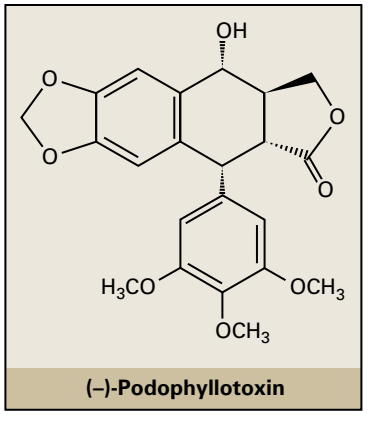
A





Podophyllum peltatum

B





Sesamum indicum

C

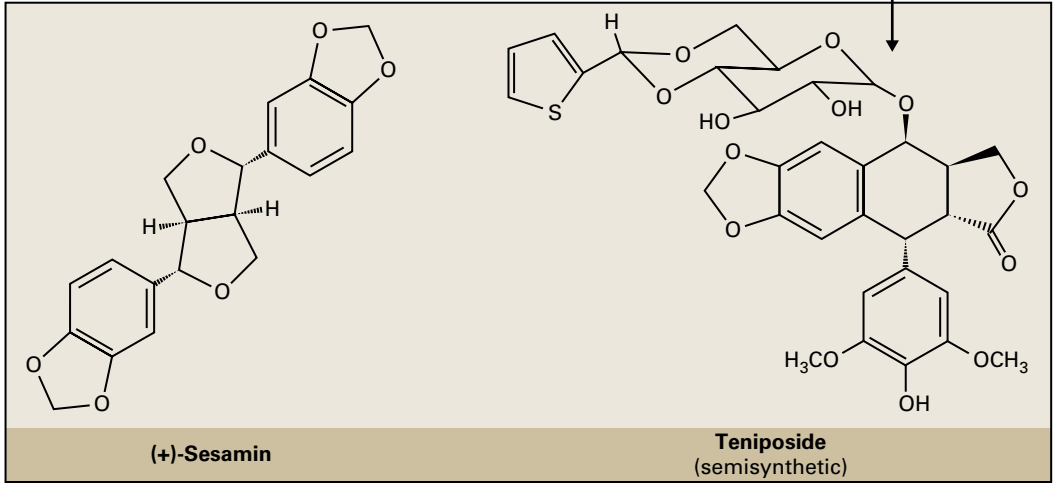


FIGURE 24.67 *Examples of 8-8′-linked lignans. (A) Plicatic acid accumulates to 3% of the dry weight of the heartwood in western red cedar. This and related compounds enable such species to survive for more than 3,000 years. (B) Podophyllotoxin, from* Podophyllum *species, such as the may apple. The teniposide, etoposide, and etophos derivatives of this compound are used in treatment of certain cancers. (C) Sesamin, from sesame seed, has antioxidant properties that prevent sesame oil from turning rancid during storage.*
Source: (A, C) Davin, Washington State University, Pullman; previously unpublished. (B) Towers, R.A. Norton, University of British Columbia, Vancouver, Canada; previously unpublished.

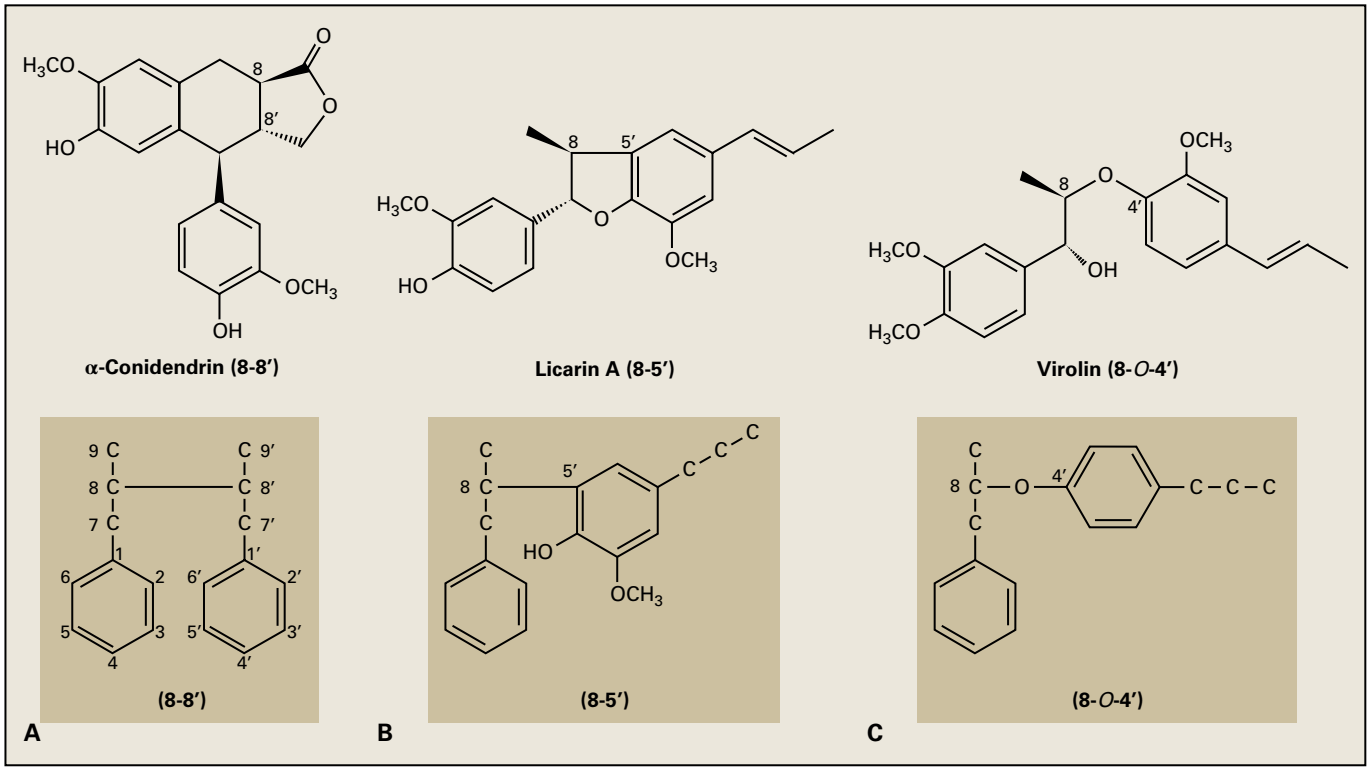


FIGURE 24.68 *Examples of lignans derived by distinct coupling modes, for example, 8-8′, 8-5′, and 8-O-4′.*

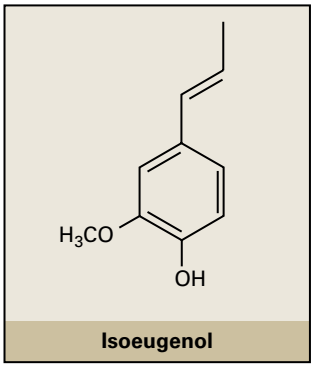


FIGURE 24.69 *Isoeugenol, an allylphenol.*

to include all monolignol-derived dimers and higher order oligomers, regardless of linkage type (e.g., 8-*O*-4′-linked, 8-5′-linked and 8-1′-linked dimers, Fig. 24.68) that do not serve the structural role of the lignins. Subclasses of lignans, called **neolignans**, have similar linkages, but are derived from allylphenol compounds, such as isoeugenol (Fig. 24.69). **Norlignans** (C_6C_3–C_6C_2) are thought to be derived from coupling of a hydroxycinnamic acid to either a monolignol or an allylphenol, with subsequent loss of the carboxyl group during coupling. Although several thousand lignans, neolignans, and norlignans are known in nature, relatively few coupling modes have been encountered.

Lignans are most often found in enantiomerically pure or enriched form in plants. The dimers are produced in plants when two monolignol radicals formed by proteins such as laccases or peroxidases are brought into close proximity in the "active site" of a directing or **dirigent protein**, which has no catalytic activity of its own, but directs the orientation of the reacting monolignol (most commonly *E*-coniferyl alcohol) radicals in a stereoselective manner so that only one enantiomeric product is typically formed (Fig. 24.70). For example, the particular optical form of pinoresinol that is formed varies with the plant species in question: whereas forsythia (*Forsythia* sp.) stem produces (+)-pinoresinol, flax (*Linum* sp.) seed produces (–)-pinoresinol. Once formed, pinoresinol can then undergo a variety of conversions, depending on the plant species (Fig. 24.71). The *Arabidopsis* genome encodes about a dozen dirigent proteins, some of which are involved in lignan production.

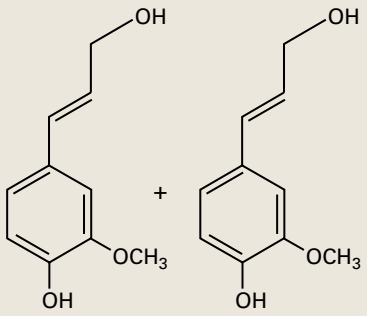
24.17.3 Plant volatiles are derived from the phenylpropanoid pathway

Four groups of related volatile compounds of particular interest are derived from phenylpropanoid-pathway intermediates. These are represented by compounds such as the benzoates benzylbenzoate, benzylacetate, and methylbenzoate; the phenylpropenes derived from eugenol, methyleugenol, methylchavicol, isoeugenol, *t*-anol and anethole (also referred to as allylphenol- and propenylphenol-derived compounds, see Table 24.3); cinnamaldehyde and methylcinnamate; and vanillin. All are important components of floral scents and/or of important spices such as cloves, cinnamon, anise, sweet basil, and vanilla bean.

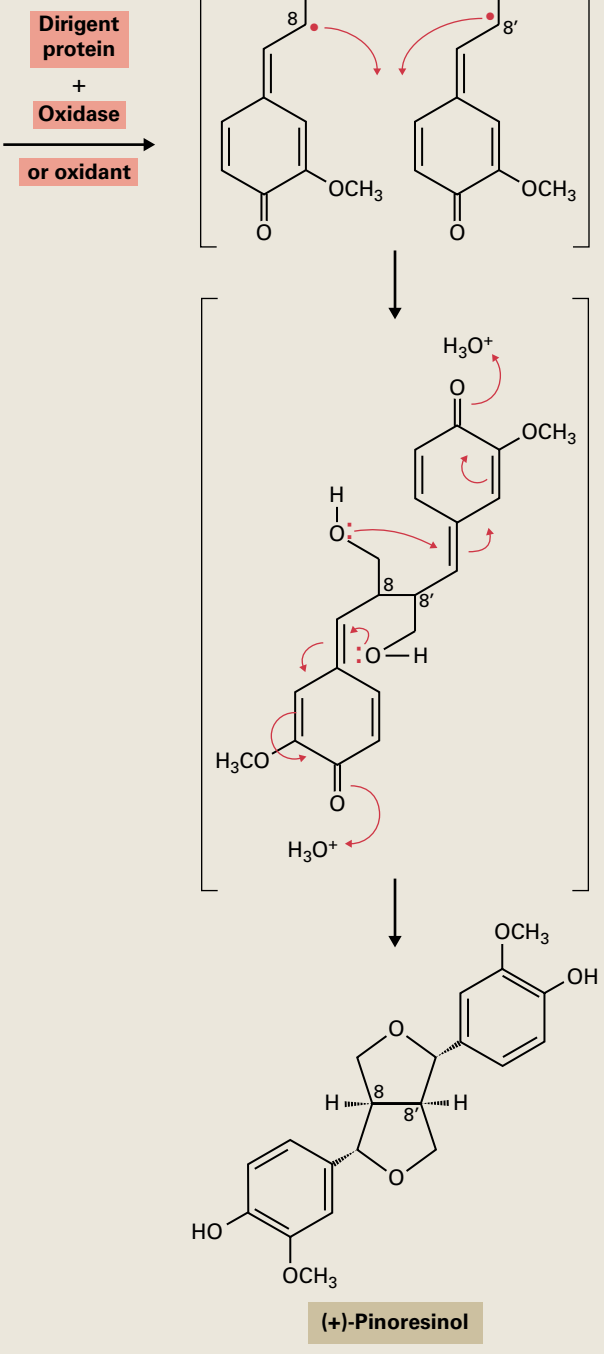
These volatile compounds are derived from intermediates in the core phenylpropanoid or phenylpropanoid pathways



Forsythia intermedia



E-Coniferyl alcohol



(+)-Pinoresinol

FIGURE 24.70 *Proposed biochemical mechanism accounting for stereoselective control (regio- and stereochemistry) of* E*-coniferyl alcohol coupling in* Forsythia *species. The particular enantiomer of pinoresinol formed can vary with plant species.*
Source: Photograph: L.B. Davin, Washington State University, Pullman; previously unpublished.

(Fig. 24.72). The benzonates are derived from cinnamyl-CoA esters and the monolignol pathway (Fig. 24.72). Methylcinnamate is derived directly from cinnamate via the action of a SABATH carboxymethyltransferase called CCMT. The phenylpropenes are derived from the monolignols via action of a BAHD acyltransferase (CCAT/CFAT) that yields the corresponding acetyl ester, which is then reduced by a member of IFR/PLR family of NADPH-dependent reductases (EGS or IGS) to yield eugenol, chavicol, isoeugenol or *t*-anol. These are further modified by cytochrome P450 enzymes and *O*-methyltransferases to a variety of structures (such as safrole, isosafrole, and myristicin; Fig. 24.72).

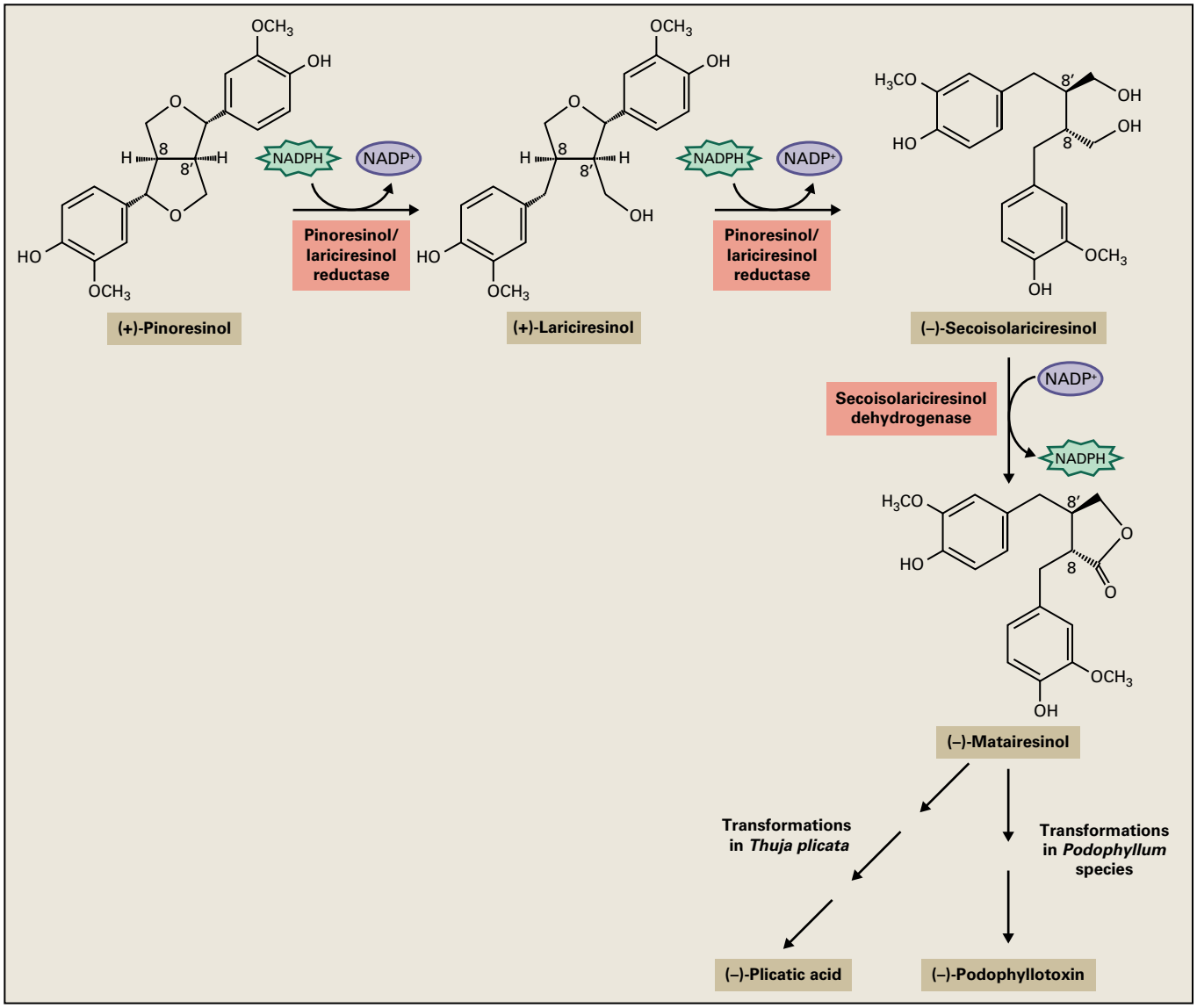


FIGURE 24.71 *Proposed biochemical pathway to the various 8-8′-linked lignan classes in* Forsythia, *western red cedar (*Thuja plicata*), and* Podophyllum *species. Similar pathways exist in many other species.*

24.18 Universal features of phenolic biosynthesis

24.18.1 Phenolic biosynthesis requires significant methylation

Despite being called phenolics or even polyphenolics, which implies the presence of free hydroxyl groups on aromatic rings, most compounds produced by the combined phenylpropanoid/phenylpropanoid-acetate pathways contain methylated hydroxyl groups (methoxy groups), and some contain methylated carboxyl groups (methyl esters). Indeed, some compound classes, such as lignans and flavonoids, are highly methoxylated, with methyl groups accounting for up to one fourth of the carbon in some molecules. As a result, the cells that produce such compounds have a very high demand for the general enzyme cofactor for methylation, *S*-adenosylmethionine (see Chapter 7).

Production of methylated phenolics requires the availability of enzymes catalyzing their formation. A large superfamily of methyltransferases has been characterized in detail; specific subfamilies are involved in methylation of specific types of functional groups. Most members of what has been called the SABATH family of carboxymethyltransferases (named after the first three enzymes identified in the gene family, salicylic acid, benzoic acid, and theobromine methyltransferases) typically methylate carboxyl groups to produce methyl esters. The majority of methylation reactions involved in formation of plant phenolics, however, are catalyzed by *O*-methyltransferases (OMTs). Most OMTs have limited substrate selectivities, although some enzymes, such as COMT ("caffeic acid" OMT), are promiscuous, which can lead to difficulties delineating biosynthetic pathways.

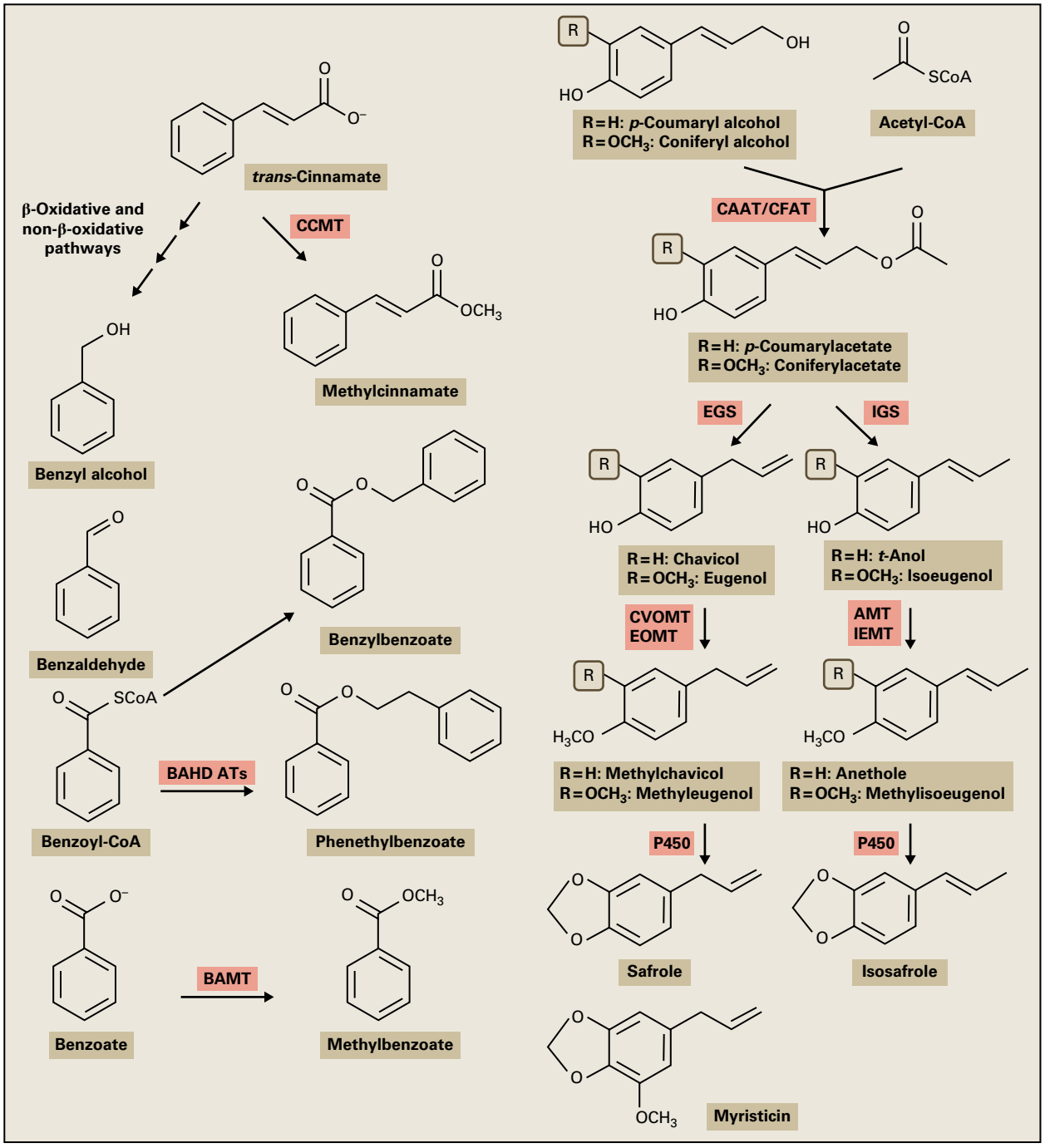


FIGURE 24.72 *Trans-cinamate, a monolignol derived from the core phenylpropanoid pathway (Fig. 24.52), is converted to a large number of volatile phenolics.*

24.18.2 Phenolic biosynthesis has a high demand for sugar moieties

Many or most of the naturally occurring plant phenolics are also modified by addition of saccharide (sugar) moieties. Many flavonoids are highly glycosylated, with the number of carbon atoms in the sugar additions often outnumbering the carbon atoms in the flavonoid core. The same is likely true for compounds of the lignan class. In contrast, the hydrolyzable tannins (see Fig. 24.73) have sugar moieties as their core, with addition of gallate or other modified benzoates to increase diversity of structure.

The sugar moieties often impart important properties to these molecules. For example, glycosylated flavonoids are more soluble in an aqueous environment than their aglycone counterparts, and it is the former that accumulate to high levels in plant vacuoles. In addition, the bitterness associated with compounds such as **naringin** (see Fig. 24.74) is eliminated when its sugar moieties are removed, leaving an aglycone with essentially no organoleptic effect.

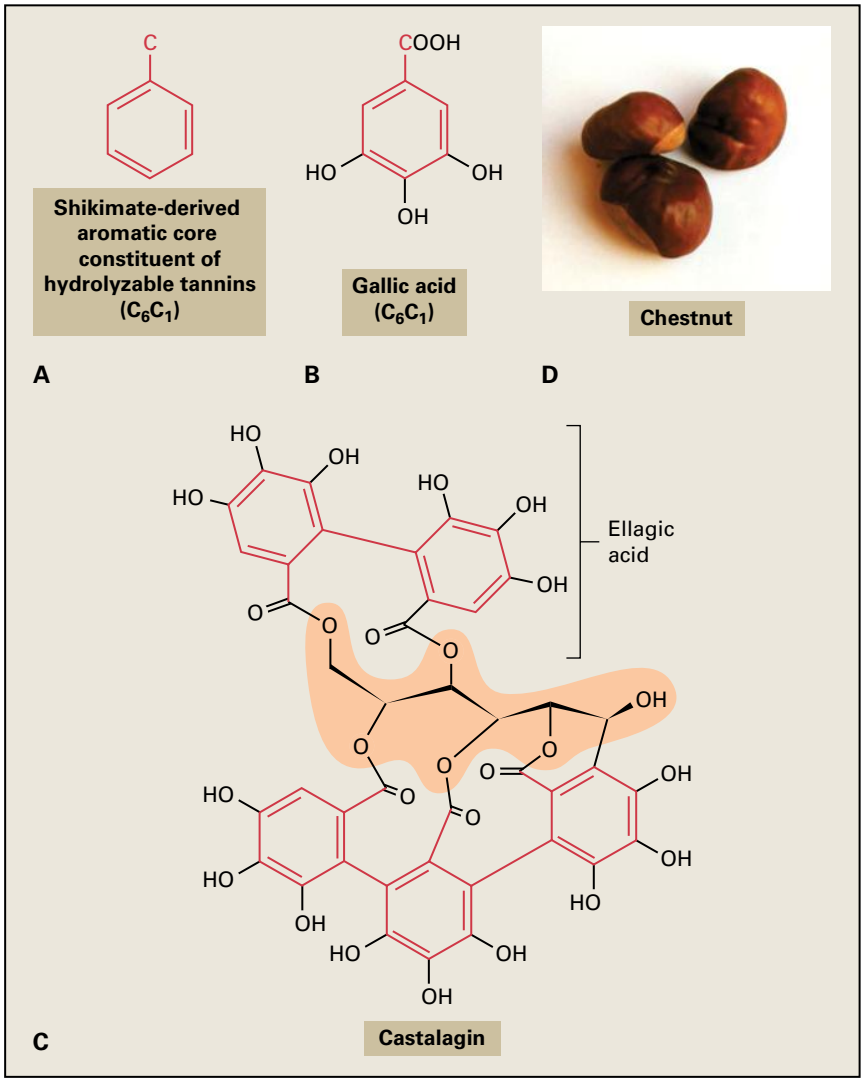


FIGURE 24.73 *The shikimate-derived skeleton (A) forms the core of gallic acid (B), a component of hydrolysable tannins, including castalagin, the core sugar moiety of which is shaded (C), from chestnut* (Castanea *sp., D).*
Source: (D) Davin, Washington State University, Pullman; previously unpublished.

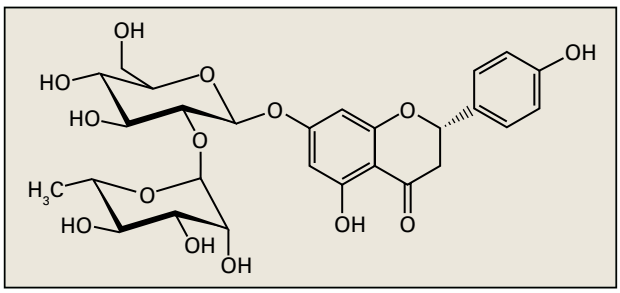


FIGURE 24.74 *The flavonone glycoside naringin. In grapefruit* (Citrus *x* paradisi*), this flavonoid gives the juice its bitter taste.*

24.18.3 Oligomers and mixed molecules are common

Lignins and suberins are not the only plant phenolics that are polymerized. Condensed tannins and oligolignans have various solubilities due to their variable states of polymerization. Proanthocyanidins with polymerization numbers in the 20s are common, as are oligolignans with varying degrees of polymerization. Other polyflavonoids are common, as are mixed flavonoid/lignan dimers/oligomers. In many instances, these compounds are again of specific absolute configurations, not being found in racemic form; a whole suite of enzymes that are involved in such dimer-/polymerization reactions are yet to be discovered.

24.18.4 Metabolons, modularity and metabolic bowties have a role in the biosynthesis of phenolics

It has long been debated whether the first three enzymes in the core phenylpropanoid pathway are associated in a metabolon (see Sections 24.8.2 and 24.12.4). Evidence for metabolon formation in the early steps of the phenylpropanoid pathway includes colocalization of PAL and 4CL on the ER in apparent close proximity to C4H, as well as measurements of flux through these early steps in some cell systems that exceed what would be expected based on the catalytic properties and diffusion rates of the enzymes and intermediates measured in a cell-free system. Assembly of the enzymes

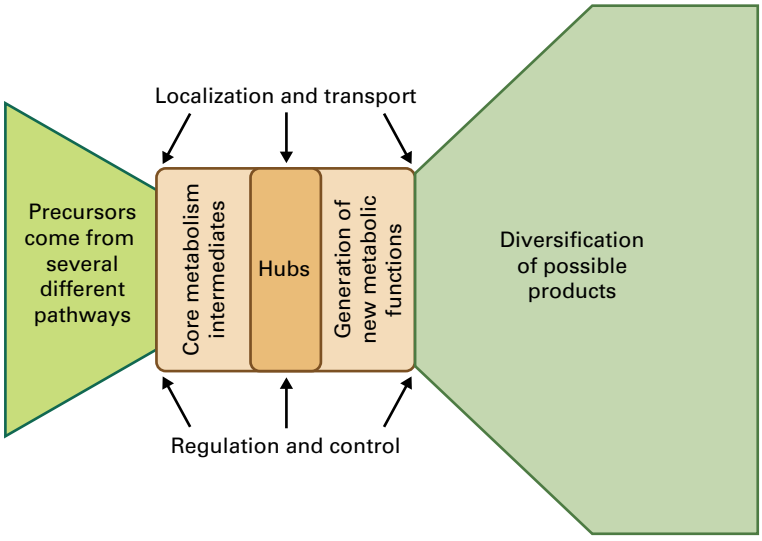


FIGURE 24.75 *Modularity and bowties are organizational features in plant specialized metabolism that include central hub metabolites, such as* p*-coumaroyl-CoA.*

of the core phenylpropanoid pathway could explain how individual plant cells differentially regulate the production of lignin precursors while simultaneously producing flavonoids under different regulatory regimes.

Another organizational principle recognized in plant metabolism in recent years, which appears to be a contributing factor in the phenylpropanoid-acetate/phenylpropanoid metabolic network, is modularity. Modularity occurs when metabolism is organized into a system that resembles "bow-ties." In such a system, selected intermediates act as hubs to connect one part of metabolism to another, and allow for great diversification in biochemical capacity (Fig. 24.75). In the phenylpropanoid-acetate and phenylpropanoid pathways, several hub molecules are clearly indicated, including *p*-coumaroyl-CoA, naringenin chalcone (flavanone), apigenin (flavone), and the monolignols (especially coniferyl alcohol). These compounds occupy key branch points that allow partitioning of one metabolite into multiple downstream pathways as a result of the action of multiple enzymes on each individual hub intermediate.

In this system, the entire phenolic biosynthetic system in plants is highly modular. Different metabolic outcomes occur in particular cells by different pathways "plugging in" to the greater phenylpropanoid/phenylpropanoid-acetate network at specific points. Partitioning between these pathways is controlled by the kinetic parameters of the enzyme that acts on the hub intermediate. Modularity thus allows for regulation of phenolic biosynthesis in a given cell, tissue, or plant.

24.19 Evolution of secondary pathways

Plants adapt to the environment by diversifying in various ways. This diversification can be reflected at the chemical level in the plethora of natural products that are produced in a species-specific manner. Selected examples of this chemical diversity have been presented in detail in the preceding sections of this chapter. Plant speciation is also linked to chemical diversification.

How do new metabolic pathways in plants evolve? As we understand more about the genes of natural product biosynthesis, a common theme has arisen that is centered on gene duplication and diversification. Those duplication and diversification events that impart fitness are then maintained through natural selection, and genes for a given secondary pathway can be either distributed throughout the plant genome or clustered. An insufficient number of plant genome sequences has been determined to date to know which of these two pathway organizations occurs most frequently.

Clustering of pathway genes may allow inheritance of the defense trait as a single functional unit. In pathways with toxic intermediates, clustering would reduce the likelihood of its disruption by segregation. At the chromatin level, clustering may also allow coordinated expression of all pathway genes. Recent advances in plant genomics and systems biology have yielded the first insights into pathway evolution in plant metabolism.

There are multiple examples of clustering of secondary pathway genes in plants. Unlike clustered microbial secondary pathways, these plant counterparts are not located in operons, but rather each gene is associated with a unique promoter. The first example of plant secondary pathway gene clustering was discovered in maize (*Zea mays*). The clustered biochemical pathway that leads to the benzoxazinones in maize was viewed as unusual at the time, but as more draft genomes are assembled, examples emerge of clustered pathways that lead to triterpenes in oat (*Avena sativa*), triterpenes in *Arabidopsis*, diterpenes in rice (*Oryza sativa*), cyanogenic glucosides in lotus (*Lotus* sp.), cassava (*Manihot esculenta*), and sorghum (*Sorghum* sp.), alkaloids in opium poppy (*Papaver somniferum*) and steroid alkaloids in tomato (*Solanum lycopersicum*). In addition, preliminary analyses of other genomes suggest that gene clusters may be present in moss, rice, and cucumber (*Cucumis sativus*). Clustering will facilitate both pathway elucidation based on signature genes and the discovery of novel plant natural products.

Summary

One of nature's greatest assets is the diversity of life forms. Although we have cataloged a large number of plant species in herbaria, we have only just begun to analyze and understand the wealth of chemical diversity that these plants produce and utilize. These chemicals constitute a largely untapped reservoir of biologically active molecules that have potential application in the emerging bioeconomy in agriculture, human health, and as renewable bioproducts for energy and manufacturing.

Although there are approximately 400,000 species of flowering plants on our planet, mankind derives 95% of food and energy needs from only 30 of these species. During human history, however, 7,000 plant species have been cultivated for consumption. A larger number, some 20,000, have been used as medicines, attesting to the unique chemical composition of plants. Plant chemicals did not, however, evolve to meet human needs. These chemicals have roles in the communication of the plant with the environment, as well as functions in plant physiology. They contribute to the fitness of the plant under varying biotic and abiotic conditions. Many answers to current, and future, societal challenges will be found in plant chemical diversity. We need only to better understand the composition of that chemical diversity, the environmental conditions that regulate it, the role played in plant fitness, and the collection of genes that underlie formation and storage of this veritable treasure trove.

Advances made in the field of plant natural products in the past decade have led to a better understanding of the intricate roles played in plant function and the interaction with the environment. We now appreciate more the *raison d'être* of plant natural products, however, we need to better understand how and where they are made and stored, why and how this biosynthesis is regulated, to fully exploit these molecules. We need more detailed knowledge of the repertoire of natural products in the plant kingdom in varying environments. With robotics and bioinformatics, the next decade of plant science will surely bring rapid advances to our understanding of how plants react to and interact with their environment. An important part of these interactions will certainly involve plant natural products.

FURTHER READING

Chapter 1

Austin JR, Staehelin LA (2011) The three-dimensional architecture of grana and stroma thylakoids of higher plants as determined by electron tomography. *Plant Physiol.* 155:1601–1611.

Bates PD, Stymne S, Ohlrogge, J (2013) Biochemical pathways in seed oil synthesis. *Curr. Opin. Plant Biol.* 16:358–364.

Boruc J, Zhou X, Meier I (2012) Dynamics of the plant nuclear envelope and nuclear pore. *Plant Physiol.* 158:78–86.

Boutté Y, Grebe M (2009) Cellular processes relying on sterol function in plants. *Curr. Opin. Plant Biol.* 12:705–713.

Bruguiere S, Kowalski S, Ferro M, et al. (2004) The hydrophobic proteome of mitochondrial membranes from Arabidopsis cell suspensions. *Phytochemistry* 65:1693–1707.

Donohoe BS, Kang B-H, Gerl M, Gergeley ZR, McMichael CM, Bednarek S, Staehelin LA (2013) *Cis*-Golgi cisternal assembly and biosynthetic activation occur sequentially in plants and algae. *Traffic* 14:551–587.

Ferro M, Salvi D, Riviere-Rolland H, Vermat T, Seigneurin-Berny D, Grunwald D, Garin J, Joyard J, Rolland N (2002) Integral membrane proteins of the chloroplast envelope: identification and subcellular localization of new transporters. *Proc. Natl. Acad. Sci. USA* 99:11487–11492.

Knaur N, Hu J (2009) Dynamics of peroxisome abundance: a tale of division and proliferation. *Curr. Opin. Plant Biol.* 12:781–788.

Kriwacki RW, Yoon, M.-Y. (2011) Fishing in the nuclear pore. *Science* 333:44–45.

Markham JE, Lynch DV, Napier JA, Dunn TM, Cahoon EB (2013) Plant sphingolipids: function follows form. *Curr. Opin. Plant Biol.* 16:350–357.

Marti L, Fornaciari S, Renna L, Stefano G, Brandizzi F (2010) COPII-mediated traffic in plants. *Trends Plant Sci.* 15:522–528.

Moellering ER, Muthan B, Benning C (2010) Freezing tolerance in plants requires lipid remodeling at the outer chloroplast membrane. *Science* 330:226–228.

Oikawa A, Lund CH, Sakuragi Y, Scheller HV (2012) Golgi-localized enzyme complexes for plant cell wall biosynthesis. *Trends Plant Sci.* 18:49–58.

Reyes FC, Buono R, Otegui MS (2011) Plant endosomal trafficking pathways. *Curr. Opin. Plant Biol.* 14:666–673.

Scheuring D, Viotti C, Krüger F, et al. (2011) Multivesicular bodies mature from the *trans*-Golgi network/early endosome in Arabidopsis. *Plant Cell* 23:3463–3481.

Segui-Simarro JM, Coronado MJ, Staehelin LA (2008) The mitochondrial cycle of Arabidopsis shoot apical meristem and leaf primordial meristematic cells is defined by a perinuclear, tentaculate/cage-like mitochondrion. *Plant Physiol.* 148:1380–1393.

Shen J, Zeng Y, Zhuang X, Sun L, Yao X, Pimpl P, Jiang L (2013) Organelle pH in the Arabidopsis endomembrane system. *Molecular Plant* doi: 10.1093/mp/sst079.

Sorek N, Bloch D, Yalovsky S (2009) Protein lipid modifications in signaling and subcellular targeting. *Curr. Opin. Plant Biol.* 12:714–720.

Sparkes IA, Frigerio L Tolley N, Hawes C (2010) The plant endoplasmic reticulum: a cell-wide web. *Biochem. J.* 423:145–155.

Staehelin LA, Kang B-H (2008) Nanoscale architecture of ER export sites and of Golgi membranes as determined by electron tomography. *Plant Physiol.* 147:1454–1468.

Viotti C, Bubeck J, Stierhof YD, et al. (2010) Endocytotic and secretory traffic in Arabidopsis merge in the *trans*-Golgi network/early endosome, an independent and highly dynamic organelle. *Plant Cell* 22:1344–1357.

Zheng H, Staehelin LA (2011) Protein storage vacuoles are transformed into lytic vacuoles in root meristmatic cells of germinating seedlings by multiple, cell type-specific mechanisms. *Plant Physiol.* 155:2023–2035.

Zhou M, Morgner N, Barrera NP, et al. (2011) Mass spectroscopy of intact V-type ATPases reveals bound lipids and the effects of nucleotide binding. *Science* 334:380–385.

Zouhar J, Rojo E (2009) Plant vacuoles: where did they come from and where are they heading. *Curr. Opin. Plant Biol.* 12:677–684.

Chapter 2

Bonawitz ND, Chapple C (2010) The genetics of lignin biosynthesis: connecting genotype to phenotype. *Annu. Rev. Genet.* 44:337–363.

Carpita NC, Gibeaut DM (1993) Structural models of primary cell walls in flowering plants: consistency of molecular structure with the physical properties of the walls during growth. *Plant J.* 3:1–30.

Cosgrove DJ (2005) Growth of the plant cell wall. *Nat. Rev. Mol. Cell Biol.* 6:850–861.

Demura T, Ye Z-H (2010) Regulation of plant biomass production. *Curr. Opin. Plant Biol.* 13:299–304.

Ellis M, Egelund J, Schultz CJ, Bacic A (2010) Arabinogalactan-proteins: key regulators at the cell surface? *Plant Physiol.* 153:403–419.

Kim S-J, Brandizzi F (2014) The plant secretory pathway: an essential factory for building the plant cell wall. *Plant Cell Physiol.* 55:687–693.

Biochemistry & Molecular Biology of Plants, Second Edition. Edited by Bob B. Buchanan, Wilhelm Gruissem, and Russell L. Jones.

© 2015 John Wiley & Sons, Ltd. Published 2015 by John Wiley & Sons, Ltd.

Companion website: www.wiley.com/go/buchanan/biochem

McCann MC, Roberts K (1991) Architecture of the primary cell wall. In *The Cytoskeletal Basis of Plant Growth and Form*. Lloyd CW, ed. New York: Academic Press, pp. 109–129.
Mohnen D (2008) Pectin structure and biosynthesis. *Curr. Opin. Plant Biol.* 11:266–277.
Olek AT, Rayon CJ, Makowski L, et al. (2014) The structure of the catalytic domain of a plant cellulose synthase and its assembly into dimers. *Plant Cell* 26:2996–3009.
Penning B, Hunter CT, Tayengwa R, et al. (2009) Genetic resources for maize cell wall biology. *Plant Physiol.* 151:1703–1728.
Popper ZA, Michel G, Herve C, Domozych DS, Willats WGT, Tuohy MG, Kloareg B, Stengel DB (2011) Evolution and diversity of plant cell walls: from algae to flowering plants. *Annu. Rev. Plant Biol.* 62:567–588.
Rose JKC, Braam J, Fry SC, Nishitani K (2002) The XTH family of enzymes involved in xyloglucan endotransglucosylation and endohydrolysis: current perspectives and a new unifying nomenclature. *Plant Cell Physiol.* 43:1421–1435.
Scheller HV, Ulvskov P (2010) Hemicelluloses. *Annu. Rev. Plant Biol.* 61:263–289.
Showalter AM, Keppler B, Lichtenberg J, Gu DZ, Welch LR (2010) A bioinformatics approach to the identification, classification, and analysis of hydroxyproline-rich glycoproteins. *Plant Physiol.* 153:485–513.
Slabaugh E, Davis JK, Haigler CH, Yingling YG, Zimmer J (2014) Cellulose synthases: new insights from crystallography and modeling. *Trends Plant Sci.* 19:99–106.
Vanholme R, Demedts B, Morreel K, Ralph J, Boerjan W (2010) Lignin biosynthesis and structure. *Plant Physiol.* 153:895–905.
Zhao Q, Dixon RA (2011) Transcriptional networks for lignin biosynthesis: more complex than we thought? *Trends Plant Sci.* 16:227–233.

Chapter 3

Amtmann A, Blatt MR (2009) Regulation of macronutrient transport. *New Phytol.* 181:35–52.
Barbier-Brygoo H, De Angeli A, Filleur S, Frachisse JM, Gambale F, Thomine S, Wege S (2011) Anion channels/transporters in plants: from molecular bases to regulatory networks. *Annu. Rev. Plant Biol.* 62:25–51.
Choi WG, Toyota M, Kim SH, Hilleary R, Gilroy S. (2014) Salt stress-induced Ca^{2+} waves are associated with rapid, long-distance root-to-shoot signaling in plants. *Proc. Natl. Acad. Sci. USA* 111:6497–6502.
Delhaize E, Gruber BD, Ryan PR (2007) The roles of organic anion permeases in aluminium resistance and mineral nutrition. *FEBS Lett.* 581:2255–2262.
Duby G, Boutry M (2009) The plant plasma membrane proton pump ATPase: a highly regulated P-type ATPase with multiple physiological roles. *Pflugers Arch.* 457:645–655.
Horie, T, Hauser, F, Schroeder JI (2009) HKT transporter-mediated salinity resistance mechanisms in Arabidopsis and monocot crop plants. *Trends Plant Sci.* 14:660–668.
Imes D, Mumm P, Böhm J, Al-Rasheid KA, Marten I, Geiger D, Hedrich R (2013) Open stomata 1 (OST1) kinase controls R-type anion channel QUAC1 in Arabidopsis guard cells. *Plant J.* 74:382–384.
Isayenkov S, Isner JC, Maathuis FJ (2010) Vacuolar ion channels: roles in plant nutrition and signalling. *FEBS Lett.* 584:1982–1988.
Kim TH, Böhmer M, Hu H, Nishimura N, Schroeder JI (2010) Guard cell signal transduction network; advances in understanding abscisic acid, CO_2, and Ca^{2+} signaling. *Annu. Rev. Plant Biol.* 61:561–591.
Kyte J, Doolittle RF (1982) A simple method for displaying the hydropathic character of a protein. *J. Mol. Biol.* 157:105–132.
Léran S, Varala K, Boyer JC, et al. (2014) A unified nomenclature of NITRATE TRANSPORTER 1/PEPTIDE TRANSPORTER family members in plants. *Trends Plant Sci.* 19:5–9.
Lin SM, Tsai JY, Hsiao CD, Huang YT, Chiu CL, Liu MH, Tung JY, Liu TH, Pan RL, Sun YJ (2012) Crystal structure of a membrane-embedded H^+-translocating pyrophosphatase. *Nature* 484:399–403.
Long SB, Campbell EB, Mackinnon R (2005) Crystal structure of a mammalian voltage-dependent Shaker family K^+ channel. *Science* 309:897–903.
Martinoia E, Meyer S, De Angeli A, Nagy R (2012) Vacuolar transporters in their physiological context. *Annu. Rev. Plant Biol.* 63:183–213.
Maurel C, Verdoucq L, Luu DT, Santoni V (2008) Plant aquaporins: membrane channels with multiple integrated functions. *Annu. Rev. Plant Biol.* 59:595–624.
Morth JP, Pedersen BP, Buch-Pedersen MJ, Andersen JP, Vilsen B, Palmgren MG, Nissen P (2011) A structural overview of the plasma membrane Na^+,K^+-ATPase and H^+-ATPase ion pumps. *Nat. Rev. Mol. Cell Biol.* 12:60–70.
Reinders A, Sivitz AB, Ward JM (2012) Evolution of plant sucrose uptake transporters. *Front. Plant Sci.* 3:22.
Schroeder JI, Raschke K, Neher E (1987) Voltage dependence of K^+ channels in guard cell protoplasts. *Proc. Natl. Acad. Sci. USA* 84:4108–4112.
Schroeder JI, Delhaize E, Frommer WB, et al. (2013) Using membrane transporters to improve crops for sustainable food production. *Nature* 497:60–66.
Schumacher K (2006) Endomembrane proton pumps: connecting membrane and vesicle transport. *Curr. Opin. Plant Biol.* 9:595–600.
Shimazaki K, Doi M, Assmann SM, Kinoshita T (2007) Light regulation of stomatal movement. *Annu. Rev. Plant Biol.* 58:219–247.
Spalding EP, Harper JF (2011) The ins and outs of cellular Ca^{2+} transport. *Curr. Opin. Plant Biol.* 14:715–720.
Tegeder M, Rentsch D (2010) Uptake and partitioning of amino acids and peptides. *Mol. Plant* 3:997–1011.
Ward JM (1997) Patch-clamping and other molecular approaches for the study of plasma membrane transporters demystified. *Plant Physiol.* 114:1151–1159.
Ward JM, Maser P, Schroeder JI (2009) Plant ion channels: gene families, physiology, and functional genomics analyses. *Annu. Rev. Physiol.* 71:59–82.

Chapter 4

Brandizzi F, Barlowe C (2013) Organization of the ER-Golgi interface for membrane traffic control. *Nat. Rev. Mol. Cell Biol.* 14:382–392.
Castilho A, Steinkellner H (2012) Glyco-engineering in plants to produce human-like N-glycan structures. *Biotechnol. J.* 7: 1088–1098.
De Marcos Lousa C, Gershlick DC, Denecke J (2012) Mechanisms and concepts paving the way towards a complete transport cycle of plant vacuolar sorting receptors. *Plant Cell* 24:1714–1732.

Ding Y, Robinson DG, Jiang LW (2014) Unconventional protein secretion (UPS) pathways in plants. *Curr. Opin. Plant Biol.* 29:107–115.
Hawes C, Schoberer J, Hummel E, Osterrieder A (2010) Biogenesis of the plant Golgi apparatus. *Biochem. Soc. Trans.* 38:761–767.
Howell SH (2013) Endoplasmic reticulum stress responses in plants. *Annu. Rev. Plant Biol.* 64:477–499.
Ibl V, Stoger E (2012) The formation, function and fate of protein storage compartments in seeds. *Protoplasma* 249:379–392.
Jarvis P, López-Juez E (2013) Biogenesis and homeostasis of chloroplasts and other plastids. *Nat. Rev. Mol. Cell. Biol.* 14:787–802.
Li R, Raikhel NV, Hicks GR (2012) Chemical effectors of plant endocytosis and endomembrane trafficking. In *Endocytosis in Plants.* Šamaj J, ed. Berlin: Springer-Verlag. pp. 37–61.
Paila YD, Richardson LGL, Schnell DJ (2013) New insights into the mechanism of chloroplast protein import and its integration with protein quality control, organelle biogenesis and development. *J. Mol. Biol.* 427:1038–1060.
Pedrazzini E, Komarova NY, Rentsch D, Vitale A (2013) Traffic routes and signals for the tonoplast. *Traffic* 14:622–628.
Reyes, FC, Buono R, Otegui MS (2011) Plant endosomal trafficking pathways *Curr. Opin. Plant Biol.* 14:666–673.
Shi LX, Theg SM (2013) The chloroplast protein import system: from algae to trees. *Biochim. Biophys. Acta* 1833:314–331.

Chapter 5

Breviario D, Gianì S, Morello L (2013) Multiple tubulins: evolutionary aspects and biological implications. *Plant J.* 75:202–218.
Cai G, Parrotta L, Cresti M (2015) Organelle trafficking, the cytoskeleton, and pollen tube growth. *J. Integr. Plant Biol.* 57:63–78.
Dumont S, Mitchison TJ (2009) Force and length in the mitotic spindle. *Curr. Biol.* 19:R749– R761.
Hamada T (2014) Microtubule organization and microtubule-associated proteins in plant cells. *Int. Rev. Cell Mol. Biol.* 312:1–52.
Henty-Ridilla JL, Li J, Blanchoin L, Staiger CJ (2013) Actin dynamics in the cortical array of plant cells. *Curr. Opin. Plant Biol.* 16:678–687.
Horio T, Murata T (2014) The role of dynamic instability in microtubule organization. *Front. Plant Sci.* 5:511.
Landrein B, Hamant O (2013) How mechanical stress controls microtubule behavior and morphogenesis in plants: history, experiments and revisited theories. *Plant J.* 75:324–338.
Lee Y-RJ, Liu B (2013) The rise and fall of the phragmoplast microtubule array. *Curr. Opin. Plant Biol.* 16:757–763.
Masoud K, Herzog E, Chabouté M-E, Schmit A-C (2013) Microtubule nucleation and establishment of the mitotic spindle in vascular plant cells. *Plant J.* 75:245–257.
McMichael CM, Bednarek SY (2013) Cytoskeletal and membrane dynamics during higher plant cytokinesis. *New Phytol.* 197:1039–1057.
Rasmussen CG, Wright AJ, Mueller S (2013) The role of the cytoskeleton and associated proteins in determination of the plant cell division plane. *Plant J.* 75:258–269.
Šlajcherová K, Fišerová J, Fischer L, Schwarzerová K (2012) Multiple actin isotypes in plants: diverse genes for diverse roles? *Front. Plant Sci.* 3:226.
Song Y, Brady ST (2015) Post-translational modifications of tubulin: pathways to functional diversity of microtubules. *Trends Cell Biol.* 25:125–136.
Szymanski DB, Cosgrove DJ (2009) Dynamic coordination of cytoskeletal and cell wall systems during plant cell morphogenesis. *Curr. Biol.* 19:R800–R811.
van Gisbergen PAC, Bezanilla M (2013) Plant formins: membrane anchors for actin polymerization. *Trends Cell Biol.* 23:227–233.
Waitzman JS, Rice SE (2014) Mechanism and regulation of kinesin-5, an essential motor for the mitotic spindle. *Biol. Cell* 106:1–12.

Chapter 6

Borsani O, Zhu J, Verslues PE, Sunkar R, Zhu J-K (2005) Endogenous siRNAs derived from a pair of natural cis-antisense transcripts regulate salt tolerance in Arabidopsis. *Cell* 123(7):1279–1291.
Brennicke A, Leaver CJ (2007) Mitochondrial genome organization and expression in plants. *eLS* doi:10.1002/9780470015902.a0003825.
Brown GG, Colas des Francs-Small C, Ostersetzer-Biran O (2014) Group II intron splicing factors in plant mitochondria. *Front. Plant Sci.* 18:5–35.
Bryant JA, Aves SJ (2011) Initiation of DNA replication: functional and evolutionary aspects. *Ann. Bot.* 107:1119–1126.
Curtin SJ, Voytas DF, Stupar RM (2012) Genome engineering of crops with designer nucleases. *Plant Genome J.* 5(2):42.
Eamens A, Wang M-B, Smith NA, Waterhouse PM (2008) RNA silencing in plants: yesterday, today, and tomorrow. *Plant Physiol.* 147(2):456–468.
Hopper AK (2013) Transfer RNA post-transcriptional processing, turnover, and subcellular dynamics in the yeast *Saccharomyces cerevisiae*. *Genetics* 194:43–67.
Jarvis P, López-Juez E (2013) Biogenesis and homeostasis of chloroplasts and other plastids. *Nat. Rev. Mol. Cell Biol.* 14:787–802.
Lee, M, Kim B, Kim VN (2014) Emerging roles of RNA modification: m6A and U-Tail. *Cell* 158:980–987.
Lieberman-Lazarovich M, Levy AA (2011) Homologous recombination in plants: an antireview. *Methods Mol. Biol.* 701:51–65.
Manavella PA, Hagmann J, Ott F, Laubinger S, Franz M, Macek B, Weigel D (2012) Fast-forward genetics identifies plant CPL phosphatases as regulators of miRNA processing factor HYL1. *Cell* 151:859–870.
Nandakumar J, Cech TR (2013) Finding the end: recruitment of telomerase to telomeres. *Nat. Rev. Mol. Cell Biol.* 14:69–82.
Reddy ASN, Marquez Y, Kalyna M, Barta A (2013) Complexity of the alternative splicing landscape in plants. *The Plant Cell* 25:3657–3683.
Sancar A, Lindsey-Boltz LA, Unsal-Kaçmaz K, Linn S (2004) Molecular mechanisms of mammalian DNA repair and the DNA damage checkpoints. *Annu. Rev. Biochem.* 73:39–85.
Takenaka M, Zehrmann A, Verbitskiy D, Härtel B, Brennicke A (2013) RNA editing in plants and its evolution. *Annu. Rev. Genet.* 47:335–352.
Waterhouse PM, Graham MW, Wang MB (1998) Virus resistance and gene silencing in plants can be induced by simultaneous expression of sense and antisense RNA. *Proc. Natl. Acad. Sci. USA* 95:13959–13964.
Wierzbicki A, Haag J, Pikaard CS (2008) Noncoding transcription by RNA polymerase Pol IVb/Pol V mediates transcriptional silencing of overlapping and adjacent genes. *Cell* 135:635–648.
Zhai J, Jeong D-H, De Paoli E, et al. (2011) MicroRNAs as master regulators of the plant NB-LRR defense gene family via the production of phased, trans-acting siRNAs. *Genes Devel.* 25:2540–2553.

Chapter 7

Galili G (2011) The aspartate-family pathway of plants. Linking production of essential amino acids with energy and stress regulation. *Plant Signal. Behav.* 6:192–195.

Hesse H, Kreft O, Maimann S, Zeh M, Hoefgen R (2004) Current understanding of the regulation of methionine biosynthesis in plants. *J. Exp. Bot.* 55:1799–1808.

Jander G, Joshi V (2010) Recent progress in deciphering the biosynthesis of aspartate-derived amino acids in plants. *Mol. Plant.* 3:54–65.

Lea PJ (1993) Nitrogen metabolism. In *Plant Biochemistry and Molecular Biology.* PJ Lea, RC Leegood, eds. John Wiley & Sons: New York, pp. 155–180.

Lea PJ, Robinson SA, Stewart GR (1990) The enzymology and metabolism of glutamine, glutamate, and asparagine. In *The Biochemistry of Plants,* Vol. 16, *Intermediary Nitrogen Metabolism.* BJ Miflin, PJ Lea, eds. Academic Press: New York, pp. 121–159.

Maeda H, Dudareva N (2012) The shikimate pathway and aromatic amino acid biosynthesis in plants. *Annu. Rev. Plant Biol.* 63:73–105.

McMurry JE, Begley TP (2005) Amino acid metabolism. In *The Organic Chemistry of Biological Pathways*, McMurry JE, Begley TP, eds. Roberts and Company Publishers: Englewood, CO, pp. 221–304.

Miller AJ, Fan X, Shen Q, Smith SJ (2007) Amino acids and nitrate as signals for the regulation of nitrogen acquisition. *J. Exp. Bot.* 59:111–119.

Nunes-Nesi A, Fernie AR, Stitt M (2010) Metabolic signaling aspects underpinning the regulation of plant carbon nitrogen interactions. *Mol. Plant* 3:973–996.

Radwanski ER, Last RL (1995) Tryptophan biosynthesis and metabolism: biochemical and molecular genetics. *Plant Cell* 7:921–934.

Slocum RD (2005) Genes, enzymes and regulation of arginine biosynthesis in plants. *Plant. Physiol. Biochem.* 43:729–745.

Stepansky A, Leustek T (2006) Histidine biosynthesis in plants. *Amino Acids* 30:127–142.

Sweetlove LJ, Felle D, Fernie AR. (2005) Getting to grips with the plant metabolic network. *Biochem. J.* 409:27–41.

Tan S, Evans R, Singh B (2006) Herbicidal inhibitors of amino acid biosynthesis and herbicidal-tolerant crops. *Amino Acids* 30:195–204.

Ufaz S, Galili G (2008) Improving the content of essential amino acids in crop plant: goals and opportunities. *Plant Physiol.* 147:954–961.

Chapter 8

Allen DK, Bates PD, Tjellström H (2015) Tracking the metabolic pulse of plant lipid production with isotopic labeling and flux analyses: past, present and future. *Progr. Lipid Res.* 58:97–120.

Badami RC, Patil KB (1980) Structure and occurrence of unusual fatty acids in minor seed oils. *Progr. Lipid Res.* 19(3):119–153.

Bates PD, Fatihi A, Snapp AR, Carlsson AS, Lu C (2012) Acyl editing and headgroup exchange are the major mechanisms that direct polyunsaturated fatty acid flux into triacylglycerols. *Plant Physiol.* 160(3):1530–1539.

Bates PD, Stymne S, Ohlrogge J (2013) Biochemical pathways in seed oil synthesis. *Curr. Opin. Plant Biol.* 16(3):358–364.

Baud S, Lepiniec L (2010) Physiological and developmental regulation of seed oil production. *Progr. Lipid Res.* 49(3):235–249.

Beisson F, Li-Beisson Y, Pollard M (2012) Solving the puzzles of cutin and suberin polymer biosynthesis. *Curr. Opin. Plant Biol.* 15(3):329–337.

Bernard A, Joubès J (2013) Arabidopsis cuticular waxes: advances in synthesis, export and regulation. *Progr. Lipid Res.* 52(1):110–129.

Browse J (2009) Jasmonate passes muster: a receptor and targets for the defense hormone. *Annu. Rev. Plant Biol.* 60:183–205.

Hölzl G, Dörmann P (2007) Structure and function of glycoglycerolipids in plants and bacteria. *Progr. Lipid Res.* 46(5):225–243.

Hurlock AK, Roston RL, Wang K, Benning C (2014) Lipid trafficking in plant cells. *Traffic*, 15(9):915–932.

Li-Beisson Y, Shorrosh B, Beisson F (2013) Acyl-lipid metabolism. *The Arabidopsis Book* 11:e0161.

Shanklin J, Guy JE, Mishra G, Lindqvist Y (2009) Desaturases: emerging models for understanding functional diversification of diiron-containing enzymes. *J. Biol. Chem.* 284(28):18559–18563.

Clemente TE, Cahoon E (2009) Soybean oil: genetic approaches for modification of functionality and total content. *Plant Physiol.* 151:1030–1040.

Theodoulou FL, Eastmond PJ (2012) Seed storage oil catabolism: a story of give and take. *Curr. Opin. Plant Biol.* 15(3):322–328.

Wallis JG, Browse J (2010) Lipid biochemists salute the genome. *Plant J.* 61(6):1092–1106.

Websites

http://aralip.plantbiology.msu.edu/
http://lipidlibrary.aocs.org/
http://www.cyberlipid.org/
http://www.lipidmaps.org/

Chapter 9

Baulcombe DC, Dean C (2014) Epigenetic regulation in plant responses to the environment. *Cold Spring Harb. Perspect. Biol.* 6:a019471.

Doyle JJ, Flagel LE, Paterson AH, et al. (2008). Evolutionary Genetics of Genome Merger and Doubling in Plants. *Annu. Rev. Genet.* 42:443–61

Farnham PJ (2009) Insights from genomic profiling of transcription factors. *Nat. Rev. Genet.* 10:605–616.

Feng S, Jacobsen SE, Reik W (2010) Epigenetic reprogramming in plant and animal development. *Science* 330:622–627.

Fransz P, de Jong H. (2011) From nucleosome to chromosome: a dynamic organization of genetic information. *Plant J.* 66:4–17.

Hirsch CD, Jiang J (2012) Centromeres: Sequences, Structure, and Biology. In *Plant Genome Diversity*, Volume 1. JF Wendel, J Greilhuber, J Dolezel, IJ Leitch, eds. Springer: Vienna, pp. 59–70.

Heslop-Harrison JS, Schwarzacher T (2011) Organisation of the plant genome in chromosomes. *Plant J.* 66:18–33.

Kelly LJ, Leitch IJ (2011). Exploring giant plant genomes with next-generation sequencing technology. *Chromosome Res.* 19:939–953.

Mardis ER (2013) Next-generation sequencing platforms. *Annu. Rev. Anal. Chem.* 6:287–303.

Morgante M, De Paoli E, Radovic S (2007). Transposable elements and the plant pan-genomes. *Curr. Opin. Plant Biol.* 10:149–155.
Paterson AH, Freeling M, Tang H, Wang X (2010). Insights from the comparison of plant genome sequences. *Annu. Rev. Plant Biol.* 61:349–72.
Riechmann JL (2002) *Transcriptional Regulation: a Genomic Overview*. The Arabidopsis Book, e0085.
Roudier F, Teixeira FK, Colot, V. (2009). Chromatin indexing in *Arabidopsis*: an epigenomic tale of tails and more. *Trends Genet.* 25:511–517.
Thomas MC, Chiang CM (2006) The general transcription machinery and general cofactors. *Crit. Rev. Biochem. Mol. Biol.* 41:105–178.
Werner F, Grohmann D (2011) Evolution of multisubunit RNA polymerases in the three domains of life. *Nat. Rev. Microbiol.* 9:85–98.
Wicker T, Sabot F, Hua-Van A, et al. (2007). A unified classification system for eukaryotic transposable elements. *Nat. Rev. Genet.* 8:973.
Zhang X (2008). The epigenetic landscape of plants. *Science* 320:489–492.

Chapter 10

Cytosolic protein synthesis and its regulation

Browning KS, Bailey-Serres J (2015) Mechanism of cytoplasmic mRNA translation. *The Arabidopsis Book* in press.
Chen X (2010) Small RNAs - secrets and surprises of the genome. *Plant J.* 61:941–958.
Dobrenel T, Marchive C, Azzopardi M, Clément G, Moreau M, Sormani R, Robaglia C, Meyer C (2013) Sugar metabolism and the plant target of rapamycin kinase: a sweet operaTOR? *Front. Plant Sci.* 4:93.
Roy B, von Arnim AG (2013) Translational regulation of cytoplasmic mRNAs. *The Arabidopsis Book* 11:e0165.
Simon AE, Miller WA (2013) 3′ Cap-independent translation enhancers of plant viruses. *Annu. Rev. Microbiol.* 67:21–42.

Protein synthesis in chloroplasts

Drechsel O, Bock R (2011) Selection of Shine-Dalgarno sequences in plastids. *Nucleic Acids Res.* 39:1427–1438.
Hirose T, Sugiura M (2004) Multiple elements required for translation of plastid atpB mRNA lacking the Shine-Dalgarno sequence. *Nucleic Acids Res.* 32:13503–13510.
Kim J, Mayfield S (1997) Protein disulfide isomerase as a regulator of chloroplast translational activation. *Science* 278:1954–1957.
Manuell A, Beligni K, Yamaguchi K, Mayfield S (2004) Regulation of chloroplast translation: interactions of RNA elements, RNA-binding proteins and the plastid ribosome. *Biochem. Soc. Trans.* 32:601–605.
Manuell A, Quispe J, Mayfield S (2007) Structure of the chloroplast ribosome. *PLoS Biol.* 5:1785–1797.
Marín-Navarro J, Manuell A, Wu J, Mayfield 3 (2007) Chloroplast translation regulation. *Photosynth. Res.* 94:359–374.
Sharma M, Wilson D, Datta P, et al. (2007) Cryo-EM study of the spinach chloroplast reveals the structural and functional roles of plastid-specific ribosomal proteins. *Proc. Natl. Acad. Sci. USA* 104:19315–19320.
Sugiura M (2014) Plastid mRNA translation. *Chloroplast Biotechnology: methods and protocols* 1132:73–91

Protein folding and post-translational modification of proteins

Boston RS, Viitanen PV, Vierling E (1996) Molecular chaperones and protein folding in plants. *Plant Mol. Biol.* 32:191–122.
Houtz RL, Portis AR (2003) The life of ribulose 1,5-bisphosphate carboxylase/oxygenase-posttranslational facts and mysteries. *Arch. Biochem. Biophys.* 414:150–158.
Jackson-Constan D, Akita M, Keegstra K (2001) Molecular chaperones involved in chloroplast protein import. *Biochim. Biophys. Acta Mol. Cell Res.* 1541(S1):102–113.
Sung DY, Kaplan F, Guy CL (2001) Plant Hsp70 molecular chaperones: Protein structure, gene family, expression and function. *Physiol. Plant* 113:443–451.
Trösch R, Mühlhaus T, Schroda M, Willmund, F (2015) ATP-dependent molecular chaperones in plastids? *More complex than expected. BBA-Bioenergetics* doi:10.1016/j.bbabio.2015.01.002.
Van Montfort R, Slingsby C, Vierling E (2002) Structure and function of the small heat shock protein/alpha-crystallin family of molecular chaperones. *Protein Fold. Cell* 59:105–156.
Walling LL (2006) Recycling or regulation? The role of amino-terminal modifying enzymes. *Curr. Opin. Plant Biol.* 9:227–233.

Protein degradation

Choi CM, Gray WM, Mooney S, Hellmann H (2014) Composition, roles, and regulation of cullin-based ubiquitin E3 ligases. *The Arabidopsis Book* 11:e0175.
Gray WM, Kepinski S, Rouse D, Leyser O, Estelle M (2001) Auxin regulates SCFTIR1-dependent degradation of AUX/IAA proteins. *Nature* 414:271–276.
Hoecker U (2005) Regulated proteolysis in light signaling. *Curr. Opin. Plant Biol.* 8:469–476.
Kapri-Pardes E, Naveh L, Adam Z (2007) The thylakoid lumen protease Deg1 is involved in the repair of photosystem II from photoinhibition in Arabidopsis. *Plant Cell* 19:1039–1047.
Müntz K (2007) Protein dynamics and proteolysis in plant vacuoles. *J. Exp. Bot.* 58:2391–2407.
Nelson CJ, Lei L, Millar AH (2014) Quantitative analysis of protein turnover in plants. *Proteomics* 14:579–592.
Nishimura K, van Wijk KJ (2014) Organization, function and substrates of the essential Clp protease system in plastids. *Biochim. Biophys. Acta* doi:10.1016/j.bbabio.2014.11.012.
Sakamoto W (2006) Protein degradation machineries in plastids. *Annu. Rev. Plant Biol.* 57:599–621.
Tan X, Calderon-Villalobos LI, Sharon M, Zheng C, Robinson CV, Estelle M, Zheng N (2007) Mechanism of auxin perception by the TIR1 ubiquitin ligase. *Nature* 446:640–645.
van der Hoom R (2008) Plant proteases: from phenotypes to molecular mechanisms. *Annu. Rev. Plant Biol.* 59:191–223.
Yoshioka-Nishimura M, Yamamoto Y (2014) Quality control of Photosystem II: the molecular basis for the action of FtsH protease and the dynamics of the thylakoid membranes. *J. Photochem. Photobiol.* 137:100–106.

Chapter 11

Barr FA, Gruneberg U. (2007) Cytokinesis: placing and making the final cut. *Cell* 30:847–860.

Cools T, De Veylder L. (2009) DNA stress checkpoint control and plant development. *Curr. Opin. Plant Biol.* 12:23–28.

De Veylder L, Larkin JC, Schnittger A. (2011) Molecular control and function of endoreplication in development and physiology. *Trends Plant Sci.* 16:624–634.

Dewitte W, Murray JA. (2003) The plant cell cycle. *Annu. Rev. Plant. Biol.* 54:235–264.

Fleming A. J. (2006) Leaf initiation: the integration of growth and cell division. *Plant Mol. Biol.* 60(6):905–914.

Gutierrez C. (2005) Coupling cell proliferation and development in plants. *Nat. Cell. Biol.* 7:535–541.

Gutzat R, Borghi L, Gruissem W. (2012) Emerging roles of the RETINOBLASTOMA-RELATED proteins in evolution and plant development. *Trends Plant Sci.* 17:139–148.

Hartwell LH. (1991) Twenty-five years of cell cycle genetics. *Genetics* 129:975–980.

Inzé D, De Veylder L. (2006) Cell cycle regulation in plant development. *Annu. Rev. Genet.* 40:77–105.

Komaki S, Sugimoto K. (2012) Control of the plant cell cycle by developmental and environmental cues. *Plant Cell. Physiol.* 53:953–964.

Lloyd C, Chan J (2006) Not so divided: the common basis of plant and animal cell division. *Nat. Rev. Mol. Cell Biol.* 7:147–152.

Marrocco K, Bergdoll M, Achard P, et al. (2010) Selective proteolysis sets the tempo of the cell cycle. *Curr. Opin. Plant Biol.* 13:631–639.

Morgan DO. (2007) *The Cell Cycle: Principles of Control*. Primers in Biology series. New Science Press.

Ten Hove CA, Heidstra R. (2008) Who begets whom? Plant cell fate determination by asymmetric cell division. *Curr. Opin. Plant Biol.* 11(1):34-41.

Chapter 12

Blankenship RE (2014) *Molecular Mechanisms of Photosynthesis*, 2nd Edition. Wiley-Blackwell.

Bordych C, Eisenhut M, Pick TR, et al. (2013) Co-expression analysis as tool for the discovery of transport proteins in photorespiration. *Plant Biol.* 15:686–693.

Bryant DA, Frigaard N-U (2006) Prokaryotic photosynthesis and phototrophy illuminated. *Trends Microbiol.* 14:488–496.

Busch A, Hippler M (2011) The structure and function of eukaryotic photosystem I. *Biochim. Biophys. Acta* 1807:864–877.

Cardona T, Sedoud A, Cox N, Rutherford AW (2012) Charge separation in photosystem II: a comparative and evolutionary overview. *Biochim. Biophys. Acta* 1817:26–43.

Christin PA, Arakaki M, Osborne CP, et al. (2014) Shared origins of a key enzyme during the evolution of C_4 and CAM metabolism. *J. Exp. Bot.* 65:3609–3621.

Cramer WA, Hasan SS, Yamashita E (2011) The Q cycle of cytochrome bc complexes: a structural perspective. *Biochim. Biophys. Acta* 1807:788–802.

Croce R, van Amerongen H (2014) Natural strategies for photosynthetic light harvesting. *Nature Chem. Biol.* 10:492–501.

Denton AK, Simon R, Weber APM (2013) C_4 photosynthesis: from evolutionary analyses to strategies for synthetic reconstruction of the trait. *Curr. Opin. Plant Biol.* 16:315–321.

Ducat DC, Silver PA (2012) Improving carbon fixation pathways. *Curr. Opin. Chem. Biol.* 16:337–344.

Florian A, Araújo WL, Fernie AR (2013) New insights into photorespiration obtained from metabolomics. *Plant Biol.* 15: 656–66.

Fuchs G (2011) Alternative pathways of carbon dioxide fixation: insights into the early evolution of life? *Annu. Rev. Microbiol.* 65:631–658.

Hagemann M, Fernie AR, Espie GS, et al. (2013) Evolution of the biochemistry of the photorespiratory C_2 cycle. *Plant Biol.* 15:639–647.

Henderson JN, Kuriata AM, Fromme R, et al. (2011) Atomic resolution X-ray structure of the substrate recognition domain of higher plant ribulose-bisphosphate carboxylase/oxygenase (Rubisco) activase. *J. Biol. Chem.* 286:35683–35688.

Hibberd JM, Covshoff S (2010) The regulation of gene expression required for C_4 photosynthesis. *Annu. Rev. Plant Biol.* 61:181–207.

Hisabori T, Sunamura E-I, Kim Y, Konno H. (2013) The chloroplast ATP synthase features the characteristic redox regulation machinery. *Antioxid. Redox Signal.* 19:1846–1854.

Hohmann-Marriott MF, Blankenship RE (2011) Evolution of photosynthesis. *Annu. Rev. Plant Biol.* 62:515–548.

Liu Z, Yan H, Wang K, et al. (2004) Crystal structure of spinach major light-harvesting complex at 2.72 Å resolution. *Nature* 428:287–292.

Nelson N, Yocum CF (2006). Structure and function of photosystems I and II. *Annu. Rev. Plant Biol.* 57:521–565.

Peterhansel C, Offermann S (2012) Re-engineering of carbon fixation in plants – challenges for plant biotechnology to improve yields in a high-CO_2 world. *Curr. Opin. Biotech.* 23:204–208.

Rochaix J-D (2014) Regulation and dynamics of the light-harvesting system. *Annu. Rev. Plant Biol.* 65:287–309.

Sage RF, Christin PA, Edwards EJ (2011) The C_4 plant lineages of planet Earth. *J. Exp. Bot.* 62:3155–3169.

Sage RF, Khoshravesh R, Sage TL (2014) From proto-Kranz to C_4 Kranz: building the bridge to C_4 photosynthesis. *J. Exp. Bot.* 65:3341–3356.

Schürmann P, Buchanan BB (2008) The ferredoxin/thioredoxin system of oxygenic photosynthesis. *Antiox. Redox Signal* 10:1235–1273.

Shikanai T (2014) Central role of cyclic electron transport around photosystem I in the regulation of photosynthesis. *Curr. Opin. Biotech.* 26:25–30.

Tanaka R, Tanaka A (2007) Tetrapyrrole biosynthesis in higher plants. *Annu. Rev. Plant Biol.* 58:321–346.

Timm S, Bauwe H (2013) The variety of photorespiratory phenotypes – employing the current status for future research directions on photorespiration. *Plant Biol.* 15:737–747.

Tobias J, Erb TJ, Evans BS, et al. (2012) A RubisCO like protein links SAM metabolism with isoprenoid biosynthesis. *Nat. Chem. Biol.* 8:926–932.

Umena Y, Kawakami K, Shen J-R, Kamiya N (2011) Crystal structure of oxygen-evolving photosystem II at a resolution of 1.9 Å. *Nature* 473:55–60.

Chapter 13

Björnberg O, Maeda K, Svensson B, Hägglund P (2012) Dissecting molecular interactions involved in recognition of target disulfides by the barley thioredoxin system. *Biochemistry* 51:9930–9939.

Buchanan BB, Balmer Y (2005) Redox regulation: a broadening horizon. *Annu. Rev. Plant Biol.* 56:187–220.
Chia T, Thorneycroft D, Chapple A, et al. (2004) A cytosolic glycosyltransferase is required for conversion of starch to sucrose in *Arabidopsis* leaves at night. *Plant J.* 37:853–863.
Denyer K, Johnson P, Zeeman SC, Smith AM (2001) The control of amylose synthesis. *J. Plant Physiol.* 158:479–487.
Fernie AR, Geigenberger P, Stitt M. (2005) Flux an important, but neglected, component of functional genomics. *Curr. Opin. Plant Biol.* 8:174–182.
Fincher G (1989) Molecular and cellular biology associated with endosperm mobilization in germinating cereal grains. *Annu. Rev. Plant Physiol. Plant Mol. Biol.* 40:305–346.
Gibon Y, Bläsing OE, Palacios-Rojas N, et al. (2004) Adjustment of diurnal starch turnover to short days: depletion of sugar during the night leads to a temporary inhibition of carbohydrate utilization, accumulation of sugars and post-translational activation of ADP-glucose pyrophosphorylase in the following light period. *Plant J.* 39:847–862.
Huber SC, Huber JL (1996) Role and regulation of sucrose-phosphate synthase in plants. *Annu Rev Plant Physiol. Plant Mol. Biol.* 47:431–444.
Kruger NJ, von Schaewen A. (2003) The oxidative pentose phosphate pathway: structure and organisation. *Curr. Opin. Plant Biol.* 6:236–246.
Michalska J, Zauber H, Buchanan BB, et al. (2009) NTRC links built-in thioredoxin to light and sucrose in regulating starch synthesis in chloroplasts and amyloplasts. *Proc. Natl Acad. Sci. USA* 106:9908–9913.
Moore B, Zhou L, Rolland F, et al. (2003) Role of the Arabidopsis glucose sensor HXK1 in nutrient, light, and hormonal signaling. *Science* 300:332–336.
Nielsen TH, Rung JH, Villadsen D. (2004) Fructose-2,6-bisphosphate: a traffic signal in plant metabolism *Trends Plant. Sci.* 9:556–563.
Ponnu J, Wahl V, Schmid M. (2011) Trehalose-6-phosphate: connecting plant metabolism and development. *Front. Plant Sci.* 2:70.
Plaxton WC, Podestá FE (2006) The functional organization and control of plant respiration. *Crit. Rev. Plant Sci.* 25:159–198.
Reinhold H, Soyk S, Simkova K, et al. (2011) Beta-amylase–like proteins function as transcription factors in Arabidopsis, controlling shoot growth and development. *Plant Cell* 23:1391–1403.
Rolland F, Baena-Gonzalez E, Sheen J (2006) Sugar sensing and signaling in plants: Conserved and novel mechanisms. *Annu. Rev. Plant Biol.* 57:675–709.
Ruan Y-L, Jin Y, Yang Y-J, et al. (2010) Sugar Input, metabolism, and signalling mediated by invertase: roles in development, yield potential, and response to drought and heat. *Mol. Plant* 3:942–955.
Satoh-Nagasawa N, Nagasawa N, Malcomber S, et al. (2006) A trehalose metabolic enzyme controls inflorescence architecture in maize. *Nature* 441: 227–230.
Stitt M, Lunn J, Usadel B (2010) Arabidopsis and primary photosynthetic metabolism—more than the icing on the cake. *Plant J.* 61:1067–1091.
Szecowka M, Heise R, Tohge T, et al. (2013) Metabolic fluxes in an illuminated Arabidopsis rosette. *Plant Cell* 25:694–714.
Tiessen A, Hendriks JHM, Stitt M, et al. (2002) Starch synthesis in potato tubers is regulated by post-translational redox-modification of ADP-glucose pyrophosphorylase: a novel regulatory mechanism linking starch synthesis to the sucrose supply. *Plant Cell* 14:2191–2213.
Weber APM, Schwacke R, Flugge UI (2005) Solute transporters of the plastid envelope membrane *Annu. Rev. Plant Biol.* 56:133–164.
Williams TCR, Miguet L, Masakapalli SK, et al. (2008) Metabolic network fluxes in heterotrophic Arabidopsis cells: Stability of the flux distribution under different oxygenation conditions. *Plant Physiol.* 148:704–718.
Zeeman SC, Smith SM, Smith AM (2007) The diurnal metabolism of leaf starch. *Biochem J.* 401:13–28.
Zeeman SC, Kossmann J, Smith AM (2010) Starch; its metabolism, evolution and biotechnological modification in plants. *Annu. Rev. Plant Biol.* 61:209–234.

Chapter 14

Buchanan BB, Balmer Y (2005) Redox regulation: a broadening horizon. *Annu. Rev. Plant Biol.* 56:187–220.
Calhoun MW, Thomas J, Gennis RB (1994) The cytochrome oxidase superfamily of redox driven proton pumps. *Trends Biol. Sci.* 19:325–330.
Day DA, Whelan J, Millar AH, et al. (1995) Regulation of the alternative oxidase in plants and fungi. *Aust. J. Plant Physiol.* 22:497–509.
Douce R, Neuburger M (1989) The uniqueness of plant mitochondria. *Annu. Rev. Plant Physiol. Plant Mol. Biol.* 40:371–414.
Dry IB, Bryce JH, Wiskich JT (1987) Regulation of mitochondrial metabolism. In *The Biochemistry of Plants*, Vol. 11. DD Davies, ed. Academic Press: London, pp. 213–352.
Ernster L (ed.) (1992) *Molecular Mechanisms in Bioenergetics*. Elsevier: Amsterdam.
Fernie AR, Carrari F, Sweetlove LJ (2004) Respiratory metabolism: glycolysis, the TCA cycle and mitochondrial electron transport. *Curr. Opin. Plant Biol.* 7:254–761.
Krömer S (1995) Respiration during photosynthesis. *Annu. Rev. Plant Physiol. Plant Mol. Biol.* 46:45–70.
Millar AH, Day DA, Whelan J (2008) Mitochondrial biogenesis and function in Arabidopsis. In *The Arabidopsis Book*, CR Somerville, EM Meyerowitz, eds. American Society of Plant Biologists: Rockville, MD.
Millar AH, Whelan J, Soole KL, Day DA (2011) Organization and regulation of mitochondrial respiration in plants. *Annu. Rev. Plant Biol.* 62: 79–104.
Moller IM (2001) Plant mitochondria and oxidative stress: electron transport, NADPH turnover, and metabolism of reactive oxygen species. *Annu. Rev. Plant. Physiol. Plant Mol. Biol.* 52:561–591.
Moore AL, Shiba T, Young L, Harada S, Kita K, Ito K (2013) unraveling the heater: new insights into the structure of the alternative oxidase. *Annu. Rev. Plant Biol.* 64:637–663.
Nicholls DG, Ferguson SJ (1992) *Bioenergetics*, 2nd ed. Academic Press, London.
Peterhansel C, Maurino VG (2011) Photorespiration redesigned. *Plant Physiol.* 155:49–55.
Rasmusson AG, Soole KL, Elthon TE (2004) Alternative NAD(P)H dehydrogenases of plant mitochondria. *Annu. Rev. Plant Biol.* 55:23–39
Siedow JN, Umbach AL (1995) Plant mitochondrial electron transfer and molecular biology. *Plant Cell* 7:821–831.
Thauer RK (2007) Microbiology. A fifth pathway of carbon fixation. *Science* 318:1732–1733.

Vanlerberghe GC, McIntosh L (1997) Alternative oxidase: from gene to function. *Annu. Rev. Plant Physiol. Plant. Mol. Biol.* 48:703–734.

Chapter 15

Ainsworth EA, Bush DR (2010) Carbohydrate transport from the leaf: a highly regulated process and target to enhance photosynthesis and productivity. *Plant Physiol.* 155:64–69.

Behnke H-D, Sjolund RD (1990) *Sieve Elements. Comparative Structure, Induction and Development.* Berlin: Springer.

Brodersen CR, McElrone AJ, Choat B, Matthews MA, Shackel KA (2010) The dynamics of embolism repair in xylem: in vivo visualizations using high-resolution computed tomography. *Plant Physiol.* 154:1088–1095

Brodribb TJ, Feild TS, Sack L (2010) Viewing leaf structure and evolution from a hydraulic perspective. *Funct. Plant Biol.* 37:488–498.

Chaumont F, Tyerman SD (2014) Aquaporins: highly regulated channels controlling plant water relations. *Plant Physiol.* 164:1600–1618.

Chen L-Q, Lin W, Qu XQ, Sosso D, McFarlane HE, Londoño A, Samuels AL, Frommer WB (2015) A cascade of sequentially expressed sucrose transporters in the seed coat and endosperm provides nutrition for the Arabidopsis embryo. *Plant Cell* (epub ahead of print).

Cramer MD, Hawkins HJ, Verboom GA (2009) The importance of nutritional regulation of plant water flux. *Oecologia* 161:15–24.

De Boer AH, Volkov V (2003) Logistics of water and salt transport through the plant: structure and functioning of the xylem. *Plant Cell Environ.* 26:87–101.

De Boer AH (1999) Potassium translocation into the root xylem. *Plant Biol.* 1:36–45.

Dechorgnat J, Nguyen CT, Armengaud P, Jossier M, Diatloff E, Filleur S, Daniel-Vedele F (2011) From the soil to the seeds: the long journey of nitrate in plants. *J. Exp. Bot.* 62:1349–1359.

Evert RF (2006) *Esau's Plant Anatomy. Meristems, Cells and Tissues of the Plant Body. Their Structure, Function, and Development.* Hoboken, NJ: Wiley.

Gilliham M, Dayod M, Hocking B, Xu B, Conn SJ, Kaiser BN, Leigh RA, Tyerman SD (2011) Calcium delivery and storage in plant leaves; exploring the link with water flow. *J. Exp. Bot.* 62:2233–2250.

Hafke JB, van Amerongen JK, Kelling F, Furch ACU, Gaupels F, van Bel AJE (2005) Thermodynamic battle for photosynthate acquisition between sieve tubes and adjoining parenchyma in transport phloem. *Plant Physiol.* 138:1527–1537.

Knoblauch M, Oparka K (2012) The structure of the phloem – still more questions than answers. *Plant J.* 70:147–156.

Lucas WJ, Ham BK, Kim JY (2009) Plasmodesmata – bridging the gap between neighbouring plant cells. *Trends Cell Biol.* 19:495–503.

Maule AJ, Benitez-Alfonso Y, Faulkner C (2011) Plasmodesmata – membrane channels with attitude. *Curr. Opin. Plant Biol.* 14:683–690.

Naseera S, Leea Y, Lapierreb C, Frankec R, Nawratha C, Geldner N (2012) Casparian strip diffusion barrier in Arabidopsis is made of a lignin polymer without suberin. *Proc. Natl. Acad. Sci. USA* 109:10101–10106.

Patrick JW (2013) Does Don Fisher's high-pressure manifold model account for phloem transport and resource partitioning? *Front. Plant Sci.* 4:184.

Patrick JW (2013) Fundamentals of phloem transport physiology. In *Phloem. Molecular Cell Biology, Systemic Communication, Biotic Interactions.* Thompson GA, van Bel AJE, eds. Chichester: Wiley-Blackwell. pp. 30–59.

Pfister A, Barberon M, Alassimone J, et al. (2014) A receptor-like kinase mutant with absent endodermal diffusion barrier displays selective nutrient homeostasis defects. *eLife* 3:e03115.

Raven JA (1977) The evolution of land plants in relation to supracellular transport processes. *Adv. Bot. Res.* 5:314–319.

Sack L, Holbrook NM (2006) Leaf hydraulics. *Annu. Rev. Plant Biol.* 57:361–381.

Slewinski TL, Zhang C, Turgeon R (2013) Structural and functional heterogeneity in phloem loading and transport. *Front. Plant Physiol.* 4:244.

Sperry JS (2003) Evolution of water transport and xylem structure. *Int. J. Plant Sci.* 164(3 suppl.):S115–S127.

Sperry JS, Hacke UG, Oren R, Comstock JP (2002) Water deficits and hydraulic limits to leaf water supply. *Plant Cell Environ.* 25:251–263.

Tegeder M, Ruan Y-L, Patrick JW (2013) Roles of plasma membrane transporters in phloem functions. In: *Phloem. Molecular Cell Biology, Systemic Communication, Biotic Interactions.* Thompson GA, van Bel AJE, eds. Chichester: Wiley-Blackwell. pp. 63–101.

Turgeon R, Wolf S (2009) Phloem transport: cellular pathways and molecular trafficking. *Annu. Rev. Plant Biol.* 60:207–221.

Turnbull CG, Lopez-Cobollo RM (2013) Heavy traffic in the fast lane: long-distance signalling by macromolecules. *New Phytol.* 198:33–51.

Tyree MT (1997) The cohesion-tension theory of sap ascent: current controversies. *J. Exp. Bot.* 48:1753–1765.

van Bel AJE (2003) The phloem, a miracle of ingenuity. *Plant Cell Environ.* 26:125–150.

van Bel AJE, Furch ACU, Hafke JB, Knoblauch M, Patrick JW (2011) Questions (n) on phloem biology. 2. Mass flow, molecular hopping, distribution patterns and macromolecular signaling. *Plant Sci.* 181:315–330.

van Bel AJE, Furch ACU, Will T, Buxa SV, Musetti R, Hafke JB (2014) Spread the news: systemic dissemination and local impact of Ca^{2+} signals along the phloem. *J. Exp. Bot.* 65:1761–1787.

Zwieniecki MA, Holbrook NM (2009) Confronting Maxwell's demon: biophysics of xylem embolism repair. *Trends Plant Sci.* 14:530–534.

Chapter 16

Amend JP, Edwards KJ, Lyons TW (eds.) (2004) *Sulfur Biogeochemistry: Past and Present*. Geological Society of America: Boulder, Colorado.

Barberon M, Berthomieu P, Clairotte M, et al. (2008) Unequal functional redundancy between the two *Arabidopsis thaliana* high-affinity sulphate transporters *SULTR1;1* and *SULTR1;2*. *New Phytol.* 180:608–619.

Bashandy T, Guilleminot J, Vernoux T, et al. (2010) Interplay between the NADP-linked thioredoxin and glutathione systems in *Arabidopsis* auxin signaling. *Plant Cell* 22:376–391.

Chan KX, Wirtz M, Phua SY, et al. (2013). Balancing metabolites in drought: the sulfur assimilation conundrum. *Trends Plant Sci.* 18:18–29.

De Angeli A, Monachello D, Ephritikhine G, et al. (2006) The nitrate/proton antiporter AtCLCa mediates nitrate accumulation in plant vacuoles. *Nature* 442: 939–942.

Desbrosses GJ, Stougaard J (2011) Root nodulation: a paradigm for how plant-microbe symbiosis influences host developmental pathways. *Cell Host Microbe.* 10:348–358.

Ehrhardt DW, Wais R, Long SR. (1996) Calcium spiking in plant root hairs responding to *Rhizobium* nodulation signals. *Cell* 85:673–681.

Erisman JW, Galloway JN, Seitzinger S, et al. (2013) Consequences of human modification of the global nitrogen cycle. *Phil. Trans. R. Soc. Lond. B Biol. Sci.* 368:20130116.

Fischer K, Barbier GG, Hecht HJ, et al. (2005) Structural basis of eukaryotic nitrate reduction: crystal structures of the nitrate reductase active site. *Plant Cell* 17:1167–1179.

Georgiadis M, Komiya H, Chakrabarti P, et al. (1992) Crystallographic structure of the nitrogenase iron protein from *Azotobacter vinelandii*. *Science* 257:1653–1659.

Giraud E, Moulin L, Vallenet D, et al. (2007) Legume symbioses: absence of Nod genes in photosynthetic bradyrhizobia. *Science* 316:1307–1312.

Gruber N, Galloway JN (2008) An Earth-system perspective of the global nitrogen cycle. *Nature* 451:293–296.

Hageman RV, Burris R (1978) Nitrogenase and nitrogenase reductase associate and dissociate with each catalytic cycle. *Proc. Natl Acad. Sci. USA* 75:2699–2702.

Hakoyama T, Niimi K, Watanabe H, et al. (2009) Host plant genome overcomes the lack of a bacterial gene for symbiotic nitrogen fixation. *Nature* 462:514–517.

Hawkesford MJ, De Kok LJ (eds.) (2007) *Sulfur in Plants – an Ecological Perspective*. Springer: Dordrecht, The Netherlands.

Hell R, Dahl C, Knaff D, Leustek T (2008) *Sulfur Metabolism in Phototrophic Organisms*. Springer: Dordrecht, The Netherlands.

Herridge DF, Peoples MB, Boddey RM (2008) Global inputs of biological nitrogen fixation in agricultural systems. *Plant Soil* 311:1–18.

Hirai MY, Klein M, Fujikawa Y. Yano M, et al. (2005) Elucidation of gene-to-gene and metabolite-to-gene networks in *Arabidopsis* by integration of metabolomics and transcriptomics. *J. Biol. Chem.* 280:25590–25595.

Ho CH, Lin SH, Hu HC, Tsay YF (2009) CHL1 functions as a nitrate sensor in plants. *Cell* 138:1184–1194.

Hoffman BM, Lukoyanov D, Dean DR, Seefeldt LC (2013) Nitrogenase: a draft mechanism. *Acc. Chem. Res.* 46:587–595.

Houlton BZ, Wang Y-P, Vitousek PM, Field CB (2008) A unifying framework for dinitrogen fixation in the terrestrial biosphere. *Nature* 454:327–330.

Hu Y, Ribbe MW (2013) Biosynthesis of the iron-molybdenum cofactor of nitrogenase. *J. Biol. Chem.* 288:13173–13177.

Khan MS, Haas FH, Samami AA, et al. (2010) Sulfite reductase defines a newly discovered bottleneck for assimilatory sulfate reduction and is essential for growth and development in *Arabidopsis thaliana*. *Plant Cell* 22:1216–1231.

Kim J, Rees D (1992) Structural models for the metal centers in the nitrogenase molybdenum-iron protein. *Science* 257:1677–1682.

Kopriva S, Mugford SG, Baraniecka P, et al. (2012) Control of sulfur partitioning between primary and secondary metabolism. *Front Plant Sci.* 3:163.

Lambeck IC, Fischer-Schrader K, Niks D, et al. (2012) The molecular mechanism of 14-3-3-mediated inhibition of plant nitrate reductase. *J. Biol. Chem.* 287:4562–4571.

Lee B-R, Koprivova A, Kopriva S (2011) Role of HY5 in regulation of sulfate assimilation in *Arabidopsis*. *Plant J.* 67:1042–1054.

Liang G, Yang F, Yu D (2010) MicroRNA395 mediates regulation of sulfate accumulation and allocation in *Arabidopsis thaliana*. *Plant J.* 62:1046–1057.

Lillo C, Meyer C, Lea US, et al. (2004) Mechanism and importance of post-translational regulation of nitrate reductase *J Exp Bot* 55:1275–1282.

Lin SH, Kuo HF, Canivenc G, et al. (2008) Mutation of the *Arabidopsis* NRT1.5 nitrate transporter causes defective root-to-shoot nitrate transport. *Plant Cell* 20:2514–2528.

Liu K-H, Tsay Y-F (2003) Switching between the two action modes of the dual-affinity nitrate transporter CHL1 by phosphorylation. *EMBO J* 22:1005–1013.

Loque D, Lalonde S, Looger LL, et al. (2007) A cytosolic trans-activation domain essential for ammonium uptake. *Nature* 446:195–198.

Ludewig U, Neuhauser B, Dynowski M (2007) Molecular mechanisms of ammonium transport and accumulation in plants. *FEBS Lett.* 581:2301–2308.

Maruyama-Nakashita A, Nakamura Y, Tohge T, Miller AJ, Fan X, Orsel M, et al. (2007) Nitrate transport and signalling. *J. Exp. Bot.* 58:2297–2306.

Maughan SC, Pasternak M, Cairns N, et al. (2010) Plant homologs of the *Plasmodium falciparum* chloroquine-resistance transporter, *Pf*CRT, are required for glutathione homeostasis and stress responses. *Proc. Natl Acad. Sci. USA* 107:2331–2336.

Muttucumaru N, Halford NG, Elmore JS, et al. (2006) Formation of high levels of acrylamide during the processing of flour derived from sulfate-deprived wheat. *J. Agric. Food Chem.* 54:8951–8955.

Oldroyd GE, Murray JD, Poole PS, Downie JA (2011) The rules of engagement in the legume-rhizobial symbiosis. *Annu. Rev. Genetics.* 45:119–144.

Op den Camp R, Streng A, De Mita S, et al. (2011) LysM-type mycorrhizal receptor recruited for rhizobium symbiosis in nonlegume *Parasponia*. *Sci. Signal.* 331:909.

Ott T, van Dongen JT, Gunther C, et al. (2005) Symbiotic leghemoglobins are crucial for nitrogen fixation in legume root nodules but not for general plant growth and development. *Curr. Biol.* 15:531–535.

Park SW, Li W. Viehhauser A, et al. (2013) Cyclophilin 20-3 relays a 12-oxo-phytodienoic acid signal during stress responsive regulation of cellular redox homeostasis. *Proc. Natl Acad. Sci. USA* 110:9559–9564.

Patron NJ, Durnford DG, Kopriva S (2008) Sulfate assimilation in eukaryotes: fusions, relocations and lateral transfers. *BMC Evol. Biol.* 8:39.

Radutoiu S, Madsen LH, Madsen EB, et al. (2003) Plant recognition of symbiotic bacteria requires two LysM receptor-like kinases. *Nature* 425, 585–592.

Rausch T, Wachter A (2005) Sulfur metabolism: a versatile platform for launching defence operations. *Trends Plant Sci.* 10:503–509.

Ravilious GE, Nguyen A, Francois JA, Jez JM (2012) Structural basis and evolution of redox regulation in plant adenosine-5′-phosphosulfate kinase. *Proc. Natl Acad. Sci. USA* 109:309–314.

Reich PB, Hobbie SE, Lee T, et al. (2006) Nitrogen limitation constrains sustainability of ecosystem response to CO_2. *Nature* 440:922–925.

Robertson GP, Vitousek PM (2009) Nitrogen in agriculture: balancing the cost of an essential resource. *Annu. Rev. Env. Resour.* 34:97–125.

Robson RL, Eady RR, Richardson TH, et al. (1986) The alternative nitrogenase of *Azotobacter chroococcum* is a vanadium enzyme. *Nature* 322: 388–390.

Rubio LM, Ludden PW (2008) Biosynthesis of the iron-molybdenum cofactor of nitrogenase. *Annu. Rev. Microbiol.* 62:93–111.

Schepers JS, Raun WR (2008) *Nitrogen in Agricultural Systems*: ASA-CSSA-SSSA. Agronomy Monograph. Vol. 49. Madison, WI.
Searle IR, Men AE, Laniya TS, et al. (2003) Long-distance signaling in nodulation directed by a CLAVATA1-like receptor kinase. *Science* 299:109–112.
Seefeldt LC, Hoffman BM, Dean DR (2009) Mechanism of Mo-dependent nitrogenase. *Annu. Rev. Biochem.* 78:701.
Stitt M, Muller C, Matt P, et al. (2002) Steps towards an integrated view of nitrogen metabolism. *J. Exp. Bot.* 53:959–970.
Takahashi H, Kopriva S. Giordano M. et al. (2011) Sulfur assimilation in photosynthetic organisms: molecular functions and regulations of transporters and assimilatory enzymes. *Annu. Rev. Plant Biol.* 62:157–184.
Tsay YF, Ho CH, Chen HY, Lin SH (2011) Integration of nitrogen and potassium signaling. *Annu. Rev. Plant Biol.* 62: 207–26.
Udvardi M, Poole PS (2013) Transport and metabolism in legume-rhizobia symbioses. *Annu. Rev. Plant Biol.* 64:781–805.
Van de Velde W, Zehirov G, Szatmari A, et al. (2010) Plant peptides govern terminal differentiation of bacteria in symbiosis. *Science* 327:1122–1126.
Vidal EA, Gutierrez RA (2008) A systems view of nitrogen nutrient and metabolite responses in Arabidopsis. *Curr. Opin. Plant Biol.* 11:521–529.
Wang D, Griffitts J, Starker C, et al. (2010) A nodule-specific protein secretory pathway required for nitrogen-fixing symbiosis. *Science* 327:1126–1129.
Wang R, Tischner R, Gutierrez RA, et al. (2004) Genomic analysis of the nitrate response using a nitrate reductase-null mutant of *Arabidopsis*. *Plant Physiol.* 136:2512–2522.
Wang YY, Hsu, PK, Tsay YF. (2012) Uptake, allocation and signaling of nitrate. *Trends Plant Sci.* 17: 458–467.
Watanabe M, Mochida K, Kato T, et al. (2008) Comparative genomics and reverse genetics analysis reveal indispensable functions of the serine acetyltransferase gene family in *Arabidopsis*. *Plant Cell* 20:2484–2496.
Wirtz M, Hell R (2006) Functional analysis of the cysteine synthase protein complex from plants: structural, biochemical and regulatory properties. *J. Plant Physiol.* 163:273–286.
Yuan L, Loqué D, Kojima S, et al. (2007) The organization of high-affinity ammonium uptake in *Arabidopsis* roots depends on the spatial arrangement and biochemical properties of AMT1-type transporters. *Plant Cell* 19:2636–2652.

Chapter 17

Argueso CT, Hansen M, Kieber JJ (2007) Regulation of ethylene biosynthesis. *J. Plant Growth Regul.* 26:92–105.
Bishop GJ (2007) Refining the plant steroid hormone biosynthesis pathway. *Trends Plant Sci.* 12:377–380.
Fujioka S, Yokota T (2003). Biosynthesis and metabolism of brassinosteroids. *Annu. Rev. Plant Biol.* 54:137–164.
Kende H (1993) Ethylene biosynthesis. *Ann. Rev. Plant Physiol. Plant Mol. Biol.* 44:283–307.
Ohnishi T, Godza B, Watanabe B, Fujioka S, Hategan L, Ide K, Shibata K, Yokota T, Szekeres M, Mizutani M (2012) CYP90A1/CPD, a brassinosteroid biosynthetic cytochrome P450 of Arabidopsis, catalyzes C-3 oxidation. *J. Biol. Chem.* 287:31551–31560.

Chapter 18

Argueso CT, Raines T, Kieber JJ (2010) Cytokinin signaling and transcriptional networks. *Curr. Opin. Plant Biol.* 13:533–539.
Belkhadir Y, Jaillais Y (2015) The molecular circuitry of brassinosteroid signaling. *New Phytol.* 206:522–540.
Bennett T, Hines G, Leyser O (2014) Canalization: what the flux? *Trends Genet.* 30:41–48.
Casal JJ (2013) Photoreceptor signaling networks in plant responses to shade. *Annu. Rev. Plant Biol.* 64:403–427.
Holt AL, van Haperen JMA, Groot EP, Laux T (2014) Signaling in shoot and flower meristems of *Arabidopsis thaliana*. *Curr. Opin. Plant Biol.* 17:96–102.
Kim TH, Bohmer M, Hu HH, Nishimura N, Schroeder JI (2010) Guard cell signal transduction network: advances in understanding abscisic acid, CO_2, and Ca^{2+} signaling. *Annu. Rev. Plant Biol.* 61:561–591.
Kudla J, Batistič O, Hashimoto K (2010) Calcium signals: the lead currency of plant information processing. *Plant Cell* 22:541–563.
Leivar P, Monte E (2014) PIFs: systems integrators in plant development. *Plant Cell* 26:56–78.
Liebrand TWH, van den Burg HA, Joosten MHAJ (2014) Two for all: receptor-associated kinases SOBIR1 and BAK1. *Trends Plant Sci.* 19:123–132.
Merchante C, Alonso JM Stepanova AN (2013) Ethylene signaling: simple ligand, complex regulation. *Curr. Opin. Plant Biol.* 16:554–560.
Miyakawa T, Fujita Y, Yamaguchi-Shinozaki K, Tanokura M (2013) Structure and function of abscisic acid receptors. *Trends Plant Sci.* 18:259–266.
Salehin M, Bagchi R, Estelle M (2015) $SCF^{TIR1/AFB}$-based auxin perception: mechanism and role in plant growth and development. *Plant Cell* 27:9–19.
Spalding EP, Harper JF (2011) The ins and outs of cellular Ca^{2+} transport. *Curr. Opin. Plant Biol.* 14:715–720.
Traas J (2013) Phyllotaxis. *Development* 140:249–253.
Urano D, Jones AM (2014) Heterotrimeric G protein-coupled signaling in plants. *Annu. Rev. Plant Biol.* 65:365–384.
Wang WF, Bai MY, Wang ZY (2014) The brassinosteroid signaling network - a paradigm of signal integration. *Curr. Opin. Plant Biol.* 21:147–153.
Xu H, Liu Q, Yao Y, Fu XD (2014) Shedding light on integrative GA signaling. *Curr. Opin. Plant Biol.* 21:89–95.
Xu J, Zhang SQ (2015) Mitogen-activated protein kinase cascades in signaling plant growth and development. *Trends Plant Sci.* 20:56–64.

Chapter 19

Andrés F, Coupland G (2012) The genetic basis of flowering responses to seasonal cues. *Nat. Rev. Genet.* 13:627–639.
Bemer M, Grossniklaus U. (2012) Dynamic regulation of *Polycomb* group activity during plant development. *Curr. Opin. Plant Biol.* 15: 523–529.
Berger F, Twell D (2011) Germline specification and function in plants. *Annu. Rev. Plant Biol.* 62:461–484.
Causier B, Schwarz-Sommer Z, Davies B (2010) Floral organ identity: 20 years of ABCs. *Semin. Cell Dev. Biol.* 21:73–79.

Chang F, Wang Y, Wang S, Ma H (2011) Molecular control of microsporogenesis in *Arabidopsis*. *Curr. Opin. Plant Biol.* 14: 66–73.
Chevalier É, Loubert-Hudon A, Zimmerman EL, Matton DP (2011) Cell-cell communication and signalling pathways within the ovule: from its inception to fertilization. *New Phytol.* 192:13–28.
Cucinotta M, Colombo L, Roig-Villanova I (2014) Ovule development, a new model for lateral organ formation. *Front Plant Sci.* 5:117.
De Smet I, Lau S, Mayer U, Jürgens G (2010) Embryogenesis - the humble beginnings of plant life. *Plant J.* 61:959–970.
Dresselhaus T, Franklin-Tong N (2013) Male-female crosstalk during pollen germination, tube growth and guidance, and double fertilization. *Mol. Plant* 6:1018–1036.
Gehring M (2013) Genomic imprinting: insights from plants. *Annu. Rev. Genet.* 47:187–208.
Graeber K, Nakabayashi K, Miatton E, et al. (2012) Molecular mechanisms of seed dormancy. *Plant Cell Environ.* 35:1769–1786.
Gutierrez L, Van Wuytswinkel O, Castelain M, Bellini C (2007) Combined networks regulating seed maturation. *Trends Plant Sci.* 12:294–300.
Gutierrez-Marcos JF, Dickinson HG (2012) Epigenetic reprogramming in plant reproductive lineages. *Plant Cell Physiol.* 53:817–823.
Gutzat R Borghi L, Gruissem W (2012) Emerging roles of RETINOBLASTOMA-RELATED proteins in evolution and plant development. *Trends Plant Sci.* 17:139–148.
Haig D (2013) Kin conflict in seed development: an interdependent but fractious collective. *Annu Rev. Cell Dev. Biol.* 29:189–211.
Hamamura Y, Nagahara S, Higashiyama T (2012) Double fertilization on the move. *Curr. Opin. Plant Biol* 15:70–77.
Hand ML, Koltunow AM (2014) The genetic control of apomixis: asexual seed formation. *Genetics* 197:441–450.
Koltunow AM, Grossniklaus U (2003) Apomixis: a developmental perspective. *Annu. Rev. Plant Biol.* 54:547–574.
Konrad KR, Wudick MM, Feijó JA (2011) Calcium regulation of tip growth: new genes for old mechanisms. *Curr. Opin. Plant Biol.* 14:721–730.
Li J, Berger F (2012) Endosperm: food for humankind and fodder for scientific discoveries. *New Phytol.* 195:290–305.
Lituiev DS, Grossniklaus U (2014) Patterning of the angiosperm female gametophyte through the prism of theoretical paradigms. *Biochem Soc. Trans.* 42:332–339.
Meng X, Sun P, Kao TH (2011) S-RNase-based self-incompatibility in *Petunia inflata*. *Ann. Bot.* 108:637–646.
Nowack MK, Ungru A, Bjerkan KN, et al. (2010) Reproductive cross-talk: seed development in flowering plants. *Biochem. Soc. Trans.* 38:604–612.
Ó'Maoiléidigh DS, Graciet E, Wellmer F (2014) Gene networks controlling *Arabidopsis thaliana* flower development. *New Phytol.* 201:16–30.
Poulter NS, Wheeler MJ, Bosch M, et al. (2010) Self-incompatibility in *Papaver*: identification of the pollen *S*-determinant *PrpS*. *Biochem Soc. Trans.* 38:588–592.
Raissig MT, Baroux C, Grossniklaus U (2011) Regulation and flexibility of genomic imprinting during seed development. *Plant Cell* 23:16–26.
Rea AC, Nasrallah JB (2008) Self-incompatibility systems: barriers to self-fertilization in flowering plants. *Int. J. Dev. Biol.* 52:627–636.
Ream TS, Woods DP. Amasino RM (2012) The molecular basis of vernalization in different plant groups. *Cold Spring Harb. Symp. Quant. Biol.* 77:105–115.
Song J, Irwin J, Dean C (2013) Remembering the prolonged cold of winter. *Curr. Biol.* 23:R807–8011.
Sprunck S, Gross-Hardt R (2011) Nuclear behavior, cell polarity, and cell specification in the female gametophyte. *Sex Plant Reprod.* 24:123–136.
Takeuchi H, Higashiyama T (2011) Attraction of tip-growing pollen tubes by the female gametophyte. *Curr. Opin. Plant Biol.* 14:614–621.
Theissen G, Melzer R (2007) Molecular mechanisms underlying origin and diversification of the angiosperm flower. *Ann. Bot.* 100 603–619
Wendrich JR, Weijers D (2013) The *Arabidopsis* embryo as a miniature morphogenesis model. *New Phytol.* 199:14–25.

Chapter 20

Archetti M, Döring TF, Hagen SB, et al. (2009) Unravelling the evolution of autumn colors - an interdisciplinary approach. *Trends Ecol. Evol.* 24:166–173.
Courtois-Moreau CL, Pesquet E, Sjodin A, et al. (2009) A unique program for cell death in xylem fibers of *Populus* stem. *Plant J.* 58:260–274.
Diggle PK, Di Stilio VS, Gschwend AR, et al. (2011) Multiple developmental processes underlie sex differentiation in angiosperms. *Trends Genet.* 27:368–376.
Fath A, Bethke P, Lonsdale J, et al. (2000) Programmed cell death in cereal aleurone. *Plant Mol. Biol.* 44:255–266.
Fracheboud Y, Luquez V, Björkén L, et al. (2009) The control of autumn senescence in European aspen. *Plant Physiol.* 149:1982–1991.
Gan S (ed.) (2007) *Annual Plant Reviews Volume 26: Senescence Processes in Plants*. Blackwell: Oxford.
Gregersen PL, Culetic A, Boschian L, Krupinska K (2013) Plant senescence and crop productivity. *Plant Mol. Biol.* 82:603–622.
Guiboileau A, Sormani R, Meyer C, Masclaux-Daubresse C (2010) Senescence and death of plant organs: Nutrient recycling and developmental regulation. *Comptes Rendus Biologies* 333:382–391.
Gunawardena AHLAN (2008) Programmed cell death and tissue remodeling in plants. *J. Exp. Bot.* 59:445–451.
Guo Y (2013) Towards systems biological understanding of leaf senescence. *Plant Mol. Biol.* 82:519–528.
Lenk A, Thordal-Christensen H (2009) From nonhost resistance to lesion-mimic mutants: useful for studies of defense signaling. *Adv. Bot. Res.* 51:91–121.
Liu Y, Bassham DC (2012) Autophagy: pathways for self-eating in plant cells. *Annu. Rev. Plant Biol.* 63:215–237.
Minina EA, Bozhkov PV, Hofius D (2014) Autophagy as initiator or executioner of cell death. *Trends Plant Sci.* 19:692–697.
Mur LAJ, Kenton P, Lloyd AJ, et al. (2008)The hypersensitive response; the centenary is upon us but how much do we know? *J. Exp. Bot.* 59:501–520.
Ohashi-Ito K, Fukuda H (2010) Transcriptional regulation of vascular cell fates. *Curr. Opin. Plant Biol.* 13:670–676.

Roberts JA, Elliott KA, Gonzalez-Carranza ZH (2002) Abscission, dehiscence, and other cell separation processes. *Annu. Rev. Plant Biol.* 53:131–158.

Rogers HJ (2013) From models to ornamentals: how is flower senescence regulated? *Plant Mol. Biol.* 82:563–574.

Thomas H (2013) Senescence, ageing and death of the whole plant. *New Phytol.* 197:696–711.

Thomas H, Huang L, Young M, Ougham H (2009) Evolution of plant senescence. *BMC Evol. Biol.* 9:163.

Thomas H, Ougham H (2014) The stay-green trait. *J. Exp. Bot.* 65:3889–3900.

Uauy C, Distelfeld A, Fahima T, et al. (2006) A *NAC* gene regulating senescence improves grain protein, zinc, and iron content in wheat. *Science* 314:1298–1301.

van Doorn WG, Beers EP, Dangl JL, et al. (2011) Morphological classification of plant cell deaths. *Cell Death Different.* 18:1–6.

Wingler A, Roitsch T (2008) Metabolic regulation of leaf senescence: interactions of sugar signaling with biotic and abiotic stress responses. *Plant Biol.* 10(Suppl. 1):50–62.

Yamauchi T, Shimamura S, Nakazono M, Mochizuki T (2013) Aerenchyma formation in crop species: A review. *Field Crops Res.* 152:8–16.

Chapter 21

Agrios GN (2005) *Plant Pathology,* 5th ed. Academic Press, San Diego, USA.

Bird DM, Williamson VM, Abad P, et al. (2009) The genomes of root-knot nematodes. *Annu. Rev. Phytopathol.* 47:333–351.

Bolton MD, Thomma BPHJ (2011) *Plant Fungal Pathogens: Methods and Protocols*. (Methods in Molecular Biology Vol 825). Humana Press Inc., UK.

Bonardi V, Cherkis K, Nishimura MT, Dangl JL (2012) A new eye on NLR proteins: focused on clarity or diffused by complexity? *Curr. Opin. Immunol* 24:41–50.

Chisholm ST, Coaker G, Day B, Staskawicz BJ (2006) Host-microbe interactions: shaping the evolution of the plant immune response. *Cell* 124:803–814.

Current Opinions in Plant Biology – Biotic Stress special issues – August 2009, 2010, 2011, 2012, 2013, and 2014.

Day P (1974) *The Genetics of Host-Pathogen Inter-relationships*. J. Wiley, San Francisco, CA.

Deslandes L, Rivas S (2012) Catch me if you can: bacterial effectors and plant targets. *Trends Plant Sci.* 17:644–654.

Dodds P.N, Rathjen JP (2010) Plant immunity, towards an integrated view of plant-pathogen interactions. *Nature Rev. Genet* 11:539–548.

Ellis JG, Dodds PN, Lawrence GJ (2007) Flax rust resistance gene specificity is based on direct resistance-avirulence protein interactions. *Annu. Rev. Phytopathol.* 45:289–306.

Fonseca S, Chico JM, Solano R (2009) The jasmonate pathway: the ligand, the receptor and the core signalling module. *Curr. Opin. Plant Biol.* 12:539–547.

Glazebrook J (2005) Contrasting mechanisms of defense against biotrophic and necrotrophic pathogens. *Annu. Rev. Phytopathol.* 43:205–227.

Gust AA, Brunner F, Nurnberger T (2010) Biotechnological concepts for improving plant innate immunity. *Curr. Opin. Biotechnol.* 21:204–210.

Hammond-Kosack KE, Jones JDG (1996) Inducible plant defense mechanisms and resistance gene function. *Plant Cell* 8:1773–1791.

Hammond-Kosack KE (2014) Biotechnology: plant protection. In *Encyclopedia of Agriculture and Food Systems*, Vol. 2, N Van Alfen editor-in-chief. Elsevier: San Diego, CA, pp. 134–152.

Hull R (2009) *Comparative Plant Virology*, 2nd ed. Elsevier Academic Press, Amsterdam, The Netherlands.

International Aphid Consortium (2010) Genome sequence of the pea aphid *Acyrthosiphon pisum. PloS Biology*, e1000313.

Jones JD. Dangl JL (2006) The plant immune system. *Nature* 444:323–329.

Llave C (2010) Virus-derived small interfering RNAs at the core of plant–virus interactions. *Trends Plant Sci.* 15:701–707.

Loebenstein G, Carr JP (2009) *Advances in Virus Research: Natural and Engineered Resistance to Plant Viruses*. Elsevier, Inc.

Maekawa T, Kufer TA, Schulze-Lefert P (2011) NLR functions in plant and animal immune systems: so far and yet so close. *Nature Immunol.* 12:817–826.

Mitchum MG, Wang X, Wang J, Davis EL (2012) Role of nematode peptides and other small molecules in plant parasitism. *Annu. Rev. Phytopathol.* 50:175–95.

Raeffaele S, Kamoun S (2012) Genome evolution in filamentous plant pathogens: why bigger can be better. *Nature Rev. Microbiol.* 10:417–430.

Robert-Seilaniantz A, Murray Grant M, et al. (2011) Hormone crosstalk in plant disease and defense: More than just JASMONATE-SALICYLATE antagonism. *Annu. Rev. Phytopathol* 49:317–343.

Schilmiller AL, Howe GA (2005) Systemic signaling in the wound response. *Curr. Opin. Plant Biol.* 8:369–377.

Scholthof HB (2005) Plant virus transport: motions of functional equivalence. *Trends Plant Sci.* 10:376–382.

Schoonhoven LM, van Loon JJA, Dicke M (2005) *Insect-Plant Biology*. Oxford University Press.

Shirasu K (2009) The HSP90-SGT1 chaperone complex for NLR immune sensors. *Annu. Rev. Plant Biol.* 60:139–164.

Spoel SH, Dong X (2012) How do plants achieve immunity? Defence without specialized immune cells. *Nature Rev. Microbiol.* 12:89–100.

Stergiopoulos I, de Wit PJGM (2009) Fungal effector proteins. *Annu. Rev. Phytopathol.* 47:233–263.

Tampakaki AP, Skandalis N, Gazi AD, et al. (2010) Playing the "Harp": evolution of our understanding of hrp/hrc genes. *Annu. Rev. Phytopathol.* 48:347–370.

Torres MA, Jones JDG, Dangl JL (2006) Reactive oxygen species signaling in response to pathogens. *Plant Physiol.* 141:373–378.

van Loon LC, Rep, M, Pieterse CM (2006) Significance of inducible defense-related proteins in infected plants. *Annu. Rev. Phytopathol.* 44:135–162.

Vleeshouwers VGAA, Raffaele S, Vossen JH, et al. (2011) Understanding and exploiting late blight resistance in the age of effectors. *Annu. Rev. Phytopathol.* 49:507–31.

Zipfel C, Robatzek S (2010)Pathogen-associated molecular pattern triggered immunity: veni, vidi… *Plant Physiol.* 154:551–554.

Chapter 22

Bailey-Serres J, Voesenek LACJ (2008) Flooding stress: acclimations and genetic diversity. *Annu. Rev. Plant Biol.* 59:313–339.

Bailey-Serres J, Fukao T, Gibbs DJ, et al. (2012) Making sense of low oxygen sensing. *Trends Plant Sci.* 17:129–138.
Bartels D, Sunkar R (2005) Drought and salt tolerance in plants. *Crit. Rev. Plant Sci.* 24:23–58.
Chinnusamy V, Zhu JK (2009) Epigenetic regulation of stress responses in plants. *Curr. Opin. Plant Biol.* 12:133–9.
Cutler SR, Rodriguez PL, Finkelstein RR, Abrams SR (2010) Abscisic acid: Emergence of a core signaling network. *Annu. Rev. Plant Biol.* 61:651–679.
Fujita M, Fujita Y, Noutosi Y, et al. (2006) Crosstalk between abiotic and biotic stress responses: a current view from the points of convergence in stress signaling networks. *Curr. Opin. Plant Biol.* 9:436–442.
Guy C, Kaplan F, Kopka J, et al. (2008) Metabolomics of temperature stress. *Physiol. Plant* 132:220–235.
Hirayama T, Shinozaki K (2010) Research on plant abiotic stress response in the post-genome era: past, present and future. *Plant J.* 61:1041–1052.
Koskull-Doering P, Scharf K-D, Nover L (2007) The diversity of plant heat stress transcription factors. *Trends Plant Sci.* 12:452–457.
Larlindale J, Mishkind M, Vierling E (2005) Plant responses to high temperature. In *Plant Abiotic Stress*. Jenks M, Hasegawa PM, eds. Blackwell Publishing Ltd: Oxford, pp. 101–144.
Mittler R, Blumwald E (2010) Genetic engineering for modern agriculture: challenges and perspectives. *Annu. Rev. Plant Biol.* 61:443–462.
Murata N, Los DA (2006) Histidine kinase Hik33 is an important participant in cold-signal transduction in cyanobacteria. *Physiol. Plant* 126:17–27.
Steponkus PL (1984) Role of plasma membrane in freezing injury and cold acclimation. *Annu. Rev. Plant Physiol.* 35:543–584.
Thomashow MF (2010) Molecular basis of plant cold acclimation: insights gained from studying the CBF cold response pathway. *Plant. Physiol.* 154:571–577.
Uemura M, Tominaga Y, Nakagawara C, et al. (2006) Responses of the plasma membrane to low temperatures. *Physiol. Plant* 126:81–90.
Umezawa T, Nakashima K, Miyakawa T, et al. (2010) Molecular basis of the core regulatory network in ABA responses: sensing, signaling and transport. *Plant Cell Physiol.* 51:1821–1839.
Wang W, Vinocur B, Shoseyov O, Altman A (2004) Role of heat-shock proteins and molecular chaperones in abiotic stress response. *Trends Plant. Sci.* 9:244–252.
Yamaguchi-Shinozaki K, Shinozaki K (2006) Transcriptional regulatory networks in cellular responses and tolerance to dehydration and cold stresses. *Annu. Rev. Plant Biol.* 57:781–803.
Yamazaki T, Kawamura Y, Minami A, Uemura M (2008) Calcium-dependent freezing tolerance in *Arabidopsis* involves membrane resealing via synaptotagmin SYT1. *Plant Cell* 20:3389–3404.
Zhu J (2003) Regulation of ion homeostasis under salt stress. *Curr. Opin. Plant Biol.* 6:441–445.
Zhu J, Dong C H, Zhu JK (2007) Interplay between cold-responsive gene regulation, metabolism and RNA processing during plant cold acclimation. *Curr. Opin. Plant Biol.* 10: 290–295.

Chapter 23

Beauclair L, Yu A, Bouche N (2010) MicroRNA-directed cleavage and translational repression of the copper chaperone for superoxide dismutase mRNA in Arabidopsis. *Plant J.* 62:454–462.
Briat J-F (2008) Iron dynamics in plants. *Adv. Bot. Res.* 46:137–180.
Briat J-F, Curie C, Gaymard F (2007) Iron utilization in plants. *Curr. Opin. Plant Biol.* 10:276–282.
Bucher M (2007) Functional biology of plant phosphate uptake and mycorrhiza interfaces. *New Phytol.* 173:11–26.
Burkehead JL, Gogolin Reynolds KA, Abdel-Ghany SE, Cohu CM, Pilon M (2009) Copper homeostasis. *New Phytol.* 182:799–816.
Deinlein U, Stephan AB, Horie T, Luo W, Xu G, Schroeder JI (2014) Plant salt-tolerance mechanisms. *Trends Plant Sci.* 19:371–379.
Delhaize E, Gruber BD, Ryan PR (2007) The roles of organic anion permeases in aluminium tolerance and mineral nutrition. *FEBS Lett.* 581:2255–2262.
Doener P (2008) Phosphate starvation signaling: a threesome controls systemic Pi homeostasis. *Curr. Opin. Plant Biol.* 11:536–540.
Gierth M, Maser P (2007) Potassium transporters in plants–involvement in K^+ acquisition, redistribution and homeostasis. *FEBS Lett* 581:2348–2356.
Gilbert N (2009) The disappearing nutrient. *Nature* 461:716–718.
Hamamoto S, Horie T, Hauser F, Deinlein U, Schroeder JI, Uozumi N (2015) HKT transporters mediate salt stress resistance in plants: from structure and function to the field. *Curr. Opin. Biotechnol.* 32:113–120.
Hiradate S, Ma JF, Matsumoto H (2007) Strategies of plants to adapt to mineral stresses in problem soils. *Adv. Agron.* 96:65–132.
Kim SA, Guerinot ML (2007) Mining iron: Iron uptake and transport in plants. *FEBS Lett.* 581:2273–2280.
Kobayashi T, Nishizawa NK (2012) Iron uptake, translocation, and regulation in higher plants. *Annu. Rev. Plant Biol.* 63: 131–152.
Kobayashi T, Ogo Y, Itai RN, Nakanishi H, Takahashi M, Mori S, Nishizawa NK (2007) The transcription factor IDEF1 regulates the response to and tolerance of iron deficiency in plants. *Proc. Natl. Acad. Sci. USA* 104:19150–19155.
Kochian LV, Hoekenga OA, Pineros MA (2004) How do crop plants tolerate acid soils? Mechanisms of aluminum tolerance and phosphorous efficiency. *Annu. Rev. Plant Biol.* 55:459–493.
Luan S, Lan W, Chul Lee S (2009) Potassium nutrition, sodium toxicity, and calcium signaling: connections through the CBL-CIPK network. *Curr. Opin. Plant Biol.* 12:339–346.
Morrissey J, Guerinot ML (2009) Iron uptake and transport in plants: the good, the bad and the ionome. *Chem. Rev.* 109:4553–4567.
Munns R, Tester M (2008) Mechanisms of salinity tolerance. *Annu. Rev. Plant Biol.* 59:651–681.
Palmer CM, Guerinot ML (2009) Facing the challenges of Cu, Fe and Zn homeostasis in plants. *Nat. Chem. Biol.* 5:333–339.
Penarrubia L, Andres-Colas N, Moreno J, Puig S (2010) Regulation of copper transport in *Arabidopsis thaliana*: a biochemical oscillator? *J. Biol. Inorg. Chem.* 15:29–36.
Puig S, Peñarrubia L (2009) Placing metal micronutrients in context: transport and distribution in plants. *Curr. Opin. Plant Biol.* 12:299–306.
Pyo YJ, Gierth M, Schroeder JI, Cho MH (2010) High-affinity K^+ transport in Arabidopsis: AtHAK5 and AKT1 are vital for seedling establishment and postgermination growth under low-potassium conditions. *Plant Physiol.* 153:863–875.
Ryan PR, Delhaize E (2010) The convergent evolution of aluminium resistance in wheat exploits a convenient currency. *Funct. Plant Biol.* 37:275–284.
Schachtman DP, Shin R (2007) Nutrient sensing and signaling: NPKS. *Annu. Rev. Plant Biol.* 58:47–69.

Schroeder JI, Delhaize E, Frommer WB, et al. (2013) Using membrane transporters to improve crops for sustainable food production. *Nature* 497:60–66.
Tran HT, Hurley BA, Plaxton WC (2010) Feeding hungry plants: the role of purple acid phosphatases in phosphate nutrition. *Plant Sci.* 179:14–27.
Tsay YF, Ho CH, Chen HY, Lin SH (2011) Integration of nitrogen and potassium signaling. *Annu. Rev. Plant Biol.* 62:207–226.
Vance CP (2010) Quantitative trait loci, epigenetics, sugars, and microRNAs: quaternaries in phosphate acquisition and use. *Plant Physiol.* 154:582–588.
Wang Y, Wu WH (2013) Potassium transport and signaling in higher plants. *Annu. Rev. Plant Biol.* 64:451–476.
Wang YY, Hsu PK, Tsay YF (2012) Uptake, allocation and signaling of nitrate. *Trends Plant Sci.* 17:458–467.
Ward JM, Maser P, Schroeder JI (2009) Plant ion channels: gene families, physiology, and functional genomics analyses. *Annu. Rev. Physiol.* 71:59–82.
Yang XJ, Finnegan P.M. (2010) Regulation of phosphate starvation responses in higher plants. *Ann. Bot.* 105:513–526.
Yruela I (2009) Copper in plants: aquisition, transport and interactions. *Funct. Plant Biol.* 36:409–430.

Chapter 24

Al-Babili S, Beyer P (2005) Golden rice- five years on the road- five years to go? *Trends Plant Sci.* 10:565–573.
Chen F, Tholl D, Bohlmann J, Pichersky E (2011) The family of terpene synthases in plants; a mid-size family of genes for specialized metabolism that is highly diversified throughout the kingdom. *Plant J.* 66:212–229.
Christianson DW (2006) Structural biology and chemistry of the terpenoid cyclases. *Chem. Rev.* 106:3412–3442.
Degenhardt J, Köllner TG, Gershenzon J (2009) Monoterpene and sesquiterpene synthases and the origin of terpene skeletal diversity in plants. *Phytochemistry* 70:1621–1637.
Kirby J, Keasling JD (2009) Biosynthesis of plant isoprenoids: perspectives for microbial engineering. *Annu. Rev. Plant Biol.* 60:335–355.
Rodríguez-Concepción M, Boronat A (2002) Elucidation of the methylerythritol phosphate pathway for isoprenoid biosynthesis in bacteria and plastids. A metabolic milestone achieved through genomics. *Plant Physiol.* 130:1079–1089.

Cyanogenic glucosides

Bjerg-Jensen N, Zagrobelny M, Hjernø K, Olsen CE, Houghton-Larsen J, Borch J, Møller BL, Bak S (2011) Convergent evolution in biosynthesis of cyanogenic defence compounds in plants and insects. *Nat. Commun.* 2:273.
Gleadow RM, Møller BL (2014) Cyanogenic glucosides: synthesis, physiology, and plant plasticity. *Annu. Rev. Plant Biol.* 65:155–185.
Møller BL (2010) Functioning dependent metabolons. *Science* 330:1328–1329.
Takos AM, Knudsen C, Lai D, et al. (2011) Genomic clustering of cyanogenic glucoside biosynthetic genes aids their identification in *Lotus japonicus* and suggests the repeated evolution of this chemical defense pathway.*Plant J.* 68:273–286.

Glucosinolates

Halkier BA, Gershenzon J (2006) Biology and biochemistry of glucosinolates. *Annu. Rev. Plant Biol.* 57:303–333.
Sønderby IE, Geu-Flores F, Halkier BA (2010) Biosynthesis of glucosinolates-gene discovery and beyond. *Trends Plant Sci.* 15:283–290.
Stauber EJ, Kuczka, P.,van Ohlen M, Vogt B, Janowitz, T.,Piotrowski M, Beuerle, T.,Wittstock,U. (2012) Turning the 'mustard oil bomb' into a 'cyanide bomb': aromatic glucosinolate metabolism in a specialist insect herbivore: *PloS One* 7: e35545.

Alkaloids

Conner WE, Boada R, Schroeder FC, González A, Meinwald J, Eisner T (2000) Chemical defense: bestowal of a nuptial alkaloidal garment by a male moth on its mate. *Proc. Natl. Acad. Sci. USA* 97:14406–14411.
Grobe N, Lamshöft M, Orth RG, Dräger B, Kutchan TM, Zenk MH, Spiteller M (2010) Urinary excretion of morphine and biosynthetic precursors in mice. *Proc. Natl. Acad. Sci. USA* 107:8147–8152.
Higashi, Y, Kutchan TM, Smith TJ (2011) The atomic structure of salutaridine reductase from the opium poppy *Papaver somniferum*. *J. Biol. Chem.* 286:6532–6541.
Kessler D, Gase K, Baldwin IT (2008) Field experiments with transformed plants reveal the sense of floral scents. *Science* 321:1200–1202.
Kutchan TM (2005) A role for intra- and intercellular translocation in natural product biosynthesis. *Curr. Opin. Plant Biol.* 8:292–300.
Ma XY, Panjikar S, Koepke J, Loris E, Stöckigt J (2006) The structure of *Rauvolfia serpentina* strictosidine synthase is a novel six-bladed beta-propeller fold in plant proteins. *Plant Cell* 18:907–920.
Minami H (2013) Fermentative production of plant benzylisoquinoline alkaloids in microbes. *Biosci. Biotechnol. Biochem.* 77:1617–1622.
Runguphan W, Qu X, O'Connor SE (2010) Intergrating carbon-halogen bond formation into medicinal plant metabolism. *Nature* 468:461–464.
Yu F, De Luca V (2013) ATP-binding cassette transporter controls leaf surface secretion of anticancer drug components in *Catharanthus roseus*. *Proc. Natl. Acad. Sci. USA* 110: 15830–15835.

Phenolics

Ayabe S, Akashi T (2006) Cytochrome P450s in flavonoid metabolism. *Phytochem. Rev.* 5:271–282.
Davin LB, Jourdes M, Patten AM, Kim K-W, Vassão DG, Lewis NG (2008) Dissection of lignin macromolecular configuration and assembly: comparison to related biochemical processes in allyl/propenyl phenol and lignan biosynthesis. *Nat. Prod. Rep.* 25:1015–1090.
Humphreys JM, Chapple C (2002) Rewriting the lignin roadmap. *Curr. Opin. Plant Biol.* 5:224–229.

Jørgensen K, Rasmussen AV, Morant M, Nielson AH, Bjarnholt N, Zagrobelny M, Bak S, Møller BL (2005) Metabolon formation and metabolic channeling on the biosynthesis of plant natural products. *Curr. Opin. Plant. Biol.* 8:280–291.

Pichersky E, Gang D (2005) Genetics and biochemistry of secondary metabolites in plants: an evolutionary perspective. *Trends Pl. Sci.* 4:439–445.

Schuurink RC, Haring MA, Clark DG (2006) Regulation of volatile benzenoid biosynthesis in petunia flowers. *Trends Plant Sci.*11:20–25.

Suzuki S, Umezawa T (2007) Biosynthesis of lignans and norlignans. *J. Wood Sci.* 53:273–284.

Vogt T (2010) Phenylpropanoid biosynthesis. *Molecular Plant.* 3:2–20.

INDEX

Please note: Page references for text are in standard font whereas *figures* appear in italics, **tables** in bold and boxes are denoted by the number appended with a "b". Compiled by INDEXING SPECIALISTS (UK) Ltd.

3-PGA *see* 3-phosphoglycerate
4E-BPs *see* eIF4E-binding proteins
5.8S RNA, gene locations 412–414, *414*
16:3 plants 342
18:3 plants 342
18S RNA, gene locations 412–414, *414*
26S proteasomes 473, *474*, 862, *862*
28S RNA 412–414, *414*
40S ribosomes 441–442, *443*
80S ribosomes *440*, 445, 447

AAA pathway 320
A-sites, protein synthesis 444, *446*
A. tumefaciens, auxin synthesis and conjugation 802, *805*
A-type cyclin-dependent kinases (CDKAs) 483–484, *483–484*
AAPS *see* amino acid permeases
AAT genes 299
ABA *see* abscisic acid
ABC (ATP-binding cassette) transporters 28, 127–128, *127*, *128*
  aluminum tolerance 1130–1131, *1131*
  wax transport 387–388, *388*
ABCB proteins, auxin transport 854, *855*
ABC model, flower organ identity 883–885, *884–887*
ABI1 genes 136
abiotic factors, oxidative stress 1090–1091, **1092**
abiotic interactions, cell death and senescence 961–964, *961–964*
abiotic stress responses 1051–1100
  crosstalk 1097–1099
  flooding and oxygen deficit 1076–1085, **1076**, *1077–1081*, *1083–1084*
  freezing/chilling 1068–1075, *1070*, *1073*, **1074**
  gene expression 1052–1054, *1053*, 1061–1068, *1063–1068*, 1073–1075, **1074**, 1082, *1083*, 1096–1097, *1098*
  heat stress 1094–1097, *1094–1095*, *1097*
  overview 1051–1054, *1052–1053*
  oxidative stress 1085–1094
  resistance mechanisms 1052, *1052*
  water deficit 1054–1068, *1055–1060*
ABP1 (auxin-binding protein 1) 179
ABRE *see* abscisic acid-responsive elements
abscisic acid (ABA) 135, 136, *137*, 170, 777–784, *778–785*
  biosynthesis 778–784, *779–783*
  gibberellin interactions 863–865, 864b, *865*
  G-protein-coupled receptors 843
  metabolic products 784, *785*
  photomorphogenesis 863–865, 864b, *865*
  programmed cell death 931, *932*
  regulation 782–784, *783*
  regulation of xylem loading 670–671
  stomatal closure 868–870, *869–870*
  structure *770*, *778*
  vivipary 778, *778*, 782–784, *783*
  water deficit 1060–1063, *1061*, *1063–1064*, *1068*
abscisic acid-responsive elements (ABRE) **428**, 1062–1063, *1063–1064*, *1068*
absorption of light, photosynthesis 511–518, *512*, *515–518*
absorption spectra of chlorophyll *518*
ACC *see* 1-aminocyclopropane-1-carboxylic acid
ACCase *see* acetyl-CoA carboxylase
accessory proteins, cytoskeleton 202–207
acclimation
  cold 1072–1073
  flooding and oxygen deficit 1076–1085, **1076**, *1077–1081*, *1083–1084*
  heat stress 1094–1097, *1094–1095*, *1097*
  senescence 961–964, *961–964*
ACC oxidase (ACO), ethylene biosynthesis 806–810, *807–809*
ACC synthase (ACS), ethylene biosynthesis 806–809, *807–808*
Acetobacter xylinum 86, *87*
acetohydroxy acid isomeroreductase *327*, 328
acetohydroxy acid synthase (AHAS) 306b, *326*, *327*, 328, *329*
acetosyringone 996–997b
acetylation of histones 433–434, *434*
acetyl-CoA
  fatty acid synthesis 344–350, *346–349*
  generation from pyruvate 616–617, *617*
  metabolic pathways *346*
  terpene synthesis mevalonate pathway 1135–1138, *1137*
acetyl-CoA carboxylase (ACCase)
  fatty acid biosynthesis 344, *347*, 348–350
  regulation 350
acetylenation, fatty acids 362–363, *363*
acetylene, reduction by nitrogenase 717
acetylenic fatty acids 362–363, *363*
N-acetylglucosamine (GlcNAc), Nod factors 722, *723*
N-acetylglutamate *332*
N-acetylglutamate synthase (NAGS) 332, 333
N-acetylornithine 333
O-acetylserine (OAS), cysteine biosynthesis 755–757, *756–757*
O-acetylserine (thiol)lyase 756, *757*
acetyltransferases, histone modification 433–434, *434*
acid-growth hypothesis 93–94, *94*
acid invertases 579
acid soils, aluminum toxicity 1127–1131, *1128–1131*
ACO *see* ACC oxidase
aconitase, citric acid cycle 617, *619*
ACP *see* acyl carrier protein
acquisition, micronutrients 1118–1123, *1121–1124*
acridone alkaloids 313b
acrylamide 300, 750
ACS *see* ACC synthase
ACT2, functions 195–196
ACT8, functions 195–196
actin
  cell shaping 218, *218*
  contractile ring 231–233
  critical concentration 197, 199–200
  cross-linking proteins *206*, 207
  directed movement of organelles 210–216, *213–216*
  elongation 197–202, *197–199*
  filament characteristics 196–202
  filament nucleation 197–198, *197*
  fluorescent imaging 208, *209*, *211*
  gel-like networks 207
  gene families 194–199
  isoforms 195–196
  microtubule cross-linking 207
  myosin interactions 203–206, *204*, *205*
  nucleation 207
  organelle anchoring 212–213, *214*
  pathogen defense 215–216, *216*
  phragmoplasts 234–237
  phragmosome 227, *227*

Biochemistry & Molecular Biology of Plants, Second Edition. Edited by Bob B. Buchanan, Wilhelm Gruissem, and Russell L. Jones.

© 2015 John Wiley & Sons, Ltd. Published 2015 by John Wiley & Sons, Ltd.

Companion website: www.wiley.com/go/buchanan/biochem

pollen tube growth 215, *216*
preprophase band 222–226, 229, *244–245*
secretory transport 215–216
sequestering, profilin 200–202b
severing proteins *206*, 207
side-binding proteins *206*, 207
structure 197–202, *197–199*
treadmilling 200, *202*
actin depolymerizing factor 207
actin filament bundles 13, 15, *17*
actinomycetes (*Frankia*), symbiotic nitrogen fixation 719
action potentials 128, *129*
action spectra, photoreceptors 858–859b, *859*
activation
ADP-glucose pyrophosphorylase 582–584, *584*
gene expression 429–430
sulfate 752–753, *752*
active peptide hormones, proteolytic processing 457–458, *460*
active sites, fatty acid desaturases 355–356, *356–357*, *360*, 362–363
active transport, mitochondrial inner membrane 639–642, *641*, *642*
acyl-ACP:*sn*-glycerol-3-phosphate acyltransferase 366, *368*
acyl-ACP thioesterases 352, *355*
acylated sterol glycosides 11, **11**
acyl carrier protein (ACP), fatty acid biosynthesis 346, *347*, 350–356, *350–355*
acyl-exchange reactions, triacylglycerol synthesis 389–390, *390*
acyltransferase, triacylglycerol synthesis 389–390, *390*
adaptation, senescence 961–964, *961–964*
ADC *see* arginine decarboxylase
addition, amino acids, protein synthesis 444–446, *446*
adenine 243
base pairing *247*
deamination *252*
intron sequences 279
in proton pumps 120, 126
structure *241*
adenosine *241*, 257b, 279, *280*
see also ADP; AMP; ATP
adenosine deaminase 245b
adenosine phosphate-isopentenyltransferase (IPT) 787, 789–790, *789*, *790*
adenosine 5′-phosphosulfate (APS) 752–753, *752*
S-adenosyl-L-homocysteine 320
S-adenosylmethionine (SAM) 318, 319, 320–321, *320*, *322*, 323, 324, 326
competing biosynthetic pathways *807*, 809–810
ethylene biosynthesis 806–810, *807–809*
adenyl cyclase, signal transduction 843–847, *844*
5′-adenylsulfate 752–753, *752*
ADH *see* arogenate dehydrogenase
adherence, pollen to stigma 903, *903*
ADH genes 308
ADP (adenosine diphosphate) *241*, *603*, 604–605, 633–634, *634*
ADP-glucose 580–584, *582*, *584*
ADP-glucose pyrophosphorylase 580–584, *584*, 746
AEC *see* *S*-aminoethyl-L-cysteine
aerenchyma 962–963, *963*, 1076, *1077*, 1082, *1083*
aerobic respiration 610–646
citric acid cycle 613–620, **615**, *617*, *619*
mitochondria 611–612, *611*
nonphosphorylating pathways 635–639
overview 610–613
Q cycle 624–627, *628*
AFM *see* atomic force microscopy
AGPs *see* arabinogalactan proteins
agriculture
acyanogenic mutants 1150–1151b
delayed senescence 948
green revolution *776*, *777*
historical diseases 986–987b
yield 750, 1051, *1052*
Agrobacterium
auxin synthesis and conjugation 802, *805*
cytokinin synthesis 789–790, *790*
-mediated T-DNA transfer 996–997b
AGs *see* type I arabinogalactans
AHA genes 124, *124*
AHAS *see* acetohydroxy acid synthase
AICAR *see* 5-aminoimidazole-4-carboxamide ribonucleotide
air seeding, cavitation 693, *694*
ajmalicine 1068, *1173*
ajmaline *1174*
AK *see* aspartate kinase
AKT1 gene 134, *135*, 145, 1109–1113, **1111**
AKT1 K^+ channel 134, *135*, *136*, **149**
Ala *see* alanine
ALA *see* δ-aminolevulinic acid
alanine (Ala) *290*, *291*, *292*, 306b
2S albumins 179, 180–181b, 184
alditol acetates 52b, 53b
aldolase 545–548, *546–547*, 589, 600–601
aldoses 45, 46
aleurone, programmed cell death 931–932, *932*
alkaline invertases 579
alkaloids 1159–1178, *1162*, *1163–1164*, 1163b, *1164*, 1165–1166b, **1167**, *1168–1169*, 1170b, *1172–1177*
berberine synthesis pathway 1169–1170, *1175*
biosynthesis 1164–1178
biotechnology 1166b, 1171–1178, *1171*, *1180*
as defense compounds 1164
historical uses 1159–1161, *1163*
insects 1165b
physiologically active **1167**
3α-(*S*)-strictosidine 1173, *1173*
alkylation of DNA bases *252*
allelic variation, resistance genes 1026–1027, *1028*
allosteric modulation
ADP-glucose pyrophosphorylase 582–584, *584*
sucrose-phosphate synthase 577, *577*
all-*trans*-violaxanthin, abscisic acid synthesis 778–784, *779–783*
ALMT gene family 141–142, **150**
ALMT transporters, aluminum tolerance 1128–1131, *1129–1131*
α-amantin 423
α-aminoadipate 320
α-amylase, starch degradation 595–596
α-1,4-glucanotransferase, starch degradation 595–596, *595*
α-glucan phosphorylase, starch degradation 596–597
α-keto acids 636–638, *636*
α-ketobutyrate 326
α-ketoglutarate dehydrogenase 618, *619*
α-ketoglutarate (α-KG) *290*
in AAA pathway 320
ammonia assimilation 642–643, *643–644*, 650, *651*
arginine N-storage 333
in GS/GOGAT pathway 293, *295*
lysine catabolism 323, 325, *325*
mitochondrial membrane shuttling 640–641, *642*
rate of production, pyruvate kinase activity *605*
reductive amination 298, *299*
α-1,4-linkages, starch *581*, 584–586
α-1,6-linkages, starch *581*, 584–586
α-linoleic acid 11, 823–824
α-linolenic acid 11, *290*, 342
α-TIP protein 28, 185
α-tocopherol (vitamin E) 309, 1088, **1088**
α-tubulin
gene families 194–199
β-tubulin dimerization 198, *200*
alternate hosts 1007
alternative NAD(P)H dehydrogenases, mitochondria 627–629, *630*
alternative oxidase (AOX) *620*, 629–632, *631*
regulation 636–638, *637*, *638*
thermogenesis 636b
thioredoxin interactions 631, 636–637, *637*
aluminum toxicity, tolerance 1127–1131, *1128–1131*
α-amantin 423
amides
conjugation 824, *824*
nitrogen fixation 720, *734*, 735
phloem loading 679–680, *680*
amination 298
amino acid permeases (AAPs), phloem loading 679–680, *680*
amino acids
aromatic 302
functions 302
phenylalanine 306, *307*, 308–309
plastids, synthesis in 316, 318
shikimate pathway 302–305, *304*
stress impacts 318, *319*
synthesis *303*, 316, 318
tryptophan 309, *311*, 312, *312*, *313*, 314–316, *314*, *316*, *317*
tyrosine 306, *307*, 308–309
aspartate-derived 299, 318–319
lysine 319–320, *321*, 325–326, *325*
methionine 320–321, *322*, 323
plastids, synthesis in *320*, 326
regulation 323–326, *323*, *324*, *325*
threonine 319, *321*
auxin conjugates 801–802, *804*
biosynthesis pathways 289, 291–292, *291*
branched-chain 326, *326*
isoleucine 326, 328–329
leucine 329–330
valine 328–329
catabolism 318
citric acid cycle 618–620
crosspathway regulation 335b
deamination 293
essential amino acids 309, 326
functions 289
gene duplications 335b
glucosinolate biosynthesis 1160–1161b

amino acids (*cont'd*)
glutamate-derived 330
arginine 331–333, *332*
proline 330–331, *331*
histidine 333–334, *334*
homeostasis 467
nitrogen assimilation 292, *292*, *295*
AS *295*, 300–301
AspAT *295*, 299
Fd-GOGAT enzyme *295*, 296–298
GDH *295*, 298–299
GS/GOGAT cycle 293, *295*, *296*
GS isoenzymes 295–296, *295*
light effects *292*, 293, 301
primary assimilation 293
regulation 301–302
secondary assimilation 293
N-transport amino acids
asparagine 300–302, *301*, *302*
aspartate 299–300, *299*, 301–302, *301*
glutamate 293–299, *294*, *295*, *296*, *297*, *298*, 301–302
glutamine 293–299, *294*, *295*, *296*, *297*, *298*, 301–302, *302*
phloem loading 679–680, *680*
protein fusions 335b
proteinogenic 289, *291*
pyridoxal phosphate mechanism *300*
research 292
senescence 954–955, *955*
sequential addition 444–446, *446*
structure 289
transporters 291–292
α-aminoadipate 320
p-aminobenzoic acid 302
1-aminocyclopropane-1-carboxylic acid (ACC) 806–810, *807–809*
S-aminoethyl-L-cysteine (AEC) 324
5-aminoimidazole-4-carboxamide ribonucleotide (AICAR) *244*, 333, *334*
δ-aminolevulinic acid (ALA) *516–517*, 518
aminotransferases (AT) 293, 299
aromatic amino acid aminotransferases 308–309
aspartate amino transferase 292, *294*, *295*, 299, *299*, *300*, *302*
branched-chain aminotransferases 329
glutamate:oxaloacetate aminotransferase 299
glutamine-2-oxoglutarate aminotransferase 293, *302*
glutamine aminotransferase activity *312*
Iso, Leu, Val synthesis *327*, 328–329
ornithine δ-aminotransferase 330, *331*
prephenate aminotransferase *307*, 308
tyrosine aminotransferases 308–309
ammonia (NH_3) 293, 295, 296, 297–298, 301, 312, 333
assimilation 642–643, *643–644*, 650, *651*, 735, *737–738*
photorespiration 650, *651*
ammonia tunnel 296, 312, *312*
ammonium (NH_4^+)
see also nitrogen fixation
asparagine synthesis *301*
photorespiratory 293, 295–296, 298
uptake 735, *737–738*
AMP (adenosine monophosphate) *241*, *244*, 300, 333
amphipathic glycerolipids 342, **343**
AMT transporters 735, *737–738*
α-amylase, starch degradation 595–596
β-amylase (BAM), starch degradation 595–596, *595*
amylopectin 580, *581*, 584–586
amyloplasts *3*, 15, *33*, 38, *38*, 112
glucose-6-phosphate/phosphate translocator 573
gravity sensation 213
hexose phosphate antiporters 573
monocotyledons, ADP-glucose transport 582, *582*
starch synthesis 580–582, *582*
amylose
starch granules *581*, 584–586
structure 580, *581*, 584
anaerobic response element (ARE) 1082
anammox reactions 711, *712*
anaphase *224*, 231, 233–234, *478*
anaphase-promoting complex/cyclosome (APC/C) 487, *488*
ancestral duplications, genome structure 415–416, *416*
anchoring
chloroplasts to actin networks 212–213, *214*
cytoskeletal functions *194*, 220–222, *221*
mitochondria 213–214
organelles 212–213, *214*
peroxisomes 213–214, *215*
ancient signaling mechanisms 836, *836*
androgenesis 891
angiosperms, xylem tissue *665*
anillin 207
animal feed 109–110, *109*, 319
animal–plant differences
brefeldin A 177b
Ca^{2+}-ATPases 126
cell cycles 476–477
cell-to-cell communication 11
centrosomes 228, *229*
complex glycans 187, *187*
endocytosis functions 24
folding helpers 175
glycerolipids 11
Golgi apparatus position 19
inward-rectifying K^+ channels 133–134
IP_3 receptors 139
miRNAs *277*
mitochondrial genomes 43, 265
mitosis *223*
necrosis 928
nuclear lamina 192–194
organelle anchoring and movement 210–211
plasma membrane 10–11
ryanodine receptors 139
storage proteins 182
anion channels 113, 117–118, 132, *137*, 140–141, *141*, **150**
anion transport, xylem parenchyma cells 669
anisotropic expansion, cortical microtubules 216–217
anomeric carbon 46–47
anomeric configuration 50, *51*, 55b, 89, *98*
anoxia
see also flooding; hypoxia
fermenting metabolism 1079–1082, *1080–1081*, *1083*
flooding 1076–1085, **1076**, *1077–1081*, *1083–1084*
metabolic acclimation 1079–1082, *1080–1081*
senescence 962–964, *963–964*
signal perception 1085
AnS *see* anthranilate synthase
antagonistic regulation of germination 863–865, 864b, *865*
antennae, photosynthetic 526–528, *527*
anterograde regulation, stromal enzymes 551
anterograde/retrograde traffic 13, *15*, 162, *166*, 175, 178, 179
anthers
microspore culture 893b
microsporogenesis 889–891, *891–892*, 893b
pollen development 889–896, *891–892*, *894*
anthocyanins, senescence 950–951, *950*
anthranilate synthase (AnS) *303*, 309, 310b, *311*, 312, *312*, 313b
antibodies *48*, 72, 89b, 99, 100b, *102*, 164b, 165b
antibody probes *48*, 100–101b
antimycin A 622, *625*
antioxidant defenses 632–633, 1086–1089, *1087*, **1088**, **1089**
antiporters 113, 142, 145, 146, 573, 639, *640*
AOX *see* alternative oxidase
AP1 *see* APETALA1 transcription factor
AP2-like transcription factors 430
APC/C *see* anaphase-promoting complex/cyclosome
AP endonucleases 252–253, *253*
APETALA1 (AP1) transcription factor 170, 881–882, *883*
apg10 mutant 334
aphids 675–676b, 1002–1003, *1003*, **1004**
APi *see* D-apiose
apical dominance 794, *794–795*, 804, *805*
D-apiose (Api) 49
apomixis 901–902, *902*
apoplast
amino acid/amide loading into phloem 679–680, *680*
biotrophic fungi 992, *995*
definition 658–659, *662*
inward-rectifying potassium channels 680, *680*
phloem loading 677–680, *678–680*
phloem unloading 685–687, *685*, **686**, *687*
polyol loading into phloem 678, *680*
sieve element loading 673–674, *673*
signaling 838
sucrose transport 577, *578*, *580*, 677–680, *678–680*, **680**
apoptosis 926–928, *927*
apoptosomes 927–928, *927*
appressorium 215–216, 990–992, *995*, 1016, *1018*
APR *see* APS reductase
APS *see* adenosine 5′-phosphosulfate
APS kinase 763, *764*
APS reductase (APR) 753–754, *753*, 766, *767*
APX *see* ascorbate peroxidase
aquaporins 12, 27, 147–148, *147*, *148*, 151, 1055–1056
Arabidopsis thalania
AHA genes 124, *124*
AKT1 gene 134, *135*, *136*

ALMT genes 142
AtHAK5 gene 145, *145*
AtSUC genes 146
CesA genes *87–88*
CM genes 306
fatty acid desaturases **358**
Fd-GOGAT deficiency 297–298
flower structures *882*, 883–885
GLR genes 139
glycerolipid synthesis mutants 366, *368*
Golgi stack-Golgi-associated TGN units 19–20
GT genes *90*
Internet resources 89b
KAT1 K^+ channel 135, *135*
leaf senescence *947*, 948
membrane transport genes 112
microsporogenesis 891
mitochondria 43, *43*
NADH-GOGAT deficiency 297–298
N-assimilation by amino acids *292*
PAI genes 315b
plant structures *882*, 883–885
root section stains *192*
SLAC1 gene 141
telomere sequence 250, *250*
tracheary element development 936–937
transcription factor binding motifs **428**
two-component signaling system 851–852, *851*
arabinans *66*, 67, 96, 99, 103, 106
arabinogalactan proteins (AGPs) 67, 69, *71*
glycans 22
GPI anchors 10
hydroxyproline 188
O-linked glycans 22–23
type I 13, *66*
type II 67, 79
arabinose 46
L-arabinose (Ara) 49, *49*, *50*, 81
arabinosidase 96
arabinoxylans 71
arabinoxyloglucans *59*
Araceae, thermogenesis 636
arachidonic acid (C_{20}) 11
ARE *see* anaerobic response element; auxin response element
ARF-GEF GNOM complex 177b, 189
ARFs *see* auxin response factors (ARFs)
arginine (Arg) *290*, *291*, *292*, 331–333, *332*, 819, *820*
arginine decarboxylase (ADC), polyamine biosynthesis 819, *820*
argininosuccinate *332*, 333
ARGONAUTE proteins 275, *276*, *277*, 285, 286, 306, *307*, 308, 899–900
ARO1 protein 335b
arogenate dehydrogenase (ADH) *307*, 308
aromatic amino acid aminotransferases 308–309
aromatic amino acid-mediated allosteric regulation 303
aromatic amino acid-rich proteins 100
aromatic cytokinins *786*, 787, 793
aromatic substances 69–70
AROM complex 304
ARP2/3 207
arrest point, cell cycle 479
ARS *see* autonomously replicating sequence
artemisinin 1143–1145, *1145*
arthropods
pathogen introduction 1002–1003, *1003*
wound healing 1002–1003, *1003*
artificial electron acceptors, photosynthesis investigations 536, *536*
artificial mini chromosomes, genetic engineering, construction 412, *413*
arylsulfatase 765
ascorbate-glutathione redox cycle, senescence 959–961, *960*
ascorbate peroxidase (APX), senescence 959–961, *960*
ascorbate (vitamin C), antioxidant systems 1088, **1088**
asexual reproduction, apomixis/apomeiosis 901–902, *902*
Asn *see* asparagine
asparagine (Asn)
functions 300
nitrogen assimilation 292, *292*, *294*, 301–302, *302*
nitrogen fixation 720, *734*, 735
senescence 954–955, *955*
structure *290*
synthesis *291*, 300–301, *301*
asparagine synthetases (ASs) 293, *295*, 300–301, *301*, *302*
aspartate amino transferase (AspAT) 293, *294*, *295*, 299, *299*, *300*, *302*
aspartate (Asp)
functions 299
nitrogen assimilation 292, *292*, *294*, 299, *299*, 301–302
structure *290*
synthesis *291*, *299*
aspartate/glutamate carrier, mitochondria 641, *642*
aspartate kinase (AK) 319, *321*, 323–324, *324*, *325*
aspartate 4-phosphate 319
aspartate-semialdehyde dehydrogenase 319, *321*
ASs *see* asparagine synthetases
assimilation
ammonia 650, *651*, 735, *737–738*
carbon dioxide 542–551, **543–544**, *544*, *546–547*, *550*
energy costs 561–563
temperature effects 653–654, *654*
variations 557–565, *557–560*, *562–564*
micronutrients 1118–1127, *1121–1127*
nitrogen *734*, 735–746, *736–741*
sulfate 752–755, *752–754*, 764–765, *764*, 766–767, *766–767*
sulfur *748*
AT *see* aminotransferases
ataxia telangiectasis mutated (ATM) proteins, checkpoint controls 495–497, *498*
AtHAK5 gene 145, *145*
AtHKT1, xylem unloading in leaves 672
ATIs *see* auxin transport inhibitors
ATM *see* ataxia telangiectasis mutated proteins
ATM and RAD-3-related (ATR) proteins, checkpoint controls 495–497, *498*
atomic force microscopy (AFM) 76b
ATP (adenosine triphosphate)
see also ATP synthase
ABC transporters 127–128, *127*
actin polymerization 197–202, *198–199*
chemiosmotic coupling hypothesis 117
chemiosmotic processes *115*
cytoplasm/nucleus trafficking 30
formation, carbohydrate metabolism *603*, 604–605
generation in thylakoid membrane system 35
hydrolysis 122, 123–124, *123*
mitochondrial transport 633–634, *634*
net stoichiometry of sucrose oxidation **615**
nitrogenase 717–718, *717–718*
production
citric acid cycle 617–618, *619*
glycolysis, number per sucrose molecule 612
structure *241*
synthesis
anoxic metabolism 1079–1082, *1080–1081*
chloroplasts 537–540, **539**, *540*, *553–558*
conformational model 120–121, *122*
mitochondria 632–633, *633–634*
pump-driven 120–121, *122*
transport, plastids 605–606, *607*
atpB-atpE transcription unit 270, *270*
ATP-binding cassette (ABC) transporters 28, 127–128, *127*, *128*
aluminum tolerance 1130–1131, *1131*
wax transport 387–388, *388*
ATP-dependent chromatin remodeling enzymes 432
ATP-dependent phosphofructokinase (PFK) 587–588, *587*, *598*
AtPLT5 transport protein 146, *146*
ATP-phosphoribosyltransferase (ATP-PRT) 333–334
ATP sulfurylase 752–753, *752*
ATP synthase
chloroplasts 36, *37*, 120–122, 537–540, **539**, *540*, *553–558*
inhibition *625*
mitochondria 41–43, *41*, 120–122, *122*, 632–633, *633–634*
ATR *see* ATM and RAD-3-related proteins
atropine 1160, *1163*
AtSUC genes 146
AttDT gene 142
attenuation, viruses 1042–1044
AtYSL1, xylem unloading in leaves 672
AUG codons 441–442, *443*, 445b
aurora B, mitosis 233b
autolysis 96, 928
autonomous endosperm formation 902, *902*
autonomously replicating sequence (ARS) 245
autophagosomes 28, *29*, 928, *929*, **929**
autophagy 468–469, 928, *929*, **929**
autotrophy 543–544b
AUX1 proteins 189

auxin 93–94, 125, 179, 189, 312, 314, 795–806, *796–800*, *802–805*
apical dominance 794, *795*, 804, *805*
bacterial synthesis and conjugation 802, *805*
biosynthesis 796–801, *796–800*
catabolism 801, *802*
cell cycle regulation *503–506*, 504–506
conjugation 801–802, *801–803*
cytokinin interactions 794–795, *795*
developmental signaling 852–857, *853–857*
embryogenesis 917–918, *918*
ethylene regulation 804, *805*
leaf epinastry 804, *805*
nodulation 730–731
regulation *800*, 801, *802*, 805
signaling and transport integration 852–857, *853–857*
signal transduction 852–857, *853–857*
structures *770*, 795–796, *796*
tracheary element development 936
transport 854–857
tryptophan-dependent synthesis 796, *797*, *799*
tryptophan-independent synthesis 798–801, *799*
ubiquitin regulation *474*, 475
vascular development 856–857, *856–857*
Auxin-Binding Protein 1 (ABP1) 854
auxin efflux carriers 189
auxin response element (ARE) **428**, 429
auxin response factors (ARFs) 177b, 429, 853–854, *853–854*
auxin transport inhibitors (ATIs), nodulation 730–731
auxotrophic mutants 312, *313*
avirulence (Avr) genes 989, 1022
axonemes 205–206, *206*
azaserine 293, *295*
azide, complex IV inhibition 622, *625*

B-type cyclin-dependent kinases (CDKBs) 483–484, *483–484*, 493, *493*
BAC *see* bacterial artificial chromosomes
bacteria
arthropod introduction 1002–1003, *1003*
auxin synthesis and conjugation 802, *805*
hypersensitive response 965–974, *966–968*, **969–970**, *972–974*
pathogen effectors **1004**
pathogenesis 992–994, 996–997b, 998
protein synthesis 450–452, *452*
virulence gene islands *1013*
bacterial artificial chromosomes (BAC)
genetic engineering 412, *413*, 53
libraries 406–408, 407–408b
bacterial translation factors, similarity to plastid translation factors **451**
bacteriochlorophyll 515, *515*
bacteroids, symbiotic nitrogen fixation 731–733, *732–734*
BAK1, brassinosteroid signaling 840–841, *840–841*
bakery products, acrylamide 750
ball-and-stick models *49*
BAM *see* β-amylase
barbed ends, actin filaments 198
bar gene 306b
basal defense 989
basal elements, promoters 427, *427*
base excision repair 252–253
basic helix-loop-helix (bHLH) proteins 429–430, *429*
basic leucine zipper (bZIP) domain proteins 174, *174*, 429–430, *429*
Basta® 306b
BC *see* biotin carboxylase
BCAT genes 329
BCCP *see* biotin carboxyl carrier protein
"beads on a string" 402, *402*
bean (Fabaceae), tRNA *273*
benzenoids 1182, **1185**
benzoxazinoid acetal D-glucosides 1010–1012, *1015*
benzoxazinoid pesticides 316
berberine synthesis pathway, alkaloids 1169–1170, *1175*
β-amylase (BAM), starch degradation 595–596, *595*
β-carotene *1147*
abscisic acid synthesis 778–784, *781*
metabolic engineering 1145, *1147*
β-glucans
during expansion/elongation 99
endoglucanase activity *85*
expansin regulation 94–95
microfibril binding *77*
in Poales order *64*, 65
synthase evolution 72
transglucanases 96
β-glucosidation, abscisic acid 784, *785*
betaines 750, *751*
β-linked polysaccharide synthase genes 86–88, *87–88*
β-oxidation
citric acid cycle 620
gluconeogenesis 643, *645*
storage lipids 393, 395, *396*
β-propeller proteins 839b, 1173, *1179*
β-transglucanases 96
β-tubulin
gene divergence *195–196*
gene families 194–199
α-tubulin dimerization 198, *200*
vascular plants 195
bHLH *see* basic helix-loop-helix proteins
BIC *see* biotrophic interfacial complex
bifunctional transcription factors 429–430
binding change mechanism, ATP synthase 539–540, *540*, 632–633, *634*
binding protein (BiP) chaperone 170, *171*, 172–173, *172*, **172**, 175, 185
binding proteins, cytoskeletal regulation 200–202b, 206–207, *206*
bioactivation, gibberellins 773–774, *775*
bioactive gibberellins 770, *771*, 773–774, *775*
bioavailability of phosphorus 1114–1116, *1115*
bioenergy 109–110
biofuels 109–110
biological nitrogen fixation 715–735, *718*, *722–724*, *732–734*
biophysical techniques, photosynthesis investigations 572–573b
biophysics of growth 93–94, *93*
biosynthesis
abscisic acid 778–784, *779–783*
alkaloids 1164–1178
auxins 796–801, *796–800*
brassinolide 810–814, *810*, *812–813*
brassinosteroids 811–818, *813*, *815–818*
cadaverine 821, *821*
carotenoids 519, *530*
chlorophyll 456–457, *516–517*, 518–519
citric acid cycle products, uses of *615*
cutin 384, *385*
cyanogenic glycosides 1152–1157, *1152*, *1155*
cysteine 755–757, *756–757*, 766–767, *766–767*
cytokinins 787–793, *788–793*
diacylglycerol 365
energy, carbohydrate metabolism 601–606
ethylene 446, 806–810, *807–809*
extracellular lipids 384–389, *385*, *387*
fatty acids 344–363
acetyl CoA 344–350, *346–349*
acetyl-CoA carboxylase 346, *347*, 348–350
acyl carrier protein 346, *347*, 350–356, *350–355*
enoyl-ACP reductase 352, *355*
3-ketoacyl-ACP dehydratase 352, *354*
3-ketoacyl-ACP reductase 351–352, *353*, *354*
3-ketoacyl-ACP synthase *347*, 351, *354*
malonyl-CoA 346–351, *347–349*, *351*
overview *347*
thioesterases 352, *355*
five carbon units of terpenoid biosynthesis 1135–1138, *1137*
gibberellins 771–776, *772–776*
glucose 573–577, *574–577*
starch degradation 595–597, *595*, *597*
glucosinolates 1159, *1159*
glutathione 758, *759*
glycolysis products, uses of *615*
heme *516–517*, 518–519
hormones 769–832
jasmonic acid 338
jasmonyl–isoleucine 824, *824*
ent-kaurine 773, *773*
lipids *338*
Arabidopsis 358–360, **358**, *359*
membrane-specific *364–375*, 365–373
lutein 519, *530*
maltose, starch degradation 595–597, *595*, *597*
membrane lipids *364–375*, 365–373
diacylglycerol pools 365
eukaryotic pathway *364–369*, 365–373, *371–373*
prokaryotic pathway *364*, 365–372, *368–370*
nitrogen 712, *713*
PAPS 746, *748*, 763, *763*
pentose phosphate/triose phosphate pool products 597–599, *598*
phenolic compounds 1185–1205
phosphatidic acids *364–366*, 365
phospholipids, phosphodiester bond formation 342, 366–368, *369*
phytochelatins 759–760, *760–761*
phytosiderophores *1121*, 1122
polyamines 819–821, *820–821*
prenyl diphosphates 1138–1141, *1140–1141*
proteins 438–463
cellular compartmentalization 438–439, *439*
cofactor insertion 456–457, *457*, 458b, *459*
elongation 444, *446–447*

frameshifting 450, 450b
initiation 441–442, *443*, 447–449, *449*, 450b, 452, *452*
pauses 456–457, *457*, 458b, *459*
plastids 450–457, *452–457*, *459*
post-translational modification 457–463, *460–466*
proteolytic processing 457–458, *460*
ribosomes 439–457, *452–457*, *459*
termination 447, *448*
viral 444b, 447–450, *449*, 450b
purine *955*
pyruvate, carbohydrate metabolism 602–604, *603*
ribulose 5-phosphate, pentose phosphate pathway 601–602, *602*
salicylic acid 827–830, *829*, 1019–1022, *1021*, *1039*
starch 580–587
storage lipids 389–393, *390*
strigolactones 832–833
suberin 385, *385*
sucrose 573–577, *574–577*, 589–590
terpenoids 771–773, *772–773*, 1135–1145, *1136–1144*, *1145–1147*
waxes 338
xanthophylls 519, *530*
biotechnology 109, 1171–1178, *1171*, *1180*
biotic factors, oxidative stress 1090–1091, **1092**
biotin carboxylase (BC), acetyl-CoA carboxylase 348, *348–349*
biotin carboxyl carrier protein (BCCP), acetyl-CoA carboxylase 348, *348–349*
biotrophic fungi
apoplastic invasion 992, *995*
pathogenesis strategies 990–992, *994–996*
biotrophic interfacial complex (BIC) 1006, *1008*
BiP chaperone *see* binding protein chaperone
bisphosphoglycerate *603*, 604
bisulfite sequencing 434
BKA1, brassinosteroid signaling 840–841, *840–841*
BL *see* brassinolide
blue light, stomatal aperture control 867–868, *867–868*
boom and bust cycle, immunity 1022–1023, *1024*
BOR1 borate transporter 189
Bradyrhizobium infection, legumes 726
branched-chain aminotransferases (BCAT) 329
branching
amylopectin *581*, 584, 585–586, *586*
shoots 831–833, *831*
Brassica, self-incompatibility 911–912, *911–912*
brassinazole 773, *774*
brassinolide (BL) 189, 810–814, *810*, *812–813*
brassinosteroids (BRs) 810–818, *813*, *815–818*
biosynthesis 811–818, *813*, *815–818*
functional groups *812*, 814
molecular genetics 814–818, *816–818*
occurrence 811
receptors 838–841, *840–841*
signal transduction 838–841, *840–841*
structures *770*, *810*, 811, *812*
brefeldin A 175, 177b, 185
BREs *see* TFIIB recognition elements
BRI1 receptor 175, 189, 839–841, *840–841*
bromodomain proteins 434
Brown, R. 193
Brownian motion 192, 193b
brown-midrib mutants 109, *109*
BRs *see* brassinosteroids
BSK kinases, brassinosteroid signaling 840–841, *840–841*
bud formation, yeast 477–479
buffering supplies, phloem transport 705, *706*
bulk flow
see also water flows
benefits 663–664, *664*
phloem 663–664, *664*, 696–697, *698–700*
phloem unloading 685–686, *686*, 688, *688*
pressure potentials 663–664, *664*
theory 660b
xylem 663–664, *664*
butterflies, alkaloids 1165b
BX1 gene, benzoxazin 317b
bypass flow, xylem loading 669
bypass reactions
Agrobacterium cytokinin synthesis 790
metabolic pathways 592–593b
bZIP *see* basic leucine zipper domain proteins

C-1 kinases 83
C_2 oxidative photosynthetic carbon cycle 648–650, *649*
C_3 photosynthetic carbon fixation *see* Calvin–Benson cycle
C_3 plants, photorespiration 653–655
C_4 plants
photorespiration 647
photosynthetic carbon concentration in mitochondria 645–646, *645*
C_4 photosynthetic carbon fixation 557–563, *558–560*
energy costs 561–563
variations 560–563, *560*, **560**, *563*
C_{16} fatty acids
desaturation 352–360, *356–361*
elongation 360, *361*
C_{18} fatty acids, desaturation 352–360, *356–361*
C_{40} precursors, abscisic acid synthesis 778–782, *779–782*
Ca^{2+}-ATPases 122, *123*, 126
cadaverine, biosynthesis 821, *821*
cADPR signaling paradigms 139
CAF-1 *see* chromatin assembly factor 1
caffeine 1168, *1168*
Ca^{2+}-independent protein kinases 141
CAKs *see* CDK-activating kinases; cyclin-dependent kinase activating kinases
CAL *see* CAULIFLOWER transcription factor
calcineurin B-like interacting kinase (CIPK) 1077–1078
Calcium-binding proteins 170
calcium–calmodulin-activated protein kinase (CCaMK), nodulation *728*, 729
calcium channels 138–139
calcium-dependent protein kinases (CDPKs) 141, 1014–1016, *1017*
Calcium–homogalacturonan junction zones *78*, 97
calcium ions (Ca^{2+})
aphid feeding 675–676b
calcium-pectate interactions *78*
deficiency *1102*
gradient 138–139
junction zones in cell walls 77–78
nodulation 723, 727, *728*
pumps 126
regulation 13, 15
sequestration of toxins 28
signal transduction 112, 843–845, *845*, 868–870, *869–870*
stomatal closure 868–870, *869–870*
tracheary element development 936
transport 17, **149**
vacuolar channels 136–138, *137*, *138*, 139–140, *139*
xylem unloading 672
calcium spiking, nodulation 724, 727–729, *728*
calcium storage 667–668, 672
callose *49*, 51, 80, 85, 1016, *1018*
callose synthase complexes 13
calmodulin (CaM) 126, 844–845, *845*, 932
calnexin 170, *171*, 173
calreticulin 170, *171*, 173, 175
Calvin–Benson–Bassham cycle 31, 32
Calvin–Benson cycle 510, 542–557, **543–544**, *544*, *546–547*, *550*, *553*, *556–557*
carboxylation 545, *546–547*, 548–551, *550*
energy costs 561–563, **652**
photorespiration 648, *648*
reduction 545, *546–547*
regeneration 545–548, *546–547*
regulation 551–557, *553*, *555–558*, 563, *563*
CaM *see* calmodulin
CAM *see* crassulacean acid metabolism
camalexin 318, *319*
cAMP *see* cyclic 3prime,5′-adenosine monophosphate
cAMP-dependent protein kinase (PKA), signal transduction 843–847, *844*
campesterol *5*, 11, 811–814, *813*
canalization hypothesis, vascular development 856, *856*
5′-cap, protein synthesis initiation 441, *443*
capacitance of cells 118
Ca^{2+}-permeable channels 139–140
capillary electrophoresis 61b
cap-independent translation enhancers (CITE), viral protein translation 447–449, *449*, 450b
carbamoyl phosphate *332*, 333
carbamoyl phosphate synthetase (CPS) *332*, 333
carbocationic reaction mechanisms, terpene synthases 1141, *1142*
carbohydrate-active enzymes (CAZy) database 89, 89b, 96
carbohydrate-binding molecules (CBMs) 97, 100–101b
carbohydrates
see also sugars
AGPs 67
chemical formula 46
gluconeogenesis 643–644, *645*
metabolism 567–609
alternative oxidase regulation 637, *637*
carbon skeletons 567, *568*, 605–606, *607*
circadian clocks 591, *591*
diurnal cycles 567, *569*
energy and reduction products 601–606
fructose-2,6-bisphosphate 588–589, *589*
gene expression 606–608
hexose phosphate pool 571–573, *571–572*

carbohydrates (*cont'd*)
metabolic pools 570–573, *571–572*
partitioning
fructose-2,6-bisphosphate 588–589, *589*
sucrose/starch 587–593
starch
degradation 591–597, 594–595b, *595*, *597*
partitioning 587–593
synthesis 580–587, *582*, 583b, *584*, 588–589, *589*
sucrose
degradation and transport 577–580, *578–580*
partitioning 587–593
synthesis 573–577, *574–577*, 588–590, *589*
triose phosphate/pentose phosphate pools 597–601, *598*, *600*
synthesis in Golgi apparatus 22–23
carbon dioxide
assimilation 542–551, **543–544**, *544*, *546–547*, *550*
energy costs 561–563
temperature effects 653–654, *654*
variations 557–565, *557–560*, *562–564*
concentration
C_4 metabolism 559–560, *559–560*
mitochondria 645–646, *645*
photosynthesis rates 646–647
production, citric acid cycle 617–618, *619*
stomatal aperture responses 869–870, *870*
carbon fluxes
alternative oxidase regulation 637, *637*
hexose phosphate pool 572
carbon monoxide (CO), complex IV inhibition 622, *625*
carbon reactions, photosynthesis 542–565, **543–544**, *544*, *546–547*, *550*, *553*, *555–558*, *562–564*
carbon skeletons 301–302, *302*
ammonia assimilation 642–643, *643–644*
carbohydrate metabolism 567, *568*, 605–606, *607*
legume/rhizobial symbiosis 733
nitrate assimilation interactions 745–746
sulfate assimilation 766–767, *766–767*
terpene synthesis 1134–1145, *1136*, *1140–1144*, *1145*
transport, plastids 605–606, *607*
CarboSource Services 89b
carboxylation, Calvin–Benson cycle 545, *546–547*, 548–551, *550*
carboxyltransferases (CT) 348, *348–349*
cardiolipin *see* diphosphatidylglycerol
CArG box **428**
β-carotene *1147*
abscisic acid synthesis 778–784, *781*
metabolic engineering 1145, *1147*
carotenes 37–38
carotenoids 519, *520*, *530*, 950
carrier-kinetic approach, potassium ions 1107
carriers, mitochondrial inner membrane 639, *641*
caryopsis *106*
Casparian bands 103, 384, *386*
caspases 927–928
castasterone (CS) *810*, 814–817, *815–817*
castor bean glycerolipid hydroxylase, transgenic expression 399–400
CAT *see* catalase
catabolism
see also degradation
auxin 801, *802*
polyamines 821, *822*
senescence 951–957, *952–956*
starch 591–597, 594–595b, *595*, *597*
storage lipids 393–395, *396*
sucrose 577–580, *578–580*
ubiquitin 469–474, *470–471*, **472**, *473–474*
catalase (CAT) 31, *32*, 1088–1089, **1089**
catastrophe, microtubule elongation 202, *203*
CAULIFLOWER (CAL) transcription factor 881–882, *883*
cavitation 691–695, *694–696*
CAZy *see* Carbohydrate-active enzymes database
CBMs *see* carbohydrate-binding molecules
CCaMK *see* calcium–calmodulin-activated protein kinase
CCs *see* companion cells
CCVs *see* clathrin-coated vesicles
cdc mutants *see* cell division control mutants
CDKAs *see* A-type cyclin-dependent kinases
CDKBs *see* B-type cyclin-dependent kinases
CDKs *see* cyclin-dependent kinases
CDP-DG *see* cytidine diphosphate–diacylglycerol pathway
CDPKs *see* calcium-dependent protein kinases
CE *see* coupling elements
cell adhesion *47*, 67, 69, 96, 100, *102*
cell biology
long-distance transport modules 664–668, *664*, **665**, *667–668*
phloem 666–668, *667*
senescence 941–942, *942*
xylem 664–666, *665*
cell–cell communication 10–11
embryo sac development 900–901, *901*
microgametogenesis 890–891, *891*
cell corners 45, *47*, *48*, *102*, *103*
cell cycle 476–506
arrest point 479
checkpoint controls 495–497, *496–497*
control mechanisms 482–487, *482–488*, 497–506, *498–506*
development 497–506, *498–506*
DNA replication 491–495, *491–494*
G1-to-S transition 488–981, *489–490*
G2-to-M transition 493, *493*
growth regulator effects 504–506, *505–506*
history of research 477–482
mitosis 493–497, *493–494*, *496*
origin of recognition complex 491, *491*
phases *478*, 479
S phase progression 491–492, *491–492*
termination 479
ubiquitin-dependent proteolysis 486–487, *488*
cell damage, oxidative stress 1086
cell death 925–982
see also programmed cell death; senescence
mutants 965–971, *966–968*, **969–970**
types 925–930
cell differentiation 99, 100, 102, *102*
cell division 476–506
see also cell cycle
animal/plant cell cycles 476–477
checkpoint controls 495–497, *496–497*
cytoskeletal dynamics 222–237
lipids 337–400
mitosis 493–497, *493–494*, *496*
theories of development 499–500, *500*
totipotency 501–502, *501–502*
cell division control (*cdc*) mutants 479–481, *480*
cell expansion, microtubules 216–219, *217–220*
cell fate determination, embryo sac development 900–901, *901*
cell fusion experiments, cell cycle research 481–482, *481*
cell membranes *see* membranes
cellobiose 50, *51*
cellodextrins 65
cellohexaose 63
cellopentaose 63
cellotetraose 63, 65
cellotriose 65
cell plates
callose 51, 80
cell wall initiation 45, 80
construction 234–237, *234–237*
formation *47*
membrane *18*, *24*
cell shaping 218, *218*
cell speciation, roots 498–499, *499*
cellular compartmentalization
see also subcellular compartmentalization
antioxidant systems *1087*, **1088**, **1089**
hexose phosphate pools 573
light harvesting complex II **540**, 541–542, *541*
lipids 337, 392
membrane lipid synthesis *364–366*, 365–366
plastid–cytosol exchanges, inner envelope transporters 467–468, *569*
proteases 468–469, *468*
protein folding 462–463
protein synthesis 438–439, *439*
sulfur assimilation 755
cellular differentiation, gene expression 426–427
cellular function, heat stress 1094–1097
cellular memory, vernalization 878–879
cellular metabolism, acetyl-CoA *346*
cellular recycling 28
cellular theory 499–500, *500*
cellulose
abundance 51
cellulose-GAX framework 77–79
cellulose-XyG framework 77
evolution 70, *75*
microfibril deposition, interphase 216–217, *217*
synthesis 80–81, *82*
cellulose/crosslinking glycan network 94–96
cellulose synthase complex 13, 80, 106–107
cell viability, programmed cell death 930
cell wall monoclonal antibodies 100b
Cell Wall Navigator 89b
cell walls *3*, 106
absence affects *46*
architecture
in angiosperms 77–79
extracellular matrix 99, *102*
polymer crosslinking 79–80
primary cell walls 73, 77, *77*, *78*, *79*
biosynthesis and assembly
cellulose microfibril formation 80, *82*
crosslinking glycan and pectin formation 83–86, *85*
glycosyl transferases 89, *90*

initiation in cell plate 80
nucleotide sugar interconversion 81, 83, *83*, *84*, *85*
synthase encoding 86–88, *87–88*
synthesis sites *81*
cytoskeletal coupling, signal transduction 220–222, *221*
environmental responses *48*
evolution *75*
extensibility 93
extracellular matrix 99, *102*
formation 45
fortification 1016, *1018*
functions 45, *46*
genomics 89b
growth *see* growth
heterogeneity probes *48*, 100–101b
human/animal uses 108–110, *109*
impact on plant development/morphology 45
internet resources 89b
locking mechanism 99
loosening 90, *91*, 99
macromolecules
arabinogalactan proteins 67, 69, *71*
aromatic substances 69–70
cellulose 51, *58*
crosslinking glycans 51–52, *59*, 63, *64*, 65, *65*
pectin matrix polymers *66*, 67, *68*
polymer evolution 70–72
structural proteins 67, *69*, *70*
in meristematic root tip cell *3*
middle lamella 45
plasma membrane connections 10, *10*, *11*, 12–13, *12*, 22, 220–221
plasmodesmata 10
polymer classes 70
polymer evolution 70–72
polysaccharides 23, 234–237, *237*
pore size 78, *79*
post-death functions 103, *104*
preprophase band 222–226, *224–225*, 229
primary 45, *47*
secondary 45, *47*
elaborations 102–103, *103*
lignin *73*, 104–106
storage function 106, *106*
suberin and cutin deposits 103–104, *104*
signal transduction 107–108, *108*
staining *192*
structures 45, *46*
sugar building blocks 45–46, 48
anomeric configuration 50, *51*
linkages 50, *51*
monosaccharides 48–49
polymer branching 51
synthesis regulation 106–107, *107*
traffic *15*
turgor pressure 24, *25*, 27
type III 65
centromeres 412, *413*
centrosomes 228, *229*
ceramide 373, *375*
cereal seed development, starchy endosperm programmed cell death 930–931, *931*
CesA genes 86–88, *87–88*, 106
chain elongation
glucosinolate biosynthesis 1159, 1160–1161b
starch synthesis 585–586, *586*
chalcones *722*, 1182, **1184**
chaperones 152–153, *153*
in chloroplasts 155, *156*
copper binding 1126
in ER *167*, *171*
heat shock proteins 1095–1096
in mitochondria *157*, 158
in peroxisomes 159
prolamins 182
protein folding *171*, 458–463, *460–465*, **461**
Rubisco folding 549, *549*
chaperonins 155, 460–463, **461**, *462–465*, 1096
Characeae, cytoplasmic streaming 211–212, *213*
charge
DNA–chromatin binding 430
ribosomal proteins 440
charge separation, chlorophyll 512, 521
chaulmoogric acid *361*
checkpoint controls, cell cycle 495–497, *496–497*
chelation, iron uptake 1121–1122, *1121*
chemical imaging 99
chemical models *49*
chemical potential 116–117b
chemical shifts 55b, 56b
chemiosmotic model *115*, 117, 537–540, **539**, *540*, *553–558*
chewing insects 1002–1003, *1003*
chilling sensitivity 376–377, *377–378*
chilling stress 376–377, *377–378*, 1068–1075, *1070*, *1073*, **1074**
ChIP *see* chromatin immunoprecipitation
chiral carbon 48
chitin, Nod factors 722, *723*
Chlamydomonas
mitochondrial DNA *266*
trans-splicing mechanism 282–283b
chlorine ions (Cl^-) 141, 145
4-chloroindole-3-acetic acid, auxin signaling 795–796, *796*
chlorophyll
absence in etioplasts 35
absorption spectra *518*
biosynthesis 456–457, *516–517*, 518–519
energy levels *512*
excitation 511–515, *512*
senescence 948–951, *949*
structures *515*
chloroplast ATP synthase 537–540, **539**, *540*, *553–558*
chloroplast chaperonin (cpn60), Rubisco folding 463, *465*
chloroplast-localized enzymes, fatty acid desaturases 358, **358**
chloroplasts *33*, 34–35, *35*, 573
see also photosynthesis
aromatic amino acid synthesis 316, 318
ATP synthase 537–540, **539**, *540*, *553–558*
Calvin–Benson cycle 542–557, **543–544**, *544*, *546–547*, *550*, *553*, *556–557*
compartments 154
diagram *3*
division 39
DNA *262*, 263
DNA-dependent RNA polymerases 269–270, *269*
electron transport chain 630b
genome 261
grana stack formation 10
grana and stroma thylakoids 35–37, *35*, *36*, *37*
hexose phosphate antiporters 573
lipid synthesis *364*, 365–372, *368–370*, 374b
membranes
lipids 337, 374b, 375–376, *375*
16:3/18:3 plants 342
mRNA *275*
optimal light absorption 212–213, *214*
peroxisome-chloroplast-mitochondrion contact *32*
photorespiration 648–650, *649*
promiscuous DNA 267, *268*
proteases 469, *469*
protein synthesis 39, 450–457, *452–457*, *459*
regulation 453–455, *454–456*, *457*
protein transport to 153–155, *155*, *156*, 157
RNA editing 288
rRNA processing *284*
senescence 37–38, 941–942, 945–948, *947*, 948–951, *949*, 952–954, *952*, *954*
starch degradation 595–597, *595*
thylakoid membrane system 35, *35*
Toc and Tic complexes 155, *156*
cholesterol *5*, *6*, 11
chorismate 302–305, *303*, *304*, *311*, 312, *312*
chorismate mutase (CM) *303*, 306, *307*, *308*, 318
chorismate synthase *304*, 305
chorismic acid 302
chromatids 494, *494*
chromatin 245, 250, 402–404, *402*
condensation 430–431, 434–435, *435*
DNA binding 430–432, *432*
genomic imprinting 920–923, *921–922*
remodeling 501–502, *501–502*
chromatin assembly factor 1 (CAF-1) 432
chromatin immunoprecipitation (ChIP) 430, 431b
chromoplasts *33*, 37, *38*, 573
chromosomal maternal effects, reproductive mutants 915
chromosome breakage, transposable elements 421
chromosomes
centromeres 412, *413*
condensation 493–495, *493–494*, *496*
euchromatic arms 411–412, *412*
kinetochore interactions 230–231, *231*
nuclear domains 28–29
nucleolar organizer regions 406, 412–414, *414*
telomeres 412
CIPK *see* calcineurin B-like interacting kinase
circadian clocks
starch synthesis regulation 591, *591*
two-component signaling system 851–852, *851*
cis-regulatory code 428–429
cis-regulatory modules (CRM) 427–429, *427*, *429*
gene expression 428–429, *428*, *429*
water stress 1062–1064, *1063–1064*
cisternae
cis-Golgi 16, *19*, *20*, 23
ER 13, 15
medial-Golgi *20*, 22, 23
trans-Golgi 18, *19*, 20–21, *20*, 21–22, 23, 26, *26*
cisternal progression 20
CITE *see* cap-independent translation enhancers

citrate
alternative oxidase regulation 637, *637*
aluminum tolerance 1128–1131, *1129–1131*
mitochondrial carriers 641–642, *641–642*, 642–643, *643*
citrate synthase, citric acid cycle 617, *619*
citric acid cycle 613–620
gluconeogenesis 643–644, *645*
intermediates, biosynthetic uses *615*
α-ketoglutarate and ammonia assimilation 642–643, *643–644*
light inhibition 646
net stoichiometry of sucrose oxidation **615**
overview 612–613
products 617–618, *619*
pyruvate dehydrogenase 616–617, *617*
pyruvate kinase synergy *605*
reaction sequence 617–618, *619*
regulation 634–635, 646
citrulline *332*, 333
CK *see* cytokinins
CKIs *see* cyclin-dependant kinase inhibitory proteins
Cladosporium fulvum, pathogen effectors 1006, **1007**
Claisen condensations, 3-ketoacyl-ACP reductase 351–352, *353*
class I transposons *see* retrotransposons
class II transposons *see* DNA transposons
classification
phospholipids 339, **343**
proteases 467
terpenoids 1147–1148b
transposable elements **418**, 419–420, 422b
clathrin-coated vesicles (CCVs) *19*
endocytosis 24, *24*, *26*, 188–189, *188*
excess membrane removal 25, *25*
trans-most Golgi cisternae 21–22
secretory pathway *166*
traffic mediation 175
CLAVATA-1 homologs, nodulation 731
CLC chloride channels **150**
CLE peptide signaling 838, 839b
climacteric 959
climate change, photorespiration 654–655
Cl^- ions 141, 145
cloud formation, oceanic algae 750, *751*
ClpAP proteases 469, *469*
clustering, cyanogenic glycoside biosynthetic genes 1153–1155, *1155*
cluster roots 1115–1116, *1116*
[4Fe–4S] clusters
see also Rieske Fe–S proteins
nitrogenase 717, *717*
CLV3-like peptides, nodulation 731
CLV3 protein 177b
CM *see* chorismate mutase
CMS *see* cytoplasmic male sterility
CNGCs *see* cyclic nucleotide-gated channels
CO *see* carbon monoxide; CONSTANS
coat protein (CP)-mediated resistance 1049, *1049*
cocaine *1168*
codeine 1160, *1164*
codon initiation 441–442, *443*, 445b
codon redefinition, viruses 450, 450b
coenocytes 919–920
coevolution
defense compounds *1150*
mycorrhizal/rhizobial symbiosis hormone signaling 721b
cofactor insertion
photosynthetic proteins 456–457, *457*, *459*
toeprinting 458b
cofactors, cytochromes *623*
cohesion–tension mechanism 691–696, *693*, *695–696*
cold acclimation 12, 1072–1073
see also chilling stress; freezing stress
collection phloem 673–681, *673–674*, *677–681*, 681, **682**
collenchyma cells 103, *103*
color variation in maize 421, *423*
commercial seed legumes 720
common body plans, floral morphologies 881–882, *881*, *884–886*
companion cells (CCs)
differentiation 664
phloem development 666–668, *667*
transport phloem interactions 682–683, *683*, *685*
comparative genomics, senescence genes 943–948, *947*
compartmentalization
fatty acid desaturation 353–358, *359*
membrane lipid synthesis *364–366*, 365–366
compartments, seed development 913–914, *914*
compatible solutes 330, 1055–1056, *1056–1057*
compensation, development 500, *500*
complex I of mitochondrial electron transport chain *620*, 621
inhibition 622–623, *625*
redox potential *621*
structure and function 621–622, *624*
complex II of mitochondrial electron transport chain *620*, 621
inhibition *625*
membrane topology 622, *626*
redox potential *621*
structure and function 622, *626*
complex III of mitochondrial electron transport chain *620*, 621
inhibition 622, *625*
proton pumping 624–627
redox potential *621*
structure and function 622, *626*
complex IV of mitochondrial electron transport chain *620*, 621
inhibition 622, *625*
redox potential *621*
structure and function 622, *627*
Complex Carbohydrate Research Center 89b, 100b
complex glycans 187
component I, nitrogenase 716–717, *716*, *718*
component II, nitrogenase *716*, 717–718, *718*
composition of membranes, lipids 373–379, *375*, 376–378, *376*, *378*, 378–379, *379*
concentration
essential mineral nutrients **1103**
oxygen, legume symbiosomes 731–733
sulfur in soils 749, *750*
xylem sap solutes **671**
condensations
chromatin 430–431, 434–435, *435*
chromosomes 493–495, *493–494*, *496*
histones 430–431, 434–435, *435*
terpenoid biosynthesis 1138–1141, *1140–1141*
conformational changes, nitrogenase 717–718, *717–718*
conformational models 46, *49*
congress, chromosomes 231
coniferyl alcohol *74*, 104
coniine 1159, *1163*
conjugation
auxin 801–802, *802–803*
cytokinins 787, *788*
isoprene units 1134–1135, *1136*
ubiquitin 469, *471*, 473–475, **472**, *473*
consensus sequences, protein synthesis initiation 441
conservation
cytoskeletal genes 194–196
energy, glycolysis 602–604
phosphate, chloroplast membrane synthesis 374b
single-copy genes 416
thioredoxin structures 552b, 554b
CONSTANS (CO), photoperiod sensing 876–878
construction of cell plates, phragmoplasts 234–237, *234–237*
contig, definition 406
contractile ring 231–233
control mechanisms, cell cycle 482–487, *482–488*
cooking, starch's usefulness 585b
cooling, retrogradation in starchy foods 585b
COPI vesicles 21, *166*, 175
COPIa vesicles 21
COPIb vesicles 21
COPII scaffold 22
COPII vesicles
budding *18*, *21*, 22, *23*
ER-to-Golgi vesicle trafficking 16, *19*, 20, *166*, 175, *178*
copper
deficiency *1102*, 1127, *1127*
uptake 1126
coregulators, gene expression 427–429, *427*, *429*
core promoters, gene expression 427, *427*
corn *see* maize
coronatine 824–825, *825*
correlation spectroscopy (COSY) 56b
cortical array, organization 218–219, *219*, *220*
cortical division sites, cytoskeleton structures 222–237, *226*
cortical endoplasmic reticulum 13, 15, *15*, *17*
cortical microtubules 88–90
cell expansion 216–219, *217–220*
organization 218–219, *219*, *220*
COSY *see* correlation spectroscopy
Cot analysis, repetitive DNA *405*
cotranslational translocation *446*, 447, 456–457, *457*, *459*
cotransporters 113
electrochemical potential 142
genes 145–146, *146*
H^+-coupled transport 143, *143*, *144*
heterologous systems 142–143
hydropathy analysis 142–143, *143*
major facilitator superfamily 145–146
metabolite specificity 145–146

Na⁺-dependent 144, *145*
regulation 144–145, *145*
SUT genes 146
transport rates 113
cotyledons, senescence 943–948, *947–948*
coumarins 1182, **1183**
p-coumaryl alcohol 104
coupling elements (CE), ABA-responsive elements 1063, *1063–1064*
covalent attachment, ubiquitin 469, *471*, 473–475, **472**, *473*
covalent modifications, histones 433–434
CP12 protein 556, *557*
CP *see* coat protein
cpn60, Rubisco folding 463, *465*
CPS *see* carbamoyl phosphate synthetase
cpSEC (chloroplast SEC) pathway *156*, 157
cpSRP (chloroplast SRP) pathway *156*, 157
crassulacean acid metabolism (CAM) 141, 557–558, *558*, 563–565, *564*
photorespiration 647
photosynthetic carbon concentration in mitochondria 645–646, *645*
C-RepeaT (CRT) proteins 175, 1063–1064, *1063–1064*
critical concentration, actin/tubulin polymerization 197, 199–200
CRM *see cis*-regulatory modules
crop yield
abiotic stress 1051, *1052*
soil sulfur content 750
crosslinking glycans 51–52, 105–106
by plant order *64*
cell walls *77*
changes during growth 97, 99
mannose-containing 65, *65*
regulation 94–96, *95*
stress relaxation *93*
structure *59*
synthesis 83–86, *85*
crosslinking proteins, cytoskeleton *206*, 207
crosspathway regulation 335b
crosstalk, abiotic stress responses 1097–1099
CRT proteins *see* C-RepeaT proteins
cryofixation 208–210, *212*
cryptochromes 858b, 875–876
CS *see* castasterone
Csl genes *87–88*, 88
CT *see* carboxyltransferases
CTP *see* cytidine 5′-triphosphate
cullin-RING ligases 470, **472**, *473*
culturing, microspores 893b
cuticles *46*, 382–388, *382*, *385*, *387–388*
cutin 104, 185–186, 382–385, *382*, **384**, *385*, *387–388*
composition 338
membrane deposition 382–385, *382*, *385*, *387–388*
monomers 384, **384**, *387*
synthesis 384, *385*
C values, flowering plant genomes 404, *404*
cyanide, complex IV inhibition 622, *625*
cyanobacteria 39, 40b, 260–261, *260*, 715
cyanogenesis 1150–1151b, 1156b, 1157
cyanogenic glycosides 1146–1158, *1148–1152*, 1150–1151b, 1153b, *1154–1155*, *1158*
biosynthesis 1152–1157, *1152*, *1155*
coevolution *1150*
diurnal cycles 1157–1158, *1158*
functions 1156b, 1157–1158, *1158*
gene clustering 1153–1155, *1155*
insects 1156b
regulation 1155–1157, *1155*
structures 1146, *1148–1149*
CYCD *see* D-type cyclins
cyclic 3prime,5′-adenosine monophosphate (cAMP), signal transduction 843–847, *844*
cyclic electron transport, photosynthesis 535–536, *535*
cyclic GMP, programmed cell death 932
cyclic nucleotide-gated channels (CNGCs) 139, **149**, 843
cyclin-dependant kinase inhibitory proteins (CKIs) 485–486, *486–487*
cyclin-dependent kinase activating kinases (CAKs) 482–483, *482*
cyclin-dependent kinases (CDKs)
cell cycle control 482–486, *482–488*, 493, *493*
classes 483–484, *483*
eukaryotic pathways 482–484, *482–484*
microgametogenesis 894, *896*
regulation 485–486, *486*
subcellular localization 484–485, *485*
cyclins, mitosis regulation 480, *480*, 482–485, *482–486*
cyclopentenyl fatty acids 363
cyclopropenoid fatty acids 363
CYCLOPS *728*, 729
CYP *see* cytochrome P450
Cys *see* cysteine
cystathionine β-lyase 320, *322*
cystathionine γ-synthase (CγS) 320, *322*, 323, *324*, *325*
cysteine (Cys) *290*, *291*
biosynthesis 755–757, *756–757*, 766–767, *766–767*
disulfide bonds 747–749
metal cluster-containing cytochromes *624*
cysteine synthase 755–757, *757*
cyst nematodes 1001
cytidine 5′-triphosphate (CTP) *242*, 243
cytidine diphosphate–diacylglycerol (CDP-DG) pathway
membrane lipid synthesis *364*, 365–372, *368–370*
phosphodiester bond formation 366–368, *369*
cytochrome b_5, fatty acid desaturases 356, *356*, 358
cytochrome b_6f complex 532–535, *532–535*, **533**
cytochrome *c*
apoptosis 927
heme C *623*
mitochondrial electron transport chain *620*, 621
photosynthesis 532–535, **533**, *534*
redox potential *621*
cytochrome-*c* oxidase *620*, 621
cytochrome *f*, photosynthesis 532–535, **533**, *534*
cytochrome oxidase, legume bacteroids 731, *733*
cytochrome P450 (CYP)
cyanogenic glycoside biosynthesis 1152–1157, *1152*, *1155*
cytokinin synthesis 787, *789*
ent-kaurine conversions 773–774, *773*
natural product biosynthesis 1146b, 1152–1157, *1152*, *1155*
cytochromes
heme groups *623*
metal clusters *624*
regulation 634–635
cytokinesis 27, 43, *43*, *47*, *478*
contractile ring 231–233
cytoskeletal dynamics 222–237
peroxisome aggregation 214
phragmoplasts 222–227, 233–237
phragmosomes 227, *227*
preprophase band 222–226, *224–225*, 229
tubular network 237, *237*
tubulovesicular network 237, *237*
cytokinins (CK) 785–795, *785–795*
apical dominance 794, *794–795*
biosynthesis 787–793, *788–793*
cell cycle regulation *503–506*, 504–506
cell death 936, 976–977, *977*
conjugates 787, *788*
degradation 793, *794*
glucosylation 795
nodulation 730–731
side chain variations *786*, 787
signal transduction 850–852, *850–851*
structures *770*, 785–788, *785–788*
tracheary element development 936
two-component system 850–852, *850–851*
cytoplasm
GS isoenzymes 293, *295*
mRNAs 274, 275
trafficking 29, 30
tRNAs 273, *273*
cytoplasmic immune receptors 1023–1026, **1024**, *1025–1027*
cytoplasmic male sterility (CMS) 896–897, *897*, 939–940
cytoplasmic maternal effects, reproductive mutants 915
cytoplasmic streaming 211–212, *213*, 663
cytosine 243
base pairing *247*
deamination *252*
dimers 254
methylation 433–434, *433*
structure *241*
cytoskeleton 191–238, *237*
see also actin; tubulin
accessory proteins 202–207
anaphase *224*, 231, 233–234
anchoring *194*
cell wall connectivity 220–222, *221*, 234–237, *237*
classes of fibrous polymers 192
cryofixation 208–210, *212*
cytokinesis 222–237
fluorescent imaging 207–208, *208–211*
functions *194*
gel-like networks 207
information flow 191–192
intermediate filaments 192–194
metabolic channeling 219–220, *220*
mitosis 222–237
mitotic spindle 227–230
motor proteins 203–206, *204*, *205*
observation 207–210, *211–212*
parallel polarity 207
phragmoplasts 222–227, *224*, *227*, 233–237, *234–237*

cytoskeleton (*cont'd*)
polarity *194*, 197–202, 207
regulation 200–202b, 205–207, *206*
remodeling 207
severing proteins *206*, 207
signal transduction 219–222
spontaneous assembly 197
treadmilling 200, *202*
cytosol
fructose-6-phosphate/fructose 1,6-bisphosphate conversions 587–588, *587*
isocitrate dehydrogenase 643, *643*
protein synthesis regulation 442, *445*
pyruvate kinase regulation *605*
starch degradation 597, *597*
cytosolic GS1 isoenzymes 295
cZ *see cis*-zeatin

D1 proteins
cofactor insertion 456–457, *457*, *459*
photosynthesis 522, *524*
proteolytic processing 457, 469
repair cycle 463, 465–466b
D2 proteins, photosynthesis 522, *524*
DAG *see* diacylglycerol
DAHP genes 303
DAHP synthase *see* 3-deoxy-D-*arabino*-heptulosonate-7- phosphate synthase
damage-associated molecular patterns (DAMPs) 1016, *1018*
DAMPs *see* damage-associated molecular patterns
DAP *see* diaminopimelate
dark reversion, phytochromes 857, *858*
daughter chromosomes, methylation 433–434
day length, flowering initiation 874–878, *876–877*, *881*
day-neutral plants 875
DBE *see* debranching enzymes
Dbf4-dependent kinase (DDK4) 492–493, *493*
DBMIB *see* 2,5-dibromo-3-methyl-6-isopropyl-*p*-benzoquinone
DCL *see* Dicer-like endonucleases
DCMU 536, *536*
DDK4 *see* Dbf4-dependent kinase
deacetylases, histone modification 433–434, *434*
deamination
amino acids 293
bases 250, *252*
debranching enzymes (DBE)
starch degradation 595–596, *595*
starch synthesis 585–586, *586*
decision to flower 872–874, *873*
deepwater rice 1077–1078, *1078–1079*, 1082–1085, *1084*
default pathway 178
defense compounds
alkaloids 1164
coevolution *1150*
cyanogenic glycosides 1156b, 1157–1158, *1158*
fatty acids 363
glucosinolates 1158–1159, *1159*
systemin production 457–458, *460*
terpenoids 1134, *1134*
threonine deaminase 328b
in vacuoles 28
defensive mechanisms 175, 984–1050
see also effector-triggered immunity; induced defense; pathogen defense mechanisms; pattern-triggered immunity
hormonal regulation 974–976, 980–981
hypersensitive response 965–974, *966–968*, **969–970**, *972–974*
membrane lipids 379–382, *380–381*
phloem parenchyma cells 682
programmed cell death 964–974
deficiencies
see also abiotic stress; water stress
essential mineral nutrients 1102–1103, *1102*, **1103**
nitrates, strigolactone signaling 833
nitrogen 712, *713*
phosphate, strigolactone signaling 833
sulfur 746, 765, *765*
deformation of kernels, ethylene 931, *931*
degeneracy, consensus sequences 441
degradation
see also catabolism
chlorophyll 948–951, *949*
cytokinins 793, *794*
DELLA proteins 861–863, *862–863*
macromolecules, senescence 951–957, *952–956*
polyamines 821, *822*
proteins 463–474
starch 593–597, 594–595b, *595*, *597*
chloroplasts 595–597, *595*
endosperm 594–595b
onset 591–593
sucrose 577–580, *578–580*
degradation followed by reductive cleavage (DFRC) method 105
dehydration, gene expression 1061–1068, *1063–1066*, *1067–1068*
dehydration responsive elements (DREB) 1063–1064, *1065*
dehydrogenation, glyceraldehyde 3-phosphate 602–603, *603*
3-dehydroquinate dehydratase 304–305, *304*, 318, 335b
3-dehydroquinate synthase 303–304, *304*
3-dehydroshikimate 304
DEL *see* DP-E2F-like proteins
delayed senescence, agricultural implications 948
DELLA proteins
gibberellin signal transduction 861–866, *862–863*, 864b, *865–866*
nuclear function 863, *863*
ubiquitination 475
DEMETER 436
dense vesicles (DVs) 184–185, *185*, *186*
density, plasmodesmata, loading phloem 674, *677*, *677*
3-deoxy-D-*arabino*-heptulosonate-7-phosphate (DAHP) synthase 302–303, *303*, *304*, 318, *319*
deoxyribonucleases 243
2-deoxyribose *241*
deoxyribosephosphodiesterase *253*
deoxysugars 49
deoxythymidine 5′-monophosphate (dTMP) 243
deoxyuridine 5′-monophosphate (dUMP) 243
dephosphorylation
phospho*enol*pyruvate *603*, 604–605, *605*
pyruvate dehydrogenase 617, *618*
sucrose-6-phosphate 575–577, *576*
depolarization, sieve tubes 679, *679–680*, 703–704, *704*
deposition
cutin 382–385, *382*, *385*, *387–388*
extracellular lipids 382–389, *382*, *385–388*
solvent-soluble waxes 385–388, *387–388*
suberin 384, *385*, *386*
depurination *252*
desaturation of fatty acids
C_{16} fatty acids 352–360, *356–361*
C_{18} fatty acids 352–360, *356–361*
membrane-localized enzymes 356–358, **358**, *359*, *360*
soluble enzymes 353–356, *356–357*
determinate nodules, legumes 725, *725*
detoxification, xenobiotics 760–762, *761–762*
development 933–937, *935–938*
see also reproductive development; vegetative development
auxin signaling 852–857, *853–857*
cell cycle control 497–506, *498–506*
cell division theories 499–500, *500*
compensation 500, *500*
embryo sacs 900–901, *901*
epigenetic control 435–436, *436*
female gametes 897–902, *897–902*
flowers, programmed cell death 939, *939–940*
homeodomain transcription factors 497–500, *498–500*
male gametes 889–897, *891–892*, 893b*894*, 895b, *896–897*
nodules, calcium spiking 724, 727–729, *728*
phloem 664, 666–668, *667*
plasmodesmata 666–668, *667*
ploidy 502–504, *503–504*
root nodules 720–733, *722–730*, **724**, *732*
seeds
compartments 913–914, *914*
embryogenesis 916–919, *917–918*
endosperm 919–920, *919*
genomic imprinting 914–915, 920–923, *921–922*
molecular regulation 913–923
parental effects 914–916, 915b, *916*
programmed cell death 930–932, *930–932*
shoot apical meristems 477, *479*
tracheary elements 933–937, *935–938*
vascular 856–857, *856–857*
xylem 664–666, 933–937, *935–938*
dextrorotatory optical rotation 48
DFRC *see* degradation followed by reductive cleavage
DHDPS *see* dihydrodipicolinate synthase
dhurrin 1150–1151b, 1152–1153, *1152*
diacylglycerol (DAG)
biosynthesis 365
galactolipid synthesis 372–373, *373*
membrane lipid synthesis 365–373, *364–369*, *371–373*
nucleotide activation 366–368, *369*
sulfolipid synthesis 372–373, *374*
diameters of xylem 665
diamine oxidase, polyamine degradation 821, *822*

meso-2,6-diaminopimelate 320
diaminopimelate (DAP) pathway 319–320, *321*
diarabinosyl 8-*O*-4-dehydrodiferulate 56–57b
diarylheptanoids 1182, **1183**
diazotrophs 715
2,5-dibromo-3-methyl-6-isopropyl-*p*-benzoquinone (DBMIB) 536, *536*
dicarboxylic acids, legume/rhizobial symbiosis 733
Dicer-like (DCL) endonucleases *276*, *277*, 285, *285*
differential gene expression 425–436
differential stability, proteins during senescence 956–957, *956*
differentiation 99, 100, 102, *102*, 426–427, 664
diffusion
  coefficients 660b
  membrane permeability coefficients 661b
  symplastic phloem unloading 688, *688*
  theory 660b
  velocity constraints 663
diffusional coupling, cytoskeleton 219–220, *220*
digestion 28
3,3′-dihexyloxacarbocyanine iodide ($DiOC^6$) 13, *15*
dihydrodipicolinate synthase (DHDPS) 320, *320*, *321*, 323, *323*, 324, *324*, 325, *325*
dihydrophaseic acid, abscisic acid metabolism 784, *785*
dihydroxyacetone phosphate, pentose phosphate/triose phosphate pool *598*
dihydroxy-acid dehydratase *327*, 328
diiron centers, stearoyl-ACP desaturases 356, *356–357*
DIMBOA (2,4-dihydroxy-7-methoxy-1, 4-benzoxazin-3-one) 317b
dimethylallyl diphosphate 1134–1141, *1137*, *1139–1141*
  cytokinin synthesis 789–792, *790*, *792*
dimethyl sulfide (DMS), cloud formation 750, *751*
dimethylsulfoniopropionate (DMSP), cloud formation 750, *751*
dinitrogen reductase (Fe protein), nitrogenase 716–718, *716–718*
$DiOC^6$ *see* 3,3′-dihexyloxacarbocyanine iodide
diphosphatidylglycerol (cardiolipin) 42, *42*, 368–369, *370*
directed movement, organelles 210–216, *213–216*
directional transport, xylem loading 669–670, *671*
direct recognition, pathogen effectors 1027–1031, *1029*
disaccharides 50, *51*
  see also sucrose
discadenine 787, *788*
disease, mechanisms of causation 989–1009, *991–993*, **992**, *995–999*, **998–999**, *1001–1003*, *1008*
disease resistance
  effector-triggered immunity 1022–1032, *1021–1035*
  heritable variation 1022, *1023–1024*
  pattern recognition receptors 1012–1014, *1016*
  salicylic acid 827–828, *827–828*
disease tolerant plants 1022–1023, *1024*
disproportionating enzymes, starch degradation 595–596, *595*, *597*
disulfide (S-S) bonds 170, 636–637, *637*, 747–749
diterpenes 1133, *1136*, 1143, *1144*
diurnal patterns
  carbohydrate metabolism 567, *569*, 590–593, *590–591*
  cyanogenic glycosides 1157–1158, *1158*
  xylem flow rates 668
divergence, actin/tubulin gene sequences *195–196*
diversity
  floral morphologies 881–882, *881*, *884–886*
  phenolic compounds 1178–1182, *1182*, **1183–1185**
  plasmodesmata structures 667, *667*
  terpenes 1142–1143, *1144*
  virus proteins 450
DMC1 genes 258
DMC1 protein 256–258
DMS *see* dimethyl sulfide
DMSP *see* dimethylsulfoniopropionate
DNA (deoxyribonucleic acid) 240, *241*
  see also nucleic acids
  base pairing 245, *247*
  chloroplasts 39, 40b
  chromatin binding 430–432, *432*
  chromosome condensation 493–495, *493–494*, *496*
  composition *246*
  Cot analysis *405*
  double helix *247*
  fluorescent in-situ hybridization 403–404b
  genomic imprinting 920–923, *921–922*
  hydrogen bonds 245, *247*
  master circles 265
  methylation 433–434, *433*, 436, 920–923, *921–922*
  mitochondria 40b, *41*
  promiscuous DNA 267, *268*
  purines 240, 243
  structure 245, *247*
  subgenomic circles 265
  sugar-phosphate backbone *246*
DNA deoxyribosephosphodiesterase 253
DNA-dependent RNA polymerases 285
dna genes 264
DNA glycosylase 252, *253*
DNA gyrase 259
DNA helicases 246, 253, *254*
DNA ligase 247, *248*, 253, *253*, *254*, 255, *255*
DNA methyltransferases 433–434, *433*
DNA polymerase holoenzymes 247–248
DNA polymerases
  DNA repair 253, *253*, 254, *254*, 255, *255*
  DNA replication 246, 247–248, *248*
  primers 250
DNA primases 246, *248*
DNA proofreading 248, 250
DNA recombination
  cell evolution 255
  double-strand break repair model 256, *256*
  homologous recombination 255, *255*, 256–258, 257b, *259*
  illegitimate recombination 259–260
  meiotic cell division 255
  one-sided invasion model *256*
  single-strand annealing model 256, *256*
  site-directed mutagenesis 257b
  site-specific recombination 258–259, *259*
  types 255, *256*
DNA repair
  damage, causes of 250–251, *252*
  error-prone repair 254
  excision repair mechanisms 252–253, *253*, *254*
  mismatch repair 253–254, *254*
  photoreactivation 251–252
  recombination repair 254–255, *255*
DNA replication 240, *241*, 245
  asymmetric replication fork 246
  cell cycle 491–495, *491–494*
  centers 248
  direction 246
  DNA polymerase holoenzymes 247–248
  DNA topoisomerases 249b
  elongation 246–248, 250
  fidelity 248
  forks 246, *247*, 248, *248*
  initiation 246, *247*
  leading and lagging strands 247, *248*
  origins of replication 245–246, *247*
  primers 246, 247
  proofreading 248, 250
  regulation 250
  semi-conservative 247
  semi-discontinuous 246–247, *248*
  stages 245
  supercoils 249b
  telomeres 250, *250*
  termination 250, *251*
  Ter sites 250
DNase hypersensitive sites 431, *432*
DNA sequences
  Arabidopsis telomeres 250, *250*
  gene promoters 427–429, **428**
DNA sequencing
  bisulfite method 434
  hidden Markov models 409–410, 410b
  projects 408, 409b
  whole genome shotgun method 408, 409b
DNA topoisomerases 246, 249b
DNA transcription 240, *241*, 268–270, **268**, *269*, *270*
DNA transposons (class II transposons) 420–422, 422b, *424*
"dock, pluck and go" model 22, *23*
dolichol 22
dolichol pyrophosphate 173
dominant recognized effectors 1022
dominant resistance genes 1022
dot plots, evolutionary analysis 415–416, *416*
cis-double bonds, fatty acids 352–353, *356*
double fertilization *902*, 907–908, *907*
double rolling-circle model 264, *264*
double-stranded RNAs (dsRNAs) 275–278, 285
downstream promoter elements (DPE) 427, *427*
DPE2 *see* α-1,4-glucosyltransferase
DP-E2F-like (DEL) proteins 489–490, *490*
DPE *see* downstream promoter elements
DREB *see* dehydration responsive elements
driving forces, phloem/xylem 663–664, *664*
drought-tolerant plants 330
dsRNAs *see* double-stranded RNAs
dTMP *see* deoxythymidine 5′-monophosphate
D-type cyclins (CYCD) 484–485, *485–486*, 505–506, *506*

dual-axis electron microscopy 75b
dual isotherm, potassium ion transport 1106, *1106*
dUMP *see* deoxyuridine 5′-monophosphate
duplications
  genes, cellular compartments 578
  genome structure 415–416, *416*
  metabolic pathways *571*
durable resistances 1022–1023, *1024*
DVs *see* dense vesicles
dynamic instability, microtubules 202, *203*
dynamin proteins 39
dynein 203–206, *204*, *205*

E2F transcription factors 488–981, *489–490*
early endosomes 26, *26*
early nodulins 729, *729–730*
early TGN cisternae 21
EB1 207
ecological roles of terpenes 1133–1134, *1134*
edible oils, metabolic engineering 395–397
EDS1 (*ENHANCED DISEASE SENSITIVITY 1*) gene *1030*, 1031
effector domains, signal transduction 836
effector-triggered immunity (ETI) 985, 1022–1032, *1021–1035*, 1047b
effector-triggered susceptibility 985, *988*
efficiency of photosynthesis with climate change 654–655, *654*
EFR *see* elf18-responsive EF-Tu receptor
EHM *see* extrahaustorial membrane
eIF1 proteins 441, **442**, *443*
eIF2 proteins 441, **442**, *443*, 443, *445*
  phosphorylation 442, *445*
eIF4E-binding proteins (4E-BPs), protein expression regulation 442, *445*
eIF4 proteins 441–442, **442**, *443*
eIF5 proteins 441, **442**, *443*
eIF6 proteins **442**, 447
eIFs *see* eukaryotic initiation factors
EIMS *see* electron-impact mass spectrometry
elaioplasts *33*, 38
electrical conductivity, sieve tubes 703–704, *704*
electrochemical gradients, ATP synthase 632–634, *634*
electrochemical potential 115, 116–117b, 117, 129, 131, *131*, 142
electrogenic transport
  mitochondria 639, *640*
  potassium ions 1109
electron carriers
  cytochrome *c* *620*, 621
  mitochondria 620–646, *620*
  photosystem I 530–535, *530–535*
  photosystem II 522–535, *524*
  ubiquinone 621, *622*
electron donors, fatty acid desaturases 356, *356*, 358
electroneutral transport, mitochondria 639, *640*
electron-impact mass spectrometry (EIMS) 52b, 54b
electron transport chains
  chloroplasts 529–536, *530–535*, 630b
  mitochondrial 620–646, *620*, 630b
    F_oF_1–ATP synthase 632–633, *633–634*
    inhibition 622–624, *625*
    substrates 622, *625*
electron transport cofactors, nitrate reductase 740–742, *742*, *744*
electrophysiology
  phosphate transport in roots 1114, *1114*
  potassium ion channels 1108–1110, *1110*
electrospray-ionization (ESI) MS 62–63b
elf18-responsive EF-Tu receptor (EFR) 175
elongases, fatty acids 360
elongation
  actin 197–202, *197–199*
  C_{16} fatty acids 360, *361*
  cytoskeleton polymerization 197
  microtubules 202, *203*
  protein synthesis 444, *446–447*
embolism repair, xylem 693–694
embryogenesis, auxin 917–918, *918*
embryo sac development 900–901, *901*
emetine 1166, *1172*
enantiomers 48
end-binding proteins *206*, 207
endocytosis 24, *24*
  actin transport 215
  FM4-64 25
  membrane compartment identification 25–27
  membrane recycling 25, *25*
  pathway 25–26, *26*
  protein sorting *166*, 188–189, *188*
  tracer uptake studies 25–27
  vesicles 189
endodermal cells 103
endogenous turnover, cyanogenic glycosides 1157–1158, *1158*
endoglucanase 60b, *64*, 85, *85*
endohydrolases 97, *97*
endomembranes 13, 161
  antiporters 142
  Ca^{2+}- permeable channels 139–140
  functions 162
  integral membrane proteins 168–169
  protein gradients 117
  symporters 142
  V-type H^+-ATPases 126–127
endomitosis 502
endoplasm, cytoplasmic streaming 211–212, *213*
endoplasmic reticulum (ER) 2
  anchoring and movement, actin networks 213
  anterograde/retrograde traffic 13, *15*
  attachment domains 16–17, *18*
  Ca^{2+}-ATPases 126
  Ca^{2+} concentrations 170
  cell wall proteins synthesis *81*
  connections to nuclear envelope 29–30
  default pathway 178
  endomembrane system 13
  enzymes synthesis *81*
  ER–Golgi trafficking 22, *23*, *166*, 178, *178*
  ER–mitochondria attachment sites 17
  ER–peroxisome attachment sites 17, *32*
  ER–plasma membrane attachment sites 17, *18*
  ER–plastid attachment sites 17, *18*
  ER–plastid lipid trafficking 17
  ER–vacuole attachment sites 17
  ethylene perception 848–849, *848–849*
  eukaryotic lipid synthesis pathway 17
  export sites 16
  folding helpers 170, **172**, 175
  functional domains 13, *14*
  N-glycosylation 173–174, *174*
  integral membrane proteins 165, 167, 168–169, *168*
  KDEL signal *178*, 179
  lipid hopping 25, *25*
  lipid transport from/to chloroplasts 366, *367*, *368*
  luminal space 165, *167*
  membrane attachment domains 16–17
  membrane lipid synthesis *364–369*, 365–373, *371–373*
  in meristematic root tip cell *3*
  non-vesicular lipid transport 16–17
  oil body synthesis 15, *17*
  oligosaccharide production 22
  protein bodies 179, 180–181b, 182, *182*
  protein folding 170–173, *171*, **172**
  protein lipid anchors 169–170, *169*
  protein quality control 170–173, 174, *174*
  protein translation 168
  protein transport to 167–168, *167*
  quality control 170–173, 174, *174*
  rearrangements 13, *15*
  secretory proteins 162, 165
  signal peptides/proteins 167–168, 178–179
  SNARE proteins 177b
  staining for microscopy 13, *15*
  storage protein synthesis 15, *17*
  structure 13
  sugar interconversion 49
  trafficking routes *19*
  translocation complex 168
  transport vesicles 16, *18*
  types of membranes 13
  vesicle budding and fusion 175–176, *176*, 178
  vesicle cycling 177b
endoplasmic reticulum (ER)-localized enzymes, fatty acid desaturases 358, **358**
endoplasmin 170, **172**
endoreplication 502–504, *503–504*
endosomal trafficking, brassinosteroid receptors 840–841, *841*
endosomes 26, 188–189, *188*
endosperm
  development 919–920, *919*
  starch degradation 594–595b
endosymbionts, definition 712
endosymbiosis theories 40b, 260–261, *260*
energy charge 305
energy conservation, glycolysis 602–604
energy conversion, light 511–518, *512*, *515–518*
energy costs, photorespiration 652
energy density, lipids 337–338, *340*
energy flow
  gluconeogenesis 643–644, *645*
  respiration 610–655
    aerobic 610–646
    citric acid cycle 613–620, 634–635, 642–643
    light-dependant 646–654
    mitochondrial electron transport 620–646
    net stoichiometry of sucrose oxidation **615**
energy metabolism, senescence 957–959, *957*
energy status, alternative oxidase regulation 637, *637*
energy transduction 112
energy transfer, chlorophyll 512
ENHANCED DISEASE SENSITIVITY 1 (*EDS1*) gene *1030*, 1031

enhancers, gene expression 428–429, *428*
ENOD genes 729, *729–730*
enolase, phospho*enol*pyruvate synthesis 604
5-*enol*pyruvylshikimate-3-phosphate (EPSP) synthase *304*, 305, 306b
enoyl-ACP reductase 352, *355*
entry receptors, rhizobial symbiosis 726–727, *726*
environmental influences
  regulation of protein synthesis 447, 453–455, *454–457*
  senescence 961–974
environmental stress
  alternative oxidase 636–638, *637*
  phenolic defense compounds **1182**
enzymes
  see also specific enzymes
  antioxidant 1086–1089, *1087*, **1088**, **1089**
  carbohydrate production 22–23
  CAZy database 89, 89b, 96
  cellulose/crosslinking glycan network regulation 96
  cellulose synthesis 80
  cell wall heterogeneity probes 100b
  fruit ripening 100, 102
  fruit softening 102
  glycan and pectin synthesis 83–86, *85*
  in Golgi apparatus 18
  herbicide tolerance 306b
  isoforms 335b
  metabolic channeling, cytoskeleton 219–220, *220*
  motor proteins, cytoskeleton 203–206, *204*
  nucleotide sugar interconversion 81, 83
  polysaccharide modification 97, *97*, *98*
  pyridoxal phosphate-dependent 299, *300*
enzymology
  cytokinin synthesis 787–793, *789–793*
  gibberellin synthesis 771–776, *772–776*
  nitrogen fixation 715–718, *716–718*
  ubiquitination 469–475, *471*, **472**, *474*
epicuticular wax, water retention 385–388
epidermal cells *46*, *95*, 103, *107*
  shaping 218, *218*
epigenetic code 435
epigenetic marks 433–435, *434–435*
epigenetics
  gene expression regulation 315b, 430–436
  growth and development 435–436, *436*
  paramutation 432–433, *433*
epigenetic states 435
epimers 48–49
epoxidation of fatty acids 362–363, *363*
EPS *see* extracellular polysaccharides
EPSP synthase *see* 5-*enol*pyruvylshikimate-3-phosphate synthase
equilibria
  metabolite pools 570, *571*
  pentose phosphate/triose phosphate pool *598*, 600–601, *600*
  phloem 696–697, *698*
equilibrium potential (E_{ion}) 116–117b, 121b, 132, 132b
Equisetum 65, 72
ER *see* endoplasmic reticulum
ER bodies 15–16, *18*
ERD2p receptor 178, *178*, 179
error-prone repair 254
Erwinia carotovora, quorum-sensing 993, *998*
erythrose-4-phosphate 302, *304*, *598*, 600
ESI *see* electrospray-ionization
E-sites, protein synthesis 444, *446*
ESKIMO1 1073
essential mineral nutrients
  adequate concentrations **1103**
  deficiencies 1102–1103, *1102*, **1103**
ester conjugates, auxin *800*, 801, *803*
ethanol production, anoxic metabolism 1079–1082, *1080–1081*
N-ethylmaleimide sensitive factor (NSF) 176
ethylene 806–810
  aerenchyma formation 963, *963*
  auxin regulation 804
  biosynthesis 446, 806–810, *807–809*
  flooding responses 1082–1085, *1083–1084*
  induced defense 1022, *1036*, 1040–1042, *1042*
  interactions 849–850, *849*
  kernel deformation 931, *931*
  necrotrophic pathogen responses 1040–1042, *1042*
  nodulation 730, *730*
  programmed cell death 931, *931*, 963, *963*, 977–979, *978–980*
  regulation 804, 808–809, *808*
  repression of biosynthesis *809*, 810
  senescence 977–979, *978–980*
  signal transduction 847–850, *848–849*
  stem elongation 804, *805*
  volatilization 810
ethylene overproducing protein (ETO1) 808–809, *808*
ETI *see* effector-triggered immunity
etiolation, gibberellin/abscisic acid regulation 863–865, 864b, *865*
etioplasts *33*, 35, *35*, *39*
ETO1 *see* ethylene overproducing protein
eubacteria 40b, 715
euchromatic chromosome arms 411–412, *412*
euchromatin 250, 431
eukaryotes
  cyclin-dependent kinase pathways 482–484, *482–484*
  gene structure 427
eukaryotic initiation factors (eIFs) 441–442, **442**, *443*, *445*
eukaryotic lipid synthesis pathway 17, *364–369*, 365–373, *371–373*
evening element **428**
evolution
  cell wall polymers 70–72
  chloroplasts 260–261, *260*
  divergence of actin/tubulin gene sequences *195–196*
  endosymbiont hypothesis 260–261, *260*
  gene homology 415b
  genetic recombination 255
  gibberellin signaling 865–866, *866*
  mitochondria 40b, 44, 260–261, *260*, 267b
  neofunctionalization 415–416, *416*
  orthology 415b
  parology 415b
  phenolic compounds 1179–1182
  plastids 40b
  polysaccharides *75*
  promiscuous DNA 267
  secondary pathways 1205–1206
  sieve elements **666**
  subfunctionalization 415, *416*
  synteny 416, *417*
excessive auxin production 803–804, *805*
excision repair mechanisms *253*, *254*
excitation of chlorophyll 511–515, *512*, 521, *522*, *524*
excitation energy transfer, photosystems 521, *522*, *524*
exclusion, aluminum tolerance 1128–1131, *1129–1131*
exoamylases, starch degradation 595–596, *595*
exocytosis 23–24, *24*, 379, *379*
exohydrolases 97, *97*
exons 278
exonucleases 248, *254*
expansins 94–96, *95*, 102
expansion *47*, 90
  see also growth
  acid-growth hypothesis 93–94
  biophysics 93
  multinet growth hypothesis 92–93
  regulation 94–96, *95*
  tip growth 91
exportin-Ran-GTP complex 161, *162*
exportins 160–161
expression *see* gene expression
extensibility 93
extensins 22, 67, *69*, 99, 188
external coincidence model, flowering initiation 876, *878*
external NAD(P)H dehydrogenases, mitochondria 627–629, *630*
extracellular auxin, signal perception 854
extracellular lipids
  functions 382–389, *382–388*
  membrane deposition 382–389, *382*, *385–388*
  synthesis 384–389, *385*, *387*
extracellular matrix proteins, signal transduction 221–222
extracellular polysaccharides (EPS), rhizobial bacteria 722–723, *724*
extrahaustorial membrane (EHM) 990–992, *995*

F_oF_1–ATP synthase *see* ATP synthase
F1 hybrids, hybrid vigor 901
F_1 complex, mitochondrial ATP synthase 539–540, *540*
FAB2 358, **358**, *359*, 374–375, *376*
fab2 mutants 374–375, *376*
facilitated diffusion
  amino acids/amides, phloem loading 679–680, *680*
  Michaelis–Menten mechanics 661b
  polyols, phloem loading 678, *680*
  proton motive force 661b
  sugars, phloem loading 677–680, *678–680*
F-actin 198, *199*
FAD2 358, **358**, *359*
FAD3 358, **358**, *359*
FAD4 358, **358**, *359*
FAD5 358, **358**, *359*
FAD6 358, **358**, *359*
FAD7 358, **358**, *359*
FAD8 358, **358**, *359*, 360
FAD *see* flavin adenine dinucleotide
farnesyl (C_{15}) 9, *9*

farnesyl diphosphate 778–779, *779–780*, 1138–1141, *1140–1141*
farnesyl transferase 170
far-red/red light sensing 776, *777*, 857–861, *858–861*
FAS *see* fatty acid synthase
fast-freeze, deep-etch, rotary-shadowed replica technique 75–76b
fast vacuolar (FV) channels 136, *137*
fatty acid acetylases 362–363, *363*
fatty acid desaturases 358, **358**, *362*
  active sites 355–356, *356–357*, *360*, 362–363
  membrane-localized 356–358, **358**, *359*, *360*
  regulation 358–360
  soluble enzymes 353–356, *356–357*
fatty acid epoxidases 362–363, *363*
fatty acid hydroxylases 362–363, *363*
fatty acid-linked membrane proteins 8, 9, *9*
fatty acids
  acetylation 362–363, *363*
  biosynthesis 344–363
    acetyl CoA 344–350, *346–349*
    acetyl-CoA carboxylase 346, *347*, 348–350
    acyl carrier protein 346, *347*, 350–356, *350–355*
    enoyl-ACP reductase 352, *355*
    3-ketoacyl-ACP dehydratase 352, *354*
    3-ketoacyl-ACP reductase 351–352, *353*, *354*
    3-ketoacyl-ACP synthase *347*, 351, *354*
    malonyl-CoA 346–351, *347–349*, *351*
    overview *347*
    thioesterases 352, *355*
    unusual products 360–363, *361–362*
  as defense mechanisms 363
  desaturation 352–360, *356–362*
    membrane-localized enzymes 356–358, **358**, *359*, *360*
    regulation 358–360
    soluble enzymes 353–356, *356–357*
    temperature 360
  cis-double bonds 352–353, *356*
  epoxidation 362–363, *363*
  hydroxylation 362–363, *363*
  industrial applications 398, **398**, 399
  lipid structures 338–344, **343**, **345**
  melting temperatures 352–353, *356*
  methylation 362–363, *363*
  methyl esters 342b
  β-oxidation 620, 643, *645*
fatty acid synthase (FAS) 346, *347*, 350–352
fatty-acid synthesizing plastids 606
FBPase *see* fructose 1,6-bisphosphatase
FC *see* fusicoccin
FdGOGAT *see* ferredoxin-dependent GOGAT enzyme
Fdx *see* ferredoxin
Fe *see* iron
feedback regulation
  gibberellin synthesis 776, *776*
  strigolactone biosynthesis 833
feeding, aphids 675–676b
feeding tubes, nematode infections 1001, *1001*
female gametes
  apomeiosis 901–902, *902*
  embryo sac development 900–901, *901*
  megagametogenesis 897, 899–900, *900*
  megasporogenesis 897, 898–899, *898*
  molecular regulation of development 897–902, *897–902*
FEN-1 nuclease *248*
Fe–O–Fe centers, stearoyl-ACP desaturases 356, *356–357*
Fe protein, nitrogenase *see* dinitrogen reductase
fermenting metabolism 1079–1082, *1080–1081*, *1083*
ferredoxin-dependent GOGAT (FdGOGAT) enzyme 293, *295*, 296–298
ferredoxin (Fdx)
  fatty acid desaturases 356, *356*, 358
  nitrite reductase 739–740, 744–745
  nitrogenase 718, *718*, 733, *734*
  photosynthesis *530*, *532*, 535–536
ferredoxin-NADP⁺ reductase (FNR) *530*, *532*, 535–536, 583–584, *584*, 744
ferredoxin-quinone oxidoreductase 536
ferredoxin-thioredoxin reductase, starch synthesis 583–584, *584*
ferredoxin–thioredoxin system (FTS) 553–556, *555–557*
fertility, surface lipids on pollen 388–389, *388*
fertilization
  molecular regulation 902–903, *902*, 906–913, *906–907*, *909–913*
  self-incompatibility 908–913, *909–913*
ferulates 105–106
Fe–S *see* iron–sulfur
FESEM *see* field-emission scanning electron microscopy
fibrous polymers, cytoskeleton 192
Fick's first law of diffusion 660b
field-emission scanning electron microscopy (FESEM) 76b
filamentous cyanobacteria, heterocycsts 715
filamin, cytoskeletal association 207
fimbrin, cytoskeletal association 207
FISH *see* fluorescent in-situ hybridization
five-carbon units
  biosynthesis 1135–1138, *1137*
  fusion 1134–1135, *1136*, 1138–1141, *1140*
fixation *see* assimilation
fix genes/Fix proteins 732–733, *733*
flagellin, signal transduction 840–841, *841*, 846–847, *846*
Flagellin Sensing 2 (FLS2) receptor 189
flavanone, structure *722*
flavin adenine dinucleotide (FAD) 358, **358**, *359*, 360, 613, *613*
flavin mononucleotide (FMN) 296, *613*
flavones *722*, 1182, **1184**
flavonoids 721, *722*, 950–951, *951*, *1182*, 1189, *1190*
flax rust disease 1006, *1008*
FLC see FLOWERING LOCUS C
fleshy fruits
  signaling of nutrient demand 706–707, *709*
  sucrose transport 689–691, *690*, **690**
flippases 6, *7*
flooding
  morphological changes 1076–1077, *1077*, 1082, *1083*
  oxygen deficit 1076–1085, **1076**, *1077–1081*, *1083–1084*
  short-term acclimation 1079–1080, *1080–1081*
  species sensitivity **1076**
flood-tolerant/sensitive plants 1078
floral morphologies, common body plans 881–882, *881*, *884–886*
florigen, flowering initiation 876, *877*
flowering
  induction, salicylic acid 826
  initiation 872–881, 880b, *881*
    external coincidence model 876, *878*
    photoperiods 874–878, *876–877*, *881*
    vernalization 874, 878–879, *879*, 880b
  programmed cell death 939, *939–940*
  regulation, epigenetic control 435–436, *436*
FLOWERING LOCUS C (*FLC*), flowering initiation 878, *879*
flowering plants
  genome size 404, *404*
  life cycle *873*
flowers
  ABC model of organ identity 883–885, *884–887*
  Arabidopsis thalania *882*, 883–885
  development
    cell death and senescence 940–943, *940–941*, **944–945**, *946–947*, *949*
    molecular regulation 881–889, *883–889*
    programmed cell death 939, *939–940*
  homeotic gene regulation 887–889, *887–889*
  molecular quartet model of organ specification 885–887, *888*
FLP recombinase *264*
FLS2 receptor, signal transduction 840–841, *841*
fluid-mosaic membrane model 4
  amphipathic nature of lipids 4, *5*, *6*
  control of lipid composition 7, **8**
  fluidity control 7, **8**, 10
  interactions 10
  lipid rafts 10
  lipid structures *5*
  membrane properties, prediction of 10
  phospholipid movement 5–6, *7*
  phospholipids 4, *6*
  proteins, membrane-bound 8–10, *8*, *9*
  sterols 7
  tethering structures 10
fluorescence microscopy 152b, 162, *192*
fluorescence resonance energy transfer (FRET), kinesin-5 232–233b
fluorescent analog cytochemistry 207–208, *208–211*
fluorescent imaging
  actin 208, *209*, *211*
  microtubules 207–208, *208–210*
fluorescent in-situ hybridization (FISH) 403–404b
4-fluoro fatty acids 363
fluorophores, cytoskeletal imaging 207–208, *208–211*
FMN *see* flavin mononucleotide
$FMNH_2$ (flavin nucleotide cofactor) 305
FMS *see* functional megaspores
FNR *see* ferredoxin-NADP⁺ reductase
FokI endonuclease 257b
folding helpers 170, *171*, *172*, **172**, 174, 175
foliar senescence-associated proteases 952–953, *953*
food industry 109
footprints, DNA transposons *419*, 420
formins, actin nucleation 207

Förster energy transfer (FRET) 519, 521
Fourier transformations 55b, 56b
Fourier transform infrared (FTIR) microspectroscopy 100–101b
fractionation of subcellular compartments 162
frameshifting, protein synthesis 450, 450b
Frankia (actinomycetes), symbiotic nitrogen fixation 719
free polysomes, protein destinations 447
free TGN cisternae 21
freeze substitution, methodology 210
freezing stress 1068–1075, *1070*, *1073*, **1074**
  gene expression 1073–1075, **1074**
  ice crystal prevention 210
  membrane lipid composition 378–379, *379*
  retrogradation in starchy foods 585b
FRET *see* fluorescence resonance energy transfer; Förster energy transfer
FRO transporters 1121, *1121*, 1124–1126
fructose 1,6-bisphosphatase (FBPase) 545–548, *546–547*, 572, 587–588, *587*
fructose 1,6-bisphosphate *588*
  fructose-6-phosphate conversions 572, 587–588, *587*
  pentose phosphate/triose phosphate pool *598*
fructose 1,6-bisphosphate aldolase 600
fructose 2,6-bisphosphatase 588–589, *589*
fructose 2,6-bisphosphate *588*
  fructose 1,6-bisphosphatase inhibition 588
  sucrose/starch partitioning 588–589, *589*
fructose-6-phosphate
  fructose-1,6-bisphosphate conversions 572, 587–588, *587*
  glucose synthesis 573–577, *576*
  hexose phosphate pool 571–573, *572*
fructose-6-phosphate-2-kinase 588–589, *589*
fruits
  ripening 100, 102, *102*, *809*, 810, 959
  senescence 941–942
  signaling of nutrient demand 706–707, *709*
  sucrose transport 689–691, *690*, **690**
FTIR *see* Fourier transform infrared microspectroscopy
FTS *see* ferredoxin–thioredoxin system
Ftsz proteins 39, 194
F-type ATPases 120–121, *122*
fuchsin 105, *105*
fucogalactoxyloglucans *59*
L-fucose (Fuc) 49, *50*, *187*
fucosidase 96
fucosyl transferases 86
fumarase, citric acid cycle 618, *619*
fumarate *332*
functional analysis
  genome annotation 408–410, 410b, 411b
  hidden Markov models 409–410, 410b
functional complementation 1108b
functional megaspores (FMS) 898–900, *899–900*
functions
  cytoskeleton *194*
  lipids 337–338, **339**, *340*
  xylem 668–672, *669–671*
fundamental forces, long-distance transport 660–661b
fungi
  abscisic acid synthesis 778–779, *779–780*
  arthropod introduction 1002–1003, *1003*
  nuclear lamina 192–194
  pathogen effectors **1004**
  pathogenesis strategies 990–992, *991*, **992**, *994–996*
furanocoumarins 1182, **1184**
furanoses 46
fusicoccin (FC) 124–125, *125*, 990
fusion, five-carbon units 1134–1135, *1136*, 1138–1141, *1140*
FV *see* fast vacuolar channels

G1 cell cycle stage 27, 43, *43*
G1-to-S transition 488–981, *489–490*
G2 cell cycle stage 27, 39, 43, *43*
G2-to-M transition 493, *493*
G3P *see* glyceraldehyde 3-phosphate
GA *see* gibberellins
G-actin 198, *199*, 200–202b
GA-insensitive dwarf-like (GID) proteins 862, *862*
galactans *66*, 67, 96
galactoglucomannans 65, *65*
galactolipids 33
  biosynthesis 372–373, *373*
  chloroplasts 337
  structure 342, **343**
galactomannans 65, *65*, 86, 106
D-galactose (Gal) 48, *50*, *187*
galactosidase 96
galactosylglycerides 4, *5*, 37
galactosyl transferases 86, 188
D-galacturonic acid (GalA) 49, *50*
galacturonosyl transferases 89
gametogenesis, programmed cell death 939–940
gametophytic apomixis 901–902, *902*
gametophytic maternal effect 914–915, 915b, *916*
gametophytic self-incompatibility (GSI) 909, 911–913, *912–913*
gamma-linolenate, biosynthesis 363
γ-TIP protein 28
γ-tubulin 207, 218–219, *219*
GAPs *see* GTPase activating proteins
gas chromatography–mass spectroscopy (GC-MS), abscisic acid synthesis 778–781
gas-liquid chromatography 52b
GATA promoter **428**
gating 120, 131, 133, 135, 140–141
GAXs *see* glucuronoarabinoxylans
GB *see* glycine betaine
G box **428**
GBSS *see* granule-bound starch synthase
GC-MS *see* gas chromatography–mass spectroscopy
GCN4p transcription factor 335b
GDH *see* glutamate dehydrogenase
GDIs *see* GDP dissociation inhibitors
GDP dissociation inhibitors (GDIs) *842*, 843
GDP-Glc 86
GDP/GTP exchange factor (GEF) 177b
GDP (guanine diphosphate), nucleotide exchange 442, *445*
GDP sugars 83
  in cell wall biosynthesis *83*
  glycans synthesis 86
  nucleotide sugar interconversion 81, 83, *85*
  substrates of glycosyl transferases **91**
GEFs *see* guanine nucleotide exchange factors
gel-like networks, cytoskeleton 207
gel-mobility shift assays, mRNA–protein binding 455b
gene complements, pathogens 1009, **1011**, *1012*, *1013*
gene expression 422–436
  abiotic stress responses 1052–1054, *1053*
  activators/repressors 429–430, *429*
  analysis 426b
  cis-regulatory modules 428–429, *428*, *429*
  DELLA proteins 863, *863*
  differential 425–436
  freezing tolerance 1073–1075, **1074**
  glycolytic fermentation 1082, *1083*
  heat shock 1096–1097, *1098*
  insulators 428–429, *429*
  Nif/Fix signaling 732–733, *733*
  nitrogenase regulation 732–733, *733*
  nitrogen reductase regulation 742–744, *743–744*
  paramutation 432–433, *433*
  regulation 427–436
    epigenetic mechanisms 430–436
    promoters 427–429, *427–428*, **428**
    transcription factors *428*, 429–430, **430**, 431b
    transposons 421–422, *423–424*
  RNA polymerases 422–425, **424**, *425*
  senescence 943–948, **944–945**, *946–947*, 952–953, *953*
  sugar-related 606–608
  tracheary element development 935, *936*
  transcription factors 434–435
  water deficit 1061–1068, *1063–1066*, *1067–1068*
gene expression profiling 426b
gene families
  actin 194–199
  potassium channels **1111**, 1112
  tubulins 194–199
gene-for-gene model 1022, *1023*
gene islands 414–415, *1013*
gene mapping 406, 943–948, *947*
general transcription factors, transcription preinitiation complex 425, *425*, **425**
genes
  cis-regulatory modules 428–429, *428*, *429*
  duplications 415–416, *416*, 578
  eukaryotic structure 427
  expression, transposons 421–422, *423–424*
  functional annotation 408–410, 410b, 411b
  housekeeping 425
  location on chromosomes 411–412, *412*
  neofunctionalization 415–416, *416*
  promoters 268, *270*, 427–429, *427–428*, **428**
  proximal promoter elements 428
  subfunctionalization 415, *416*
  synteny 416, *417*
  virus resistance 449b
gene silencing, viral resistance 1042–1044
gene targeting 257b
genetic analysis 309

genetic engineering
Agrobacterium-mediated T-DNA transfer 996–997b
aluminum tolerance 1131
artificial mini chromosomes, construction 412, *413*
golden rice 1145, *1147*
high-lauric-content rapeseed 398–399
knowledge-based approaches 1049
lipids 395–400
pathogen defense mechanisms 1044–1049
resistance genes 1032, 1044–1048, 1047b
transcription activator-like effectors 1048–1049
transgenic ricinoleic acid expression 399–400
virus coat protein resistance 1049, *1049*
genetic recombination 255
genetics
see also molecular genetics
aluminum tolerance 1130–1131
autophagy 928, **929**
cyanogenic glycoside biosynthesis 1153–1155, *1155*
disease resistance 1022, *1023–1024*
flooding responses 1084–1085
hypersensitive response 965–971, *966–968*, **969–970**
potassium ion channels 1109–1113, **1111**
preformed defenses 1009–1012, **1010**, **1011**, *1012*, *1013*
programmed cell death 965–971, *966–968*, **969–970**
self-incompatibility 908–909, *909*
senescence 943–948, **944–945**, *946–947*
genetic screening 292, 1068, 1071b
genomes 240
annotation 408–410, 410b, 411b
DNA movement between 267, *268*
mitochondrial 43–44, 264–265, *265*, *266*, 267, **267**
nuclear 260, 261, 264
organellar 260
pathogens **1011**, *1013*
plastid 261, *262*, 264
replication and maintenance 504
tobacco mosaic virus 994, *999*, *1000*
genome-sequencing projects 408, 409b
genome size
flowering plants 404
retrotransposons 420–421, *420*
genome structure 401–437
ancestral duplications 415–416, *416*
annotation 408–410, 410b, 411b
centromeres 412, *413*
differential expression 426–427
euchromatic arms 411–412, *412*
genome-sequencing projects 408
hidden Markov models 409–410, 410b
high-resolution microscopy 401–404
larger genomes 414–415
nucleolar organizer regions 406, 412–414, *414*
optical mapping 406, 407–408b
organization 404–416, *412–413*
physical maps 406–408, 407–408b
promoters 427–429, *427–428*, **428**
synteny 416, *417*
telomeres 412
totipotency 426
transcription, preinitiation complexes 424–425, *425*, **425**
transposable elements 416–422, **418**, *419–420*, 422b, *423–424*
genomic imprinting 436, 914–915, 920–923, *921–922*
genomic resources 89b
geranium (*Pelargonium*) 39
geranyl diphosphate 1138–1141, *1140*
geranylgeranyl 9, *9*
geranylgeranyl diphosphate 1138–1141, *1140–1141*
ent-kaurine synthesis 773, *773*
geranylgeranyl transferase 170
germination
antagonistic regulation 863–865, 864b, *865*
DELLA proteins 861–866, *862–863*, 864b, *865–866*
gibberellin 776, *777*
molecular regulation 903, *903*
programmed cell death 930–932, *930–932*
seed oil catabolism 393–395, *396*
starch degradation 594–595b
strigolactones 830–833, *830–832*
gerontoplasts 37–38
GFP *see* green fluorescent protein
GH3 enzymes, auxin conjugation 801–802, *804*
giant cells, nematode infections *1001*, 1002
gibberellins (GA) 93, 769–776, *770–777*
abscisic acid interactions 863–865, 864b, *865*
auxin regulation 805
bioactivation 773–774, *775*
biosynthesis 771–776, *772–776*
feedback-regulation 776, *776*
green revolution 776, *777*
inactivation 774, *775*
pathogen signaling 1042, *1042*
photomorphogenesis 863–865, 864b, *865*
plant/fungal synthesis pathways 774–776
programmed cell death 931, *932*
signaling pathway evolution 865–866, *866*
signal transduction 861–866, *862–863*, 864b, *865–866*
structure *770*, *771*
ubiquitin 475
GID *see* GA-insensitive dwarf-like proteins
GlcNAc *see N*-acetylglucosamine
7S globulins 180–181b
11S globulins 180–181b, *181*
globulins 15, 180–181b
GLR gene family 139
GLT gene 296
glucan chains, starch synthesis 586
α-1,4-glucanotransferase, starch degradation 595–596, *595*
glucanotransferases
starch degradation 595–596, *595*
starch synthesis 586
α-glucan phosphorylase, starch degradation 596–597
β-glucans
during expansion/elongation 99
endoglucanase activity *85*
expansin regulation 94
microfibril binding *77*
in Poales order *64*, 65
synthase evolution 72
transglucanases 96
glucan, water dikinase (GWD) 593–595, *595*
glucocerebrosides 4, *5*, **11**, 12
glucomannans 65, *65*, 81, 86, 106
gluconeogenesis 572, 643–644, *645*, *958*, 959
glucose 46, 187, *187*
biosynthesis 572, 573–577, *574–577*, 595–597, *595*, *597*, 643–644, *645*, *958*, 959
hexose phosphate synthesis 597, *597*
starch polymers *581*, 584–586
glucose conjugates, abscisic acid metabolism 784, *785*
D-glucose (Glc) 48, *49*, 50, *50*
glucose-1-phosphate 573, 595–596
glucose-6-phosphate 571–573, *572*, 601–602, *602*
glucose-6-phosphate dehydrogenase 601–602, *602*
glucose-6-phosphate isomerase 571–572, *572*
glucose-6-phosphate/phosphate translocator (GPT) 573
glucose sensing, kexokinase 1 607
glucosidases 170, *171*, **172**
β-glucosidation, abscisic acid 784, *785*
glucosinolates 1010, *1014*, 1158–1159, *1159*, 1160–1161b
α-1,4-glucosyltransferase (DPE2), starch degradation 597, *597*
glucosyltransferases 86
D-glucuronic acid (GlcA) 49, *50*
β-glucuronidase (GUS), gene expression analysis 426b
glucuronoarabinoxylans (GAXs) 51, *59*, 65, 70, 79, 95
glucuronoxylans 71–72, 103
GLU genes 296, 297–298
glutamate:oxaloacetate aminotransferase (GOT) 299
glutamate/aspartate carrier 641, *642*
glutamate dehydrogenase (GDH) 293, 618–620
amino acid oxidation 618–620
genes 298–299, *299*
glutamate catabolism 298, *298*, *302*
glutamate synthesis 298, *298*, *302*
NH_4^+ assimilation 293, *294*, 298
regulation *302*
glutamate (Glu)
asparagine synthesis *301*
aspartate synthesis *299*
catabolism 298
GDH activity 298
GS/GOGAT cycle 293, *295*
mitochondrial membrane shuttling 641, *641*
nitrogen assimilation and transport 292, *292*, *294*, 301–302
oxidation, citric acid cycle 618–620
photorespiration *649*, 650
senescence 954–955, *955*
structure *290*
synthesis *291*
glutamate receptors 139, **149**
glutamate synthase 293, *295*
glutamic γ-semialdehyde (GSA) 330, 331
glutamine amidotransferase 296, 312, *312*, 333
glutamine (Gln)
GS/GOGAT cycle 293–299, *295*, *296*, *297*
nitrogen assimilation 292, *292*, *294*, 301–302, *302*, 720, *734*, 735
senescence 954–955, *955*

structure *290*
synthesis *291*
glutamine-glutamate shuttle 293
glutamine:2-oxoglutarate aminotransferase (GOGAT) 293, *295*, *302*, 650, *651*
glutamine-PRPP amidotransferase 245b
glutamine synthetase (GS) 293, 295–296, *295*, *296*, *302*, 650, *651*, 712
γ-glutamylcysteine synthetase 758, *759–760*
γ-glutamyl kinase 330, 331
γ-glutamyl phosphate 293
γ-glutamylphosphate reductase 331
glutaredoxin 554b
glutathione 758–762, 764–765
biosynthesis 758, *759*
senescence 959–961, *960*
sulfate assimilation 764–765, *764*
xenobiotic detoxification 760–762, *761–762*
glutathione conjugates (GS-conjugates) 128, *128*
glutathione synthetase 758, *759*
glutelins 184–185
glycan hydrolases 102
glycans
carbohydrate production 22–23
complex 187
high-mannose 187, *187*
N-glycosylation 173–174, *174*
N-linked 173–174, *173*, 187
O-linked 22–23, 188
processing in Golgi apparatus 187–188, *187*
glyceraldehyde 3-phosphate dehydrogenase 602–604, *603*
glyceraldehyde 3-phosphate (G3P)
dehydrogenation 602–603, *603*
pentose phosphate/triose phosphate pool *598*
systemic acquired resistance 1036–1037, *1039*
terpene synthesis methylerythritol-4-phosphate pathway 1138, *1139*
glycerolipid hydroxylases, transgenic ricinoleic acid expression 399–400
glycerolipids 11
see also galactolipids; phospholipids; sulfolipids; triacylglycerols
de novo synthesis, phosphate attachment 366–368, *369*
desaturation 352–360, *356–361*, 358–360
structures 339–344, **343**, *344*, **345**
glycine betaine (GB) 1057–1058, *1058*
glycine decarboxylase, photorespiration *649*, 650
glycine (Gly)
nitrogen assimilation *292*
photorespiration *649*, 650
structure *290*
synthesis *291*
uptake 119, *120*
glycine-rich proteins (GRPs) 67, *69*, *70*, *71*, 103
glycinin 180–181b
glycolate oxidase, photorespiration *649*, 650
glycolipids 11, **11**
glycolysis
energy conservation 602–604
intermediates, biosynthetic uses *615*
net stoichiometry of sucrose oxidation **615**
overview 612
pentose phosphate/triose phosphate pool 600–601, *600*
regulation 605
glycolytic fermentation 1079–1082, *1080–1081*, *1083*
glycoproteins 22–23, 80, 173, 187, 188
glycosidases 18
glycosides **11**
glycosidic linkage 50
glycosylation 22–23
N-glycosylation 170, 173, *173*
O-glycosylation 188
glycosyl hydrolases 96, *98*
glycosyl lyases 96, *98*
glycosylphosphatidylinositol (GPI) 10
glycosyl transferases (GTs) 18, 89, *90*, **91**, 187
glycosyl transfer mechanisms 89
glyoxylate, photorespiration *649*, 650
glyoxysomes 32, *32*, 941–942
glyphosate 305, *305*
glyphosate-resistant transgenic crops 305
GMP (guanosine monophosphate) *244*
GOGAT *see* glutamine:2-oxoglutarate aminotransferase
golden rice, metabolic engineering 1145, *1147*
Golgi apparatus 18, *81*
AGPs 67
anchoring and movement, actin networks 213–214
carbohydrate production 22–23
crosslinking glycan synthesis 83–86
ER–Golgi trafficking *23*, *166*, 178, *178*
functions 18
glycoproteins 80
glycosylation 22–23
Golgi scaffold/matrix 22
Golgi stack-Golgi-associated TGN units 19–21, *20*, *21*
noncellulosic polysaccharide synthesis 80, *81*, 83–86
nucleotide sugar interconversion 81, 83
pectin synthesis 83–86
protein sorting 182–185, *183*, *184*, *185*
sugar interconversion 49
TGN cisternae 21–22
trafficking *15*, *19*, 22
vacuolar signal receptors 184
Golgi body *3*
Golgi cisternae
cis-Golgi 16, *19*, *20*, 23
medial-Golgi *20*, 22, 23
trans-Golgi 18, *19*, 20–21, *20*, 21–22, 23, 26, *26*
trans-Golgi networks (TGNs) 18, *19*
anterograde/retrograde traffic 162
clathrin-coated vesicles 175
endocytosis 188–189, *188*
function 21
Golgi stack-Golgi-associated TGN units 19–21, *20*, *21*
traffic *15*
trafficking routes *19*, 162
Golgi scaffold/matrix 19, *19*, *20*, *21*, 22, *23*
Golgi stacks 18
docking to ER export site *21*, 22, *23*
Golgi stack-Golgi-associated TGN units 19–21, *20*, *21*
in meristematic root tip cell *3*
pauses at ER export sites 22
trafficking routes *19*
GOT *see* glutamate:oxaloacetate aminotransferase
GPC *see* grain protein content
GPCRs *see* G-protein coupled receptors
GPCR-type G proteins (GTG) 843
GPI (glycosylphosphatidyl-inositol) anchored proteins 69, *71*, *168*, 169–170, *169*
G-protein coupled receptors (GPCRs) 838, 841–843, *842*
GPT *see* glucose-6-phosphate/phosphate translocator
grain protein content (GPC), senescence 948
gram-negative bacteria, nitrogen fixation 718–735, *720*, **721**, 721b, *722–730*, **724**, *732–734*
granal thylakoids *35*, *36*, *37*, 510, *510*
grana stack formation 10
granule-bound starch synthase (GBSS) 585–586, *586*
granules, starch *581*, 585
gravitational potential 660b
gravitropic signalling 15, 213
GRD *see* GROUNDED transcription factor
green fluorescent protein (GFP) 16, *18*, 33, 152b, 426b
green revolution, gibberellins 776, *777*
GroEL proteins 461–462, *462*, *464*, 1096
GroES proteins 461–462, *462–464*
GROUNDED (GRD) transcription factor 917, *917*
growth
acid-growth hypothesis 93–94, *94*
actin 197–202, *197–199*
auxin 730–731, 794, *795*, 804, *805*, 852–857, *853–857*, 936
biochemical changes 97, 99
biophysics 93–94, *93*
cell cycle regulation 504–506, *505–506*
cellulose/crosslinking glycan network 94–96, *95*
DELLA protein regulation 861–866, *862–863*, 864b, *865–866*
direction, change in 93
end of growth 99
epigenetic control 435–436, *436*
growth mechanisms 90–91, *91*
microtubules 197–202, *203*
multinet growth hypothesis 92–93, *92*
pectin network 96
pollen tubes 215, *216*, 904–905, *904–905*
polysaccharide structure modification 97, *97*, *98*
rate, change in 93
rate equations 93
regulation 93, 94–96, *95*, 607–608, *608*
tip growth 91, *92*
Type 1 walls 96
growth sinks
post-SE transport 684–691, *686–690*, **686**, *692*
signaling 705, *708*
GrpE 460, *462*
GRPs *see* glycine-rich proteins
GS *see* glutamine synthetase
GSI *see* gametophytic self-incompatibility
GTG *see* GPCR-type G proteins
GT (glycosyl transferase) genes 89, *90*, **91**
GTPase activating proteins (GAPs) 842, *842*
GTPases 176, *176*

GTP (guanine triphosphate)
protein synthesis 441–447, *443*, *445–446*, *448*
tubulin polymerization 197–202, *198*
GTs *see* glycosyl transferases
GU-AG rule 279, 280
guanine *241*, 243, *247*
guanine diphosphate *see* GDP
guanine methyltransferase *274*
guanine nucleotide exchange factors (GEFs) 843, *842*
guanine triphosphate *see* GTP
guanosine-based sugars 81, *83*, 83, *85*, 86, **91**
guanylyltransferase *274*
guard cells *46*
anion channels 140–141, *141*
ion channels 129, 133, *134*, 135–136, *135*, 138, *138*, 140–141, *141*
light responses 867–870, *867–870*
pumps 124
wall thickening 103
guidance, pollen tubes *904–905*, 905
guide RNAs 286
GUS *see* β-glucuronidase
GWD *see* glucan, water dikinase

H^+ *see* proton…/hydrogen…
Haber–Bosch process 714b
Hagen–Poiseuille equation/law 660b
hap1 mutants 334
haploid plant generation, microspore culture 893b
haploinsufficiency 914–915, 915b, *916*
HATs *see* histone acetyl transferases
haustorium 990–992, *995*
Haworth projections 46, *49*
hcsiRNAs *see* heterochromatic siRNAs
HDACs *see* histone deacetylases
HDEL retention signal 178
"head-to-tail" addition
cytoskeletal polymers 197–198, *198*
five-carbon units of terpenoid biosynthesis 1134–1135, *1136*
heat shock elements (HSEs) 1096–1097
heat shock factors (HSFs) 1096–1097, *1098*
heat shock proteins (HSPs) 153, 1094–1097, *1094–1095*, **1095**, *1097–1098*
chaperones 1095–1096
osmotic stress protection 1058–1059
heat stress responses 1094–1097, *1094–1095*, *1097*
Hechtian strands 12–13, *12*
helix-loop-helix proteins, gene expression 429–430, *429*
heme
biosynthesis *516–517*, 518–519
cytochromes *623*
heme A *623*
heme C *623*
hemibiotrophic fungi 992, *996*
hemi-methylated sites on daughter chromosomes 433–434
hemiterpenes 1133
herbicides
AHAS inhibitors 328, *329*
and amino acid synthesis 306b
tolerance 306b, 760–762, *761–762*
heritable variation, disease resistance 1022, *1023–1024*
heroin 1161, *1164*
heterochromatic siRNAs (hcsiRNAs) 276, *276*, 277, **278**, 285–286
heterochromatin 250, 431
heterocysts, cyanobacteria 715
heteronuclear multiple-quantum coherence (HMQC) 56b
heteronuclear single-quantum correlation (HSQC) 56b
hexapyranoses 49
hexokinase, starch degradation 597, *597*
hexose phosphate antiporters 573
hexose phosphate pool 571–573, *571–572*
cellular compartmentalization 573
fructose-2,6-bisphosphate level modulation 588–589
pyrophosphate-dependent phosphofructokinase 572, 575–576b
hexose phosphorylation, ATP independent pathways 579
hexoses 46
HG *see* homogalacturonan
HGPRTase *see* hypoxanthine-guanine phosphoribosyltransferase
hidden Markov models (HMMs), genome sequencing 409–410, 410b
high-affinity potassium transporters 1106–1107, *1106*, 1109
high-lauric-content rapeseed, genetic engineering 398–399
highly substituted GAX (HS-GAX) 97, 99
highly vacuolated cells
cytoplasmic streaming 211–212, *213*
phragmosomes 227, *227*
high-mannose glycans 187
high-performance liquid chromatography (HPLC) 60b
high-pressure freezing, methodology 210
high-resolution microscopy, genome structure 401–404
high-throughput mutant screening, cyanogenesis 1150–1151b
histidine (His)
nitrogen assimilation *292*
structure *290*
synthesis *291*, 333–334, *334*
histidine kinase, cytokinin signal transduction 850–851, *850–851*
histidine phosphotransfer protein (HPt), cytokinin signal transduction 851, *851*
histidine-rich sequences, fatty acid desaturases 358, *360*
histone acetyl transferases (HATs) 434, *434*
histone chaperones 432
histone code hypothesis 435
histone deacetylases (HDACs) 434–435, *434–435*
histone methyl transferases (HMTases) 434
histones 402–404, *402*
acetylation 433–434, *434*
cell cycle 492–493, *492*
condensation 430–431, 434–435, *435*
covalent modifications 433–434
methylation 434
historical nitrogenous soil amendments 714b
H^+/K^+-exchanging ATPase 122
see also proton pumps
HKT transporter gene family 144
HMMs *see* hidden Markov models
HMQC *see* heteronuclear multiple-quantum coherence
HMTases *see* histone methyl transferases
hnRNP (heterogeneous ribonucleoprotein) proteins 161, *161*
homeodomain-type transcription factors 497–500, *498–500*
homeostasis
amino acids 467
copper 1126–1127
phosphate 1116–1118, *1118*
homeotic gene regulation, flowers 887–889, *887–889*
L-homoarginine, cadaverine biosynthesis 821, *821*
R-homocitrate, molybdenum-iron binding, nitrogenase 716
homocysteine 320
homodimers, transcription factors 429–430, *429*
homogalacturonan (HG) *66*, 67, 72, 77–78, 86, 96, 99, 100
see also Ca^{2+}-HG junction zones
homogentisate 309
homology
active sites of fatty acid modifying enzymes 362–363
electron transport chains 630b
gene evolution 415b
prenyltransferases/terpene synthases 1141–1142, *1143*
homoserine 319
homoserine dehydrogenase (HSDH) 319, *320*, *321*, 323, *324*, *325*
homoserine kinase 319, *321*
homoserine 4-phosphate 319, 324
hormones
see also individual hormones
biosynthesis 769–832
flooding responses 1082–1085, *1083–1084*
nodulation 730, *730*
pathogen resistance 974–976, 980–981
phloem transport 706, *709*
senescence regulation 974–981
ubiquitin regulation *474*, 475
xylem loading 670–671, *671*
housekeeping genes 425
HPAEC 60b
HPLC *see* high-performance liquid chromatography
H^+-PPase *see* hydrogen pyrophosphatase
HPt *see* histidine phosphotransfer protein
HR *see* hypersensitive response
HRGPs *see* hydroxyproline-rich glycoproteins
HSDH *see* homoserine dehydrogenase
HSEs *see* heat shock elements
HSFs *see* heat shock factors
HS-GAX *see* glucuronoarabinoxylans
Hsp40 proteins 460, *462*
Hsp60 proteins *156*, 158, 461–462, *462–464*
Hsp70 proteins 155, *156*, *157*, 158, 459–462, *460–462*
HSPs *see* heat shock proteins
HSQC *see* heteronuclear single-quantum correlation
human/animal uses of plants 108–110, *109*
human benefits of phenolic compounds 1185

HXK1 *see* hexokinase 1
HXXHH motifs, fatty acid desaturases 358, *360*
hybrid nucleases 257b
hybrid vigor, F1 hybrids 901
hydraulic conductance
  cavitation 691–693, *694–695*
  cohesion–tension mechanism 691, *693*
  phloem 681, **682**, 685–689, *686–689*, 691
  theory 660b
  xylem 668–669, *670*, 691–696, *694–696*
hydrogen (H^+) pumps *see* H^+-ATPases
hydrogen peroxide, immunity 1016, *1017*
hydrogen pyrophosphatase (H^+-PPase) 27
hydrolysis
  glucosinolates 1158–1159, *1159*
  triacylglycerols 393–395, *394*, *396*
hydropathy analysis 113, 114–115b
13-hydroperoxylinolenic acid, metabolism 379, *380–381*
hydrophilic domains 4, *5*, *6*
hydrophobic domains 4, *5*, *6*
hydrostatic pressure (Ψ_p) 146–147
  phloem **682**, 697–700, *698–700*
  sieve tubes **682**
3-hydroxyacyl-ACP, dehydration to enoyl-ACP 352, *354*
hydroxycinnamates 70, *72*
hydroxylation, fatty acids 362–363, *363*
p-hydroxyphenylpyruvate 306, *307*, 308
hydroxyproline 188
hydroxyproline-rich glycoproteins (HRGPs) 67, *69*, *70*, 99, 103, 188, 1016, *1018*
hypersensitive response (HR) 965–974, *966–968*, **969–970**, *972–974*, 989, *989*
hypoxanthine-guanine phosphoribosyltransferase (HGPRTase) 245b
hypoxia 447, 1081–1085, *1083*
  see also anoxia; flooding; oxygen deficit

IAA *see* indole-3-acetic acid
IB *see* inclusion bodies
IBA *see* indole-3-butyric acid
ice crystals, preventing formation 210
identity genes, meristems 879–881, *882*
IGL *see* indole-3-glycerolphosphate lyase
IGP *see* imidazole glycerol phosphate
IGPS *see* indole-3-glycerolphosphate synthase
Ile *see* isoleucine
illegitimate recombination 259–260
imidazole glycerol phosphate (IGP) 333, *334*
imidazolinones 306b, 328, *329*
immunity
  see also defense....; effector-triggered immunity; pattern-triggered immunity
  nucleotide-binding-leucine rich repeat proteins 1024–1032, *1026–1027*, *1029–1031*
  overview 985–989, *988*
immunocytochemistry 152b
IMP *see* inosine 5′-monophosphate
importin-Ran-GTP complex 161, *162*
importins 160–161
inactivation
  see also inhibition
  gibberellins 774, *775*
inclusion bodies (IB) *48*
indeterminate nodules, legumes 725, *725*
indirect recognition, pathogen effectors 1027–1031, *1029*
indole 316, 317b
indole-3-acetic acid (IAA) *770*, 795–796, *796*
  see also auxin
indole-3-butyric acid (IBA) 795–796, *796*
indole glycerol phosphate 333
indole-3-glycerolphosphate lyase (IGL) 316
indole-3-glycerolphosphate synthase (IGPS) *311*, 314, 315, 316, *316*
indole ring 309, *309*, 314, *316*
induced defense 1012–1032, *1015–1031*, **1024**
  cell wall fortification 1016, *1018*
  effector-triggered immunity 1022–1032, *1021–1035*
  nucleotide-binding-leucine rich repeat proteins 1024–1032, *1026–1027*, *1029–1031*
  pattern-triggered immunity 1012–1022, *1016–1020*
induction of flowering, salicylic acid 826
industrial applications
  fatty acids 398, **398**, 399
  nitrogen fixation 714b
  starch 585b
infection threads, legume nodulation 724–726, *725*, *732*
inflorescence
  LEAFY 881–882, *881*, *883*, 887–888
  meristems 879–881, *882*
  programmed cell death 939, *939–940*
information flow
  cytoskeleton 191–192
  gel-like networks 207
in-frame stop codon readthrough 450, 450b
inheritance 39
  see also genetics
inhibition
  ADP-glucose pyrophosphorylase 582–584, *584*
  alternative oxidase 629–631, *631*
  brassinosteroid synthesis 814
  chloroplast electron transport 536, *536*
  cyclin-dependent kinase 485, *486*
  ethylene biosynthesis *809*, 810
  invertase 579–580
  ent-kaurine oxidase 773, *774*
  mitochondrial electron transport chain 622–624, *625*
  ribosomes 439, 441b
  RNA polymerases 423
  sulfate uptake 750–751
initiation
  flowering 872–881, 880b, *881*
    external coincidence model 876, *878*
    photoperiods 874–878, *876–877*, *881*
    vernalization 874, 878–879, *879*, 880b
  leaves, auxin signaling 856–857, *856–857*
  protein synthesis 441–442, *443*
    cytosolic regulation 442, *445*
    plastids 452, *452*, *453*
    viruses 447–449, *449*, 450b
inner membranes of mitochondria 611, *611*, 639
inorganic nitrogen compounds 711, **712**
inorganic phosphate (P_i)
  chloroplast transport *569*, 573
  mitochondrial transport 633–634, *634*
  starch synthesis 582–584, *584*
inosine 5′-monophosphate (IMP) *244*
insects
  alkaloids 1165b
  cyanogenic glycosides 1156b
  wound healing 1002–1003, *1003*
insensitivity, pathogen effectors 1033
in situ hybridization, gene expression analysis 426b
insulators, gene expression 428–429, *429*
integral membrane proteins
  F_oF_1–ATP synthase 632–633, *633–634*
  lipid bilayer association 8–10, *8*
  mitochondrial electron transport chain 620–633, *620*, *624–631*, *633–634*
  orientation in ER membrane 168–169, *168*
  retention signals 178, *178*, 179
  selective permeability 113
  topogenic sequences 168–169, *168*
  types *168*
integration, pentose phosphate/triose phosphate pool 597–599, *598*
integrins
  cytoskeleton–cell wall coupling 221–222
  signal transduction 221–222
intercellular transport, trans-membrane 661b
intercisternal elements *19*, 21
intermediate filaments, cytoskeleton 192–194
intermediate repeat DNA 406
intermembrane space, mitochondria 611, *611*
intermolecular tunnel 314, *317*, 317b
internal reorganizations, senescence 941–942, *942*
internal vesicles 26
interphase 477, *478–479*
  anisotropic expansion 216–217
  chromosome transcription 29
  cortical endoplasmic reticulum 13, 15
  nucleoli 29
  nucleus 29
  vacuole dispersion 27
intracellular auxin, signal transduction 852–854, *853–854*
intracellular signaling 843–847, *844–846*
  calcium ions 843–845, *845*
  calmodulin 844–845, *845*
  cyclic 3prime,5′-adenosine monophosphate 843–847, *844*
  MAPK cascades 846–847, *846*
  osmotic stress 1065–1068, *1067–1069*
intrinsic proteins (PIPs) 147
introns 278
  Group I introns 278–280, **279**, *282*
  Group II introns 278–279, **279**, 280, *282*, 282–283b
  Group III introns 279
  GU-AG rule 279, 280
  homing 280
  nuclear pre-mRNA introns 278, 279, **279**, *280*
  nuclear pre-tRNA introns 278, 279, **279**, *281*
  self-splicing 279–280, *282*
  splicing 279, *280*, *281*
  trans-splicing mechanism 282–283b
invertase 577–580, *578–580*
inward-rectifying potassium channels 680, *680*, 1112

ion channels 113
see also individual channels and pores
action potentials 128, *129*
anion channels 140–141, *141*
electrochemical potential 129, 131, *131*
gating 120, 131–132, 133, 135
inward-rectifying 133–135, *135*
ionic selectivity 131–132, 132b
malate channels 141–142, *142*
mechanical stimuli transduction 843
open and closed states 133, *133*
permeability ratios 132b
reversal potential 120
Shaker family 135, *136*, **149**, 1109–1113, *1110*, **1111**
study techniques
lipid bilayers 129, *131*
microelectrode impalement 129, *131*
patch clamp 129, 130b
threshold voltage 133, *134*
transport rates 113
two-pore channel family 140, *140*
ubiquitousness 129
vacuolar channels 136–138, *137*, *138*, 139–140, *139*, *140*
voltage sensors 135, *136*
ion fluxes, radiotracers **1105–1106**
ionic currents 130b
ionic homeostasis 28
ionic selectivity 131–132, 132b
ions, phloem loading 680, *680*
ion traps 62–63b
IPMDH *see* isopropylmalate dehydrogenase
IPMI *see* isopropylmalate isomerase
IPMS *see* 2-isopropylmalate synthase
Ipomoea tricolor, flower senescence 940, *941*
IP_3 receptors 139
IPT *see* adenosine phosphate-isopentenyltransferase
iron
see also diiron
cellular storage 1124–1125, *1125*
deficiency *1102*, 1122
transport 1120–1125
uptake 1120–1124, *1121–1125*
iron ions (Fe^{2+}) **149**
iron-molybdenum (FeMo) cofactor, nitrogenase 716–717, *716–718*
iron-nicotinamide transporter (AtYSL1), xylem unloading in leaves 672
iron protein, nitrogenase 717–718
iron protoporphyrin IX *623*
iron–sulfur (Fe–S) clusters 296, 717, *717*
iron–sulfur (Fe–S) proteins 532–533, **533**, *624*
isoamylase 3, starch degradation 596
isocitrate dehydrogenase
citric acid cycle 617–618, *619*
cytosolic 643, *643*
isoenzymes 292
isoflavone, structure *722*
isoforms, actin/tubulin evolution 195–196
isoleucine (Ile) 323
nitrogen assimilation *292*
precursor to metabolites *326*
structure *290*
synthesis *291*, *320*, 326, *327*, 328–329
synthesis regulation *323*
isopentanes *1133*
isopentyl diphosphate 1134–1141, *1137*, *1139–1141*
methylerythritol-4-phosphate pathway biosynthesis 1138, *1139*
mevalonate pathway biosynthesis 1135–1138, *1137*
isoprenes *1133*
see also dimethylallyl diphosphate; five-carbon units; isopentyl diphosphate
isoprenoid cytokinins *786*, 787–793, *788–793*
isopropylmalate dehydrogenase (IPMDH) *327*, 329–330
isopropylmalate isomerase (IPMI) *327*, 329
2-isopropylmalate synthase (IPMS) *327*, 329

JA *see* jasmonic acids
JA–Ile *see* jasmonyl–isoleucine
jasmonic acids (JA) 821–825, *823–825*
biosynthesis 338, 379, *381*, 823–824, *824–825*
induced defense 1022, 1040–1042, *1042*
metabolic products 825, *825*
necrotrophic pathogen responses 1040–1042, *1042*
senescence 980–981
signaling 379–382
structure *770*, 822–823, *823*
jasmonyl–isoleucine (JA–Ile) 824, *824*

K^+ *see* potassium…
KAS *see* 3-ketoacyl-ACP synthase
KAT1 gene 1109–1113, **1111**
katanin, microtubule severing 207
ent-kaurine 773, *773*
ent-kaurine oxidase (KO) 773, *774*
KDEL retention signal 178, *178*, 179, 185
kernel deformation, ethylene 931, *931*
α-keto acids 636–638, *636*
3-ketoacyl-ACP dehydratase 352, *354*
3-ketoacyl-ACP reductase 351–352, *353*, *354*
3-ketoacyl-ACP synthase (KAS) *347*, 351, *354*
α-ketobutyrate 326
α-ketoglutarate dehydrogenase 618, *619*
α-ketoglutarate (α-KG) *290*
in AAA pathway 320
ammonia assimilation 642–643, *643–644*, 650, *651*
arginine N-storage 333
in GS/GOGAT pathway 293, *295*
lysine catabolism 323, 325, *325*
mitochondrial membrane shuttling 640–641, *642*
rate of production, pyruvate kinase activity *605*
reductive amination 298, *299*
2-ketoisovalerate 329
ketoses 45
kexokinase 1 (HXK1), glucose sensing 607
α-KG *see* α-ketoglutarate
kinase LRE1 174, *174*
kinases 485, *486*, 835
see also individual enzymes
leucine-rich repeats 107, *108*, 189, 839–840, 1023–1026, *1025–1026*
kinesin-5 232–233b, 234
kinesin *204*, 205, 232–233b, 234
kinetics
actin elongation 197–202, *197–199*
nitrate uptake *740*
potassium ion transport 1106–1107, *1106–1107*
kinetin *785*
kinetochores 230–231, *231*, 494–495, *494*
Kip-related proteins (KRPs) 486, *487*
knock-in/knock-out experiments 257b
knowledge-based approaches, disease control 1049
KO *see ent*-kaurine oxidase
Kranz anatomy 558, *559*
krebs cycle *see* citric acid cycle
KRPs *see* Kip-related proteins
K^+ transporters 138
KUP/HAK/KT family of transporters 134, 138, **149**

laballenic acid *361*
laccases 105
lactate, anoxic metabolism 1079–1082, *1080–1081*, *1083*
lactate dehydrogenase (LDH) 1079, *1080*
laevorotatory optical rotation 48
lag phase, cytoskeleton nucleation 197–198, *197*
lamellae 34
laminar flow 660b
laminaribiose 50, *51*
large subunit of Rubisco (LSU) 463, *465*
late embryogenesis abundant (LEA) proteins 1058–1059, 1073–1075, **1074**
late endosomes 26
lateral exchange of nutrients from transport phloem 682–683, *684–685*
lateral heterogeneity 35–37, 540–541, *540–541*, **540**
lateral inhibition, megaspore development 899
late TGN cisternae 21
LAX transporters 854, *855*, 857, *857*
LDH *see* lactate dehydrogenase
LEA *see* late embryogenesis abundant proteins
leaf cell diagram *3*
leaf epinastry 804, *805*
LEAFY (LFY) transcription factor 881–882, *881*, *883*, 887–888
leaky scanning 444b
leaves
auxin signaling 856–857, *856–857*
ion delivery 671–672, *672*, 680
morphology 934b
senescence 945–951, *946–947*, *949*, *952*, *958*, 959
terminal development 940–948, *941–942*, **944–945**, *946–947*, *949*
xylem unloading 671–672, *672*
legumes
bacteroids 731–733, *732–734*
Bradyrhizobium infection 726
commercial species 720
nitrogen assimilation *734*, 735–746, *736–741*
nitrogen transport 720, *734*, 735–739, *736–741*
Nod factors 722–724, *722–723*
nodulins 729, *729–730*
root hairs 724, **724**, *725*, 727, *728*, *732*
root nodules 720–735, *721*, *724–730*, *732–734*, *736*
bacteroids 731–733, *732–734*
calcium spiking 724, *728*, 729
development 720–733, *722–730*, **724**, *732*

hormone signaling 729–731
microaerobic environment 731–733, *732–733*
molecular genetics 726–733, *726–730*, *732–733*
symbiotic nitrogen fixation 718–735, *720*, **721**, 721b, *722–730*, **724**, *732–734*
lenticels 1076, *1077*
Lesch-Nyhan syndrome 245b
lesion mimic mutants 971, *972*
leucine (Leu)
nitrogen assimilation *292*
precursor to metabolites *326*
synthesis *291*, *327*, 329–330
leucine-rich repeat receptor-like kinases (LRR-RLK) 189
leucine-rich repeats (LRR) 107, *108*, 189
brassinosteroid receptors 839–840
R-proteins 1023–1026, *1025–1026*
leucine zipper proteins 429–430, *429*
leucoplasts 33, *33*, 38, *38*
Lewis antigen 187
LFY *see* LEAFY
LHC *see* light-harvesting complexes
life cycles
flowering plants *873*
liverwort 889, *890*
ligand-binding domains, signal transduction 836
light
absorption and energy conversion 511–518, *512*, *515–518*
chlorophyll synthesis 35
critical C_4 enzyme modulation 563, *563*
magnesium ions 556–557
N-assimilation by amino acids 301–302, *302*
nitrogen reductase regulation 743–744, *743–744*
optimal absorption, chloroplasts 212–213, *214*
phytochrome signaling 860–861, *861*
properties 511
stromal enzyme modulation 453–454, *454–457*, 551–557, *553*, *555–558*, 563, *563*
stromal pH 556–557
light-harvesting complexes (LHC) 35, 526–528, *527*, 540–542, *540–541*, **540**
organization and regulation 540–542, *540–541*, **540**
phosphorylation **540**, 541–542, *541*
light-induced germination, lettuce seeds 776, *777*
light microscopy 75b, 76b, 402, *402*
light perception 857–861, *858–861*
light periods 589–591, *591*
light reactions of photosynthesis 510–542, *511–512*, *518*, *524–526*, *530–532*, *534–535*, *541–542*
lignans 1182, **1183**
lignins 1181
analysis methods 55–58b, 105, *105*
aromatic amino acids 302
induced defense 1016, *1018*
interaction types *73*
metabolic pathways *72*
reducing content 109, *109*
secondary walls 104–106
xylem structure 664, 666
LIM15 protein *259*
limit dextrinase 596
LINEs *see* long interspersed elements
α-1,4-linkages, starch *581*, 584–586
α-1,6-linkages, starch *581*, 584–586
β-linked polysaccharide synthase genes 86–88, *87–88*
linoleate desaturase 358
α-linoleic acid 11, 823–824
α-linolenic acid 11, *290*, 342
lipid bilayers 2
see also membranes
cross-section *4*
ion channel research 129, *131*
lipid structures *5*
organization of lipid molecules *6*
phospholipid movement 5–6, *7*
phospholipids 4, *6*
proteins, associated 8–10, *8*, *9*
spontaneous assembly 4
sterols 7
temperature impacts 7, **8**
lipid hopping 25, *25*
lipid micelle *4*
lipid rafts 10
lipid recycling 17
lipids
see also galactosylglycerides; glucocerebrosides; membrane lipid synthesis; membranes; phospholipids; sterols; storage lipids
amphipathic nature 4, *5*, *6*
biosynthesis *338*, 358–360, **358**, *359*, *364–375*, 365–373, 392–393
cell reproduction 337–400
cellular compartmentalization 337, 392
classes 4
cold acclimation 12, 1072–1073
definition 337
desaturation 352–360, *356–361*
elongation 360, *361*
energy density 337–338, *340*
eukaryotic synthesis pathway 17, *364–369*, 365–373, *371–373*
extracellular 382–389, *382–388*
fatty acid composition 365
genetic engineering 395–400
gluconeogenesis 643–644, *645*
membrane deposition 382–389, *382*, *385–388*
nomenclature 342b
oil bodies 391–392, *391*
phase transition 7
physical states 7
in plant membranes 4, *5*, *6*
prokaryotic synthesis pathway 17, *364*, 365–372, *368–370*
roles in plants 337–338, **339**, *340*
stearoyl-ACP desaturases 353–356, *356–357*
storage 339–342, 389–393, *390*
structures 338–344, *344–345*
temperature of melting 7, **8**, 352–353, *356*
transport to/from endoplasmic reticulum and chloroplasts 366, *367*, *368*
turnover 7
lipid-transfer proteins 17
lipooligosaccharides, Nod factors 722–724, *722–723*
lipopolysaccharides, rhizobial bacteria 722–723, *724*
lipoxygenase pathway 379, *380–381*
liquefaction 100
liverwort, lifecycles 889, *890*
LjNFR1 receptor 727, *726*
LKR *see* lysine-ketoglutarate reductase
loading
phloem 673–681, *673–674*, *677–681*
xylem 668–669, 670–671, *671*, 739
LOG *see* LONELY GUY
LONELY GUY (LOG) 788–789, *789*
long-day plants 875
long-distance transport 658–710
cell biology 664–668, *664*, **665**, *667–668*
fundamental forces 660–661b
phloem
cell biology 666–668, *667*
functional sectors 673, *673*
regulation 705–709, *706–709*
short-distance transport to nonvascular cells 673–691, *673*, *677*, *679–681*, *684–685*, *687–690*, *692*
whole-plant organization 696–704, *698–704*
selection pressures and systems 658–664, 660–661b
xylem
cell biology 664–666, *665*
functional properties 668–672, *669–671*
whole-plant organization 691–696, *692–697*
long interspersed elements (LINEs) 421
long terminal repeats (LTR) 419–421
loosening of cell walls 90, *91*, 99
Lotus japonicus, nodulation 726–727, *726*
low-affinity potassium transporters 1106–1107, *1106*, 1109
low oxygen concentrations, legume symbiosomes 731–733
low-temperature sensing systems 1072
LRR *see* leucine-rich repeats
LRR RLK *see* leucine-rich repeat receptor-like kinases
Lsi1/2, silicon transport in roots 670–671, *671*
LSU *see* large subunit of Rubisco
LTR *see* long terminal repeats
lupinic acid 787, *788*
lutein biosynthesis 519, *530*
lycopene *38*
lysigeny 933, *933*
lysine-ketoglutarate reductase (LKR) 325, *325*
lysine-ketoglutarate reductase-saccharopine dehydrogenase 335b
lysine (Lys) 299
cadaverine biosynthesis 821, *821*
catabolism 325, *325*
level regulation 325–326, *325*
nitrogen assimilation *292*
structure *290*
synthesis *291*, 319–320, *320*, *321*
synthesis regulation 323–324, *323*, *324*, *325*
lysine-sensitive AK 323–324
lytic vacuoles *15*, 26, *26*, 28, *29*, 182

macromolecular enzyme complexes, cyanogenic glycoside biosynthesis 1155–1157, *1155*
macromolecular signaling proteins, phloem transport 700–703, *701–703*

macromolecules
  degradation 951–957, *952–956*
  phloem transport 700–703, *701–703*
  plasmodesmata 701, *702*
macronutrients, definition 1102
MADS domain transcription factors 430, 886–887, *888*
Magnaporthe oryzae 1006, *1008*
magnesium–ATP hydrolysis, nitrogenase 717–718, *717–718*
magnesium ions 556–557, *1102*
maize (*Zea mays*)
  auxin ester conjugation 801, *803*
  CesA genes *87–88*
  color variation 421, *423*
  genome 420–421, *420*
  GT genes *90*
  internet resources 89b
  mitochondrial genome *265*, **267**
  retrotransposons 420–421, *420*
  vivipary 778, *778*, 782–784, *783*
major facilitator superfamily (MFS) 145–146
major intrinsic protein (MIP) family 147
malate
  alternative mitochondrial oxidation pathways 616, *616*
  aluminum tolerance 1128–1131, *1129–1131*
  oxidation 616
  transport 141–142, *142*, **150**
malate-aspartate shuttle 299
malate channels 141–142, *142*, **150**
malate dehydrogenase 618, *619*
MALDI–TOF *see* matrix-assisted laser desorption ionization-time of flight MS
male gametes
  apomixis 901–902, *902*
  cytoplasmic sterility 896–897, *897*
  formation 889–897, *891–892*, 893b*894*, 895b, *896–897*
  microgametogenesis 889–896, *891–892*, *894*
  microspore culture 893b
  microsporogenesis 889–891, *891–892*, 893b
  segregation ratio distortion 896b
  surface lipids 388–389, *388*
malic enzyme, plastids 605–606, *607*
malonyl-CoA:ACP transacylase 351, *351*, *352*
malonyl-CoA 346–351, *347–349*, *351*
maltose 595–597, *595*, 597, *597*
malvalic acid 363
manganese, deficiency *1102*
mannan hydrolases 96
mannans 65, *65*, 72, 96, 106, *106*
mannan transglycosylases 96
mannose 187, *187*
D-mannose (Man) 48, *50*
mannosidase I 22
mannosidase I-green fluorescent protein fusion protein *20*, 22
mannosidases 187
D-mannuronic acid (ManA) 49, *50*
MAP65 207
MAPK *see* mitogen-activated protein kinases
master circles 265, *265*, *266*
MATE transporters *see* multidrug and toxic efflux transporters
matrix, mitochondria 611, *611*
matrix-assisted laser desorption ionization-time of flight (MALDI–TOF) MS 62–63b
matrix-oriented NAD(P)H dehydrogenases, mitochondria 627–629, *630*
maturation of seeds, molecular regulation 923, *923*
Mäule reagent 105, *105*
MCM *see* minichromosome maintenance helicase
mechanical stress, freezing stress 1069–1072, *1070*
mechanical transduction 220–222, *221*, 843
mechanochemical enzymes *see* motor proteins
mediators of gene expression 427–429, *427*, *429*
Medicago truncatula, nodulation 726–727, *726*
medicines *see* pharmaceuticals
megagametogenesis 897, 899–900, *900*, 939–940
megaspore mother cells (MMC) 898–899, *899*
megasporogenesis 897, 898–899, *898*
melting temperatures of fatty acids 352–353, *356*
membrane anchor sequences 169
membrane-bound polysomes 447, 452–453, *453*
membrane destabilization
  chilling stress 1068–1069
  freezing stress 1069–1072, *1070*
membrane lipid synthesis 17, *364–375*, 365–373
  diacylglycerol pools 365
  endoplasmic reticulum–chloroplast transport pathways 366, *367*, *368*
  eukaryotic pathway *364–369*, 365–373, *371–373*
  prokaryotic pathway *364*, 365–372, *368–370*
membrane potential (V_m) 117–119, *118*, 119b, 141, 661b
membrane proteins
  apoplastic sieve element loading 677–680, *678–680*, **680**
  folding 462–463
  thylakoid localized 452–453
membrane receptor kinases 838–841, 839b, *841–842*
membrane recycling 24–25, *25*, *26*
membranes 111
  see also endoplasmic reticulum; fluid-mosaic membrane model; lipids
  bilayers 342, **343**
  cell reproduction, lipids 337–400
  chilling sensitivity 376–377, *377–378*, 1068–1069
  chloroplasts 337, 374b, 375–376, *375*
  cold acclimation 1072–1073
  composition 373–379, *375*
  destabilization 1068–1072, *1070*
  domains 10
  extracellular lipid deposition 382–389, *382*, *385–388*
  freezing stress 378–379, *379*, 1069–1072, *1070*
  functions 2, 373–382
  inheritance 3
  ion channel receptors 843
  lipid composition 373–379, *375*, *376–379*
  lipid micelles *4*
  major classes **343**
  mitochondria *364*, 365–372, *368–370*, *375*
  permeability 111, *112*
  permeability coefficients 661b
  phospholipids 342, **343**
  photosynthesis impairment 375–376, *377*
  plasma membrane *see* plasma membrane
  properties 2
  signaling pathways 379–382, *380–381*
  structure 2, *3*
  traffic 13, *15*
  types 2, **4**
membrane stabilization, cold acclimation 1072–1073
membrane topology, complex II of the mitochondrial electron transport chain 622, *626*
membrane transport/trafficking
  see also aquaporins; ion channels; loading; uptake
  biological processes 111–112
  chemiosmotic processes *115*
  electrochemical potential 115, *115*, 116–117b, 117
  hydropathy analysis 113, 114–115b
  ionic selectivity 132b
  membrane potential 117–119, *118*
  membrane potential changes 119b
  mitochondrial metabolites 639–646
  oil:water partition coefficient 111, *112*
  patch clamp technique 130b
  proteins *see* protein sorting
  proton gradients 117, 118b
  proton motive force 118b
  pumps *see* pumps
  selective permeability 113
  solute uptake energetics 121b
  transporter interactions 119–120, *120*
  transporters 113, **149–150**
  viruses 998, *1000*
  water deficit/salinity 1060, *1060*
  water transport 146–148, *147*, *148*
Mendel, G., pea phenotypes 583b
MEP *see* methylerythritol-4-phosphate
meristems
  development 477, *479*
  identity gene expression 879–881, *882*
  inflorescence 879–881, *882*
MeSA *see* methylsalicylic acid
mesophyll cells 218, *218*, 673–674, *673*
messenger ribonucleoprotein (mRNP) complex 161
messenger RNA (mRNA) 240, 273
  5′cap formation 273, *274*
  chloroplasts *275*
  editing 286–288, *288*
  functions 270
  introns 279
  leaky scanning 444b
  modification 273, *274*, 275
  photosynthesis-encoding genes 261
  poly(A) tails and segments 275
  polycistronic plastid mRNAs 286, *286*
  regions 273, *274*
  storage protein sorting 185
  structural proteins 67
  structure *274*
  transcription 423
  translation 439–457, *452–457*, *459*
  upstream open reading frames 445b
  viral 447–449, *449*, 450b
Met *see* methionine
metabolic acclimation, oxygen deficit 1079–1082, *1080–1081*
metabolic bypasses, alternative oxidase 629–631, *631*, 635–639, 636b, *638*

metabolic channeling, cytoskeletal organization 219–220, *220*
metabolic dysfunction, chilling stress 1068–1069
metabolic engineering
  alkaloid synthesis 1174–1178, *1180*
  edible oils 395–397
  natural product pharmaceuticals 1174–1178, *1180*
  terpenoids 1145, *1147*
metabolic pathways
  abscisic acid 784, *785*
  brassinosteroids 811–818, *813*, *815–818*
  bypass reactions 592–593b
  carbohydrates
    alternative oxidase regulation 637, *637*
    circadian clocks 591, *591*
    energy and reduction products 601–606
    gene expression 606–608
    starch degradation 591–597, 594–595b, *595*, *597*
    starch synthesis 580–587, *582*, 583b, *584*
    sucrose 577–580, *578–580*
    triose phosphate/pentose phosphate pools 597–601, *598*, *600*
  cellular, acetyl-CoA *346*
  duplications *571*
  integration 597–599, *598*, 658–710
  jasmonic acid 825, *825*
  long-distance transport 658–710
  malonyl-CoA *349*
  metabolomics 599b
  pentose phosphate pathway *598*, 601–602, *602*
  phosphatidic acid synthesis 365
  pyrophosphate 575–576b
  ubiquitin proteolysis 469–474, *470–471*, **472**, *473–474*
metabolite pools
  carbohydrate metabolism 570–573, *571–572*
  concept 570–571, *571*
  equilibria 570, *571*
  hexose phosphate 571–573, *571–572*
  pyrophosphate 575–576b
  triose phosphate/pentose phosphate 597–601, *598*, *600*
metabolite profiles, cold-induced changes 1073
metabolites
  compartmentalization 112
  distribution 112
  exchanges from mitochondria 639–646, *641*, *642*
  sulfo-group transfers 763–764
metabolite shuttling, mitochondria 640–642, *642*
metabolomics 599b
metabolon 1155–1157, *1155*
metacaspases 928
metal clusters, cytochromes *624*
metaphase 231, 402–404, *478*
metaphase plate 231
metastable compartments, cytoskeleton 219–220
methanethiol 323
methionine chain elongation 329
methionine cycle (Yang cycle), ethylene biosynthesis 806–808, *807*
methionine γ-lyase 323, 326
methionine (Met) 299
  nitrogen assimilation *292*
  seed crops 749–750
  structure *290*
  synthesis 3, *291*, 320–321, *320*, *322*, 323, 326
  synthesis regulation 323–324, *323*, *324*, *325*
methionine sulfoximine (MSO) 293, *295*, *296*
methionine synthase (MS) 320, *322*, 326
methylation
  analysis 51, 52b, 53b
  cytosine 433–434, *433*
  daughter chromosomes 433–434
  DNA 436, 920–923, *921–922*
  fatty acids 362–363, *363*
  genomic imprinting 436
  histones 434
methylerythritol-4-phosphate (MEP) pathway 1138, *1139*
4-O-methylglucuronoxylans 103
methyl jasmonate, necrotrophic resistance 1040–1042, *1042*
methylsalicylic acid (MeSA) 828–830, 1035, *1036*
L-*O*-methylthreonine 326
methyltransferase *322*
Met-tRNA, protein translation initiation 441–442, *443*
mevalonate pathway 1135–1138, *1137*
MFS *see* major facilitator superfamily
MGD *see* monogalactosyl diacylglycerol
MIA *see* mitochondrial import and assembly machinery
mice, morphine synthesis 1166b
Michaelis–Menten mechanics 661b
microaerobic environments, legume root nodules 731–733, *732–733*
microarrays, gene expression analysis 426b
microelectrode impalement 129, *131*
microfibrils 51, *58*
  cell walls *77*
  evolution 70
  mannans 65
  multinet growth hypothesis 92–93, *92*
  orientation during growth 92–93
  particle rosettes 80, *82*, 86
  separation *95*
  stress relaxation *93*, 94
  synthesis 80, *82*, 86–88
  terminal complexes 80, *82*
microgametogenesis 889–896, *891–892*, *894*
micronutrients
  acquisition 1118–1123, *1121–1124*
  assimilation 1118–1127, *1121–1127*
  definition 1102
microRNAs (miRNAs) 276–277, *277*, **278**, 285, *285*
  copper homeostasis 1126–1127, *1127*
  protein synthesis initiation regulation 442
  transcription 423
microscopy 75–76b
  atomic force microscopy 76b
  dual-axis electron microscopy 75b
  field-emission scanning electron microscopy 76b
  fluorescence 152b, 162, *192*
  genome structure 401–404
  optical 75b, 76b, 402, *402*
  staining 13, *15*
microspore culture 893b
microsporocytes 890, *891*
microsporogenesis 889–891, *891–892*, 893b, 939–940
microtubules
  actin cross-linking 207
  cell expansion 216–219, *217–220*
  cell shaping 218, *218*
  characteristics 196–202
  cortical array organization 218–219, *219*, *220*
  cross-linking proteins *206*, 207
  dynamic instability 202, *203*
  dynein interactions 203–206, *204*, *205*
  end-binding proteins *206*, 207
  fluorescent imaging 207–208, *208–210*
  gel-like networks 207
  kinesin interactions *204*, 206
  mitotic spindle 227–230
  nucleation 197–199, *197*, 207
  organelle movement and anchoring 214–215
  phragmoplasts 234–237, *234–237*
  phragmosome 227, *227*
  phrophase spindle 228–231, *230*
  severing proteins *206*, 207
  side-binding proteins *206*, 207
  structure 198, *200*
  treadmilling 200
middle lamella *3*, 45, *47*, 67, *77*, 96, *102*, *103*
mineral deficiency 833, 1102–1103, *1102*, **1103**
mineral toxicity, tolerance 1127–1131, *1128–1131*
minichromosome maintenance helicase (MCM) 491–492, *491*
MIP *see* major intrinsic protein family
MIRNA genes 285
miRNAs *see* microRNAs
mismatch repair 253–254, *254*
mitochondria
  aerobic respiration 611–612, *611*, 620–646, *620*
  alternative NAD(P)H dehydrogenases 627–629, *630*
  alternative oxidase *620*, 629–631, *631*, 636–638, 636b, *637*, *638*
  anchoring and movement, actin networks 213–214
  apoptosis 927
  cell volume occupied 43
  changes during cell cycle 43, *43*
  compartments 611, *611*
  composition 41, *41*
  cristae 41, *41*, 42
  cytoplasmic male sterility 896–897, *897*
  diagram *3*
  electrogenic transport 639, *640*
  electroneutral transport 639, *640*
  ER attachment sites 17
  evolution 40b, 260–261, 267b
  F_oF_1–ATP synthase 632–633, *633–634*
  functions 39, 41
  gene promoters 270
  genomes 43–44
    Chlamydomonas *266*
    conservation of genetic content 265, 267, **267**
    size/arrangement 264–265, *265*, *266*
    Zea mays *265*
  gluconeogenesis 643–644, *645*
  GS isoenzymes 293

mitochondria (*cont'd*)
inner membrane 41, *41*, 42, 157, *157*, 639
intermembrane space 41, *41*, 157, *157*
malate-aspartate shuttle 299
matrix 41, *41*, 157, *157*
membrane lipids *364*, 365–372, *368–370*, *375*
in meristematic root tip cell *3*
metabolite exchanges 639–646, *641–645*
mRNA 275
nonphosphorylating pathways 635–639, *637*, *638*
outer membrane 41, *41*, 157, *157*
oxidative phosphorylation *614*
peroxisome-chloroplast-mitochondrion contact *32*
phosphatidic acid synthesis *364–366*, 365
photorespiration 648–650, *649*
photosynthetic carbon concentration 645–646, *645*
plastid tRNA genes 44
porins 41, *41*
presequences 157–158, *157*
programmed cell death 957–961, *958*
promiscuous DNA 267, *268*
protein complexes 41–42, *41*
protein synthesis 43–44
protein transport to 157–159, *157*, *158*
Q cycle 624–627, *628*
respirasomes *624*, 627, *629*
RNA 44, 273, 282, 285, 288
senescence 957–961, *958*
shoot apical meristem cells 42–43, *42*
substrate transporters 639, *641*
symports/antiports 639, *640*
tRNAs 44, 273
mitochondrial ATP synthase 41–42, *41*, 537–540, **539**, *540*, *553–558*
mitochondrial DNA (mtDNA) 43–44, 260, 264–265, *265*, *266*, 267, 267b, *268*
mitochondrial electron transport chain 620–646, *620*
equivalent chloroplast complexes 630b
F_oF_1–ATP synthase 632–633, *633–634*
inhibitors 622–624, *625*
nonphosphorylating pathway integration 635–639, *637*, *638*
proton translocation 621–624, *624*
Q cycle 624–627, *628*
redox potential of complexes *621*
respirasomes *624*, 627, *629*
substrates 622, *625*
mitochondrial import and assembly (MIA) machinery 159
mitochondrial superoxides 632–633
mitogen-activated protein kinases (MAPKs)
intracellular signaling 846–847, *846*
pattern-triggered immunity 1014–1016, *1017*
seed development 916–917, *917*
mitosis 476–506, *478–479*, 493–497, *493–494*, *496*
checkpoint controls 495–497, *496–497*
cytoskeletal dynamics 222–237, *231*
ER changes 15
metaphase chromosomes 402–404
microgametogenesis 891–896
mitochondria changes *43*
nuclear envelope changes 31
mitosis-promoting factor (MPF) 480–481, *480*
mitotic catastrophe 495
mitotic spindle, dynamics 227–230
mixed-linkage β-glucan synthase 85
mixed-linkage (1→3),(1→4)-β-D-glucans *64*, 65, 72, 85, *88*, 96, 99, *106*
MMC *see* megaspore mother cells
Mn_4CaO_5cluster, photosystem II 525–526, *527*
mobile signals, flowering initiation 875–876, *877*
mobilization, storage lipids 393–395, *394*, *396*
model organisms, photosynthesis 509b
models of cytoskeletal gene family evolution 195–196
model systems, mineral transport 1108–1109
MoFe protein *see* molybdenum-iron (MoFe) protein
molecular genetics
brassinosteroid synthesis 814–818, *816–818*
disease resistance *1021–1035*, 1022–1032
nodulation 726–733, *726–730*, *732–733*
oil yield improvements 397
self-incompatibility 908–913, *909–913*
molecular quartet model, flower organ specification 885–887, *888*
molecular regulation
endosperm development 919–920, *919*
fertilization 902–903, 906–908, *906–907*
male gamete formation 889–897, *891–892*, 893b*894*, 895b, *896–897*
megagametogenesis 897, 899–900, *900*
megasporogenesis 897, 898–899, *898*
pollination 902–905, *903–905*
reception of pollen tubes 906–907, *906–907*
reproductive development
female gametes 897–902, *897–902*
fertilization 902–903, 906–908, *906–907*
flower development 881–889, *883–889*
initiation of flowering 872–881, 880b, *881*
male gamete formation 889–897, *891–892*, 893b*894*, 895b, *896–897*
photoperiods 874–878, *876–877*, *881*
pollination 902–905, *903–905*
seeds 913–923
self-incompatibility 908–913, *909–913*
vernalization 874, 878–879, *879*, 880b
seed maturation 923, *923*
sporophyte development 916–918, *917–918*
transition from vegetative to reproductive development 872–881, 880b, *881*
molten globules, protein folding 458
molybdenum cofactors (MoCo), nitrate reductase 740–742, *742*
molybdenum-iron (MoFe) protein, nitrogenase 715–717
monoclonal antibodies *48*, 72, 89b, 100b, *102*
monocotyledons, amyloplasts, ADP-glucose transport 582, *582*
monogalactosyl diacylglycerol (MGD), biosynthesis *364*, 365, *368*, *373*
monolignols *73*, *74*, 104–106
monomeric G-proteins 842, *842*
mononucleotides 243
monosaccharides 48–49
monoterpenes 38, *38*, 1133, *1136*, *1142*
morphine 1161, *1164*, 1166b
morphology
flooding responses 1076–1077, *1077*, 1082, *1083*
leaves, programmed cell death 934b
membrane lipid composition 373–375, *376*
plasma membranes, freezing stress 378–379, *379*
trans-most Golgi cisternae 21
moths, alkaloids 1165b
motifs, gene promoters 427–429, **428**
motility, cytoskeletal functions *194*
motion, brownian 192, 193b
motor proteins 203–206, *204*, *205*
MPF *see* mitosis-promoting factor
MreB, prokaryotes 194–195
mRNAs *see* messenger RNAs
mRNP *see* messenger ribonucleoprotein complex
MS *see* methionine synthase
MSA element 493, *493*
MSO *see* methionine sulfoximine
mtDNA *see* mitochondrial DNA
MtLYK3 receptor 727, *726*
multidrug and toxic efflux (MATE) transporters 146, 1128–1131, *1129–1131*
multinet growth hypothesis 92–93, *92*
multistep system, cytokinin signal transduction 850, *850*
multivesicular bodies (MVBs) *15*, 26–27, *26*, 162, 175, 184, 188–189, *188*
Münch flow, phloem 697
μ-oxo bridges, fatty acid desaturases *357*
mustard oil bombs 1158
mutarotation 47, 48
mutations 250–251, *252*, 421–422, *423–424*
mut genes 253–254
MutS-MutL-MutH complex 253–254, *254*
MVBs *see* multivesicular bodies
MYB3RA 493, *493*
mycorrhizal symbiosis 721b, 1115, *1115*
myosin
cytoplasmic streaming 211–212, *213*
cytoskeletal interactions 203–206, *204*, *205*
directed organelle movement 210–216, *213–216*
organelle anchoring 212–213, *214*
polarity *205*
myristic acid (C_{14}) 9, *9*
myxothiazol *625*

NAC *see* N-terminal amino acid domains
NAD^+ *see* nicotinamide adenine dinucleotide
nad genes 282–283b
NADH
mitochondrial respiration control 635
production 602–603, *603*, 612–613
NADH dehydrogenase-like (NDH) complex *535*, 536
NADH dehydrogenases, mitochondria 627–629, *630*
NADH hydrogenase *620*, 621
NAD-ME photosynthesis *see* NADP-malic enzyme C_4 photosynthesis
$NADP_+$ *see* nicotinamide adenine dinucleotide phosphate
NADP-glyceraldehyde 3-phosphate dehydrogenase (NADP-GAPD) 556, *557*
NADPH
alternative oxidase 631
carbohydrate metabolism 601–602, *602*, 605–606, *606*

mitochondrial respiration control 635
pentose phosphate pathway 601–602, *602*
plastids 605–606, *606*
synthesis 35
NADPH dehydrogenases 627–629, *630*
NAD(P)H-dependent GOGAT (NAD(P)H-GOGAT) 293, 296, *296*
NADP-malic enzyme (NAD-ME) C_4 photosynthesis 561, *562*
NADP-thioredoxin reductase C (NTRC) 583–584, *584*
NAGS *see* *N*-acetylglutamate synthase
Na^+ ions 142, 144, *145*
Na^+/K^+-exchanging ATPase 122
Na^+/K^+ transport 122, 144, *145*
NAM *see* NO APICAL MERISTEM protein
natural-antisense si RNAs (natsiRNAs) 276, *276*, 277, **278**, 285
natural products 1132–1206
alkaloids 1159–1178, *1162*, 1163b, *1164*, 1165–1166b, **1167**, *1168–1169*, 1170b, *1172–1177*
cyanogenic glycosides 1146–1158, *1148–1152*, 1150–1151b, 1153b, *1154–1155*, *1158*
glucosinolates 1158–1159, *1159*, 1160–1161b
metabolic engineering 1174–1178, *1180*
phenolic compounds 1178–1206, *1181–1187*, *1189–1191*, *1193–1204*
sulfur-containing compounds **748**, 749, *749*
terpenoids 1113–1145, *1135–1137*, *1145*, 1147–1148b
NB *see* nucleotide-binding sites
NDH *see* NADH dehydrogenase-like complex
necrosis 926, *927*, 928, 973–974, *974*
necrotrophic pathogens
defense strategies 1033, 1040–1042, *1042*
pathogenesis strategies 990, *993*
nematodes, pathogenesis *1001*, 1002, **1004**
neo cell theory 500, *500*
neofunctionalization, evolution and speciation 415–416
Nernst potential 116–117b
net stoichiometry of sucrose oxidation **615**
Ni *see* nickel
nickel (Ni) tolerance 333–334
nicotinamide adenine dinucleotide (NAD^+)
redox chemistry *612*
reduction 602–603, *603*
structure *612*
nicotinamide adenine dinucleotide phosphate ($NADP^+$) 601–602, *602*, 605–606, *606*, *612*
nicotine 1161, *1168*, 1170b
nif genes/Nif proteins 732–733, *733*
NIPs *see* nodulin 26-like intrinsic membrane proteins
NiR *see* nitrite reductase
nitrate (NO_3^-) 735–746, *739–746*
carbon metabolism interactions 745–746
deficiencies 833
homeostasis 738
reduction 739–744, *739–745*
signaling 745, *746*
transport 145, 738–739
transporters **150**
uptake 119, *120*, 735–738, *739–741*
nitrate reductase (NR) *295*, 301, 739–744, *739–744*
nitric oxide dioxygenase (NOD) 972–973
nitric oxide (NO) 332, 622, *625*, 932
nitrite reductase (NiR) *295*, 301, 739, 744–745, *745*
nitrogen
see also nitrogen compounds; nitrogen fixation; nitrogen metabolism
deficiency phenotypes 712, *713*
remobilization in senescence 954–955, *955*
storage compounds 331, 333
transport in legume roots 720, *734*, 735–739, *736–741*
uptake *712*
nitrogenase 715–718, *716–718*, 732–733
acetylene reduction 717
iron protein 717–718
molybdenum-iron protein 715–717
redox states *718*
nitrogen compounds
of biological importance *713*
inorganic 711, **712**
nitrogen cycle 711–712, *712*
nitrogen fixation
amides 720, *734*, 735
bacteroids 731–733, *732–734*
biological 715–735, *718*, *722–724*, *732–734*
enzymology 715–718, *716–718*
filamentous cyanobacteria 715
industrial 714b
legumes *734*, 735–746, *736–741*
microaerobic environments 731–733, *732–733*
overview 711, *712–713*
oxygen effects 715
rates 711, **713**
symbiotic 718–735, *720*, **721**, 721b, *722–730*, **724**, *732–734*
ureides 720, 735, *736*
nitrogen metabolism 711–746, *712–713*, 714b, *716–730*, *732–734*, *736–746*
overview 711–715, *712–713*, 714b
sulfate assimilation 766–767, *766–767*
nitrogenous soil amendments, history 714b
N-linked glycans 22, 173–174, *173*, 187–188, *187*
NLSs *see* nuclear localization signals
NMP *see* nucleoside monophosphate
NMR *see* nuclear magnetic resonance spectroscopy
NO_3^- *see* nitrate
NO *see* nitric oxide
NO APICAL MERISTEM (NAM) protein, senescence 948
NOD *see* nitric oxide dioxygenase
NodD proteins, rhizobia 722, *722*
Nod factors, legumes 722–724, *722–723*
nodulation 722–733, *722–730*, **724**, *732*
auxin 730–731
calcium spiking 724, *728*, 729
cytokinins 730–731
hormone signaling 730, *730*
molecular genetics 726–733, *726–730*, *732–733*
nodules
bacteroids 731–733, *732–734*
calcium spiking 724, *728*, 729
hormone signaling 730, *730*
legumes 720–735, *721*, *724–730*, *732–734*, *736*
microaerobic environment 731–733, *732–733*
molecular genetics 726–733, *726–730*, *732–733*
symbiotic nitrogen fixation 718–735, *720*, **721**, 721b, *722–730*, **724**, *732–734*
nodulin 26-like intrinsic membrane proteins (NIPs) 147
nodulins 729, *729–730*
Nomarski optics, root cells *192*
nomenclature, lipids 342b
noncyclic electron transport chain, photosynthesis 529–531, *530–532*
nonenzymatic antioxidant systems 1086–1089, *1087*, **1088**, **1089**
NONEXPRESSOR OF PATHOGENESIS-RELATED GENES (NPR) protein 1037–1038, *1039*
nongreen plastids, biosynthesis and respiration 605–606, *607*
nonheme iron centers, stearoyl-ACP desaturases 355–356, *356–357*
nonpermissive high temperatures 1094–1095
nonphosphorylating pathways
see also alternative oxidase
aerobic respiration 635–639, *637*, *638*
nonphotochemical quenching (NPQ) 542, *542*
nonphotosynthetic plants 568–570
nonreducing sugars 573, *574*
nonselective proteolysis 467
nonvascular cells, short-distance transport 673–691, *673*, *677*, *679–681*, *684–685*, *687–690*, *692*
NORs *see* nucleolar organizer regions
NPA (Asn-Pro-Ala) residues 147, *147*, *148*
NPCs *see* nuclear pore complexes
NPQ *see* nonphotochemical quenching
NPR1 175
NPR *see* NONEXPRESSOR OF PATHOGENESIS-RELATED GENES
NR *see* nitrate reductase
NRAMP transporters **149**
NSF *see* *N*-ethylmaleimide sensitive factor
N-terminal amino acid (NAC) domains 106, *107*
NTPs *see* nucleotide triphosphates
NTRC *see* NADP-thioredoxin reductase C
nuclear envelope 13, *29*
changes during mitosis 31
connections to ER 29–30
functions 29–30
inner nuclear membrane 29, 160
nuclear lamina 160
nuclear pore complexes 160, *161*, *162*
outer nuclear membrane 29, 160
perinuclear space 160
traffic *15*
nuclear gene products, chloroplast protein synthesis regulation 453–454, *455*, 455b
nuclear genomes, repetitive and single-copy sequences 404–406, *405*
nuclear lamina 30, 160, 192–194
nuclear localization signals (NLSs) 30, 160–161, **161**
nuclear magnetic resonance (NMR) spectroscopy 51, 55–58b, 77
nuclear membranes *3*, 727–729, *727*
see also nuclear envelope
nuclear pore complexes (NPCs) 30, 160, *161*, *162*, 727, *727*

nuclear pores 29, *29*, 30, *30*, 31, 727, *727*
nuclear spin 55–58b
nuclear translocation, phytochromes 859–861, *860*
nucleases 257b, 953–954
nucleation
  actin filaments 197–198, *197*, 207
  cytoskeleton polymerization 197–198, *197*, 207
  microtubules 197–199, *197*, 207
nucleic acids, *see also* DNA; nucleotides; RNA
nucleic acids 240
  composition *241*
    nucleotides 240, 243
    phosphodiester bonds *241*, 243, 245, *246*
    polynucleotide chains 243
    sugar-phosphate backbone *241*, 243, *246*
  3′ end 243
  5′ end 243
  notation convention *246*
  remobilization in senescence 954–955, *955*
  reverse transcription 240, *241*
  of viruses 240, *241*
nucleolar organizer regions (NORs) 406, 412–414, *414*
nucleoli *3*, 29, 30–31
nucleoplasm 29
nucleoporins (Nups) 30, 160, 161
nucleoside kinase 243
nucleoside monophosphate (NMP) kinase 305
nucleoside phosphorylase 243
nucleosides *241*, 243
nucleosome arrays 404
nucleotidases 243
nucleotide-binding-leucine rich repeat (NB-LRR) proteins, pathogen defense 1024–1032, *1026–1027*, *1029–1031*
nucleotide-binding (NB) sites, R-proteins 1024–1026, *1026–1027*
nucleotide conversion editing 286–287, **287**, *288*
nucleotide diphosphate-sugar pyrophosphorylases 83
nucleotide exchange, protein synthesis initiation 442, *445*
nucleotide excision repair 252–253
nucleotide insertion/deletion editing 286, *287*, **287**
nucleotides 240, 243
  base pairing 245
  catabolism 243
  composition 240
  notation convention *241*, 243
  phosphodiester bonds 243, 245
  salvage pathways 243, 245b
  synthesis *242*, 243, *244*
nucleotide sugar interconversion 81, 83, *83*, *84*, *85*
nucleotide synthesis, pentose phosphate/triose phosphate pool 600, *600*
nucleotide triphosphates (NTPs), cytoskeletal polymerization 197–202, *198–199*
nucleus 28–29
  DELLA protein functions 863, *863*
  diagram *3*
  in meristematic root tip cell *3*
  photosynthesis genes 261, 263
  promiscuous DNA 267
  protein transport in/out 160–161, *161*, **161**, *162*
  ubiquitin pathway 469–470
Nup107 complex, nodulation 727, *727*
Nups *see* nucleoporins
nutrient acquisition 112
nutrient concentrations, regulation in xylem 671
nutrient deficiency, strigolactone signaling 833
nutrients
  autotrophy 543–544b
  essential minerals 1102–1103, *1102*, **1103**
  fleshy fruit development 689–691, *690*, **690**, 706–707, *709*
  lateral exchange, transport phloem 682–683, *684–685*
  phloem loading 673–681, *673–674*, *677–681*
  post-SE transport 684–691, *685–690*, *692*
  salvage, senescence 954–957, *955–956*
  seed development *690*, 691
  transport, phloem loading 673–674, *673*
  xylem loading pathways, roots 668–671, *669–671*

OAA *see* oxaloacetate
O-acetylserine (OAS), cysteine biosynthesis 755–757, *756–757*
OAS *see O*-acetylserine
δOAT *see* ornithine δ-aminotransferase
observation of cytoskeleton 207–210, *211–212*
oceanic algae, cloud formation 750, *751*
OCT *see* ornithine carbamoyl transferase
ODC *see* ornithine decarboxylase
O-glycosylation 188
oil bodies (oleosomes) 15, *17*, 391–392, *391*
  gluconeogenesis 643
  senescence 941–942
oil glands 15, 933
oil seeds, engineering 398–399
oil storage 38
oil yields 397
Okazaki fragments 247, 248, *248*
oleate desaturases 358
oleate Δ12-hydroxylase 362
oleosins 15, *17*, 391–392, *391*
oleosomes *see* oil bodies
oligomycin B, ATP synthase inhibition *625*, 632
oligomycin-sensitivity-conferring protein (OSCP), F_oF_1–ATP synthase 632
oligonucleotides 243
oligosaccharides 22, 60–61b, 62–63b, 173–174, *174*
oligosaccharins 22
oligosaccharyltransferase 170, *171*, **172**, 173
O-linked glycans 22–23, 188
OMP *see* orotidine 5′-monophosphate
oomycetes 990–992, *991*, **992**, **1004**
open reading frames (ORFs) 257b, 261, 287–288
  leaky scanning 444b
  protein synthesis 443–444, 445b, 450
  viral protein synthesis 444b, 450, 450b
operons 261, *263*
opines 996–997b
opium 1159–1161, *1162*, 1163b
optical mapping of genomes 406, 407–408b
optimal light absorption, chloroplasts 212–213, *214*
ORC *see* origin of recognition complex
ORFs *see* open reading frames
organellar DNA 260
  chloroplasts and mitochondria evolution 260–261, *260*
  DNA movement between genomes 267
  encoding sites 261, 263
  mitochondrial genomes *265*, *266*
    conservation of genetic content 265, 267, **267**
    size/arrangement 264–265, *265*, *266*
  plastids genome 261, *262*, 263–264, **263**, *264*
  promiscuous DNA 267, *268*
organelles
  anchoring
    actin 212–213, *214*
    microtubules 214–215
  antioxidant systems *1087*, **1088**, **1089**
  cell plate construction 235–237, *236–237*
  directed movement
    actin 210–216, *213–216*
    microtubules 214–215
  fractionation 152b
  protein synthesis 438–439, *439*
organic acids, mitochondrial respiration control 635
organic anions, aluminum tolerance 1128–1131, *1129–1131*
organ identity, ABC model 883–885, *884–887*
organismal theory 499–500, *500*
organization of cortical array 218–219, *219*, *220*
organization of photosynthetic complexes 218–219, *219*, *220*, 540–542, *540–541*, **540**
organ specification, flowers, molecular quartet model 885–887, *888*
orientation, cellulose microfibrils, interphase 216–217, *217*
origin of recognition complex (ORC), cell cycle 491, *491*
origins of replication 245–246, *247*
ornithine 330, 332–333, *332*, 819, *820*
ornithine δ-aminotransferase (δOAT) 330–331, *331*
ornithine carbamoyl transferase (OCT) 333
ornithine-citrulline shuttle 293
ornithine decarboxylase (ODC) 819, *820*
orotate *242*, 243
orotic acid pathway *242*, 243
orotidine 5′-monophosphate (OMP) *242*
orthology, gene evolution 415b
orthovanadate 122
Oryza sativa
  CesA genes *87–88*
  chloroplast DNA *262*
  GT genes *90*
  Internet resources 89b
  promiscuous DNA *268*
OSCP *see* oligomycin-sensitivity-conferring protein
osmolytes, osmotic adjustment 1055–1056, *1056–1057*
osmoprotection 1055–1057
osmotic adjustment 1055–1056, *1055–1057*
osmotic potential 93
osmotic pressure 146–147
  sieve tubes 681, **682**
  water potential 660–661b
  xylem 672, *672*, 695
osmotic stress
  membrane destabilization 1069–1072, *1070*
  signaling 1065–1068, *1067–1069*
outer membranes, mitochondria 611, *611*
outward-rectifying potassium channels 1112
overflow model, starch synthesis 590–591

overproduction, auxin 803–804, *805*
over-ripening prevention *809*, 810
ovules, development 897–898, *897*
oxalate 28
oxalic acid, necrotrophic pathogenesis 990
oxaloacetate (OAA) *290*, 299, *299*
  citric acid cycle 613, *616*
  mitochondrial carriers 641–642, *641–642*, 642–643, *643–644*
oxidation
  amino acids 618–620
  glutamate 618–620
  malate 616
  sucrose, net stoichiometry **615**
  water, photosystem II 525–526, *525*
β-oxidation
  citric acid cycle 620
  gluconeogenesis 643, *645*
  storage lipids 393, 395, *396*
oxidative amination 298
oxidative bursts 971–973, *973*, 1091
oxidative metabolism *958–960*, 959–961
oxidative phosphorylation *614*, **615**
  F_oF_1–ATP synthase 632–633, *633–634*
  net stoichiometry of sucrose oxidation **615**
  regulation 634–635, *635*
  respirasomes *624*, 627, *629*
oxidative photosynthetic carbon cycle 648–650, *649*
oxidative stress
  abiotic/biotic stressors 1090–1091, **1092**
  antioxidant systems 1086–1089, *1087*, **1088**, **1089**
  environmental factors 1085–1086, *1085*
  ozone exposure 1089–1090, *1090–1091*
  protein expression 1091–1092
  responses 1085–1094
  tolerance 1091–1092, **1092**
μ-oxo bridges, fatty acid desaturases *357*
oxygen
  aerobic respiration 612–613, *612*
  concentration, photosynthesis rates 646–647
  low concentration in legume symbiosomes 731–733
  nitrogen fixation effects 715
oxygenase activity, Rubisco 654
oxygen deficit
  see also anoxia; flooding; hypoxia
  flooding 1076–1085, **1076**, *1077–1081*, *1083–1084*
  root structure adaptation 1076–1078, *1077–1079*
  short-term acclimation 1079–1080, *1080–1081*
  signal perception 1085
oxygenic photosynthesis 510–542, *511–512*, *518*, *524–526*, *530–532*, *534–535*, *541–542*
  see also chlorophyll; photosystem…
oxylipins, signaling 379–382
ozone, oxidative stress 1089–1090, *1090–1091*

P2C reductase *331*
P3 P-protein *see* plant-specific ribosome protein
P5C *see* Δ^1-pyrroline-5-carboxylate
P5CS *see* Δ^1-pyrroline-5-carboxylate synthetase
PAC *see* precursor accumulating vesicles
paclobutrazol 773, *774*
PADs *see* pulsed amperometric detectors
PAI *see* phosphoribosylanthranilate isomerase
PAL *see* phenylalanine ammonia lyase
palmitic acid 9, *9*, 11
palmitoylation 170
palmitoyl-CoA, sphingolipid biosynthesis 373, *375*
PAO *see* polymaine oxidases
papillae *48*
PAPS *see* 3′-phosphoadenosine 5′-phosphosulfate
para-chloromercuribenzenesulfonic acid (PCMBS), phloem loading studies 677, *678*
parallel deposition, cellulose microfibrils/cortical microtubules 216–217, *217*
parallel polarity, cytoskeletal polymer bundles 207
parallel β-sheets, leucine rich repeats 1023, *1026*
paramutation 432–433, *433*
parasitism, strigolactone signaling 830–833, *830–832*
Parasponia (Ulmaceae), symbiotic nitrogen fixation 720
parenchyma *46*
  phloem 682, *684*, *685*
  xylem *665*, 666, 669
parental effects, seed development 914–916, 915b, *916*
parology, gene evolution 415b
parthenogenesis 902, *902*
partitioning
  sucrose/starch 587–593
    diurnal cycles 590–593, *590–591*
    fructose-2,6-bisphosphate 588–589, *589*
    photosynthate control 590–592, *592*
PAs *see* polyamines
Pasteur effect 1079
PAT *see* phosphoribosylanthranilate transferase
patch clamp technique 129, 130b, 1109
pathogen defense mechanisms 175, 984–1050
  basal defense 989
  genetic engineering 996–997b, 1032, 1044–1049
  hormonal regulation 974–976, 980–981
  hypersensitive response 965–974, *966–968*, **969–970**, *972–974*
  induced 1012–1032, *1015–1031*, **1024**
  necrosis 973–974, *974*
  necrotrophic pathogens 1033, 1040–1042, *1042*
  overview 985–989, *988*
  pathogen recognition 1023–1030, **1024**, *1025–1029*
  pattern-triggered immunity 1012–1022, *1016–1020*
  preformed 1009–1012, *1013–1015*
  programmed cell death 964–974
  reactive oxygen species 990
  R-proteins/genes 1023–1032, **1024**, *1025–1031*, **1034**
  signaling 1033–1042, *1035–1037*, **1038**, *1039–1042*
  systemic acquired resistance 1033–1038, *1035–1037*, **1038**, *1039*
  viruses 1042–1044
  zig-zag-zig scheme 955, *988*
pathogen effectors 1003–1007, **1004**, *1005*, **1007**, *1008*
  insensitivity 1033
  recognition 1027–1031, *1029–1031*
pathogenesis 989–1009, *991–993*, **992**, *995–999*, **998–999**, *1001–1003*, *1008*
  Agrobacterium 996–997b
  arthropod 1002–1003, *1003*
  bacteria 992–994, 996–997b, *998*, **1004**
  effectors 1003–1007, **1004**, *1005*, **1007**, *1008*
  fungal pathogens 990–992, *991*, **992**, *994–996*, **1004**
  necrotrophic pathogens 990, *993*
  nematodes *1001*, 1002, **1004**
  viruses 994–1000, *999*, *1000*, **1004**
pathogenesis-related (PR) proteins 1035–1038, **1038**
pathogens
  agriculture 986–987b
  cytoskeletal resistance mechanisms 215–216
  gene complements/virulence-factor repertoires 1009, **1010**
  genomes **1011**, *1013*
  specialization 1007
patterning, embryos 916–919, *917–918*
pattern-recognition receptors (PRRs) 985, *988*, 1012–1014, *1016*, 1044, *1044*
pattern-triggered immunity (PTI) 985, *988*, 1012–1022, *1016–1020*
  genetic engineering 1044–1048, 1047b
pauses in protein synthesis 456–457, *457*, 458b, *459*
PC *see* plastocyanin
PCD *see* programmed cell death
PcG proteins 888–889, *889*
P-cluster of nitrogenase *716–717*, 717–719
PCMBS *see* para-chloromercuribenzenesulfonic acid
PCNA (proliferating cell nuclear antigen) 248, *248*
PDC *see* pyruvate decarboxylase
PDI *see* protein disulfide isomerase
PE *see* phosphatidylethanolamine
peak flow velocities, xylem 668
pea phenotypes, starch deposition 583b
pectate lyases 97
pectic polysaccharides 23
pectin glucuronyltransferases 96
pectin lyases 97
pectin matrix 77, *79*
pectin methylesterase (PME) 77, 100, 102
pectin network 96
pectins
  calcium-pectate interactions *78*
  cell corners 45, *47*
  cell walls 77, *77*
  constituents *66*, 67, *68*
  fruit ripening 100, 102, *102*
  functions 67
  human and animal food 109
  pit membranes 666
  pore size *79*
  synthesis 85–86, 321
  Type II walls 99
  uronic acid-rich polysaccharides *66*, 67
pentapyranose 49
pentose phosphate pathway *598*, 601–602, *602*
pentose phosphate/triose phosphate pool 597–601, *598*, *600*
pentose sugars 46, 240, *241*

PEP *see* phospho*enol*pyruvate
PEP carboxykinase (PEPCK) C_4 photosynthesis 561, *562*
PEP carboxylase *see* phospho*enol*pyruvate carboxylase
PEPCase *see* phospho*enol*pyruvate carboxylase
PEPCK *see* phospho*enol*pyruvate carboxykinase
pericentromeric regions 412, *413*
perinuclear space 29, 30, 160
peripheral membrane proteins 8–9, *8*
permissive high temperatures 1094–1095
peroxidases 105
peroxisomes *3*, 17, 31–32, *32*, 159, *160*
  aggregation during cytokinesis 214
  anchoring and movement, actin networks 213–214, *215*
  gluconeogenesis 643
  lipid β-oxidation 395, *396*
  photorespiration 648–650, *649*
  senescence 957–959
peroxisome targeting signals (PTSs) 159, *160*
pesticides 316
pests, pathogen introduction 1002–1003, *1003*
petals
  see also flower…
  senescence 826
Petunia hybrida, β-tubulins 195
Petunia spp., self-incompatibility 912–913, *913*
PEX10 protein 32
PEX genes 159
PEX receptor proteins 159, *160*
PFK *see* phosphofructokinase
PFP *see* pyrophosphate-dependent phosphofructokinase
PG *see* phosphatidylglycerol
3-PGA *see* 3-phosphoglycerate
PGIPs *see* polygalacturonase-inhibiting proteins
PGPs *see* phosphoglucan phosphatases
pH
  acid-growth hypothesis 94
  anoxic metabolism 1079–1081
  apoplastic space 80
  cystolic 123
  KDEL signal *178*
  proton motive force 117
  stroma 556–557
  vacuolar 28, 126, 137, *137*
  vacuolar channels 137, *137*
pharmaceuticals 162, 165b, 187
  alkaloids 1159–1161, *1163*, **1167**
  metabolic engineering 1174–1178, *1180*
phaseic acid, abscisic acid metabolism 784, *785*
phaseolin 172, *172*
phases of transcription 424
phase transitions 7
phenolic compounds 1178–1206, *1181–1186*
  biosynthesis 1185–1205
  diversity 1178–1182, *1182*, **1183–1185**
  evolution 1179–1182
  human benefits 1185
  L-phenylalanine 1185–1188, *1186–1187*
  phenylpropanoid-acetate pathway 1188–1195, *1190–1191*, 1192b, *1193–1195*
  phenylpropanoid pathway 1195–1201, *1196–1203*
  universal features of biosynthesis 1202–1205, *1205*
phenotypes, reproductive mutants 915b
phenylacetic acid, auxin signaling 795–796, *796*
L-phenylalanine, phenolic compound synthesis 1185–1188, *1186–1187*
phenylalanine ammonia lyase (PAL) 318, 1186–1188
phenylalanine hydroxylase 309
phenylalanine (Phe)
  nitrogen assimilation *292*
  structure *290*
  synthesis *291*, *303*, 306, *307*, 308–309
phenylpropanoid-acetate-derived flavonoids *1182*
phenylpropanoid-acetate pathway, phenolic compound synthesis 1188–1195, *1190–1191*, 1192b, *1193–1195*
phenylpropanoid pathway, phenolic compound synthesis 1195–1201, *1196–1203*
phenylpropanoids *48*, 79, 104–105, 950–951, *951*
phenylpropenes 1182, **1184**
phenylpyruvate 306, *307*, 308
phloem
  see also sieve elements
  amino acid concentrations 292
  bulk flow 663–664, *664*, 696–697, *698–700*
  cell biology 666–668, *667*
  development 664, 666–668, *667*
  differentiation 664
  driving forces 663–664, *664*
  functional sectors 673, *673*
  hormonal control 706, *709*
  hydrostatic pressure **682**, 697–700, *698–700*
  loading 673–681, *673–674*, *677–681*
    amino acids/amides 679–680, *680*
    apoplastic pathways 677–680, *678–680*
    inward-rectifying potassium channels 680, *680*
    polyols 678, *680*
    RFO sugars 681, *681*
    sucrose 677–680, *678–680*, **680**
    symplastic pathways 681, *681*
    water flows 681, **682**
  macromolecular signaling proteins 700–703, *701–703*
  potassium ion transport 1104, *1104*, 1112
  regulation of nutrient flows 705–709, *706–709*
  sap composition 674–676, **676**
  short-distance transport in nonvascular cells 673–691, *673*, *677*, *679–681*, *684–685*, *687–690*, *692*
  sieve pore occlusion 698–700, *700*
  unloading 673, 684–691, *685*
    apoplastic transport 685–687, *685*, **686**, *687*
    plasmodesmata 685–686, *686*, 706, **708**
    symplastic transport 685–691, *685–690*, **686**, *692*
    water flows 691, *692*
  viral transport 703, *703*, 998–1000, *999*
  whole-plant organization *659*, 696–704, *698–704*
phloem parenchymal cells (PPC)
  nutrient loading 673–674, *673*
  nutrient transport regulation 705, *708*
  sink cells 684–691, *686–690*, **686**, *692*
  transport phloem 682, *684*, *685*
phloroglucinol *105*
phosphatases 243
phosphates
  see also inorganic phosphate
  chloroplasts *569*, 573
  conservation 374b
  deficiencies 833
  mitochondrial transport 633–634, *634*
  transporters **150**, 633–634, *634*, 1114, *1114*, *1118*
  uptake 1114–1118, *1115–1118*
phosphatidate 368, *369*
phosphatidic acids **8**, *364–366*, 365, 368, *369*
phosphatidylcholine (PC) *6*, **8**, 25, *344*, 369, *371*, 379, *379*
phosphatidylethanolamine (PE) *6*, **8**, 17, *364*, *368*, 369–372, *370–372*
phosphatidylglycerol (PG) *363*, 368–369, *368*, *370*
phosphatidylinositol-anchored membrane proteins 8, 9–10, *9*
phosphatidylinositol 4,5-biphosphate (PIP_2), hydrolysis 379, *380*
phosphatidylinositol (PI)
  biosynthesis *364*, 369, *370*
  signaling pathways 379, *380*
phosphatidylserine decarboxylase 372, *372*
phosphatidylserine (PS) 17, *364*, 369–372, *370*, *372*
phosphinothricin acetyltransferase 306b
L-phosphinothricin (L-PPT) 293, *295*, *296*, 306b
3′-phosphoadenosine 5′-phosphosulfate (PAPS), sulfur assimilation 746, *748*, 763, *763*
phosphodiesterases 243
phosphodiester bonds *241*, 243, 245, *246*, 366–368, *369*
phospho*enol*pyruvate carboxykinase (PEPCK) C_4 photosynthesis 561, *562*
phospho*enol*pyruvate carboxylase (PEP carboxylase) 558–560, 563–565, *563*, 613, *616*, 746
phospho*enol*pyruvate (PEP) *290*, 302, *304*, *603*, 604–605, *605*, 613, *616*
phospho*enol*pyruvate/phosphate translocator 334
phosphofructokinase (PFK) 572, 575–576b, 587–588, *587*, *598*
phosphoglucan phosphatases (PGPs), starch degradation 595–596, *595*
phosphoglucan, water dikinase (PWD) 593–595, *595*
phosphoglucomutase, hexose phosphate pool 571–572, *572*
phosphogluconate dehydrogenase 601–602, *602*
2-phosphoglycerate, 3-phosphoglycerate conversions *603*, 604
3-phosphoglycerate (3-PGA) *290*
  ADP-glucose pyrophosphorylase regulation 582–584, *584*
  Calvin–Benson cycle 545, *546–547*
  2-phosphoglycerate conversions *603*, 604
  photorespiration *649*, 650
  Rubisco-mediated synthesis 393
3-phosphoglycerate kinase 545, *546–547*, *603*, 604
phosphoglyceromutase, carbohydrate metabolism 604
phosphoglycolate phosphatase, photorespiration 640–650, *649*
phosphohydrolase *274*
phospholipase C 69, 379, *380*
phospholipids 4
  biosynthesis 342, *364–375*, 365–373

classes 339, **343**
flipping 6, *7*
movement in lipid bilayer 5–6, *7*
phosphodiester bond formation 366–368, *369*
in plasma membrane 11, **11**, 12
in plastid membranes 33
structure *5*, *6*, 342, **343**, *344*
phosphopantetheine groups, acyl carrier protein *350*, 351
5-phosphoribose 333
5-phosphoribosyl-1-pyrophosphate (PRPP) *242*, 243, 245b, *334*
phosphoribosylanthranilate isomerase (PAI) *311*, 314, *314*, 315b
phosphoribosylanthranilate transferase (PAT) *311*, 312, *313*
phosphoribosyltransferase 243
phosphoribulokinase (PRK) *546–547*, 548, 556, *557*
phosphorus
bioavailability 1114–1116, *1115*, 1118
deficiency *1102*, 1115–1116
nutrition 1113–1118, *1114–1116*
remobilization in senescence 953–954, *955*
transport, roots 1114, *1114*, 1118
phosphorylation
ADP, carbohydrate metabolism *603*, 604–605
cyclin-dependent kinase regulation 485, *486*
initiation factors, protein synthesis regulation 442, *445*
light harvesting complex II **540**, 541–542, *541*
proteins, cortical array organization 218–219, *220*
pyruvate dehydrogenase 617, *618*
signal transduction 838–841, 839b, *841–842*
photochemistry
see also light…
reaction centers 519
photoinhibited D1 protein, repair cycle 463, 465–466b
photoinhibition 542
photolyases 252
photons 511
photo-oxidative damage 28
photoperiods
flowering initiation 874–878, *876–877*, *881*
partitioning responses 591, *591*
photophosphorylation 537–540, **539**, *540*, *553–558*
photoprotection, carotenoids 519, *520*
photoreactivation 252
photoreceptors 858–859b
phytochromes 857–861, *858–861*
photorespiration 646–655
ammonia 650, *651*
biochemical basis 646–648
climate change 654–655
energy costs 652, **652**
Fd-GOGAT enzyme 296–298
pathway 648–652
peroxisome-chloroplast-mitochondrion contact 32, *32*
peroxisomes role 31–32
physiological roles 652–654
Rubisco 549–551, *550*, 647–648
photorespiratory ammonium 293, 296
photosynthates, glucose/starch synthesis regulation 589–591
photosynthesis 508–566
biophysical investigations 572–573b
Calvin–Benson cycle 542–557, **543–544**, *544*, *546–547*, *550*, *553*, *556–557*
carbon reactions 542–565, **543–544**, *544*, *546–547*, *550*, *553*, *555–558*, *562–564*
chloroplasts 510, *510*
citric acid cycle effects 646
cyclic electron transport 535–536, *535*
efficiency, climate change 654–655, *654*
energy costs **652**
genes 261, 263
impairment, membrane lipid compositions 375–376, *376*
Kranz anatomy 558, *559*
light reactions 510–542, *511–512*, *518*, *524–526*, *530–532*, *534–535*, *541–542*
overview 508–511, 509b, *510–511*
PEP carboxylase 558–560, 563–565, *563*
photorespiratory energy cost 652, **652**
photosystem organization and regulation 540–542, *540–541*, **540**
photosystems 519–529, *522–528*, **522**, **523**, **529**
Q-cycle 53–55, *534*
quantum yield 512–515
regulation, hexokinase 1 607
Z-scheme 530–531, *531–532*
photosynthetic membrane system, lateral heterogeneity 35–37, *35*
photosynthetic proteins, cofactor insertion 456–457, *457*, *459*
photosystem I 521–522, **522**, 528–529, **529**, *530–531*, 535–536, *536*
stroma thylakoids 35
photosystem II 521–528, **522**, *524–528*, **527**
D1 protein synthesis 456–457, *457*, *459*
electron carriers 522–535, *524*
grana thylakoids 35
subunits 522–523, *524*, **524**
synthesis 456–457, *457*
photosystems 519–529, *522–528*, **522**, **523**, **529**
organization and regulation 540–542, *540–541*, **540**
reaction centers 519–522, *522*, *524*, *527*, *530–531*, *535*
variable stoichiometry 540–544, *540–541*, **540**
phototropins 858b
stomatal aperture control 867–868, *867–868*
phragmoplasts 27, 80
cytoskeletal structures 222–227, *224*, *227*, 233–237, *234–237*
tubulovesicular network 237, *237*
phragmosomes 80
formation 227, *227*
PHT transporters **150**
PhyA *see* phytochrome A
Physcomitrella patens 204b
physical mapping, genome structure 406–408, 407–408b
physiologically active alkaloids **1167**
physiological roles, protein degradation 463–467, 465–466b, *467*
phytoalexins *48*
phytochelatins, biosynthesis 759–760, *760–761*
phytochelatin synthase 760, *761*
phytochrome A (PhyA), proteolytic regulation 466–467, *467*
phytochromes
nitrogen metabolism 301
nuclear translocation 859–861, *860*
photoperiod sensing 875–876
red/far-red photoreversibility 857–859, *858–860*
signal transduction 857–861, *858–861*
transcription factor stability 860–861, *861*
phytochromobilin isomers *868*
phytoferritin 34, *34*
phytopathogenic bacteria 992–993, *998*
phytoplankton–climate connection 750, *751*
phytosiderophores 1121–1122, *1121*
P_i *see* inorganic phosphate
PI *see* phosphatidylinositol
Pictet–Spengler reaction 1173
PID gene *see PINOID* gene
pigmentation 28, 37–38
pigment metabolism, senescence 948–951, *949*, *951*
pigments, excitation 511–515, *512*
PII protein 333
PINOID (*PID*) gene, auxin signaling 856
PIN proteins 189, 854–857, *855*
PIP_2 *see* phosphatidylinositol 4,5-biphosphate
PIPs *see* intrinsic proteins
pit hairs, xylem 665–666, *665*
pit membranes, xylem 665–666, *665*
plant cells, mitosis *224*
plant pathogens
see also pathogens
definition 984
plant pests
see also pests
definition 984
PlantProbes 89b, 100b
16:3 plants 342
18:3 plants 342
plant-specific ribosome protein (P3 P-protein) 440
plant volatiles, pest feeding 1003
plasma membranes 2, *10*
anion channels 132, 140–141, *141*
antiporters 113
aquaporins 12, 147
Ca^{2+}-ATPases 126
Ca^{2+} channels 138–139
callose synthesis *81*
cellulose synthesis *81*
cell wall connections 12–13, *12*
cell wall cross-linkage 220–221
cold acclimation 12
diagram *3*
electrochemical gradients 115, 117
endocytosis 24, *24*
ER-plasma membrane attachment sites 17
exocytosis 23–24, *24*
functions 10
G-protein coupled receptors 838, 841–843, *842*
H^+-ATPases
effects 12
free energy relationship 123–124
genes 124
P-type *123*
regulation 124–125, *125*
K^+ channels 133, *134*, 135–136, *136*
K^+ transporters 138

plasma membranes (*cont'd*)
lipid composition 11, **11**
membrane potential 117–119, *118*, 119b
membrane recycling 24–25, *25*, *26*
in meristematic root tip cell *3*
morphology, freezing stress 378–379, *379*
physical continuity 10
plasmodesmata production 10
proteins 12–13
proton gradients *115*
P-type ATPases 122, 123–124
receptor classes 838
receptor kinases 838–841, 839b, *841–842*
recycling pathway 24
Shaker family of channels 135, *136*, **149**, 1109–1113, *1110*, **1111**
signal perception 838–843, 839b, *840–842*
sucrose transporters 146
traffic *15*
transmembrane signaling receptors 12
transporters 142, 143, 144, *144*, *145*
transport types *120*
turgor pressure 11, 24–25, *25*
voltage 117, 133, *134*
water permeability 148
plasmids, *Agrobacterium*-mediated T-DNA transfer 996–997b
plasmodesmata 10, *11*
density, loading phloem 674, 677, *677*
development 666–668, *667*
macromolecular trafficking 701, *702*
phloem loading 673–674, *673*
phloem unloading 685–686, *686*, 706, **708**
solute flux 663–664, *663*
structural diversity 667, *667*
substructures *662*
symplasmic transport, sucrose 577, *580*
symplastic transport 659, 661b, *662*
viral transport 994–998, *999*
plasmolysis, cell wall–plasma membrane coupling 220–221
plastids 32–33
see also specific type
aspartate-derived amino acids *320*, 326
cofactor transport from cytosol 567–568, *570*
division 39, *39*
DNA 260
DNA-dependent RNA polymerases 269–270, *269*
DNA enzymes 264
DNA replication 263–264, *264*
DNA transcription 270
envelope membranes 33–34
evolution 40b, 260–261
functions 32–33
gene promoters 270, *270*
general properties 567–568
genomes 261, *262*, **263**
gibberellin biosynthesis 771, *772*
glucose-6-phosphate/phosphate translocator 573
gravity sensation 213
GS isoenzymes 293, *295*
hexose phosphate antiporters 573
inheritance 39
inner envelope membrane 34
intermembrane space 33
malic enzyme 605–606, *607*
mRNA 275
nuclear-encoded gene products 261, 263
outer envelope membrane 33–34
phytoferritin storage 34, *34*
plasticity 33
plastid-encoded gene products 261, 263
polycistronic mRNAs 286, *286*
polycistronic transcription units 261, *263*
prokaryotic lipid synthesis pathway 17
promiscuous DNA 267, *268*
proteases 469, *469*
protein sorting to 153–155, 157
protein synthesis 450–457, *452–457*, *459*
pyrimidine biosynthesis 243
RNA processing 282
sieve elements 667–668, *668*
starch synthesis 580–584, *584*
stromules 33, *34*
structure 33
tRNA *273*
types *33*, 34
plastid-specific ribosomal proteins (PSRPs) 452
plastid translation factors 450–452, **451**, *454*
plastocyanin-ferredoxin oxidoreductase activity of photosystem I 528–529, **529**, *530–531*
plastocyanin (PC), cytochrome b_6f complex 533–535, *534*
plastoglobules 34, *34*, 35, *35*, 37, *37*, *38*
plastoglobulins 37
plastoquinone (PQ), cytochrome b_6f complex 309, 522–528, *524–528*, **524**, **527**, 533–535, *534*
ploidy, development 502–504, *503–504*
P-loops, potassium ion channels 1110, *1110*
PME *see* pectin methylesterase
pmf see proton motive force
pneumatophores 1077, *1077*
Poales 65, 72
poikilothermic organisms 7
pointed ends, actin filaments 198
polarity
cytoskeleton *194*, 197–202
dynein 206
kinesins 206
myosins 203
polar transport stream, auxin 855–856, *855*
pollen *46*
adherence and hydration 903, *903*
allergies 202b
fertility, surface lipids 388–389, *388*
microgametogenesis 889–896, *891–892*, *894*
self-incompatibility 910, *910*
pollen–pistil interactions, surface lipids 388–389, *388*
pollen tubes
callose 51, 80
growth, actin 215, *216*
guidance *904–905*, 905
molecular regulation 904–905, *904–905*
reception 906–907, *906–907*
tip growth *49*, 91
pollination
molecular regulation 902–905, *903–905*
seed oil catabolism 393–395, *396*
polyamines (PAs) 332, 818–821, *820–821*
biosynthesis 819–821, *820–821*
degradation 821, *822*
structures *770*, *819*
polycistronic transcription units 261
polycomb repressive complex 1 (PRC1) 888–889
polycomb repressive complex 2 (PRC2) 434, 922–923, *922*
reproductive development 879, 880b, 920–923, *921–922*
polygalacturonase-inhibiting proteins (PGIPs) 1016, *1018*
polygalacturonase (PGase) 67, 100, 102
polyketides 1182, **1185**
polymaine oxidases (PAO), polyamine degradation 821, *822*
polymer crosslinking 80
"polymer trap" model, RFO sugar transport 681, *681*
polyols, phloem loading 678, *680*
polypeptides
see also proteins
chain elongation 444, *446–447*
polyploidy, development 502–504, *503–504*
polyproline II 67
polyproline stretches, profilin 207
polysaccharide hydrolases 94, 96, *97*, *98*
polysaccharides 45–46
analysis methods
alditol acetates 53b
electron-impact mass spectrometry 54b
ESI MS 62–63b
MALDI-TOF MS 62–63b
methylation analysis 52b, 53b
NMR spectroscopy 55–58b
temperature gradient chromatography 52b, 53b
cell wall–cytoskeletal coordination 234–237, *237*
cell wall heterogeneity probes *48*, 100–101b
evolution *75*
functions 22
glycosyl transferases 89, *90*
β-linked synthase genes 86–88
nomenclature 50
storage 106
structural diversity 89
structure modification 96, *97*, *98*
synthesis in Golgi apparatus 22
polysomes, classes 447
polyteny, development 502–504, *503–504*
polyunsaturated fatty acids
chloroplasts 375–376, *377*
structures 338, **341**, **345**
poppies, gametophytic self-incompatibility 911–913, *912–913*
Populus trichocarpa
tracheary element development 936–937, *938*
β-tubulins 195
pore-plasmodesma units (PPUs) 666–668, *667*
porins 41
mitochondria 611
post-SE transport 684–691, *685–690*, *692*
apoplastic transport 685–687, *685*, **686**, *687*
symplastic transport 685–691, *685–690*, **686**, *692*
post-translational modification 457–463, *460–466*
proteolytic processing 457–458, *460*
ribosomal proteins 440

stromal enzymes 551–553
tubulins 196
potassium (K^+) channels 113, *120*, 138
AKT 134, *135*, *136*, **149**, 1109–1113, *1110*, **1111**
genes 134–135, *135*
HAK channels 145, *145*, **149**
inward-rectifying 133–135, *134*, 135–136, **136**, **149**
KAT 134, 135, *135*, 1109–1113, **1111**
KUP/HAK/KT family of transporters **149**
membrane potential 117–119, *118*
outward-rectifying 133, *134*, 135–136, *138*, **149**
regulation 135–136
Shaker family of channels 135, *136*, **149**, 1109–1113, *1110*, **1111**
TPK1 channels 138, *138*, **149**
two-pore channels 138, **149**
voltage-dependent 133, *134*
potassium (K^+) ions
deficiency *1102*
gene families **1111**, 1112
phloem loading 680, *680*
symplastic transport 1104, *1104*
transport **149**, 1103–1113, *1104*, **1105–1106**, *1106–1107*, *1110*
uptake 119, **136**
vacuolar channels 136–138, *137*, *138*
xylem loading 669–671, *671*
PPC *see* phloem parenchymal cells
PP_i *see* pyrophosphate
L-PPT *see* L-phosphinothricin
PPUs *see* pore-plasmodesma units
PQ *see* plastoquinone
PRC1 *see polycomb* repressive complex 1
PRC2 *see polycomb* repressive complex 2
precocious germination, abscisic acid 778, *778*
precursor accumulating (PAC) vesicles 185
precursor RNAs (pre-RNAs) 278, 279, 280, 282, 285
predator protection, alkaloids 1165b
preformed defenses 1009–1012, *1013–1015*
pre-initiation complex (preIC) 424–425, *425*, **425**, 491–492, *491*
prenyl diphosphates, biosynthesis 1138–1141, *1140–1141*
prenyl group-linked membrane proteins 8, 9, *9*
prenylquinones 37
prenyl transferases 170, 1140–1142, *1141*, *1143*
prephenate aminotransferase *307*, 308
prephenate dehydratase 308
prephenate dehydrogenase 308
preprophase band 222–226, *224–225*, 229
prereplication complex (preRC) 491–492, *491*
presequences 157–158, *157*
pressure-flow mechanism, phloem transportation 696, *698*
pressure potentials 93
bulk flow 663–664, *664*
primary cell walls 45, *47*
defining 102
structural networks 73, 77, *77*
Type I walls 77–79, *77*
Type II walls *77*, 79
primary metabolites, terpenoids 1132–1133, *1132*
PRK *see* phosphoribulokinase
(pro)cambial progenitor cells, vascular differentiation 664
processivity, motor proteins 205
products, citric acid cycle 617–618, *619*
profilin, cytoskeletal regulation 200–202b
programmed cell death (PCD) 925–982
abiotic interactions 961–964, *961–964*
apoptosis 926–928, *927*
cell viability 930
cytokinins 936, 976–977, *977*
defensive bodies 932–937, *935–937*
environmental influences 961–974
ethylene 931, *931*, 963, *963*, 977–979, *978–980*
genetics 965–971, *966–968*, **969–970**
hypersensitive response 965–974, *966–968*, **969–970**, *972–974*
jasmonic acid 980–981
mitochondria 957–961, *958*
mutants 965–971, *966–968*, **969–970**
necrosis 926, *927*, 928, 973–974, *974*
organ shapes 932–948, 934b, *935–940*, **944–945**, *946–947*
pathogen attack 964–974
pathogen defense mechanisms 1037–1038, *1039*
plant-pathways 928, *929*
reproductive development 937–940, *939–940*
salicylic acid 980, *981*
secretory body development 932–933, *933*
seed development and germination 930–932, *930–932*
senescence 940–982
tracheary element development 933–937, *935–938*
victorin-induced 974, *975*
xylogenesis 933
prokaryotes
axonemes 205–206, *206*
cell shape 194–195
prokaryotic lipid synthesis pathway 17, *364*, 365–372, *368–370*
prolamellar bodies 35, *35*
prolamins 15, *17*, 180–181b, 182, 184–185
proline dehydrogenase 331
proline-glutamate exchange 331
proline (Pro)
regulation 330–331
stress tolerance 330
structure 289, *290*
synthesis *291*, 330, *331*
proline-rich proteins (PRPs) 67, *69*, *71*, 99, 103
prolyl *cis-trans*-isomerases 170
prometaphase 27, 31, *478*
promiscuous DNA 267, *268*
promitochondria of the embryo 42
propagative cell death mutants **970**, 971
β-propeller proteins 839b, 1173, *1179*
propeptides 182–183, *183*
properties of light 511
prophase 31, *478*
prophase spindles 228–231, *230*
proplastids *33*, 34, *34*
n-propylgallate, alternative oxidase inhibition 629–631, *631*
prosystemin, defense responses 682
proteases
autophagy 468–469
cellular compartmentalization 468–469, *468*
chromosome separation *494*, 495
classification 467
plastids 469, *469*
regulation 468
selectivity 467
senescence 952–953, *954*, 955–957, *956*
tracheary element development 936
ubiquitin pathways 469–474, *470–471*, **472**, *473–474*
proteinaceous channels 152, *153*
in chloroplasts 155, *156*
in mitochondria *157*
in peroxisomes 159, *160*
proteinase inhibitors, wound healing 1040
protein bodies 15, 179, 180–181b, 182, *182*, 185
protein disulfide isomerase (PDI) 170, *171*
protein import translocons 155
14-3-3 proteins, nitrogen reductase expression regulation 743–744, *744*
proteins
see also secretory proteins; *specific proteins*; storage proteins; structural proteins
conjugation, ubiquitin 469, *471*, 473–475, **472**, *473*
cysteine 747–749
degradation 173, 463–474, 465–466b
physiological roles 463–467, 465–466b, *467*
ubiquitin 463–467, 465–466b, *467*
differential stability, senescence 956–957, *956*
disulfide bonds 747–749
diversity
leaky scanning 444b
viruses 450
encoding sites 152
expression with oxidative stress 1091–1092
folding 170–173, *171*, **172**, 432, 458–463, 1095–1096
chaperonins 460–463, **461**, *462–465*
Hsp70 proteins 459–462, *460–462*
membrane/secretory proteins 462–463
molecular chaperones 458–463, *460–465*, **461**
grana and stroma thylakoids 36–37
hydropathy analysis 113, 114–115b
hydrophilic domains 114–115b
hydrophilic surfaces 152
hydrophobic domains 114–115b
lipid modifications 169–170, *169*
as membrane components 2, 8–10, *8*, *9*, 113
in mitochondria 41–42
molten globule form 458
multifunctional 335b
nucleotide-binding-leucine rich repeat motifs 1024–1032, *1026–1027*, *1029–1031*
phosphorylation, cortical array organization 218–219, *220*
in plasma membrane 12–13
post-translational modification 457–463, *460–466*
proteolytic processing 457–458, *460*
ribosomal 439–440, **440**
sucrose density gradient analysis 163–164b
synthesis 438–463
cellular compartmentalization 438–439, *439*, 452–453
cofactor insertion 456–457, *457*, 458b, *459*
elongation 444, *446–447*

proteins (*cont'd*)
in ER 15–16
frameshifting 450, 450b
initiation 441–442, *443*, 447–449, *449*, 450b, 452, *452*, *453*
in mitochondria 43–44
pauses 456–457, *457*, 458b, *459*
plastids 450–457, *452–457*, *459*
in plastids 39
regulation 442, *445*, 453–455, *454–457*
ribosomes 439–457, *452–457*, *459*
stress conditions 447
termination 447, *448*
viral 444b, 447–450, *449*, 450b
translocation 152
transport 30
ubiquitinylation 469–474, *470–471*, **472**, *473–474*
protein sorting
analysis
pulse-chase experiments 164b
sucrose density gradient analysis 163–164b
cellular machinery
chaperones 152–153, *153*
folding 152–153
multistep process 153
proteinaceous channels 152, *153*
secretory pathway 153, *154*
sorting machinery 151–152
targeting domains 151–152, **153**
targeting pathways 153, *154*
targeting signals 152b
dual targeting 159
endocytosis 188–189, *188*
targeting to mitochondria 159
import apparatus 158
presequences 157–158
targeting to nucleus 30
targeting to peroxisomes 159, *160*
targeting to the plastids
proteinaceous channels and chaperones 155
targeting into thylakoid lumen 155, 157
transit peptides 153–155
transport in/out of nucleus 160–161, *161*, **161**, *162*
protein storage vacuoles (PSVs)
aleurone cells 931–932, *932*
endocytic pathway *26*
protein bodies 182, *182*
protein sorting 179, *179*, 184–185, *186*
protein transport to 182–183, *183*
seed storage proteins 180–181b
traffic *15*, 184–185
vacuolar sorting receptors 183–184, *184*
vacuole transformation pathways 28, *29*
protein turnover, ethylene biosynthesis 808–809, *808*
proteobacteria 40b, 260, *260*, 720
proteoglycans 22
proteolysis
senescence 952–953, *954*, 955–957, *956*
ubiquitin 469–474, *470–471*, **472**, *473–474*
proteomics, redox regulation 554b
protochlorophyllide 35
protofilaments, microtubules 198
proton-coupled transport 143, *143*, 144–145, *144*, *145*
proton gradients *115*, 117, 118b, 123–124, 632–633, *634*
proton leakage, respiratory control 635, *635*
proton motive force (pmf) 117, 118b, 119–120
ATP synthase 632–633, *634*
chloroplast ATP synthase 537–540, **539**, *540*, *553–558*
facilitated diffusion 661b
photosynthesis 510–511, *511*
proton-pumping ATPases 113, *120*, 576b
AHA genes 124, *124*
ATP hydrolysis 123–124, *123*
ATP synthesis 120–121, *122*
binding protein 172
Ca^{2+}-ATPases 126
F-type 120–121, *122*
import into mitochondria *157*
membrane potential 117–119, *118*
in plasma membrane 11, 12
P-type 122, 123–124, *123*, 126
regulation 124–125, *125*
V-type 22, 27, 126–127, *126*
proton translocation
see also ATP synthase
complex III 624–627
cytochrome b_6f complex 533–535, *534*
mitochondrial electron transport chain 621–624, *624*
Q cycle 624–627, *628*
protoplasts 25, 45, *46*
prototrophic mutants 312
proximal promoter elements, gene expression 428
PRPP *see* 5-phosphoribosyl-1-pyrophosphate
PR proteins *see* pathogenesis-related proteins
PRPs *see* proline-rich proteins
PRRs *see* pattern recognition receptors
PS *see* phosphatidylserine
psaA gene 282–283b
psbB operon *263*, *286*
pseudogamy 902, *902*
Ψ_p *see* hydrostatic pressure
P-sites, protein synthesis 444, *446*
PSRPs *see* plastid-specific ribosomal proteins
Ps. savastanoi, auxin synthesis and conjugation 802, *805*
PSVs *see* protein storage vacuoles
PTI *see* pattern-triggered immunity
PTR transporters **150**
PTSs *see* peroxisome targeting signals
P-type ATPases 122, 123–124, *123*
pulp and paper industry 109
pulse-chase experiments 152b, 164b
pulsed amperometric detectors (PADs) 60–61b
pumps 113
see also ATP synthase
ABC-type 127–128, *127*, *128*
Ca^{2+}-ATPases 126
electrogenic 117
H^+-PPases 127
transport rates 113
PUPs *see* purine permeases
purine 240, *241*, 243, *244*, *955*
purine-nucleoside phosphorylase 245b
purine permeases (PUPs) 146
purine salvage pathways 793, *793*
putrescine 819–821, *820*
PWD *see* phosphoglucan, water dikinase
pyranoses 46
pyridoxal phosphate mechanism *300*
pyrimidine dimers 251–252
pyrimidine nucleotides 240, *241*, *242*, 243
pyrimidyl-oxy-benzoates 328, *329*
pyrophosphatase 243
pyrophosphate-dependent phosphofructokinase (PFP) 572, 575–576b, 587–588, *587*, *598*
pyrophosphate (PP_i), metabolic roles 575–576b
Δ^1-pyrroline-2-carboxylate 330
Δ^1-pyrroline-5-carboxylate (P5C) 330, 331
Δ^1-pyrroline-5-carboxylate reductase *331*
Δ^1-pyrroline-5-carboxylate synthetase (P5CS) 330, *331*, 335b
pyrrolizidine alkaloids 1161–1162, *1169*
pyruvate *290*, 326
acetyl-CoA generation 616–617, *617*
carbohydrate metabolism 602–604, *603*
mitochondrial transport 613
terpene synthesis 1138, *1139*
pyruvate decarboxylase (PDC) 1079–1081, *1080*
pyruvate dehydrogenase 616–617, *617*
pyruvate dehydrogenase kinase 617, *618*
pyruvate dehydrogenase phosphatase 617, *618*
pyruvate ferredoxin/flavodoxin oxidoreductase 718, *718*, 733, *734*
pyruvate kinase *603*, 604–605, *605*, 613, *616*

Q cycle 53–55, *534*, 624–627, *628*
qRT-PCR *see* quantitative real time reverse transcriptase PCR
QTL *see* quantitative trait loci
quality, seed crops, sulfur content 749–750
quantitative real time reverse transcriptase PCR (qRT-PCR), gene expression analysis 426b
quantitative trait loci (QTL), flooding responses 1084–1085
quantized angular momentum 55b
quantum yield
photosynthesis 512–515
C_3 plants 653–654, *654*
C_4 plants 653–654, *654*
quaternary structures, Rubisco **549**
quiescence strategy, flooding tolerance 1078
quinine 1160, *1167*
quinolizidine alkaloids 1162, *1169*
quorum-sensing 993, *998*

Rab proteins 176
race-specific resistance 1023–1026, **1024**, *1025–1027*
RAD51 genes 258
RAD51 protein 256–258
radial flow pathway, xylem loading 669, *670*
radioactive pulse-chase experiments 162
radio frequency (RF)-pulses 55b, 56b
radiotracers, ion flux experiments 1104–1107, **1105–1106**, *1107*
raffinose family oligosaccharides (RFOs) 1057–1058, *1059*
symplastic SE loading 681, *681*
RAM *see* root apical meristems
Raman imaging 100–101b
Ran 160–161, *162*
rapeseed, high-lauric-content engineering 398–399
rates of nitrogen fixation 711, **713**
rbcL gene 261

RBCS gene 261
RBR see RETINOBLASTOMA-RELATED gene
RBR/E2F pathway, cell cycle control 488–981, *489–490*, 501–502, *501–502*
RCD *see* reduced cell death mutants
RD29A gene 1068–1075, *1070*, *1073*, **1074**
rDNA *see* ribosomal DNA
RdRPs *see* RNA-dependent RNA polymerases
reaction centers, photosystems 519–522, *522*, *524*, *527*, *530–531*, *535*
reaction mechanisms, alkaloid biosynthesis enzymes 1172–1174
reactive oxygen species (ROS) 330
  biosynthesis 1016, *1017*
  hypersensitive response 971–973, *973*
  molecular structures *1086*
  pathogen defense mechanisms 990
  signaling 1092–1094, *1093*
  stress responses 1085–1094
RecA protein 258, *258*
reception of pollen tubes, molecular regulation 906–907, *906–907*
receptor kinases 838–841, 839b, *841–842*
  self-incompatibility 910, *910*
receptor-like kinases (RLKs) 107, *108*, 189, 838–841, 839b, *841–842*
  fertilization 906–907, *906–907*
  self-incompatibility 909–911, *910*
receptor-like proteins (RLP), immunity *1025*, 1025
recessively inherited resistance genes 1033, **1034**
recoding mechanisms, viral protein synthesis 450, 450b
recognition, TATA boxes 425, *425*
recombinant DNA, vectors 996–997b
recombination repair 254–255
recycling endosomes 26
recycling pathway 24
red/far-red light sensing 776, *777*, 857–861, *858–861*
red/far-red photoreversibility, phytochromes 857–859, *858–860*
redox activation, ADP-glucose pyrophosphorylase 583–584, *584*
redox chemistry
  mitochondrial respiratory complexes *621*
  NAD^+ *612*
  nitrogenase cycles *718*
  ubiquinone 621, *622*
redox conditions, senescence 959–961, *960*
redox regulation
  ferredoxin–thioredoxin system 553–556, *555–557*
  γ-glutamylcysteine synthetase 758, *760*
  proteomics 554b
reduced cell death (RCD) mutants 968, **969**
reducing equivalents, citric acid cycle 617–618, *619*
reducing sugars *574*
reduction
  acetylene 717
  Calvin–Benson cycle 545, *546–547*
  NAD^+ 602–603, *603*
  NADP 601–602, *602*, 605–606, *606*
  nitrate 739–744, *739–744*
  nitrite 739, 744–745, *745*
  sugars, nonenzymatic 573, *574*
  sulfate 753–754, *753*
  sulfite 754
reductive amination 298
reductive phase of Calvin–Benson cycle 545, *546–547*
reductive sulfate assimilation 752–754, *753*, 755–757, *756–757*
regulation
  see also molecular regulation
  abscisic acid synthesis 782–784, *783*
  acetyl-CoA carboxylase 350
  ADP-glucose pyrophosphorylase 582–584, *584*
  alternative oxidase 636–638, *637*, *638*
  apoptosis 926–928, *927*
  brassinolide biosynthesis 814
  Calvin–Benson cycle 551–557, *553*, *555–558*
  citric acid cycle 634–635, 646
  cyanogenic glycoside biosynthesis 1155–1157, *1155*
  cyclin-dependent kinases 485–486, *486*, 493, *493*
  cysteine synthase 757, *757*
  cytokinins 793, *794*
  cytoskeleton 200–202b, 206–207, *206*
  epigenetic mechanisms 430–436
  ethylene biosynthesis 446, 808–809, *808*
  flowering, epigenetic control 435–436, *436*
  gene promoters 427–430, **428**
  gibberellin synthesis 774–776, *776*
  glycerolipid desaturation 358–360
  glycolysis 605
  G-proteins 842, *842*
  mitochondrial cytochrome pathways 634–635, *635*
  nitrogenase expression 732–733, *733*
  nitrogen reductase expression 742–744, *743–744*
  phloem nutrient concentration 705–709, *706–709*
  phosphate uptake and homeostasis 1116–1118, *1118*
  photosynthesis 540–542, *540–541*, **540**
  photosystems 540–542, *540–541*, **540**
  phytochrome A 466–467, *467*
  profilin 200–202b
  proteases 468, 952–953, *954*
  protein synthesis 442, *445*, 453–455, *454–457*
  pyruvate dehydrogenase 616–617
  Rubisco 463, 553–555, *553*
  seed oil biosynthesis 392–393
  senescence 943–948, **944–945**, *946–947*
  senescent macromolecule recycling 955–956
  starch biosynthesis 582–584, *584*
  starch/sucrose partitioning 588–591, *589–590*
  strigolactone biosynthesis 833
  sucrose-phosphate synthase 577, *577*
  sucrose/starch partitioning 588–589, *589*
  sugar signaling 607–608, *608*
  sulfate assimilation 764–765, *764*
  ubiquitin attachment 473–475
  xylem nutrient concentration 671
regulons, water stress 1062
reinitiation, protein synthesis 445b
relative water content (RWC) 1054–1055
release factors (RFs), protein synthesis 447, *448*
release phloem 673, 684–691, *685*
  apoplastic transport 685–687, *685*, **686**, *687*
  symplastic transport 685–691, *685–690*, **686**, *692*
remobilization, senescence 953–956
remodeling
  chromatin 432, 501–502, *501–502*
  cytoskeleton 207
repair
  D1 protein 463, 465–466b
  embolized xylem 693–694
repeat-variable diresidues (RVDs) 257b
repetitive DNA 404–406, *405*
  Cot analysis *405*
  larger genomes 414–415
replication, DNA, cell cycle 491–495, *491–494*
replication forks, cell cycle 491, *491*
replication licensing, DNA 491–492, *491*
replication protein A (RP-A) 246
replicons 246
replisome 491, *491*
repression, ethylene biosynthesis *809*, 810
repressors, gene expression 429–430
reproductive development
  apomixis/apomeiosis 901–902, *902*
  megagametogenesis 897, 899–900, *900*
  megasporogenesis 897, 898–899, *898*
  molecular regulation 872–924
    female gametes 897–902, *897–902*
    fertilization 902–903, 906–908, *906–907*
    flower development 881–889, *883–889*
    initiation of flowering 872–881, 880b, *881*
    male gamete formation 889–897, *891–892*, 893b, *894*, 895b, *896–897*
    photoperiods 874–878, *876–877*, *881*
    pollination 902–905, *903–905*
    seeds 913–923
    self-incompatibility 908–913, *909–913*
    vernalization 874, 878–879, *879*, 880b
  mutant phenotypes 915b
  programmed cell death 937–940, *939–940*
  seeds, molecular regulation 913–923
  transition from vegetative development 872–881, 880b, *881*
rescue, microtubule elongation 202
resistance genes (*R*-genes) 985–989, *988*, 1023–1027, **1024**, *1025–1028*
  see also R-proteins
  allelic variation 1026–1027, *1028*
  genetic engineering 1032, 1044–1048, 1047b
  recessively inherited 1033, **1034**
resistance mechanisms, stress tolerance 1052, *1052*
resonance frequency 55b
respirasomes *624*, 627, *629*
respiration 610–655
  see also Calvin–Benson cycle; citric acid cycle; glycolysis; photorespiration
  aerobic 610–646
    mitochondrial electron transport 620–633
    mitochondrial electron transport chain 620–646, *620*
    nonphosphorylating pathways 635–639, *637*, *638*
    overview 610–613
  citric acid cycle 613–620
  fermenting metabolism 1079–1082, *1080–1081*, *1083*
  gluconeogenesis 643–644, *645*
  legume bacteroids 731, *733*
  light-dependent 646–654

respiration (*cont'd*)
biochemical basis 646–648
pathway 648–652
mitochondrial electron transport 620–646, *620*
nonphosphorylating pathways 635–639, *637*, *638*
overview 610–613
oxidative phosphorylation *614*, **615**
oxygen deprivation effects **1076**
Q cycle 624–627, *628*
respiratory control 634–635, *635*
response regulator protein, cytokinin signaling 850–851, *850–851*
(*S*)-reticuline 1170, *1176*
RETINOBLASTOMA-RELATED (*RBR*) gene, microgametogenesis 894
retrogradation, starchy foods 585b
retrograde regulation, stromal enzymes 551
retrograde traffic 13, *15*
retromer-coated vesicles 26, 175
retrotransposons (class I transposons) 419–421, *419*, 422b
maize genome 420–422, *420*, 422b, *424*
reversal potential (E_{rev}) 132, 132b
reverse transcriptase PCR (RT-PCR), gene expression analysis 426b
reverse transcription 240, 426b
RF *see* radio frequency
RFOs *see* raffinose family oligosaccharides
RFs *see* release factors
RGD peptides 221–222
R-genes *see* resistance genes
RG I *see* rhamnogalacturonan I
RG II *see* rhamnogalacturonan II
rhamnogalacturonan I (RG I) *66*, 67, 72, 77, 96, 99, 100
rhamnogalacturonan II (RG II) 67, *68*, 77
rhamnogalacturonan lyases 97
L-rhamnose (Rha) 49, *50*, 85
rhizobial bacteria
extracellular polysaccharides 722–723, *724*
nitrogen fixation 718–735, *720*, **721**, 721b, *722–730*, **724**, *732–734*
NodD proteins 722, *722*
Nod factors 722–724, *722–723*
rhizosphere, phosphate bioavailability 1114–1116, *1115*
RHO of plant (ROP) GTPases
anoxia sensing 1085
pollen tubes 904–905, *904–905*
ribonucleases 243
ribonucleotide reductase 243
ribonucleotides *241*
ribose *241*
ribose 5-phosphate, pentose phosphate/triose phosphate pool *598*
ribose 5-phosphate isomerase *546–547*, 548
ribosomal DNA (rDNA) 30
ribosomal RNA (rRNA) 271, 439, **440**
assembly in nucleoli 30
chloroplasts 40b
evolution 260, *260*
functions 270
gene locations 406, 412–414, *414*
mitochondria 40b
processing 282, *283*, *284*
remobilization in senescence 953–954
structure *272*
transcription 423
ribosome inactivating proteins (RIPs) 439, 441b
ribosomes
A-sites 444, *446*
chloroplasts 40b
classes 271
E-sites 444, *446*
frameshifting 450, 450b
functions 270
mitochondria 40b
plastids **440**, 450–452
post-translational modification 440
production in nucleoli 30–31
protein composition 439–440, **440**
protein synthesis 439–457, *452–457*, *459*
pauses 456–457, *457*, 458b, *459*
P-sites 444, *446*
ribosomal RNA 439, **440**
RNA encoding genes 406, 412–414, *414*
scanning 441–442, 444b
subunits 271
toeprinting 458b
ribozymes 270, 279–280, 439, **440**
ribulose-1,5-bisphosphate carboxylase/oxygenase (Rubisco) 31–32, 39, 261, 545, *546–547*, 548–551, *550*, 557
activation 553–555, *553*
carboxylase/oxygenase activity ratios 648
climate change 654–655
energy costs **652**
folding 463, *465*
modulation 553–555, *553*
oxygenase activity 549–551, *550*, 654
photorespiration 647–648
regulation of accumulation 463
seed oil biosynthesis 393
ribulose-1,5-bisphosphate (RuBp), Calvin–Benson cycle 545–548, *546–547*
ribulose 5-phosphate *598*, 601–602, *602*
ribulose 5-phosphate epimerase *546–547*, 548, *598*, 601
ribulose 5-phosphate isomerase *598*, 601
rice
CesA genes *87–88*
chloroplast DNA *262*
germination in flooded environments 1077–1078, *1078–1079*
GT genes *90*
Internet resources 89b
leaf senescence 945–948, *946–947*
promiscuous DNA *268*
silicon transporters, roots 670, *671*
rice blast fungus, pathogenesis 1006
ricinoleic acid *361*, 362, 399–400
Ricinus communis 439, 441b
Rieske Fe–S proteins 532–533, **533**, *624*
ripening of fruits 100, 102, *102*, *809*, 810, 959
RIPs *see* ribosome inactivating proteins
RISC *see* RNA-induced silencing complex
RLKs *see* receptor-like kinases
RLP *see* receptor-like proteins
RMR proteins 184
RNA-dependent RNA polymerases (RdRPs) 275, 285
RNA editing 286–288, *287*, **287**, *288*
RNAi *see* RNA interference
RNA-induced silencing complex (RISC) 275–276
RNA interference (RNAi) 275, *276*
RNAPI 423, **424**
RNAPII 423, **424**, *425*, **425**
RNAPIII 423, **424**
RNAPIV 423, **424**
RNAPV 423, **424**
RNA polymerases (RNAPs) 422–425, **424**, *425*
DNA-dependent 268–270, **268**, *269*, 285
eukaryotic vs. prokaryotic 268, *269*
illegitimate recombination 259
nuclear 268–269
plastid 269–270, *269*
RNA-dependent 285
RNA editing *287*
RNA processing 280, 282, 285
RNA processing 278
exons 278
polycistronic plastid mRNAs 286, *286*
pre-RNAs 280, *281*, 282, *283*, *284*, 285
RNA editing 286–288, *287*, **287**, *288*
small regulatory RNAs 285–286, *285*
RNAPs *see* RNA polymerases
RNA (ribonucleic acid) 240
see also nucleic acids; *specific types of RNA*
biochemical properties 270
classes 275
classification by size 270–271, *271*
functions 270
gene silencing 275–278
purines 243
ribosomes, gene locations 406, 412–414, *414*
self-replication 270
structures 245
synthesis 268–270, *269*
translation 439–457, *452–457*, *459*
RNase H 247, *248*
RNase P 277–278, **278**
RNA sequencing 426b
RNA silencing 1043–1045
RNA splicing 278
RNA translation 240, *241*
RNA viruses 240
root apical meristems (RAM) 477, *479*, 497, *498*
root hairs 91, 724, **724**, *725*, 727–729, *728*, *732*
root nodules
bacteroids 731–733, *732–734*
legumes 720–735, *721*, *724–730*, *732–734*, *736*
bacteroids 731–733, *732–734*
calcium spiking 724, 727–729, *728*
development 720–733, *722–730*, **724**, *732*
flavonoid signaling 721, *722*
hormone signaling 730, *730*
microaerobic environment 731–733, *732–733*
molecular genetics 726–733, *726–730*, *732–733*
nitrogen assimilation *734*, 735, *736*
roots
aerenchyma 962–963, *963*, 1076, *1077*, 1082, *1083*
ammonium uptake 735, *737–738*
architecture, nitrate regulation 745
cell speciation 477, *479*, 497–499, *498–499*
clustered 1115–1116, *1116*
extracellular lipids 384–385, *386*
nitrate regulation 745

phosphate transporters 1114, *1114*, *1118*
potassium transporters 1103–1113, *1104*, **1105–1106**, *1106–1107*, *1110*
sodium–potassium transporters 1112–1113
sodium transporters 1112–1113
stained sections, *Arabidopsis thalania* *192*
xylem loading 668–671, *669–671*
ROP *see* RHO of plant GTPases
ROS *see* reactive oxygen species
rosette complex 80, *82*, 86
Rosid I lineage 719, *720*
rotenone, complex I inhibition 624, *625*
rough endoplasmic reticulum *3*, 13, 15, *16*, 162, 165
round peas, starch granules 583b
Roundup 306b
RP-A (replication protein A) *248*, 258
rpl21 gene 267
R-proteins 1023–1032, **1024**, *1025–1031*
see also resistance genes
allelic variation 1026–1027, *1028*
associated proteins *1030–1031*, 1031–1032
leucine rich repeats 1023–1026, *1025–1026*
nucleotide-binding sites 1024–1026, *1026–1027*
unique 1032
rps12 gene 282–283b
5.8S rRNA 278, 282, *283*
17S rRNA 282, *283*
25S rRNA 282, *283*
rRNA *see* ribosomal RNA
5s rRNA gene 267b, 278
RT-PCR *see* reverse transcriptase PCR
Rubisco *see* ribulose-1,5-bisphosphate carboxylase/oxygenase
Rubisco activase 553–555, *553*
RuBp *see* ribulose-1,5-bisphosphate
Ruta graveolens 313b, 335b
RVDs *see* repeat-variable diresidues
RWC *see* relative water content
ryanodine receptors 139

SA *see* salicylic acid
Saccharomyces cerevisiae
complementation 142
membrane-associated genes 111
membrane transport genes 111–112, 145
origins of replication 245
saccharopine 325, *325*
saccharopine dehydrogenase (SDH) 325, *325*
sac genes 765
SAG *see* SA 2-*O*-β-glycoside
SA β-glucosyl ester (SGE) 828, *829*
SA 2-*O*-β-glycoside (SAG) 828, *829*
salicylhydroxamic acid (SHAM) 629–631, *631*
salicylic acid (SA) 302, *770*, 826–830, 826b, *827–829*
biosynthesis 827–830, *829*, 1019–1022, *1021*, *1039*
disease resistance 827–828, *827–828*
induced defense 1019–1022, *1021*, 1033–1038, *1037–1039*, 1042, *1042*
pathogen signaling *1030*, 1033–1038, *1037–1039*, 1042, *1042*
petal senescence, flowering induction 826
senescence 980, *981*
structure *770*
voodoo lily thermogenesis 826–827
salinity, membrane transport effects 1060, *1060*
S-alleles, self-incompatibility 911, *912*
SALT OVERLY SENSITIVE 1 (SOS1) channel 1060, *1060*
salt tolerance 1112–1113
salvage of nutrients in senescence 954–957, *955–956*
SAM *see* *S*-adenosyl-L-methionine
SAMs *see* shoot apical meristems
SAM synthetase *322*, 323
sap composition, sieve tubes 674–676, **676**
saponins 1009–1012, *1013–1014*
sap-sucking insects, pathogen introduction 1002–1003, *1003*
SAR *see* systemic acquired resistance
saturated fatty acids **341**
scalar coupling 55b
scanning
leaky 444b
protein synthesis initiation 441–442, 444b
SCARECROW (SCR) 498–499, *499*
S cell cycle stage
DNA replication 245, 246, 250
mitochondria changes 43, *43*
vacuole changes 27
SCF *see* Skp1-Cullin-Fbox ligases
Schiff base formation *300*
schizolysigeny 933, *933*
SCR *see* SCARECROW
SD *see* spontaneous death mutants
SDH *see* saccharopine dehydrogenase
secondary cell walls 45
cellulose 51
CesA genes 86, *87*, *88*
elaborations *47*, 102–103
lignins *73*, 104–106
storage function 106, *106*
synthesis regulation 106–107, *107*
thickening patterns *103*
secondary metabolites, terpenoids 1132–1133, *1132*
secondary pathways, evolution 1205–1206
second messengers, signal transduction 843–847, *844–846*
secreted vesicles 186, *186*
secretory immunoglobulin A (SIgA) 165b
secretory pathway 161–162, *166*
see also secretory proteins; secretory vesicles
anterograde/retrograde traffic *166*
coat types 175
default pathway 178
dense vesicles 184–185, *185*
ER entry 168
integral membrane protein orientation in ER membrane 168–169, *168*
KDEL signal *178*, 179
lipid anchors 169–170, *169*
membrane anchor sequences 169
N-glycosylation 173, *173*
N-linked glycan processing 187–188, *187*
non-Golgi vacuolar pathways 185–186, *186*
O-linked glycan processing 188
protein bodies 179, 182, *182*
protein folding 170–173, *171*, *172*, **172**
protein retention 178–179, *178*
protein synthesis 162
protein targeting to vacuoles 182–183, *183*
signal peptides 167–168
signal proteins 177b, 178–179
signal recognition particles 168
traffic route 162
translation 162
unfolded protein response 174–175, *174*
vacuolar sorting receptors 183–184, *184*
vacuolar sorting signals 182–183, *183*
vesicle budding and fusion 175–176, *176*, 177b, 178
vesicles 162
secretory proteins 161–162
folding 170–173, *171*, *172*, **172**, 462–463
signal peptides 167–168
secretory vesicles
actin transport 215–216
AGPs *67*
anterograde/retrograde traffic *166*
cell wall growth *81*, 90, *91*
endocytosis 26, *26*, *166*
exocytosis 23–24, *24*
functions 21–22
numbers 21
protein sorting 162
vesicle budding and fusion 175–176, *176*, 178
vesicle cycling 177b
sedoheptulose-1,7-bisphosphatase *546–547*, 548
sedoheptulose 7-phosphate, pentose phosphate/triose phosphate pool *598*
seed crops, methionine content 749–750
seed oils, unusual fatty acids 363
seeds
defense mechanisms, fatty acids 363
development
compartments 913–914, *914*
embryogenesis 916–919, *917–918*
endosperm 919–920, *919*
genomic imprinting 914–915, 920–923, *921–922*
molecular regulation 913–923
parental effects 914–916, 915b, *916*
programmed cell death 930–932, *930–932*
sporophytes 916–918, *917–918*
sucrose transport *690*, 691
maturation 923, *923*
scattering 103, *104*
secondary cell walls 106
signaling of nutrient demand 706–707, *709*
storage oils 15
storage proteins 15, 180–181b
triple response to ethylene 847, *847*
segregation ratio distortion, gametophytic mutations 896b
selection pressures, long-distance transport 658–664, 660–661b
selective permeability, mitochondrial inner membranes 639
selective proteolysis 467
selectivity, potassium transporters 1106–1107, *1107*
self-incompatibility
genetics 908–909, *909*
molecular genetics 908–913, *909–913*
programmed cell death *939*, 940
senescence 925, 940–982

abiotic interactions 961–964, *961–964*
agricultural implications 948
cell biology 941–942, *942*
chloroplasts 941–942, 945–948, *947*, 948–951, *949*, 952–954, *952*, *954*
cytokinins 976–977, *977*
energy metabolism 957–959, *957*
environmental influences 961–964, *961–964*
ethylene 977–979, *978–980*
flower development 940–943, *940–941*, **944–945**, *946–947*, *949*
gene expression 952–953, *953*
genetics 943–948, **944–945**, *946–947*
gluconeogenesis *958*, 959
hormonal regulation 974–981
internal reorganizations 941–942, *942*
jasmonic acid 980–981
leaves *958*, 959
macromolecule degradation 951–957, *952–956*
mitochondria 957–961, *958*
nutrient salvage 954–957, *955–956*
oxidative metabolism *958–960*, 959–961
peroxisomes 957–959
petals, salicylic acid regulation 826
phenylpropanoid metabolism 950–951, *951*
pigment metabolism 948–951, *949*, *952*
proteases 952–953, *954*, 955–957, *956*
rice leaves 945–948, *946–947*
salicylic acid 980, *981*
as a stress response 962–964, *963–964*
sequence-dependent glycanases 60b
sequencing
bisulfite method 434
hidden Markov models 409–410, 410b
projects 408, 409b
whole genome shotgun method 408, 409b
sequential addition, amino acids, protein synthesis 444–446, *446*
sequestering, actin 200–202b
sequestration of toxins 28
SERAT *see* serine acetyltransferase
serine acetyltransferase (SERAT) 756–757, *757*
serine:glyoxylate aminotransferase *649*, 650
serine (Ser) 188, *290*, *291*, *292*
photorespiration *649*, 650
SEs *see* sieve elements
sesquiterpenes 1133
sessility of plants 570
severing proteins, cytoskeletal polymers *206*, 207
sexual identity, unisexual flowers 939, *939*
SGE *see* SA β-glucosyl ester
SGR see Stay Green gene
shade avoidance, tryptophan aminotransferase 798
Shaker family of channels 135, *136*, **149**, 1109–1113, *1110*, **1111**
SHAM *see* salicylhydroxamic acid
SH-EP proteases 179, *179*, 185
shikimate 304
shikimate dehydrogenase 304–305, *304*, 318, 335b
shikimate kinases *304*, 305
shikimate pathway 302–305, *303*, *304*, 600
shikimate 3-phosphate 305
Shine–Dalgarno sequence, mRNA translation 452
shoot apical meristems (SAMs) 42–43, *42*, 477, *479*, 497, *498*
shoot branching
hormones 831–833, *831*
strigolactone signaling 831–833, *831*
SHOOT MERISTEM-LESS (*STM*) genes 498, *498*
short-day plants 875
short-distance transport, nonvascular cells 673–691, *673*, *677*, *679–681*, *684–685*, *687–690*, *692*
short interfering RNAs (siRNAs) 275–278, *276*, **278**
short interspersed elements (SINEs) 421
SHORT ROOT (SHR), root cell speciation 498–499, *499*
SHORT SUSPENSOR (*SSP*) gene, seed development 916, *917*
short-term acclimation, flooding and anoxia 1079–1080, *1080–1081*
SHR *see* SHORT ROOT
sHSPSs *see* small heat shock proteins
sialic acid *187*
side-binding proteins, cytoskeleton *206*, 207
side chain variation
brassinosteroids *812*, 814
cytokinins *786*, 787
sieve elements (SEs) *46*, 99
see also companion cells; phloem
calcium storage 667–668
cell biology 666–668, *667*
cell structures and metabolism 676–677, *677*
differentiation 664
loading 673–681, *673–674*, *677–681*
plastids 667–668, *668*
ultrastructural elements **666**
sieve pore occlusion, phloem 698–700, *700*
sieve tubes (ST)
depolarization and sucrose transport 679, *679–680*
electrical conductivity 703–704, *704*
hydrostatic and osmotic pressures **682**
sap composition 674–676, **676**
SIgA *see* secretory immunoglobulin A
signaling cassettes, signal transduction 836
signaling pathways
see also signal integration; signal perception; signal transduction
classes 837–838
common characteristics 836–837
interactions and integration 837
jasmonate 379–382
membrane lipids 379–382, *380–381*
nitrate 745, *746*
phosphatidylinositol 379, *380*
pollen tube guidance *904–905*, 905
pollen tube reception *902*, 906–907, *906–907*
pollen tubes 904–905, *904–905*
reactive oxygen species 1092–1094, *1093*
systemic acquired resistance 1033–1038, *1035–1037*, **1038**, *1039*
water deficit 1065–1068, *1067–1069*
signaling receptors, rhizobial symbiosis 726–727, *726*
signal integration
abiotic stress responses 1097–1099
characteristics 837
ethylene 849–850, *849*
flowering initiation 874
stomatal aperture control 866–870, *867–870*
signal peptidase *167*, 168, 170
signal peptides 167–168, *167*, **167**, 169, *171*, *183*
signal perception
characteristics 834–838, *835*, *836*
ethylene 848–849, *848–849*
extracellular auxin 854
low-temperature sensing 1072
oxygen deprivation 1085
pathogen effectors 1027–1031, *1029–1031*
phytochromes 857–861, *858–861*
plasma membranes 838–843, 839b, *840–842*
signal recognition particles (SRPs) 157, *167*, 168, 169
signal transduction 107–108, *108*, 112, 174, 834–871
see also signaling pathways; signal integration; signal perception
auxin 852–857, *853–857*
calcium ions 843–845, *845*, 868–870, *869–870*
carbon dioxide 869–870, *870*
characteristics 834–838, *835*
common pathway characteristics 836–837
cytokinins 850–852, *850–851*
ethylene 847–850, *848–849*
fertilization 906–907, *906–907*
gibberellins 861–866, *862–863*, 864b, *865–866*
G-protein coupled receptors 838, 841–843, *842*
intracellular 843–847, *844–846*
membrane receptor kinases 838–841, 839b, *841–842*
pathway interactions 837
phytochromes 857–861, *858–861*
plasma membranes 838–843, 839b, *840–842*
RGD peptides 221–222
second messengers 843–847, *844–846*
silencers, gene expression 275–278, 428–429, *428*, 1042–1045
silicon transport, xylem loading 670–671, *671*
sinapyl alcohol *74*, 104
SINEs *see* short interspersed elements
single-copy DNA 404–406, 416
single-strand RNAs (ssRNAs) *276*, 285
singlet states, chlorophyll 512, *512*
SIPs *see* small basic intrinsic proteins
siRNAs *see* short interfering RNAs
site-directed mutagenesis 257b
site-specific recombination 258–259, *259*
sitosterol *5*, 11
SK genes 305
SKOR protein 669–671, *671*
Skp1-Cullin-Fbox (SCF) ligases 487, *488*
auxin signaling 853, *853*
SLAC1 gene 141
SLIM1 gene 764–765, *765*
S-locus receptor kinase (SRK), self-incompatibility 910–911, *910–911*
slow vacuolar (SV) channels 139–140, *139*, *140*
SLs *see* strigolactones
small basic intrinsic proteins (SIPs) 147
small G-proteins, functions 842, *842*
small heat shock proteins (sHSPs) **1095**, 1096
small nuclear RNAs (snRNAs) 275, **278**, 423
small nucleolar RNAs (snoRNAs) 275, **278**
small ribonuclear-proteins (snRNPs) 275
small RNAs 275–278, *276*, **278**, 285–286

smooth endoplasmic reticulum *3*, 13, 15, *16*
SMYRK gene 727
SNARE *see* soluble *N*-ethylmaleimide-sensitive factor attachment protein receptor
SNARE genes 175, 177b
snoRNAs *see* small nucleolar RNAs
SnRK1 protein kinase, sugar sensing 608
snRNAs *see* small nuclear RNAs
snRNPs *see* small ribonuclear-proteins
SOD *see* superoxide dismutase
sodium ions (Na^+) 142, 144, *145*, 1060, *1060*, 1112–1113
sodium–potassium transporters 1112–1113
sodium transporters 1112–1113
soil amendments, nitrogenous 714b
soils, sulfur content 749, *750*
solid-state NMR 56b
soluble *N*-ethylmaleimide-sensitive factor attachment protein (SNARE) receptor 175–176, *176*, 177b, 178, 928
soluble oligomeric complexes, folding 463, *465*
solute potential (Ψ_s) 146–147
solute uptake energetics 121b
solvent-soluble wax deposition 385–388, *387–388*
somatic embryogenesis 436
SOS1 *see* SALT OVERLY SENSITIVE 1 channel
specialization of pathogens 1007
speciation
  orthology and parology 415b
  roots 498–499, *499*
specificity factors, Rubisco 648
specific transcription factors
  see also trans-acting factors
  gene expression 427–429, *427*, *429*
spermidine 819–821, *820*
spermine 819–821, *820*
S phase 491–492, *491–492*
sphingolipids 342, **345**, 373, *375*
sphingomyelin 11
spindle midzone 232–233b
spliceosomes *280*
spontaneous assembly, cytoskeleton 197
spontaneous death (SD) mutants 968, **969**
spontaneous pathway *156*, 157
sporophyte development 916–918, *917–918*
sporophytic maternal effect 914
sporophytic self-incompatibility (SSI) 909–911, *910–911*
SPS *see* sucrose-phosphate synthase
SRK *see S*-locus receptor kinase
S-RNAases *see* stylar ribonucleases
SRPs *see* signal recognition particles
SSI *see* sporophytic self-incompatibility
SSP see SHORT SUSPENSOR gene
ssRNAs *see* single-strand RNAs
S-state model, photosystem II 525–526, *526–527*
ST *see* sieve tubes
stability regulation, transcription factors 860–861, *861*
standard chemical potential 116–117b
standard electrochemical potential 116–117b
starch
  biosynthesis 580–587, *582*, 583b, *584*
    regulation 582–584, *584*, 588–589, *589*
  degradation
    chloroplasts 595–597, *595*
    endosperm 594–595b
    metabolic pathways 593–597, 594–595b, *595*, *597*
    onset 591–593
  diurnal accumulation/utilization regulation 590–593, *590–591*
  granules *581*, 584–586
  Mendels' pea phenotypes 583b
  partitioning 587–593, *589*
  retrogradation 585b
  storage 38, 564–565, *564*, 590–593, *590–591*
  structure 580, *581*, 584–585
  transitory 564–565, *564*
starch branching enzymes 585–586, *586*
starch debranching enzymes 585–586, *586*
starch synthase 585–586, *586*
starchy endosperm seeds, programmed cell death 930–931, *931*
STAR proteins 1130–1131
start codons 441–442, *443*, 445b
starvation responses 469, 765, *765*
statoliths 15
Stay Green (*SGR*) gene 945, *947*, 948
steady state, cytoskeleton polymerization 197
stearic acid 11, 353–356, *356*
stearolic acid *361*
stearoyl-ACP desaturases 353–356, *356–357*
stele, xylem loading 668–671, *669–671*
stem elongation, ethylene 804, *805*
sterculic acids 363
sterculynic acid *361*
sterility, male gametes 896–897, *897*
sterol biosynthesis *813*
sterol esters 11
sterol glycosides 11, **11**
sterol glycosylation 11
sterols 4, *5*, 7, 11, **11**
steryl glucosides **11**
stigma, pollen adherence 903, *903*
stigmasterol *5*, 11
stilbenes 1182, **1183**
STM see SHOOT MERISTEM-LESS genes
stoichiometry
  photosystem organization 540–544, *540–541*, **540**
  Q cycle 625–627
  sucrose oxidation **615**
stomata 103, 124, 133, 137, *137*, 141
  abscisic acid signaling 868–870, *869–870*
  aperture regulation 866–870, *867–870*
stop codons 447, *448*, 450, 450b
storage
  iron 1124–1125, *1125*
  starch 38, 564–565, *564*, 590–593, *590–591*
storage lipids 339–342
  catabolism 393–395, *396*
  gluconeogenesis 643–644, *645*
  oil bodies 392–393
  β-oxidation 393, 395, *396*
  synthesis 389–393, *390*
storage parenchyma cells 184, *185*
storage proteins
  classes 15, *17*, 180–181b
  protein bodies 179, 182, *182*
  synthesis 15
  transport to vacuoles 182–183, *183*, 185–186, *186*
  vacuolar sorting receptors 183–184, *184*
storage sinks
  post-SE transport 684–691, *686–690*, **686**, *692*
  signaling 705, *708*
straight chain models 46, *49*
strawberries, essential mineral deficiencies *1102*
streaming, cytoplasm 211–212, *213*
stress granules, hypoxia 1082, *1083*
stress relaxation 93, *93*
stress responses
  see also abiotic stress responses
  abiotic factors 1051–1100
  alternative oxidase 636–638, *637*
  aromatic amino acid synthesis 318, *319*
  protein translation regulation 447
  resistance mechanisms 1052, *1052*
  senescence 962–964, *963–964*
stress tolerance 330
3α-(*S*)-strictosidine 1172, 1173, *1173*, *1179*
strictosidine synthase 1173, *1179*
strigolactones (SLs) 830–833, *830–832*
stroma
  protein transport to 34, 154, 155, *155*, *156*, 157
  structure 34, *35*
  thylakoids *see* grana thylakoids; stroma thylakoids
stromal enzymes, light modulation 551–557, *553*, *555–558*
stromal thylakoids 35–37, *35*, *36*, *37*, 510, *510*
stromules 33, *34*
structural diversity, plasmodesmata 667, *667*
structural motifs, race-specific resistance 1023–1026, **1024**
structural proteins *67*, *69*, *70*, *73*, 79, 103
structure
  actin 197–202, *197–199*
  F_oF_1–ATP synthase 632–633, *633*
  microtubules 198, *200*
  mitochondria 611, *611*
  plasmodesmata *662*
  tubulins *200*
stylar ribonucleases (S-RNAases), self-incompatibility 912–913, *913*
subcellular compartmentalization
  alkaloid biosynthesis 1171
  antioxidant systems *1087*, **1088**, **1089**
  cyclin-dependent kinases 484–485, *485*
  glucosinolates 1158
  Rubisco genes **549**
suberin 103–104, *104*
  biosynthesis 385, *385*
  deposition 384, *385*, *386*
  monomers 384–385, **384**, *387*
subfunctionalization 415, *416*, 578
subgenomic circles 265, *266*
substrate specificity
  3-ketoacyl-ACP synthase isoforms *347*, 351, *354*
  potassium transporters 1106–1107, *1107*
substrate supply, mitochondrial respiration 635, 639, *641*
substructures of plasmodesmata *662*
subunits
  chloroplast ATP synthase 538–539, *538*, **539**, *540*
  cytochrome b_6f complex 532–535, **533**, *534–535*
  photosystem I **529**
  photosystem II 522–523, *524*, **524**
  plastid ribosomes **440**, 450–452

succinate dehydrogenase
citric acid cycle 618, *619*
membrane topology 622, *626*
mitochondrial electron transport chain *620*, 621
structure and function 622, *626*
succinyl-CoA synthetase, citric acid cycle 617–618, *619*
sucrose
aerobic respiration 612–613, *612*
apoplast transport 577
biosynthesis 573–577, *574–577*
at photosynthesis onset 589–590
regulation 588–589, *589*
degradation 577–580, *578–580*
density gradient analysis 163–164b
diurnal synthesis/starch conversion regulation 590–593, *590*
metabolism 577–580, *578–580*
oxidation, net stoichiometry **615**
partitioning 587–593, *589*
symplasmic transport 577, *580*
transport 677–680, *678–680*, **680**, 689–691, *690*, **690**
sucrose facilitators (SUFs) 689–691, *690*
sucrose/H^+ symporters (SUTs/SUCs) 146, 677–680, *678–680*, **680**, 689–691, *690*
sucrose-phosphate phosphatase 575–577, *576*
sucrose-phosphate synthase (SPS) 575–577, *576–577*, 589
sucrose synthase 80, 577–579, *578–580*
SUCs *see* sucrose/H^+ symporters
SUFs *see* sucrose facilitators
sugars
see also carbohydrates
α configuration 47, 48
β-linked polysaccharide synthase genes 86–88
carbon conformations 46, 48
carbon numbers 46
cell walls 45–46, *50*
chair formations 46
D[A]/[A]L designation 48
equatorial/axial positions 46
formula 45–46
GDP sugars 81–86, *83*, *85*, **91**
gluconeogenesis 643–644, *645*
hydroxyl groups 46, 48
interconversion *50*, 81, 83, *83*, *84*, *85*
monosaccharides 48–49
N-assimilation by amino acids 301, *302*
nomenclature *49*
nonreducing 573, *574*
oligosaccharides *see* oligosaccharides
pentose sugars 46, 240, *241*
polymer branching 51
polymer linkages 50, *51*
polysaccharides *see* polysaccharides
raffinose oligosaccharides 681, *681*, 1057–1058, *1059*
reducing/nonreducing 50
uridine diphosphate-glucose 573–577, *576–577*
sugar signaling 607–608, *608*
sulfate **150**
activation 752–753, *752*
assimilation 752–755, *752–754*, 764–767, *764*, *766–767*
reduction 753–754, *753*
sulfated compounds 763–764
sulfate permeases 751–752
sulfhydryl/disulfide regulation, alternative oxidase 636–637, *637*
sulfite oxidase activity 755, *755*
sulfite reductase activity 754
sulfolipid biosynthesis 372–373, *374*
sulfonylamino-carbonyltriazolinones 328, *329*
sulfonylureas 306b, 328, *329*
sulfotransferases 763–764
sulfur 320–321, 323, 746–767
assimilation *748*
chemistry 747–950, *748–751*, 768
cycle *712*
deficiency 746, 765, *765*
remobilization in senescence 954–955, *955*
soil concentrations 749, *750*
transport 750–752, *751*
uptake 746, *747*, 750–752, *751*
sulfur acclimation (*sac*) genes 765
sulfur-containing compounds **748**, 749, *749*
Sulfur–Sulfur (disulfide) bonds 170, 636–637, *637*, 747–749
SULTR transporters **150**
supercomplexes, mitochondrial electron transport chain *624*
superoxide dismutase (SOD)
abiotic stress responses *1087*, 1088–1089
copper deficiency 1127, *1127*
immunity 1016, *1017*
superoxides, mitochondrial, antioxidant defenses 632–633
surface lipids, male fertility 388–389, *388*
survival promotion, virulent pathogens 990
susceptibility, pathogen effectors 1003–1007, **1004**, *1005*, **1007**, *1008*
SUTs *see* sucrose/H^+ symporters
SV *see* slow vacuolar channels
SWRPs *see* systemic wound response proteins
symbiosis, strigolactone signaling 830–833, *830–832*
symbiosis receptor kinase, legumes 727
symbiosomes, legumes 731–733, *732–734*
symbiotic nitrogen fixation 718–735, *720*, **721**, 721b, *722–730*, **724**, *732–734*
amides 720, *734*, 735
bacteroids 731–733, *732–734*
commercial species 720
cyanobacteria 719
gram-positive bacteria 719
microaerobic environment 731–733, *732–733*
molecular genetics 726–733, *726–730*, *732–733*
nodulins 729, *729*
similarity to mycorrhizal symbiosis 721b
ureides 720, 735, *736*
symplasm
definition 659, *662*
phloem loading 681, *681*
plasmodesmata 659, *662*
symplasmic transport
nutrients, roots 669, *669*
phloem unloading 685–691, *685–690*, **686**, *692*
plasmodesmata 659, 661b, *662*
potassium ions 1104, *1104*
sieve element loading 673–674, *673*
sucrose 577, *580*
viruses 994–1000, *999*, *1000*
xylem unloading in leaves 671–672, *672*
symporters 113, 119, *120*, 142, 145
mitochondrial membranes 639, *640*
synaptonemal complex *259*
synaptotagmin, virus trafficking 998, *1000*
synchronization, cell cycle regulation 479–481, *480*
syncytial feeding structures, nematodes *1001*, 1002
syntaxins 175–176
synteny 416, *417*
synthesis *see* biosynthesis
systemic acquired resistance (SAR) 828–830, 1033–1038, *1035–1037*, **1038**, *1039*
systemic wound response proteins (SWRPs) *1036*, 1039–1040
systemin 457–458, *460*, 1039

TAA1 *see* tryptophan aminotransferase
tabtoxinine-β-lactam 293, *296*
tagging, transposons 421
tail-anchored (TA) proteins 169
TALENs *see* transcription activator-like effector nucleases
TALEs *see* transcription activator-like effectors
tandem repeats 406
TANGLED 222–225, *226*
TA proteins *see* tail-anchored proteins
targeted protein degradation, auxin transduction 852–854, *853–854*
target genes, chromatin immunoprecipitation 430, 431b
targeting domains 151–152, **153**
chloroplasts *156*, 157
dual targeting 159
mitochondria 157–158, *157*
multiple 153, *156*, 157, 159
targeting signals 152b
target of rapamycin (TOR) kinase, autophagy 928
ta-siRNAs *see trans*-acting small interfering RNAs
TATA binding protein (TBP) 425, *425*
TATA boxes
gene expression 427, *427*
heat shock factors 1096–1097
recognition 425, *425*
TAT (twin arginine translocation) pathway *156*, 157
TBP *see* TATA binding protein
TD *see* threonine deaminase
T-DNA *see* transferred DNA
telomerase 250, *251*, 412
telomeres 250, *250*, *251*, 412
telophase *478*
nuclear envelope reassembly 31
nucleoli reformation 31
vacuole volume reduction 27
temperature
carbon dioxide assimilation 653–654, *654*
cell membrane fluidity 7
cold acclimation 12
fatty acid desaturation 360
photosynthetic quantum yield 653–654, *654*
temperature gradient chromatography 52b, 53b
temperature of melting (T_m) 7, **8**, 352–353, *356*
terminal development, leaves 940–948, *941–942*, **944–945**, *946–947*, *949*

terminal dUTP nick end labeling (TUNEL) assay 926–927, *927*
terminal flower 1 (*tfl1*) mutants 881–882, *883*
termination
  cell cycle 479
  protein synthesis 447, *448*
ternary complexes 441, *443*
terpenes
  diversity 1142–1143, *1144*
  pest feeding 1002
  skeleton modification 1143–1145, *1145*
  terpenoid cyclizations 1141–1143, *1142–1144*
terpene synthases 1141–1143, *1142–1144*
terpenoids 1113–1145, *1135–1137*, *1145*, 1147–1148b
  biosynthesis 771–773, *772–773*, 1135–1145, *1136–1144*, *1145–1147*
  classification 1147–1148b
  five carbon unit fusion 1134–1135, *1136*, 1138–1141, *1140*
  functions 1133–1134
  identification 1147–1148b
  metabolic engineering 1145, *1147*
  metabolites 1132–1133, *1132*
  methylerythritol-4-phosphate pathway 1138, *1139*
  mevalonate pathway 1135–1138, *1137*
  prenyl diphosphate biosynthesis 1138–1141, *1140–1141*
  prenyltransferases 1140–1142, *1141*, *1143*
  skeleton modification 1143–1145, *1145*
  terpene formation 1141–1143, *1142–1144*
Ter sites 250
TEs *see* tracheary elements
tethering structures 10
tetrahydrodipicolinate 320
tetrapyrrole rings in chlorophyll 515, *515*
TFIIB recognition elements (BREs) 427, *427*
TFIIH transcription factor 269
tfl1 mutants *see terminal flower 1* mutants
TGN cisternae 21
TGNs *see trans*-Golgi networks
Theriak 1159–1161, *1162*, 1163b
thermal noise, Brownian motion 192, 193b
thermogenesis 636b, 826–827
thermotolerance 1094–1097, *1094–1095*, *1097*
thioesterases, fatty acid biosynthesis 352, *355*
thioester linkages, acyl carrier protein *350*, 351
thioredoxin (Trx) 552b, 553, 554b, 555, *555–557*
  ADP-glucose pyrophosphorylase regulation 583, *584*
  alternative oxidase 631, 636–637, *637*
Thr *see* threonine
three-dimensional (3D) NMR 56b
threonine deaminase (TD) 326, *326*, *327*, 328b
threonine-rich proteins *69*, 99, 103
threonine synthase (TS) 319, *321*, 323, *324*, *325*
threonine (Thr)
  nitrogen assimilation *292*
  O-glycosylation 188
  precursor to Ile, Leu, Val *326*, *327*
  structure *290*
  synthesis *291*, 319, *320*, *321*
  synthesis regulation 323–324, *323*, *324*, *325*
threshold voltage 133, *134*
thylakoid ATP synthase 537–540, **539**, *540*, *553–558*
thylakoids 2, 35–37, *35*, *36*, *37*, 155, *156*, 157
  electron transport pathways 529–536, *530–535*
  photosynthesis 510, *510*
  photosystem organization and regulation 540–542, *540–541*, **540**
  protein biosynthesis 452–453
  proton gradients 537–540, **539**, *540*, *553–558*
thymidylate synthase 243
thymine *241*, 243, *247*
Ti *see* tumor-inducing
Tic complex 155, *156*
TIM complex *157*, 158, 159
tip growth 91, *92*
α-TIP protein 28, 185
γ-TIP protein 28
TIPs *see* tonoplast intrinsic proteins
TIR1, auxin signal transduction 853, *853*
tissue printing *70*
TKRP125 *see* tobacco kinesin-related protein of 125 kDa
TMV *see* tobacco mosaic virus
tobacco kinesin-related protein of 125 kDa (TKRP125) 234, *236*
tobacco mosaic virus (TMV) 965–968, *966–967*, 994, *999*, *1000*
tobacco (*Nicotiana tabacum*) *272*, 282–283b, 1161, *1168*, 1170b
Toc complex 155, *156*
tocopherol 309
α-tocopherol (vitamin E) 309, 1088, **1088**
TOCSY (total correlation spectroscopy) 56–57b
toeprinting 458b
tolerance
  aluminum toxicity 1106–1107, *1106*, 1109
  flooding 1076–1085, **1076**, *1077–1081*, *1083–1084*
  oxidative stress 1091–1092, **1092**
  viruses 1042–1045
TOM complex *157*, 158, 159
tonoplast
  anion channels 132, *141*
  H^+-PPases 127
  malate channel 142
  membrane 27, 1117
  pH *141*
  proton gradients *115*, 576b
  sucrose transporters 146
  TPK1 channels 138
  V-type H^+-ATPases 126–127
  water permeability 148
tonoplast intrinsic proteins (TIPs) 147, 735
topogenic sequences 168–169, *168*
topoisomerase *248*, 259
TOR *see* target of rapamycin kinase
total correlation spectroscopy (TOCSY) 56–57b
totipotency 426, 501–502, *501–502*
toxin sequestration 28
TPC (two-pore channel) family 140, *140*
TPK1 channels 137–138, *138*, **149**
TPP *see* trehalose phosphate phosphatase
TPS *see* trehalose phosphate synthase
TPT *see* triose phosphate translocator
tracheary elements (TE)
  see also xylem
  cell biology 664–666, *665*
  development 933–937, *935–938*
  differentiation 664
tracheids *47*, 103, 665
trafficking *15*
  see also endoplasmic reticulum; Golgi…; protein sorting; secretory pathway; transport; transporters
  cell walls 79–80
  cytoplasm/nucleus 29, 30
  cytoplasm/vacuoles 28
  cytosol/chloroplasts 34
  ER/Golgi/TGN-associated vesicles 13, 16, *19*, 20–21, 22, *23*
  ER/mitochondria 17
  ER/plasma membrane 17
  ER/plastids 17
  mitochondria 41
  nuclear pores 30, *30*
  plastid/plastid 33
trans-acting factors, gene expression 423, 427, *427*, *429*
trans-acting small interfering RNAs (ta-siRNAs), transcription 276, *276*, 277, **278**, 285, 423
transaldolase *598*, 601
transaminases 299
transcellular routes, intercellular transport 659
transcription
  phases 424
  preinitiation complexes 424–425, *425*, **425**
  RNA polymerases 422–425, **424**, *425*
transcription activator-like effector nucleases (TALENs) 257b, 1048–1049, *1048*
transcription activator-like effectors (TALEs) 1003–1006, *1005*, 1048–1049
transcriptional co-repressors 435, *435*
transcriptional regulation
  brassinolide biosynthesis 814
  DELLA proteins 863, *863*
  ethylene biosynthesis 808, *808*
  signal perception 835–836, *835*
transcription factors 170, 174, *174*, 268, 269, 335b
  copper homeostasis 1126–1127, *1127*
  flower organ specification 885–887, *888*
  G1-to-S transition 488–981, *489–490*
  gene expression *428*, 429–430, **430**, 431b, 434–435
  MADS domain 430, 886–887, *888*
  regulation of seed oil biosynthesis 393
  seed development 916–918, *917–918*
  signal perception 835, *835*
  stability regulation, phytochromes 860–861, *861*
  water stress 1062–1068, *1063–1065*, *1067–1068*
transcription preinitiation complex 424–425, *425*, **425**
transduction, mechanical, cytoskeleton 220–222, *221*
transfer cells *46*
transferred DNA (T-DNA), plant transformation 996–997b
transfer RNA-isopentenyltransferase (tRNA-IPT) 791–792, *792*

transfer RNAs (tRNAs) 271, *272*, 273
cytokinin synthesis 791–792, *792*
cytoplasmic vs. plastid 273, *273*
functions 270
genomic locations 439
introns 279
mitochondrial 44, *266*
nuclear 160
plastid 261
processing *281*, 282, 285
transcription 423
transgenic plants 165b
β-transglucanases 96
transition element nutrition and uptake 1125
transitory starch 564–565, *564*
transit peptides 154–155, *156*, 157
transketolase *546–547*, 548, *598*, 601
translation of messenger RNA 439–457, *452–457*, *459*
translesion replication 254
translocation complex 168
transmembrane signaling receptors 12
transmembrane transport 639–646, *640–645*, 661b
see also active transport; facilitated diffusion; ion channels; pumps; transporters
transport
see also electron carriers; ion channels; transporters
anions, xylem parenchyma cells 669
ATP in plastids 605–606, *607*
auxin 854–857
carbon skeletons, plastids 605–606, *607*
electrons
mitochondria 620–646, *620*
ubiquinone 621, *622*
iron 1120–1125
lipids, endoplasmic reticulum to/from chloroplasts, membrane lipid biosynthesis 366, *367*, *368*
metabolites, from mitochondria 639–646, *640–645*
nitrate 738–739
nitrogen, legume roots 720, *734*, 735–739, *736–741*
nutrients, phloem loading 673–674, *673*
phloem, whole-plant organization *659*, 696–704, *698–704*
potassium ions 1103–1113, *1104*, **1105–1106**, *1106–1107*, *1110*
vesicles 16, *205*
viruses 994–1000, *999*, *1000*
xylem, whole-plant organization *659*, 691–696, *692–697*
transporters 111–112, 113, 146, *146*
see also cotransporters; ion channels; pumps
amino acids 291–292
apoplastic sieve element loading 677–680, *678–680*, **680**
interactions 119–120, *120*
iron, roots 1121–1122, *1121–1122*
micronutrients 1121–1126, *1121–1126*
phosphate, roots 1114, *1114*
potassium ions 1104–1113, **1105–1106**, *1106–1107*, *1110*
sodium 1112–1113
sodium–potassium 1112–1113
sulfur 750–752, *751*
transport rates 113
types 113
transport phloem 673, 682–683, *683–685*
transport rates 113
transport vesicles 16, *205*
transposable elements
chromosome breakage 421
classification **418**, 419–420, 422b
footprints *419*, 420
genome structure 416–422, **418**, *419–420*, 422b, *423–424*
transposons, mutation and expression modification 421–422, *423–424*
transposon tagging 421
trans-sulfuration pathway 320
trans-zeatin (tZ) *785–786*, 787–792, *788–792*
traumatin, signaling 382
treadmilling, cytoskeleton 200, *202*
trehalose-6-phosphate, growth regulation 607–608, *608*
trehalose phosphate phosphatase (TPP) 608, *608*
trehalose phosphate synthase (TPS) 608, *608*
triacylglycerols 15
biosynthesis 389–393, *390*
hydrolysis, germination/pollination 393–395, *394*, *396*
lipid storage 339–342
oil bodies 391–392, *391*
properties 338
structure 339, *344*
triazolopyrimidines 306b, 328, *329*
tricarboxylic acid cycle *see* citric acid cycle
trichomes 45, *46*, *104*, *107*
TRiC proteins, protein folding 461–462, **461**, *462–464*
triglycerides, gluconeogenesis 643–644, *645*
triose phosphate isomerase 545, *546–547*, *598*, 600–601
triose phosphate/pentose phosphate pool 597–601, *598*, *600*
triose phosphate pools
fructose-2,6-bisphosphate level modulation 588–589
fructose-1,6-bisphosphate level modulation 589
pyrophosphate-dependent phosphofructokinase 575–576b
triose phosphate translocator (TPT) *569*, 573, 590–591
trioses 46
triple response, ethylene signaling 847, *847*
triplet states, chlorophyll 512
triterpenes 1133, *1136*, 1143, *1144*
tRNA-IPT *see* transfer RNA-isopentenyltransferase
tRNAs *see* transfer RNAs
tropomyosin 207
Trx *see* thioredoxin
tryptophan aminotransferase (TAA1) 798
tryptophan analogs 312
tryptophan-independent synthesis of auxin 798–801, *799*
tryptophan insensitive AnS 313b
tryptophan synthase (TS) *311*, 314–316, *316*, *317*
tryptophan (Trp) *290*, 309, *309*
nitrogen assimilation *292*
synthesis
anthranilate synthase 309, 312, *312*
biosynthesis pathway *291*, *303*, *311*
genetic analysis 309
indole-3-glycerol-phosphate synthase 314, *316*
phosphoribosylanthranilate isomerase 314, *314*
phosphoribosylanthranilate transferase 312, *313*
tryptophan synthase 314–316, *316*, *317*
L-tryptophan (L-Trp), auxin biosynthesis 796, *797*, *799*
TS *see* threonine synthase; tryptophan synthase
TSA genes 315–316, 317b
TSB genes 315–316
TTTAGGG repeats 412
tubular network, cytokinesis 237, *237*
tubulin
see also microtubules
critical concentration 197, 200
gene families 194–199
isoforms 195–196
microtubule characteristics 196–202
nucleation 197–199, *197*
post-translational modification 196
structure *200*
α-tubulin
gene families 194–199
β-tubulin dimerization 198, *200*
β-tubulin
gene divergence *195–196*
gene families 194–199
α-tubulin dimerization 198, *200*
vascular plants 195
γ-tubulin 207, 218–219, *219*
tubulovesicular network of phragmoplasts 237, *237*
tufA gene 267
tumor-inducing (Ti) plasmids 996–997b
TUNEL *see* terminal dUTP nick end labeling assay
turgor pressure 11
anion channels, regulation by 141
biophysics of growth 93
cell expansion 90, 92
generation of 112
impact on membrane events 24–25, *25*
vacuole expansion 27
turnover, cyanogenic glycosides 1157–1158, *1158*
twin arginine translocation (TAT) pathway *156*, 157
two-component system, cytokinin signal transduction 850–852, *850–851*
two-dimensional (2D) NMR 56b, 57b, 58b
two-pore channel (TPC) family **149**
type I arabinogalactans (AGs) 67
type I DAHP synthases 303
type I walls 77–79, *77*, 95, 96, 99, 104
type II DAHP synthases 302–303
type II walls *77*, 79, 96, 97, 99, 104, 105
type III walls 65
type I fatty acid synthase 350
type II fatty acid synthase 350–352
typeIII/typeIV secretion systems, legume–rhizobial symbiosis 723
tyrosine aminotransferases 308–309
tyrosine (Tyr)
nitrogen assimilation *292*
structure *290*
synthesis *291*, *303*, 306, *307*, 308–309
tZ *see trans*-zeatin

ubiquinol (UQH_2) *622*
ubiquinone (UQ) 621, *622*
  alternative oxidase regulation 638, *638*
  redox chemistry 621, *621*, *622*
  structure *622*
ubiquitin 469–474, *470–471*, **472**, *473–474*
  auxin signaling 852, *853*
  cell cycle control 486–487, *488*
  regulation 473–475
  senescence 957
  structure 469, *470*
ubisemiquinone anion ($UQ^{\bullet-}$) *622*
UDP *see* uridine diphosphate
UDP-Glc-glycoprotein glucosyltransferase (UGGT) 170, *171*, **172**, 173
UDP-glucose:sterol glycosyltransferase 11
UDP-glucose *see* uridine diphosphate-glucose
UDP-glycosyltransferases (UGT) 1152–1157, *1152*, *1155*
UDP (uridine) sugars **91**
  cellulose synthase genes 86
  cellulose synthase substrate 80
  in cell wall biosynthesis 81, *83*
  glycans synthesis 86
  mixed-linkage β-glucan synthase substrate 85
  nucleotide sugar interconversion 81, 83, *84*
  substrates of glycosyl transferases **91**
UGGT *see* UDP-Glc-glycoprotein glucosyltransferase
UGT *see* UDP-glycosyltransferases
ultrastructural elements, sieve elements **666**
UMP *see* uridine 5′-monophosphate
umu genes 254
Umu proteins 254
uncoupling proteins
  respiratory control 635, *635*
  thermogenesis 636b
unfolded protein response (UPR) 174–175, *174*
uniconazole 773, *774*
unique R-proteins 1032
unisexual flowers, sexual identity 939, *939*
unloading
  phloem 673
    apoplastic transport 685–687, *685*, **686**, *687*
    symplastic transport 685–691, *685–690*, **686**, *692*
  xylem, leaves 671–672, *672*
unsaturated fatty acids **341**
5′-untranslated regions (UTR) 441–442, 444b, 447–449, *449*, 450b
unusual fatty acids
  biosynthesis 360–363, *361–362*
  seed oils 363
UPR *see* unfolded protein response
UPS *see* ureide permease
upstream open reading frames 441–442, 445b
uptake
  copper 1126
  iron 1120–1124, *1121–1125*
  phosphate 1114–1118, *1115–1118*
  potassium ions 1104–1113, **1105–1106**, *1106–1107*, *1110*
  sulfur 746, *747*, 750–752, *751*
  transition elements 1125
UQ *see* ubiquinone
UQH_2 *see* ubiquinol
uracil *241*, 243
urea 146, 332
urea permease AtDUR3 146
ureide permease (UPS) 146
ureides, nitrogen fixation 720, 735, *736*
uric acid 245b
uridine 5′-monophosphate (UMP) *242*
uridine diphosphate-glucose (UDP-glucose)
  glucose-1-phosphate interconversions 573
  glucose synthesis 573–577, *576–577*
  structure *575*
uridine diphosphate (UDP), galactolipid/sulfolipid biosynthesis 372–373, *373–374*
uridine triphosphate (UTP) *242*, 243
uronic acids 52b
UTP *see* uridine triphosphate
UTR *see* 5′-untranslated regions
UV light 251–252, *252*
UVR8 859

V *see* vanadium
VAC2 construct 177b
vacuolar K^+ (VK) channels 136–137, *137*, *138*
vacuolar processing enzymes (VPEs) 928, 965–968, *967*
vacuolar sorting receptors (VSRs) 183–184, *184*
vacuolar sorting signals (VSSs) 177b, 182–183, *183*
vacuoles *3*
  see also lytic vacuoles; protein storage vacuoles
  ABC transporters 127–128, *127*
  cation channels 136–138, *137*, *138*
  cell expansion 27
  cell volume occupied 27, *27*
  changes during cell cycle 27
  energy conservation 27
  ER attachment sites 17
  functions 27–28
  gluconeogenesis 643–644, *645*
  invertase activity 579
  malate transport 141–142, *141*, *142*
  membrane voltage 117
  in meristematic root tip cell *3*
  osmolarity 27
  pH 126
  proteases 468–469, *468*
  sequestration of amphipathic metabolites 127–128, *128*
  sequestration of xenobiotics 127–128, *128*
  slow vacuolar channels 139–140, *139*, *140*
  solutes 27
  traffic *15*, 175
  transformation pathways 28
  types 28, *29*
  V-type H^+-ATPases 126–127, *126*
valine (Val)
  nitrogen assimilation *292*
  precursor to metabolites *326*
  structure *290*
  synthesis *291*, *327*, 328–329
VAM *see* vesicular-arbuscular mycorrhizae
vanadium (V), alternative nitrogenases 716
variable flow rates, xylem 668
variable stoichiometry, photosystem organization 540–544, *540–541*, **540**
vascular development
  auxin 856–857, *856–857*
  canalization hypothesis 856, *856*
vascular plants, β-tubulins 195
VDAC *see* voltage-gated anion channels
vectors
  arthropods 1002–1003, *1003*
  recombinant DNA 996–997b
vegetative development
  see also development
  transition to reproductive development 872–881, 880b, *881*
velocity
  diffusion 663
  xylem flow rates 668
VEN genes 333
vernalization
  cellular memory 878–879
  flowering initiation 874, 878–879, *879*, 880b
vernolic acid *361*
vesicles, transport *205*
vesicular-arbuscular mycorrhizae (VAM) 1115, *1115*, 1118
vessel elements 665
victorin-induced programmed cell death 974, *975*
vira RdRPs 275
virulence-factor repertoires of pathogens 1009, **1011**, *1012*, *1013*
virulent pathogens, survival promotion 990
virus-encoded protein (VPg) 449b
viruses
  cap-independent translation enhancers 447–449, *449*, 450b
  hypersensitive response 965–974, *966–968*, **969–970**, *972–974*
  introduction by insects 1002–1003, *1003*
  leaky scanning 444b
  nucleic acids 240, *241*
  pathogen effectors **1004**
  pathogenesis 994–1000, *999*, *1000*, **1004**
  phloem transport 703, *703*
  protein diversity 450
  protein synthesis 444b, 447–450, *449*, 450b
  resistance, tolerance and attenuation 449b, 1042–1045, 1049
  transport 994–1000, *999*, *1000*
vitamin C (ascorbate), antioxidant systems 1088, **1088**
vitamin E (α-tocopherol), antioxidant systems 309, 1088, **1088**
vivipary
  abscisic acid 778, *778*, 782–784, *783*
  Zea mays 778, *778*, 782–784, *783*
VK *see* vacuolar K^+ channels
volatile indoles 316
volatile terpenes *1136*
volatilization, ethylene 810
voltage 140–141, *141*
  threshold 133, *134*
voltage-gated anion channels (VDAC), mitochondria 611
voltage-sensing potassium ion channels 1104–1113, **1105–1106**, *1106–1107*, *1110*
voltage sensors 135, *136*
volume flow rate 660b
voodoo lily, thermogenesis 636b, 826–827
VPEs *see* vacuolar processing enzymes
VPg *see* virus-encoded protein
VSRs *see* vacuolar sorting receptors
VSSs *see* vacuolar sorting signals
VTI snares 177b
V-type H^+-ATPases 126–127, *126*

WAKS *see* wall-associated kinases
Walker A and B motifs 127, *127*
wall-associated kinases (WAKs) 107, 108
WallBioNet 89b
Warburg, O. 646–647
warts *47*
waste product excretion 112
water
  membrane permeability 4, 111, *112*, 148
  oxidation by photosystem II 525–526, *525*
  polymer conformation impacts 79–80
  vacuole expansion 27
water deficit *see* water stress
water flows
  see also bulk flow
  collection phloem 681, **682**
  phloem unloading 691, *692*
  xylem loading 668–669, *670*
water–plastoquinone oxidoreductase activity of photosystem II 522–528, *524–528*, **524**, **527**
water potential 93, 94, 660–661b
  phloem 681, **682**, 685–691, *686–689*
  plant health 1054
  xylem 668–669, *670*, 672
water retention, epicuticular wax 385–388
water stress
  abscisic acid 1060–1063, *1061*, *1063–1064*, *1068*
  cavitation 695, *696*
  gene expression 1061–1068, *1063–1066*, *1067–1068*
  osmolytes 1055–1056, *1056–1057*
  osmotic adjustment 1055–1056, *1055*
  physiological and cellular responses 1054–1061, *1055–1060*
  signaling pathways 1065–1068, *1067–1069*
  wilting 27
water transport 146–148, *147*, *148*
water uptake equations 93
waxes
  biosynthesis 338, 386–388, *387*
  membrane deposition 385–388, *387–388*
WEE1 kinase, cyclin-dependent kinase regulation 485, *486*
Welwitchia mirabilis, leaf senescence 941, *941*
WGS *see* whole genome shotgun sequencing
wheat (*Triticum* spp.), tRNA *272*
whole genome profiling 406, 407–408b
whole genome shotgun (WGS) sequencing 408, 409b
whole-plant organization
  phloem transport *659*, 696–704, *698–704*
  xylem transport *659*, 691–696, *692–697*
Wiesner reagent (phloroglucinol-HCl) 105
wilting 27
Wollaston, H. 193
wound healing 457–458, *460*, *1036*, 1039–1040
wound-signaling pathways 379, *382*
WOX (WUSCHEL-RELATED HOMEOBOX) transcription factors 916–918, *917–918*
WRINKLED1 (WRI1) 393
wrinkled pea starch granules 583b
WRKY genes 106
WUSCHEL-RELATED HOMEOBOX (WOX) transcription factors 916–918, *917–918*
WUSCHEL (WUS) 498, *498*, 887–888

xanthophyll cycle 519, *520*
xanthophylls 37–38, 519, *520*, *530*
xenobiotics 28, 127–128, *128*, 760–762, *761–762*
Xenopus laevis oocytes 142–143, *143*, 145, *146*, 147
XET *see* xyloglucan endo-β-transglucosylases
XTHs *see* xyloglucan endotransglycosylase/hydrolases
XyGs *see* xyloglucans
Xyl *see* D-xylose
xylem
  air seeding 693, *694*
  amino acid concentrations 293
  angiosperms *665*
  bulk flow 663–664, *664*
  cell biology 664–666, *665*
  cohesion–tension mechanism 691, *693*
  development 664–666, 933–937, *935–938*
  differentiation 664
  driving forces 663–664, *664*, 691, *693*
  embolism repair 693–694
  functional properties 668–672, *669–671*
  hydraulic conductance 668–669, *670*, 691–696, *694–696*
  lignin functions 664, 666
  loading 668–669, 670–671, *671*, 739
  osmotic pressure 672, *672*, 695
  parenchyma cells *665*, 666, 669
  peak flow velocities 668
  pit hairs/membranes 665–666, *665*
  regulation 670–671, *671*
  sap solute concentrations **671**
  transport of potassium ions 1104, *1104*, 1112
  unloading, leaves 671–672, *672*
  variable flow rates 668
  vessel diameters 665
  whole-plant organization *659*, 691–696, *692–697*
xylogalacturonan *66*, 67
xylogenesis 933
xyloglucan endo-β-transglucosylases (XET) 95, *95*, 96, 102
xyloglucan endotransglycosylase/hydrolases (XTHs) 96, 1084
xyloglucans (XyGs)
  backbone 50
  cellulose/crosslinking glycan network regulation 94–95
  evolution 70–71, *75*
  side groups **63**
  storage 106
  structures 51–52, *59*, 63
  synthesis 86
  Type I walls 77
D-xylose (Xyl) 49, *50*, 83, *187*
xylosidase 96
xylosyltransferases 86

Yang cycle (methionine cycle) 806–808, *807*
Yariv reagent 69
YDA *see* YODA
yeast 477–479, 1108b, 1111b
yellowing of rice leaves 945–948, *946–947*
yield
  see also quantum yield
  abiotic stress 1051, *1052*
  soil sulfur content 750
  thresholds 93
YODA (YDA) 916–917, *917*
YUCCAs, auxin biosynthesis 796–798

cis-zeatin (cZ) *785*, 787, 791–793, *792*
zeatin *O*-glucosyltransferase 795
trans-zeatin (tZ) *785–786*, 787–792, *788–792*
zein *17*
zeitlupes 858–859b
ZFNs (zinc-finger nucleases) 257b
zig-zag-zig scheme, immunity 955, *988*
zinc, deficiency *1102*
zinc finger proteins 257b, 429–430, *429*
Zinnia elegans 933–936, *935–937*
ZIP transporters **149**
Z-scheme 530–531, *531–532*

WILEY END USER LICENSE AGREEMENT

Go to www.wiley.com/go/eula to access Wiley’s ebook EULA.